4th Meeting on
Chemistry & Life

BRNO, Czech Republic
September 9–11, 2008

Organised by Faculty of Chemistry
Brno University of Technology

The Fourth Meeting on Chemistry & Life was held in the beautiful city of Brno which is the educational and cultural centre of the South Moravian part of the Czech Republic. It draws upon the tradition of three annual meetings providing a forum for exchange of ideas on recent advances in research and development in chemistry, biotechnology, materials science and environmental technology for people from industry, research and academia. The conference was held at the Faculty of Chemistry, Brno University of Technology under the auspices of the rector of the Brno University of Technology, prof. Karel Rais, MBA.

THE SUBJECT SESSIONS
- Environmental Chemistry & Technology (head of the session: Josef Čáslavský)
- Food Chemistry & Biotechnology (head of the session: Jiřina Omelková)
- Chemistry of Inorganic Materials (head of the session: Jaromír Havlica)
- Chemistry of Organic Materials (head of the session: Zdeněk Friedl)
- Photochemistry (head of the session: Michal Veselý)
- Physical & Applied Chemistry (head of the session: Miloslav Pekař)
- Polymers & Polymer Composites (head of the session: Josef Jančář)

SCIENTIFIC COMMITTEE

Chairman:
Jaromír Havlica

Vice-Chairman:
Ladislav Omelka

Members:
Josef Čáslavský   (Brno University of Technology, Czech Republic)
Zdeněk Friedl   (Brno University of Technology, Czech Republic)
José Luis Gómez-Ariza   (Universidad de Huelva, Spain)
Josef Jančář   (Brno University of Technology, Czech Republic)
Frank Jones   (University of Sheffield, United Kingdom)
Branimir Jovančićević   (University of Belgrade, Serbia)
Alan J. Lesser   (University of Massachussetts, USA)
Ivan Mašek   (Brno University of Technology, Czech Republic)
Jiřina Omelková   (Brno University of Technology, Czech Republic)
Miloslav Pekař   (Brno University of Technology, Czech Republic)
Juhani Peuravuori   (University of Turku, Finland)
Jan Schwarzbauer   (Aachen University Lochnerstr, Germany)
Andrej Staško   (Slovak Technical University Bratislava, Slovakia)
Michal Veselý   (Brno University of Technology, Czech Republic)
Martin Weiter   (Brno University of Technology, Czech Republic)

ORGANIZING COMMITTEE

Chairman:
Radek Přikryl

Vice-Chairman:
Renata Herrmannová

Members:
Hana Alexová
Petr Dzik
Miroslav Geršl
Martin Moos
Ilona Pipková
František Šoukal
Roman Varmuža
Eva Vitoulová

The Faculty of Chemistry, Brno University of Technology
thanks to the following partners and companies, supporting the
4th Meeting on Chemistry & Life:

Amedis, spol. s r.o.
Anamet s.r.o.
AutoCont CZ a.s.
Brněnské vodárny a kanalizace, a.s.
Dopravní podnik města Brna a.s.
Labimex s.r.o.
LECO Instrumente Plzeň s.r.o.
Merci s.r.o.

Nicolet CZ s.r.o.
PLIVA d.d.
Sigma-Aldrich spol. s r.o.
Veletrhy Brno, a.s.
Verkon s.r.o.
Vysoké učení technické v Brně
2 Theta ASE, s.r.o.

TABLE OF CONTENTS

PREFACE

Dear participants of the Chemistry and Life 2008 conference,

like three years ago, this year a special issue of the Chemické listy Journal with contributions presented at this 4th successive conference Chemistry and Life has been delivered to you again. Unlike the previous conference contributions, this year's ones have been published electronically on a CD, which might be appreciated by many of you, dear participants.

Since 1999 the conference Chemistry and Life has regularly been organized by Faculty of Chemistry of Brno University of Technology (BUT). It has become one of the most significant items in the field of science and research activities implemented by the faculty. Specialists have shown increasing interest in the conference and the present Organizing Committee has received almost 300 contributions that will be presented in 7 sessions. Besides the traditional attendance of Czech and Slovak chemists we also appreciate increasing number of contributing scientists and researchers from abroad.

Fruitful cooperation with industry enables implementation of the conference in broad extent designed by the organizers. The conference committees are pleased to offer accompanying social programme that might contribute to successful course of the conference.

Dear participants of the 4th Chemistry and Life conference, on behalf of both the Organizing and Scientific Committees I feel honoured to welcome you to the grounds of Faculty of Chemistry of BUT. At the same time let me express the hope that the conference outcomes will contribute to development of knowledge in various branches of chemistry.

Assoc. Prof. Jaromír Havlica, Ph.D.
Dean of Faculty of Chemistry of BUT Brno
Chairman of the Scientific Committee of the Chemistry and Life 2008 conference

Explanatory note:

The contributions published in this journal supplement are numbered in accord with accepted abstracts. Based on the requests of some authors several full text contributions were not published in the journal even if they were presented in the form of either conference posters or lectures. Abstracts of all the conference contributions were published in the Book of Abstracts of the 4th Chemistry and Life 2008 conference that is available at the www.fch.vutbr.cz/chl_2008 website.

1. PLENARY LECTURES

L01 FUNCTIONAL DAIRY PRODUCTS – FROM TRADITIONAL TO MODERN BIOTECHNOLOGY

IRENA ROGELJ and BOJANA BOGOVIČ MATIJAŠIĆ

University of Ljubljana,Biotechnical faculty
Jamnikarjeva 101, 1000 Ljubljana, Slovenia
Irena.rogelj@bfro.uni-lj.si

Introduction

There are many aspects of functional food concept and as a consequence this term has no exact definition. It is usually described as "food which promotes health beyond providing basic nutrition".

In order to establish a scientific basis to the new areas of functional foods, the European Functional Food Science Programme (FUFOSE) was set up. The following definition was proposed[1]: »A food can be regarded as "functional" if it is satisfactorily demonstrated to affect beneficially one or more target functions in the body, beyond adequate nutritional effects, in a way that is relevant to either an improved state of health and well-being and/or reduction of risk of disease«. Some additional conditions were stressed as well: »Functional foods must remain foods, and they must demonstrate their effects in amounts that can normally be expected to be consumed in a diet. According to this definition a functional food can be[2]:

- A natural food in which one of the components has been naturally enhanced through special growing conditions.
- A food to which a component has been added to provide benefits
- A food from which a component has been removed so that the food has less adverse health effects.
- A food in which the nature of one or more components has been chemically modified in order to improve health.
- A food in which the bioavailability of one or more components has been increased to provide greater absorption of a beneficial component.
- Any combination of the preceding possibilities.

Dairy Products in the Light of Functional Food

Milk and dairy products have long been seen as a »healthy food« and an essential component of a diet. Yoghurt is perhaps the most popular of all fermented milks. The belief in its beneficial influence on human health has existed in many civilizations over a long period of time. In Ayurveda, one of the oldest medical sciences that date from around 2500 BC, the consumption of yoghurt has been recommended for the maintenance of overall well being[3]. In 76 BC the Roman historian Plinius recommended the administration of fermented milk for treating the gastrointestinal (GIT) disturbances[4]. Therefore, fermented milk could be regarded as nature's original functional food. However, not earlier than nearly 2000

years later man started to recognize the agents which convert milk to the sour milk - the Lactic Acid Bacteria (LAB).

Whey, a co-product of cheese-making, was discovered about 3000 years ago. There are historical references about the use of whey as aphrodisiac and for medical purposes, including sepsis, wounds' healing, and 'stomach disease'[5,6]. Nowadays, sound scientific substantiation of the nutritional and biological qualities of whey components, notably the proteins, is increasing and whey-based ingredients have become prominent representatives of the functional foods.

Today we know that milk contains an array of bioactive peptides and is rich in antioxidants, highly absorbable calcium, conjugated linoleic acid (CLA) and other biologically active components. Nutritional and genetic interventions to alter the milk composition for specific health and/or processing opportunities are gaining importance in dairy biotechnology. Less fat in milk, altered fatty acid (FA) profiles with less saturated FA and more healthy FA such as CLA, improved amino acid profiles, less lactose, and absence of β-lactoglobulin are some examples of milk »designing«[7,8]. Furthermore, a wide range of products can be obtained from this nourishing liquid.

"The variety of functional foods that can be developed is limited by our imagination" wrote Spence[9] who grouped functional foods in four types (Table I). Although dairy products can be found in each type, it has to be stressed that we may use the term "functional" only for products with proven health benefits.

Table I
Different types of functional foods

Type	Characteristics	Example of dairy products
Fortified products	Increased content of existing nutrients	Products fortified with Ca, vitamins or antioxidants (Q10)
Enriched products	New nutrients or components added (not normally found in particular food)	Products enriched with pro-, pre-biotics
Altered products	Existing components replaced or chemically modified	Products with fat replacers (fat free) Hydrolysed milk
Enhanced commodities	Changes in the raw commodities that have altered nutrient composition	Milk with altered FA profile (less saturated FA, more omega-FA and CLA. Milk with higher level of melatonin.

Bioactive Components of Functional Dairy Products

Milk is a natural source of a variety of beneficial nutrients and biologically-active compounds with potential impacts on the human health. Designing and developing functionality

in dairy products simply means modifying and/or enriching the healthy nature of the original base. In addition, progress in food processing and biotechnology offers new possibilities in creating foods with special characteristics and functionality. Among the most prominent representatives of functional dairy products are certainly fermented products.

The health promoting effects of the fermented dairy foods may be related to the biological activity of the lactic acid bacteria (LAB) used in the production of these products.

In theory, LAB can exert beneficial effects through two mechanisms: direct effects of the live microbial cells or indirect effects via biogenics. The special type of bacteria associated with "healthy" gastro intestinal tract (GIT) has been classified as "probiotic" bacteria. By FAO/WHO[10] definition, probiotics are live microorganisms which, when ingested in adequate amounts, deliver measurable physiological benefits, which are usually strain specific. Biogenics are defined as food components derived from microbial activity which provide health benefits without involving intestinal microflora[11]. According to this definition the biogenics of fermented milk are the substances such as lactic acid, butyric acid, bioactive

Table II
Health benefits of probiotic cultures

Health benefit	Mechanisms
Prevention/treatment of GIT infections, diarrhea	Antimicrobial activity (organic acids, hydrogen peroxide, bacteriocins) Depletion and/or competition for substrates Occupation specific binding-sites Reduction of luminal pH
Improvement in lactose metabolism	Production of β-D-galactosidase
Antimutagenic properties	Binding of mutagens Reduction of faecal enzymatic activity (β-glucuronidase, azoreductaze, nitroreductaze) Production of butyric acid
Anticarcinogenic activity	Reduction of faecal enzymatic activity (β-glucuronidase, azoreductaze, nitroreductaze) Production of short chain fatty acid Normalization of intestinal permeability Strengthening of intestinal barrier Boosting of immune system
Reduction in serum cholesterol	De-conjugation of bile salts Taken up cholesterol during growth
Prevention/treatment of *Helicobacter pylori* infection	Reduction of bacterial load Inhibition of growth of *H. pylori*
Stimulation of immune system	Directly or indirectly stimulation by changing the composition or activity of intestinal microflora

peptides, β-galactosidase, and exopolysaccharides produced by LAB during fermentation.

Functional Cultures

In the dairy biotechnology, the LAB are the most important bacteria that lead all fermentations. LAB inhabit two main ecological niches: the mucous surfaces of man and animals, and fermented foods. The acidification and enzymatic processes accompanying the growth of LAB impart the key flavour, texture, and preservative qualities to a variety of fermented foods. The LAB, notably lactobacilli, which occupy important niches such as the gastrointestinal tracts (GIT) are considered to contribute a number of probiotic benefits to general health and well being[12] (Table II).

The search for a starter culture has until recently been relying on the screening of a large number of isolates in small-scale food fermentations. Molecular biology has fostered the development of genetically based selection tools allowing us to specifically target the individual genes and metabolic pathways responsible for desired performance parameters of a starter culture. Specific targeting makes screening by high throughput methods possible, and it opens the possibility to use mutant selection and genetic engineering to construct novel starters. The engineering of recombinant starter cultures by the aid of food grade techniques can now be done on a safety level matching or even exceeding the safety level of "natural" screening and selection[13,14,15].

Examples of novel strains obtained by the use of modern techniques are:
- a spontaneous roseoflavin-resistant mutant derived from *Propionibacterium freudenreichii* B374 that shows increased riboflavin production and was used as adjunct culture for production of yoghurt with improved nutritional value[16],
- a non-D-lactate-producing variant of probiotic *Lactobacillus johnsonii* La1, convenient for the patients suffering from short bowel syndrome and intestinal failures[13].

Probiotic cultures production technologies should provide in a cost effective manner high quality, safe end-products with long shelf life. Working with living microbes is demanding since viability losses occur easily if microbial cultures are exposed to stressful conditions. Technological robustness can be improved by activating the stress genes of bacterial cells during processing by suitable sub- lethal treatments, or by genetically modifying the strain to make it more robust[17].

Biogenics

During the milk fermentation by LAB the main chemical change is fermentation of lactose into lactic acid. The functional properties of lactic acid are numerous: it reduces pH, influences the physical properties of casein and promotes digestibility, improves the utilisation of calcium and other minerals, and inhibits the growth of potentially harmful bacteria.

The liberation of short- and medium-chain free fatty acids during fermentation and in the stomach after milk fat ingestion, contributes to a lowering of the pH which facilitate digestion of proteins and inhibit the pathogenic bacteria. In addition, the fatty acids and monoglycerides with chain lengths varying from 8 to 12 carbon atoms display antibacterial and antiviral activity[18]. Recent studies confirmed the potential of these FAs to reduce body weight, particularly body fat[19]. Butyric acid formed during fermentation in milk or in the colon, affects intestinal cell differentiation, apoptosis and cell growth control. It is also known that butyrate displays anti-colorectal cancer properties, probably by enhancing apoptosis of mutant colonic cells[20].

Much attention has been directed toward conjugated linoleic acid (CLA) since the discovery of its anticarcinogenic properties. Strong evidence from animal trials supports an influence of CLA on body composition, i.e. lowering of body weight and fat mass and a relative increase in the lean body mass. Results from human trials do not support a weight loss-inducing effect of CLA but indicate a body fat lowering effect associated with an increase in the lean body mass[21]. Cows' milk fat is the richest natural source of CLA and its quantity can be raised by cow's nutrition. Possibilities to increase the CLA content of dairy products with microbial cultures have been studied by many authors however, their contribution in increasing CLA in dairy products seems to be minor[22]. Enrichment of dairy products with encapsulated CLA seems more perspective way for producing CLA rich dairy products[23].

Many LABs are known to produce exocellular polysaccharides or EPSs. Their precise function still remains unclear, although it is considered to be related to cell adhesion and cell protection in different ecosystems. LAB that produce EPSs play an important role in dairy industry because of their contribution to the texture, mouthfeel and stability of fermented milk. Besides their technological functionality, certain EPSs produced by LAB are also claimed to have beneficial physiological effects. It is speculated that the increased viscosity caused by EPSs may increase the residence time of ingested fermented milk in the GIT and in this way also enable transient colonisation of probiotic bacteria. Because of the special composition and low degradability, EPSs can act as prebiotics and thus beneficially affect the host by selectively stimulating the growth and activity of beneficial intestinal bacteria in the colon. Suggested health benefits of some EPSs are antitumor, antiulcer, immunomodulating and cholesterol-lowering activities[24,25,26].

Probably the most important as well as thoroughly studied biogenics in dairy products are whey proteins and bioactive peptides. Whey proteins have been implicated in a variety of nutritional and physiological effects, including physical performance, recovery after exercise, and prevention of muscular atrophy, satiety and weight management, cardiovascular health, anti-cancer effects, wound care and repair, management of infections, infant nutrition and healthy aging[6].

Milk proteins are rich source of bioactive peptides. Milk proteins-derived bioactive peptides are inactive as long as are a part of parent protein and can be released by enzymatic proteolysis. Once they are liberated, bioactive peptides may act in the body as regulatory compounds (Table III). Many of bioactive peptides demonstrate multifunctional activity. For example, some regions in the β-casein contain overlapping peptide sequences which exert different biological effects. These regions are called "strategic zones" and are partially protected from proteolytic breakdown[27,28,29].

Table III
Physiological functionality of milk-derived bioactive peptides[29]

Activity	Target system
Antihypertensive Antioxidative Antithrombotic Hypocholesterolemic	CARDIOVASCULAR SYSTEM
Opioid • agonist activity • antagonist activity	NERVOUS SYSTEM
Mineral-binding Anti-appetizing Antimicrobial	GASTROINTESTINAL SYSTEM
Antimicrobial Immunomodulatory Cytomodulatory	IMMUNE SYSTEM

Functional Dairy Products and Health

H y p e r t e n s i o n

High blood pressure is one of the most important risk factors of coronary heart disease. Studies have shown that during fermentation of milk ACE-inhibitory peptides arise from caseins[29]. The best known ACE-inhibitory peptides are Val-Pro-Pro (VPP) and Ile-Pro-Pro (IPP). At present, at least two fermented sour-milk products containing the ACE-inhibitory three-peptides VPP and IPP have been launched commercially. The Japanese product "Calpis" fermented by *L. helveticus* and *Saccharomyces cerevisiae* contains two ACE-inhibitory peptides derived from β-casein f84-86 (VPP) and f74-76 (IPP) and one from κ-casein f108-110 (IPP)[30]. The Finnish product "Evolus" contains the same three-peptides produced by *L. helveticus* LBK-16H strain. Both of these fermented drinks have proven effects in the reduction of blood pressure in hypertensive human subjects[29].

G a s t r o i n t e s t i n a l H e a l t h a n d
G e n e r a l W e l l - B e i n g

The intestinal microflora is important for maintenance of host health, providing energy, nutrients and protection against pathogens. Although the colonic microflora is relatively stable throughout life, age-related changes in the GIT as well as changes in diet and host immune system reactivity affect population composition[31]. Since the LAB are essential in

the maintenance of intestinal homeostasis and consequently in general human health, functional fermented dairy products have been proposed as healthy foods to control intestinal disorders. The results of an extensive research work have confirmed their beneficial effect in the case of lactose intolerance, GIT infections, viral diarrhoea, antibiotic-associated diarrhoea, in prevention and treatment of traveller's diarrhoea and *Heliobacter pylori* gastritis. Less consistent results have been obtained studying the effects of functional dairy products on the side effects of radiotherapy, constipation and in cancer prevention[32].

Lactose Intolerance

The most documented beneficial effect of fermented milks, especially yoghurt, on the intestinal function is observed in the case of lactose intolerance[33,34]. Lactose intolerance is caused by a deficiency in the enzyme beta-galactosidase, resulting in the inability to digest the disaccharide, lactose. The symptoms of lactose intolerance are diarrhoea, flatulence and abdominal pain after consumption of milk. The mechanisms involved in the beneficial effects of LAB and fermented milks in case of lactose intolerance are: lower lactose concentration in the fermented milk, high lactase activity of LAB used as starter cultures and active lactase present in fermented milk or entering the small intestine within the bacterial cells able to survive gastric and bile conditions.

Diarrhea

One of the main applications of probiotics has been the treatment and prevention of antibiotic-associated diarrhoea, which is often caused by occurrence of *Clostridium difficile* after an antibiotic treatment. The application of probiotics in the clinical setting significantly reduced antibiotic-associated diarrhoea by 52 %, reduced the risk of travellers' diarrhoea by 8 % and that of acute diarrhoea of diverse causes by 34 %. Moreover, the associated risk of acute diarrhoea among children or adults was reduced by 57 % and 26 %, respectively[35]. Several possible mechanisms by which fermented dairy foods containing probiotics or cultures containing milks reduce the duration of diarrhoea, are competitive exclusion, translocation/barrier effect and improved immune response[34].

Conclusions

Development of functional dairy products requires various groups of experts including medical experts, nutritionists, microbiologists and food technologists. By using an individual's unique genetic makeup and nutritional requirements, consumers may have in the future a greater possibility to choose between different functional dairy food products and to consequently reduce their risk of disease.

REFERENCES
1. Diplock A. T.: Br. J. Nutr. *81*, S1 (1999).
2. Ashwell M.: *Concepts of functional foods*. ILSI Press, Belgium, 2002.
3. Chopra A., Doiphode V.V. Med. Clin. North Am. *86*, 75 (2002).
4. Bottazzi, V.: Biotechnology *5*, 315 (1983).
5. Kosikowski F. V. in: *Whey and whey foods* (Kosikowski F. V., ed.), Cheese and Fermented Milk Foods, p. 446. Edwards Brothers, New York 1982.
6. Smithers G. W.: Int. Dairy J. *18*, 695 (2008).
7. Sabikhi L.: Curr. Sci. *87*, 1530 (2004).
8. Sabikhi L.: Adv. Food Nutr. Res. *53,* 161 (2007).
9. Spence J. T.: J. Food Compos. Anal. *19,* S4 (2006).
10. FAO/WHO Guidelines for the evaluation of probiotics in food (London, Ontario) 2002, 11.
11. Mitsuoka T.: Biosci. Microflora *19*, 15 (2000).
12. Shah N. P.: Int. Dairy J. *17,* 1262 (2007).
13. Mollet B.: Int. Dairy J. *9*, 11 (1999).
14. Hansen E. B.: Int. J. Food Microbiol. *78*, 119 (2002).
15. Beloqui A., de María P. D., Golyshin P. N., Ferrer M.: Curr. Opin. Microbiol. *11*, 1 (2008).
16. LeBlanc J. G., Rutten G., Bruinenberg P., Sesma F., de Giori G. S., Smid E. J.: Nutrition *22,* 645 (2006).
17. Meng X. C.,Stanton C.,Fitzgerald G. F., ,Daly C., Ross R. P.: Food Chem. *106*, 1406 (2008).
18. Schaafsma G., Steijns J. M. in: *Essentials of Functional Foods* (Schmidl M. K., Labuza T. P. ed.), Dairy Ingredients as a Source of Functional Foods, p. 181. Aspen Publishers, Inc., Gaithersburg, Maryland (2000).
19. Marten B., Pfeuffer M., Schrezenmeir J.: Int. Dairy J. *16*, 1374 (2006).
20. Pouillart P.R.: Life Sci. *63*, 1739 (1998).
21. Collomb M., Schmid A., Sieber R., Wechsler D., Ryhänen E-L.: Int. Dairy J. *16*, 1347 (2006).
22. Sieber R., Collomb M., Aeschlimann A., Jelen P., Eyer H.: Int. Dairy J. *14*, 1 (2004).
23. Jimenez M., Garcia H. S., Beristain C. I.: LWT *41*, 1047 (2008).
24. DeVuyst L., De Vin F., Vaningelgem F., Degeest B.: Int. Dairy J. *11*, 687 (2001).
25. Ruas-Madiedo P., Hugenholtz J., Zoon P.: Int. Dairy J. *12*, 163 (2002).
26. Jolly L., Vincent S. J. F., Duboc P., Neeser J-R.: Antonie van Leeuwenhoek *82*, 367 (2002).
27. Meisel H.: Int. Dairy J. *8*, 363 (1998).
28. Schanbacher F. L., Talhouk R. S., Murray F. A., Gherman L. I., Willett L. B.: Int. Dairy J. *8*, 393 (1998).
29. Korhonen H., Pihlanto A.: Int. Dairy J. *16*, 945 (2006).
30. Yamamoto N, Maeno M, Takano T.: J. Dairy Sci. 82, 1388 (1999).
31. Woodmansey E. J.: J. Appl. Microbiol. *102*, 1178 (2007).
32. Reid, G.: Int. Dairy J. *18*, 969 (2008).
33. Sanders M. E.: J. Nutr. *130*, 384S (2000).
34. Vasiljevic T., Shah N. P.: Int. Dairy J. *18*, 714 (2008).
35. Sazawal S., Hiremath G., Dhinga U., Malik P., Deb S., Black R. E.: Lancet Infect. Dis. *6*, 374 (2006).

L02 ALKALI-ACTIVATED ALUMINOSILICATES: PAST, PRESENT AND FUTURE

PAVEL KRIVENKO

V. D. Glukhovsky State Scientific Research Institute for Binders and Materials, Kiev National University of Civil Engineering and Architecture, Vozdukhoflotsky prospect, 31, Kiev, 03037, Ukraine,
pavlo.kryvenko@gmail.com

Introduction

Beginning from 1957, a scientific school in Kiev, USSR, headed by Professor Victor Glukhovsky has been developing a new direction in the binding materials, the background of which was the discovery of binding properties of the alkali metals. The alkali metals compounds act not only as activators of hardening but are responsible for the formation of main structural elements of the alkali-activated cements – zeolite-like compounds of different types.

Just these hydration products, analogues to natural zeolites of the $Na_2O(K_2O) \cdot Al_2O_3 \cdot (2\text{-}4)SiO_2 \cdot 2H_2O$ type, have been discovered in ancient concretes (Ancient Greece, Ancient Rome, Egypt, Syria). Durability of the ancient concretes and similarity of their structure with that of the alkali-activated cement concretes allowed to predict their high durability. Effectiveness and high performance properties of the alkali-activated cement concretes are supported by over 50-year experience of service of the structures made from them.
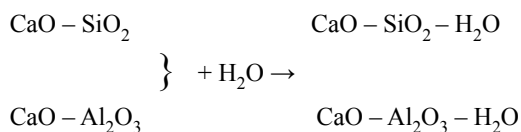
Theoretical Background

Less than a century ago just an idea of the presence of free alkalis in a cement composition was treated by cement people as absurd one and this was a basic postulate of fundamentals of exhibiting hydraulic by mineral systems. The alkali metal compounds were excluded from the traditional hydraulic cements because of their high solubility.
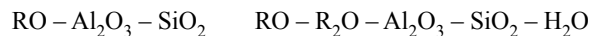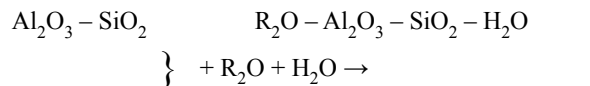
At the same time, the studies held to reveal the reasons for excellent durability of ancient cements in combination with the data collected on stability and composition of natural mineral formations testified that this postulate was not correct.

In 1957 the scientist from the Soviet Union Victor Glukhovsky has discovered that compounds of alkali metals (Li, Na, K, Rb, Cs) – the elements of the first group of the Periodic Table, exhibit hydraulic binding properties similar to compounds of the alkali earth metals (Mg, Ca, Sr, Ba)- the elements of the second group.

Thus, an idea of creation of the cementitious systems was transformed as the following:

$$\left.\begin{array}{l} CaO - SiO_2 \\[1em] CaO - Al_2O_3 \end{array}\right\} + H_2O \rightarrow \begin{array}{l} CaO - SiO_2 - H_2O \\[1em] CaO - Al_2O_3 - H_2O \end{array}$$

"Old scheme" (ordinary Portland cement, high-alumina cement)

$$\left.\begin{array}{l} Al_2O_3 - SiO_2 \\[1em] RO - Al_2O_3 - SiO_2 \end{array}\right\} + R_2O + H_2O \rightarrow \begin{array}{l} R_2O - Al_2O_3 - SiO_2 - H_2O \\[1em] RO - R_2O - Al_2O_3 - SiO_2 - H_2O \end{array}$$

"New scheme" (alkali- activated cement)
where R – Na, K, Li, Rb, Cs

The idea itself of using these systems as cementitious ones was based, first of all, on geological data that sodium-potassium- calcium aluminosilicate compounds, which are known to have the higher stability and resistance to atmospheric reagents, are present in the Earth. Secondly, this idea was based on the results of experimental studies, which proved that alkali hydroxides and salts of alkali metals came into interaction with clay minerals, aluminosilicate glasses and crystalline substances of natural and artificial origin with the formation of water resistant alkaline and alkaline- alkali-earth aluminosilicate hydration products analogous to natural minerals of the zeolite and mica types.

Terminology

The established possibility of modelling the processes taking place in the Earth's crust based on an interaction between the decay products of rock-forming minerals: clays and alkalis, followed by synthesis of these minerals, suggested using natural soils as starting materials for producing a binder. This explains why the binders/cementitious materials/ developed as long ago as in 1957 have been called "soil cements" and the concretes "soil silicates"[1].

The alkaline and alkali-earth hydroaluminosilicates analogous to natural minerals (hydronepheline, analcime, natrolite, thompsonite, hydrosodalite, etc.) are formed in the soil cement stone during the process of hardening along with calcium hydrosilicates and carbonates.

The soil silicates contain alkalis in large amounts (1–20 % wt. calculated on R_2O). Just the alkaline oxides are the components which determine their binding properties. The alkali earth oxides are either absent in them (fly ashes, cakes, clays, field spur minerals) or are present in the aluminosilicate component (cakes, fly ashes, slags) or may be introduced from the outside as the components of the traditional binding materials (lime, Roman-, Portland-, slag Portland or high alumina cements).

In 1973, Professor J. Davidovits was granted his first patents for the geopolymers[2]. The technology for manufacturing these cements included the following steps: mixing kaolinite, lime stone, dolomite; burning of a mix and introduction of alkaline compound solutions. During these processes, the kaolinite converts to the metakaolinite ($Al_2O_3 \cdot 2SiO_2$), gaining the pozzolanic properties, while calcium and magnesium carbonates form calcium and magnesium oxides. Being added to a cement mix, silica or soda or its mixture with potash incorporated with a mixing water produce sodium and potassium hydroxides. The last initiates a chemical reaction with

polysilicate and aluminosilicate oxides with the formation in a composition of the hydration products, represented by analcime and hydrosodalite. Some of these products are known as commercial products (trade names: Pyrament, Geopolycem, Geopolymite, etc.). The cements of this type are known in the art under a general name "geopolymers".

The alkali-activated cements are known among cement people also under other names: alkali-activated cements[3] SKJ-binder[4], F-cement[5], gypsum-free Portland cement[6], geocements[7].

Classification

The classification proposed by[8] is based on the characteristic features of the products of hydration and hardening of the alkali-activated cements, the "edge" variants of which may be represented by the compounds of two types: the alkaline hydrosluminosilicates of the system $R_2O - Al_2O_3 - SiO_2 - H_2O$ and the earth hydrosilicates.

A variety of blended alkaline-alkali-earth hydroaluminosilicates may exist within these "edge" variants. A phase composition of the hydration products of the cement stone is determined by a kind of the initial raw material (Table I).

Table I
Mineralogical composition of the cement hydration products vs type of initial aluminosilicate component

Cement type	Initial soild phase	Alkali content R_2O [%]	Hydration product
OPC	OPC clincker	<0.6	
Alkali-activated OPC	OPC clinker + R_2O	1–5	
Alkali-activated blended OPC	OPC clinker + additive (slag, ash, basalt) + Me_2O	2–5	
Slag alkali-activated cement	Metallurgical slag + R_2O	4–8	
Ash alkali-activated cement	Ash – product of coal combustion	5–10	
Geocement	Clay + R_2O	10–20	

Principles of Compositional Build-up of the Alkali-Activated Cements

The following postulates have been laid down in their creation:

- alkalis act not only as activators but as structure- forming elements included into the formed phases as well;
- the formed phases (of hydration products) are characteristic of the presence of new formations of the $R_2O–Al_2O_3 – SiO_2 – H_2O$ and $R_2O – CaO – Al_2O_3 – SiO_2 – H_2O$ types;
- the quantities of alkalis to be introduced are caused by a necessity to meet a stoichiometric composition /stoichiometry requirement/ of the alkaline and alkaline-alkali-earth hydroaluminosilicates analogous to natural zeolites.

In compliance with these principles the alkali content in the cement will be determined by an Al_2O_3 content of the aluminosilicate component (Fig. 1.).
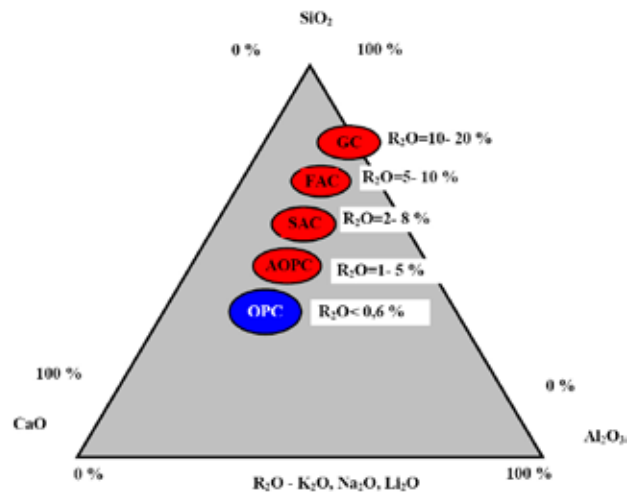

Fig. 1. **Comparative chemical analysis of different types of OPC and alkali-activated cements. Abbreviations: OPC – ordinary Portland cement; AOPC – alkali-activated ordinary Portland cement; SAC – slag alkali-activated cement; FAC – ash alkali-activated cement; GC – geocement**

The introduction into a cement composition of the alkali metal compounds in much larger quantities than was permitted in compliance with the principles of compositional build-up of the traditional cements based on calcium and magnesium compounds suggested to consider that the alkali metal compounds not only act as activators of hardening but as self-functioning components of the binding system $Me_2O – MeO – Me_2O_3 – SiO_2 – H_2O$, the main structure-forming products of which are low-basic calcium hydrosilicates and zeolite-like products. A low basicity of the hydration products is caused by specific features of the structure-forming processes taking place in the slag alkali- activated cements, namely: a hydrolytic destruction of the solid phase of the low-basic phases is caused, first of all, by the break of the covalent

bonds $Si - O - Si$, $Me^{3+} - O - Me^{3+}$, $Si - O - Me^{3+}$ according to a scheme $\equiv Si - O - Si \equiv \leftrightarrow [\equiv Si - O - Si \equiv] - \leftrightarrow \equiv Si - OH + \equiv Si - O -$ with protonization of the ion $Me^{2+} - O$ bonds taking place in parallel, as it is known to happen in the high-basic systems[9].

An alkaline cation that provides the flow of the hydrolytic destruction of the low-active low-basic phases, acts at early stages of structure formation as a catalyst of destruction. Then, as soon as the condensation processes evolve, it takes an active part as a co-partner of the Ca^{2+} and Mg^{2+} in the structure formation processes. This facilitates its modification due to the formation of the alkaline and alkaline-alkali-earth hydroaluminosilicates that are morphologically homogeneous to low-basic calcium-magnesium hydrosilicate phases.

At early stages of hydration and hardening (for example, of the slag alkali-activated cements), the structure formation is caused, chiefly, by the formation and crystallization of the low- basic hydrosilicates and hydrogarnets. The alkaline and alkali-earth hydro-aluminosilicates, as a result of their slower crystallization, occur at the later stages. Being formed, chiefly, in the pore space, they fill it and promote strong crystallization contacts with primary phases to occur, as well as initiate the formation of more homogeneous and dense structure.
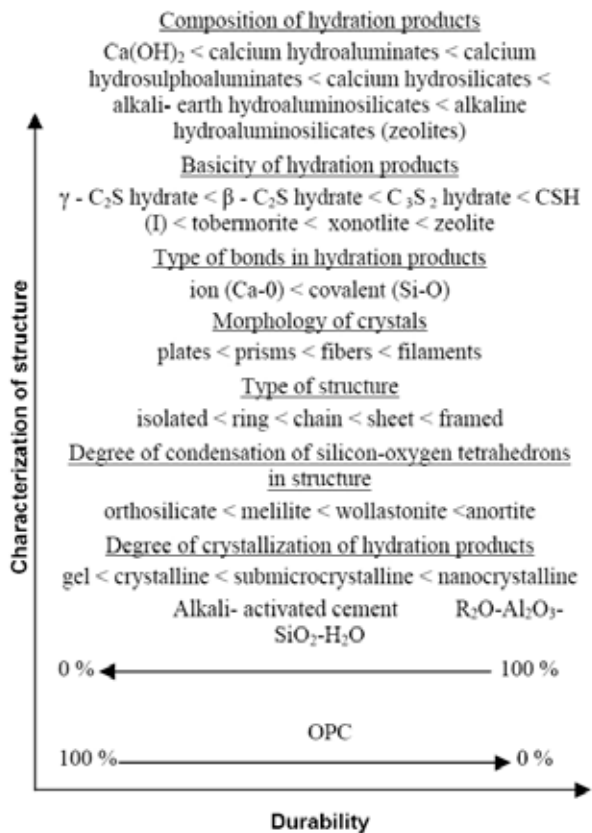

Fig. 2. **Dependence between phase compositions of the hydration products, their structure and durability of the cement stone**

Besides, high pH-values of the medium at which the hydration process takes place block a transfer of the Ca-ions into the solution, thus explaining the absence of $Ca(OH)_2$ and the fact that the resulted calcium hydrosilicate has, as a rule, a basicity over 1.

Table II
Comparative data on solubility of new formations of the slag alkali-activated and portland cement stones.

Cement type	New formations		Solubility
	Mineral	Stoichiometric formula	[$kg\,m^{-3}$]
Slag alkaline cement	CSH(B)	$5CaO\ SiO_2\ nH_2O$	0.05
	Xonotlite	$6CaO\ 6SiO_2\ H_2O$	0.035
	Riversideite	$5CaO\ 6SiO_2\ 3H_2O$	0.05
	Plombierite	$5CaO\ 6SiO_2\ 10.5H_2O$	0.05
	Gyrolite	$2CaO\ 3SiO_2\ 2.5H_2O$	0.051
	Calcite	$CaCO_3$	0.014
	Hydrogarnet	$3CaO\ Al_2O_3\ 1.5SiO_3\ 3H_2O$	0.02
	Na-Ca hydrosilicate	$(Na,Ca)\ SiO_4\ nH_2O$	0.050
	Thomsonite	$(Na,Ca)\ Si_2O_3\ Al_2O_3\ 6H_2O$	0.05
	Hydronepheline	$Na_2O\ Al_2O_3\ 2SiO_2\ 2H_2O$	0.02
	Natrolite	$Na_2O\ Al_2O_3\ 3SiO_2\ 2H_2O$	0.020
	Analcime	$Na_2O\ Al_2O_3\ 4SiO_2\ 2H_2O$	0.02
	Calcium hydroxide	$Ca(OH)_2$	1.3
Portland cement	C_2SH_2	$2CaO\ SiO_2\ nH_2O$	1.4
	CSH(B)	$5CaO\ 6SiO_2\ nH_2O$	0.05
	Tetra calcium hydroaluminate	$4CaO\ Al_2O_3\ 13H_2O$	1.08
	Tricalcium hydroaluminate	$3CaO\ Al_2O_3\ 6H_2O$	0.56
	Hydrosulpho-aluminate	$3CaO\ Al_2O_3\ 3CaSO_4\ 31H_2O$	high

Durability

Specific features of the mechanism of hydration and hardening of the alkali-activated cement determine formation of the more effective microstructure of the cement stone at different levels as compared with the Portland cement stone (Fig. 2.). This is also clearly seen from comparison of the data on solubility of new hydration products of the alkali-activated and Portland cement stone (Table II).

Industrial Uses

The experience from the small and large scale industrial uses of the alkali-activated cements gained starting the 1960s in construction (hydropower engineering, road, agricultural, industrial, civil engineering, mining, etc.) gave proofs to high performance properties of the concretes on them. The use of the alkali-activated cement-based materials was found to be especially effective one for specially intended use in many fields besides construction[11].

Below are given some fields of the manufacture and use of the alkali-activated aluminosilicates (Table III).

Table III
Some examples of practical uses of the alkali- activated aluminosilicates

	Hydraulic	Road	Agricultural	Industrial	Residential	Mining
2007		Heavy-duty road pavements, access roads and storage sites of chemical plants				
2000	Inorganic adhesives and glues, protective coatings against action of corrosive environments and high temperatures					
1990			Articles and structures from acid resistant concretes	High-rice building from precast and cast-*in-situ* concrete		Compounds for radioactive waste immobilization Bodies of precise machine tools
1985			Floors, landings from cast-*in-situ* concretes	Blocks for buildings, garages, storage houses, etc.		Dies, moulds
1980			Articles and structures from hest resistant concrete	Floor slabs, foundation wall blocks, foundation blocks, piles	Oil well mortars and grouts	Linings of MD-pumps for aluminium melts
1975		Road bases from strengthened soils				
1970	Tubings of anti-slide systems	Pavements from cast-*in-situ* concrete and precast reinforced concrete slabs	Pasture sites, storage sites for fertilizers, silo pits from cast-*in-situ* and precast concrete	Foundation blocks, floor slabs, columns, beams, foundation wall blocks, elements of cleaning-up systems		Reinforced pit props, sleepers
1960	Sea breakwaters, elements of irrigation systems from cast-*in-situ* and precast pre-stressed concrete	Pedestrian way slabs, edges of pavement, landing field slabs				
	Hydraulic	**Road**	**Agricultural**	**Industrial**	**Residential**	**Mining**
	Constructional engineering					**Non-constructional engineering**

Over 45 years passed since the alkali-activated cements appeared in the field and their efficiency and potential have been proved by extensive researches held not only in the Soviet Union but in many countries over the world: Poland, Finland, The Netherlands, Germany, Czech Republic, Romania, Slovak Republic, Bulgaria, Japan, China, USA, Canada, India, Brazil, Spain, the UK. The experience collected for this period of commercial- scale manufacture and use of structures and articles made from slag alkali-activated cement concrete in various fields of construction testifies to their higher service properties as compared with those of Portland cement. These materials were found to be the most highly effective ones when used in extremely severe conditions as well as in non-civil engineering fields (Fig. 3.).

More than 50 years practical experience of the Kiev school is connected with a TECHNOLOGY under which the alkaline activator was introduced into a concrete in a form of aqueous solution, namely:

- "Concrete" – an aluminosilicate component, an alkaline activator and modifying additives are introduced in a dry form or in a form of a solution during mixing concrete ingredients similar to conventional concrete technology.
- "Cement" – an aluminosilicate component, an alkaline activator and modifying additives are interground for further use in concrete under traditional OPC based concrete technology (Fig. 4.).

Standard Test Procedures

Determination of mechanical and physical properties of alkali- activated cements is carried out according to DSTU B V 2.7-24-95 and ASTM C 109/C 109M. According to these standards a water to cement ratio (W/C) is chosen in order to provide a flow value (cone measurement) = 106–115 mm.

In case of using these test methods according to EN standards (EN 196-1, 196-3, and 196-6, under which the
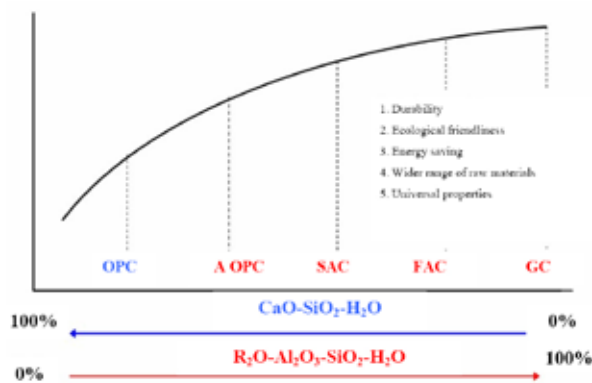
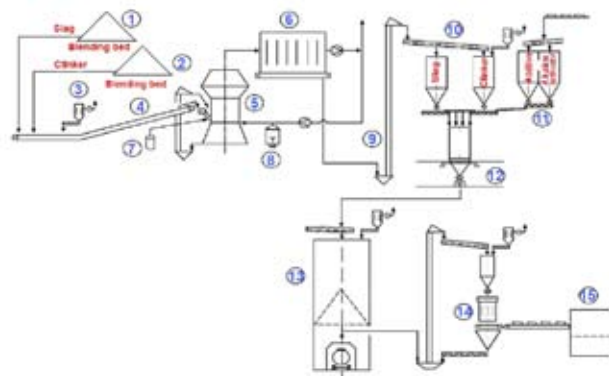Fig. 3. **Benefits of the alkali-activated cements as compared to Portland cements**

Fig. 4. **"Cement" technology of slag alkali-activated cement manufacture. 1 – blending bed for slag, 2 – blending bed for clinker, 3 – dust collector, 4 – belt conveyer, 5 – vertical roller mill, 6 – fabric filter, 7 – metering equipment for water repellent, 8 – heat generator for drying, 9 – elevator, 10 – silos for cement constituents, 11 – bunker for additives and alkaline activator, 12 – mixer for dry cement constituents, 13 – ready product storage silo, 14 – packer for bags, 15 – palletizer agent**

W/C is restricted to a value of 0.5) the following amendments should be introduced: in determination of flowability of the cement/sand mortar the alkaline solution/solid constituents or water/solid constituents ratio should be chosen experimentally in such a way that to provide the flow values between 160–180 mm.

Conclusions

At the moment Ukraine has all normative documentation required for a large-scale application of the alkali-activated cements and materials.

In order to bring this technology into large-scale worldwide application, the RILEM Technical Committee organized in 2007 "Alkali activated materials" should fulfil the following tasks:

To collect and summarize the experience on:
- raw materials
- cements
- concretes
- structures
- production
- test procedures
- durability
- field of application

To develop basic recommendations "Preparation of a performance-based specification for cast-in-place alkali-activated cements and concretes".

The results of this work will allow to develop and approve the national standards for the alkali-activated materials.

REFERENCES

1. Glukhovsky V. D.: *Soil Silicates* (*Gruntosilikaty*). Budivelnik Publish, Kiev 1967.
2. Davidovich J.: US Patent 3950470.
3. Silic. Ind. *9*, 175 (1983).
4. Changgo Lu: Concr. Cem. Prod. *6*, 1991.
5. Forss B.: *Proceedings of 6 th Int. Conference on Alk. Concrete*, p. 101. Denmark, 1983.
6. Odler R, Skalny J., Brunauer S: *Proceedings of 6th Int. Congress on the Chemistry of Cements*, p. 142. Stroiizdat, Moscow 1983.
7. Krivenko P, Skurchinskaja Zh.: *Int. Conference on the Utilization of Fly-Ash and Other Coal Combustion By-Products*, p. 64-1–64-7. Shanghai, China 1991.
8. Krivenko P.: *10th Int. Congress on the Chemistry of Cements*, 4iv046. Sweden, 2–6 June 1997.
9. Krivenko P.: Dissertation. Kiev Polytechnic University, Ukraine, 1986.
10. Shi C., Krivenko P., Roy D.: *Alkali-Activated Cement and Concretes*. Taylor & Francis, London, New York, 2006.

L03 ORGANIC ANTHROPOGENIC CONTAMINANTS IN RIVER SYSTEMS – AN OVERVIEW ON COMPLEMENTARY ENVIRONMENTAL APPROACHES

JAN SCHWARZBAUER

Institute of Geology and Geochemistry of Petroleum and Coal, RWTH Aachen Unievrsity, Lochnerstrasse 4–20, 52056 Aachen,
schwarzbauer@lek.rwth-aachen.de

Introduction

Rivers are sensitive but also complex ecosystems hosting a wide spectrum of organisms. Anthropogenic activities and the resulting discharge of contaminants have resulted in increasing river pollution over decades. Especially, in industrialized, densely populated or agricultural strongly affected regions the natural riverine organic matter is superimposed by huge anthropogenic emissions.

Organic contaminants discharged to the aquatic environment exhibit a high diversity with respect to their molecular structures and the resulting physico-chemical properties. Although the chemical analysis of anthropogenic contamination in river systems is still an important feature, especially with respect to the identification and structure elucidation of novel contaminants, the focus of environmental studies has changed. In recent times the research on the environmental behaviour of organic pollutants became more and more important in order to assess their risk as a result of their emission to natural systems. Consequently, the knowledge not only about the occurrence and amount of anthropogenic contaminants but also about bioavailability, their exchange within different compartments, as well as on molecular aspects of degradation or metabolism processes increases significantly. Further on, environmental studies on the anthropogenic pollution of aquatic systems do not remain on the analysis of pre-selected substances. Considering the currently use of over 1,000,000 man-made chemicals in the EU it has to be assumed, that analytical investigations on environmental systems solely focussed on a few pollutants still do not depict the 'real' pollution level. Therefore, the number of more extensive and detailed investigations considering a wide spectra of relevant organic pollutants increases slowly. Such investigations reveal a more comprehensive view on the state of pollution of a natural system[1]. For all the described purposes, a complementary application of different analytical strategies and methods have to be applied to reveal a better understanding of environmental processes affecting the riverine pollution by organic substances. Examples of such approaches are presented following.

River Water

Within river systems two quite differing compartments exist, the particulate matter as well as the water phase, representing a hydrophilic and a more lipophilic phase, respectively. Most of the organic substances accumulate either in the water phase or in the sediments depending on their polarity and the resulting hydro- or liphophilicity. This partition also determines the principal transport processes and, consequently, the distribution of the organic contaminants. The water phase of riverine systems is characterized by more polar and frequently less stable contaminants.

Non-Target Screening

A huge proportion of riverine contamination is caused by low-molecular weight organic compounds, like pesticides plasticizers, pharmaceuticals, personal care products, technical additives etc. Some of them, like PCB or PAH have already been investigated thoroughly and, consequently, their behaviour in aqueous systems is very well described. Since analyses on organic substances in river water traditionally focused on selected pollutants, in particular on common priority pollutants which are monitored routinely, the occurrence of further contaminants, e.g. pharmaceuticals, personal care products or chelating agents has received increasing attention within the last decade. Screening analyses revealed recently an enormous diversity of low-molecular weight organic contaminants in wastewater effluents and river water.[2–5] Since many of these substances have been rarely noticed so far, it will be an important task for the future to study their occurrence and fate in natural environments.

An outstanding example for an early screening study dated back to the 70'ies. Sheldon and Hites published detailed GC-MS based analyses applied to water samples from the Delaware river[6]. This study presents more than 100 organic river water constituents. A similar approach was used by Franke et al.[2] in order to investigate the organic pollution of the Elbe river. Contributions of several tributaries were characterized by indicative organic compounds derived from industrial, municipal or agricultural sources. Additionally screening analyses were applied to sewage effluents as a major anthropogenic contribution to the riverine environment[3]. All these approaches revealed a high number of organic contaminants and lead to the structure elucidation and identification of numerous still unknown or unreported organic contaminants.
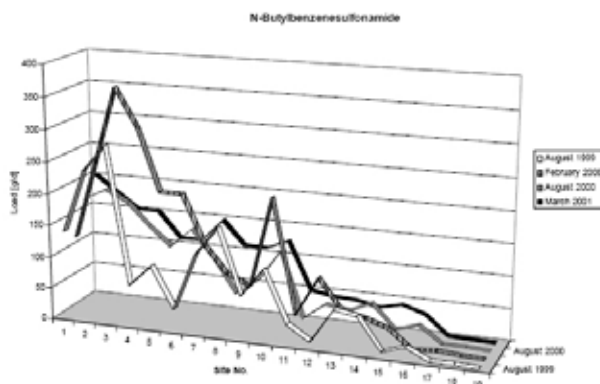

Fig. 1. **NBBS in the longitudinal profile of the Lippe river (according to ref.[7])**

Therefore, it should be a main issue of environmental studies to provide a comprehensive view on the state of pollution of river water, in particular with respect to lipophilic low molecular weight organic contaminants. Such non-target-screening analyses has been performed only rarely in the past.
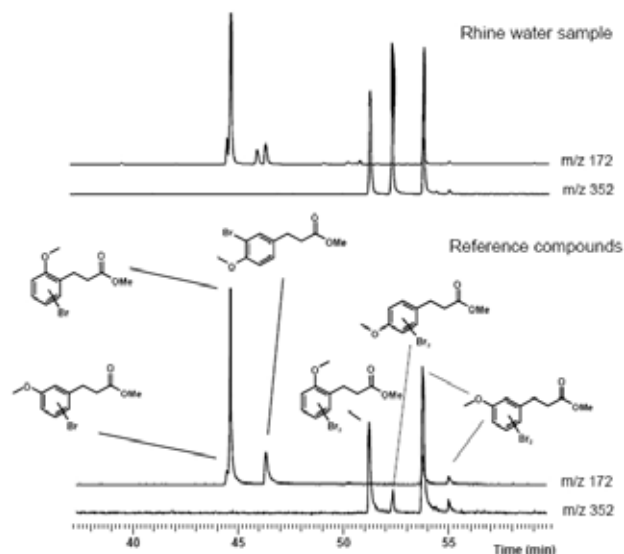

Figure 2: Brominated contmainants identified in Rhine water (according to ref.[8])

Screening analyses on longitudinal section of the rivers Rhine and Lippe (Germany) revealed complex pattern of anthropogenic contaminants comprising a lot of still unnoticed pollutants (e.g. N-butylbenzenesufonamide NNBS, see Fig. 1.) or still unidentified compounds such as brominated aromatics as depicted in Fig. 2.

These investigations demonstrated the need to expand our analytical focus on a broader spectrum of organic contaminants, because such comprehensive investigations can build up an adapted base for advanced monitoring studies.

Point vs Non-Point Sources

High attention has been given to non-point and multiple source emissions especially to agricultural contamination (e.g. pesticides) and to sewage effluents derived from treatment plants. The contamination by these sources is characterized by a widespread distribution of environmental stable compounds. However, the emission of point sources like industrial effluents exhibit frequently higher concentration of contaminants and a more complex mixture of substances. Nevertheless, these contaminations are normally restricted to a local importance. Therefore, source point emission are frequently underestimated or neglected, although they can have dramatical impact on river sections.

Investigations performed on industrial emissions contaminating river systems revealed significant contributions of harmful substances. These compounds exhibit frequently molecular structural moieties of high environmental rele-

vance or interest like halogen substitution or aromatic parts see (Fig. 3.). Most of these compounds occurred with elevated concentrations and corresponding loads (examples see Table I) at the outflow from the industrial sites representing a high environmental impact on the connected river system.

Table I
Specific compounds in two different types of industrial effluents and their emission rate

Industry	Compound	Load at outflow [g d^{-1}]
Petrochemical industry	Triphenylphosphine oxide	> 10
Chemical industry	Phenylmethylsulfone	ca 0.5
	2,6-Dithiohexane	ca. 20
	Dichlorobenzenes	ca. 5
	Trichorobenzoic acid	ca. 3

Riverine Particulate Matter

River water phase includes the suspended particulate matter representing an aerobic environment, whereas the sedimentary compartment is mainly more anaerobic. Therefore, particle associated pollutants underly quite different degradation pathways as the result of different microbial communities.

Anthropogenic Marker

In addition to pollutants, characterized by harmful ecotoxicological or toxicological effects, further anthropogenic contaminants were analysed frequently, the so-called ‚anthropogenic markers'. An impressive review on the evaluation and use of anthropogenic marker compounds has been published[9].

These substances are useful to reflect anthropogenic emissions to natural systems especially in terms of source specificity. Anthropogenic marker compounds are both natural substances derived from human feces or urine and xenobiotics. Apart from information on the emission sources they also provide information on transport pathways and fate of anthropogenic contaminants.

This approach has been applied e.g. to sediment samples from the Lippe river in order to point out the general contamination situation of this riverine system (Kronimus et al. 2005). It was able to differentiate individual industrial emission sources from agricultural and municipal contamination as depicted in Fig. 4.

Geochronology

During flood events riverine particulate matter can be deposited on flood plains and riparian wetlands. Accordingly these areas can act as ecological archives in case of undisturbed and periodical sedimentation. The dating of these sediment deposits can be performed by gamma spectrometric analysis of the radio-nuclides ^{210}Pb and ^{137}Cs. Organic geo-
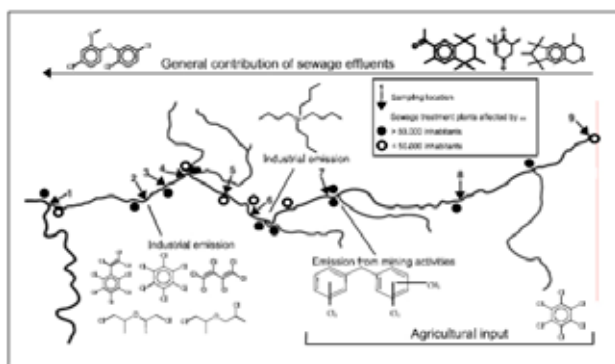
Fig. 4. **Emission situatiuon at the Lippe river as reflected by anthropogenic marker (according to ref.[10])**

chemical investigations on anthropogenic contaminants in these dated layers allow a detailed description of the emission of organic contaminants into the corresponding riverine system[11]. However, this approach is restricted to substances, which are characterized by a sufficient environmental stability and immobility in the particulate phase.

An example was published for the Lipper river system revealing interesting insights into different time periods of contamination and of technical application of additives. Important emission periods are reflected by the geochrnoligical profiles as presenetd in Fig. 5.
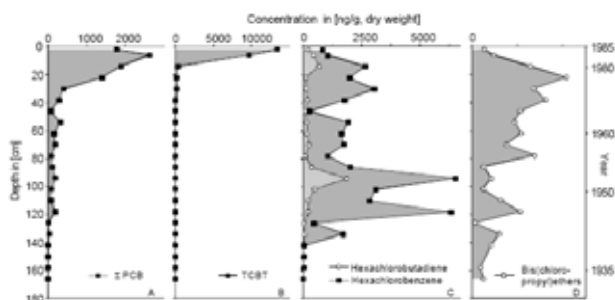
Fig. 5. **Geochronological profiles of selected pollutants in a core from riparian wetlands of the Lippe river (according to ref.[12])**

Carbon Stable Isotopes

Compound specific carbon isotope analyses are increasingly applied in environmental studies. Investigations the aquatic environment focused mainly on polycyclic aromatic hydrocarbons, monoaromatic compounds and halogenated aliphatics.[13–16] Further on, laboratory studies investigated the isotopic fractionation as a result of environmental processes, in particular transport and transformation processes (e.g. vaporization, adsorption, abiotic and biotic degradation) .[17–20] Carbon isotope ratios are not only useful data for evaluating the environmental fate of organic pollutants but also for distinguishing different emission sources discharging the same contaminants.

Interestingly, all applications reported so far avoid the two major limitations of compound-specific isotope analyses: *(i)* the lower sensitivity as compared to traditional GC/MS

analyses and *(ii)* the requirement of complete gas chromatographic separation of the contaminants. On the contrary, natural river systems are mostly low or moderately contaminated and, accordingly, concentrations of individual contaminants are also low. Consequently, information on the isotopic characterization of contaminants existing in these water systems are highly restricted.

However, studies dealing with carbon stable isotope values of organic contaminants in Rhine river and Lippe river water samples allowed interesting insights into the environmental fate of selected plasticizers, technical additives and musk fragrances[21,22] (Kronimus and Schwarzbauer, Schwarzbauer.as examplified in Fig. 6.
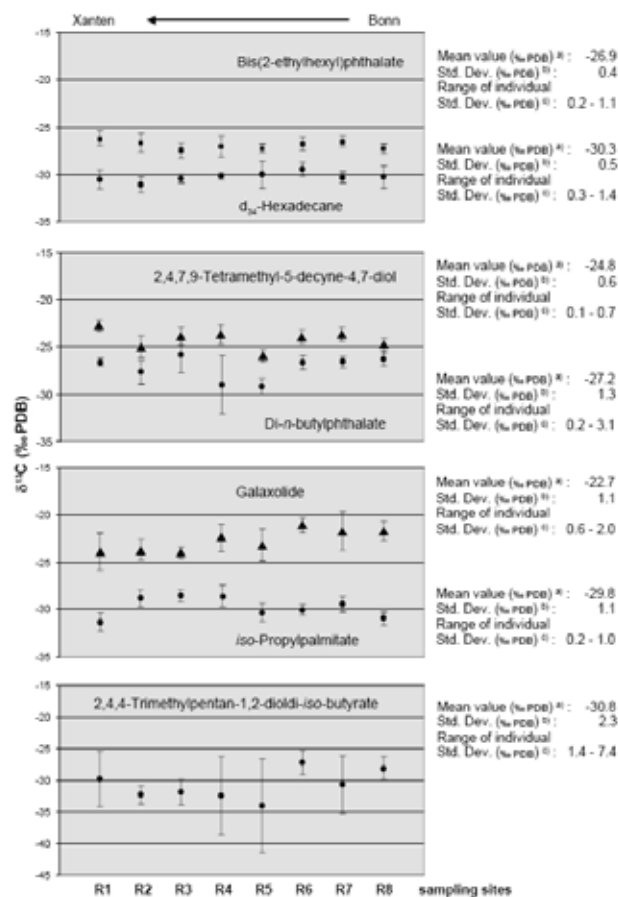

Fig. 6. **Carbon stable isotope values of selected pollutants in Rhine river water (according to ref[21])**

Perspectives

This short overview on recent research activities in the field of riverine organic pollution shall demonstrate the need to broaden the spectra of analytical approaches and strategies in order to meet the challenge to obtain the most detailed and most precious view on the anthropogenic impact on the aquatic environment. Such approaches comprise as described non-target screening, consideration all type of emission source (point/non-point), geochronology, stable isotope analyses as

well as anthropogenic markers. Additionally, also non-mentioned topics like the bound fraction of pollutants immobilised in particulate matter or the contamination by polymers open new insights and expand our knowledge on riverine contaminations and pollutant pathways in rivers.

Noteworthy, major parts of this outline have been recently published more comprehensively as well as in more detail[1].

REFERENCES

1. Schwarzbauer J.: *Organic contaminants in riverine and groundwater systems – aspects of the anthropogenic contribution*, Springer Verlag, 2006.
2. Franke S., Hildebrandt S., Schwarzbauer J., Link M., Francke W.: Fresenius J. Anal. Chem. *353*, 39 (1995).
3. Paxeus N.: Wat. Res. *30*, 1115 (1996).
4. Espadaler I., Caixach J., Om J., Ventura F., Cortina M., Pauné F., Rivera J. Wat. Res. *31*, 1996 (1997).
5. Castillo M., Barceló D.: In: Sample Handling and Trace Analysis of Pollutants: Techniques, Applications and Quality Assurances, Barceló D (Ed.). Elsevier Science B. V. 1999, p 537.
6. Sheldon L. S., Hites R.A.: Environ. Sci. Technol. *13*, 574 (1979).
7. Dsikowitzky L., Schwarzbauer J., Kronimus A., Littke R.: Chemosphere *57*, 1288 (2004).
8. Schwarzbauer J., Heim S.: Water Res. *39*, 4735 (2005).
9. Takada H., Eganhouse R. P.: Molecular markers of anthropogenic waste. In: *Encyclopedia of Environmental Analyses and Remediation*, Meyers R. A. (Ed.), John Wiley & Sons 1998, p 2883.
10. Kronimus A., Schwarzbauer J., Dsikowitzky L., Heim S., Littke R.: Wat Res *38*, 3473 (2004).
11. Heim S., Schwarzbauer J., Kronimus A., Littke R., Hembrock-Heger A.:. Environ. Chem. Lett. *1*, 169 (2003).
12. Heim S., Schwarzbauer J., Kronimus A., Littke R.: Org. Geochem. *35*, 1409 (2004).
13. Dempster H. S., Sherwood Lollar B., Feenstra S.: Environ. Sci. Technol. *31*, 3193 (1997).
14. Mazeas L., Budzinski H., Raymond N.: Org. Geochem.. *33*, 1259 (2002).
15. Stark A., Abrajano jr T. A., Hellou J., Metcalf-Smith J. L.: Org. Geochem. *34*, 225 (2003).
16. Sturchio N. C., Clausen J. L., Heraty L. J., Huang L., Holt B. D., Abrajano T. A.: Environ. Sci. Technol. *32*, 3037 (1998).
17. Mazeas L., Budzinski H.: Org. Geochem. *33*, 1253 (2002).
18. Sherwood-Lollar B., Slater G. F., Ahad J., Sleep B., Spivack J., Brennan M., Mackenzie P.: Org. Geochem *30*, 813 (1999).
19. Yanik P. J., O'Donnell T. H., Macko S. A., Qian Y., Kennicutt II M. C.: Org. Geochem *34*, 291 (2003b).
20. Harrington R. R., Poulson S. R., Drever J. I., Colberg P. J. S., Kelly E. F.: Org Geochem *30*, 765 (1999).
21. Schwarzbauer J., Dsikowitzky L., Heim S., Littke R.: Intern. J. Environ Anal. Chem. *85*, 349 (2005).
22. Kronimus A., Schwarzbauer J., Dsikowitzky L., Littke R.: Environ Chem Letters *4*, 23 (2006).

L05 CHALLENGES OF THE ANALYSIS OF FOOD AND ENVIRONMENTAL MATRICES BY GC-TOF MS AND GC × GGC-TOF MS

TOMÁŠ KOVALCZUK, JITKA ZROSTLÍKOVÁ, JANA HAJŠLOVÁ, JAKUB SCHŮREK and MARK LIBARDONI

Leco Corporation, Apllication Laboratory Prague, Sokolovská 219, Pratur 9-Vysočany, 190 00

Tomas.kovalczuk@leco.cz

Introduction

The demands on the analysis of organic contaminants' residues have been increasing recently, taking into account the number of compounds analysed in a single run, number of matrices handled within one method, requirements on detection limits as well as requirements on the analysis speed. Accordingly, considerable progress in both sample preparation techniques and in the instrumentation has been done recently. As for the instrumental part, gas chromatography still remains a widely used separation technique in such residue analysis, thanks to its high separation potential and wide range of applicability. Mass spectrometry is becoming to be used more as primary detection technique in GC, instead of being a confirmatory tool only.

Time-of-flight mass spectrometry offers several important benefits over conventional (scanning) MS detectors: *(i)* With TOF MS full mass spectral information is available across the whole chromatogram, while the achieved detectability is comparable to the one typical for conventional MS detectors. Therefore, unambiguous confirmation of analyte identity is possible according to full mass spectrum. *(ii)* The absence of spectral skewing and the constant ratios of ions across a chromatographic peak allow the application of software data mining algorithms of peak finding and true signal deconvolution. This enables the applications for non-target screening analysis. *(iii)* Being the fastest MS detector, time-of-flight can be used for the applications in fast and ultra-fast GC and comprehensive two-dimensional gas chromatography (GC × GC), as discussed below.

Within the data mining software routines the Peak Find algorithm automatically and effectively locates all peaks in the chromatogram. Co-eluting analytes, peaks buried beneath the background of the TIC, and even small peaks buried beneath large matrix interferences are automatically detected and reported. After the Peak Find algorithm has located all of the analytes, the true mass spectra for each analyte are automatically extracted from the system background, matrix background, and co-eluting components. Even ions that are shared between co-eluted analytes are accurately proportioned to provide a complete mass spectrum. The resulting spectrum is then used for analyte identification by spectral interpretation or by library search using any number of commercially available or operator-prepared databases. Fig. 2. shows the overlap of the tolylfluanide and penconazole peaks with a time difference of 0. s between the peak apexes. Although,

it is impossible to distinguish the two peaks in the combined TIC, the peaks can be resolved by plotting the individual ion masses. Apex non-deconvoluted spectra A) contain some ions originating in co-eluted peak (red and green arrows). After applying the deconvolution agorithm these spectra are then missing all these contaminating ions B) and can be then identified by matching to mass spectral libraries C). This ability to separate and identify closely eluting peaks decreases the need for highly resolved peaks and permits faster analysis.
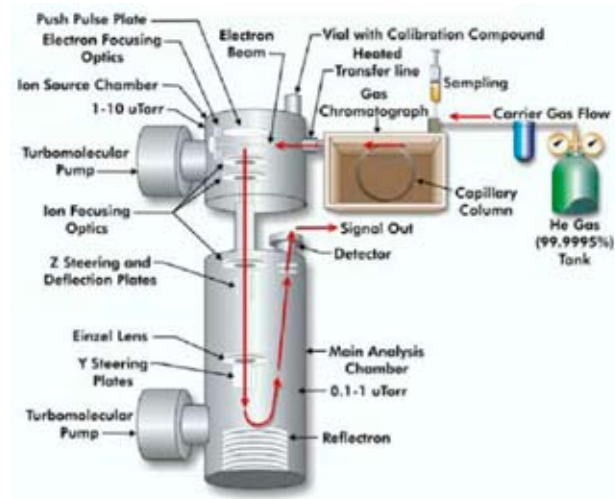

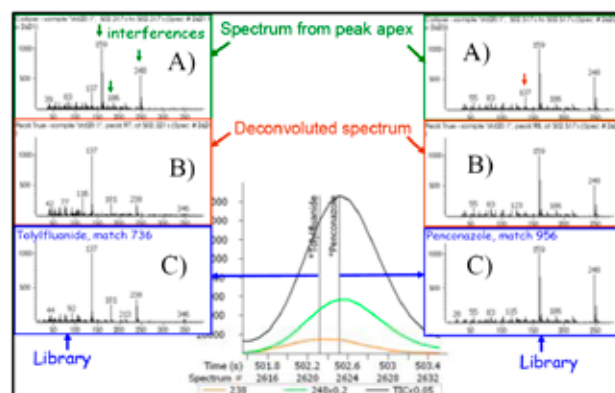Fig. 1. **TOF MS design (Pegasus HT, LECO, USA)**

Fig. 2. **True signal deconvolution demonstrated on closely co-eluted peaks of penconazole and tolylfluanide**

Comprehensive two-dimensional gas chromatography (GC × GC) has been a subject of attention in recent years, because of its enormous separation ability. In GC × GC, two columns of different selectivity are connected via a thermal modulator, which cuts small parts of the first column eluate, focuses them to sharp zones and samples them onto the second column, where a very fast "flash" separation (100–150 times faster compared to separation in first column) is performed. Each compound of a sample is therefore subjected to two independent separation mechanisms (see Fig. 3.).

The considerably increased peak capacity of GC × GC over one dimensional GC provides not only improved sepa-
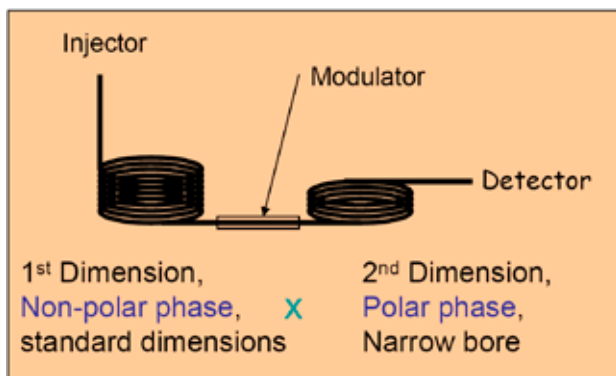
Fig. 3.　**GC×GC diagram**

ration of target analytes (see Fig. 4.) but also target analytes from matrix which allow more accurate identification and quantification of analytes.

Results

In the presented contribution applications focusing on GC-TOF MS and GCxGC-TOF MS examination of difficult environmental samples will be shown.

REFERENCES
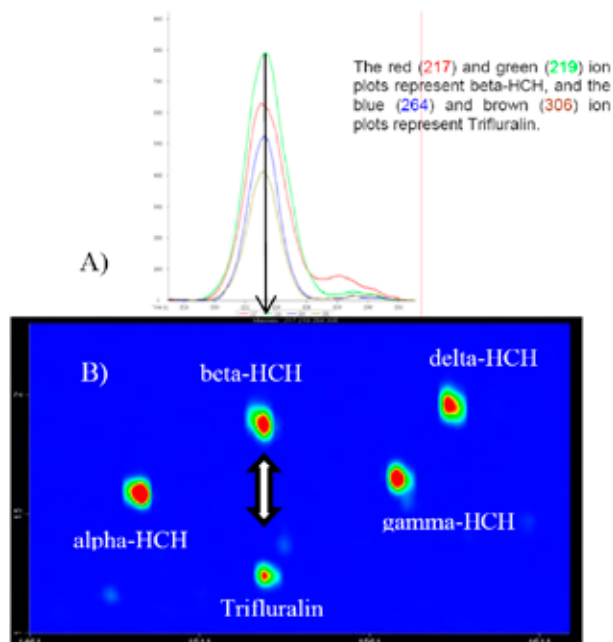1. Application Note Leco Corp. Acessed by internet via: http://www.leco.com/resources/application_note_subs/ pdf/separation_science/-252.pdf

The red (217) and green (219) ion plots represent beta-HCH, and the blue (264) and brown (306) ion plots represent Trifluralin.

A)

B)　　delta-HCH

beta-HCH

alpha-HCH

gamma-HCH

Trifluralin

Fig. 4.　**Contour plot showing chromatographic separation of beta-HCH and Trifluralin in the second dimension as noted by the white arrow (B), however, they co-elute in the first dimension (A) (ref.[1])**

L08   TRANSFORMATION OF PETROLEUM POLLUTANT IN THE ENVIRONMENT

BRANIMIR JOVANČIĆEVIĆ[a,b]

[a]*Department of Chemistry, University of Belgrade, Studentski trg 12–16, Belgrade, Serbia,*
[b]*Center of Chemistry, IChTM, Sudentski trg 12-16, Belgrade, Serbia, bjovanci@chem.bg.ac.yu*

Introduction

Petroleum and its refining products continue to be one of the most abundant environmental pollutants. Consequently, transformation processes of petroleum-type pollutants in soils, recent sediments, alluvial sediments, ground and surface waters were studied by numerous authors: in coastal marine environment[1], in estuarine sediments[2], under arctic marine conditions[3], on the East Mediterranean coast[4] etc.

The fate of an oil type pollutant in the environment can be monitored most accurately by determining its quantity and studying its composition in the polluted samples from the same or close locality, and during different periods of time. On that way a number of experiments were carried out in order to define the intesity and optimal conditions for the most efficient biodegradation (temperature, humidity, nutrients) e.g., [5-11].

On the other side, simulation of the natural conditions in the laboratory or by *ex situ* bioremediation with simultaneous intensification of only specified factors affecting the intensity and rate of transformation made it possible to save time and to come to relevant conclusions. Applications of biodegradation processes foccussed primarily on bioremediation of different sections of the environmental compartments have been described, e.g.[12–14]

In this paper our recent results will be reviewed observed by investigating tranformation processes of petroleum-type pollutant 1) by determining its quantity and studying its composition in the polluted samples from different distance of oil spill; 2) by determining its quantity and studying its composition in the polluted samples during different periods of time from oil spill; 3) by simulation of the natural conditions in the laboratory and 4) by *ex situ* bioremediation with simultaneous intensification of only specified factors affecting the intensity and rate of transformation.

Tranformation Processes of Petroleum Pollutant by Determining its Quantity and its Composition in the Samples from Different Distance of Oil Spill

In order to gain insight into oil transformations which occur during migration and to contribute to the elucidation of migration mechanisms in water-wet environments, the content and composition of heavy fuel oil from an accidental oil spill near a railway station was determined in crushed rock samples from various depths and distances from the oil spill[15]. The observed differences in the group composition (increase in NSO-compounds content with depth and distance), and in the distribution of n-alkanes and isopreno-

ids C_{19}, pristane (Pr) and C_{20}, phytane (Phyt) (the shift of the n-alkane-maximum and the shift of Pr/n-C_{17} and Phyt/n-C_{18}-ratios towards higher values with depth and distance; Fig. 1.) lead to the conclusion that heavy fuel oil migration through the crushed rock environemnt occured in the presence of water by the colloidal micelle mecahnisms. Namely, higher n-alkane homologues and pristane and phytane incorporated into the micelles of petroleum NSO-compounds and water and thus they are "transported" preferentially, compared to shorter-chain n-alkanes.

Tranformation Processes of Petroleum Pollutant by Determining its Quantity and its Composition in the Samples During Different Periods of Time from Oil Spill

The process of biodegradation of petroleum-type pollutants in underground waters from Danube alluvial sediments (the locality of Pančevo Oil Refinery) was followed through a period from November 1997 to February 2000 by GC analyses of isolated alkane fractions[16,17] (Fig. 2.).

In the period from November 1997, when first samples were taken, to February 2000, when fifth samples were taken, important changes of the chemical composition were obvious, especialy in well I. Relative contribution of n-alkanes as compared to pristane and phytane in sample Ia indicated changes defined as "initial petroleum biodegradation".
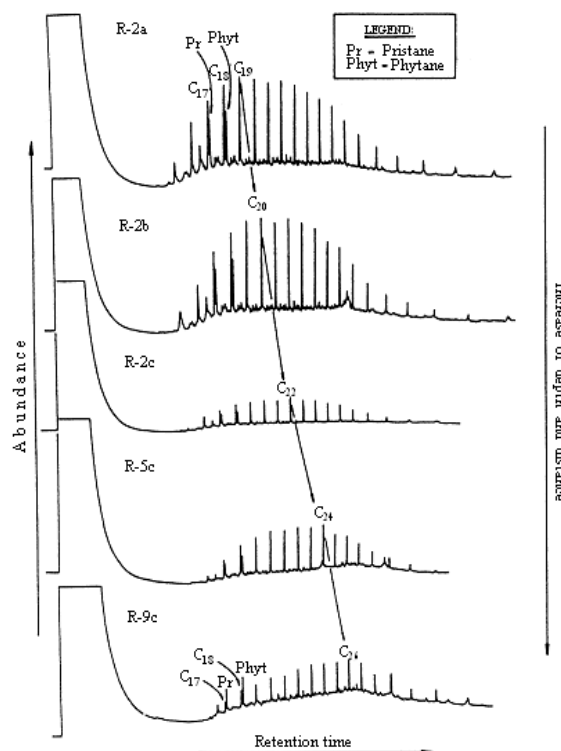

Fig. 1.   **Gas chromatograms of saturated hydrocarbon fractions isolated from emptied heavy fuel oil (R-2a → R-9c, increase the depth and distance from oil spill)[15].**
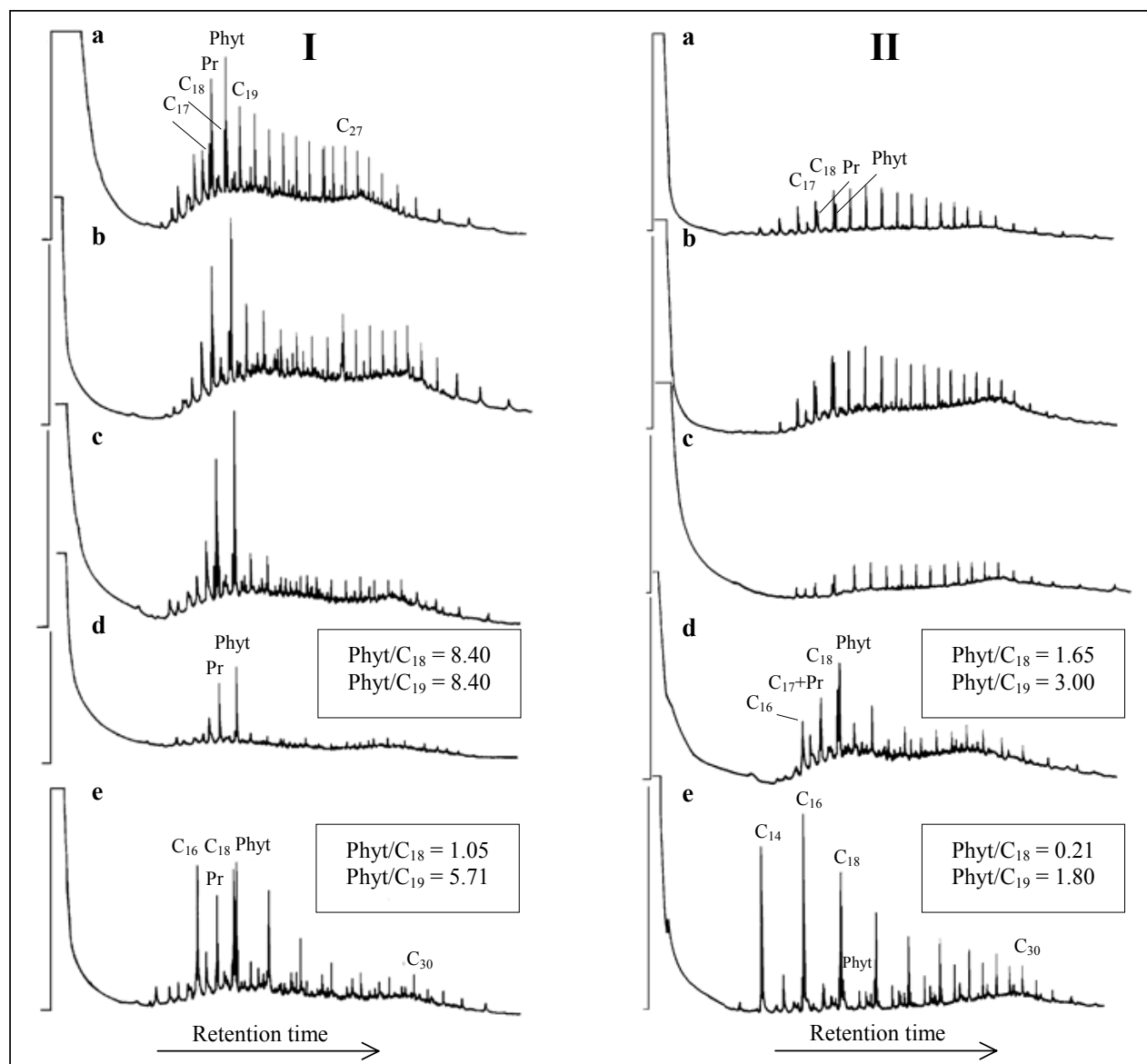
Fig. 2.　**Gas chromatograms of alkanes isolated from oil polluted alluvial ground waters (Pančevo Oil Refinery locality, I and II wells). Samples were taken in November 1997 (a), May 1998 (b), in September 1998 (c), September 1999 (d) and in February 2000 (samples e)[16,17].**

The abundance of C_{17} and C_{18} n-alkanes was somewhat smaller than the abundance of pristane (C_{19}) and phytane (C_{20}). Gas chromatogram of sample Ib showed that in the period from November 1997 to May next year the amount of n-alkanes relative to isoprenoids was reduced, a phenomenon typical for biodegradation intensity in geochemical literature defined as "very slight" or "minimal biodegradation"[18–20]. Later, in September 1998 (sample Ic), the amount of n-alkanes was still smaller. Finally, during next one year, n-alkanes were almost completely degraded (sample Id). Pristane and phytane remained nonbiodegraded.

Comparison of Pr/n-C_{17} and Phyt/n-C_{18} ratios observed in samples Ia-c (winter 1997 – autumn 1998) suggested that

biodegradation was considerably more intensive during the summer period than during the winter or spring periods. On the other hand, by comparing these degradation intensities with those observed in samples originating from close but deeper localities, it was concluded that biodegradation of the petroleum-type pollutant was more intensive in shallow underground waters[21]. In a relative short period of time, from September 1999 to February 2000, the alkane fraction of the petroleum-type pollutant suffered an unexpected change (sample Ie, Fig. 2.). Namely, while pristane and phytane were found in the same amounts characterized by approximately the same ratios, in this fraction of the pollutant new even carbon-number C_{16} to C_{30} n alkanes were observed. It was
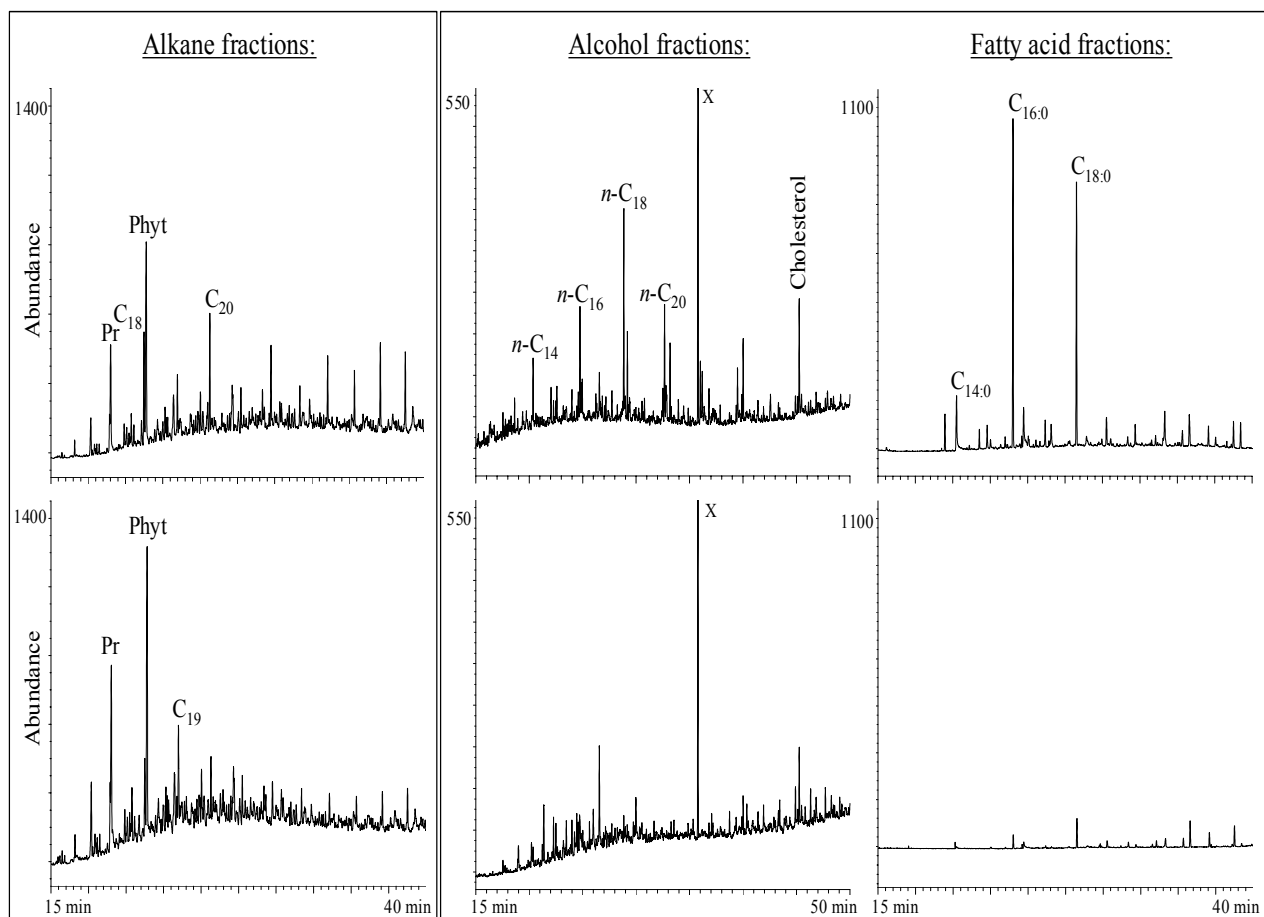
Fig. 3. **Chromatograms of GC-MS analyses of fractions of alkanes, alcohols and fatty acids (their methyl-esters), isolated from extracts I d (below) and Ie (above)[24].**

supposed that these even carbon-number n-alkanes were biosynthesized by some microorganisms. According to literature data, the following organisms are known to synthesize such compounds: Desulfovibrio desulfuricans, Corynebacterium sp., Escherichia coli, Rhizopus stolonifer or Penicillium sp.[22]. These are all micro-organisms which have grown on different organic basal medium (for example sewerage waste[23]). Consequently, the biosynthesis of even carbon-number C_{16}–C_{30} n-alkanes was tried to confirm by detailed analysis of extracts obtained from samples d and e[24] (Fig. 3.).

It was found that sample Ie, containing remarkable amounts of even *n*-alkane homologues, contained, as well, in the alcoholic fraction, a homologous series of even carbon-number alcohols in a C_{14} to C_{20} range and a relatively significant amount of cholesterol. On the other hand, sample Id, which did not contain any significant amounts of neither odd nor even n-alkane homologues, did not contain alcohols or higher fatty acids.

Even carbon-number alcohols and fatty acids observed in sample Ie were taken as a proof of the presence of particular microorganisms, i.e., of unicellular, nonphotosynthetic algae of *Pyrrophyta* type. These types of microorganisms,

also known under a popular name of "fire algae", are known to be able to synthesize even *n*-alkane homologues on a suitable base such as petroleum or petroleum-type pollutants[25].

Tranformation Processes of Petroleum Pollutant by Simulation of the Natural Conditions in the Laboratory

The fate of a petroleum-type pollutant in environmental water may be foreseen on the basis of laboratory simulation experiments of microbiological degradation of petroleum using microorganism consortiums similar to those typical for the natural environment, activated on a corresponding nutrient base[26]. As an example, Figure 4 shows a gas chromatogram of the alkane fraction of a paraffinic-type crude oil originating from Serbia oil field (Sir-1C), and gas chromatograms of alkane fractions of the same crude oil isolated after 90 days of simulated biodegradation on an inorganic "Knop" base (Ca(NO$_3$)$_2$·4H$_2$O, K$_2$HPO$_4$, MgSO$_4$·7H$_2$O, KCl, FeCl$_3$, H$_2$SO$_4$, H$_2$O; pH ≈ 8) under daylight (Sir-1) and in absence of light (Sir-2), as well as on a "Bujon" organic base (tryptone, yeast extract, glucose, distilled water, pH ≈ 7) under daylight (Sir-3) and in darkness (Sir-4). The experiments were carried out with microorganisms consortium similar to that one iden-

tified as dominant in the investigated surface sewage water in the channel of the Pančevo Oil Refinery (*Phormidium foveolarum, Achanthes minutissima, Nitzschia communis, Chlorella communis*)[27].

In an experiment on a Knop base, which maximally correspond to natural conditions, by biodegradation under daylight (Sir-1), n-alkanes were almost completely degraded. In darkness, the degradation was less effective (Sir-2). In experiments on a Bujon base, *n*-alkanes were found to be much less degraded (Sir-3 and Sir-4).
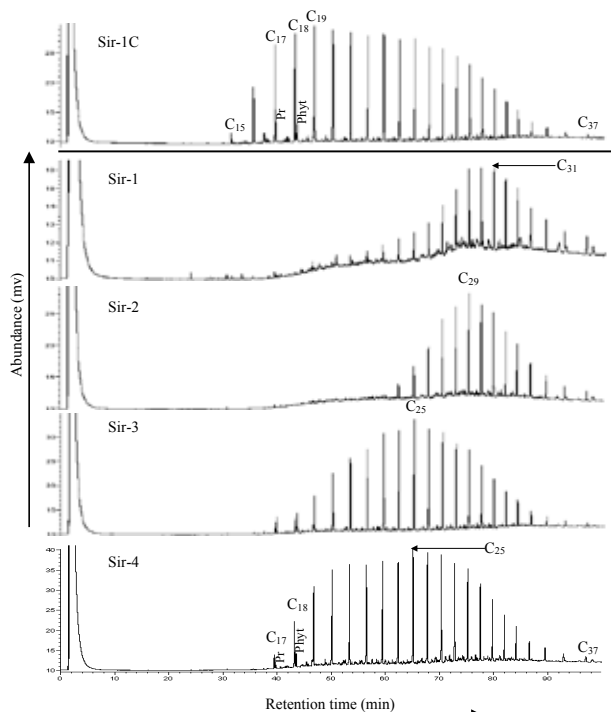
Fig. 4. **Gas chromatograms of the alkane fractions derived from paraffinic type petroleum of Sirakovo after 90 days of simulated biodegradation with *Phormidium foveolarum*, *Achanthes minutissima*, *Nitzschia communis* and *Chlorella communis* with Kp medium in the light (Sir-1), with Kp medium in the dark (Sir-2), with Bh medium in the light (Sir-3), with Bh medium in the dark (Sir-4) together with chromatogram of alkane fraction typical for the control experiments (Sir-1C)[27].**

On the other hand, in experiments carried out in the same way, using the same nutrient bases and identical microorganisms, but with a naphthenic-type crude oil originating also from Serbia, it was possible to follow the degradation of isoprenoid aliphatic compounds27 (Table I). Comparison of Phyt/C30-hopane ratios observed in the investigated samples after 90 days of simulated biodegradation (Ve-1 – Ve-4) with those observed in control tests (Ve-1C – Ve-4C; Table I), showed the degradation of isoprenoids to be also most pronounced on the Knop inorganic nutrient base and under daylight. Under identical experimental conditions, polycyclic alkanes of sterane and triterpane types retained their original distributions.

Table I
Parameters based on gas chromatograms of naphthenic-type crude oil alkane fractions[27]

	Pr/Phyt	Phyt/C30-hopane
Ve-1C	0.21	1.68
Ve-1	ND	ND*
Ve-2C	0.37	3.81
Ve-2	ND	ND*
Ve-3C	0.46	4.00
Ve-3	0.52	1.67
Ve-4C	0.10	0.50
Ve-4	0.30	0.32

ND – parameter was not calculated due to total degradation of pristane and phytane
ND* – parameter was not calculated due to total degradation of phytane

The experiment of *ex situ* soil bioremediation was performed at the locality of the Oil Refinery in Pančevo (alluvial formation of the Danube river, Serbia) polluted with the oil type pollutant[28]. The experiments of biostimulation, bioventilation and reinoculation of autochthonous microbial consortium were carried out during the six-month period (May – November 2006). The changes in the quantity and composition of the pollutant, or the bioremediation effect, were monitored by analysis of the samples of the polluted soil taken in time spans of two weeks. In that way, from the beginning until the end of the experiment, 12 samples were collected and marked with P_1–P_{12} (Pančevo 1 – Pančevo 12). The results obtained showed that more significant changes in the composition of the oil pollutant occurred only during the last phases of the experiment (P_8–P_{12}; Fig. 5.). The activity of microorganisms was reflected in the increase of quantity of the polar oil fractions, first of all fatty acid fractions. In that way the quantity of total eluate increased, and the quantity of the insoluble residue was reduced to minimum, by which the oil pollutant was transferred to a form which can be removed more efficiently and more completely from the soil, as a segment of the environment.

Also, these experiments presented atypical transformations of saturated hydrocarbons of petroleum type pollutants[29]. Namely, organic substance from P_1, P_8 and P_{12} samples were extracted by Soxhlet's method and quantified. Isoprenoid aliphatics, in particular pristane and phytane, and polycyclic aliphatics of sterane and triterpane types in saturated hydrocarbon fractions were analysed by GC-MS (SIM method). Significant amounts of *n*-alkanes have not been detected. The MS-chromatogram revealed only marginal amounts of pristane and phytane in sample P_1. Pristane and phytane occurred in sample P_8, and in even higher quantities in the final sample P_{12} (Fig. 6.). The proceeding bioremediation process was accompanied by the decrease of the relative amounts of pentacyclic terpanes of hopane type, compared to tri- and tetracyclic terpanes[29]. In the initial sample P_1 the distribution
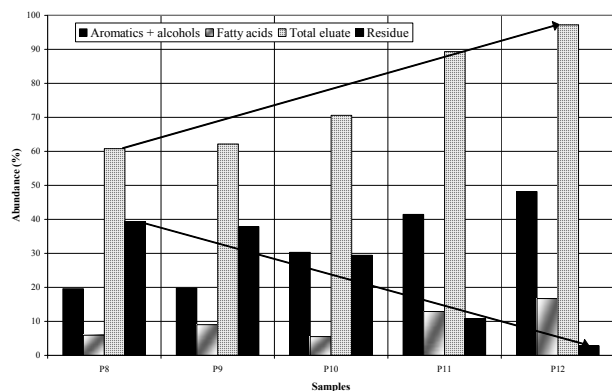
Fig. 5. **Contents of total aromatics and alcohols, fatty acids, total eluate and the column residue for samples P_8–P_{12} (ref.[28]).**

of steranes and hopanes follows a pattern, which is characteristic for crude oils. However, their identification by SIM method was not possible in samples P_8 and P_{12} because of the reduced concentration[29].

The observed changes in the alkane fractions' compositions may be considered as atypical, referring to the fact that during oil biodegradation under natural conditions, decomposition of isoprenoids occurs much easier and faster than decomposition of polycyclic alkanes of tri-, tetra- and pentacyclic terpane, sterane and diasterane types, after the decomposition of *n*-alkanes has been almost completed.

Instead Conclusions

In spite of remarkable advancement of petroleum exploitation, transport and refining technologies, petroleum and its refining products continue to be one of the most abundant environmental pollutants. Consequently, studies on the environmental fate of petroleum-type pollutants remain to be an actual scientific interdisciplinary problem.

Fig. 6. **Ion chromatogram characteristical for isoprenoids (m/z 183) of samples P_1, P_8 and P_{12} (full mass spectra of phytane peak for P_1 sample is also given)[29].**

REFERENCES

1. Readman J. W., Bartocci J., Tolosa I., Fowler S.W., Oregioni B., Abdulraheem M. Y.: Marine Pollut. Bull. *32*, 493 (1996).
2. Oudot J., Merlin F. X., Pinvidic P.: Marine Pollut. Bull. *45*, 113 (1998).
3. Garrett R. M., Rothenburger S. J., Prince R. C.: Spill Sci. Tech. Bull. *8*, 297 (2003).
4. Ezra S., Feinstein S., Pelly I., Baumen D., Miloslavsky I.: Org. Geochem. *31*, 1733 (2001).
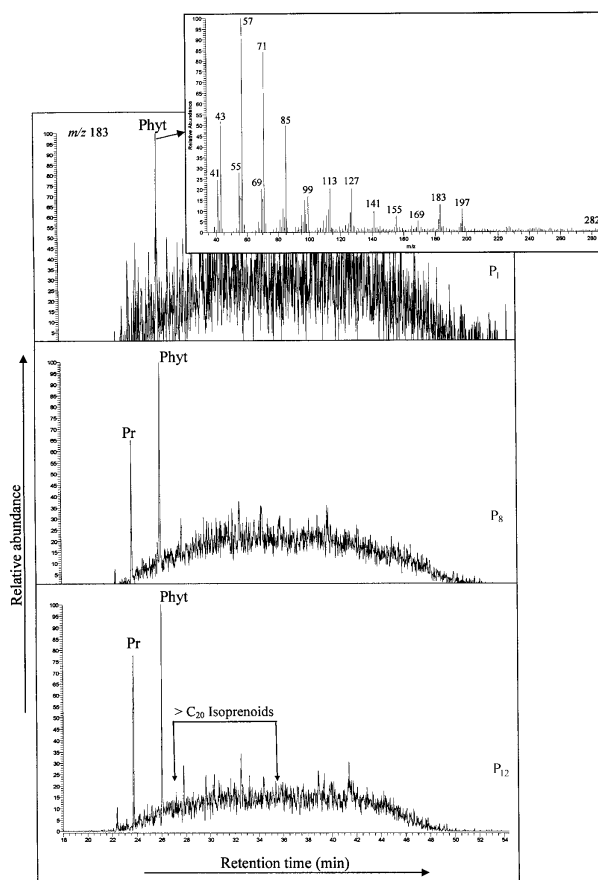5. Prince R. C.: Critic. Review. in Microbiol. *19*, 2514 (1993).
6. Blanke M., Wibbe M. L.: Environ. Sci. Pollut. Res. *6*, 2 (1999).
7. Brandsch R., Nowak K-E., Binder N., Jastorff B.: J. Soil. Sed. *1*, 234 (2001).
8. Kahru A., Maloverjan A., Sillak H., Põllumaa L.: Environ. Sci. Pollut. Res. *9*, 27 (2002).
9. Truu J., Heinaru E., Talpsep E., Heinaru A.: Environ. Sci. Pollut. Res. *9*, 8 (2002).
10. Hallberg R., Trepte B.: J. Soil Sed. *3*, 21 (2003).
11. Rosolen V., Herpin U., Fräncle S., Breulmann G., Camargo P. B.de, Paganini W. S., Cerri C. C., Melfi A.J. Markert B.: J. Soil. Sed. *5*, 112 (2005).
12. Atlas R. M.: Marine Pollut. Bull. *31*, 178 (1995).
13. Al-Hadhrami M. N., Lappin-Scott H. M., Fisher P. J.: Marine Pollut. Bull. *34*, 969 (1997).
14. Chaîneau C. H., Yepremian C., Vidalie J. F., Ducreux J., Ballerini D.: Water, Air, Soil Pollut. *144*, 419 (2003).
15. Jovančićević B., Tasić Lj., Vujasinović S., Matić I., Malović D., Pfendt P.: J. Serb. Chem. Soc. *61*, 1025 (1996).

16. Wehner H., Jovančićević B., Polić P., Vrvić M., Scheeder G., Teschner M.: *20th International Meeting on Organic Geochemistry, Nancy, 10 – 14 Sept. 2001*, Book of Abstracts (Landais P., ed.), p. 265 (resp. Poster no., P/THU/02).

17. Jovančićević B., Polić P, Vitorović D., Scheeder G., Teschner M., Wehner H.: Fresenius Envir. Bull. *10*, 178 (2001).

18. Volkman. J. K., Alexander R., Kagi R. I., Woodhouse G. W.: Geochim. Cosmochim. Acta, 47, 785 (1983).

19. Head I.M., Jones D.M., Larter S.: Nature. *426*, 344 (2003).

20. Peters K. E., Walters C. C., Moldowan J. M.: *The biomarker guide*. Cambridge University Press, Cambridge, New York, Melbourne, Madrid, Cape Town 2005.

21. Jovančićević B., Polić P.: Fresenius Envir. Bull. *9*, 232 (2000).

22. Grimalt J., Albaigés J.: Geochim. Cosmochim. Acta, *51*, 1379 (1987).

23. Jovančićević B., Tasić Lj., Wehner H., Marković D., Polić P.: Fresenius Envir. Bull. *7*, 320 (1998).

24. Jovančićević B., Polić P., Vrvić M., Scheeder G., Teschner T., Wehner H.: Envir. Chem. Lett. *1*, 73 (2003).

25. Blaženčić J.: *Algal systematic*. Naučna knjiga, Beograd 1988. (in Serbian)

26. Hurst C. J.: *Manual of environmental microbiology*. ASM Press, Washington 1997.

27. Antić M., Jovančićević B., Ilić M., Vrvić M., Schwarzbauer J.: Environ. Sci. Pollut. Res. *13*, 320 (2006).

28. Jovančićević B., Antić M., Vrvić M., Ilić M., Novaković M., Saheed R.M., Schwarzbauer J.: J. Serb. Chem. Soc. *73*, 601 (2008a).

29. Jovančićević B., Antić M., Pavlović I., Vrvić M., Beškoski V., Kronimus A., Schwarzbauer J.: Water, Air, and Soil Pollut. *190*, 299 (2008b).

2. ENVIRONMENTAL CHEMISTRY & TECHNOLOGY

2.1. Lectures

L02 DEGRADATION PRODUCTS OF SYNTHETIC POLYMERS AS EMERGING ENVIRONMENTAL CONTAMINANTS

JOSEF ČÁSLAVSKÝ, MILADA VÁVROVÁ, DANIELA MÁCOVÁ and LUDMILA MRAVCOVÁ

Institute of Chemistry and Technology of Environmental Protection, Faculty of Chemistry, Purkyňova 118, 612 00 Brno, Czech Republic,
caslavsky@fch.vutbr.cz

Introduction

Synthetic polymers belong to attributes of modern life; it is hard to imagine contemporary lifestyle without them.

These materials came into existence before almost 200 years. In 1811 french pharmacist Henry Braconnot prepared the first man-made material by treating of wood and cotton by concentrated nitric acid. This material was called "xyloidin" and it hasn't found any practical use. The term "polymer" was proposed later in 1833 by Jöns Jakob Berzelius. The first semi-synthetic polymer, vulcanized rubber, was synthesized by Charles Goodyear in 1839. Very popular and widely used celluloid was discovered in 1870 by John Wesley Hyatt; it was prepared from nitrocellulose and camphor. All these polymers were based on raw materials of natural origin. The first fully synthetic (and also very popular) polymer was bakelite, which was prepared between years 1907–1909 by Belgian chemist Leo Baekeland.
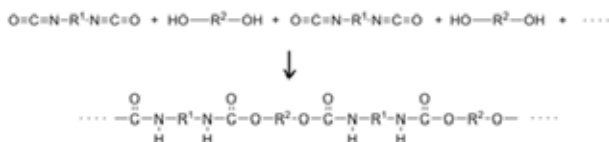

Fig. 1.   **Polyurethane synthesis**

In our study we focused our attention on polyurethanes. Thesse polymers were discovered in 1937 by german chemist Otto Bayer. Their synthesis is quite simple; by reaction of diisocyanate with diol the polymeric chain is formed containing both monomer units connected by urethane bonds:

Toluene diisocyanate is most often used raw material; if polyols are used instead of diols then 3-dimensional and more firm polymer network is formed.

Nowadays, polyurethanes are very popular and widely used due to their extremely flexible properties, which can be "tailored" with respect to their planned use. Flexible low density foams ($6\ kg\,m^{-3}$) are used in bedding and upholstery, semi-rigid ones serve as packaging foams and rigid are used as insulation foams. High density foams ($400\ kg\,m^{-3}$) in fle-

xible version serve as footwear midsoles and outsoles, rigid ones are used as integral skin in vehicle interiors and rigid foams are produced as simulated wood. Microcellular foams and elastomers (density $800\ kg\,m^{-3}$) are used for fabric coatings and synthetic fibers production and also for vehicle facia and other exterior parts of cars and also as structural foam. Solid polyurethane elastomers - RIM (density $1,200\ kg\,m^{-3}$) are used for example in production of printer rolers.

The worldwide production of polyurethane is constantly increasing and in 2003 it overcame 10 million of tons. From this amount 1/3 is produced in Europe, another 1/3 in North America and the last 1/3 in the rest of the World[1].

The mass flow of polyurethanes in Europe in 2000 was described by Ron Zevenhoven[2]. The total PU consumption was approx. $3\ Mt\,yr^{-1}$ (cca $1.8\ Mt\,yr^{-1}$ of PU foams, cca $0.8\ Mt\,yr^{-1}$ of rigid foams, cca $0.4\ Mt\,yr^{-1}$ of RIM and elastomers). From this amount only cca $150\ kt\,yr^{-1}$ is recycled and approximately the same amount is incinerated. Remaining cca 90 % of the amount produced end in landfills, where it can undergo various decomposition reactions. Therefore, it would be useful to enhance biodegradability of these materials; on the other side, the products of decomposition could be environmentally dangerous.

In our study we focused our attention on the identification of degradation products of polyurethane with enhanced biodegradability. Either natural conditions or simulatend ageing were used, both volatile and non-volatile compounds were analysed.

Experimental

Polyurethane foams (PUFs) were prepared at the Institute of Material Science by reaction of diisocyanate and polyol; part of the synthetic polyol (up to 10 %) was replaced by biodegradable biomass originated polyol (cellulose acetate, wheat protein, acetylated potato starch, carboxymethylcellulose, 2-hydroxyethylcellulose). In parallel, control PUF was prepared by standard procedure (i.e. without addition of biomass polyol).

H y d r o l y t i c   D e g r a d a t i o n
3 g of PUFs were refluxed with $150\ dm^3$ of deionized water for 8 hours. Leachates were analyzed by LC/ESI-MS.

N a t u r a l   P h o t o d e g r a d a t i o n
Flat pieces of PUFs were placed into flower window box on the top of soil layer and fixed by small stone. These pieces were let outside for 2 months. After this period the PUFs were extracted by ultrasonication in acetonitrile or n-hexane; acetonitrile extracts were analysed by LC/ESI-MS, hexane extracts by GC/MS.

A c c e l e r a t e d   A g e i n g – D e t e c t i o n   o f   N o n - V o l a t i l e   C o m p o u n d s
Flat pieces of PUF were placed under the UV-discharge tube and irradiated for 6 hours. Exposed PUFs were sonicated in *n*-hexane, the extract was volume reduced and analyzed by GC/MS.

Accelerated Ageing – Detection of Volatile Compounds

Flat pieces of PUFs were placed into accelerated ageing device (Fig. 2.) composed of quartz tube open on one end (length 24.5 cm, I.D. 3.5 cm) with input tubing and Teflon cover. The device was placed under UV discharge tube. Two SPME devices were inserted into both input and output tubing (the first with polydimethylsiloxane fibre, the second with polyacrylate fibre) and the ends of the device together with SPME holders were covered by aluminium foil to protect them against the UV light. The irradiation tooks place for 6 hours. After this period, SPME devices were directly analyzed by GC/MS.
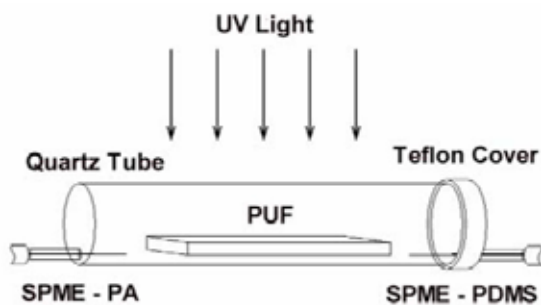
Fig. 2.　**Accelerated ageing device**

HPLC/MS

For HPLC/MS the Esquire-LC instrument (Bruker Daltonics, Bremem, Germany) was used. This system consists of the Agilent HPLC 1100 Series with binary gradient pump, electrospray ion source and spherical ion trap analyzer. A Supelcosil™ LC-18DB column (2.1×250 mm, 5 μm particles) was used (Supelco, USA). Gradient elution from 30 to 100 % acetonitrile in water in 30 min was used at constant flow rate of 0.25 ml min^{-1}. For the detection both UV-VIS detector of DAD type, and mass spectrometry were used. Drying temperature in electrospray was 350 °C, nebuilizing gas (N_2) pressure was 50 psi, and drying gas (N_2) flow was 14 dm^3 min^{-1}. Both positive and negative ions were registered (in separate runs).

GC/MS

System Agilent 6890N GC/5973 MSD (Agilent Technologies, Waldbronn, Germany) was employed. The column was HP-5MS 5 m×0.25 mm×0.25 μm, helium at a flow of 1 ml min^{-1} was used as carrier gas in constant flow mode. Temperature program was as follows: 50 °C for 1 min, then to 280 °C at 5 °C min^{-1}, final isotherm 5 min. 1 μl of sample was injected in splitless mode at a temperature of 280 °C with
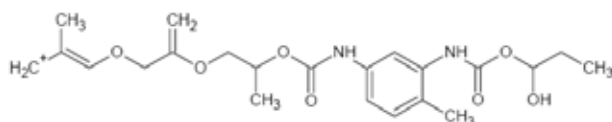

Fig. 3.　**Structure of PUF hydrolytic degradation product**

splitless time of 1 min. Interface temperature was 260 °C, temperature of ion source and quadrupole 230 and 150 °C, respectively. Electron ionization at 70 eV electron energy was used, spectra were registered in scan mode within the range of 50–450 amu. NIST 05 spectral library was used for the identification of separated compounds.
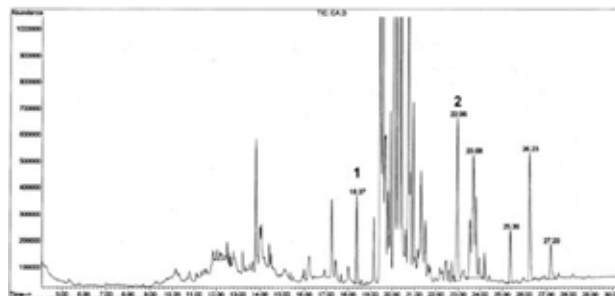

Fig. 4.　**PUF non-volatile degradation products. Compound identification: 1: bis(2-ethylhexyl) ester of hexanedioic acid; 2: di-tolyl-isocyanate**

Results

Typical LC chromatograms of PUF extract show only two peaks at the beginning. Using the LC/MS/MS experiments and MS^n with direct insfusion of the sample, the probable structure of main degradation product was proposed (see Fig. 3.).

This structure is evidently a fragment of polyurethane polymer chain.

Fig. 4. shows the chromatogram of hexane extract of polyurethane after UV irradiation. Using the database search several peaks were successfully identified, but in many cases the identification was unsuccessfull, in spite of the fact that the experimental spectrum was of good quality. The most probable explanation is that the NIST05 database doesn't contain
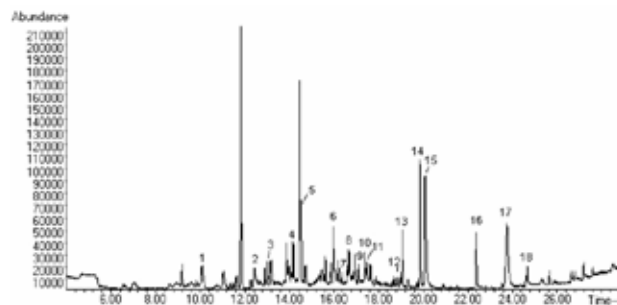

Fig. 5.　**Volatile degradation products (PDMS fibre). Compound identification: 1: 2-methyl-1,3-dioxane; 2: 2,6-diisocyanatotoluene; 3: 6,10-dimethyl-5,9-undecadiene-2-one; 4: 2,5-diterc-butyl-1,4-benzochinone; 5: pentadecane; 6: hexadecane; 7: 2,6-bis(1,1-dimethyethyl)-4-(1-oxopropyl)phenol; 8: dodecanoic acid methylester; 9: 4-decyl-morpholine; 10: heptadecane; 11: 2,6,10,14-tetramethyl-pentadecane; 12: ?? (isoprenoid alkane); 13: tetradecanoic acid isopropylester; 14: 4-undecyl-morpholine; 15: N,N-dimethyl-1-hexadecanamine; 16: 4-tetradecyl-morpholine; 17: squalene; 18: 4-hexadecyl-morpholine**
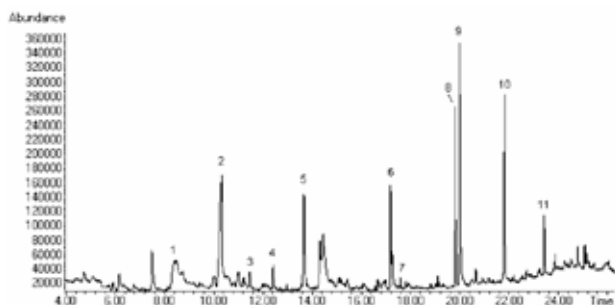
Fig. 6.   **Volatile degradation products (PA fibre). Compound identification: 1: 2-(2-ethoxyethoxy)-ethanol; 2: 2-ethyl-hexanoic acid; 3: 1,3-dioxane; 4: 2-methyl-1,3-dioxolane; 5: 2-methyl-1,3-diisocyanatobenzene; 6: 2,6-bis(1,1-dimethyethyl)-4-(1-oxopropyl)phenol; 7: 4-decyl-morpholine; 8: 4-undecyl-morpholine; 9: N,N-dimethyl-1-hexadecanamine; 10: 4-tetradecyl-morpholine; 11: 4-hexadecyl-morpholine**

mass spectra of compounds of this type. The only possibility of structure revealing in these cases remains the manual interpretation using the common fragmentation rules[3].

Fig. 5. shows the chromatogram of volatile degradation products of PUF with addition of hydroxyethylcellulose adsorbed by SPME on PDMS fibre. Various classes of compounds were found – alkanes, esters of fatty acids, morpholine derivatives, but also poisonous 2,6-diisocyanatotoluene. Fig. 6. depicts the same degradation products adsorbed on polyacrylate fibre. In this case more polar compounds are preferred like morpholine derivatives, but again toxic 2,6-diisocyanatotoluene (compound 2) was found.

Composition of the degradation products also depends on the type of biodegradable filler. Toluene diisocyanate was found only when hydroxyethylcellulose and cellulose acetate were applied.

Conclusions

Degradation products of polyurethane foams with enhanced biodegradability were studied. Both degradation under natural conditions and accelerated ageing were used, both non-volatile and volatile compounds were analysed using liquid and gas chromatography interfaced to mass spectrometry. The composition of degradation products was influenced by the type of biodegradable filler used instead of 5 % of polyether polyol in the polyurethane synthesis. When modified cellulose was used, poisonous toluene diisocyanate was identified as volatile degradation product. The identification of products separated by GC by library search was unsuccessfull in many cases; the reason is problably caused by the fact that the used MS library is commonly oriented and doesn't contain the spectra of PUF degradation products.

Following research will be focused on the quantitative analysis of PUF degradation products, either using SPME and suitable surrogates, or using adsorption tubes with suitable adsorbent.

REFERENCES

1   http://www.poliuretanos.com.br/Ingles/Chapter1/11Market.htm
2. Zevenhoven R., Ph.D. Thesis, Helsinki University of Technology, Helsinki, Finland, 2004
3. McLafferty F., Tureček F.: *Interpretation of Mass Spectra*. University Science Books, USA, 1993.

L03 USAGE OF GAS CHROMATOGRAPHY AND IMS DETECTION FOR EVALUATION OF POLYMER BARRIER MATERIAL PROPERTIES

JANA DVOŘÁKOVÁ[a] and IVAN MAŠEK[b]

[a]*VOP-026 Šternberk, s.p., division VTÚO Brno, Veslařská 230, 637 00 Brno, Czech Republic,*
[b]*Faculty of Chemistry, VUT, Purkyňova 118, 612 00 Brno, Czech Republic,*
dvorakova.j@vtuo.cz

Introduction

The protective properties are the most important parameters for selection of well-suited materials for construction of individual protective equipment (IPE). These properties determine ability of a given IPE against the highly toxic agents and industrial harmful substances under short time and/or long time contamination in the gaseous and liquid phases.

The most frequently used protective materials for IPE are polymer barrier materials. Their numerous advantages such as easy availability, possibility of mass production, relative low cost as well as the broad range of manufactured qualities determine their use for different protective purposes. Single-layer or laminated polymers and textile with polymeric or elastomeric layer are used as barrier materials. It is possible to use metallic film, PET sheet with layer of SiOx (e.g. material CERAMIX from company ALCAN) or other nanolayers, adsorption textile (e.g. SARATOGA with spherical sorbent or Charcoal Cloth made from activated carbon fibres) eventually special membranes (e.g. NAFION, GORE-TEX, POROTEX, PURTEX etc.) with specific diffusion properties for toxic agents.

Resistance of polymer barrier materials against harmful substances is defined as parameter called breakthrough time (BT)[1,2,3,4]. Breakthrough time is the most widespread way of barrier materials evaluation in term of constructional usage of materials, their manufacture and conditions of their selection.

Experimental

The procedures for evaluation of protective properties are elaborated in accordance with the Czech Technical Standard ČSN ISO EN 6529 (October 2001) which results from American Standard ASTM F 739-99a (August 1999)[5,6]. The above-mentioned standard describes experimental methods used for testing of barrier materials resistance against permeation of liquid and gaseous substances and, among other things (e.g. conditions of measurement for closed-loop or open-loop, continual and discontinual measurement, preparation of samples etc.) recommends suitable analytical techniques for evaluation of permeation toxic vapors. The gas chromatography (GC) is one of these techniques which is commonly used for detection and identification of chemical warfare agents (CWA) as well as ion mobility spectrometry (IMS)[7,8,9,10]. The 2, 2'-dichlorodiethylsulfide (sulphur mustard, HD) was used for measurement of permeation as testing chemical. The double-sided butyl rubber polyamide fabric was used as the used tested material.

Permeation Method

The following methods were selected for evaluation of barrier properties of polymer materials[11,12,14,15]. The principle of these methods is illustrated by visual demonstration on Fig. 1. where the scheme of alternative permeation cell that is used for measurement at aerodynamics conditions. The alternative permeation cell respects requirements of standard ČSN EN ISO 6529. This cell is made from stainless steel. The clamping system is solved by the one central withdrawal nut (see scheme on Fig. 1.) that makes possible not only quick clamping and exchange of tested materials but also total obturation of samples. The tested material separates the alternative cell into two parts. Upside of cell contains testing chemical (here sulphur mustard) and on the other side the permeating gas or vapor is swept away into the carrier gas leading to detector. The carrier gas and agent vapors mixture is then analyzed by suitable detection techniques.
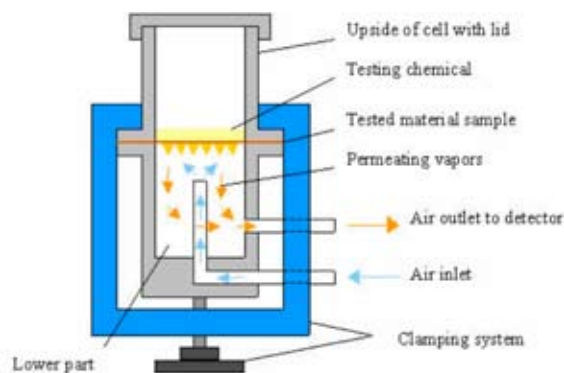

Fig. 1. **Scheme of alternative permeation cell used for measurement at aerodynamics conditions**

Composition of Experimental System

The experimental system for permeation measurement of toxic agents was designed in accordance with the standard ČSN EN ISO 6529. The clean air comes through drying column (the clean air is represented by blue arrows) washes lower part of tested material. The air stream carry away permeating vapors of testing chemical to the given detector (the air containing vapors of testing chemical is represents by red arrow). This system was modified according to the used kind of detection (see scheme on Fig. 2.).

GC and IMS detector GID-3 were used for analysis of permeating sulfur mustard vapors. The GC equipped with FID detector, Agilent 6890, was used for separation of gases and vapors between mobile and stationary phase. The components are separated on the basis of holding ability of the stationary phase into the chromatographic column. This analytical method enables evaluation of taken samples using
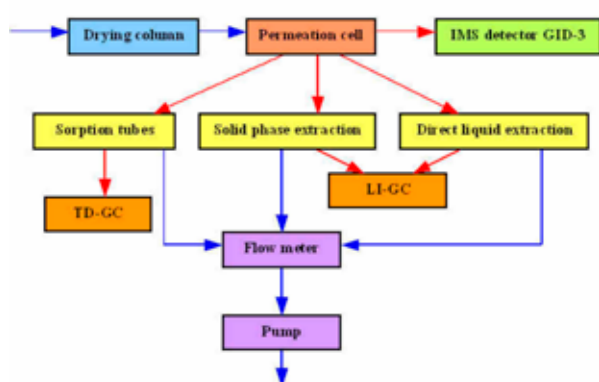
Fig. 2.   **Composition of usable experimental system for measurement of permeation of toxic agent through protection barrier materials**

thermal desorption from solid phase sorbent (Tenax™ TA), direct solvent liquid extraction (n-hexane) and solid phase extraction (SPE) method. The IMS detector GID-3 operates on the basis of the different mobility of ions in gaseous phase in the homogeneous electric field.

The investigated barrier material sample was fixed inside the alternative permeation cell (see scheme on Fig. 1.) and contaminated from the upper side with defined amount of liquid HD agent. The permeating agent vapors were sampled from the permeation cell space under the material sample by the IMS detector. The air-drying column was connected at the front end of the permeation cell inlet to protect IMS detector against moisture. IMS detector was connected to the PC where the measured data was continually acquired, saved and graphically evaluated (see chart on Fig. 3. and Fig. 4.) with using the software BarieraSW2006 especially designed for this purpose.

The scheme of LI/GC and TD/GC testing system is shown on Fig. 2. The same configuration of permeation cell including the investigated material sample placing and contamination procedure was used. The special sampling device equipped with a controlled air pump and flow meter was used for permeating agent sampling by the solid phase extraction ASSET-32™ tubes, direct solvent liquid extraction (DSLE) by n-hexane (for GC, ≥99.0 %) and DAAMS Tenax™ thermal desorption tubes. Air flow of 100 mL/min was set up. Agilent GC equipped with FID detector was used for analysis of liquid sample.

Results

The results of sulphur mustard permeation through tested materials obtained by IMS detector and GC (thermal desorption, direct liquid extraction and solid phase extraction) are compared in the chart on Fig. 3. and Fig. 4. Observed concentration shift shown in the chart is probably caused by different sensitivity of used methods. SPE method is more sensitive than direct solvent liquid extraction and direct solvent liquid extraction method is more sensitive than IMS method.
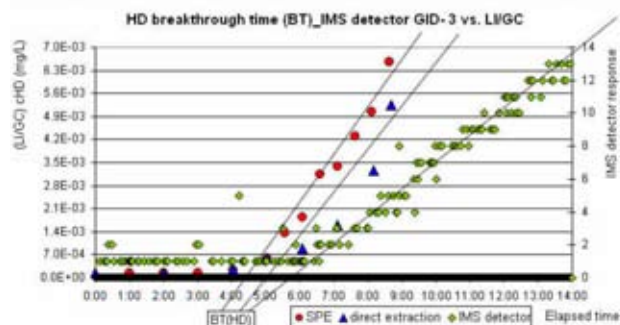

Fig. 3.   **he IMS and LI/GC techniques (direct solvent liquid extraction and solid phase extraction) results comparison**
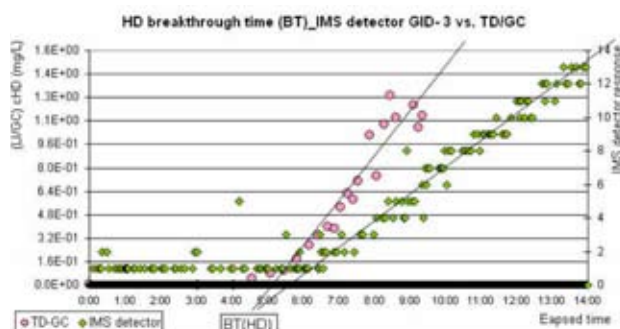

Fig. 4.   **The IMS and TD/GC techniques (thermal desorption) results comparison**

Breakthrough time of HD was determined on the basis of graphical analysis of permeation curves called time-lag. The permeation curve was interlayed by line13–19. The point where the line is crossing the x-axis represents the HD breakthrough time of investigated material (see Table I).

Table I
The values of HD breakthrough time obtain time-lag method

The used techniques	Breakthorough time of HD	
	minutes	hours
IMS	350	5 : 50
TD-GC	310	5 : 10
LI-GC (SPE)	270	4 : 30
LI-GC (DSLE)	300	5 : 00

Basically the breakthrough time is dependent also on the other factors then the used analytical method. Temperature is one of the most important factors, which strongly influences the permeation process. The following experiments, held under the same conditions, have been performed to quantify the temperature dependence. The course of permeation was monitoring by the IMS detector GID-3, which is preferable for long continual measurement. The measurement was proceeded in temperature range from 15 °C to 40 °C by 5 °C. The lower range limit was defined by freezing point of sulphur mustard, which is 14.5 °C. The upper limit was restricted by

tolerable ness of protection means. The fatal overheating of human body can happen at the temperatures over 40 °C.

The charts of all permeation curves are shown on Fig. 5. The permeation of HD agent through polymer membrane is faster with increasing temperature and permeation will be sharper course.
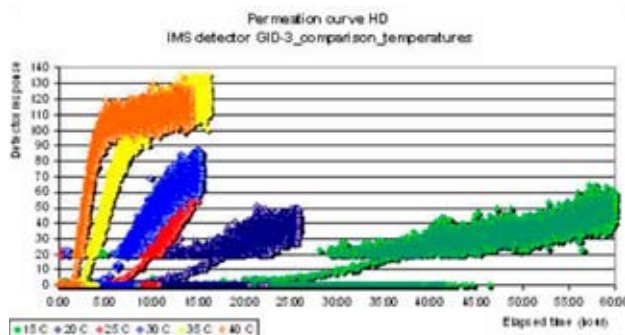

Fig. 5.   **The comparison of permeation curves obtained at different temperatures**

The related values of breakthrough times evaluated with using time lag method are presented in Table II.

Table II
The values of HD breakthrough time obtained with using the time-lag method for measurement under various temperatures by IMS detector

Temperature	Breakthorough time of HD	
	minutes	hours
15 °C	1485	22 : 20
20 °C	600	12 : 00
25 °C	440	7 : 20
30 °C	285	4 : 45
35 °C	150	2 : 30
40 °C	90	1 : 30

The dependence of HD breakthrough time on temperature is plotted in chart shown on Fig. 6. The points in the chart were interlaced by exponential curve and this curve was expressed by regression equation. The exponential equation can be used for breakthrough time on temperature depen-
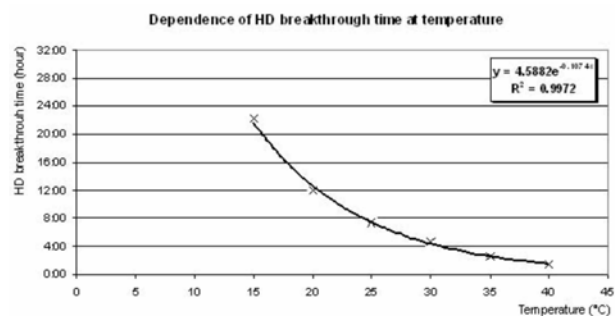

Fig. 6.   **The chart of HD breakthrough time dependence on the temperature**

dence quantification and the parameters could be used for different materials resistance comparison.

Conclusions

The main purpose of this measurement was to compare the analytical methods and/or detection techniques used for the breakthrough time's evaluation. On the basis of obtained results comparison it is possible to submit that the value of HD breakthrough time is strongly dependent on sensitivity of used analytical method. The IMS detector enables to perform the continual measurement of permeation HD in real time. The result is permeation curve represented by increase of permeating vapors amount in time. The GC method providing an exact determination of kind and amount of permeating compound and products of interaction between tested polymer and permeating toxic agent, i.e. qualitative a quantitative analysis in contrast to IMS. However, the GC method does not enable to perform the continual measurement and is not so suitable for long term measurement. Otherwise, the IMS method indicates course of permeation vapor through polymer membrane but is not able to determine kind and amount of permeated compound.

But simultaneous use of both detection methods used simultaneously enable to perform the more exact definition of tested polymer barrier material character.

References
1. Slabotinský J.: Dissertation, VÚ 070 Brno, 1981.
2. Rozsíval V.: Dissertation, VAAZ Brno, 1961.
3. Obšel, V., Dvořáková, J.: Průběžná zpráva, VTÚO Brno, 2006.
4. Obšel, V., Dvořáková, J.: Průběžná zpráva, VTÚO Brno, 2007.
5. ASTM F 739-99a: *Standard Test Method for Resistance of Protective Clothing Materials to Permeation by Liquids or Gases Under Conditions of Continuous Contact* (August 1999)
6. ČSN EN ISO 6529: *Ochranné oděvy – Ochrana proti chemikáliím – Stanovení odolnosti materiálů ochranných oděvů proti permeaci kapalin a plynů* (říjen 2002).
7. Hill, H. H., Martin, Jr. and S. J.: Pure Appl. Chem. *74*, 2281 (2002).
8. Lancaster, P. A.: *Gas chromatography analysis of sulfur mustard in diethyl phthalate*. Melbourne, Australia, 1998.
9. Jareman, F.: Master`s Thesis. , Lulea University of technology, 1999
10. Gary D. Sides <gary.sides@gastechnology.org> Detection of chemical warfare agents, IUPAC Workshop, Croatia [on line]. 2007, 16.8.2007 [cit. 20.09.2007]. Dostupný z: <http://www7.nationalacademies.org/IUPAC-OPCW_Workshop/Sides.pdf>.

11. Duncan, B., Urquhart, J., Roberts, S.: *Review of Measurement and Modelling of Permeation and Diffusion in Polymers*. NP Laboratory, UK, 2005.

12. Rozsíval, V.: Habilitační práce, Brno 1966.

13. Ye, X., Lv, L., Zhao, X. S., Wang, K.: J. Membr. Sci. *283*, 425 (2006).

14. Crank, J.: *The Mathematics of Diffusion*, Clarendon press, Oxford, 1956.

15. Dhingra, S. S.: *Mixed Gas Transport Study through Polymeric Membranes: A novel technique.* Faculty of the Virginia Polytechnic Institute and State University, Blacksburg, Virginia, 1997.

16. Laot, Ch.M.: *Gas Transport Properties in Polycarbonate*. Faculty of the Virginia Polytechnic Institute and State University Blacksburg, Virginia, 2001.

17. Flaconneche, B., Martin, J., Klopffer, M. H.: Oil Gas Sci. Technol, *56*, 261 (2001).

18. Wang, P., Schneider N. S., Sung N.: J. Appl. Polym. Sci. *71*, 1525 (1999).

19. Holzmuller, W., Alternburg, K.: *Fyzika polymerů*. Praha, SNTL, 1966.

L04　COMPLEX ESSESSMENT OF ORGANOPHOSPHATES LOW DOSE CHRONIC EXPOSURE ON ENDOTHELIUM, MACROPHAGES, PLATELETS AND ESTERASES

E. ERMOLAEVA, N. GONCHAROV, A. RADILOV, L. GLASHKINA, I. MINDUKSHEV[a], P. AVDONIN[b], I. DOBRYLKO and V. REMBOVSKIY

Research Institute of Hygiene, Occupational Pathology and Human Ecology, Saint-Petersburg, Russia,
[a]*I. M.Sechenov Institute of Evolutionary Physiology and Biochemistry, Saint-Petersburg, Russia,*
[b]*N. K. Koltzov Institute of Developmental Biology, Moscow, Russia,*
nvgoncharov@mail.ru

Introduction

Morphofunctional disturbances of circulation in rat embryos intoxicated by derivatives of organophosphates (OP), a role of endothelium directly affected by OP under acute intoxications[1,2], and various data on the role of endothelium in development of peripheral neuropathies of various genesis[3,4,5] were the basis for consideration of endothelium as one of the main targets under chronic intoxication with OP. In this research work, an attempt has been undertaken to clarify an impact of circulatory disturbances, the cellular component of haemostasis, and neuropathy target esterase (NTE) activity upon reaction of rat organism under intoxication with low doses of OP.

Materials and Methods

In these experiments diisopropylfluorophosphate (DFP), which can induce the delayed polyneuropathy, and paraoxon which has no such effect, were applied with drinking water at doses 10^{-2} mgkg^{-1} (1/100 LD$_{50}$) and 10^{-4} mgkg^{-1} (1/10,000 LD$_{50}$). The intoxication was conducted daily 5 times in a week for 3 months. Esterases of choline and non-choline substrate specificity[6,7,8,9] were studied; for rat brain, the enzyme activity was calculated per mg of protein[10]. To investigate the OP effects upon NADPH-oxidase system, we used the functional state of peritoneal macrophages with fluorescent microscope and fluorescent probe dichlorfluorescein diacetate (DCF)[11]. Kinetic parameters of platelet aggregation were studied by low angle light scattering technique[12]. The functional activity of endothelium under OP intoxication was studied with rat aorta by method of endothelium-dependent relaxation[13,14]. The results obtained were processed by variation statistics and MS Excel software.

Results and Discussion

Comparing the level of inhibition of esterases in blood plasma after 3 months' intoxication with the OP, we have found that the residual activity of NTE was much lower than that of red blood cells' acetylcholine esterase (AChE). Inhibition of NTE activity in rat brain 2 months after stopping intoxication with DFP gives an indirect evidence for development of neurotoxic effects. Activity of esterases after chronic intoxication demonstrates a switch of inhibition from one enzyme to another, embracing both choline specific and non-specific esterases. It is noticeable that the most prolonged neurotoxic effect (20–30 % reduction of NTE activity after 6 months' period of the post-intoxication recovery) remained in the platelet-rich plasma (PRP).

The next method demonstrating its efficacy for diagnostics of the low dose intoxication with OP was estimation of the level of generation of reactive oxygen species (ROS) during "respiratory burst" by professional phagocytes (macrophages). It is a widely known fact that macrophages
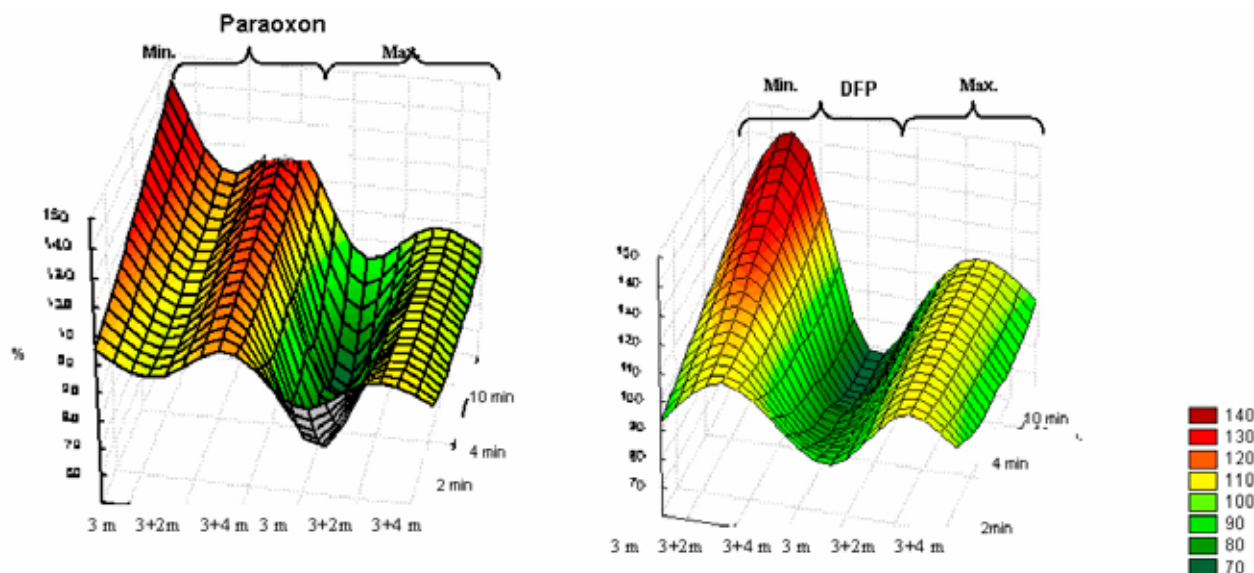

Fig. 1.　**Generation of ROS by mice macrophages after 3 months' chronic intoxication and 2 and 4 months after cessation of the intoxication with paraoxon and DFP at doses 10^{-4} mgkg^{-1} (min) and 10^{-2} mgkg^{-1} (max)**

are not only scavengers and alarm cells but they also have important functions to occupy key positions in every kind of immune response: production of antibodies, induction of cell immune reactions, development of immunologic memory and tolerability, thus correctly being named "dispatcher cells". In our experiments, the functional activity of mouse macrophages was activated under intoxication with OP at 10^{-4} mg kg^{-1} (Fig. 1.). Activation of phagocytes affected by low doses of OP leads to production of ROS (hydrogen peroxide, superoxide anion, singlet oxygen and hydroxyl anions), which cause modification of tissue and serum proteins and lipids to further cause their obtaining of antigenic properties. Thus, activation of phagocytes is an autocatalytic process and can lead to formation of the vicious circle. On the other hand, absence of macrophages' activation under exposure to large doses of OP indicates a suppression of antigen-presenting function of these cells; it is also known that chemical agents inhibiting this function in most cases cause suppression of immune response[16].

The animals' immune status was further tested with low angle light scattering technique and studies of functional activity of blood platelets. Besides of a leading role in haemostasis, blood platelets play also an important role in immune reactions being a mediator between these two physiologic systems[17,18]. For the expense of binding with C1q receptor, the platelets can adhere to endothelium of capillaries, where local interaction of platelets with activating agents can take place[19,20].

Peroral chronic administration of DFP and paraoxon to laboratory animals for 3 months with the following examination at 2, 4 and 5 months after cessation of the intoxication demonstrated that in both cases a pronounced disturbance of the functional activity of platelets was observed, followed by a prolonged period of recovery of kinetic parameters of platelet aggregation (Fig. 2.). In 3 months of chronic intoxication with DFP a marked increase of EC_{50} was registered, similar to the case with Russian VX[21]. In contrast to DFP and RVX, paraoxon did not have a visible effect on sensitivity of platelets, but affected the maximal velocity of aggregation to the greater extent.

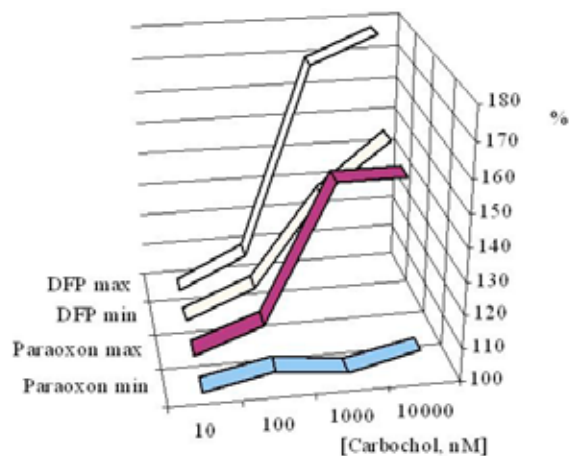Investigation of blood vessel endothelium revealed that

Fig. 3.　**Relative excess over control (100 %) of the blood vessel contracting force in 3 months of intoxication with DFP and paraoxon at doses 10^{-2} and 10^{-4} mg kg^{-1} (carbachol was administered at the background of pre-constriction with norepinephrine)**

under chronic intoxication with OP an inhibition of endothelium-dependent relaxation occurs with both DFP and paraoxon, though the former was more potent at the same doses (Fig. 3.). Moreover, the level of pre-constriction with epinephrine under exposure to DFP was significantly different from that observed under exposure to paraoxon. So not only the level of relaxation following pre-constriction did change but also the background tonus of blood vessels and dynamics of the pre-constriction *per se*. In 2 months after cessation of the intoxication, inhibition of the endothelial function was nevertheless rather pronounced in both groups of rats that were exposed to DFP and paraoxon at 10^{-2} mg kg^{-1}. In 5 months, there were significant changes only in rats exposed to DFP, being at the same level in both groups of intoxicated rats administered to DFP at doses 10^{-4} and 10^{-2} mg kg^{-1}.

Conclusions

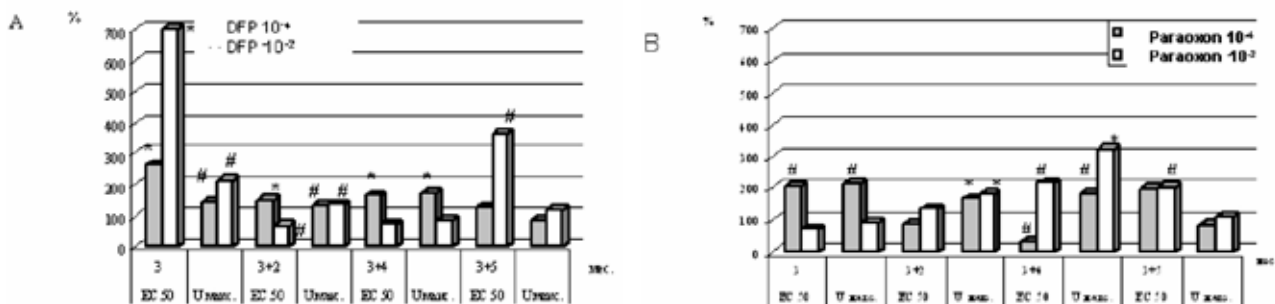Esterases of various geneses, localization and functional specialization should be molecular targets for OP.

Fig. 2.　**Relative changes of the medium effective concentration of activator (EC50) and maximal velocity of platelet aggregation (Umax) after peroral administration of DFP (A) and paraoxon (B) at doses 1×10^{-2} (max) and 1×10^{-4} (min) mg kg^{-1}: after 3 months of intoxication, then at 2, 4 and 5 months of the "recovery period"; (# – P < 0.1; *P < 0.05)**

Changes in activity of esterases under prolonged exposure have a phase character with predominant inhibition of NTE as a delayed effect.

Endothelium should be one of the main tissue targets in case of chronic low dose intoxication with OP.

Blood platelets and phagocytes could be sensitive testing models to estimating effects of the low level exposure to OP.

The pathogenesis of low dose chronic intoxication with OP is probably based upon the two complementary factors: development of immunoreactivity and tissue/circulatory hypoxia.

REFERENCES

1. Прозоровский В. Б., Скопичев В. Г.: Экспериментальная и клиническая фармакология № *3*, 64 (2005c).
2. Carvalho F. A., Graca L. M., Martins-Silva J., Saldanha C.:FEBS J. *272*, 5584 (2005).
3. Myers R. R., Powell H. C., Shapiro H. M., Costello M. L., and Lampert P. W.: Ann. Neurol. *8*, 392 (1980).
4. Low P. A., Tuck R. R., Dyck P. J., Schmelzer J. D., Yao J. K.: Proc. Natl. Acad. Sci. U S A *81*, 6894 (1984).
5. Ollson Y. Peripheral Neuropathy P. *1984*, 579.
6. Ellman G. L., Courtney D. K., Andres V. Jr., Featherstone R. M.: Biochem. Pharmacol. *7*, 88 (1961).
7. Johnson M. K.: Biochem. J. *111*, 487 (1969).
8. Johnson M. K., Glynn P.: Toxicol. Lett. *82–83*, 459 (1995).
9. Брик И. Л., Мандельштам Ю. Е, Немец В. И.: Химия в сельском хозяйстве. *15*, 40 (1977).
10. Досон Р., Элиот Д., Эддиот У., Джонс К. Справочник биохимика. – М.: Мир. *1991,* 544.
11. Гамалей И. А., Каулин А. Б., Кирпичникова К. М.: Цитология. *30,* 1426 (1988).
12. Деркачев Э.Ф., Миндукшев И. В., Кривченко А. И., Крашенинников А. А.: Патент RU 2108579 C1 6 G01 N 33/49, Б.И. №10 (II). C.29 (1998).
13. Mulvany M. J., Halpern W.: Circ. Res. *41*, 19 (1977).
14. Angus J. A., Broughton A., Mulvany M. J.: J. Physiol. (Lond.). *403*, 495 (1988).
15. Дранник Г. Н.: Курс лекций. 2007. http://immuno. health-ua.com/article/9.html
16. Hamrah P., Dana M. R.: Chem. Immunol. Allergy. *92*, 70 (2007).
17. Spycher M. O., Nydegger U. E.: Infusionsther. Transfusionsmed. *22*, 36 (1995).
18. Mindukshev I., Goncharov N., Shabanova E., Ermolaeva E., Mironova M.,Radilov A., Jenkins R., Krivchenko A.: Spectroscopy. *20*, 57 (2006).
19. Galdal K. S.: Haemostasis.*14*, 378 (1984).
20. Козинец Г. И., Макарова В. А. Исследование системы крови в клинической практике. - М.*1998,* 480.
21. Ермолаева Е. Е., Гончаров Н. В., Радилов А. С., Глашкина Л. М., Кузнецов А. В., Миндукшев И. В., Авдонин П. В., Добрылко И. А., Рембовский В. Р.: Токсикологический вестник. № 2., С. 3 (2008).

L05 INFLUENCE OF CLIMATE CONDITIONS AND AIR CONTAMINATION ON VILLAGE INHABITANTS HEALTH

SLAVOMÍRA KAŠIAROVÁ[a] and MELÁNIA FESZTEROVÁ[b]

[a]Trenčín University of A. Dubček, Department of Public Management, Študentská 2, 911 50 Trenčín,
[b]Constantine the Philosopher University, Faculty of Natural Sciences, Department of Chemistry, Tr. A. Hlinku 1, 949 74 Nitra,
kasiarovas@azet.sk

Introduction

The understanding of health as a main component of environment quality accrues from the Agenda 21 concerning the right of human beings to healthy and productive life[1]. Air, one of the components of environment, is polluted primarily by anthropogenic factors. Generally, the countryside is considered a healthy environment[2]. However, there are very few studies to prove this assumption since the air monitoring is a long-term and expensive method and therefore carried out only on a few monitoring points[3].

The aim of the study was to assess the state of climatic conditions and state of air quality in relation to the rate of diseases among the inhabitants of Královce-Krnišov village by a simple method, based on a comparison of potential conditions of contamination with real state of population health. The Southern Sitno micro region is important for tourism development and geographical conditions.

Experiment and Methods

Using the reconnaissance of the place was carried out terrain research. Information and sources of contaminants were observed together with the perception of problems related to air quality and environmental health. The obtained data were further processed by the statistical method of contingential tables, on the basis of which the individual mutual relations were evaluated, at the free scope degree of 1 and the level of importance 0.01 (χ quadrate). An assessment of the state and movement of air required the analysis of the relief as well as sunshine input as well as the regional state and movement of air for which GIS tools (geomedia) were used. Contamination was interpreted from the map of the secondary landscape structure and sources of contaminants. The relation between movement and quality of air and environmental health was worked out on the basis of the basic data parametric analysis with the subsequent table synthesis and mathematic statistics

Results and Discussion

On the territory of the Kráľovce–Krnišov village (the Štiavnické Mountains) cold, mild warm and warm mountain climate prevails. The average yearly temperature spans are from 5.5 °C to 8 °C. The average cloud amount is around 62 %. The number of sunny days is around 48 a year and the number of cloudy days is around 125. The territory is characterized by regional northern, north-west air circulation with a low year and day amplitudes prevailing all the year round. There are frequent temperature inversions during the radiation weather with a depression circulation. There is also an intensive effect of a "temperature island" with a distinctive increase of day amplitudes supported by the effect of winds of low intensity. Negative influences on environmental health are diseases caused by contamination from regional emissions resulting from the type of climate and skin diseases as a consequence of contamination of anthropogenic and natural factors – frequent and concentrated air circulation especially in winter time. Frequent skin diseases and flu are typical for inversion type of weather. Respiratory diseases and diseases related to increased stress conditions due to the amplitudes changes, such as blood pressure disorders, stress and cardiovascular diseases, were confirmed. The increase of the all above diseases was statistically confirmed.

The territory of the Southern Sitno micro region is exposed to the influence of industry confirmed by the considerable damage of the environment by pollutants distributed in conditions of mesoclimate. The contamination of the regional type concerns mainly average annual NO_2 and SO_2 concentrations. The contamination in the settlement is therefore of integrated character from the following sources:

- *transport related emissions* – the contamination intensity is lower in winter and spring season, no statistical importance with any disease was shown;
- *heating related emissions* – at inversion type of weather there is an increased intensity of contamination especially during the winter season (most inhabitants use wood for heating, some of them waste and electricity), an influence on the occurrence of blood pressure disorders was confirmed;
- *radiation* (high volume activity of radon from the geological background, radon is considered the carcinogenic element causing lung cancer and respiratory diseases);
- *emissions from rural zone* (agriculture – a smell from the animal husbandry, excrements of animals, liquid manure).

A demographic structure of Kráľovce – Krnišov village population represents a regressive type, lift the biggest age groups in the village between 20–40 and 40–60. Based on the analysis of microclimate, mesoclimate and macroclimate, contamination and illness rate considering the statistic importance, the population group and factors originating from the environment. The occurrence of health problems (Statistically important relations illustrated in Tables I, II, III, IV) could be specified as follow:

- an increased occurrence of the blood pressure disorders in the local population: people using electricity for heating, people using electric appliances at home, women and children, age group over 60, inhabitants suffering from obesity, cardiovascular diseases, occupational diseases and people living mainly on the slopes exposed

Table I
The relation of the diseases occurrence to the sex and age of Kráľovce – Krnišov village population (χ quadrant)

Age/Sex/Affections	Man/age [years]			Woman/age [years]			Child/age [years]		
	20–40	41–60	Over 60	20–40	41–60	Over 60	0–0.5	0.5–12	13–19
Blood pressure disorders	0.76	0.08	0.76	6.17[d]	0.11	10.05[c]	0	0	0
Stress	0.08	0.08	0.76	4.16[e]	0.03	0.50	0.05	0.05	20[c]
Influenza	0.04	0.04	0.33	1.39	0.06	1.08	0.45	0.16	0.01
Eczema	0.04	0.04	0.33	0.67	0.33	2.49	0.19	0.06	0.01
Bronchitis	0	1.37	0.52	0.01	2.27	3.40	0.12	0.09	0.22
Affection from work	0.08	0.08	0.76	1.22	3.26	0.69	0	0	0
Cardiovascular disease	0.83	1.37	0.15	2.67	0.20	1.76	0	0	0
Asthma	0.83	1.37	0.15	0	0	0	0	0	0
Allergies	0	0	0	0	0	0	0.05	0.70	0.57

[c]Relation is at statistically high level of significance (degrees of free1), χ quadrant = 6.63<
[d]Relation is at statistically medium level of significance (degrees of free1), χ quadrant = 5.02–6.63
[e]Relation is at statistically low level of significance (degrees of free1), χ quadrant = 3.84–5.02

Table II
The relation of the diseases occurrence in Kráľovce – Krnišov village (χ quadrant)

Affections	Blood pressure disorders	Stress	Influenza	Eczema	Bronchitis	Affection from work	Cardiovascular disease	Asthma	Allergies
Blood pressure disorders	–	0.09	1.81	1.66	1.33	8.84[d]	19.44[d]	0.28	0.28
Stress	0.03	–	0.07	0.99	1.65	0.33	0.00	3.99[e]	0.28
Influenza	1.81	0.07	–	0.00	2.46	0.34	1.14	0.22	0.21
Eczema	1.66	0.99	0.00	–	1.56	8.75[d]	2.67	0.18	0.18
Bronchitis	1.33	1.64	2.46	1.57	–	1.09	0.47	8.36[d]	8.36[d]
Affection from work	8.84[d]	0.33	0.34	8.75[d]	1.09	–	13.45[d]	0.12	0.12
Cardiovascular disease	19.44[d]	0.00	1.14	2.68	0.47	13.45[d]	–	0.07	0.07
Asthma	0.28	3.99[e]	0.22	0.18	8.36[d]	0.12	0.07	–	0.01
Allergies	0.28	0.28	0.22	0.18	8.36[d]	0.12	0.07	0.01	–

Table III
The relation of the diseases occurrence to type of dwelling of Kráľovce – Krnišov village pollution (χ quadrant)

Physical, chemical, biological hazards/affections	Chemicals in work	Manures	Dry toilet	Moisture of house	Electrical appliances	Electrical	Heating		Mateiral of house	
							Waste	Coal	Stone	Brick
Blood pressure disorders	0.09	1.74	4.61[e]	0.30	10.78[c]	12.86[c]	5.07[d]	4.08[e]	0.09	2.25
Stress	4.06[e]	3.13	5.78[d]	4.80[e]	1.36	1.84	2.30	0	0.39	0.27
Influenza	0.00	6.09[d]	4.80[e]	6.09[d]	1.14	3.68	0.03	7.06[c]	0.64	1.54
Eczema	0.04	0.09	0.04	2.12	2.67	0.58	0.47	0.09	0.11	0.39
Bronchitis	1.74	4.30[e]	1.05	2.32	0.65	0.24	0	0.89	0.73	0.90
Affection from work	7.53[c]	4.30[e]	0.05	0.62	13.45[c]	11.11[c]	0.51	0.33	0.04	0.99
Cardiovascular disease	0.06	0.37	0.09	0.01	1.49	5.90[d]	0.03	0.94	0.94	0.08
Asthma	0.20	0.48	1.59	1.66	0.07	0.24	1.76	0.69	5.81d	1.19
Allergies	0.19	0.48	0.51	0.62	0.07	0.24	0.58	0.69	0. 18	1.19

Table IV

The relation of the diseases occurrence to the nutrition and physical work of Kráľovce – Krnišov village population (χ quadrant)

Various/Affections	Finish food	Finish food Smoke	Medicine (ache)	Physicalwork	Sucklening
Blood pressure disorders	4.47[e]	1.17	5.57[d]	0.67	3.16
Stress	0.00	16.63[c]	0.16	2.28	0.99
Influenza	1.08	0.90	0.00	0.34	6.60[d]
Eczema	0.00	0.74	4.54[e]	0.73	0.32
Bronchitis	2.40	0.51	2.45	1.09	0.56
Affection from work	0.96	0.51	2.45	0.03	0.63
Cardiovascular disease	0.13	0.30	3.26	0.47	0.72
Asthma	2.74	0.06	0.62	0.12	0.62
Allergies	0.37	0.06	1.66	0.12	1.66

to the south and on the territory of the "thermal island" effect;

- an increased occurrence of frequent flu in the local population: people living on the slopes exposed, to the age group of children 0–5 months, store-bought meat and house produced eggs consumers;
- an increased occurrence of skin diseases in the local population: the age group of children 0–5 months, adults of the age group 20–40, people living on the places with frequent valley circulation, and people living on the territory with the top climate as a result of the regional air pollution; - an increased occurrence of respiratory diseases in thelocal population: people living on the slopes exposed to the north, on the places with valley climate with important changes of amplitudes and places exposed to the transport emissions, especially with regard to people suffering from allergies, asthma, frequent injuries, radon radiation from the geological background;
- an increased occurrence of cardiovascular diseases in the local population: people living on the slopes exposed to the south, on the territory of "the thermal island "effect, on the territory with the strong changes of amplitudes in the valley climate, people suffering from blood pressure disorders and occupational diseases;
- an increased occurrence of occupational diseases in the local population: people who are in contact with toxic stuff at their workplace and people suffering from blood pressure disorders, skin diseases and cardiovascular diseases.

Conclusions

To determine the relation between climatic conditions and environmental health of the inhabitants of the Královce - Krnišov model village in the Štiavnické Mountains, a new method based on confrontation of potential conditions of selected factors of an environment – climate and real state of the environmental health – was used. Statistical results have shown the relation, which had been theoretically assumed.

After the additional implementation and verification, the model can be considered as a good, quick, cheap and informative method for the assessment of the environmental health in rural settlements.

REFERENCES

1. Hilbert H.: *Action Plan for the environment and health of population of the Slovak Republic II.* Ministry of Health Care SR Bratislava 2000.
2. Kukkonen E., Sklret E., Sundell J., Valbjrn O.: *Indoor Climate Problems -Investigation and Remedial Measures.*NT Techn. Report 204, Nordtest, Espoo, Finland 1993.
3. Samešová D., Ladomerský J.: Evaluation environmentalaspects. Mech. Acta *2-B*,150 (2005).

L06   INTEGRATION METALLOMICS, PROTEOMICS AND TRANSCRIPTOMICS IN ENVIRONMENTAL ISSUES

JOSE LUIS GÓMEZ-ARIZA, MACARENA GONZALEZ-FERNANDEZ, TAMARA GARCIA-BARRERA, JUAN LOPEZ-BAREA and CARMEN PUEYO

Universidad de Huelva, Departamento de Química y Ciencia de los Materiales; Facultad de Ciencias Experimentales; Campus de El Carmen; 21007-Huelva (Spain), ariza@uhu.es

Introduction

Metallomics is one of most recent *-omics* whose importance is associated to the presence of metals or any other heteroelement (e.g. elements different of C, H, N, or O) in biomolecules. These metal-linked molecules play important roles in the cells and by extension in the biological behaviour of the organisms.

Some of these elements are essential for life, marked in green in the Fig. 1, other are non-essential or toxic, marked in red. This is the case of transition elements, such as Fe in Cytochrome P450, a superfamily of enzymes that regulate the metabolism of pollutants, drugs and steroids. As well as Fe in transferrin, that transport and deliver this element. Cobalt is the key-element of B12 vitamin and Ni in urease (the enzyme for urea hydrolysis into carbon hydroxide and ammonia). Other transition elements such as Cu and Zn are responsible for the activity of the superoxide dismutase, which is involved in the elimination of superoxide radical.

Fig. 1.   **Essential (green) and non-essential (red) elements**

Together with elements linked to these proteinous molecules other non-proteinous molecules of high molecular weigh, such as DNA is characterized by the presence of phosphorus, or boron in polysaccharides from vegetal cell walls.

Therefore, the chemistry of a cell and by extension of living tissues and biological fluids can be characterized, not only by its typical genome and proteome, but also by the metallome, the distribution of metals and metalloids among the different biomolecules. The metallome describes, per analogy with genome and proteome, the entirety of metal and metalloid species within a cell or tissue type.[1–4] The scope of metallomics is very broad, focusing on developments of new analytical techniques and instruments, as well as innovative applications focused on environmental, food or health issues.

Instrumental Approaches in Metallomics

Three-dimensional systems should be at least used in Metallomics: *(i)* a separation component by gel electrophoresis or HPLC; *(ii)* an very sensitive elemental monitoring system, for metal or non-metal quantification, mainly ICP-MS; and *(iii)* a component for the structural characterization of the molecules, generally based on mass spectrometry. Therefore, the metal or heteroelement act as tag of the experiment, heteroatom-tagged proteomics[5].

Interest of *−omics* Integration

The benefit that Metallomics produces due to the simplification introduced by the metal tag can be insufficient when an overall appraisal of complex real problems, such as those related to environmental, food or health issues is considered.

If we consider a contamination problem, genetic responses to stress conditions are often regulated at transcriptional level that can be checked by using the microarray technology to generate genome-wide transcriptional profiles. The changes detected by microarrays can be confirmed by RT-PCR (reverse transcription–PCR). In addition, modifications in the proteome can also used as markers of pollution as consequence of protein expression alteration triggered by contamination. However, these changes in proteins profiles can not necessarily reflect alterations in gene expression at the transcript level, but changes from post –transductional modifications.

Therefore, the three *-omics* are complementary and integration among them is advisable. However, the difficulties in integrating data from different *-omics* technologies in non-laboratory strains should not be under-estimated, and the use of non-inbred strains/species induce a variety of confusing factors can complicate interpretation. To avoid these problems in environmental studies we propose the use in parallel of sequenced model species and proved bioindicators with gentic sequence homologous to the model. In the present study we have selected two mouse species: *(i)* a model organism used in many studies in the laboratory, whose genetic sequence can be easily obtaine from database, *Mus musculus*, and *(ii)* an aboriginal species checked as useful sentinel organism in monitoring programs, *Mus spretus*[6].

In the present work a combined application of transcriptomics, proteomics and metallomics approaches has been performed in Doñana Natural Park, one of the most important European biological reserves, in which millions of migrating birds land each year in their way to/from Africa. The couple *M. musculus/M. Spretus* was used for this integration.

Experimental

Sampling Areas

Mice were collected in February 2004 at six sites from Doñana surroundings and the Domingo Rubio Stream, both at Huelva province (Fig. 2.). Animals were captured with live traps and taken alive to the nearest laboratory (Huelva University or Doñana Biological Reserve-CSIC). Their sex and

weight were determined and those of 11–12 g were killed by cervical dislocation and dissected. Individual livers and kidneys were frozen in liquid nitrogen and stored at –80 °C.

Transcript Quantifications

Primer design, RNA preparation, reverse transcription, and absolute quantification by real-time PCR. Briefly, PCR reactions were performed in quadruplicate. No primer dimers were detected. Primers showed optimal (~ 100%) PCR efficiencies in the range of 20 to 2×10^5 pg of total RNA input with high linearity (r > 0.99). An absolute calibration curve was constructed with an external standard in the range of 10^2 to 10^9 RNA molecules. The number of mRNA molecules was calculated from the linear regression of the calibration curve (y = –3.326x + 39.693; r = 0.998).

Microarray-based transcript quantification was performed by using the "Whole Mouse Genome Oligo Microarray Kit" (Agilent), which includes 60-mer oligonucleotide probes representing all known genes and transcripts (~ 41,000) of the model *M. musculus* species. Approximately, 20 µg of total RNA were converted to fluorescently labelled cDNA (with Cy3-dCTP or Cy5-dCTP) following the "Agilent Fluorescent Direct Label Kit" instructions. Hybridization was carried out in Agilent's SureHyb Hybridization Chambers at 65 °C for 17 hours using the Agilent's "Gene Expression Hybridization Kit". The hybridized microarrays were then disassembled and washed at room temperature, as described in the Agilent Microarray Based Gene Expression Analysis protocol. To eliminate dye-bias, dye swap replicates were performed. Microarrays were scanned at 532 and 635 nm using a confocal scanner (Axon 4000B). The ratio of Cy5 to Cy3 was adjusted to 1 varying PMT gain as a global normalization of each array. The images were analysed using GenePix Pro v4.1 software (Axon) and data were subsequently input to Genespring v7.3 software (Agilent) for further analysis.

2-DE Analysis and Protein Identification

Around 50 mg of livers from four male mice/site were pooled and homogenized in 20 mM Tris-HCl, pH 7.6, with 0.5 M sucrose, 0.15 M KCl, 20 mM DTT (Dithiothreitol), 1 mM PMSF (phenylmethanesulfonyl fluoride), and protease inhibitors, at a ratio of 3 ml g^{-1}. Cell debris was cleared by centrifugation, and the supernatant treated with benzonase and ultracentrifuged. Protein extract (115 µg) was incubated 30 min in 450 µl rehydration buffer (7M urea, 2% CHAPS, 20 mM DTT, 0.5% Pharmalyte 3–10, bromophenol blue traces), spun and loaded on 24 cm (pH 4–7) Amersham Immobiline Dry-Strips®. After 6 h passive and 6 h active (50 V) rehydration in a BioRad Protean IEF cell (20 °C, 50 mA strip^{-1}), the voltage was raised until obtain ootimum separation. After freezing at –80 °C, the strips were soaked 20 min in equilibration mix (50 mM Tris-HCl, pH 8.8, 6M urea, 30% glycerol, 2% SDS, bromophenol blue traces) with 65 mM DTT, drained and again soaked 20 min in this mix with 25 mM

iodoacetamide. SDS-PAGE was done in 12.5% gels using the BioRad Protean® Plus Dodeca cell (20 °C) at 2.5 W gel^{-1}, 10 min, and 10 W gel^{-1} until separation was finished. Gels were silver-stained following a standard protocol compatible with MS analysis. Analytical quality chemicals and Milli-Q water (Millipore®) were used throughout.

Gel images of three replicates/sample were obtained with a BioRad GS-800 densitometer. Spot volumes were quantitated using the PDQuest software (v7.1, BioRad). Initially, only spots exhibiting in "Santa Olalla" lagoon (SOL) an over/underexpression ratio of at least threefold with respect to any other sampling site were considered. One-way analysis of variance followed by the Student–Newman–Keuls post-test was then used for a definitive selection of the spots showing altered expression patterns between the different animal groups. Differentially expressed spots were manually excised, reduced (10 mM DTT), alkylated (55 mM iodoacetamide), digested overnight at 30 °C with trypsin (Promega) and the peptides extracted with ACN/TFA (Acetonitrile/ Trifluoroacetic acid). Aliquots of 0.5 µl were analyzed by MALDI-TOF-PMF (Matrix Assisted Laser Desorption- Time of Flight-Peptide Mass Fingerprint) in a Voyager DE-PRO instrument (Applied Biosystems) in reflectron mode. PMF data were contrasted against mammalian sequences included at Swiss-Prot (EBI, Heidelberg, Germany) and nonredundant NCBI (Bethesda, MD, USA) databases using ProteinProspector (California University, San Francisco, CA, USA) and MASCOT (Matrix Science, London, UK) softwares.

Analysis of Extracts by SEC Coupled with ICP-MS

Extracts were twofold diluted with the mobile phase and centrifuged at (11,000 rpm) $15.5572 \times 1g$ for 1 h at 4 °C, and latterly filtered through Iso-Disc poly(vinylidene difluoride) filters (25-mm diameter, 0.2-µm pore size) to avoid column overloading or clogging. Elemental fractionation profiles were obtained by size exclusion chromatography (SEC) coupled to ICP-MS as detector. Two columns were used in the experiment: Hiload 26/60 Superdex 30 Prep column for a separation range below 10 kDa (low molecular mass, LMM) and a Superdex 75 Prep column for a separation range of 3–70 kDa (high molecular mass, HMM), both from Amersham Biosciences (Uppsala, Sweden). These columns were calibrated using standards of known molecular mass, such as bovine serum albumin (67 kDa), metallothionein I (7 kDa), gastrin rat I (2,126 Da) and Gly6 (360 Da) for LMW column, and bovine serum albumin (67 kDa), chymotrypsinogen A (25 kDa), ribonuclease A (13.7 kDa) and metallothionein I (7 kDa) for HMW column. The void retention time was estimated with bovine serum albumin (67 kDa) and blue dextran (2,000 kDa), for LMW and HMW, respectively.

Results

The three *-omics* approaches (transcriptomics, proteomics and metallomics) have been applied to Doñana Natural Park and the surrounding areas. Doñana is an impor-

Fig. 2.   **Sampling area**

tant ecological area, which covers 543 km^2 with a great variety of ecosystems and shelters wildlife including thousands of European and African migratory birds, fallow deer, Spanish red deer, wild boar, European badger, Egyptian mongoose, and endangered species such as the Spanish Imperial Eagle and Iberian Lynx. This non-contaminated area was used as
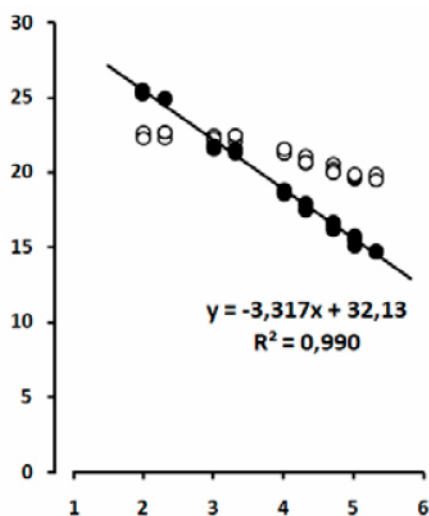
negative reference (SOL) in comparison to the neighbouring "Domingo Rubio" stream (DR1 to DR6) and the positive references (PS and ARZ). These areas are contaminated by mining, agricultural and industrial effluents (DR1 to DR6 and PS) and by pesticides and fertilizers (ARZ) (Fig. 2.).

The mouse *Mus spretus* is an aboriginal species that has been commonly used for environmental assessment of this area (x) by means of classical biomarkers, but new tools based on recent –omics, such as transcriptomimcs and proteomics constitute a promising alternative. However, the molecular biology methodologies present problems by the fact of poor inclusion of typical bioindicators in gene/protein sequences database. For this reason we use species close to model organisms that are well covered in public databases. This is the case of *M. musculus*, which is studied comparatelly with *M. spretus*. These comparisons are only possible if genetic homology between both species is proved.

Genetic Homology Between *M. musculus* and *M. spretus*

A crucial start-point in quantitative RT-PCR is primer design. For absolute transcript quantification it is necessarily to design primers that amplify the targets and the calibrator with optimal (100 %) PCR efficiencies. This fact requires a great genetic homology between target and calibrant species. Primers for RT-PCR quantification of *M. spretus* Cyp and Gst mRNAs were designed based on known gene sequences from *M. musculus*. Remarkably, these primers, when amplified in *M. spretus*, gave single products exhibiting in most cases 100% nucleotide sequence identity. Therefore, most designed primers were exactly complementary to the desired M. spretus templates and amplified them with 100% efficiency. In few cases, however, primers should be redesigned based on nucleotide sequences of PCR fragments from *M. spretus*. Fig. 3 ref.[8].

Therefore, genetic homology between model and bioindicator species was clearly proved.

$$y = -3,317x + 32,13$$
$$R^2 = 0,990$$

Fig. 3.   **Efficiency curves in genetic correlation between *M. musculus* and *M. spretus* for Gsta3 transcript. ● specific primers, ○ non-specific primers. X-axis, log total mNRA (pg); Y-axis, threshold cycle (Ct)**
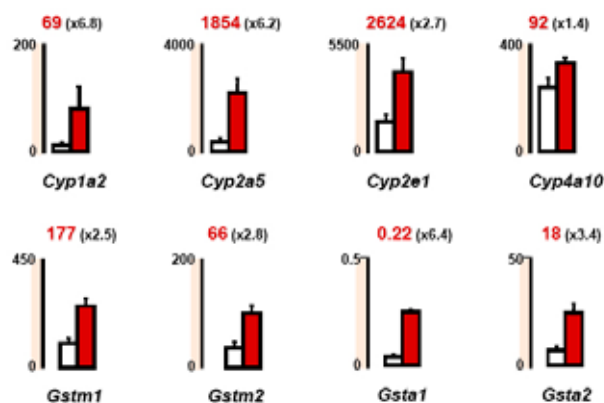
Fig. 4.   **Sampling area-associated differences in *M. spretus* hepatic mRNA levels. Y-axis, nRNA molecules/pg total RNA. White bar, SOL non-polluted area; red bar, polluted area**

M u s   S p r e t u s   T r a n s c r i p t   E x p r e s s i o n   S i g n a t u r e s   i n   C o n t a m i n a e d   A r e a s

We have used the absolute measurement of mRNA levels from selected key genes (CYPs and GSTs) to biomonitoring the exposure and biological effects of pollutants on free-living nonmodel *M. spretus*. For this purpose the mRNA molecules of genes coding for different cytochrome P450 and glutathione transferases were quantified in mice dwelling at both the non-contaminated point SOL and contaminated area PS.

As an example, Fig. 4. shows the concomitant up-regulation of some *Cyp* transcripts in *M. spretus* PS population, as compared to that at SOL in the Doñana Biological Reserve. The possibilities of transcription quantification to assess the level of contamination are clearly demonstrated. In addition, the absolute Cyp transcript expression signature is depending on the type of contaminant (Fig. 5.), which can use to identify the nature of contamination under consideration.
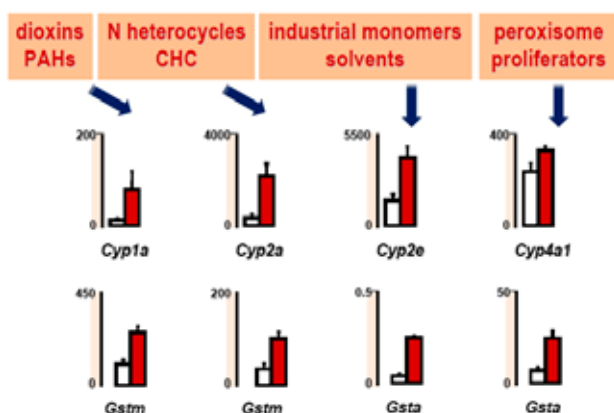
Fig. 5.　**Transcripts expression signature related to the type of contaminants. Y-axis, nRNA molecules/pg total RNA**
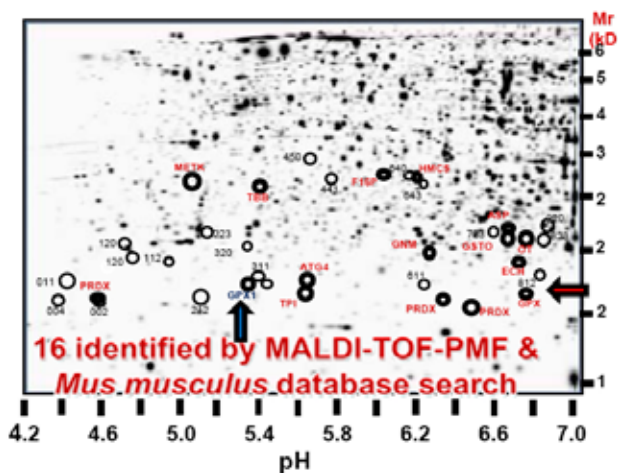
Fig. 6.　**Protein expression of liver cytosolic extract from *Mus spretus***

P r o t e o m i c s   S t u d y   o f   *M u s   s p r e t u s*

The homology between *M. musculus* and *M. spretus*, at DNA sequence level allows the proteomics evaluation of protein expression differences caused by contamination episodes in *Mus spretus*, but usinf the gnetinc sequence of *Mus musculus* in protein identificacion by MALDI-TOF-PMF. A comparative study at proteomic level of cytosolic fractions of liver from *M. spretus* sampled in Doñana and Domingo Rubio stream were performed analysing the extracts by 2-DE and searching the protein expression differences. Over 2500 spots were resolved in the pH range 4–7 and 14–70 kDa M_r. Image analysis of the gels yielded 36 spots with significantly altered expression. Of them, 16 proteins were identified by MALDI-TOF-PMF and heterologous search against *Mus musculus* databases. When this approach is applied to contaminated and non-contaminated points a clear diference in spots intensities corresponding to differentially expressed protreins was observed, which can be used for the environmental pollution assessment of proteomics.

M e t a l l o m i c s   A p p r o x i m a t i o n   t o   t h e   M o u s e   *M u s   m u s c u l u s*

In this study the presence of unknown metallobiomolecules in *M. musculus* was studied for the first time. Firstable, a general evaluation of the presence of total concentration of metal in different organs of the mouse (lung, liver, spleen, kidney, brain, testicle, heart and muscle) was performed.The experiments were carried out on inbred *M. musculus* specimens. An you can see the elements considered. Fe is the element most abundant in the different organs with an averaged concentration of 7,500 µg dm^{-3} in thecytosolic extracts. Other elements are Zn (about 2,300 µg dm^{-3}), Cu (550 µg dm^{-3}), Ni (165 µg dm^{-3}), Se (145 µg dm^{-3}), and a toxic element such as Pb (26 µg dm^{-3}). These elements are differentially distributed in the organs, for example, Cu and Zn are mainly present in the liver, but Pb in the muscle. An similar comments can be addressed to the other elements.

Metal-biomolecules profiles was obtained with ICP-MS as metal tracer, using couplings with size exclusion chroma-
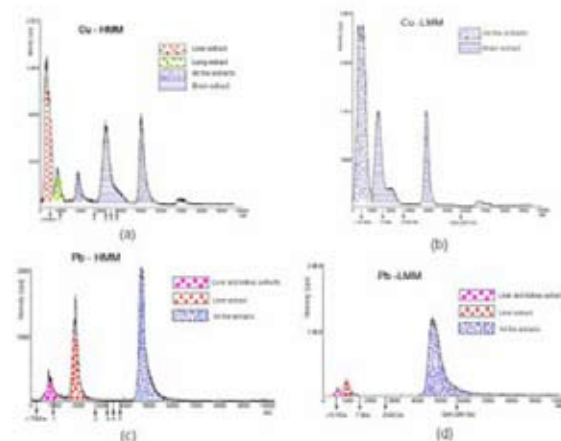

Fig. 7.　**SEC-ICP-MS metal profiles in *Mus musculus* corresponding to Cu and Pb. HMM size exclusion column for 3,000 to 70,000 Da; LMM, size exclusion column for 300 to 10,000 Da**

tography to characterize metalbiomolecules molecular mass profile, and subsequently in series, on the fractions isolated in the previous separation, reverse phase chromatography for a further purification of the extracts and biomolecule isolation. Two SEC columns were used to discriminate molecules with molecular mass range under 10,000 (360 to 10,000 Da) and between 3,000 and 70,000 Da. The results for Cu and Pb, this latter as example of toxic are shown as examples in Fig. 7.

The results obtained for Cu and Pb can be summarized in the following items:

- All extracts showed peaks in the range of 300 and 2,000 Da whatever metal or organ considered.
- A peak was observed in the void volume of the LMM column ($M_r < 10$ kDa) for all profiles, although they showed low intensities except for Cu that was studied in more detail.
- A Cu-containing fraction (7–10 kDa) was found in the brain which was absent in all other M. musculus organs. Other elements, e.g. Pb, do not have peaks equivalent in that range of masses. Therefore, further studies involving subsequent purification by another chromatography technique and isolation of this Cu-bound biomolecule for MS identification is being considered.
- The Cu and Pb fractions resolved in the HMM column were mainly associated with molecules with molecular masses from 25 to 67 kDa, which are present in all the organs for Cu and only in liver for Pb.
- A chromatographic peak associated to Cu was detected in the molecular mass range 67 to 70 kDa for the lung extract, and in liver and kidneys for Pb.
- A Cu-peak can be observed in liver extract at the void volume of the HMM column.

In Fig. 8. is shown the chromatograms corresponding to the cytosolic extracts. The main fraction is associated to liver and is eluted in the void volume of HMM column. Additional experiments with reverse phase chromatography of this isolated fraction and ICP-MS detection reveal that tow peaks can result from additional purification of this fraction.
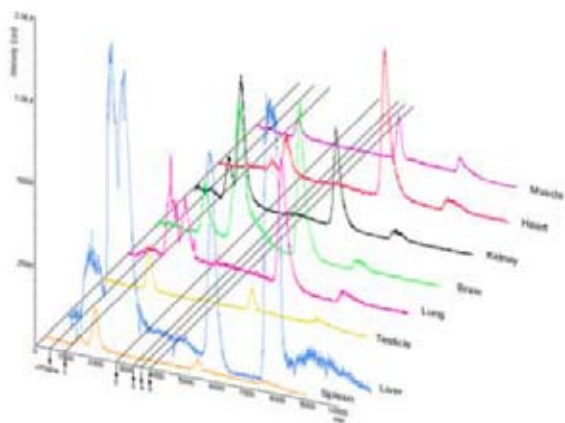
Fig. 8. **Chromatographic profiles with HMM column (3,000 to 70,000 Da)**

Integration of Metallomics with Proteomics and Transcriptomics

The complementary character of the different approaches presented in relation to *Mus musculus/Mus spretus* and the environmental assessment considered prevously claims for the integration of these three -*omics*.

The availability of the complete sequence of an increasing number of genomes allows the developments in proteomics, which can be achieved by electrospray and MALDI-TOF mass spectrometry. However, many proteins can be sensitively detected by ICP-MS due to the presence of ICP-ionizable elements (heteroelements). Therefore the three -omics are complementary, and in this context the combination of validated metallomic data with the transcriptome and proteome knowledge of a cell is one of the largest challenges for future research in this topic.

A crucial question is that better established -*omics* (transcriptomics and proteomics) support their studies on model organisms whose gene/protein sequence are well collected in databases. On the contrary, bioindicators currently used in environmental studies are non-model organisms absent from public databases. The design of primers that allows the confirmation of homology in gene expression at the transcript level between bioindicators used in environmental studies and sequenced model specimens is a very good tool to perform environmental metallomics and proteomics.

This new triple-omics approach (MEPROTRANS-*triple*-OMICS) is being applied to the *M. musculus-M. spretus* couple in Doñana Natural Park for environmental assessment, following the steps listed below:

- Extraction of RNA for transcriptomic and of proteins for proteomic and metallomic analyses.
- Quantification of changes at the transcriptome level by means of commercially available microarrays and further validation of selected microarray results by absolute quantification using real-time RT-PCR.
- Quantification of changes at the proteome level by 2-DE analysis and subsequent protein identification by MALDI-TOF-PMF.
- Integration of transcriptomic and proteomic results to distinguish transcriptional from post-transcriptional changes.
- Isolation of heteroatom-tagged molecules by size exclusion chromatography fractionation of tissue extracts guided by ICP-MS (First Dimension) and further purification by reverse phase and/or ion exchange chromatography with ICP-MS on the previous selected fractions (Second Dimension). This metallomic scheme will be assisted by 2-DE analysis to reveal the complexity of the successive sub-proteomes. The purification steps involving metallomics and proteomics will be repeated until the final isolation of target metal-biomolecules for identification by tandem mass spectrometry.

- Validation of metallomic results by Western hybridization and/or enzymatic assays, and by absolute quantification of transcripts coding the identified metalloproteins.
- Integrative multidisplinary decision on the optimal assay (high sensitivity, low cost and easy to perform) to be recommend for routine assessment of differentially expressed metalloproteins as novel biomarker in ecotoxicological studies.

Conclusions

The study of complex systems related with living organisms, such as the environment or health, in which many variables are involved, requires multidisciplinary tools for a comprehensive assessment of these issues.

Several –*omics*, such as transcriptomics, proteomics and metallomics, offer a valuable alternative in environmental studies since they provide massive information about biomolecules in cells and organisms that help to overcome these problems. An overall evaluation of changes that contaminants induce in cells is only possible by integration of -*omics*:

- Transcripts induced by pollutants (transcriptomics) encode proteins with altered expression profiles, which undergo post-traductional modifications (proteomics).
- Many proteins related to enviromental issues are bound to metals (i.e. CYPs, SODs, GPXs, metallothioneins) that make advisable the use of metal-tagged techniques (metallomics) as preliminary step to simplify proteomic and transcriptomic approaches.

Proteomics can guide metallomics by checking the presence of molecules in extracts obtained with the chromatography-ICPMS couplings:

- This assists metal biomolecules isolation for mass spectrometry identification.
- 2D analysis provide an image of the number of molecules in the extract and their molecular mass

This triple -*omic* approach (MEPROTRAN-*triple-*OMICS) is a very useful and comprehensive alternative in the study of environmental issues and the diagnosis of contamination problems. In addition, MEPROTRANS-*triple-*OMICS can assist in the validation of traditional biomarkers and a more simple cheap and fast assessment of environmental issues.

REFERENCES

1. Haraguchi H., Matsura H.: In: Enomoto S (rd) Bitrel, Wako (Saitama). Fujiyoshida (Yamanashi), Japan, 2003.
2. Szpunar J., Lobinski R., Prange A. Appl. Spectros. *57*, 102 (2003).
3. Szpunar J.: Anal. Bioanal. Chem. *378*, 54 (2004).
4. Gómez-Ariza J. L., Garcia Barrera T., Lorenzo F., Bernal V., Villegas M. J., Oliveiras V.: Anal. Chim. Acta. *524*, 15 (2004).
5. Sanz-Medel A.: Anal. Bioanal. *381*, 1 (2005).
6. Bonilla-Valverde D., Ruiz-Laguna J., Muñoz A., Ballesteros J., Lorenzo F., Gómez-Ariza J. L., López-Barea J.: Toxicology *197*, 123 (2004).
7. Ruiz-Laguna J., Garcia-Alfonso C., Peinado J., Moreno S., Leradi L., Cristaldi M., López-Barea J.: Biomarkers *6*, 146 (2001).
8. Ruiz-Laguna J., Abril N., García-Barrera T., Gómez-Ariza J. L., López-Barea J., Pueyo C.: Environ. Sci. Technol. *40*, 3646 (2006).

L07 HEAVY METALS IN SOLID IMMISIONS IN THE VICINITY OF IRON ORE MINING AND PROCESSING PLANT IN NIŽNÁ SLANÁ

JOZEF HANČUĽÁK, ERIKA FEDOROVÁ, OĽGA ŠESTINOVÁ, TOMISLAV ŠPALDON, JÁN BREHUV and PAVEL SLANČO

Institute of Geotechnics of the Slovak Academy of Sciences Watsonova 45, 043 53 Košice, Slovak Republic,
hanculak@saske.sk

Introduction

The content of hazardous substances in atmospheric deposition significantly contributes to the pollution of environment. A lot of studies deals with the research of atmospheric deposition, mostly using methods monitoring wet deposition, wet and dry deposition (bulk deposition), but also methods using fog and low cloud sampling[1]. The solid emissions from the technologies of ores and industrial minerals processing by their specific composition influence constitution of atmospheric deposition, especially in the areas of processing plants. The main emission source in the area of Nižná Slaná is iron-ore mining and processing plant. The plant exploits the siderite ore. The run-off-mine ore is through several technological centres processed into the blast furnace pellets as a final product of the plant. The contribution deals with the evaluation of results obtained from monitoring of atmospheric deposition in the form of dust fallout (modified method bulk deposition). The research was carried out by the Institute of Geotechnics of the SAS in the area of the Siderite, Ltd. from 2001 to 2007, predominantly from viewpoint of heavy metals deposition (Fe, Mn, Zn, Pb, Cu, Cr, Cd, and As).

Characteristics of the Plant

The plant is situated in the Slaná river valley in the Slovak Republic. The valley has an orientation of north-south and northwest-southeast, respectively. The wind circs are influencing by an orography of given territory. Distribution of wind directions and the occurrence of calm in the near-by Rožňava town are shown in Table I.

Exploited deposit is located in the Revúca upland Mts., the Dobšiná foothill belt Mts. of the Slovak Ore Mts. Utility mineral is siderite. The average content of iron and manganese in ore is 33.5 % and 2.8 %, respectively. Manganese is bonded isomorficaly in the siderite lattice. There are also unfavourable elements (As, S, Pb, Zn) that occur as, sulphides, sulphates, sulphosalts and oxides. The most significant unacceptable impurity is arsenic that is present in the form of arsenopyrite. The average content of As in the run-off-mine ore is approximately of 0.01–0.1 %. Ore processing consists of crushing, magnetizing roasting, wet milling, magnetic separation and pelletizing. Primarily, thermal technologies, i.e. pelletizing and magnetizing roasting are responsible for the amount of dust outlet. Flue gases are exhausted to the environmental air through 120-meter high chimney after several stages of dedusting. Table II presents the average concentrations of the selected elements in the dust outlet from pelletizing plant and rotary furnaces. The emissions of solid pollutants from 1998 to 2007 are shown in the Table III.

Material and Methods

The samples of dust fallout were taken in the 30 days (± 3 days) intervals from the seventeen sampling stations. The cylindrical plastic sedimentation containers (inside diameter – 12.5 cm), put in two support stands in the height of 2.5 to 3 m, were used for the sampling. The containers were filled with 250 ml of pure water with addition of isopropanol. After sampling, the content of containers was quantitatively located to evaporating dishes and evaporated. The organic mass was removed by annealing of dry matter at 450 °C. The chosen temperature prevented carbonate degradation and in such way enables to avoid the misinterpretation of dust fallout gravimetry results. The samples were gravimetrically evaluated before and after annealing, in the mass units recalculated for the area and the respective time period. Inorganic portion determined by annealing from twelve month period was cumulated to the one sample and after mineralization it was analysed using AAS (SpectrAA – 30 VARIAN). On the basis of these chemical analyses and mass yield of the dust fallout, the average annual depositions by observed heavy metals were calculated for each of the seventeen sampling points. The localization of sampling stations is illustrated in Fig. 1.
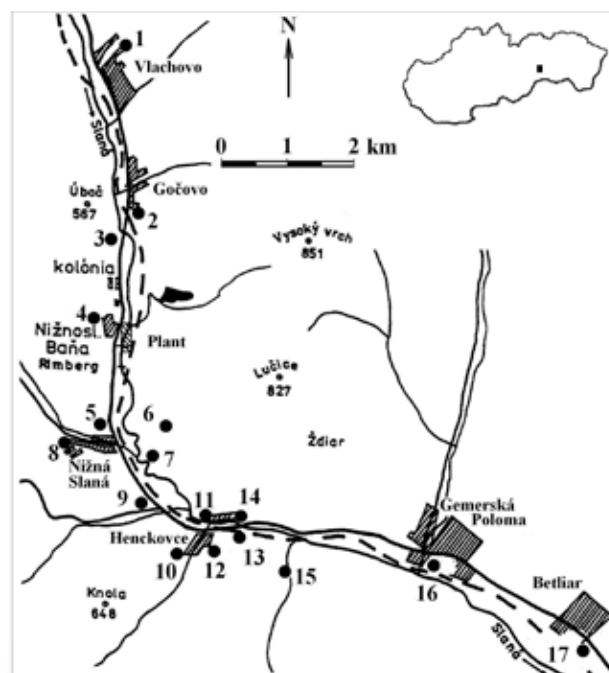

Fig. 1.　**Sampling locations in the area of Nižná Slaná**

Results and Discussion

The average year values of total deposition for whole monitored period determined for individual sampling points

Table I
Percentage of the wind directions and calm in the Rožňava town [%]

N	N-E	E	S-E	S	S-W	W	N-W	Calm
38	8	6	2	25	2	3	6	10

Table II
The content of the selected elements in the solid dust outlets from thermal technologies

Technologies	Fe [%]	Mn	Zn	Pb	Cu [ppm]	Cr	Cd	As
Pelletizing	30.4	3.48	94	32.6	99	39	25	636
Rotary furnaces	27.8	2.12	200	127	170	63	24	176

Table III
The emissions of solid pollutants from the plant (1998–2007) [t year^{-1}]

1998	1999	2000	2001	2002	2003	2004	2005	2006	2007
156.4	116.3	116.9	86.7	32.9	63.3	63.8	121.5	155.8	148.4

Table IV
The average deposition of selected heavy metals and total deposition in the area of Nižná Slaná (2001–2007)

Parameter	Total dep.	Fe	Mn	Zn	Pb [mg m^{-2} year^{-1}]	Cu	Cr	Cd	As
Minimum	8,621.0	1,221.0	60.9	9.54	0.35	1.67	1.09	0.033	1.49
Maximum	32,537.0	9,636.0	631.3	63.12	2.81	5.73	4.36	0.078	28.84
Average (n = 17)	18,155.0	4,543.0	272.7	23.34	0.93	3.38	2.58	0.050	11.07
Median	17,173.0	4,423.0	265.0	17.68	0.68	3.27	2.59	0.048	8.77
SD	6,996.0	2,288.0	160.6	16.59	0.65	1.05	1.05	0.012	7.50

were in the interval 8.6–32.5 g m^{-2} y^{-1}. In most of sampling points a significant increase of solid pollutant emissions in 2005 till 2007 comparing with previous years was not detected (total dust fallout). On the other hand, the significant increases of Fe, Mn and As deposition values were recorded using dust fallout analysis in the most of sampling stations. The samples of dust fallout were also subjected to X-ray diffraction (XRD) analysis. Thus, minerals such as quartz, chlorite, siderite, ankerite were detected. These minerals come from raw ore handling but also as a result of aeolation from surrounding environment. On the other side hand there are minerals, namely hematite, maghemite, magnetite and wüstite coming from the thermal technologies of the plant[2].

Table IV presents average values of deposition of selected heavy metals and basic statistic parameters for the whole monitored period and all sampling points. Qualitative composition of dust fallout unlike of its quantity significantly contributed to the ecological load of the individual sampling points that was caused by plant activities. Between various sampling points high differences in the deposition were determined mainly for Fe, Mn and As. There were not so high differences in the deposition with others elements. The most

ecological load was situated in the south of the plant, in the central part of the valley. The statistical dependence between emissions of solid pollutants and deposition of observed metals (annual median) in the individual years by correlation analysis was evaluated. Relatively high positive values of correlation coefficient were calculated for manganese, iron and arsenic, namely 0.794, 0.764 and 0.749, respectively. Correlation coefficients for other elements were relatively low. The development of selected metal deposition (median) and the emissions of solid pollutants for the whole monitoring period is showed in Fig. 2.

In the Slovak Republic there are not determined allowable limits for heavy metals deposition from dust fallout. That is the reason why relative comparison of heavy metal depositions for different localities is used for assessment of immission load.

In the Nižná Slaná locality, Fe deposition achieves high values because of solid pollutants emissions consist mainly of iron minerals. Fe depositions monitored in the individual stations were in the range from 1.221 to 9.636 mg m^{-2} y^{-1}. In Košice town with metallurgy industry, the values varied from 232 to 7.568 mg m^{-2} y^{-1} (ref.[3]). In the Czech Republic
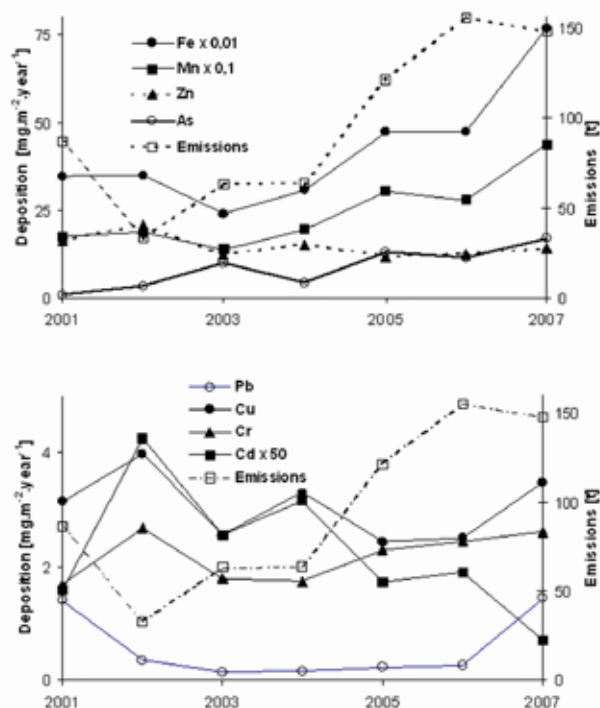
Fig. 2. **Development of selected metal deposition (median) and the emissions of solid pollutants (2001–2007)**

in 2005 (measured for subsystems of basic and contaminated areas), ten times lower Fe deposition was determined in comparison with area of Nižná Slaná (69–1,002 $mg\,m^{-2}\,y^{-1}$) (ref.[4]).

The highest contents of manganese in dust fallout were detected in the area of Nižná Slaná and Jelšava with maximum deposition values of Mn 631.3 and 406.4 $mg\,m^{-2}\,y^{-1}$, respectively[3]. Average values exceeded 200 $mg\,m^{-2}\,y^{-1}$. In past, the most manganese loaded territory was the locality Dolný Kubín that is located nearby iron-alloy factories Istebné, where the maximum deposition Mn value from dust fallout was 668 $mg\,m^{-2}\,y^{-1}$(ref.[5]). In other parts of Slovakia, average deposition of Mn from dust fallout were 3.6 and 34.4 $mg\,m^{-2}\,y^{-1}$ in the Slovak Paradise and Košice, respectively[3]. In the case of Nižná Slaná and Jelšava, the main manganese sources were iron-ore mining factories, magnesite factories and raw materials (siderite, magnesite) treated in these factories. In the Czech Republic in the monitored territories the average deposition of Mn was 13.6 $mg\,m^{-2}\,y^{-1}$ and the maximum deposition was 68.3 $mg\,m^{-2}$ per year[4].

The deposition values of Zn in the Nižná Slaná area were in the interval 9.5–63.1 $mg\,m^{-2}\,y^{-1}$ with the average value of 23.3 $mg\,m^{-2}\,y^{-1}$. In general, these values are not very high. In the Czech Republic, the average atmospheric depositions of Zn were 50.6 and 54.3 $mg\,m^{-2}\,y^{-1}$ and the maximum was 206 $mg\,m^{-2}\,y^{-1}$(ref.[4]). In the agricultural area Austria and England, the measured values of zinc deposition were

in range from 21.4 to 48.9 $mg\,m^{-2}\,y^{-1}$ respectively 22.1 to 35.6 $mg\,m^{-2}\,y^{-1}$(refs.[6,7]).

The deposition of Pb was relatively low (0.11–2.44 $mg\,m^{-2}\,y^{-1}$) in the locality of Nižná Slaná. The maximum content of Pb (21.89 $mg\,m^{-2}\,y^{-1}$) from dust fallout was measured in Krompachy, while the main source of solid pollutions was cooper smeltery[3]. In past, in Slovakia, there was determined the maximum content of Pb in dust fallout (380 $mg\,m^{-2}\,y^{-1}$) in the locality of Prievidza, that was caused by steam brown coal combustion[5]. The deposition of Pb was 5.4 to 13.9 $mg\,m^{-2}\,y^{-1}$ in England and Wales[6]. In Austria, the measured values were 1.90–5.44 $mg\,m^{-2}\,y^{-1}$(ref.[7]).

The deposition of Cu achieved low values in Nižná Slaná (1.74-5.68 $mg\,m^{-2}\,y^{-1}$). High copper deposition (128.26 $mg\,m^{-2}\,y^{-1}$) was measured in Krompachy[3]. The values in Austria and England were in range from 6.24 up to 14.70 respectively 22.1 to 35.6 $mg\,m^{-2}\,y^{-1}$(refs.[6,7]).

The average depositions of chromium in Nižná Slaná were in the interval from 1.19 to 4.77 $mg\,m^{-2}\,y^{-1}$. The average depositions of chromium from dust fallout in the Slovak Paradise and Jelšava were 0.64 and 10.52 $mg\,m^{-2}\,y^{-1}$, respectively. The maximum measured value was detected in Košice (14.62 $mg\,m^{-2}\,y^{-1}$)(ref.[3]). In the Czech Republic, atmospheric deposition monitoring revealed values in the range from 0.21 to 2.81 $mg\,m^{-2}\,y^{-1}$ and in Austria in the interval from 0.72 to 1.95 $mg\,m^{-2}\,y^{-1}$(refs.[4,7]). In England and Wales, the Cr values were in range from 0.75 to 2 $mg\,m^{-2}\,y^{-1}$(ref.[6]).

The deposition values of cadmium in the Nižná Slaná were in the range from 0.033 to 0.084 $mg\,m^{-2}\,y^{-1}$. This is relatively low value. In Košice and Jelšava, the measured average values were 0.678 and 0.742 $mg\,m^{-2}\,y^{-1}$, respectively[3]. In the Czech Republic, the atmospheric deposition monitoring detected values in the range from 0.025 to 1.230 $mg\,m^{-2}\,y^{-1}$ and n Austria in the interval 0.146–0.325 $mg\,m^{-2}\,y^{-1}$(refs.[4,7]). The deposition of Cd was 0.19 to 0.61 $mg\,m^{-2}\,y^{-1}$ in England and Wales[6].

Relatively high values of arsenic deposition were registered in the locality of Nižná Slaná. The average values in the monitored areas were in the interval of 1.28–29.28 $mg\,m^{-2}\,y^{-1}$. The source of arsenic is arsenopyrite that is present in siderite batch. The maximum arsenic value was detected from sampling station no.5 that is close to the factory. This value is two fold times higher that the maximum value from Krompachy, where the measured value was 14.588 $mg\,m^{-2}\,y^{-1}$(ref.[3]). In the relative pure area of Slovak Paradise, the recorded values of arsenic deposition were from 0.044 to 0.155 $mg\,m^{-2}\,y^{-1}$(ref.[3]). The atmospheric deposition monitoring in the Czech Republic registered values from 0.21 to 2.81 $mg\,m^{-2}\,y^{-1}$(ref.[4]). In past, in the Slovak Republic, maximum content of As in dust fallout was 35 $mg\,m^{-2}\,y^{-1}$ in the locality of Prievidza (effect of steam brown coal combustion with high concentration of As)[5]. The average values for atmospheric deposition in the Czech Republic were 0.50–0.67 $mg\,m^{-2}\,y^{-1}$ and maximum arsenic value was 2.11 $mg\,m^{-2}\,y^{-1}$ in 2005(ref.[4]). In England and Wales, the As values were in range from 0.31 to 1 $mg\,m^{-2}\,y^{-1}$(ref.[6]).

Conclusions

The detailed analysis of dust fallout from the locality of Siderite, Ltd. factory revealed the extent of ecological load. In comparison with others localities, this area is the most influenced with heavy metals (iron, manganese and arsenic). This fact reflects the composition of siderite and applied technological treatments of siderite ore in the factory. Although relatively small territory was monitored, the significant differences are detected. There are many different factors, for example: meteorological, orographic, emissive, binding and particle sedimentation mechanisms with linkage to impurities and also others factors. Although the method of measuring of dust fallout is laborious with some mistakes, the relative evaluation of individual localities imission load provides applicable results.

REFERENCES

1. Fišák J., Tesař M., Řezáčová D., Eliáš V., Weignerová V., Fottová, D.: Atmos. Res., *64*, 75 (2002).
2. Baluchová B., Fejdi P., Bobro M.: Mineralia Slovaca, *36*, 357 (2004).
3. Hančuľák J., Bobro M., Brehuv J., Slančo P.: Acta Montanistica Slovaca, *10*, 246 (2005).
4. Prášková L., Kubík, L., Malý, S.: *Annual report 2005*. Central institute for supervising and testing in agriculture. Brno 2006.
5. Ursíniová M., Vaňová R., Paľušová O.: Acta Hygienica et Epidemiologica et Microbiologica. Praha, *21*, 1 (1992).
6. Nicholson F. A., Smith S. R, Alloway B. J., Carlton-Smith C., Chambers B. J.: Sci. Total Environ. *311*, 205 (2003).
7. Spiegel H., Böhm K.E., Roth K. Sager M.: *Proceedings 7th Intern. Conf. on the Biogeochem. of Trace Elements; Uppsala '03, 15 -19 June 2003* (Gobran G., Lepp N., ed.)*, p.19, Uppsala 2003.*

L08   COMPARISON OF ENERGY DISPERSIVE X-RAY FLUORESCENCE SPECTROMETRY, INDUCTIVELY COUPLED PLASMA OPTICAL EMISSION SPECTROMETRY AND LASER ABLATION WITH PLASMA SPECTROMETRY IN THE ELEMENTAL ANALYSIS OF SOILS

IVONA HUBOVÁ[a], MARKÉTA HOLÁ[a], VLASTIMIL KUBÁŇ[b], ILSE STEFFAN[c] and VIKTOR KANICKÝ[a]

[a]Laboratory of Atomic Spectrochemistry, Department of Chemistry, Faculty of Science, Masaryk University, Brno 611 37, Czech Republic,
[b]Department of Chemistry and Biochemistry, Faculty of Agronomy, Mendel University of Agriculture and Forestry, Brno 613 00, Czech Republic,
[c]Department of Analytical Chemistry and Food Chemistry, Faculty of Chemistry, University of Vienna, Vienna 1090, Austria,
41396@mail.muni.cz

Introduction

Agricultural soils represent complex multiphase multicomponent material which requires adequate methods of chemical analysis. Content of elements represents important parametre which relates to nutrition of plants on one side and a contamination with toxic elements on the other side. For intake of elements by plants only selected elemental forms (species) are bioavailable. Speciation or fractionation based on selective leaching of particular species followed by atomic absorption spectrometry or inductively coupled plasma optical/mass spectrometry (ICP-OES, ICP-MS) analyses of resulting solutions are employed for this purpose. Nevertheless, total elemental contents, which comprise also elemental forms that are insoluble in leaching media or by the action of plants, might be interesting for overall characterisation of a particular soil. In this case, total sample decomposition procedures based on the action of a mixture of mineral acids or a sample fusion with a suitable melt are applied to dissolve resistant minerals and desintegrate possibly present silicate lattice.

However, some methods for direct analysis of solids are more advantageous because of elimination of possible analytes losses and minimization of risk of contamination. For this purpose, X-ray fluorescence (XRF) spectrometry[1] is frequently and routinely used. Laser-assised plasma spectrometry techniques, such as laser induced breakdown spectroscopy[2], and ICP-OES or ICP-MS in connection with laser ablation (LA) seem to be promising tool for soil analysis.[3–7]

The aim of this work consists in establishing new methods of soil elemental analysis using LA-ICP-OES/MS. Artificially intentionally contaminated archive soil samples were employed. Toxic metals Cr, Ni, Cu, Zn and Pb were considered in the method developement. For the method validation, these soil samples were subjected to ICP-OES analysis of solutions obtained by total decomposition using mineral acids. Seleted soil standard reference materials were also analyzed. Independent results acquired by XRF analysis of soil sample pellets were used for confirmation of accuracy of solution analysis by ICP-OES.

Besides the total elemental content determination, selected soils were characterized by means of the five-step extraction procedure to asses elemental fractions bound to particular soil phases. This information might be important for explanation of possible matrix effects associated with processes of LA.

A selection and preparation of a suitable binder represents the indispensable step in the development of ablation – based methods. In our work we investigated a silica sol-gel matter preparation and its mixing with soil samples. The binder was then successfully applied in LA-ICP-OES/MS methods. The accuracy of the developed methods was confirmed by analysis of certified reference materials of soils (GBW07405 – 07).

Experimental

Soil Samples

Experimentally contaminated agricultural soils representing various soil types belong to archived materials of the Central Institute for Supervising and Testing in Agriculture (UKZUZ), Brno, Czech Republic.

Studied trace elements Cr, Ni, Cu, Zn, Pb occur in the concentration ranges as shown in Table I.

The soil samples were ground in a ball mill and dried to constant weight. The particle size of ground samples was measured by laser diffractometry and the particle diameter did not exceed 30 µm.

Table I
Concentration range of tested soils and RSD values for PN-ICP-OES

Element	C range [mg kg⁻¹]	RSD [%]
Cr	21–590	3.7–1.7
Ni	3.5–262	14–0.9
Cu	11–242	2.5–3.2
Zn	51–1355	2.7–0.5
Pb	22–1015	2.7–1.6

The solution analysis by ICP with pneumatic nebulization, (PN-ICP-OES) was carried out after the sample decomposition with a mixture of HF and $HClO_4$(ref.[5]) The soil-wax pellets for XRF analysis were prepared as a mixture of 4 g of a soil powder and 0.9 g of wax. The mixture was homogenized in a ball mill and then pressed by a hydraulic press to a pellet with a diameter of 32 mm. Sequential extraction was performed using five reagents with a different strength (Table II)[8,9]. The sol-gel method, allowing homogenous dispersion of internal standard (Sc) and analytes in calibration pellets, was applied for analysis of tested soils by LA-ICP-MS[10].
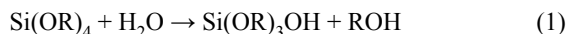
Table II
Sequential extraction procedure

Step	Metal phase	Reagent
1	Exchangeable	1 M NaOAc (pH = 8.2)
2	Carbonate	1 M NaOAc (pH = 5)
3	Mn-Fe oxides	0.04 M $NH_2OH \cdot HCl$ in 25 % HOAc
4	Organic	0.02 M HNO_3, 30% H_2O_2(pH = 2), 3.2 M NH_4OAc in 20% HNO_3
5	Residual	conc. HF, $HClO_4$, HCl

Sol-Gel Technique

Sol-gel is an amorphous solid prepared via sol-gel processing, in which a colloidal suspension (sol) is first formed by mixing a silicon (e.g. tetraethoxysilane-TEOS) alkoxide precursor, water, a co-solvent and an acid or base catalyst. Alkoxyl groups are removed by acid- or base-catalysed hydrolysis reactions (Eq. (1)), and networks of O−Si−O linkages (gel) are formed in subsequent condensation reactions, which can produce either water or alcohol as shown in equations (2) and (3), involving hydroxyl groups[11]. Internal standard is integrated with the sample during gelation process.

Hydrolysis:

$$Si(OR)_4 + H_2O \rightarrow Si(OR)_3OH + ROH \qquad (1)$$

Condensation:

$$X_3SiOH + HOSiX'_3 \rightarrow X_3Si-O-SiX'_3 + H_2O \qquad (2)$$

$$X_3SiOR + HOSiX'_3 \rightarrow X_3Si-O-SiX'_3 + ROH \qquad (3)$$
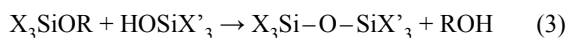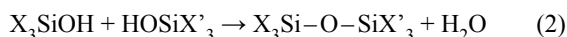
An archive soil sample with the lowest content of Cr, Ni, Cu, Zn and Pb spiked with solutions of elements of interest was used for the preparation of calibration samples. Twenty-two soil samples and three certified reference material of soils (GBW07405 – 07) were analyzed by developed LA-ICP-MS method and the obtained contents were compared with results of independent methods (XRF, ICP-OES).

The real soil samples were treated by the following procedure: 1.2 g of soil was weighed into a 50 ml beaker and 3 ml of TEOS, 6 ml of ethanol, 1.5 ml of water, 20 µl of the Sc standard solution (100 mg ml^{−1}) and two drops of 0.01 mol dm^{−3} HNO_3 were added. The beakers were put into a thermostated water bath maintained at ∼ 75 °C under ultrasonic stirring for ∼ 1.5 h to reach the complete gelation. After 20 min., 5 ml of water was added. The gelled materials were dried overnight in an oven at 110 °C. The sol-gel samples were manually ground and pressed into pellets with 12 mm in diameter and 1 mm thickness[10].

Instrumentation

A Jobin Yvon 170 Ultrace with laterally viewed ICP was used for solution analysis. The ICP system combines a monochromator and a polychromator. The monochromator was set on the Pb II 220.353 nm line and other four studied analytes were measured with the polychromator of a Paschen Runge montage using analytical lines Cr II 267.720 nm, Ni II 231.608 nm, Cu II 324.759 nm and Zn I 213.860 nm.

The XRF analysis was performed on an energy-dispersive XRF spectrometer (SPECTRO XEPOS) by polarized radiation, equipped with a Pd X-ray tube and a Si-detector. The real unknown samples were analyzed by the TUR-BOQUANT method, which is able to analyze the elements Na-U.

The LA-ICP-MS was performed with a laser ablation system UP 213 (New Wave, USA) and an ICP-MS spectrometer Agilent 7500 CE (Agilent, Japan). A commercial Q-switched Nd:YAG laser, operated at the wavelength of 213 nm with the 5th harmonic frequency, was used for ablation. The ablation device is equipped with programmable XYZ-stages that allowed sample movements during the ablation process. The samples were placed into the SuperCell (New Wave, USA) and were ablated by the laser beam, which was focused onto the sample surface through a quartz window. The ablated material was transported by flowing He to the ICP.

Results

The total contents of trace elements were determined using ICP-OES after total decomposition. XRF spectrometry was chosen for result comparison. Relative standard deviation of the total decomposition method and concentration range of tested soils can be found in Table I. Higher RSD value might be due to sample inhomogeneity and uncertainty of the measurement at low element concentration. Satisfactory agreement was found for ICP-OES solution analysis and XRF spectrometry. Correlation coefficient r values exceeded 0.994. Comparison of PN-ICP-OES and XRF determination of zinc as an easily leachable element is presented in Fig. 1.

A five-stage sequential extraction procedure was used for the determination of the speciation of extractable heavy
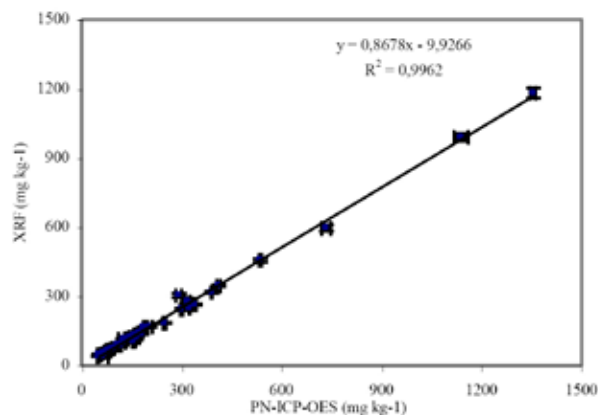

Fig. 1. **Comparison of results obtained by XRF analysis and PN-ICP-OES of soil extracts for Zn I 213.860 nm**

Table III
Comparison of efficiency of extraction by PN-ICP-OES to XRF analysis

Element	Efficiency [%]
Cr	63
Ni	82
Cu	80
Zn	102
Pb	96

Table IV
Comparison of CRM GBW07407 soil analysis results by LA-ICP-MS and certified values; the uncertainty intervals are calculated on a 95 % confidence level

Method [mg kg^{-1}]	LA-ICP-MS	Certified value
Cr	432 ± 28	410 ± 23
Ni	269 ± 27	276 ± 15
Cu	84 ± 8	97 ± 6
Zn	139 ± 15	142 ± 11
Pb	15 ± 3	14 ± 3

metals by PN-ICP-OES. The results as a sum of the five extraction steps were compared with those obtained after total decomposition and by XRF spectrometry. Efficiency of soil extracts to pressed pellets together with correlation coefficients are presented in Table III. The best efficiency of extraction can be observed for lead and zinc. Efficiency of extraction depends on the binding to minerals with different solubility. Low efficiency of chromium can be explained by binding to poorly soluble chromspinels and chromite[12,13].

The soil samples were analysed to evaluate the possibility of quantitative elemental analysis by laser ablation. The results for LA-ICP-MS were compared with the results of XRF as a method representing another type of direct analysis and with the results of solution analysis by ICP-OES as an ordinary method. In the case of Cr, slightly lower concentration values were yielded for the total decomposition using PN-ICP-OES than for both direct analysis methods, which can be caused by the incomplete decomposition of Cr in acids (Fig. 2.).
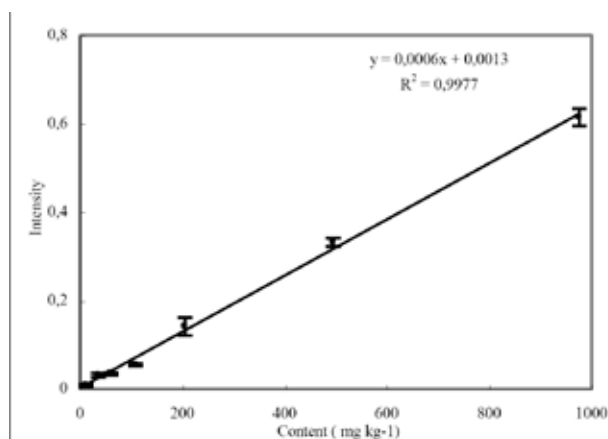
Fig. 2. **Comparison of LA-ICP-MS and PN-ICP-OES after total decomposition results for Cr as a barely leachable element**

The calibration was performed using spiked sample pellets. The soil with a low content of elements of interest was spiked with seven concentration levels to obtain a calibrated range from 24 to 965 mg kg^{-1}. The calibration curves were fitted by a computer program WinStat. All calibration plots were linear over the whole concentration range. Intercepts of the regression lines were tested by t-test and were statistically insignificant ($t_a < t_{0.05;n-2}$) for all studied elements. Correla-

tion coefficient r values were in the range of 0.997–0.999. Calibration line for copper with scandium as internal standard is presented in Fig. 3.

Repeatability of ablation was described as RSD % which was calculated from three measurements of ablation signal on the different locations of each pellet. The RSD values did not exceed 8%.

The accuracy of the method was confirmed by analysis of three CRM soils. Results of CRM GBW 7407 by LA-ICP-MS and certified values are given in Table IV.
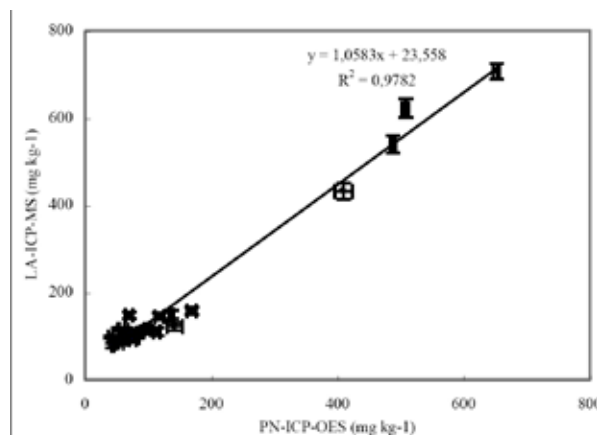
Fig. 3. **Calibration graph for Cu with internal standardization by Sc**

Conclusions

Monitoring of the heavy metals in agricultural soils is gaining the importance because these elements can be accumulated by plants and thus enter the food chain. To obtain total elemental content of Cr, Ni, Cu, Zn, Pb the decomposition with HF and HClO$_4$ by ICP-OES was used. The sequential extraction procedure providing more information than total concentration determination was used to study bioavailability of metals. Methods of total decomposition are very lengthy and sometimes even not fully efficient therefore direct methods are more convenient in such a case. XRF analysis of soil pellets prepared with a wax binder and LA-ICP-MS of perfectly homogenized pellets using sol-gel method represented the direct methods.

The results of direct methods were compared with those obtained by PN-ICP-OES. A satisfactory agreement was

found for all three methods applied to the studied elements, except for chromium as was mentioned.

REFERENCES

1. dos Anjos M. J., Lopes R. T., de Jesus E. F. O., Assis J. T., Cesareo R., Barradas C. A. A.: Spectrochim. Acta B *55*, 1189 (2000).
2. Capitelli F., Colao F., Provenzano M. R., Fantoni R., Brunetti G., Senesi N.: Ž. Geoderma *106*, 45 (2002).
3. Kanicky V., Mermet J. M.: Fresenius' J. Anal. Chem. *363*, 294 (1999).
4. Musil P., Otruba V., Kanicky V., Mermet J. M.: Spectrochim. Acta B *55*, 1747 (2000).
5. Mikoláš J., Musil P., Stuchliková V., Novotný K., Otruba V., Kanický V.: Anal. Bioanal. Chem. *374*, 244 (2002).
6. Lee Y. L., Chang Ch. Ch., Jiang S. J.: Spectrochim. Acta B *58*, 523 (2003).
7. Baker S. A., Bi M., Aucelio R. Q., Smith B. W., Winefordner J. D.: J. Anal. At. Spectrom. *14*, 19 (1999).
8. Hlavay J., Prohaska T., Weisz M., Wenzel W. W., Stingeder G. J.: Pure Appl. Chem. *76*, 415 (2004).
9. Mester Z., Cremisini C., Ghiara E., Morabito R.: AnalyticaChimica Acta *359*, 133 (1998).
10. Hubová I.: J. Anal. At. Spectrom. *22*, 1 (2007).
11. Wright J. D., Sommerdijk A. J. M.*: Sol-Gel Materials Chemistry and applications,* 2001.
12. Medved J., Sterško V., Kubová J., Polakovičová J.: Fresenius´ J. Anal. Chem. *360*, 219 (1998).
13. Doležal J., Povondra P., Šulcek Z.: *Rozklady základních anorganických surovin*, SNTL Praha, 1966.

L09 TISSUE-SPECIFIC DISTRIBUTION AND ACCUMULATION OF ORGANOCHLORINE POLLUTANTS IN SELECTED RAPTOR SPECIES FROM THE CZECH REPUBLIC

RADIM LÁNA[a], MILADA VÁVROVÁ[a,b], VLADIMÍR VEČEŘEK[b] and STANISLAV KRÁČMAR[c]

[a]*ICTEP, Faculty of Chemistry, Brno University of Technology, Purkyňova 118, 612 00 Brno, Czech Republic,*
[b]*University of Veterinary and Pharmaceutical Science Brno, Palackého 1–3, 612 42 Brno, Czech Republic,*
[c]*Mendel University of Agriculture and Forestry in Brno, Zemědělská 1, 613 00 Brno, Czech Republic,*
lana@fch.vutbr.cz

Introduction

Organochlorine compounds such as polychlorinated biphenyls (PCBs) or organochlorine pesticides (OCPs) are known as persistent organic pollutants (POPs). Despite the ban on production or restrictions on use many years ago the POPs still continue to be found in various samples from the environment and accumulate through the food chains. For their top position within the food chain and the sensitivity to environmental changes birds of prey are very suitable bio-accumulation markers. The amount of pollutants accumulating in the raptors' tissues is related not only to their diet and corresponding trophic position, but also to the differences in accumulation among habitats and ecosystems (aquatic vs. terrestrial)[1]. Moreover, sensitivity also varies greatly between compound and species[2].

However, it is difficult to use birds for the assessment of pollutant transfers within the food web, except for those species partly associated with the aquatic habitats where the transfer can be documented in some measure. For instance the cormorant or heron are fish feeders and top predators in aquatic ecosystems, have relatively high levels of POPs in the adipose tissue, and hence are suitable bioindication species[3].

Because practical and ethical reasons, low numbers and often legal protection inhibit the sacrifice of free-living animals, methods for non-destructive biomonitoring have been developed. Whereas many studies have previously focused on the use of eggs or hair, feathers, on the other hand, have an advantage that they can be collected irrespective of season, age or sex[4]. Another simple approach consists in the use of specimens found dead.

In the Czech Republic, the levels of PCBs in unhatched eggs from raptors were monitored. No intra- or interspecies differences were found and the findings corresponded to those from Germany, Canda or the USA, where the CB 153 was the most abundant congener[5].

This study deals with the levels of organochlorine pollutants in various tissues of raptor species from the Czech Republic and compares the results with those from foreign surveys.

Experimental

The sampling area as well as the raptor and fish species and their detailed description have already been published[6].

Selected tissue samples of investigated specimens were homogenized and dessicated by activated anhydrous sodium sulphate. Two different extraction techniques were employed for the isolation of lipids from the tissues. The samples of muscles, kidneys and liver were extracted by petrolether (SupraSolv, Merck) by means of accelerated solvent extraction (140 °C, 12 MPa, 3×5 min static extraction + N_2 purge). The samples of brain, skin, feathers and intestinal content were extracted by petrolether:acetone (1:1, v/v) for 6 h in a Soxtec apparatus. The removal of lipids from raw extracts was carried out on an adsorption column packed with Florisil (5 g; 60/100 mesh, Sigma-Aldrich, activated at 600 °C for 6 h). The samples were then eluted with 90 ml of n-hexane: diethylethere (94:6, v/v), evaporated to dryness using a rotary evaporator, and dissolved in 1 ml of *n*-hexane.

The quanification of target analytes was carried out by HP 6890N high resolution gas chromatograph with two micro-electron capture detectors (63 Ni m-ECD) and two capillary columns (HT-8 and DB-17ms) operated in parallel (H_2 as the carrier gas). Nine-point calibration curves in a linear range from 0.5 to 1,000 ng ml^{-1} were used and the limit of quantification (LOQ) for all analytes was calculated as 2.5 ng g^{-1} of lipids (i.e. about 0.13 ng g^{-1} d.w. for 4% lipid content in a tissue).

Results

The levels of organochlorine pollutants found in the muscle tissue of cormorants from the Záhlinice area (2007)
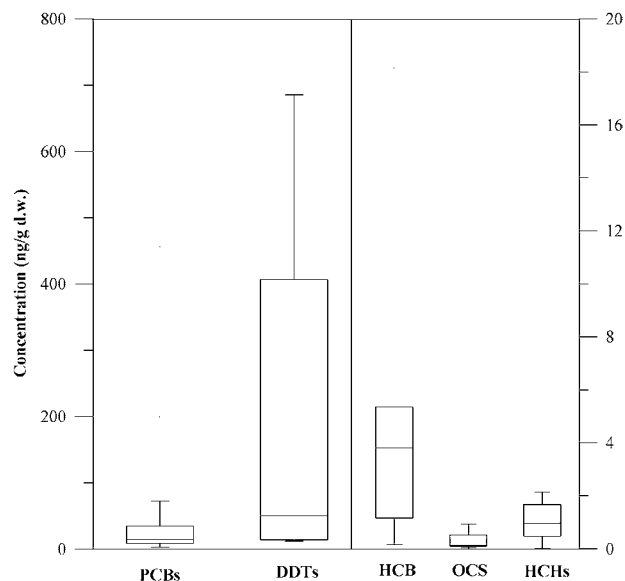

Fig. 1. **Organochlorine pollutants in muscle tissue of common cormorant from the Záhlinice area (n = 8). Horizontal lines represent median, rectangles delimit the 1st and 3rd quartiles, and error bars represent the min/max values. Outlying values are marked as "+" (2007).**

are presented in Fig. 1. PCB congeners 138, 153 and 180, and the p,p'-DDE were the most abundant compounds. As can be read in this graph, there are significant differences in the levels of organochlorines in samples of different specimens. Due to its higher content of lipids, compared with the other tissues, skin was by far "the most contaminated" tissue (approx. five times higher levels of PCBs and OCPs). Extreme values exceeded 5,000 ng g^{-1} w.w. for the sum of 7 PCB congeners, and DDT and its metabolites reached even higher levels. Interspecies differences in the concentrations of POPs are shown in Fig. 2.
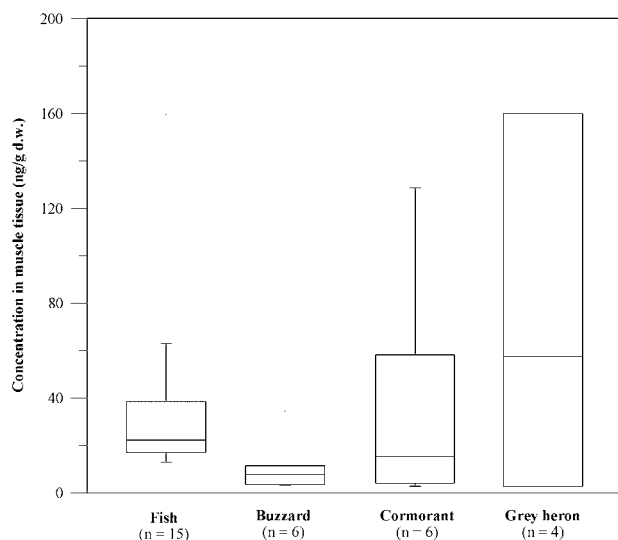
Fig. 2.   **PCBs in muscle tissue of species from the Záhlinice area. Horizontal lines represent median, rectangles delimit the 1st and 3rd quartiles, and error bars represent min/max values. Outlying values are marked as "+" (2003).**

Comparison of fish and raptors' tissues from the Záhlinice area showed an increase in the concentrations of POPs towards higher levels of the food chain and the process of accumulation of POPs was clearly illustrated.

Conclusions

Investigated raptor species including cormorant, grey heron and buzzard lived up to their reputation of being the most contaminated members of food chains. Cormorants and grey heron top the aquatic food chain and hence the levels of organochlorines found in their tissues were significantly higher than those in their fish prey. The results can be well compared with other findings not only within the Czech Republic a prove fish and birds of prey to be suitable bioaccumulation markers.

REFERENCES
1. Borgå K., Fisk A.T., Hoekstra P.F., Muir D.C.G.: Environ. Toxicol. Chem. *23*, 2367 (2004).
2. Hoffman D.J., Melancon M.J., Klein P.N., Eisemann J.D., Spann J.W.: Environ. Toxicol. Chem. *17*, 747 (1998).
3. Ryckman D.P., Weseloh D.V., Hamp P. et al: Environ. Monitor. Assess. *53*, 169 (1998).
4. Dauwe T., Jaspers V., Covaci A., Schepens P., Eens.: Environ. Toxicol. Chem. *24*, 442 (2005).
5. Kubištová I.: Dissertation. University of Veterinary and Pharmaceutical Sciences Brno, Brno, Czech Republic, 2002.
6. Houserova P., Kubáň V., Kráčmar S., Sitko J.: Environ Pollution *145*, 185 (2007).

L11 POTENTIAL APPLICABILITY OF A HIGH PERFORMANCE CHELATION ION CHROMATOGRAPHIC METHOD TO THE DETERMINATION OF ALUMINIUM IN ANTARCTIC SURFACE SEAWATER

JULIETTE TRIA, PAUL R. HADDAD and PAVEL NESTERENKO

Australia Centre for Research on Separation Science (ACROSS), School of Chemistry, University of Tasmania, Private Bag 75, Hobart, Tasmania, Australia, 7001, jtria@utas.edu.au

Introduction

In oceanography, aluminium is used as a tracer to fingerprint the location and magnitude of atmospheric dust deposition. Aluminium is particularly suitable as a tracer because of its short residence time in surface seawater, its relatively simple seawater chemistry and the fact that primary input to the open ocean is by atmospheric deposition. The information supplied by surface aluminium concentrations is vitally important to understanding the role that aeolian deposition plays in supplying trace elements to the surface ocean and subsequent effects on biological processes. The information is especially important for furthering knowledge of the biogeochemistry of iron. Iron is of particular interest because it is an essential element for the growth and metabolism of all marine organisms despite only being available in extremely low concentrations (0.1–0.5 nM)[1]. Iron has been shown to limit phytoplankton growth, which in turn may have implications on global climate through drawdown of gases used in photosynthesis, such as carbon dioxide. An accurate and robust method for determining aluminium is thus vital for continuing studies into atmospheric deposition and subsequently climate control.

Flow injection analysis (FIA), has typically been used for the quantification of aluminium in seawater, due to its portability for shipboard use, suitable limit of detection and relative ease of use. However, this technique still requires preconcentration of as much as 10 ml of seawater in order to achieve the required sensitivity[2]. Other common techniques for the determination of trace concentrations of aluminium, such as ICP-MS, are unsuitable for use at sea due to the size of the instrumentation as well as the amount of sample pretreatment required.

Chromatographic techniques have become increasingly popular for the quantification of aluminium in recent years. Ion chromatography has successfully been used for the separation of aluminium in a selection of matrices including natural waters[3–6] and biological samples[7]. The technique is relatively simple and can be coupled with a variety of detection methods such as UV-VIS and mass spectrometry, allowing for both high selectivity and sensitivity.

Chelation ion chromatography (CIC) offers an alternative to traditional ion-exchange IC, particularly for samples of high ionic strength. CIC functions by retaining metal ions according to the stability of the corresponding complexes and allows for the separation and preconcentration of aluminium in complex samples. In addition, CIC also offers the advantages of using only one type of material for both preconcentration/matrix elimination and separation and also the ability to acquire a simplified chromatogram identifying only kinetically-labile and chemically inert species[8,9]. Ion-exchange interactions are likely to occur simultaneously; however, high ionic strength eluents are typically used to ensure chelation is the dominant mechanism.

The iminodiacetic acid functional group has been shown to be a highly promising ligand for the separation of metal ions by CIC[10]. Our previous work has shown the applicability of iminodiacetic acid functionalised silica (IDAS) to the determination of aluminium in paper mill process water[11]. This work detailed the optimised separation conditions of an IDAS packed column including eluent composition, flowrate and column temperature. Good separation in a complex matrix was achieved, with high column efficiency.

The most commonly used method for the detection of aluminium at low concentrations is the highly sensitive fluorescent detection of its lumogallion complex. This approach has been applied successfully to the determination of aluminium in a wide range of samples, including those with a high salt content, e.g. saline water and body fluids. Nishikawa and co-workers were the first to describe application of the technique to seawater and the batch method has since been incorporated into FIA systems [12]. The limit of detection for the technique has been improved through the addition of surfactants and through optimisation of conditions such as pH and temperature.

This paper is a continuation of our work with IDAS but for the specific purpose of the direct determination of aluminium in seawater. The determination of Al in seawater poses a myriad of potential problems including sample matrix interferences and extremely low concentrations. We have developed a HPCIC method coupled with fluorescent detection of the aluminium-lumogallion complex. The system has been successfully applied to seawater samples obtained in the Ross Sea, Antarctica.

Experimental

A p p a r a t u s

A Metrohm 844 UV/VIS Compact IC was used for all analyses. The system delivered the eluent at 0.3 ml min^{-1} and was set up with a post-column reactor, consisting of a 2 m PTFE reaction coil (1/16" × 0.02"). This reactor was immersed in a water bath for heating above room temperature. Peristaltic pump tubing delivered the PCR reagent at a constant flow-rate of 0.36 ml min^{-1}. A 20 μl sample loop was used unless specified.

A column heater set to 71 °C housed a 200 × 4 mm i.d. column packed with 5 μm IDAS (JPP Chromatography Ltd, UK). Detection was carried out using a Varian Prostar 363 fluorescence detector fitted with a xenon lamp. The excitation and emission wavelengths were set to 500 and 550 nm

respectively. The detector and Compact IC were connected through a Metrohm 830 IC Interface.

Reagents

All reagents were of an analytical grade. A NaCl-HNO₃ eluent (unless otherwise indicated) was made from stock 2M and 1M solutions respectively. All solutions were prepared from a Milli-Q Element purification system, (Millipore, North Ryde, NSW, Australia). A stock 1M MES (Sigma, Castle Hill, NSW, Australia) buffer was made and pH adjusted to 6.05 (unless otherwise stated) with concentrated NaOH. A stock 2M NH₄OAc buffer was prepared from trace metal grade concentrated acetic acid (GFS Chemicals, Powell, Ohio, USA) and ammonia solution (isopiestic distilled concentrated NH₄OH) and pH adjusted to 6.8. A stock 3mM lumogallion (Pfaltz and Bauer, Waterbury, CT, USA) solution was prepared and refrigerated in dark conditions for up to 2 months. Working lumogallion buffers were prepared daily as were aluminium standards.

Samples

Surface seawater was collected aboard the Research Vessel Nathaniel B Palmer (USA) by means of a towed fish. Samples were collected at a depth of approximately 7 m using trace metal clean procedures. The seawater was filtered (0.25 μm) and acidified to pH 2 using trace metal clean HCl.

Results

Separation Conditions

Optimum operating conditions for the separation of aluminium in complex matrices using IDAS have previously been detailed elsewhere[11]. The only modification to these conditions was the use of NaCl rather than KCl in the eluent. The reason for this was the availability of high grade chemical reagent in order to ensure low background fluorescence. In summary these conditions were a 0.25M NaCl–40mM HNO₃ eluent delivered at 0.3 ml min⁻¹ with separation on a 200×4 mm i.d. column packed with 5 μm IDAS at 71 °C.

Background Fluorescence

A significant dip in fluorescence away from the baseline before the elution of aluminium was observed in preliminary experiments. This dip was up to one fifth the size of the peak of a 0.1 ppm aluminium standard. It was decided that the probable cause was high background fluorescence due to the reagents used to prepare the eluent, in particular the chloride salt. Initially, KCl was used for the preparation of the eluent and despite choosing an analytical grade KCl, the level of aluminium contamination was obviously high. A solution to this was the addition of a trap column positioned before the separation column. The column was packed with Eichrom Diphonix® resin (particle size 100–200 mesh). This resin has diphosphonic and sulfonic acid groups bonded to a polystyrene/divinylbenzene matrix. It is capable of extraction of a range of metals from both neutral and highly acidic solutions. The column, measuring 250×4 mm i.d., effectively removed

the majority of the aluminium from the eluent, reducing the dip by a factor of 25. In addition, trace metal grade sodium chloride and nitric acid were used in the eluent for subsequent experiments.

Optimisation of Lumogallion Chemistry

Buffer and pH

Work by Howard and co-workers[13] previously reported the optimum pH of the aluminium-lumogallion reaction to be between 4 and 5.5. Resing and Measures later found the maximum response to be in a much narrower range between pH 5 and 5.5(ref.[12]). Based on this fact, MES was chosen as the buffer for initial experiments given its pK_a of 6.27 at 25 °C and subsequent useful buffering range[14]. Although initial chromatograms of a 1 ppm aluminium standard, using a 40mM MES solution at pH 6.2, were promising in terms of sensitivity and efficiency, the pH of the effluent was found to be only 2.9. Increasing the MES concentration to 120mM served to improve this situation, but also resulted in an increase in baseline noise and reduction in both sensitivity and efficiency. Consequently, it was decided to continue investigations using ammonium acetate, a buffer extensively used for the aluminium-lumogallion reaction.

Firstly, the effect of varying the concentration of the ammonium acetate buffer on sensitivity was observed. This was carried out by diluting a stock 3M buffer (pH 6.7) to 0.25. 0.5 and 1 M. The results indicated that a concentration of 0.25 M gave the best result in terms of peak area and also for achieving an effluent pH closest to optimum for the lumogallion reaction. It was shown that peak area of a 0.1 ppm aluminium standard increased almost 1 times through the use of 0.25M compared with 1M ammonium acetate and over 8 fold compared with 40mM MES.

Seawater samples intended for quantification of aluminium require acidification to between pH 1.8–2. Consequently, the buffer utilised in the lumogallion reaction needs to be able to maintain an optimum pH even on mixing with the acidified sample. The 0.25M ammonium acetate buffer was shown to have insufficient buffering capacity when mixed with an acidified sample. Not only did the retention time decrease but a loss in sensitivity also resulted. Given that a decrease in sensitivity was also previously observed with an increase in buffer concentration for ammonium acetate, the only alternative was to increase the pH of the buffer. This was attempted but it appeared that even increasing the buffer pH to 8 resulted in little improvement. This meant that short of sacrificing sensitivity for buffering capacity, ammonium acetate was not the best choice for the analysis of acidified seawater.

The choice of buffers capable of maintaining a pH of approximately 5.5 is fairly limited. This led to the decision to reinvestigate MES. For comparative proposes, a 0.25M solution of MES (pH adjusted to 6.05 with NaOH) was firstly trialed. The result was an equivalent sensitivity to ammonium acetate but with the added advantage of no loss in sensitivity

between acidified and non-acidified samples. Similarly, changes in retention times were negligible. The remaining issue with the use of MES was the increase in baseline noise and subsequent increase in detection limits. This problem was overcome by pre-cleaning the buffer using a column packed with Eichrom Diphonix® resin. The resulting baseline noise reduced approximately three times and the corresponding background fluorescence was almost seven times less.

It was thus determined that a pre-cleaned buffer of 0.25M MES adjusted to a pH of 6.05 with NaOH, was the optimum choice for the determination of aluminium in acidified seawater samples.

Temperature

The response of the reaction between aluminium and lumogallion has been investigated in both batch techniques and flow systems. In the batch method, an optimal temperature of 80 °C is generally accepted[13,15], whereas FIA methods tend to use 50 °C. The latter is based on investigations carried out by Resing and Measures which concluded that most of the temperature-based reaction rate gain had been achieved by this temperature[12]. Independent investigation into the effect of temperature on the rate of reaction was undertaken by us due to the fact a different buffer was used. It was found that the highest response, in terms of peak area, was obtained at temperatures between 65 and 75 °C (Fig. 1.). Based on this response, 70 °C was chosen as the temperature at which to operate the post column reactor for all subsequent anlyses.
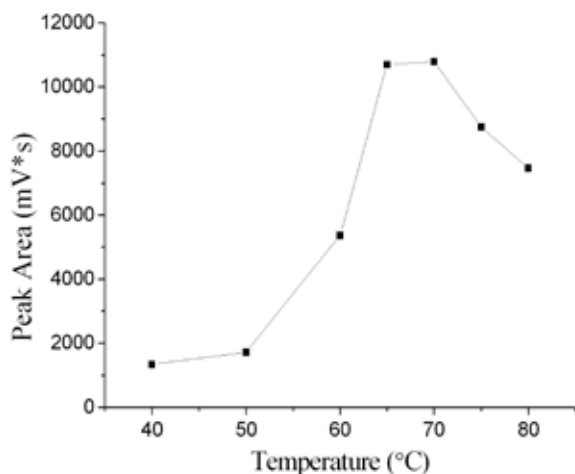
Fig. 1. **Dependence of fluorescence response on temperature**

Lumogallion and Reaction Coil

The extent of chemical reaction needs not be complete for an analytical technique to be valid. However, it is desirable to obtain as high a reaction yield as possible in order to ensure the technique has good precision. For the reaction between aluminium and lumogallion, the concentration of post-column reagent may be changed, along with temperature and reaction time, in order to control the extent of reaction. Three concentrations of lumogallion (0.03, 0.04 and

0.05 mM) were tested in order to exhaust possible improvements to the system via this approach. The concentrations chosen were based on those used in flow systems. It was found that at concentrations higher than 0.03 mM, no significant improvements were achived. Additionally, the effect of increasing the length of the post column reaction coil from 2m to 4m was also studied. The result, however, was a slight reduction in fluorescence. A MES buffer containing 0.03 mM lumogallion together with a 2m reaction coil were thus used in all subsequent analyses.

Surfactant

Howard and co-workers reported an increase in the fluorescence intensity of the aluminium-lumogallion complex of as much as 5-fold through the addition of a non-ionic surfactant[13]. Further investigation has been carried out by Resing and Measures[12], which showed that Brij-35 enhanced fluorescence to a greater extent than other surfactants, such as Triton X-100 and cetylammonium bromide (CTAB). In order to ensure the lowest limit of detection was achieved for this system, an investigation into the effect of surfactants was also carried out. The results differed substantially from those discussed earlier. It was found that although the addition of Brij-35 enhanced fluorescence marginally, a simultaneous increase in baseline noise negated any improvement achieved. Interestingly, when CTAB was tested, the aluminium peak disappeared altogether. This was considered to be an effect of the surfactant adhering to the tubing walls and effectively stripping the aluminium from the reagent stream. The system required flushing with methanol in order to resume normal operation. Consequently, further investigation into the possible use of surfactants was abandoned, with the decision to explore other approaches to lowering the detection limit being deemed more favourable.

Sample Volume

A more attractive approach for achieving a low LOD was increasing the sample loop volume. All previous experiments had been carried out using a volume of 20 µl. The response of the system to higher volumes was investigated and the results are depicted in Fig. 2. It can be seen that for volumes between 20 and 500 µl, the system follows a linear response, as expected. It was also noteworthy that no reduction in column efficiency was experienced at higher volumes. The highest efficiency was achieved for a 100 µl sample loop, which was unexpected considering that band broadening is generally associated with increased sample size and is often responsible for an observed reduction in performance of the chromatographic column as injection volume is increased.

Another unexpected result of increasing the sample volume was an increase in retention time. Generally, a decrease in retention time would be expected due to competition from other analytes for chelation sites, especially in such a complex matrix as seawater. This was shown not to be the case for IDAS and may be explained in terms of the forma-

tion of negatively charged aluminium complexes in seawater (e.g. fluoro complexes) and the high ionic strength of the eluent. The effect of ionic strength has been reported to affect the retention of ions in chelation IC[8,16]. In an environment of sufficiently high ionic strength the repulsion between negatively charged aluminium species and the iminodiacetic acid functional groups may be reduced. This can result in a subsequent increase in retention time as observed in our studies. This response is actually considered favourable as it allows for additional stabilisation of the baseline between the minor dip in fluorescence and elution of the aluminium.
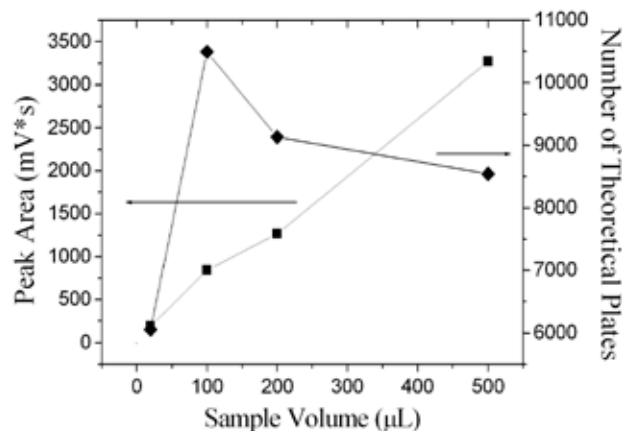
Fig. 2. **Effect of increasing sample volume on column performance and fluorescence response**

Seawater Samples

At this stage, the optimised HPCIC system coupled with fluorescence detection had been shown to be applicable to the determination of aluminium in acidified standards prepared in Milli-Q water. Previous work by us has shown that IDAS can be successfully applied to the analysis of samples with a complex matrix but it had not yet been used for the detection of aluminium in seawater. Seawater is difficult to analyse not only in terms of the high salt content, but also due to the number of other potentially interfering ions, such as iron and magnesium. However, preliminary chromatograms showed no co-elution problems and there was only one additional peak (at ~ 8 min) other than aluminium. Based on previous findings this peak is likely to be due to iron and/or a mixture other analytes e.g. sodium and calcium.

Calibration of the system using a 500 µl sample loop was carried out by means of standard addition to an Antarctic seawater sample containing low levels of aluminium. The limit of detection was determined from the standard deviation of clean seawater and determining the signal equivalent to three times this value (i.e. 3σ). A LOD of 0.39 nM was achieved using a 500 µl sample loop. Good linearity of the system was observed between 1.8 and 36 nM.

Chromatograms of Antarctic seawater for different injection volumes are given in Fig. 3.
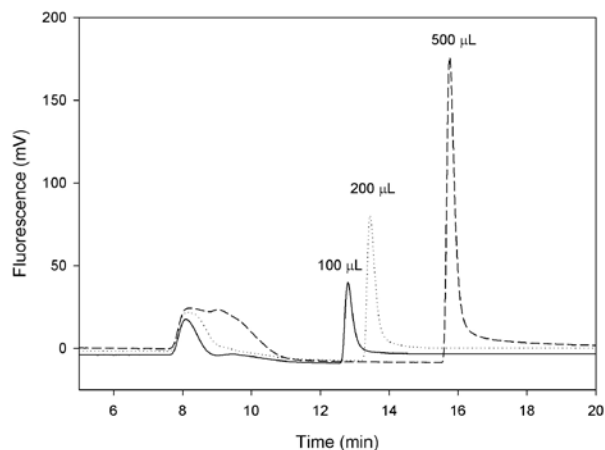
Fig. 3. **Chromatogram of Antarctic seawater for different injection volumes**

Conclusions

The optimised HPCIC system with fluorescence detection of the aluminium-lumogallion complex shows promise for the quantification of aluminium in Antarctic seawater. The IDAS chromatographic column does not suffer from issues such as co-elution of species with aluminium and produces peaks of good efficiency in a reasonable timescale. The response of the system to standard addition is linear and is applicable over a concentration range valid to seawater analysis. Additionally, the LOD achievable with the system means it should be capable of handling the low concentrations of aluminium expected in Antarctic seawater.

At this stage, the system has not been successfully applied to the quantification of aluminium in a seawater sample. The method currently suffers from an enhanced fluorescent response most likely due to matix interferences of seawater. It is difficult to determine the extent of this enhancement since there is not a certified seawater reference material for aluminium; but it is believed that, at present, the system produces a response approximately three times higher than the true value. Studies are underway to eliminate this problem and are currently focusing on the removal or adequate separation of aluminium from the remainder of the seawater matrix.

REFERENCES

1. Johnson K. S., Gordon R. M., Coale K. H.: Mar. Chem. *57*, 137 (1997).
2. Brown M. T., Bruland K. W.: Limnol. Oceanogr.: Methods. *6*, 87 (2008).
3. Drabek O., Mladkova L., Boruvka L., Szakova J., Nikodem A., Nemecek K.: J. Inorg. Biochem. *99*, 1788 (2005).
4. Mitrovic B., Milacic R., Pihlar B., Simoncic P.: Analusis. *26*, 381 (1998).
5. Fairman B., Sanz-Medel A., Jones P., Evans E. H.: Analyst. *123*, 699 (1998).

6. Kozuh N., Milacic R., Gorenc B., Abollino O., Sarzanini C.: Int. J. Enviro. Anal. Chem. *67*, 27 (1997).
7. Lian H. Z., Kang Y. F., Bi S. P., Yasin A., Shao D. L., Chen Y. J., Dai L. M., Tian L. C.: Anal. Bioanal. Chem. *376*, 542 (2003).
8. Jones P., Nesterenko P. N.: J. Chrom. A. *789*, 413 (1997).
9. Nesterenko P. N., Jones P.: J. Sep. Sci. *30*, 1773 (2007).
10. Nesterenko P. N., Shpigun O. A.: Russ. J. Coord. Chem. *28*, 726 (2002).
11. Tria J., Butler E. C. V., Haddad P. R., Bowie A. R.: Anal. Chim. Acta. *588*, 153 (2007).
12. Resing J. A., Measures C. I.: Anal. Chem. *66*, 4105 (1994).
13. Howard A. G., Coxhead A. J., Potter I. A., Watt A. P.: Analyst. *111*, 1379 (1986).
14. Martell A. E., Smith R. M.: NIST Critically selected stability constants of metal complexes database. Version 8.0. Texas A & M University, Texas 1998.
15. Hydes D. J., Liss P. S.: Analyst. *101*, 922 (1976).
16. Saldadze K. M., Kopylova-Valova V. D.: *Kompleksoobrazyushie Ionity* (Complexing Ion Exchangers). Khimiya, Moscow 1980.

L12 DIRECT ANALYSIS IN REAL TIME – TIME-OF-FLIGHT MASS SPECTROMETRY: ANALYSIS OF PESTICIDE RESIDUES AND ENVIRONMENTAL CONTAMINANTS

LUKÁŠ VÁCLAVÍK, JAKUB SCHŮREK, TOMÁŠ ČAJKA and JANA HAJŠLOVÁ

Department of Food Chemistry and Analysis, Institute of Chemical Technology Prague, Technicka 5, 166 28 Prague 6 – Dejvice, Czech Republic,
lukas.vaclavik@vscht.cz

Introduction

Ambient desorption ionization mass spectrometry (MS) is a rapidly growing area representing an attractive alternative to conventional analytic approaches. Recently introduced ionization techniques, such as direct analysis in real time (DART)[1], desorption electrospray ionization (DESI)[2] or atmospheric pressure solids analysis probe (ASAP)[3], allow direct examination of various types of samples in the open atmosphere and at ground potential. Little or no sample treatment prior to analysis is required. Additionally, time-consuming separation of sample components, which is usually employed by chromatographic methods, can be omitted with ambient MS.[4]

The ionization process with DART is based on interactions of metastable atoms of gas with atmosphere (H_2O, O_2) and sample components. The gas (usually helium) flows through a tube divided into several compartments. In a discharge chamber, ions, electrons and metastables are formed. In the next step, charged species are removed from the gas stream and heated gas promotes the desorption process. Ionization of the sample occurs in the area between the ion source and a mass spectrometer inlet (sampling gap). DART provides relatively simple mass spectra characterized mainly by $[M + H]^+$ and $[M]^+$ in positive-ion mode or $[M−H]^-$ and $[M]^-$ in negative-ion mode.[1] It is worth to notice, that DART technique has common features with atmospheric pressure chemical ionization (APCI) as the formation of metastables take place in an electrical discharge.[1,4]

DART ion source can be hyphenated to any type of mass spectrometer. However, when coupled to a high-resolution time-of-flight mass spectrometer (TOFMS), accurate mass measurement is enabled, allowing the confirmation of target analyte identity and calculations of elemental compositions of "unknowns". For correct identification of "unknowns", it is essential to gain knowledge about the examined matrix to allow discrimination of potential compounds suggested by the software.

Until now, very few papers dealing with applications of DART have been published.[5-9] In following examples, the potential of DART–TOFMS technique for qualitative and quantitative analysis of *(i)* pesticide residues, in particular case, strobilurins in wheat grains, *(ii)* thiabendazole on cut-flower leaves, and *(iii)* rapid screening of brominated flame retardants (BFRs) in in-door dust extract, will be demonstrated.

Experimental

C h e m i c a l s

Pesticide standards (≥ 99 %) were obtained from Dr. Ehrenstorfer (Germany), decabromodiphenyl ether (BDE-209) standard (≥ 98 %) was provided by Cambridge Isotope Laboratories (USA). Solvents used for sample extractions and preparations of standard solutions were HPLC-grade. Poly(ethylene glycol) 600 was from Sigma-Aldrich (Germany), anhydrous Na_2SO_4 was supplied by Merck (Germany).

S a m p l e   P r e p a r a t i o n

(i) An amount of 12.5 g of milled wheat grains was spiked with an internal standard (prochloraz) at a concentration of 250 ng g^{-1} and extracted by shaking with 50 ml of ethyl acetate and 10 g of anhydrous Na_2SO_4. The suspension was filtered and the volume was reduced by evaporation to 25 ml. Similarly, wheat grain extracts spiked with strobilurins (azoxystrobin, kresoxim methyl, pyraclostrobin, trifloxystrobin, dimoxystrobin and picoxystrobin) in the range from 12 to 1200 ng g^{-1} were prepared. Wheat grains with incurred residues of azoxystrobin, kresoxim methyl and pyraclostrobin (reference material) were processed as described above.

(ii) Flowers (roses) were purchased from local florists shop. The leaf was separated from the rest of flower and its surface was directly analyzed.

(iii) In-door dust containing BFRs (mainly BDE-209) was extracted using ASE 300 pressurized liquid extraction system (Dionex, USA): a hexane–acetone (1 : 1, v/v) mixture was used for extraction. The residues of extract were dissolved in isooctane.

D A R T – T O F M S   A n a l y s i s

For DART–TOFMS analyses, the system consisting of a DART ion source (IonSense, USA), a JEOL AccuTOF LP high-resolution mass spectrometer [JEOL (Europe) SAS, France], and an AutoDART HTC PAL autosampler (Leap Technologies, USA) was used. Helium gas was flowed at 2.9 dm^3 min^{-1}, discharge needle voltage was ± 3000 V, while perforated and grid electrode voltages were set to ± 150 V and ± 250 V, for positive and negative-ion mode, respectively. Other system parameter settings were changed depending on examined analytes, as summarized in Table I. To monitor bromine fragment ions originated from BDE-209, the cone voltage of the mass spectrometer was adjusted as described in results section.

Automated introduction of liquid samples was carried out with the use of Dip-it™ tips (IonSense, USA). Solid samples (flower leaves) were introduced manually by placing them in front of DART source. Poly(ethylene glycol) 600 solution (200 µg ml^{-1}) was introduced at the end of each sample analysis to perform internal mass calibration (mass drift compensation). The mass resolution of the instrument

Table I
DART–TOFMS parameter settings

Analytes	Polarity	Beam temp. [°C]	Ion guide voltage [V]
Strobilurins	Positive	300	1000
Thiabendazole	Positive	150	800
BDE-209	Negative	300	600
Bromine ions	Negative	350	400

during the measurements was typically 6,000 full width at half maximum (fwhm).

Results

Analysis of Strobilurins

The strobilurins and prochloraz (internal standard) were detected as $[M + H]^+$ ions (see Fig. 1.). A high mass resolving power of TOFMS instrument enabled the identity confirmation of target analytes on the basis of elemental composition calculations; the differences between measured (accurate) and calculated (exact) masses ranged from –2.27 to 5.10 ppm.

Fig. 2. shows the total ion current (TIC) record of six injections of wheat grain extract spiked with strobilurins (240 ng g^{-1}) and prochloraz (250 ng g^{-1}). Unfortunately, the
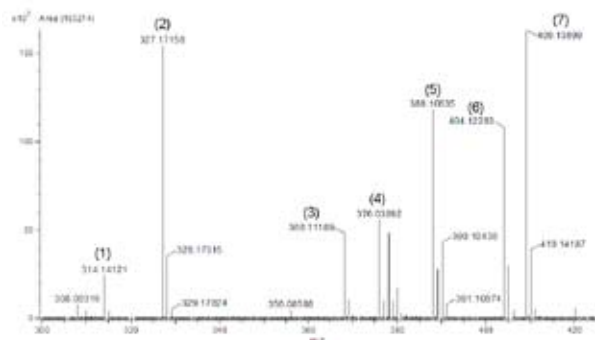
Fig. 1.   **Dart positive mass spectrum of wheat grain extract spiked with strobilurins (240 ng g^{-1}) and prochloraz (250 ng g^{-1}); (1) Kresoxim methyl, (2) Dimoxystrobin, (3) Picoxystrobin, (4) Prochloraz, (5) Pyraclostrobin, (6) Azoxystrobin, (7) Trifloxystrobin**
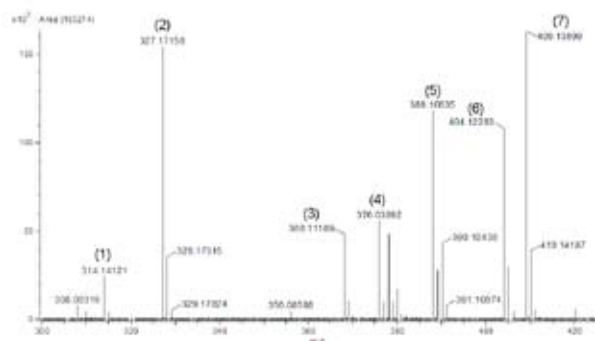
Fig. 2   **TIC chromatogram of six repeated wheat grain extract introductions [(1)–(6)] followed by PEG 600 solution (7)**
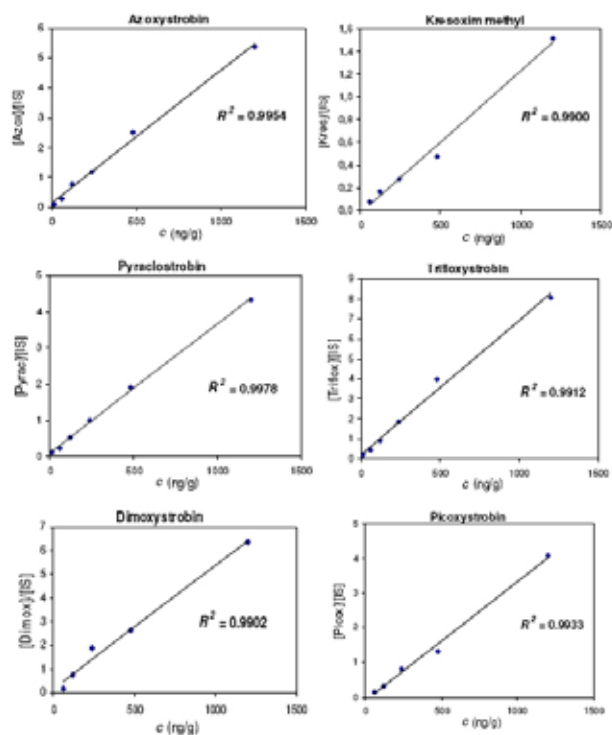
Fig. 3.   **Examples of calibration curves of matrix-matched strobilurin standards**

absolute response of the detector, even when employing autosampler, was poorly repeatable because of the dependence of position of the sampling tip and the sampling gap. Therefore, an internal standard had to be used for quantification of strobilurin residues. Calibration plots obtained by analyses of matrix-matched standards (see Fig. 3.) were constructed by plotting the ratio of analyte/internal standard ion intensity *vs.* concentration of particular analyte. Acceptable linearity was obtained for tested concentration range, regression coefficients of calibration curves were higher than 0.99.

In the next step, basic performance characteristics of the method were estimated using spiked samples. The repeatability was in the range from 8 to 15 % (n = 6, 60 ng g^{-1}), LOQs (limits of quantification) ranged from 12 to 30 ng g^{-1}. Considering the European regulation requirements, this method can be useful for rapid control of strobilurin residues in wheat grains[10]. For comparative purposes, wheat grain sample containing incurred residues of strobilurins was analyzed using

Table II
DART–TOFMS and LC–MS/MS methods: Analysis of incurred residues in wheat grains

Analyte	Concentration [ng g^{-1}]	
	DART–TOFMS	LC–MS/MS
Azoxystrobin	445	429
Kresoxim methyl	45	52
Pyraclostrobin	202	190

in-house validated method employing liquid chromatography–tandem mass spectrometry (LC–MS/MS). A good agreement of the results generated by two alternative approaches is documented in Table II.

Direct Detection of Thiabendazole in Plant Leaf

In this experiment, the possibility to monitor pesticide residues directly from the surface of the flower leaf was examined. For this purpose, the temperature of gas beam was decreased to 150 °C. Fig. 4.(A) shows positive mass spectrum of the leaf surface obtained by DART–TOFMS. In zoomed mass spectrum (Fig. 4.(B)), ion m/z 202.04410 corresponding to protonated thiabendazole molecule $[C_{10}H_8N_3S]^+$ (theoretical mass m/z 202.04389) was observed. No other pesticide compounds were detected in examined sample.
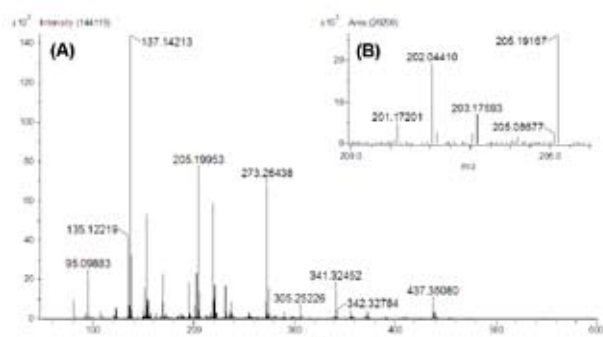
Fig. 4.   **DART positive mass spectrum of flower leaf; (A) m/z 50–600, (B) m/z 200–206. The ion m/z 202.04410 corresponds to thiabendazole**

Screening of BFRs in In-Door Dust

The most common methods used in analysis of BFRs employ gas chromatography coupled to mass spectrometry (GC–MS) operated in negative chemical ionization mode (NCI)[11]. The ions $[^{79}Br]^-$ and $[^{81}Br]^-$ are typically the base peaks in NCI mass spectra of these compounds and due to their selectivity they are frequently used for quantification purposes[12]. Supposing some similarity of BFRs fragmentation under NCI conditions in GC–MS and negative APCI,
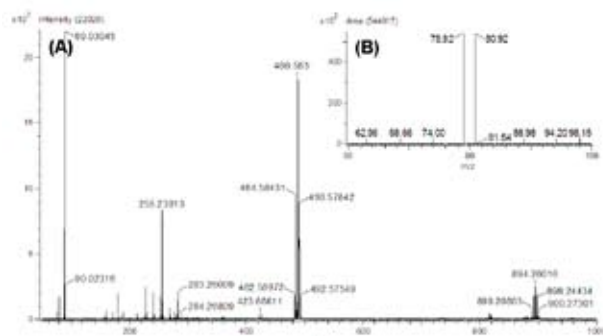
Fig. 5.   **DART negative mass spectrum of BDE-209 standard solution (50 µg ml^{-1}); (A) beam temp.: 300 °C, cone volt.: –20 V, (B) beam temp.: 350 °C, cone volt.: –140 V**

DART–TOFMS was proposed as a suitable approach for rapid screening of BFRs.

In the first phase of this experiment, the ionization of BDE-209 by DART was investigated. As documented in Fig. 5.(A), phenolate anions resulting from the cleavage of the ether bridge and anions resulting from bromine abstraction were observed after introduction of BDE-209 standard solution. To induce fragmentation, the cone voltage was decreased from -20 V to -140 V. Under these conditions, intensive $[^{79}Br]^-$ and $[^{81}Br]^-$ ions were the only ions in recorded mass spectrum (Fig. 5.(B)).
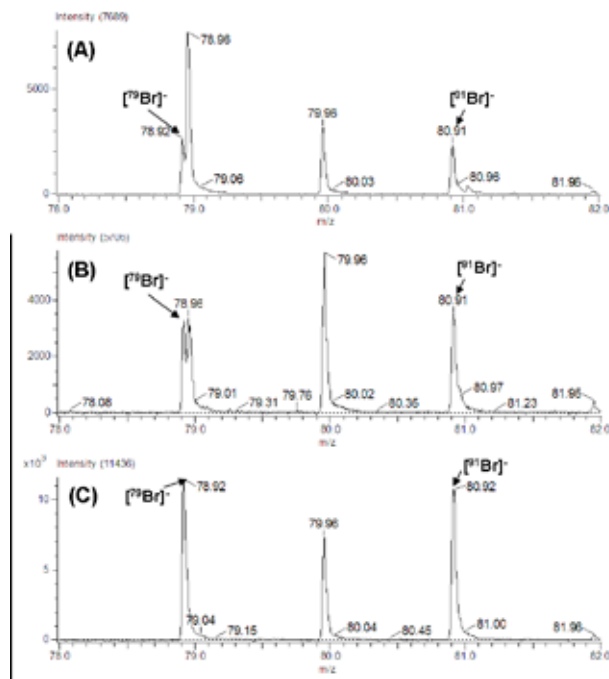
Fig. 6.   **DART negative mass spectrum of in-door dust extract; (A) cone volt.: –140 V, (B) cone volt.: –200 V, (C) cone volt.:–240 V**

While it was not possible to detect BFRs in dust extract due to high chemical noise, both bromine ions were distinctly recognized when fragmentation was induced (Fig. 6.(A)). To remove interfering ion with a mass close to $[^{79}Br]^-$, an attempt to induce its fragmentation was undertaken. As shown in Fig. 6.(B) and Fig. 6.(C) this was achieved by further decrease of cone voltage value.

Conclusions

DART–TOFMS technique can be used for determination of strobilurin fungicides in milled wheat grain extracts obtained by simple extraction procedure without time-consuming chromatographic separation. This method withstands the regulation demands of the European Union for the control of pesticide residues; moreover, simplified workflow enables examination of many samples within a short time period.

Qualitative analysis of solid samples without any sample preparation is a challenging application of this novel technique. DART–TOFMS was shown to be a useful tool enabling rapid examination of plant surface and detection of pesticide used for flower treatment.

Preliminary results indicate the potential to introduce new concepts into rapid screening of BFRs by employing DART–TOFMS. In addition, the information provided by both negative and positive mass spectra should be exploited with the aim to detect the presence of other contaminants. Of course, more follow-up research is needed, with a special focus on quantification of target compounds and identification of unknowns.

REFERENCES
 1. Cody R. B., Laramee J. A., Durst H. D.: Anal. Chem *77*, 2297 (2005).
 2. Takats Z, Wiseman J. M., Gologan B., Cooks R. G.: Science *306*, 471 (2004).
 3. McEwen C. N., McKay R. G., Larsen B., S.: Anal. Chem. *77*, 7826 (2005).
 4. Venter A., Nefliu M., Cooks R. G.: Trends Anal. Chem. in press (2008).
 5. Williams J. P., Patel V. J., Holland R., Scrivens J. H.: Rapid Commun. Mass Spectrom. *20*, 1447 (2006).
 6. Petucci C., Diffendal J., Kaufman D., Mekonnen B., Terefenko G., Musselman B.: Anal. Chem. *79*, 5064 (2007).
 7. Haefliger O. P., Jeckelmann N.: Rapid Commun. Mass Spectrom. *21*, 1361 (2007).
 8. Morlock G., Ueda Y.: J. Chromatogr. A *1143*, 243 (2007).
 9. Cajka T., Vaclavik L., Riddellova K., Hajslova J.: LC GC Eur. *21*, 250 (2008).
10. EC (European Communities), Council directive 97/57/EC establishing Annex VI to directive 91/414/EC *concerning the placing of plant protection products on the market* Off. J. Eur.Commun. L265 (1997).
11. Xie Z., Ebinghaus R.: Anal. Chim. Acta *610*, 156 (2008).
12. Cajka T., Hajslova J., Kazda R., Poustka J.: J. Sep. Sci. *28*, 601 (2005).

L13　APPLICATION OF NEEDLES AS BIOINDICATORS FOR THE EVALUATION OF PERSISTENT ORGANIC POLLUTANTS ENVIRONMENTAL CONTAMINATION LEVEL

M. VÁVROVÁ[a,b], R. LÁNA[a], M. HROCH[a], J. ČÁSLAVSKÝ[a], I. HLAVÁČKOVÁ[a] and B. TREMLOVÁ[b]

[a]*Brno University of Technology, Faculty of Chemistry; Purkyňova 118, 612 00 Brno, Czech Republic*
[b]*University of Veterinary and Pharmaceutical Sciences Brno, Faculty of Veterinary Hygiene and Ecology,*
vavrova@fch.vutbr.cz

Introduction

Bioindicators are living organisms in which concentrations of organic pollutants considerably exceed those found in air, water, sediments, or soil. Bioindicators, which are frequently used in monitoring studies and screenings, should allow selective and specific determination of contaminants not only in all compartments of the environment, but also in all links of food chains of species living in the area under study. Contaminants detectable by the use of bioindicators include also PCB indicator congeners 28, 52, 101, 118, 138, 153, 180 which rank with priority pollutants monitored in the Czech Republic[1]. Plant bioindicators are used in environmental studies of agrarian ecosystems in our country where they can yield information for both conventional monitoring and biomonitoring. The most frequently used plant species are alfalfa, cereals, and oil plants[2]. The source of contamination is of great importance. Monitoring of PCBs can often identify long-distance transport as one of the contamination sources. Airborne volatile PCBs can originate from various sources including agricultural production[3]. Thus, PCBs penetrate into plant tissues and influence the contamination level. Papers dealing with the contamination of crops by xenobiotics are rather scarce. Most of the respective investigations were carried out in fodder plants and were oriented rather on effects of feeding of contaminated crops to farm animals[1].

Of all above-mentioned plant bioindicators, coniferous plants except for larch have the greatest informative value when the leaf analysis method is used. Needles do not fall off every year as compared to deciduous trees, and one may monitor a degree of burden using different methods such as the discoloration of assimilatory organs, sudden changes in coloration, excessive leaf-fall, crown thinning, partial or complete dieback of trees, and particularly the above-mentioned methods of leaf analysis.

Knowledge of the level of contamination of this link of the food chain is therefore necessary for studies of xenobiotic transfer[1,4]. Comprehensive studies of plant contamination were completed in Moravian areas affected by disastrous floods in 1997 and 1998. Effects of floods on the contamination of soil and vegetation by persistent organic substances are summarized in the „Report on the 1998 Monitoring Results - Hazardous Substances within Food Chains and Influencing Imputes published by the Ministry of Agriculture of the Czech Republic in 1998[2].

Synthetic xenobiotics are included in persistent organic pollutants (POPs) group; they represented a significant risk to the environment owing to their physico-chemical and toxicological properties.

PBDEs are aromatic substances whose structures resemble that of PCBs (see Fig. 1.).
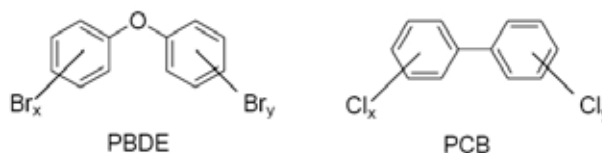
Fig. 1.　**PBDEs and PCBs**

The numbering of individual PBDE congeners, whose total sum is 209, complies with the IUPAC nomenclature used in the numbering of PCBs.

Physicochemical Properties of PBDEs

Tri- (major congener 28), *tetra-* (47), *penta-* (99, 100), *hexa-* (153, 154), *hepta-* (183) and *deka-*(209) are the most commonly used PBDE groups which also occur most frequently in the environment.

PBDEs are lipophilic and persistent substances that show low solubility in water. Because of their high resistance against acids, bases, heat, light, and redox reactions, they pose a significant risk to the environment. When they enter the environment, they remain there for a prolonged period of time due to their physical-chemical properties. The octanol/water partition coefficient ($\log K_{ow}$) is another important characteristic of these compounds. The values of their $\log K_{ow}$ vary in a range of 5.98 (28)–9.97 (209), which indicates that these substances are highly hydrophobic.

Upon excessive heating and burning, PBDEs will decompose to very toxic substances such as polybrominated dibenzo-p-dioxins (PBDD) and dibenzofuranes (PBDF). The melting point of PBDEs varies from 64 °C (BDE 28) to 302.5 °C (BDE 209) whereas many congeners are liquids at standard conditions.

PBDEs are used as fire retardants. In this application the ideal situation is when a retardant decomposes at a temperature by about 50 °C lower than that of a polymer – PBDEs meet this requirement with a number of polymers.

Production

The industrial synthesis of PBDEs usually proceeds through catalytic reaction between a diphenyl ether and bromine, yielding a mixture of different isomers. Alternatively, PBDE may also be prepared from phenolate and bromobenzene or by allowing diphenyliodonium salt to react with bromophenolate.

Novel synthetic procedures have been recently developed. One of the most significant developed procedures uses 2,5-dibromo-4-fluoronitrobenzene as a precursor to produce congeners 153 and 154 or employs a modified Sinaki reaction to prepare congener 81.

Industrial Use of PBDEs

DekaBDE

This compound is extensively used in "high-impact" polystyrenes, thermoplastic polyester resins, acrylonitrile-butadiene-styrene rubber, nylon, PVC, and elastomers. BDE 209 is also widely used in isolation materials for electric cables. There is a large number of commercial products based on BDE 209 such as widely used Bromkal 81, DE 83, FR-1210, Chemflam 011, Hexcel PF1.

***Okta*BDE**

*Okta*BDE congeners are mainly used in computer components and the components of office instruments. Furthermore, they are also known to be used in various thermoplastics, adhesives and coating compositions. Bromkal 79-8 DE, FR 143, Tardex 80, etc. are commercial names of widely used mixtures.

***Hexa*BDE**

*Hexa*BDE together with *penta*BDE congeners are contained in commercial mixtures (for example BR 33 A).

***Penta*BDE**

Commercial mixtures are used as additives in epoxy-resins, phenol resins, and textiles. This particularly applies to DE 71, FR 1205/1210, Bromkal 70, Bromkal 61. The Bromkal 70-5 DE mixture (34 % *tetra*BDE, 60 % *penta*BDE and 6 % *hexa*BDE) was widely used in the past.

***Tetra*BDE**

T*etra*BDE congeners have identical applications as *pen-*

*ta*BDE. The average levels of congeners in the commercially used mixture are as follows: 41 % of *tetra*BDE congeners, 45 % *penta*BDE congeners, 6 % *hexa*BDE congeners, and about 8 % of PBDE of unknown structure. Some groups of BDEs are not produced individually but occur as impurities in commercial mixtures (for example nonaBDE or heptaBDE). The least brominated classes of congeners such as triBDE, diBDE, and monoBDE, are neither produced commercially, nor used otherwise.

General use of BDEs

More than one half of PBDEs is used in the production of electric and electronic devices and components, with *Deka*BDE, *Okta*BDE and *Penta*BDE being used most widely, as mentioned above. The highest levels of PBDEs occur in domestic appliances. The reason is that the devices of this kind (TV sets, vacuum cleaners) contain the highest portion of plastics, as compared to other above-mentioned classes of devices, with fire retardants being usually bound to such plastic materials.

Experimental

Samples were taken in several locations. Organochlorine pesticides (DDT and its metabolites, γ-HCH and HCB), polychlorobiphenyls (PCB) and polybromodiphenylethers (PBDE) were selected for analysis. The isolation of tracked analytes from plant matrices was performed by the means of extraction processes, namely via sonication and Soxhlet extraction, extract purification was realized by column chromatography. The final determination was performed by gas chromatography with μECD detection and the confirmation analyses by gas chromatography and mass spectrometric detection. The procedure is summarized in following Scheme 1.

Table I
Polychlorinated biphenyls in needles

| | Concentration [ng g^{-1}] | | | | | | |
	CB 28	CB 52	CB 101	CB 118	CB 138	CB 153	CB 180
Pine	0.25	0.10	0.07	0.06	0.06	0.07	–
Fir	0.33	0.12	0.09	0.10	0.07	0.12	0.05
Blue Spruce	0.30	0.09	0.07	0.08	0.10	0.09	0.04

Table II
Organochlorinated pesticides in needles

| | Concentration [ng g^{-1}] | | | | | | | |
	4,4'-DDT	4,4'-DDE	4,4'-DDD	2,4'-DDT	2,4'-DDE	2,4'-DDD	γ-HCH	HCB
Pine	0.08	0.17	<LOQ	<LOQ	ND	ND	0.15	0.15
Fir	0.21	0.24	0.07	0.14	<LOQ	ND	0.12	0.09
Blue Spruce	0.11	0.11	0.04	0.11	ND	ND	0.13	<LOQ

Table III
Polybrominated diphenyl ethers in needles

| | Concentration [ng g^{-1}] | | | | | | | | | |
	BDE 3	BDE 15	BDE 28	BDE 47	BDE 99	BDE 100	BDE 118	BDE 153	BDE 154	BDE 183
Pine	0.80	0.40	4.50	1.50	ND	<LOQ	1.20	1.00	1.60	1.70
Fir	1.30	ND	2.20	<LOQ	0.70	ND	ND	<LOQ	ND	ND
Blue Spruce	0.50	ND	1.80	1.40	2.50	1.20	0.80	0.80	2.10	<LOQ

Collecting needles
(10 g each sample)
↓
Grounding/extraction
3 × 20 min. with n-hexane-acetone (3 : 2)
↓
Clean-up on Florisil column
elution with n-hexane-acetone (94 : 6)
↓
GC/μECD analysis of extracts
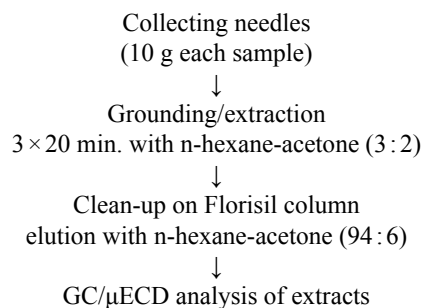
Scheme 1

Results

The study submitted deals with problems of the utilization of spruce, pine and fir needles for the evaluation of ecosystems' primary organic pollutants (POPs) load.

Tables I, II and III show the obtained results – concentrations of polychlorinated biphenyls, organochlorinated pesticides and polybrominated diphenyl ethers in needles, respectively.

On the basis of acquired results, it could be stated that level of needles contamination is not negligible. Within the group of PCBs the highest concentrations were found at PCB 28 with highest volatility. Pesticide 4,4'-DDT and 4,4'- DDE, γ-HCH and HCB were dominant from study groups of organochlorinated compounds. It was surprise that PBDE levels were considerably higher than those of other POPs, especially BDE 28.

Conclusions

Needles of pine, fir and blue spruce were used as bioindicators of the atmospheric contamination by persistent organic pollutants. These needles are covered by waxy layer, which effectively concentrates the vapour phase pollutants from surrounding atmosphere. The results proved the suitability of the conifera needles for the estimation of atmospheric contamination by persistent organic pollutants.

REFERENCES

1. Zima S., Vávrová M.: *Project Monitoring of Food Chains (transfer study "Feeding – snímal")*. Veterinary and Pharmaceutical University Brno, 65 p. (1994) (in Czech).
2. Ministry of Agriculture of the Czech Republic. *Report on the 1998 monitoring results – hazardous substances within food chains and influencing inputs*, Praha 1999, 47 pp. (1999).
3. Oehme M., Haugen J. E., Schlabach M.: Environmental Science and Technology, *30*, 2294 (1996).
4. Samuillah Z.: *Global environment monitoring system. Biological monitoring of environmental contaminants.* University of London, Technical report (1990).

2.2. Posters

P01   ULTRATRACE DETERMINATION OF SILVER IN PRECONCENTRATED WATER SAMPLES BY ELECTROTHERMAL ATOMIC ABSORPTION SPECTROMETRY

SEYED HAMID AHMADI[a], JAVAD DIDEHVAR ASL[a], MOHAMMAD HASAN AMINI[a] and ROYA BAHADORI[b]

[a]*Chemistry & Chemical Engineering Research Center of Iran P.O. Box 14335-186, Tehran, Iran,*
[b]*Research Center for Conservation of Cultural Relics, Tehran, Iran,*
ahmadi@ccerci.ac.ir

Introduction

Silver is one of the industrially important elements. It is used for the preparation of corrosion-resistance alloys and its compounds are extensively used in the processing of foods, drugs and beverages and in filters and other equipments to purify water. It also has an important role in electrical and electronic application, photographic film production and the manufacturing of fungicides[1,2]. These widespread applications have resulted in increased silver content of environmental water samples. In turns, owing to the toxicity of silver to many aquatic organisms even at low concentrations, the serious environmental problems may occur. Therefore, simple and highly sensitive methods are needed to monitor the Ag levels in water samples at ever decreasing concentrations.

Several atomic spectrometric techniques such as flame and electrothermal atomic absorption spectrometry (FAAS and ETAAS) [3,4], inductively coupled plasma atomic emission spectrometry (ICP-AES)[5] and inductively coupled plasma mass spectrometry (ICP-MS)[6] have been proposed for the determination of silver in different environmental samples. In order to improve the detection limit, various preconcentration procedures have also been used in combination with the above-mentioned techniques. These include solvent extraction[7], solid phase extraction[8], precipitation[9], adsorption on tungsten wire [10] and cloud point extraction[11]. However, most of these procedures are laborious, time-consuming and may cause sample contamination.

Recently, Assadi and co-workers introduced a novel microextraction method called dispersive liquid–liquid microextraction (DLLME) as a highly sensitive, efficient and powerful method for the pre-concentration and determination of traces of organic and inorganic compounds in water samples[12,13]. In the present work, the DLLME was combined with ETAAS for determination of silver for the first time. In this method, an appropriate mixture of extraction solvent and disperser solvent is injected rapidly into an aqueous sample containing silver ions and sodium diethyldithiocarbamate (DDTC) by a syringe. Then, the resulting cloudy solution is centrifuged and the fine droplets sedimented in a few-μl volume at the bottom of the conical test tube are finally introduced into the ETAAS for the determination of its silver content. The applicability of this approach was validated for the determination of silver in water samples. The proposed method was also applied to the determination of silver in several water samples with satisfactory results.

Experimental

R e a g e n t s   a n d   S o l u t i o n s

Reagent grade carbon disulfide, carbon tetrachloride and chloroform, as extraction solvents, and acetone, acetonitrile, methanol and ethanol as disperser solvents from Merck chemical company. Doubly distilled deionized water was used throughout. Analytical grade nitrate salts of silver and other cations (all from Merck) were of the highest purity available and used without any further purification except for vacuum drying. The stock solution of silver ($1,000$ mg dm^{-3} for atomic spectroscopy standard) was prepaed by dissolving 0.1575 g of silver nitrate (Merck) in deionized water containing 1 ml concentrated nitric acid (Merck) in a 100 mlvolumetric flask and diluting to mark with deionized water and stored in the dark. Working standard solutions were prepared by serial dilutions of the stock solution with ultrapure water prior to analysis. The chelating agent, 0.001M sodium diethyldithiocarbamate (DDTC) solution was prepared daily by dissolving the appropriate amount of DDTC (analytical grade, Merck) in methanol (suprasolv, Merck).

Tap, underground and river water samples used for development of the method were collected in PTFE containers from the Tehran and added appreciated amount of HNO$_3$ to adjust pH 3 and stored in dark at 4 °C and analyzed within 48 h of collection without previous treatment or filtration.

I n s t r u m e n t a t i o n

The experiments were performed using a Perkin Elmer atomic absorption spectrometer (AA 1100B), equipped with a graphite furnace atomizer HGA-700. Deuterium background correction was employed to correct non-specific absorbances. All measurements were performed using the peak height. An Intensitron™ silver hollow cathode lamp and a pyrolytic coated graphite tube (Perkin Elmer) were used. The sample injection volume was 10 μl in all experiments. The instrumental parameters and temperature program for the graphite atomizer are listed in Table I. Argon gas with 99.95% purity was purchased from Roham Gas Co. (Tehran, Iran) was used as protected and purge gas. A Kendro 1020D centrifuge (Germany) was used for centrifugation. All 15-ml screw cap falcon test tubes with conical bottom (extraction vessel) were maintained into 0.1 mol dm^{-3} HNO$_3$ for cleaning of any inorganic compounds and washed with doubly deionized water and then with acetone for proper sedimentation of fine droplets of the extraction solvent in the centrifuging step.

G e n e r a l   P r o c e d u r e

A 10.0 ml of aqueous solution contaning 0.2 ppm Ag and 0.01mM DDTC was placed in a 15 ml screw cap falcon test tube with conic bottom. 0.8 ml methanol, as disperser solvent, containing 60 μl carbon tetrachloride, as extraction sol-

vent, was injected rapidly into the sample solution by using a proper Hamilton syringe and the mixture was gently shaken. A cloudy solution (water/methanol/carbon tetrachloride) was formed in the test tube, Ag-DDTC complex is extracted into the fine droplets of carbon tetrachloride. The mixture was then centrifuged for 3 min at 3,500 rpm. After this process, the dispersed fine droplets of carbon tetrachloride were sedimented at the bottom of test tube (25 ± 1 μl). Finally, 10 μl of 0.05% Pd(NO$_3$)$_2$, as chemical modifier, followed by 10 μl of the sedimented phase were consecutively pipetted into the same auto-sampler device and the content was injected into the graphite tube and the silver content is determined by electrothermal atomic absorption spectrometry

Results

S t u d y   o f   t h e   E T A A S   C o n d i t i o n s

In order to reduce interferences and increase the accuracy, the use of a chemical modifier or a modifier mixture has become indispensable in ETAAS measurements. In the present work, we used Pd(NO$_3$)$_2$ as a chemical modifier. When the palladium modifier was not added, the analytical signal was gradually decreased until 50 % of the initial signal. The influence of the palladium modifier on the background level was also important. Based on the experimental results, addition of 0.05% (w/v) Pd(NO$_3$)$_2$ solution allowed increasing the analytical signal with considerable background reduction, without increasing the pyrolysis temperature. Because for portions larger than 10 μl the signals were not further improved, the palladium modifier injection volume was chosen as 10 μl.

The selection of an appropriate pyrolysis temperature is very important for removing as much the matrix as possible and preventing the pyrolysis loss of the analytes prior to atomization. The influence of pyrolysis temperature was studied on the absorbance, in the range of 300–1,100 °C. The maximum absorbance was achieved in the range of 300–450 °C in the presence of chemical modifier. However, when the pyrolysis temperature was over 500 °C, the signal of analyte decreased rapidly with the increase of the pyrolysis temperature. Therefore, 450 °C was selected as the optimized pyrolysis temperature for the determination of silver.

In the selected pyrolysis temperature of 450 °C, the effect of pyrolysis time on the absorbance of Ag was investigated. The results showed that the absorbance was increased when the pyrolysis time was changing from 10 to 40 s and no appreciable improvements were observed for longer times. As a result, a pyrolysis time of 40 s was chosen.

Using a pyrolysis temperature of 450 °C and pyrolysis time of 40 s, the effect of the atomization temperature, in the range of 1,000–1,500 °C, on analytical signal of Ag was also studied, The maximum signal . in the presence of chemical modifier was obtained at about 1,200 °C and remained unchanged with the further increasing of temperature up to 1,500 °C. So, the atomization temperature of 1,300 °C was selected for the further experiments. The experimental results show that atomization time has little effect on the atomic sig-

nal of Ag. Therefore, an atomization time of 3 s was selected. The unusual low pyrolysis and atomization temperatures used in this work is probably due to the fact that the components used in the dllme procedure are reducing the thermal stability of Ag.

Table I
The graphite furnace temperature program for silver determination

Step	Temperature [°C]	Ramp time [s]	Hold time [s]	Argon flow rate [ml min^{-1}]
Drying	100	1	20	250
Pyrolysis	400	5	30	250
Atomization	1,400	0	3	0
Cleaning	1,800	0	2	1,000

E f f e c t   o f   T y p e   a n d   V o l u m e   o f   t h e   E x t r a c t i o n   S o l v e n t

Careful attention should be paid to the selection of the extraction solvent. It should have higher density rather than water, extraction capability of the interested compounds and low solubility in water. Chloroform, carbon tetrachloride and carbon disulfide were compared in the extraction of silver. A series of sample solution were studied by using 500 μl methanol containing different volumes of the extraction solvent to achieve 25 μl volume of the sedimented phase. The solubility of the extraction solvents in water is different. Therefore to recover 25 μl volume of the sedimented phase at the bottom of the test tube, it is necessary to add an excess to account for this solubility. Thereby, 75, 50 and 60 μl of chloroform, carbon disulfide and carbon tetrachloride were used, respectively.

In this experiment chloroform, carbon disulfide and carbon tetrachloride as extraction solvents obtained enrichment factors of 122.9 ± 9.4, 119.1 ± 10.5 and 127.7 ± 6.7, respectively. According to these results, variations of the enrichment factors using different extraction solvents are not statistically significantly different. Carbon tetrachloride forms a well stable cloudy solution, its sedimented phase can easily be removed by sampler to be introduced into the graphite furnace and has less consumption volume, while chloroform forms an unstable cloudy solution and carbon disulfide is difficult to be removed by sampler. Therefore, carbon tetrachloride was the best to be used.

To examine the effect of the extraction solvent volume, solutions containing different volumes of carbon tetrachloride were subjected to the same DLLME procedures. The experimental conditions were fixed and include the use of 500 μl methanol different volumes of carbon tetrachloride (40, 50, 60, 70 and 80 μl). By increasing the volume of carbon tetrachloride from 40 to 80 μl, the volume of the sedimented phase increases from 20 to 50 μl. Enrichment factor decreases with increasing the volume of carbon tetrachloride, because of the volume of the sedimented phase increases. Subsequently, at

low volume of the extraction solvent high enrichment factor was obtained. Thereby, the gain in sensitivity was achieved by using 60 μl of carbon tetrachloride.

E f f e c t   o f   T y p e   a n d   V o l u m e   o f   t h e
D i s p e r s e r   S o l v e n t

The main criterion for selection of the disperser solvent is its miscibility in the extraction solvent and aqueous sample. For this purpose, different solvents such as acetone, acetonitrile, methanol and ethanol were tested. A series of sample solutions were studied by using 800 μl of each disperser solvent containing 60 μl of carbon tetrachloride (extraction solvent). The enrichment factors obtained for acetonitrile, acetone, methanol and ethanol were 108.7 ± 9.1, 125.2 ± 8.8, 120.4 ± 5.3 and 115.6 ± 7.5, respectively. The results show no statistical significant differences between disperser solvents; however, the solubility of DDTC in methanol makes it a better choice.

The effect of the volume of methanol on the extraction recovery was also studied. Since, variation of the volume of methanol makes change in the volume of sedimented phase at constant volume of carbon tetrachloride (extraction solvent). Thereby, to avoid this matter and in order to achieve a constant volume of sedimented phase (25 μl) the volume of methanol and carbon tetrachloride were changed, simultaneously. The experimental conditions were fixed and include the use of different volumes of methanol 0.50, 0.8, 1.00 and 1.50 ml containing 45, 60, 75 and 100 μl of carbon tetrachloride, respectively. Under these conditions, the volume of the sedimented phase was constant (25 ± 1 μl). It is clear that by increasing the volume of methanol, the solubility of complex in water increases. Therefore, the extraction recovery decreases. Thus, 800 μl of methanol was selected as optimum volume in order to achieve better and more stable cloudy solution.

E f f e c t   o f   p H

The separation of metal ions by dispersive liquid–liquid microextraction involves prior formation of a complex with sufficient hydrophobicity to be extracted into the small volume of the sedimented phase, thus, obtaining the desired preconcentration. pH plays a unique role on metal–chelate formation and subsequent extraction. The effect of pH on the complex formation and extraction of silver from water samples was studied in the range of 1–6 by using concentrated H_2SO_4 solution(note that DDTC is a weak base). The results illustrated in Fig. 1. reveal that the absorbance is nearly constant in the pH range of 3.5–4.0. Therfore the pH 4 seems a proper choice. Moreover, to make pH 4 adjustment, the use of buffer (which are sources of contamination) is not necessary and sulfuric acid can simply be used to make the pH adjustment.

E f f e c t   o f   D D T C   C o n c e n t r a t i o n

The effect of the DDTC concentration on the absorbace was studied in the range of 0.001-1mM of DDTC. The
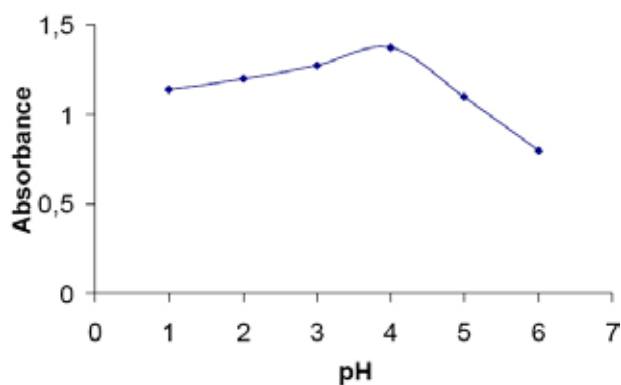
Fig. 1.　**Effect of pH on silver extraction**

absorbace was increased by increasing the DDTC concentration, which is well expected. It seems that slight reduction of extraction in high concentration of DDTC is due to the extraction of DDTC itself, which can easily saturate the small volume of extraction solvent. Also, at high concentration of DDTC (1mM) the background absorbance was increased. Therefore, the concentratiion of 0.01 mM DDTC was selected as the best choice to prevent any interference.

E f f e c t   o f   S a l t

For investigating the influence of ionic strength on performance of DLLME, various experiments were performed by adding different amount of $NaNO_3$ (0–8 % (w/v)). Other experimental conditions were kept constant. By increasing the $NaNO_3$ from 0 to 8 %, the volume of sedimented phase increases slightly from 25 to 27 μl. The results showed that salt addition has no significant effect on the enrichment factor. It is maybe because of two opposite effects of salt addition in DLLME of silver. One of them is increasing the volume

Table II
Effect of foreign ions on the pre-concentration and determination of silver (20 ng ml^{-1})

Ion	Ion/Au ratio	Extraction recovery [%]
Li^+	10,000	103.5 ± 3.7
K^+	10,000	103.8 ± 4.8
Mg^{2+}	10,000	94.3 ± 1.9
Ca^{2+}	10,000	102.3 ± 7.3
Mn^{2+}	1,000	96.3 ± 4.7
Ni^{2+}	1,000	89.7 ± 8.7
Hg^{2+}	1,000	104.5 ± 3.8
Cu^{2+}	1,000	93 ± 1.2
Co^{2+}	1,000	101.2 ± 4.0
Cd^{2+}	1,000	93.6 ± 3.8
Pb^{2+}	1,000	95.9 ± 1.3
Bi^{3+}	1,000	94.6 ± 3.7
Cr^{3+}	1,000	94.8 ± 5.0
NO_3^-	1,000	105.8 ± 4.6
SO_4^{2-}	1,000	101.0 ± 6.2
Cl^-	10,000	103.3 ± 4.6

of sedimented phase that decreases the enrichment factor and another is salting-out effect that increases the enrichment factor. Therefore, the enrichment factor is nearly constant by increasing the amount of sodium nitrate. Therefore the experiments were performed in absence of the salt.

Effect of Coexisting Ions

The effects of common coexisting ions in natural water samples on the recovery of silver were studied. In these experiments, 10.0 ml of solutions contains 20 ng ml^{-1} of silver and various amounts of interfering ions were treated according to the recommended procedure. A given spices was considered to interfere if it resulted in a ± 5 % variation of the AAS signal. The results obtained are given in Table II.

Figures of Merit

Table. III summarizes the analytical characteristics of the optimized method, including linear range, limit of detection, reproducibility, and enhancement factor. The calibration graph was linear in the range of 6–120 ng ml^{-1} of silver. The limit of detection, defined as $C_L = 3 S_B/m$ (where C_L, S_B and m are the limit of detection, standard deviation of the blank and slope of the calibration graph, respectively), was 1.2 ng ml^{-1}. The relative standard deviation (R.S.D.) for ten replicate measurements of 20 ng dm^{-3} Ag was 3.6 %. The enhancement factor was obtained from the slope ratio of calibration graph after and before extraction, which was about 66.

Table III
Analytical characteristics of DLLME-ETAAS for determination of Ag

Element condition	DLLME–ETAAS	ETAAS
Linear range [ng ml^{-1}]	6–120	500–20,000
Correlation coefficient (r)	0.995	0.997
Slope	2.65	0.04
Enhancement factor[a]	66	–
RSD [%], (n = 8)[b]	3.6	3.5
LOD [ng ml^{-1}][c]	1.2	80

[a]Calculated as the ratio of slope of pre-concentrated samples to that obtained without pre-concentration.
[b]At a silver concentration of 20 ng ml^{-1}.
[c]Determined as three times of the standard deviation of the blank signal, and slop of calibration curve after pre-concentration

Analysis of Natural Waters

The proposed DLLME–ETAAS methodology was applied to the determination of silver in several water samples. Tap, underground and river water were collected from the Tehran and were analyzed by DLLME combined with ETAAS for determination of silver. The concentration of silver in the tap, underground and river water samples were determined to be 17.2 ± 0.6 ng ml^{-1}, 24.7 ± 0.6 ng ml^{-1} and 30.10 ± 0.4 ng ml^{-1} respectively (Table IV). The water sam-

ples were spiked with silver standards to assess matrix effects. The relative recoveries of silver from these waters at spiking level of 10 and 20 ng ml^{-1} were 102, 98, and 100 %, respectively (Table IV). These results demonstrated that the tap, underground and river water samples matrices, in our present context, had little effect on DLLME of silver.

Table IV
Determination of Ag in real samples

Sample	Added [ng ml^{-1}]	Found [ng ml^{-1}][a]	Recovery [%]
Tap water[b]	–	17.2 ± 0.6	–
	10	27.3 ± 0.4	101
	20	37.5 ± 0.6	103
Underground water[c]	–	24.7 ± 0.5	–
	10	34.6 ± 0.6	99
	20	44.4 ± 0.5	97
River water[d]	–	30.1 ± 0.4	–
	10	40.0 ± 0.5	99
	20	50.2 ± 0.8	101

[a]Mean of three experiments ± standard deviation.
[b]From drinking water system of Tehran, Iran.
[c]Obtained from Vardavard, Iran.
[d]From Karaj river, Iran.

Conclusions

In this paper we introduced a DLLME–ETAAS method for the analysis of ultra trace amounts of Ag in real samples such as tap water, river water and underground water. The important features of DLLME method are low cost, use of minimized toxic organic solvents, simplicity of operation, rapidity, high enrichment factor and high sensitivity and selectivity. High preconcentration factor was obtained easily through this method and a detection limit at ng ml^{-1} level was achieved with only 10.00 ml of sample. In this method sample preparation time as well as consumption of toxic organic solvents was minimized without affecting the sensitivity of the method..This method is characterized with simplicity, rapidity, reliability, safety and low cost, and is suitable for the determination of ultra-trace silver in environmental water samples.

REFERENCES

1. Grayson M. : *Kirk–Othmer Encyclopedia of Chemical Technology* ,.(3rd ed.), vol. 21, Wiley, New York 1980.
2. Smith I.C., Carson B. L.:, *Trace Metals in the Environment* , vol. 2, Ann Arbor Science Publisher's Inc., Ann Arbor 1977.
3. Šràmkovà J., Kotrlý S., Jakoubková P.: Anal. Chim. Acta *408*, 183 (2000).
4. Baron M. G., Herrin R. T., Armstrong D. E.: Analyst *25*, 123 (2000).
5. Singh R. P., Pambid E. R.: Analyst *115*, 301 (1990).
6. Ndung'u K., Ranville M. A., Franks R. P., Flegal A. R.: Mar. Chem. *98*, 109 (2006).

7. Koh T., Sugimoto T.: Anal. Chim. Acta *333*, 167 (1996).
8. Dadfarnia S., Haji Shabani A. M, Gohari M.: Talanta *64*, 682 (2004).
9. Sant'Ana O. D., Wagener A. L. R., Santelli R. E., Cassella R. J., Gallego M., Valcarcel M.: Talanta *56*, 673 (2002).
10. Rahman M. A., Kaneco S., Amin M. N., Suzuki T., Ohta K.: Talanta *62*, 1047 (2004).
11. Stalikas C. D.: Trends Anal. Chem. *21*, 343 (2002).
12. Rezaee M., Assadi Y., Milani Hosseini M. R., Aghaee E., Ahmadi F., Berijani S.: J. Chromatogr. A *1116*, 1 (2006).
13. Zeini Jahromi E., Bidari A., Assadi Y., Milani Hosseini M. R., Jamali M. R.: Anal. Chim. Acta *585*, 305 (2007).

P02 REMOVAL OF 2-MERCAPTO-BENZOTHIAZOLE FROM SYNTHETIC WASTEWATER

BEÁTA ALMÁSIOVÁ, JÁN DERCO, ANGELIKA KASSAI and EVA HÁSOVÁ

Slovak University of Technology, Faculty of Chemical and Food Technology, Institute of Chemical and Environmental Engineering, Radlinského 9, 812 37 Bratislava 1, Slovak Republic,
beata.almasiova@stuba.sk

Introduction

2-Mercaptobenzothiazole (MBT) is the most important member of the benzothiazole group of heterocyclic aromatic compounds. It is a pale yellow, crystalline substance with an unpleasant odor and a bitter taste. This xenobiotic compound is used mainly in the manufacture of rubber additive chemicals but also has other uses, notably as a corrosion inhibitor, antifreeze for automobiles. It is known as a toxic and poorly biodegradable pollutant. It is able to pass conventional treatment systems, widespread with surface and underground waters and enters into organisms[1]. Data concerning biodegradation of MBT are inconclusive. Some authors[2] have suggested it is recalcitrant to biodegradation.

Genotoxicity investigations in bacterial and mammalian test systems provide some evidence indicating that MBT has the potential to induce mutations and chromosomal aberrations. Toxicity studies in rats and mice chronically exposed to MBT identified increases in various tumors[3]. Epidemiological investigations indicate that workers occupationally exposed to MBT have an increased risk of death from bladder cancer. MBT interfered with the nitrification processes and exhibited biocidal effects. MBT inhibits the degradation of easily degradable organics[4].

This work was aimed at study biodegradation of MBT and effect of this compound on activated sludge. Degradation of MBT by ozone was also studied.

Experimental
Biodegradability of MBT

Adaptation of activated sludge to MBT was carried out in semicontinuos bioreactor. We were adapted MBT with maximal concentration 25 and 50 $mg\,dm^{-3}$ on the activated sludge. Time of adaptation was 3 weeks. During the adaptation we measured inhibition effect of MBT on the activated sludge by respirometric measurements.

Adsorption tests were performed both with adapted and nonadapted activated sludge to MBT. Adsorption of MBT on activated sludge was studied at various concentration values of MBT. We were measured the specific sorptive capacity of sludge at low (10, 20 and 60 $mg\,dm^{-3}$) and high concentration of MBT (100, 200 and 500 $mg\,dm^{-3}$).

Ozonation of MBT

The feasibility of utilisation of ozone for degradation of MBT was investigated in laboratory scale equipment. The experiments were performed in bubble ozonation column. The ozonation equipment consists of two glass columns, 0.04 m diameter and 1.70 m height. The first column was filled with synthetic water with MBT, and the other one was filled with solution of potassium iodide to destroy residual ozone in the outlet of the first ozonation column. The system was operated in batch mode. Synthetic wastewater containing MBT was added into ozonation reactor at the beginning of trials. Continuous flow of oxygen 30 $dm^3\,h^{-1}$ was applied for generation of ozone. The Lifetech ozone generator with the maximum ozone production 5 $g\,h^{-1}$ and Lifetech ozone UV detector were used. Ozonation trials were carried out at 70 % of the power maximum of ozone generator. Initial concentration of MBT in synthetic water was 50 $mg\,dm^{-3}$.

Results

MBT is not consumed by non adapted activated sludge. Decrease of respiration rate of non adapted activated sludge was observed with the increase of 2-MBTconcentration. Rapid decrease of respiration activity was observed for activated sludge after adaptation. The endogenous respirometric rate decreased by 6 % at concentration 25 $mg\,dm^{-3}$ MBT in comparison with reference model. The endogenous respirometric rate decreased by 39 % at concentration 50 $mg.dm^{-3}$ MBT in comparison with reference model.

The decrease of dissolved MBT concentration was observed at the low concentration levels. The value of COD and TOC increased after 10 days, which is caused by increase of concentration of MBT in solution.

Table I shows the results of adsorption test carried out at lower concentration values of MBT. Negligible adsorption of MBT on activated sludge was observed at MBT concentration higher than 100 $mg\,dm^{-3}$.

According to results shown in the Fig. 1. the highest COD removal was observed during the first 20 minutes of ozonation. The initial COD value conversion achieved about 98 % after 50 minutes. The efficiency of TOC removal was 54 % after 50 minutes of ozonation. Almost total removal (96 %) of 2-MBT from the sample was achieved after 5 minutes of ozonation. Simultaneously the presence of benzothiazole was identified as ozonation intermediate. The presence of benzothiazole (BT) was identified in the sample after 50 minutes of ozonation. Fien et al.[5] show, that MBT and its breakdown products had a high affinity towards ozone as indicated by the

Table I
Specific sorptive capacity of activated sludge

c_{MBT} at solution [$mg\,dm^{-3}$]	MTB decrease by adsorption [$mg\,dm^{-3}$]	MTB decrease by adsorption [$mg\,g^{-1}$]
10	4.2	42
20	5.9	59
60	6.8	68

rates for partial oxidation and mineralization. Benzothiazole was identified as the first ozonation product, reaching up to 60 mol% of the original MBT concentration, followed by low concentration of 2(3-H) benzothiazolone.

The results of absorption of ozone in the fresh water and in the synthetic wastewater containing MBT are given in Fig. 2. The saturation concentration of ozone 23.1 mg dm^{-3} was achieved in fresh water after 35 minutes. Specific ozone consumption values were 0.78 g g^{-1} for COD and 1.88 g g^{-1} for TOC.
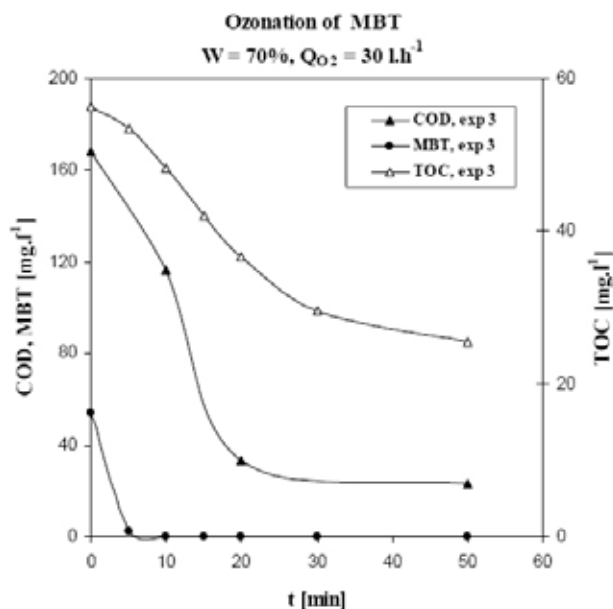
Fig. 1.   **COD, TOC and MBT as a function of ozonation time at oxygen flow rate 30 dm^3 h^{-1} and W = 70 %**

Conclusions

Respirometric tests confirmed that this compound is not biodegradable. Activated sludge showed adsorption affinity to MBT at concentration values up to 60 mg dm^{-3}. Significant decrease of MBT content was observed after five minutes of ozonation. Correspondent efficiency values for COD and TOC removal were 55 and 16 %. COD removal rate 5.2 mg dm^{-3} min^{-1} was observed at 70 % of maximum ozone
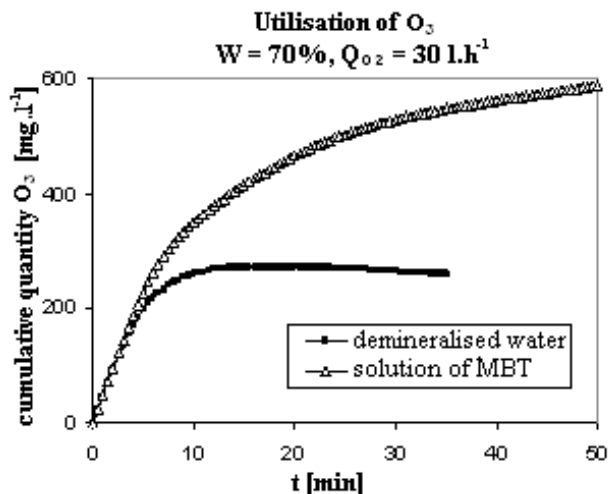
Fig. 2.   **Utilization of ozone in demineralised water and in synthetic wastewater contentaining MBT**

generator power. The presence of benzothiazole was identified as ozonation intermediate. It can be concluded that MBT is readily transformed by ozonation.

REFERENCES

 1. De Wever H., Verachtert H.: Water Research *31*, 2673 (1997).
 2. Chudoba J., Tuček F., Zeis K:. Acta Hydrochim. Hydrobiolo. *5*, 495 (1977).
 3. Whittaker M. H., Gebhart A. M., Miller T. C., Hammer F.: Toxicol And Health. *2004*, 49.
 4. Reemtsma T., Fiehn O., Kalnowski G. and Jekel M.: Environ. Scien. Technol. *29*, 478 (1995).
 5. Fiehn O., Wegener G., Jochimsen J. and Jekel M.: Water Research *32*, 1075 (1998).

P03 HEALTH RISK ASSESSMENT BY INDOOR AIR QUALITY MONITORING

EKATERINA ANDREEVA, IVAN MAŠEK and MILADA VÁVROVÁ

Brno University of Technology, ICTEP, Czech Republic, Purkyňova 118, 612 00 Brno, Czech Republic,
xcandreeva@fch.vutbr.cz

Introduction

The risk is an inseparable part of working activity. That is why a general duty of employer is to ensure health and safety at work for all employees. They are protected by the main framework Directive 98/391/EEC, which basic principle is risk prevention, which requires risk assessment by the responsible employer.

Dangerous substances can be found in many workplaces. A recent European survey shows that 16 % of workers reported handling hazardous products and 22 % being exposed to toxic vapours[1]. As far as work accidents concern according to OSHA facts[1]:

- Every 3 and a half minutes somebody in the European Union dies from work-related causes
- Every year 142,400 people in the EU die from occupational diseases and 8,900 from work-related accidents
- Up to third of these 150,000 fatalities each year can be attributed to hazardous substances at work in the EU (including 21,000 to asbestos)

Exposure to dangerous substance occurs at any industry workplace, on farms, in vehicles, especially at chemical plants and at smaller areas, such as high school, universities, in laboratories and also at home or in office.

Dangerous substances affect human's health by different ways. Some can cause cancer, affect the reproductive function or cause mutagenic effects. Other agents may cause brain damage, be harmful to the nervous system, respiratory airways or skin.

Quality of workplace environment includes not only safety conditions at work, achieved by continual risk assessment and elimination of these risks, but also means a clean and healthy environment. The working environment is formed by different microclimatic conditions, such as level of noise, lighting, quality of indoor air, surrounding temperature, level of humidity etc. Each of these factors has a great influence on worker's health and productivity of his work.

Since many people spend a large part of their lives in closed areas – in an office, at school, in transport – clean air becomes essential for good health and this is especially true when speaking about indoor air.

Posing the Problem

As it was mentioned above among different workplaces, school's environment can be found. Nowadays school area consists of not only usual class-rooms, but also covers wide range of specialized working facilities, for example chemical laboratories.

In this article we will focus on chemical hazards in the laboratories. People who work or study in a chemical laboratory are exposed to many kinds of hazards, e.g. chemical substances, mechanical hazards, biological agents, physical factors, psychological conditions and so on.

Special feature of such work environment is that level of chemical threats rises steeply, since the quantity and range of chemicals are higher than in any other place of usual life. Many agents are highly flammable and explosive, their careless handling and storage may result in fire ignition and explosions. Toxic gases, fumes and liquids may be produced and cause poisoning or infection of personnel and students. Some chemical agents have carcinogenic or mutagenic properties.

Indoor air quality is also one of the important factors in the working space and shouldn't be underestimated. The influence of air quality which we breathe can be extended on two main problems: long-term health affection and work-related accidents. The first problem is connected with long-term exposure of workers and students to low concentrations of different substances in the air (the most followed are carbon and nitrogen oxides, radon and Volatile Organic Compounds – VOCs). Usually it can be solved by periodical measuring of concentration, assessing the possible risks of this exposure and taking correcting measures, for example improving ventilation, changing working regime, and using proper personal protective equipment.

The second problem concerns working-related accidents. On the one hand any laboratory worker or student can be exposed to toxic gases and fumes, which may unexpectedly escape from their container or come out from the by-side effect of reaction. These substances in the air can cause different effects:

- Acute poisoning or injury of the organism
- Cause allergies
- Irritate eyes or breathing system

Usually there are few people in laboratory at the same time. If one of them will lose self-control under certain conditions, such as bad vision, suffocation, pain, his behavior becomes dangerous for others and can lead to emerging other hazards for surrounding people.

Objects of Research

According to EC Directive 1999/13/EC (Solvent Emissions Directive), Volatile Organic Compounds (VOCs) are functionally defined as organic compounds having at 293.15 K (i.e., 20 °C) a vapor pressure of 0.01 kPa or more, or having a corresponding volatility under particular conditions of use.

In a majority solvents need to be managed carefully due to their volatility and general flammability, in particular during loading and unloading, storage and when using large quantities.

Commonly, producers enclose Safety Data Sheets to their products with necessary using, handling and storage recommendations:

- Safe exposure limits and techniques for managing flammability
- Information on the main hazards, how to protect against them and the steps to take in an emergency
- Occupational exposure limits (OELs)
- Handling, storage, transport, spills and disposal advice
- Regulatory information such as classification and labeling
- Toxicity and environmental information

In chemical laboratory among other used chemicals one of the most famous are organic solvents, which usually referred to as group of Volatile Organic Compounds (VOCs). VOCs are compounds given off by a number of other indoor sources. Concentrations of most volatile organic compounds is higher in indoor than outdoor air. They commonly can be found in household, institutional, and industrial cleaning and maintenance products, and in building and finishing materials. Other sources of VOCs include the burning of fuels such as gas, wood and kerosene, as well as tobacco products. VOCs can also come from personal care products (perfume and hair spray), cleaning agents, dry cleaning fluid, paints, lacquers, varnishes, hobby supplies, and from copying and printing machines[2].

In enclosed spaces, VOCs can cause eye, nose, and throat irritation, dizziness, headache, memory and visual impairment. Higher concentrations may cause irritation of the lungs, as well as damage to the liver, kidney, or central nervous system. Some VOCs are suspected to cause cancer in humans and have been shown to cause cancer in animals. The health effects caused by VOCs depend on the level and length of exposure.

The real concentrations of VOCs are usually orders of magnitude below the occupational threshold limit values (TLVs). However, some VOCs may be present above their human odor thresholds (OTs). Beside odor annoyance, VOCs at sub-TLV level may cause non-specific health effects such as eye and upper respiratory airway irritation, headache and increased weariness[3].

The main route of exposure to solvents is via inhalation. Occupational exposure limits (OELs) set the airborne concentration of a substance that workers can be exposed to, day after day without any adverse health effects. OELs are normally set for an 8 hour day^{-1} and a 40 hour week^{-1} and are continuously reviewed by national and EU authorities. OELs for the majority of hydrocarbon and oxygenated solvents are set between 10 and 1,000 parts per million depending on the volatility and toxicity of an individual substance[4].

According to what was stated above as objects of research were chosen some organic solvents which are frequently used in chemical laboratories of the Faculty of Chemistry, Brno University of Technology. Acquired data will be used for the following health risk assessment in chosen workplaces.

Managing the Problem

A four-step approach to risk assessment exists[4].

- Make an inventory of the substances used in the processes in the workplace and those generated by the process such as welding fumes or wood dust.
- Collect information about these substances, i.e. the harm they can do and how this can happen. Safety data sheets (SDS), which must be provided by the supplier of a chemical, are an important source of information.
- Assess exposure to the identified dangerous substances, looking at the type, intensity, length, frequency and occurrence of exposure to workers, including combined effects of dangerous substances used together and the related risk.
- Rank the severity of the established risks.

As we can see from this list of steps, assess exposure is one of the important parts. Exactly, this direction was chosen to exposure prevent and control of the dangerous substances in chemical laboratories.

The purpose of this study is to measure the concentration of VOCs, which are used in chosen chemical laboratories and to assess possible occupational health risks. The aim is to protect people who are supervising the practice work and working in the harmful environment for a long time (occasionally more than 8 hours). This research work is supposed to be conducted for a long-term period.

The measurements will be taken in different working areas (for example laboratory of organic chemistry, storage area). For conducting the analysis a passive air sampling by Radiello cartridges with charcoal is chosen with followed CS_2 desorption and GC with FID or GC-MS analysis.

Method used to sample collection and analysis, passive sampling (by means of new trade product Radiello®), is considered to be a simple and rather cost-effective. Unlike active sampling, passive samplers require no expensive pumps and are simple to use (no calibration is needed). Other advantages are:

- Compact, portable
- Offer indication of average pollution levels over time periods of 8 hour to weeks/months
- Relatively low-cost in compare with other methods
- Applicable for personal monitoring and indoor air analysis

Conclusions

Important point of view for assessing acceptable working place is its safety requirements and conditions which will surround the employees, what means working environment, which consists of physical, chemical and other factors. These factors can unfavorable affect worker's health by their poor quality or quantity, as well as duration of this affection.

Everybody wants to work in the safety and high-quality working environment. This statement enclosed in the European legislation and imposes some obligations on employers:

- Assess the possible risks
- Take measures to eliminate or reduce the risks
- Effectiveness control of the preventive measures and their review

A healthy work environment means the monitoring and maintenance of hygienic limits in the workplace, such as temperature, humidity of air, proper chemical composition, intensity of working process etc.

University area with its laboratories is a special working environment. Students and other workers, who is working or studying in such laboratories, are exposed to many kinds of hazards. But the main difference is that laboratory work involves a greater variety of possible chemical hazards. There are many agents, which have flammable, explosive, toxic and other characteristics.

Besides obvious risks, which can emerge during laboratory work, there are also non-evident ones, for example, air quality.

Among different chemical agents, there is a group of the most used, such as organic solvents. Some of them could be very harmful for human's health, but usually for assessing their affection it'simportant take into account their features, time of exposure and concentration during exposure.

For this purpose the methodology of indoor air analysis is going to be developed, which is supposed to help in assessing possible occupational health risks, posed by quality of indoor air in chemical laboratories. The indoor air analysis is conducting by passive sampling with following GC with FID or GC-MS analysis on long-term conditions.

REFERENCES
1. Statistics – OSHA – European Agency for Safety and Health at Work [online]. c1998–2008 , 06.06.2008 [cit. 2008-06-07]. Available from : <http://osha.europa.eu/en/statistics>.
2. Indoor Air Quality – Volatile Organic Compounds (VOC\'s) - BC HealthFile #65d [online]. c2006 , 07-2006 [cit. 2008-06-07]. Available from WWW: <http://www.bchealthguide.org/healthfiles/hfile65d.stm>.
3. Reiser, R., et al. Indoor air pollution by volatile organic compounds (voc) emitted from flooring material in a technical university in Switzerland. Proceedings: indoor air [online]. 2002 [cit. 2008-06-07], pp. 1004-1009. Available from www: <http://www.chps.net/manual/iaq_download.htm>.
4. ESIG : Health & Safety – European Solvents Industry Group ESIG: Solvents industry in Europe [online]. 08-05-2008 , 08-05-2008 [cit. 2008-06-07]. Availabnnle from: <http://www.esig.org/content.php?level1=1&level2=29&page=79&mode=1>.
5. Factsheet – 33 – An introduction to dangerous substances in the workplace : Facts. Facts [online]. no. 33, (2003) [cit. 2008-06-07]. Available from WWW: <http://osha.europa.eu/en/publications/factsheets/33/view>.
6. Radiello – The radial simmetry diffusive sampler [online]. Fondazione Salvatore Maugeri IRCCS , 2006 , March 22th 2007 [cit. 2007-06-07]. Available from WWW: <http://www.radiello.it/english/index_en.html>.

P04   NITROGEN IN BREEDING LAYING HENS AND ENVIRONMENT PROTECTION

MÁRIA ANGELOVIČOVÁ, MAREK ANGELOVIČ and MIROSLAVA KAČÁNIOVÁ

Faculty of Biotechnology and Food Sciences, Slovak University of Agriculture, Tr. A.Hlinku 2, Nitra, 949 76 Slovakia, maria.angelovicova@uniag.sk

Introduction

At EU–15 level the gross nitrogen balance in 2000 was calculated to be 55 kg ha^{-1}, which is 16 % lower than the balance estimate in 1990, which was 66 kg ha^{-1}. In 2000 the gross nitrogen balance ranged from 37 kg ha^{-1} (Italy) to 226 kg ha^{-1} (the Netherlands). All national gross nitrogen balances show a decline in estimates of the gross nitrogen balance (kg ha^{-1}) between 1990 and 2000, apart from Ireland (22% increase) and Spain (47% increase). The following Member States showed organic fertilizer application rates greater than the threshold of 170 kg ha^{-1} specified by the Nitrates Directive in 2000: the Netherlands (206 kg ha^{-1}) and Belgium (204 kg ha^{-1}). The general decline in nitrogen balance surpluses is due to a small decrease in nitrogen input rates (–1.0 %) and a significant increase in nitrogen output rates (10 %). The gross nutrient balance for nitrogen provides an indication of potential water pollution and identifies those agricultural areas and systems with very high nitrogen loadings. As the indicator integrates the most important agricultural parameters with regard to potential nitrogen surplus it is currently the best available approximation of agricultural pressures on water quality. High nutrient balances exert pressures on the environment in terms of an increased risk of leaching of nitrates to groundwater. The application of mineral and organic fertilizers can also lead to emissions to the atmosphere in the form of nitrous dioxide and ammonia, respectively. Gross nitrogen balances are above 100 kg per ha in the Netherlands, Belgium, Luxembourg and Germany. They are particularly low in most Mediterranean countries given the overall lower livestock production in this part of Europe. It is currently not possible to provide gross nitrogen balance estimates for the new EU Member States and the accession as the relevant statistical data are under elaboration. National balances, however, can mask important regional differences in the gross nutrient balance that determine actual nitrogen leaching risk at regional or local level. Individual Member States can thus have acceptable gross nitrogen balances at national level but still experience significant nitrogen leaching in certain regions, for example in areas with high livestock concentrations. There are a number of regions where pig livestock units have increased by more than 25 % between 1990 and 2000 (for example, north-western Denmark, north-western France, north-eastern Spain and northern Belgium). These are likely to be regional 'hotspots' for high gross nitrogen balances that can lead to environmental pressures. Member States with high nitrogen balances are making efforts to reduce these pressures on the environment. These build on a range of different policy instruments, requiring considerable political effort to succeed given the significant social and economic consequences of reducing livestock production in many affected areas[3,4].

Experimental

We realized experiments with laying hens *Shaver Starcross* 288, which ingested feed mixture with different protein content. In six experiments laying hens fed feed mixture with protein contents 173.10 g per kilogram and in four experiments were used feed mixture with protein contents 146.12 or 146.68 g per kilogram. It is soya cereal type assigned for laying hens. The laying hens ingested fodder *ad libitum*.

Within experiments were researched:
- protein contents in feed mixture in one kilogram (chemical analysis – Kjeldahl method and calculation),
- excreted nitrogen [g kg^{-1}] in dropping per bird and day (chemical analysis – Kjeldahl method and calculation).

Results

Higher protein contents 173.10 g per kilogram of feed mixture resulted in excreted dropping at laying hens higher nitrogen contents in compare with protein contents 146.40 g per kilogram feed mixture. After ingestion of feed mixture with protein content 173.10 g per kilogram was nitrogen content in dropping from 1.88 g per bird and day. The laying hens, which fed feed mixture with protein contents 146.40 g per kilogram, excreted the nitrogen in dropping 1.38 g per bird and day. From these results follows that near decrease protein contents in feed mixture from 173.10 to 146.40 g per kilogram is possibility of nitrogen decrease in excreted dropping at laying hens about 26.60 % per bird and day. This different of decrease of excreted nitrogen in dropping at layers is statistically significant (P<0.001). Correlation coefficient between content of crude protein in feed mixture and content of nitrogen in dropping at layers has high level r = 0.99.

Low-protein diet system for layers with addition of amino acids is beside biologically-cattle-breeding, economical and ecological too.

Progressive decrease of proteins content to 146.0 g per 1 kg feeding mixture set up the order of limiting amino acids for layers: methionine, lysine, tryptophane and threonine[5].

On bases of results model trials on layers were concluded that feeding, fat-enriched mixture supplied DL-methionine, choline chloride and vitamin B$_2$ by need of the effective

Table I
Excreted nitrogen [g kg^{-1}] in dropping at laying hens, which ingestion of feed mixture with different protein contents

Trial	Index		SD	v$_{\%}$	t-test
1st	CP [g kg^{-1}]	173.10	0.91	0.52	55.68[+++]
2nd	CP [g kg^{-1}]	146.40	0.32	2.68	
1st	N [bird day^{-1}]	1.88	0.005	0.22	18.52[+++]
2nd	N [bird day^{-1}]	1.38	0.02	1.57	

substance possible reach adequate the laying, egg weight and their quality on the economical using of the feedstuff and lower environment load[1]. In order experiment autors confirmed results of decrease of excreted nitrogen in dropping at laying hens[2].

Conclusions

The research results about nitrogen in breeding of laying hens in relationship to environment protection confirmed the possibility its decrease. One of the possibilities is decrease of protein contents in feed mixture. The decrease of crude protein content in feed mixture from 173.10 into 146.40 g per kilogram (about 15.43 %) is possibility of decrease of excreted nitrogen in dropping at laying hens about 26.60 %, which is statistically significant (P<0.001). Correlation dependency between content of nitrogen in dropping at laying hens and content of crude protein is high, r = 0.99.

REFERENCES

1. Angelovičová M.: Živočíšna výroba *42*, 263 (1997).
2. Angelovičová M., Angelovič M.: *Proceedings of scientific conference Food Safety and Control,* p. 153. Nitra, 2008.
3. Van Grinsveen H., van Eerdt M., Willems J., Ulleneers E.: *Paper presented at OECD workshop on evaluating agri-environmental policies*, Paris, December 2004.
4. Mikkelsen S., Iversen T.M., Kjaer S., Feenstra P.: *Paper presented at OECD workshop on evaluating agri-environmental policies*, Paris, December 2004.
5. Kočí Š.: Poultry *33*, 117 (1991).

P05　TESTING OF VARIOUS SORBENTS FOR COPPER REMOVAL FROM ACID MINE DRAINAGE

MAGDALENA BÁLINTOVÁ and NATÁLIA KOVALIKOVÁ

Civil Engineering Faculty, Technical University of Košice, Vysokoškolská 4, 042 00 Košice,
magdalena.balintova@tuke.sk

Introduction

The elimination of the consequences of mining activities belongs to the most serious environmental problems nowadays. Acid mine drainage (AMD) with high metal concentrations and usually with low value of the pH (about 2–4) is mainly a result of chemical oxidation of sulphides and other chemical processes in overflowed mines, mining waste dumps and tailings. This water may transfer various heavy metals in a dissolved form, such as Fe, Cu, Al.

The abandoned Smolník mine is regarded as an environmental loading in the Central Europe region, where AMD is generated and discharged from abandoned mine and contaminates the Smolník Creek catchment. This acid mine drainage (AMD) with pH 3–4 contents high metal concentrations that vary in dependence on rainfall intensity (e.g. Fe 500–400 $mg\,dm^{-3}$; Cu 3–1 $mg\,dm^{-3}$; Zn 13–8 $mg\,dm^{-3}$ and Al 110–70 $mg\,dm^{-3}$) (ref.[1]).

There are various physical-chemical methods of treatment such polluted water e.g. neutralisation, ion exchange, precipitation, sorption, membrane processes, filtration. The choice of the suitable methods is based not only on concentration of heavy metals in surface water but also on economical factors.

Sorption belongs to effective and economically acceptable methods for heavy metals removal. Deorkar and Tavlarides[1] developed an adsorption process of inorganic chemically active adsorbents (ICAAs) to selectively recover Fe^{3+}, Cu^{2+}, Zn^{2+}, Cd^{2+} and Pb^{2+} from AMD solutions without neutralization. More than 75 % of copper was removed from solutions by active carbon and biosorbents prepared from mosses, the highest sorption capacity had active carbon. On the other hand, pH values in the presence of active carbon increased almost to 9, thus copper was precipitated from the solution[3].

The paper deals with utilization of four types of sorbents (zeolite, active carbon and an atypical sorbents usually used for oil pollutants removal from surface water: turf brush PEATSORB – a hydrophobic material and universal crushed sorbent ECO-DRY) for cooper removal from AMD Smolník and presents influence of them on Cu decreasing under various conditions. The change of pH has been monitored, too.

Experimental

For study of Cu ions removal from acid mine drainage by adsorption, zeolites (granularity 0.5–1 mm, 2.5–5 mm, 4–8 mm) (Zeocem, a.s., Bystré, Slovakia), active carbon (granularity ≤ 0.1 mm), turf brush PEATSORB and universal crushed sorbent ECO-DRY (REO AMOS Slovakia) were used.

Because the experiments were carried out using untreated AMD (shaft Pech, locality Smolník, Slovakia), which is very unstable, new sampling of AMD for every experiment was realised. Copper removal efficiency by sorptive materials was tested at laboratory temperature under static conditions. 5 g zeolites, 1 g active coal, 5 g turf brush PEATSORB and 5 g universal crushed sorbent ECO-DRY, were overflowed with 100 ml of raw AMD for 24 h, then the mixtures were filtrated.

The dependence of Cu concentration decreasing on time (1; 3; 5; 10 min) was investigated under dynamic conditions using turf brush PEATSORB. In filtrate was determined pH (METTLER TOLEDO) and Cu by Bicinchoninate method (Colorimeter DR 890, HACH LANGE). Test of Cu precipitation in AMD was carried out by raw AMD samples of 100 ml, each were titrated to pH end points ranging from 4 to 8 using NaOH (0.5 $mol\,dm^{-3}$). During titration, the AMD solution was continuously stirred and the pH was monitored. When the preset pH end point was reached, the titrated solution was filtered to remove precipitated metals. The filtrate was used for characterizaton of copper solubility as a function of pH.

Results and Discussion

The untreated AMD (pH 3.72, Cu 2.22 $mg\,dm^{-3}$) was taken for adsorption efficiency determination of various sorbents. In Table I efficiencies of used sorbents on Cu removal from AMD are presented. In case of zeolite (2.5–5.0 mm), there was irregularity obserwed because the best adsorption effect was expected in the finest one. This fact can be explained as the structure faillure of the finest zeolite by acidity of environment. Turf brush PEATSORB was the most efficient (54.5 %) from tested sorbents.

Table I
Efficiency of various sorbents on Cu removal

adsorbent	pH	Cu $[mg\,dm^{-3}]$	efficiency [%]
zeolite (0.5–1.0 mm)	3.5	1.94	12.6
zeolite (2.5–5.0 mm)	3.7	1.79	19.4
zeolite (2.5–5.0 mm)	3.6	1.93	13.1
active coal	4.3	1.98	10.8
ECO DRY	3.7	2.17	2.2
PEATSORB	3.1	1.01	54.5

All used sorbents resulted in slightly pH decrease (exepting active coal) that was positive fact because as it is seen in Fig. 1. pH above 4 is connected with precipitation of copper (for AMD pH 3.92, Cu 1.38 $mg\,dm^{-3}$).

As Fig. 2. shows 55.8 % of copper were removed after 3 minutes and the longer time of stirring wasn't efficient. The pH decreasing can be explained as ion exange process by humic acid in turf brush[4].
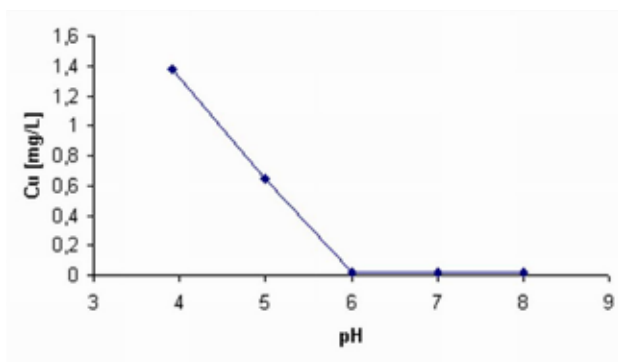
Fig. 1.　**Influence of pH on Cu precipitation from AMD**
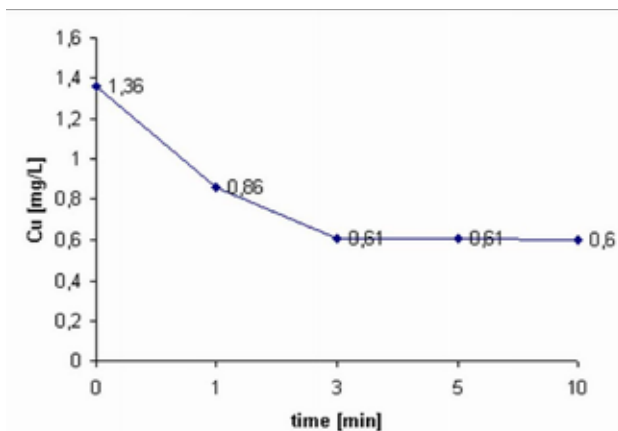
Fig. 2.　**Dependence of Cu removal from AMD versus adsorption time**

Conclusions

　　This study shows possibility of the natural adsorbents utilisation for Cu removal from acid mine drainage. Turf brush PEATSORB was the most efficient for copper removal – decreasing of Cu concentration in AMD was about 54.5 % under static conditions and 55.8 % in stirred sample during
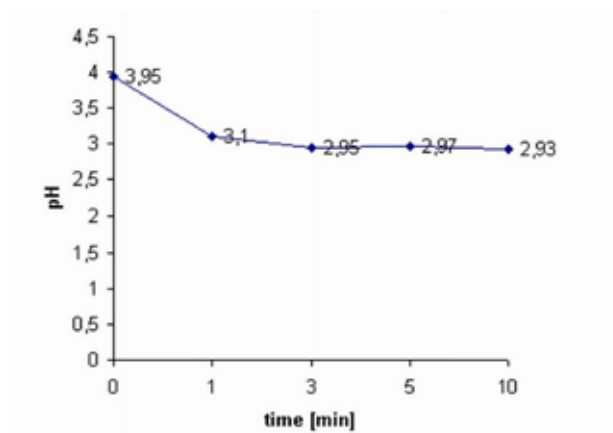
Fig. 3.　**Dependence of pH change during Cu removal from AMD by PEATSORB**

3 minutes. Based on experimental results we can state that chosen adsorbents haven't influenced pH increasing above 4 excepting active coal hence the Cu removal can be the result of adsorption proces.

REFERENCES

　1. Lintnerová, O., et al: Geologica Carpathica. *57*, 311 (2006).
　2. Deorkar, N. V., Tavlarides, L .L.: Environ.Prog. *17,* 120 (1998).
　3. Kadukova, J., et al: Acta Metallurgica Slovaca. *12*, 174 (2006).
　4. Panday, A. K., et al: Ecotoxicology and Environmental Safety. *47*, 195 (2000).

P06 INFLUENCE OF THE COMPOSITE SORBENT ON THE CONTENT OF SELECTED ELEMENTS IN THE SEDIMENT LOAD OF THE WATER RESERVOIR AND SLUDGE BED

JÁN BREHUV, OĽGA ŠESTINOVÁ, TOMISLAV ŠPALDON, PAVEL SLANČO, JOZEF HANČUĽÁK and ERIKA FEDOROVÁ

Institute of Geotechnics of Slovak Academy of Sciences, Watsonova 45, 045 53 Košice,
brehuv@saske.sk

Introduction

Sediment load of the streams and water reservoirs (hereinafter as WR) are a result of erosive and sedimentation processes of the respective basins. The term "sediment load" is used in hydrology according to the norm actually in force[1]. Geology and geochemistry[2] use the terms "river and bottom sediments". The mining waste deposited in mine sludge beds[3] constitute a residue of mining and treatment processes. Pollution of WR with sediment load causes problems in the decreasing of water content in the WR[4] aggravating the protection of the surrounding territory against floods, etc. That is why the sediment load (bottom sediments) need to be removed from the WR[5]. Due to great amounts of sediments it needs to be decided not only on how to extract the sediments, but also on how to store or dispose of them.

Sludge beds are objects where waste created at mining extraction of raw materials and mainly created as a result of the following treatment technologies is deposited or sedimented. They are designed and built so that they do not constitute a danger for the surrounding environment. Despite the facts mentioned above the unwilling seepage of waters from the sludge beds to the ground water occurs. The waters from the sludge bed draining containing various elements flow into the surface streams. Depending on their level of contamination by various elements, mainly heavy metals (HM) the water in the surface streams and then their sediments are contaminated[6,7].

The sediment load of streams and reservoirs may be classified as hydromorphic, subhydric soils[8]. However, there is a difference resting in the method of their contamination by various elements. They are situated in a different aquatic environment and catch contaminants from several sources. They are contaminated by a wider spectrum of elements than soils what makes their use[9] or treatment more complicated. That is fully true also about the sediment load and the mining waster in the basins of the Hornád River (Fig. 1.) treatment of which is using a composite sorbent is the subject of this paper (poster).

The literature proves that only the treatment of drinking waters[10], industrial waters[10,11] and soils using natural zeolites was successful. There are published results of an experimental testing of other natural materials, but they relate to soil treatment[12,13] only. However, it seems that there is a need to find a specific technological procedure with a specific sorbent[14]

Fig. 1. **Situation map of the Hornad river basin**

for the treatment of soil, sediment or mining waste deposited on the dumping sites (dumps) or sludge beds (Fig. 2.) for a longer period of time.
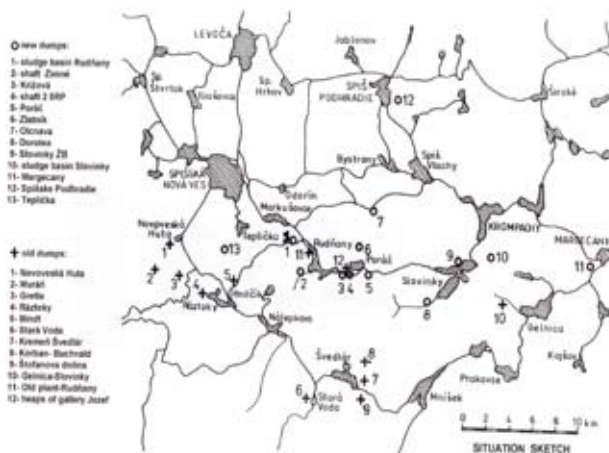
Fig. 2. **Situation map of the dumps localities in Hornad river basin**

Experimental Works

The most suitable solution of the problem of HM contaminated sediments should be their extraction after previous solution of reduction of the content or stabilization of dangerous HM contained in the sediment load (bottom sediments). That is why the first laboratory experiments were carried out at the beginning of 2007 monitoring the impact of the inorganic composite sorbent to reduce the content or stabilization of the elements in the sediment load of the water reservoir "Ružín I". According to the producer of this sorbent it is made from natural raw materials. It is mixture of atomically clays, smectite basalt tuffs, alginate, dolomite, gypsum, zeolite, coal and others. Proportion of individual components is trade secret. Qualitative mineralogical analysis of this sorbent was made by X-ray diffraction analysis. It contain amorphous phase, calcite ($>15\%$) as dominant minerals and quartz, sericite, chlorit-caolinite, dolomite ($3–15\%$)

as accompanying minerals. The impact of the mentioned sorbent on the reduction of the HN content in the sediment load was observed in laboratory conditions in compliance with the producer's recommendation in form of a 120 and 333 days experiment

The procedure of the 120-day experiment was as follows. First, 9.5 g of the sediment were weighted and 0.5 g of the sorbent added corresponding to 5 per cent by weight. The samples were put in 250 ml PVC bottles for 120 days and poured with 10 ml of the destilled water. After expiration of 120 days to each of the samples a 100 ml of 2M HNO_3 were added as a leaching agent. Then, the samples were shaken for 6 hours and sedimented for 1 hour.

A similar procedure was carried out in connection with the 333 days experiment. First 9.5 g of the sediment were weighted and 0.5 g of the mentioned sorbent added corresponding to 5 per cent by weight in accordance with producer´s recommendation. The samples were put in 250 ml PVC bottles for 333 days and poured with 10 ml of the destilled water. After expiration of 333 days to each of the samples a 100 ml of 2M HNO_3 were added as a leaching agent. Then, the samples were shaken for 6 hours and sedimented for 1 hour.

In both cases the contents of selected elements Cu, Cr, Ni, Pb and Zn were ascertained using AAS methods. For determination of the content of Cu and Zn flame atomic absorption spectrometry and for Cr, Ni and Pb graphite tube atomizer were used.

Results and Discussion

The results of the experiment when the composite sorbent affected the samples of sediment load from water reservoir for 120 and 333 days are contained in Table I.

The results of the experiment when the composite sorbent affected the samples of mining waste from sludge bed for 120 and 333 days are contained in Table II.

The content of elements of Ni, Cr and Pb in the samples marked like 1C–4C as well as in the samples containing the composite sorbent (CS) is under the lowest limit TV, norm for environment[15] and that is why the results are not in Table I and are not commented. The remaining samples marked like 120 d CS have shown the decrease of Cu from 4.53 to 8.20 % and from 11.55 to 38 % for Zn after 120 days. After 333 days the decrease of the content of Cu was ascertained from 5.55 to 15.83 % and Zn showed the content decrease from 11.26 to 37.1 %.

The cont ent of Ni and Cr in procured control samples (C) as well as in samples containing the composite sorbent (CS) was under the lowest limit TV, of the norm for environment15 and that is why the results are not commented.

The remaining samples marked as CS have shown the decrease of Cu from 7.25 to 11.65 %, Pb from 7.10 to 13.81 % and Zn from 15.36 to 19.68 % after 120 days. After 333 days the decrease of the content of Cu was ascertained from 11.23 to 14.76 %, Pb from 5.87 to 11.57 % and the content of Zn decreased from 7.67 to 9.81 %.

Table I

Influence of composite sorbent on content of heavy metals of sediment load from the water reservoir

Sample	Cu	Zn
	[mg kg^{-1}]	
1 C	151	76.4
120 d CS	140.5 (7 %)	47.35 (38 %)
333 d CS	127.1 (15.83 %)	48.05 (37.1 %)
max. % of decrease	15.83	38
2 C	168	386.8
120 d CS	157 (6.55 %)	306.6 (20.57 %)
333 d CS	142.9 (14.94 %)	311.7 (19.25 %)
max. % of decrease	14.94	20.57
3 C	48.8	54.9
120 d CS	44.8 (8.20 %)	36.3 (33.88 %)
333 d CS	44.0 (9.84 %)	38.8 (29.33 %)
max. % of decrease	9.84	33.88
4 C	342	310.8
120 d CS	326.5 (4.53 %)	274.9 (11.55 %)
333 d CS	323 (5.55 %)	275.8 (11.26 %)
max. % of decrease	5.55	11.55

1C–4C control sample of sediment load without composite sorbent;

120 d CS a 333 d CS – samples of sediment load with composite sorbent after 120 and 333 days

Table II

Influence of the composite sorbent on the content of heavy metals in the waste from the mining sludge bed

Sample	Cu	Pb	Zn
	[mg kg^{-1}]		
Dam C	103	1,296	1,382
120 d CS	91 (11.65 %)	1,117 (13.81 %)	1,110 (19.68 %)
333 d CS	87.8 (14.76 %)	1,146 (11.57 %)	1,276 (7.67 %)
max. % of dec.	14.76	13.81	19.68
Lagoon C	552	2,351	2,364
120 d CS	512 (7.25 %)	2,184 (7.10 %)	2,001 (15.36 %)
333 d CS	490 (11.23 %)	2,213 (5.87 %)	2,132 (9.81 %)
max. % of dec.	11.23	7.10	15.36

C – control sample from the mining sludge bed without composite sorbent

120 d CS a 333 d CS – samples with composite sorbent

Application of the composite sorbent also decreased the contents of Cu, Pb and Zn in both samples but the percentage of the content of HM is insignificant. Due to very significant exces of the content of Cu, Pb and Zn compared to the highest limit – IV, of the norm for environment[15]. Recycling of the waste deposited in the sludge bed should be considered

as more favorable aiming at gaining Cu, Pb and Zn. It has been the very first experiment and so our opinion may not be considered as a decisive one.

Conclusions

- When verifying the content of the composite sorbent on the content of heavy metals in the WR sediment load and wastes in the sludge bed, the decrease of the content of Cu, Pb and Zn has been ascertained. The decrease is not significant. NO other sorbents were used for the experiment and so composite sorbent cannot be recommended for the HM decreases.
- A long-term verification is needed for the recommendation of the application of used sorbent to decrease the content of HM in sediment load as well as the mining waste. The results need to be considered as preliminary and they require further verification in the conditions "in situ" for the minimum of 2 years.
- Further experiments should focus on the comparison of the used sorbent with sorbents that are accessible and experimentally tested, such as zeolites, bentonites, kaolinites and based on experimental results the most suitable sorbents should be proposed for the sediment load, wastes from sludge beds or soil.
- Today, the verification of the respective sorbent is underway in various foreign institutes. It would be useful to study the results, if they are published. Later after further experimental verification it using in our condition can be recommended.

REFERENCES

1. ČSN 73 65 11: *Nomenclature in Hydrology* (1.7.1977)
2. Šutriepka M.: *Geochemical Research of Contamination of Bottom Sediments of Water Reservoirs of Ružín and Veľké Kozmalovce.* Doctoral Thesis. Faculty of Natural Sciences, Department of Geochemistry of the Comenius University in Bratislava 2007, 168 s.
3. Peter P. and all: *Designing and building up of the sludge beds.* ALFA Bratislava, 312 p.
4. Bobro M. , Brehuv J., Hančuľák J., Merva M.: *Development of Erosive and Sedimentation Processes in the Water Reservoir Ružín. Final Report.* ČÚ B-3 pre ESPRIT Banská Štiavnica. ÚGt SAV Košice, October 1996.
5. Brehuv J., Bobro M., Hančuľák J.: *Distribution of Several Risk Elements in the Sediments of the Water Reservoir Ružín I.* Acta Montanistica Slovaca. Year 2 3/1997, TU Košice, p. 295-297. ISSN 1335-1788.
6. Brehuv J.: *Contamination of Sediments of the Water Reservoir Ružín I by heavy metals in Relation to Slime Pits.* Acta Montanistica Slovaca. Košice, Vol.5, 3/2000, p. 306-309. ISSN 1335-1788. 1.
7. Šutriepka M.: *Contamination of Bottom Sediments of Selected Water Reservoirs by Potentially Toxic Elements:* Workshop: "Creation and Assessment of Dangerous Mining Pollution" Modra-Harmónia, 15. – 17. 5. 2006. KÚ, Prír. fak. Bratislava.
8. Hraško J: *Soil Analyses.* Slovenské vydavateľstvo pôdohospodárskej literatúry, Bratislava, 1962.
9. Bobro M., Brehuv J., Hančuľák J., Slančo P., Špaldon T., Šestinová O., Lucová K.: *FinalReport – Quality and Quantity Research Related to Sediments and Erosive Processes in the Basin of Hornád and Hnilec to the Water Reservoir Profile of Ružín I.* in 2002 –2005 - for Slovenský vodohospodársky podnik š.p. Banská Štiavnica, Odštepný závod Košice. ÚGt SAV Košice, október 2006. 56 s.
10. Horváthová E.*: Ion Exchange on Natural Zeolites in the Technologies of Water Treatment and Cleaning.* Research Institute of Water Economy, Bratislava, 1990, 69.s.
11. Jablonovská K., Štyriaková I.: *Absorption of Zinc and Lead to Clay Minerals.* Acta Montanistica Slovaca, 11, Mimoriadné číslo 2, 304 (2006).
12. Szabová T., Bugel M., Leščinská M.: *Possibility of the Use of Zeolites in the Protection of Environmental Components.* Acta Montanistica Slovaca. Ročník 4, 1/1999, p. 61-65.
13. Reháková M., Čuvanová S., Gavaľová Z., Rimár J.: Chem. Lett. *97*, 260 (2003).
12. Decision of the Ministry of Environment of the Slovak Republic *on the Highest Tolerated Values of Harmful Substances in the Soil and on Identification of Organisation Eligible to Assess Real Values of those Substances No. 531/1994-540.* (1994)
14. Kafka Z., Punčochářová J.: Chem. Lett. *96*, 800 (2002).
15. Metodological Instruction of the Ministry of Environment of the Slovak Republic No. 549/1998-2 for *Assessment of Risks from Pollution of Sediments of Streams and Water Reservoirs.* (1998)

P08 ENGLISH FRO CHEMISTS CAN BE PHUN

GABRIELA CLEMENSOVÁ

Faculty of Chemistry, Brno University of Technology, Purky-ňova 118, 612 00 Brno, Czech Republic,
clemensova@fch.vutbr.cz

"To teach or not to teach any special English tailored to serve a particular profession which in our case means English for chemists? ...Isn't deep, substantial knowledge of general English everything one needs to be able to communicate?"

Such questions are often ask by many a technically oriented colleague I meet at my workplace. To answer them, I always remember Elaine Horowitz, PhD from the School of Education of UT at Austin (TX). She openes her doctoral classes on Foreign Language Acquisition with the following definition of language competence:

"Foreign language competence can be defined as the ability of authentic self presentation in that language. In other words, you can be called competent in L2 if the level of your education is reflected in the way you use this language. That means if a native speaker finds out who you are from the way you communicate."

Accepting this approach to competency we can say with confidence that English for specific purposes has its irreplaceable position in a postsecondary curriculum.

ESP may not always focus on the language of one specific discipline or occupation, but it is supposed to introduces students to common features of academic discourse in the sciences or humanities, frequently called English for Academic Purposes (EAP),

I would like to communicate some ideas and experience of teaching ESP classes at the Faculty of Chemistry of BUT. Our mission of teaching English for future chemists is more or less challenged by these phenomena:

(i) Absence of appropriate teaching materials on the market. We have not found any material in bookstores which would fit our specific needs and could be used as an English textbook for the chemistry students. (This said with no intention to blame any bookstore, of course!)

(ii) The different language experience of the students who come to our school. Their language proficiency often ranges from the true novice level to the advanced. The beginners and lower intermediate students have the possibility to attend two semesters of general English classes before they register for ESP. However, the different level of their language knowledge in the ESP classes cannot be fully eliminated as you could hardly expect them to make the leap from the beginner level to the upper intermediate or even advanced one in one year.

(iii) The absolute majority of our students strongly oppose and almost detest memory based learning as they are used almost entirely to rely on their ability of logical reasoning. ("We would not have been here at BUT if we had been able to memorize. If we had been able to memorize, we would sure have studied law or humanities!)

(iv) Students, especially in the previous years, had often a feeling that English was not their major specialization. That they did not come here to study English but chemistry. Despite the gradual change in this approach, there are always some who enter to the English classroom saying: "We are so tired from the previous instructions ...," The laboratory classes we have just had were so tedious...", We are just after organic chemistry/physics, math, ... classes and tests, absolutely drained both intellectually and physically, please, do not want us to talk…" etc, etc.

(v) Last but not least challenge is that the technically oriented students are not such good "natural speakers" even in their mother language as the students of the humanities. ("My goodness gracious, I do not know what to say even in Czech. And now you want me to communicate it in English on top of it…!")

What have we done to cope with the above mentioned challenges?

Ad *(i)* The first step to overcome the gap in the teaching materials on the market was the creation and implementation of the teaching material of our own. At the earlier stages of our professional lives at our school we always prepared handouts and distributed them at the beginnings of the lessons. The dramatic change in our work occurred when the internet was installed into most of our classrooms. The availability of this medium made a great stimulus for us to create an internet based textbook which we called English for Chemists www.fch.vutbr.cz/ang2. When creating this material we had the following objectives in minds:

The structure of our faculty – it is reflected in the selection of the topics as the subject matter of the individual lessons corresponds with the specialization of our institutes...

Proportional balancing of the lesson content so that all four major skills could be developed equally. The use of 4 different icons (indicating writing, talking, listening and reading) to label the individual exercises gives us a quick orientation.

We tried hard to bring sound into the reading activities. – Why do we emphasize sound so much? Everybody will agree that priority number 1 in foreign language instructions is to reach fluency. Fluency can be defined as the ability to understand and speak instantly, e.g. without translating. Fluency enables us to talk easily with native speakers. They easily understand us and we easily understand them The only way how to reach it goes through listening. That means we shall not get fluency in English just by reading English articles or learning grammar rules. To become fluent, students must have a lot of understandable, repetitive listening. It means, they will not learn English only with their eyes, but they must learn English with their ears. It is important to know that powerful listening must be repetitive and understandable (A. J. Hoge). We managed to answer this demand by the following ways:

- the reading sections of the textbook have been vocalized by a native lecturer

- each vocabulary section is competed with a hyperlink going to Merriam-Webster on-line dictionary which is soundtracked
- each lesson is completed with a substantial number of hyperlinks going to various sound tracked specific articles, animations, video recordings, demonstrations etc. that can be utilized for this purpose.

Exposing students to the culturally authentic sources as much as possible. (e.g. videotapes, radio and TV broadcasts, films, songs etc.) – this material has long been advocated by foreign language educators as stimulating pedagogical aids. One of the best sources of the authentic materials for classroom instructions is the Internet. Target language sites accessed through the Internet offer both teachers and students a wealth of authentic materials. The advantage of such materials is that they are current and readily available. Their topicality can be easily maintained by the regular visits of these web sites. That is why we completed the individual lessons with hyperlinks going to various specific video sections, songs, soundtracked animations, classroom instructions etc.

However, it is important to remember, that the documents found on the Web, like all authentic materials, have been created by and for native speakers of the language. That means they are not written with the language learning in mind. For this purpose we assessed these documents from the perspective of their general understandability first. Then we have completed these materials with the tasks that suit even the less proficient students.

Ad *(ii)* The different language experience of our students

We tried to meet the needs of the less proficient students by creating each textbook lesson in two versions. Firstly it is a printable version which the student will print and bring with him/ her to the class. Its format leaves plenty of space for writing down student's own answers. Secondly, each unit has also the version completed with the clues to all exercises. This serves mainly to the less advanced ones to go through the explain subject matter at home again and check their answers or possibly to look up the correct answers.

Besides, each lesson is ended with a short self test enabling the students to evaluate their comprehension.

Ad *(iii)* Unwillingness to learn vocabulary and idioms by memorizing

Experts say that most of people must hear a new word 30 times to remember it forever. To know a word and instantly understand it, you probably need to hear it 50–100 times. The students must know that it is not enough to listen to a new word just once or twice. As the time allocation of our classes do not allow to practice repetitive listening to much at school, the students are strongly recommended to go to all the listening material again at their leisure, e.g. at home, and repeat all the listening activities as many times as possible.

Ad *(iv)* How to engage the students who are tired from the previous "more important" classes? The answer is: make the English for chemists fun.

Here the Internet makes a great aid again. We can use various science/chemistry oriented humor, interactive quizzes, crossword puzzles and various songs created by native students and teachers with the aim to bring fun and entertainment into their chemistry classes. Songs make excellent memory boosters. AS most people have strong musical memory, we take can advantage of this fact to make memorization and learning easier. Putting words to music instantly makes those words more memorable.

Besides memorizing song verses our learners can profit from retelling the jokes, playing memory boosting quizzes (e.g. flash cards), solving crosswords etc.

This can be effectively completed with the popular game based on the repetition of the words. Everybody who has ever visited a language school will sure the remember the game called: In our local super market we can buy/I will pack into my suitcase … Its variations on the premises of our school sound: In our chemistry laboratory we have … (the names of various laboratory equipment follow) .../Breathing carbon monoxide will cause… (Symptoms of CO poisoning)/Iodine deficiency causes… etc, etc.

Ad *(v)* Shyness to speak

During a semester students must prepare their own minipresentations to meet one of the necessary conditions of getting a credit. Prior this activity they are provided with all the necessary phrases and expressions so that they learn how to address the audience, introduce themselves, express the purpose of the paper/presentation, signpost the presentation, move on in the course of it, describe the pictures, verbalize graphical data, ask checking-up questions, invite questions, finish the presentation… Though the students are encouraged to use the topics which have been explained in the classes, they widely use the Internet again as a rich source of additional information.

We managed to incorporate two funny chemistry oriented dramas into a lesson. The plays come from the Internet and where created by the native authors without the language learning objective. However, our students find them very entertaining and participate enthusiastically in dramatic readings.

This activity also fits a multilevel class as the students are given the freedom in adapting the sentences. So the less advanced can make their entries less complicated and simpler, while the more advanced ones enjoy the full versions of their roles. Dramatization engages students emotionally and socially, as well as intellectually. The students thoroughly enjoy it, and it leaves strong, memorable impressions which can later help recall and improve learning. Thus at the end of the activity they are able to repeat various catch phrases by heart (e.g. thanks to the plays "Becoming an alcohol – a sad story of good oxygen becoming bad", or "Electrophilic Addition" they will long remember structures as: "My mom has always warned me against organic acids", "It is against the rule. What rule? Markovnikov's rule!" Aren't my electrons good enough for you? "Along comes electron hogging

chlorine" "Keep your precious electrons for yourself, you …
!" etc).

The students are encouraged to role play the authentic professional dialogues videotaped for instructional purposes as well as those which are found on the ESL web pages.

After all, we can say that English for chemists is pHun!

P09　VOLATILE DEGRADATION PRODUCTS OF POLYURETHANE FOAMS

DANIELA MÁCOVÁ, TEREZA TOBIÁŠOVÁ and JOSEF ČÁSLAVSKÝ

Institute of Chemistry and Technology of Environmental Protection, Faculty of Chemistry, Brno University of Technology, Purkyňova 118, 612 00 Brno, Czech Republic, xcmacova@fch.vutbr.cz

Introduction

Polyurethanes are the world's sixth most abundant synthetic polymer. The most of their production represent flexible polyurethane foams. At the end of their life-cycle they are often deposited on waste dumps, where they degrade under the influence of various environmental factors; photodegradation and hydrolysis are the main routes. After that, their degradation products can be distributed in the environment. In common, synthetic polymers are not prone to environmental degradation. Therefore, they could stay there for a long time. Their degradability can be improved by addition of the biodegradable filler.

The generation of volatile products has been reported from the photo- and thermal degradation of many polymers.[1–4] Complex mixtures of degradation products of this type were for example identified in starch-based polymers[5]. Till now, there is no information about volatile compounds generated during photodegradation of synthetic polyurethane with biodegradable filler. Several studies have been developed on the UV degradation of aromatic polyurethane. Such photo-degradation has already exhibited formation of free radicals, recombination, scission of bonds, crosslinking and oxidation reactions[6,7].

This paper is focused on the identification of volatile photodegradation product of polyurethanes modified by biodegradable filler using Solid Phase Microextraction (SPME) and Gas Chromatography linked to Mass Spectrometry. The SPME method was selected in the experiment for its fastness, simplicity and environmental friendness.

Experimental

Material and Sampling

Polyurethane foam modified with biodegradable filler like carboxymethyl cellulose, acetylated potato starch, cellulose acetate, 2-hydroxyethyl cellulose and wheat protein were prepared at the Institute of Material Chemistry at Faculty of Chemistry, Brno University of Technology.

For sampling of volatile compounds the system consisting of quartz tube with Teflon cover and two SPME holders, the first with polyacrylic fibre (PA) 85 μm and the second with polydimethylsiloxane fibre (PDMS) 100 μm (both Supelco, USA) and UV lamp (high-pressure mercury discharge tube, $\lambda = 254$ nm), was set-up. The system is shown on Fig. 1.
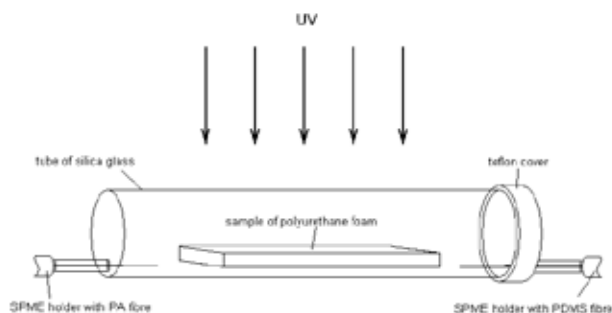
Fig. 1.　**System for sampling of VOCs formed by photodegradation of polymer**

GC-MS analysis

Separation and identification of volatile compouds from UV-induced polyurethane foam photodegradation was realized using Agilent 6890N gas chromatograph coupled with Agilent 5973 mass selective detector (Agilent Technologies, Germany). HP-5MS column 30.0 m × 0.25 mm × 0.25 μm was used for the separations. The injector and transfer line temperature was 270 °C. The GC oven temperature program for PDMS fibre was: 4 min at 40 °C, then increased at 15 °C min^{-1} to 100 °C, then 8 °C min^{-1} to 270 °C, then 15 °C min^{-1} to 280 °C. For the compounds desorbed from PA fibre the column temperature program was slightly modified: 4 min at 40 °C, increased at 10 °C min^{-1} to 230 °C, then 15 °C min^{-1} to 280 °C. Injection/desorption of analytes from SPME fibres was realized in splitless mode. Helium was used as the carrier gas at a constant flow of 1 ml min^{-1}. Ion source temperature was 230 °C, electron ionization at 70 eV was used. Quadrupole analyzer of the MSD was operated in scan mode within a range 30–550 amu, solvent delay was 4 min. Identification of separated compounds was based on NIST 05 spectral library search.

Results

Seven types of polyurethane foams with different fillers and reference foam without filler were irradiated by UV lamp during this study. Volatile compounds were sorbed on PA and PDMS fibers and desorbed, separated and detected by GC-MS technique.

All identified compound are listed under chromatograms (Figs. 2. and 3.). Many various compounds have been identified.

Group of branched and non-branched aliphatic hydrocarbons containded: pentadecane, hexadecane, heptadecane, 2,6,10,14-tetramethylpentadecane, 2,6,10,15,19,23-hexamethyl-2,6,10,14,18,22-tetracosahexaene (Squalene). These compounds are probably formed by homolysis of bonds in soft part of polyurethane.

Group of ketone and fatty acid esters contained: 6,10-dimethyl-5,9-undecadiene-2-one, methylester of dodecanoic acid and isopropylester of tetradecanoic acid.

By photo-oxidation of alkenes hydroperoxides were formed – 1,3-dioxane and 2-methyl 1,3-dioxane.
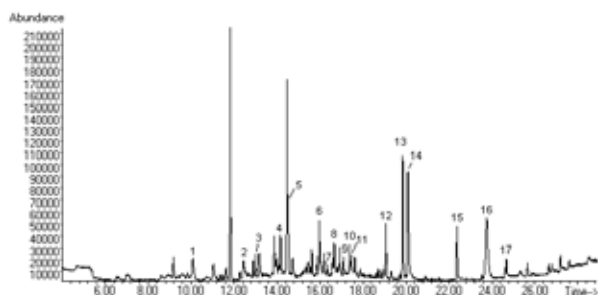
Fig. 2. **Volatile degradaction products of polyurethane foam sorbed on PDMS fibre**
1: 2-methyl-1,3-dioxane, 2: 2,4-diisocyanatotoluene, 3: 6,10-dimethyl-5,9-undecadiene-2-one, 4: 2,5-diterc-butyl-1,4-benzochinone, 5: pentadecane, 6: hexadecane, 7: 2,6-bis(1,1-dimethyethyl)-4-(1-oxopropyl)phenol, 8: 1-methylester dodecanoic acid, 9: 4-decyl-morphline, 10: heptadecane, 11: 2,6,10,14-tetramethylpentadecane, 12: isopropylester tetradecanoic acid, 13: 4-undecyl-morpholine, 14: N,N-dimethyl-1-hexadecanamine, 15: 4-tetradecyl-morpholine, 16: squalene, 17: 4-hexadecyl-morpholine

Also nitrogen derivates were detected, namely line of alkyl-substitued morpholines and N,N-dimethyl-1-hexadecanamine.

By the photolysis of hard segment of polyurethane foam 2,5-diterc-butyl-1,4-benzochinone, 2,6-bis(1,1-dimethyethyl)-4-(1-oxopropyl)phenol and 2,4-diisocyanatotoluene (2,4-TDI) were formed.

2,4-TDI is very volatile and toxic. The compound is used as main reagent at synthesis of polyurethane. 2,4-TDI was detected in case of all polymers modified by celulose derivate fillers. It is difficult to say whether that compound is photodegradation product of polyurethane foam or unreacted raw material residue. It will be studied in the next research.

All the compounds were detected in most polyurethane samples. There was observed qualitative change only.

Quantitative differences were found in the case of minority distribution compounds. Their identification using library search in NIST 05 was unsuccessful in most cases. Probably small concentrations of analyte and resulting low-intensity mass spectra could be the reason, or – due to specific character of volatile compound made by irradiation of polyurethane foam – their mass spectra are not included in this library.

PA fibre shows higher selectivity in comparison with PDMS fibre which in opposite gives more complex information about volatile compounds formed during photodegradation of polyurethane.
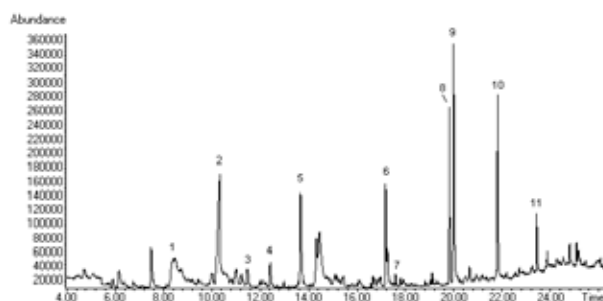
Fig. 3. **Volatile degradaction products of polyurethane foam sorbed on PA fibre**
1: 2-(2-ethoxyethoxy)-ethanol, 2: 2-ethyl-hexanoic acid, 3: 1,3-dioxane, 4: 2-methyl-1,3-dioxolane, 5: 2-methyl-1,3-diisocyanatobenzene, 6: 2,6-bis(1,1-dimethyethyl)-4-(1-oxopropyl)phenol, 7: 4-decyl-morpholine, 8:4-undecyl-morpholine, 9: N,N-dimethyl-1-hexadecanamine, 10: 4-tetradecyl-morpholine, 11: 4-hexadecyl-morpholine

Conclusions

In this study the SPME method was applied for the identification of volatile compounds formed by irradiation of polyurethane foams modified by biodegradable fillers. A wide range of compounds was detected and most of them were succesfully identified by library search. The identification of the remaining compounds will be a subject of the next research.

REFERENCES

1. Philippart J. L., Posada F., Gardette J. L.: Polym. Degr. Stab. *285*, 49 (1995).
2. Albertsson A. Ch., Karlsson S.: Polym. Degr. Stab. *245*, 41 (1993).
3. Khabbaz F., Albertsson A. Ch., Karlsson S.: Polym. Degr. Stab. *329*, 61 (1998).
4. Carlsson D. J., Krzymien M., Worsfold D. J., Day M.: J. Vinyl. Add. Techn. *3,* 2 (1997).
5. Hakkarainen M., Albertsson A. Ch., Karlsson S.: J. chromatogr. A. *741*, 251 (1996).
6. Dannoux A., Esnouf S., Begue J., Amekraz A., Moulin C.: Nucl. Instr. Meth. Phys. Res. B. *236*, 488 (2005).
7. Irusta L., Fernandez-Berridi M.J.: Polymer *40*, 4821 (1999).

P10   DYNAMIC SIMULATION OF BIOLOGICAL NITROGEN REMOVAL PROCESSES

LENKA ČERNOCHOVÁ[a], JÁN DERCO[a] and MANFRED SCHÜTZE[b]

[a]*Faculty of Chemical and Food Technology, Institute of Chemical and Environmental Engineering, Slovak University of Technology, Radlinského 9, 812 37 Bratislava, Slovakia,*
[b]*ifak – Institut für Automation und Kommunikation e.V. Magdeburg, Werner-Heisenberg-Str. 1, 39106 Magdeburg, Germany,*
lenka.cernochova@stuba.sk

Introduction

With rising requirements for protection water resources and thereby for quality of effluent wastewater too, more complex technologies for wastewater treatment are applied as well. These technologies are characterised by more processes with different reaction rates and requirements in term of reaction conditions, interactions and generally by more complex structure of treatment lines. The complexity of these systems is also related to mutual interaction between wastewater treatment plant (WWTP) and others parts of the urban wastewater system, e.g. sewer system and receiving water (Derco and Schütze, 2004). Consequently, designing of processes and technologies and their efficient operation are also significantly complex.

Mathematical models and simulations programs belong to prospective and currently more often utilised tools. They offer a simple way how to analyse changes in technologies at WWTP by optimisation or intensification already existed plants or it can help by designing new WWTPs as well.

The results of application of the Activated Sludge Model No. 1 (ASM1) (Henze et al., 1987) using dynamic simulations for verification of steady state design with regard to dynamic behaviour of the WWTP and for prediction dynamic effluent concentration values are presented.

Dynamic Simulation of WWTP

ASM1 was used for modelling of the biological stage at real WWTP in Nové Zámky (Fig. 1.). Two series of measurements included diurnal variations of wastewater flow and composition in input and output at the biological stage were carried out. The first set of measurement was perfomed in May 2002, when the nitrification process was operated. Because of expected more stringent requirements in effluents, this activated sludge plant was upgraded in 2003 applying a pre-denitrification system. The second measurements were realised after the reconstruction (in March 2007). The results of measurements were transformed into organic and nitrogen pollution fractions according to structure of the ASM1.

For comparison of the experimental and the calculated resultant concentration values in the WWTP effluent were chosen criteria according the Regulation of the Slovak government (2005). The model ASM1 and the default parameter values included in the SIMBA program have been used for performing dynamic simulations. The calculated concentration values for individual pollutants in daily composite samples were calculated based on pollutant mass balancess.
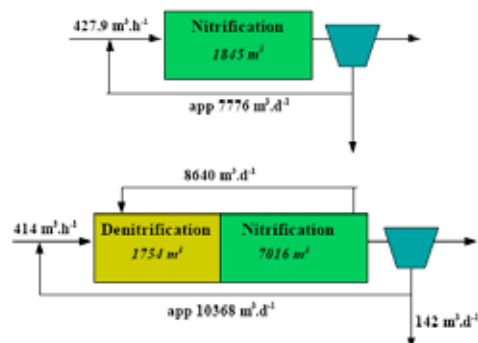
Fig. 1.   **Schemes of WWTP setups; Above: WWTP before reconstruction (2002); Below: WWTP after reconstruction (2007)**

Results

Model Suitability

First step of simulations was to verify suitability of ASM1 to describe WWTP. From the results (Fig. 2) it can be concluded that the dynamic simulations describe the experimental effluent values quite well.

Verification of Steady State Disign by Dynamic Simulation

The purpose was to verify the results of conventional steady-state design of the WWTP biological stage (Derco *et al*, 2004) for future upgrading with regard to expected load in 2036. The data for this scenario were obtained from the operator of the WWTP – Západoslovenská vodárenská spoločnosť, a.s. Resulting values (7 mg dm^{-3} ammonium nitrogen and 9.3 mg dm^{-3} total nitrogen) of dynamic simulations are lower than today's effluent standards (10 mg dm^{-3} ammonium nitrogen and 15 mg dm^{-3} total nitrogen). It can be summarised that the steady state design for the WWTP upgrading
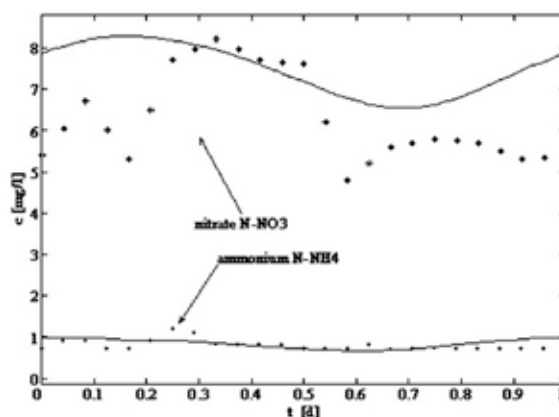
Fig. 2.   **Effluent concentrations of ammonium nitrogen at WWTP after reconstruction (*experimental and ‾calculated values)**

with perspective for 2036 follows also the dynamic effluent standard values. It can be expected that upgraded WWTP will meet current legislation also with regard to dynamics of the processes.

The first task was to investigate what could happen if the reconstruction in 2003 had not been carried out. The effluent concentration values are shown in Table I. The load in 2007 and consequently the effluent concentration values are lower than in 2002 due to industrial activities reduction. This result could lead to the conclusion that there had been no need for the reconstruction of the WWTP in 2003. However, because of the more stringent requirements (Regulation of the Slovak government, 2005) which permits $10.0 \, \text{mg} \, \text{dm}^{-3}$ for ammonium nitrogen for effluent of WWTP with corresponding load, it was necessary to carry out the reconstruction. Therefore, it should be stressed that the WWTP without this reconstruction would not be able to meet current effluent standards.

The second task was to study what would happen if the pollution load of actual biological stage of the WWTP increased to values expected in 2036. The results of dynamic simulations show that even if the load will increase, the WWTP will be able to meet current effluent requirements.

Table I
Results of simulations

	WWTP 2002	1st task	WWTP 2007	2nd task
plant layout	2002	2007		
load situation	2002	2007	2007	2036
N-NH$_4$ [mg dm^{-3}]	25.06	20.89	0.81	4.05
N-NO$_3$ [mg dm^{-3}]	0	0	7.47	3.91

Conclusions

Two time-variable influent and effluent data sets of wastewater flow and composition were measured for different technological arrangements of the WWTP and were applied for dynamic simulations.

It can be concluded from the work that the mathematical model ASM1 is suitable for the description of the process dynamics of the WWTP biological stage. Good fit between experimental and calculated effluent concentration values resulted from performed dynamic simulations.

The results of dynamic simulation confirmed the necessity of the WWTP reconstruction carried out in 2003 in order to comply with actual legislation requirements.

Compliance with actual effluent limits follows for previous steady state design and upgrading of the WWTP when investigating dynamics of the process.

According to results of dynamic simulations it can be expected that the existing WWTP will comply with actual discharge standards also for pollution load as expected in 2036.

REFERENCES
1. Chem. Pap. *56,* 117 (2002).
2. Derco J., Kovács A., Gulyásová A., Dercová K., Horňák M.: *Reserch report No. 4272*, Bratislava, Slovakia, 2002
3. Derco J., Drtil M., Bodík I., Hutňan M.: *Technológia vody a ochrana vodných zdrojov I. Časť.* ÚVTIP Nitra, Bratislava 2004.
4. Derco J., Schütze M.: *Odpadové vody 2004. Október 20–22, Tatranské Zruby 2004*, p. 111
5. Henze M., Grady Jr. C. P. L., Gujer W., Marais G. R., Matsuo T.: *Activated Sludge Model No. 1*, Scientific and Technical Report No. 1., IAWPRC, London 1987.
6. ifak. *SIMBA 5 – Manual.* Institut für Automation und Kommunikation e. V., Magdeburg 2005.
7. Regulation of the Government of the Slovak Republic N° 296/2005 on *Quality Objectives of Surface Waters and on Limit Values for Pollution Indicators of Waste Waters and Special Waters.*

P11　APPLICATION OF A 6-MERCAPTOPURINE FUNCTIONALIZED SORBENT FOR DIFFUSIVE GRADIENTS IN THIN FILMS TECHNIQUE

PAVEL DIVIŠ, ROMAN SZKANDERA and PETER MATÚŠ

Brno University of Technology, Faculty of Chemistry, ICTEP Purkyňova 118, BRNO, 612 00 Czech Republic, divis@fch.vutbr.cz

Introduction

The diffusive gradients in thin films technique (DGT)[1] is used more than 10 years for determination of kinetically labile metal species in natural waters, soils and sediments[2]. However this technique is at the present time validated for measurement of more than 50 metals, only few attention was applied to measurement of mercury.

As we reported in our previous studies[3,4], combination of agarose diffusive gel together with the sorption gel containing resin with thiol functional groups is the best choice for measuring of mercury by DGT. Nevertheless, at the present time there is almost no resin of this type for direct use in DGT on the market. For DGT, strictly defined size of resin about 100 µm is used. As the resins available on the market have particle size about 1 mm, there is need to crush their particles and separate the required fraction by sieving. This activity can seriously contaminate the resin or it can change its properties.

In presented study we try to prepare needful resin by our self in laboratory. The Iontosorb AV resin (Iontosorb, Czech Republic) with particle size 50–100 µm was used in advance. This resin contains free amino group which can be easily diazotated (Fig. 1.). Resulted diazonium salt can be subsequently used for raction with specific reagent containing thiol groups. In this work we used 6-mercaptopurine as this reagent. New modified Iontosorb AV was characterised in laboratory and then it was used to prepare sorption gels for DGT technique. The performance of DGT with modified Iontosorb AV was then tested in model mercury solution.
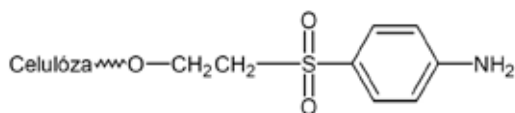
Fig. 1.　**Chemical formula of Iontosorb AV**

Experimental

Modification of Iontosorb AV Resin

Iontosorb AV was modified using diazotation and copulation reactions[5,6]. The amount of 5 g Iontosorb AV was washed with hydrochloric acid and then with ultrapure water to neutral pH. After washing, diazotation was performed at 0–5 °C using 1M solutions of hydrochloric acid and sodium nitrite. Diazotation was stopped after adding of 40 ml of rea-gents. Yellow product was filtered out and washed several time with ultrapure water. Diazonium salt was then placed to the continuously mixed and cooled reactor containing 3.5 g of 6-mercaptopurine dissolved in 10% (v/w) sodium carbonate. After 24 h new red-brown product was filtered out, washed several time with ultrapure water and dried in exicator.

Analytical Control of New Functionalised Resin

Qualitative test was done using an infrared spectroscopy (Impact 400, Nicolet, USA). Infrared spectrum of new functionalized resin was compared with blank infrared spectrum of Iontosorb AV.
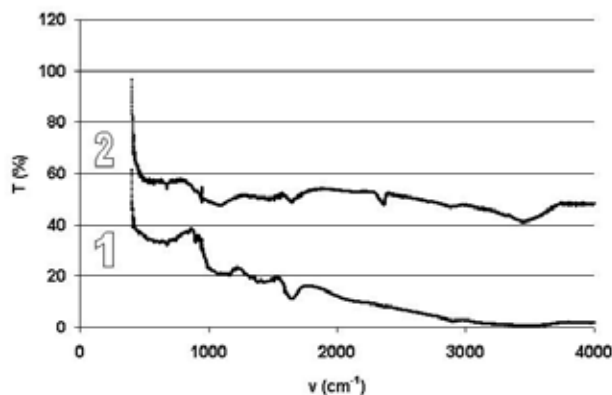
Fig. 2.　**Infrared spectrum of Iontosorb AV (1) and new functionalized resin (2)**

Quantitative test of thiol groups was done by iodometric titration at pH ~ 9. To 50 mg of modified Iontosorb AV, 25 ml of 0.001M potassium iodine was added, and after 5 min of shaking and 30 min of standing in the dark, resulted solution was titrated by 0.001M ammonium thiosulphate.

Testing of New Functionalised Resin for Use in DGT Technique

Sorption gels for DGT technique were prepared by incorporation of modified Iontosorb AV into the agarose gel. The amount of 0.2 g of modified Iontosorb AV was added to a hot agarose solution (4% (v/w)) and the hot solution was casted between two glass plates separated by 0.4 mm plastic spacers. The disks 2 cm in diameter were cuted out from the gels after cooling down and washig of the gel sheets.

Diffusive gels were prepared by similar way, the only one difference was that clear hot agarose solution (3% (v/w)) and 0.8 mm plastic spacers were used.

The agarose sorption and diffusive gels were used to assembly the DGT unit. Four DGT units were exposed in a 5 dm^3 beaker containing well mixed 10 µg dm^{-3} mercury solution for 3 h to perform basic DGT test. Simultaneously to the exposition of DGT units, mercury concentration in the solution was measured by atomic absorption spectrometry (AMA 254, Altec, CZ).

Results

Sucessful incorporation of 6-mercaptopurine to Iontosorb AV was proved by chage in resin colour from white to red-brown. Infrared spectroscopy has shown a new peak in Iontosorb AV spectra with wave nuber 2,362 cm⁻¹ (Fig. 2.). This is a characteristic peak for thiol groups. The amount of thiol groups was determined by iodometric titration to be 0.5 mmol g⁻¹. This should be enough to prevent the saturation of functional groups when DGT sampling units are deployed in natural waters. New resin was successfully incorporated into the agarose gel. The agarose gel as a support for resin was chosed because of problems associated with commonly used polyacrylamide gel. In polyacrylamide gel, the new resin aggregated and it was difficult to prepare homogenous gel. In agarose gel there was no problem with aggregation of resin particles. After optimalization of sorption gel preparation procedure, basic DGT test was performed. Results from this experiment are shown in Table I. It can be seen that the difference between real mercury concentration measured by AAS and mercury concentration calculated from accumulated mass of mercury in resin gels extracted from DGT sampling units is less than 10 %. This result matches the requirements of DGT Research Ltd. for right function of DGT.

Conclusions

This study proved that the 6-mercaptopurine functionalised Iontosorb AV is useable for measuring of mercury in natural waters by DGT and it provided useful informations for further experiments in which better characterization of new sorbent will be carried out and more extensive investigation of its use in DGT will be done. For example, experiments

Table I
Results from basic DGT performance test

DGT concentration [μg dm⁻³]	Real concentration [μg dm⁻³]	Difference [%]
7.5	8.0 ± 0.4	6
8.2	8.0 ± 0.4	3
8.7	8.0 ± 0.4	8
8.2	8.0 ± 0.4	3

in solutions containing natural ligands and experiments in real sytems will be realized during the next years and a comparison with other sorbents usable in DGT will be done.

REFERENCES

1. Zhang H., Davison W.: Anal. Chem. *67*, 3391 (1995).
2. Diviš P., Dočekalová H., Smetková V. : Chem. Listy. *99*, 640 (2005).
3. Dočekalová H., Diviš P.: Talanta *65*, 1174 (2005).
4. Diviš P., Leermarkers M., Dočekalová H., Gao Y.: Anal. Bioanal Chem. *382*, 1715 (2005).
5. Davies R. V., Kennedy J., Lane E. S., Willans J. L.: J. Appl. Chem. *8*, 68 (1958).
6. Mondal B. C., Das D., Das A. K.: Anal. Chim. Acta *450*, 223 (2001).

P12 THE DETERMINATION OF METHYLMERCURY IN WATER ECOSYSTEMS

LENKA TUHOVČÁKOVÁ, HELENA DOLEŽALOVÁ WEISSMANNOVÁ, JOSEF ČÁSLAVSKÝ and MILADA VÁVROVÁ

Brno University of Technology, Faculty of Chemistry, Purkyňova 118, Brno, Czech Republic,
dolezalova@fch.vutbr.cz

Introduction

Alkyl mercury compounds belong to a group of organometallic compounds with a high bioaccumulation potential. They are formed from inorganic forms in a methylation process and exhibit 100 times higher toxicity than inorganic forms[1]. Methyl mercury is a neurotoxin which attacks the central nervous system (CNS). The most frequent pathway by which methyl mercury enters the body is through the gastrointestinal tract which may absorb up to 95 % of methyl mercury received by a man via fish meat. It may also penetrate through the skin. It is well soluble in fat which explains its transport through blood-brain barrier and diffusion into cell membranes. It also passes the foetal placenta; the risk of damage to the foetus occurs at a mercury concentration in hair as low as 15–20 mg kg^{-1}. The tolerated dose of mercury in man is 33 µg per 70 kg of body weight[2,3,4]. Methyl mercury was responsible for a large number of intoxications in the past. For example, fish living in water polluted with waste from a chemical company producing chlorine caused intoxication by methyl mercury in Japan while mercury intoxications in Iraq were caused by the grain treated with methyl-mercury-containing fungicides that was originally intended as seed[5]. Methyl mercury is the most common organic form occurring in biological systems. It is soluble in water and is relatively stable. It passes biological membranes easily and has a long half-time of decomposition up to 70 days[4]. Methyl mercury has the highest partition coefficient K$_{ow}$, which explains its high affinity towards fat. Methylation is one of the mercury's most important environmental reactions. Methylation takes place in the sediment as well as in sea water and fresh water. The fastest rate of methylation was observed on the sediment's surface that was in contact with water [6,7].

Experimental

The optimization of the method was carried out using the Certified Reference Material CRM 464; tuna fish containing a total amount of THg = 5.24 µg g^{-1} and methyl mercury MeHg = 5.5 µg g^{-1}. The sample weighed 0.1 g. A total of 5 samples were extracted and each sample was subjected to three parallel measurements. Extraction was performed according to the published method[8]. Gas chromatography was used as the final analytical method. The results of parallel measurements were evaluated as mean values and their standard deviation was calculated.

Table I
The conditions of the GC/µECD analysis

Parametrers of GC/µECD	
Column	DB-608, 30 m × 0.530 mm × 0.5 µm
Injection	splitless
Injector temperature	250 °C
Carrier gas	He, 3 ml min^{-1}, constant flow
Detector temperature	250 °C
Make-up gas	N2, 20 ml min^{-1}

Results

The Certified Reference Material was used particularly for the determination of metrological parameters of the method. The mean recovery of extraction was found to be 64.9 ± 2.0 %. The lower recovery rate as compared to the literature(ref.[8]) could be caused by the certified reference material used which just passed the expiry date. As a result, the content of methyl mercury might differ from that provided in the certificate. Fig. 1. shows the chromatogram of the analysis of MeHg isolated from the certified reference material.
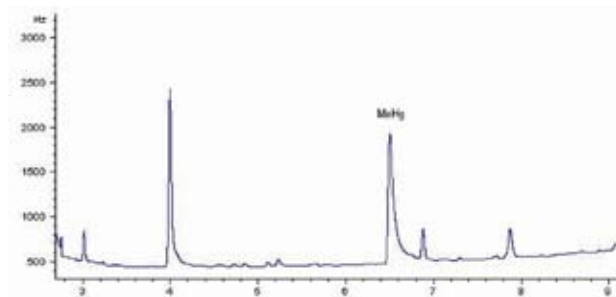
Fig. 1. **Chromatogram for the certified reference material**

Table II contains the results of recovery from individual parallel measurements of methyl mercury levels in the CRM (Marked as 1–5).

To determine the accuracy of methyl mercury determination using GC/µECD, 5 parallel measurements of the certified reference material were carried out. The results are provided in Table III.

Table II
Recoveries for 5 parallel samples of certified reference materials. Declared value of MeHg – 5,500 [ng g^{-1}]

CRM	Mean peak area	c [ng ml^{-1}]	MeHg [ng g^{-1}] exper.	Recovery [%]
1	6,163.81	40.05	3,559.60	64.72 ± 0.51
2	7,030.21	45.67	3,653.96	66.44 ± 3.80
3	6,938.18	45.08	3,606.12	65.57 ± 1.71
4	6,884.60	44.73	3,578.27	65.06 ± 0.61
5	6,625.99	43.05	3,443.86	62.62 ± 3.59

Table III
The accuracy of methyl mercury determination using GC/μECD

	Mean level [ng g^{-1}]	RSD [%]
MeHg	3,568.36	1.79

Conclusions

The method of determining the level of methyl mercury in fish muscles using GC/μECD was modified. The optimization of the method was performed using the Certified Reference Material. On the basis of recovery and accuracy, it was concluded that the test procedure without sample pre-treatment can be applied with this method of analysis.

REFERENCES

1. Remy S., Prudent P., Probst J. L.: Appl. Geochem. *21*, 1855 (2006).
2. Faro L. R .F., et al.: Neuropharmacology *42*, 612 (2002).
3. Goméz-Ariza J. L., Lorenzo F., Garcia–Barrera T.: Chemosphere *61*, 1401 (2005).
4. Faro L. R. F., et al.: Ecotox. Environ. Safe. *55*, 173 (2003).
5. Maršálek P., Svobodová Z.: Czech J. Food Sci. *24*, 138 (2006).
6. Carro A. M., Mejuto M. C.: J. Chromatogr. A *882*, 283 (2000).
7. Mishra S., et al.: Anal. Chim. Acta *551*, 192 (2005).
8. Castillo A., Roig-Navarro A. F., Pozo O. J.: Anal. Chim. Acta *577*, 18 (2006).

P13　ECOTOXICOLOGICAL TESTING AND TEST METHODS OF CHEMICALS

HELENA DOLEŽALOVÁ WEISSMANNOVÁ, HELENA ZLÁMALOVÁ GARGOŠOVÁ and MILADA VÁVROVÁ

Brno University of Technology, Faculty of Chemistry, Purkyňova 118, Brno, Czech Republic
dolezalova@fch.vutbr.cz

Introduction

Ecotoxicity involves the identification of chemical hazards to the environment. The Globally Harmonized System of Classification and Labeling of Chemicals (GHS) describes testing for hazards to the aquatic environment in Part 3, Chapter 3.10 (UNECE, 2004a). Annex 8, Guidance on Hazards to the Aquatic Environment (UNECE, 2004). Ecotoxicity tests can be classified into two following categories: standard and alternative tests.

The ecological testing according to US EPA and UNECE includes many tests; however, several methods of ecotoxicological testing are used in the Czech Republic. For the typical standard and alternative aquatic ecotoxicological tests crustacea (*Daphnia magna, Thamnocephalus platyurus, and Artemia salina)*, aquatic plant (*Lemna minor*), algae (*Desmodesmus subspicatus, Scenedesmus subcapitatus, Selenastrum capricornutum)* are used. In accordance with OECD, UNECE and Czech legislation the standard tests include these organisms in following tests – *Daphnia magna* (OECD Test No. 202: Daphnia sp. Acute Immobilizations Test, EN ISO 6341:1996), *Desmodesmus subspicatus* (OECD – Test No. 201: Alga, Growth Inhibition Test, ISO 8692:2004). The aquatic organism *Lemna minor* (OECD Test No. 221: Lemna sp. Growth Inhibition Test, ISO 20079:2005) is application in OECD and ISO standard methods for the testing of chemicals.

Experimental

The general principle of ecotoxicological tests is the determination of effective concentration (EC50), eventually lethal concentration (LC50) or inhibition concentration (IC50). The limit test corresponds to one dose level of $100\,\text{g}\,\text{dm}^{-3}$. A stepwise procedure involves four steps: the limit test, confirmatory test, basic test and definitive test.

These types of studies produce end points such as LC50, EC50 and NOEC. EC50, LC50 and IC50 are the effective concentrations (i.e., the concentration of material in water that is estimated to produce a specifically quantified effect to 50 % of the test organisms). The EC50 and its 95 % confidence interval are usually derived by statistical analysis of a quantal, "all or nothing", response (such as death, fertilisation, germination, or development) in several test concentrations, after a fixed period of exposure. End point means the variables (i.e., time, reaction of the organisms) that indicate the termination of a test, and also means the measurement(s) or value(s) derived, that characterise the results of the test (EC50). LOEC (lowest observed effect concentration) is the lowest concentration tested causing a statistically measurable effect to the test system. NOEC (no observed effect concentration) is the highest concentration tested causing no statistically measurable effect to the test system. The parameters LOEC and NOEC may be statistically determined.

The aim of statistical analysis of ecotoxicological data is to obtain a quantitative concentration-response relationship by regression analysis. For this purpose many models could be used such as: linear interpolation, polynomial regression, log–logistic regression, probit model, Weibull model, Dunnett test, William test, Jokheere-Terpstra test.

Ecotoxicological Tests for Determination of Ecotoxicity of Standard K_2CrO_4

The standard chemical K_2CrO_4 was used for the determination of ecotoxicity, for th estimation of sensitivity of testing organisms *Dapnia magna Strauss*, (Daphtoxkit F™ magna – standard test) *Thamnocephalus platyurus* (Thamnotoxkit F™ – alternative test) and *Lemna minor* (standard test OECD) and for validation and comparison of obtained results with the declared values. Table I performs the basic parameters of tests in coordinance with the directive.

Table I
The parameters of tests

Parameters	Daphtoxkit F™	Thamnotoxkit F™	*Lemna minor*
$c\,[\text{mg}\,\text{dm}^{-3}]$	0.32–3.20	0.032–0.320	10–160
$T\,[°C]$	22 ± 2	20 ± 2	24 ± 2
$I\,[\text{lx}]$	6,000	4,000	–

Results

On the base of analysis of obtained ecotoxicological results for studied tests the values of EC50, LC50 and IC50 were determined for standard chemical K_2CrO_4. The experimental data with the basic statistic characteristics are summarized in Table II. The EU-Directive 93/67/EEC classifies substances according to their ecotoxicological value (EC50). On the base of obtained data from ecotoxicological tests (crustacea tests Daphtoxkit F™ and Thamnotoxkit F™) the study chemical belongs to very toxic for aquatic organisms. The studied chemical K_2CrO_4 is also toxic to aquatic organisms for macrophyta *Lemna minor*.

The *Thamnocephalus platyurus* was found as the test organism of highest sensitivity with LC50 = $0.092 ± 0.002\,\text{mg}\,\text{dm}^{-3}$. The effective concentration (EC50/24 h) from Daphtoxkit F™ for exposure 24 hours was $0.99 ± 0.022\,\text{mg}\,\text{dm}^{-3}$ and the effective concentration (EC50/48 h) was confirmed $0.79 ± 0.031\,\text{mg}\,\text{dm}^{-3}$ The inhibition concentration for *Lemna minor* (IC50/168 h) was calculated from average specific growth rate and confirmed via percent reduction in yield, IC50/168 h was equal to $20.52 ± 0.399\,\text{mg}\,\text{dm}^{-3}$. For validation and confirmation of experimental data the probit model was used for determina-

tion of ecotoxicological parameters. Calculated values from probit model and experimental values were in very good correlation with declared value of tests.

Table II
The ecotoxicity of K_2CrO_4 (n = 9; concentration in mg dm^{-3})

| | Daphtoxkit F™ | | Thamnotoxkit F™ | *Lemma minor* |
	EC50/ 24 h	EC50/ 48 h	LC50/24 h	IC50/168 h
Declared values	1.03	0.75	0.10	–
Experim. value	0.99	0.79	0.092	20.52
Probit model	0.96	0.69	0.093	–
Median	0.99	0.75	0.093	20.00
s	0.0286	0.0411	0.0035	0.5200

Conclusions

The ecotoxicity of the tested chemical was confirmed by the application of ecotoxicological tests. In the majority of cases, on the base of the obtained results of the study tests with chemical, the tests perform very suitable way for the study of ecotoxicity and can be used for evaluation of ecotoxicity of other chemicals and wastes. This study confirmed declared value and all data were statistical evaluated in detail, and the sensitivity of testing organism was also confirmed.

REFERENCES

1. UNECE:*Globally Harmonized System of Classification and Labeling of Chemicals*. ST/SG/AC.10/C.3/40/ Add.221 December 2001.
2. van Straalen N. M.: Environ. Toxicol. Pharmacol. *11*, 167 (2002).
3. Isnard P., Flammarion P., Roman G. et all: Chemosphere *45*, 659 (2001).
4. OECD *Environmental health and Safety Publications: Series on testing and Assesssmnet* No.10, ENV/MC/ CHEM (98)18.
5. OECD Environmental health and Safety Publications: OECD *Guidelines for Testing Chemicals* No 201 (2006, 2004, 1992)
6. ISO 8692:2004: *Water quality – Freshwater algal growth inhibition test with unicellular green algae*
7. ISO 6341:1996: *Water quality – Determination of the inhibition of the mobility of Daphnia magna Straus (Cladocera, Crustacea) – Acute toxicity test*
8. ISO 20079:2005: *Water quality – Determination of the toxic effect of water constituents and waste water on duckweed (Lemna minor) – Duckweed growth inhibition test*
9. Commission of the European Communities, 1996. *Technical guidance document in support of commission directive 93/67/EEC on risk assessment for new notified substances and commission regulation (EC) No 1488/94 on risk assessment for existing substances. Part II; Environmental Risk Assessment.* Office for official publications of the European Communities, Luxembourg.

P14　INDOOR AEROSOL EXAMINING

ADRIANA EŠTOKOVÁ, NADEŽDA ŠTEVULOVÁ and
LENKA KUBINCOVÁ

*Technical University of Košice, Civil Engineering Faculty,
Institute of Building and Environmental Engineering, Vysoko-
školská 4, 042 00 Košice, Slovak Republic,*
Adriana.Estokova@tuke.sk

Introduction

Aerosol particles are generally considered to be one of the principal indoor risk factors. Operation, number and behavior of occupancy i.e. type, emission intensity and amount of indoor contamination sources (building materials, combustion processes, smoking, cleaning)[1,2] determine temporal and spatial variations of indoor aerosol distribution. The particulate matter (PM) cause the negative health effect, when they are inhaled and deposited in the respiratory tract[3].

This paper is primarily concerned with suspended PM_{10} concentrations and indoor settled PM monitoring with regard to the chemical composition and shape of PM_{10} particles.

Experimental

M e t h o d s

Suspended particulate matter investigation was focused on thoracic fraction PM_{10} monitoring in various types of residential and non-residential buildings. Measurement includes integral particles sampling onto a collection material (membrane filter Synpor 0,8 μm pore size, 35 mm in diameter) by sampling equipment VPS 2000 (Envitech, Trenčín) at air flow of 960 $dm^3 h^{-1}$ during sampling period of approximately 24 hours. The sampling was carried out in the middle of the room at the height of 1,500 mm from the floor. The windows and the door were closed during the monitoring period. The particulate mass concentrations were determined by gravimetric method from the increase of filter weight. Because of minimisation of humidity interference, the filters were dried at 105 °C for 8 h before and after sampling and than were equilibrated at a constant temperature and humidity (e.g. 20 °C and 50 % RH) for 24 h before and after sampling.

The monitoring of indoor settled PM was performed in selected flat building. Sampling was carried out by passive methods based on PM settling into Petri dishes during 28 days. The particle surface concentrations were determined by gravimetric method.

The PM_{10} samples were characterized by scanning electron microscopy/energy-dispersive X-ray analysis (SEM/ EDX) and atomic absorption spectroscopy (AAS) as the main techniques. Particle morphology was determined by SEM on the equipment Tesla BS 340. The elemental EDX analysis were carried out on the micro-analytical system LINK ISIS 300 (Oxford Instruments) operating in secondary mode at a potential 25 kV and at extension 600–30,000. The chemical analysis of the selected metals samples content was realised by SpectrAA-30 (Varian).

Results

The results of indoor PM_{10} monitoring in different types of residential and non-residential buildings are illustrated as average mass concentrations in the Fig. 1.
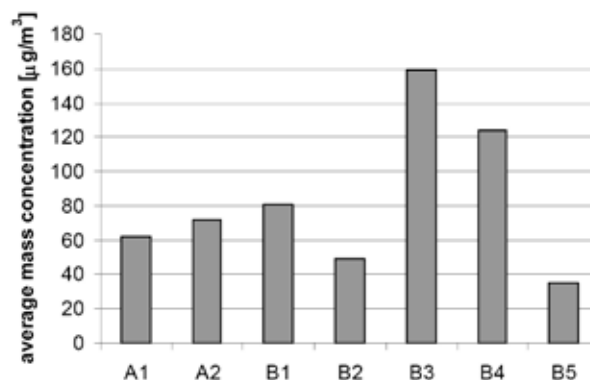
Fig. 1.　**The average mass concentrations of PM10 in residential (A) and non-residential (B) buildings: A1 – single family residences, A2 – flat-residences, B1 – school buildings; B2 – offices; B3 – commercial buildings; B4 – buildings for culture and ntertainment, B5 – hospitals and sanitary facilities**

The highest mass PM_{10} concentration was observed in non-residential public buildings. The PM_{10} hygienic limit for indoor air in Slovak republic – 50 $\mu g\,m^{-3}$ was exceeded in all monitored types of residential and non-residential buildings excepting B2 (offices) and B5 (hospitals). The concentrations of settled PM were measured at various heights and were ranged from 21.0 $\mu g\,cm^{-2}$ to 86.6 $\mu g\,cm^{-2}$. The trend of gradual decreasing of particulate matter occurrence with the raise of height was observed (Fig. 2.).
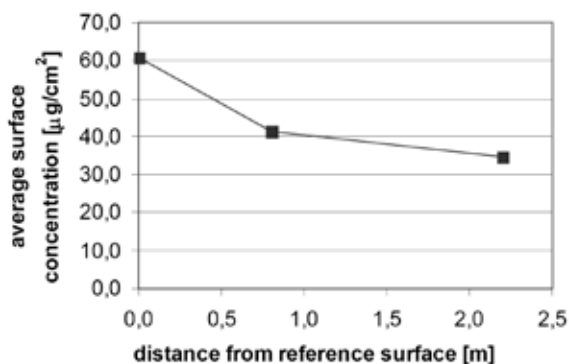
Fig. 2.　**Average mass surface concentration of settled PM in dependence on the height**

The mass concentrations of metals in PM_{10} samples investigated by AAS are summarised in Table I.

The obtained mass concentrations of metals in indoor particle samples correspond with those of in typical urban aerosol[5]. The individual particles in irregular shape of the various particle size as well as particles aggregates were observed on the SEM micrographs (Fig. 3.).

Table I
The mass concentrations of metals

Element	Average [$\mu g\,m^{-3}$]	Minimum [$\mu g\,m^{-3}$]	Maximum [$\mu g\,m^{-3}$]
Cu	0.704	0.03	3.38
Pb	0.094	0.007	0.666
Cd	0.094	0.002	0.625
Ni	0.050	0.007	0.29
Cr	0.058	0.007	0.35
Zn	0.408	0.08	2.01
As	0.007	0.0001	0.019
Fe	1.818	0.36	9.23
Sb	0.115	0.0001	1.47
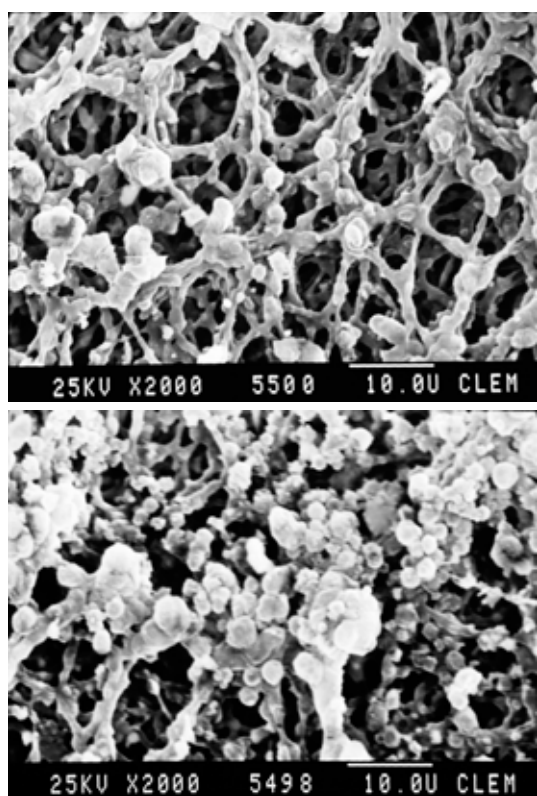
Fig. 3.   **SEM micrograph of particles**

The majority of PM_{10} particles are non-spherical in shape with strong division of the surface. The occurrence of the spherical particles as well as of fibrous particles was not obvious[4].

The energy-dispersive X-ray system interfaced to the SEM provides preliminary information on the elemental composition of the samples. Fig. 4. represents EDX spectrum of the selected solid aerosol sample. The principal inorga-
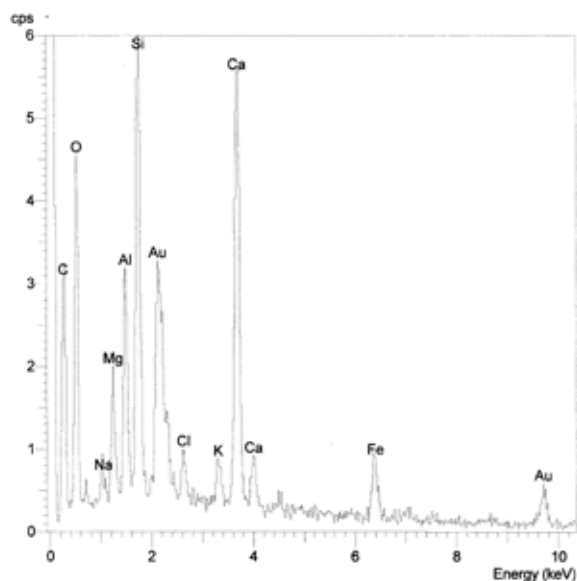
Fig. 4.   **EDX spectrum of suspended PM_{10}**

nic elements constituting the particles in order of decreasing peak intensity were Ca ≈ Si > O > Al > C > Mg > Fe > Cl > Na ≈ K.

Conclusions

High indoor PM_{10} concentrations exceeding the hygienic limit (excepting offices and hospitals and sanitary facilities) were found out in this study. The trend of gradual decreasing of settled particulate matter concentration with height rising was observed. The determined metal mass concentrations in PM_{10} correspond with the typical metal concentration range of the urban aerosol. SEM investigation refers the presence of majority particles non-spherical in shape, in primary as well as secondary form (aggregates).

REFERENCES

1. Eštoková, A. et al.: *Proceding of the 4th International Conference: Praticulate matter*, p. 124. Slovakia, Košice: TU, 2003.
2. Owen, M. et al: J. Atmos. Environ *26*, 2149 (1992)
3. Gwynn, R.CH. et al: J.Environmental Health perspectives *108*, 125 (2000).
4. Eštoková, A., Števulová, N.: J. Chemické listy *96*, 8 (2002).
5. Hovorka J.:*Aktuálni otázky znečistení ovzduší*. UK, Praha 2004.

P15 ATMOSPHERICAL DEPOSITION AND IMMISSION SITUATION IN THE NIŽNÁ SLANÁ AREA

ERIKA FEDOROVÁ, JOZEF HANČUĽÁK, OĽGA ŠESTINOVÁ, JÁN BREHUV and TOMISLAV ŠPALDON

Institute of Geotechnice of the Slovak Academy of Sciences, Watsonova 45, 043 53 Košice,
fedorova@saske.sk

Introduction

Owing the positive results of geological survey, the Nižná Slaná region has become during last 35 years the most important basis of Fe-ore. Potential of industrial siderite is 63 mil. t[1,2].

The biggest of the polution sources is the chimney which is 120 m high. The dust fallout was monitored by means of 17 sampling points located maximally up to 8 km from main source of pollution. The pollutants have municipal as well as industrial origin[5]. The range of plant emission by chemical data processing and by their comparision with dust deposition was investigated. In the present time the communal and the natural sphere causes the air pollution[3,7].

Experimental

Samples of the dust deposition were taken in monthly intervals from seventeen sampling places in the intervals of 30 ± 3 days. To take the samples of the dust deposition plastic sedimentation containers having a cylinder shape with the internal diameter of 12.5 cm were used and located on two holders in the height of 2.5 to 3 m[1,4,7]. The containers were filled with 250 ml of distilled water with additives of substances preventing creation of algae in the summer period and antifreeze additives in the winter period. After sampling the content of the containers was quantitatively transferred to the evaporating dishes and evaporated. To remove the organic mass the evaporation residue was annealed at the temperature of 450 °C. The temperature was selected not to cause degradation of present carbonates and so possible distortion of gravimetry of the dust deposition. The gravimetry was made separately for each of the containers[6]. The result for each month and individual sampling places is calculated in units of $g\,m^{-2}(30\,days)^{-1}$ and it is the average of alues from two exposed containers. The inorganic part from twelve months set by annealing was cumulated into one sample and after mineralization analysed for individual monitored elements using the AAS method and the SpectrAA – 30 VARIAN unit[4,7].

Results

Localisation of the sampling places of deposition is shown in Table I.

The results are the values acquired from deposition samples after drying and annealing. The specific values of dust fallout are shown on Table II. As it is evident from these results, the highest values of the dust fallout were recorded in summer months and the vegetation period and that is

Table I
Localisation and the samples quantity in the year of 2007

Number of locality	Locality	The samples quantity
1	Vlachovo – swimming pool	12
2	Gočovo – playground	11
3	N. Slaná – colony	12
4	Above plant	12
5	Before plant	12
6	N. Slaná – agrarian cooperative	12
7	N. Slaná – playground	12
8	Direction to Kobeliarovo	12
9	Crossroad – Štítnik	11
10	Henckovce – before village	12
11	Henckovce – upper part	12
12	Henckovce – cemetary	12
13	Henckovce – near railway	12
14	Henckovce – lower part	12
15	Between H. a G. Polomou	11
16	Gemerská Poloma	12
17	Betliar	12

reflected in the percentage representation of the annealed organic part.

According to Table II and Fig. 1. the highest average values were recorded on sampling places no. 7 and 5 in 2007 being directly influenced by the dust deposition from the spot source of the plant and localized in the central part of the valley (4.40 an 2.77 $g\,m^{-2}$ (30 days)$^{-1}$ accordingly). Just to compare, the average value from the sampling place no. 8 that is localized relatively close to the plant, but on the west side of the valley (west side of Nižná Slaná in the direction to Kobeliarovo) achieves only 0.57 $g\,m^{-2}(30\,days)^{-1}$. Some of the increased values mainly from the summer period need to be ascribed also to the extremely dry weather in 2007 and blowing out of the inorganic particles from the uncovered horizonts of the farmland.
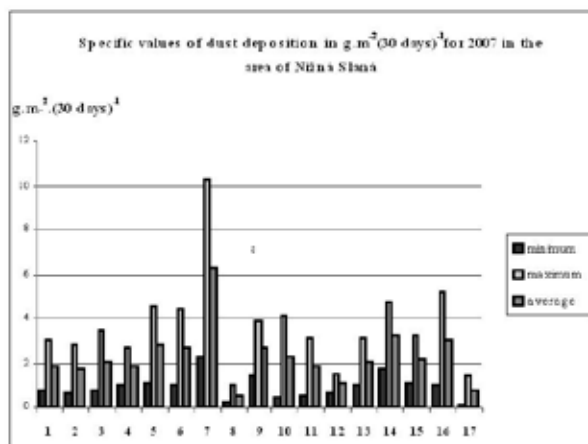
Fig. 1. **Specific values of dust deposition in $g\,m^{-2}(30\,days)^{-1}$**

Table II
Specific values of dust deposition in $g\,m^{-2}(30\ days)^{-1}$

No.	Locality	After dying			After annealing		
		min.	max.	aver-age	min.	max.	aver-age
1	Vlachovo – swimming pool	1.08	4.72	2.90	0.73	3.00	1.87
2	Gočovo – playground	1.07	12.13	6.60	0.70	2.82	1.76
3	N. Slaná – colony	1.28	5.76	3.52	0.72	3.43	2.07
4	Above plant	1.32	8.29	4.80	0.98	2.71	1.84
5	Before plant	2.10	5.24	3.67	1.10	4.52	2.81
6	N. Slaná – agranian cooperative	2.65	8.80	5.72	0.93	4.41	2.67
7	N. Slaná – playground	3.01	13.22	8.12	2.29	10.23	6.26
8	Direction to Kobeliarovo	0.34	3.97	2.16	0.18	0.98	0.58
9	Crossroad – Štítnik	1.69	9.82	5.76	1.38	3.92	2.65
10	Henckovce – before village	0.79	9.11	4.95	0.42	4.08	2.25
11	Henckovce – upper part	0.94	8.65	4.79	0.55	3.10	1.83
12	Henckovce – cemetary	0.96	5.08	3.02	0.61	1.49	1.05
13	Henckovce – near railway	1.21	8.62	4.92	0.94	3.12	2.03
14	Henckovce – lower part	2.07	12.71	7.39	1.68	4.79	3.24
15	Between H. and G. Polomou	1.67	6.07	3.87	1.09	3.23	2.16
16	Gemerská Poloma	1.37	7.83	4.60	0.96	5.16	3.06
17	Betliar	0.55	6.37	3.46	0.13	1.42	0.77

Conclusion

Monitoring of the dust deposition in 2007 year has shown a relative increase of dustiness in the monitored area influenced by the activity of the Siderit plant. The increased
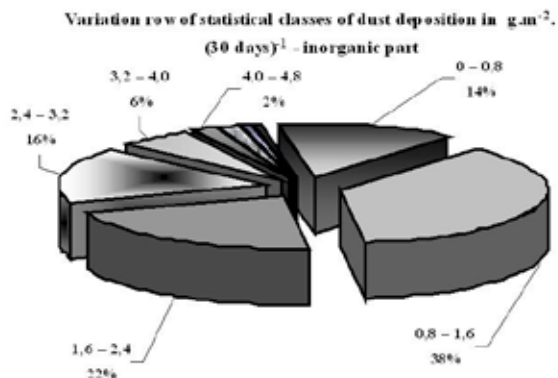
Fig. 2. **Variation row of statistical classes in $g\,m^{-2}(30\ days)^{-1}$ - inorganic part**

impact can be observed in the area of the farm where the smoke plume touches the terrain immediately.[4] Specific sources of gaseous and solid substances exhaled to the move with air flows in the heights of 100 – 250 m. The research in this area will enable to highlight the positive activity of the plant management in relation to the public in the interest of improvement of environment quality in the given area.

REFERENCES

1. Kyntera F., Nevyjel E., Leško O.: *The pollutants measurements in the Nižná Slaná area*, Košice 1984.
2. Grecula P. et al: Mineralia Slovaca, *829*, 1 (1995).
3. Mihók J.: *Mining – processing establishment.* SIDERIT Nižná Slaná, p. 125, (1997).
4. Fedorová E.: Dissertation. Slovac Academy of Sciences at Košice, Košice, Slovakia, 2003.
5. Baluchová B., Fejdi P., Bobro M.: Mineralia Slovaca 36, 357 (2004).
6. Ursíniová M., Vaňová R., Paľušová O.: Acta Hygienica et Epidemiologica et Microbiologica 21, 1 (1992).
7. Hančuľák J., Bobro M., Brehuv J., Slančo P.: Acta Montanistica Slovaca 10, 246 (2005).

P16 THE NATURAL AND ANTHROPOLOGICAL CONTAMINATION SOURCES OF THE HALČIANSKY WATER RESERVOIR

SLAVOMÍRA KAŠIAROVÁ[a] and MELÁNIA FESZTEROVÁ[b]

[a]*Trenčín University of A. Dubček, Department of public management, Študentská 2, 911 50 Trenčín, Slovakia*
[b]*Constantine the Philosopher University, Faculty of Natural Sciences, Department of Chemistry, Tr. A. Hlinku 1, 949 74 Nitra, Slovakia*
kasiarovas@azet.sk

Introduction

Many technical sights, as an integral part of a landscape structure, are at the same time its dominant features as they are directly related to its history. In the Banská Štiavnica region they are mostly related to mining traditions. Importance of water reservoirs, also called "tajchy", in the region stems their recreational utilisation. The cleanliness of water is therefore a key issue[1].

This study has focused on the identification of possible natural and anthropogenic sources[2] of pollution in the model territory of the Halčiansky water reservoir and consequently on its contamination. Water reservoirs built to provide the water energy for driving mining machinery are a part of a mining history. As such they are a typical landscape-ecological component of the Banská Štiavnica landscape. Because of their significance they are listed on The State List of Cultural Monuments as sights of technical development and on The World Catalogue of Water Reservoirs.

Experiment and Methods

In the model territory of the Halčiansky Water Reservoir, conditions of potential movement of water and related contaminants were analysed in relation to natural and anthropogenic sources of contaminants with the use of GIS (Geomedia Professional) tools. The aim of the analysis was to determine the vector of the transport and representative sampling points. Based on the system analysis of the above conditions, the selection of sampling points was proposed with the sampling points for the transport system set as transparent. Samples of water taken at the representative points (period 2006–2007) were analysed in situ by spectrophotometer (Hach DR 2000, Horiba) and related to an assumed model of contamination. The results of physical-chemical analysis were further compared with the expected transit and interpretation of the contamination in the territory.

Results and Discussion

The following characteristics have been derived from the results and water quality monitoring:

(i) Water reaction, conductivity, turbidity, temperature, salinity, nitrates (1.3–2.2 $mg\,dm^{-3}$) and amount of chlorides (1.6–9.3 $mg\,dm^{-3}$) and sulphates (18–33 $mg\,dm^{-3}$) complied with the norm No. 490/2002 Z. z. during all seasons, and no measured value exceeded the norm.

(ii) An increase of ammonia, nitrites, phosphates concentrations and of chemical consumption of oxygen exceeding the limit value set by the norm No. 491/2002 Z. z. was recorded during all four seasons.

- Free ammonia – concentration values of NH_3 were in a range of 0.07–1.07 $mg\,dm^{-3}$ them exceeding the limits of the norm (<0.3 $mg\,dm^{-3}$). In the vicinity of the sampling points 2 and 3 there were grazing grounds foraged by cattle and sheep and an agricultural land fertilized by ammoniac, sulphate ammonia or liquid manure, increasing concentration of ammonium salts in water. Cattle excrements and fertilizers are entering water reservoir by the run-off flowing down the surrounding slopes. The directions of run-off conditions also confirm this. Another source of pollution at the sampling points 5 and 6 was stabled cattle and cesspools from the residential or recreational areas.
- The most distinctive representation of pollution in the form of nitrites 0.004–0.226 $mg\,dm^{-3}$ was detected in spring when the concentration of those contaminants exceeded the value set up by the norm almost eleven times. Mutual comparison of sampling points indicated the highest concentration of nitrites at the sampling sites 3, 4, 5 and 6. Nitrites are products of biochemical oxidation of ammonia and to lesser extent products of the reduction of nitrates. Their sources are household sewage and wastewater.
- There were also excessive concentrations of phosphates 0.6–2.1 $mg\,dm^{-3}$, which exceeded limits set up by the norm five times, with maximum concentrations registered in autumn at the sampling site 2. Main sources of phosphates are household sewage and wastewater together with dead bodies of plants and animals.
- Chemical consumption of oxygen 10–2,800 $mg\,dm^{-3}$ had the highest value in winter, at the sampling site 1 (the dam), exceeding the limit value set up by the norm eighty times. Organic water pollution can be both of natural (leaches from the organically rich soil, forest, peat bog, etc.) and artificial origin (pesticides, fertilisers).

The above results have shown that the selection of sampling points based on the system analyses and GIS outcomes confirmed assumptions of physical-chemical analysis of water in natural and residential zones. The exceptions were nitrates and chlorides concentrations, in case of which the higher values were expected especially in the agricultural areas or residential zones.

Conclusions

Results of potential conditions of contaminants in the territory of the vector movement of water and gravitation confronted with results of physical-chemical analyses show the relevance of the model. This will enable an effective

and rational selection of sampling places in the future, ensuring the representativeness of sampling in the professional analysis of water contamination.

REFERENCES

1. Samešová D., Melichová Z., Šikulová Z.: Séria environ. ekol. 1, 104 (2002).
2. Samešová D., Ladomerský J.: Ekologia, 2006 (in press).

P17   BIOMODIFIED FORMS OF NATURAL ZEOLITE AND THEIR ENVIRONMENTAL APPLICATION

MÁRIA REHÁKOVÁ[a], ĽUBICA FORTUNOVÁ[a], SILVIA ČUVANOVÁ[b], LUCIA GABEROVÁ[c] and MÁRIA KUŠNIEROVÁ[b]

[a]*Faculty of Science, P.J.Šafárik University, Moyzesova 11, 041 54 Košice, Slovac Republic,*
[b]*Institute of Geotechnics, Slovak Academy of Sciences, Watsonova 45, 043 53 Košice, Slovac Republic,*
[c]*Université de Provence, Centre de Saint-Jérôme, Marseille, France,*
maria.rehakova@upjs.sk

Introduction

The increasing levels of heavy metals in the environment represent a serious threat to human health, living resources, and ecological systems. Mobile and soluble heavy metal species are not biodegradable and tend to accumulate in living organisms, causing various deseases and disorders. Amongst various treatment methods, ion exchange and sorption seem to be the most attractive in case those nontoxic, low cost zeolites are used.

Natural zeolite of clinoptilolite type (CT) from East Slovakian deposit in Nižný Hrabovec has been studied with respect to its feasibility of application in environmental area in combination with biotechnological methods.

This recent investigation presents a continuation of our previous study[1,2] of the decrease of content of heavy metal and other toxic compounds (polychlorinated biphenyls-PCB) in plants growing on heavily contaminated soils in industrial areas. Natural zeolite as well as zeolitic fertilizers was used in this study. The results of study of growing certain agricultural plants in contaminated soils with varying dosages of natural zeolite (CT), zeolitic fertilizer and standard NPK fertilizer confirmed the favorable influence of both zeolite and the zeolite based fertilizer. Analysis of plant material showed that the lowest content of heavy metals (Zn, Cu, Pb, Cd and Cr) as well as of PCB was found in plants grown in contaminated soils with the application of CT. The content of heavy metals and PCB was lower almost of a half in comparison with plants grown on untreated contaminated soils[2]. Plants grown in contaminated soils with the addition of zeolitic fertilizer showed a somewhat higher content. Natural clinoptilolite by ion exchange of heavy metals and sorption of toxic substances into its cavities and channels blocked their reception into the plants.

The aim of the recent study is the enlarging of clinoptilolite sorption surface by the effect of microorganisms and obtaining more efficient results of its application in the process of reducing the residual content of heavy metals and other toxic compounds in industrial contaminated soils.

According to the literature[3–5], certain species of microorganisms have been found to absorb surprisingly large quantities of heavy metals. The removal of heavy metals from municipal and industrial wastes by biological treatment systems has continued to be of interest. Bacterial surfaces have great affinity to sorb and precipitate metals resulting in metal concentration on the surface. All microbes, which expose negatively charged groups on their cell surface, have the capacity to bind metal ions. Complexolysis is a process corresponding to microbial formation of complexing and chelating agents that solubilize metal ions. The microorganisms are able to transform toxic compounds to less toxic. Biosorption of copper (II) ions by Thiobacillus ferrooxidans were studied and is shown to be an effective bacterial bioaccumulation process[3]. Acidithiobacillus and Thiobacillus cultures are used for biological reduction of chromium (VI)-containing wastes[4]. The attention is paid also to the utilization of combination of microorganisms and microporous materials (active carbon, zeolite) to achieve better sorption properties for adsorption of toxic compounds[5].

Our recent study is aimed to biomodification of the surface of natural zeolite of the clinoptilolite type using the microorganisms Thiobacillus ferrooxidans. Studied are also model forms of zeolites containing copper ions, and the influence of microorganisms on the biosorption of these ions as well as other changes connected with metabolic activity of the microorganisms present. The main motivation of this study is the remediation of soils contaminated with high concentrations of the residual of heavy metals and other toxic compounds.

Experimental

In order to study modified forms of natural zeolite, the natural zeolite of clinoptilolite type (CT) was used from the Eastern Slovakia deposit in Nižný Hrabovec. Two various granulometric classes were taken for the experiments: fine-grained one of the particle size up to 200 µm, denoted as CT1, and coarse-grained of the particle size 0.4–0.6 mm, denoted as CT2. Both granulometric classes of clinoptilolite was thermally activated at 100–110 °C for 1 hour. So prepared zeolitic samples were used for the synthesis of copper forms as well as for cultivation by microoganisms.

All chemical agents used at the synthesis of modified copper forms of the natural clinoptilolite, at the analyses and preparation of nutrition medium were analytical grade (Merck and Fluka).

Preparation of Copper Forms of Natural Zeolite

Copper forms of natural clinoptilolite were prepared by the reaction of fine- and coarse thermally activated fraction of natural clinoptilolite by a reaction with $CuSO_4$ solution of two concentrations: 0.1 and 1.0 $mol\,dm^{-3}$. By this way, both copper forms, fine-grained denoted as CuCT1 and coarse-grained one, denoted as CuCT2, were obtained in consequence of an ionic-exchange mechanism. These heterogeneous mixtures were after 2 hours of stirring decanted several times and centrifuged in order to get rid of sulphate ions and then dried for 1 hour at 100 °C.

Determination of Copper Content in CuCT Samples

The copper content in the copper forms of CuCT1 and CuCT2 was determined indirectly by determination of copper content in the solution unadsorbed by the zeolitic structure, both by AAS spectroscopy at Varian Spectr AA-30, Australia and by SPECOL 11, Carl Zeiss, Jena.

The amount of Cu (II) in the zeolitic samples was determined by the energy dispersive spectroscopy (EDS) analysis using a TESLA BS 340 scanning electron microscope (TESLA ELMI a.s. with a LINK ISIS 300 microanalyser).

Contamination of the Zeolitic Material by Microorganisms

The zeolitic samples the CT1 and CT2 fractions and the copper forms were contamined in a parallel process of cultivation of microorganisms Thiobacillus ferrooxidans (TF) for different time 3,4,5 and 12 months. Before the contamination, all zeolitic samples were irradiated by a germicide lamp for sterilization. The microorganisms used were sufficiently multiplicated in a nutrition medium 9K according to Silverman and Lundgren[6]. In order to compare the surface areas and the pore volumes, a control abiotic sample (denoted as CTF) was used after application only of nutrition medium, without microorganisms.

Analysis of the Surface Areas and the Pore Volumes

The analysis of surface areas and the pore volumes of the zeolitic samples prior to the contamination and after contamination by microorganisms were realized by GEMINI 2360 (Micrometrics USA). The specific surface area was determined by low-temperature adsorption of nitrogen. Before measurements the samples were heated for 2 hours at 105 °C.

Results and Discussion

Biomodified zeolitic samples were prepared by using microorganisms in order to achieve larger sorption surface at natural zeolite of the clinoptilolite type and thus obtain more efficient results at its application in reducing the content of heavy metal residuals and other toxic materials in industrially contamined soils. Two grain- size fractions of natural clinoptilolite were studied: fine-grained (CT1) and coarse-grained (CT2). Both fractions were cultivated by microorganisms Thiobacillus ferrooxidans (TF) after thermal activation. This type of microorganism was chosen from the collection of soil microorganisms due to its accessibility as well as to the fact that some laboratory methods were available developed at the Institute of Geotechnics of the Slovak Academy of Sciences in Košice. Experimental experiences were obtained with using this type of microorganisms in the extraction of heavy metals from aluminosilicate structure. Thiobacillus ferrooxidans are applied in mineral biotechnologies for the extraction of Cu, Fe and other metals[7] and they are also present in low concentrations in the soil.

In our first studies of the biomodified forms[8] of the natural zeolite of clinoptilolite type (CT) the microorganisms Actinomycetes were used too. However, we had observed only negligibly small changes caused by these microorganisms in the studied time interval so that we did not continue in that study.

The zeolitic samples were cultivated at dynamic conditions for different time intervals: 1,3,4,5 months and 1 year. The analyses of the surface area size and pore volumes were realized also after short time intervals during the activity of the microorganisms and nutrition medium: after 3 hours and one day. The surface area and pore volumes decreased in these short time intervals.

In our previous studies[2] the content of heavy metals and PCB in the plants (spring barley-Hordeum vulgare) that were grown in contaminated soils decreased (e.g. content of $Cu = 16\ mg\,kg^{-1}$, $Zn = 52.4\ mg\,kg^{-1}$, $PCB = 2524\ \mu g\,kg^{-1}$) compared with the plants grown in contaminated soils without an added zeolite (content of $Cu = 33.1\ mg\,kg^{-1}$ $Zn = 107\ mg\,kg^{-1}$, $PCB = 4765\ \mu g\,kg^{-1}$). For this reason we have prepared also some model forms of the natural CT with a copper cations content, which forms could be analogically obtained in natural conditions too, if the clinoptilolite sorbs the copper cations that are in the industrially contaminated soils.

Via the contamination of the copper forms of the clinoptilolite by the mentioned microorganisms we pursued the changes of the surface, the volume of the pores and the bioleaching of copper from the zeolitic material as well.

The results of the study of the surfare areas changes of the clinoptilolite, its fine-grained CT1 and coarse-grained CT2 and its some copper forms CuCT1 and CuCT2 are in the Table I and Figs. 1. and 2. The results of the pore volumes were in a good agreement with the results of the surface

Table I
Summary of the size of the surfaces (Sa) of the fine-grain fraction CT1, coarse-grain fraction CT2 and some copper forms before and after the contamination by microorganisms *Thiobacillus* ferrooxidans (TF), and the reference sample (CTF) containing only the nutrition medium without the microorganisms

Sample	Samples contaminated with microorganisms TF	Sa [$m^2\,g^{-1}$]	Control sample CTF Sa [$m^2\,g^{-1}$]
CT1	starting sample without TF	24.2117	24.2117
	after 3 months with TF	29.635	30.6734
CT2	starting sample without TF	25.4622	25.4622
	after 3 months with TF	30.3999	28.6739
CuCT1 (0.1M)	starting sample without TF	25.1931	25.1931
	after 3 months with TF	33.0535	32.6870
	after 1 year with TF	38.2758	37.4310
CuCT2 (0.1M)	starting sample without TF	25.6817	25.6817
	after 3 months with TF	33.154	33.6086
	after 1 year with TF	42.7652	39.6286

areas. The surface areas are relatively low because they were measured only for comparison of the changes. These samples were heated only at temperature 105 ºC for two hours. In our next study the surface area will be measured also after heating at the higher temperatures up to 400 °C.
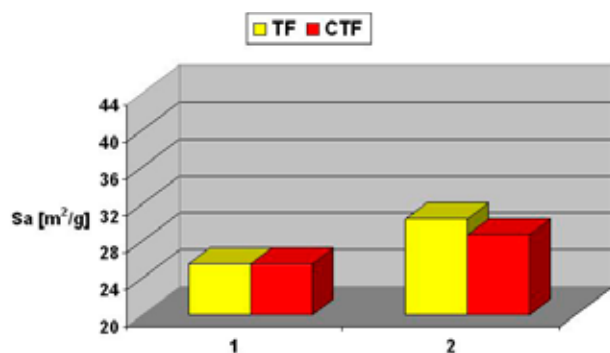
Fig. 1. **Diagram of surface area changes Sa [m^2 g^{-1}] of zeolitic sample CT2, *vs*. its control (CTF): 1) starting sample, 2) three months after the contamination by the *Thiobacillus ferrooxidans***
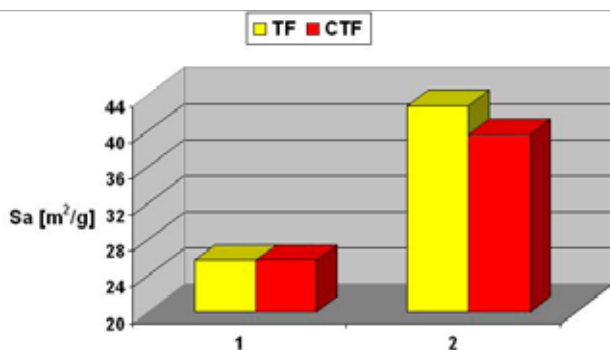
Fig. 2. **Diagram of surface area changes Sa [m^2 g^{-1}] of zeolitic sample CuCT2, *vs*. its control (CTF): 1) starting sample, 2) one year after the contamination by the *Thiobacillus ferrooxidans***

After the comparison of the samples before the contamination by the microorganisms TF and the reference samples CTF it was found out that even the nutrition medium itself, pH = 1.57, contributes to the enlargement of the surface area. The changes of the surface size and the pore volumes were related also with the grain size. At the fine-grain fraction CT-1 the enlargement of the surface of the reference sample (CTF) was higher compared to the sample contaminated by microorganisms. But at the coarse-grained fraction CT-2 which was contaminated by microorganisms the enlargement of the surface area was higher compared with the reference sample. However, more study is still necessary to confirm it and to find out if a change of the grain-size has not occured because such a change can cause an enlargement of the surface size.

At the copper forms CuCT the activity of the microorganisms caused enlargement of the surface area and the pore volumes at both the fine-grain and the coarse-grain fraction, compared to the reference samples.

The copper forms were studied also with respect to a copper bioleaching. According to the analyses of the copper content in the samples contaminated by microorganisms for one year their activity decreased the copper content about 60–75 % (e.g. Cu = 2.17 % in CuCT1 (0.1M) without TF; Cu = 0.58 % in CuCT1 (0.1M) with TF after 1 year). The bioleaching decreased the copper content in the copper forms of the zeolitic samples (CuCT) depending on its starting concentration and on other conditions of the bioleaching process. *Thiobacillus ferrooxidans* utilises copper ions for its metabolic processes. *T. ferrooxidans* contains in the periplasmic space the small blue copper proteins – rusticyanin, which are the principal component in the iron respiratory electron transport chain[9].

The study of the surface area changes and of the bioleaching of copper continues with the aim to obtain more detailed results after more time intervals and under various conditions.

Conclusions

The results of the analyses of the surface area size and the pores volume of the clinoptilolite and its copper forms both before and after the contamination by microorganisms Thiobacillus ferrooxidans confirmed the changes caused by the presence of the microorganisms. The results of the copper bioleaching too indicated that via the influence of the nutrition media and metabolic activity of the microorganims there occured changes of the zeolite surface and decrease of the copper content in the samples. At the present we continue in the study with the aim to obtain more experimental results about the activity of the microorganisms acting for various time intervals and at various conditions.

The combination of application of the zeolites and bioremediate technologies, which use the metabolic activity of the microorganisms looks to be a perspective ecological alternation of the contaminants degradation.

REFERENCES

1. Reháková M., Čuvanová S., Gavaľová Z., Rimár J.: Chem. listy *5*, 260 (2003).
2. Reháková M., Čuvanová S., Dzivák M., Rimár J., Gavaľová Z.: Curr. Opin. Solid State Mater. Sci. *8*, 397 (2004).
3. Masud Hussain S., Anantharaman N.: J. Univ. Chem. Technol. Metall *40*, 227 (2005).
4. Allegretto P., Furlong J., Donati E.: J. Biotechnol. *122*, 55 (2006).
5. Lameiras S., Quintelas C., Tavares T.: Bioresour. Technol. *99*, 801 (2008).

6. Silverman M. P., Lundgren D. G.: J. Bacteriol. *78,*326 (1959).
7. Kušnierová, M., Fečko, P. *Minerálne biotechnológie I.,* VŠB–TU, Ostrava 2001, p. 143.
8. Reháková M., Kušnierová M., Gaberová L., Fortunová Ľ., Čuvanová S.: Chem. listy *100*, 717 (2006).
9. Kanbi D. L., Antonyuk S., Hough M. A., Hall J. F., Dodd F. E., Hasnain S. S.: J. Mol. Biol. *320*, 263 (2002).

P18　DISTRIBUTION PATTERNS OF ORGANIC POLLUTANTS IN BRNO LAKE WITH RESPECT TO ITS DEPOSITIONAL HISTORY

EVA FRANCŮ[a], JAN SCHWARZBAUER[b], MATHIAS RICKING[c], RADIM LÁNA[a], PAVEL MÜLLER[a], JURAJ FRANCŮ[a] and SLAVOMIR NEHYBA[d]

[a]*Czech Geological Survey, Leitnerova 22, 658 69 Brno, Czech Republic,*
[b]*Institute of Geology and Geochemistry of Petroleum and Coal, Aachen University of Technology (RWTH), Lochnerstr. 4–20, 52056 Aachen, Germany,*
[c] *Working Group Hydrogeology and Applied Geochemistry, Free University Berlin, Malteserstr. 74–100 – Raum B117, 12249 Berlin, Germany,*
[d]*Department of Geology and Mineralogy, Masaryk University, Kotlarska 2, 611 37 Brno,*
eva.francu@geology.cz

Introduction

The contamination of the environment with persistent organic pollutants (POPs) has been of great concern since the 1960s. Polychlorinated biphenyls (PCBs) or organochlorine pesticides (OCPs) are found mainly in water, sediments and aquatic biota throughout the world[1,2]. Owing to an intensive agricultural and industrial production in past few decades, in particular, river and lake sediments in the Czech Republic are loaded with POPs and their levels are only partly decreasing[3]. Brno Lake is situated on the Svratka River upstream from the city of Brno and belongs to the most important water reservoirs in the SE Czech Republic. Undisturbed sediment deposits in lacustrine systems can act as environmental archive after radiodating [4,5]. Since there are only a few studies dealing with the levels of organochlorine contaminants in dated sediment cores [6–9], this pilot study is focused on the occurrence of risk elements and organic pollutants in vertical profiles of the sediment layers of the Brno Lake in order to restore the pollution history of these trace organic pollutants.

Experimental

The first sampling campaign in Brno Lake covered nine 1m-deep cores with 52 sediment samples. A 3 m-long core was drilled during the period of time when the reservoir was empty in the early 2008. The detailed sampling includes 120 samples in total; detailed sedimentological investigation and geochemistry were applied to the whole 3 m profile.

All samples were analyzed using screening methods such as magnetic susceptibility (Kf) measured on KLY-2,3 and 3S kappabridges, elemental analysis of total organic and inorganic carbon (TOC, TIC, respectively), high performance liquid chromatography (HPLC) of 16 EPA priority polycyclic aromatic hydrocarbons (PAH), and gas chromatography with flame ionization detector (GC-FID) to measure the total extractable hydrocarbons (TEH). Seven indicative PCB congeners and organochlorine pesticides were determinated by means of gas chromatograph HP 6890 equipped with μECD

[63]Ni, cool-on-column injector and capillary column HP-5ms (60 m × 0.25 mm i.d.). From the screening results 20 samples were selected for gas chromatography coupled with mass spectrometry (GC/MS) in full scan mode to characterize the distribution of the alkylated aromatic and parent hydrocarbons and in selected ion monitoring mode (SIM) for the saturated fraction (SAT).

Results

The sedimentological visual examination together with elemental analysis of the total organic and inorganic carbon (TOC and TIC) and of the magnetic susceptibility (Kf) indicate a stratigraphic archive with roughly 5 cycles each about 60 cm thick marked by increased magnetic susceptibility, increased sand content and lowered organic carbon (Fig. 1.). These coarser grained intervals formed probably during major flooding events and migration of the lake bottom channel.
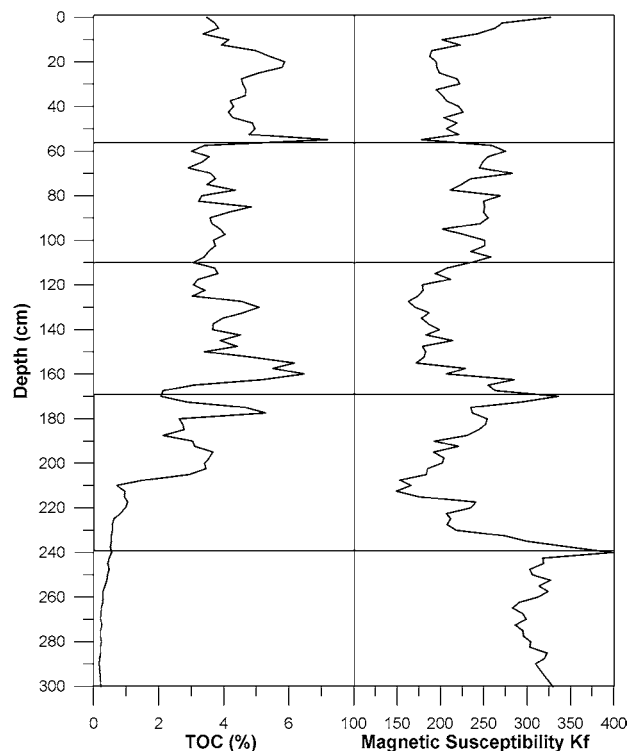
Fig. 1.　**Total organic carbon and magnetic susceptibility in the deep well core profile from the Brno Lake (2008)**

The early phase of the depositional history has sedimentary structures suggesting more fluviatile environment and sandy lithology. The later phases are characteristic by increasing portion of fine-grained sediments. Laminated sediments with organic carbon of up to 7.18 % mark the highstand phases with stratified water column, which persisted over long periods of the existence of the lake. A Th-U(Ra)-K gamma-spectrometric survey shows that a probable source of these elements is in the weathered granitic material of the Brno Massif while the contribution from the U-mines is negligible.

The dating using ^{137}Cs indicates the position of the 1986 and 1961-2 events. The organic carbon, total sulphur, PAHs and PCBs provide a tentative pattern related to depositional history and flow rate. The geochemical profiles show a general upward increase in eutrophication and organic matter accumulation associated with increased cyanobacterial blooms. The sum of nine PAHs often exceeds the 10 mg kg^{-1} EPA limit value and their pyrogenic character suggests an origin in low-quality fuel and furnaces used in the villages and recreational facilities in the watershed.
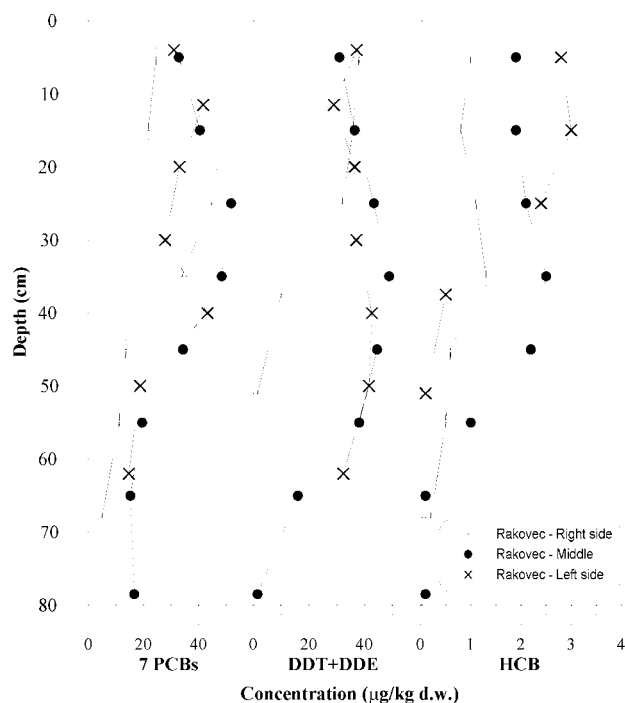
Fig. 2.   **Vertical changes in organochlorine pollutants levels in one-meter-deep well core profiles from the Brno Lake (2001)**

The higher-chlorinated PCB congeners 138, 153 and 180, and *p,p*-DDE (a highly stable aerobic metabolite of the notorious insecticide *p,p*-DDT) are the most abundant organochlorine compounds detected in the sediments. PCBs show upward increase from a depth of 0.6 (0.8–0.5) m (Fig. 2.), which marks the beginning of the use of PCBs and DDT. A

stagnation in the PCB and DDT concentration is observed in the upper part of the profile (0.25–0.00 m) deposited during the last decade. The differences in POP concentrations found in individual cores and layers are closely associated with variable sedimentation rates and occurrences of bottom currents affecting the organic matter deposition.

Conclusions

The pollution archive related to the depositional history of the Brno Lake suggest at least 5 cycles, each about 60 cm thick, defined by the maxima in magnetic susceptibility and minima in total organic carbon which are associated with major floods or migration of bottom currents. The amount of POPs is low in more sandy early sediments, increases at a specific depth and age throughout the basin and finally stagnates during the last decade of mud deposition indicating decreased input of POPs into the environment.

REFERENCES
1. Sapozhnikova Y., Bawardi O., Schlenk D.: Chemosphere *55*, 797 (2004).
2. Luder B., Kirchner G., Lucke A., Zolitschka B.: J. Paleolimnol. *35*, 897 (2006).
3. Müller, P., Hanák, J., Boháček, Z., Toul, J., Müllerová, H., Kovářová, M.: Final Report of the project VaV/630/4/02, MS, Czech Geological Survey, Praha. Brno. MŽP Praha (2005a in Czech).
4. Bollhöfer A., MAngini A., Lenhard L., Wessels M., Giovanoli F., Schwarz B.: Environ Geol *24*, 267 (1994).
5. Heim S., Schwarzbauer J., Kronimus A., Littke R., Woda C., Mangini A.: Org. Geochem. *35*, 1409 (2004).
6. Heim S., Ricking M., Schwarzbauer J., Littke R.: Chemosphere *61*, 1427 (2005).
7. Catallo W.J., Schlenker M., ambrell R.P., Shane B.S.: Environ Sci Technol *29*, 1436 (1995).
8. Wei S. et al: Mar. Pollut. Bull. (in press, 2008).
9. Heim, S., Schwarzbauer, J., Kronimus, A., Littke, R., Hembrock.-Heger, A.: Envir.. Chem. Lett. *1*, 169 (2003).

P19　NEW RESIN GEL FOR DIFFUSIVE GRADIENTS IN THIN FILM (DGT) TECHNIQUE

MICHAELA GREGUŠOVÁ[a,b], BOHUMIL DOČEKAL[b] and HANA DOČEKALOVÁ[b]

[a]*Institute of Analytical Chemistry of the ASCR, v. v. i. Veveří 97, 60200, Brno, Czech Republic,*
[b]*Faculty of Chemistry, Brno University of Technology Purkyňova 118, 61200 Brno, Czech Republic,*
xcgregusova@fch.vutbr.cz

Introduction

The diffusive gradients in thin film technique (DGT) represents a relatively new approach to *in situ* determination of labile metal species in aquatic systems. The DGT device accumulates labile species *in situ* from the solution, and thus problems associated with conventional collection and filtration procedures can be eliminated. After diffusing through a layer of polyacrylamide gel of known thickness (Fig. 1.), metal species are trapped by an immobilized binding agent (usually Chelex 100) incorporated in a resin gel layer[1]. Concentration gradient established in the diffusive layer is a basis for quantitative measurement of metal concentrations in the solution. The mass of accumulated metals in the resin gel is usually determined by AAS or ICP-MS after elution of resin gel with acid.

This paper reports on the performance of a new resin gel based on alternative binding agent with 5-sulphophenyl-azo-8-hydroxychinoline groups, specific sorbent Spheron-Oxin® (ref.[2]).

Experimental

Diffusive and resin gels were based on polyacrylamide hydrogel, prepared according to the conventional procedures (DGT Research Ltd., Lancaster, UK)[1]. Chelex 100 was substituted by Spheron-Oxin® in the resin gel. DGT probe was loaded with resin gel, diffusive gel and filter on the cylindric body and sealed with a plastic top with an exposition window of 2 cm in diameter (Fig. 1.). DGT probes were deployed in the test solutions at 24 ± 1 °C.

Elution efficiency of Cd, Cu, Ni, Pb and U was obtained from subsequent elution experiments with 1 ml 1 mol dm^{-3} nitric acid. The sorption capacity of discs was estimated from accumulated mass of a metal in resin discs immersed in solutions of 25–790 mg dm^{-3} Cu. The effect of solution acidity was investigated within the range of pH 3–8. The effect of ionic strength and potential interferents of alkali earth elemets to heavy metals was tested with model solution of sodium (2.5×10^{-5}–0.6 mol dm^{-3}) and magnesium (0–0.05 mol dm^{-3}) nitrate. The effect of competitive ligands on DGT metal uptake was investigated in solutions containing iminodiacetic acid (0–1 × 10^{-4} mol dm^{-3}) and humic substance Fluka (product No. 53680) (0–316 mg dm^{-3}).
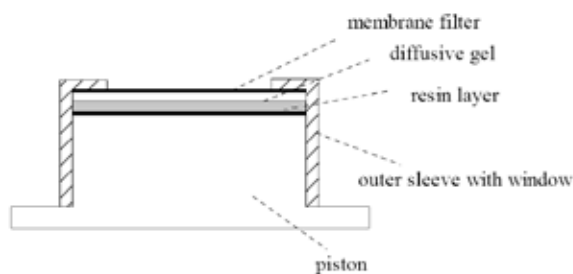
For estimation of specific sorption capabilty to uranium, sorbents Chelex 100, Spheron-Oxin® and Spheron-Salicyl® were exposed to 5 mg dm^{-3} U solutions (pH ~ 6,7) of various carbonate concentration (0–100 mg dm^{-3}).

Results

Quantitative analysis by DGT requires reproducible elution of metal ions from the resin. The elution efficiency for the Spheron-Oxin® resin gel, calculated as the ratio of the amount eluted from the gel and the amount taken up by the gel, was 0.98, 0.66, 0.86, 0.93 and 0.90 for Cd, Cu, Ni, Pb and U, respectively.

Since DGT can be used as a long-term monitoring tool, it is important to assess the sorption capacity of the resin gel. Maximum sorption capacity of 3 µmol disk^{-1} Cu was determined from the isotherm. Because the linear part of the sorption isotherm relates to aproximatelly 10 % of the capacity, discs can be deployed in natural waters for a long time period of several months.

Uptake experiments in the pH range of 3–8 showed that resin gel with Spheron-Oxin® can be used in DGT technique within the pH range of 6–8, typical for most of the natural waters.

The effect of ionic strength was investigated with solution of cadmium (40 µg dm^{-3}). Concentration of Cd measured by DGT was independent of ionic strengths up to 0.6 mol dm^{-3} NaNO$_3$.

Fig. 1.　**Scheme of the DGT unit**
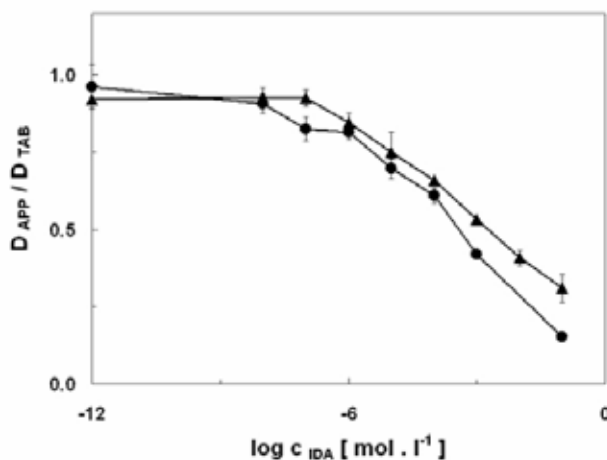
Fig. 2.　**Influence of IDA concentration c$_{IDA}$ on the normalized values of the apparent diffusion coefficients (D$_{APP}$/D$_{TAB}$) for Ni (pH ~ 7). ●Chelex 100, ▲Spheron Oxin®**

In real water systems, several other ions are present, which can compete with metals measured by DGT. The Ca and Mg are dominant cations in hard waters. Although the stability constant for magnesium is lower than for Cd, Cu, Ni and Pb, magnesium can affect DGT measured metals concentrations. Uptake of Cd, Cu, Ni and Pb was not influenced by magnesium nitrate in the whole concentration range up tu 0.05 mol dm^{-3}. New discs can be also used in high salinity waters.
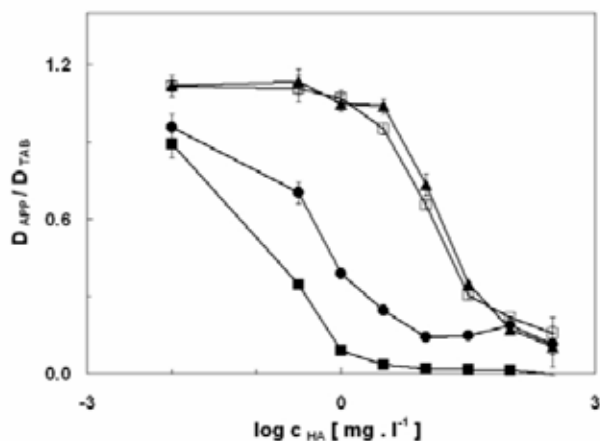
Fig. 3.　**Ifluence of HA concentration c$_{HA}$ on the normalized values of the apparent diffusion coefficients (D$_{APP}$/D$_{TAB}$) for Spheron-Oxin® resin gel (pH ~ 7). ▲Cd, ●Cu, □Ni, ■Pb**

In natural waters, variety of ligands occurs that can affect concentration measured by DGT technique. Iminodiacetic acid (IDA) was used as a model strong ligand influencing the uptake of metals. The results of deployment of DGT units, packed with Spheron-Oxin® and Chelex 100 resin gels, in Ni solutions containing IDA in the concentration range of 0–0.1 mol dm^{-3} are shown in Fig. 2.

Diffusion coefficients (D) can be calculated when taking into account diffusion area (3.14 cm^2) and thickness of the diffusive layer. Those diffusion coefficients can be considered as apparent diffusion coefficients (D$_{APP}$) of the metal under specific conditions. Their values represent the metal fluxes per unit deployment time, unit diffusion area, unit metal concentration in the external solution and unit thickness of the diffusive gel layer. The difference between both curves relates to stability constants of both funcional groups. This difference can be employed in speciation measurements.

Humic acids (HA) are the most widespread natural complexing ligands. Influence of the concentration of the humic substance on the D$_{APP}$ is shown in Fig. 3., in which element-specific effect of HA can be observed. Similar results were also obtained in Refs.[3,4], in which Chelex 100 and Spheron-Thiol® resin gels were used. Due to competitive reactions,
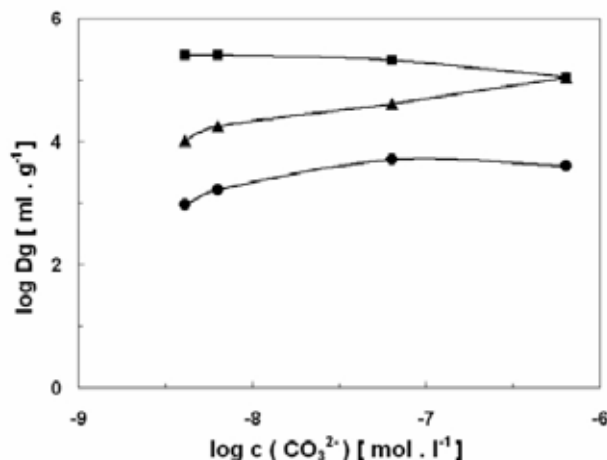
Fig. 4.　**Influence of carbonate concentration on distribution coefficient of uranium for ■ Spheron-Oxin®, ▲ Spheron-Salicyl®, and ● Chelex 100 sorbents (pH ~ 6.7)**

the complex formation with HA decreases the concentration of metal species in external solution that can be measured by DGT.

Uranium, analogously to other heavy metals, forms various complexes in natural waters with a variety of ligands. Depending on pH of the solution, uranyl ions are bound in stable hydroxocomplexes and, especially carbonate complexes due to dissolved atmospheric CO$_2$. Influence of equilibrium carbonate concentration on distribution coefficient (D$_g$) of uranium is shown in Fig. 4. It is evident that the resin gel based on Spheron-Oxin® appears to be a new useful resin gel for speciation analysis of uranium in natural waters.

Conclusions

The new resin gel based on Spheron-Oxin® with anchored 5-sulphophenyl-azo-8-hydroxychinoline functional groups exhibits very strong afinity to Cd, Cu, Ni, Pb and U. In addition to conventional Chelex 100 based gels it can be applied in DGT technique and provide more information on heavy metals speciation, especially of uranium in aquatic systems.

REFERENCES

1. Dawison W., Zhang H.: Nature *367*, 546 (1994).
2. Slovák Z.: Bulletin of n.p.Lachema Brno, 1979, 30 p.
3. Dočekal B., Řezáčová-Smetková V., Dočekalová H.: Chem. Pap. *59*, 298 (2005).
4. Trávníčková J.: *Diploma Thesis.* Brno University of Technology, Brno, Czech Republic, 2008.

P21　CHALLENGES IN THE ANALYSIS OF HEXABROMOCYCLODODECANE IN THE ENVIRONMENTAL SAMPLES

PETRA HRÁDKOVÁ, JAN POUSTKA, JANA PULKRABOVÁ, MICHAELA NÁPRAVNÍKOVÁ and JANA HAJŠLOVÁ

Department of Food Chemistry and Analysis, ICT Prague, Technická 3,166 28 Prague 6, Czech Republic, petra.hradkova@vscht.cz

Introduction

Brominated flame retardants (BFRs) are compounds widely used in commercial products to reduce and prevent the extent of fire. Hexabromocyclododecane (HBCD) is the third most produced BFR worldwide and the second most used BFR in Europe. HBCD is mainly applied as an additive flame retardant for the expanded and extruded polystyrene which are used as insulation materials in buildings and in the upholstery textile.

As the HBCD is not chemically bound to the material to which is added, it could leak into the environment through emission during a production or use of various materials, from final products or following disposal. Similarly to other BFRs, HBCD is a persistent, bioaccumulative and toxic chemical.

There are theoretically 16 HBCD diastereoisomers, however, the technical mixture consists mainly from three diastereomeric pairs of enantiomers (α-, β- and γ-HBCD), the latter one is the most abundant (75–85 %).

Both GC-MS and LC-MS are commonly used techniques for the quantitative determination of HBCD. Total-HBCD (sum of α-, β- and γ-HBCD) may be measured by GC-MS, but it does not allow the quantification of the individual isomers, because the HBCD diastereoisomers can rearrange above oven temperature of 160 ℃ and also resolution of GC separation is not sufficient. The individual HBCD diastereoisomers can be determined using LC-MS/MS. On the other hand, the response in this system may be influenced by matrix ion suppression especially in the electrospray ionisation MS[1,2,3,4].

In this study, the both types of analytical systems were tested to assess the ways of HBCD determination in the environmental samples.

Experimental

The choice of environmental samples was based on: *(i)* a representativeness of both biotic and abiotic components and *(ii)* origin from Czech environment. The final extracts of tested samples including target analytes were analysed by two different chromatographic systems:

- GC-MS (using negative chemical ionization mode (NCI) with quadrupole analyzer)
- LC-MS/MS (using negative electron spray ionization (ESI–) with tandem quadrupole analyzer).

Sample Treatment

The fish muscles of species chub (*Leuciscus cephalus*) and bream (*Abramis brama*) represented biotic environmental samples. The chub and bream frequently occur in Czech rivers, are very suitable as a bioindicator of the aquatic environment contamination and were caught in the Vltava River. Also sediment and sewage sludge represented other analysed samples. The sewage sludge was collected in a sewage treatment plant (STP) and the river sediment was collected downstream from this STP, both in Hradec Králové. The individual standards of α-, β- and γ-HBCD diastereoisomers were obtained from Cambridge Isotope Laboratories (CIL, UK).

The samples (sediment and sludge after drying) were desiccated with anhydrous sodium sulphate and then extracted in a Soxhlet apparatus using a solvent mixture *n*-hexane: dichloromethane (1 : 1, v/v) for fish and DCM in case of sediment/sludge. The crude extracts were rotary-evaporated to dryness. Lipid content of fish samples was determined gravimetrically. In next analytical step, the samples were re-dissolved in 10 ml of ethylacetate: cyclohexane (1 : 1, v/v). The fat and other co-extracted compounds were removed by a gel permeation chromatography (GPC). Finally, a target fraction was rotary-evaporated and concentrated in isooctane and in acetonitrile for GC and LC analysis, respectively. GC extract was in addition treated with concentrated sulphuric acid prior the analysis.

Instrumental Determination

The target analytes were separated using either gas or liquid chromatography. An Agilent 6890N gas chromatography (GC) coupled to an Agilent 5975 Inert XL mass spectrometer (MS) was operated in NCI mode (both Agilent, USA). The system was equipped with a 15 m × 0.25 mm × 0.1 μm DB XLB capillary column (J&W Scientific, USA). The temperature of the column was programmed from 80 ℃ (2 min) to 325 ℃ at a rate of 50 ℃ min^{-1} and held for 5 min. Helium was used as a carrier gas at ramping flow from 1.5 ml min^{-1} (7.2 min) to 3 ml min^{-1} at a rate of 50 ml min^{-1}(ref.[2]). The ion source, quadrupole and interface temperature were 150 ℃, 150 ℃ and 300 ℃, respectively. Bromine isotopic ions [Br]$^-$ at m/z 79, 81 and molecular ions [Br$_2$] at m/z 158 and 160 were monitored for confirmation HBCD in selected ion monitoring (SIM) mode.

A high performance liquid chromatograph carried out with a Waters Alliance 2695 HPLC instrument (USA) together with a Quattro Premier XE tandem-quadrupole mass spectrometer (Waters, USA) was operated in negative electrospray ionization (ESI–). The LC separation of the compounds was performed on a NUCLEODEX beta-PM chiral column (200 × 4 mm id, 5 μm, Macherey-Nagel), kept at 40 ℃, using an (A) methanol, (B) acetonitrile and (C) deionized water gradient. The gradient was programmed as follow: 30 % (A), 30 % (B) and 40 % (C), 0–3 min linear change to 30 % (A), 60 % (B) and 10 % (C), 3–20 min kept this composition.

Specific mass transitions (m/z 640 → 79, 81) were used for a MS/MS determination.

Results and Discussion

The levels of HBCD in selected environmental samples were monitored using both types of previously described analytical systems. As mention above, HBCD consists of three diastereoisomers – α-, β-, and γ-HBCD. Fig. 1. documented the result of a GC-MS application, this technique does not enable the isomers separation, all isomers are eluted in one broaden peak. For this reason, α-isomer is used as a calibrant. Furthermore, individual diastereomers have different response factors which can cause that the less accurate results are obtained in case of higher content of β- and γ-isomers.
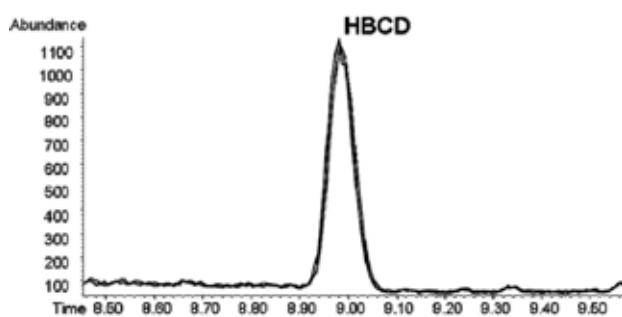
Fig. 1.　**GC-MS chromatogram of HBCD (m/z 79 and 81)**

On the other hand, the LC-MS/MS allows separation of six individual enantiomers as demonstrates Fig. 2.a. The LC chromatograms show diverse patterns of the isomeric composition. In the sediment samples (abiotic matrix), as shows Fig. 2.b, γ-diastereoisomer is usually predominant, followed by α- and β-HBCD, what reflects the diastereomeric profile in various technical products. The content of the first isomer in the biota samples is the inverse and α-HBCD is the most abundant (no figure). It could be caused by biotransformation process in live organisms[5]. In addition to ability of excellent separation of individual enantiomers, LC-MS/MS provides lower limit of detection (0.5 ng g^{-1} lipid weight, 0.7 ng g^{-1} dry mass) in comparison with GC-MS system (0.8 ng g^{-1} lipid weight, 0.8 ng g^{-1} dry mass) in case of fish samples, sediment and sewage sludge, respectively.

The first results obtained from the analysis of the Czech environmental samples are resumed in Table I. The chub and bream livers contained both α-HBCD enantiomers and at the low concentration also β-enantiomers. The high level of γ-HBCD was determined in the sample of chub muscle from Podolí. This significantly higher level of γ-isomer in biota sample may indicate there is an emission source in particular locality present, because as mention above, γ-isomer dominates in technical mixture. The similar pattern of diastereomers was found also in the sediment and sewage sludge samples where only γ-HBCD was detected as shows Fig. 2.b. Comparing the results obtained within our study, it was found that the GC levels of target analytes are just a
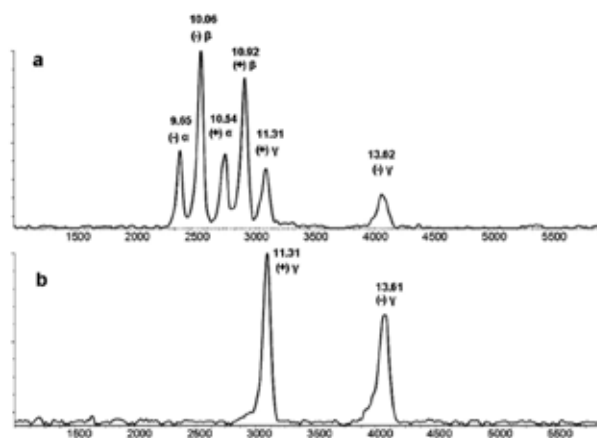
Fig. 2.　**LC-MS/MS chromatogram of (a) a standard of HBCD individual enantiomers and (b) a real sample of river sediment from Hradec Králové**

slightly overevaluated by about 13 % in case of α-diastereomers. Total differences in the results between LC-MS/MS and GC-MS can be cause by usage of α-HBCD as a calibrant together with diverse response factor of individual diastereomers in GC-MS.

Table I
The results of diastereoisomers obtained by LC-MS/MS and sum of HBCD as a result of application GC-MS in fish samples (ng g^{-1} lipid weight) and sediment/sewage sludge (ng g^{-1} dry mass)

Fish	Locality	HBCD Diastereoisomers			Results of GC-MS
		α	β	γ	
Chub	Němčice	34	1.4	n.d	36
Bream	Němčice	68	0.4	n.d.	80
Chub	Klecany	6.6	n.d.	n.d.	7.5
Bream	Lysá	59	1.1	n.d.	69
Chub	Podolí	16	6	105	58
Sediment	Hradec Králové	n.d	n.d	28.1	17.7
Sewage sludge	Hradec Králové	n.d	n.d	103.9	156

Conclusions

In presented study, two different analytical techniques (GC/MS and LC-MS/MS) were tested for the analysis of HBCD isomers in environmental samples. The potential of the first system is particularly in the determination of the total HBCD occurrence in samples. On the other hand, the latter one using chiral permethylated β-cyclodextrine stationary phase allows the separation and quantification of individual diastereomers. Comparing the results obtained within our study, it was found that the GC levels of target analytes are just little overevaluated. For this reason, the need for further investigations into differences between GC and LC results are necessary.

HBCD profiles in fish are different from those observed in sediment and sewage sludge. In fish, usually α-HBCD is the major diastereomer, whereas in sediment and in sewage sludge is most abundant γ-HBCD. The processes affecting these differences in isomer composition are not fully investigated yet. LC-MS/MS is an appropriate for monitoring changes of diastereomers pattern.

REFERENCES

1. Haug L. S., Thomsen C., Liane V. H., Becher G.: Chemosphere *71*, 1087 (2007).
2. Heeb N. V., Schweizer W. B., Mattrel P., Haag R., Kohler M., Schmid P., Zennegg M., Wolfensberger M.: Chemosphere *71*, 1547 (2008).
3. Gómara B., Lebrón-Aguilar R., Quintanilla-López J. E., González M. J.: Anal. Chim. Acta *605*, 53 (2007).
4. Van Leeuwen S. P. J., De Boer J.: Mol. Nutr. Food Res. *25*, 194 (2008).
5. Yegers B. N., Mets A., Van Bommel R., Minkenberg C., Hamers T., Kamstra J. H., Pierce G. J., Boon J. P.: Environ. Sci. Technol. *39*, 2095 (2005).

P22　THE CONTENT OF POLYBROMINATED DIPHENYL ETHERS IN FRESHWATER FISH FROM BRNO WATER RESERVOIR

M. HROCH, M. VÁVROVÁ and **V. VEČEREK**

Faculty of Chemistry, University of Technology Brno, Purkyňova 118, 612 00 Brno, Czech Republic,
hroch@fch.vutbr.cz

Introduction

One group of "new" persistent halogenated contaminants is represented by brominated flame-retardants (BFRs). BFRs are chemicals widely used in various products such as plastics and textiles to prevent a fire hazard. Generally two types of these compounds are in use. The *reactive* BFRs represented mainly by tetrabromobisphenol A (TBBPA) are incorporated into the polymeric materials by covalent binding, whereas the *additive* types, represented by polybrominated diphenyl ethers (PBDEs), polybrominated biphenyls (PBBs) and hexabromocyclododecane (HBCD) are embedded into a matrix of appropriate polymer.

PBDEs are similar to polychlorinated biphenyls (PCBs) in structure and characteristics such as hydrophobic and semi-volatile and/or nonvolatile. Theoretically 209 congeners (5 majorities) of PBDEs exist with specific chemical and physical properties, which lead to various biological and toxicological effects. Alike other organohalogen compounds such as PCBs, DDT and other organochlorine pesticides, PBDEs are lipophilic, very stable and resist to acids and basis, heat and light and biodegradation.

Table I
Physical and chemical characteristics of majority congeners

Congener	No. of Br atom	Log K_{ow}	Melting point [°C]	Slb. in water [mg ml^{-1}, 25°C]
47	4	6.55	83.5–84.5	0.015
99	5	7.13	90.5–94.5	0.0094
100	5	6.86	102	0.04
154	6	7.39	131–132.5	8.7×10^{-7}
209	10	9.97	302.5	4.17×10^{-9}

The concern over these anthropogenic compounds is that they can be released into the environment from products as they are not chemically bounded to the materials, and more importantly, they are persistent with a high bioaccumulation potential.

PBDEs are being found as contaminants of indoor and outdoor environments. The presence of PBDE was proved in all the components of the environment such as air, sediment and sewage sludge as well as biological samples including biota, human blood, adipose tissues and breast milk. Quite high concentrations were found in the dust in flats and offices.

Experimental

This study presents results of measuring concentration of ten PBDE congeners (BDE-3, 15, 28, 47, 99, 100, 118, 153, 154 and 183) in different species of fish using gas chromatography with electron captured detector (GC-ECD). These samples were collected from Brno water reservoir, which is situated near the Brno city.

Five head of each kind were detected and the total PBDE congener concentrations (Σ PBDEs) in the fish were amur < bream < crucian < carp.

C h e m i c a l s

PBDE standards, all with declared 99% purity, were purchased from AccuStandard, Inc. (New Haven, USA). Working standard mixtures in isooctane contained following congeners: 4-BDE (BDE 3), 4,4'-diBDE (BDE 15), 2,4,4'-triBDE (BDE 28), 2,2',4,4'-tetraBDE (BDE 47), 2,2',4,4',5-pentaBDE (BDE 99), 2,2',4,4',6-pentaBDE (BDE 100), 2,3',4,4',5-pentaBDE (BDE 118), 2,2',4,4',5,5'-hexaBDE (BDE 153), 2,2',4,4',5,6'-hexaBDE (BDE 154), 2,2',3,4,4',5',6-heptaBDE (BDE 183).

M e t h o d

A homogenized fish tissue was desiccated with mixture of sea sand and anhydrous sodium sulphate. Soxhlet extraction carried out (6 hours) with hexane/petrolether solvent mixture (96 : 4, v/v) for isolation of target analytes from the sample. Concentrated crude extracts were purified by using multi layer column (300 × 8 mm; florisil, silica, alumina). The collected fraction was evaporated to dryness and re-dissolved in 1 ml of isooctane. After addition of a few drops of sulphuric acid the organic layer was used for GC analysis. Quantification of target analytes was carried out by high-resolution gas chromatography, where two capillary columns (DB-17 MS column and HT-8 column) operated in parallel mode were used. Experiments were carried out on Agilent 6890 GC system and the analytes were identified by retention times.

Results

This paper reports PBDEs levels in freshwater fish. These were determined by gas chromatography with ECD. The identification of PBDEs in the fish samples was based on comparison of the retention times with those of the available authenticated standards. All results are summarized in
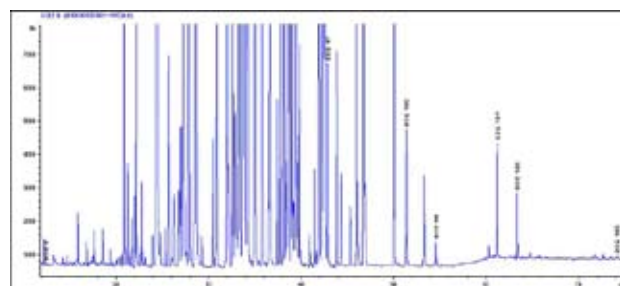
Fig. 1.　**Chromatogram of carp-skin sample analysed by GC with electron captured detector in capillary column DB-17 MS**

Table II
Concentrations of PBDE detected in carp skin and muscle [µg kg^{-1}]

Cong./ Carp	Skin Range	Skin Mean	Muscle Range	Muscle Mean
BDE 3	21.2–26.3	24.8	14.6–17.0	15.2
BDE 15	nd[*]	–	nd	–
BDE 28	nd	–	nd	–
BDE 47	66.7–188	118	54.5–78.2	66.4
BDE 99	26.3–50.0	33.3	nd	–
BDE 100	49.8–136	98.2	37.9–55.1	46.3
BDE 118	nd	–	nd	–
BDE 153	42.5–77.1	52.2	nd	–
BDE 154	37.1–98.6	69.3	28.6–34.1	30.5
BDE 183	18.9–24.5	21.0	nd	–

[*]not detected

Table III
Concentrations of PBDE detected in crucian skin and muscle [µg kg^{-1}]

Cong./ Crucial	Skin Range	Skin Mean	Muscle Range	Muscle Mean
BDE 3	69.6–175	–	81.3	81.3
BDE 15	nd	–	nd	–
BDE 28	nd	–	nd	–
BDE 47	49.9–68.2	57.4	31.3	31.3
BDE 99	nd	–	16.5–27.9	24.4
BDE 100	40.0–62.3	57.8	nd	–
BDE 118	nd	–	nd	–
BDE 153	62.2	62.2	31.8–106	85.5
BDE 154	23.6–25.1	24.7	nd	–
BDE 183	nd	–	nd	–

Tables II–IV. The levels of PBDEs in amur were bello tho limits of detection, therefore they were left out in the table summary. Fig. 1. shows representative chromatogram of carp skin sample analysed in capillary column DB-17 MS with 50 % diphenyl- 50 % dimethylsiloxane stationary phase.

The most abundant congeners determined in skin of investigated species were BDE 3, BDE 47, BDE 100 and BDE 153. Greater mean levels were observed in skin then muscle tissues.

Table IV
Concentrations of PBDE detected in bream skin and muscle [µg kg^{-1}]

Cong./ Bream	Skin Range	Skin Mean	Muscle Range	Muscle Mean
BDE 3	42.2–62.2	48.3	26.0–31.5	29.8
BDE 15	nd	–	nd	–
BDE 28	nd	–	nd	–
BDE 47	35.2	35.2	nd	–
BDE 99	nd	–	nd	–
BDE 100	19.8	19.8	13.2	13.2
BDE 118	nd	–	nd	–
BDE 153	20.6–22.8	21.7	18.6	18.6
BDE 154	nd	–	nd	–
BDE 183	nd	–	nd	–

Polybrominated diphenyl ethers are very resistant to biodegradation and also show carcinogenic and mutagenic effects. Due to unavoidable emissions into the environment PBDEs have been found throughout the world both in abiotic (air, water, soil, sediment) and biotic (fish tissue, bird eggs, marine mammals) compartments. Into the future, will be very important and necessary monitoring these compounds in the environment and food chain especially.

REFERENCES
1. Marsh G., Hu J., Jakobsson E., Rahm S.; Bbergman A.: Environ. Sci. Technol. *33*, 3033 (1999).
2. de Boer K., Boom J. P.: *Polybrominated biphenyls and diphenyl ethers. The handbook of environmental chemistry 3*, New types of persistent halogenated compound, 61–95, 2000.
3. Kazda R., Hajšlová J., Poustka J., Čajka T.: Anal. Chim. Acta *520*, 237 (2004)
4. WHO/ICPS: Environmental health kriteria 162, Brominated diphenyl ethers, World health organization, Geneva, 1994.

P23   EXAMINATION OF ABANDONED Sb DEPOSITS BY MINERALOGICAL METHODS IN POPROČ (SLOVAKIA)

MICHAL JANKULÁR[a], TOMÁŠ KLIMKO[b], ĽUBOMÍR JURKOVIČ[a], BRONISLAVA LALINSKÁ[b], PETER ŠOTTNÍK[c], OTÍLIA LINTNEROVÁ[c] and MICHAL ŠUTRIEPKA[c]

Faculty of Natural Sciences Comenius University
842 15 Bratislava, Slovak Republic,
[a]*Department of Geochemistry,*
[b]*Department of Mineralogy and Petrology,*
[c]*Department of Economic Geology,*
jankular@fns.uniba.sk

Introduction

The Poproč region has long been recognized as an important source of antimony in Europe. Mining began in the 17th century and finished in 20th century[1]. The abandoned Poproč Sb deposit is situated in the SE part of the Spišskogemerské Rudohorie Mts. (Slovakia). Geologically, the area consists of Paleozoic metamorphic rock complexes – graphitic and sericitic phyllites, metapsammites and metarhyolitic tuffs and granites. The Sb mineralization occurs as quartzcarbonate veinlets and impregnation in the host rocks. Antimony is the main ore mineral; others are pyrite, arsenopyrite, and various sulphides of Pb-Zn-Cu. The main non-metallic vein minerals are quartz, carbonates, tourmalines, albites, sericites, and chlorites. Extensive contamination related to the Sb deposit in Malé Karpaty Mts. was described previously[2,3]. The study of arsenic and antimony bindings to ferrous ochres[4,5], concentrations and distribution of As and Sb in oxidation rims of destabilized sulphides of impoundment sediment, and experimental investigation of geochemical barrier media were important. An investigation of biological and chemical oxidation was also conducted[6]. Rapid dissolution of Sb from impoundment sediment was studied at the nearby Dúbrava deposit[7]. Description of significant influence of long term mining activity and the potential effects of abandoned deposits on population health quality were described in the Zlatá Idka community (Spišsko-gemerské Rudohorie Mts.)[8]. Finally, a study of the Poproč area and its surroundings reported highly contaminated surface waters, soils, and stream sediments[9]. The As in soil samples exceeded class C standards of the Ministry of Agriculture of the Slovak Republic No. 531/1994-540 by 400 times, all stream sediment samples exceeded class C As and Sb limits, and concentrations of Sb were 100 times higher than sanitary regulatory limits for drinking water[10,11].

Experimental

Samples were collected of geological materials and natural media (groundwater, surface waters, stream sediments, soils and ochres) and selected plant species (roots and shoots) in the field area shown in Fig. 1. Samples were preferentially collected in areas near potential local contamination sources (outflow from mines, tailings ponds and theirs surroundings, and mining wastes). Samples of soils, stream sediments, impoundment material, and plant tissues were dried and homogenized under laboratory conditions by standard procedure. Special techniques were needed to selectively dissolve the solid ochre samples from the Agnes and Filip adits outflow. Selective dissolution analysis is based on the different dissolution rates of various mineral phases and compounds[12]. Based on the Fe_{OX}/Fe_{DT} ratio in analyzed ochre samples, it was possible to evaluate the relative crystallinity of the Fe^{III} oxides and oxyhydroxides. Samples were dissolved by three different methods:

- dissolution of Fe oxides and oxyhydroxides in hydrochloric acid
- dissolution of Fe oxides and oxyhydroxides in dithionate-citronate-bicarbonate (DCB)
- dissolution of Fe oxides and oxyhydroxides in ammonium acetate

Samples of soils, sediments, waters, impoundment material, ochre, and plant tissues were analyzed in the geochemical laboratories of the State Geological Survey of the Slovak Republic. Selected chemical parameters (As, Sb, Zn, Cu, Pb, Fe, Al, Mn) were analyzed by atomic absorption spectrometry in the <0.125 mm mesh size fraction.

Results

Chemical analyses of the various environmental media sampled confirm the previous field investigation findings that the area surrounding the abandoned Poproč Sb deposit is highly polluted.

Results of selected chemical analysis data for soils are shown in Table I. The most important contaminants in the area are antimony and arsenic; their association is in accordance with the fact that the two elements are chemically similar[13,14]. Their toxicology is also similar, and they are both carcinogenic[15,16]. Extremely high concentrations of Sb were recorded in the area surrounding the Agnes adit, with values ranging from 4,700 mg kg^{-1} to 10,000 mg kg^{-1}. The highest As level measured 56,900 mg kg^{-1}. These extreme Sb and As concentrations in soils near the Agnes adit are both a result of recent contamination. A 2 m thick layer of ochre precipitates was observed over a 200 m^2 area coming from the Agnes adit until the year 2004 when stable conditions were provided. The ochre precipitate, which potentially contained similarly high concentrations of toxic elements were in the past mechanically removed by water outflowing from the Agnes adit, discharging to the catchment of the Olšava River. Chemical analysis of ochre samples collected from the Agnes adit and dissolved in HCl show high content of As and Sb in ochre material (Table II); these toxic elements have long contaminated the surface water and stream sediments of the Olšava and Bodva Rivers.

Antimony, analogous to arsenic, has an ability to bind to plant tissues and can be phytotoxic[17]. Considering the often-described mobility of these elements likely controlled by

Fig. 1.　Schematic map of investigated area

Table I
Selected chemical parameters of soil samples from surrounding of Sb deposit Poproč [mg kg⁻¹]. Fe, Mn, Al, SO4 expressed in %

	Adit Filip	Adit Filip-subs	Adit Agnes OU	Adit Agnes OA1	Adit Agnes OA2	Im-pound-ment	Im poundment (cover)
As	72	298	11,060	26,380	56,900	1,898	2,800
Sb	3,270	86,230	9,254	4,697	9,993	4,747	4,190
Pb	274	1723	25	<5	<5	351	352
Zn	122	352	135	1,655	3,272	71	60
Cu	54	155	48	34	52	15	13
Fe	4.23	4.29	17	30.8	35.6	0.92	5.67
Mn	0.174	0.106	0.262	0.073	0.02	<0.001	0.002
Al	7.97	6.92	4.73	1.44	0.07	5.06	3.38
SO₄	0.13	0.11	0.14	0.27	0.24	0.27	1.97

Fe, Mn oxides and pH[18], their biosorption into organisms or biovolatilization in organisms[19,20] is important. Plant tissues were sampled in the area of interest and high concentrations

of As and Sb were detected in selected plant species. Near the Agnes adit, the maximum As and Sb values of plant tissue were, respectively, 45.8 mg kg⁻¹ and 1.9 mg kg⁻¹ (dry weight).

Table II
Ochre samples chemical analyses (mg.kg-1)

Chemical parameter	Spring 300 m NW from adit Agnes	Adit Agnes
Fe	106,000	336,000
As	8,600	34,000
Sb	5,200	6,100
Pb	104	97
Zn	160	831
Cu	44	0
Mn	1,580	210
Hg	0.4	1
Cd	0	12
Na	8,540	1,360
K	1,720	420
Ca	10,600	2,460
Mg	6,070	830
Al	7,660	2,560
S	23,300	5,950

Conclusions

The results of preliminary mineralogical and geochemical sampling near the abandoned Poproč Sb deposit reveal significant contamination of the surrounding environment. The most important toxic elements in the study area are As and Sb. High concentration levels measured in adit estuaries could be caused by inadequate mine closure/rehabilitation. Deposition of highly contaminated ochre precipitates near the Agnes adit and outflow are indicative of contaminated mine waters; inadequate recultivation has caused ochre precipitates (containing As and Sb) to be resuspended and to flow into the Olšava river catchment. The next step should be research into geochemical and mineralogical mobility and the bioavailability of the main contaminants in the environmental media.

REFERENCES

1. Chovan M., Háber M., Jeleň S., Rojkovič I.: *Ore textures in the Western Carpathians*. Slovak Academic Press, Bratislava 1994.
2. Miner. Slov. *35*, 131 (2003). (in Slovak)
3. Ministry of Education of the Slovak Republic: *Risk contamination assessment of surroundings of Sb, Au and sulphide deposit in Pezinok and proposition for remediation: toxicity of As and Sb, acidification*, AV/901/2002 (VTP25) (2006 ME SR). (in Slovak)

4. Slov. Geol. Mag. *5*, 179 (1999).
5. Geochim. Cosmochim. Acta *71*, 4206 (2007).
6. Andráš P., Milovská S., Kušnierová M., Adam M., Šlesarová A., Chovan M., Hajdušková Ľ., Lalinská B.: *7th International Symposium on Environmental Geotechnology and Global Sustainable Development: Environmental hazards at the Sb-Au-S deposit Pezinok* (Slovakia) in relation to the chemical and biological-chemical oxidation processes, Helsinki, 8. – 10. June 2004, p. 10
7. Slov. Geol. Mag. *6*, 61 (2000).
8. Env. Geol. *51*, 387 (2007).
9. Ministry of Environment of the Slovak Republic: *Poproč – tailings piles, ore dumps, impoundments, search investigation*, state by April 1996, (1996 ME SR). (in Slovak)
10. Ministry of Agriculture of the Slovak Republic: *Maximum permissible values of harmful pollutants in soil and definition of qualified organizations to determine real values of these pollutants*, No. 531/1994-540 (MA SR 1994). (in Slovak)
11. Government Directive of the Slovak Republic: *Demands on water assigned to human usage and quality control assigned to human use*, No. 354/2006 (2006). (in Slovak)
12. Geochim. Cosmochim. Acta *45*, 421 (1981).
13. WHO: Guidelines for Drinking Water Quality: Health Criteria and Other Supporting Information, (WHO 1996).
14. Earth-Science Rev. *59*, 125 (2002).
15. Water Res. *34*, 4304 (2000).
16. J. Clean. Prod. *13*, 19 (2005).
17. Ann. Rev. Plant Physiol. *29*, 511 (1978).
18. J. Hydrol. Hydromech. *55*, 223 (2007).
19. Environ. Pollut. *124*, 93 (2003).
20. Environ. Sci. and Pollut. Res. *14*, 31 (2007).

P24   DETERMINATION OF VOLATILE COMPOUNDS AND SACCHARIDES AT ALDER WOOD HYDROLYSIS

FRANTIŠEK KAČÍK[a], MARTA LAUROVÁ[a] and DANICA KAČÍKOVÁ[b]

[a]*Department of Chemistry and Chemical Technologies,*
[b]*Department of Fire Protection,*
Faculty of Wood Sciences and Technology, Technical University in Zvolen, T. G. Masaryka 24, 960 53 Zvolen, Slovak Republic,
kacik@vsld.tuzvo.sk

Introduction

A pretreatment of lignocellulosic biomass at the production of pulp, ethanol and other technically important chemicals, is a subject of research for a long time. The pretreatment main goal is to remove lignin and hemicelluloses, to decrease celullose crystallinity and to increase porosity of the lignocellulosic material. The various physical, physico-chemical an biological processes of pretreatment are used for this purpose at present[1,2].

One method is a high-pressure water prehydrolysis. It is realized at a wide range of temperatures (160–260 °C), but in the short time intervals (0.42–7 min) in dependence on wood species[3].

The hydrothermal pretreatments of lignocellulosic materials have got a different effect on their main components. Extractives, hemicelluloses and watersoluble lignin are released from wood in the temperature range 150–230 °C. The cellulose fraction depolymerises at the higher temperatures (210–280 °C)[3,4].

At wood hydrolysis also other compounds arise except saccharides. They can be processed (methanol, acetic acid, propionic acid, 2-furaldehyde), resp. their negative environmental influence must be solved[5]. Their concentration in the hydrolysates depends on wood species and the hydrolysis conditions, mainly on the temperature and the time of the treatment.

The water prehydrolysis of biomass (by saturated water steam and hot high-pressure water) can be considered as a environmentally friendly technology, where it is not necessary to add any chemicals[6].

This paper aim was to research the release of saccharidic part and volatile compounds from alder wood (*Alnus glutinosa* (L.) GAERTN.) during the water hydrolysis.

Experimental
M a t e r i a l
Wood samples preparation

The samples from the trunk wood of 59 years old alder (*Alnus glutinosa* (L.) GAERTN.) were chipped to the dimensions $2 \times 2 \times 10$ mm.

Wood analyses

The amount of extractives soluble in the mixture toluene-ethanol (1 : 2) was determined in accordance with ASTM Standard D 1107-96[7], the amount of cellulose by Seifert method[8] and the amount of holocelluse by Wise method[9]. Lignin amount was determined in accordance with ASTM Standard D 1106-96[10].

H y d r o l y s i s

Wood chips (2 g) were put into the stainless autoclaves with internal volume 12 cm^3 and they were refilled by distilled water. The solid/liquor ratio was 1 : 4.

The prehydrolysis was performed in the thermostate at the temperatures 160, 180 and 200 °C. The time of treatment was 30, 60, 120 and 240 min. Then the autoclave was cooled into the temperature 20 °C and the hydrolysate was filtrated.

H y d r o l y s a t e s   A n a l y s e s
pH value

Hydrolysates pH values were determined by the potenciometric method with pH meter inoLab pH 720 (WTW GmbH).

Saccharides

Saccharides amount in the hydrolysates was determined in the form of aldonitrilacetates by GC method[11] at the following conditions: column – 5 % PEGA Chromaton N-AW-DMCS (0.16–0.2 mm) 240 cm × 0.35 cm, column temperature – 200 °C, injector temperature – 260 °C, detector temperature – 250 °C, detector – FID, carrier gas – N_2.

Volatile compounds

The volatile compounds in the hydrolysates (methanol, acetic acid, propionic acid, 2-furaldehyde) were determined by the method of GC[12] at the following conditions: column – Chromosorb 102 (80–100 mesh) 120 cm × 0.35 cm, column temperature – 195 °C, injector temperature – 250 °C, detector temperature – 250 °C, detector – FID, carrier gas – N_2.

Results

During the hydrothermal treatment of wood, various acid compounds are released. It is confirmed by the measured values of pH (Table I). The increase of the hydrolysates acidity causes next degradation of wood matter and the glycosidic bonds in the polysaccharides are cleavaged.

The hydrolysates acidity is due to the formation of so-called nascent organic acids (formic, acetic, propionic e.g.), which are formed by the cleavage of some functional groups from the polysaccharides and also by the decomposition of arised monosaccharides. These acids have got an important influence on the next course of the hydrolysis, therefore they catalyse the glycosidic bond cleavage in the polysaccharides[13,14].

The used alder wood contained 84.06 % of holocellulose, 41.26 % of cellulose, 21.45 % of lignin and 4.97 % of extractives.

Table I
Hydrolysates pH value

Temperature [°C]	Time [min]	pH
160	30	4.14
160	60	3.46
160	120	3.29
160	240	3.18
180	30	3.61
180	60	3.18
180	120	3.03
180	240	3.09
200	30	3.17
200	60	2.95
200	120	2.92
200	240	2.97

Table II
Yield of monosaccharides in hydrolysates

Temperature [°C]	Time [min]	Monosaccharides [g dm^{-3}]
160	30	1.56
160	60	2.84
160	120	4.46
160	240	9.12
180	30	2.46
180	60	14.40
180	120	7.96
180	240	3.15
200	30	3.05
200	60	4.71
200	120	2.23
200	240	1.92

Table III
Yield of total saccharides in hydrolysates

Temperature [°C]	Time [min]	Total saccharides [g dm^{-3}]
160	30	2.43
160	60	3.35
160	120	15.06
160	240	14.06
180	30	3.83
180	60	30.48
180	120	12.36
180	240	3.29
200	30	14.97
200	60	6.40
200	120	3.57
200	240	1.23

Table IV
Yield of volatile compounds in hydrolysates

Temperature [°C]	Time [min]	Methanol [g dm^{-3}]	Acetic acid [g dm^{-3}]	Propionic acid [g dm^{-3}]	2-Fur-aldehyde [g dm^{-3}]
160	30	0.11	0.28	0.10	0.02
160	60	0.31	1.35	0.53	0.14
160	120	0.63	4.46	1.17	0.63
160	240	0.54	5.77	0.94	1.64
180	30	0.18	0.67	0.18	0.05
180	60	0.47	5.35	0.92	0.89
180	120	0.82	7.73	0.74	7.24
180	240	0.84	7.52	0.65	9.23
200	30	0.29	3.41	0.61	0.46
200	60	0.40	7.72	0.59	6.43
200	120	0.97	10.03	0.66	8.17
200	240	1.13	2.95	0.82	5.12

At the temperature 160 °C the monosaccharides amount in the hydrolysates increased during the total time range (Table II). At the higher temperatures the maximum yield of monosaccharides was determined during 60 min of the hydrolysis. It is in accordance with 2-furaldehyde amount increase in the hydrolysate (Table IV). The highest concentration of monosaccharides was observed at the temperature 180 °C and the time of the hydrolysis 60 min.

The similar trend we can see at the determination of total saccharides amount (Table III) determined after the hydrolysis by 3 % sulfuric acid. At the biggest yields of the saccharides (180 °C, 60 min) approximately one half of the saccharides amount is present in the form of monosaccharides and second half in the form of oligosaccharides and polysaccharides.

In the hydrolysates there are various volatile compounds. Their amounts increase in dependence on the temperature and the time of treatment in most cases (Table IV).

Methanol, arising mainly by the methoxyl group cleavage, is extreme toxic. In some cases it is necessary to remove it before the next treatment of the hydrolysate. In hardwoods there are 3–5 % of acetyl groups (CH_3CO-), they give rise

acetic acid at the hydrolysis. The acetic acid amount increases mainly at the first 120 min of the hydrolysis, then their increase is retarded. It corresponds with the results of birch wood hydrolysis, where the increase of acetic acid amount was slowed or decreased in the hydrolysis at the temperature 200 °C[15,16].

2-Furaldehyde arises by pentose dehydratation and it can be isolated as a valuable product under certain conditions. The temperature of 180 °C causes the heavy increase of 2-furaldehyde, its concentration increases due to the condensation reactions at the temperature 200 °C.

Conclusions

From the experimental results obtained at the hydrolysis of alder wood can be concluded that at the mild conditions of hydrolysis the acetic acid and 2-furaldehyde concentration increases due to the saccharides deacetylation and dehydration, respectively. The amount of 2-furaldehyde decrease is

due to its participation in the condensation reactions at the temperature 200 °C.

The maximum of both monosaccharides and total saccharides contents were found at the temperature 180 °C and the time 60 min of the treatment.

REFERENCES

1. Sun Y., Cheng J.: Bioresour. Technol. *83*, 1 (2002).
2. Mosier N., Wyman Ch., Dale B., Elander R., Lee Y.Y., Holtzapple M., Ladish M.: Bioresour. Technol. *96*, 673 (2005).
3. Garrote G., Domínguez H., Parajó J. C.: Holz Roh Werkst *57*, 191 (1999).
4. Sasaki M., Adschiri T., Arai K.: Bioresour. Technol. *86*, 301 (2002).
5. Horbaj P.: Energia *3*, 52 (2001).
6. Garrote G., Domínguez H., Parajó J. C.: J Chem Tech Biotechnol. *74*, 1101 (1999).
7. ASTM Standard D 1107-96: *Standard test method for ethanol toluene solubility of wood* (1998).
8. Seifert V. K.: Das Papier *1960*, 104.
9. Wise L. E., Murphy M., D'Addieco A. A.: Paper Trade J. *122*, 35 (1946).
10. ASTM Standard D 1106-96: *Standard test method for acid insoluble lignin in wood* (1998).
11. Kačík F., Solár R. : *Analytická chémia dreva*. Technická univerzita vo Zvolene, Zvolen 2000.
12. Kačík F.: *Tvorba a chemické zloženie hydrolyzátov v systéme drevo-voda-teplo*. Technická univerzita vo Zvolene, Zvolen 2001.
13. Conner A. H., Lorenz L. F.: Wood Fiber Sci. *18*, 248 (1986).
14. Garotte G., Domínguez H., Parajó J. C.: Holz Roh Werkst *59*, 53 (2001).
15. Sundqvist B., Karlsson O., Westenmark U.: Wood Sci. Technol. *40*, 549 (2006).
16. Kačík F., Výbohová E., Kačíková D.: Acta Facultatis Xylologiae *49*, 39 (2007).

P26 MODELING OF DISPERSION OF WINDBORNE MATERIAL IN ATMOSPHERE

MICHAL KAPOUN[a], RADIM DVOŘÁK[b], FRANTIŠEK ZBOŘIL[b] and IVAN MAŠEK[a]

Brno University of Technology,
[a]Faculty of Chemistry,
[b]Faculty of Information Technology,
kapoun@fch.vutbr.cz

Introduction

Air pollution modeling is an attempt to describe the functional relation between emissions and occurring concentrations and deposition. Air pollution measurements present these occurring concentrations and deposition, but they can only give a snapshot at specific locations and times. In principle, the air pollution modeling can give a more complete and consistent description, including an analysis of the causes-the emissions sources-which have led to these concentrations/deposition.

Air pollution models play an important role in science, because of their capability to investigate the importance of the relevant processes, and they play a major role in application (e.g. fire brigade intervention during chemical accidents)[1].

The atmospheric dispersion modeling, where the air pollution modeling belongs to, has a long history and it dates back to the end of 19th century, when Reynolds in 1895(ref.[2]) formulated criterion for the change from laminar to turbulent flow, in other words the diffusion, in pipes. During the next few decades, the huge progress was done in the describing of mathematical formulas and their correspondences to observations. These formulas were evaluated in analytical way and they were restricted to simple cases where the solution could be found. Nowadays, the trend of atmospheric dispersion evolution is based on the numerical solution of diffusion equation.

The diffusion equation is expressed in a form of partial differential equation (PDE). The solution of the equation can be derived by analytical process that is often very difficult to find. There exist many cases of PDE where the analytical solution to the PDE does not even exist. Thus, many kinds of numerical methods have been developed and they have been used next to the analytical ones. However, the problem exists in this kind of evaluation and it is the arising of numerical error. The only ways to check the accuracy is either to compare the results with the exact analytical solution or to compare it with the observation.

In our work we have used the first case thus the form of diffusion equation had to be simplified so as its analytical solution can be calculated. The reason originates from the fact that it is not possible to find the exact analytical solutions in the majority of cases where the solutions are looked for[2].

Mathematical Models

The general form of the diffusion equation describing atmospheric dispersion can be expressed as follows[1]:

$$\frac{\partial C}{\partial t} + \nabla C \bar{u} = \nabla (\mathbf{D} \nabla C) + \\ + chemistry + emmisions + \\ + dry\_deposition + \\ + wet\_deposition \tag{1}$$

where C is a pollution concentration, $\bar{u}$ is a wind velocity, $\mathbf{D}$ are diffusion coefficients (their coordinate axes are D_x, D_y and D_z, respectively).

The chemistry term presents atmospheric chemistry term that is used for the determination of a chemical substance influence to the atmosphere and to the dispersion process itself. The emissions term expresses the rate of the emissions in the atmosphere and its relation to the atmospheric dispersion of the specific pollutant. The last two terms, dry and wet depositions, are the major sink terms in the model and besides they determine the pollutant behavior above the terrain surface.

In our case, we have used the advection-diffusion equation (A-DE) which is a part of equation (1) and where the terms chemistry, emissions and wet deposition are neglected. The reasons for this choice were that the chemistry and emissions terms are complex to find the analytical solution for them. The wet deposition plays an important role for water-soluble species only and it is not our primary concerns at this moment.

Full form of A-DE can be expressed as follows:

$$\frac{\partial C}{\partial t} = -\nabla C \bar{u} + \nabla (\mathbf{D} \nabla C) + W \frac{\partial C}{\partial z} \tag{2}$$

where C, $\bar{u}$ and $\mathbf{D}$ symbols have the same meanings as in equation (1). W is a pollutant gravitational settling velocity.

Equation (2) can be furthermore simplified if we apply following assumptions. When the wind speed value is sufficiently large, a diffusive transport is negligible in wind direction with respect to advection (Ermak[3]). Moreover, the coefficients D_y, and D_z, depend on the downwind distance x only and they are therefore independent on the crosswind distance y and height distance z. From these facts, the diffusive terms can be simplified - the brackets are not needed anymore and the second derivatives appear. Last assumption is the stationary source with constant strength during time. Thus, the result of our simplification is a steady state form of equation (2):

$$u_x \frac{\partial C}{\partial x} = D_y(x)\frac{\partial^2 C}{\partial y^2} + D_z(x)\frac{\partial^2 C}{\partial z^2} + W\frac{\partial C}{\partial z} \qquad (3)$$

Here u_x is a wind speed in the *x* direction; all other variables are the same as in equation (2).

To be completed, the PDE (3) needs to have specified boundary conditions. The first condition follows from an assumption of continuous point source with constant strength located in (0,0,*h*) coordinates:

$$C(0,y,z) = \frac{Q}{u}\delta(y)\delta(z-H). \qquad (3a)$$

The next two conditions follow from the natural assumption that pollutant concentration approaches zero far from the source in the lateral *y* directions and high above the source:

$$C(x,+\infty,z) = 0 . \qquad (3b)$$

$$C(x,-\infty,z) = 0 . \qquad (3c)$$

$$C(x,y,+\infty) = 0 . \qquad (3d)$$

The last boundary condition is that pollutant deposition onto the ground occurs at a rate proportional to local air concentration[3] (for simplicity, the flat ground is taken into account only):

$$\left[D_z(\infty)\frac{\partial C}{\partial z} + WC \right]_{z=0} = \left[vC \right]_{z=0} . \qquad (3e)$$

The deposition velocity *v* depends on many factors such as type and size of pollutant particles, the roughness of terrain and its other surface properties and the meteorological conditions.

A n a l y t i c a l   m o d e l
The analytical solution of equation (3) with respect to boundary conditions (3a-e) is derived in (refs.[3,5,6]), and it is done by expression (4):

$$C(x,y,z) = \frac{Q}{2\pi u_x \sigma_y \sigma_z} e^{\frac{-y^2}{2\sigma_y^2}} e^{\left[\frac{-v(z-h)}{2D} \frac{v^2\sigma_z^2}{8D^2} \right]} \times$$

$$\times \left\{ e^{\frac{-(z-h)^2}{2\sigma_z^2}} + e^{\frac{-(z+h)^2}{2\sigma_z^2}} - \sqrt{2\pi}u_x \frac{\sigma_z}{D} e^{\left[\frac{u_x(z+h)}{D} + \frac{u_x^2}{2D^2} \right]} \times \right. $$
$$\left. \operatorname{erfc}\left[\frac{u_x\sigma_z}{\sqrt{2}D} + \frac{z+h}{\sqrt{2}\sigma_z} \right] \right\} . \qquad (4)$$

The standard deviations of plume width and height, σ_y and σ_z, are defined in terms of their respective diffusion coefficients[3,6]:

$$\sigma_i^2(x) = \frac{2}{u_x}\int_0^x D_i(x)dx . \qquad (5)$$

The error function erfc (ξ) is defined in (ref.[4]) as:

$$\operatorname{erfc}(\xi) = \frac{2}{\sqrt{\pi}}\int_\xi^\infty e^{-z^2} dz . \qquad (6)$$

N u m e r i c a l   M o d e l
In our model we have decided to use the well know method of lines, which was frequently used for solving different kinds of PDEs by classical analog and hybrid computers. In order to perform this method the given PDE (3) must be transformed into the system of ordinary differential equations (ODEs). To do that the discretization of all variables except one must be done. In our case we have discretized *y* (points *j*, step Δy) and *z* (points *k*, step Δz) variables and we have let the *x* variable continuous (because of the assumed wind direction).

The obtained system of ODEs is as follows:

$$\frac{dC(x,j,k)}{\partial x} =$$
$$\frac{D_y(x)}{u_x}\cdot\frac{C(x,j+1,k)-2C(x,j,k)+C(x,j-1,k)}{\Delta y^2} +$$
$$+\frac{D_z(x)}{u_x}\cdot\frac{C(x,j,k+1)-2C(x,j,k)+C(x,j,k-1)}{\Delta z^2} + \qquad (7)$$
$$+\frac{W}{u_x}\cdot\frac{C(x,j,k+1)-C(x,j,k-1)}{2\Delta z} .$$

The system of ODEs (6) is solved inside the $<N_j;N_j>$ interval along the *y* direction, and inside the $<0;N_k>$ along the *z* direction, where N_j and N_k are natural numbers. Thus the total number of ODEs is $(2N_j + 1)\times(N_k + 1)$ and all equations can be solved for current time point in parallel.

The boundary condition (3a) is transformed to new initial conditions (7a):

$$C(0,0,H) = \frac{Q}{u_x\Delta y\Delta z} \qquad (7a)$$
$$C(0,j,k) = 0 \quad \text{otherwise}.$$

And new boundary conditions (7b–e) for the ODEs system (7) with respect to (3b–e) are:

$$C(x, +N_j, k) = 0 . \tag{7b}$$

$$C(x, -N_j, k) = 0 . \tag{7c}$$

$$C(x, j, +N_k) = 0 . \tag{7d}$$

$$C(x, j, 0) = \frac{D_z(\infty)}{2\Delta z(v - W) + D_z(\infty)} C(x, j, 2) . \tag{7e}$$

For integration of the system of ODEs (7) the 4th order Runge-Kutta method was chosen. It has sufficient accuracy as is shown in the next chapter.

Results

As was mentioned above equation (3) supposes one point source that has constant strength. It means that the amount of pollutant is constant during time. The wind flows along *x* axis with constant speed and the ground is flat everywhere. In our experiments, all diffusion coefficients were constant in every space points during time, for simplicity.

Now everything is defined to solve our model of PDE (3) with boundary conditions (3a–e). The experiment has been done with following coefficient setting. The diffusion coefficients has been set like that: $D_y = 0.23$ m^2 s^{-1}, $D_z = 0.23$ m^2 s^{-1} which is the parameter of ammonia, other coefficients has been: $v = 2$ m s^{-1}, $W = 3$ m s^{-1}, $u_x = 2$ m s^{-1}, $Q = 0.1$ kg s^{-1} and $H = 1.5$ m.

The space discretization has been chosen as follows: $N_i = 600$, $N_j = 50$, $N_k = 50$, $\Delta x = 0.005$ m, $\Delta y = 0.05$ m and $\Delta z = 0.05$ m. In this case the assumed space 3 m × 2.5 m × 2.5 m has been discretized into 1,500,000 points in which the equations have been calculated.

V i s u a l i z a t i o n

We made simple program/tool for solving given A-DE and for the visualization of the results with possibility of comparison the analytical and the obtained numerical soluti-

ons. The program has possibility to make the cuts through the perpendicular grid in XY, XZ and YZ planes in any depth and the appropriate grid points can be plotted.

Fig. 1. and Fig. 2. show the XY and XZ cuts for our above-defined experiment. The level of gray (the lighter the more concentrated) expresses the amount of concentration of pollutant at each point - the most concentrated means approximately 0.5% of source concentration.

Fig. 2.　**XZ plane cut in depth of 25 of overall depth 50 which means that the cut in depth of point source is shown. The wind flows from left to right**

Scales of axes (*x* is horizontal, *y* is vertical) in figures above are these:
- Fig. 1.: *x* axis: <0, 3.8> m, *y* axis: <–0.8, +0.8> m
- Fig. 2.: *x* axis: <0, 3.3> m, *y* axis: <0, 2.5> m

The three-dimension (3D) visualization is another way to represent the calculated data in space. It has many advantages and gives to the user tool for fast investigation of the result. Many methods of gas or fluid visualization were developed however not all are suitable for our purpose. We can mention the stream ribbons, stream surfaces, particle traces, vector fields etc.[7]

Fig. 1.　**XY plane cut in zero depth, which means that the ground pollutant dispersion is shown. The wind flows from left to right**
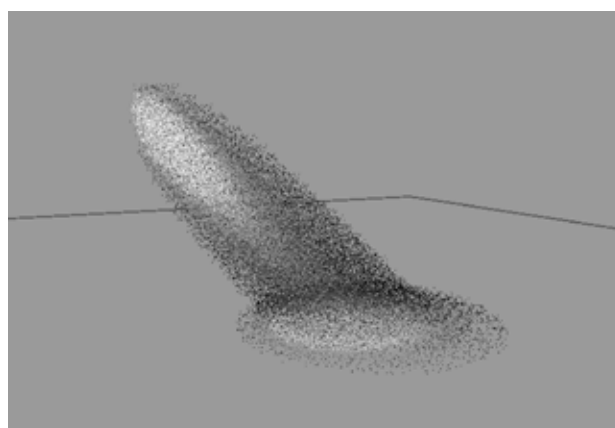
Fig. 3.　**3D visualization of pollutant dispersion in the atmosphere. The white color points show the highest concentration of pollutant, the black color points show its low concentration**

In our case, we have inspired in particle visualization of pollutant concentration. After many experiments of different ways of visualization, we conclude to the one showed in Fig. 3. The concentration is expressed by two basic methods – by color and by particle count. The level of the top concentration can be adjusted – in Fig. 3. the white means approximately 1 % of source concentration, thus the user can see that this level of concentration will occurs in the presented scenario on the ground too. For the better perception of depth, the further particles are darkened, they do not interfere with the foreground particles.

A c c u r a c y

The problem of numerical calculation is the stability of the system and the accuracy of the calculation. Both depend especially on the size of calculation steps. In our case, when we have transformed the PDE (3) into the system of ODEs (7), three calculation steps exist.

The first step Δx is a step along x axis and it is used as integration step in described experiment. Thus, its size primarily influences the accuracy of obtained results.

Last two steps Δy and Δz discretize y and z variables and they have impact on the size of ODEs system (7). These steps subdivide the space in lateral directions and both are used for approximation of the second derivatives appearing in PDE (3). Therefore, they influence both the stability and the accuracy and they thus indirectly affect the size of Δx.
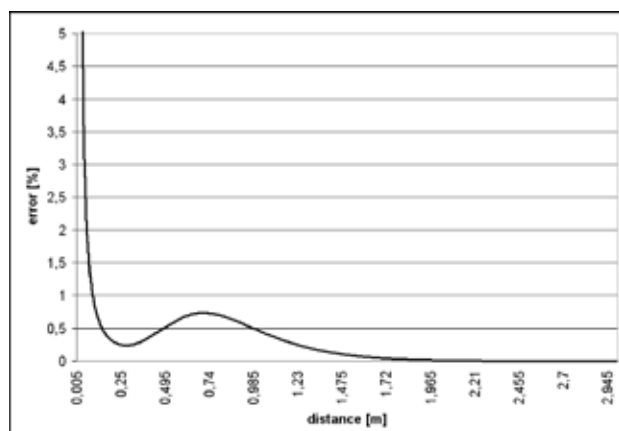
Fig. 4. **The absolute error of the numerical calculation. The vertical axis shows the error, the horizontal axis shows the distance from source along x axis (in wind direction)**

In case of our numerical solution of A-DE there exist specific properties of the calculation behavior, as you can see from our error measurement shown in Fig. 4., where the absolute error is shown. The error evolution is shown along the wind direction. More specifically the error is the mean error in all points (one plane) of the specific x distance.

The greatest error along x axis has been measured close to the source, which is caused by definition of the initial condition (7a). Fig. 4. shows other peak of error which is around 0.7 m distance from the source. That is the place where the plume reaches the ground. The boundary condition (7e) which is the approximation of boundary condition (3e) is the main reason of this error existence. It must be noted that the numerical calculations were stable in spite of measured errors.

Conclusion

The numerical method of A-DE solution has been proposed and implemented and the results have been presented. In addition, the accuracy of our model has been verified by comparison with the analytical solution.

Presented method is relatively simple and easy to implement, therefore, it can be relatively easy extend to more general form of the A-DE which will be the main goal of the future project progress. The extensions could be the general wind direction and speed, the non-flat ground with obstacles (trees, buildings etc.), non-stationary point source/sources etc. Moreover, other atmospheric parameters such as temperature and humidity and substance chemical properties will be added to the model for even more physically and chemically correct behavior.

This preliminary work will be served as a base for more sophisticated model that will be a part of the intelligent system for human protection against consequences of industrial accidents and its analysis. To do that many experiments and measurements of real substance outflows, gas dispersion etc. will have to be done.

REFERENCES
1. Builtjes P. J. H.: *Air Pollution Modeling and Its Application XIV* (Gryning S.E., Schiermeier F.A., ed,), p. 3, Major Twentieth Century Milestones in Air Pollution Modelling and Its Application, Springer US, 2004.
2. Reynolds O.: Philos. Trans. R. Soc. London, Ser. A , *1895*, 123.
3. Ermak D. L.: Atmos. Environ. *11*, 231 (1977).
4. Jacobson M. Z.: *Fundamentals of Atmospheric Modeling*. Cambridge University Press, New York 2005.
5. Slanco P., Bobro M., Hanculak J., Geldova E.: Acta Montanistica Slovaca,, 313 (2000).
6. Roussel G., Delmaire G., Ternisien E., Lherbier R.: Environmental Modelling & Software *15*, 653 (2000).
7. Pagendarm H. G.: *Visualization and Intelligent Design in Engineering and Architecture*, p. 315, Scientific Visualization in computational fluid dynamics, Computational Mechanics Publications, 1993.

P27   REPROCESSING OF DANGEROUS PUT-OUT CHEMICALS AND WASTES

JURAJ KIZLINK

*Faculty of Chemistry, Brno University of Technology, Purky-
ňova 118, 612 00 Brno,*
kizlink@fch.vutbr.cz

Introduction

The possibilities of reprocessing of some dangerous put-out chemicals and wastes are described. The usual way for the disposal of these compounds and wastes is the effective combustion in the suitable incinerator. However, this facility must be equipped with effective furnace, vigorous supplier for air-oxygen, hold-up of waste gases for at least six seconds and also with effective cleaning of emissions[1–4]. Procedure is relatively simple, however too expensive. Some of these chemicals and wastes can be disposed by total decomposition by means of strong reactive chemical agents[5–10]. We suggested and also elaborated the chemical reprocessing of these chemicals or their wastes into some non-toxic chemicals, suitable for technical praxis.

Proposed Procedures

Benzidine (4,4'-diaminodiphenyl) (92-87-5)

Benzidine as dangerous proved chemical cancerogen is already put out from chemical praxis and usually its diposal is due to combustion in suitable mixtures of more combustible materials[1–4]. This compoun is possible to change by reprocessing into aromatic etherical compound. The base of this reprocessing is diazotation of benzidine (base, hydrochlorine, sulfate) in the methanolic solution by dry hydrochlorine and then with addition of concentrated water solution or finelly powdered alkaline nitrite in the ice bath. When diazotization is over, another methanol is added and the reaction mixture is very slowly heated (simmered) in the large flask under reflux water-cooled condenser. The diazonium salt is slowly decomposed, the nitrogen gas escape and in the methanol solution after heating up to boiling is converted into the 4,4'-dimethoxydiphenyl compound (fragrance). NOTE: The volume in the flask must be at least twice larger than volume of reaction mixture because the escape of nitrogen gas is vigorous and it is possible to reach explosion hazard of the flask. This compound often contains 4,4'-dihydroxydiphenyl as impurity, especially if this reaction is carried out in the presence of water.

When we need the pure compound, it is possible to apply alkalization by means of alkaline lye and then to use some methylating agent, such as methyl iodide or dimethyl sulfate[11,12]. In the case we use ethanol as solvent, after boiling the diphenyl compound is obtained.

The similar procedure is possible to use for other aromatic amines and diamines, such as 1,4-diaminobenzene known as p-phenylene diamine (Ursol S, alergen, harmful substance) and other aromatic diamines as 1-aminonaphtalene (alfa-naphtyl amine) and 2-aminonaphtalene (beta-naphtyl amine, Feba, Fenyl-beta, PBN), which is also very potent carcinogen!

Hydrazine (Diazane) /302-01-2/ and Also Hydrazine-Hydrate (10217-52-4)

Hydrazine in the salts (hydrochloride, sulphate) is relatively stable substance and its disposal is quite safe[5–10]. Hydrazine in the form of base or hydrate is also effective carcinogen and its disposal is usually realized by the means of combustion[1–4]. This substance is possible to convert to prosperous compound by boiling with benzaldehyde resulting into substituted hydrazone, known in the cosmetic industry under trade name Benzalazine (cheap UV-absorber for suncreams).

Hydrogen Cyanide (Formonitrile, Zyklon B) (74-90-08) and Alkaline Cyanides KCN (151-50-8) and NaCN (143-33-9)

Hydrogen cyanide and alkaline cyanides are very toxic substances. They could be totally decomposed under influence of strong oxidative agents, such as alkaline hypochlorites, hydrogen peroxide and fumic nitric acid, even to nitrogen, carbon dioxide and water[13–15]. However all concentrated alkaline cyanides could be converted by heating of their ethanolic solution together with benzyl chloride and the benzyl cyanide (phenylacetonitrile). After addition of toluene into reaction mixture, followed by azeotropical distillation and removal of reaction water the phenylacetic acid ethyl ester is obtained. This compound is possible to obtain as pure substance (fragrance) after suitable drying (calcium chloride or sodium sulphate) and distillation. After reduction by hydrides it is possible to obtain 2-phenylethanol (fragrance) as the chemical substitute of natural rose oil.

REFERENCES

1. Brunner C. D.: *Incineration Systems, Selection and Design*, Van Nostrand - Reinhold, New York 1984.
2. Dawson G. W., Mercer B. W.: *Hazardous Waste Management*, Wiley, New York 1986.
3. Bilitewski B., Hardtle G., Marek K.: *Abfallwirtschaft*, Springer Verlag, Berlin 1991.
4. LaGrega M. D., Buckingham P. L., Evans J. C.: *Hazardous Waste Management*, McGraw-Hill, New York 2001.
5. Lunn G., Sansone B.: *Destruction of Hazardous Chemicals in the Laboratory*, Wiley, New York 1990.
6. Luxon S. G.: *Hazards in the Chemical Laboratory*, Royal Society of Chemistry, London 1992.
7. Richardson M. L.: *Risk Management of Chemicals*, Royal Society of Chemistry, London 1992.
8. Stricoff R. S., Walters D. B.: *Handbook of Laboratory Health and Safety*, Wiley, New York 1995.

9. Chereminisoff N. P.: *Handbook of Solid Waste Management and Waste Minimization Technologies*, Elsevier Science, Burlington 2003.

10. Shafer D. A.: *Hazardous Material Characterization*, Wiley, New York 2006.

11. Černý J. V., Černý M., Paleček M., Procházka M.: *Organická syntéza – Organikum*, Academia, Praha 1971.

12. Večeřa M., Panchartek J.: *Laboratorní příručka Organické chemie*, SNTL, Praha 1987.

13. Kizlink J.: *Nakládání s odpady*, Fakulta chemická VUT, Brno 2007

14. Kuraš M.: *Odpady – jejich využití a zneškodňování*, VŠCHT, Praha 1994

15. Kuraš M.: *Odpadové hospodářství*, Ekomonitor, Chrudim 2008.

P28　APLICATION OF CHITOSAN FOR WATER TREATMENT

ZUZANA KLÍMOVÁ[a], PETR DOLEJŠ[a,b] and MILADA VÁVROVÁ[a]

[a]*Institute of Chemistry and Technology of Environmental Protection, Faculty of Chemistry, Brno University of Technology, Purkyňova 118, 612 00 Brno, Czech Republic,*
[b]*W&ET Team, box 27, Písecká 2, 370 11 České Budějovice, Czech Republic,*
klimova-z@fch.vutbr.cz

Abstract

Results of experimental study focused on the removal of humic substances and turbidity by cationic biopolymer chitosan are presented. Chitosan is a natural high-molecular-weight polymer prepared from chitin, which is a polysaccharide found in the exoskeleton of shellfish like shrimps or crabs. The high content of amino groups provides very interesting heavy metals chelating properties to chitosan. Chitosan is partially soluble in diluted mineral acids such as HNO_3, HCl, H_3PO_4. We have used 0.5% solutions of chitosan diluted in 0.1M HCl. Aggregates of humic substances after inorganic coagulant or chitosan addition were separated by centrifugation. Tests were made with model humic water. The aim of this work was to found optimal use of chitosan and to compare its coagulative effectivity with that of standard coagulants – ferrous and clayey sulphate.

Introduction

Chitosan is a derivative of chitin, a polysaccharide that is the major component of the shells of crustaceans and insects. Chitin consists of long chains of acetylated D-glucosamine, that is, glucosamine with acetyl groups on the amino groups (N-acetylglucosamine). Chitosan is N-deacetylated chitin, although the deacetylation in most chitosan preparations is not complete (see Fig. 1.). Chitin itself is usually prepared from crab or shrimp shells or fungal mycelia. Treatment with an alkali then produces chitosan with about 70% deacetylation[1,2].
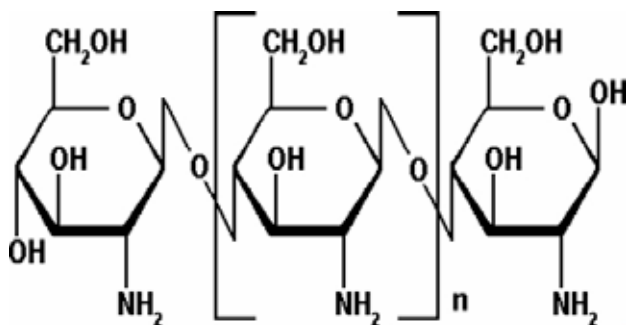
Fig. 1.　**Structure of chitosan**

Chitosan as cationic polysaccharide is an important polymer flocculant in water treatment. It is known that in chitosan's molecular structure contains many amino groups ($-NH_2$) and hydroxyl groups ($-OH$) on the molecular chain. These $-OH$ and $-NH_2$ groups contain single-pair electrons that can offer the electron pair to empty d-trajectories of metal ions. Chitosan can therefore be used for removal of many unwanted metal ions from water such as Al^{3+}, Zn^{2+}, Cr^{3+}, Hg^{2+}, Ag^+, Pb^{2+}, Ca^{2+} and Cu^{2+} etc. Because the active amino groups in chitosan molecule can be protonated with H^+ in water into a cationic polyelectrolyte[3] the molecule shows effects of static attraction and adsorption. Thus chitosan can also flocculate particles into digger flocs which become deposited. Chitosan can be effectively used for removing COD (organic contaminant) and SS (solid suspending substances) in water treatment.

Compared with traditional chemical flocculants, chitosan has the following advantages: the required dosage is lower, a the depositing velocity is higher, also the efficiency of removing COD, SS and metal ions is better, sludge treatment is easier and there is no further pollution. Chitosan as a flocculant for treating of water will be more expensive than traditional flocculants. The objective opf our work was to prepare a cheaper composite based on the chitosan flocculant material and to make this up from lobster shells[4] and other chemical flocculants. This composite chitosan flocculant was planned not only to reduce flocculation cost but also to improve flocculating function, in comparison with single chitosan flocculant and traditional chemical flocculant poly-aluminium chloride (PAC)[5].

Impurities present in the raw water are in suspended, colloidal, and dissolved form. These impurities are dissolved organic and inorganic substances, microscopic organisms, and various suspended inorganic materials. It is necessary to destabilize and bring together (coagulate) the suspended and colloidal material to form particles. Afterwards these particles are removed by filtration.

Coagulation is accomplished by the addition of ions having the opposite charge to that of the colloidal particles. Since the colloidal particles are almost always negatively charged, the ions which are added should be cations or positively charged. Typically, two major types of coagulants are added to water. These are aluminium salts and iron salts. The most common aluminium salt is aluminium sulphate, the most common iron salt is ferric sulphate. Iron and aluminium salts are used as primary coagulants and the reactions that occur after addition of these coagulants are fairly well elucidated. More recently, organic polyelectrolyte coagulants have become also used. Organic coagulants are sometimes used in combination with inorganic coagulants. Depending on the specific chemistry of the target water, polymer use can vary from as little as 5 % of the total coagulant dosage to as much as 100 % ref.[6].

Chitosan has been widely used in vastly diverse fields, ranging from waste management to food processing, medicine and biotechnology. It becomes an interesting material in pharmaceutical applications due to its biodegradability and biocompatibility, and low toxicity. The protonization of amino groups in solution makes chitosan positively char-

ged, and thereby very attractive for flocculation and different kinds of binding applications. Since most natural colloidal particles, including bacteria and macromolecules, are negatively charged, attractive electrostatic interactions may lead to flocculation[1,2,4].

Experimental

C h i t o s a n   S o l u t i o n s

Chitosan is partially soluble in dilute mineral acids such as HNO_3, HCl, H_3PO_4. We have used 0.5% solutions of chitosan TM 324 (Primex, Island) diluted in 0.1M HCl. The solution was prepared fresh before each set of experiments for consistency.

M e t a l - B a s e d   C o a g u l a n t s

Ferric sulphate $[Fe_2(SO_4)_3]$ and aluminium sulphate $[Al_2(SO_4)_3 \cdot 18H_2O]$, supplied by Kemifloc a.s. (Přerov, Czech Republic) or Kemwater ProChemie s.r.o., (Bakov nad Jizerou, Czech Republic) respectively were used for the experiments.

M o d e l   H u m i c   W a t e r s

Tests were made with model humic water. Model water was mixtures of distilled water, tap water and natural concentrate of humic substances sampled from a peatbog near Radostín. Selected model humic water parameters are given in Table I.

Turbidity was formed by addition of bentonit. Absorbance at 254 nm was measured in 1-cm cell and absorbance at 387 nm and at 820 nm were measured in 5-cm cell[7].

C o a g u l a t i o n   T e s t s

Coagulation test using centrifugation as the separation method was employed. This test did allow us to study formation of NOM particles by Brownian motion (perikinetic coagulation) and has the highest possible degree of reproducibility (in any place in the world) as temperature is the only parameter influencing the kinetics of particles formation. Aggregation time was 10 and 40 minutes. Absorbance at 254 nm, 387 nm and 820 nm were evaluated.
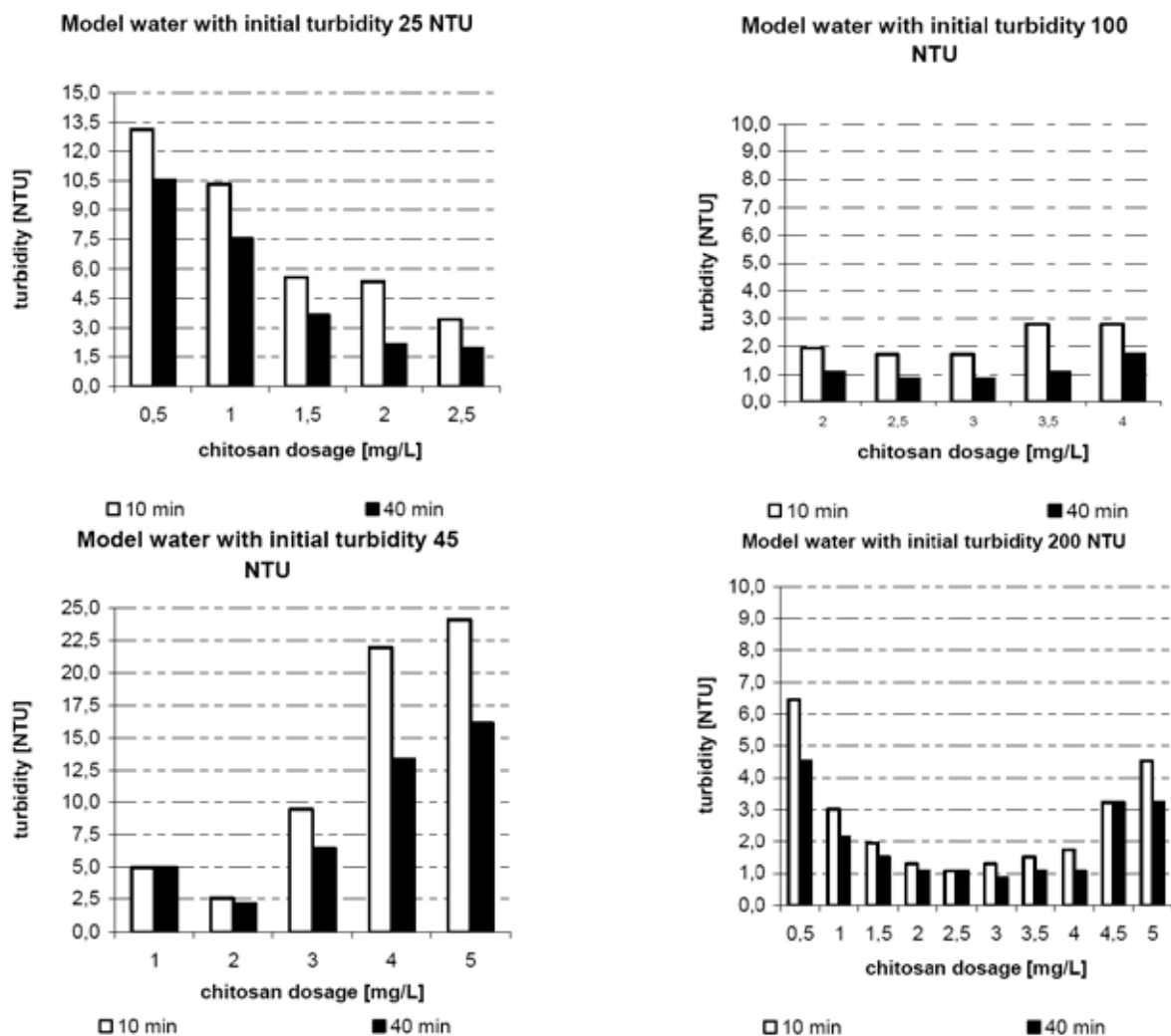
Fig. 2.   **Turbidity removal comparison between different initial turbidity levels**

Table I
Parameters of starting model humic waters

pH	6.3
$ANC_{4.5}$ [mmol dm^{-3}]	0.4
χ [mS m^{-1}]	16.7
A_{254} (1 cm)	0.178
A_{387} (5 cm)	0.196
A_{820} (5 cm)	0.015
turbidity [NTU]	2.4

χ – conductivity; $ANC_{4.5}$ – acidic neutralising capacity to pH 4,5; A_{254} – absorbance at 254 nm; A_{387} – absorbance at 387 nm; A_{820} – absorbance at 820 nm

Results

Chitosan solution was dosed into model waters with values of initial turbidity 25, 45, 100 a 200 NTU. The dosages of chitosan were from 0.5 to 5.0 mg dm^{-3}.

Figs. 2 and 3. show comparison of removal of turbidity between different initial turbidity. Optimum coagulant dose ranged from 2.0 to 3.0 mg dm^{-3} of chitosan. Removal of turbidity was more than 90 % in optimum dose. Application of higher dosages induced lower efficiency of turbidity removal. Values of turbidity were lower than 2.0 NTU after treatment[8].

Conclusion

Generally, the results show very good removal of humic substances and turbidity by chitosan. The optimum pH value for chitosan coagulation was between 6–7 ref.[9].

Almost 100% removal was reached when using relatively low dosages of chitosan. Value of turbidity lower than 10 NTU was measured already at dosage of 0.5 g dm^{-3}. The results show that chitosan is a promising substitute of metal-based coagulants, which are traditionally applied in treatment of turbid humic waters.

Fig. 3.   **Dependence of absorbance and pH at chitosan dosage**

REFERENCES

1. Divakaran R., Sivasankara Pilla V. N.: Water Res. *36*, 2414 (2002).
2. Dalwoo Corporation: *Chitin, chitosan and chitosan oligomer from Crab Shells*. [online]. cit. 2008-07-21 http://members.tripod.com/~dalwoo/
3. Safari,K., Elmaleh S., Coma J., Bankhouja K.: Chem. Eng. J. *27*, 9 (2004).
4. Defang Z., Gang Y., Penvi Z.: Chin. J. Environ. Sci. *1*, 62 (2002).
5. Defang Z., Wu J., Kennedy J., F.: Carbohydr. Polym. *71*, 135 (2008).
6. Gulbrandsen: Organic polymers [online]. 2002. cit. 2008-05-13. http://www.gulbrandsen.com/GTI_prod_4_3_06.shtml.
7. Dolejš P.: *In Sborník konference „Hydrochémia '83"*. Bratislava: ČSVTS VÚVH, p. 361, 1983.
8. Klímová Z., Dolejš P.: *In Sborník konference PITNÁ VODA 2008*, České Budějovice: W&ET Team, p. 213, 2008.
9. Klímová Z.: *In Sborník konference VODA ZLÍN 2008*, Zlínská vodárenská, a.s., Voding Hranice s.r.o., p. 65.

P30　THE EFFECT OF WASTE BASALT WOOLS ON THE CHEMICAL, AGROCHEMICAL, PEDOLOGICAL AND HYGIENIC-TOXICOLOGICAL SOIL PARAMETERS

PETER KOVÁČIK, ALENA VOLLMANNOVÁ and JAROSLAV NOSKOVIČ

Department of Agrochemistry and Plant Nutrition, Faculty of Agrobiology and Food Resources, Slovak University of Agriculture in Nitra, Tr. A. Hlinku 2, 949 76 Nitra, Slovak Republic,
Peter.Kovacik@uniag.sk

Introduction

The range of soil amendments applying in agriculture of European countries, and Asia as well is considerably wider than the one in Slovakia. However, after Slovak accession to EU it has started to diversify year by year, as many soil amendments affect positively on weathering of the mineral soil elements and mineralization of organic soil elements. They reduce production of non-soluble phosphorus compounds, thereby affect positively on the level of available soil nutrients. Consequently they are alternative sustaining harvest stabilization due to the financial shortage for purchase of the industrial and organic fertilizers[1].

The trial aim was to ascertain the affect of two almost identical recycled waste rock wools produced for hydroponic plant growing (Agroban) and for building industry (Nobasyp) by the company Izomat Nová Baňa on many soil parameters.

Experimental

Characteristics of the Waste (Rock) Basalt Wools

Nobasyp is a commercial name for loose minced thermo-insulating material sold as Nobasil. It is produced as a result of milling (recycling) of Nobasil which has not met the requirements of the consumer (shape, thickness, colour, etc.). Agrodrap can be obtained by scrapping the pieces of rock wool (basalt wool) commercially sold as Agroban. In a similar way like Nobasyp, Agrodrap is produced with the aim to evaluate Agroban which is made with different parameters than the particular buyer requires. Appropriate agrochemical and hygienic-toxicological parameters of used waste rock (basalt) wools were the condition for their inclusion in biological tests.

Vegetation Trials

The pot trial was realized in a vegetation cage located at the Slovak Agricultural University in Nitra. 25 kg of Haplic Luvisol with a low content of C, accessible N and P and a high content of K were weighed out into 30 kg pots^{-1}. Every pot was sown with 100 spring barley grains. After the germination the number of the individuals was united to 75 plants per pot. There were 8 treatments repeated four times (0 – control; NS_1 – Nobasyp dose of 20 t ha^{-1}, AD_1 – Agro-

drap dose of 20 t ha^{-1}; NPK – the dose of NPK fertilizers consisting of N dose – 140 kg ha^{-1}, P dose – 50 kg ha^{-1} and K – 40 kg ha^{-1}; NPK + NS_1 – fertilizers + the basic dose of Nobasyp 20 t ha^{-1}; NPK + $NS_{1/2}$ – fertilizers + half a dose of Nobasyp 10 t ha^{-1}, NPK + AD_1 – fertilizers + the basic dose of Agrodrap 20 t ha^{-1}; NPK + $AD_{1/2}$ – fertilizers + half a dose of Agrodrap). The doses of NPK nutrients (N – 3 g pot^{-1}, P – 1 g pot^{-1}, K – 2 g pot^{-1}) were calculated taking into account the N_{an} and accessible P, K contents in the Haplic Luvisol as well as the requirements of the nutrients for planned yield (6 t ha^{-1} of the grain).

Nitrogen was added in the fertilizer DAM 390, P in a form of simple superphosphate and K in a form of 60 % KCl. Nobasyp and Agrodrap doses were chosen on the basis of knowledge[2].

The spring barley harvest was performed in a growth phase DC 91. After the harvest the soil samples were taken from the whole profile of each pot where was given a research in the effect of waste rock wools on many soil parameters.

Analytical Methods

Specific electric conductivity (EC) was determined by the conductometer Hana HI 8820 N. The hydrogen ions activity was sensed potentiometrically by the glass electrode (in a soil suspension) after 24 hours of effect 1M KCl on the soil. The cation exchange capacity was detected as a sum of the base of saturation and the total acidity of soil[3]. The total carbon content was sensed oxidometrically, oxidation with $K_2Cr_2O_7$ in the environment H_2SO_4. Composition of humic substances was detected by Kononova – Beltchikova method[3]. The content of Cd, Pb, Cr, Ni was detected after mineralization with $HF + HClO_4$ by atomic absorption spectrophotometry.

Results and Discussion

The application of Nobasyp or Agrodrap (20 t ha^{-1}) has statistically significantly increased the cation exchange capacity (+ 35.7 % and + 17.2 %), the sum of exchange basic cations (+ 42 % and + 21.4 %) and the base of saturation of the soil (+ 4.7 % and + 3.6 %). The bulk density of the soil has been decreased significantly as well (–5.7 % and –2.5 %), whereas Nobasyp has determined the parameters more importantly than Agrodrap. Established results are at disagreement with the contention[4] which assert that the use of the mineral wool do not improve physical parameters of the soil. The assertion is irrational, because their experiments were narrowly focused on the effect of the wools on the water reserves increase of eroded soil.

Both materials have had a positive effect on the total carbon content (+ 2.1 % and + 9.3 %) and and the organic matter quality, thereby have increased the humic acid share in the soil, whereas Agrodrap has had more significant effect on these parameters than Nobasyp. The combined application with NPK fertilizers has increased the positive effect of the wools on the increase of the organic matter quality of the soil.

Both waste rock wools have had an alcalic effect on the soil and have deadened acidic effect of the fertilizers and the negative effect on the increase of salt content in the soil as well. They have had the same effect on the content of nine determined heavy metals in the soil (Cd, Pb, Cr, Zn, Cu, Co, Ni, Mn, Fe) as NPK fertilizers application.

At the end of the trial was the content of six heavy metals (Cd, Pb, Cr, Cu, Co and Ni) in all the treatments lower than before the start of the trial.

Conclusions

Due to the neutral effect of wools on the heavy metals content in the soil and the positive effect on the remaining soil parameters can be Nobasyp and Agrodrap regarded as soil amendments.

REFERENCES
1. Marschner H.: *Mineral nutrition of higher plants*. Elsevier Academic press, San Diego, California, 889 p, 2005.
2. Kovacik P.: Acta fytotechnica et zootechnica *9*, 5 (2006).
3. Hanes J.: *Analyses of soil sorption properties*. VUPOP Bratislava a SPU Nitra, 136 p, 1999.
4. Orlik T., Marzec M.: Acta cientarium Polonorum – Formatio Circumiectus *3(1)*, 81 (2004).

P31 INFLUENCE OF WATER EROSION PROCESSES ON THE BOTTOM SEDIMENT QUALITY

NATÁLIA KOVALIKOVÁ and MAGDALÉNA BÁLINTOVÁ[a]

[a]*Civil engineering Faculty, Technical university of Košice, Vysokoškolská 4, 042 00 Košice,*
natalia.kovalikova@tuke.sk

Introduction

Erosion processes in watersheds belong to serious ecological and economical problems because of negative consequences in terms of soil and water deterioration as well as on the environment as a whole. Sediments, detached by the erosion, bind nutrients (particularly nitrogen and phosphorus), that can significantly affect the balance of the aquatic ecology, resulting in eutrophication of lakes and rivers[1].

More studies in Slovakia have been focused on the assessment of soil erosion, based upon principles and parameters defined in the Universal Soil Loss Equation, but neither from them has dealt with nutrient transport assessment in consequence of water erosion.

This contribution deals with the nutrient transport from eroding upland fields by the small water basin Kľušov.

Experimental

M a t e r i a l   a n d   M e t h o d s

The study of nutrient transport assessment in consequence of water erosion has been realized in vicinity of small water basin (SWB) Kľušov situated at the Tisovec stream in the east of Slovakia. Average depth of SWB is 3.5 m and its total capacity is 72,128 m^3

According to last measuring, the quantity of sediments in reservoir caused the decreasing of SWB capacity about 33 % during 18 years. Therefore this reservoir was run the water off from 2005 to 2007 and has been chosen as model basin for our study.

For bottom sediment quality assessment, there was realized sampling of bottom sediments and also sampling of arable land in vicinity of reservoir.

Soil samples were taken according the modified methodology for nutrient transport assessment in consequence of water erosion. This methodology comes out from Decree of the Ministry of Agriculture of the Slovak Republic No. 338/2005 Coll. combine with Soil Sampling according to Mahler and Tindall[2], because Slovak decree doesn't assess soils in term of total phosphorus and nitrogen concentrations, it considers only with plant available nutrients.

Soil samples were taken from arable land in period 2006–2007.

Together with soil samples also one composite sediment sample was taken from each selected locality – along the reservoir and by the dyke.

Localities for sediment and soil sampling are shown in Fig. 1.

Fig. 1.　**Sediment and soil sampling localities**

In the first stage of our research, the granularity impact of soil and sediment particles on the nutrient concentration was followed, because pollutants are preferentially attached to the finest particles (fractions below 63 microns)[3].

Samples of bottom sediments and soils were analyzed for total N and P in accredited laboratory of State Geological Institute of Dionyz Stur Spišská Nová Ves.

Results

From chemical analyses (Table I) follows that nutrient concentrations in average soil sample (P1, P2) were nearly identical with concentrations of followed compounds in fractions below 63 microns (P1', P2').

The concentrations of P, N in chosen sediment samples (S1–S8) were diverse due to irregular sediment deposition in the reservoir (Table II). These concentrations increase with proportion of the finest particle fraction and the higher concentrations are by the dyke (Fig. 2.). In this case the literary information[3] about higher concentrations of the followed compounds (N, P) in sediment samples in fraction below 63 microns has been confirmed. Because we found[4] that nutrient concentrations in sediment average sample (S1, S2, S5) and sediment fractions below 0.063 mm (S1', S2', S5') are nearly identical, in the next research we have focused only on concentration in average sediment and soil sample (Table I, II).

Table I
Concentration of N and P in the arable land

Sample	N_{tot} [%]	P_{tot} [%]
P1	0.08	0.069
P1'	0.09	0.068
P2	0.12	0.065
P2'	0.13	0.066
P3	0.18	0.082
P4	0.16	0.055
P5	0.22	0.075
P6	0.23	0.06
P7	0.20	0.077
P8	0.22	0.058

Nutrient transport assessment from soils to surface water was studied through transport of dissolved and adsorbed forms of N and P.

Table II
Concentration of N and P in SWB sediments

Sample	N_{tot} [%]	P_{tot} [%]
S1	0.26	0.112
S1' (100 %)	0.26	0.112
S2	0.24	0.113
S2' (97.65 %)	0.24	0.110
S3	0.22	0.066
S4	0.23	0.066
S5	0.24	0.112
S5' (89.24 %)	0.25	0.115
S6	0.20	0.090
S7	0.17	0.049
S8	0.14	0.070
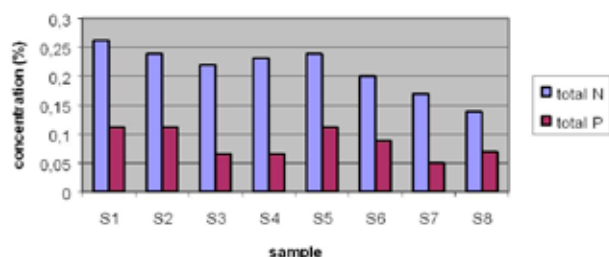
Fig. 2.　**Influence of sampling distance from the dyke on the N and P sediment concentration**

For determining nutrient concentrations in dissolved phase several leaching experiments were realized. Expe-riment results have shown that portion of dissolved phase represented 0.46–0.65 % of total P and 0.37–0.46 % of total N in the soil sample. According these findings, dissolved phase weren't considered.

As follows from Table I, nitrogen concentrations in adsorbed phase of soils varied from 0.08 % to 0.23 % and phosphorus concentrations were in range 0.054 % to 0.082 %. It depends on rates and date of fertilizer application and also on type of grown crop and its uptake rates (samples P1–P4 before and P5–P8 after nitrogenous fertilizer application).

Conclusions

The concentration of nutrients in studied soil samples wasn't influenced by their granularity and depends on the applicable fertilizer rates and grown plant uptake.

The results from chemical analyses confirmed the lite-rary information that the concentrations of P, N in chosen sediment samples are diverse due to irregular sediment depo-sition in the reservoir and increase with proportion of the finest particle fraction.Concentrations of P, N in sediments correspond to their concentrations in soils what is in accord with our results about their maximal portion in adsorbed phase.

REFERENCES

1. Bálintová M., Kovaliková N.: Sel. Sci. Pap. *1*, 189 (2005).
2. Mahler R. L., Tindall T. A.: Coop. Ext. Bull.*1997,* 704
3. Methodological instruction of Ministry of environment SR No. 549/98-2
4. Kovaliková N., Bálintová M.: Acta Facultatis Ecologiae *16*, 129 (2007).

P32 MODELLING AND DIAGNOSING OF MECHANICAL ENGINEERING LIFE CYCLE PRODUCTION PROCESS

RUŽENA KRÁLIKOVÁ and ALENA PAULIKOVÁ

Technical University in Košice, Faculty of Mechanical Engineering, Department of Environmental Studies and Control Processes, Park Komenského 5, 041 87 Košice, Slovak Republic,
ruzena.kralikova@tuke.sk

Introduction

Competing business challenges to interest in production process as determined factor for quality products, environment protection, production machinery condition, required parameters for machining and elaborateness for given accuracy. One of solution is the implementation modern simulating devices and applications of analogs in production practice.

It is necessary to pay attention to production process as a determined factor for product quality, environment protection, production machinery state, required parameters for machining and elaborateness, which is given for achievement of required accuracy. One of solution is implementation of modern simulation devices and application of models in production operation.

Environmental Strategies

Environmental aspects, its loading and protection give production enterprises the possibility of evaluation of their production methodology, used technology, raw material and energy management in term of environmental influence reduction.

However, the quality of these solutions dependes on project quality for new building-up or reconstruction of production, there is need to add ecological aspects to ordinary methods of projecting.

The ecological ones in determined term ensure sustainable development of environment. Policy, economy and ecology have got significant function. Works, function and possibilities in environmental creation and protection could be outlined in points which represent strategy of mechanical engineering development in environmental view at present:
- production of environmental suitable products,
- using of environmental acceptable technologies for their production,
- energy and raw material economy – low-waste, non-waste and recycling technologies,
- machinery and devices production for environmental protection and creation (water treatment plants, filters, separators, traps, eco-technology).

Model Creation of Mechanical Engineering Production Process

Production process is the collection of human activity, machinery and physical processes and its results are particu-

lar kinds of products. At every production process there are three factors:
- systematic activity – human work,
- work objects which are transformed to products – basic mechanical engineering products are machines, function groups, nodal points and components,
- means of work, which are production machines, devices, tools, accessories, helpers, transport and handling equipments, control technology[1].

During production process shape and composition materials are changed so that the result is the new utility value. The production process can start if production factors, inputs are disposable. One of inputs can be also the creation of production process model. That is why is necessary to have concrete data, which characterize given production process.

By analysing of process activity there are scheme where particular phases of phenomena observation or object perform these activities that are each other connected and regulated by producer's and customer's decision.

In accordance to environmental view the mechanical engineering production process is open system with its relation to surroundings. It has got full interaction among subjects. In accordance to relations this system is quite open which makes possible the full interaction to surroundings. In Fig. 1. and Fig. 2. there is the comparison of production process from the point of the view:
- influence on the environment
- renewable and unrenewable resources exploitation of raw materials and energy
- interaction with other processes
- waste production[4].
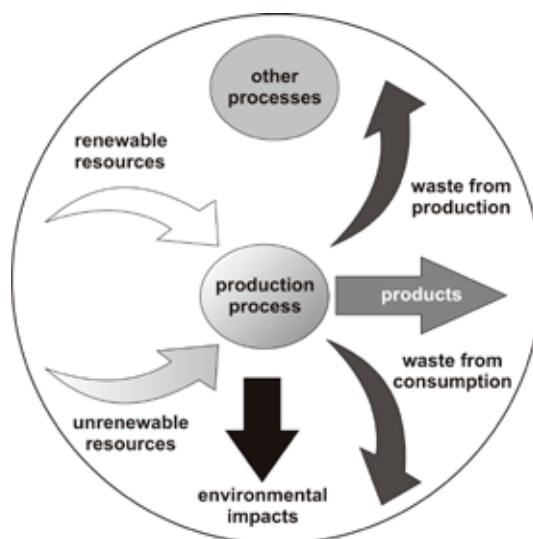
Fig. 1.   **Nonenvironmental production process**

Environmental suitable production has to follow the main aim. Production process is regarded as system which creates closed structure with interaction of system environ-
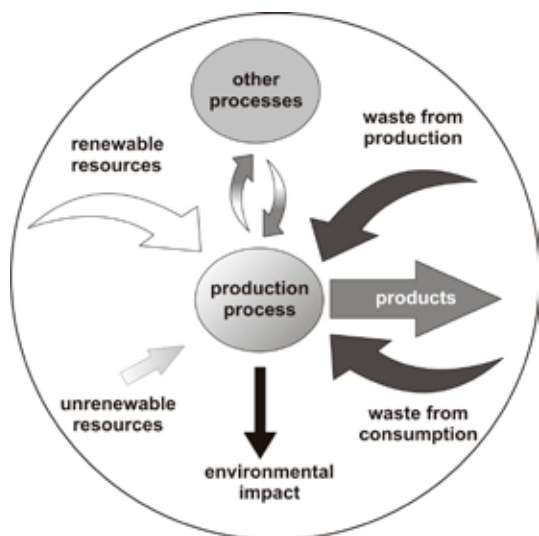
Fig. 2.　**Environmental production process**

ment, i.e. Closed Loop Systems, Fig. 3. This system demonstrates renewable energy, nontoxic materials in a closed loop and sustainable product design. It is rooted within circular concepts of the product life cycle.

Production process has also got its life cycle. There are characterized its production, system, technological and environmental phases. According to production aspects the process can be in beginning phase of its cycle. However according to environmental impact view can be out-of-date or according to qualitative parameters in leading countries "outsider". Working out of equivalent model of production process is has got several phases as followings:
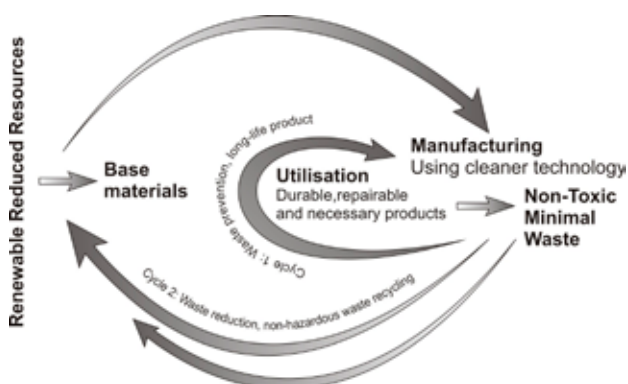
Fig. 3.　**Closed Loop Systems**[4]

Prediction　Analysis

Estimation of production running, its inputs and outputs is possible to make or by considering that production has got the same way eventually similar way or quite new and different way. The way is determined as kind of application, its evaluation, modification or change of production, systemic, technological and environmental approaches. It is important to establish the reliable obtained information. It can reach

to use accurate methods of data collecting or application of measurement methods if there is an existing operation plant where it is possible to obtained parameters.

Development　of　Method

According to number of inputs and outputs, we can choose strategy or methods for model development. We obtained various types of models with the combination of individual parameters. If we choose the main point as economical point and inputs will be reduced only gains, expenses, costs per hour, costs per piece, etc. Very simply model comes into existence but in real operation there is not applied. Many customers ask for quality, ecology, and modern technology not only low price.

Model　Implementation

There is a verification of prediction and correctness of used methods. If the preparation is worked out in details then the implementation is simple and the model can be applied in short time. Implementation makes possible to modify a model and it creates other opportunity to regulate and to adjust the model.

Controlling　of　Model

After successful implementation of model there is final period – i.e. control. It is the adjusting according to external and internal operational demands. All feedback relations in system can be used and following modifications, which do not influence the model creation but only they simulate all changes in production.

Application　of　Model

Model, which is created in this way, exists from its beginning to its end and this model makes possible to eliminate or minimize mistakes. These mistakes would be developed directly in operation without the using of previous simulation.

Model becomes the control tool for production process. Mistakes in model are cheaper than real production and changes, which are done in model, are reversible as well. Production enterprises can use Model for improving or representation for customers, contact persons from state institutions, for certification of quality of environmental management, for training and courses of employees or for comparison of product quality to competing product. In model there are all accessible methods and technologies, which product operator requires. One of methods is Life Cycle Assessment (LCA)[2].

Life Cycle Assessment

Life Cycle Assessment is very often term predominately in environmental management field. Every mechanical engineering product shows environmental "track" in environment and this way these environmental impact are evaluated during all its life cycle – from the cradle to grave. It is complicated to obtain enough data number from operation. Or obtained data are different values, units or time and accuracy of obtaining.

Production process is also concerned hundreds of products and its characters are complicated. In LCA there are assessed for example harmful substances released into the air and water, amount of solid waste as well, energy and raw material consumption, human environmental effects, who are in production. Tools of LCA cover general matters as well as localizations independent from evaluation methods.

Modelling of process means the using of all available methods from LCA, SEM, standards ISO 14000 and 9000 and technological processes, LCA technologies and likewise. Complex model can also simulate production accidents[3].

Multicriterial Environmental Evaluation of Using Chemicals in Individual Plants

This evaluation is based on quantification of parameters for environment quality by means of unbalanced evaluating effects of production process.

Fig. 4. **Multicriterial evaluation for using of chemicals in production process**

Objectivity of solution has got number of evaluating coefficients, their optimal number in interval 20–25. Deriving from following relations it is possible to determine Q_j – value of environmental chemical load:

$$Q_j = \sum_j \frac{a_{ij} - \bar{a}_j}{s_j} \times k_j, \qquad (1)$$

where:

Q_j – value of environmental load,
a_{ij} – value j-element of vector,

$\bar{a}_j$ – average value of j-element
s_j – standard deviation of modified j-descriptor,
k_j – reduction constants.

Example for application of multicriterial evaluation for using of chemicals in production process is in Fig. 4.

It is possible to determine from application of multicriterial evaluation which operational plant is the most loaded, i.e. the plant with the higher Q_j- value.

Conclusions

Methods for monitoring and checking of technological, chemical and environmental aspects for production can have other applications as well.

There are in various enterprises for development of technology or optimalization of operation according to customer's, producer's or environmental engineer's demands. This period is period IT technologies and it could show that environmental pollution is slowing because operation plats of individual productions began to behave more understanding.

Model of life cycle for production process is one of tools that helps producers made with optimal technology, develop products with optimal balanced performance and costs, characters which are up to standards for environment, health and safety.

REFERENCES

1. Králiková, R., Pauliková, A.: *In: SYM-OP-IS 2006: Simpozijum o operacionim istraživanjima*: Banja Koviljača, Beograd: Instirut Mihailo Pupin, 2006. p. 45-48.
2. Králiková, R., Pauliková, A., Wessely, E.: In: *Industrial engineering – adding innovation capacity of labour force and entrepreneur: 5th international DAAAM Baltic conference,* p. 203. Tallinn, Estonia 2006.
3. Kozáková, Ľ.: *In: 11th Conference on Environment and Mineral Processing*, p.23. Ostrava, Czech Republic 2007.
4. www.cleanproduction.org/images/closed-loop-diagram. gif, citated on 28th May, 2008.

P33　SIMULATION OF CHEMICAL FACTORS IN WORKING ENVIRONMENT

ALENA PAULIKOVÁ and RUŽENA KRÁLIKOVÁ

Technical University in Košice, Mechanical Engineering Faculty, Department of Environmental Studies and Control Processes, Park Komenského 5, 04187 Košice, Slovak Republic,
ruzena.kralikova@tuke.sk

Introduction

Mechanical engineering has not got so many environmental impacts as chemical industry but its technologies often use various chemicals to improve its operations. Working environment of mechanical engineering is also a subsystem of global geosphere environment.

People spend so long term that they identify this working environment with their microenvironment. People are often influenced by several factors in this "small world" of them. These factors categorize some working activities from point of view the environmental and health risks. The categorization of our working activities involves the known details about factors of work and working environment.

At industry plants there is most of workers exposed to a combination of multiple factors of working environment which influence their health and comfort. The category is determined separately for individual factors but there is no methodology of working activities assessment for any combination of individual factors[1].

By means of modern software simulation there is designed the methodology with the look-up functions of program Vensim for a complex assessment of working environment in specific conditions of mechanical engineering enterprises.

Chemical Parameters in Cutting Process

In cutting processes there are a lot of chemical parameters which improve or make worse human working environment. These chemicals exist in various form and states. The liquids and aerosols create predominant part of the states.

Cutting Fluids

Cutting emulsion is a dispersion system of two insoluble liquids. One creates microscopical drops dispersed in the other liquid. At machining only emulsion type: *oil in water* is used. Milk appearance or transparent appearance depends on size of oil drops. For the first case the drops are larger and for the second case the drops are smaller than 10 mm^3.

Mineral oil and water almost do not generate an emulsion. That is why the other component is needed – emulator which covers oil drops with absorption coat protecting their repeated mergence. Soaps, organic amino compounds, sulphonate compounds and the like are used as emulators.

Mineral oils conditioned with emulators are called emulsive oils. They also contain anticorrosive, antibacterial and high-pressure additives. The content of mineral oils in emulsive oils is 50–75 %.

The second component of basic emulsion compounds is water which has got very good cooling effect. However, raw water has got a lot of defaults for a preparation of industrial emulsions, i.e. presence of limestone and magnesium which are liquated and they create hard-removable sediments on metal surfaces. The sediments silt up piping, sieves, tanks and also seal the functional parts of machinery[2].

As well the corrosive influences and high contents of micro-organisms are harmful in water for an emulsion preparation. An anticorrosive protection is performed by the anticorrosive additives, i.e. soda, borax, sodium phosphate or sodium silicate. These additives soft water and decrease its surface tension. They improve wettability, cooling effects and create alkaline environment. Alkaline environment is suitable from point of view an anticorrosive protection of ferrous metals. There are pH under 9.0 because safety and health reasons. If pH is higher then there is a damage of protective coats and rubber parts of machines.

The main default is an inclination to micro-organism contamination what makes short cutting fluid durability by decisive way. If there is an emulsion value of pH 9.5 and higher then micro-organism development is decelerated. However, in this condition the emulsion is health unsuitable, irritate skin and airways.

Additive BIOSTAT® for Cutting Fluids

BIOSTAT® is a common name for new generation set of antibacterial and fungicidal preparations which have been developed for 8 years in the framework of environment friendly production.

Preparation set BIOSTAT® is inorganic origin and its influence is based on three activity principles:

- the strong electrochemical influence of Ag ion operating directly with energy reaction in an electron-transportation string of cellular proteins
- the irreversible denaturation of sulfhydryl groups of micro-organism proteins by means of the ion exchange H by Ag
- the strong oxidation possibility of product of BIOSTAT®, which causes the catalytic oxidation H_2O molecule and air oxygen generating hydrogen peroxide. Hydrogen peroxide is fissioned consequently into H_2O molecule and oxygen radical[3].

Determination of Parameters for Model

Simulation software Vensim is a graphical model tool. By means of it, we can draft, document, simulate, analyse and optimize various simulation models of industrial technologies. One of the technologies is also machining with using of chemicals, which belongs to the difficult tasks solved in environmental engineering protection.

The keystone of s model imulation is determination and application of following variables in the sketch with nodes and connecting curves:

- level parameters – amounts of cutting fluids
- rates – operations or technological processes
- constant variable – chemical factors
- auxiliary variables – derived parameters for chemical and environmental impacts.

Model for Cutting Fluid Chemicals

In Fig. 1. there is the sketch of applied parameters for using of cutting liquids in machining and in Fig. 2. there is the simulation of these parameters.
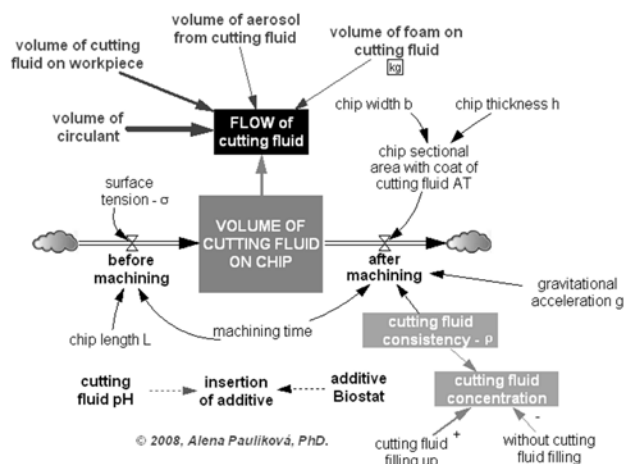
Fig. 1.   **Used parameters of cutting liquids in machining**

Simulation for Cutting Fluid Chemicals
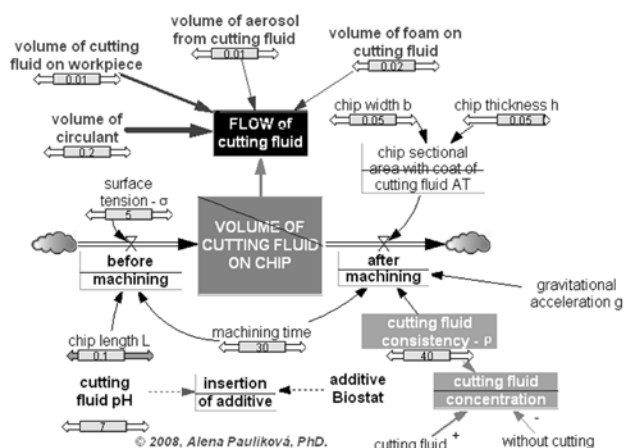
Fig. 2.   **Simulation parameters of cutting liquids**

There is a chemical world of systems driven by cause and affect. Those systems include production, protection, biological, chemical, thermodynamic or workflow.

Environmental or chemical systems can be modelled as nodes representing system variables and connecting lines representing causal effects. The changing value of one variable can cause another to increase or decrease. Understanding how a system really works is the first step towards using, improving or automating[4].

Results

We can change chemical status of the overall machining process with the movement of slider. Every constant has got its own slider. The change of constant value influences the value of auxiliary variables and then they influence value of level parameters.

This similar model can help the technicians or workers to properly dose various additives, to fill up fresh cutting fluids, to increase total productivity and to save expenses.

Conclusions

By the assessment of individual quantitative indicators of cutting fluid chemical status we can draw these conclusions:

- used cutting fluids began to spoil the most often by long term of cleaning of individual machines and cutting fluid reservoirs
- the insertion of additive BIOSTAT® into cutting fluids to lengthen their durability and cleaning intervals.
- the declination of Ag is caused its sedimentation of undissolved additive in the cutting fluid reservoirs and its removal by means of workflows or waste-flows of cutting fluids
- the cutting fluids flows need for their cycle the segment of sedimentation reservoir and filters to improve working environment
- additive BIOSTAT® does not cause allergic reaction of respiratory or dermal characters.

REFERENCES

1. Pauliková A.: Habilitation Thesis, Technical University, Košice, 2008.
2. Ruiz J. M, Kollár V, Brokeš P.: *Priemyselné technológie*, Grafické štúdio Ing. Peter Juriga, Bratislava 2000.
3. Ansil: *Manuál pre aplikáciu prípravku Biostat®* (Slovenská republika), 2006.
4. www.excelsoftware.com, August 8, 2007.

P34　MULTI-RESIDUE METHOD FOR THE ANALYSIS OF PESTICIDES AND MYCOTOXINS IN CEREALS BY LC-MS/MS

ONDŘEJ LACINA, JANA URBANOVÁ, ALEXANDRA KRPLOVÁ and JANA HAJŠLOVÁ

Institute of Chemical Technology Prague
Technická 5, 166 28 Prague 6,
ondrej.lacina@vscht.cz

Introduction

In the recent decade, liquid chromatography–tandem mass spectrometry (LC MS/MS) operated in a selected reaction monitoring mode, has become the main tool for the analysis of food and environmental contaminants presenting wide range of physico-chemical properties. This approach allowed the introduction of multiresidue methods with up hundreds target analytes determined in a single run. However, most of these methods are focused only on one group of food contaminants such as pesticides, veterinary drugs, mycotoxins, plant toxins, etc. Considering the fact, that sample preparation/detection principles are basically similar for most of these methods, we attempted to determine pesticide residues and mycotoxins - contaminants representing different sources of origin in single run. The comprehensive LC-MS-MS multi-residue method has been developed and validated for 14 *Fusarium* toxins, 4 aflatoxins, ochratoxin A, 3 *Alternaria* toxins and 200 pesticides.

Experimental

Chemicals and Reagents

Certified pesticide and mycotoxins standards were purchased from Dr. Ehrenstorfer GmbH (Germany), Riedel de Haen (Germany) and/or Biopure (Austria). Individual analyte stock solutions (concentrations in the range 0.3–3 mg ml^{-1}) were prepared in either methanol or acetonitrile, depending on the solubility of particular analyte. These solutions were used for preparation of mixed standard solution in acetonitrile (10 µg ml) and stored in −18 °C. Deionized water for preparation of a mobile phase was produced by Milli–Q apparatus (Millipore, Germany). Ammonium formate for mass spectrometry was obtained from Fluka (Buchs, Germany). Acetonitrile (Sigma-Aldrich, Germany) and methanol (Merck, Germany) were HPLC gradient grade solvents for pesticide residue analysis.

Sample Preparation

5 g of sample were weighted into 50 ml PTFE centrifugation tube. Then, 20 ml of extraction mixture of acetonitrile/water/formic acid (75 : 24 : 1, v/v/v) were added and the tube was placed onto laboratory shaker for 90 min. After this time, the tube was centrifuged (Hettich, Germany) at 11,000 rpm for 5 min and aliquot of extract was diluted by a water in a ratio 2 : 1 and filtered through a 0.45 µm PTFE filter Iso-DiscTM (Supelco, USA), and transferred into a vial.

HPLC-MS-MS Analysis

The HPLC analyses of selected pesticides and mycotoxins were performed using an Alliance LC system (Waters, USA) equipped with an Atlantis T3 column (100 × 2.1 mm I.D., 3 µm particle size, Waters, USA) maintained at 30 °C. The mobile phase contained 0.005M ammonium formate in deionized water (A) and methanol (B), flow rate was 0.3 ml min^{-1}. The optimized chromatographic method started at mobile phase composition of 5 % of B and was hold for 0.5 min, then rising linearly to 60 % of B and then 100 % at 15 min. This composition was held for 8 min to remove co-extracted matrix from column, 6min re-equilibration to initial mobile phase composition followed. Sample injection volume 8µl was used in all experiments.

HPLC system was connected to tandem mass spectrometer Quattro Premier XE (Waters, USA) operated in positive electrospray ionization mode. The capillary voltage was set to 3,500 V, source temperature was maintained at 120 °C and desolvation temperature was 380 °C. The masses of parent and daughter ion, cone voltage and collision energy were tuned previously for each analyte and two MS/MS transitions were acquired for each of them.

Results

Optimization of Sample Preparation

QuEChERS extraction method published and extensively tested in a recent years[1–3] has become the widely used method for isolation pesticide residues from various matrices. QuEChERS method employs acetonitrile (MeCN) extraction followed by partition induced by added salts. If necessary dispersive SPE clean-up is performed. The partition step discriminate a lot of bulk matrix compounds such as sugars and/or acids, which would interfere with determinative step, however also recovery of polar target analytes is reduced. For this reason, the QuEChERS has not become an extraction method of choice for mycotoxins, especially for relatively polar B trichothecenes.

It should be noted, that existing multi-mycotoxins methods are based on the extraction by MeCN i.e. use similar solvent as QuEChERS. Although the sources of food contamination by pesticides and mycotoxins are fairly different in their nature, from analytical point of view there are a large number of representatives of these two groups, possessing similar physico-chemical properties. On this account, it is a conscionable concept to put together analysis of mycotoxins and pesticide residues in one multi-toxin method.

The bottleneck of such method might be the sample preparation step, since it is necessary to achieve acceptable recovery for all analytes and at the same time discriminate extraction of matrix components, which could cause suppression of ionization as far as electrospray (ES) is employed in LC-MS method. In principle, achieving simultaneously these two requirements is impossible, and, therefore the only feasible approach is to examine extract directly without any purification[4–5].

Several extraction solvents including MeCN, methanol (MeOH) and their mixtures with water were tested to achieve good recovery for a wide range of analyte polarities. MeOH and its mixtures with water offered good extraction efficiency for polar and semi-polar compounds, however high amount of matrix was also co extracted. Only aqueous MeCN was used, because of poor extraction of polar analytes by pure solvent. It is a common practice in many multi-mycotoxin methods to employ azeotropic mixture of 84 % MeCN and 16 % water. This approach was developed for easy purification by Mycosep and subsequently solvent evaporation, nevertheless omitting purification step enabled improvement of extraction efficiency of polar compounds (such as DON-3-glucoside, acephate, propamocarb) by increasing of water content in extraction mixture up to 25 % (v/v). At the same time, acceptable recoveries were still obtained for relatively non-polar analytes represented e.g. by zearalenon and pyrethroid insecticides.

It should be noted that the addition of water prior to extraction into low moisture samples as cereals is also recommended by a document N° SANCO/2007/3131. To improve recovery of fumonisin mycotoxins and protect unstable base-sensitive pesticides against the hydrolysis, addition of 1 % of formic acid into extract mixture was necessary.

The final extract was diluted by water to decrease content of MeCN and consequently to reduce matrix effects. Different ratios of MeCN and water in a vial were tested, nevertheless the content of water higher than 50% caused precipitation of matrix components and consequently decreasing of recovery of non-polar analytes.

O p t i m i z a t i o n   o f   L C - M S - M S

As mentioned above, no purification step was employed, so chromatographic separation plays an important role to separate analytes and matrix to decrease matrix effects. Although slow gradient was used, very strong signal suppression (over 80 % lower signal of matrix matched standard as compared to solvent standard) still occurred for some of later eluting compounds.

Many LC-MS pesticide multi-residues method use only ESI$^+$ ionization, because almost of analytes ionize only in positive mode or better sensitivity/selectivity is achieved under these conditions. Although B-trichothecenes offer better sensitivity in a negative mode by formation adducts with acetic or formic anion (depends on composition of mobile phase), ionization in positive mode is also possible. The main advantage of positive mode is a compatibility with more than 95 % pesticides and other mycotoxins (aflatoxins, fumonisins) which do not give any ions in ESI$^-$.

M e t h o d   V a l i d a t i o n

The distribution of recoveries of all analytes in wheat is shown in Fig. 1. The recovery and repeatability of particular analyte was obtained from analysis of spiked wheat material at 100 μg kg^{-1}. The extraction method offers a good recovery for both, acids and bases and covered a wide range of pola-

rities. The trueness of method was demonstrated by analysis of reference materials for mycotoxins (ochratoxin A, deoxynivalenol, nivalenol, T-2 and HT-2 toxins) and proficiency testing materials obtained from FAPAS 0950 and EUPT-C1/SRM2. For all reference materials and positive findings in proficiency tests were achieved satisfactory score |z|<2.
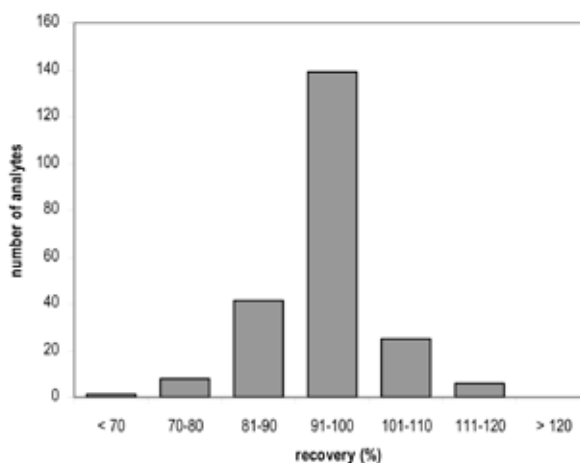
Fig. 1.   **Distribution of recoveries of all 222 pesticide residues and mycotoxins at concentration level 100 μg kg^{-1} in wheat**

Conclusions

The multi-toxin LC-MS-MS method for simultaneous analysis of 200 pesticide residues and 22 mycotoxins in cereals has been developed and fully validated. Acceptable recoveries and repeatabilities have been achieved for most of analytes. The trueness of generated data was also documented. The authors are convinced that this high throughput approach will find a wide use in many control laboratories in close future.

REFERENCES

1. Annastasiades M., Lehotay S. J., Štajnbaher D., Schenck F. J.: J. AOAC *86*, 412 (2003).
2. Lehotay S. J., Maštovská K., Lightfield A. R.: J. AOAC *88*, 615 (2005).
3. Lehotay S. J., Maštovská K., Yun S. J.: J. AOAC *88*, 630 (2005).
4. Sulyok M., Krska R., Schuhmacher R.: Anal Bioanal Chem *389*, 1505 (2007).
5. Sulyok M., Berthiller F., Krska R., Schuhmacher R.: Rapid Commun. Mass Spectrom. *20*, 2649 (2006).

P35   AEROBIC MTBE BIODEGRADATION BY
PAECILOMYCES VARIOTII

BLAZO LALEVIC[a], VERA RAICEVIC[a], LJUBINKO
JOVANOVIC[b], DRAGAN KIKOVIC[c] and MIOMIR
NIKSIC[a]

[a]*Faculty of Agriculture, Nemanjina 6, 11080 Belgrade-
Zemun,*
[b]*Institute for Multidisciplinary Research, Kneza Viseslava,
11000 Belgrade,*
[c]*Faculty of science, Lole Ribara 29, 38220 Kosovska Mit-
rovica*
lalevicb@yahoo.com

Introduction

Methyl *tert*-butyl ether (MTBE) has been used since the
1970s as a gasoline additive and octane booster to replace
lead and other toxic additives and to improve combustion
efficiency of gasoline. Because of useful properties, MTBE
has become one of the organic compounds with the highest
production in the world[1]. In 1999, about 3.3 million tons had
produced in the European Union[2]. In the United States, in
1998, MTBE was the fourth-most-produced chemical[3]. How-
ever, its extremely water solubility, mobility and volatiliza-
tion have resulted in its contamination of surface soils, groun-
dwater and sediments mainly from leaky tanks and spills[4]. A
report by the U.S. Geological Survey identified MTBE as the
second most common contaminant of urban aquifers in the
USA[5]. The U.S. Environmental Protection Agency[6] has listed
MTBE as a possible human carcinogen and recommended
concentration in drinking water below 40 $\mu g\,dm^{-3}$.They also
proposed the methods for removal of MTBE from environ-
ments.

Bioremediation is methods, which use natural biolo-
gical activity of microorganisms and plants to transform or
destroy different toxic contaminants[7]. Previous bioremedi-
ation studies reported little or no biodegradation of MTBE
under aerobic[8,9] and anaerobic[10,11] condition. However,
authors[4,9,12,13] reported that pure and mixed bacterial cultures
have been capable for MTBE biodegradation. There are only
a few reports of fungal strains capable of biodegradation of
MTBE[14,15,16] so far.

The aim of this paper was to investigate the capacity of
fungal strain *Paecilomyces variotii,* isolate 129b, for MTBE
biodegradation at different MTBE concentration in labora-
tory conditions.

Material and Methods
Isolation and Identification of Fungus *Paecilomyces Variotii*

The fungal strain of *Paecilomyces variotii*, isolate
129b, was isolated from the wastewater of API separator in
Oil Refinery Pancevo, Serbia. The cultures maintained onto
rose bengal streptomycin agar (RBSA) plates[17] at 26 °C. The
identification based on fungal morphological characteristics
growing in malt agar and Czapek yeast agar (CYA), using the
key for identification[18].

Degradation Experiment

Liquid suspension cultures grown axenically in 250ml
glass bottles. The growth medium (80 ml) was mineral salts
medium[14]. The medium sterilized at 121 °C for 15 min and
inoculated with 10 % (v/v) of suspension of *Paecilomyces
variotii* conidia (13.8×10^5). After addition of different MTBE
concentrations, the liquid suspension cultures incubated for
19 days at 26 °C and shaken at 120 rpm. All the experiments
were conducted in triplicate.

The Yield of *Paecilomyces Variotii* Mycelia

The yields of mycelia measured after 19 days by means
of dry weight. Liquid suspension cultures were vacuum filte-
red onto filter papers. Mycelia and filters were dried at 65 °C
for 24 h and reweighed. The control variant was without
MTBE as an sole energy and carbon source. The experiments
were conducted in triplicate.

Analytical Methods

The MTBE used in these experiments originates from
industrial facilities of Oil Refinery Pancevo. Consumption of
MTBE was monitored by a Agilent Technologies 6890N gas
chromatograph (GC) fitted with a flame ionization detector. A
30 m × 0.53 mm ID, 3.0 μm DB-624 column was used (J&W
Scientific, Folsom, CA, USA). The temperature program was
50 °C for 2 minutes, ramp 8 °C min⁻¹ to 100 °C, hold 3 minu-
tes. The injector temperature was 170 °C and detector (FID)
temperature 300 °C. The flow hydrogen was 40 ml min⁻¹,
flow air 450 ml min⁻¹ and make up gas N_2 25 ml min⁻¹.

The headspace (Agilent 7694E Head Sampler) was:
vial equilibration time 30 min; bath temp. 80 °C; valve/temp
loop 85 °C; transfer line temp. 120 °C; loop size 1 ml; pres-
sure time 0.00 min; loop fille time 0.050 min; loop eq. time
0.05 min; inject time 1.0 min. Internal standard was acetoni-
trile (retention time 2.951 min). The MTBE retention time
was 3.310 min. In experiment, headspace samples (100 μl)
were taken with gas-tight syringes.

The consumption of MTBE was measured in the begin-
ning of the experiment and after 5; 12; 15 and 19 days.

Results

The soils of Oil Refinery Pancevo are heavy polluted
with different organic substances and it can be expected to
find out big diversity of fungus and bacteria whose use pol-
lutants there as sole source of carbon and energy. During dif-
ferent experiments, about 40 bacteria and 14 different fungi
strains were identified and isolated. One of the fungi founded
there, after testing, showed high ability to consume MTBE.
That fungus is isolated and identified as *Paecilomyces vari-
otii*, isolate 129b, and used in experiments. Ours results
showed that degradation rate was depending on initial MTBE
concentration (10.85; 34.34 and 83.15 ppm used) and time

of sampling. After 19 days of incubation, the degradation of initial middle (34.34) and high (83.15) MTBE concentration stopped, while the degradation of lowest MTBE concentration (10.85) continued after incubation period (Table I).

Table I
The decreasing of MTBE concentration (ppm) caused by fungal strain *Paecilomyces variotii* isolate 129b

MTBE [ppm]	5th day	12th day	15th day	19th day
10.85	6.6	6.08	2.45	1.55
34.34	33.5	23.34	19.19	20.2
83.15	74.3	46.92	38.25	40.7

Moreover, even different pattern of degradation the fungal strain of *Paecilomyces variotii*, isolate 129b, decreased MTBE concentration in all treatments used (Table II). The highest degradation rate (2.23 ppm per day) was in the treatment with the highest concentration used, (from 83.15 to 40.70). In the middle treatment, the degradation rate decreased to 0.744 ppm per day and in lowest concentration the degradation rate further decrees to 0.490 ppm per day. However, the total MTBE degraded by fungi is to be in highest concentration used (42.7 ppm for 19 days). From the Table III it can be seen that there is no substantial change in the fungus yields (mg/ml) compared treatments and control.

Table II
The MTBE degradation rate [%] caused by fungal strain *Paecilomyces variotii* isolate 129b

MTBE [ppm]	5th day [%]	12th day [%]	15th day [%]	19th day [%]
10.85	39.2	44.0	77.4	85.7
34.34	2.4	32.0	44.1	41.2
83.15	10.6	43.6	54.0	51.1

The highest yield of *Paecilomyces variotii* mycelia was noticed at lowest initial MTBE concentration. The addition of MTBE slightly affects mycelia yield and is similar to control. The results of mycelia yield is in correlation with degradation results, because the highest mycelia yield is noticed in variant with lowest concentration used, but even that the difference among treatments are not statistically significant.

Table III
Paecilomyces variotii mycelia biomass after 19 days of MTBE treatments

MTBE initial concentration [ppm]	repeats [mg ml^{-1}]			average [mg ml^{-1}]
	I	II	III	
10.85	0.010	0.026	0.037	0.024
34.34	0.019	0.022	0.012	0.018
83.15	0.018	0.025	0.014	0.019
control	0.013	0.022	0.016	0.017

The results of experiments showed that the fungal strain *Paecilomyces variotii* isolate 129b, is capable of MTBE utilization as sole source of carbon and energy to support growth. The highest MTBE degradation rate was at the lowest initial MTBE concentration. The addition of MTBE had a negative effect on degradation rate but total MTBE degraded was higher.

Discussion

Fungi are highly successful in survival because of their great physiological versatility. Their ability to produce extracellular enzymes is of great survival value. Fungi are involved in the biodegradation processes of undesirable materials (waste, pesticides, detergents, oil spills etc.) into harmless products[19]. The utilization of filamentous fungi for bioremediation processes has been limited compared with bacteria. Because of enzyme production in different environmental conditions, the fungi perform the degradation of broad spectrum of pollutants[20]. One of enzyme that is responsible for MTBE degradation is alcohol dehydrogenase[14], who affects the TBF formation during the MTBE oxidation. Because of its gelatinolytic and cellulolytic activity, the fungus *Paecilomyces variotii* is capable of biodegradation of some aromatic volatile organic compounds (VOC) like toluene[21], formaldehyde[22] and alkylbenzenes[23]. In addition, recent reports showed that *Paecilomyces variotii* could be use in cadmium biosorption[24] and for bioremediation of aflatoxine[25]. Previous mycoremediation studies indicated that different fungal cultures have capability of MTBE biodegradation[15,16].

The results of investigation shown that *Paecilomyces variotii* mycelia can grow in the presence of different MTBE concentration. MTBE degradation rate is lowest in the latest phase of incubation period. This conclusion is in accordance with previous MTBE studies[14], where the MTBE degradation rate progressively declined during the mycelia incubation with MTBE alone. Our experiments showed that the degradation rate was lower than in previous studies[14], but the initial MTBE concentration was lower than in our investigation. The slower degradation rate was also possibly due to presence of methanol, which was solvent for MTBE. Other authors[15] also reported similar conclusion.

The low degradation rate and yield of mycelia indicates that MTBE may be a poor substrate and energy source and/or that an intermediate during degradation may inhibit the microbial growth[12]. During the MTBE degradation, intermediates concentrations increased, while concentration of MTBE was decreased[26]. This conclusion confirms the MTBE degradation by microbial pure cultures. The results showed that ether bonds could be cleavage by certain microorganisms, although some investigations showed that this bond is not biodegradable or resistant to biodegradation[27]. According to this conclusion is a result of yield of *Paecilomyces variotii* mycelia, which was comparatively low. The low yield of microbial cultures in the presence of MTBE was also reported in earlier studies[28], probably because this compound is metabolic and electron transport inhibitor[9].

This investigation confirms that the fungus *Paecilomyces variotii* isolate 129b can utilize the MTBE as a sole source of energy and carbon and could be use in degradation of recalcitrant contaminants such as the fuel oxygenates.

Conclusions

Based on these results following conclusions are obtained:

- The degradation capability of *Paecilomyces variotii* isolate 129b depend on initial MTBE concentration and on time of sampling.
- During the experiment, the highest degradation rate was conducted at lowest initial MTBE concentration. After incubation period, the degradation of initial middle and high MTBE concentration stopped, while the degradation of lowest MTBE concentration continued.
- The highest yield of *Paecilomyces variotii* mycelia was notices at lowest initial MTBE concentration, but even that the difference among treatments are not statistically significant.
- The fungus *Paecilomyces variotii* isolate 129b can utilize the MTBE as a sole energy and carbon source and could be use in degradation of recalcitrant contaminants such as the fuel oxygenates.

REFERENCES

1. Schmidt, T. C., Schirmer, M., Weiß, H., Haderlein, S. B.: J. Contam. Hydrol. *70*, 173 (2004).
2. Krayer von Krauss, M., Harremoës, P.: *Late Lessons from Early Warnings: The Precautionary Principle 1896–2000*. Environmental Issue Report, Vol. 22. Office for Official Publications of the European Communities, Copenhagen. (2001).
3. Johnson, R., Pankow, J., Bender, D., Price, C., and Zogorski, J.): Environ. Sci. Technol. *34*, 210A. (2000).
4. Hanson, J. R., Ackerman, C. E., Scow, K. M.: Appl. Environ. Microbiol. *65*, 4788 (1999).
5. Squillace, P. J., Zogorski, J. S., Wilber, W. G., Price, C. V. Environmental Science and Technology *30*, 1721 (1996).
6. U.S. Environmental Protection Agency: Overview. EPA 510-F-97-014. Office of Solid Waste and Emergency Response, Washington, DC (1998).
7. Vidali, M.: Pure Appl. Chem. *73*, 1163 (2001).
8. Jensen, H. M., Arvin, E.: *Contaminated soils '90F* (Arndt, M. Hinsenveld, and W. J. van den Brink (eds.),. Kluwer Academic Publishers, Dordrecht, The Netherlands. 445–448 (1990).
9. Salanitro, J. P., Diaz, L. A., Williams, M. P., Wisniewski, H. L.: Appl. Environ. Microbiol. *60*, 2593 (1994).
10. Mormile, M. R., S. Liu, and J. M. Suflita.: Environ. Sci. Technol. *28*, 1727 (1994).
11. Yeh, C. K., and J. T. Novak: Water Environ. Res. *66*, 744 (1994).
12. Mo, K., Lora, C. O., Wanken, A. E., Javanmardian, M., Yang, X., Kulpa, C. F.: Appl. Environ. Microbiol. *47*, 69 (1997).
13. Lalevic, B., Raicevic Vera, Kikovic, D., Jovanovic Lj.: *Proceedings of XI Eco-conference*, p. 271. Novi Sad, (2007).
14. Hardison, L. K., Curry, S. S., Ciuffetti, L. M., Hyman, M. R.: Appl. Environ. Microbiol. *63*, 3059 (1997).
15. Magaña-Reyes, M., Morales, M., Revah, S.: Biotechnol. Lett *27*, 1797 (2005).
16. Lalevic, B., Dabic, D., Raicevic, V., Kikovic, D., Jovanovic, Lj., Niksic, M.: Mater. Prot. *3*, 45 (2006).
17. Peper, I. L., Gerba, C. P., Brendencke, J. W.: Acad. Press, San Diego, 11-33 (1995).
18. Samson, R. A., Hoekstra, E. S., Frisvad, J. C. Baarn-Delft: Centraalbureau voor Schimmelcultures, Seventh edition (2004).
19. Gopinath, S. C. B., Anbu, P., Hilda, A.: Mycoscience *46*, 119 (2005).
20. Bennett, J. W., Faison, B. D.: *Manual of Environmental Microbiology*, Washington DC: ASM Press, 758–765 (1997).
21. Estevez, E., Veiga, M. C., Kennes, C.: J. Ind. Microbiol. Biotechnol. *32*, 33 (2005).
22. Kondo, T., Morikawa, Y., Hayashi, N.: Appl. Microbiol. Biotechnol. *77*, 995 (2008).
23. Kennes, C., Veiga, M. C.: J. Biotechnol. *113*, 305 (2004).
24. Chatterjee, N.: Thapar Institute of Engineering and Technology (Deemed University) PATIALA- 147 004 (2006).
25. El-Shiekh, H., Mahdy, H. M., El-Aaser, M.: Pol. J. Microbiol. *56*, 215 (2007).
26. Alimohammadi, M., Mesdaghinia, A. R., Mahmoodi, M., Nasseri, S., Mahvi, A. H., Nouri, J.: Iran J. Environ. Health Sci. Eng. *2*, 237 (2005).
27. Erika, L. J., Christy, A. S., Kirk, T. O., Michael, R. H.: Appl. Environ. Microbiol. *70*, 1023 (2004).
28. Hristova, K., Gebreyesus, B., Mackay, D., Scow, K. M.: Appl. Environ. Microbiol. *69*, 2616 (2003).

P36   BIOLEACHING OF ANTIMONY MINERALS BY BACTERIA *ACIDITHIOBACILLUS FERROOXIDANS* AND *DESULFOVIBRIO DESULFURICANS*

ALENA LUPTÁKOVÁ[a], EVA MAČINGOVÁ[a], STEFANO UBALDINI[b] and JANA JENČÁROVÁ[a]

Institute of Geotechnics of Slovak Academy of Sciences, Watsonova 45, 043 53 Kosice, Slovak Republic,
luptakal@saske.sk

Introduction

In several gold ores, gold is trapped in the matrix in of metallic sulphides (FeS_2, Sb_2S_3 etc.). In such cases recovery of gold from refractory ores requires a pre-treatment to liberate the gold particles from the host mineral. For the pre-treatment of gold ores exist several hydro- and biohydrometallurgical processes[1]. The fundamental of biohydrometallurgical processing for sulphide minerals is the application of microorganisms, which on the basis of their metabolic processes can increase or decrease mobility of metals[2,3,4].

In the area of biohydrometallurgical processing of gold-bearing antimony sulphide minerals and concentrates the iron- and sulphur-oxidising bacteria have the very important function as well as on the ground the new knowledge also the sulphate-reducing bacteria[5,6,7]. Using involved bacteria to catalyse the breakdown of sulphides that host the gold is an important biological method for the pre-treatment of refractory gold ores. Following this biological treatment a combination of chemical and physical methods are used for leaching (e.g. the cyanide process) and concentration (e.g. the electrowinning) of gold. Although these methods are well accepted by industry, they harbour limitations in the processing of low-grade refractory ores, and regulatory agency/public acceptance of cyanide use. The objectives of this work were to evaluate the use of iron- and sulphur-oxidising bacteria *Acidithiobacillus ferrooxidans* (*At. ferrooxidans*) and sulphate-reducing bacteria *Desulfovibrio desulfuricans* (*Dsv. desulfuricans*) in the biohydrometallurgical processing of gold-bearing antimony sulphide minerals. Experiments were conducted at laboratory scale on a refractory gold-bearing stibnite coming from Santa Rosa de Capacirca Mine, Bolivia. Involved bacteria were used separately at different conditions for the pre-treatment of the aforementioned sample in order to increase the subsequent gold recovery during cyanidation processes. The *At. ferrooxidans* application is based on the their ability to oxidize and dissolve pyrite and stibnite, thus releasing the entrapped gold particles. The using of the bacteria *Dsv. desulfuricans* is based on their ability of the bacterially H_2S production for the alkaline leaching of stibnite.

Experimental

Microorganisms

In the experiment were used bacteria *At. ferrooxidans* isolated from the acid mine water[8] (deposit Smolník, Slovakia) and *Dsv. desulfuricans* isolated from the potable mineral water[9] (Gajdovka spring, Kosice, Slovakia). The isolation was performed by the modified dilution method[10].

Samples of Ore

The sample of gold-bearing antimony sulfide minerals used was obtained from Bolivia[6] (Santa Rosa de Capacirca Mine). Mineralogical characterisation by X-ray Diffraction (XRD) showed the presence of quartz (SiO_2), stibnite (Sb_2S_3) and pyrite (FeS_2). Their chemical composition includes 21.93 % Si, 4.94 % Sb, 4.28 % Fe and 3.77 % (S). Quantitative chemical analysis was performed by Inductively Coupled Plasma Spectrometry (ICP).

Bioleaching Test by Bacteria

Bacteria *At. ferrooxidans* and *Dsv. desulfuricans* were used separately. The experimental tests were conducted in a fed batch reactor at 30 °C under aerobic and dynamic conditions (with *At. ferrooxidans*) and anaerobic and static conditions (with *Dsv. desulfuricans*). The weight of the sample of gold-bearing antimony sulfide minerals was of 10 g. The total volume of feed solution consisted of 100 ml selective nutrient medium[1] 9K(A) for *At.f.* with pH 2.5; and DSM-63 medium[10] for *Dsv. desulfuricans* with pH 7.5. The abiotic control was carried out without the bacteria application at the same conditions. Dissolved metals in liquid phase during the experiments were determined using an atomic absorption spectrophotometer. After 120 days the solid phases were recovered by filtration and were saved for the consequently test of cyanidation.

Results

The results of the bioleaching i.e. the pre-treatment of gold-bearing antimony sulphide minerals are demonstrated by Figs. 1.–4.
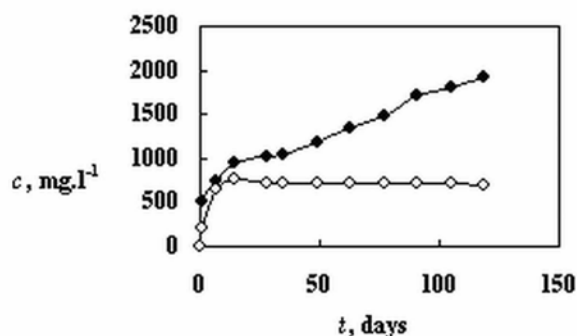
Fig. 1.   **Dissolution of Fe by bacteria *Acidithiobacillus ferrooxidans* from the sample of gold-bearing antimony sulfide minerals. c – concentration of Fe, t – time of bioleaching, ● – Acidithiobacillus ferrooxidans, ○ – abiotic control**

Fig. 1. presents the dissolution of the Fe by bacteria *At. ferrooxidans* and in the cases from the start until the end of experiments the concentration of Fe in liquid phase increase. From beginning, probably due to interaction between

the mineral and the cultural medium and after 14 days by direct and indirect influence of bacteria *At. ferrooxidans*. This fact demonstrates the comparison of the Fe dissolution curve shape of *At. ferrooxidans* and abiotic control. It confirms the bioleaching of pyrite (FeS$_2$).
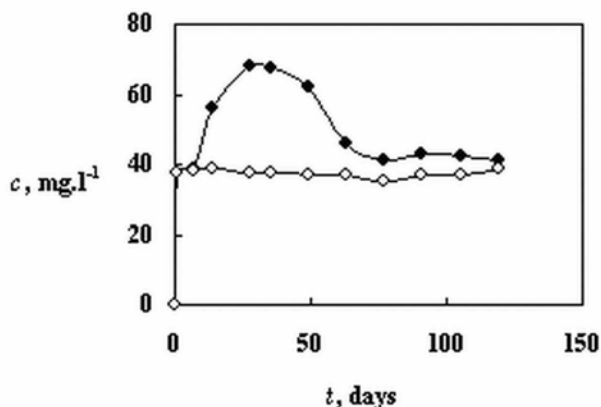
Fig. 2. **Dissolution of the Sb by bacteria *Acidithiobacillus ferrooxidans* from the sample of gold-bearing antimony sulfide minerals. . c – concentration of Sb, t – time of bioleaching, ● – Acidithiobacillus ferrooxidans, ○ – abiotic control**
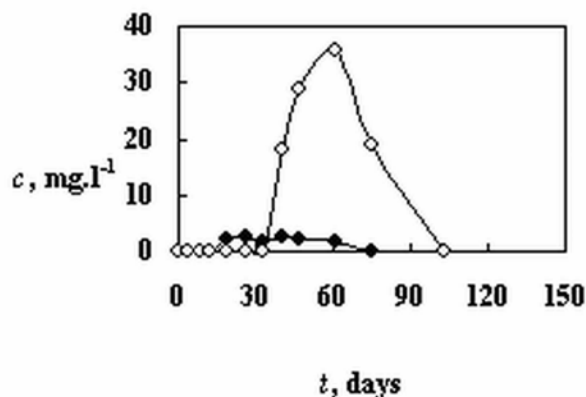
Fig. 3. **Influence of bacteria *Desulfovibrio desulfuricans* for the Fe dissolution under the alkaline leaching of gold-bearing antimony sulfide minerals. c – concentration of Fe, t – time of bioleaching, ● – Desulfovibrio desulfuricans, ○ – abiotic control**

Fig. 2. shows the trend of the Sb dissolving. Initially, during 7 days the concentration of Sb increases in the *At. ferrooxidans* presence and abiotic control, probably due to interaction between the mineral and the cultural medium. After 7 days the abiotic control allocated the circa constant Sb concentration in liquid phase until the end. After 35 days was recorded the depression as follows was observed the decreasing of the Sb concentration until the end of experiments in the *At. ferrooxidans* presence. This fact can be interpreted on the bases the creation of the insoluble antimony oxosulphates – (SbO)$_2$SO$_4$ according the reaction (1)[11]:

$$Sb_2S_3 + 6O_2 + 2H_2O \rightarrow (SbO)_2SO_4 + 2H_2SO_4 \qquad (1)$$

Figure 3 presents the Fe concentration in liquid phase at the using bacteria *Dsv. desulfuricans* that was from beginning until the end almost zero. Although the little increase was observed after 19 days. This situation can be resolve by the Fe precipitation with bacterially produced hydrogen sulphide under the influence of bacteria *Dsv. desulfuricans* After 40 days it's the intense increase was recorded in the experiments without bacteria. Just now concerning this fact we have not the adequate understanding. At the end of the experiments the Fe concentration at presence SRB and abiotic control were again almost zero.

Figure 4 shows the Sb concentration in the liquid phase at the using bacteria *Dsv. desulfuricans* From the confrontation of the Sb concentration curve shape in the abiotic control and in the presence bacteria you can see that the influence of bacteria *Dsv. desulfuricans* was not significant. The contamination of the abiotic control by bacteria *Dsv. desulfuricans* was not evidence. After 20 days was observed the formation of the shined cover on the reactor wall in the presence bacteria. Its can be explain to the Sb concentration decreasing.
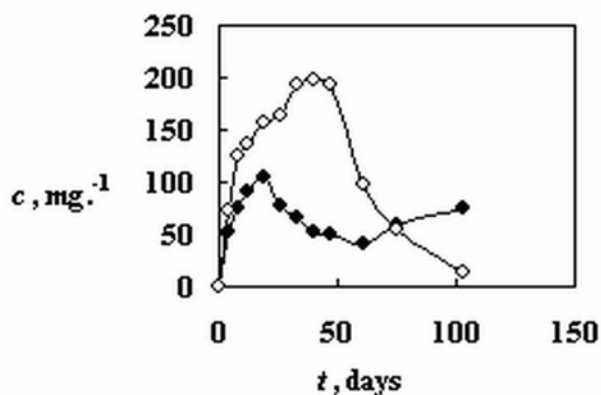
Fig. 4. **Influence of bacteria *Desulfovibrio desulfuricans* for the Sb dissolution under the alkaline leaching of gold-bearing antimony sulfide minerals. c – concentration of Sb, t – time of bioleaching, ● – Desulfovibrio desulfuricans, ○ – abiotic control**

After ending the solid phases were recovered by filtration from solution. The solid phases were saved for the consequently test of cyanidation and liquid phases for the electrowinning.

Conclusions

Experimental studies confirmed:
- the bacteria *At. ferrooxidans* have the positive influence on the dissolving of pyrite (FeS$_2$) and stibnite (Sb$_2$S$_3$) to occur in the used sample of gold-bearing antimony sulphide minerals,
- the increase, subsequent the depression and the decreasing of the Sb concentration during the bioleaching

experiments with bacteria *At. ferrooxidans* can be interpret on the bases the creation of the insoluble antimony oxosulphates – $(SbO)_2SO_4$,

- the bacteria *Dsv. desulfuricans* does not show the expressive influence for the alkaline leaching antimony-bearing materials.

REFERENCES

1. Karavajko G. I., Rossi G., Agate A. D., Groudev S. G., Avakyan Z. A.: *Biogeotechnology of metals*. Centre of projects GKNT, Moscow 1988.
2. Gadd G. M.: Curr. Opin. Biotechnol. *11*, 271 (2000).
3. Kadukova J., Stofko M.: *Environmetálne biotechnológie pre hutníkov.* Equilibria s.r.o., Kosice 2000.
4. Poulin R., Lawrence R. W.: Miner. Eng. *9*, 799 (1996).
5. Solozhenkin P. M., Lyalikova-Medvedeva N. N.: J. of Mining Sci. *37*, 534 (2001).
6. Ubaldini S., Veglio F., Toro L., Abbruzzese C.: Miner. Eng. *13*, 1641 (2000).
7. Solozhenkin P. M., Nebera V. P.: *Proc. of 15th International Biohydrometallurgy symposium: Biohydrometallurgy: a sustainable technology in evolution* (Tsezos M., Hatzikioseyian A., Remoudaki E., eds.), p.10. National Technical University of Athens, Zografou, Athens 2004.
8. Luptakova A., Kusnierova M.: *Proceedings of 2nd International Conference on Environmental Research and Assessment* (Patroescu M., Matache M., ed.), p. 254. Bucharest 2006.
9. Luptáková A., Kušnierová M., Fečko P.: *Minerálne biotechnológie II., sulfuretum v prírode a v priemysle.* ES VŠB – TU Ostrava, Ostrava 2002.
10. Ronald M. A.: *Principles of Microbiology.* Mosby, New York 1995.
11. Postgate J. R.: *The sulphate-reducing bacteria*. Cambridge University Press, Cambridge 1984.
12. Lyalikova N. N.: Trans. Mosc. Soc. *24*, 11 (1966).

P37　THE RECLAMATION OF CALCIUM SULPHATE SLUDGES BY SULPHATE-REDUCING BACTERIA

ALENA LUPTÁKOVÁ[a] and MÁRIA KUŠNIEROVÁ[a]

Institute of Geotechnics of Slovak Academy of Sciences, Watsonova 45, 043 53 Kosice, Slovak Republic,
luptakal@saske.sk

Introduction

Combustion of fossil fuels containing sulfur releases sulfur oxides to the atmosphere. If lime or limestone scrubbing desulfurizes combustion gases, calcium sulfates sludges are generated and these must be disposed of. Many processes for their treatment have been developed. Under appropriate conditions these sulfate can be converted to sulfide by the anaerobic bacterial sulfate reduction, which is the basic metabolic process of sulfate-reducing bacteria (SRB).

The SRB represent a group of chemoorganotrophic and strictly anaerobic bacteria that may be divided into four groups based on rRNA sequence analysis[1]: Gram-negative mesophilic SRB, Gram-positive spore forming SRB, thermophilic bacterial SRB and thermophilic archaeal SRB. They include genera like *Desulfovibrio, Desulfomicrobium, Desulfobacter, Desulfosarcina, Desulfotomacullum, Thermodesulfobacterium, Archaeoglobus*, etc.

Considering the inorganic or organic character of energy source of SRB there are two types of anaerobic respiration of sulfates authotrophic and heterotrophic[2]. SRB produce a considerable amount of gaseous hydrogen sulfide, which reacts easily in the aqueous solution with heavy metal, forming metal sulfides that have low solubility. In the bacterial anaerobic reduction of sulfates the organic substrate (lactate, malate, etc.) or gaseous hydrogen is the electron donor and sulfates is the electron acceptor.

The industrial technologies for the desulfurization of combustion products produced during the generation of electric energy by combustion of fossil fuels use limestone ($CaCO_3$) as an absorption agent. The desulfurization of combustion products proceeds in the absorber in several stages. This process results in the formation of gypsum suspension ($CaSO_4 \cdot 2H_2O$) which is incorporated into the final stored product – "stabilizate" – after being treated together with other wastes (ash, burnt lime, desulphurization waste water, etc.).

The objective of our study was to verify experimentally the possibility of using gypsum contained in the above-mentioned "stabilizate" as the source of electron acceptors for the growth of SRB with the prospect of the recycling of desulfurization agent – limestone.

Experimental

Microorganisms

A culture of SRB (genera *Desulfovibrio* and *Desulfotomaculum*) was obtained from drinking mineral water Gajdovka (locality Kosice-north, Slovak Republic). For the isolation and cultivation of these bacteria a selective nutrient medium (DSM-63 – Postgate′s C medium) was used[3].

Liquid Phase

The feed solution (the selective nutrient medium (DSM-63 – Postgate's C medium without sulfates) was prepared by dissolving analytical grade salts such as: K_2HPO_4 0.5 g dm^{-3}, NH_4Cl 1 g dm^{-3}, $CaCl_2 \cdot 6H_2O$ 0.1 g dm^{-3}, $MgCl_2 \cdot 6H_2O$ 0.3 g dm^{-3}, $C_3H_5O_3Na$ 2.0 g dm^{-3}, $C_2H_3O_2SNa$ 0.1 g dm^{-3} and $C_6H_8O_6$ 0.1 g dm^{-3} in distilled water.

Solid Phase

The sample of "stabilizate" from Vojany power plant (Slovak Republic) was used in the experiments. Mineralogical characterisation by X-ray Diffraction (XRD) showed the presence of $CaSO_4$ 40.84 %, SiO_2 22.70 %, Al_2O_3 10.70 %, Fe_2O_3 4.26 % and CaO 3.00 %.

Analytical Procedures

A turbidimetric method was used to measure the concentration of soluble sulfate ion concentrations in the liquid phase[4]. Samples were centrifuged for 10 minutes at 10,000 rpm before performing the analysis. Digital pH-meter GPRT 144 AGL was used. Qualitative changes of "stabilizate" were performed by the qualitative X-ray diffraction analysis using Dron-2 instrument and energy dispersive spectrometry (EDS) analysis using instruments, which consisted of a scanning electron microscope BS 300 and an X-ray microanalyser EDAX 9100/60. Samples of solid phase were dried and coated with gold before the EDS analysis.

Biological Utilization of Gypsum from "Stabilizate"

Series of anaerobic tests were studied in a fed batch reactor in the thermostat at 30 °C. Samples of "stabilizate" were kept in static conditions for a period of 40 days at pH 7.5. The weight of "stabilizate" was 20 g. The stock culture of SRB was used as an inoculum (10 %, v/v). The total volume of feed solution consisted of 200 ml distilled water and 300 ml selective nutrient medium for SRB (DSM-63 – Postgate's C medium without sulfates). The abiotic control was carried out without the SRB application at the same conditions. After 40 days the solid phase was filtered, dried and analyzed using the qualitative X-ray analysis and energy dispersive spectrometry (EDS) analysis.

Results

The formation of black precipitates and the sensorial detection of classical strong H_2S smell were observed after 3–4 days from the beginning of the process. These remarks were not detected in the abiotic control until the end of the experiment. Changes of sulphates concentration during the discontinuous cultivation of sulphate-reducing bacteria using gypsum contained in the "stabilizate" as the source of electron acceptors for the growth of SRB are shown in Fig. 1. The results of qualitative X-ray diffraction analysis of original "stabilizate",

bacterially treated "stabilizate" and "stabilizate" of abiotic control are shown in Figs. 2.–4. They show the significant qualitative changes in the "stabilizate" initiated by SRB. The sulfates from the original major component of "stabilizate" – $CaSO_4 \cdot 2H_2O$ (Fig. 2.) – were reduced according by SRB forming hydrogen sulfide as proved by the sensorial detection of classical strong H_2S smell. This is indirectly confirmed by Fig. 3, which proves the extinction of $CaSO_4$ and formation of $CaCO_3$ according to equation (1):

$$2C_3H_5O_3Na + CaSO_4 \xrightarrow{SRB} 2CH_3COONa + CO_2 + CaCO_3 + H_2S + H_2O \quad (1)$$
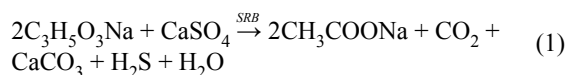
The above-mentioned changes have not been observed in abiotic control as documented by the comparison of qualitative X-ray analysis of "stabilizate" before applying SRB (Fig. 2.) with the qualitative X-ray analysis of "stabilizate" in abiotic control (Fig. 4.). The results of energy dispersive spectrometry (EDS) analysis and scanning electron microscope of original "stabilizate", bacterially treated "stabilizate" and "stabilizate" of abiotic control are shown in Figs. 5.–7. They fall into line with Figs. 2., 3. and 4. and suggest on the

elimination of $CaSO_4 \cdot 2H_2O$ form "stabilizate". The element composition of solid phases (Figs. 5., 6. and 7.) accepts with this fact.
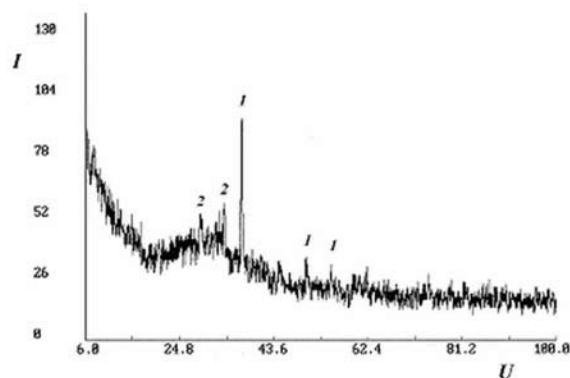
Fig. 3. **Qualitative X-ray analysis of solid phase formed by the effect of SRB on "stabilizate". I – intenzity, U – 2-theta uhol, 1 – CaCO$_3$, 2 – SiO$_2$**
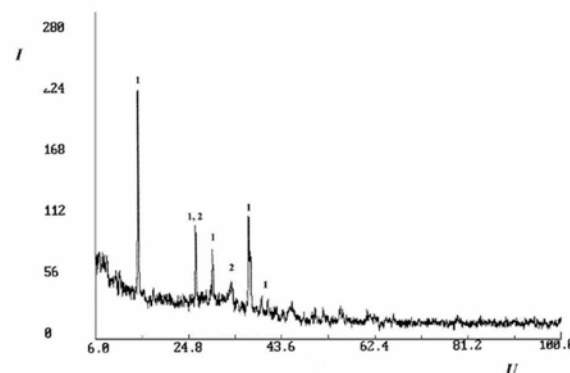
Fig. 4. **Qualitative X-ray analysis of solid phase in abiotic con-**

Fig. 1. **Changes of sulfates concentration during the discontinuous cultivation of sulfate-reducing bacteria.**
c – sulfates concentration, t – time of sulfate-reducing bacteria cultivation, ● – "stabilizate" with SRB, ○ – "stabilizate" without SRB (abiotic control)
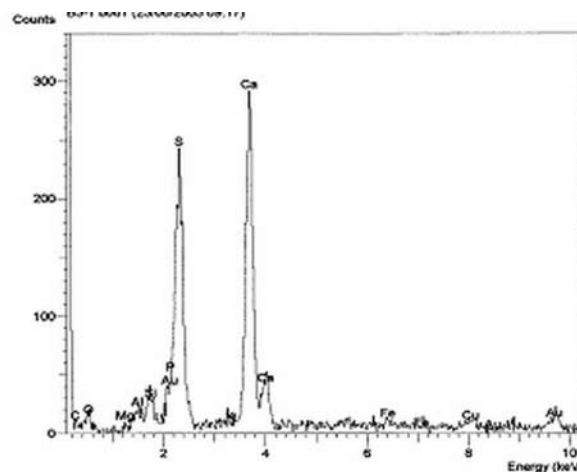
Fig. 5. **EDS qualitative analysis of "stabilizate" before application of sulfate-reducing bacteria**

Fig. 2. **Qualitative X-ray analysis of "stabilizate" before application of sulfate-reducing bacteria. I – intenzity, U – 2-theta uhol, 1 – CaSO$_4$·H$_2$O, 2 – SiO$_2$**
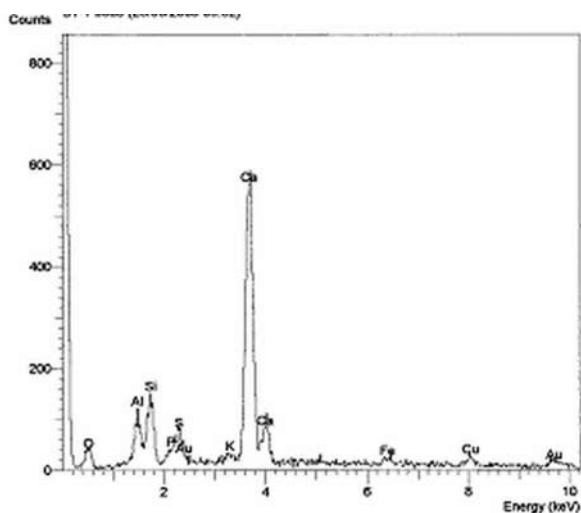
Fig. 6.   **EDS qualitative analysis of solid phase formed by the effect of SRB on "stabilizate"**

Conclusions

The results confirmed the theoretical assumptions on the use of gypsum, which forms the substantial component of "stabilizate", as the source of sulphate for sulphate-reducing bacteria, which produce hydrogen sulphide in the process of bacterial reduction of sulphates. They also showed the possibility of recycling desulphurization agent – limestone.
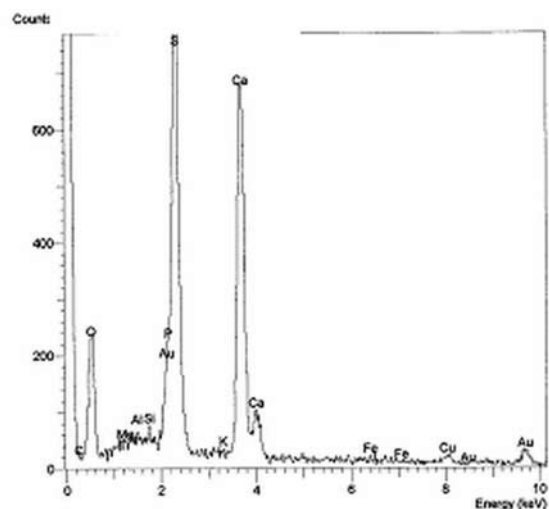
Fig. 7.   **EDS qualitative of solid phase in abiotic control**

REFERENCES

1. Castro H. F., Williams N. H., Ogram A.: FEMS Microbiol. *31*, 1 (2000).
2. Odom J. M., Rivers Singleton J. R.: *The sulphate-reducing bacteria Contemporary Perspectives*, Springer-Verlag, New York 1993.
3. Karavajko G. I., Rossi G., Agate A. D., Groudev S. G., Avakyan Z. A.: *Biogeotechnology of metals*. Centre of projects GKNT, Moscow 1988.
4. APHA, *Standard Methods for the Examination of Water and Wastewater*, 17th edition, American Public Health Association, USA, Washington D. C., 1989.

P38 BIOLOGICAL-CHEMICAL REGENERATION OF DESULPHURIZATION SORBENTS BASED ON ZINC FERRITE

MÁRIA KUŠNIEROVÁ, ALENA LUPTÁKOVÁ, VLADIMÍR ŠEPELÁK and MÁRIA PRAŠČÁKOVÁ

Institute of Geotechnics SAS, Watsonova 45, 043 53 Kosice, Slovak Republic,
kusnier@saske.sk

Introduction

The energetic demands of people in present, as well as in the future will be supplied mainly by the energy from the fossil sources, which is accompanying with the negative impact on the environment in the form of emissions of sulphate and carbonate compounds. For desulphurization and decarbonization of these emissions more commercial technological methods have been developed, to which belongs also the utilization of solid sorbents (filters) based on the zinc ferrite. The studies of Grindly[1] and Krisham[2] helped to clear up the high-temperature process of desulphurization of waste gases after coal combustion which can be described by the chemical equation:

$$3ZnFe_2O_4 + 3\,H_2S + H_2 \rightarrow ZnS + 2FeS + 4H_2O \quad (1)$$
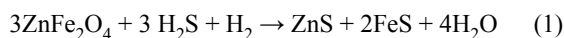
In dependence on the conditions of the combustion process there is according to the Lamoreaux[3] a possibility of a occurring of another reaction of the iron (occurring in the solid sorbents) with waste gases of carbon, leading to formation of carbide. This is governed by the equations:

$$3FeO + CO \rightarrow Fe_3C + 2O_2 \quad (2)$$

$$3Fe + CO \rightarrow Fe_3C + \tfrac{1}{2}O_2 \quad (3)$$
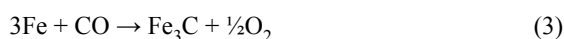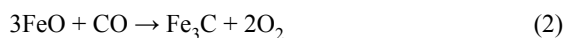
The phase composition of sulphurized (amortised) sorbents shows the presence of sulphidic and carbidic structures located mainly on the surface of particles of zinc ferrite (respectively $Zn\,Fe_2O_3$ – micropellets of zinc ferrite). They became inactive and the further utilization is constrained to their regeneration. In relation with the most effective methods of manifold recycling of sorbents, several methods of their regeneration were studied.

The literature shows two methods of regeneration of sulphatizing sorbents based on zinc ferrite. The first method commercially used, is a oxidising pyrolysis of sulphides[2]. In this process are the sulphidic structures in dependence on the temperature of the oxidising rousting transformed step by step at the first stage to the sulphates and at the second stage which corresponds to the temperature of sulphates decomposition (in the temperature range from 480 to 600 °C) to the oxides, according to the equations (4) and (5):

$$2FeS + 3.5O_2 \rightarrow Fe_2O_3 + 2SO_2 \quad (4)$$

$$ZnS + 1.5O_2 \rightarrow ZnO + SO_2 \quad (5)$$
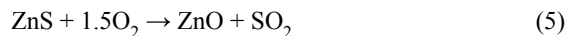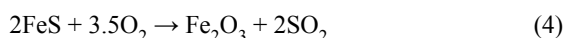
The second method of the regeneration of desulphurization sorbents which is introduced by Sakao[4], is based on the principle of pressure leaching of ZnS in water environment at the temperature over 550 °C. This method is described by the equation, almost identical with the Eq. (5):

$$ZnS + 1.5O_2 \rightarrow ZnO + SO_2 \quad (6)$$
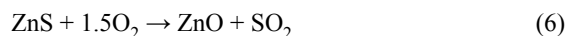
The commercially available technologies of sulphides processing and treatment (as sources of colour and rare metals) have nowadays started with utilization of biological-chemical processes (bio-leaching); where the physical and chemical base of degradation of sulphidic structures is identical with the methods of regeneration of desulphurization sorbents mentioned above.

The principle of all mentioned methods is the process of sulphides oxidation with utilization of various methods of catalysis. In the process of thermic regeneration is the oxidising reaction catalysed by the thermic energy, at pressure leaching by the pressure and temperature.

The aim of this paper is to testify the biological-chemical method as a new method of sorbents regeneration, utilising the catalytic effect of the metabolism of an acidophilous bacteria – *Thiobacillus ferrooxidans,* oxidising the sulphate and iron[8].

Experimental

Material

Zinc ferrite

For biological-chemical regeneration, zinc ferrite after sulphurization test was used. The powder sample containing 90 % zinc ferrite and 10 % bentonite binder by weight was pelletized to cylindrical pellets, calcined in air from room temperature to 970 K, and crushed and sieved to the size of a stainless steel cylinder, in which 25 g of pelletized sorbent was packed. The simulated coal gas had the following composition: 30 % vol. CO, 50 % vol. N_2, 19.5 % vol. H_2, and 0.5 % vol. H_2S. Total gas flow-rate diring absoption was 5,000 $cm^3\,min^{-1}$. The desulphurization tests were stopped when the H_2S concentration of the effluent gas was above 50 ppm. The details of the sulphurization experiments are described also in our previous papers[6,7].

Bacteria

The bacteria used in experiments was: *Thiobacillus ferrooxidans*, isolated from the mining drainage waters of sulphides deposits, which is cultivated for a long time on the sphalerite (ZnS) substrates. The leaching solution was formed by cultivated medium according to the Silverman and Lundgren[5], in which the cells of bacteria were scattered. The pH value of the solution at the beginning of the reaction was 1.6.

Methods

The experiments of biological-chemical way of regeneration were realized by the form of charge leaching tests at the suspension density 5 % at the temperature of 30 °C, under continuos stirring for the period of 19 days. The qualitative changes of investigated zinc ferrite during the process of biologico-chemical way of regeneration were evaluated by:

- RTG diffraction analysis (diffractometer DRON 2,0 Technsabexport, Russian, FeKa radiation),
- particle size distribution (granulometer Helos and Rodos, Sympatec GmbH Claustahl Zellerfeld),
- BET adsorption method for measuring the adsorption surface (Micromeritics, Gemini 2360, in nitrogen atmosphere),
- chemical analysis of the content of Zn and Fe in the leach (atom absorption spectroscopy on the instrument Spectra AA-30 ,Varian, Australia).

Results

RTG diffraction analysis of amortised sorbents revealed except of the rest ferrite zinc (Franklinite, $ZnFe_2O_4$), which represents probably the nonreacted cores of micropelets, also the presence of the formed sulphidic, sulphate, oxidic and carbidic compounds: b-sphalerite (ZnS), wurtzite (ZnS with addition of Fe), pyrite (FeS_2), melanterite ($FeSO_4 \cdot 9H_2O$), elemental sulphur (S), magnetite (Fe_3O_4), hematite (a-Fe_2O_3) and cohenite (Fe_3C).

The bio-leaching of this product leads to the biologico-chemical degradation of amortised layers located on the surface, which is accompanied by the extraction of Zn and Fe to the leach. The changes of the concentration of introduced elements in the leach in dependence on the time of leaching are shown in Table I.

The concentration of Zn in the leach during the observed time interval showed the arising trend, while in the Fe concentration dependence has been appeared the maximum (after 15 days the concentration of the leached ferrite decreased). As the realized experiments represent the spontaneous non-regulated process of biologico-chemical oxidation, it is possible to assume that the decrease of the Fe concentration

Table I

The time dependence of changes of Zn and Fe concentration in the leach during the biological-chemical regeneration of amortised sorbents based on zinc ferrite

Time leaching [days]	Concentration Fe [g dm^{-3}]	Concentration Zn [g dm^{-3}]
0	0.37	0.62
3	0.37	1.21
5	1.48	1.56
7	1.50	1.73
10	1.39	2.68
14	0.52	2.81
17	0.55	2.97
19	0.61	3.19
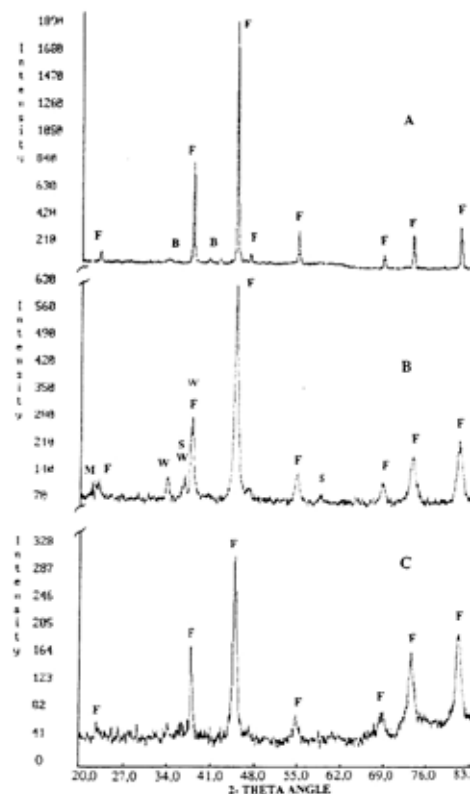
Fig. 1. **Comparison of X-ray phase analysis of zinc ferrite sorbent, A – primary, B – pasivated, C – biologically and chemicaly regenerised**
Legend: W – wurtzite, F – franclinite, S – sphalerite

was caused by the precipitation of the secondary oxidic compositions of the iron. This assumption has been confirmed by the RTG diffraction analysis of the leach. After finishing the biological-chemical leaching of amortised sorbent the extinction of the most of secondary structures formed by sorption of sulphate compositions was observed by the RTG method (Fig. 1.).

The regenerated sample contained the franklinite, addition of magnetite, metal zinc and the rest of wurtzite, which during the observed period manifested itself as refractory mineral and to its destruction the longer period or the change of electrochemical conditions of leaching should be needed[9].

Referring to the reality, that the effectivity (the sorption capacity) of sorbents is directly connected with the sizes of their surfaces and inversely with the particles sizes, the changes of these parameter were also studied (Fig. 2.). The process of biological-chemical regeneration caused intense changes in the adsorption surface of sorbents, it has changed from the value of 2.8245 m^2 g^{-1} at amortised sample to the value of 6.2543 m^2 g^{-1} at the regenerated sample.

The expressive change was also registered at the distribution of the particles sizes. The value of mean particle diameter has decreased from the value of 9 mm at amortised sorbent to 2.19 mm at the regenerated sorbents (Table II).
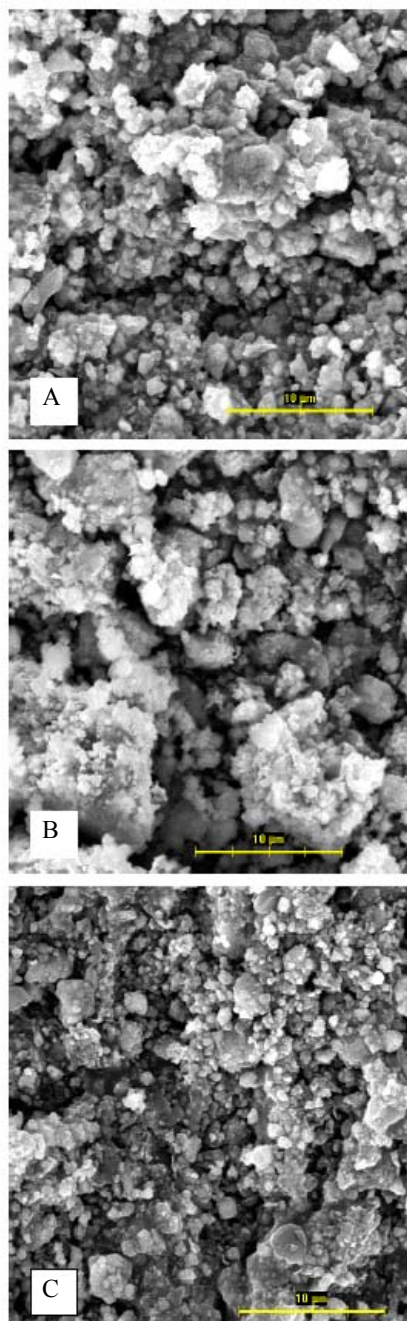
Fig. 2. **Mophology of surface of the zinc ferrite sorbent, A – primary, B – pasivated, C – biological and chemical regenerised**

Conclusions

The presented results confirm the possibility of utilization of the biological-chemical method as a new regeneration method of desulphurization sorbents based on zinc ferrite. The big advantage of this process in comparison with conventional regeneration methods is the lowering of the temperature of leaching from 500°C to 30°C. The period of the duration of the regeneration seems to be an disadvantage, its lowering requires the additional research aimed at the con-

Table I
Comparison of the selected fysical and chemical charakteristic of the zinc ferrite sorbents before and after biological and chemical regeneration

Sample	Specific surface SA $[m^2 g^{-1}]$	Surfaces factor f* $d_{50}[\mu m]$	Average of particles
primary sorbent	2.6	1.022	4.77
pasivated sorbent	2.8	1.478	9.10
regenerised sorbent	6.2	1.797	2.19

tinual optimalization of conditions for biologico-chemical regeneration.

REFERENCES

1. Grindley T., Steinfeld G.: *Proceedings. 4th Annual Contractor ́s Meeting on Contaminant Control in Hot Coal-Derived Gas Streams. U. S. Department of Energy/ METC. Morgantown, WV.* DOE/ METC, 85-3, pp. 314-446. Morgantown 1984.
2. Krishan G. N.,Tong G. T., Lamoreaux R. H., Brittain R. D.: Wood B.J.: *Proceedings of Fifth Annual Contractor ́s Meeting on Contaminant Contro in Hot Coal-Derived Gas Streams. U. S. Department of Energy/METC.* Morgantown, WV. DOE/ METC-85/6025, pp. 6-18. Morgantown 1985.
3. Lamoreaux R.M., Brittain R.D., Zieger J., Leach. S.C.: *Determination of Solid Phase Boundaries in Coal Gas Desulfurization by Zinc Ferrite., U. S. Department of Energy/METC.* Technical Report DOE/MC 21096-2192. Morgantown, WV, 1986.
4. Sasaoka E., Hatori M., Sada N., Uddin A.: Ind. Eng. Chem. Res. *39*, 3844 (2000).
5. Buchanan R. E. and Bigons N. E. *Bergy ́s Manual of Determinative Bacteriology.*, 8th ed., Baltimore, 1974.
6. Wutzer R., Steinike U., Lorenz P., Rossahl,B.: Brennstoff-Wärme-Kraft *45*, 477 (1993).
7. Šepelák V., Rogachev Yu., Steinike U., Uecker D. Ch., Krumeich F., Wissmann S., Becker K. D.: Brennstoff-Wärme-Kraft *48*, 1996, 28.
8. Barret J., Hughes M. N., Karavajko G. I., Spencer P. A.: *Metal extraction by bacterial oxidation of minerals.* Eôis Horwood, New York, London, Toronto, Sydney, Tokyo, Singapore, 1996.
9. Baláž P., Kušnierová M., Varencova V. I., Mišura B.: J. Miner. Process. *40*, 273 (1994).

P42　CAUSES OF ACCIDENTS REGARDING TRANSPORT OF DANGEROUS GOODS

JANA VICTORIA MARTINCOVÁ[a], IVAN MAŠEK[a] and JIŘÍ MARTINEC[b]

[a]*Faculty of Chemisty Brno, University of Technology, Purkyňova 118, 612 00 Brno, Czech Republic,*
[b]*Clean Energies Unit, Institute for Energy, JRC, 1755 ZG Petten, The Netherlands,*
platina@email.cz

Introduction

Transport of dangerous substances can be characterized by a permanent or relative contact with the population and represents in all possible stages a potential hazard. Related to human health, injury or death people during accidents also damage to property and the affected environment, the transport of dangerous goods is very serious problem. Road – accidents in hazardous materials transportation have increased 95 % in the last 30 years. This negative feature of the excessive traffic is evident due to available statistics of the accidents in the whole Europe. Besides the noticeable number of accidents in the cases related to the transport of dangerous substances the economical point of view in increasing costs is under general concern.

The most frequented transportation regarding dangerous goods is on the roads in the Europe.

Results

Accident registration has been launched in 2000 in the Czech Republic by the traffic police. Data from 2000 to 2002 are not very precise because of administration faults. Data registered since 2003 has been more precise.

As an example of main causes of accidents the accident frequency in 2003 and 2004 were used – regarding accidents conform to the directive ADR (European Agreement Concerning the International Carriage of Dangerous Goods by Road). There was a new code system regarding causes of accidents used. Previous code system included causes and their consequences related to the hazard. The new system is focused only on the main cause of accident. The aim of the system is the minimal and concise list of codes.

All results regarding causes of accidents were worked out by cooperation with Police of the Czech Republic.

Figs. 1. and 2. show the main causes of ADR accidents which are evident.
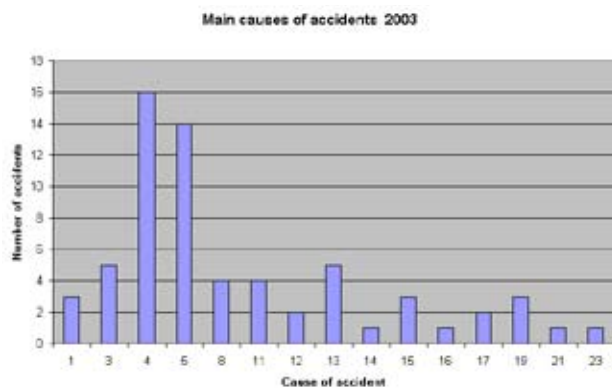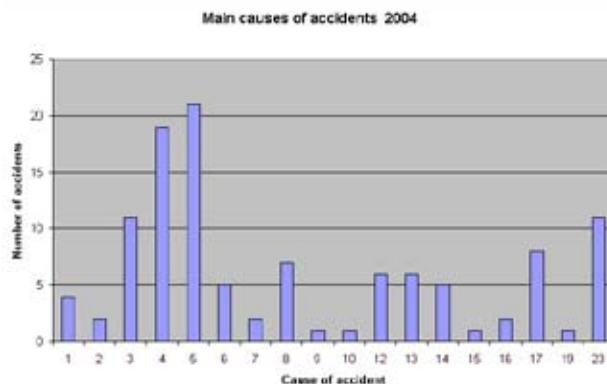
Fig. 2.　**Main cause of accident, 2004**
1 – overtaking, 2 – side-on crash, 3 – speeding (not keep a safe distance), 4 – driver did not adapt speed (to condition and character of a road, cargo character, skills of a driver, character of a car), 5 – poor attention of a driver (skid, crashing into a barrier, off the road, collision with a car, a stationary car, a driving car, collision with a pedestrian, collision with a bicycle), 6 – while reversing, 7 – uncontrolled driving of truck set, 8 – driving roadside, 9 – not respecting railway signals, 10 – turning round, 11 – technical fault (on the vehicle, on the vehicle set), 12 – turning off, 13 – non-acquaintance with or bad judgment of the size of the truck, 14 – crash with upstream driving car, 15 – bad fixation of a cargo, 16 – falling asleep, micro-sleep, 17 – not respecting traffic signs ("right of way", prohibitive), 18 – not giving right of way, 19 – bad driving in the traffic lane (side-on crash, inadvertence of the parallel driving car), 20 – character of the road, damage of the road, 21 – contrary climatic conditions, 22 – impaired driving, 23 – cause is unknown

Reasons of accidents are mostly the same when considering small cars or trucks. The main reasons are human error; poor attention of drivers and their reactions and no acceptance of the speed limit.

The experience of drivers is crucial and each company (transporting dangerous goods according to the ADR) should have a possibility to check driver's crime sheet regarding accidents and other offences.

From the figures below the age of drivers causing accidents is evident. The statistic results from years 2003 and 2004 for construction of Figs. 3. and 4. were used.

From the mentioned results is evident, that the age of drivers has no effect on the accident frequency (ADR) or the cause. In fact many of available studies show relation between frequency of accidents (regarding total number of car accidents) and age drivers.

Fig. 1.　**Main cause of accident, 2003**
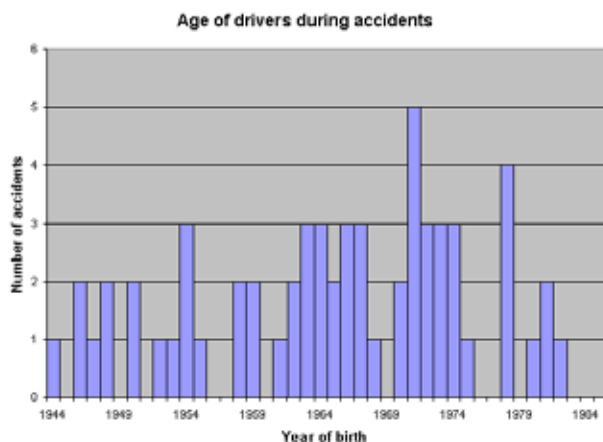
Fig. 3.   **Age of drivers during accidents, 2003**
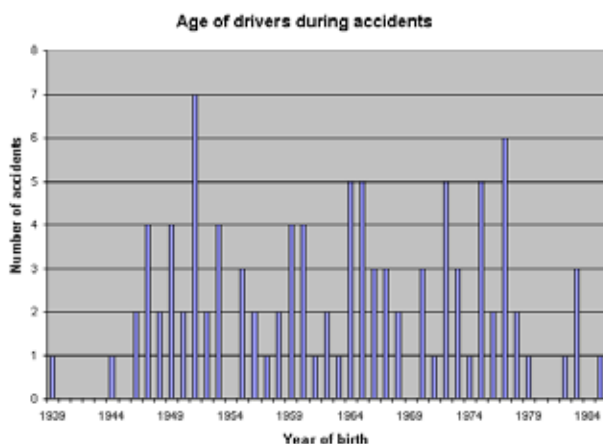
Fig. 4.   **Age of drivers during accidents, 2004**

Conclusions

The Czech Republic is one of the countries with the largest accident frequency and high number of deaths of people

during accidents. Reasons for accidents are mostly the same when considering small cars or trucks. The main reason is human error – insufficient attention of drivers and their reactions, further more no acceptance of the speed limit.

Substances included in the group of flammable substances (according with European ADR directive) represent the most frequently transported dangerous materials on the roads. A risk assessment for dangerous substances is performed using different kinds of methods. In order to propose and create methods for the safe transport of dangerous goods is at first necessary to perform an extensive analysis of the existing situation. Methods must be also focused, made relevant to different localities and the industry to represent different surroundings. More strict penalties could be applied. The experience of drivers is crucial and each company (transporting substances according to ADR) should have to check drivers' crime sheet regarding accidents and other offences and also prove their skills.

There is possibility to improve the situation through our preparedness, self-education, and interest regarding the problem.

REFERENCES
1. Police of the Czech Republic, Statistics.
2. United Nations Economic Commission for Europe: Directive ADR – European Agreement Concerning the International Carriage of Dangerous Goods by Road, United Nations, New York and Geneva, 2006.
3. Lees, F. P.: *Prevention in the Process Industries*, Butterworths, London, 1980.
4. Scenna N. J., Santa Cruz A. S. M.: Reliab. Eng. Syst. Saf. *90*, 83 (2005).
5. Martincova, Masek, NBC 2006, *Symposium on chemical, biological, nuclear and radiological threats – a safety and security challenge*, Tampere, Finland 2006.
6. Martincova J., Masek I.: *34th International Conference of SSCHE*, Tatranské Matliare, May 2008.

P43 RISKS FACTORS OF SOCIAL DEVELOPMENT AS ENVIRONMENT FOR MANAGEMENT

IVAN MAŠEK[a] and JAROMÍR NOVÁK[b]

[a]*Brno University of Technology, Faculty of Chemistry, Purkynova 118, Brno, 612 00, Czech Republic,*
[b]*Palacký University Olomouc, Philosophical Faculty, Krizkovskeho 12, Olomouc, 771 80, Czech Republic,*
masek@fch.vutbr.cz

Introduction

All things, phenomena, and processes have their own causes and consequences. They bring along pros and cons; they can be controlled and chaotic, can and cannot be influenced. Social development has been getting more and more complicated, undergoing fast changes; being difficult to predict. If the last century was said to be a century of changes, this feature will be more significant and determining for further development. There is more and more urgent need to ask questions about further development and search for answers to them. What is our future going to be like? What factors are there going to become determinants for further phenomena and processes management? It is necessary to deal with negative consequences of our decision making processes. For the purpose of this contribution, concerning the topic of the conference, We are going to try to briefly describe some of the crucial factors development, which could be considered as risks.

Authors think that everybody can be influenced by them, as well as influence them him/herself. This concerns especially those people who manage.

Risk factors

Factor 1 – Population Accumulation Dynamics

The number of the Earth population grows unevenly, especially in materially immature countries. In materially mature countries the birth rate is descending, there are a growing number of seniors. This will evoke changes in processes as well as in number and quality of human population, its behaviour and migration.

Population aging will influence its integration into economic and other socially significant processes. Social and health systems, material and non-material needs, such as boarding, dressing, hygiene, travelling, free time, home equipment; relationship between people and generations will change. Country defence potential will change, too.It is a big difference between the needs to negate poverty with a lack of capital and material production, and, on the contrary, to offer capital and material production to poverty.

Factor 2 – Inequality of the World Wealth

There are a few countries that experience a relative prosperity. On the other hand it is estimated that up to two billions of people suffer absolute poverty. There are about fifteen countries on the planet which record growth, but more than a hundred countries record descent or stagnation. According to some records there are 85 % shopping expenses for 20 % of the richest people. On the other hand 20 % of the poorest people must settle for 1.1 % of the world incomes (as compared to 1.4 % in 1991 and 2.3 in 1960).

More than a billion people do not have access to medical services, basic education or drinkable water, two billions do not have electricity and 80 % of the world population do not have the slightest possibility to telecommunicate and this access new information and communication technologies, which can, for example, enable distant studies.

It has also been found out that if the world population used the same ways of development and consumption as North America, we would need three planets like the Earth is.

The gap between the rich and the poor is getting bigger. On one side there are great chances to balance the inequalities, and on the other side they are being deepened. The problems of justice are to be seriously dealt with. The poor can not pay for the prosperity of the rich.

The inequalities are deepened not only among countries, or the North and the South, but also among people inside the countries. For instance, in the USA the rate between the highest and the lowest salaries has risen from 35 multiple up to 150 multiple within the last 20 years. We witness deepening of inequalities even here in our republic. Is it right for the poor to contribute the rich? How long will it last to the poor to start taking from the rich or at least make their wealth less pleasant? There are such cases and most probably there will be more and more of them.

Factor 3 – The Environment

Pressure caused by human activities having impact on nature systems is huge. Generally, it is connected with great material movement. Unrenewable resources are being fatigued, wasted, species of fauna and flora perish, water and air are being polluted, and number of natural as well as human-caused disasters is growing.

There have been mostly warning and non-optimistic statements published in the last few years. They are often contradictory. Yet, they have something in common – they make us think and act. Acting in the sense of adequate performance does not appear very often. It is so for many reasons.

Europe, as well as other continents, is going to face droughts and floods. Water level of seas can rise up to one meter. There is a threat of devastating winds. World map is expected to change.

According to the Living Planet Report, published by the World Wildlife Fund (WWF), standards of our lives can collapse in three decades. It is because we have been withdrawing from the planet every year up to one fifth more than the planet is able to renew. If the development continues this way, the biological capacity withdrawal deficit will reach up to 220 % in the half of the century.

The report states that the life expectancy will rapidly decline around the year 2030. Level of education and world economy will irrefutably collapse.

Unrenewable resources are being fatigued and wasted, species of fauna and flora perish, water and air are being polluted, and number of natural as well as human-caused disasters is growing. Environment knows no frontiers. In the past years at international conferences attention was paid to greenhouse gases emissions, yet no success was reached. For example – the USA produce 2.5 multiple of carbonic oxide emissions per person than Europe. In the USA the emissions production growth is eighteen per cent; the world average is nine per cent.

A hectare of tropical forests disappears every two seconds. The species disappear from hundred to thousand times faster then they would when living in a harmonic environment.

Water problems are increasingly urgent. What may happen is that this century will even become a century of a war over water, food and raw materials. Water means life. Lack of water is more and more apparent. Rivers, streams, swamps and moor land dry up.

Unrenewable resources are being fatigued, wasted, species of fauna and flora perish, water and air are being polluted, and number of natural as well as human-caused disasters is growing. Environment knows no frontiers. In the past years attention was paid to greenhouse gases emissions at international conferences, yet no success was reached. For example – the USA produce 2.5 multiple of carbonic oxide emissions per person than Europe. Water problems are increasingly urgent. Maybe this century will even become a war over water, food and raw materials.

Factor 4 – Globalization

Consequently to almost complex globalization the world is really or relatively diminishing, with no regard to continents, countries, districts. Mutual dependency of population is growing incredibly; consequences of individual's mistakes significantly affect others.

Here an essential question is to be asked: What is the connection between often absurdly defended freedom of individuals and at the same time the growing mutual dependence of people? Apart from freedom there is also justice and stability, balance and equality. So far we have been witnessing more of globalization of power, profit and exploitation. It is necessary to globalize responsibility for nature and people in it.

Great attention is being paid to globalization in various discussions. It has its positive features as well as big negatives. We must find a way to tame it to avoid a great disaster.

If we manage to run the globalization processes there is a chance for a positive development. It is good that Movements against wild globalization start to appear.

Factor 5 – Integration and Disintegration

Various groups come into being and on the contrary, states decay, therefore the there is bigger and undesirable atomization. People, regions and countries have their own interests, often of vital importance, which can be and are in contradiction with interests and aims of other countries. It is difficult do make compromise solutions. Politics and economics deal more often with the consequences than causes. Almost 20 new countries have arisen within the past 10 years, which have different political systems and aims, which are, apart from other, based on nationalistic principles.

The role of international organisations changes – UN, EU, International monetary fond, World Bank, WTO, NATO and others. We can not say that the changes are always positive, transformation is essential.

Factor 6 – NCB Weapons

There are a growing number of countries which have or will have nuclear weapons. That increases the world insecurity as well as opportunities to destroy. Here is important to note the proliferation of military equipment and technologies of ambiguous use, like NBC weapons. Gun trade volume is not low. For example, in the last three years, American companies sold weapons for nearly 19 milliard dollars; French companies for 4 milliards dollars, and German ones for 1 milliard dollars.

Besides official, by governments approved gun trades there is a trade that is being tolerated and concluded by governments. There is also illegal gun trade.

A big threat of today is a black market dealing with nuclear material and nuclear equipment. Gaining theoretical knowledge in the way of overpaying the specialists or documents is a current problem, too. Non-proliferation of all kinds of weapons, especially NBC weapons has another side, too. It is that they are kept by countries that have already had them. The logic is simple – why do some countries have them, and why the others do not? Why can you have them but we cannot? Once these weapons exist, it is a question of time and money for the others to get them. The "others" can potentially mean terrorists. Why have these weapons actually been developed and why do they exist? If the development does not change, the world will take a risk of self-destruction. The danger can be bigger than it was during the cold war time. During the cold war time, these weapons "helped" keep peace, though the peace was unstable and faulted.

There is a growing number of countries which have or will have nuclear weapons. That increases the world insecurity as well as a chance to destroy. Here is important to note the spread of military equipment and technologies of ambiguous use, like NBC weapons.

Factor 7 – Violence Growth

It is easily provable that there is a quantitative as well as qualitative growth of violence. Here it is appropriate to remember Erich Fromm who defines violence as an urgent

consequence of a non-lived and crippled life. A person who is not able to create must destroy. We have been witnessing growth of violence. The violence has many forms – human (physical and mental), military, economy, financial, political, etc. Difference between war and peace has been becoming less apparent as seen from many contemporary examples. The volume of gun-running is not small. For example, in the last three years American companies sold weapons for nearly 19 milliard dollars, French companies for 4 milliard dollars and German ones for 1 milliard dollars. People tend to feel insecure. Violence has negative influence on mental, physical, and social health.

F a c t o r   8   –   P e r m a n e n t   D e v e l o p m e n t

Probably never in human history was people's ability to self destroy as high as it is today. Will we control the ability or cope with it? Is permanent development possible? Is there and will there be enough sources for needs filling? Values and needs vary with individuals, regions, states and continents – will the differences be apparent? One of many world principles is stability and balance. Let us admit that something like this exists in materially developed world. The situation, however, can rapidly change into misbalance and dramatic value, visions and ideology conflicts.

The world has been changing fast and dramatically. Is mankind able to accept these changes throughout its physical and mental essence? Probably everybody must admit that mere existence of modern technologies brings along civilisation risks that were unthinkable several years ago. How can the modern technologies be used and controlled for general use? Do modern technologies serve people or do people serve modern technologies?

F a c t o r   9   –   A b i l i t y   t o   M a n a g e

To be able to cope with development and suppress negative factors as much as possible, the problems have to be recognised and described openly and impartially. It also necessary to find consensual solution – to manage. Management is, in its essence, optimal use of available sources. The main group of sources include: human, financial, material, information and time sources.

Risk factors are unpleasant parts of life. They can, however, work as challenge for searching for solution. Individual and social scruples make people tend to avoid thinking about unpleasant things. This phenomenon can be seen every day. However, burying heads into sand and pursuing ostrich-like policy will not lead to success. This policy will lead to postponing and not solving the problems and, in its consequences, will be nonreturnably harmful.

It is necessary to independently examine the risk factors and, if necessary, to establish an independent institution for these purposes. Avoiding unpleasant things can cause their outbreak. Political institutions have to be included in this

work in larger extent than they are today. Without wearing ideological blinkers must we ask questions like: "Is it true? Can it be true?" instead of "who and why said that?".

If we characterise contemporary and, especially, future environment as turbulent, it will not be an empty or just interesting concept. In various studies there have been characterised dozens of risks that can reach different levels of significance and different levels of development. It is probable that there may quickly appear new unexpectable, and, from today's point of view, unpredictable risks. Unfortunately, we make some decisions using logic of today or even yesterday. Environment has been becoming more and more complicated; technologies have been in progress. People and their understanding, thinking and behaviour are changing, too.

It is necessary to ask the main question: Is there (do we have) any visions, plans, and directions for the new century? Are there any devices for them? Don't we focus on short-term, purpose-made, selfish solutions, which will chase us into a trap? Don't we remove consequences instead of causes of our decisions?

We are certain that the crucial key matter of future is regulation, management, ability and willingness to manage even within international standards, as well as balanced unity of managing items. It is necessary to solve problems within international standards without selfishness, using the principles of solidarity and balanced values substitutions. It will take us a long time to do so.

Conclusions

The above stated factors are mutually interconnected; they influence each other, change their content and extent. There is a possibility of chaotic and unrestrained development along with uncontrollable, unpredictable changes resulting from these factors. In their consequences, these changes create risks and threats. It is very important for the top management representatives to realise the characters of development factors. These factors concern each of us, too.

REFERENCES

1. Beck, U.: *Riziková společnost.* Sociologické nakladatelství, Praha 2004.
2. Huntington, Samuel P. *Střet civilizací.* Rybka publishers, Praha 2001.
3. Němeček, P., a kol.: *Možné trendy rozvoje podniků.* Akademické nakladatelství CERM, Brno 2004.
4. Novák, J.: Možné vývojové tendence okolí managementu. *In Sborník konference GEMAN 04 „General management".* Plzeň: Sdružení EVIDA Plzeň, 2004.
5. Rašek, A.: *Zpráva o stavu České republiky-oblast bezpečnosti.* CESES, UK Praha, 2004.
6. Souček, Z.: Sežer! Nebo budeš sežrán?! ? *In Sborník konference PEMAN 05 „Personal management".* Plzeň: Sdružení EVIDA Plzeň, 2005.

P44 CAN WE ENSURE SAFER ENVIRONMENT FOR CULTURAL HERITAGE?

IVAN MAŠEK[a] and ZDENA ROSICKÁ[b]

[a]Brno University of Technology, Faculty of Chemistry, Purkynova 118, Brno, 612 00, Czech Republic,
[b]Universita of Pardubice, Faculty of Restoration, Jiraskova 3, Litomysl, 570 01, Czech Republic,
masek@fch.vutbr.cz

Introduction

Books should be kept in a stable environment. This is best effected by preventing temperature changes around the collection or ensuring that any changes made will be very gradual. In addition, books in fragile condition should be placed in close-fitting, nearly airtight enclosures. They protect materials from dust and airborne pollutants; reduce the exchange of moisture between the paper in the books and the air. Slow changes in air temperature around a book will not cause harm, even sudden upward temperature changes are not too damaging. In case the book in a protective enclosure is suddenly cooled, water will condense on the enclosure's interior walls when the temperature drops bellow the dew point of the air within the enclosure.

The climate maintained in a library is the result of a compromise between the needs of the readers and the staff, maintenance demands and the structure of the building which should result in minimizing the deterioration rate of the collection. It is believed that that the rate of deterioration of library materials doubles with every 10°C increase of temperature. This belief is based on the fact that the speed of chemical reactions depends in large part of temperature. Recommended temperature ranges for a variety of library materials.

A certain amount of relative humidity is necessary for paper to retain its flexibility but scientists disagree about the optimum relative humidity desirable because increased moisture content increases the rate of deteriorative chemical reactions and mold will grow. The recommended level of relative humidity is a compromise among several requirements:

• level of moisture high enough to maintain flexibility,
• level low enough to slow deterioration of materials and control insects and mold,
• level that will do no structural harm to library buildings due to condensation in cold weather.

Molds cause a downy or furry growth on the surface of organic matter; they can develop on leather, cloth, paper, etc., especially in the presence of relatively high heat and relative humidity. Every cubic meter of air contains thousands of molds spores that cover surface of library objects. Mold and mildew eat books and papers. The cellulose, adhesives and starches in the sizing provide a source of nutrition that enables the fungi to excrete digestive enzymes that convert these materials into forms they can digest. Molds usually attack bindings before the text block because it lands on the binding first, the cellulose is more difficult to digest and the text block is tightly closed.

Salvage of Flood Damage Papers

It should be noted that flood damage to some items may be irreversible. The treatment of objects of high monetary, historic or sentimental value should only be performed in consultation with a conservator.

Many people are sensitive to mold and some mold species are toxic. The best way to prevent or stop the outbreak of mold is to remove items from environmental conditions that encourage mold growth: high temperature, high relative humidity, stagnant air and darkness. If wet and moldy materials cannot be dried immediately they may be stabilized by freezing. Placing damaged items in a personal or commercial freezer will not kill mold, however, it will put the mold in a dormant state until time and the appropriate treatment environment are available. Active mold look fuzzy or slimy. Dormant mold is dry and powdery. Mold which remains active after freezing or after the host material appears dry may be treated with exposure of 1–2 hours to ultraviolet radiation from the sun. Extreme caution must be exercised when treating material outdoors: too much radiation will accelerate deterioration and may cause fading, wind may cause physical damage, and high relative humidity or condensation caused by rapid temperature changes may also exacerbate mold growth. Dormant mold spores will reactivate as soon as conditions are favorable. They should, therefore be removed from items and may be brushed or vacuumed away.

There are both chemical and non-chemical means to kill mold. Effective treatment can be fungi-static or fungicidal. Fungi-static treatments are those preventing the mold spores from germinating but do not kill the mold. Freezing is one of methods. Fungicidal treatment kills the mold and its spores. No safe large-scale treatment imparts lasting or residual mold control. That is why it is important to change the environment so it inhibits mold growth. In addition, there is some evidence that books and papers treated with fungicides may be more susceptible to mold after treatment than they were prior to the outbreak.

Fig. 1. **Flood damaged book**

Paper is very fragile when it is wet. In some cases it may be desirable to remove caked-on mud and dirt as dirt left by receding water may be contaminated. Wet documents or photographs which cannot be air dried within two days should be frozen to inhibit mold growth. Circulating air will effectively dry most items. Physical distortions may result but information will be saved. Blotting materials for air drying should be clean and absorbent. Screening material such as window screens, well supported and stacked with spaces between them provide an excellent compact drying surface. The porous surface assists air circulation and promotes drying.

Without intervention glossy materials such as paperback book covers, art books, etc. are likely to stick together. Loose glossy materials should be spread out in one layer for air drying. Bound glossy materials must be interleaved between every page to prevent sticking.

As to books, interleaving material should be placed between the text block and the front back covers. If time and supplies allow interleaving material should be placed intermittently throughout the text as well. Evaporation of water as it wicks into the interleaving paper will enhance drying.

Several classes of photographs are highly susceptible to water damage and the recovery rate will be very low. Old photographs and negatives can never be frozen. Most prints, negatives and slides may successfully be individually air dried face up. Contemporary photographic prints and negatives which are still wet and have stuck together may separate after soaking in cold water, however, this type of treatment could cause irreversible damage. Highly valued items, particularly prints, for which there is no longer a negative, should be referred to a conservator immediately.

Conclusions

The most critical element affecting the longevity of library materials is the environment in which they are used and stored. The sitting of the building, its orientation to the sun, building's location in areas safe from flooding and other natural disasters, planted areas and trees near perimeter walls, the design of roofs, basements, and location of windows considering stack areas. But it is not only buildings and their design that cause problems: libraries house millions of books published on acidic paper, high temperatures and humidity cause chemical reactions between the cellulose in paper, the acids residing in the fibers, and pollutants in the atmosphere, all of which accelerate deterioration.

Adjusting the environment near the building can help considerably in reducing problems inside.

REFERENCES
1. Ritzenthaler M. L.: *Archives and Manuscripts: Conservation: A Manual on Physical Care and Management.* SAA Basic Manual Series. Chicago: Society of American Archivists, 1993.
2. Padfield T.: Climate Control in Libraries and Archives. In *Preservation of Library Materials: Conference held the National Library of Austria, Vienna, 1986.* IFLA Publications, 41. Munchen:K.G.Saur, 1987.
3. Nyberg S.: *The Invasion of the Giant Spore.* SOLINET Preservation Program Leaflet No 5: Southeastern Library Network, Inc., November 1, 1987.

P47 CIVIL PROTECTION IN THE CZECH REPUBLIC AND ITS PERSPECTIVES

OTAKAR J. MIKA and LENKA FIŠEROVÁ

Faculty of Chemistry, Brno University of Technology, Purky-ňova 118, 61200 Brno, Czech Republic,
mika@fch.vutbr.cz

Introduction

From the legal, institutional and structural points of view the history of the conception of civil protection in the Czech Republic was relatively complicated during 90-ties. The above development accompanied fundamental social-political changes in the country after 1989 without being completed with adaptation of legislation focused on civil protection. Even if the importance of civil protection reflecting increasing risks of anthropogenic, natural and mixed origin in peace conditions was fully accepted by specialists and the responsible state authorities passed individual measures aimed on gradual change of the state then, the global conception of civil protection was approved by the Czech government as late as in 2002.

The Act No. 239 of June 28, 2000 on integrated rescue system introduced the term civil protection into the Czech legal code. According to the above act civil protection is understood as fulfillment of civil protection tasks, especially warning, evacuation, sheltering and emergency survival of civilian population and further measures to ensure protection of their lives, health and possessions with reference to the article No. 61 of Protocol Additional to the Geneva Conventions of August 12, 1949 on protection of international armed conflicts victims (Protocol I).

Civil protection has become an integral and priority domain of emergency planning and management. In connection with its systematical implementation and practical realization the necessity of university education for qualified emergency managers mastering thoroughly both theoretical and practical background of civil protection has been proved.

History of Civil Defense and Protection

Purposeful and qualified attention has been paid to the practical and theoretical problems of civil protection in the Czech Republic (former Czechoslovakia) for more than seventy years.

As early as in 1929, after World War I, the Centre for Civil Defense was established by the Czechoslovak Ministry of Defense as a response to both complicated international political situation then and to growing fears of danger from air force war activities threatening civilians especially with chemical warfare agents. The Centre was run as a voluntary organization via local bodies with the semi-official support of central authorities and with active participation of organizations whose program was concentrated on defense activities. One year later the organization Protection of Civilians against Air Raids arose.

A remarkable change of situation was noticed in the first half of 30-ties of the previous century. At that time the attempt of Nazi Germany to realize its political aims aggressively by all the available means expressed by its intensive building military and air forces was becoming more and more apparent.

The authorities of the Czechoslovak Republic reflected the above situation by introduction of a series of individual precautions resulting in passing the Act No. 82/1935 Coll. on protection from and on defense against air raids. The base for system of legal regulations for civil protection was set both by promulgation of the above law and by establishment of Civil Air Defense (referred to as CAD). Amending the above law another Act No. 75 of April 1938 represented a reaction to immediate threat of the Czechoslovak Republic by fascist Germany. The conception of CAD in the pre-war Czechoslovak Republic fulfilled requirements then and under given conditions it comprised the first historical phase of systematic and effective attempt to solve the problems of civil protection.

During the occupation of the Czechoslovak Republic by Nazis the CAD was liquidated and its compartments, units and material equipment were taken over by the German Air Defense in 1941. After liberation in 1945 the CAD passed out of existence. The first attempts to re-establish it were realized after 1948.

Regardless of certain individual measures the work on institutionalization of a civil defense (referred to as CD) organization culminated in 1951 by acceptance of Government resolution on civil defense fixing gradual organizational, personal and material building of civil defense in the legal code.

Between 1951 and 1970 civil defense was focused solely on protection against conventional weapons and on priority ensurance of protection against weapons of mass destruction effects (referred to as WMD). In 1955 the Research Institute of Civil Defense was established. Transfer of civil defense subject to protection against weapons of mass destruction expressed crucial qualitative change that resulted in acceptance of the new Resolution of Government of the Czechoslovak Republic No. 49/1958 Coll. on civil defense of the Czechoslovak Republic. For its support the following services were founded: medical, energy, gas, transport, fire, order, road and bridge, municipal, shelter, water-technical, agricultural, camouflage, construction-technical and supply ones. Operative control of civil defense was ensured by CD staffs whose members were mainly regular soldiers.

Based on the legal resolution of Federal Assembly No. 17/1976 Coll. drawing on doctrinal theory of Warsaw pact countries the subordination of CD was transferred from the Federal Ministry of Interior to the Federal Ministry of National Defense effective January 1, 1976. The State Defense Council became the supreme body for state defense control. Federal Ministry of National Defense was entrusted to become the central body of state administration for organization, coordination and control of CD on the whole area of the

Czechoslovak Republic. Local authorities at all levels were responsible for provision of tasks and needs of CD. Between 1976 and 1989 CD followed directives of the State Defense Council.

In June 1991 the State Defense Council approved the Conception of Civil Defense in the Czech and Slovak Federative Republic reflecting trends of CD development abroad with the aim to focus on protection of population against non-military emergency events. For the first time in the Czechoslovak history clear differentiation of functions and tasks of CD in times of peace and during military alerts was expressed.

Substantial changes were implemented after division of the federal state into two independent ones and after the establishment of the Czech Republic on January 1, 1993. Effective that day the operation of the former Federal CD staff was transferred to the Staff of Civil Defense of the Czech Republic. On March 17, 1993 the Resolution of the Government of the Czech Republic No. 126/1993 Coll. on the state of civil protection in the Czech Republic, its structure and material needs ensurance was passed. The government states there that the formation of the new civil protection system (referred to as CP) will be realized together with the new conception of the Army of the Czech Republic with full respect to the Protocols Additional I and II to the Geneva Conventions. On September 1, 1993 the Central Body for Civil Protection of the Czech Republic was established by the directive of then minister of defense. The body became an authority of the Ministry of Defense responsible for execution of state administration in CP affairs and at the same time it replaced the Staff of Civil Protection of the Czech Republic.

In 1997 the Government of the Czech Republic confirmed the resolution No. 710/1997 Coll. transferring the authority to execute state administration on CP from the Ministry of Defense to the Ministry of Interior and set the effective date on January 1, 2000 in the resolution No. 53/1999 Coll. In the new organization structure the Central Body for Civil Protection of the Czech Republic and regional CP bodies were united with the Fire Rescue Service of the Czech Republic (referred to as FRS). This way the activities of CP of the Czech Republic as an institution was terminated and the General Directorate of FRS of the Ministry of Interior became central authority entrusted with civil protection.

Effective Legislation Focused on Ensurance of Civil Protection

The government of the Czech Republic approved the Conception of Civil Protection until 2006 with the Prospect to 2015 (referred to as conception 2006) in its resolution No. 417/2002. The conception solves protection of civilians systematically. The government obliged ministers and heads of other authorities, governors and city mayors of Prague, Brno, Ostrava and Plzeň to implement fully the measures comprised in the above conception 2006 that emphasizes responsibility of ministries, central state authorities, local authorities, persons and physical persons for CP specified by laws. The

conception was revised by the resolution of the Czech government No. 21/2005 Coll.

In the above conception 2006 civil protection was characterized as a system of activities and procedures, subject related authorities, other subjects and individual citizens resulting in minimization of impacts of emergencies on lives and health of inhabitants, on possessions and environment.

At the beginning of 2008 (on February 25) the Government of the Czech Republic passed the resolution No. 165 "On Evaluation of the State of Implementation of the Conception of Civil Protection until 2006 with the Prospect to 2015 and on the Conception of Civil Protection until 2013 with the Prospect to 2020" giving more details on CP in the Czech Republic. This resolution contains 25 pages of specialized text from the field of CP and the Schedule of Implementation of Provisions on CP until 2013 with the Prospect to 2020 (referred to as conception 2013 and schedule). Inspite of the attempt to design the conception 2013 and schedule from the contemporary point of view it is necessary to point at inconsistent solutions of some problems concerned.

Civil protection represents an extremely important aspect of life of modern society. The supreme legislative regulation of the Czech Republic, the Constitution, ensures protection of lives, health, possessions of Czech citizens and protection of environment. Similarly to other developed European countries the security-political situation in the Czech Republic has been re-evaluated during the last decade of the 20th century. As the result of substantial political changes at the beginning of 90-ties military threat in Europe and global war conflict became less probable. Attention was focused on non-military risks important from the point of view of individual countries and security of their citizens.

Regarding the importance of civil protection its problems should be specified and expressed in a special law. Possible content and extent of the suggested law on civil protection follows:

- Introductory provisions
- Definitions and basic terms
- General provisions
- Emergency events and crisis states
- Basic organization and technical measures for civil protection
- Protection of citizens against impacts and effects of emergency events and crisis states
- Preparedness of citizens for emergency events and crisis states
- Execution of state administration in the field of civil protection
- Effectiveness of the act

Besides the above mentioned legislative regulation a project "Who is Who in Civil Protection" should be implemented. Authors and proposers will appreciate inspiring and constructive ideas and comments concerning the project.

Project: Who is Who in Civil Protection in the Czech Republic

Aim of the project:
- to compile a database of specialists in the fields related to civil protection in the Czech Republic
- to support preparedness and capacity of action of professional and voluntary bodies related to civil protection
- to list bodies or people in the database based on voluntary principle (protection of personal data of listed participants of the project)

Project outcomes:
- Proceedings (printed publication)
- Implementation and update of a website

Participating organizations – initial suggestion:
- Universities: e.g. Technical University of Ostrava – Faculty of Safety Engineering; University of Defense Brno – Institute of NBC Defense Vyškov; Police Academy of the Czech Republic, Prague, Department of Crisis Management; Brno University of Technology, Faculty of Chemistry; Tomas Bata University Zlín; University of South Bohemia, České Budějovice; Palacky University Olomouc; University of Pardubice; University of Economics, Prague etc.
- Research institutes and specialized institutions: e.g. Population Protection Institute Lázně Bohdaneč; Military Technical Institute of Protection Brno; National Institute for Nuclear, Chemical and Biological Protection Kamenná; State Office for Nuclear Safety, Prague etc.
- Companies and firms manufacturing and marketing materials for civil protection (e.g. syndicate of companies Czech NBC team etc.)
- Ministries: Ministry of Interior – General Directorate of Fire Rescue Service and Police of the Czech Republic; Ministry of Health – Department of Crisis Preparedness, Emergency Medical Service, Air Rescue Service, selected hospitals; Ministry of Defense; Ministry of Industry and Trade; Ministry of Transport; Ministry of Education, Youth and Sport; Ministry of Environment; voluntary bodies, e.g. Czech Red Cross, Mountain Rescue Service of the Czech Republic etc.

Proposed personal data of specialists to be listed in the "Who is Who in Civil Protection in the Czech Republic" database:

- First name and surname, academical degrees
- Employment history/accomplishments
- Major contemporary professional orientation
- Major supervised projects and publications in the field of CP in recent 5 (10) years
- Contact information for communication: address, telephone and fax numbers, e-mail address etc.

Implementation of the above process makes sense when its outcomes are accessible e.g. on a special website available for selected specialists assigned with passwords and when the database is regularly updated.

Conclusions

Contradictory and contrary character of civilization activities accompanied with permanent proliferation of security risks results in increasing danger for citizens caused by growing number and types of emergency events. The development of corresponding security system lags behind the above described process, which makes the problems of civil protection permanently unresolved.

Civil protection as a system of specialized measures remains an integral part of crisis management and represents its priority in non-military emergency events. Concerning the systematic approach to solve individual types and kinds of emergency events civil protection is understood as a separately controlled and coordinated domain.

With regard to growing importance of civil protection nowadays and in future preparation of and negotiation on special legislative regulations (see the proposed law on civil protection above) based on a "set of acts on crisis states" passed in the half of 2000 year and effective January 1, 2001 can be highly recommended. The field of civil protection deserves proper background in thorough legislation.

REFERENCES
1. Zeman M., Mika O. J.: *Protection of Citizens*. Brno University of Technology, Faculty of Chemistry, Brno 2007
2. Silhanek B., Dvorak J.: *Short History of Civil Protection*. Ministry of Interior, General Directorate of FRS of the Czech Republic, Prague 2003
3. Kratochvilova, D.: *Protection of Citizens*, Society of Safe and Fire Engineering, Ostrava 2005
4. Krulik O., Masek I., Mika O. J.: *Phenomenon of Current Terrorism*. Brno University of Technology, Faculty of Chemistry, Brno 2008

P48 APPLICATION OF DGT METHOD FOR ASSESMENT OF AVAILABILITY OF HEAVY METALS TO PLANTS

Z. MLÁDKOVÁ[a], K. PEŠKOVÁ[a,b], B. DOČEKAL[b], H. DOČEKALOVÁ[a] and P. ŠKARPA[c]

[a]*Department of Environmental Chemistry and Technology, Faculty of Chemistry, Brno University of Technology, Purky-ňova 118, 612 00 Brno, Czech Republic,*
[b]*Institute of Analytical Chemistry, Czech Academy of Science, Veveří 97, 602 00 Brno, Czech Republic,*
[c]*Mendel University of Agriculture and Forestry, Faculty of Agronomy, Zemědělská 1, 613 00 Brno, Czech Republic,*
mladkova@fch.vutbr.cz

Introduction

At present time problems of toxic metal contamination of soils are often solved. The form of metals present in the environment is an important factor affecting their bioavailability. Metals are often bound to various organic complexing ligands as humic substances, which influences their mobility. Therefore, studies of metal speciation are necessary for understanding how metals can move in nature systems.

Leaching procedures are especially used for determination of toxic metals concentration in soils. Simple leaching procedures using aqua regia, ethylenediaminetetraacetic acid (EDTA), nitric acid or sodium nitrate are usually recommended and applied. However, leaching procedures give no information about the metal fraction which is really available for the root system of plants. Therefore, new approaches are still being searched to obtain a better characterization of bioavailable forms of metals and their transport in soils.

Recently an *in situ* technique capable of quantitatively measuring labile metal species has been developed[1]. This technique, known as diffusive gradients in thin films (DGT), has been successfully used to measure the *in situ* concentrations of metals in natural waters, sediments and soils and has been shown to be a promising tool to assess metal phytoavailability in a wide range of soils. The technique is based on accumulation of solutes in a resin layer after passing through a well-defined diffusive gel layer. The mass of solutes accumulated in the resin during a period of deployment time is measured.

The aim of this work was to assess the heavy metal uptake of radish and to test the capability of DGT to predict phytoavailability of the metals for this plant.

Experimental

Soil Treatment and Leaching Procedures

Homogenized and sieved soil, which had been sampled in Zabcice site, was used in the experiment. Content of Cd and Cu extractable with nitric acid, acetic acid, EDTA, sodium nitrate and water was determined in the soil according to the recommendation of the Community of Bureau of Reference (BCR)[2] and Gupta[3]. Portion of 6 kg of the soil was weight into each of 40 pots. Soil portions in individual pots were spiked by adding solution of Cd and Cu, so that the concentration of the metal in the soil was increased by 1 ppm Cd, 2 ppm Cd, 100 ppm Cu and 200 ppm Cu. The pots with non-spiked soil portions served as control samples. After 3 months, leaching with the same agents was carried out with artificially contaminated samples.

DGT Experiment

The gels for DGT were prepared according to the conventional procedures (DGT Research, Ltd., Lancaster, UK)[4]. The DGT piston probes were deployed at 24 ± 1 °C in each soil sample in triplicate with the moisture content of 150 % of maximum water holding capacity MWHC for 24 hours. After elution of the resin gel with 1M HNO_3, the accumulated mass of Cd or Cu was determined.

Pot Experiment

Radish (*Raphanus sativa*) was sown both in the control and contaminated soils. Five plants of radish were grown in each of four pots with the same soil sample. Six weeks after sowing the radishes were harvested, rinsed with deionized water; the root divided into the white inner part and the red outer part and digested using the dry mode mineralizer (APION). Dry matter content in both parts was determined by drying samples in a oven at 105 °C.

Determination of Metals

Content of Cu and Cd was determined by electrothermal atomic absorption spectrometry (ETAAS) employing Perkin-Elmer Model 4110 Zeeman atomic absorption spectrometer. Recommended conditions were applied.

Results

Concentration of Cd and Cu found in soil samples by leaching with $NaNO_3$ and water and in dry matter of radish edible parts are summarized in Tables I and II. The test sample was also characterized by other leaching agents. Content of elements in this soil related to nitric acid, acetic acid and EDTA leachate fractions was 49.1 ± 2.8; 45.5 ± 1.9; 11.8 ± 0.8 µg kg^{-1} Cd and 6.80 ± 0.50; 0.256 ± 0.051; 3.10 ± 0.17 mg kg^{-1} Cu.

The content of both metals is significantly higher in contaminated soils as intended. The results show that added metals are strongly bound to the soil matrix. The amount of extractable Cd and Cu with $NaNO_3$ reaches only 10 % and even only 0.1 % of added metal, respectively. The concentrations found by means of DGT technique are within 1–2 orders of magnitude lower than the concentrations in sodium nitrate leachates for both metals.

The dry matter content was determined in both analyzed parts of radishes. The red outer part and the white inner part contained on average 11 % and 5 % of dry matter, respectively. Cd and Cu concentration in both parts of radish increases with increasing content of these metals in soils. The Cd and Cu uptake in red outer part of radish is higher than

in white inner part. The fluctuation of individual results indicates higher biological variability among the plants grown in the experimental pots.

Table I
Cadmium content in soils and in dry matter of plant samples grown in these soils

	Concentration of Cd $[\mu g \, kg^{-1}]$		
	Control soil	Cd 1 ppm soil	Cd 2 ppm soil
Leaching – NaNO₃	0.47 ± 0.10	46.7 ± 8.5	249 ± 32
Leaching – water	0.85 ± 0.10	1.89 ± 0.73	3.77 ± 0.51
DGT unit	0.015 ± 0.003	1.54 ± 0.26	3.38 ± 0.96
Radish – white part	86.0 ± 20.0	$2,430 \pm 212$	$4,860 \pm 1,230$
Radish – red part	282 ± 67	$3,543 \pm 762$	$6,260 \pm 1,420$

Conclusions

Metal concentration (Cd, Cu) in radish depends on the concentration of the metal in soils in which the plants were grown. DGT technique can provide relevant information on accessible form of elements in the soil.

Table II
Copper content in soils and in dry matter of plant samples grown in these soils

	Concentration of Cd $[\mu g \, kg^{-1}]$		
	Control soil	Cu 100 ppm soil	Cu 200 ppm soil
Leaching – NaNO₃	10.9 ± 2.1	210 ± 11	202 ± 39
Leaching – water	7.71 ± 0.40	75.9 ± 18.9	77.9 ± 6.3
DGT unit	0.191 ± 0.030	3.71 ± 0.19	4.96 ± 0.33
Radish – white part	$2,340 \pm 440$	$7,220 \pm 1,160$	$11,600 \pm 4,600$
Radish – red part	$3,520 \pm 505$	$15,200 \pm 1,830$	$42,800 \pm 21,400$

REFERENCES

1. Davison W., Zhang H.: Nature *367*, 545 (1994).
2. Ure A. M., Quevauviller P., Muntau H., Griepink B.: Int. J. Environ. Anal. Chem. 51, *135* (1993).
3. Gusta S. K., Aten C.: Int. J. Environ. Anal. Chem. *51*, 25 (1993).
4. DGT measurements in waters, soils and sediments; DGT Research Ltd., Lancaster, UK http://www.dgtresearch.com, (January 2008).

P49　SPECTROPHOTOMETRIC MICRODETERMINATION OF PHOSPHATE BASED ON THE ION ASSOCIATION COMPLEX WITH RHODAMINE B IN WATER

MARTIN MOOS and LUMÍR SOMMER

Brno University of Technology, Chemistry and Technology of Environmental Protection, Purkyňova 118, 612 00 Brno,
xcmoos@fch.vutbr.cz

Introduction

Phosphate may be a serious problem for the ecosystem[1,2] since it is the main reason for the eutrophication of natural surface waters. In the presence of phosphate, a considerable growing of anabaena is observed which release toxins after their extinction. Moreover, the phosphates cause a considerably growing of water plants which consume the oxygen contents in water, and interfere with the aquatic life. The visual spectrophotometry[3,4] often based on the interaction of molybdatophosphate or molybdatovanadato-phosphate with some basic dyes is often used for its determination.[5–8] The formation of an ion associate with the sensitive Rhodamine B (Tetraethylrhodamine) was studied in detail in this paper.

Experimental

Chemicals

All chemicals used were in analytical grade quality.

$0.01 \ mol \ dm^{-3}$ standard solution of phosphate was prepared from $0.3402 \ g \ KH_2PO_4$ (Lachema, Brno, Czech Republic) in 250 ml, previously dried 1h at 130 °C.

$0.3 \ mol \ dm^{-3}$ solution of sodium molybdate, (Lachema, Brno, Czech Republic) and $1 \times 10^{-3} \ mol \ dm^{-3}$, solution of Rhodamine B (Tetraethylrhodamine), (Merck, Darmstadt, SRN) in milli Q water were stock solutions.

Brij 35 (Aldrich, Steinheim, SRN), Triton X 100 (Calbiochem Co., San Diego, USA) and Polyvinylalcohol (PVA) (Sigma, Steinheim, SRN) surfactants were in 1 % wt. aqueous solutions.

Astasol standard solutions with $1 \ g \ dm^{-3}$ of SiO_3^{2-}, Ca^{2+}, Al^{3+}, Fe^{3+}, K^+, Na^+, Mg^{2+}, As^{3+}, Cl^-, SO_4^{2-}, NH_4^+, NO_3^-, NO_2^- (Analytika, Praha, ČR), were used for studying interferences.

Real Waters Samples

Surface water from the River Sázava, mineral water Korunní, drinking water from the Brno water supply and sea water from the Mediterranean Sea were sampled. The water samples were filtered by using membrane filter with pore size 0.45 μm.

Instrument

Spectrophotometer Spectronic UNICAM UV 500 (Spectronic Unicam, UK, Cambridge).

Calibration plots and limits of detection

All linear calibration plots were evaluated according to the standard ČSN ISO 8466-1[10] characterizing necessary statistical characteristics for evaluation of linear calibration plots (variation range homogeneity test and linearity test).

The detection limits were expressed according to Graham[9], Miller[11] and to IUPAC[13].

The method of continuous variation[12] was used for the evaluation of the mol ratio of components.

Results

The sequence of mixing components has an important effect for the sensitivity and reproducibility of the method. The maximal absorbance was reached for the following order of mixied components: phosphate → non-ionic surfactant → sodium molybdate → sulphuric acid → Rhodamine B. The absorbance of the ternary species of 12–molybdatophosphate with Rhodamine B reaches its maximum value for $8.3 \times 10^{-5} \ mol \ dm^{-3}$ Rhodamine B and $0.03 \ mol \ dm^{-3}$ sodium molybdate after 20 min. at 572 nm. The higher concentrations of both components are responsible for the absorbance decreases.

Effect of Acidity

In the following range 0.1–$3.0 \ mol \ dm^{-3}$, the absorbance considerably decreased with the increasing concentration of sulphuric acid. $1 \ mol \ dm^{-3}$ of H_2SO_4 was optimal for obtaining stable absorbance of the associate in time. Hydrochloric acid has a similar effect but $1.5 \ mol \ dm^{-3}$ was used for further measurements.

Effect of surfactants

Three non-ionic surfactants were used, Brij 35, Triton X 100 and PVA respectively, from which 0.01 % wt. of Brij 35 was optimal. In the presence of Triton X 100 the adsorption of the ion associate on glass surface was observed. PVA 30,000–70,000 mol. weight does not prevent turbidity in solution.

Calibration Plots and Detection limits (LOD)

The strictly linear calibration plots were evaluated for six concentration levels between 1×10^{-6}–$7 \times 10^{-6} \ mol \ dm^{-3}$. The points were measured in triplicate for the optimal conditions $1 \ mol \ dm^{-3}$ sulphuric acid, 0.01 % wt. Brij 35, $0.03 \ mol \ dm^{-3}$ sodium molybdate and $8.3 \times 10^{-5} \ mol \ dm^{-3}$ Rhodamine B for the evaluation were used.

Effect of ions

$1,000 : 1 \ Mg^{2+}$, K^+, Na^+, NH_4^+, NO_3^- SO_4^{2-}, Cl^-, HCO_3^- did not interfere the determination of $1 \times 10^{-6} \ mol \ dm^{-3}$ H_2PO_4 and $100 : 1 \ Al^{3+}$, Fe^{2+}, Ca^{2+}. As (III, V) and NO_2^- interfered above concentrations only which are not present in natural waters. The SiO_3^{2-} was successfully masked with $6.7 \times 10^{-4} \ mol \ dm^{-3}$ tartaric acid.

Table I
Calculated values from calibration plots

$y = 0.1421x + 0.0104$		$R^2 = 0.9987$
$X_\Delta^{\alpha\,a}$	0.40×10^{-6} mol dm^{-3}	1.24×10^{-5} g dm^{-3}
$X_\Delta^{\beta\,a}$	1.18×10^{-6} mol dm^{-3}	3.66×10^{-5} g dm^{-3}
$X_m^{\,b}$	0.79×10^{-6} mol dm^{-3}	2.44×10^{-5} g dm^{-3}
$X_{3\sigma}^{\,c}$	0.83×10^{-6} mol dm^{-3}	2.56×10^{-5} g dm^{-3}
$\varepsilon_\sigma^{\,d}$	142123 ± 3767	mol^{-1} cm^{-1} dm^3

The Stoichiometry of the Ternary Species of 12-Molybdatophosphate with Rhodamine B

The molar ratio of components in the ion associate was expressed from the method of continuous variations[12].

$$n = \frac{x_{max}}{1 - x_{max}}. \text{ The resulting value of n was } n = \frac{0,5}{1-0,5} = 1 .$$
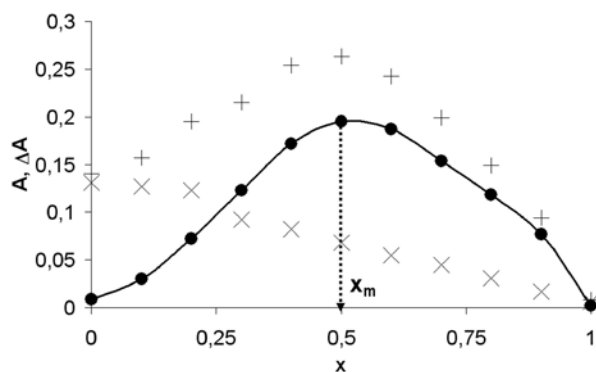
Fig. 1. **The point 0 on the Jobs curve corresponds with the maximal concentration of the Rhodamine B and zero concentration of phosphate, the point 1 with the maximal concentration of phosphate and zero concentration of Rhodamine B. + points belong to the total absorbance of solution, × points belong to the Rhodamine B blank**

This molar ratio corresponds with the ratio between phosphate and Rhodamine B as 1 : 1. Which describes the composition of the ion associate such as $H_2P[Mo_3O_{10}]_4^- \cdot RhB^+$ in 1 mol dm^{-3} H_2SO_4.

Applications For the Real Samples of Water

For all kinds of water, the method of standard additions in six concentration levels which are 1, 2, 4, 6, 7×10^{-6} mol dm^{-3} was used. The concentration of phosphate was found 0.1 ± 0.02 mg dm^{-3} triplicate the values in the
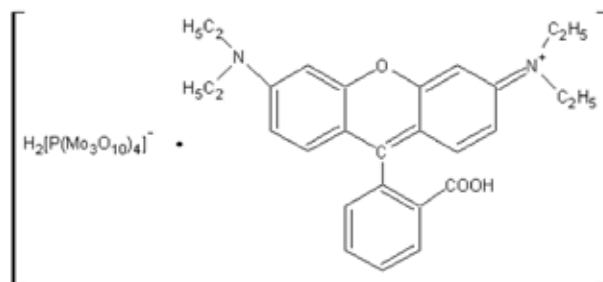
Fig. 2. **The supposed structure of the ion associate**

river water and 0.16 ± 0.007 mg dm^{-3} phosphate in the drinking water. The determination could not be carried out by this approach for mineral water because of increased contents of silicate in solution. The optimal concentration of 6.7×10^{-4} mol dm^{-3} tartaric acid is not effective for masking but the necessary higher concentration of tartaric acid would interfere with the determination of phosphate. The concentration of phosphate in the analyzed sea water was under the detection limit and the method of standard addition can not be used.

REFERENCES

1. Klein G., Perera P.: *Eutrophication and health*. WHO and EC, Luxembourg 2002.
2. Pitter P.: *Hydrochemie*. VŠCHT, Praha 1999.
3. Marczenko Z.: *Separation and spectrophotometric deter-mination of elements*. Ellis-Horwood, Chichester 1986.
4. Malát M.: *Absorpční anorganická fotometrie*. Academia, Praha 1973.
5. Xiao L. H., Jia Z. Z.: Anal. Chim. Acta *55*, 580 (2006).
6. Sommer L., Doležal J.: Scripta fac. Sci. Nat. Univ. Purk. Brun *19*, 159 (1989).
7. Kratochvíla J., Sommer L.: Scripta Fac. Sci. Nat. Univ. Purk. Brun *10*, 53 (1980).
8. Kartikeyan S., Rao T. P., Iyer C. S. P., Damodaran A. D.: Microchimica Acta *71*, 113 (1994).
9. Graham R. C.: *Data Analysis for the Chemical Science*. VCH Publisher, New York 1993.
10. ČSN ISO 8466-1: *Kalibrace a hodnocení analytických metod a určení jejich charakteristik* -Část 1: *Statistické hodnocení lineární kalibrační funkce* (březen 1994).
11. Miller J. N., Miller J. C.: *Statistics and Chemometrics for Analytical Chemistry*. Pearson Education Limited, New York 2005.
12. Sommer L., Hniličková M.: Bull. Soc. Chim. France 1959, 36.
13. MacDougall D.: Anal. Chem. *52*, 2242 (1980).

P50 DETERMINATION OF URANIUM BY ICP-AES IN THE ABSENCE AND PRESENCE OF PRECONCENTRATION ON MACROPOROUS SORBENTS

MARTIN MOOS, KRISTÝNA URBÁNKOVÁ and LUMÍR SOMMER

Brno University of Technology,Chemistry and Technology of Environmental Protection, Purkyňova 118, 612 00 Brno, xcmoos@fch.vutbr.cz

Introduction

Determination of uranium at very low concentrations often needs preconcentration in order to meet the detection limit of a given analytical method. Matrix interferences are another problem when using AAS and ICP-AES. The preconcentration by solid phase extraction is simple, rapid and usually help to eliminate interferences from the matrix elements. Several sorbents were used for preconcentration and separation of trace uranium (VI)[1], among them the macroporous Amberlite XAD resins[2,3], silica[4,5], active carbon[6] and polyurethane foam[7] which can be loaded with completing reagents. The modified Amberlite XAD 4 resin in various particle size was studied for the sorption of uranium in this paper prior to the final determination by ICP-AES[1–3].

Experimental

Chemicals

All chemicals used were of analytical grade quality.

1 $g\,dm^{-3}$ standard solution of uranium (VI) Astasol (Analytika, Praha, Czech Republic)

0.5 $g\,dm^{-3}$ solution of 4-(2-pyridylazo)resorcinol (PAR) from, Lachema, Brno, Czech Republic, the ammonium salt of pyrrollidincarbodithioate (APDC) from, Lachema, Brno, Czech Republic, 8-hydroxyquinoline-5-sulphonic acid (8-HQS) from Aldrich, Steinheim, Germany and 1,2-dihydroxybenzene (PYR) from Lachema, Brno, Czech Republic in distilled water were stock solutions.

Cationic surfactants 1-ethoxycarbonylpentadecyl-trimethylammonium bromide (Septonex®) from Tamda, Oloumouc, Czech Republic, benzyldimethyltetradecyl-ammonium chloride (Zephyramin®) from Merck, Darmstadt, Germany and benzyldimethyldodecyl-ammonium bromide (Ajatin®) from Fluka, Buchs, Switzerland were in 0.1 $mol\,dm^{-3}$ aqueous solutions.

The macropourous sorbent Amberlite® XAD 4 (Fluka, Buchs, Switzerland) was previously dried 24 h at 100 °C, milled and sieved; the fraction 0.32–0.63 μm was used and ctivated in methanol for 24 hours. 200 mg of activated sorbent was filled into empty cartridges. The columns were finally washed by 10 ml of acetone and 10 ml of distilled water.

Solutions for the sorption or the eluent were aspirated through the sorbent-filled plastic cartridges using the vacuum pump operated vacuum suction device Dorcus™ (Tessek, Praha, Czech Republic). A peristaltic pump UNIPAM 315™ (Scientific instrument, Warszawa, Poland) was attached with 3 mm wide silicon tubing to the cartridges and operated at a solution flow rate of 1 $ml\,min^{-1}$.

Instrument

An echelle-based ICP-spectrometer with a prism pre-disperser IRIS AP™ (Thermo Jarell Ash, U.S.A.) containing a CID detector with 512×512 pixels for 195–900 nm, axial plasma discharge and echelle grating with 54.4 lines mm^{-1} was used. The plasma source was a generator with 27.12 MHz with the power output of 1.35 kW. The plasma argon flow rate was 12 $dm^3\,min^{-1}$. The integration time was 30 s. The results were the average of 3 measurements. Spectral lines (nm) in high orders: U 385.958 and U 409.014 nm were tested for the determination and the spectral line 385.958 was used for future measurement.

Calibration Plots and Limits of Detection

All linear calibration plots were evaluated according to the ČSN ISO 8466-1 standard including the variation range homogeneity test and linearity test[8]. The confidence limits of the plot are also expressed.

The recovery was calculated by the expression

$$R = {c(U)_{eluted}} \Big/ {c(U)_{applied\ onto\ the\ column}} \cdot f \qquad (1)$$

where f is the enrichment factor.

The detection limit was expressed according to Graham[9], Miller[10] from the calibration plots and to IUPAC[11] from 10 points of the blank.

Results

Determination of Uranium by ICP-AES in the Absence of Preconcentration

Some determination in geological samples was earlier described[12]. A 10% signal decrease was observed for 0.75 $mol\,dm^{-3}$ HNO_3, but for 1 $mol\,dm^{-3}$ HCl the decrease reaches 20 %. In the presence of various 3×10^{-3} $mol\,dm^{-3}$ surfactants, Brij 35, Zephyramine, Ajatin and dodecylsuphate the 5–15 % increase of the calibration slope was observed. Similarly, the slope of calibration plots increased by 5 % in the presence of 6×10^{-5} $mol\,dm^{-3}$ PAR, 9×10^{-5} $mol\,dm^{-3}$ APDC or 2.2×10^{-5} $mol\,dm^{-3}$ 8-HQS. (cf. Table I)

Calibration plots and effect of interfering ions

The strictly linear calibration plots were evaluated for seven concentration levels between 0.1 $mg\,dm^{-3}$– 50 $mg\,dm^{-3}$. The points were measured in triplicate. The detection limits were $X_\Delta^\alpha = 1.26$ $mg\,dm^{-3}$, $X_\Delta^\beta = 3.69$ $mg\,dm^{-3}$ according to Graham, $X_\Delta^m = 1.13$ $mg\,dm^{-3}$ according to Miller and 0.30 $mg\,dm^{-3}$ according to IUPAC.

For 1–3 $mg\,dm^{-3}$ U, no interference were observed for $100:1$ NO_3^-, Cl^-, SO_4^{2-}, SiO_3^{2-}, NH_4^+, Na^+, K^+, Ca^{2+}, Mg^{2+},

Table I
The regression equation for different selected systems

U (VI) Solution	regression equation
Basic[a]	$y = 4.48x + 1.29$
Septonex[b]	$y = 4.49x + 0.23$
Dodecylsulphate[c]	$y = 5.37x + 1.08$
0.75 mol dm^{-3} HNO3	$y = 4.04x + 2.18$
1 mol dm^{-3} HCl	$y = 3.75x + 3.18$
PAR[d]	$y = 4.95x + 1.32$
APDC[e]	$y = 4.83x + 0.43$

[a]calibration plots for 1 mg dm^{-3}–15 mg dm^{-3} U without organic reagents ;
[b]3×10^{-3} mol dm^{-3} Septonex;
[c]3×10-3 mol dm^{-3} sodium dodecylsulphate;
[d]2×10^{-5} mol dm^{-3} PAR;
[e]3×10^{-5} mol dm^{-3} APDCin solution

Al^{3+}. The 10 : 1 excess of multicomponent standards containing Br$^-$, Cl$^-$, Br$^-$, SO$_4^{2-}$, PO$_4^{3-}$ or Cd^{2+}, Co^{2+}, Cr^{3+}, Cu^{2+}, Mn^{2+}, Pb^{2+}, V^{5+} and Zn^{2+} (each of metal ion) in the absence or presence of Y^{3+} internal standard (1 mg dm^{-3}) did not interfere. 10 : 1 excess of Fe^{3+} interferes strongly by the 50% signal decrease in the presence of Y^{3+}.

Determination of Uranium by ICP-AES After the Preconcentration on Modified Amberlite XAD 4

Prior to the sorption, the column was conditioned by 10 ml of 5×10^{-3} mol dm^{-3} Septonex whose pH was adjusted by hydrochloric acid and sodium hydroxide. This procedure was always used for the sorption.

Effect of Surfactants and Organic Reagents

The retention efficiency of 3 mg dm^{-3} U from 50 ml volume with the optimal pH 9 without surfactants and organic reagents was 56 % only. The elution of uranium from the column was carried out with 10 ml acetone and 1 mol dm^{-3} nitric HNO$_3$ (1 : 1). The various surfactants were used such as non-ionic Brij 35, cationic Septonex or Zephyramine and anionic dodecyl sulphate respectively, from which 5×10^{-3} mol dm^{-3} of Septonex was optimal for conditioning and allowed the recovery of 96 % U. The recovery with dodecylsulphate was 81 % U. Brij 35 produced a foam in the column and Zephyramine did not prevent turbidity during evaporation, when HNO$_3$ was used for elution.

Moreover the sorption of 1.5–15 mg dm^{-3} of U was quantitative by using 6×10^{-5} mol dm^{-3} PAR and 9×10^{-5} – 1.8×10^{-4} mol dm^{-3} APDC which corresponds with the 5 or 10 fold excess of reagent and the recovery nearly 100 % was obtained in the presence of 1.3×10^{-4} mol dm^{-3} 8-HQS and 1.4×10^{-4} mol dm^{-3} PYR. Thus, 6×10^{-5} mol dm^{-3} of PAR was recommended for following preconcentration.
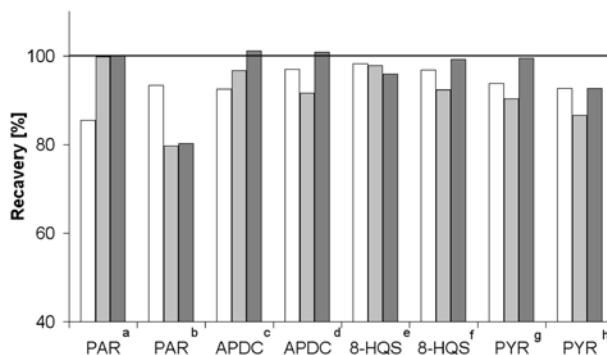
Fig. 1. **Effect of organic reagents.** □ pH = 5; ▨ pH = 7; ■ pH = 9; [a]6×10^{-5} mol dm^{-3} PAR, [b]1.2×10^{-4} mol dm^{-3} PAR, [c]9×10^{-5} mol dm^{-3} APDC, [d]1.8×10^{-4} mol dm^{-3} APDC, [e]6.7×10^{-5} mol dm^{-3} 8-HQS, [f]1.3×10^{-4} mol dm^{-3} 8-HQS, [g]1.4×10^{-4} mol dm^{-3} PYR; [h]2.7×10^{-4} mol dm^{-3} PYR, 3 mg dm^{-3}U was sorbed after conditioning the sorbent with 5×10^{-3} mol dm^{-3} Septonex solution

Effect of pH

The influence of pH on the sorption follows from Table II. The sorption was quantitative in the interval of pH 7–9.

Table II
Effect of pH on the sorption[a]

pH	recovery [%]
9	100.0 ± 3.6
8	99.5 ± 3.7
7	100.6 ± 2.4
6	89.6 ± 4.8
5	88.6 ± 5.3
4	82.7 ± 0.9

[a]From 50 ml of sample with 3 mg dm^{-3} U, in the presence of 6×10^{-5} mol dm^{-3} PAR and after conditioning the sorbent with 5×10^{-3} mol dm^{-3} Septonex solution. The sorption was carried out in triplicate

Effect of Eluents

For the quantitative elution of the complex of uranium (VI) with the used reagents, acetone, ethanol and methanol in different ratio with 1 mol dm^{-3} nitric acid were tested. The most effective eluent with 100% recovery of U was 10 ml of 1 : 1 acetone and 1 mol dm^{-3} nitric acid or the 1 : 1 mixture of acetone and 4 mol dm^{-3} HNO$_3$ mixtures. The best eluents are compared in Table III.

Conclusions

The sorbent XAD-4 in the presence of 4-(2-pyridylazo)resorcinol or pyrrollidincarbodithioate was observed for the separation and preconcentration of Uranium (VI) at pH 9. The column of Amberlite XAD 4 of particle size 0.32–0.63 μm was washed with 10 ml of acetone and 10 ml of distilled water, and conditioned with

Table III
The recovery with different eluents

Elution reagent	Recovery of U [%][a]
Ethanol-HNO$_3$ [1 mol dm^{-3}]	92 ± 5
Aceton-HNO$_3$ [1 mol dm^{-3}]	100 ± 3
Methanol-HNO$_3$ [1 mol dm^{-3}]	94 ± 2

[a] eluted with 10 ml of eluent in triplicate

5×10^{-3} mol dm^{-3} Septonex solution. The sample solution containing 1.5–15 mg dm^{-3} U with 6×10^{-5} mol dm^{-3} of PAR was applied on the column with 1 ml min^{-1}. The column was then washed with 15 ml of distilled water and uranium eluted with a mixture of acetone : 1 mol dm^{-3} HNO$_3$ (1 : 1). The organic solvent was removed by evaporation under an IR lamp to 2 ml in a suitable Teflon® dish. The residue was then diluted to 10 ml by distilled water and analyzed by ICP-AES. (cf. Table IV)

REFERENCES

1. Rao T. P., Metilda P., Gladis J. M.: Talanta *68*, 1064 (2006).
2. Ramesh A., Mohan K. R., Seshaiah K.: Talanta *57*, 243 (2002).
3. Singh B. N., Maiti B.: Talanta *69*, 393 (2006).
4. Leepipatpiboon V.: J. Chromatography A *697*, 137 (1995).
5. Ueda K., Koshino Y., Yamamoto Y.: Anal. Lett. *18*, 2345 (1985).
6. Okamota Y., Murata T., Kumamaru T.: Anal. Sci. *7*, 879 (1991).

Table IV
The efficiency for uranium (VI) in the presence of org. reagent at pH 9 on Amberlite XAD 4

Org. reagent	Uranium (VI)		
	1.5 mg dm^{-3}	3 mg dm^{-3}	15 mg dm^{-3}
PAR[a]	1.53 ± 0.02	2.99 ± 0.05	14.75 ± 0.12
APDC[b]	1.65 ± 0.09	3.05 ± 0.05	15.69 ± 0.15
APDC[c]	1.43 ± 0.07	3.01 ± 0.05	14.48 ± 0.69

[a] 6×10^{-5} mol dm^{-3} PAR,
[b] 9×10^{-5} mol dm^{-3} APDC,
[c] 1.8×10^{-4} mol dm^{-3} APDC,
[d] The sorbent conditioned with 5×10^{-3} mol dm^{-3} Septonex and the sorption carried out in triplicate

7. Ferreira S. L. C.: Spec. Chim. Acta Part B *62*, 4 (2007).
8. ČSN ISO 8466-1: Kalibrace a hodnocení analytických metod a určení jejich charakteristik -Část 1: Statistické hodnocení lineární kalibrační funkce (březen 1994).
9. Graham R. C.: *Data Analysis for the Chemical Science. A Guide to Statistical Techniques*, VCH Publisher, New York 1993.
10. Miller J.N., Miller J. C.: *Statistics and Chemometrics for Analytical Chemistry*. Pearson Education Limited, New York 2005.
11. MacDougall D., Crummett W.B.: Anal. Chem. *52*, 2242 (1980).
12. Kanický V., Abu-Ajamieh Y., Awadat A. W.: Scripta Fac. Nat. Univ. Masaryk. Brun. *25*, 21 (1995).

P51 SIMULTANEOUS SPECIATION OF SELENIUM AND MERCURY IN ENVIRONMENTAL SAMPLES BY USING A COLUMN SWITCHING SYSTEM WITH LIQUID CHROMATOGRAPHY COUPLED TO ICP-MS

F. MORENO, T. GARCÍA-BARRERA and J. L. GÓMEZ-ARIZA

Departamento de Química y Ciencia de los Materiales "Prof. J. C. Vílchez Martín". Facultad de Ciencias Experimentales. Universidad de Huelva, Campus de El Carmen. 21007 Huelva (Spain),
fernando.moreno@dqcm.uhu.es

Introduction

Mercury is a very toxic element which damages the central nervous system, endocrine system, kidneys, and other organs. Exposure over long periods of time or heavy exposure to mercury vapour can result in brain damage and ultimately death. Mercury and its compounds can produce serious birth defects.Compounds of mercury tend to be much more toxic than the element itself.[1–3]

On the other hand selenium is an essential micronutrient for animals with biological functions as cofactor. However it is toxic in large doses. Selenium deficiency can lead to Keshan and Kashin-Beck diseases. If it is taken in excess it can lead to seleniosis. In addition, several studies have suggested a link between cancer and selenium deficiency[4].

It has been issued that Se-methionine inhibits some neurotoxic effects of methylmercury.[5–7]

For this reason, the development of new analytical strategies for multielemental speciation is a primordial issue.

In the present study, a new method for the detection of Se- and Hg- species has been developed, including chiral species.

Experimental

I n s t r u m e n t a t i o n

The HPLC system is an Agilent 1100 series. The columns used were a Phenomenex Bondclone C18, 300 mm × 3.90 mm, 10 μm; and an Astec Chirobiotic T column, 250 mm × 4.6 mm.

An inductively coupled plasma mass spectrometer Model HP 4500 (Hewlett Packard, Yokogawa, Analytical System, Tokyo, Japan) equipped with a Babington nebuliser was used in this study.

R e a g e n t s   a n d   S t a n d a r d s

All reagents were of analytical reagent grade. Deionized water (18 MΩ cm^{-1}) was obtained from a Milli-Q water purification system (Millipore, UK). 2-mercaptoethanol 98% was purchased from Sigma–Aldrich (Steinheim, Germany) and tetraethylammonium chloride from Fluka (Switzerland). Ammonium acetate and nitric acid were obtained from Merck (Darmstadt, Germany).

Stock standard solutions of 1,000 mg Se dm^{-3} were prepared in deionized water from selenocystine (SeCys$_2$, Sigma), seleno-DL-methionine (Se-DL-Met, Sigma), seleno-L-methionine (Se-L-Met, Sigma), selenomethylselenocysteine (SeMeSeCys, Sigma), selenocystamine (SeCA, Sigma), sodium selenate (Na$_2$SeO$_4$) and sodium selenite (Na$_2$SeO$_3$).

Methylmercury chloride stock standard solution was prepared at 1,000 mg Hg dm^{-3} by dissolving methylmercury chloride (Merck (Darmstadt, Germany) into 2% HNO$_3$. Mercury chloride stock standard solution was prepared as 1,000 mg Hg dm^{-3} solution by dissolving mercury chloride (Merck (Darmstadt, Germany) into 10% HNO$_3$.

P r o c e d u r e

A 0.075% tetraethylammonium chloride water solution at pH 4.5 (mobile phase A) and a 5% (v/v) methanol-water solution containing 0.06 mol dm^{-3} ammonium acetate and 0.1% (v/v) 2-mercaptoethanol (mobile phase B) were used as the mobile phases for HPLC. The flow rate was 1 ml min^{-1} and the sample injection volume was 100 μl. The columns were connected using three valves to build a column swithching system and species were on-line detected by ICP-MS. The columns outlets were connected directly to the nebulizer of the ICP-MS system.

Elemental detection was performed using a model 4500 ICP-MS system. The plasma and auxiliary argon flow rates were 15 and 1 dm^3 min^{-1}, respectively. The nebulizer gas flow rate was 1.28 dm^3 min^{-1}. The forward RF power was fixed at 1,266 W. The dwell time was 3 seconds per isotope and ^{77}Se, ^{82}Se and ^{202}Hg were monitored.

Table I
HPLC conditions

Time	Mobile phase	Columns
0–5.1	A	RP
5.1–6.15	A	RP + Chiral
6.15–8.3	A	RP
8.3–13.3	A	RP + Chiral
13.3–25	B	RP

RP = Phenomenex Bondclone C18 column,
300 mm × 3.90 mm, 10 μm
Chiral = Astec Chirobiotic T column, 250 mm × 4.6 mm,

In our study of selenium and mercury speciation have been successfully separated six selenium compounds and two major mercury compounds in biological samples using a reversed-phase column. The chiral species of selenium was later separated with the second column.

After the injection in the loop, all species go into the reversed phase column and later directly to the ICP-MS, using the mobile phase A. With this program, SeCM, SeCys, SeMeSeCys and Se (IV) elute before 5.1 minutes. At 5.1 minutes we active the second column, and D-selenomethionine and L-selenomethionine go throught the chiral column. After that, at 6.15 minutes we switch off the chiral column,

then Se (VI) go out from reversed phase column to the ICP-MS. At 8.3 minutes we switch on the chiral column again going out D-Selenomethionine and L-Selenomethionine. At this moment, MeHg and inorganic mercury are still inside the reversed phase column and to get their separation, at 13.3 minutes we disconnect the chiral column again and the mobile phase B is pumped. With this change we get the elution of MeHg and inorganic mercury.

Results

Fig. 1. illustrates the chromatograms obtained with the method proposed and the Table II show the species detected, their retention times, detection limits and linear range. The detection limits vary between 0.3 and 9.7 ng depending of the species. The Relative Standard Deviation (% RSD) for the retention time is below 1 % for all species and for peak area is below 19 % for all species.
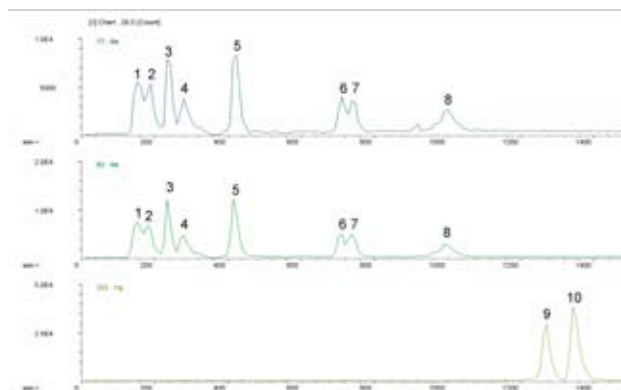
Fig. 1. **Chromatogram obtained by the proposed method for [77]Se, [82]Se and [202]Hg isotopes**

Conclusions

This work reports for the first time an analytical methodology for the chromatographic separation of mercury and selenium species including chiral ones.

The methodology proposed for the simultaneous speciation allows a deeper insight into the interaction between Se and Hg-species which is a key question due to the beneficious effect of Se-species into Hg toxicity.

Table II
Retention times, detection limits and linear range of the species

Peak	Species	Retention time [s]	Detection limit [ng]	Linear range [ppb]
1	Se-cystamine	162.2	6.24	62.4–1,000
2	Se-cystine	189.2	4.03	40.2–500
3	Se-methyl-selenocysteine	243.3	7.78	77.8–1,000
4	Se (IV)	279.3	7.26	72.6–1,000
5	Se (VI)	420.8	6.63	66.3–1,000
6	Se-L-methionine	717.3	9.67	96.7–1,000
7	Se-D-methionine	752.4	4.78	47.8–1,000
8	Peak due to mobile phase change			
9	Methylmercury	1,265.1	4.40	44.0–10,000
10	Inorganic mercury	1,344.4	0.30	3–10,000

The developed methodology allows high sample throughput and low sample consumption that is highly important for the application to food and biological samples.

This method don't has memory effect in the system.

REFERENCES
1. Devi M., Fingerman M.: B Environ. Contam. Tox. *55*, 746 (1995).
2. Drevnick P. E., Roberts A. P., Otter, R. R., Hammerschmidt C. R., Klaper, R., Oris, T.: Comp. Biochem. Phys. C *147*, 331 (2008).
3. Zahir F., Rizwi S. J., Haq S. K., Khan R. H.: Environ. Toxicol. Phar. *20*, 351 (2005).
4. Whanger P. D.: J. Nutr. *119*, 1236 (1989).
5. Weber D. N., Connaughton V. P., Dellinger J. A., Klemer D., Udvadia A., Carvan III M. J.: Physiol. Behav. *93*, 250 (2008).
6. Dos Santos A. P. M., Mateus M. L., Carvalho C. M. L., Batoréu M. C. C.: Toxicol. Lett. *169*, 121 (2007).
7. Wen-Xiong W., Wong R. S. K., Wang J., Yu-fong Y.: Aquat. Toxicol. *68*, 39 (2004).

P53 VOLATILE ORGANIC SUBSTANCES PRESENT IN SPICES AND SPRUCE NEEDLES

LUDMILA MRAVCOVÁ, MILADA VÁVROVÁ, JOSEF ČÁSLAVSKÝ, MICHAELA STOUPALOVÁ, ILONA HLAVÁČKOVÁ and HANA VÍTEČKOVÁ

Brno University of Technology, Faculty of Chemistry, Purkyňova 118, 612 00 Brno,
mravcova@fch.vutbr.cz

Introduction

Essential oils are volatile lipophilic substances, usually colorless. Most often, essential oils consist of terpenes, namely monoterpenic hydrocarbons, aldehydes, alcohols, ketones, acids, esters. Their content substances are usually classified as isoprenoids and phenylpropanoids groups[1]. Their characteristic scent is conditioned by terpenic compounds, in general[2].

The TLC (thin layer chromatography) method can be used for the identification of essential oil present in spice[1]. This method is simple, without need of sofisticated and expensive instrumentation. Defined amount of the analysed mixture is applied on the starting line of a plate covered by a thin layer of sorbent (stationary phase). Chromatographic plate is then placed into the developing chamber with mobile phase, which rises slowly and evenly through the thin layer, transporting the individual components of the analyzed mixture by various speed. Dried thin layer with perceptible stains of particular compounds of the mixture situated in different distances from the start – represents TLC chromatogram. The identification of compounds is performed either via comparison of their migration distances with standards, or by comparison of their R_F values with those obtained from the literature[3].

Another option to identify essential oils is application of SPME (Solid phase microextraction) in connection with GC/MS. Solid phase microextraction is simple and efficient sorptive – desorptive technique used for solventless isolation/ preconcentration of target analytes from the sample matrix[4]. In the field, this procedure could be also used as passive sampling method. During this procedure, analytes are sorbed by thin layer of stationary phase placed on the SPME fiber. The SPME process continues until the equilibrium in the system is reached. In physical-chemical terms, the SPME technique state of equilibrium depends on the analyte properties and on the type and thickness of polymer covering the silica fiber[4].

Experimental

For the identification of essential oils present in spice (caraway, cardamom, pepper, sweet pepper, calamint, cinnamon and muscat), two methods were used[5]:
- TLC
- SPME, GC/MS

T L C

Spice essential oils isolation proceeded in the following manner. Spice samples were extracted by ethanol for 10 minutes. After that, the extract was filtered and the spice was reextracted twice for 20 minutes by petroleum ether. Extracts were concentrated on the vacuum rotary vaporizer to the defined volume.

By means of micropippete, concentrated extracts were applied on the chromatographic plate (Alugram Sil G). The distance of applied stains was between 0.5–1 cm, the volume of applied sample was always 10 μl and 20 μl. Ethanol and petroleum ether extracts I and II were applied on plates.

Plates were developed in a closed chromatographic chamber, which was filled with a developing agent – mobile phase formed by the mixture of toluene and ethyl acetate (ratio 93 : 7). Developing was ascensive and was let in progress until the mobile phase reached the distance of 1 cm from the top of the plate. Plates were let to dry and then they were sprayed by developer for the purpose of visualization of stains created by separated substances. The used developer consisted of ethanol and sulphuric acid (ratio 95 : 5), which was mixed in 1 : 1 ratio with one-percent solution of vanillin in ethanol. After the chemical detection, plates were dried again in the drier at the temperature of 105 °C for 5 minutes. Identification of vizualized stains was performed via comparison of experimental R_F values with those published in the literature[6].

S P M E – G C / M S

Weighted amounts of individual spices (1 g) were put into vials. Substances from spice were sorbed from the headspace by SPME fiber at the temperature of 40 °C. The compounds were then directly injected into the gas chromatograph.

The SPME fiber used was 65 μm polydimethylsiloxan/ divinylbenzene (PDMS/DVB) from Supelco. Gas chromatograph with mass spectrometric detector was Agilent 6890N GC/5973 MSD. The HP-5MS column (Agilent Technologies, USA), 30 m × 0.25 mm × 0.25 μm was used, the injector temperature was 270 °C, oven program was: 45 °C, 2 min, 5 °C to 200 °C, hold 2 min. He at a flow of 1 ml min⁻¹ (constant flow mode) was used as a carrier gas, transferline temperature was 250 °C, ion source temperature was 230 °C, quadrupole temperature was set to 150 °C. Direct interface connection was applied, electron ionization at 70 eV was employed.

Results

TLC chromatograms evaluation was performed in accordance with requirements of the Pharmaceutical Codex[6], which is valid for phytopharmaca and recomends TLC as an optimum screening method. R_F values were calculated for each of detected stains. This factor was also used for the identification. Besides the retention factor, also the colours of the stains were compared. For example, the comparison of all sweet pepper extracts shows Table I. In column "Identified Compound", unambiguously identified content substance

is presented in bold; where no compliance existed, "n.i." is stated, which stands for "not identified". Concerning results, it is evident that not all the content substances were present in all extracts. Mostly, they were detected in the ethanolic extract and in the first petroleum extract and their presence in these two extracts was influenced by the chemical nature of these substances.

Table I
Identification of volatile compounds in sweet pepper extracts

RF Ethanol	RF Petroleum ether I	RF Petroleum ether II	Identified compound
–	0.17	–	pinene
0.23	0.22	–	cymene
0.28	–	–	terpinene
0.38	0.41	0.39	n.i.
0.52	0.65	0.67	n.i.
0.69	0.68	–	n.i.
0.93	–	–	n.i.
0.96	–	–	n.i.
0.99	–	–	n.i.

As the second method of essential oils components analysis, SPME in connection with GC/MS was used. The method was optimalized and measurements were performed under conditions mentioned above. Also by this method, not the concentration of substances, but their identification was the matter of concern. In contrast to TLC, the isolation/pre-concentration of target compounds was performed via head-space method. To confirm the presence of a given substance NIST spectral library search was used. The Fig. 1. shows chromatogram of sweet pepper spice. In Table II is a summary of substances identified via spectral library search in this spice.
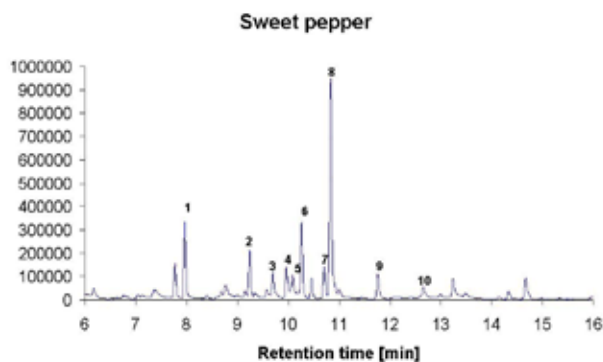
Sweet pepper

Fig. 1. **Chromatogram of sweet pepper**

By comparison of Tables I and II it is obvious, that more single volatile substances and their isomers can be recognised

Table II
Retention times and identification of compounds present in sweet pepper

Peak Number	Retention Time	Identification
1.	7.97	α-pinene
2.	9.24	β-pinene
3.	9.71	β-myrcene
4.	10.09	α-felandrene
5.	10.26	3-karene
6.	10.46	α-terpinene
7.	10.71	p-cymene
8.	10.84	limonene
9.	11.76	γ-terpinene
10.	12.66	4-karene

by means of SPME in connection with GC/MS. Similar comparison could be made at all spices used.

Conclusion

Analytical separation-based methods were used for the identification of content substances present in essential oils of seven spice species. Following results were obtained:
- The isolation of essential oils content substances can be performed by the means of either appropriate solvent extraction, or passive sampling via SPME.
- Screening chromatography method on the thin layer (TLC) is appropriate for the quick identification of content substances in essential oils. This method is also recommended by the Pharmaceutical Codex[6].
- Decisive GC/MS method enabled the identification of more content substances, including some isomers, at all spice and herbal tea samples analysed.

REFERENCES

1. Marsili, R.: *Techniques for Analyzing Food Aroma.* CRC 1996.
2. Podlech, D.: *Kapesní atlas léčivé rostliny*, Slovart 2007.
3. Wager, H., Bladt, S., Zgainski, E. M.: *Plant drug analysis.* Springer – Verlag 1984.
4. Pawliszyn, J.: *Solid Phase Microextraction: Theory and Practice.* Wiley-VCH 1997.
5. Sides, S., Robards, K., Helliwell, S.: Trend.Anal.Chem., *19*, 322 (2000).
6. *Český farmaceutický kodex*. X-EGEM 1993.

P54　CHANGES IN CAROTENOIDS PATTERN IN *MOUGEOTIA SP.* ALGAE INDUCED BY HIGH LIGHT STRESS

EDWARD MUNTEAN, VICTOR BERCEA, NICOLETA MUNTEAN and NICOLAE DRAGOȘ

University of Agricultural Sciences and Veterinary Medicine Cluj-Napoca, 3–5 Calea Mănăştur, 400372 Cluj-Napoca, Romania,
edimuntean@yahoo.com

Introduction

When exposure to light exceeds a maximum that can be used productively by the photosynthesys, a violaxanthin de-epoxidation leads to antheraxanthin and finally to zeaxanthin, the excessive energy being then dissipated as heat[1]. At lower irradiance, zeaxanthin is re-epoxidated back to violaxanthin by zeaxanthin-epoxidase (Fig. 1.).
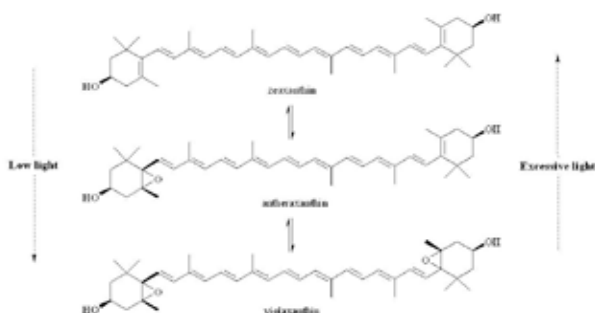
Fig. 1.　**The xanthophyll cycle**

This reversible interconversion of zeaxanthin and violaxanthin via antheraxanthin was called xanthophyll cycle or violaxanthin cycle, being initially studied in higher plants[6,7]; further researches established that it has a photoprotective role, removing the excess excitation energy from the photosynthetic antennae[1-4], protecting in this way photosynthetic organisms from dammage by excessive light. The aim of this research was to establish the way in which the carotenoid biosynthesis is influenced by high light stress in the green algae *Mougeotia sp.* Agardt.

Experimental

The carotenoid standards were kindly provided by F. Hoffmann – La Roche, Basel, Switzerland. All solvents were HPLC grade purity (ROMIL Chemicals). The green algae *Mougeotia sp.* Agardt (AICB 560) originated from the collection of the Institute of Biological Researches Cluj-Napoca; it was grown in a Bold nutritive solution mixed by introducing air containing 5 % CO_2, under continuous illumination (300 $\mu mol\,m^{-2}\,s^{-1}$, measured with a Hansatech Quantum Sensor QSPAR), at an average temperature of 20 °C for 15 days. Extraction and high performance liquid chromatography analysis (HPLC) were conducted according to a previous published procedure[5]. Separations were performed on an Agilent 1100 system, using a Nucleosil 120-5 C_{18} column and the following mobile phases: A – acetonitrile : water (9 : 1) and B – ethyl acetate. The flow rate was 1 ml min^{-1}. and the solvent gradient was as follows: from 0 to 20 min. – 10 % to 70 % B, then from 20 to 30 min. – 70 % to 10 % B. Carotenoids identification was completed based on HPLC co-chromatography with authentic carotenoid standards.

Results

The HPLC chromatogram from Fig. 2.a reveals the carotenoid pattern for the saponified extract of *Mougeotia sp.* control sample, dominated by two major carotenoids: lutein and β-carotene. Besides, four xanthophylls (violaxanthin, lutein, zeaxanthin and 5,6-epoxy-β-carotene) and four carotenes (α-carotene, β-carotene, 9Z-β-carotene and 15Z-β-carotene) were also identified.

When the *Mougeotia* culture was exposed to a high light irradiation (4,500 $\mu mol\,m^{-2}\,s^{-1}$), the content of antheraxanthin increased strongly as a result of de-epoxidation (Fig. 2.b, Table I), the carotenoid pattern being dominated by lutein and antheraxanthin, while among minor carotenoids 5,6-epoxy-β-carotene moved out and zeaxanthin appeared.

Table I
The carotenoid concentrations of target carotenoids [$\mu g\,ml^{-1}$ algal suspension]

Carotenoids	Control sample	Irradiation with 4,500 [$\mu mol\,m^{-2}\,s^{-1}$]	Recovery after irradiation
Violaxanthin	0.02	0.01	0.10
Antheraxanthin	0.10	0.60	0.05
Lutein	1.00	0.56	0.37
Zeaxanthin	0.00	0.05	0.02
5,6-epoxy-β-carotene	0.04	0.00	0.03
α-carotene	0.04	0.01	0.02
β-carotene	0.19	0.03	0.10
9Z – β-carotene	0.04	0.01	0.02
15Z – β-carotene	0.01	traces	0.01

The whole carotenoid pattern was affected by the light stress (Fig. 2.a and 2.b), not only the xanthophylls involved in the xanthophyll cycle. Chromatograms emphasize another important aspect in the studied matrix: the xanthophyll cycle converts violaxanthin mainly in antheraxanthin, not in zeaxanthin; this finding agrees with results reported for *Mantoniella squamata*[3], where they were attributed as consequences for the mechanism of enhanced non-photochemical energy dissipation. The recovery after the light stress leads to a reversible epoxidation to violaxanthin, revealed by the chromatogram from Fig. 2.c, the final higher violaxanthin level being correlated with a strong decrease in antheraxanthin concentration (Fig. 2.c, Table I), while the new chromatographic pattern is dominated by four major carotenoids: lutein, β-carotene, violaxanthin and 5,6-epoxy-β-carotene.
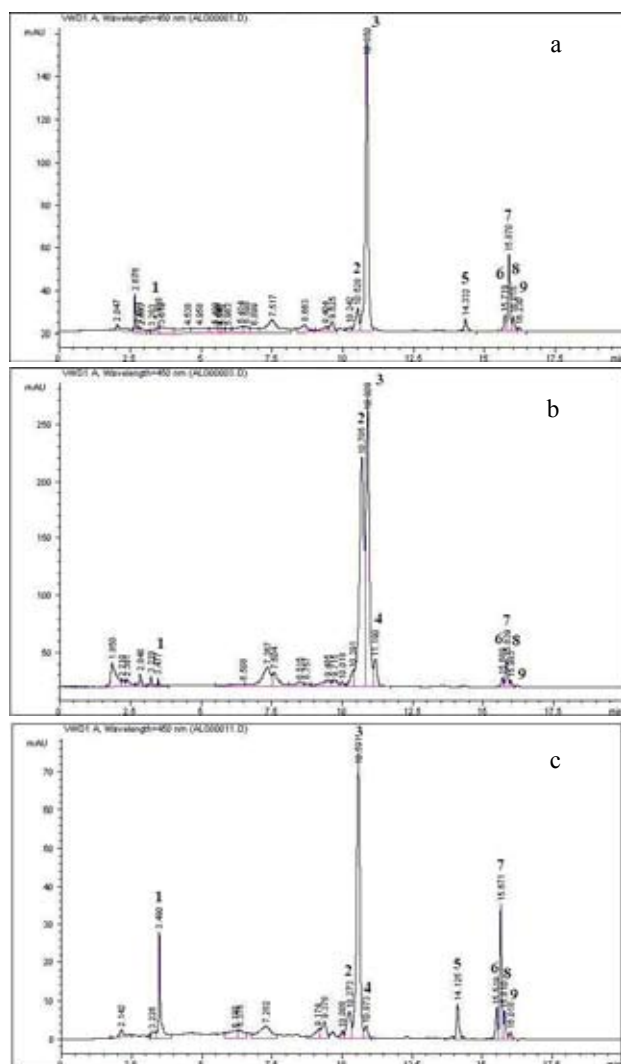
Fig. 2.   **HPLC chromatograms of carotenoids from the Mougeotia sp. samples: a – control sample; b – illumination with 4,500 μmol m⁻² s⁻¹; c – recovery after illumination. Peak identities are: 1: violaxanthin, 2: antheraxanthin, 3: lutein, 4: zeaxanthin, 5: 5,6-epoxy-β-carotene, 6: α-carotene, 7: β-carotene, 8: 9Z – β-carotene, 9: 15Z – β-carotene**

Conclusions

The obtained data reveals the way in which the carotenoid pattern is affected by high light stress in the analyzed algal strain, as well as the way this reacts during the recovery stage.

They proved that the xanthophyll cycle's regulatory mechanism is functional in *Mougeotia sp.* algae, leading to an almost complete interconversion of violaxanthin to antheraxanthin and zeaxanthin. However, its contribution to non-photochemical quenching is not as significant as in higher plants; the small amounts of zeaxanthin recorded during experiments suggesting that this strain posses another dissipation mechanism(s) which operates together with xanthophyll cycle.

Hence, HPLC analysis revealed a particular behavior of *Mougeotia spp.* algae under intense illumination: the major de-epoxidation product of violaxanthin is not zeaxanthin, but antheraxanthin. More than that, the high light stress affects the whole carotenoid biosynthesis, starting with the violaxanthin cycle's precursor: β-carotene.

REFERENCES
1. Darko E., Schoefs B., Lemoine Y.: J. Chromatogr. A. *876*, 111 (2000).
2. Demmig-Adams B.: Trends Plant Sci. *1*, 21 (1996).
3. Goss R., Böhme K., Wilhelm C.: Planta *205*, 613 (1998).
4. Masojídekl J., Kopeckýl J., Koblížek M., Torzillo G.: Plant Biol. *6*, 342 (2004).
5. Muntean E., Bercea V.: Studia Universitatis Babeş-Bolyai, Physica, L, *4b*, 668 (2005).
6. Sapozhnikov D. I., Krasnovskaya T. A., Mayevskaya A. N.: Dok.Acad.Nauk.SSSR, *113*, 465 (1957).
7. Yamamoto H., Nakayama O. M., Chichester C. O.: Arch. Biochem.Biophy. *97*, 168 (1962).

P55   SIMULTANEOUS ION CHROMATOGRAPHIC DETERMINATION OF ANIONS AND CATIONS IN SURFACE WATERS FROM FIZES VALLEY

EDWARD MUNTEAN, TANIA MIHĂIESCU, NICOLETA MUNTEAN and RADU MIHĂIESCU

University of Agricultural Sciences and Veterinary Medicine Cluj-Napoca, 3–5 Calea Mănăştur, 400372 – Cluj-Napoca, Romania,
edimuntean@yahoo.com

Introduction

Water Framework Directive[11] demands a concerted approach in order to achieve a good ecological state for all water bodies across Europe. The objectives agreed must be coordinated beyond the level of individual survey areas and consolidated for the river basin district as a whole.

Fizes catchment, part of Somes catchment tributary of Tisa watershed, is located in Transylvania Plain, in the northern part of Romania. A distinctive feature of this area is the presence of ponds, mainly used for fishery. The major pollution sources are represented by sediments (generated by erosional processes and transported in the water bodies) and diffuse pollution sources (originated from agricultural activities and the improper septic systems of the localities). Fizes catchment, through its features of relatively low antropic pressures and with little structural changes, represents a natural laboratory for designing and implementing programs of restorations of watersheds in agricultural landscapes.

In such a context, chemical analysis is usually employed to identify the aquatic system characteristics including the assessment of inputs, distribution of various chemical species and characterization the outputs generated by the physical, chemical and biological processes developed within the water bodies. Among the specific chemical indicators, the inorganic species hold an important place, determining largely the behavior and evolution of the aquatic system.

The new analytical techniques, generated by the advent of ion chromatography (IC) deliver a more precise measurement of the various inorganic species present in the water body. IC is a high-performance ion-exchange chromatography technique for the separation and quantification of low-molecular-weight ions[1–8], being in use since 1975, from the time of the development of the eluent suppressor[6]. Because of its high accuracy and reliability, IC is nowadays the one of the most powerful tool for analysis of environmental samples[1,5], becoming an important technique for the determination of ionic species for monitoring water quality. This technique was used for the system of fishing ponds, streams and ground waters from Fizes Valley watershed (Fig. 1.), which was studied in order to assess the effects of antropic pollution through leaching of fertilizers from soils and waste waters from the villages within its catchment.

An IC method with conductivity detection was developed, enabling the simultaneous determination of six cations (Li^+, Na^+, K^+, NH_4^+, Mg^{2+} and Ca^{2+}) and seven anions (F^-, Cl^-, Br^-, NO_2^-, NO_3^-, PO_4^{3-} and SO_4^{2-}) in a single run, saving thus analytical time, sample pre-treatment and reagents.

Fig. 1.   **Fizes catchement river network map, with sampling points' locations**

Experimental

Chemicals for mobile phases' preparation were of analytical grade: 4-hidroxybenzoic acid (Acros Organics), lithium hydroxide (Scharlau) and nitric acid (Merck). Ultrapure water with a specific resistance of 18.2 MΩ cm^{-1} was utilized for preparation of mobile phases as well as for sample dilution, being obtained from a Direct Q 3UV Smart (Millipore). All solutions were stored in polyethylene bottles which had been thoroughly rinsed with ultrapure water. Mobile phases were filtered through a 0.45 μm membrane (Millipore), and then degassed using an Elmasonic S30 H ultrasonic bath before use. Standard working calibration solutions were prepared from a "six cation standard-II" (Dionex Corporation) and from "seven cation standard-II" (Dionex Corporation). The external standard method was used for quantification.

Water samples were collected from seven sources located in Fizes watershed; samples were passed through a 0.45 μm membrane filter (Millipore), and then were stored for 24 hours at 4 °C in 0.5 dm^3 polyethylene containers[9,10], each sample was analyzed in triplicates. The samples with ion concentrations exceeding the calibration range were diluted accordingly and re-analyzed.

Analyses were performed on a Shimadzu system, consisting from: a Proeminence DGU 20As online degasser, a Proeminence LC-20AP solvent delivery module, an automatic sample injector SIL-10AF, a conductivity detector CDD-10Avp, a Proeminence CTO-20A column oven, a FCV-10AH$_2$ valve unit, an Allsep Anion 7u column (150×4.6 mm), an Universal Cation 7u (100×4.6 mm) and a Proeminence CBM-20A system controller in a configuration which is represented schematically in Fig. 2. Instrument control, data acquisition and data analysis were accomplished by a computer running "LCsolution" ver.1.2. software.

300 μl samples were injected in each case; using a temperature of 40 °C, a total separation of 23 min. was effective for a good resolution for all seven anions from the mixed
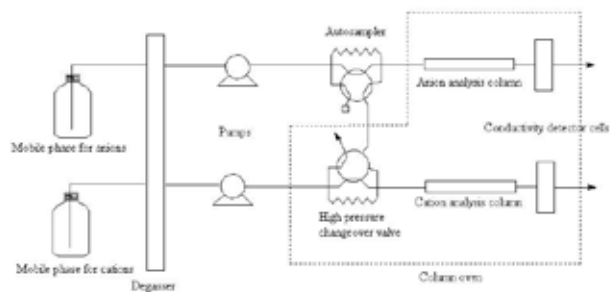
Fig. 2. **Schematic representation of the IC system configuration used for simultaneous analysis of cations and anions**

standard solution (fluoride, chloride, nitrite, bromide, nitrate, phosphate and sulphate – Fig. 3.) and for all six cations (lithium, sodium, ammonium, potassium, magnesium and calcium – Fig. 4.), all peaks being baseline separated.
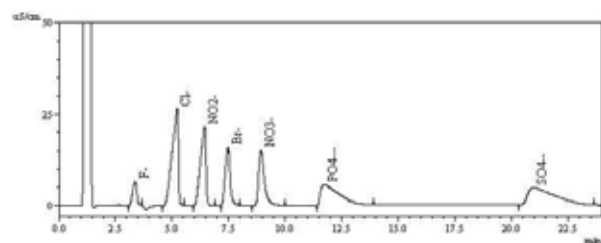
Fig. 3. **Separation for a standard mixture of anions (Allsep Anion 7u column, using as mobile phase a 4-hidroxybenzoic acid 4mM solution with pH-ul adjusted to 7.5 with LiOH 0.1M, the flow rate being 0.85 ml min⁻¹)**
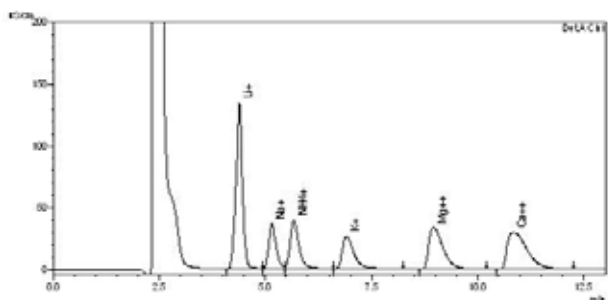
Fig. 4. **Separation for a standard mixture of cations (Universal Cation 7u column, using as mobile phase a 3 mM HNO3 solution, the flow rate being 0.5 ml min⁻¹)**

A LGC certified reference material (LGC6020, SPS ww2) was used for validation.

Results

Calibrations were achieved using five levels of concentration, for accurately determine the concentration of target ions. The calibration curves show a good linearity with $R > 0.99$ as indicated in Table I, Figs. 5. and 6.

Table I
Results of regression analysis for calibrations

Anion	Linearity range [ppm]	Regression equation	R
F^-	4.02–20.10	$C = 0.000130278A + 0.83973$	0.9978
Cl^-	20.40–102.00	$C = 0.000117938A - 0.523926$	0.9997
NO_2^-	20.20–101.00	$C = 0.000156194A + 0.11461$	0.9997
Br^-	20.00–100.00	$C = 0.000230581A + 1.34467$	0.9995
NO_3^-	20.00–100.00	$C = 0.000214872A + 0.28929$	0.9999
PO_4^{3-}	40.00–200.00	$C = 0.00023591A - 0.68846$	0.9994
SO_4^{2-}	9.94–79.52	$C = 0.0001677A - 1.1364$	0.9994
Li^+	0.99–4.99	$C = 0.00000262A - 0.7806$	0.9993
Na^+	4.06–20.30	$C = 0.000015644A - 2.12366$	0.9997
NH_4^+	10.30–50.60	$C = 0.000015822A + 1.04561$	0.9999
K^+	5.02–25.10	$C = 0.000000898A + 0.62187$	0.9997
Ca^{2+}	5.04–25.20	$C = 0.000000475A + 0.41618$	0.9998
Mg^{2+}	10.18–50.90	$C = 0.000011512A + 1.09553$	0.9998
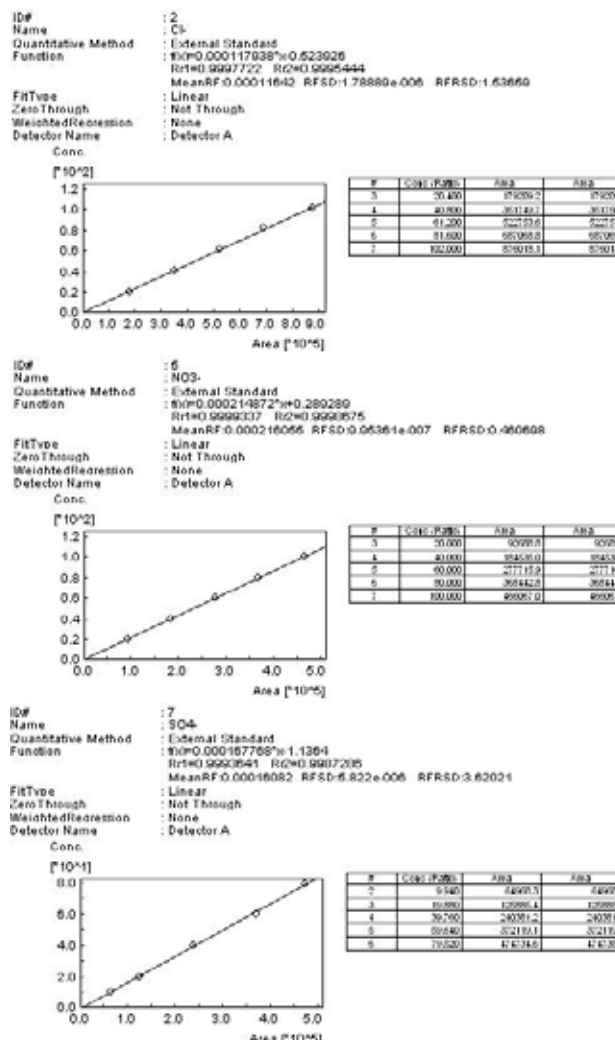
Fig. 5. **Calibrations for the reported anions**

ID# : 9
Name : Na+
Quantitative Method : External Standard
Function : f(x)=1.56448e-005*x+2.12366
Rr1=0.9997851 R2=0.9995702
MeanRF:1.28137e-005 RFSD:1.48142e-006 RFRSD:11.5612
FitType : Linear
ZeroThrough : Not Through
WeightedRegression : None
Detector Name : Detector A

ID# : 10
Name : NH4+
Quantitative Method : External Standard
Function : f(x)=1.5022e-005*x+1.04561
Rr1=0.9999162 R2=0.9998354
MeanRF:1.55908e-005 RFSD:4.74992e-007 RFRSD:2.86298
FitType : Linear
ZeroThrough : Not Through
WeightedRegression : None
Detector Name : Detector A

ID# : 11
Name : K+
Quantitative Method : External Standard
Function : f(x)=9.98236e-006*x+0.621866
Rr1=0.9997949 R2=0.9994899
MeanRF:9.48513e-006 RFSD:2.70407e-007 RFRSD:2.85087
FitType : Linear
ZeroThrough : Not Through
WeightedRegression : None
Detector Name : Detector A

ID# : 12
Name : Mg++
Quantitative Method : External Standard
Function : f(x)=1.15119e-005*x+1.09553
Rr1=0.9997815 R2=0.9995230
MeanRF:1.20631e-005 RFSD:2.8424e-007 RFRSD:2.35628
FitType : Linear
ZeroThrough : Not Through
WeightedRegression : None
Detector Name : Detector A

ID# : 13
Name : Ca++
Quantitative Method : External Standard
Function : f(x)=4.75257e-006*x+0.416179
Rr1=0.9990905 R2=0.9997811
MeanRF:4.92053e-006 RFSD:9.23013e-008 RFRSD:1.87350
FitType : Linear
ZeroThrough : Not Through
WeightedRegression : None
Detector Name : Detector A

Fig. 6.　**Calibrations for the reported cations**

From the 13 quantifiable ions, only eight were found in the analyzed water samples: Na^+, K^+, NH_4^+, Mg^{2+}, Ca^{2+}, Cl^-, NO_3^-, PO_4^{3-} and SO_4^{2-}, within a concentration range of 6.64 ppm (for K^+) to 346.27 ppm (for SO_4^{2-}). Calibrations for these ions are presented in figures 5 and 6.

Table II provides information on the anion concentration while Table III reveals the cation concentration from the investigated surface waters.

Table III
The anions' concentrations in the studied water sources (mean values ± SD)

Location	Cl^- [ppm]	NO_3^- [ppm]	SO_4^{2-} [ppm]
Draw well near Tăul Popii lake	66.99 ± 3.29	79.97 ± 3.97	343.28 ± 17.14
Spring near Tăul Popii lake	27.53 ± 1.39	–	141.17 ± 7.03
Cătina lake	66.54 ± 3.37	25.63 ± 1.21	346.27 ± 17.31
Geaca lake	57.21 ± 2.81	23.69 ± 1.15	264.03 ± 13.29
Ţaga lake	94.11 ± 4.70	23.02 ± 0.93	279.85 ± 13.85
Ştiucii lake	60.28 ± 2.96	–	63.69 ± 2.91
Fizeş river	191.53 ± 9.46	–	254.32 ± 12.62

The higher nitrate concentration in the draw well is due to the fact that a relatively high nitrate concentration is a general characteristic for underground water resources in Fizes catchment; this catchment has substantial diffusion pollution sources originated by manure and animal breeding. The chloride concentration ranges from 27.53 ppm (in a spring located near Tăul Popii lake) to 191.53 ppm (Fizes river), possible to explain due to the geological substrate of the area, salt being present as outcrops in the lower part of the catchment. The sulfate concentration was high in all samples, ranging from 63.69 ppm (in Stiucii lake) to 347.26 ppm (in Cătina lake).

All the concentration values are consistent with the general geological composition of the area. Slightly different values measured in different points of water surface sampling points in the same collector (Fizes valley) stream could be explained as consequence of normal variation due to different water contact duration among the watershed, during precipitation events.

Conclusions

This research revealed the state of the water quality and also clarified some aspects related to the process of self purifications of the water system in the considered area. The upstream ponds retain most of the sediment and pollutants through mechanisms of sedimentation and self-purification, most of the pollution sources being also located in the upper part of the catchment.

Data gathered will serve as beneficial experience for future rehabilitation measures. Using the proposed IC configuration, the laboratory productivity increases much, as there is no longer necessary to prepare two sample sets – one for

Table III
The cations' concentrations in the studied water sources (mean values ± SD)

Location	Na$^+$ [ppm]	NH$_4^-$ [ppm]	K$^+$ [ppm]	Mg^{2+} [ppm]	Ca^{2+} [ppm]
Draw well near Tăul Popii lake	121.60 ± 6.03	15.28 ± 0.73	20.96 ± 1.03	108.05 ± 5.33	76.17 ± 3.80
Spring near Tăul Popii lake	25.93 ± 1.26	12.02 ± 0.51	6.64 ± 0.30	69.27 ± 3.42	65.43 ± 3.25
Cătina lake	168.31 ± 8.41	12.31 ± 0.44	15.54 ± 0.72	156.96 ± 7.79	76.27 ± 3.73
Geaca lake	158.05 ± 7.84	14.62 ± 0.70	17.52 ± 0.86	151.21 ± 7.53	71.25 ± 3.48
Ţaga lake	103.47 ± 5.15	13.03 ± 0.63	19.15 ± 0.94	104.22 ± 5.19	54.07 ± 2.65
Ştiucii lake	28.79 ± 1.40	12.65 ± 0.59	18.43 ± 0.90	18.80 ± 0.93	9.10 ± 0.41
Fizeş river	275.94 ± 13.78	11.11 ± 0.36	15.52 ± 0.74	142.90 ± 7.17	74.97 ± 3.74

anion analysis, the other for cation analysis. With one injection, the autosampler introduces the sample in both analysis channels. The method has potential to be used in water quality surveys in the purpose of correlating diffuse pollution inputs with changes in water quality. Specific self purification processes can also be operatively estimated.

REFERENCES
1. Cickarik D., Dersek-Timotic I., Onjia A., Rajakovic I.: J. Serb. Chem. Soc. *70*, 995, (2005).
2. Gjerde D. T., Fritz J. S., Schmuckler G.: J. Chromatogr. *187*, 35 (1980).
3. Gjerde D. T., Fritz J. S.: *Ion Chromatography*. Hüthig, Heidelberg, 2000.
4. Helaleh M. I. H., Al-Omair A., Tanaka K., Mori M.: Acta Chromatogr. *15*, 247, (2005).
5. Shpigun O. A., Zolotov Y: *A. Ion Chromatography in Water Analysis*. West Sussex, England, Ellis Horwood Ltd., 1988.
6. Small H., Stevens T. S., Bauman W. C.: Anal. Chem. *47*, 1801 (1975).
7. Smith F. C., Chang R. C.: *The practice of ion-chromatography*. Wiley, 1984.
8. Weiss J.: *Ion Chromatography*, VCH, Weinheim, 1995.
9. ISO 5667-1: 1980: Water quality – sampling, part 1: guidance on the design of sampling programmes.
10. ISO 5667-2: 1991: Water quality – sampling – part 2: guidance on sampling techniques.
11. Directive 2000/60/EC of the European Parliament and of the Council of 23.11.2000 establishing a framework for Community action in the field of water policy.

P56 STRATEGIES TO REDUCE DETECTION LIMITS IN THE ANALYSIS OF BROMINATED FLAME RETARDANTS IN ENVIRONMENTAL SAMPLES

MICHAELA NÁPRAVNÍKOVÁ, JANA PULKRABOVÁ, PETRA HRÁDKOVÁ, JAKUB SCHŮREK, JAN POUSTKA and JANA HAJŠLOVÁ

Institute of Chemical Technology, Prague, Department of Food Chemistry and Analysis, Technická 3, 166 28 Prague 6, Czech Republic,
michaela.napravnikova@vscht.cz

Introduction

Polybrominated diphenyl ethers (PBDEs) represent an important class of brominated flame retardants (BFRs) which are widely used in various consumer products such as electronic equipment, textiles and plastics[1]. These chemicals are highly persistent and bioaccumulative what leads to their ubiquitous occurrence in the environment[2], both in abiotic and biotic matrices.

Compared to major group of organohalogenated persistent organic pollutants (POPs) such as polychlorinated biphenyls (PCBs), the levels of PBDEs in respective environmental compartments are typically lower by one order of magnitude. On this account, low detection limits (LODs) are needed for their reliable control.

Gas chromatography coupled to mass spectrometry (GC/MS) operated in either electron ionization mode (EI) or in negative chemical ionization (NCI) are commonly employed analytical procedures of determination these compounds[3]. In NCI mode monitoring of abundant bromine ions (m/z 79 and 81) provides a more sensitive and selective option compared to EI. Nowadays, comprehensive two-dimensional (orthogonal) gas chromatography coupled to time-of-flight mass spectrometry (GC×GC/TOFMS) has become another challenging alternative to analyze very complex PBDEs mixtures[4].

In any case, achieving low LODs is also associated with the amount of sample introduced into GC system. The most commonly used GC injection technique for PBDEs is a splitless injection mode[3], however, several studies were reported a possibility to employ a large-volume programmed-temperature vaporizer injection (PTV) in the determination of these compounds[5].

This paper presents the method performance characteristics obtained in several GC systems used for quantification of PBDEs.

Experimental

For our experiments a standard mixture of most common PBDE congeners (BDEs No. 28, 47, 49, 66, 85, 99, 100, 153, 154 and 183) purchased from AccuStandard inc. (USA) was used. The real-life sample containing trace amount of PBDEs was a purified extract obtained from fish tissue by procedure described by Hajšlová et al.[6]. To assess LODs achievable under various GC conditions following set-up were tested:
- PTV-GC/MS (EI),
- PTV-GC/MS (NCI),
- GC/TOFMS (EI),
- PTV-GC/TOFMS (EI).

PTV-GC/MS (EI) and PTV-GC/MS (NCI)

GC/MS analyses were performed on an Agilent 6890N gas chromatograph coupled to a mass selective detector (Agilent 5975XL Inert MSD) equipped with quadrupole analyzer operated in NCI or EI mode using splitless or PTV injection. The GC conditions were as follows: a DB-XLB capillary column (15 m × 250 μm i.d. × 0.1 μm, J&W Scientific); a oven temperature program: from 105 °C (held for vent time) to 260 °C (held for 1 min) at 50 °C min^{-1} then to 300 °C at 20 °C min^{-1} and held for 3 min; carrier gas: helium with constant flow 1.5 ml min^{-1}. The MS was operating in the selected ion monitoring (SIM) mode (monitored ions were m/z 79, 81, 159, 161 and m/z 406, 484, 564, 484, 562 for NCI and EI mode, respectively). The MS (NCI) parameters were as follows: reagent gas: methane; temperatures of MSD interface, ion source, and quadrupole: 280 °C, 150 °C, and 150 °C, respectively. The temperatures of MSD interface, ion source and, quadrupole for MS (EI) system were 280 °C, 230 °C and, 150 °C, respectively.

Four parameters for PTV injection were tested: vent time (*VT*), vent flow (*VF*), injection volume (*IV*) and splitless period. Starting injection temperature was 50 °C (held 4.6 min) and it was ramped to 350 °C at 500 °C min^{-1}.

GC/TOFMS and PTV-GC/TOFMS

The analyses were performed on a Pegasus 4D instrument (Leco, USA) consisting of an Agilent 6890N gas chromatograph equipped with splitless and/or PTV injector and a Leco Pegasus III high-speed time-of-flight mass spectrometer.

The same, DB-XLB capillary column was used for determination of analytes. The GC conditions were similar to PTV–GC/MS system. The interface temperature was 280 °C. The MS acquisition rate was 11 Hz, the mass range 35–850 amu, the ion-source temperature 300 °C, and the detector potential −1875 V.

Results

In the first part of this study, the implementation and optimalization of a PTV injection coupled with GC/MS (EI and/or NCI mode) was realized. A solvent standard solution of above mentioned PBDE congeners was used for optimalization PTV injection conditions. Optimal parameters assessed by the comparison of a peak height of individual analytes were as follows:
- vent time: 90 s
- vent flow: 60 ml min^{-1}

Table I
LODs of individual PBDE congeners [ng ml^{-1} isooctane] for the GC/MS techniques tested

Analyte	GC/MS (EI) (splitless)	GC/MS (NCI) (splitless)	PTV–GC/MS (EI)	PTV–GC/MS (NCI)	GC/TOFMS (EI)	PTV–GC/TOFMS
BDE 28	1.0	0.05	0.1	0.01	2.3	0.3
BDE 47	1.0	0.1	0.1	0.01	3.1	0.6
BDE 49	1.0	0.1	0.1	0.01	2.5	0.4
BDE 66	1.0	0.1	0.1	0.01	3.7	0.6
BDE 85	2.0	0.2	0.3	0.01	1.3	0.7
BDE 99	1.5	0.1	0.3	0.01	3.0	0.4
BDE 100	1.5	0.1	0.1	0.01	0.6	0.6
BDE 153	5.0	0.1	0.6	0.02	3.2	0.9
BDE 154	3.5	0.1	0.3	0.02	2.5	0.7
BDE 183	3.0	0.2	0.2	0.06	7.1	1.5

- injection volume: multiple injection 2×10 µl
- splitless period: 2 min.

The repeatability of the PTV–GC/MS injection, expressed as a relative standard deviation (RSD, n = 10) ranged from 3.8 to 6.3 % and 3.8 to 10.3 % for NCI and EI mode, respectively. Similar RSD values for multiple injections were obtained (3.8–9.2 % and 1.7–10.8 % for NCI and EI mode, resp.) were determined for spiked fish lipid extract (1 ng g^{-1} lipid weight).

LODs calculated as a quantity of analyte that generates a response 3-time higher than the noise level of the detection system (based on the injection of solvent standard solution mixture) are summarized in Table I. LOQs were the minimum concentrations of analytes that was possible to quantify with acceptable accuracy and precision. Under these conditions, the LOQ was the lowest calibration level and corresponded for particular analyte to $3 \times$ LOD. Generally, in NCI mode, significantly lower LODs were obtained compared to EI mode. On the other hand, the identification of individual PBDEs was only based on their retention times. PBDEs are eluted in order of increasing bromine number and intensity

of appropriate responses was obtained in following order in case of GC/MS (NCI) system: BDE 28 > BDE 49 ~ BDE 47 ~ BDE 66 ~ BDE 100 > BDE 99 ~ BDE 85 ~ BDE 154 ~ BDE 153 > BDE 183 (see Fig. 1.). Similar chromatogram obtained by PTV-GC/TOFMS (EI) is documented in Fig. 2.
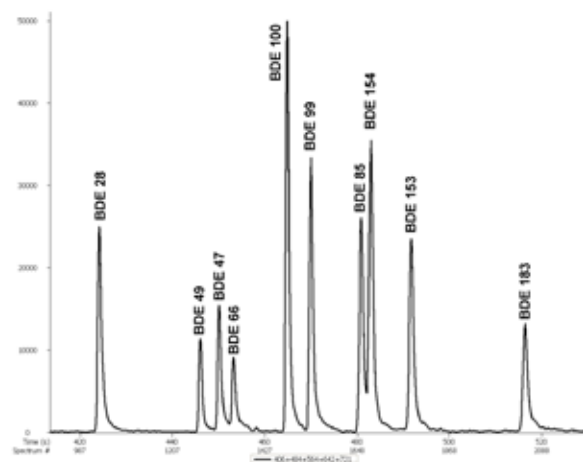
Fig. 2. **Chromatogram of mixed standard of PBDEs obtained by PTV–GC/TOFMS (EI)**

Table I shows a significant reduction of LODs by almost one order of magnitude (to values 0.01–0.06 ng ml^{-1} by the use of PTV which allowed introduction of 1–250 µl of sample (only 1–5 µl were injected by pulsed splitless).

PTV–GC/TOFMS provide LODs similar to PTV–GC/MS (EI) and values were ranged from 0.3 to 1.5 ng ml^{-1}. The main advantage of this technique is availability of full mass spectral information for all sample components, i.e. confirmation of target analytes.

Conclusions

In the present work, LODs of individual PBDE congeners were reduced using various GC systems in analysis of these analytes in various matrices such as environmental samples (fish muscle, sediment etc.). Four different injection

Fig. 1. **Chromatogram of mixed standard of PBDEs obtained by GC/MS (NCI)**

techniques, three of them employing PTV, were tested in our study.

- Generaly, the NCI mode provided signifficantyl lower LODs compared with EI mode coupled to all tested GC/MS system.
- The lowest LODs were obtained by GC/MS coupled to the PTV injection operated in NCI mode, under these conditions large quantity of analytes without solvent (due to PTV injection) and high selectivity for bromine ions (due to MS-NCI mode) could be performed.
- PTV-GC/TOFMS employing splitless injection provided similar results in comparison with GC/MS (NCI) using splitless injection.

REFERENCES

1. Čajka T., Hajšlová J., Kazda R., Poustka J.: J.Sep.Sci. *28*, 601 (2005).
2. Mariani G., Canuti E., Castro-Jiménez J., Christoph E. H., Eisenreich S. J., Hanke G., Skejo *H*., Umlauf G.: Chemosphere (2008)*, in press.*
3. Covaci A., Voorspoels S., de Boer J.: Environ. Int. *29*, 735 (2003).
4. Dallüge J., Beens J., Brinkman U. A. Th.: J. Chromatogr. A. *1000*, 69 (2003).
5. Tollbäck P., Björklund J., Östman C.: J. Chromatogr. A 991, 241 (2003).
6. Hajšlová J., Pulkrabová J., Poustka J., Čajka T., Randák T.: Chemosphere *69*, 1195 (2007).

P58　SIMULTANEOUS DETERMINATION OF MERCURY, LEAD AND CADMIUM IN AQUEOUS SAMPLES USING PECTIC ACID-MODIFIED CARBON PASTE ELECTRODE

JOSE H. SANTOS and SEAN GERARD WARD

Department of Chemistry, University of Brunei Darussalam, Tungku Link, Gadong BE1410, Brunei Darussalam, joey@fos.ubd.edu.bn

Introduction

Anodic stripping voltammetry (ASV) and its variants are the most sensitive electroanalytical techniques employed for trace heavy metal analysis. Mercury electrodes have been widely used for ASV due to their ease of use and compatibility with a number of heavy metal species. Recently, however, there are major concerns regarding the use of mercury in the laboratory because of hazards it poses to humans and other living organisms. Prompted by environmental issues, some of the applications of modified carbon paste electrodes (CPE) are aimed at the development of mercury-free electrodes for ASV[1]. In this paper, we investigated the use of pectic acid as a modifier for CPE and its utilization for the analysis of some representative heavy metal species.

Pectic acid, also known as polygalacturonic acid, is a natural polymer found in citrus rinds. It consists of chains of 300 to 1000 units of galacturonic acid monomer joined with $\alpha 1 \rightarrow 4$ linkages. When incorporated in a CPE, the exposed carboxylic acid groups are responsible for the accumulation of heavy metal ions on the electrode surface presumably through ion-exchange or complex-formation processes.

The aim of this study is to fabricate pectic acid-modified CPE and examine various experimental conditions that affect the analytical signal when used as a working electrode for the ASV of mercury, lead and cadmium in aqueous samples.

Experimental

Pectic acid isolated from orange peel was obtained from Fluka and used without further purification. Mineral oil, graphite powder were purchased from Sigma-Aldrich while 1,000-ppm standard solutions of Hg (II), Pb (II) and Cd (II) were from Sharlau (Spain). All other chemicals used were at least AR grade.

All electrochemical experiments were carried out using a BAS 100B Electrochemical System (BioAnalytical System) in the Osteryoung square wave stripping voltammetry mode (OSWSV) or cyclic voltammetry (CV) utilizing Ag/AgCl reference electrode and a Pt wire counter electrode.

Modified carbon paste was prepared by thoroughly mixing 4:1 (w/w) ratio of graphite powder to powdered pectic acid and enough mineral oil to form a paste typical for conventional CPEs. A portion of prepared paste was then tightly packed on the cavity (2-mm dia.) of previously cut 200-ml pipette tip where a copper rod was inserted on the other end to establish electrical contact.

The modified CPE was first immersed in a sample solution containing the heavy metal ion being analyzed. After a predetermined period of time, referred to as accumulation time, the electrode was removed from the sample and rinsed thoroughly with water. The electrode was then transferred into a voltammetric cell containing deoxygenated 0.1M HCl for ASV. The accumulated metals were first reduced by applying a sufficiently negative potential of –800 mV for 60 s, then re-oxidized while anodically scanning the potential. The peak-type *I-E* plots resulting from the anodic scan were recorded and evaluated.

Results and Discussion

P r e l i m i n a r y　S t u d i e s

Cyclic voltammetric experiments revealed that pectic acid-modified CPE possesses a useful potential window ranging from –900 mV to 1200 mV relative to the Ag/AgCl reference electrode when the supporting electrolyte used was deoxygenated 0.1M HCl. Preliminary investigations also showed that Cd, Pb and Hg undergoes redox transformations at about –690, –470 and +100 mV, respectively, using the above CPE and electrolyte combination. In principle, these metal species may be simultaneously detected and conveniently analyzed with well resolved analytical peaks using the modified CPE.

I n d i v i d u a l　A n a l y s i s

Results of ASV experiments using laboratory prepared solutions containing a single metal species are consistent with the literature[2,3]. For all the three heavy metal species, as the concentration increases or the accumulation time is prolonged, the peak current also increases in a linear fashion until such an instance where current signal plateaus and further increase in concentration or accumulation time does not anymore amplify the peak height. This is due to the fact that the higher the concentration or the longer the electrode is immersed into the solution containing the analyte; more metal ions are able to accumulate on the surface, which consequently provides a higher current. Saturation point is attained when the active sites for metal accumulation are maximized resulting to levelling of current response. Using an accumulation time of 2 min and other parameters described in the experimental section, the sensitivities and detection limits are reported in Table I. Sensitivities were calculated from the slopes of individual calibration curves within the linear dynamic range while detection limits (LOD) were estimated based on three times the standard deviation of the blank. Further

Table I
Analytical data for pectic acid-modified CPE

Metal	Sensitivity [$\mu A\,ppm^{-1}$]	LOD [ppm]	LOL [ppm]
cadmium	20	0.25	20
lead	50	0.15	50
mercury	10	0.40	50

improvements in LOD and limits of linearity (LOL) were observed upon increasing or decreasing the accumulation time, respectively.
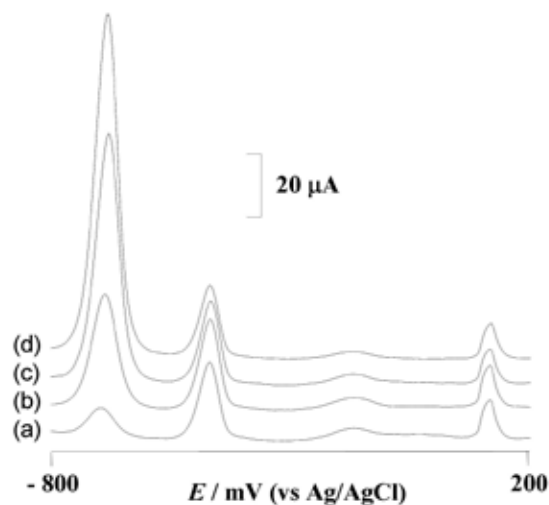
Fig. 1.   **ASV for solutions containing 1 ppm Pb, 3 ppm Hg and varying Cd: (a) 1, (b) 3, (c) 5, (d) 10 ppm**
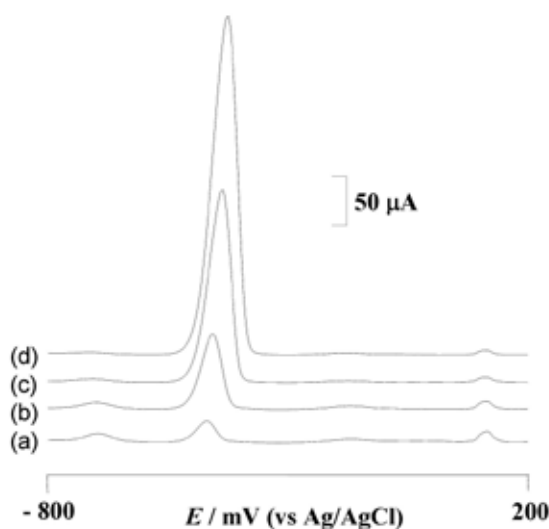
Fig. 2.   **ASV for solutions containing 1 ppm Cd, 3 ppm Hg and varying Pb: (a) 1, (b) 3, (c) 5, (d) 10 ppm**
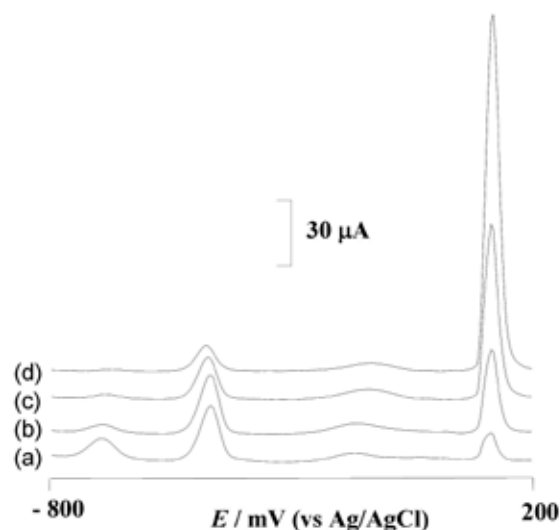
Fig. 3.   **ASV for solutions containing 1 ppm Cd, 1 ppm Pb and varying Hg: (a) 3, (b) 5, (c) 10, (d) 20 ppm**

S i m u l t a n e o u s   A n a l y s i s

When two or three metals studied in this project are present in the same solution, well resolved peaks with characteristic potentials corresponding to specific metal species are observed as shown in Figs. 1., 2. and 3.

Although linearity between peak height and concentration is maintained, careful inspection of individual peaks revealed that sensitivity decreases when the three metal ions co-exist. Moreover, as the concentration of one metal increases, the current signal for the other two decreases. This is presumably due to competition for binding sites among the metal ions and their varying affinities to carboxylate groups in pectic acid.

REFERENCES
1. Wang J.: Electroanalysis *3*, 255 (1991).
2. Yantasee W., Lin Y., Fryxell G. E., Busche B. J.: Anal. Chim. Acta *502*, 207 (2004).
3. Ghiaci M., Rezaei B., Kalbasi R. J.: Talanta *73*, 37 (2007).

P59   DETECTION OF FOREIGN ORGANIC SUBSTANCES IN WATER AND BIOLOGICAL SAMPLES

E. SAVELIEVA, N. KORYAGINA, N. KHLEBNIKOVA,
N. GONCHAROV and A. RADILOV

*Research Institute of Hygiene, Occupational Pathology and
Human Ecology, Saint-Petersburg, Russia,*
esavelieva59@mail.ru

Introduction

The chemical analysis of biomedical samples (bodily fluids, tissues) aimed at revealing exposure to toxic chemicals (TCs) can be directed to the following targets:

(i) TCs themselves, when their metabolism is slow enough,

(ii) Low-molecular metabolites of TCs,

(iii) High-molecular adducts of TCs with proteins.

Right choice of target (marker) with account for the life cycle of a TC (adsorption–distribution – metabolism – excretion) predetermines success of analysis. The targets *(i)* and *(ii)* are more convenient to determine by conventional GC-MS methods but are unsuitable for retrospective analysis in view of their short life time in the organism. We developed procedures for the determination in biomedical samples of all the three groups of biomarkers of TCs.

Results and Discussion

Direct analysis of a TC in biomedical samples was considered to be a rational approach in toxicokinetic research on fluoroacetic acid, one of the most potent metabolic poisons (FAA). Salts of FAA are still used in some countries for rodent population control; deadly poisoning of humans and farm animals was also described. At our laboratory, procedures for the determination of O-alkyl esters of methylphosphonic acid (low-molecular metabolites of organophosphorus warfare agents, OPWAs) and thiodiglycol (metabolite of sulfur mustard) were also developed. These metabolites are products of both biogenic and abiogenic hydrolysis of the parent agents, and, therefore, their determination in environmental samples is actual for retrospective analysis aimed at establishing the fact and degree of environmental pollution with the corresponding agents. Of particular importance for forensic analysis are universal procedures suitable both for water and for biological fluids. We developed universal procedures for the determination of FAA, methylphosphonic acid (MPA), ethyl MPA (marker of VX), isopropyl MPA (marker of sarin), isobutyl MPA (marker of Russian VX), pinacolyl MPA (soman marker), and thiodiglycol in water, urine, and blood plasma.

For retrospective establishment of exposure to TCs, procedures for the determination of reactivation products of blood plasma butyryl cholinesterase (BChE) inhibited by OPWAs and of thiodiglycol isolated by alkaline hydrolysis from albumin adducts. These procedures all are based on GC/MS combined with solid-phase microextraction (SPME).

Solid-phase microextraction is a unique method that allows one to combine on a single stage extraction from a matrix, concentration, and injection of a sample. SPME offers a great advantage of analyzing the whole sample rather than its aliquot, and, therefore, is more than about an order of magnitude more sensitive compared with traditional separation and concentration methods. SPME poses no threat of contamination of a GCMS system by matrix components. Of key importance for successful SPME analysis is right choice of microfiber, conditions for sorption (temperature, time, sample mixing mode, ionic strength of analyzed solution) and desorption (temperature, delay time).

Therefore, in developing an SPME procedure, one should optimize the following parameters:
- Type of microfiber
- Sorption and thermodesorption temperatures of target analytes
- Sorption and thermodesorption times
- Ionic strength of the solution.

Before GC/MS analysis nonvolatile target compounds were derivatized either in situ with subsequent concentration of the volatile derivative on microfiber (analysis for FAA) or directly on microfiber with vapors of derivatizing agents (analysis for MPA and its O-alkyl esters).

In what follows we schematically represent certain of the mentioned procedures. Fig. 1. shows the block scheme of the determination of sodium fluoroacetate in various media. In view of the fact that the volatile derivative, ethyl fluoroacetate, is sampled from equilibrium vapor, the sample matrix scarcely affects the results of analysis. The developed procedure is universal and can be applied both for control of drinking water and for toxicokinetic and forensic investigations.
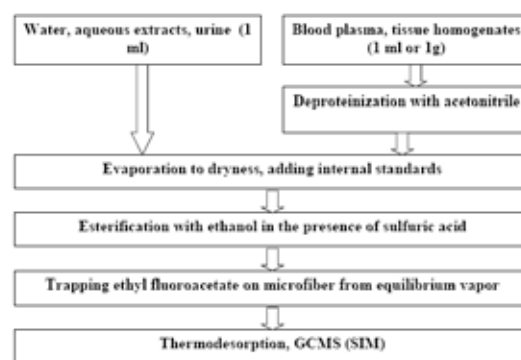
Fig. 1.   **Block scheme of the unified procedure for the determination of sodium fluoroacetate in water and biomedical samples by SPME-GCMS**

The detection limits are 0.001 mg ml^{-1} for drinking and natural waters, 0.01 mg ml^{-1} for blood plasma, and 0.01 mg ml^{-1} for organ homogenates (without recounting for dry weigh). The procedure is described in detail in ref.[1].

For the determination of the low-molecular metabolites of organophosphorus warfare agents, MPA and its alkyl

esters, in urine we suggested a procedure involving extraction of the analytes on microfiber, their silylation with *N*-tert-butyldimethylsilyl-*N*-methyltrifluoroacetamide (MTBSTFA) directly on microfiber, thermodesorption of the resulting derivatives in a hot GC injector, GC separation, and MS detection in the SIM mode. Three types of microfibers of various polarities were tested: 50/30 μm DVB/Carboxen/PDMS, 85 μm Carboxen/PDMS, and 70 μm Carbowax/DVB (Fig. 1.). The best results were obtained on the first microfiber.

Unlike certain related techniques, SPME provides a unique possibility for experimenting with various types of microfibers differing from each other in chemical nature and micropore size. Development of an SPME procedure always begins with searching for an optimal microfiber. This process is illustrated in Fig. 2.
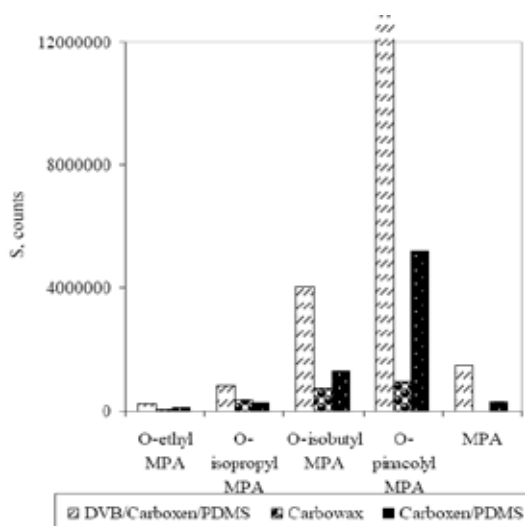
Fig. 2.　**Efficiency of various microfibers for the determination of MPA and O-AMPAs as tert-butyldimethylsilyl derivatives**

In vivo animal (rats) experiments gave evidence for the possibility of revealing exposure to OPWAs at the ≥0.5 LD$_{50}$ level within no less than 48 h after exposure. Urinary metabolites of OPWAs could, in principle, be detected within two weeks after exposure, but even if sufficiently high doses of OPWAs were applied. The procedure is schematically represented in Fig. 3 and described in detail in ref.[2].

For retrospective establishment of exposure to OPWAs we developed an SPME-GCMS procedure based on reactivation of inhibited BChE (Fig. 4.). Reactivation of blood BChE inhibited by OPWAs by the action of fluoride ion gives rise to the parent compounds in the case of G-type agents or fluoroanhydrides in te case of V-type agents. SPME is especially efficient in this case, since the reactivation products are trapped by microfiber and thus eliminated from the reaction zone, which drives the reactivation process. Soman is best retained by microfiber. In should be noted that the developed procedure is feasible for the determination of total soman and for the separate determination of reactivated and intact soman.
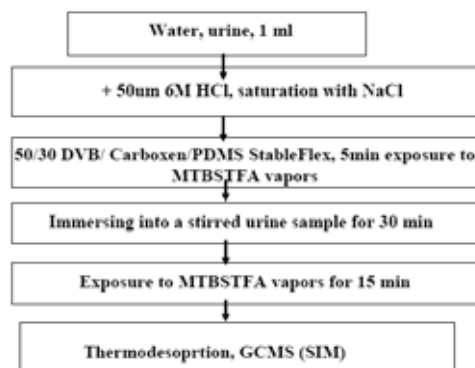
Fig. 3.　**Block scheme of the procedure for the determination of O-AMPAs in urine by SPME-GCMS**

Conclusions

Procedures for the determination in biomedical samples of biomarkers of TCs have been developed. For fluoroacetic acid, the detection limits are 0.001 mg ml^{-1} for drinking and natural waters, 0.01 mg ml^{-1} for blood plasma, and 0.01 mg g^{-1} for organ homogenates (without recounting for dry
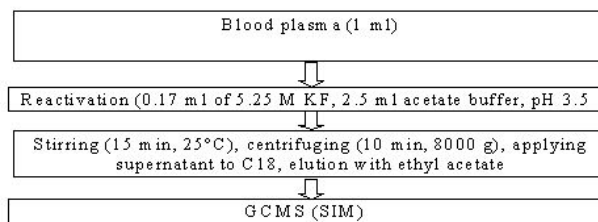
Fig. 4.　**Block scheme of the determination of blood plasma BChE reactivation products by SPME-GCMS**

weigh). For organophosphorus warfare agents, the detection limits in the analyzed sample volumes are 0.01 mg dm^{-3} for sarin and 0.002 mg dm^{-3} for soman. The analysis time (including sample preparation) is 2.5 h. Exposure to OPWAs by the results of analysis for inhibited BChE reactivation products can be revealed within 2 and more weeks after intoxication with high doses.

REFERENCES

1. Koryagina N. L., Savelieva E. I., Khlebnikova N. S., Goncharov N. V., Jenkins R. O., Radilov A. S.: J. Anal. Bioanal. Chem. *386*, 1395 (2006).
2. Savelieva E. I., Koryagina N. L., Khlebnikova N. S., Feld V. E., Radilov A. S.: *Sixth International Chemical and Biological Medical Treatment Symposium*. p. 64, Spiez, Switzerland 2006.
3. Savelieva E. I., Koryagina N. L., Radilov A. S., Khlebnikova N. S., Feld V. E.: *Fourth World Congress on Chemical, Biological and Radiological Terrorism*. p. 18, Dubrovnik 2007.

P60 DETERMINATION OF SULFONAMIDES IN WATER USING MULTI-WALLED CARBON NANOTUBES SPE AND HPLC WITH FLUORESCENCE DETECTOR

STEFANIA SIMON[a], DAN LUPU[a], ALEXANDRU BIRIS[a] and CONSTANTIN BELE[b]

[a]*National Institute for Research and Development of Isotopic and MolecularTechnologies, R-400293, Cluj-Napoca, Romania,*
[b]*University of Agricultural Sciences and Veterinary Medicine,R-400372,Cluj-Napoca, Romania,*
stefania@itim-cj.ro

Introduction

Multi-walled carbon nanotubes (MWCNTs) are a novel carbon material, repeatedly discussed in the literature for the solid phase extraction (SPE) of several organic contaminants.[1–3]

In this paper a sensitive method was developed for the determination of six commonly sulfonamides (SAs) in water by SPE using MWCNTs as adsorbent. Final analysis was carried out by HPLC coupled with fluorescence detection.

Experimental

Reagent and Water Samples

Sulfadimethoxine (SDM), sulfadiazine (SDZ), sulfamethoxazole (SMX), sulfamerazine (SMR), sulfanilamide (SNA), sulfaguanidine (SGN) and fluorescamine were obtained from Sigma-Aldrich. MWCNTs were purchased from Institute for Research and Development of Isotopic and Molecular Technologies Cluj-Napoca, Romania. Deionized and redistilled water was prepared on Milli-Q Plus (Millipore). Acetonitrile, ortophosphoric acid (H_3PO_4) and dipotassiumphosphate (K_2HPO_4) were purchased from Merck. A river water sample was collected from Somes (Cluj-Napoca) and filtered through 0.45 μm nylon membrane and stored at a temperature of 4 °C.

Chromatographic System and Conditions

All experiments were carried out by using Shimadzu VP Series liquid chromatograph equipped with a degasser and a mixer of mobile phase. A fluorescence (FL) detector FR-10 AXL with excitation wavelength of 405 nm and emission wavelength of 495 nm was used to analyse the tested solutions. Chromatographic separation was performed on a Alltima RP C-18 column (250 mm × 4.6 mm, 5 μm). Gradient elution with a mixture of acetonitrile (solvent A) – phosphate buffer pH 3.5 (solvent B) at a flow rate of 1 ml min^{−1} was applied. The initial gradient conditions were: 65 % solvent B for the first 25 min, decreasing to 50 % in 25 min, finally it was brought back to 65 % in 5 min and held for 5 min until the next injection.

Extraction Procedure

The cartridge packed with 200 mg MWCNTs was prepared in a 6ml polypropylene syringe and the sorbent was retained by two polyethylene frits. The solutions (water sample or water sample spiked with analytes) adjusted to pH 6 were loaded at a flow rate of 4 ml min^{−1}.Then, SAs were eluted using a mixture of 3 ml ammonium acetate water solution (0.2M) and 6 ml acetonitrile.The eluate was evaporated to about 3 ml under nitrogen stream in a 35 °C block heater. Then 3 ml of methylene chloride was added and each samples was mixed and separated. The lower layer was evaporated to near dryness. The extract was reconstituted in 1.0 ml mobile phase. The analytes were quantified by HPLC with a pre-column derivatization with fluorescamine (400 μl of sample + 400 μl of fluorescamine 0.1 %).The whole solution was mixed with a vortex mixer. The sample was filtered through a 0.45 μm nylon filter and after standing for 30 min at ambient temperature was ready for analysis.

Results

The effect of the pH was investigated over the range of pH 4–8 and it was found that the pH of sample solutions in the whole range nearly had no influence on the extraction of SAs.

To investigate the influence of sample volume, different volumes of pure water were spiked with a constant mass of 0.25 μg of each analyte. It was found that the recoveries of SAs
decreased slightly with the increase of sample volume. When the volume was 200 ml, the recoveries of 55–93 % were obtained for the six SAs.

For elution of SAs we selected a mixture of ammonium acetate and acetonitrile 1 : 2 (v/v) and better recoveries were obtained when eluent volume amounted to 9 ml.

The results of the linearity of SAs determined under the optimized conditions and using 200 ml of spiked pure water are reported in Table I. The linearity of each compound measured by HPLC method was good from 0.05 to 5 ng ml^{−1}.

The correlation coefficient of the calibration curves were above 0.999.

Table I
Retention time (t_R) and linearity of SAs

Sulfonamide	t_R [min]	b[a]	a[b]
SMX	11.23	21.694	0.564
SNA	17.69	20.944	0.574
SDZ	20.43	9.402	0.245
SMR	22.94	16.644	−0.192
SGN	42.32	8.021	0.071
SDM	46.68	5.560	0.104

b[a]: Slope
a[b]: Intercept

The recoveries of analytes were evaluated using 200 ml of environmental water samples (Somes river) spiked with

the mixture of SAs at 0.25 and 2.5 ng ml^{-1} and enriched and analyzed by this system. The results are listed in Table II.

Table II
Recoveries of SAs spiked water samples (n = 3)

Sulfonamides	Spiked [ng ml^{-1}]	Recovery [%]
SMX	0.25	57 ± 5.2
	2.5	55 ± 6.4
SNA	0.25	74 ± 7.3
	2.5	73 ± 6.8
SDZ	0.25	82 ± 4.3
	2.5	77 ± 3.7
SMR	0.25	58 ± 5.4
	2.5	56 ± 7.6
SGN	0.25	93 ± 4.1
	2.5	88 ± 6.9
SDM	0.25	87 ± 2.5
	2.5	79 ± 5.3

The chromatogram of the river water sample spiked with SAs is shown in Fig. 1.

Conclusions

The HPLC method with fluorescence detection characterized by a good reliability for quantitative determination of six different kinds of SAs from environmental samples has been developed. The results showed that MWCNTs could be used as a potent SPE sorbent for SAs.
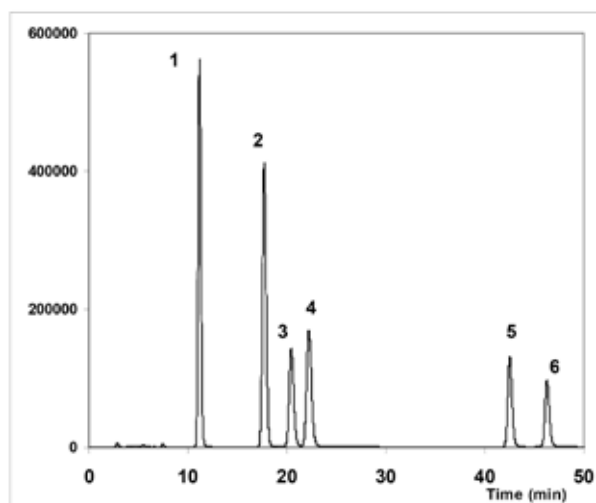
Fig. 1.   **SPE-LC-FL chromatogram of river water sample spiked with 2.5 ng ml^{-1} of each compound. (1) SMX; (2) SNA; (3) SDZ; (4) SMR; (5) SGN; (6)SDM**

REFERENCES
1. Niu H., Cai Y., Shi Y., Wei F., Liu J., Mou S., Jiang G.: Anal. Chim. Acta *594* , 81(2007).
2. Fang G.Z., He J.X., Wang S.: J. Chromatogr. A *1127*, 12 (2007).
3. Zhao H., Wang L., Qiu Y., Zhou Z., Zhong W., Li X.: Anal. Chim. Acta *586*, 399 (2007).

P61　MICROBIOLOGIAL REMEDIATION OF METAL-CONTAMINATED SOIL

VALÉRIA SNOPKOVÁ

Department of Biotechnology, Institute of Geotechnics the Slovak Academy of Sciences,
Watsonova 45, 043 53 Košice, Slovak Republic.
snopkova@saske.sk

Introduction

Soil contamination with anthropogenic heavy metals, which mainly comes from industrial activity, atmospheric deposition and land application of sewage sludge, has received much attention in the recent years. The anthropogenic heavy metals are to be easily accumulated in the topsoil1, resulting in potential problems such as toxicity to plants and animals[1,2], accumulation in food chain, perturbation of the ecosystem and adverse health effects[4,5]. Metals, which are significantly toxic to human beings and ecological environment, include chromium (Cr), cooper (Cu), lead (Pb), mercury (Hg), zinc (Zn), manganese (Mn), cadmium (Cd), nickel (Ni), arsenic (As) and iron (Fe), etc.[6].

Contaminated soil is notoriously difficult to treat because the contaminants are often tightly bound to the soil particles. Conventional remediation technologies are becoming less popular due to the high treatment costs and bioremediation processes to improve the contaminant removal efficiency and cost effectiveness. However, as an innovative technology, there are many factors to be investigated with the future development[7].

Bioremediation

Bioremediation is defined as a method using living organisms, or their particles (enzymes) to reduce, eliminate, fixate or transform contaminants presented in the soil, in sediments, in waters or in the air[8,9]. In the bioremediation processes bacteria, fungi, yeasts and plants present the most imposed organisms. Recently, the ability of algaes and planktons are being researched. Some technologies are based on the use of general or genetically modified organisms[8]. Bioremediation works by either transforming or degrading contaminants to non-hazardous or less hazardous chemicals. These processes are called, respectively, biotransformation and biodegradation. Biotransformation is any alteration of the molecular or atomic structure of a compound by microorganisms. Biodegradation is the breaking down of organic substance by microorganisms into smaller organic or inorganic components[9].

Metal – Microbe Interactions

Microorganisms, especially bacteria, exist in complex biogeochemical matrices in subsurface sediments and soils[9] and are known to mediate many geochemical processes[10,11]. They can interact with metals via many mechanisms, some of which may be used as the basis of the potential bioremediation strategies[9]. Microbes can mobilize metals through autotrophic and heterotrophic leaching, chelation by microbial metabolites and siderophores, and methylation, which can result in volatilization. Conversely, immobilization can result from sorption to cell components or exopolymers, transport into cells and intracellular sequestration or precipitation as insoluble organic and inorganic compounds, e.g. oxalates[12,13] sulphides or phosphates[14,15].

Metal　Mobilization

Bioleaching. Metals can be leached from solid matrices via autotrophic and heterotrophic leaching. Chemolitotrophic and heterotrophic bacteria have the major role.

Most autotrophic leaching is carried out by chemolithotrophic, acidophilic bacteria which fix carbon dioxide and obtain energy from the oxidation of ferrous iron or reduced sulfur compounds, which causes the solubilization of metals because of the resulting production of Fe(III) and H_2SO_4[16,17]. The microorganisms involved include sulfur-oxidizing bacteria, e.g., *Acidihiobacillus thiooxidans*, iron- and sulfur-oxidizing bacteria, e.g., *Acidithiobacillus ferrooxidans* and ironoxidizing bacteria, e.g., *Leptospirillum ferrooxidans*[18,19].

In the case of oxide, carbonate and silicate ores, limits are set for the use of thiobacilli. For such ores, research is being done on the use of heterotrophic bacteria. In this case, metals are dissolved by organic acids, or complexing, or chelating agents produced by the bacteria. Heterotrophic bacteria require organic supplement for growth and energy supply. Among the bacteria, members of the genus Bacillus are most effective in metal solubilization[19].

Siderophores are low molecular weight Fe(III) coordination compounds that are excreted under iron-limiting conditions by microorganisms, particularly bacteria and fungi, to enable accumulation of iron from the environment[20,21]. Although primarily produced as a means of obtaining iron, siderophores are also able to bind other metals such as magnesium, manganese, chromium (III), gallium (III) and radionuclides such as plutonium (IV)[22,23].

Biomethylation of Hg, As, Se, Sn, Te and Pb can be mediated by a range of bacteria under aerobic and anaerobic conditions. Methyl groups are enzymatically transferred to the metal, and the given species may transform a number of different metal(-loid)s. Methylated metal compounds formed by these processes differ in their solubility, volatility and toxicity [23].

Metal　Imobilisation

Bioacumulation and **biosorption**. Bacteria can physically remove heavy metals from solution through association of these contaminants with biomass. Bioaccumulation is the retention and concentration of substance within an organism. In bioaccumulation, metals are transported from the outside of the microbial cell trough the cellular membrane, into the cell cytoplasm, where the metals are sequestred[9,24]. Biosorption describes the association of soluble substances with the cell surface. Sorption does not require an active metabolism. The amount of metal biosorbed to the exterior of bacterial

cells often exceeds the amount predicted using information about the charge density of the cell surface[9,25].

Bioprecipitation. Sulfate reduction is an example for the precipitation of metals ions in solution. Sulfate-reducing bacteria form metal sulfides that are insoluble. The stability of these sulfides depends on maintenance of anoxic conditions[7,24], and nutrients are also inevitable. Stimulating sulfate reducion can increase pH also and form metal hydroxides and oxides that precipitate and do not migrate in soil and groundwater[7].

Biooxidation, **bioreduction**. Microorganisms are also known to oxidize and reduce metal contaminants. Mercury and cadmium can be oxidized while arsenic and iron can be reduced by microorganisms. Cr(VI) can be oxidized to Cr(III) that is less mobile and toxic. Bacteria such as *Bacilus subtilis* and SRB in the presence of sulfur can perform this reaction[7].

Bioremediation Technologies

According to the site, bioremediation technologies are divided to:

- ***in-situ*** – are carried out at the place of the contamination,
- ***ex-situ*** – the contaminated matter is taken off from the natural locality and it is consequently processed[26].

Ex situ bioremediation is usually realized on the specific revised place or in the reactor. The pre-treating of contaminated matter increases the efficiency of this process[26]. *Ex-situ* methods have been around longer and are better understood, and they are easier to contain, monitor, and control. However, *in-situ* bioremediation has several advantages over *ex-situ* techniques. *In-situ* treatment is useful for contaminants that are widely dispersed in the environment, present in dilute concentrations, or otherwise inaccessible (e.g., due to the presence of buildings or structures). This approach can be less costly and less disruptive than *ex-situ* treatments because no pumping or excavation is required. Moreover, exposure of site workers to hazardous contaminants during *in-situ* treatment is minimal[27].

Broadly, bioremediation strategies can be further divided into natural attenuation, biostimulation, and bioaugmentation strategies[27].

Bioaugmentation presents an addition of microorganisms or their products, such as biosurfactants or enzymes[28]. Thus, inoculation of 'specialized' biomass may allow for an increased biodegradation of target pollutants as well as a more effective detoxification of the solid matrix[29] . Another common result of bioaugmentation is the dramatic reduction of remediation times[30,31]. Indigenous or exogenous, standard or modified microorganisms are used[32,33]. Generally, they present mixed cultures of microorganisms, but it could be also pure bacterial strains adapted onto the aimed contaminant in the laboratory[34,35].

Biostimulation can be aggressive or passive, in that electron donors, electron acceptors, and trace nutrients can be injected into the environment to stimulate indigenous organisms to increase biomass or activity to affect the contaminant. Passive biostimulation techniques include simple infiltration galleries or simply spreading fertilizer on surface without any pumping or mixing[25,27].

Natural attenuation relies on the intrinsic bioremediation capabilities of that environment. Environments high in organic carbon and energy sources, low contaminant concentrations, and without significant nutrient deficiencies may be able to degrade or transform the contaminants of concern without any intervention [27].

Conclusions

Environmental biotechnologies with applications of bacteria are eco-friendly and cost effective. They present natural technologies for treatment of toxic metals from soil. The following development is desirable, because of the high specificity and the time-consuming of biological processes and because of the difficulty to control them.

REFERENCES

1. Samsoe-Petersen L., Larsen E.H., Larsen P.B., Bruun P.: Environ. Sci. Technol. *36*, 3057 (2002).
2. Ma Y., Dickinson N.M., Wong M.H.: Biol. Fertil. Soils *36*, 79 (2002).
3. Berti W.R., Jacobs L.W.: J. Environ. Qual. *25*, 1025 (1996).
4. Forstner U., 1995. In: *Metal Speciation and contamination of Soil*. (Allen H.G., Huang C.P., Bailey G.W., Bowers A.R. ed.), CRC Press, Boca Raton, FL, (1995).
5. Stalikas C.D., Mantalovas Ach., Pilidis G.A.: Sci. Total Environ. *206*, 17 (1997).
6. Meena A.K., Mishra G.K., Rai P.K., Rajagopal Ch., Nagar P.N.: J. Hazard. Mater. *112*, 161 (2005).
7. Mulligan C.N., Yong, R.N, Gibbs B.F.: Eng. Geol. *60*, 193 (2001).
8. Dercová K., Makovníková J., Barančíková B., Žuffa J.: Chemické listy *99*, 682 (2005).
9. Tabak H.H., Lens P., van Hullebusch E.D., Dejonghe W.: Environ. Sci. Technol. *4*, 115 (2005).
10. Ehrlich H.L.: Appl. Microbiol. Biotechnol. *48*, 687 (1997).
11. Ledin M.: Earth Scien. Rev. *51*, 1 (2000).
12. Gharieb M.M., Sayer J.A., Gadd G.M.: Mycol. Res. *102*, 825 (1998).
13. Sayer J.A., Gadd G.M.: Mycol. Res. *101*, 653 (1997).
14. White C., Gadd G.M.: Microbiol. *142*, 2197 (1996).
15. Yong P. Macaskie L.E.: J. Chem. Technol. Biotechnol. *63*, 101 (1995).
16. Rawlings D.E.: in: *Biomining: Theory, Microbes and Industrial Processes* (Rawlings D.E., ed.) Springer-Verlag, Berlin, 1997.

17. Schippers A., Sand W.: Appl. Environ. Microbiol. *65*, 319 (1999).
18. Ewart D.K., Hughe, M.N.: Adv. Inorg. Chem. *36*, 103 (1991).
19. Bosecker K.: FEMS Microbiol. Rev. *20*, 591 (1997).
20. John S.G.: Environ. Sci. Technol. *35*, 2942 (2001).
21. White Ch., Wilkinson S. C., Gadd G.M.: Internat. Biodet. Biodeg. *35*, 17 (1995).
22. Birh L., Bachofen R.: Experienta *46*, 827 (1990).
23. Gadd G.M.: Geoderma *122*, 109 (2004).
24. Gaszó L.G.: Cejoem *7*, 178 (2001).
25. Palmisan A., Hazen T., Bioremediation of metals and radionuclides. Prepared for the NABIR, LBNL – 42595 (2003).
26. Kubal M., Burkhard J., Březina M.: in *Dekontaminační technológie*. VŠCHT, Praha 2002.
27. Hazen T.C., Tabak H.H.: Environ. Sci. Technol. *4*, 157 (2005).

28. Gentry T.J, Josephson K.L., Pepper I.L.: Biodegrad. *15*, 67 (2004).
29. Silva E., Fialho A.M., Sá-Correia I., Burns R.G., Shaw L.J.: Environ. Sci. Technol. *38*, 632 (2004).
30. Zhang C., Hughes J.B., Nishino S.f., Spain J.C.: Environ. Sci. Technol. *34*, 2810 (2000).
31. Robles-Gonzales I.V., Fava F., Poggi-Voraldo H.M.: Microb. Cell. Fact. *7*, 1 (2008).
32. Boon N., Goris J., de Vos. P., Verstraet W., Top E.M.: Appl. Environ. Microbiol *66*, 2906 (2000).
33. Vidali M., Pure Appl. Chem. *73*, 1163 (2001).
34. Ramasamy K., Parwin Banu K., Parwin Banu S.: in: *Enviromental bioremediation technologies*. (Singh S.N., Tripathi R.D., ed.), p.7. Springer, New York 2004.
35. Dercová K.: Odpady *4*, 16 (2004).

P62　DISTRIBUTION OF PHTHALIC ACID ESTERS (DEHP, DBP) IN CHICKEN TISSUES AND ORGANS

VLASTA STANCOVÁ[a], ALŽBETA JAROŠOVÁ[a], LENKA KRÁTKÁ[a], JIŘÍ HARAZIM[b] and PAVEL SUCHÝ[c]

[a]*Mendel University of Agriculture and Forestry Brno Faculty of Agronomy, Zemědělská 1, 613 00, Brno, Czech Republic,*
[b]*Central Institute for Supervising and Testing in Agriculture, Hroznová 2, 656 06, Brno, Czech Republic,*
[c]*University of Veterinary and Pharmaceutical Sciences Brno, Palackého 1/3, 612 42, Brno, Czech Republic,*
xwegsch0@node.mendelu.cz

Introduction

Phthalates, ubiquitous food and environmental contaminants, are the most frequently used plasticizers for PVC. Due to the widespread use of plasticized PVC for a vast number of technical purposes and for some food contact materials, the phthalates are produced in huge amounts. Several million tons of phthalates are used per year worldwide in the production of soft polyvinyl chloride and other plastics. Phthalates are not chemically bound in to the products and are released continuously into the air or leach from the products[1]. The migration of phthalates from packaging materials containing these compounds to fatty foodstuffs is a well-known source of food contamination[2]. Major and most toxic phthalic acid esters (PAEs) associated with food are di-2-ethylhexyl phthalate (DEHP) and di-n-butyl phthalate (DBP). PAEs entering the human body are rapidly hydrolyzed to the monoesters and than metabolized and excreted with urine and feces[1].

PAEs are considered highly hazardous to human health because they disrupt the hormonal balance and impair reproduction and development. Some of them are considered as potential carcinogens, teratogens and mutagens. Additionally, phthalates are suspected to trigger asthma and dermal diseases in children. The main objective of the present work is to investigate the real content of DEHP and DBP in samples of chicken's muscle, skin, fat and liver[3].

Experimental

M e t h o d s

Phthalates content measurement in lyophilisated chicken tissues is made in four separate steps, where every sample is analyzed in parallel which brings additional measurement correctness check. Blank is important for glass cleaness check and to specify chromatography background. First step consists of fat extraction from tissues using mixture of organic solvents (acetone : hexane; 1 : 1). In second step, after dissolving co-extracts in mobile phase (dichlormethane: cyclohexane; 1 : 1), they are separated by Bio-Beads S-X3 gel-permeation chromatography. Third step comprise of cleaning of eluate with usage concentrated sulfuric acid. High performance liquid chromatography on Separon SGX C 18 with UV detection at 224 nm was last, fourth step. The mobile phase was acetonitrile – water (1 : 1) pumped at a flow-rate of 1.0 ml min^{-1}. Retention time of DBP was ca. 3.5 min. and DEHP ca 8 min.

M a t e r i a l s

32 chickens ROSS 308 were used in our work. Chickens were separated into four groups of eight Chickens depending on ingredients in feeding mixture. Chickens in second group were fed common feeding mixture fortificated by 3% coleseed oil with low phthalate content into BR2 and 5% into BR3. In this case, vegetative oil was stored in the tin container. Common feeding mixture with 3% coleseed oil with high phthalate content added into BR2 and 5% into BR3 was fed by third group. Coleseed oil for third group was stored in plastic wrapping. The fourth group was comprised by chickens fed by routine feeding mixture with addition 3% animal fat into BR2 and 5% into BR3. 42 days old chickens were butchered and their muscles, skin, fat and liver were used for making samples for analysing. Samples were lyophilisated and before next analysing were hold in freezer in −18 °C. Table I illustrates contents of both phthalates in feeding mixture used in our work.

Table I
Contents of both phthalates in ingredients added to feeding mixture

	DBP [mg kg^{-1}]	DEHP [mg kg^{-1}]	ΣDBP+DEHP [mg kg^{-1}]
Coleseed oil (tin)	15.56	2.25	17.81
Coleseed oil (plastic)	51.35	<0.20	51.35
Animal fat	43.28	2.10	45.38

Results

Figs. 1.–4. represents chickens separated into four groups groups depending on kind of ingredients in feeding mixture. Each figure expresses average value of contents DEHP and DBP in edible part of chicken's body. Fig. 1. demonstrates real average contents of phthalates in muscle (0.35 mg kg^{-1} DEHP; 0.22 mg kg^{-1} DBP), skin (1.18 mg kg^{-1} DEHP; 0.36 mg kg^{-1} DBP), fat (1.36 mg kg^{-1} DEHP; 0.47 mg kg^{-1} DBP) and liver (0.16 mg kg^{-1} DEHP; 0.02 mg kg^{-1} DBP) in group of chickens fed by common feeding mixture without phthalate addition. Findings in muscle (0.08 mg kg^{-1} DEHP; 0.08 mg kg^{-1} DBP), skin (1.10 mg kg^{-1} DEHP; 0.51 mg kg^{-1} DBP), fat (1.92 mg kg^{-1} DEHP; 0.49 mg kg^{-1} DBP) and liver (0.24 mg kg^{-1} DEHP; 0.11 mg kg^{-1} DBP) of second group is depicted in Fig. 2. Contamination of muscle (0.32 mg kg^{-1} DEHP; 0.15 mg kg^{-1} DBP), skin (1.38 mg kg^{-1} DEHP; 0.57 mg kg^{-1} DBP), fat (3.27 mg kg^{-1} DEHP; 1.28 mg kg^{-1} DBP) and liver (0.16 mg kg^{-1} DEHP; 0.03 mg kg^{-1} DBP) of chickens of third group shows Fig. 3. In fourth group we determined following contents of phthalates: muscles (0.39 mg kg^{-1} DEHP; 0.22 mg kg^{-1} DBP), skin (1.60 mg kg^{-1} DEHP;

0.44 mg kg^{-1} DBP), fat (1.85 mg kg^{-1} DEHP; 0.74 mg kg^{-1} DBP) and liver (0.23 mg kg^{-1} DEHP; 0.13 mg kg^{-1} DBP).
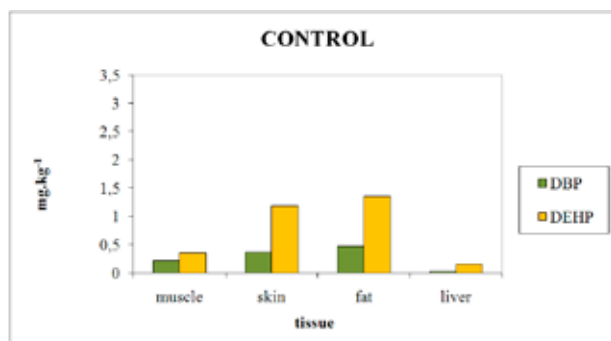
Fig. 1.   **First group of chickens fed by common feeding mixture**
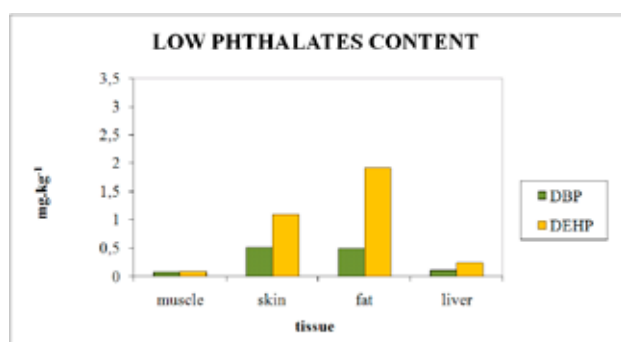
Fig. 2.   **Second group of chickens fed by common feeding mixture with addition of coleseed oil with low phthalates content**

Conclusions

Our measurements proved lipophilic character of phthalates, which were accumulated in chicken's fat tissue and skin. That means that fat tissue is useful indicator of phthalates contamination. Liver, despite containing more fat than muscles, had lower values of phthalates mainly because of their enzymatic base, which were transforming phthalates to metabolites. Relatively high contents of phthalates in control group points at ubiquitous content of these contaminants. The values of DEHP and DBP were identically higher in all samples.
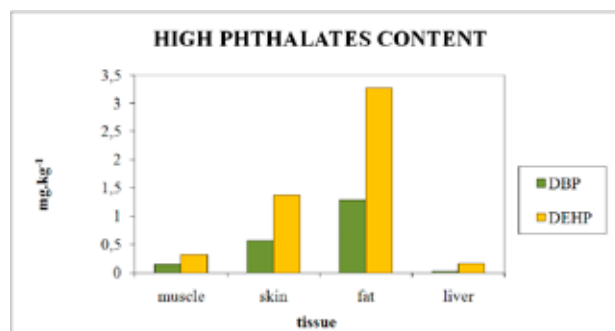
Fig. 3.   **Third group of chickens fed by common feeding mixture with addition with coleseed oil with high phthalates content**
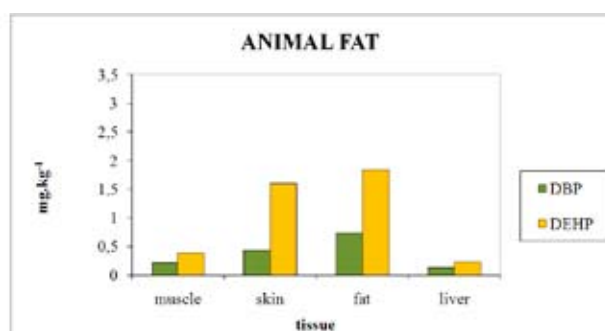
Fig. 4.   **Fourth group of chickens fed by common feeding mixture with addition of animal fat**

REFERENCES
1. Wormuth M., Scheringer M., Vollenweider M., Hungerbuhler, K.: Risk Anal. *26*, 803 (2006).
2. Schmidt R. H., Rodrick G. E.: *Food Safety Handbook.* Wiley, New Jersey 2003.
3. Schettler T.: Int. J. Androl. *29,* 134 (2006).

P63 PURIFICATION PROCESS INFLUENCE ON THE PAH DETERMINATION IN REAL SOIL SAMPLES

MICHAELA STOUPALOVÁ, MILADA VÁVROVÁ, LUDMILA MRAVCOVÁ and VLADIMÍR VEČEREK

University of Veterinary and Pharmaceutical Sciences Brno, Faculty of Veterinary Hygiene and Ecology
Palackého 1–3, 612 42 Brno, Czech Republic,
stoupalovam@vfu.cz

Introduction

The analytical procedure usually consists of several partial steps: the isolation of analytes, extract purification, and the concentration of monitored analytes[1]. Environmental analysis currently tends to use such analytical procedures to allow the reliable and fast determination of monitored substances at the lowest possible costs. In the field of sample preparation, attention is devoted particularly to the combination of methods which enable the selective extraction of analytes followed by their concentration. The accuracy and precision of measurement in particular are monitored in the instrumental end-point as they are closely linked to the selectivity and sensitivity of analytical instruments. A special emphasis is laid on the confirmation techniques which should prove the results obtained using a typical method and reduce the risk of false-positive and false-negative results[2,3].

Polycyclic aromatic hydrocarbons (PAHs) are formed in the incomplete combustion of organic matter, for example during combustion of fossil fuel or wood, in running engines of motor vehicles, during fire and during free incineration of biomass or municipal waste[4]. They are also produced naturally, for example in active volcanoes.

Individual PAHs differ significantly by their properties which define their potential risks. They are characterized by great variability in terms of toxic, physicochemical and chemical properties that may affect the environment. They produce different effects on individual species and the link between toxicity of individual PAHs and their structure is currently being investigated[5].

Experimental

The effect of the purification procedure on the content of analytes was investigated in samples of soil. The isolation of PAHs from soil was performed using microwave extraction. Samples were purified using column chromatography. HPLC was used as final analytical method.

E x t r a c t i o n

The isolation of PAHs from soil was performed using microwave extraction. The extraction step lasted 25 minutes, at a temperature of 120 °C and an input of 1,200 W, by using 20 ml of a hexane/acetone (1 : 1) mixture. Microwave extraction provided two sets of samples; each set was subsequently subjected to a different purification method.

P u r i f i c a t i o n

We monitored influence of the purification process on the determination of monitored analytes. We carried out comparison of two purification process.

Purification 1: Samples were cleaned-up using column chromatography on a silica column (5 g). The sample was applied on the top of the column; 10 ml of hexane were applied on the top of the column prior to the complete adsorption of the sample on the column, followed by elution with 5 ml of an eluting mixture consisting of hexane : dichloromethane (1 : 1) and finally with 10 ml of the same mixture. The last fraction was collected.

Purification 2: The samples in the second set were purified using column chromatography on a column with silica gel (4 g) and florisil (4 g). The sample was applied directly on the prepared column. The column was washed with 60 ml of a hexane : dichloromethane (1 : 1) mixture prior to the complete adsorption of the sample into the sorbent. The whole eluate was collected.

H P L C

The determination itself was performed using the HPLC Agilent 1100 Series with a DAD and FLD detectors. The HPLC determination was carried out under following conditions: gradient elution (A = 60 % water/40 % acetonitrile; B = 100 % acetonitrile); 0 min A, 30 min B, 40 min. B, 42 min A For separation SUPELCOSIL™ LC-PAH column was used (25 cm × 2.1 mm × 5 μm). The flow-rate of the mobile phase was constant, 0.4 ml min^{-1}, temperature 30 °C. FLD settings were: 0–17.4 min λ_{ex} = 260 nm, λ_{em} = 350 nm; 17.4–42 min λ_{ex} = 260 nm, λ_{em} = 420 nm. DAD setting was: λ = 225 nm.

Results

The main aim of this work was to investigate the effect of the purification process on the content of monitored PAHs in the real samples of soil. For better clarity, the results are provided in graphs and expressed in percentage; for assessment, the values determined in the first set of samples (purification on silica) were chosen as 100 % for assessment purposes. The results are presented in Figs. 1.–3. for individual samples of soil.

It follows from Fig. 1. that both purification techniques provided comparable results. Fig. 2. shows the results for
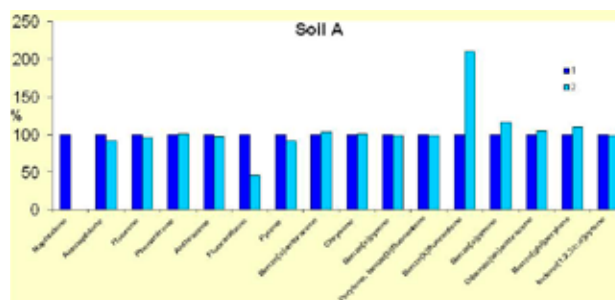
Fig. 1. **Influence of a purification procedure – soil A**
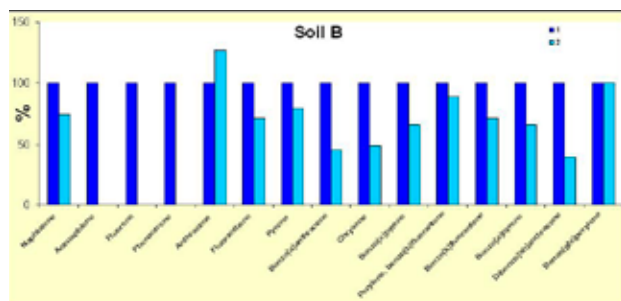
Fig. 2. **Influence of a purification procedure – soil B**
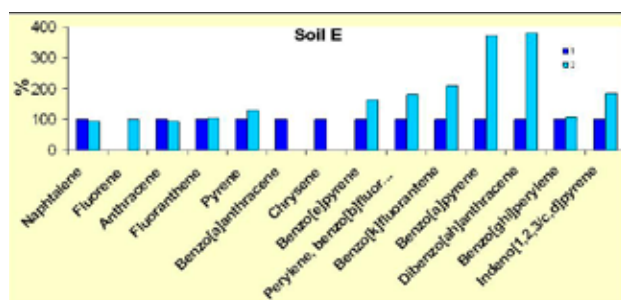
Fig. 3. **Influence of a purification procedure – soil E**

soil B, better results were obtained using the first purification method where the third fraction was the only fraction analysed. Samples of soil C exhibited a common trend for lower-molecular-weight PAHs where the method of extract

purification had hardly any effect on the final content in the given matrix. On the contrary, the second purification method using two sorbents (silica gel and florisil) was proven optimal for the PAHs with higher molecular weight.

Conclusions

However, in this context it is important to point out that the yield of pre-analytical techniques is significantly influenced by the sample matrix by the way of matrix effects. The structure and chemical qualities of individual PAH also plays an important role.

REFERENCES

1. Poustka J.: *Dissertation*. VSCHT Prague, Prague, Czech Republic, 1995.
2. Kocourek V., Hajšlová J., Holadová K.: *Methods of xenobiotics determination in food. Laboratory Manual. Part III*. VÚPP, STIPP Prague, 1992.
3. Kocourek V., Vávrová M., Uhnák J.: *Methods of xenobiotics determination in food. Laboratory Manual. Part II*. VÚPP, STIPP Prague, 1990.
4. Jech L. *Polycyclic aromatic hydrocarbons (PAHs)*. AXYS-VARILAB s.r.o., Prague, 2006.
5. Jelínková G.: *Diploma thesis*. VUT Brno, Brno, Czech Republic, 2003.

P64 OPTIMALIZATION OF SPME METHOD FOR SPICE CONTENTUAL SUBSTANCES DETERMINATION

MICHAELA STOUPALOVÁ, MILADA VÁVROVÁ, HANA PLESKAČOVÁ, LUDMILA MRAVCOVÁ and VLADIMÍR VEČEREK

University of Veterinary and Pharmaceutical Sciences Brno, Faculty of Veterinary Hygiene and Ecology Palackého 1–3, 612 42 Brno, Czech Republic stoupalovam@vfu.cz

Introduction

The SPME method can be used to extract analytes from different matrices. It has been employed in the isolation of analytes from the air, food, water, and other matrices[1]. The SPME method has a number of major advantages such as fast rate, high sensitivity and good accuracy; the detection limit regularly achieved for the above-mentioned matrices ranges in $ng\,kg^{-1}$. First published in 1989, the SPME method is now a well established extraction method whose application has been assessed and documented[2].

The analyses of organic, fragrant, and flavouring components as well as sample preparation are usually started with the concentration of an analyte. If one considers a time demand, the passive SPME sampling technique is the quickest, with sample preparation not exceeding 30 minutes[3].

The consistency of the results and the reliability of detection with SPME as well as repeatability and reproducibility are influenced by a number of factors, like polymer polarity and the thickness of a polymer layer (stationary phase) on the surface of a fibre, the sampling method, the pH, the ionic strength of a solution, sample temperature, agitation, etc.

Experimental

The objective of this paper was the optimization of solid phase microextraction (SPME) method, which is used for determination of the essential oils in spice. Analytes were analysed by GC/MS.

S P M E

The SPME method was investigated with different fibers (polydimethylsiloxane – 100 μm thickness and polydimethylksiloxayne-divinylbenzene – 65 μm), extraction time (1; 2; 5; 10; 15; 20; 30; 40 and 60 minutes), extraction temperature (30; 40 and 50 °C) and incubation of sample (0; 5; 10; 15; 20 minutes).

G C / M S

The determination itself was performed using the GC 6890N (Agilent Technologies, USA) with a mass-spectrometric detector 5973N MSD (Agilent Technologies, USA); for separation HP-5MS capillary column was used (30 m × 0.25 mm × 0.25 μm). The injector temperature was 270 °C, the ion source temperature was 230 °C and the Transfer Line temperature was 250 °C. The temperature programme was 45 °C for period of 2 minutes, 5 °C min⁻¹ to 200 °C, 200 °C for period of 2 minutes; the total analysis time was 35 minutes. The flow-rate of the carrier gas (He) was constant, $1\ ml\,min^{-1}$.

Results

The aim hereof was to optimise the SPME method for determination of the essential oils in spice. We monitored influence of the stationary phase on the sorption of monitored analytes. We carried out comparison of two PDMS fibres (100 μm) and PDMS-DVB (65 μm). The results obtained are stated in Fig. 1. From it follows that the PDMS-DVB fibre (65 μm) shows higher sorption effectivity for all the monitored pesticides.
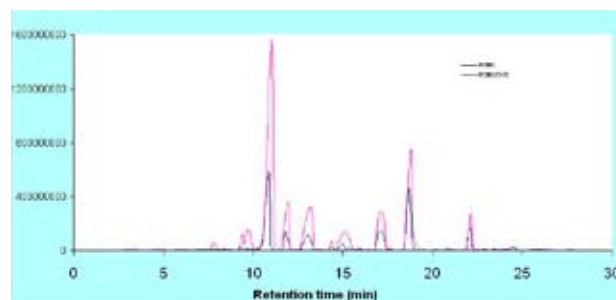
Fig. 1. **Influence of the fibre type on response of detectors for the monitored analytes**

Also the influence of temperature on sorption of the target compounds was monitored. The following temperatures were tested: 30, 40 and 50 °C. Lower-molecular-weight terpenes were shown to have the best responses at a temperature of 30 °C while for the medium-molecular-weight terpenes (around $150\ g\,mol^{-1}$), the effect of different temperature on the adsorption of analytes wasn't so strong. Terpenes with the highest molecular weight ($204\ g\,mol^{-1}$) exhibited the highest response at a temperature of 50 °C. On the basis of the results and literature data, the sorption value at 30 °C was selected.

Various sorption times were measured (1; 2; 5; 10; 15; 20; 30; 40, and 60 minutes) at temperature of 30 °C. The time of 15 minutes seems to be suitable for both the sensitivity and a good repeatability.

This study also investigated the effect of sample conditioning before analyte sorption. The conditions of analysis
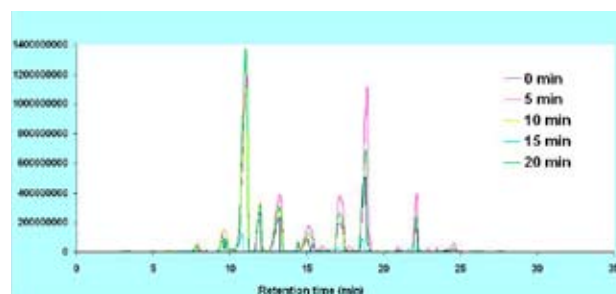
Fig. 2. **Influence of the incubation time on response of detectors for the monitored analytes**

Table I
RSD in determination of analytes

Analyte	RSD	Analyte	RSD
α-pinene	13	menthone	32
camphene	11	borneol	18
sabinene	14	estragol	28
β-pinene	9	α-cubebene	12
β-myrcene	7	thymol acetáte	38
α-phellandrene	10	ylangene	31
3-carene	7	copaene	27
α-terpinene	7	α-bourbonene	34
2-nitro-p-cymene	3	isocaryophyllene	35
limonene	23	β-caryophyllen	26
eucalyptol	8	humulene	31
γ-terpinene	4	α-caryophyllen	36
β-terpineol, cis-	15	isoledene	32
linalool	13	α-muurolene	36
thujone	22	epizonarene	36
camphor	12	karyophyllene oxide	34

were as follows: the duration of sorption was 15 minutes at a temperature of 30 °C. This temperature was also used for sample conditioning. Fig. 2. shows the comparison between the different durations of sample conditioning (0; 5; 10; 15; 20 minutes) and it is seen that the 5-minute conditioning is the most suitable as it gives the highest response for the majority of target analytes.

The repeatability of the method was determined based on 5 repetitions and is expressed as a relative standard devi-ation (Table I). Terpenes are listed in the table according to their increasing molecular weight. It follows from the results that lower-molecular-weight terpenes have better repeatability than more volatile terpenes with higher molecular weight. Standard deviations vary in a rather wide range of 28–38 % for substances with higher molecular weight which may be attributed to the optimalization of the SPME method where some parameters (particularly the duration and temperature of sorption) were chosen at such levels to match for the whole group of 32 monitored substances.

Conclusions

SPME conditions used for optimalization of head-space method were follows: 15 min exposition of PDMS-DVB (65 μm) fiber at 30 °C in head-space above 0.5 g of spice sample in vial. The incubation of sample was 5 minutes at extraction temperature 30 °C.

REFERENCES
1. Shao Y. et al.: Flavour and Fragrance Journal *18*, 5 (2003).
2. López P., et al.: Analytica Chimica Acta *559*, 97 (2006).
3. Holadová K., Prokůpková G., Hajšlová J., et al.: Analytica Chimica Acta *582*, 24 (2007).

P65　DTA AND FLUORESCENCE SPECTRA OF HUMIC ACIDS AS INDICATORS OF HUMAN INFLUENCE ON SOIL

NORA SZOMBATHOVÁ[a], JÖRG LUSTER[b], BOŽENA DEBSKA[c], ANTON ZAUJEC[a], MILAN MACÁK[a], VLADIMÍR ŠIMANSKÝ[a], ERIKA TOBIAŠOVÁ[a] and JURAJ CHLPÍK[a]

[a]*Department of pedology and geology, Slovak University of Agriculture, Tr. A. Hlinku 2, 949 76 Nitra, Slovakia,* [b]*Swiss Federal Research Institute WSL, Zürcherstrasse 111, CH-8903 Birmensdorf, Switzerland,* [c]*Department of Environmental Chemistry, University of Technology and Agriculture, Bernardynska 6, 85-225 Bydgoszcz, Poland,* nora.szombathova@uniag.sk

Introduction

Humic substances (HS) are the most abundant and stable organic C forms found in soil. Based on their solubility in alkaline and acid solutions they can be divided into humic acids (HA), fulvic acids (FA) and humin. Spectroscopic measurements provide valuable information on the nature of soil HS, they are nondestructive, require only small amounts of sample, and are experimentally simple as referred by Stevenson[6]. Thermal analysis curves, heat fluxes, absorption and fluorescence properties can provide useful information on nature, origin, chemistry and structure of HS Blaser et al.[2]; Gonet et al.[3], Senesi et al.[5].

In this study we investigated differences in absorptive, fluorescence and thermal characteristics between humic acids isolated from humus horizons of soils with different land use (agroecosystem and forest ecosystem).

Experimental

Samples were collected from A-horizons of soil pits dug on cultivated and nearby oak-hornbeam forest soils from locality Báb (south-western Slovakia). The parent material was calcareous loess. Samples were compared in two pairs:
- Profiles 1 and 2 – located at an upland position, 80 m apart: 1 – forest soil, Luvic Phaeozem, 2 – cultivated soil, Haplic Chernozem
- Profiles 3 and 4 – located at a colluvial foot slope, 60 m apart: 3 – forest soil, 4 – cultivated soil, both on Orthic Luvisol

Humic acids (HA) were isolated by Orlov[4] method. Total luminescence spectra (TLS) of HA were recorded on a Shimadzu RF5000 spectrometer, and absorption spectra on a Shimadzu UV 240. For measuring, the stock solutions were diluted to organic C concentration 10 mg dm^{-3}, and adjusted to pH 7. TLS excitation slit width was set to 5 nm, emission to 3 nm. TLS were recorded as a series of 10 synchronous scan spectra with differences between excitation and emission wavelength ($\lambda_{ex}/\lambda_{em}$) of 25 nm.

Thermal properties were recorded on Derivatograph C – MOM Hungary. Detailed information concerning differential thermal analysis (DTA) was presented by Gonet et al.[3]. Based on the results, value "Z", proportional to "aliphaticity" of HA was calculated. It expresses the ratio of weight loss in low temperature (endo + exo1) to weight loss in high temperature range (exo2).

Results and Discussion

The absorbance ratios of UV-VIS spectra are listed in Table I. Stevenson[6] stated that UV-VIS spectra of HA are broad, featureless and monotonously decreasing with increasing wavelength, thus absorbance ratios were used in determining their chemical structure. $A_{280/465}$ ratio reflects the proportion between the lignin structures more resistant to humification and materials at the initial stage of transformation, $A_{280/665}$ – ratio between groups resistant to humification and strongly humified ones, $A_{465/665}$ decreases with increasing molecular weight and condensation. In our study, higher values of absorbance ratios indicated that HA from forest soil content more lignin type compounds and had lower degree of aromatic structures condensation than that from the cropped soil.

Table I
Ratios of humic acid absorbances, fluorescence peak positions and intensities

Profile	$A_{280/665}$	$A_{280/465}$	$A_{465/665}$	$\lambda_{ex}/\lambda_{em}$ 455/515	$\lambda_{ex}/\lambda_{em}$ 310/480
				peak intensities [a.u]	
forest, upland	5.25	28.33	5.40	280	245
cultivated, upland	4.53	22.46	4.96	>350	<350
forest, slope	5.06	28.00	5.53	315	280
cultivated, slope	4.67	21.54	4.62	>350	315

Table II
Thermal properties of humic acids

Profile	Area under DTA effects [% of total]			Z
	endo	exo1	exo2	
forest, upland	4.1	57.6	38.3	1.61
cultivated, upland	2.6	35.6	61.8	0.62
forest, slope	4.4	51.6	44.0	1.27
cultivated, slope	5.7	31.3	63.0	0.59

Three-dimensional total luminescence spectra (TLS) enable detailed view with more complete information than simple excitation, emission, or synchronous scan spectra Blaser et al.[2]. TLS of studied HA (Table I) performed two

major peaks, a first at $\lambda_{ex}/\lambda_{em} = 455/515$ indicating highly conjugated aromatic compounds, like disubstituted coumarins, xanthones and quinones and a second peak at $\lambda_{ex}/\lambda_{em} = 310/480$ nm indicating simple phenolics like hydroxysubstituted benzoic and cinnamic acid derivatives Senesi et al.[5]. Peaks occured at the same positions, and differed only in fluorescence intensity, which was the highest at $\lambda_{ex}/\lambda_{em} = 455/515$ nm. This is evidence that HA from cultivated soils were more humified and polycondensed. Alberts et al.[1] reported, that the peak with similar $\lambda_{ex}/\lambda_{em} = 455.7/510.6$ nm was observed in HA form Hungarian soils.

Thermal properties, mainly the degree of aliphaticity "Z" (Table II) was lower in HA isolated from cultivated soil (0.62 and 0.59) than HA from forest soil (1.61 and 1.27), what confirmed higher condensation of aromatic structures or humification degree of HA from cultivated soil.

Conclusions

Results of the present study confirmed that absorbance, fluorescence and thermal characteristics of HA can be a sensitive index of structural changes between cultivated and natural soils, thus, they can be used as an indicator of anthropogenic influence on soil.

REFERENCES

1. Alberts J. J., Takács M.: Org. Geochem. *35,* 243 (2004).
2. Blaser P., Heim A., Luster J.: Environ. Int. *25,* 285 (1999).
3. Gonet S. S., Cieslewicz, J.: Environ. Int. *24,* 629 (1998).
4. Orlov D. S., Grischina L. A.: *Praktikum po chimii gumusa.* MGU, Moskva, 1981.
5. Senesi N., Miano T., Provenzano M. R., in: *Humic Substances in the Aquatic and Terrestrial Environment.* (Allard B., Borén H., Grimvall A., ed.), chapter V, p. 63. Springer, Berlin 1991.
6. Stevenson F. J.: *Humus chemistry. Genesis, composition, reactions.* Wiley, New York 1994.

P66   EVALUATION OF HEAVY METALS MOBILITY IN SEDIMENTS FROM THE HNILEC RIVER, SLOVAKIA

OĽGA ŠESTINOVÁ, JÁN BREHUV, JOZEF HANČUĽÁK, TOMISLAV ŠPALDON and ERIKA FEDOROVÁ

Institute of Geotechnics, Slovak Academy of Sciences, Watsonova 45, 043 53 Košice, Slovak Republic,
sestinova@saske.sk

Introduction

The contribution deals with the content and mobility of heavy metals: copper, nickel and lead in the samples of sediment load from drainage basin of the Hnilec River.

The former mining activities with the following treatment of iron and copper ores have had negative effect on the region of Middle Spiš. The main anthropogenic sources of the contamination of environment come from the localities Krompachy, Rudňany and the surroundings of Spišská Nová Ves, and also the river-basin of the Hnilec, the Ružín No. 1, the Palcmanská Maša reservoirs and an old environmental loads after mining activities in Smolník area. The flooded deposit in Smolník produces heavily mineralized acid waters that contaminate water and sediments of Smolník stream, Hnilec River and even Ružín reservoir. The deposit is not stable and negatively influences the surroundings[1].

Many sequential extraction methods were employed for the determination of particular forms of heavy metals contained in the sediments, differing in the number of the extraction steps, extraction solvents used extraction procedures. Leachate contains a group of elementary forms with similar physical and chemical properties. The extraction process evaluates the strength of bonding of the metal forms to different soil phases, to ion-renewable, carbonated, reducible, oxidable and finally to resistant residue[2]. The best known is the five-step sequential extraction of soil published by Mc Laren and Crawford and Tessier[3]. This method can differentiate heavy metals held in the sediments in five steps. It can be applied to provide a quick indication of changed element mobility in the monitored locality[4].

Experimental

C h a r a c t e r i s t i c   o f   t h e   S e d i m e n t s

The one-shot sequential extraction procedures were applied on eight sediment samples collected from the industrially polluted region of Central Spiš, Slovakia, localities of the Ružín No. 1 reservoir, the Palcmanská Maša reservoir and stream Smolník situated on the Hnilec River. The reference material of sediment from river Labe was also used for analysis. Sampling was realized in the year 2007 and total content of copper, nickel and lead were determined. Finally, the samples were dried, quartered, sieved under 1 mm and mineralised in a microwave pressure digestion system MWS-3.

S e q u e n t i a l   E x t r a c t i o n

The sequential extraction was conducted under the following procedures: **Fraction: A** – released forms were determined in the extract of extraction solvent – 2M HNO_3. The supernatant was filled up to 100 ml. The rest was used in the second step. This fraction contains metals bonded to sulphide and phosphate. **Fraction: B** – potentially mobile forms were determined in the extract of extraction solvent – 0.05M EDTA. This fraction contains metals in ion-changing form and bonded to carbonates. **Fraction: C** – mobile forms were determined in the extract of extraction solvent 0.1M $CaCl_2$. This fraction contains metals in ion-changing form. **Fraction: D** – residual forms presents extracted phase e. g. metals bonded to silicate structure and to a crystal lattice of primary minerals. The residuals were dried at room temperature. After drying and homogenization, the single extracts were measured by the absorption spectrometry method. Copper was determined by flame atomization and nickel and lead by graphite furnace atomic absorption spectrometry (VARIAN, Australia).

Results

Active soil reaction (pH) and oxidation-reduction potential is presented in Table I. It has shown that only sample SP (stream Smolník – mine Pech) was an acid sediment and the rest are slightly alkaline sediments. The increase of pH causes the growth of copper adsorption by colloid, clayey and organic material and thereby the mobility of copper in soil decreases[5].

Table I

The description of sampling places and chemical composition of sediments taken in area of the Hnilec Rriver in 2007

Locality		pH	Redox potential [mV]	Organic portion [%]	Dry basis [%]
Ruzin	VDR1	7.55	259	10.02	36.40
Ruzin	VDR2	7.25	254	10.18	54.52
Ruzin	VDR3	7.52	257	4.50	42.40
Pal. Masa	PM1	7.52	257	18.85	29.54
Pal. Masa	PM2	7.60	259	13.78	34.86
Pal. Masa	PM3	7.73	262	15.89	31.25
Pal. Masa	PM4	8.06	265	18.20	39.9
Smolník	SP	3.3	355	26.01	53.7

The results of copper, zinc, nickel and cadmium content determined in extraction solvents after extraction of sediments using sequential extraction are given in Table II.

The results of sequential extraction are presented as the percentage yield of metal from sequential extraction, where 100 % is total concentration of metal in sediment.

The results in cumulation histogram (Fig. 1.) show that the highest concentrations of copper were determined in the fraction A in released forms and the highest percentage yield in sample VDR1, 2 with values 65.7 and 60.3 % respectively. The yields in the potentially mobile and mobile forms were
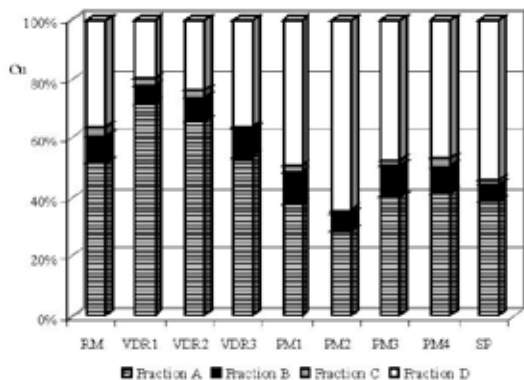
Fig. 1. **Cumulation histogram of the copper yields in fractions A–D of the sequential extracts of the sediments, RM – Reference Material-sediment, VDR1 – 3 Ružin No. 1 reservoir, PM1–4 Palcmanska Masa reservoir, SP – stream Smolník, mine Pech**

Fig. 3. **Cumulation histogram of the lead yields in fractions A–D of the sequential extracts of the sediments, RM – Reference Material-sediment, VDR1 – 3 Ružin No. 1 reservoir, PM1–4 Palcmanska Masa reservoir, SP – stream Smolník, mine Pech**

Fig. 2. **Cumulation histogram of the nickel yields in fractions A–D of the sequential extracts of the sediments, RM – Reference Material-sediment, VDR1 – 3 Ružin No. 1 reservoir, PM1–4 Palcmanska Masa reservoir, SP – stream Smolník, mine Pech**

low. In fraction D the highest values of yield were confirmed in samples PM2 64.1 % and SM 55.2 %.

The Fig. 2. presents the distribution of nickel in fractions. The highest concentration of nickel was determined in fraction D, where the highest yield was in sample PM4 80 % and the least in sample SP 16 %. In the other forms, the nickel content in yield was very low.

According to Fig. 3., the highest concentrations of lead were found in fraction A, where the highest values of yield were in samples PM 3 64.2 % and PM 2 – 1 (54.4–51.6 %). In fraction B–C, the content of was in low percentage yield and the yield was higher in fraction D.

The results of yield are given in Table III, where the total content of particular heavy metals Cu, Ni, Pb in sediments were compared with the sum of metal concentrations in fraction A–D from sequential extraction. In sample PM2, 100 % yield of copper was determined.

Table II
Copper, nickel and lead content determined in extraction solvents after extraction of sediments using sequential extraction method, RM – Reference Material-sediment, VDR1 – 3 Ružin No. 1 reservoir, PM1–4 Palcmanska Masa reservoir, SP – stream Smolník, mine Pech

Fraction	Element	Sediment contents [mg kg^{-1}]								
		RM	VDR1	VDR2	VDR3	PM1	PM2	PM3	PM4	SP
A	Cu	33.5	160.0	178.2	166.0	14.6	10.0	19.6	18.4	216.0
	Ni	3.3	9.6	4.6	5.7	7.0	5.1	7.4	4.5	0.3
	Pb	33.9	34.7	40.4	35.3	26.3	55.5	18.0	17.1	34.9
B	Cu	6.0	13.4	22.6	29.4	4.0	1.8	5.0	4.0	35.0
	Ni	2.0	0.6	07	1.3	2.4	1.4	5.4	5.0	0.1
	Pb	4.1	2.9	4.2	6.4	3.7	6.7	2.7	2.1	4.4
C	Cu	2.0	5.2	6.8	2.8	0.8	0.5	1.0	1.2	6.2
	Ni	1.3	1.2	1.6	0.6	0.6	0.4	1.1	1.4	0.3
	Pb	1.7	1.6	2.3	0.8	0.8	1.1	0.8	0.6	1.2
D	Cu	23.7	45.2	64.2	11.2	18.9	22.0	0.3	20.8	306
	Ni	26.7	38.5	27.3	27.4	47.2	42.6	51.3	47.4	7.1
	Pb	15.6	5.4	7.3	9.8	4.4	2.7	2	2.4	8.7

Table III

Analysis comparison of total dissociation and the sum of metal concentrations in the sequential extraction procedure of the sediment samples

Element		Sediment [mg kg^{-1}]								
		RM	VDR1	VDR2	VDR3	PM1	PM2	PM3	PM4	SP
	Sum of ex.st.	65.2	223.8	271.8	309.4	38.3	34.3	48.6	44.4	563.2
Cu	Total cont.	79.9	243.5	295.5	353.9	45.8	34.3	49.5	47.9	572.0
	Yield %	81.6	91.9	92.0	87.4	83.6	100	98.2	92.7	98.5
	Sum of ex.st.	33.3	49.9	34.2	35.0	57.2	49.5	65.2	58.7	7.8
Ni	Total cont.	35.5	66.0	82.3	67.4	79.6	60.1	80.0	59.2	44.2
	Yield %	93.8	75.6	41.5	51.9	71.8	82.4	81.5	98.5	17.6
	Sum of ex.st.	55.3	44.6	54.2	52.3	35.2	66	23.5	22.2	49.2
Pb	Total cont.	77.6	108	121	80	51	102	28	37	92
	Yield %	71.3	41.3	44.8	65.4	69	64.7	83.9	60	53.5

The comparison of the sum of metal concentrations in the sequential extraction procedure with of total dissociation verified the suitability of the used method. Moreover, the RM LGC River Sediment was applied, where metal contents are copper – 83. 6 mg kg^{-1}, zinc – 439 mg kg^{-1}, nickel – 34.7 mg kg^{-1} and cadmium – 2.7 mg kg^{-1}.

Conclusions

The one-shot sequential extraction, which characterise the individual forms of heavy metals bonds in the sediments, was used for the determination of heavy metals mobility in the contaminated sediments from the Hnilec River (Slovakia) area. 2M HNO$_3$ was used to define the released content including different fractions of elements according to their solubility. Potentially mobile and mobile forms represent the sum of risk element forms for the evaluation of sediment biotoxicity. In this connection, the sediments had low content of copper, nickel and lead in potentially mobile and mobile forms (fractions B–C). This fraction contains metals in ion-changing form and bond to carbonates.

Lead and copper reached higher values and nickel was in the least concentration in fraction A (realised forms) in order Pb > Cu > Ni. This fraction contains metals bonded to sulphide and phosphate.

REFERENCES

1. Luptakova A.,: *Flowed deposit Smolnik – the source of acid mining waters, 3rd Conference on Environment engineering*, 81-85, 2006.
2. Zavadska M., Zemberyova M., Farkasovska I.: Chem. papers *93*, 391 (1999).
3. Tessier A., Campbell P. G. C., Bisson M.: Anal. Chem. *57*, 844 (1979).
4. Vojtekova V., Krakovska E.: Chem. papers *100*,1096 (2006).
5. Takac P., Kozakova L., Valkova M., Zelenak F.: Acta Montanistica Slovaca *13(1)*, 82 (2008).

P67 ELIMINATION OF SULPHATES FROM WASTE WATER OF OLD MINING LOADS

TOMISLAV ŠPALDON, JÁN BREHUV, JOZEF HANČUĽÁK, OLGA ŠESTINOVÁ and ERIKA FEDOROVÁ

Institute of Geotechnic of the Slovak academy of science, Watsonova 45, 043 53 Košice, Slovak republic, spaldon@saske.sk

Introduction

Heavy industry and the impact of mining, although being in decay, significantly facilitate the deterioration of quality of surface waters. Besides the technological water from the existing plants, there is a huge amount of secondarily polluted mining waters due to the rainfall. The rainfall water in the underground areas in old mining works gradually chemically and chemically and biologically reacts with the surrounding rock environment and brings amounts of harmful substances to the surface that pollute the surface waters. They include mainly heavy metals, sulphates, chlorides, phosphates and other substances.

From the point of view of quality of surface waters the area in the vicinity of the municipality of Smolník has been known as one of the worst in Slovakia for a longer period of time and the brook of Smolník is ranked in the worst – the fifth degree of quality as a highly polluted brook.

This work aims at the following: study the possibility of reduction of the concentration of the content of sulphates and other heavy metals set by the EU directives in the mining waters flowing from the old mining load of the deposit of Smolník.

Table I
Trend of mine water quality from Smolník in period from 1986 to 2004[2]

Year	SO_4^{2-} [mg dm^{-3}]	Fe [mg dm^{-3}]	Cu [mg dm^{-3}]	Mn [mg dm^{-3}]
1986	6,004	72.0	37.2	43.3
1987	4,634	51.2	39.4	65.8
1991	1,155	7.0	11.1	12.3
1992	1,233	19.9	10.7	13.5
1993	1,481	61.3	5.3	12.8
19941	1,350	57.8	7.2	11.3
19942	4,000	155.0	11.8	11.0
19943	9,512	914.7	51.3	104.7
1995	5,825	772.4	7.4	136.2
1997	4,133	421.4	3.9	37.2
2000	4,170	137.6	4.3	41.3
2001	3,461	556.0	2.8	37.9
2002	2,296	620.0	1.7	38.4
2003	2,680	501.0	1.5	33.4
2004	2,723	425.0	1.5	27.9

Physical and Chemical Characteristics of the Mining Water from the Deposit of Smolník

Qualitative parameters of the running mining water were monitored systematically. The values often move significantly. They depend on the amount of rainfall, rainfall intensity, period of being held in the mining areas, place (depth), etc. A large number of floods and mainly fires in the mine caused huge increases of presence of Fe and Cu in the mining water. The mining fire by spontaneous combustion of pyrite in 1896–97 caused the increase of the Cu concentration up to 150 g dm^{-3}, in 1910 the Cu concentration increased even to 180 g dm^{-3} due to the fire! In 1923 57.6 tonnes of copper flew into the recepient.[1]

Table I evidently shows the gradual increase, culmination and finally the decrease of value of almost all indicators. Those changes were caused due to flooding and its completion. After almost four-year exposition of mining waters in the rock environment a strong mineralisation occurred and concentration of all components exceeded all permissible concentrations (they are exceeded today as well).

Elimination of Sulphates using Precipitation and Al-Ions.

The concentration of sulphate ions in the tested water was 2,984 mg dm^{-3} and pH 3.34. When making experiments with the mining water a HACH spectrophotometer, type DR 2000 and a digital pH-meter WTW 330i were at our disposal.

Precipitation of SO_4^{2-} Ions Only at Presence of $Ca(OH)_2$ Without Al^{3+} Ions

Methodological procedure of precipitation:
- $Ca(OH)_2$ – 15 minutes of mixing at 200 rpm,
- suspension filtering,
- determination of the content of sulphates and the pH value (see in Table II).

Table II
Results of mine water desulphatation by $Ca(OH)_2$, Pech pit

Sample no.	$Ca(OH)_2$ [mg dm^{-3}]	pH	SO_4^{2-} [mg dm^{-3}]	Effect des. [%]
1	6	12.59	2,400	19.6
2	8	12.60	2,362	20.8
3	10	12.61	2,385	20.1
untreated water	0	3.34	2,984	–

As the required pH value is 12.4 and more, Table II shows that the sufficient amount of $Ca(OH)_2$ is 5–6 g dm^{-3}. Higher amounts do not impact the pH values any longer. At the same time, one can observe that adding of lime itself has no significant impact on the reduction of the content of sulphates either. Out of the original approximate amount of 2,984 g only 600 g were precipitated and that constitutes the efficiency of only about 20 %.

Precipitation of SO_4^{2-} Ions at Presence of $Ca(OH)_2$ and Sodium Aluminate (ALR-F)

Methodological procedure of precipitation is based on long range experiments of the scientific group from Technical university in Ostrava[3]: Best results of sulphates precipitation were obtained at pH value close to 12.5.

- $Ca(OH)_2$ – 15 minutes of mixing at 200 rpm
- ALR-F –30 minutes of mixing at 200 rpm
- suspension filtering
- determination of the content of sulphates and the pH value

Al ions changes to form hydrated calcium aluminates and part of arisen mineral ettringite, Fe ions change from bivalent to trivalent ferrous hydroxide and also remain in the mud.

The results of those experiments are shown in Table III[5].

Table III

Results of mine water desulphatation from Pech pit at optimal reagents dosing[4]

Sample No.:	$Ca(OH)_2$ [$g\,dm^{-3}$]	ALR-F [$ml\,dm^{-3}$]	pH	SO_4^{2-} [$mg\,dm^{-3}$]	Effect desul. [%]
1	5.2	3.2	12.56	118.28	96.03
2	5.2	3.4	12.56	199.60	93.31
3	5.2	3.6	12.56	49.92	98.32
4	5.2	3.8	12.56	45.28	98.48
5	5.4	3.2	12.56	64.40	97.84
6	5.4	3.4	12.56	123.28	95.87
7	5.4	3.6	12.55	65.00	97.82
8	5.4	3.8	12.55	49.64	98.33
9	5.6	3.2	12.58	114.40	96.17
10	5.6	3.4	12.58	42.96	98.56
11	5.6	3.6	12.58	0.48	99.98
12	5.6	3.8	12.58	0.97	99.97

Elimination of Sulphates Using Sorbents and Ion Exchangers

As opposed to the static regime when a sorbent or precipitation reagents are added to the water container when they are slowly mixed for a certain optimal time, in case of a dynamic regime the treated water continuously flows through the column the bed of which consists of a sorbent, a ion exchanger or a mixture with the sorbent. Experiments with the mining water from the shaft of Pech – Smolník were performed. The water was stabilised in the ratio of 5 ml HNO_3 (2M) per 1 litre. Elimination of sulphates can be realised using the following methods:

- raw stabilised mining water,
- sorbent – active coal,
- ion exchanger – mixture 50 : 50 catex and anex,
- sorbent – zeolite (Nižný Hrabovec) mineral form –clinoptilolite, structure - tectosilicate, empiric formula – $(Ca,K_2,Na_2,Mg)_4Al_8Si_{40}O_{96} \cdot 24H_2O$,

- mixture of 80 % of zeolite, 20 % cent of A–C,
- mixture 80 %of zeolite, 20 % of C–A,
- ion exchanger – cation exchanger – catex-strog acid Ostion,
- ion exchanger – anion exchanger – anex – light basic annex with styrene-DVB skeleton – Amberlite IRA-96,
- sorbent – slovakite (inorganic composite sorbent) – it is sorbent based on advantages of various minerals properties.
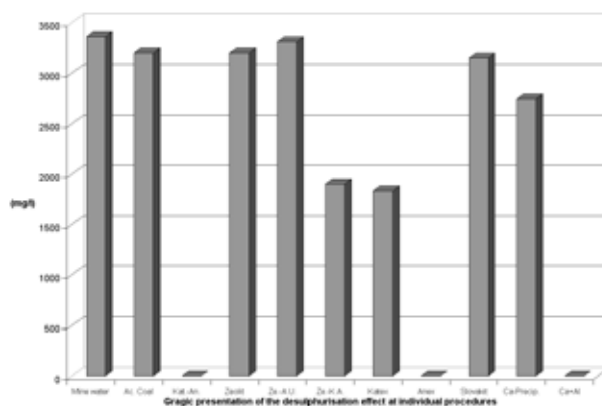
Fig. 1.　**Graphic presentation of the desulphurisation effect at individual procedures**

Discussion to the Measured Results.

Sulphates reduction is possible by various methods, like reversing osmosis, electrodialysis, ultrafiltration, diaphragm processes, but these methods are too expensive. Biological methods are long-lasting, that is why we used chemical processes, i.e. sorption by active coal, various sorbents and ion exchangers and precipitation by Al and Ca ions.

Based on the results shown in Fig. 1. the success rate of individual reagents can be definitely set. The inorganic component sorbent slovakite may be considered as relatively successful. It was tested in the static regime as well and it was rather unsuccessful there. The result was surprising in case of the dynamic sorption. The efficiency of elimination of sulphates reached approximately 60 %. The efficiency of 43 % in case of the mixture of zeolite and the cation exchanger and the anion exchanger was caused only due to the small amount of the anion exchanger in the reagent. There was no practical effect of zeolite itself. Almost 100% efficiency was achieved by means of the anion exchanger what is in case of anion elimination logical[6].

Conclusion

As the strict limits for waters discharged to the surface flows set by the European Union begin to come into force also in the recently acceded EU countries the issue of waters discharged from the old mining load of Smolník will have to be dealt with seriously very soon. Several options are offered. The use of ion exchangers would be probably very costly although a very efficient solution. The most probable solu-

tion will be the use of physical and chemical methods, and namely their different combinations, such as neutralisation, precipitation by means of Al ions or sorption by means of composite sorbents.

REFERENCES
1. Jaško V.: Smolník: *Komplexné hydrogeologické a hydrochemické posúdenie ložiska Cu – Fe rúd*, Štúdia, Bratislava 1966.
2. Šlesárová A.: Doktorandská dizertačná práca. Košice 2007.
3. Vidlář J., Schejbal C. : *Důlní vody s nadlimitním obsahem síranů a možnosti jejich čištění*, Sborník vědeckých prací Vysoké školy báňské-Technické univerzity Ostrava, 1999.
4. Heviánková S., Vidlář J., Špaldon T.: *Tests of precipitation of sulphates from mining water*, kwartalnik Górnictwo i Geoinżynieria, zeszit 3/2, Krakow 2005.
5. Luptáková A., Špaldon T., Bálintová M.: *Remedation of acid mine drainage by means of biological and chemical methods*, IBS 2007, Frankfurt am Main, Biohydrometallurgy: From the single cell to the environment, p. 285, ttp Trans Tech publications Switzerland, 2007.
6. Špaldon T.: Doktorandská dizertačná práca, Vysoká škola báňská, Ostrava 2007.

P68   ARSENIC REMOVAL FROM WATER BY SYNTHETIC AKAGANEITE

MIROSLAVA VÁCLAVÍKOVÁ[a,c], KATARÍNA
ŠTEFUSOVÁ[a], GEORGE P. GALLIOS[b] and ŠTEFAN
JAKABSKÝ[a]

[a]Institute of Geotechnics, Slovak Academy of Sciences, Watsonova 45, 043 53 Košice, Slovakia,

[b]Laboratory of General. & Inorganic Chemical Technology, School of Chemistry, Aristotle University, 540 06 Thessaloniki, Greece,

[c]School of Chemistry, Royal Military Academy, Renaissancelaan 30, 1000 Brussels, Belgium,
vaclavik@saske.sk

Introduction

Arsenic is considered one of the most toxic contaminants found in water-streams. It poses serious health risks to humans (e.g. cancer, cardiovascular and neurological effects). There are two main groups of arsenic pollution sources; natural (dissolution of As containing mineral ores) and anthropogenic sources (e.g. arsenic-based insecticides and pesticides, fertilizers, coal combustion, mining, semiconductor industies). The maximum contaminant level of arsenic in drinking water (both in EU and USA) is 10 $\mu g\,dm^{-3}$.

Arsenic has several oxidation states (-3, 0, $+3$, $+5$) but the most common forms in natural waters are trivalent arsenite [As (III)] and pentavalent arsenate [As (V)]. The pH and the redox potential (Eh) of the aqueous system determine the predominant form of As; As (III) is dominant in reducing conditions while As (V) in oxidizing conditions. Generally, As (III) is considered to be more toxic than As (V)[1].

There are various methods for arsenic removal from water streams, such as sorption, ion-exchange, precipitation, coagulation and flocculation, reverse osmosis, membrane technologies, electrodialysis, biological processes as well as lime softening. A good overview[2] and a critical review[3] of the available methods are given recently. An effective and commonly used method for water treatment is sorption of arsenic on natural or synthetic sorbents. The most commonly used sorbents can be classified in two main groups: *(i)* sorbents based on iron compounds, which are the most frequently used (e.g. several iron (III) oxides/hydroxides, materials based on iron oxides/hydroxides, natural iron ores and waste materials containing iron particles) and *(ii)* sorbents based on aluminium compounds (e.g. activated alumina or gibbsite). Several other sorbents (clays, manganese dioxide, activated carbon, ion-exchange resins, biosorbents, etc.) have also been studied for As removal[2].

Experimental

Reagents

Analytical grade chemicals were used in all experiments. Model solutions were prepared by dissolving $AsHNa_2O_4 \cdot 7H_2O$ in deionized water, 0.01 M $NaNO_3$ and 0.1 M $NaNO_3$. The pH of the solutions was adjusted with suitable concentrations of NaOH and HNO_3.

Preparation and Characterization of Sorbent

Synthetic akaganeite was prepared by hydrolysis of partially neutralized $FeCl_3$ by addition of NaOH. The precipitate thus obtained was centrifuged and it was subsequently submitted to dialysis to remove Cl^- ions. The material was dried and used for arsenic sorption. XRD analysis[4] confirmed that the material produced was akaganeite. The specific surface area (measured by BET) was 151.3 $m^2\,g^{-1}$.

Sorption Experiments

The effect of pH, initial arsenic concentration, sorbent dose and temperature as well as ionic strength effect at arsenic sorption were studied in batch type experiments. The experiments were performed in a rotary shaker set at 30 rpm and equilibrium time 24 hours. Preliminary experiments have shown that equilibrium was established. The arsenic quantity in solutions was determined by AAS and spectrophotometry before and after the sorption experiments. The sorption capacity (Q) of akaganeite was calculated using the equation:

$$Q = \frac{C_0 - C_{eq}}{C_s} \tag{1}$$

where C_0 and C_{eq} are the initial and equilibrium arsenic concentration, respectively and C_s is the sorbent concentration in solution.

Results

Effect of Solution pH

It is well known that the solution pH plays an important role in all sorption experiments in aqueous systems. It determines the aquatic chemistry of the system under study (in this case As speciation) and also the charge density of the solid surface (sorbent). It is related to the sorption mechanisms and reflects the nature of the physicochemical interactions of the species in solution and the active sites on the sorbent[5].

The effect of solution pH on As (V) sorption on akaganeite was examined at pH values 2.0–9.0 at ambient temperature. Sorbent concentration in solution was 2 $g\,dm^{-3}$ and initial arsenic concentration was 100 $mg\,dm^{-3}$. The results are given in Fig. 1. for various electrolyte ($NaNO_3$) concentrations. The best sorption is observed at pH 2.0. However, in this case, akaganeite is dissolved and iron was determined in filtrates. For this reason, all sorption experiments were carried out at pH 3.5, where no iron was found in solution. At this pH, the sorption capacity was a bit smaller than at pH 2.0 and around 40 mg As (V) g^{-1} of sorbent. This is considered quite good compared to the average value reported in the literature[3]. The effect of the ionic strength was also studied by adding 0.01 and 0.1 M $NaNO_3$. It is shown that (Fig. 1.) the

effect can be considered as negligible. In a previous study[4] the zeta potential of akaganeite was studied and the point of zero charge was found at pH 7.5. At pH 3.5, the zeta potential was around +20 mV and the predominant As (V) species is $H_2AsO_4^-$. So, attractive electrostatic forces favour sorption. However, at pH 8.0, the zeta potential is negative and the predominant species is $HAsO_4^{-2}$. Electrostatic forces are repulsive but still sorption is achieved due to the existence of specific forces. Calculations with Geochemist Workbench (data not shown here) show that in the presence of iron mineral As (V) can form scorodite (iron arsenate) on the mineral surface and the maximum is obtained at pH 2.0, This coincides very well with the maximum sorption at pH 2.0 in our experiments (Fig. 1.). The existence of scorodite on akaganeite surface was also proved by FTIR spectra[6]. The chemical nature of the sorption can also explain the sorption of As (V) at pH 8.0. In our results, the effect of ionic strength was negligible. However, in the literature[6] a significant effect was observed, but with KNO_3 and in smaller sorbent concentrations (<2 $g\,dm^{-3}$). The effect was decreasing with increasing sorbent concentrations. This was attributed to the elimination of the negative charge of akaganeite by the potassium cations and the easier approach of As (V) species to the surface of the sorbent. It is well known that the increase of the ionic strength decreases the effective radius of the electric double layer. The arsenate species can come closer to the surface so that the attractive chemical forces overcome the electrostatic repulsion forces and sorption is achieved.
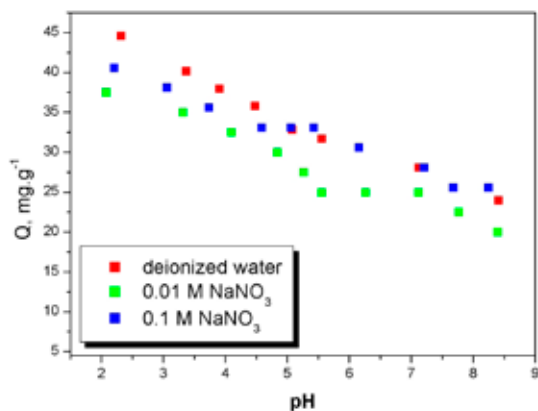
Fig. 1. **Effect of solution pH on As (V) sorption**

Effect of Initial Arsenic Concentration

The effect of initial arsenic concentration (20–200 $mg\,dm^{-3}$) was studied with 2 $g\,dm^{-3}$ sorbent concentration, ambient temperature and pH values 3.5 and 7.0. The results are given in Fig. 2. (data points: experimental data, lines: isotherms). Sorption isotherms were evaluated (from experimental data) using the Freundlich model:

$$Q = K C_{eq}^b \qquad (2)$$

where Q is amount sorbed per unit mass of sorbent, K and b are constants and C_{eq} is the equilibrium concentration. Freundlich sorption parameters (K, b, R^2) were calculated and are given in Table I. The maximum sorption capacity was around 53 and 37 $mg\,g^{-1}$ for pH values 3.5 and 7.0 respectively. The R^2 values show a good agreement of the model to the experimental data. As is expected, the K value (which shows the affinity of akaganeite to As (V)) decreases with the increase of the pH.
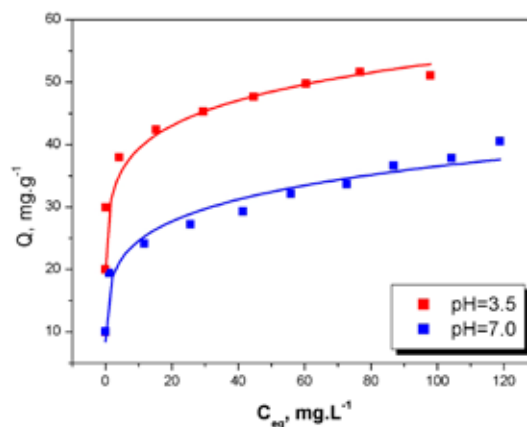
Fig. 2. **Sorption isotherms**

Table I
Freundlich adsorption parameters

pH	Freundlich parameters		
	K	b	R^2
3.0	32.26	0.10	0.98
7.5	12.84	0.23	0.97

Effect of temperature

The effect of temperature on arsenic sorption was investigated at initial arsenic concentration 100 $mg\,dm^{-3}$, sorbent concentration 2 $g\,dm^{-3}$ and 4 different temperatures (ambient, 30, 40 and 50 °C). The experimental results are presented in Table III. The maximum sorption capacity increased with increasing temperatures indicating an endothermic reaction[6]. The maximum sorption capacity (at 50 °C) was around 43 $mg\,g^{-1}$.

Table II
The effect of temperature

T [°C]	Q [$mg\,g^{-1}$]
ambient temperature	37
30	38
40	40
50	43

Effect of Sorbent Dose

The effect of sorbent dose was studied at ambient temperature, initial arsenic concentration 100 $mg\,dm^{-3}$ and sorbent

concentration range 0.5–10 $g\,dm^{-3}$. The results are presented in Table II. Increase of the sorbent dose in solution caused a decrease of akaganeite sorption capacity. However, this is not a good indicator of sorption ability, because with bigger sorbent concentrations all the available active sorption sites are not occupied. It is important to see what is the remaining As (V) concentration after treatment. In a real system this is the important factor; the remaining concentration should be below the limits. In the last column of Table III the remaining concentrations are given. It is observed a significant decrease of the remaining As (V) conc. with increase of the sorbent dose. It seems that a good dose is 5 $g\,dm^{-3}$, which gives a 96 % removal and a satisfactory final As concentration of 4 $mg\,dm^{-3}$.

Table III
The effect of sorbent dose

$C_S\,[g\,dm^{-3}]$	$Q\,[mg\,g^{-1}]$	$C_{eq}\,[mg\,dm^{-3}]$
0.5	43.0	78.5
1.0	41.4	58.6
2.0	36.3	27.4
5.0	19.2	4.0
10.0	9.6	4.0

Conclusions

Synthetic akaganeite is a suitable sorbent for arsenic removal, especially at acidic environment. It is a low cost sorbent, as it is prepared from easily available cheap inorganic materials and has a good efficiency (above the average reported in the literature). It removes arsenic by chemical sorption favored by an increase of temperature and the best results are obtained at pH 3.5. However, at pH 7.0, gives also satisfactory results. This is important for the treatment of drinking water. The capacity of the material was not affected significantly with increased ionic strength (up to 0.1 M $NaNO_3$). The experimental data follow (with good agreement) the Freundlich isotherm.

REFERENCES
1. Smedley P. L., Kinniburgh D. G.: Appl. Geochem. *17*, 517 (2002).
2. Vaclavikova M., Gallios G. P., Hredzak S., Jakabsky S.: Clean. Techn. Environ. Policy. *10*, 89 (2007).
3. Deliyanni, E. A., Peleka, E. N., Gallios, G. P., Matis, K. A.: Int J Envir & Waste Manag, (in press).
4. Štefušová K., Václavíková M., Gallios G. P., Jakabský Š., Kozáková I., Ivaničová L., Gešperová D.: *Proceedings of the 11th International Conference on Environment and Mineral Processing, Ostrava, 31 May –2 June 2007*, (Fečko P., Čablík V., ed.), Part II, p. 71 (Lecture).
5. Aksu Z., Gönen F.: Process Biochem *39*, 599 (2004).
6. Deliyanni, E. A., Bakoyannakis, D. N., Zouboulis, A. I., Matis, K. A.: Chemosphere *50*, 155 (2003).

P69 THE EPR STUDY OF PARTICULATE MATTER

NADEŽDA ŠTEVULOVÁ, ADRIANA EŠTOKOVÁ and PAVEL STOPKA

Technical University of Košice, Civil Engineering Faculty, Institute of Building and Environmental Engineering, Vysokoškolská 4, 042 00 Košice, Slovak Republic, Nadezda.Stevulova@tuke.sk

Introduction

In recent years the role of particulate matter in environmental and health areas has come under increased attention of experts and public. The PM_{10} and $PM_{2.5}$ (particle fractions related to their size) concentrations show higher correlation to the negative health effects in comparison to the total suspended particulate matter[1]. Building constructions and materials play an important role in indoor particulate matter contamination due to particles infiltration through joint construction leakages and material distribution and deposition processes[2].

The dust particles are dangerous not only because of their high concentrations in dependence on their particle size but also because of their nature[3]. The surface of the inhaled particles which determines the biological response is large. The surface reactivity of particles depends on the number of reactive spots on the dust particles surface and on the distribution of various sites (free radicals and paramagnetic species) at the surface[4]. It determines the pathogenic potential of inhaled particles.

This work is concerned with the particulate matter reactivity investigation by concentration of surface active centres.

Experimental

Both total suspended particles (TSP) and PM_{10} measurement includes integral sampling onto a collection material (membrane filter Synpor 0.8 µm pore size, 35 mm in diameter) by sampling equipment VPS 2000 (Envitech, Trenčín) at flow rate of 960 $dm^3\,h^{-1}$ during sampling period of approximately 24 hours.

The surface reactive spots concentrations of suspended particulate matter were detected on the spectrometer ERS 220 (GAS, Berlin) with a resonator RSX 216 at room temperature under following conditions: the microwave power 10 mW, modulation amplitude 0.02 mT, time constant 0.5 s. The relative intensity of the signals measured for investigated dust samples was determined by comparing them with those of Mn(II)/ZnS a Cr(III)/MgO as standard samples. The EPR spectrum was recorded as the first derivation of the absorption spectrum at the speed record 14.3 $mT\,min^{-1}$.

The quantitative and qualitative interpretation of obtained spectra was performed by computer software Origin.

Results

Typical EPR spectra of investigated total suspended particulate mater and PM_{10} samples are illustrated in Figs. 1.–3.
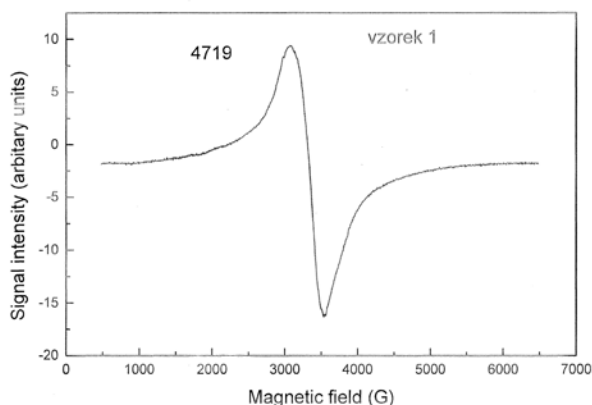
Fig. 1. **EPR spectra of total suspended particulates**
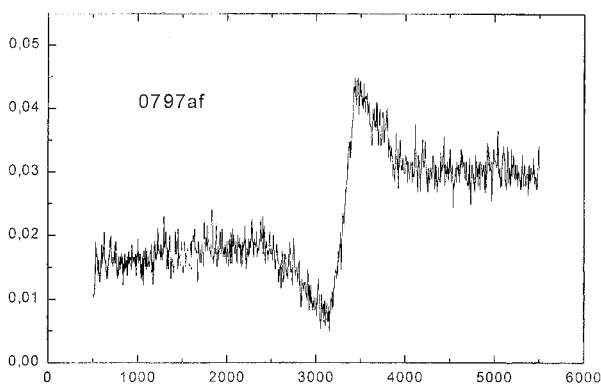
Fig. 2. **EPR spectrum of PM_{10}**
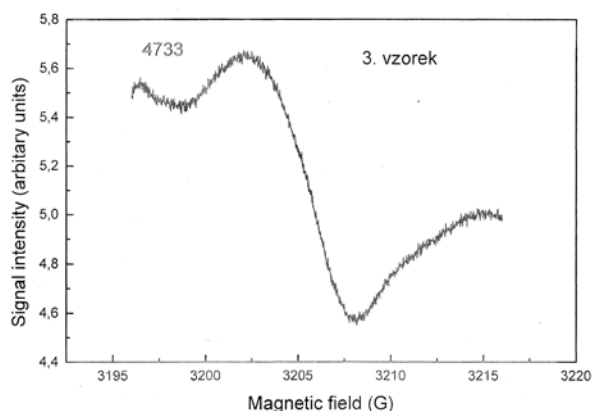
Fig. 3. **Detail of PM_{10} EPR spectrum**

Wide singlet peak centered at g factor value was identified in EPR spectra of particulates. The g factors range from 2.010 to 2.093 for measured particle samples as the Table I shows.

Singlet peak superponed by triplet peak with factor values $g_1 = 2.1162$, $g_2 = 2.0700$, $g_3 = 2.0191$ was identified in EPR spectrum of total particulate matter in Fig. 1. It could be an isotropic triplet (g = 2.07) with splitting constant a = 7.6375 +/ 0.5495 mT.

Table I
G-factor values, ΔH_{pp} and spin concentrations

Sample	g-factor	ΔH_{pp} [mT]	Spin concentration [spin mg^{-1}]
TSP	2.070	34.6	3.84×10^{18}
TSP	2.015	40.0	3.68×10^{17}
TSP	2.020	40.0	1.64×10^{18}
TSP	2.010	40.0	2.22×10^{18}
PM10	2.093	472	2.01×10^{18}
PM10	2.080	554.9	2.02×10^{17}
PM10	2.055	410.8	2.06×10^{17}
PM10	2.070	345.65	1.09×10^{19}

The signals on EPR spectra recorded on the particulate samples were identified as a superposition of signals arising from various paramagnetic species. It is mainly the presence of transition metal ions in a low oxidation state, typically iron, which have to be regard as a possible cause of toxicity. In accordance with results obtained in paper[4], the appearance of Fe^{2+} on the surface of the dust particles and its subsequent oxidation to Fe^{3+} in octaedric configuration leads to production of free radicals at solid-liquid interphase by direct reduction of atmospheric molecular oxygen. These sites may be implicated in the formation of dangerous active oxygen species in vivo.

The total surface spin concentrations of particulate samples were determined in range from 3.68×10^{17} to 3.84×10^{18} spin.g^{-1} for total suspended particulate matter and from 2.02×10^{17} to 1.09×10^{19} spin g^{-1} for PM_{10}. The significant difference between spin concentrations values of total

suspended particulate matter and PM_{10} was not found. The determined spin concentrations values are approximately 10^2 times higher than spin concentrations values of mechanically activated quartz and silicon powders[5].

Conclusions

The determined surface spin concentrations obtained from EPR spectra were high. But based on these experimental results of paramagnetic centres occurrence study explicitly, it cannot be expressily considered particulate matter to have toxic properties. The paramagnetic ions testing in special chemical reactions[6] used for this purpose may more accurately indicate potential risk of particulate matter toxicity.

REFERENCES

1. Marconi A.: *Proceeding of Conference Healthy Buildings*, p. 531. Helsinky, 2000.
2. Sverak T.: Int. J. Mineral. Proces. *74*, S379 (2004).
3. Seinfeld J. H.: *Atmospheric Chemistry and Physics of Air Pollution*. Wiley, New York 1985.
4. Volante M., Giamello E. et al: *Proceeding of the 1st International Conference on Mechanochemistry*, p.125. Cambridge Interscience Publishing, Cambridge, 1994.
5. Tkáčová K., Števulová N.: J. Mater. Res. *10*, 2728 (1995).
6. Fenoglio I., et al: J. Mater. Synth. Proces. *8*, 145 (2000).

P70 SELECTION OF PACKING MATERIALS FOR BIOFILTER DEVELOPMENT

IVETA ŠTYRIAKOVÁ and ALEXANDRA VAŠKOVÁ

Institute of Geotechnics of the Slovac Academy of Sciences, Watsonova 45, 043 53 Košice, Slovakia,
bacil@saske.sk

Introduction

Natural materials that are available in large quantities may have potential as inexpensive sorbents. Cost effective alternative technologies or sorbents for treatment of metals contaminated waste streams are needed. A study[1] reported that zeolites, clinoptilolite in particular, demonstrate strong affinity for Pb and other heavy metals. Adsorbing Cd and Zn examined by both modifications with natural bentonite[2]. Results showed that the acid-treatment decreased the adsorption capacity, while the heat treatment did improve capacity. Retention of Pb and Zn on pure calcite was the subject of a number of investigations[3,4]. On the contrary, the number of sorption studies of both ions on magnesite is very limited.

Investigations on the biosorption mechanism of heavy metals show that the metal ions are deposited by adsorption to the functional groups present on the cell wall. Dead as well as living cells are used in the removal of metal ions[5,6]. The batch adsorption experiments demonstrate that the surface complexation approach can be used successfully to quantify the adsorption of Cd in a mixed *B. subtilis* – quartz system as functions of both pH and solute/sorbent ratios[7].

We are interested in the surface complexation approach of zeolite, bentonite, calcite, magnezite and also these materials with bacteria in the behavior various heavy metals in the batch experiments. The objectives of this work were to determine the differences of mineral/water and mineral-bacteria/water interface in sorption capacities of metals.

Experimental

The biosorption experiments were carried out in Erlenmeyer flasks which contained 10 g samples and 100 ml medium. The medium contained (per liter) 0.5 g NaH_2PO_4, 1.0 g $(NH_4)_2SO_4$, 0. g NaCl, and 2 g glucose. The flasks were inoculated with a mixture of *Bacillus cereus* and *B. megaterium* (0.1 g wet bacteria dm^{-3}) that had been previously isolated from Horná Prievrana. The two strains were purified by heat treatment at 80 °C for 15 min followed by streak plating on nutrient agar cultures. The isolates were identified with the BBL Crystal Identification System (Becton, Dickinson and Co., Franklin Lakes, NJ). For identification, the isolates were cultivated on Columbia agar plates per manufacturer's instructions.

The flasks were incubated under dynamic conditions (150 rev min^{-1}) for 3 hours at 25 °C. The liquid phase was contained individual metals in 0.5mM concentration in the forms $ZnSO_4$, $CuSO_4$, $PbCO_3$. The spent media (leachates) were sampled for metal analysis. The chemical controls did not receive an inoculum but were incubated under otherwise similar conditions.

Solid residues were analyzed by X-ray diffraction using a Philips X'Pert SW–binary diffractometer with CuKα radiation (40 kV, 50 mA), equipped with an automatic divergence slit, sample spinner, and a graphite secondary monochromator. Data were collected for 2–60 °2Θ with a step width of 0.05 ° and a counting time of 30 s per 0.05 °. The mineralogy has been evaluated in quantitative terms from X-ray powder diffraction patterns using a Rietveld-based data processing technique.

Quantitative changes in the liquid phase were measured with a Model 30 Varian atomic absorption spectrometer (Varian, Inc., Melbourne, Vic., Australia).

Batch experiments were conducted to measure:
- Zn, Cu, Pb and zeolite adsorption in a mixed singly metals – zeolite – *Bacillus* system
- Zn, Cu, Pb and bentonite adsorption in a mixed singly metals – bentonite – *Bacillus* system second
- Zn, Cu, Pb and quartz sands adsorption in a mixed singly metals – quartz sands – *Bacillus* system
- Zn, Cu, Pb and calcite adsorption in a mixed singly metals – calcite – *Bacillus* system
- Zn, Cu, Pb and magnezite adsorption in a mixed singly metals – magnezite – *Bacillus* system

Zeolite

The natural materials, zeolite was obtained from Nižný Hrabovec location in Slovakia. The mineralogical composition of zeolite was clinoptilolite 51–68 %, quartz + cristobalite 9–20 %, feldspars 8–13 %, mica 13 % and iron minerals 0.3 %.

Table I
Chemical composition of zeolite

Components	SiO_2	Al_2O_3	Fe_2O_3	MgO	Na_2O
% wt.	67.0	12.3	1.3	0.7	0.7

Bentonite

The natural materials, zeolite was obtained from Lastovce location in Slovakia. The mineralogical composition of bentonite was smectite 63%, quartz 21%, kaolinite 11%, feldspars 4-6% and calcite 2%.

Table II
Chemical composition of bentonite

Components	SiO_2	Al_2O_3	Fe_2O_3	MgO	Na_2O
% wt.	59.2	18.6	2.8	4.2	0.7

Quartz Sands

The natural materials, zeolite was obtained from Nižný Hrabovec location in Slovakia. The mineralogical composi

tion of zeolite was quartz 85 %, kaolinite 8 %, mica 6 % and iron minerals 3–5 %.

Table III
Chemical composition of quartz sands

Components	SiO$_2$	Al$_2$O$_3$	Fe$_2$O$_3$	MgO	Na$_2$O
% wt.	96.1	1.7	0.4	0.05	0.03

C a l c i t e

The natural materials, calcite was obtained from Horné Srnie location in Slovakia. The mineralogical composition of rock was calcite 80 %, quartz 5 %, kaolinite 2 %, plagioclase 0.5 %, and iron minerals 0.7 %.

Table IV
Chemical composition of calcite

Components	SiO$_2$	Al$_2$O$_3$	Fe$_2$O$_3$	MgO	Na$_2$O
% wt.	11.8	3.9	1.2	0.8	0.05

M a g n e z i t e

The fired material of magnezite was obtained from Jelšava location in Slovakia. The mineralogical composition of sample was periclase 98 %.

Table V
Chemical composition of fired magnezite

Components	SiO$_2$	CaO	Fe$_2$O$_3$	MgO	K$_2$O
% wt.	0.02	0.11	0.01	97.3	0.06

Results

The individual mineral phases of silicates (zeolite, bentonite, quartz sands) and carbonates (magnezite, calcite) can control the efficiency of biofiltration when sorption and precipitation of metals occurs. Moreover, in both cases, Zn, Cu, Pb were accumulated at the mineral and cell surface as precipitates. An important parameter for packing material is the removal capacity of the minerals.

Removal of Zn from solution by silicate was of lower efficiency, 20 % Zn by zeolite, 46 % by bentonite, 21 % by quartz sands was removed, while up to 55 % by calcite and 88 % by magnezite (Fig. 1.).

Removal of Cu was similar approximately 24 % by these minerals (Fig. 2.).

Pb was very effective removed 93 % by bentonite and magnezite and 74 % by zeolite and calcite (Fig. 3.).

The experimental results of the selected natural mineral materials showed that bentonite has higher adsorption capacities than zeolite for Pb and Zn. However, magnezite appear to be more effective than calcite in precipitation of Pb and Zn.

The affinity series for bacterial removal of these metals decrease in the order Pb > Zn > Cu with the low sorption capacity only approximately 0.06 mM dm^{-3}. At 0.1 g bacte-

ria dm^{-3} is a small amount of cells for adsorption metals onto the bacterial surface.
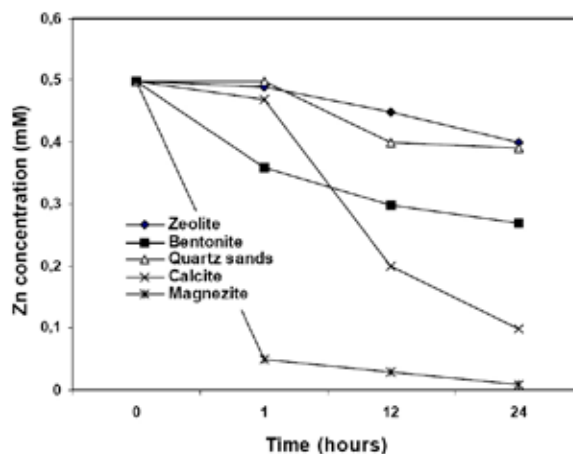
Fig. 1. **Time dependence of Zn biosorption and precipitation by minerals and bacterial cells**
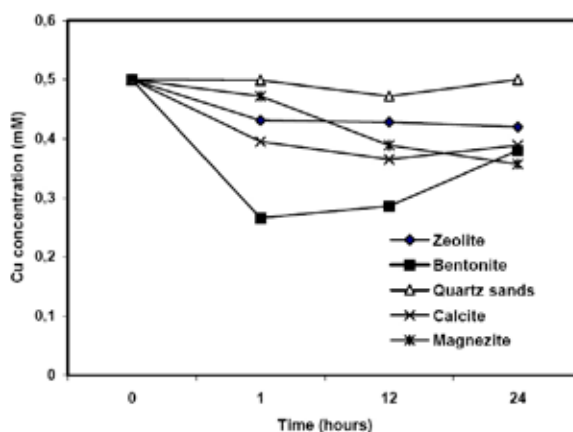
Fig. 2. **Time dependence of Cu biosorption and precipitation by minerals and bacterial cells**
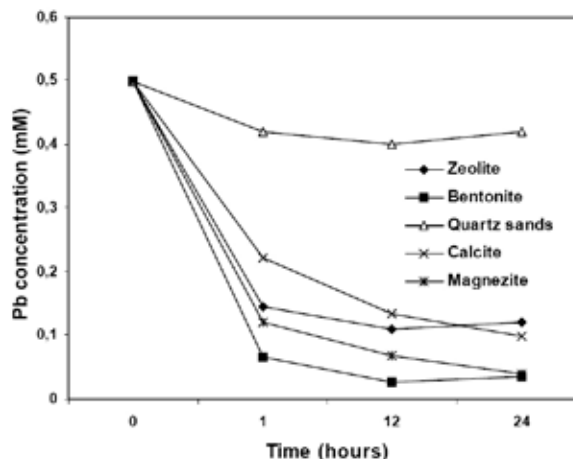
Fig. 3. **Time dependence of Pb biosorption and precipitation by minerals and bacterial cells**

This biosorption batch experiment represents a minerals-dominated regime in which the bacterial concentration is low, and therefore the difference of mineral and cell adsorption is big in the biological processes of pH change from 7 to 4 during silicate biofiltration and of pH change from 7 to 9 during carbonate biofiltration.

The result dominantly involves decreasing metal concentration in solution in dependence of time and kind of minerals. This indicates that the contact time between the metal solution and the mineral kind and also the bacterial amount is of crucial importance.

Conclusions

The batch adsorption experiment in ternary and binary systems with individual sorbents, ternary metal-mineral-bacteria and binary metal-bacteria interaction can be used to ascertain the effect of bacteria and selected of minerals like packing materials in development of biofilters. The results suggest that the adsorption observed in the 0.1 g dm^{-3} bacterial dm^{-3} system dominantly involves the mineral surface that is why biofiltration need to increase bacterial amount in packing filter.

REFERENCES
1. Leppert D.: Mining. Eng. *42*, 604 (1990).
2. Pradas E. G., Sánchez M. V., Cruz F. C., Viciana M. S., Pérez M. F.: J.Chem. Tech. Biotechnol. *59*, 289 (1994).
3. Elzinga E. J., Reeder R. J.: Geochimica et Cosmochimica Acta *66*, 3943 (2002).
4. Godelitsas A., Astilleros J. M., Hallam K., Harissopoulos S., Putnis A.: Environ. Sci. Technol. *37*, 335 (2003).
5. Panchanodikar V. V., Das R. P.: Int. J. Environ. Stud. *44*, 251 (1993).
6. Kuyucak N., Volesky B.: Biotechnol. Lett. *10*, 137 (1988)
7. Yee N., Fein J. B.: Chem. Geol. *185*, 303 (2002).

P71 ANTIBIOTIC EFFECTS OF THE NAPHTOQUINONIC DERIVATIVE ON GRAM-POSITIVE AND GRAM-NEGATIVE GERMS

RADU TAMAIAN[a], NADIA PĂUN[a], VIOLETA NICULESCU[a], ANDREEA IORDACHE[a], RALUCA VREMERĂ[a] and ŞTEFANIA BROSCĂŢEAN[b]

[a]*Research and Development Department, National Research and Development Institute for Cryogenics and Isotopic Technologies – ICIT Râmnicu Vâlcea, Uzinei Street No. 4 240050, Râmnicu Vâlcea, Romania,*

[b]*S.C. IMOFARM S.R.L., Piscului Street No. 15 040403, Bucureşti, Romania,*

tradu@icsi.ro

Introduction

Intestinal motile bacteria *Enterobacter aerogenes* and nonmotile coccus *Enterococcus faecalis* are known as being contaminating pathogenetic agents of aliments[1–3] and drinking water[4]. Pathological agents: coccus and bacteria have a significant multiple-antibiotic resistance at natural drugs and also at chemically obtained drugs.[5–10]

The naphthoquinones are a wide class of plants' metabolites, which are currently used for manufacturing cosmetics, foods or for medicinal purposes[11,12]. Also the natural naphthoquinones were tested for antitumoral[13], antiinflamatory[14] and antimicrobial[15,16] activity. For antibiotic activity is being responsible the compound structure, therefore the aim of any structure-activity relationship should be to find the most potent and least toxic compound. In this respect, we studied the antibiotic effect of dichlor derivative of 1,4-naphthoquinone: 2,3-dichloro-1,4 naphthoquinone (dichlone – Fig. 1.) on Gram-positive nonmotile coccus *Enterococcus faecalis*, and Gram-negative motile bacteria *Enterobacter aerogenes*.
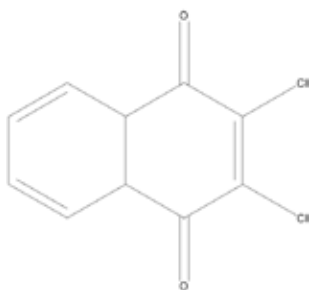
Fig. 1. **Dichlone structure**

In order to identify dichlone's grade of remanence, in the inoculated culture mediums, it was used HPLC technique.

Experimental

M a t e r i a l s   a n d   E q u i p m e n t s

Dehydrated culture media: primary culture media TSA (tryptic soy agar) from Fluka (Buchs, Switzerland) and M-H broth (Müeller-Hinton broth) from Fluka (Buchs, Switzerland) for antibiotic susceptibility testing.

Both culture media were rehydrated with ultrapure water made with water ultra-purifier TKA Smart2Pure UV6 from TKA Wasseraufbereitungssysteme GmbH (Niederelbert, Germany).

Used microbial strains were made by MicroBioLogics Inc. (Saint Cloud, USA), as following:
- KWIK-STIK™: *Enterococcus faecalis* (ATCC 29212);
- KWIK-STIK™: *Enterococcus faecalis* (ATCC 19433);
- KWIK-STIK™: *Enterobacter aerogenes* (ATCC 13048).

Culture media were sterilised with a Raypa AES-75 autoclave from R.ESPINAR, S.L. (Barcelona, Spain).

All cultures were incubated in a Raypa Incuterm ID-50 incubator from R.ESPINAR, S.L. (Barcelona, Spain).

Barium chloride from Utchim S.R.L. (Râmnicu Vâlcea, Romania) and sulfuric acid from Utchim S.R.L. (Râmnicu Vâlcea, Romania) were used for preparation of McFarland turbidity standards.

Odyssey DR/2500 spectrophotometer from Hach Company (Loveland, USA) was used for inoculums' and prepared McFarland turbidity standards' OD (optical density) determination.

For antimicrobial susceptibility testing it was used dichlone from Merck (Darmstadt, Germany).

Dichlone's grade of remanence was detected with HPLC equipment: Thermo Finnigan Surveyor system from Thermo Fisher Scientific Inc. (Waltham, USA). PDA detector set to 254 nm. Hypersil™ GOLD Column 100×4.6 mm.

Dichlone standard for HPLC: dichlone standard from Supelco (Bellefonte, USA).

Other reagents for HPLC technique:
- Acetonitrile from Merck (Darmstadt, Germany);
- Water Chromasolv from Honeywell International Inc., Riedel-de Haën (Seelze, Germany).

M e t h o d s

Primary and secondary cultures: the KWIK-STIK™ lyophilized microorganisms' strains (*Enterococcus faecalis* ATCC 29212 and ATCC 19433; *Enterobacter aerogenes* ATCC 13048) were transferred on Petri dishes with sterile TSA and incubated at 35 °C for 24 hours (primary cultures); then, subcultures were made from primary cultures and incubated also on sterile TSA for 24 hours at 35 °C.

Antimicrobial susceptibility testing by broth microdilution technique: dichlone's MIC (minimal inhibitory concentration – defined as drug concentration at which no growth is visible) was determined by broth microdilution technique. A sterile culture tube with M-H broth was inoculated with an aliquot from the three types of secondary growth. Inoculated broth's OD was adjusted at 0.5 McFarland standard with prepared turbidity standards – aproximatively 1×10^8 CFU ml^{-1}. Standardised inoculums' aliquots from all three types of secondary culture were transferred on culture tubes with sterile liquid medium: M-H broth. Dichlone's MIC was tested on those standardised inoculums, on M-H broth.

Table I
Concentration of dichlone used in MIC testing

Dilution 1	Dilutions 2	Dilutions 3
0.001 µg ml^{-1}	0.125 µg ml^{-1}	16.0 µg ml^{-1}
0.002 µg ml^{-1}	0.25 µg ml^{-1}	32.0 µg ml^{-1}
0.004 µg ml^{-1}	0.5 µg ml^{-1}	64.0 µg ml^{-1}
0.008 µg ml^{-1}	1.0 µg ml^{-1}	128.0 µg ml^{-1}
0.016 µg ml^{-1}	2.0 µg ml^{-1}	256.0 µg ml^{-1}
0.032 µg ml^{-1}	4.0 µg ml^{-1}	
0.064 µg ml^{-1}	8.0 µg ml^{-1}	

HPLC technique: for the identification of 2,3-dichloro-naphtoquinone in the samples a 1 mg ml^{-1} solution was prepared in acetonitrile and 10 µl injected into the HPLC system. The sample was injected three times.

Mobile phase was 60 % acetonitrile with 40 % water.

Chromatograms were registered at 254 nm.

Results

Antimicrobial susceptibility testing results show that the dichlone have no antimicrobial activity on Gram-negative bacteria *Enterobacter aerogenes*; in the same time the growth of Gram-positive coccus *Enterococcus faecalis* (both strains) was completly inhibited, as in Table II.

Table II
Dichlone's MIC on Enterococcus faecalis strains

Strain	MIC [µg ml^{-1}]
E. faecalis – ATCC 29212	0.5
E. faecalis – ATCC 19433	0.5

As we mentioned in introduction, dichlone's grade of remanence, in the inoculated culture mediums for MIC was determined by HPLC. The chromatograms of the mentioned naphtoquinone obtained at the most effective chromatographic conditions are shown in Figs. 2. and 3.

The height and area of PDA signal (254 nm) for this naphtoquinone confirmed the calculated value for MIC.
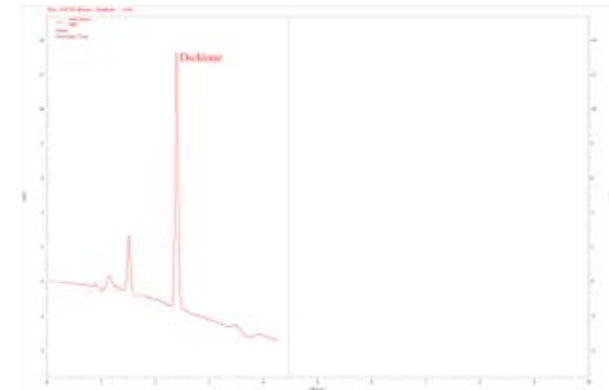
Fig. 2.   **HPLC chromatogram for dichlone's MIC (*E. faecalis* – ATCC 29212)**
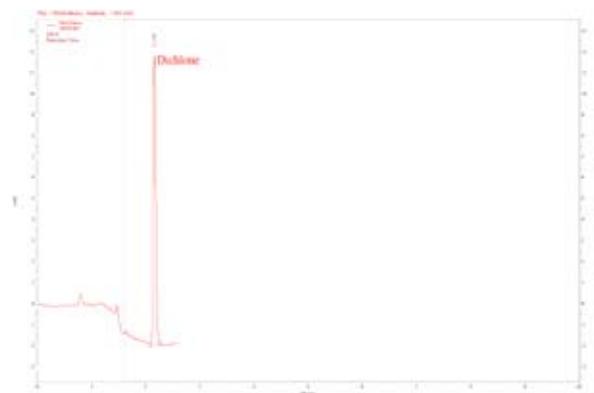
Fig. 3.   **HPLC chromatogram for dichlone's MIC (E. faecalis – ATCC 19433)**

Conclusions

The results of this study show that dichlone has no antimicrobial activity on Gram-negative germs (*Enterobacter aerogenes*). In the mean time, dichlone's MIC on Gram-positive germs (*Enterococcus faecalis* – both strains) it was at 0.5 µg ml^{-1} in liquid culture media (M-H broth). This concentration was confirmed by HPLC determination.

REFERENCES

1. Clark J. A., Burger C. A., Sabatinos L. E.: Can. J. Microbiol., *28*, 1002 (1982).
2. Baudart J., Coallier J., Laurent P., Prévost M.: Appl. Environ. Microbiol., *68*, 5057 (2002).
3. Filipkowska Z.: Acta Microbiol. Pol., *52*, 57 (2003).
4. Delbés C., Ali-Mandjee L., Montel M. C.: Appl. Environ. Microbiol., *73*, 1882 (2007).
5. Johnston L. M., Jaykus L. A.: Appl. Environ. Microbiol., *70*, 3133 (2004).
6. Hayes J. R. English L. L. Carr L. E., Wagner D. D., Joseph S. W.: Appl. Environ. Microbiol., *70*, 6005 (2004).
7. Morosini M. I., Garciá-Castillo M., Coque T. M., Valverde A., Novais A., Loza E., Baquero, Cantón R.: Antimicrob. Ag. Chemoth., *50*, 2695 (2006).
8. Sawant A. A., Hegde N. V., Straley B. A., Donaldson S. C., Love B. C., Knabel S. J., Jayarao B. M.: Appl. Environ. Microbiol., *73*, 156 (2007).
9. Macovei L., Zurek L.: Appl. Environ. Microbiol., *72*, 4028 (2006).
10. Macovei L., Zurek L.: Appl. Environ. Microbiol., *73*, 6740 (2007).
11. Masuda K., Funayama S., Komiyama K., Umezawa, I., Ito K.: J. Nat. Prod., *50*, 418 (1987).

12. Papageorgiou V. P., Assimopoulou, A. N., Couladouros E. A., Hepworth D.; Nicolaou K. C.: Angewdte Chem. Int., *38*, 270 (1999).
13. Gokhale1 N., Padhye S., Newton C., Pritchard R.: Metal-Based Drugs, *7*, 121 (2000).
14. Steihberg F. M., Gershwin M. E., Rucker R. B.: Jour. Nutr., *1994*, 744.
15. de Paiva S. R., Figueiredo M. R., Aragão T. V., Coelho Kaplan M. A.: Mem. Inst. Oswaldo Cruz, *98*, 959 (2003).
16. Brandelli A., Bizanim D., Martinelli M., Stefani V., Gerbase A. E.: Braz. Jour. Pharm. Sci., *40*, 247 (2004).

P72 PRACTICAL APPLICATION IN AGRICULTURE OF THE MAGNESIUM PRODUCTS INDUSTRY WASTE

LIDIA TAUBERT, HORTENSIA RADULESCU, SÁNDOR A. KISS, RUDOLF KASTORI, ECATERINA PRINCZ and ÉVA STEFANOVITS-BÁNYAI

Chemistry Institute – Timisoara of the Romanian Academy, Bv. Mihai Viteazu No.24, 300223 – Timisoara, Romania.
lidiat@acad-icht.tm.edu.ro

Introduction

The industrial processes of manufacturing magnesium compounds – oxide and carbonates mainly, from dolomites, by carbon dioxide leaching, generate important amounts of waste[1,2]. The composition of this waste includes calcium carbonate and precipitated magnesium carbonates (in ratio of 3:1 till 4:1) together with other impurities, presents in the raw material such as iron, manganese, copper and zinc[3,4].

The alkaline reaction and the important mineral content – essential and trace elements – of this waste can be valuated in agriculture as soil amendment and fertilizer for acid soils with low fertility[5-7].

The main objective of this study is to present the influence of waste types and doses on the fertility characteristics of an acid soil. The improve of the soil fertility was established by studying some vegetation characteristics and the protein content of green oat plants. The paper reports the effects of several waste doses and types on luvosoil with and without nitrogen contribution. Two types of waste were experimented, one from the industrial process (A) and the second resulted as crusts deposed on the equipment walls (B).

Experimental Part

Luvosoil, having a pH_{H2O} of 6.94 and pH_{KCl} of 5.76 and a rather low soil fertility, was collected, air-dried, crushed, mixed and put into pots, each containing 1 kilogram soil. The soil was treated with two types of waste in different amounts, having each the composition presented in Table I.

Table I
Composition of the two experimented industrial waste

Specification	Waste A	Crusts B
Ca, %	28	19
Mg, %	7	14
Fe, $mg\,kg^{-1}$	1850	880
Cu, $mg\,kg^{-1}$	1.9	51
Mn, $mg\,kg^{-1}$	136	51
Zn, $mg\,kg^{-1}$	2.6	50

The experimental alternatives pursued by this research consist of four different doses for each waste (A, B), namely A_1, A_2, A_3, A_4 and B_1, B_2, B_3, B_4 and also a control alternative (C_0), represented by untreated soil. All the experimental alternatives took place in three replicates (R_1, R_2, R_3). At the replicates R_2 and R_3, 134 mg nitrogen kg^{-1} soil as ammonium nitrate was added in each pot. The description of the experimental alternatives is shown in Table II, in which R represent the replicate without nitrogen treatment (R_1) and R_N – the average of replicates R_2 and R_3, treated with nitrogen.

All the pots were sown with thirty oat grains. The vegetation period was that of green plant, pursued for 8 weeks. The pots were placed in laboratory near the window and watered every second day by 100 ml water. Along the vegetation period, some morphological parameters, like number of risen plants, plant size, fresh and dry weight were pursued. Some composition features like dry matter and protein content were determined too. At harvest time, soil samples were collected in order to establish the impact of waste treatment on soil fertility. Soil characteristics like pH, essential and trace elements were analysed.

Soil pH in watery and salin extracts was determined by a pH-meter. The metal element content in soil at harvest time was established by AAS-ICP method. The protein content in oat plants was analysed by using the Kjeldahl method.

Results and Discussion

The impact of waste treatment on soil reaction and macroelements content is shown in Table III.

Soil reaction was analysed using two analytical methods, in watery and salt extract. The extraction in KCl solution hinders salts hydrolysis in soil and therefore the obtained pH values are more stable but lower by 1.7 pH units in comparison with those of the watery extract. For both methods, a buffer process of the soil reaction was established, turning the low acid soil reaction to an alkaline reaction, proportional with the increase of the waste dose. The increase of the pH value took place slowly by adding waste A and suddenly in case of waste B, which composition contains more magnesium than that of waste A. The highest pH values were established for A_4 (pH = 8.354) and B_4 (pH = 8.290). The nitrogen contribution decreases the pH-values because of the acid reaction of ammonium nitrate.

Analysing the soil calcium content, a proportional increase was established once with the growth of the waste dose. The increase of the calcium content took place suddenly for waste of type A and slowly for the waste B, remarking a suddenly growth only for the highest B dose. The highest waste doses for type A and B generate a calcium content of 2.674 $g\,kg^{-1}$ (A_4) and 2.717 $g\,kg^{-1}$ (B_4) respectively.

A growth of the magnesium soil content was established once with the increase of the waste dose (A, B). Higher values were determined for waste type B. Alike as for the calcium content in soil, a nitrogen contribution decreases the magnesium content values for the alternatives with waste of type A.

Table II
Description of the experimental alternatives

Experimental alternative		Waste dose, mg kg^{-1}	Nitrogen contrib., mg kg^{-1}	Mineral Suplimentation					
				Ca, mg kg^{-1}	Mg, mg kg^{-1}	Fe, mg kg^{-1}	Cu, μg kg^{-1}	Mn, μg kg^{-1}	Zn, μg kg^{-1}
A$_1$	R	179	-	50	13	0.33	0.34	24.3	0.47
	RN	179	134	50	13	0.33	0.34	24.3	0.47
A$_2$	R	357	-	100	25	0.66	0.68	48.7	0.93
	RN	357	134	100	25	0.66	0.68	48.7	0.93
A$_3$	R	714	-	200	50	1.32	1.36	97.4	1.86
	RN	714	134	200	50	1.32	1.36	97.4	1.86
A$_4$	R	1429	-	400	100	2.64	2.72	194.7	3.72
	RN	1429	134	400	100	2.64	2.72	194.7	3.72
B$_1$	R	263	-	50	37	0.23	13.40	13.4	13.20
	RN	263	134	50	37	0.23	13.40	13.4	13.20
B$_2$	R	526	-	100	74	0.46	26.80	26.8	26.40
	RN	526	134	100	74	0.46	26.80	26.8	26.40
B$_3$	R	1053	-	200	147	0.93	53.60	53.6	52.60
	RN	1053	134	200	147	0.93	53.60	53.6	52.60
B$_4$	R	2105	-	400	295	1.85	107.30	107.3	105.20
	RN	2105	134	400	295	1.85	107.30	107.3	105.20

Table III
Impact of waste treatment on soil reaction and macroelements content

Experimental alternative		Soil reaction				Ca content		Mg content	
		pH$_{H2O}$		pH$_{KCl}$,					
		pH unit	D	pH unit	D	g kg^{-1}	%	g kg^{-1}	%
C$_0$	R	6.939	-	5.763	-	2.136	100.0	0.327	100.0
A$_1$	R	6.887	−0.052	6.093	0.330	2.267	106.1	0.348	106.4
	RN	7.054	0.115	5.934	0.171	2.222	104.0	0.343	104.9
A$_2$	R	7.718	0.779	6.565	0.802	2.261	105.8	0.352	107.6
	RN	7.229	0.290	6.174	0.411	2.168	101.5	0.337	103.1
A$_3$	R	8.178	1.239	6.468	0.705	2.440	114.2	0.400	122.3
	RN	8.291	1.352	6.983	1.220	2.280	106.7	0.371	113.5
A$_4$	R	8.354	1.415	7.307	1.544	2.674	125.2	0.464	142.2
	RN	8.435	1.496	7.257	1.494	2.607	122.0	0.449	137.3
B$_1$	R	7.771	0.832	6.216	0.453	2.122	99.3	0.343	104.9
	RN	7.386	0.447	5.908	0.145	2.151	100.7	0.330	100.9
B$_2$	R	7.734	0.795	6.556	0.793	2.164	101.3	0.361	110.4
	RN	7.677	0.738	6.536	0.773	2.270	106.3	0.380	116.2
B$_3$	R	8.016	1.077	6.881	1.118	2.254	105.5	0.412	126.0
	RN	8.215	1.276	6.944	1.181	2.390	111.9	0.427	130.6
B$_4$	R	8.290	1.351	7.082	1.319	2.717	127.2	0.566	173.1
	RN	8.222	1.281	7.360	1.597	2.547	119.2	0.480	146.8

Table IV
Influence of waste type and doses on the soil trace elements content

Experimental alternative		Fe content		Mn content		Zn content		Cu content	
		$\mu g\,kg^{-1}$	%	$\mu g\,kg^{-1}$	%	$g\,kg^{-1}$	%	$g\,kg^{-1}$	%
C_0	R	234.7	100.0	87.84	100	11.400	100.0	3.402	100.0
A_1	R	249.6	106.3	84.20	95.9	33.100	290.4	3.491	102.6
	RN	251.4	107.1	84.30	96.0	25.080	220.0	3.639	107.0
A_2	R	244.6	104.2	80.06	91.1	31.200	273.7	3.669	107.8
	RN	245.1	104.4	95.00	108.2	11.900	104.4	3.669	107.8
A_3	R	260.3	110.9	86.97	99.0	13.960	122.5	3.462	101.8
	RN	253.6	108.1	85.44	97.3	11.910	104.5	3.609	106.1
A_4	R	257.0	109.5	73.42	83.6	12.920	113.3	3.669	107.8
	RN	264.5	112.7	88.00	100.1	6.721	59.0	3.821	112.3
B_1	R	232.5	99.1	75.56	86.0	4.418	38.8	3.462	101.8
	RN	251.1	107.0	95.77	109.0	4.407	38.7	3.609	106.1
B_2	R	242.5	103.3	70.53	80.3	4.832	42.3	3.358	98.7
	RN	236.6	100.8	81.62	92.9	4.821	42.3	3.462	101.8
B_3	R	235.0	100.1	94.39	107.5	4.567	40.1	3.787	111.3
	RN	237.8	101.3	73.76	84.0	19.300	169.3	3.506	103.1
B_4	R	253.8	108.1	92.62	105.4	4.425	38.8	3.728	109.6
	RN	237.8	101.3	76.49	87.1	10.210	89.6	3.402	100.0

Table V
Influence of waste and nitrogen contribution on some vegetation characteristics of green oat

Experimental alternative		Risen plants		Size of green plants		Fresh weight	
		number	%	cm	%	$mg\,piece^{-1}$	%
C_0	R	21	70	51	100	362	100
A_1	R	22	73	54	106	327	90
	RN	23	77	73	143	591	163
A_2	R	27	90	53	104	352	97
	RN	22	73	72	141	623	172
A_3	R	28	93	56	109	332	92
	RN	22	73	75	147	650	180
A_4	R	23	77	59	116	387	107
	RN	19	63	77	151	737	204
B_1	R	22	73	53	104	300	83
	RN	27	90	70	137	537	148
B_2	R	24	80	60	118	350	97
	RN	22	73	78	153	600	166
B_3	R	25	83	52	102	404	112
	RN	28	93	70	137	464	128
B_4	R	30	100	53	104	370	102
	RN	22	73	58	114	582	161

Table VI
Impact of waste treatment on some composition features of green oat plants

Experimental alternative		Dry weight		Dry matter	Protein content	
		mg piece^{-1}	%	D.M. %	P%	%
C_0	R	162	100	44.8	10.08	100
A_1	R	159	98	48.1	5.42	53.8
	RN	248	153	41.9	12.56	124.6
A_2	R	167	103	46.9	4.75	47.1
	RN	255	157	41.0	12.65	125.5
A_3	R	161	99	47.9	5.01	49.7
	RN	255	157	39.2	13.68	135.7
A_4	R	183	113	47.3	5.03	49.9
	RN	300	185	41.0	12.78	126.8
B_1	R	155	96	51.3	5.41	53.6
	RN	233	144	43.0	12.31	122.1
B_2	R	158	98	45.6	4.98	49.4
	RN	273	169	46.0	11.89	118.0
B_3	R	184	114	46.5	4.63	45.9
	RN	200	123	43.4	12.59	124.9
B_4	R	150	93	40.8	5.83	57.8
	RN	250	154	42.9	12.99	128.9

Because of their trace elements content, the soil treatment with waste of type A and B generates in soil a different trace element level in comparison to the control alternative, presented in Table IV.

Analysing the iron content of the experimental alternatives, it was established that unimportant increases of the iron content took place once with the growth of both waste type doses. The highest iron concentrations were found in alternative A_4 and B_4 representing the highest waste doses and having an increase of 12.7 % (A) and 8.1 % (B).

The manganese content in soil has lower values for all the experimental alternatives than that of the control alternative. An exception is represented by A_2 registering an increase of 8.2 % and B_1 of 9.0 %, both with nitrogen contribution.

The zinc content in soil decreases once with the increase of the waste dose. The highest value was registered for A_1 and the increase was of 190.4 %. By addition of waste B, the zinc content in soil decreases having lower values than the control alternative.

The copper content in soil remains almost constant after waste addition. The highest increase was registered for A_4 representing 12.3 %. Treating soil with waste B, the highest registered increase was 11.3 % for B_3.

The effects of soil treatment with waste A and B show an important influence on the development and nutrition of green oat plants. The results are presented in Table V and Table VI.

The enhance of the waste A amounts in soil treatment had a beneficial effect on the grain germination praised by a higher number of risen plants. Adding nitrogen to soil, the number of risen plants remained low. The effects are similar for soil treatment with waste B, except for B_1 and B_3, where the nitrogen contribution increases the number of risen

plants. The highest number of risen plants was established for B_4, 30 representing 100 % of the sown oat grains.

Green oat plants grew taller once with the increase of the waste dose in both cases (waste A and waste B). Adding nitrogen, an obvious increase of the plant size was established. The tallest plants were find for alternatives A_4 (highest waste A dose + nitrogen contribution), namely 77 cm and 78 cm for B_2 (second waste B dose + nitrogen contribution).

At harvest time, green oat plants for all alternatives were thinner, having a reduced fresh weight in comparison with the control alternative for those without nitrogen contribution. The nitrogen supplement makes the plants more vigorous having a higher fresh weight and dry weight for all the experimental alternatives. The fresh weight increase was more evident for soil treatment with waste A; for the highest waste dose (A_4), the increase was of 104 % in comparison with the control alternative. Similar to the fresh weight increase, took place the dry weight increase. The most evident results were established for the alternatives treated with waste A. The increase of the dry weight was the highest of 85 % for the alternative A_4.

The altering of dry matter was increasing for the alternatives without nitrogen treatment and decreasing for those with nitrogen treatment. The highest dry matter value was of 51.3 % for B_1 (lowest waste B dose) and the lowest value was 39.2 % for A_3 (waste A + nitrogen contribution).

The protein content of green oat plants shows, at harvest time, two different aspects comparative with the control alternative. For the alternatives in which no nitrogen was added, the protein content represents half of the control alternative content. Adding nitrogen, the protein content has increased and became double given to the alternatives without nitrogen contribution. The highest protein level was found for

A$_3$, namely 13.68 % and 12.99 % for B$_4$. The increase of the waste dose and nitrogen contribution generates an enhance of the plant protein content.

Conclusions

Considering the obtained results, the two experimented industrial waste can be used in certain doses as soil amendment for low fertile acid soil, with or without nitrogen addition.

Treating soil with different doses of waste, a buffering effect was established, which rises the pH values from low acid to low alkaline.

The presence of magnesium and calcium in the waste composition increases the soil content, proportional with the growth of the waste dose.

The enhance of the trace elements content in soil is representative for iron, copper and zinc (waste A).

The experimental waste doses (waste A, waste B) had a beneficial effect on grain germination improving the number of risen oat plants by 23 % (waste A) and 30 % (waste B).

At harvest time, the size of green oat plants was taller by 8 cm (waste A) and 9 cm (waste B) comparative to the control alternative with untreated soil. Nitrogen additions increased their size by 51 % (waste A) and by 53 % (waste B).

The fresh weights of the plants show a decrease proportional with the increase of the waste doses (A, B) only for the alternatives without nitrogen addition.

The dry matter values are increasing once with enhance of dose for both waste in all alternatives without nitrogen contribution. The addition of nitrogen decreases the dry matter value at harvest time for all the alternatives comparative to the control. The decrease of dry matter is more severe for the alternatives treated with waste A.

Adding nitrogen, the protein content has increased and became double given to the alternatives without nitrogen contribution.

REFERENCES
1. Kohn D., Taubert L., Policec S.: Filtrieren und Separieren F&S *12*, 161 (1998).
2. Taubert L., Policec S., Kohn D.: *Proceedings of International Symposium "Regional Multidisciplinary Research"* (Mirton, ed.), p.521 Timisoara, Romania 1998.
3. Taubert L.: *Proceedings of the 12th Romanian International Conference on Chemistry and Chemical Engineering: Inorganic Chemical Technology* (Printech, ed.), p. 201Bucharest, Romania 2001
4. Taubert L.: *Proceedings of 9th Symposium on Analytical and Environmental Problems* (SZAB, ed.), p. 41, Szeged, Hungary 2002..
5. *Radulescu H, Kiss A. S., Taubert L., Princz E.: Proceedings of 12th Symposium on Analytical and Environmental Problems* (SZAB, ed.), p. 467, Szeged, Hungary 2005.
6. Taubert L., Kiss A. S., Radulescu H., Princz E.: *Proceedings of 13th Symposium on Analytical and Environmental Problems* (SZAB, ed.), p.261, Szeged, Hungary 2006.
7. Taubert L., Princz E., Radulescu H., Kiss A. S., Stefanovits-Bányai É.: *5th International Conference of the Chemical Societies of the South-East European Countries: Chemical Sciences at the European Crossroads, Ohrid-Macedonia, 10–14 Sept. 2006*, p. 203, Book of Abstracts (Grafotissok, ed.),

P73 POSSIBILITY OF OBJECTIVE CONTROL OF NATURAL GAS ODORISATION

DANIEL TENKRÁT, ONDŘEJ PROKEŠ and JAN BERÁNEK

Institute of Chemical Technology Prague, Department of Gas, Coke and Air Protection, Technická 5, 166 28 Prague, Daniel.Tenkrat@vscht.cz

Introduction

Natural gas is one of the most important energy carriers in Europe (in the Czech Republic as well). Total consumption of natural gas (NG) in the Czech Republic in 2006 was $9,269 \times 10^6$ m³. Within the distribution to end users and also during natural gas utilization the most important requirement is the safety of customers.

Natural gas odorisation means operations involving the addition of odorant to gas to ensure characteristic odour of NG so that a person can judge the odour to be distinctive and unpleasant so that the presence of gas in air (in concentrations below lower explosive limit – LEL) is readily detectable. By the odorant addition any physical or chemical property (except the smell) of NG cannot be changed. As odorants organic sulfur compounds are often use (mercaptans and sulfides). Nowadays a new type of sulfur free odorant is being introduced to the NG market.

The NG odorisation in fact does not have any technological purpose; its main sense consist in evoking psychological effect, because the odour of NG must be alarming and incommutable with any common smell.

In the Czech Republic the odorisation process is specified by the technical regulation TPG 918 01. This regulation lists as odorants just organic sulfur compounds. However, it does not mean that sulfur-free odorants can not be used.

Experimental

The main task of natural gas odorisation is to ensure such operating condition when natural gas in every part of the distribution grid fulfils the requirement of a "warning odour level". In case of a gas leakage the warning odour level (see Table I.) must be reached until the 20 % of lower explosive limit (LEL; L_d) is reached. Odorisation level can be verified by:

- The odorisation level control – which can be done by olfactometry in selected points on distribution grid or by means of questionnaires at selected representative sample of customers. In both cases indirect indicators are taken into account so that both forms are considered to be subjective methods.
- Odorant concentration measurement – in natural gas can be estimated continuously or discontinuously in selected points on grid. In this case particular concentration of odorant in NG is measured. This is so called objective method.

The aim of this work was a critical comparison of the subjective odorisation control (according to TPG 91801) with the objective odorisation control. It means direct measurement of an odorant concentration in NG using modern analytical techniques and comparison with results from olfactometry measurement.

Analytical Equipment

The accurate odorant concentration in NG was estimated by gas chromatograph HP 6890 equipped with mass detector MSD 7393 (Hewlett-Packard). For the analysis Supelco 24158 SPB-1 Sulfur (30 m × 320 μm × 4 μm) column was used. Starting temperature was 30 °C with heating rate 15 °C min⁻¹. The analysis terminated at 110 °C.

The odorisation level control was estimated by dynamic olfactometry using olfactometer Ecoma TO 8-8. The procedure is based on step-by-step evaluation of olfactory perception of at least four (max. eight) observers. A sample of odorised natural gas is diluted by synthetic air in ratios between 1 : 131,072 and 1 : 8 (NG:air). As soon as the observer indicates olfactory perception to be odour treshold (or warning odour level) the actual dilution of the sample is recorded.

Terminology

Minimal odorant concentration represents the odorant content in NG [mg m⁻³] which fulfill the requirement for creating warning odour level – grade 3 (see Table I).

Estimation of the minimal odorant concentration is determined by:

- K value [mg m⁻³] which represents the minimal concentration of an odorant in natural gas-air mixture which reliably ensures the warning odour level,
- lower explosive limit (L_d) –expressed by % vol. of natural gas in air,
- and from the requirement to evoke the warning odour level before one fifth (i.e. 20 %) of LEL of natural gas in air is reached.

Minimal odorant concentration c_n can estimated according to the following formula:

$$c_n = \frac{100 \cdot K}{0.2 \cdot L_d} \ [\mathrm{mg\,m^{-3}}]. \qquad (1)$$

Typical K values of commonly used odorants are 0.08 for tetrahydrothiophene, 0.03 for mercaptans and 0.07 mg m⁻³ for the GASODOR S-free odorant.

Odour intensity is the extent of odour perception which is by the odour evoked. Commonly the odour intensity is evaluated as an odorisation level. List of odorisation levels can be found in the Table I.

Results

Two samples of a real odorised "Russian" natural gas sampled directly from natural gas pipeline into tedlar sam-

ple bags were used for all experiments. Both samples were analyzed by GC-MS and an overview of obtained odorant concentrations is given in Table II.

Table I
Odorisation Levels according to TPG 918 01(ref.[2])

Odorisation level (grade)	Olfactory perception	Comment
0	Odour not detected	–
1	Very low intensity	Odour threshold
2	Weak odour	–
3	Mean odour	Warning odour level
4	Strong odour	–
5	Very strong odour	–
6	Extremely strong odour	Upper limit of intensity

Table II
Samples overview

	DMS	TBM	Total
		[$mg\,m^{-3}$]	
Sample 1	2.71	3.31	6.02
Sample 2	3.32	4.35	7.67

For the estimation of odorisation level shortened examination described in technical norm ČSN 38 5550[1] was applied. In this test the odour threshold (grade 1) is estimated as a first point and the warning odour level (grade 3) as a second point. From obtained data (mean value from all observers mean values) the dependence of odorisation level on odorant concentration in natural gas was created.

The measurement was carried out by two different groups of observers.

The first one (GROUP 1), consisted of professional observers who satisfied the conditions listed in ČSN EN 13725[3] for performing the olfactometry measurement.

The second one (GROUP 2), consisted of observers who are performing the subjective odorisation control in gas distribution companies.

Obtained data are given in Figs. 1. and 2. Each of them represents the dependence of odorisation level on the odorant concentration in natural gas – air mixture.

Conclusions

Performed measurement shows considerable subjectivity of an olfactometry measurement of the odorisation level. While observers from Group 1 respond accurately with minimal deviations, observers from Group 2 respond in wide range of dilution with considerably scattered results. This result is connected with the sensitivity threshold across population and to some extent with professional deformation of
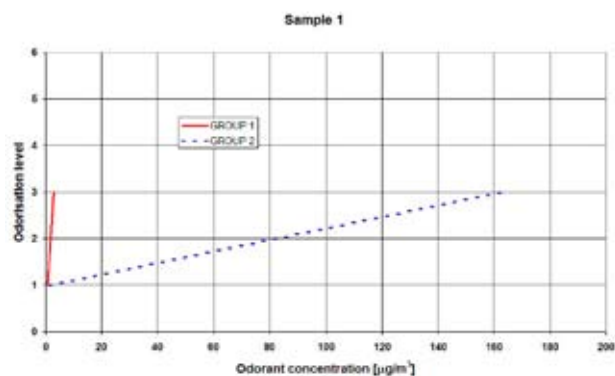
Fig. 1.　**Dependence of odorisation level on the odorant concentration for Sample 1**
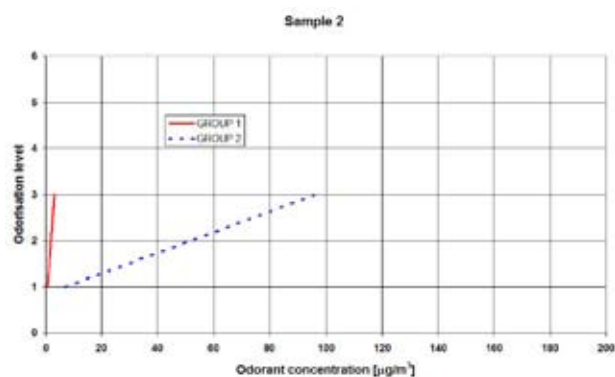
Fig. 2.　**Dependence of odorisation level on the odorant concentration for Sample 2**

employees carrying out the on-site olfactometry odorisation control of NG at selected points on natural gas grid.

From the data obtained from Group 1, the *K* value for the odorant used in samples can be estimated. This value is considerably lower than the *K* value, which is currently used in the Czech Republic (the obtained *K* value lies under $0.003\,mg\,m^{-3}$ comparing to published $0.07\,mg\,m^{-3}$ in the national technical regulation[2]).

As a main result of accomplished experiments it can be strictly recommended to prefer objective method for periodic odorisation control. Nowadays gas distribution companies slowly change the way of odorisation control considering the objective control as the guarantee of safe gas distribution and utilization up to end customers.

REFERENCES

1. ČSN 38 5550; *Odorizace topných plynů*, 1986.
2. TPG 918 01; *Odorizace zemního plynu*, 2002.
3. ČSN EN 13 725; *Kvalita ovzduší. Stanovení koncentrace pachových. látek dynamickou olfaktometrií*, 2003.

P74 CONTAMINATION OF SOIL AND ALIMENTARY WHEAT IN ZEMPLÍNSKA POLLUTED AREA

JÁN TOMÁŠ, JURAJ ČÉRY, LADISLAV LAHUČKÝ and JANETTE MUSILOVÁ

Departmentt of Chemistry, Faculty of Biotechnology and Food Sciences, Slovak University of Agriculture, Tr. A. Hlinku 2, 949 01 Nitra, Slovak Republic,
jan.tomas@uniag.sk

Introduction

Soil is a determining component of environment by its range and function that belongs to the basic technologic instruments and it is not an only revealing resource. Agrocosystems and mainly soil of these actively react on entries of polluted substances, which cause its biological degradation. Inorganic contaminants belong to main factors of biological degradation, heavy metals and metalloids are cummulated in soil environment. Our soils situated in key area (Strednozemplínska area) are exposed to an emissions effect from many sources for a long time period. It is proved mainly by acidification of soil horizons, exceeded content of heavy metals in soil and consequently in above-ground mass in this contaminated were found.

Experimental

We have collected the soil samples from exactly given places by the GPS system. Then we have processed information in the OziExplorer program, where the gained points were also evaluated. We have gained the soil samples from two depths 0–0.1 m (A horizon) 0.2–0.35 (B horizon). The soil samples have been taken by geological probe GeoSampler. The contents of the risky elements has been elevated on areas with active agricultural activity in Humenné location where we could assume that the observed area is contaminated by the reason of widespread industrial activity in this region. The contents of risky elements were determinated in *aqua regia* as a pseudototal content in 2M HNO_3 as the potential mobilized forms.

Results

The total content of the risky elements in soils includes all forms of the occurrence of exact element in soil. In our soil samples we have determined the contents of these chosen risky elements Cd, Pb, Ni, Zn, Cu, Cr, Co. We have evaluated the measured results by law No. 220/2004 about protection and exploitation of agricultural soil and resolution No. 531/1994. The evaluated area has exceeded the limit values in *aqua regia* solution in A horizon in the case of four following risky elements Cd, Ni, Zn and Co. Content of Cd was increased in all gained points in the observed horizon. The interval of values has been in range of 1.10 to 1.90 mg Cd kg^{-1} soil. The highest value presented was exceeding 171 % to the limit value. The content of Ni moved in wide interval of 40.4–70.4 mg Ni kg^{-1} of soil. At the highest content the limit value has exceeded by

40.8 %. The limit value of Zn enhanced in one gained point where the value presented 153.2 mg kg^{-1} that means exceeding at 2.1 %. The content of Co moved in wide interval from 19.6–29.6 mg kg^{-1}. The limit value for Co exceeded in all gained points. Limit value was at the highest concentration enhanced by 97.3 %.

In B horizon in digestion of *aqua regia* the limit values of all metals also exceeded. The content of Cd was increased in the observed horizon by all gained points. The interval of the value moved from 1.30 to 2.0 mg Cd kg^{-1} of soil. The content of Pb moved in wider range 39.6–114.8 mg Pb kg^{-1} of the soil and it was measured in two gained points. The highest content means increase at 64 %. The content of Ni exceeded in six gained points. The highest content presented the value 52.8 %. The increased content of Cu and Cr at the present area has a detailed character; the highest value of Cu exceeded the limit value at 12.6 %. The highest measured value of Cr, 86.8 mg kg^{-1} soil means increasing by 24 %. Measured values of Co we have found were in a range from 19.2–40.0 mg kg^{-1}. The limit value for Co was exceeded in all gained points. The content of heavy metals in 2M HNO_3 solution represented the potential mobilized content which includes different fraction of elements from the view of their solubility. The content of Cd in A horizon in Humenné area has moved in the range of interval 1.9–3.2 mg kg^{-1}. The value 3.2 mg kg^{-1} presented 10.6 fold increasing towards the reference value. The contamination by Cd has a broad character and affects all the gained points. The measured value of Pb was in the range 13.1–185.0 mg kg^{-1}. Other values of the heavy metals which were measured in A horizon doesn't express the enhanced potential mobility and their contents were under the limit value. The content of Cd in B horizon was in the range 1.9–3.5 mg kg^{-1}. Its highest value is increased at 11.6 fold to the reference value. The content of Pb in potential available form was in the range 100.4–253.6 mg kg^{-1} in B horizon. Risky elements have ability to get from the foodstuffs from soil, water and air as contaminants, some of them could be natural compounds of foodstuffs. By evaluation of grinding fractions from the standpoint of heavy metals we have found out that the limit value of Co has been exceeding. The value of Co was in the range 0.047–0.287 mg kg^{-1} the area of Humenné. The highest acceptable amounts exceeded in the I. and IV. milling fractions. The limit value has been enhanced at 218.5 %. The content of Pb was 2.5 fold higher than the limit value in the analyzed wheat grain. The cultivated winter wheat is not suitable for food processing from the point of Foodstuff Codex.

Conclusions

The contamination in the monitored area has an anthropogenic character which is caused by the industrial emissions produced by chemical factories situated in the surroundings Strážske and Humenné. With the observation of pseudototal (total) and potentially mobile contents of the risky and trace elements in area of Humenné, we can state that the contents of risky elements in A horizon exceeded in the case of Cd,

Ni, Co and Zn. The pseudototal contents of the determined elements show the local enhancement of all heavy metals in B horizon. The potentially mobilized forms of the risky elements were assessed in 2M HNO_3 these limit values exceeded in horizons A and B in the case of Cd and Pb. The highest acceptable amounts were increased in the I. and IV. milling fractions.

REFERENCES

1. Linkes V.: *Monitoring of soils of the Slovak Republic.* The Research Institute of Soil Fertility, Bratislava, 1997.
2. Vollmannová A., Tóth T., Lazor P., Stanovic R., Trebichalský P.: *Input of risk metals into the agricultural crops cultivated near of old environmental burdens.* 12th Inter. Sci. conf. Nitra, 2008.
3. Toth T., Lazor P., Melichacova Arvay J., Harangozo L.: *Risk of application of sludge on soil hygiene.* Science of younger researchers. MZLU, Brno, 2006.

P75 DETERMINATION OF CHANGES IN SOIL ORGANIC MATTER CONTENT THROUGH CARBON AND NITROGEN LABILE FRACTIONS

E. TOBIAŠOVÁ, T. TÓTH, and V. ŠIMANSKÝ

Slovak Agricultural University in Nitra, Tr. A. Hlinku 2, 949 76 Nitra, Slovak Republic,
Erika.Tobiasova@uniag.sk

Introduction

The quantity and quality of soil organic matter (SOM) are the most important characteristics, which influence the sustainable development. Much more sensitive indicators of dynamic changes of C and N are their fractions, labile carbon or potentially mineralizable nitrogen[1]. Techniques for isolating individual carbon fractions are different. Usually there is acid hydrolysis by H_2SO_4 with different concentrations[2] or HCl[3]. Other developed method was a fractionating method of SOM and fractions or substrates of SOM based on the susceptibility to oxidation by permanganate[4]. Modification and standardization of $KMnO_4$ oxidation technique[5] has increased the precision and simplified the technique, using only one concentration of $KMnO_4$, thereby dividing soil carbon into labile (C_L) and non-labile (C_{NL}) carbon. Research focuses on possibilities of SOM changes evaluation through the C_T – total organic carbon, C_L – labile carbon, C_{NL} – non-labile carbon, L_C – lability of soil organic carbon, LI_C – lability index of carbon, CPI – carbon pool index, CMI – carbon management index, N_T – total nitrogen, N_L – potentially mineralizable nitrogen, N_{NL} – non-labile nitrogen, L_N – lability of soil nitrogen, LI_N – lability index of nitrogen, NPI – nitrogen pool index, NMI – nitrogen management index and selection of suitable parameters for sensitive reaction on SOM changes also in agro-ecosystems.

Experimental

The studied territory of Malanta (lat. 18°08'N and long. 18°08'E) is located in the lower part of Selenec creek basin and its tributaries which belong to the central part of Nitra river basin. The geological substratum is created of few existing rocks with high quantities of fine materials. The soil is Orthic Luvisol. The average annual temperature of air was 9.6 °C and mean annual precipitation was 633 mm. The project with ecological (ES) and integrated (IS) farming systems was established in 1990. We collected the soil samples in the period 2005–2007. We determined C_T[6], C_L[4], N_T[7] and N_L[8] in soil samples. We calculated C_{NL}, L_C, LI_C, CPI and CMI[5]. We used this procedure for evaluating changes of soil nitrogen, as well. Data were analyzed using analysis of variance and differences were determined using the Duncan test. We used correlation to determine the relationships between studied parameters.

Results

Statistically significant higher average contents of C_L were determined in ES than IS. Higher content of C_L was in fertilized variants than in variants without fertilization (Table I).

In our study contents of phosphorus (r = 0.599, *P* < 0.01) and potassium (r = 0.488, *P* < 0.05) had statistically significant influence on C_L. L_C was higher in fertilized variants (0.223) than in variants without fertilization (0.202). L_C was in negative correlation with pH_{KCl} (r = –0.452, *P* < 0.05). Values of LI_C were in correlation with pH_{KCl} (r = –0.471, *P* < 0.05). On average, statistically significant higher average CMI value was in IS (1.38) than in ES (1.13), which showed on higher changes in organic carbon sources in ES. CMI values showed whether dominant processes are carbon losses or processes of new organic substances production. Statistically significant differences of N_L contents were also found between farming systems. On average higher N_L content was in ES 129 mg kg^{-1} than in IS 100 mg kg^{-1}. Values of N_L were in negative correlation with base exchangeable cations (r = –0.416, *P* < 0.05) and degree of saturation (r = –0.404, *P* < 0.05). Content of N_{NL} was in positive correlation with content of phosphorus (r = 0.564, *P* < 0.01) and potassium (r = 0.664, *P* < 0.01).

Conclusions

The results focused on the necessity of application, predominantly of carbon and nitrogen fractions on the evaluation of quality changes and losses of SOM. According to statistical assesment suitable parameters for sensitive reaction on SOM changes in agro-ecosystems seems to be mainly parameters C_L, L_C, CMI and N_L.

Table I
Mean values of parameters of SOM quality

| | Farming system | | Plot | |
	ESa	ISb	5	7
LC	0.216ac	0.229a	0.224a	0.222a
LIC	1.045a	1.170a	1.100a	1.117a
CPI	1.076a	1.182a	1.162a	1.095a
CMI	1.126a	1.380b	1.274a	1.232a
LN	0.109a	0.078a	0.103a	0.085a
LIN	2.304a	1.167a	2.079a	1.392a
NPI	1.090a	0.997a	1.132a	0.955a
NMI	2.542a	1.123a	2.359a	1.306a
	[g kg^{-1}]			
CT	12.885bc	11.422a	12.205a	12.102a
CL	2.289a	2.122a	2.220a	2.191a
CNL	8.963a	9.299a	8.352a	9.910a
	[mg kg^{-1}]			
NT	1338.2a	1168.3a	1341.7a	1164.8a
NL	129.2b	100.2a	122.5a	106.8a
NNL	1209.0a	1068.2a	1219.2a	1058.0a

[a]Ecological farming system,
[b]Integrated farming system,
[c]Values followed by the same letter within each column are not significantly different at *P* < 0.05

REFERENCES

1. Schjonning P., Munkholm L., Elmholt S., Olesen J. E.: Agric. Ecosyst. Environ. *122*, 157 (2007).
2. Rovira P., Vallejo V. R.: Geoderma *107*, 109 (2002).
3. Silveira M. L., Comerford N. B., Reddy K. R., Cooper W. T., El-Rifai H.: Geoderma *144*, 405 (2008).
4. Loginov W., Wisniewski W., Gonet S. S., Ciescinska B.: Pol. J. Soil Sci. *20*, 47 (1987).
5. Blair G. J., Lefroy R. D. B., Lisle L.: Austr. J. Agric. Res. *46*, 1459 (1995).
6. Nelson D. W., Sommers L. E., in: *Total carbon, organic carbon and organic matter*. (Sparks, D. L., ed.), chapter III, p. 961. ASA & SSSA, Madison 1996.
7. Bremmer J. M. *Nitrogen-total*. (Sparks D. L., ed.), chapter III, p. 1085. ASA & SSSA, Madison, 1996.
8. Standford G., Smith S. J.: Soil Sci. *126*, 210 (1978).

P76   DISTRIBUTION OF HEAVY METALS IN SOILS

TOMÁŠ TÓTH, JURAJ ČÉRY, JÁN TOMÁŠ, ALENA
VOLLMANNOVÁ and PETER LAZOR

*Department of Chemistry, Faculty of Biotechnology and Food
Sciences, Slovak Univeristy of Agriculture, Tr. A. Hlinku 2,
949 01 Nitra, Slovak Republic,*
tomas.toth@uniag.sk

Introduction

The soil quality is derived from its loading by hazardous
substances. The loading of soil occurs when the soil is not
able to lower the negative influences of the heavy metals. The
reference value, which represents natural content of heavy
metals in soil, forms the basis for evaluation of the content of
heavy metals in soil. The important parameters for the input
of heavy metals from soil into plants are: the soil reaction,
the content and the quality of organic matter, the nutrition
of plants, cation exchange and sorption capacity, the micro-
biological activity, the oxidation and reduction potential, the
amount and the quality of the clay fraction of soil and the
methods of soil cultivation, etc.

Experimental

The hazardous heavy metals were determined in eight
soil subtypes. Their choice was concentrated on the lowland
regions (Trnovec n/V. – haplic chernozems, Imeľ – eutric
fluvisols, Čičarovce – luvic stagnosols, Dolný Štál – mollic
fluvisols, Veľké Leváre – haplic arenosols, Malanta – haplic
luvisols). We took four parallel soil samples to be able to exa-
mine the soil homogenity of the monitored area. The sam-
ples from the pedological probe were taken from the depth
of 0–0.1 m; 0.20–0.30 m; 0.35–0.45 m. The state of the soil
hygiene was examined by evaluation of the total contents of
Cd, Pb, Cr, Cu and Zn. The total contents were determined af-
ter the mineralization by wet way H_2SO_4, HNO_3 and $HClO_4$
using the method of atomic absorption spectrometry. We also
determined the heavy metals in the pedological probe to be
able to estimate the anthropogenical and geochemical ori-
gin of the heavy metals. The above mentioned heavy metals
were determined in the extract of 2M HNO_3 and in cold. The
mobilizable forms of heavy metals were determined in the
extract with 0.05M EDTA. The mobile heavy metal forms
were determined in extract of 0.01M $CaCl_2$.

Results

The valid legislation was used for the evaluation of soil
hygiene. The evaluation is influenced by determination of the
total contents of heavy metals and by the determination of
heavy metals in 2M HNO_3 leach. Contents of heavy metals
in 2M HNO_3; 0.05M EDTA and 0.01M $CaCl_2$ and the per-
centage abundance of Zn, Cu, Cr, Pb and Cd in individual
extractants. The following order of extractability for indi-
vidual extractants is evident. The results of determination
of actual mobilizable forms are considered to be the most
acceptable. The percentage contents of individual heavy

metals and the total content of heavy metals in highly conta-
minated soil are as follows: Zn 1.7–13.9 %; Cu 14.1–62.6 %;
Cr 0.1–1.3 %; Pb 14.6–24.1 %; Cd 12.9–22.8 %. EDTA and
natrium and ammonium of EDTA are able to form stable
and defined complexes with heavy metal cations and they
cause the solubility of carbonates and oxides Fe and Al. The
exctracted contents of heavy metals were measurable during
the use of flame AAS. The mutual interactions of Zn, Cu, Cr,
Pb and Cd with the soil components influence the pH value,
content and quality of organic substances. Apart from the
above mentioned soil properties, there are many other varia-
ble soil properties. The lowest Zn solubility was determined
in subtypes of luvic stagnosols and eutric cambisols with pH
values in the acid part and the quality of mould expressed
by the ratio of humic acids to fluvic acid was the lowest but
on the other hand the percentage of mould has one of the hi-
ghest values. The solubility of Cu in 2M HNO_3 and in 0.05M
EDTA was in all soil subtypes the highest and it is especially
valid for haplic arenosols, haplic chernozems, mollic fluvi-
sols (FL_m). The order of solubility for the determined ele-
ments and and extractants was as follows: 2M $HNO_3 > 0.05$M
EDTA > 0.01M $CaCl_2$.

The lowest amount of Cd and Pb from haplic areno-
sols (RM_g) were extracted by extraction with 2M HNO_3 and
0.05M EDTA and the highest amounts of Cd were obtained
from mollic fluvisols, haplic chernozems. The evaluation of
heavy metal contents extracted from individual extractants
at different pH values, the content of mould and its qualita-
tive composition is not unequivocal and dependence between
variable soil properties and conditions of environment
disappear.

The solubility of Cu in 2M HNO_3 and in 0.05M EDTA
was in all soil subtypes the highest and it is especially valid
for haplic arenosols, haplic chernozems, mollic fluvisols.
The order of solubility for the determined elements and and
extractants was as follows: 2M $HNO_3 > 0.05$M EDTA > 0.01M
$CaCl_2$. We think that the best extractant is 0.05M EDTA with
restriction to Cd, Pb, Cu and partially for Zn. It is not possible
to find an universal extractant for evavalution of heavy metals
mobility in soil.

Conclusions

(i) The extractability for individual ectractans is evident:
2 mol dm^{-3} HNO_3 : Cu > Cd > Pb > Zn > Cr; 0.05 mol dm^{-3}
EDTA: Cu > Cd > Pb > Zb > Cr; 0,01 moldm^{-3} $CaCl_2$:
Cd > Cu > Pb > Zn > Cr. *(ii)* It is necessary to emphasize the
differences in solubility between the highly contaminated
eutric cambisols of Stredný Spiš and other analyzed soils.
The different solubility is in all extractants and heavy metals
except the solubility of chromium in 0.05M EDTA and
0.01M $CaCl_2$. It is probably connected with the high portion
of heavy metals of immissional origin. The other analyzed
soil subtypes have a low solubility of Zn in HNO_3 and EDTA
in luvic stagnosols.

REFERENCES

1. Arvay J., Melichacova S., Lahucky L., Musilova J., Bystricka J.: *Food safety and control: The crops quality cultivated on heavy metals contaminated soil from Region Hont, Nitra, March 28–29, 2008,* Book of Works, Nitra, 2007.
2. Bajcan D., Lahucky L., Stanovic R., Arvay J.: *IX Banskostiavnicke Days: Agricultural plants hygiene growed on metalic loaded aluvial soils.* Zvolen 2007.
3. Bujnovsky R., Jurani B.: *Plant and soil: Quality of soil its determination and evaluation.* The Research Institute of Pedology and Soil, Bratislava, 1998, 150 p.
4. Linkes V.: *Monitoring of soils of the Slovak Republic.* The Research Institute of Soil Fertility, Bratislava, 1997.
5. Makovnikova, J.: Dissertation. The Research Institute of Soil Fertility, Bratislava, 1998
6. Stanovic R., Harangozo L., Arvay J.: *59th Chemical Congress: Influence of sulphur to arsen toxicity in agricultural plants*, ChemZi 1/3 2007.

P77 MULTICOMPONENT MICRODETERMINATION OF ARSENIC, ANTIMONY, TELLURIUM, SELENIUM BESIDES OF THALLIUM BY ICP-MS IN WATERS

KRISTÝNA URBÁNKOVÁ, JIŘÍ MACHÁT and LUMÍR SOMMER

Brno University of Technology, Chemistry and Technology of Environmental Protection, Purkyňova 118, 612 00 Brno,
urbankova@fch.vutbr.cz

Introduction

The concentration of As and Tl in the environment is controlled by strict guidelines. Since considerable affection of the human organism is described for As and Tl[1,2]. Te is more toxic than Se but little is known about its requirements. Se is longely known for its ambivalency and particular essentiality for the human and animal organism and its implication in various enzymes on trace levels. Arsenic compounds are an important dopant for the semiconductor silicon production and a modifier of mechanical properties in lead and copper alloys. Complicated hydrolytic equilibria can be present in dilute aqueous solutions in dependence on pH[3].In fact, these equilibria in aqueous solutions have little influence on the results of ICP-MS only. The multicomponent microdetermination of inorganic As, Sb, Se, Te and Tl with ICP-MS is remarkable selective and sensitive and has not been studied in detail[4].

Experimental

C h e m i c a l s

Standard solutions of Se, Te, As, Sb and Tl with 100 µg dm^{-3} were prepared by dilution from original solutions containing 1.000 ± 0.002 g dm^{-3} metals which were purchased from Analytica s.r.o., Prague.

A multicomponent standard containing 1.000 ± 0.002 g dm^{-3} Al, Ba, Ca, Cd, Co, Cr, Cu, Fe, Mg, Mn, Na, Ni, Pb, Ti, Zn was also from Analytica s.r.o. Prague.

The tuning solutions for ICP-MS were 1 mg dm^{-3} of Ce^{3+}, Li, Y, and Tl$^+$ in 2% HNO$_3$. In such solution must be the ratio CeO$^+$/Ce$^+$≤1.5 % and Ce^{2+}/Ce$^+$≤3 % for bivalent ions. The solution containing 1 mg dm^{-3} of Co^{2+} in 1% HCl was used for tuning with the Helium collision cell.

I n s t r u m e n t a t i o n

An ICP-MS spectrometer Agilent 7500ce Japan was used with a plasma generator of 27.12 MHz and the power output 1,500 W. The sample nebulized by a concentric silica nebulizer MicroMist™ with a cooled Scott chamber entered by an injector of 2.5 diameters into the plasma.

The flow of the carrier argon trough the nebulizer was 1 dm^3 min^{-1} and contained the make up argon 0.33 dm^3 min^{-1}. A constant temperature 2 °C of the nebulising chamber was maintained.

Results

No polyatomic interferences were observed for selected isotopes ^{75}As, ^{82}Se, ^{121}Sb, ^{125}Te and ^{205}Tl such as Ar^{2+}, ArH$^+$, ArO$^+$ and ArN$^+$. Six-points calibration plots for selected element isotopes were strictly linear for concentrations less than 1,000 µg dm^{-3} in solutions containing 0.5% HNO$_3$. The signal intensity considerably decreases with the increasing concentration of acids. For the hydrochloric acid the decrease is 6 % for ^{205}Tl and 11% for ^{75}As with 5% HCl, With HNO$_3$, the decrease is 30% for ^{82}Se and ^{125}Te but for ^{75}As and ^{205}Tl 15%. The medium of 0.5% HNO$_3$ is optimal and recommended for the measurement.

I n t e r f e r e n c e s

The effect of 1–250 mg dm^{-3} of Na, K, Ca, Mg, Al, Fe(III), on the signal intensity was evaluated for 100 µg dm^{-3} in 0.5 % HNO$_3$. For 1–10 mg dm^{-3} of the matrix element the error for the microelement signal does not exceed 5 %. For 50 mg dm^{-3} of the matrix element, the error for the microelements increased to 15–20 % in the presence to Ca, Mg, Al and Fe(III). On the other hand, 250 mg dm^{-3} of Na and K cause less than 10% error for 100 µg dm^{-3} As, Se, Sb, Te, Tl.

In the presence of 1–100 µg dm^{-3} of multicomponent solution containing Al, Ba, Ca, Cd, Co, Cr, Cu, Fe, Mg, Mn, Na, Ni, Pb, Ti, Zn with 100 µg dm^{-3} of ^{75}As, ^{82}Se, ^{121}Sb, ^{125}Te and ^{205}Tl a considerable interference was observed and the signal decreased up to 70 %. The error can be decreased in the presence of 100 µg dm^{-3} of internal standard. ^{72}Ge was suitable for ^{75}As in the He mode and ^{82}Se in the normal mode and ^{209}Bi was suitable for the remaining elements measured in normal mode (Fig. 1.).

A p p l i c a t i o n   o f   W a t e r   S a m p l e s

Five-point strictly linear calibration plots with spiked microelements were carried out for all kinds of waters. The slopes of the regression lines were compared with that of ultra pure water to evaluate the influence of the matrix which cause some signal decrease by 5 %. This error can be diminished by using internal standards especially for sea and mine waters.
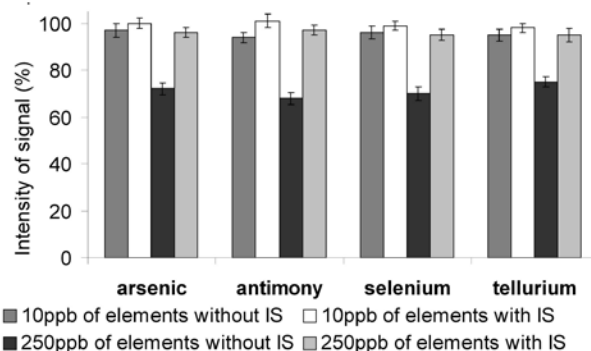
Fig. 1.　**The influence of multicomponent standard on the intensity of signal of 100 µg dm^{-3} of ^{75}As, ^{82}Se, ^{121}Sb, ^{125}Te and ^{205}Tl in the presence or absence of internal standard (^{72}Ge and ^{209}Bi)**

The detection limits were expressed according to UPAC[5]. For ^{75}As was the limit of detection 0.05–0.08 $\mu g\,dm^{-3}$, for ^{82}Se 0.04–0.03 $\mu g\,dm^{-3}$, ^{121}Sb 0.03–0.01 $\mu g\,dm^{-3}$, ^{125}Te 0.3–0.02 $\mu g\,dm^{-3}$ and for ^{205}Tl 0.005–0.2 $\mu g\,dm^{-3}$.

The evaluation of the contents of microelements resulted form spikes 1, 3 and 5 $\mu g\,dm^{-3}$ in solutions containing 0.5% HNO_3. The proper contents of the microelements in the sea and mine waters resulted from the corrected calibration plot by the standard addition method since their contents is higher than the detection limit of these elements.

For the drinking, surface and mineral waters, the evaluation was realized directly from the spikes, comparing the corrected regression equation of the calibration plot. This was because the amounts of microelements were below their detection limit.

Selected internal standards ^{72}Ge for ^{75}As in the He mode and ^{82}Se in the normal mode and ^{209}Bi for the remaining elements, measured in normal mode were always used during evaluation. The confidence intervals according to Dean and Dixon statistics[6] for triplicate analyses were used.

Table I
Evaluation of results from 1, 3 and 5 $\mu g\,dm^{-3}$ spikes used

	Drinking water	Surface water	Mineral water
^{205}Tl	1.004 ± 0.005	3.006 ± 0.010	5.004 ± 0.009
^{125}Te	1.003 ± 0.004	3.004 ± 0.009	5.005 ± 0.012
^{121}Sb	1.003 ± 0.004	3.003 ± 0.008	5.003 ± 0.009
^{82}Se	1.003 ± 0.002	3.004 ± 0.006	5.004 ± 0.007
^{75}As	1.001 ± 0.003	3.001 ± 0.005	5.001 ± 0.004

Conclusions

^{75}As, ^{82}Se, ^{121}Sb, ^{125}Te and ^{205}Tl were determined in the concentration range ≤1,000 $\mu g\,dm^{-3}$ in solution with 0.5% HNO_3 in the absence and presence of internal standards ^{72}Ge for ^{75}As in the Helium mode, ^{72}Ge for ^{82}Se in the normal mode and ^{209}Bi for ^{121}Sb, ^{125}Te and ^{205}Tl when the normal mode was used. 100 $\mu g\,dm^{-3}$ of the microelement can

Table II
Evaluation of results by the method of standard deviation in the sea and mine water[a]

	Sea water	Mine water
^{205}Tl	0.017 ± 0.025	0.811 ± 0.036
^{125}Te	0.022 ± 0.019	0.421 ± 0.032
^{121}Sb	0.020 ± 0.013	0.229 ± 0.029
^{82}Se	0.054 ± 0.015	1.012 ± 0.014
^{75}As	0.020 ± 0.033	0.537 ± 0.041

[a]Five-points calibration plots used

be determined in the presence of 50 $mg\,dm^{-3}$ of Ca, Mg, Al, Fe(III) with 15–20% error but in the presence of 200 $mg\,dm^{-3}$ of Na, K with 10% error only. In the presence of 250 mg of a multicomponent sample with 100 $\mu g\,dm^{-3}$ of studied elements the signal decrease. The error was decreased in the presence of 100 $\mu g\,dm^{-3}$ of internal standard.

For water samples the standard addition method was used for sea and mine water only to evaluate the microelements because the concentration of microelements exceeds the practical detection limits from the IUPAC recommendation. For surface and potable waters with the amounts of microelements below the detection limit three spikes were directly evaluated in triplicate according to Dean and Dixon statistics in the presence of internal standards.

REFERENCES

1. Vercruysse A (ed.): *Hazardous Metals in Human Toxikology Part B, Techniques and Instrumentatiton in analytical Chemistry*, Elsevier Press, Amsterdam 1984.
2. Das A. K., Chakraborty R., Cervera M. L., De la Guardia M., Anal.Bioanal.Chem. *385*, 665 (2006).
3. Bayes Ch. F., Messner R. E.: *The Hydrolysis of Cations*, Wiley, N. York 1976.
4. Balaram V.: Atom. Spectroscopy *14*, 174 (1993).
5. Currie L. A.: Pure Appl. Chem *67*, 1699 (1995).
6. Dean R. B., Dixon W. J.: Anal. Chem *23*, 636 (1951).

P78　SEPARATION AND PRECONCENTRATION OF ARSENIC, ANTIMONY, SELENIUM AND TELLURIUM ON MODIFIED SILICAGELS FOR THEIR DETERMINATION BY ICP-AES

KRISTÝNA URBÁNKOVÁ, LUMÍR SOMMER and MARTIN MOOS

Brno University of Technology, Chemistry and Technology of Environmental Protection, Purkyňova 118, 612 00 Brno,
urbankova@fch.vutbr.cz

Introduction

The determination of toxic or ambivalent microelements arsenic, antimony, selenium and tellurium in water samples requires inevitably a preconcentration prior to the determination by ICP-AES. The separation and preconcentration by various solid phase extractions were earlier studied and such technique widely used for water samples. The complexation of these elements with organic reagents is of particular interest when interacting with various kinds of silica sorbent used.[1–5] The combination of organic reagent with cationic surfactant was examined for sorption in this paper.

Experimental

Chemicals

All chemicals and solvents used were of analytical grade quality.

Astasol standards for arsenic, antimony, selenium and tellurium containing 1.000 ± 0.002 g dm^{-3} of element were from Analytica™ Prague, Czech Republic.

The cationic surfactant 1-ethoxycarbonylpentadecyltrimethylammonium bromide (Septonex®) from Aventa, Czech Republic and organic reagents 4-(2-Pyridylazo)resorcinol (PAR), Pyrrollidincarbodithioate (APDC), thiourea (THU) and 1,2-dihydroxybenzene (PYR) from Lachema, Czech Republic, diethyldithiocarbamidate (DTC) from Fluka, Switzerland and 8-hydroxyquinoline-5-sulphonic acid (8-HQS) from Aldrich, Germany were used.

Modified sorbents were Separon™ SGX C18, C8, SGX NH$_2$, SGX CN, SGX RPS and SGX Phenyl with particle size 60 μm, from Tessek™ Prague, Czech Republic.

Instrumentation

An echelle based ICP-spectrometer with a prism-predisperser IRIS AP™, (Thermo Jarell Ash) and CID detector with 512×512 pixels for 195–900 nm, axial plasma discharge of 1.35 kW and echelle grating with 54.4 lines were used.

The following spectral lines [nm] As 228.8, Sb 231.1, Se 190.6 and Te 214.2 were suitable for final evaluation only because of their high intensity, selectivity and low background influences.

Results

Sorption of Elements on the Silica Sorbent in the Presence of Surfactant

Prior to the sorption, the column was conditioned successively with 10 ml of distilled water and 10 ml of 5×10^{-4}–$\times 10^{-2}$ mol dm^{-3} aqueous solution of surfactant. 50 ml of solution containing 1 mg dm^{-3} of As, Sb, Se and Te (each of them) was always sorbed by a flow rate 1.0–3.0 ml min^{-1} at pH 7. The column was then rinsed with 10 ml of distilled water and the elements eluted with 10 ml of acetone-ethanol (1 : 1) mixture in the presence of 0.1 mol dm^{-3} HCl which showed the highest elution efficiency. The organic eluent was always removed by evaporation under an infra-red lamp to 1 ml in a suitable Teflon dish.

5×10^{-3} mol dm^{-3} Septonex® is optimal for the retention of inorganic form of As, Sb, Se and Te. The recovery values decrease from concentration larger than 1×10^{-2} mol dm^{-3} Septonex® because of the competing influence of micelles formed under these conditions in solutions. The recovery was nearly 100 % on SGX C18 (C8) for Sb, Se and Te but for As it reaches 60 % only. On the other sorbents, the sorption efficiency decreased. As was retained from 4 % on SGX Phenyl to 15 % on SGX CN. 70 % retention of Sb was on SGX NH$_2$. The recoveries for Se were about 90 % for SGX NH$_2$, RPS and Phenyl. On the other hand, more than 40 % of Te was retained on sorbent SGX RPS and NH$_2$.

Effect of Organic Reagents

The retention of monitored microelements was carried out from 50 ml of solutions containing 1 mg dm^{-3} of each metal with organic reagents when the column was previously conditioned by 5×10^{-3} mol dm^{-3} Septonex® only.

The sorption from solution containing 0.85×10^{-4}–3.35×10^{-4} mol dm^{-3} PAR was quantitative for Separon™ SGX C18, SGX C8, SGX CN for Sb, Se and Te. On SGX C18 and C8 the retention of complexes was nearly 100 % for 2.77×10^{-4}–1.1×10^{-3} mol dm^{-3} 8-HQS and also 6.25×10^{-4}–8.33×10^{-3} mol dm^{-3} PYR. The recoveries about 90 % were observed for 4.86×10^{-4}–7.29×10^{-4} mol dm^{-3} APDC and about 80 % for 4.90×10^{-4}–1.50×10^{-3} mol dm^{-3} DTC or 1.05×10^{-3}–4.20×10^{-3} mol dm^{-3} THU for Sb, Se and Te. The sorption of As was far from being quantitative. 1.70×10^{-4} mol dm^{-3} PAR can be used for the retention of As, Sb, Te on SGX NH$_2$ and SGX RPS for As, Sb, Se. On the other hand, 2.77×10^{-4} mol dm^{-3} 8-HQS is optimal for Se on SGX NH$_2$ and SGX Phenyl and 2.43×10^{-4} mol dm^{-3} DTC was suitable for the retention of Te on SGX RPS, SGX Phenyl and for As on SGX Phenyl.

Effect of Sample Volume

The influence of sample volume was tested for the retention from 50–1,000 ml solution containing 0.2–0.01 mg dm^{-3} each of element in the presence of the particular organic reagents after conditioning. This corresponds to a 5–100-fold

enrichment of As, Sb, Se and Te which enables the final use of ICP-AES.

Volumes of up to 1,000 ml have no effect on the retention efficiency on Separon™ SGX C18, C8 and SGX RPS. The sorption is however quantitative from 500 ml only on SGX NH$_2$, SGX CN and SGX Phenyl. The weakening of the retention forces of ionic associate or complexes on the surface of sorbent may supports the subsequent washing out of the element species from the column.

Application for Water Samples on Separon™ SGX C18

Standards of folowing elements were spiked to equilibrated drinking, mineral and river water samples containing no detectable amounts of these elements. The Separon™ SGX C18 was previously conditioned by 10 ml of distilled water and 10 ml of 5×10^{-3} mol dm^{-3} Septonex®. The sorption was provided from 250 ml of sample solutions in the presence of 1.68×10^{-4} mol dm^{-3} PAR.

Table I
The recovery (%) of arsenic and antimony in water samples[a]

Spikes [mg dm^{-3}]	$c_{element}$[b] [mg dm^{-3}]	Arsenic	Antimony
Mineral water			
0.25	0.01	58.30 ± 2.44	98.74 ± 2.70
0.50	0.02	60.02 ± 2.60	101.3 ± 3.40
1.00	0.04	60.23 ± 3.36	99.54 ± 2.87
River water			
0.25	0.01	59.71 ± 3.14	100.9 ± 2.39
0.50	0.02	60.90 ± 2.69	97.26 ± 3.53
1.00	0.04	62.34 ± 2.43	100.9 ± 3.09

[a]The analysis was carried out in triplicate and evaluated according Dean and Dixon[6]
[b]Concentration in 250 ml of water sample

Table II
The recovery (%) of selenium and tellurium in water samples[a]

Spikes [mg dm^{-3}]	$c_{element}$[b] [mg dm^{-3}]	Selenium	Tellurium
Mineral water			
0.25	0.01	100.5 ± 2.57	100.5 ± 3.06
0.50	0.02	98.60 ± 3.00	99.50 ± 3.07
1.00	0.04	99.23 ± 2.66	99.78 ± 2.33
River water			
0.25	0.01	99.78 ± 2.71	100.8 ± 2.35
0.50	0.02	98.90 ± 2.80	99.64 ± 2.47
1.00	0.04	101.7 ± 2.11	100.2 ± 1.73

[a]The analysis was carried out in triplicate and evaluated according Dean and Dixon[6]
[b]Concentration in 250 ml of water sample

Conclusions

The separation and preconcentration of arsenic, antimony, selenium and tellurium in the presence of 1.68×10^{-4} mol dm^{-3} 4-(2-Pyridylazo) resorcinol after previous conditioning with 5×10^{-3} mol dm^{-3} Septonex® was described in this paper. This procedure was successfully used for determination of these elements by ICP-AES in real water samples.

REFERENCES

1. Sturgeon R. E., Willie S. N., Berman S. S.: Anal. Chem. *57*, 6 (1985).
2. Jitmanee K., Oshima M., Motomizu S.: Talanta *66*, 529 (2005).
3. Gabros S., Rzepecka M., Bulska E., Hulanicki A.: Spectrochim. Acta Part B *54*, 873 (1999).
4. Zhang L., Merita Y., Sakuragawa A., Isozaki A.: Talanta *72*, 723 (2007).
5. Dressler V. L., Pozebon D., Curtius A. J.: Spectrochim. Acta Part B, 1527 (1998).
6. Dean R. B., Dixon W. J.: Anal. Chem. *23*, 636 (1951).

P79 TREATING WASTEWATER BY USING OF BIOCERAMIC FILTERS

A. VAŠKOVÁ, I. ŠTYRIAKOVÁ and V. SNOPKOVÁ

Department of Biotechnology, Insitute of Geotechnics of the Slovac Academy of Sciences , Watsonova 45, 043 53 Košice, Slovakia,
avaskova@saske.sk

Introduction

Nowadays, the control and treatment of industrial effluents has become one of the most important steps of the productive process, since the regulatory offices have been very rigorous about this subject[1].

Heavy metals are a group of contaminants that are high toxic to humans, animals, and aquatic lives and are commonly found in many munic pal and industrial wastes[4]. The toxicity of copper released into the environment has triggered a number of studies aimed at its removal from aqueous solutions. As a treatment approach, sorption in columns has widely been used in water treatment[2]. The using of bioceramic filters based on iron oxides, quartz sand, clay minerals, and bacteria could be an alternative way to remove heavy metals from industrial effluents. Iron oxides, a common constituent of soils, sediments, and aquifers, have high surface areas and are capable of adsorbing a significant quantity of metals. They are dominant adsorbents in many environments because of their capability to be finely dispersed and act as coatings on other particles[3]. A number of studies on metal uptake using quartz sands and clay minerals, have been conducted and results have shown good adsorption properties due to its metal-binding capacity and high surface area. Bacteria, in particular, are effiecient sorbents of heavy metals, although subtle differences can be seen between species and under various physicochemical conditions. Previous studies showed that the gram-positive bacteria *Bacillus sp*. was able to retain several heavy metals as silicate minerals or as oxyhydroxides at 20 and 4 °C under laboratory simulations of natural conditions.

The concentration of some of the toxic metals are higher than permissible discharge levels in effluents. It, therefore, becomes necessary to remove these heavy metals from these wastewaters by an appropriate treatment before releasing them into the enviroment.

Experimental

The adsorption of copper by bioceramic filters was studied by column technique. In this study two types of filters were used and compared in sorption efficiency.

Magnetite Preparation

Iron oxides can be easily synthetize in laboratory conditions. Synthetic magnetite (Fe_3O_4) used in this work was prepared by partial oxidation of Fe^{2+} solution at temperature 90 °C under anoxic conditions in the presence of nitrogen ions -oxidizing agent. The surface area was 13 $m^2 g^{-1}$ and particle

size range from 0.05–0.2 μm. The main mineral phase was confirmed by RTG diffraction, IR spectroscopy and Mössbauer spectroscopy method.
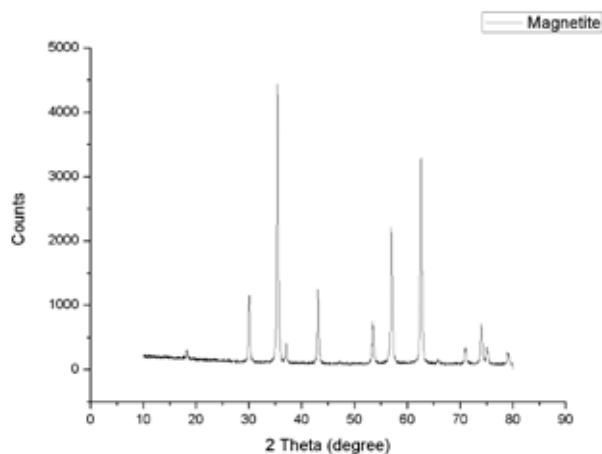
Fig. 1.   **XRD-pattern of synthetic magnetite**

Characterization of Quartz Sand and Clay Minerals

Quartz sand used in this work was obtained from Šaštín Stráže deposit (Slovakia) and composed of quartz (88–90 %), feldspar (8–10 %), heavy minerals (1 %) and clay minerals (1 %) of grain size 0–1 mm. The clay mineral used in this study was bentonit composed of montmorillonite (60–80 %) obtained from Jelšový potok deposit.

Table I
Chemical composition of quartz sand

Element [%]	QS
SiO_2	92.7
Al_2O_3	3.95
Fe_2O_3	0.32
TiO_2	0.06
CaO	0.16
MgO	0.15
Na_2O	0.93
K_2O	1.32
Cr_2O_3	0.004
MnO	0.02

Bacteria

In this study two bacterial strains were isolated from the copper pollluted waste water of industry plant: *Bacillus megaterium* and *Pseudomonas diminuta*. The resistance of bacterial strains to copper was tested. The bacterial isolate *Bacillus megaterium* could grow at a concentration ranging from 52–260 mg Cu dm^{-3} and *Pseudomonas diminuta* at a concentration max 52 mg Cu dm^{-3}, at temperature 25 °C. Therefore *Bacillus sp*. isolate was used for this study. The bacterial isolate *Bacillus sp*. was inoculated into flask containing Nutrient broth (Merck) and aerobically cultivated

at 25 °C by the agitating at the speed of 150 rpm. The cells were harvested from the growth medium by membrane filtration (pore size 0.85 μm). Bacteria suspension was prepared with concentration of bacteria 1.2×10^9 ml^{-1} in accordance to MacFarland standards.

Preparation of Copper Model Solutions

The model solution of Cu (II) was prepared by dissolving of $CuSO_4 \cdot 5H_2O$ in deionized water in various concentrations ranging from 0.01; 0.02; 0.04; 0.06; 0.1; 0.5; 1; 1.5; 2; 2.5; 3 to 5 mM. Previous studies showed that at pH 5 is the most effective copper sorption. The initial pH of the solutions was adjusted to 5 by adding 0.1M HNO_3 or 0.1M NaOH for the biosorption experiments. Various Cu(II) concentrations and concentration after sorption process were measured by atomic absorption spectrofotometer (Varian AA240 Z, AA240 FS, Australia).

Column Studies

In this study glass columns were used for experiments. The filtration column was 130 mm high with an inner diameter of 40 mm. Column was packed with appropriate amounts of each sorbent in layers (100 g of quartz sand, 0.5 g of bentonite and 0.1 g of synthetic magnetite). 50 ml of bacteria suspension was passed through the column to adjusted the adhesion of bacteria cells. Two types of filtration columns were prepared. In both types there was 45 mm depth of ceramic medium, one reached with bacteria (biotic filter) and another filter without bacteria medium (abiotic filter). Then 50 ml of Cu(II) model solution was passed through the column at a constant flow rate of 1.5 ml min^{-1}.

Fig. 3.   **Sorption columns**

Results

Bioceramic filters composed of quartz sand + bentonite + synthetic magnetite + bacteria were used for the sorption of copper. These two types of filters were compared in sorption efficiency. The effect of initial concentration on the percentage removal of copper by biotic and abiotic filters is shown in Fig. 2. Fig. 2. demonstrates that sorption was more effective in case of biotic filters. The work was carried out at the pH (5) of model solution because this pH value is for copper sorption optimum. The maximum removal of Cu(II) was attained at a concentration 63.5 mg dm^{-3} Cu. High removal efficiency (> 95 %) was obtained over the copper (II) concentration range 1–100 mg dm^{-3}. However the removal percentage decreased with increasing the copper (II) concentration (> 100 mg dm^{-3}). Therefore this method seems to be suitable for the removal of relatively lower concentration of copper.
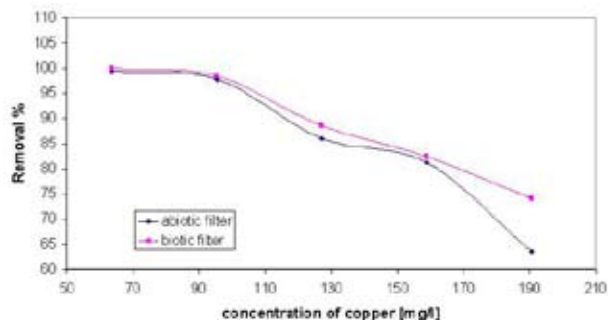
Fig. 2.   **Effect of initial copper concentration on percent removal of copper by biotic and abiotic filter**

Conclusions

The present study showed that the bioceramic filters based on quartz sand, bentonite, synthetic magnetite and bacteria can be used as an effective adsorbent of copper. The results of experiments showed high removal of copper by both types of model filters at concentrations ranging from 0.01 to 1.5 mM Cu(II). At higher concentrations removal of copper decreased. The percentage removal was more effective in biotic filters with baceria medium; however the difference compared with abiotic filter was not so marked. Therefore in further experiments bacteria medium with higher concentration of bacteria cells is needed. In the further study various iron oxides (hematite, goethit) and clay minerals (zeolite, kaolinite) will be used in experiments and their sorption efficiency will be compare.

REFERENCES
1. Cassela R. J.: Microchem. J. *72*, 17 (2002).
2. Meena A. K., Mishra G. K., Rai P. K., Rajagopal Ch., Nagar I.: J. Hazard. Mater. *B122*, 161 (2005).
3. Kooner Z. S.: Environ. Geol. *21*, 242 (1993).
4. Wu. G., Li L. Y.: J. Contam. Hydrol. *33*, 313 (1998).

P81　DETERMINATION OF SURFACTANTS INCLUDED IN SEWAGE WATER

MILADA VÁVROVÁ[a,b], LENKA LANGOVÁ[a], KRISTÝNA KUBÍČKOVÁ[b], HELENA ZLÁMALOVÁ GARGOŠOVÁ[a], MICHAELA STOUPALOVÁ[b] and VLADIMÍR VEČEREK[b]

[a]*Brno University of Technology, Faculty of Chemistry, Purkyňova 118, 612 00 Brno,*
[b]*University of Veterinary and Pharmaceutical Sciences Brno, Faculty of Veterinary Hygiene and Ecology,*
vavrova@fch.vutbr.cz

Introduction

Surfactants or detergents belong to a group of organic substances that adsorb at a low concentration in the interface, thereby decreasing interfacial or surface energy. Detergents therefore show surface activity which manifests itself by the formation of foam in aqueous solutions[1]. Such properties facilitate the wetting of surfaces and the removal of impurities[2].

Detergents can be divided according to their dissociation properties into the following groups: anionic detergents, cationic detergents, ampholytic detergents, and non-ionogenic detergents[2]. There are many kinds of individual detergents.

During wastewater treatment, detergents account for a high percentage of chemical oxygen demand. Detergents are also able to increase the solubility of other toxic organic components in water and soil. When adsorbed in sludge, they may impair sludge dewatering. Generally, the concentration of detergents at the outflow from a wastewater treatment plant depends on the efficiency and technological parameters of the facility.

Wastewater usually contains different kinds of detergents. For biological treatment, the level of detergents in wastewater should not exceed 1,000 mg dm^{-3}(ref.[4]). In countries where the consumption of washing powders and cleaning agents is high, the concentration of anion-active detergents in municipal wastewater varies in a range of 10–20 mg dm^{-3}. Increased concentrations of detergents can be detected in wastewater from textile industry, the production of washing and cleaning agents and cosmetic production plants, and may exceed 100 mg dm^{-3}. High levels of detergents are also present in wastewater originating from laundries and car washes[5]. The limit concentration of anion-active detergents in drinking water is 0.2 mg dm^{-3}. This parameter is used to indicate the level of pollution in underground water or treated surface water with sewage[2].

Experimental

The samples of wastewater to be analysed were collected at both the inflow and outflow of the wastewater treatment plant of the University of Veterinary and Pharmaceutical Sciences (VFU Brno). The samples of wastewater taken at the outflow were collected before chlorination to prevent the distortion of the results. The sample of water was measured immediately after collection; the transfer of the sample took approximately 10 minutes.

Detergents were determined using Merck spectrophotometric cuvette tests. The method for the determination of anion-active detergents can be used for concentrations ranging from 0.05 to 2.0 mg dm^{-3}. This method is similar to EPA 425.1, US Standard Methods 5540 and EN 903. Cation-active detergents are determined using a spectrophotometric method in a concentration range of 0.05–1.5 mg dm^{-3}. The determination of non-ionogenic detergents was carried out in a range of 0.1–7.5 mg dm^{-3}.

Results

The levels of anion-active, cation-active and non-ionogenic detergents were measured at both the inflow and outflow of the wastewater treatment plant during one week. It follows from the overview of the results provided in Table I that the samples of wastewater contain mainly anion detergents whose level is three orders higher than that of other detergents. The results in the table also demonstrate that the level of detergents in water – particularly anion-active detergents – decreased significantly as a result of wastewater treatment; the highest level detected was 0.97 mg dm^{-3} and was determined on Friday while the lowest level (0.29 mg dm^{-3}) was found on Tuesday. The highest concentration of cationic detergents (0.24 mg dm^{-3}) was detected on Monday and decreased markedly on other days (0.025 mg dm^{-3}). The presence of highly toxic cationic detergents is alarming.

Table I
Comparison of the levels of anion-active detergents in the inflow and outflow [mg dm^{-3}]

	Inflow	Outflow
1	20.00	0.40
2	12.90	0.29
3	18.30	0.49
4	13.90	0.49
5	14.00	0.97

Table II
Comparison of the levels of cation-active detergents in the inflow and outflow [mg dm^{-3}]

	Inflow	Outflow
1	0.400	0.240
2	0.020	0.025
3	0.690	0.025
4	0.025	0.025
5	0.025	0.025

The levels of non-ionogenic detergents in wastewater collected at the outflow were the same in all cases – 0.05 mg dm^{-3}. The differences between individual findings (the highest and the lowest levels) are difficult to explain; it is

possible that other biologically active compounds such as pharmaceuticals may also be present in wastewater affecting the biological stage of wastewater treatment in the respective wastewater treatment plant.

Table III
Comparison of the levels of non-ionogenic detergents in the inflow and outflow [$mg\,dm^{-3}$]

	Inflow	Outflow
1	0.69	0.05
2	0.89	0.05
3	2.40	0.05
4	1.40	0.05
5	2.61	0.05

Conclusions

Detergents are closely related to the environment. From an environmental point of view, the impact of detergents on water resources management, their biodegradability, toxicity and eutrophication caused by detergents is very significant. Since a large number of synthetic detergents exhibits insufficient biodegradability, water courses are becoming polluted with these substances. Even low concentrations of surfactants were shown to endanger the organisms in the environment.

In order to minimize their concentrations in the environment, generally valid rules should be implemented to help protect our environment.

REFERENCES

1. Kizlink, J.: *Technologie chemických látek II. Zpracování ropy, paliva a petrochemie, chemické speciality, pesticidy, dezinfekční látky, tenzidy, plasty a kaučuk, aditiva a pomocné chemikálie, výbušniny, biotechnologie, organizace pro chemii.* VUT Brno, Brno, 2001.
2. Pitter, P.: *Hydrochemie.* VŠCHT, Praha, 1999.
3. Venhuis S. H., Mehrvar M.: Int. J. Photoenergy *6*, 115 (2004).
4. Dhouib, Hamad, Hassaï̈ri, Sayadi. Process Biochem. *38*, 1245 (2003).
5. Nařízení vlády č. 61/2003, o ukazatelích a hodnotách přípustného znečištění povrchových vod a odpadních vod, náležitostech povolení k vypouštění odpadních vod do vod povrchových a do kanalizací a o citlivých oblastech. *Sbírka zákonů*, No. 24, p. 898, 2003.

P82　EXAMINATION OF THE MUTUAL INTERACTION OF HEAVY METALS IN COURSE OF ADSORPTION FROM MODEL SOLUTIONS

JÁN VEREŠ[a], TOMÁŠ BAKALÁR[b], MILAN BÚGEL[b] and MARTIN SISOL[b]

[a]*Institute of Geotechnics, Slovak Academy of Science, Watsonova 45, 043 53 Kosice, Slovakia,*
[b]*Technical University of Kosice, Faculty of Mining, Ecology, Process Control and Geotechnology, Letna 9, 042 00 Kosice, Slovakia,*
veres@saske.sk

Introduction

Heavy metals contamination occures in aqeous waste streams of many industries, such as metal plating facilities, mining operations, tanneries etc. Heavy metals are not biodegradable and tend to accumulate in living organisms, causing various diseases and disorders and environmental problems. Treatment processes for metals contaminated waste streams include chemical precipitation, ion exchange, membrane separations (ultrafiltration, reverse osmosis, electrodialysis) and adsorption. Natural materials that are available in large quantities, or certain waste products from industrial or agricultural operations, may have potential as inexpensive sorbents. Due to their low cost, after these materials have been expended, they can be disposed of without expensive regeneration. Cost is an important parameter for comparing the sorbent materials. Adsorption is considered to be the simplest and most cost-effective technique. The removal of heavy metal ions from industrial wastewaters using different adsorbents is currently of great interest[1].

Zeolites are naturally occuring hydrated aluminosilicate minerals. They belong to the class of minerals known as "tectosilicates". The structures of zeolies consist of three-dimensional frameworks os SiO_4 and AlO_4 tetrahedron. This structure causes zeolite to have negatively charged surface. The negative charge is balanced by the exchangable cation (calcium, sodium or potassium). The fact that zeolite exchangeable ions are relatively harmless makes them particularly suitable for removing undesirable heavy metal ions from industrial effluent waters.[2–4]

The zeolite samples from different regions show different behaviour in ion-exchange processes[5]. The ion exchange process in zeolites is influenced by several factors such as concentration and nature of cations and anions, pH value and crystal structure of the zeolite. In this study, the adsorption properties of the natural zeolite and synthetic zeolite Slovakite® with respect to some heavy metal cations in solution were investigated[6].

Experimental

Materials and Chemicals

A natural zeolite was obtained from Slovakia (Nizny Hrabovec). The main phase is clinoptilolite and the chemical compositions are SiO_2 (73.42 %), Al_2O_3 (12.43 %), CaO (2.94 %), K_2O (2.61 %) and Fe_2O_3 (1.05 %). The synthetic zeolite Slovakite® is patented product and the chemical composition is unrevealed by the producent.

Inorganic chemicals were supplied as analytical reagents and deionized water was used. The studied metal ions were Pb^{2+}, Ni^{2+}, Cu^{2+} and Zn^{2+}. Solution of lead and nickel was prepared by using their nitrate salts, $Pb(NO_3)_2$, $Ni(NO_3)_2.6H_2O$. The solution of copper and zinc was prepared from their sulphate salts, $CuSO_4.5H_2O$, $ZnSO_4.7H_2O$.

Adsorption Tests

The ion exchange of heavy metals on natural zeolite and on synthetic zeolite Slovakite® were carried out using the batch metod. Batch adsorption experiments were conducted using 2 g of adsorbent with 200 ml of solutions in flasks containing heavy metal ions of desired concentrations at constant temperature (25 °C). The initial concentration of heavy metals in stock solutions was in the range at 5–1,000 mg dm⁻³. Sorption experiments were carried out at pH 5.5. The flasks were then agitated in an orbital shaker at a speed of 200 rpm for a period of 2 h. The quantity of elements in solution has been determined both before the introduction of sorbent and after the equilibrium time of 24 hours by AAS.

The amount of adsorbed metal was calculated using the equation:

$$q_{eq} = \frac{c_0 - c_{eq}}{c_s} \qquad (1)$$

where c_0 and c_{eq} [mg dm⁻³] are the concentrations of the metal ion in initial and final solutions and c_s [g dm⁻³] is the sorbent concentration.

Results and Discussion

Adsorption of Metals on Natural Zeolite

The adsorption of Pb^{2+}, Ni^{2+}, Cu^{2+}, and Zn^{2+} onto natural zeolite as a function of their concentrations was studied at 25 °C by varying the metal concentration from 5 to 1,000 mg dm⁻³ while keeping all other parameters constant. The experimental data were modeled with Langmuir, Freundlich and Redlich-Peterson isotherms. The adsorption isotherms which are the most suitable to fitting the adsorption processes on natural zeolite in single system are shown in Figs. 1. and 2. The isotherm analyses showed different adsorption behaviour for Pb^{2+}, Ni^{2+}, Cu^{2+} and Zn^{2+}. Metal adsorption increased in the following order: $Pb^{2+} > Ni^{2+} > Cu^{2+} > Zn^{2+}$ (Figs. 1. and 2.). Fig. 1. illustrates the dynamic adsorption process of Cu^{2+} and Zn^{2+} on natural zeolite. As shown Fig. 1., the maximum sorption capacity of natural zeolite was already exhausted (the equilibrium capacity was achieved) when the metal concentration in solution was in low range. Fig. 2. presents that the sorption capacity of sorbent was not expended even by the highest initial concentration of Pb^{2+} and Ni^{2+} in solution.

Fig. 1.　**Adsorption isotherms of Cu^{2+} and Zn^{2+} on natural zeolite**
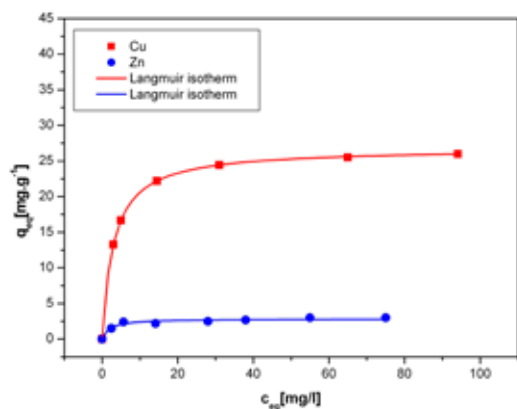
Fig. 3.　**Adsorption isotherms of Cu^{2+} and Zn^{2+} on synthetic zeolite Slovakite®**

Fig. 2.　**Adsorption isotherms of Pb^{2+} and Ni^{2+} on natural zeolite**
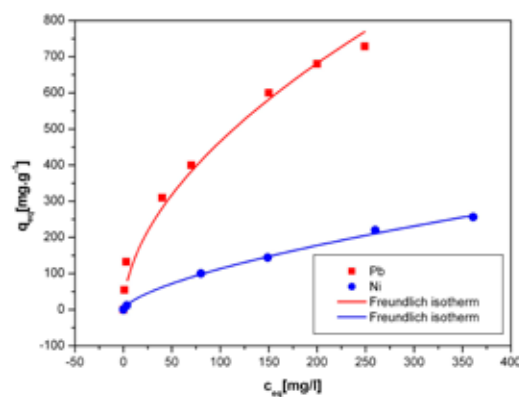
Fig. 4.　**Adsorption isotherms of Pb^{2+} and Ni^{2+} on synthetic zeolite Slovakite®**

　　The Langmuir and Freundlich models effectively described the sorption data with all R^2 values >0.95.

A d s o r p t i o n　o f　M e t a l s　o n　S y n t h e t i c Z e o l i t e　S l o v a k i t e ®

　　The adsorption of Pb^{2+}, Ni^{2+}, Cu^{2+}, and Zn^{2+} onto synthetic zeolite Slovakite® as a function of their concentrations was studied in the same conditions as on natural zeolite. Figs. 3. and 4. illustrate the adsorption isotherms of selected heavy metals on Slovakite® in single component system. Comparing the two isotherms on Fig. 3., Cu^{2+} adsorption is usually higher than Zn^{2+}. For Zn^{2+}, equilibrium adsorption approaches the value of 42 mg g^{-1} while for Cu^{2+} equilibrium adsorption still shows higher value than 130 mg g^{-1}. Fig. 4. shows a comparison of Pb^{2+} and Ni^{2+} adsorption. For both metals, equilibrium adsorption still shows an increasing trend at higher equilibrium concentrations. The cations sorbed from the solutions followed the same order as on natural zeolite but the sorption capacity of Slovakite® was much higher.

　　The Langmuir and Freundlich models effectively described the sorption data with all R^2 values >0.98.

Conclusions

　　These results show that natural zeolite from Nizny Hrabovec and Slovakite® can be used effectively for the removal of heavy metal cations from solutions. Best sorption capacity was obtained on synthetic zeolite Slovakite®, decrease in this order $Pb^{2+}>Ni^{2+}>Cu^{2+}>Zn^{2+}$. The selectivity sequence of cations is the same on both sorbents, but the sorption capacity of synthetic zeolite is much higher. The main disadvantage of synthetic zeolite Slovakite® its higher cost.

REFERENCES

1.　Bailey S. E., et al.: Wat. Res. *33(11)*, 2469 (1999).
2.　Barer R. M.: *Zeolites and Clay Minerals as Sorbent and Molecular Sieves*, Academic Press, New York, 1987.
3.　Breck D. W.: J. Chem. Edu. *41*, 678 (1964).
4.　Hafez M. B., Nazmy A. F., Salem F., Eldesoki M.: J. Radioanal. Chem. *47*, 115 (1978).
5.　Matik M., Václavíková M., Gallios G., Hredzák S., Ivanicova L.: Chem.listy *99*, 49 (2005).
6.　Vereš J.: Diploma thesis. Technical University in Košice, Slovakia, Košice 2007.

P83　FUNGICIDAL EFFECT OF PRINTED TITANIUM DIOXIDE LAYERS

MÁRIA VESELÁ, MICHAL VESELÝ, PETR DZIK, JANA CHOMOUCKÁ and LENKA ŠUPINOVÁ

Brno University of Technology, Faculty of Chemistry, Purkyňova 118, 612 00 Brno, Czech republic,
vesela@fch.vutbr.cz

Introduction

Microorganisms are crucial and inevitable part of life on Earth. They are found basially everywhere – in air, soil, in animal and human bodies, even in places with extreme conditions. Microbial contamination is a serious issue which has to be dealt with in numerous cases of everyday life. Various sterilization and dissinfecting methods have therefore been developed so far.

Photocatalytic processes on thin layers of titanium dioxide represent a new approach to the everlasting struggle against microbial contamination. Reactive oxygen species generated on the surface of irradiated TiO_2 inactivate most type of microbes[1]. Apparently, titanium dioxide coated surfaces self-reducing the population of microbes to minimal level and preventing their growth would be of a great importance.

Most photodegradation reactions on organic substrates are based on the oxidative power of photoinduced electronic holes or are mediated by $HO^{\bullet}$ radicals. Such reaction usually lead to a complete mineralization of organic substrate to carbon dioxide and water. However, it is necessary to provide a reducible reactant (i.e. electron acceptors) which would react with photogenerated electrones. In most cases of photocatalytic degradation reactions, oxygen is present and it acts as primary electron acceptor. Oxygen is thus transformed to superoxide radical ($O_2^{\bullet-}$) and in this way a hydroxyl radical can be produced:

$$TiO_2 \xrightarrow{h\nu} TiO_2(e_{cb}^-, h_{vb}^+) \rightarrow \text{recombination} \tag{1}$$

$$TiO_2(h_{vb}^+) + H_2O_{ads} \rightarrow TiO_2 + HO_{ads}^{\bullet} + H^+ \tag{2}$$

$$TiO_2(e_{cb}^-) + O_{2\,ads} + H^+ \rightarrow TiO_2 + HO_2^{\bullet} \leftrightarrow O_2^{\bullet-} + H^+ \tag{3}$$
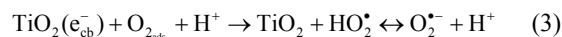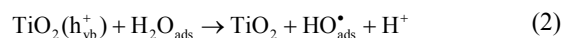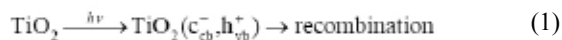
Experimental

Material and Methods

Sol and substrate preparation. Sol-gel technique was applied to titanium dioxide thin films preparation using titanium(IV) propoxide as titanium precursors. A mixture of absolute ethanol and acetylacetone (ACAC) was added to titanium(IV) propoxide (TTP) under continuous stirring. Then a small amount of water in ethanol was dropped at last to the previously mixed solution. Soda lime glass plates with sizes of $50 \times 50 \times 1.5$ mm were chosen as a substrate for immobilization of TiO_2 thin films. Soda lime glasses were treated in boiling 9M sulphuric acid. Before the preparation of the thin films, each glass was pre-treated in order to eliminate the dust, grease and other residues using liquid surfactants and dried under air flow.

Sol application was performed in a novel innovative way utilizing a modified office inkjet printer. Ink cartridges were removed from the printer and the ink tubing and printhead were flushed and purged with anhydrous propanol. "Virgin empty" spongeless carts were supplied by MIS Associates, USA. Sol was filtered through 0.2 μm mesh size syringe filter and loaded into one "virgin empty" cart. This cart was installed into the printer in the black position and after a series of head cleaning cycles a perfect nozzle check pattern was obtained. Cleaned glass plates were then mounted into a modified CD holder, fed into the printer and printed with "black only" driver setting. The colour of the printed pattern was varied in different shades of grey (100 %, 95 %, 90 %, 80 %, 70 %, 60 %) and thus glasses with varying sol loading were printed. The resolution, print speed and media settings were also varied and their influence on the resulting TiO_2 layer properties was evaluated. Two way of printer setting were chosen for thin layer of TiO_2 preparation – slow (S) and rapid (R). The sample marked as 100 R corresponds to 100 % of sol loadings printed by rapid way.

Layer treatment. After this procedure, the coated glass plates were dried in the oven at 110 °C for 30 min. Finally, the deposited layers were thermally treated in a calcination furnace at 450 °C for 4 hours.

Photocatalytic Inactivation of Yeasts

A 24-hour culture of yeast *Candida vini* CCY 29-39-3 (provided by Slovak Yeast Collection, Bratislava) was prepared at 25 °C. After the cultivation, 10 ml of culture medium was sampled into a plastic test tube, rinsed twice and centrifuged at 4,000 rpm for 6 minutes. The supernatant was discarted and the yeast sediment was diluted with 1 ml of distilled water an throroughly mixed.

A titanum dioxide coated glass plate was irradiated by UV lamp for 30 minutes in order to obtain a superhydrophilic surface. 25 μl of diluted yeast suspension was pipetted onto the glass plate and evenly spread across its surface. Then the glass plate with yeast suspension was placed in a sreaction chamber. The chamber consisted of a Petri dish with reflective aluminum foil bottom and quartz glass cover. A few drops of water were aplse placed into the reaction chamber in order to maintain the humidity.

The reaction chamber was irradiated by 4 fluorescent lamps Sylvania Lynx-S 11 W with emission maximum at 350 nm. The irradiation intensity was 1 mW cm^{-2} within 290–390 nm spectral region. Irradiated samples were dyed and observed by fluorescent microscopy.

Survival Ratio Calculation

The exposed yeast suspension was mixed with 25 μl acridine orange solution (1×10^{-4} mol dm^{-3}) in phosphate buffer of pH = 6. After thorough mixing, the sample was observed with epi-fluorescent microscope Nikon Eclipse E200.

20 digital images of randomly chosen different places ocross the glass plate were recorded using CCD camera PixeLINK PL-A662 mounted on the Nikon microscope. At every recorded image, the number of living cells N_L (green flurescence) and dead cells N_D (orange fluorescence) was counted. Then, the survival ratio *SR* was calculated:

$$SR = \frac{N_L}{N_{L+D}} \qquad (4)$$

Results

After irradiating *Candida vini* suspension deposited on the 100 R glass plate a significant inactivation was observed – the SR dropped to 0.032 ± 0.023 within 70 minutes. On the other hand, the non-irradiated sample showed no inactivation within 70 minutes. These observations are in a good compliance with the results of Seven et al.[4], who also observed no inactivation of microbes on titanium dioxide in darkness. Only very small inactivation was observed on an irradiated bare glass without the catalyst layer. (Figs. 1., 2.).

These results are in agreemnet with the observations made by Kühna et al.[3], who irradiated bacteria *Pseudomonas aeruginosa* on a glass plate covered with titanium dioxide. They found out that bacreial cell inactivation takes place. This phenomenon was explained to be caused by the oxidative stress of oxygen radicals inside cells during the exposure by UV-A radiation. Once the stress rises over a certain threshold, the cell dies.
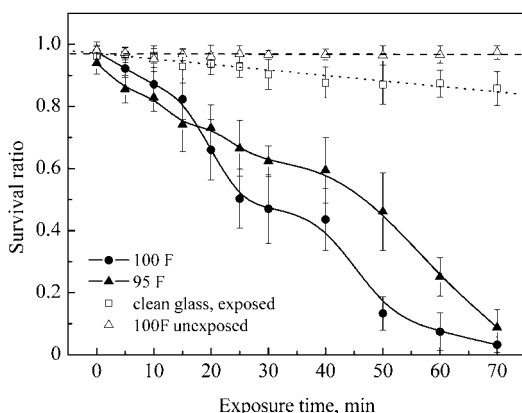
Fig. 1.   SR comparison for *Candida vini* at different conditions on R substrates

A constant decrease of SR in a certain time from the reaction start was observed by Benabbou et al.[2] in the case of *Escherichia coli*. Cell mebrane damage resulting from photocatalytical processes leads to an increase in membrane permaebility and eventually to free outflow of cell fluids. Therefore both bacterial cells as well as molecules of intracellural organels can become the substrate of reactive oxygen species (ROS) attack. ROS react simultaneously with the cytoplasmatic membrane of living cells and with the remains of dead
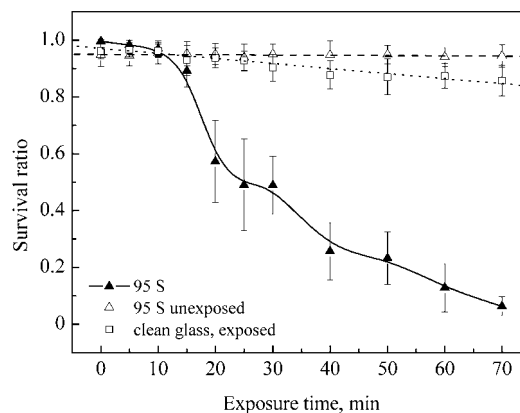
Fig. 2.   SR comparison for *Candida vini* at different conditions on S substrate

cells (polysycharides, lipids) at the same time. Our results also confirm this hypothesis.

When we compare the inactivation rates for *Candida vini* on R and S substrates (Fig. 2. and Fig. 1.) it becomes clear that the inactivation rate of *Candida vini* does not depent on the structure and topology of the catalyst layer, as long as the glass surface is well couted by titanium dioxide.

Conclusions

When comparing the photocatylic inactivation rate of *Candida vini* on two types of immobilised catalyst (rapidly printed and slowly printed titanium dioxide layers) it is possible to conclude that significant inactivation was observed on glass plates with very high sol loading, i.e. with very well covered surface (samples 100 R, 95 R, 95 S). We also observe a certain decrease in the inactivation rate after reachicg the SR value of appr. 50 %. This might be caused by the simultaneous consuption of ROS both by the still living cells membrane as well as the organic remains of already killed cells. Almost constant SR value between 25 and 35 minutes suggest a competitive reaction pathway.

REFERENCES

1. Huang N., Xiao Z., Huang D., Yuan Ch.: Supramol. Sci. *5*, 559 (1998).
2. Benabbou A. K., Derriche Z., Felix C., Lejeune P., Guillard C.: Appl. Catal. B Environ. *76*, 257 (2007).
3. Kühn K. P., Chaberny I. F., Massholder K., Stickler M., Benz V. W., Sonntag H-G., Erdinger L.: Chemosphere *53*, 71 (2003).
4. Seven O., Dindar B., Aydemir S., Metin D., Ozinel M. A., Icli S.: J. Photochem. Photobiol. Chem. *165*, 103 (2004).

P84 PHOTOCATALYTIC DISINFECTION OF WATER USING Ag/TiO$_2$

MÁRIA VESELÁ, MICHAL VESELÝ, JANA CHOMOUCKÁ and MICHAELA LIPENSKÁ

Brno University of Technology, Faculty of Chemistry, Purkyňova 118, 612 00 Brno,
vesela@fch.vutbr.cz

Introduction

Photocatalytic oxidation of organic compounds represents a major potential to be applied in environmental technologies. The photocatalytic process is capable to decompose most organic matter to water and carbon dioxide. Conventional cleaning technologies such as ozonization or chlorination have their limits. For example, ozone decomposes readily and chlorine, which is used widely for the dissinfection of drinking water, can react with organic compounds to form toxic byproducts[1.] Methods utilizing ozone a UV radiation are expensive and often technically challenging.

Reactive oxygen radicals are are produced in the presence of adsorbed oxygen and electron donor. These radical can cause rapid microbe cell death and at the same time decompose organic compounds.

The fungicidal effect of TiO$_2$ can be mediated by the presence of a noble metal, such as silver, at the catalyst surface[1]. Therefore, the deposition of silver nanoislets on the catalyst surface can lead to the production of a highly effective dissinfecting agent.

Experimental

Multi-Tube Flow Reactor

Suspension of yeast was colected in 3-neck flask and was circulated with peristaltic pump through tubes irradiated by 4 Sylvania LYNX lamps with total power output 44 W (Fig. 1.). A flow rate was 50 ml min^{-1}. A transmitance of glass wall of tubes was 93 % at maximum light output of Sylvania LYNX lamp at 350 nm. Irradiance was maintained at 1.0 mW cm^{-2} by lamp distance adjustment.

The inner walls of reactor were covered by titanium dioxide layer using sol-gel process based on tetraisopropoxide solution stabilized with acetoecetone. The inner glass walls were coated by dip-coating method. For experiment with Ag/TiO$_2$ the metallic silver was deposited on TiO$_2$ layer by photocatalytic process from silver nitrate solution wih ethanol.

Tubes with 1.2 % mol. and 2.4 % mol. of silver were prepared.

Yeast Suspension and CFU Evaluation

The yeast *Hansenula anomala* CCY 38-1-30, supplied by Slovak Collection of Yeasts, Bratislava, was cultivated in malt extract at 28 °C. After 24 hours a 10 ml was taken into test-tube for centrifugation. The pelets were washed with sterile distilled water and centrifugated. This process was repeated twice. The pelets were resuspended in 10 ml of
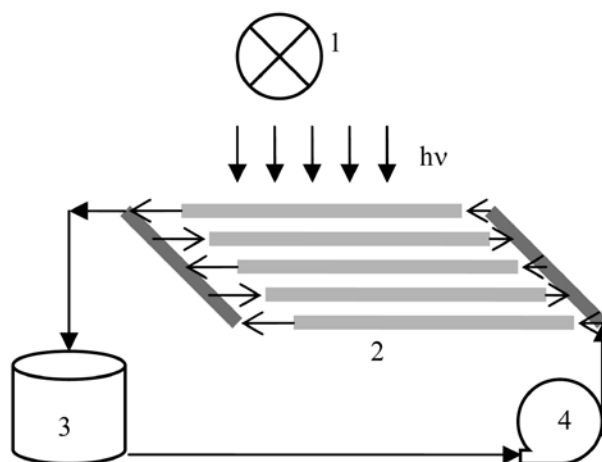
Fig. 1. **Multi-tube flow reactor: 1 – Sylvania LYNX lamps (4 × 11 W), 2 – tubes, 3 – multi-neck flask with yeast suspension (250 ml), 4 – peristaltic pump**

water and number of cells was calculated using Bürker chamber. This suspension was used for preparation of suspnesions with various cell concentration.

From the multi-tube flow reactor were taken samples in regular intervals. Number of colony forming units (CFU) was evaluated by indirect way: 100 µl of sample was spread on malt extract agar in 3 Petri dishes. After 48 hours of cultivation a number of colonies were enumerated and an average value was expresed as CFU ml^{-1}.

Results

We conducted experiments with photocatalytic inactivation of yeast cells in a multi-tube flow reactor with varying concentrations of cells (500 to 5,000 CFU ml^{-1}). We showed that during the experiment, the number of viable yeast cells decreases. The cell wall of *Hansenula anomala* is quite thick with a rigid structure, therefore we can expect it to be very resistant against ROS attact. Nevertheless, a total cell inactivation was achieved within 160 minutes.

We also observed the photocatalytic inactivation of *Hansenula anomala* (Fig. 2.) on TiO$_2$ photocatalyst layer overcoated with a very small amount of metallic silver. We also observed a decrease in the size of colonies grown from survivng cells. This phenomenon was noted also by Erkan et al.[6], who described diminishing colonies of *Saccharomyces cerevisiae* after irradiation in TiO$_2$. In this case, however, the titanium dioxide was overcoated with paladium and the diminishment is believed to be caused by the weakening of surviving cells.

It is well known that pure silver, copper, zinc and their ions pose antimicrobial properties. If these metals are deposited onto TiO$_2$ thin films, their antimicrobial effect will act together with the antimicrobial effect of bare TiO$_2$. We can expect the metallic silver to prevent elcetron-hole recombination on the surface of the photocatalyst and thus improve the efficiency of the photocatalytic process. In this case the pho-

tocatalyst would ensure the surface sterility upon the irradiation by UV and metal ions will do their job in the darkness[7]. According to Semikin a Skulachev, the interaciton of Ag^+ a SH groups of respiratory enzymes can lead to cell membrane permeability changes, resulting into major disorders in the whole cell. Apart from the membrane permaebility change, a cell-membrane separation is possible as well. Eventually, the possibility of Ag^+ addition to the bacterial genetic material was reported, too[4].
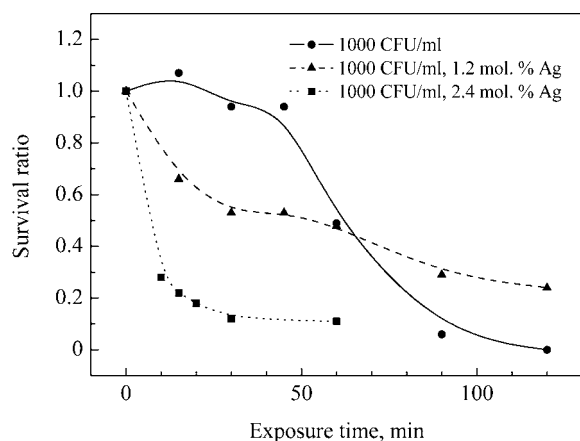
Fig. 2. **Photocatalytic inactivation of *Hansenula anomala* cells on TiO$_2$ and Ag/TiO$_2$ layers in multi-tube flow reactor**

We showed that yeast cells of *Hansenula anomala* are not capapble of regeneration, which is otherwise usual, especially in the case of bacteria. The cells are probably damaged in such extend that they loose their reproduction ability. Identical effect was observed on combined surface of Ag/TiO$_2$ (Fig. 3.).

Conclusions

The collected result indicate that it is possible to photocatalytically inactivate cells even with a very rigid cell wall (*Hansenula anomala*). In this way, a complete photocatalytic dissinfection of water can be performed. A very small amount of metallinc silver deposited on the surface of titanium dioxide photocatalyst enhanced the inactivation rate.
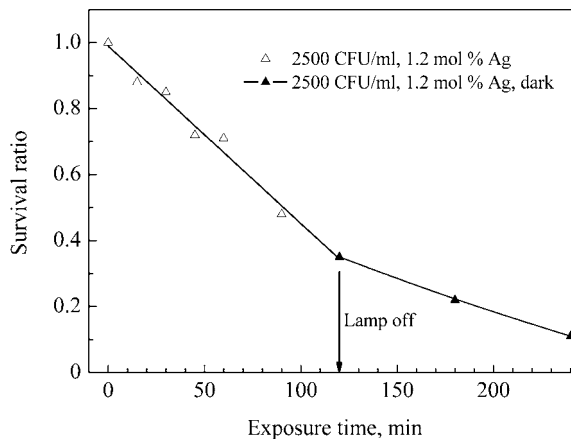
Fig. 3. **Photocatalytic inactivation of *Hansenula anomala* cells on Ag/TiO$_2$ layer in multi-tube flow reactor. The lamp was powered off after 120 minutes**

We also showed that in the case of *Hansenula anomala*, the surviving cells are not able to reproduce after the irradiation is terminated. The cells lose their reproduction ability. Similarly, the cells lose their reproduction ability after their irradiation on TiO$_2$ surface doped with silver islets (1.2 a 2.4 % mol. silver).

REFERENCES
1. Kubacka A., Ferrer M., Martínez-Arias A., Fernández-Garciá M.: Appl. Catal. B Environ. 2007, in press
2. Yip H. Y., Yu J. C. M., Chan S. C., Zhang L. Z., Wong P. K.: J. Water Environ. Tech. *3*, 47 (2005).
3. Keleher J., Bashant J., Heldt N., Johnson L., LI Y.: World J. Microbiol. Biotechnol. *18*, 133 (2002).
4. Semeykina A. L., Skulachev V. P.: FEBS Lett. *269*, 69 (1990).
5. Pratap Reddy M., Venugopal A., Subrahmanyam M.: Water res. *41*, 379 (2007).
6. Erkan A., Bakir U., Karakas G.: J. Photochem. Photobiol. Chem. *184*, 313 (2006).

P85　LABORATORY STUDY OF ARSENIC MOBILITY IN STREAM SEDIMENTS AND IMPOUNDMENT MATERIAL USING COLUMN EXPERIMENTS

VERONIKA VESELSKÁ and EDGAR HILLER

Comenius University in Bratislava, Faculty of Natural Sciences, Department of Geochemistry, Mlynská dolina, 842 15 Bratislava, Slovak Republic,
veselska@fns.uniba.sk

Introduction

High arsenic contents in the impoundment situated near the village of Poša in the upper part of the catchment of the Kyjov brook in eastern Slovakia, represent an environmental problem because of As mobilization and transport from the impoundment material and significant contamination of surface water of the Kyjov brook (the mean As values of $11{,}385\ \mu g_{As}\,dm^{-3}$, $1{,}778\ \mu g_{As}\,dm^{-3}$ and $295\ \mu g_{As}\,dm^{-3}$ measured in the Kyjov brook during 2000, 2005 and 2007 respectively)[1]. Decreasing concentrations of As in surface water are involved in delimited using of impoundment in last few years.

Arsenic distribution in different stream sediment constituents and its mobilization determine As concentration in aquatic environment and affect its bioavailability and toxicity to the biosphere[2,3].

The major processes controlling As leaching from sediments to natural waters include mineral (co)precipitation/ dissolution, adsorption/desorption, chemical and biological transformations. The conditions present such as pH, redox potential, solution composition, the sediment properties and mineralogical composition of the sediment determine the dominant processes affecting the environmental fate of As in the stream sediments and ist leaching behaviour[4,5].

The main objective of this study was to investigate leaching behaviour of As from the heterogeneous impoundment material and the three stream sediments and the evaluation of the total As mobility.

Experimental

The samples used in this work are either the stream sediments of the Kyjov brook taken at the distance of 100, 1,000 and 2,000 m from the impoundment (denoted as KY-100, KY-1000 and KY-2000) or the impoundment material (denoted as KY-0).

Continuous column leaching experiments were conducted under standard conditions ($25 \pm 3\,°C$, 101,325 Pa) to provide information about As release, its binding and desorption kinetic. The experiments were run in duplicates. Each of the two glass columns per one sample was filled with 50 g of a dry sample (a < 1 mm fraction) and columns were during five days flushed with 1.3 dm^3 of 0.0125M solution, that was prepared to resemble the composition of surface waters of the Kyjov brook and contained by 2×10^{-5} M PO$_4^{3-}$, 2.8×10^{-3} M Cl$^-$ and 3.2×10^{-3} M SO$_4^{2-}$. The upward flow was regulated at

a rate of 0.2 ml min^{-1}. During the experiment, 14 samples of leachates were collected from each of the columns, pH values were measured and the concentrations of As were determined by graphite furnace atomic absorption spectrometry (Perkin-Elmer 4110 ZL).

Results

The results of the column experiments showed that theAs release from the solid samples was likely controlled by Fe and Mn oxohydroxides, pH values of the geosorbents and leachates and also organic carbon content. It was also observed that the time was an important factor influencing the As release.

Significant correlations of the amounts of As released from the solid samples with its total contents (r = 0.975, P < 0.05) (Fig. 1.) as well as with total organic carbon contents (r = 0.942; P < 0.05) were found. The total organic carbon content was measured using a Leco RC-412 multiphase determinator at 550 °C.

The impoundment material (KY-0) has the highest total organic carbon content (37 %), which is likely attributed to the fact that stored sludge consists of fly ashes derived from coal and chemical waste combustion. Alkaline character of the KY-0 (pH = 8.55) as well as high leachate pH (pH ~ 9.0) enhance release of As and its transport to the liquid phase. The results of various studies showed that the amounts of As oxyanions released from different solid geosorbents increase in alkaline conditions, mainly when pH > 8(ref.[6]) The maximum As concentration in column leachates from KY-0 was determinated after 25 hours, when the easily soluble fraction of As weakly bound on the solid surface was released. The late hindered As release from KY-0 could be caused by the presence of mullites and vitreous phases. It is suggested here that some fraction of As may be only hardly available to be released because of its strong binding within the heterogenous components.
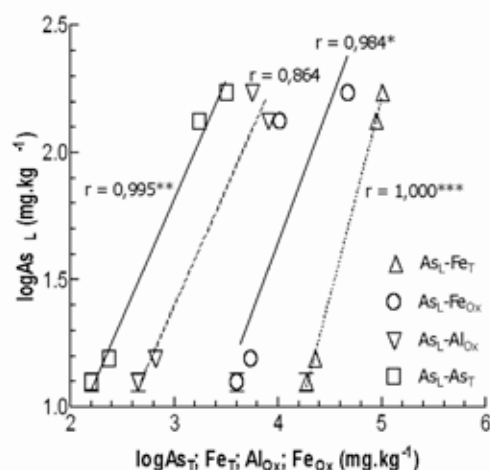
Fig. 1.　**Relationships between the amounts of As released and total contents of As, Fe as a ammonium-oxalateextractable Alox, Feox in the log-log form**

Notably high accumulation of trace elements including As in the most contaminated sample KY-100 (3,208 $mg_{As} kg^{-1}$) with the lowest relative mobility, is likely due to high contents of the Fe, Al, Mn oxohydroxides. The relative mobility of As was inversely related to the oxalate-extractable Mn content (r = –0.960, P < 0.05) and not significantly to the oxalate-extractable Fe content such that diffusion in hydrated micropores of amorphous Fe and Mn oxides might be the rate limiting mechanism of the As release (Fig. 2.).
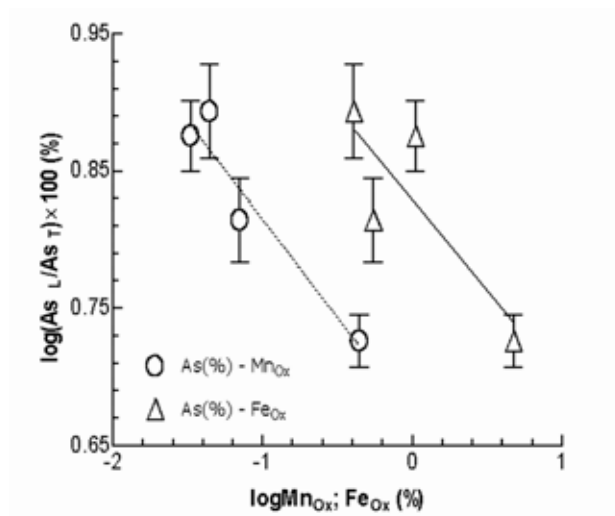
Fig. 2.　Relationship between the relative mobility of As and the ammonium oxalate-extractable Mn, Fe contents in the log-log form

The amount of As released from samples KY-1000 and KY-2000 increased rapidly within short extraction times, reaching the apparent equilibrium after 174 min. The relative mobility of As in KY-1000 and KY-2000 was approximately the same as in impoundment material although the total Fe, Mn contents in KY-1000, 2000 are 2-times lower as compared with KY-0. The total contents of elements Cd, Cr, Fe, Hg, Mn, Pb, Zn, Al, As and Sb were determined after digestion with acid mixture.

Conclusions

The fractions of As released in column experiments were generally less than 10 % (5.32–7.83 %) of its total contents, but they represented high absolute amounts of readily available and water-soluble As (83 $mg kg^{-1}$). The fraction released from the source impoundment material (132 $mg kg^{-1}$) represented high As concentration in its leachates, reaching up to 8,000 $\mu g dm^{-3}$. As concentrations in the leachates from all the samples exceed maximum permissible level in drinking water (10 $\mu g dm^{-3}$; Decision of the Slovak Health Ministry No. 151/2004).

REFERENCES
1. Jurkovič Ľ., Kordík J., Slaninka I.: Slovak Geol. Mag. *12,* 31 (2006).
2. Tao Y., Zhang S., Jian W., Yuan CH., Shan X.: Chemosphere *65,* 1281 (2006).
3. Williams L. E., Barnett M. O., Kramer T. A., Melville J. G.: J. Environ. Qual. *32,* 841 (2003).
4. Gao S., Fujii R., Chalmers A. T., Tanji K. K.: Soil Sci. Soc. Am. J. *68,* 89 (2004).
5. Smith E., Naidu R., Alston A.M.: J. Environ. Qual. *31,* 557 (2002).
6. Ganne P., Cappuyns V., Vervoort A., Buvé L., Swennen R.: Sci. Total Environ. *356,* 69 (2006).

P86   ANTIBIOTICS IN THE ENVIRONMENT

H. VÍTEČKOVÁ, L. VYDROVÁ, D. VELEBOVÁ, M. VÁVROVÁ and L. MRAVCOVÁ

Brno University of Technology, Faculty of Chemistry, Purkyňova 118, Brno 612 00, Czech Republic,
viteckova@fch.vutbr.cz

Introduction

Tetracyclines (TC) present a class of antibacterial drugs. Due to their broad antibacterial spectrum and economic advantages, tetracyclines have been commonly used in veterinary medicine and in human medicine for the purpose of prevention and treatment of disease. However, their widespread utilization could lead to TC residues in animal-originated food and in the environment. The antibiotics in food and water consumed for long periods can also cause problems regarding the spread of drug-resistant microorganisms[1].

It is well known that the principal pathway of antibiotics into the aquatic environment is via wastewater systems following consumption and excretion by humans, and via effluents from landfills and farms[2]. Presently conventional wastewater treatment plants (WWTPs) were designed without consideration of antibiotics removal from wastewater. Many previous studies have shown that, while some antibiotics may be eliminated in the WWTPs, some other may be hardly removed in the process, therefore they can reach the aquatic environment[3,4]. Due to irremovable antibiotics, wastewater treatment plants become an important point source of emissions into the environmen[1,2,3].

Experimental

To monitor the tetracycline residues a reliable method is needed. SPE for purification and preconcentration of analytes was used. Spectrophotometric method for antibiotic determination was used.

S a m p l i n g

Waste water samples have been taken from the waste water treatment plant (WWTP) in the University of Veterinary and Pharmaceutical Sciences Brno campus in one-day intervals into amber glass sampling bottles. In this WWTP, we decided to deal with the antibiotics in particular because these drugs samples were taken from the WWTP inlet and compared with the samples taken from WWTP outlet.

The samples were processed immediately or stored in a refrigerator till the following day.

R e a g e n t s

During the process, the following chemicals have been used: oxalic acid, p.a. sulfuric acid p.a., dinatrium phosphate dodecahydrate p.a., all from Lachema, CZ; acetonitrile for HPLC, methanol for HPLC, from Riedel-de-Haen, SRN; citric acid, p.a. Onex, CZ; Chelaton III, p.a. Penta,CZ;

Tetracycline, Chlorotetracycline and Oxytetracycline, standards for HPLC, were from Sigma Aldrich, CZ.

McIlvain buffer: citric acid (12.9 g dm^{-3}), natrium salt of ethylenediaminetetraacetate (37.2 g dm^{-3}), dodecahydrate of dinatrium phosphate (30.2 g dm^{-3}) in deionized water

Elution mixture: 20 mmol dm^{-3} oxalic acid in methanol.

S a m p l e   T r e a t m e n t

Samples were filtered using paper filters to remove particles. Volume of 200 ml samples were extracted 20 minutes with McIlvain buffer in an ultrasonic bath.

A Phenomenex Strata C18-E SPE column (55 μm, 500 mg 6 ml^{-1}) was conditioned with 4 ml of methanol followed by 3 ml of McIlvain buffer. After sample loading, the column was washed with 3 ml deionized water. The column was dried using the vacuum of the SPE manifold. Then the tetracyclines were eluted with 10 ml of elution mixture.

S p e c t r o p h o t o m e t r i c   A n a l y s i s

The analyses were carried out on UV-VIS spectrophotometer Spectronic Helios (UK). Deuterium and wolfram lamp was used for determination.

At first the absorption spectrum was measured in the range 230–450 nm step by step 2 nm. Tetracyclines have two absorption maximas as resulting from absorption spectrum and with accordance to published data: 246 nm and 360 nm[4]. Spectrophotometer was adjusted to zero value through the use of elution reagent. Subsequently, real samples were measured to determine the absorbance value at absorption maximum. Quartz cuvette with optical path 1 cm was used.
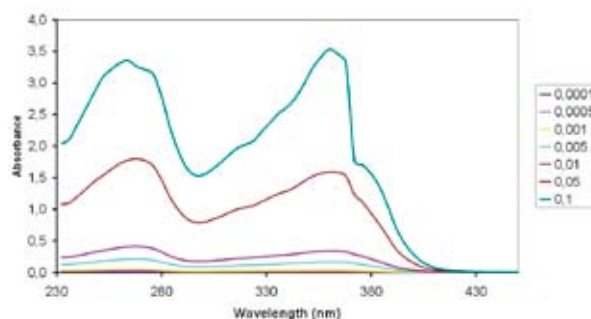
Fig. 1.   **Absorption spectrum of tetracycline in various concentrations [mg ml^{-1}]**
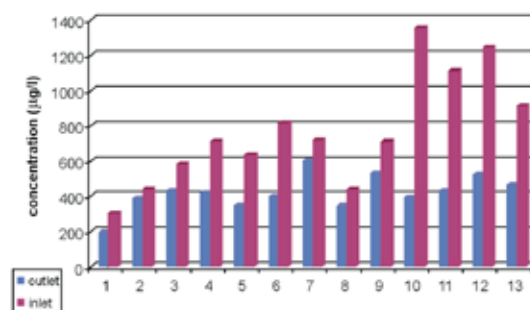
Fig. 2.   **Concentration of tetracycline in real samples**

Results

All tetracyclines have typical absorption spectrum. They have two characteristical absorption maximas, 264 nm and 360 nm. Due to their characteristic we could determinate tetracyclines and their metabolites together by spectrophotometry.

Inlet concentrations of analytes were always higher than outlet concentrations. This indicates that these pharmaceuticals are removed partially in the wastewater treatment plant. The change of tetracycline concentration may be caused by photodegradation.

Conclusions

As the use of pharmaceuticals is increasing, fast sample preparation and determination method is required.

Samples were taken from wastewater treatment plant placed in Veterinary and Pharmaceutical university Brno campus, from inlet and outlet.

Samples were filtered before extraction.

SPE was optimized for preparation and preconcentration of wastewater samples.

An efficient method for determination of tetracyclines in wastewater, using spectrophotometry, was developed.

Spectrophotometry was used because this is commonly used in laboratories and machine operation is cheap.

REFERENCES

1. Pavlović D. M. et al.: Trends Anal. Chem. *26*, 1062 (2007).
2. Hirsch R. et al.: Sci. Tot. Env. *225*, 109 (1999).
3. Hernando M. D. et al.: Talanta *69*, 334 (2006).
4. Fritz J. W.: Food. Chem. *105*, 1297 (2007).

P87 THE FLUORIMETRIC DETERMINATION OF ALUMINIUM, GALLIUM AND INDIUM WITH 8-HYDROXYQUINOLINE-5-SULPHONIC ACID IN AQUEOUS AND SUBMICELLAR MEDIUM

ŠIMON VOJTA and LUMÍR SOMMER

Institute of Environmental Protection, Faculty of Chemistry, Brno University of Technology, Purkyňova 118, 612 00 Brno, Czech Republic,
halapaloosa@email.cz

Introduction

The complexing and analytical properties of 8-Hydroxyquinoline-5-sulphonic acid (QSA) are similar to 8-Hydroxyquinoline but the solubility of complexes in aqueous solutions increases and no fluorescence of the reagent in the large pH interval has been observed. The QSA was formerly used as a fluorogenic reagent for a number of metal ions including Mg^{2+}, Zn^{2+}, Cd^{2+}, Ce^{3+} and Al^{3+}(ref.[1]). The fluorimetry of Gallium and Indium complexes in aqueous solutions was only briefly mentioned.

The fluorescence of metal complexes with QSA can be considerably enhanced in the presence of surfactants in submicellar and micellar medium[2,3]. The fluorescence properties of the metal species with QSA were tested in the presence of surfactants and exploited chromatographically in very low concentrations.

Thus the cationic surfactants were widely used for the enhancement of fluorescence of metal complexes with QSA[4]. The attention was also paid to the fluorimetric determination of Al with QSA also in mixtures with Zn using derivative synchronous scan in the presence of surfactant[5]. The Partial Least Square Method (PLS) in combination with pH gradient FIA was used in binary mixtures of ions in complexes with QSA whose fluorescence was enhanced by the surfactant[6].

In this paper the fluorescent Al^{3+}, Ga^{3+} and In^{3+} complexes with QSA were studied in detail in the absence and presence of surfactants and optimal conditions were recommended for the determination of particular metals in the presence of Zephyramine. Normal and first derivative spectra were evaluated.

Experimental

Instruments

Spectrofluorimeter Aminco Bowman, Series 2 with 1 cm quartz cells, 4 nm exit slits, photomultiplier under 450–850 V. Sample cell was tempered to 20 °C.

The calculation of the first derivative was made by using the instrument software using Golay-Savitzky 11-point convolution.

Chemicals
• Standards used, Analytica s.r.o., Prague:
Aluminium chloride 1.000 ± 0.002 g dm^{-3} containing 5 % HCl
Gallium chloride 1.000 ± 0.002 g dm^{-3} containing 10 % HCl
Indium chloride 1.000 ± 0.002 g dm^{-3} containing 10 % HCl

• 8-Hydroxyquinoline-5-sulphonic acid hydrate (QSA), Sigma–Aldrich was used without purification
• 0.1M Benzyldimethyltetradecylammonium chloride (Zephyramine®) – Sigma-Aldrich Co.
• 0.1M 1-ethoxykarbonylpentadecyltrimethylammonium bromide (Septonex®)–Sigma-Aldrich Co.
• 0.1M Dodecylbenzyldimethylammonium bromide (Ajatin®) – Sigma-Aldrich Co.
• 1% Didodecyldimethylammonium bromide – Sigma-Aldrich Co.
• 1% Polyoxyethylene(23) lauryl ether (Brij 35) – Sigma-Aldrich Co.
• 1% Hexadecyltrimethylammonium chloride – Fluka.
• 1% 4-(1,1,3,3-Tetramethylbutyl)phenyl-polyethylene glycol (Triton X-100) – Calbiochem Co.
• 0.1 M Sodium dodecylsulphate (SDS) - BDH Chemicals, England.

Evaluation of Data

The limits of detection X_D^α and X_D^β calculated according to Graham[7] follow from the calibration plots and their confidence intervals were compared with those from multiple measurements of the background according to IUPAC[8].

The stoichiometry of complexes was evaluated by using the modified continuous variations method[9] in the absence and presence of cationic surfactant Zephyramine. The fluorescence was measured for several sums of equimolar solutions, where $c_o = c_M + c_L$.

Results

The complexes of 8-Hydroxyquinoline-5-sulphonic acid with Al, Ga, and In produce an outstanding fluorescence for wavelengths over 430–600 nm with λ_{max} at 495 nm for Al, λ_{max} at 504 nm for Ga and λ_{max} at 519 nm for In. The corresponding excitation λ_{max} are 360 nm, 365 nm and 367 nm. The fluorescence shows considerable pH dependence which reaches the maximum in solution with $c_L = 7.4 \times 10^{-5}$ M
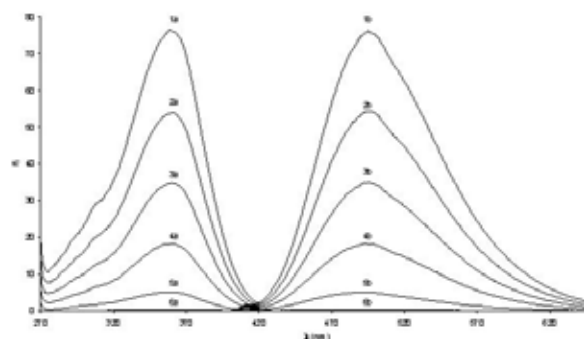
Fig. 1. **Excitation(a) and emission(b) spectra of Aluminium(III) in the presence of 7.4×10^{-5} mol dm^{-3} QSA at 620 V in dependence on concentration of Al(III) at pH 4**
1 – 1.6 µg cm^{-3}, 2 – 0.8 µg cm^{-3}, 3 – 0.4 µg cm^{-3}, 4 – 0.2 µg cm^{-3}, 5 – 0.05 µg cm^{-3}, 6 – 0 µg cm^{-3}

at pH 4 for Al^{3+}, $c_L = 1.5 \times 10^{-5}$ M at pH 3 for Ga^{3+} and $c_L = 3.5 \times 10^{-5}$ M at pH 8 for In^{3+} (Figs. 1. and 2.).

No fluorescence was observed for the sole reagent in this pH interval.
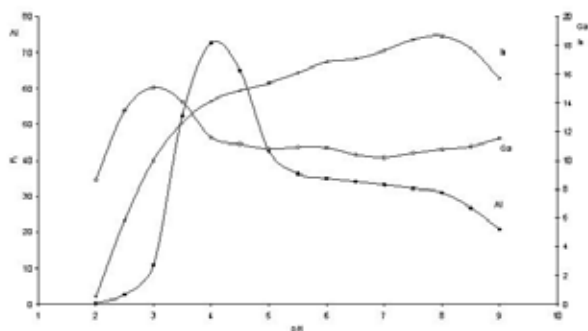
Fig. 2.   **Fluorescence intensity dependence on pH for each complex (0.3 μg cm⁻³ of each element) at optimal conditions**

The first derivations of the fluorescence and excitation spectra under the same conditions as the normal spectra with $\lambda_{max(em)} = 460$ nm (AlQSA), $\lambda_{max(em)} = 472$ nm (GaQSA) and $\lambda_{max(em)} = 478$ nm (InQSA)are given in Fig. 3. Higher derivations could not be used because of a big noise of the instrument.

The calibration plots are stricly linear in solution with $c_L = 7.4 \times 10^{-5}$ M for Al^{3+} at pH 4 or $c_L = 5.8 \times 10^{-5}$ M QSA for Ga^{3+} at pH 3 and $c_L = 1.78 \times 10^{-5}$ M and pH 8 for In^{3+}.

Although the calibration plots are strictly linear till 2 μg cm⁻³, the meaningful metal concentration range was 0.04–1 μg cm⁻³. The decrease of QSA concentration in solution negatively influence the extent of the linear part of the calibration plot, the increase of QSA concentration causes quenching.

There is no considerable difference in the values of detection limits for normal spectra, derivative spectra and values in the presence of 0.0012 M cationic surfactant Zephyramine
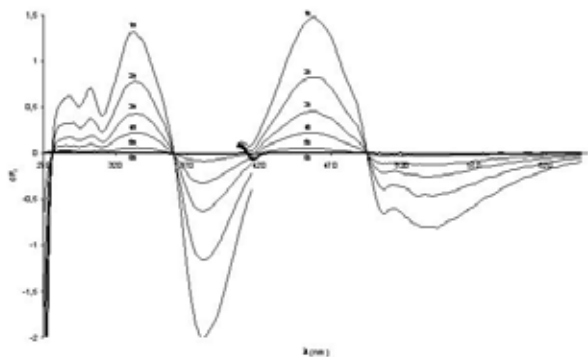
Fig. 3.   **The first derivative excitation(a) and emission(b) spectra of Aluminium(III) in the presence of 7.4×10^{-5} mol dm⁻³ QSA at 620 V in dependence on concentration of Al(III).**
1 – 1.6 μg cm⁻³, 2 – 0.8 μg cm⁻³, 3 – 0.4 μg cm⁻³, 4 – 0.2 μg cm⁻³, 5 – 0.05 μg cm⁻³, 6 – 0 μg cm⁻³

when values according to Graham and IUPAC recommendation are compared.

Cationic surfactants increase considerably the intensity of fluorescence with no λ_{max} shift, but some little bathochromic shift (lesser than 20 nm) of excitation maximum is observed. The fluorescence increase is time dependent and takes 1 hour either during radiation or when the sample is left in darkness. Since the largest effect of the cationic surfactant is often observed for the CMC the formation of a fluorescent ion associate is assumed with the anionic metal complexes. The fluorescence, however, slowly decreases after reaching the micellar concentration of the surfactant.

The largest positive effect was found for 0.0012 M Zephyramine but for the subsequent increase of concentration a considerable decrease of fluorescence is observed for all cationic surfactants.

The anionic surfactants such as dodecylsulphate have a negative influence with the increasing concentration. No effect is observed for selected non ionic surfactants such as Triton X 100 and Brij 35, and β-cyclodextrine.

The effect of various surfactants follows from the Fig. 4. which shows relative fluorescence intensity dependence on surfactant concentration for GaQSA. The influence of surfactants for the AlQSA and InQSA is similar to that of GaQSA complex.
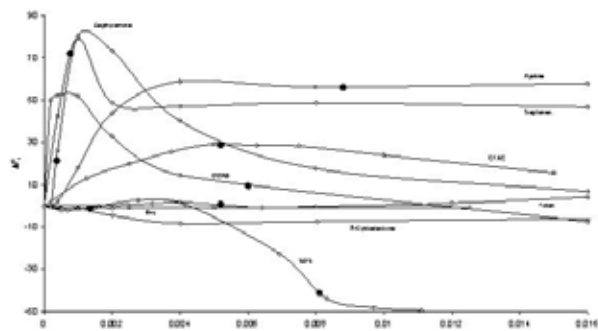
Fig. 4.   **Surfactants influence on the GaQSA complex at pH 3. Septonex, Zephyramine, Ajatine, SDS – mol dm⁻³, CTAC (Hexadecyl trimethyl ammonium chloride – c/4 [mol dm⁻³], DDAB (Didodecyldimethyl ammonium bromide), β-Cyklodextrine – c/5 [mol dm⁻³], Triton X 100 – c/4 × 10⁻⁵ [ppm], Brij – c/15 [mol dm⁻³].**
Critical micellar concentrations are highlighted by the fulfilled marks

The fluorimetric method of continuous variations for at least two concentrations c_o gives unambiguously the simple mole ratio M : L = 1 : 1 in the Al^{3+}, Ga^{3+} and In^{3+} complexes at pH 3–4. For the increasing pH 8 and In^{3+} a higher complex is also indicated (Fig. 5.).

In the presence of constant concentration 0.0012 M of cationic surfactant Zephyramine a ratio M : L = 1 : 3 appears which may indicate the formation of a ternary species, ML_3^{3-} .3 T^+.

Fig. 5. **Continuous variations of AlQSA complex at pH 4. 1 – $c_0 = 1.1 \times 10^{-4}$ M, 635 V, 2 – $c_0 = 5.6 \times 10^{-5}$ M, 705 V, 3 – 5.6×10^{-5} M, 0.0012 M Zephyramine, 660 V**

There are no interferences observed for Na^+ and K^+ at 1,000 : 1 molar ratio. The effects of some other ions at optimalized conditions are summarized in Fig. 6. No considerable difference in the interferences is observed for the absence or presence of cationic surfactant Zephyramine (Fig. 6.).

Fig. 6. **Interferences for 0.3 $\mu g\,cm^{-3}$ of each element at optimal conditions in the presence of 0.0012 M Zephyramine**

For the application, 0.04–1 $\mu g\,cm^{-3}$ of Al^{3+}, Ga^{3+} and In^{3+} are determined in the excess of QSA in the presence of 0.0012 M Zephyramine and 0.05 M hexamethylentetramine at pH 4 for Al, pH 3 for Ga and in the presence of 0.05 M tetraborate at pH 8. In the presence of 0.05 M hexamethylentetramine or sodium tetraborate 10% lower fluorescence intensity is observed. 0.05 M MES is not suitable because of larger fluorescence intensity decrease about 15 %.

Conclusions

The collinear fluorescence spectra of complexes with 8-Hydroxyquinoline-5-sulphonic acid were used for the study of Al, Ga, In complexes and determination of these elements at pH 4, 3 or 8. Strictly linear calibration plots for 0.04 – 1 $\mu g\,cm^{-3}$ of the metal ion are observed under optimized conditions for the normal and first derivative spectra or in the presence of cationic surfactant.

The efficiency of fluorescence intensity increases in the presence of submicellar concentrations of cationic surfactants, especially Zephyramine. The detection limits from normal or first derivative spectra and in the submicellar media are practically identical (0.03–0.05 $\mu g\,cm^{-3}$), but sensitivity is significantly increased in the presence of Zephyramine. Fatal interferences are observed from Fe^{3+} and PO_4^{3-} only.

For the individual determination of Al, Ga and In with QSA hexamethylentetramine or sodium tetraborite buffers are suitable. The multicomponent determination of these ions can be carried out by approaching the PLS method[10].

REFERENCES
1. Bishop J. A.: Anal. Chim. Acta *29*, 172 (1963).
2. Alonso J. I. G., Garcia M. E. D., Medel A. S.: Talanta *31*, 361 (1984).
3. Prat M. D., Compañó R., Beltrán J. L., Codony R.: Journal of Fluorescence *4*, 279 (1994).
4. Soroka K., Vithanage R. S., Phillips D. A., Walker B., Dasgupta P. K.: Anal. Chem. *59*, 629 (1987).
5. Salinas F., Delapena A. M., Duran M. S.: Anal. Letters *21*, 1457 (1988).
6. Porter N., Hart B. T., Morrison R., Hamilton I. C.: Anal. Chim. Acta *308*, 313 (1995).
7. Graham R. C.: *Data Analysis for the Chemical Sciences. A Guide to Statistical Techniques*. VCH Publishers (1993).
8. Currie L. A.: Pure and Applied Chemistry *67*, 1699 (1995).
9. Vosburgh W. C., Cooper G. R.: J. Am. Chem. Soc *63*, 437 (1941).
10. Vojta S., Jančář L., Sommer L.:, Journal of Fluorescence *18*, 339 (2007).

P88 SURGICAL POLYESTER FABRIC IMPREGNATED BY CROSS-LINKED COLLAGEN

PAVEL FILKA, LUCY VOJTOVÁ and JOSEF JANČÁŘ

Brno University of Technology, Faculty of Chemistry, Institute of Materials Chemistry, Purkyňova 464/118, 612 00 Brno, Czech Republic,
xcfilka@fch.vutbr.cz

Introduction

Collagen is a widely applicable protein in medical applications. The main advantage of this biomaterial is its ability to create fibers with a high strength and stability by using different cross-linking agents or physical methods. Collagen's significant properties are biocompatibility and resorbability in organism, which might be particularly used at surface modification of surgical fabrics based on polyester silk (PES). The collagen modified PES nets used in surgery for longtime fixation or reinforcing different organs may accelerate healing injury as well as reduce inflammation of a tissue surrounding the implanted fabrics[1].

Natural crosslinking gives collagen special properties, namely higher rigidity and endurance against proteolytical cleavage. However, during processing and utilization the collagen loses those particular properties. That is why the collagenous material is additionally cross-linked by chemical or physical methods in order to regenerate original net behaviours.

Chemical methods employ bifunctional compounds (e.g. aldehydes, epoxides, isocyanides, carbodimides, acrylic acid etc.) which can react with amino groups of collagen in two different places resulting in generation of a new strengthing bond. Their main disadvantage is toxicity of used chemicals[2]. Instead of toxic aldehydes it might be used nontoxic 1-ethyl-3-(-dimethylaminopropyl) carbodiimide (EDC), which is soluble in water. For reaction acceleration the N-hydroxysuccinimide (NHS) as catalyst can be added to the system with EDC[3].

In this work cross-linking agents based on melamin-formaldehyde resin (named as LYOFIX and MH – 83) as well as carbodiimide (system EDC/NHS) were used for crosss-linking collagen impregnated on the polyester surgical net CHS 100. Swelling behaviours in the water and degradation at 37 °C in physiological solution with the purpose of increasing biocompatibility of commercial surgical net were examined.

Experimental

Modified derivative of alkylmelamineformaldehyde in aqueous solution (LYOFIX, Ciba, Hungary), hexamethylolmelamineformaldehyde resin (MH-83, Draslovka a.s. Kolin, CZ), 1-ethyl-3-3-dimethylaminopropyl)-carbodiimide hydrochloride (EDC, Sigma-Aldrich s.r.o.), N- hydroxysukcinimide (NHS 98 %, Sigma-Aldrich s.r.o.), $Na_2HPO_4 \cdot 12H_2O$ (Lach-Ner a.s. CZ), collagen type I (8 %, VÚP a.s., Brno), net for surgical purposes (CHS 100 – knitwork made from polyester silk, VÚP a.s., Brno), ultra - clean demineralize and deionize MILIQ water (prepared in arrangement of Millipore S.A. at FCH BUT, CZ).

Preparation of a Collagen Films

Polyester fabric CHS 100 was cut into same size square pieces of about 1 cm² which were diped layed on the 5 ml of 1% collagen solution (prepared from 100% freeze – dried collagen) embedded with extra 5 ml of 1% collagen solution. This sample was air-dried for approximately 48 h to the constant weight.

Cross-Linking

Collagenous films were cross-linked by 2% solution of LYOFIX and MN-83 resins for a period of 12 mins. Subsequently the samples were five times washed by the distilled water for 5 mins and dryied by air to the constant weight.

Collagenous films were cross-linked by the ethanol solution containing 50 mmol dm⁻³ of EDC and 25 mmol dm⁻³ of NHS. After 4 h of cross-linking the samples were washed out for 2 h in 0.1M solution of $Na_2HPO_4 \cdot 12H_2O$ and finally four times for half an hour in the distilled water followed by air-drying to the constant weight.

Swelling

Swelling characteristics were evaluated to compare the cross-linking effectivity by each agent. Swelling proceeded for a period of 40 min to 1 h in MILIQ water at a laboratory temperature. Quantity of absorbed water was weighted in five minute intervals. Both water content (OV) and swelling ratio (SB) of each sample were calculated according to equation (1) and (2), where m_C is weight of swollen sample in a given time and m_S is weight of dry sample prior the swelling[4].

$$OV\,[\%] = \frac{m_C - m_S}{m_C} \cdot 100 \qquad (1)$$

$$SB\,[-] = \frac{m_C}{m_S} \qquad (2)$$

Degradation

Each sample was placed in the physiological solution with addition of sodium azide (0.1% NaCl + 0.02% Na_3N) and placed into the incubator set to 37 °C to determine the hydrolytic degradation. Prepared samples were every day taken out from the incubator, dried by the filtration paper, consequently weighted and immediately placed back with fresh physiological solution. Degradation was expressed as percentual decrease of collagen weight in certain time having the zero point at the maximum of swelling according to equations (3) and additionaly (4)–(6).

$$\text{Degradation} = 100 - ((\text{Wk} \cdot 100)/\text{Wb}) \qquad (3)$$

$$\text{Wk} = W - W_{sb} \qquad (4)$$

$$\text{Wsb} = W_{ss} + W_{ss} \cdot OV_{13} \qquad (5)$$

$$OV_{13} = \frac{W_{sb} - W_{ss}}{W_{sb}} \cdot 100 \qquad (6)$$

W_k represents weight of swollen collagenous sample without wet net, W_b is weight of swollen collagenous sample at maximum of swelling, W_{sb} is weight of wet net, W_{ss} is weight of dry net, W is weight of swollen collagenous sample with net and OV_{13} is water in net after 13 days of swelling (%).

Morphology

Morphology of samples was observed by the scanning electron microscope Philips Quanta 200. On the sample surface conductive lay of 3–4 nm were steamed by the sputter Polaron SC7640 prior the analysis.

Result and Discussion

Swelling Ratio

Swelling ratio (SB) of all prepared samples shows Fig. 1. It can be seen that the highest swelling ratio attained non cross-linked collagen (SB = 42 in 25 min), then non cross-linked collagen coated on the net (SB = 14 in 25 min). Cross-linked collagens have almost same swelling ratio (SB = 3–4 in 25 min). The lower amount of water absorbed polyester net (SB = 1 in 25 mine).
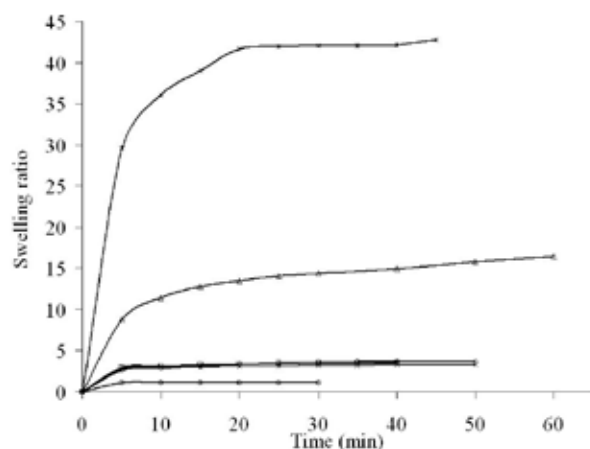
Fig. 1.   **Dependence of swelling ratio on time for samples cross-linked by the EDC – NHS (◇), LYOFIX (□), MH-83 (×), non cross-linked collagen with net (△), non cross-linked collagen without the net (∗) and the net without collagen (○).**

Degradation

From the degradation behavior dependence of collagen in the physiological solution at 37 °C on time (Fig. 2.) it is assumed that the fastest degradation yielded non cross-linked collagen within 21 days of incubation. After 23 days degraded non cross-linked collagen coupled to the net resulting in net maintain. The slowest degradation in the physiological solution showed the collagen cross-linked by EDC-NHS which recorded 59 % of degradation in 78 days of incubation. The shortest degradation of cross-linked collagen embodied sample treated by LYOFIX resin (17 % of degradation in 24 days) followed by MH-83 resin (32 % of degradation in 35 days).
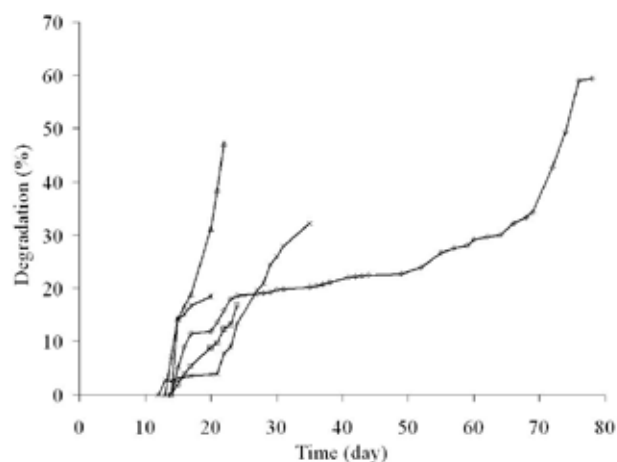
Fig. 2.   **Dependence of degradation on time of collagenous samples coss-linked by the EDC – NHS (◇), LYOFIX (□), MH 83 (×), non cross-linked collagen on the net (△), non cross-linked collagen without the net (∗)**

Morphology

Scanning electron microscope picture in Fig. 3.a (sight angle of 54 °) shows good adhesion between the non cross-linked collagen coated on the PES net as well as between the collagen cross-linked by the EDC-NHS and the PES fabric (Fig. 3.b).

Cross-linked samples after the degradation were observed in environmental mode. From the Fig. 4. it is evident the separation of collagen from the polyester net in this case

(a)   (b)
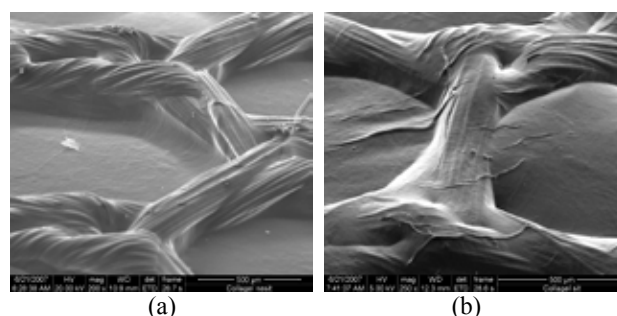
Fig. 3.   **Morphology of collagen built – up on the net CHS100 non cross-linked (a) and cross-linked by the EDC – NHS (b)**

cross-linked by the EDC – NHS after the 78 days of incubation in the physiological solution.
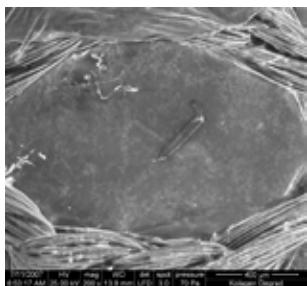
Fig. 4. **Morphology of degraded collagen coated on the net and cross-linked by the EDC – NHS**

Conclusions

The all cross-linked collagen samples embodied very good adhesion to the net when coated and did not show any separation until the total degradation. Samples cross-linked by the new system of EDC-NHS attained approximately the same swelling ratio like samples cross-linked by the resins of LYOFIX and MH-83. The biggest strength of polymeric net and hydrolytic degradation resistivity showed sample cross-linked by the EDC-NHS system, which were stable against the degradation for 78 days in physiological solution at 37 °C (confirmed by microscopy). Due to the obtained properties the new cross-linked collagen might enhance the biocompatibility of commercially used net CHS 100 since it is coated and implanted. Moreover, collagen itself might be modified (e.g. with hyaluronic acid) in order to speed up the wound healing process or reduce the tissue inflammation in the net surrounding environment.

REFERENCES

1. Lee Chi H., Singla A., Lee Y.: Int. J. Pharm. *221*, 1 (2001).
2. Dijkstra P. J., Damink L. H. H., Feijen J.: Cardiovasc. Path 01. *5*, 286 (1996).
3. Damink L. H. H., Dijkstra P. J., Van Luyn M. J. A., Van Wachem P. B., Nieuwenhuis P., Feijen J.: Biomaterials *17*, 765 (1996).
4. Nam K., Kimura T., Kishida A.: Biomaterials *28*, 1 (2007).

P89 SOIL HYGIENE IN OLD ENVIRONMENTAL BURDEN AREAS

ALENA VOLLMANNOVÁ[a], JÁN TOMÁŠ[a], DANIEL BAJČAN[a] and PETER KOVÁČIK[b]

[a]*Department of Chemistry, Faculty of Biotechnology and Food Sciences,*
[b] *Department of Agrochemistry and Plant Nutrition, Faculty of Agrobiology and Food Resources, Slovak University of Agriculture, Tr. A. Hlinku 2, 949 01 Nitra, Slovak Republic*
Alena.Vollmannova@uniag.sk

Introduction

The necessity of old environmental burden areas remedy is one of present environmental problems. The negative effect of the anthropogenic breach into the environment arised in the past still exists. It can be often a potential source of risk element input into the all components of the environment. The old scrap-heaps, mines, landfills, industrial, biological[1] and chemical wastes, heavy metals[2] and oil products are important factors of the environment contamination.

In our research work the soil hygiene of three various old environmental burden areas of Slovakia is evaluated.

The first one is the wider surrounding of previous Nickel smeltery in Sereď situated in the loaded region Dolný Váh, one of 12 regions of the Slovak Republic with the most contaminated soils by risk elements[3]. The second observed region is the alluvial area near of Štiavnica river running through the area long-time burden by intensive mine activity[4]. The third surveyed locality is the wider surrounding of Iron ore mines in Rudňany. This enterprise belonged in the past to the one of determining sources of the emission contamination of the environment in loaded area of Stredný Spiš.

The risk of heavy metal input from residual metallic burden soil into the food plants as well as into the whole human food chain is in observed regions evident.

Experimental

The observation of risky elements in soils were realized on parcels in cadasters of villages: Zavar, Križovany, Vlčkovce, Hoste, Malá Mača and Veľká Mača in the distance of 5 to 9 km in northern and nort-western direction and in cadasters of villages Veľká Mača, Šintava and Vinohrady nad Váhom in the distance of 2 km south-western, 2.8 km eastern and 3.5 km north-eastern from former emmission source of Nickel smeltery Sereď.

In longitudinal north-southern direction of river Štiavnica alluvium 11 soil samples from cadastres of villages Prenčov, Hontianske Nemce, Hontianske Tesáre, Terany, Dudince, Hokovce, Horné Semerovce, Tupá, and Hrkovce were taken. The river length is 54.6 km. The distance between Prenčov and Hrkovce is about 36 km.

In the Stredný Spiš region the soil samples were taken in cadaster of Markušovce in the distance of 10–12.5 km north-western, Matejovce 7.6 km northern, Chrasť nad Hronom 10 km north-eastern and Poráč 6 km eastern of former emmission source ŽB Rudňany.

The samples with pedological probe from surface soil layer were taken from 33 experimental sites. Analyses were conducted in samples of soil ground on fine soil I. and from this fine soil the representative sample was taken and sieved through the sieve with average 0.2 mm (fine soil II). The total content of risky elements was determined by the AAS method in soil extract gained after total decomposition of soil by wet way with the mixture of acids $HF + HNO_3 + HClO_4$.

Results

The soil hygiene was evaluated after Resolution of the Ministry of Agriculture of the Slovak Republic No. 531/1994--540, which determines the hygienic limits for soil contents of 15 selected risk elements. The reference value A means that the soil is not contaminated if the substance concentration is below this value, the indicative value B means that soil contamination was analytically proven, the indicative value C means the necessity of the soil sanitation. The soils surround of previous Nickel Smeltery Sereď could be considered from the standpoint of risky metals contents as relatively „clean", in spite of moderately enhanced contents of Cd, Cu, Ni and Co. There was no content value meaning analytical proof of soil contamination. The Cd content was in the range from 1.6 to 2.5-fold of background value A (0.8 mg $Cd\,kg^{-1}$) in all observed parcels. The Ni content exceeded the value A (35 mg $Ni\,kg^{-1}$) in all parcels with the exception of Vinohrady nad Váhom locality, while it was enhanced from 1.1 to 1.4-fold. The Cu content was increased in all localities with the exception of Zavar and Veľká Mača (1.03 to 1.93-fold of value A 36 mg $Cu\,kg^{-1}$). The enhanced soil content of Co was observed in Zavar, Hoste, Veľká Mača and Šintava (1.06 to 1.22-fold of value A 20 mg $Co\,kg^{-1}$). All of the determined values were deeply under the hygienic limit for the soil contamination.

In soils of the second observed region of alluvium Štiavnica river the soil contamination by high contents of Cu, Zn, Cd and Pb was confirmed. The determined Pb contents were extremely high in all of analysed soil samples and they even markedly exceeded the indicative limit value for soil sanitation C (600 mg $Pb\,kg^{-1}$) given by valid legislative.The Cu and Pb contents in observed soils were the highest in Prenčov (2.6-fold of indicative value B 100 mg $Cu\,kg^{-1}$ resp. 5.4-fold of indicative value C for Pb), the highest Zn and Cd contents were determined in soil of Hontianske Nemce (5.52-fold resp. 4.24-fold of indicative values B 500 mg $Zn\,kg^{-1}$ resp. 5 mg $Cd\,kg^{-1}$). The lowest Cu soil content was determined in Horné Semerovce (on the level of the indicative value B), the lowest Zn, Cd and Pb contents were determined in Hontianske Tesáre (Zn on the level of the limit value B, Cd 30% under the limit and Pb 1.78-fold of the indicate value B 150 mg $Pb\,kg^{-1}$).

The situation in the wider surrounding of the third surveyed site of the former emmission source was different. The enormly high content of Hg was found out in Markušovce

in locality Olšanské pole, which was even exceeding the hygienic limit determining the soil sanitation (1.9 to 3.8-fold of value C 10 mg Hg kg^{-1}). Similarly the extremely high content of Hg was determined in Poráč, where the 3.2-fold higher exceeding of this limit value was determined. The contamination of soil by Hg was obvious also in localities: Pod horky, Zemkovské (Markušovce) and Na stráni (Matejovce because of the exceeding of limit value B (2 mg Hg kg^{-1}) for the soil contamination at 4.65-fold. Similarly the soil contamination by As was proved in Markušovce (locality Olšanské pole), where the limit value B (30 mg As kg^{-1}) was exceeded 1.45-fold and Poráč (locality Pasienky) with 1.06-fold In Poráč the soil contamination by Cu was evident (1.15-fold of limit B).

Conclusions

The residual soil burden by heavy metals and potential follow contamination of the food chain in observed areas presents the potential risk for the human health. Therefore it is important to monitor the risk metal contents as in soils as in agricultural plants and in case that it is necessary to realise the remedy for the inhibition of the risk heavy metal input into the human food chain.

REFERENCES
1. Toth, T.: Acta Envir. Univ. Comenianae *15(1)*, 66 (2007).
2. Hegedusova, A., Hegedus, O., Musilova, J.: *Risks of soil contamination by cadmium.* Monograph. CPU Nitra, 2006
3. Bedrna, Z.: *Environmental pedology.* SAS Bratislava, 2002
4. Arvay, J., Melichacova, S., Lahucky, L., Musilova, J., Bystricka, J.: *Food safety and control : The crops quality cultivated on heavy metals contaminated soil from Region Hont*, Nitra, 28–29. 3. March 2008, Book of Works, SAU Nitra, 2007.

P90　EPR STUDY ON PHOTOINDUCED PROCESSES OF NOVEL QUINOLONE DERIVATIVES

ZUZANA VRECKOVÁ, VLASTA BREZOVÁ, MAROŠ BELLA, VIKTOR MILATA and SOŇA JANTOVÁ

Institute of Physical Chemistry and Chemical Physics, Faculty of Chemical and Food Technology, Slovak University of Technology in Bratislava, Radlinského 9, 812 37 Bratislava, Slovak Republic,
zuzana.vreckova@stuba.sk

Introduction

4-Oxo-1,4-dihydroquinoline derivatives (4-quinolones) represent one of the largest classes of antimicrobial agents used nowadays in the medical care[1]. Specific members of this drug family display also high activity against eukaryotic type II topoisomerases, as well as against cultured mammalian cells[2]. These antineoplastic quinolones represent a prospective source of new anticancer agents. The presence of extended π-electron system of quinolone derivatives results in their photosensitive properties; therefore UVA irradiation can induce their photosensitive reactions with phototoxic responses. Previously we demonstrated that excitation of nitrogen heterocycle molecules by UVA radiation may significantly enhance their biological activities[3].

Novel 7-substituted 6-oxo-6,9-dihydro[1,2,5]selenadiazolo[3,4-*h*]quinoline derivatives were synthesized as potential anticancer and antimicrobial agents and their ability to produce Reactive Oxygen Species (ROS) upon irradiation was tested using Electron Paramagnetic Resonance (EPR) spectroscopy. Additionally, their cytotoxic/phototoxic effects on human leukemia cells HL60 were characterized.

Experimental

The synthesis of 7-substituted 6-oxo-6,9-dihydro[1,2,5]-selenadiazolo[3,4-*h*]quinoline derivatives was performed according to the reaction pathways published in ref.[4].

Table I summarizes the structure, substitution and abbreviation of the synthesized selenadiazoloquinolones.

E P R　P h o t o c h e m i c a l　E x p e r i m e n t s

EPR measurements at the X-band were performed with an EMX EPR spectrometer (Bruker, Germany) using a TE_{102} (ER 4102ST) resonator. Samples were irradiated at 295 K directly in the EPR spectrometer cavity using HPA 400/30S lamp (400 W, $l_{max} = 365$ nm, Philips, UVA irradiance 3 mW cm^{-2}). A Pyrex glass filter was applied to eliminate the radiation wavelengths below 300 nm. The experimental EPR spectra acquisition and simulation was carried out using *WIN EPR* and *SimFonia* programs (Bruker).
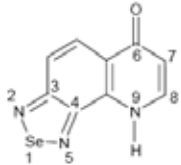
The photoinduced generation of free radicals was monitored by spin trapping technique with 5,5-dimethyl-1-pyrroline N-oxide (DMPO) and 5-(diisopropoxyphosphoryl)-5-methyl-1-pyrroline N-oxide (DIPPMPO) as the spin traps. The selective oxidation of 4-hydroxy-2,2,6,6-tetramethylpiperidine (TMP) *via* singlet oxygen to the paramagnetic nitroxyl radical 4-hydroxy-2,2,6,6-tetramethylpiperidine N-oxyl (Tempol) was applied for $^1O_2$ detection by EPR spectroscopy. The aerated solutions of 7-substituted [1,2,5]selenadiazolo[3,4-*h*]quinolo-nes in dimethylsulphoxide (DMSO) mixed immediately before EPR experiments, were transferred into a flat cell (WG-808-Q, Wilmad) suitable for TE_{102} cavity, and the EPR spectra were monitored *in situ*.

UV/visible spectra were recorded in DMSO by means of a Shimadzu UV-3600 spectrophotometer.

Table I
Structure, substitution and abbreviation of investigated 7-substituted 6-oxo-6,9-dihydro[1,2,5]-selenadia-zolo[3,4-*h*]quinoline derivatives

Structure	7-Substitution	Abbreviation
	H	7-H-SeQ
	$COOC_2H_5$	7-COOEt-SeQ
	$COOCH_3$	7-COOMe-SeQ
	COOH	7-COOH-SeQ
	$COCH_3$	7-Ac-SeQ
	CN	7-CN-SeQ

C y t o t o x i c / P h o t o t o x i c　E f f e c t

The murine leukemia cell line HL60 (obtained from American Type Culture Collection, Rockville, MD, USA) was used. These cells were grown in RPMI medium in 5 % CO_2 at 37 °C under conditions specified in ref.[4]. A starting inoculum 2.6×10^5 HL60 cells ml^{-1} in the exponential phase of growth was used. 5 ml of the suspension were added into Petri dishes (diameter 60 mm), then 20 μl of derivative 7-Ac-SeQ at various concentrations were added to the cells. One part of the dishes was irradiated with HPA 400/30S lamp upon UVA dose of 0.4 J cm^{-2}. After 24, 48 and 72 h cultivation, the number of cells per culture dishes was counted in a Bürker chamber and viability of treated and control irradiated/non irradiated cells were determined by 0.4 % trypan blue staining.

Results

7-Substituted 6-oxo-6,9-dihydro[1,2,5]selenadiazolo[3,4-*h*]quinoline derivatives absorb UV radiation with three absorption maxima about 400, 340 and 300 nm, which are only slightly influenced by the substituents properties, as is shown in Fig. 1. The presence of acetyl substituent in 7-Ac-SeQ derivative caused bathochromic shift of the low-energy band to 410 nm with a shoulder at 485 nm.

Upon photoexcitation, all 7-substituted 6-oxo-6,9-dihydro[1,2,5]selenadiazolo[3,4-*h*]quinoline derivatives demonstrated the ability to generate super-oxide anion radicals trapped as •DMPO-O_2^- or •DIPPMPO-O_2^- spin adducts.

Fig. 2.a shows the time-course of 11 individual EPR spectra monitored upon continuous UVA irradiation of 7-COOEt-SeQ, indicating the efficient generation of twelve-line EPR signal with spin Hamiltonian parameters corresponding to •DMPO-O_2^- ($a_N = 1.275$ mT; $a_H^\beta = 1.032$ mT;
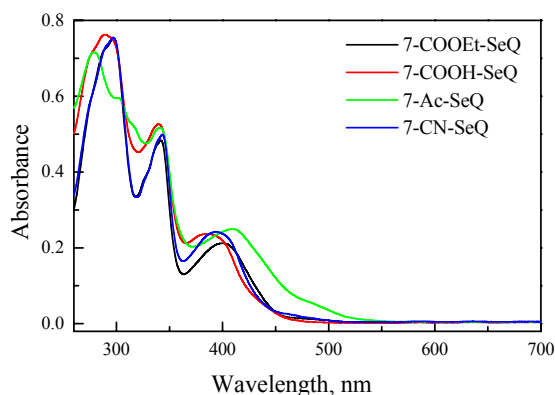
Fig. 1. **UV/VIS spectra of 7-substituted 6-oxo-6,9-dihydro[1,2,5]selenadiazolo[3,4-h]quinoline derivatives measured in DMSO (concentration 40 µM; cell length 1 cm)**

$a_H^\gamma = 0.135$ mT and g-value = 2.0058). Additionally, Fig. 2. b illustrates the formation of typical three-line EPR signal of Tempol ($a_N = 1.575$ mT; g = 2.0060) produced from TMP *via* singlet oxygen. However, photogenerated paramagnetic Tempol is upon prolonged irradiation decomposed to diamagnetic products, most probably by the termination of its nitroxyl group with super-oxide anion radicals ($>NO^\bullet + O_2^{\bullet-}$).
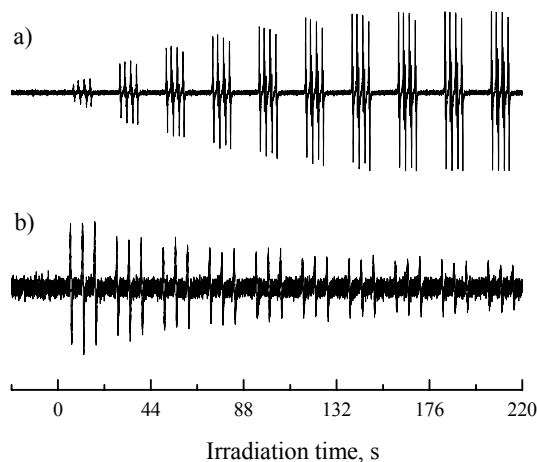
Fig. 2. **The time-course of EPR spectra monitored upon photoexcitation of aerated DMSO solutions of 7-COOEt-SeQ ($c_0 = 3.2$ mM) in the presence of: a) DMPO spin trap (magnetic field sweep, SW = 10 mT); b) TMP (SW = 6 mT)**

The EPR experiments confirmed that the photoexcitation of selenadiazoloquinolones in the presence of molecular oxygen resulted in the formation of $O_2^{\bullet-}$ and $^1O_2$, and

these processes perform simultaneously. The photoactivity of 7-sub-stituted 6-oxo-6,9-dihydro[1,2,5]selenadiazolo[3,4-h]quinoline derivatives upon irradiation of polychromatic UV source was evaluated using *(i)* quantum efficiency of spin-adduct formation of superoxide radical with DMPO spin trap ($^\bullet DMPO-O_2^-$), and *(ii)* quantum efficiency of Tempol generation from TMP by singlet oxygen. The values of quantum efficiencies reflect the donor/acceptor properties of substituents; the highest value of $^\bullet DMPO-O_2^-$ quantum efficiency was found for 7-acetyl 6-oxo-6,9-dihydro[1,2,5]selenadiazolo[3,4-h]quinoline (7-Ac-SeQ).

The *in vitro* cytotoxic effect of six 7-substituted 6-oxo-6,9-dihydro[1,2,5]selenadiazolo[3,4-h]quinoline derivatives was investigated on cell proliferation of human leukemia HL60 cells. Derivatives demonstrated different cytotoxic effects, which were time- and concentration- dependent, and the highest impact was found for 7-Ac-SeQ. The application of UVA irradiation caused an escalation of 7-Ac-SeQ effects on cell proliferation; the percentage of growth inhibition was increased in the range of 10–50 %.

Conclusions

EPR and UV/Vis experiments confirmed UVA-induced excitation of 7-substituted 6-oxo-6,9-dihydro[1,2,5]selenadiazolo[3,4-h]quinoline derivatives, which is coupled with electron or energy transfer to molecular oxygen *via* Type I and Type II photooxidation mechanisms producing super-oxide anion radical and singlet oxygen.

REFERENCES

1. Oliphant C. M., Green G. M.: Am.. Family Physician *65,* 455 (2002).
2. Robinson M. J., Martin B. A., Gootz T. D., Mc-Guirk P. R., Moynihan M., Sutcliffe J. A., Osheroff N.: J. Biol. Chem. *266,* 14,585 (1991).
3. Jantová S., Letašiová S., Brezová V., Čipák Ľ., Lábaj J.: J. Photochem. Photobiol. B: Biol. *85,* 163 (2006).
4. Bella M., Jantová S., Brezová V., Kučerák J., Ondrušová Ľ.: *Industrial Toxicology 07, 27th International Symposium Proceedings*, p. 127. Bratislava, 2007.

P91 THE BORON IN KRAFT PULP MILL AND INFLUENCE IN WASTE WATER

EVA GEMZICKÁ and MILAN VRŠKA

Department of Chemical Technology of Wood, Pulp and Paper, Slovak University of Technology, Radlinského 9, 812 37 Bratislava, Slovak Republic,
milan.vrska@stuba.sk

Introduction

The elemental boron almost is not occurred in nature and it usually is component only its different compounds. The boron forms boranes with hydrogen. It forms acids of these types: $(HBO_2)_n$ and H_3BO_3. The borides are boron compounds with metals (Me) and boron forms BX_3 with halides (X_3). The oxycompounds are formed with boron and oxygen, i.e. B_2O_3 and $(BO)_n$. $B_2O_3(l)$ [molten] dissolves oxides of metals (borax pearls). Wide range of boron compounds exists with different stoichiometry and structure (see Fig. 1.). The boron more often exists as borax in nature. The molten borax covers molten other metal and so it is protective compound against oxidation. The mixture boron and Na_2CO_3 is used for dissociation of geological and hard dissolving samples[1,2].
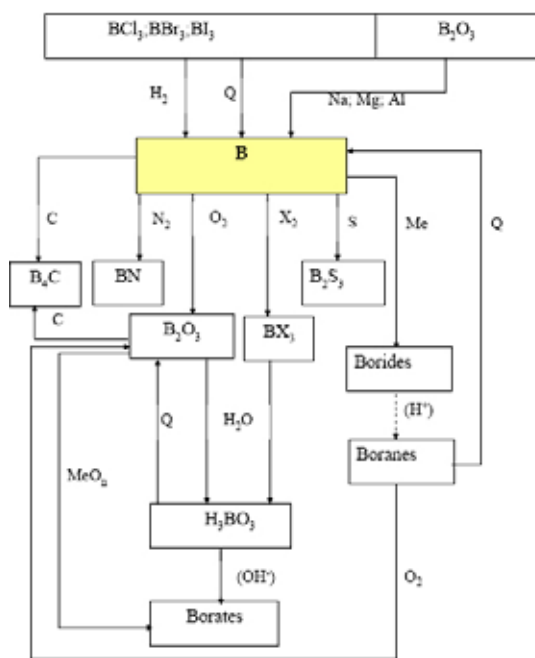
Fig. 1.　**Chart for Boron reaction**

Borax is used in recovery line for process improvement in kraft pulp mill too. The conventional recovery cycle with addition of borates; this produces 10 % of the formed NaOH (partial autocaustification). The borates react in two places in the recovery cycle: the recovery boiler and the smelt dissolver. In the former sodium carbonate reacts with a sodium-lean borate, forming a sodium-rich borate formed:

$NaBO_2(l) + Na_2CO_3(l) = Na_3BO_3(l) + CO_2(g)$. In this reaction, the borates and the sodium carbonates are in a smelt phase, which implies that the reaction rate is high. In the dissolver, Na_3BO_3 reacts with water: $Na_3BO_3(l) + H_2O = 2NaOH(aq) + NaBO_2(aq)$(ref.[3]).

Fig. 2.　**Borax $Na_2B_4O_7\cdot 10H_2O$ i.e. Sodium tetraborate. It is applied in different industry: metallurgy, glass industry, ceramic industry and in some pulp mill**

Boron compounds are occurred in fresh/salt water and in waste water too. Concentration of boron compounds is app. 5 $mg\,dm^{-3}$ in salt water[4]. Boron occurs naturally in fresh water at an average of 1 $mg\,dm^{-3}$ or less many times. High boron concentrations may be toxic to freshwater fish regarding concentration of 10–300 $mg\,dm^{-3}$ (e.g. for Rainbow trout 24-day LC50 is 88 $mg\,dm^{-3}$) in flowing water. Mainly borate is hazardous for water plants (e.g. for Green algae 96-hr IC10 is 24 $mg\,dm^{-3}$). Any definitive ecotoxicological conclusions don't exist about genotoxic, carcinogenic or mutagenic effects to water organisms, but still under investigation[5].

Experimental

The autocaustification was realized in kraft pulp mill. Trial was started on December 1, 2007 till December 14, 2007 and restarted again on January 4, 2008. This trial was finished on February 25, 2008. Waste water was monitored for boron concentrations in two different laboratories. The boron concentration was determined in the first laboratory (spectrophotometry with azomethin at 415 nm) as calculation from borates. The boron also was analyzed using OES ICP method (in 2nd laboratory) the first time in different samples of waste water, which were from different pH and COD. Alkali waste water, acid waste water, waste water of sewage water treatment plant, water from river and output to river were analyzed for boron in two steps, i.e. during trial and after trial in 2nd laboratory with OES ICP.

Borax was added into dissolvent tank for green liquor step by step. Boron concentration was increased in waste water in February, when borax was added more in recovery line.

Results

Boron analysis was difficult because of small particulates, which were filtrated from samples, but boron concentration was estimated from samples, which were not filtrated.
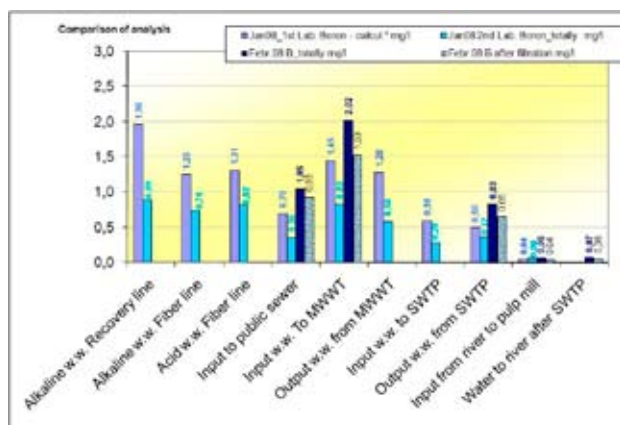
Fig 3.   **Comparison of B analysis**

Note : w.w. = waste water, MWWT = mechanical waste water treatment, SWTP = sewage water treatment plant
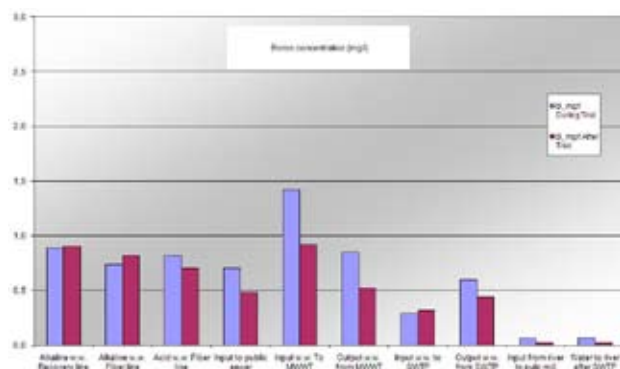
Fig. 4.   **Boron concentrations**

The results are from these samples, because boron could be component in small particulates of waste water samples. Boron concentration is low in waster water which is cleaned in SWTP. The limits are not specified by low for boron concentration in waste water to the water recipient.

In the Danube, water (Komárno – Bratislava) was determinate to have a natural concentration on the level of 39 $\mu g\,dm^{-3}$(ref.[6]) and for river is the level of 20 $\mu g\,dm^{-3}$ in the river after the biological waste water treatment plant and 20 $\mu g\,dm^{-3}$ in recipient to pulp mill. Boron concentration was low in lime sludge too. Boron was accumulation in system and its output was waste water, but boron concentration was low.

Conclusions

In this work was studied effect of adding boron compound to recovery line on the water quality.

- Boron is component in very small particulates in waste water, therefore boron concentration is better without filtration of samples for boron determination. Boron concentration is not total in waste water by filtration.
- Boron concentration is low in output - waste water to river, what corresponding accumulation of boron compounds in system of pulp mill.
- There was little decreasing of boron concentration after trial, but boron compounds were in system.

Open question:

- What about deposits in recovery line and pipeline of waste water?

REFERENCES

1. Internet: Referat – prvky p1 a p2
2. www.chtf.stuba.sk/kach/support/ACh_prednaska06.pdf
3. Richards T., Nohlgren I., Warnqvist B., Theliander H.: Nordic Pulp and Paper Research Journal *17(3)*, 213 (2002).
4. http://sk.wikipedia.org/wiki/B%C3%B3r
5. Safety data sheet for commercial product [borax]
6. www.gabcikovo.gov.sk/vvb/vr2004/priloha%20D/text.pdf

P92 CONTENTS OF DIFFERENT FRACTIONS OF SULPHUR IN SLOVAKIA SOILS

ANTON ZAUJEC[a], LÝDIA JEDLOVSKÁ[a] and MELÁNIA FESZTEROVÁ[b]

[a]*Faculty of Agrobiology and Food Resources, Slovak University of Agriculture, Tr. A. Hlinku 2, 949 76 Nitra, Slovakia,*
[b]*Faculty of Natural Sciences, Constantine the Philosopher University, Tr. A. Hlinku 1, 949 74 Nitra,*
Anton.Zaujec@uniag.sk

Introduction

In the past there were high sulphur contents in the soil, mostly from the atmospheric inputs. Nowadays, in some localities deficit of sulphur was observed. In the last time advanced quality of environment is required by society. The aim of this work was to identify the distribution of sulphur fractions in different soil types of Slovakia.

Experimental

Basic sulphur fractions that we assessed in soil samples were: chloride soluble sulphur (CISS), sulphate sulphur (SS), heat soluble sulphur (HSS) by Williams-Steinbergs. Soil samples were taken from similar depths from 52 localities including basic soil types: Haplic Chernozems (CHH), Haplic Luvisols (LVH), Phaeozems (PH), Eutric Cambisols (CME), Dystric Planosols (PLD), in 1999–2006 years. Analytical methods of sulphur fractions determination were described by Jedlovská, Feszterová[1].

Results and Discussion

Chloride Soluble Sulphur Fraction (ClSS)

The chloride soluble sulphur values (ClSS) were determined as extremely hight in Phaeozems, in localita Maňa, Žitavský luh 2,744.5 mg kg^{-1} (depth: 0–0.1 m) and in locality Okoč 1,173.6 mg kg^{-1} (0–0.4 m). Generally, the contents of ClSS varied with depth, the highest values were observed in subsoil layers. The minimum values were determined in vineyard on Eutric Cambisols 3.2 mg kg^{-1} (0.3–0.6 m; Tokaj) and in textural light Haplic Luvisols 4.4 mg kg^{-1} (0.5–0.6 m; Rišňovce).

Sulphate Sulphur Fraction (SS)

The highest sulphate sulphur content was in Haplic Luvisols locality Golianovo (1,191.7 mg kg^{-1}; depth: 0–0.2 m) and Nové Sady (856.1 mg kg^{-1}; 0.2–0.4 m). The content of sulphate sulphur varies by soil types and depth of soil profiles. The minimum values (from 1.2 mg kg^{-1} to 3.7 mg kg^{-1}) were observed in topsoil of Haplic Chernozems (locality Štefanovičova), Eutric Cambisols (locality Viničky) and Haplic Luvisols (Rišňovce).

Table I
Contents of chloride soluble sulphur (ClSS)

Soil types/ (numbers)	Depth [m]	Mean [mg kg^{-1}]	Standard deviation
Haplic Chernoyems (14)	0.0–0.2	192.5	175.2
	0.2–0.4	92.8	61.2
	0.4–0.6	151.0	132.5
	0.6–0.8	98.7	71.8
	0.8–1.4	70.0	66.1
Phaeozems (6)	0.0–0.2	234.0	151.4
	0.2–0.4	373.7	271.5
	0.4–0.6	358.0	220.4
	0.6–0.8	453.2	303.0
	0.8–1.4	261.7	81.8
Haplic Luvisols (17)	0.0–0.2	305.3	274.3
	0.2–0.4	299.9	259.8
	0.4–0.6	299.1	254.7
	0.6–0.8	375.3	333.6
	0.8–1.0	384.4	299.7
	1.0–1.2	395.5	275.0
	1.2–1.4	244.3	201.6
Dystric Planosols (5)	0.0–0.2	82.0	77.0
	0.2–0.4	45.4	32.5
	0.4–0.6	63.7	20.3
	0.6–0.8	106.2	72.4
	0.8–1.4	121.8	118.5
Eutric Cambisols (10)	0.0–0.2	130.0	125.9
	0.2–0.4	157.4	157.3
	0.4–0.6	159.2	154.3
	0.6–0.8	171.8	156.4
	0.8–1.4	187.7	115.0

Heat Soluble Sulphur Fraction (HSS)

The lowest values of HSS fraction were determined in comparison to the mentioned sulphur fractions. The highest HSS content was in Phaeozems locality Žitavský luh (1,837.4 mg kg^{-1}; depth: 0–0.1 m), in Haplic Luvisols locality Revúca (617.5 mg kg^{-1}; 0–0.3 m) and in Haplic Chernozems locality Sládkovičovo- Nový Dvor (433.8 mg kg^{-1}; 0.5–0.7 m). The minimum of HSS (from 0.28 mg kg^{-1} to 1.2 mg kg^{-1}) were observed in topsoil of Eutric Cambisols (Tokaj), of Haplic Luvisols (Tesárske Mlyňany) and in sandy loam Haplic Chernozems (Dulovce).

Conclusions

The contents of sulphur fractions (ClSS, SS, HSS) varied by depth of soil profiles and soil types. The maximumn values of ClSS fraction were observed in Phaeozems (336.1 mg kg^{-1}) and Haplic Luvisols (329.1 mg kg^{-1}). The values under average values of ClSS (206.2 mg kg^{-1}) were in Eutric Cambisols (161.2 mg kg^{-1}), Haplic Chernozems (121.0 mg kg^{-1}) and Dystric Planosols (83.8 mg kg^{-1}). The highest contents of SS fraction were determined in Haplic Chernozems

Table II
Contents of sulphate sulphur (SS)

Soil types/ (numbers)	Depth [m]	Mean [mg kg^{-1}]	Standard deviation
Haplic Chernozems (14)	0.0–0.2	162.1	134.2
	0.2–0.4	184.2	144.9
	0.4–0.6	116.9	97.9
	0.6–0.8	149.7	108.7
	0.8–1.4	120.9	87.0
Phaeozems (6)	0.0–0.2	213.2	125.7
	0.2–0.4	218.4	52.0
	0.4–0.6	263.2	140.7
	0.6–0.8	428.9	187.2
	0.8–1.4	377.3	145.5
Haplic Luvisols (17)	0.0–0.2	323.0	320.3
	0.2–0.4	389.5	234.6
	0.4–0.6	234.2	117.7
	0.6–0.8	242.0	124.3
	0.8–1.0	223.7	46.7
	1.0–1.2	281.4	64.6
	1.2–1.4	310.0	62.2
Dystric Planosols (5)	0.0–0.2	38.7	35.9
	0.2–0.4	53.5	64.3
	0.4–0.6	53.9	46.7
	0.6–0.8	50.3	36.8
	0.8–1.4	42.2	30.5
Eutric Cambisols (10)	0.0–0.2	92.4	79.0
	0.2–0.4	103.1	91.6
	0.4–0.6	101.2	87.3
	0.6–0.8	154.3	59.9
	0.8–1.4	125.0	82.8

Table III
Contents of heat soluble sulphur (HSS)

Soil types/ (numbers)	Depth [m]	Mean [mg kg^{-1}]	Standard deviation
Haplic Chernozems (14)	0.0–0.2	93.4	89.0
	0.2–0.4	143.8	115.8
	0.4–0.6	132.4	130.7
	0.6–0.8	110.4	89.1
	0.8–1.4	115.8	93.4
Phaeozems (6)	0.0–0.2	207.4	109.5
	0.2–0.4	249.8	92.7
	0.4–0.6	227.7	96.1
	0.6–0.8	213.3	36.2
	0.8–1.4	214.7	31.2
Haplic Luvisols (17)	0.0–0.2	145.3	106.7
	0.2–0.4	161.5	84.8
	0.4–0.6	152.9	86.8
	0.6–0.8	163.5	127.2
	0.8–1.0	146.9	51.8
	1.0–1.2	131.3	71.2
	1.2–1.4	127.7	48.1
Dystric Planosols (5)	0.0–0.2	53.5	52.5
	0.2–0.4	76.5	46.2
	0.4–0.6	77.1	24.3
	0.6–0.8	89.1	31.2
	0.8–1.4	56.8	32.0
Eutric Cambisols (10)	0.0–0.2	203.6	140.4
	0.2–0.4	130.0	134.6
	0.4–0.6	166.1	144.7
	0.6–0.8	239.8	173.7
	0.8–1.4	131.0	83.2

(300.2 mg kg^{-1}) and in Haplic Luvisols (286.3 mg kg^{-1}), while in Dystric Planosols the values were only 47.7 mg kg^{-1}.

The differences between soil types were determined in HSS fraction, where the highest mean values observed in Phaeozems and Eutric Cambisols. The lowest value of HSS fraction was in Dystric Planosols.

Decreasing contents of ClSS fraction, in monitoring of soils types where: PH > LVH > CH > CME > PLD, the decreasing contents of SS fraction was LVH > PH > CH > CME > PLD. Presented results show the possibilities how to evaluate

the different fractions of sulphur in different soils types in Slovakia.

REFERENCES

1. Jedlovská, L., Feszterová, M.: *Proceedings of 10th Intern. Scientific Workshop: Topical tasks solved in agro-food sector.* (Vavrišinova K., ed.) p.16, Nitra 2004.

P93 FACTORS INFLUENCING THE SORPTION BEHAVIOUR OF HERBICIDE ACETOCHLOR IN SOILS AND SEDIMENTS

LENKA ZEMANOVÁ, EDGAR HILLER and ZOLTÁN KRASCSENITS

Comenius University in Bratislava, Faculty of Natural Sciences, Department of Geochemistry, Mlynská dolina, 842 15 Bratislava, Slovak Republic,
zemanoval@fns.uniba.sk

Introduction

Acetochlor (2-chloro-*N*-(ethoxymethyl)-*N*-(2-ethyl-6-methylfenyl)acetamide) is a selective systematic herbicide used in the production of maize, soybean and other crops[1]. Ability to predict its mobility in the environment is of major importance as US EPA has classified acetochlor as a probable human carcinogen[2].

The aim of this study was to investigate the sorption and desorption of acetochlor in various types of natural sorbents (soils, bottom and river sediments). The attention was paid to the effect of soil/sediment properties on acetochlor sorption and desorption.

Experimental

Chemicals and Sorbents

Experiments were conducted with analytical grade acetochlor (purchased from Sigma Aldrich Kft.), a relatively non-polar compound ($\log K_{ow} = 2.5$) with water solubility 223 $mg\,dm^{-3}$ at 20 °C[1].

Eight surface soils (denoted as A1–8) were collected from cultivated sites in Slovakia. Moreover, one soil collected from C horizon at the depth of 2 m (SS), three bottom sediments (BS1–3), and two river sediments (RS1–2) were used. Basic properties of the soils and sediments studied are shown in Table I.

Sorption/Desorption Experiments

Sorption experiments were conducted using a batch equilibration method, with two initial concentrations of acetochlor used (1 and 10 $mg\,dm^{-3}$). The acetochlor concentration in supernatant solutions after equilibration was measured using high performance liquid chromatography with ultraviolet detection (HPLC-UV) in the National Water Reference Laboratory for Slovakia (Bratislava).

Desorption experiments followed immediately after the sorption experiments with an initial concentration of 10 $mg\,dm^{-3}$.

Results

Sorption coefficients for acetochlor are given in Table II. TOC was found to be the main soil/sediment property correlating with the extent of acetochlor sorption ($r = 0.774$; $P < 0.01$). Strong affinity of acetochlor to soil organic matter was reported also by other researchers[2,3].

Table I
Properties of soils and sediments used in the study

	TOC [%]	C_{HA}/C_{FA}	Clay [%]	pH (H_2O)	$CaCO_3$ [%]
A1	4.59	1.09	11.13	6.93	1.40
A2	1.92	1.12	15.32	7.99	2.00
A3	0.89	0.72	22.08	6.76	0.30
A4	2.49	1.07	9.08	7.86	12.2
A5	1.21	1.16	5.75	6.32	N.D.
A6	1.19	1.53	11.00	7.96	2.74
A7	0.48	0.90	0.60	5.76	0.20
A8	1.57	1.12	37.20	6.11	N.D.
SS	0.60	0.95	4.05	8.20	4.10
RS1	2.46	0.42	2.16	7.17	0.30
RS2	3.46	0.87	1.89	7.22	3.60
BS1	3.05	0.89	6.41	7.56	3.80
BS2	1.64	1.62	7.85	7.46	2.20
BS3	6.39	0.78	2.03	6.45	N.D.

The relationship between K_d and total organic carbon content was improved after excluding the soil A8 from the data set ($r = 0.902$; $P < 0.001$). This could be explained by the significantly higher clay mineral content (especially smectites) of this soil as compared with other sorbents. Previous studies of the sorption of organic pollutants in soils have shown that in soils with the high clay mineral/organic matter ratio, the mineral fraction can play an important role in binding organic compounds such as pesticides[4].

The humic/fulvic acid ratio (C_{HA}/C_{FA}) is one of the characteristics of the soil organic matter quality[5]. The results of this study showed a positive correlation between the K_{oc} and the C_{HA}/C_{FA} ratio ($r = 0.578$; $P < 0.05$). Its signifi-

Table II
Sorption coefficients of acetochlor (K_d and K_{oc}) and percentage of acetochlor desorbed (P_{des})

	Initial concentration $C_0 = 1\ mg\,dm^{-3}$		Initial concentration $C_0 = 10\ mg\,dm^{-3}$		
	K_d [$dm^3\,kg^{-1}$]	K_{oc} [$dm^3\,kg^{-1}$]	K_d [$dm^3\,kg^{-1}$]	K_{oc} [$dm^3\,kg^{-1}$]	P_{des} [%]
A1	7.108	155	5.871	128	12.0
A2	3.248	169	2.537	132	27.9
A3	1.358	152	1.036	116	37.5
A4	3.406	137	2.635	106	19.1
A5	2.109	174	1.551	128	35.6
A6	3.344	281	2.999	252	23.0
A7	1.018	212	0.840	175	34.3
A8	6.265	399	5.145	328	27.7
SS	1.062	177	0.918	153	41.0
RS1	3.463	141	2.579	105	27.0
RS2	4.218	122	3.353	97	22.5
BS1	3.020	99	3.081	101	26.4
BS2	3.854	235	3.378	206	26.2
BS3	6.577	103	5.491	86	16.0

cance increased after excluding the soil A8 from the data set ($r = 0.766$; $P < 0.01$).

The method of step-down multiple regression analysis was used to determine the soil properties significantly contributing to the overall acetochlor sorption. The soil A8 appeared to have specific sorption properties, thus it wasn't included in the analysis. The analysis yielded the following equations:

$$K_d = 1.043(\text{TOC \%}) + 1.725(C_{HA}/C_{FA}) - 0.777 \qquad (1)$$
$$R^2 = 0.888; \text{n} = 12; P < 0.001; \text{SE} = 0.67$$

$$K_d = 0.891(\text{TOC \%}) + 1.723(C_{HA}/C_{FA}) - 1.011 \qquad (2)$$
$$R^2 = 0.914; \text{n} = 12; P < 0.001; \text{SE} = 0.497$$

The equations (1) and (2) were acquired when the results obtained at initial acetochlor concentrations of 1 and 10 mg dm^{-3} were used, respectively. The K_d of acetochlor was found to depend significantly on the total organic carbon content of the soil/sediment. The distribution of humus components expressed as the C_{HA}/C_{FA} ratio is also a significant factor influencing the acetochlor affinity to the sorbents.

Desorption of acetochlor from all soils and sediments was less than the amount initially sorbed (Table II). Desorption extent is significantly ($r = -0.81$; $P < 0.01$) influenced by total organic carbon content, with greater organic carbon contents reducing the desorption. Significant inverse correlations were also found between the humic components (C_{HA} and C_{FA}) and P_{des}, but no other significant correlations between P_{des} and soil/sediment properties were observed.

Conclusions

Organic matter appears to be the main sorbent constituent responsible for acetochlor retention in soils/sediments, with both quantitative and qualitative parameters playing important role in its ability to bind acetochlor. The specific appearance of the clay-rich soil A8 in whole analysis implies that mineral surfaces can also significantly contribute to acetochlor immobilization under favourable conditions.

REFERENCES

1. Tomlin C. D. S.: *The e-pesticide manual, 12th ed*. CD-ROM form, Version 2.0. British Crop Protection Council 2001.
2. Ye C.: Bull. Environ. Contam. Toxicol. *71*, 919 (2003).
3. Ferri M. V. W., Gomes J., Dick D. P., de Souza R. F., Vidal R. A.: Rev. Bras. Ci. Solo *29*, 705 (2005).
4. Sheng G., Johnston C. T., Teppen B. J., Boyd S. A.: J. Agric. Food Chem. *49*, 2899 (2001).
5. Dousset S., Mouvet C., Schiavon M.: Chemosphere *28*, 467 (1994).

P94 ECOTOXICOLOGICAL EVALUATION OF THE SLUDGES FROM WASTE WATER TREATMENT PLANTS

HELENA ZLÁMALOVÁ GARGOŠOVÁ, LUCIE HELLINGEROVÁ and MILADA VÁVROVÁ

Institute of Chemistry and Technology of Environmental Protection, Faculty of Chemistry, Brno University of Technology, Purkyňova 118, 612 00 Brno, Czech Republic,
zlamalova@fch.vutbr.cz

Introduction

The tendency to improve the water quality in the Czech Republic is linked with building up new waste water treatment plants (WWTP), what results in growing production of sewage sludges. Multi-purpose way for efficient utilization or sludge disposal hasn't existed till now.

Sewage sludges are very rich in nutrients and organic matter. This makes the spreading of this kind of waste on land as a fertilizer or an organic soil improver very suitable. Unfortunately, the sludge tends to concentrate heavy metals and organic compounds present in waste waters. The Sewage Sludge Directive (86/278/EEC) regulates sludge use in such way to prevent harmful effects on soil, vegetation, animals and man. In the Czech Republic almost one third of sewage sludges ends as a waste; this could be hazardeous. In Europe hazardous wastes are classified by 14 criteria including ecotoxicity (H 14). Environmental ecotoxicology deals with the potentially harmful effects of chemicals and wastes on organisms. For this purpose various testing organisms and various type of bioassays are used.

The aim of our study was the ecotoxicological testing of sewage sludges from different waste water treatment plants by selected ecotoxicity tests with respect to their intended use. We used following organisms: crustacea *Daphnia magna* and *Thamnocephalus platyurus* and seeds of terrestrial plant *Sinapis alba*. The values of 24h-LC50 and 48h-LC50 obtained for *Thamnocephalus platyurus* and *Daphnia magna* and 72h-IC50 values gained for *Sinapis alba* are the basic data for the ecotoxicological assessment of the sewage sludges and for their classification following the Czech legislation[1,2].

Experimental

Samples of sewage sludges from high-capacity municipal WWTP, situated in Brno, Modřice and from small WWTP in Veterinary and Pharmaceutical University Brno were evaluated. From WWTP Brno, Modřice following sewage sludges were tested:

- anaerobic stabilized sewage sludges (AS)
- dewatered anaerobic stabilized sewage sludges (DWAS)
- dessicated anaerobic stabilized sewage sludges (DSAS)

From local WWTP in Veterinary and Pharmaceutical University Brno primary sludges were tested (PS).

Samples Preparation

All samples were collected in pure plastic bottle and untill testing stored in the dark at 4 °C for less than four days prior the bioassay experiment. Samples were dried at temperature 105 ± 5 °C and sludge dry residue was determinated gravimetrically. Two types of water leaches were prepared from studied sewage sludges. The first batch of samples was prepared in accordance with Czech legislation; the samples were mixed in ratio 1 : 10 (sludge dry residue: deionised water). The second one was diluted with deionised water to have the same dry matter content as anaerobic stabilized sewage sludges from WWTP Modřice (3.89 %). Sample tubes filled with defined quantity of sample and water were shaken at 5–10 rpm (revolutions per minute) for 24 hour at temperature 15–25 °C. After centrifugation the leaches supernatants were removed and filtered using paper filter (5 μm). To assure suitable surroundings for each testing organism the supernatants were enriched by adding specific amounts of salts following OECD Guidelines[3,4].

Principle of Ecotoxicological Tests

The general principle of ecotoxicological tests is the determination of effective concentration (EC50), eventually lethal concentration (LC50) or inhibition concentration (IC50). These concentrations of tested compound (substance, sewage water or leaches of sewage sludges) cause the mortality of 50 % of testing organisms or 50% inhibition of growth rate in relation to control tests. The organisms are exposed to the test substance for a period of 24, 48, and 72 hours in agreement with requirements of a given test. At least five test concentrations should be used. A stepwise procedure involves three steps: the preliminary test, the confirmatory test and the definitive test. The confirmatory test confirms or disconfirms results of limit test. In preliminary test undiluted sewage sludges leaches are used. If results of preliminary test indicate possible ecotoxicity the definitive test follows. The highest concentration in definitive test should preferably result in 100% immobilization (mortality or inhibition) and the lowest concentration tested should preferably give no observable effect.

Application of Ecotoxicity Tests for Sewage Sludges Evaluation

Testing organisms (Daphnia magna, Thamnocephalus platyurus, Sinapis alba.) were used in preliminary test with raw water sewage leaches (WSL) and in definitive tests with various testing concentrations of WSL; 50, 100, 200, 500, 700 ml dm^{-3}. Under the same conditions tests with control group of the same organisms in standard freshwater but without WSL were conducted.

The Daphtoxkit FTM makes use of the dormant eggs of the crustaceans Daphnia magna, which are protected by chitinous capsule called ephippium. Ephipia can be stored for long time without losing their viability. When the testing organisms are needed it is necessary to put chitinous capsule

into specific environmental conditions and during period of about 3 days testing organisms are ready for use. Daphnids aged less than 24 were exposed to the sewage leaching at a range of concentrations 50, 100, 200, 500, 700 ml dm^{-3} in definitive tests for a period of 24 and 48 hours at 20–22 °C and light intensity of 6,000 lux. Immobilization was recorded at 24 hours and 48 hours and compared with control values. The results were analyzed in order to calculate the EC50 at 24 and 48 h. Determination of the EC50 at 24 h is optional.

The Thamnotoxkit FTM uses the testing organism Thamnocephalus platyurus, aged less than 24 hours. The exposition was 24 h at a range of the same concentrations at 20–22 °C and 4,000 lux. The obtained results were analysed and the values LC50 at 24 h were calculated. Two above mentioned tests are alternative tests, whilst the test on Sinapis alba represents standard phytotoxicity test. This root growth inhibition toxicity test was used as a standard OECD test. The high quality seeds of Sinapis alba were exposed for 78 hours to tested solution, at temperature 20 ± 2 °C in the dark. After 78 hours the lengths of hypocotyls of seeds in tested and in control group were measured and values of IC50 were evaluated. For a validation of test it is necessary to apply the following performance criteria; Daphnotoxkit FTM and Thamnotoxkit FTM – number of dead and immobile organisms should not exceeded 10 % in control. In root growth inhibition toxicity test germinability should be more than 90 %.

Results

On the base of the analysis of obtained ecotoxicological data the values of EC50, LC50 and IC50 were evaluated for various samples of sewage sludges. These values made possible the evaluation of sludges ecotoxicity and also facilitated their categorization from the point of view of the leacha-

Table I
The ecotoxicity of sewage sludges and their classification

Sewages sludges	24h-EC50 or 24h-LC50 [ml dm^{-3}]	Class of leachability
AS	22.81	III
DWAS	39.57	II
DSAS	139.64	III
PS	38.17	III
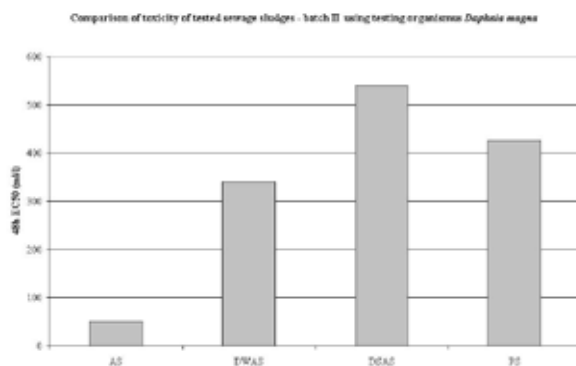
Fig. 1.　**Comparison of ecotoxicity of tested sewage sludges using testing organisms *Thamnocephalus platyurus***

bility. Table I summarizes values of 24h-EC50 or 24h-LC50 for the most sensitive testing organisms, which form the basis for evaluation and categorization of sewage sludges.

Conclusions

Different sewage sludges were tested in respect to their possible hazardous characteristic - ecotoxicity. On the bases of obtained results sewage sludges were classified in term of their leachability. No sample of sewage sludge exhibit ecotoxicity following the Czech legislation.

REFERENCES

1. Wilke, B. M., Riepert, F., Christiane Koch., Kühne, T.: Ecotoxicol. Environ. Saf., *70*, 283 (2008).
2. Kubík, V., Hofman, J., Holoubek, I.: *Abstract Book of SETAC Europe the 16th Annual Meeting*. Hague, Netherlands: SETAC, 2006. p. 79. 7.5.2006, Hague, The Netherlands., Issue 2, June 2008, pp 283
3. OECD Environmnetal health and Safety Publications: OECD Guidelines for Testing Chemicals No. 202 (2004).
4. OECD Environmnetal health and Safety Publications: OECD Guidelines for Testing Chemicals No. 208 (2006).

P95 MICROWAVE DESULPHURIZATION OF COAL

INGRID ZNAMENÁČKOVÁ, MICHAL LOVÁS, SILVIA ČUVANOVÁ and ŠTEFAN JAKABSKÝ

Institute of Geotechnics, SAS, Watsonova 45, 043 53 Košice, Slovakia,
znamenackova@saske.sk

Introduction

Microwave heating has been used in several studies of the coal desulfurization. Desulphurization by microwaves is closely related to the form of sulphur compound in the coal, the physical and chemical structure, as well as the chemical activity of the leachant. The ability of molten NaOH to desulfurize the coal has been known for more than three decades. The process known as molten caustic leaching (MCL) was tested for the first time in the USA. The objective was the removing of the mineral components, pyritic and organic sulfur by the reaction of coal with a mixture of molten sodium and potassium hydroxides. The MCL process was effectively applied for the treatment of the Slovak brown coal[1]. Balaz et al. reported the use of simultaneous grinding and alkaline chemical leaching process (GACL) on brown coal and found that more than 41 % of total sulphur reduction was achieved.

Magnetic methods of mineral removal from coal depend on the difference in the magnetic moment associated with mineral particles and coal. The microwave heating enhances the magnetic susceptibility of the iron mineral, thus rendering it more amenable to the magnetic separation. The effect of microwave heating on magnetic processing of the pyrite was investigated[2], where different size fractions of the pyrite were heated in a microwave oven at 2.45 GHz frequency and different power levels. Ability of coal desulfurization by magnetic separation following microwave heating was also investigated[3]. The microwaves were found as an effective method to selective heating of pyrite in the coal causing the formation of pyrrhotite. It was stated that pyrrhotite could be removed by low-intensity magnetic separation.[4–6]

Experimental

Coal Sample Characterization

In this study, five different coal samples were used. They were ground to less than 3 mm and the representative samples were prepared. The results of analyses of the total sulphur content are listed in Table I.

Microwave and Classical Heating

The microwave heating of investigated coal samples was realized in the microwave oven Whirlpool AVM 434 and Panasonic NN 5251 B with maximum power of 900 W, adjusted for the laboratory purposes for continuos temperature measuring of heated material. The temperature was measured using the contactless thermometer Raynger MX4 in the range 30–900 °C. The classical heating of coal in the mufle oven was realized as well.

Table I
Total sulphur content in the coal samples

Locality	Grain size [mm]	S_{tot} [%]
Handlová (SR)	–3	1.5
Nováky (SR)	–3	3.0
Cígeľ (SR)	–3	2.27
	1–3	5.35
Sokolov (CR)	0.07–0.5	6.85
	–0.07	7.52
	1–3	0.5
	0.5–1	0.5
Donbas (R)	0.2–0.5	0.49
	0.07–0.2	0.53
	–0.07	0.52

Magnetic Separation

The magnetic separation of the coal samples was carried out by means of a roll-type electromagnetic separator Mechanobr, type 138 T-SEM, intended for dry separation.

Microwave Radiation and Molten Caustic Leaching – RMCL

A mixture of 15 g coal + 15 g NaOH + 10 ml H_2O was used as an input to microwave oven operating in nitrogen atmosphere. Microwave desulphurizastion of coal was realised according to the Scheme 1.
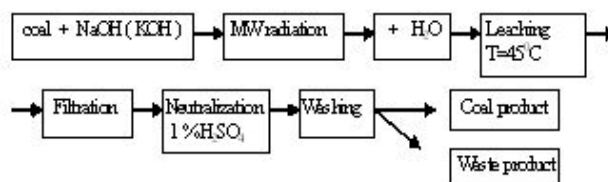
Scheme 1
The RMCL (Radiation and Molten Caustic Leaching) desulphurization of coal

Results

Magnetic Separation of Coal

Coal sample of the grain size 0.05–0.2 mm was heated before magnetic separation in the microwave oven for 10 minutes at the power 900 W and frequency 2.45 GHz. The results of the magnetic separation after microwave radiation are listed in Table II.

The magnetic separation of the coal sample was ineffective for our conditions.

The Molten Caustic Leaching of Coal

Effect of ratio of NaOH and coal

The effect of ratio of NaOH and coal from the Cígeľ locality after the microwave radiation (2.5 minutes) on reduction of the total sulphur content is displayed in Fig. 1.

Table II
The results of coal magnetic separation after the microwave radiation

Grain size [mm]	Magnetic induction [T]	Mass yield of magnetic product [%]	Recovery of S_{pyr} in mag. prod. [%]
	0.13	4.32	39.6
	0.24	4.72	43.2
0.05–0.2	0.42	10.80	44.7
	0.51	11.54	45.5
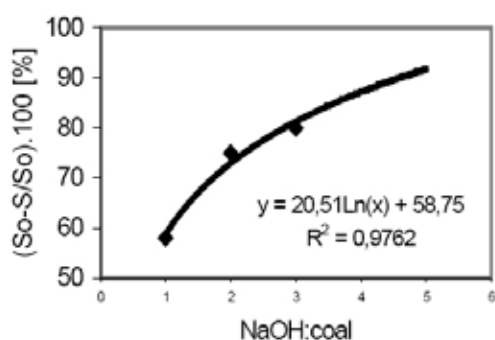
Fig. 1. **The influence of ratio of NaOH and coal on the total sulphur content in coal sample (Cígeľ) after RMCL process, So-content of sulphur basic sample**

From the obtained results, it is possible to state, that 80 % of the total sulphur content is possible to remove by ratio of NaOH : coal = 3 : 1.

Effect of reaction time

The time dependence of microwave heating on decrease of the total sulphur content in coal from the Cígeľ locality by ratio of NaOH : coal = 1 : 1 is displayed in Fig. 2. The sulfur removal increased to 76 % within 5 minutes and reached 85 % at 10 minutes, but after 10 minutes, the change was not significant.

The total sulphur content decreased from 2.27 % to 1.0 % (56 %) in the mufle oven at the temperature 380 °C (within reaction time 40 minutes). The main difference between the

thermal and microwave heating was the extremely short time for desulphurization in the case of microwave experiments.

Effect of the coal deposits

The dependence of sulphur content in the coal samples from the localities Cígeľ, Handlová, Nováky in RMCL proces is displayed in Fig. 3. The conditions of the microwave heating were following: temperature 380–400 °C, time 3 minutes, the ratio of NaOH : coal = 1 : 1.

It can be seen, that the effect of microwave pretreatment on reduction of the total sulfur content in samples from Nováky and Cígeľ (52–56 %) is higher than in sample from Handlová (28 %).
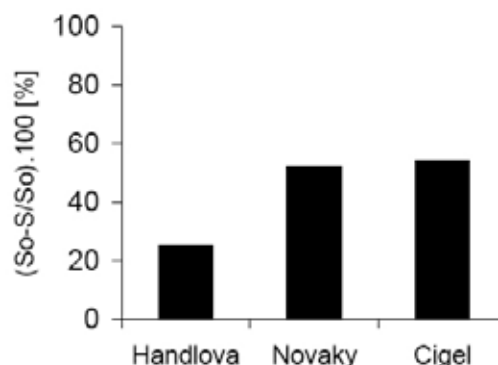
Fig. 3. **RMCL for coal samples from Handlová, Nováky, Cígeľ**

Effect of the particle size

The influence of particle size on chemical desulfurization process was also studied. The representative samples were divided in fractions of 1–3, 0.5–1, 0.07–0.5, <0.07 mm and microwave heating of samples from Donbas (500 W and 6 minutes) and Sokolov (750 W and 3 minutes) was realized. The results are given in Figs. 4. and 5.

The decrease about 25 % of the total sulphur content was in the sample from Sokolov eminent. The influence of graine size was negligible.

The decrease about 35 % of the total sulphur content in black coal from Donbas locality for graine size 1–3 mm was observed.

Fig. 2. **The change of total sulphur content of the coal samples with time**
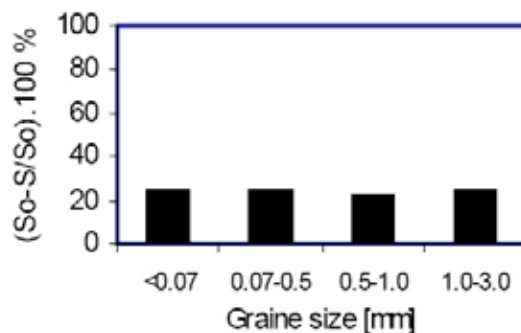
Fig. 4. **The decrease of the total sulphur content in sample from Sokolov versus different size fraction in RMCL process**
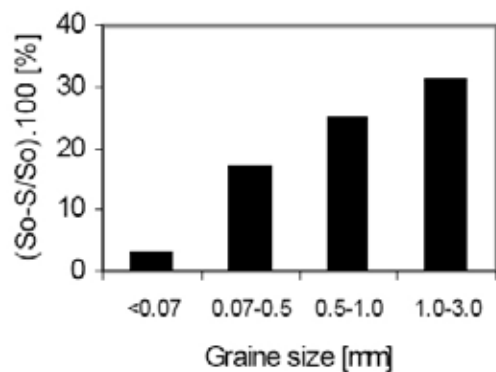
Fig. 5.   **The decrease of the total sulphur content in sample from Donbas versus different size fraction in RMCL process**

Conclusions

Microwave heating of the coal is advantageous for the subsequent desulphurization. Conventional procedure of coal desulphurization requires heating period about 40 minutes and microwave procedures reduces this heating period for a few minutes. The use of microwave radiation for the desulphurisation of coal displays potential and may be soon a commercial reality. This would allow the use of high sulphur coals in an environmentally and economically sound way.

REFERENCES
1. Balaz, P., LaCount, R. B., Kern, D. G., Turcaniova, L: Fuel *2001, 80.*
2. Uslu U, Atalay A. I. Arol A I: Colloids Surf. A, Physico-chem. Eng. Asp. *225*, 1 (2003).
3. Uslu U, Atalay A: Fuel Process. Technol. *85*, 1 (2004).
4. Jorjani, E., Rezai, B., Vossoughi, M., Osanloo, M: Fuel *83*, 7 (2004).
5. Kingman S. W., Rowson N. A.: Min. Eng. *11*, 11 (1998).
6. Kingman S. W., Rowson N. A.: J. Microwave Power Electromagn. Energ. *35*, 3 (2000).

P96   THE BIOLOGICAL ACTIVITY OF 16α(*H*)-PHYLLOCLADANE ISOLATED FROM SLOVAK BROWN COAL

ANTON ZUBRIK[a], ANDREA LAUKOVÁ[b], ALENA GÁBELOVÁ[c], ZUZANA VALOVIČOVÁ[c], ĽUDMILA TURČÁNIOVÁ[a] and JOSEF CVAČKA[d]

[a]*Institute of Geotechnics, Slovak Academy of Sciences, Watsonova 45, 043 53 Košice, Slovakia,*
[b]*Institute of Animal Physiology, Slovak Academy of Sciences, Šoltésovej 4–6, 040 01 Košice, Slovakia,*
[c]*Cancer Research Institute, Slovak Academy of Sciences, Vlárska 7, 833 91, Bratislava, Slovakia,*
[d]*Institute of Organic Chemistry and Biochemistry v.v.i., Academy of Sciences of the Czech Republic,*
Flemingovo nám. 2, 166 10 Prague 6, Czech Republic,
zubant@saske.sk

Introduction

The coal research brings novel opportunities for non-fuel utilization. One of the promising ways is extraction and isolation of organic compounds (diterpenes, humic acids) with potential biological activity. The Slovak coals (Nováky lignite and Handlová brown coal) contain high amounts of tetracyclic diterpene hydrocarbons[1,2], which can be valuable precursors for pharmaceutical products. Kauranes and phyllocladanes are important diastereoisomeric tetracyclic diterpene biomarkers. Tetracyclic diterpene derivates isolated from plants show a strong biological activity and they are active components of many plant medicaments and extracts used in folk medicine. Kauranes exhibit an anti-microbial, anti-HIV, anti-inflamatory, anti-fertility, antiparasitic, insect anti-feedant, antifungal and cytotoxic activities[3]. Phyllocladanes are very rare in the nature; nevertheless, they were also identified and isolated from several plants. Orizaterpenol (phylloklad-15-en-6β,14βdiol) from the rice hull of *Oryza sativa* shows cytotoxicity against murine leukemia cells[4]. The use of phyllocladane diterpenoids for plant growth promotion and/or retardation is already patented[5].

The biological activity of tetracyclic diterpenoids isolated from the geological samples has not been studied yet, therefore the main goal of our work was to isolate tetracyclic diterpane from the coal and test its biological activity *in vitro*.

Experimental

Isolation of 16α(*H*)-Phyllocladane from Slovak Brown Coal

The brown coal (50 kg) was collected in several places of the Handlová mining area (Fig. 1.) and a representative sample was obtained by quartation.

Before the extraction; the Slovak brown coal from Handlová was physically treated on hydrocyclone[7] to obtain quality carbon product with A^d (ash content) = 7.70 % wt., W^a (moisture) = 12.26 % wt., C^d = 61.6 %, H^d = 5.6 %, N^d = 0.7 %, S^d = 1.2 %, O^d = 23.2 %. Further, the coal (20 g)
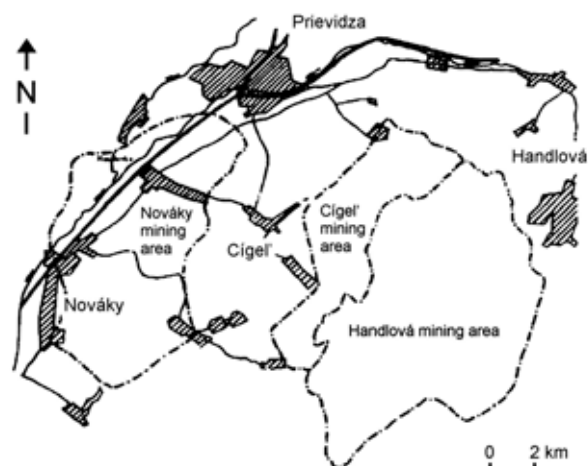
Fig. 1.   **The situation map of Handlová-Nováky coal basin with Handlová mining area in central part of Slovakia (adapted from ref.[6])**

was extracted with dichloromethane (250 ml) in microwave oven (Wirlpool AVM 434, 500 W, 2.45 GHz) in distilling flask with reversing reflux system (20 min). After the extraction, the mixture was filtered and the solvent was evaporated. The crude extract (367 mg) was re-extracted on SPE column (Chromabond SiOH, Macharey – Nagel GmbH + Co. KG) with n-hexane (100 ml). The solvent was evaporated and the purified SPE extract (112 mg) was further separated by column chromatography on silica gel (5 g of Kieselgel 60, granularity 0.06 – 0.2 mm, Carl Roth GmbH + Co. KG) with 4×20 ml of hexane to four fractions denominated as F1–F4. All fractions were analyzed by TLC and GC/MS. 16α(*H*)-phyllocladane was found in the F1 fraction. TLC analysis of F1 showed presence of a single spot with $R_F = 0.91$, that contained three compounds: the most abundant component (81.6 %) was 16α(*H*)-phyllocladane; second one was isopimarane (11.2 %) and finally 18-norisopimarane (3.9 %). Unambiguous identification as 16α(*H*)-phyllocladane was achieved by coinjection of the sample and standards in the laboratory of Prof. Bernd Simoneit (Oregon State University, USA). The final isolate (36.7 mg) named as TD1 containing 81.6 % of 16α(*H*)-phyllocladane was used for further biological tests.

Bacterial Strains

All tested Gram[+] and Gram[−] bacteria (*Enterococcus* spp., β-hemolytic streptococci, *Staphylococcus aureus* CCM 3953, *S. aureus* SA5, *Listeria innocua* LMG 13568 *Enterobacter cloacae* 5139, 19259, 4417, *Klebsiella pneumoniae* 1962, 12506, 5182, 1366, *Serratia marcescens* 19194, *Salmonella enterica* serovar Duesseldorf SA31, *S. enterica* ser. Enteritidis PT4, *Shewanella putrefaciens, E. coli* K88, *E. coli* 6295, 5765) were of human or veterinary origin (isolated from the various wounds, blood, sputum and faeces). The strains were maintained on the appropriate selective media according to ISO.

S p o t   T e s t

The antimicrobial activity was determined by the diffusion agar spot test[8]. For the testing, TD1 was dissolved in n-hexane and the various concentration ranges of TD1 (600 mg ml^{-1}; 300 mg ml^{-1}; 150 mg ml^{-1}; 75 mg ml^{-1}) and several volume doses were used; 5 µl is optimal dosage to test on solid agar containing the indicator strain. The solvent n-hexane was used as a control. After 24 hours of incubation at 37 °C, the inhibitory zones were evaluated. MICs (minimal inhibitory concentrations) were expressed as the lowest concentration of TD1 inhibiting the growth of the indicator bacteria (mg ml^{-1}).

C e l l   L i n e

The human hepatoma cell line HepG2 was generously provided by Prof. Andrew R. Collins (University of Oslo, Norway). HepG2 cells were maintained in William´s modified medium supplemented with 10% fetal calf serum and antibiotics (penicillin 200 U ml^{-1}, streptomycin and kanamycin 100 µg ml^{-1}) at 37 ºC in humidified 5% CO_2 atmosphere.

C e l l   T r e a t m e n t

Hep G2 cells were grown for 48 h until semi-confluency, prior to exposition to TD1 and positive control. TD1 was dissolved in ethanol at 40 ºC freshly before use and added to culture medium to reach the final concentrations ranging from 0.045 to 0.5 mg ml^{-1} for 24 hours. The concentration of the solvent never exceeded 0.1 %. Control cells were exposed to 0.1% ethanol. Cells were exposed to hydrogen peroxide (150 µM), the positive control, on ice in dark for 5 minutes.

S i n g l e   C e l l   G e l   E l e c t r o p h o r e s i s   (S C G E)

The procedure of Singh et al.[9], modified by Collins et al.[10] and Slameňová et al.[11] was followed. The data were evaluated statistically by the Student's t-test.

Results and Discussion

The details of isolation and structure elucidation of 16α(*H*)-phyllocladane (Fig. 2.) was published previously[2,12].
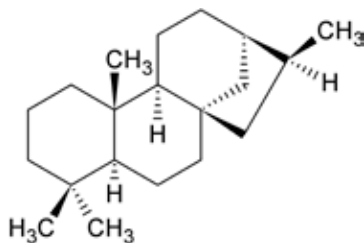
Fig. 2.   **The structure of 16α(H)-phyllocladane**

A n t i m i c r o b i a l   A c t i v i t y

TD1 inhibited the growth of 3 Gram$^-$ bacteria (*Kl. pneumoniae* 5182, 1366; *E. coli* 5765) among 19 tested strains. MIC value for these strains is 300 mg ml^{-1}. Others tested bacteria were not sensitive to TD1. The antibacterial activity of

tetracyclic diterpene (ent-kauren-19-oic acid) was detected particularly against Gram$^+$ bacteria[13]. In our case, this is the primary and first unique result associated with inhibitory activity of phyllocladane against Gram$^-$, pathogenic bacteria such as *Klebsiella* spp. It is necessary to note that for the further practical usage, the selectivity of the potential pharmaceutical compound is one of the principal conditions.

G e n o t o x i c i t y

Based on previous cytotoxicity experiments (data not shown), the genotoxic activity of TD1 was evaluated at concentrations 0.045–0.5 mg ml^{-1} (Fig. 3.). In general, only a weak cytotoxicity (~ 20%) was determined at these highest concentrations.

A linear dose dependent increase of DNA migration was detected in TD1-exposed cells ($r^2 = 0.8732$). A mild but statistically significant increase of DNA damage was found at concentrations 0.25–0.5 mg ml^{-1} ($p < 0.05$–0.01). There are limited data concerning the toxicity of phyllocladane-type diterpenes. Recently, Chung et al.[4] reported a strong cytotoxicity of orizaterpenol in P388cells.
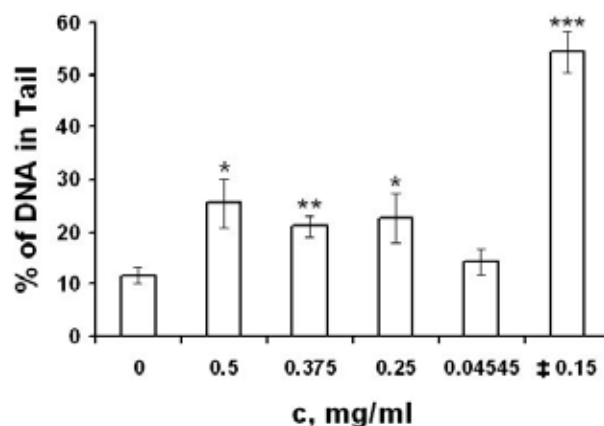
Fig. 3.   **The level of DNA damage induced by TD1 in HepG2 cells. Cells were exposed to various concentrations of TD1 for 24 hours. ‡ – positive control – H_2O_2 (0.15 mM). Significantly different from control cells determined by Student's t-test, * $p < 0.05$, **$p < 0.01$ and ***$p < 0.001$**

Conclusions

Biological activity of TD1 (containing 81.4 % of 16α(*H*)-phyllocladane) from Handlová brown coal was assayed in vitro using pathogenic bacteria and the human hepatoma cell line HepG2. The selective antimicrobial effect against Gram$^-$ strains of *Kl. pneumoniae* 5182, 1366, *E. coli* 5765 was determined with MIC up to 300 mg ml^{-1}. In addition, TD1 induced DNA damage in human tumor cell line HepG2 without strong cytotoxicity. Further search for biological active compounds from Slovak coal and others biological tests will be carried out.

REFERENCES

1. Streibl M., Kristín M., Krupčík J. Stránsky K.: An. Quim. *68*, 879 (1972).
2. Zubrik A.: *Dissertation*. Institute of Geotechnics of Slovak Academy of Sciences, Košice, Slovakia, 2007.
3. Guisalberti E. L.: Fitoterapia *68*, 303 (1997).
4. Chung I. M., Ali M., Hahn S. J., Siddiqui N. A., Lim Y. H., Ahmad A.: Chem. Nat. Compd. *41*, 182 (2005).
5. Singh A. K., Bagchi G. D., Singh S., Dwivedi P. D., Gupta A. K., Khanuja S. P. S.: USP 6673749 (2004).
6. Machájová Z., Verbich F., Sýkorová I.: Acta Montanistica Slovaca *5*, 261 (2000).
7. Hredzák S.: Gospodarka Surowcami Mineralnymi *15*, 221 (1999).
8. De Vuyst L., Callewaert R., Pot B.: Syst. Appl. Microbiol. *19*, 9 (1996).
9. Singh N. P., McCoy M. T., Tice R. R., Schneider E. L.: Exp. Cell Res. *175*, 184 (1988).
10. Collins A. R., Duthie S. J., Dobson V. L.: Carcinogenesis *14*, 1733 (1993).
11. Slameňová D., Gábelová A., Ružeková L., Chalupa I., Horváthová E., Farkašová T., Bozsakyová E., Stetina R.: Mutat. Res. *383*, 243 (1997).
12. Zubrik A., Šaman D., Vašíčkova S., Simoneit B. R. T., Turčániová Ľ., Lovás M., Cvačka J.: Organic Geochemistry (submitted).
13. Mendoza L., Wilkens M., Urzúa A.: J. Ethnopharmacol. *58*, 85 (1997).

3. FOOD CHEMISTRY & BIOTECHNOLOGY

3.1. Lectures

L01 NONSACCHAROMYCES YEAST IN GRAPE MUST – ADVANTAGE OR SPOILAGE?

JAROSLAVA KAŇUCHOVÁ PÁTKOVÁ[a], EMÍLIA BREIEROVÁ[b] and INGRID VAJCZIKOVÁ

[a]*Institute for viticulture and enology of SARC Matuškova 25, 831 01 Bratislava, Slovak republic,*
[b]*Institute of ChemistrySAS, Dúbravská cesta 9, 845 38 Bratislava, Slovak republic,*
chememi@savba.sk

Introduction

The fresh grape must consists of spontaneous microflora formed from 90 to 99 % by yeasts. The most important genus is without doubt *Saccharomyces cerevisiae* which is responsible for successive fermentation and good wine quality. Recently the contribution of non-*Saccharomyces* yeasts have been widely discussed as there is not definitive opinion on their contribution to the wine quality, especially aroma. *Hanseniaspora osmophila* and *Kloeckera apiculata* should be considered detrimental yeast species, by higher acetic acid, acetaldehyde, ethyl acetate and acetoin production[1]. To avoid spoilage it is recommended to inoculate the grape must by *Saccharomyces cerevisiae* immediately after pressing. On the other hand, the apiculate non-*Saccharomyces* yeast is a natural indigenous microflora which contributes to the wine origin. Thus the question wheather to allow the apiculate microflora to start fermentation or not has not yet been solved.

The aim of this study work was to determine the aroma profile of isolated non-*Sacaharomyces* yeast from the chemical as well as the sensorial viewpoints. The yeasts of the genera *Rhodotorula*, *Sporobolomyces*, *Pichia*, *Hansenula*, *Issat-chenkia*, and *Torulospora*, were tested from the viewpoint of their contribution to the wine aroma. The results were than exploited and tested in the real wine-making process.

Experimental

Following yeast strains were isolated from the grape must and degraded products: *Rhodotorula mucilaginosa* (2 strains), *Sporobolomyces pararoseus*, *Pichia membranefaciens*, *Pichia anomala* (2 strains), *Candida intermediata*, *Torulospora delbruecki,* and *Issatchenkia orientalis*. For comparison 3 *Saccharomyces cerevisiae* strains were also used. Two of them were isolated from the grape must, the third was a commercial one (Lallemand).

Consequently the isolated yeast strains were inoculated to the first cultivation medium: the sterile grape must had been femented for 10 days at 10 °C under semiaerobic conditions or 4–6 weeks at 10 °C under anaerobic conditions.

Second cultivation medium: the sterile Vinea drinks were inoculated by studied yeast strains and cultivaited at 20 °C for 10 days under semiaerobic conditions.

The samples were than sensorially evaluated by a group of degustators. The same samples were than analysed by gas chromatography for the aroma compounds production. Each sample was analysed on the GC MS (Shimadzu QP 2010) equipment and also on the GC FID equipment (GC 8000 CE Instruments).

Two methods of sample preparation were done:

The samples (20 ml) were extracted by ether (2 ml), and centrifuged prior to analysis. The etheric extract was used for analysis (liquid – liquid extraction). This method was used for higher alcohols (propanol, isoamylacohol, ethyl ester and higher alcoholos esters) determination

The samples were extracted by Tenaq (solid phase microextraction) and than 10 min sampling according to[6]. This method was used for monoterpenic compounds determination.The same column and the same conditions were used by both analysis: Column: DB WAX 30 m, 0.25 × 0.25, temperature programme: 30 °C, hold 2 min, increase by 4 °C min^{-1} up to 230 °C, hold 10 min, 1 ml of sample was injected to injection port at 200 °C, detector temperature 220 °C, carrier gas: helium, injektion mode: split 1 : 100, flow control mode: pressure 70 kPa

Results

After inoculation and fermentation of the grape must and Vinea drink the number of aroma compounds increased significantly, in both cases and more than 60 compounds were found. Most of them were recognized as typical fermentation products, etc. ethanol, izoamylacohol, propanol, etylester of caproic, caprylic and caprinic acids, ethylacetate, isovaleric acid, pentylacetate, 2,3-butandiol, furfural, 3-hydroxybutyrate, methionon, 1,4-butandiol. 2-metyl a 3-metylbutanoic acid, 2-phenyletylacetate, izoamylacetate, cis 3-hexenylacetate, etylbenzoate, α-terpineol, etyl isobutyrate, etyl butyrate, etyl 2-metylbutyrate, etyl isovalerate, isoamyl acetate, ethyl hexanoate, cis-3-hexenol, ethyl octanoate, furfural, linalool, ethyl furoate, ethyl decanoate, ethyl benzoate, α-terpineol, fenylethyl acetate, and geraniol. The increased production of typicall glycolysis products were also confirmed by several authors[2,3,4]. Ethyl propionate and propyl acetate, characterized the sample of the grape must fermented by *Kloeckera apiculata*, and 2-propanol and 2-hexanone characterized the sample of the grape must fermented by *Pichia membranefaciens*[2]. Rojas[3] studied analysis of non-*Saccharomyces* yeast fermentation products and found higher acetate content, especially 2-phenylacetate and isoamylacetate for *Pichia* yeasts. Albertazzi[4] also described higher levels of phenylacetate by other yeast - *Pichia pastoris* and *Kloeckera saturnus* (700–1700 mg dm^{-3}). From our results we can confirm incereased ester production by all studied microorganisms, especially increased content of ethyl acetate.

However, we have found that some microorganisms produced special compounds, which were not recognised by other yeasts. After the fermentation of the grape must by *R. mucilaginosa* and *Sp. pararoseus,* aroma compounds significantly increased. Acetate, hexanal, heptanal, octanal, cyclopentanone, thiazole, decalactone, propyl-3-dimethyl aminopropyl, nonanone, heptanon, and butanediol were formed. *P. anomala* produced especially isoamyl benzyl ether. The medium fermented by *Sporobolomyces* was rich in sabinylacetate, 3,4-hexandion and eicosane. *R. mucilaginosa* generated cyklopentanol and, α-cyklogeraniol. *S. cerevisiae* produced vericaldehyd and γ-nonalakton.

We have found out that yeasts of the genera *Pichia, Rhodotorula*, and *Sporobolomyces* did not produce the linalool acetate, contrary to *S. cerevisiae.*

The differences in the compound production within the same yeast species were also observed. *S. cerevisiae* strain 8 produced caproic aldehdyd, trans-pinocamphon, dodecanal, 5-methyl-3-heptanon, izo-menthylacetate, contrary to *S. cerevisiae* strain 5 which did not produce any of these compounds. *R. mucilaginosa* strain 11 produced higher amounts of 2,3-butandiol, but did not produce any izopen-

Table I
Aroma compounds typically produced by various yeast species and flavoural characterisation of founded compounds

Yeast strain	compound	Flavour fragrance
R. mucilaginosa	cyklopentanol, alfacyklogeraniol	mint aroma spice flavour carnation odour
Pichia anomala	izoamyacetat	banana flavour
Sp. pararoseus	sabinylacetate	fruity aroma
S. cerevisiae	valericaldehyd, γ-nonalakton	coffee aroma coconut odour

Table II
Sensorial evaluation of fermented grape must by various yeast strains, +positive impression, −negative impression

Yeast strain	Anaerobic conditions aroma	perc.	Semiaerobic conditions aroma	perc.
C.intermediata	yeast	+	acidic	−
R.mucilaginosa 3	socks smelly	−	acethone	−
T.delbruecki	pleasant	+	vanilla	+
I.orientalis	autolyses	−	acethone	−
Pichia anomala	acethone	−	lime	+
P.membranefaciens	autolyses	−	yeasty	+
R. mucilaginosa 11	autolyses	−	honey	+
Pichia anomala	acethone	−	honey	+
Sp. pararoseus	not recognised	−	yeasty	+
S.cerevisiae 5	acidic	−	ferment	+
S.cerevisiae 8	fruity	+	ferment	+
S.cerevisiae 16	honey	+	ferment	+

Table III
Evaluation of Vinea fermented under semiaerobic conditions

	Semiaerobic conditions Vinea	
Yeast strain	20 °C Aroma	Percept
C. intermediata	acidic	+
R. mucilaginosa 3	acethone	+
T. delbruecki	yeasty	+
S. cerevisiae 5	yeastly	+
I. orientalis	grape must	+
S. cerevisiae 8	honey	+
P. membranofaciens	vinea	−
R. mucilaginosa 11	acethone	+
P. anomala	honey	+
Sp. pararoseus	acethone	+

tylformiate and 3,4-hexandion. These compounds produced strain *Rhodotorula mucilaginosa* strain 3.

One of the most important factors in wine proofing is the sensorial evaluation of wine aroma. It is very difficult to estimate which from all above mentioned compounds will prevail over the other ones and wheather the wine could give positive or negative impression. It is due to the complexity of wine aromas, the heterogenity of perception and recognition thresholds for each one compound as well as many interactions occuring within and after fermentation[5].

As shown in Table II, under anaerobic conditions only *T. delbruecki* from apiculate microflora developed a pleasant aroma. All the other yeast strains evolved unpleasant, smelly aroma. However, the situation was radically changed when the fermentation occured under semi-aerobic conditions. *Torulospora delbruecki* produced the pleasant aroma, exactly defined as vanilla. Also both strains of *P. anomala*, *Pichia membranefaciens, Sp. pararoseus* and one strain of *R. mucilaginosa* evoked very pleasant aroma, some of them with honey notes, some of them fruity or increased fermetative impression.

The results of better sensorial evaluation under semiaerobic conditions were subsequently tested by real wine-making fermentation. The problem which usually occurs in real process is that the present microfloras consists of several yeast genera which can possitively or negatively contribute to the wine quality.

The group of degustators confirmed that the wines were better evaluated when they were fermented under semiaerobic conditions, with the inocoluation by *S. cerevisae* not directly after fermentation, but several hours after grape pressing. The main advantage of this system is its ability to improve the originality of the wine.

Conclusions

We have found compounds which were typically produced by some non-*Saccharomyces* yeast strains – cyklopentanol, alfacyklogeraniol for *R. mucilaginosa,* sabinylacetate, for *Sp. pararoseus,* and izoamylbenzylether for *P. anomala*.

We can confirm that under anaerobic conditions, most of the apiculate microflora, except *T. delbruecki*, negatively affected wine aroma because they produced higher amounts of aldehydes – pentanal, hexanal, heptanal, 3,4-hexanedione, eicosene which caused the buttery and waxy odour.

However under semiaerobic conditions apiculate yeast species promoted positive aroma perception in products. *Torulospora* and *Pichia* yeast strains increased the fruit and/ or coconut aroma by higher production of sabinyl res. isoamylacetate.

Semiaerobic conditions applied several hours prior inoculating by *S. cerevisiae* improve sensorial evaluation of wine and increase the support of originality and variety typicity.

However, the fermentation under such conditions is still very hazardous because oxidative defects or microbiological defaults of wine could occured.

REFERENCES

1. Granchi L., Ganucci D., Messini A, Vincenzini M.: FEMS Yeast Res. *2*, 403 (2002).
2. Romano P., Fiore C., Paraggio M., Caruso M., Capece A.: Int. J. Food Microbiol, *86*, 169 (2003).
3. Rojas V., Gil J.V., Pinaga F., Manzanares P.: Inter. J. Food Microbiol. *70*, 283 (2001).
4. Albertazzi E, Cardillo R., Servi S.: Biotechnol. Lett. *16*, 491 (1994).
5. Ribereau-Gayon P., Glories Y., Dubordieu D., Maujean A., Handbook of Enology, Ed. Wiley, Chicester, 404 (2000).
6. Kruzlicova D., Mocak J., Hrivnak J.: J. Food Nutr. Res. *47*, 37 (2008).

L02 APPROACHES TO MINIMIZATION OF ACRYLAMIDE LEVEL IN FOODS

ZUZANA CIESAROVÁ

VÚP Food Research Institute
Priemyselná 4, 824 75 Bratislava, Slovak Republic,
ciesarova@vup.sk

Introduction

Thermal treatment of foods is a common way for improvement of digestibility, safety, quality and sensory properties of many foods which is used for ages. Besides unambiguous desirable aspects of this treatment some detrimental effects are still emerging e.g. a loss of nutrition-worthy compounds and an undesirable generation of contaminants.

In 2002, Swedish researchers have first reported the formation of acrylamide in foods processed at elevated temperatures[1]. Recent assessment by the Joint FAO/WHO Expert Committee on Food Additives (JECFA) in 2005[2] confirmed that a risk cannot be excluded for dietary intake of acrylamide because it is classified as a probable human carcinogen by the International Agency for Research on Cancer (IARC)[3]. In that assessment JECFA concluded that the margin of exposure for average and high consumers were low for compound that is genotoxic and carcinogenic and that this may indicate a human health concern. Therefore the Commission Recommendation since 2007 announced that "appropriate efforts to reduce acrylamide concentrations in foodstuffs should continue"[4]. Moreover, with respect to the last observations confirming the association between acrylamide intake and endometrial, ovarian[5], and breast[6] cancer risk, the concern on the acrylamide mitigation activity is very urgent.

Occurrence of Acrylamide in Thermally Treated Foods

After the discovery of acrylamide, a lot of studies confirmed the presence of acrylamide in nearly all fried, baked and roasted foods. Acrylamide exposure varies depending upon the population´s eating habits and the way the foods are processed and prepared. Generally, fried potato products, ready-to-eat breakfast cereals, baked goods and roasted coffee are the most important food categories that contribute most to acrylamide exposure. An average long-term exposure of acrylamide was estimated of 0.3 to 0.8 µg (kg body weight) $^{-1}$ day^{-1} on the base of the few data which were available at the FAO/WHO Consultation in 2002[7]. Based on the reported data, the Committee JECFA in 2005[2] noted that children may have intakes of acrylamide around two or three times higher those of adult consumers when expressed on a body weight basis. It is expected that children and adolescents have consumption patterns different from adults. Most of the types of foods in which acrylamide was detected are popular among children and adolescents, such as French fries, snacks, biscuits and breads. Moreover, they have a lower average body weight and, consequently, a higher average food intake per kilogram body weight than adults. For that, acrylamide intake by these individuals is considered a concern.

Mechanism of Acrylamide Formation

Initial results on acrylamide content indicated carbohydrate-rich foods to generate relatively more acrylamide[1]. Several researchers have established that the main pathway of acrylamide formation in foods is linked to the Maillard reaction and, in particular, the amino acid asparagine[8,9]. The link of acrylamide to asparagine, which directly provides the backbone of the acrylamide molecule, has been established by labelling experiments[9,10]. Study to date clearly shows that the amino acid asparagine is mainly responsible for acrylamide formation in heated foods after condensation with reducing sugars or a carbonyl source. Moreover, the sugar-asparagine adduct, N-glycosylasparagine, generates high amounts of acrylamide, suggesting the early Maillard reaction as a major source of acrylamide[9]. In addition, decarboxylated asparagine (3-aminopropionamid), when heated can generate acrylamide in the absence of reducing sugars[10]. A good evidence supporting the early Maillard rection as a main reaction pathway involving early decarboxylation of the Schiff base, rearrangement to the resulting Amadori product, and subsequent beta-elimination to release acrylamide has been presented[11].

Factors Affecting Acrylamide Formation in Foods

The resulting acrylamide concentration in foods ultimately depends on both products and process variables. Acrylamide formation requires the amino acid asparagine and a carbonyl compound as the Maillard reaction precursors. The concentration of acrylamide precursors and temperature mainly affect the rate of acrylamide formation. It is a fact that formation and degradation of acrylamide occurs in the same time during heating at elevated temperatures, it means that measured acrylamide content of a food is net result of two consecutive reactions occurred during thermal processing[12].

Based on the current knowledge of the mechanism of acrylamide formation, many parameters affecting the level of acrylamide in foods were investigated, e.g. heat intake, the level and type of saccharides and amino acids, moisture and water activity, additives, processing steps etc.[13], and consequently various ways of acrylamide minimization in foods have been proposed. Many of them are summarized in a "living" document "The Acrylamide Toolbox" published by experts associated in the Confederation of the Food and Drink Industries of the European Union (CIAA)[14].

The mitigation approach is divided in two strategies:
- Prevention of acrylamide formation through a modification of food composition (a decline of asparagine and reducing saccharides contents), processing conditions (thermal input, pH, moisture), an addition of compounds suppressing the formation of acrylamide (acids, enzymes, proteins, antioxidants etc.) and an enhancement of processing steps (pre-treatment, blanching, fermentation etc.)[15].
- Facilitation the acrylamide elimination through storage conditions or the initialization of acrylamide polymerization[16,17].

Temperature plays an important role in the formation and elimination of acrylamide. It is well known that acrylamide forms in foods that are cooked at high temperatures (> 120 °C)[8,13,18]. For shorter heating times as in the frying operation of potato chips or strips, lowering the frying temperature may significantly reduce the amount of acrylamide formed (Fig. 1.). The same may not be true for longer heating periods as in the roasting of coffee beans where extending the operation may result in a decrease in the amount of acrylamide persisted in the final product[19]. They may be a critical temperature/time zone where acrylamide is formed at a greater rate than it is destroyed, at temperatures outside of this zone little acrylamide is present.
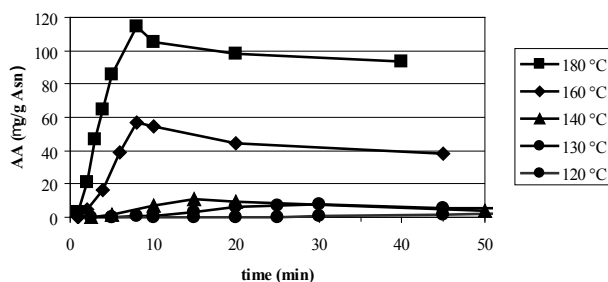
Fig. 1. **Amount of acrylamide after heating of equimolar mixture of glucose and asparagine at different temperatures**

The fact that acrylamide is not formed during boiling indicates that higher temperatures and/or low moisture conditions are needed for its formation. During heating under atmospheric conditions, higher temperatures can be reached only if simultaneous drying takes place, which is the case in frying, baking and roasting. The loss of water as the food dries during heating extracts a large amount of the incoming energy, and hence a bulk of the product is at a temperature very much lower than that of the heating medium. In this respect, temperature, time and moisture are key drivers of acrylamide formation in foods during heating (Fig. 2.). The moisture content determines the physical state and mobility of chemical constituents in food matrix. In addition, water alone affects the chemical route and the mechanistic pathway for acrylamide formation[13].

Concerning reducing sugars as carbonyl source, fructose has been found more effective than glucose in forming acrylamide (Fig. 2.). Both the chemical reactivity of sugars and their physical state play an important role in acrylamide formation. The melting point of fructose and glucose are 126 °C and 157 °C, respectively[13]. This explains why fructose is more reactive than glucose on acrylamide formation during heating. Frying, baking and roasting are simply characterized as open processes in which heat and mass transfer occur simultaneously. As the moisture reduces due to evaporation, sugars initially dissolved in water begin to form a saturated solution and then crystallize. After crystallization, melting

is required to change their state to liquid, so to make them chemically reactive. In this respect, reducing sugars having a lower melting point is expected to form acrylamide earlier during heating.
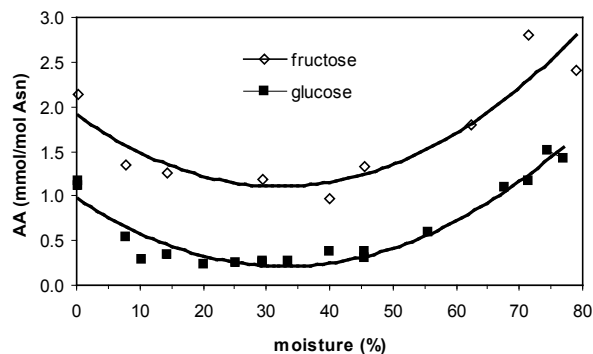
Fig. 2. **Amount of acrylamide after heating of equimolar mixture of asparagine and glucose/fructose at 180 °C for 20 min with different addition of water**

Enzyme Treatment Leading to Acrylamide Reduction

One of the most effective ways to avoid acrylamide formation is removing the precursors, particularly amino acid L-asparagine. L-asparaginase as an enzyme of the hydrolases group (EC 3.5.1.1.) selectively hydrolyses the amide bond of L-asparagine which results in the formation of aspartic acid and ammonia. Because the acrylamide formation correlates strongly with a free asparagine concentration, the reduction of L-asparagine in raw materials leads to the reduced level of acrylamide in final products[20]. The safety of asparaginase application is guaranteed by approving of GRAS status of *Aspergillus oryzae* asparaginase enzyme from Novozymes A/S[21], and *Aspergillus niger* asparaginase enzyme from DSM[22], and a positive evaluation from the JECFA in 2007[23] as well. Moreover, this enzyme is inactivated by high temperature in the process of proteolysis.

The application of L-asparaginase solution in a simulated potato matrix resulted in 50 to 90 % reduction of acrylamide content depending on the conditions (enzyme dose, time and temperature of incubation). No significant differences in impacts on L-asparagine conversion into L-aspartic acid in model samples between bacterial and fungal originated enzymes were observed. The positive effect of enzyme on the decrease of acrylamide content was confirmed also after L-asparaginase application on raw potato mash as well as dehydrated potato-wheat semi-products (Fig. 3. and Fig. 4.)[20].

It is known that each intervention in the technology can be accompanied with consequences on the quality and sensory properties of final products which are strongly connected with the acceptability by consumers. For that reason the preliminary sensory evaluation of thermally and enzymatically treated products was done by a panel of trained judges. They described the main properties important for

these kinds of products such as darkness, yellowness, appearance, stickiness, crispness, oiliness, flavour, off-flavour, saltiness, sweetness and overall acceptability. Changes in colour were observed in pancakes prepared under different heating programmes, where darkness and crispness were more intensive in pancakes prepared at higher temperature of frying. No differences in evaluated sensory properties mentioned above were found out in any case of L-asparaginase application (P = 99 %) that was consider as a great advantage of the presented effective way of acrylamide reduction in food products[24].
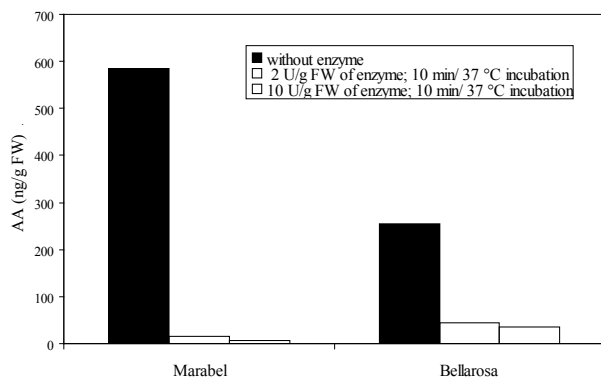
Fig. 3. **Amount of acrylamide (AA) in raw potatoes (varieties Marabel and Bellarosa) after enzymatic treatment (L-asparaginase produced by A. oryzae applied at concentration of 2 and 10 U g^{-1} FW and incubated at 37 °C for 10 min) and following heat treatment at 180 °C for 20 min**
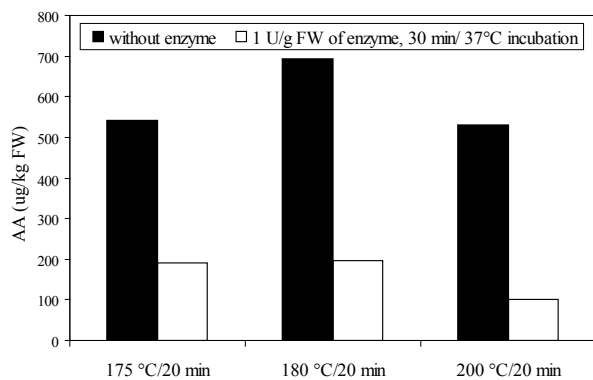
Fig. 4. **Amount of acrylamide (AA) in pancakes prepared from potato-wheat powder at different heating temperatures (175 °C, 180 °C and 200 °C) for 20 min with previous enzymatic treatment (L-asparaginase produced by A. oryzae applied at concentration of 1 U g^{-1} FW and incubated at 37 °C for 30 min)**

Conclusions

Since the acrylamide occurrence in foods and its potentiality to cause detrimental affects on human health attracts attention in all over the word, the effort to minimize its level in foods and consequently the human exposure to acrylamide is extremely advisable. Among many ways of acrylamide reduction the application of enzyme in order to prevent acry-

lamide formation is feasible and effective without any undesirable effect on sensory quality of final products. For that reason, this procedure is protected by the patent application filed with the Industrial Property Office of the Slovak Republic under the number 5027-2006.

REFERENCES

1. Tareke E., Rydberg P., Karlsson P., Eriksson S., Tornqvist M.: J. Agric. Food Chem. *50*, 4998 (2002).
2. JECFA 2005 64th meeting Rome, 8-17 February 2005: http://www.who.int/ipcs/food/jecfa/summaries/summary_report_64_final.pdf
3. IARC. Acrylamide. In IARC Monographs on the evaluation of carcinogen risk to humans: some industrial chemicals. International Agency for Research on Cancer, 60, p. 389, Lyon, France 1994.
4. Commission Recommendation of 3 May 2007 on the monitoring of acrylamide levels in food (notified under document number C(2007) 1873).
5. Hogervorst J. G., Schouten L. J., Konings E. J., Goldbohm R. A., Van Den Brandt P. A.: Cancer Epidemiol. Biomarkers Prevent. *16*, 2304 (2008).
6. Olesen P. T., Olsen A., Frandsen H., Frederiksen K., Overvad K., Tjonneland A.: Int. J. Canc. *122*, 2094 (2008).
7. FAO/WHO (2002): *Opinion of the Scientific Committee on Food on new findings regarding the presence of acrylamide in food*, Brussels, 3 July 2002.
8. Mottram D. S., Wedzicha B. L., Dodson A. T.: Nature *419*, 448 (2002).
9. Stadler R. H., Blank I., Varga N., Robert F., Hau J., Guy P. A., Robert M. C., Riediker S.: Nature *419*, 449 (2002).
10. Zyzak D. V., Sanders R .A., Stojanovic M., Tallmadge D. H., Eberhart B. L., Ewald D. K., Gruber D. C., Morsch T. R., Strothers M. A., Rizzi G. P., Villagran M. D.: J. Agric. Food Chem. *51*, 4782 (2003).
11. Yaylayan V. A., Wnorowski, A., Perez-Locas C.: J. Agric. Food Chem. *51*, 1753 (2003).
12. Biedermann M., Grob K.: Mitt. Geb. Lebensmitt. Hyg. *94*, 406 (2003).
13. Ciesarová Z., Kiss E., Kolek, E.: Czech J. Food Sci. *24*, 133 (2006).
14. CIAA Acrylamide Toolbox [on-line]. Brussels : Confederation of the Food and Drink Industries of the European Union, 11 December 2007.
15. Ciesarová Z.: Chem. Listy *99*, 483 (2005).
16. Kolek E., Šimon P., Šimko P.: J. Food Sci. *72*, E341 (2007).
17. Kolek E., Šimko P., Šimon P., Gatial, A.: J. Food Nutr. Res. *46*, 39 (2007).
19. Senyuva H. Z., Gökmen V.: Food Add. Contam. *22*, 214 (2005).

20. Ciesarová Z., Kiss E., Boegl P.: J. Food Nutr. Res. *45*, 141 (2006).

21. FDA 2006 Agency Response Letter GRAS Notice No. GRN 000201.

22. FDA 2007 Agency Response Letter GRAS Notice No. GRN 000214.

23. JECFA 2007 68th meeting Geneva, 19-28 June 2007: http://www.who.int/ipcs/food/jecfa/summaries/summary68.pdf

24. Ciesarová Z., Kukurová K.: Proc. ICC International Conference Bosphorus 2008, Istanbul 24-26 April 2008, p. 197.

L03 SOLID STATE FERMENTATION AS A TOOL FOR PREPARATION OF BIOPRODUCTS ENRICHED WITH POLYUNSATURATED FATTY ACIDS

MILAN ČERTÍK, ZUZANA ADAMECHOVÁ and LINDA NÉMETH

Department of Biochemical Technology, Faculty of Chemical and Food Technology, Slovak University of Technology, Radlinského 9, 812 37 Bratislava, Slovak Republic,
milan.certik@stuba.sk

Introduction

Increasing demand for high-value lipids has focused commercial attention on the provision of suitable biosynthetic framework for their production. One of the main target for microbial oil transformation is construction of healthy and dietary important polyunsaturated fatty acids, such as γ-linolenic acid (18 : 3 ω-6; GLA), dihomo-γ-linolenic acid (20 : 3 ω-6; DGLA), arachidonic acid (20 : 4 ω-6; AA), eicosapentaenoic acid (20 : 5 ω-3; EPA) and docosahexaenoic acid (22 : 6 ω-3; DHA). Their applications in biomedical, nutritional and pharmaceutical fields coupled with their inadequacy from conventional agricultural and animal sources has looked for developing suitable biotechnologies to produce these compounds[1].

Particularly active in the synthesis of PUFAs are species of fungi belonging to *Zygomycetes*[2]. Oleaginous fungi producing PUFA could be economically valuable because the most of their PUFAs occur in the triacylglycerol fraction of their lipids. Two basic processes have been developed for microbial production of PUFAs: submerged and solid state fermentations[3,4]. However, the principal difficulty that has been experienced with submerged PUFA-riched oil production has been in its marketing rather than in developing the large-scale fermentation and oil extraction process. Therefore, the association of oleaginous fungi with solid state fermentations (SSF) has been developed in order to improve commercial potential of microbial oils and thus to create new perspectives for the economic competitiveness and market of microbial polyunsaturated fatty acids (PUFAs). Solid state fermentation is a process in which microorganisms grow on a moist solid substrate in the absence of free water[5]. SSF simulates fermentation reactions occurring in the nature and allows microbial utilization of raw agro-materials or byproducts of the agro-food industries. Because some oleaginous fungi simultaneously decrease anti-nutrient compounds in the substrates (e.g. phytic acid) and partially hydrolyze substrate biopolymers, prefermented mass with a high content of PUFAs may be used as inexpensive food and feed supplement[6]. Thus, SSF might provide the other opportunity to fill marketing claims in food, feed, pharmaceutical, veterinary and environmental fields.

This paper deals with effectivity of several lower filamentous fungi to synthesize various PUFAs during their utilization of cereals by solid state fermentations.

Experimental

Microorganisms

Thamnidium elegans CCF 1456, *Cunninghamella echinulata* CCF-103, *Cunninghamella elegans* CCF-1318, *Mortierella isabelina* CCF-14, *Mortierella isabelina* CCF-1098, *Mortierella alpina* CCF 185 were obtained from the Culture Collection of Fungi (Charles University, Prague, Czech Republic). The culture was maintained on modified Czapek-Dox agar slants with yeast extract (2.5 g dm⁻³) at 4 °C.

Substrates and Cultivation Conditions

Depending on the microorganism, various types of substrates were employed during SSF experiments. Spent malt grains (SMG) were added to some substrates. Autoclavable microporous polypropylene bags (160 × 270 mm²) were filled with 10 g of dry substrate, moistened by the addition of 10 ml distilled water, soaked for 2 h at laboratory temperature and sterilized in autoclave (120 kPa, 120 °C, 20 min). In order to increased yield of PUFAs, sunflower or linseed oils were added to some substrates. In addition, various amounts of 10% acetone or ethanol solutions of selected plant extracts were tested with the aim to activate enzymes involved into PUFA biosynthesis. The substrates were inoculated and mixed with 2 ml of spore suspension (1–2 × 10⁶ spores per ml). Then each bag was closed with sterile cotton plugs, inoculated substrate was spread in the bags to obtain substrate layer of about 1 cm and incubated statically at 25 °C for 4–6 days (*T. elegans*, *C. echinulata*, *C. elegans*, *M. isabellina*) and 10–14 days (*M. alpina*). Triplicate SSF experiments for each substrate were prepared to assess reproducibility and average results are presented.

Lipid Extraction and Fatty Acid Analysis

Prefermented cereal materials (bioproducts) were gently dried at 65 °C for 10 h and weighed. Lipids from homogenized bioproducts were isolated with chloroform/methanol (2 : 1, v/v) and purified according to Čertík et al.[7] and total lipids were determined gravimetrically. Fatty acids of total lipids were analyzed as their methyl esters[8] by gas chromatography according to Čertík et al[9]. Gas chromatograph (GC-6890 N, Agilent Technologies) was equipped with a capillary column DB-23 (60 m × 0.25 mm, film thickness 0.25 μm, Agilent Technologies) and a FID detector (constant flow, hydrogen 35 ml min⁻¹, air 350 ml min⁻¹, 250 °C). Analyses were carried out under a temperature gradient (130 °C for 1 min; 130–170 °C at program rate 6.5 °C min⁻¹; 170–215°C at program rate 2.7°C min⁻¹; 215 °C for 7 min; 220–240 °C at program rate 2 °C min⁻¹; 240 °C for 2 min) with hydrogen as a carrier gas (flow 2.1 ml min⁻¹, velocity 49 cm s⁻¹, pressure 174 kPa) and a split ratio of 1/50 (inlets: heater 230 °C, total hydrogen flow 114 ml min⁻¹, pressure 174 kPa). The fatty acid methylester peaks were identified by authentic standards of C₄–C₂₄ fatty acid methylesters mixture (Supelco, USA) and quantified by an internal standard of heptadecanoic acid

(C17:0, Supelco, USA). Fatty acid concentration was evaluated with ChemStation software B0103 (Agilent technologies, USA).

Results and Discussion

The extensive research and development of PUFA production by SSF is basically aimed at improving the economic competitiveness of that microbial process compared to plant- and animal-derived oils. Emphasis is put on increasing the product value, using inexpensive substrates, screening for more efficient strains and reducing the processing steps. Therefore, it is necessary to optimize the potential of microorganisms for transformation of agroindustrial materials and oil residues into desired metabolites.

Screening of microorganisms has led to selection of *T. elegans*, *C. echinulata*, *C. elegans* and *Mortierella isabellina* as producers of GLA[6,9] and *Mortierella alpina* as a producer of DGLA, AA and EPA[10]. Generally, the surface of substrates was not only covered by the fungal mycelium during cultivation, but the fungal hyphae also penetrated into the substrates. Thus, fungal PUFAs were accumulated in the newly formed bioproduct and their amount depended on the substrates, microorganisms and cultivation conditions used.

Depending on the microorganism, various types of cereal substrates were employed during SSF experiments (Table I). Spent malt grains (SMG) served as an internal support. Substrates without SMG in most cases led to agglomeration of substrate particles and created more compact mass which in turn interfered with microbial respiration and affected substrate utilization negatively. Presence of SMG improved bioconversion of linoleic acid from substrates to GLA[9]. Substrates with internal support not only provided better respiration and aeration efficiency due to an increased inter-particle space but also helped to remove the heat generated during fermentation. It should be noticed that although PUFAs were synthesized more effectively by SMG addition to substrates, total PUFAs yield was also dependent on substrate/SMG ratio. Unbalanced substrate/SMG ratio might provide limited surface for microbial attack and thus poorer availability of assimilable compounds (including oils) from substrates.

Growth of fungi on a carbohydrates-containing substrates resulted after optimization of cultural conditions in constant lipid yield with the demanded fatty acid profile. Further improvement of PUFAs formation was achieved by physiological regulation of the SSF process employing following steps[10]: a) gradual elevation of carbon/nitrogen ratio with addition of appropriate carbon source; b) optimization of water activity, temperature and oxygen availability; c) transformation of exogenously added oils consisting of precursor of PUFAs. There is a stock of relatively cheap vegetable oils containing individual fatty acid precursors and SSF was applied for microbial utilization of renewable agricultural oils with the aim to modify their properties for production of value-added bioproducts with enhanced biological characteristics. Thus the ability of the strains to utilize exogenous fatty acids opens new possibilities to prepare PUFAs in high

yield. Moreover, because fungi possess active oil-biotransforming system, these strains were also tested for their ability to convert directly oil-rich substrates (corn, sunflower seeds, linseeds, rapeseeds) to PUFAs.

Table I
Production of γ-linolenic acid (GLA), dihomo-γ-linolenic acid (DGLA), arachidonic acid (AA) and eicosapentaenoic acid (EPA) by solid state fermentations of selected fungi utilizing various cereal substrates. Ratio of susbtrate/SMG was 1:3 (w/w)

Strain	Substrate	PUFA	Yield [g kg⁻¹ BP]
T. elegans	oat flakes/SMG	GLA	5.9
	wheat bran/SMG	GLA	5.0
	wheat bran/SMG/ sunflower oil	GLA	10.0
	crushed corn	GLA	10.0
	rye bran/SMG	GLA	4.2
	buckwheat/SMG	GLA	4.7
	millet/SMG	GLA	6.5
	amaranth/SMG	GLA	4.7
C. echinulata	barley	GLA	6.1
C. elegans	barley	GLA	7.0
M. isabellina	barley	GLA	18.0
M. alpina	rice	AA	21.4
	wheat sprout/SMG	AA	36.1
	wheat bran/SMG	AA	42.3
	rye bran/SMG	AA	21.9
	peeled barley	AA	16.2
	oat flakes	AA	31.2
M. aplina	cresed sesame seeds	DGLA	21.3
M. alpina	peeld barley/linseed oil/SMG	EPA/AA	23.4/36.3

Biosynthesis and profile of fatty acids is controlled by enzymes involved in lipogenesis, so activation or inhibition of these metabolic steps is also useful tool for improving carbon flux to individual PUFAs[11]. For example, bioconversion of DGLA to AA is catalyzed by ,Δ⁵' desaturase and inhibition of this enzyme by crushed sesame seeds was accompanied by rapid increase of DGLA/AA ratio[11]). In addition, application of various plant extracts possessing bioactive compounds seems to be promising way how to regulate fatty acid biosynthetic machinery in order to gain bioproduct with high yield of preferred PUFA. Application of ethanol extracts from ginger or sweet flag improved GLA yield by 30 % or 25 %, respectively. On the other hand, biosynthesis of GLA was reduced by 70 % when acetone extract from tansy was employed to the substrate.

Conclusions

Naturally prepared cereal based bioproducts enriched with PUFAs may be used as an inexpensive food and feed supplement. Thus, the association of selected microorganisms

with solid state fermentations has created new perspectives for the economic competitiveness and market of cereal based bioproducts containing PUFAs.

REFERENCES
1. Gill I., Valivety R.: Trends Biotechnol. *15*, 401 (1997).
2. Čertík M., Shimizu S.: J. Biosci. Bioeng. *87*, 1 (1999a).
3. Čertík M., Shimizu S.: Agro Food Industry Hi-Tech. *10*, 26 (1999b).
4. Čertík M., in: *Biocatalysis and Bioenergy* (Hou C.T., Shaw J.-F., ed),p 571-585, Wiley, New York 2008
5. Pandey A.: Biochem. Eng. J. *13*, 81 (2003).
6. Slugeň D., Streďanský M., Streďanská S., Čertík M., Grego J.: Czech Patent 279043 (1994).
7. Čertík M., Andráši P., Šajbidor J.: J. Am. Oil Chem. Soc. *73*, 357 (1996).
8. Christoperson S.W., Glass R.L.: J. Dairy Sci. *52*, 1289 (1969).
9. Čertík M., Sláviková L., Masrnová S., Šajbidor J.: Food Technol. Biotechnol. *44*, 75 (2006).
10. Sláviková L., Čertík M.: Chem. Listy, *99*, 234 (2005).
11. Čertík, M, Sakuradani, E, Shimizu S.: Trends Biotechnol. *16*, 500 (1998).

L05 PHYSIOLOGICAL REGULATION OF BIOTECHNOLOGICAL PRODUCTION OF CAROTENOID PIGMENTS

VLADIMÍRA HANUSOVÁ[a], MARTINA ČARNECKÁ[b], ANDREA HALIENOVÁ[b], MILAN ČERTÍK[a], EMÍLIA BREIEROVÁ[c] and IVANA MÁROVÁ[b]

[a]*Department of Biochemical Technology, Faculty of Chemical and Food Technology, Slovak University of Technology, Radlinského 9, 812 37 Bratislava, Slovak Republic;*
[b]*Faculty of Chemistry, Brno University of Technology, Purkyňova 118, 612 00 Brno, Czech Republic;*
[c]*Institute of Chemistry, Slovak Academy of Sciences, Dúbravská cesta 9, 845 38 Bratislava, Slovak Republic,*
milan.certik@stuba.sk

Introduction

Carotenoids represent one of the broadest group of natural antioxidants (over 600 characterized structurally) with significant biological effects and numerous of industrial applications. Because the application of synthetically prepared carotenoids as food additives has been strictly regulated in recent years, huge commercial demand for natural carotenoids has focused attention on developing of suitable biotechnological techniques for their production.

There are many microorganisms including bacteria, algae, yeast and fungi, that are able to accumulate several types of pigments; but only a few of them have been exploited commercially[1]. From the view of yeasts, a range of species such as *Rhodotorula*, *Rhodosporidium*, *Sporidiobolus*, *Sporobolomyces*, *Cystofilobasidium*, *Kockovaella* and *Phaffia* have been screened for carotenoids formation. Yeast strains of *Rhodotorula* and *Sporobolomyces* formed β-carotene as the main pigment together with torulene and torularhodine as minor carotenoids. In contrast, *Phaffia* strains accumulated astaxanthin as a principal carotenoid. Comparative success in yeast pigment production has led to a flourishing interest in the development of fermentation processes in commercial production levels. However, in order to improve the yield of carotenoid pigments and subsequently decrease the cost of this biotechnological process, optimizing the culture conditions including both nutritional and physical factors have been performed. Factors such as carbon and nitrogen sources, minerals, vitamins, pH, aeration, temperature, light and stress showed a major influence on cell growth and yield of carotenoids.

This paper summarizes our experience with physiological regulation and scale-up of biotechnological production of carotenoid pigments by yeasts.

Experimental

Microorganisms and Cultivation Conditions

All strains investigated in this study (*Sporobolomyces roseus* CCY 19-6-4, *S. salmonicolor* CCY 19-4-10, *Rhodotorula glutinis* CCY 20-2-26, *R. glutinis* CCY 20-2-31, *R. glutinis* CCY 20-2-33, *R. rubra* CCY 20-7-28, *R. aurantiaca* CCY 20-9-7 and *Phaffia rhodozyma* CCY 77-1-1) were obtained from the Culture Collection of Yeasts (CCY; Institute of Chemistry, Slovak Academy of Sciences, Bratislava) and maintained on malt slant agar at 4 °C.

The basic cultivation medium for flasks experiments for *Rhodotorula* and *Sporobolomyces* strains consisted of (g dm^{-3}): glucose – 20; yeast extract – 4.0; $(NH_4)_2SO_4$ – 10; KH_2PO_4 – 1; $K_2HPO_4 \cdot 3H_2O$ – 0.2; NaCl – 0.1; $CaCl_2$ – 0.1; $MgSO_4 \cdot 7H_2O$ – 0.5 and 1 ml solution of microelements [(mg dm^{-3}): H_3BO_4 – 1.25; $CuSO_4 \cdot 5H_2O$ – 0.1; KI – 0.25; $MnSO_4 \cdot 5H_2O$ – 1; $FeCl_3 \cdot 6H_2O$ – 0.5; $(NH_4)_2Mo_7O_{24} \cdot 4H_2O$ – 0.5 and $ZnSO_4 \cdot 7H_2O$ – 1]. The basic cultivation medium for flasks experiments for *Phaffia* strain consisted of (g dm^{-3}): glucose – 20, yeast autolysate – 2.0, KH_2PO_4 – 0.4, $(NH_4)_2SO_4$ – 2.0, $MgSO_4 \cdot 7H_2O$ – 0.5, $CaCl_2$ – 0.1, NaCl – 1.0. All strains grew under a non-lethal and maximally tolerated concentration of Ni^{2+}, Zn^{2+}, Cd^{2+} and Se^{2+} ions. Also, stress conditions were induced by addition of various conventrations of NaCl and H_2O_2. The cultures were cultivated in 500 ml flasks containing 250 ml cultivation medium on a rotary shaker (150 rpm) at 28 °C to early stationary grow phase. All cultivation experiments were carried out at triplicates and analyzed individually.

Flasks results were verified in bioreactors and these scale-up experiments were carried out in 2 L fermentor (B. Braun Biotech), 20 L (SLF-20) and 100 L (Bio-la-fite) fermentors with an agitation rate of 250–450 rpm and a temperature of 20–22 °C. The pH was controlled at pH 5.0 by the addition of NH_4OH and the dissolved oxygen concentration was maintained by supplying sterile air at a flow rate equivalent to 0.3–0.7 vvm.

Pigment Isolation and Analysis

Pigments from homogenized bioproducts were isolated by organic extraction and analyzed by high-performance liquid chromatography (HPLC). Analysis was carried out with an HP 1100 chromatograph (Agilent) equipped with a UV-VIS detector. Pigments extracts (10 µl) were injected onto LiChrospher® 100 RP-18 (5 µm) column (Merck). The solvent system (the flow rate was 1 ml min^{-1}) consisted of solvent A, acetonitrile/water/formic acid 86 : 10 : 4 (v/v/v), and B, ethyl acetate/formic acid 96 : 4 (v/v), with a gradient of 100 % A at 0 min, 100 % B at 20 min, and 100 % A at 30 min.

Gel Electrophophoresis

1D PAGE-SDS electrophoresis of proteins was carried out by common procedure using 10% and 12.5% polyacrylamide gels. Proteins were staining by Coomassie Blue and by silver staining. For comparison, microfluidic technique using 1D Experion system (BioRad) and P260 chips was used for yeast protein analysis too. 2D electrophoresis of proteins was optimized in cooperation with Laboratory of Functional Genomics and Proteomics, Faculty of Science, Masaryk University of Brno. 2D gels were obtained from protein pre-

paratives isolated from lyophilized cells. After optimization of separation conditions proteomes from stressed *R.glutinis* and *R.rubra* cells were isolated, lyophilized and analyzed. Quantitative analysis was done using BioRad Laboratories 2D software. Identification of some spots was done using LC-MS/MS.

Results and Disscussion

To find suitable conditions for carotenoids production, several pigment forming yeasts have been tested for their ability to modify carotenoid biosynthesis based on media composition. Kinetic analysis revealed that yeasts strains differed from the view of growth rates and pigments formation. It must be emphasized that overall yield of carotenoids is directly related to the total biomass yield, thus, to keep both high growth rates and high flow carbon efficiency to carotenoids by optimal cultivation conditions is essential in order to achieve the maximal pigment productivity.

Carotenoid accumulation in cells was significantly activated when yeasts were treated by selected stress conditions and their combinations (heavy metals, hydrogen peroxide and salt). However, such stimulation of pigment biosynthesis was more effective if stress factors were employed to the medium in exponential growth phase than from the beginning of cultivation[2–4]. It may be explained by hypothesizing a possible activation or inhibition mechanism by metal ions on specific carotenogenic enzymes, in particular, on specific enzymes involved in carotenoid biosynthesis, in agreement with previous studies reporting activation or inhibition by metal ions in microbial enzymes. The other explanation is based on observations that presence of heavy metals results in formation of various active oxygen radicals what, in a turn, induces generation of protective carotenoid metabolites that reduce negative behaviour of free radicals[5].

During environmental stress response many red yeasts exhibit cross-protective mechanisms. Preincubation of yeast culture with low concentration of one stress factor in inoculum media (e.g. salt, hydrogen peroxide) induces adaptation pathways resulted in enhanced carotenoid production[6]. Further addition of higher concentration of either the same or other stress factor can lead to significant (5–10 times) increase of β-carotene production in *Rhodotorula glutinis* and *Sporobolomyces salmonicolor*[2]. Simple preincubation of *R. glutinis* in presence of 2% NaCl in inoculation medium followed by fermentation in inorganic production medium led to increased formation of biomass with accumulated carotenoids. This combined environmental stress using mild stress effect of salt or hydrogen peroxide could be industrially used for production of carotene enriched biomass. The results from flasks experiments are summarized in Table I.

Laboratory flasks experiments were verified in semi-scale conditions (from 2 dm^3 to 100 dm^3 fermentors). It was confirmend that glucose utilization was followed by increased pigment biosynthesis. Therefore, fed-batch fermentations were applied to enhanced carotenoid production. In addition, combination of aimed environmental condition resulted in activated accumulation of selected carotenoids (Table I).

Enhancement of carotenoid production by environmental stress is also associated with changes in expression levels of various genes. Therefore, molecular changes in yeast cells on genome, proteome and metabolome level were studied using PFGE, 2D-GE, LC/MS/MS and EPR techniques. Presence of stress factors was accompanied by changes in carotenoid production as well as by alternations in protein levels. However, further analyses have to be focused on more precise characterization of proteins those displayed significant changes under increased biosynthesis of carotenoids.

REFERENCES

1. Bhosale P.: Appl. Microbiol. Biotechnol. *73*, 351 (2004).
2. Márová I., Breierová E., Kočí R., Friedl Z., Slovák B., Pokorná J.: Annals of Microbiology *54*, 73 (2004).
3. Breierová E., Márová I., Čertík M.: Chem. Listy *99*, 109 (2005).
4. Čertík M., Masrnová S., Sitkey V., Minárik M., Breierová E.: Chem. Listy *99*, 237 (2005).
5. Rapta P., Polovka M., Zalibera M., Breierová E., Žitňanová I., Márová I., Čertík M.: Biophys. Chem. *116*, 1 (2005).
6. Kočí R., Drábková M., Márová I.: Chem. Listy *99*, 297 (2005).

Table I
Production of carotenoids in flask and fermentation experiments

Strain	Pigment	Pigment yields
Flasks experiments		
S. roseus	β-carotene	30 mg dm^{-3} (by $Zn^{2+} + H_2O_2$)
R. glutinis	torulene	6 mg dm^{-3} (by $Zn^{2+} + H_2O_2$)
R. glutinis	torularhodin	1 mg dm^{-3} (by Cu^{2+})
P. rhodozyma	astaxanthin	20 mg dm^{-3} (by Se^{2+})
Scale-up fermentations		
S. salmonicolor.	total carotene	41 mg dm^{-3} (by $NaCl + H_2O_2$)
R. glutinis	β-carotene	35 mg dm^{-3} (by $NaCl + H_2O_2$)
P. rhodozyma	astaxanthin	110 mg dm^{-3} (by $NaCl + NaCl$)

L06 ENZYMATIC SACCHARIDE ACETYLATIONS IN WATER – COMPARATION OF CATALYSTS

VLADIMÍR MASTIHUBA[a], TATIANA KRAKOVÁ[b] and MÁRIA MASTIHUBOVÁ[a]

[a]*Institute of Chemistry, Center for Glycomics, Slovak Academy of Sciences, Dúbravská cesta 9, 845 38 Bratislava, Slovak Republic,*
[b]*Institute of Molecular Biology, Slovak Academy of Sciences, Dúbravská cesta 21, 845 51 Bratislava, Slovak Republic,*
chemvrma@savba.sk

Introduction

Enzymatic esterification of various hydroxy compounds is studied for about 40 years. Such reactions are usually performed in reaction systems comprising controlled amount of water to prevent product hydrolysis. Followingly, enzymatic esterification of unprotected saccharides is hampered by their decreased solubility in low water environment.

We had recently described acetyl esterase from *Trichoderma reesei* to catalyze acetylations of several carbohydrates and alcohols in bulk water phase[1]. Acetyl esterases may be found in several raw commercial preparations of enzymes dedicated for biomass degradation since acetylation occurs widely on natural polysaccharides and plant cell wall fragments[2]. Acetyl hydrolyzing activity occurs quite frequently in lipases (which may be result either of wider acyl specifity or of protein impurity) and some reports describe also esterase activity of serum albumins[3].

Our present work explores performance of several enzymes/crude enzyme preparations and proteins (Celluclast 1.5 L FG, Ultraflo L, lipases from *Candida antarctica, Candida rugosa, Aspergillus niger* and *Thermomyces lanuginosus*, bovine serum albumin) in acetylations of glucose (**1a**) and methyl α-D-glucopyranoside (**1b**), comparing product yields and position selectivity of the reaction.

Experimental

Assays of acetyl esterase activity in enzyme preparations were performed as previously described[1]. Synthetic reactions were routinely performed by dissolving 1.2 g of glucose or *alpha* methyl glucoside in 10 ml mixture of water and acetyl donor (vinyl acetate or isopropenyl acetate, 4 : 1) and the reaction was started by adding 1 ml or 300 mg of the enzyme. Reaction mixture was then stirred at 37 °C for 1–3 days and the course of the reaction was followed by t.l.c. on silica gel plates (chloroform – methanol, 3 : 1, visualisation by pouring into 5% sulphuric acid in ethanol and drying in hot air). Reaction mixture was then concentrated *in vacuo*, products separated by chromatography on silicagel column (chloroform – methanol, 3 : 1) and identified by NMR. For every reaction, a parallel experiment was executed without addition of enzyme to check occurence of a spontaneous acetylation. The spontaneous reactions were tested also separately in 0.1M acetate and phosphate buffers.

Results

Table I presents level of acetyl hydrolysing activities in enzyme preparations. Although water insoluble Lipolase 100 was not active in photometric assay, it catalyzed acetylations of aliphatic alcohols in stirred low water reactions (data not shown).

Table I
Acetyl hydrolysing activity of enzyme preparations

enzyme (souce)	activity [U ml^{-1}]	activity [U g^{-1}]
Celluclast 1.5 L FG (*Trichoderma reesei*)	18.4	
Ultraflo L (*Humicola insolens*)	31.5	
Novozym 735 (*Candida antarctica*)	55.6	
BSA (*Bos taurus*)		4.0
Amano Lipase A (*Aspergillus niger*)		219.1
Lipase AYS (*Candida rugosa*)		621.1
Lipolyve CC (*Candida rugosa*)		319.0
Lipolase 100T (*Thermomyces lanuginosus*)		not estimated

Since phosphate buffer catalyzes acetylation of saccharides by vinyl acetate[4], we tried to assess the extent of this process in our reactions (Table II).

Table II
Sponatneous acetylation of glucose by vinyl acetate (VA) and isopropenyl acetate (IPA) in buffered solutions and water

pH	Acetyl donor	Monoacetates	Diacetates
4.01	VA	+	−
4.51	VA	++	−
5.02	VA	++	+/−
5.51	VA	+++	+
5.72	VA	+++	+
6.03	VA	+++	+
Water	VA	−	−
Water	IPA	−	−
5.72	IPA	+/−	−

Increasing pH of the buffer resulted in increased creation of glucose monoacetates and eventually diacetates when vinyl acetate was used as acetyl donor. To avoid such unselective acetylations, all enzymatic reactions were executed using water instead of the buffer.

Scheme 1 summarizes in general the scale of products identified in reaction mixtures.
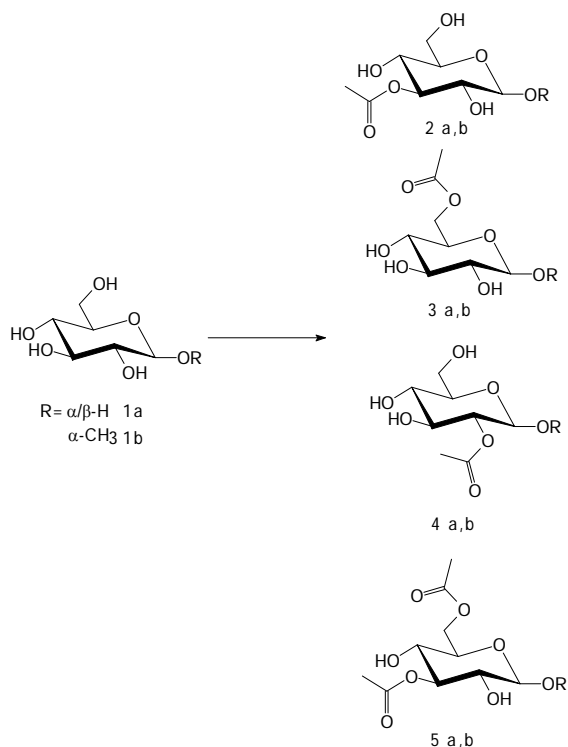
Scheme 1
Summarization of products created by enzymatic acetylations of glucose and methyl α-D-glucopyranoside with vinyl acetate or isoprenyl acetate

Yeast lipases gave low yields of pure **3 a,b**, thus showing high specifity for acetylation of primary hydroxyl (Tables 3,4). However, Lipolyve CC was reactive only with the glucoside **1 b** and did not acetylate free glucose within 3 days.

On the other side, Amano Lipase A (*Aspergillus niger*) as a representative of fungal lipases gave 10% yield of an equimolar mixture of **2 a**, and **3 a**. Interestingly, acetylation

Table III
Enzymatic acetylations of glucose by vinyl acetate (VA) and isopropenyl acetate (IPA) in water

enzyme	acetyl donor	mono-acetates [%]	diacetates [%]	reaction time [days]
Celluclast	VA	19.7 **2 a : 3 a** 12 : 1	0	1
Lipolyve CC	IPA	0	0	3
Novozym 735	VA	2.0 **3 a**	9.6 not determined	3
Amano Lipase A	IPA	10.0 **2 a : 3 a** 1 : 1	4.2 **5 a**	2

did continue to create only one diacetate (3,6-di-O-acetyl glucose, **5 a**), thus keeping the original specifity for positions 3-O- and 6-O- (Table III). Acetylations of methyl α-D-glucopyranoside (**1 b**) with isopropenyl acetate proceeded with the same positional specifity to produce **2 b** and **3 b**. When isopropenyl acetate was replaced by vinyl acetate as acetyl donor, selectivity increased markedly in favor of **2 b** (Table IV). No reaction was observed when another fungal lipase – Lipolase 100T – was used as biocatalyst.

Acetylations of **1 b** catalyzed by bovine serum albumin and Ultraflo L (an enzyme cocktail from *Humicola insolens*) were unselective, giving mixtures of three monoacetates (Table IV).

The best results were achieved by use of Celluclast, a cellulase preparation from *Trichoderma reesei* RUT C-30 comprising the same acetyl esterase as reported earlier[1]. Acetylations gave 19.7 % and 10 % of monoacetylated glucose and methyl glucoside, respectively (Tables III, IV). The selectivity was exclusively to position 3-O- in acetylation of **1 b** while in acetylation of glucose, almost 8% of 6-O- acetate **3 a** was found in the monoacetate fraction.

Table IV
Enzymatic acetylations of methyl glucoside by vinyl acetate (VA) and isopropenyl acetate (IPA) in water

enzyme	acetyl donor	mono-acetates [%]	diacetates [%]	reaction time [days]
Celluclast	IPA	10.0 **2 b**	0	1
Lipolyve CC	IPA	2.2 **3 b**	0	0.9
Lipase AYS	IPA	1.9 **3 b**	0	0.16
Amano Lipase A	IPA	10.5 **2 b : 3 b** 2,5 : 1	1.7 **5 b**	1
Amano Lipase A	VA	6.4 **2 b : 3 b** 13 : 1	0.7 **5 b**	1
BSA	VA	2.1 **3 b : 4 b : 2 b** 2.0 : 1.3 : 1.0	0	5
Ultraflo L	IPA	3.9 **3 b : 4 b : 2 b** 4.5 : 2.5 : 1.0	0	1

Conclusions

Our results proved Celluclast to be the best catalyst for acetylations of glucose and methyl α-D-glucopyranoside according to its selectivity, product yields, availability and price. Since Celluclast has significantly lower acetyl esterase activity comparing to the other enzymes tested in this study, the enzyme seems rather unique. The enzyme selectivity to position 3-O- gives a promiss of its use in two step enzymatic

esterifications of saccharides, in which acetylation provides organic solvent-soluble sugar derivatives possessing free primary hydroxyls.

REFERENCES

1. Kremnický Ľ., Mastihuba V., Côté G. L.: J. Mol. Catal. B: Enzymatic *30*, 229 (2004).
2. de Vries R. P., Visser J.: Microbiol. Mol. Biol. Rev. *65*, 497 (2001).
3. Sedlacek M., Manoharan I., Boopathy R., Duysen E. G., Masson P., Lockridge O.: Biochem. Pharmacol. *70*, 1673 (2005).
4. Shi C., Zhang J. B., Fu H., Tang J.: Lett. Org. Chem. *3*, 932 (2006).

L07   PREPARATION OF BIODIESEL FROM TALL OIL

RADOSLAV MIKULÁŠIK[a], IGOR ŠURINA[a],
SVETOZÁR KATUŠČÁK[a], JÁN CVENGROŠ[b] and
MARTIN POLOVKA[c]

*Department of Chemical Technology of Wood, Pulp and
Paper, [a]Institute of Polymer Materials,
[b]Institute of Physical Chemistry and Chemical Physics, Faculty of Chemical and Food Technology, Slovak University of
Technology,Radlinského 9, 812 37, Bratislava, Slovakia,
[c]Food Research Institute, Department of Chemistry and Food
Analysis, Priemyselná 4, 824 75, Bratislava, Slovakia,
radoslav.mikulasik@stuba.sk*

Introduction

It has known that after delignification kraft pulping process almost all extractable dissolved or emulsified substances of wood pass into black liquor. Evaporation of water from black liquor causes an increase in sodium salts content. Soaps are settled on all places, where liquor remains motionless. Tall soaps flowing on surface are separated in the form of foam in all tanks and their amount increases with density of black liquor[1–3]. Tall soap may be incinerated together with higher-density black liquor within chemicals recovery or separated and utilised to high value chemicals. The latter alternative is more cost effective[4]. Kraft tall soap (TS) may be converted by acidification to tall oil (TO) and individual components isolated from it by vacuum distilation.

TO is a dark brown, viscous and odorous liquid[5] containing mainly higher fatty acids (HFA), resin acids (RA), sterols and many other extractable substances[6].

Very interesting is HFA content ranging from 26 to 58 % wt.[7] and depending mainly on the sort of wood. Given the high amount of wood, which is delignificated in paper mill in Central-european region, it represents a cheap raw material for biodiesel production. Biodiesel is exclusively produced from expensive vegetable oil.

This work is focused on biodiesel production from tall oil and testing of selected biodiesel properties and their comparison with EN 14214[8]. A method based on esterification straight by methanol and subsequent vacuum distillation of methylesters HFA from mixture was chosen. The method seems to be more advantageous than that based on esterification of HFA fraction obtained preferentially by vacuum distillation of TO. Namely, boiling point of HFA methylesters is lower than that of HFA.

Our method is more efficient from the viewpoint of energy demands when compared with the method realised, e.g., by AltÂparmak D., Keskin A., Koca A., Gürü M., [9].

Experimental

Materials

Chemicals: sulphuric acid, 96 % wt., Microchem, SR,
Tall oil was prepared from aqueous solution of tall soap supplied by MONDI Packaging Paper Štětí, ČR.

Instruments, Facilities, Methods

Gas chromatography and mass spectrometry (GC/MS). Analysis of tall oil composition was performed by GC/MS with a Hewlett – Packard 5890A/5790B equipment.

GC conditions: column: PTE–5, 30 m, 0.25 mm ID, 0.25 μm film, carrier gas: helium, flow-rate 1 ml min^{-1}, pressure 50 kPa , purge off: 0 min (split), injection temperature: 275 °C, temperature of detector: 280 °C, temperature program: 170 °C (3 min), 5 °C min^{-1} – 270 °C (9 min), 15 °C min^{-1} – 300 °C (3 min)

MS conditions: mass range: 43–550 amu, EMV: 2400 V, threshold setting: 1000, SD: 3 min

IR spectroscopy. Infrared spectra of all specimens were obtained by Digilab Excalibur FTS 3000MX – FTIR method. Samples were measured by diffusion scatter method (DRIFT) in KBr powder (5 % wt.).

Vacuum (molecular) distillation. A laboratory molecular vacuum evaporator MO15[10] was used to isolate methylesters HFA and also to purify this product.

Other laboratory equipment: furnace, balance, centrifuge, vacuum rotary evaporator.

TO preparation from TS was carried out at following conditions:

Table I
Conditions of tall oil preparation from tall soap

Mass TS	~ 1,000 g
Heating time TS 25 → 95 °C	~ 15 min.
H_2SO_4 concentration	43.6 wt. %
Volume of added H_2SO_4 solution	1.5 dm^3
Reaction time	200 min. (3.3 h)
Agitation	intensive (3.3 h)

TO was consequently esterified at conditions:

Table II
Conditions of tall oil esterification by CH_3OH

Conc. sulphuric acid [H_2SO_4, 96 % wt.] of the mass of HFA in TO	5 % wt.
Temperature of reaction mixture	60 °C
Molar ratio of CH_3OH to HFA in TO	6 : 1
Reaction time	5.5 h
Intensive agitation of reaction mixture	5.5 h

Table III
Properties of tall soap and tall oil

Dry matter [% wt.]	65.56
Ash [% wt.]	11.36
TO in TS [% wt.]	84.00
Acid number of prepared TO [mg KOH g^{-1} TO]	154.70

Results and Discussion

Preparation of TO

TO was prepared by TS acidification by sulphuric acid at conditions given in Table I. Sulphuric acid was added in excess. Reaction mixture undergoes vigorous agitation during the process.

At the beginning, about 1,000 g TS (one batch) was heated in a 4,000 ml beaker in water bath. Temperature of water bath was kept in the range of 90–95 °C by adjustable cooker. After heating of TS at the water bath temperature, sulphuric acid was added and a blender activated. The blender ensured intensive agitation during the whole process. At TO preparation, the following reaction proceeded:

$$R—COONa + H_3O^+ \rightarrow R—COOH + H_2O + Na^+$$
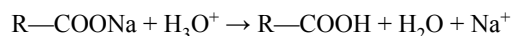
Scheme 1
Conversion of saponified HFA to acid form

Volume of obtained tall oil after separation of aqueous and a lignin phase from one batch was 482 ml or 465 g, and the yield in % wt. was 70.9.

Having concluded the process, phase separation was performed. TO was separated from aqueous and lignin phases by separatory. Subsequently, warm water was used to wash TO, until pH of waste water reached ~ 6–7 due to necessity to eliminate H_2SO_4 residues from esterified oil. Finally, TO was dehydrated in a vacuum rotary evaporator.

Preparation of tall oil was performed using two apparatus simultaneously. For totally 3.3 h, 2×482 ml of oil after separation of aqueous and lignin phase was obtained. This process was repeated 6 times and a total amount of prepared oil was ~ 5,784 ml (5,580 g). A total amount of TS used in the process was ~ 7,867 g (besides moisture).

Average batch yield reached 70.93 % wt. Theoretical yield was 84.0 % wt., i.e. weight loss was 13.07 % wt. This amount included the matter remaining on the beaker and funnels walls owing to a decrease in temperature and increase in viscosity of tall oil. The inner surface of 4,000 ml beaker and 2,000 ml separatory funnel was significant.

Moreover, not all saponified HFA and RA were converted to their acid form by the reaction shown in Scheme 1.

GC/MS Analysis of TO

The prepared TO contained 30 % wt. HFA, 20 % wt. RA, ~ 18.5 % sterols. Non-analysed portion represented ~ 44.2 % wt. and contained higher fatty alcohols, hydrocarbons, lignin and cellulose fragments, non-methylated fatty and resin acids and inorganic compounds. These substances cannot be classified into the above three groups. In addition, these substances could be modified by the preparation process or its conditions.

Table IV
GC/MS analysis – composition of tall oil

Extractives	[% wt.]
Fatty acids	29.8
Resin acids	20.0
Sterols	6.0
Analysed portion	55.8
Non-analysed portion	44.2
Total	100.0

Esterification of Tall Oil
– Preparation of Tall Oil
Methylesters (TOME)

The prepared TO, after washing by water and dehydratation were subjected to esterification at optimal conditions based on Neaves D.E.[11].
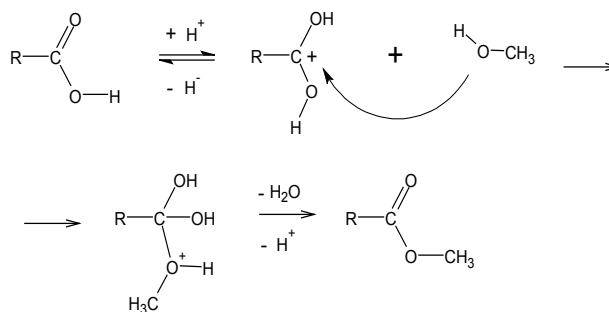
Scheme 2
Mechanism of HFA esterification with methanol in acid media

Mechanism of acid catalysed esterification by methanol is proposed in Scheme 2. Conditions of esterification are summarized in Table II.

1,000 g TO with HFA content ~ 30 % wt. i.e. ~ 300 g was processed. As catalyst, suphuric acid ~ 15 g (8.2 ml at density 1.835 g cm^{-3}) was used. The total amount of methanol added to the reactor was ~ 204.8 ml (methanol was added in excess to HFA, in molar ratio 6 : 1)

Average molar mass of fatty acids was estimated as 281.55 g mol^{-1}. Stemming from the fact that optimal conditions (time 2–3 h) given by literature concern only the fraction HFA isolated from TO and not the fraction included in TO, reaction time was prolonged to 5.5 h to ensure maximum conversion.

The process was repeated 3 times and total volume of prepared TOME approached 3,000 ml (2,835 g).

Vacuum Distillation of TOME

Data on amounts of obtained distillates (D1, D2), residues (Z1, Z2) and weight losses (WL) from 1st and 2nd distillation stage are listed in Table V and VI.

Table V
Vacuum Distillation material balance: 1st stage

TOME	D1		Z1		WL
[g]	[g]	[wt. %]	[g]	[wt. %]	[wt. %]
2362	845	35.8	1419	60.0	4.2

Table VI
Vacuum distillation material balance: 2nd stage

TOME	D2		Z2		WL
[g]	[g]	[wt. %]	[g]	[wt. %]	[wt. %]
845.3	712	84.2	101.4	12.0	3.8

The prepared amount of TOME was heated and then let settle. Formed water and unreacted methanol were removed with a vacuum (molecular) evaporator.

Then 2.5 dm^3 TOME was withdrawn from 3 dm^3 volume of TOME and distilled at the folowing conditions: pressure 10–50 Pa and temperature 135–140 °C. 955 ml (~ 845 g) of distillate (D1) was obtained which represented ~ 38 % vol. (~ 36 % wt.). During this distillation D1 was polluted by RA.

Destillate D1 955 ml (~ 845 g) was consequently distillated at pressure 2–20 Pa and temperature 130–135 °C. Under these conditions, we obtained 835 ml (711.8 g) of distillate D2, i.e. ~ 87 % vol. from D1, (84 % wt.)

The total yield of these processes: from 2,500 ml TOME (2,363 g) we obtained 835 ml (711.8 g) which represented 33.4 % vol. (30.1 % wt.).

Acid number parameter of D2 (19.610 mg KOH g^{-1}) did not comply with European standard EN 14214 for biodiesel (stipulating less than 0.5 mg KOH g^{-1}), D2 had to undergo further treatment. D2 included some RA. They were neutralised and precipitated and D2 (tall oil fatty acids methyl esthers – TOFAME) after this treatment had acid number 0.3 mg KOH g^{-1}. This value fully meets EN 14214. However, total volume of the final product decreased from 835 to 630 ml (566.6 g) which represented – when comparing to the TOME amount – 25.2 % vol., (~ 24 % wt.).

The final product prepared in such a mode was subjected to analyses in laboratory of VÚRUP, which was accredited for analyses of biofuels. Results are assembled in Table VII.

Results Obtained by Fourier Transform Infrared Spectrometry (FTIR)

FTIR spectra of our product and a sample of soybean oil methylesters (SOME) were scanned and were found to comply with EN 14214. We observed very good similarity in absorption peaks of our product and SOME sample. Both spectra are almost identical. This may mean that both speci-
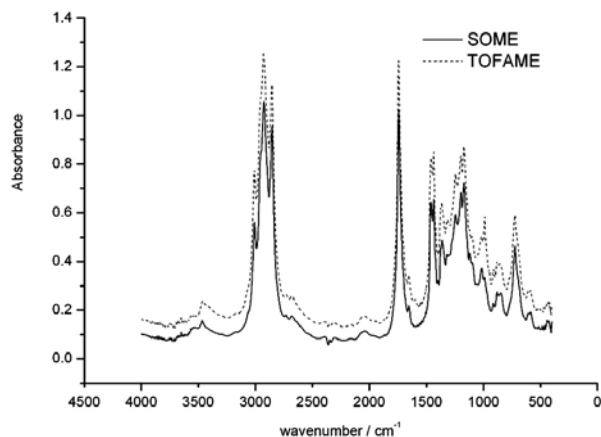
Fig. 1.　**Comparison of FTIR spectra: TOFAME and SOME**

mens have similar physical and chemical properties.
Test Results for Biodiesel from

Table VII
Values of prepared biodiesel compared with EN14214 standard values

Properties	Units	Determined value	EN 14214 value	Uncertainty
Density at 15 °C	kg m^{-3}	**899.3**	875–900	0.1 %
Carbon residue (10% distillation residue)	wt. %	**<0.010**	max. 0.3	10 %
Kinematic viscosity at 40 °C	mm^2 s^{-1}	**3.932**	3.5–5	1.5 %
Cold filter plugging point	°C	**–12**	0 to –13 –13 to –20 (winter)	3 °C
Ester content	wt. %	**95.7**	min. 96.5	2.5
Linolenic acid methyl ester	wt. %	**0.7**	max. 12	–
Sulphur content	mg kg^{-1}	**1208**	max. 10	2 %

Accredited Laboratory
Conclusions

Prepared tall oil was esterified by methanol at optimal conditions in the presence of acid catalyst. Tall oil fatty acids methyl esters were isolated from TOME mixture by vacuum distillation.

Total yield of these processes: from 2,500 ml TOME (2,363 g), 630 ml (566.6 g) resulted which represents

25.2 % vol. (~ 24 % wt.). Biodiesel prepared in this procedure complies with EN 14214 except of chemicaly bonded sulphur.

REFERENCES
1. Košík M. , Blažej A.: *PHYTOMASS: A Raw Materials for Chemistry and Biotechnology*, Veda-Ellis Horwood Ltd., Chichester, Great Britain, 1993.
2. Lužáková V., Vrška M.: Cellul. Chem. Technol. *39*, 237 (2005).
3. Lužáková V., Marcincinová T., Vrška M.: Chemické listy *94*, 880 (2000).
4. Šutý L.: *Výroba a vlastnosti buničín*, p.147, ALFA, Bratislava, 1982.
5. Lee S.Y., Hube M. A., Saka Sh.: BioResources *1*, 150 (2006).
6. Bokis C. P., Chen Ch. Ch., Orbey H.: Fluid Phase Equilibria *155*, 193 (1999).
7. Košík M., Blažej A.: *Fytomasa ako chemická surovina*, p. 340, VEDA, Bratislava, 1985.
8. EN 14214, EUROPEAN STANDARD – Automotive fuels – Fatty acid methyl esters (FAME) for diesel engines – Requirements and test methods, http://www.acbiodiesel.net/docs/FAME%20Euro %20standard%20draft%20Oct02.pdf http://www.biopalivo.sk/EN%2014214.pdf
9. AltÂparmak D., Keskin A., Koca A., Gürü M.: Bioresour. Technol. *98*, 241 (2007).
10. Cvengroš J.: Chem. Prům. *40,* 135 (1990).
11. Neaves D. E.: *Evaluation of fatty acid fraction derived from tall oil as a feedstock for biodiesel production,* Master thesis, Faculty of Mississippi State University, School of Chemical Engineering, May 2007.

L08 ARTIFICIAL NEURAL NETWORKS IN FOOD ANALYSIS

JÁN MOCÁK[a,b], VIERA MRÁZOVÁ[a], DÁŠA KRUŽLICOVÁ[b] and FILIP KRAIC[a]

aDepartment of Chemistry, University of Ss. Cyril & Methodius, Nám. J. Herdu 2, 917 01 Trnava, Slovakia,
bInstitute of Analytical Chemistry, Slovak University of Technology, Radlinskeho 9, 812 37 Bratislava, Slovakia, jan. mocak@ucm.sk

Introduction

During the last twenty years the chemists have get accustomed to the use of computers and consequently to the exploitation of various complex mathematical and statistical methods, by which they have been trying to explore multivariate correlations between the output and input variables more and more in detail. Input variables of different kind are often continuous and represent usually the results of instrumental measurements but also other observations, sometime discrete or categorical, are important for characterizing the investigated objects. Such kinds of input variables are for example the results of sensorial assessment of foodstuffs or simply some qualitative attributes like odour or colour (agreeable/disagreeable or clear/yellowish/yellow). The output variables are the targets of the corresponding study, which again can be represented by some continous variable or a categorical one with two or more levels. With the increasing complexity of analytical measurements, and the analysed sample itself, it becomes clear that all effects that are of interest cannot be described by a simple univariate relation but they are multivariate and often they are not linear. A set of methods, which allow study of multivariate and non-linear correlations that have recently found very intensive use among chemists are the artificial neural networks (ANNs for short)[1].

The ANNs are difficult to describe using a simple definition. Perhaps the closest description would be a comparison with a black box having multiple input and multiple output which operates using a large number of mostly parallel connected simple arithmetic units. The most important thing to characterize about all ANN methods is that they work best if they are dealing with non-linear dependence between the inputs and outputs. They have been applied for various purposes, e.g. optimisation[2,3] quantification of unresolved peaks[4,5], estimation of peak parameters, estimation of model parameters in the equilibria studies, etc. Pattern recognition and sample classification is also an important application area for the ANN[6–8], which is important and fully applicable in food chemistry.

The most widespread application areas of implementing the ANNs for solution of foodstuff problems are: *(i)* wine characterization and authentification, *(ii)* edible oil characterization and authentification, *(iii)* classification of dairy products and cheese, *(iv)* classification of soft drinks and fruit products, *(v)* classification of strong drinks. In this paper two examples are given, which exemplify the application of artificial neural networks for authentification of varietal wines and olive oils.

Theory

The theory of the ANN is well described in monographs[9–13] and scientific literature. Therefore only a short description of the principles needed for understanding the ANN application will be given here. The use of the ANN for data and knowledge processing can be characterized by analogy with biological neurons. The artificial neural network itself consists of neurons connected into networks. The neurons are sorted in an input layer, one or more hidden layer(s) and an output layer. The input neurons accept the input data characteristic for each observation, the output neurons provide predicted value or pattern of the studied objects, and the hidden neurons are interconnected with the neurons of two adjacent layers but neither receive inputs directly nor provide the output values directly. In most cases, the ANN architecture consists of the input layer and two active layers – one hidden and one output layer. The neurons of any two adjacent layers are mutually connected and the importance of each connection is expressed by weights.

The role of the ANN is to transform the input information into the output one. During the training process the weights are gradually corrected so as to produce the output values as close as possible to the desired (or target) values, which are known for all objects included into training set. The training procedure requires a pair of vectors, *x* and *d*, which together create a training set. The vector *x* is the actual input into the network, and the corresponding target - the desired pre-specified answer, is the vector *d*. The propagation of the signal through the network is determined by the connections between the neurons and by their associated weights, so these weights represent the synaptic strengths of the biological neurons. The goal of the training step is to correct the weights w_{ij} so that they will give a correct output vector *y* for the vector *x* from the training set. In other words, the output vector *y* should be as close as possible to the vector *d*. After the training process has been completed successfully, it is hoped that the network, functioning as a black box, will give correct predictions for any new object x_n, which is not included in the training set.

The hidden x_i and the output y_i neuron activities are defined by the relations:

$$\xi_i = t(\xi_i) \tag{1}$$

$$\psi_i = t(\xi_i) \tag{2}$$

$$\xi_i = \sum_{j=1}^{p} w_{ij} x_j + \upsilon_i \tag{3}$$

where $j = 1, \ldots, p$ concern neurons x_j in the previous layer which precede the given neuron *i*. ξ_i is the net signal – the sum of the weighted inputs from the previous layer, υ_i is the bias (offset), w_{ij} is the weight and, finally, $t(\xi_i)$ is *transfer function,* expressed in various ways, usually as the threshold

logic function, sigmoid function or hyperbolic tangent function. The most common sigmoid function is of the form

$$\pi(\xi_i) = \frac{1}{1+e^{-k\xi_i}} \tag{4}$$

where k is a constant. The aim of the neural network training is to *minimize the error E* by changing the weights and offsets

$$E = \sum_{i=1}^{r} E_i = \sum_{i=1}^{r} (y_i - d_i)^2 \tag{5}$$

where r is the number of the input-output vector pairs in the training set, d_i is the respective component of the required output vector and y_i is the response to the adequate component x_i of the input vector. The error E is minimized most often by the steepest descent method or another gradient method. The described theory is adequate mainly for the multilayer perceptron algorithms like Back Propagation, Quick Propagation and Quasi-Newton, with some differences in details.

The ANN calculations can be effectively made using several commercial software packages like Trajan[14], Statistica Neural Networks[15], SAS JMP[16] and others[17,18].

Experimental

Description of Wine Samples and Instrumentation

72 wine samples of 6 varieties originated from Small Carpathian region (Slovakia) and produced in West Slovakia in 2003 were quantitatively analysed by gas chromatography using headspace solid-phase microcolumn extraction. The set of samples contained 11 samples of Frankovka Blue (code FM), 12 samples of Chardonnay (Ch), 16 samples of Műller Thurgau (MT), 9 samples of Welsch Riesling (RV), 7 samples of Sauvignon (Sv) and 17 samples of Gruener Veltliner (VZ). Wine aroma compounds were extracted from the headspace into a microcolumn; the microcolumn was then transferred into a modified GC injection port for thermal desorption and the released compounds were analysed. Areas of chromatographic peaks of the same retention time corresponding to the selected 65 volatile aroma compounds were used in all samples. Wines were characterised by a set of identified compounds with corresponding relative abundances. Analyses were carried out on a GC 8000 Top Series, CE Instruments (Rodano-Milan, Italy) equipped with a modified split-splitless inlet and flame ionization detector. The inlet was modified so that it was possible to insert a glass microcolumn (1 mm i.d., packed with 5.0 mg of 60–80 mesh Tenax TA). The fused silica capillary column Omegawax 250, 30 m × 0.25 mm × 0.25 μm film thickness (Supelco, Bellefonte, Pennsylvania, USA) was used. The GC inlet and the detector temperatures were 250 °C and the initial column temperature was maintained at 25 °C. The thermal desorption was performed at 10 kPa pressure for 5 min, then the pressure was increased to 50 kPa and the column tempera-

ture was programmed at a rate of 4 °C min^{-1} up to 210 °C and maintained at 210 °C for 10 min. Helium was used as the carrier gas. A computer program Class-VP 7.2, SP1 (Shimadzu, Columbia, Maryland, USA) was used for data acquisition. Analyses of each wine sample were repeated twice.

Description of Drinking Water Samples and Instrumentation

93 water samples containing potable, spring and mineral waters, originated from Croatia (54 samples), Slovenia (30), the Czech Republic (6), and France (3) were studied. From each brand 3 specimens were sampled so that the analyses were finally made for 15 tap water samples, 51 spring water samples, of which 12 samples were carbonated, and 27 mineral water samples, of which 9 samples were carbonated. Experiments were performed using a high-resolution inductively-coupled plasma mass spectrometer (ICP MS) Element 2 (Thermo, Bremen, Germany) equipped by autosampler (ASX 510, Cetac Technologies, USA), the sample introduction kit with a conical nebulizer (Thermo, Bremen, Germany) and a Scott-type glass spray chamber (Thermo, Bremen, Germany) for transporting the analytes into the plasma of the ICP MS unit. The investigated water samples were analysed and characterized by thirty one continuous variables – nuclide concentrations determined by the ICP MS measurements: Ag107, Ag109, Al27, As75, B11, Ba138, Be9, Bi209, Cd111, Cd114, Co59, Cr52, Cu63, Fe56, Li7, Mn55, Mo95, Mo98, Ni60, Pb208, Sb121, Sb123, Se77, Sn118, Sn120, Sr86, Ti47, Tl205, U238, V51, and Zn66. The standard solutions and the blank solutions were prepared by adding of 1 % high purity nitric acid (Fluka, Steinheim, Switzerland) and 1 % high purity hydrochloric acid (Merck, Darmstadt, Germany).

Results

Classification of Varietal Wines

For quantitative analysis, based on the integrated peak area, 65 chromatographic peaks were selected. A complete assignment of the analysed compounds to the selected peaks was not necessary in the applied approach, however, for 19 peaks the corresponding species were identified. It is very important to note that the retention time order for all selected compounds was the same for all 72 samples and the way of chromatographic signal evaluation was identical. The obtained final data matrix suitable for chemometrical processing contained 72 rows (objects) and 65 columns (variables). Since the number of variables was too large compared to the number of objects, selection of the best variables, based on the F-test, was performed by stepwise feature selection. In this way, 30 best variables were chosen enabling best discrimination among the six studied wine varieties. For comparison purposes, the wine classification was performed not only using the ANNs but also several techniques of discriminant analysis were implemented.

The classification model was calculated using the training set of samples containing all samples but one when the leave-one-out validation was used or without three samples in

case of using the leave-three-out validation. Thus, the remaining one sample or three samples were not included in the training procedure but were used for inspecting the quality of prediction whether the predicted variety of wine matches the real wine variety. The results achieved by several classification techniques and different software are summarized in Table I. The presented ANN results were achieved after optimising the neural network; the lowest error was obtained when using a three layer perceptron with 30 input neurons (areas of the selected best peaks), 3 hidden neurons and one six-level output neuron (representing the predicted wine variety).

All wine samples (100 %) were correctly classified into six classes by variety when the calculated multidimensional model is considered – no one sample was allocated to a wrong class. Considering the validation results, the performance in leave-one-out validation depend on the applied multivariate technique. The leave-three-out manual technique can be used also in the case when the automatic leave-one-out validation is not enabled for the given method and software. All validation results shown in Table I are above 90 %, which justifies very good ways of wine variety prediction enabling to confirm or reject wine authenticity.

Classification of Drinking Water

Three classification criteria were used for the classification of drinking waters: (1) by three types of water – potable, mineral and spring water, (2) by five types of water – potable, mineral, mineral carbonated, spring and spring carbonated water, (3) by three countries of origin – Slovenia, Croatia and Czechia (the category of French waters was not used due to a very low number of samples). Before the calculations new categorical variables were created, which correspond to the first, second and third classification criterion: WType 3, WType 5 and Country, resp. In addition, a special categorical variable Carbon was created in order to mark whether the sample is carbonated or not (c/n). When using the ANNs it is possible to utilize this variable at the input to provide some

additional information about the sample. It is worth noting that the discriminant analysis techniques, except logistic regression, do not permit the use of non continuous input variables. The mentioned additional information cannot be of course used when the classification by the second criterion is used.

Table II shows the classification results for five cases using categorization by water type into 3 and 5 classes, the same categorization but with the help of additional categorical variable Carbon, and finally categorization by 3 countries of origin. Intelligent Problem Solver is an extremely useful module of Trajan software facilitating the selection of the optimal neural network. For the sake of place, Table II exhibits only five best networks, automatically selected by this module, but a good possibility is to make a choice among a larger nuber of networks. Moreover, the networks belonging to different ANN variants can be examined in this way (e.g. Radial Base ANN). In Table II, the ordinal number of the network is marked by No, the number of neurons in individual layers is marked by I (input), H (hidden), and O (output); Err. indicates the sum of squares error obtained both for the training and test sets. The most important results are

Table I
Success in prediction of wine variety using 72 varietal wines, 30 optimally selected chromatographic peaks, 5 classification and 2 validation techniques

Method	Classif. success	Leave-1-out	Leave-3-out	Software
LDA	Correct/all	69/72	69/72	SAS
	%	95.8	95.8	
QDA	correct/all	66/72	65/72	SAS
	%	91.7	90.3	
KNN	correct/all	72/72	67/72	SAS
	%	100.0	93.1	
LR	correct/all	–	69/72	SPSS
	%	–	95.8	
ANN	correct/all	–	68/72	JMP
	%	–	94.4	

Table II
ANN – selection of the best network for 5 different criteria of water classification using Intelligent Problem Solver of software Trajan 6.0

Categor variables	MLP networks Neurons				Train. set Err.	Test set Err.	Success [%]
	No	I	H	O			
Country	1	31	6	1(3)	0.009	3.759	77.3
	2	31	6	1(3)	0.023	4.706	81.8
	3	31	5	1(3)	0.023	2.801	77.3
	4	31	6	1(3)	0.017	3.464	81.8
	5	31	6	1(3)	0.0044	5.239	86.4
Country c/n	1	32	5	1(3)	0.0079	3.215	86.4
	2	32	6	1(3)	0.001	3.921	81.8
	3	32	6	1(3)	0.100	2.242	86.4
	4	32	6	1(3)	0.0032	1.829	86.4
	5	32	6	1(3)	0.144	0.480	90.9
WType3	6	31	6	1(3)	0.0054	0.0026	100.0
	7	31	6	1(3)	0.0008	1.602	86.4
	8	31	6	1(3)	0.0002	0.649	95.5
	9	31	6	1(3)	0.0010	0.204	95.5
	10	31	6	1(3)	0.0000	0.935	86.4
WType3 c/n	1	32	6	1(3)	1.4×10^{-5}	$2. \times 10^{-5}$	100.0
	2	32	6	1(3)	1.1×10^{-6}	5.8×10^{-6}	100.0
	3	32	5	1(3)	5.9×10^{-6}	0.0029	100.0
	4	32	6	1(3)	1.2×10^{-9}	8.2×10^{-6}	100.0
	5	32	6	1(3)	1.5×10^{-8}	9.1×10^{-3}	100.0
WType5	1	31	6	1(5)	0.2946	0.744	90.9
	2	31	6	1(5)	0.215	0.599	86.4
	3	31	6	1(5)	0.424	1.154	81.8
	4	31	6	1(5)	0.197	0.4498	59.1
	5	31	6	1(5)	0.480	0.934	90.9

in the last column, which expresses the ratio between the numbers of correct classifications to the total number in per cents. The results are excellent when categorization by the type of water is concerned. A bit less successful but still very good is classification by the country of origin, however, some difficulty here is cause by the fact that drinking waters cannot be strictly differentiated by the country borders but the geological factors can be more important.

Conclusions

Theoretical background and practical examples of exploitation of artificial neural networks were given.

Quantitative results facilitating characterization, classification and authentification of Slovak varietal wines using artificial neural networks and other multidimensional chemometrical techniques were acquired. Six studied wine varieties were correctly categorized on the basis of the areas of chromatographic peaks corresponding to the selected 65 volatile aroma compounds in all samples. In all studied cases the calculated classification performance was higher than 90 %. A higher classification performance was achieved when instead of all peaks 30 optimally selected peaks were used in the training procedure. Applied approach is suitable mainly when many analytical data and complex analytical signals are obtained. The established classification models are fully applicable for the prediction of the category of an unknown wine sample.

Using the nuclide concentration determined by the ICP MS method, five types of drinking water from different European countries were classified. The classification results corresponding to the selected classification criteria were very good – from 90 to 100 % for classification by the water type and about 85 % for classification by the country of origin. A detailed study may also enable to find the nuclides, which concentration level is characteristic for the given kind of the water sample. Some details concerning implementation of neural networks were also referred.

REFERENCES

1. Zupan J.: Acta Chim. Sloven. *41*, 327 (1994).
2. Havel J., Madden J. E., Haddad P. R.: Chromatographia *49*, 481 (1999).
3. Havlis J., Madden J. E., Revilla A. L., Havel J.: J. Chromatography B *755*, 185 (2001).
4. Bocaz-Beneventi G., Latorre R., Farková M., Havel J.: Anal. Chim. Acta *452*, 47(2002).
5. Dohnal V., Farková M., Havel J.: Chirality *11*, 616 (1999).
6. Fidencio P. H., Ruisanchez I., Poppi R. J.: Analyst *126*, 2194 (2001).
7. Sanni O. D., Wagner, M. S., Briggs, D.: Surf. Interface Anal. *33*, 715 (2002).
8. Ball G., Mian S., Holding F., Allibone R.O., Lowe J., Ali S., Li G., McCardle S., Ellis I.O., Creaser C., Rees R.C.: Bioinformatics *18*, 395 (2002).
9. Gasteiger J., Zupan J.: Angew. Chem. *32*, 503 (1993).
10. Devillers J.: *Neural Network in QSAR and Drug Design*. Academic Press, San Diego 1996.
11. Kvasnička V., Beňušková L., Pospíchal J., Farkaš I., Tiňo P., Kráľ A.: *Introduction into the Theory of Neural Networks* (in Slovak). IRIS, Bratislava 1997.
12. Zupan J., Gasteiger J.: *Neural Networks in Chemistry and Drug Design*. 2nd Ed., Wiley, Weinheim 1999.
13. Bishop C.M.: *Neural Networks for Pattern Recognition*. Oxford Univ. Press, Oxford 2004.
14. Trajan Software: *Trajan Neural Network Simulator, Release 6.0.* Trajan Software Ltd., Durham, U.K. 2004.
15. Statistica ver. 7.0: Statsoft, Inc., Tulsa, OK, U.S.A. 2004.
16. JMP ver. 6.0.2: SAS Institute, Cary, NC, U.S.A. 2006.
17. NeuroSolutions ver. 5.0.3: NeuroDimension, Inc., Gainesville, FL, U.S.A. 2005.
18. Matlab: *Neural Network Toolbox*. The MathWorks, Inc., Natick, MA, U.S.A. 2005.

L09 DETECTION OF SPICES' IRRADIATION BY MODERN SPECTROSCOPIC TECHNIQUES

MARTIN POLOVKA and MILAN SUHAJ

Department of Chemistry and Food Analysis, VÚP Food Research Institute, Priemyselná 4, P. O. Box 25, 824 75 Bratislava, Slovak Republic,
polovka@vup.sk

Introduction

Herbs and spices are daily used condiments, frequently undergoing the microbial contamination (average contamination by microorganisms and/or their spores can reach up 10^5–10^8 microorganisms per gram)[1]. Thus γ-irradiation treatment is accepted as one of the most effective sterilization technique.

Toxicological and nutritional tests proved the safety of γ-radiation doses below 10 kGy, which was accepted by Codex Alimentarius (CA) General Standard for irradiated foods as the maximum legal/allowed absorbed dose for dried aromatic herbs, spices and vegetable seasonings sterilisation, with the exception for cases when the higher dose application is necessary to achieve a legitimate technological purpose[2]. In contradiction to CA standards, the limitation of US Food and Drug Administration (FDA) set the maximum allowed dose for culinary herbs and spices to 30 kGy[3].

Besides the positive effects of γ-radiation, its negative impact on environment or even on human health forces the food control authorities to develop reliable and sensitive methods applicable for dosimetric purposes even long time after the radiation process.

It is well known, that γ-radiation of food samples results in the formation of free radical species. Thus, Electron Paramagnetic Resonance (EPR) spectroscopy represents a suitable tool to investigate the irradiated spice.[5–12] As follows from several recently published data, the application of EPR spectroscopy for dosimetric purposes is limited by several factors, mostly by limited lifetime and thermal stability of γ-radiation induced radicals.[5–13]

Our previous investigations were focused on the monitoring of radiation-induced changes e.g., in black pepper, oregano, allspice, ginger, or clove.[5,9–12]

The aim of the present study was to monitor the effect of γ-irradiation on the microbiological quality of powder samples of ground dry caraway seed (*Carum carvi*, L.) and ground dry laurel leaves (*Laurus nobilis*, L.). The influence of absorbed dose on the character of formed paramagnetic structures, as well as their life-time was investigated by means of EPR spectroscopy. Moreover, antioxidant properties of individual spice extracts were characterized using both EPR and UV-VIS spectrophotometer by means of 1,1-diphenyl-2-picrylhydrazyl (˙DPPH), 2,2'-azinobis (3-ethylbenzothiazoline-6-sulfonic acid) diammonium salt (ABTS⁺˙) radicals, ferric reducing power (FRP) and thiobarbituric acid reactive substances (TBARS) assays. Total contents of polyphenols (TPC) in each extract was also monitored and expressed as Gallic acid equivalent. In addition, multivariate statistical methods were used for the discrimination of native (non-irradiated) samples from that exposed to γ-radiation.

Experimental

Samples Characterisation

Samples of ground dry caraway seed (dry matter content, 92.1 %) originating from Austria and laurel leaves (dry matter content, 92.5 %) from Turkey were provided by Kotanyi, GmbH, Vienna, Austria. Spice samples were irradiated using ^{60}Co source at average doses of 5, 10, 20 and 30 kGy (dose rate, 2 kGy h⁻¹) according to commercial practices at Artim, Ltd. (Prague, Czech Republic). After the irradiation, all the samples were stored in closed bags in the darkness at ambient conditions.

Microbiological Analysis

Elementary microbiological analysis of all spice samples (total counts of microorganisms, presence of coliform bacteria, yeasts and moulds) was carried out following the relevant STN ISO standards two times: immediately after the irradiation and after 6 months of post-irradiation storage.[14–16]

EPR Experiments

EPR experiments with solid samples were performed identically as previously described elsewhere, using a portable X-band EPR spectrometer e-scan (Bruker, GmbH, Karlsruhe, Germany).[5,10–12] Spice sample (100 mg) was placed in the thin-wall EPR quartz tube (internal diameter, 3 mm) and cylindrically shaped column was formed (sample column heights: 2.1 ± 0.2 cm (caraway) and 2.0 ± 0.2 cm (laurel tree), respectively; and then inserted into the standard rectangular cavity of EPR spectrometer.

Ethanolic extracts of spice samples were prepared identically as described in our previously published papers, by mixing 0.4 g of respective spice sample with 8 ml ethanol of spectroscopic grade.[5,10,12] Their ability to terminate ˙DPPH and ABTS⁺˙ radicals was monitored.[5,10,12,17,18]

Experimental EPR spectra were recorded at 298 K. The response and settings of EPR spectrometers were checked by means of solid DPPH and Strong pitch standards (Bruker) daily before the experiments, The obtained spectra were evaluated using WIN EPR and SimFonia software (Bruker) as described e.g. in.[5,9–11,19,20]

UV-VIS Experiments

Extracts used in UV-VIS experiments were prepared by mixing 2.0 g of respective spice sample with 50 ml methanol/water (80 %, v/v) solvent[9,11]. Double-beam UV-VIS spectrometer Specord M40 (Carl Zeiss, Jena, Germany) with accessories was used for the monitoring of antioxidant properties. All the experiments were carried out in the same square quartz UV-VIS transparent cells (path length, 1 cm). The monitoring of antioxidant ability of spices' extracts was performed

identically as described in our previous papers, involving the DPPH, TBARS and FRP assays. Total phenolic compounds content of extracts was evaluated, as well. [9, 11]

M u l t i v a r i a t e   S t a t i s t i c a l   A n a l y s i s

Canonical discriminant analysis of all results obtained from UV-VIS experiments was performed using the Unistat® software in order to distinguish the native (non-irradiated) spice samples from that exposed to γ-radiation.

Results

Microbiological analysis performed immediately after the irradiation process proved, that as a result of γ-irradiation, the total count of microorganisms in caraway sample irradiated at dose of 5kGy decreased considerably from 2.8×10^4 colony forming unit (CFU) detected in reference sample, to less than $10\, CFU\, g^{-1}$. The same effect of γ-irradiation on laurel leaves was achieved using the dose of 10 kGy, still fulfilling the requirements of international standards on irradiation[3,4].

Table I
Microbiological analysis of ground caraway seeds (C) and laurel bay leaves (L) samples, γ-irradiated at doses of <0-30> kGy using 60Co-source performed one day after the γ-irradiation

Radiation dose [kGy]	Total count of microorganisms [CFU g⁻¹]		Coliform bacteria [CFU g⁻¹]		Moulds [CFU g⁻¹]	
	C	L	C	L	C	L
0	2.8×10^4	1.7×10^5	1.0×10^4	8.6×10^3	9.8×10^3	5.7×10^3
5	<10	5.7×10^3	<10	5.0×10^1	2.5×10^2	<10
10	<10	<10	<10	<10	<10	<10
20	<10	<10	<10	<10	<10	<10
30	<10	<10	<10	<10	<10	<10

As follows from data presented in Table I, the presence of oliform bacteria as well as of yields and moulds was effectively suppressed by the irradiation. Analysis performed 6 months of post-irradiation storage confirmed, that microbial status of both spices remained practically unchanged.

EPR spectrum of both reference (non-irradiated) samples represents broad singlet line with unresolved hyperfine splitting, attributable mostly to Mn^{2+} ions, upon which the additional sharp EPR line ($g_{eff} = 2.0022$, $\Delta B_{pp} \sim 1\, mT$) is superimposed, previously assigned to stable semiquinone radicals produced by the oxidation of polyphenolic compounds present in plants. In addition, the presence of low-intensive EPR singlet line was noticed in caraway reference sample, attributable to radicals generated during the grinding process (Table II).[5,9–11]

EPR spectra of γ-radiation treated spices showed the formation of additional paramagnetic structures. As follows from detail simulation analysis of obtained spectra (Table II), different, mostly cellulosic and carbohydrate radical structures were identified.

Table II
Identification of radical structures found in reference and γ-irradiated samples of ground caraway and laurel leaves

EPR signal origin	g-value	Hyperfine splittings [mT]	ΔB_{pp} [mT]
Reference samples			
Semiquinones	$g_\perp = 2.0042$	–	0.52
	$g_\parallel = 2.0030$		
Carbohydrate I	$g_\perp = 2.0041$	–	0.06
	$g_\parallel = 2.0028$		
γ- irradiated samples			
Carbohydrate II	$g_\perp = 2.0041$	$A_\perp = 0.7$	0.45
	$g_\parallel = 2.0033$	$A_\parallel = 0.6$ (2H)	
Carbohydrate III	$g_\perp = 2.0032$	$A_\perp = 0.85$	0.67
	$g_\parallel = 2.0025$	$A_\parallel = 0.7$ (2H)	
Carbohydrate IV	$g_\perp = 2.0030$	$A_\perp = 0.45$	0.59
	$g_\parallel = 2.0038$	$A_\parallel = 0.40$ (1H)	
Cellulosic	$g_\perp = 2.0029$	$A_\perp = 3.00$	1.20
	$g_\parallel = 2.0014$	$A_\parallel = 1.70$ (2H)	
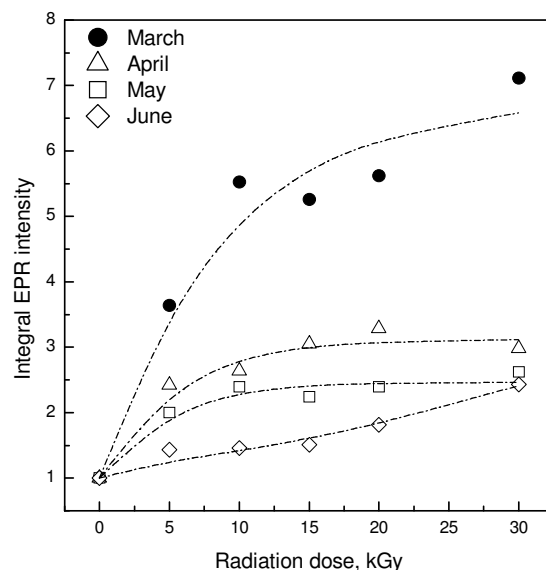
Fig. 1. **Dependence of integral EPR intensity of ground caraway seed on γ-radiation dose measured immediately after the irradiation (March) and during three month of post irradiation storage (April-June). EPR spectra were recorded using 0.633 mW microwave power at 298 K**

These radicals originate either from cleavage processes of cellulose matter (laurel leaves) and/or of other polysaccharides forming the skeleton of plant structures and their cells, as the cellulosic radicals were not detected in γ-irradiated caraway samples.

In accord with our previously published papers, the dose-dependent formation of radical structures' in γ-irradiated samples of both spices under study was found (Fig. 1.).

The obtained dependence can be effectively used as calibration curve enabling the estimation of previously absorbed dose.[5,9–11]
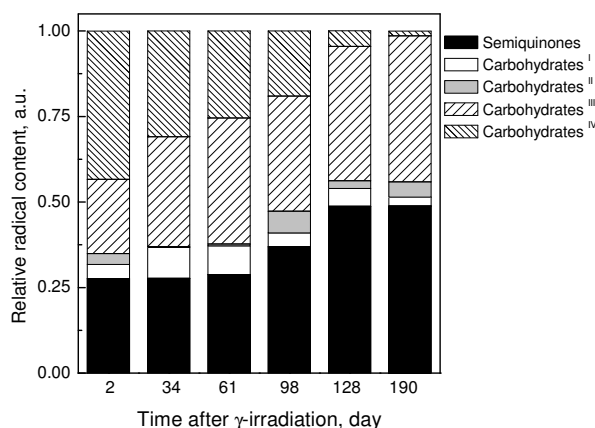
Fig. 2. **The dependence of relative radicals' content on time after the γ-irradiation obtained from the simulation analysis of experimental EPR spectra of caraway sample treated at dose of 30 kGy**
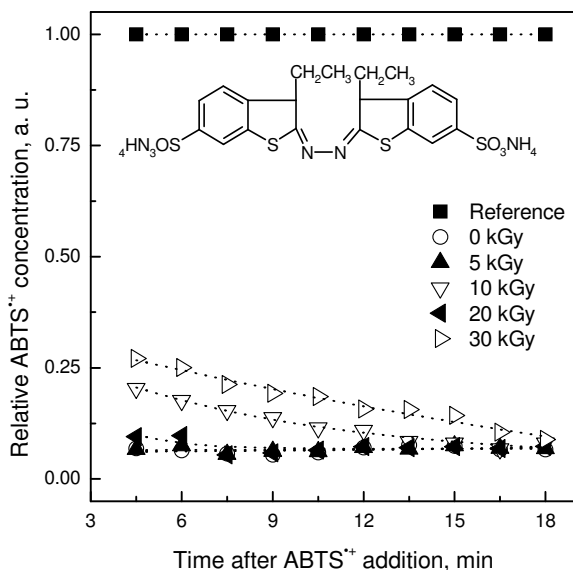
Fig. 3. **The dependence of relative ABTS⁺ concentration on time after its mixing with caraway ethanolic extracts prepared from samples exposed to different doses of γ-radiation. Inset represents the structural formula of ABTS. Extracts were prepared 2 days after the irradiation. Pure ethanol was used as reference**

As a result of irreversible decay of radical structures induced by γ-radiation, the integral EPR spectra intensity of irradiated samples decreased gradually as is clearly demonstrated on Fig. 1. and Fig. 2. for caraway samples. On the contrary, the signal intensity of both reference samples remains practically unchanged.

Detail evaluation of experimental spectra revealed the lowest stability of cellulosic radicals in laurel leaves (half life ~ 10 weeks) followed by carbohydrate radicals, which stability ranged from 20 up to 60 weeks. These results are in good agreement with our previously published papers.[5,9–11]

Ethanolic extracts of both reference spices revealed significant ability to terminate ˙DPPH as well as ABTS˙⁺ radicals. As demonstrated on Fig. 3., it is only slightly influenced by the absorption of γ-radiation. Results obtained moreover showed, that radical-scavenging ability of laurel leaves' extracts is significantly higher than that of caraway; probably due to the differences in types and concentrations of polyphenolic compounds.

UV-VIS experiments proved, that radiation treatment resulted in significantly increased ˙DPPH radical-scavenging activity of bay leaves methanolic extracts. In addition, the TBARS value of caraway extracts, representing a measure of oxidative products concentration, was slightly increased. As a result of post-irradiation storage, a minor increase of ferric reducing power, ˙DPPH radical-scavenging ability as well as content of polyphenolic compounds of bay leaves extracts was noticed, whereas the TBARS values of both, caraway and bay leaves extracts, was somewhat reduced.

Discriminant analysis of all variables obtained from UV-VIS experiments was used to differentiate the studied spices according to the absorbed dose. As depicted on Fig. 4., the effective discrimination was achieved only when non-irradiated samples and samples treated by dose of 30 kGy were compared. Using this approach, 93% correctness of caraway classification was found, influenced mostly by TBARS values and TPC content. In the case of bay leaves, 73% correct differentiation of non-irradiated sample from sample γ-irradiated at 30 kGy was found.
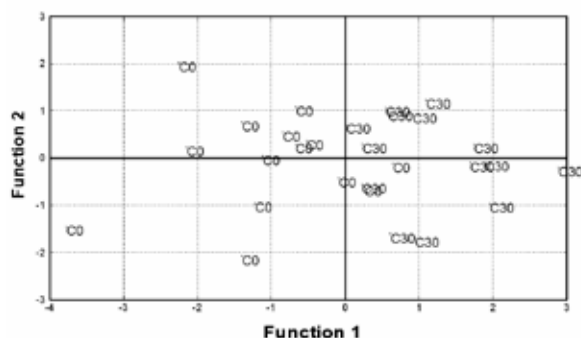
Fig. 4. **Canonical discriminant analysis of non-irradiated caraway samples (C0) and of samples γ-irradiated at 30 kGy (C30). Characteristics obtained from UV-VIS experiments (˙DPPH, TBARS, FRP, TPC) immediately after the irradiation and during the storage of samples at ambient conditions were used as variables**

Conclusions

It was proved, that γ-irradiation of caraway and bay leaves samples even at doses of 5 kGy and 10 kGy, respectively, is an efficient microbiological decontamination tool.

The consideration of γ-radiation impact on spices is a multi-component problem. As follows from results presented in this study, EPR spectroscopy represents a valuable dosimetric tool. In addition, the canonical discriminant analysis based on UV-VIS characteristics of spices' extracts can be effectively used for the differentiation of spices treated at higher doses of γ-radiation from the unaffected ones.

REFERENCES

1. Grecz N., Al-Harity R., Jaw R.: J. Food Saf. *7*, 241 (1986).
2. Thayer D. W., Josephson E.S., Brynjolfsson A., Giddings G.G.: *Radiation pasteurization of food*. Council for Agricultural Science and Technology CAST Issue Paper No. 7. Ames, Iowa, USA 1996.
3. CODEX STAN 106-1983: General standard for irradiated foods.
4. Code of Federal Regulations 21CFR179: Irradiation in the production, processing and handling of food.
5. Polovka M., Brezová V., Šimko P.: J. Food Nutr. Res. *46*, 75 (2007).
6. Raffi J., Yordanov N. D., Chabane S., Douifi L., Gancheva V., Ivanova S.: Spectrochim. Acta A *56*, 409 (2000).
7. Yordanov N. D., Aleksieva K.: Radiat. Phys. Chem. *69*, 59 (2004).
8. Korkmaz M., Polat M.: Radiat. Phys. Chem. *62*, 411 (2001).
9. Suhaj M, Rácová J., Polovka M., Brezová V.: Food Chem. *97*, 696 (2006).
10. Polovka M., Brezová V., Staško A., Mazúr M., Suhaj M., Šimko P: Radiat. Phys. Chem. *75*, 309 (2006).
11. Horváthová J., Suhaj M., Polovka M., Brezová V., Šimko P.: Czech J. Food Sci. *25*, 131 (2007).
12. Sádecká J., Polovka M.: J. Food Nutr. Res. *47*, 51 (2008).
13. Franco R. W. A., Martin-Neto L., Kato M. S. A., Furlan G. R., Walder J. M. M., Colnago L. A.: J. Food Sci. Technol. *39*, 395 (2004).
14. ISO Standard 4833:2003: *Microbiology of food and animal feeding stuffs – Horizontal method for the enumeration of microorganisms – Colony-count technique at 30 °C.*
15. ISO Standard 4832:2006: *Microbiology of food and animal feeding stuffs – Horizontal method for the enumeration of coliforms – Colony-count technique.*
16. ISO Standard 7954:1987: *Microbiology – General guidance for enumeration of yeasts and moulds – Colony count technique at 25 °C.*
17. Pellegrini N., Simonetti P., Gardana C., Brenna O., Brighenti F., Pietta P.: J. Agric. Food Chem. *75*, 339 (2001).
18. Staško A., Brezová V., Biskupič S., Rapta P.: J. Food Nutr. Res. *46*, 145 (2007).
19. Polovka M.: J. Food Nutr. Res. *45*, 1 (2006).
20. Polovka M., Brezová V., Staško A.: Biophys. Chem. *106*, 39 (2003).

L10   APPLICATION POTENTIAL OF NOVEL GAS CHROMATOGRAPHY HIGH THROUGHPUT TIME-OF-FLIGHT MASS SPECTROMETERY SYSTEM (TRU TOF) IN FOOD AND ENVIRONMENTAL ANALYSIS

JAKUB SCHŮREK, JANA PULKRABOVÁ and JANA HAJŠLOVÁ

Department of Food Chemistry and Analysis, Faculty of Food and Biochemical Technology, Institute of Chemical Technology, Technická 5, Praha 166 28, Czech Republic, jakub.schurek@vscht.cz

Introduction

In last years, analytical approaches employing gas chromatography coupled to time-of-flight mass spectrometry (GC-TOF MS) proved to be a useful tool in assessment of quality and safety of food[1–4] and also environmental matrices[5]. But only recently, at the end of 2007, new time-of-flight mass spectrometric (TOF MS) detector specialy designed for high-throughput of samples, has been introduced. High throughput is the key to increased profitability of the analyses, while obtaining faster results and optimization. The need for selected ion monitoring (SIM) operation and low dynamic range associated with traditional quadrupoles and ion traps may take time and money away from laboratory's bottom-line. The assessed instrument (GC-HT TOF MS) is combining fast acquisition mass spectrometer (80 Hz) with specific data-mining algorithms. The aim of this benchtop instrumental set-up is to achieve the speed and resolution necessary to accomplish Time-Compressed Chromatography. Using such detector, sufficient data density is obtained to accurately characterize even the narrowest GC peaks produced under conditions of fast chromatography separation. The acquisition of the full mass spectral information of the sample with comparable sensitivity as obtained by selected ion monitoring (SIM) mode with quadrupole or ion trap instruments makes feasible the application of a deconvolution algorithm obtaining pure mass spectra even for coeluting compounds and achieving reliable confirmation. Consequently, trace level analysis of unknown sample components can be performed.

The schematic view of GC-HT TOF MS is shown in Figure 1. Within the mass spectrometer source, the filament continuously generates an electron beam. The GC effluent is introduced into the source through a heated transfer line. Electron ionization (EI) occurs as a result of interactions between an electron beam with an analyte molecule from the GC effluent. Chemical ionization (CI) occurs as a result of EI interactions between the electron beam with the CI reagent gas which creates charged reagent ions that ionize the analyte molecules from the GC effluent. Ions are pulsed from the orthogonal accelerator at a nominal frequency of 20 kHz. Each pulse of ions into the flight tube results in a mass spectrum which is referred to as a transient. The transients are then summed to provide mass spectral acquisition rates up to 80 spectra second[−1]. The focusing optics are used to direct

ions through the system and ensure a high recovery of signal at the detector. Deflection optics are used to prevent unwanted signals, such as ions from a solvent front or unwanted background ions generated by carrier gas or residual gas, and extend the life of the detector. The ions are pulsed into the flight tube with equal kinetic energies (K.E. = 1/2 mv^2). Therefore, ions of varying mass-to-charge ratios will have different velocities as they move through the flight tube. Fragment ions with different velocities traveling over the same fixed distance will have different arrival times at the end of that distance (velocity = distance/time). Masses are resolved in time-of-flight mass spectrometers by the time each mass takes to reach the detector at the end of the flight path (time = constant x $m^{1/2}$). For example, a mass of 100 mu will take approximately 15 microseconds to reach the detector while a mass of 1,000 mu will take 50 microseconds to travel the same distance.

In this work we aimed to evaluate new GC-HT TOF MS instrumentation in analysis of pesticides, pharmaceuticals, poly-chlorinated biphenyls (PCBs) and poly-brominated dibenzo ethers (PBDEs). The best GC-MS settings has been optimized in order to obtaine fast and reliable analytical methods for routine control of purified extracts of different food-stuffs, or sediment, and water. Appraisal of mentioned technique with respect to the cost and time demands was also done.
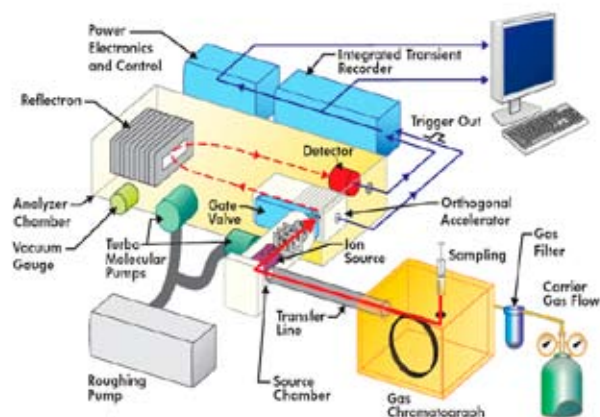
Fig. 1.   **Schematic diagram of GC-HT TOF MS**

Experimental

R e a g e n t s   a n d   M a t e r i a l

Tested compounds (listed in Table II) with purity ranging from 95 to 99 % were purchased from Dr. Ehrenstorfer (Augsburg, Germany) in case of pesticides and PCBs. PBDEs and estrogenic pharmaceuticals were obtained from Cambridge Isotope Laboratories (CIL, UK). All solvents used within sample preparation (see Table I) were of analytical grade (Scharlau, Barcelona, Spain). Working solutions (concentration 1.25–250 µg dm^{−3}) were prepared by series of dilutions of the stock solutions (10 mg dm^{−3}) with appropriate solvent.

Table I
Sample preparation and GC-HT TOF MS instrumental set-up

Instrumental set-up	Analytes group			
	Pesticides (baby food)	PCBs (fat)	PBDEs (sewage water)	Pharmaceuticals (river sediment)
Sample preparation	Ethyl acetate extraction of baby food followed by HPGPC clean-up.[6]	Soxhlet extraction of adipose tissue using hexane:dichlormethane (1 : 1, v : v) followed by HPGPC clean-up.[7]	Filtration of water followed by microextraction in packed siringe (MEPS, C-18).[8]	Hexane:acetone (1 : 1, v : v) extraction followed by SPE clean-up.9
GC	Injection: splitless 1 μl, 250 °C Column: forte BPX-5 (40 m × 0.18 mm × 0.18 μm) Temperature programming: 70 °C (1 min), 45 °C min^{-1} to 300 °C (3 min) Column flow: 1 ml min^{-1}	Injection: pulse splitless 1 μl, 250 °C, 1.5 min at 50 p.s.i. Column: forte BPX-5 (30 m × 0.25 mm × 0.25 μm) Temperature programming: 80 °C (1.5 min) 45° C min^{-1} to 340 °C (6 min) Column flow: 1 ml min^{-1}	Injection: PTV, 10 μl, 50 °C (2 min) 400 °C min^{-1} to 300 °C Column: DB-XLB (15 m × 0.25 mm × 0.1 μm) Temperature programming: 80 °C (2 min) 50 °C min^{-1} to 320 °C (4 min) Column flow: 1.5 ml min^{-1}	Injection: pulse splitless 1 μl, 250 °C, 2 min at 90 p.s.i. Column: forte BPX-5 (30 m × 0.25 mm × 0.25 μm) Temperature programming: 80 °C (2 min) 55 °C min^{-1} to 330 °C (5 min) Column flow: 2 ml min^{-1}
TOF MS	Detector voltage: 1,750 V Time of analysis: 10 min	Detector voltage: 1,875 V Time of analysis: 14 min	Detector voltage: 1,800 V Time of analysis: 11 min	Detector voltage: 1,875 V Time of analysis: 12 min

For optimization and validation purposes blank matrix (pork fat, apple based baby food) was chosen. Sewage water was obtained from local water treatment facility (Prague) and sediment was sampled at Podoli site (river Vltava).

Sample Analysis

Different sample preparation procedures for each analytes group were applied.[6–9] Their brief overwiev can found in Table I. The GC-HT TOF MS system consisted of a HP 6890 (Agilent Technologies, Palo Alto, CA, USA) gas chromatograph with split-splitless injector (or Agilent PTV Inlet) and LECO TruTOF™ HT time-of-flight mass spectrometer (LECO, St Joseph, MI, USA). The detector operated in electron impact ionisation mode (EI) or positive chemical ionization mode (CI+). GC-TOF MS was performed using set-up and conditions summarized also in Table I.

Results

Fast Analysis and Spectral Deconvolution

To demonstrate the application potential of TruTOF HT system and ChromaTOF software for detection/identification, selected contaminats and residues were analyzed under optimized conditions shown in previous chapter. All of the analyzed sample has been processed by automated peak finding and deconvolution function. Within peak finding, the Chroma TOF software automatically detects peaks at all acquired single masses (*m/z* 35–650 in our work) above certain signal-to-noise level (S/N = 25 was used in the given cases). After that, deconvolution alghoritm mathematically separates mass spectra of chromatographically coeluted compounds. Deconvoluted spectra are then compared to NIST

library and the identification is performed automatically. As the example Fig. 2. shows the Deconvoluted Total Ion Chromatogram (DTIC) for matrix matched standard (25 μg dm^{-3}). Due to rapid analysis (fast temperature programming rate 45 °C), several coelutions occured (see Fig. 2.A). Successful spectral deconvolution followed by positive identification of overlapping chromatographic peaks have been enabled by data acquisition rate of 15 Hz offered by the Tru TOF (see Fig 2.B–C). Althought, within all tested analytes groups and matrices certain coelutions occured, the quantification
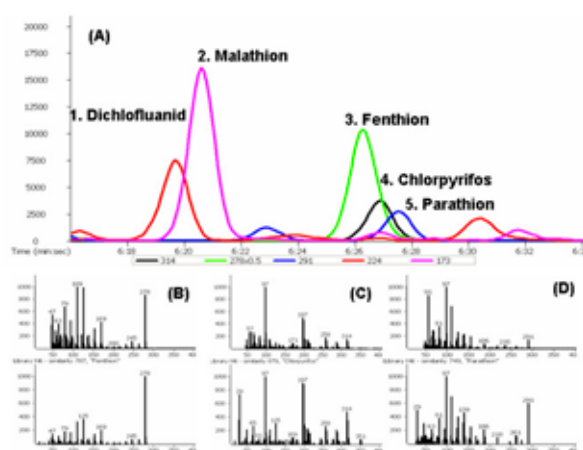
Fig. 2. **GC-HT TOF MS analysis of matrixe match standard of pesticides at 25 μg dm^{-3}(apple based baby food). (A) Deconvoluted TIC chromatogram. Measured mass spectrum (upper line) of Fenthion (B), Chlorpyrifos (C) and Parathion (D) along with respective NIST library hits (bottom line)**

of target compouds was possible using peak abundancies of deconvoluted peaks at their particular uniqu masses.

Methods Performance Characteristics

Relevant performance characteristics of the analytical methods (repeatability, LOD/LOQ and linearity) were tested on spiked samples in three replicates. As long as this work was mainly focused at the final determinative step of the whole analytical process, issues associated with sample preparation (such as recoveries) were not discussed. The results are summarized in Table II.

Table II
Method performance characteristics of selected analytes in various food matrices analyzed by GC-HT TOF MS. LOQs were estimated in purified matrix extracts or in water (for BPDEs). Repeatability (RSD) was measured at 25 $\mu g\,dm^{-3}$

Compound	Linearity (R2)	LOQ [$\mu g\,dm^{-3}$]	RSD (n =3 , [%])
Pesticides in baby food			
HCB	0.9991	2.5	2
DDT	0.9994	5	5
DDE	0.9981	5	7
DDD	0.9980	5	9
lindan	0.9995	2.5	4
endrin	0.9993	5	4
chlorpiryfos	0.9975	5	6
heptachlor	0.9972	5	8
PCBs in pork fat			
PCB 28	0.9983	2.5	5
PCB 52	0.9963	5	9
PCB 101	0.9955	5	6
PCB 118	0.9959	5	10
PCB 138	0.9960	5	5
PCB 153	0.9942	10	12
PBDEs in water			
BDE-28	0.9987	0.005	2
BDE-47	0.9954	0.001	4
BDE-66	0.9891	0.025	3
BDE-85	0.9930	0.010	4
BDE-99	0.9912	0.010	5
BDE-153	0.9854	0.025	7
BDE-183	0.9900	0.050	12
Pharmaceuticals in sediment			
Ethinylestradiol	0.9880	5	6
Dienestrol	0.9947	5	4
Diethylstilbestrol	0.9962	5	3

The limits of detection (LOD), were defined as the lowest detectable concentration (S/N≥3). The limits of quantification (LOQ) were estimated as a lowes calibration level (LCL).

Analysis of Real-life Samples

The ability of the presented technique to determine target analytes in real life samples was tested at various food extracts (for pesticides, PCBs) and water samples (for PB-DEs).

As the example, case of PDBEs in sewage water is presented. It should be noted that the trace level target analysis as well as analysis of unknown sample components could be facilitated when working with TOF mass spectrometers due to their excellent confirmation power.[10] The identification of BDE-28 is documented in Fig. 3. Full mass spectrum obtained as a result of electron ionization (70 eV) was obtained after automatic spectral deconvolution. This fact proved, that coupling MEPS with PTV-GC TOF MS would express good potential for quantification of BFRs at their native concentration range (10^0–10^1 $ng\,dm^{-3}$) in releases of a waste water treatment plant effluent or sewage water.[11,12] Moreover, such results showed new possible concepts in rapid water analysis by employing microextraction in packed sirynge (MEPS) coupled to PTV-GC TOF MS. This approach minimizes sample handling and reduces time/cost of measurement.
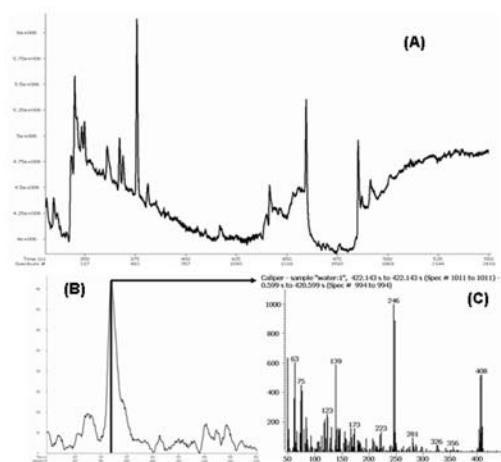
Fig. 3. **MEPS-GC TOF MS analysis of sewage water sample. (A) TIC chromatogram of sewage water. (B) Zoomed part of chromatogram – masses 406 + 408 are displayed.(C) Measured mass spectrum of natively present BDE-28**

Conclusions

This study briefly described a relatively fast separation for analysis of different microcontaminants in food and environmental samples. High-speed temperature programming significantly reduced the overall analysis time as compared to traditional methods. Detection by TOF MS gives all of the sensitivity needed in order to identify trace level components while at the same time providing the data density needed to define narrow GC peaks and deconvolute overlapping peaks.

Further tests will be facilitated in order to create ultra fast multimethod for simultaneous detection of wide spectrum of contaminants by GC-HT TOF MS. The hyphenation of this

technique to microextraction sample preparations (MEPS, SPME) is the possible option to enlarge spectrum of HT TOF MS applications.

REFERENCES
1. Lehotay S.J., Hajslova J.: TrAC *21*, 686 (2002).
2. Hajslova J., Zrostlikova J.: J. Chromatogr. A *1000*, 181 (2003).
3. Schureka J., Portoles T., Hajslova J., Riddellova K., Hernandez F.: Anal. Chim. Acta *611*, 163 (2008).
4. Agustin M.R.R., Park H., Hong S., Ryu J., Lee K.: J. of Chromatogr.A *1085*, 278 (2005).
5. Ticha J., Hajslova J., Jech M., Honzicek J., Lacina O., Kohoutkova J., Kocourek V., Lansky M., Kloutvorova J., Falta V.: Food Control *19*, 247 (2008).
6. Hajslova J., Zrostlikova J.: J. Chromatogr. A *1000*, 181 (2003).
7. Suchan P., Pulkrabová J., Hajšlová J., Kocourek V., Anal. Chim. Acta *520*, 193 (2004).
8. Schurek J., Pulkrabova J., Hajslová J., Lahoutifard N.: Organohalogen Compd. *2008,* 70.
9. Hájková K., Pulkrabová J., Schůrek J., Hajšlová J., Poustka J., Nápravníková M., Kocourek V.: Anal. Bioanal. Chem. *387*, 1351 (2007).
10. Schurek J., Portoles T., Hajslova J., Riddellova K., Hernandez F.: Anal. Chim. Acta *611*, 1636 (2008).
11. Hale R. C., Guardia M. J. L., Harvey E., Gaylor M. O., Mainor T. M.: Chemosphere *64*, 181 (2006).
12. North K. D.: California. Environ. Sci. Technol. *38*, 4484 (2004).

L12 INTERACTIONS BETWEEN ORGANIC FOOD CONTAMINANTS AND PLASTIC PACKAGING MATERIALS

P. ŠIMKO[a], B. SKLÁRŠOVÁ[a], P. ŠIMON[b] and
B. DROBNÁ[c]

[a]*Food Research Institute, Priemyselna 4, P. O. Box 25, 824 75 Bratislava,*
[b]*Institute of Physical Chemistry and Chemical Physics, Faculty of Chemical and Food Technology, Slovak University of Technology, Radlinského 9, 812 37 Bratislava, Slovakia,*
[c]*Department of Toxic Organic Pollutants, Research Base of the Slovak Medical University, Limbova 12, 833 03 Bratislava, Slovakia,*
simko@vup.sk

Introduction

Polychlorinated biphenyls (PCBs) are a group of 209 man-made organic chemicals containing carbon, hydrogen and differing amounts of chlorine. The commercial production of PCBs started in 1929 but their use had been banned or severely restricted in many countries since the 1970s and 80s because of serious risks to human health and the environment. PCBs have been used in a wide range of products such as plastics, paints, and adhesives. Since PCBs are resistant to acids and bases as well as to heat, they have mainly been used in electric equipment as heat transfer fluids, or lubricants, respectively. Disposal of waste that contains PCBs in landfills or incinerators can lead to environmental contamination. PCBs were first detected in environmental samples in 1966[1]. PCBs can persist in the environment and accumulate in animals and along the food-chain. A human organism may be exposed to PCBs by ingestion of contaminated food and water, or inhaling contaminated air. PCBs have been shown to cause cancer and a number of serious non-cancer health effects in animals, including effects on the immune system, reproductive system, nervous system, endocrine system, more frequent infections, and changes of the skin, particularly rashes and chloracne. Their harmful effects to man and the environment are well documented in a number of reviews.[2–7] Therefore, the elimination of PCBs from foods and the environment is important. Adsorption of organic contaminants on plastic packaging materials is a promising way of decreasing levels of organic contaminants in foods.[8–13] For example, on the basis of interactions with plastic package, the concentrations of polycyclic aromatic hydrocarbons (PAHs) in a liquid smoke flavour stored in low density polyethylene (LDPE) bottles were lowered by two orders during 14 days[8]. The rate-limiting step was diffusion in the liquid media[14]. PAHs were primarily adsorbed on the LDPE surface, with migration into the bulk of the polymer, intensifing the effectiveness of the removal process[15]. This process is also effective for removal of PAHs from solid media, e.g. benzo[a]pyrene content in duck meat was lowered by 75 % after 24 hours of interaction with LDPE[16]. The ability of polyethylene terephtalate (PET) to decrease PAH concentrations in polar and non-polar liquid media has already been unambiguously proven[9]. However, the removal was limited only to surface adsorption which led to equilibrium between liquid and solid phase. Moreover, this process was also affected by other compounds (vitamins, synthetic antioxidants, fytosterols, etc.) present in such liquid media as vegetable oils[12]. The aim of this work was to study the possibilities of PCB removal from water and rapeseed oil by adsorption onto PET and polystyrene (PS) receptacles.

Experimental

PET Receptacles

In the experiment, pre-bubbled PET receptacles of cylindrical shape with i.d. of 21.4 mm and height 150 mm were used. The receptacles were provided by Palma-Tumys. The company uses them for oil and fruit syrup packaging after blowing to volume of 2 dm^3.

PS Receptacles

PS tubes with i.d. of 23 mm and height 120 mm were supplied by Čechvalab (Bratislava, Slovakia).

PCB

PCB congeners (PCB 28 – 2,4,4'-trichlorbiphenyl; PCB 52 – 2,2',5,5'-tetrachlorbiphenyl; PCB 101 – 2,2',4,5,5'-pentachlorbiphenyl; PCB 103 – 2,2',4,5',6-pentachlorbiphenyl; PCB 138 – 2,2',3,4,4',5'-hexachlorbiphenyl; PCB 153 – 2,2',4,4',5,5'-hexachlorbiphenyl; PCB 174 – 2,2',3,3',4,5,6'-heptachlorbiphenyl; PCB 180 – 2,2',3,4,4',5,5'-heptachlorbiphenyl) were purchased from LABSERVICE (Spišská Nová Ves, Slovakia) each with the concentration of 100 µg ml^{-1} in hexane.

Solvents

Hexane of analytical grade was purchased from Merck, Darmstadt, Germany. The solvents were rectified just before use in a distillation apparatus.

Other Chemicals and Materials

Anhydrous Na$_2$SO$_4$, was also purchased from Merck.

Experiment

Distilled water was spiked with six PCB congeners solutions diluted in acetone to obtain final concentration in water between 1–7 µg dm^{-3}. Then the water was heated to 40 °C for 1 hour and occasionally shaken to evaporate residual acetone. After cooling to 19 °C, the water was sampled for initial PCB concentration. Then the PET and PS receptacles were filled with the spiked water and placed into a polystyrene box to protect them from light and to keep constant temperature of 19.2 °C. The temperature was monitored and recorded by a thermometer (ThermoScan, BDV, mesto, Netherlands). The samples for analysis were taken after 1; 3; 5; 7; 11; 24; 72 h. To maintain the same conditions, a new set of receptacles was taken for each analysis.

Sample Preparation

5 ml of water were extracted with hexane four times. Hexane layers were combined, dried with anhydrous Na_2SO_4 and evaporated until nearly dry. Remaining solvent was evaporated at room temperature just before analysis. The residuum was dissolved in a known volume of standard solution of PCB-103 and analysed by GC.

GC Analysis

Analysis were performed on gas chromatograph Agilent Technologies 6890N equipped with electron capture detector using capillary GC column DB-5, 60 m × 0.25 mm (i.d.), 0.25 μm film thickness (purchased from J&W Scientific, Folsom, California, USA) using splitless technique with temperature program as follows: isothermal at 110 °C for 1.5 min., then temperature elevation to 200 °C at 30 °C min^{-1}, hold for 0.2 min, then temperature elevation to 300 °C at 2.5 °C min^{-1}. Helium was used as carrier gas with a constant flow rate of 0.8 ml min^{-1}.
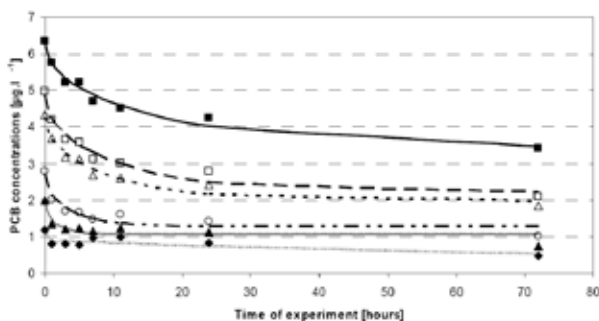
Fig. 1. **Changes in PCB concentration in water stored in PET receptacles (experimentally obtained data compared with data calculated using the kinetic equation of adsorption[1])**
(♦) – PCB 28 c_{exp}, (▨) – PCB 28 c_{cald}, (▲) – PCB 52 c_{exp}, (▨) PCB 52 c_{cald}, (○) –PCB 101 c_{exp}, (— — —) – PCB 101 c_{cald}, (Δ) – PCB 138 c_{exp}, (-) – PCB 138 c_{cald}, (□) – PCB 153 c_{exp}, (— —) – PCB 153 c_{cald}, (■) – PCB 180 c_{exp}, (——) – PCB 180 c_{cald}

Results

At experiments the concentration of PCBs started to decrease immediately after filling the receptacles in both systems studied as seen from Figs. 1 and 2.

The observed dependences of PCBs concentration *vs.* time were modelled using the kinetic equation (1), which has been derived for the diffusion of PAHs in non-stirred liquids placed into cylindrically shaped receptacles[9]:

$$c_t = c_\infty + (c_0 - c_\infty)\sum_{n=1}^{\infty}\frac{4}{a^2\alpha_n^2}\exp\left[-D\alpha_n^2 t\right], \qquad (1)$$

where c_0 is the initial concentration of PCBs in water, c_t is the concentration of PCBs in the medium at time t, and c_∞ is the concentration of PCBs corresponding to infinite time (equilibrium), a is the radius of the cylinder, α_n are the roots
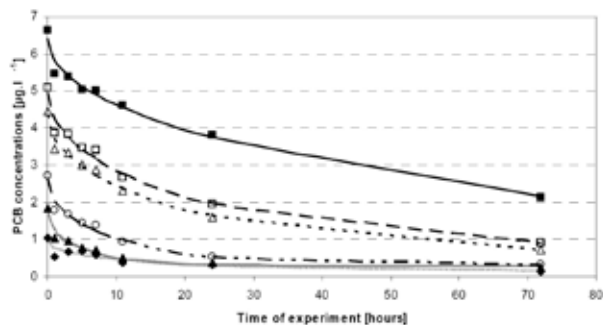
Fig. 2. **Changes in PCB concentration in water stored in PS receptacles (experimentally obtained data compared with data calculated using the kinetic equation of adsorption[1]).**
(♦) – PCB 28 c_{exp}, (▨) – PCB 28 c_{cald}, (▲) – PCB 52 c_{exp}, (▨) PCB 52 c_{cald}, (○) –PCB 101 c_{exp}, (— — —) – PCB 101 c_{cald}, (Δ) – PCB 138 c_{exp}, (-) – PCB 138 c_{cald}, (□) – PCB 153 c_{exp}, (— —) – PCB 153 c_{cald}, (■) – PCB 180 c_{exp}, (——) – PCB 180 c_{cald}

of the zero-order first-kind Bessel function and D is the diffusion coefficient of PCB in water. The parameters c_∞, $c_0 - c_\infty$ and D were identified by the non-linear least squares method by minimizing the sum of squares of differences between the PCB concentrations measured experimentally and those calculated by equation (1). The values of identified parameters are listed in Skláršová et al.[17].

The extent of PCBs removal can be characterized by the distribution coefficient expressed by the formula:

$$\beta = \frac{c_0 - c_\infty}{c_\infty}. \qquad (2)$$

The higher is the value of β, the greater part of PCBs is removed from water after reaching the equilibrium. The values of β are listed in Skláršová et al.[17]. The values of β for PS are much higher than the corresponding values for PET. This implies a much higher affinity of PCBs to PS in comparison with PET.

For understanding the sorption process, it is useful to quantify the ratio of the "total PCBs area" to the contact area of the plastic receptacles. The surface areas S of the molecules of the congeners were calculated using the Savol program (Tripos, St. Louis, Missouri, USA) and are summarised in Skláršová et al.[17]. The number of PCB molecules adsorbed on the polymer surfaces was calculated from the differences between the initial and the equilibrium concentrations of PCBs in water. The following formula gives C, the coverage of the plastic surface by the PCB monolayer:

$$C = \frac{N_A a (c_0 - c_\infty) S}{2M}, \qquad (3)$$

where M is the molar mass of the PCB, N_A is the Avogadro number. The results showed that the total area composed from partial PCB areas adsorbed onto PET is equal to 30.2 %

of the total PET area, while the total area adsorbed onto PS from water is equal to 50.7 %. These values indicate that the PCBs removal from water could be classified as monomolecular adsorption on the plastic surfaces. The values of PCB diffusion coefficients in water, calculated from equation (1) for both experimental systems are not very different which indicates that the same physicochemical processes take place in the PCB removal process from water. The curves of PCBs concentration *vs*. time are subject to measurement uncertainties that propagate into the values of *D*.

Conclusions

The results and findings of this work lead to the following conclusions:

- The PCB concentration in the water filled into PET and PS receptacles decreases due to adsoption of PCBs onto the surface of plastics.
- The interaction PCB – plastics can be classified as a monomolecular adsorption of PCBs on the polymer surface so that it can be expected that the adsorption equilibrium will obey the Langmuir isotherm.
- The values of diffusion coefficients obtained enable to predict the rate of PCB elimination at any time of the interaction; the values of the distribution coefficients characterize the extent of the PCBs removal.
- Although both polymers are suitable for PCB removal, PS is far more effective in comparison with PET.

REFERENCES

1. Jensen S.: *Report of a new chemical hazard. New Scientist, 32*, pp. 116, 1966.
2. IARC Monographs on the evaluation of the carcinogenic risk of chemicals to humans. Vol. 18. Polychlorinated biphenyls and polybrominated biphenyls. Lyon : International Agency for Research on Cancer, 140 p, 1978.
3. IARC Monographs on the evaluation of the carcinogenic risk of chemicals to humans. Supplement 7. Overall evaluation of carcinogenicity: An updating of IARC monographs, Vol 1 to 42. Lyon : International Agency for Research on Cancer, 440 p, 1987.
4. Lorenz H., Neumeier G.: *Polychlorinated biphenyls (PCBs)*. A joint report of the Federal Health Office and the Federal Environmental Agency. BGA Publication No.4/83. Munich: mmV Medizin Press, 1983.
5. Kimbrough R. D.: Annu. Rev. Pharmacool. Toxicol. *27*, 87 (1987).
6. Toxicological profiles for polychlorinated biphenyls. Washington, D.C. : U.S. Department of Health and Human Services, Agency for Toxic Substances and Disease Registry, 1993.
7. Environmental Health Criteria 140. Polychlorinated biphenyls and Terphenyls. 2nd ed. Geneva : World Health Organization, 682 p, 1993.
8. Šimko P.,Brunncková B.: Food Addit. Contam. *10*, 257 (1993).
9. Šimko P.,Šimon, P., Belajová, E.: Eur. Food Res. Technol. *219*, 273 (2004).
10. Šimko P., Skláršová B., Šimon P., Belajová E.: Eur. J. Lipid Sci. Technol. *107*, 187 (2005).
11. Šimko P., Skláršová B., Šimon P., Belajová E.: Czech J. Food Sci. *24*, 143 (2006).
12. Skláršová B., Šimko P., Šimon P., Belajová E.: J. Food Nutr. Res. *45*, 12 (2006).
13. Šimko P., Kolek E., Skláršová B., Šimon P.: J. Food Nutr. Res. *45*, 179 (2006).
14. Šimko P., Šimon P., Khunová V., Brunncková B., Drdák M.: Food Chem. *50*, 65 (1994).
15. Šimko P., Šimon P., Khunová V.: Food Chem. *64*, 157 (1999).
16. Chen J., Chen S.: Food Chemistry *90*, 461 (2005).
17. Skláršová, B., Šimko, P., Šimon, P., Drobná, B.: J. Food Nutr. Res. *46*, 128 (2007).

L13 ANALYSIS OF *FUSARIUM* MYCOTOXINS: A CRITICAL ASSESSMENT

MILENA ZACHARIÁŠOVÁ[a], JANA HAJŠLOVÁ[a], JAN POUSTKA[a], MARTA KOSTELANSKÁ[a], ALEXANDRA KRPLOVÁ[a] and LUKÁŠ VÁCLAVÍK[a]

[a]*Institute of Chemical Technology, Prague, Faculty of Food and Biochemical Technology, Department of Food Chemistry and Analysis, Technicka 3, 166 28 Prague 6, Czech Republic, milena.zachariasova@vscht.cz*

Introduction

Mycotoxins, secondary metabolites of microscopic filamentary fungi, are compounds generally considered to be very toxic. Their occurrence in agricultural commodities represents a major health concern for humans and animals. One of the most important fungi genera, that produce mycotoxins, is *Fusarium*. *Fusarium* species are able to produce lots of structurally different mycotoxins including trichothecenes, zearalenones and fumonisins. Trichothecenes are a group of tetracyclic seskviterpene alcohols and can be divided into two groups: type A and type B (they differ from each others in the existence of ketone at C8 in trichothecene type B molecule). The main representatives of type A trichothecenes include e.g. T-2 toxin, HT-2 toxin, diacetoscirpenol, 15-acetoscirpenol and neosolaniol. The most important naturally occurring type B trichothecenes is deoxynivalenol representing the most abundant trichothecene found in cereals, followed by 15 acetyldeoxynivalenol, 3-acetyldeoxynivalenol, nivalenol and fusarenone-X. Other mycotoxins belonging to the genus Fusarium are fumonisins (esters of 20-carbone backbone and two tricarballylic acids) and zearalenone (substituted lacton of resorcyclic acid).[1–3] Beside free mycotoxins, the existence of mycotoxin conjugates, toxins bound to more polar compounds like glucose, which originate as a result of mycotoxins metabolism by plants, was proved[4,5]. Deoxynivalenol-3-glucoside (DON-3-Glc) was found to be dominating[6].

Because of relatively high incidence of mycotoxins, there is an urgent need for effective monitoring of these compounds in foodstuffs. Over the past 15 years, a great progress in mycotoxins analysis area has been made. Sampling contributes to the largest variability in the analysis of mycotoxins , thus, obtaining of a representative sample represents a crucial step. Sampling strategies of agricultural commodities within mycotoxin analysis are defined by the European legislation EC/401/2006.[7–9]

There are various criteria typically considered when analytical method is developed. Not only the overall cost, but also other factors such as speed of the analysis, level of technical skills of an analyst, and the type of results provided by the method (qualitative or also quantitative) need to be balanced and the relative importance of each criterion evaluated. Especially for multidetection methods, when a large number of mycotoxins possessing a wide range of physicochemical properties considered, a compromise between the factors mentioned above is usually needed.[8–10]

The first step in multimycotoxin analysis includes the isolation of particular analytes. The extraction should perform a compromise between the solvent strength required for the transfer of analytes from the matrix to the solution and the compatibility of solvent with further analytical process. An acetonitrile – water (84 : 16, v/v) mixture is commonly used providing sufficient recoveries, and simultaneously minimises number of co-extracted matrix compounds. Additionally, this solvent mixture represents an azeotropic composition and thereby its evaporation within further sample preparation procedure is facilitated[11].

Once the sample extract is obtained, the clean-up step should be performed to remove impurities potentially interfering during the determination step. Beside this, the clean-up procedure helps to concentrate the mycotoxins prior to their analysis; especially immunoaffinity columns based on specific immunochemical reaction of analyte and antibody present in the cartridge are very convenient for this purpose. The specificity of immunoaffinity clean-up for only one target mycotoxin or class of mycotoxins can be in some respect a limiting factor, particularly in the case of multimycotoxin analysis[9,12]. However, multimycotoxin immunoaffinity clean-up cartridges specific to a wide range of analytes are already available[13,14]. Additionally, common SPE approaches representing by e.g. MycoSep columns are also widely used. The main advantage of MycoSep clean-up is the speed of procedure: no time-consuming rinsing steps as in the case of immunoaffinity and/or other SPE clean-up are required.[15–17]

The final step of the analytical procedure is the determinative step. Nowadays, reference methods for mycotoxins determination involve almost exclusively liquid chromatography coupled to tandem mass spectrometry (LC-MS/MS), which provide both selectivity and sensitivity of the detection.[7–9] There are no limitations in sample preparation such as derivatisation step, which is needed within the gas chromatographic approaches GC-ECD or GC-MS (*Note*: derivatisation of hydroxyl groups in order to attain the volatility is typically performed using heptafluorobutylimidazole or trimethylsilylether).[18–20] A challenging option in the field of LC-MS analysis is the use of high-resolution system LC-TOFMS, which provides a feasible tool for non target masked mycotoxin screening.

Beside classical confirmatory chromatographic methods mentioned above, there are also methods based on immunological assays. Especially ELISA as rapid quantitative tools for mycotoxin analysis is very suitable. However, possible overestimation of results caused by cross-reactions with compounds similar to target analytes could be a limitation of this approach.[7–9,17]

In the following text, three different analytical approaches are discussed. Firstly, performance characteristics of GC-ECD and LC-MS/MS methods are compared. Secondly, results obtained by means of two commercial ELISA assays and reference LC-MS/MS method are introduced. A proof of ELISA capability in terms of its cross-reaction potential is presented.

Experimental

Materials and Methods

Standards of mycotoxins nivalenol (NIV), deoxynivalenol (DON), deoxynivalenole-3-glucoside (DON-3-Glc), 3-acetyldeoxynivalenol (3-ADON), 15-acetyldeoxynivalenol (15-ADON), fusarenone-X (fus-X), T-2 toxin (T-2), HT-2 toxin (HT-2) and zearalenone (ZEA) were purchased from Biopure (Tulln, Austria). A Synergi Hydro RP column (Phenomenex, Torrance, CA, USA), a liquid chromatograph HP1100 Binary Series LC system (Agilent Technologies, Palo Alto, CA, USA) coupled to an ion trap mass analyser LCQ Deca (Finnigan, San Jose, CA, USA) were employed for LC separation and MS/MS detection. For GC–ECD method, a gas chromatograf HP 5890 Series II with an electron capture detector (^{63}Ni) and a capillary column HP-35 (30 m × 0,25 mm I.D. × 0,25 μm phase) with (35%-fenyl)-methylpolysiloxan stationary phase (Agilent Technologies, Palo Alto, CA, USA) were used. For ELISA analysis, two commercial available DON kits, i.e. Ridascreen® DON (R-Biopharm, Darmstadt, Germany) and AgraQuant® DON Assay 0.25/5.0 Test Kit (Romer Labs, Tulln, Austria), were purchased.

GC-ECD method: An amount of 10 g of homogenised ground sample was extracted by shaking with 100 mL of an acetonitrile–water mixture (84:16, v/v) for one hour and extract was filtered (Filtrak No. 390, VEB Freiberger, Berlin, Germany). The crude extract was passed through MycoSep™ #225 and four millilitres of cleaned extract was evaporated. Residue after evaporation was redissolved in methanol, transferred into the derivatisation vial, and after methanol evaporation using a gentle stream of nitrogen, derivatisation for 20 min at 60 °C using 100 μl trifluoracetanhydride with addition of 10 mg NaHCO$_3$ was performed. Further, 500 μl of isooctane, 1 ml of deionised water and 0.5 g of anhydrous sodium sulphate was added followed by removing of 300 μl of the organic layer and addition of 200 μl of isooctane to the vial for GC–ECD analysis.

LC-MS/MS method: An amount of 12.5 g of homogenised ground sample was extracted by shaking with 50 mL of an acetonitrile–water mixture (84:16, v/v) for one hour and the crude extract was filtered (Filtrak No. 390, VEB Freiberger, Berlin, Germany). Eight millilitres of filtered extract were passed through the MycoSep™ #226 column and four millilitres of filtered extract were evaporated to dryness and dissolved in 1 mL of a water–methanol mixture (50:50, v/v). Finally, the sample was passed through a 0.2 μm microfilter (Alltech, Deerfield, IL, USA) prior to analysis.

ELISA: In case of immunochemical assays, both sample preparation and the ELISA analysis itself were carried out strictly according to manufacturer recommendations. An amount of 20 g of ground sample was extracted with 100 ml of deionised water and vigorously shaken for 3 minutes. Further, the extract was filtered and an appropriate aliquot was placed into the microwell.
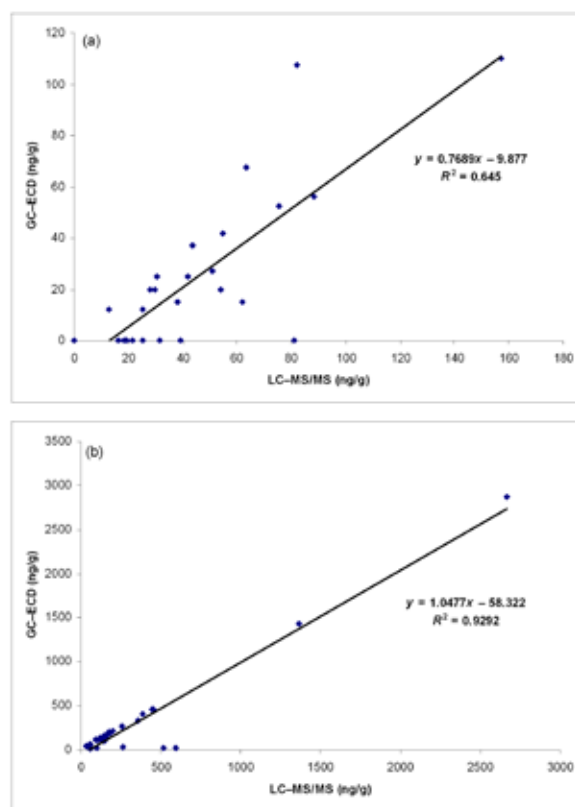
Fig. 1.　**Correlation of the results of wheat samples obtained by LC–MS/MS and GC–ECD methods for a) NIV b) DON.**
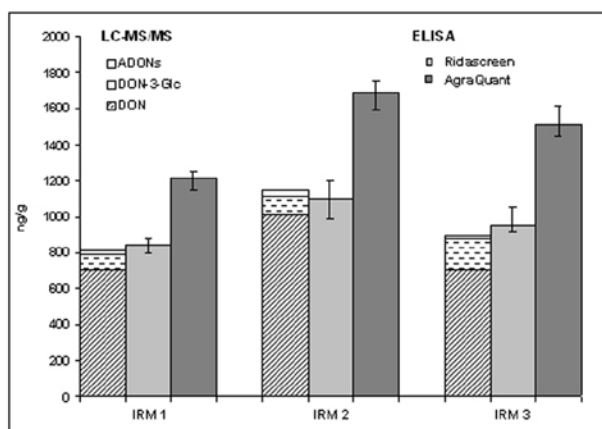
Fig. 2.　**DON content in reference materials measured by LC–MS/MS and two types of commercial ELISA kits.**

GC-ECD vs. LC-MS/MS

Using the previously used GC–ECD method, NIV, DON, FUS-X, 3-ADON, 15-ADON, HT-2 and T-2 were analysed within a single run. Recoveries 68–97% and relative standard deviations (RSDs) ≤16 % were obtained for all of analytes analysed. As regards LC–MS/MS method, the scope of target analytes has been extended for ZEA and "masked" mycotoxin DON-3-Glc. Recoveries of LC-MS/MS

ranged between 76–95 % with exception of NIV and DON-3-Glc, where recoveries were somewhat lower (approx. 65 and 43 %, respectively). The low recoveries of NIV and DON-3-Glc can be contributed to their partial adsorption onto the polar MycoSep™ #226 column cartridge. In spite of somewhat recoveries for NIV and DON-3-Glc, the RSDs of LC-MS/MS method were ≤10%.

The detection limits (LODs) were 2–10 times lower for LC-MS/MS compared to GC-ECD. In addition, for T-2, the LOD decreased even less (from 130 to 1 ng g^{-1}) by employing LC-MS/MS procedure.

With respect to our effort to increase the DON-3-Glc recovery, the LC-MS/MS analytical procedure was performed without MycoSep clean-up step. Although the LODs of LC-MS/MS method were approximately 5 times higher compared to LC-MS/MS method with MycoSep™ #226 clean-up. , the recovery of NIV and DON-3-Glc increased to 78 and 89 %, respectively. Since a higher amount of matrix components is introduced to the MS system (causing the ionisation suppression in ESI ion source), it is important to use for quantification purposes the matrix-matched standards to avoid quantification errors.

For comparison purposes, the data obtained by GC-ECD (with MycoSep™ #225 clean-up) and LC–MS/MS methods (with MycoSep™ #226 clean-up), a set of 25 naturally contaminated wheat samples has been analysed. With regard to low incidence of other mycotoxins than DON and NIV in the investigated samples, correlation of results was carried out for these two analytes only (see Fig. 1.). As shown in Fig. 1.a, GC-ECD method provided systematically underestimated results for NIV compared to LC-MS/MS. This phenomenon can be explained by decomposition of NIV during derivatisation[18]. For DON, acceptable correlation between GC-ECD and LC-MS/MS results was achieved (except of five outliers). Discrepancies between the results presumably lies also in the crucial derivatisation step[21,22].

E L I S A *v s .* L C - M S / M S

Once the immunochemical assay was performed, comparison with results obtained by LC-MS/MS was accomplished. We should note that LC-MS/MS analyses were performed without MycoSep clean-up to avoid the discrimination of DON-3-Glc caused by its trapping on MycoSep cartridges. As shown in Fig. 2., the results obtained by ELISA (Ridascreen) are comparable to that of LC-MS/MS (*Note*: total DON content calculated from DON-3-Glc and acetylated DONs contribution is considered). Whereas AgraQuant kit provided overestimated results compared to LC-MS/MS (overestimation 49, 46 and 69 % for if total DON obtained by LC-MS/MS is considered 100 %). This trend could be explained by cross-reaction of kit antibodies with matrix components and/or with other DON conjugates. Similar phenomenon was observed during the analysis of beer samples by AgraQuant ELISA kit (overestimation compared to total DON determined by LC-MS/MS was up to 600 %)[23].

Conclusions

Different analytical strategies for sample preparation and instrumental analysis for the determination of mycotoxins were investigated. The choice of method used depends on various factors such as overall cost, detection level required, complexity of matrix and available instrumentation. Obtained results differed by method used, which was demonstrated especially for DON and partially also for NIV. For GC-ECD, derivatisation step was shown to the most critical part of the method; losses of analytes were demonstrated compare to LC-MS/MS approach. As regards ELISA assays (determination of DON), they tended to overestimate the results compare to LC-MS/MS method. We hypothesis that this can be partially explained by the cross-reactivity to DON conjugates (acetylated DONs and DON-3-Glc shown in our recent study)[23], however further research is needed to fully explain this phenomenon.

REFERENCES

1. Moss M. O., Thrane U.: Tox. Lett. *153*, 23 (2004).
2. Cumagun C. J. R. Rabenstein F., Miedaner T.: Plant Pathol. *53*, 446 (2004).
3. Yu K., Yuan X., Huang B.: Siliao Yanjiu, *2006*, 35.
4. Berthiller F., Lemmens M., Werner U., Krska R., Hauser M. T., Adam G., Schuhmacher R.: Mycotoxin Res. *23*, 68 (2007).
5. Berthiller F., Werner U., Adam G., Krska R., Lemmens M., Sulyok M., Hauser M. T., Schuhmacher R.: Ernaehrung *30*, 477 (2006).
6. Berthiller F., Krska R., Dall'Asta C., Lemmens M., Adam G., Schuhmacher R.: Mycotoxin Res. *21*, 205 (2005).
7. Krska R., Molinelli A.: Anal. Bioanal. Chem. *387*, 145 (2007).
8. Pittet A.: Mitteilungen aus Lebensmitteluntersuchung und Hygiene *96*, 424 (2005).
9. Krska R., Schubert-Ullrich P., Molinelli A., Sulyok M., MacDonald S., Crews C.: Food Addit. Contam. *25*, 152 (2008).
10. Miller J. D.: Food Addit. Contam. *25*, 219 (2008).
11. Sulyok M., Krska R., Schuhmacher R.: Anal. Bioanal. Chem. *389*, 1505 (2007).
12. Barricelli M., Schmidt K., Boerner B.: Deutsche Lebensmittel-Rundschau *104*, 22 (2008).
13. Lattanzio V. M. T., Solfrizzo M., Powers S., Visconti A.: Rapid. Commun. Mass Spectrom. *21*, 3253 (2007).
14. MacDonald S., *XII IUPAC Symposium on Mycotoxins and Phytotoxins, Istanbul, 21-25 May 2007* (Poster no. 1438).
15. Liang Y., Liu L., Zhang Ch.: Zhongguo Liangyou Xuebao *21*, 160 (2006).

16. Pussemier L., Pierard J. Y., Anselme M., Tangni E. K., Motte J. C., Larondelle Y.: Food Addit. Contam. *23*, 1208 (2006).
17. Krska R.: J. Chromatogr. A *815*, 49 (1998).
18. Croteau S. M., Prelusky D. B., Trenholm H. L.: J. Agric. Food Chem. *42*, 928 (1994).
19. Razzazi-Fazeli E., Rabus B., Cecon B., Bohm J.: J. Chromatogr. A *968*, 129 (2002).
20. Langseth W., Rundberget T.: J. Chromatogr. A *815*, 103 (1998).
21. Welzig E., Drs E., Josephs R. D., Schothorst R. C., van Egmond H. P., Pettersson H., Chan D., Krska R.: Mycotoxin Res. *21*, 224 (2005).
22. Krska R., Welzig E., Drs E., Josephs R. D., Schothorst R. C., van Egmond H. P., Pettersson H., Chan D., MacDonald S.: J. AOAC Int. *89*, 1573 (2006).
23. Zachariasova M., Hajslova J., Kostelanska M., Poustka J., Krplova A., Cuhra P., Hochel I.: Anal. Chim. Acta (paper submitted).

3.2. Posters

P01　DETERMINATION OF B-CAROTENE IN THE GELATIN CAPSULE

ZUZANA KOLAJOVÁ[a], BAYANMUNKH ALTANGEREL[a], DANIELA KRAMÁŘOVÁ[a], OTAKAR ROP[a] and IGNÁC HOZA[a]

[a]Department of Food Engineering Faculty of Engineering, Faculty of Technology, TBU in Zlin, Czech Republic, bayanmunkh_mn@yahoo.com

Introduction

β-carotene is the most well known of the carotenoids, a phytonutrients family that represents one most of the widespread groups of naturally occurring pigments. Steenbock suggested that the plant pigment carotene was responsible for the vitamin A activity and that carotene could not be vitamin A, it may be converted metobolitically to the actual vitamin in the 1919[1]. β-carotene consists of a chain of 40 carbon atoms, with conjugated double bonds and a ring structure at each end of the chain. Depending on the positions of the molecular groups attached to the carbon chain, naturally occurring beta carotene may be: *cis-trans* and all *trans* isomers. The most common carotenoid in all green plants is β-carotene. Animal and our body cannot synthesis β-carotene and they depend on feed for their supply. There are many studies showing β-carotene can show role of antioxidant potency. Also several studies have been focused on the content of β-carotene in food products, food supplements and biological fluids.[2–4]

One of the vitamin supplement package products is gelatin capsule. Gelatin capsule has a very rapid dissolution property, usually 90 seconds in water at 37 °C. So, this protein is a very useful raw material for emulsifier in food, pharmaceutical and others products. Previous studies show that gelatin is used as a carrier, coating or separating agent for other substances. Supplemental intake of β-carotene probably should not exceed 3–15 mg per day. β-carotene supplements are found on the Generally Recognized as Safe (GRAS) list issued by the Food and Drug Administration.

The purpose of this study was to find new method for determination of β-carotene and isolation process, of course.

Experimental

High-performance liquid chromatography is generally accepted as the modern method of choice to separate, identify, and quantify carotenoids. Specially, it combined with ECD, UV-VIS and fluorescence detector are the common method for determination and identification of β-carotene in vegetables and other samples.

C h e m i c a l s   a n d   M a t e r i a l s

β-carotene was obtained from personal prepared tablet materials (at TBU in Zlin). Methanol (purity: 99.8 %), acetonitrile (purity: 99.9 %) were obtained from Merck KGa (Darmstadt, Germany). Phosphoric acid (purity: 85 %) was obtained from Chemapol (Prague, Czech Republic). All solvents were of HPLC grade. Deionized water, purified by Aqua osmotic system (Aquaosmotic, Tisnov, Czech Republic) was used for solve sample preparation stages. Hexan (purity: 99.9 %) was obtained from Penta (Prague, Czech Republic), was used in extraction of sample. Ethanol was obtained from Chemapol (Prague, Czech Republic), used to solve sample after evaporation.

E q u i p m e n t   a n d   C h r o m a t o g r a p h i c
C o n d i t i o n s

HPLC separation was performed using HPLC with ECD detection (Coulochem III, ESA). Potentials of the cells for detector were 500 and 600 mV.

β-carotene was separated on the Supelcosil LC18 DB (250×4.6 mm,5 μm) with a mobile phase of methanol/acetonitrile/phosphoric acid (70 : 29.5 : 0.5, v/v/v) at a flow rate of 1.1 ml min^{-1}. The separation was carried out ambient temperature. In this experiment we used isocratic elution.

S a m p l e   P r e p a r a t i o n

Filling from gelatin capsule was dissolved into 10 ml of deionized water and after that extracted using 10 ml of n-Hexan solution and extraction process was repeat six times. After extraction, sample solution was evaporated to dryness in rotary evaporator at 35–40 °C. After evaporation, the residue was dissolved in 10 ml of ethanol and was filtered trough 0.45 μm filter (Nylon) before injected into column. Sample (20 μl) was injected into a column that has been equilibrated with solvent mixture of mobile phase.

Results

The total carotenoid content of the tested gelatin capsule of vitamin supplement (β-carotene, extract from blueberries) was 6 mg (Table I).

Table I
β-carotene content in the gelatin capsules

Name	Weight [g]	β-Carotene [mg]	Extraction of blueberries [mg]
	0.3156	6	150
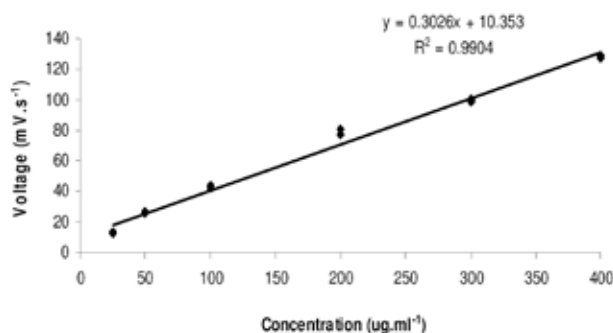
Fig. 1.　**Calibration curve of β-Carotene**

Standard curve of β-carotene are shown in Fig. 1. We prepared standard solution from 25 µg ml^{-1} to 400 µg ml^{-1} for construction of a standard curve in our study.

We were interested to quantification of real value of β-Carotene in oil matrix gelatin capsule vitamin supplement. We were conducting extraction process at water bath at 30 °C for 2 min and at ambient temperature. The samples were completely extracted 6 times after 30 minute extraction using n-hexane.
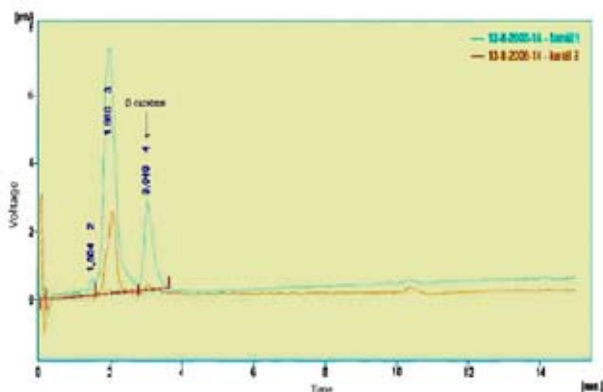
Fig. 2.　**Chromatograms of a gelatin capsule vitamin supplements**

Peak 3 were positively identified like β-carotene. Each sample was measured five times (Table II).

Result of our study shows 5.83±0.02 mg per capsule β-carotene in examined samples.

Table II
Content of β-carotene in a gelatin capsule vitamin supplement

Sample	Average peak area [mV s^{-1}]	Content of β-caroten in tablet [mg]
1	52.00	5.804
2	51.25	5.700
3	53.30	5.986
4	52.45	5.867
5	53.40	5.999
Average	52.48	5.83±0.020

Conclusions

This study shows that the gelatin capsule vitamin supplement analyzed here contains 5.83 ± 0.02 mg of β-carotene. Producer declares 6.00 mg in each capsule. Must be checked it, if producer has a right vehicle for mixture of β-carotene and blueberry extract, because we have verified our method with standard addition. Finally we can conclude that HPLC with ECD method have shown to be acceptable for determination and quantification of β-carotene in a gelatin capsule vitamin supplements.

REFERENCES
1. Gerald F.: Jr. "The vitamins" fundamental aspects in nutrition and health *1999*, 23.
2. Hiroshi Iwase.: J. Anal. Chem. Act. *463*, 21 (2002).
3. Olives Barba A. I., Camara Hurtado M, Sanchez Mata M. C., Fernandez Ruiz V., Lopez Saenz de Tejada M.: J. Food Chem. *95*, 328 (2006).
4. Ferruzzi M., Mario G.: J. Anal. Biochem. *256*, 74 (1998).

P02 DETERMINATION OF B-CAROTENE IN TOMATO BY HIGH PREFORMANCE LIQUID CHROMATOGRAPHY WITH ELECTROCHEMICAL DETECTOR

PETRA VOJTÍŠKOVÁ[a], BAYANMUNKH ALTANGEREL[a], DANIELA KRAMÁŘOVÁ[a], OTAKAR ROP[a] and IGNÁC HOZA[a]

[a]*Department of food Engineering, Faculty of Technology, T.Bata University in Zlin, Czech Republic,*
bayanmunkh_mn@yahoo.com

Introduction

Commonly studied carotenoid in the human diet is β-carotene because of its antioxidative and provitamin A activities. Provitamin A carotenoids, particularly β-carotene in fruits and vegetables, are the major source of vitamin A for its deficiency is a serious health problem in many developing countries. The abundant sources of β-carotene are sweet potatoes, carrots, spinach, tomato and other vegetables and fruits. Since tomatoes are major use for human dietary in many countries, it is becoming a prevention of deficiency of antioxidant vitamins. Many studies have been focused on antioxidant vitamins content in tomatoes. Abdulnabi et al.[1] investigated the antioxidative vitamin (vitamin E, vitamin C and β-carotene) content in tomatoes cultivated in Hungary, using HPLC. This study suggests that the highest values of β-carotene were found in Gitana, Katinka and Delfino cultivars (3.13–3.79 $\mu g\,g^{-1}$) and the lowest levels of β-carotene were in Tampo and Selma cultivars. Therefore, β-carotene occurs in tomatoes and various tomato products in amount of 0.23–2.83 mg 100 g^{-1}(ref.[2]).

The objective of this work was to estimate, using modern analytical techniques (ESA Coulochem III Multi-Electrode Detector), and the β-carotene content of tomatoes.

Experimental

High performance liquid chromatography (HPLC) is the most commonly used method for the separation, quantitation, and identification of carotenoids found in vegetables samples.

Sample Preparation

Initially a 10 g sample of tomato was placed in a 50 ml flask and mixed with 26 ml of extraction solvent (acetone : hexane, 50 : 50, v/v). The mixture was shaken in a water bath at 35 °C for 20 min. The upper phase was collected and poured into a 50 ml flask. The lower phase was extracted again with same solvent and shaken for 30 min. The upper phase was also collected and poured into the same flask. After filtration through Filtrak No.390 filter paper. The filtrate was poured into a 250 ml flask and evaporated under vacuum at 30 °C and residues were redissolved in 5 ml of ethanol. The solution was filtrated through a 0.45 µm nylon filter and 20 µl was injected into HPLC system. HPLC separation was performed using ESA HPLC with ECD detection

(Coulochem III) which is equipped with analytical column Supercosil LC18-DB (250 × 4.6mm, particle size 5 µm). Separation took place at 30 °C, flow rate of mobile phase (methanol : acetonitrile : phosphoric acid) was 1.0 ml min^{-1}. Potentials of the cells for detector were 500 and 600 mV.

β-carotene standard solution concentrations ranging from 25 to 400 µl ml^{-1} were prepared for the standard curve.

Identification and Quantification of β-carotene in Tomato

The identification of β-carotene was carried out by the retention time. The equation from the calibration curve was used for the calculation of the amount of β-carotene in tomatoes. The regression equation and correlation coefficient (R^2) were obtained using Microsoft Excel 2003 software to calculate the quantity of β-carotene in tomatoes.

Results

Typical chromatogram depicting the separation of a β-carotene standard solution is shown in Fig. 1. We were interested in checking chromatographic condition and retention time of β-carotene using a selected method in this investigation.
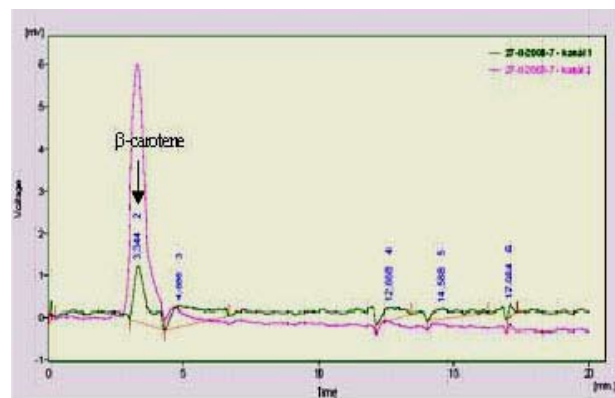
Fig. 1.　**Chromatogram of standard β-carotene**

The predominant peak at approximately 3.3 min is β-carotene. This value is used for identification of β-carotene in samples. The calibration curve was measured with the
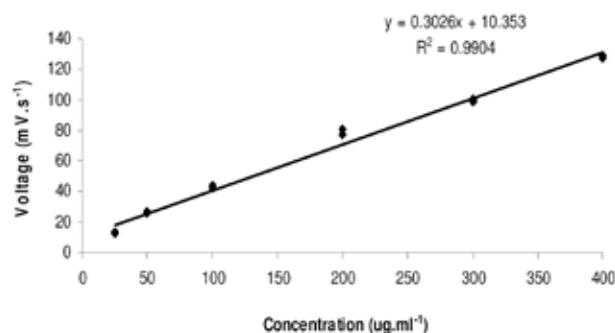
Fig. 2.　**Calibration curve of β-Carotene**

standard of β-carotene that was dissolved in ethanol. Fig. 2. shows calibration curve of a standard β-carotene.

The regression equation was obtained from the calibration curve of β-carotene, $y = 0.3026 x + 10.353$ ($R^2 = 0.9904$). This studied range was appropriate to calculate concentration of β-carotene in tomatoes.

The small peak showing the β-carotene on Fig. 3. (very closely at 2.912 min) has not been identified, because it is an admissive peak area that matches β-carotene's peak in chromatograms.
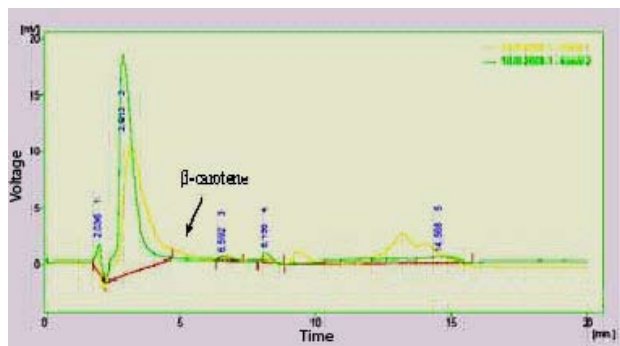
Fig. 3.　**Chromatograms from tomato extract**

However, this does not pose any problem; usually tomatoes do not contain high concentration of β-carotene. Result of this chromatogram suggests the presence of other organic compounds in tomato. Many study indicated that lycopene and/or other common cartenoids's levels are higher than β-carotene in tomatoes.

Table I shows the results obtained from the analysis of β-carotene in different samples. The first sample was immediately extracted with extraction solution after purchased from supermarket. The second sample was stored 2 weeks in a refrigerator before extraction.

The higher value of β-carotene (1.197 mg 100 g^{-1}) was obtained with the first sample. The values obtained in this

Table I
Tomato concentration of β-carotene

Sample	Weight [g]	Peak area [mV s^{-1}]	Amount of β-carotene [mg 100 g^{-1} of fresh mass]
1	10.0707	14.0	1.197
2	10.1726	1.6	0.024

study are very close to those reported by Olives Barba et al.[3], who reported a range of 0.6–1.2 mg per 100 g for β-carotene in 4 tomato varieties.

Bender (1993) has summarised the contradictory results of published studies designed to estimate the magnitude of vitamin loss during frozen storage of vegetables and fruits. Thus, we presumed that the content of β-carotene was reduced in second sample during storage period.

Conclusions

The present study shows that the measured levels of β-carotene (1.197 mg 100 g^{-1}) were low compared to the recommended intake. European epidemiological studies revealed 6–10 mg β-carotene as the recommended daily intake to provide good health and a reduction in risk of diseases (Lachance, 1998; National Research Council, 1989). Accordingly, one serving 100 g tested tomato contributes 11.97–19.95 % of the recommended daily intake of β-carotene.

REFERENCES

1. Abdulnabi A. Abushita, Emhemed, A, Hedshi, Hussien G, Daood, Reter A. Biacs: J. Food Chem. *60*, 207 (1997).
2. Barenska M., Schutze W., Schulz H.: J. Anal. Chem. *15*, 78 (2006).
3. Olives Barba. A. I., Camara Hurtado M., Sanchez Mata M. C., Fernandez RuizV., Lopez Saenz de Tejada M.: J. Food Chem. *95*, 328 (2006).

P03　PROTECTIVE EFFECT OF LYCOPENE FROM TOMATOES POWDER IN OXIDATIVE STRESS INDUCED BY ADMINISTRATION OF L-THYROXIN IN RATS

SANDA ANDREI, ADELA JOANTA, ADELA PINTEA and M. MERCA SARLEA

University of Agricultural Sciences and Veterinary Medicine, Faculty of Veterinary Medicine, Department of Biochemistry 3–5 Mănăştur Street, Cluj-Napoca, Romania,
sandrei@usamvcluj.ro

Introduction

Accumulating evidence has suggested that the hyperthyroidism is associated with increases in radical oxygen species (ROS) production and lipid peroxidation products in some tissues of rats. The response of the antioxidant systems is unclear. The changes in the levels of antioxidant enzymes in various tissues were found to be imbalanced and often opposite[1]. Lycopene, the main carotenoids in tomatos, has been shown to be a potent antioxidant in vitro and in vivo. Recent interest in lycopene is due to the finding of an inverse association between dietary lycopene and risk of some types of cancer and cardiovascular disease[2].

There are few literature data, which present studies regarding the effect of nonenzymatic antioxidants administration on oxidative stress induced by thyroid hyper function. In the present work, effects of the ingestion of tomatoes powder, rich in lycopene, on the activities of antioxidant enzymes (superoxid dismutase – SOD, catalase, and glutathion peroxidase), the oxidation of lipids and on fatty acids composition on liver, thyroid and myocardium were examined in rats intraperitonial injected with L-thyroxin.

Experimental

Experimental Procedure

Experiments were performed on three groups of male white Wistar rats: control (C – nontreated animals, normal diet); H group (treated animals with thyroxin and normal diet) and HT group (animals treated with thyroxin and tomatoes powder enriched diet). We induced hyperthyroidism by intraperitoneal L-thyroxine administration, $10\ \mu g\,(100\ g$ bodyweight$)^{-1}$, daily for a week. Daily dietary for group HT diet was supplemented with a natural product, tomato powder, obtained by Kunding Food Company. These powders contain $62.5\ \mu g$ lycopene $(1\ g\ powder)^{-1}$. Each rats from HT group received $25\ \mu g$ lycopene $(100\ g\ wet)^{-1}\ day^{-1}$ corresponding to $0.4\ g$ tomato powder $(100\ g\ wet)^{-1}\ day^{-1}$ during 7 days. After 8 days the animals were sacrificed and thyroid, liver and myocardium tissue were collected.

Biochemical Determinations

Protein extracts was obtained using potassium phosphate buffer (pH = 7.35). The activities of SOD, catalase, glutathion peroxidase and lipids oxidation were estimated in this protein extract using photometric methods[3].

Lipids extracts from different tissues was obtained with methanol and chloroform, based on Folch procedure The fatty acids analysis was made on total lipids extracts using gas-chromatography (GC)[4].

Results

In all biological samples we can observed an increase of antioxidant enzymes activities in H – rats compared with control. In the case of rats treated with diet rich tomatoes powder it can be observed a diminution of antioxidant activities probably due the antioxidant properties of lycopene (Table I). The increase of antioxidant enzymes activity in thyroidian tissue could be explained due to stimulation effect of thyroid hormones on protein shynthesis.

Table I
Antioxidant enzymes activity

Tissue/ Experimental groups	Catalase Ncat [g wet tissue^{-1}]	Glutathone peroxidase U GPx [g wet tissue^{-1}]	Superoxid dismutase U SOD [g wet tissue^{-1}]
Liver			
C	5068.79	62.93	225.69
H	8499.99	40.30	243.61
HT	5891.08	61.64	206.23
Thyroid			
C	410.10	4.66	58.87
H	793.33	7.66	83.99
HT	424.99	5.16	100.96
Myocardium			
C	717.64	20.18	53.84
H	835.08	28.55	11.33
HT	690.62	23.67	95.14

Lipid peroxides levels were significantly increased compared with control group. Oral administration of lycopene resulted in a significant reduction of lipid peroxides levels in HT-group compared with rats treated only with thyroxin (Table II).

Table II
Lipids peroxides level (MDA μmoles g wet tissue^{-1})

Experimental groups	Liver	Thyroid	Myocardium
C	1239.44	4.98	912.11
H	1750.40	12.91	1201.92
HT	1294.74	7.96	988.24

The results of the analysis of fatty – saturated fatty acids (SFA), monounsaturated fatty acids (MUFA) and polyunsaturated fatty acids (PUFA) – are showed in detail by Table III.

In thyroid gland, compare with the control, we can observed a decrease of total fatty acids content in experimental group treated with L-thyroxin. The determination of content

in PUFA and the ratio between UFA and SFA are the other methods that can be used in order to determinate the level of lipids peroxidation process. These ratio decrease in T group (so in this case appear a rise of lipids peroxidation level) but increase in group supplemented with lycopene.

Table III
Fatty acids contents in total lipids extract [mg g^{-1} wet tissue]

Tissue/FA	C group	H group	HT group
Liver			
SFA	1.56	3.59	10.07
MUFA	1.03	3.52	5.81
PUFA	1.36	5.70	18.15
Thyroid			
SFA	11.91	2.26	16.14
MUFA	5.85	1.20	7.95
PUFA	16.13	2.88	26.34
Myocardium			
SFA	4.02	2.23	5.32
MUFA	2.69	2.26	4.33
PUFA	4.35	3.08	8.68

Thyroid hormones stimulated the biosynthesis of FA in liver[5]. In the case of rats treated with L-thyroxin the FA content is higher compare with the control. The highest level apear in the case of rats from HT group because the administration of L-thyroxin as an effect the stimulation of FA synthesis and lycopene protect these acids against oxidation.

In myocardium fatty acids content decrease in T group compared with the control because in this tissue the lypogenic activities of thyroid hormones is lower compared with other tissue.

Conclusions

Tomatoes powder reduces the burden of oxidative stress in hyperthyroidism and led to reduction in lipid peroxidation and to increase in antioxidant level.

The administration of L-thyroxin has an effect a decrease of FA content in thyroid gland and myocardium. The content of FA in hepatic tissue prelevated from rats treated with L-thyroxin is higher compared with the control because this thyroid hormone stimulate the synthesis of these acids.

In all analyzed tissue the tomatoes powder administration has an effect an increase of FA content.

REFERENCES
1. Joanta A., Filip A., Andrei S.: Acta Physiol. Hung., *93*, 347 (2006).
2. Andrei S., Pintea A., Catoi C.: Bulletin USAMV-MV Cluj, *60*, 24 (2003).
3. Andrei S., Pintea A., Bunea A.: Bulletin USAMV-MV Cluj, *64*, 32 (2007).
4. Andrei S., .Pintea A., Catoi C.: Bulletin USAMV-MV Cluj, *62*, 17 (2005).
5. Blennemann B., Moon Y., Freake H: Endocrinology, *130*, 637 (1992).

P04 THERMOPHILIC BACTERIA APPLICATION TO WHEY BIODEGRADATION

LIBOR BABÁK and RADKA BURDYCHOVÁ

Institute of Food Science and Biotechnology, Faculty of Chemistry, Brno University of Technology
Purkyňova 118, 612 00 Brno, Czech Republic,
babak@fch.vutbr.cz

Introduction

In former times the whey was thought as valueless waste of dairy industry rising in cheese, cottage and casein production. Its application was in feed only. In these days, the whey meaning inceases simultaneously with new knowledges of nutrition, with sepative methods development, envirtonment protection endeavour and rapid progress of food and pharmaceutical industry. Environmental aspect is purity rivers maintenance and it means the prohibition of waste-water disposal (the whey too). It is possible to make the whey „liquidation" by the help of microbial systems. Several microbial systems were used for these purposes but they are still pure described. Testing of new microbial systems for the degradation ot the whey is in progress. In this work, the testing of degradation of the whey medium using the mixture of thermophilic bacteria is described.

Experimental

Experiments were practised with thermophilic aerobic culture, the mixture of bacteria of the genus *Bacilus* and the genus *Thermus* (sludge from waste treatment plant Bystřice pod Hostýnem). The whey from cheese production (type ermine) was used as the medium. Casein (0.1 mol dm^{-3} H_2SO_4) and α,β-lactoglobulins (20 min at 85 °C) were taken out before cultivations. The whey was centrifuged and pH value was adjusted. All cultivations were practised in the laboratory fermentor BIOSTAT B (B. Braun Biotech.) with working volume 2 dm^3.
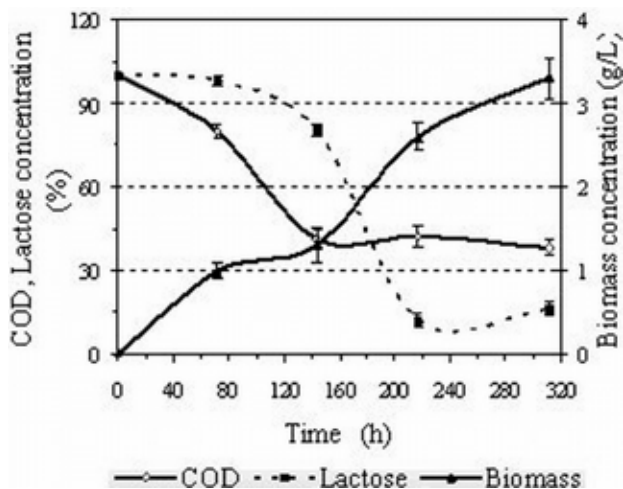
Fig. 1. **Batch cultivation progress in longer time (312 hours)**

Cultivation conditions: multiple turbo-stirrer 250 min^{-1}, aeration 10 dm^3 min^{-1}, pH adjusted on value 6.5, medium temperature 60 °C, vessel isolation Mirelon. The batch was selected as the cultivation method. The cultivation time was 66 h (1st experiments) and 312 h (2nd experiments). The process characteristics were determined direct by fermentor system (dissolved oxygen concentration) or by the help of samples taking and their analyses (biomass – turbidimeter, COD – spectrofotometer at 600 nm, lactose – HPLC after microfiltration, 100 % lactose ≈ 46 g.dm^{-3}. The statistical analyse was realized in the relevancy level 0.05.

Results

The experimental results are summarized in Fig. 1. & 2.
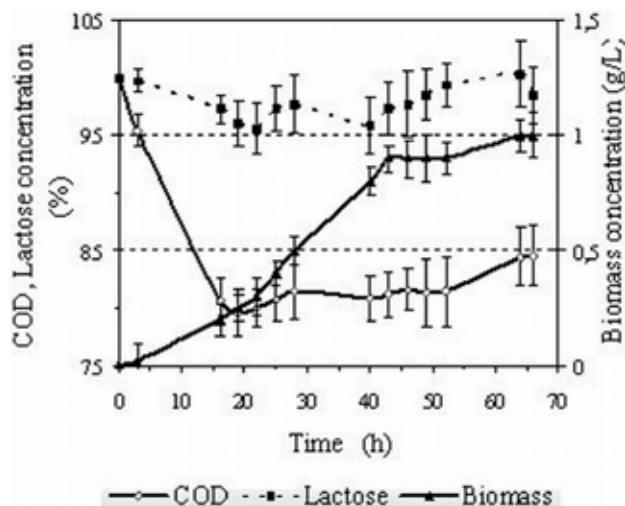
Fig. 2. **Batch cultivation progress in shorter time (66 hours)**

Hence it follows:
- Lactose was not used as primary substrate source (Fig. 2.), consequently the exponential growth phase in time 3–43 hours (specific growth rate μ = 0.05 ± 0.01 h^{-1}) is a result of simpler whey compound utilization probably, for example lactate.
- Lactose metabolisation was combined with the 2nd growth phase in time 120–260 hours (specific growth rate μ = 0.010 ± 0.006 h^{-1}) (Fig. 1.).
- The biomass accrument was very slow. It was probably an inhibition effect of concentrated substrate, especially in the 1st cultivation period (Fig. 1., Fig 2.). Total biomass concentration after 312 hours: (3.3 ± 0.3) g dm^{-3} at productivity 0.01 g.dm^{-3} h^{-1}.
- The oxygen limitation can contibute to slow biomass growth (primarily in the 1st growth phase).
- Maximum COD elimination was in the 1st half of every exponetial growth phase: 15 ± 3 % after the 1st growth phase and ± 4 % after the 2nd growth phase.
- The oxygen transfer coefficient was determined too, $k_L a$ = (270 ± 21) h^{-1}.

Conclusions

It was achieved total COD elimination 62 % after 312 hours of the batch cultivation with thermophilic culture on waste whey. The biodegradation process rate is limited of lower biomass concentration and oxygen insufficiency. The correspondence between the time of exponential bacteria growth and the main COD elimination period was demonstrated. In conclusion, the mixture of termophilic bacteria population has significant whey biodegradation abilities in view of its application to dairy wastes.

REFERENCES

1. Babak L., Rychtera M.: J. Biotechnol. *118*, S184 (2005).
2. Brock T. D.: Thermophiles: General, Molecular and Applied Mikrobiology, Wiley, New York 1986.
3. Drbohlav J.: Mlékařské Listy *41*, 4 (1990).
4. Jeppsson U.: Ph. D. Thesis, Lund Inst. of Technology 1996.
5. Kaštánek F.: *Bioinženýrství*, Academia, Praha 2001.
6. Kittner Z.: *Průmyslové vody, jejich úprava a čištění*, VUT, Brno 1980.
7. Kristjansson J. K.: *Thermophilic Bakteria*, CRC Press Inc., New York 1992.
8. La Para T. M., Alleman J. E.: Wat. Res. *33*, 895 (1999).
9. LaPara T. M. et al.: J. Environ. Eng. 126, 739 (2000).
10. Lopez Zavala, M. A. et al.: Wat. Res. *38*, 5 (2004).
11. Mullin W. J., Emmons, D. B.: Food Res. Int. *30*, 2 (1997).
12. Rychtera M., Páca J.: *Bioinženýrství kvasných procesů*, SNTL, Praha 1985.
13. Vismara R.: Wat. Res. *4*, 441 (1985).

P05 GROWTH CURVES OF MIXED THERMOPHILIC BACTERIA

LIBOR BABÁK, RADKA BURDYCHOVÁ and VLASTIMIL DOHNAL

Institute of Food Science and Biotechnology, Faculty of Chemistry, Brno University of Technology, Purkyňova 118, 612 00 Brno, Czech Republic,
babak@fch.vutbr.cz

Introduction

Temperature is one of the most important enviromental factors controlling the activities and evolution of organisms and is one of the easiest variables to measure. Not all temperatures are equally suitable for the growth and reproduction of living organisms. Most of animals, plants and eucaryotic microorganisms are not able to exist at temperatures above 50 °C. It contrast to this fact, some procaryotic microorganisms can grow at temperatures above 60 °C commonly. We call them thermophiles. The most thermophilic microorganisms live in the thermal zone of the Earth. Their industrial use is various, from food industry to waste-water treatment. The important knowladge for any application of these microorganisms is their basic growth characteristics. The aim of this work was testing of growth of the mixture of thermophilic bacteria with possible potential to be used in waste-water industry.

Experimental

Experiments were carried out using the mixture of thermophilic bacteria of the genus *Bacilus* and genus *Thermus* (sludge from waste treatment plant Bystřice pod Hostýnem). The substrates composition: C-source 4 g dm^{-3}, MgSO$_4$·7H$_2$O, 1. g dm^{-3}, (NH$_4$)$_2$SO$_4$ 0.3 g dm^{-3}, KH$_2$PO$_4$ 7 g dm^{-3}, yeast extract 2.4 g dm^{-3}, Peptone 8.5 g dm^{-3}. Glucose, lactose, sacharose and maltose were tested as the main source of carbon in succesive steps. Inoculum was prepared in the same conditions as tested cultivations. Inoculation rate: 1 : 10. Cultivations were practised 50 hours in two different systems – in 1.5 ml vials (anaerobic conditions) and in 1.5 dm^3 laboratory fermentor (aerobic conditions).

The vials, with magnetic bar and tightly screw capped, were placed into autosampler plate thermostated at 60 °C. Flow injection analysis (FIA) was used for measurement of microorganism quantity. The amount of 10 μl of the sample was injected into water stream (0.2 ml min^{-1}) and the absorbance at 600 nm was measured. The area under the curve of chromatogram was used for microorganism quantification. The sample was drawn and analysed each 5 minutes for 50 hours. The HPLC system HP 1100 (Agilent Technologies, Palo Alto, USA) consisted of vacuum degasser unit (model G1322A), quaternary pump (G1311A), autosampler (G1313A) and quadrupole mass spectrometer (G1946VL) with electrospray ionization was used. The ChemStation software (Rev. A 10.02) controlled the chromatographic system and it was used for chromatogram evaluation. The vials with

cultivation media were placed in thermostated plate KEVA (Ing. Pavel Krásenský, Brno, Czech Republic) and stirred using magnetic stirrer.

The cultivations in bioreactor were practised in a laboratory batch fermentor BIOSTAT B (B. Braun Biotech.) Cultivation conditions: multiple turbo-stirrer 250 min^{-1}, aeration 10 dm^3 min^{-1}, pH adjusted on value 6.5, medium temperature 60 °C, vessel isolation Mirelon. Biomass concentration was determined by the help of samples taking and their analyses in turbidimeter.

Results

The experimental results are summarized in Fig. 1. & 2.
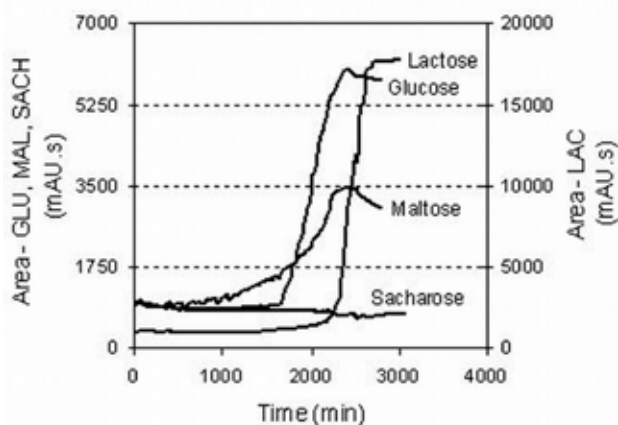
Fig. 1. **Growth curves on different substrates into vial (10,000 mAU.s ~ 1 g dm^{-3} (biomass concentration)**
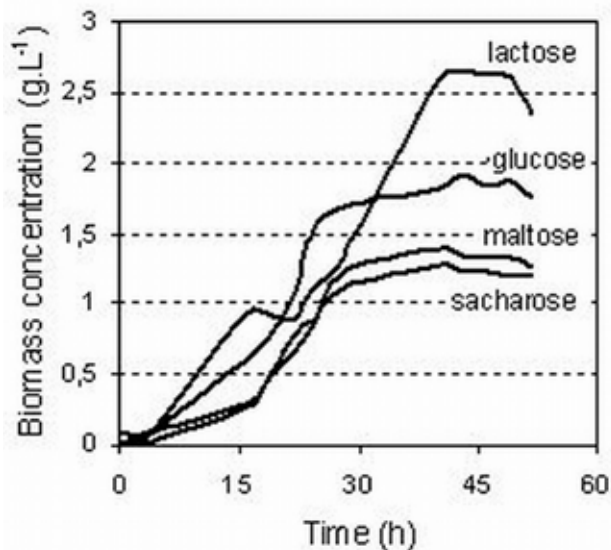
Fig. 2. **Growth curves on different substrates in fermentor**

Hence it follows (Fig. 1.):
• Sacharose was not utilised by mixed thermophilic bacteria in anaerobic system only. Enzyme decomposed sacha-

rose (invertase) was probably not formed (Fig. 1.).

- In both systems, maximal cells growth was achieved on lactose (Fig. 1., 2.). Total biomass concentration after 50 hours: 1.7 ± 0.2 g dm^{-3} in vials and 2.7 ± 0.4 g dm^{-3} in the fermentor.
- Total biomass concentration on others substrates was as follows (Fig. 1., 2.): glucose 0.6 ± 0.2 g dm^{-3} (vials) and 1.9 ± 0.5 g dm^{-3} (fermentor), maltose 0.3 ± 0.1 g dm^{-3} (vials) and 1.4 ± 0.3 g dm^{-3} (fermentor), sacharose 0.1 g dm^{-3} (vials) and 1.3 ± 0.2 g dm^{-3} (fermentor).
- The difference between total biomass concentration in the vials and in the fermentor is statistically significant on statistic level 0.05. It follows from these results that tested culture has mainly aerobic character.
- The biggest biomass productivity was reached in cultivation in fermentor, on lactose: 0.054 ± 0.009 g dm^{-3} h^{-1}.
- Lag-phase period (Fig. 1., Fig 2.) was the shortest in cultivations in the aerobic fermentor sytems ($\sim$ 3h on all substrates). In anaerobic vials was this phase very long: on maltose $\sim$8h, on lactose ($\sim$25h). (Sacharose is not comparised).
- Specific growth rates: glucose 0.19 ± 0.05 h^{-1} (vials) and 0.10 ± 0.05 h^{-1}, maltose: 0.05 ± 0.01 h^{-1} (vials) and 0.06 ± 0.02 h^{-1} (fermentor), sacharose 0.06 ± 0.02 h^{-1} (fermentor only). The difference between specific growth rates in the vials and in the fermentor is not statistically significant on statistic level 0.05.
- It is possible to differ two exponential growth phases (I: 3–15 h., specific growth rate 0.25 ± 0.03 h^{-1} and II: 22–38 h. specific growth rate 0.12 ± 0.02 h^{-1}) in the bioreactor cultivation on lactose. Lactose served as the main carbon source in the first phase of cultivation, in the second phase lactose was consumed immedately and the growth proceeds on organics acids by metabolic way generated (Fig. 2.).
- In vials on lactose was observed different situation, there was one exponential growth phase with specific growth rate: 0.31 ± 0.01 h^{-1}.(Fig. 1.).
- It follows from our experiments that the biggest growth rate was achieved in bacteria cultivation on lactose (in both systems – in the fermentor and in the vials).

Conclusions

The dramatically differences between growth rate and total biomass concentration in cultivations on lactose and others substrates were detected. Lactose was the most suitable substrate in growth aspect in both aerobic and anaerobic conditions. With regard to better growth results in the fermentor cultivations, the main population of the mixture of bacteria tested is aerobic.

Maltose and glucose were utilised by thermophilic microorganisms too, but growth was slower. Sacharose was not utilised in anarobic vials, thermophilic bacteria was not able to decompose this substrate.

In conclusion, this work described growth and growth characteristics of tested microorganisms and contributed to better knowledge of thermophilic mixed bacteria cultures.

REFERENCES
1. Andrade C.M.M.C. et al.: Rev. Microbiol. *30*, 4 (1999).
2. Babak L., Rychtera M.: J. Biotechnol. *118*, 184 (2005).
3. Brock T. D.: Thermophiles: *General, Molecular and Applied Microbiology*, Wiley, New York 1986.
4. Brock T. D.: *Thermophilic microorganisms and life at high temperatures*, Springer-Verlag, New York 1978.
5. Frank R. et al.: *Thermophiles: Biology and Technology at high temperature*, CRC Press Inc., New York, 2007.
6. Jeppsson U.: Ph. D. Thesis, Lund Inst. of Technology 1996.
7. Kaštánek F.: *Bioinženýrství*, Academia, Praha 2001.
8. Kristjansson J. K.: *Thermophilic Bacteria*, CRC Press Inc., New York 1992.
9. Lopez Zavala, M. A. et al.: Wat. Res. *38*, 5 (2004).
10. Pozmogova I.N.: Mikrobiologiia *44*, 3 (1975).
11. Reysenbach A-L. et al.: *Thermophiles: Biodiversity, Ecology and Evolution*, Springer, New York, 2001.

P06 MONITORING OF ACRYLAMIDE LEVELS USING LC-MS/MS: MALTS AND BEERS

VERONIKA BARTÁČKOVÁ, LUKÁŠ VÁCLAVÍK, KATEŘINA RIDDELOVÁ, VLADIMÍR KOCOUREK and JANA HAJŠLOVÁ

Institute of Chemical Technology Prague,
Department of Food Chemistry and Analysis,
Technicka 5, Prague 6 – Dejvice, 166 28,
veronika.bartackova@vscht.cz

Introduction

Acrylamide (AA), a hazardous chemical, is classified as a probable human carcinogen (IARC, 1994)[1]. AA is formed during Maillard reaction in starch-rich foods. Its occurrence in human diet was for the first time reported by Swedish scientists in 2002[2].

Alike many other heat processed foods prepared from cereals, malts may contain AA, originated from sugar and asparagin contained in barley. Besides of other factors, AA levels depend on the temperature and the time employed for treatment.

In our study, various types of malts, commonly used as additives (colorants, aroma donors etc.) in bakery and/or in brewing industry were examined for AA levels using LC-MS/MS.

In the next phase of our experiments the transfer of this processing contaminant into the beer was studied. The analytical procedure used for the analysis consists of cleanup step employing solid-phase extraction (SPE) followed by liquid chromatography coupled to tandem mass spectrometry (LC–MS/MS). A wide range of bottled beers obtained at the Czech retail market was examined within this monitoring study.

Experimental

Chemichals and Materials

AA (purity 99,5 %) was from Sigma/Aldrich/Fluka (Switzerland). $^{13}C_3$-AA (isotopic purity ≥ 99 %) was purchased from CIL (USA). Magnesium sulphate was from Sigma/Aldrich/Fluka (Switzerland). Sodium chloride was from Penta (Czech Republic). Aluminium oxide (basic) was from Merck (Germany). All organic solvents were of HPLC grade quality.

Calibration standard solutions were prepared in water by diluting stock standard solutions in concentration range 1–250 ng ml^{-1} with fixed amount of $^{13}C_3$–AA– 100 ng ml^{-1}.

Isolute Multimode® (6 ml, 500 mg) and Isolute ENV+® (6 ml, 500 mg) SPE cartridges were purchased from IST (U.K.).

Samples

Czech special roasted malts (4 from barley and 1 from wheat) were employed for the study. In addition to the malt samples, intermediates collected during processing (that was conducted under different time and temperature conditions) were examined.

The German set of samples included 12 malts (brew, special, caramel, wheat and rye), used in beer industry.

Thirty beer samples representing various typical brands were purchased from the Czech retail market.

Malt Sample Preparation

The key step of this method is the transfer of AA from the primary aqueous extract into acetonitrile forced by added salts (MgSO$_4$ and NaCl); separation of aqueous and organic phases is induced[3]. Most matrix interferences are then removed from organic phase by dispersive solid phase extraction (MgSO$_4$ and basic Al$_2$O$_3$ are used for this purpose). Acetonitrile is evaporated under a gentle stream of nitrogen and solvent is exchanged to water.

Beer Sample Preparation

After decarbonization the beer sample undergoes cleanup with two subsequent SPE cartridges. Final extract is in 60% methanol in water (v/v solution). The methanol is evaporated by a gentle stream of nitrogen[4].

Analysis of AA by LC-MS/MS

LC-MS/MS measurements were accomplished with the use of a separation module Alliance 2695 (Waters, USA) interfaced to a Quattro Premier XE mass spectrometer (Micromass, UK). Chromatographic separation was carried out using an Atlantis T3 column (3 mm × 150 mm × 3 μm). Isocratic elution of AA was achieved with mobile phase composed of acetonitrile and water (3 : 97, v/v).

The mass spectrometer, equipped with pneumatically assisted electrospray interface (ESI), was operated in a positive ionization mode.

LOD´s and LOQ´s for malt samples were 10 μg kg^{-1} and 30 μg kg^{-1}, respectively. LOD´s and LOQ´s for beer samples were 2 μg dm^{-3} and 5 μg dm^{-3}, respectively.

Results

AA levels in malt corresponded to the temperatures employed for their production. In dark malts AA content was relatively high, clearly due to advanced Maillard reaction induced by heating process.

Table I
Czech malts

Malt	AA (μg kg^{-1})
Semi-finished light caramel	35
Light caramel	37
Semi-finished dark caramel	404
Dark caramel	243
Coloured	111
Czech	25
Wheat	<10

The overview of this processing contaminant in various Czech and German malts is summarized in Table I and II.

The AA levels as high as 900 $\mu g\,kg^{-1}$ were found in German caramel rye malt used for the production of the speciality beers. Generally, only low AA levels were found in pale malts.

Table II
German malts

Malt	AA ($\mu g\,kg^{-1}$)
Rye	<30
Chocolate wheat	49
Wheat malt	<10
Munich dark	150
Red caramel	81
Caramel rye	909
Light caramel	<30
Caramel aromatic	409
Melanoidin	105
Smoked	<30
Pilsner	<30
Munich	67

Some transfer of AA into beer was shown by analysis of beers collected at the Czech detail market (Table III). About 30 % of examined samples contained levels above limit of quantification of the LC-MS/MS method. The range of AA level was between 5–10 $\mu g\,dm^{-3}$. The measured mean concetratin was 7 $\mu g\,dm^{-3}$. Two samples of non-alkoholic beer contained AA. In the 1 of 2 semi-dark beers was determined AA. Only 2 from the all (16) light beers were positive for AA. The most percentage of positive samples were in the group of dark beers. 4 from 5 dark beers contained acrylamide in mean level 9 $\mu g\,dm^{-3}$. No AA was detected in two special beers.

Conclusions

The levels of AA in malts vary in a wide range. Generally, the highest level of this proccesing contaminant occurred in caramel rye malt used for production of special beers.

The examination of semi-finished malts indicates possible degradation of AA during roasting of malts. After reaching a maximum, the levels successively decrease.

Predictably, the highest levels of AA were found in dark beers. In a few of light beer samples was AA detected too.

Table III
Czech beers

Beer	AA $\mu g\,dm^{-3}$
Light	6
Light, non-alcoholic	6
Light	<5
Light, lager	<5
Special lager	<2
Light	<2
Light, lager	<2
Light, low sugar content	<2
Dark, lager	10
Light	<2
Light, lager	<5
Light, lager	<5
Light, lager	<5
Light, non-alcoholic	<2
Light	<5
Light, lager	<5
24% Special, dark	<2
Light, non-alcoholic	6
16% Special,	<2
Dark, lager	10
Light, lager	<5
Dark, lager	8
Light, lager	<2
Light	<5
Dark, lager	<5
Semi-dark, lager	<5
Semi-dark, lager	5
Light	<2
Light, lager	7
Dark, lager	8

REFERENCES

1. IARC: *IARC Monographs on the Evaluation of Carcinogenic Risks to humans.* Lyon, France, 1994.
2. Report from Swedish Scientific Expert Comittee: Acrylamide in food – *Mechanisms of formation and influencing factors during heating of foods*, June 30 2002.
3. Mastovska K., Lehotay S. J.: J. Agric. Food Chem. *54*, 7001 (2006).
4. Rosén J., Hellenäs K.-E.: Analyst *127*, 880 (2002).

P07 CONTENT OF POLYCYCLIC AROMATIC HYDROCARBONS IN HONEYS FROM THE CZECH REPUBLIC

PETRA BATELKOVÁ, IVANA BORKOVCOVÁ, KLÁRA BARTÁKOVÁ and LENKA VORLOVÁ

University of Veterinary and Pharmaceutical Science Brno Palackého 1/3, 612 42 Brno,
pbatelkova@vfu.cz

Introduction

Polycyclic aromatic hydrocarbons (PAHs) belong to the family of persistent organic pollutants having many properties with a negative impact on human organism (carcinogenicity, mutagenicity).

In addition to the inhaled air the main exposition source of polycyclic aromatic hydrocarbons for the most of population are foodstuffs. PAHs were found in many foodstuffs both of animal origin (mainly as a result of culinary treatment) and plant origin (due to atmospheric deposition and growing in the contaminated soil). The data about PAHs content in honey are rare[1]. In the study dealing with the PAHs content in honey considerably high concentrations are reported[2], especially for the honeydew honey, not only for those PAHs with 3–4 aromatic rings (acenaphten 187 $\mu g\,kg^{-1}$, fluoren 163 $\mu g\,kg^{-1}$, phenanthren 625 $\mu g\,kg^{-1}$, anthracen 635 $\mu g\,kg^{-1}$) predominantly occurring in foodstuffs ant materials of plant origin[3], but also for the toxic PAHs (benzo-k-fluoranthen 58 $\mu g\,kg^{-1}$, benzo-a-pyren 126 $\mu g\,kg^{-1}$).

The aim of this study was to estimate content of PAHs in Czech honeys whose high quality is known (absence of antibiotics, minimal content of hydroxymethylfurfural). The content of 15 priority pollutants according to the US EPA was monitored, namely naphtalen (NAPT), acenaphten (ACENAPT), fluoren (FLU), anthracen (ANT), fluoranthen (FLT), pyren (PY), benzo-a-anthracen (BaA), chrysen (CHRY) benzo-b-fluoranthen (BbF), benzo-k-fluoranthen (BkF), benzo-a-pyren (BaP), dibenzo-a,h-anthracen (DBahA), benzo-g,h,i-perylen (BghiPE) and indeno-1,2,3-cd-pyren (IPY).

Experimental

I n s t r u m e n t s

The Waters 2695 Alliance chromatographic system was equipped with the Waters 2475 fluorescence detector. A column PAH C18 (250 mm × 4.6 mm I.D. 5 μm (Waters, Germany) was used. The column was held at 30 °C with a column heater. Mobile phase A: water, B: acetonitrile, flow 1.4 ml min^{-1}, linear gradient were used. PAHs were detected by the fluorescent detector using an excitation and emission wavelength program (λ_{exc} ranged from 232 nm to 300 nm and λ_{em} from 330 nm to 500 nm). The HPLC system was controlled and the data were processed by Waters Empower 2 software.

C h e m i c a l s a n d R e a g e n t s

Acetonitrile (Merck KGaA), dichloromethane (Merck KGaA) and hexane (Scharlau), the PAHs standard mixture (PAH mix 9, Dr. Ehrenstorfer), sodium sulphate anhydrous, sodium chloride, HPLC water. All solvents were HPLC grade or for residual analysis, other chemicals p.a. quality at least.

S a m p l e s

10 samples of honey obtained directly from Czech beekeepers and 10 samples of honey from shops with the Czech Republic declared as a country of origin were analysed. Each sample was analysed in at least duplicates, blank samples in each series were performed.

P r o c e d u r e

Three kinds of procedures of sample preparation were used.

The first procedure: 10 g sample of honey was dissolved in 100 ml of deionised water, 1 g NaCl and 10 ml hexane added and thoroughly shaken for 30 min. By means of separatory adapter an aliquot of organic layer was taken and evaporated to dryness. The residue was dissolved in 1 ml of acetonitrile, filtered through nylon membrane filter (0.45 μm) and analysed by HPLC.

The second procedure: 10 g of honey sample was mixed with anhydrous sodium sulphate, added 40 ml of dichloromethane and extracted by means of ultrasonic bath and Ultra Turrax. After filtration the solvent was evaporated and next process was the same as in the first procedure.

The third procedure: 10 g of sample was dissolved in 100 ml of deionised water and extracted by means of solid phase of SPE cartridges. The next process was as in the first procedure.

Results

Fig. 1. represents typical chromatogram obtained with honey sample. The average concentrations of each PAHs ranged from 0,02 to 2.22 $\mu g\,kg^{-1}$ (Table I). Recoveries, which were calculated by using observed and spiked concentrations for PAHs, ranged from 60 to 90 %. Limit of quanti-

Table I
Concentrations of PAHs [μg.kg^{-1}] in samples of honey

honey from	NAPT	ACENAP	FLU	PHE
bee-keepers	0.29	0.20	0.66	0.32
shops	0.82	0.45	0.49	2.22
	ANT	FLT	PY	BaA
bee-keepers	0.07	0.02	0.15	0.55
shops	0.07	0.07	0.05	0.16
	CHRY	BbF	BkF	BaPY
bee-keepers	0.15	0.04	0.08	0.05
shops	0.02	0.02	0.02	0.02
	DBahA	BghiPE	IPY	
bee-keepers	0.26	0.10	0.07	
shops	0.09	0.0	0.02	
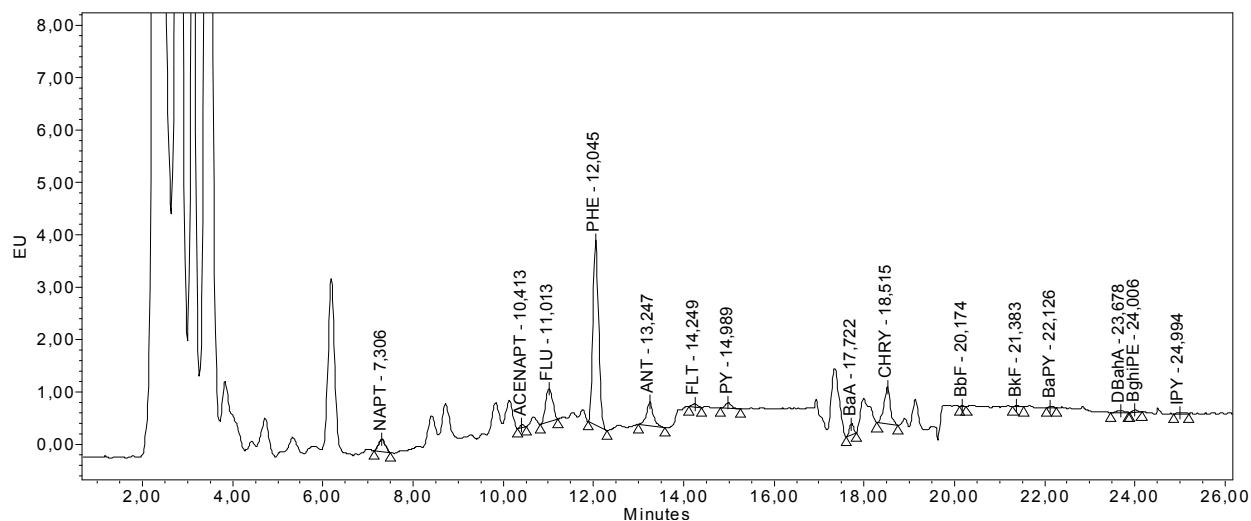
Fig. 1. **Chromatogram of PAHs in honey from shops. The conditions of analysis are shown in Section 2**

fication, which was obtained from blank experiments, was 0.01 µg kg^{-1}. RSD ranged from 0.01 to 20 %. These results were similar for each type of procedures.

Conclusions

The content of polycyclic aromatic hydrocarbons in analysed samples were very low, they ranged between 0.02 to 2.22 µg kg^{-1} for individual PAHs. These values are usually found in uncontaminated foodstuffs. In conclusion we can say that Czech honeys proved their traditional safety and high quality.

REFERENCES

1. Albero B., Sanchez-Brunete C., Tadeo J. L.: J. AOAC Int. *86*, 576 (2003).
2. Dobrinas S., Birghila S., Coatu V.: J. Food Compost. Anal. *27*, 71 (2008).
3. EC (European Commission) 2002: *Opinion of the Scientific Committee on Food on the risks to human health of Polycyclic Aromatic Hydrocarbons in food.* http://ec.europa.eu/food/fs/sc/scf/out153_en.pdf. Date of download 20.5.2008.

P08   QUANTITATIVE DETERMINATION OF SULFONAMIDE RESIDUES IN CHICKEN MEAT BY A NEW SOLID PHASE EXTRACTION AND HPLC-UV FOR DETECTION

CONSTANTIN BELE[a], OCTAVIAN NEGREA[a], ADELA PINTEA[a], FRANCISC VASILE DULF[a], DAN LUPU[b] and ALEXANDRU R. BIRIS[b]

[a]*University of Agricultural Sciences and Veterinary Medicine, R- 400372 Cluj-Napoca, Romania,*
[b]*National Institute for Research and Development of Isotopic and Molecular Technologies, R-400293 Cluj-Napoca, Romania,*
cbele2002@yahoo.com

Introduction

Sulfonamides (SAs) are a group of synthetic antibiotics that have been used in food-producing animals for therapeutic and prophylactic purposes[1]. There is a risk of occurrence of unwanted residues in animal products if these antimicrobials have been improperly administered or if the proper withdrawal period has not been observed. To safeguard human health, the European Community has adopted for SAs safe maximum residue limits (MRLs) at the total level of $100 \ \mu g \, kg^{-1}$ in food of animal origin[2].

Many methods such as LC and LC-MS, GC and GC-MS, ELISA, biosensor immunoassay (BIA) and high performance capillary electrophoresis (HPCE) have been developed for the determination of SA residues in food[3]. Solid phase extraction (SPE) was used as clean-up or enrichment method for SAs in tissues. The main sorbents used for the extraction of SAs are C18, aluminium oxide, strong cation-exchange[4].

Multi-walled carbon nanotubes (MWCNTs) are a novel carbon material used as an effective solid phase adsorbent for organic compounds (including SAs)[5].

In this paper, a sensitive method was developed for the determination of six SAs in chicken meat using MWCNTs and aluminium oxide as solid phase adsorbents followed by HPLC with UV detector.

Experimental

Materials and Reagents

Chicken muscle tissues were purchased from local food market and deep frozen until analysis. Organic solvents such as acetonitrile, acetic acid and 1- propanol were all pesticide residue grade , commercially available from Merck . Anhydrous sodium sulfate was analytical grade (Bucarest, Romania). Deionized and redistilled water was prepared from Milli-Q Plus (Millipore). Sodium acetate trihydrate (Merck) was used as buffer for HPLC mobile phase. Sulfadiazin (SDZ), sulfamerazine (SMR), sulfapyridine (SPY), sulfisoxazole (SIO), sulfamethoxazole (SMO) and sulfadimethoxine (SDM) were purchased from Sigma.

MWCNTs were purchased from Institute for Research and Development of Isotopic and Molecular Technologies Cluj-Napoca, Romania.

Standard stock solutions were prepared by accurately dissolving approximately 10 mg of SAs in 10 ml of acetonitrile LC grade and stored at 4 °C. Working standards were prepared weekly by appropriate dilution in acetate buffer at pH 4.5.

Chromatografic System and Conditions

All experiments were carried out by using Shimadzu VP Series liquid chromatograph equipped with a UV-VIS detector.

The chromatographic separation was accomplished in 30 min with gradient elution on a C 18 (250 mm × 4.6 mm, 5 μm) analytical column (Alltima) with a mobile phase 0.01M acetate buffer pH 4.5 (A) and acetonitrile (B). Flow 1 ml min^{-1} was used for the separation of analytes at the following program: 20 % B to 50 % within 22 min, back to 20 % in 3 min, equilibration for 5 min. The injection volume was 20μl and the detection of SAs was conducted at 266 nm.

Sample Preparation and Sample Clean-up

Ten grams of minced chicken tissue was placed into a 50 ml polypropylene tube. 20 ml acetonitrile and 5 grams baked anhydrous sodium sulfate was then added. The sample was homogenized with an Ultraturax for about 1 min., and then centrifuged at 5,000 rpm for 5 min. The residue was extracted by sonication with 20 ml acetonitrile and then centrifuged at 5000 rpm for 5 min. The extracts were combined and the solvent was concentrated to 5 ml. The solution was passed through the Alumina N SPE cartridge preconditioned by 10 ml acetonitrile. The analytes were eluted with 5 ml acetonitrile : water (80 : 20, v/v). The eluent and loading solvents were combined and transferred to concentration bottle. Then 5 ml 1-propanol was added and the solution was evaporated to near dryness. The residue was dissolved by ultrasonication for 1 min with 30 ml acetate buffer (pH 5). A second SPE cartridge (200 mg MWCNTs) was utilized to remove potential interferences. The SPE was conditioned with acetonitrile (5 ml) and water (5 ml) prior to loading the sample. The analytes were eluted with a mixture of 2 ml acetate buffer (pH 4.5) and 4 ml acetonitrile. The eluate was evaporated to 1 ml under nitrogen stream in a 40 °C block heater and filtered through a 0.45 μm disposable syringe filter.

Results

The present procedure uses two SPE cartridges for clean-up because acetonitrile extracted a lot of endogenous compounds from meat sample. The first one, Sep-Pak Alumina N, is a polar sorbent SPE cartridge. The second SPE cartridge (MWCNTs) is a non-polar sorbent and was utilized to further cleanse the extract.

The calibration graphs obtained by plotting peak area versus drug concentration in $0.1–10 \ \mu g \, ml^{-1}$ range are reported in Table I.

Table I
Retention time (t_R) and linearity of SAs

Sulfonamide	t_R [min]	b^a	a^b
SDA	7.51	127301	−3582
SPY	8.82	108274	−24580
SMR	9.65	121645	−9957
SIO	12.88	97992	2987
SMO	13.37	112048	18902
SDM	20.79	83942	−14029

b^a: Slope
a^b: Intercept

The linear correlation coefficient (r^2) are all above 0.999.

Chromatograms of a blank sample and of a spiked sample of chicken muscle are shown in Fig. 1. and 2.
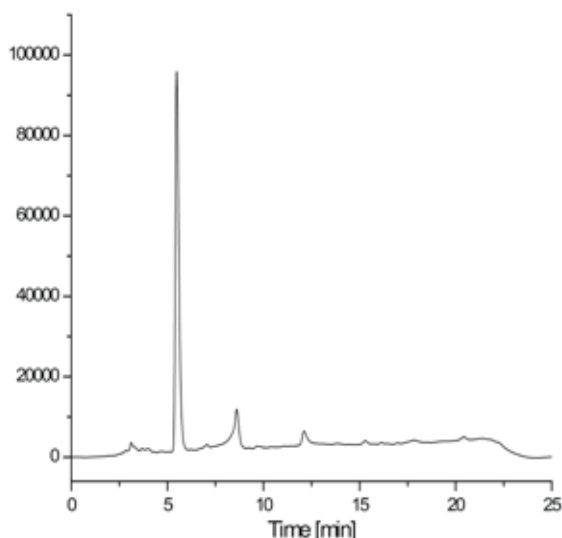
Fig. 1.   **The chromatogram of blank chicken muscle**

Table II
Recoveries of SAs in chicken meat tissue (n = 3)

Sulfonamides	Spiked [µg kg^{-1}]	Recovery [%]
SDA	50	78. ± 2.3
	100	80.4 ± 4.7
SPY	50	72.6 ± 6.8
	100	75.3 ± 7.2
SMR	50	65.6 ± 4.3
	100	67.9 ± 2.5
SIO	50	77.8 ± 1.2
	100	79.4 ± 3.4
SMO	50	74.7 ± 5.6
	100	76.5 ± 6.4
SDM	50	76.3 ± 7.6
	100	78.7 ± 6.9
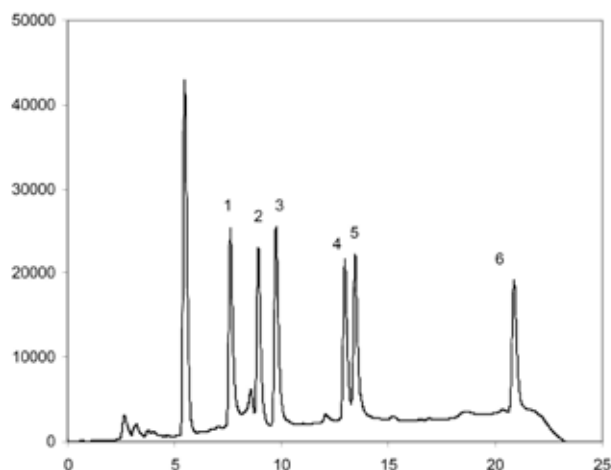
Fig. 2.   **The chromatogram of the spiked sample with 50 µg kg^{-1} of the following sulfonamides: 1:SDA, 2: SPY, 3: SMR, 4: SIO, 5: SMO, 6:SDM**

Under this extraction and pre-treatment procedure , the sulfonamide fortified chicken sample did not induce peaks interfering with SAs peaks. The recoveries of analytes were evaluated by spiking 0.5 and 1 µg of each standard analyte to 10.0 g tissues. The results are listed in Table II.

Good recoveries ranging from 65.6 to 80.4 % were determined, which indicated that sample preparation procedure was suitable for the analysis of SAs in chicken meat sample.

As an application, 30 samples of commercial chicken meat purchased from local food market were analysed using the present method. No residue sulfonamide was detected in all meat sample. All HPLC chromatograms were free from interferences.

Conclusion

In this study , an analytical method to determine six SAs in chicken meat was developed utilizing two SPE cartridges for sample clean-up and pre-concentration of analytical components prior to HPLC analysis. The newly developed sample pre-treatment procedure effectively removed the potential matrix interferences from endogenous compounds of meat. Average recoveries of analytes from spiked meat ranging from 65.6 to 80.4 % of six SAs were determined.

REFERENCES
1. Kim D. S., Park M. S.: Yonsei Med. J. *39*, 595 (1998).
2. Establishment of Maximum Residue Levels of Veterinary Medical products in foodstuffs of animal origin, Council Regulation No. 2377/90 of EEC.

3. Shao B., Dong D., Wu Y., Hu J., Meng J., Tu X., Xu S.: Anal. Chim. Acta *546*, 174 (2005).
4. Kishida K., Furusawa N.: J. Chromatogr. A *937*, 49 (2001).
5. Fang G. Z., He J. Z., Wang S.: J. Chromatogr. A *1127*, 12 (2006).

P09 MONITORING OF SENSORIALLY ACTIVE SULPHUR SUBSTANCES IN MALT AND BEER

RENATA MIKULÍKOVÁ, SYLVIE BĚLÁKOVÁ, ZDENĚK SVOBODA and SIMONA MACUCHOVÁ

Research Institute of Brewing and Malting, Plc., Malting Institute Brno, Mostecká 7, 614 00 Brno,
mikulikova@brno.beerresearch.cz

Introduction

Recently, a great deal of research effort has been devoted to sensorially active substances affecting beer quality. Quality of brewing materials, unhopped wort and hopped wort production technology, fermentation technology, beer maturation and beer ageing contribute significantly to analytical and sensorial beer characteristics.

Heterocyclic and sulphur compounds, some of them with high sensorial activity even in extremely low concentrations, belong to sensorially active substances affecting beer quality principally[1]. Trace amounts of these compounds commonly detectable in food contribute to their flavor, therefore this effect can be generally assessed as favourable. In malt and beer, however, it is true to a limited extend only and the presence of heterocyclic and sulphur substances is evaluated rather negatively[2]. Sulphur compounds get into beer either with initial materials (malt, hop) or they are formed in the course of chemical or enzymatical reaction during the respective production phases (mashing, brewing, fermentation, ageing). Content of sulphur compounds in barley and hop depends not only on a variety but on a growing locality, course of weather and growing technology employed as well. In malt, content of sulphur substances depends first of all on malting technology and possible contamination with undesirable microorganisms[3]. Most of the sulphur compounds present in barley, malt and beer are non-volatile substances (amino acids, proteins, inorganic sulphates). These substances do not directly account for unfavourable beer flavours and odours but under certain conditions they may be important precursors of sensorially active substances. These substances are, in majority of cases, volatile and their amount is usually less than 1 % of the total amount of the sulphur containing substances in beer, i.e. actual amounts of substances responsible for sulphur odours are extremely low[4].

Experimental

Sensorically Active Sulphur Substance

Following volatile sulphur substances were monitored: dimethylsulphide [75-18-3], dimethyl disulphide [624-92-0], dimethyltrisulphide [3658-80-8], carbondisulphide [75-15-0], ethylsulphide [75-08-1], diethyldisulphide [111-81-6], methionol [505-10-2], 3-methylthiophen [616-44-4], ethylthioacetate [625-60-5], 2-methyl-1-buthanthiol [1878-18-8].

Selection of the Analyzed Samples

Sensorially active sulphur substances were determined in beers bought in retail stores. Six pale dispensed beers, 4 dark, 6 lager and 3 non alcoholic beers were selected for the analyses.

The analyzed malt samples were produced from different barley varieties (Bojos, Jersay, Malz, Prestige, Tolar, Xanadu), from 3 growing stations (Branišovice, Věrovany, Vysoká).

Determination of Volatile Sulphur Substances

Direct analysis of sulphur sensorially active substances is not easily applicable regarding their very low concentrations ($\mu g\,kg^{-1},dm^{-3}$ – $ng\,kg^{-1},dm^{-3}$) in the analyzed matrixes (malt, beer)[5,6]. Prior to the analysis, the analytes must be extracted from the matrix and concentrated. The HS-SPME method was used for extraction and concentration[7,8]. The CAR/PDMS fibre was chosen as the optimum fibre for this technique. The gas chromatographic analysis with flame photometric detection was employed to determinate sensorially active sulphur substances.

HS-SPME/ GC/ FPD conditions:

Sample:	2 ml of beer (vial 4 ml)
	6 ml of malt extract (vial 50 ml)
Sample temperature:	45 °C, 10 min
SPME fiber:	85 μm CAR™/PDMS
Extraction:	HS-SPME, 30 min, 45 °C
Desorption:	3 min, 250 °C

Chromatographic conditions:

Capillary column:	GS-Gaspro (30 m × 0.32 mm)
Thermal program:	from 40 °C to 235 °C
Flow of carrying gas He:	1.5 ml min⁻¹
PTV injector:	250 °C, splitless (3 min)
FPD detector:	T detector – 150 °C,
	T base – 250 °C

Results and Discussion

Two types of fibres (PEG, CAR/PDMS) were tested for the HS-SPME analysis. Fig. 1 shows higher affinity to the CAR/PDMS fiber for the analytes studied. This fibre was chosen for the analysis of sulphur substances, sorption time was optimized at 45 °C. Optimum sorption time was 30 minutes.

Validation parameters for the relevant analytes are given in Table I.

Carbon disulphide, methionol, dimethylsulphide, 3-methylthiophen and diethyldisulphide were detected in beers. Table II shows results of beer sample analyses.

In malt samples only dimethylsulphide was determined. Results of malt analyses are given in Fig. 2.

Table I
Validation parameters of the analyzed sulphur substances

Analyte	Range of calibration concentrations [μg dm⁻³]	R^2	LOQ [μg dm⁻³]	Extended relative uncertainty [%]
carbon disulphide	0.04–0.15	0.9809	0.01	22
methionol	2.4–10.0	0.9308	0.5	25
ethylsulphide	0.15–0.70	0.9845	0.01	30
dimethylsulphide	0.10–0.50	0.9898	0.005	3
3-methylthiophen	0.05–0.20	0.9945	0.001	4
dimethyldisulphide	0.03–0.15	0.9918	0.01	13
2-methyl -1- buthanthiol	0.10–0.55	0.9768	0.05	29
diethyldisulphide	0.2–0.8	0.9782	0.05	28
dimethyltrisulphide	0.03–0.15	0.9956	0.005	25
ethylthioacetate	0.03–0.15	0.9867	0.01	15

Table II
Contents of sulphur substances in beer

[μg dm⁻³]	Pale dispensed beers (n=6)	Pale lager beer (n=6)	Dark beer (n=4)	Nonalcoholic beer (n=3)
carbon disulphide	0.02–0.05	<0.01	0.05	<0.01
methionol	4.30–6.20	2.0–3.34	2.03–4.01	<0.5
ethylsulphide	<0.01	<0.01	<0.01	<0.01
dimethylsulphide	0.85–1.45	0.29–0.67	0.9–1.29	1.0
3-methylthiophen	0.10–0.16	<0.001	0.18	<0.001
dimethyldisulphide	<0.01	<0.01	<0.01	<0.01
2-methyl -1-buthanthiol	<0.05	<0.05	<0.05	<0.05
diethyldisulphide	0.08–0.20	0.05–0.25	0.12–0.19	0.36
dimethyltrisulphide	<0.005	<0.005	<0.005	<0.005
ethylthioacetate	<0.01	<0.01	<0.01	<0.01
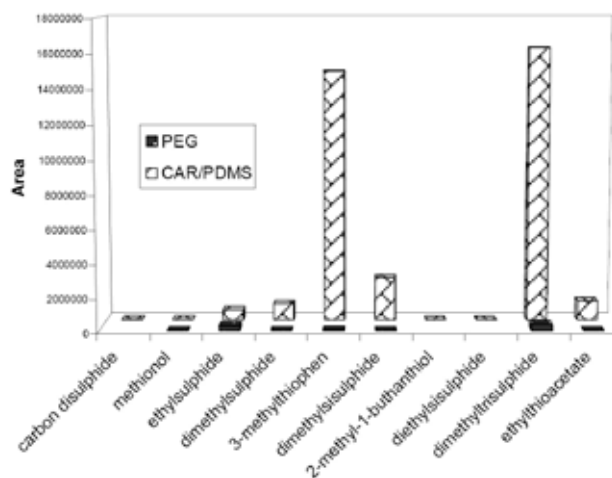
Fig. 1. **Comparison of suitability of SPME fibres for the analysis of sulphur substances**
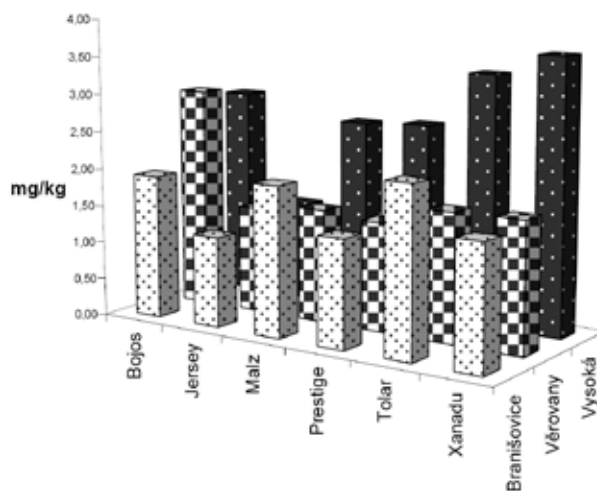
Fig. 2. **DMS content in the analyzed malts**

Conclusions

The HS-SPME/GC/FPD method was optimized and validated for the assay of sulphur volatile substances in malt and beer. This method determined following volatile sulphur substances in the beer sample: carbon disulphide, carbon disulphide, and dimethylsulphide in the sample of malt.

REFERENCES

1. Soltoft M.: Brygmesteren, *2*, 18 (1988).
2. White F. H., Parsons R.: *European Brewery Convention Proceedings of the 15th Congress*, Nice, *1975*, p. 721-734.
3. Anness B. J., Bamforth C. W.: J Inst. Brew., *88*, 244 (1982).
4. Werkhoff P., Guntert M., Krammer G., Sommer H., Kaulen J.: J. Argic. Food Chem., *46*, 1076 (1998).
5. Mestres M., Busto O., Guasch J.: J. Chromatogr. A, *773*, 261 (1997).
6. Pawliszyn J.: *Solid phase Microextraction: theory and practice*. 1997.
7. Hill P. G., Smith R.M.: J. Chromatogr. A, *872*, 2003 (2000).
8. Scarlata Ch. J., Ebeler S. E.: J. Agric. Food Chem., *47*, 2505 (1999).

P10　MONITORING OF FERULIC ACID CONTENT DURING MALT PRODUCTION

SYLVIE BĚLÁKOVÁ, RENATA MIKULÍKOVÁ, ZDENĚK SVOBODA and SIMONA MACUCHOVÁ

Research Institute of Brewing and Malting, Malting Institute Brno, Mostecká 7, 614 00 Brno, Czech Republic, belakova@brno.beerresearch.cz

Introduction

Antioxidant activity of ferulic acid plays an important role in a biochemical process of beer production. Currently, causes of wort haze have been investigated and relationships between wort haze, filterability and beer quality have been studied. Information on ferulic acid may help elucidate causes of haze formation[1].

Ferulic acid (4-hydroxy-3-methoxycinnamic acid) belongs to phenolic acids derived from cinnamic acid. It is a natural antioxidants and inhibitors of enzymatic browning. In plant cell walls it protects cells from the effect of pathogens, controls expansibility of cells, growth and affects biological digestibility. Ferulic acid is frequently a part of fibre where it is bound by ester linkage to hemicelluloses.

Generally, ferulic acid plays a principal role in breakdown of barley caryopsis cell walls. High content of ferulic acid in walls can serve as a protection against premature hydrolysis. The presence of ferulic acid protects cell walls against microbial attack. It stops lipid peroxidation and is effective at suppression of hydroxyl radicals[2,3].

The aim of our project was to determine the dependence of ferulic acid content on a barley variety and malting technology.

Experimental

Ferulic acid was determined in samples of eight barley varieties (Jersey, Maltz, Bojos, Radegast, Sebastian, Prestige, Tolar, and Xanadu). Barleys were from harvest 2007 and they came from two different growing localities – Krásné Údolí (forage area, worse growing conditions for spring malting barley) and Věrovany (sugar-beet area, good growing conditions for spring malting barley). Malts were prepared in the micro malting plant of the Malting Institute of the RIBM in Brno using the method with short steep and sucking off CO_2. Wort was made by a so-called congress method, i.e. standard mashing procedure with finely ground malt.

Alcalic hydrolysis with 2 M of natrium hydroxide was used to release ferulic acid from compact homogenized samples. After pH adjustment, the extract was purified using the SPE (Solid Phase Extraction).

The purified extract was microfiltered and transferred to a vial. In liquid samples extraction with alcalic hydrolysis was omitted, following procedure remains the same.

The samples were then analyzed using gradient elution on the UPLC WATERS ACQUITY liquid chromatograph equipped with WATERS 2996 PDA detector. Mobile phase consisted of 0.05M phosphate buffer (pH 3.5) and acetonitrile. Column used was ACQUITY UPLC BEH C18 1.7 μm 2.1 × 50 mm.

Results

Content of total ferulic acid was determined in a series barley – malt – wort. Results are presented in the Table I.

Conclusions

The results of measurement prove the dependence of content of total ferulic acid on a variety and growing locality in the series barley – malt – wort.

Concentration of total ferulic acid in barley samples varied in the range of 650–950 mg kg^{-1} in dependence on a variety and growing locality.

Concentration of total ferulic acid in malt samples varied in the range of 900–1,740 mg kg^{-1} in dependence on a variety and growing locality.

Concentration of total ferulic acid in wort samples varied in the range of 6–9 mg dm^{-3} in dependence on a variety and growing locality.

Table I
Content of total ferulic acid in a barley – malt – wort chain from the localities Krásné Údolí and Věrovany

	Krásné údolí			Věrovany		
	Barley [mg kg^{-1}]	Malt [mg kg^{-1}]	Wort [mg dm^{-3}]	Barley [mg kg^{-1}]	Malt [mg kg^{-1}]	Wort [mg dm^{-3}]
Jersey	746.1	1,012.6	7.99	825.1	1,537.0	8.09
Maltz	693.7	1,044.6	7.42	803.1	1,613.2	8.01
Bojos	672.9	970.5	6.14	682.0	1,392.1	5.52
Radegast	806.7	1,067.0	6.05	844.1	1,361.6	5.91
Sebastian	712.2	948.7	8.87	832.9	1,737.4	6.96
Prestige	733.5	1,113.9	7.90	911.0	1,428.6	7.23
Tolar	734.3	1,153.7	6.11	825.4	1,563.2	5.57
Xanadu	648.8	905.9	6.44	692.4	1,263.0	8.45

REFERENCES
1. Kanauchi M., Bamforth C. W.: J.Inst Brew. *108*, 73 (2002).
2. Sun R. S., Sun X. F., Wang S. Q., Zhu W., Wang X. Z.: Industrial Crops and Products *15*, 179 (2002).
3. Lee I. Y., Volm T. G., Rosazza J. P. N.: Enzyme Microb. Technol. *23*, 261 (1998).

P11 CONTENT OF STROBILURIN FUNGICIDES IN BARLEY, MALT AND BEER

RENATA MIKULÍKOVÁ, SYLVIE BĚLÁKOVÁ, ZDENĚK SVOBODA and SIMONA MACUCHOVÁ

Research Institute of Brewing and Malting, Plc., Malting Institute Brno, Mostecká 7, 614 00 Brno
mikulikova@brno.beerresearch.cz

Introduction

Strobilurin pesticides represent an important group of fungicides with a broad efficiency spectrum. These fungicides began to be used commercially in 1996 and they were produced by the companies Syngenta (azoxystrobin) and BASF (kresoxim-methyl)[1].

Natural strobilurins (*Strobilurus* and *Oudemansiella*) were isolated from wood-rotting bracket fungi (Basidiomycetes). These wood decay fungi produce fungicidially acting substances in defense against lower fungi. The name strobilurine comes from *Strobilurus tanacetus*, one of the first fungi from which they were isolated (strobilurin A)[1].

Strobilurins represent an important group of efficient fungicides and together with oxazoline-diones (famoxadone) and imidazolinones (fenamidone) they are Qo inhibitors (Quinone outside Inhibitors). Their action is based on inhibition of mitochondrial respiration, they bind Qo instead of cytochrom b, which is a part of cytochromal complex bc1 localized in the inner mitochondrial membrane of fungi. Binding blocks the transfer of electrons between cytochrom b and cytochrom c1, inhibiting thus production of ATP and disrupting the energy cycle of fungi. Originally, strobilurins are natural substances produced by higher fungi, e.g. *Strobilurus tanacetus* (strobilurin A), *Oudimansiella mucida* (oudemansin A). Chemically they belong to methoxyacrylates (e.g. azoxystrobin and picoxystrobin), methoxycarbamates (pyraclostrobin), oximino acetates (kresoxim – methyl, trifloxystrobin), ozimino-acetamides (dimoxystrobin, etc.), and dihydro-dioxazinones (fluoxastrobin). Their characters, including efficiency spectrum, are very variable. They affect mainly preventively, but also curatively and some even have eradicative effects. All of them act in contact, some of them in depth or translaminarily or systemically (azoxystrobin and picoxystrobin). They move acropetally in a plant. Their efficacy is very wide, they are active against sac fungi (Ascomycetes), bracket fungi, imperfect fungi and oomycetes. They are highly imperiled by the origin of resistance (cross resistance within the QoI fungicides)[1,2].

Resistance was proved in more pathogenic fungi. In cereals, powdery mildew (*Blumeria graminis* f.sp. *tritici*, *Blumeria graminis* f.sp. *hordei*), septoria blotch (*Mycosphaerella graminicola*), net blotch (*Pyrenophora teres*), helminthosporioses in wheat (*Pyrenophora tritici – repentis*), and in the other crops, e.g. in apple, scab (*Venturia inaequalis*), grapevine downy mildew (*Plasmopara viticola*), and grapevine powdery mildew (*Erysiphe necator*). When applying strobilurins, observance of all provisions is highly recommended to avoid the development of resistance[1,2,3].

Following fungicides are used against fungal diseases of barley in the Czech Republic azoxystrobin (Amistar), picoxystrobin (Acanto, Acanto Prima), trifloxystrobin (Sfera 267.5 EC), fluoxystrobin (Fandango 200 EC), and kresoxim-methyl (Juwel, Juwel Top). Azoxystrobin (Ortiva) is registered against fungal diseases of hop in the CR.

Considering the increase in the extent of strobilurin use in the protection of barley and hop and their stability in a plant, it is necessary to introduce monitoring of their residues, intermediaries and final product.

Experimental

25 samples of beer, 50 samples of malt and 50 samples of barley were analyzed.

60 ml of methanol/acetone mixture was added to 20 g of ground matrix. Disintegration of the mixture was performed in an ultrasound bath for 30 minutes. The disintegrated mixture was centrifuged at 6,500 rev min^{-1} for 15 min at 10–15 °C. The obtained solutions were transferred to boiling flasks (250 ml) and evaporated to dryness on a vacuum evaporator. The obtained dry residue was dissolved with 20 ml of distilled water in the ultrasound bath for 1 minute. Mixture was purified through the SPE column ENVI™CarbII/PSA.

pH of the beer sample (100 ml) is adjusted to pH 6 by adding NaOH solution and the sample is then purified through the LiChrolut column.

The analyses of samples were performed on a gas chromatograph (Trace GC Ultra, Thermo Finnigan) connected to a mass detector (Trace DSQ, Thermo Finnigan). To separate the analyzed substances a DB5-MS capillary column (30 m × 0.25 mm i.d., 0.25 mm) with following thermal program was used: initial temperature 70 °C for 1 min., increase in temperature 10 °C min^{-1} to 280 °C, maintained for 5 min.

Table I
Barley, malt (SPE-EnviCarbII/PSA)

	SPE recovery [%]	LOQ [mg kg^{-1}]	RSD [%]
azoxystrobin	83–88	0.003	8–12
kresoxym - methyl	80–84	0.002	5–7
picoxystrobin	85–90	0.002	5–7
trifloxistrobin	82–87	0.002	7–10

Table II
Beer (SPE-LiChrolut)

	SPE recovery [%]	LOQ [mg kg^{-1}]	RSD [%]
azoxystrobin	88–90	0.003	<8
kresoxym – methyl	87–90	0.002	<5
picoxystrobin	90–95	0.002	<5
trifloxistrobin	87–91	0.002	<5

Table III
Content of strobilurin residues in the analyzed samples

	Number of analyzed samples	azoxystrobin	kresoxym – methyl	picoxystrobin	trifloxistrobin
barley	50	<LOQ	<LOQ	<LOQ	<LOQ
malt	50	<LOQ	<LOQ	<LOQ	<LOQ
beer	25	<LOQ	<LOQ	<LOQ	<LOQ

Programmed flow of carrying gas He was from 1.5 ml min^{-1} to 3 ml min^{-1}. Temperature of PTV injector 280 °C, splitlless regime for 0.8 min. Temperature in the transfer line between GC and MSD was 200 °C. Mass spectrometer was adjusted in SCAN (50–450 m/z) and SIM (Selected Ion Monitoring) mod (EI+ − positive electron ionisation) and selected values (m/z) for relevant analytes were as follows:

- azoxystrobin – 344, 388 (m/z)
- trifloxistrobin – 116, 131, 222 (m/z)
- picoxystrobin – 145, 335 (m/z)
- kresoxym – methyl – 116, 131, 222 (m/z)

Results

The method for determination of strobilurins in barley, malt and beer was optimized. Validation parameters for the individual matrices and SPE columns are given in Table I and Table II. Contents of strobilurins in all the analyzed samples were below the limit of quantification (Table III).

REFERENCES

1. Bartlett D. W., Clough J. M., Godwin J. R., Hall A. A., Hamer M., Parr-Dobrzanski B.: Pest. Manag. Sci. *58*, 649 (2002).
2. Beautement K., Clough J. M., de fraine P. J., Godfrey C. R. A.: Pestic. Sci. *31*, 499 (1991).
3. de Melo Abreu S., Correia M., Hebbert P., Santos L., Alves A.: Food. Addit. Contam. *22*, 549 (2005).

P12　THE EFFECT OF FERMENTATION CONDITIONS ON THE YEAST AROMA PROFILE

JAROSLAVA KAŇUCHOVÁ PÁTKOVÁ[a], EMÍLIA BREIEROVÁ[b], KORNÉLIA NEMCOVÁ[a] and INGRID VAJCZIKOVÁ[c]

[a]*Institute for viticulture and enology of SARC Matuškova 25, 831 01 Bratislava, Slovak republic,* [b]*Institute of Chemistry SAS, Dubravska cesta 9, 845 38 Bratislava, Slovak republic,* chememi@savba.sk

Introduction

Several factors influence the aroma profile during the alcoholic fermentation of the grape must. One of the widely discussed topics is the using of apiculate microflora and its contribution to the aroma of wine. Several authors have studied[1–3] the behaviour of various yeast genera – *Kloeckera, Pichia, Bretanomyces* and their contribution to the wine aroma, considering the apiculate microflora as spoilage. Our previous results[4] confirmed the role of apiculate microflora in the wine aroma production under semiaerobic conditions and support of the original character of wine by apiculate microflora.

The aim of this work was to determine the effect of changes in external conditions – oxygen, temperature or substrate composition on the sensorial expression of genera *Rhodotorula, Sporobolomyces, Pichia, Hansenula Issat-chenkia,* and *Torulospora* under the winemaking process. All above mentioned factors influence positively or negatively the final wine product. Multivariate analysis of variance was used to determine the overall weight of each one factor.

Table I
Sensorial evaluation of fermented grape must by various yeast strains under various fermentation conditions

Yeast strain	Anaerobic conditions grape must				Anaerobic conditions synthetic medium			
	10°C		25°C		10°C		25°C	
	aroma	percept	aroma	percept	aroma	percept	aroma	percept
C. intermediata	yeast	+	sulphuric	–	grape	+	acetic	–
R.mucilaginosa	socks smelly	–	yeast	+	yeast	+	socks smelly	–
T.delbruecki	yeast	+	acetic	–	sweety	+	bread	–
S. cerevisiae	acidic	–	fruity	+	sulphuric	–	sulphuric	–
I. orientalis	autolyses	–	acethone	–	yeast	–	Not recognised	–
Pichia anomala	acethone	–	acidic	–	fruity	+	acethone	–
S.cerevisiae	yeast	–	sulphuric	–	fruity	+	acethone	–
P. membranofaciens	autolyses	–	sulphuric	–	socks smelly	–	Not recognised	–
R.mucilaginosa	autolyses	–	acidic	–	corny	+	sweet	–
P. anomala	acethone	–	fruity– apple	+	candy floss	+	Not recognised	–
Sp.pararoseus	Not recognised	+	fruity	+	socks smelly	–	acethone	–
S.cerevisiae	acidic	–	sulphuric	–	rubber smell	–	autolyses	–
S.cerevisiae	fruity	+	sulphuric	–	acidic	+	autolyses	–
	Semiaerobic conditions grape must				Semiaerobic conditions synthetic medium			
	10°C		25°C		10°C		25°C	
	aroma	percept	aroma	percept	aroma	percept	aroma	percept
C. intermediata	acidic	–	fruity	+	floral	+	fruity	+
R. mucilaginosa	acethone	–	fruity	+	frowstilly	–	vanilla	+
T.delbruecki	vanilla	+	vanilla	+	honey	+	fruity	+
S. cerevisiae	autolyses	–	grape	+	sulphuric	–	acetic	–
I. orientalis	acethone	–	fruity	+	autolyses	–	autolyses	–
P. anomala	honey	+	fruity	+	fruity	+	fruity	+
S. cerevisiae	honey	+	acetic	–	yeast	+	floral	+
P. membranofaciens	yeast	+	acetic	–	medical	–	yeast	+
R.. mucilaginosa	honey	+	fruity	+	sulphuric	–	Not recognise	–
P. anomala	honey	+	fruity	–	sweety	+	yeast	+
S. pararoseus	yeast	+	fruity	+	sweety	+	Not recognise	+
S. cerevisiae	yeast	+	yeast	+	sweety	+	Not recognised	+
S. cerevisiae	yeast	+	fruity	–	Not recognised	+	Not recognised	+
S. cerevisiae	yeast	+	fruity	–	autolyses	–	Not recognised	+

Experimental

Following yeast strains were isolated from the grape must: *Rhodotorula mucilaginosa* (2 strains), *Sporobolomyces pararoseus, Pichia membranefaciens, Pichia anomala* (2 strains), *Candida intermediata, Torulospora delbruecki,* and *Issatchenkia orientalis*. For comparison 4 *Saccharomyces cerevisiae* yeast strains were also used. Two of them were isolated from the grape must; two of them were commercial active dry yeast strains (Lallemand).

Fermentation media: grape must or semisynthetic medium (10 $g\,dm^{-3}$ glucose, 5 $g\,dm^{-3}$ $(NH_4)_2SO_4$, 2 $g\,dm^{-3}$ KH_2PO_4, 1 $g\,dm^{-3}$ $MgSO_4 \cdot 7H_2O$, 0.1 $g\,dm^{-3}$ $CaCl_2 \cdot 2H_2O$, 0.1 $g\,dm^{-3}$ NaCl, 3 $g\,dm^{-3}$ yeast autolysate, were used. The fermentation processed under semiaerobic and anaerobic conditions at the temperature 10 and 25 °C, respectively.

At the end of fermentation process the samples were sensorially evaluated by a group of degustators.

The identical samples were subsequently analysed by gas chromatography for the aroma compounds production. Each sample was analysed on the GC MS (Shimadzu QP 2010) equipment and also on the GC FID equipment (GC 8000 CE Instruments).

Two methods of sample preparation were done:
- Samples (20 ml) were extracted by ether (2 ml), and centrifuged prior to analysis. The etheric extract was used for analysis. (liquid – liquid extraction). This method was used for higher alcohols (propanol, isoamylacohol, ethyl esterand esters determination.
- Samples were extracted by Tenaq (solid phase microextraction) and than 10 min sampled in the GC according to[5].

The same column and the same conditions were used by both analysis: Column: DB WAX 30 m, 0.25 × 0.25, temperature programme: 30 °C, hold 2 min, increase by 4 °C min⁻¹ up to 230 °C, hold 10 min, 1 ml of sample was injected to injection port at 200 °C, detector temperature 220 °C, carrier gas: helium, injektion mode: split 1 : 100, flow control mode: pressure 70 kPa

Results

MANOVA test was used to explain the variation in the aroma compounds produced by various yeast strains under aerobic/anaerobic conditions. The aerobic conditions influ-enced the variance in several compounds like ethylacetate, izoamylacete, and propanol.

The other important factor was the temperature. When the temperature increased more compounds were produced by all yeast strains, but the effect of higher temperature was negative. From the statistical view point the less important factor was evaluated by the media composition, interpreting only 5 % of data variance.

Table I shows the sensorial evaluation of fermented grape must by various yeast strains. There were differences in the specific aroma in several cases. For example Rhodotorula mucilaginosa was recognized as fruity aroma in fermenting grape must, and as vanillic aroma fermenting the synthetic media under semiaerobic conditions, however socks smelly and yeasty under anaerobic ones. Similar results were obtained by Torulospora delbruecki, fermenting semiaerobically grape must, however "only" honey and fruity aroma fermenting synthetic medium.

Conclusions

Using statistical data, we confirmed that the aroma compounds production is strongly influenced by the presence of oxygen. The temperature affected the production of aroma compounds to the lower extend and the media composition had the minor impact.

The changes in the sensorial evaluation of aroma are more intensive and important than changes in the chemical composition.

Under defined conditions the apiculate microflora can produce aromas which directly contribute to the variety or origin character and highly improve them.

REFERENCES
1. Granchi L., Ganucci D., Messini A, Vincenzini M.: FEMS Yeast Res. *2*, 403 (2002).
2. Romano P., Fiore C., Paraggio M., Caruso M., Capece A.: Int. J. Food Microbiol. *86*, 169 (2003).
3. Rojas V., Gil J.V., Pinaga F., Manzanares P.: Inter. J. Food Microbiol. *70*, 283 (2001).
4. Pátková-Kaňuchová J., Nemcová K., Vajcziková I., Bre-ierová E.: *In proceedings from 36ᵗʰ Annual Konference on Yeasts*, (2008).
5. Kruzlicova D., Mocak J., Hrivnak J.: J. Food Nutr.. Res.. *47*, 37 (2008).

P13 BIOGENIC AMINES REDUCTION BY PROBIOTIC *L. CASEI* DURING RIPENING OF FERMENTED SAUSAGES

RADKA BURDYCHOVÁ, VLASTIMIL DOHNAL and PETRA HOFERKOVÁ

Department of Food Technology, Mendel University of Agriculture and Forestry in Brno, Zemedelska 1, 613 00 Brno, Czech Republic,
burdycho@node.mendelu.cz

Introduction

Fermentation technology is one of the oldest food technology applications. The use of starter cultures in the field of meat fermentation has been reviewed several times[1–3]. Starter cultures have been used in the sausage production to reduce fermentation time, ensure low residual nitrate and nitrite contents in the end product and standardize the organoleptic characteristics[2]. Starter microorganisms can also improve safety and stability of the product, extending the shelf life and provides diversity resulting in new sensory properties. Metabolic activities of the microorganisms used as starters are essential for the desirable changes determining the particular characteristics of the fermented meat product. Lactic acid bacteria represent the most important group of starter microorganisms as they are well adapted to the meat environment and are involved in all changes occuring during fermentation and ripening[3].

In the last years, the adding of probiotics into fermented sausages became more and more popular. It has confronted new challenge in the area of functional food. Probiotics are defined by the FAO/WHO as live microorganisms which when administered in adequate amounts confer a health benefit on the host. When ingested in sufficient numbers regularly, probiotics are believed to play an important role in the control of host intestinal microbiota and maintenance of its normal state[4]. The presence of adequate number of live probiotic cells in fermented sausages in the time of consumption represents the first challenge for the development of such probiotic product, taking the recommended dose of at least 10^8 cells a day[1].

Biogenic amines are organic molecules which occur in wide variety foods, mainly fermented foods like meat and dairy products[5–8]. They are formed mainly by decarboxylation of amino acids or by amination and transamination of aldehydes and ketones[9]. When high amounts of biogenic amines are consumed or when normal methabolic pathways of amine catabolism are inhibited, various negative effects like hypertension or hypotension, nausea, headache, cardiac palpitation or other complications can occur[10]. When applied into fermented foods, some probiotic were described to decrease biogenic amines formation (Sacco, Italy). To evaluate this theory, this study was carried out.

Experimental

The aim of this work was to study the effect of probiotic bacteria *L. casei* in the mixture with two different starter cultures (1 – *Staphylococcus carnosus*, *Lactobacillus curvatus*; 2 – *Pediococcus acidilactici*) on biogenic amine formation during fermentation, ripening and storage of typical Czech fermented sausages „Herkules". Other parameters like pH, total counts of microorganisms, LAB, counts of probiotic *L. casei* and the amounts of biogenic amines tyramine, histamine, putrescine and kadaverine were determined.

Bacterial Cultures

Probiotic culture *L. casei* 431 (Sacco, Italy) was obtained in lyofilized form. Two different starter cultures *(i) Lactobacillus curvatus*, *Staphylococcus carnosus* and *(ii) Pediococcus acidilactici* were used for production of fermented sausages.

Sausages Production

Two batches of sausages called „Herkules" were made using as follows: mixture of frozen pork and pork fat (80 %), beef (20 %), sugars (0.6 % dextrose), 2.5 % nitrate salt (with 0.9 % nitrite), E 250, E 316 and spices were added according to traditional receptture. Furthermore, 0.025 % starter (1 and 2) and the same amount of probiotic bacteria (*L. casei*) were added. Two control batches (starters 1 and 2) with no probiotic bacteria were included. The sausages were smoked for 6 days at 26–24 °C and processed in climate chamber in accordance with a traditional four weeks programme (11–13 °C, 75 % relative humidity). After fermentation, sausages were ripened at 15 °C for further 21 days.

pH Measurement

pH was measured directly from the sausages as the mean value of three measurements in the day of production and after 3, 5, 7, 14, 21, 28 and 49 days of fermentation and ripening.

Microbiology Analysis of Sausages

Three sausages from each batch were analyzed at the day of production and after 14, 28 and 49 days after production to observe probiotic counts. Ten grams of each sample were homogenized in 90 ml of Ringer solution (Noack, France) using Stomacher. 1 ml of appropriate dilution was plated on: *(i)* Plate count agar (PCA, Noack, France) to determine total microbial count; *(ii)* MRS agar (Merck, Germany) to count lactic acid bacteria (LAB); *(iii)* MRS agar (Noack, France) containing 112 mg dm^{-3} moxalactam (Sigma-Aldrich, Germany) for selective enumeration of *L. casei*. Plates for enumeration of total microbial count were incubated at 30 °C for 72 hours. All other plates were incubated anaerobically for 3 days at 37 °C.

Biogenic Amines Determination

The analytical determinations of biogenic amines were performed in triplicate. The amount of 10 g of each sausage

sample was weighted into the plastic test tube. A volume of 0.5 ml of an internal standard, 1,7-diaminoheptane, with concentration $1\,mg\,ml^{-1}$ was added to the sample and it was extracted with 20 ml of 5% trichloroacetic acid for two minutes using a disintegrator Heidolph Diax 900 (Heidolph Instruments, Germany). Suspension was then centrifuged for 10 minutes (3,000 rpm, 4 °C). The supernatant was filtered through paper filter (Filtrak no. 390) and the solid residue was extracted for the second time (using method described above). Both extracts were collected into one tube, filled in 50 ml with 5% trichloroacetic acid and filtered through the nylon membrane filter (13 mm, 0.45 μm, Chromatography research Supplies, Edison, USA). An aliquot 1 ml of an extract was mixed with 0.5 ml of saturated sodium carbonate solution (Sigma-Aldrich, s.r.o, Prague, Czech Republic) and derivatized with 1 ml of acetonic solution of dansyl chloride ($5\,mg\,ml^{-1}$) for 1 hour at 40 °C. The excess of unreacted derivatisation agent was removed by reaction with 250 μl 10mM ammonia solution. Derivatized biogenic amines were then extracted into diethyl ether (3×1 ml); etheric extract was evaporated to dryness and dissolved in 500 μl of acetonitrile. The same procedure was applied on standard solution of biogenic amines (Sigma-Aldrich). Biogenic amines were determined as described in Burdychova and Komprda[11] and Burdychova and Dohnal[12] by high performance liquid chromatography with UV detection at 254 nm. The formation of biogenic amines by starter and probiotic cultures was screened as described by Burdychova and Dohnal[12].

Results

Microbial Counts

A number of health benefits have been claimed for probiotic bacteria such as *Lactobacillus casei*. Because of the potential health benefits, this organism is increasingly incorporated into fermented foods. However, studies have shown low viability of this probiotic in market preparations[13].

In both bathes with probiotic bacteria, *L. casei* was detected at concentration of 10^4 $CFU\,g^{-1}$ during ripening period and stayed at this level during the whole storage period. The changes in probiotic flora during ripening and storage of sausages are shown in Fig. 1. Initial LAB counts in probiotic batches were significantly higher than in the control samples without probiotics ($p < 0.05$), due to the inoculation of starter strains. During first 14 days of ripening LAB numbers reached levels up to 10^7 $CFU\,g^{-1}$ in all batches; thereafter, during next 14 days of ripening, the counts of LAB significantly decreased in all batches to the level of 10^6 $CFU\,g^{-1}$. The total microbial count reached levels up to 10^8 $CFU\,g^{-1}$ in all batches during first 14 days of ripening and their counts gradually decreased to the level of 10^7 $CFU\,g^{-1}$ during next 14 days of ripening and 21 days of storage (data not shown).

To provide health benefits, the suggested concentration for probiotic bacteria is 10^6 $CFU\,g^{-1}$ of a product[13] and daily consummation of 100 g of such product is recommended. However, the minimal dose is depended on several factors such as individual person, probiotic strain and type of food

product[14]. On the other hand, dry sausages are products, which may be suitable carriers for probiotics into the human gastrointestinal tract. The question still is, if those types of meat products can be called functional foods and consumed daily.
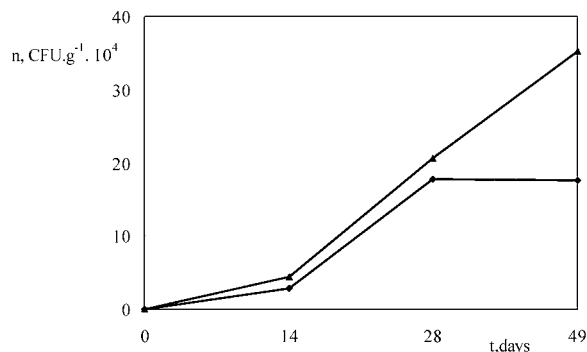
Fig. 1.   **Changes of probiotic *L. casei* during ripening (0–28) and storage (28–49) of sausages „Herkules", ▲ starter + probiotic *L. casei*, ♦ starter 2 + probiotic *L. casei***

Biogenic Amines Formation

Biogenic amines are formed by the microbial decarboxylation of free amino acids in food[15] and they are generally present in dry sausages as reviewed by Maijala[16] and Eerola et al.[17] As described by Buckenhüskes[18], the absence of biogenic amines formation should be a selection criterion for strains used as meat starter cultures. In our study was confirmed that neither starter nor probiotic cultures formed biogenic amines (results not shown). All sausages were analyzed for biogenic amines by HPLC. The concentrations of BA in the raw material were low but during ripening, fermentation and storage period a sharp rise occurred in both control and probiotic batches. The only BA which were at low levels during the whole ripening and storage periods was histamine, which concentrations varied from 0.5 to 2.5 $mg\,kg^{-1}$ in all batches (data not shown). Nout[19] pointed out that histamine contents should be in the range of 50–100 $mg\,kg^{-1}$ in sausages processed according to „Good Manufacturing Practice", the amount of histamine measured in this study is in agreement with this rule.

Putrescine was the main amine formed in both control batches, followed by cadaverine and tyramine. The concentration of putrescine increased from 1.9 to 101.2 $mg\,kg^{-1}$ (control batch 1) and from 4.6 to 350.5 $mg\,kg^{-1}$ (control batch 2). The amount of cadaverine increased from 2.0 to 39.9 $mg\,kg^{-1}$ (control batch 1) and from 11.7 to 81.6 $mg\,kg^{-1}$ (control batch 2). The level of tyramine increased from 6.3 to 204.4 $mg\,kg^{-1}$ (control batch 1) and from 10.5 to 300.4 $mg\,kg^{-1}$ (control batch 2), respectively. In this study, putrescine, cadaverine and tyramine accumulation was significantly inhibited in probiotic sausages when compared with controls without probiotic *L. casei* culture. Putrescine concentration increased gradually during ripening and storage period, reaching levels 53.7 $mg\,kg^{-1}$ (probiotic batch 1) and 163.5 $mg\,kg^{-1}$ (probio-

A
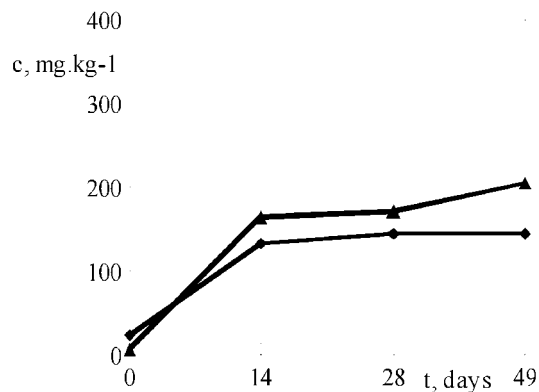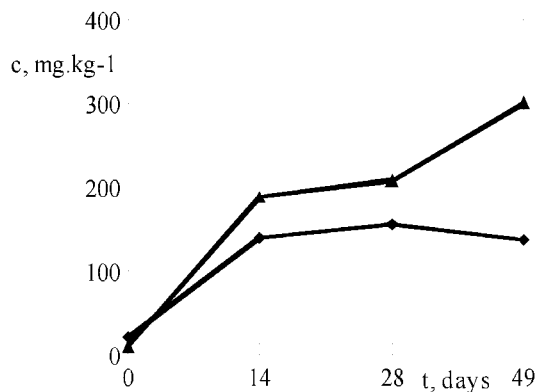
B
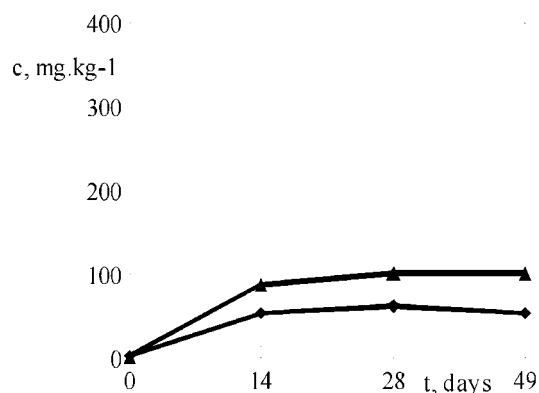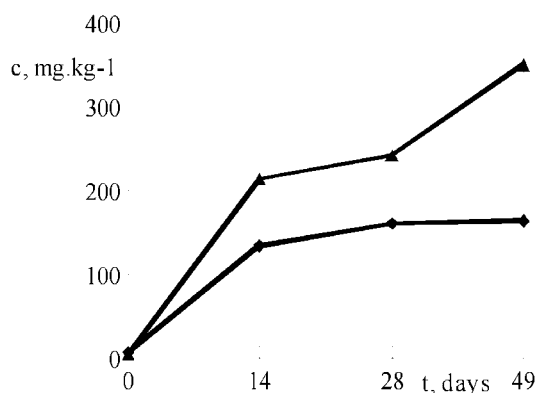
C
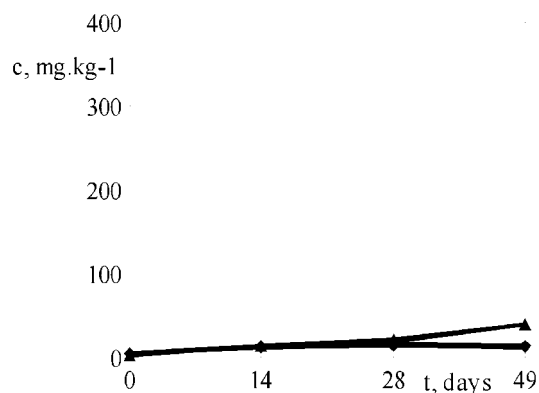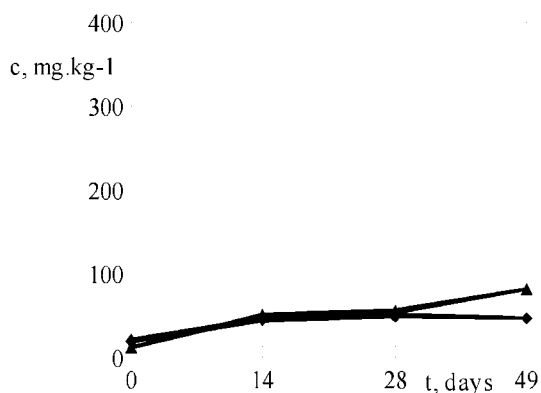
Fig. 2. **Changes of BA during ripening (0–28) and storage (28–49) of sausages „Herkules". (A) tyramine concentrations, (B) putrescine concentrations, (C) cadaverine concentrations. ▲ starter 1, ♦ starter 1+probiotic *L. casei* (control batch 1)**

Fig. 3. **Changes of BA during ripening (0–28) and storage (28–49) of sausages „Herkules". (A) tyramine concentrations, (B) putrescine concentrations, (C) cadaverine concentrations. ▲ starter 2, ♦ starter +probiotic *L. casei* (control batch 2)**

tic batch 2) and at the end of storage. Cadaverine amounts increased gradually during ripening period, during storage period level down to 13.2 mg kg^{-1} (probiotic batch 1) and 46.3 mg kg^{-1} (probiotic batch 2). The levels of tyramine fol-

lowed the same trend reaching concentrations 144.6 mg kg^{-1} (probiotic batch 1) and 137.5 mg kg^{-1} (probiotic batch 2) at the end of storage period. The results are shown in Fig. 2. and Fig. 3.

The allowable maximum level of tyramine in foods is 100–800 mg kg^{-1} and 1,080 mg kg^{-1} is toxic[20]. The tyramine contents were lower than these values in all cases. Nout[19] concluded that for „Good Manufacturing Practice", the amount of tyramine should be in the range of 100–800 mg kg^{-1}. I was described[21–23] that with occurrence and accumulation of biogenic amines putrescine and cadaverine largely contributes the contaminant microbial population (such as enterobacteria). Probiotic *L. casei* has evidently inhibitory effect on the growth of this bacteria or formed metabolites which influence the production of BA.

p H

pH profiles of control and probiotic batches were almost the same (data not shown). During the first 3 days of ripening, the pH of all sausages decreased (P<0.05) to about 4.1–4.5 due to production of lactic acid and other organic acids by lactic acid bacteria as described by Lücke[3]. After that, pH increased (P<0.05) due to decomposition of acids to become almost constant. Some authors have reported that the main reason for low levels of biogenic amines is the low pH during r ipening period[6]. In this study, no correlation between pH and biogenic amines formation was found.

Conclusions

Some authors published that the inoculation of competitive and decarboxylase-negative starter cultures has been shown to be a useful tool to inhibit spontaneous aminogenic microflora and thus considerably reduce aminogenesis[24,22]. It seems that the lowering of BA concentrations by probiotic *Lactobacillus casei* described in this study is in agreement with these statements. Evidently, *L. casei* 01 (Sacco, Italy) was well adapted to meat fermentation and could have inhibitory effect on microorganisms producing BA.

REFERENCES
1. Hammes W. P., Hertel C.: Meat Sci. *49*, 125 (1998).
2. Hugas M., Monfort J. M.: Food Chem. *59*, 547 (1997).
3. Lücke F. K. Meat Sci. *56*, 105 (2000).
4. Fuller R., in: Probiotics 2: *Applications and practical aspects* (Fuller R., ed.), chapter I, p.1. Chapman Hall, New York 1997.
5. Santos M. H. S.: Int. J. Food Microbiol. 29, 213 (1996).
6. Maijala R., Eerola S.: Meat Sci. *35*, 387 (1993).
7. Stratton J. E., Hutkins R. W., Pylor S. L.: J.. Food Prot. *54*, 460 (1991).
8. Vitova E. Loupancova B., Zemanova J., Stoudkova H., Brezina P., Babak L.: Czech. J. Food Sci. *24*, 268 (2006).
9. Maijala R., Nurmi E., Fischer A.: Meat Sci. *39*, 9 (1995).
10. Rawles D. D., Flick G. J., Martin R. E.: Adv. Food Nutr. Res. *39*, 329 (1996).
11. Burdychova R., Komprda T.: FEMS Mikrobiol. Lett. *276*, 149 (2007).
12. Burdychova R., Dohnal V.: Chem. listy *101*, 907 (2007).
13. Shah N. P.: J. Dairy Sci. *83*, 894 (2000).
14. Perdigon G., Maldonado-Galdeano C., Valdez C., Medici M.: Eur J Clin Nutr, *56*, 21 (2002).
15. Askar A., Treptow, H.:
16. Maijala R.: Academic dissertation. Helsinki, Finland, 1994.
17. Eerola S., Hinkkanen R., Lindfors E., Hirvi T.: J. AOAC Int. *76*, 575 (1993).
18. Buckenhüskes H.: FEMS Microbiol. Rev. *12*, 253 (1993).
19. Nout M. J. R.: Food Res. Int. *27*, 291 (1994).
20. Shalaby A. R. Food Res. Int. *29*, 675 (1996).
21. Bover-Cid S., Holzapfel W. H.: Int. J. Food Mikrobiol. *53*, 33 (1999).
22. Bover-Cid S., Izquierdo-Pulido M., Vidal-Carou M. C.: J. Food Prot. *64*, 367 (2001).
23. Halász A., Bárách A., Simon-Sarkadi L., Holzapfel W.: Trends Food Sci. Technol. *5*, 42 (1994).
24. Bover-Cid S., Hugas M., Izquierdo-Pulido M., Vidal-Carou M. C.: J. Food Prot. *63*, 237 (2000).

P14 TESTING OF DIFFERENT *SACHAROMYCES* SPECIES FOR THE ABILITY TO SORB DEOXYNIVALENOL

RADKA BURDYCHOVÁ, VLASTIMIL DOHNAL and DANA VRÁNOVÁ

Mendel University of Agriculture and Forestry in Brno Zemedelska 1, 613 00 Brno, Czech Republic, burdycho@node.mendelu.cz

Introduction

Mycotoxin contamination of food and feed is a high risk to human and animal health[2]. The majority of the causal organisms are producers of mycotoxins such as highly toxic trichothecenes[4]. Four types of trichothecenes are described, type A and type B, which differ in the presence or absence of a keto group at C-8 of the trichothecene skeleton, type C with additional epoxydic group and macrocyclic type D. The most common trichothecene in cereals is type B trichothecene deoxynivalenol (DON).

Deoxynivalenol, also called vomitoxin, is produced by *Fusarium fungi*, such as *F. graminearum* or *F. culmorum*. It has negative effect on animal growth and health. DON inhibits the synthesis of DNA, RNA and proteins at the ribosomal level. High doses causes the vomiting in pigs, lower concentrations in the diet reduces feed intake and animal growth[5]. Different physical and chemical methods have been recommended for detoxification of mycotoxin-contaminated food and feed. Nevertheless, only a few of them have been accepted for practical use. Thermal degradation of trichothecenes is not so effective, because they are relatively stable and they decomposes at 210 °C within 30–40 min[10]. From physical methods are the most frequently used feed additives on sorbent basis, such as bentonite or active charcoil. The disadvantages of adsorbents are their relatively high dosage and sorption of biologically active compounds, e.g. vitamins or trace metals. In addition, the sorbents can bind to only a limited group of mycotoxins and in some cases does not provide required effect[7]. Biological decontamination of mycotoxins using microorganisms is one of the well-known strategies for the management of mycotoxins in food and feed. Biological decontamination of mycotoxins by different microorganisms was reviewed several times.[1,8,11,15] There are two ways of action – sorption on cell walls or enzymatic degradation, for example using epoxydase. De-epoxylated form is less toxic than original DON. Among the different potential decontaminating microorganisms, the genus Saccharomyces represent the unique group, which is widely used in food fermentation and preservation. The aim of this study was screening of ability of different Saccharomyces species to remove deoxynivalenol from liquid medium.

Experimental

Microbial Cultures and Culture Conditions

All cultures were obtained from Culture Collection of Yeast (Bratislava, Slovakia). The cultures were *Saccharomyces cerevisiae* 20_1; isolated from loaf of hornbeam, *Saccharomyces bayanus* 21-31-12; isolated from mushrooms, *Saccharomyces paradoxus* 2 isolated from needles of spruce, *Saccharomyces paradoxus* 21-53-2 isolated from soil and *Saccharomyces paradoxus* isolated from the loaf of locust. All cultures were cultivated in Plate Count Broth (PCB; Merck, Germany) at 30 °C for 48 hours and then subcultured by transfering 4 ml of the culture to the cultivation test tube. Three replicates per sample of inoculum were used at each measuring. On the base of O. D. (600 nm) values that have been taken during the cultivation of yeasts with deoxinyvalenol the analysis of their counts has been done.

Preparation of Yeast Cultures for Testing of DON Sorbtion

All used chemicals were analytical or gradient grade. Standard of deoxynivalenol (DON) was obtained from Sigma-Aldrich, s.r.o. (Czech Republic). The stock solution of DON was prepared by dissolution of 1 mg of DON in 5 ml of acetonitrile to give solution with concentration $0.2\ \mathrm{mg\,ml^{-1}}$. The solution was stored at –18 °C. Working solutions for calibration curve measurement were prepared by dilution of stock solution.

The amount of 0.5 μg of DON was transferred to test tube and evaporated to dryness. In the next step, 4 ml of cultivation media (PCB) with yeasts were added to the test tube and the sample was cultivated in thermostated box at 30 °C for 4 hours. The concentration of free DON was measured at the beginning of cultivation and after 4 hours of cultivation.

Prior the DON determination it was necessary to remove yeasts from culture medium using ultrafiltration through polytetrafluoroethylene membrane filter (SMI-LabHut Ltd., UK) with pore size 0.20 μm. After this step, the filtrate was diluted with acetonitrile (in ratio 16 : 84). Next, the clean-up with MycoSep® 225 Trich was applied. Briefly, 5 ml of solution was transferred to the glass tube and pushed through the MycoSep® 225 Trich column. 2 ml of this eluate were evaporated to dryness and redissolved in 400 μl of HPLC mobile phase. Mobile phase consisted of 1mM formic acid/acetonitrile (90 : 10, v:v) with flow rate $1\ \mathrm{ml\,min^{-1}}$.

Chromatographic Determination of DON

The HPLC system HP 1100 (Agilent Technologies, Palo Alto, USA) consisted of vacuum degasser unit (model G1322A), quaternary pump (G1311A), autosampler (G1313A) and quadrupole mass spectrometer (G1946VL) with electrospray ionization was used. The ChemStation software (Rev. A 10.02) controllig chromatographic system and was used for chromatogram evaluation.
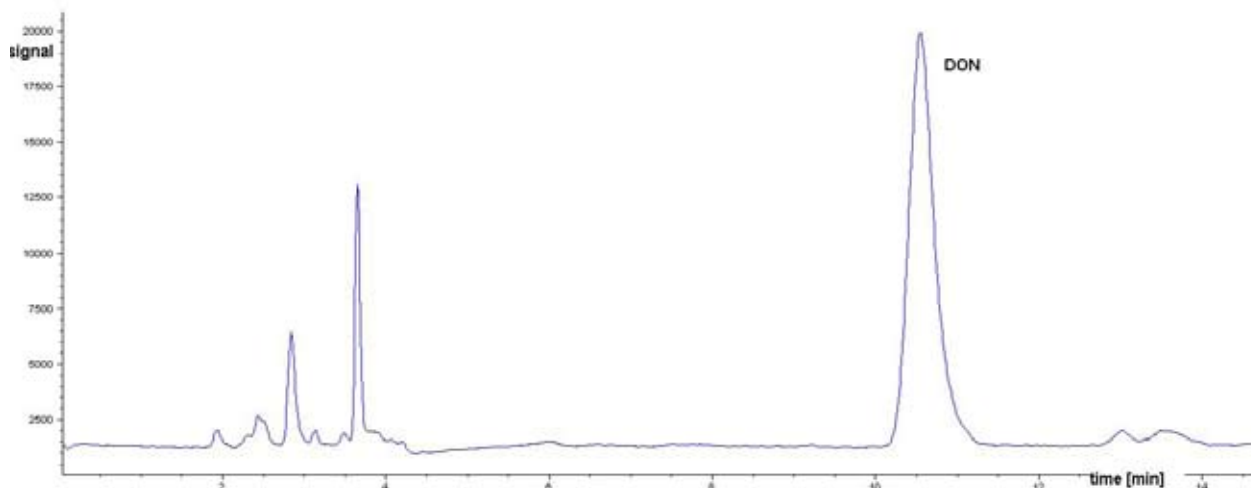
Fig. 1.   **Elution of DON in mobile phase**
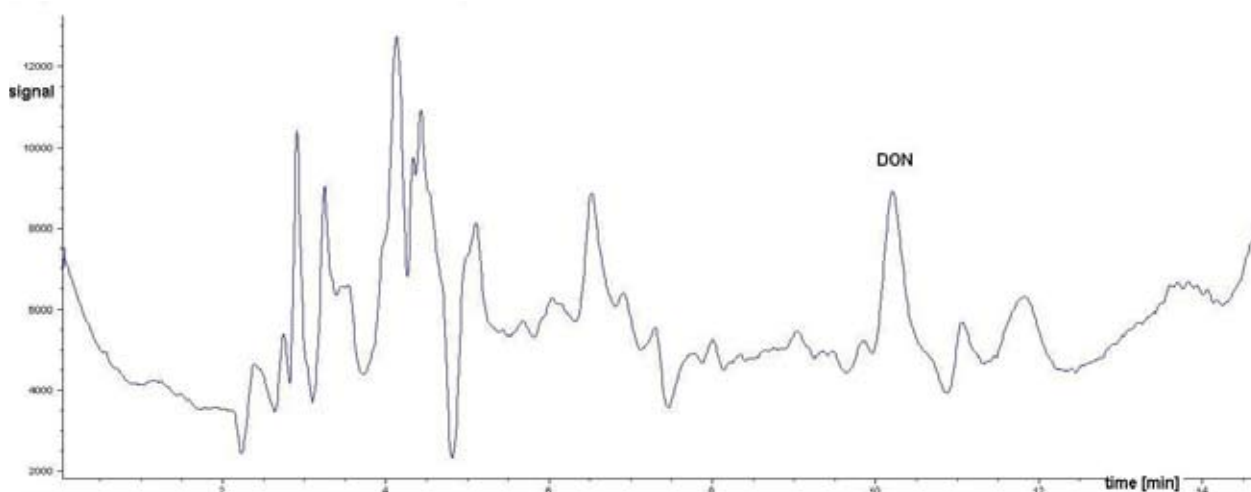
Fig. 2.   **Elution of DON in culture medium (Plate Count Broth)**

Analytical determination of DON was performed on reverse-phase chromatographic column LUNA (250 × 4.6 mm, particle size 5 μm; Phenomenex, USA). DON was detected on mass spectrometric detector (MS) as positively charged ions: [DON+H]$^+$, m/z = 297 and [DON+Na]$^+$, m/z = 319). The time of analysis was 15 min, DON was eluted at 10.9 minutes. The separation was performed at laboratory temperature.

The calibration curve was measured using standard addition method. The appropriate amount of DON was added into pure cultivation media solution and processed in the same way as the real samples.

Results

Knowledge on interaction of yeasts with mycotoxins goes back more than three decades[6,12].

The yeast of the genus *Saccharomyces* were described as capable to bind different types of mycotoxins, like aflatoxins[14], ochratoxin A[13], T2 toxin and zearalonon[9].

In this study, isolates of yeasts belonging to different species of the genus *Saccharomyces* were tested for deoxinyvalenol binding.

First of all, the detection of DON in culture medium was tested. It was observed that the detector signal is much lower when analyzed DON in culture medium (PCB) than when analyzed it in pure mobile phase (see Fig. 1. and 2.).

The reason of this phenomenon could be the lowering of deoxynivalenol inonization caused by interfering compounds in culture medium.

The detector signal of initial concentration of deoxynivalenol in culture medium was taken as 100 % for futher calculations.

In all culture batches there was observed decrease in the concentration of DON, which was measured using HPLC.

Of the 5 *Saccharomyces* isolates, all of them were able to sorbe DON.

The percentages of lowering of DON concetrations after cultivation with all *Saccharomyces* isolates are shown in Table I.

Table I
Lowering of DON concentration [%] in culture media with different *Saccharomyses* strains

Yeast strains	Incubation time [hours]		
	0	4	8
	Concentration [%]		
S. cerevisiae	67.71	71.12	78.15
S. bayanus	67.75	68.07	72.05
S. paradoxus	66.04	67.92	75.65
S. paradoxus	5.83	12.67	18.95
S. paradoxus	57.77	62.61	76.25

The maximum sorbtion of deoxinyvalenol was observed in all yeasts strains immediately after DON addition to culture medium with cultured yeasts.

The next cultivation did not significantly influenced further lowering of DON concentration.

Most of the yeast strains bound more than 70 % (w/w) of deoxinyvalenol. The only isolate from soil (*Saccharomyces paradoxus* 21-53-2) bound less than 20 % (w/w) of the added toxin in PCB.

It follows from Table II that the most significant decrease of live yeast cells was detected at isolate of *S. bayanus* (isolated from muschrooms).

This strain was the most sensitive to deoxynivalenol. On the other hand, the most resistant to deoxynivalol was *S. paradoxus* (isolated from the loaf of locust).

From results obtained in this study it is clear that the ability to sorb deoxynivalenol by several strains of the genus *Saccharomyces* was demonstrated. Commertially, the yeast

Tabulka II
The yeasts concentration in cultivation media after addition of DON

Yeast strains	Incubation time (hours)		
	0	4	8
	Yeast concentration [CFU ml^{-1}]		
S. cerevisiae	1.4×10^7	1.3×10^6	1.1×10^5
S. bayanus	1.9×10^7	1.6×10^5	1.5×10^4
S. paradoxus	1.7×10^6	1.6×10^5	1.3×10^5
S. paradoxus	9.9×10^4	4.0×10^4	5.5×10^3
S. paradoxus	4.5×10^5	1.5×10^5	1.1×10^5

cell walls are applied as feed additives (Mycosorb). Their detoxifying activity is based on complex formation between glucomannan and mycotoxins.

Conclusions

It seems that, according to results of experiments realized till present time, microorganisms are the main living organisms applicable of mycotoxin biodegradation. Further screening of microorganisms for their ability to sorbe deoxynivalenol may lead to detection of more efficient and better applicable yeasts and bacteria.

REFERENCES
1. Bata A., Lasztity R.: Trends Food Sci. Technol. *10*, 223 (1999).
2. Bennett J. W., Klich M.: Clin. Microbiol. Rev. *16*, 497 (2003).
3. Bhatnagar D., Lillehoj E. B., Bennet J. W.: In J. E. Smith and R. S. Henderson (Eds.) *Mycotoxins and animal foods,* p. 816, MA: CRC Press, Boston, 1991.
4. Bottalio A., Perrone G.: Eur. J. Plant Pathol. *108*, 611 (2002).
5. Canady R. A., Coker R. D., Egan S. K., Krska R., Kuiper-Goodman T., Olsen M., Pestka J., Resnik S., Schlatter J.: *Deoxynivalenol* (JECFA 47, 2001). http://www.inchem.org/documents/jecfa/jecmono/v47je05.htm.
6. Ciegler A., Lillehoj E. B., Peterson R. E., Hall H. H.: Appl. Microbiol. *14*, 934 (1966).
7. Danicke S., Valenta H., Doll S., Ganter M., Flachowsky G.: Anim. Feed Sci. Technol *114*, 141 (2004).
8. Dohnal V., Ježková A., Jun D., Kuča K.: Curr. Drug Metab. *9*, 77 (2008).
9. Freimund S., Sauter M., Rys P.: J. Environ. Sci. Health *B38*, 243 (2003).
10. Kamimura H. (1989) Removal of mycotoxins during food processing. In: Natori, S., Hashimoto, K. & Ueno, Y., eds, *Mycotoxins and Phycotoxins '88,* p. 169, Amsterdam: Elsevier Science Publisher.
11. Karlovsky P.: Nat. Toxins *7*, 1 (1999).
12. Mann R.: Zeitschrift für Lebensmittel Forschung *163*, 39 (1977).
13. Raju M. V., L. N. and Devegowda G.: Br. Poultry Sci. *41*, 640 (2000).
14. Shetty P. H. and Jespersen L.: Trends Food Sci. Technol. *17*, 48 (2006).
15. Styriak I., Concova E.: Vet. Hum. Toxicol. *44*, 358 (2002).

P15 SEPARATION OF COMPLEX OLIGOSACCHARIDES FROM WORT AND BEER USING HPLC

JANA CABÁLKOVÁ and JANETTE BOBÁĽOVÁ

Institute of Analytical Chemistry of the AS CR, v. v. i., Veveří 97, 602 00 Brno, Czech Republic,
cabalkova@iach.cz

Introduction

Oligosaccharides (OS) including maltooligosacharides (MOS) are essential non-volatile compounds in fermentation processes appeared in a wide range of food products and beverage production involving beer. Specifically, monitoring of changes in carbohydrate pattern before, during, and after the malting is of great fundamental and practical significance for brewing technologies and the sensory characteristics of the beer.[1–3]

The intent of the study was to optimize analytical conditions for separation and quantification of the OS in the congress wort, hopped worth, green beer, and lager beer.

Experimental

Materials and Methods

Standards of MOS (Sigma-Aldrich, St. Louis, USA) with degree of polymerization (DP) from maltotriose (MA3) up to maltoheptaose (MA7) were used for the primal identification and column calibration. Separation was achieved on 1100 Series HPLC system equipped with refractive index (RI) detector (Agilent Technologies) on Prevail Carbohydrate ES analytical column (250 × 4.6 mm, 5 μm; Alltech) using a mixture of acetonitrile (ACN)/water 3 : 2 (v/v) with a flow rate of 1 ml min^{-1} and 10 μl injection loop.

Samples

Eleven defined varieties of wort samples (congress wort, hopped worth, and green beer) were harvested during the year 2006 in different regions all around the Europe. For comparison one sample of home-made lager beer with 5.0 % (v/v) of ethanol was used. Samples were sonicated for 10 minutes, centrifuged and filtered with 0.22 μm PVDF Millipore filter (Millipore, Bedford, USA) before analysis.

Results

Standards of non-derivatized MOS from MA3 up to MA7 were separated using different ratio of ACN/water to find optimal separation conditions. The ratio of 3 : 2 (v/v) enabled simultaneous and sufficiently selective separation in 20 minutes duration. Then, calibration dependencies were determined. Standard solutions of MOS in the concentration range of 0.25–10.0 mg ml^{-1} for MA3, 0.25–5.0 mg ml^{-1} for MA4, and 0.2–2.0 mg ml^{-1} for MA5, MA6, and MA7 were prepared by dissolving in mixture of ACN/water 1 : 1 (v/v). Triple injections were used for each standard solution and the peak areas were plotted against the corresponding concentration. The concentration dependencies were linear with correlation coefficients about 0.99 for all standards.

After optimization, samples of eleven different barley varieties of congress wort, hopped worth, green beer, and the lager beer were separated using HPLC according to their DP. Elution time below 45 minutes for all wort samples was observed (Fig. 1.).

Individual peaks in chromatogram (Fig. 1.) were labeled by DP in their increasing order. In general, the retention times
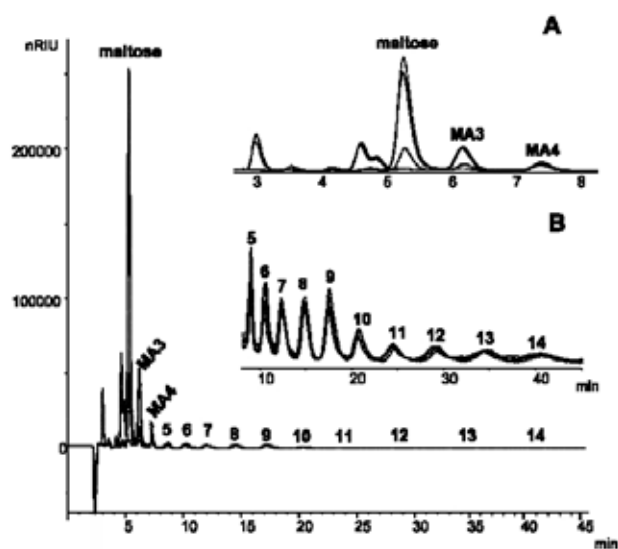
Fig. 1. **Separation of congress wort (full line), hopped worth (dotted line), green beer (dashed line) of the same variety and lager beer (broken line) using HPLC. Detail of separation in the low-weight range (A) and higher oligosaccharides (B). Peak numbers correspond to the DP**
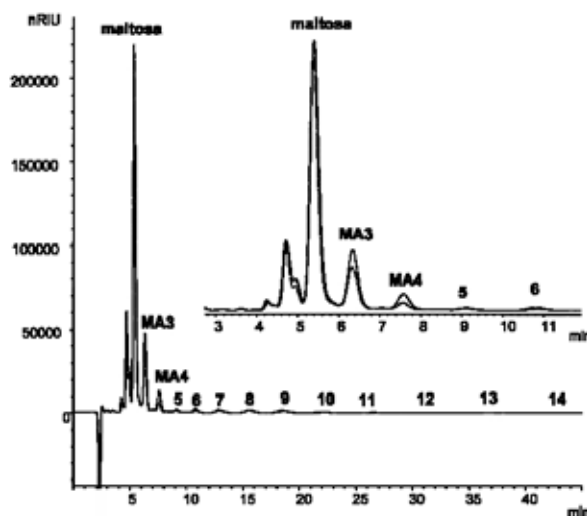
Fig. 2. **Differences in concentration profiles of OS in the congress wort prepared from variety Maltasia (full line) and Quench (dashed line) using HPLC. Detail of separation for low-weight OS. Peak numbers same as in Fig. 1.**
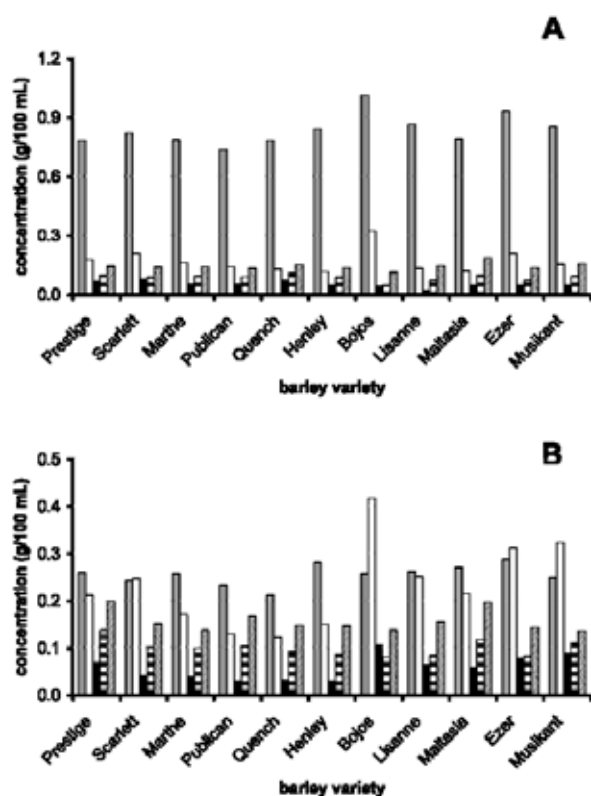
Fig. 3. **Concentration profile of individual OS in the congress wort (A) and green beer (B) for different barley varieties. Symbols: DP 3 (vertical lines), DP 4 (white), DP 5 (black), DP 6 (horizontal lines), and DP 7 (transversal lines).**

of eluted OS with DP<4 corresponded exactly to the retention times of standards of MA3, MA4 respectively, while small shifts in the retention times for OS with DP>4 compared to the standards of MOS were observed. It seems that OS with DP<4 are mostly consisted of linear α-(1 → 4)-linked glucose chains, while higher OS can be substituted by maltose/maltotriose residues of α-(1 → 6)-linked chains to form hardly fermentable saccharides so called dextrins. To identify the actual chain position, combination of HPLC with mass spectrometry has to be applied.

Beside the quality differences, noticeable changes in the quantity of OS for multiple DP were observed. There was high concentration of mono-, di-, and trisaccharides in the congress wort and hopped worth, while green beer and beer revealed significant decrease of these saccharides as expected after fermentation process. Especially maltose – the most abundant saccharide in the congress wort – was mostly fermented, so its concentration significantly decreased in the green beer (Fig. 1.A). In comparison, the concentration of OS with DP>4 did not show any significant changes neither in the wort nor in the beer samples. Their concentration remained on the same levels in all wort samples (Fig. 1.B).

Beside concentration changes in the wort samples of the same variety, significant changes in the content of low-weight saccharides (up to DP 4) in the congress wort of different barley varieties were found (Fig. 2.).

Obtained calibration data were used for quantification of OS corresponded to those with DP 3 to DP 7. The content of individual OS from different barley varieties is shown in Fig. 3.

The highest concentration of MA3 and MA4 was found in the Bojos variety, while Maltasia revealed the lowest concentration. Observed changes in the saccharide concentration can serve as the indicator of the quality and the usefulness of individual barley varieties; therefore, is essential in the development and production of new sort of beer.

Conclusions

ACN/water 3 : 2 (v/v) with flow rate of 1 ml min^{-1} provided for good separation of oligosaccharides up to tetradecasaccharides in 45 minutes duration. Significant changes in the quantity of low oligosaccharides in eleven different wort samples were found. The changes in the concentration and pattern of OS are important knowledge for development of the new brewing technologies.

REFERENCES

1. de Keukeleire D.: Quim. Nova *23*, 108 (2000).
2. Vinogradov E., Bock K.: Carbohydr. Res. *309*, 57 (1998).
3. Nogueira L. C., Silva F., Ferreira I. M. P. L. V. O., Trugo L. C.: J. Chromatogr. A *1065*, 207 (2005).

P17 EXTENSION OF ASPARAGINASE APPLICATION TO ACRYLAMIDE MINIMIZATION FROM POTATO TO CEREAL PRODUCTS

ZUZANA CIESAROVÁ[a], KRISTÍNA KUKUROVÁ[a], ALENA BEDNÁRIKOVÁ[a] and FRANCISCO J. MORALES[b]

[a]*VÚP Food Research Institute, Priemyselná 4, 824 75 Bratislava, Slovak Republic,*
[b]*CSIC Consejo Superior De Investigaciones Cientificas, Instituto Del Frio, José Antonio Novais 10, E-28040 Madrid, Spain,*
ciesarova@vup.sk

Introduction

Acrylamide is a suspected human carcinogen, formed in fried and baked carbohydrate-rich foodstuffs such as potatoes and cereals. The free amino acid asparagine and reducing sugars are considered as the main precurosrs[1].

A number of raw material pre-treatments were investigated which could mitigate acrylamide formation. Unfortunately, most of them may also have an impact on the product sensory quality. For example, the acidification may result in a sour product taste, the addition of amino acids may generate unpleasant off-flavours upon heating or in the case of calcium chloride addition, product texture might be improved, but on the other hand it causes a bitter aftertaste[2]. However, the application of L-asparaginase enzyme before heat treatment results in a sufficient decrease of acrylamide amount with no undesirable impact on sensory quality of final products[3].

The aim of this work was an extension of enzymatic way of acrylamide elimination in potato products[3] to cereal of *rosquillas* type in collaboration with CSIC Institute del Frio in Spain. In addition, the impact on the sensory quality of products prepared with L-asparaginase was evaluated.

Experimental

L-asparaginase (Novozymes, Denmark) produced by *Aspergillus oryzae* was applied in simulated potato and cereal matrices and food products on potato and cereal base such as potato pancakes and typical Spanish cereal product named *rosquillas* (Spanish doughnuts), respectively. Following analytical parameters were determined:
- Saccharides using HPLC/RI according to ref.[4]
- Amino acids using LC/MS/MS according to ref.[5]
- Acrylamide using LC/MS/MS according to ref.[6]

The content of main acrylamide precursors (monosaccharides and amino acid asparagine) were analysed in raw material. The conversion of asparagine to aspartic acid and final acrylamide content after heat treatment was observed.

In potato pancakes the preliminary sensory evaluation was done using a dual method. An appearance, colour, texture and selected descriptors of taste and aroma were deter-mined using 0–5 point scale. Five trained assessors payed an extraordinary attention to offlavour detection.

Potato Matrix

Before the enzyme application in food products, the appropriate conditions of L-asparaginase incubation (time and temperature) were tested in simulated matrices. Potato matrix consisted of the main acrylamide precursors (asparagine and glucose), potato starch and water in typical proportions: asparagine and glucose were used in equimolar ratio and content of water was 80 %. Potato starch was dried before the application to matrix in the ratio of 1 : 0.2 with mixture of asparagine and glucose.

Cereal Matrix

Cereal matrix simulated Spanish cereal products recipe for *rosquillas* preparation and was composed of asparagine, glucose, fructose, wheat starch and water. Glucose and fructose were used in equimolar ratio and in 1 : 4 ratio with starch in a final mixture. Potency of 3 levels of asparagine (0.1, 0.5 and 1.0 %) were compared. Content of water in cereal matrix was 50 %.

Asparaginase Application

L-asparaginase was applied in concentrations of 2 and 10 U g⁻¹ to simulated potato matrix or 0.1, 0.5 and 1.0 U g⁻¹ to simulated cereal matrix. The enzyme was incubated at 20, 37, 50, 60 and 70 °C for 5, 10, 20, 30 and 60 min in thermostat (Fried Electric, Haifa, Israel). Subsequently L-asparaginase was applied to different potato varieties (*Marabel* and *Bellarosa*) purchased from local Slovak market in concentrations of 1 and 2 U g⁻¹, respectively, to potato pancakes (potato-cereal food product) in concentration of 1 U g⁻¹, and to cereal product rosquillas in concentrations of 100 and 500 U kg⁻¹ of flour. L-asparaginase in food samples was incubated at 37 °C for 10 and 15 min, respectively.

Thermal Treatment

For potato matrix 0.2 g of glucose and asparagine mixture, 1 g of potato starch was weighed into the vial and 4 ml of water (control sample) or 4 ml of enzyme solution with required concetration was added and in next step, after enzyme incubation, treated at 180 °C for 20 min in thermoblock (Liebisch Labortechnik, Bielefeld, Germany).

For cereal matrix 0.24 g of glucose and fructose mixture and 0.76 g of wheat starch was weighed into the vial, 0.76 ml of asparagine solution (concentration of 0.1, 0.5 and 1.0 g in per 100 ml) in control sample or 0.38 ml of asparagine solution (concentration 0.2, 1.0 and 2.0 g per 100 ml) and 0.38 ml of enzyme solution with demanded concentration was added. Vials were incubated and heated at 190 °C for 15 min in thermoblock.

Then, samples were cooled to room temperature and final content of acrylamide was determined.

Potato Pancakes Preparation

Potato-cereal powder for pancakes preparation was purchased from local market (Bramborák, Amylon, Czech Republic). Dough was prepared with water (control sample) and L-asparaginase solution (1 U g^{-1}). 4 pancakes with weight of 35 ± 1 g were fried on teflon pan (Tescoma, Czech Republic) in one run in microwave MW 800 HW 25 (Orava, Slovak Republic) using convection programme (170, 185 and 200 °C), 10 min for each side of pancake.
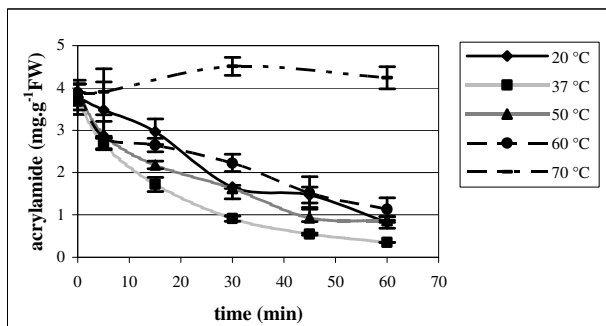
Fig. 1. **L-asparaginase efficiency to acrylamide mitigation in dependence on the incubation temperature (20, 37, 50, 60 and 70 °C) in a model system**
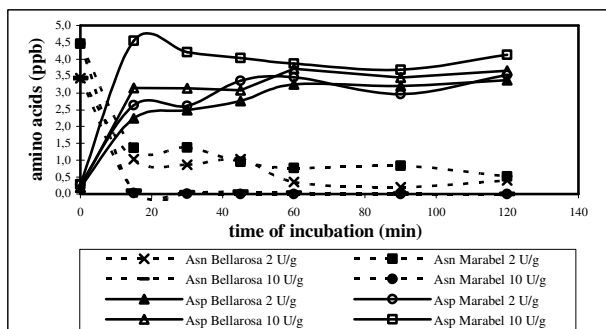
Fig. 2. **Conversion of asparagine to aspartic acid by L-asparaginase application (2 and 10 U g^{-1}, 37 °C) in 2 varieties of potatoes (Marabel, Bellarosa)**

Cereal Products Preparation

Typical Spanish cereal products *rosquillas* were preapared from dough according to three different and simplified recipes consisted of flour, sugar or equimolar mixture of glucose and fructose, in water (flour : sugar : water was in 4 : 1 : 2 ratio). In one recipe also sodium bicarbonate was added. From the dough samples of 10.0 ± 0.5 g weight and stick shape were formed and fried in sunflower oil in a fryer (Taurus, Spain). 4 samples in one run and also in duplicate were prepared for each temperature (180 and 200 °C), time (4, 6, 8 min) for each recipe (control and two levels of L-asparaginase: 100 and U kg^{-1} of flour). The dough with enzyme was incubated at 37 °C for 15 min in thermostat (Memmert, Germany).

Results

The content of asparagine in potato varies in the range from 2.3 to 39.4 mg g^{-1} of dry weight[7] that was comprised in a simulated potato matrix construction. Using different concentration of enzyme (2, 10 and 20 U g^{-1}), time and temperature of enzyme incubation (at 20, 37, 50, 60 and 70 °C for 5–60 min) the efficiency of L-asparaginase activity was compared. It was found out that temperature of 37 °C was the most suitable for sufficient acrylamide content elimination (Fig. 1.). In the case of potato matrix the time of enzyme incubation was reckoned as a limiting factor. After 30 min at 37 °C acrylamide reduction in final heated samples in levels of 8, 25 and 46 % was achieved and 91 % using 60 min of enzyme incubation.

The content of asparagine in the used potato samples was determined on 4.42 mg g^{-1} of fresh weight for variety *Marabel* and 3.52 mg g^{-1} of fresh weight for variety *Bellarosa*. Two levels of L-asparaginase (2 and 10 U g^{-1}) were applied and incubated at 37 °C. In potatoes the conversion of asparagine to aspartic acid was observed to be very fast (Fig. 2.) resulting in a sufficient acrylamide elimination (98–99 % in *Marabel* and 84–86 % in *Bellarosa*) after 10 min of enzyme incubation.

The content of asparagine in potato pancakes was 2.2 mg g^{-1} of powder. Using 1 U g^{-1} of L-asparaginase and 15 min of enzyme incubation at 37 °C, the 86% reduction of acrylamide content in a final product was achieved. No differences in sensory properties caused by enzyme were observed in the appearance (colour, texture) as well as in the taste and the aroma.

The asparaginase application in the simulated cereal matrix resulted in 18, 90 and 96% reduction of acrylamide using enzyme concentration of 0.1, 0.5 and 1.0 U g^{-1}, respectively, which was followed by enzyme treatment of cereal products. This time the determination of final acrylamide reduction in these products is in progress.

Conclusions

L-asparaginase application is proved to be an effective way of acrylamide reduction in potato and cereal products. In the presented study the 80–98 % of acrylamide elimination was achieved in dependence on matrix composition. Unambiguously, the distinctive advantage of L-asparaginase application is the avoiding undesirable changes in organoleptic properties of final products.

REFERENCES

1. Stadler R. H. et al.: J. Agric. Food Chem. *52*, 5550 (2004).
2. Mestdagh F. et al.: Food Chem. *106*, 914 (2008).
3. Ciesarová Z., Kiss E., Boegl P.: J. Food Nutr. Res. *45*, 141 (2006).

4. Ozcan S., Senyuva H. Z.: J. Chromatogr. A *1135*, 179 (2006).
5. Wilson A. M. et. al.: J. Food Sci. *46*, 300 (1981).
6. Ciesarová Z., Kiss E., Kolek E.: Czech J. Food Sci. *24*, 133 (2006).
7. Tayemans D. et al.: Crit. Rev. Food Sci. Nutr. *44*, 323 (2004).

P18   AMINO ACIDS PROFILE OF SELECTED WHOLEGRAINS IMPORTANT TO ACRYLAMIDE FORMATION IN CEREAL-BASED PRODUCTS

ZUZANA CIESAROVÁ[a], KRISTÍNA KUKUROVÁ[a], ALENA BEDNÁRIKOVÁ[a], PETER HOZLÁR[b] and ĽUBOMÍR RUCKSCHLOSS[b]

[a]*VÚP Food Research Institute, Priemyselná 4, 824 75 Bratislava, Slovak Republic,*
[b]*Research and Breeding Station at Vígľaš-Pstruša, 962 12 Detva, Slovak Republic,*
ciesarova@vup.sk

Introduction

Acrylamide as a suspected carcinogen attracts great attention due to its widespread occurrence in many staple foods of daily usage[1] as well as due to the recommendation of the European Commission since 2005 to minimize its level[2]. It is known that acrylamide arises from naturally occurred compounds in plants such as reducing saccharides and amino acids during the commonly used process of heat treatment of foods[3,4]. Acrylamide is preferably formed from amino acid L-asparagine, only in a less extent from aspartic acid, glutamine, and glutamic acid in the presence of saccharides during baking[5]. It is well established that the amount of reducing sugars is more important than free asparagine for the formation of acrylamide in potato-based products[6]. However, in cereal foods including bread, the main determinant of acrylamide formation during baking is free asparagine amount in raw material and ingredients, in particular cereal flour.

The concentration of free asparagine have been studied in different commercial milling fractions of wheat and rye[7]. Whole grain flours showed higher amounts of asparagine (for wheat and rye 0.5 g kg^{-1} and 1.1 g kg^{-1}, respectively) versus sifted flours. Of the wheat fractions, wheat germs was reported to have the highest level of asparagine (4.9 g kg^{-1}).

However, agronomical factors (e.g. crop variety, climatic conditions fertilizer regimes) may significantly impact the amount of free asparagine in cereal crops[8] and consequently the concentration of acrylamide in the final product. Regional differences may account for levels that vary by more than fivefold, and today the scientific data that may explain this variability is lacking.

Based on this knowledge it can be said that in the cereal sector the main way of acrylamide reduction is through amino acids control responsible for acrylamide formation. From the point of view of acrylamide formation, the selected 10 sorts of wholegrains appointed for human usage in bread and cereal breakfast production which are bred in Slovakia as well as 6 kinds of wheat flours from different milles in Slovakia were assorted according to profile of amino acids asparagine, aspartic acid, glutamine, and glutamic acid.

Experimental

Raw Materials

Wheat grains of 5 varieties (PS-3/05, PS-11, PS-9/06, PS-27/06, PS-51/06) and oat grains of 5 registrated varieties (Vendelin, Valentin, Zvolen, Atego, Detvan) were obtained from the Research and Breeding Station at Vígľaš-Pstruša. Wheat flours originated from Slovak milles (PMD Bratislava, Kolárovo, Sládkovičovo, Šurany) were purchased from local markets.

Reagents

Asparagine (Asn) standard (99.5%) was supplied by Fluka (Steinheim, Germany) and aspartic acid (Asp), glutamic acid (Glu), glutamine (Gln) standards (99%) were supplied by Merck (Darmstadt, Germany). D3-glutamic acid (d3-Glu) standard (97%) was supplied by Cambridge Isotope Laboratories (Andover, USA). Acetic acid (glacial) was HPLC reagent grade and obtained from Fisher Scientific (Loughborough, UK). Perfluorooctanoic acid (PFOA) (96%) and HPLC gradient grade acetonitrile were obtained from Sigma-Aldrich (Steinheim, Germany). Deionized water from a PURITE Select system (Oxon, UK) was used for preparation of amino acid and ion-pairing reagent solution.

Instrumentation

The LC/ESI-MS-MS apparatus for quantification of 4 free amino acids were performed by Agilent 1200 HPLC system (Waldbronn, Germany) consisting of a binary pump, an autosampler and a temperature controlled column oven, coupled to an Agilent 6410 Triple Quad detector equipped with ESI interface. The analytical separation was performed on a Purospher® STAR RP-8ec column (150 mm × 4.6 mm, 3 μm) using isocratic mixture of 100 ml of acetonitrile and 900 ml of aqueous solution of PFOA (0.05mM) at a flow rate 0.5 ml min^{-1} at room temperature. All parameters of the ESI-MS-MS system were based on in-source generation of the protonated molecular ions of the 4 amino acids measured and the internal standard (d3-Glu), as well as collision-induced production of amino acid-specific fragment ions for multiple reaction monitoring (MRM) experiments.

Sample Preparation

Stock solution of amino acids 1,000 μg ml^{-1} were prepared by dissolving 25 mg of each in 25 ml of deionized water. Working standards were prepared by diluting the stock solution of amino acids to concentrations of 0.05–2.00 μg ml^{-1}. Each working standard solutions consist of 0.5 μg ml^{-1} of internal standard (d3-Glu). Finely ground or homogenized sample (1 g) was extracted by 10 ml of 0.2mM acetic acid and after mixing in a vortex mixer for 2 min the mixture was centrifuged at 5,000 rpm for 10 min at −5 °C and filtered through 0.45 μm nylon syringe filter prior to LC/MS analysis[9].

Results

In this study, 5 varieties of wheat grains, and 5 varieties of oat grains as well as 6 kinds of wheat flours were used

for determination of amino acids profile. Since particularly free amino acid L-asparagine (Asn) and in a less extent also L-aspartic acid (Asp), glutamine (Gln) and glutamic acid (Glu) are responsible for the formation of acrylamide in cereal products during baking, the amino acids mentioned above were determined in the samples of wheat flours (Table I), wheat grains (Table II), and oat grains (Table III).

Table I
The amount of asparagine, aspartic acid, glutamine and glutamic acid in the samples of wheat flours

Wheat flours	Asn [mg kg^{-1}]	Asp [mg kg^{-1}]	Gln [mg kg^{-1}]	Glu [mg kg^{-1}]
A	78.51	130.86	25.01	45.53
B	115.22	154.14	39.12	77.82
C	56.14	106.85	22.28	51.68
D	92.56	133.03	32.38	67.73
E	88.37	117.11	24.62	56.20
F	81.75	121.87	31.03	59.59

Table II
The amount of asparagine, aspartic acid, glutamine and glutamic acid in the samples of wheat grains

Wheat grains	Asn [mg kg^{-1}]	Asp [mg kg^{-1}]	Gln [mg kg^{-1}]	Glu [mg kg^{-1}]
PS-51/06	221.71	79.46	24.74	76.41
PS-11	228.88	218.43	44.08	126.72
PS-27/06	290.86	181.67	121.25	187.29
PS-9/06	222.07	137.94	51.61	142.20
PS-3/05	188.04	117.02	32.76	113.39

Table III
The amount of asparagine, aspartic acid, glutamine and glutamic acid in the samples of oat grains

Oat grains	Asn [mg kg^{-1}]	Asp [mg kg^{-1}]	Gln [mg kg^{-1}]	Glu [mg kg^{-1}]
Detvan	792.24	268.85	396.91	468.79
Vendelin	567.55	144.62	211.15	261.89
Valentin	546.22	156.83	240.65	269.36
Zvolen	720.76	160.05	312.94	285.28
Atego	522.36	201.01	199.48	305.56

It is evident that in the wheat flour there is the aspartic acid which has the highest portion among determined amino acids. The amount of free L-asparagine varies between 78.51 mg kg^{-1} and 115.22 mg kg^{-1}. On the other hand, in the whole grains of wheat and oat the free L-asparagine occupies the highest ratio of free amino acids. Moreover, the oat grains contain approx. two or three fold higher amount of L-asparagine comparing to wheat grains. It is important from the point of view of the next usage of these grains at their heat treatment in the process of production of bakery ware or breakfast cereals. Furthermore, there were observed some differences between the amino acid profile in the similar kinds of wheat flour. These differences should be considered at the choice of flour which should be used for production of high heat treated products.

Conclusions

Human exposure of acrylamide from cereal products represents approx. one half of daily exposure of this contaminant. The determination of amino acids in flours as well as in the whole grains which are responsible for acrylamide formation after heat treatment could be helpful at the choice of suitable flour and cereal variety with the lowest asparagine amount and could decrease of human exposure of acrylamide from cereal products.

REFERENCES

1. Tareke E., Rydberg P., Karlsson P., Eriksson S., Tornqvist M.: J. Agric. Food Chem. *50*, 4998 (2002).
2. JECFA 2005 64th meeting Rome, 8-17 February 2005: http://www.who.int/ipcs/food/jecfa/summaries/summary_report_64_final.pdf
3. Mottram D. S., Wedzicha B. L., Dodson A. T.: Nature *419*, 448 (2002).
4. Stadler R. H., Blank I., Varga N., Robert F., Hau J., Guy P. A., Robert M. C., Riediker S.: Nature *419*, 449 (2002).
5. Yaylayan V. A., Wnorowski, A., Perez-Locas C.: J. Agric. Food Chem. *51*, 1753 (2003).
6. Amrein T. M., Bachman S., Noti A., Biedermann M., Barbosa M. F., Biedermann-Brem S., Grob K., Keiser A., Realini P., Escher F., Amado R.: J. Agric. Food Chem. *51*, 5556 (2003).
7. Frederiksson H., Tallving J., Rosen J., Aman P.: Cereal Chem. *81*, 650 (2004).
8. Taeymans D., Wood L., Ashby P., Blank I., Studer A., Stadler R. H., Gonde P., van Eijck P., Lalljie S., Limgnert H., Lindblom M., Matissek R., Muller D., Tallmadge D., O´Brien J., Thompson S., Silvani D., Whitmore T.: Crit. Rev. Food Sci. & Nutr. *44*, 323 (2004).
9. Ozcan S., Senyuva H. Z.: J. Chromatogr. A 1135, 179 (2006).

P19　CHARACTERIZATION OF BETA-CAROTENE ENRICHED BIOMASS PRODUCTION BY RED YEASTS

MARTINA ČARNECKÁ[a], ANDREA HÁRONIKOVA[a], TEREZIE DVOŘÁKOVÁ[a], ANDREA HALIENOVÁ[a], IVANA MÁROVÁ[a] and EMÍLIA BREIEROVÁ[b]

[a]Brno University of Technology, Faculty of Chemistry, Department of Food Chemistry and Biotechnology, Purkyňova 118, 612 00 Brno, Czech Republic,
[b]Institute of Chemistry, Slovak Academy of Sciences, Dúbravská cesta 9, 845 38 Bratislava, Slovak Republic,
carnecka@fch.vutbr.cz

Introduction

During the last decades fast progress has been made within the field of biochemistry of carotenoid biosynthesis in bacteria, fungi, and plants. Although more than 600 different carotenoids have been identified in nature, only a few are used industrially. There are many yeast strains able to produce different carotenoids. However, the heterobasidiomycetous yeast *Xanthophyllomyces dendrorhous*, are the only microbial systems with commercial potentials for the production of astaxanthin. Several genes involved in the astaxanthin biosynthetic pathway of *X. dendrorhous* have been cloned and characterized recently. Analysis of DNA in other red yeast is very complicated and only several genes were described yet.

There are many yeast strains able to produce different carotenoids, mainly as a part of stress response. In this work three different red yeast strains (*Sporobolomyces roseus, Rhodotorula glutinis, Rhodotorula rubra*) were enrolled into a comparative study. To increase the yield of carotenoid pigments at improved biomass production, several types of exogenous as well as nutrition stress were tested. Each strain was cultivated at optimal growth conditions and in medium with modified carbon and nitrogen sources. Synthetic media with addition of complex substrates (e.g. yeast extract) and vitamin mixtures as well as some waste materials (whey, potato extract) were used as nutrient source. Some types of exogenous stress – peroxide, salt were applied too. The production of carotene-enriched biomass was carried out in flasks as well as in laboratory fermentor. Changes in yeast cells on metabolome level were studied using LC/MS techniques to carotenoid analysis.

Materials and Methods

S t r a i n s

In the study following red yeast strains were tested: *Rhodotorula glutinis* CCY 20-2-26, *Sporobolomyces roseus* CCY 19-4-8; *Rhodotorula rubra* CCY 20-7-31; *Phaffia rhodozyma* CCY 77-1-1, *Sporobolomyces salmonicolor* CCY 19-4-10.

C u l t i v a t i o n

Red yeasts were cultivated in a simple glucose medium aerobically at 28 °C. Physiological stress was induced by nutrition components (C and N source) and by addition of 5 mM peroxide and 2% and/or 5 % NaCl. Stress cultivations with *S. salmonicolor*, *R. glutinis* and *P. rhodozyma* were realized in flasks as well as in 2 L-laboratory fermentor (B.Braun Biotech).

Three series of cultivations were realized with each strain. Two-step inoculation was done. All strains were firstly inoculated into a medium containing yeast autolysate (7 g), $(NH_4)_2SO_4$ (5 g), glucose (40 g), KH_2PO_4 (5 g), $MgSO_4$ (0.34 g) per liter (INO I) and cultivated at 28 °C for 24 hours at permanent shaking and lighting. Second inoculum (INO II) was prepared similarly, in 1st series was used the same medium as INO I, in 2nd series lyophilized whey was added (7 g dm^{-3}) and in 3rd series potato extract (7 g dm^{-3}) was added into INO II. Cultivation in INO II undergo at 28 °C for 24 hours at permanent shaking and lighting. Production media contained $(NH_4)_2SO_4$ (5 g), glucose (40 g), KH_2PO_4 (5 g), $MgSO_4$ (0.34 g) per liter. Several waste substrates were added and cultivation was done for 80 hours at 28 °C under permanent lighting and shaking. Production media were prepared according to following scheme:

- 1st series: INO I --- INO II --- production: 1 – control, 2 – 5 mM peroxide, 3 – 2% NaCl, 4 – 5% NaCl, 5 – lyophillized whey non-processed (7 g dm^{-3}), 6 – lyophillized whey processed by deproteination agent (7 g dm^{-3}), 7 – liquid whey (250 ml dm^{-3}), 8 – potato extract (Hi Media; 7 g dm^{-3})
- 2nd series: INO I --- INO II (whey, 7 g dm^{-3}) --- production: 1 – control, 2 – 5 mM peroxide, 3 – 2% NaCl, 4 – 5% NaCl, 5 – lyophillized whey non-processed (7 g dm^{-3}), 6 – lyophillized whey processed by deproteination agent (7 g dm^{-3}), 7 – liquid whey (250 ml dm^{-3})
- 3rd series: INO I --- INO II (potato extract 7 g dm^{-3}) --- production: 1 – control, 2 – 5 mM peroxide, 3 – 2% NaCl, 4 – 5% NaCl, 5 – potato extract (7 g dm^{-3}).

A n a l y z e d　P a r a m e t e r s

In all samples biomass and carotenoid content were evaluated. Biomass was determined gravimetrically. Levels of carotenoids – lycopene and beta-carotene were analyzed using HPLC/VIS (450 nm) and verified by HPLC/MS. Ergosterol and phytoene were analyzed by RP-HPLC (280 nm).

Results

In this work the growth of some red yeasts on waste substrates and subsequent effect of these substrates on beta-carotene production was studied. It was observed that addition of non-processed or deproteined whey or potato extract to media can increase beta-carotene production.

In *Rhodotorula glutinis* addition of deproteined whey into production medium led to 3.5 × increased production of beta-carotene without changes in biomass. Non-processed whey or potato extract added to production media led to about 3 × increase of beta-carotene production but it was accompanied by lost in biomass. The highest yield was reached after addition of lyophillized whey to INO II as well as

Table I
Production of biomass and beta-carotene by stressed red yeasts in laboratory flasks

	R. glutinis biomass	*R. glutinis* Beta-carotene	*S. roseus* biomass	*S. roseus* Beta-carotene
control	11.1	0.18	11.5	0.16
2 mM peroxide/INO	10.6	0.17	10.6	0.26
2% salt/ INO	11.8	0.38	11.6	0.05
2% salt/ INO/ 5 mM peroxide/prod.	10.1	0.56	11.7	0.17
2 mM peroxide/INO/ 5 mM peroxide/prod.	10.0	0.29	10.0	0.29

to production media. Liquid whey exhibited negative effect. Also potato extract added into INO II led to increased beta-carotene production, while biomass yield was lower.

Rhodotorula rubra is poor producer of carotenoids when compared with other strains. However, cultivation in presence of potato extract in INO II combined with salt stress in production medium led to the highest biomass as well as beta-carotene production observed yet.

Sporobolomyces roseus exhibited substantial changes in biomass : carotene ratio dependent on whey addition. Substantial biomass decrease in presence of lyophillized whey in INO II (under 5 g dm^{-3}) was accompanied by very high beta-carotene yield.

In flasks combined stress led to induction of carotenoid production in all studied strains; 3 × increase of beta-carotene (*R.glutinis*) was obtained. Addition of stress factor into inoculation medium induced slight increase of biomass production (salt - *R.glutinis*) and beta-carotene production (*R. glutinis*).

Conclusions

Changes in medium composition can lead to substantial changes in biomass as well as carotenoid production. Waste substrates can be used as medium component, which can in particular strains and conditions induce carotenoid as well as biomass production. Thus, waste substrates could be used industrially for carotenoid-rich biomass production.

Predominantly strain *Rhodotorula glutinis* CCY 20-2-26 can be used for industrial production of carotenoid-rich biomass using processed waste substrates and/or mild physiological stress.

REFERENCES

1. Breierová E., Márová I., Čertík M.: Chem. Listy *99*, 109 (2005).
2. Schmidt-Dannert C., Umeno D., Arnold F. H.: Natur. Biotechnol. *18*, 750 (2000).
3. Lee P. C., Momen A. Z. R., Mijts B. N., Schmidt-Dannert C.: Chem. Biol. *10*, 453 (2003).
4. Marova I., Breierova E., Koci R., Friedl Z., Slovak B., Pokorna J.: Ann. Microbiol. *54*, 73 (2004).

P21 BIOGENIC AMINES IN CHEESES AND HUMAN HEALTH

ZUZANA DIČÁKOVÁ and EVA DUDRIKOVÁ

University of Veterinary Medicine, Komenského 73, 041 81 Košice, Slovak Republic,
dicakova@uvm.sk

Introduction

Food safety is an increasingly important public health issue. Governments all over the world are intensifying their efforts to improve food safety. These efforts are in response to an increasing number of food safety problems and rising consumer concerns[1]. Like of other processed foods, also cheeses result from a manufacturing process involving the selection of raw material (e.g. milk, lactic acid bacteria, rennet), preparatory treatments such as milk pasteurization, renneting, drainage, salting, the ripening operation proper, preservation (if needed), packaging and storage. Last but not least, treatment of the food by the consumer influences its condition. Thus, an integral approach should be taken when assign the implications of individual risk factors for the safety of the consumer[2].

Cheeses are among those high-protein-containing foodstuffs in which enzymatic and microbial activities cause the formation of biogenic amines from amino acid decarboxylation (Innocente et al., 2007). Codex Alimentarius of the Slovak Republic stated the maximum limit only for the tyramine in hard cheeses, in which the concentration of tyramine must not exceed value of 200 mg kg^{-1}.

The aim of this study was to determine cadaverine (CAD), histamine (HIS), tyramine (TYR) and putrescine (PUT) in some commercial cheeses commonly consumed in Slovakia using ion-exchange chromatography. Chemical analyses were carried out in parallel with determination of sensory assessment of cheeses and their microbiological quality with the respect of *Enterobacteriaceae*.

Experimental

In total 31 samples of five cheese typologies were taken from supermarkets and retail shops: 5 high cooked cheeses, like Emmental, 8 low cooked cheeses, like Edam, 9 mozzarella like cheeses, 5 mould cheeses, and 4 sour natural ripened cheeses containing yeasts and *Brevibacterium linens*. All products were sampled during the correct their shelf life. Samples were stored at 4 °C until to analysis.

B i o g e n i c   A m i n e s   A n a l y s i s

The five biogenic amines (BA) studied were: cadaverine (CAD), histamine (HIS), tyramine (TYR) and putrescine (PUT). Ion exchange chromatography with amino acid analyzer (AAA 339 – T Microtechna, Czech Republic) was used for both qualitative and quantitative studies of biogenic amines in cheeses[3].

Each sample (100–200 g) was homogenised and mixed thoroughly with a Moulinex blender on a day of collection or purchase. A 10 g sample was extracted with 5% trichloracetic acid, centrifuged and filtrated through a membrane filter with a pore size of 0.45 μm. All the samples were prepared and analysed in duplicates.

M i c r o b i o l o g i c a l   A n a l y s i s

All cheese samples were subjected to microbiological routine analysis: Enterobacteriaceae, E. coli, Staphylococcus aureus, yeasts and moulds. The cultured selective agar plates (blood agar, VRBG Agar, Endo Agar, Baird-Parker Agar; Oxoid, UK) were used. Petri dishes were inoculated with 0.1 ml of diluting sample and cultivated in aerobic conditions 24–48 h at 37 °C and 25 °C for five days, respectively. Pure cultures were identified at species by routine microscopical, cultivation and biochemical methods. Micromycetes were identified macroscopically and microscopically, using the method according to St-Germain and Summerbell[4].

S e n s o r y   E v a l u a t i o n

Six volunteers (all women) were evaluated attributes related to the flavour and mount feel of all type of cheeses used in the experiment. The descriptor chosen were: colour, consistency, mouth couting, cheese flavour intensity, sourness, bitterness, off-flavour, and overall acceptability.

Results

The mean value of biogenic amine sum (CAD + HIS + TYR + PUT) concentration in mg kg^{-1} varied from 9.82 in cheese with moulds to 1,092.33 in sour natural ripened cheeses. In both groups of hard cheese the mean value of the sum biogenic amine concentration was very similar (175.05 mg kg^{-1} in high cooked cheeses *versus* 198.32 mg kg^{-1} in low cooked cheeses). The prevailing amine in all cheeses included into the experiment was tyramine, following by histamine, although HIS was not detected in any case of mozzarella-like cheeses evaluated.

Enterobacteriaceae count ranged from 1.12 × 10^3 CFU g^{-1} (high cooked cheese samples) to 21 × 10^3 CFU g^{-1} in cheese with mould. Totally, *Enterobacteriaceae* were isolated in 19 (61.29 %) of 31 evaluated cheese samples in this study.

According to the sensory assessment, 87.01 % of evaluated cheese had characteristic organoleptic properties depending on the kind of cheese. In four of 31 evaluated cheeses, the cheese samples did not show excellent sensory qua-

Table I

Concentration of BA in low cooked cheeses and *Enterobacteriaceae* count (Ent) (CFU × 10^3 g^{-1})

Col. stats	HIS	TYR	PUT [mg kg^{-1}]	CAD	Sum	Ent
Mean	8.5	134.8	13.2	18.0	173.5	8.2
sd	10.6	128.6	16.5	25.0	138.9	12.1
Minimum	1.0	1.30	0.0	0.0	8.00	0.0
Maximum	33.2	305.1	39.9	64.8	324.0	32.5
Median	4.5	111.7	3.9	8.2	173.5	1.0

lity mainly in the flavour. In one of did not accepted cheeses from sensory viewpoint, the cheese sample from high cooked smoked and grate cheese, the original packing of cheese from the hypermarket we detected large defects in sensory cheese characteristic.

Table II
Concentration of BA in high cooked cheeses and *Enterobacteriaceae* count (Ent) (CFU $\times 10^3 \, g^{-1}$)

Col. stats	HIS	TYR	PUT	CAD	Sum	Ent
		[mg kg^{-1}]				
Mean	24.7	150.7	13.5	9.3	196.6	1.1
sd	28.9	180.6	18.4	12.1	168.5	1.5
Minimum	1.0	1.30	0.0	0.0	62.5	0.0
Maximum	67.7	432.6	43.2	29.7	464.0	3.1
Median	12.8	102.6	4.9	4.9	174.0	0.0

Table III
Concentration of BA in mould cheeses and *Enterobacteriaceae* count (Ent) (CFU $\times 10^3 \, g^{-1}$)

Col. stats	HIS	TYR	PUT	CAD	Sum	Ent
		[mg kg^{-1}]				
Mean	2.4	1.6	0.0	0.35	3.7	21.1
sd	1.7	2.5	0.0	0.7	3.5	46.3
Minimum	1.0	0.0	0.0	0.0	1.0	0.0
Maximum	4.9	5.3	0.0	1.4	9.0	104.0
Median	1.9	0.6	0.0	0.0	2.5	0.6

Table IV
Concentration of BA in mozzarella like cheeses and *Enterobacteriaceae* count (Ent) (CFU $\times 10^3 \, g^{-1}$) (*p < 0.05)

Col. stats	HIS	TYR	PUT	CAD	Sum	Ent
		[mg kg^{-1}]				
Mean	0.0	1.2	3.7	2.0	6.7*	1.2*
sd	0.0	2.6	5.8	4.3	11.5	1.5
Minimum	0.0	0.0	0.0	0.0	0.0	0.0
Maximum	0.0	8.0	14.1	12.6	34.0	4.0
Median	0.0	0.0	0.0	0.0	0.0	0.5

Table V
Concentration of BA in sour natural ripened cheeses and *Enterobacteriaceae* count (Ent) (CFU $\times 10^3 \, g^{-1}$) (*p < 0.05)

Col. stats	HIS	TYR	PUT	CAD	Sum	Ent
		[mg kg^{-1}]				
Mean	66.2	249.2	207.4	673.2	1,194.0*	2.0*
sd	51.2	169.2	194.3	462.8	783.4	4.1
Minimum	14.2	83.8	18.2	190.9	443.0	0.0
Maximum	152.1	454.2	526.5	1,408.0	2446.0	8.2
Median	168.1	151.4	653.9	907.0	2446.0	0.0

Cheese consisted of the gross crust of dark brown colour with a rare presence of cheese curd of golden – yellow colour. The consistency of cheese was dry and hard, odour expressive smoked and taste was biter and tarry (sum of BA = 466.3 mg kg^{-1}, *Enterobacteriaceae* were not isolated).

According to the sensory assessment, 87.01 % of evaluated cheese had characteristic organoleptic properties depending on the kind of cheese. In four of 31 evaluated cheeses, the cheese samples did not show excellent sensory quality mainly in the flavour. In one of did not accepted cheeses from sensory viewpoint, the cheese sample from high cooked smoked and grate cheese, the original packing of cheese from the hypermarket we detected large defects in sensory cheese characteristic. Cheese consisted of the gross crust of dark brown colour with a rare presence of cheese curd of golden – yellow colour. The consistency of cheese was dry and hard, odour expressive smoked and taste was biter and tarry (sum of BA = 466.3 mg kg^{-1}, *Enterobacteriaceae* were not isolated).

Conclusions

From a "good manufacturing practice" point of view, total of 100–200 mg kg^{-1} of biogenic amines in fermented foods are regarded as acceptable[2]. The major BA producers in foods are except some lactic acid bacteria which do not produce significant levels of BA, the undesirable bacteria mostly *Enterobacteriaceae* and *Enterococcus* sp.[5] According to our results, the count of Enterobacteriaceae and sum of biogenic amines was statistically significant only in mozzarella like cheeses and in sour natural ripened cheeses (p < 0.05).

From a health point of view the sum BA as well as the concentration of individual biogenic amines should not to increase some certain levels. According to Spanier et al. (1991) the sum of BA (HIS+TYR+PUT+CAD) 900 mg g^{-1} in cheese is recommended as the highest acceptable concentration. This limit was exceeded in sour natural ripened cheeses in which the sum of BA was determined in a value of 1,194 ± 783.4 mg kg^{-1} of cheese sample.

REFERENCES

1. WHO: Food safety and foodborne illness. Fact sheet No. 237, 2007.
2. Nout M. J. R.: Food Chem., *101*, 1285 (2007).
3. Innocente N., Biasutti M., Padovese M., Moret S.: Determination of biogenic amines in cheese using HPLC technique and direct derivatization of acid extract.
4. St-Germain G., Summerbell R.: *Identifying filamentous fungi: A clinical laboratory handbook.* Belmont California, USA, 1996.
5. Spanier M. C., Bruin T. J. F., van Roode B. A. S. W.: Nutr. Technol. Anal. Saf. *VI. 15*, 213 (1991).

P22 PHYTOSTEROL AND FATTY ACID PROFILE OF FOUR EDIBLE OILS PROCESSED IN ROMANIA

FRANCISC VASILE DULF[a], CARMEN SOCAIU[a], CONSTANTIN BELE[a], ADELA PINTEA[a] and MIHAELA UNGURESAN[b]

[a]University of Agricultural Sciences and Veterinary Medicine, 3–5 Mãnãstur Str., 400372, Cluj-Napoca, Romania, [b]Technical University of Cluj-Napoca, Chemical Department, 103–105 Muncii Bvd., 400641, Cluj-Napoca, Romania, francisc_dulf@yahoo.com

Introduction

Triglycerides represent the principal component (95–98 %) of most edible oils obtained from seeds and fruits. Small amounts of sterols, free fatty acids, hydrocarbons, tocopherols, phospholipids and triterpenic acids are also present.

Fatty acids occur predominantly as esters of glycerol, i.e., triacylglycerol, in natural fats of animal and plant origin. Two distinct families of essential fatty acids exist in the human body: the ω-3 family (derived from α-linolenic acid) and ω-6 family (derived from linoleic acid)[1].

Phytosterols are a group of natural compounds found in all plants and in food products of plant origin. In vegetable oils, sterols are found primarily as free and esterified forms[2].

Four edible oils: walnuts, sesame, peanut and poppy seed oil, processed by minimal technologies (cold pressing) in Romania were investigated. The goal of the present study was the identification and quantification of fatty acids as FAMEs (fatty acid methyl esters), in the total lipid extracts (TLE) and in the esterified sterol fractions (ESF). Total, free and esterified sterols were also quantified as trimethylsilyl ether derivatives (TMS), using gas-chromatography (GC) with flame ionization detector (FID).

Experimental

Sample Preparation

The FAMEs were prepared by transesterification of the oil samples and the esterified sterol fractions by sodium methoxide catalysis[1].

Saponification, extraction, purification and preparation of TMS derivatives of the total, free and esterified sterols were made according to Phillips et al.[3].
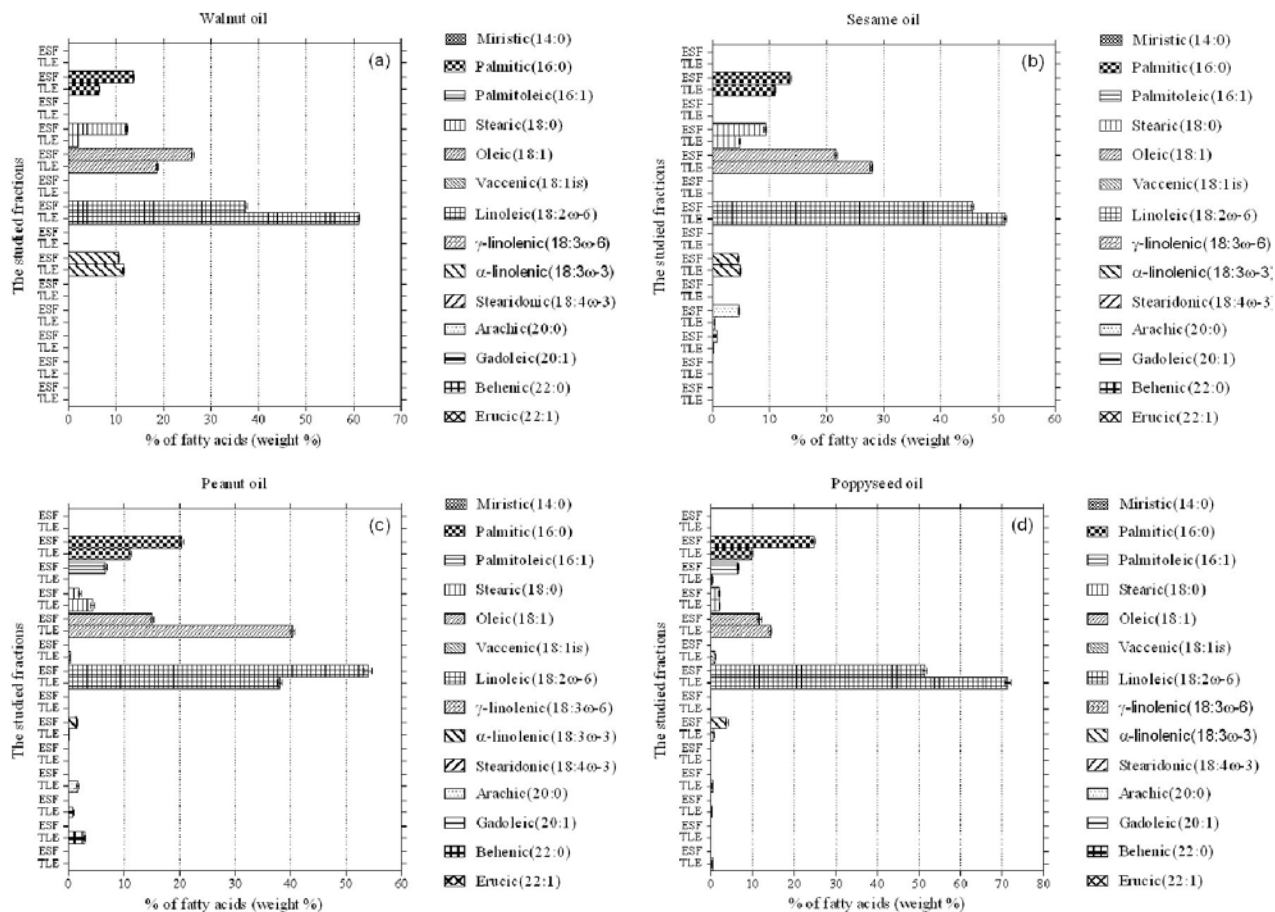
Fig. 1. **The fatty acid compositions [weight %] in total lipid extracts (TLE) and esterified sterol fractions (ESF) of: (a) walnut, (b) sesame, (c) peanut and (d) poppysed oils**

GC Analysis

GC conditions (for FAMEs): gas chromatograph SHIMADZU GC-17-A equipped with FID detector and capillary column Alltech ATWAX (30 m × 0.25 mm × 0.25 μm) with temperature programme 150 °C held for 5 min, ramp 4 °C min⁻¹ up to 235 °C, held for 5 min. The flow rate of the carrier gas helium was 1.8 ml min⁻¹ (split ratio 1 : 20). The injector and the FID temperature was 260 °C. The identification of FAMEs was based on retention times and comparison with those of standard FAMEs.

GC conditions (for derivatized sterols): GC-FID apparatus was the same. An RTX-5™ fused silica capillary column (30 m × 0.25 mm × 0.25 μm) was used. The temperature programme was: 200 °C held for 5 min, ramp 10 °C min⁻¹ up to 300 °C (held 20 min); injector temperature 280 °C; detector temperature 300 °C. The flow rate of the carrier gas helium was 0.58 ml min⁻¹ (split ratio 1 : 17). Identification of sterols was based on comparison of their relative retention times (RR_t to β-sitosterol) with data from the literature[4, 5]. A mixture of sterol standards was studied in the same conditions and the retention times (R_t) were used to assist the peak identification. The sterol concentrations were calculated using the area of the internal standard peak.

All extractions and GC-FID runs were performed in triplicate. The mean values and standard deviations were calculated.

Results

The fatty acid and sterol compositions reported in this study are in good agreement with those reported in the literature.[3,4,6,7]

Table I
Total sterol concentrations after direct saponification of the oils (mg 100g⁻¹)

Sterols	Walnut	Sesame	Peanut	Poppyseed	RR_t
1.	1.01 ± 0.12	n.d.	n.d.	n.d.	0.80
2.	n.d.	n.d.	n.d.	n.d.	0.83
3.	13.10 ± 0.74	71.00 ± 0.32	23.90 ± 0.34	41.18 ± 0.25	0.90
4.	0.60 ± 0.07	1.11 ± 0.11	1.53 ± 0.06	4.09 ± 0.11	0.91
5.	0.42 ± 0.05	34.10 ± 0.63	14.60 ± 0.32	11.44 ± 0.57	0.94
6.	147.00 ± 1.03	345.00 ± 0.66	114.00 ± 0.86	187.40 ± 0.56	1.00
7.	7.15 ± 0.23	2.71 ± 0.15	2.46 ± 0.10	2.33 ± 0.08	1.02
8.	28.00 ± 0.94	50.70 ± 0.50	15.30 ± 0.49	23.29 ± 0.70	1.03
Total	197.28 ± 3.18	504.62 ± 2.37	171.79 ± 2.17	269.73 ± 2.27	
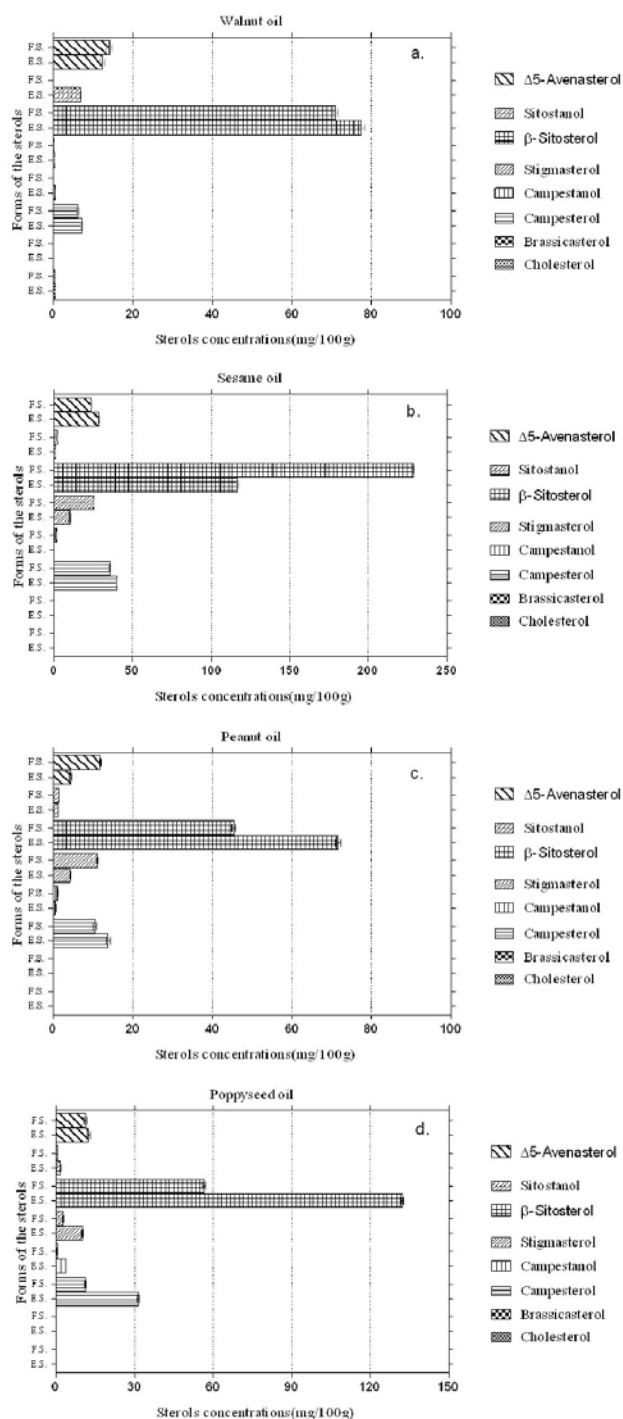
Fig. 2.   **Free and esterified sterol concentrations in four edible oils: (a) walnut, (b) sesame, (c) peanut and (d) poppysed oil**

Fatty Acid Composition

Fig. 1. illustrates the fatty acids compositions of edible oils used in this study. Three fatty acids were predominant in the analyzed oils (TLE) and theirs subfractions (ESF): linoleic acid (37.27–71.41 %), oleic (11.58–40.36 %) and palmitic acid (6.54–24.62 %).The unsaturated fatty acids/saturated

fatty acids ratios varied from 3.96 to 10.62 for the total lipid extracts. For the studied ESF's, these ratios varied from 2.64 to 3.44.

The polyunsaturated fatty acids were the most abundant out of the unsaturated fatty acids of TLE's, in all studied oils, except for peanut oil. The polyunsaturated/monounsaturated fatty acids ratios ranged from 0.92 to 4.49 for the analyzed TLE's and from 1.83 to 3.06 for ESF's, respectively.

Sterol Composition

The predominant phytosterols in all four samples were sitosterol, campesterol and Δ5-avenasterol (see Table I).The proportion of free and esterified sterols varied widely among samples (see Fig. 2.). In all oils except sesame oil, most of the β-sitosterol was esterified.

Conclusions

The determination of fatty acids and sterols' composition is essential for the analytical assessment of the quality, origin, extraction method, refining procedure and possible adulteration of the vegetable oils.

REFERENCES

1. Christie W. W.: *Gas Chromatography and Lipids*. The Oily Press Ltd., Glasgow 1989.
2. Abidi S. L.: J. Chromatogr. A *935*, 173 (2001).
3. Phillips K. M., Ruggio D. M., Toivo J.I., Swank M.A., Simpkins A. H.: J. Food Comp. Anal. *15*, 123 (2002).
4. Phillips K. M., Ruggio D. M., Ashraf-Khorassani M.: J. Agric. Food Chem. *53*, 9436 (2005).
5. Yang B., Karlsson R. M., Oksman P. H., Kallio H.P.: J. Agric. Food Chem. *49*, 5620 (2001).
6. Dubois V., Breton S., Linder M., Fanni J., Parmentier M.: Eur. J. Lipid Sci. Tehnol. *109*, 710 (2007).
7. Beardsell D., Francis J., Ridley D.: J. Food Lipids *9*, 1 (2002).

P23   ANTIOXIDANT ACTIVITY OF FLAVANOLS FROM GRAPE SEED EXTRACTS

RUGINA DUMITRITA, SIMONA VICAS, CARMEN MOMEU and CARMEN SOCACIU

Univeristy of Agricultural Sciences and Veterinary Medicine, Cluj-Napoca, Calea Manastur Street, No. 3–5, Romania, oliviapreda@gmail.com

Introduction

Natural antioxidants, particularly from fruits and vegetables, have gained increased interest among consumers and scientific community, due to their lower risk for cardiovascular diseases and cancer demonstrated by many studies[6].

Grape seeds are a rich source of flavanols, having monomers such as catechin, epicatechin, epicatechin-3-*o* gallate and dimers, trimers, teramers. Extracts from four varieties of Romanian grapes: Merlot, Mustoasa, Feteasca, and Chasla were first analyzed by HPLC (high performarce liquid chromatography) regarding their flavonol content.

The aim of this research was to evaluate the efficiency of ORAC, DPPH and ABTS radicals and to estimate the antioxidative capacity of grape seed extracts. The antioxidative activity of the extracts was determined through:

- Oxygen radical absorbance capacity assay (ORAC)
- 2,2'-diphenyl-1-pichrylhydrazyl assay (DPPH)
- Trolox equivalent antioxidant capacity assay (TEAC)

Total phenolic compounds content was determinated colorimetrically using Folin-Ciocalteu reagent.

Material and Methods

Preparation of Grape Seed Extracts

Seeds of the Vitis vinifera grape were obtain from Recas area (Bihor, RO). Grape seed were first grinded until a powder was obtained, which was afterwards deoiled with hexan (1 part of powder to 10 parts of hexane w/v). The solid residue was kept under the hood in the dark to evaporate the hexane. Seed extracts were prepared for analysis by mixing the powder with metanol/water/acetic acid (70 : 29.05 : 0.5, v/v/v) for a ratio of 1 part powder to 10 parts solvent (w/v). The mixture was sonicated for 15 min and shaken for 30 min at 4,000 rpm. The extract was concentrated in vacuum rotary evaporator at 40 °C. Volume of the concentrate was then adjusted to obtain a concentration of 1 g solids ml^{-1} by adding a predetermined volume of methanol[7].

ORAC Assay

ORAC assay measures antioxidant inhibition of peroxyl radical induced oxidation, reflecting classical radical chain breakage of antioxidant activity, by hydrogen atom transfer. The ORAC assay was performed as described by Ou et. al.[4].

DPPH Assay

DPPH assay is based on the measurement of the reduction ability of antioxidants toward DPPH$^{\bullet+}$. The kinetics of 400 µl grape seed extract in 2.8 ml of DPPH (80 µM in etanol) were registered in 30 min by monitoring DPPH disappearance at 515 nm.

TEAC Assay

TEAC assay asseses the capacity of a compound to scavenge ABTS radical (ABTS$^{\bullet+}$). Intensely colored radical cation ABTS$^{\bullet+}$ is formed by peroxyl radical oxidation of ABTS. The antioxidant ability is measured as the ability of test compounds to decrease the color formation. Using the method of Arnao et. al. (2002)[1] the interaction between the antioxidants and the ABTS$^{\cdot+}$ was monitored spectrophotometricaly at 734 nm.

Folin-Ciocalteu Assay

In Folin-Ciocalteu assay 250 µl extract were mixed with 1.25 ml of Folin-Ciocalteu reagent and 1.9 ml of sodium carbonate respectively and allowed to react for 2 hours. The absorption was measured with a Biotek Synergy HT spectrophotometer. The total phenolic compounds content was expressed as gallic acid equivalents (GAE mg g^{-1} dry weight DW).

Results and Discussion

The four grape seed extracts were analyzed by HPLC-UV, Merlot variety having 80 % of flavanols content, Feteasca 50 %, Mustoasa 40 %, and the poorest flavanol content was for Chasla, only 20 % (data not shown). Table I and Fig. 1. shows the value obtained for the antioxidant capacity assays. ORAC, TEAC and DPPH values are expressed in µM Trolox g^{-1} DW. The antioxidant activity using TEAC and ORAC ranged from 86 to 280, and respectively from 100–183 µM Trolox g^{-1} DW. From the four grape seed extracts, Merlot and

Table I
Antioxidant activity of grape seed extracts as determined by ORAC, DPPH, TEAC and Folin-Ciocalteu assay

| Sample name | µM Trolox g^{-1} DW | | | mg GAE 100 mg^{-1} DW |
	ORAC	DPPH	TEAC	Folin-Ciocalteu
Merlot	183.73 ± 2.4	1,140 ± 0.08	280.3 ± 1.8	651.2 ± 0.02
Mustoasa	123.1 ± 0.2	424 ± 0.09	129.6 ± 0.6	467.5 ± 0.04
Feteasca	155.3 ± 2.1	656.1 ± 1.3	202.1 ± 0.6	645.2 ± 0.01
Chasla	100.7 ± 1.8	67.2 ± 1.1	86.18 ± 3.1	423.2 ± 0.01

Chasla varieties have the highest (280.3 ± 1.8), and respectively the lowest (86.18 ± 3.1) TEAC values. Chasla have also the lowest ORAC value (100.7 ± 1.8).

The antioxidant activities determined by TEAC and ORAC showed a very good correlation (r = 0.99). A good correlation was obtained also for ORAC and DPPH assay (r = 0.97). Both assays are based on Trolox (a water soluble derivative of vitamin E) equivalents, although the ORAC assay represents a hydrogen atom transfer reaction mechanism and the TEAC assay represents a single electron transfer-based method[5]. Ou et al. (2002) reported no correlation between the FRAP and ORAC techniques among most of 927 freeze and dried vegetable samples, whereas these methods reveald a hight correlation in blueberry fruit (Connor et al, 2002)[3,4]. Similarly, Awika et al, 2003 observed high correlation between ABTS, DPPH, ORAC among sorghum and its products[2]. DPPH assay values shows significant differences between the flavanol richest Merlot sample (1,140 ± 0.08) and the flavanol poorest Chasla sample (67.2 ± 1.1) respectively. The amounts of total phenolic compounds were of the same order of magnitude among the studied grape seed varieties from 423 mg GAE 100 g^{-1} DW to 651 mg GAE 100 g^{-1} DW material (Table I). This is most probably due to the presence of the same type of phenolic compounds in the samples[5].

Conclusions

The flavanols contribute to the antioxidant activity of grape seed extracts. Ranking of antioxidant capacity was higly consistent across the different methods used, obtaining the same following ranking from the varities of the grapes seed extracts tested:

Merlot> Feteasca> Mustoasa > Chasla

This study confirms also the correlation between ORAC, DPPH and TEAC assays, their values being proportional with phenolic compounds contents.
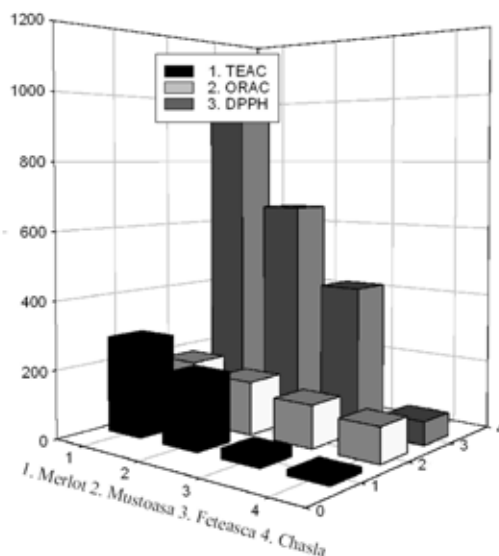
Fig. 1. **The antioxidant activity of grape seed extracts determined by TEAC, ORAC, DPPH assays**

REFERENCES

1. Arnao M. B., Cano A., Alcolea J. F., Acosta M.: Phytochem. Anal. *12*, 138 (2001).
2. Awika J. M., Rooney L. W., Wu X., Prior R. L., Cisneros-Zevallos L.: J Agric Food. Chem. *51*, 6657 (2003).
3. Connor A. M., Luby J. J., Hancock J. F., Berkheimer S., Hanson E. J.: J. Agric. Food. Chem. *50*, 893 (2002).
4. Ou B., Huang D., Hampsch-Woodill M., Flanagan J. A., Deemer E. K.: J. Agric. Food. Chem. *50*, 3122 (2002).
5. Prior R. L., Cao G.: Proc. Soc. Exp. Biol. Med. *220*, 255 (1999).
6. Thaipong K.: J. Agric. Food. Comp. Anal. *19*, 659, (2006).
7. Yilmaz Y., Toledo R. T.: J. Agric. Food. Chem. *52*, 255 (2004).

P24 INFLUENCE OF LONG-TERM STORAGE CONDITIONS ON ANTIOXIDANT AND OTHER ACTIVE COMPONENT CONTENT IN SEVERAL SORTS OF APPLES

KATEŘINA DUROŇOVÁ[a], KATEŘINA PAŘILOVÁ[a], ANDREA HALIENOVÁ[a], JITKA DVOŘÁKOVÁ[a], RADKA KOČÍ[a], JAN GOLIÁŠ[b] and IVANA MÁROVÁ[a]

[a]Institute of Food Science and Biotechnology, Brno University of Technology, Purkyňova 118, 612 00 Brno, Czech Republic,
[b]Department of Post-Harvest Technology of Horicultural Products, Valtická 337 691 44 Lednice, Czech Republic,
katka.duronova@centrum.cz

Introduction

Apples are one of the most common sources of natural antioxidants in Czech population. This work was focused on study of changes of antioxidant content, enzyme activities, and protein composition in several local sorts of apples stored for a long time under controlled atmosphere with reduced oxygen content.

To qualitative as well as quantitative analysis of individual low-molecular weight antioxidants RP-HPLC/UV-VIS and LC/MS were used. Activites of superoxide dismutase, peroxidase and polyphenoloxidase were measured spectrophotometrically, antioxidant activity was measured by Randox kit. Proteins were analyzed by 1D microfluidic system Experion, saccharides by HPLC/RI. Except long-term storage conditions also influence of some other commonly used technological processes were tested (freezing, drying).

Material and Methods

P l a n t   M a t e r i a l

Apples of three cultivars (Idared, Golden Delicious and Jonagored) were harvested and stored under Regular Atmosphere (RA) and controlled atmosphere-Fluctuated ANaerobiosis (FAN) for 158 days at 1 °C.

T o t a l   P h e n o l i c ,   F l a v o n o i d   a n d   A n t i o x i d a n t   C a p a c i t y   A s s a y s

Total solube phenolics were analyzed colometrically with Folin Ciocalteu reagent using photometric detection (750 nm) and results were expressed as mg gallic acid per 1 g of apple.

Total flavonoid content was analyzed colometrically with $NaNO_2 + AlCl_3$ using photometric detection (510 nm). Results were expressed as mg catechin per gram of apple tissue.

Total antioxidant capacity was measured by Randox kit. This colorimetric method use radical $ABTS^{·+}$ (2,2'-Azinobis(3-ethyl-2,3-dihydroBenzoThiazol-6-Sulphonate))and photometric detection (600 nm). Results were expressed as mmol Trolox (6-hydroxy-2,5,7,8-tetramethylchroman-2-carboxylic acid) per liter of raw apple juice.

I n d i v i d u a l   A n t i o x i d a n t s   A s s a y s

Individual flavonoids were analyzed using RP- HPLC method with the extrenal standarts ((–)catechin, catechin gallate, chlorogenic acid, epicatechin, morin, phlorizin, quercetin, rutin). Spectrophotometric detection (UV-VIS) after their extraction was used. In these assays two types of extraction were used:
- water extraction
- extraction by mixture of 1% HCl + ethylacetate

Samples (20 µl) were injected into the RP-18 column (Biospher PSI 200 C18, 7 µm, 150 mm × 4.6 mm). Mobile phases were methanol/water (55 : 45) for water extraction and methanol/acetonitrile/water with 1% phosporic acid (20 : 30 : 50) for organic extration. The flow rate was maintained at 0.75 ml min^{-1}, analysis was performed at 30 °C.

Carotenoids (beta-carotene, lycopene, luteine) were analyzed by RP-HPLC with spectrophotometric detection, organic extraction (acetone + diethylether) was used for pigment isolation. Samples (20 µl) were injected into the RP-18 column (Hypersil C18, 5 µm, 250 mm × 4.6 mm). As mobile phase for isocratic elution methanol was used. The flow rate was 1.1 ml min^{-1}, analysis was done at 45 °C.

A s c o r b i c   A c i d   A s s a y

Ascorbic acid was determined using RP-HPLC on Hypersil APS-2, NH_2, 5 µm, 150 mm × 4.6 mm column. Samples were stabilized by 2% HPO_3, 20 µl was injected. Mobile phase was natrium acetate/acetonitrile (95/5). Analysis was performed at flow rate 0.6 ml min^{-1} and 30 °C.

Microtitration method with 2,6-dichlorindofenol was used as comparative method too. The end point of titration was determined by pink colour.

Results were expressed as mg of ascorbic acid per kg of apples.

S u r f a c e   M i c r o f l o r a   A s s a y

Natural microflora was determined using Evirocheck® kit (Merck). Two types of kit were used:
- Contact TVC – Total Viable Counts
- Contact YM(R) – Yeasts and Mould

These tests can be used for analysis of liquid material as well as for surface testing. Results were expressed as KBE cm^{-2} or cfu cm^{-2}. Artificial injection of *Gloeosporium* and *Penicillium* moulds was done for comparison of effect of surface infection on apple quality. Infected apples were stored in darkness and cold (6 °C). After 4–8 weeks surface changes were observed and surface microscopy of apples was done too.

S e n s o r y   A n a l y s i s

A group of 21 respondents were enrolled into orientation sensory study. They tested several apple varieties and evaluated basic sensory parameters. Apple variety preferences and apple intake was studied too. The group of respondents was divided into two age-different groups:

- seniors: total 13, age 68.5 ± 7.16; 10 F/3 M,
- juniors: total 8, age 27.13 ± 3.63; 6 F/2 M.

Results

Antioxidant levels in apples are relatively low. Differences were observed according to fruit colour (variety) – high content was found mainly in yellow sorts (Golden Delicious). Freezing led to very low changes of antioxidant levels. Controlled drying caused concentration of all antioxidants including ascorbate.

Apple surface natural microflora contained mostly moulds and yeasts. Artificial infection of long-term stored apples (158 days) was more intensive in apples stored under normal atmosphere than under controlled storage conditions (fluctuated anaerobiosis).

Total phenolic and flavonoid levels differed according to apple sort and colour. A part of phenolics formed by flavonoids was in range of 30–60 %. Ascorbate levels detected in apples were in range 12–51 $mg\,kg^{-1}$. In Idared apples about 4× higer content of ascorbate was found when compared with Jonagored apple. Concentrations of individual flavonoids (chlorogenic acid, morin, quercetin, rutin) carotenoids (lycopene, beta-carotene) and catechins ((–)catechin, catechin gallate, epicatechin) differed slighty according to apple sort. These substances exhibited significant contribution to final colour of apple fruits. Their content in apples was relatively low. TAS levels were related to the content of phenolics and flavonoids, no direct correlation was found. Antimutagenicity corresponded to TAS.

Freezing is very suitable procedure for long-term conservation without significant changes of active substance content. After drying under regulated conditions (12 hours, 50 °C) the highest decrease was observed in ascorbate level (62 %), TAS level decreased by 42 %, flavonoids and phenolics content decreased by 40–50 %. Regulated drying has probably no significant negative effect on biological activity of apples with regard to amount of dried fruit intake.

Long-term storage (158 days) led to some increase in levels of total as well as individual antioxidants in all studied sorts. The highest level of all antioxidants was found in Idared variety, which is characteristic by the lowest long-term stability. Levels of most of antioxidants in apples stored under modified atmosphere were also lower than under RA. It seems that great group low molecular weight as well as high molecular weight antioxidants is mobilized in overriped or damaged fruits, the higest response was observed in Idared apples. Simultaneously, this variety was very sensitive to artificial mould infection, fruit damage after artificial infection was in this sort the highest from all studied apple varieties. Thus, some unbalance in apple antioxidant status could be accompanied with increased sensitivity to mould infection.

In stored apples some antioxidant enzymes were analyzed too. The highest activity exhibited catalase (CAT) followed by superoxide dismutase (SOD). Level of polyphenoloxidase (PPO) was very low. Activities of CAT and PPO were lower in apples stored under regular than under modified atmosphere, while SOD activity was higher in apples stored under FAN. In red varieties the antioxidant enzymes exhibited higher values than in the green ones. Mainly CAT and PPO are mobilized on overriped and/or slightly damaged apples.

Sensory analysis results obtained in two gorups of age-different subjects showed that in both groups no significant differences in evaluation taste, aroma, colour and texture in 4 sorts of apples were found. The lowest degree of consumer acceptance was found in Idared apple, while Jonagold was the most prefferd sort from analyzed apples. In general, red apple sorts were better accepted than green sorts. Both group preffered fresh apples than dried fruits. Apple intake in senior group (1 apple daily, on average) was about 2× higher than in junior group.

Conclusions

In general, apples contain a large number of different low-molecular weight as well as enzyme antioxidants, but levels of individual derivatives are relatively low. However, high intake of apples confirmed by questionnaire analysis can lead to cumulative effect. Thus, apples are one of the most important sources of natural antioxidants in Czech population (average intake in population is about 600 g per week).

At present, more than 90 % of produced apples are being stored and the losses range from 5 % to 25 %. Study of modern storage technologies and their influence of fuit quality and consumer acceptability is very important problem.

P25   CONTENT OF POLYPHENOLS AND ANTIRADICAL ACTIVITY OF BEE POLLEN

KATARÍNA FATRCOVÁ-ŠRAMKOVÁ[a], JANKA NÔŽKOVÁ[b], MAGDA MÁRIÁSSYOVÁ[c], MIROSLAVA KAČÁNIOVÁ[d] and EVA DUDRIKOVÁ[e]

[a]*Department of Human Nutrition, Slovak University of Agriculture in Nitra (SUA), Tr. A. Hlinku 2, 949 76 Nitra,* [b]*Institute of Biodiversity Conservation and Biosafety, SUA Nitra,* [c]*Food Research Institute, Centre in Modra,* [d]*Department of Microbiology, SUA Nitra,* [e]*University of Veterinary Medicine in Košice, Slovak Republic,*
katarina.sramkova@uniag.sk

Introduction

Recently, many investigations have been concerned with antioxidant properties of different nutritional products. Bee gathered pollen is regarded as valuable special food and is used also in apitherapy[1]. This beehive product also has several useful pharmacological properties, such as antibiotic, antineoplastic, antidiarrhoeatic and as an antioxidant agent[2]. The antioxidant activity of honeybee-collected pollen has been recognized as a free radical scavenger and as a lipid peroxidation inhibitor[2,3]. This activity has been associated with the phenolic pollen content[2].

The aim of the study was to measure content of polyphenols and the antiradical activity of dried bee pollen.

Materials and Methods

The pollen loads were collected by 20 honey bee colonies (*Apis mellifera*) settled in hives with bottom-fitted pollen traps, from different areas of Slovakia, during the season 2007.

The fresh bee pollen was stored at –18 °C for approximately half of year, with moisture 20 %, until analysed. The dried pollen samples were dried (moisture 9–11 %). The moisture was tested by thermo-gravimetric analyzer. The pollen loads for analysis were taken from the following plant species: *Papaver somniferum* L., *Brassica napus* subsp. *napus* L., *Helianthus annuus* L.

The pollen samples (10 g) were milled, homogenized and diluted in 100 ml 90% ethanol. The ethanol extracts of pollen were stored at 5 °C for further analysis.

The modified method by Brand-Williams was used[4,5]. Antiradical activity of various bee pollen samples was determined using the free DPPH• radical. Absorbance at 515.6 nm was measured at different time intervals using Shimadzu 1601 UV/VIS spectrophotometer (UV-1601, Shimadzu, Tokyo, Japan) until the reaction reached a plateau. The absorbance of the 2,2-diphenyl-1-pikrylhydrazyle radical (DPPH•) without an antioxidant (i.e. the control), was measured first. The percent of inhibition of the DPPH• radical by the sample was then calculated according to the formula:

$$\% \text{ inhib} = [(A_{C0} - A_{At})/A_{C0}] \cdot 100, \qquad (1)$$

where A_{C0} is the absorbance of the control at t = 0 minute, A_{At} is the absorbance of the antioxidant at time t minutes, % inhib equals percentage of free DPPH• radicals.

Total polyphenols content was quantified according to the Folin-Ciocalteau spectrophotometric method using tanin as reference standard[6]. Results were expressed as milligrams of tanins equivalent per kilogram of pollen and were presented as the mean of triplicate analyses. All values of antioxidant and antiradical activity are expressed as mean ± standard deviation.

Results and Discussion

The antiradical activity was in the particular samples in range from 48.83 to 86.12 % (average 71.39 ± 16.45 %). Antiradical activity as determined by the DPPH radical scavenging method decreased in the order: *Brassica napus* > *Papaver somniferum* > *Helianthus annuus*. In samples of bee pollen was the polyphenol content in the range from 763.67 to 1377.67 mg kg^{-1} (average 1026.67 ± 258.31 mg kg^{-1}). Antiradical activity increased in the same order than content of polyphenols (Table I). In present investigations, great variability regarding content of polyphenols as well as antiradical activity in 3 pollens was found.

Table I
Antiradical activity and content of polyphenols in pollen

Pollen	DPPH [% of inhibition]	Polyphenols [mg kg^{-1}]
H. annuus	48.43 ± 0.29	763.67 ± 5.56
P. somniferum	79.61 ± 0.45	938.67 ± 3.09
B. napus	86.12 ± 0.48	1377.67 ± 3.68

Almaraz-Abarca et al.[7] reported that antioxidant activities were different for each species and were not clearly associated to the flavonol content in pollen. Pollen from different botanical origin had different antioxidant capacity. The flavonol and phenolic acid composition, rather than the concentration, could be the determinant factor.

Great variability of phenolic contents was observed in the pollen of 12 plant species. Great differences in the radical-scavenging activity (RSA) were observed and were not correlated with the content of phenolic compounds. The pollen species can be divided into three groups: those of high (61–91.3 %), medium (23.5–29.6 %), and low RSA (8.6–16 %). In some of them a very high RSA corresponded to high levels of total phenols, phenylpropanoids and flavonols.[8]

In the present investigations very high and high antiradical activity in the case of *Brassica napus* and *Papaver somniferum*, respectively, were manifested by very high and high content of polyphenols. The above results are partially in agreement with the Leja et al.[8] reports. *Helianthus annuus* pollen integrated to second group with medium RSA reported

by Leja et al. (2007). None of investigated pollens from our research is being possible to integrate to third category with the low RSA. High levels of phenolic constituents are often accompanied by high antioxidative capacity of pollen; however, according to reports of Campos et al.[9,10], no direct correlation between flavonoids and radical-scavenging activity was found.

Conclusions

Further studies of the antioxidant properties (include antiradical activity) and the antioxidant components of bee pollen from different botanical origins are required, especially identification and quantification of individual antioxidants contained in pollen.

REFERENCES

1. Bogdanov S.: Apiacta *38*, 334 (2004).
2. Campos R. M. G.: Thesis. School of Pharmacy. Universidade de Coimbra. Portugal. 318 pp. (1997).
3. Campos M. G. et al.: Polyphenols *94*, 415 (1994).
4. Brand-Williams W. et al.: Lebensm. Wiss. u. Technol. *28*, 25 (1995).
5. Sánchez-Moreno C. et al.: J. Sci. Food Agric. *76*, 270 (1998).
6. Singleton V. L. et al.: Meth. Enzymol., *299*, 152 (1999).
7. Almaraz-Abarca N. et al.: Interciencia *29*, 574 (2004).
8. Leja M. et al.: Food Chem. *100*, 237 (2007).
9. Campos M. G. et al.: J. Agric. Food Chem. *51*, 742 (2003).
10. Campos M. G. et al.: Free-radical scavenging properties of bee-pollens – the non-involvement of flavonoids? Polyphenols Communications 2000, September 11-15. Freising-Weihenstephan Germany.

P26   REDUCTION POWER, POLYPHENOLS CONTENT AND ANTIMICROBIAL ACTIVITY OF HONEY

KATARÍNA FATRCOVÁ-ŠRAMKOVÁ[a], JANKA NÔŽKOVÁ[b], MAGDA MÁRIÁSSYOVÁ[c], MIROSLAVA KAČÁNIOVÁ[d] and EVA DUDRIKOVÁ[e]

[a]*Department of Human Nutrition, Slovak University of Agriculture in Nitra (SUA), Tr. A. Hlinku 2, 949 76 Nitra,*
[b]*Institute of Biodiversity Conservation and Biosafety, SUA Nitra,*
[c]*Food Research Institute, Centre in Modra,*
[d]*Department of Microbiology, SUA Nitra,*
[e]*University of Veterinary Medicine in Košice, Slovak Republic,*
katarina.sramkova@uniag.sk

Introduction

Recent views propose honey not only as a health-promoting dietary supplement, but shed light on its antioxidant properties. Honey has been reported to have antifungal activity, but not many species of fungi have been tested[1]. Superficial fungal infections are amongst the most difficult diseases to successfully treat, antibiotics which successfully combat bacterial diseases being largely ineffective against fungi. So a treatment which has both antifungal and antibacterial activities would be most beneficial. Therefore the effectiveness of honey against the dermatophyte species which most frequently cause superficial mycoses (tineas such as ringworm and athletes foot) was investigated[2]. The aim of the study was to measure the reduction power, content of polyphenols and antimicrobial activity of honey.

Materials and Methods

Two honey samples were obtained directly from beekeepers during the 2007 harvest, from different locations across Slovak Republic. The floral origin of the samples was specified by microscopic analyses of pollen grains at Institute of beekeeping in Liptovsky Hradok. Honeys were derived from different plant species namely *Castanea sativa* Mill. and *Brassica napus* subsp. *napus* L. Honey samples were stored at 4 °C in the dark until analysed.

Reduction power was evaluated by the method of Prietto et al.[3]. This method is established on reduction of Mo (VI) to Mo (V) with an effect of reduction parts in the presence of phosphor under formation of green phosphomolybdenum complex. Solution absorbance of reducing sample was measured at 705 nm (UV-1601, Shimadzu, Tokyo, Japan) toward black experiment (distilled water). Reduction power of compounds (RP_{AA}) expressed as quantity of ascorbic acid necessary to achieve the same effect in $\mu g\,ml^{-1}$ was calculated using the equation (1).

Total polyphenols content was quantified according to the Folin-Ciocalteau spectrophotometric method using tanin as reference standard[4].

$$RP_{AA} = (A_{705\,nm} - 0.0011)/0.00236 \qquad (1)$$

The potential antimicrobial activity of selected honey samples against *Alternaria infectoria*, *Scopulariopsis brevicaulis*, *Trichophyton ajelloi* and *Saccharomyces cerevisiae* was studied using the agar well diffusion method. The strains of fungi were maintained on Czapek-Dox agar (CDA, HiMedia). Honey solutions were prepared in three fractions: 50, 25 and 10 % (by mass per volume). Experimental results were expressed as means ± standard deviation. All tests were performed in triplicate.

Results and Discussion

Reduction power of chestnut honey compounds was higher ($4,083.67 \pm 4.50\ \mu g\,ml^{-1}$) than of rape honey ($3,618.33 \pm 3.30\ \mu g\,ml^{-1}$). Comparison of polyphenols content also refers on higher values in chestnut honey than in rape honey ($65.33 \pm 3.86\ mg\,kg^{-1}$ versus $41.00 \pm 2.16\ mg\,kg^{-1}$). The value of polyphenols for chestnut honey was approximately 1.6-fold higher than that for rape honey.

Bertoncelj et al.[5] reported that total phenolic content (determined by the modified Folin-Ciocalteu method), antioxidant activity and colour parameters differ widely among 7 different Slovenian honey types. In the case of chestnut honey the phenol content was $199.9 \pm 34.1\ mg\,kg^{-1}$, i.e. 3-fold more than in our present study. The results obtained from the study by Beretta et al.[6] showed that the total phenol content in chestnut honey was $211.2\ mg\,kg^{-1}$, i.e. 3.2-fold more than in our present study.

Vela et al.[7] observed that the phenolic compounds are partly responsible for the antioxidant effects of honey, but obviously there are other factors involved.

Table I
Antimicrobial effect of honey samples

	Honey concentration [%]		
	10	25	50
Castanea sativa Mill.			
A. infectoria	11.46 ± 0.45	15.83 ± 0.99	18.21 ± 0.40
S. brevicaulis	11.70 ± 0.67	14.40 ± 0.99	18.75 ± 0.25
T. ajelloi	14.55 ± 1.12	18.11 ± 0.39	21.75 ± 0.35
S. cerevisiae	8.15 ± 0.18	10.32 ± 0.30	12.84 ± 0.93
Brassica napus subsp. *napus* L.			
A. infectoria	10.94 ± 1.59	15.77 ± 0.12	17.22 ± 0.35
S. brevicaulis	9.93 ± 0.09	12.36 ± 0.44	17.37 ± 0.43
T. ajelloi	13.77s628 ± 1.01	17.38 ± 0.83	20.99 ± 0.52
S. cerevisiae	7.51 ± 0.47	11.83 ± 0.89	14.48 ± 0.86

Antifungal activities of the two honey samples with different concentration against fungi *Alternaria infectoria*, *Scopulariopsis brevicaulis*, *Trichophyton ajelloi* and *Saccharomyces cerevisiae* strains are presented in Table I. The obtained results characterize honey samples as a product with a broad antimicrobial effect.

A comparative method of adding honey to culture media was used to evaluate the action of starch on the antifungal activity of honey[8]. Brady et al.[9] studied antifungal activity of honey to dermatophytes. The results of this investigation show that the common dermatophytes are sensitive to the antimicrobial activity of honey, indicating that clinical evaluation of honey in the treatment of tineas is warranted.

Conclusions

Phenolic compounds appear to be responsible for the antioxidant activity of honey. Further studies are necessary to clarify the antioxidant effect of honey.

REFERENCES

1. Prietto P. et al.: Anal. Biochem., *269*, 337 (1999).
2. Singleton V. L. et al.: Methods Enzymol. *299*, 152 (1999).
3. Brady N. F. et al.: Pharm. Sci. *2*, 471 (1996).
4. Boukraâ L., Bouchegrane, S.: Rev. Iberoam. Micol. 31, 309 (2007).
5. Rademaker M.: N. Z. Med. J. *106*, 14 (1993).
6. Bertoncelj J. et al.: Food Chem. *105*, 822 (2007).
7. Beretta G. et al.: Anal. Chim. Acta *533*, 185 (2005).
8. Vela L. et al.: J. Sci. Food Agric. *87*, 1069 (2007).

P27 COMPARISON OF PECTATE HYDROLASES FROM PARSLEY ROOT CELLS

DANA FLODROVÁ[a,b], EVA STRATILOVÁ[b], SOŇA GARAJOVÁ[b] and JIŘINA OMELKOVÁ[a]

[a]*Brno University of Technology, Faculty of Chemistry, Purkyňova 118, 612 00 Brno,*
[b]*Institute of Chemistry, Slovak Academy of Sciences, Dúbravská cesta 9, 845 38 Bratislava, Slovakia,*
flodrova@fch.vutbr.cz

Introduction

Plant pectate hydrolases are in general supposed to be bound on primary cell wall where they cause the homogalacturonan degradation. Polygalacturonases can be classified into two groups depending on action pattern; enzymes randomly cleaving substrate (polygalacturonases, EC 3.2.1.15) and enzymes terminally cleaving substrate (exopolygalacturonases, EC 3.2.1.67)[1]. The biological function, structure as well as gene-expression of polygalacturonases have been studied in detail, while the research of exopolygalacturonases (exoPGs) is still on its beginning. ExoPGs have not yet been fully characterized in terms of developmental roles but could clearly have significant involvement in cell expansion processes. These enzymes are supposed to play a key role in the turnover of biologically active oligogalacturonates as signalling molecules affecting plant growth and development.

Plant exoPGs were supposed to prefer only polymeric substrate and the ability for cleaving substrate with lower degree of polymerization (DP) was strictly attributed to enzymes produced by microorganisms. First description of plant enzyme preferring oligogalacturonates (oligogalacturonate hydrolase, OGH) appeared in 2005 when an enzyme from carrot roots was described[2].

Experimental

Purification of Exopectate Hydrolases

In this work, exopectate hydrolases were isolated from parsley root juice and pulp extracts. The pulp protein mixture presents a very heterogeneous material what requires more complicated purification process. Accordingly, two different purification pathways were developed using different separation methods involving gel-permeation, affinity chromatography, chromatofocusing as well as preparative IEF (Scheme 1.).

Characterization of Exopectate Hydrolases

Activities of pectate hydrolases, utilizing substrates with various DP and different pHs, were determined by Somogyi assay[3]. The zymogram technique after IEF[4] with a colourless D-galacturonan DP 10 followed by staining of non cleaved substrate with ruthenim red was used for determination of pI. Molecular mass analysis of native and deglycosylated enzymes was done using SDS-PAGE with silver or Commasie Blue staining method for band visualization. Presence of
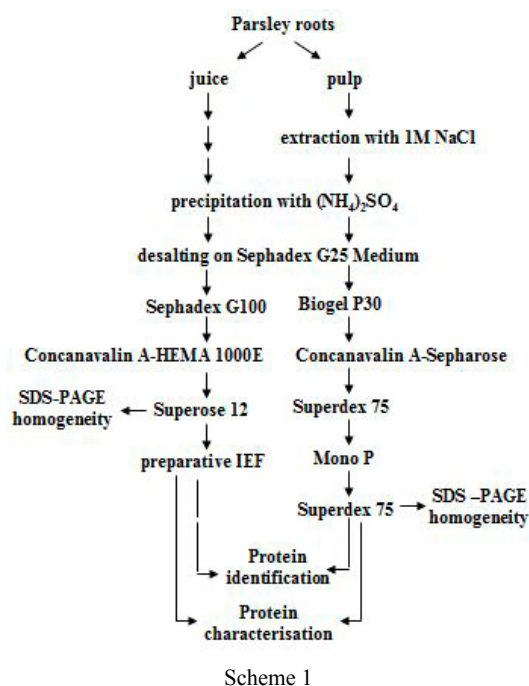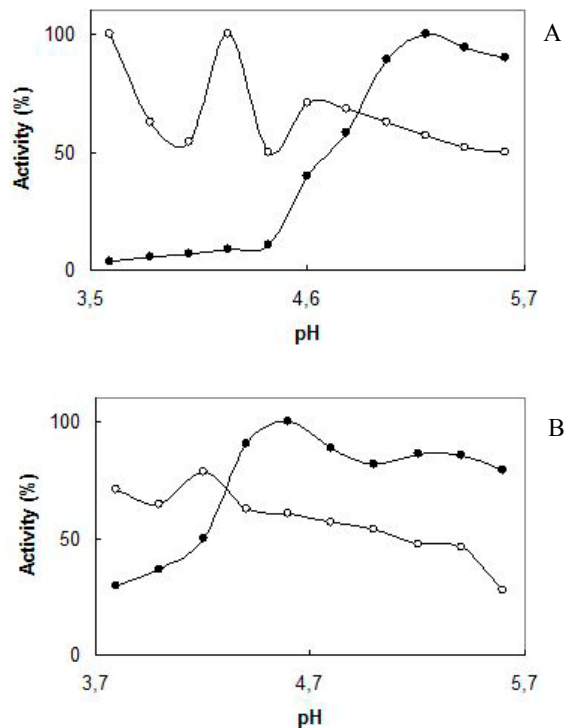
Fig. 1. **The pH optima of pectate hydrolases in parsley roots; enzyme activity on: • – 0,5% sodium pectate, ○ – 1 µmol ml⁻¹ pentagalacturonate, A – enzymes from parsley juice, B – enzymes from parsley pulp**

Scheme 1

these enzyme forms in individual cell structures was determined using the differential centrifugation method[5].

Results

Only pectate hydrolases with terminal action pattern on substrate were found in parsley roots cells[6,7]. ExoPG and two types of OGH were isolated, partially purified, further characterized and in-between compared. The comparison of their molecular masses, isoelectric points (Table I), temperature optima, thermal stability and also action pattern showed very similar results. On the other hand there were observed differences in their pH optima (Fig. 1., Table I) and substrate specificity in respect to DP of substrate (Fig. 2., Table I). In addition, the individual enzyme forms occurred in different cell structures as is partially shown (Fig. 3.).
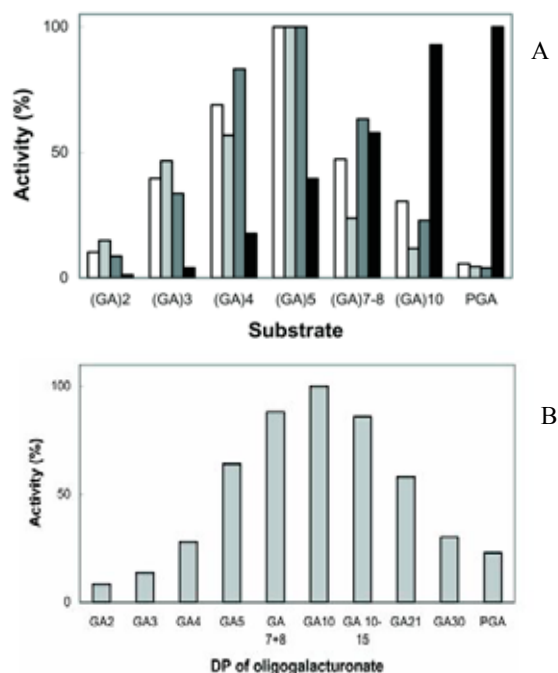
Fig. 2. **The initial rates of pectate hydrolases from parsley roots on substrates with various DP: A – enzymes isolated from parsley juice with pH optimum 3.6 – □, 4.2 – ▨, 4.6 – ▦ and 5.2 – ■, B – enzyme found in parsley pulp with pH optimum 4.7**

Table I
Characterization of pectate hydrolases from parsley root cells

Enzyme	pH optimum	DP of preferred substrate	M_r	pI	Occurrence
OGH6a	3.6	6	55.3	5.45	organelles
OGH6b	4.2	6	55.3	5.35	plasts, walls
OGH6c	4.6	6	55.3	5.60	intracel. comp.
OGH10	4.7	10	53.5	5.30	wall
exoPG	5.2	PGA	55.3	5.55	wall, ER
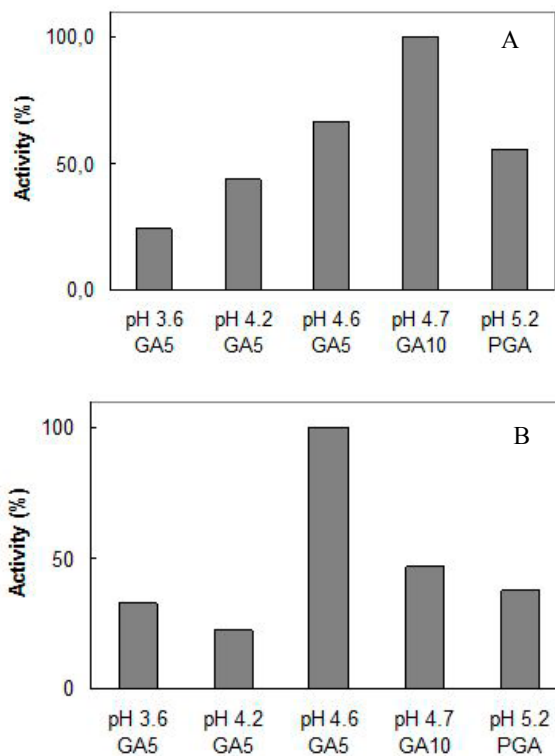
Fig. 3. **Abundance of individual exopectate hydrolase activities in different cell component: A – cell wall, B – cytosol**

ExoPG preferring the polymeric substrate has its pH optimum at 5.2. In contrast, the other types of pectate hydrolases, OGHs, favour oligomeric substrates, hexagalacturonate (OGH6) and decagalacturonate (OGH10) respectively. OGH10 has its pH optimum at 4.7.

OGH6 includes three isoforms with pH optima at 3.6, 4.2 and 4.6 (Table I). All forms showed temperature optima between 60–70 °C and were 100% stable at 55 °C (all unbound forms) and 50 °C (OGH10) respectively.

Conclusions

Five forms of pectate hydrolases purified from parsley root cells were described[6,7]. The main difference between these enzymes is mainly the substrate preference in relation to the chain length. It is accompanied by the sharp decrease of pH optima with decrease in DP of preferred substrate. The relationship between pH decrease in primary cell wall during auxin activation of proton pump bound on plasmatic membrane[8] and DP decrease in linear parts of pectin molecule side chains[9] regulated by pectate hydrolases with terminal action pattern can be indicated.

One enzyme only (OGH10), with preference to decameric substrate, was strictly bound to the cell wall. Next three forms, with preference to hexagalacturonate, were found in other cell structures. Only one typical form of exoPG with preference to polymeric substrate was identified; partially bound to the cell wall and partially free in the cytosol.

The OGH10 enzyme with unique substrate preference to decamer could also be important in determining the half-live of oligogalacturonic acids in the infected plant tissue. It could be the endogenous signals regulating aspect of programmed developmental events or responses to "invanders". Therefore, this enzyme and other pectate hydrolases may be of importance to the plant from several perspectives.

REFERENCES
1. Rexová-Benková Ľ., Markovič O.: Adv. Carbohydr. Chem. *33*, 323 (1976).
2. Stratilová E., Dzúrová M., Malovíková A., Omelková J.: Z. Naturforsch *60c*, 899 (2005).
3. Somogyi M. J.: Biol. Chem. *195*, 19 (1952).
4. Radola B. J.: Electrophoresis *1*, 43 (1980).
5. Garajová S., Flodrová D., Ait-Mohand F., Farkaš V., Stratilová E.: Biologia *63*, 313 (2008).
6. Flodrová D., Dzúrová M., Lišková D., Ait Mohand F., Mislovičová D., Malovíková A., Voburka Z., Omelková J., Stratilová E.: Z. Naturforsch. *62*, 382 (2007).
7. Flodrová D., Garajová,S., Malovíková A., Mislovičová D., Omelková J., Stratilová E.: Biologia, submitted
8. Rayle D.L., Clealand R. E.: Plant Physiol. *99*, 1271 (1992).
9. Vincken J. P., Schols H. A.,Oomen R. J., McCann M. C., Ulvskov P., Voragen A. G. J., Visser R. G. F.: Plant Physiol. *132*, 1781 (2003).

P28 REACTION MECHANISM OF XYLOGLUCAN ENDOTRANSGLYCOSYLASE (XET) FROM *PETROSELINUM CRISPUM* ROOTS

SOŇA GARAJOVÁ, DANA FLODROVÁ, VLADIMÍR FARKAŠ and EVA STRATILOVÁ

Institute of Chemistry, Slovak Academy of Sciences, Dúbravská cesta 9, 845 38 Bratislava, Slovakia
chemsong@savba.sk

Introduction

Plant xyloglucan endotransglycosylases (XETs, EC 2.4.1.207) catalyze the random cleavage of β-1,4-polyglucose backbone of the donor molecule (xyloglucan, XG) and the transfer of part of XG carrying the newly created reducing end to hydroxyl group at C-4 on the non-reducing end of another XG molecule or XG-derived oligosaccharide (acceptors). The process of transglycosylation can be described by Bi Bi reaction mechanism. Generally, there are two possible models of Bi Bi reaction mechanism: Pin-Pong and Sequential. In the Ping-Pong mechanism, the cleavage and transfer of part of polyglycan chain to the acceptor run in two steps. The first product (represented by the part of polyglycan chain carrying the original reducing end) is released from the stable enzyme-substrate complex before the acceptor substrate can bind. In contrast to the Ping-Pong mechanism, the sequential mechanism is observed like one step reaction, where a ternary complex of enzyme with the both substrates is formed. The products are released at the same time.

The main XET form of parsley roots with the isoelectric point 4.6 has a broad pH optimum in the region of its stability (pH 4.5–9.0) with one maximum in acidic (pH 5.8) and the second one in alkalic (pH 8.8) region[1]. The kinetic analysis at these two pH optima was performed using radioactive alditols of XG octasaccharide (XLXGol+XXLGol) as an acceptor substrate as well as in dependence on the degree of polymerization (DP) of reducing xyloglucan oligosaccharides (XGOs). XGOs with DP 7, 8 and 9 were used.

The mechanism of BiBi reaction was suggested from the nonlinear regression of kinetic data.

Experimental

Extraction of XTH from Parsley Roots

XET from parsley roots (*Petroselinum crispum* cv. Olomoucká dlouhá) was isolated and partially purified as described previously[1].

Substrates

Tamarind seed xyloglucan used in this study was from Dainippon Pharmaceutical Co., Ltd, Osaka, Japan.

XGOs with DP 7–9 were prepared by digestion of tamarind xyloglucan with *Trichoderma* cellulase[2]. They were purified on Biogel P2 column and further fractionated by preparative HPLC on TSK Gel Amide column (Tosoh) as described[3]. XG octasaccharide was converted to the corresponding 1-deoxy-1-aminoalditols (glycamines) by reductive amination[4]. Radioactive alditol of XG octasaccharide or reducing XGOs with DP 7, 8 and 9 were prepared by their reduction with Na-borotritide [^{3}H]NaBH$_4$ (ICN Radiochemicals, San Diego, CA) as described earlier[5].

Kinetic Parameters

Standard XET assays were performed at 29 °C utilizing the radiometric method according to Fry et al. The initial rates were determined at pH 5.8 and 8.8 using five different concentrations of xyloglucan (0.5–5 g dm^{-3} at pH 5.8 and 0.5–1.5 g dm^{-3} at pH 8.8, respectively) and of radioactive alditols of XG octasaccharide (0.6–3.1 μM). Further experiments were all performed at pH 5.8 using the same XG concentration range as described previously for this pH. Reducing XGOs with DP 7, 8 and 9 were used in the range of 5–200 μM. The incorporation of each [1–^{3}H]-labelled XGOs was measured by scintillation counting (Liquid Scintillation Analyzer Tri-Carb 2800TR, PerkinElmer, Illinois, USA) as described previously (Sulová et al., 1995). The K_M values were calculated from nonlinear regression using Origin 6.0.

Results

XET as a member of glycoside hydrolase family GH16 utilize a double displacement/retaining mechanism of transfer. This mechanism involves the formation of a covalent enzyme-substrate intermediate[6], what is characteristic for
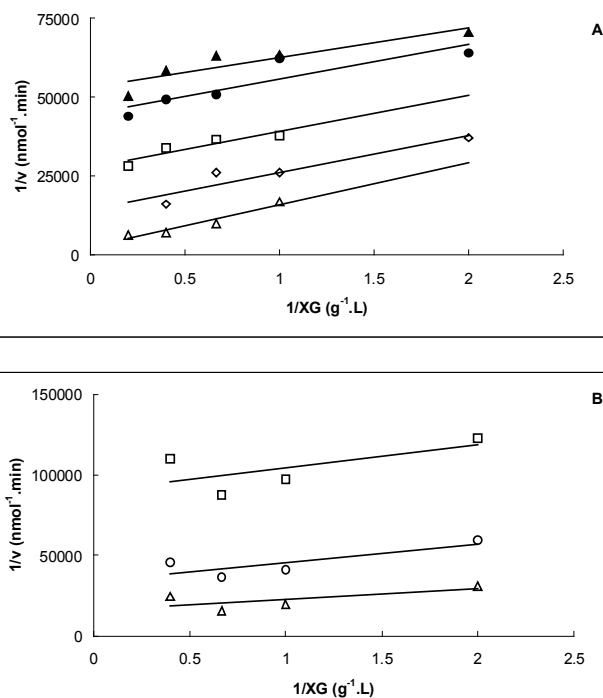
Fig. 1. **Plot of 1/v = f(1/XG) at different concentrations of mixture of XLXGol+XXLGol: 0.86 μM (▲), 1 μM (●), 1.24 μM (□), 1.54 μM (◊), 2.1 μM (○) and 3.1 μM (△). Michaelis parameters were determined at pH 5.8 (A) and 8.8 (B), respectively**

retaining glycanase operating by Ping-Pong mechanism. This is supported by the most of works published to this date[3,7,8]. On the other hand, the kinetic data of XET isolated from suspension-culture poplar cells are consistent with the sequential mechanism[9].

Table I
Kinetic parameters calculated from nonlinear regression

Acceptor substrate	Parameter values ± S.D.	
	K_{MXG} [g dm^{-3}]	K_{MXGO} [μmol dm^{-3}]
nonasaccharide	0.854 ± 0.21	42.199 ± 6.546
octasaccharide	0.589 ± 0.22	92.396 ± 10.120
heptasaccharide	0.755 ± 0.08	117.612 ± 5.588

this reason the further study of kinetic parameters was carried out only at acidic pH using reducing XGOs.

The Lineweaver-Burk plots for XET showed parallel lines at higher concentrations of reducing XGOs with DP 7, 8 and 9 as acceptor substrates (Fig. 2. A, B, C).

The kinetic parameters K_M were determined by measuring initial transfer rates of reducing XGOs with DP 7, 8 and 9 into XG (Table I). The data concluded in Table I show that the K_M values for acceptor substrates increase with their decreasing DP. On the other hand the lowest K_M value for donor substrate was calculated for octasaccharide as an acceptor.

Conclusions

The kinetic study analyzed at both pH optima of XET (pH 5.8 and 8.8, respectively) indicate that the affinity of enzyme to acceptor substrate (mixture of XLXGol + XXLGol) is independent on pH unlike the K_M values for XG, where significant differences can be seen.

The relationship between the K_M values and DP of acceptor substrates shows the decrease of enzyme affinity to reducing XGOs with their decreasing DP. As a consequence, the best acceptor substrate seems to be the nonasaccharide.

The comparison of K_M values for octasaccharides indicates that parsley XET has a higher affinity for reducing oligosaccharide than to its alditol.

In all cases excepting the kinetic analysis using low concentrations of XGOs, the Lineweaver-Burk plots for XET showed parallel lines. These results indicated that the enzyme catalyzed the reaction utilizing a Ping-Pong (Bi Bi) mechanism rather than a sequential one. Hence, the non-parallel lines at lower concentrations of XGOs can be explained by the stronger influence of side reactions like interpolymeric transglycosylation and inhibitions at such concentrations of acceptor substrate.

Fig. 2. **Plot of 1/v = f(1/XG) at different concentrations of nonasaccharide (A), octasaccharide (B) and heptasaccharide (C): 5 μM (■), 10 μM (♦), 20 μM (▲), 30 μM (●), 50 μM (□) and 200 μM (◊)**

Kinetic analysis was performed at both pH optima of XET (Figure 1 A, B) using radioactive alditols of XG octasaccharide (XLXGol + XXLGol).

While K_M values for mixture of XLXGol + XXLGol were very similar at both pH optima (123 μM at pH 5.8 and 137 μM at pH 8.8, respectively) for XG they differed (0.565 g dm^{-3} at pH 5.8 and 2.42 g dm^{-3} at pH 8.8, respectively). A strong inhibition with higher concentrations of XG was observed especially at pH 8.8 where the linearity of reaction in dependence on XG concentration was limited. From

REFERENCES
1. Garajová S., Flodrová D. Ait-Mohand F., Farkaš V., Stratilová E.: Biologia *63*, 313 (2008).
2. Sulová Z., Lednická M., Farkaš V.: Anal. Biochem. *229*, 80 (1995).

3. Baran R., Sulová Z., Stratilová E., Farkaš V.: Gen. Physiol. Biophys. *19*, 427 (2000).
4. Fry S. C.: Plant J. *11*, 1141 (1997).
5. Sulová Z., Takáčová M., Steele N. M., Fry S. C., Farkaš V.: Biochem. J. *330*, 1475 (1998).
6. Sinnott M. L.: Chem. Rev. *90*, 1171 (1990).
7. Nakamura A., Haga K., Yamane K.: FEBS Lett. *337*, 66 (1994).
8. Saura-Valls M., Faure R., Ragas S., Piens K., Brumer H., Teeri T. T., Cottaz S., Driguez H., Planas A.: Biochem. J. *395*, 99 (2006).
9. Takeda T., Mitsuishi Y., Sakai F., Hayashi T.: Biosci. Biotech. Biochem. *60*, 1950 (1996).

P29　MULTIELEMENTAL PROFILING AS FINGERPRINT OF WINES BY SIZE-EXCLUSION COUPLED TO UV AND ICP-MS

TAMARA GARCÍA-BARRERA and JOSÉ LUIS GÓMEZ-ARIZA

Departamento de Química y Ciencia de los Materiales, Facultad de Ciencias Experimentales, Campus de El Carmen, Avda. de Fuerzas Armadas S/N, 21007-Huelva, Spain, tamara@dqcm.uhu.es

Introduction

A number of studies describes the levels of metals in wines[1,2] and organic compounds with high complexation capacity with them like anthocyanins[3], phenolic compounds[4,5], and so on. Correlation of metals and organic compound has been pointed out but it can not be probed since the measurements were performed off-line. Only in the case of Pb, the size exclusion chromatography coupled to an inductively coupled plasma mass spectrometry (SEC-ICP-MS) was used to determine biomolecular complexes[6]. However, the multielemental profiling of wines by SEC-ICP-MS has not been performed until now. This approach has been successfully applied to the fractionation of several elements in nuts[7,8], soybean flour[9], and organs from *Mus musculus*[10]. Multielemental fractionation studies have also been performed by SEC-ICP-MS in premature human[11,12] and whey milk[13]. The aim of this work is to determine the metal-binding molecules profiles in red and white wines from different grape varieties as a preliminary step to find key compounds that can be used as fingerprint as well as to know all the metallospecies present in wines. The analytical methodology to obtain the distribution patterns of these elements was based on SEC online coupled to UV and ICP-MS.

Experimental

Samples

Samples of red and white wines were purchased in a local supermarket. All the samples were stored al 4 °C until analysis. Table I shows the list of wines analyzed and the assigned codes.

Procedures

The SEC was carried out in a 26/70 XK column packed with Sephadex LH-20 (hydroxypropylated dextran beads crosslinked to yield a polysaccharide network) all from Amersham Biosciences (Uppsala, Sweden). An AKTA-Prime system (pump and UV detector at 254 nm) (Amersham) was used as the eluent delivery system, equipped with a 200 µl sample loop. ICP-MS Agilent, Model 7500 ce (Agilent Technologies, Tokyo, Japan). The instrumental operating conditions are given in Table II. Samples were two-fold diluted with mobile phase and 200 µl was injected in the SEC-UV-ICP-MS system. The mobile phase for SEC was daily prepared with a pH 4 methanol-buffer (50 : 50, v/v) solution.

Table I
Analysed samples

Sample	Origin	Grape Variety	Comments
1	NAVARRA	Tempranillo, Garnacha	Red
2	NAVARRA	Not determined	Red
3	JUMILLA	Monastrell	Red
4	NAVARRA	Garnacha	Red
5	RIOJA	Tempranillo, Garnacha, Graciano	Red
6	JUMILLA	Monastrell, Tempranillo	Red
7	PENEDÉS	Tempranillo, Garnacha, Carieña	Red
8	RIOJA	Tempranillo, Garnacha	Red
9	VALDEPEÑAS	Tempranillo	Rosé
10	CAMPO DE BORJA	Tempranillo, Garnacha	Red
11	PENEDÉS	Garnacha, Cariñena	Red
12	LA MANCHA	Tempranillo	Red
13	RIBERA DEL DUERO	Not determined	Red
14	JUMILLA	Monastrell	Red
15	RIOJA	Tempranillo, Garnacha	Red
16	CATALUÑA	Macabeo	White
17	CONDADO DE HUELVA	Zalema	White
18	CONDADO DE HUELVA	Zalema, Palomino	White
19	PENEDÉS	Chardonnay, Parellada	White

Table II
Instrumental operating conditions for SEC-UV-ICP-MS

SEC-UV	
Column	Sephadex LH-20
Exclusión limit	5,000 Da
Mobile phase	Methanol-water (pH 4.0)
Flow rate	2 ml min^{-1}
Injection volumen	200 µl
UV-visible wavelength	254 nm
ICP-MS	
Forward power	1,500 W
Carrier gas flow rate	0.8 dm^3 min^{-1}
Make up gas	0.1 dm^3 min^{-1}
S/C temperature	–2 °C
Sampling depth	8 mm
Sampling and skimmer cones	Pt
Dwell Time	0.1 s per isotope
Isotopes monitored	^{55}Mn, ^{60}Ni, ^{63}Cu, ^{66}Zn, ^{75}As, ^{208}Pb, ^{53}Cr, ^{57}Fe, ^{59}Co, ^{82}Se, ^{111}Cd

Results

The fractionation profiles of the elements in wines are shown in Figs. 1.–4. Only the most interesting profiles are discussed in this paper.

Manganese Fractionation Profiles

Fig. 1 shows the chromatographic profiles of ^{55}Mn in the studied samples. The typical molecular mass distribution pattern of this element is the presence of only one highly abundant fraction between 2,126–7,000 Da. This fact indicates that manganese in wines is mainly associated with polysaccharides, peptides, proanthocyanidins or low molecular mass proteins. Condensed tannins and anthocyanins are the most important metal ligands, since these species have numerous coordination sites capable of binding metal cations. In addition, the molecular mass indicates that the organic compound is not an anthocyanin. It has been reported that cyanidin-3-O-glucoside anthocyanin with two –OH groups in the ortho position can complex Mn at the ratio 2:1 ref.[4], but the chromatograms shows the absence of Mn in the retention time of this anthocyanin or the abundance is too low.
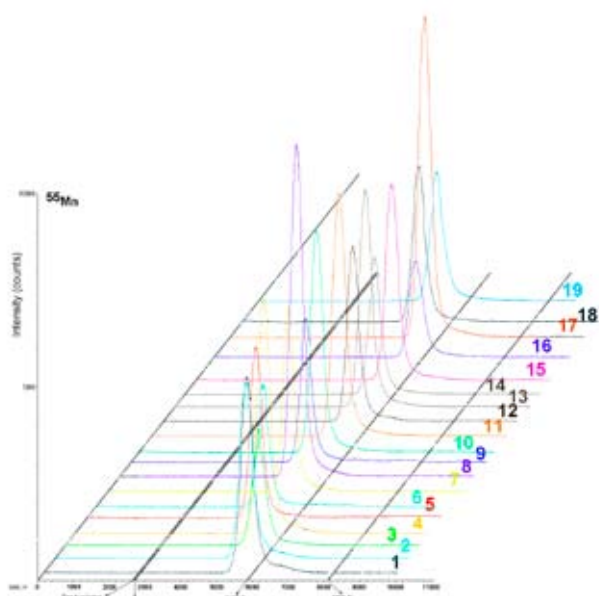
Fig. 1.   **Molecular mass distribution of manganese species in wines**

Lead Fractionation Profiles

Fig. 2. shows the superimposed chromatographic profiles of ^{208}Pb in wines. Lead is mainly bound with high molecular mass compounds as can be concluded from the co-elution with Metallothionein I (7,000 Da). All the samples present around the same abundance of this Pb-containg fraction. It is remarkable the presence of two peaks in this molecular mass region in sample 5. Sample 10 is the only one that presents a Pb-containing fraction of about 2,126 Da. In several samples[1,4,11,17,18], a low abundant fraction with a molecular mass from 1,325 to 2,126 Da, have also been detected. Experiments with untreated wine passed through a minicolumn packed with polyurethane foam modified by 2-(2-benzothiazo-lylazo)-p-cresol indicated that Pb(II) is strongly associated to other constituents, possibly bound with pectic polysaccharides and/or other related high-molecular-
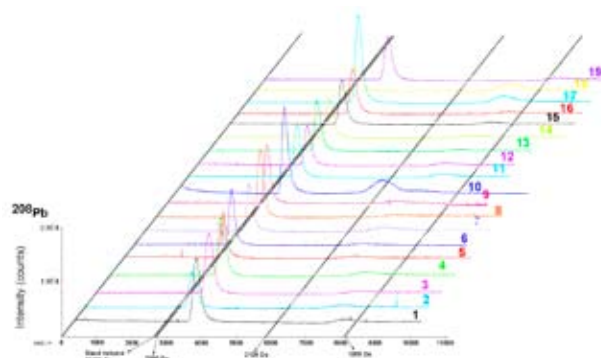
Fig. 2.   **Molecular mass distribution of lead species in wines**

weight natural organic species[14]. As previously reported[6], lead in wine can be bound with a structurally complex pectic polysaccharide (rhamnogalacturonan II-RG II) that present the ability to form dimmers cross-linked by 1:2 borate diol esters (dRG II). RG-II is a major polysaccharide of wine and is mainly present as a dimmer, although the monomeric form can also be detected. The molecular mass of dRG II is about 10 kDa, so the presence of B and Pb in this region is a marker of the presence of the complex. For this reason 11B was monitored together with ^{208}Pb and they were detected in all the samples in the fraction of about 7,000 Da. Fig. 3 shows the presence of both elements in the most abundant fraction of lead in wines (about 7,000 Da) in sample 1.
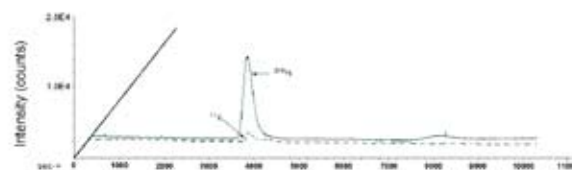
Fig. 3.   **Coelution of Pb and B in sample 1**

Arsenic Fractionation Profiles

The molecular mass fractionation profiles of arsenic (Fig. 4.) are very different to those previously considered for other elements. Although the abundance of As-containing peaks is low and not all the samples present this element above the detection limits, we can find that arsenic is present in two fractions, one of low molecular mass (526–1,355 Da) and other of about 2,126 Da. It has been reported (15) that the inorganic arsenic, As (III) (arsenite) is the major arsenic specie in wines but the organic species such as dimethylarsinic acid (DMAA) and monomethylarsonic acid (MMAA), are under the detection limits of hidride generation-atomic spectroscopy fluorescence (HG-AFS). Other papers report that, in most of wines, DMAA is the most abundant specie, but the total inorganic aresenic fraction is considerable[16]. Some arsenosugars have also been determined in wines with a molecular mass from 326 to 478 Da[17]. However, the association of As in wines with an organic compound of high molecular mass (2,126 Da) have not been reported until now.
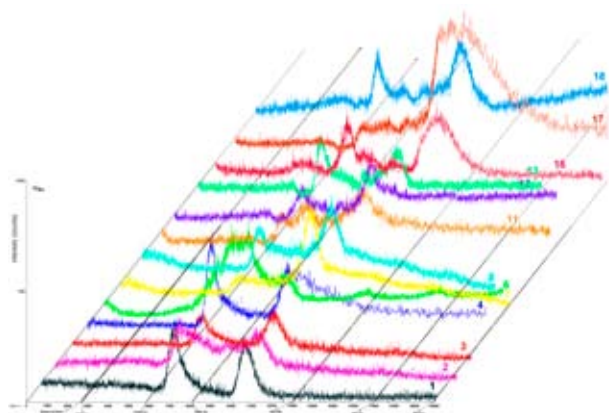
Fig. 4.   **Molecular mass distribution of arsenic species in wines**

Conclusions

The identification of chemical forms of elements in wine enables their toxicity and bioavailability to be estimated. The use of ICP-MS allows the multielement speciation in wines in only one chromatographic run, which constitutes a reliable technique with high throughput. The possibility to screen many elements in a given chromatographic peak from a sample is critical since there are no errors associated with different measurements. On the other hand, food samples are complex and the selectivity of the ICP-MS avoids the tedious sample preparation. Therefore, ICP-MS is an excellent guide for further studies of the fraction of interest like reversed phase coupled to ICP-MS, refractive index and UV detectors. The simultaneous determination of elements, carbohydrates, polysaccharides and polyphenols will be allowed. Finally, complexes will be identified by organic mass spectrometry.

REFERENCES

1. Jos, A.; Moreno, I.; González, A.G.; Repetto, G.; Cameán, A.M.: Talanta *63*, 377 (2004).
2. Serapinas, P.; Venskutonis, P.R.; Aninkevicius, V.; Ezerinskis, Z.; Galdikas, A.; Juzikiene, V.: Food Chem. *107*, 1652 (2008).
3. Gómez-Ariza, J.L.; García-Barrera, T.; Lorenzo, F.: Anal. Chim. Acta *570*, 101, (2006).
4. Esperanza, I.; Salinas, I.; Caballero, I.; Santamaría, C.; Calvo, I.; García-Minac J.M.; Fernandez J.M.: Anal. Chim. Acta *524*, 215 (2004).
5. Karadjova, I.; Izgi, B.; Gucer, S.: Spectrochim. Acta Part B *57*, 581 (2002).
6. Szpunar, J.; Pellerin, P.; Makarov, A.; Doco, T.; Williams, P.; Medina, B.; Lobinski, R.: J. Anal. At. Spectrom. *13*, 749 (1998).
7. Wuilloud, R.G.; Kannamaumarath, S.S.; Caruso, J.A.: Anal. Bioanal. Chem. *379*, 495 (2004).
8. Gómez-Ariza, J.L.; Arias-Borrego, A.; García-Barrera, T.: J. Chromatogr. A *1121*, 191 (2006).
9. Fingerová, H.; Koplíc, R.: Fresenius J. Anal. Chem. *363*, 545 (1999).
10. González-Fernández, M.; García-Barrera, T.; Arias-Borrego, A.; Bonilla-Valverde, D.; López-Barea, J.; Pueyo, C.; Gómez-Ariza, J.L.: Anal. Bioanal. Chem. *390*, 17 (2008).
11. de la Flor St Remy, R.R.; Fernández Sánchez, M.L.; López Sastre, J.B.; Sanz-Medel, A.: J. Anal. At. Spectrom. *19*, 1104 (2004).
12. Michalke, B.; Schramel, P.: J. Anal. At. Spectrom. *19,* 121 (2004).
13. Rivero-Martino, F.A.; Fernández-Sánchez, M.L.; Sanz-Medel, A.: J. Anal. At. Spectrom. *17*, 1271 (2002).
14. Pyrzynska, K.: Crit. Rev. Anal. Chem. *34*, 69 (2004).
15. Karadjova, I.B.; Lampugnani, L.; Onor, M.; D'Ulivo, A.; Tsalev, D.L.: Spectrochim. Acta Part B *60,* 816 (2005).
16. Herce-Pagliai, C.; Moreno, I.; González, A.G.; Repetto, M.; Cameán, A.M.: Food Addit. Contam. *19,* 542 (2002).
17. Wangkarn, S.; Pergantis, S.A.: J. Anal. At. Spectrom. *15,* 627 (2000).

P30 SOLATION OF Cu-METALLOPROTEINS IN *MUS MUSCULUS* BRAIN EXTRACTS BY REVERSE PHASE-HPLC COUPLED TO ICP-MS

M. GONZÁLEZ-FERNÁNDEZ, T. GARCÍA-BARRERA, J. LÓPEZ-BAREA, C. PUEYO and J. L. GÓMEZ-ARIZA

Dpto. Química y Ciencias de los Materiales. Facultad de Ciencias Experimentales. Universidad de Huelva, Campus de El Carmen, 21007 (Huelva), Spain,
macarena.gonzalez@dqcm.uhu.es

Introduction

Orthogonal chromatography systems coupled to ICP-MS and organic mass spectrometry has been widely used for metal-biomolecules characterization in biological samples connected with in environmental issues. The use of these analytical approaches provides very interesting information to deep insight on toxicological concern of metals in the environment. The use of heteroatoms can be used as markers that simplify the traditional proteomic approaches[1,2].

In a previous study, several organs of *Mus musculus* mice were extracted and analyzed by size exclusion chromatography coupled to UV and inductively coupled plasma mass spectrometry (SEC-UV-ICP-MS)[3]. Some differences were found in the molecular mass distribution patterns of elements in the studied organs as in the case of a Cu-containing fraction that was only present in the brain. This fraction was collected, lyophilized and separated by reversed-phase (RP) high performance liquid chromatography (HPLC) following the Cu with the ICP-MS.

2D-PAGE study of the extracts was performed in parallel, for the identification of overall proteins, after tryptic digestion of the spots. Comparison of metallomics and proteomics results was performed and correlated with *Mus musculus* genome information from data base.

Experimental

Standard Solutions and Reagents

Methanol (Teknokroma, Barcelona, Spain) was of LC gradient grade. Double de-ionized water (18.2 MΩ CM) obtained from a Milli-Q water system (Millipore, Bedford, MA, USA) was used throughout. All the reagents used were of the highest available purity.

The buffer solution was prepared by dissolving 100 mM of ammonium acetate (Merck, Darmstadt, Germany) in water containing 1 % (v/v) methanol (buffer A) and in methanol (buffer B), adjusting the pH to 7.4. Suprapur acetic acid (100% m/m) and ammonia (25% m/m) used for pH adjustment of the mobile phases were purcharsed from Merck[4].

Instrumentation

HPLC was performed with an Agilent 1100 Series (Waldbronn, Germany). Reversed-phase HPLC was performed with a Spherisorb ODS 2 column (250 mm × 4.6 mm, 5 μm particle size: type PEEK) (Waters, Massachusetts, USA). The reversed-phase HPLC column was directly connected to the nebulizer of the ICP-MS instrument via PEEK tubing.

Elemental detection was performed using a model Agilent 7500ce ICP-MS instrument (Waldbronn, Germany)

Table I
Instrumental conditions for (RP-HPLC) and (ICP-MS)
Instrumental operating conditions

Reverse phase-HPLC conditions	
Columns Spherisorb ODS 2 (250 mm × 4.6 mm, 5 μm)	
Mobile phase Concentration gradient methanol (pH 7.4)	
A: 100 mM NH₄Ac in 1% methanol	
B: 100 mM NH₄Ac in methanol	

Time [min]	Buffer [%]
0	0
5	30
15	30
25	0
Flow rate	0.4 ml min⁻¹
Injection volume	50 μl

ICP-MS conditions	
Forward power	1,500 W
Plasma gas flow rate	15.0 dm⁻³ min⁻¹
Auxiliary gas flow rate	1.00 dm⁻³ min⁻¹
Carrier gas flow rate	0.86 dm⁻³ min⁻¹
Sampling depth	6.5 mm
Sampling and skimmer cones	Platinum
Dwell time	0.3 s per isotope
Isotopes monitored	^{63}Cu

Procedures

Animals and sample preparation

Mus musculus (inbred BALB/c strain) mice were from Charles River Laboratory (Spain). Mice of 7 weeks of age were fed ad libitum with feed conventional pellets. This feed contained 11.9 % moisture, 16.1 % crude protein, 3.1 % crude oil, 60 % N-free extract (including starch, sugars, crude fibre, etc.) and 5.1 % total minerals. Cu concentrations included in the feed were as follows (the limits recommended for this element is indicated in parentheses): 17 mg kg⁻¹ Cu (10–35 mg kg⁻¹).

Mice were individually killed by cervical dislocation and dissected. Individual organs were excised, weighed in Eppendorf vials, cleaned with 0.9% NaCl solution, frozen in liquid N₂ and stored at –80 °C until they were used for extract preparation. Mice were handled according to the norms stipulated by the European Community. The investigation was performed after approval by the Ethical Committee of the University of Córdoba (Spain). Entire organs of each type (lungs, livers, spleens, kidneys, brains, testicles, hearts and muscles) from 20 different animals were pooled. The weight of the brain in the pool was 3.265 g. After that a solution (3 ml g⁻¹) was added containing the following: 50 mM Tris-HCl buffer solution at pH 8, 1 mM DTT, 1 mM PMSF and protease inhibitors (100 μl ml⁻¹). Later, benzonase was added (500 U ml⁻¹)

to the extracts, they were incubated for 30 min at room temperature and, finally, were centrifuged at 80,000 rpm for 1 h. Extracts were stored at −80 °C until analysis.

Results

The profiles of different elements, such as Cu, Pb, Zn, Ni, As, Mn were obtained with two SEC: High molecular mass (HMM) for a separation range of 3–70 kDa and low molecular mass (LMM) for a separation range below 10 kDa ref.[3].

This work focuses the profile of copper from different organs with the LMM column. In this figure, a differential peak between 2,126 to 7,000 Da was observed in the brain extract.
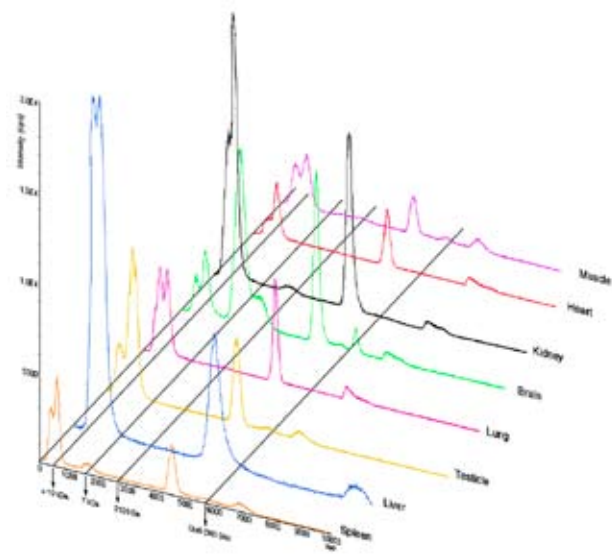
Fig. 1. **Molecular size distribution patterns of Cu obtained by SEC-ICP-MS with the LMW column**

For this reason, the copper fraction from brain was isolated for a preliminary study and was used a second chromatographic separation to purify the fraction previously mentioned by using (RP)-HPLC and ICP-MS.

In Fig. 2., we can observe the two peaks obtained.

The mass balance corresponding to both chromatography separation of this element was performed. A good recovery is obtained which de notes an acceptable isolation of the Cu molecules. For SEC the recovery of cooper from the total injected was 44.40 % and for (RP)-HPLC 76.5 %. The first peak contains 44.43 % of cooper from the total recovery for (RP)-HPLC and the second one 32.07 %. The total concentrations of cooper have been reported elsewhere[3].

Conclusions

Previous works report the molecular size distribution patterns of elements in *Mus musculus* mice. In spite of Mus *musculus* is well known since a great number of proteomic
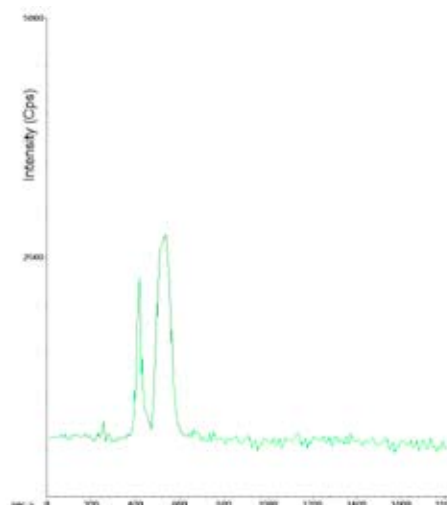
Fig. 2. **Elution profiles of Cu by (RP)-HPCL-ICPMS from the brain extract**

and genomic studies have been performed (i.e., the genome is completely known), the metallome has not been reported until now. The most interesting fraction is that from Cu in brain extract which is not present in any other organ. This fraction has been latterly purified by RP-HPLC-ICP-MS. The pure extracts from RP-HPLC present only two peaks that can be related to Cu-biomolecules. Future works will be focused in the identification of these copper-compounds by organic mass spectrometry.

The ICP-MS constitutes a powerful technique to obtain the patterns of many elements in complex biological tissues and it is an excellent guide for further studies of the fraction of interest like further separations by orthogonal techniques, molecular mass-spectrometric elucidations of the metallospecies involved and so on.

REFERENCES

1. Gómez-Ariza, J.L.; García-Barrera, T.; Lorenzo, F.; Bernal, V.; Villegas, M. J.; Oliveira, V.: Anal Chim Acta *524*, 15 (2004).
2. Szpunar, J.: Anal Bioanal Chem 378, 54 (2004).
3. González-Fernández, M.; García-Barrera, T.; López-Barea, J.; Puedo, C.; Gómez-Ariza, J.L.: Anal. Bioanal. Chem. *390*, 17 (2008).
4. Goenaga-Infante, H.; Cuyckens, F.; Van Campenhout, K.; Blust, R.; Claeys, M.; Van Vaeck, L.; Adams, F.: J. Anal. At. Spectrom. *19*, 156 (2004).

P31　ANALYSIS OF FLAVOR COMPOUNDS IN FRUITS BY GC WITH TWO DIMENSIONAL DETECTION BY FID AND MS

R. JARA BIEDMA, T. GARCÍA-BARRERA and J. L. GÓMEZ-ARIZA

Dpto. de Química y CC.MM. Facultad de Ciencias Experimentales. Universidad de Huelva. Campus de El Carmen, 21007 Huelva, Spain,
tamara@dqcm.uhu.es

Introduction

The fruit juice industry has become one of the world´s major agricultural businesses with world trade in fruit juices annually exceeding 10 billion $[1]. A key characteristic of this product is the flavour.[2–7] Sweet orange (*Citrus sinensis*) typical aroma is attributed to alcohols, hydrocarbons, esters and aldehydes considering solely the number of compounds involved. Among these compounds, citral, limonene, linalool, α-pinene, ethyl butanoate, acetaldehyde and octanal have been identified as most contributing to orange flavour, and can be used in orange juice authentication. In addition, some orange juice off-flavours can be developed such as α-terpineol that is a well known off-flavour compound present in stored citrus products formed from d-limonene or linalool[8].

In this work, a method based on liquid-liquid extraction with ethyl acetate and later preconcentration has been optimised for the extraction of about twenty flavour compounds in orange juice. The method is complemented by a chromatographic separation (GC) for the identification of different compounds based on the retention times obtained by gas chromatography.[4–9] with flame ionization detector (GC-FID) and the mass spectra of each analyte (GC-MS). Quantification data was obtained with both detectors. The levels of the flavour compounds have been used to enhance the quality of oranges for industrial juice production and authentication purposes.

Experimental

Materials

The gas chromatograph used for this study is an Agilent 6890N.

Chromatographic parameters:
- Column: HP-5MS. 30 m in length 0.25 mm ID. 0.25 μm film.
- Stationary phase (5% phenyl)-methylpolysiloxane
- Injector Temperature: 250 °C
- Oven Programme (Table I):

Table I
Oven program for the chromatographic separation

Temperature [°C]	Rate [°C min⁻¹]	Hold [min]	Total [min]
50		5	5
225	3	10	73.33

- Detector temperature: 300 °C.
- Column flow rate: 1 ml min⁻¹
- Carrier gas: Helium
- Injection volume: 5 μl

Analytical Methods

Sample preparation

An aliquot of 30 ml of juice, previously tempered and homogenized by manual or mechanical shaking, was measured using a test tube of 50 ml Class A and transferred using a funnel tapered to a 100 ml separating funnel, provided with a Teflon key.

After that, 20 ml of juice was extracted with a mixture of ethyl ether: methanol: ethyl acetate (18.5 : 1 : 0.5) and centrifuged to 5 °C and 4000 rpm for 5 minutes. Supernatant was withdrawn and passed to a 100 ml bottle with screw cap. The juice was extracted again with 20 ml of pentane and centrifuge to 5 °C and 4,000 rpm for 5 minutes. Supernatant was withdrawn and passed to 100 ml container together with the previous organic phase.

The third extraction was carried out with 20 ml of dichloromethane: methanol (19 : 1) mixture and centrifuged to 5 °C and 4,000 rpm for 5 minutes. The contents of the centrifuge tube were transferred carefully to a 100 ml separating conical funnel. After few minutes the organic phase (bottom) was separated in a vial. Anhidrous sodium sulphate was added and the content was stirred and centrifuged under the same conditions above described.

The total of all three phases was passed to a functional round-bottoned flask for evaporation with a rotary evaporator, keeping the bath temperature at 70 °C to eliminate the most volatile solvents (all of them with boiling point lower than 70 °C except ethyl acetate). The extract was transferred to an eppendorf tube and the internal standard (α-ionone) was added to achieve a final concentration 50 mg dm⁻³. The extract was concentrated to a final volume of 1 ml.

Chromatographic analysis

5 μl of the extract with the internal standard were injected in the gas chromatograph with a FID detector. For the inequi-
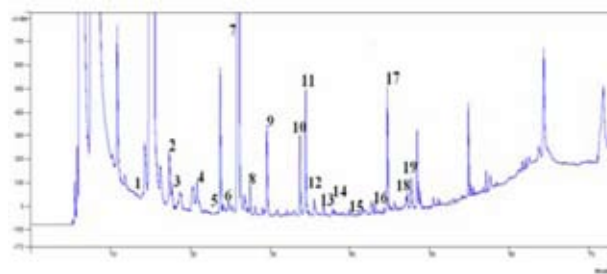
Fig. 1.　**Chromatogram of a sample of orange juice using GC-FID: 1. Hexanal + ethyl butyrate, 2. Cis-3-hexen-1-ol, 3. Hexanol, 4. α-Pinene, 5. (-) β-Pinene, 6. Ehyll hexanoate, 7. Limonene, 8. γ-Terpinene, 9. L-linalool, 10. (+)Terpinen-4-ol, 11. S-α-terpineol, 12. Decanal, 13. Neral, 14. Carvone, 15. Geranial, 16. Dodecanal, 17. α-ionone (internal standard), 18. β-ionone, 19. Valencene**

vocal identification of some compounds in the sample, the mass spectrometer detector was used.

Results
Calibration and Detection Limits

Fig. 1 shows the typical chromatogram of a sample of orange juice. As we can see, 19 compounds responsible of the flavour were identified depending on their retention times using standards.

Presence of Volatile Compounds in Juices Studied

Fig. 2 shows the concentration of minority compouns present in the analysed oranges juices.

Fig. 3 shows the major flavour compounds found in the analysed samples. As we can see, the concentration of limonene is very high (with concentrations up to 72 ppm) and lower concentrations of S-α-Terpineol, a compound that comes from the degradation of limonene and is responsible of unpleasant odors at concentrations greater than 2 ppm.
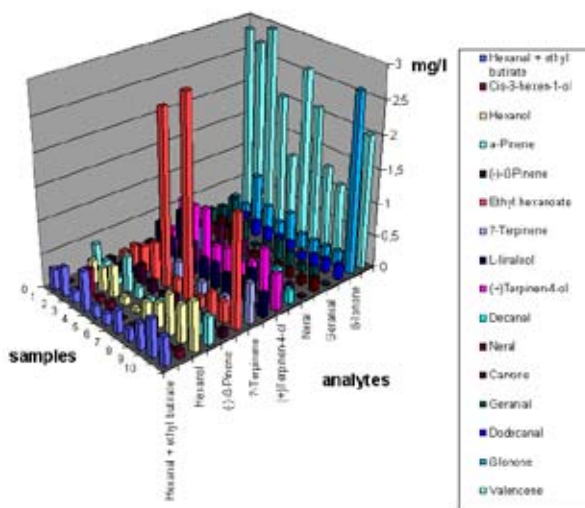
Fig. 2.   **Three-dimensional bar chart that represents the concentration of the compounds responsible for the aroma minority ten samples of orange juice**

Conclusions
- It has been optimized a fast, accurate and sensible methodology for the quantification of volatile compounds responsible for the flavour of the orange juice.
- It has developed a procedure for extraction of these compounds with recoveries around 80%.
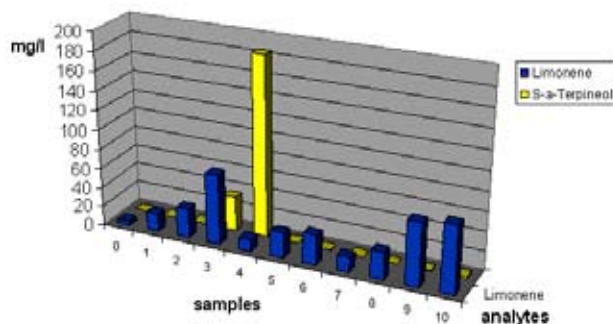
Fig. 3.   **Three-dimensional bar chart that represents the concentration of the compounds majority responsible for the scent of ten samples of orange juice**

- The methodology developed is transferable to the food industry and can contribute to the development of a new products of enhanced quality
- The method allows monitoring the process of maturation of the orange (*Citrus sinensis*) by assessing the concentrations of aromas.

REFERENCES
1. Robards, K.; Antolovich, M.: Analyst *120*, 1 (1995).
2. Mussinan C. J.; Morello M. J.; Flavour Analysis, Developments in Isolation and Characterization, American Chemical Society, Washington, DC, 1998.
3. Hinterholzer, A.; Schieberle, P.: Flavour Fragr. J. *13*, 49 (1998).
4. Högnadottir, A.; Rouseff, R. L. J.: Chromatogr. A *998*, 201 (2003).
5. Brat, P.; Rega, B.; Reynes, M.; Brillouett, J.M. : J. Agric. Food Chem.*1*, 3442 (2003).
6. Buettner, A.; Schieberle, P.: J. Agric. Food Chem. *49*, 2387 (2003).
7. Porto, C. D.; Pizzale, L.; Bravin, M.; Conte, L.S.: Flavour Fragr. J. *18*, 66 (2003).
8. Gómez-Ariza, J. L.; García-Barrera, T.; Lorenzo, F.: J. Chromatogr. A *1047*, 313 (2004).
9. Naim M.; Rouseff, R.L.; Zehavi, U.; Schutz, O.; Halvera-Toledo, E. in: Mussinan, C. J.; Morello, M. J. (Eds.): *Flavour Análisis, Developments in Isolation and Characterization*, American Chemical Society, Washington, p. 30, 1998.

P32 CONTENT OF CADMIUM IN SELECTED MEAT PRODUCTS SUPPLIED ON THE SLOVAK MARKET

JOZEF GOLIAN, BRANISLAV ŠIŠKA, ROBERT TOMAN and MICHAL BOŠIAK

Department of Food Hygiene and Safety, Faculty of Biotechnology and Food Sciences, Slovak Agricultural University in Nitra,Trieda A. Hlinku 2, 949 76 Nitra
Jozef.Golian.AF@uniag.sk

Introduction

One of the most important aspects of environmental pollution to humans is that a significant intake of heavy metals occurs through diet. Food-producing animals are a rich source of food, but they are also a source of various contaminants. Heavy metals are natural components of the environment, but in recent years industrial, agricultural and zootechnic development has been responsible for the diffusion of these substances in the environment[1]. The toxicity and metabolism of metals may be influenced by number of factors, which vary in importance for different metals. Many factors, such as sex, age, metal interaction and diet, can affect the absorption and accumulation of these metals[2]. The cadmium levels in meat from muscle are of the order of 0.01 mg kg^{-1} for animal at slaughter, although they may be higher in older animals. Cadmium concentrations in liver, and particularly, kidney are substantially higher than that in muscle. In livers of calves, pigs and poultry, Cadmium levels range from 0.02 to 0.2 mg kg^{-1}, these levels may also be higher in older animals. Cadmium levels found in kidneys from calves and pork pigs from 0.05 to 0.5 mg kg^{-1}, while the concentration in ox kidneys may approach 1 mg kg^{-1}. Horse kidney and liver may have cadmium concentrations exceeding 10 mg kg^{-1}(ref[3]). The levels of cadmium and other elements were determined in beef and pork imported to Sweden from six different countries. All results for cadmium were below the detection limits of 0.001 mg kg^{-1} fresh weight[4].

Experimental

In this study we analysed 360 samples of meat products – sausages, hams and frankfurters. The 90 of samples descended from Slovak Republic, 90 of samples from Czech Republic, 90 of samples from Austria and 90 of samples from Germany. The samples were collected of the Slovak market in 2007.

Cadmium in food samples was determined by pressure mineralisation in the combination with atomic absorption spectrophotometry. The samples were separately packed in polyethylene bags and stored at –20 °C until the analysis. Samples were weighed in glass digestion tubes on a precision balance. Prior to analyses the samples were homogenised and then 1.5 g of sample was taken for pressure decomposition. A 10 ml high purity nitric acid (HNO$_3$) added to the tube and enclosed into pressure cooker, and stationed into pre-heat drier. The pressure decomposition insisted 3 hour at 150 °C.

The measurements of cadmium were performed on an atomic absorption spectrophotometer VARIAN AA-175.

Results

We evaluated the content of cadmium in three kinds of the meat products: sausages, hams and frankfurters, which descended from different producers. The basic variance-statistical characteristics of cadmium in meat products are showed in Table I. The highest mean value of cadmium in sausages (0.0589 mg kg^{-1}) was found at products supplied from Austria. The lowest mean value of cadmium (0.0525 mg kg^{-1}) was found in Slovak sausages. The highest mean value of cadmium (0.0583 mg kg^{-1}) was found in Slovak hams, and the lowest average value of cadmium (0.046 mg kg^{-1}) was detected in Austria hams. The highest mean value of cadmium (0.0679 mg kg^{-1}) was found in Slovak frankfurters and lowest value of cadmium (0.0513 mg kg^{-1}) was found in Austria frankfurters. Variability content of cadmium in individual meat products was very different and varied from 69.32 % to 111.03 %. At sausages was the highest variability (111.03 %) at products made in Slovak republic, the lowest variability content of cadmium (70.28 %) was found in products made in Austria. At hams was the highest variability (96.77 %) of the content of cadmium at products made in the Slovak Republic, and the lowest variability at hams (69.32 %) was at products made in Germany. At frankfurters was found the highest variability of cadmium from Austria (107.5 %) and the lowest variability of cadmium was at frankfurters of Czech Republic (77.99 %). The number of samples for individual meat products and countries, which suitable respectively unsuitable applications of Food Codex Slovak Republic are shown in Table II. The number of unsuitable samples in the each group of meat products, ranged from 2 to 6. From total number 360 of samples were an excess of the allowable limit in 57 cases. Content of selected chemical element in the followed meat products was different. The origin of cadmium in the meat products is from raw material (meat and organs of animals), additive material (condiment) and water. Due to this, it has to be stated, that differences in the content of chemical elements are of reason. Meat from different animals, of different conditions and breeding was used for products. They were fed with different feed. Therefore content of selected metal in their muscle is different. Meat has been minced and mixed together, therefore content of cadmium in the meat products is dependent on the level of mince or homogenisation respectively. Different occurrence of studied chemical element in the meat products is dependent on the level of meat and organs contaminant.

Many of previous reports has followed the content of chemical elements in the muscle, kidney and liver. From the point of view of human exposure it is necessary to follow the content of toxic substance in meat products, as all slaughtered animals are not examined individually. Therefore monitoring of distribution and occurrence of chemical elements in the meat products is necessary.

The occurrence of cadmium in meat and meat products studied other authors; referred to toxic effects of cadmium[5,6,7]. The obtained results content of cadmium in meat products are comparing with the results of other authors[8,9].

Table I
Basic variance-statistical characteristics of cadmium in meat products

Parameters	x [mg kg^{-1}]	S. D[*] [mg kg^{-1}]	C. V[**] [%]	x$_{min}$	x$_{max}$
Slovak republic					
Sausages	0.0525	0.0583	111.03	0.004	0.241
Hams	0.0583	0.0564	96.77	0.005	0.217
Frankfurters	0.0679	0.0636	93.67	0.008	0.247
Czech republic					
Sausages	0.0544	0.0518	95.35	0.002	0.168
Hams	0.0534	0.0427	79.83	0.004	0.146
Frankfurters	0.0547	0.0427	77.99	0.001	0.174
Austria					
Sausages	0.0589	0.043	73.0	0.006	0.147
Hams	0.046	0.0424	92.18	0.002	0.156
Frankfurters	0.0513	0.0552	107.5	0.002	0.241
Germany					
Sausages	0.034	0.0375	70.28	0.002	0.141
Hams	0.047	0.0353	69.32	0.006	0.144
Frankfurters	0.0562	0.0459	81.63	0.004	0.212

Table II
Numbers of samples suitable and unsuitable by Food Codex in the Slovak Republic

Products	Suitable samples	Unsuitable samples
Slovak republic		
Sausages	24	6
Hams	25	5
Frankfurters	24	6
Czech republic		
Sausages	25	5
Hams	25	5
Frankfurters	25	5
Austria		
Sausages	24	6
Hams	26	4
Frankfurters	26	4
Germany		
Sausages	27	3
Hams	28	2
Frankfurters	24	6

Conclusions

We found, that meat product were contaminated by cadmium. From evaluated 360 samples (salami, hams and sausages) was 15.8 % (57 of samples) evaluated as over-limit in comparison with the highest allowable value (0.1 mg kg^{-1}) by Food Codex Slovak Republic. The highest values of cadmium were detected in sausages made in the Slovak Republic (0.247 mg kg^{-1} respectively 0.224 mg kg^{-1}). As primary source of cadmium in meat products can be regarding liver, kidney and meat. The high variability content of cadmium is given mainly thereby, that products descended from different producers.

REFERENCES

1. Miranda M., Lopéz M. A., Castillo C., Hernández J., Benedito J. L.: Vet. Hum. Toxicol. *42,* 265 (2000).
2. Goyer R. A., in: *Metal toxicology* (Goyer R. A., Klaassen C. D., Waalkes M. P.ed.). Academic Press, London 1995.
3. Satarug S., Haswell-Elkins M. R., Moore R. M.: Brit. J. Nutr. *84,* 79 (2000).
4. Jorhem L., Sundstrom B., Engman J., Astrand-Yates C., Olsson I.: Food Add. Contam. *13,* 737 (1996).
5. Miranda M., Lopéz M. A., Castillo C., Hernández J., Benedito J. L.: Eur. Food Res. Technol. *212,* 426 (2001).
6. DPIE/NFA. *Sources of cadmium in agricultural products.* (Rayment G. E.). Queensland Department of Natural Resources, Brisbane 1995.
7. Ysart G., Miller P., Croasdale M., Crews H., Robb P., Baxter M., De L´Argy Ch., Harrison N.: Food Add. Contam. *17,* 755 (2000).
8. Sola S., Barrio T., Martin A.: Food Add. Conatam. *15,* 580 (1998).
9. Lopez A. M., Benedito J. L., Miranda M., Castillo C., Hernandez J., Shore R. F.: Food Add. Contam. *17,* 477 (2000).

P33 CHIRAL SPECIATION OF IODINE IN THYDOID HORMONES BY USING HPLC/MS/MS AND HPLC-ICP-MS

ELISA GOMEZ DE LAS HERAS, JOSE LUIS GÓMEZ-ARIZA and TAMARA GARCÍA-BARRERA

Universidad de Huelva, Departamento de Química y Ciencia de los Materiales, Facultad de Ciencias Experimentales, Campus de El Carmen, 21007-Huelv, Spain
pippinheroe@hotmail.com

Introduction

Iodine is a key-element in the thyroid functions as active centre of the thyroid hormones, which activity depend on the number of iodine atoms into the molecule. These hormones are involved in the regulation of different important biological processes.

Thyroxine (T_4 or 3,5,3',5'-tetraiodothyronine) is the major hormone produced and secreted in the follicular cells of the thyroid gland by the protein thyroglobulin (Tg). Other compounds homologues have also been subsequently characterized.

In addition, thyroid hormones have enantiomeric forms which affect their biological activities[1,2]. Therefore, these species have to be determined separately to know their real metabolic behaviour and action on living organisms.

There are a number of problems associated with the analysis of thyroid hormones. The use of liquid chromatography/mass spectrometry presents several advantages over the currently used radio-immunoassay (RIA) and gas chromatography-mass spectrometry methods. The use of a UV detector to monitoring chromatographic separations allows a good sensitivity. There is an increasing interest for the use of HPLC coupled to MS, which increases the selectivity with acceptable sensitivity that is advisable for the complex biological matrices. However, the most sensitive analytical approach for iodinated hormones is HPLC-ICP-MS, which has been proposed by Michalke and other authors[3].

In the present study an analytical method for eight thyroid-related compounds has been performed. The coupling of HPLC-UV(PDA)-MS allows the identification and quantification of all the compounds and HPLC-ICP-MS the analysis of very low level of these hormones. A procedure for the analysis of these substances in human serum samples has been optimized and method reliability validated by recovery experiments.

Experimental

All the calibrants: L-thyronine – T_0; 3,5-diiodo-L-thyronine – L-T_2; 3,3',5-triiodo-L-thyronine – L-T_3; 3,3',5'-triiodo-L-thyronine – L-r-T_3; L-Thyroxine – LT_4; D-thyroxine – D-T4; 3,5-diiodo-L-tyrosine – DIT; 3-iodo-L-tyrosine – MIT were obtained from Sigma-Aldrich Chemie (Steinheim, Germany). Stock solutions were prepared at a concentration of 1 mg ml^{-1} in a mixture of MeOH and 10 nM NaOH (1:1 (v/v)).

Chromatographic Conditions and Instrumetation

A SpectraSYSTEM P4000 (HPLC) coupled in series with a SpectraSYSTEM UV6000LP photo diode array detector (PDA) and a LCQ Advantage mass spectrometer from Thermo-Finnigan (San José, CA, USA) with electrospray ionization (ESI) as ion source was used with a CHIRAL-PAK® QN-AX column. The mobile phase was 3% acetic acid in 40 % acetonitrile and 60 % water mixture; flow rate 0.7 ml min^{-1}.

HPLC-ICP-MS Coupling

An ICP-MS (HP 7600e, Hewlett-Packard, USA) was used with the same chromatographic conditions of previous paragraph. Iodine was determined at m/z 127. The operational conditions were the followings: forward power 1500 W, plasma gas flow rate 15.0 ml min^{-1}, auxiliary gas flow rate 1.0 ml min^{-1}, carrier gas flow rate 0.6 ml min^{-1}, optional gas (O_2) 6%, sampling depth 6.5 mm, sampling and skimmer cones of platinum. The dwell time was set to 0.3 s.

Hormones Extraction from Serum

A ClinChek®-Control serum (RECIPE, Chemicals+ Instruments GmbH, Munich, Germany) serum was used for hormone extraction. A volume of sample between 300 and 450 µl of serum was treated with a triple volume of 1% formic acid in acetonitrile. The mixture was vortexing for 5 min and centrifugated at 3,000 rpm for 10 min. The supernatant was filtered by 0.2 µm before to inject into the chromatographic column.

Results

The use of the in series coupling HPLC-PDA (UV-vis)-MS intents to combine the sensitivity of UV detector with the PDA system and the selectivity of MS. However, the very low levels of these hormones in healthy and hypothyroid people require more sensitive detection that can be reached with HPLC-ICP-MS.

A chiral separation of these hormones was performed using a *tert*-butyl carbamoylated quinine stationary phase.
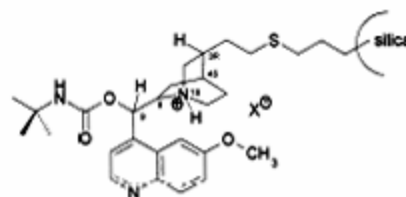
Fig. 1. **Tert-butyl carbamoylated quinine stationary phase**

Several solvent mixtures were tested as mobile phases. The optimum separation was obtained with 3 % of acetic in acetonitrile:water (40:60) at a flow rate 0.7 ml min^{-1}.

In Fig. 2 is shown a typical chromatogram obtained with the HPLC-(PDA)UV system for 20 mg dm^{-3} of each compound. The different compounds are well resolved but

overlapping of T0 and L-MIT was observed. For this reason MS/MS mode detection was tested for selective extraction of the ion $[M + H]^+$ of To (m/z 274.1) against L-MIT (m/z 308.1) – Fig 3.

A similar chromatogram was obtained with HPLC-ICP-MS, but limits of detection decreased drastically and the mixtures of hormones were traced at 5 µg dm^{-3} (Fig. 4).
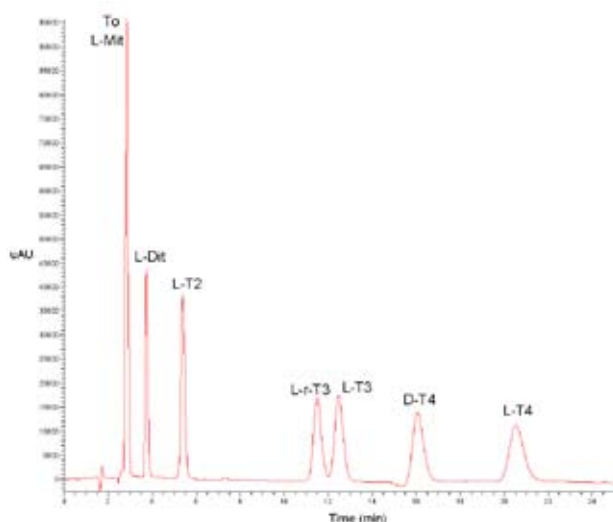
Fig. 2.　Chromatogram of thyroid hormones with HPLC-(PDA)UV
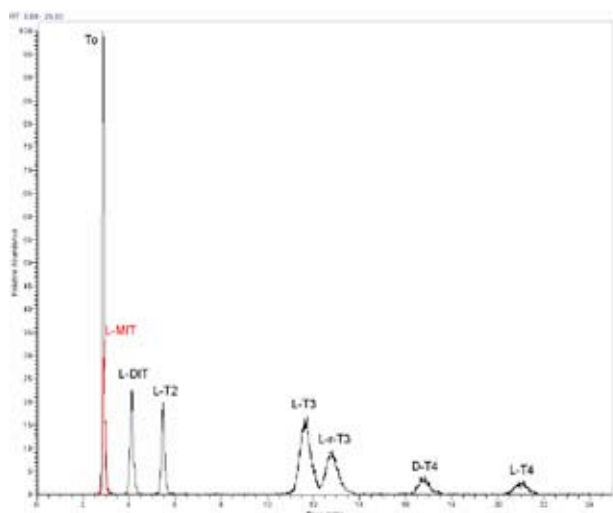
Fig. 3.　Chromatogram of thyroid hormones with HPLC-MS/MS

M e t h o d s　P e r f o r m a n c e

The method based on HPLC-(PDA)UV present a linear range between 1 and 25 mg dm^{-3}, with detection limits between 0.04 to 0.1 mg dm^{-3}.

For the HPLC-ICP-MS method the linear range was obtained between the detection limit and 100 µg dm^{-3}, and detection limits between 0.15 and 2.0 µg dm^{-3}, depending of compound considered.
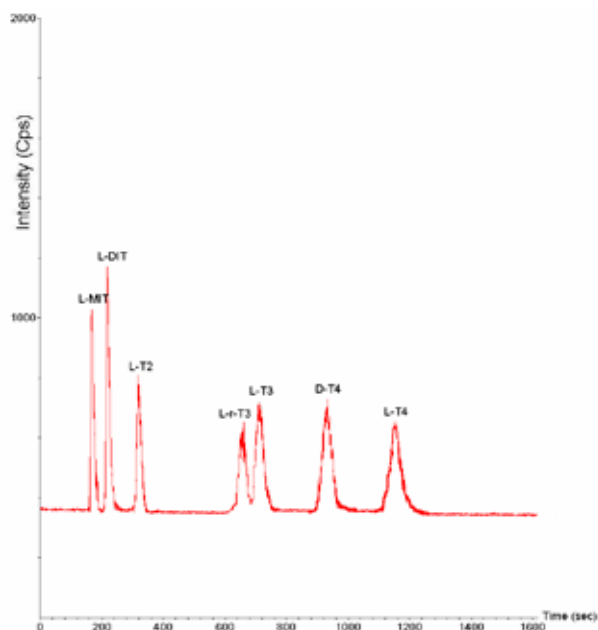
Fig. 4.　Chromatogram of thyroid hormones with HPLC-ICP-MS

H o r m o n e s　E x t r a c t i o n　f r o m　S e r u m

Proteins present in the serum were eliminated by precipitation with 1 % of formic acid in acetonitrile.

The final approach were appplied to a control human serum (ClinChek®-Control serum), usually used in the hospital for quality control, with good recoveries.

C o n c l u s i o n s

The combination of HPLC-PDA-UV-MS and HPLC-ICP-MS allows identification and cuantification of thyroid hormones in human serum. The use t-BuCQN colunm allows chiral speciation of these hormones. Proteins elimination from serum is necessary for the analysis of thyroid hormones in human serum. The method is suitable for the analysis of these hormones in control serum samples. Further studies are necessary to check the applicability of the approach to real human serum.

REFERENCES

1. Gorman C. A., Jiang N. S., Elldfson R. D., Elveback L. R.: J.Clin. Endocrinol. Metab. *49*, 1 (1979).
2. Eisdorfer I. B., Post A., J. Pharm. Sci. *56*, 1092 (1967).
3. Simon R., Tietge J. E., Michalke B., Degitz S., Schramm K. W.: Anal. Bioanal. Chem. *372*, 481 (2002).

P35 COMPARISON OF PROTEOME AND METABOLOME CHANGES IN STRESSED YEAST STRAINS *RHODOTORULA GLUTINIS* AND *RHODOTORULA RUBRA*

ANDREA HALIENOVÁ[a], IVANA MÁROVÁ[a], ZBYNĚK ZDRÁHAL[b], HANA KONEČNÁ[b], MARTINA ČARNECKÁ[a], KATEŘINA PAŘILOVÁ[a] and EMÍLIA BREIEROVÁ[c]

[a]*Department of Food Chemistry and Biotechnology, Faculty of Chemistry, Brno University of Technology, Purkyňova 118, 612 00 Brno, Czech republic,*
[b]*Laboratory of Functional Genomics and Proteomics, Faculty of Science, Masaryk University of Brno, Czech Republic,*
[c]*Institute of Chemistry, Slovak Academy of Sciences, Dúbravská cesta 9, 845 38 Bratislava, Slovak Republic,*
halienova@fch.vutbr.cz

Introduction

Exogenous stress and other environmental factors can induce many changes in cell composition. Some of these changes involved in stress response may lead to over- or underexpression of cell proteins. Identification of metabolic markers characteristic for certain events provides important insight into the metabolism control. Additionally, this information could be used to the biotechnological production of some industrially significant metabolites.

Carotenogenic yeasts produce high amount of lipidic compounds. Carotenoids are membrane-bound lipid-soluble pigments, which can act as effective antioxidants and scavenge singlet oxygen. In red yeasts they probably act as adaptive and/or protecive mechanism against exogenous oxidative stress and UV-irradiation. Carotenoids are produced by a specific branch of common isoprenoid pathway and accumulated in particular cell organelles.

In this work, protein and metabolic profiles of salt- and peroxide- stressed carotenogenic yeasts of the genus Rhodotorula were analyzed. Yeast cells *Rhodotorula glutinis* CCY 20-2-26 and *Rhodotorula rubra* CCY 20-7-29 were cultivated in glucose medium in presence of 2–5% NaCl and 2–5 mM hydrogen peroxide. In yeast cells carotenoids and ergosterol as specific stress metabolites were measured using HPLC/DAD. Proteins were separated by 1D and 2D electrophoresis. Some spots were identified by LC/MS/MS.

Materials and Methods
Strains

Industrial yeasts *Rhodotorula glutinis* CCY 20-2-26 and *Rhodotorula rubra* CCY 20-7-29 were used as tested strains. As a comparative strain *Saccharomyces cerevisiae* CCY 21-4-88 was used. Red yeasts were cultivated on glucose medium aerobically at 28 °C. Exogenous stress was induced by 2–5 mM peroxide and 2–5% NaCl.

Cell Fractination

Protein fractions of red yeast cells were obtained by gradually separation using combination of chemical (NaOH and detergents) and mechanical (glass beads; 100 μm) lysis. Protein fraction for 2D analysis was isolated mainly from lyophilized cells.

Carotenoid Analysis

Levels of carotenoids – lycopene, beta-carotene, torulen and phytoene were analyzed using HPLC/MS. Ergosterol was analyzed by RP-HPLC (280 nm).

1D Gel Electrophoresis

1D PAGE-SDS electrophoresis of proteins was carried out by common procedure using 10% and 12.5% polyacrylamide gels. Proteins were staining by Coomassie Blue and by silver staining. For comparison, microfluidic technique using 1D Experion system (BioRad) and P260 chips was used for yeast protein analysis too.

2D Gel Electrophoresis and LC-MS/MS

2D electrophoresis of proteins was optimized in cooperation with Laboratory of Functional Genomics and Proteomics, Faculty of Science, Masaryk University of Brno. 2D gels were obtained using protein preparatives isolated from lyophilized cells. After optimization of separation conditions proteomes from stressed *R. glutinis* and *R. rubra* cells were isolated, lyophilized and analyzed. Quantitative analysis was done using BioRad Laboratories 2D software. Identification of some spots was done using LC-MS/MS.

Results

Proteins from red yeast species were isolated with cell lysis combined with mechanical disintegration and protein profiles were obtained by 1D and 2D electrophoresis. Meta-
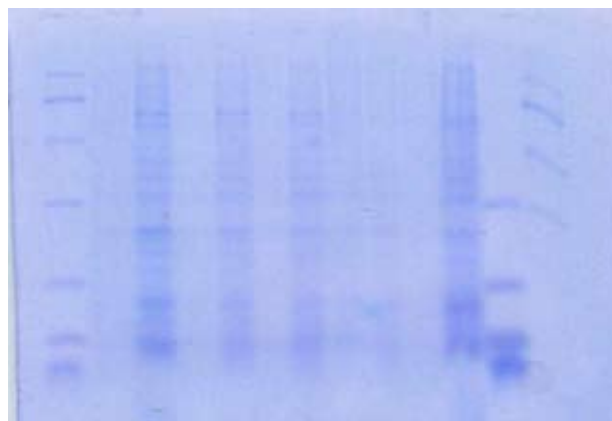
Fig. 1. **1D protein profiles – stressed *R. rubra* (NaOH); lane 1 – standard 6, 2 – proteome from lyofilized cells, 3 – proteome from non-lyofilized cells, 4 – proteome 2% NaCl, lyo, 5 – 2 % NaCl, non-lyo, 6–7 – 5 % NaCl, 8–9 – 2 mM hydrogen peroxide, 10–11 – 5 mM peroxide; 12, 13 – standards 4, 5**

bolome changes connected with proteome changes were observed. Presence of exogenous stress factor led to overproduction of carotenoids.
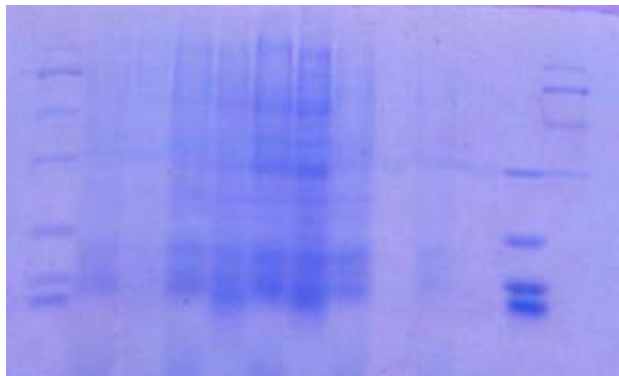
Fig. 2.   **1D protein profiles – stressed *R. glutinis*; lane 1 – standard 6, 2 – proteome isolated by NaOH, 3 – proteome isolated by SDS, 4 – proteome 2% NaCl, NaOH, 5 – 2 % NaCl, SDS, 6–7 – 5 % NaCl, 8–9 – 2 mM hydrogen peroxide, 10–11 – 5 mM peroxide; 12, 13 – standards 4, 5**
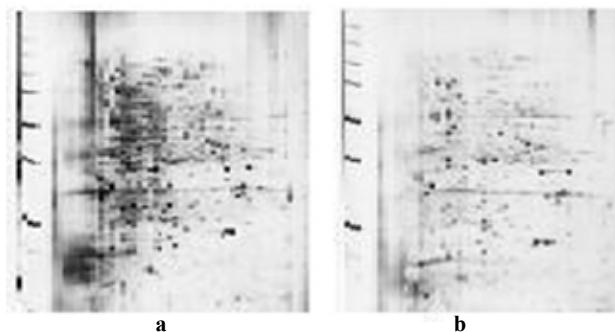
Fig. 3.   **Protein profiles of *Rhodotorula glutinis* a) control b) peroxide stress**
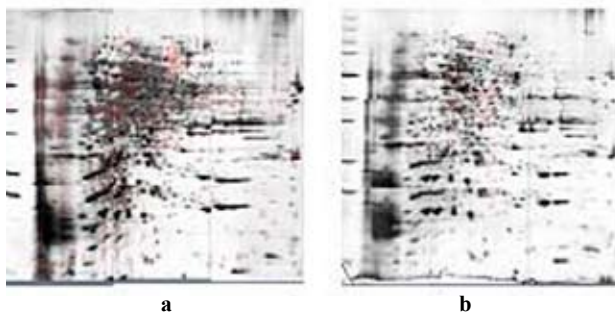
Fig. 4.   **Protein profiles of *Rhodotorula rubra* a) control b) peroxide stress**

Conclusions

In this work proteome changes in two *Rhodotorula* strains grown under salt and peroxide stress was studied. Isolation of proteins from red yeast cells is extremely complicated by unusual character of cell wall. Combination of several glycosidases and glucuronidases was the most common procedure. However, this method can lead to high interference of lytic enzymes during electrophoretic separation. In this work isolation of proteome using detergent SDS or alcalic lysis (NaOH) combined by mechanical disintegration by glass beads was optimized.

1D electrophoresis PAGE-SDS exhibited relatively good separation of proteins. Better results were obtained by alcaline lysis.

2D electrophoresis was done using stressed yeasts *Rhodotorula glutinis* and *Rhodotorula rubra*. Proteomic profiles differed according to strain and stress type.

In *R. glutinis* proteome more spots were evaluated. Significant 2D proteome changes were observed mainly in peroxide stress. Relatively well-balanced response to stress influence was observed in presence of 2 % salt; it seems that *R.glutinis* cells could exhibit long-term adaptation to this stress factor.

In *R. rubra* proteome less protein spots were detected and changes in stress conditions were not such intensive as in *R.glutinis*.

Proteome changes corresponded to some metabolome changes in *Rhodotorula* cells. Presence of some exogenous stress factor led to important overproduction of beta-carotene and ergosterol. Both these industrially significant metabolites are induced by the same way through the common isoprenoid pathway. In presence of salt well-balanced adaptation mechanisms were probably activated and, thus, salt stress could be used industrially to enhanced production of beta-carotene enriched biomass. *R. rubra* produced substantially lower amount of beta-carotene, this production was quite independent on stress factor.

Further experiments are needed for detailed characterization of molecular changes connected with exogenous stress and for identification of proteins involved in stress response of red yeasts.

REFERENCES

1. Halienova A., Marova I., Carnecka M., Konečná H., Hanusova V., Hezinova V.: J. Biotechnol. *131*, 202 (2007).

P36 (1→3)(1→4)-B-D-GLUCAN: VARIABILITY AND FACTORS AFFECTING ITS CONTENT IN OAT GRAIN

MICHAELA HAVRLENTOVÁ, MILAN ČERTÍK and JÁN KRAIC

Agricultural Biotechnologies Department, Slovak Agricultural Research Center – Research Institute of Plant Production Piešťany, Bratislavská cesta 122, 921 68 Piešťany, Slovak Republic,
havrlentova@vurv.sk

Introduction

β-D-glucan is major polysaccharide constituent of cell walls in the *Poales*, an order that includes cereals as well as other grass species. It is a linear and partially water-soluble polysaccharide that consists only of glucose linked through both β-(1→3)- and β-(1→4)-glykosidic linkages in various ratios. β-D-glucan plays an important role in cell wall architecture and plant development[1]. It has a positive impact on human health in terms of lowering cholesterol and blood glucose levels[2], increasing immunity against infection and positive influencing of bowel function[3].

Heritability estimates for β-D-glucan content have ranged from 0.27 to 0.58(ref.[4]). β-D-glucan content is affected by environmental factors. Genotype and the environment are significant sources of variation for its content; the ranking of genotypes is generally consistent over the environments[5].

Experimental

Mature grains of 99 oat genotypes were milled and passed through 0.5 mm sieve. The level of β-D-glucan was determined using Mixed-linkage Beta-glucan assay procedure, Megazyme (Ireland)[6]. Samples were suspended and dissolved in a 0.02M sodium phosphate buffer (pH 6.5), incubated with purified lichenase enzyme, and an aliquot of filtrate was reacted with purified β-glucosidase enzyme. The glucose product was assayed using an oxidase/peroxidase reagent. The measurement of the amount of β-D-glucan was performed in three parallel assays and expressed on a dry weight basis.

Results and Discussion

The β-D-glucan content ranged from 1.73 to 5.70 %, with 3.44 % as a mean value. The result is consistent with the determined values of β-D-glucan content in the set of European oat genotypes (3.90 %, 3.64 %, respectively)[7,8]. Our results show, likewise the literature[8], that naked genotypes dispose of higher levels of this metabolite (4.38 % on average) in comparison with the hulled oat, where the mean content was 3.26 % (Table I). The majority (90 %) of naked genotypes contain higher level of β-D-glucan than is the average in analysed oat set. The increased value of β-D-glucan is connected with the presence of gene *nud* for a hulless type of grain[9]. Naked oats are the feed that provide the largest welfare benefits[10] and their demand as a food crop is on a world-wide scale increasing[11]. Genotypes Terra,

Avenuda, SV-5, Arnold, Neon, Izak, Salomon, Saul, Bandicoot, and Ábel with the highest level (>4.00 %) observed can be therefore used as a convenient material in breeding and food industry.

In our work a relation between the oat glume colour (yellow, white, black) and the content of β-D-glucan was found. Our results indicate that the black genotypes show the lowest standard deviations in the content of evaluated metabolite. The degree variance of β-D-glucan level expressed as a coefficient of variation displayed the highest value in white hulled oat, next in yellow, and the lowest values were calculated for the genotypes with black glume colour (Table I). Because higher value of variation coefficient directly correlates with lower variance of metabolite biosynthesis within a set, we could state, that black hulled oat with low variation coefficient are characterized by markedly stable biosynthesis of β-D-glucan in the comparison with yellow and white types. Similarly, biosynthesis of other biochemical parameters (proteins, fatty acids, and lipids) also shows to by more stabile in black hulled oat[12].

Analysis of variance suggested that oat morphological and biochemical parameters depend on the environment and the genotype variously[13,14]. Test weight, groat percentage and weight, protein, and β-D-glucan content were about equally influenced by the environment and genotype[13], whereas oat lipids, total starch, and amylose content were more strongly influenced by genotype.

The content of monitored parameter according to the year of genotype registration is documented on the Fig. 1. The mean value of β-D-glucan in oats with the breeding date before the year 1960 was 2.53 %, moreover a stabilisation was observed during the period of years 1961–2000. At the beginning of the 21st century a gradually raising of β-D-glucan content in oat seeds was detected.

Table I
Mean values of the β-D-glucan content in naked and hulled oat and in individual groups according to the glume colour

Group of oat	Mean value [%]	Standard deviation	Variation coefficient
Naked	4.38***	0.96	22.03
Hulled	3.26	0.60	18.34
Yellow	3.28	0.62	18.97
White	3.46	0.71	20.55
Black	3.31	0.46	13.89***

*** significant at P≤0.001

Conclusions

Naked genotypes dispose of higher β-D-glucan content in comparison with the hulled. Genotypes Terra, Avenuda, SV-5, Arnold, Neon, Izak, Salomon, Saul, Bandicoot, and Ábel with the highest level of monitored health beneficial polysaccharide can be used in breeding programs and seed processing in food industry as its donors. Genotypes with black colour of the glumes account significantly lower stan-

dard deviation and variation coefficients in the content of β-D-glucan, what indicates markedly stable biosynthetic mechanism of the studied metabolite.
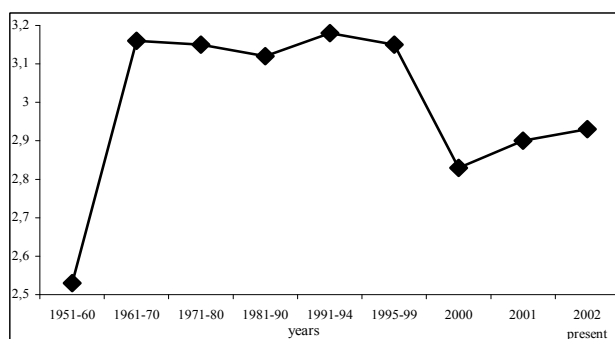
Fig. 1.   **Mean content of β-D-glucan [%] according to the breeding date**

REFERENCES

1. Buckeridge M. S., Rayon C., Urbanowicz B., Tiné M. A. S., Carpita N. C.: Cereal Chem. *81*, 115 (2004).
2. Kerckhoffs D. A. J. M., Hornstra G., Mensink R. P.: Am. J. Clin. Nutr. *78*, 221 (2003).
3. Mälkki Y., Virtanen E.: Lebensmittel-Wissenschaft Technol. *34*, 337 (2001).
4. Kibite S., Edney M. J.: Can. J. Plant Sci. 78, 245 (1998).
5. Peterson D. M., Wesenberg D. M., Burrup D. E.: Crop Sci. *35*, 965 (1995).
6. McCleary B. V.: http://secure.megazyme.com/ downloads/en/data/K-BGLU.pdf
7. Redaelli R., Sgrulleta D., DeStefanis E.: Cereal Res. Comm. *31*, 185 (2003).
8. Grausgruber H., Scheiblauer J., Schönlechner R., Ruckenbauer P., Berghofer E.: *Genetic variation for plant breeding,* Proceedings of the 17th EUCARPIA General Congress, Tulln, 8–11 Sept. 2004, Proceedings Book (Vollmann J., Grausgruber H., Ruckenbauer P., eds.,) p. 23.
9. Swanson J. S.: J. Cereal Sci. *22*, 157 (1995).
10. Brennan J. P., Singh R. P.: Econ. Res. Rep. *3*, 1 (2000).
11. Stevens E. J., Armstrong K. W., Bezar H. J., Griffin W. B., Hampton J. G.: www.fao.org/docrep/008/y5765e/y5765e0i.htm
12. Čertík M., Havrlentová M., Ješko D., Bieliková M., Hozlár P., Kraic J.: Agric. *54*, 2 (2008).
13. Doehlert D. C., McMullen M. S., Hammond J. J.: Crop Sci. *41*, 1066 (2001).
14. Rhymer C., Ames N., Malcolmson I., Brown D., Duguid S.: Cereal Chem. *82*, 197 (2005).

P37 EXTRACTION AND DETERMINATION OF FLAVONOIDS IN PLANT MATERIALS

BARBORA HOHNOVÁ[a,b], PAVEL KARÁSEK[b] and MILENA VESPALCOVÁ[a]

[a]*Faculty of Chemistry, Brno University of Technology, Purkyňova 118, Brno 612 00,*
[b]*Institute of Analytical Chemistry of the ASCR, v.v.i.,Veveří 97, Brno 602 00,*
hohnova@fch.vutbr.cz

Introduction

Flavonoids are one of the largest groups of secondary metabolites and they are responsible for coloration of plants. They are found in fruits, vegetables, beverages like tea, wine, beer, and large amount of flavonoids was also found in several medicinal plants. Flavonoids play important role in human diet because of their antioxidant properties, estrogenic action and wide range of antimicrobial and pharmaceutical activities[1].

Extraction of flavonoids from the samples is usually performed by maceration with aqueous methanol[2], solid-phase extraction[3], sonication[4], and supercritical fluid extraction (SFE)[5]. High-performance liquid chromatography (HPLC)[6], capillary electrophoresis (CE)[7], capillary electrochromatography (CEC)[8] or gas chromatography (GC)[9] are commonly used for their determination and quantification.

Since rapid and efficient extraction technique prior to chromatographic analysis is nowadays of primary interest, the liquid extraction at high temeperature and pressure – *Pressurized fluid extraction* (PFE), was introduced. PFE offers several advantages over conventional extraction procedures. The use of higher temperature increases the diffusion rate, solubility and mass transfer of the compounds and decreases the viscosity and surface tension of the extraction solvent. These changes improve the contact of analytes with the solvent and enhance extraction, which can be achieved more rapidly with less solvent consumption as compared with conventional extraction methods. The elevated pressure not only maintains the extraction solvents in liquid state, but also improves the contact of solvent with analytes trapped in matrix pores. The absence of light and air significantly reduces degradation and oxidation of compounds during extraction[10].

In the last years, pressurized fluid extraction has been succesfully applied to the extraction of flavonoids from plant materials and foods. This application of PFE as powerful sample preparation step was recently reviewed by Mendiola et al.[11]

Recently, intense attention has been paid to *Stevia rebaudiana* Bertoni (Asteraceae) because of content of low-caloric high intensity sweet diterpene glycosides (50–400 times sweeter than sucrose)[12]. Besides sweet glycosides also flavonoids have been isolated from *Stevia*. Rajbhandari et al. determined that *Stevia* contains apigenin, luteolin, quercetin, kaempferol and quercitrin. The flavonoids were extracted by classical maceration and their structures were determined by standard methods of uv, nmr, and ms spectroscopy[13].

In this study, we focused on optimalization of liquid chromatografic conditions after extraction step for rapid and succesful determination and quantification of quercetin, luteolin, apigenin and kaempferol contained in *Stevia* leaves.

Experimental

Chemicals and Standard Solutions

Stevia leaves were obtained from Ukraine. Acetonitrile, methanol and formic acid, all HPLC-grade, were purchased from Riedel-de Haën (Prague, Czech Republic). Water was purified with a reverse osmosis system Ultra Clear UV (Barsbüttel, Germany).

Flavonoid standards quercetin, kaempferol, luteolin and apigenin were obtained from Sigma-Aldrich (Prague, Czech Republic). Stock solution of all flavonoids (1 g dm^{-3} each) was prepared in methanol and stored in the fridge at 5 °C.

PFE of Stevia Rebaudiana Leaves

A static PFE of Stevia leaves was performed using a onePSE extractor (Applied Separations, Allentown, PA, USA). A portion (1 g) of leaves was placed into 22 ml extraction cell that contained inert material (glass beads (570–700 μm)) at the bottom of the cell. The PFE parameters were set as follows, temperature 60–120 °C, pressure 15 MPa, extraction time 3×5 minutes, rinsing time 20 s, and nitrogen purge time 90 s after each cycle and 120 s after extraction run. After PFE run, the extract was cooled to 5 °C and stored in the fridge until HPLC analysis.

Chromatographic Conditions

HPLC apparatus was eqCipped with LC 1150 pump (GBC Scientific Equipment Pty Ltd, Dandenong, Australia), injection valve with 20-μl sample loop (Ecom, Praha, Czech Republic), column oven LCO 101 (Ecom, Praha, Czech Republic) and Linear UVIS-206 Multiple Wavelength detector (Linear Instruments, Fremont, CA). The wavelength was set at 360 nm. Mobile phase was composed of acetonitrile (A) and water (B) adjusted at pH 2.3 by formic acid. Several reversed-phase columns were tested: 1) 4.6 mm i.d., 150 mm long Symmetry C18 5 μm stationary phase (Waters, USA); 2) 3.0 mm i.d., 150 mm long Xbridge C18 3.5 μm stationary phase (Waters, USA); 3) 3.0 mm i.d., 150 mm long Atlantis T3 C18 3 μm stationary phase (Waters, USA); 4) 3.0 mm i.d., 150 mm long Xterra RP C18 3.5 μm stationary phase (Waters, USA); and 5) 4.6 mm i.d., 250 mm long Supelcosil LC-18 5 μm stationary phase (Supelco, USA). Gradient programme was employed at flow rate 0.5 ml min^{-1}: 0 min 10 % A; 20 min 70 % A. When Xterra C18 column was used, the flow rate was set to 0.3 ml min^{-1} because of high backpressure. LC systems were connected to PC and controlled by Clarity software (DataApex, Czech Republic).

Results

Since luteolin, quercetin, apigenin and kaempferol have very similar structures (Fig. 1.), the main point of view of this study was to find optimal analytical conditions for their efficient separation.

Several single columns with different column lengths and different sorbent parameters were tested. The gradient of water/acetonitrile mixture was used as mobile phase. The replacement of acetonitrile with methanol as mobile phase component was also investigated, but the separations didn't show satisfactory results. After modification of mobile phase compositions by formic acid at pH = 2.3, significant peak shape improvement of the observed compounds was noticed. In all experiments, the flow rate of mobile phase was 0.5 ml min^{-1}, only when Xterra C18 column was tested, the flow rate was set to 0.3 ml min^{-1} because of the high column backpressure. The experiments were performed with flavonoid standard solution (c = 30 μg ml^{-1}). Injected amount of analyte was 20 μl.

compounds	R¹	R²
quercetin	- OH	- OH
luteolin	- H	- OH
apigenin	- H	- H
kaempferol	- OH	- H
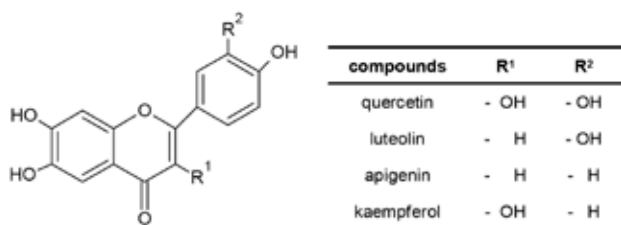
Fig. 1. **Chemical structures of analyzed flavonoids**

The comparison of column efficiency for separation of the above compounds is shown in Fig. 2. First, two hybrid C18 columns with the same column parameters were compared: (a) 3.0 mm i.d., XBridge 150 mm long column, 3.5 μm particle size, (b) 3.0 mm i.d., Xterra 150 mm long column, 3.5 μm particle size. Both separations showed only three peak. In separation (a) very nice separation of apigenin and kaempferol was observed, while in separation (b) the separation of apigenin and kaempferol was slightly poor. However, the column performance of both columns was too poor to separate luteolin and quercetin, the peak coelution was observed. Nevertheless, neither the utilization of longer column, (c) 4.6 mm i.d., Supelcosil C-18 250 mm long column, 5 μm particle size, didn't show the improvement of luteolin and quercetin separation and also the separation of kaempferol and apigenin wasn't very acceptable. Further, (d) 3.0 mm i.d., Atlantis T3 C18 150 mm long column, 3.0 μm particle size was tested. The column separated not only apigenin and kaempferol but also luteolin and quercetin. However, although the column proved to separate single flavonoids, the peak shapes didn't match our ideas. The efficient separation of observed compounds was achieved by (e) 4.6 mm i.d., Symmetry C18 150 mm long column 5 μm stationary phase. The kaempferol and apigenin were separated to baseline and separation of luteolin and quercetin was sufficient for succesful determination and quantification of both compounds present in the sample.
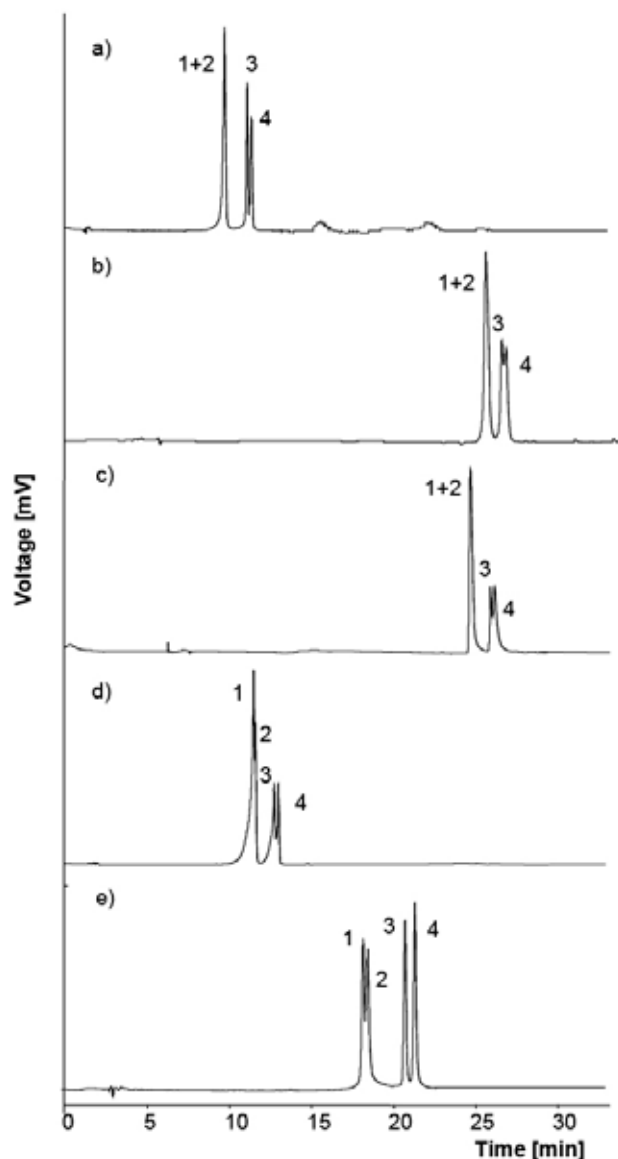
Fig. 2. **HPLC chromatogram of comparison column separation of flavonoid standards. (1) quercetin, (2) luteolin, (3) apigenin, (4) kaempferol. (a) Xbridge C18 column (3.0 × 150 mm length), (b) Xterra C18 column (3.0 × 150 mm length), (c) Supelcosil C18 column (4.6 × 250 mm length), (d) Atlantis T3 C18 column (3.0 × 150 mm length), (e) Symmetry C18 column (4.6 × 150 mm length). For chromatographic conditions see the experimental part**

Conclusion

The data presented in this report indicate that there are wide variations in the effectiveness of different reversed-phase HPLC columns when used to analyse flavonoids. High efficiency separation was obtained with Symmetry C18 column. Gradient elution with acetonitrile in water adjusted to pH 2.3 by formic acid facilitated the separation of luteolin, quercetin, kaempferol and apigenin. In the future, this procedure will be used for quantitative analysis of Stevia flavono-

ids after PFE and appropriate pre-cleaning step of the extracts prior to HPLC analysis.

REFERENCES

1. Carlo G., Mascolo N., Azzo A. A., Capasso F.: Life Sci. *65*, 337 (1999).
2. Molnár-Perl I., Füzfai Z.: J. Chromatogr. A *1073*, 201 (2005).
3. Michalkiewicz A., Biesaga M., Pyrzynska K.: J. Chromatogr. A *1187*, 18 (2008).
4. Ogawa A., Arai H., Tanizawa H., Miyahara T., Toyooka T.: Anal. Chim. Acta *383*, 221 (1999).
5. Lin M. C., Tsai M. J., Wen K. C.: J. Chromatogr. A *830*, 387 (1999).
6. Fang F., Li J. M., Pan Q. H., Huang W. D.: Food Chem. *101*, 428 (2007).
7. Lee B. L., Ong C. N.: J. Chromatogr. A *881*, 439 (2000).
8. Rodriquez-Delgado M. A., Pérez M. L., Corbella R., Gonzalez G., Garcia Montelongo F. J.: J. Chromatogr. A *871*, 427 (2000).
9. Deng F., Zito S. W.: J. Chromatogr. A 986, 121 (2003).
10. Richter B. E., Jones B. A., Ezzell J. L., Porter N. L.: Anal. Chem. *68*, 1033 (1996).
11. Mendiola J. A., Herrero M., Cifuentes A., Ibañez E: J. Chromatogr. A *1152*, 234 (2007).
12. Brandle J. E., Starratt A. N., Gijzen M.:Can. J. Plant Sci. *78*, 527 (1998).
13. Rejbhandari A., Roberts M. F.: J. Nat. Prod. *46*, 194 (1983).

P39 *TRICHOSPORON CUTANEUM*: CELL ADHESION ON CELLOPHANE SURFACE

JITKA HRDINOVÁ, TEREZA KRULIKOVSKÁ, VLADIMÍR JIRKŮ, OLGA SCHREIBEROVÁ, ALENA ČEJKOVÁ and JAN MASÁK

Institute of Chemical Technology Prague, Technická 5, 166 28 Praha 6 – Dejvice, Czech Republic, jitka.hrdinova@vscht.cz

Introduction

Recently we have faced the problem of increasing amount of solid cellulose wastes that come mainly from agriculture activities, food industry as well as from municipal waste[1,2].

Cellulose is considered to be a solid nontoxic pollutant; however, its recalcitrant nature causes many difficulties in removal of cellulosic waste. The microbial degradation is one of the possibilities how it could be solved.

Colonization of solid material by microbial cells is the crucial step in their biodegradation. Biofilm formation by cellulolytic microorganisms is not investigated enough. Therefore, establishing more efficient arrangement for technological solubilization of solid cellulosic wastes could be achieved using cellulolytic biofilms, formed by direct colonization of these wastes by cell populations. In this association, cellophane was chosen as a representative of solid cellulosic substrates (carrier) and the yeast *Trichosporon cutaneum* as a relatively little researched cellulolytic strain.

Experimental

The yeast *Trichosporon cutaneum* CCY 30-4-5 was obtained from Department of Genetics and Microbiology, Faculty of Science, Charles University, Czech Republic.

Inoculum was grown in complex medium and after 2 days it was replaced in minimal medium supplemented with 1% cellulosic substrates as a sole source of carbon. Sigmacell Type 101, carboxymethylcellulose – CMC, hydroxyethylcellulose – HEC, cellophane and filter paper was used as the representatives of these substrates. Minimal medium composition in $g\,dm^{-3}$: KH_2PO_4 – 1.7; $Na_2HPO_4 \cdot 7H_2O$ – 0.75; $(NH_4)_2SO_4$ – 5.0; $MgSO_4 \cdot 7H_2O$ – 0.02; $CaCl_2$ – 0.02; $FeSO_4 \cdot 7H_2O$ – 0.001; $MnSO_4 \cdot H_2O$ – 0.001, pH 5.8. The temperature was maintained at 28 °C. Cultures were harvested during the exponential phase; at 48–72 hr. Separated and rinsed cells were used for experiments.

FC 81 Flow Cell Description

The FC 81 Flow Cell in Fig. 1. is a flat plate flow cell designed for use with transmitted light microscopes and it was used for observation of biofilm formation by yeast *Trichosporon cutaneum*. The capability of the yeast cells to colonize cellophane as well as the effect of shear stress was investigated.

Experiment conditions:
- Cell suspension – $OD_{400\,nm}$ 0.1
- Temperature – 22 °C
- Flow rate – 2-20 ml min^{-1}
- Time period – 2 hr.
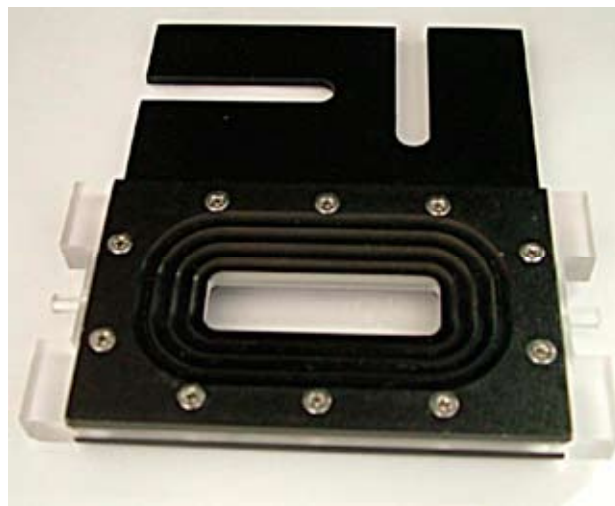
Fig. 1. **Photograph of the FC 81 Flow Cell (Biosurface Technologies, Corp., USA)**

Experiments were carried out as shown by Fig. 2.; Fig. 3. illustrates an emplacement of cellophane stripe in the flow cell.

Hydrophobity of Yeast Cells

The yeast populations were prepared in cultivation medium supplemented with different types of cellulosic substrates. Hydrophobity of yeast cell surface was determined using MATH method[3].

Microscopy and Image Analysis

The colonization of cellophane was observed with transmitted light microscopy and analysis of the images was accomplished with Lucia (Laboratory Imaging, Ltd., UK). The areal parameters of objects (colonies, cells) such as length, width and colonized area were measured with image analysis4. The observation area of the flow cell was divided into three fields (inflow, middle, and outflow). Ten images were taken in every field.

- Microscope – NIKON Eclipse E400, Plan Fluor objective, 10×/0.30, Ph1 DLL, ∞/0.17 WD 16.0 (Japan)
- Filter – 45 mm, NCB11
- Camera and software – Canon PowerShot A620, ZoomBrowser EX 5.5

1 – Aeration
2 – Stock bottle with mineral medium
3 – Pump
4 – Flow Cell FC 81
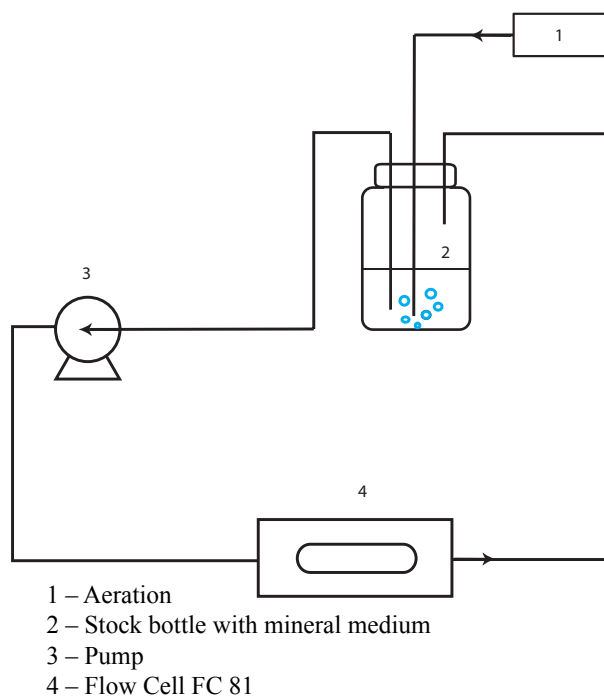
Fig. 2. **Scheme of the FC 81 Flow Cell connection during the experiment**

1 – Cover Glass
2 – Slide
3 – Cellophane
4 – Space for medium flow
5 – Parts of the flow cell
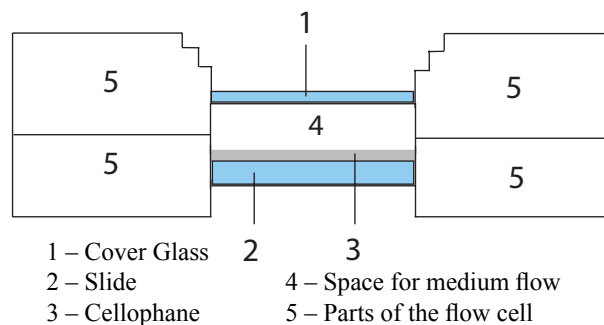
Fig. 3. **Cross-section of the FC 81 Flow Cell**

Results

Character of Cell Envelopes of *Trichosporon Cutaneum*

The results obtained by MATH method are summarized in Table I. The cell envelopes of the population *Trichosporon cutaneum* grown in the presence of filter paper had the most

Table I
Hydrophobity of cell envelopes in dependence on using different types of cellulosic substrates as sole of carbon

Cellulosic substrate	Cell hydrofobity [%]
filter paper	83.8
cellophane	51.8
carboxymethylcellulose	76.4
hydroxyethylcellulose	79.3
Sigmacell Type 101	9.6
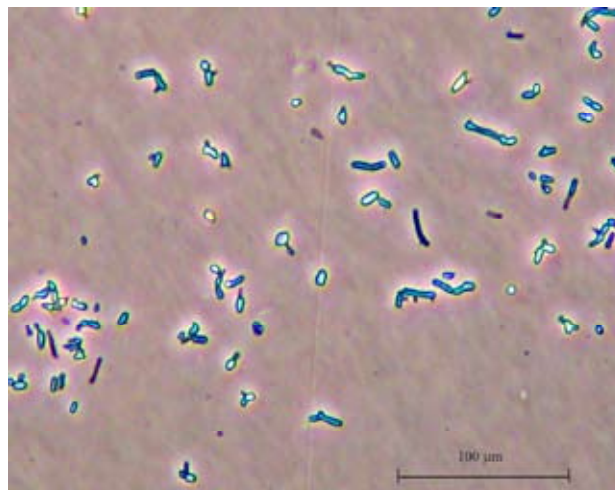
Fig. 4. **Cells of *Trichosporon cutaneum* attached on cellophane (phase contrast)**

hydrophobic character (83.8 %), whereas the population cultivated on Sigmacell had very hydrophilic cell surfaces. The hydrophobity of cellophane stripes (95.6 %) was determined at Department of Polymers, ICT Prague. We wanted to choose cells with similar surface characters as the cellophane stripes. Filter paper could not be used for biomass preparation because of low biomass concentration. For this reason HEC was used for following experiments.

Influence of Shear Stress on Cellophane Colonization

Low flow rates of medium are less favourable for the cellophane colonization (Table II). Also small areas

Table II
Influence of shear stress on the cellophane colonization and object morphology changes

Flow rate [ml min^{-1}]	Colonized area [%]	Objects in field	Area [µm^2]	Lenght [µm]	Width [µm]	Elongation*
2	4.86	12	180.98	27.92	5.94	1.76
4	4.42	12	176.64	24.00	6.33	1.81
6	16.07	27	194.27	29.56	5.40	1.76
8	8.49	40	80.42	15.02	5.01	1.69
10	4.25	21	97.32	15.69	5.50	1.74
15	2.38	15	86.32	15.79	5.25	1.97
20	6.08	24	117.22	20.90	5.65	2.18

(on an average 4 %) were colonized as long as the rates are higher than 8 ml min^{-1} (probably the influence of shear stress). 8–16 % area was colonized using the flow rates between 6 and 8 ml min^{-1}. The increase of shear stress had not significant influence on morphological parameters of objects – width and elongation with exception of length and area of objects.

Conclusions

The capacity of *Trichosporon cutaneum* cells to colonize cellophane (used as a carrier and the source of carbon) was proved (Fig. 4.). FC 81 Flow Cell appears to be suitable apparatus for microscopy study of biofilm formation. Image analysis is favourable tool for monitoring and evaluation of biofilm formation.

The flow rate 10 ml min^{-1} was appropriate for study of biofilm formation. However, for the purpose of cellophane degradation more colonized areas are required (6 ml min^{-1}).

The effect of shear stress is one of required information needed for optimalization of these processes. Nutrient starvation, cell suspension density, medium composition etc. are factors that could probably affect biofilm formation.

REFERENCES

1. Lynd R. L., Weimer J. P., Zyl W. H., Pretorius I. S.: Microbiol. Mol. Biol. Rev. *66*, 505 (2002).
2. Šulák M., Šmogrovičová D.: Chem. listy *102*, 108 (2008).
3. Rosenberg M. D., Gutnick E.: Fems Microbiol. Lett. *9*, 29 (1980).
4. Yang X., Beienal H.,: J Microbiol Methods *39*, 109 (2000).

P40 SEASONAL CHANGES OF RUBISCO ACTIVITY AND ITS CONTENT IN NORWAY SPRUCE EXPOSED TO AMBIENT AND ELEVATED CO_2 CONCENTRATIONS

MIROSLAV HRSTKA[a], LUCIE ZACHOVÁ[a], OTMAR URBAN[b] and MARTINA KOŠVANCOVÁ[b]

[a]*Department of Food Chemistry and Biotechnology, Faculty of Chemistry, Brno University of Technology, Purkyňova 118, 612 00 Brno, Czech Republic,*
[b]*Institute of Systems Biology and Ecology AS CR, Poříčí 3b, 603 00 Brno, Czech Republic,*
htka@fch.vutbr.cz

Introduction

Ribulose-1,5-bisphosphate carboxylase/oxygenase, Rubisco (EC 4.1.1.39) is the most abundant protein on the Earth. This enzyme catalyses carboxylation of D-ribulose-1,5-bisphosphate (RuBP), the first step of the Calvin cycle in competition with oxygenation of RuBP that leads to the photorespiratory pathway. Rubisco is a key enzyme of photosynthesis regulation[1]. It must be reversibly activated with CO_2 and Mg^{2+} before catalysis can occur. The activation in vivo must be facilitated by the presence of a second protein, Rubisco activase[2].

Rubisco activity depends on the amount of enzyme and the activation state of its active sites and changes within several minutes depending on temperature, RuBP supply, irradiance, CO_2 concentration, inorganic phosphate content, and presence of inhibitors in the active site[3]. Rubisco content varies over the time scale of hours and days in dependence on specific saccharide contents (e.g. glucose, sucrose). Increased contents of these sugars lead, via a hexokinase-related signal, to the repression of Rubisco gene expression and subsequent decrease in the content of Rubisco protein[4,5]. Decrease in Rubisco amount may be also the result of non-selective decrease in leaf nitrogen content[6,7]. Many authors[8–10] present that Rubisco content reaches a maximum soon after full expansion of the leaf. Then Rubisco is gradually degraded and its nitrogen is translocated into growing organs during senescence.

Short-term exposure of higher plants to elevated CO_2 concentrations usually increases photosynthetic CO_2 uptake. Long-term growth in elevated CO_2 usually leads to decrease of content and activity of Rubisco. This biochemical adjustment, which is often termed acclimation or down-regulation, reduces photosynthetic capacity[11].

In this work we measured seasonal changes of Rubisco initial and total activities in vitro as well as Rubisco content in Norway spruce needles to answer following quesions:

- Is there a decrease of Rubisco activity and content in Norway spruce during the growing season?
- Is there a down-regulation of Rubisco activity and content in Norway spruce cultivated in elevated CO2 concentration?

Experimental

Materials

The experiment was conducted in 2007 at the experimental site Bílý Kříž in Beskydy Mts. Five-year old seedlings of Norway spruce (*Picea abies* [L.] Karst.) were grown under ambient (A = 375 μmol (CO_2) mol^{-1}) and elevated (E = 700 μmol (CO_2) mol^{-1}) CO_2 concentrations using the glass domes with adjustable windows. Last year needles were sampled between 11 a.m. and 3 p.m. at the following dates: 15th May, 23th July and 10th October. About 0.06 g of needles were weighed and the projected area of these needles was estimated according[12]. Needles were inserted into microtube Eppendorf and put into liquid nitrogen.

Methods

Rubisco activity assay. Needles from one microtube were homogenized in a chilled mortar with 0.02 g inert sand and 5 ml extraction buffer composed of: 50 mM HEPES, 5 mM Na_2EDTA, 5 mM dithiothreitol (DTT), and 1 % insoluble polyvinylpolypyrrolidone, all at pH 8.0. The homogenate was centrifuged at 10,000 × g for 30 s and an aliquot of the supernatant was used immediately for spectrophotometric Rubisco activity assay, based on the continuous measurement of 3-phosphoglycerate-dependent NADH oxidation in a coupled enzyme system[13]. The initial Rubisco activity was determined by adding 20 μl of extract to 100 μl of activation solution which contained 25 mM $KHCO_3$ and 20 mM $MgCl_2$ and 850 μl of assay solution composed of: 50 mM HEPES (pH 8.0), 25 mM $KHCO_3$, 20 mM $MgCl_2$, 5 mM Na_2EDTA, 5 mM DTT, 3.5 mM ATP, 0.35 mM NADH, 3.5 mM phosphocreatine, 80 nkat glyceraldehyde-3-phosphate dehydrogenase, 80 nkat 3-phosphoglyceric phosphokinase, and 80 nkat creatine phosphokinase. The reaction was started by the addition 30 μl of ribose-5-phosphate (R5P) at final concentration 0.4 mM and the changes in absorbance at 340 nm were immediately measured at 25 °C using Helios γ (Spectronic Unicam, UK) spectrophotometer.

The total activity was measured after 15 min incubating 20 μl of the extract with 100 μl of activation solution. 850 μl of assay solution were added, the reaction was again started by adding 30 μl of R5P at final concentration 0.4 mM and the changes in absorbance at 340 nm were measured.

Rubisco content determination. Needles from one microtube were homogenized in a chilled mortar with 0.02 g inert sand and 2 ml extraction buffer containing 62 mM Tris, 2% (w/v) sodium dodecyl sulphate (SDS), 65 mM DTT, and 10% (v/v) glycerol, all at pH 6.8. The homogenate was centrifuged at 10,000 × g for 2 min, 0.5 ml of the supernatant were added to 0.5 ml sample buffer composed of 3% (w/v) Tris, 5% 2-mercaptoethanol, 10% (w/v) SDS, 20% (v/v) glycerol, and 0.2% (w/v) bromophenol blue and the mixture was incubated 5 min at 100 °C.

Rubisco content was determined by SDS-PAGE with a Mini-PROTEAN 3 system (Bio-Rad). Resolving gels contained 10 % (w/v) acrylamide, 0.27 % (w/v) N,N´-methy-

lene-bis-acrylamide, 0.37M Tris-HCl (pH 8.8) 0.1 % (w/v) SDS, 0.04 % (v/v) N,N,N',N'-tetramethylethylene-diamine (TEMED), and 0.1 % (w/v) ammonium persulphate. Stacking gels contained 5 % (w/v) acrylamide, 0.13 % (w/v) N,N'-methylene-bis-acrylamide, 0.19M Tris, 0.02 % (v/v) TEMED, and 0.1 % (w/v) ammonium persulphate.

A 5 μl of sample solution were loaded on polyacrylamide gel. Electrophoresis ran 60 min at the constant voltage 140 V. The large subunit of Rubisco was detected by staining with Coomassie brilliant blue and its identity was confirmed by co-electrophoresis of Rubisco standard (Sigma-Aldrich) (Fig.1). Quantification of individual bands was performed on HP Scanjet 5590P with programme Advanced Image Data Analyzer, ver. 3.23.001 (Raytest, Germany).

Results
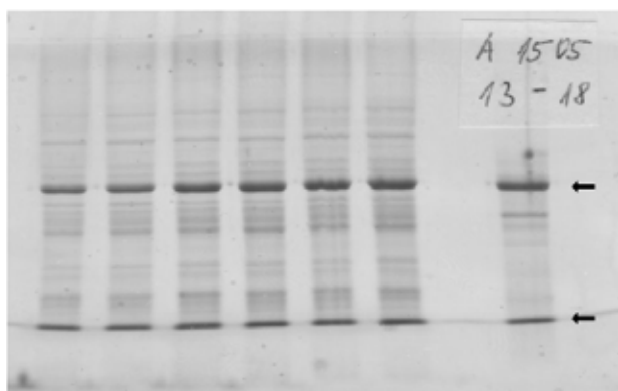
Fig. 1. **A representative SDS-PAGE gel with separated proteins from Norway spruce needles (six left columns) and Rubisco standard 1 mg ml^{-1} (the first column from the right). The upper arrow indicates the large subunit of Rubisco protein and the lower arrow indicates the small one**

Both initial and total activities in E were lesser than those in A with the exception of autumn. It is in good accordance with data of other authors[14–16]. Maximum of activities we measured in May and then they gradually decreased. Rubisco initial activity in A decreased about 57 % while in E dropped about 41 % during the growing season. Total activity decreased about 66 % in A and about 44 % in E. Rubisco content dropped about 55 % in A and about 50 % in E. The sharp diminution of Rubisco content in E in July could be caused by enormous drought in the first half of summer in combination with the phenomenon that elevated CO_2 concentrations accelerate the senescence of leaves[6,8,10]. Both initial and total activities as well as content decreased less in E than in A (Fig. 2.). We hypothesised that down-regulation in E – if there was any – proceeded in the first year of needles life.
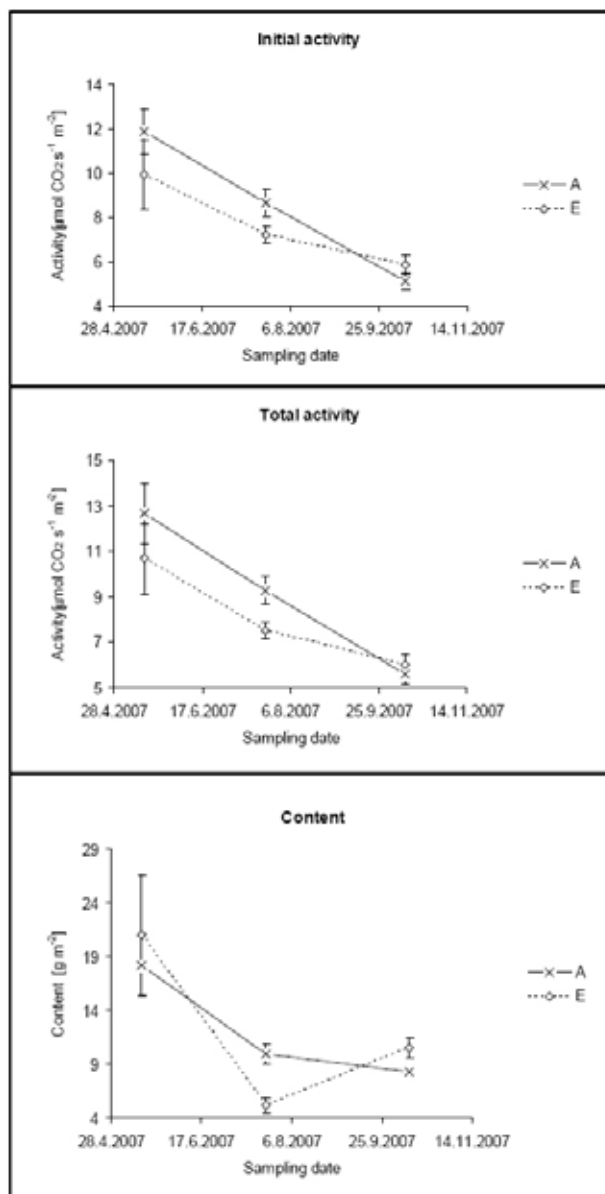
Fig. 2. **Rubisco activity and content in Norway spruce, A – ambient [CO$_2$], E – elevated [CO$_2$], n = 10**

Conclusions

We confirmed a decrease both Rubisco initial and total activities as well as Rubisco content in Norway spruce during the growing season. According to our measurements, there is not down-regulation of Rubisco activity and its content in last year needles in Norway spruce during the growing season.

REFERENCES
1. Farquhar G. D., von Caemmerer S., Berry J. A.: Planta *149*, 78 (1980).
2. Portis A. R. Jr.: Biochim. Biophys. Acta *1015*, 15 (1990).
3. von Caemmerer S., Quick P.W.: Rubisco:Physiology in vivo. – In: Leegood R.C., Sharkey T.D., von Caemmerer S.: Photosynthesis: Physiology and Metabolism. Kluwer Acad. Publ., Dordrecht (2000).
4. Drake B. G., Gonzales-Meler M.A., Long S.P.: Annu. Rev. Plant Physiol. Plant. Mol. Biol. *48*, 609 (1997).
5. Moore B. D., Cheng S. H., et al.: Plant Cell Environ. *22*, 567 (1999).
6. Makino A., Harada M., et al.: Plant Physiol. *115*, 199 (1997).
7. Curtis P. S. Vogel C. S., at al.: Ecol. Appl. *10*, 3 (2000).
8. Suzuki Y., Makino A., Mae T.: Plant Cell Environ. *24*, 1353 (2001).
9. Nie G. Y, Long S. P., et al.: Plant Cell Environ. *18*, 855 (1995).
10. Makino A.: Soil Sci. Plant Nutr. *49*, 319 (2003).
11. Urban O.: Photosynthetica, *41*, 9 (2003).
12. Kalina J., Slovák V.: Ekológia *23*, 163 (2004).
13. Lilley R. M., Walker D. A.: Biochim. Biophys. Acta *358*, 226 (1974).
14. Griffin K. L., Tissue D. T., et al.: Plant Cell Environ. *23*, 1089 (2000).
15. Myers D. A., Thomas R. B., DeLucia E. H., et al.: Plant Cell Environ. *22*, 473 (1999).
16. Rogers A., Ellsworth D. S.: Plant Cell Environ. *25*, 851 (2002).

P41 LIPID DEGRADATION AND ITS APPLICATION TO LIPID-CONTAINING WASTEWATER

KATEŘINA ILLKOVÁ, JIŘINA OMELKOVÁ and BOHUMILA VLČKOVÁ

Institute of Food Chemistry and Biotechnology, Faculty of Chemistry, Brno University of Technology, Purkynova 118, 612 00 Brno, Czech Republic,
xcillkova@fch.vutbr.cz

Introduction

Food industry and restaurants produce each year about 15 % of the total wastewater and 50 % of the organic pollution. Character and composition of wastewater depends on manufacturing technology and current raw material. Wastewater from food industry and restaurants contain lipids. These lipids are present in the wastewater. They are difficult to remove and degrade, because they are difficult to dissolve in the water[1].

For facilitation of production unit and treatment wastewater fats and oils, enzymatic preparations (EP), which are used, they are accelerated decomposition of organic material lipids matter. These EP mix of lipases, proteases, amylases and cellulases, some of them contain suitable combination of bacteria, and they contain detergents and surfactants, as well.

In this study was evaluated 5 EP for their ability to degraded lipids in the wastewater. It was made isolation of lipid-degrading bacteria and the proof of lipolytic bacteria. They investigated their lipolytic activities at agar plates by aerobic and anaerobic conditions. Further ability of lipid degradation and fatty acids utilization at submerged cultivation and chemical oxygen demand was followed.

Experimental

Enzymatic preparations are mixtures of enzymes and bacteriological cultures. These preparations were inoculated agar plates with tributyrin agar (tributyrin agar base). Plates were incubed for 7 days at 27 °C for aerobic and anaerobic conditions. The growth colonies were used for determination of the lipolytic activity.

Samples for determination of lipid degradation and utilization fatty acids were taken from submerged cultivation The medium for submerged cultivation contained per liter distilled water 1.12 g K_2HPO_4; 0.48 g KH_2PO_4; 5 g NaCl; 0.1 g $MgSO_4 \cdot 7H_2O$; 2 g $(NH_4)_2SO_4$ and 100 µl EDTA. Medium was autoclaved at 121 °C for 20 min and then the medium was supplemented with 1 ml olive oil, as the natural substrate. In the end, the medium was inoculated by enzymatic preparations. Medium were incubated under aerobic conditions at 27 °C and agitated at 160 rev min⁻¹ for 14 days in Erlenmeyer flasks in a shaker. The % free fatty acids were determined as an indication of the olive oil degradation by the tested enzymatic preparations[1].

Spirit Blue Agar (Detection of Lipolytic Activity)

Microoragnisms was grown on spirit blue agar plates, to which tributyrin and tween 80 were added as a lipase substrate in ratio 1 : 1. Plates were incubated at 27 °C. Lipolytic activity was identified the plates as a transparent halo around the colonies after 7 days of incubation[2].

Enzyme assay

The activity was determined by using culture in 0, 65 ml 0, 05 M phosphate buffer (pH 7.2) a 0.1 ml 0.025M pNP-laurate in ethanol. The hydrolytic reaction was carried out at 37 °C for 30 min, after which 0.25 ml 0.1M Na_2CO_3 was added. The mixture was centrifuged and the activity determined at 420 nm. One unit of lipase activity is defined as the amount of enzyme which liberates 1 µg p-nitrophenol from p-NP-laurate, as a substrate in 30 min under assay condition[3,4].

Determination Lipid Degradation and fatty Acids Utilization

From each Erlenmeyer flasks 20 ml culture medium was aseptically drawn and transferred to a separating funnel, where it was mixed with 20 ml of hexane. The mixture was agitated for 2 min and the upper layer was put to the clean and weight beaker. The lower layer was re-extracted by a fresh 20 ml of hexane and the upper layer after the extraction was collected to the beaker again. The extract in the beaker was evaporated by heating at 100 °C. Then the dry extracted lipids were weight and dissolved in 50 ml of alcohol in the presence of phenolphthalene indicator. The solution was titrated with 0.1M KOH until the developing of pink color. The same procedure was repeated within 2, 6, 8, 10 and 14 days. The free fatty acids % in the sample was indicated lipid degradation and fatty acids utilization, which was calculated according to this equation:

$$\%\text{free fatty acids} = \frac{V_{KOH} \cdot c_{KOH} \cdot M \cdot 100}{1000 \cdot m}, \qquad (1)$$

where V_{KOH} is the volume of 0.1M KOH at the end point, c_{KOH} actual concentration of the 0.1M KOH, M is the molecular weight of the oleic acid and m is the weight of the dry extract[1].

Chemical Oxygen Demand (COD)

Chemical oxygen demand (COD) is a measure of the capacity of the water to consume oxygen during the decomposition of organic matter and the oxidation of inorganic chemicals such as ammonia and nitrite. COD measurements are commonly made with samples of wastewater or natural water, contaminated by domestic or industrial waste.

COD was determined by the standard potassium dichromate method, descrieved in the Methods for the Examination of Waters and Associated Materials (2007).

At 80 ml of water, 2 ml of the oil and 50 µl enzymatic preparations was added in to the separatory funnel. One of the separatory funnel was used as a control. The volume of the separatory funnel was mixed and within 20 min the sample of the water phase was taken to determine chemical oxygen demand (COD).

Results

Spirit Blue Agar (Detection of Lipolytic Activity)

The lipolytic microorganisms metabolized the lipid in the medium and form colonies with halos indicating lipolysis. It was found out, that in all tested microorganism preparations were presented and formed colonies with halos indicated lipolysis.
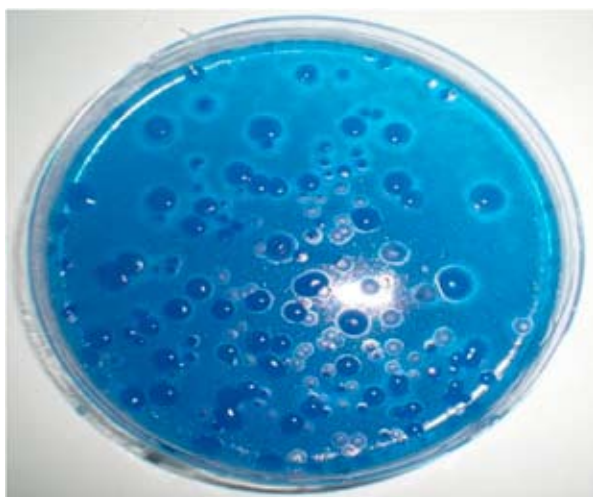
Fig. 1. **Bacterial colonies with halos indicating lipolysis**

Lipolytic Activity

Cultivation on agar plates. The highest value of the lipolytic activity was determined at EP 1, the lowest lipolytic activity was determined at EP 3.

The highest calculated value was found in supernatant of EP 1 by anaerobic conditions, value of the activity was $a = 9. 16 \times 10^{-3}$ mmol min^{-1}, the lowest value was in sediment of EP 3 by aerobic conditions, $(a = 1 \times 10^{-4}$ mmol min$^{-1})$. Lipolytic activity was detected at all five enzymatic preparations.

Table I

Lipolytic activity in 5 of enzymatic preparations (expression $a \times 10^{-3}$ mmol min^{-1})

EP	aerobe		anaerobe	
	supernatant	sediment	supernatant	sediment
1	7.11	1.96	8.79	2.95
2	6.59	1.40	8.51	2.86
3	5.04	0.10	7.25	1.77
4	5.44	1.19	7.42	2.48
5	8.52	2.32	9.16	3.28
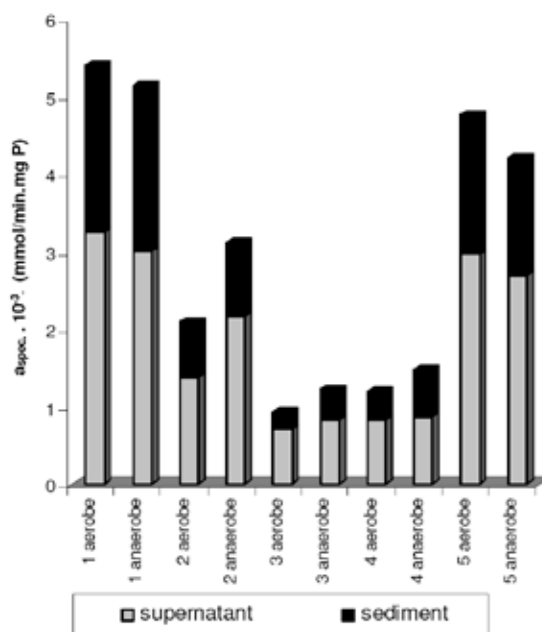
Fig. 2. **Comparsion values of the lipolytic activity for the individual enzymatic preparations**

Submers cultivation. The highest activity was measured on the 10th day of the cultivation. The decrease of activity was registered on the 10th day. The highest activity had the enzymatic preparation 5 and the lowest had the enzymatic preparation 3.

Table II

Relativic activity a_{rel} [%] in enzymatic preparations during submers cultivation

EP [days]	1	2	3	4	5
2	62.97	53.09	46.06	50.32	73.56
6	83.26	74.35	66.98	68.69	85.46
8	84.73	78.74	75.54	77.82	94.15
10	100.00	100.00	100.00	100.00	100.00
14	75.52	68.73	62.23	63.50	90.00

3.3 Lipid Degradation and Fatty Acids Utilization

Results of the determination demonstrate at Table III and at Fig. 3.

Table III

% free fatty acids of EP during submers cultivation

EP1	EP2	EP3	EP4	EP5	days
9.69	10.07	14.87	3.68	3.72	2
13.04	37.74	19.02	4.75	25.43	6
48.91	48.42	33.28	7.13	39.02	8
66.57	56.5	40.75	37.66	48.04	10
20.1	22.83	26.49	20.38	26.15	14
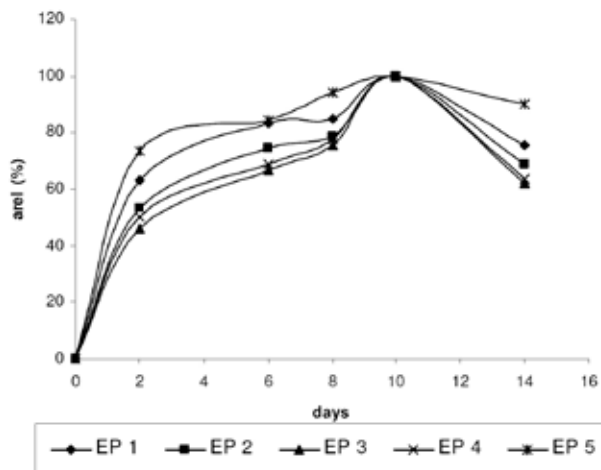
Fig. 3.　**Comparsion individual EP during 14 day's submerged of cultivation**

D e t e r m i n a t i o n   o f   C O D

Results of determination of COD show Table IV, the best values were reached at the EP 1 and EP 5.

Table IV
Chemical oxygen demand

EP	1	2	3	4	5	control sample
c [mg O_2 dm^{-3}]	61	89	143	94	64	31

Conclusions

There were tested 5 commercial preparations with aim to find out, if they have lipolytic activity and if they have ability to degrade fats. Samples were cultivated at the agar plates and submerged cultivation in Erlenmeyer flasks. The comparison results of lipolytic activities of both cultivations were followed. The submerged cultivation, after 2 days of EP demonstrated approximately the same value of activities as cultivation on agar plates after 7 days.

All tested EP had ability to degraded olive oil and released fatty acids. The best degrading ability had EP 1, the lowest ability EP 4.

It was made a laboratory verification of function 5 EP for liquefaction and decomposition of fats and oils in the wastewater. On the basis obtained by dates, it might be choosen the best EP for suggestion technology. Biotechnology effects were made out for EP 1 and 5, the lowest efficiency was made out by EP 4.

REFERENCES
1. El-Bestawy E., El-Masry M. H., El-Adl N. E.: World J. Microbiol. Biotechnol. *21*, 815 (2005).
2. Costas M., Deive F. J., Longo M. A.: Process Biochem. *39*, 2109 (2004).
3. Nawani N., Dosanjh N. S., Kaur J.: Biotechnol. Lett *20*, 997 (1998).
4. Sigurgísladóttir S., Konráösdóttir M., Jónsson A., Kristjánsson J. K., Matthiasson E.: Biotechnol. Lett *15*, 361.(1993).

P42 GAS CHROMATOGRAPHY-MASS SPECTROMETRY CHARACTERIZATION OF SEA BUCKTHORN

ANDREEA IORDACHE, RADU MINEA, MONICA CULEA and CAMELIA LEHENE

Babes-Bolyai University, Str. Kogalniceanu, nr.1, 3400 Cluj-Napoca, Romania,
mculea@phys.ubbcluj.ro

Introduction

Besides naturally growing plants, sea buckthorn (*Hippophae rhamnoides)* hybrids of different subspecies are cultivated in order to prevent desertification, since it forms strong root and it is resistant to extreme temperature, drought and poor soil. There is a long tradition in Asia for using sea buckthorn berries in folk medicine. It was demonstrated that the oils extracted from pulp and seeds have regenerating, anti-inflammatory, anti-ulcerogenic, hepatoprotective, cytoprotective properties.[1–4] Sea buckthorn berries are exceptionally rich in both lipophilic and hydrophilic bioactive compounds and represent an important resource for pharmacy and food industry. The pulp oil has a special composition with a very high content of unusual palmitoleic acid, up to 54 % of total fatty acids, while the seeds oil is rich in linoleic and α-linolenic acids. Other important compounds of sea buckthorn oil are sterols, tocopherols and tocotrienols and their content depend on the berries origin, growth condition and oil processing method.

The aim of this study was to develop a sensitive analytical method for determination of fatty acids, vitamin F and E and sterols in sea buckthorn oil, by gas chromatography/mass spectrometry (GC/MS). The method was applied for testing the lipophilic compounds after the treatment at different kGy doses with accelerated electrons.

Experimental

Materials and Methods

Standards of fatty acids methyl esters and acetyl chloride were from Fluka (Buchs, Switzerland), α-tocopherol standard was from Sigma-Aldrich (Munich, Germany). All other chemicals were from Comchim (Bucharest). The oil and plant samples were from Hofigal (Bucuresti).

GC-MS and HPLC

A Trace DSQ ThermoFinnigan quadrupol mass spectrometer coupled with a Trace GC was used. The methyl esthers of the fatty acids were separated on a Rtx-5MS capillary column, 30 m × 0.25 mm, 0.25 μm film thickness, using a temperature program from 50 °C (1 min) to 310 °C, at 8 °C min^{-1}; then kept 8 minutes at 310 °C. The conditions used for GC-MS were: transfer line temperature 250 °C, injector temperature 200 °C; ion source temperature 250 °C; Splitter: 10 : 1. Electron energy was 70 eV and emission current, 100 μA.

Extraction and Derivatization

Fatty acid methyl esters (FAME) were obtained by esterification reaction of known quantities of oil with 100 μl 3M HCl methanol at 100 °C for 60 min followed by evaporation to dryness under N$_2$ stream 0.1 mg of the internal standard C11 : 1 was added at 20 μl oil. Then the sample was solved in 100 μl DCM or ethyl acetate, and 3 μl were injected into GC-MS. Vitamin E and sterols were also determined in the different samples.
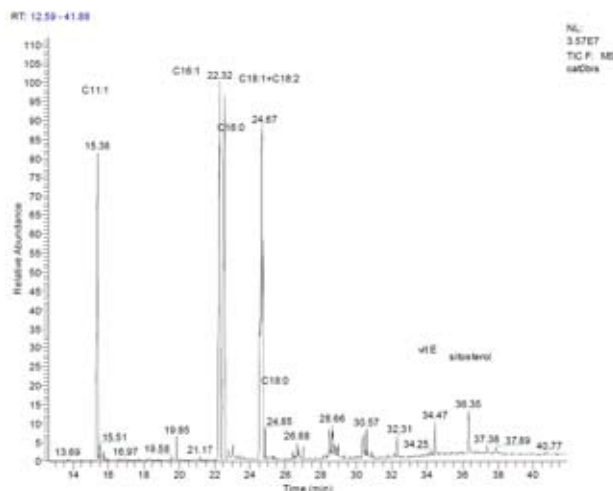
Fig. 1. **FAME, vitamin E and sterols separation in sea buckthorn oil**

HPLC Analysis of α-tocopherol

The sea buckthorn oil samples were injected into HPLC for vitamin E determination. The sea buckthorn oil was saponified with 60% KOH in ethanol, in the presence of ethanol and pyrogallol, at 75 °C for 45 min. The sample mixture

Table I
The compounds identified in sea buckthorn oil

Compounds	RT [min]	area [%]
Methyl myristate (C14 : 0)	19.85	0.79
methyl palmitoleate(C16 : 1)	22.36	30.68
methyl palmitate(C16 : 0)	22.63	24.53
methyl oleate +linoleat (C18 : 1+C18 : 2)	24.73	37.18
methyl stearate (C18 : 0)	24.89	0.63
C20 : 1	26.83	0.55
methyl arachinate (C20 : 0)	27.01	0.3
C22 : 1	28.93	0.86
behenic acid methyl ester (C22 : 0)	29.03	0.22
C24 : 1	30.57	0.41
methyl lignocerate (C24 : 0)	30.89	0.14
C26 : 0	32.31	0.26
vitamin E	34.47	0.6
sitosterol	36.36	2.13
lupeol	37.41	0.42
urs-12-en-28-ol	40.8	0.31

was extracted with hexane: ethyl acetate (9 : 1). The organic layer was washed with 5% sodium chloride solution and then evaporated to dry and dissolved in methanol. HPLC system contained LC20 AT Shimadzu pumps and a Waters 990 PDA detector. A Supelco Discovery C18 (25 cm × 4.6 mm, 5 μm particle diameters) HPLC column was used. The mobile phase consisted in methanol: water (98 : 2) and the chromatogram was monitored at 292 nm. Tocopherol identification was based on the retention time of α-tocopherol standard (Sigma) and UV-VIS spectra. Quantitative analysis was done using a calibration curve with α-tocopherol (0.01–0.2 mg ml^{-1}), r = 0.989.

Results

The results obtained for the sea buckthorn oil by GC-MS are presented in Table I. The results obtained for sea buckthorn vitamin E at different doses are shown in Table II.

Table II

Vitamin E determination in sea buckthorn oil by HPLC at different doses [kGy]

Dose [kGy]	α-tocopherol [mg 100 ml oil^{-1}]
0	57.75
0.03	50.52
0.07	29.1
0.38	26.8
0.72	25.9
1.05	25.8
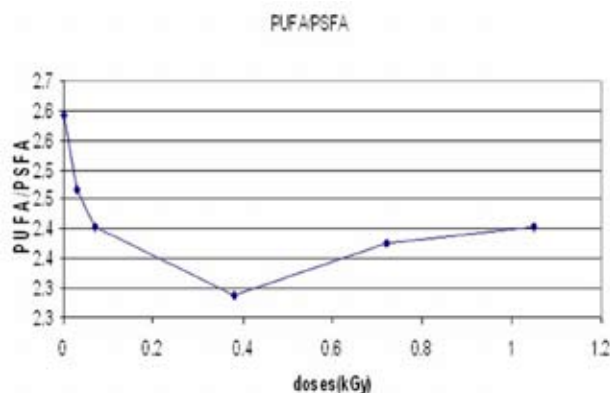
Fig. 2.   **The ratio between unsaturated and saturated fatty acids evolution with doses [kGy] in sea buckthorn oil**

Vitamin E decreased two times at 1.05 kGy treatment (Table II). In sea buckthorn oil, at the highest dose applied, the ratio between unsaturated and saturated fatty acids has decreased at half value of control (Fig. 2.). Also the sterols and vitamin E values have decreased with irradiation more than two times, as presented in Fig. 4. Similar results have been obtained in juice of the fruits. In sea buckthorn leaves the changes are not significant (Fig. 3. and Fig. 5.).
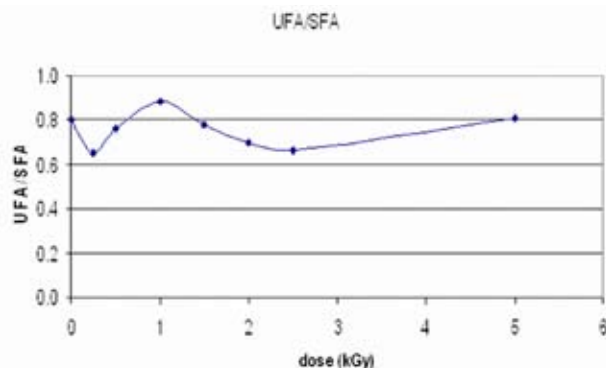
Fig. 3.   **The ratio between unsaturated and saturated fatty acids evolution with doses [kGy] in sea buckthorn leaves**
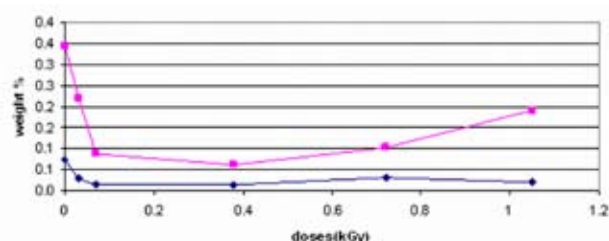
Fig. 4.   **Vitamin E and sitosterol [% weight] versus applied doses (GC-MS determination)**
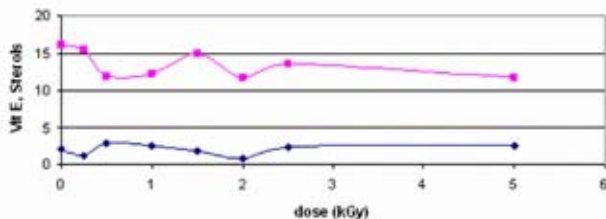
Fig. 5.   **E vitamin and sterols [area %] with doses [kGy] in sea buckthorn leaves**

Conclusions

The GC-MS and HPLC methods developed showed significant changes of antioxidants as vitamins E, F and sterols with doses after the treatment of sea buckthorn oil, juice but not in leaves at different kGy doses with accelerated electrons. The treatment for decontamination needs to be optimized to avoid loses of its important nutrients.

REFERENCES

1. Roussi A.: Annales Botanici Fennici *8*, 177 (1971).
2. Geetha S., Sai Ram M., Singh V., Ilavazhagan, G., Sawhney, R.C.: J. Ethnopharmacol. *79*, 373 (2002).
3. Eccleston C., Yang B., Tahvonen R., Kalli, H., Rimbach G. H., Minihan A. M.: J. Nutr. Biochem. *13*, 346 (2002).
4. Yang B., Kallio H.: Trends Food Sci. Technol. *13*, 160 (2002).

P43   RAPID AUTHENTIFICATION OF NATURAL JUICES BY GC-MS

ANDREEA IORDACHE, MONICA CULEA and ONUC COZAR

Babes-Bolyai University, Str. Kogalniceanu, nr.1, 3400 Cluj-Napoca, Romania
mculea@phys.ubbcluj.ro

Introduction

A simple and rapid GC-MS method for the detection of adulteration of natural fruit juices is presented. The method consists of the analysis of sterol patterns and it is a useful rapid approach for the fruit juices control by GC-MS[1].

A GC-MS analytical method is described for some natural juices analysis. The fingerprint of sterols was used to characterize the natural juice.

Experimental

A rapid liquid-liquid extraction method was used. The fruit juices were extracted by using petrol ether as a solvent. The fruit juice extracts were separated on a capillary column, and identified with a mass spectrometer.

A p p a r a t u s

The sterols were separated on a Rtx-5MS capillary column, 15 m × 0.25 mm, 0.25 μm film thickness, in a temperature program from 50 °C for 1 min, then ramped at 15 °C min^{-1} to 300 °C and held for 15 min. Identification of sterols and their patterns were used for juice characterization.

A Trace DSQ ThermoFinnigan quadrupol mass spectrometer in the EI mode coupled with a Trace GC was used. The following conditions were used: ion source temperature 250 °C, injector temperature 200 °C, transfer line temperature 250 °C, splitter 10 : 1, electron energy 70 eV and emission current 100 μA.

E x t r a c t i o n   P r o c e d u r e

Ethanol, fruit juice and petrol ether 2 : 2.5 : 0.4, v/v/v, were mixed in a cap vial for 2 minutes. Then the mixture was centrifugated 2 minutes. 1μl was injected twice into the GC. Ethanol was used for pectine and emultion agents precipitation.

Results

Different compounds such as volatile aroma compounds, fatty acids and sterols have been identified into the cromatograms of the extracts of orange (Fig. 1.), grapefruit and pineapple juices. A NIST library was used for compounds identification from the mass spectra obtained after gas chromatographic separation. The sterols identified from the fruits juices were the following: cholesterol, campesterol, ergostanol, stigmasterol, beta-sitosterol, the main sterol, isofusterol and citrostadienol. Limonen was the main volatile compound extracted from citrus fruits.
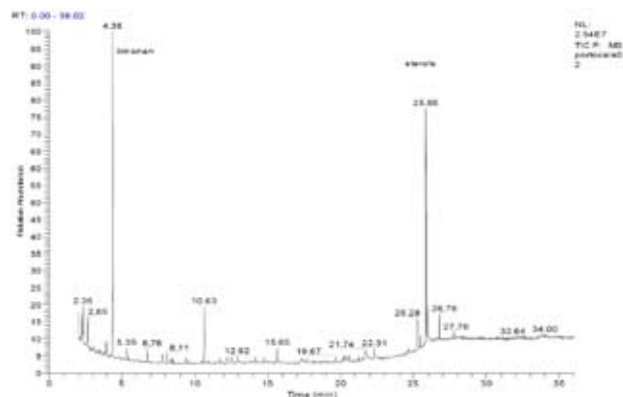
Fig. 1.   **Compounds separation from orange extract**

Fig. 2. presents the separation of sterols from the fruit juice extract (orange). The fingerprint chromatograms of different fruits differ in the concentration of this sterols, but there are also few variation of the sterols identified in orange, grapefruit and pineapple juices In pineapple was identified stigmastenone at the retention time of citrostadienol (alpha 1 sitosterol).
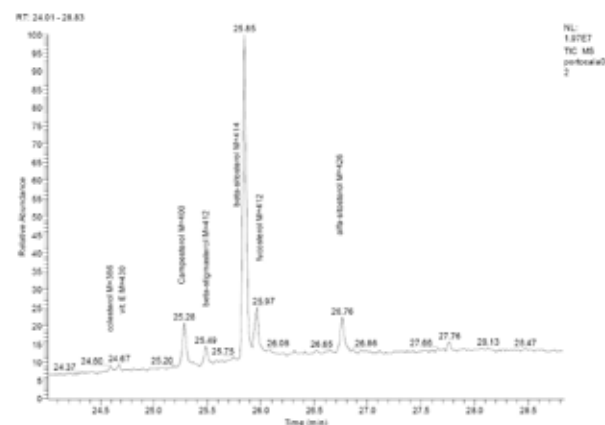
Fig. 2.   **Separation of sterols from orange extract**

Table I
Sterols identified in orange juice extract

Tr [min]	Compound	M	m/z
11.3	Valencene	204	161
14.6	Nooklactone	218	147
25.3	Campesterol	400	400
25.4	Ergostanol	402	233
25.5	beta-stigmasterol	412	412
25.9	beta-sitosterol	414	414
25.97	isofucosterol	412	314
26.8	citrostadienol	426	285

Table I presents the compounds identified into the chromatogram of the orange juice extract.

Table II presents the important ions of the compounds identified in juices. The ratio of different peaks area from
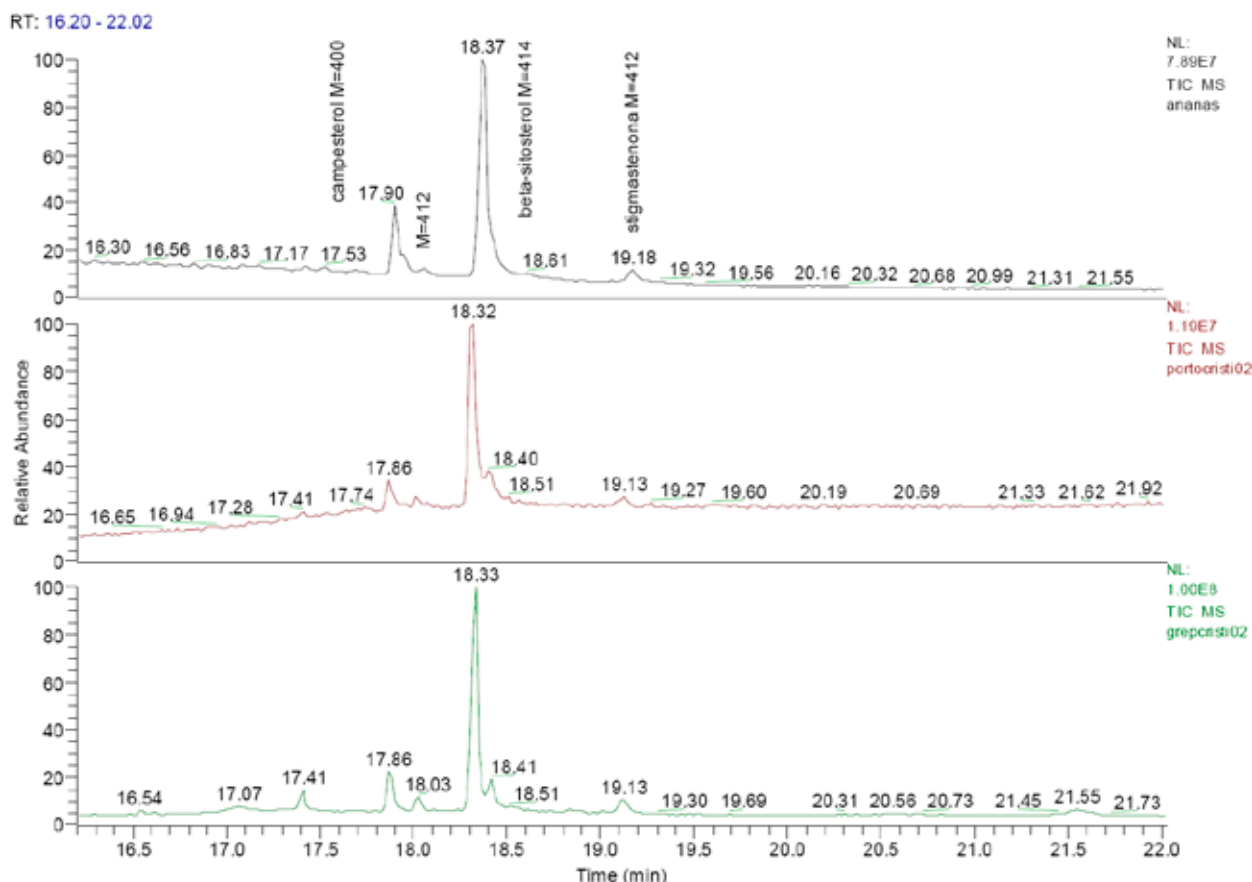
Fig. 3. **Comparison of sterol profiles from pineapple, orange and grapefruit extracts in a faster temperature program**

Table II
Relative intensity of the important ions of the sterols identified in orange juice extract

Compound	Base peak, m/z	Important ions m/z, rel. intensity [%]
Valencene	161	91, 93 (65); 105, 107 (60), 133, 204 (50); 147, 189 (37)
Nooklactone	147	79, 121 (84); 91, 133 (65), 105, 175, 203(56)
Campesterol	400	315, 382, 367, 289 (50), 145, 213, 255 (30)
Ergostanol	233	424(99), 203, 205 (20), 397 (30)
beta-stigmasterol	412	255, 271, 300 (50), 351 (33)
beta-sitosterol	414	329, 396 (50), 303, 381 (40)
isofucosterol	314	281 (34), 229 (26), 315(25)
citrostadienol	285	328, 286, 267 (35)

the mass spectrum can be used for a better evaluation of the differences among juices, the base peak but also some other important ions could be used for authenticity evaluation of the natural juice, as adulteration of grapefruit more expensive juice with orange juice.

The sterol profile is a useful approach for confirming the presence of juices of orange, grapefruit, pineapple and passion fruit in compounded beverages and for detecting of adulteration of fruit juices.

Conclusions

The developed method is very useful for fruit juices authentification. The method can be used in the control of adulteration of juices in the food industry. Sensitivity of the method could be 100 times improved in the SIM mode.

REFERENCES

1. Ng L.-K., Hupe M.: J. Sci. Food Agric. *76*, 617 (1998).
2. Ronards K., Antolovich M.: Analyst *120*, 1 (1995).

P44 COMPARATIVE EXTRACTION METHODS OF SOME BIOLOGIC ACTIVE COMPOUNDS IN HERBS

ANDREEA IORDACHE, MONICA CULEA and ONUC COZAR

Babes-Bolyai University, Str. Kogalniceanu, nr.1, 3400 Cluj-Napoca, Romania,
mculea@phys.ubbcluj.ro

Introduction

Many studies are made for the optimization of the experimental design approach for obtaining the best recoveries, low solvent consumption and reduced extraction times. In the last years the number of procedures using extraction of organic compounds from different matrices has increased[1,2].

The aim of the present work is to present a comparison between some extraction methods, for qualitative characterization of flavors extracted from herb plants of different sources.

Experimental

A liquid-liquid extraction method (LLE), compared with two different solid-phase extraction methods (SPE- on 300 mg RP-18, C-18 silica bonded and 300 mg TCS), a microwave one (MWE) and an ultrasonic extraction one (USE) were compared using an aroma compounds standard mixture. The analytical method chosen were gas chromatography and gas chromatography – mass spectrometry (GC-MS).

Materials and Methods

A Hewlett Packard GC 5890 couplet with a MS engine 5989B in the EI mode was used for compounds identification. The GC was equipped with a HP-5MS capillary column 30 m × 0.25 mm diameter, 0,25 μm film thickness, in the temperature program: 50 °C for 2 min, then increased to 250 °C with a rate of 8 °C min⁻¹, helium flow rate 1 ml min⁻¹. Deactivation by treating the injector glass liner with 5% dimethyldichlorosilane in toluene was very important for a better sensitivity. The GC/MS interface line and the ion source were maintained to 200 °C, and quadrupol analyser at 100 °C. Electron energy was 70 eV and electron emission 300 μA.

Methanol, methylen chloride, hexane, ethyl acetate, acetone were purchased from Comchim (Bucharest, Romania). The standards were from Fluka, Sueden: 1. 3-Hepten-2-one, used as external standard (ES), 2. 1,8-cineol (eucalyptol) 3. linalool 4. geraniol 5. alpha-terpinyl-acetate 6. geranyl acetate 7. amyl salicylate 8. myristic acid (C14:0) 9. palmitic acid (C16:0) 10. Stearic acid (C18:0) . FAME were from Polyscience Corporation, Evantson, Illinois, USA. The standards, 100 μl each, formed the *mixture M*, except of the external standard, 3-hepten-2-one, added separately before extraction. Cartridges of 300 mg RP-18 and TSC were obtained from Merck. A stock solution was obtained by diluting 100 μl of each compound. Working standard was prepared by diluting the stock solution to obtain a concentration of 3.3 % vol.

LLE Extraction

A mixture of three solvents (S) was prepared: ethyl acetate: hexane: methylen chloride (5:1:1, v/v/v). The LLE extraction procedure was: 30 μl *mixture M* in 1 ml solution distilled water: ethanol (1:1, v/v), or 1 ml hydroalcoholic flavour extract), 1 ml distilled water and 0.33 ml *solvent S*, (3:3:1, v/v/v) were mixed 1.5 minutes and then centrifugated 2 minutes. 1 μl 3-hepten-2-one, was added to the supernatant and then 1 μl was injected two times by using the autosampler injector.

SPE Extraction

The solid phase was conditioned with 3 ml methanol and 3 ml distilled water. After sample application, washing and drying 10 minutes at vacuum, the sample was eluted with 3 × 0.3 ml solvent. The solvent was *solvent S* in the case of RP-18 cartridges and chloroform-acetone (1:1, v/v), in the case of TSC cartridges. After adding of 1 μl of the external standard to the eluate, 1 μl was injected by using the autosampler injector. Each sample was injected twice.

MWE Extraction

The microwave extraction procedure was performed at 2,45 GHz for 4 sec, to a temperature of 60 °C, in a screw cap vessel. 30 μl *mixture S* was added to 1 ml hydroalcoholic solution, 1 ml distilled water and 0.33 ml *solvent S* were placed in the microwave funnel and extracted. Then 1 μl 3-hepten-2-one (ES), was added to the supernatant and analyzed twice.

USE Extraction

The ultrasonic extraction procedure was performed 1min, at a temperature of 60 °C. The ultrasonic probe was placed in the vessel containing 30 μl *mixture S* in 1 ml hydroalcoholic solution, 1 ml distilled water and 0.33 ml *solvent S*. After extraction, 1 μl 3-hepten-2-one (ES) was added to the supernatant and analyzed.

Table I
Recovery [%] obtained by different procedures

Component	LLE	SPE	SPE	MW	US
heptenone					
1,8-cineole (eucalyptol)	98.97	81.47	68.54	100.84	99.75
linalool	96.67	86.96	72.07	100.98	100.50
geraniol	94.31	87.54	77.91	111.48	112.12
alfa-terpenyl acetate	97.57	86.13	73.52	102.26	100.37
geranyl acetate	96.28	83.14	72.75	102.57	99.86
amyl slicilate	97.23	85.72	73.99	120.91	118.03
C14:0	100.82	86.24	75.07	98.02	95.04
C16:0	97.14	86.73	75.87	96.91	92.95
C18:0	96.93	85.54	74.68	95.74	92.07

Results

The average values resulted from two or three extraction procedures and two injections of each extract. The relative standard deviation values were bellow 3 % for each extraction procedure. The mean values for the recoveries found for each aroma compound studied are presented for different extraction modes in Table I. The best values for recovery were found for MWE (103 %) and USE (101 %), followed by SPE (85.5 %) on RP-18 and LLE (97.3 %).

Table II
LLE precision characterization for vermut extracts

Compound	mean	SD	RSD [%]
eucalyptol	8.86	0.14	1.58
fenchone	2.34	0.05	2.35
linalool	30.65	0.31	1.02
terpinen	2.96	0.06	2.16
geraniol	2.12	0.05	2.35
cinnamaldehyde	0.56	0.05	8.89
trans-anethole	4.2	0.09	2.22
thymol	1.55	0.06	4
alpha-terpenyl acetate	1.74	0.07	4.06
isobornyl isovalerate	2.07	0.14	6.76
eugenol	2.9	0.11	3.73
miristicin	1.14	0.05	4.8
elemicin	1.08	0.03	3.16
herniarine	0.93	0.05	5.24
bisabolol oxid A	1.04	0.03	3.17
myristic acid	1.24	0.07	5.7
ethyl miristate	1.39	0.14	9.78
lactone	0.78	0.05	6.37

Separation chromatogram is presented in Fig. 1. The LLE method (3 : 3 : 1, v/v/v) was used for studies on vermut, bitter and herbs aroma compounds. The relative standard deviation values found for four different extraction procedures injected twice were bellow 5 % in the case of vermut and also for bitter aroma compounds (n = 4).

Tables II and III present the precision obtained for different aroma compounds extracted by LLE from vermut and respectively from bitter (n = 4). The identification of the compounds was obtained by GC/MS.
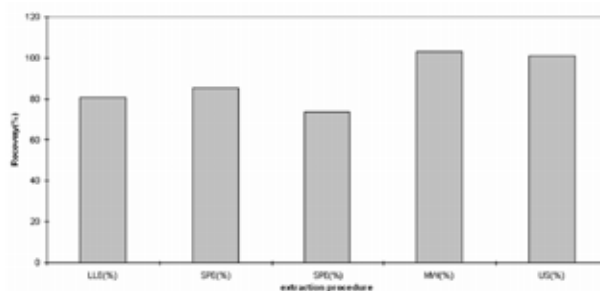
Fig. 2. **Recovery comparison for different extraction methods for the standard mixture**

Table III
LLE precision characterization for bitter extracts

Compound	mean	SD	RSD [%]
eucalyptol	0.34	0.001	0.29
fenchone	2.51	0.03	1.05
trans-sabinene hydrate	1.23	0.04	2.93
p-anis aldehyde	1.35	0.15	10.76
cinammaldehyde	1.61	0.05	2.79
trans anethol	8.87	0.42	4.68
eugenol	71.79	0.71	0.98
coumarin	0.86	0.05	6.15
miristicin	1.11	0.01	1.04

Conclusions

This work presents a comparison of different extraction methods for the characterization of some aroma compounds. The methods are suitable for the determination of trace amounts of aroma compounds in plant extract.

Fig. 1. **Separation chromatogram for the standard mixture**

Good recovery mean values were obtained by LLE (97 %) using an appropriate mixture of solvents comparable with the recoveries of the other extraction methods as SPE (86 %), MWE (103 %) and USE (101 %). The characterization of bitter and vermut aroma by LLE method showed R.S.D. lower than 5 %. The comparison of flavours of herbs from different sources showed qualitative and quantitative differences.

REFERENCES
1. Gherman C., Culea M., Cozar O.: Talanta *53*, 253 (2000).
2. Hu, S. G., Li L., He X. W.: J Chromatogr A. *1062*, 31 (2005).

P45 BIOREMEDIATION OF BOTTON SEDIMENTS USING *BACILLUS MEGATERIUM* AND *BACILLUS CEREUS*

KATARÍNA JABLONOVSKÁ and IVETA ŠTYRIAKOVÁ

Department of Biotechnology, Institute of Geotechnice of Slovac Academy of Sciences, Watsonova 45, 043 53 Kosice, Slovak Republic
jablonov@saske.sk

Introduction

The water reservoir Ružín I. lies in an area, which for several centuries has been known for mining and metallurgical activities. The bottom sediments are contaminated with heavy metals, in the concrete with Hg, Cu, Mn, Zn, Ni and Cd, which were washed away into the water reservoir from locations of former mining activities (Cicmanova et al., 2003). Enhanced amounts of heavy metals preclude of direct utilization of sediments in agricultural and building industry and also in ground shaping (Brehuv, J., 2000).

The availing of bioleaching techniques on mobilization of heavy metals from sediments seems to be an appropriate manner of retreatment. In this attempt, besides indigenous microflora bacterial species *Bacillus megaterium* and *Bacillus cereus* was used. These bacterial species were izolate from the soil matrix of sampling place Hornád-inlet. Because heavy metals are increasingly found in microbial habitats due to natural and industrial processes, microbes have envolved several mechanisms to tolerate the presence of heavy metals (by either efflux, complexation, or reduction of metal ions) or to use them as terminal electron acceptors in anaerobic respiration (Senenska-Pobel S. et al, 1998). The objectives of this work were to determine the differences of influence *Bacillus cereus* and *Bacillus megaterium* on leachibility Ni and Cd ions from polluted sediments.

Experimental

Sediment samples were obtained from the botton of water reservoir Ružín I in Slovakia at differend depths (20 and 40 cm). Heavy metals composition is given in Table I.

Biological leaching of the sample material was carried out in conical flasks with 30 g sediment and 600 ml Ashby´s medium. The Ashby´s medium contained (per liter) 0.2 g urea, 1 g K_2HPO_4, 0.075 g NaCl. Glucosse (2 g dm^{-3}) was added as the organic substrate. The flasks were inoculated with *Bacillus megaterium* and *Bacillus cereus* cultures, originally isolated from the sediment of water reservoir Ružín I. in Slovakia. The two strains were purified and followed by streak plating on nutrient agar cultures. The isolates were identified with the BBL Crystal Identification System (Becton Dickinson, USA).

The flasks were incubated under static conditions for 6 months at 25 °C in the dark. Appropriate abiotic controls were included in these experiments. Changes in the chemical composition of solid and liquid phases were measured by atomic absorption spectrometry (Varian AA240-Z with GTA-

120 a AA240-FS). The particle size distribution was measured by the laser radiation scattering using a model 22 Laser-Particle – Sizer Analysette (Fritsch GmbH, Idar-Oberstein, Germany).

Results

The Ni and Cd concentrations of sediments taken from 20 and 40 cm depth layers are shown in Table I. The amount of investigated heavy metals overrun the limit values given by Metodical Instruction ministry of Environment – Slovak Republic No. 491/2002. The established values give information about the potential risk of Ni and Cd releasing and about surrounding and outlying contamination ecosystems.

Table I
The results of surface layer analysis of sediments from 20 cm depth and their comparison with Metodical Instruction Ministry of Environment – Slovak Republic No. 491/2002

Element Depth		Ni	Cd
		[mg kg^{-1}]	
20 cm		87	1.2
40 cm		86	0.9
MIME-SR	MPC	44	12.0
No. 491/2002	TV	35	0.8

Table II
Effectivity of bioleaching process with application of *Bacillus megaterium* and *Bacillus cereus*

Element	Before BL [mg kg^{-1}]	After BL *Bacillus megaterium* [mg kg^{-1}]	After BL *Bacillus cereus* [mg kg^{-1}]
Ni	86.0	79.0	70.0
Cd	1.2	0.8	1.0

Fig.1. depicts the kinetic of the bioleaching process of Ni from sediment sample taken from the depth 20 cm. Ni concentration was observed during bioleaching in soluble form. The curves present the differences between the effectivity of bioleaching processes in two bacterial systems, *Bacillus megaterium* and *Bacillus cereus*. The above mentioned processes took 54 days. The maximum concentration of eluted Ni was achieved in the 21th day (*B. megaterium*) and by *B. cereus* in the 14th day. The maximum concentration Ni in *B. cereus* system achieved 1,247.3 ng ml^{-1} and in *B. megaterium* system 1,087.5 ng ml^{-1}. The results refer to the higher effectivity in the case of application of the bacterial strain *Bacillus cereus*.

Fig. 2. presents the kinetic curves of the bioleaching process of Cd from the sediment sample (20 cm depth). The Cd leaching processes were carried out under the same conditions as in the case of the Ni leaching. In the presence of Bacillus megaterium an increased concentration of Cd was detected. The medium in the 14th day contained
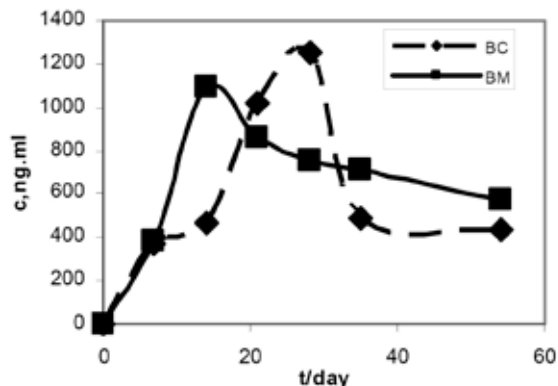
Fig. 1. Basic kinetic of the bioleaching Ni, sediment depth – 20 cm, BM – *Bacillus megaterium*, BC – *Bacillus cereus*

14.2 ngml^{-1} Cd. These experiments give a considerable evidence about the differences of metabolic activity of two bacterial strains, Bacillus cereus and Bacillus megaterium. The results show more effective application of Bacillus megaterium, because of the shorter time needed to Cd releasing into the solution. The concentration of Cd in the medium is approximately 3 times higher as in the case of obtained from the depth 40 cm were proved through the same experimental processes as the sediment from the 20 cm, but the behaviour and the results of bioleaching Ni and Cd were in both cases the same (Data not showed).
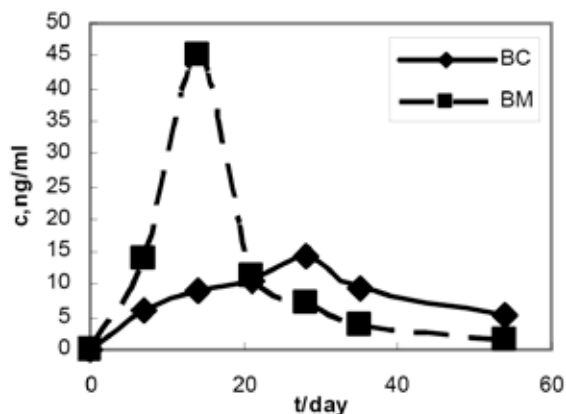
Fig. 2. Basic kinetic of the bioleaching Cd, sediment depth – 20 cm, BM – *Bacillus megaterium*, BC – *Bacillus cereus*

pH of bioleaching system has a direct relationship to the mobility of metals relating to their solubility. The concentration of cations in sediment solution usually increase greatly under a low pH condition (Wu et al., 2006). The decrease of pH values was achieved through bacterial production of acetic acid, butyric acid, pyruvic acid, lactic acid and formic acid (Styriakkova et al, 99). Fig. 5 presented the decreasing of pH values in both *B. cereus* and *B. megaterium* bioleaching
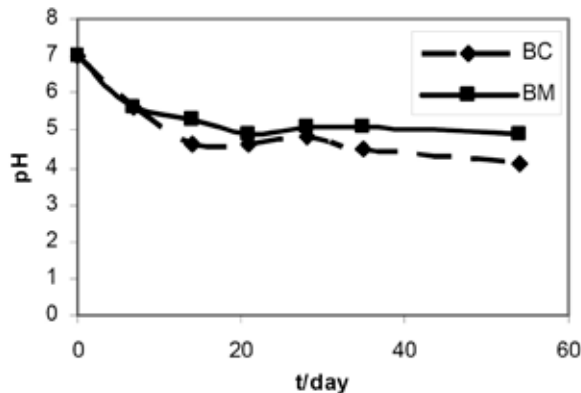
Fig. 3. The decrease of pH in course of bioleaching. BM – Bioleaching system with the application of *Bacillus megaterium* inoculum BC – Bioleaching system with the application of *Bacillus cereus* inoculum

systems. The measurements indicate a markedly change in the pH solution during the first 20 days from pH 7 to 4.6 (*B. cereus*) and 4,9 (*B. megaterium*). In the next experiment a relatively constant level pH values are shown.

Conclusions

Our study demonstrated that *Bacillus spp*. related to the species *Bacillus megaterium* and *Bacillus cereus,* presented and isolated from heavy metals contaminated sediments, are able to release Ni and Cd ions from polluted sediments. This kind of heterotrophyc microorganisms may pose positive impact on the availability and mobility of Ni and Cd and other heavy metals in sediments from water reservoir Ružín I . In this study Cd ions seems to be easier leached through *Bacillus megaterium* strain than *Bacillus cereus* according to their metabolic activity and adaptablity to the Cd polluted environment. The Ni ions was easier leached with application of *Bacillus cerus* strain. In general, the bacteria innoculation enhanced the leachability of Ni and Cd. The possible mechanisms may also be responsible for the integrated effects of lowering pH through bacteria metabolism and production of organic acids.

REFERENCES

1. Cicmanova S., Lučivjanska V.: Ekototox. Char. Rizikik. Obl., MŽP SR and ŠGÚDŠ (2003).
2. Brehuv J.: Act. Mont. Slov. *5,* 3006, (2000).
3. Selenska – Pobell S., Panak P., Miteva V., Boudakov I., Bernard G., Nitsche I.: FEMS Micr.Ecol. *29*, 66 (1998).
4. Wu S. C., Luo Y. M., Cheby K. C., Won M. H.: Env. Pollut. *144*, 772 (2006).
5. Štyriakova I., Štyriak I., Kušnierova M.: Biohydr. Environ. the Env. IBS *,99*, 595, (1999).

P46　BIOSORBENTS PREPARATION FOR HEAVY METALS REMOVING FROM WATERS

JANA JENČÁROVÁ and ALENA LUPTÁKOVÁ

*Institute of Geotechnics of Slovak Academy of Sciences
Watsonova 45, 043 53 Kosice, Slovakia,
jencarova@saske.sk*

Introduction

Heavy metals are very important pollutants in waters. They are non-degradable and therefore continue to accumulate in water bodies. Because of their toxic properties and the tendency for bioaccumulation in the food chain, it is imperative to take effective precautions and to reduce the concentration levels of heavy metals in waters[1].

Current methods in order to remove the toxic metal ions from wastewater are: chemical precipitation, ion exchange, extraction, adsorption, reverse osmosis techniques[2].

Adsorption is understood to involve the interphase accumulation or concentration of substances at a surface or interface. Absorption is a process in which the molecules or atoms of one phase interpenetrate nearly uniformly among those of another phase to form a solution with it[3]. A specific type of sorption based on the used solid phase that is derived from various types of biomaterials or biomass is biosorption[4].

Microbial biomass is frequently used for the bioremediation of heavy metals polluted waters as the biomass capable absorb, adsorb and in some cases precipitate the metals out of solution[5].

Sulphate reducing bacteria (SRB) are genera of dissimilatory bacteria, which utilise sulphate as a terminal electron acceptor and perform dissimilatory reduction of sulphate ions (SO_4^{2-}) to hydrogen sulphide (H_2S) gas. The hydrogen sulphide produced by the SRB, as part of their metabolic processes is capable to react with metal cations to form stable sulphide precipitates[6].

Microbial iron sulphide is well known as an adsorbent for the treatment of metallic ion polluted wastewater[5].

Material and Methods

Cultivating Medium

For sulphate-reducing bacteria cultivation was modified nutrient medium DSM-63 (ref.[7]) with the addition of $Fe_2(SO_4)_3 \cdot 9H_2O$ used. This medium creates optimal conditions for SRB growth genera *Desulfovibrio* and *Desulfotomaculum*.

Sulphate-Reducing Bacteria

Bacteria were isolated from a mixed culture obtained from potable mineral water collected at Gajdovka spring (Košice, Slovak republic) with pH 7.5 and H_2S odour.

Sorbents Preparation

The iron sulphides preparation was realized in the bioreactor filled with 500 ml of modified nutrient medium DSM-63 and inoculated with 100 ml of a culture of SRB during 21 days at 30 °C under anaerobic conditions. These conditions were generated by introducing an inert gas (N_2) and chemically with sodium thioglycollate. The pH of the medium was adjusted to the value 6.8 with sodium hydroxide.

Preparation was realized under 2 different modes. During first mode the bioreactor worked at 30 °C under anaerobic conditions without addition of fresh nutrient medium during 21 days. During second process of preparation the bioreactor worked 4 days in batch mode and then 3 days in continuous mode (i.e. fresh medium was supplied into reactor for more intensive SRB growth and iron sulphides production). We realized 3 periods (21 days).

Model Solutions

Model solutions were prepared by dissolving $ZnSO_4 \cdot 7H_2O$ and $CuSO_4 \cdot 5H_2O$ analytical grade salts. For sorption experiments were solutions with contain of Zn^{2+} and Cu^{2+} 100 mg dm^{-3} used.

Sorption Experiments

Batch sorption experiments were realized in Erlenmeyer flasks filled by 100 ml of model solution of Zn^{2+} or Cu^{2+} and the sorbent. The sorbent dose was 0.1 g. For the best contact between sorbent and model solution were samples agitated by mechanical laboratory shaker at 250 oscillations per minute. Sampling was conducted during 90 minutes. The concentration of zinc and copper was determined by atomic absorption spectrometry.

Results and Discussion

The process of the iron sulphides preparation by SRB was successful in both modes, demonstrated by black precipitates in Fig. 1. and the sensorial detection of H_2S odour.
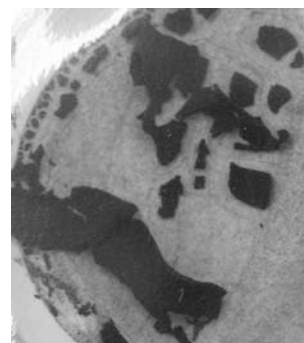
Fig. 1.　**Bacterially produced iron sulphides**

Sorption of Cu and Zn cations from model solutions by biogenic sorbents prepared in batch-continuous mode was studied. Fig. 2. shows removal of Zn^{2+} and Cu^{2+} during 90 minutes. All copper ions were removed. In the same time only 50 % of zinc ions were removed.
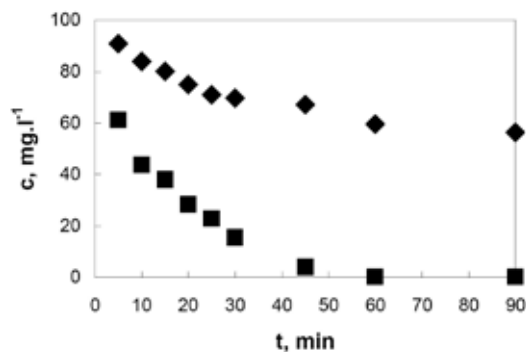
Fig. 2.   **Removal of copper and zinc ions from model solutions.
c – concentration of copper and zinc ions, ■copper, ◆ zinc,
t – time**

In Fig. 3. are present quantities of copper and zinc ions
that iron sulphides were able to capture from 100 ml of solu-
tion in calculation on 1 g weights of dry the sorbent.
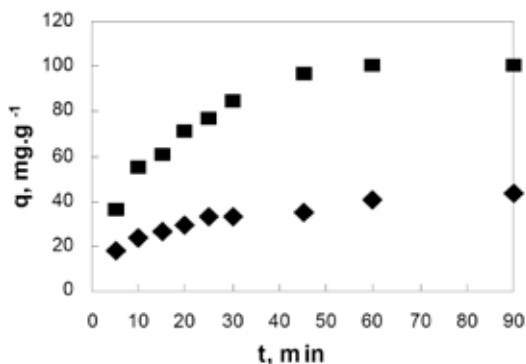
Fig. 3.   **Sorption of copper and zinc ions from model solutions.
q – sorption, ■copper,◆ zinc, t – time**

Fig. 4. shows sorption of zinc ions by iron sulphides pre-
pared in batch-continuous mode (BCM) and in discontinuous
mode (DM) from model solutions. We can see, that "batch-
continuous sorbent", which production process is possible to
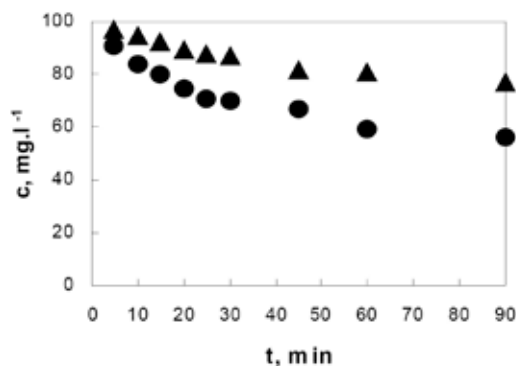
Fig. 4.   **Removal of zinc ions using sorbent prepared in 2 diffe-
rent modes. c – concentration of zinc ions, ● batch-continuous
sorbent, ⊘ discontinuous sorbent, t – time**

see in Fig. 5., was able to remove more ions in the same times
than "discontinuous sorbent".

Fig. 5.   **Bioreactor during continuous mode**

In Fig. 6. are present quantities of zinc ions that sorbents
captured from solutions in calculation on 1 g weights of dry
the sorbent.
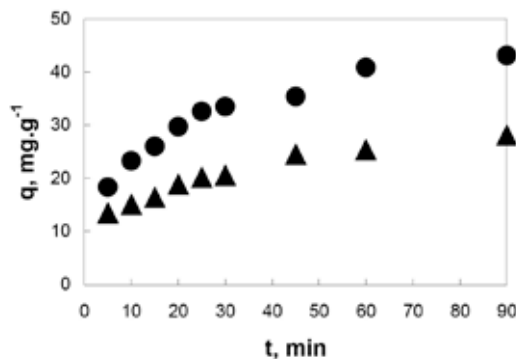
Fig. 6.   **Sorption of zinc ions using sorbents prepared in 2 diffe-
rent modes. q – sorption ● batch-continuous sorbent ⊘ discon-
tinuous sorbent, t – time**

Conclusions

This work was oriented on preparation of iron sulphides
sorbents by sulphate-reducing bacteria for the heavy metals
removing from waters and realization sorption experiments.
From results it is clear that sorpion of copper ions was higher
than sorption of zinc ions after 90 minutes of experiments.
We can also conclude that different mode of iron sulphides
preparation reflects in sortpive capability of sorbent, because
batch-continuous prepared sorbent was more effective than
discontinous prepared.

REFERENCES

1. Ozverdi A., Erdem M.: J. Hazard. Mater. *B137*, 626 (2006).
2. Erdem M., Ozverdi A.: Sep. Purif. Technol. *51*, 240 (2006).
3. Volesky B.: *Sorption and Biosorption*. BV-Sorbex, Inc., St.Lambert, Quebec 2004.
4. Kaduková J., Virčíková E.: *Minerálne biotechnológie III- biosorpcia kovov z roztokov*. ES VŠB TU Ostrava 2003.
5. Marius M. S., James P. A. B., Bahaj A. S., Smallman D. J.: J. Magn. Magn. Mater. *293*, 567 (2005).
6. Marius M. S., James P. A. B., Bahaj A. S., Smallman D. J.: J. Phys.: Conference Series *17*, 65 (2005).
7. Bergey´s *Manual of Determinative Bacteriology*. Willians & Wilkins, USA, Baltimore 1989.

P47 GENOTYPE VARIABILITY OF FATTY ACIDS IN CEREAL GRAINS

DALIBOR JEŠKO[a] and MILAN ČERTÍK[b]

[a]Slovak Agricultural Research Centre – Research Institute of Plant Production Piešťany, Bratislavská 122, 921 68 Piešťany, Slovak Republic,
[b]Department of Biochemical Technology, Faculty of Chemical and Food Technology, Slovak University of Technology, Radlinského 9, 812 37 Bratislava, Slovak Republic,
jeskod@vurv.sk

Introduction

Cereals are important part of human and animal nutrition. From the view of lipids, cereal grains are quite low in fats (averaging 3.6 %) that consist of mainly palmitic, oleic and linoleic acids. Oat (*Avena* spp) includes many species of which *Avena sativa* L is the most commonly cultivated[1]. It is mainly grown for feed use, but due to its high nutritional value, much interest is now focused on expanding its food applications. Among cereal grains, oat has the best protein quality and quantity and is a valuable source of minerals and vitamins, especially thiamine and pantothenic acid[2]. Moreover, the lipid content of oat is high with very good balance between polyunsaturated and saturated fatty acids[3,4] and, therefore it is important crop from the nutritional point of view[5]. Significant levels of other lipid compounds, such as phospholipids, glycolipids, and phytosterols, may also find application in various pharmaceutical, medical, food, and industrial fields.

Buckwheat is annual melliferous crop. For many years cultivation of buckwheat declined, but recent interest in old, traditional foods have led to resurgence in its cultivation. Buckwheat belongs to pseudo-cereals together with amaranth and millet. These grains have been important food crops in various parts of the world and have potential for much greater and more widespread use[6].

Because lipids are essential compounds of cereal grains, this study was focused on genotype variability of fatty acid composition in following cereal grains: oat, millet, amaranth and buckwheat. The research in this field could significantly help in cereal classification.

Experimental

Oil content and fatty acid composition in following cereal grains have been determined in this study: oat (85 varieties), millet (29 varieties), amaranth (20 varieties) and buckwheat (10 varieties).

Total lipids were extracted from oat grains 2-times by 100 ml chloroform/methanol (2 : 1, v/v) for 60 min at laboratory temperature with occasional stirring. After extraction the mixture was filtered and 0.97% KCl (1.2-fold of total extract volume) was added. The mixture was stirred vigorously for 1 min and centrifuged (5 min, 3,000 g) to effect phase separation. The chloroform – lipid containing layer was filtered through anhydrous Na_2SO_4 and evaporated under vacuum[7].

Table I
Average amounts (AV), standard deviation (SD) and variation coefficient (VC) of lipid content and fatty acids in studied cereal grains

Cereals (number)		Lipids [%]	Fatty acids [%]				
			C16:0	C18:0	C18:1	C18:2	C18:3
Oat (79)	AV	4.5	16.0	1.7	37.8	38.5	1.6
	SD	1.2	0.8	0.4	2.5	2.2	0.4
	VK	26.9	4.9	22.2	6.6	5.6	21.9
Millet (29)	AV	3.8	7.5	1.9	21.3	63.6	1.2
	SD	0.57	0.35	0.63	1.83	2.65	0.25
	VK	14.9	4.6	33.5	8.6	4.2	20.7
Buckwheat (10)	AV	2.3	13.3	2.1	36.3	35.2	1.9
	SD	0.54	0.52	0.07	0.97	0.53	0.07
	VK	23.5	3.9	3.4	2.7	1.5	3.5
Amaranth (10)	AV	5.2	17.1	2.7	23.6	43.0	0.7
	SD	0.79	2.50	0.29	4.34	6.34	0.11
	VK	15.1	14.6	10.8	18.4	14.8	15.3

Fatty acids of total lipids were analyzed as their methyl esters by gas chromatography (GC-6890 N, Agilent Technologies) using a capillary column DB-23 (60 m × 0.25 mm, film thickness 0.25 μm, Agilent Technologies) and a FID detector (constant flow, hydrogen 35 ml min^{-1}, air 350 ml min^{-1}, 250 °C) under a temperature gradient (130 °C for 1 min; 130–170 °C at program rate 6.5 °C min^{-1}; 170–215 °C at program rate 2.7 °C min^{-1}; 215 °C for 7 min; 220–240 °C at program rate 2 °C min^{-1}) with hydrogen as carrier gas (flow 2.1 ml min^{-1}, velocity 49 cm s^{-1}, pressure 174 kPa) and a split ratio of 1/50 (Inlets: heater 230 °C, total hydrogen flow 114 ml min^{-1}, pressure 174 kPa)[8]. The fatty acid methylester peaks were identified by authentic standards of C_4–C_{24} fatty acid methylesters mixture (Supelco, USA) and evaluated by ChemStation 10.1 (Agilent Technologies). The variation coefficient (VC) of individual fatty acids was calculated from the equation: VC = (δ_{n-1}/average value of selected fatty acid) × 100, where δ_{n-1} is a decisive deviation.

Results
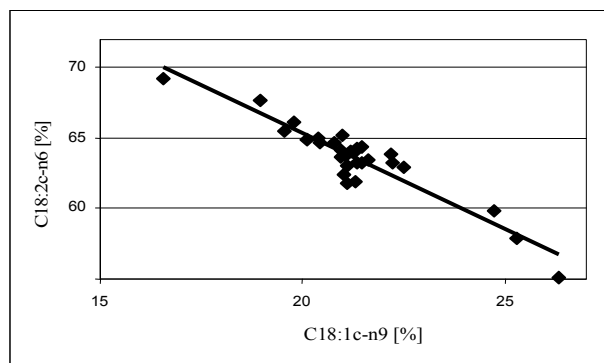
Fig. 1. **Relationship between oleic and linoleic acid in millet lipids**
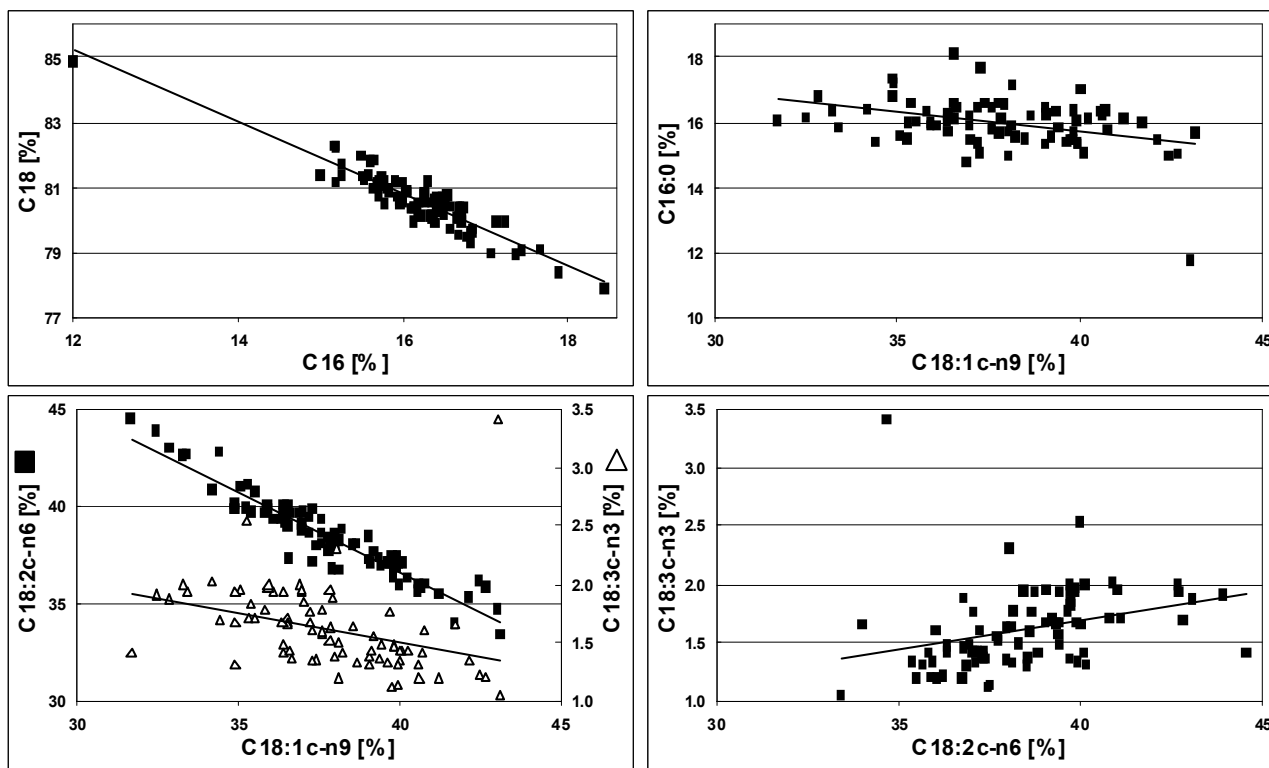
Fig. 2.   **Relationship between main fatty acids in oat lipids**

Lipid amounts in investigated cereals varied between 1.5 to 8.2 %. Linoleic (C18:2c-n6), oleic (C18:1c-n9) and palmitic (C16:0) acids were the major fatty acids whereas α-linolenic acid (C18:3c-n3) and stearic acid (C18:0) were minor fatty acids (Table I).

Correlation between levels of oleic and linoleic acids
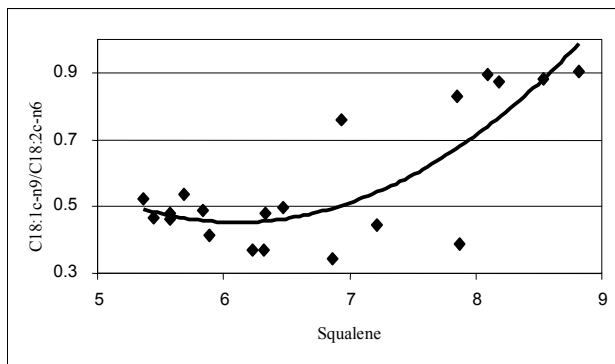
Fig. 3.   **Relationship between C18:1c-n9/C18:2c-n6 ratios and squalene amounts in amaranthus grains**

indicated that activity of Δ^{12}-desaturase might be controlled genotypically (Fig. 1.). The results indicate that elevation amount of total C16 fatty acids is related with loss of amount total C18 fatty acids in oat lipids. Also decrease of oleic acid amount is accompanied with higher linoleic and α-linolenic acid amounts. Accumulation of linoleic acid amount is

related with accumulation of α-linolenic acid amount as well (Fig. 2.). Variations in individual fatty acid levels also demonstrated deviation in biosynthesis stability of these compounds in selected cereal genotypes. Moreover, relationship between C18:1c-n9/C18:2c-n6 ratios and squalene amounts were found in amaranthus varieties (Fig. 3.).

Conclusions

Although fatty acid composition in all varieties of individual cereal type was similar, statistical analysis and calculation of various ratios among fatty acids clearly showed that fatty acid profile can be used for more precise description of single cereal genotypes. Oats containing lower lipids amounts were characterized by increased fatty acid unsaturation due to elevated concentrations of both linoleic and α-linolenic acids and reduced levels of oleic acid. Fatty acid composition together with calculated fatty acid parameters offers not only valuable taxonomic and physiologic information for classification of various cereal varieties, but also may be used by farmers and producers for aimed applications of cereals from the view of desired lipid attributes.

REFERENCES

1. Schrickel D. J.: *Oats production, value, and use, In Oats - Chemistry and Technology*. Ed by Webster F. H., American Association of Cereal Chemists Inc, St Paul, Minnesota, USA, 1 (1986).
2. Lockhart H. B., Hurt H. D.: *Nutrition of oats In Oats - Chemistry and Technology*. Ed by Webster F. H., American Association of Cereal Chemists Inc, St Paul, Minnesota, USA, 297 (1986).
3. Cordain L.: World Rev. Nutr. *84*, 19 (1999).
4. Molteberg E. L., Vogt G., Nilsson A., Frolich W.: Cereal Chem. *72*, 88 (1995).
5. Zhou M., Robards K., Holmes M. G., Helliwell S.: J. Am.. Oil Chem..Soc.. *76*, 159 (1999).
6. Belton P. S., Taylor J. R. N.: *Pseudocereals and less common cereals*. Springer, 269 (2002).
7. Čertík M., Andráši P., Šajbidor J.: J. Am. Oil Chem. Soc. *73*, 357 (1996).
8. Čertík M., Sláviková L., Masrnová S., Šajbidor J.: Food Technol. Biotechnol. *44*, 75 (2006).

P48 PRELIMINARY STUDIES ON THE ANTIFUNGAL ACTIVITY AND COMPOSITION OF THE HEXANE EXTRACT OF THE BRAZILIAN *CHENOPODIUM AMBROSIOIDES* L.

GULAB NEWANDRAM JHAM, CAROLINA MARANGON JARDIM, ONKAR DEV DHINGRA and MARCELO MOREIRA FREIRE

Federal University of Viçosa (Universidade Federal de Viçosa), Department of Chemistry, Minas Gerais, 36571-000, Brazil,
gulab@ufv.br

Introduction

Extracts of several edible botanicals are reported to have antifungal activity. However, little work has been carried out to manage fungal deterioration of stored products by plant derived bioactive compounds.

Epazote (*Chenopodium ambrosioides* L.) is an herb native to South America and although there are a few reports on fungicidal properties of its dichloromethane extracts[1,2], no studies have been conducted on its chemical compositions. In this study, we report our preliminary results on antifungal activity of the crude hexane extract hexane extract (HE) of the Brazilian epazote against four fungi (*Aspergillus flavus, A. glaucus, A. niger, A. ochraceous*) and identification of volatiles in the hexane extract by gas chromatography (GC) and gas chromatography combined with mass spectrometry (GC-MS).

Experimental

Plant Material and Hydrodistillation

The epazote leaves were harvested from shrubs in Viçosa, Minas Gerais, Brazil, and extracted with hexane (200 ml) for 12 h. The organic phase was collected, dried over anhydrous sodium sulfate; hexane was evaporated in a rotatory evaporator at 30 °C under reduced pressure, weighed and evaluated.

Antifungal Activity

The antifungal activity of the hexane extract was tested on potato-dextrose agar (PDA) with use of poison food assay. Percent growth inhibition was calculated by dividing radial growth in the treatment plates by growth in the control plates and multiplying by 100. The data were analyzed by ANOVA and the means compared by the Tukey test ($p = 0.05$).

Identification of Compounds

The volatiles in the crude hexane extract were identified by GC using RI (Kováts retention index) and GC-MS. The peaks were first identified by GC-MS library system based on similarity indexes (SI). RI was obtained for most GC peaks. The final identification was based on the best SI and RI fits

Results and Discussion

Depending upon the fungus an inhibition of 25–100 % was obtained (Fig. 1.). In this study, at concentration of 0.3 %, 100% inhibition of four important post-harvest fungi was obtained. The minimum concentration of 0.1 % was reported for complete inhibition of *Rhizoctonia solani*[1].
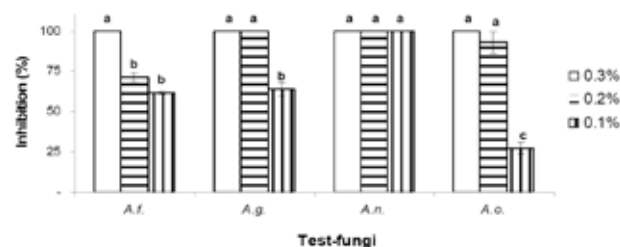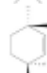
Fig. 1. **Percent radial growth inhibited by crude *Chenopodium ambrosioides* hexane extract after 6-day incubation (25 °C) at concentrations of 0.3 %, 0.2 and 0.1 %. Mean of three replications. For each concentration the histograms of different fungi, headed by the same letter do not differ at ($p = 0.05$). The bars represent the standard deviation within the treatment. A.f. = *Aspergillus flavus*, A.g. = *A. glaucus*, A.n = *A. niger*, A.o = *A. ochraceous***

Table I
Identification, based on gas chromatography (RIs-Kováts retention indexes) and gas chromatography-mass spectrometry and % composition of the crude hexane extract of the Brazilian Chenopodium ambrosioides

		Crude hexane extract		
Peak no	KI	%	Compound	Structure
1	1019	11.2	α-terpinene	
2	1026	6.0	*p*-cymene	
3	1031	0.4	benzyl alcohol	
4	1247	54.0	(*Z*)-ascaridole	
5	1287	2.3	carvacrol	
6	1305	17.3	(*E*)-ascaridole	
Other identified compounds		8.8	–	–

The composition of the hexanic extract has not been reported in the literature. About 91.8 % of the volatiles in the hexane extract were identified by GC and GC-MS (Table I,

Fig. 2.). In adddition, other non-volatiles such as mono, di and triacylglycerides etc., which would not be dectected under our GC conditions were presumably also present.

The % composition and antifungal activities were similar to those reported for the *C. ambrosioides* essential oil (EO) reported by us[3].
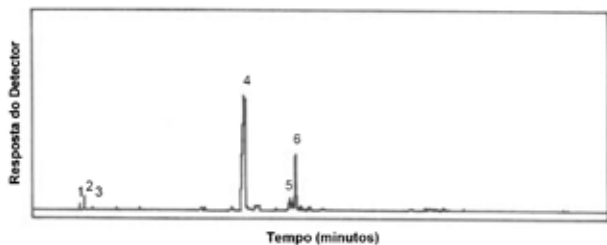
Fig. 2.   **Reconstructed gas chromatogram obtained on analyses of crude Chenopodium ambrosioides hexane extract**

Conclusions

The antifungal activities of the *C. ambrosioides* essential oil[3] and hexane extract were very high and were attributed to terpene-like compounds. We are now conducting studies to isolate the active fraction of the hexane extract as well as extend our studies to other common storage fungus.

REFERENCES
1. Arispuro I. V., Bernal S. A. Tellez M. A. M., Nieblas M. O.: Rev. Mex. Fitopatolo. *15*, 91 (1997).
2. Dubey N. K., Kishore N., Srivastava O. P., Dikshit A., Singh S. K.: Plant Soil *72*, 91 (1983).
3. Jardim C. M., Jham G. N. Dhingra O. D., Freire M. M. J.: Chem. Ecol. (2008, in press).

P49 EVALUATION OF ANTIOXIDANT AND ANTIMICROBIAL ACTIVITIES OF NATURAL HONEYS

MIROSLAVA KAČÁNIOVÁ, MARTINA FIKSELOVÁ, SOŇA FELŠÖCIOVÁ, VLADIMÍRA KŇAZOVICKÁ, KATARÍNA FATRCOVÁ-ŠRAMKOVÁ, JANKA NÔŽKOVÁ and IVETA UBREŽIOVÁ

Faculty of Biotechnology and Food Sciences, Slovak University of Agriculture, Tr. A.Hlinku 2, Nitra, 949 76 Slovakia, miroslava.kacaniova@uniag.sk

Introduction

In general, the antioxidant capacity of honey appeared to be a result of the compounds including phenolics, peptides, organic acids, enzymes and other phytochemicals (Gheldof et al., 2002). The phenolic compounds contribute significantly to the antioxidant capacity in many studies. Reports on honey as antifungal agent were comprehensively reviewed by Molan (1992). The "inhibine number" is the degree of dilution to which a honey retains its antibacterial activity, representing a sequential dilution of honey in steps of 5 %, from 25 to 5 %. Allen *et al.*, (1991) found many honeys with low activity and 36 % of samples with activity near or below detectable levels. In this study, antioxidant effects (by DPPH method) as well as the antifungal effects of natural honeys on five species of fungi collected, were tested.

Experimental

Honey was extracted from the hives of bees and kept at 4 °C away from direct light before use. Samples were derived from different plant species of Acacia (2 samples), Brassica (1 sample), Thyme (1 sample) and the rest of samples (5 samples) were of floral origin. Samples originated from different places of Slovakia and one sample came from Rodos

Antioxidant Activity

A method was adapted according to Sanches Moreno et al. (1998) and Brand-Wiliams et al. (1995). Honey (10 g) was dissolved in 100 ml of ethanol (90%), and 0.1 ml of solution was taken to 3.9 ml of DPPH methanolic solution (25 mg dm^{-3}) and mixed. Absorbance at 515 nm was measured at different time intervals. The blank reference cuvette contained DPPH methanolic solution. Results were expressed as % inhibition.

Antifugal Activity

All samples were prepared aseptically and handled protected from direct sunlight. Honey solutions were prepared in three fractions: 50, 25 and 10 % (by mass per volume). Five species of fungi were isolated from wheat samples collected from different locations in Slovakia: *Penicillium crustosum, P. expansum, P. griseofulvum P. raistrickii* and *P. verrucosum* by the agar well diffusion method. All fungal isolates were identified microscopically, and samples of each fungus were deposited in the fungal collection bank. The strains of fungi were maintained on Czapek yeast extract agar (CYA, HiMedia). All plates were incubated at 25 °C in the dark and inhibition zones were measured after 3 days. The statistical processing of the data obtained was implemented by means with SAS software.

Results

In term of antioxidant activity of honeys the best results were found at thyme honey from Rodos (11.84 %) and floral honeys from different places of Lučenec (10.09 %, 10.19 %). The lowest antiradical activity was determined at Acacia honey (7.615 %). Kücük et al. (2007) studied three different Turkish honeys and found high levels of polyphenolics and high antioxidant activity in three antioxidant assays. Radical scavenging assay was the highest at chestnut honey, then followed heterofloral honey and the least at rododendron one.

Table I
Antioxidant activity [%] of honey samples

Honey/Place of origin	Inhibition [%] ± SD
Acacia/Nitra	8.53 ± 0.08
Brassica/Nitra	9.89 ± 0.33
Floral/Smrečany	8.39 ± 0.11
Thyme/Rodos	11.84 ± 0.35
Floral/Nitra	8.98 ± 0.24
Floral/Hlohovec	9.96 ± 0.40
Floral/Lučenec	10.19 ± 0.53
Acacia/Lučenec	7.62 ± 0.56
Floral/Lučenec	10.09 ± 0.34
All	9.50 ± 1.25

Al-Mamary et al. (2002) showed a linear positive relationship with the extract concentration. The antioxidant activity of diluted honey samples increased with increasing the levels (50 µl, 100 µl, 200 µl) of honey samples. The total antioxidant activities of diluted samples varied from −6.48 % (prooxidant activity) to 65.44 % inhibition. In our case determined antioxidant activity (Table I) was low, varied from 7.62 % (Acacia/Lučenec) to 11.84 % (Thyme/Rodos).

The results obtained characterize honey samples as a product with a broad antimicrobial effect. The strongest antifungal effect was shown by honey samples of 50 % concentration against *Penicillium raistricki* strains. The least antifungal effect was shown by honey samples of 10 % concentration against to *Penicillium expansum* strains. No inhibitory activity was detected with any of the seven species with the pasture honey at any concentration up to the highest tested 50 % (v/v). Maughrabi (2003) found that wild honey was effective against *Alternaria solani* and *Phytophthora infestanns*, also against *Rhizoctonia solani* and *Fusarium oxysporum*, and to a less extent against *Stemphylium solani* and *Colletotrichum sp.*

Table II
Antimicrobial effect of honey samples against *Penicillium* strains

Microscopic fungi	Honey concentration [%]		
	10	25	50
Penicillium crustosum	11.67 ± 3.00	22.22 ± 8.38	28.67 ± 8.11
Penicillium expansum	7.22 ± 5.63	12.22 ± 4.79	24.22 ± 16.54
Penicillium griseofulvum	10.78 ± 1.92	15.11 ± 3.62	21.56 ± 5.53
Penicillium raistrickii	8.67 ± 2.87	16.22 ± 5.07	33.11 ± 14.59
Penicillium verrucosum	7.67 ± 1.94	12.78 ± 3.67	23.44 ± 9.84

Conclusions

Selected honeys showed low scavenging ability to DPPH radical, but can be classified as a product with a broad anti-microbial effect. The strongest antifungal effect was shown by honey samples of 50% concentration against *Penicillium raistricki* strains.

REFERENCES

1. Al-Mamary M., Al-Meeri A., Al-Habori M.: Nutr. Res. *22 (9)*, 1041 (2002).
2. Allen K. L., Molan P. C., Reid G. M.: J. Pharm. Pharmacol. *43*, 817 (1991).
3. Brady N. F., Molan P. C., Harfoot C. G.: Pharm. Sci. *2*, 471 (1996).
4. Brand-Williams W., Cuvelier M. E., Berset C.: Lebensm. − Wiss. U.- Technol. *28*, 25 (1995).
5. Gheldof N., Wang X. H., Engeseth N. J.: J. Agric.Food Chem., *50 (21)*, 5870 (2002).
6. Kücük M., Kolay S., Karaoglu S.,et al.: Food Chem., *100*, 2526 (2007).
7. Molan P.C.: Bee World *73*, 5 (1992).
8. Molan P.C.: Bee World *73*, 59 (1992).
9. Mughrabi K. I. A.: Phytopathol. Mediterr. *42*, 280 (2003).
10. Sánchés-Moreno C., Larruri A., Saura-Calixto F.: J. Sci. Fd Agric. 270 (1998).

P50 COMBINED TECHNIQUE LC/MS IN ANALYSES OF ANTIOXIDANT COMPOUNDS

RADKA KOČÍ, MARIE TRČKOVÁ, LUKÁŠ MÜLLER and IVANA MÁROVÁ

Department of Food Chemistry and Biotechnology
Faculty of Chemistry,Brno University of Technology
Purkyňova 118, 612 00 Brno, Czech Republic,
koci-r@fch.vutbr.cz

Introduction

Antioxidants constitute a large group of plant and microbial secondary metabolites (for exemple carotenoids, phenolics, oligopeptides, saccharidic derivates etc.) with major interest because of their anti-inflammatory effects and of their potential anti-atherogenic properties[1,2]. Many foods are good sources of antioxidants: vegetables, legumes, whole-grain cereals, tea extracts, honey etc. The best source of these physiologically active compounds with rapid effects on human health is represented by some sorts of fruit[1]. Especially citrus fruit contain high-levels of phenolics and/or ascorbic acid[3]. Widely consumed apples are rich on polyphenols too with the most abundant chlorogenic acid[4].

Phenolics in human plant nurtur play important roles in sensory properties of food, because of its influence on colour and/or flavour. Moreover major part of phenolic substances occure as physiologicaly active components with very hight antioxidative capability as well as effective protection against cancer growth and/or other degenerative diseases[3,4].

Analysis of phenolic substances could be realised using many different instrumental methods starting with TLC and ending with GC (some special applications). In the present the most preffered technique in separation of non-volatile compounds, such as phenolics are, is modern instrumental method LC/MS combining perfect separation with universal detection of individual sample components[5].

Experimental

Presented work was focused on characterisation of several substances (phenolics, carotenoids) with antioxidant activity containned in biologic materials and on their distribution in individual sample fractions (juice, pulp, peel).

Antioxidants were isolated *(i)* by ethylacetate-ether (phenolics) and/or aceton-ether (carotenoids) extraction, *(ii)* by SPE method with amide-2 (phenolics) and/or C18 AR columns (carotenoids).

Separation and detection of phenolics were optimalized using followed conditions: Restek C18 Ultra aqueous column heated on 30 °C, gradient elution using 1% acetic acid: acetonitril in range 60-45 : 40-55 with flow of mobil phase 0.4 ml min^{-1}, UV-VIS detection (280 nm and/or 370 nm), MS tune file on chlorogenic acid (negative ion mode).

Identification of carotenoids was gone on column Polaris C18 A heated on 45 °C, using isocratic elution with LC/MS methanol (flow 0.25 ml min^{-1}), UV-VIS detection (450 nm) and/or MS detection (tune file on β-carotene in positive ion mode).

Standard compounds as well as food samples were determined by MS full scan and/or MS/MS full scan mode.

Results

Standards of antioxidants were analysed using off-line and/or on-line HPLC/UV-VIS/ESI-MS. However reported results were obtained by on-line LC/UV-VIS/MS, because of low response of off-line method.

Table I

Precursors (MS full scan) and fragments (MS^{2}full scan) of standards

Compound	m/z [M-H]$^-$ or [M]$^{+\bullet}$	Fragments (m/z)
β-carotene	537	–
epicatechin	289	217, 245, 271
catechin	289	227, 245, 271
quercetin	301	107, 121, 151, 239, 257, 273
morin	301	229, 257, 273
fisetin	285	163, 213, 229
kaempferol	285	151, 229, 257
acid gallic	169	–
acid chlorogenic	353	191, 309, 339
myricetin	317	179, 245, 289, 299
naringenin	271	–
rutin	609	301
procyanidin	577	–

In Table I determined parent ions (MS full scan) and/or typical fragments obtained by tandem mass spectrometry are resumed. MS full scan spectra of chosen phenolic standards are demonstrated on Fig. 1. and Fig. 2.
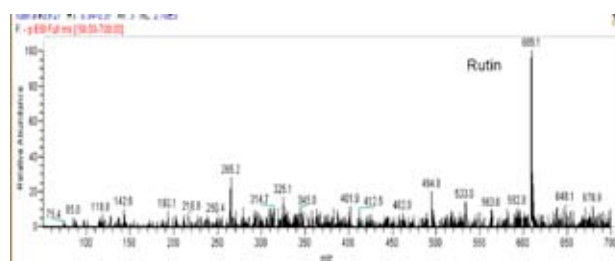
Fig. 1. **MS full scan spectrum of rutin**
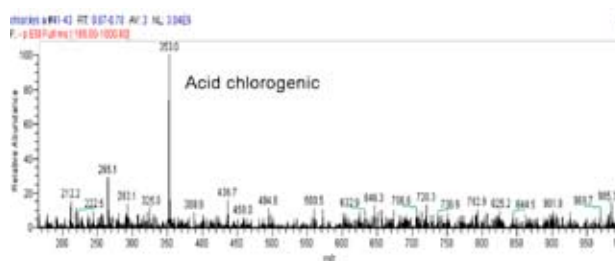
Fig. 2. **MS full scan spectrum of acid chlorogenic**

Compounds in food samples are identified in MS spectra according to m/z values of determined standards (Table I). Phenolic substances were analysed with higher sensitivity than carotenoids, because of its moderate polarity – general condition of electrosprey use[3,5].

Fig. 3. shows an exemple of chromatogram of several phenolics contained in orange.
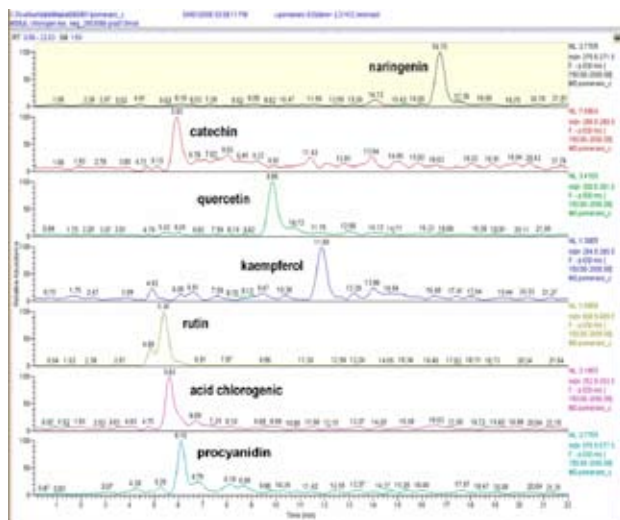
Fig. 3. **Phenolics in orange juice: naringanin, catechin, quercetin, kaempferol, rutin, acid chlorogenic and procyanidin**

Table II
Antioxidants in food samples

Sample	Total phenolics [mg 100 g^{-1}]	β-carotene [μg 100 g^{-1}]
orange	572 ± 13	264.3 ± 1.2
lemon	388 ± 12	218 ± 8
tangerine	148 ± 13	720 ± 25
grapefruit	172 ± 6	714 ± 36
apple	2181 ± 43	593 ± 70
carrot	1352 ± 46	5289 ± 123
tomato	13.4 ± 0.8	14.1 ± 2.1
sweet pepper	4.37 ± 0.03	4660 ± 27
onion	16.3 ± 1.0	40.1 ± 1.9
garlic	1.32 ± 0.04	–
potato	379 ± 16	2077 ± 127
gourd – seeds	1898 ± 28	–
sunflower-seeds	517 ± 10	–

Fruit samples were observed as the best and complex sources of phenolics (Table II). Amount of total phenolics was highest in apple, the mostly consumed fruit. But considerable yield was observed in orange as well as in sunflower-seeds. Very important food source of phenolics are also carrot and/or gourd-seeds.

Antioxidant capacity of carrot is increaced by high-level of β-carotene (carotenoids). Important concentration of

carotenoids was observed also in sweet pepper and/or potato (Table II).

Studied samples contained rutin and/or acid chlorogenic as principal phenolics, their distribution in individual fractions of food is demonstrated on Fig. 4 and Fig. 5.

General part of phenolic substances is presented in fruit and/or vegetable juice, while higher amount of selected phenolics was observed in pulp.
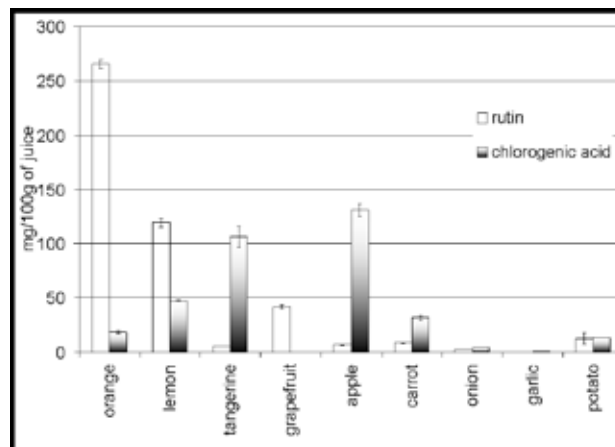
Fig. 4. **Occurrence of rutin and acid chlorogenic in juice**
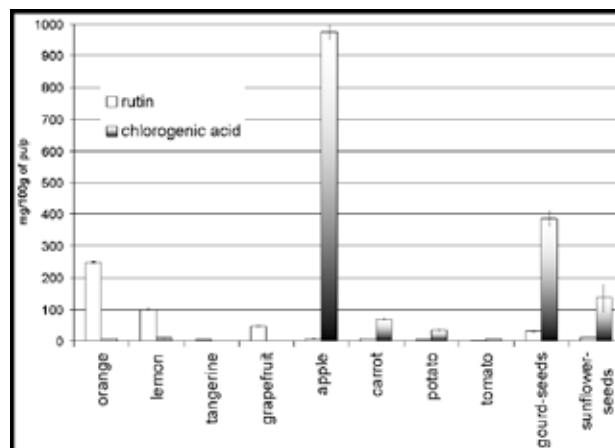
Fig. 5. **Presence of rutin and acid chlorogenic in pulp**

Peel was analysed in apple and potato only (data not show). This fraction was characteristic by higher amount of chlorogenic acid, while other analysed phenolics were presented in very lower concentration and/or was not determined.

Conclusions

Combined instrumental technique LC/ESI-MS is more suitable for analysis of phenolics than in identification of carotenoids. Carotenoid are lipid-soluble pigments, so ionisation process with ESI source is insufficient. More important method for carotnoid analysis is LC/APCI-MS.

Analysis of compound distribution is surely influenced

by extraction method, however results demonstrate that fruit and/or vegetable should be used as whole product. The one fraction consummation (for exemple fruit juice only) reduces conciderable antioxidant yields contained in pulp as well as in peel of fruit and/or vegetable sources.

REFERENCES

1. Abad-Garcia B., Berrueta, L. A., Berrueta, L. A., Crespo-Ferrer, I., Gallo, B., Vicente, F.: J. Chromatogr. A *1154*, 87 (2007).
2. Li H., Tyndale S. T., Heath D. D., Letcher R. J.: J. Chromatogr. B *816*, 49 (2005).
3. Bilbao M.D.M., Andres-Lacueva C., Jauregui O., Lamuela-Raventos R.M.: Food Chem. *101*, 1742 (2007).
4. Oszmiański J., Wolniak M., Wojdylo A., Wawer I.: Food Chem. *107*, 1473 (2008).
5. de Rijke E., Out P., Niessen W.M.A., Arbese F., Gooijer C., Brinkman U.A.Th.: J. Chromatogr. A *1112*, 31 (2006).

P51 INFLUENCE OF CHEMICAL TREATMENT ON FUSARIUM TOXINS IN BARLEY HARVESTED 2005–2007

JANA KOHOUTKOVÁ, KATEŘINA LANCOVÁ, ALEXANDRA KRPLOVÁ, ONDŘEJ LACINA, JANA HAJŠLOVÁ, JANA MARKOVÁ and JAROSLAVA EHRENBERGEROVÁ

Department of Food Chemistry and Analysis, Institute of Chemical Technology, Technická 5, 166 28 Prague 6
Jana.Kohoutkova@vscht.cz

Introduction

Mycotoxins are toxic secondary metabolites produced by certain toxigenic microscopic fungi in various crops used as raw materials for the production of foodstuffs and fodder.

Fusarium toxins have been shown to cause a variety of toxic effects (both acute and chronic) in humans and animals (vomiting, dermal irritation, haemorragic lesions, weight reduction, etc.).

The main objective of this study was to investigate the influence of key agricultural practices (resistance of barley cultivars, chemical treatment use, pre-crop and different growing locality) on *Fusarium* mycotoxins in barley. Field trials were realized in cooperation with the Agricultural Research Institute Kroměříž (harvest 2005, 2006 and 2007).

For the determination of the most important *Fusarium* mycotoxins, the high-performance liquid chromatography coupled to tandem mass spectrometry (LC–MS/MS) was used. The trueness of the generated data was successfully demonstrated in proficiency test (Food Analysis Performance Assessment Scheme, FAPAS®) organized by Central Science Laboratory (CSL, York, UK).

Experimental

M y c o t o x i n s

Characterisation of analytical method: isolation of the most important *Fusarium* mycotoxins from sample was carried out using an acetonitrile/water mixture for one hour by a shaker. Extract was analysed by LC–MS/MS (LCQ Deca, Finnigen, USA), on column Synergi Hydro RP (150 mm ×3 mm × 4 μm) after clean-up by solid phase extraction employing the MycoSep 226® cartridges.

Target mycotoxins:
- trichothecenes *type B* – deoxynivalenol (DON), nivalenol (NIV), fusarenon-X (Fus-X), sum of 13-acetyldeoxynivalenol and 15-acetyldeoxynivalenol (expressed as ADON)
- trichothecenes *type A* – HT-2 toxin (HT-2), T-2 toxin (T-2)
- zearalenone (ZON)

P e s t i c i d e s

Characterisation of analytical method: Isolation of target pesticides from sample was carried out using a acetonitrile after addition 1% formic acid. Extract was analysed by LC–MS/MS (Quattro Premier XE, Waters, USA) on column Discovery C18 (100 mm × 3 mm × 5 μm).

Table I
Used pesticides

Active compound	Type	Product
Amidosulfuron	Herbicid	Secator
Mefenpyr-diethyl	Herbicid	Secator
Iodosulfuron-methyl-sodium	Herbicid	Secator
Fenpropimorph	Fungicid	Cerelux
Flusilazole	Fungicid	Cerelux
MCPA	Herbicid	Optica trio
Mecoprop	Herbicid	Optica trio
Tebuconazole	Fungicid	Falcon
Triadimenol	Fungicid	Falcon
Spiroxamin	Fungicid	Falcon

G r o w i n g   L o c a l i t y

Harvest 2005:
Žabčice
- chemical treatment (pesticide)
- no chemical treatment (pesticide)

Kroměříž
- no chemical treatment (pesticide)

Harvest 2006:
Kroměříž
- no chemical treatment (pesticide)

Branišovice
- chemical treatment (pesticide)
- no chemical treatment (pesticide)

Uherský Ostroh
- chemical treatment (pesticide)
- no chemical treatment (pesticide)

Harvest 2007:
Žabčice
- chemical treatment (pesticide)
- no chemical treatment (pesticide)

Kroměříž
- chemical treatment (pesticide)
- no chemical treatment (pesticide)

E x a m i n e d   S a m p l e s

Varieties of barley: Amulet, Bojos, Jersey, Malz, Prestige, Sebastián, Tolar and other

Harvest 2005:
6 barley samples
30 malt samples prepared from tested barley

Harvest 2006:
40 barley samples

Harvest 2007:
36 barley samples

Results

Table II

	Positive samples:	
	Toxin	[%]
	Harvest 2005	
Barley	DON (major mycotoxin)	100.0
	HT-2 toxin	86.0
	NIV	28.0
	T-2 toxin	17.0
Malt	DON (majority mycotoxin)	100.0
	ZON	13.3
	HT-2 toxin	23.3
	T-2 toxin	10.0
	sum ADON	10.0
	Harvest 2006	
Barley	DON (major mycotoxin)	100.0
	NIV	33.0
	T-2 toxin	65.0
	HT-2 toxin	22.5
	Harvest 2007	
Barley	DON (major mycotoxin)	94.0
	NIV	92.0
	HT-2 toxin	86.0
	T-2 toxin	58.0
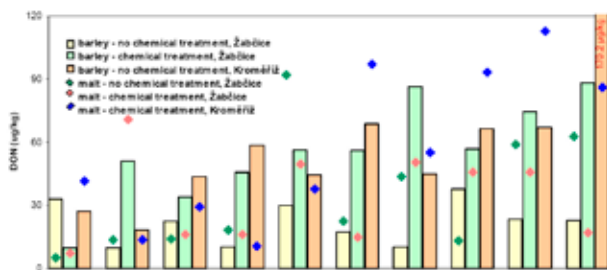
Fig. 1.   **Changes of DON concentrations after malting process**

Conclusions
- Influence of pesticide treatment has not been documented. Highest and lowest incidence of DON were detected at "no - chemical treatment" samples.
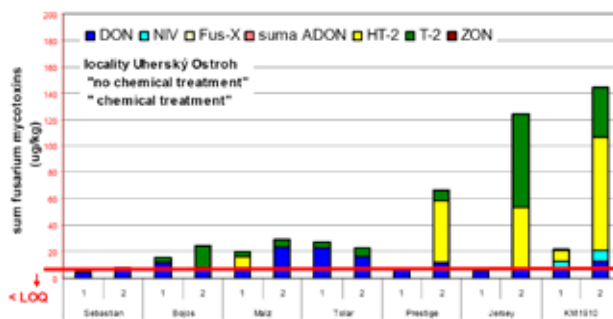
Fig. 2.   **Influence of barley variety on trichothecene levels**
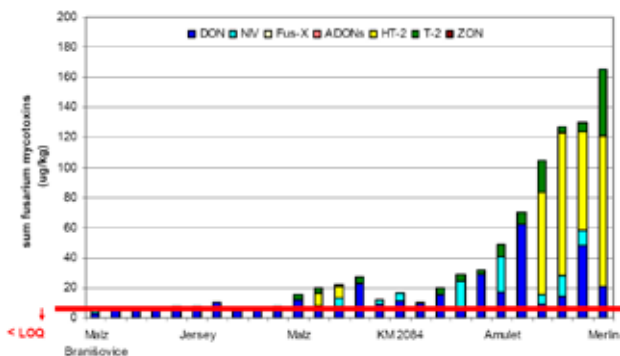
Fig. 3.   **Influence of chemical treatment on production of fusarium toxins in barley samples**

- The differences among localities were significant, that could be caused by different weather conditions and different spectrums of trichothecenes indicated a contamination of barley by various fusarium fungi.
- Influence of barley variety was significant. Highest incidences of mycotoxins were detected at Amulet and Merlin varieties.

REFERENCES
1. Obst A., Lepschy J., Beck R., Bauer G., Bechtel A.: Mycotoxin Res., *16A*, 16 (2000).
2. Šíp V., Chrpová J., Leišová L., Sýkorová S., Kučera L., Ovesná J.: Czech Genet. J. Genet. Plant Breeding (2007).

P52 MONITORING OF ACRYLAMIDE IN FOODS IN THE CZECH REPUBLIC

JANA KOLÁŘOVÁ, IRENA ŘEHŮŘKOVÁ and JIŘÍ RUPRICH

National Institute of Public Health – Centre for Hygiene of Food Chains, Palackeho 3a, 612 42 Brno, Czech Republic, kolarova@chpr.szu.cz

Introduction

Acrylamide is a substance that is produced, first of all (but not exclusively), in starch foods as a result of high temperature (> 120 °C) used during culinary processes, particularly during baking, grilling, frying or microwaving. Acrylamide can cause cancer in animals and experts assume that acrylamide can probably cause cancer also in humans[1,2].

The main mechanism of acrylamide formation in food is expected via a reaction between the amino acid asparagine and reducing sugars, e.g. glucose, under high temperature[1,3].

Methodology

Since 2004, content of acrylamide has been monitored within the framework of "The Project on Dietary Exposure of the Czech Population to Selected Chemical Substances" carried out by the Centre for the Hygiene of Food Chains in Brno with the objective to describe the dietary exposure of the Czech population to chemical substances.

Sample collection is designed to cover current diet composition and also various regions in the country. Important feature of the monitoring project is a fact that samples are culinary treated so that they could be analysed in the same stage as they are consumed[4].

The determination of acrylamide is conducted in starch-rich foods but also othercomm. commodities, where acrylamide was previously detected[5] (for example olives, coffee and so on) within the range of so-called "Food basket for the Czech population". Individual commodities were purchased four times per year.at a retail market of twelve towns in the CR[6].

The acrylamide is isolated from a matrix by the extraction to 100 ml demineralised warm water (60 °C). After 20 min. mixing the sample is centrifuged at 11,000 rpm for 10 min. 7 ml of supernatant is then transferred into a stoppered flask containing 2 g anhydrous potassium bromide. Derivatization (conversion of acrylamide into 2,3-dibromopropionamide) is a next step. 2.5 ml saturated solution bromine (100 ml H_2O + 3 ml bromine) were added into stoppered flask with sample. A product of bromination (over night reaction) was extracted with 2.5 ml ethylacetate and converted into stable 2-bromopropenamide by dehydrobromination with triethylamine. The ethylacetate extract is filtered and analysed by gas chromatography (HP 5890) coupled with mass spectrometry (HP 5972) employing $^{13}C_3$ acrylamide as the internal standard.

The m/z 149 and 151 were used in the method of quantification (SIM) of 2-bromopropenamide and the m/z 152 and

154 for labelled 2-bromopropenamide. The ions separated by two mass units are due to the contribution of the two isotopes of bromine. The ratio of 79Br to 81Br is 1 : 1, which enables us to choose between the above m/z in the process of quantification. The m/z value, which isn't influenced by interference, is chosen.

The method was validated and accredited according to CSN EN ISO/IEC 17025 (Czech Accreditation Institute). The quality control was implemented by participating in proficiency testing organised by Food Analysis Performance Assessment Scheme (FAPAS).

In addition, FAPAS samples of known acrylamide content were used as reference materials for internal testing.

Results and Discussion

In total 803 various samples were analysed during 2005–2007. The highest content of acrylamide was found in potato crisps (range 268–3,817 µg kg^{-1}), french-fries (range < 15–705 µg kg^{-1}), honey gingerbread (73–429 µg kg^{-1}), cocoa powder (56–567 µg kg^{-1}). Relatively high acrylamide levels were detected in spices (147–1,076 µg kg^{-1}).

Table I
Acrylamide content in food samples (2005–2007)

Commodity	n	µg kg^{-1}
Potato crisps	36	267.88–3817.48
French fries	33	< 15–704.65
Ground paprika	12	147.39–1075.98
Pepper	12	182.06–456.48
Biscuits	36	50.19–1337.24
Savoury biscuits	24	68.70–708.38
Gingerbread	24	73.36–429.18
Cocoa powder	24	55.63–566.91
Wafers	36	22.00–420.94
Plain chocolate	12	61.11–246.86
Cornflakes	24	< 15–299.48
Cake	24	15.59–190.24
Muesli	24	< 15–195.36
Flaky pastry	12	22.54–146.93
Wheat-rye bread	24	19.84–83.58
Rye bread	36	< 15–92.67
Cream cake	26	< 15–97.51
Wholemeal bread	36	< 15–87.09
Wholemeal rolls	36	< 15–98.19
Pizza	12	< 15–66.29
Chocolate sweets	36	< 15–83.01
Chocolate bars	36	< 15–123.22
Wheat rolls	24	17.78–70.26
French loaf	24	16.17–53.67
Milk chocolate	12	28.19–63.49
Coffee (infusion)	12	4.42–21.81
Peanuts	12	< 15–48.97
Sponge biscuits	24	< 15–34.79
Cocoa instant drink	12	< 15–20.84

Concentration in peanuts, chocolate sweets, bread, rolls, sponge biscuits ranged from 15 µg kg^{-1} (LOQ = 15 µg kg^{-1}) to 100 µg kg^{-1}. The results in Table I summarize results of work at the Centre for the Hygiene of Food Chains during 2005–2007.
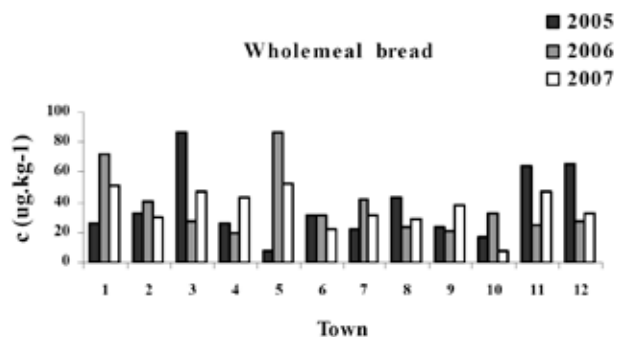
Fig. 1.   **Acrylamide content in wholemeal bread**
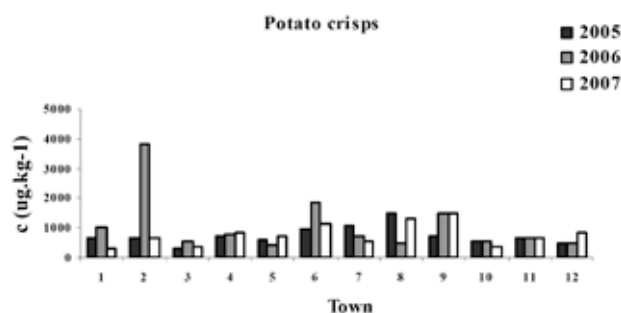
Fig. 2.   **Acrylamide content in potato crisps**

The variation of acrylamide levels were recorded between individual samples of same commodities. It can be explained by fluctuation of acrylamide precursors (asparagine and sugars) in raw materials (potatoes, cereales – .), technology, storage conditions, etc. . For example Fig. 1. and Fig. 2. document variability of results for wholemeal breads and potato crisps.

Conclusion

The results will be used for both a point and probabilistic assessment of dietary exposure doses and consequently for health risk characterization. For more precise estimate of exposure doses more acrylamide concentration results are still required.

REFERENCES

1. Eriksson S.: *Acrylamide in food products: Identification, formation, and analytical methodology*, doctoral thesis. Department of Environmental Chemistry, Stockholm University, Sweden 2005.
2. Acrylamide : withdraw: www.acrylamide-food.org
3. Acrylamide : withdraw: http://www.ciaa.be/documents/others/biscuits-EN-final.pdf.
4. Ruprich J.: *The Health Risk Assessment of Dietary Exposure to Selected Chemical Substances in year 2002.* National Institute of Public Health, Prague, 2003.
5. Kolářová J., Hradilová J., Řehůřková I., Ruprich J.: Český Těšín, 55 2006.
6. Ruprich J., Dofková M., Kopřiva V., Resová D., Řehůřková I.: *Spotřební koš potravin pro ČR*. SZÚ Praha, 289 p., 2000.
7. Kolářová J., Řehůřková I., Ruprich J.: *Konference XXX-VII. Lenfeldovy a Hoklovy dny, Brno, Sborník přednášek*, p. 90. 2007.

P53　TRANS FATTY ACIDS IN DIET OF THE CZECH POPULATION DURING YEAR 2007

JANA HRADILOVÁ, IRENA ŘEHŮŘKOVÁ, JIŘÍ RUPRICH, SYLVA SALÁKOVÁ and DAGMAR PEČINKOVÁ

National Institute of Public Health, Centre for the Hygiene of Food Chains, Palackého 3a, 612 42 Brno, Czech Republic, hradilova@chpr.szu.cz

Introduction

The topic "*trans* fatty acid" recently appears as a problem of growing interest. This is especially due to the relationship to negative health impact of these fatty acids.

Unsaturated fatty acids can have the same chemical formula but different chemical and consequently also physiological properties due to different geometrical configuration. The double bond of the unsaturated fatty acid can be in either *cis* or *trans* configuration. In nature most unsaturated fatty acids are in a *cis* configuration. This means that the hydrogen atoms are on the same side of the two carbons of the double bond. In the *trans* configuration, the hydrogen atoms are on the opposite side of the two double bond carbons.

Trans fatty acids (TFA) are formed in technological and microbiological processes by isomerization of *cis* double bonds to *trans* double bonds. Small amounts of *trans* fat are produced in the rumen of ruminants and then found in dairy and beef fat. *Trans* fats are predominately and not-intentionally produced commercially in large quantities through a process called partial hydrogenation used to protect foods from spoilage. The goal of partial hydrogenation is to add hydrogen atoms to unsaturated fats, making them more saturated. These more saturated fats have a higher melting point, which makes them attractive for baking and extends their shelf-life. These more stable fats are used in margarines and shortenings. Most of the *trans* fats are found in foods made with or fried in partially hydrogenated oils (margarines, high-fat baked goods, especially doughnuts, cookies, pastries and crackers). The *trans* fat content of these foods may be as high as 45–50 % of the fat.

High intakes of TFA may have an influence on total cholesterol. *Trans* fats increase levels of LDL (so-called "bad" cholesterol) and also lower levels of HDL (so-called "good" cholesterol). TFA increase the risk of coronary heart disease and of other chronic health problem (cancer, diabetes, obesity, interfility).

Several countries and the World Health Organization (WHO) have taken regulatory initiatives on the intake of TFA levels and proposed revisions to the criteria for nutrient content claims. The United States Food and Drug Administration (FDA) issued a regulation requiring manufacturers to list *trans* fat on the Nutrition Facts panel of foods and some dietary supplements. With this rule, consumers will have more information to make healthier food choices that could lower their consumption of *trans* fat as a part of heart-health diet. The WHO has tried to balance public health goals with a practical level of *trans* fat consumption, recommending in 2003 that trans fat be limited to less than 1 % of overall energy intake.[1–7]

The important input highlighting problems and questions around TFA in the Czech diet was an opinion of the Scientific Committee on Foods (VVP)[8,9]. This opinion was requested by the Czech Ministry of Health as a reaction on the open letter written by the group of Czech researchers criticizing content of TFA in some foods (shortening fat, cakes and biscuits, where TFA is main element – 50 % of all fatty acids content) placed on a market and requesting obligatory labeling similar to that used in the USA or in Denmark. The VVP repeated some ideas of EFSA and measures which can help to reduction the amount of TFA in foods. The VVP also recommended to analyse food samples representing current Czech diet to estimate main dietary sources and their influence on the total TFA intake[8,9].

The National Institute of Public Health in Prague, Centre for the Hygiene of Food Chains in Brno, is responsible to organize and perform longitudinal monitoring project named "Dietary Exposure to Selected Chemical Substances". In the framework of this project fatty acids have been monitored since 2005[10].

Material and Methods

Fatty acids were determined in food samples representing so-called food basket of the Czech population. 268 various food samples were collected for analyses of FA in 2007 (food samples are collected in 12 places which create 4 regions in the Czech Republic). Samples were culinary treated so that they could be analysed in the same stage as they are consumed. The result of the preanalytical treatment is a homogenous sample of cooked foods, which is then analysed[11]. One sample (mixture of samples from 3 places) represents composite sample for each region (A, B, C, D).

The analytical procedure consists of the three consequent steps - extraction of the triacylglycerols from the matrix, saponification and ester interchange with methanol and finally analyse methylesters of fatty acid using the GC – FID method. After culinary treatment and pre-homogenisation the samples were homogenized and extracted with mixture of petroleum ether/acetone (ratio 2 : 1) as a solvent by homogenizator (high frequency of revolutions) or by using of a hot solvent. Triacylglycerols of the extracted fat were saponified and ester interchanged with methanol. Methylesters of fatty acid were shaken out with hexan, dried, filtrated and then were analysed by gas chromatograph (TRACE GC) with flame ionization detection, split/splitless injection and capillary column (SP™ 2560, 100 m × 0,25 mm, thickness of film 0,2 μm). Standard Supelco 37 Component FAME Mix was used.

The method was validated using EffiValidation 3.0 software. The accuracy of the method was confirmed by analysing CRMs. Analytic quality control was implemented by participating in proficiency testing organised within Food Analysis Performance Assessment Scheme (FAPAS) of the Central Science Laboratory York (UK). Used method is

Table I
Results of the monitoring of fat and TFA in 2007 in food samples collected in 4 regions (n = 4)

Name of sample	Fat [%]	TFA [%]	Name of sample	Fat [%]	TFA [%]
Gingerbread	8.2–16.6	24.8–32.51	Cocoa	2.2–3.3	not detected
Wafers	26.6–30.9	0.23–12.14	Semolina	0.2–0.4	0.07–1.11
Chocolate sweets	16.1–31.3	0.25–14.34	Soya products	1.4–2.2	0.05–0.05
Biscuits	14.8–20.1	0.85–5.73	Smoked fish	15.8–23.0	0.17–0.20
French fries	4.9–6.7	0.77–1.12	Freshwater fish	11.1–16.5	0.49–0.66
Potato crisps	29.3–36.7	0.93–1.10	Canned fish	15.2–18.8	0.09–0.92
Wheat-rye bread	0.2–0.3	0.14–0.45	Sea fish	0.29–0.29	0.07–0.07
Rye bread	0.6–2.1	0.27–0.34	Marinated fish	4.2–12.6	0.06–0.07
Wholemeal bread	1.5–5.7	0.21–0.33	Poultry offal	3.3–7.9	0.09–0.18
Wheat rolls	2.6–3.4	0.09–1.73	Pork liver	3.5–5.1	0.10–0.14
Sponge biscuits	3.0–10.6	0.34–4.26	Sausages	14.8–22.2	0.14–0.24
Flour	0.7–0.7	0.08–0.12	Black and white pudding	12.8–24.7	0.19–0.21
Milk	0.8–1.1	1.95–2.41	Beef	10.7–14.2	1.46–2.70
Condensed milk	7.4–10.5	1.73–2.25	Rabbit	3.0–7.9	0.24–0.30
Infant milk formula	15.1–21.9	0.74–1.05	Turkey	1.1–1.6	0.38–0.47
Butter	81.3–82.4	1.94–2.20	Chicken	12.3–20.0	0.22–0.24
Butter spread	28.2–32.6	2.0–9.87	Minced meat	22.5–29.8	0.76–1.14
Margarines	41.2–59.3	0.13–1.15	Hen	7.7–11.4	0.13–0.23
Milk pudding	1.4–1.7	0.97–1.43	Smoked meat	10.1–19.8	0.22–0.89
Whole milk yoghurt	4.9–5.6	1.65–1.78	Pork	9.7–13.3	0.17–0.22
Curd dessert	1.0–4.4	1.76–1.98	Pork flank	22.2–35.8	0.15–0.22
Whipping cream	24.8–31.3	1.40–1.70	Frankfurters	14.7–38.9	0.51–1.0
Cream	10.2–11.2	1.09–1.50	Liver sausage	19.6–28.6	0.17–0.21
Sour cream	11.5–14.0	2.03–2.27	Cooked salami	14.7–23.2	0.13–0.59
Ice cream	5.7–8.0	1.24–7.13	Dry salami	25.1–48.9	0.21–0.32
Cream dessert	11.3–15.3	1.94–2.24	Bacon	45.7–62.1	0.15–0.22
Processed cheese	15.0–19.5	1.90–4.15	Poultry specialities	6.8–17.2	0.14–0.25
Blue cheese	25.2–39.0	1.64–1.81	Knackwurst	31.0–34.4	0.26–0.41
Camembert cheese	18.7–24.1	1.54–2.0	Pork ham	2.9–4.3	0.10–0.60
Hard cheese Edam	14.0–21.0	1.51–2.87	Head cheese	17.0–24.7	0.30–0.44
Eggs	7.6–9.4	0.24–0.47	Lard	86.2–97.9	0.15–0.18

accredited according to EN ISO IEC 17025 by the Czech Accreditation Institute.

Results and Discussion

Fatty acids were determined in food samples representing current diet consumed by the Czech population. The highest concentrations of TFA have been found in gingerbread, wafers, chocolate sweets and biscuits. Relatively high concentrations of TFA were also determined in butter spread, sour cream and ice cream. Very low concentrations of TFA have been found in poultry offal, pork liver, marinated fish, sea fish, flour and cocoa. In the Table I the name of sample, the ranges of content of fat and TFA are shown.

In total 268 individual food samples were analysed in 2007 (food samples are collected in 12 places which create 4 regions A, B, C, D) in the Czech Republic. In most of them the content of TFA did not exceed concentration 1 % TFA in fat (in 65 % of samples). The TFA concentration > 10 % in fat was observed in 2 % of samples. (Fig. 1.).
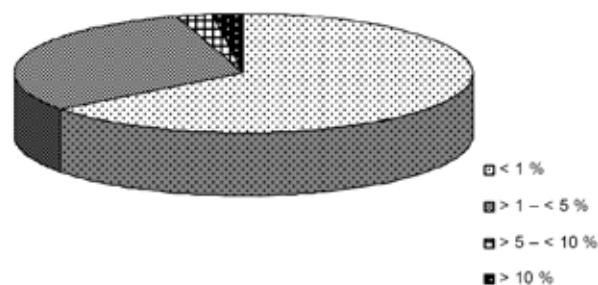
Fig. 1. **The content of the TFA as % of fat in samples collected in 2007**

In Fig. 2. an example of the comparison four kinds of sweet food samples from 4 regions (A, B, C, D) is shown. In this samples were measured the highest concentrations of TFA; it is possible to see differences between individual measures.
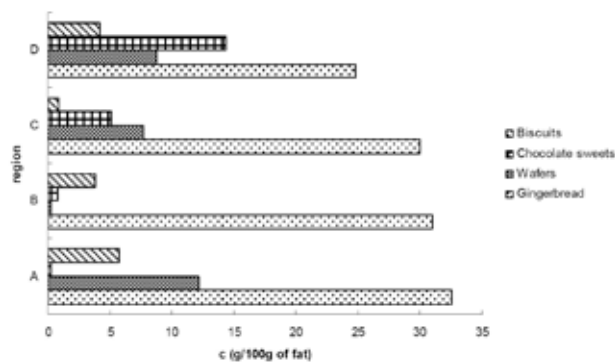
Fig. 2. **The content of the TFA in samples with the highest measured concentrations of TFA in 2007 from 4 regions**

As an example the average content of the TFA in meat (pork, hen, chicken, turkey, rabbit and beef) samples collected in 2007 from 4 regions is shown in Fig. 3.
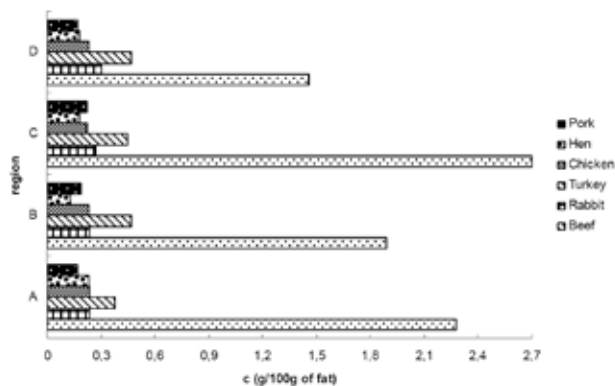
Fig. 3. **The content of the TFA in selected meat samples collected in 4 regions**

Conclusions

The topic "*trans* fatty acid" has importance for public health protection and promotion.

The content of TFA in the samples representing food basket for the Czech population was monitored in the year 2007. The highest concentrations of TFA were found in gingerbread, wafers and biscuits. Very low concentrations of TFA were found in pork liver, sea fish, flour and cocoa.

Ongoing monitoring program can cumulate new data which could be used for point and also probabilistic assessment of usual intake of FA/TFA. Results can considerably contribute to open public discussion focused on this important area of human nutrition.

REFERENCES

1. *Fatty Acids*, http://www.cyberlipid.org/fa/acid0001.htm, loaded May 7, 2008.
2. Brát J.: Potravinářská rev. *3*, 23 (2005).
3. *Trans fat*, http://en.wikipedia.org/wiki/Trans_fat, loaded May 7, 2008.
4. *Trans Fatty Acids and the Heart*, http://heartdisease. about.com/cs/cholesterol/a/Transfat.htm, loaded May 7, 2008.
5. *Trans Fatty Acids*, http://www.americanheart.org/presenter.jhtml?identifier=3030450, loaded 7.5.2008.
6. World Health Organization, http://www.who.int, loaded May 7, 2008.
7. Steinhart H., Rickert R., Winkler K.: Eur. J. Med. Res. *8*, 358 (2003). Review.
8. *Trans-mastné kyseliny v potravinách*, http://www.chpr. szu.cz/vedvybor/dokumenty/stanoviska/stan_2004_11_ deklas_TFA_info1rev.pdf, loaded September 25, 2006.
9. Vědecký výbor pro potraviny, http://www.chpr.szu.cz loaded September 25, 2006.
10. Ruprich J.: *The Health Risk Assessment of Dietary Exposure to Selected Chemical Substances in year 2002*. National Institute of Public Health, Prague 2003.
11. Ruprich J.: *Food basket for CR: Exposure Factors – CR 1997*. National Institute of Public Health, Prague 2000.

P54　DIETARY EXPOSURE MONITORING OF PERSISTENT ORGANIC POLLUTANTS FOR THE CZECH POPULATION

SYLVA SALÁKOVÁ, JANA KOLÁŘOVÁ, IRENA ŘEHŮŘKOVÁ and JIŘÍ RUPRICH

National Institute of Public Health – Centre for Hygiene of Food Chains, Palackého 3a, 612 42 Brno, Czech Republic, salakova@chpr.szu.cz

Introduction

Persistent organic pollutants (POPs) are organic compounds that are resistant to environmental degradation through chemical, biological and photolytic processes. They are highly persistent, lipophilic and bioaccumulative industrial contaminants. POPs accumulate in fat of organisms. Some of them are classified as possible human carcinogens. Therefore POPs have been controlled as contaminants in the Czech environment for many years.

The Centre for the Hygiene of Food Chains in Brno guarantees "the Project on Dietary Exposure to Selected Chemical Substances" whose objective is to describe dietary exposure to selected chemical substances for the Czech population. In the framework of this project 26 OCPs – *p,p´*-DDD, *o,p´*-DDD, *p,p´*-DDT, *o,p´*-DDT, *p,p´*-DDE , *o,p´*-DDE, endosulfan I + II, endosulfan sulfate, HCH(alpha-, beta-, gamma-, delta-,), aldrin, endrin and its metabolite endrinketone, dieldrin, methoxychlor, heptachlor and its metabolites heptachlorepoxide (A + B), HCB, alpha and gamma chlordane, mirex and the seven most significant indicators of PCBs (28, 52, 101, 118, 153, 180) have been monitored since 1994. Cis- and trans- chlordane, oxychlordane and mirex were quantified since 2002.

Experimental

PCBs and OCPs were determined in samples which represent more than 95 % of composition (by weight) of current diet for the Czech population. First of all the samples bought on the Czech market were subjected to culinary treatment so that they could be analyzed under the same conditions as they are consumed. The result of the preanalytical treatment was a homogenous sample, which was then analyzed. The analytical procedure consisted of: *(i)* isolation (extraction) of the analytes from the matrix, *(ii)* removal of co-extracted compounds of the matrix and *(iii)* analysis using the GC method. The procedure was optimized as a multiresidual analysis for determination of polychlorinated biphenyls (PCBs) and organo-chlorine pesticides (OCPs).

Standards

We used a single standard solution of PCBs and OCPs (concentration 10 ng µl^{-1}, Dr. Ehrenstorfer) for preparation of calibration standard. Internal standards (PBB1, PCB 209 and 2,4,5,6-Tetrachloro-m-xylene, concentration 10 ng µl^{-1}, Dr. Ehrenstorfer) were used to determine the extent of recovery of the analytical procedure.

Sample Preparation

The amount of the food samples for the analysis was 50–200 g. Samples were ground with anhydrous sodium sulphate and spiked with PBB1, PCB 209 and 2,4,5,6-Tetrachloro-m-xylene as recovery standards. The first step of the preparation is the extraction. The type of extraction depends on the matrix of sample. The fat samples were extracted on automatic extraction device (Buchi Extraction System B-811) by hot solvents, non-fat samples were extracted at high speeds homogenizator (Polytron PT 3100) and the liquid samples were extracted in the liquid/liquid system. The mixture of petroleum ether/acetone (ratio 2 : 1) or dichloromethane was used as a solvent for liquid samples. The extracts were evaporated to constant weight in a rotary evaporator and the lipids were determined gravimetrically. The sample extracts were purified by a gel permeation chromatography (GPC) on column "Envirogel GPC cleanup column" fy Waters and by column chromatography on Florisil.

GC Analysis

The cleaned samples were analyzed by gas chromatograph (GC-Hewlett-Packard 5890) with two column system using different stationary phases and ECD detectors. For analyses were used following conditions:

column: DB 5 (30 m × 0.25 mm × 0.25 µm)
column: DB 17(30m × 0.25 mm × 0.25 µm)
initial temperature:　90 °C
initial time:　2 min
temperature rate 1:　15 °C min^{-1}
final temperature:　180 °C
temperature rate 2:　3 °C min^{-1}
final temperature:　220 °C
temperature rate 3:　1 °C min^{-1}
final temperature:　250 °C, final time 0.67 min
run time:　52 min

The method for the determination of POPs is accredited by the Czech Accreditation Institute by the CSN EN ISO/IEC 17025 Standard. Quality control of the results was conducted by the means of testing materials (TM) and certified reference materials (CRM). Certified reference material for PCBs was BCR 350 (mackerel oil) and certified reference material for OCPs was BCR 598 (cod liver oil) and BCR 430 (pork fat). Limits of quantification, depending on the type of the matrix, ranged between 0.002 and 0.05 µg kg^{-1}.

Results

Every year from 1994 to 2007 the content of 37 POPs was determined in the samples of foodstuffs. 110 samples of foodstuffs are analyzed per year. The highest content of POPs was observed in fishes, meat products, butter and milk products.

The results showed that the most abundant of all the measured analytes were *p,p´*-DDE and PCB 138, 153,180. The highest concentrations of these analytes were repeatedly

found in freshwater fish and fish products. Their occurrence was also observed in meat. A common source of them is also milk fat. Selection of the highest sums of analytical findings in 2007 (n = 110) is shown in the Fig. 1. and Fig. 2. The non-fat samples are logically less contaminated groups concerning these analytes. The data were used for assessment of dietary exposure of the population of the Czech Republic (Fig. 3., Fig. 4.).

Conclusions

　　As the PCBs can accumulate in animal tissues, the foods of animal origin are one of the most significant sources of exposure. Higher exposure doses can be particularly expected in persons with high intake of animal fats. Hence, the decrease in consumption of animal fat can significantly contribute to lowering exposure doses.
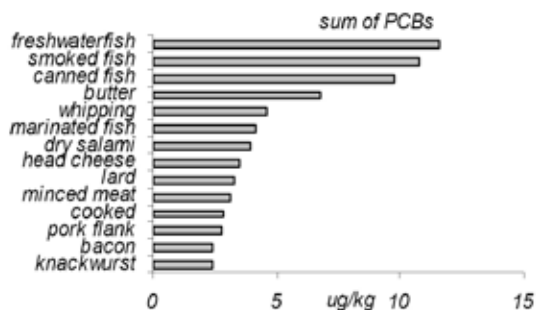
Fig. 1.　**Selection of foods with the highest concentrations of PCBs (sum of PCB 28, 52, 101, 118, 138, 153, 180) in 2007**
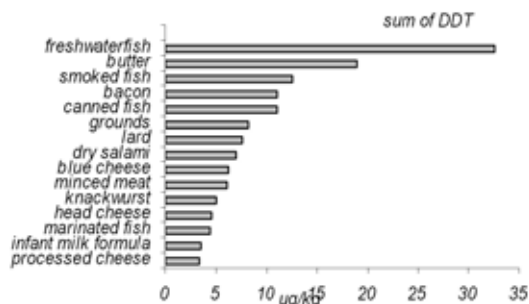
Fig. 2.　**Selection of foods with the highest concentrations of sum of DDT + DDE + DDD in 2007**

　　The trends in population exposure to DDT isomers and its analogues (DDD, DDE) and PCBs have been investigated since 1994. The found results expressed as the dietary exposure for the average Czech population (considering food consumption and the culinary factor) did not even reach the acceptable daily intake for any monitored POPs. The found exposition doses of individual POPs probably do not present a serious health risk for the average population of the Czech Republic. Detailed information about the monitoring can be found in publications of the National Institute of Public
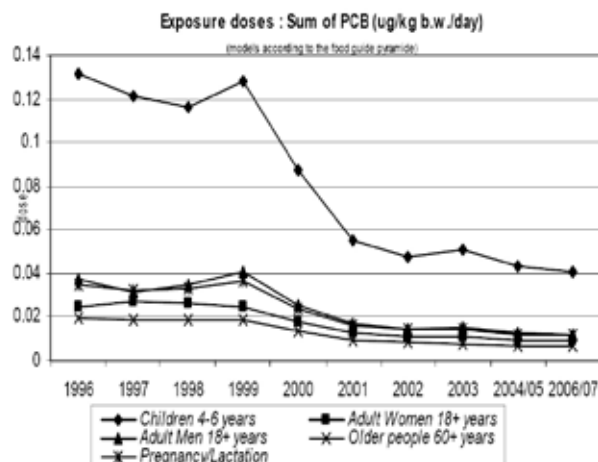
Fig. 3.　**The trend of exposure doses for a sum of 7 PCBs (28, 52, 101, 118, 138, 153, 180) since 1996 to 2007**
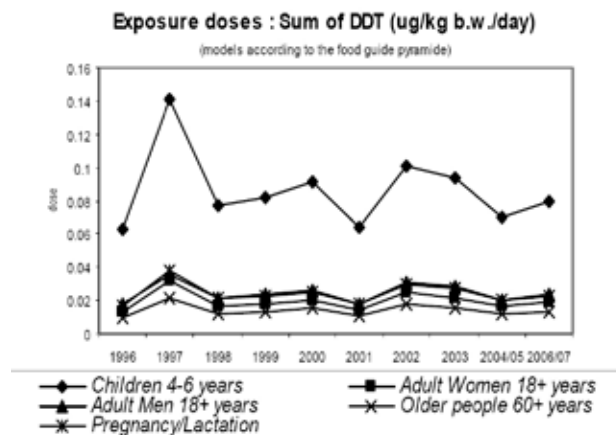
Fig. 4.　**The trend of exposure to sum DDT (= DDT + DDE + DDD) since 1996 to 2007**

Health in Prague, describing human dietary exposure in the Czech Republic.

REFERENCES
  1. Ruprich J.: *The Health Risk Assessment of Dietary Exposure to Selected Chemical Substances in year 2002*. National Institute of Public Health, Prague 2003
  2. Ruprich J.: *Food basket for CR: Exposure Factors – CR 1994* . Natinal Institute of Public Health, Prague 1997
  3. Ruprich J., Dofková M., KOPŘIVA V., Resová D., Řehůřková I.: *Spotřební koš potravin pro ČR*. Praha: SZU Praha, 2000.
  4. Ruprich J., et al.: *Zdravotní důsledky zátěže lidského organizmu cizorodými látkami z potravinových řetězců v roce 2005*: Státní zdravotní ústav Praha, 2006. hppt://www.chpr.szu.cz/monitor/tds05c/tds05c.htm
  5. Řehůřková I.: Cent. Eur. J. Publ. Health *10*, 174 (2002).

P55 OCCURRENCE OF FUSARIUM MYCOTOXINS AND THEIR CONJUGATED FORMS IN CEREAL-BASED FOODS

M. KOSTELANSKÁ, J. HAJŠLOVÁ, M. ZACHARIÁŠOVÁ, A. KRPLOVÁ, J. POUSTKA and J. KOHOUTKOVÁ

Institute of Chemical Technology Prague,
Technická 3, 166 28 Prague 6 – Dejvice, Czech Republic,
marta.kostelanska@vscht.cz

Introduction

Cereal-based foodstuff such as bread and beer belong in many countries to the most important items in markets´ basket. Trichothecene mycotoxins, the toxic secondary metabolites produced by species of *Fusarium* genus, are the common "natural" contaminats of cereals worldwide. Furthermore, these toxins are relatively stable, surviving household/industrial processing, thus transferred into the final food products[1,2,3].

Deoxynivalenol (DON) is one of the most abundant *Fusarium* mycotoxin. Recently, it has been shown, that besides the native form, DON also occures in cereals conjugated to glucose[1]. This "masked" DON-3-Glucoside (DON-3-Glc) is produced by metabolism of living plants and therefore, the consumers are exposed to both these mycotoxins that occur in food. The recent studies have shown that, alike the DON, "masked" forms can be transmitted thoughout the processing to food products[3]. With regard to the above mentioned, the special attention should be paid to control maximum limits established for toxins in unprocessed grains as well as food products.

Several studies concern with mycotoxin contamination of cereal-based commodities such as bread or beer, have been published up to now[4,5], however, only very limited information is known about the occurrence of conjugated forms of trichothecenes, especially DON in processed cereal-based foodstuff. The current study concern with analysis of DON-3-Glc in bread and beer is aiming at fillig the gap in this area. The aim of study was to determine: *(i)* the influence of baking technological times on levels of mycotoxins in bread and *(ii)* the average contamination of commercially available beers.

Experimental

Chemicals and Reagents

Pure crystalline standards of analysed mycotoxins deoxynivalenol (DON), DON-3-Glucoside (DON-3-Glc), 3-acetylDON and 15-acetylDON (ADONs), nivalenol (NIV), fusarenon-X (Fus-X) HT-2 toxin (HT-2), T-2 toxin (T-2) and zearalenone (ZON) were purchased from Biopure (Austria). Organic solvents in HPLC grade used for LC-MS/MS analysis were products of Sigma-Aldrich (Germany). Cellite for beer samples purification was obtained from Sigma-Aldrich as well. Ultra-pure water was produced by Milli-Q systém. Working composite standards stock solution prepared in acetonitrile at concentration 1,000 ng ml^{-1} was stored at 4 °C. Matrix-matched standards used for analysis were prepared by procedure described below (see sample preparation) at concentration range 1–1,000 ng ml^{-1}.

Samples

Bread samples (n = 9) were prepared in laboratory scale from whole-wheat flour, which was ground from naturaraly infected wheat grains. The loaves of bread were prepared in 3 variants differing in times of proofing, fermentation and baking (variant 1: 40 min. proofing and fermentation, variant 2: 45 min. proof. + ferment., variant 3: 50 min. proof. + ferment). For the dough-making process flour (300 g), yeasts (5.4 g), salt (4.5 g), saccharose (6 g), vegetable oil (4.5 g) and distilled water (150–165 ml) were used. Immediately after farinographic kneading the dough was placed into the laboratory thermostat for 40 or 50 min. After the proofing the dough was divided into three pieces that were allowed to ferment for 40 or 50 min. The bread loaves were baked in an electric laboratory oven at 240 °C for 15 or 20 min.

23 light and 7 dark beer samples, which were collected in Czech retail market in the year 2008. All of beers analysed within this monitoring study were derived only from barley malts and contained 4–6 volume % of alcohol.

Sample Preparation

Whole-wheat flour and bread samples after the drying were processed as follows: 12.5 g of homogenised samples were extracted with 50 ml of acetonitril-water mixture (84 : 16, v/v) for 30 min using an automatic laboratory shaker (IKA Laboratortechnik, Germany). Crude extract was then filtered (Filtrak No.390, VEB Freiberger, Germany) and 4 ml aliquot were evaporated to dryness, the residue was transfered into 1 ml of mobile phase in HPLC grade, consisted of water-methanol (1 : 1, v/v) and passed through a 0.2 μm microfilter (Alltech, USA).

The extraction step of beer samples was carried out by analogous procedure. To 16 ml of degassed beer were added 3.2 g of Cellite and 84 ml of acetonitrile. This heterogenous mixture was shaken for 30 min and then filtered. 5 ml of extract were evaporated to dryness and residue again redissolved in mixture of methanol-water (1 : 1, v/v).

LC-MS/MS Mycotoxins Analysis

Separation and quantification of target analytes were carried out by means of procedure described in detail in our previous study[2]. Briefly, HPLC separation (HP 1100 LC system, Agilent Technologies, USA) with reversed phase hyphenated to tandem mass spectrometer (Finnigan LCQ Deca, USA) were used for chromatographic separation of analytes. Mobile phase consisted of methanol and water acidified with ammonium acetate. Further MS/MS identification and quantification of analytes was carried out by ion trap analyzer with APCI ion source in both positive and negative mode.

The sample analysis was carried out in three repetitive. Matrix-matched standards of samples were prepared as described above with the only one difference, residue after crude extract evaporation was dissolved in toxins standard solution (methanol: water, 1 : 1, v/v). By means of described analytical method the limits of detection were achieved in range 0.5–5 ng ml^{-1} for measured mycotoxins.

Results

The levels of *Fusarium* toxins found in wheat grains, whole-wheat flour and breads prepared by three alternative procedures are summarized in Table I. Out of 8 monitored target mycotoxins only NIV, DON and its conjugates ADONs and DON-3-Glc were present at levels exceeded method detection limits. No Fus-X, HT-2, T-2 and ZON were found in examined samples. It should be noted, that conjugated DON was contained in experimental wheat at relatively high level, in this particular case the DON-3-Glc: DON ratio value was approximately 3 : 10, while in previous studies the ratio was reported to be 1 : 10 ref.[2].

Within the baking experiments decrease of both DON and DON-3-Glc occurred (up to 33 % and 49 %, respectively), ADONs and NIV decreased below the limits of detection. Although no significant differences in mycotoxins levels were obtained in bread loaves prepared under various experimental conditions, some indirect correlation between DON and DON-3-Glc concentrations could be seen. The longer was fermentation and proofing phase the lower was DON decrease, while decline DON-3-Glc was higher. These results indicate a potential breakdown of DON-3-Glc during bread-making yielding in free DON. At the same time other unknown transformations of these mycotoxins take place resulting in overall lower trichothecenes levels in bread in comparison with wheat taken into the process.

Table I
Levels of mycotoxins in wheat, flour and bread variations

| Sample | Mycotoxins [μg kg^{-1}] | | | |
	DON	DON-3-Glc	ADONs	NIV
Wheat	469	162	73	47
Flour	337	102	23	15
Bread-var.1	263	29	<5	<5
Bread-var.2	278	25	<5	<5
Bread-var.3	292	22	<5	<5

The data obtained in the second part of experiments concerned with beers are presented in Table II. The majority of beers contained detectable levels of DON, ADONs and DON-3-Glc. Occurrence of DON-3-Glc was shown in all of light

Table II
Levels of mycotoxins in beers

Beer	Mycotoxin [μg dm^{-3}]	Incidence [%]	Mean [μg dm^{-3}]	Range [μg dm^{-3}]
Light	DON	82	12.9	1.5–33.7
	DON–3–Glc	100	16.3	3.2–38.0
	ADONs	69	8.1	3.9–27.8
Dark	DON	84	9.3	1.0–29.5
	DON–3–Glc	92	11.0	2.5–40.2
	ADONs	71	8.8	5.1–19.8

beer samples. Interestingly, its mean levels exceeded DON levels in light as well as dark beers. Although bioavailability of DON-3-Glc has not been documented until now, question arises whether this "masked" DON does not increase the healt risk associated with trichothecenes dietary intake. The relative ratio of DON-3-Glc and DON in beers ranged from 0.8 to 1.3.

Conclusions

The results obtained in this study can be summarized as follows:

(i) Some decrease of *Fusarium* mycotoxins including DON and its major conjugates ADONs and DON-3-Glc occurred during baking.

(ii) No significant impact of the tested technological times (proofing and fermentation) was observed.

(iii) Extensive contamination of beers obtained at Czech market demonstrated. The levels of DON, ADONs and DON-3-Glc in light and dark beers were comparable, the later compound was dominating.

REFERENCES

1. Berthiller F, Dall'Asta Ch, Schuhmacher R, Lemmens M, Adam G, Krska R.: J. Agric. Food Chem. *53,* 3421 (2005).
2. Lancova K., Hajslova J., Kostelanska M., Kohoutkova J., Nedelnik J., Moravcova H., Vanova M.: Food Addit. Contam. *25*, 650 (2008).
3. Lancova K., Hajslova J., Poustka J., Krplova A., Zachariasova M., Dostalek P., Saschambula L.: Food Addit. Contam. *25*, 732 (2008).
4. Schollenberger M., Suchy S., Terry Jara H., Drochner W., Miller H.M.: Mycopathologia *147*, 49 (1999).
5. Papadopolou-Bouraoui A., Vrabcheva T., Valzacchi S., Stroka J., Anklam E.: Food Addit. Contam. *21*, 607 (2004).

P56 LIGNANS IN FLAXSEED – LC-MS/MS DETERMINATION

ANNA KRAJČOVÁ[a], VĚRA SCHULZOVÁ[a], JANA HAJŠLOVÁ[a] and MARIE BJELKOVÁ[b]

[a]Department of Food Chemistry and Analysis, Faculty of Food and Biochemical Technology, ICT Prague, Technická 5, 166 28 Prague 6, Czech Republic,
[b]Agritec Plant Research s. r. o., Šumperk
anna.krajcova@vscht.cz

Introduction

Lignans constitute a group of important biologically active plant phenols, structually characterized by the coupling of two phenylpropanoid units by a bond between β-positions in propane side chains. Lignans were identified in trees already in the 19th century. Currently, wide occurrence of lignans in various vascular plants has been well documented[1].

The interest in lignans and other phytoestrogens has grown in the recent years because of their putative beneficial health effects[2]. They have been suggested to induce a various effects, such as antioxidant, antitumor, estrogenic, and antiestrogenic activities, and the protection against coronary heart disease[3].

The reachest dietary source of lignans are flaxseeds, with glycosides of secoisolariciresinol (SECO) (Fig. 1.) and matairesinol (MAT) (Fig. 2.) as the major representatives of this group[2]. After ingestion, these lignans are deglycosylated and partly converted to the mammalian enterodiol and enterolactone by colonic bacteria. These forms are considered as the biologically active substances responsible for the beneficial effects in humans[4].

In the presented study, a quantitative method (LC MS/MS) for determination of the plant lignans, secoisolariciresinol and matairesinol, in flaxseed has been developed. The study of variation in SECO and MAT content was based on examination of various cultivars of flaxseed.
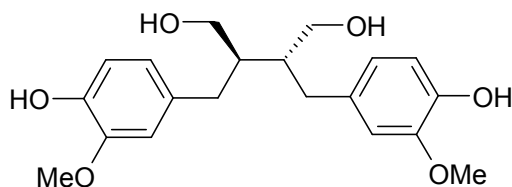
Fig. 1. **SECO**
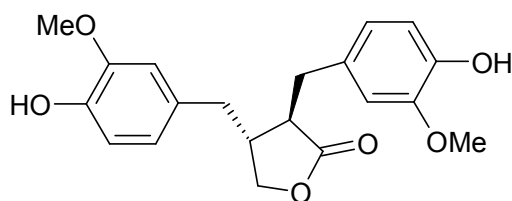
Fig. 2. **MAT**

Experimental

C h e m i c a l s

The lignan standards, secoisolariciresinol and mataresinol were purchased from Sigma Aldrich (Germany). The β-glucuronidase/sulfatase was purchased from Sigma-Aldrich (Germany).

Ethylacetate, cyclohexane, and acetic acid glacial were purchased from Sigma-Aldrich (Germany). Sodium hydroxide was purchased from Penta Chrudim (Czech republic). The deionised water was prepared using Milli-Q water system (Millipore, USA).

S a m p l e s

The flaxseeds were obtained from Agritec Plant Research s.r.o. (Šumperk, Czech republic). The levels of SECO and MAT were monitored in different cultivars. Cultivars AGT, Alaska, Astral, Atalante, Bajkal, Baladin, Flanders, Lola, Oural, Recital represented oil cultivars. Cultivar Venica represented fibre flax.

S a m p l e   P r e t r e a m e n t

Defated flaxseeds were incubated overnight with enzyme of Helix pomatia β glucuronidase/sulfatase in sodium acetate buffer at 37 °C. Subsequently the enzymatic hydrolysates were extracted with ethylacetate/cyclohexane. After removing the solvent, the residue was transfered into mobile phase.

A n a l y s i s

LC-MS/MS method was employed for examination of extracts. The system consisted of Alliance chromatography separation Module 2695 (Waters, USA) equipped with Discovery C 18 column (Supelco, Germany) (50 mm × 3.0 mm i.d., 5 μm), and Quattro Premier XE (Waters, UK) mass spectrometer detector employing an electrospray ionization source operating in negative mode.

M e t h o d   V a l i d a t i o n

Analytes were quantified by the standard addition method to compensate the influence of the co-isolated matrix on the effectivity of the ionisation process. Matrix standards could not be used due to unavailability of blank flaxseeds.

Repeated measurements were carried out to get performance characteristic of the method.

Results

Optimization of extraction and hydrolysis. The release of aglycones (SECO, MAT) from their glycosidic forms prior to analysis is necessary. Enzymatic hydrolysis was tested, and optimized. β glucuronidase/sulfatase (Helix pomatia) in sodium acetate buffer was used for hydrolysis of defated ground flaxseeds. Subsequent extraction of target analytes was carried out with ethylacetate/cyclohexane solvent mixture.

Chromatografic and detection conditions. The LC MS/MS method earlier described by Milder at al. (2004) was

tested in the first stage. However, due to relatively high limits of detection, the composition of mobile phase was modified using acetic acid to enhance MS ionisation.

Performance characteristics. The quantification was carried out using the standard addition method. The crude flaxseed extracts were spiked with analytes to increase the analytical signal by a factor of 1.5 to 3.

The limits of detection (LOD) were determined by five repetitive analysis of standard solutions, the found values were for SECO 0.020 $mg\,kg^{-1}$ and for MAT 0.025 $mg\,kg^{-1}$.

The repeatability was determined by six times analysis of flaxseed extracts and was expressed as relative standard deviation (RSD, %), the value for MAT was 3.2 % and for SECO 4.7 %.

Table I
Average levels of SECO and MAT in different cultivars of flaxseed

Cultivar	MAT [$mg\,kg^{-1}$]	SECO [$mg\,kg^{-1}$]
AGT	13	1157
Alaska	22	2317
Astral	14	1955
Atalante	14	1317
Bajkal	13	1172
Baladin	11	1197
Flanders	14	1193
Lola	12	1150
Oural	11	716
Recital	12	1030
Venica	16	682

Concentration of lignans in flaxseeds. The mean levels of lignans are shown in Table I. Their amount in various flaxseed samples ranged for SECO from 219 (Venica) to 2610 (Alaska) $mg\,kg^{-1}$, and for MAT from 5 (AGT 984) to 22 (Alaska) $mg\,kg^{-1}$ with average levels 1031 $mg\,kg^{-1}$ of SECO and 13 $mg\,kg^{-1}$ of MAT. The levels of SECO were significatly lower in fibre flax cultivar Venica (220–860 $mg\,kg^{-1}$) compared to linseed oil cultivars (280–2600 $mg\,kg^{-1}$). The differences in MAT content were comparable in both types of linseeds.

Conclusions

LC-MS/MS method for determination of plant lignans, SECO and MAT, in flaxseed has been developed and validated. Flaxseeds were shown to be a rich dietary source of lignans. The dominating phytoestrogens representing this biologically active compounds were SECO and MAT. The highest lignans content was in cultivar Alaska.

REFERENCES

1. Willför S. M., Smeds A. I., Holmbom B. R.: J.: Chromatogr. A. *64*, 1112 (2006).
2. Sicilia T., Niemeyer H. B., Honig D. M., Metzler M.: J. Agric. Food. Chem. *51*, 1181 (2003).
3. Smeds A. I., Eklund P. C., Sjohölm R. E., Willför S. M., Nishibe S., Deyama T., Holmbon B. R.: J. Agric. Food. Chem. *55*, 1337 (2007).
4. Charlet S., Bensaddek L., Raynaud S., Gillet, F., Mesnard F., Fliniaux M.-A: Plant Physiol. Biochem. *40*, 225 (2002).

P57 THE OCCURENCE OF PHTHALIC ACID ESTERS IN SELECTED FEEDSTUFFS

LENKA KRÁTKÁ, ALŽBETA JAROŠOVÁ, JANA MALYSZOVÁ, VLASTA STANCOVÁ and JIŘÍ HARAZIM

Mendelova zemědělská a lesnická univerzita v Brně
Zemědělská 1, 613 00 Brno,
krtaska@seznam.cz

Introduction

Phthalate acid esters (PAEs) are used in large quantities as softeners in many plastic products, paint, glue, putty, pharmaceutical products and cosmetics.[1–3] Significant migration into the environment is demonstrated during their production, manufacture, use and disposal.[4–5] Phthalates are not chemically bound to these products and are therefore continuously released into the air or through leaching into liquids.[6–11] Humans can be exposed to vinyl plasticizers through ingestion, inhalation, direct injection, or by skin contact. Exposures to phthalates range from milligrams to micrograms[12]. The occurrence of di-(2-ethylhexyl) phthalate (DEHP) ranks over 50 % of total PAEs. Butyl-benzyl phthalate (BBP) and di-*n*-butyl phthalate (DBP) are common occurrence[13].

Experimental

The aim of this investigation was to determine the occurance and content of phthalate acid esters (DBP and DEHP) in feedstuffs and oils.

M a t e r i a l

Samples of feedstuffs, premixes and feed additives for livestocks were collected by qualified expert from ÚKZÚZ (Central Agricultural Control and Testing Institute) in years 2005 (n = 73) and 2006 (n = 59). These samples were collected from received feeds, dispatch stores, reception stores and multicomponent scales and stocked in polyethylene bags and glass bottles. Samples of oils A, B, C (n = 23) were collected during technological production processing in 2007. Oils A were stored in glass bottles, B and C in plastic barrels.

M e t h o d s

Proved methods were used for PAEs determination in feedstuffs[14]. Samples were stored in refrigerator after sampling and transporting.

Before starting the analyses, glass and laboratory materials were washed and rinsed with acetone. Samples were sufficiently homogenized, extracted by organic solvents mixture hexan:acetone (1 : 1). PAEs were separated from co-extracts by GPC (gel permeation chromatography) in a Bio-beads S-X3 filling. After GPC, the eluate was cleaned with hydrated sulphuric acid. PAEs were determined by HPLC and UV detection at 224 nm in a Cogent e-Column, C 18, using acetonitrile:water (9 : 1) as the mobile phase. The detection limit for PAEs in feeds is 0.03 mg kg^{-1}.

Table I
Concentrations of DBP, DEHP and ΣDBP+DEHP in feedstuffs in 2005

Sample	DBP [mg kg^{-1}]	DEHP [mg kg^{-1}]	ΣDBP+DEHP [mg kg^{-1}]
Wheat	0.91	3.15	4.06
Soybean oil	110.96	20.46	131.42
Natrium chloride	0.12	0.79	0.91
Vitamin K3	0.30	0.22	0.52
Vitamin D3	0.09	0.99	1.08
L-lysin	<0.03	<0.03	<0.03
Vegetable soybean oil	19.89	8.60	28.49
Alimet-methionine	38.36	<0.03	38.36
Animal fat	47.29	11.58	58.87
Animal fat	26.22	15.33	41.55
Folic acid	0.07	1.46	1.53
Corn	1.02	1.01	2.03

Results

Detected concentrations of DBP, DEHP and ΣDBP+DEHP in the first year of study (2005) are digested in Table I. The highest concentration of ΣDBP+DEHP was found in soybean oil (131.42 mg kg^{-1}) and animal fat (58.87 mg kg^{-1}). The lowest concentration was measured for L-lysin (<0.03 mg kg^{-1}). In 2006 (n = 59) levels of ΣDBP+DEHP ranged from 0.04 mg kg^{-1} (Wheat – start of processing) to 32.4 mg kg^{-1} (Rapeseed oil – end. plastic). A list of results in 2006 is given in Table II. PAEs in oils are listed in Table III. The highest concentrations of PAEs were measured in oils C (ΣDBP+DEHP = 61.55 mg kg^{-1}), whereas lowest levels were found in oils A (5.14 mg kg^{-1} ΣDBP+DEHP).

Table II
Concentrations of DBP, DEHP and ΣDBP+DEHP in feedstuffs in 2006

Sample	DBP [mg kg^{-1}]	DEHP [mg kg^{-1}]	ΣDBP+DEHP [mg kg^{-1}]
Vitamin D3	0.08	0.28	0.36
Vitamin K3	<0.03	0.19	0.19
Biotin	0.21	1.68	1.89
Nicotinic acid	0.04	2.98	3.02
L-lysin	0.05	1.71	1.76
Vitamin E	0.62	1.53	2.15
Wheat - start of processing	<0.03	0.04	0.04
Rapeseed oil – start	2.43	18.55	20.98
Rapeseed oil – end	4.68	17.19	21.87
Rapeseed oil – end plastic	26.63	5.77	32.4
Alimet	1.29	3.23	4.52
Mycocarb	0.05	0.04	0.09

Table III
Concentration of DBP, DEHP and ΣDBP+DEHP in oils

Sample	DBP [mg kg^{-1}]	DEHP [mg kg^{-1}]	ΣDBP+DEHP [mg kg^{-1}]
Oil A	1.11	5.71	6.82
Oil C	2.13	37.38	39.51

Conclusions

Samples of feedstuffs for livestock (complementary feeds, premixes, feed additives and raw materials) were collected in years 2005 and 2006, oils in 2007. Various levels of contamination were determined in feedstuffs. Feed additives, premixes and complementary feeds as well are poor in phthalates. Raw materials have higher amounts of PAEs, but the highest concentrations were measured in materials with high fat content. Because of phthalate´s lipophilic nature, they are released mainly into feedstuffs containing fat[15]. Phthalic acid esters determined in this investigation are similar to RASZYK et al. (1998)[16], where was DBP level in feed additives 0.207 mg kg^{-1} and DEHP 0.216 mg kg^{-1}. Oils before technological production processing (in plastic barrels) contained lower levels of PAEs than after processing, so this study confirmed, that PAEs can easily migrate from platics to fat.

REFERENCES

 1. Agency for Toxic Substances and Disease Registry. 2001. *Toxicological Profile for Di-n-butyl Phthalate.* Atlanta, GA: Agency for Toxic Substances and Disease Registry.
 2. Agency for Toxic Substances and Disease Registry. 2002. *Toxicological Profile for Di(2-ethylhexyl) Phthalate (DEHP).* Atlanta, GA: Agency for Toxic Substances and Disease Registry.
 3. Schettler T.: Int. J. Androl. *29*, 134 (2006).
 4. Polo M., Llompart M., Garcia-Jares C., Cela R.: J. Chromatogr. A *63*, 1072 (2005).
 5. Staples C. A., Peterson D. R., Parkerton T. F., Adams W. J.: Chemosphere *35*, 667 (1997).
 6. Afshari A., Gunnarsen L., Clausen P. A., Hansen V.: Indoor Air. *14*,120 (2004).
 7. Fujii M., Sinohara N., Lim A., Otake T., Kumagai K., Yanagisawa Y.: Atmos. Environ. *37*, 5495 (2003).
 8. Elsisi A. E., Carter D. E., Sipes I. G.: Fundam. Appl. Toxicol.. *12*, 70 (1989).
 9. McKee R. H., El-Hawari M., Stoltz M., Pallas F., Lington A. W.: J. Appl. Toxicol. *22*, 293 (2002).
10. Wormuth M., Scheringer M., Vollenweider M., Hungerbuhler K.: Risk. Anal. *26*, 803 (2006).
11. Schettler T.: Int. J. Androl. *29*:134, 181 (2006).
12. http://www.reason.org/peg2.html
13. Lopez-Jimenez F. J., Rubio S., Perez-Bendito D.: Anal. chim. acta *142*, 551 (2005).
14. Jarošová A. Habilitační práce. MZLU. Brno, 2004, p.137
15. Tsumura Y., Ishimitsu S., Namakura Z., Yoshii K., Kaihara A., Tonogai Y.: J. Food Hyg. Soc. Jap. *42*, 128 (2001).
16. Raszyk J., Gajdůšková V., Jarošová A., Salava J., Palac J.: Veterinární Medicína – Czech *43*, 93 (1998).

P58　NEW APPROACH IN ANALYSIS OF FUSARIUM MYCOTOXINS AND THEIR "MASKED" FORMS: IMMUNOAFFINITY COLUMN CLEAN-UP

ALEXANDRA MALACHOVÁ (KRPLOVÁ), MARTA KOSTELANSKÁ, MILENA ZACHARIÁŠOVÁ, JANA KOHOUTKOVÁ and JANA HAJŠLOVÁ

Institute of Chemical Technology Prague, Technická 5, 166 28 Prague 6 – Dejvice, Czech Republic, alexandra.malachova@vscht.cz

Introduction

Mycotoxins are classified as toxic, low molecular weight secondary metabolites of microscopic filamentous fungi. Fusarium toxins are the most common contaminants in cereals. Recently several research study have been focused on masked deoxynivalenol and other mycotoxins of these group. The hyphothesis on existence of "masked" mycotoxins was postulated as soon as in mid-1980s. Mycotoxicosis cases were observed in farm animals although the laboratory examination of a feeding stuff did not indicate high levels of toxins. It was concluded that hydrolysis of precursor toxins in digestive tracts of animals occurs. Follow up research showed that mycotoxins can be partly metabolized by living plants as a result of detoxification process. "Masked" mycotoxins escape routine analysis for several reasons. These substances are more polar than the precursor toxins, they are difficult to extract with the common organic solvents or get lost in the clean-up procces. In addition, standards of these substances are not commercially available. Currently deoxynivalenol-3-glucoside (D3G) representing the "masked" form of the most common mycotoxin deoxynivalenol (DON) is available.

The most common method in mycotoxin analysis is liquid chromatography coupled with tandem mass spectrometry (LC-MS/MS). To reduce interferences due to matrix coextracts various clean-up procedures are involved in sample processing step.

This study assessed the afficacy of several immunoaffinity columns (IACs) designed either for single fusarium toxins (DONPREP®, EASI EXTRACT HT-2 T-2®, EASI EXTRACT ZON®) and DZT Multi Myco IACs for multimycotoxin analysis. Based on our recent research we investigated occurence of this phenomenon that documented cross reactivity of D3G in DON dedicated ELISA kits in the above IACs.

MycoSep® 226 AflaZoṇ columns clean-up based on adsorbtion chromatography usage were used for crude extract processing.

Experimental

C h e m i c a l s

Standards of analysed mycotoxins DON, D3G, HT-2 toxin (HT-2), T-2 toxin (T-2) and zearalenone (ZON) were purchased from Biopure (Austria).

Calibration standard solutions were prepared in the LC mobile phase methanol:water (50 : 50, v/v) by diluting of stock standard solutions in concentration range 5–1000 ng ml^{-1}. While standards in solvent were employed for calibration in case of purified samples, matrix-matched standards were used for unpurified extract.

S a m p l e s

Naturaly contaminated maize containing several fusarium toxins (see Table I) was used for our experiments.

Table I
Contents of trichothecene mycotoxins

Trichothecene	Mean [µg kg^{-1}]	s.d. [µg kg^{-1}]
deoxynivalenol	620	21
deoxynivalenol-3-glucoside	100	26
HT-2 toxin	27	18
T-2 toxin	52	15
zearalenone	462	23

I m m u n o a f f i n i t y　C o l u m n s　a n d　M y c o S e p

Immunoaffinity columns DONPREP®, EASI EXTRACT HT-2 T-2®, EASI EXTRACT ZON® and DZT Multi Myco IACs were purchased from R-Biopharm Rhône Ltd (Germany). DONPREP® columns contain a highly specific monoclonal antibodies purifying and concentrating DON from a sample extract. EASI EXTRACT HT-2 T-2® columns are made for determination of HT-2 and T-2 and EASI EXTRACT ZON® are specified for ZON analysis. DZT Multi Myco IACs are designed as multi-mycotoxins columns. MycoSep® 226 AflaZoṇ columns (Romer Labs®, Austria) are designed for complex matrices with more interference such as gluten, meal feed and processed food.

S a m p l e　P r e p a r a t i o n　(E x t r a c t i o n　a n d　C l e a n - u p)

For preparation of purified extract column application instructions recommended by producers were followed. Extraction processes and all subsequented steps – diluting, passing through column and eluting are summarized in Table II.

In addition, the acetonitrile:water (84 : 16, v/v) crude extract was prepared for LC-MS/MS analyses. This procedure is accredited to according ČSN EN ISO/IEC 17025:2005 for direct LC-MS/MS analysis and accuracy of generated data is regularly documented through proficiency tests (FAPAS®).

A n a l y s i s　o f　M y c o t o x i n s　U s i n g　L C - M S / M S

High performance liquid chromatograph (HP1100 binary series LC system, Agilent Technologies, USA) coupled with tandem mass spetrometer (Finnigan LCQ Deca, USA) were employed. Chromatographic separation of

Tabulka II
Procedures employed for sample processing (according to producer recommendation)

| Step of sample preparation | DONREP® | Immunoaffinity columns | | | SPE columns MycoSep® 226 |
		Easi exctract HT-2 & T-2®	Easi exctract ZON®	DZT Multi MyCo	
extraction solution	deionised water	methanol : water (90 : 10, v/v)	acetonitrile : water (75 : 25, v/v)	methanol : water (75 : 25, v/v)	acetonitrile : water (84 : 16, v/v)
dilution crude extract	no	phosphate buffered saline	phosphate buffered saline	phosphate buffered saline (PBS)	no
mLs of extract passed through comumn	2 ml extract	25 ml diluted extract	25 ml diluted extract	25 ml diluted exctract	8 ml of extract
washing	5 ml deionised water	20 ml deionised water	20 ml PBS	10 ml deionised water	no
elution	3×1.5 ml methanol	3×1.5 ml methanol	3×1.5 ml methanol	3×1.5 ml methanol	no

samples components was carried out in a reverse phase system using the column with polar endcapping (Synergi Hydro RP, 150 mm × 3mm × 4 μm).

MS-detector was operated in atmospheric pressure chemical ionization (APCI) mode, selective negative ions were aquired for DON, D3G and ZON, while for HT-2 and T-2 positive ions were monitored.

Results

The recoveries of fusarium toxins obtained within validation process employing spiked samples (200 μg kg^{-1}) for repeated analysis procedures (n = 3) characterized in Table II were summarized in Table III. The cross reactivity value for D3G is higher than recovery for DON in DONPREP®. Similarly D3G crossreacted in DZT Multi Myco IACs, nevertheless, it was fairly lower than aprox. 40 %. These DZT Multi Myco IACs provided good recoveries for HT-2 and T-2 even higher than in EASI EXTRACT HT-2T-2® IACs dedicated

these two toxins. Similarly, higher recovery was achieved in DZT Multi Myco IACs than in EASI EXTRACT ZON® IACs.

The levels of fusarium toxins determined in analysis of contaminated maize corrected to recoveries are shown in Table IV. When taking the results in Table I obtained by direct LC-MS/MS as a reference (= 100 %), some more pronounced differences for results were seen. The most pronounced are higher concentration determined for HT-2 and T-2 by DZT Multi Myco IACs and ZON by EASI EXTRACT ZON® IACs. On the other hand, underestimation of D3G content accords when it is used IACs clean-up step. We can see good agreement of generated data for most of tested approaches.

Conclusions

The usage of immunoaffinity columns represent the challenging approach in selective pre-concentration of target

Table III
Recoveries of mycotoxins for various columns

Columns	Analyte	Recovery [%]
DONPREP®	DON	76
	D3G	103
EASI EXTR. HT-2T-2®	HT-2	90
	T-2	73
EASI EXTR. ZON®	ZON	66
DZT Multi MyCo	DON	79
	D3G	40
	HT-2	102
	T-2	106
	ZON	94
MycoSep® 226	DON	94
	D3G	40
	HT-2	92
	T-2	84
	ZON	98

Table IV
Data of different extraction and clean up process corrected to reference values noted in Table I

Columns	Analyte	%
DONPREP®	DON	86
	D3G	44
EASI EXTR. HT-2T-2®	HT-2	93
	T-2	125
EASI EXTR. ZON®	ZON	151
DZT Multi MyCo	DON	97
	D3G	35
	HT-2	152
	T-2	131
	ZON	101
MycoSep® 226	DON	98
	D3G	25
	HT-2	104
	T-2	110
	ZON	124

mycotoxins, moreover, isolation of same metabolite of parcial toxins is possible depending on cross reactivity of particular antibodies. Thanks to removing most of interferences with ionization process (resulting in signal suppression) and on this account, a lower detection limits can be obtained in LC-MS/MS. In addition, the improvement of method performance characteristics, the usage of standards in net solvent is possible for calibration. On the other hand, the cost of analysis is fairly increased by using immunoaffinity columns. Therefore, for analysis of sample containing relatively high levels of mycotoxins such as maize used in this study, the direct analysis of crude extract is better option. Moreover, more accurate quantification of D3G is obtained in this extract. As far as, usage of IACs is prefered to obtained high sensitivity of analysis then DZT Multi MyCo IACs are recommended for reliable pre-concentration of trichothecenes and ZON.

REFERENCES

1. Berthiller F., Dall'Asta Ch., Schuhmacher R., Lemmens M., Adam G., Krska R.: J. Agric. Food Chem. *53*, 3421 (2005).
2. Lattanzio V. M. T., Solfrizzo M., Powers S., Visconti A.: Rapid Commun. Mass Spectrom. *21*, 3253 (2007).

P59 THE EFFECT OF CELL ADHESION ON POLLUTANT BIODEGRADATION

TEREZA KRULIKOVSKÁ, OLGA SCHREIBEROVÁ, JITKA HRDINOVÁ, JAN MASÁK, ALENA ČEJKOVÁ and VLADIMÍR JIRKŮ

Institute of Chemical Technology Prague, Department of Fermentation Chemistry and Bioengineering
Technicka 5, 166 28 Prague, Czech Republic,
tereza.krulikovska@vscht.cz

Introduction

The unicellular microorganisms naturally form multicellular communities called biofilm. Bacterial biofilms are generally described as surface associated community consisting of microcolonies surrounded by a matrix of exopolymers (EPS) with varied composition. The characteristics of biofilm which are in focus of present research are the ability to withstand and degrade high concentration of various toxic substances.

Phenol and catechol are toxic and persistent pollutants of the environment. They enter the environment from a number of industrial sources, namely from the production of pesticides, herbicides and many others. The method of removal by bacterial population is one of the possible solutions[1].

For our experiments gram-positive *Rhodococcus erythropolis* was chosen as a bacterium with a broad degradation potential, owning to its highly versatile metabolism.

Experimental

Rhodococcus erythropolis CCM 2595 was cultivated in BSM[2] medium at 28 °C. Carbon source was added (phenol or catechol 0.7 g dm^{-3}) after sterilisation.

Phenol and catechol concentration in media were determined by HPLC: Watrex column 250 × 4 mm, Nucleosil 100 C18, acetonitrile/deionized water (40/60), 1.0 ml min^{-1}, UV detection 254 nm.

Changes in biomass concentration were measured by spectrophotometric method at 595 nm as a total protein concentration[3].

The cell surface hydrophobicity was assayed using a procedure according to Rosenberg[4] – BATH test. Polymer material surface hydrophobicity was measured by a contact angle measurement method[5].

For EPS composition analysis the biomass was removed from carrier by ultrasound and 2% EDTA addition. Saccharides were assayed according to Dubois[6], proteins according to Bradford[3].

Rate of adhesion during initial period of cultivation was determined by fluorescent microscopy (Microscope Nikon Eclipse E400). After staining of biofilm by SYTO 13 the part of colonized area was measured by the method of image analysis (LUCIA, Laboratory Imaging Ltd., CZ).

Results

Suspended Cells

Experiments were carried out in shaken flasks (120 rpm) in medium with phenol or catechol as a sole carbon source. The concentration of 0.7 dm l^{-3} of the pollutant was chosen as a stressed concentration according to previous experiments (data not shown). The changes of biomass concentration during cultivation were expressed as a total protein concentration. The results are presented in the Fig. 1. The biomass concentrations at the end of both cultivations were 13 mg dm^{-3}. The phenol (0.7 g dm^{-3}) was totally degraded after 49.5 h, catechol (0.7 g dm^{-3}) after 119.4 h.

Experiments have shown that catechol biodegradation is affected by day light. During cultivation catechol was decomposed to compounds which interacted with glass. The repeated use of glass vessels was impossible.
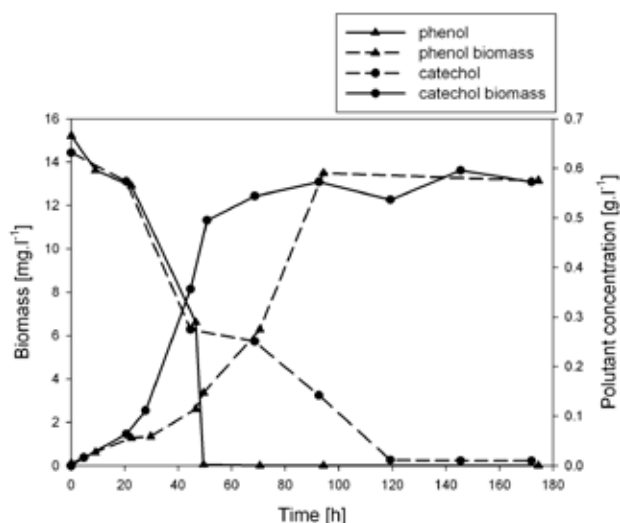
Fig. 1. ***Rhodococcus erythopolis* suspended cells growth and pollutant biodegradation. The cells were cultivated in shaken flasks in BSM medium at 28 °C. The phenol or catechol was used as sole carbon source (concentration 0.7 g dm^{-3}). The phenol/catechol and biomass (expressed as a total protein) concentration were monitored.**

Biofilm

The cell adhesion on solid materials is significantly affected by cell envelope composition and by hydrophobic/hydrophilic interactions between cells and carrier materials. The hydrophobicity and variance in EPS composition were studied.

Table I
Carrier materials hydrophobocity

Material hydrophobicity	Contact angle [°]
Glass (microscopic slide)	26.4 ± 6.6
Silicone	97.0 ± 3.6

The material hydrophobicity was determined by contact angle measurement. The results are summarised in the Table I. If value of contact angle is less than 90 ° the material is considered to be hydrophilic, if contact angle is greater than 90 ° the material is hydrophobic.

The cell hydrophobicity was determined by the BATH test. It was found that *Rhodococcus erythropolis* belongs to microorganisms with hydrophobic cell envelope character; the determined hydrophobicity is 89.0 ± 6.3 %.

The quantity of proteins and saccharides in EPS is shown in the Table II. Both proteins and saccharides amount is approximately two times higher in biofilm EPS from silicon carriers.

Table II
The concentration of saccharides and proteins in EPS

EPS composition		silicon	glass
Saccharides	$\left[\dfrac{mg_{EPS}}{g_{biomass}}\right]$	4.9	2.7
Proteins	$\left[\dfrac{\mu g_{EPS}}{g_{biomass}}\right]$	4.8	2.5

Rate of adhesion during initial period of cultivation was determined by the method of image analysis. Results have shown (Table III) that silicone is colonized more rapidly and better that glass. Small colonies were visible on silicone materials immediately after beginning of cultivation. Their area increased in time.

Table III
Portion of carrier occupied area by biofilm

	Image analysis	1h	24h
glass	colonized area [%]	0.0	0.2
	number of objects in the measured area	0	46
silicone	colonized area [%]	12.5	47.9
	number of objects in measured area	1,394	1,103

The biofilm experiments were carried out in glass columns ($\emptyset = 5$ cm, volume 220 ml). The silicone and glass tubes (external diameter 0.5 cm, 1.0 cm length) were chosen as carriers. The biofilm growth was the first stage of the process. The cells were cultivated in columns in mineral medium (BSM) with phenol (concentration 0.3 g dm^{-3}, changed at regular intervals) for 3 weeks at 20 °C. After this period the stabilized biofilm was used for phenol degradation. The results are summarised in the Fig. 2. The biofilm concentration on glass (silicone) tubes was 4.1 (8.7) g dm^{-3}, respectively. The concentration of suspended cells in medium

was lower in column with silicon tubes than in column with glass ones. The phenol was totally degraded in column with glass/silicone after 65 h/90 h, respectively.
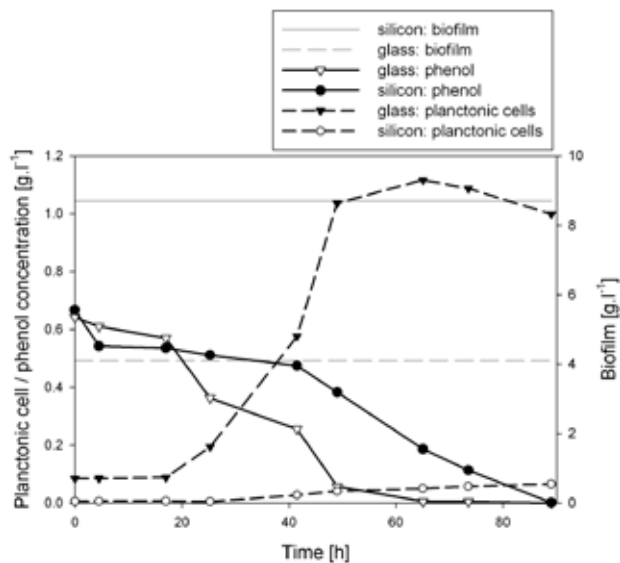
Fig. 2. **Phenol biodegradation by biofilm of *Rhodococcus erythopolis*. The cultivation was carried out in glass columns with two types of carrier (glass and silicone tubes, external diameter 0.5 cm, length 1 cm). The biomass was measured as total protein concentration at 595 nm**

The comparison of the biodegradation rates of the pollutants are summarised in the Table IV. Results indicate that catechol has a lower degradation rate than phenol. The highest biodegradation rate is reached in biofilm system with glass carriers.

Table IV
Comparison of biodegradation rate of the pollutants by suspended and sessile cells

Biodegradation rate $\left[\dfrac{mg_{pollutant}}{g_{protein} \cdot h \cdot l}\right]$			
		Phenol 0.7 g dm^{-3}	Catechol 0.7 g dm^{-3}
Suspended cells		3.89	1.61
Biofilm	glass	silicon	not tested in
	12.01	4.09	glass collums

Conclusions

It was found out that *Rhodococcus erythroposlis* cells better colonize silicone carriers to glass ones. Although the biomass concentration on glass carriers was two times lower the biodegradation rate was three times higher than in system with silicone. This indicates that only a part of biofilm is metabolically active. Results confirmed the hypothesis of higher biodegradation velocity of pollutants in biofilm system.

REFERENCES

1. Melenova I., Demnerova K.: Chem. Listy *98*, 908 (2004).
2. Masak J., Cejkova A., Jirku V.: J. Microbiol. Methods *30*, 133 (1997).
3. Bradford M. :Anal. Biochem. *72*, 248 (1976).
4. Rosenberg M.: FEMS Microbiol. Lett. *22*, 289 (1984).
5. Masak J., Cejkova A., Jirku V., Kotrba D., Hron P., Siglova M.: Environ. Int. *31*,197 (2005).
6. Dubois M, Gilles KA, Hamilton JK, Rebers PA, Smith F: Anal. Chem. *28*, 350 (1956).

P60 CATEGORIZATION OF OLIVE OILS

DÁŠA KRUŽLICOVÁ[a], JÁN MOCÁK[a,b] and ERNST LANKMAYR[c]

[a]*Institute of Analytical Chemistry, Slovak University of Technology, Radlinskeho 9, 812 37 Bratislava, Slovakia,*
[b]*Department of Chemistry, University of Ss. Cyril & Methodius, Nám. J. Herdu 2, 917 01Trnava, Slovakia,*
[c]*Institute for Analytical Chemistry, University of Technology Graz, A-8010 Graz, Austria,*
dasa.kruzlicova@stuba.sk

Introduction

Olive oil is an important food component, which enjoys special and increasing popularity in many countries not only due to its delicate taste but also because of its nutrition value. Depending on regional conditions a variety of oils are produced in different quality.

Olive oil has several favourable health effects related to: reducing the content of adversely acting blood LDL cholesterol causing risk of cardiovascular diseases, decreasing the blood pressure, glucose content in blood, and increasing absorption of vitamins A, D, E, and K. The beneficial health effects of olive oil are connected to high contents of mono-unsaturated fatty acids and antioxidative substances.

Chemical analysis of olive oil is cumbersome since it consists of a complex mixture of chemical compounds and due to enormous matrix effect[1]. In this study, olive oil samples of different oil types were characterized by absorbances in their UV-VIS spectra and by sensorial assessment. Using a new chemometrical approach[2], based on the absorbances at the most informative wavelengths, neither the standard materials nor assignment of chemical compounds were necessary so that it is cheaper, requires less laboratory work but demands more computations.

Experimental

Olive Oil Samples and Their Characteristics

193 olive oil samples of Greek origin were studied belonging to five different oil types coded by M (31 samples), K (37 samples), E (13 samples), N (94 samples), and T (18 samples); these codes were used instead of commercial brand on demand. The sensorial assessment of the oils was made in a ten-point scale. Absorbances were measured at 2001 wavelengths in the range 200–700 nm. Acidity, the peroxide value, and traditional measurements K232 and K270 were used as further characteristics of the oil quality.

Instrumentation and Chemometrical Techniques

UV-Vis spectra of olive oil samples were measured by spectrophotometer Varian, Cary 50 Conc (Varian, Vic., Australia) and software Cary Win UV was used for data acquisition and processing. Absorption spectra of diluted (1 : 300, v/v) olive oil were measured in isooctane (spectroscopy grade);

then they were digitized using a 0.25 nm step and saved to the PC.

For classification purposes new categorical variables *Sens*, *Variety* and *Location* were used denoting sensorial quality, oil type and geographical origin of the sample, resp. Linear discriminant analysis, quadratic discriminant analysis, logistic regression, the K-th nearest neighbour method and artificial neural networks were utilized as the classification techniques. The classification performance was evaluated for: *(i)* the *training set* used for computing the classification model, *(ii)* the *test set* created by the individual samples excluded from the training set by the "leave-one-out" principle[3].

Results

Categories of Olive Oils

According to sensorial characteristics, the collected samples were categorized into three classes using categorical variable *Sens*: the highest quality oils (6.5–9.0 points, denoted as "best"), the medium quality samples (3.5–6.4, "good"), and not acceptable quality (1.0–3.4, "worst").

Two further categorization principles were applied: *(i)* the type of olive oil using categorical variable *Variety* - five categories M, K, E, N, and T, *(ii)* the geographic locality, Peloponnese, Central Greece, and Crete, using the three-class categorical variable *Location*.

Classification of Olive Oils by Different Criteria

Linear discriminant analysis (LDA) and other classification techniques need an optimal reduction of the original number of variables eliminating unimportant ones. For this purpose the stepwise variable selection was used, by which 60 optimal wavelengths were selected in the case of the oil type categorization, 37 wavelengths were selected when sensorial quality was categorized, and 60 wavelengths when categorizing the oils by geographical origin.
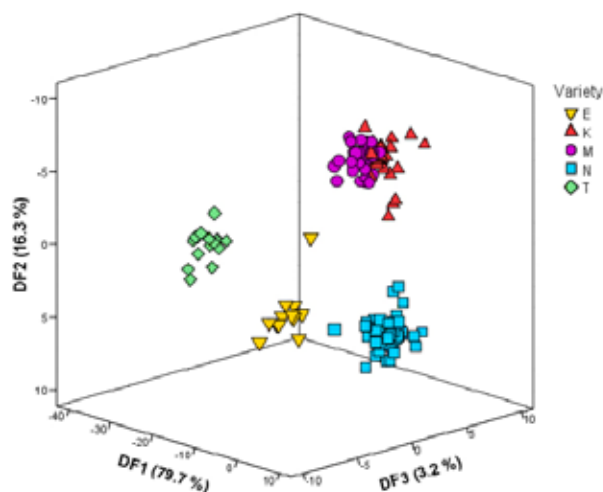
Fig. 1. **3D LDA plot of 5 different varieties of olive oils**

Display of the olive oils discrimination by the oil type (*Variety*) in 3D space of first three discriminant functions is shown in Fig. 1. Analogical 2D displays in Fig. 2. and Fig. 3. depict the oils classification by sensorial quality and geographic origin. A very good separation of the oil classes is evident in all three studied cases.

Plot of Discriminant Functions
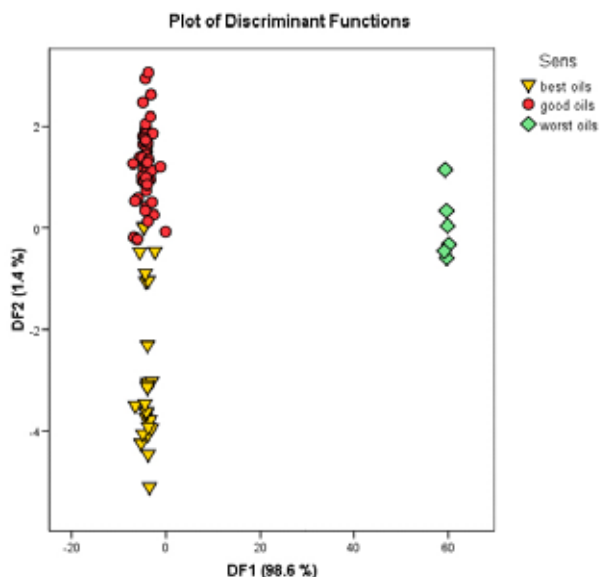
Fig. 2. **2D LDA plot of three olive oil classes differing by the sensorial quality**
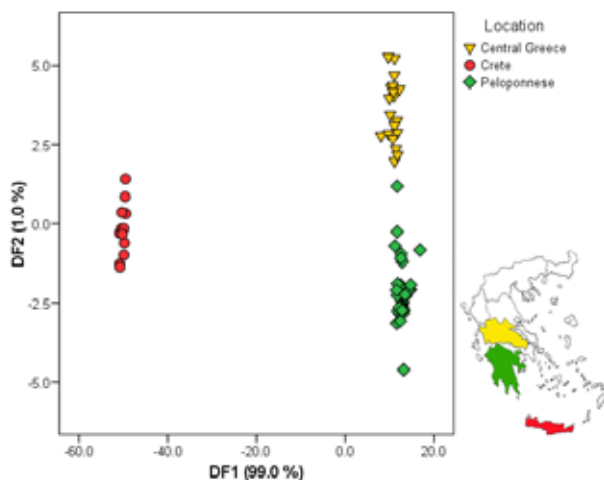
Fig. 3. **2D LDA plot of three olive oil classes differing by geographical origin**

Quadratic discriminant analysis (QDA), logistic regression (LR) and K-th nearest neighbour method (KNN) are further frequently used classification techniques[4]. They were used together with LDA and artificial neural networks (ANN)[5] for a complex classification of olive oils. A very good separation of the olive oil samples according to two selected criteria is shown in Table I and Table II.

Table I
Results of classification of 187 olive oils by variety

Method	Classification success	Model	Leave-1-out	Software
LDA	Number of correct	186	177	SPSS
	%	99.5	94.7	
QDA	Number of correct	187	131	SAS
	%	100.0	70.1	
KNN	Number of correct	186	185	SAS
	%	99.5	98.7	
LR	Number of correct	187	–	SPSS
	%	100.0	–	

The effectivity of classification using different classification techniques and software is here expressed by the ratio of the successfully categorized objects to all objects in per cents. The most important are the results of cross-validation achieved here by leave-one-out method. They show the effectivity of prediction new objects (olive oils) not involved in the training procedure; the best techniques are close to 100 %.

Table II
Results of classification of 93 olive oils by sensorial quality

Method	Classification success	Model	Leave-1-out	Software
LDA	Number of correct	87	81	SPSS
	%	95.6	89.0	
QDA	Number of correct	91	60	SAS
	%	100.0	65.9	
KNN	Number of correct	85	80	SAS
	%	93.4	87.9	
LR	Number of correct	91	–	SPSS
	%	100.0	–	
ANN	Number of correct	91	–	JMP
	%	100.0	–	

Classification of the oil samples by geographic origin was performed only by the LDA technique, which categorized 98.4 % of samples by leave-one-out technique in a correct way (consistent with Fig. 3.).

Conclusions

Classification of olive oils by variety, sensorial quality and geographic location was successfully performed by several chemometrical techniques using modern commercial software. The classification effectivity was in best cases close to 100 %. A speciality and novelty of the applied approach is processing of spectral data without the need to utilize standards representing the most important components of olive oils. Therefore a very complex quantitative multicomponent analysis is not necessary and the expenses for it and for the standard materials are saved.

REFERENCES

1. Kruzlicova D., Mocak J., Lankmayr E.: *Proc. YISAC 2006*. Zagreb University, Zagreb 2006, p. 43.
2. Lankmayr E., Mocak J., Serdt K., Balla B., Wenzl T., Bandoniene D., Gfrerer M., Wagner S.: J. Biochem. Bioph. Methods *61*, 95 (2004).
3. Vandeginste B. G. M., Massart D. L., Buydens L. M. C., de Jong S., Lewi P. J., Smeyers-Verbeke J.: *Handbook of Chemometrics and Qualimetrics: Part B*. Elsevier, Amsterdam 1998.
4. Khattree R., Naik D. N.: *Multivariate data reduction and discrimination*. SAS Institute, Cary, N.C. 2000.
5. Zupan J., Gasteiger J.: Neural Networks in Chemistry and Drug Design. 2nd Ed. Wiley-VCH, Weinheim 1999.

P61　THE PROTEOMIC ANALYSIS OF BARLEY ALBUMINS AND GLOBULINS

MARKÉTA LAŠTOVIČKOVÁ and JANETTE BOBÁĽOVÁ

Institute of Analytical Chemistry of the ASCR, v.v.i., 602 00 Brno, Veveří 97, Czech Republic,
lastovickova@iach.cz

Introduction

The proteins and glycoproteins play many important roles not only in nature, but also in technologies (*e.g.* food chemistry, medical technologies).

The characterization of glycoproteins is not an easy task and several techniques have to be used for the resolving of their total chemical composition. Today, methods including gel electrophoresis, LC, and MS together with the database searches have been increasingly used. MS has become a widely used method in protein analysis after the invention of MALDI and electrospray ionization techniques[1].

Proteomics is increasingly used to address questions of development, physiology and quality of crop plants[2,3]. Modern analytical techniques are used for the characterization of cereal seed composition in order to increase basic knowledge about these plants for economical and nutritional aspects. One of the most important crops is barley (*Hordeum Vulgare*), which is used mainly for malting and animal feed[4]. The production of (glyco)proteins in barley seed is of particular interest, because this approach can be utilized to produce barley lines with improved properties, such as malting quality due to expression of thermotolerant enzymes[5].

Experimental

Extraction of Proteins

The grains of malting barley (cultivar Jersey) were obtained from Research Institute of Brewing and Malting (Brno, Czech Republic). 250 mg of flour was mixed with 2 ml of extraction reagent (TRIS buffer – 0.1 M, pH 7.8 containing 0.5 M NaCl; 1 mM $MnCl_2$; 1 mM $CaCl_2$) and shaken 2 h. The suspension was centrifuged (20 min; 14,000 rpm). The supernatant containing the proteins was filtered using 0.45 μm microfilter (Millipore) and used for the following experiments.

Affinity Chromatography (AC)

A glycoprotein enriched fraction was obtained by Concanavalin *A* (Con *A*) lectin chromatography (Calbiochem). 4 ml of TRIS extract was applied on the column. Purified glycoproteins were released by 500 mM glucose.

1 D - G E

The proteins were separated by 12.5 % SDS gels. SDS-PAGE separations were performed on 16 × 14 cm gels (OWL SEPARATION SYSTEMS).The visualization was carried out by Coomassie Brilliant Blue R-250 (CBB).

In-Gel Trypsin Digestion and Mass Spectrometry

The particular barley proteins and glycoproteins separated by 1-D GE were subjected to in-gel trypsin digestion[6]. Peptides, obtained by trypsin digest, were analyzed by MS. MS experiments were carried out on an *Applied Biosystems 4700 Proteomics Analyzer* mass spectrometer. α-Cyano-4-hydroxycinnamic acid (10 mg m^{-1} 0.1% trifluoroacetic acid/acetonitrile (1 : 1, v/v)) was used as a matrix for MALDI-TOF MS analysis of peptides obtained by trypsin in-gel digestion. Nitrogen was used as the collision gas for MS/MS experiments. Protein identification was performed by searching the peptide masses and MS/MS sequence stretches against the sequence databases using the MASCOT or ProFound search engines.

Results

This work was focused on the systematic proteomic study of barley grains. Barley was selected as a model sample because it contains a complex mixture of proteins and glycoproteins and has a lot of analogies in other plant materials.

In general, it is not possible to identify the proteins without previous combination of MS with the separation techniques. Therefore especial attention was paid to the optimization of extractions and following separation methods. The different extraction reagents, selected on the basis of Osborn's protein classification, were tested and obtained protein patterns were compared. Fig. 1. showed noticeable differences between individual extract. The attention was focused
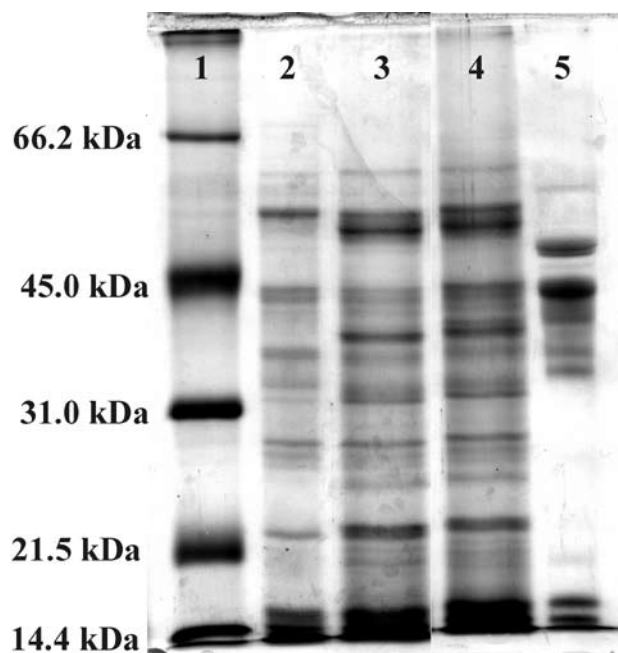
Fig. 1.　**CBB stained 12.5 % 1-D SDS gel of barley proteins extracted by different extraction reagents. Lane 1 – molecular weight markers, Lane 2 – aqueous extract; Lane 3 – salt extract; Lane 4 – TRIS extract, Lane 5 – ethanol extract**
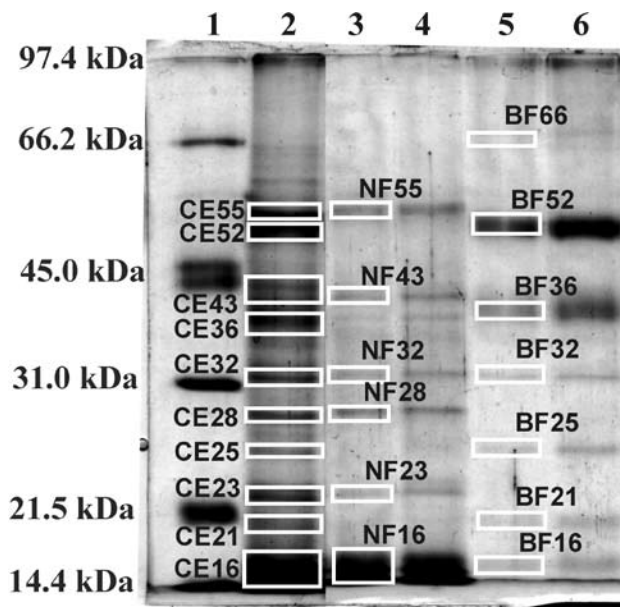
Fig. 2. **CBB stained 12.5 % 1-D SDS gel of TRIS extracts and its AC fractions. Lane 1 – molecular weight markers, Lane 2 – crude TRIS extract (CE); Lanes 3, 4 – Con A non-bound protein fractions of TRIS extract (NF); Lanes 5, 6 – Con A bound glycoprotein fraction of TRIS extract (BF)**

on albumin/globulin fraction extracted by TRIS buffer (see Experimental) that is important for food industry, because the proteins belonging to this fraction survive malting and brewing procedures and influence beer quality.

Lectin AC, one of the most effective glycoprotein isolation methods, was used for other simplification of albumins/ globulins mixture and for the acquisition of fraction containing a high degree of barley glycoproteins. Since a common feature of plant seed glycoproteins is the presence oligosaccharide chains having an affinity for Con *A*, it was used to enrich the fraction of barley high-mannose and hybrid-types *N*-glycoproteins having affinity for this kind of lectin. The particular proteins (Con *A* non-bound fractions) and glycoproteins (Con *A* bound fraction) were subjected to SDS-PAGE. 1-D gel of AC fractions is shown in Fig. 2. Major bands were cut out (Fig. 2.) and exposed to the trypsin in-gel digestions. Extracted mixture of peptides was subjected to MS and MS/MS analyses. Subsequent database searching led to the identification of numerous groups of barley proteins with molecular masses ranges from about 70 to below 20 kDa. Their summary is shown in Table I.

Conclusions

These experiments confirmed that combination of AC, SDS-PAGE and MALDI-TOF MS is convenient for the characterization of barley (glyco)proteins. The developed procedures can be used for the solution of important industrial (*e.g.* brewing) problems.

Table I
Identified proteins from TRIS extract and its AC fractions

Indication of gel spots (extract)	Indication of gel spots (AC fractions)	Molecular mass (theor.) [kDa]	Molecular mass (exp.) [kDa]	Accession number	Protein name
–	BF66	72.5	~ 66	gi|421978	BEG1
CE55	NF55	57.9 59.6	~ 57	gi|38349539 gi|10953877	β-Amylase
CE55	BF52	57.7	~ 57	gi|804656	β-Glycosidase
CE 52	BF52	72.5	~ 55	gi|421978	BEG1
CE43	NF43	43.3	~ 43	gi|1310677 P06293	Protein Z serpin Protein Z
CE36	BF36	72.5	~ 36	gi|421978	BEG1
–	BF32	31.5 25.6	~ 31	gi|15824660 gi|72333	Con A
CE32	NF32	30.0	~ 32	gi|132577	rRNA N-glycosidase
CE28	NF28	28.5	~ 28	gi|116316	Endochitinase
CE25	BF25	72.5	~ 25	gi|421978	BEG1
CE23	NF23	20.0–22.4	~ 23	gi|439275 gi|4699834 gi|18920 gi|18916	Mixture of α-amylase/subtilisin inhibitors
–	BF21	72.5	~ 21	gi|421978	BEG1
CE16	NF16	16.1	~ 16	gi|439275	CMa-α-amylase inhibitor
CE16	NF16	17.9	~ 16	gi|452325	CMd-α-amylase inhibitor
–	NF16	16.7	~ 16	gi|6634471	CMe-α-amylase inhibitor
–	BF16	72.5	~ 16	gi|421978	BEG1

REFERENCES
1. Finnie Ch., et al.: Phytochemistry *65*, 1619 (2004).
2. Østergaard O., et al.: Proteomics *4,* 2437 (2004).
3. Silva F., et al.: Food Chem. *106*, 820 (2008).
4. McGregor A.W., Bhatty R.S.: *Barley: Chemistry and Technology.* American Association of Cereal Chemists, Inc. St. Paul 1993.
5. Clark S.E., Muslin, E.H., Henson C.A.: Protein Eng. Des. Sel, *17*, 245 (2004).
6. Shevchenko A.; Wilm M.; Vorm O.; Mann. M.: Anal. Chem. *68*, 850 (1996).

P62 COMPARATIVE STUDY OF THE PROTEIN COMPOSITION INDUCED BY MALTING BARLEY OF TWO VARIETIES

MARKÉTA LAŠTOVIČKOVÁ, MARTINA ŠOPÍKOVÁ and JANETTE BOBÁĽOVÁ

Institute of Analytical Chemistry of the ASCR, v.v.i., 602 00 Brno, Veveří 97, Czech Republic,
lastovickova@iach.cz

Introduction

The selection of barley cultivar has great importance for the malting and brewing industries, as well as for breeders, because malting properties and resistance of barley plant to fungal or viral diseases is cultivar-dependent. Since protein content is one of the most important barley character related to malt qualities, proteomics is ideal tool for both differentiation of barley cultivars and description of malting course. Proteomic analysis usually includes some separation technique connecting with MS and the database searches. SDS-PAGE has been commonly used as a separation step before MS analysis of proteins. Moreover, it seems to be convenient tool for the study of qualitative differences between barley cultivar.[1–3]

The aim of this study was the characterization of protein changes and the identification of major proteins that undergo some modifications during malting process. For these experiments two barley cultivars were selected.

Experimental

Extraction of Proteins from Barley Grains

Barley grains in different malting degrees (cultivar "Jersey" and KM1910) were obtained from Research Institute of Brewing and Malting (Brno, Czech Republic). 50 mg of sample was mixed with 1 ml of deionized water and shaken 1 hr. The suspension was centrifuged (10 min; 13,000 rpm). The supernatant containing the proteins was lyophilized.

Protein Separation

Lyophilized extracts were resuspended in 150 μl sampling buffer (Laemmli Sample Buffer (Bio-Rad) with β-mercaptoethanol, 19:1) and denaturated (10 min, 95 °C). SDS-PAGE separations were performed on 15 % TRIS-HCl (Bio-Rad) or gradient (4–20 % TRIS-HCl, Bio-Rad) gels. The visualization was carried out by Coomassie Brilliant Blue (CBB) R-250, CBB G-250 and silver staining.

Protein Identification

The selected proteins separated by 1-D GE were digested in-gel by chymotrypsin[4]. Obtained peptides were analyzed by MALDI-TOF MS (*Applied Biosystems 4700 Proteomics Analyzer*). α-Cyano-4-hydroxycinnamic acid (CHCA; 10 mg ml⁻¹ 0.1% trifluoroacetic acid/acetonitrile (1:1, v/v)) was used as a MALDI matrix. Air was used as the collision gas for all MS/MS experiments. Protein identification was performed by searching the peptide masses and MS/MS sequence stretches against the sequence databases using the MASCOT search engine (database NCBInr).

Results

Protein Changes During Malting

Water-soluble proteins were extracted from barley mature grains, grains after 1–5 days of malting and from green and ready malt. 1-D GE was performed to obtain a complex characterization of changes of protein profiles during malting. The gradient gel (4–20 %) was used to acquire the results covering the largest interval of molecular masses. Since the demand for a protein staining (sensitivity, compatibility with MS) is one of the most important tasks in GE, especial attention was paid to the selection of protein visualization. Two types of CBB (R-250 and G-250) and silver staining were compared (data not shown). The best results were obtained with CBB-G of which using the differences between protein patterns during malting were distinct (Fig. 1.).

A visual inspection of gradient gel confirmed significant modifications observed after three days of malting at minimal five protein bands at molecular masses about 53 kDa, 43 kDa, 26 kDa, and 23 kDa (see arrows in Fig. 1.). The major changes were noticed at the band with molecular mass about 43 kDa. Therefore it was cut out, digested by chymotrypsin and obtained mixture of peptides was subjected to MS and MS/MS analyses (Fig. 2. a, b). Database searching revealed its identity as *Protein Z* (gi/131091). This protein is important for the brewers, because due to its posttranslational modifications (glycations) influence the sensory and technological properties of beer (e.g. foam).

Protein Pattern for Different Barley Cultivars

Extracts from mature grains and malt of two different varieties, Jersey and KM, were separated via 15 % 1-D SDS-
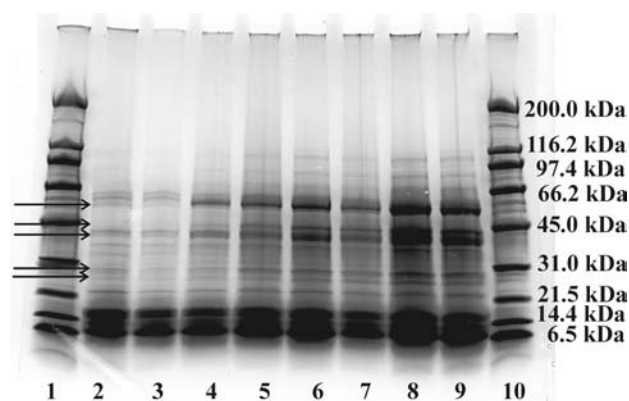
Fig. 1. **CBB-G stained gradient 1-D SDS gel of protein extracts from mature grains (Lane 2), one day malting grains (Lane 3), two days malting grains (Lane 4), three days malting grains (Lane 5), four days malting grains (Lane 6), five days malting grains (Lane 7), green malt (Lane 8) and ready malt (Line 9). Molecular weight markers are in Lanes 1 and 10**
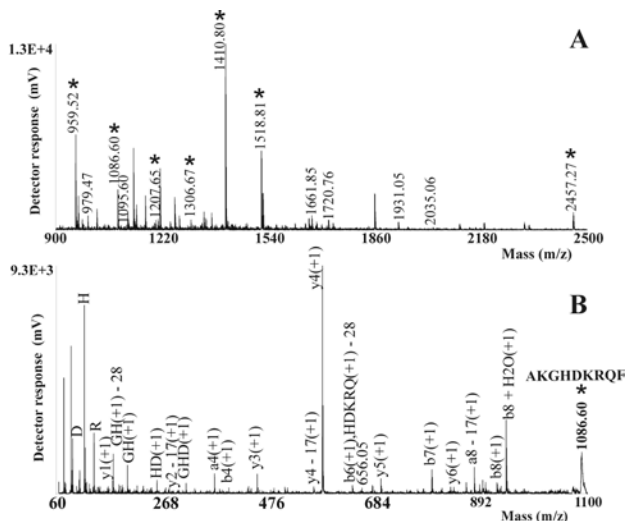
Fig. 2.　**A) MALDI-TOF mass spectrum of peptide mixture from in-gel tryptic digest of a protein band 43 kDa. The asterisks (*) mark peptides coming from barley Z protein (confirmed by MS/MS). B) Representative MALDI-TOF fragmentation spectrum of [M+H]$^+$ ion peptide at m/z 1086**

Fig. 3.　**CBB-G stained 15 % 1-D SDS gel of protein extracts from mature grains (Lane 2 – variety Jersey; Lane 3 – variety KM), and ready malt (Lane 4 – variety Jersey; Lane 5 – variety KM). Molecular weight markers are in Lane 1**

PAGE in order to compare their protein profile. An example of differences in the protein pattern between cultivars is given in Fig. 3. The most relevant changes were observed between mature grains. As Fig. 3 showed, some of perceptible differences are in the protein concentrations (e.g. bands about 40 kDa), some bands were not present in KM cultivar, others in Jersey (see arrows in Fig. 3.).

Conclusions

　　　Combination of 1D-GE and MALDI-TOF MS was successfully used for the revealing of characteristic changes in protein profile during malting process as well as the differences between two selected barley cultivars.

REFERENCES

1. Cooke R.J.: J. Chrom. A *698*, 281 (1995).
2. Hao J. et al.: J. Am. Soc. Brew. Chem *64*, 166 (2006).
3. Bobalova J., Chmelik J.: J. Chrom. A *80*, 1163 (2007).
4. Shevchenko A., Wilm M., Vorm O., Mann M.: Anal. Chem. *68*, 850 (1996).

P63   FATTY ACIDS LIKE MARKERS OF PROCESSED CHEESE CHANGES DURING STORAGE

BLANKA LOUPANCOVÁ, EVA VÍTOVÁ, HANA ŠTOUDKOVÁ and FRANTIŠEK BUŇKA

Institute of Food Science and Biotechnology, Faculty of Chemistry, Brno University of Technology, Purkyňova 118, 612 00 Brno
blankaloupancova@seznam.cz

Introduction

Pasteurized processed cheese products are cheese-based food produced by comminuting, blending and melting one or more natural cheeses and optional ingredients into a smooth homogenous blend with the aid of heat, mechanical shear and usually emulsifying salts.

Optional ingredients which are determined by the product type include dairy ingredients, vegetables, meats, stabilizers, emulsifying salts, flavours, colours, preservatives and water[1,2]. Dairy ingredients means butter, cottage cheese, milk concentrates (e.g. skimmed milk powder, whey powder, caseinates).

Chemical composition of processed cheese depends on a processed cheese type and raw materials used[3].

Although the dairy products fall into the class of so called non-acid foodstuffs and suitable methods must be used to prolong their durability, the processed cheese was proposed as a part of Combat Ratio. The Combat Ratio serves for nutrition of soldiers in specific combat situations such as separation from a unit, battle, etc.[3]. There are special requirements for a minimum durability of individual components of Combat Ration which has been set as 24 months depending on an ambient temperature[4].

Practically the only method of achieving the 24 month durability of processed cheese is the thermo-sterilization. In the article the effect of a defined sterilization heating and storage conditions, such as temperature and time, on changes of fatty acids contents in sterilized processed cheese was investigated.

Experimental

Processed cheese (40 % dry matter, 45 % fat in dry matter) was manufactured following the traditional technology process in a selected dairy. The processing temperature was 91 °C, total time of heating was 5 minutes. Cheeses were than sterilized at 117 °C for 20 minutes and then cooled down to 10 °C in 2 hours.

Cheese samples were stored at 6 ± 2 °C, 23 ± 2 °C and 40 ± 2 °C during 24 month.

Extraction of Fat

The cheese sample (5.0 g) was heated with 15 ml of hydrochloric acid in boiling water bath until it dissolves and then still 20 minutes.

Ethanol (15 ml), diethyl ether and petrol ether (both 30 ml), were added into stirred mixture after cooling down. Closed flask was shaken and then allowed to separate the water and organic phases. The upper (organic) phase was displaced by the pipette to dried weighed flask. Next the water phase was reextracted with 15 ml of diethyl ether and 15 ml of petrol ether two times.

The rest of organic solvent was evaporated in 60 °C water bath (to dispose smell). Flask with fat sample was dried at 105 °C for one hour[1].

Methanol Esterification Method

The fat sample (5.0 g) was saponified with 50 ml methanolic solution of potassium hydroxide ($c = 0.5$ mol dm^{-3}) for 30 minutes in distilling flask with condenser and was esterified after neutralization by sulphuric acid on methyl orange for 30 minutes again.

After cooling methyl esters were shaken with 10 ml of heptane three times. The extract was dried by anhydrous sodium sulphate and filtered to a 50 ml volumetric flask again. Both heptane portions were rinsed with 20 ml of water twice. The extract was dried by anhydrous sodium sulphate and filtered to a 50 ml volumetric flask and filled up to the mark with heptane[5].

GC Analysis

Prepared heptane methyl esters solutions were injected to gas chromatograph using autosampler.

GC conditions: gas chromatograph TRACE GC (ThermoQuest Italia S. p. A., I) equipped with flame ionization detector, split/splitless injector and capillary column SPTM 2560 (100 m × 0.25 mm × 0.2 µm) with the temperature programme 60 °C held for 2 min, ramp 10 °C min^{-1} up to 220 °C, held for 20 min. The injector temperature was 250 °C and the detector temperature was 220 °C. The flow rate of the carrier gas N$_2$ was 1.2 ml min^{-1}.

Results

This work deals with the fatty acids included in processed cheese. The most abundant fatty acids such as lauric,
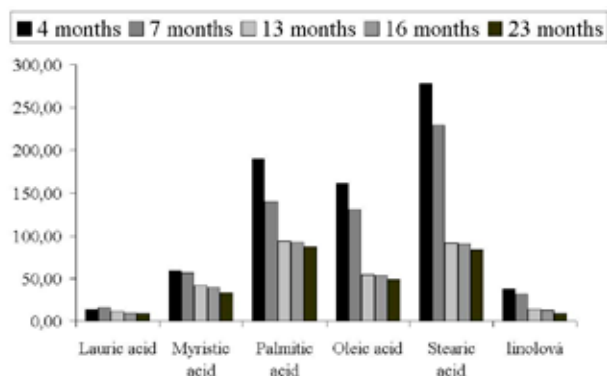
Fig. 1.   **Influence of the storage time on the amount of fatty acids (cheeses stored at 6 ± 2 °C) (mg g^{-1} of cheese)**
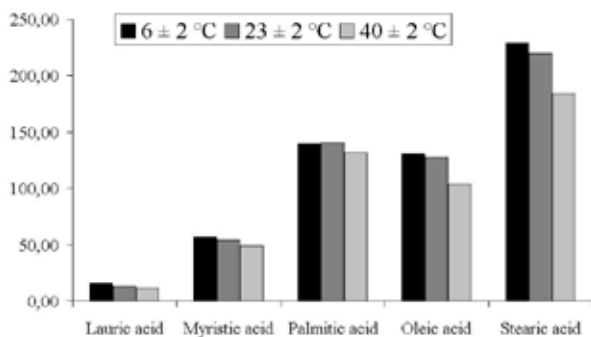
Fig. 2. **Differences between amounts of fatty acids in cheeses stored at different temperature (storage time 23 months) (mg g⁻¹ of cheese)**

myristic, palmitic, stearic and oleic acid were elected like markers of changes during storage. The differences between amounts of these fatty acids depending on the storage temperature and time of storage were observed in this experiment.

In the Fig. 1 there are showed the differences between the processed cheeses stored at 6 ± 2 °C. By the increasing time of storage the amouths of elected fatty acids decrease. This can be explained by autooxidation process which can not be averted.

Since the first months the volume of fatty acids decreased with the temperature. In the Fig. 2. we can see differences

between the cheeses stored for 23 months at different conditions. The temperature promotes the oxidative process.

Conclusions

The changes of fatty acids inclued in sterilized processed cheeses during storage were observed in these experiments. The cheeses were stored at different conditions for the 24 months.

We can conclude that the storage conditions significantly influence the content of individual fatty acids in cheeses. The contents of fatty acids in cheeses decreased as the consequence of longer time and higher temperature of storage. This fact can be probably caused by oxidation reactions of cheese fat.

REFERENCES

1. Guinee T. P., in: *Encyclopedia of Dairy science* (Roginski H., ed.). Academic press, 411, London 2003.
2. Kristensen D, Hansen E, Arndal A., Trinderup R. A., Skibsted L. H.: Int. Dairy J. *11*, 837, 2001.
3. Buňka F., Vítová E., Hrabě J., Zemanová J.: Int. Dairy J., Volume *14*, 9 (2004).
4. Standardization Agreement 2937 (2001): *Survival, Emergency and Individual Combat Ration – Nutritional Values and Packaging*. 3. ed., NATO/MAS, Brussels.
5. Sunesen L. O., Lund P., Sörensen J., Hölmer G.: Technol *35*, 128 (2002).

P64 DETERMINATION OF SELECTED ANTIOXIDANT ENZYMES IN BARLEY AND MALT

SIMONA MACUCHOVÁ[a], RENATA MIKULÍKOVÁ[a], IVANA MÁROVÁ[b] and SYLVIE BĚLÁKOVÁ[a]

[a]*Research Institute of Brewing and Malting, Plc., Mostecká 7, 614 00 Brno, Czech Republic,*
[b]*Institute of Food Chemistry and Biotechnology, Faculty of Chemistry, University of Technology Brno*
Purkyňova 118, 612 00 Brno, Czech Republic,
macuchova@brno.beerresearch.cz

Introduction

Presence of Reactive Oxygen Species (ROS) negatively affects the sensory stability of beer, thus, final quality of beer is related to its antioxidant activity. Antioxidant content in beer is substantially dependent on anti-oxidative activity of the primary raw materials – barley and malt. In barley antioxidants prevent the undesirable and generally negative changes of grain quality during the cropping and stocking. Generally, antioxidants can act against ROS by radical trapping, by inhibition of their formation or by decreasing of their effects. Complex antioxidant system acts as a well-coordinated complex of low molecular weight- and enzyme antioxidants. In barley antioxidant enzymes are represented mainly by superoxide dismutase, catalase and peroxidase.

Superoxide dismutase (SOD) is the main antioxidative enzyme in plant cells, where it stands for catalyse of dismutation of superoxide to dioxygen and hydrogen peroxide. This hydrogen peroxide is subsequently decomposed to dioxygen and water; catalases and peroxidases stand in this reaction as catalyzators.

In this work the influence of selected biological and chemical factors on superoxide dismutase and catalase activity in barley and malt were studied. As the part of the work was the optimization of enzyme activity determination methods associated.

Methods

Samples of Barley and Malt

The enzyme activities were studied in two sets of 24 samples (6 barley varieties – Bojos, Jersey, Malz, Radegast, Sebastian and Tolar, cultivated on 4 localities – Branišovice, Hrubčice, Lednice and Krásné Údolí): the first set treated by standard spraying, the second was not treated. The malts originated from these samples were analysed using the same methods as for barley grain analysis.

Determination of Superoxide Dismutase

The modified method using the diagnostic kit RANSOD (Randox Laboratories, UK) was used for superoxide dismutase activity determination. This method employs xanthine oxidase to generate superoxide radicals, which react with 2-(4-iodophenyl)-3-(4-nitrophenol)-5-phenyltetrazolium chloride forming a formazan dye. The superoxide dismutase activity is then calculated by the degree of this reaction's inhibition.

Because the original method was developed for superoxide dismutase determination from human blood, the modification for SOD analysis in barley and malt consists in extract preparation from smashed and homogenized samples (Belcredi *at al.*, 2006): The sample is grinded and compounded in distilled water at 45 °C. The mixture is compounded for 15 minutes in the tub at the same temperature of water bath. After half-hour chilling the mixture is filtered. The filtrate is analysed for SOD activity according to the RANSOD kit manual.

Determination of Catalase

The most frequently used method for catalase activity determination (Bergmeyer, 1970) modified by Góth (1991) was used in this work. Góth's modification is based on fact, that the catalytic action of catalase could be stopped by addition of ammonium molybdate forming stable coloured complex with hydrogen peroxide.

Grinded sample is mixed with phosphate buffer at $pH = 7.0$ and than is this mixture compounded for one hour at the temperature of 5 °C. After subsequent centrifuging is supernatant filtered and used for analysis: hydrogen peroxide (at 12 mmol dm^{-3} concentration) is added to specimen and after 1.5 minutes is also added ammonium molybdate (at 16.2 mmol dm^{-3} concentration). The absorbance of formed yellow complex is measured at 375 nm. The concentration of remaining hydrogen peroxide is observed at calibrating curve. Calculated amount of used hydrogen peroxide (in mmol min^{-1}) agree with catalase activity (in U-units).

Results

SOD activity determination in chosen samples of barley and malts shows significant differences. The highest values of SOD activity were obtained in Bojos variety samples, the lowest in Radegast variety; concerning locality differences the highest values were founded in Branišovice.

Activity of catalase is corresponding with SOD activity – also these values were the highest namely for Bojos variety

Table I
SOD and catalase activity ($U g^{-1}$ of dry matter) in barley and malt, depending on the localities

Locality	Treatment	SOD activity		Catalase activity	
		Barley	Malt	Barley	Malt
Branišovice	non-treated	120	143	114	166
	treated	128	149	115	148
Hrubčice	non-treated	108	129	116	118
	treated	116	118	116	120
Krásné Údolí	non-treated	112	109	78	92
	treated	97	106	71	85
Lednice	non-treated	90	119	86	105
	treated	86	117	90	138

Table II
SOD and catalase activity (U g^{-1} of dry matter) in barley and malt, depending on the varieties

Variety	SOD activity		Catalase activity	
	Barley	Malt	Barley	Malt
Bojos	128	133	114	140
Jersey	114	127	109	135
Malz	93	126	97	110
Radegast	92	113	107	123
Sebastian	110	127	113	115
Tolar	106	116	110	112

and field in Branišovice; the lowest values were observed in Malz variety. Used method for catalase activity determination shows itself to be easy and quick. Above referred method was slightly modified for this work's purposes: original concentration of ammonium molybdate (32.4 mmol dm^{-3}) recorded non-linear dependence on analyzed hydrogen peroxide depletion, therefore it had to be halved, and hence the absorbance of formed yellow complex is measured at 375 nm instead of original 405 nm.

REFERENCES
1. Bergmeyer, H. V.: *Methods of enzymatic analysis*. 636 Verlag Chemie, Weinheim, Bergstre, 1970.
2. Góth, L.: Clinica Chim. Acta *196*, 143 (1991).
3. Belcrediová, N., Ehrenbergerová, J., Havlová, P.: Acta Universitatis Agriculturae et Silviculturae Mendelianae Brunensis *24*, 7 (2006).

P65 FAT CONTENT AND ITS QUALITY IN RAPESEED (*BRASSICA NAPUS* L) DURING STORAGE

JÁN MAREČEK, MARTINA FIKSELOVÁ, HELENA FRANČÁKOVÁ and ZDENKA MUCHOVÁ

Department of Plant Processing and Storage, Faculty of Biotechnology and Food Sciences, Slovak University of Agriculture, Tr. A. Hlinku 2, Nitra, 949 76 Slovakia,
Jan.Marecek@uniag.sk

Introduction

Fats and oils contain unsaturated fatty acids bound with triacyglycerols. Plant oils consist of polyunsaturated fatty acids which are susceptible for oxidation (Pokorný, 2001).

Colza oil is low in saturated fatty acids content (6–8 %), but is source of linolenic acid, oleic acid (60 %), and has favourable ratio of n-3 and n-6 fatty acids.

By the influence of higher temperatures the fat is decomposed. Chemical and physical changes of fat during frying cause an increase of fat viscosity, free fatty acids content, color changes, decrease of iodine value, and tendency to foaminess of fat (Venskutonis et al., 2000, Salková, 2002).

The aim of this work was evaluation of the influence of storage time on fat stability in rapeseed (oxidation changes of fat fraction).

Material and Methods

Rapessed was stored in silo. Samples (15 kg) were continuosly taken and analysis were performed - at the begining of storage (after harvest), during the storage and at the end of storage time. Rapeseed was stored in Poľnonákup Hont in Hontianske Nemce, as the mixture of variants. Analysis were performed at Department of Plant Processing and Storage, Faculty of Biotechnology and Food Sciences (SUA Nitra), then at Slovak Agricultural Research Centre in Nitra and at Food Research Institute, Biocenter Modra. Results are present from 3 years of observations (2003–2005).

Methods

Determined parameters of the rapeseed quality were the content of dry matter by Slovak Technical Standard (STS 560116), ash content (combustion at 900 °C), fat content (STS 560116), peroxide value (STS 580130), iodine value (by Hanuš), acid value (STS 580130), thiobarbituric value (distilling method), nitrogen compounds (by Kjeldahl). Fatty acids representation (chromatographically) was determined as follows: myristic, palmitic, palmitoleic, stearic, oleic, linoleic, linolenic, arachidonic, behenic and erucic.

Terms of samplings:
- year 2003:1st July 10, 2003, 2nd October 12, 2003, 3rd January 15, 2004, 4th April 20, 2004
- year 2004: 1st August 23, 2004, 2nd October 28, 2004, 3rd January 24, 2005, 4th April 20, 2005
- year 2005: 1st August 10, 2005, 2nd November 15, 2005, 3rd February 15, 2006, 4th May 20, 2006

Results and Discussion

Mean dry matter content varied from 94.34 % (2005) to 94.81 % (2003). Higher content of dry matter is important point for storage stabilize. In term of rapeseed storage it is important to take into account that water is situated in the hydrophilic part of the seeds, in the direction to the skin. In the middle of the seed there is the fat.

Nutritional compunds were found to be stabile. Mean nitrogen compounds were determined more than 22.42 %. Mean ash content of the rapeseed was 3.83 %, ranged from 3,65 (2004)–3,93 % (2003).

Evaluation of Oxidative Changes in Lipid Fraction of Rapeseed

Mean fat content ranged from 43.16 (2003) to 45.52 % (2004). Linhart (2006) declared that colza oil was for its benefits on immune system evaluated more favourable than the rest of edible oils. Biodiesel production from rapeseeds makes this more preferable compared to another oils. Both advantages increased the price of rapeseed.

Peroxide value is optimal up to 10 mmol $O_2 kg^{-1}$. Our mean results showed 2.4 mol $O_2 kg^{-1}$. Acid value was more than 2 mg $KOH g^{-1}$ of fat (2.28 mg $KOH g^{-1}$ fat). According to the STS (46 2300-2) acidity of rapeseed during the storage got higher during the years 2004–2005. Higher content of free fatty acids can cause problems with oil refining.

Mean iodine value was 102.3, then this fat can be classified as semi-drying. Thiobarbituric value is desired to be low

Table I
Oxidative changes of lipid fraction of rapeseed during the storage

Rape seed	Fat [%]	Peroxide value [mmol $O_2 kg^{-1}$]	Acid value [mg $KOH g^{-1}$]	Thiobarbituric value [mg $MDA kg^{-1}$]
		2003		
1.	39.83	2.90	1.77	0.081
2.	44.83	3.71	1.75	0.088
3.	44.80	3.87	1.77	0.092
4.	43.16	3.85	1.79	0.096
Mean	43.16	3.58	1.77	0.089
		2004		
1.	45.20	1.82	2.02	0.058
2.	44.18	2.21	3.19	0.056
3.	46.50	3.08	3.09	0.066
4.	46.20	3.75	3.20	0.063
Mean	45.52	2.72	2.86	0.061
		2005		
1.	42.63	1.72	1.95	0.043
2.	43.60	1.95	1.95	0.051
3.	44.15	1.98	2.42	0.056
4.	44.26	2.24	2.52	0.064
Mean	43.66	1.97	2.22	0.053

during the storage, our mean value (0.0068 mg MDA kg^{-1}) showed the stability in oxidative changes (Table I).

The highest representation of fatty acids was found at oleic acid content (61.658 %), followed by linoleic acid (24.112 %) and linolenic (6.690 %). Mean content of erucic acid was found 0.399 %.

Conclusion

Storage conditions affect quality of raw materials. We can conclude that during observed years were not found any important oxidative changes in fat of rapeseed, seems due to optimal conditons during its storage.

REFERENCES
1. Baranyk P., Fábry A., Škerík J.: Výživa a potraviny *59,* 137 (2004).
2. Linhart Z.: Farmář *12*, 11 (2006).
3. Pokorný J.: Výživa a potraviny *56*, 39 (2001).
4. Salková, Z.: Trendy v potravinárstve *9*, 6 (2002).
5. STN 46 23 00 – 2. *Požiadavky na repku olejnú pri nákupe.*
6. STN 56 01 16. *Stanovenie sušiny.*
7. STN EN ISO 659. *Stanovenie obsahu tuku.*
8. STN EN ISO 665. *Stanovenie vlhkosti a obsahu prchavých látok.*
9. STN 58 01 01. *Stanovenie jódového čísla.*
10. STN 58 01 30. *Stanovenie peroxidového čísla. Stanovenie čísla kyslosti.*
11. Venskutonis R., Pokorný J.: Czech J. Food Sci. *18*, 148 (2000).

P66   ANALYSIS OF ACTIVE SUBSTANCES IN HONEY – A CONTRIBUTION TO HONEY AUTHENTICITY

IVANA MÁROVÁ[a], ZUZANA JELÉNKOVÁ[a], KATEŘINA DUROŇOVÁ[a], RADKA KOČÍ[a], PETRA ŽDÁNSKÁ[b] and VERONIKA EHRENBERGEROVÁ[b]

[a]Institute of Food Science and Biotechnology, Brno University of Technology, Purkyňova 118, 612 00 Brno, Czech Republic,
[b]The Secondary Technical School of Chemisty, Vranovská 65, 614 00 Brno, Czech Republic,
marova@fch.vutbr.cz

Introduction

Honey belongs to the oldest delicacies of natural origin. Moreover, honey contains many biologically active substances with positive effect on human health. This work was focused on study of antioxidant content, enzyme activities, protein and saccharide composition in 26 sorts of honey, which differed in geographical and botanical origins. Several qualitative as well as quantitative parameters were determined with the aim to contribute to identification of these compounds which could be considered as markers of the floral origin of honey.

Material and Methods

26 samples of honey, one sample of propolis and one sample of royal jelly were analyzed. Honey were harvested in year 2006 and 2007 and bought in retail chain, special shops and directly from bee-keeper. The study was focused on analysis of antioxidants. Followed groups of antioxidants were determined: flavonoids, catechins, carotenoids, vitamins E, C, A. Authenticity of quality were determined by hydroxymethylfurfural analysis.

Active Substances Analysis

Total phenolics were analyzed colometrically with Folin Ciocalteu reagent (750 nm). Total flavonoid content was analyzed colometrically with $NaNO_2 + AlCl_3$ (510 nm). Total antioxidant capacity was measured by Randox kit.

Individual flavonoids were analyzed by RP- HPLC/UV-VIS method. Using extrenal standards concentration of ((-)catechin, catechin gallate, chlorogenic acid, epicatechin, morin, quercetin, rutin was done. Samples (20 µl) were injected into the RP-18 column (Biospher PSI 200 C18, 7 µm, 150 mm × 4.6 mm). Mobile phases were methanol/water (55 : 45) for catechins and methanol/acetonitrile/water + 1% phosporic acid (20 : 30 : 50) for flavonoid analysis. The flow rate was maintained at 0.75 ml min⁻¹, analysis was performed at 30 °C. Carotenoids (beta-carotene, lycopene, luteine) were analyzed by RP-HPLC with spectrophotometric detection using Hypersil C18, 5 µm, 250 mm × 4.6 mm column, isocratic elution by methanol at the flow rate 1.1 ml min⁻¹ and at 45 °C.

Identifiaction of individual flavonoids and catechins was performed by on-line LC/MS/ESI analysis (Mass spectrometer LCQ Advantage Max). Optimalization of mass spectrometry analysis in negative mode was done using chlorogenic acid. Samples of beer were mixed with 5 times higher amount of 2% HCl and extracted by SPE (Amid-2 column). Isocratic elution was performed by mobile phase acetonitrol:1% acetic acid 50 : 50 at flow rate 0.4 ml min⁻¹ at 30 °C. Individual components were detected in full scan module.

Ascorbic acid was determined usin RP-HPLC on Hypersil APS-2, NH2, 5 µm, 150 mm × 4.6 mm column. Samples were stabilized by 2% HPO_3, 20 µl was injected. Mobile phase was natrium acetate/acetonitrile (95 : 5). Analysis was performed at flow rate 0.6 ml min⁻¹ and 30 °C. Microtitration metod with 2,6-dichlorindofenol was used as comparative mthod too. The end point of titration was determined by pink colour.

5-hydroxymethylfurfural Assay

Concentration of 5-HMF was analyzed by RP- HPLC/UV-VIS method using external calibration. Honey extracts (20 µl) were injected into the RP-18 column (Kromasil C18, 7 µm, 150 × 4.6 mm). Isocratic elution was performed by mobile acetonitrile/water + 1% acetin acid (3:97). The flow rate was maintained at 1 ml min⁻¹, analysis was performed at 30 °C, UV detection was done at 284 nm.

Sensory Analysis

A group of 21 respondents were enrolled into orientation sensory study. They tested several fruit tea and evaluated basic sensory parameters. The droup of respondents was divided into two age-different groups:
- seniors: total 13, age 68.5 ± 7.16; 10 F/3 M,
- juniors: total 8, age 27.13 ± 3.63; 6 F/2 M.

Additionally, consumer questionnaire was completed by 35 student respondents. Preferences and consumption of dried fruit and cereal bars were evaluated.

Results

Average values of total antioxidant capacity ranged (12.75–137.49) mmol 100 g⁻¹. Average values of total phenolic ranged (8.51–61.34) mg 100 g⁻¹ and average values of total flavonoids ranged (0.75–6.04) mg 100 g⁻¹. Honey samples contained (41.83–585.10) µg 100 g⁻¹ of rutin, (9.30–313.40) µg 100 g⁻¹ of myricetin, (6.5–171.90) µg 100 g⁻¹ of luteolin, (3.19–436.37) µg 100 g⁻¹ of quercetin, (2.10–242.66) µg 100 g⁻¹ of apigenin, (0.15–105.12) µg 100 g⁻¹ of caempferol and (0.07–17.52) mg 100 g⁻¹ of naringenin. From group of catechins there were measured (5.98–310) µg 100 g⁻¹ of catechin, (17.77–486.29) µg 100 g⁻¹ of epicatechin, (0.18–64.90) µg 100 g⁻¹ of catechin gallate and (0.59–140.56) µg 100 g⁻¹ of epicatechin gallate. From lipophilic compounds the most abundant in honey samples was tocopherol, its value ranged (29.20–8531.17) µg 100 g⁻¹.

Table I
Total antioxidant activity of several kinds of honey

Honey kind	TAS [mmol 100 g^{-1}]
linden	45.01 ± 0.51
floral (whisked) 2007	26.86 ± 0.38
floral (whisked) 2006	51.34 ± 0.61
sunflower	55.76 ± 0.58
rape (natural)	16.51 ± 0.31
rape (pasted)	40.23 ± 0.50
meadow (floral) (supermarket 1)	22.31 ± 0.35
forest (floral mixed) (supermarket 1)	37.84 ± 0.49
meadow (floral) (supermarket 2)	16.20 ± 0.30
forest (supermarket 2)	44.61 ± 0.48
thyme and herbal	55.04 ± 0.58
acacia	16.73 ± 0.32
royal jelly in honey	3,118.93 ± 11.02
meadow (meadow flora)	21.99 ± 0.34
eucalyptus	62.14 ± 0.67
meadow	47.09 ± 0.44
acacia	33.28 ± 0.45
orange flower honey	12.75 ± 0.29
cereal	58.63 ± 0.55
raspberry leaves	40.20 ± 0.42
Floral – bee-keeper	146.68 ± 1.28
honydew	137.49 ± 1.16
Royal yelly	198.62 ± 1.33
propolis	57,355.93 ± 300.42

Table II
5-HMF concentration in several kinds of honey

Honey kind	5-HMF [mg 100 g^{-1}]
linden	0.24 ± 0.00
floral (whisked) 2007	0.52 ± 0.01
floral (whisked) 2006	1.46 ± 0.00
sunflower	3.09 ± 0.00
rape (natural)	0.23 ± 0.01
rape (pasted)	0.38 ± 0.00
meadow (floral) (supermarket 1)	0.26 ± 0.00
forest (floral mixed) (supermarket 1)	0.20 ± 0.00
meadow (floral) (supermarket 2)	1.79 ± 0.01
forest (supermarket 2)	0.88 ± 0.00
thyme and herbal	0.89 ± 0.02
acacia	4.06 ± 0.00
royal jelly in honey	0.76 ± 0.01
meadow (meadow flora)	0.56 ± 0.00
eucalyptus	1.64 ± 0.01
meadow	1.13 ± 0.00
acacia	1.63 ± 0.00
orange flower honey	0.73 ± 0.00
cereal	2.09 ± 0.01
raspberry leaves	0.66 ± 0.00
Floral – bee-keeper	0.38 ± 0.00
honydew	0.50 ± 0.02
Royal yelly	0.41 ± 0.00
propolis	0.54 ± 0.01

Ascorbate content ranged (0.65–4.65) mg 100 g^{-1}. Content of hydroxymethyl furfural ranged (0.26–4.06) mg 100 g^{-1}.

By LC/MS method luteolin, naringenin, protocatechin acid, coffee acid and p-cumaric acid in honeydew were detected and, furthermore, kyanidin and pinocembrin in floral honey were found.

Mono-floral honey contained biologically active compounds the most, imperceptibly less contained multi-floral honey and honeydew honey. Acacia honey contained the lowest amount of biologically active compounds.

Conclusions

According to our analytically obtained data there is no possible to say which kind of honey (meadow or forest) exhibited more beneficial health effect. It seems that honey quality is more significantly influenced by processing and storage conditions than by honey origin alone.

REFERENCES
1. Fallico, B., Zappala, M., Arena, E., Verzera, A.: Food Chem. *85*, 305 (2004).

P67 ANTIOXIDANT AND ANTIMUTAGENIC ACTIVITY OF DRIED FRUIT, DRUIT TEAS AND CEREAL FRUIT PRODUCTS

IVANA MÁROVÁ[a], MICHAELA BAROŠOVÁ[a], MARTINA TOMKOVÁ[a], HEDVIKA VONDRÁČKOVÁ[a], KATEŘINA DUROŇOVÁ[a] and RADKA KOČÍ[a]

[a]*Institute of Food Science and Biotechnology, Brno University of Technology, Purkyňova 118, 612 00 Brno, Czech Republic,*
marova@fch.vutbr.cz

Introduction

Cereal products form important par of human nutrition. They contain high amount of saccharides, proteins, fiber, vitamins, minerals and other nutrients. There are many studies about benefitial healt effect of cereals in prevention of cardivascular diseases, cancer and hyperlipidaemia. At this time cereals are recommended mainly in the form of complex natural saccharides digested for a long time. Many cereals are mixed with other components as cocoa, nuts, seeds, hioney, chocolade, and also dried fruit. Addition of several kinds of dried fruit could enhance beneficial effect of cereal product.

In this work some biologically active substances in dried fruit, fruit teas and cereal products were analyzed.

Material and Methods

8 kinds of fruit teas (apple, pear, black currant, lemone, cherry etc.) were erolled into this study. 14 kinds of dried fruits were analyzed (apple, pear, plum, berries, tropical kinds etc). 9 kinds of cereal müsli bars with addition of dried fruit (e.g. berries, bear, apple, pear, plum, orange etc.) were analyzed too.

Antioxidant Analysis

Total phenolics were analyzed colometrically with Folin Ciocalteu reagent (750 nm). Total flavonoid content was analyzed colometrically with $NaNO_2 + AlCl_3$ (510 nm). Total antioxidant capacity was measured by Randox kit.

Individual flavonoids were analyzed by RP-HPLC/UV-VIS method. Using extrenal standards concentration of ((–)catechin, catechin gallate, chlorogenic acid, epicatechin, morin, quercetin, rutin was done. Samples (20 μl) were injected into the RP-18 column (Biospher PSI 200 C18, 7 μm, 150 mm × 4.6 mm). Mobile phases were methanol/water (55 : 45) for catechins and methanol/acetonitrile/water + 1% phosporic acid (20 : 30 : 50) for flavonoid analysis. The flow rate was maintained at 0.75 ml min^{-1}, analysis was performed at 30 °C. Carotenoids (beta-carotene, lycopene, luteine) were analyzed by RP-HPLC with spectrophotometric detection using Hypersil C18, 5 μm, 250 mm × 4.6 mm column, isocratic elution by methanol at the flow rate 1.1 ml min^{-1} and at 45 °C.

Identifiaction of individual flavonoids and catechins was performed by on-line LC/MS/ESI analysis (Mass spectrometer LCQ Advantage Max). Optimization of mass spectro-metry analysis in negative mode was done using chlorogenic acid. Samples of beer were mixed with 5 times higher amount of 2% HCl and extracted by SPE (Amid-2 column). Isocratic elution was performed by mobile phase acetonitrol:1% acetic acid 50 : 50 at flow rate 0.4 ml min^{-1} at 30 °C. Individual components were detected in full scan module.

Ascorbic acid was determined usin RP-HPLC on Hypersil APS-2, NH2, 5 μm, 150 mm × 4.6 mm column. Samples were stabilized by 2% HPO_3, 20 μl was injected. Mobile phase was natrium acetate/acetonitrile (95 : 5). Analysis was performed at flow rate 0.6 ml min^{-1} and 30 °C. Microtitration metod with 2,6-dichlorindofenol was used as comparative mthod too. The end point of titration was determined by pink colour.

Antimutagenity Assay

Test strain *Saccharomyces cerevisiae* D7 was used for antimutagenic effect trstiny. The frequency of spontaneous convertants at the tryptophan locus (trp5-12/trp5-27) and revertants at the isoleucine locus (ilv-1-92/ilv1-92) was tested. In each assay positive and negative controls were included. For positive controls 4-nitroquinoline-1-oxide was used as standard mutagen. Experiments were carried out by 1-day treatment of the growing cells with tested samles. After treatment the cells were washed with with phosphate buffer and plated on a solid medium. After 5-days cultivation at 28 °C Ile-revertants and Trp-convertants colonies were counted. Five consecutive experiments were performed.

Sensory Analysis

A group of 21 respondents were enrolled into orientation sensory study. They tested several fruit tea and evaluated basic sensory parameters. The droup of respondents was divided into two age-different groups:
- seniors: total 13, age 68.5 ± 7.16; 10 F/3 M,
- juniors: total 8, age 27.13 ± 3.63; 6 F/2 M.

Additionally, consumer questionnaire was completed by 35 student respondents. Preferences and consumption of dried fruit and cereal bars were evaluated.

Results

Analysis of dried fruits showed high level of vitamins and phenolics mainly in berries. High level of carotenoids was observed in dried apricots and plums. High antioxidant activity was found mainly in dried apples, cranberries and blueberries (Table I).

The highest content of total phenolics, total flavonoids, total antioxidant capacity, procyanidin B2 and chlorogenic acid was measured in plums and blueberry bars (Table II). The highest level of reduced saccharides was evaluated in raspberry and cereal bars.

Higher antioxidant content was found in herbal teas than in fruit teas. Comparing bag teas with loose leaf teas higher antioxidant activity was shown in loose leaf teas. In all tea samples catechins – catechin, epicatechin, epicatechin gallate

and other flavonoids – rutin, morin, quercetin, kaempferol, myricetin and luteolin were determined. In most of teas high level of catechin and rutin was detected. Higher vitamine C level was found in most of fruit teas and in rose hip tea.

High antimutagenic activity exhibited dried cranberries and blueberries. Most of tested dried fruits with high anti-mutagenic effect exhibited also high antioxidant activity as well as high content of some antioxidants. No direct correlation was found among these parameters. High antimutagenic activity showed most of fruit teas, mainly pear tea.

Table I
Total antioxidant activity of dried fruit

Dried fruit	TAS [mmol dm^{-3}]
apple	123.194 ± 1.280
pear	55.020 ± 0.440
apricot	37.380 ± 0.480
plum	56.640 ± 0.980
cherry	54.998 ± 3.840
blueberry	92.396 ± 3.570
cranberry	87.996 ± 4.280
strawberry	59.874 ± 1.350
raisin	82.862 ± 1.280
date	40.456 ± 1.257
fig	28.342 ± 1.100
pineapple	46.198 ± 2.560
mango	1.1568 ± 0.230
papaya	17.9304 ± 0.985

Table II
Total antioxidant activity of cereal bars with dried fruit

Fruit cereal bar	TAS [mmol dm^{-3}]
plum	8.15 ± 1.28
apple	4.02 ± 0.64
apricot	5.26 ± 0.75
raspberry	4.96 ± 0.52
tropical	2.85 ± 0.48
blueberry	8.76 ± 1.76
pear	6.24 ± 1.02
mixed	6.45 ± 1.14
orange	6.02 ± 0.96

During long-term storage of fruit teas (1 year, 20 °C, darkness) a significant decrease of all analyzed antioxidant parameters was followed.

Conclusions

In this work selected kinds of dried fruit, fruit teas and cereal fruit bars were compared. The hioghest values of active substances were found in dried berries, apples and apricote. Similarly, the highest amount of antioxidant substances was found in cereal bars with berries. Cereal part of bars exhibited also important contribution to total antioxidat activity. In fruit teas similar content of active substances was found because of identical basic composition of most teas (apple, rose hip, ibis).

It can be concluded that cereal products, dried fruit ant their mixtures could be important foods recommended for modern human nutrition

P68 CHARACTERIZATION OF "CZECH BEER" – A PILOT STUDY

IVANA MÁROVÁ[a], RENATA MIKULÍKOVÁ[b],
ZBYNĚK ZDRÁHAL[c], HANA KONEČNÁ[c], KATEŘINA
PAŘILOVÁ[a] and ANDREA HALIENOVÁ[a]

[a]*Institute of Food Science and Biotechnology, Brno University of Technology, Purkyňova 118, 612 00 Brno, Czech Republic,*
[b]*Malting Institute, Brno, Czech Republic,*
[c]*Laboratory of Functional Genomics and Proteomics, Faculty of Science, Kamenice 5, Brno, Czech Republic,*
marova@fch.vutbr.cz

Introduction

The healthful and nutritive properties of beer have been recognized by the medical profession for thousands of years. Clinical and statistical evidence and laboratory studies have shown that active substances in beer could influence immune system, block cancer formation, protect against coronary disease and even prolong life. Total benefitial effect of beer and malt samples is a result of many individual contributions of natural substances present in such complicated biological material.

Within the last few years, development of modern instrumental analytical methods has gained increasing importance in authenticity control of food and food ingredients. The characterization of beer samples has a lot of interest because their composition can affect the taste and stability of beer and consumer health. Many substances could contribute to final taste of beer. To the most important probably belong proteins and phenolic substances.

Polypeptides and proteins that influence, direct or indirectly, beer foam quality are protein Z, LTP1 and hordein/glutelin fragments, which originated from malt and have a direct influence on beer foam quality. Other proteins, like malt hordeins and albumins and wheat are, to some degree, also important for beer quality. Protein hydrophobicity is pointed out as a key parameter to enhance foam quality. Electrophoretic, chromatographic and immunological analytical methods are currently used to study polypeptides and proteins present in barley, malt, wort, beer, and foam. Best results are obtained when combinations of these methods are applied.

The aim of this pilot study is to compare composition and to find specific and/or characteristic components in several kinds of beer, malt and other brewing materials.

Material and Methods

13 samples of several types of malt (2× Czech malt, 2× German malt, 2× carapils, 2× caramel, 3× dark-caramel, 2× wheat) were gained from Malting Institute in Brno. 10 kinds of analyzed beer samples were obtained from retail chain, additional 6 samples of Czech beer were gained from breweries.

Antioxidant Analysis

Total phenolics were analyzed colometrically with Folin Ciocalteu reagent (750 nm). Total flavonoid content was analyzed colometrically with $NaNO_2 + AlCl_3$ (510 nm). Total antioxidant capacity was measured by Randox kit.

Individual flavonoids were analyzed by RP-HPLC/UV-VIS method. Using extrenal standards concentration of ((-)catechin, catechin gallate, chlorogenic acid, epicatechin, morin, quercetin, rutin was done. Samples (20 µl) were injected into the RP-18 column (Biospher PSI 200 C18, 7 µm, 150 mm × 4.6 mm). Mobile phases were methanol/water (55 : 45) for catechins and methanol/acetonitrile/water + 1% phosporic acid (20 : 30 : 50) for flavonoid analysis. The flow rate was maintained at 0.75 ml min^{-1}, analysis was performed at 30 °C. Carotenoids (beta-carotene, lycopene, luteine) were analyzed by RP-HPLC with spectrophotometric detection using Hypersil C18, 5 µm, 250 mm × 4.6 mm column, isocratic elution by methanol at the flow rate 1.1 ml min^{-1} and at 45 °C.

Identifiaction of individual flavonoids and catechins was performed by on-line LC/MS/ESI analysis (Mass spectrometer LCQ Advantage Max). Optimalization of mass spectrometry analysis in negative mode was done using chlorogenic acid. Samples of beer were mixed with 5 times higher amount of 2% HCl and extracted by SPE (Amid-2 column). Isocratic elution was performed by mobile phase acetonitrol:1% acetic acid 50 : 50 at flow rate 0.4 ml min^{-1} at 30 °C. Individual components were detected in full scan module.

1D Gel Electrophoresis

1D PAGE-SDS electrophoresis of proteins was carried out by common procedure using 15% and 17.5% polyacrylamide gels. Proteins were staining by Coomassie Blue and by silver staining. For comparison, microfluidic technique using 1D Experion system (BioRad) and P260 chips was used for yeast protein analysis too.

2D Gel Electrophoresis and LC-MS/MS

2D electrophoresis of proteins was optimized in cooperation with Laboratory of Functional Genomics and Proteomics, Faculty of Science, Masaryk University of Brno. 2D gels were obtained using protein preparatives isolated from lyophilized cells. After optimization of separation conditions proteomes from lyophilized beer samples were analyzed. Quantitative analysis was done using BioRad Laboratories 2D software. Identification of some spots was done using LC-MS/MS.

Results

The content of total phenolics in malt was about 1.4× higher than in wort and hop wort and 1.5–2.5× higher than in beer samples. Phenolic content decreased in sequence dark caramel – caramel – Czech – German – wheat malt. The main flavonoid detected in most of malt and wort samples was (–) catechin followed by rutin and quercetin. Czech malt con-

tained about 14 µg g^{-1} of (–)catechin, 2 µg g^{-1} of rutin and 1.4 µg g^{-1} of caempherol, while wort contained about 5x higher (–)catechin level. The ration of individual flavonoids changed with malting temperature. Levels of flavonoids changed similarly as phenolic content. TAS levels were several times higher in dark types of malt than in wheat or Czech malt.

Barley and malt proteins are relatively well-documented and their analysis belongs to commercially used tests for barley variety authenticity. Beer proteome has been not studied in detail. In this work main protein fractions (40 kDa, lower than 8–10 kDa, peptides – see Fig. 1. and Fig. 2.) were determined in lyophillized beer samples. Pilot 2D electrophoretic analysis of some beer samples was done mainly for optimization of analysis conditions.
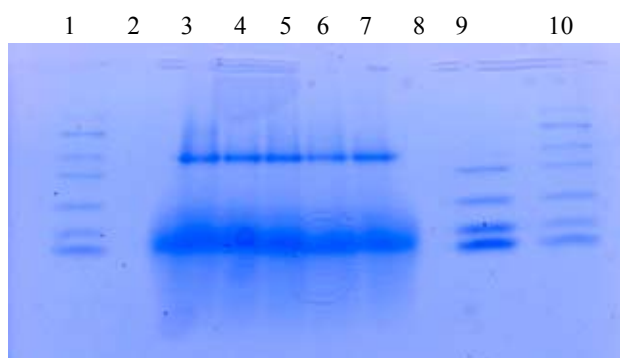
Fig. 1.   **1D PAGE-SDS analysis of beer proteins. 1 – standard 6 (97.4, 67.0, 45.0, 29.0, 21.0, 12.5, 6.5 kDa; 3-7 – proteome from lyofilized beer; 9 – standard 5 (29.0, 21.0, 12.5, 6.5 kDa); 10 – standard 6**

Conclusions

The aim of presented pilot study was to use modern techniques to qualitative and quantitative analysis of characteristic components of Czech beer. One of the main goals is separation and analysis of specific proteins and peptide fragments and changes of their content during beer processing. Based on analysis of barley variety purity using standard 1D
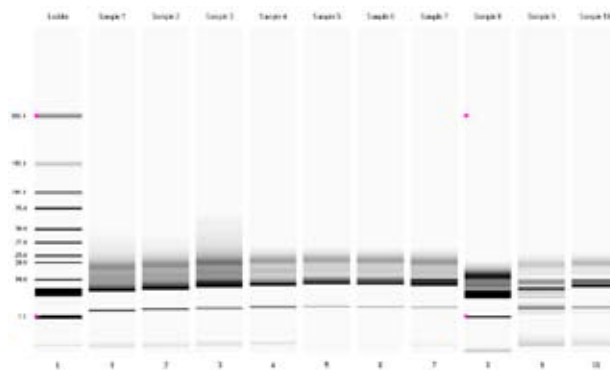
Fig. 2.   **Microfluidic 1D electrophoresis of beer proteins**

PAGE-SDS detailed characteristics of proteins by microfluidic techniques, 2D-electrophoresis, LC/ESI-MS, LC/MS/MS was tested. Further aim was qualitative and quantitative analysis of individual phenolics in Czech beer by chromatographic techniques (RP-HPLC, LC/MS). All analyses will be performed in several kinds of Czech beer in comparison with beers processed by different technology. All results will be compared to obtain a set of parameters suitable to final characterization of Czech beer. This set could be used in food control to authenticity assesment of Czech beer.

REFERENCES

1. Leiper K. A., Stewart G. G., McKeown I. P.: J. Inst. Brew. *109*, 57 (2003).
2. Zimmermann B. F., Galensa R.: Eur. Food. Res. Technik. *224(3)*, 385 (2007).
3. Perrocheau L., et al.: Proteomics *5*, 2849 (2005).
4. Boren M., Larsson H., Falk A., Jansson C.: Plant Sci. *166*, 617 (2004).
5. Vundla W., Torline P.: J. Am. Soc. Brew. Chem. *65*, 21 (2007).

P69 TOCOPHEROL AND FATTY ACIDS CONTENTS OF SELECTED ROMANIAN CEREAL GRAINS

CRISTIAN TUDOR MATEA, OCTAVIAN NEGREA,
IOAN HAS, SIMONA IFRIM and CONSTANTIN BELE
University of Agricultural Science and Veterinary Medicine,
R-400372,Cluj-Napoca, Romania,
a426401@yahoo.com

Introduction

Cereals grains are one of the main sources of tocopherols (Ts) for humans[1]. These compounds are recognized for their inhibition of lipid oxidation in biological systems and each isomer shows , to a different extent, vitamin E activity in the order $\alpha - T > \beta - T > \gamma - T > \delta - T$(ref.[2]). The interest in the relationship between Ts and fatty acids (FA) is outlined by the fact that fats are carriers for Ts and they have at the same time a prooxidant effect since they are susceptible to oxidation[3].

The objective of this study is to determine the content of tocopherols (α– , $\beta+\gamma$ and δ–) and FA composition in 19 elected Romanian cereal grain varieties (wheat, maize and oat).

Experimental

C e r e a l   S a m p l e s

Cereal grain samples harvested in 2006 and 2007 were obtained from Agricultural Research Institute Turda. The samples included eight wheat, eight maize and three oat varieties (var.). Samples from two replicates were chosen for analysis. All samples were ground in a laboratory mill. Ground samples were stored at –20 °C until extracted.

M e t h o d s

Total lipids (TL) were determined according to a routine procedure 4.

The tocopherols were analysed using a Shimadzu VP Series liquid chromatograph equipped with a degasser and a fluorescence detector FR-10 AXL with excitation wavelength of 290 nm and emission wavelength of 325 nm. Chromatographic separation was performed on a Alltima RP C-18 column (250 mm × 4,6 mm, 5 μm). The column was used at 40 °C. The mobile phase was a mixture of acetonitrile and methanol (50 : 50 , v/v) and eluted at a flow rate of 1.0 ml min^{-1}.

Sample treatment included saponification of 0.5 g cereal flour in a Pyrex glass tube with 0.5 ml 50% KOH and a mixture of 5 ml + 2 ml water in the presence of 0.1 g ascorbic acid. The tube was transferred to a boiling water bath for 30 min. Then 6 ml of ethanol 50% was added to the cooled tube. Unsaponified lipids were extracted by using three portions (each 10 ml) of n-hexane: diethyl ether (7 : 3, v/v). After separation of the phases, the organic layers were collected in a separatory funnel. Organic extracts were washed three times with water and then evaporated in a vacuum rotary evaporator at 35 °C. The dried residue was extracted with 2 ml methanol + 2 ml acetonitrile by mixing on a vortex mixer for 2 min. The tocopherol contents were calculated from the peak areas using standard curves of tocopherols ($\alpha - T$, $\beta - T$, $\gamma - T$ and $\delta - T$) obtained from Merck and Sigma.

FA were analyzed by gas-liquid chromatography (GLC) with flame ionization detection (FID). The sample (1 μl) was injected into gas-chromatograph, a Shimadzu GC-17 A series equipped with a 30 m Alltech AT-WAX coated with polyethylene glycol (0.25 mm I.D., 0.25 μm film thickness).The oven temperature was programmed as follows : 70 °C for 2 min, then raised to 150 °C at 10 °C, held at 150 °C for a further 3 min, then raised to 235 °C at 4 °C min^{-1} . The final oven temperature was maintained for 5 min. The injector and detector temperature was 260 °C. The carrier gas was helium at a pressure of 147 kPa.

FA were converted to methyl esters by reaction with boron trifluoride/methanol at 80 °C for 2 h in a Pyrex glass tube. Esters were extracted twice with 1 ml n-hexane, the extracts were combined, neutralized with sodium carbonate and dried with anhydrous sodium sulfate and filtered. Finally the filtrate was concentrated under a stream of nitrogen.

Table I
The content of tocopherols in different cereal grains

Cereal	Tocopherols [mg 100 g^{-1}] range		
	α	β+γ	δ
Wheat	0.77	0.23	–
	0.64–0.98	0.16–0.31	–
Maize	0.26	0.96	0.08
	0.16–0.34	0.75–1.21	0.05–0.12
Oat	0.31	0.03	–
	0.27–0.37	0.02–0.04	–

Results

The means and ranges of tocopherols in different cereal grains are shown in Table I.

α-tocopherol was the main isomer found among analysed tocopherols in wheat and oat var. The content of α-T in wheat var. was similar to that reported by other authors[1,5]. Maize had the highest $\beta+\gamma$ tocopherol content. Small quan-

Table II
Total lipids and fatty acid profiles of selected cereals

TL and fattyacids [g 100 g^{-1}] food	Wheat	Maize	Oat
TL	1.6	5.2	5.8
SFAs[1]	0.17	0.55	0.74
MUFAs[2]	0.18	1.32	1.80
PUFAs[3]	–	–	–
Total cis	0.67	2.66	1.75
n-6 (as 18 : 2)	0.64	2.59	1.70
n-3	0.03	0.07	0.05

[1] Saturated fatty acids
[2] Monounsaturated fatty acids
[3] Polyunsaturated fatty acids

tities of δ–T was found in maize whereas in wheat and oat it was not found.

Table II presents the mean values for the analysis of TL and fatty acid profile of selected cereals. Lipids are only a minor component of cereals, with the amount varying from a lipid content of 1–3 % in wheat , to 5–9 % in maize and 5–10 % in oats[6].

Total unsaturated fatty acids (UFAs) ranged from 57–86 % of total fatty acids with linolenic and oleic acid predominant for wheat var. Total UFAs ranged from 72–87 % respectively 62–83 % for maize and respectively oat var. and the same predominant fatty acids. The content of linoleic acid was significantly higher in maize var. than in wheat and oat var.

The lower content of α–T in maize var. does not correlate with the standpoint that higher PUFA content is accompanied by higher content of α–T (ref.[7]).

Conclusions

This study focused on the quantification of tocopherols and fatty acids in 19 selected Romanian cereal grain varieties. The results of this study should be helpful in updating the national database for food composition and for assessment of the nutritional intake of the population.

REFERENCES

1. Zielinski H., Ciska E., Kozlowska H.: Czech J. Food Sci. *19*, 182 (2001).
2. Cavallero A., Gianinetti A., Finocchiaro F., Delogu G., Stanca A. M.: J. Cereal Sci. *39*, 175 (2004).
3. Ribarova F., Zanev R., Shishkov S., Rizov N.: J. Food Comp. Anal. *16*, 659 (2003).
4. Folch J., Lees M., Stanley G. H. S.: J. Biol. Chem. *226*, 497 (1957).
5. Holasova M., Velisek J., Davidek J.: Potrav. Vedy *13*, 409 (1995).
6. McKevith B.: Nutr. Bull. *29*, 111 (2004).
7. Thomas M. J.: Nutr *16 ,*716 (2000).

P70 MONITORING OF BARLEY STARCH AMYLOLYSIS BY GRAVITATIONAL FIELD FLOW FRACTIONATION AND MALDI-TOF/ TOF MS

KAREL MAZANEC and JANETTE BOBÁĽOVÁ

Institute of Analytical Chemistry of the ASCR, v. v. i.Veveří 97, 602 00 Brno, Czech Republic,
mazanec@iach.cz

Introduction

In barley grain, starch occurs in form of granules with bimodal size distribution. The oval large starch granules (A) have diameters in the range from 10 to 40 μm and they prevail in weight. On the other hand, the spherical small starch granules (B) have diameters from 1 to 10 μm and they prevail in number[1]. Enzymatic starch granule hydrolysis is one of the most important reactions occurring during malting and mashing.

In this study, the capacity of gravitational field flow fractionation (GFFF) to monitor the amylolysis of starch granules was investigated. In previous works[2-6] GFFF was successfully used for study of size distribution of starch granules in different barley varieties. Degradation of starch particles from wheat was monitored by sedimentation FFF[7]. Lower saccharides released during amylolysis can be studied by MALDI-MS.

Experimental

Kernels of barley variety Jersey were used for isolation of starch granules. Kernels were graded and the fractions over 2.5 mm were used. The isolation procedure is described in detail elsewhere[8]. It combines classical approaches (incl. crushing of barley kernels by a roll crusher, steeping in 0.02M HCl, repeated rubbing and filtering through sieve 0.08 mm) and present knowledge (treatment with ß-glucanase and cellulase).

Starch granules were hydrolyzed by 2 units of α-amylase mg^{-1} starch (Sigma-Aldrich) added to 2 ml of 3% (w/v) starch suspension at 35 °C. Aliquots were removed in time interval during hydrolysis and centrifuged. Supernatant was mixed with 2,5-dihydroxybenzoic acid (DHB) and measured by 4700 Proteomics Analyzer (Applied Biosystems, USA) MALDI-TOF/TOF mass spectrometer (equipped with Nd/YAG laser; 355 nm).

Starch granules were resuspended in 10^{-3} % sodium dodecyl sulphate (SDS) (Fluka, Germany), sonicated and analyzed by GFFF. Apparatus for GFFF is described in[6]. The channel dimensions were $360 \times 20 \times 0.150$ mm. The highpressure pump HPP 4001 (Laboratory Instruments, Prague, Czech Republic) was used to introduce the carrier liquid into the channel via an inlet capillary situated at the channel head. UV/VIS Spectra 100 (Spectra Physics, San Jose, USA) operated at 470 nm was used as a detector. The samples were injected at the stopped flow by using a Hamilton microsyringe. Just after injection, a loading flow rate of 0.2 ml min^{-1}

was applied for 10 s. Then a relaxation time (stopped-flow period) was 1.5 min. After this time period, a linear flow rate of 0.8 ml min^{-1} was applied.

Results

Experimental conditions of GFFF separation were chosen in order to elute starch particles in focusing or lift-hyperlayer elution mode[6]. In this elution mode, starch granules do not interact with the channel bottom; therefore particle-wall interactions are negligible.

Fig. 1. shows a representative GFFF elution fractogram obtained for native starch of barley variety Jersey. Three major peaks can be seen: the first corresponding to unretained species (void volume), the second corresponding to the large A starch granules and the third peak corresponding to the small B starch granules.
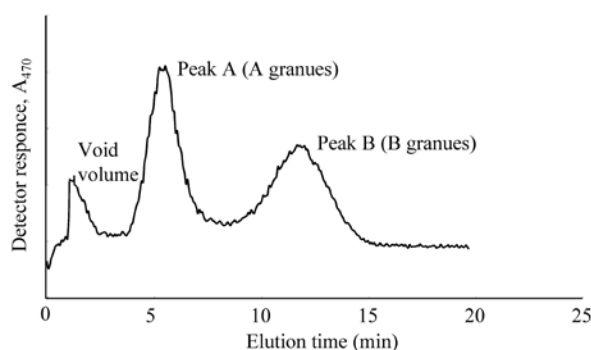
Fig. 1. **Representative fractogram of native starch from barley variety Jersey after GFFF elution**

The α-amylase type VIII-A from barley (Sigma) was chosen for starch granule attack. In the case of bimodal starch population, the amylolysis mechanisms are more complex than those for small monomodal starches. Amylases start enzymatic digestion on specific points of the large A starch granules. Degradation then continues towards the centre of the granule by the formation of channels leading to particle
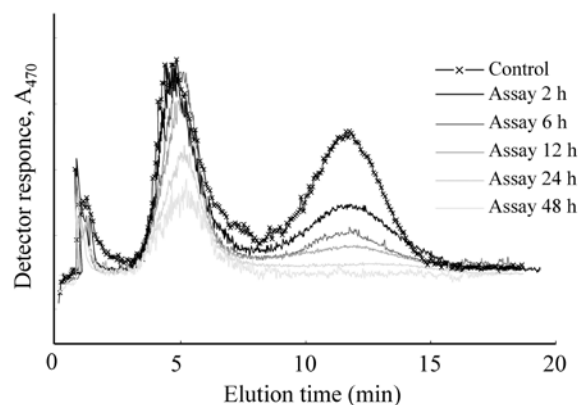
Fig. 2. **GFFF monitoring of barley starch enzymatic hydrolysis. Starch was isolated from barley variety Jersey**
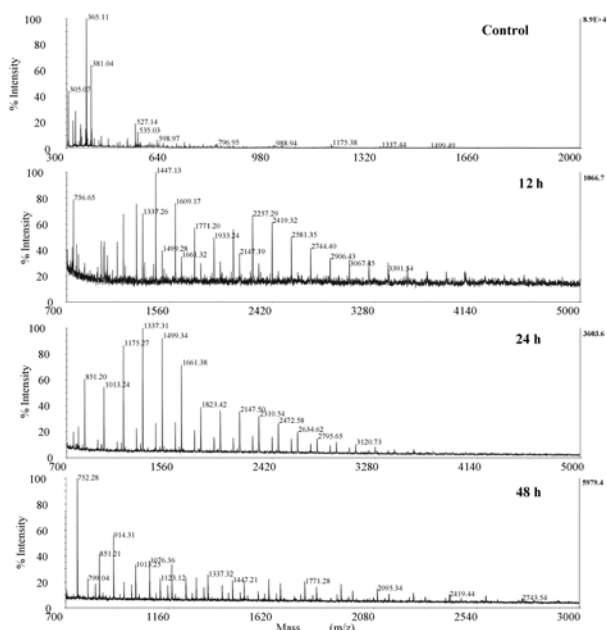
Fig. 3. **MALDI-TOF mass spectra of saccharides released during amylolysis. DHB was used as a matrix**

disruption and fragmentation after certain time[9]. Contrary, B granules are gradually digested from the whole surface.

Fig. 2. shows fractograms of native barley starch incubated with amylase. Changes in GFFF fractogram profiles were observed during amylolysis. The rapid decrease of the intensity of B peak corresponds to the greater susceptibility of B granules to amylolysis[9]. The time depended decrease in peak A signal after certain incubation period is also well-marked. On the other hand, the fractograms of the control starch sample showed minimal changes through experiment. The results of experiments well reflects concept of pitting degradation of large A starch granules and pheripheral hydrolysis of small B granules.

Lower sugars released during amylolysis were studied by MALDI-MS. The spectra of the control sample and digestion mixture during amylolysis are shown in Fig. 3. Increasing

intensities of peaks related to sugars correspond to released saccharides during amylolysis. With progress of hydrolysis several series of +162 Da peaks can be seen in mass spectra (see the last spectrum in Fig. 3.).

Conclusions

The results of incubation of native starch granules isolated from Jersey barley variety with amylases confirmed that GFFF appeared to be a good tool for monitoring of degradation progress of native barley starch. MALDI-MS of lower sugars released during amylolysis showed its potential for study of products of starch hydrolysis.

REFERENCES

1. Tillet I. J. L., Bryce J. H.: *European Brewery Convention: Proceedings of the 24th Congress* (van Wijngaarden M. ed.), p.45. Oslo, Norway1993.
2. Chmelík J., Krumlová A., Budinská M., Kruml T., Psota V., Bohačenko I., Mazal P, Vydrová H.: J. Inst. Brew. *107*, 11 (2001).
3. Chmelík J., Krumlová A., Čáslavský J.: Chem. Pap.-Chem. Zvesti *52*, 360 (1998).
4. Janoušková J., Budinská M., Plocková J., Chmelík J.: J. Chromatogr. A *914*, 183 (2001).
5. Reschiglian P., Zattoni A., Casolari S., Krumlová A., Budinská M., Chmelík J.: Anal. Chim. *92*, 457 (2002).
6. Chmelík J., Mazanec K., Bohačenko I., Psota V.: J. Liq. Chromatogr. Related Technik. *30*, 1289 (2007).
7. Salesse C., Battu S., Begaud-Grimaud G., Cledat D., Cook-Moreau J., Cardot P. J. P.: J. Chromatogr. A *1129*, 247 (2006).
8. Bohačenko I., Chmelík J., Psota V.: Czech J. Food Sci. *24*, 11 (2006).
9. Lindeboom N., Chang P. R., Tyler R. T.: Starch/Stärke *56*, 89 (2004).

P72 THERMOGRAVIMETRIC ANALYSIS OF LIQUID PYROLYSIS PRODUCTS OF WOODY BIOMASS

RADOSLAV MIKULÁŠIK, JANA KOSINKOVÁ, ALEŠ HÁZ, SOŇA FIGEDYOVÁ and IGOR ŠURINA

Department of Chemical Technology of Wood, Pulp and Paper, Faculty of Chemical and Food Technology, Slovak Technical Univerzity Radlinského 9, 812 37 Bratislava, Slovak Republic,
Radoslav.Mikulasik@stuba.sk

Introduction

Thermal analysis (TA) represents a set of methods, used to study the changes of investigated material by measuring some physical properties as a function of temperature.

Nowadays, several thermoanalytical methods are used, differing in monitored physical property (mass, volume, length, magnetic susceptibility, temperature difference between sample and reference sample), etc.

In thermogravimetric analysis (TGA), mass changes of sample are determined as a function of temperature.

Data obtained from TG measurements are used to investigate thermal stability of substances, determination of relative volatility and determination of other physical and chemical parameters. First derivative of TGA curve according to temperature is denoted as DTGA or DrTGA and represents the rate of reaction.

TGA is used very frequently to study thermal behavior of different kinds of biomass (in inert or oxidative atmospheres), mainly agricultural crops or their residues[1], woody wastes[2], some fossil fuels – coal and blend fuels (biomass/coal)[3,4].

Pyrolysis of plant or woody materials generates solids, liquids and gaseous fuels or products. Their composition depends on the pyrolysis process conditions.[5–8]

Thermal behaviour of liquid and solid pyrolysis products – bio-oil and wood coal – usable as fuels or for energetic purposes – can be studied by means of thermoanalytical methods. Experimental part of this work is focus on TGA, which was used for study of thermal behaviour and thermal stability of fractions of bio-oil in inert atmosphere.

Experimental

Materials

Bio-oil fractions originating at industrial pyrolysis of beech wood – pyrolysis condensate (PC), pyro-oil (PO), and wood tar (WT) were suplied from SLZ Chémia, Slovakia.

Methods and Instruments

Thermogravimetric analysis (TGA) was performed on a Mettler Thermoanalyzer 2, in inert gas atmosphere (nitrogen).

Conditions: flow rate: 60 ml min^{-1}, temperature program was 10 °C min^{-1} from 25 to 600 °C, analysis time 60 min, and sample amount was ~ 20 mg.

Results

As can be seen from TGA results (Fig. 1.) of pyrolysis condensate (PC), temperature rise up to ~ 120 ºC resulted in more than 90 % weight loss. PC is formed of a mixture of compounds which distilled with the highest rate at 97 ºC.

This fraction of bio-oil according to TGA curve contains mainly volatile organic compound (VOC) and water. VOC is defined as a compound which has boiling point equal or less than 250 °C at pressure 101.3 kPa[9].
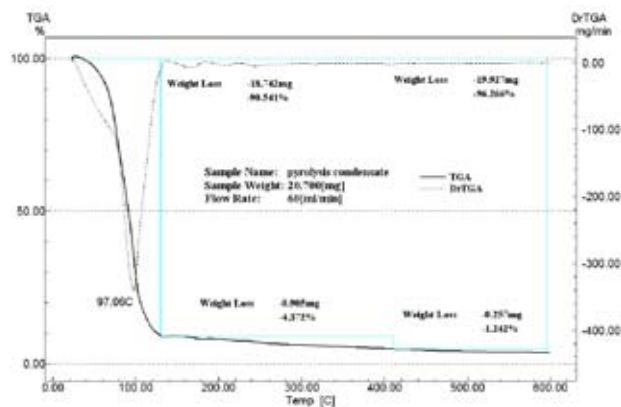
Fig. 1. **TG analysis of pyrolysis condensate**

The results of TGA analysis of pyro-oil (PO) document (Fig. 2.) that PO still contains VOC (6 %), but their amount is much lower than that present in the fraction of PC. Increasing the temperature to ~ 410 ºC leads to ~ 93 % weight loss and so the most part of PO distilled off or is thermally decomposed.
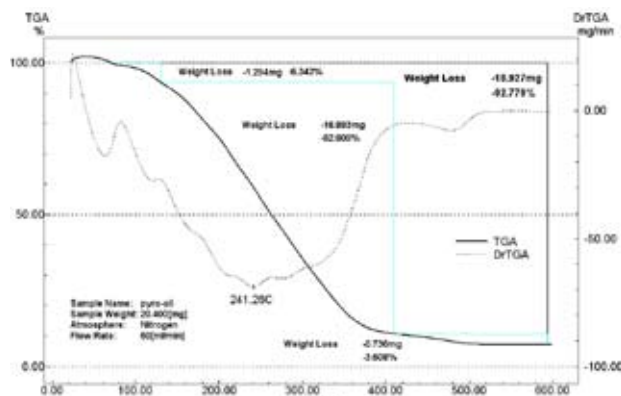
Fig. 2. **TG analysis of pyro-oil**

The results of TGA analysis of wood tar (Fig. 3.) led to a conclusion that reaching temperature ~ 400 ºC, 75 % of wood tar fraction (WT) underwent decomposition.

This fraction contains also thermally stable compounds as evidenced by residual more than 20 % amount at 600 ºC.

The individual phases of the thermal decomposition or degradation – namely I. dehydratation and volatilisation, II. active pyrolysis and III. passive pyrolysis[10] were analysed.
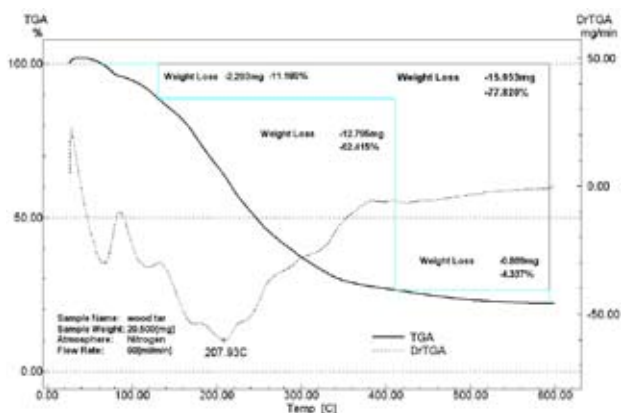
Fig. 3.   **TG analysis of wood tar**

Fig. 4. shows comparison of TGA curves of fractions of bio-oil. It is obvious from this comparison that the least stable fracion is PC, followed by PO and ending with WT.
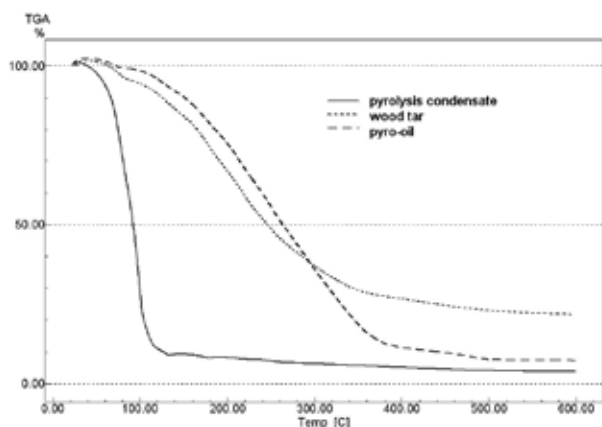
Fig. 4.   **Comparison of TG analysis of bio-oil fractions at the same conditions**

Temperatures and weight losses for individual stages are listed in Table I.

Table II indicates total weight losses for individual fraction of bio-oil and corresponding decomposition temperatures at which the maximum weight loss per minute occurs.

Data in tables for individual stages differ because every fraction contains other compounds and in different quantitative amounts.

Table I
Decomposition stages of bio-oil fractions and weight loss

Stage	I.		II.		III.	
T [°C]	25–130		130–410		410–600	
Sample	[mg]	[%]	[mg]	[%]	[mg]	[%]
PC	18.80	90.8	0.91	4.4	0.26	1.3
PO	1.29	6.3	16.89	82.8	0.74	3.6
WT	2.29	11.2	12.80	62.4	0.89	4.3

PC contains mainly water, VOC and hydrocarbons with short chains. PO contains hydrocarbons with longer chains, benzene and phenolic structures. WT is composed mainly of condensed aromatic substances, benzene and phenolic structures.

Table II
Total weight loss of bio-oil fractions and decomposition temperature at max. weight loss

Sample	Weight [mg]	Loss [mg]	Loss [%]	t_{max} [°C]
PC	20.7	19.963	96.4	97.1
PO	20.4	18.927	92.8	241.3
WT	20.5	15.953	77.8	207.9

Conclusions

In this work, we investigated three liquid fractions of bio-oil generated in process of woody biomass pyrolysis beechen wood.

TGA measurements indicated different composition of individal fraction of bio-oil.

Pyrolysis condensate contains substantially volatile compounds (VOC) and water than pyro-oil and wood tar. Pyro-oil contains more VOC than wood tar, which is confirmed by total weight losses of these fractions. Pyrolysis condensate has total weight loss 96.4 %, pyro-oil 92.8 % and wood tar 77.8. So the residue of wood tar is highest at 600 °C.

At all fractions it is possible to deduce from TGA curves that if temperature increases gradually, then distillation of volatile compounds and their exothermal decomposition occur.

Distillation and decomposition process proceed in different temperature intervals and weight losses at these intervals are different for individual fractions, which means that each fraction contains different substances with different ratio.

Based on TGA results it can be concluded that the least thermal stability has fraction of pyrolysis condensate, followed by pyro-oil and, finally, the most stable was wood tar.

REFERENCES

1. Šimkovic I., Csomorova K.: J. Appl. Polym. Sci. *100*, 1318 (2006).
2. Lapuerta M., Hernández J. J., Rodríguez J.: Biomass Bioenergy *27*, 385 (2004).
3. Vuthaluru H. B.: Bioresour. Technol. *92*, 187 (2004).
4. Jones J. M., Kubacki M., Kubica K., Ross A. B., Williams A.: J. Anal. Appl. Pyrolysis *74*, 502 (2005).
5. Czernik S.: *Review of Fast Pyrolysis of Biomass Mississippi Bioenergy Thermochemical Conversion Technologies Roundtable*, Jackson, MS, January 28, 2004, National Renewable Energy Laboratory 1617 Cole Boulevard, Golden, CO 80401, presentation.

6. Bridgwater A.V., Meier D., Radlein D.: Org. Geochem. *30*, 1479 (1999).
7. Mohan D., Pittman Ch. U. Jr., Steele Ph. H.: Energy Fuels *20*, 848 (2006).
8. Bridgwater A. V., Peacocke G. V. C.: Renewable Sustainable Energy Rev. *4*, 1 (2000).
9. Directive 2004/42/CE of the European parlament and of the Council of 21 April 2004 on *the limitation of emissions of volatile organic compounds due to the use of organic solvents in certain paints and varnishes and vehicle refinishing products and amending* Directive 1999/13/EC, Official Journal of the European Union, L 143/89
10. Kumar A., Wang L., Dzenis Y. A., Jones D. D., Hanna M. A.: Biomass Bioenergy (2007).

P73　ANALYTICAL MEASUREMENTS AND PHISICOCHEMICAL PARAMETERS DETERMINATION IN STRAWBERRIES AND RASPBERRIES ENHANCE PRODUCTION

A. GAGO, F. MORENO, T. GARCÍA-BARRERA and J. L. GÓMEZ-ARIZA

Dpto. de Química y CC.MM, Facultad de Ciencias Experimentales, Universidad de Huelva, Campus de El Carmen, 21007 Huelva, Spain,
amanda.gago@dqcm.uhu.es

Introduction

Strawberry is one of the most delicious fruits of the world, which is a rich source of vitamins and minerals[1].The strawberry harvest in Huelva was included in the main group of agricultural activities in which Spain have an important position in the framework of the European Union. Huelva offers adequate climatic characteristics and soil composition as well as water disponibility for irrigation that is exceptional in the national territory. Contemporany history of cultivating strawberry de Huelva started in 60's in Moguer city.

In recent years, several day-neutral varieties have been introduced and different agro-techniques were standardized at various research stations[2]. In addition, strawberry has become the most favourite fruit crop among the growers, especially near towns and cities, which has resulted a phenomenal increase in its area and production. In Huelva, many varieties of strawberry and raspberry are grown, but (*Fragaria vesca* var. *Camarosa* and *Rubus idaeus* var. *Glen Lyon)* has become the most popular dessert variety due to its high production potential and because it is an attractive red medium-sized fruit of better quality.

The safeguard of quality characteristics from harvest up to consumption is an essential requirement for the fruit sector. Quality control and authentication of fruits and derivatives is a key aspect for consumers and producers. Food authentication is the process by which a food is verified as complying with its label description. Labeling and compositional regulations, which may differ from country to country, have a fundamental place in determining which scientific tests are appropriate for a particular issue[3] Thus the availability of sound analytical methods which can ensure the authenticity of foods plays a fundamental role in the operation of modern society. In this sense, several analytical parameters have to be taken into account.

In this work, we have analysed several samples of strawberries and raspberries (*Fragaria vesca* var. *Camarosa* and *Rubus idaeus* var. *Glen Lyon*) in relation with phisicochemical parameters (elements such as Ca, Mg, K, Na, B, Cu, Fe, Ni and Zn; anions: phosphates, nitrates, sulphates, carbonates; solids in suspension, pH, redox potential). The experiment was carried out during six months in which several agrochemical experiments have been developed such as the use of new plastics for the harvest and the pollination with bumblebees.

Experimental

S a m p l e s

Samples of soils and leaves were analysed in this study. The samples of leaves were taken during the months of major production of both plants and the samples of soil at the beginning and at the end of the harvest.

P r e p a r a t i o n   o f   t h e   S a m p l e

(i) Samples of leaves: The samples were dried in an oven at 100 °C. After that they were extracted by using a microwave oven: 0.2 g of sample was weighted and 4 ml of HNO_3 (65%) were added. The program was from room temperature to 170 °C at 20 °C min^{-1}.

(ii) Samples of soil: the same parameters that for the leaves were analyzed, but different extractant solutions were used[4,5]:

- Phosphorus: Extraction with sodium bicarbonate at pH 8.5
- Manganese and iron: Extraction with ammonium acetate pH 4.8
- Sodium, potassium, calcium and magnesium: Extraction with ammonium acetate at pH 7
- Organic matter: was determined by a redox process using potassium dichromate and sulphuric acid, to measure the excess of dichromate with a salt-ferrous

M e a s u r e d   E l e m e n t s   a n d   M e t h o d s   o f   A n a l y s i s :

- ^{63}Cu and ^{66}Zn: measured with an Inductively Coupled Plasma Mass Spectrometry (ICP-MS) Model 4500 (Agilent Technologies, Tokyo, Japan)
- Orthophosphates: measured with the molybdenum blue method[4].
- Mn, Fe, Ca, Mg: they were measured with Atomic Absorption Spectroscopy (AAS).
- K and Na: Atomic Emission Spectroscopy (AES).
- Determination of the soil texture: it was measured by using the Mastersizer 2000, a laser diffraction instrument.

I C P - M S   P a r a m e t e r s :

- RF power: 1,370 W
- Plasma gas flow-rate: 15 dm^3 min^{-1}
- Auxiliary gas flow-rate: 1.00 dm^3 min^{-1}
- Nebulizer gas flow-rate: 1.15 dm^3 min^{-1}
- Sampling depth: 6.5
- Sampler and skimmer cones: Ni
- Time per isotope: 0.3 s per isotope
- Isotopes monitorized: ^{63}Cu and ^{66}Zn

Results

The results of analyses of soil throughout the study are collected in the Table I.

- At the beginning of the study (February).
- At the end of the harvest, in June.

Table I
Results of analyses of soil throughout the study

	Strawberry		Raspberry	
	February	June	February	June
Carbon [%]	0.24	0.14	0.26	0.20
Oxidable organic matter [%]	0.42	0.24	0.44	0.34
Organic matter total [%]	0.54	0.31	0.57	0.45
N [%]	<D.L	<0.3	<D.L	<0.4
H [%]	<D.L.	<0.7	<D.L.	<0.8
P [mg kg^{-1}] Extraction NH$_4$-Ac pH 7	158.94	89.73	144.63	185.2
K [mg kg^{-1}]	62.55	35.64	86.24	95.37
Na [mg kg^{-1}]	14.5	N.D.	19.19	N.D.
Ca [mg kg^{-1}]	167.61	520	188.6	640
Mg [mg kg^{-1}] Extraction NH$_4$-Ac pH 4.8	30.91	33.1	39.67	62.09
Mn [mg kg^{-1}]	8.47	8.50	7.09	8
Fe [mg kg^{-1}]	14.78	6.91	10.54	8.41
Principio del formulario Soil texture[4] Final del formulario	Loamy sand		Loamy sand	
Clay	5 %		15 % Final del formulario	
Silt	17 %		37 %	
Sand	73 %		37 %	
Graves Final del formulario	5 %		11 %	

D.L. – Detection Limit; N.D. – Not determined

The results of the analyses of leaves throughout the study are represented in the Figs. 1., 2. and 3.

Once we have obtained the results of the measured concentrations of elements in leaves and soil, it is required to get conclusions of the analysis comparing the obtained values with the common known concentrations for each specie[6,7]. It is important that the levels of the elements in the plants are the required ones in each stage of the growing.

As it is shown in Fig. 1., the levels of copper and zinc are between required levels in both species. In this sense, we can observe that the level of zinc is major at the beginning of the harvest. Similar conclusions can be drawn for the concentration of lements in Figs. 2. and 3.

As it is shown in Fig. 2., in the leaves from strawberries the levels an

As it is shown in Table I, the levels of organic matter are low that is a characteristic of sand soils. In addition, the levels go down through the harvest. Although levels are low, the results of production has been good in both cases.
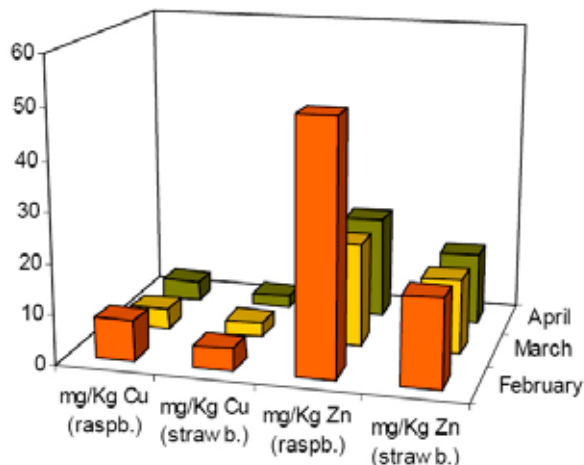
Fig. 1.   **Evolution of copper and zinc in leaves of strawberries and raspberries**
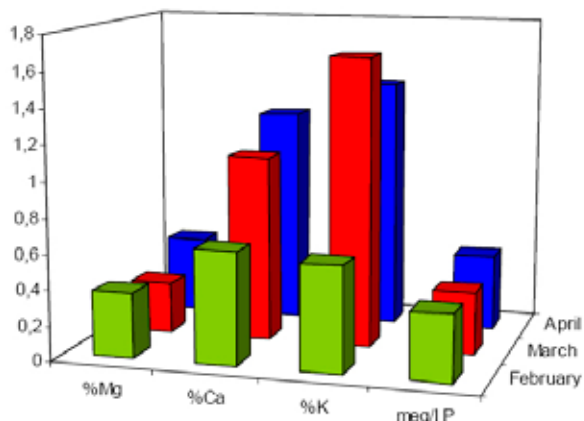
Fig. 2.   **Evolution of magnesium, calcium, potassium and phosphorus in leaves of strawberries**
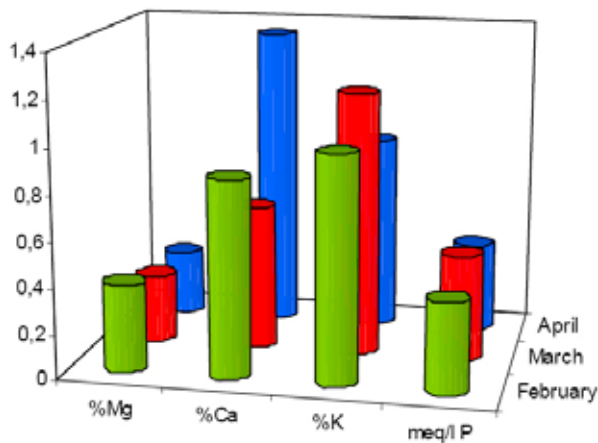
Fig. 3.   **Evolution of magnesium, calcium, potassium and phosphorus in leaves of raspberries**

The samples were taken monthly, and they covered all stages of development of the crop: vegetative growth, flowering and fruiting.

These measured parameters were used to know the evolution of these two varieties and to observe the requirements of the plants. Future works will be focused in a discussion of a parelell study carried out to observe the evolution of the fruit, ºBrix, potential deformations, and other parameters such as pollination using bumble bees as well as the experimentation with new biodegradable plastic.

Conclusions
- An analytic methodology for the determination of a great number of analytical parameters of agronomic interest has been developed in this study.
- The obtained analytic data are of great utility to evaluate the experiences of the use of biodegradable padding plastics in the cultivation of raspberry.
- The use of pollination by bumblebees increases the production and improves the quality of the fruit.

REFERENCES

1. Singh, R.; Sharma, R. R.; Tyagi, S. K.: Sci. Hort. *112*, 215 (2007).
2. Sharma, R. R.; Sharma, V. P.; Pandey, S. N.: Acta Hort. *662*, 187 (2004).
3. Gómez-Ariza, J. L.; García-Barrera, T.; Lorenzo, F.: J. Chromatogr. A. *1047*, 313 (2004).
4. Clescerl, L.; Greenberg, A.; Eaton, A.: Standard *Methods for the Examination of Water & Wastewater: 21st edition*. American Water Works Association (2005).
5. Doménech, X.: *Química del suelo*. Miraguano, (1995).
6. Primo-Yúfera, E.; Carrasco-Dorrién, J. M.: *Química Agrícola I "Suelos y Fertilizantes"*. Alhambra (1981).
7. López-Ritas, J.; López-Mélida, J.: *El diagnóstico de suelos y plantas*. Ed. Mundi Prensa (1985).
8. Dodd, M.B.; Lauenroth W. K.: Vegetatio *133*, 13 (1997).

P74 MULTIVARIATE METHODS IN FOOD ANALYSIS

VIERA MRÁZOVÁ[a], JÁN MOCÁK[a], KATJA ŠNUDERL[b] and ERNST LANKMAYR[c]

[a]*Department of Chemistry, University of Ss. Cyril & Methodius, Nám. J. Herdu 2, 917 01 Trnava, Slovak Republic,*
[b]*Faculty of Chemistry and Chemical Engineering, Smetanova 17, SI-2000 Maribor, Slovenia,*
[c]*Institute for Analytical Chemistry, University of Technology Graz, A-8010 Graz, Austria,*
viera.mrazova@ucm.sk

Introduction

Chemometrical processing of the results of instrumental analytical measurements takes advantage of modern statistical methods and advanced software and creates new possibilities for solution of problems in various practical fields of application, e.g. in assessing quality of raw and processed food[1,2], or in advancement of diagnosis in laboratory medicine, which we have studied in recent years[3,4].

Wine belongs to the commodities, which are very frequent objects of falsification[1]. Therefore it is necessary to develop procedures which make possible wine classification and authentication[5,6], i.e. verification of the selected sample with regard to the wine variety, producer/locality as well as the year of production.

Pumpkin seed oils enjoy special and increasing popularity mainly due to their characteristic taste. The oil is contained in the seeds, consists of approx. 70 % unsaturated fatty acids and contain a number of important compounds like triterpenoides, carotenoides, tocopheroles and phytosteroles[2]. The oil quality also depends on the geographical origin, seasonal variations and climatic influences.

This study was focused on the classification of white varietal wines based on the results of chemical analyses. Another goal was spectral characterization of different sorts of pumpkin seed oils accompanied by the sensory evaluation, which after chemometrical data processing facilitated detecting the properties most informative about the oil quality.

Experimental

Wine Samples

Altogether 46 samples of Slovak varietal wines, Welsch Riesling, Grüner Veltliner and Chardonnay, were analyzed during two years using 18 traditionally analysed variables like SO_2, total acids, citric acid, malic acid, tartaric acid, lactic acid, sugars by Shoorle, glucose, fructose, polyphenols, density, etc. The wines were produced by two producers in Bratislava and Hlohovec. Sensorial analysis of all examined wine samples was also provided.

Pumpkin Oil Samples

36 commercially available pumpkin oil samples of Steyrian origin were studied. The samples were examined by sensorial analysis and spectroscopically using 38 variables representing the maximum fluorescence signal.

Sensorial Analysis

Sensorial analysis of wines was made by a group of experts who assessed in a twenty-point scale colour, bouquet, taste, and the total points. Two or three wine categories were made by sensorial quality according to the median or the lower and upper terciles of total points. Smell, taste and visual character of oils were concerned when rating the sensory quality of oils. The collected oil were categorized into two basic classes: fully satisfactory ("good") *vs.* not fully satisfactory ("bad").

Statistical Analysis

Statistical treatment of the obtained data was performed using program packages SPSS (SPSS Inc., Chicago, U.S.A.) and STATGRAPHICS Plus 5.0 (Manugistics, Inc., Rockville, U.S.A.).

Results

Wine

Principal Component Analysis (PCA)

Fig. 1. depicts the PCA representation of the samples of three wine varieties and two vintages where some natural grouping of the studied wines is visible. It is worth to note that the observed natural wine clusters are not created by the wine varieties but correspond mainly to the vintage categories: the 1999 samples are below –1.0 on the PC1 axis, the 2,000 samples are above + 1.0.
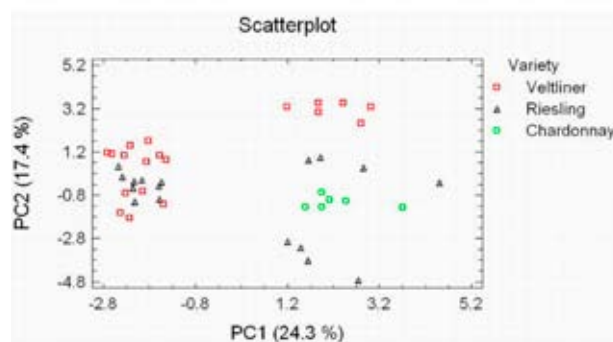
Fig. 1. **PCA scatterplot of the studied wine samples**

Discriminant Analysis (LDA)

LDA is a supervised learning method, in which the classification model is constructed using the the training data set. Then the developed model is used to classify the test samples data set. Three ways of classification were used: by variety, year of vintage, total sensorial quality. In addition, partial sensorial characteristics were used: colour, taste and bouquet of wine. The LDA results using different criteria are summarized in the last two columns of Table I. Success of classification for the set of 46 wine samples was close to 100 %. Fig. 2. exemplifies the successful classification by variety.
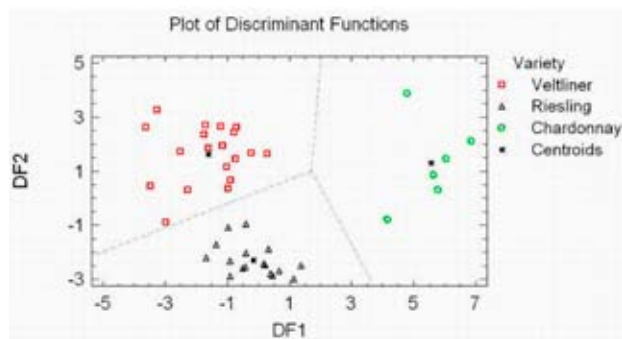
Fig. 2. **LDA plot of three wine varieties**

Fig. 3. **PCA loadings plot showing the interposition of the used wavelengths for fluorescence measurements.**

The stepwise discriminate analysis was applied to the complete set of variables in order to select the variables most important regarding the classification criterion. The classification performance was evaluated for the best group of variables, the number of which is given in brackets.

When the leave-one-out validation technique was applied for classification of wine by *sensorial quality* ("good" or "bad") a 78 % and 87 % success were obtained for all and five best variables, resp.

Table I
Criteria for wine classification and success in classification when all or best variables were used

Criterion	Number of classes	Classification success in %	
		All*	Best*
Variety	3	100.00	95.65 (3)
Vintage	2	100.00	100.00 (2)
Quality	2	93.48	93.48 (5)
Quality	3	86.96	78.26 (9)
Colour	2	91.30	89.13 (7)
Colour	3	76.09	78.26 (6)
Bouquet	2	97.83	93.48 (8)
Bouquet	3	93.48	84.78 (10)
Taste	2	91.30	91.30 (10)
Taste	3	86.96	91.30 (7)
Producer	2	100.00	100.00 (4)

* "All" refers to 18 originally used variables; "Best" refers to the optimally selected variables with their number in brackets

P u m p k i n   O i l s
Principal Component Analysis
The data set of pumpkin oils characterized by 38 variables (maximal intensity of fluorescence using exitation wavelengths 280–650 nm) was used for this study. The inspection of the PCA scatterplot (not shown) has revealed that two oil samples as outliers. The remaining oils are located in two natural clusters at negative values of PC1 and positive values of PC2, resp. In the loadings plot (Fig. 3.), all excitation wavelenghts are divided into three groups. A reasonable assignment of these groups is a task of our current study.

Discriminant Analysis
Fig. 4. represents the LDA graphical output, which shows that very good quality oils samples are located in a cluster at positive values of the first discriminant function (DF1) whilst the lower quality oils form a cluster at negative DF1 values. The separation of two sorts of oils differing by the sensorial quality is remarkable. The classification performance was 100 % for *cross-validation* using the leave-one-out procedure.
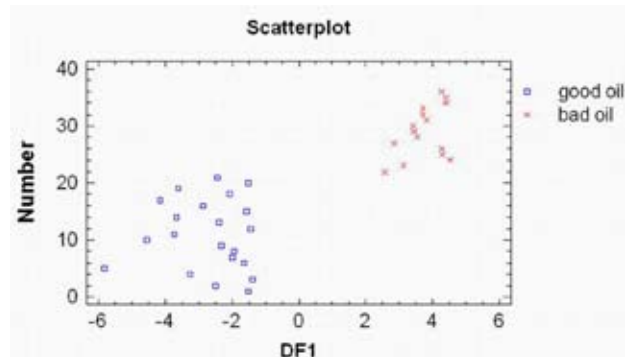
Fig. 4. **LDA plot of the oil sample number vs. the sole discriminant function DF1**

Conclusions
White varietal wines were succesfully classified according to several classification criteria: by variety, vintage, producer as well as partial sensorial descriptors. A very good quantitative separation of the wine samples according to all chosen criteria was obtained by discriminant analysis.

Stepwise variable selection enabled to find an optimal reduced set of variables. The established and validated discriminant models are fully applicable for the category prediction of the unclassified wine samples.

Fluorescence analysis can be successfully applied for classification of commercial pumpkin oils according to their sensorial quality. The investigation of the species causing the most important fluorescent signals reflecting the oil quality is the object of our further study.

REFERENCES

1. Petka J., Mocak J., Farkas P., Balla B., Kovac M.: J. Sci. Food Agr. *81*, 1533 (2001).
2. Lankmayr E., Mocak J., Serdt K., Balla B., Wenzl T., Bandoniene D., Gfrerer M.: J. Biochem. Biophys. Meth. *61*, 95 (2004).
3. Kavkova D., Varmusova E., Tudik I., Mocak J., Balla B., Berezova M.: Europ. Respirat. J. *18*, 397 (2001).
4. Balla B., Mocak J., Pivovarnikova H., Balla J.: Chemometrics Intell. Lab. Systems *72*, 259 (2004).
5. Penza M., Cassano G.: Food Chem. *86*, 283 (2004).
6. Ferreira A. P., Lopes J. A., Menezes J. C.: Anal. Chim. Acta *595*, 120 (2007).

P75 PHYTOCHEMICAL STUDY OF FLAVONOIDES FROM *MELAMPYRUM CRISTATUM* L. SPECIES

MELANIA FLORINA MUNTEANU[a], LAUREAN VLASE[b] and CLAUDIA TOMA[a]

[a]*"Vasile Goldis" West University, 1 Feleacului Str., 300041, Arad, Romania,*
[b]*University of Medicine and Pharmacy „Iuliu Hateganu" Cluj-Napoca, Emil Isac street No. 13, Cluj-Napoca,*
anaionescuro@yahoo.com

Introduction

The Melampyrum genus is not studied in Romania that is why there had been chosen the study of *Melampyrum cristatum* L. species with the help of HPLC couplet with MS. A modification to this method achieved by a group of young researchers from Cluj was brought change of the mobile phase, from a mobile was brought phase with elements that are not volatile, there are arrived at a volatile one, the element from the chromatography column can be inserted in mass spectrometry being obtained supplementary information about the elements because the spectrum is registering the molecular mass and mass spectrum from the elements found.[1–4]

Experimental part

Method of Analysis

In a Sox let device the plant powder is treated, leaves respectively flowers from *Melampyrum cristatum* L., to remove the chlorophyll. There were taken work 10 g leaves, flowers, cut up sieve IV with 460 ml clorophorm, the extraction was carried out for 48 hours at 60 °C, until the solvent becomes completely colorless. The powder is subjected to another extraction with 140 ml methanol; the solution resulted being the basic one from which the qualitative determinations will be made.

For the analysis of the polyphenol compounds from vegetable extracts the high performance liquid chromatography coupled with mass spectrometry (LC/MS) was used.

Devices

HPLC coupled with mass spectrometer; binary pump**;** autosampler; thermostat HP 1100 Series; detector UV HP 1100 Series; mass spectrometer Agilent Ion Trap 1100 VL.

MS working conditions: source of ions- ESI (electrospray); ionization manner-negative ; nebulizer-nitrogen , pressure 60 PSI ; drying gas-nitrogen , flow rate 12 $dm^3 min^{-1}$, temperature 300 °C , capillary potential: +3000 V; method of analysis-monitoring specific ions (poly phenol carboxylic acids) or AUTO MS (flavonoides and their aglycons)

HPLC working conditions: analytical column Zorbax SB-C18 100 mm × 3.0 mm i.d., 3.5 μm (Waters); Precolumn Zorbax SB-C18; the mobile phase: mixture methanol: acetic acid solution 0.1% (v/v) elution in gradient (start 5% methanol, up to 35 min 42% methanol, up to 45 min 5% methanol – re-equilibration); flow rate: 1 ml min^{-1}, temperature: 48 °C; detection: UV 330 nm up tu 17 minutes, 370 nm up to 38 minutes; volums of injection: 5 μl.

Polyphenol Analysis by UV Detection

Every category of elements were detected at the wavelength corresponding to maximum of absorbtion of UV spectrum. So, the polyphenolcarboxilic acids were detected at the wave-length from 330 nm, but the flavonoides and their aglycons at 370 nm.

Processing of Samples to be Analysed

There were analyzed in parallel two samples of each vegetable extract, one as such, but another one hydrolyzed. The reason for which hydrolysis achieved is the fact that, in general, some floavonoide aglycons or some polyphenolicarboxilic acids are not free, but on bound (glycosides, esters, etc).

So, carrying out on acid hydrolysis will lead to freeing there compounds from the bound form and it would bring more information about the chemical composition of the studied product.

The samples that are analyzed as such are diluted 1 : 10 before the injection. The hydrolysis was performed following the procedure: one part of the extract is diluted with one part of HCl solution and it is maintained on water bath at 80 °C for 40 min. It is brought at 10 ml (measuring flask) and it is injected in the chromatographic system.

Thin layer Chromatography was Performed in the Following Conditions

Solution to analyzed: extract from *Melampyrum cristatum* flowers and leaves 25 μl applied.

Standard solution: methanol solution from rutozid 1.22 mg ml^{-1} (Roth), hiperozid 1.1 mg ml^{-1} (Merck), clorogenic acid 1 mg ml^{-1} (Fluka) and cafeic acid 1 mg ml^{-1} (Roth) − 10 μl applied; stationary phase: Kieselgel 60F254 (Merck); mobil phase: ethylacetate (Merck) – ethylmethylketone (Merck) – formic acid (Merck) – water (50 : 30 : 10 : 10, vol.); migration distance 10 cm: 12 cm; migration time: 60 minute.

The application of solution in layers was carried out in bands of 1 cm at 1.5 cm distance from the lower border of the plate.

Reveal of plate it has realized with iron clorure 10 % in ethanol.

The chromatogram analysis is realized in UV la 254 nm, after the revelation in visible light spectrum.

TLC Coupled with Photo Densitometry

The chromatographic plate was scanned with a Shimadzu CS9000 photo densitometer after pulverization with iron clorure. The photo densitometer parameters are: way

of functioning in reflexion, wolfram lamp, scanning method: zig zag, λ = 550 nm.

Results and Discussions

Workings in the described condition there are presented the flavonoid concentrations in leaves, respectively in flowers from *Melampyrum cristatum L.*

After the photodensitometric evaluation for the *Melampyrum cristatum* leaves, the sample which is more concentrated in flavonoides, the densitogram from Fig. 4 was obtained. The height of the drops in densitogram, the low flavonoide concentration.
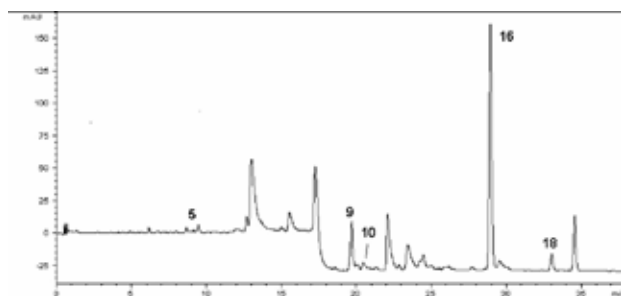
Fig. 2. **Mass spectrum of methanolic hydrolysed extract from** *Melampyrum cristatum L.* **leaves**
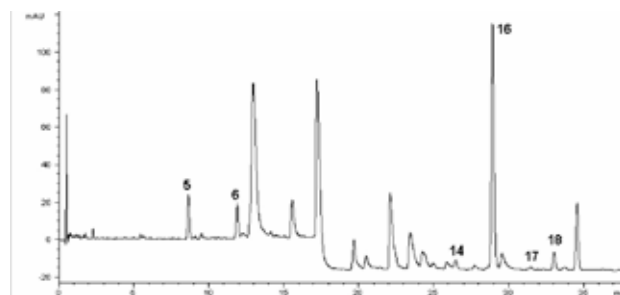
Fig. 1. **Mass spectrum of methanolic unhydrolysed extract from** *Melampyrum cristatum L.* **leaves**
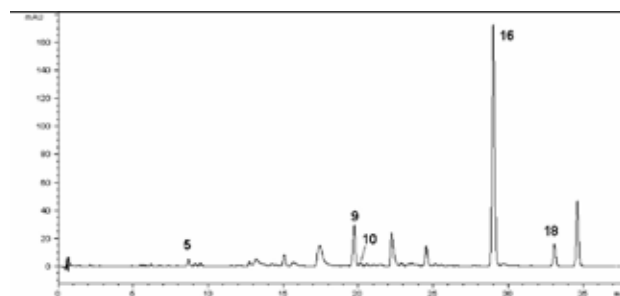
Fig. 3. **Mass spectrum of methanolic unhydrolysed extract from** *Melampyrum cristatum L.* **flowers**

Table I
Concentration of methanolic unhydrolyzed extract from *Melampyrum cristatum L.* leaves

Compound	Nr.	Identification UV	Confirmation MS	Concentration in extract [μg ml^{-1}]	The quantity in vegetable drug [mg g^{-1}]
Isoquercitrin	9	yes	yes	60.838	0.30419
Rutozid	10	yes	yes	3.715	0.01858
Luteolina	16	yes	yes	153.390	0.76695
Apigenina	18	yes	yes	15.195	0.07598

Table II
Concentration of methanolic hydrolysed extract from *Melampyrum cristatum L.* leaves

Compound	Nr.	Identification UV	Confirmation MS	Concentration in extract [μg ml^{-1}]	The quantity in vegetable drug [mg g^{-1}]
Quercetol	14	yes	yes	3.380	0.01690
Luteolina	16	yes	yes	131.092	0.65546
Kaempferol	17	yes	yes	1.439	0.00720
Apigenina	18	yes	yes	11.235	0.05618

Table III
Concentration of methanolic unhydrolysed extract from *Melampyrum cristatum L.* flowers

Compound	Nr.	Identification UV	Confirmation MS	Concentration in extract [μg ml^{-1}]	The quantity in vegetable drug [mg g^{-1}]
Isoquercitrin	9	yes	yes	46.930	0.23465
Rutozid	10	yes	yes	2.876	0.01438
Luteolina	16	yes	yes	140.680	0.70340
Apigenina	18	yes	yes	18.190	0.09095

Table IV

Concentration of methanolic hydrolysed extract from *Melampyrum cristatum L.* flowers

Compound	Nr.	Identification UV	Confirmation MS	Concentration in extract $[\mu g\,ml^{-1}]$	The quantity in vegetable drug $[mg\,g^{-1}]$
Quercetol	14	yes	yes	2.659	0.01330
Luteolina	16	yes	yes	11.122	0.05561
Kaempferol	17	yes	yes	1.642	0.00821
Apigenina	18	yes	yes	13.479	0.06740
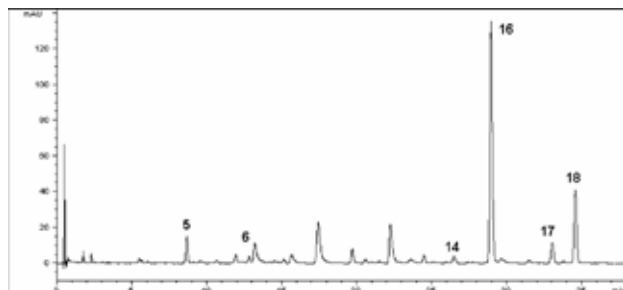
Fig. 4. **Mass spectrum of methanolic hydrolysed extract from *Melampyrum cristatum L.* flowers**

Table. V

The apigenin and luteolin concentration obtained by TLC

Test	Apigenina Area	$c\,[mg\,ml^{-1}]$	Luteolina Area	$c\,[mg\,ml^{-1}]$
M.cristatum flowers	21,474.6	0.82	102,253.9	0.74
M.cristatum leaves	18,528.3	0.71	107,944.8	0.78

Table VI

The concentration found in rutozid and hiperozid by *Melampyrum cristatum L.* flowers and leaves

	Melampyrum cristatum leaves	flowers
Rutozid %	1.850 %	1.750 %
Hiperozid %	0.43125 %	0.71875 %

The quantitative analyses are made after the method from *Cynarae folium* monography and *Crategus folium* cum flore monography by FR IX and FR X.

REFERENCES

1. Vlase L., Radu L., Fodorea C., Leucuţa S., Gocanj S.: Liq. Chromatogr. Related Technol. *28*, 3109 (2005).
2. Fodorea C. S., Vlase L, Leucuţa S., Tămaş M.: Clujul Medical, *4*, 923 (2003).
3. Suciu S., Vlase L., Fodorea C. S., Tămaş M., Leucuţa S.: Revista de Medicină şi Farmacie *50*, 52 (2004).
4. Suciu S., Vlase L., Fodorea C. S., Tămaş M., Leucuţa S.: Clujul Medical *3*, 604, (2004).
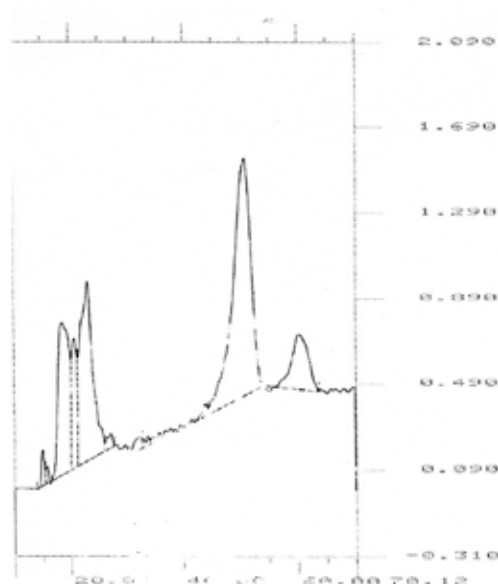
Fig. 5. **Densitogram by *Melampyrum cristatum* flowers**
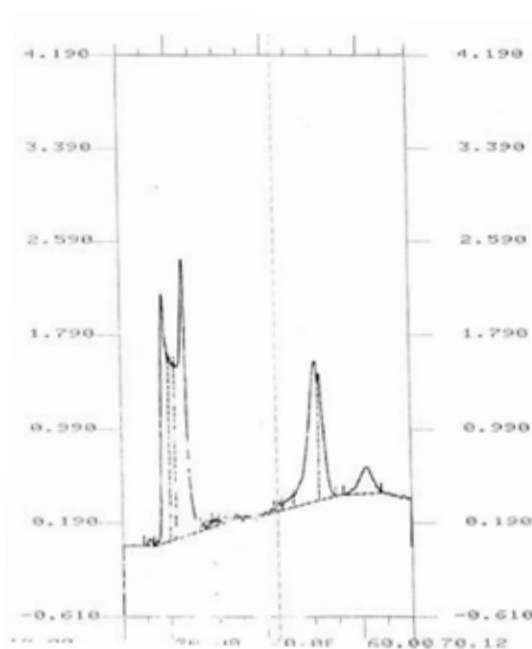
Fig. 6. **Densitogram by *Melampyrum cristatum* leaves**

P76 THE INFLUENCE OF CHOICE FACTORS ON FERMENTATION OF RED WINE

JIŘINA OMELKOVÁ and LUCIE ZECHMEISTROVÁ

*Faculty of Chemistry, Brno University of Technology, Purky-
ňova 118, 612 00 Brno, Czech Republic,*
omelkova@fch.vutbr.cz

Introduction

Winemaking can be summarized as the biotransforma-
tion of must into wine, which performed principally by *Sac-
charomyces cerevisiae* strains during the primary alcoholic
fermentation. A secondary fermentation, the so-called malo-
latic fermentation is biodeacidifacation that is often encou-
raged, since it improves wine stability and quality. Malolatic
fermentation (MLF) usually occurs either spontaneously or
after inoculation with selected bacteria after fermentation.
MLF, the enzymatic decarboxylation of L-malic acid to L-
lactic acid, is an important secondary fermentation process
carried out by lactic acid bacteria (LAB) during the vinifica-
tion of red must, and certain white and sparkling wine styles.
In addition to deacidification, MLF can increase microbiolo-
gical stability and enhance the flavour and aroma of wine. The
study was focused on the composition of microflora during
the extraction of flavour components from grape solids and
during fermentation as well. In this way the two technology
processes for the production of red wine from Velké Pavlo-
vice region were monitored.

Experimental

Three different media were applied for the cultivation
of microorganisms; first for monitoring of total volume of
microorganisms, second for yeasts and third for lactic acid
bacteria. The indirect method was used for the determination
of the amount of viable cells. This method consists of the
enumeration of visible macroscopic colonies grown up on
agar plates. When the cells grew up, the forms of colonies
were analyzed visually and the morphology of microorga-
nisms was microscopically detected.

Cultivation media:
- *Plate Count Agar*. Suitable for the determination of total
  number of microorganisms in foodstuffs.
- *Malt Agar with the addition of antibiotics*. Into the cul-
  tivation medium streptomycine 80 µg/l and propionic
  acid 0, 25 ml/l was added. Suitable for the isolation and
  identification of yeasts and fungi.
- *Tomato Juice Medium Base (for Lactobacillus from
  wine)*. Suitable for the isolation and identification of lac-
  tic acid bacteria occurring in wine.

Results

Two technological procedures in wine manufacturing,
which differ in technological steps shown in the Table I, were
compared.

Since the start of wine manufacturing, till the last addi-
tion of SO_2, the total number of yeasts in wine factory No. 1

Table I

Technological procedure	Preliminary fermentation				Alcoholic fermentation	
Application	SO_2	CE	CY	CB	Mode of heating	SO_2
Wine factory No. 1	–	×	×	–	regulated	×
Wine factory No. 2	×	×	×	×	non regulated	×

CE – Commercial Enzymes
CY – Commercial Yeasts
CB – Commercial Bacteria

was monitored. Number of cells in dependence on time is
shown in Fig. 1. It is known[1], that the yeasts *Saccharomyces
cerevisiae* do not start the fermentation. The yeasts starting
the fermentation are *Hanseniaspora* (*Kloeckera*), *Candida
Metschnikowia*. From Fig. 1. follows that the number of
starting yeasts and yeast microorganisms reached the value
$1.2 \times 10^6 \pm 1.3 \times 10^5$ cells in 1 ml. Other yeasts than *Sac-
charomyces* growing at the start of the fermentation, utilize
aminoacids and vitamins for their growth and reduce the
growth of *Saccharomyces cerevisiae*. These play an impor-
tant role in the second half of the fermentation time[1]. From
the Fig. 1. it is evident that even though the commercial cul-
ture of *Saccharomyces cerevisiae* was inoculated into the
mash during the day of crushing, the increase of total number
of yeasts occurred 4 days after the inoculation. The whole
period of preliminary fermentation lasted 8 days and the hi-
ghest value of total number of yeasts was achieved in a day
of pressing. After that the decrease was observed. This effect
can be attributed to the autolysis of yeasts after the alcoholic
fermentation[1]. The decrease is also caused by the inhibition
of starting population of bacteria *Oenococcus oeni* and malo-
latic fermentation, as shown in Fig. 2. After the alcoholic
fermentation the autolysis of yeasts occurs, followed by the
liberation of nutrients important for the growth of bacteria
and the growth of present yeasts, as well. The decrease is
also caused by the inhibition of starting population of bacte-
ria *Oenococcus oeni* and malolactic fermentation, as shown
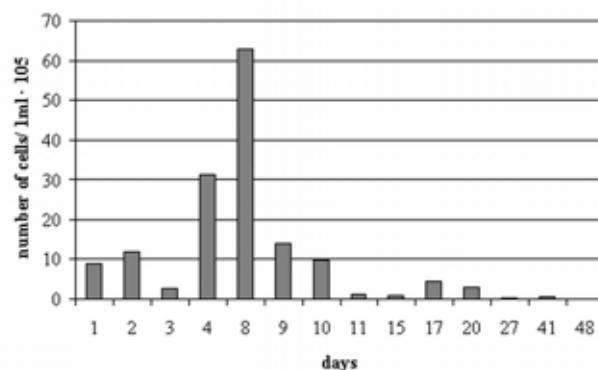
Fig. 1.   **Number of yeasts – Wine factory No. 1**

in Fig. 2. After the alcoholic fermentation the autolysis of yeasts occurs, followed by the liberation of nutrients important for the growth of bacteria and the growth of present yeasts, as well.
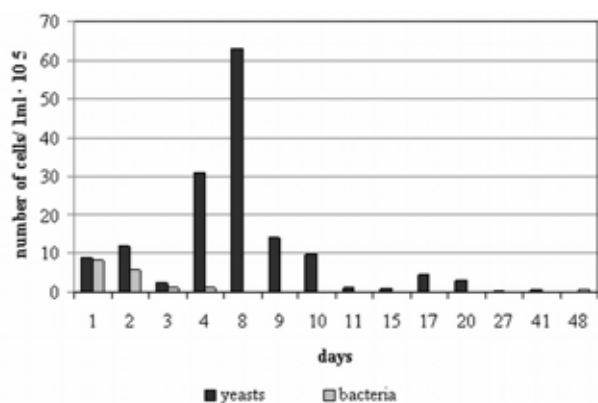
Fig. 2.   **The comparison of the number of yeasts and lactic bacteria wine factory No. 1**

From the comparison of the number of yeasts in both wine factories (Fig. 3.) follows that after the pressing the total number of yeasts in wine factory No. 2 was lower. This difference is probably a result of the application of small amount of SO^2 in factory No. 2 by the start of the preliminary fermentation of the juice. The application of SO_2 was carried out to eliminate the development of undesirable microflora. The difference can also result from the difference in heating of the must in tank.
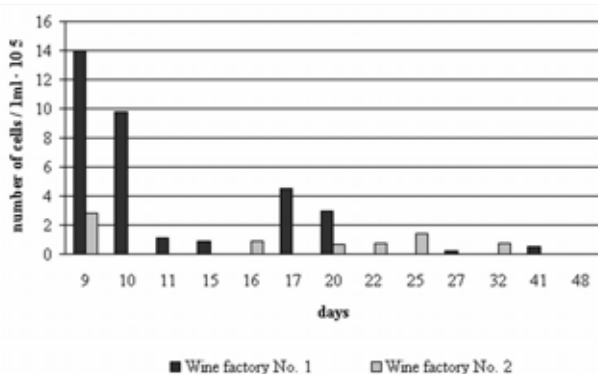
Fig. 3.   **The comparison of the number of yeasts in wine factories No. 1 and No. 2**

After the alcoholic fermentation the start of malolactic fermentation is supposed. In wine factory No. 1 the amount of bacteria of malolactic fermentation was studied (Fig. 4.). In the case of wine factory No. 2 the commercial culture of bacteria *Oenococcus oeni* was applied. The heating of the must was realized using the heating rod. This procedure implies that the local overheating can occur, which destroys the microflora. In wine factory No. 2 by the application of malolactic bacteria no bacteria of lactic fermentation were detected.
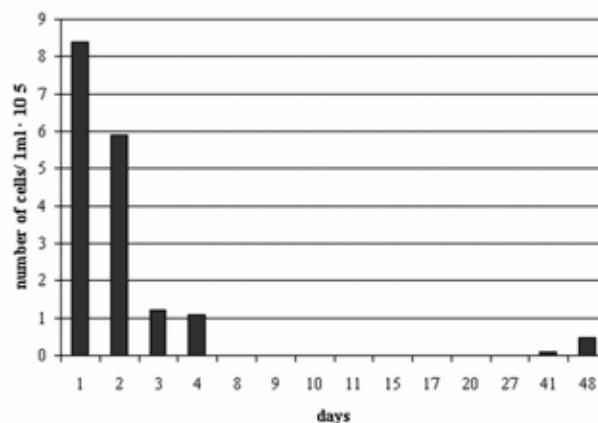
Fig. 4.   **Number of lactic bacteria – wine factory No. 1**

During the study of the fermentation process the attention was also focused on the fungi in red wine manufacturing. From the results based on the visual evaluation of the increase on Petri dishes can be supposed that the fungi *Penicillium* and *Aspergillus* dominate. These can produce the different micotoxins. Fig. 5. presents the mixed culture of microorganisms, which grew from the grape juice in the day of crushing. The important result is the presence of the fungi *Botrytis*.
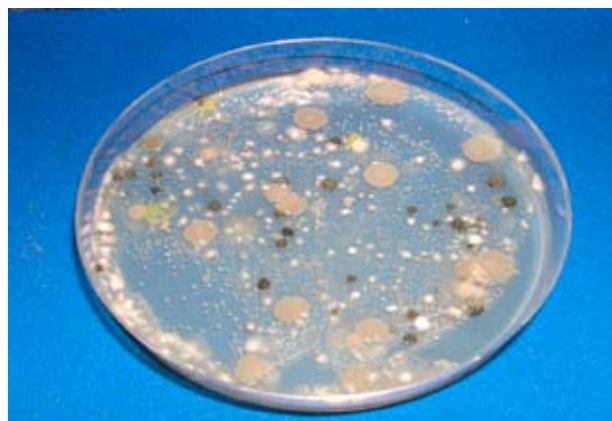
Fig. 5.   **The mixed culture of microorganisms, which grew from the grape juice in the day of crushing**

Fig. 6. is an example of the growing blue-green colony of yeasts with the white edge, which appeared on plates with the grown population of the yeasts. This figure is also an example of the fungi, which during its development colonized the population of the yeasts

In Fig. 7. the blue-green fungi with the white edge can be seen again. In difference to Fig. 6. this fungi during its development did not colonize the site, where the population of yeasts was grown. These effect is in accordance with the observation[1] that the yeasts *Metschnikowia pulcherrima, Pichia*, *Candida*, *Cryptococcus* and some *Saccharomyces* and *Zygosaccharomyces* have strong antifungal aktivity
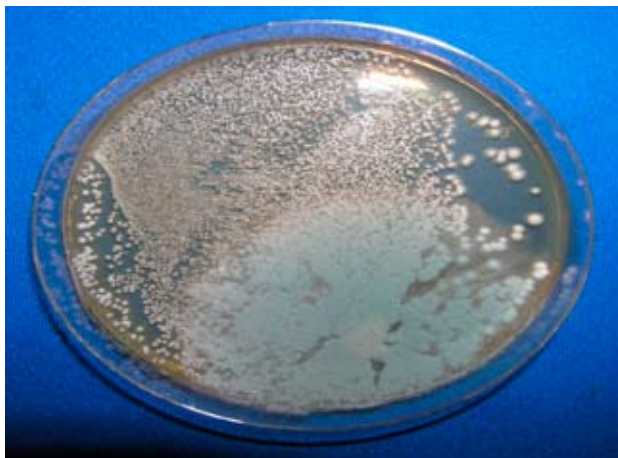
Fig. 6. **The fungi, which during its development colonized the population of the yeasts**

Fig. 7. **The blue-green fungi with the white edge**

In the framework of the study it was confirmed that the wine is the product of many diverse interactions between yeasts, fungi and bacteria. This microflora can be positively and negatively influenced by the different technological interventions
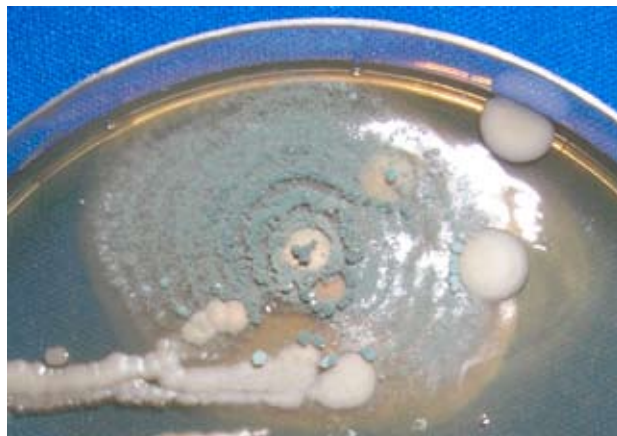
REFERENCES
1. Fleet G. H.: Intern. J. Food Microbiol. *86*, 11 (2003).

P77 OPTIMALIZATION OF CULTIVATION MEDIA AND HYDROXYLASE ENZYME PRODUCTION BY *AUREOBASIDIUM PULLULANS*

STANISLAVA MATALOVÁ, JIŘINA OMELKOVÁ and IVAN ŠIMKOVIČ

Mendel University of Agriculture and Forestry, Zeměděl-ská 1, 602 00 Brno, Czech Republic,
matalovas@volny.cz

Introduction

In many countries, wheat straw is an abundant lignocellulosic by-product from farming, consisting of cellulose (35–40 % wt.) and hemicellulose (25–30 % wt.) in close association with lignin (10–15 % wt.)[1].

Lignin is a natural, complex, heterogenous, phenylpropanoid polymer comprising 25–30 % of plant biomass. Primarily three enzymes, i.e., lignin peroxidase (LiP), manganese peroxidase (MnP) and laccase[2,3,4] have been held responsible for lignin degradation.

Laccase (benzenediol: oxygen oxidoreductase, EC 1.10.3.2) belongs to a group of polyphenol oxidases containing copper atoms in the catalytic centre and usually called multicopper oxidases.

Laccases catalyze the reduction of oxygen to water accompanied by the oxidation of a substrate, typically a p-dihydroxy phenol or another phenolic compound. It is difficult to define laccase by its reducing substrate due to its very broad substrate range.

Although laccase was also called diphenol oxidase, monophenols like 2,6-dimethoxyphenol or guaiacol are often better substrates than diphenols, e.g. catechol or hydroquinone. Syringaldazine[N,N0-bis(3,5-dimethoxy-4-hydroxybenzylidene hydrazine)] and ABTS are often considered to be a unique laccase substrates[5].

Laccase activity has been demonstrated in many fungal species, but laccase production has never been demonstrated in lower fungi. There are many records of laccase production by ascomycetes. Yeasts are a physiologically specific group of both ascomycetes and basidiomycetes. This basidiomycete yeast produces a true laccase capable of oxidation of phenols and aminophenols and unable to oxidize tyrosine[6]. The production of laccase was not demonstrated in ascomycetous yeasts.

In this study, the method suitable for production laccase as lignin-degrading enzymes by Aureobasidium pullulans was optimized. Wheat straw was the only carbon source and only the most essential nutrients were added.

Experimental Microorganism

The fungal strain *Aureobasidium pullulans* F 8189 used in the present study was obtained from the culture collection of the Culture Collection of Yeasts (CCY), SAV, Institute of Chemistry. The tested culture was maintained at 26 °C on malt slant agar for 10 days.

Cellulolytic Substrate

Wheat straw from local sources (0.3–0.5 mm particle size) was used as natural substrate. This substrates was sterilized in autoclave at 120 °C for 20 minutes.

Optimalization of Culture Conditions

Growth of *A. pullulans* was studied in three cultivation media – glucose medium (GM), glucose medium with wheat straw (GSM) and basal medium with wheat straw (BSM) during solid-state (SSF) and submerged (SF) fermentation.

The glucose medium contained in grams per 1,000 g: KNO_3, 2; K_2HPO_4, 1; $MgSO_4$, 0.5; glucose, 50. The basal medium has the same composition as glucose medium but without glucose. The pH of the both media was adjusted to 5.6. These media were then autoclaved for 30 min at 121 °C and poured into Petri dishes with diameter of 9 cm and in 100 ml Erlenmayer flasks. Cultivation media with wheat straw also contained sterilized wheat straw (1 g wheat straw 100 ml^{-1} of medium).

Petri dishes and Erlenmayer flasks were inoculated by three ways – with fungal spores obtained from 4 days grown cultures on malt agar, with three mycelial discs (each 1×1 cm) obtained from 4 days fungal culture grown on glucose agar and inoculation by loops. Growth of *A.pullulans* was observed at 26 and 32 °C.

Enzyme Assay

Laccase (EC 1.10.3.2) activity was determined by the oxidation of 2,2'-azino-bis(3-ethylthiazoline-6-sulfonate) (ABTS) according to Buswell et.al.[7] The reaction mixture for the standard assays contained 100 µl ABTS solution (1mM), 300 µl sodium acetate buffer pH 5.0 (0.1M) and 600 µl enzyme extract. Oxidation was followed via the increase in absorbance at 420 nm ($\varepsilon_{420} = 36,000$ M^{-1} cm^{-1}). All enzyme assays were performed in triplicate.

Protein concentration was determined by Lowry et al. method[8] with bovine serum albumin as standard.

Results

A comparison of growth pattern of *A.pullulans* in various cultivation conditions as medium composition, temperature or method of inoculation was made and the results are presented in Table I. As Table I demonstrates, *A. pullulans* were grown in different type of solid media. In the course of liquid cultivations less growth was observed regardless of temperature. The best growth rate was obtained in GSM or BSM medium in comparison to GM during solid-state fermentation.

The effect of method of inoculation varied from inoculation with fungal spores (maximum growth) to inoculation by loops (minimum growth).

For testing of production of hydroxylase were chosen microorganism Aureobasidium pullulans by methods of Azure-B agar and ABTS agar[9]. In an attemp to compare the production laccase during solid-state and submerged

Table I
Growth rate of *A. pullulans* on different cultivations media – glucose medium (GM), glucose medium with wheat straw (GSM) and basal medium with wheat straw (BSM)

Incubation time [days]	Type of inoculation	Solid state fermentation		
		GM 26/32 °C	GSM 26/32 °C	BSM 26/32 °C
3	Loop	0/+	0/0	0/+
	Fungal spores	+/+	+/+	0/+
	Mycelial discs	0/0	0/0	0/0
5	Loop	0/+	0/0	0/+
	Fungal spores	+/+	+/+	+/+
	Mycelial discs	+/0	+/0	+/0
10	Loop	0/+	++/0	++/+
	Fungal spores	++/+	++/0	++/+
	Mycelial discs	+/+	+/0	++/+
14	Loop	0/+	++/+	+/+
	Fungal spores	++/+	++/+	++/+
	Mycelial discs	+/+	+/+	++/++

0 = no growth, + = growth, ++ = extremelly growth

fermentation, *A. pullulans* was studied in various solid and liguid media. No laccase activity could be detected in any solid media. In contrast to solid-state fermentation, this strain proceeded the maximum activity in liquid GM, but low level of laccase was detected in BSM. Laccase production reached its maxima on 8 and 15 day for GM and 7 day for GSM and BSM. (Fig. 1.).
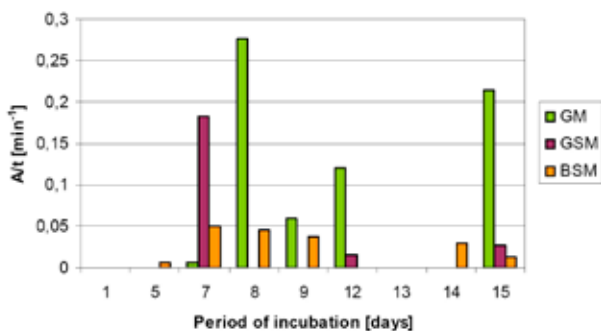
Fig. 1.   **Comparison of the production of laccase by *A. pullulans* grown on three different culture media during submerged cultivation**

Conclusions

Our results indicated, that the conditions optimal for *A. pullulans* growth were determined for glucose medium with wheat straw, temperature 26 °C, inoculation by fungal spores and solid state fermentation. The results reported here also showed that optimal growth of *A. pullulans* and production of laccase were not be detected for the same cultivation conditions.

During the optimalization of the culture medium hydroxylase activity reached higher level in the presence of yeast *Aureobasidium pulllulans* in the glucose medium without wheat straw during submerged cultivation. Relatively higher laccase production on GM showed twin peaks during their incubation.

Reapperance of enzyme activity during later stage of wheat straw degradation might be attributed to fungal autolysis resulting in the release of cell membrane bound on intracellular enzymes in the medium[10].

REFERENCES

1. Zaldivar J., Nielsen J., Olsson L.: Appl. Microbiol. Biotechnol. *56*, 17 (2001).
2. Glenn J. K., Morgan M. A., Mayeld M. B., Kuwahara M., Gold M. H.: Biochem. Biophys. Res. Commun. *114*, 1077 (1983).
3. Hatakka A.,Uusi-Rauva A. K.: Eur. J. Appl. Microbiol. Biotechnol. *17*, 235 (1983).
4. Glenn J. K.,Gold M. J.: Arch. Biochem. Biophys. *242*, 329 (1985).
5. Harkin J. M., Larsen M. J., Obst J. R.: Mycologia *66*, 469 (1974).
6. Williamson P. R.: J. Bacteriol. *176*, 656 (1994).
7. Buswell J. A., Cai Y., Chang S.: FEMS Microbiol. Lett. *128*, 81 (1995).
8. Lowry O. H., Rosebrough N. J., Farr A. L., Randall R. J.: J. Biol. Chem. *193*, 265 (1951).
9. Matalová S., Omelková J., Šimkovič I.: *International Conference of Applied Natural Sciences, Trnava, 7-9 Nov. 2007, Book of Abstracts* (Pipíška M., ed.), p. 15.
10. Arora D.S., Chander M., Gill P. K.: Intern. Biodeter. Biodegr. *50*, 115 (2002).

P78　INFLUENCE OF MODIFIED BIOCOMPOSITES ON PRODUCTION OF EXTRACELLULAR POLYSACCHARIDES BY IMMOBILIZED *AUREOBASIDIUM PULLULANS*

VLADIMÍR ONDRUŠKA, IVANA MÁROVÁ, JAN DAVID AND LUCY VOJTOVÁ

Faculty of Chemistry, Brno University of Technology, Purkyňova 118, 612 00 Brno, Czech Republic, xcondruska@fch.vutbr.cz

Introduction

Pullulan is an extracellular water-soluble polysacharid produced by yeast-like strain *Aureobasidium pullulans*. It is a linear homopolysaccharide usually described as an a-(1–6) lincagen polymer, consisting mainly of maltotriose units[1]. The regular alternation of alpha-1,4 and alpha-1,6 bonds results in two distinctive properties, such as structure flexibility, enhanced water-solubility and excellent film- and fiber forming properties[2]. Thanks these characteristic pullulan can be used in low-calorie food aidtives, cosmetic emulsions, oxygen-impermeable film for packaging, adhesives, and thickening and extending agents. Recently, pullulan has been getting renewed attention as an excellent material for pharmaceutical and biomedical application[3].

Fermentation can be affected by different types of carbon and nitrogen source resulted in varying pullulan yields during the culture growth process, since the philamentous forms or chlamydospores are less productive than the yeast or pigment-free blastospores[4].
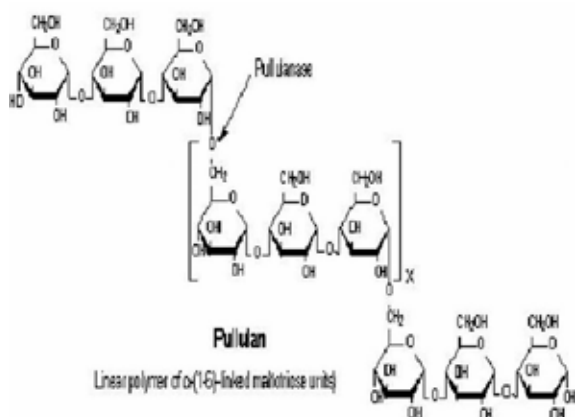
Fig. 1.　**Chemical structure of polysaccharide pullulan**

In this work, several media with different type of carbon and/or nitrogen source were used for *A. pullulans* cultivation. PUR foams modified by 10 % of carboxymethyl cellulose, 2-hydroxyethyl cellulose, acetylated starch and acetyl celulose, respectively were used as immobilization agents. A. pullulans cells were cultivated in Erlenmeyer flasks at 28° C for 120 to 480 hours. First, all materials were tested as potential carbon/nitrogen source. Further, microorganisms were cultivated for 4–6 weeks in presence of PUR under permanent shaking. Samples were taken in 24-hour intervals, quantitative changes of biomass and pullulan content were determined gravimetrically and/or spectrophotometrically. Additionally, surface microscopy of all degraded polyurethanes was tested.

Material and methods

Microorganism and Culture Conditions

Strain of *A. pullulans*, CCM F-148 was purchased from Czech Collection of Microorganisms. The culture was stored on medium with malt extract and yeast malt agar, respectively, at 4° C. For biodegradation experiments 100 ml of inoculum was prepared in 500 ml Erlenmayer flask. Cultivation was performed at 28 °C and 150 rpm for 24 hours. Inoculum as well as production medium contained ($g\,dm^{-3}$): yeast extract 7, potassium phosphate 5, ammonium sulphate 5, magnesium sulphate 0.34, glucose 40 was used as carbon source, distilled water. Initial pH was 6.5 before autoclaving. All flasks were incubated in an incubator shaker operating at 28–30 °C and 150 rpm for 120 hours.

Materials

General chemicals: polyether polyol, tolylene diisocyanate 80/20 (TDI), tin and amine based catalysts, surfactant and water. Biodegradable fillers: acetylated starch (AS), acetylcellulose (AC) Mn = 30,000 Da and 2-hydroxyethyl-cellulose (HEC) Mn = 90,000 Da. The foams were prepared by a three-step reaction process. The chemical composition of the pulverized BIO-PU foams was proved by an infrared spectroscopy on the Nicolet Impact 400D Fourier Transform InfraRed (FTIR) spectrometer using the KBr technique.

Measuremend of Dry Cell Weight and Pullulan Production

Samples for analyses (10 ml) were taken from each flask in regular 24-hour intervals. Total biomass (summ of mycelial and yeast cells) was determined after centrifugation of the culture sample at $12,000 \times g$ for 20 min and washing the sediment with distilted water gravimetrically (drying at 105 °C for 2 hours).

To analysis of pullulan production, supernatant was mixed with 2 volumes of absolute ethanol for 20 min. Precipited polysaccharide was separated by centrifugation or filtration and dried at 80 °C. Pullulan precipitate was purified twice by hot water and by ethanol. Crude pullulan yield was measured gravimetrically.

Pure polysaccharide content was determined by analysis of products of its enzymatic hydrolysis (effect of pullulanase resulted in maltotriose). The content of maltotriose was determined by Somogyi-Nelson method[5], calibration with maltotriose was performed.

Results

Fig. 2. shows biomass and pullulan production in presence of modified PUR foams. It seems that the highest pullulan production was observed in control medium (without PUR), so, PUR presence exhibited negative effect on pullan production.
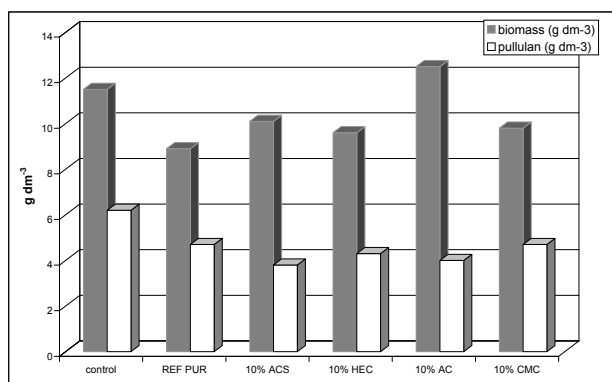
Fig. 2.   **Biomass and pullulan production by *A. pullulans* grown in presence of modified PUR foams**

Conclusions

Yeast strain Aureobasidium pullulans can grow in presence of modified polyurethane foams. Degradation degree of BIO-PUR corresponded with growth of yeast culture. The highest degree of degradation was found in PUR modified by 40 % carboxymethyl cellulose; degree of degradation decreased with CMC concentration.

According to our results of *A. pullulans* grown in PUR presence it seems that most of modified polyurethane foams exhibited slight negative effect on pullullan (4.3 g dm^{-3} control, 4.9 g dm^{-3} 1% ACS-PUR, 3.2 g dm^{-3} REF-PUR) as well as biomass production (11.5 g dm^{-3} control, 7.8 g dm^{-3} 1% ACS-PUR, 8.9 g dm^{-3} REF-PUR). Acetyl cellulose was the only modification agent, which was able to enhance pullulan (6.5 g dm^{-3}) as well as biomass (12.5 g dm^{-3}) production.

REFERENCES
1. Leathers T. D.: Appl Microbiol Biotechnol. *62*, 468 (2003).
2. Lee J. H., Kim J. H., Zhu I. H., Zhan X. B., Lee J. W., Shin D. H. et al.: Biotechnol Lett. *23*, 817 (2001).
3. Shingel K. I.: Carbohydrate Res. *339*, 447 (2004).
4. Audet J., Lounes M., Thibault J.: Bioprocess. Eng. *15*, 209 (1996).
5. Káš J., Kodíček M., Valentová O.: *Laboratorni techniky biochemie*. Praha 2005.

P79 FATTY ACIDS DISTRIBUTION IN THE LIPID FRACTIONS OF *CALENDULA OFFICINALIS* L. SEEDS OIL

ADELA PINTEA, FRANCISC VASILE DULF, CONSTANTIN BELE and SANDA ANDREI

University of Agricultural Sciences and Veterinary Medicine, Manastur 3–5, 400372, Cluj-Napoca, Romania,
apintea@usamvcluj.ro

Introduction

Plant oils are important renewable resources used as food; feed or as industrial feedstocks[1]. The C*alendula* seeds oil is currently considered a potential oilseed crop with industrial or other functionalities. It is characterized by a high content of the unusual conjugated octadecatrienoic acid – calendic acid (18 : 3c 8t, 10t, 12c) and some other conjugated isomers, which give special chemical and physical properties[2]. There is an increasing interest for conjugated fatty acids since some of them were proved to have anticancer and lipid-lowering effects[3,4]. Calendic acids have inhibitory effect on human colon cancer cells, decrease body fat content and have hepatoprotective effect[5,6,7]. Here we present the fatty acids distribution in the lipid fractions of *Calendula* seeds and the fatty acids variation during seeds maturation.

Experimental

Extraction and Lipid Fractionation

Total lipids were extracted using Folch method[8]. Neutral lipids were separated by TLC with a solvent mixture of hexane: ethyl ether: acetic acid (95 : 15 : 1). Polar lipids were scratched, extracted and separated according to Heape method[9].

Fatty Acids Analysis

The total lipid extract and the lipid fractions were transesterified with BF3/methanol. The methyl esters of fatty acids (FAME) were dissolved in hexane and injected for GC analysis. A Shimadzu GC 17A with FID detector and a Crompack Silica 25 MXO capillary column (25 m × 0.25 mm i.d., film thickness 0.25 µm) was used. The temperature program was: 5 min at 70°C, 4 °C/min to 235 °C (hold 5 min). The injector temperature was 260 °C and the detector temperature – 260˚C. The carrier gas was helium.

Sterols Analysis

A part of total lipid extract was saponified by refluxing with 1M KOH ethanol/water (8 : 2, v/v) solution for 1 h. The unsaponifiables, containing total sterols, were then extracted first with petroleum ether and diethyl ether. The ether phases were combined, washed and evaporated to dryness.

The sterols were derivatized trimethyl silyl ether (TMS) derivatives and separated on fused silica capillary column coated with 5% phenyl/95% dimethylpolysiloxane (30 m × 0.25 mm i.d., film thickness 0.25 µm; Rtx-5; Restek Corporation, Bellefonte, PA, USA) and using the same

GC system mentioned above. The temperature program was: 5 min at 200 °C, 10 °C/min to 300 °C (hold 20 min).

FAME and sterols peaks were identified by comparison of their retention times with those of commercially available standards (Sigma). All extractions and GC-FID runs were performed in triplicate and mean values were calculated.

Results

Calendula seeds were analyzed in different stages during their maturation, seeds collected: immediately after flower drops (0), one week after (1) and two weeks after flower drops. (2). The fatty acids composition is presented in Fig. 1. The calendic acid represents – 8.62 % at first stage, it increased at 26.6 % one week after and reached the maximum content of 53 % in the mature seeds. The increasing of 18 : 3c content occurs in the same time with the fast decreasing of linoleic acid and a slow decrease of oleic acid, while stearic and linolenic acid remain almost to the same values during seeds maturation.
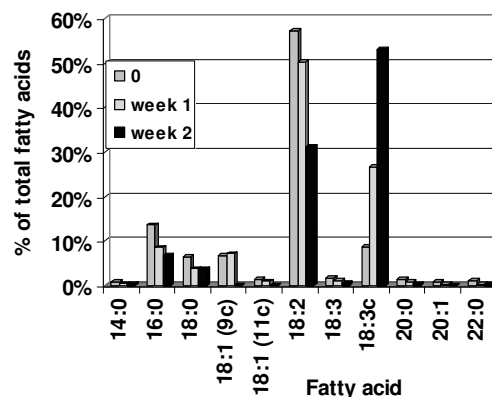
Fig. 1. **Fatty acids variation during seeds maturation**

Triacylglycerols (TAG) contain the highest amount of conjugated fatty acids (33 %), while in diacylglycerols (DAG) and monoacylglycerols (MAG) contain less than 10 % (data not shown). The polar lipid (PL) fraction is highly unsaturated, with more than 65 % of linoleic acid. Conjugated acids are present in polar lipids fraction fact which can

Table I
Fatty acids distribution in lipid fractions

Fatty acid	TAG	SE	PL
Miristic 14 : 0	0.75	1.58	0.34
Palmitic 16 : 0	6.41	21.25	12.88
Stearic 18 : 0	2.47	2.65	2.84
Oleic 18 : 1 (9c)	7.33	10.02	7.21
Linoleic 18 : 2 (9c, 12c)	47.2	47.8	65.56
α-linolenic 18 : 3 (9c, 12c, 15c)	1.17	3.15	3.13
Conjugated acids 18 : 3c	33.33	11.5	6.56
Arachidic 20 : 0	0.65	2.25	0.31
Gadoleic 20 : 1 (9c)	0.49	0.65	0.30

Table II
Sterols composition in *Calendula* seeds

Component	Retention time [min]	[mg 100 g^{-1}] seeds
5-α-cholestane-3-β-ol (Internal standard)	40.23	–
Cholesterol	39.63	4.23
Campesterol	45.07	9.21
Campestanol	45.60	0.42
Stigmasterol	46.50	17.6
Δ-7-Campesterol	48.57	1.42
β-Sitosterol	49.78	38.9
(Sitostanol + β-amyrin)	50.63	0.97
Δ-5-Avenasterol	51.05	3.72
Δ-7-sitosterol	53.95	13.98
Δ-7-avenasterol	55.13	2.91
Citrostadienol	61.33	1.56
Total sterol content		94.92

be explained by the implication of phosphatidylcholine and some of his derivatives in the desaturation and transacylation processes. The esterified sterols (SE) contain the highest amount of palmitic acid, but also more than 11 % conjugated fatty acids (Table I). β-Sitosterol is the major phytosterol of seeds, representing 41 % of total sterols, followed by stigmasterol with 18 %, Δ7 – sitosterol – 15 % and campesterol – 10 % (Table II)

Conclusions

The fatty acids composition of *Calendula* seeds is strongly influenced by the degree of seeds maturation. Conjugated fatty acids reached maximum content in mature seeds. Conjugated fatty acids are concentrated in triacylglycerols and they are present in lower amount in other lipid fractions. Beside the industrial application, *Calendula* seeds oil can be considered as a nutraceutical due to his high content (over 80 %) of biologically active polyunsaturated fatty acids and phytosterols.

REFERENCES

1. Dyer J. M., Stymne S., Green A. G., Carlsson A. S.: Plant J. *54*, 640 (2008).
2. Chisholm M. J., Hopkins C. Y.: Can. J. Chem. *38*, 2500 (1960).
3. Igarashi M., Miyazawa T.: Cancer Lett. *148*, 173 (2000).
4. Koba k., Imamura J., Akashoshi A., Kahno-Murase J., Nishizono S., Iwabuchi M., Tanaka K., Sugano M.: J. Agric. Food Chem. *55*, 3741 (2007).
5. Yasui Y., Hosokawa M., Kohno H., Tanaka T., Miyashita K.: Anticancer Res. *26*, 1855 (2006).
6. Chardigny J. M., Hasselwander O., Genty M., Kraemer K., Ptock A., Sébédio J. L.: Lipids *38*, 895 (2003).
7. Pintea A., Bara A., Andrei S., Bele C.: *Bulletin USAMV 61*, 116 (2004).
8. Folch J., Lees M., Sloane-Stanley, G. H.: J. Biol. Chem., *226*, 497 (1957).
9. Heape A. M., Juguelin H., Boiron F., Cassagne C.: J. Chromat. *322*, 391 (1985).

P80 LIPID PEROXIDATION PRODUCTS IN PLASMA OF PATIENTS WITH CHRONIC PANCREATITIS

MARTINA PODBORSKÁ[a], ANTONÍN LOJEK[a], LUKÁŠ KUBALA[a], RADKA BUŇKOVÁ[a], IVANA MÁROVÁ[b], ARONA ŠEVČÍKOVÁ[c], JAN TRNA[c] and PETR DÍTĚ[c]

[a]Institute of Biophysics of the Academy of Sciences of The Czech Republic, v.v.i., Královopolská 135, 612 65 Brno, [b]Faculty of Chemistry, University of Technology Brno, [c]Clinic of Internal Medicine – Gastroenterology, Faculty Hospital Brno (Faculty of Medicine of MU Brno),
podborska@ibp.cz

Introduction

The chronic inflammation of human pancreas (chronic pancreatitis) is known to be associated with an increased generation of reactive oxygen species damaging pancreatic tissue[1,2]. One of the primary targets of these radicals are unsaturated fatty acids. The lipid peroxidation leads to formation of mutagenic compounds such as malondialdehyde (MDA) and 4-hydroxynonenal (4-HNE). Therefore, the main aim of the study was to determine MDA and 4-HNE plasma levels in patients with chronic pancreatitis using HPLC-DAD.

Experimental

Materials

EDTA tubes 7.5 ml (Sarstedt) were used for blood collection. Water G CHROMASOLV® (for gradient elution), methanol G CHROMASOLV® (for gradient elution, ACS), acetonitrile CHROMASOLV® (for HPLC, gradient grade) and butylated hydroxytoluene (BHT) were purchased from Sigma-Aldrich Ltd. Solid Phase Extraction (DSC-C18; Discovery®, 1 ml Tube, 50 mg) tubes were obtained from Supelco. EDTA disodium salt (EDTA-Na$_2$) and trichloroacetic acid (TCA) were from Fluka – Biochemika. 2,4-dinitrophenylhydrazine (DNPH) and potassium dihydrogen-phosphate (KH$_2$PO$_4$) were purchased from Lachema and 35% hydrochloric acid (HCl) from Penta. All reagents and chemicals were analytical grade of highest purity. All organic solvents were HPLC grade.

Plasma Collection

A total of 105 patients (range 20 to 60 years; 69 males and 36 females) with chronic pancreatitis was included in the study. Blood samples were collected by venipuncture into EDTA tubes twice from each patient. The second blood collection was performed six months after the first round. Whole blood was immediately centrifuged (3,500 rpm, 22 °C for 10 min) and plasma was removed. Aliquots of plasma in test tubes (1.5 ml, with 1.96 mM BHT) were snap frozen in liquid nitrogen and then stored at –80 °C. The same procedure for plasma collection was used for the healthy male and female volunteers (range 20 to 60 years, 10 males and 17 females).

Plasma Preparation

Hydrolysis of protein bound MDA and 4-HNE was achieved by incubating 500 µl plasma with 250 µl 0.25 N hydrochloric acid in 60 °C water bath for 40 min. Then, protein was precipitated with 250 µl 15% trichloracetic acid, and the mixture was centrifuged (16,000 G, 4 °C for 10 min). The supernatant was further used for HPLC analysis.

HPLC Analysis

For derivatization, 100 µl or 200 µl of DNPH reagent (5 mM solution in 2 M HCl) was added to 600 µl of supernatant for MDA-DNPH products or to 1,000 µl of supernatant for 4-HNE-DNPH products. This reaction mixture was incubated for 60 min at room temperature protected from light. 4-HNE-DNPH adducts were extracted with SPE tubes – DSC-C18 which were conditioned with 1 ml of methanol, then with 1 ml 25 mM KH$_2$PO$_4$ for adjustment acidic pH 3 of the sample matrix. Concentrated 4-HNE-DNPH adducts were eluted with 300 µl of acetonitrile. The adducts of 4-HNE-DNPH and MDA-DNPH after reaction with DNPH were directly injected onto Cogent™ Bidentate C18 column (4.2 µm, 4.6 × 150 mm I.D.) with pre-column MetaGuard Polaris-C18 (5 µm, 4.6 mm). Chromatography was performed using Agilent 1100 series and DNPH derivates of aldehydes (MDA-DNPH and 4-HNE-DNPH) were detected with Agilent 1100 photo-diode detector at 310 nm (MDA) or 350 nm (4-HNE) at flow-rate 1 ml min^{-1} with an isocratic elution acetonitrile-water-acetic acid (40 : 60 : 0.2, v/v/v) for MDA-DNPH detection and with linear gradient of acetonitrile-water-acetic acid (50 : 50 : 0.2, v/v/v) to acetonitrile-water-acetic acid (80 : 20 : 0.2) in 20 min (for 4-HNE-DNPH determination). The amounts of MDA and 4-HNE were quantified by performing peak area analysis using external calibration curve. The plasma concentrations of MDA and 4-HNE were expressed as µmol dm^{-3}.

Statistical Analysis

Data are reported as mean ± S.E.M. The data were statistically analyzed by Student´s *t*-test. A *P* value of less than 0.05 was considered significant.

Results

Fig. 1.(a) and Fig. 1.(b) demonstrate the concentration of MDA and 4-HNE in plasma of patients with chronic pancreatitis in the 1st and 2nd blood collection compared with healthy volunteers (control). MDA concentrations (mean 0.29 ± S.E.M. 0.01 µmol dm^{-3}) in plasma from the 1st blood collection were significantly higher in comparison with healthy controls. Moreover, MDA levels (mean 0.41 ± S.E.M. 0.02 µmol dm^{-3}) in the plasma from the 2nd blood collection were significantly higher not only in comparison with healthy controls but also in comparison with MDA levels in plasma from the 1st blood collection. Similarly, the concentrations of 4-HNE were significantly increased in plasma from the 1st blood collection (mean 0.31 ± S.E.M. 0.05 µmol dm^{-3}) in comparison with healthy controls.
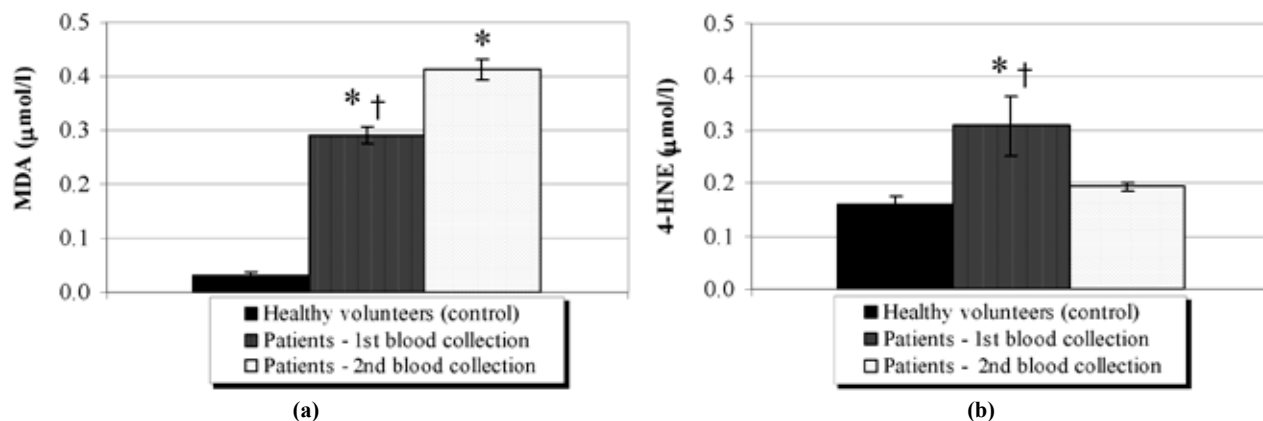
Fig. 1. **Effect of the chronic inflammation of human pancreas on lipid peroxidation expressed as MDA concentration (a) and 4-HNE concentration (b); values are the mean ± S.E.M. * Symbol shows significant difference compared to the control, † symbol shows significant difference between the 1st and 2nd blood collection**

However, the levels of 4-HNE in the 2nd blood collection (mean $0.19 \pm$ S.E.M. $0.01\ \mu mol\,dm^{-3}$) were only slightly elevated in comparison with healthy controls. The concentration trend of 4-HNE is not correlated with MDA between the 1st and 2nd blood collection.

Conclusions

In the present study, we demonstrated that the chronic inflammation in pancreas is accompanied with an increased concentration of secondary products of lipid peroxidation as MDA and 4-HNE in blood plasma. This observation is in agreement with published studies of other authors[3,4].

In contrast with 4-HNE, the concentration of MDA in plasma increased gradually during the followed time period. It can be suggested that MDA rather then 4-HNE could be a good biomarker[5,6,7] for monitoring of oxidative stress in patients with chronic pancreatitis and a progress of the disease.

To confirm this suggestion, these patients will be examined periodically in the consequent two years.

REFERENCES

1. Frossard J. L., Dumonceau J. M., Pastor C., Spahr L., Hadengue A.: World J. Gastroenterol. *14*, 2596 (2008).
2. Schoenberg M. H., Birk D., Beger H. G.: Am. J. Clin. Nutr. *62*, l306 (1995).
3. Verlaan M., Hennie M. J. R., Van Schaik A., Wanten J. A. G., Jansen B. M. J. J., Peters H. M. W., Drenth P. H. J.: World J. Gastroenterol. *12*, 5705 (2006).
4. Casini A., Galli A., Pignalosa P., Frulloni L., Grappone C., Milani S., Pederzoli P., Cavallini R., Surrenti C.: J. Pathol. *192*, 81 (2000).
5. Negre-Salvayre A., Coatrieux C., Ingueneau C. and Salvayre R: Br. J. Pharmacol. *153*, 6 (2008).
6. Dalle-Donne I., Rossi R., Colombo R., Giustarini D., Milzani A.: Clin. Chem. *52*, 601 (2006).
7. Nair U., Bartsch H., Nair J.: Free Radic. Biol. Med. *43*, 1109 (2007).

P81 THE EFFECT OF LIPOPHILICITY ON ANTIFUNGAL ACTIVITY OF SOME 2-AMINO AND 2-METHYLBENZIMIDAZOLE DERIVATIVES

SANJA O. PODUNAVAC-KUZMANOVIĆ, DRAGOLJUB D. CVETKOVIĆ and DIJANA J. BARNA

University of Novi Sad, Faculty of Technology, Bulevar cara Lazara 1, 21000 Novi Sad, Serbia
sanya@uns.ns.ac.yu

Introduction

Benzimidazole and its derivatives have a long history as antimicrobial agents. Several thousands of benzimidazole analogs have been synthesized and screened for pharmacological activity. They are of wide interest because of their diverse biological activity and clinical applications. These heterocycle systems have different activities as they can act as bacteriostats or bactericides, as well as fungicides[1–5] and they are present in numerous antiparasitic, antitumoral and antiviral drugs.[6–7] Also, some of them exhibit appreciable antiprotozoal activity[8]. It was confirmed to have a moderate in vitro anti-HIV activity[9]. The success with these group of molecules stimulated the search for new biologically active derivatives. Understanding the role of chemical structure on biological activity is very important. Predictions of biological and physicochemical properties of molecules based on their structure are the fundamental and most interesting objectives of chemistry.

The conception that there exists a close relationship between bulk properties of compounds and the molecular structure of those compounds is quite rooted in chemistry. This idea allows one to provide a clear connection between the macroscopic and the microscopic properties of matter, and thus has been firmly established as one of the central foundations of chemistry. Therefore, it is the basic tenet of chemistry to attempt to identify these assumed relationships between molecular structure and physico-chemical properties and then to quantify them.

A large number of research studies are nedded to analyze the pharmacophore present in these compounds using the Three Dimensional QSAR (quantitative structure-activity relationship) methods.[10–12] The physicochemical properties predicted from structure are helpful in the search for new molecules of similar or increased biological activity. QSAR studies enable the investigators to establish reliable quantitative structure-activity relationships, to derive a QSAR model and predict the activity of novel molecules prior to their synthesis.[13–16]. These studies reduce the trial- and error element in the design of compounds by establishing mathematical relationships between physical, chemical, biological, or environmental activities of interest and measurable or computable parameters such as physicochemical, electronic, topological, or stereochemistry. 3D-QSAR methodology has been succesfully used to generate models for various chemotherapeutic agents.

Progress in the use of QSAR methods has shown the importance of the hydrophobic or lipophilic nature of biologically active molecules. The lipophilicity modifies the penetration of bioactive molecules through the apolar cell membranes. This property is usually characterized by partition coefficient ($\log P$), which is essentially determined from distribution studies of the compound between an immiscible polar and non-polar solvent pair. To measure $\log P$ by the conventional "shake-flask" technique[17] is difficult and time resuming. It is complicated to determine $\log P$ for substances that are not very soluble in water or can not be detected by conventional techniques. Instead of measuring the $\log P$ values by equilibrium methods, partition chromatographic data can be determined.

One of the most frequently used methods for lipophilicity measuring is reversed-phase thin-layer chromatography (RP TLC)[18–22]. Lipophilicity can be expressed in terms of many different descriptors ($\log P$, π, f, $\log k_w$, R_M, R_M^0) obtained experimentally or calculated. Most frequently used experimental parameters are retention constants, R_M^0 (RP TLC) and $\log k_w$ (RP HPLC), whilst the calculated factor is $\log P$. Samples of pure compounds are not always available, so it is important to develop QSAR methods that can efficiently predict biological activity by using theoretical descriptors computed from the chemical structure. $\log P$ is also used in many environmental studies to determine the environmental fate of chemicals. By knowing exact values for this parameter, it is possible to predict the inhibitory activity of a drug.

In this context, the aim of the present study was to investigate the activity of different substituted 2-amino and 2-methylbenzimidazoles against yeast *Saccharomyces cerevisiae* and study the quantitative effect of lipophilicity on antifungal activity. The main objective was to establish a quantitative lipophilicity-inhibitory activity relationships and derive a high-quality model which would link the lipophilicity of these compounds with their inhibitory activity.

Experimental

The structures of the benzimidazoles tested in this study are presented in Table I. All the compounds, except (1) and (8) were synthesized by a general procedure described by Vlaović[23]. 2-aminobenzimidazole (1) and 2-methylbenzimidazole (8) were of analytical reagent grade, commercially available.

Antifungal Activity

All the benzimidazole derivatives were tested for their *in vitro* growth inhibition activity against yeast *Saccharomyces cerevisiae* (ATCC 24860). For the evaluation of the antifungal activities of the samples, agar disc diffusion method was used as described by NCCLS[24].

The strains were grown on Sabouraud Dextrose slants for 24 hours at 25 °C and checked for purity. After incubation the cells were washed from the surface of agar and suspended in a sterile phisyological solution. The number of cells in 1 ml of suspension for inoculation, measured by Mc Farland

Table I
The structures of the compounds studied

Compound	R_1	R_2
1	NH_2	H
2	NH_2	$C_6H_5–CH_2$
3	NH_2	$4–CH_3–C_6H_4–CH_2$
4	NH_2	$4–Cl–C_6H_4–CH_2$
5	NH_2	$C_6H_5–CO$
6	NH_2	$4–CH_3–C_6H_4–CO$
7	NH_2	$4–Cl–C_6H_4–CO$
8	CH_3	H
9	CH_3	$C_6H_5–CH_2$
10	CH_3	$4–CH_3–C_6H_4–CH_2$
11	CH_3	$4–Cl–C_6H_4–CH_2$
12	CH_3	$C_6H_5–CO$
13	CH_3	$4–CH_3–C_6H_4–CO$
14	CH_3	$4–Cl–C_6H_4–CO$
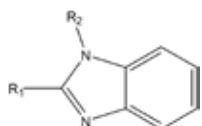
nefelometer, was $1 \times 10^7 \, CFU \, cm^{-3}$. The 1 ml of this suspensions was homogenized with 9 ml of melted (45 °C) Sabouraud Dextrose Agar and poured into Petri dishes. On the surface of the agar the 6 mm diameter sterile paper discs (Hi Media, Mumbai, India) were put and impregnated with 10^{-3} ml of samples. The plates were incubated for 24–47 hours at 25 °C, and the diameter of the resulting inhibition zone (including the disc) was measured (in mm). The evaluation of antifungal activities of samples was carried out in three repetitions.

Minimum inhibitory concentration (MIC) was determined by the agar dilution method according to guidelines established by the NCCLS standard M7-A5[25]. The MIC of tested benzimidazoles is defined as the lowest concentration of the compound at which no growth of the strain is observed in time and under specified experimental conditions. Stock solutions of the compounds were prepared in dimethylformamide (DMF). Further dilutions were performed with distilled water. The inoculated plates were then incubated at 35 °C for 16–20 h. A control (using DMF without any test compound) was included for each organism. It was determined that the solvent had no activity against any of the test microorganisms. The negative logarithms of molar MICs ($\log 1/c_{MIC}$) were determined and used for further calculations.

Molecular Modeling and log *P* Calculations

Molecular modeling studies were performed by using CS Chem-Office Software version 7.0 (Cambridge software) running on a P-III processor[26]. All molecules were constructed by using Chem Draw Ultra 7.0 and saved as the template structure. For every compound, the template structure was suitably changed considering its structural

features, copied to Chem 3D 7.0 to create a 3-D model and, finally, the model was cleaned up and subjected to energy minimization using molecular mechanics (MM2). The minimization was executed until the root mean square (RMS) gradient value reached a value smaller than 0.1 kcal mol^{-1}·A. The Austin Model-1 (AM-1) method was used for re-optimization until the RMS gradient attained a value smaller than 0.0001 kcal mol^{-1}·A using MOPAC. The lowest energy structure was used for each molecule to calculate lipophilicity parameters (Table II).

Statistical Methods

The complete regression analysis was carried out by PASS 2005, GESS 2006, NCSS Statistical Softwares[27].

Table II
Data of the lipophilicity parameters

Compound	$\log P$
1	0.99
2	2.96
3	3.44
4	3.52
5	2.84
6	3.32
7	3.39
8	1.48
9	3.45
10	3.94
11	4.01
12	3.33
13	3.81
14	3.89

Results

The results of antifungal studies of benzimidazoles tested against *Saccharomyces cerevisiae* are summarized in Table III. As indicated, all the compounds show antifungal activities against the tested yeast. Consequently, compounds with high $\log 1/c_{MIC}$ are the best antifungals. The MICs were compared with Ketoconazole and Amphotericin which were screened under similar conditions as reference drugs.

In order to identify the effect of lipophilicity on the inhibitory activity, QSAR studies of title compounds were performed.

A set of benzimidazoles consisting of 14 molecules was used for multilinear regression model generation. The reference drugs were not included in model generation as they belong to a different structural series. An attempt has been made to find structural requirement for inhibition of *Saccharomyces cerevisiae* using QSAR Hansch approach on benzimidazole derivatives. To obtain the quantitative effects of the lipophilicity parameter of benzimidazole derivatives on their antifungal activity, QSAR analysis with $\log P$ was operated.

Table III
Antifungal screening summary

Compound	$\log 1/c_{MIC}$ exp.	$\log 1/c_{MIC}$ predict.	Residuals
1	3.726	3.772	−0.046
2	4.854	4.946	−0.092
3	4.579	4.498	0.081
4	4.615	4.632	−0.017
5	4.880	4.986	−0.106
6	4.604	4.657	−0.053
7	4.638	4.568	0.07
8	4.325	4.231	0.094
9	4.551	4.483	0.068
10	3.277	3.435	−0.158
11	3.313	3.229	0.084
12	4.577	4.645	−0.068
13	3.602	3.778	−0.176
14	3.637	3.573	0.064
Ketoconazole	4.628	–	–
Amphotericin	4.869	–	–

Usually, lipophilicity parameters are linearly related to pharmacological activity (MICs), but in the more general case this relationship is not linear[28]. Therefore, it was made a complete regression analysis resorting to linear, quadratic and cubic relationships. The statistical quality of the resulting models is determined by correlation coefficient (r), standard error of estimation (s), and probability factor related to F-ratio (F). Good quality of mathematical models was obtained in cases of quadratic and cubic relationships, as depicted in Eqs.(1) and (2). It is noteworthy that both equations were derived using entire data set of compounds (n = 14) and no outliers were identified. The F-value obtained in Eqs.(1) and (2) is found statistically significant at 99 % level since all the calculated F values are higher as compared to tabulated values. It is apparent from the data that fitting equations improve when resorting to second order polynomial.

$$\log 1/c_{MIC} = -0.748 \log P^2 + 3.654 \log P + 0.712 \quad (1)$$
r = 0.962; s = 0.171; F = 69.32

$$\log 1/c_{MIC} = -0.201 \log P^3 + 0.863 \log P^2 - 0.263 \log P + 3.382 \quad (2)$$
r = 0.979; s = 0.134; F = 77.56

For the estimation of the quality with regard to predictive ability of the best model (2), the cross-validation statistical technique has been applied. The simplest and most general cross-validation procedure is the leave-one-out technique (LOO technique). This method uses cross-validated fewer parameters: PRESS (predicted residual sum of squares), SSY (total sum of squares deviation), r^2_{CV} and r^2_{adj} (Table IV). PRESS is an important cross-validation parameter as it is a good approximation of the real predictive error of the models. Its value being less than SSY points out that the model pre-

dicts better than chance and can be considered statistically significant. The present models have PRESS << SSY. From the PRESS and SSY, r^2_{CV} can be easily calculated:

$$r^2_{CV} = 1 - PRESS/SSY \quad (3)$$

But, the only way to estimate the true predictive power of a model is to test their ability to predict accurately the biological activities of compounds. In order to verificate the predictive power of the developed model, predicted $\log 1/c_{MIC}$ values of benzimidazoles investigated were calculated by using Eq.(2) and compared with the experimental values.

Table IV
Cross-validation parameters

Eq.(2)	
PRESS	1.317
SSY	4.370
PRESS/SSY	0.301
r^2_{CV}	0.699
r^2_{adj}	0.946

Based on the magnitude of residue, there is a close agreement between the observed and calculated inhibitory activity (Table III). Further the plot of linear regression predicted $\log 1/c_{MIC}$ values against the observed $\log 1/c_{MIC}$ values also favor the model expressed by Eq.(2) (Fig. 1.).
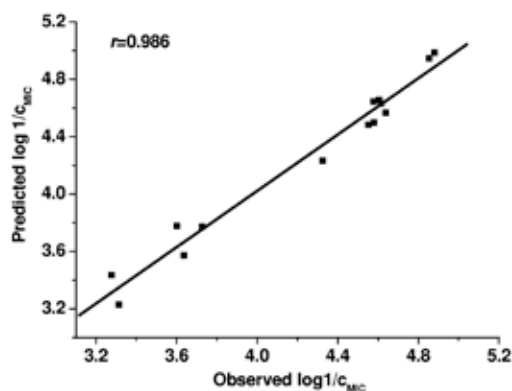
Fig. 1. **Plots of predicted versus experimentally observed inhibitory activity against *Saccharomyces cerevisiae***

In order to investigate the existence of a systemic error in developing the QSAR models, the residuals of predicted $\log 1/c_{MIC}$ were plotted against the observed $\log 1/c_{MIC}$ values (Fig. 2.). The propagation of the residuals on both sides of zero indicates that no systemic error exists in the development of regression models as suggested by Jalali-Heravi and Kyani[29].

From the derived model, it can be concluded that strong influence of the partition coefficient, $\log P$, is important for the antifungal activity and this parameter is usually related to

pharmacological activity. This evidence was clearly described in lipid theory advanced by Meyer and Overton. According to this theory, log P is a measure of hydrophobicity which is important for the penetration and distribution of the drug, but also for the interaction of drug with receptors. Therefore, it can be suggested that lipophilic properties have to be checked for designing of potent antifungal agents as they are deciding factors for its activity.
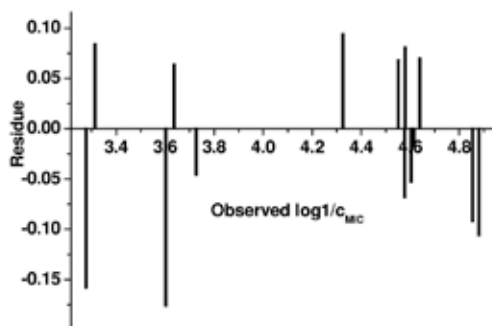
Fig. 2.   **Plot of residual values against the experimentally observed log 1/c_{MIC} values**

Conclusions

QSAR analysis was performed to estimate the quantitative effects of the lipophilicity parameter, log$P$, of the different substituted 2-amino and 2-methylbenzimidazole derivatives on their antifungal activity against *Saccharomyces cerevisiae*. log P values were calculated for each molecule, and high-quality mathematical model relating the inhibitory activity, log 1/c_{MIC}, and log P was defined . For the estimation of the predictive ability of this model, the cross-validation statistical technique was applied. Comparison of the linear, quadratic and cubic relationships showed that the cubic equation was the most appropriate for prediction of antifungal activity of the investigated class of molecules. It is concluded that strong influence of the partition coefficient, log P, is important for the inhibitory activity and this parameter is usually related to pharmacological activity. The obtained mathematical model was used to predict antifungal activity of the benzimidazoles investigated and close agreement between experimental and predicted values was obtained. It indicates that this model can be successfully applied to predict the antifungal activity of these class of molecules.

REFERENCES

1. Goker H., Alp M., Yildiz S.: Molecules *10*, 1377 (2000).
2. Nguyen P. T. M., Baldeck J. D., Olsson J., Marquis R. E.: Oral Microbiol. Immunol. *20*, 93 (2005).
3. Podunavac-Kuzmanović S. O., Leovac V. M., Perišić-Janjić N. U., Rogan J., Balaž J.: J. Serb. Chem. Soc. *64*, 381 (1999).
4. Podunavac-Kuzmanović S. O., Cvetković D.: J. Serb. Chem. Soc. *75*, 381 (2007).
5. Ayhan-Kilcigil G., Altanlar N.: Turk. J. Chem. *30*, 223 (2006).
6. Boiani M., Gonzalez M.: J. Med. Chem. *5*, 409 (2005).
7. Garuti L., Roberti M., Cermelli C.: Bioorg. Medicinal Chem. Letter *9*, 2525 (1999).
8. Kazimierczuk Z., Upcroft J. A., Upcroft P., Gorska A., Starosciak B., Laudy A.: Acta Biochim. Polon. *49*, 185 (2002).
9. Akbay A., Oren I., Temiz-Arpaci O., Aki-Sener E., Yalcin I.: Arzneim.-Forcsh./Drug Res. *53*, 266 (2003).
10. Bevan D.: *QSAR and Drug Design*. Network Science, http://www.netsci.org/Science/Compchem/feature12.html.
11. *QSAR*, The Australian Computational Chemistry via the InternetProject,www.chem.swin.edu.au/modukes/mod4/index.html.
12. Hansch C.: J. Med. Chem. *19*, 1 (1976).
13. Vasanthanathan P., Lakshmi M., Babu M. A., Gupta A. K., Kaskhedikar S. G.: Chem. Pharm. Bull. *54*, 583 (2006).
14. Melagraki G., Afantitis A., Sarimveis H., Igglessi-Markopoulou O., Supuran C. T.: Bioorg. Med. Chem. *14*, 1108 (2006).
15. Podunavac-Kuzmanović S. O., Markov S. L., Barna D. J.: J. Theor. Comp. Chem. *6*, 687 (2007).
16. Podunavac-Kuzmanović, S. O., Barna, D. J., Cvetković D. M.: Acta Periodica Technol. *38*, 139 (2007).
17. Leo A., Hansch C., Elkins D.: Chem. Rev. *71*, 525 (1971).
18. Nasal A., Siluk D., Kaliszan R.: Curr. Med. Chem. *10*, 381 (2003).
19. Tiperciuc B, Sarbu C.: J. Liq. Chrom. Rel. Technol. *29*, 2257 (2006).
20. Perišić-Janjić N. U., Podunavac-Kuzmanović S. O.: J. Planar Chromatogr. *21*, 135 (2008).
21. Perišić-Janjić N. U., Podunavac-Kuzmanović S. O., Balaž, J. S., Vlaović Dj.: J. Planar Chromatogr. *13*, 123 (2000).
22. Slawik T., Paw B.: J.Liq. Chromatogr. *27*, 1043 (2004).
23. Vlaović Đ., Čanadanović-Brunet J., Balaž J., Juranić I., Đoković D., Mackenzie K.: Biosci. Biotech. Biochem. *56*, 199 (1992).
24. National Committee for Clinical Laboratory Standards, NCCLS *Approval Standard Document M2-A7*. Vilanova, Pa, U.S.A. 2000.
25. National Committee for Clinical Laboratory *Standards, NCCLS Approval Standard Document M7-A5*. Vilanova, Pa, U.S.A. 2000.
26. CS. Chem. Office, Version 7.0, Cambridge Soft Corporation, 100 Cambridge Park Drive, Cambridge, MA 02140-2317, U.S.A. 2001.
27. www.ncss.com.
28. Lien E.J.: *Side Effects and Drug Design*. Marcel Dekker, New York 1987.
29. Jalali-Heravi M., Kyani A.: J. Chem. Inf. Comput. Sci. *44*, 1328 (2004).

P82 QSAR MODELS FOR PREDICTING THE ANTIBACTERIAL ACTIVITY OF SOME 1-BENZYLBENZIMIDAZOLE DERIVATIVES

SANJA O. PODUNAVAC-KUZMANOVIĆ, DRAGOLJUB D. CVETKOVIĆ and DIJANA J. BARNA

University of Novi Sad, Faculty of Technology, Bulevar cara Lazara 1, 21000 Novi Sad, Serbia,
sanya@uns.ns.ac.yu

Introduction

Quantitative structure-activity relationships (QSAR) represent an attempt to correlate structural or property descriptors of compounds with activities. These physico-chemical descriptors, which include parameters to account for hydrophobicity, topology, electronic properties, and steric effects, are determined empirically or, more recently, by computational methods. Activities used in QSAR include chemical measurements and biological assays. For example, biological activity can be expressed quantitatively as in the concentration of a substance required to give a certain biological response. Additionally, when physiochemical properties or structures are expressed by numbers, one can form a mathematical relationship, or quantitative structure-activity relationship, between the two. The mathematical expression can then be used to predict the biological response of other chemical structures. QSAR currently are being applied in many disciplines, with many pertaining to drug design and environmental risk assessment. Using QSAR, it can be obtained an estimate of the activity of a chemical from its molecular structure only.[1–7] QSAR offers the possibility for screening a large number of chemicals in a short time and with low cost.
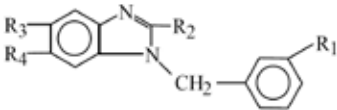
The benzimidazole nucleus, which is a useful structure for further research and for development of new pharmaceutical molecules, has received much attention in last decade. Because of their antimicrobial activities, new benzimidazoles have been synthesized and investigated for medical applications. Position and type of the substituents on the benzimidazole ring are responsible for the variety of biological activity. Many derivatives of benzimidazole are well known as antibacterial agents, as well as this class of compounds have been found to show antimicrobial activities against Gram-positive and Gram-negative bacteria, primarily because of the potential bio-activity of benzimidazole-based ligands.[8–15] So, the incorporation of the imidazole and benzimidazole nuclei is an important synthetic strategy in drug discovery.

Synthesis of benzimidazoles fused to another heterocyclic ring has attracted wide spread attention due to their diverse application as antioxidant[16,17], antifungal[18], antitubercular[19], anticancer[20,21] and antiallergic drugs[22]. Various benzimidazoles are also effective inhibitors of the growth of HIV-virus[23,24].

In view of above and in continuation of our studies on inhibitory activities of benzimidazole derivatives[4–7,11–14], as well as on correlation of molecular properties with activity, the objective of this investigations was to study the usefulness of QSAR in the prediction of the antibacterial activity of benzimidazole derivatives against Gram-negative bacteria *Pseudomonas aeruginosa*. The multiple linear regression (MLR) models have been developed as a mathematical equations which relate chemical structure to the inhibitory activity.

Table I
Structural formulae of the compounds

Cmpd	R_1	R_2	R_3	R_4
1	CH_3	H	CH_3	CH_3
2	Cl	H	CH_3	CH_3
3	F	H	CH_3	CH_3
4	OCH_3	H	CH_3	CH_3
5	CH_3	NH_2	H	H
6	Cl	NH_2	H	H
7	F	NH_2	H	H
8	OCH_3	NH_2	H	H
9	CH_3	NH_2	CH_3	CH_3
10	Cl	NH_2	CH_3	CH_3
11	F	NH_2	CH_3	CH_3
12	OCH_3	NH_2	CH_3	CH_3

Experimental

The investigated compounds (Table I) were synthesized by procedure described earlier[25].

Antibacterial Investigations

All the benzimidazole derivatives were evaluated for their *in vitro* growth inhibitory activity against bacteria *Pseudomonas aeruginosa* (ATCC 27853). Antibacterial activities of the compounds were tested by the disc-diffusion method under standard conditions using Mueller-Hinton agar medium as described by NCCLS[26].

The investigated isolate of bacteria was seeded in the tubes with nutrient broth (NB). It was taken 1 ml of seeded NB and homogenized in tubes with 9 ml of melted (45 °C) nutrient agar (NA). The homogenous suspension was poured out in Petri dishes. The discs of filter paper (diameter 5 mm) were ranged on cool medium. After cooling on formed solid medium, 2×10^{-5} dm^3 of the investigated compounds were placed by micropipette. After incubation of 24 hours in thermostat at 25–27 °C, inhibition (sterile) zone diameters (including disc) were measured (in mm). Inhibition zone diameter over 8 mm indicates the tested compound is active against microorganism. Every test was done in three replications.

Minimum inhibitory concentration (MIC) was performed by the agar dilution method according to guidelines established by the NCCLS standard M7-A5[27].

The MIC of tested benzimidazoles is defined as the lowest concentration of the compound at which no growth of the strain as observed in a period of time and under specified experimental conditions. Stock solutions of the compounds were prepared in dimethylformamide (DMF). Further dilutions were performed with distilled water. The concentration range of the compounds tested was between 6.25–125 μg ml^{-1}. The inoculated plates were than incubated at 35 °C for 16–20 h. A control using DMF without any test compound was included for each organisms. There was no inhibitory activity in the wells containing only DMF. The MIC values of the benzimidazoles tested were obtained as μg ml^{-1}. In order to classify the antibacterial activity, we established comparisons with antibacterial agents currently employed in therapeutic treatment. The MICs were compared with Ampicillin and Gentamicin which were screened under similar conditions as reference drugs.

Molecular Modeling

All molecular modeling studies were performed by using HyperChem 7.5 software (HyperCube Inc, Version 7.5) running on P-III processor[28]. HyperChem includes a model builder that turns a rough 2Dsketch of a molecule into 3D. The created 3-D models were cleaned up and subjected to energy minimization using molecular mechanics (MM$_2$). The minimization is executed until the root mean square (RMS) gradient value reaches a value smaller than 0.1 kcal mol^{-1}·A. The Austin Model-1 (AM-1) method was used for re-optimization until the RMS gradient attains a value smaller than 0.0001 kcal mol^{-1}·A using MOPAC. The lowest energy structure was used for each molecule to calculate molecular descriptors.

Descriptors Generation

The numerical descriptors are responsible for encoding important features of the structure of the molecules and can be categorized as electronic, geometric, hydrophobic, and topological characters. Descriptors were calculated for each compound in the data set, using the software HyperChem[28], Dragon[29], and CS Chem Office Software version 7.0(ref.[30]). Since there was a large number of desriptors for each compound, Pearson's correlation matrix was used as a qualitative model, in order to select the suitable descriptors for MLR analysis. The eight descriptors which were showing maximum correlation with inhibitory activity were chosen for further evaluation. The values of descriptors selected for MLR model are presented in Table II (molar refractivity (*MR*), polarizability (*P*), molar volume (*MV*), hydration energy (*HE*), total energy (*TE*), surface area grid (*SAG*), and partition coefficient (log *P*)).

Statistical Methods

The complete regression analysis were carried out by PASS 2005, GESS 2006, NCSS Statistical Softwares[31]. The Elimination Selection Stepwise regression (ES-SWR) algorithm was used to select the most appropriate descriptors. ES-

Table II

Values of molecular descriptors used in the regression analysis

Cmpd	MR	P	MV	HE
1	87.25	30.78	811.60	−1.00
2	87.69	30.87	804.81	−1.86
3	83.10	28.85	777.39	−2.23
4	89.34	31.42	841.79	−3.68
5	81.56	28.46	744.54	−6.39
6	81.99	28.55	736.31	−7.16
7	77.40	26.53	704.51	−7.31
8	83.65	29.1	771.05	−8.95
9	90.12	32.13	844.29	−4.26
10	89.24	32.22	833.57	−5.38
11	85.97	30.2	802.16	−5.21
12	92.27	32.77	871.99	−6.83
	TE	DM	SAG	log *P*
1	27.17	3.98	490.32	4.24
2	26.87	3.974	429.54	4.31
3	27.02	3.976	477.14	3.91
4	28.92	3.978	507.17	3.63
5	26.35	4.464	458.41	3.44
6	26.03	4.427	450.08	3.52
7	26.07	4.428	433.17	3.12
8	27.94	4.429	470.97	2.83
9	27.67	4.428	503.71	4.42
10	27.18	4.409	498.16	4.49
11	27.46	4.410	480.77	4.09
12	29.38	4.406	517.74	3.80

SWR is a popular stepwise technique that combines Forward Selection (FS-SWR) and Backward Elimination (BE-SWR). It is basically a forward selection approach, but at each step it considers the possibility of deleting a variable as in the backward elimination approach, provided that the number of model variables is greater than 2.

Results

The substituted benzimidazoles were first evaluated for *in vitro* antibacterial activity against Gram-negative bacteria *Pseudomonas aeruginosa*. The values of MIC are summarized in Table III. The screening results reveal that all the compounds exhibited *in vitro* activity against the tested strain.

In an effort to determine the role of structural features, QSAR study was undertaken. A set of benzimidazoles consisting of 12 molecules was used for multilinear regression model generation.

The reference drugs were not included in model generation as they belong to a different structural series. Different physicochemical, steric, electronic, and structural molecular descriptors were used as independent variables and were correlated with antibacterial activity.

Developing a general model requires a diverse set of data, and, thereby a large number of descriptors have to be considered. Desriptors are numerical values that encode diff-

Table III
Antibacterial screening summary

Compound	$\log 1/c_{MIC}$ exp.	$\log 1/c_{MIC}$ predict.	Residuals
1	4.602	4.636	–0.034
2	4.637	4.636	0.001
3	4.609	4.518	0.091
4	4.328	4.373	–0.045
5	4.278	4.213	0.065
6	4.314	4.235	0.079
7	3.981	3.993	–0.012
8	3.704	3.732	–0.028
9	4.627	4.607	0.020
10	4.659	4.591	0.068
11	4.333	4.433	–0.100
12	4.352	4.372	–0.020
Ampicillin	4.446	–	–
Gentamicin	5.787	–	–

erent structural features of the molecules. Selection of a set of appropriate descriptors from a large number of them requires a method, which is able to discriminate between the parameters. Pearson's correlation matrix has been performed on all descriptors by using NCSS Statistical Software. The analysis of the matrix revealed 8 descriptors for the development of MLR model (Table II).

Mathematical models were formed by a stepwise addition of terms. A delition process was then employed where each variable in the model was held out in turn and using the remaining parameters models were generated. Each descriptor was chosen as input for the software package of NCSS and then the stepwise addition method implemented in the software was used for choosing the descriptors contributing to the antibacterial activity of benzimidazole derivatives.

The partition coefficient ($\log P$) tends to correlate with antibacterial activity exclusively and the best monoparametric model was found to be the following:

$$\log 1/c_{MIC} = 0.518 \log P + 2.391 \qquad (1)$$
$$n = 12; \; r = 0.932; \; s = 0.085; \; F = 66.43$$

Addition of HE as an additional parameter to $\log P$, increased the correlation coefficient from 0.932 to 0.951 (Eq.(2)).

$$\log 1/c_{MIC} = 0.415 \log P + 0.031 \, HE + 2.940 \qquad (2)$$
$$n = 12; \; r = 0.951; \; s = 0.010; \; F = 42.21$$

It should be noted that the addition of other parameters to $\log P$ and HE does not significantly improved the correlation coefficients. However, if quadratic values of descriptors were included in the stepwise multiple regression procedure, the best correlation was found as depicted in Eq.(3).

For the testing the validity of the predictive power of selected MLR model (3) the leave-one-out technique

$$\log 1/c_{MIC} = -0.201 \log P^2 + 1.930 \log P - \qquad (2)$$
$$0.001 \, HE^2 + 0.014 \, HE + 0.082$$
$$n = 12; \; r = 0.967; \; s = 0.008; \; F = 25.41$$

(LOO technique) was used. The developed model was validated by the calculation of following statistical parameters: predicted residual sum of squares (PRESS), total sum of squares deviation (SSY), cross-validated correlation coefficient (r^2_{CV}), and adjusted correlation coefficient (r^2_{adj}) (Table IV).

Table IV
Cross-validation parameters

Eq.(2)	
PRESS	0.151
SSY	0.942
PRESS/SSY	0.160
r^2_{CV}	0.840
r^2_{adj}	0.900

PRESS is an important cross-validation parameter as it is a good approximation of the real predictive error of the models. Its value being less than SSY points out that the model predicts better than chance and can be considered statistically significant. Thus, in view of this, model 3 is statistically significant. Further, to be a reasonable QSAR model, PRESS/SSY ratio should be lesser than 0.4. The data presented in Table IV indicate that for the developed model this ratio is 0.160. The high value of r^2_{CV} and r^2_{adj} are the essential criteria for qualifying the QSAR model 3 as the best one.

To confirm the predictive power of a model the inhibitory activitiy of 12 molecules included in the study was calculated by the model 3. The data presented in Table III show that the observed and the estimated activities are very close to each other. It indicates the good predictability of the established model 3. Fig. 1. shows the plots of linear regression predicted *versus* experimental values of the antibacterial activity of benzimidazoles investigated. To investigate the existence of a systemic error in developing the QSAR models, the residuals
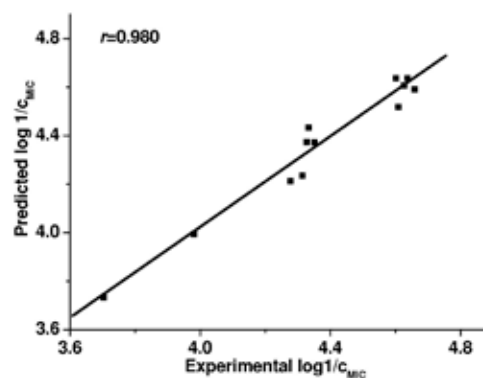
Fig. 1. **Plots of predicted versus experimentally observed inhibitory activity against *Pseudomonas aeruginosa***

of predicted values of inhibitory activity were plotted against the experimental values in Fig. 2. The propagation of the residuals on both sides of zero indicates that no systemic error exists in the development of regression models as suggested by Jalali-Heravi and Kyani[32]. It indicates that these models can be successfully applied to predict the antibacterial activity of these class of molecules.
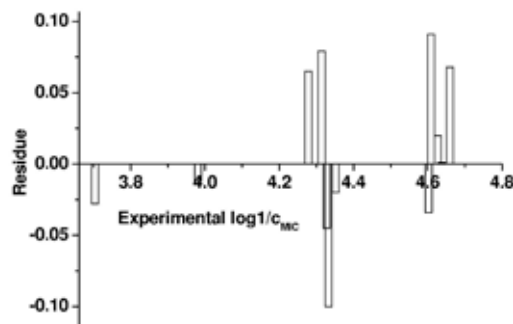
Fig. 2.   **Plot of residual values against the experimentally observed log $1/c_{MIC}$ values**

Conclusions

From the results and discussion made above, we conclude that the 1-benzylbenzimidazole derivatives are effective in vitro against the Gram-negative bacteria Pseudomonas aeruginosa. Molecular modeling and QSAR analysis were performed to find the quantitative effects of the molecular structure of the compounds on their antibacterial activity. The problem of selecting the appropriate descriptor as input for theoretical model was overcome by Pearson correlation matrix, which can be used as a tool for identifying the appropriate descriptors when a large number of them with different features are available. An accurate mathematical model was developed for predicting the inhibitory activity of some benzimidazole derivatives. The validity of the model has been established by the determination of suitable statistical parameters. The established model was used to predict inhibitory activity of the benzimidazoles investigated and close agreement between experimental and predicted values was obtained. The low residual activity and high cross-validated r^2 values (r^2_{CV}) observed indicated the predictive ability of the developed QSAR model. It indicates that the antibacterial activity of series of 1-benyzlbenzimidazole derivatives can be successfully modeled using different molecular descriptors.

REFERENCES

1. Bevan D.: *QSAR and Drug Design*. Network Science, http://www.netsci.org/Science/Compchem/feature12. html.
2. *QSAR*, The Australian Computational Chemistry via the InternetProject,www.chem.swin.edu.au/modukes/ mod4/index.html.
3. Hansch C.: J. Med. Chem. *19*, 1 (1976).
4. Podunavac-Kuzmanović S. O., Markov S. L., Barna D. J.: J. Theor. Comp. Chem. *6*, 687 (2007).
5. Podunavac-Kuzmanović, S. O., Barna, D. J., Cvetković D. M.: Acta Periodica Technol. *38*, 139 (2007).
6. Perišić-Janjić N. U., Podunavac-Kuzmanović S. O.: J. Planar Chromatogr. *21*, 135 (2008).
7. Perišić-Janjić N. U., Podunavac-Kuzmanović S. O., Balaž, J. S., Vlaović Dj.: J. Planar Chromatogr. *13*, 123 (2000).
8. Kazimierczuk Z., Upcroft J. A., Upcroft P., Gorska A., Starosciak B., Laudy A.: Acta Biochim. Polon. *49*, 185 (2002).
9 . Goker H., Kus C., Boykin D. W., Yildiz S., Altanlar N.: Bioorg. Med.Chem. *17*, 2233 (2007).
10. Ozden S., Atabey D., Yildiz D., Goker H.: Bioorg. Med. Chem. *13*, 1587 (2005).
11. Podunavac-Kuzmanović S. O., Cvetković D. M.: Centr. Eur. J. Occupat. Environ. Med.. *12*, 55 (2006).
12. Podunavac-Kuzmanović S. O., Markov S. L.: Centr. Eur. J. Occupat. Environ. Med. *12*, 61 (2006).
13. Podunavac-Kuzmanović S. O., Leovac V. M., Perišić-Janjić N. U., Rogan J., Balaž J.: J. Serb. Chem. Soc. *64*, 381 (1999).
14. Podunavac-Kuzmanović S. O., Cvetković D.: J. Serb. Chem. Soc. *75*, 381 (2007).
15. Kucukbay H., Durmaz R., Orhan E., Gunal S.: Il Farmaco *58*, 431 (2003).
16. Kus C., Ayhan-Kilcigil G., Can-Eke B., Iscan M.: Arch. Pharm. Res. *27*, 156 (2004).
17. Ayhan-Kilcigil G., Kus C., Coban T., Can-Eke B., Iscan M.: J. Enz. Inhib. Med. Chem. *19*, 129 (2004).
18. Ayhan-Kilcigil G., Altanlar N.: Turk. J. Chem. *30*, 223 (2006).
19. Mohamed B. G., Hussein M. A., Abdel-Alim A. M., Hashem M.: Arch. Pharm. Res. *29*, 26 (2006).
20. El-Hawash S. A., Badawey E. A., Kappe T.: Pharmazie *54*, 341 (1999).
21. Soderlind K. J., Gorodetsky B., Singh A., Bachur N., Miller G., Lown J.: Anti Canc. Drug Des. *14*, 19 (1999).
22. Nakano H., Inoue T., Kawasaki N., Miyataka H., Matsumoto H., Taguchi T., Inagaki N., Nagai H., Satoh T.: Chem. Pharm. Bull. *47*, 1573 (1999).
23. Demirayak S., Abu-Mohsen U., Cagri Karaburun A.: Eur. J. Med. Chem. *37*, 255 (2002).
24. Rida S. M., El-Hawash S. A., Fahmy H. T., Hazzaa A. A., El-Meligy M. M.: Arch. Pharm. Res. *29*, 826 (2006).

25. Vlaović Đ., Čanadanović-Brunet J., Balaž J., Juranić I., Đoković D., Mackenzie K.: Biosci. Biotech. Biochem. *56*, 199 (1992).

26. National Committee for Clinical Laboratory Standards*, NCCLS Approval Standard Document M2-A7*. Vilanova, Pa, U.S.A. 2000.

27. National Committee for Clinical Laboratory Standards, *NCCLS Approval Standard Document M7-A5*. Vilanova, Pa, U.S.A. 2000.

28. HyperChem 7.5, Hypercube, Inc., 419 Phillip St., Waterloo, Ontario, Canada N2L 3X2.

29. Dragon 5 Evaluation version, 2004, Talete SRL, Milano, Italy.

30. CS. Chem. Office, Version 7.0, Cambridge Soft Corporation, 100 Cambridge Park Drive, Cambridge, MA 02140-2317, U.S.A. 2001.

31. www.ncss.com.

32. Jalali-Heravi M., Kyani A.: J. Chem. Inf. Comput. Sci. *44*, 1328 (2004).

P83 ANTIMICROBIAL INVESTIGATIONS OF NICKEL(II) COMPLEXES WITH SOME 1-BENZYLBENZIMIDAZOLE DERIVATIVES

SANJA O. PODUNAVAC-KUZMANOVIĆ and DRAGOLJUB D. CVETKOVIĆ

University of Novi Sad, Faculty of Technology, Bulevar cara Lazara 1, 21000 Novi Sad, Serbia,
sanya@uns.ns.ac.yu

Introduction

Physiological activity and commercial applications of many benzimidazole derivatives have received much attention. Benzimidazole and its derivatives have different activities as they can act as bacteriostats or bactericides and fungicides.[1–10] Extensive biochemical and pharmacological activities have confirmed that these molecules are effective against RNA viruses and inhibit the formation of virus induced RNA polymerase, thereby preventing or retarding RNA synthesis various strains of microorganisms.[11–14] Antimicrobial activity of these class of compounds against *Helicobacter pylori*[15] and oral *Streptococci*[16] was also reported. Synthesis of benzimidazoles fused to another heterocyclic ring has attracted wide spread attention due to their diverse application as antioxidant[17,18], antifungal[19], antitubercular[20], anticancer[21,22], and antiallergic drugs[23]. Also, some of these compounds exhibited anti-HIV activity[24,25].

The complexes of transition metals with benzimidazole and related ligands have been extensively studied as models of some important biological molecules[26]. It was found that the complexes showed larger antimicrobial activitiy than the ligands applied alone.

Following our studies of the reactivity of benzimidazole derivatives with metallic halides[5–8], we evaluated the antibacterial activity of this type of complexes in this study. We report *in vitro* inhibitory activities of 1-benzylbenzimidazoles and their nickel (II) complexes against three gram-positive bacterial strains: *Bacillus cereus, Staphylococcus aureus* and *Sarcina lutea,* one gram-negative isolate: *Pseudomonas aeruginosa.*

Experimental

In the present paper we evaluated the antibacterial activity of nickel (II) complexes with the following starting ligands: 1-(3-chlorobenzyl)-2-aminobenzimidazole (L^1), 1-(3-fluoro-benzyl)-2-aminobenzimidazole (L^2), 1-(3-chlorobenzyl)-2-amino-5,6-dimethylbenzimidazole (L^3), 1-(3-fluorobenzyl)-2-amino-5,6-dimethylbenzimidazole (L^4) and 1-(3-methylbenzyl)-2-amino-5,6-dimethylbenzimidazole (L^5).

All the ligands were synthesized by Vlaović et al. according to a procedure described earlier.[27] Nickel (II) complexes were prepared following the same procedure described in our previous paper[7].

Antibacterial activity

All the nickel (II) complexes were tested for their in vitro growth inhibitory activity against Bacillus cereus ATCC 10876, Staphylococcus aureus ATCC 25923, Sarcina lutea ATCC 9341 and Pseudomonas aeruginosa ATCC 27853.

Antibacterial activities of the complexes were tested by the disc-diffusion method under standard conditions using Mueller-Hinton agar medium as described by NCCLS[28]. Each of the investigated isolates of bacteria was seeded in the tubes with nutrient broth (NB). 1 ml of seeded NB was homogenized in tubes with 9 ml of melted (45 °C) nutrient agar (NA). The homogenous suspension was poured out in Petri dishes. The discs of filter paper (diameter 5 mm) were ranged on cool medium. After cooling on formed solid medium, 0.02 ml of the investigated compounds ($\gamma = 1000$ µg ml^{-1}) were placed by micropipette. After incubation of 24 hours in thermostat at 25–27 °C, inhibition (sterile) zone diameters (including disc) were measured (in mm). Inhibition zone diameter over 8 mm indicates the tested compound is active against microorganisms. Every test was done in three replications. Antimicrobial activities of the free ligands against the same bacteria were tested in our previous studies[8].

Minimum inhibitory concentration (MIC) was performed by the agar dilution method according to guidelines established by the NCCLS standard M7-A5[29]. MIC was described as the lowest concentration of the compound that visibly inhibited colony's growth. Stock solutions of the compounds were prepared in dimethylformamide (DMF). Further dilutions were performed with distilled water. The concentration range of the compounds tested was between 60–750 µg ml^{-1} in two-fold dilution steps. The inoculated plates were than incubated at 35 °C for 16–20 h. A control using DMF without any test complex was included for each organisms. It was determined that the solvent had no activity against any of the test microorganisms.

Results

The results of antibacterial studies of the nickel (II) complexes with two series of 1-benzylbenzimidazole derivatives tested by the agar disc-diffusion method are summarized in Table I.

As can be seen from the data, all the investigated compounds displayed *in vitro* inhibitory activity against very persistent bacteria. The complexes investigated were found

Table I
In vitro antibacterial activity of complexes at a concentration of 1,000 µg ml^{-1}

Complex	Inhibition zone diameter [mm]			
	P.aeruginosa	*B. cereus*	*S. aureus*	*S. lutea*
Ni(L^1)$_2$Cl$_2$	22	26	26	29
NI(L^2)$_2$Cl$_2$	17	24	24	25
Ni(L^3)$_2$Cl$_2$	9	17	17	18
Ni(L^4)$_2$Cl$_2$	8	16	17	17
Ni(L^5)$_2$Cl$_2$	5	16	17	16

to be more active against Gram-positive than Gram-negative bacteria (*Pseudomonas aeruginosa*).

In the case of Gram-negative isolate only complexes of 2-aminobenzimidazole derivatives exhibited significant inhibitory activity. Nickel (II) complexes of L^3, L^4 and L^5 were slightly active against the *Pseudomonas aeruginosa*. In the case of *Bacillus cereus* and *Staphylococcus aureus* nickel (II) complexes of ligands L^1 and L^2 also express higher activity than another complexes. Gram-positive bacteria *Sarcina lutea* was persistent in all investigated cases, too. Nickel (II) complexes containing L^1 and L^2 were very highly or highly active, respectively. On the other hand, complexes of L^3, L^4 and L^5 were moderately active against the same bacteria.

In the next phase, MIC of the tested compounds was performed by the agar dilution method. From the results presented in Table II, it is seen that nickel(II) complex containing L^1 was active against *Pseudomonas aeruginosa* with a MIC value of 250 μg ml^{-1}, whilst Ni(L^2)$_2$Cl$_2$ was less toxic. However, Ni(L^3)$_2$Cl$_2$ and Ni(L^4)$_2$Cl$_2$ were same active, but complex of L^5 has the low activity against the same bacteria.

In the case of *Bacillus cereus* and *Staphylococcus aureus* complexes containing 2-aminobenzimidazole derivatives as ligands were more active (MIC = 125 μg ml^{-1}) than complexes of 2-amino-5,6-dimethylbenzimidazole derivatives. Ni(L^3)$_2$Cl$_2$ was equally active as Ni(L^4)$_2$Cl$_2$ with higher MIC value of 250 μg ml^{-1} against the same bacteria, whilst complex containing L^5 expressed MIC of 500 μg ml^{-1}.

On the other hand, all the complexes were more active against *Sarcina lutea*. The complex of L^3 with a MIC value of 125 μg ml^{-1} has the same activity as Ni(L^4)$_2$Cl$_2$, but complexes of 2-aminobenzimidazole derivatives were the most active. Ni(L^5)$_2$Cl$_2$ has the lowest activity against these two Gram-positive bacteria.

Comparing the activities of the tested complexes it was found that 1-substituted-2-aminobenzimidazole derivatives (L^1, L^2) formed the nickel (II) complexes which were more active than complexes of 1-substituted-2-amino-5,6-dimethyl-benzimidazoles (L^3, L^4, L^5). Consequently, it is suggested that methyl groups at the 5 or 6 position decreases the general inhibitory activity of the tested complexes. Also, antibacterial results shows that if the benzimidazole nucleus was substituted with a 3-chlorobenzyl group at the N1 atom, the antibacterial activity was increased.

The differences found in the activities of the nickel (II) complexes and the non-complexed ligands obtained in our previous investigations[8], suggest that the coordinated Ni(II) may play a significant role in the antibacterial potency. A possible explanation may be offers by the chelation theory stating a relationship between decreasing polarizability of the metal and increasing lipophilicity of the complexes. This property is now seen as an important parameters related to membrane permeation in biological system. Many of the processes of drug disposition depend on the ability or inability to cross membranes and hence there is a high correlation with measures of lipophilicity. Moreover, many of the proteins involved in drug disposition have hydrophobic binding sites

further adding to the importance of lipophilicity. The latter might promote inhibitory activity.

Moreover, the results of this study revealing that the compounds tested displayed higher activity against the Gram-positive than the Gram-negative one bacteria, likely point to the relevance of the structure of the bacterial cell wall in the antimicrobial potency of the substances. It is prospective because the cell wall is essential to the survival of many bacteria and some antibiotics are able to kill bacteria by inhibiting a step in the synthesis of peptydoglycan. Gram-positive bacteria possess a thick cell wall containing many layers of peptidoglycan and teichoic acids, but in contrast, Gram-negative bacteria have a relatively thin cell wall consisting of a few layers of peptidoglycan surrounded by a second lipid membrane containing lipopolysaccharides and lipoproteins. These differences in cell wall structure can produce differences in antibacterial susceptibility and some antibiotics can kill only Gram-positive bacteria and is ineffective against Gram-negative pathogens.

Table II
MIC tested of complexes

Complex	MIC [μg ml^{-1}]			
	P.aeruginosa	*B. cereus*	*S. aureus*	*S. lutea*
Ni(L^1)$_2$Cl$_2$	250	125	125	62.5
Ni(L^2)$_2$Cl$_2$	500	125	125	62.5
Ni(L^3)$_2$Cl$_2$	750	250	250	125
Ni(L^4)$_2$Cl$_2$	750	250	250	125
Ni(L^5)$_2$Cl$_2$	1000	500	500	250

Conclusions

The antibacterial activity of the nickel (II) complexes with two series of 1-benzylbenzimidazole derivatives was tested against very persistent microorganisms: *Pseudomonas aeruginosa*, *Bacillus cereus*, *Staphylococcus aureus* and *Sarcina lutea*. All the complexes displayed *in vitro* inhibitory activity, but 1-substituted-2-aminobenzimidazole derivatives formed the nickel (II) complexes which were more active than complexes of 1-substituted-2-amino-5,6-dimethyl-benzimidazoles. The basic antibacterial activity of the benzimidazoles was produced by the presence of an amino group at the position 2 of the benzimidazole ring. Methyl groups at the 5 or 6 position decreases the general inhibitory activity of the relevant benzimidazoles. Also, the results indicated that tested complexes were more active against Gram-positive than Gram-negative bacteria. It may be concluded that the antibacterial activity of the compounds is related to cell wall structure of the bacteria. It is possible because the cell wall is essential to the survival of many bacteria and some antibiotics are able to kill bacteria by inhibiting a step in the synthesis of peptidoglycan.

REFERENCES

 1. Pandey V. K., Bishnoi A., Saxena R., Joshi M. N., Bajpai S. K.: Indian J. Chem. *41*, 1978 (2002).
 2. Kucukbay H., Durmaz R., Orhan E., Gunal S.: Il Farmaco *58*, 431 (2003).
 3. Perišić-Janjić N. U., Podunavac-Kuzmanović S. O.: J. Planar Chromatogr. *21*, 135 (2008).
 4. Perišić-Janjić N. U., Podunavac-Kuzmanović S. O., Balaž, J. S., Vlaović Dj.: J. Planar Chromatogr. *13*, 123 (2000).
 5. Podunavac-Kuzmanović S. O., Cvetković D. M.: Centr. Eur. J. Occupat. Environ. Med.. *12*, 55 (2006).
 6. Podunavac-Kuzmanović S. O., Markov S. L.: Centr. Eur. J. Occupat. Environ. Med. *12*, 61 (2006).
 7. Podunavac-Kuzmanović S. O., Leovac V. M., Perišić-Janjić N. U., Rogan J., Balaž J.: J. Serb. Chem. Soc. *64*, 381 (1999).
 8. Podunavac-Kuzmanović S. O., Cvetković D.: J. Serb. Chem. Soc. *75*, 381 (2007).
 9. Podunavac-Kuzmanović S. O., Markov S. L., Barna D. J.: J. Theor. Comp. Chem. *6*, 687 (2007).
10. Ozden S., Atabey D., Yildiz D., Goker H.: Bioorg. Med. Chem. *13*, 1587 (2005).
11. Pandey V.K., Upadhay M., Dev Gupta V.,Tandon M.: Acta Pharm. *55*, 47 (2005).
12. Garuti L., Roberti M., Cermelli C.: Bioorg. Med.Chem. Lett. *9*, 2525 (1999).
13. Pandey V. K., Joshi M. N., Tandon M., Bajpai S.K.: Acta Pharm. *50*, 293 (2000).
14. Pandey V. K., Tusi Z., Tusi S., Joshi M.N., Bajpai S.K.; Indian J. Het. Chem. *111*, 309 (2002).
15. Gata L., Perna F., Figura N., Ricci C., Holton J., D′Anna L., Miglioli M., Vaira D.: J. Antimicrob. Chemother. *51*, 439 (2003).
16. Nguyen P. T. M., Baldeck J. D., Olsson J. R., Marquis R. E.: Oral Microbiol. Immunol. *20*, 93 (2005).
17. Kus C., Ayhan-Kilcigil G., Can-Eke B., Iscan M.: Arch. Pharm. Res. *27*, 156 (2004).
18. Ayhan-Kilcigil G., Kus C., Coban T., Can-Eke B., Iscan M.: J. Enz. Inhib. Med. Chem. *19*, 129 (2004).
19. Mohamed B. G., Hussein M. A., Abdel-Alim A. M., Hashem M.: Arch. Pharm. Res. *29*, 26 (2006).
20. Ayhan-Kilcigil G., Altanlar N.: Turk. J. Chem. *30*, 223 (2006).
21. Soderlind K. J., Gorodetsky B., Singh A., Bachur N., Miller G., Lown J.: Anti Canc. Drug Des. *14*, 19 (1999).
22. El-Hawash S. A., Badawey E. A., Kappe T.: Pharmazie *54*, 341 (1999).
23. Nakano H., Inoue T., Kawasaki N., Miyataka H., Matsumoto H., Taguchi T., Inagaki N., Nagai H., Satoh T.: Chem. Pharm. Bull. *47*, 1573 (1999).
24. Fukuda T., Saito T., Tajima S., Shimohara K., Ito K.: Arzneim.-Forsch./Drug Res. *34*, 805 (1984).
25. Demirayak S., Abu-Mohsen U., Cagri Karaburun A.: Eur. J. Med. Chem. *37*, 255 (2002).
26. Rida S. M., El-Hawash S. A., Fahmy H. T., Hazzaa A. A., El-Meligy M. M.: Arch. Pharm. Res. *29*, 826 (2006).
27. Vlaović Đ., Čanadanović-Brunet J., Balaž J., Juranić I., Đoković D., Mackenzie K.: Biosci. Biotech. Biochem. *56*, 199 (1992).
28. National Committee for Clinical Laboratory Standards, *NCCLS Approval Standard Document M2-A7*. Vilanova, Pa, U.S.A. 2000.
29. National Committee for Clinical Laboratory Standards, *NCCLS Approval Standard Document M7-A5*. Vilanova, Pa, U.S.A. 2000.

P84 CHEESE SPECIES IDENTIFICATION BY MULTIVARIATE ANALYSIS OF ELEMENTAL DATA

MARTIN POLOVKA, MILAN SUHAJ AND MÁRIA KOREŇOVSKÁ

Department of Chemistry and Food Analysis, VÚP Food Research Institute, Priemyselná 4, P. O. Box 25, 824 75 Bratislava, Slovak Republic,
polovka@vup.sk

Introduction

To guarantee cheeses' authenticity, responsible food control authorities need to dispose of reliable analytical traceability techniques that enable to check whether the products are correctly described and labelled, or not.

In the recent years, extensive literature data on the methods of analysis applicable to the detection of mixtures of milk from different species either in raw or even in processed milk products are available. A large number of methods are applicable to detect the presence of different milk species in cheeses, as well.[1–4]

Multivariate analysis represents valuable tool, making possible the categorization of different food samples via the consideration of many variables that can be measured, often in a single analytical level. In addition, multivariate analysis of chromatographic, electrophoretic or elemental data is considered to be the powerful method for the discrimination of cheeses based on the different geographical origin, varieties and quality or for the consideration and monitoring of cheese maturation.

As follows from previously published data, the concentration ranges of some elements in milk and cheese are strongly dependent on animal species and feeding, season of sample collection, environmental conditions and manufacturing processes, as well.[5–11] Coni et al. revealed, that the concentration of selected trace elements (e. g., of Al, Ba, Cd, Co, Cr, Cu, Fe, Mg, Mn, Ni, Pb, Pt, Sr and Zn) differ significantly for sheep and goat milks and for their related products[5]. The mineral composition of ewes', cows', and goats' milk and of samples of different pure-milk cheeses made from them was analysed by Martin-Hernandéz using the stepwise discriminant analysis, reaching the 76 % correct classification of cheeses according to milk species[6]. Another statistical study dealt with the comparison of metal composition of different types of milks based on the presence of Se, Fe, Cu, Zn, Na, K, Ca, Mg, brought 98% correct classification of the samples for each type of milk[7]. Discriminant analyses of some elemental data were successfully used by Koreňovská et al. for the identification of cheeses' region of origin.[8–10] Using the same approach, 94.1 % of Mahon cheese samples were correctly classified into traditional and industrial groups, and 89.7 % of samples into fresh, half-ripened, ripened and old-ripened groups. [11]

As follows from the above-presented data, the authentification of cheeses using the elemental markers requires reliable data, obtained by analytical methods of high specificity and sensitivity, e. g. by atomic absorption spectrometry (AAS).

In this paper, the identification and discrimination of cows', sheeps' and goats' cheeses from different Slovak regions using the selective elemental data and pattern recognition analysis is presented.

Experimental

Samples Characterisation

Commercially available samples of 54 cow hard cheeses of Emmental and Edam type, 116 sheep (40 hard and 76 bryndza type) and 20 goat cheeses, all of the Slovak origin were analyzed to the content of selected elemental markers (Ba, Cr, Cu, Hg, Mg, Mn, Ni and V) by AAS. These markers were chosen on the base of geochemical characterization of Slovak regions[12].

Reagents

All chemicals were of analytical grade. Nitric acid of suprapure quality and stock solutions of respective metal (Ba, Cr, Cu, Hg, Mg, Mn, Ni, and V at the concentration of 1.00 g dm^{-3}, each) were purchased from Merck (Darmstadt, Germany). Lanthanum chloride (5%) used as ionic suppressor was delivered from SMÚ (Bratislava, Slovakia).

AAS Conditions

Respective cheese sample (0.5 g) was digested in a mixture of 4 ml of 65 % HNO$_3$ and 0.5 ml H$_2$O$_2$, using the Milestone MLS 1200 MEGA (Sorisole, Italy) microwave digestion system.

Perkin Elmer 4100 atomic absorption spectrometer (Norwalk, CT, USA) equipped with a deuterium lamp background-correction system and HGA 700 graphite tube atomizer with pyrolytically coated graphite tubes and flame was used. The presence and concentration of Mg and Mn metals were determined from atomic spectrometry measurements, using an air/acetylene flame. Metal elements of Ba, Cr, Cu, Ni, and V were detected on graphite tube atomizer, as previously described by Koreňovská and Suhaj.[8–10]

The accuracy of results was verified by standard addition method. The accuracy of method used for metal elements determination was estimated by means of two reference materials (NCS ZC 73008, rice and NCS ZC 73013, spinage) to be 98–125 %. Recovery of the method was assessed by the analysis of fortified cheese samples; mean recoveries of elements reached 96–109 %. Finally, the combined standard uncertainty was 5.3–14 %.

Determination of Hg

For the determination of mercury in cheeses, single – purpose mercury analyser AMA 254 (Altech, Prague, Czech Republic) was used. The BCR-150 skim milk powder (Brussels, Belgium) served as reference material.[8–10]

S t a t i s t i c s

Multivariate statistical methods, e.g., cluster analysis, factor analysis, and canonical discriminant analysis, were performed using the Unistat® software.

Results

Fig. 1. shows the preliminary predisposition of cows', sheeps' and goats' cheese samples under the study to natural grouping, obtained by hierarchical cluster analysis of determined elemental markers. Clusters were constructed using Ni, Cu and Mg variables, as they were found to have the most discriminating impact on cheeses distinction. As follows from data presented, samples are grouped into two major clusters: the first one correspond mostly to sheeps' cheeses and the second to cow and goat cheese samples, respectively.
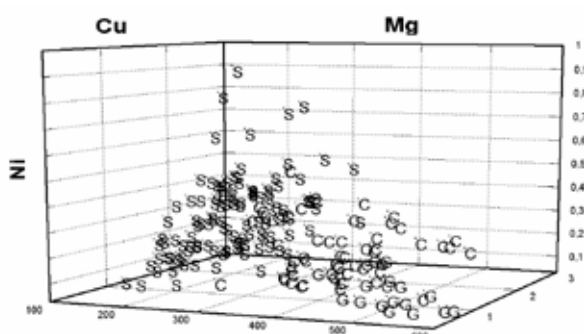
Fig, 1.   **Cluster graph of sheeps' (S), cows' (C) and goats' (G) cheeses, constructed using the Ni, Cu and Mg content as variables. Distance measure: Block; Method: Median**

Although there is a clear differentiation tendency, both groups of clusters contain some incorrectly classified samples. In order to achieve the better differentiation of examined cheese species, factor analysis using the principal component factoring with the varimax-rotation was performed to describe the main variations between the Ba, Cr, Cu, Hg, Mg, Mn, Ni and V content.

Using this approach, mathematical model explaining the mutual correlation between a large set of variables was
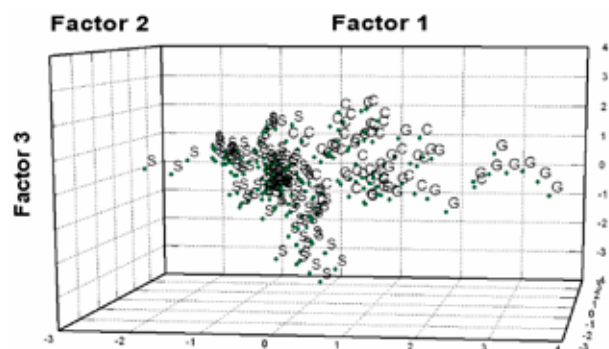
Fig. 2.   **Principal component factoring of sheeps' (S), cows' (C) and goats' (G) cheeses; Rotation: Varimax; Variables selected: Ba, Cr, Cu, Hg, Mg, Mn, Ni and V**

constructed. As we found, first factor, related mainly to the content of Hg, Mg and Ni, explain 26 % of the total markers' variation; the second one (18.5 %) is strongly influenced by Cu and Mn variability, and the last factor (15.4 %) by the variability of Ba and V. These three factors sufficiently explain more than 60 % of overall elemental data variations. Visualisation of data obtained (Fig. 2.) suggest, that the most effective differentiation of cows', sheeps' and goats' cheeses can be achieved following the first factor axis.

Results of canonical discriminant analysis (Fig. 3.) demonstrated very high potential to distinguish the differences among the cows', sheeps' and goats' cheeses.
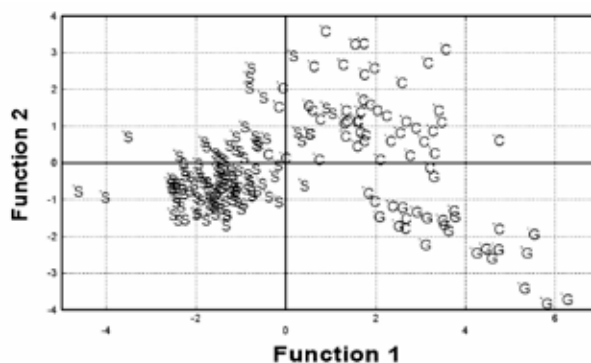
Fig. 3.   **Canonical discriminant analysis of sheeps' (S), cows' (C) and goats' (G) cheeses; Plot of discriminant score; Variables selected: Ba, Cr, Cu, Hg, Mg, Mn, Ni and V**

Discriminant functions correctly classified 92.6 % of all samples according to the species' origin. First discriminant function reveals the highest canonical correlation (89.5 %) and explains up to 83.6 % of the total variance. As follows from the values of standardized coefficients, Mg, Mn and Ni markers most significantly influence the discrimination at first function, whereas for the second discriminant function, the presence of Cu and Hg is essential.

In addition, K[th]-neighbour discriminant analysis provided 100 % correctness of samples classification at k = 1; and 91.1 % at k = 2. Stepwise discriminant analysis, which sorts the used markers according to their descending influence on the discrimination, gives the following order: Mg, Cu, Ni, Mn, Hg, V, Ba and Cr.

Some of the markers used in this work, e.g. Cu, Mg, and Mn, were previously successfully used for cheeses' origin authentification also by other authors.[5–7,13,14] Significant discrimination of cheeses' species presented in this work can be effectively explained by the geochemical differences in sheeps', cows' and goats' pasture soils. Sheeps' pastures are located in the mid-mountain regions whereas cows' and goats' ones are to be found predominantly in lowland agricultural areas. Thus, the content of minerals and other trace elements in feeding diet vary significantly, subsequently influencing their content in cattle milk and milk products.

Conclusions

Multivariate statistical methods of elemental markers analyses involving both the principal factor analysis and canonical discriminant analysis represent effective tools to discriminate Slovak commercial cows', sheeps' and goats' cheeses and to identify their origin. Results obtained enable the development of simple and rapid protocols for cheeses' classification and quality ensurance.

REFERENCES

1. Commission Regulation (EC) No 1081/96. *Official Journal of the European Union*, *L 142*, 15 (1996).
2. Moio L., Chianese L., Rivemale M., Addeo F.: Lait *72*, 87 (1992).
3. Addeo F. L., Moio L., Chianese - Nota G.: Ital. J. Food Sci. *1*, 71 (1989).
4. Moio L., Sasso M. L., Chianese L., Addeo F.: Ital. J. Food Sci. *3*, 185 (1990).
5. Coni E., Bocca A., Copplelli P., Caroli S., Cavallucci C., Marinucci M. T.: Food Chem. *57*, 253 (1996).
6. Hernández C. M., Amigo L., Martín-Alvarez P. J., Juárez M.: Z. Lebensm. Forsch. *194*, 541 (1992).
7. Rodríguez E. M., Alaejos M. S., Romero C. D.: J. Agric. Food Chem. *47*, 1520 (1999).
8. Koreňovská M., Suhaj M.: Eur. Food Res. Technol. *225*, 707 (2007).
9. Koreňovská M., Suhaj M.: Eur. Food Res. Technol. *221*, 550 (2005).
10. Suhaj M., Koreňovská M.: J. Food Nutr. Res. *46*, 174 (2007).
11. Frau M., Simal S., Femenia A., Rosselló C.: Z. Lebensm. Forsch. *207*, 164 (1998).
12. Čurlík J., Šefčík P.: Geochemical Atlas of the Slovak Republic. Part V: Soils. Soil Science and Conservation Research Institute, Bratislava (1999).
13. Rincon F., Moreno R., Zurera G., Amaro M.: J. Dairy Res. *61*, 151 (1994).
14. Fresno J. M., Prieto B., Urdiales R., Sarmiento, R. M., Carballo J.: J. Sci. Food Agric. *69*, 339 (1995).

P85 OPTIMALIZATION OF METHOD FOR QUANTIFICATION OF *STREPTOCOCCUS* MUTANS TO DENTAL MATERIALS

ILONA PRUDÍKOVÁ, STANISLAVA MATALOVÁ and JOSEF JÁNČÁŘ

Faculty of Chemistry, Brno University of Technology Purkyňova 118, 612 00 Brno, Czech Republic,
xcprudikova@fch.vutbr.cz

Introduction

The attachment of certain microorganisms to specific surfaces in the human oral cavity and the resulting formation of dental plaque on teeth and dental materials are primary causes for oral diseases such as denture stomatitis, gingival inflammation, and secondary caries, which may consequently lead to unhealthy complications[1]. Secondary caries is the most frequent reason for the replacement of restorative materials including resin composites. That is reason, why antimicrobial agents are incorporated and bacterial adhesion has to be measured.

In the literature, several methods for quantification of deposited oral microorganisms were described, but a lot of them could be characterized as time, materials, instruments and financially – consuming.

The amount of sorbed bacteria could be expressed using radio-labelled microorganisms. Cells were radio-labelled using $[3H]$ – thymidine[2–7], $[3H]$ – uridine or $[35S]$ – methionine. The amount of adsorbed bacteria was measured in a scintillation counter and was determined as radioactive counts per minute (CPM) of the labelled bacteria after washing them with buffer (KCl) to remove unbound bacteria.

Other tests for microorganisms quantification were carried on examine dental materials. Discs from this dental materials were inserted in petri dishes or tubes that contained cell suspension and than they were incubated for 24 hours. After incubation discs were removed and rinsed with distilled water or PBS. Adherent bacteria were fixed with methanol or glutaraldehyd and stained with acridine orange, crystal violet or modified Gram stain. Quantitative analysis was performed using a fluorescence microscope. The number of adherent cells in several random fields was counted on each sample and bacterial adhesion was expressed as percentage area coverage[8].

These methods were used the most often, but except them, other minor methods were tested. Capopreso at.al.[9] analysed bacterial adhesion to dental alloys spectrophotometrically in a microplate reader at 570 nm. The bacterial adhesion of each specimen was quantified as the ratio between the optical density at 570 nm and the surface area of the specimen. Blunden[9], Duskova[10,11] expressed the amount of deposited microorganisms as percentage weight gain. Wu-Yuan[12] and Wilbershausen[13] examined the attachment of oral bacteria by SEM. For SEM, the samples were fixed in formaldehyd or glutaraldehyd and dehydrated through a graded series of aceton or ethanol. Boeckh[14] placed bacterial suspensions

in conical cavities within the material and after incubation, the suspensions were removed form the restoratives and the numbers of viable bacteria were counted.

F. Ozer at al. used for testing antibacterial activity Tooth cavity model. They prepared three cylindrical cavities in the flat surface of human extracted tooth. Cell suspension and brain heart infusion (BHI) broth were put in cavities and incubated for 24 h at 37 ºC. The number of *S. mutans* recovered was determined by the classical bacterial counting method using 5% sheep blood agar[8].

Experimental

The spectrophotometric Biuret method was used to quantified amount of bacteria *S. mutans* adhering to the polymer surface. In order to optimise Biuret method the composition of liquid culture medium, the amount of bacteria suspension used for the samples inoculation, the samples incubation time and methods for the bacteria releasing from the samples were tested.

Biuret Method

Under alkaline conditions substances containing two or more peptide bonds form a purple complex with copper salts in the reagent. Upon complexation, a violet color is observed. The absorbance of the Cu^{2+} protein complex is measured at 540 nm and compared to a standard curve. Bovine serum albumin is used as a standard. This method was employed for the quantification of the S. mutans in both culture medium and on the discs.

Biuret agent was prepared by dissolving 1.5 g $CuSO_4 \cdot 5H_2O + 6$ g $C_4H_4O_6KNa \cdot 4H_2O$ in 500 ml H_2O. 300 ml 10% NaOH was added to the solution and distilled water to make 1,000 ml.

When studying the amount of bacteria in the suspension following procedure was used: 1 ml of the tested suspension was mixed with 4 ml of Biuret agent and 1 ml distilled water. Upon 10 seconds shaking period and 30 minute incubation, absorbance was measured against a blank at 540 nm.

To evaluate the amount of bacteria adhered to the disc, the bacteria had to be released from the disc. The samples were placed into 2 ml distilled water and ultrasonic bath were used. The time of ultrasonic bath was varied up to 8 minutes (2, 4, 6 and 8 minutes) in order to find out conditions when both the highest amount of bacteria is released and still no damage of the disc occurs. Further the procedure is same as in case of quantification of bacteria in suspension.

Dental Materials and Prepare of Samples

The discs were prepared from the commercially available microhybrid composites (Adoro, Ivoclar Vivadent), D3MA resin-based materials (Advanced Dental Materials) and ceramic materials (Ivoclar Vivadent) as reference material.

The material was placed in a metal mold between a layer of transparent foil and metal. It was cured in the Vectris cur-

ing machine for 20 minutes at 60 °C, 460 nm. After curing, the discs were removed from the mold and sterilized in autoclave.

Microbial Work

An oral cavity isolant *Streptococcus mutans* P2093 has been chosen as a tested microorganism. *S. mutans* is oral bacteria, that is assumed to be the main infander of the dental caries. The bacterial strain *S. mutans* used in this study was clinical isolates from child mouth (obtained from prof. MUDr. Martina Kukletová, CSc., Brno Masaryk University). The microorganism was stored in commercially available Petri dish with Blood agar IMA VLAC and IMA VLGP (Laboratory of Medical Microbiology, Třinec).
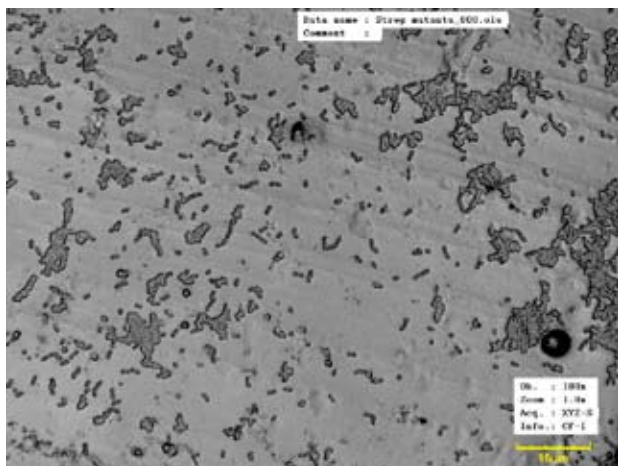
Fig. 1.   **S.mutans growing on composite polymer disc**

The microorganisms were cultivated in liquid culture medium BHIB. In order to improve the bacteria growth a certain amount of further source of sugar was added into the medium. 0.1; 1; 5 and 10 wt% of sacharose and glucose were tested.

The samples were prepared by placing the sterilized disc in 5 ml BHIB medium in test tube and inoculating with bacteria suspension. The appropriate volume of bacteria suspension and incubation time had to be tested. First one was tested by inoculation of 0.2; 0.4; 0.6; 0.8 a 1.0 ml of bacteria suspension into 5 ml BHIB and evaluation of bacterial growth. The incubation time was varied up to 28 hours and appropriated incubation time was evaluated from the growing curve.

Results

First of all the appropriate composition of the culture medium was investigated. 0,1; 1; 5 and 10 wt% of sacharose and glucose were added to BHIB and the influence of additives on bacteria growth were evaluated see Fig. 2. Best growing results were obtained for the medium with 1 wt% of glucose.

When testing the influence of inoculated volume on bacteria growth, the volume was varied up to 1.0 ml. The results are presented in Table I. The highest absorbance was mea-
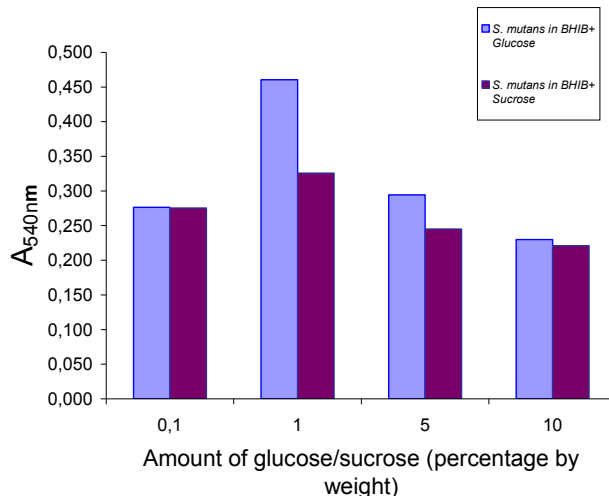
Fig. 2.   **S. mutans growing in BHIB with glucose or sacharose**

Table I
Influence of suspension volume on S. mutans growth

Inoculated volume [ml]	Absorbance [540 nm]
0.2	0.290
0.4	0.288
0.6	0.285
0.8	0.286
1.0	0.270

sured when using 0.2 ml of bacteira suspension. This volume was used for further testing.

Growing curve (Fig. 3.) presents influence of incubation time on the bacterial growth respectively on absorbance. It could be seen that the amount of bacteria increases with increasing of the incubation time until it reached maximal value. In our experiment the maximal absorbance resp. amount of bacteria was obtained for the samples incubated for 18 hours. When incubating the bacteria in medium for longer time the nutriens in medium are exhausted. This results in dying out of bacteria and thus decreasing of absorbance.
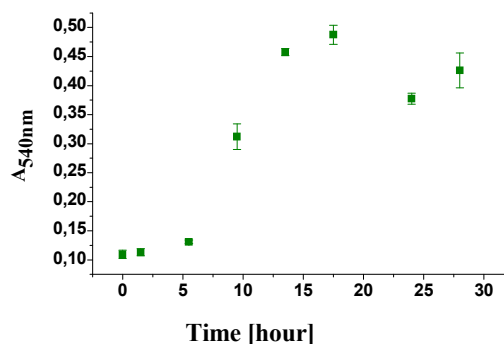
Fig. 3.   **S.mutans growing curve**

Finally appropriated method for releasing the bacterial cells from disc had to be worked out. The ultrasonic bath was used and the working time was varied up to 8 minutes. The amount of released bacteria and effect of ultrasonic waves on the tested material was evaluated see Fig. 4. The best results were obtained for the working time of 6 minutes. Longer working time causes irreversible material damage while shorter treatment time did not released all bacteria.
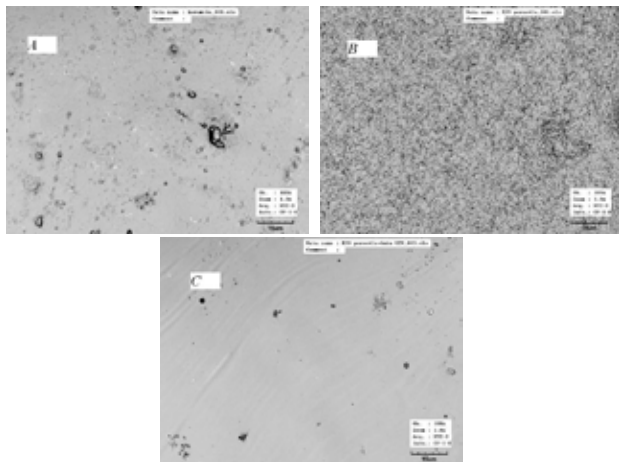
Fig. 4. **Ceramic materials: A = without *S. mutans*, B = with *S. mutans*, C = after ultrasonig bath for 6 minutes**

The main goal of this work was to find out appropriate method for the studying of the microbial adhesion to new dental materials. The spectrofotometric techniques based on Biuret reagent were employed. The method was optimised in order to fulfill requirements for further material testing.

According to our measurement the BHIB medium with 1 wt% of glucose gives the best growing results. Samples placed in BHIB-glucose medium was further inoculated with 0,2 ml of *S. mutans* suspension. This volume fulfil both requirement – low volume and good growing results. Further the appropriate incubation time was investigated. The highest absorbance was obtained for the samples incubated for 18 hours.

Finally time neccessary for releasing bacteria from the disc samples in ultrasonic bath was evaluated. The best results were obtained after 6 minutes. The highest amount of bactery was released while the disc still remained undamaged.

This optimised method will be employed for testing new dental materials. Our further studies will be focused on testing various antimicrobial additives that will improve microbial resistance of dental restorative materials.

REFERENCES
1. Buergers R., Rosentrirr M., Hande G.: *RUMC*, Regensburg, Germany
2. Steinberg D., Eyal S.: J. Dent. 30, (2002).
3. Saito T., Takatsuka T., Kato T., Ishihara K., Okuda K.: Archs. Oral Biol. 42, (1997).
4. Steinberg D., Mor C., Dogan H., Zacks B., Rotstein I.: Dent. Mater. *15*, 14 (1999).
5. Orstavik J., Orstavik D.: Acta Odontol. Scand. 42, (1982).
6. Fine D. H., Furgang, D., Kaplan J., Charlesworld J., Figursky D. H.: Arch. Oral Biol. 44, (1999).
7. Shahal Y., Steinberg D., Hirschfeld Z., Bronstheyn M., Kopolovic K.: J. Oral Rehabil. 25, (1998).
8. Matalová S.: Dissertation. Brno University of Technology, Brno, Czech Republic, 2004.
9. Blunden R. E., Orth D., Orth M., Oliver R. G., Okane C. O.: Brit. J. Orth. 21, (1994).
10. Dušková J., Broukal Z.: Česk. Stomat. 82, (1983).
11. Dušková J., Broukal Z.: Česk. Stomat. 84, (1984).
12. Capopreso S., Cerroni L., Frangini S., Barlattani A., Condo S. G.: Minerva Stomatol. 48, (1999).
13. Wu-Yuan Ch. D., Eganhouse K. J., Keller J. C., Walters K. S.: J. Oral Implant. 21, (1995).
14. Willershausen B., Callaway A., Ernst C. P., Stender E.: Inter. Dent. J. 49, (1999).

P86　BROMINATED FLAME RETARDANTS PROFILES IN BREAST MILK AND ADIPOSE TISSUE SAMPLES: CASE STUDY CONCERNED WITH CZECH POPULATION

JANA PULKRABOVÁ, PETRA HRÁDKOVÁ, MICHAELA NÁPRAVNÍKOVÁ, JANA HAJŠLOVÁ and JAN POUSTKA

ICT, Prague, Department of Food Chemistry and Analysis
Technická 3, 166 28 Prague 6, Czech Republic,
jana.pulkrabova@vscht.cz

Introduction

Brominated flame retardants (BFRs) are chemicals that are extensively used in various polymers and especially in electronic equipment, plastics, electronic, textiles and other furniture[1]. Due to their persistence and bioavailability in combination with their large consumption and disposal, they are becoming emerging environmental contaminants. Now they have become ubiquitous in the environment and magnify in the biological tissue as seen in classical organochlorine compounds (OCs).

The Czech population body burden of halogenated persistent organic pollutants (POPs) is of a great concern due to incautious handling of hazardous chemicals in the past time. A monitoring of human matrices, including polybrominated diphenyl ethers (PBDEs) and hexabromocyclododecane (HBCD) has been employed for this purpose in the recent decade.

The main aim of the presented study was to investigate levels and profiles of (*i*) BFRs represented by PBDEs and HBCD and (*ii*) "classical" organochlorine contaminants occurring in the adipose tissue of people living in the Czech Republic and in human breast milk from Czech mothers. To our knowledge, this is the very first study reporting PBDEs levels in adipose tissue samples of Czech citizens together with similar studies conducted elsewhere in the world.

Experimental

B r e a s t　M i l k

Samples of breast milk were obtained from 56 Czech women living in Olomouc region (located in the north-east part of the Czech Republic) during the autumn 2007 in the co-operation with the Gynaecological-maternity Clinic, Faculty Hospital in Olomouc. The age of mothers participating in this study ranged from 21 to 45 years (mean and median 29 year). The breast milk was expressed manually into the glass bottles and stored at −18 °C until analysis according to WHO methodology.[2] The analytical procedure used for analysis of human breast milk samples was described in detail in our earlier study.[3,4]

H u m a n　A d i p o s e　T i s s u e

Adipose fat tissue samples for determination of selected POPs were collected from patients (n = 98) who underwent a tumescent liposuction for aesthetic reasons. The mean age of

the group was 35.5 years with a range of 17–60 years. The analytical procedure used for analysis of adipose tissue samples has been described in detail in our earlier study[5]; therefore, there is only a brief summary of procedure steps. Approximately 5 g of adipose fat tissue sample was homogenized with anhydrous sodium sulphate (20 g) and and extracted in a Soxhlet apparatus for 8 h using a hexane : dichlormethane mixture (1 : 1, v/v, 150 ml). The extract was rotary evaporated at 40 °C and residues were weighted for a lipid determination. An aliquot of isolated fat (cca 750 mg) was dissolved in 10 ml of an internal standard (PCB 112) solution (cyclohexane: ethylacetate, 1 : 1, v/v). Sample extracts were then purified on a Bio Beads S-X3 column using cyclohexane : ethylacetate (1 : 1, v/v) as a mobile phase. A fraction corresponding to a elution volume of 14–30 ml was collected.

Results

The first data on the occurrence of BFRs in Czech humans employing breast milk as a bioindicator matrix were reported by Kazda et al. in 2004[4], however, the information on the other major POPs, such as PCBs and DDTs was not provided.

An overview of the most abundant PBDE and PCB congeners together with OCP levels in both types of examined matrices collected in the Czech Republic within presented study is shown in Table I. The results clearly document ubiquitous occurrence of PBDEs emission sources in the environment of general Czech population.

BDE congeners 47 (tetrabromo-), 153 (hexabromo-) and 183 (heprabromo-) were predominant and accounted up to 80 % of the total PBDEs. Other relatively abundant representatives of this group were congeners BDE 99 and 100 (both pentabromo-). BDEs 28, 49, 66, 85 and 154 were detected only in several samples, mostly close to the limit of quantification.

Interestingly, PBDE profile in human adipose tissue found in our present study was not identical to that one observed in breast milk samples. While in the latter matrix BDE 47 was the most abundant congener followed by BDE 153, opposite ratio of these major PBDEs was found in adipose tissue samples (see Fig. 1.). Biotransformation and accumulation kinetic properties of individual PBDE congeners after human exposure may contribute to these differences. As shown in Fig. 1., a similar trend was observed in a recent Japanese study[6], while this was not reported in a study conducted in Sweden, which documented, in both human milk and adipose tissue, the levels of BDE 47 to be approximately 4-times higher than BDE 153. The use of Penta-BDE technical mixture with a majority of BDE 47 was probably dominating in this country[7]. In this Scandinavian country this difference could be attributed to different uses of these products or a different in the diet of individuals. On the other hand, no significant differences were found by a comparison PCB profiles in both examined matrices.

Table I
Levels of PBDEs, PCBs and OCPs determined in breast milk and adipose tissue collected in the Czech Republic during the year 2007 (ng g^{-1} lipid)

Analyte	Breast milk (n = 56)		Adipose tissue (n = 98)	
	Mean	Median	Mean	Median
BDE 28	0.31	0.12	0.1	0.05
BDE 47	1.52	1.11	1.1	0.7
BDE 49	0.22	0.14	0.05	0.05
BDE 66	0.13	0.13	0.1	0.05
BDE 85	0.19	0.12	0.05	0.05
BDE 99	0.73	0.53	0.5	0.2
BDE 100	0.3	0.17	0.5	0.3
BDE 153	0.54	0.21	1.3	1
BDE 154	0.14	0.11	0.2	0.1
BDE 183	0.32	0.15	0.7	0.4
BDE 209	2.93	1.52	5.4	<2
HBCD	0.22	0.13	1.2	<0.5
PCB 28	2.3	1.56	2	1.8
PCB 52	2.36	1.64	1.6	1.3
PCB 101	2.73	2.34	4.2	1.9
PCB 118	17.84	13.43	17.7	14.3
PCB 138	143.61	119.84	121.6	110.1
PCB 153	229.81	202.76	233.6	219.8
PCB 180	192.98	166.67	245	230.7
HCB	40.78	34.72	120.4	72.1
b-HCH	11.28	8.31	23.9	17.5
p,p´-DDE	178.95	148.81	582.5	478.8
p,p´-DDD	4.26	3.94	1.7	1.3
p,p´-DDT	22.04	16.64	24.9	20.4
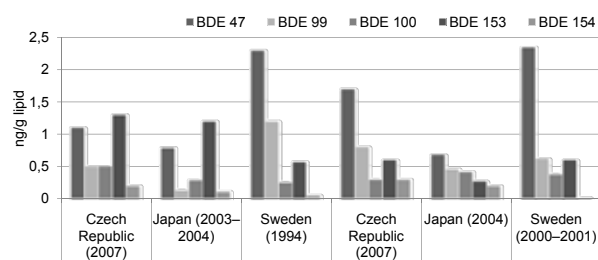
Fig. 1. **PBDE congener profile in both examined matrices from various countries**

Generally, based on available studies, PBDE levels in breast milk and adipose tissue samples collected within this study were comparable to those reported in other European countries but considerably lower (by almost one order of magnitude) than results from the United States, probably due to a less extensive use of this group of BFRs in common goods and products[6-11].

As compared to PBDEs, the levels of OCs (PCBs and OCPs) were up to 2–3 orders of magnitude higher, obviously, due to a relatively longer history of their intensive use in a wide range of areas. Although PCBs, DDT and several other persistent OCs were banned many decades ago, and, in spite of their decline witnessed in the Czech Republic alike worldwide, these POPs are still persisting in very high quantities in the environmental compartments. Not surprisingly, their transfer into the food chain still continues, what was documented also in this study. The OCs pattern found in Czech breast milk was: PCBs>DDTs>HCB>HCHs. The following PCBs profile was found: CB 153>CB 138>CB 180> CB 118>CB 101 ~ CB 52 ~ CB 28. The dominating PCB congeners No. 153, 138 and 180 contributed together to the total PCBs content by almost 80 %.

Regarding to other chlorinated POPs, p,p´-DDE was their major representative in all analyzed samples. The contamination input in the food chain obviously occurred many years ago since the parent compound, p,p´-DDT, was significantly lower. Other OCPs like HCB (hexachlorobenezene) and β-HCH (hexachlorocyclohexane), were apparently in all samples at levels above LOQs (see Table I).

The levels of PCBs were similar to those found in other European countries. While no age dependency was found for PBDEs, an increase of PCB and OCP levels with age was observed. Different exposure routes of donors were documented by the absence of the relationship between PCBs and OCPs.

Conclusions

This study reports the residue levels of PBDEs and HBCD together with "classical" OCs in human adipose tissue and breast milk samples obtained in the Czech Republic.

The results clearly show the ubiquitous occurrence of BFRs in the general Czech population, BDE 153 and BDE 47 being the most abundant congeners in examined biotic samples. Despite its broad use, BDE 209 was detected in only a few adipose tissue samples.

The mean values of PBDEs in human fat from Czech donors did not largely differ from those recorded from other European countries

Also PCB and OCP levels were comparable to those reported in similar studies conducted outside of the Czech Republic. It should be noted that the production and use of PCBs has been banned for three decades, whereas the use and production of PBDEs still continues. In spite of the fact, that penta- and octa-BDE technical mixtures were banned in the EU four years ago, humans are still exposed in their daily lives from food and emissions from various products into their environment.

REFERENCES

1. de Wit C. A.: Chemosphere *46*, 583 (2002).
2. World Health Organization, 1991.
3. Čajka T., Hajšlová J.: Bull. Environ. Contam. Toxicol. *70*, 913 (2003).

4. Kazda R., Hajšlová J., Poustka J.,Čajka T.: Anal. Chim. Acta *520*, 237 (2004).
5. Hajšlová J., Pulkrabová J., Poustka J., Čajka T., Randák T.: Chemosphere *69*, 1195 (2007).
6. Kunisue T., Takayanagi N., Isobe T., Takahashi S., Nose, Yamada T., et al.: Environ. Inter. *33*, 1048 (2007).
7. Guvenius D. M., Bergman Å., Norén K.: Arch. Environ. Contam. Toxicol. *40*, 564 (2001).
8. Eslami B., Koizumi A., Ohta S., Inoue K., Aozasa O., Harada K. et al.: Chemosphere *63*, 554 (2006).
9. Kalantzi O. I., Martin F. L., Thomas G. O., Alcock R. E., Tang H. R., Drury S. C., et al.: Environ. Health Perspect. *112*, 1085 (2004).
10. Lind Y., Darnerud P. O., Atuma S., Aune M., Becker W., Bjerselius R., et al.: Environ. Res. *93*,186 (2003).
11. Johnson-Restrepo B., Kannan K.; Rapaport D. P., Rodan B. D.: Environ. Sci. Technol. *39*, 5177 (2005).

P87　IODINE IN MILK ON THE CZECH MARKET

RADEK KAVŘÍK, IRENA ŘEHŮŘKOVÁ and JIŘÍ RUPRICH

National Institute of Public Health – Centre for Hygiene of Food Chains, Palackého 3a, 612 42 Brno, Czech Republic
kavrik@chpr.szu.cz

Introduction

Iodine is an essential trace element. Biological role of this trace element is related to the hormonal system of thyroid gland where iodine is a constituent of thyroid hormones. Therefore iodine is very important element also for human population. Natural sources of iodine are e.g. seaweed, seafood and also plants grown on iodine-rich soil[1].

Iodine deficit is typical problem for areas where there is low content of iodine in the diet especially in areas where seafood consumption is low[2]. It is well known that Europe and therefore also the Czech Republic belong between countries with known iodine deficiency. Usual public health protection measure is fortification of salt with iodine.

Many studies have been published about problem of dietary intake of iodine for the Czech population. Summary study about situation in the Czech Republic published Scientific Committee on Food in 2007[3].

The National Institute of Public Health in Prague, Centre of Hygiene of Food Chains in Brno is involved in "The Project on Dietary Exposure to Selected Chemical Substances"[4]. The objective of the project is to describe the dietary exposure of the population of the Czech Republic. In the framework of this project iodine has been monitored since 1998.

Since year 2000 to 2003 has been observed increasing trend of iodine intake. This effect causes mainly usage of fortified salt in kitchen and during industrial food processing. Doses observed in the 2003 reached 3.59 μg kg^{-1} b.w./day (230 μg/person/day)[5]. This value matches 153 % of recommended daily intake by Czech law (Regulation 446/2004).

As a biomarker of short term (24 hours) intake of iodine the urinary level is mostly used. The National Institute of Public Health in Prague and some other institutes monitor urinary level of iodine for many years. It was recognized that average iodine concentration in adult's urine increased from 85 μg dm^{-3} to 251 μg dm^{-3}(ref.[6]) during years 1995–2005.

This increase can be attributed to some specific foods in our diet. High concentrations of iodine were measured in fish, meat products, instant soups, milk and milks products. It was recognized that significant exposure sources are mainly milk and milks products, bread, meat products and eggs (descending order to total exposure dose).

Probabilistic modelling was used to estimate usual daily intake of iodine from various kinds of foodstuffs for age groups in the Czech population[3,7]. It was observed that milk is the most important source of iodine for various age groups in the Czech Republic. Results of that modelling (it did not take added salt after cooking into account) also support an idea that high intake of iodine can be a certain risk for young children (< 10 years) where milk and dairy produces represent very important parts of their diet[7].

That was the reason why our laboratory focused its research on iodine concentration in marketed consumer milk.

Experimental

Twice a year, in May and November, 24 samples of milk (12 semi-skimed and 12 skimed milks) were purchased from markets in twelve towns in the Czech Republic. These samples were analyzed as one composite sample. Milk samples have been also analysed as individual samples since 2007 to get better imagination about distribution of iodine concentrations.

For determination of iodine was used Sandell-Kolthoff method. The principle of this method is in catalytic function of iodide in oxidation-reduction reaction Ce(IV) and As(III).

Samples are transferred to refractory glass tube. Solutions of potassium hydroxide and zinc sulphate are added. These mixtures are stirred and tubes are placed in an oven at 105 °C to dry the samples and then in a cold muffle furnace where are left until temperature gradually rises to 600 °C. The tubes are taken out. At this stage the food samples are not completely digested. The samples are soaked with 0.5 ml of water and then placed in a cold muffle furnace and digestion process is repeated. Now the samples are completely digested. Into each tube containing the digest, 6 ml of water is added and stirred to dissolution of the water-soluble part of the digest. The suspension is transferred into a centrifuge tube and centrifuged for 10 min at 2500 rev min^{-1}.

Aliquot of the supernatant liquid is transferred to the glass tube and refilled with water to 2 ml. Then 2 ml of arsenic(III) solution is added and the tube is placed in the cooling bath (10 min). Then 2 ml of cerium(IV) solution is added and the tube is placed in the water bath at 40 °C (20 min) and then in the cooling bath (10 min). Then 0.5 ml of brucine is added and the tube is placed in an oven at 105 °C (15 min). After adding of every solution thorough stirring is important.

Finally, a light absorption is measured by spectrometer at 430 nm. Limit of quantification is 15 μg kg^{-1}. This method is accredited according to CSN EN ISO/EC 17025:2005 by the Czech Accreditation Institute.

Results

Average concentration of iodine in milk analysed since 1998 to 2007 is 268 μg kg^{-1}. The results are shown in Fig. 1. Average concentration of iodine in milk composite samples has been higher since 2003.

In 2007, after publishing of results clarifying a key role of milk in iodine intake, we analyzed all of 24 samples from the Czech market individually. Results for semi-skimed milks are shown in Fig. 2. and for skimed milk in Fig. 3. Semi-skimed milk from town No. 7 (May, 07) has not been determined.

Average content of iodine in semi-skimed milk was 344 μg kg^{-1} in May and 277 μg kg^{-1} in November. Average
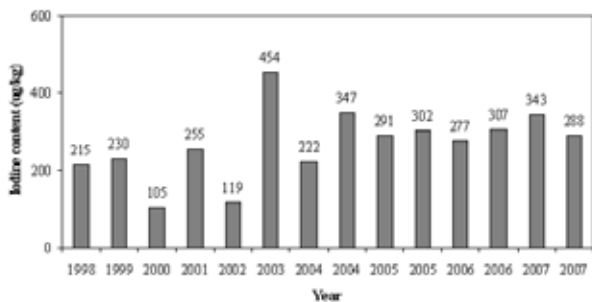
Fig. 1. **Average iodine content in milk (1998–2007)**
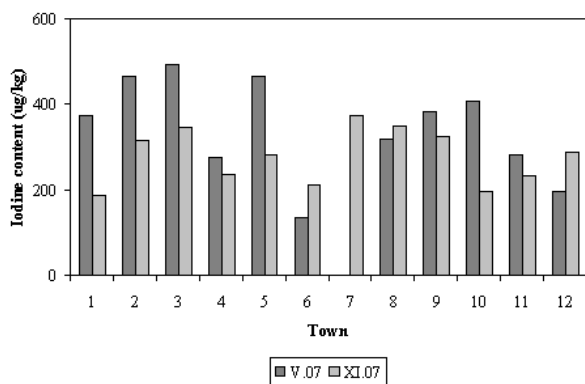
Fig. 2. **Iodine content in semi-skimed milk (2007)**
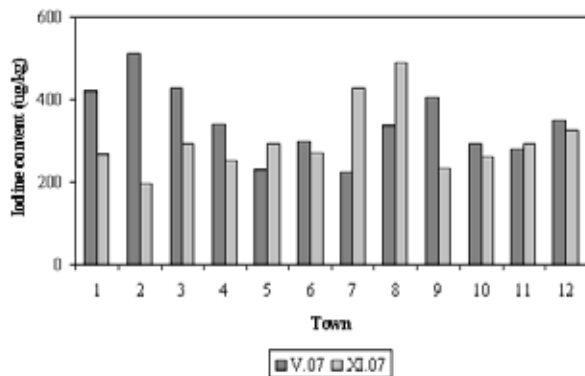
Fig. 3. **Iodine content in skimed milk (2007)**

content of iodine in skimed milk was 343 µg kg⁻¹ in May and 299 µg kg⁻¹ in November. These data can signalize decreasing trend of iodine content in milk available at the Czech market in 2007 in comparison to previous years. Semi-skimed milk contain slightly higher average amount of iodine than skimed milk. Fig. 2. and Fig. 3. show relatively high concentration variability between individual milk samples. Maximal concentration of iodine in milk was 509 µg kg⁻¹ (skimed milk, XI/07, town No. 2) and minimal concentration was 135 µg kg⁻¹ (semi-skimed milk, V/07, town No. 6) in year 2007.

Conclusions

The dietary intake of iodine has monitored since 1998. The monitoring of the dietary exposure requires information about iodine content in individual foodstuffs and extends of their consumption[7]. At the present information is available and therefore we can calculate both a point and a probabilistic estimate of intake for different age categories of the Czech population.

It was found that milk is the most important source of iodine which can present certain health risk for high consumers mainly for children. According to the EC Regulation No. 1459/2005 allowed amount of iodine in complete feed for dairy cows and layers decreased from 10 mg kg⁻¹ to 5 mg kg⁻¹. Results of feed control are not known at the moment in the Czech Republic. Then samples of milks have been analysed individually since 2007 to clarify possible exposure doses dominy from milk.

Average content of iodine in milk (period 1998–2007) was 268 µg kg⁻¹. Over the last years was this value about 300 µg kg⁻¹. Average content of iodine in milk in May and November 2007 was 343 µg kg⁻¹ and 288 µg kg⁻¹ respectively. We found large variability of concentrations between individual milk samples. High concentration variability can be problem for food operators and also for consumers due to not standard iodine content (e.g. production of infant and baby milk formulas). Optimal content of iodine in milk in context of overall dietary exposure is about 200 µg kg⁻¹. It would be advantage for all to keep variability of iodine content in individual milk samples as much as close to this value.

Optimal iodine intake is important for good health of Czech population. The most endangered group is children. These are reasons why monitoring of iodine content in individual samples of milk from the Czech market will continue.

REFERENCES

1. *Iodine*, http://en.wikipedia.org/wiki/Iodine, loaded May 14, 2008
2. *Sources of iodine*, International Council for the Control of Iodine Deficiency Disorders, http://www.iccidd.org/pages/iodine-deficiency/sources-of-iodine.php, loaded May 15, 2008.
3. Ruprich J., Řehůřková I.: *Informace vědeckého výboru pro potraviny ve věci: Jód, část I: obvyklý dietární přívod pro populaci ČR*, Státní zdravotní ústav, Centrum hygieny potravinových řetězců Brno, 2007, http://www.chpr.szu.cz/vedvybor/dokumenty/informace/Info_2006_18_deklas_JOD%20cast1.pdf.
4. Ruprich J.: *The Health Risk Assessment of Dietary Exposure to Selected Chemical Substances in year 2002*. National Institute of Public Health, Prague 2003.
5. Ruprich J. a kol.: *Zdravotní důsledky zátěže lidského organizmu cizorodými látkami z potravinových řetězců v roce 2003, Odborná zpráva za rok 2003,* Státní zdravotní ústav Praha, 2003, http://www.chpr.szu.cz/monitor/tds03c/tds03c.htm.

6. *Biologický monitoring – Odborná zpráva za rok 2006*, Státní zdravotní ústav Praha, 2006 http://www.szu.cz/tema/zivotni-prostredi/odborne-zpravy-1.

7. Ruprich J, Dofková M., Řehůřková I., Slaměníková E., Resová D.: *Individuální spotřeba potravin - národní studie SISP04*, Státní zdravotní ústav, Centrum hygieny potravinových řetězců Brno http://www.chpr.szu.cz/spotrebapotravin.htm.

P88 MONITORING OF MERCURY CONTENT IN THE FOOD BASKET FOR THE CZECH POPULATION DURING 1994–2007

J. ŘEHÁKOVÁ, I. ŘEHŮŘKOVÁ, J. RUPRICH, J KALVODOVÁ and D. MATULOVÁ

National Institute of Public Health – Centre for the Hygiene of Food Chains, Palackého 3a, Brno 612 42 Czech Republic,
rehakova@chpr.szu.cz

Introduction

Mercury belongs to group of heavy metals. In nature mercury can be found in various forms (organic and inorganic compounds, elementary Hg^0) with different toxicity. For human organism all mercury forms can be toxic. The most important and the most danger forms are alkyl-mercury compounds like methylmercury (MeHg) and inorganic compound like Hg^{2+}. The hazard is connected also with cumulative properties of mercury. The highest concentrations are measured in kidneys, liver and spleen.

Less frequent acute intoxication causes vomit, diarrhea and abdominal ache. More important is a risk of chronic intoxication. Exposure can lead to cerebral paralysis, cephalonia, deafness, blindness and high blood pressure (Minamata disease)[1]. MeHg as the most danger mercury form comes through blood-brain barrier and via placenta can be transported into fetal brain.

Main exposure routes for mercury are inhalation and digestion... Disputative question is long-term influence of amalgam fillings. Mercury is very well absorbed after oral exposure (95 % MeHg is absorbed). Due to potential health risks it is necessary to monitor the mercury content in foodstuffs of vegetable and as well as animal origin. Plants and animal contamination can be caused by growing in contaminated environment (industry wastes and exhalation). Important source of mercury exposure especially in seaside countries are fish.

Many studies have been published about the determination of mercury in foods. Centre for the Hygiene of Food Chains in Brno has been involved in the monitoring of the content of total mercury in foods (see "The Project on Dietary Exposure of the Czech Population to Selected Chemical Substances" [2,3]). This project has been started in 1994 and the third period runs in this time. The aim of this monitoring programme is an assessment of dietary exposure, comparison with toxicological reference points, and characterization of health risks. To achieve these goals it is necessary to perform a systematic monitoring of the mercury content in the food basket of the Czech population as well as to know consumption of individual foods.

This work summarizes the mercury content found in individual foods in our laboratory during past 14 years. Also their contribution to the total dietary exposure and validation by using of biomarkers are included.

Methodology

The analyzed foods were selected according to the knowledge of their consumption by the average person in the Czech population[4,5]. In total 143 kinds of foodstuffs were selected and studied in specific time periods. Food samples were collected in 4 regions (12 sampling towns) and delivered to Centre of Hygiene of Food Chains in Brno. This organization represents 572 food samples that have been processed during two-year period. Some kind of foodstuffs (more frequently consumed) are sampled repeatedly and measured every year (e.g. milk or potatoes even $2 \times$ per year and town), others (less frequently consumed) are sampled and measured only once in the whole two-years period. In total 880 individual samples were measured in this period. After delivery of samples into the Centre of Hygiene of Food Chains in Brno, the samples undergo the culinary treatment in pre-analytical laboratory so that they are analyzed in the same state as they are consumed. The samples are then homogenized and delivered into the central analytical laboratory for further treatment and analyses.

In analytical laboratory mercury content (as a total mercury) is determined by AAS method using principle of selective system AMA 254 with solid sample dosing without previous analytical preparation. Optimized method provides adequate sensitivity for the determination of the mercury in foods. The limit of quantification is 0.1 $\mu g\,kg^{-1}$ for a minimal sample weight 200 mg. The degree of recovery ranged from 95 to 105 %. The RSD of repeatability does not exceed 10 %. This method is accredited according to ČSN EN ISO/IEC 17025:2005. To ensure accuracy of the results matrix reference materials as well as various internal test materials are used. In addition our laboratory participates in proficiency testing (FAPAS, IMEP etc.).

Results

The content of total mercury was monitored in 143 kinds of food representing so called food basket of the Czech population. Based on previous experience only fifteen kinds of food with the highest measured mercury content were selected and visualized in Fig. 1. This figure shows foods with their corresponding concentration values. The dietary exposure is influenced not only by the content of mercury in the given food, but also by the quantity of consumed foods To calculate the dietary exposure doses it is also necessary to take into account the changes caused by the culinary treatment of the given food which are described by the so called culinary factor[3]. The influence of both the consumption and culinary factor on the final exposure dose is demonstrated by the following figure. The fifteen most significant exposure sources of total mercury are given in Fig. 2. In both figures (1.,2.) concentration data are used from the last monitoring period 2006–2007.

Foodstuffs listed in Fig. 1. and Fig. 2. are traditionally highlighted in first places during whole period of monitoring program (1994–2007). Fig. 3. shows the changes in measured content of total mercury [$\mu g\,kg^{-1}$] in five selected most
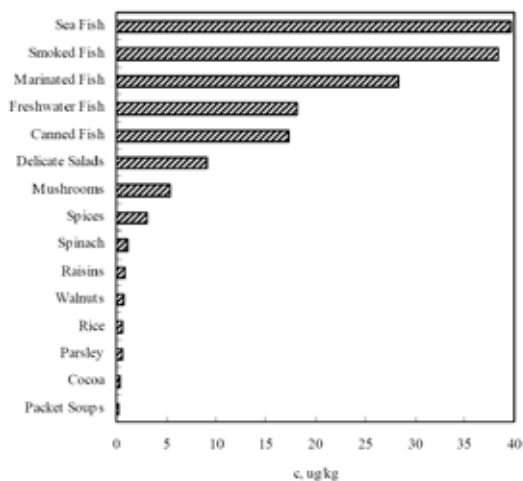
Fig. 1.　**Total mercury concentration in selected foods in the Czech Republic in 2006/2007**
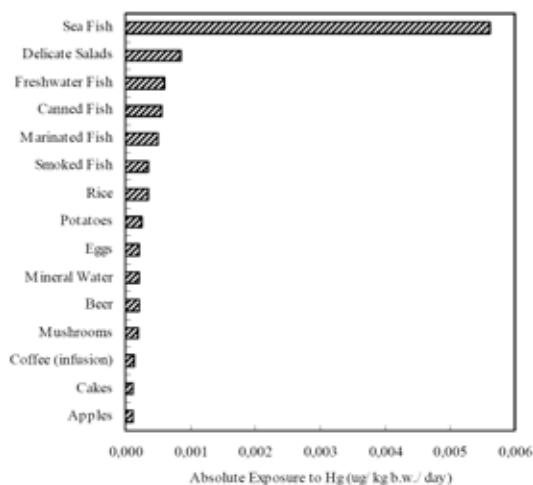
Fig. 2.　**Dietary exposure sources for total mercury in the Czech Republic in 2006/2007**

Fig. 3.　**Content of total mercury in selected foods**
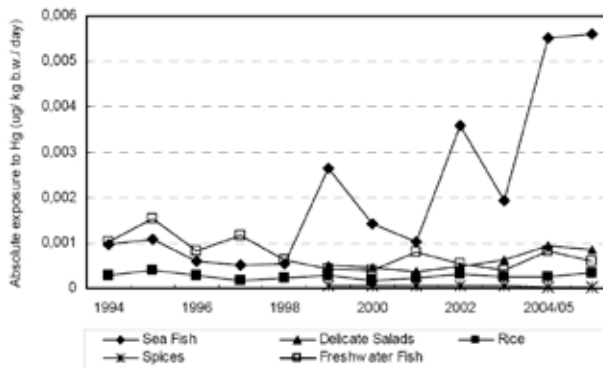
Fig. 4.　**Contribution of selected foods to the overall exposure doses for total mercury**

Discussion

The results from whole monitored period (1994–2007) support an idea that foods containing the highest amounts of total mercury are fish and fish products, delicate salads, mushrooms, spices and rice (Fig. 1.). With regard to the significance of foods as dietary exposure sources the most important foods are as well fish and fish products, delicates salads
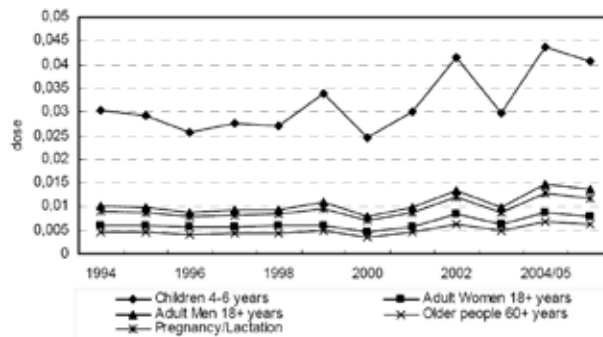
Fig. 5.　**Exposure doses: total mercury [µg kg⁻¹ b.w. day⁻¹] (consumption models according to the food guide pyramid)**

contaminated foods in time (years) and their contribution to the exposure doses is plotted in Fig. 4.

The trend of exposure doses to total mercury is shown in Fig. 5. There are included exposure doses for different population groups in the Czech Republic during monitoring period 1994–2007. The point estimate of health risk indicates fluctuating trend with a slight tendency to increasing. The most exposed group are children due to higher usual intake of foods per kg of their body weight.

For assessment of human exposure and better health risk characterization are often used also biomarkers (human blood, urine or hair). This special approach is also used by the National Institute of Public Health in the monitoring project called "Biological monitoring"[6,7]. In Fig. 6. the behaviour of the total dietary exposure with time is shown for monitored period 1994–2007. Also in this figure the levels of mercury in blood samples in selected years for adult Czech population in the same period are shown.

and rice. (Fig. 2.). It support an idea that the most hazardous foods from exposure point of view are fish meat and fish products. 80–90 % of total mercury in fish is expected as MeHg in muscle[8,9]. Then total mercury content is suitable indica-
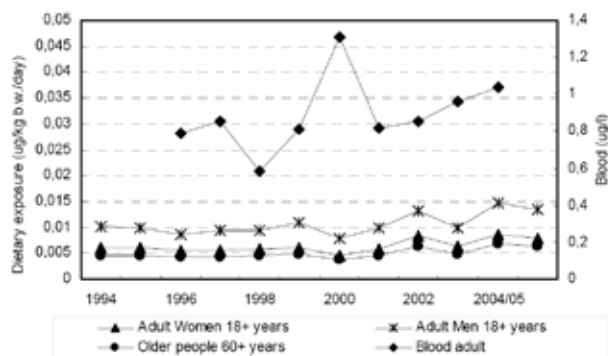
Fig. 6.　**Comparison of measured overall dietary exposure doses of total mercury and levels measured in Blood (point estimate)**

tor of possible exposure to MeHg in this case. Other groups of foods are not of so important for exposure of the Czech population.

The estimate of the dietary exposure from the most significant samples (sea fish) show tends to increase. This tendency to increase may be due to the trend of growing consumption this commodity given by development of business and import from seaside countries. The monitoring also showed an increasing tendency for the dietary exposure to mercury which was in correspondence with the levels of mercury in human blood in the same period. In the Fig. 5. are included data found for adult. The same trend can be seen for children too.

Conclusion

The content of total mercury in the samples of the food basket of the Czech Republic has been monitored since 1994. Produced data enabled the calculation of both - the exposure dose coming from individual samples and the total dietary exposure dose. The average value of the total dietary exposure in the period 1994–2007 is 0.0126 $\mu g\,kg^{-1}$ b.w. day^{-1} It represents 0.0882 $\mu g\,kg^{-1}$ b.w. week^{-1}.

In 1978 the FAO/WHO JECFA evaluated total mercury and set PTWI at 5 $\mu g\,kg^{-1}$ b.w. week^{-1} from which MeHg should not be higher than 3.3 $\mu g\,kg^{-1}$ b.w. week^{-1}. US EPA defined RfD 0.1 $\mu g\,kg^{-1}$ b.w. day^{-1}. PTWI set by FAO/WHO JECFA for MeHg was revised into 1,6 $\mu g\,kg^{-1}$ b.w. week^{-1}(ref.[9,10,11]) in June 2003. According to longitudinal monitoring results it was proved that average value of overall dietary exposure to total mercury has not been breaking toxicological reference points set by FAO/WHO JECFA or US EPA in none of different population groups in the Czech Republic. Potentially risky groups are children and pregnant women or nursing mothers due to highest sensitivity of embryo/neonates in combination with dietary habit involving highly contaminated kinds of fish (mainly predator fish meat). Therefore it is important regularly evaluate dietary habit of the Czech population, analyse possible food sources of (at least) total mercury and do relevant advices to consumers. We should not forget that hazard of mercury in fish is

in unknown extent balanced by benefits of some important nutrients coming from that food sources.

REFERENCES

1. Masazumi Harada, M.D., Ph.D.: *Minamata Disease and the Mercury Pollution of the Globe*, http://www.einap.org/envdis/Minamata.html#name.
2. Ruprich J., Řehůřková I., Dofková M., in: *.Environmental Health Monitoring System in the Czech Republic* (Denková P., Puklová V., ed.), chapter VII, p. 58. National Institute of Public Health, Prague 2004.
3. Ruprich J.: *The Health Risk Assesment of Dietary Exposure to Selected Chemical Substances in year 2002.* National Institute of Public Health, Prague 2003.
4. Černoevičová, M., Kořiva, V., Ostý, V., Resová, D., Řehůřková, I., Walterová, D.: *Food Basket – Czech Republic*(Ruprich J., ed.), National Institute of Public Health 1993.
5. Ruprich J. a kol.: *Individuální spotřeba potravin v ČR – národní studie SISP04,* Státní zdravotní ústav, Centrum hygieny potravinových řetězců Brno, http://www.chpr.szu.cz/spotrebapotravin.htm.
6. *Zdravotní důsledky expozice lidského organismu toxickým látkám ze zevního prostředí (biologický monitoring)*, Odborná zpráva za rok 2005, SZÚ Praha, Ústředí monitoringu zdravotního stavu, June 2006, http://www.szu.cz/uploads/documents/chzp/biomonitoring/biologicky_monitoring_05.pdf.
7. *Zdravotní důsledky expozice lidského organismu toxickým látkám ze zevního prostředí (biologický monitoring), Odborná zpráva za období 1994–2004*, Státní zdravotní ústav Praha, Praha, June 2005. http://www.szu.cz/uploads/documents/chzp/biomonitoring/biologicky_monitoring_94_04.pdf.
8. Řehůřková I., Ruprich J. a kol.: *Dietární expozice rtuti populace ČR, Snížení PTWI pro methyl rtuť,* Státní zdravotní ústav, Centrum hygieny potravinových řetězců , Brno, www.chpr.szu.cz .
9. Ruprich J., Řehůřková I., Drápal J., Kozáková M.: *Stanovisko vědeckého výboru pro potraviny ve věci: Methylrtuť v rybách a rybích výrobcích,* Státní zdravotní ústav, Centrum hygieny potravinových řetězců Brno, 2004, http://www.chpr.szu.cz/vedvybor/dokumenty/stanoviska/stan_2004_5_deklas_Hg_rev1.pdf.
10. World Health Organization, Food and Agriculture of the United Nations Organization: *Joint FAO/WHO expert committee on food additives, Sixty-first meeting, Summary and conclusions,* Rome, 10-19 June 2003, ftp://ftp.fao.org/es/esn/jecfa/jecfa61sc.pdf, loaded May 19, 2008.
11. Ruprich J. a kol.: *Zdravotní důsledky zátěže lidského organizmu cizorodými látkami z potravinových řetězců v roce 2005, Odborná zpráva za rok 2005,* Státní zdravotní ústav Praha, 2006, http://www.chpr.szu.cz/monitor/tds05c/tds05c.htm.

**P89 THE INFLUENCE OF SURFACE
CHARACTERISTICS ON BACTERIAL CELL
ADHESION**

OLGA SCHREIBEROVÁ, TEREZA KRULIKOVSKÁ,
JITKA HRDINOVÁ, JAN MASÁK, ALENA ČEJKOVÁ,
VLADIMÍR JIRKŮ and PETR HRON

*Institute of Chemical Technology Prague, Technická 5,
166 28, Praha 6, Czech Republic,*
olga.schreiberova@vscht.cz

Introduction

Bacterial cell adhesion is the first step in the formation of multicellular structure called biofilm. Biofilm is a dynamic community of cells which display distinct properties from the planktonic cells. These can be utilized in bioremediation technologies[1], however the stability of adhesion must be ensured. For this purpose, the principles of initial adhesion must be investigated and understood.

Experimental

- Microorganism.

Gram-positive pollutant degrading bacteria *Rhodococcus erythropolis* CCM 2595 was obtained from the Czech Collection of Microorganisms (Masaryk University Brno, Czech Republic).

- Cultivation and biomass determination.

Cells were cultivated in 200 ml of medium in shaked Erlenmeyer flasks. The growth of suspended cells was monitored as optical density at 400 nm (O.D.). Either a complex medium nutrient broth (HiMedia, India) or minimal medium was used (KH_2PO_4 0.17 $g\,dm^{-3}$, K_2HPO_4 0.13 $g\,dm^{-3}$, $(NH_4)_2SO_4$ 0.71 $g\,dm^{-3}$, $MgCl_2$ 0.34 $g\,dm^{-3}$, $MnCl_2$ 1 m $g\,dm^{-3}$, $CaCl_2$ 0.26 m $g\,dm^{-3}$, $FeSO_4$ 0.6 m $g\,dm^{-3}$, Na_2MoO_4 2 m $g\,dm^{-3}$, pH 7). In minimal medium phenol or glucose was used as the only carbon and energy source.

- Cell hydrophobicity.

Hydrophobicity of cells was determined by the MATH test[2].

- Cell fatty acids.

For fatty acids determination the cells were harvested by centrifugation, washed and lyophilized. Fatty acids were esterified to methyl esters, extracted to hexan and analysed by GC-FID.

- Adhesion monitoring.

The Flow cell 81 (BioSurface Technologies, USA) was used for assessing the adhesion of cells. Materials with different hydrophobicity and other properties were evaluated. Three types of glass were employed: microscope slide (labeled glass in following text), coated glass and hydrophobized glass. Also polymeric materials silicone and teflon were evaluated. The glass and silicone materials were prepared at the Department of Polymers, Faculty of Chemical Technology, Institute of Chemical Technology, Prague.

- Material hydrophobicity.

The material hydrophobicity (except teflon) was deter- mined by the Surface Energy Evaluation system (Department of Physical Electronics, Faculty of Science, Masaryk University, Czech Republic).

Results

The External Conditions Influence on Cell Hydrophobicity

Cell wall hydrophobicity reflects the cell physiological state and is one of the most important cell characterictics that determine the ability to adhere[3]. Cell hydrophobicity can be influenced by the type of the source of carbon and energy.

In our study we investigated the effect of medium composition (complex and minimal media, optimal and stressful cultivation conditions). We found that the initial phenol concentration 0.3 $g\,dm^{-3}$ can be considered as optimal and that phenol concentration 0.7 $g\,dm^{-3}$ partially inhibits the growth and can be called stressful (data not shown). Concentration 1.0 $g\,dm^{-3}$ caused considerable inhibition of the growth. Nutrient broth was chosen as a complex medium. Also glucose (as a C source) in minimal medium was tested. During the experiments, hydrophobicity of cells in different growth phases was determined to ascertain the influence of this factor, which according to literature, can be considerable[4].

The *Rhodococcus erythropolis* cells were proven to be highly hydrophobic in all monitored media (see Fig. 1.). The medium composition influence on variation of cell hydrophobicity was significant. The changes in cell hydrophobicity during the growth (exponential, stationary phase) were not considerable and therefore the subsequent experiments were carried out with cells in stationary phase.
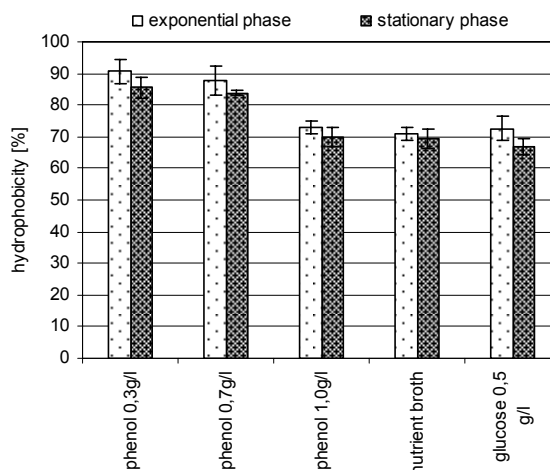
Fig. 1. **The dependence of *R. erythropolis* cells hydrophobicity on media composition**

The fatty acid composition of cells cultivated in media with different phenol concentration is presented in the Table I. Results indicate that there is dependency of fatty acid composition on initial phenol concentration.

Table I

Cell envelope fatty acid composition. Cells were harvested by centrifugation and lyophilized fatty acids were esterified to methyl esters, extracted to hexan and analysed by GC-FID

	Fatty acid (methyl ester)	t_R [min]	Carbon atoms	Phenol [g dm^{-3}]	
				0.3	0.7
	not identified	7.6	x		
14:0	tetradecanoate	13.3	14		4.8
i-15:0	13-methyltetradecanoate	14.9	15		
	not identified	17.8	x		
16:1	cis-9-hexadecanoate	17.9	16	8.3	12.7
16:0	hexadecanoate	18.3	16	41.8	51.7
	not identified	19.4	x	3.2	
17:0$^\Delta$	cis-9,10-methylenhexadecanoate	20.6	17	8.8	
17:0	heptadecanoate	20.9	17		
18:1^9	cis-9-oktadecanoate	22.7	18		
18:0	oktadecanoate	23.4	18	2.1	8.0
	not identified	24.2	x	33.6	24.5
	not identified	26.8	x	2.1	

Cell Adhesion

The determination of material hydrophobicity and other surface characteristics influence on cell adhesion was the aim of our work. Five materials were tested, both hydrophilic and hydrophobic. The hydrophilic materials were: glass without any modifications (strictly hydrophilic) and coated glass with slightly less hydrophilic surface. The hydrophobic materials were: hydrophobized glass and silicone with equal hydrophobicity, to ascertain the influence of surface moieties. The last material was teflon, known for its extreme hydrophobicity[5] and antiadhesion properties.

Experiments were carried out using cells precultivated in Erlenmeyer flasks. The hydrophobicity of these cells was approximately 85 % (Fig. 1.). Initial adhesion experiments (see Table II) were carried out in the presence of phenol (0.3 g dm^{-3}). The adhesion was monitored after one hour and after 24 hours. The results confirmed that hydrophobic cells do not adhere to hydrophilic surface. The results also verified our assumption that beside hydrophobicity there are other important factors in the process of cell adhesion. The teflon was proven to be an unfavourable material for cell adhesion.

Table II

The adhesion of *Rhodococcus erythropolis* cells on different materials after one and twenty-four hours

Experiment duration [h]		1	24
material	material hydrophobicity	colonized area [%]	
glass	26.4 ± 6.6	0	0.2
coated glass	55.9 ± 8.2	4.9	3.2
hydrophobized glass	97.0 ± 2.0	12.1	12.9
silicone	97.0 ± 3.6	39.5	40.1
teflon	108 [5]	7.6	4.9

The colonized area was three times higher on silicone than on the hydrophobized glass with the same hydrophobicity. The influence of the experiment duration was not significant.

Also the adhesion of cells with different inoculation origin was evaluated (see Table III). The cells were precultivated in inoculum medium (nutrient broth or mineral medium with phenol) and then transferred to experiment medium. This was proven to be substantial in cell attachment. The cells adhered the most to silicone, but only in medium with phenol concentration 0.3 g dm^{-3}. When transferred from either nutrient broth or minimal medium to minimal medium with phenol concentration 0.7 g dm^{-3}, cells adhered considerably less.

Table III

The influence of inoculum cultivation conditions on Rhodococcus erythropolis cells adhesion on different materials

	Experiment set-up		
inoculum medium	n.broth	n.broth	phenol 0.7 g dm^{-3}
experiment medium	phenol 0.3 g dm^{-3}	phenol 0.7 g dm^{-3}	phenol 0.7 g dm^{-3}
material	material hydrophobicity	colonized area [%]	
glass	26.4 ± 6.6	0	0.2	0.04
silicone	97.0 ± 3.6	39.5	4.5	9.2
teflon	108	7.6	5.5	6.0

Conclusions

In our study the influence of cultivation conditions on cell hydrophobicity and cell adhesion was confirmed. It was found that not only hydrophobicity of materials plays important role in colonization, but also other surface characteristics are significant.

REFERENCES
1. Melenová I., Demnerová K.: Chem. Listy *98*, 908 (2004).
2. Rosenberg M. D., Gutnick D., Rosenberg E.: FEMS Microbiol. Lett. *9*, 29 (1980).
3. Masák J., Čejková A., Jirků V., Kotrba D., Hron P., Siglová M.: Environ. Int. *31*, 197 (2005).
4. Walker S. L., Hill J. E., Redman J. A., Elimelech M.: Appl. Environ. Microbiol. *71*, 3093 (2005).
5. Tarasevich Y. I.: Theor. Exp. Chem. *42* (2006).

**P91   SELECTION OF SUITABLE OF
       MICROORGANISMS FOR PREPARATION OF
       LACTIC ACID FERMENTED CABBAGE JUICE**

IVANA ŠIMONOVÁ, JOLANA KAROVIČOVÁ, MÁRIA
GREIFOVÁ and ZLATICA KOHAJDOVÁ

*Institute of Biotechnology and Food Science, Faculty of Chemical and Food Technology, Slovak University of technology, Radlinského 9, 812 37 Bratislava, Slovak Republic,
ivana.simonova@stuba.sk*

Introduction

The vegetable juices processed by the lactic acid fermentation introduce change in the beverage assortment. During fermentation, a great amount of another substances useful for health is produced by lactic acid bacteria and by other microorganisms[1]. Most probiotic microorganisms are lactic acid bacteria such as *Lactobacillus plantarum*, *Lactobacillus casei*, *Lactobacillus acidophilus*, and *Streptococcus lactis*[2].

The term *probiotic* refers to live microorganisms that survive passage through the gastrointestinal tract and have beneficial effects on the host[3].

Prebiotics are an alternative for probiotics or their cofactors. They are defined as non-digestible or low-digestible food ingredients that benefit the host organism by selectively stimulating the growth or activity of one or a limited number of probiotic bacteria in the colon[4]. Inulin and oligofructose are the most studied and well-established prebiotics[5]. Inulin is a polydisperse fructan and it is a mixture of oligomers and polymers of chain of fructosyl units with one glucosyl unit at the end of a chain. The non-digestibility of inulin is the reason for the reduced caloric value of this natural polysaccharide.

Inulin is frequently used as an additive in functional ood articles, especially as substitute for lipid compounds and upplement for sugar. It can also be used in products with increased dietary fibre content, e.g. bread or food product, with a bifidogenic effect[6].

The conditions for lactic acid fermentation based on a cabbage juice and four probiotic lactic acid bacteria has been studied. All cultures showed good biochemical activity in the cabbage juices. Addition of prebiotic preparation into the cabbage juices has been studied also.

Experimental

B a c t e r i a l   S t r a i n s   a n d   G r o w t h
C o n d i t i o n s

Lactobacillus plantarum CCM 7039, *Lactobacillus amylophillus* CCM 7001, *Lactobacillus amylovorus* CCM 4380 and *Bifodobacterium longum* CCM 4990 (obtained from Czech Collection of Microorganisms, Faculty of Sciences, Masaryk University, Brno, Czech Republic) were cultivated at 30 °C 2 day in the three medium (medium A-MRS broth, medium B-MRS broth with addition 2 % prebiotic preparation and medium C-MRS broth, the glucose was substituted

prebiotic preparation). For fermentation we used night culture with initial concentration 10^6 CFU per milliliter. The pH of MRS medium was adjusted to 5.8 ± 0.2, and the medium was autoclaved 120 °C for 20 min.

A n a l y s i s   o f   G r o w t h

Cellular growth was followed by plate counting throughout the fermentation. The number of CFU per milliliter were obtained through enumeration on MRS agar after anaerobic incubation at 37 °C for 48 h.

A n a l y s i s   o f   M e t a b o l i t e   P r o d u c t i o n

The concentration of lactic acid, citric acid and acetic acid were determined through high-performance liquid chromatography with RI detector (K-2301. Knauer). An Polymer IEX H form (250 × 8 mm, Watrex) column was used with 9 mM of H_2SO_4 as the mobile phase at a flow rate of 1 ml min^{-1}. The column temperature was kept constant at 50 °C. Before injection the samples were filtred (pore size 0,20 μm). All samples were analyzed triplicate. The measurement of pH was performed using a LABOR-pH-meter CG-834 SCHOTT, Germany[7].

F e r m e n t a t i o n   o f   C a b b a g e   J u i c e s

The fresh raw material (cabbage – *Brassica oleracea* L. convar. *capitata* (L.) *Alef. var. alba*, variety HOLT was purchased in a local market in Slovakia. Fresh sample juices were obtained by extracting the juice from cabbage using a kitchen juicer. Subsequently, the juices were gauze-filtered, fortified by adding 2% D-glucose and 0.5% NaCl, and inoculated with a culture of the lactic bacteria. Thus treated juices were poured into 250 ml graduated flasks, which were stoppered with sterile stoppers and left to ferment in a thermostat for 168 hours at 21 °C. During the fermentation, samples at specified intervals were taken for analytical determinations.

Results

In this study we applied *Lactobacillus plantarum* CCM 7039, *Lactobacillus. amylophillus* CCM 7001, *Lactobacillus amylovorus* CCM 4380 for preparation of lactic acid fermented cabbage juices. The suitability of *Bifidobacterium longum* CCM 4990 was also tested because study of Lukačová et. al., describes this bacterium as a potential probiotic culture[8].

In this work, we also tested influence lactic acid bacteria on the prebiotic preparation Frutafit® IQ (90–95 % instant inulín).

At the first, we tested the grow lactic acid bacteria in the tree MRS medium. We find out, that the lactic acid bacterie during the 48 h of cultivation has suitable condition for grow in the MRS medium with glucose and 2% inulin than in the MRS medium (without glucose) with 2% inulin. The Fig. 1. describe the grow *Lactobacillus amylophilus* CCM 7001 in the free various medium. The Fig. 2. describe decrease of pH during cultivation of *Lactobacillus amylophilus* CCM 7001.
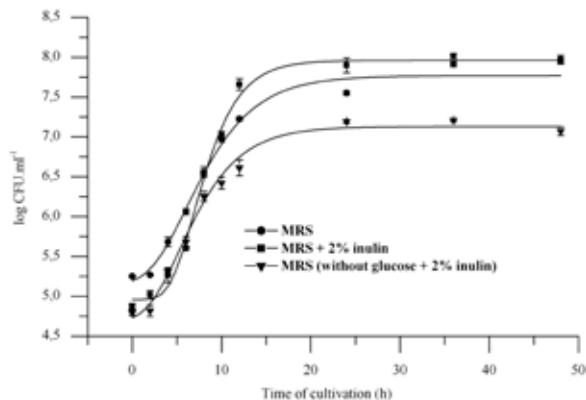
Fig. 1.   **The growth of *Lactobacillus amylophilus* CCM 7001 in the tree various medium**
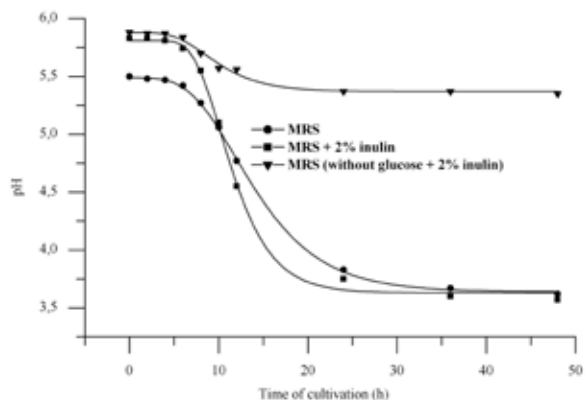
Fig. 2.   **The pH of *Lactobacillus amylophilus* CCM 7001 in the tree various medium**

From this result we conclude that the *Lactobacillus plantarum* CCM 7039, *Lactobacillus. amylophillus* CCM 7001, *Lactobacillus amylovorus* CCM 4380 and *Bifodobacterium longum* CCM 4990 were not capable utilised inulin from Frutafit® IQ during 48 h of cultivation.

During the fermentation, pH of the juices decreases usually from 6–6.5 to 3.8–4.5. A rapid decrease of pH at the beginning of fermentation has decisive importance for the quality of the final product[9]. At the beginning of fermentation

process, the cabbage juices had pH 6.3–6.1. At the end of fermentation process (after 168 h) the samples had pH 4.2–3.86. Formation of lactic acid is considered to be the key factor of the preserving effect in lactic acid fermentation[10]. After 168 h of fermentation, the cabbage juices containing 5.5–11.7 g dm^{-3} of lactic acid.

Conclusions

From the results it could be concluded that cabbage could be an effective raw material for prepared lactic acid fermented juices inoculated with microorganisms *Lactobacillus plantarum* CCM 7039, *Lactobacillus. amylophillus* CCM 7001, *Lactobacillus amylovorus* CCM 4380 and *Bifidobacterium longum* CCM 4990.

Also the results show, that tested probiotic bacteria and addition of 2 % prebiotic preparation were suitable for preparation lactic acid fermented cabbage juice with functional properties.

REFERENCES

1. Kohajdová Z., Karovičová J.: Chem. Pap. *59*, 1 (2005).
2. Yoon K. Y., Woodams E. E., Hang Y. D.:Bioresource technol. *97* (2006).
3. De Roos M. N., Katan M. B.: Am. J. Clin. Nutr. *71* (2000).
4. Grajek W., Olejnik A., Sip A.: Acta Biochim. Pol. *52*, 3 (2005).
5. Roberfroid M. B.: Brit. J. Nutr. *93* (2005).
6. Golobi T., Mičović E., Bertoncelj J.: Acta Agricult. Slov. *83*, 2 (2004).
7. Karovičová J., Drdák M., Polonský J., Rajniaková A.: J. Chrom. A, *665* (1994).
8. Lukáčová D., Karovičová J., Greifová, M., Šovčíková A.: J. Food Nut. Res. *2* (2006).
9. Montaňo A., Sánchez A. H., Rejano L., De Castro A.:Int. J. Food Microbiol. *35* (1997).
10. Kuchta T., Radošovská R., Glončáková B., Belicová A., Lopašovská J.: Bull. Potrav. Výsk. *33* (1994).

P92   USING OF HYDROCOLLOIDS FOR DELAYNG STALING OF BAKERY PRODUCTS

ZLATICA KOHAJDOVÁ, IVANA ŠIMONOVÁ and JOLANA KAROVIČOVÁ

Institute of Biochemical and Food Technology, Department of Food Technology, Slovak University of Technology Radlinského 9, 812 37 Bratislava, Slovak Republic
zlatica.kohajdova@stuba.sk

Introduction

One group of the most extensively used additives in the food industry are the hydrocolloids[1]. The most well know and applied in the industry polymers included in this kind of substances are alginates, carrageenans, agar, guar gum, arabic gum, methyl cellulose and carboxymethyl cellulose[2]. These compounds used in food products and processing can serve as processing aids, provide dietary fiber, impart specific functional properties or perform a combination of these roles. Guar and xanthan gums, for instance, have been used at 7 % and 2 % levels, respectively, in bread to provide dietary fiber for therapeutic purposes. At a lower level of incorporation, gums have served as additives to improve the quality of bread[3].

In the baking industry, hydrocolloids are of increasing importance as bread improvers as they can induce structural changes in the main components of wheat flour systems along the breadmaking steps and bread storage[1]. The hydrocolloids are added to bakery products for control water absorption and consequently dough rheology[4], improving their shelf life by keeping the moisture content and retarding the staling[5]. It is well known the effect of hydrocolloids on starch pasting properties[5,6]. These starch properties, that include gelatinization temperature, paste viscosity and retrogradation of the starch, affect baking and final quality and staling behaviour of baking products[6].

The present study was done to examine the effect of different hydrocolloids on retarding the staling process of baked goods.

Experimental

A wheat flour T650 (containing 11.20 ± 0.2 % of proteins, 0.68 ± 0.001 % of ash in dry matter and 31.55 ± 0.4 % of wet gluten in dry matter) and wholemeal spelt flour (containing 17.30 ± 0.3 % of proteins, 2.21 ± 0.002 % ash in dry matter and 40.99 ± 0.5 % of wet gluten in dry matter) and of local origin was used in the study. Blend flour was obtained mixing of wheat and wholemeal spelt flours in ratio 85:15.

The hydrocolloids used were: guar gum, gum arabic, xanthan gum and methyl 2-hydroxyethyl celullose. The dough was prepared according to formulation, which was 100 % blend flour, salt 2 %, sugar 1 %, yeast 4 %, sunflower oil 2.5 %, hydrocolloid 1 % on flour weight basis and water to farinographic consistency 400 BU (Brabender Units). All raw materials were procured from the local market in Slovakia.

The ingredients were mixed during 6 minutes in farinographic mixing bowl. After 20 min fermentation, the dough was divided into 100 g loaves, formed on dough former, proofed 45 min and baked in an electric oven during 12 min at 230 °C. Baking trials were performed in triplicate.

Determination of Crumb Hardness

Crumb hardness was measured on freshly baked loves (2 h after baking) and on loaves that were stored for 24, 48 and 72 hours at ambient temperature using a manually operating penetrometer AP 4/1 when 1 penetrating unit represented 0.1 mm.

Results

Bakery products have a very short shelf life and their quality is highly dependent on the period of time between baking and consumption[7].

Firming of bread crumb during storage is a common phenomenon and leads to a crumbly texture, and lower consumer acceptance. Staling of bakery products is generally defined as an increase in crumb firmness and a parallel loss in product freshness[8]. Firming is the preferred parameter used to evaluate staling development[9].

In this study, the anti-staling potential of various hydrocolloids was investigated. We concluded that all from applied hydrocolloids expect methyl 2-hydroxyethyl cellulose reduced firmness during 72 h storage period, given softer crumb than control samples (without hydrocolloids). The reason for the softer texture with gum treatments might be that the hydrophylic gums were holding more water, which led to higher moisture content in the final baked product and as a consequence, retrogradation of the starch and bread firming is retarded[10]. Guar gum had the greatest effect in decreasing crumb hardness (see Fig. 1.). This hydrocolloid has a softening effect due to a possible inhibition of the amylopectin retrogradation, since guar gum preferentially binds to starch[11]. Effect addition of different concentration of guar gum (from 0 to 2 %) on shelf life of baked products was also
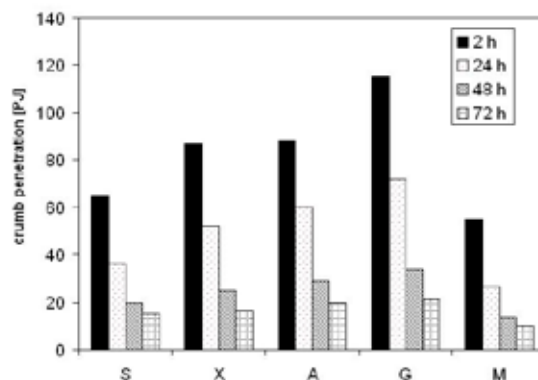
Fig. 1.   **Effect hydrocolloids on crumb penetration (S-control sample, × – xanthan gum, A – gum arabic, G – guar gum, M-methyl 2-hydroxyethyl celullose**

studied. From results concluded that addition 0.75–2 % of this compound significantly delaed baked goods staling process. Expect these positive effects, the incorporation of guar gum also improved palatability of final products.

Conclusions

Nowadays, the use of additives has become a common practice in the baking industry. Baked goods staling evaluated during 72 h storage period through bread firmness values showed, that loaves prepared with hydrocolloids extent products contained celullose derivate were soften when control sample. Guar gum was showed as good bakery improver owing to its good crumb softening effects.

The incorporation of hydrocolloids into the loaves also influenced rheological parameters of dough and sensory acceptance of final products in different ways.

REFERENCES

1. Selomulyo V. O., Zhou W.: J. Cereal Sci. *45*, 1 (2007).
2. Gómez-Diaz D., Navaza J. M.: Food Agricult. Environ. *1*, 98 (2003).
3. Onweluzo J. C., Leelavathi K., Rao P. H.: Plants Foods for human Nutr. *54*, 173 (1999).
4. Mandala I., Karabela I., Kostaropoulos A.: Food Hydrocol. *21*, 1397 (2007).
5. Rojas J. A., Rosell C. M., De Barber B.: Food Hydrocol. *13*, 27 (1999).
6. Gómez M., Ronda F., Caballero P. A., Blanco C. A., Rosell C. M.: Food Hydrocol. *21*, 167 (2007).
7. Barcenas M. E., Haros M., Benedito C., Rosell C. M.: Food Res Int. *36*, 863 (2003).
8. Ji Y., Zhu K., Qian H., Zhou H.: Food Chem. *104*, 53 (2007).
9. Ribotta P. D., Le Bail A.: LWT - Food Sci. Technol. *40*, 879 (2007).
10. Sharadanant R., Khan K., Cereal Chem. *80*, 773 (2003).
11. Shalini K. G., Laxmi A.: Food Hydrocol. *21*, 110 (2007).

P93 INFLUENCE OF PH ON THE RHEOLOGY PROPERTIES OF TOMATO KETCHUPS

JARMILA LEHKOŽIVOVÁ, JOLANA KAROVIČOVÁ, JARMILA HOJEROVÁ, ZLATICA KOHAJDOVÁ and IVANA ŠIMONOVÁ

Institute of Biotechnology and Food Science, Faculty of Chemical and Food Technology, Slovak University of Technology, Radlinského 9, 812 37 Bratislava, Slovak Republic, jarmila.lehkozivova@stuba.sk

Introduction

A large part of the world tomato crop is processed into tomato paste, which is subsequently used as an ingredient in many food products, mainly soups, sauces and ketchup[1]. Tomato ketchup is concentrated dispersion of insoluble matter in aqueous medium[2].

By definition, rheology is the study of the deformation and flow of matter. So, rheological properties are based on flow and deformation responses of foods when subjected to stress[3]. The flow properties of food products significantly influence not only technology processes during the production, but the texture of final products, too[4]. Tomato ketchup viscosity is very important from both engineering and consumer viewpoints[5].

The aim of this work was investigated the influence of pH on the rheological properties of 3 samples of the formulated tomato ketchups at pH levels 3.5, 4.0 and 4.5. This pH range is most common for tomato ketchups. In recent years rheological properties of food products have become increasingly important in the formulation of food and the optimization of food processing.

Experimental

Three samples of tomato ketchup were prepared in laboratory conditions. The tomato paste with tomato soluble solids 30 % and guar gum cames from the company Kolagrex Int., s.r.o., Kolárovo, Slovak Republic. Some ingredients such as

Fig. 1. **Flow curves of the studied ketchup samples at shear rate 0–1,000 s^{-1} and temperature 25±1 °C**

Isosweet and Resistamyl 348 were from Amylum Slovakia, s.r.o., Boleráz, Slovak Republic and other were purchased from local market.

Tomato Ketchup Preparation

The 100 g of tomato ketchup samples were prepared following the recipe: 35 g of tomato paste (TSS 30 %) mixed with ingredients typically used in ketchup preparation (15 g of isosweet, 11.5 g of vinegar, 1.5 g of salt, 2 g of resistamyl 348, 0.1 g of guar gum and 34.9 g of water). The pH level of the mixture was modified at level 3.5 (A1), 4.0 (A2) or 4.5 (A3) and followed by stirring for 5 min. The mixture was heated and stirred constantly until temperature between 80–85 °C reached. Ketchup samples were then stored at ambient temperature (25 °C) for 24 h before analyses.

Rheological Measurement

The rheological measurements of this study were carried out using the rotational viscometer (controlled rate mode) HAAKE Viscotester VT 550 (Haake, Karlsruhe, Germany) with coaxial cylinder measuring sensor systems MV DIN 53019. The Viscotester VT 550 was computer-operated with the application software RheoWin Job Manager and data evaluation software RheoWin Data Manager (ThermoHaake, Karlsruhe, Germany).

Flow curves (the graphical correlation between shear stress τ and shear rate D) were measured at a continuously increasing shear rate ramp over 3 min from 0 to 1000 s^{-1}. The apparent viscosity:

$$\eta_a = \tau/D \tag{1}$$

The thermal stability of the studied samples was measured at the low shear rate of 10 s^{-1} after 3 min of shearing.

Results

From the shape of the flow curves, which are demonstrated on the Fig. 1., it is possible to get the important information about rheological character of each ketchup sample. All 3 samples behave as non-Newtonian fluids, of which shear stress and apparent viscosity was changed with rate of dynamic strain. Rheograms confirmed their pseudoplastic characters too.

Viscosity curves (Fig. 2.) were constructed by conversion of values of flow curves. From their shape it is possible to set viscosity of the product at specific shear rates to which will be product exposed during dispersion, mixing, pumping, and filling to container as well as during application with consumer. The highest apparent viscosity during shear rate range 10–1,000 s^{-1} was determined in ketchup sample A1 with pH 3.5. Decreasing in the apparent viscosity was followed by sample A2 with pH 4.0 and then by sample A3 with pH 4.5. The requirement putting on some food products exposed to the specified temperature range is that its viscosity changed minimally. The effect of temperature on viscosity of ketchup samples is showed in Fig. 3. Ketchups should have
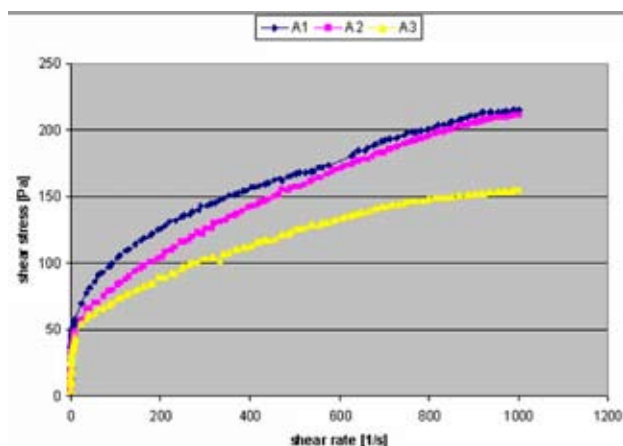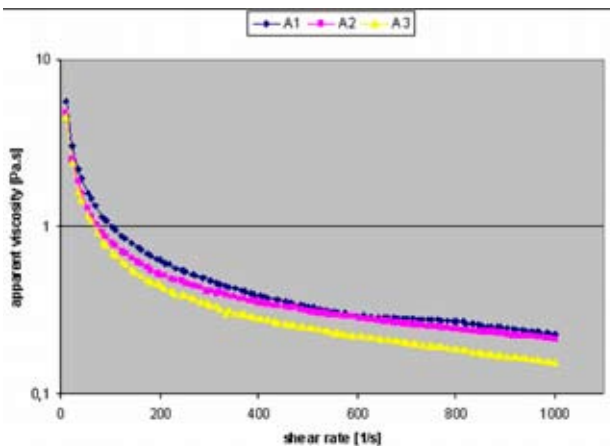
Fig. 2. **Viscosity curves of the studied ketchup samples at shear rate 10–1,000 s^{-1} and temperature 25±1 °C**

Fig. 3. **Effect of temperature on viscosity of the studied ketchup samples at shear rate D = 10 s^{-1} and temperature range from 5 ± 1 °C to 90 ± 1 °C**

small viscosity sensitivity between refrigerator and room temperature[6]. The smallest change in the apparent viscosity about 11.4 % was found in sample A1 with pH 3.5.

Conclusions

Rheological properties are next to colour and flavour the important criterion of sensory evaluation of the food product and its acceptation by consumer. The necessity to set the flow behaviour of product so that their characteristics, standard and quality would be maintained during transportation, storage and application is important from aesthetical and practical point too.

Three samples of the formulated ketchup with different pH level were investigated. The pH level of analysed tomato ketchups varied from 3.5 to 4.5, the most common pH range in ketchups.

The results indicated that studied samples of tomato ketchup behave as non-Newtonian fluids with pseudoplastic characteristics. The apparent viscosity was decreased with increasing pH level of tomato ketchups samples at all temperature range from 5 °C to 90 °C and at all shear rate range from 10 s^{-1} to 1,000 s^{-1}.

REFERENCES

1. Valencia C., Sánchez M. C., Ciruelos A., Latorre A., Madiedo J. M., Gallegos C.: Food Res. Int. *36*, 911 (2003).
2. Sharoba A., Senge B., El-Mansy H., Bahlol H., Blochwitz R.: Eur. Food Res. Tech. *220*, 142 (2005).
3. Rao M. A.: *Rheology of fluid and semisolid foods: principles and applications*. Aspen Publishers Inc., Gaithersburg, Maryland 1999.
4. Štern P., Hojerová J.: Bull Food Res. *39*, 167 (2000).
5. Valencia C., Sánchez M. C., Ciruelos A., Gallegos C.: Food Sci. Tech. Int. *10*, 95 (2004).
6. Hojerová J., Štern P., Zsemlye R.: Bull Food Res. *44*, 83 (2005).

**P94 DISTRIBUTION OF DIAZINON IN
VARIOUS TISSUES AND ITS EFFECT ON
SERUM CHOLINESTERASE AFTER AN
INTRAPERITONEAL ADMINISTRATION**

BRANISLAV ŠIŠKA, JOZEF GOLIAN, ROBERT
TOMAN and ANDREA KRAJČÍROVÁ

Department of Food Hygiene and Safety, Faculty of Biotechnology and Food Sciences, Slovak Agricultural University in Nitra, Trieda A. Hlinku 2, 949 76 Nitra,
branislav.siska@gmail.com

Introduction

Diazinon (O,O-diethyl O-2-isopropyl-6-methylpyrimidin-4-yl phosphorothioate) belongs to the group of organophosphate insecticides used to control cockroaches, fleas and ants. It is also used to control a wide variety of sucking and leaf eating insects and it has also veterinary use[1].

Diazinon has toxic effect on nervous system. This effect is achieved through the inhibition of acetylcholinesterase[2]. This enzyme has a key role in process for controlling of nervous signal transfer. Lack of acetylcholinesterase causes accumulation of acetylcholine. Accumulation of this neurotransmitter on the connections between nerves and muscles causes uncontrolled muscular contraction and algospasmus, between nerves and glands causes continual secretion of these glands, while acetylcholine cumulation between certain nerve cells in a brain causes sensory behavior disorders[3].

Diazinon is also able to cause oxidative stress of the organism through the forming of free radicals that are formed during the increased overextension of the organism by pesticides[4,5].

LD 50 (letal dose for 50 % of tested animals) for diazinon is very different depending up to the species of used laboratory animal. For rats, this value was established to be 1250 mg kg^{-1} after peroral administration and for laboratory mice 80–135 mg kg^{-1} of diazinon after peroral administration. ADI value (acceptable daily intake) was established on 0.002 mg kg^{-1} of diazinon per day[3,6]. Typical symptoms of poisoning are weakness, headaches, tightness in the chest, blurred vision, nonreactive pinpoint pupils, salivation, sweating, nausea, vomiting, diarrhea, abdominal cramps, and slurred speech. Some researches pointed out that diazinon has also mutagenic effect, however current evidence is inconclusive[3,7]. When it comes for a carcinogenic effect, diazinon is not considered to be a carcinogenic compound[7].

Metabolism and excretion rates for diazinon are rapid. The half-life of diazinon in animals is about 12 hours. The product is passed out of the body through urine and in the feces. The metabolites account for about 70 % of the total amount excreted. Diazinon does not belong to the group of chemicals that is characteristic with the long-lasting cumulation in human or animal tissues. However, in some cases could be diazinon detected in the samples of fat tisse, because this tissue has certain ability to cumulate organophosphate insecticides for relatively short period of time. Cattle exposed to diazinon may store the compound in their fat over the short term[8].

In this assay, we studied the effect of diazinon intraperitoneal administration on rat serum cholinesterase catalytic activity and the distribution of diazinon in various tissues of organs of experimental animals.

Experimental

Laboratory rats in the age of 135 days were randomly divided into 2 groups. Each group consisted of 10 males. Animals in the first group were administrated with diazinon (Sigma, USA) 20 mg kg^{-1} b.w. intraperitoneally in physiological solution. The second group served as a control group and was administrated only with the physiological solution. 24 hours after the administration of tested substance, animals were sacrificed, blood samples were taken from hearts and samples of livers, kidneys, muscles and fat tissue were taken during the autopsy.

Catalytic activity of cholinesterase was determined with using of Bio-La-Test®. The amount of diazinon in tissues was determined with using of gas chromatography with mass spectrometry.

Basic statistical characteristics – arithmetic mean, standard deviation and variation coefficient were calculated for cholinesterase catalytic activity and for amount of diazinon in each group. Obtained data were then processed in order to determinate statistical significance of the results. The Student's t-test was finally used for establishment of statistical significance.

Results

No deaths were observed in any of groups of experimental animals. However, animals from diazinon treted group approximately 12 hours after the administration of diazinon showed symptoms connected with depression of cholinesterase activity and did not react on external stimuli. Results of the determination of cholinesterase activity are presented in Table I.

Table I
Cholinesterase activity (μkat dm^{-3}) in different groups

Group of animals	Cholinesterase activity activity (X ± SD)	Variation coefficient [%]
Dizinon group	1.81 ± 0.79*	44
Control group	3.69 ± 0.51	14

X – arithmetic mean, SD – standard deviation,
*p-value < 0.05

Changes of cholinesterase catalytic activity were observed in diazinon treated animals. We observed significant decrease of cholinesterase catalytic activity from 3.69 μkat dm^{-3} in control group to 1.81 μkat dm^{-3} in experimental group. Muscular weakness, confuse and lethargy were typical symptoms that were observed on experimental animals in our assay.
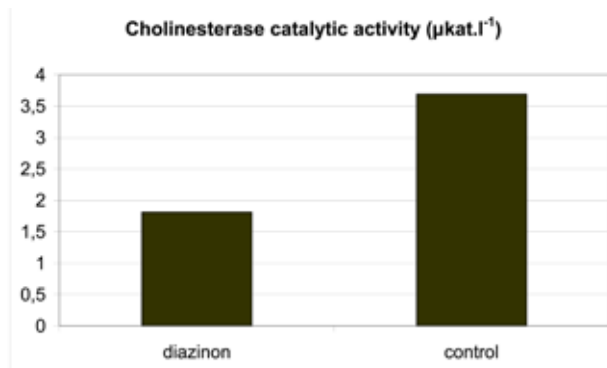
Fig. 1.   **Cholinesterase activity in different groups**

Fig. 2.   **Amount of diazinon in various tisuues**

Results of the determination of diazino amount in various tissues of control animals in comparison with experimental group of animals are presented in Table II.

Table II
Amount of diazinon in various tissues $[\text{mg kg}^{-1}]$

	Amount of diazinon $[\text{mg kg}^{-1}]$)		
Tissue	Control	Experimental (X ± SD)	Variation coefficient [%]
Liver	0	0	0
Kidney	0	0.072 ± 0.036	49
Muscle	0	0.067 ± 0.041	62
Fat	0	3.717 ± 3.749[*]	100

X – arithmetic mean, SD – standard deviation,
[*]p-value<0.05

After analyzing samples of livers, kidneys, muscles and fat tissue for amount of diazinon we observed significant increasing of dizinon amount in samples of fat tissue. Inconsiderable incease of diazinon amount was detected in samples of kidneys and musled. On the other hand we did not detect any amount of diazinon in liver samples of experimental animals.

Conclusions

Itraperitoneal administration of diazinon in amount of 20 mg.kg⁻¹ caused significant depression of cholinesterase cata-

lytic activity. Significantly increased amount of diazinon was detected only in samples of fat tissue. On the other hadn, we did not detect any amount of diazinon in samples of liver.
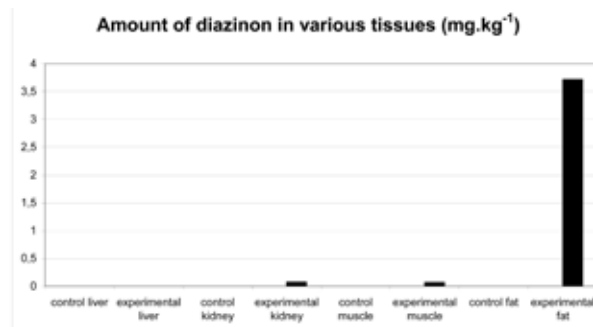
REFERENCES

1. Watterson A. E.: Toxicoll. Lett. *107*, 241 (1999).
2. Üner N., Oruç E. Ö., Sevgiler Y., Şahin N., Durmaz H., Usta D.: Effect of diazinon on acetylcholinesterase activity and lipid peroxidation in the brain of *Oreochromilis niloticus*. Env. Tox. Pharmacol. *21*, 241 (2006).
3. Tomlin C. D. S.: *The Pesticide Manual: A World Compendium.* British Crop Protection Council, Farnham 1997.
4. Hazarika A., Sarkar S. N., Hajare S., Kataria M., Malik J. K.: Toxicol. *185*, 1 (2003).
5. Oruç E. Ö., Üner N.: Comp. Biochem. Physiol. *127*, 291 (2000).
6. Lu, F. C. A.: Regul. Toxicol. Pharmacol. *21*, 352 (1995).
7. Gallo M. A., Lawryk N. J., in: *Handbook of Pesticide Toxicology* (Hayes W., J., Jr., Laws E., R., Jr.), p. 3-5. Academic Press, New York 1991.
8. United States Public Health Service: *Hazardous Substance Data Bank.* Washington, DC 1995.

P95   IDENTIFICATION OF BACTERIAL STRAINS OF *LACTOCOCCUS LACTIS* SPECIES IN HARD CHEESES USING PCR

ALENA ŠPANOVÁ, JITKA HERZOGOVÁ, PETR PTÁČEK and BOHUSLAV RITTICH

Brno University of Technology, Faculty of Chemistry, Department of Food Chemistry and Biotechnology, Purkyňova 118, 612 00 Brno, Czech Republic,
spanova@fch.vutbr.cz

Introduction

Lactococci are the most prominent group of lactic acid bacteria applied in dairy fermentations. Strains of *L. lactis* ssp. *lactis* have been used in the manufacture of different types of cheese. Moreover, some lactococcal strains produce bacteriocins which show activity against food pathogens. Differentiation of these strains on the basis of phenotypic tests is time-consuming and can lead to misclassification. Due to the wide use in dairy industry and different technological properties, fast and reliable PCR-based methods were developed which enable identification of *L. lactis*[1] and distinction between the two subspecies *lactis* and *cremoris*[2]. False-negative results can occur due to the presence of extracellular PCR inhibitors in real tested samples of dairy products.[3–5] The problem of pure DNA preparation can be resolved by means of various isolation and purification methods. Solid phase systems based on non-selectively adsorbing DNA have been developed. It was shown that PCR-ready DNA can be isolated using magnetic microspheres P(HEMA-*co*-EDMA) containing carboxyl groups[4,5] in the presence of high concentrations of PEG 6000 and NaCl.

The aim of this work was to develop a method for PCR-ready DNA isolation from different hard cheese samples. Carboxyl-functionalised magnetic poly(2-hydroxyethyl methacrylate-*co*-ethylene dimethacrylate) microspheres (P(HEMA-*co*-EDMA)) were used for DNA isolation. The quality of extracted DNA was checked by PCR amplification.

Material and Methods

Chemicals and Equipment

Primers for PCR were synthesised by Generi-Biotech (Hradec Králové, Czech Republic); *Taq*I DNA polymerase was from Bio-Tech (Prague, Czech Republic), DNA ladder 100 bp from Malamité (Moravské Prusy). The PCR reaction mixture was amplified on an MJ Research Programme Cycler PTC-100 (Watertown, USA).

Magnetic nonporous poly(2-hydroxyethyl methacrylate-co-glycidyl methacrylate) P(HEMA-*co*-GMA) microspheres containing carboxyl groups were prepared according to the previously described procedure[6] in the Institute of Macromolecular Chemistry (Academy of Sciences of the Czech Republic) in Prague. Magnetic particles were separated on a Dynal MPC-M magnetic particle concentrator (Oslo, Norway).

Methods

The type strain *Lactococcus lactis* subsp. *lactis* CCM 1877[T] from the Czech Collection of Microorganisms was used as a control strain. It was cultivated on MRS agar with 0.5 % of glucose at 30 °C for 48 h. The cells from 1.5 ml culture were centrifuged (14,000 g 5 min^{-1}), washed in water, and resuspended in 500 µl of lysis buffer (10mM Tris, pH 7.8, 5mM EDTA pH 8.0, lysozyme 3 mg ml^{-1}). After 1 hour, 12.5 µl of 20% SDS and 5 µl of proteinase K (10 µg ml^{-1}) was added and incubated at 55 °C overnight. DNA was extracted using phenol methods[7], precipitated with ethanol, and dissolved in TE buffer (10 mM Tris-HCl, 1mM EDTA, pH 7.8).

The DNA from hard cheese samples was isolated from crude cell lysates from cheese filtrates by the phenol extraction procedure[7] (control) and by magnetic microspheres (see later). Magnetic microspheres P(HEMA-*co*-EDMA) containing carboxyl groups (100 µl, 2 mg ml^{-1}) were added to the crude cell lysates (100 µl) together with 5M NaCl (400 µl), 40% PEG 6000 (200 µl) and water to a volume of 1,000 µl (200 µl). After 15 minutes of incubation at laboratory temperature, the microspheres with bound DNA were separated using magnet, washed in 70% ethanol, and DNA was eluted into 100 µl of TE buffer.

Species-specific PCR primers PALA4 and PALA14 (targeted on *acm A* gene encoding *N*-acetylmuramidase specific to *Lactococcus lactis*, 1131 bp long PCR products)[1] were used for the identification of *Lactococcus lactis* species. The PCR mixture contained 1 µl of each 10mM dNTP, 1 µl (10 pmol µl^{-1}) of each primer, 1 µl of Taq 1.1 polymerase (1 U µl^{-1}), 2.5 µl of buffer (1.5mM), 1–3 µl of DNA matrix, and PCR water was added up to a 25 µl volume. The amplification reactions were carried out using the following cycle parameters: 5 min of the initial denaturation period at 94 °C (hot start), 60 s of denaturation at 94 °C, 60 s of primer annealing at 45 °C, and 60 s of extension at 72 °C. The final polymerisation step was prolonged to 10 min. PCR was performed in 30 cycles. The PCR products were separated and identified using electrophoresis in 1.5% agarose gel. The DNA on the gel was stained with ethidium bromide (0.5 µg ml^{-1}), observed on a UV transilluminator (305 nm), and documented.

Results and Discussion

Pre-PCR processing procedures have been developed to remove or reduce the effects of PCR inhibitors from hard cheese samples. Ten different cheese samples were used. The method of DNA isolation using magnetic microspheres was evaluated. Different amounts of cheese and different procedures of their homogenisation were tested at first. The best results were achieved with cheese samples (1 g of cheese 1.5 ml^{-1} of sterile water) homogenised in a grinding mortar. The hard pieces of cheese samples were removed using filtration through sterile gauze. The fat layer was removed from the filtrates by pipetting. The cells in the filtrates (1.5 or 3 ml) were centrifuged (10,000 g 5 min^{-1}), washed with 1 ml of ste-

rile water, and resuspended in 1 ml of lysis buffer with lysozyme and treated with laboratory temperature (see above). Then, the procedure of DNA isolation using magnetic microspheres was used (see above). In PCR 1 and 3 µl of DNA matrix were used. The results with 3 µl of DNA matrix are shown in Fig. 1. In all samples prepared from 3 ml of filtrate, PCR products specific to *Lactococcus lactis* were amplified.
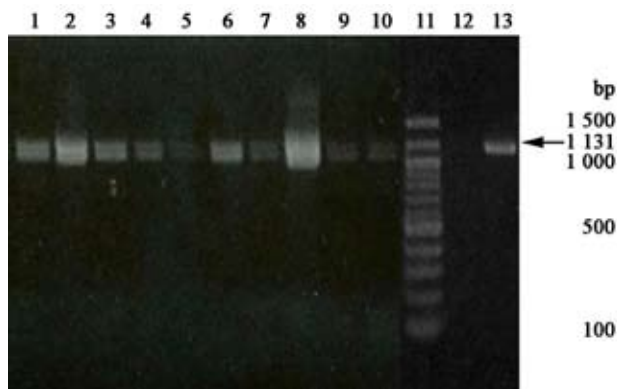
Fig. 1. **Agarose gel electrophoresis of PCR products obtained after amplification of *Lactococcus lactis* DNA (3 µl) isolated from hard cheese samples by magnetic microspheres. Lanes 1-10: hard cheese samples, lane 11: DNA standards (100 bp ladder), lane 12: negative control without DNA, lane 13: positive control with purified *Lactococcus lactis* subsp. lactis CCM 1877T DNA (c_{DNA} = 10 ng µl^{-1})**

Conclusion

The evaluated procedure of hard cheese sample preparation for DNA isolation using magnetic microspheres was verified on 10 different cheese samples with success. The quick and more simple method of DNA isolation with magnetic microspheres gave results comparable to those with DNA isolated using phenol extraction.

REFERENCES

1. Buist G., Kok J., Leenhouts K.J., Dabrowska M., Venema G., Haandrikman A.J.: J. Bacteriol. *177*, 1554 (1995).
2. Barakat R.K., Griffiths M.W., Harris L.J.: Int. J. Food Microbiol. *62*, 83 (2000).
3. Burdychova R., Komprda T.: FEMS Microbiol. Lett. *276*, 149 (2007).
4. Rittich B., Španová A., Horák D., Beneš M.J., Klesnilová L., Petrová K., Rybnikář A.: Colloids Surf. B: Biointerfaces *52*, 143 (2006).
5. Španová A., Rittich B., Štyriak I., Štyriaková I., Horák D.: J. Chromatogr. A *1130*, 115 (2006).
6. Španová A., Horák D., Soudková E., Rittich B.: J. Chromatogr. B *800*, 27 (2004).
7. Sambrook J., Russel D.W.: *Molecular Cloning* (3rd ed.), Cold Spring Harbor Laboratory Press, New York, 2001.

P96 IDENTIFICATION OF BACTERIAL STRAINS OF *STREPTOCOCCUS THERMOPHILUS* SPECIES USING PCR

ALENA ŠPANOVÁ, MARTINA TYCOVÁ, ŠTĚPÁNKA TRACHTOVÁ and BOHUSLAV RITTICH

Brno University of Technology, Faculty of Chemistry, Department of Food Chemistry and Biotechnology, Purkyňova 118, 612 00 Brno, Czech Republic,
spanova@fch.vutbr.cz

Introduction

Most molecular diagnostic studies of lactic acid bacteria have been focused on the strains of *Lactobacillus* and *Bifidobacterium*[1–4] genera due to their probiotic potential and commercial exploitation in food industry. Undeservedly less attention has been devoted to the identification of *Streptococcus thermophilus* in the literature. *Streptococcus thermophilus* is namely one of the most widely used lactic acid bacteria in the dairy industry as a starter culture component in the manufacture of fermented dairy products, such as yoghurt and cheese, and in probiotic preparations. Identification of *Streptococcus thermophilus* is therefore important. Classical methods based on biochemical characterisation are in many cases insufficient. For this reason, specific PCR primers for identification *of Streptococcus thermophilus* cells were described in the literature[5,6].

The aim of this work was to isolate PCR-ready DNA from yoghurt and milk drink samples containing PCR inhibitors. Carboxyl-functionalised magnetic poly(2-hydroxyethyl methacrylate-*co*-ethylene dimethacrylate) microspheres (P(HEMA-*co*-EDMA)) were used for DNA isolation. The quality of extracted DNA was checked by PCR specific to *Streptococcus thermophilus*.

Material and Methods

C h e m i c a l s a n d E q u i p m e n t

Primers for PCR were synthesised by Generi-Biotech (Hradec Králové, Czech Republic); *Taq*I DNA polymerase was from Bio-Tech (Prague, Czech Republic), DNA ladder 100 bp from Malamité (Moravské Prusy). The PCR reaction mixture was amplified on an MJ Research Programme Cycler PTC-100 (Watertown, USA).

Magnetic nonporous poly(2-hydroxyethyl methacrylate-co-glycidyl methacrylate) P(HEMA-*co*-GMA) microspheres containing carboxyl groups were prepared according to the previously described procedure[7] in the Institute of Macromolecular Chemistry (Academy of Sciences of the Czech Republic) in Prague. Magnetic microspheres were separated on a Dynal MPC-M magnetic particle concentrator (Oslo, Norway).

M e t h o d s

The strain *Streptococcus thermophilus* CCM 4757 from the Czech Collection of Microorganisms was used as a control strain. It was cultivated on MRS agar with 0.5 % of glucose at 30 ºC for 48 h. The cells from 1.5 ml culture were centrifuged (14,000 g 5 min^{-1}), washed in water, and resuspended in 500 µl of lysis buffer (10mM Tris, pH 7.8, 5mM EDTA pH 8.0, lysozyme 3 mg ml^{-1}). After 1 hour, 12.5 µl of 20% SDS and 5 µl of proteinase K (10 µg ml^{-1}) were added and incubated at 55 °C overnight. DNA from these crude cell lysates was extracted using phenol method[8], precipitated with ethanol and dissolved in TE buffer (10mM Tris-HCl, 1mM EDTA, pH 7.8).

Altogether 2 g of yoghurt (milk drink) samples resuspended in 2 ml water was centrifuged (12,000 g 5 min^{-1}) to sediment the bacteria cells. The cells in the sediments were washed with 1 ml of sterile water and lysed. DNA from yoghurt samples was isolated from crude cell lysates by the phenol extraction procedure (control) (see above) and by magnetic microspheres (see later). Magnetic microspheres P(HEMA-*co*-EDMA) (100 µl, 2 mg ml^{-1}) containing carboxyl groups were added to the crude cell lysates (100 µl) together with 5M NaCl (400 µl), 40% PEG 6000 (200 µl) and water to a volume of 1,000 µl (200 µl). After 15 minutes of incubation at laboratory temperature, the microspheres with bound DNA were separated using magnet, washed in 70% ethanol, and DNA was eluted into 100 µl of TE buffer.

Species-specific PCR primers were used for the identification of *Streptococcus thermophilus* species[9]. The PCR mixture contained 1 µl of each 10 mM dNTP, 1 µl (10 pmol µl^{-1}) of each primer, 1 µl of Taq 1.1 polymerase (1 U µl^{-1}), 2.5 µl of buffer (containing 1.5 mM Mg^{2+} ions), 1–5 µl of DNA matrix, and PCR water was added up to a 25 µl volume. The amplification reactions were carried out using the following cycle parameters: 5 min of the initial denaturation period at 95 °C (hot start), 60 s of denaturation at 95 °C, 60 s of primer annealing at 58 °C, and 60 s of extension at 72 °C. The final polymerisation step was prolonged to 10 min. PCR was performed in 30 cycles. The PCR products were separated and identified using electrophoresis in 1.5% agarose gel. The DNA on the gel was stained with ethidium bromide (0.5 µg ml^{-1}), observed on a UV transilluminator (305 nm), and documented on a TT667 film using a CD34 camera.

Results and Discussion

Fermented diary products (8 white and fruit yoghurts and 2 milk drinks) from the market were used for the analysis. Pre-PCR processing procedures have been developed to remove or reduce the effects of PCR inhibitors from tested samples. The quality of DNA in crude cell lysates of bacteria from yoghurt (milk drink) samples was proved (see Material and methods) using agarose gel electrophoresis. DNA in amounts from approximately 70 to 350 ng was detected. Then, the method of DNA isolation using magnetic microspheres was evaluated. The amounts of eluted DNA in all samples tested were smaller than the detection limit for gel electrophoresis, but these amounts were sufficient for PCR. Detection of specific 968 bp long PCR products is given in Fig. 1. in which PCR product intensities for different amounts of DNA matrix are compared. PCR products of higher inten-
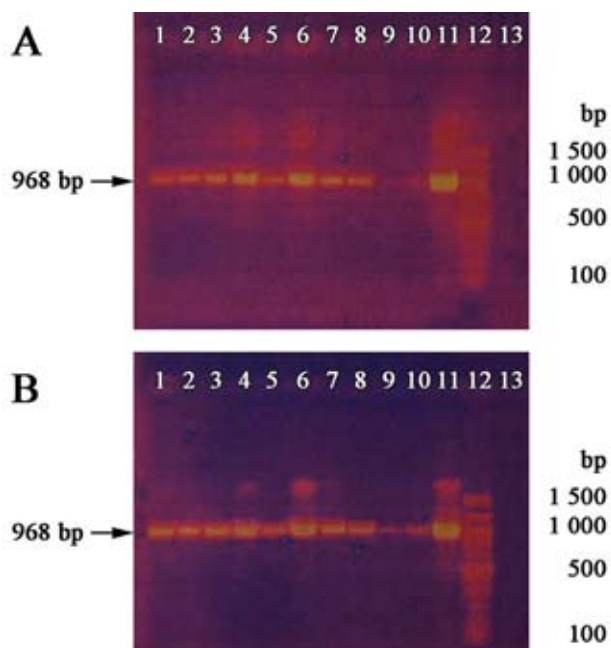
Fig. 1. **Agarose gel electrophoresis of PCR products obtained after amplification of *Streptococcus thermophilus* DNA isolated from yoghurt and milk drink samples by magnetic microspheres. Lanes 1-8: yoghurt samples, lanes 9,10: milk drinks, lane 11: positive control with purified Streptococcus thermophilus CCM 4757 DNA (c_{DNA} = 10 ng µl^{-1}), lane 12: DNA standards (100 bp ladder), lane 13: negative control without DNA. A: 1 µl of DNA matrix, B: 2 µl of DNA matrix**

sity were detected using higher amounts of DNA matrix. From these results it follows that the negative influence of PCR inhibitors in tested products on the PCR course was thus eliminated. DNA was isolated in a quality suitable for PCR.

Conclusion

The method of DNA isolation from yoghurt samples by magnetic microspheres was evaluated. Using the proposed DNA isolation process, PCR products specific to *Streptococcus thermophilus* were amplified in all samples. The results presented here show that the simple method proposed is suitable for the isolation of whole DNA from yoghurt and milk drink samples, which can be used for PCR.

REFERENCES

1. Haarman M., Knol J.: Appl. Environ. Microbiol. *72*, 2359 (2006).
2. Ward P., Roy D.: Lait *85*, 23 (2005).
3. Masco L., Vanhoutte T., Temmerman R., Swings J., Huys G.: Int. J. Food Microbiol. *113*, 351 (2007).
4. Burdychova R., Komprda T.: FEMS Microbiol. Lett. *276*, 149 (2007).
5. Brigidi P., Swennen E., Vitali B., Rossi M., Matteuzzi D.: Int. J. Food Microbiol. *81*, 203 (2003).
6. Timisjarvi A. T., Alatossava T.: Int. J. Food Microbiol. *35*, 49 (1997).
7. Španová A., Horák D., Soudková E., Rittich B.: J. Chromatogr. B *800*, 27 (2004).
8. Sambrook J., Russel D. W.: *Molecular Cloning* (3rd ed.), Cold Spring Harbor Laboratory Press, New York, 2001.
9. Lick S., Drescher K., Heller K. J.: Appl. Environ. Microbiol. *67*, 4137 (2001).

P97 STUDY OF OXIDATION STABILITY OF SELECTED VEGETAGLE OILS

HANA ŠTOUDKOVÁ, MONIKA MAXOVÁ, JIŘÍ KUČERÍK and JANA ZEMANOVÁ

Brno University of Technology, Faculty of Chemistry, Purkynova 118, 61200 Brno, Czech Republic,
stoudkova@fch.vutbr.cz

Introduction

Vegetable oils are obtained from different parts of oil-seed plants by cold expression and subsequent extraction and purification. Since long ago, oils belong to among basic cosmetic preparations and use in pharmaceuticals, food industry and other industrial purposes. They embody the whole series of authenticated positive efects on human organism and they are used as a part of food supplements[1].

Food lipids undergo a chain of changes due to ripening, harvesting, processing and storage. These changes are caused by several factors including browning reactions, microbial spoilage and lipid autoxidation. Lipid oxidation is a free-radical chain reaction that causes a total change in the sensory properties and nutritive value of food products[2].

Oxidation processes influence quality of oils and fats. Characteristic changes associated with oxidative deterioration include development of unpleasant tastes and odours as well as changes in color, viskosity, density or solubility[3]. The others of the effects of lipid oxidation can be loss of vitamins, and damage to proteins[2].

Differential scanning calorimetry (DSC) is the technique used for establishing the oxidative stability of oils and fats and characterizion of their physical properties[4,5]. Oxidative stability and deterioration of oils depend on initial composition, concentration of minor compounds with antioxidant or prooxidant characteristics, degree of processing, and storage conditions[6]. Quality and stability of vegetable oils are important factors that influence its acceptability and market value.

The induction period (IP) is measured as the time required to reach an endpoint of oxidation corresponding to either a level of detectable rancidity or a sudden change in the rate of oxidation[7].

Experimental

S a m p l e s

Different vegetable oils from various plant origins were used in this study. These were Grape Seed oil refined, Crude Linseed oil, Castor oil, Almond oil refined, Soya Bean oil refined, Avocado oil refined, Apricot Kernel oil refined, Corn oil refined and Olive oil refined.

Samples were obtained from M + H, Míča and Harašta, s.r.o. After opening the bottles with oils there were stored at 4 °C.

M e t h o d

Differential Scanning Calorimetry (DSC) of each sample in oxygen atmosphere were performed several times until reproducible results were obtained. For this purpose Shimadzu DSC-60 (Kyoto, Japan) was used connected through TA-60WS with computer, where the data were collected.

The furnace was calibrated by using transition temperatures of fusion of indium and zinc (melting point: 156.6 °C for indium, 419.6 °C for zinc).

Samples were measured out 2.5 µl (0.2, 0.5 °C min^{-1}), 5.0 µl (1.0, 3.0, 5.0, 7.0 °C min^{-1}) and 10 µl (10.0, 15.0 °C min^{-1}) and measured in open aluminum pan. Flow rate of oxygen was set at 15 ml min^{-1} and rate of heating 0.2, 0.5, 1.0, 3.0, 5.0, 7.0, 10.0 and 15.0 °C min^{-1} from room temperature (25 °C) to 300 °C was applied. Obtained results were treated by means of enclosed software TA-60.

Results

For the using vegetable oils, the kinetic parameters important to the determination of induction period were obtained for non-isothermal DSC measurements. The onset temperatures of oxidation for various using oils were measured with scan rates 0.2, 0.5, 1.0, 3.0, 5.0, 7.0, 10.0 and 15.0 °C min^{-1}.

The parameters A and B were obtained by a comparison of experimental and theoretical values of onset temperatures of the oxidation peaks using the program TIND. The values of kinetic parameters A and B are listed in the Table I.

Table I
Values of the kinetic parameters A and B

Oils	A [min]	B [K]
Castor	2.72×10^{-13}	1.38×10^{4}
Olive	6.62×10^{-13}	1.32×10^{4}
Soya Bean	1.54×10^{-11}	1.16×10^{4}
Avocado	4.69×10^{-11}	1.12×10^{4}
Grape Seed	4.43×10^{-12}	1.19×10^{4}
Almond	5.26×10^{-11}	1.10×10^{4}
Corn	1.00×10^{-10}	1.08×10^{4}
Apricot Kernel	1.29×10^{-10}	1.06×10^{4}
Crude Linseed	8.99×10^{-12}	1.12×10^{4}

The temperature dependence of the induction period can be expressed according to the Equation (1):

$$t_i = A \exp (B/T) \tag{1}$$

Providing that parameters A [min] and B [K] were obtained by minimizing the sum of squares between experimental and theoretical values of heating rate and T [K] is specific temperature, induction period t_i [min] can be determined.

Induction period values (t_i) of various using vegetable oils calculated for temperature 25 °C and 100 °C are shown in Table II.

Table II
Values of the induction periods – extrapolation to 25 °C (t_i^{25}) and extrapolation to 100 °C (t_i^{100})

Oils	t_i^{25} [min]	t_i^{100} [min]
Castor	3.00×10^7	2.81×10^3
Olive	1.28×10^7	1.70×10^3
Soya Bean	1.34×10^6	5.29×10^2
Avocado	1.03×10^6	5.37×10^2
Grape Seed	9.87×10^5	3.22×10^2
Almond	5.93×10^5	3.52×10^2
Corn	5.44×10^5	3.80×10^2
Apricot Kernel	3.31×10^5	2.65×10^2
Crude Linseed	1.79×10^5	9.49×10^1

In the case low temperature (25 °C), sequence of stability vegetable oils was falled: castor > olive > soya bean > avocado > grape seed > almond > corn > apricot kernel > crude linseed.

Enormously high induction period values, especially castor and olive oil, appeared unreal. By this reason, the extrapolation on high temperature (100 °C) was applied.

From the determined values it is obvious that castor and olive oil had the longest induction period and apricot kernel and crude linseed oil had the shortest induction period. In the case soya bean and avocado oil, it was obtained the similar results and the values of the both oils differed about 8 minutes.

Induction periods for individual oils were determined from the known values onset temperatures and parameters A and B. Equation 1 was used for calculation. Dependences of the experimental calculated induction periods on the temperatures are demonstrated in Fig. 1.
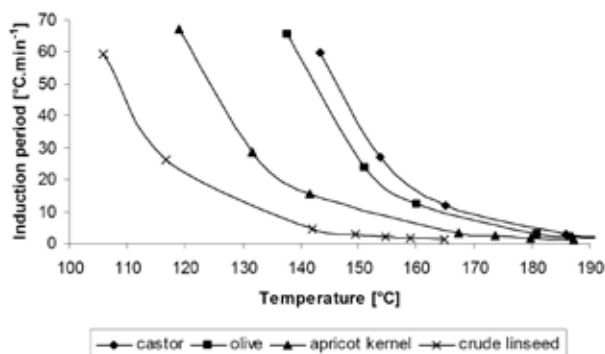
Fig. 1. **Temperature dependences of the induction periods for the most stable (castor and olive oil) and the least stable (apricot kernel and crude linseed oil) vegetable oils**

Conclusions

The order of stability of vegetable oils was identified by statistical comparison of record gained from various temperature extrapolation and reciprocal comparison of stability of given oils. The order of the most stable oils (castor and olive oil) and the least stable oil (linseed oil) depending on extrapolation and reciprocal comparison did not differ. The non-isothermal method DSC was employed with the aim to determine the induction period of vegetable oils.

REFERENCES

1. Dugo G. et al.: Food Chem. *87*, 639 (2004).
2. Coni E., et. al.: Thermochim. Acta *418*, 11 (2004).
3. Šimon P. Kolman L., et al.: JAOCS *77*, 639 (2000).
4. Tan C. P., Che Man Y. B.: Trends Food Sci. Technol. *13*, 312 (2002).
5. Giuffrida F., et al.: Food Chem. *101*, 1108 (2007).
6. Crapiste G. H., et al: JAOCS *77*, 1437 (1999).
7. Frankel E. N.: Trends Food Sci. Technol. *4*, 220 (1993).

P98 ANTIOXIDANT PROPERTIES OF GRAPE SKINS EXTRACTS INVESTIGATED BY EPR AND UV-VIS SPECTROSCOPY

LENKA ŠŤAVÍKOVÁ[a] and MARTIN POLOVKA[b]

[a]*Department of Food Chemistry and Biotechnology, Faculty of Chemistry, Brno University of Technology, Purkyňova 118, 612 00 Brno, Czech Republic,*
[b]*Department of Chemistry and Food Analysis, VÚP Food Research Institute, Priemyselná 4, 824 75 Bratislava, Slovak Republic,*
stavikova@fch.vutbr.cz

Introduction

The growing attention is recently focused on the improvement of human health by the consumption of food or food supplements rich in antioxidants. Grape skins contain a plenty of different flavonoids, e.g., quercetin, catechins, flavonols, anthocyanidins, phenolic acid derivatives and other compounds. Anthocyanins, as the most abundant of them, are associated with the colour of several aerial and subterranean organs in many plants. In grapevines, anthocyanins are accumulated in leaves during senescence and are responsible for the colouration of grape skins in red and rosé cultivars, and in the grape pulp, respectively. These pigments are water soluble and reveal the beneficial effects on human health, including the enhancement of visual acuity, but evinced also anticarcinogenic, antimutagenic or anti-inflammatory action. The reduction of coronary heart disease and thus the phenomenon known as the "French Paradox" is attributed to them, as well.[1-5]

Main interest is paid to the isolation of phenolic compounds from grapes and wine. A great effort is given to choose a suitable extraction system for anthocyanins isolation, as they are highly reactive compounds and exceptionally sensitive to pH changes[6,7]. Supercritical fluid extraction with carbon dioxide and pressurized liquid extraction with acidified water, sulphured water or acidified organic solvents were successfully applied for the extraction of different phenolic compounds from grapes and wines in the past.[8-11]

In this contribution, the complex study of grape skin methanolic extracts, prepared by Pressurized Fluid Extraction (PFE)[12,13] from two wine grape varieties, St. Laurent and Alibernet from Velké Pavlovice and Mikulov sub-regions (South Moravia region, Czech Republic) is presented.

Experimental

Respective methanolic extracts were prepared from three different amounts (0.5 g, 1.0 g and 1.5 g) of either crude dried grape skins (St. Laurent) or lyophilized grape skin powders (Alibernet) using the PFE extraction at different temperature (40 °C–120 °C) and pressure of 15 MPa[12, 13].

Antioxidant activity of extracts was tested by EPR spectroscopy using the Bruker portable EPR spectrometer e-scan with accessories in Fenton system (H_2O_2/Fe^{2+}), generating reactive hydroxyl radicals (•OH) followed by spin trapping technique, using the 5,5-dimethylpyrroline-N-oxide (DMPO) as spin trap[14]. In addition, radical scavenging activity of extracts was assessed applying 2,2-diphenyl-1-picrylhydrazyl (•DPPH) free radical and 2,2'-azino-bis-(3-ethylbenzthiazoline-6-sulfonic acid) cation radical (ABTS•+) assays. All the experiments were performed at 298 K, using the same quartz flat cell. EPR spectra were processed similarly as previously described elsewhere[15].

Total phenolic compounds' content (TPC) of individual extracts was determined using the Folin-Ciocalteu assay and their tristimulus colour values (CIE Lab) were estimated, using the UV-VIS spectrophotometer Specord (Carl Zeiss, Jena, Germany)[16,17].

In addition, pH values of all extracts were also measured using the combined glass electrode.

All the data obtained were subsequently correlated and discriminated, using the multivariate statistics, involving the canonical discriminant analysis, principal component analysis, and canonical correlation analysis, respectively.

Results

EPR Experiments

Antioxidant properties of grape skin extracts were tested in experimental systems, in which free radicals were generated via Fenton reaction. Fig. 1. shows typical time evolution of EPR spectra recorded in system containing respective
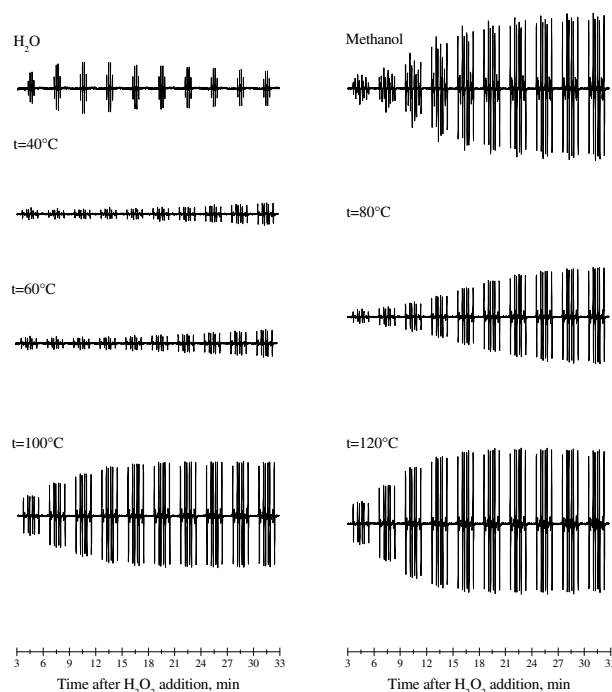
Fig. 1. **The time evolution of EPR spectra recorded in system containing deionised water, methanol (reference) and methanolic extracts of St. Laurent variety prepared from 1.5 g of crude grape skins at 40–120 °C, respectively; Fenton's reagents and DMPO spin trap. Spectra were recorded at 298 K using magnetic field sweep, SW = 8 mT**

grape skin extract of St. Laurent wine variety and Fenton's reagents, in the presence of DMPO spin trap. As follows from simulation analysis, in the presence of pure water, dominantly the formation of $^{\bullet}$OH radicals is observed, whereas in pure methanol (reference sample), the formation of different types of carbon-centred radicals is to be found, in accord with our previous experiments and already published data.[14,15,18] The addition of grape skin extracts into system resulted in the decrease of spin adduct concentration as a result of competitive reactions between the antioxidants, generated free radicals and spin trap.[15,18,19]

Staško et al., suggested previously the expression of antioxidant activity of Tokay wines as the relative amounts of radicals scavenged[19]. Using this approach, we can conclude that antioxidant properties of St. Laurent variety extract is significantly lower than that of Alibernet (66 % and 89 %, respectively, for extracts prepared from 1.0 g at 40 °C). As we moreover proved, antioxidant activity of extracts is in both cases strongly dependent on extraction temperature, falling down to 9 % for St. Laurent extract prepared from 1.0 g at 120 °C, whereas that of Alibernet descended practically to zero.

$^{\bullet}$DPPH and ABTS$^{\bullet+}$ radicals assays are traditionally used for food samples radical-scavenging ability (RSA) evaluation. They were previously successfully used, e. g., for tea or wine samples characterisation.[15,18-20] As we confirmed, extracts of both varieties prepared at 40 °C demonstrated significant ability to terminate $^{\bullet}$DPPH and ABTS$^{\bullet+}$.

Pellegrini et al. suggested the effective comparison of RSA for different food products, based on Trolox-equivalent antioxidant capacity (TEAC) calculation[21]. Following this approach, TEAC value of each extract was calculated for reactions with both $^{\bullet}$DPPH and ABTS$^{\bullet+}$. As follows from the results obtained, the increasing extraction temperature TEAC$_{ABTS^{\bullet+}}$ values of St. Laurent variety (Fig. 2.) are slightly

lower in comparison to that of Alibernet, only slightly influenced by extraction temperature. On the other hand, TEAC$_{DPPH^{\bullet}}$ values differ significantly, in the case of St. Laurent extracts prepared from 1.0 g, they range from 1.50 to 1.75, whereas in the case of Alibernet from 3.7 to 4.0.

U V - V I S   E x p e r i m e n t s

The TPC content of all extracts under study was monitored and expressed as Gallic acid equivalent (GAE)[16]. The results obtained indicate that the content of polyphenols in Alibernet variety extracts is more than two times higher than that of St. Laurent. This would explain generally higher antioxidant and radical-scavenging activities of Alibernet extracts. Significant correlation (>85%, P>0.01) between the TPC and TEAC for both types of extracts was achieved, in dependence on the mass of grape skins used for the extract preparation. As follows from data presented in Table I, correlation is better for St. Laurent varieties, probably due to different composition of polyphenols.

Table I
Correlation matrices between the TPC content and radical-scavenging abilities of grape skin extracts

	TPC	TEAC$_{ABTS^{\bullet+}}$	TEAC$_{\bullet DPPH}$
St. Laurent			
TPC	1	0.9778	0.9518
TEAC$_{ABTS^{\bullet+}}$	0.9778	1	0.9060
TEAC$_{\bullet DPPH}$	0.9518	0.9060	1
Alibernet			
TPC	1	0.8650	0.9220
TEAC$_{ABTS^{\bullet+}}$	0.8650	1	0.6909
TEAC$_{\bullet DPPH}$	0.9220	0.6909	1

As a result of growing extraction temperature from 40 °C up to 120 °C, approx. 20% and 40% decrease of the TPC content in extracts of St. Laurent and Alibernet varieties was noticed, respectively.

Fig. 2. **Trolox equivalent antioxidant capacity (TEAC) of St. Laurent extracts, prepared at different temperature from different mass of crude grape skins in the reaction with ABTS$^{\bullet+}$**
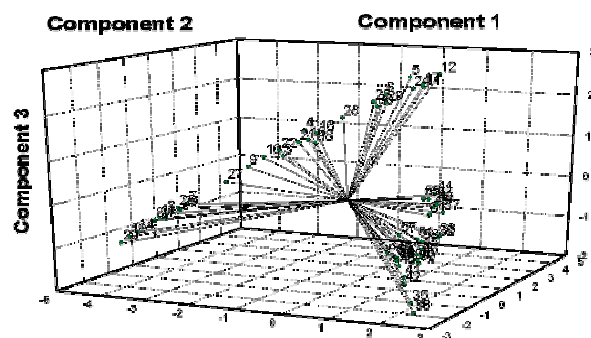
Fig. 3. **Classification – recognition of both wine grape varieties (1–30 – St. Laurent, 31–60 – Alibernet) based on principal component analysis**

The influence of extraction temperature on CIE L[*], a[*], b[*] colour characteristics or on pH values was only negligible.

S t a t i s t i c a l   E v a l u a t i o n

All the above mentioned characteristics were used for the classification and mutual recognition of both wine grape varieties using the principal component analysis (Fig. 3.) and canonical discrimination analysis[22].

Both statistical approaches provided practically 100% correct classification of both varieties. As also follows from discriminant analysis, all the monitored characteristics are dependent on the mass of grape skins used for respective extract preparation.

Additional experiments are in progress to evaluate the influence of solvent on the above-mentioned characteristics as well as to analyze the profile of polyphenols in both grape skin varieties.

Conclusions

Multi-experimental analysis performed with methanolic extracts prepared from grape skins of two varieties (St. Laurent and Alibernet) by PFE, revealed their significant antioxidant and radical-scavenging abilities, in significantly positive correlation with the TPC content. The influence of extraction temperature on radical – scavenging abilities, tristimulus values or TPC content is non-significant.

REFERENCES

1. Ju Z. Y., Howard L. R.: J. Agric. Food Chem. *51*, 5207 (2003).
2. Garcia-Alonso M., Rimbach G., Sasai M.: Mol. Nutr. Food Res. *49*, 1112 (2005).
3. Longo L., Vasapollo G.: Food Chem. *94*, 226 (2006).
4. Cantos E., Espín J. C., Tomás-Barberán F. A.: J. Agric. Food Chem. *50*, 5691 (2002).
5. Czyzowska A., Pogorzelski E.: Eur. Food Res. Technol. *214*, 148 (2002).
6. Durán N., Minussi R. C., Rossi M..: Food Chem. *82*, 409 (2003).
7. Kähkönen M. P., Heinämäki J., Ollilainen V.: J. Sci. Food Agric. *83*, 1403 (2003).
8. Roth M., Karásek P., Planeta J.: J. Chromatogr. A *1002*, 13 (2003).
9. Postecu I. D., Tatomir C., Chereches G..: J. Optoel. Adv. Mater. *9*, 564 (2007).
10. Luque-Rodríguez J. M., Luque de Castro M. D., Pérez-Juan P.: Biosource. Technol. *98*, 2705 (2007).
11. Ju Z. Y., Howard L. R.: J. Food Sci. *70*, S270 (2005).
12. Richter E. B., Jones B. A., Ezzell J.L.: Anal. Chem. *68*, 1033 (1996).
13. http://www.epa.gov/SW-846/pdfs/3545a.pdf.
14. Polyakov N. E., Kruppa A. I., Leshina T. V., Konovalova T. A., Kispert L. D.: Free Rad. Biol. Med. *31*, 43 (2001).
15. Polovka M.: J. Food Nutr. Res. *45*, 1 (2006).
16. Suhaj M, Rácová J., Polovka M., Brezová V.: Food Chem. *97*, 696 (2006).
17. Horváthová J., Suhaj M., Polovka M.: Chem. Pap. *61*, 1 (2007).
18. Polovka M., Brezová V., Staško A.: Biophys. Chem. *106*, 39 (2003).
19. Staško A., Polovka M., Brezová V., Biskupič S., Malík F.: Food Chem. *96*, 185 (2006).
20. Staško A., Brezová V., Biskupič S., Rapta P.: J. Food Nutr. Res. *46*, 145 (2007).
21. Pellegrini N., Simonetti P., Gardana C., Brenna O., Brighenti F., Pietta P.: J. Agric. Food Chem. *75*, 339 (2001).
22. Koreňovská M., Suhaj M.: Eur. Food Res. Technol. *221*, 550 (2005).

P99   THE IMPACT OF FERMENTATION PROCESS ON AMINO ACID PROFILE OF GRÜNER VELTLINER WHITE WINE

LENKA ŠŤAVÍKOVÁ and MIROSLAV HTKA

Department of Food Chemistry and Biotechnology, Faculty of Chemistry, Brno University of Technology, Purkyňova 118, 612 00 Brno, Czech Republic,
stavikova@fch.vutbr.cz

Introduction

Amino acids represent 30–40 % of total wine nitrogen. It is generally accepted, that they may act as nutrients for both yeast and malolactic bacteria during the wine fermentation. In the yeasts' growing phase, they can be either partially or totaly metabolised, excreted by living yeasts at the end of the fermentation or released by proteolysis during the autolysis of the dead yeasts. In addition, amino acids can serve as substrate for the production of aroma compounds [3–5] or biogenic amines[6,7] in wine. On the contrary, their production by enzymatic degradation of the grape proteins was described[1,2].

There is no doubt, that their content in wines is dependent on the fertilization and climatic conditions, duration of skin maceration in the must, field treatments and on other factors[2,6–8]. Recently, amino acids' content in wines is studied extensively for several reasons, e. g, due to the differentiation of Champagnes and sparkling wines[2], the determination of geographic origin, variety and vintage[2,7,8], the assessment of substances with enological interest (e.g., of aroma compounds)[3–5], or toxicological interest (biogenic amines etc.)[6,7,9,10], the monitoring of nitrogen metabolism during the fermentation[5,11] or their changes during the ageing of wines[12,13].

The determination of amino acid in wines is usually employed by HPLC with precolumn derivatization using *o*-phthaldialdehyde (OPA), fluorenylmethyl-chloroformate (FMOC) or 6-aminoquinolyl-N-hydroxysuc-cinimidyl carbamate (AQC).[2,4,6–8,10–14] Ion-exchange chromatography with post-column derivatization with ninhydrin reagent[1,9,15] or comprehensive two-dimensional gas chromatography[16] was successfully applied, as well.

In this contribution, the impact of spontaneous and inoculated fermentations on amino acids profile of Grüner Veltliner (*Vitis vinifera*) white wine is presented, applying an ion exchange chromatography with post-column derivatization with ninhydrin and spectrophotometric detection system.

Experimental

Wine Sample

Grüner Veltliner (*Veltlínské zelené*) white wine variety from Velké Pavlovice sub-region (South Moravia region, Czech Republic) was investigated. Wine samples were prepared by two different technological processes. In the first one, the spontaneous fermentation was used, whereas in the second, wine was prepared by inoculated fermentation. The sampling procedure was performed every other day continuously, starting from cider up to the final young wine.

Chromatographic Conditions

Respective wine sample was analysed to free amino acids (FAA) content after its filtration and dilution in Li-citric buffer (pH 2.2), employing the AAA T339 amino acid analyser (Mikrotechna, Prague, Czech Republic) equipped with Ostion LG ANB ion-exchange resin column. Amino acids separation was achieved by stepwise gradient elution using the Li-citric buffer system. Post-column derivatization with ninhydrin reagent and spectrophotometric measurement was used for their determination.

Results

Concentration profile of the following 36 compounds potentially present in wine samples under study was investigated: cysteic acid (CystAC), tautine (Tau), phosphoethanolamine (PE), urea, aspartic acid (Asp), hydroxyproline (Hpro), threonine (Thr), serine (Ser), asparagine (Asn), glutamic acid (Glu), glutamine (Gln), α-aminoadipic acid (α-AAD), proline (Pro), glycine (Gly), alanine (Ala), citrulline (Cit), α-aminobutyric acid (α-ABA), valine (Val), cysteine (Cys), methionine (Met), cystathionine (Cysne), isoleucine (Ile), leucine (Leu), tyrosine (Tyr), phenylalanine (Phe), α-alanine (α-ALA), β-aminobutyric acid (β-ABA), γ-aminobutyric acid (GABA), ethanolamine (EA), ammonium (NH_3), ornithine (Orn), lysine (Lys), histidine (His), 1-methyl histidine (1-met His), 3-methyl histidine (3-met His), arginine (Arg).

Results obtained showed, that total FAA concentration in wine samples prepared by spontaneous fermentation ranged from 302.30 mg dm^{-3} up to 1,578.25 mg dm^{-3}, whereas in those prepared by inoculated fermentation, from 289.64 mg dm^{-3} up to 1,371.41 mg dm^{-3}.

In the sample prepared by a spontaneous fermentation, the total concentration of free amino acids slowly increased during the first three days from 1,299.75 g dm^{-3} to the maximum of 1,371.47 mg dm^{-3}, then in next six days of fermen-
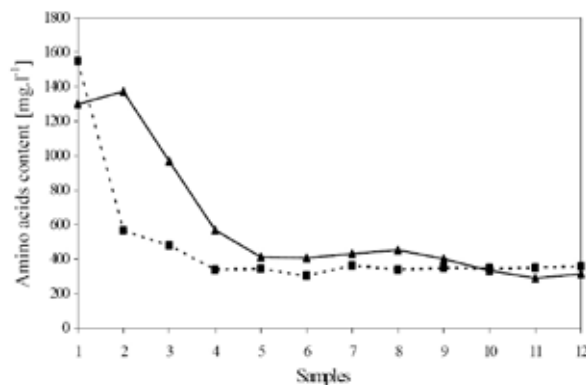
Fig. 1.   **Total free amino acids content monitored during 24 days in the wine samples prepared by spontaneous (▲) and inoculated (■) fermentation processes**
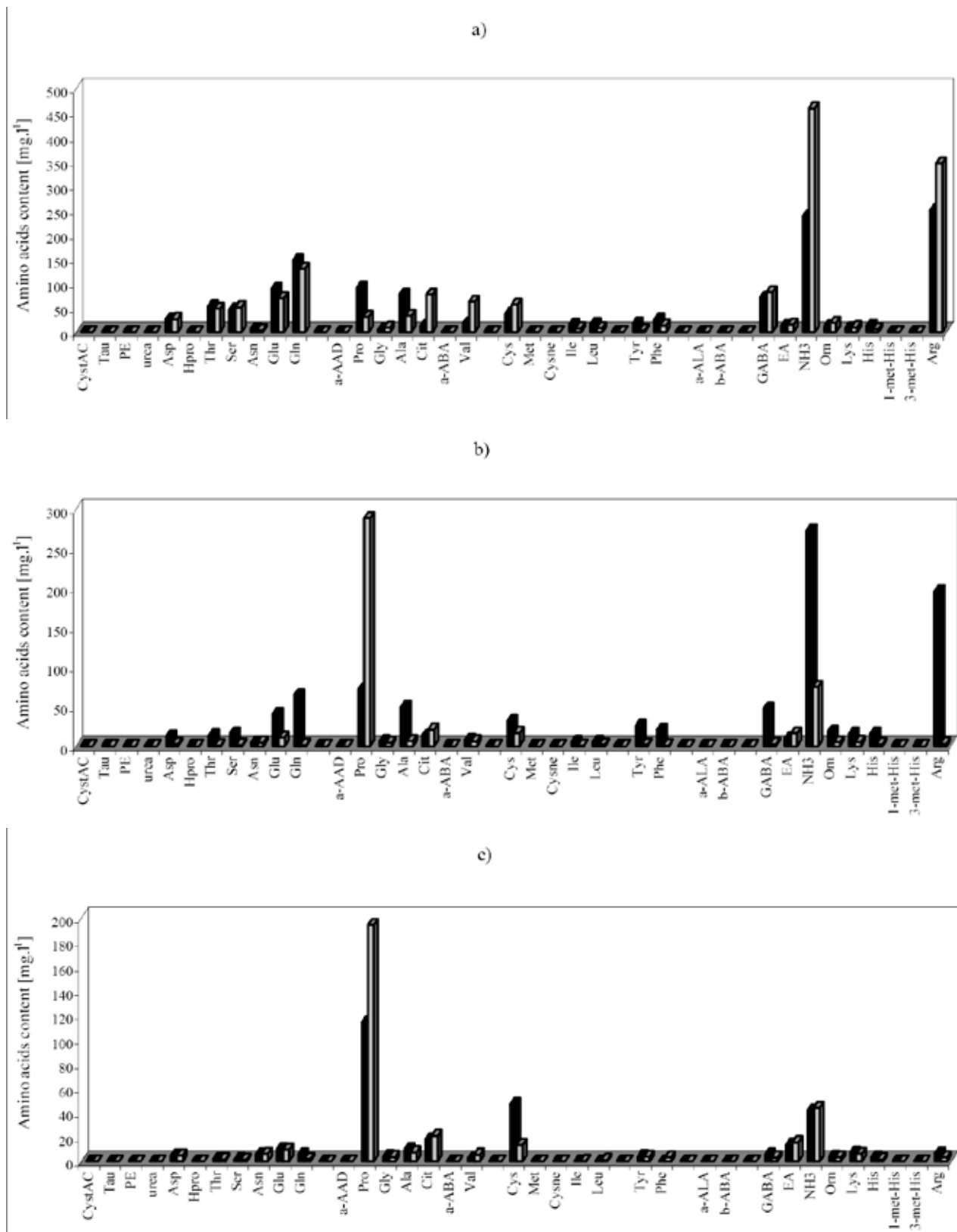
Fig. 2.　**The content of individual amino acids in a) cider, b) semi – fermented product, c) young wine prepared by spontaneous (black fill) and inoculated (gray fill) fermentation**

tation, the gradual decrease was noticed, falling down to 412.92 mg dm^{-3}. The continous fermentation proces caused their decrease to 289.64 mg dm^{-3} (Fig. 1.). The content of some amino acids, e.g. of Asp, Thr, Ser, Glu, Gln, Val, Ile, Leu, Ala, GABA, Orn, His and Arg revealed exactly the same decreasing trend as described above, whereas the content of Asp, Thr, Ser, Glu, Gln, Ala, Leu and Ile decreased after seven days of fermentation practically to zero.

In the so-obtained young wine, the total amino acids content was found to be 313.38 mg dm^{-3}. Proline was identified as the most abundant of them (113.86 mg dm^{-3}), followed by cysteine (47.18 mg dm^{-3}) and citrulline (18.32 mg dm^{-3}). Majority of amino acids identified in young wine reached the concentration level of 3–15 mg dm^{-3}, with the exception only for Tyr, Ser and Phe with the concentration lower than 3 mg dm^{-3}.

In the sample prepared by inoculated fermentation, a rapid decrease of total amino acids concentration from 1,578.25 mg dm^{-3} to 567.37 mg dm^{-3} was observed right at the begining of the fermentation process. During the next four days, only slow decrease of the amino acids content was detected, as also depicted on Fig. 1.

The same amino acids as in the case of spontaneous fermentation were found to influence the decrease of the total FAA content. On the other hand, the concentration of Asp, Tyr, Gly, Lys, Orn and EA amino acids remained practically unaffected by the fermentation.

Total amino acids content in young wine after twenty four days of fermentation was 358.13 mg dm^{-3} (Fig. 1., Fig. 2.).

The results obtained are in good agreement with the amino acid values determined in other wine varieties and viticultural regions[15,22].

Conclusions

Twenty-three different amino acids were positively identified in Grüner Veltliner white wine. For the first time, the dependence of the amino acids' profile on wine-making technologies is presented. The type of fermentation influences also the concentration of amino acids. This approach could be effectively used for the classification and identification of wines.

REFERENCES

1. Héberger K., Cosmós E., Simon-Sarkadi L.: J. Agric. Food Chem. *51*, 8055 (2003).
2. Souflerous E. H., Bouloumpasi E., Tsarchopoulos C., et al.: Food Chem. *80*, 261 (2003).
3. Hernández-Orte P., Cacho J. F., Ferreira V.: J. Agric. Food Chem. *50*, 2891 (2002).
4. Hernández-Orte P., Ibarz M. J., Cacho J., et al.: Food Chem. *98*, 300 (2006).
5. Ardö Y.: Biotechnol. Adv. *24*, 238 (2006).
6. Torrea D., Ancín C.: J. Agric. Food Chem. *50*, 4895 (2002).
7. Herbert P., Cabirta M. J., Ratola N., et al.: J. Food Eng. *66*, 315 (2005).
8. Bouloumpasi E., Soufleros E.H., Tsarchopoulos C., et al.: Vitis *41*, 195 (2002)
9. Cosmós E., Simon-Sarkadi L.: Periodica Polytechnica Ser. Chem. Eng. *46*, 73 (2002).
10. Bauza T., Kelly M.T., Blaise A.: Food Chem. *105*, 405 (2007).
11. Arias-Gil M., Garde-Cerdan T., Ancin-Azpilicueta C.: Food Chem. *103*, 13152 (2007).
12. Alcaide-Hidalgo J. M., Moreno-Arribas M. V., Martin-Alvarez P. J., et al.: Food Chem. *103*, 572 (2007).
13. Alcaide-Hidalgo J. M., Moreno-Arribas M. V., Polo M. C., et al.: Food Chem. *107*, 622 (2008).
14. Callejon R. M., Tesfaye W., Torija M. J., et al.: Eur. Food Res. Technol. *227*, 93 (2008).
15. Triebel S., Sproll C., Reusch H., et al.: Amino acids *33*, 451 (2007).
16. Mayadunne R., Nguyen T. T., Marriott P. J.: Anal. Bioanal. Chem. *382*, 836 (2005).

P100 CHARACTERIZATION OF NEUTRAL LIPID COMPOSITION OF *NIGELLA SATIVA* L. SEEDS OIL

CLAUDIA TOMA[a], ADELA PINTEA, CONSTANTIN BELE and FRANCISC V. DULF

[a]*Department of Pharmacognosy Faculty of Pharmacy, "Vasile Goldis" West University, 1 Feleacului Str., 300041, Arad, Romania,*
claudiatoma2004@yahoo.com

Introduction

Nigella sativa L. is an annual herbaceous plant which belongs to the family of *Ranunculaceae,* widely cultivated in Middle East, Asia and Northern Africa. The seeds, known as black cumin, are used for culinary purposes, as a spice for pastry and bakery. *Nigella* seeds and oil are used in arabian folk medicine for the treatment of asthma, as carminative, diuretic or lactogogue[1,2]. More recently *Nigella sativa* fixed oil showed gastroprotective, hepatoprotective and antitumour effects *in vivo*[3,4]. The biological effects of the oil are mainly atributable to thymoquinones, known as powerfull antioxidants. Other components such are polyunsaturated fatty acids, phytosterols and tocopherols can contribute to the beneficial effects of the black cumin seeds.

The lipid composition, including lipid classes, fatty acids and sterols of *Nigella* seeds of various geographical origins were reported[5,6,7]. The fixed oil contains high levels of unsaturated fatty acids and an unusual fatty acid – 20 : 2 (11c, 14c) – considered as a chemotoaxanomic marker for *Nigella* species. The main sterols reported in black cumin seeds were β-sitosterol, stigmasterol and campesterol[6,7]. The aim of this work was the study of lipid fraction in the oil of *Nigella* seeds cultivated in Romania, as a potential nutraceutical or ingredient of functional food.

Experimental

Extraction and Lipid Fractionation

Total lipids were extracted with chloroform : methanol (2 : 1; v/v), evaporated to dry and kept –20 °C in use. Neutral lipids were separated by TLC with a solvent mixture of hexane: ethyl ether: acetic acid (95 : 15 : 1).

Fatty Acids Analysis

The fatty acids methyl esters of total lipids and lipid fractions (FAME) were obtained by transesterification with BF_3/methanol. A Shimadzu GC 17A with FID detector and a Crompack Silica 25 MXO capillary column (25 m × 0.25 mm i.d., film thickness 0.25 μm) was used. The temperature program was: 5 min at 150 ºC, 4 ºC min⁻¹ to 235 º C (hold 5 min). The injector temperature was 260 °C and the detector temperature –260 °C. The carrier gas was helium.

Sterols Analysis

A part of total lipid extract was saponified by refluxing with 1M KOH ethanol/water (8 : 2, v/v) solution for 1 h. The unsaponifiables were then extracted first with petroleum ether and diethyl ether.

The sterols were derivatized BSTFA containing 1% TMCS in pyridine and separated on fused silica capillary column coated with 5% phenyl/95% dimethylpolysiloxane (30 m × 0.25 mm i.d., film thickness 0.25 μm; Rtx-5; Restek Corporation, Bellefonte, PA, USA). The same GC system mentioned above was used, with the following temperature program: 5 min at 200 °C, 10 °C min⁻¹ to 300 °C (hold 20 min).

FAME and sterols peaks were identified by comparison of their retention times with those of commercially available standards (Sigma). All extractions and GC-FID runs were performed in triplicate and mean values were calculated.

Results

Nigella seeds are characterized by high oil content, ranging between 30–40 % of fresh weight. The Romanian cultivar investigated has a total lipid (TL) content of 30.1 g 100 seeds⁻¹. For German cultivar a value of 39.2 % oil in fresh seeds was reported[8]. The major fraction is the neutral lipids, representing 96.6 % of the oil while the polar lipids (PL) count for 3.4 %. The total sterols were found at 87 mg 100g⁻¹ seeds, value which is lower than those reported for German cultivar but higher than for the Tunisian one (Table I)[6,7].

Table I
Nigella seeds oil composition

Fraction	Amount
Neutral lipids	29.1 ± 0.05 g 100 g⁻¹ seeds
Polar lipids	0.9 ± 0.01 g 100 g⁻¹ seeds
Total sterols	87.2 ± 0.02 mg 100 g⁻¹ seeds
Total oil	30.1 ± 0.05 g 100 g⁻¹ seeds

In the total lipids extract the major fatty acid was linoleic acid – 56.6 %, followed by oleic acid – 23.5 %. The most important saturated fatty acid was palmitic acid – 12.66 %. Saturated fatty acids represent 16 %, monounsaturated fatty acids – 23.8 % and polyunsaturated fatty acids account for more than 59 % of total lipids. The unusual eicosadienoic acid 20 : 2 (11c, 14c) was found at 2.5 %, value which is close to that reported for other cultivars.

The fatty acids composition of triacylglycerols (TAG) was closed to that of the TL. Diacylglycerols (DAG) and monoacylglycerols (MAG) contains lower palmitic and linoleic acid and higher oleic and eicosadienoic acid. The esterified sterols (SE) and the polar lipds (PL) contain the highest concentration of saturated fatty acids: palmitic (more than 17 %) and stearic (more than 4 %). The PL class also has the highest level of eicosadienoic acid. Miristic, linolenic and gadoleic acids were present in negligible amount in all lipid classes (Table II). Only traces of arachidic acid 20 : 0 were found. The sterol fraction contains: 37 % β-sitosterol, 11 % stigmasterol and 10 % campesterol as major compunds.

Tabulka II
Fatty acids composition of lipid classes [% of total fatty acids]

Fatty acid	TL	TAG	DAG	MAG	SE	PL
14:0	0.20	0.21	0.20	0.20	0.22	0.24
16:0	12.66	12.21	11.43	11.36	17.59	17.88
18:0	3.15	1.12	3.35	3.67	4.57	4.33
18:1 n-9	23.52	21.93	24.49	24.98	22.84	20.26
18:2 n-6	56.61	57.05	51.34	50.21	46.52	47.28
18:3 n-6	0.22	0.21	0.26	0.3	0.73	0.44
20:1 n-9	0.26	0.26	0.19	0.27	0.29	0.26
20:2 n-6	2.52	2.39	3.36	4.227	2.14	4.75

Conclusions

Black cumin seeds oil is exceptionally rich in biologically active polyunsaturated fatty acids, mainly linoleic acid. The presence of lipid-lowering phytosterols increases the nutritional value of the oil. There are small but non significant variations in the oil content and fatty acids composition in seeds of various origins which can be explained by genetic and environmental factors.

REFERENCES

1. Ali B. H., Blunden G.: Phytoter. Res. *17*, 299 (2003).
2. Houghton P .J., Zarka R., De las Hera, B., Hoult J. R.: Planta Med. *61*, 33 (1995).
3. El-Abhar H. S., Abdallah D. M., Saleh S.: J. Ethnopharmacol. *84*, 251 (2003).
4. Kanter M., Coskun O., Budancamanak M.: World J. Gastroenterol. *11*, 6684 (2005).
5. Saleh Al-Jasser M.: Food Chem. *45*, 239 (1992).
6. Ramadan M. F., Mörsel J. T.: Eur. Food Res. Technol. *214*, 521 (2002).
7. Cheikh-Rouhou S., Besbes S., Blecker C., Deroanna C., Attia H.: Food Chem. *101*, 673 (2007).
8. Ramadan M. F., Mörsel J. T.: Nahrung/Food *46*, 240 (2002).

P101 IDENTIFICATION OF VIABLE *LACTOBACILLUS* CELLS IN FERMENTED DIARY PRODUCTS

ŠTĚPÁNKA TRACHTOVÁ, ALENA ŠPANOVÁ and BOHUSLAV RITTICH

Brno University of Technology, Faculty of Chemistry, Department of Food Chemistry and Biotechnology
Purkyňova 118, 612 00 Brno
trachtova@fch.vutbr.cz

Introduction

Lactobacillus and *Bifidobacterium* species are commonly found in foods and are members of the gastrointestinal tract of humans and animals. They are the most commonly used group of lactic acid bacteria (LAB) in the production of human probiotics. Methods for qualitative and quantitative control of probiotic products are required due to the growing interest in their commercial exploitation. Differentiation of viable and non-viable cells of LAB from a product is still problematic. Culture-dependent enumeration is relatively time-consuming and the results may be influenced by poor viability or low densities of the target organisms[1]. Rapid and reliable methods are needed for routine determination of initial cell counts in the inoculum or for viable cell estimation during the time period of storage. Therefore, culture-independent analysis as an alternative and/or complementary method for quality control measurements of probiotic products was developed. The combination of PCR and the ethidium monoazide (EMA-PCR) dye is a new method for selective distinction between viable and dead bacterial cells[2-4]. The general application of EMA is based on EMA penetration into dead cells with compromised cell-membrane (cell-wall) integrity. EMA is covalently linked to DNA by photoactivation and this DNA cannot be amplified in PCR. Viable cells remain intact and only DNA from these cells can be amplified and gives a PCR product.

The aim of this work was to optimise and use EMA-PCR for distinction between viable and dead *Lactobacillus* cells in real samples of dairy products (yoghurts).

Materials and Methods
Chemicals and Equipment

The primers for PCR were synthesised by Generi-Biotech (Hradec Králové, Czech Republic); *Taq*I DNA polymerase was from Bio-Tech (Prague, Czech Republic); DNA ladder 100 bp (Malamité, Moravské Prusy), and EMA from Sigma (St. Louis, USA). The *Lactobacillus paracasei* CCDM strain (obtained from the Czech Collection of Dairy Microorganisms, CCDM, Tábor, Czech Republic) was used for DNA isolation. The dairy products (white yoghurts before and after expiration date) were obtained from the market. The PCR reaction mixture was amplified on an MJ Research Programme Cycler PTC-100 (Watertown, USA).

Methods

Bacterial cells of *Lactobacillus paracasei* were cultivated at 37 °C aerobically in liquid MRS medium for 24 h or on MRS agar up to 48 hours, respectively. Altogether 1 ml of the cells was washed by water and resuspended in 500 μl lysis buffer (10 mM Tris-HCl, pH 7.8, 5 mM EDTA, pH 8.0, lysozyme 3 mg ml^{-1}), and incubated at laboratory temperature for 1 h; 10 μl proteinase K (1 μg ml^{-1}) and 2.5 μl SDS (20 %) (end concentration 0.5 %) was added and the mixture was incubated at 55 °C for 18 h. DNA was extracted from crude cell lysates with phenol[5] and dissolved in TE buffer (10 mM Tris-HCl, pH 7.8; 1 mM EDTA, pH 8.0). The concentration of DNA was estimated spectrophotometrically and DNA was dissolved to a concentration of 10 μg ml^{-1}.

Yoghurt samples (Klasik white yoghurt OLMA Olomouc from the trade network before and after expiration date, 1 g) was resuspended in 1 ml sterile water. The cells were washed twice with sterile water and treated with EMA (0.1 mg ml^{-1}) for 10 min at laboratory temperature. Photoactivation was performed using light exposure (halogen lamp, 500 W) for 5 minutes on ice. Then the cells were washed with 1 ml of water to remove EMA from the sample. The cells without EMA treatment were used as control. Afterwards the cells were lysed by boiling (10 min) and crude cell lysates (5 μl) were used as DNA matrix in EMA-PCR.

PCR was performed with LBLMA 1 and R16 primers specific to the *Lactobacillus* genus[6], which enabled the amplification of a 250 bp long amplicon. Briefly: the PCR mixture contained 0.5 μl of each 10 mM dNTP, 0.5 μl (10 pmol μl^{-1}) of each primer, 0.5 μl of Taq 1.1 polymerase (1 U μl^{-1}), 2.5 μl of buffer (1.5 mM), 1–5 μl of DNA matrix, and PCR water was added up to a volume of 25 μl. The amplification reactions were carried out using the following cycle parameters: 5 min of the initial denaturation period at 94 °C (hot start), 60 s of denaturation at 94 °C, 60 s of primer annealing at 55 °C, and 60 s of extension at 72 °C. The final polymerisation step was prolonged to 10 min, the number of cycles was 30. The EMA-PCR products (250 bp) were detected using agarose gel electrophoresis (1.8 %) in 0.5 × TBE buffer (45 mM boric acid, 45 mM Tris-base, 1 mM EDTA, pH 8.0). The DNA was stained with ethidium bromide (0.5 μg ml^{-1}), observed on a UV transilluminator (305 nm), and photographed on a TT667 film using a Polaroid CD34 camera.

Results and Discussion

The ability of EMA to covalently bind to DNA and to inhibit PCR was confirmed using purified DNA isolated from *Lactobacillus paracasei* cells. As a result of EMA activity, DNA treated with EMA was not amplified in PCR in contrast to DNA without EMA treatment. The results are shown in Fig. 1. The method developed was applied for the discrimination of viable and dead *Lactobacillus* cells from dairy products (yoghurt). The results are shown in Fig. 2. and Table I. Non-expired or shortly expired (12 days) yoghurts contained both dead and viable *Lactobacillus* cells because intensities of EMA-PCR products amplified from EMA treated and
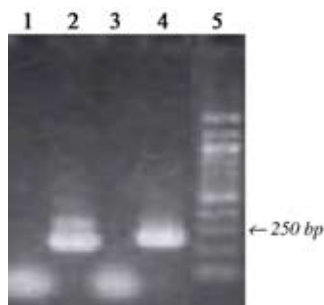
Fig. 1. **Agarose gel electrophoresis of EMA-PCR products obtained after amplification of purified *Lactobacillus* DNA: lane 1: EMA treatment, lane 2: no EMA treatment, lane 3: negative control without DNA, lane 4: positive control with purified *Lactobacillus* DNA ($c_{DNA} = 10\ ng\,\mu l^{-1}$), lane 5: DNA standard (100 bp ladder)**
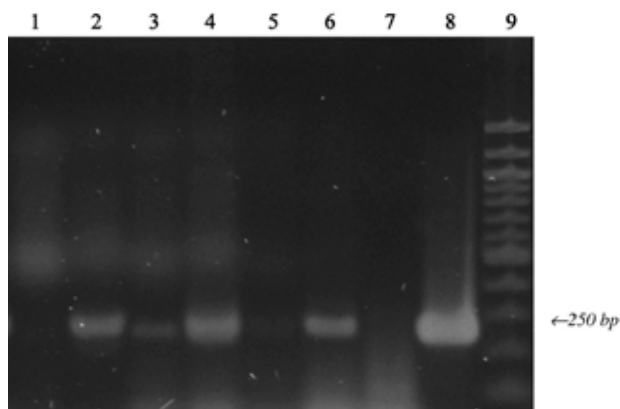
Fig. 2. **Agarose gel electrophoresis of EMA-PCR products obtained after amplification of *Lactobacillus* DNA from yoghurt: lanes 1, 3, and 5: cells with EMA treatment, lanes 2, 4, and 6: cells without EMA treatment, lane 9: DNA standard (100 bp ladder); lanes 1 and 2: 32 days after yoghurt expiration, lanes 3 and 4: not expired, lanes 5 and 6: 12 days after yoghurt expiration, lane 7: negative control without DNA, lane 8: positive control with purified *Lactobacillus* DNA ($c_{DNA} = 10\ ng\,\mu l^{-1}$)**

not treated cells deffered. On the contrary, in longer expired yoghurts only dead cells were detected. This is in agreement with the presumption that non-expired yoghurt samples contain more viable cells.

Table I
Identification of viable and dead *Lactobacillus* cells in yoghurt samples

Yoghurt expiration [days]	EMA treatment	EMA-PCR product	Viability of cells
Non-expired	+	++	viable and dead
	–	+++	
12	+	+	viable and dead
	–	++	
32	+	–	dead
	–	+++	

Conclusions

The results presented here show that the method proposed (ethidium monoazide treated cells in combination with polymerase chain reaction) is suitable for the distinction of viable and dead *Lactobacillus* cells. The method developed was applied for the analysis of real dairy products (yoghurts). More viable cells were detected in non-expired yoghurt samples.

REFERENCES

1. Roy D.: Int. J. Food Microbiol. *69*, 167 (2001).
2. Rudi K., Moen B., Drømtorp S. M., Holck A. L.: Appl. Environ. Microbiol. *71*, 1018 (2004).
3. Lee J. L., Levin R. E.: J. Microbial Methods *67*, 456 (2006).
4. Soejima T., Iida K., Qin T., Taniai H., Seki M., Takade A., Yoshida S.: Microbial Immunol. *51*, 763 (2007).
5. Sambrook J., Russel D. W.: Molecular Cloning (3rd ed.), Cold Spring Harbor Laboratory Press, New York, 2001.
6. Dubernet S., Desmasures N., Guéguen M.: FEMS Microbiol. Letters *214*, 271 (2002).

P102 DYNAMICS OF SELECTED PESTICIDES APPLIED TO APPLE PROTECTION DURING PRE-HARVEST AND POST-HARVEST PERIOD

JANA URBANOVÁ[a], ONDŘEJ LACINA[a], JAKUB SCHŮREK[a], MIROSLAV LÁNSKÝ[b] and JANA HAJŠLOVÁ[a]

[a]*Department of Food Chemistry and Analysis, Institute of Chemical Technology in Prague, Technicka 3, Prague 6, 166 28, Czech Republic,*
[b]*Research and Breeding Institute of Pomology, Holovousy, Czech Republic,*
jana.hajslova@vscht.cz

Introduction

Pesticides represent an important group of agrochemicals used for food crop protection. However, their residues can often be detected in treated crops at the harvest time. Because of the health hazard, this issue is of high concern, mainly when crops containing residues are intended for baby food production. Infants and young children are the most vulnerable group of human population; therefore, uniform maximum residue limit (MRL) 0.01 mg kg^{-1} has been established in EU for any pesticide residue occurring in processed baby food. Currently, most of producers require raw materials complying with this (low) residue limit, although it applies to processed product. Under real-life conditions, this may pose a problem, since many pesticide preparations even when used in accordance with Good Agriculture Practice (GAP) may leave residues exceeding the "baby food" MRL[1].

Apples are the key raw material for production of fruit-based baby food. Unfortunately apples can be attacked by various disorders not only during pre-harvest period but also during storage. Sometimes incipient infection is too small to be seen prior to fruit storage but may develop under favourable conditions (high humidity) as a result of sporulation from older lesions. Particular treatment strategy should be applied to apples intended for storage because the decline of pesticide residues within a post-harvest time might be slower (depending on the storage conditions) than during the pre-harvest period when the drop is relatively rapid due to various environmental factors[2].

Experimental

Field Experiments

Four different apple varieties, Golden Delicious, Gloster, Idared and Melrose, were examined in this study. The same treatment schedule was applied to all studied varieties. The overview of pesticide preparations and some relevant characteristics of active ingredients are listed in Table I.

In the first phase, the experimental apple trees obtained specific pesticide treatment from April to June, see Table I. In the second phase, the orchard was divided into four sections (S1–S4). In the S1 no pesticides were used, while in S2–S4, fungicides against storage pests were applied according to the scheme shown in Table II.

The first set of samples was taken for analysis at the time of harvest (October 10, 2007) and the next two after three (January 8, 2008) and five (March 19, 2008) months of cold storage (1–3 °C).

Table I
Schedule of the pre-harvest treatment

Application date	Pesticide preparation/ dosage [per hectare]	Active ingredient	Mode of action	Safety period [days]
April 12, 2007	Chorus 75 WG/0.2 kg	cyprodinil	fungicide	28
	Cascade 5 EC/1.5 kg	flufenoxuron	insecticide	-
April 19, 2007	Clarinet 20 SC/1.5 dm³	fluquinconazole pyrimethanil	fungicide fungicide	28
April 26, 2007	Thiram Granulo/3.0 kg	thiram	fungicide	14
May 3, 2007	Dithane Neotec/3.0 kg	mancozeb	fungicide	21
	Calypso 480 SC/0.2 dm³	thiacloprid	insecticide	14
May 11, 2007	Delan 700 WDG/0.6 dm³	dithianon	fungicide	21
	Score 250 EC/0.2 dm³	difenoconazole	fungicide	49
May 18, 2007	Polyram WG/3.0 kg	metiram	fungicide	21
	Insegar 25 WP/0.3 kg	fenoxycarb	insecticide	60
May 25, 2007	Integro/0.5 dm³	methoxyfenozide	insecticide	14
June 1, 2007	Baycor 25 WP/1.0 kg	bitertanol	fungicide	35
	Score 250 EC/0.2 dm³	difenoconatole	fungicide	49
June 7, 2007	Domark 10 EC/0.4 dm³	tetraconazole	fungicide	14
June 14, 2007	Syllit 400 SC/1.7 dm³	dodine	fungicide	21
	Trebon 10 EW/0.5 dm³	etofenprox	insecticide	28
June 26, 2007	Mythos 30 SC/1.0 dm³	pyrimethanil	fungicide	28
	Mospilan 20 SP/0.25 kg	acetamiprid	insecticide	28

Table II
Schedule of the treatment against storage diseases

Code	Pesticide preparation [kg ha^{-1}] active ingredient – safety period	Application date
S1	–	–
S2	Delan 700 WG (0.7) dithianon – 21 days	September 19, 2007
S3	Thiram Granuflo (3.0) thiram – 14 days	September 26, 2007
S4	Zato 50 WG (0.15) trifloxystrobin – 14 days	September 26, 2007

A n a l y t i c a l　M e t h o d s

Most of pesticides were liquid chromatography (LC) amenable, so for isolation of 14 from 17 examined analytes the QuEChERS method[3] was applied. Crude extract (without cleanup step realized with primary-secondary amine (PSA)) was examined by LC coupled with tandem mass spectrometry (MS/MS). Limits of quantitation (LOQ) for these pesticides were 0.002 mg kg^{-1}, only for dodine LOQ was 0.005 mg kg^{-1}. Ethylenbisdithiocarbamates (EBDC), in this study represented by mancozeb, metiram and thiram, were determined as a sum by solid phase micro-extraction (SPME) of their degradation product (carbon disulfide), identification/quantitation was performed by gas chromatography coupled with mass spectrometry (GC-MS), LOQ was 0.001 mg kg^{-1}.

Results

At the time of harvest, residues of some pesticides (acetamiprid, cyprodinil, flufenoxuron, fluquinconazole, fenoxycarb, tetraconazole and thiacloprid) used for treatment (Table I) were not detected. Other pesticides exceeding the method LOQ could be grouped into three categories based on their concentration levels: *(i)* compounds with residues below 0.01 mg kg^{-1} at the time of harvest (i.e. difenoconazole, dithianon, methoxyfenozide, EBDC), *(ii)* compounds with residues exceeding the "baby food" limit at the harvest time, but declining below the limit at the end of the storage period (i.e. bitertanol, etofenprox) and *(iii)* compounds with residues not significantly declining and exceeding the 0.01 mg kg^{-1} all the time (i.e. dodine, pyrimethanil). No generalization on the relationship between residues dynamics and apple variety could be drawn. The highest amount of bitertanol residues occurred in variety Golden Delicious (Fig. 1. A) and etofenprox residues was the highest in variety Idared (Fig. 1. B) in all experiments. Worth to notice that the changes of pesticides classified as concentration category *(iii)* were not dependent on apple variety.

Treatment for post-harvest disease protection was carried out before the harvest in compliance with required safety period. For this purpose three fungicide preparations with different active ingredients (dithianon, thiram and trifloxystrobin) were tested (Table II). Thiram, although applied only 14 days before the harvest, did not exceed "baby food" limit,
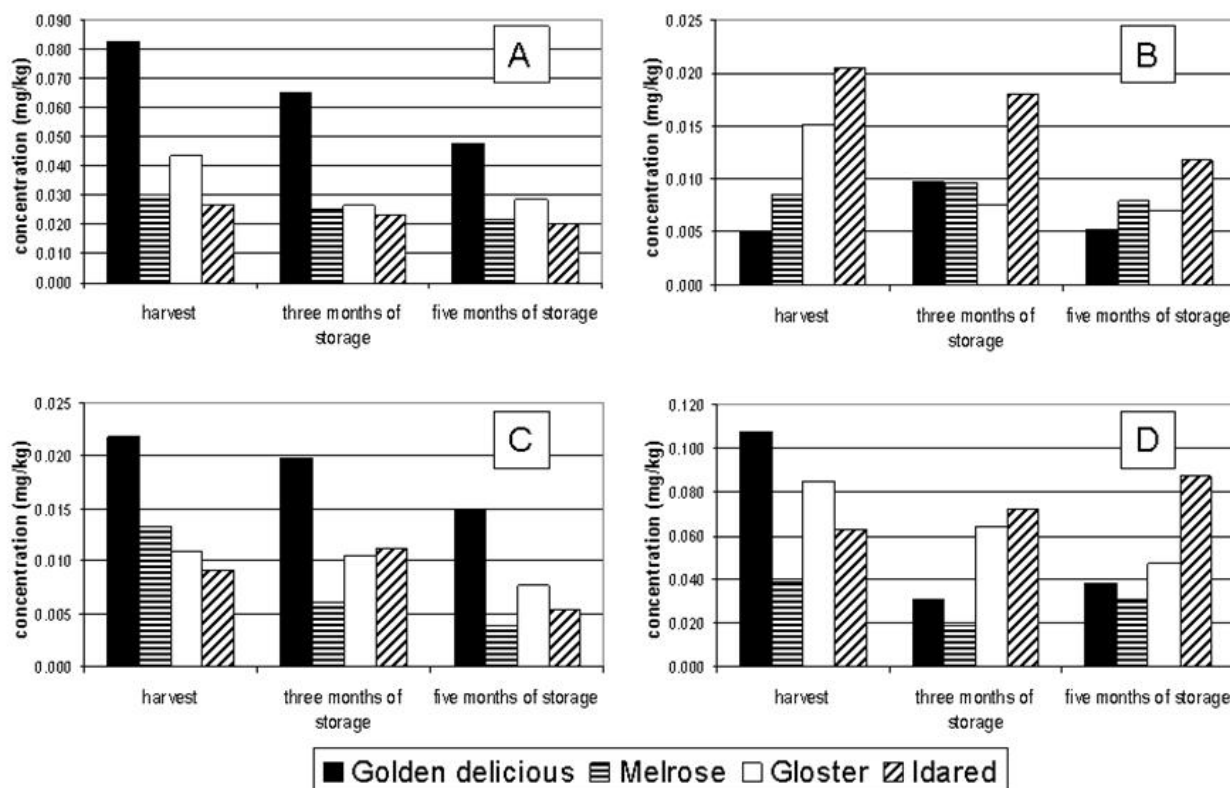
Fig. 1.　**The dynamics of selected pesticides during cold storage (1–3 °C); A: bitertanol, B: etofenprox, C: trifloxystrobin, D: dithianon**

whereas residues of dithianon and trifloxystrobin exceeded $0.01 \, \mathrm{mg \, kg^{-1}}$ during the entire storage period. As shown in Fig. 1. C, residues of trifloxystrobin were the highest in variety Golden Delicious. Different concentration trend was observed with dithianon residues, the lowest levels were detected in variety Melrose (Fig. 1. D) and similar dynamics of its residues could be observed although in apples treated five months before storage.

Conclusions

The presented study has documented relatively large variation of pesticide residues in various apple varieties obtained the same treatment. Interestingly the residues tended to be the highest in Golden Delicious while in Melrose were in most experiments the lowest. This may be associated with different wax content in these varieties. In any case, weather conditions before harvest play a key role in levels of residues occurring in apples at the start of storage period. Only repeated experiments may give more general conclusions.

REFERENCES
1. Ticha J., Hajslova J., Kovalczuk T., Jech M., Honzicek J., Kocourek V., Lansky M., Kloutvorova J., Falta V.: Food Addit. Contam. *24*, 605 (2007).
2. Ticha J., Hajslova J., Jech M., Honzicek J., Lacina O., Kohoutkova J., Kocourek V., Lansky M., KloutvorovaJ., Falta V.: Food Control *19*, 247 (2008).
3. Anastassiades M., Lehotay S., Stajnbaher D., Schenck AOAC 2, 86 (2003).

P103 RELATIONSHIP BETWEEN XANTHOHUMOL, POLYPHENOLS, AND FLAVONOIDS CONTENT IN HOP LEAVES AND CONES WITH REGARD TO CULTIVAR AND VEGETATION PERIOD

EVA ÜRGEOVÁ, PETER KULACS, MÁRIA VAŠKOVÁ
and ĽUDOVÍT POLÍVKA

Department of Biotechnologies, Faculty of Natural Sciences, University of SS Cyril and Methodius in Trnava, Nám. J. Herdu 2, 917 01 Trnava, Slovakia,
eva.urgeova@ucm.sk

Introduction

Some secondary metabolites are present in plant cells in the form of precursors and are activated after pathogen attack[1]. Secondary metabolites having biocide effect include isoprenoids, phenol substances, organic sulphur compounds, saponins, alkaloids, proteins, and peptides[2].

In this perspective, increasing attention is being paid to the plant called common hop (*Humulus lupulus* L.). The plant is diecious. Wild-growing hop grows on wet soils, mainly in riparian zones, in shrubberies, on the edges of canals and in similar places[3,4]. All the main components are contained in lupuline glands[3,5], although some components, e.g. essential oils, were also identified in the leaves of the plant[6]. Concerning the chemical composition, hop resins are prenylated derivates of floroglucinol, comprising alpha-bitter acids and beta-bitter acids[5]. In recent years, antibiotic[7], antifungal[8], and antioxidant activities of humulone[9] have been identified. One of the big groups of substances contained in the hop plant is the group of polyphenol compounds[10], phenol acids, chalkones, flavanols, flavonols, antocyanides, catechines and proantocyanides. Flavonoids as a group of organic compounds display a wide range of biological and pharmacological properties[11], including antiviral, antimicrobial, antioxidant, and anticancer properties[12,13]. Stevens[14] identified three main groups of flavonoids in the hop plant including prenylflavonoids. The content of prenylated flavonoids in the hop plant fluctuates between 0.2–0.6 %[15]. The chemical composition of hop is not constant; it changes with time and depends on the conditions of post-harvest storage[4,15]. Regarding the chemical composition, an important role was played by such factors as the plant development stage, location, growing practices, weather, and pressure of pathogens. Langezaal[6] reports that in hop leaves there are essential oils in much lower concentrations than in cones. To our knowledge, the content of low-molecular polyphenyls in hop leaves has not been studied yet.

Experimental

Materials and Methods

We tested the samples of hop, cones and leaves taken from the Gene Bank of the Slovak Republic in the Institute of Plant Production, Piešťany (SCPV–VÚRV). The samples of different cultivars of hop were dried and homogenized. We used the following cultivars of hop: Osvald's clones 31, (K-31), and 72 (K-72), Bor, Sládek, Aromat, Zlatan, and Pre-

miant. We collected the samples before flowering and at the end of vegetal period.

The content of phenol substances was determined by Singelton's method[16]. The amount of 0.2 ml of methanol extract was mixed with 1 ml of Folin-Ciocalteu's reagent and 0.8 ml of 7.5 % (w/v) Na_2CO_3. Absorbance was measured at 750 nm wave-length after 30 minutes of incubation in dark. The content of polyphenols was compared with the absorbance of galic acid.

Flavonoids were determined by Rakotoarison's method[17]. 1 ml of methanol extract was added to 1 ml of methanol solution of $AlCl_3 \cdot 6H_2O$, 2% (w/v), and absorbance was measured after 10 minutes at 394 nm. Quercetin was taken as the standard.

Xanthohumol was determined by HPLC. Dry material was homogenized with methanol in a sonificator (Bandelin Electronic, Germany) for about 10 minutes, and then purified by centrifugation and filtration on a column (Waters, USA). Eluate (5 µl) was injected into the HPLC instrument and detected at 370 nm. The mobile phase consisted of 900 ml of methanol with 100 ml of water. The analytical column was Nucleodur Sphinx RP EC 150/4.6 (5 µm). Xanthohumol was purchased form Sigma, Germany.

Results

The concentration ranges of phenol substances, flavonoids and xanthohumol in hop cultivated in the Slovak Republic are summarized. The content of polyphenols and flavonoids was monitored during the vegetal period of plant growth. All cultivars showed different contents of secondary metabolites during the vegetal period, their content in leaves decreased from the end of June to September (Table I).

Table I
Polyphenols content in hop leaves during the vegetal period

Cultivar	Polyphenols [mg g^{-1} DM]	
	06/07*	09/07*
K-31	8.83	1.22
Bor	5.00	2.25
Sládek	5.76	2.04
K-72	7.46	0.99
Aromat	6.56	0.98
Premiant	5.52	0.90
Zlatan	6.23	1.82

*06/07 and 09/07 – date of sampling

Phenol substances were in the interval between 0.90–2.25 mg g^{-1} of dry matter in leaves, and from 4.0 to 21.1 mg g^{-1} of dry matter in cones (Table II) at the end of the vegetal period.

The content of polyphenols was dependent on the type of cultivar and on climatic conditions as well. Comparison of the contents of polyphenols in extracts from hop cones in 2006 and 2007 is shown in Fig. 1. The content of phenol substances in leaves did not basically relate to the content of phe-

nol substances in cones. The highest content of polyphenols was detected in the aromatic cultivar Osvald's clone K-72.

Table II
Phenol substances content in hop cones at the end of the vegetal period

Cultivar	Polyphenols [mg g^{-1} DM]
K-31	16.2
Bor	17.4
Sládek	18.8
K-72	21.1
Aromat	11.2
Premiant	20.0
Zlatan	17.0
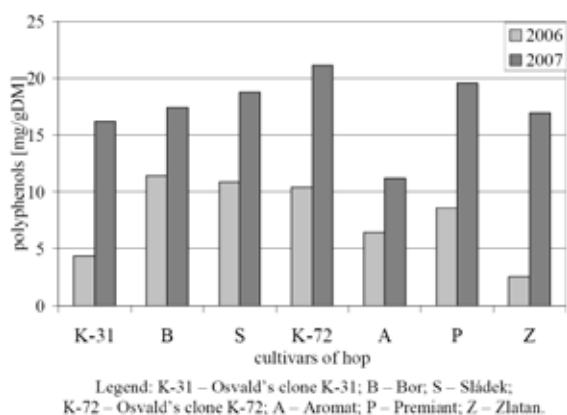
Fig. 1. **Comparison of the content of polyphenols in hop cones in 2006 and 2007**

Table III
Flavonoids content in hop leaves during the vegetal period

Cultivar	Flavonoids [mg g^{-1} DM]	
	06/07*	09/07*
K-31	6.37	0.65
Bor	3.45	0.71
Sládek	3.24	0.76
K-72	6.31	0.48
Aromat	5.89	0.50
Premiant	2.13	0.72
Zlatan	5.03	0.61

*06/07 and 09/07 – date of sampling

Table III and Table IV show the data on flavonoid content in leaves, compared with xanthohumol content. We noted a decline during the vegetal period in both cases, so as in phenol substances.

Xanthohumol, prenylated flavonoid, was defined in extracts from hop cones. Its content, like the content of phenol substances and flavonoids, was the highest at the end of

Table IV
Averaged content of xanthohumol in hop leaves during the vegetal period

Cultivar	Xanthohumol [% wt.]		
	9/2006	6/2007	9/2007
K-31	0.009	0.055	0.014
Bor	0.012	0.067	nd
Sládek	0.013	0.068	0.014
K-72	0.010	0.060	0.015
Aromat	0.011	0.041	0.013
Premiant	nd	0.047	0.009
Zlatan	0.011	0.039	0.016

nd – no data
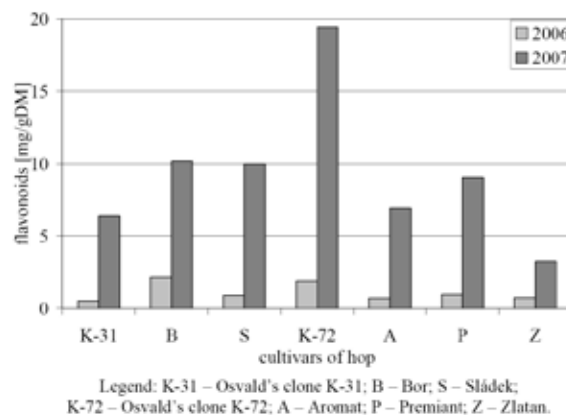
Fig. 2. **Flavonoids content in hop cones for 2006 and 2007**

Table V
Averaged content of xanthohumol in hop cones for 2006 and 2007 (cones sampled on September 22, 2006 and September 24, 2007)

Cultivar	Xanthohumol [mg g^{-1} DM]	
	2006	2007
K-31	0.39	1.14
Bor	1.98	3.11
Sládek	1.11	8.87
Aromat	0.49	0.62
Zlatan	0.29	2.32

vegetal period in cones (Figure 2). The level of xanthohumol was influenced by the climatic conditions (Table V).

Conclusions

The concentrations of secondary metabolites, phenol substances, and flavonoids depended on the vegetal period at first.

The quantity of phenol substances was within the range of 5.00–8.83 mg g^{-1} of dry matter, for flavonoids 2.13–6.37 mg g^{-1} of dry matter in the leaves before flowering. The ranges decreased to 0.90–2.25 mg g^{-1} of dry matter of phenol

substances, and to 0.48–0.76 mg g^{-1} of dry matter at the end of vegetation.

The climatic conditions influenced the content of secondary metabolites; the contents of xanthohumol were very different in identical cultivars, compared to the years 2006 and 2007.

REFERENCES

1. Morrissey J. P., Osbourn A. E.: Microbiol. Mol. Biol. Rev. *63*, 708 (1999).
2. Masarovičová E., Repcák M., Erdelský K., Gašparíková O., Ješko T., Mistrík I.: *Fyziológia rastlín*. Univerzita Komenského Bratislava 2002.
3. Hornsey I.: R. Soc. Chem. *58*, (1999).
4. Moir M.: J. Am. Soc. Brew. Chem. *58*, 131 (2000).
5. De Keukeleire D.: Química Nova *23*, 108 2000.
6. Langezaal C. R.: Pharm. World Sci. *15*, 178 (1993)
7. Simpson W. J., Smith A. R. W.: J. Appl. Bacteriol. *72*, 327 (1992).
8. Mizobuchi S., Sato Y.: Agric. Biol. Chem. *49*, 399 (1985).
9. Tagashira T., Watanabe M., Uematsu N.: Biosci. Biotechnol. Biochem. *59*, 740 (1995).
10. Inglis T.: http://www.nzhops.co.nz/articles/flavours.htm
11. Hollman P. C., Katan M. B.: Arch. Toxicol. *20*, 237 (1998).
12. Bylka W., Matlawska I., Pilewski N. A.: J. Am. Nutr. Assoc. *7*, 24 (2004).
13. Papadopoulou CH., Soulti K., Roussis I. G.: Food. Technol. Biotechnol. *43*, 41 (2005).
14. Stevens J. F., Miranda C. L., Buhler, D. R.: J. Am. Soc. Brew. Chem. *56*, 136 (1998).
15. De Keukeleire J., Ooms G., Heyerick, A., Roldan-Ruiz I., Van Bockstaele E., De Keukeleire D.: J. Agric. Food Chem. *51*, 4436 (2003).
16. Sigleton V. L., Rossi J. A.: Am. J. Enol. Viticult. *16*, 144 (1965).
17. Rakotoarison D. A., Gressier B., Trotin F., Bruner C., Dine T., Luyckx M., Vasseur J., Cazin M., Cazin J. C., Pinkas M.: Pharmazia *52*, 60 (1997).

P105 SEA BUCKTHORN – SOURCE OF VITAMIN C

MILENA VESPALCOVÁ[a], DANA VRÁNOVÁ[a], JIŘINA ENDSTRASSEROVÁ[a] and VOJTĚCH ŘEZNÍČEK[b]

[a]*Faculty of Chemistry, Brno University of Technology, Institute of Food Science and Biotechnology, Purkynova 118, 612 00 Brno,*
[b]*Faculty of Horticulture, Mendel University of Agriculture and Forestry, Department of Breeding and Propagation of Horticultural Plants, Valtická 337, 691 44 Lednice,*
vespalcova@fch.vutbr.cz

Introduction

Sea buckthorn (*Hippophae rhamnoides*) is a bush giving small orange fruits. The bush comes from Asia but it has spread almost all over the world during last century because it can be grown even in harsher climate conditions without special agrotechnical technology. The largest producers of sea buckthorn are China, Russia, Finland and Germany at present.

Sea buckthorn has been used as a natural drug in Asia to treat heart diseases, digestive tract diseases, cough, etc. Today, sea buckthorn extract is added not only in homeopathic remedies and food supplements, but also into syrups, jams, sweets, oils, face creams, shampoos, soaps, teas and many other products all over the world. Sea buckthorn contains many substances beneficial to human health, particularly vitamin C in amount larger than in other kinds of fruit or vegetable. Among other substances, also carotenoids, flavonoids, essential unsatured fatty acids and phytosterols should be mentioned. Their content depends not only on individual genotypes and cultivars of this plant but also on the site at which the plant is growing. This, naturally, holds also for the vitamin C, which frequently serves as one of basic indicators of alimentary and economical attractivity of planted sea buckthorn cultivars.

The aim of the presented work is therefore the comparison on the vitamin C content in the sea buckthorn cultivars and genotypes growed by Faculty of Horticulture, Mendel University of Agriculture and Forestry Brno. Two methods have been applied for the determination of the vitamin C content in the sea buckthorn juice: HPLC with photometric detection and the direct coulometric determination of the vitamin C.
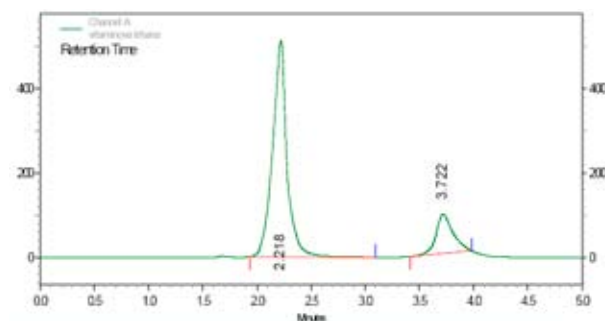
Fig. 1.   **Analysis of the Vitaminová cultivar**

Experimental

The HPLC Determination

The Liquid chromatograph Spectra System equipped with the UV 6000 LP detector and the Chromquest software (Thermo Separation Products, USA) were used. for analyses of sea buckthorn juices prepared from the sea buckthorn cultivars as described below. The juices were injected on the TESSEK Separon SGX RPS Column (TESSEK, Praha, Czech Republic). The separation bed of 5 μm particles was of 5 mm in diameter and of 250 mm in length. 0.01M oxalic acid was the mobile phase. The column effluent was monitored at 254 nm.

Direct coulometry

The coulometric analyser PCA/C-Vit (ISTRAN, Bratislava, Slovak Republik) equipped with porous working electrode served for direct coulometric determination of vitamin C without preliminary separation of the compound from sea buckthorn juices. The determination utilizes oxidation of ascorbic acid to dehydroascorbic acid

$$C_6H_8O_6 - 2e \rightarrow C_6H_6O_6 + 2H^+ \tag{1}$$
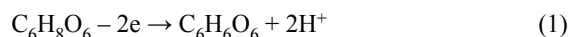
The Preparation of Juices

We analysed 12 cultivars of sea buckthorn listed in Table I. The cultivars were planted in the breeding station of the Horticulture Faculty, Mendel University of Agriculture and Forestry Brno in Žabčice. Fruits harvested October 4, 2006 were immediately frozen to −18 °C and stored at this temperature in the freezing box till the analyses started April 2007. Approximately 5 grams of dry fruits freely warmed to room temperature was weighed to five digits and homogenized in the mortar with small amount oxalic acid, quantitatively transfered to the 100 ml volumetric flask by 2 % (w/v) solution of oxalic acid in water and than filled with the acid solution to the division line. For chromatographic analyses, aliquot part of solution was filtered using the Büchner slit-sieve funnel and by cellulose 3-μm microfilter. The filtered sample was enriched by the special reaction solution R-020T (ISTRAN, Bratislava, Slovak Republic) for coulometric analyses. The analysed sample were prepared daily just before use and stored in dark during analyses.

Results and Discussion

A typical chromatogram of C vitamin analysis at conditions specified in Experimental is given on at Fig. 1. Vitamin C is in second peak, first peak is a mixture of unidentified impurities.

Main validation parameters of successively repeated chromatographic analyses are as follows: LOD and LOQ of ascorbic acid is 0.2 and 0.7 mg dm^{-3}, respectively. Correlation coefficient of ascorbic acid is $R^2 = 0.9942$ for the concentration range of vitamin C from 0.0007 to 500 mg dm^{-3}. Repeatability of analyses in concentration ranges 151–200 mg dm^{-3}, 51–150 mg dm^{-3} and 10–50 mg dm^{-3} given by RSD vaules is 4 %, 6 % and 10 %, respectively. Mean recovery of used analysis is 89.5 %. However, repeatability

Table I
Content of C vitamin in sea buckthorn cultivars and geno-types determined by HPLC

Cultivar or genotype	Content of C vitamin [mg 100 g^{-1}]			
	1st run[**]	2nd run[**]	3rd run[**]	Mean content
Aromat[*]	18.2	25.7	22.4	22.1
Buchlovice I[*]	69.7	62.7	79.3	70.6
Buchlovice III[*]	41.5	46.1	44.6	44.1
Hergo	32.0	24.1	27.7	27.9
Kyjevský	105.2	92.9	94.0	97.2
Leicora	158.0	137.0	136.1	143.7
Olejová	56.0	57.4	56.3	56.6
Trofimovskaja	22.4	15.2	17.3	18.3
Velkoosecký I	183.4	187.3	168.9	179.9
Velkoosecký II	167.9	166.3	168.5	167.6
Velkoosecký III	161.3	165.0	152.1	159.5
Vitaminová	98.0	91.0	103.5	97.5

[*]genotype
[**]mean value from three subsequent analyses

of the whole method including the juice preparation was lower as expected. This show columns 2, 3 and 4 in Table I. The yield variation in the preparation of the filtered juice is the reason for differences in paralel determinations that exceed repeatability of chromatographic analyses. Data summarized in Table I evidence that the vitamin C content differes by one order of magnitude in individual cultivar. Coulometic measurements summarized in Table II prove this principal finding of liquid chromatgraphy analyses Total error of analyses with the coulometric determination of the vitamin C content is

Table II
Content of C vitamin in selected sea buckthorn cultivars and genotypes determined by direct coulometry

Cultivar or genotype	Mean content [mg 100 g^{-1}]	Total measurement error [%]
Buchlovice I[*]	60.2	21
Hergo	20.9	29
Leicora	120.4	18
Olejová	40.5	26
Trofimovskaja[*]	10.3	35

rougly one order of magnitude higher than total error of analyses with the vitamin C content determined chromatographically. Moreover, the error of the coulometric determination increases with the decreasing vitamin C content in the filtered juice as indicate data in Table II. This evidences that columetry without vitamin C separation may be utilized as the final analytical step in need however only if semiquantitative precision of the whole method is acceptable, e.g., in preliminary analyses. For precise analyses, liquid chromatography has to be used as the final step.

REFERENCES

1. Sava, C., Chirila, E., Bucurt, L.: Forest Res. 98 (2001).
2. Tang, X., Tigerstedt, M. A. P.: Sci. Hort. *88*, 203 (2001).
3. Kafkas, E., Kosar, M., Türemis, N., Baser, K. H. C.: Food Chem. *97*, 732 (2006).
4. Hernández, Y., Lobo, M. G., Gonzálet, M.: Food Chem. *96*, 654 (2006).

P106 ARSENIC SPECIATION IN FISH USING HIGH PERFORMANCE LIQUID CHROMATOGRAPHY COUPLED WITH HYDRIDE GENERATION ATOMIC FLUORESCENCE SPECTROMETRY

EVA VITOULOVÁ[a], VERONIKA HARKABUSOVÁ[a] and BLANKA MACHARÁČKOVÁ[b]

[a]*Department of Food Chemistry and Biotechnologies, Faculty of Chemistry, Brno University of Technology, Purkyňova 118, 612 00 Brno, Czech Republic,*
[b]*Department of Biochemistry, Chemistry and Biophysics, Faculty of Veterinary Hygiene and Ecology, University of Veterinary and Pharmaceutical Sciences,Palackého 1–3, 612 42 Brno, Czech Republic,*
vitoulova@fch.vutbr.cz

Introduction

Investigations of the chemical constituensts of aquatic organisms can provide useful informations about the environment as well as toxicologically relevant data about the composition of biological species consumed by humans[1]. Arsenic causes a variety of adverse health effects to humans after acute and chronic exposures[2]. Toxicity, environmental mobility and accumulation in living organisms usually depend on the form in which the element is present. Information on the chemical forms is important for understanding the role of the element present as well as revealing its environmental cycle[3]. In the environment arsenic can be found as several compounds ranging from inorganic arsenite and arsenate to methylated compounds like monomethylarsonic acid, dimethylarsinic acid, trimethylarsine oxide, arsenobetaine, tetramethylarsonium ion and arsenocholine. In biologic samples several arsenosugars and arsenolipids can be present as well[4].

The determination of arsenic compounds is mostly carried out by hyphenated techniques, the main parts being liquid chromatographic separation and element specific detection. By far the most used systems are liquid chromatography inductively coupled plasma mass spectrometry (LC-ICP-MS) and liquid chromatography hydride generation atomic fluorescence spectrometry (LC-HG-AFS)[5]. Atomic fluorescence spectrometry (AFS) can be a good alternative to inductively coupled plasma mass spectrometry (ICP-MS) detector, with the advantage of a lower cost of investment and handling[5,6].

Experimental

Standards and Reagents

All solutions were prepared with deionized water (18.2 MΩcm). Stock solutions of 1,000 mg(As)dm^{-3} were prepared by dissolving $NaAsO_2$ (Fluka, Switzerland), $Na_2HAsO_4 \cdot 7H_2O$ (Fluka, Switzerland), $CH_4AsNaO_3 \cdot 1.5H_2O$ (Chem. Service, USA), $(CH_3)_2AsHO_2$ (Fluka, Switzerland) and arsenobetaine (Fluka, Switzerland). All arsenic solutions were stored in the dark at + 4 °C. These stock solutions were diluted with deionized water to the desired concentrations before use.

For the analytical procedures the following chemicals were used: potassium dihydrogen phosphate (Fluka, Switzerland), potassium monohydrogen phosphate (Fluka, Switzerland), hydrochloric acid (Analytika, Czech Republic), potassium persulfate (Fluka, Switzerland), sodium borohydride (Riedel-de Haën, Germany), sodium hydroxide (Riedel-de Haën, Germany), nitric acid (Analytika, Czech Republic), hydrogen peroxide (Lach-Ner, Czech Republic), ascorbic acid (Riedel-de Haën, Germany), potassium iodide (Analytika, Czech Republic), magnesium nitrate (Merck, Germany). All chemicals were at least of analytical grade.

Instrumentation

A Gynkotek P508 (Gynkotek, Germany) HPLC pump and six-port injection valve (Ecom, Czech Republic) were used in conjunction with a strong anion-exchange column Hamilton PRP X-100 (Hamilton, USA). An Excalibur atomic fluorescence detector (PS Analytical, UK) equipped with a boosted discharge hollow cathode lamp (Photron, Australia) was used for detection. The measurements are carried out on the resonance line of As 193.76 nm. For data collection and evaluation was used CSW software – version 1.7 (Data Apex, Czech Republic).

Sample Preparation

The muscle of commercially available fish samples were homogenized and freeze-dried.

For the determination of total arsenic by AFS the microwave digestion (using HNO_3 and H_2O_2) was employed; followed by the addition of $Mg(NO_3)_2$ to complete the destruction.

Triplicate of samples were extracted with 10 ml of deionized water using ultrasonic bath at 50 °C for 2 hours. The extraction vessels were shaken every 15 min to ensure dispersion of the sample. After extraction the samples were centrifuged and extract was filtered through a 0.45 μm membrane filter and kept at 4 °C till speciation analysis.

Conditions of Total Arsenic Determination

A KI/ascorbic acid reducing solution was employed to reduce arsenic species to As (III). The reducing solution was added at least 30 minutes before analysis. Conditions for hydride generation: 1 % $NaBH_4$ in 1 % NaOH at flow rate the 4.5 ml min^{-1} and 4.9 mol dm^{-3} HCl at flow rate 9 ml min^{-1}.

Speciation analysis conditions

The mobile phase was 10 mM K_2HPO_4/KH_2PO_4 adjusted to pH 6.1 at flow rate 1 ml min^{-1}. The hydride generation of the arsines was carried out by adding 6 mol dm^{-3} HCl and 1.4 % $NaBH_4$ in 1 % NaOH, both at the 3 ml min^{-1} flow rate. 1 % $K_2S_2O_8$ in 1 % NaOH at the flow rate 0.3 ml min^{-1} was used as oxidation solution, oxidation was supported by UV.

When analysing a samples containing arsenobetaine (AsB) it is necessary to analyse the sample twice, once with the UV lamp switched off and once with it switched on. This is due to the fact that AsB coelutes with arsenite. If the UV lamp is off AsB don't react with $NaBH_4$ and don't give a signal.

Results and Discussion

Total Arsenic Concentrations

The total arsenic concentrations in fish muscle are summarized in Table I. These results are lower than limits given by legislative of Czech Republic. All samples were also measured by atomic absorption spectrometry with hydride generation to ensure quality results. Results obtained by HG-AAS were comparable to HG-AFS results.

Table I
Total arsenic concentrations in the investigated samples determined by AFS

Sample	Total arsenic [µg kg^{-1}]	RSD [%]
Salmon 1	186	2
Salmon 2	741	4
Trout 1	968	0
Trout 2	966	1
Trout 3	618	4
Tunny	2059	1

Speciation Analysis of Arsenic

The influence of pH of mobile phase on the separation efficiency has been investigated. The pH values were in the range of pH 4–8. The best results were obtained with pH 6.1. Separation of the five arsenic standards is shown in the Fig. 1.

Typical chromatogram of fish extract *(Thunnus atlanticus)* is presented in Fig. 2. All analysed samples of fish contained only non-toxic arsenobetaine.

The results of the speciation analysis are shown in the Table II. Comparision with total arsenic content reveals that extraction efficiencies ranged from 66 to 106 %.
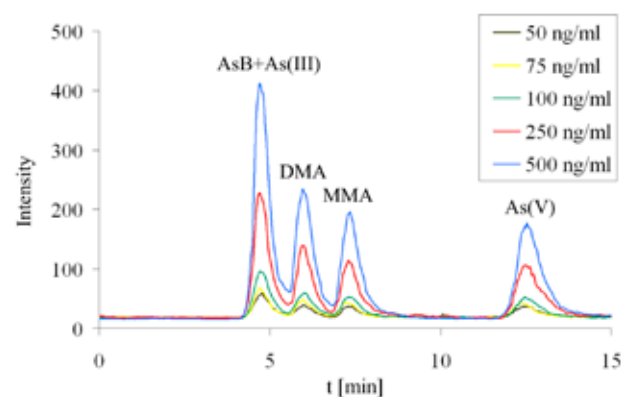
Fig. 1. **Standard chromatogram of five arsenic species**

Fig. 2. **Peak of arsenobetain in the chromatogram of tunny**

Table III
Arsenobetaine concentrations in the investigated samples determined by HPLC-UV-HG-AFS

Sample	Extractable arsenic [µg kg^{-1}]	RSD [%]
Salmon 1	170	9
Salmon 2	783	4
Trout 1	714	0
Trout 2	644	1
Trout 3	407	4
Tunny	1760	2

Conclusions

Amount of total arsenic in the samples was lower than limits for arsenic given by legislative of Czech Republic. Arsenic was present in the form of nontoxic arsenobetaine in all analysed samples of fish.

REFERENCES

1. Schaeffer R., Francesconi K. A., Kienzl N., Soeroes C., Fodor P., Varadi L., Raml R., Goessler W., Kuehnelt D.: Talanta *69*, 856 (2006).
2. Mandal K. B., Suzuki K. T.: Talanta *58*, 201 (2002).
3. McSheehy S., Szpunar J., Morabito R., Quevauviller P.: Trends Anal. Chem. *22*, 191 (2003).
4. Slejkovec Z., Bajc Z., Doganoc D. Z.: Talanta *62*, 931 (2004).
5. Schaeffer R., Soeroes C., Ipolyi I., Fodor P., Thomaidis N. S.: Anal. Chim. Acta *547*, 109 (2005).
6. Gomez-Ariza J. L., Sanches-Rodas D., Giraldez I., Morales E.: Talanta *51*, 257 (2000).

P107 COMPARISON OF AROMA PROFILES OF SEVERAL TYPES OF DARK CHOCOLATE

EVA VÍTOVÁ[a], BLANKA LOUPANCOVÁ[a], HANA ŠTOUDKOVÁ[a], JANA ZEMANOVÁ[a], LIBOR BABÁK[a] and IVANA MACKŮ[b]

[a]*Faculty of Chemistry, Brno University of Technology Purkyňova 118, 612 00 Brno, Czech Republic,*
[b]*Faculty of Technology, University of Tomas Baťa, T.G. Masaryk square 588, 760 01 Zlín, Czech Republic,*
evavitova@post.cz

Introduction

Chocolate (CHC) aroma has been the subject of extensive research. Most of the research work deals with cocoa beans, powder, liquor and CHC. CHC aroma is very complex and is determined by the cocoa plant variety and the fermentation and roasting process. Unfermented cocoa beans are nearly without odour and have a bitter and astringent flavour. Cocoa specific aroma precursors are formed during fermentation by acid induced proteolytic processes[1]. Correct fermentation is essential to produce a good flavour in the final CHC. The different ways of fermenting will give rise to different flavour, unfermented beans do not develop any CHC flavour and are excessively astringent and bitter[2].

The following roasting decreases water content and a full CHC flavour is developed. The high temperatures remove many of the volatile acids and other aroma compounds are formed, in particular as a result of caramelization of sugars, Maillard reaction, protein degradation and sulphur compounds synthesis. The sources of hundreds of volatiles found in roasted beans are the reducing sugars, free amino acids and oligopeptides[3,4]. Several hundreds compounds have been found in roasted cocoa, the most significant are N- and O-containing heterocyclic compounds – alkylpyrazines, furans and pyrroles. Roasting is the most important step for flavour development, it is possible that cocoa subjected to an improper roasting generates undesirable aroma[5].

Finally, conching ends flavour development. The conching is the mixing and shear of the CHC and results in the removal of some undesirable volatiles[2].

Current European legislation allows the addition of vegetable fats to CHC up to a level of 5 % of the product weight, provided that the addition is indicated on the label[6]. However, this addition can influence flavour of CHC. The aim of this work was to compare aroma profiles of three types of dark CHC, produced with or without addition of vegetable fat.

Experimental

Samples

Three types of plain CHC: Figaro plain CHC (min. 48 % cocoa), Figaro for cooking (min. 37 % cocoa) and Kaumy CHC glaze (min. 35 % cocoa) were tested in this work.

Methods

Aroma compounds were determined by the SPME-GC. The SPME fibre CAR™/PDMS 85 μm, extraction 20 min 35 °C. GC conditions: gas chromatograph TRACE™ GC (ThermoQuest Italia) equipped with FID and split/splitless injection port, DB-WAX capillary column (30 m × 0.32 mm × 0.5 μm). The injector 250 °C, splitless mode, the desorption time 5 min, linear purge closed for 5 min. The detector 220 °C. The carrier gas (N_2) 0.9 ml min^{-1}. The oven temperature program: 40 °C, 1 min, 5 °C min^{-1} to 200 °C, 7 min.

Results

SPME-GC was used for the analysis of volatile aroma compounds in three types of dark CHC with different content of vegetable fat. This method is simple, rapid and very mild, so it is suitable for the characterization of the food aroma. The reproducibility, linearity and detection limits of the method were determined in previous work[7]. Aroma active compounds were identified and quantified using standards, in total 56 compounds were found in CHC samples: 14 acids, 9 aldehydes, 8 ketones, 17 alcohols, 7 esters and 1 nitrogen compound. According to the literature, the main cocoa flavour components are alcohols, ethers, hydrocarbons, furans, thiazoles, pyridines, acids, esters, aldehydes, imines, amines, oxazoles, pyrazines and pyrroles[5,8].

The total contents of aroma compounds of CHC tested were compared. This comparison is presented in Fig. 1. The comparison of single groups of compounds is in Fig. 2.

Figaro plain CHC is classic CHC, produced without addition of vegetable fat. In total 50 aroma compounds were identified in this type of CHC, the most abundant were ethanol, propan-1-ol, butan-2,3-diol and phenylacetaldehyde. These compounds arise during fermentation of cocoa beans by the activity of present microflora[3].

Figaro for cooking is plain CHC, intended for making of various CHC sweets, glazes etc. It contains certain amount of vegetable fat up to 5 %. In total 47 compounds were identified here, the most abundant were methanol, ethanol, propan-1-ol, butan-2,3-diol, acetic acid, acetone and phenylacetaldehyde.

Kaumy is CHC imitation, in which cocoa butter is completely replaced by vegetable fat. Although its appearance is very similar to CHC, different fat influences taste, it is not so delicious thus is not suitable for direct consumption. Kaumy is best for making of CHC sweets, where its unpleasant off flavour is not so obvious. In total 46 aroma compounds were found here, the most abundant were methanol, ethanol, propan-1-ol, butan-2,3-diol and acetic acid.

All types of CHC contained the significantly high concentrations of alcohols and fatty acids (Fig. 2.). The highest content of alcohols and also quite high content of fatty acids was in Kaumy glaze, so several these compounds probably contribute to its unpleasant off flavour. Kaumy surprisingly had also the highest total content of aroma compounds (Fig. 1.), plain CHC, which is supposed to have the best cocoa flavour, the lowest.
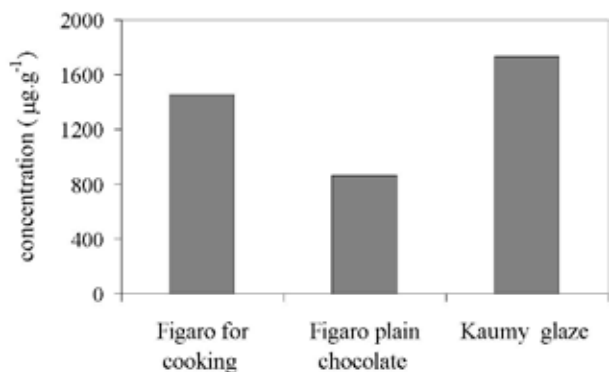
Fig. 1.   **The comparison of total contents of aroma compounds of three types of dark chocolate**
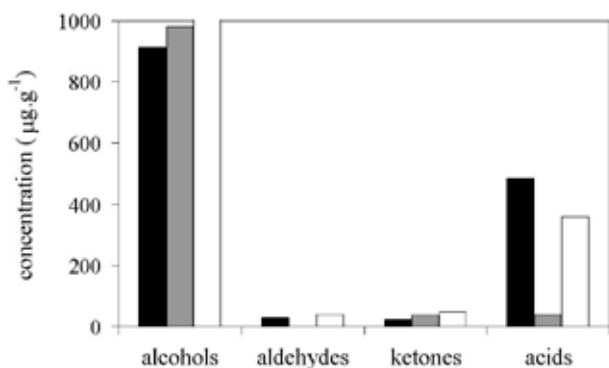
Fig. 2.   **The comparison of single groups of aroma compounds of three types of dark chocolate. Figaro for cooking ■, Figaro plain chocolate ▨ Kaumy glaze   □**

Conclusions

Some important aroma compounds were found in three types of dark CHC. CHCs have similar aroma profiles, but owing to their different composition (cocoa butter, vegetable fat, cocoa dry matter) concentration of several aroma compounds is different. Fatty acids and alcohols were quantitatively the most important compounds in all types of CHC. The highest total content of all aroma compounds was in Kaumy glaze, so several these compounds probably contribute to its unpleasant off flavour.

REFERENCES
1. Voight J., Biehl B., et al.: Food Chem. *49*, 173 (1994).
2. Beckett T. S.: *The Science of chocolate*. RSC Paperbacks, Cambridge 2004.
3. Schwan R. F., Wheals A. E.: Crit. Rev. Food Sci. *44*, 205 (2004).
4. Zemanová J., Vítová E., et al.: Czech J. Food Sci. *22*, 314 (2004).
5. Bonvehí J. S.: Eur. Food Res. Technol. *221*, 19 (2005).
6. Ulberth F., Buchgraber M.: Eur. J. Lipid Sci. Technol. *105*, 32 (2003).
7. Vítová E., Loupancová B., et al.: Czech J. Food Sci. *24*, 268 (2006).
8. Komprda T., Burdychová R., et al.: Food Microbiol. *25*, 219 (2008).

P108 MONITORING OF CHANGES IN POPULATION OF YEASTS DURING FERMENTATION OF GRAPE MUST

DANA VRÁNOVÁ, MICHAELA ZDEŇKOVÁ and RENATA VADKERTIOVÁ

Faculty of Chemistry, Brno University of Technology, Purkyňova 118, 612 00 Brno, Czech Republic,
vranova@fch.vutbr.cz

Introduction

Traditionally, wine fermentation has been carried out in spontaneous way by indigenous yeasts present on the grapes when harvested, or introduced from the equipment and cellar during the fermentation process. At present most wine producers carry out the fermentation process by adding a pure Saccharomyces strains to the must to improve final wine quality[1,23].

The strains at the species level can be identified using conventional methods based on biochemical and physiological characteristic or molecular techniques. Over the last decade molecular techniques for the identification of yeast strains have been widely studied[4,5,8]. The applicability of techniques as the RAPD method and restriction enzyme analysis of PCR amplified DNA fragments (PCR-RFLP) has been demonstrated as a tool for taxonomic purposes[11,16,19].

The fermentation of grape must into wine is a complex microbiological process characterized by the presence of a large number of different microorganisms. The composition of yeasts population on grape berries and leaves plays an important role in wine fermentations, as different genera, species and strains with their metabolic activity influence the sensory quality and organoleptic characteristics of wine.[3,7,8,13,15,16,18] Yeasts associated with grape or wine ecosystem are usually classified in 15 different genera[21]: *Brettanomyces/ Dekkera, Candida, Cryptococcus, Debaryomyces, Hanseniaspora/Kloeckera. Kluyveromyces, Pichia, Metschnikowia, Rhodotorula, Saccharomyces, Saccharomycodes, Schizosaccharomyces, Zygosaccharomyses*.

The aim of this study was monitoring of the changes in yeast population during spontaneous alcoholic fermentation of cider of *Veltlin green* cultivar. We isolated yeasts in different period of grape cider fermentation. Identification of the individual strains was carried out using PCR-RFLP analysis of 5.8S-ITC region.[6,7,11,12]

Experimental

Sample Preparation

The samples analyzed in this study were isolated from white wine cider ("*Veltlin green*") obtained from local producer from wine region Velke Pavlovice. Control yeast strains used in this study were from the Culture Collection of Yeasts, Bratislava, Slovakia (CCY).

Sampling at different stages of fermentations was performed at days: 1, 3, 5, 7, 9, 11, 13, 15, 17, 19, 21, 23 Aliquots of each sample (several dilutions) were spred on to plates of wort agar. Cells were directly collected from a fresh yeast colony using a microbiological loop.

DNA was extracted and purified by Ultra Clean Microbial DNA Isolation Kit – obtained from Elizabeth Pharmacon spol. s.r.o., CR. 3–10 ng of DNA in 1–2 μl of TBE buffrer were used in a 50 μl amplification reaction.

PCR Amplification of the Yeast DNA

The amplification reaction of the rDNA region spannding the 5.8 rDNA gene and the ITS regions were carried our under the following conditions: 50 μl of reaction mixture contained 5–20 ng template DNA, polymerase buffer, 0.2 mM of dNTP (N = A, T, G, C) 0.5 μM of each primer and 1 U Taq DNA polymerase. The amplification protocol included the following steps: Initial denaturation at 94 °C for 4 min, 25 cycles of amplification: denaturation at 94 °C for 1 min, annealing at 48 °C for 30 sec, and extension at 72 °C for 1 min. The final extension was at 72 °C for 10 min. Amplification products were analysed on 0.7% (w/v) agarose gel in TBE buffer. PCR amplification was carried out in a PTC-100™ thermocycler (MJ.Research,Inc.). Upper primer: (ITS1) 5'-TCC GTA GGT GAA CCT GCG G-3',Lower primer: (ITS4) 5'-TCC TCC GCT TAT TGA TAT GC-3' (VBC BIOTECH, GmbH)[6]. With these two primers a different products (900, 800, 700, 500 and 450 bp) were obtained after amplification with DNA template from species of genus *Saccharomyces* (Fig. 1.).

Restriction Analysis and Gel Electrophoresis

PCR products (20 μl) were digested in 20 μl of reaction volume with 1U of restriction endonuclease using the manufacturers conditions.

The restriction enzymes used: Alu I, Hae III, Hinf I and Mse I. (Fermentas, Lithuania)

The producst of digestion were analysed by horizontal gel electroforesis system (OWL, USA) in 2% (w/v) agarose gels and comparison with yeasts from CCY. After electroforesis the gels were stained with EtBr and visualized under UV light (Fig. 2.).

Results

The restriction fragments of amplified part of DNA from 27 yeasts isolated from wine must were compared with those of 40 yeasts from the Collection of yeasts of Chemical institute of Slovak Academy of Sciences in Bratislava.

Based on the identity of length and number of restriction fragments the taxonomic assignment of yeasts was performed. In some cases no species, but only genus assignment was carried out. Samples No. 83, 107, 70, 9, 30, 62 and 102 were identified as Pichia fermentans, the sample No. 6 and 106 were identified as Hanseniaspora uvarum.

Table I
Yeasts identification during fermentation of wine cider

Different stages of fermentation [days]	Number of samples	Identification
1	83, 107	*Pichia fermentans*
	106	*Hanseniaspora uvarum*
3	9, 70	*Pichia fermentans*
	6	*Hanseniaspora uvarum*
	104	*Rhodosporium sp.*
5	30	*Pichia fermentans*
	40	*Saccharomyces sp.*
7	7	*Saccharomyces mangini*
	62, 102	*Pichia fermentans*
	95A	*Saccharomyces cerevisiae*
9	95B, 96	*Pichia sp.*
	22, 87	*Saccharomyces mangini*
11	67, 58	*Saccharomyces mangini*
13	90, 72	*Saccharomyces mangini*
15	73, 88	*Saccharomyces mangini*
17	63	*Saccharomyces mangini*
19	18, 97	*Saccharomyces mangini*
	46	*Metschnikowia pulcherrima*

After restriction analysis with enzyme HinfI the sample No. 106 was identified as Pichia fermentans.

Nevertheless, the detailed analysis of restriction fragments with enzyme AluI and microscopic analysis led to the attribution to Hanseniaspora uvarum. (TableI)

After the restriction analysis of the sample No. 40 was assigned to the genus *Saccharomyces* without the determination of species. The sample No. 7 was identified as *Saccharomyces mangini*.Using the restriction analysis with enzymes HinfI, HaeIII and AluI the adherence to the genus *Saccharomyces* was proved by the samples 18, 22, 58, 63, 67, 72, 73, 87, 88, 90 and 97. The analysis of these samples with enzyme MseI enabled the species identification. The simila-
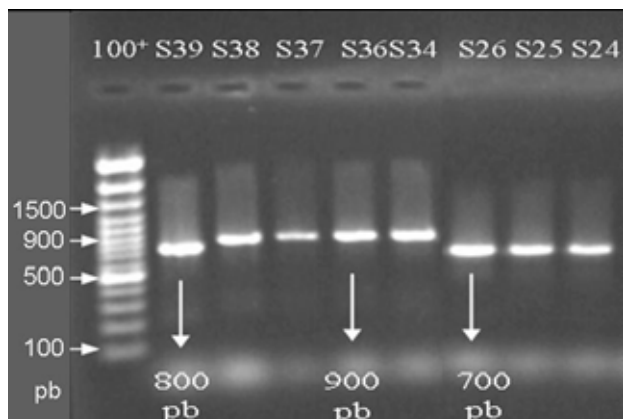
Fig. 1. **Example of agarose gel with PCR products of an amplification of the 5.8S-ITS rDNA (S24–S39 = CCY yeasts, 100⁺ – size marker**

rity with the collection species *Saccharomyces mangini* was evidenced.

The restriction analysis using enzyme HinfI proved the similarity with the genus of Pichia in the case of the sample No. 96. Applying endonuclease HinfI the probe No. 96 was consequently assigned as *Pichia fermentans*. The submission to the genus of *Pichia* was determined also by the sample No. 95B using the enzyme HaeIII. By the sample No.95A the similarity with the collection species S*accharomyces cerevisiae* was proved. The result of restriction analysis using the enzymes HinfI, MseI, HaeIII and AluI documented the identity with the collection species *Metschnikowia pulcherrima* by the sample No. 46.
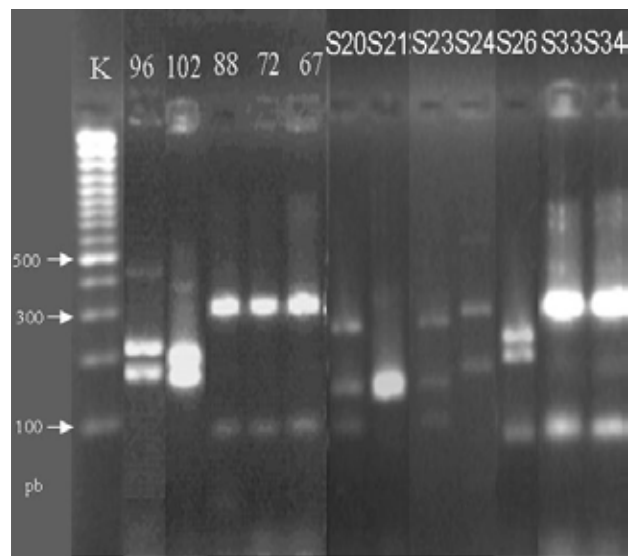
Fig. 2. **Example of digestion products of the amplificates obtained using the restriction enzyme HinfI (S20–S34 = CCY yeasts, 67, 72, 88, 96, 102 – wine yeasts,K – size marker 100pb)**

Conclusions

The result of the analysis is the identification of yeasts of genus *Pichia*, *Hanseniaspora* and *Rhodotorula* in the initiation stages of fermentation and that of Saccharomyces in the further stages of fermentation. The species assignment is *Pichia fermentans* and *Hanseniaspora uvarum*. The unambiguous taxonomic assignment can be performed with *Saccharomyces mangini*. By other yeasts of genus *Saccharomyces* the determination of species was not possible.

It was proved that in the stage of late time of must fermentation and of the formation of young wine the yeasts of genus *Saccharomyces* prevail. The presence of *Saccharomyces cerevisiae* was proved. The interesting result was identification of yeasts species *Metschnikowia pulcherrima*. This yeasts appears in the first stages of fermentation.

The method PCR-RFLP is suitable for taxonomic assignment of yeasts of different genus. Nevertheless, for the exact assignment the selection of primers and restriction enzymes plays the important role.

REFERENCES

1. Boekhout T., Robert V.: *Yeast in food*. Cambridge England: Woodhead publishing limited, 2003.
2. Capece A., Salzano G., Romano P.: Int. J. Food Microbiol. *84*, 33 (2003.
3. Clemente-Jimenez, et al.: Food Microbiol. *21*, 149 (2004).
4. Deák T.: Trends Food Sci. Technol. *12*, 165 (1995).
5. Dlauchy D., Tornai-Lehoczki J., Péter G.: Syst. Appl. Microbiol. *22*, 445 (2003).
6. Esteve-Zarzoso B., Bellech C., Uruburu F., Querol A.: Int. J. Syst. Bacteriol. *49*, 329 (1999).
7. Espinosa J. C., et al.:I Food Technol.Biotechnol *40*, 157 (2002).
8. Fernández-Espinar M. T., et al.: Int. J. Food Microbiol. *70*, 1 (2001).
9. Fernández-Espinar M. T., Barrio E.,Querol A.: Yeasts *20*, 1213 (2003).
10. Gomes L. H., et al.: Food Microbiol. *17*, 217 (2000).
11. Heras-Vazquez F. J., Mingorance-Cazorla L., Clemente-Jimenez J. M., Rodriguez–Vico F.: Federation of European Microbiological Societes *3*, 3 (2003).
12. Hiero N., Gonzáles Á., Mas A., Guillamón J. M.: J. Appl. Microbiol. *97*, 792 (2004).
13. Ivannikova Yu. V.,Naumova E. S.,Martynenko N. N., Naumov G. I.: Microbiol. *76*, 194 (2007).
14. Josepa S., Guillamon J. M., Cano J.: FEMS Microbiol. Lett. *193*, 255 (2000).
15. López V., Fernandéz-Espinar T., Barrio E., Ramón D., Querol A.: Int. J. Food Microbiol. [online] *81*, 63 (2003).
16. Masneuf I., Aigle M., Dubourdieu D.: FEMS Microbiol. Lett. *138*, 239 (1996).
17. Možina S., Raspor P.: Food Technol. Biotechnol. *35*, 55 (1997).
18. Nikolaou E., et al.: Food Control *18*, 1458 (2007).
19. Nguyen Huu-Vang, Gaillardin C.: Syst. Appl. Microbiol. *20*, 286 (1997).
20. Pulvirenti A., Nguyen H. V., Caggia C., Giudici P., Zambonelli C.:FEMS Mikrobiol. Lett. *192*, 191 (2000).
21. Raspor P., Damjana M., Polanc J., Možina S., Čadež N.: Int. J. Food Microbiol. *109*, 97 (2006).
22. Santos S. K. B., Basílio A. C. M., Brasileiro B. T. R., Simões D. A., Silva-Filho E. A., Morais Jr. M.: World J. Microbiol. Biotechnol. *23*, 1613 (2007).
23. Senses-Ergul S., Ágoston R., Belák A., Deák T.: Int. J. Food Microbiol. *108*, 120 (2006).

4. CHEMISTRY OF INORGANIC MATERIALS

4.1. Lectures

L01 SOME NON-TRADITIONAL BINDERS AND COMPOSITES TESTED AT THE STUDENT LABORATORIES OF THE INSTITUTE OF MATERIALS CHEMISTRY, BRNO UNIVERSITY OF TECHNOLOGY

JIŘÍ BRANDŠTETR, JAROMÍR HAVLICA, TOMÁŠ OPRAVIL and FRANTIŠEK ŠOUKAL

Department of Materials Chemistry, Faculty of Chemistry, Brno University of Technology, Purkynova 118, 612 00 Brno, Czech Republic,
brandstetr@fch.vutbr.cz

Introduction

At present, the effort to increase the productivity of materials results a.o. in the utilization of different non-traditional cements and composites based preferably on mineral "wastes" – secondary industrial products/fly ashes, metallurgical slags, energogypsum...) These activities save natural mineral resources and decreas the amount of discharged materials on the dumping sites. Novel chemical and mineral admixtures enable the preparation of "tailored" material of demanded special properties. Very often, lack of information and/or unstable quality of secondary materials is the real reason of their unsufficient use. Therefore, better publicity, adequate education at schools of all types, meetings and and conferences can play very important role. At the University of Technology in Brno, the students in their diploma and postdoctoral theses solve in the laboratories many of these problems mostly from chemical point of view with the final objective to enlarge the assortment of binders and mineral composites. Many projects are solved in the cooperation with the industry, where the increasing interest to use "green" material is stil more emphasized. Very often, these activities are connected with the effort to decrease the carbon dioxide emission, solving ecological and economical problems at the same time.

Long Term Durability Of Concrete?

Portland cement (PC) will be our binder No. 1 for next decades, but we know this material only from the year 1824 and its wider use dates to the end of 19th century. The phase composition of concrete based on PC differs from the natural minerals considerably. In the earth crust, we cannot find hydrates of high-calcium minerals, nature does not like such a relatively unstable compounds. From the Table I, the differences between the content of CaO, SiO_2 and Al_2O_3 are especially remarkable.

The CSH gel, portlandite, ettringite and monosulfate incline to sulfatation and/or carbonatation, the content of pores

is high (Fig. 1.), the long-term phase changes can bring about the structure decomposition. Therefore, R & D of concrete based on different chemical and phase composition including non-clinker ones is urgently demanded.

High-Performance Concrete (HPC)

For many years, high-strength concrete was only perceived as a new concrete for the construction of high-rise buildings, bridges, offshore platforms etc. Now, high-performance concrete is viewed as an emerging type of new concrete whose applications are growing both in volume and diversity. It is becoming a high-tech material according to the

Table I
Chemical composition of some mineral materials

	Earth crust	Portland cement	BF slag	Siliceous fly ash
SiO_2	64	16–26	28–38	55
Al_2O_3	17	4–8	8–24	26
Fe_2O_3	7	2–5	1–3	7
CaO	6	59–67	30–50	8
Na_2O	2	1–4	1–20	1
MgO	2	0.5–1.5	0.2–1	0.5
K_2O	2	0.5–1.5	0.5–3	0.6
SO_3	<1	<0.5	1–3	0.6
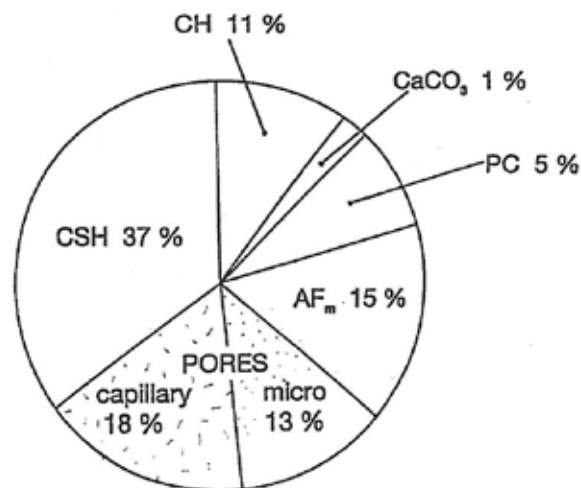
Fig. 1. **Phase composition of the PC paste after 1 year at w/c = 0.5 (Taylor, 1981)**

needs of the users, where the decisive role is played by the mineral and especially chemical additives controlling the tailored properties. As a mineral additive into HPC, microsilica is routinely used, which can be substituted by cheaper microground siliceous fly ash. In the R&D, modern instrumental techniques enables the essential study of the chemical bonds of the constituents and the micro-(nano)structure[1].

Chemical Admixtures,
Superplasticizers

Very important influence on the production of high-performance concrete exhibit the chemical admixtures of different composition and purpose. Most important, even undispensible, are superplasticizers (SP) enabling to lower considerably the water/cement ratio and thus to increase the strengths or to reduce the cement consumption[2]. At present, broad interest is put on polycarboxylate types SP, which are usually available in solutions, but some newer types of cements (e.g. Danish Secutec) contain the SP in the solid form, which diminish possible mistakes in the preparation of concrete or mortar. Very important is the use of compatible SP in a proper amount, which can be assessed by calorimetric measurement (ref.[3], see next chapters) and slump flow tests.

Self-Compacting Concrete (SCC)

In last decade, self-compacting concrete containing adequate amount of SP are widely used in many different constructions - high-rise buildings, self-leveling floors, in hybrid steel-concrete constructions etc. The viscosity, workability and setting times of superplasticized concrete or mortars are reliably controlled by the slump flow minicone test. By these SCC, steel tubes are filled to reduce the steel consumption at maintaining the total strengths[4]. The use of fine aggregate prevents the segregation.

Reactive Powder Concrete (RPC)

Concrete of ultra-high strengths can be prepared by emitting of coarse aggregate, using only very fine sand under 0.4 mm[5]. This reactive powdered concrete is in fact mortar, RPM. The use of bauxite is recommended, the content of steel microfibers (0.14×3 mm) up to 30–50 % to the cement content and thermal treatment enhances the compressive strengths up to 400 MPa[6]. By replacing part of fine sand by steel powder, the strengths can exceed 700 MPa[7]. The first hours of setting under a certain pressure and temperature around 70 °C is recommended.
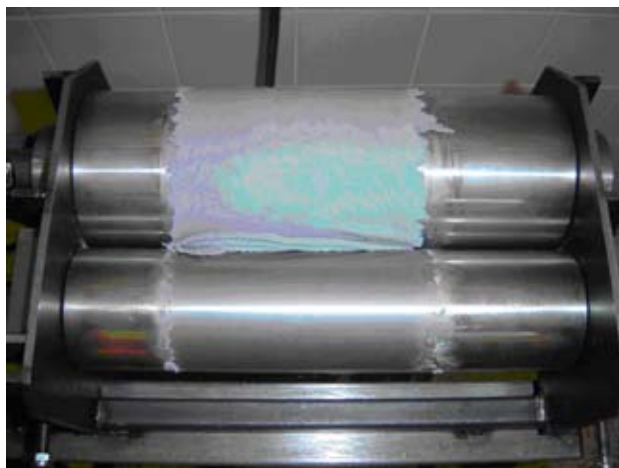
Fig. 2.   **Two-cylinder high-shear mixer (mechanochemical activation)**

Gypsum-Free Concrete

Gypsum mixed with the clinker as a retarder of of portland cement setting can be replaced by a higher amount of compatible superplasticizer. Because the start of setting is thus shifted too much, a certain amount of sodium or potassium carbonate must be added[8]. The presence of SP lowers the w/c, the addition of alkalis controls the setting times and the workability of the fresh mixture.

Macro-Defect Free (MDF) Concrete

This composites are in fact inorganic-organic copolymers. The mineral part is cement (portland or aluminate), the organic constituent is polyvinylacohol or certain polyacrylates. MDF materials possess ultra-high flexural strengths up to 150 MPa. Due to very low w/c under 0.15, special high-shear mixing of components is necessary (mechano-chemical activation)[9]. The special two-cylinder mixer (Fig. 2.) will be used also for other composites.

Fig. 3.   **Nest of termites (Gambia)**

Green Binders for the Production of Foundry Molds and Cores

The use of water glas as binders in molds for metal casting was introduced in Brno in fifties by prof. Petržela. Some years ago, water glass containing 2 % of sodium aluminate was produced in Poland and introduced on the market under the name Rudal, which can be succesfully used also for the alkali-activation of aluminosilicates in the production of

geopolymers. From organic binders, proteins[13], enzymes and polysaccharides[14,15] can be used. The broad use of these ecologically friendly organic binders enables radical improvement of the hygienic conditions in the casting houses, where due to organic plastics used in the production of cores, toxic emissions are in a high concentration.

Binders for Clayey Materials (Proteins, Polysaccharides, Enzymes)

Clayey materials are usually stabilized by lime or fly ashes (subbases of roads or buildings). Good possibilities show also organic binders on the different bases. In last years, promising applications show enzymes, decomposing as catalyzers organic constituents in clays forming proteins and saccharides, which act as binders[10,11,12]. This effect is used by the termites - soil eaters building in this way their nests (Fig. 3.) stable against tropical rains. Important is the ratio of siliceous sand to clay. Enzymes used in the construction of roads are available on the market.

Inorganic-Organic Copolymeric Materials

In nature, inorganic – organic copolymers possessing outstanding properties are synthetized succesfully for billions of years and we try in to imitate at least some of them in the R & D by many teams all over the world[16]. To this group of materials, the products of polycondensation of cement with superplasticizers of can be inserted as well as MDF concrete. On the surface of mineral constituents, free cations primarily react with the hydroxyl and/or carboxyl groups of different organic admixtures forming thus copolymers of demanded properties. The mineral admixtures like slag, fly ashes, different aggregate etc. enlarge markedly the assortment of composites possessing tailored properties. The inorganic-organic non-traditional copolymeric materials can be coined without exaggeration as composites for the 21st century.

Geopolymers (Alkali-Activated Alumino-Silicates)
The Activation of Granulated Blast-Furnace Slag (GBFS)

As soon as in seventies, in cooperation with the Research Institute of Building Materials in Kiew, slag-alkaline cements and concrete were prepared[17]. The GBF slag was activated by sodium hydroxide or silicate, forming precursors of zeolites possessing dense amorphous micro(nano)structure and high short-term strengths. Because of efflorescence brought about by sodium carbonate, potassium compounds were succesfully used. These composites of zeolitic character were coined as geopolymers[18], because they are in fact imitation of natural minerals. In the geopolymeric structure silicate and aluminate tetrahedra are connected via oxygen bridges, which can be considered as nanofibers. The calcium compounds present in the slag form preferably CSH gel. Instead of BF slag, other aluminosilicates (fly ashes, metakaolin...) can be succesfully used – see next paragraphs. It is possible to prepare on slags high-strength geopolymers possessing the compressive strengths over 150 MPa[19]. The zeolitic character of geopolymers gives to these amorphous materials ion-exchanging properties. According to the nature and concentration of the alkaline compound used, the times of setting and strengths can be controled (see Fig. 5.). These composites are very promising from ecological as well as economical points of view, because as a base component, industrial by-products ("wastes") are used, saving thus mineral natural resources – limestone and lowering considerably the carbon dioxide emissions. Newer research shows that in many ancient buildings (pyramids), geopolymeric material was used and compacted by tamping, similarly to our concrete[20]. Without any doubts, geopolymers can be considered as material for the 21st century.

Geopolymers From Fly Ashes (FA)

The utilization of siliceous fly ashes from high-temperature coal combustion is prefered, the calcium content is rather small. The reaction rate with alkalis is accelerated at higher temperatures[21]. The production of the geopolymers using fly ashes can have regional character due to the wide occurence of this by-product. The possibility of producing lightweight FA geopolymers introduces very interesting and cheap building material[21] resisting to higher temperatures.

Geopolymers From Metakaolin

By burning kaolin at the temperatures around 750 °C, metaolin is formed, which in the very fine form reacts with alkali hydroxides, carbonates or silicates. These products do not contain calcium oxide and are coined "pure" geopolymers. Preferably, some silica can be added to increase the SiO_2 content. The mutual ratio of the components is aproximately $Na(K)_2O \cdot Al_2O_3 \cdot 4SiO_2 \cdot 10H_2O$. The amorphous character of this zeolite precursor has ion-exchanging properties and can be used for the immobilization of potentially toxic components. The mixture of potassium hydroxide activated metakaolin (10 %) with fine quartz sand (90 %) was succesfully used for the production of sculptures resembling sandstone[22].

The Use of Solid Residues After Fluidized Bed Coal Combustion (FBCC)

Due to lower combustion temperature (around 850 °C) of coal, the solid residues – coarse bed ash and fine fly ash from separators – have different chemical and phase composition in comparison to the high-temperature fly ashes. These residues contain rather high amount of free lime and calcium sulfate (up to 15–20 %) and possess hydraulic properties[23]. The addition of superplasticizers makes it possible to lower the w/c under 0.30, the 28 days compressive strengths are without any further admixtures up to 70 MPa. The possibility to replace gypsum in portland cement production by this material was very succesful, the long-term strengths of the pastes or composites with the addition of FBCC ashes were increased. The presence of solfites in these FA does not interfere. The alkali activation of the FBCC fly ashes can be used for the immobilization of toxic wastes.
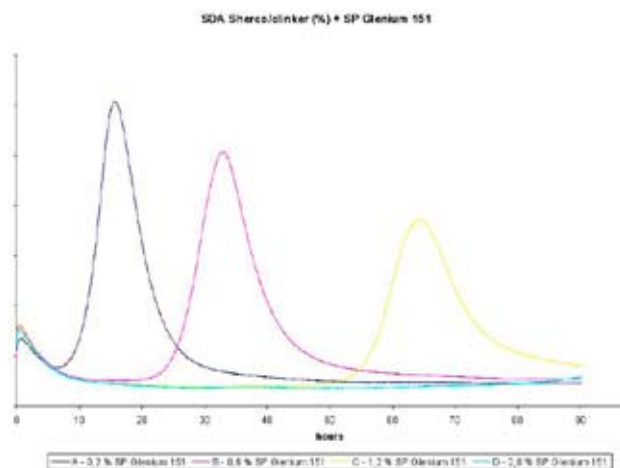
Fig. 4. **Calorimetric measurement of FBCC FA paste containing increasing amount of superplasticizer Glenium 151**
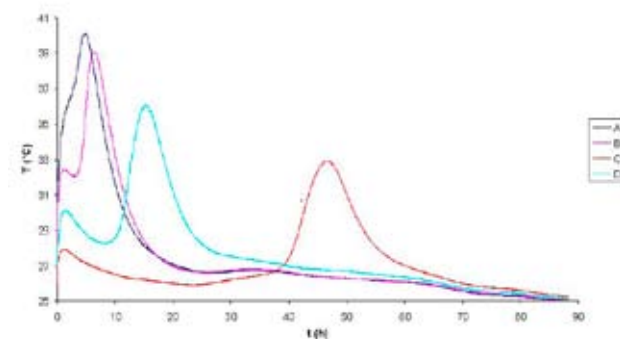
Fig. 5. **Calorimetric measurement of mixtures of BF slag containing decreasing amount of alkali activateing water glass solution (see next Table II)**

Lightweight Composite Based on the Formation and Decomposition of Ettringite, AF_t

Non-traditional composites based on FBCC ashes, energogypsum and lime were developed. According to the chemical composition of the ashes, lime hydrate is added to form CSH gel. At higher temperature, in superplasticized mixture ettringite AF_t is formed, which is due to the consequently enhanced temperature decomposed under the formation of bassanite and monosulfate AF_m. For the compressive strenghts 6–15 MPa, CSH gel is responsible. The volume density is 1,300–1,500 $kg\,m^{-3}$.

Application of Calorimetric Methods, Kinetics of Reactions

In optimization of compositions of concrete and mortars, one of the main role sis played by the proper type and amount of admixtures, especially superplasticizer. The use of calorimetery proved to be very suitable metod measuring the hydration heat evolution in time, influenced by the admixtures, w/c, starting temperature etc. The course of reactions enable to assess start and time of setting. The semiadiaba-

Table II
Composition of mixtures to the Fig. 5.

	A	B	C	D
BF slag [g]	450	500	460	325
Alkal.activator [ml]	120	90	37.5	50
Water [ml]	30	60	112.5	50
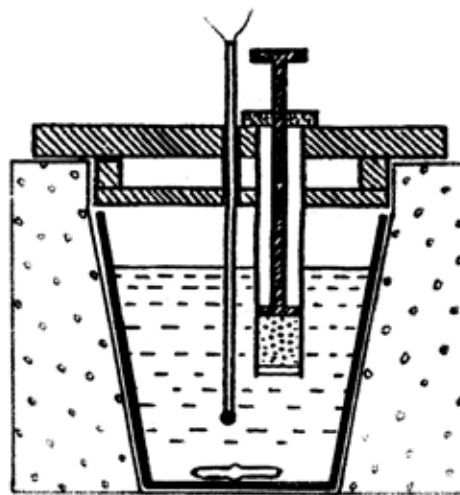
Fig. 6. **Solution calorimeter (enthalpimeter)**

tic calorimeter[3] makes it possible to measure series up to 16 samples at the same time. The samples of the fresh mixture (usually 300.0 g) in styrofoam thermoinsulated beakers contain thermoelements connected to the measuring card of the computer enabling to evaluace the results. On next figures, curves ilustrate the influence of the SP content on the start and time of setting (Fig. 4.) and effect of the different amount of sodium component on the activation of blast turnace slag (Fig. 5.).

Very useful information can be obtained by the solution calorimetry (enthalpimetry, Fig. 6.), enabling rapid determination of the quality or composition of powdered samples. The thermal impulse of the reaction of the sample with a reagent (e.g. dil. HCl) depends not only on the chemical composition, but also on the fineness of the sample – the specific surface area. This metod enables the rapid determination of some constutuents, which are by other methods time consuming, e.g. determination of the SiO_2 content, sulfates, activity of lime etc.The producers of different binders or metakaolin use enthalpimetric metod for the determination of the effect of grinding.

Discussion and Conclusions

The published papers and different printed matters contain a great amount of novel information, but to find really progressive ones in a given branch is not easy. I tis a pleasure to present, that the effort of increasing the productivity of materials is still more often a main topics of R & D of many

teams all over the world. In the building industry, the utilization of solid by-products of metallurgy and energetic industry ("wastes" like fly ashes, slags, energogypsum etc.) are in fact important raw materials, bringing about marked lowering of carbon dioxide emissions at the same time. These and related problems are solved by our students in diploma and doctoral theses. It is necessary to improve the information activities including the specialized education at all types of schools and thus to contribute to the sustainable development of the society.

REFERENCES

1. Aitcin P. C.: *High-Performance Concrete*. E & FN Spon, Routledge, London, 1998.
2. Brandštetr J., Krátký J., Szklorzová H.: Superplasticizers in concrete and mortars (in Czech). Part I: Silika *13(7–8)*, 214 (2003), Part II: Silika *14(1–2)*, 40 (2004).
3. Brandštetr J., Polcer J., Krátký J., Holešinský R., Havlica J.: Cem. Concr. Res. *31*, 941 (2001).
4. Lukáš J., Brandštetr J., Hela R.: *Proceedings of the International Conference on Bridges*, p. 1032. Dubrovnik, 2006.
5. Brandštetr J.: Minerální suroviny *1*, 23 (1999).
6. Brandštetr J., Havlica J., Opravil T., Frank V.: Silika *17*, 212 (2007), *Proceedings of the III. Conference Non Traditional Cements and Concrete* (V. Bílek and Z. Kyršner, Ed.), p. 119. Brno 2008.
7. Richard P., Cheyrezy M.: *In : Concrete Technology, Past, Present and Future* (Mehta P. K., Ed.). ACI SP p. 144. Detroit 1993.
8. Škvára J., Brandštetr J., Krátký J. : *Plasticizer for the production cement pastes, mortars and concrete*. CZ. pat. No. 297 701 (2007)
9. Šoukal F., Brandštetr J., Havlica J., Odler I.: Silika *17*, 45 (2007).
10. Cagášková L.: Diploma project, FCH BUT, Brno 2006.
11. Horák J. : Diploma project. FCH BUT, Brno 2005.
12. Horák J., Omelková J., Cagášková L., Brandštetr J.: Silika *26*, 146 (2006).
13. Kramářová D., Brandštetr J., Rusín K.: Chem. Listy *99*, 1234 (2008).
14. Laichman L.: Doctoral thesis, FCH BUT, Brno 2008.
15. Laichman L., Brandštetr J., Rusín K. : *Proceedings of the 8th Internat. Foundryman Conference*, p. 1. Zagreb, 2008.
16. Wegner G.: Acta Mater. *48*, 253 (2000).
17. *Proceedings of the conference „Slag-alkaline Cements, Concrete and Constructions*"(Glukhovskiy V.D. and Krivenko P.V., Ed.s). SRIBM, Kiew 1984.
18. Davidovits J.: J. Thermal Anal. *37*, 1533 (1991).
19. Shi C., Krivenko P. V., Roy D. M.: *Alkali-Activated Cements and Concretes*. Taylor & Francis, 2006.
20. Davidovits J.: *Geopolymer*. Institut Geopolymér, Saint Quentin, 2008. pp. 596.
21. Škvára F., Kopecký L. Němeček J., Bittner J.: Ceramics-Silikáty *50*, 208 (2006).
22. Opravil T., Brandštetr J., Havlica J., Šrámková E.: *Proceedings of the III. Conference Non-Traditional Cements and Concrete* (V. Bílek and Z.Keršner, Ed.), p. 508. Brno 2008.
23. Opravil T., Ptáček P., Šoukal F., Brandštetr J.: *Proceedings of the X. conference "Ecology and New Building Materials"*. p. 99, Brno 2006.

L03 THE EFFICACY OF DEACIDIFICATION BY AEROSOLS OF MgO AND DOLOMITE MICROPARTICLES

SILVIA HOLÚBKOVÁ[a], MICHAL JABLONSKÝ[a], MARTINA BAJZÍKOVÁ[b], JOZEF HANUS[c], JOZEF RYCHLÝ[d], VLADIMÍR BUKOVSKÝ[b] and SVETOZÁR KATUŠČÁK[a]

[a]*Institute of Polymer Materials, Department of Chemical Technology of Wood, Pulp and Paper, Faculty of Chemical and Food Technology, Slovak University of Technology, Radlinského 9, 831 07 Bratislava, Slovak Republic,*
[b]*Slovak National Library, Nám. J. C. Hronského 1, 036 01 Martin, Slovak Republic,*
[c]*Slovak National Archives, Drotárska cesta 42, 81 701 Bratislava, Slovak Republic,*
[d]*Polymer Institute, Slovak Academy of Sciences, Dúbravská cesta 9, 842 36 Bratislava, Slovak Republic,*
silvia.holubkova@stuba.sk

Introduction

It has long been widely acknowledged that paper which is produced in an industrial way is endangered by acid decomposition or oxidation[1]. The degradation process can be stopped effectively by neutralisation and the insertion of an alkaline buffer[2].

Application of mass deacidification process is connected with problems in controlling its efficacy and quality. There are no unified criteria for evaluating particular processes of mass deacidification[3]. Alkaline reserve, pH, their homogenity and effect of deacidification agents are among those used within the scope of evaluation[4,5,6,7]. Nowadays, each organization brings own new parameters to evaluating the deacidification process. Evaluation according to the criteria of 'Library of Congress, Pittsburgh'[4] is one of the options. Another option is evaluation of the process efficacy according to criteria of Swiss National Library, Bern[3,7,8,9].

Deacidification processes produce specific side effects on treated materials, according to their chemistry and method of application. Organic solvents used in, or produced during, liquid-phase processes can cause bleeding of dye stuffs (especially red dyes) in textile book covers, in inks, and stamps. All the deacidification methods using liquid can cause deformation and cockling of paper and binding[8].

Alkaline particles, such as MgO and dolomite micro-particles in the air (SoBu)[10], MgO and CaO in the air (Libertec)[11] and MgO in a perfluoralkanes (Bookkeeper)[4] are also used in deacidification of books and archival documents containing cellulose base. The most significant effect of deacidification methods based on the application of sub-micron particles is a whitish powdery deposit on paper and binding surfaces, obviously the deacidification agent (magnesium oxide, calcium oxide, dolomite microparticles and calcium carbonate). It can be easily removed by brushing, but this creates additional and time-consuming work. If it remains in the book, it can spray out during the use with the risk of health problems for the user[8].

Experimental

Raw Material

Wood containing newsprint paper (grammage 45 g m^{-2}, surface pH: 5.6) containing mechanically bleached, groundwood (55 %), bleached sulphite pulp (20 %), cought trash fibres (15 %) and clay (10 %) was used in experiments. The test books (format A5) were sent for treatment to Sobu (Fürth) company providing commercial mass deacidification.

Accelerated Ageing Procedure

Samples of paper were conditioned according to TAPPI T402 om – 93[12] at 23 ± 1 °C, and at relative humidity of air RH = 50 ± 2 %. Seventy-five sheets of paper (A5 format) were encapsulated inside a PET/Al/PE bag. The samples were aged at 96 ± 2 °C for 0, 2, 5, 10 and 15 days according to ASTM D 6819 – 02: Standard test method for accelerated aging of printing and writing paper by dry oven exposure apparatus, in which sealed glass tubes were replaced by a composite foil made of polyethylene / aluminium / polypropylene (TENOFAN Al / 116S). After ageing, the papers were conditioned for testing according to TAPPI T402 om - 93[12].

Mechanical Properties

Breaking length was determined according to TAPPI T494 om – 88[13] and the folding endurance was determined using the MIT apparatus according to TAPPI T511 om – 96[14] with a tension of 0.3 kg instead of the standard 1 kg.

Evaluation of Treatment Effectiveness

The comparison of treated/modified ($X_{t, m}$) and non-treated/non-modified ($X_{t,n}$) samples after the same period and conditions of ageing is expressed as:

$$S_{X, t} = \frac{X_{t, m}}{X_{t, n}}, \tag{1}$$

where $S_{X, t}$ stands for permanence coefficient by given treatment, X – examined properties (the breaking length (l_t) and the folding endurance (ω)), t– ageing period
If $S_{X,t} > 1$, the permanence is increased; if $S_{X,t} = 1$, it is not changed; $S_{X,t} < 1$, the permanence is decreased[15].
Linear dependence was obtained after calculating the logarithm of double folds. Time values for log ω = 0 were calculated from linear equation. Values were used for relative comparison the efficacy of deacidification process to non-treated control sample.

The lifetime of the paper ends when logarithm of the folding endurance becomes zero ($t_{\log \omega} = 0$)

The coefficient of relative increase of the lifetime for folding endurance ($S_{\tau, \omega}$) is to be expressed as eq (2).

$$S_{\tau,\omega} = \frac{t_{\log \omega = 0, m}}{t_{\log \omega = 0, n}} \; . \qquad (2)$$

Results

Kinetic dependences of changes in mechanical properties of paper were evaluated. Average values and average divergences that only indicate the variability recorded in measurement, are given for all kinetic dependences.

Stability of paper treated by aerosols of MgO and dolomite microparticles was compared to non-treated paper.

The loss of breaking length under ageing is shown in Fig. 1.
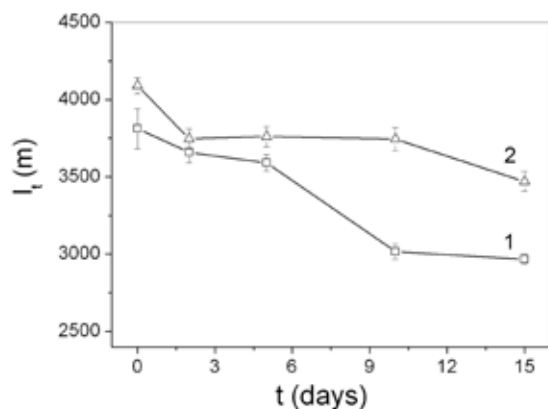
Fig. 1. **Effect of ageing time [days] on breaking length [m]:**
1 – non-treated newsprint paper
2 – newsprint paper treated by aerosols of MgO and dolomite microparticles

The breaking length of unaged non-treated paper was 3,811 m. After 15 days of ageing, the loss of strength decreased by approx. 22 % (2,968 m). After deacidification by aero-
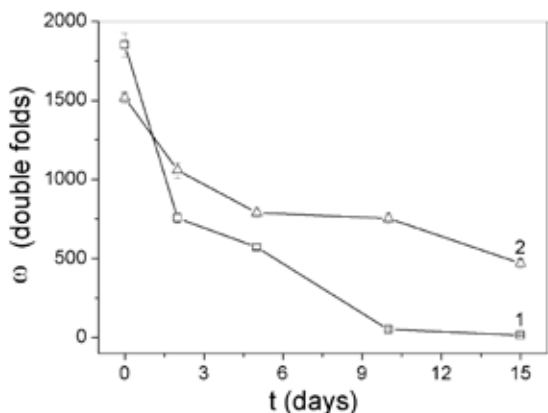
Fig. 2. **Effect of ageing time [days] on folding endurance [double folds]:**
1 – non-treated newsprint paper
2 – newsprint paper treated by aerosols of MgO and dolomite microparticles

sols of MgO and dolomite microparticles, the measured breaking length was 4,090 m. After 15 days of ageing, the loss of strength decreased by approx. 15 % (3,470 m). Permanence coefficient of the breaking length for unaged paper was evaluated $S_{lt,0} = 1.1$, the modification caused slight strengthening effect. The permanence of breaking length after 15 days of ageing was $S_{lt,15} = 1.2$, hence the modification caused positive stabilization effect.

The following picture (Fig. 2.) shows folding endurance (ω, double folds, load 0.3 kg) as a function of ageing time.

The number of double folds of untreated paper was 1850. After 2 days of ageing, the number of double folds decreased rapidly (754). After 15 days of ageing, the folding endurance was reduced to 51 double folds. After the deacidification by aerosols of MgO and dolomite microparticles 1515 double folds were determined. The number of double folds kept decreasing during the ageing process, however, the decrease rate was slower comparing to non-treated sample. After 15 days of ageing, the folding endurance was reduced to 470 double folds. The permanence coefficient of folding endurance for unaged paper was evaluated $S_{\omega,0} = 0.8$, which implies that the modification process did not result in strengthening effect, however, stability increased significantly after 15 days of ageing reaching $S_{\omega,15} = 33.6$.

The logarithm of folding endurance related to ageing time is shown in Fig. 3.
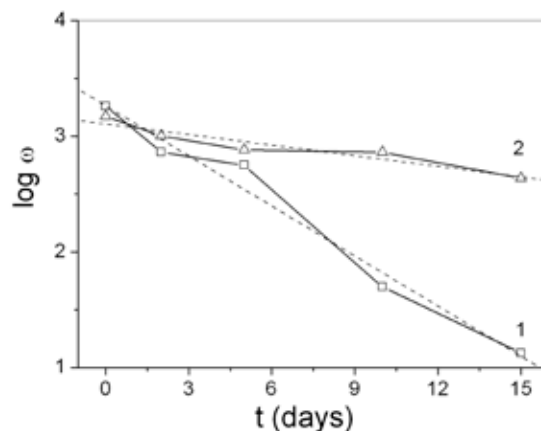
Fig. 3. **Effect of ageing time [days] on logarithm of folding endurance:**
1 – non - treated newsprint paper
2 – newsprint paper treated by aerosols of MgO and dolomite microparticles

Time values for $\log \omega = 0$ were calculated from linear equation. The coefficient of relative increase of the lifetime was calculated from formula (2) $S_{\tau,\omega} = 4.7$; which means that stability of modified paper increased by 470%.

To compare the air−MgO−dolomite microparticles technological platform (TP) to other recent TPs, the following criteria of multifactorial evaluation system of Consortium Kniha[SK] and Library of Congress[4] have been used:

- Innovation potential. Potential of the future development, research, and further education.
- Efficacy in term of increase stability of mechanical properties and life-time prolongation.

  It is the criterion of efficacy of deacidification process according to the Library of Congress[4] on tested paper, which is expressed as the rate at which paper loses strength upon accelerated ageing at 90°C / 50 RH for up to 30 days, shall be decreased by at least a factor of 3.0, when the logarithm of the folding endurance is plotted against time in days ($S_{\tau, \omega}$). The permanence of the treated paper shall be increased by a factor of 300%.

- pH and alkaline reserve,
- Price
- Risk:

  Deterioration of documents, possibility of deacidification of books without their damage, sensorial properties
  Explosion hazard
  Flammability hazard
  Health hazard
  Environmental hazard

On the basis of criteria of multifactorial evaluation system the air–MgO–dolomite TP deacidification fulfills the Consortium Kniha[SK] and Library of Congress[4] requirements for the lifetime increase ($S_{\tau,\omega} = 4.7$), improves the mechanical permanence sufficiently ($S_{\omega,15} = 33.6$; $S_{lt,15} = 1.2$). It is the most advanced, the cheapest and safest one as well (in terms of danger of fire or explosion). Platform HMDO is progressive, however, danger of fire or explosion is significant and is severalfold more expensive. The other TPs are less suitable for deacidification or not suitable for deacidification of books.

The most ecological methods are based on platform water/air regarding the environmental quality, tenability and future prospects. Freons are used in less eco-perspective TPs of which global warming potential is by 320–8,400 times higher than that of CO_2.

Conclusions

The paper was aimed at evaluating the deacidification by aerosols of MgO and dolomite microparticles. The research was based on examination of mechanical properties through multifactorial evaluation according to the requirements of Consortium Kniha[SK] and Library of Congress[4].

The air–MgO–dolomite deacidification TP fulfills requirement for the lifetime increase ($S_{\tau,\omega} = 4.7$), it does improve the mechanical permanence sufficiently ($S_{\omega,15} = 33.6$; $S_{lt,15} = 1.2$). It is most advanced, the cheapest, the most ecological and safest one as well (in terms of danger of fire or explosion or health hazards).

REFERENCES

1. Liers, J.: Restaurator *20* (1999).
2. Liers, J.: Restaurierung *2* (2001).
3. Swiss National Library: *International Conference: SAVE PAPER,* p. 94. *Bern, 15–17.Feb. 2006* (Banik, G., Doering, T., Hähner, U.).
4. Buchanan, S., Bennett, W., Domach, M. M.: *An evaluation of the Bookkeeper mass deacidification process.* Pittsburgh 1994.
5. Harris, K., E.: *A paper chase saving the written word at the Library of Congress.* Washington DC 1999.
6. Swiss National Library: *Quality standards for the paper-save Swiss process used for the deacidification of the collections of the Swiss federal archives and the Swiss federal office of culture.* Bern 2004.
7. Swiss National Library: *International Conference: SAVE PAPER,* p. 7. *Bern 15–17. Feb 2006* (Grossenbacher, G).
8. Banik, G.: Restaurator *26*, 1 (2005).
9. Bluher, A.: Papier Restaurierung *4*, 4 (2003).
10. www.sobu.de, 2008 – 05 – 19.
11. www.libertec.de, 2008 – 05 – 19
12. TAPPI T402 om – 93: *Standard conditioning and testing atmospheres for paper, board, pulp handsheets, and related products.*
13. TAPPI T494 om – 88: *Tensile breaking properties of paper and paperboard (using constant rate of elongation apparatus).*
14. TAPPI T511 om – 96: *Folding endurance of paper (MIT tester).*
15. Vrška, M., Katuščák, S., Polovka, M., Vizárová, K., Cedzová, M., Hanus, J., Mináriková, J., Bukovský, V.: Wood Res. *49,* (2004).

L04 DISTRIBUTION OF HEAVY METALS IN THE PRODUCTS OF MAGNETIC SEPARATION OF SIDERITE ORE FROM NIŽNÁ SLANÁ

SLAVOMÍR HREDZÁK, MICHAL LOVÁS, ŠTEFAN JAKABSKÝ, DANA GEŠPEROVÁ and MARIÁN BALOG

Institute of Geotechnics of the Slovak Academy of Sciences, Watsonova 45, 043 53 Košice, Slovak Republic, hredzak@saske.sk

Introduction

The mining company Siderite, Ltd. Nižná Slaná is only one producer of iron ore in Slovakia. The mining field of the company is located in the southeast part of the Slovak Ore Mts. and it consists of two near one another placed deposits (their distance is about 2,500 m), namely Manó and Kobeliarovo.

The ore from the first of one contains in the average 33.5 % of Fe, 2.18 % of Mn, 8.5 % of SiO_2, 0.001–0.2 % of As, 0.001–0.03 of Pb, 0.002–0.009 % of Zn and 0.5–1.5 of S. The average quality of ore from the Kobeliarovo deposit is as follows: 33.98 % of Fe, 1.71 % of Mn, 3.71 of SiO_2 and 0.02 % of As[1]. The ores from the both deposit are characterized by fine intergrowth of utility minerals and gangue.

The company exploits siderite ore by underground method, namely sublevel caving. The run-off-mine ore is subjected to crushing and classifying. The coarser classes are pre-treated using a dry high intensity magnetic separation. Only class with a grain size of 0–4 mm is led through bypass and directly added to magnetic product obtained by separation of coarser classes. In such way obtained material is roasted in rotary furnaces with the aim to improve the magnetic properties of main utility Fe-bearing mineral, i.e. siderite. Thus, during magnetizing roasting, siderite is changed into magnetite and/or maghemite with much higher magnetic susceptibility. After cooling the roasted ore is wet ground to a grain size 90 % under 63 μm and subjected to wet low intensity magnetic separation. Magnetic product is filtered and led to pelletizing plant. Final product – blast furnace pellets usually contain 55.4 % of Fe, 3.4 % of Mn and 5 % of SiO_2.

Currently, an annual production of ore is running about 720,000 tons. Subsequently, 320,000 tons of blast furnace pellets are made from the ore[2]. Maximal annual production, i.e. 1,010,365 tons of ore and 447,810 tons of pellets, was attained in 2000[3].

As it was mentioned above, up to now, the ore fraction with a grain size of 0–4 mm is not magnetically pre-treated and it is directly led to rotary furnaces. Its mass yield usually ranges 15–20 %[3], but at some time it can attain up to 45 %, in dependence on grain size quality of run-off-mine ore, resulting from conditions at exploitation. The coarser ore pre-treatment by dry high magnetic separation is aimed at the decreasing of free quartz and accompanying rocks amount in the feed to rotary furnaces. After running-in of this technological line the management of company has begun to pay higher attention to the possibilities of quality improvement of the 0–4 mm class, which can significantly influence the quality of final product especially concerning undesirable components content.

Thus, under laboratory conditions, a dry grain size analysis and tests of dry magnetic separation were performed at the Institute of Geotechnics of the SAS in Košice with the aim to determine the distribution of chemical components as a function of grain size and to verify the possibilities of dry separation of this class.

Experimental

Condition of Dry Magnetic Separation

Dry magnetic separation was carried out using a universal laboratory magnetic separator JONES (Fig. 1.), in a cassette intermediate between of poles separator. The cassette was equipped by two plates, grooved and flat ones, made of carbon-free iron owing to ensuring of required induction and gradient of magnetic field with regard to maximal grain size of a feed (Fig. 2.).
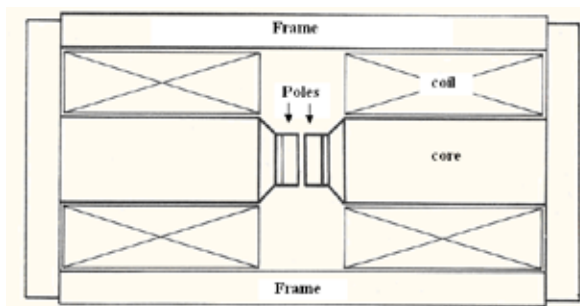
Fig. 1. **Design of the JONES separator**

Fig. 2. **The cassette equipped by plates**

Thus, the conditions of magnetic separation at three values of magnetizing current and appropriate inductions of magnetic field are introduced in Table I.

Methods of Assessment

After determination of mass yields the products of classifying and separation were subjected to chemical analyses and measurements of volume magnetic susceptibility. Loss

Table I
Conditions of magnetic separation

Magnet. current [A]	Induction of magnetic field [T]	
	Top of groove	Flat plate
1.50	0.60	0.47
1.75	0.70	0.54
2.00	0.75	0.60

on ignition (LOI) at 900 °C and SiO_2 content were assayed gravimetrically. Other elements have been determined by atomic absorption spectroscopy using the device VARIAN with accessories: Fast Sequential AAS AA240FS, Zeeman AAS AA240Z with Programmable Sample Dispenser PSD120, Graphite Tube Atomizer GTA120 and Vapor Generation Accessory VGA-77. Mercury in the products of magnetic separation was assayed using a Trace Mercury Analyser TMA 254.

The volume magnetic susceptibility "κ" measured using the device Kappabridge KLY-2, Geofyzika Brno at the following conditions: a magnetic field intensity of 300 A m^{-1}, a field homogeneity of 0.2 %, an operating frequency of 920 Hz, measurement range of device $-1,999 \times 10^{-6}/650,000 \times 10^{-6}$ SI units[4].

On the basis of mass yields and chemical analyses the recoveries of observed components into products of classifying and separation were calculated according to the method of classical material balance.

Results

G r a i n S i z e A n a l y s i s

The results are introduced in Tables II and III, respectively. As to values in Table II, it is clear, that content of Fe is higher in coarser classes. The iron content corresponds with content of manganese, magnesium and LOI. Thus, at increasing of Fe content, the contents of all mentioned components increase too. Conversely, contents of SiO_2 and Al are higher in finer classes. Similarly, the highest values of main undesirable elements such as As, Cu, Zn and Ni were detected in the finest classes. Mercury was determined only in the finest class and its content was of 1.5 ppm. As it implies from Table III, the recoveries of observed components into individual classes are strongly influenced by mass yield values as a result of small differences among contents of given component in various classes. But recoveries of utility components, namely Fe and Mn, into coarser classes (2 mm) are higher than recoveries of SiO_2 and Al. Thus, it can be stated, that main utility mineral, i.e. siderite slightly concentrates in classes 2 mm and free quartz and quartz-bearing rocks in finer classes.

Table II
Chemical composition of grain size classes

Grain size [mm]		Yield [%]	κ	Fe [%]	SiO$_2$ [%]	Mn [%]	LOI [%]	As [ppm]	Al [%]	Mg [%]	Ca [%]	Cu [ppm]	Zn [ppm]	Pb [ppm]	Ni [ppm]
4.0		15.40	873	29.90	8.32	1.79	29.51	630	0.80	3.84	0.44	115.00	70.00	45.00	14.50
3.0	−4.0	15.15	882	29.28	10.94	1.64	28.78	410	1.07	3.70	0.36	100.00	75.00	20.00	16.80
2.0	−3.0	6.99	894	29.52	10.69	1.75	28.71	820	1.08	3.70	0.35	65.00	100.00	20.00	17.80
1.0	−2.0	23.08	891	28.49	11.89	1.68	28.01	700	1.27	3.59	0.32	145.00	115.00	10.00	19.50
0.5	−1.0	16.80	861	27.83	12.11	1.63	27.72	710	1.35	3.55	0.43	95.00	85.00	20.00	21.90
0.25	−0.5	10.39	865	26.64	13.51	1.59	27.11	770	1.67	3.45	0.59	145.00	100.00	15.00	24.90
0.125	−0.25	6.47	863	25.72	12.74	1.52	26.85	980	2.01	3.36	0.45	300.00	140.00	10.00	32.80
0.063	−0.125	4.06	872	26.46	12.13	1.53	26.59	970	1.72	3.52	0.70	185.00	170.00	25.00	34.50
	−0.063	1.66	862	25.15	13.36	1.38	24.80	1160	2.61	3.25	0.38	150.00	125.00	15.00	34.50
	feed	100.00	876	28.28	11.40	1.66	28.08	699	1.30	3.61	0.42	131.30	98.38	20.49	20.88

Table III
Recoveries of observed components into grain size classes

Grain size [mm]		Fe [%]	SiO$_2$ [%]	Mn [%]	LOI [%]	As [%]	Al [%]	Mg [%]	Ca [%]	Cu [%]	Zn [%]	Pb [%]	Ni [%]
4.0		16.28	11.23	16.65	16.18	13.87	9.49	16.39	16.20	13.48	10.95	33.80	10.69
3.0	−4.0	15.68	14.53	15.04	15.52	8.88	12.49	15.54	13.04	11.54	11.55	14.78	12.18
2.0	−3.0	7.30	6.55	7.37	7.15	8.20	5.82	7.16	5.85	3.46	7.11	6.82	5.96
1.0	−2.0	23.25	24.05	23.41	23.02	23.10	22.59	22.94	17.67	25.49	26.98	11.26	21.55
0.5	−1.0	16.54	17.84	16.49	16.59	17.06	17.49	16.55	17.29	12.16	14.52	16.40	17.62
0.25	−0.5	9.79	12.31	9.98	10.03	11.44	13.38	9.95	14.67	11.48	10.56	7.61	12.39
0.125	−0.25	5.88	7.22	5.93	6.19	9.06	10.02	6.02	6.96	14.78	9.20	3.16	10.16
0.063	−0.125	3.80	4.32	3.75	3.85	5.64	5.39	3.97	6.80	5.72	7.02	4.96	6.71
	−0.063	1.47	1.94	1.39	1.46	2.75	3.34	1.49	1.51	1.89	2.11	1.21	2.74
	feed	100.00	100.00	100.00	100.00	100.00	100.00	100.00	100.00	100.00	100.00	100.00	100.00

Magnetic Separation

The quality of separation products obtained at three values of magnetizing current or more precisely induction of magnetic field is described in Tables IV–VI. Subsequently, the recoveries of observed components into separation products, i.e. magnetic (M) and nonmagnetic (N) ones, are introduced in Tables VII–IX.

An increasing of the value of magnetizing current resulted above all in a rising of mass yield into magnetic product. Understandably, the highest Fe content in magnetic product was achieved at the smallest induction of magnetic field, when grains of liberated siderite with the highest magnetic susceptibility are collected in this product. However, the recovery of iron under such conditions is minimal. Thus, with gradually enhancing of induction, the magnetic product is slightly contaminated by waste components, mainly SiO_2, but the recoveries of iron and manganese significantly rise.

Conclusions

Present results of the research on benefication of the class 0–4 mm of siderite ore can be recapitulated as follows:

Table IV
Properties and quality of products obtained at magnetizing current of 1.5 A

Product	Yield [%]	$\kappa \times 10^6$ [SI unit]	Fe [%]	SiO_2 [%]	Mn [%]	LOI [%]	As [ppm]	Hg [ppm]	Al [%]	Mg [%]	Ca [%]	Cu [ppm]	Zn [ppm]	Pb [ppm]	Ni [ppm]
M	33.36	1011	32.31	5.37	1.64	30.46	370	1.30	0.99	3.24	0.28	110	75	15	15
N	66.64	791	25.12	14.60	1.36	26.62	710	1.60	1.64	3.40	0.35	195	100	10	27
feed	100.00	864	27.52	11.52	1.45	27.90	597	1.50	1.42	3.34	0.33	167	92	12	23

Table V
Properties and quality of products obtained at magnetizing current of 1.75 A

Product	Yield [%]	$\kappa \times 10^6$ [SI unit]	Fe [%]	SiO_2 [%]	Mn [%]	LOI [%]	As [ppm]	Hg [ppm]	Al [%]	Mg [%]	Ca [%]	Cu [ppm]	Zn [ppm]	Pb [ppm]	Ni [ppm]
M	58.01	956	30.62	7.23	1.59	29.70	370	1.00	0.94	3.11	0.29	80	80	15	15
N	41.99	720	23.10	17.96	1.27	25.80	890	1.80	1.57	3.21	0.38	130	105	10	26
feed	100.00	857	27.46	11.74	1.46	28.06	588	1.34	1.20	3.15	0.32	101	91	13	19

Table VI
Properties and quality of products obtained at magnetizing current of 2 A

Product	Yield [%]	$\kappa \times 10^6$ [SI unit]	Fe [%]	SiO_2 [%]	Mn [%]	LOI [%]	As [ppm]	Hg [ppm]	Al [%]	Mg [%]	Ca [%]	Cu [ppm]	Zn [ppm]	Pb [ppm]	Ni [ppm]
M	84.20	1003	29.39	8.53	1.56	29.08	570	1.20	1.15	3.46	0.30	135	87	15	21
N	15.80	549	18.04	27.05	1.00	21.37	1200	3.60	2.34	3.16	0.64	145	110	10	26
feed	100.00	931	27.60	11.45	1.47	27.86	669	1.58	1.34	3.41	0.35	137	91	14	22

Table VII
Recoveries of components into separation products at magnetizing current of 1.5 A

Product	Fe [%]	SiO_2 [%]	Mn [%]	LOI [%]	As [%]	Hg [%]	Al [%]	Mg [%]	Ca [%]	Cu [%]	Zn [%]	Pb [%]	Ni [%]
M	39.16	15.55	37.68	36.42	20.69	28.91	23.21	32.31	28.59	22.02	27.30	42.89	21.50
N	60.84	84.45	62.32	63.58	79.31	71.09	76.79	67.69	71.41	77.98	72.70	57.11	78.50
feed	100.00	100.00	100.00	100.00	100.00	100.00	100.00	100.00	100.00	100.00	100.00	100.00	100.00

Table VIII
Recoveries of components into separation products at magnetizing current of 1.75 A

Product	Fe [%]	SiO_2 [%]	Mn [%]	LOI [%]	As [%]	Hg [%]	Al [%]	Mg [%]	Ca [%]	Cu [%]	Zn [%]	Pb [%]	Ni [%]
M	64.68	35.74	63.35	61.40	36.48	43.42	45.27	57.21	51.32	45.95	51.28	67.45	44.83
N	35.32	64.26	36.65	38.60	63.52	56.58	54.73	42.79	48.68	54.05	48.72	32.55	55.17
feed	100.00	100.00	100.00	100.00	100.00	100.00	100.00	100.00	100.00	100.00	100.00	100.00	100.00

Table IX
Recoveries of components into separation products at magnetizing current of 2 A

Product	Fe [%]	SiO$_2$ [%]	Mn [%]	LOI [%]	As [%]	Hg [%]	Al [%]	Mg [%]	Ca [%]	Cu [%]	Zn [%]	Pb [%]	Ni [%]
M	89.67	62.68	89.26	87.88	71.68	63.98	72.36	85.35	71.41	83.22	80.82	88.88	81.14
N	10.33	37.32	10.74	12.12	28.32	36.02	27.64	14.65	28.59	16.78	19.18	11.12	18.86
feed	100.00	100.00	100.00	100.00	100.00	100.00	100.00	100.00	100.00	100.00	100.00	100.00	100.00

- utility components of ore, i.e. Fe and Mn, a slightly more concentrate into coarser fractions 2 mm,
- conversely, gangue represented above all by SiO$_2$ and Al concentrates into finer ones bellow 2 mm,
- a relative high content of As from 980 to 1,160 ppm was detected in fines bellow 0.25 mm,
- similarly, higher contents of other heavy metals such as Cu, Zn and Ni were also determined in fines, while the highest content of Pb was identified in the coarsest fraction,
- an increasing of magnetic field induction at separation resulted in slight reduction of Fe and Mn content in magnetic product, but also in significant enhancement of their recoveries.

Finally, it can be recommended:
- to reject the fraction with a grain size of 0–0.25 mm from technological flowsheet and in such way to prevent the contamination of final product by heavy metals,
- to apply magnetic induction about 0.7–0.8 T at separation process to avoid losses of iron and manganese in nonmagnetic product.

REFERENCES
1. Boláček O., Mihók J.: Iron Ore Works, Nižná Slaná, 1994. In: Grecula P. et al.: *Mineral deposits of the Slovak Ore Mountains*, Vol. 1., Geocomplex, Bratislava 1995.
2. Investment project: Innovation of technological process of the Siderit, Ltd. Nižná Slaná and development of reserves of the Nižná Slaná – Manó – Kobeliarovo deposit, Attachment 3.
3. Lukáč S.: Acta Montanistica Slovaca 7, 227 (2002).
4. Kappabridge KLY-2: Instruction manual for magnetic susceptibility bridge, Geofyzika Brno.

L05 MAGNETICALLY MODIFIED BENTONITE AND STUDY OF ITS IMPROVED SORPTION PROPERTIES

ZUZANA OROLÍNOVÁ and ANNAMÁRIA MOCKOVČIAKOVÁ

Institute of Geotechnics, Slovak Academy of Sciences, Watsonova 45, 043 53, Košice, Slovak Republic,
orolinova@saske.sk

Introduction

Clays are naturally occurring aluminosilicates having sheet structure. Natural clays are low-cost and available materials functioning as cation exchangers. They have often been used to adsorb metallic contaminants. Among the three basic classes of clays – kaolinite, micas, smectites, the last mentioned have the largest surface area and the highest cation exchange capacity. If the major mineral in clay is montmorillonite or a member of other smectites, than, it is called bentonite[1]. For evaluation its behaviour against chemical attack, bentonite attracted the researcher's concern for a long time and has been studied extensively[2].

Use of natural bentonite in treating aqueous waste containing heavy metals and organic matter has been previously reported in many works.[3–5] Natural bentonites are usually activated or modified with the aim to improve their sorption properties.[6–7]

It is documented that nano-scaled magnetic particles could be also used for sorption purpouses and they are good sorbents of contaminants from aqueous or gaseous effluents[8].

In this work the natural bentonite was modified by the magnetic particles with the aim to enhance its sorption properties. The structural, surface, porous and sorption properties of composite materials were studied.

Experimental

Materials

The natural bentonite originated from the locality Stará Kremnička – Jelšový potok. It was first treated by sedimentation method to obtain monomineral fraction with the particle size below 20 μm.

The composite materials were prepared from the solutions of ferric and ferrous salts, where bentonite was added before the iron oxide precipitation. The magnetic particles were precipitated by NH_4OH added dropwise. The bentonite dosage was adjusted in order to obtain different bentonite/iron oxide wight ratios 1 : 1, 5 : 1 denoted as A, E respectively. The modification process was realized at two selected temperatures 293 and 358 K.

Methods

The nitrogen adsorption experiments were realized with Micrometrics ASAP 2400 apparatus (Slovakia). The specific surface area S_{BET} was calculated from the adsorption isotherms according to the BET (Brunauer, Emmett, Teller) method in

a range of relative pressure 0.03–0.2 p/p_0. The value of total pore volume V_a was determined from the amount of adsorbed volume at relative pressure close to saturation pressure. The micropore volume V_{micro} and value of external surface S_t were obtained from the *t*-plot analysis. The pore size distribution of studied materials was calculated using the BJH (Barett-Joyner-Halenda) method from the desorption isotherms.

Powder X-ray diffraction (XRD) patterns were collected using a Philips PW1820 (Germany) equipped with a CuKα radiation (40 kV, 40 mA). The JCPDS PDF database was used for the phase identification.

Mössbauer spectroscopy measurements were carried out with a $^{57}Co/Rh$ γ-ray source (Germany) at the room temperature. The velocity scale was calibrated relative to ^{57}Fe in Rh. Recoil spectral analysis software was used for the quantitative evaluation of the Mössbauer spectra[9].

The value of magnetization of the samples was determined by the superconducting quantum interference device (SQUID) magnetometer measurement (Germany) at the maximum field of 50 kOe.

The scanning electron microscopy (SEM) analyses were made in JEOL JSM-6400 (Germany). Elements present in composites surface were determined using the energy dispersive analyzer of X-rays (EDAX) on the SEM.

The sorption of zinc from model aqueous solutions by the natural and magnetically modified bentonite was carried out using batch-type equilibrium experiments in a rotary shaker for 24 hours at constant ambient temperature. The initial total metal ion concentration range was 10–100 mg dm^{-3}. Sorption experiments were realized at pH = 5 and the sorbent concentration was 2 g.dm^{-3}. The final metal concentration was determined by atomic absorption spectroscopy (AAS using a Varian Spectr AA-30) and the metal uptake was calculated from the difference. Sorption isotherms have been fitted with Langmuir equation. The sorption capacities of the natural and modified bentonite were compared.

Results

The adsorption and desorption isotherms of the natural and modified bentonite, shown in Fig. 1.(a), (b), were obtained from the adsorbed and desorbed gas plotted against the relative pressure. The hysteresis loops are associated with the capillary condensation that is typical for mesoporous materials. The final arising part of the isotherms assigns the occurrence of macropores in the structures[10]. The values of BET surface area calculated from the adsorption isotherm, values of external surface and pore volume are included in Table I. The composite materials showed once more higher values of specific surface area compared to the bentonite. The value of total pore volume has the increasing tendency in dependence of the higher content of iron oxide in the composites. The higher values of the specific surface area and increasing values of total pore volumes should be explained by the secondary pore structure formation caused by the creating of agglomerates on the bentonite surface during the iron oxide precipitation. The *t*-plot method is a transformation of adsorption

isotherm in which relative pressure is replaced by t (estimated statistical thickness of adsorbed layer of nitrogen). Plot of V (adsorbed gas volume) versus t was linearized in the range from 0.354 nm (thickness of adsorbed monolayer) to 0.5 nm (corresponding roughly to the range of relative pressures 0.1–0.2) and the extrapolation of this plot to $t = 0$ gave the values of specific volume of micropores. As follows from the Fig. 2. the contribution of small pores to the total pore volume is not significant because the values of the micropore volume obtained by this method were almost equal to zero.

Table I
Structural parameters of the investigated samples

Sample	S_{BET} [$m^2 g^{-1}$]	V_a [$cm^3 g^{-1}$]	V_{micro} [$cm^3 g^{-1}$]	S_t [$m^2 g^{-1}$]
Bentonite	39.4	0.096	0.005	27.6
A293	73.7	0.216	0.004	64.2
E293	90.7	0.187	0.002	83.9
A358	82.8	0.251	0.004	73.7
E358	84.8	0.183	0.003	77.5
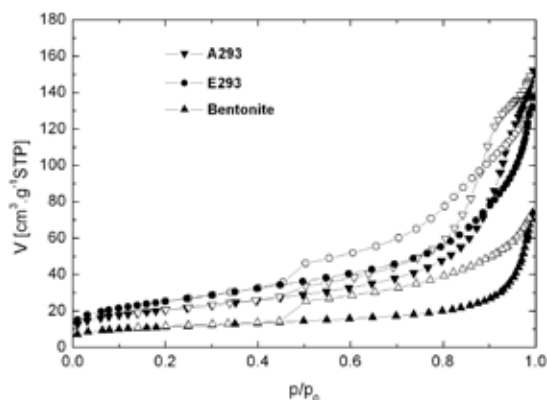
Fig. 1.(a) **Adsorption – desorption isotherms of natural and modified bentonite at 293 K (filled symbols – adsorption isotherms, open symbols – desorption isotherms)**
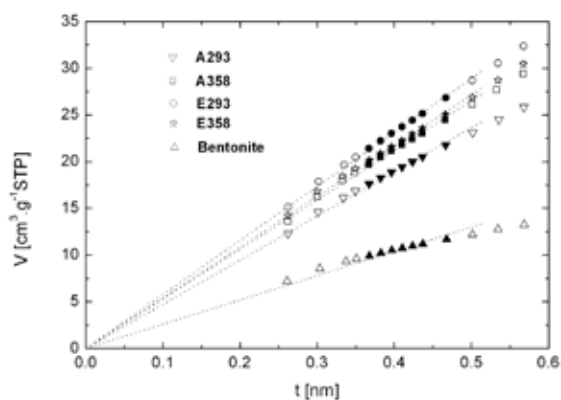
Fig. 2. **t-plot of the investigated samples (filled symbols – linearized parts)**
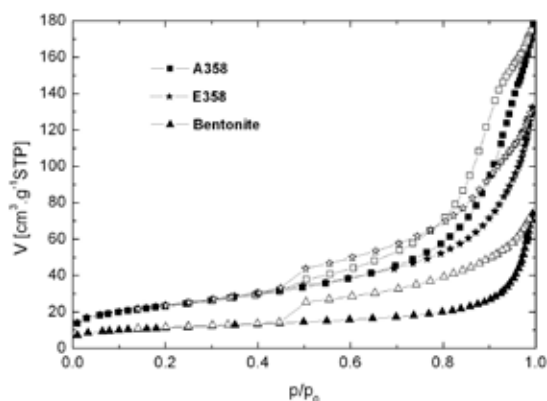
Fig. 1.(b) **Adsorption – desorption isotherms of natural and modified bentonite at 358 K (filled symbols – adsorption isotherms, open symbols – desorption isotherms)**

Fig. 3. **Pore size distribution of the investigated samples**

Distribution of adsorbed volume in the investigated samples was estimated by the BJH method from the desorption isotherms. Fig. 3. shows the dependence of the volume density distribution on the average pore diameter of the natural bentonite and its modified samples.

The curves of the composite materials indicate the increase in the volume in mesopores in comparison to the natural bentonite. The analysis has shown that the porosity of modified samples varied with the different content of magnetic

particles in composite. The stronger formation of secondary mesopore structure showed the samples A293 and A358, especially in the range 11–25 nm. The curve of pore size distribution of the E293 sample is shifted left that signifies occurrence of smaller pores in comparison with E358.

The XRD analysis of the composites confirmed the presence of montmorillonite and Fe oxidized phase, but it was not able to determine the iron oxide phase because of strongly overlapping of magnetite and maghemite diffraction lines. Therefore the Mössbauer spectroscopy was used to identify this phase. Except the maghemite, goethite in the samples synthesized at 293 K was observed too, Fig. 4.
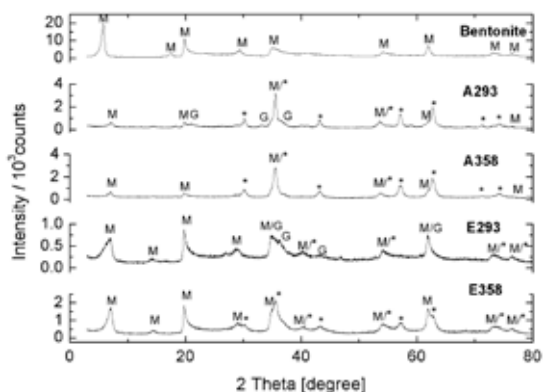
Fig. 4. **X-ray diffraction pattern of natural bentonite and modifiet samples (M – montmorillonite, * - iron oxide diffraction, G – goethite)**

The room temperature Mössbauer spectra of composites A293, A358 and E358 are complexes consisting of paramagnetic doublet and one sextet. The analysis of the A293 sample, Fig. 5.(a), confirmed the presence of γ-Fe_2O_3 (average hyperfine magnetic field for the octahedral site: $B^{Oct} = 41.8$ T, isomer shift IS = 0.25 mm s^{-1}, relative spectral area RA = 40.15 %; for the tetrahedral site: hyperfine magnetic field $B_{hf}^{Tet} = 47.6$ T, IS = 0.13 mm s^{-1}, RA = 24.1 %)
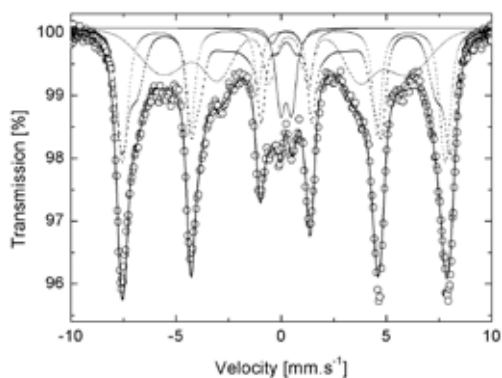
Fig. 5.(a) **Fitted Mössbauer spectrum of the sample A293**
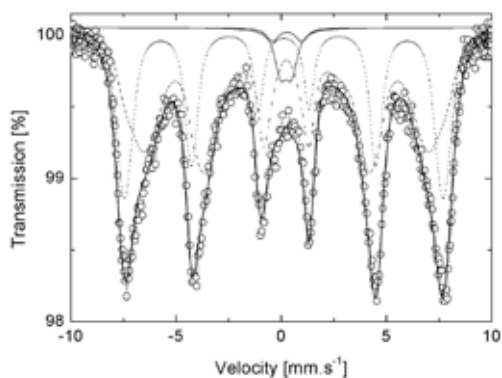
Fig. 5.(b) **Fitted Mössbauer spectrum of the sample A358**

and small amount of goethite ($B_{hf} = 35.8$ T, IS = 0.26 mm s^{-1}, quadrupole splitting QS = –0.08 mm s^{-1}, RA = 28.7 %) in composite sample. The Mössbauer spectrum analysis of the samle A358 showed only the presence of maghemite (average hyperfine magnetic field for the octahedral site: $B^{Oct} = 38.8$ T, isomer shift IS = 0.25 mm s^{-1}, relative spectral area RA = 59.7 %; for the tetrahedral site: hyperfine magnetic field $B_{hf}^{Tet} = 47$ T, IS = 0.13 mm s^{-1}, RA = 35.8 %) in composite, Fig. 5.(b). The similar results were obtained for the sample E358. The relative spectral area of maghemite was lower that was confirmed by its lower content in composite. More expressive paramagnetic doublet of bentonite was observed for this sample. The Mössbauer spectrum of the E293 sample has shown only a paramagnetic doublet. It was fitted with two paramagnetic doublets, Fig. 5.(c). In the case of very small magnetic particles, they do not show magnetic properties and their sextet structure is bowing into paramagnetic doublet structure.
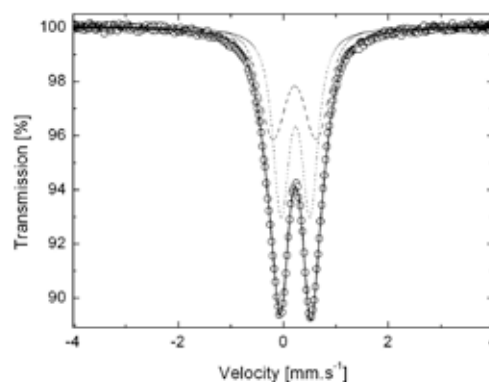
Fig. 5.(c) **Fitted Mössbauer spectrum of the sample E293**

In all investigated composite samples two paramagnetic positions of Fe^{3+} in bentonite were detected.

The magnetization σ of nanosized iron oxide synthesized at 293 K and 358 K without the bearer was measured by SQUID magnetometer. The obtained values were 83.59 emu g^{-1} and 80.95 emu g^{-1} respectively. These measured values were used to calculate the expected theoretical values of magnetization for the modified samples.

The measured magnetization for the composites increases in dependance on the increasing maghemite content in the samples. The measured values do not respond to theoretical. That should be explained by the contribution of measured bentonite magnetization and in the case of samples A293 and E293 also by the presence of goethite in their structures. The value of magnetization of the E293 sample is almost equal to zero. It was confirmed by the Mössbauer spectroscopy that composite E293 contain small particles. The obtained values are listed in Table II.

Fig. 6.(a) shows the morphology of the sample E293 observed by SEM in Compo mode. The white spots belong to maghemite agglomerates on the bentonite surface. It was also confirmed by the EDAX analysis illustrated on Fig. 6(b)

where the presence of Fe and O elements on the bentonite surface was detected.

Table II
Measured and theoretical values of magnetization of the investigated samples

Sample	$\sigma\,[\mathrm{emu\,g^{-1}}]$	Theoretical $\sigma\,[\mathrm{emu\,g^{-1}}]$
Bentonite	4.02	–
A293	37.02	41.80
E293	0.69	13.93
A358	46.22	40.48
E358	15.07	13.49
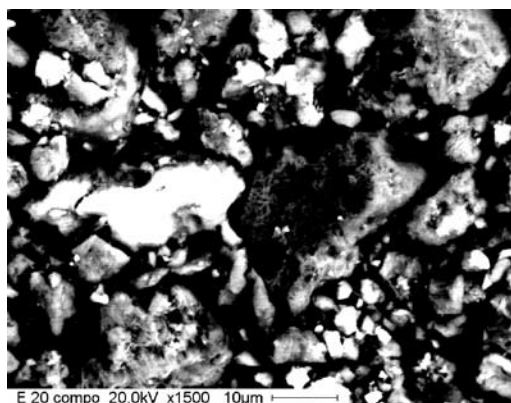
Fig. 6.(a)   **SEM Compo mode image of the composite sample E293. White parts signify the presence of iron oxide on the bentonite surface**
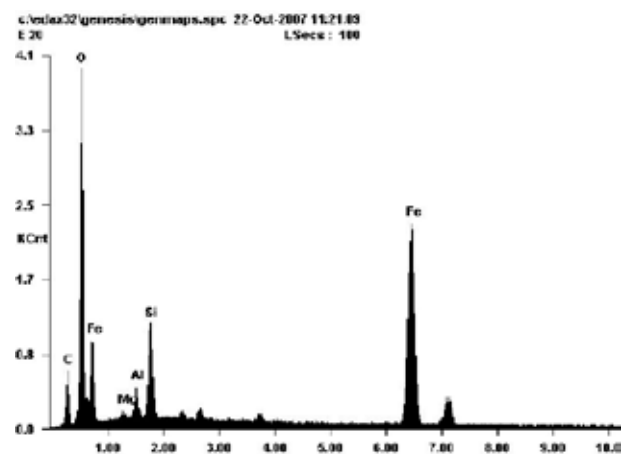
Fig. 6.(b)   **EDAX analysis of the composite sample E293**

The sorption experiments of zinc were realized on the natural bentonite and composite material. From all obtained results of previous studies two samples were interesting from the sorption point of view. A358 showed the highest value of pore volume and magnetic property, E293 had the largest specific surface area. On the basis of the result of zeta potential measurement, the last mention sample was used for sorption experiment. The effect of metal ion concentration on

zinc adsorption was investigated over the concentration range 10–100 mg dm^{-3} at room temperature. The sorption isotherms obtained at constant temperature are shown in Fig. 7. From this, it is observed that the adsorption capacity q_e increases as a function of metal concentration. The maximum sorption capacity of sorbents has not been reached yet. The experimental data of sorption were fitted with linearized Langmuir type model, Fig. 8.(a), (b), according to the equation (1).

$$\frac{C_e}{q_e} = \frac{1}{Q_m \cdot K} + \frac{C_e}{Q_m},\qquad(1)$$

where C_e is the equilibrium concentration of metal in solution, q_e is the corresponding amount of metal ions sorbed onto sorbent, Q_m and K are Langmuir constants related to sorption capacity and sorption energy, respectively. Maximum sorption capacity Q_m represents monolayer coverage of sorbent with sorbate and K represents enthalpy of sorption and should vary with temperature.

The maximum sorption capacity of bentonite and E293 calculated from the slope of the plot was 22 mg Zn g^{-1} and 23 mg Zn g^{-1}, respectively.
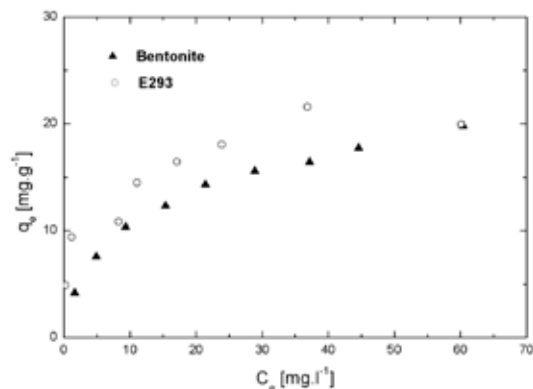
Fig. 7.   **Sorption isotherms of Zn^{2+} ions by the natural bentonite and E20 composite sample**
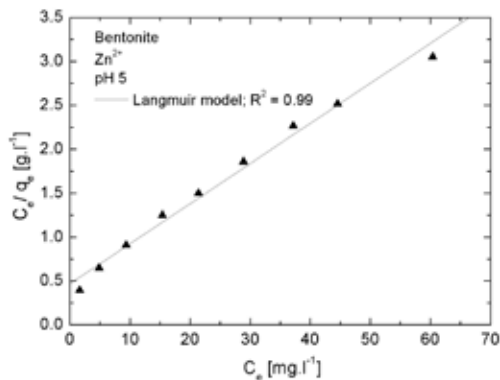
Fig. 8.(a)   **Linearized form of Langmuir sorption isotherm of Zn2+ on natural bentonite**
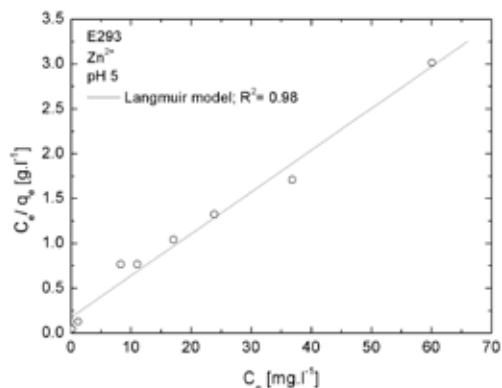
Fig. 8.(b)   Linearized form of Langmuir sorption isotherm of Zn^{2+} on composite E293

Comparing the efficiency of the natural and modified bentonite towards zinc cations it seems the composite material E293 to be more convenient in removing of this metal from solutions.

Conclusion

Magnetic modification of natural bentonite seems to be a perspective way of enhancing its sorption properties and offers an easy separation and recovery of sorbents[11].

The natural bentonite was modified by iron oxide particles and its improved properties were studied. The natural bentonite as well as composites showed mesoporous structure, the occurrence of macropores was observed from their hysteresis loops. The BET surface area of the composite materials was twice higher in comparison to the natural bentonite. The total pore volume had the increasing tendency in dependance on the higher content of iron oxide in the composite materials because of textural porosity created between the iron oxide particles.

The composite materials exhibited the magnetic properties, which were confirmed by magnetization measurements. The XRD analysis showed the diffractions of Fe oxidized phase in composites materials, in case of the composites synthesized at 293 K, goethite diffractions were observed. Fe oxidized phase was identified by the Mössbauer spectroscopy and it belonged to maghemite. Only the composite sample E293 showed the paramagnetic property that it was caused probably by small iron oxide particles in the composite. The presence of the iron oxide particles on the bentonite surface was observed by SEM and analyzed by EDAX. Maghemite particles were nonhomogenously distributed on the bentonite surface, creating agglomerates.

The sorption properties of the natural bentonite and composite E293 were studied. The composite sample showed the higher adsorption capacity of Zn^{2+} over the whole concentration range in comparison to the natural bentonite. The experimental data were well fitted by the Langmuir type model. Comparing the efficiency of both materials, magnetically modified bentonite seems to be a promise candidate for practical use in heavy metals removal.

REFERENCES
1. Önal, M., Sarikaya, Y., Alemdaroğlu, T.: Turk. J. Chem., *25*, 2412 (2001).
2. Kaya, A., Ören, A.H.: J. Hazard. Mater. *B125,* 183 (2005).
3. Bereket, G., Aroğuz, A. Z., Özel, M. Z.: J. Colloid Interface Sci. *187*, 338 (1997).
4. Tsai, S. Ch., Ouyang S., Hsu, Ch. N.: Appl. Radiat. Isot. *54*, 209 (2001).
5. Tachi, Y., Shibutani, T., Sato, H., Yui, M.: J Contam. Hydrol. *47*, 171 (2001).
6. Volzone, C., Garrido, L. B.: Cerâmica *48*, 153 (2002).
7. Karahan, S., Yurdakoç, M., Seki, Y. Yurdakoç, K.: J Colloid Interface Sci. *36*, 293 (2006).
8. Václavíková, M., Jakabský, Š., Hredzák, S.: Nanoengineered Nanofibrous Materials, NATO Sci. Ser. II. Math. Phys. Chem. *169*, 479 (2004).
9. Lagarec, K., Rancourt, D. G.: *Recoil - Mössbauer Spectral Analysis Software for Windows, version 1.02*, Ottawa, ON 1998.
10. Sing, K. S. W., Everett, D. H., Haul R. A. W., Moscou, L., Pierotti, R. A., Rouquérol, J., Siemieniewska, T.: Pure Appl. Chem. *57*, 603 (1985).
11. Bourlinos, A. B., Zboril, R., Petridis, D., Microporous Mesoporous Mater. *58*, 155 (2003).

L06 REDUCTIVE DISSOLUTION OF SYNTHETIC FERRIC IRON MINERALS BY ACIDOPHILIC BACTERIUM *ACIDIPHILIUM* SJH

ZUZANA PÁLLOVÁ[a], DANIEL KUPKA[a], ALEXANDRA VAŠKOVÁ[a], ZUZANA OROLÍNOVÁ[a], VLADIMÍR ŠEPELÁK[b] and JANA ŠKRLÍKOVÁ[c]

[a]*Department of Biotechnology, Institute of Geotechnics of Slovak Academy of Sciences, Watsonova 45, 043 53 Kosice, Slovak Republic,*
[b]*The Institute of Physical and Theoretical Chemistry, Braunschweig University of Technology, Hans-Sommer-Str. 10, 38106 Braunschweig, Germany,*
[c]*Department of Analytical Chemistry, University of P. J. Šafárik, Moyzesova 16, 041 54 Kosice, Slovak Republic,*
pallova@saske.sk

Introduction

Iron oxides are ubiquitous in soils and rocks, lakes and rivers, on the sea floor, in air, and in organisms. They are abundant in soils and aquifers, where they act as a sorbent of heavy metals and of other components. Iron oxides have a substantial impact on the quality of underground waters and porous water in sediments[1].

In an aquatic environment, iron occurs in two oxidative states; Fe^{3+} and Fe^{2+}. Ferric iron is stable in aerobic conditions, especially in neutral and alkaline pH. The concentration of free ferric ions in these conditions is approximately 10^{-17} M. On the other hand, ferrous iron is highly soluble in a wide range of pH and in anoxic conditions[2]. Ferrous iron rapidly oxidizes in the presence of oxygen to ferric iron, which rapidly precipitates above pH 2.5. Below pH 2.5, both iron species are soluble and the oxidation of Fe^{2+} to Fe^{3+} is extremely slow[3].

Dissimilative reduction of ferric iron is an alternative way of respiration of microorganisms in anaerobic conditions. Trivalent iron that could occur in a form of soluble or insoluble compounds can act as a final acceptor of electrons taken during the oxidation of organic matter (heterotrophic organisms) or inorganic matter (autotrophic organisms)[4]. Iron is a redox-active element and it easily transforms from one oxidative state to another. Redoxpotential of the pair Fe^{3+}/Fe^{2+} at pH 2 is 0.77 V. This value (0.84 V) is close to the standard redox potential of the system O_2/H_2O(ref.[5]).

The bacterial reduction of solid state ferric iron causes the dissolution of iron minerals including associated elements[6]. Reductive dissolution of iron can be applied in elimination of undesirable ferric minerals from nonmetalics or in bioremediation of acid mine drainage.

This work presents the behavior of solid as well as liquid ferric iron reduction by bacteria *Acidiphilium* SJH. The bacteria of genus Acidiphilium are heterotrophic, aerobic or facultative anaerobic organisms. These thrive in acidic and neutral range of pH, with an optimum at pH 3 [7]. They oxidize organic substratum to CO_2 and as an oxidant they utilize oxygen or trivalent iron [8]. Acidophilic heterotrophic bacteria have unique properties, therefore they seem to have the possibility for reductive leaching of solid ferric iron compounds[9].

Bacteria Acidiphilium SJH reduce Fe(III) to Fe(II) even at the presence of oxygen[10,5]. The obligatory anoxic environment is not a necessary term in the above mentioned processes of iron reduction. In addition, some strains of the genus Acidiphilium can simultaneously utilize both oxygen and trivalent iron during the oxidation of organic material. The co-respiration of O_2 and Fe^{3+} at acidophilic heterotrophs is an interesting phenomenon. The absence of oxygen is an obligatory requirement for many neutrophilic microorganisms to reduce ferric iron. Iron respiration is inhibited even at a trace amount of oxygen.

Experimental

Iron Oxide Preparation and Characterization

Five pure synthetic iron minerals were prepared as follows:

- Goethite – α-FeO(OH) was prepared from an alkaline system by the hydrolysis of 1M $Fe(NO_3)_3$ with 5M KOH. The synthesis took 60 hours at 70 °C. Yellow-brown colored goethite powder was obtained.
- Lepidocrocite- γ-FeO(OH) was synthesized by oxidizing a Fe^{2+} ($FeCl_2 \cdot 4H_2O$) containing solution at a pH close to neutral. By this method crystalline reddish-yellow lepidocrocite was obtained.
- Magnetite – Fe_3O_4 was prepared from the solution of $FeSO_4 \cdot 7H_2O$ flushed with N_2 gas. The solution of KNO_3 and KOH was used as an oxidizing agent. The oxidation proceeded at 90 °C. The black precipitate occurred after several minutes.
- Maghemite – γ-Fe_2O_3 was prepared by the heating of the sample of synthetic lepidocrocite in a furnace at 250 °C. The thermal transformation was carried out for 2 hours.
- Hematite – α-Fe_2O_3 was being synthesized by acid hydrolysis from the solution of $FeCl_3$ and HCl at 78 °C for ten days.

The resulting products were separated from the liquid phase by centrifugation and then washed with distilled water. The iron oxide powders were finally dried at laboratory temperature and stored in the exicator.

The specific surface area of each iron mineral was measured by the BET (GEMINI 2360, Micromeritics, USA). This method is based on the adsorption of nitrogen molecules on the solid state's surface.

The XRD patterns were collected using a Philips PW 1820 powder diffractometer with CuK_α radiation. The JCPDS PDF database[11] was utilized for phase identification.

Mössbauer spectra of the samples were taken in transmission geometry at temperature T = 293 K. A ^{57}Co/Rh γ-ray source was used. The velocity scale was calibrated relative to ^{57}Fe in Rh. The Recoil spectral analysis software was used for the quantitative evaluation of the Mössbauer spectra[12].

Bacterial Iron-Reduction

Bacterial strain *Acidiphilium* SJH was obtained as a gift from Dr. Barrie Johnson (University of Wales, Bangor, School of Biol. Sci.). It was incubated aerobically in an acidic medium that contained (per liter) 6.25 g $(NH_4)_2SO_4$, 2.5 g $MgSO_4 \cdot 7H_2O$, 0.13 g tryptic soy broth, 0.9 g D-galactose, and 1 ml solution of trace elements. The medium was adjusted at pH 2.5 with 5M H_2SO_4. The bacteria were cultivated in a thermostat at 25 °C under aerobic conditions. The bacterial growth was measured as optical density, recorded at λ = 600 nm. The grown bacterial cultures were collected by Milipore membrane filters with a pore size 0.22 μm. Cell pellets were suspended in fresh medium and adjusted to final cell concentration equal to OD_{600} = 1.0. The cell suspension was poured into special tubes with a screw cap and a septum. Each tube contained m = 0.05 g of iron mineral. The experiments were done in triplicates and each series included one abiotic control. The tubes were closed airtight and incubated statically at 25 °C.

In order to keep anoxic conditions within the tubes and to avoid the contamination, the samples were taken through the cap's septum with sterile needles and syringes. The samples were filtered in order to separate the solid and liquid phases. The leaching solutions were immediately stabilized by sulfuric acid to prevent abiotic oxidation of ferrous iron. The ferrous iron concentration was measured by the o-phenantroline colorimetric method[13], ferric iron by UV- spectrophotometric method at λ = 300 nm[14].

Bacterial reduction of soluble ferric iron was carried out in a stirred laboratory bioreactor with working volume of 1 dm^3. The innoculum was prepared identical as in the aforesaid experiments. During the incubation, the samples of medium were withdrawn in intervals for the chemical analyses and optical density measurements. Iron speciation and bacterial cell concentration were measured as stated above. The specific iron reduction rates were normalized for cells density equivalent to 1.0 absorbance unit (OD_{600}).

Results

The XRD analyses and Mössbauer spectroscopy confirmed the purity of prepared synthetic minerals. The XRD pattern of the hematite sample is presented in Fig. 1. The positions of all experimental diffraction lines are the same as those for the theoretical diffraction lines of the α-Fe_2O_3 phase. Thus, the as-synthesized sample corresponds to pure α-Fe_2O_3 phase[11].

The room-temperature Mössbauer spectrum of the hematite sample is characterized by symmetric sextet structure (Fig. 2.). The spectrum is well fitted by one sextet component with the hyperfine parameters: isomer shifts IS = 0.24 mm/s, quadrupole splitting QS_{M1} = –0.10 mm s^{-1} and hyperfine magnetic field B = 51.2 T. These parameters are characteristic of ferric (Fe^{3+}) ions[15, 16] in octahedral coordination of oxygen ions in α-Fe_2O_3.

Significant differences in specific surface areas were measured for individual iron minerals (Table I).
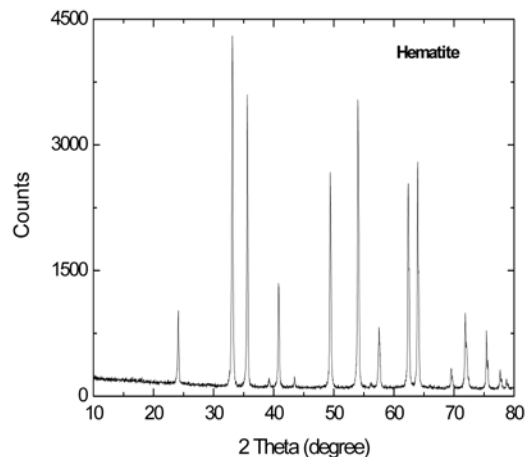
Fig. 1. **XRD patterns of the hematite sample**

Fig. 3 shows the time course of bacterial leaching of goethite and hematite. Non-linear regression was used to calculate initial leaching rate, because the instantaneous rate decreased with time. Goethite and hematite have well ordered crystalline structure and are rather refractory towards leaching. Their stability could also be assumed in natural environment. The samples of lepidocrocite and maghemite possessed the highest specific surfaces. They also proved the highest rates of chemical and bacterial leaching (Fig. 4). The lepidocrocite is a less stable mineral in comparison with goethite and hematite. This was validated by the results of our experiments. The initial rate of iron reduction at lepidocrocite was 3.0 mg dm^{-3} h^{-1}, at maghemite 2.83 mg dm^{-3} h^{-1}. The highest observed concentrations of Fe^{2+} in leaching solutions reached approximately 600 mg dm^{-3}, which corresponds to 20% yield. The rate of the leaching was gradually decreasing. The reason of this decelerating could be the passivation of mineral surface, adsorption of Fe^{2+} ions from solution onto mineral surface or bacterial cells. In addition, the inhibition could be caused by the change of sorption affinity of bacterial cells to mineral surface[17].
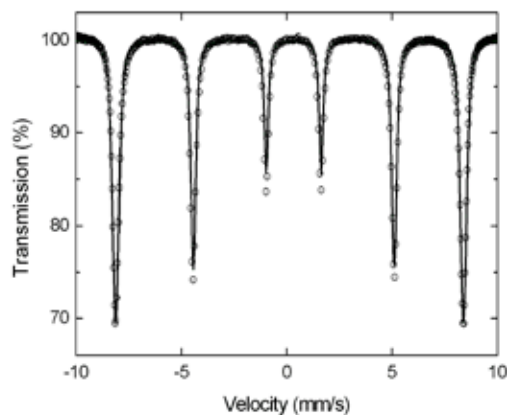
Fig. 2. **Room-temperature ^{57}Fe Mössbauer spectrum of hematite**
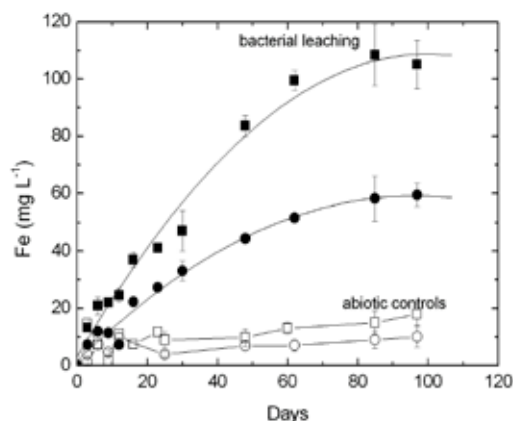
Fig. 3. **Bacterial leaching of goethite (squares) and hematite (circles). Symbols represent the means of triplicate incubations ± standard deviation. Open symbols indicate chemical leaching of minerals in abiotic controls**

Table I
Specific surface area, initial rates of iron reduction and [*]specific rates of iron reduction normalized for surface area of 1 m^2 and cells density equivalent to 1.0 absorbance unit (OD_{600})

Mineral	$S_A [m^2 g^{-1}]$	$r_0 [mg\, dm^{-3} h^{-1}]$	$rsp [\mu g\, m^{-2} h^{-1}]$[*]
Goethite	30	0.095	0.89
Hematite	5	0.053	3.03
Lepidocrocite	73	3.0	11.64
Maghemite	87	2.83	9.24
Magnetite	13	1.44	31.45

The bacterial activity is limited by the availability of Fe^{3+}. When solid substrates are utilized, the linear bacterial growth is commonly observed. The growth is limited by the rate of iron dissociation from the solid surface. The specific rates of leaching were calculated for a unit of mineral surface and a unit of bacterial cells (Table I). For the quantification of leaching rates for various minerals initial rates were calculated from non-linear regression, using a second-order power function.

In anoxic conditions, bacteria utilized Fe^{3+} cation as an electron acceptor from the oxidation of organic matter (saccharides). The rate of bacterial reduction of Fe^{3+} to Fe^{2+} in the solution highly exceeds the dissociation rate of Fe^{3+} from mineral surface, which is the rate-determining step. Therefore, in the presence of iron reducing bacteria, almost all soluble iron occurs in the form of Fe^{2+} ions.

In solutions without bacteria both iron species were detected (Fig. 5.). The sterile acidic medium (pH 2.2) brought about the chemical leaching of iron from oxihydroxides because of the adsorption H^+ protons to mineral surface followed by the extraction of Fe^{3+} from the crystal lattice[18]. The acid leaching is a reversible process of the hydrolytic reaction connected with the formation of Fe(III) precipitate: $2Fe^{3+} + 3H_2O \leftrightarrow Fe_2O_3 + 6H^+$. The presence of Fe^{2+} in aci-

dic leaching liquors in the absence of Fe-reducing bacteria could be a result of chemical reduction of Fe^{3+} with organic substances obtained in media (D-galactose and tryptic soy broth).

Magnetite contains both Fe^{2+} and Fe^{3+} ions in its crystal structure. Under anoxic conditions, two potential mechanisms exist for aqueous release of iron from magnetite. One is the reaction resulting in maghemite formation and incongruent release of Fe (II) to solution (1)[19].

$$[Fe^{2+}Fe^{3+}{}_2]O_{4(mn)} + 2H^+ \rightarrow \gamma[Fe^{3+}{}_2]O_{3(mh)} + Fe^{2+} + H_2O \quad (1)$$
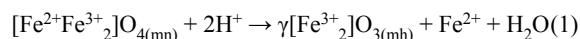
In addition, in extremely acidic solutions pH < 1 congruent dissolution was observed, which releases both Fe^{2+} and Fe^{3+} from magnetite (2) corresponding to Fe^{3+}/Fe^{2+} ratios of 2 : 1 (ref.[20]).

$$[Fe^{2+}Fe^{3+}{}_2]O_{4(mn)} + 8H^+ \rightarrow Fe^{2+} + 2Fe^{3+} + 4H_2O \quad (2)$$
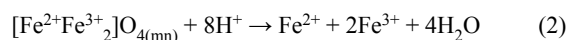
In our experiments, sterile controls containing magnetite proved high concentrations of Fe^{2+} in leaching liquor, according to (1). The presence of trivalent iron points out the possibility of leaching according to (2). Fig. 4. presents the behavior of chemical and bacterial leaching of magnetite. The initial rate of the iron extraction from this mineral was 1.44 $mg\, dm^{-3} h^{-1}$. Recounted values to magnetite's specific surface (13 $m^2 g^{-1}$) showed the highest specific rate of iron extraction.
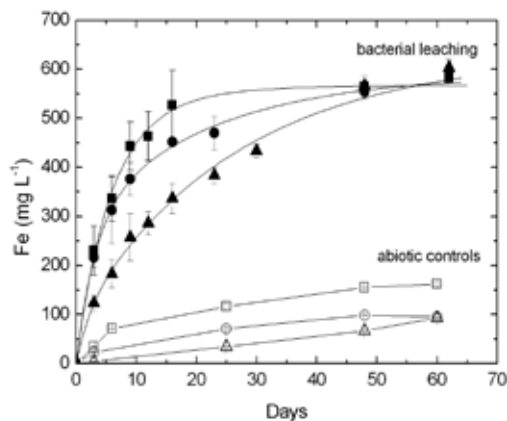
Fig. 4. **Bacterial leaching of lepidocrocite (squares), maghemite (circles) and magnetite (triangles). Symbols represent the means of triplicate incubations ± standard deviation. Curves indicate the fit of a second order power function used to determine initial rates. Open symbols indicate chemical leaching of these minerals in abiotic controls**

Fig. 6. depicts the bacterial reduction of soluble ferric iron in the bioreactor. After the innoculation of bacteria into the fresh medium, the dissolved oxygen was consumed within 2 hours and ferric iron became the only terminal electron acceptor for the bacterial oxidation of organic substratum (3).
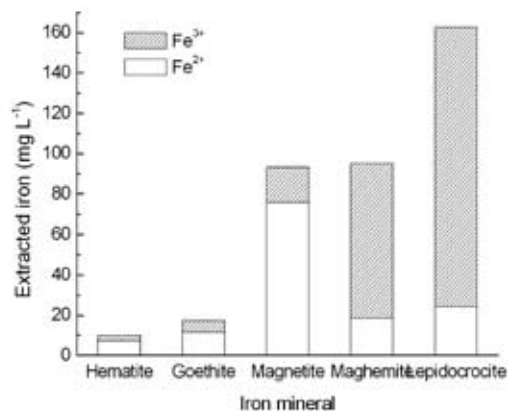
Fig. 5. **Concentration of Fe^{3+} and Fe^{2+} in leaching liquors of sterile controls after 60 days of incubation**

$$C_6H_{12}O_6 + 24\,Fe^{3+} + 6\,H_2O \rightarrow 6\,CO_2 + 24\,Fe^{2+} + 24\,H^+ \;(3)$$
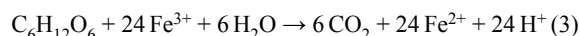
The bacteria grew exponentialy with a specific growth rate $\mu = 0.024\ h^{-1}$. In this period, the specific rate of iron reduction calculated to an absorbance unit was $250\ mg\,dm^{-3}\,h^{-1}$. After the exponential growth phase, the specific rate of iron reduction started decreasing. The bacteria completely reduced fer-

ric iron to ferrous iron within 48 hours. After the depletion of Fe^{3+} the bacterial growth has stopped because of the absence of any available electron acceptor in the medium.
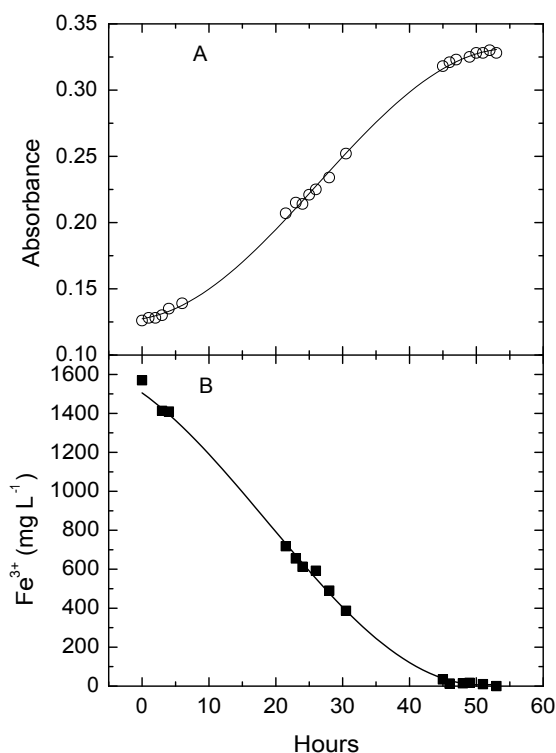
Conclusions

Iron reduction in natural conditions, in suboxic zones and aquifers, is caused by several abiotic and biotic processes. Iron reducing bacteria make use of Fe(III) as an electron acceptor from the oxidation of organic matter. Solid iron compounds undergo reductive dissolution, which affects the persistence and mobility of metals, phosphates, radionuclides, and organic pollutants[4].

The rate and the extent of bacterial reduction of Fe(III) oxihydroxides could be affected by several factors, mainly by the composition of microbial population, the kind of the iron mineral, and the sorption affinity of bacterial cells to mineral surface[17]. In addition, the rate of iron reducing could be inhibited by adsorption of Fe^{2+} ions from the solution onto the mineral surface or the surface of bacterial cells. This work deals with the kinetics of five synthetic iron minerals´ leaching by acidophilic heterotrophic iron- reducing bacteria. The kinetics of chemical and bacterial leaching depends on the solubility of minerals that follows from the degree of crystal structure's coordination. The initial rates of solid Fe(III) reduction normalized to a biomas and mineral surface unit were in the range from 0.89 to $31.45\ \mu g\,m^{-2}\,h^{-1}$. The leaching rates decreased in the following order: lepidocrocite > maghemite > magnetite > goethite > hematite (Table I). According to these results, hematite presents the most refractory from the studied minerals.

The maximal observed specific rate of solid ferric iron reduction calculated to biomas unit was $4.3\ mg\,dm^{-3}\,h^{-1}$. The specific rate of bacterial reduction of soluble Fe^{3+} calculated to biomas unit reached $250\ mg\,dm^{-3}\,h^{-1}$. The rate of soluble iron reduction was incomparably higher than the rates observed at solid ferric compounds rates reduction. In the case of solid phases, the rate determining step is the dissolution of iron ions from the solid phase into the solution.

Fig. 6. **Anaerobic incubation of *Acidipjilium* SJH in the medium containing soluble ferric iron. A: The bacterial growth measured as the absorbance. B: The bacterial reduction of soluble ferric iron in the course of incubation**

REFERENCES

1. Tessier A., Fortin D., Belzile N., DeVitre R., Leppard, G. G.: Geochim. Cosmochim. Acta *60*, 387 (1996).
2. Johnson D. B.: Biodeter. Abstr *9*, 1 (1995).
3. Stumm W., Morgan, J. J.: *Natural Waters*, New York, 1996.
4. Lovley D. R.: FEMS Microbiol. Rev. *20*, 305 (1997).
5. Johnson D. B., Bridge T. A. M.: J. Appl. Microbiol *92*, 315 (2002).
6. Lovley D.R.. Microbiol. Rev *55*, 259 (1991).
7. Johnson D. B., McGinness S.: Appl. Environ Microniol. *57*, 207 (1991).

8. Küsel K., Dorsch T., Acker G., Stackebrandt E: Appl. Environ. Microbiol *65*, 3633 (1999).

9. Bridge T.A.M., Johnson D.B.: Geomicrobiol. J. *17*, 193 (2000).

10. Küsel K., Roth U. Drake H. L. D.: Environ. Microbiol. *4*, 414 (2002).

11. JCPDS PDF, International Centre for Diffraction Data, Newton Square, PA, 2004.

12. Lagarec K., Rancourt D. G.: RECOIL. *Mössbauer Spectral Analysis Software for Windows.* University of Ottawa, Ottawa 1998.

13. Herrera L., Ruiz P., Aguillon J. C., Fehrmann A.: J. Chem. Tech. Biotechnol *44*, 171 (1989).

14. Basaran A. H., Tuovinen O. H.: Appl. Microbiol. Biotechnol *24*, 338 (1986).

15. Menil F. J.: Phys. Chem. Solids *46*, 763 (1985).

16. Goulart A. T., de Jesus Filho F., Fabris J. D. Coey J. M. D.: Hyperfine Interact. *83*, 451 (1994).

17. Caccavo F. Jr.: Appl. Environ. Microbiol. *65*, 5017 (1999).

18. Suter D., Banwart S., Stumm W.: Langmuir, *7* 809 (1991).

19. White A. F., Peterson M. L., Hochella M. F. Jr.: Geochim. Cosmochim. Acta *58*, 1859 (2004).

20. Bruyere V. I. E., Blesa M. A. . J. Electrochem. Soc. *132*, 141 (1985).

L07 THE EFFECT OF HYDROGEN ON COMBUSTION OF NATURAL GAS

ONDŘEJ PROKEŠ, DANIEL TENKRÁT and ALEŠ DOUCEK

Ústav Plynárenství, Koksochemie a Ochrany Ovzduší, VŠCHT Praha, Technická 5; 166 28 Praha 6, prokeso@vscht.cz

Introduction

Due to oncoming fossil fuel depletion, attention is nowadays paid to alternative resources, especially the renewable ones. Their major handicap is a limited possibility of the utilization compared to current resources. Hydrogen, owing to great properties to easy and high-efficient conversion to electricity, is consequently regarded as a universal energy carrier. On this account, R & D of new methods to produce hydrogen, its transport, storage and utilization are the priorities.

Recapitulation of Current State

Production and consumption of hydrogen is gradually increasing nowadays and it is expected to increase by 6 to 10 % annually in next few years. Currently the hydrogen consumption exceeds 50 billion normal cubic meters per year. In connection with changing conditions of world energy market, the structure of particular national energetic conceptions is also changing, leading in an effort to employ the sources with high efficient energy conversion and simultaneously small or even no amount of produced pollutants. It is creditable that these changes are demanded and widely supported also at the politic level. The technology of fuel cells is closely connected with hydrogen utilization and generally works at high efficiency and upon zero emissions of carbon dioxide and also other pollutants. Another hydrogen advantage is high variability of its production. It can be produced from all fossil or regenerative fuels and also nuclear energy. This flexibility and high efficient and clean utilization give hydrogen its giant power and promising future. Concerning distribution of hydrogen, it can be transported as a compressed gas or liquefied. Liquefied hydrogen is preferred for big amounts and for long distances because of higher energy cost for liquefaction. Compressed hydrogen can be transported in pressure flasks or gas pipelines. Co-distribution of hydrogen and natural gas is discussed as a possibility of distribution hydrogen during a transition period to hydrogen economy.

Co-Distribution of Hydrogen with Natural Gas

For a transport of the gaseous hydrogen pipelines can be used similarly to natural gas. However there is not sufficiently wide distribution net nowadays. That is reason why hydrogen and natural gas co-distribution is considered in existing pipelines system. There were several practical experiments, which confirmed possibility to co-distribute up to 5 % vol. hydrogen in natural gas, without any influence on gas industry devices. It means no essential modification on transit pipelines, regulating stations etc. In case of local pipelines it is not necessary to fear of hydrogen addition, since in the past, coal gas, which contains up to 50 % vol., was successfully distributed. Co-distribution of hydrogen with natural gas may be in transition period very advantageous because of several reasons: *(i)* current gas pipelines are able to provide sufficient capacity for hydrogen supply without additional costs, *(ii)* emission of pollutants (CO, NO_x) produced by existing gas appliance can be considerable lowered, causing positive environmental effect especially in bigger agglomerations.

Table I
Composition of used gas mixtures

Component	NG	10 % H_2	20 % H_2	30 % H_2
$\varphi(CH_4)$ [% mol]	97.93	90.58	78.41	69.97
$\varphi(C_2H_6)$ [% mol]	0.777	0.719	0.772	0.684
$\varphi(C_3H_8)$ [% mol]	0.263	0.243	0.262	0.233
$\varphi(i–C_4)$ [% mol]	0.044	0.041	0.044	0.040
$\varphi(n–C_4)$ [% mol]	0.049	0.045	0.049	0.044
$\varphi(i–C_5)$ [% mol]	0.010	0.009	0.010	0.009
$\varphi(n–C_5)$ [% mol]	0.008	0.007	0.008	0.007
$\varphi(C_6)$ [% mol]	0.002	0.002	0.002	0.001
$\varphi(H_2)$ [% mol]	–	7.26	19.52	28.26
$\varphi(CO_2)$ [% mol]	0.059	0.055	0.068	0.061
$\varphi(N_2)$ [% mol]	0.855	0.984	0.81	0.676
$\varphi(O_2)$ [% mol]	–	0.054	0.043	0.024

Table II
Properties of used gas mixtures

Attribute	NG	10 % H_2	20 % H_2	30 % H_2
Hi (15 °C) [MJ m^{-3}]	34.15	32.32	29.48	27.40
Hs (15 °C) [MJ m^{-3}]	37.91	35.93	32.88	30.63
W (15 °C) [MJ m^{-3}]	50.34	49.27	47.85	46.82
d (15 °C) [–]	0.567	0.532	0.472	0.428

Related Legislation

Considering addition of hydrogen to natural gas, safe and trouble-free operation of gas appliances must be ensured. There are two main regulations in the Czech Republic: TPG 902 02 regarding requirements for gas quality and ČSN EN 437 regarding gas appliances testing. TPG 902 02 defines quality grade and testing of gaseous fuels with high methane content. It restricts hydrogen content to 2 % mol. It implies impossibility of distributing hydrogen in natural gas in higher concentrations. According to ČSN EN 437 a gas with hydrogen content 23 % vol. is applied during testing to examine appliance for flame stability or in different word danger of backfiring. Up to 2% difference in Wobbe index is allowed.

Experimental

The main purpose of the research was an evaluation of emission characteristics of various hydrogen–natural gas

mixtures. Furthermore, the determination of optimal volume concentration interval that can be reliable operated under conditions in the Czech Republic were demand. Results should be a basis for evaluation of possibility to co-distribute hydrogen with natural gas. It should be possible also to prove expected lowering of pollutants production. Conclusions should be applicable especially in relation to end user and their gas appliances.

Experimental Arrangement

Measurements were carried out on two standard and one condensing boiler, which should also provide data about benefit of using condensing boilers in respect of specific emission of CO and NO_x. Standard boilers were represented by top supported Therm 12 S with nominal heat output 15 kW and stationary Viadrus G27 ID with nominal heat output 32–37.5 kW. Condensing boilers were represented by Junkers ZSB 16-1 A CERASMART with nominal heat output 16.1 kW. Several model mixtures from 1.5 % vol. up to 40 % vol. of hydrogen in natural gas were examined.
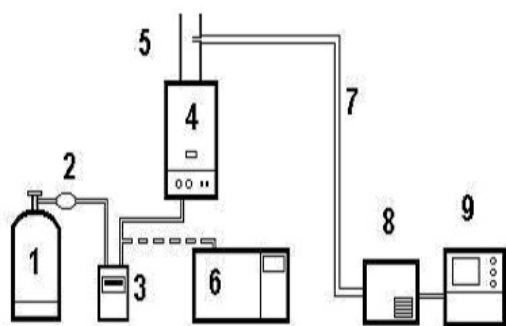
Fig. 1. **Scheme of experimental installation: 1 – pressure cylinder with gas sample, 2 – pressure regulator, 3 – gas meter, 4 – gas boiler, 5 – duct system, 6 – gas chromatograph, 7 – heated sampling track, 8 – sample treatment, 9 – flue gas analyzer**

The Therm boiler was observed in two operational regimes: half and full heat output, the Viadrus boiler was examined at full heat output. Measured quantities were composition of inlet gas (gas chromatography Hewlett-Packard 6890 with TCD and FID), composition of flue gas (analyzer Horiba PG 250, O_2, CO_2, CO, NO_x) and continuous heat output measurement. Flue gas was sampled by portable sample treatment unit PSS-5 with heated inlet filter, heated teflon hose, teflon membrane gas pump and Poltier gas cooler. Experimental arrangement is shown on Fig. 1.

Results

In Table I, compositions of inlet gases are summarized. Also values of lower heat value (H_i), higher heat value (H_s), relative density (d) and Wobbe index (W) calculated according to ISO 6976 are shown.

The results of experiment are average weight concentrations of carbon monoxide $\bar{\rho}_N^{3\%O_2}$ (CO) and nitrogen oxides

$\bar{\rho}_N^{3\%O_2}$ (NO_x) (expressed as NO_2) for normal reference state ($t = 0\ °C$, $p = 101325\ Pa$), dry gas and reference oxygen content 3% vol. measured during 15 to 30 minutes intervals of steady state. The Results are summarized in Table III and IV.

Table III
CO emissions:　$\bar{\rho}_N^{3\%O_2}$ (CO) $[mg\,m^{-3}]$

Boiler	NG	10 % H_2	20 % H_2	30 % H_2
Therm	19.8	15.8	10.8	10.2
Therm (1/2)	44.8	20.8	24.0	30.9
Viadrus	6.4	2.0	0.5	1.7

Table IV
NO_x emissions:　$\bar{\rho}_N^{3\%O_2}$ (NO_x) $[mg\,m^{-3}]$

Boiler	NG	10 % H_2	20 % H_2	30 % H_2
Therm	175	154	162	142
Therm (1/2)	182	134	139	127
Viadrus	150	126	132	120

Table V
CO specific emissions:　$\bar{\xi}$ (CO) $[mg\,kWh^{-1}]$

Boiler	NG	10 % H_2	20 % H_2	30 % H_2
Therm	22.1	17.4	11.8	11.0
Therm (1/2)	50.0	23.1	26.2	33.5
Viadrus	7.1	2.2	0.5	1.8

Table VI
NO_x specific emissions:　$\bar{\xi}$ (NO_x) $[mg\,kWh^{-1}]$

Boiler	NG	10 % H_2	20 % H_2	30 % H_2
Therm	195.7	170.5	177.3	154.0
Therm (1/2)	202.9	147.8	152.5	137.1
Viadrus	167.6	139.6	144.2	130.2

Conclusions

The results prove lowering of weight concentrations of CO by hydrogen addition with an optimum concentration of hydrogen about 20 % vol. Emission of CO was lowered to half for Therm and to less than 10 % for Viadrus in the optimal case (Table III). In all occasions, the highest concentration of CO and NO_x was for natural gas without hydrogen addition, which proves possibility to add hydrogen to natural gas to lower emission of pollutants. Emissions of NO_x showed decreasing tendency with hydrogen addition in the whole interval. Therefore extension of measure interval is desirable in future to at least 40 % vol. of hydrogen. Even more interesting for evaluation of hydrogen effect on emissions are specific emissions per 1 kWh summarized in Table V and VI. It also proved the highest CO and NO_x emission by combustion of natural gas without hydrogen addition.
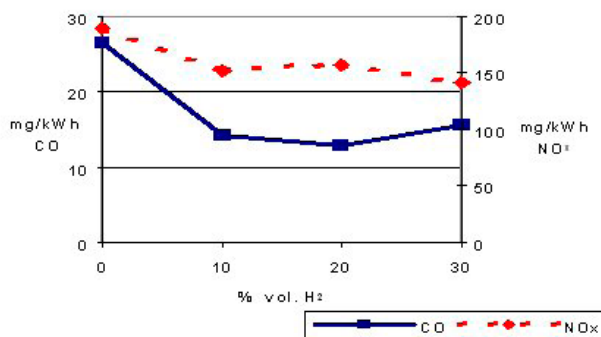
Fig. 2.   **Average specific emissions of CO and NO$_x$**

In the case of NO$_x$ there was lowering up to 30 %, for CO even up to 70 %. Performed experiment showed possibility to combust mixtures of natural gas and hydrogen (up to 30 % vol.) without operational problems i.e. backfiring. Hydrogen addition causes CO and NO$_x$ emission lowering in all observed cases.

REFERENCES

1. Palmová I., Schöngut J.: Chem. listy *98*, 205 (2004).
2. Čapla L., Buryan P., Prokeš O., Fík J., Žahourek J.: Abhangigkeit der Emission der alten Hauslichen Gasgerate von der Zusammensetzung des Erdgases, 52. Berg- und Huttenmanischen Tag 2001, p.49, Freiberg (2001)
3. Dicks A. L.: J. Power Sources *61*, 113 (1996).
4. Doucek A.: Diploma Thesis, VŠCHT Praha (2007).
5. Prokeš, O., Doucek, A., Tenkrát, D.: Chemické zvesti *61* (2007).
6. Yanga, C., Ogdena, J.: International Journal of Hydrogen Energy *32*, 268 (2007).

L08　EFFECT OF PARTICLE SIZE ON DEHYDROXYLATION OF KAOLIN – AN INFRARED SPECTROSCOPY STUDY

PETR PTÁČEK, DANA KUBÁTOVÁ, JAROMÍR HAVLICA, FRANTIŠEK ŠOUKAL and TOMÁŠ OPRAVIL

Institute of Materials Chemistry, Brno University of Technology, Purkyňova 118, 612 00, Czech Republic,
ptacek@fch.vutbr.cz

Introduction

Kaolinite ($Al_2(Si_2O_5)(OH)_4$) dehydroxylation processes have been studied for many years by many ways including thermal analysis[1–8], molecular spectroscopy[1], structural analysis[1,9] and electron microscopy[7,10].

The dehydroxylation of kaolinite is determined by different factor, such as degree of structural ordering, particle size and shape, adsorbed and substituted ions, mineral admixtures, etc. Also the influence of instrumental conditions (especially sample mass, heating rate and sample pre-treatment) on the decomposition is often discussed. Another important experimental factor is the pressure[2,5,6]. It was observed that the temperature of the dehydroxylation effect shifts to lower temperatures as the reduction of particle size takes place[2].

The thermal dehydration of hydroxyl-containing compounds like kaolinite occurs in a formation of water molecules due to an interaction of neighboring OH groups. The water release from the octahedral coordinated Al^{3+} ion could generate isolated OH groups[5].

The reaction path, which gives orthorhombic mullite from kaolinite, can be simplified to following simultaneous reactions[7,11]:

$$Al_2O_3 \cdot 2SiO_2 \cdot 2H_2O \xrightarrow{400-700\,°C} Al_2O_3 \cdot 2SiO_2 + 2H_2O \quad (1)$$

$$2(Al_2O_3 \cdot 2SiO_2) \xrightarrow{925-1,050\,°C} 2Al_2O_3 \cdot 3SiO_2 + SiO_2 \quad (2)$$

$$3(2Al_2O_3 \cdot 3SiO_2) \xrightarrow{>1,100\,°C} 2(3Al_2O_3 \cdot 2SiO_2) + 5SiO_2 \quad (3)$$

$$SiO_2 \xrightarrow{>1,200\,°C} SiO_2 (cristobalite) \quad (4)$$
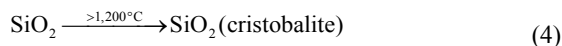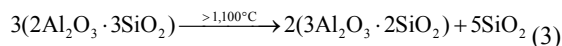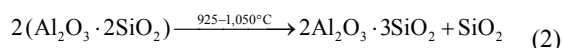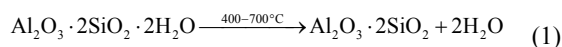
Dehydroxylation is splitting into two separate processes with T_{max} about 550 and 600 °C. The first step was explained due to loss of "structural water" and destruction of the kaolinite sheet structure. The second step was discussed as a kinetically controlled recombination of alumina and silica to the meta-kaolinite structure[5].

The effect of particle size on course of dehydroxylation processes of washed Na-kaolin Sedlec Ia were investigated by mid-infrared spectroscopy via series of isothermal experiment on temperature range from 150 to 650 °C. Ralatioship between particle size and primary spectroscopic variables, i.e. amplitude, peaks wavelength and half-width, of kaolinite spectral bands were evaluated.

Experimental

K a o l i n

Washed Na-kaolin Sedlec Ia from region Karlovy vary (Czech Republic) produced by Sedlecký kaolin a.s. was used in this study. Content of kaolinite is higher than 90 % wt. with equivalent diameter grain median in range 1.2–1.4 µm. The main impurities are mica group minerals and quartz. The colorant oxides content – hematite (α-Fe_2O_3) and tetragonal TiO_2 (rutile), is lower than 0.85 and 0.2 % wt., respectively.

The kaolin grain fraction with particle diameter 90–80 µm (f_{90-80}), 80–71 µm (f_{80-71}), 71–63 µm (f_{71-63}), 63–50 µm (f_{63-50}), 50–40 µm (f_{50-40}) and undersize ($f_{<40}$) were used for FT-IR experiments. This fraction was previously dried for 2 h at 150 °C due to removing of adsorbed water. The specific surface area of sample was 16.6 $m^2 g^{-1}$ (Chembet – 3000). Thermogravimetric weight loss (TG-DTA analyzer Setaram 92–18) of applied kaolin is about 13.15 % wt.

I n f r a r e d　S p e c t r o s c o p y

Infrared spectra of samples were recorded in KBr pellets using FT-IR spectrometer Nicolet Impact 400 in the wavelengths range from 4,000 to 400 cm^{-1}. Measurements were done under resolution 8 cm^{-1}.

Heat threaded samples were mixed with KBr with mass ratio 1 : 100. Mixtures were homogenized by grinding in mortar dish. Weighted amount of these mixtures were pressed under 40 kPa for 20 s and next 80 kPa for 30 s.

D a t a　P r o c e s s i n g

All correction of spectra (smoothing, subtracting and fitting), mathematic and statistic operations were made with OriginPro 7.0 and Statistica 8.0 software.

Results

The FT-IR spectrum of dray kaolin is shown on Fig. 1. The data from refs.[12–14] were used for interpretation of measured infrared spectra. The quadruplet of IR bands in X-H stretching region (X = O, N, C) are v_1, v_2, v_3 a v_4 vibration modes of hydroxyl groups in kaolinite structure. The first three bands at 3,697, 3,669 and 3,655 cm^{-1} belong to stretching of so-called outer hydroxyls (ouOH, inner-surface hydroxyls). The rest v_4(OH) vibration mode is assigned to stretching of inner surface hydroxyl (inOH). These groups are located on the shared plane between the octahedral and tetrahedral sheets of the same kaolinite layer.

The inner-surface hydroxyl groups show a strong in-phase symmetric stretch at 3,697 cm^{-1} (v_1) with transition moment close to c^* and two weak out of phase vibrations at 3,669 (v_2) and 3,655 cm^{-1} (v_3) with transition moment in the (001) plane[12]. The OH groups bending and translation vibrations are located at 935 δ_1(ouOH), 910 δ_2(inOH) and 791, 754 cm^{-1}, respectively.

There are three sharp bands at Si–O stretching region belonging to vibration of Si–O(apical) at 1,115 cm^{-1}, symmetric stretching of Si–O–Si (siloxane bridge) at 1,033 cm^{-1}
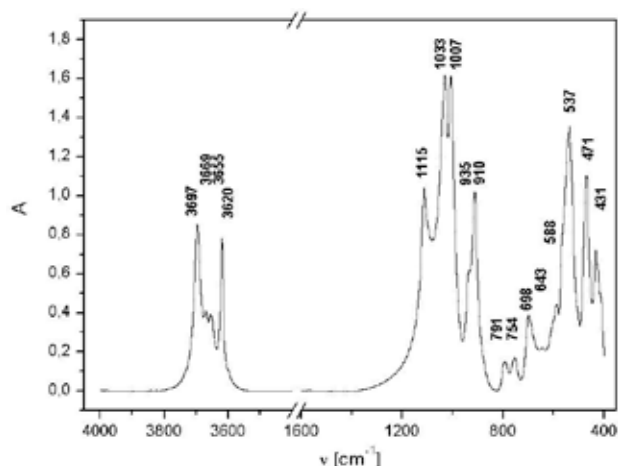
Fig. 1. **Subtracted FT-IR spectrum of kaolin Sedlec Ia for the f$_{50-40}$ fraction**

and asymmetric of Si–O–Si at 1,007 cm^{-1}, respectively. Band of Si–O bending is located at 431 cm^{-1}.

The other kaolinite bands in the spectrum on Fig. 1. are relatet to O–Al–OH (698 cm^{-1}) and Si–O–Al (537 and 470 cm^{-1}) in kaolinite structure. Bands at 643 and 588 cm^{-1} probably belong to admixture of illite.

O H   S t r e t c h i n g   R e g i o n

IR spectrum fitted over hydroxyl stretching region by Lorentz function is shown on Fig. 2. In addition to fundamental modes of OH groups (a–d) there was found small band at 3,599 cm^{-1} (e), which probably belongs to admixtures in the sample – illite or goethite.

S i – O   S t r e t c h i n g   a n d   O H
D e f o r m a t i o n   R e g i o n

Loretz function gave no good results over this region thereby the first type Voight function was applied:

$$y = y_0 + A\left[m_u \frac{2}{\pi} \frac{w}{4(x-x_c)^2 + w^2} + (1-m_u)\frac{\sqrt{4\ln 2}}{\sqrt{\pi} w} e^{-\frac{4\ln 2}{w^2}(x-x_c)^2} \right] \quad (5)$$

where y$_0$ is offset, x$_c$ peak center, A amplitude, w width and m$_u$ shape factor of peak. Fitted spectrum is shown on Fig. 3.

D e h y d r o x y l a t i o n   o f   K a o l i n

The change of the spectra shape during thermal treatment of sample in static oven atmosphere is shown on Fig. 4. for 50–40 µm fraction and on Fig. 5. for 71–63 µm fraction.

Dehydroxylation process is in generally accompanied with decrease OH stretching and bending bands. Stretching and bending modes of Si–O and Al–O bond show loses of their selectivity. The details about kaolinite spectra changes during course of dehydroxylation process we are already described in ref.[15].
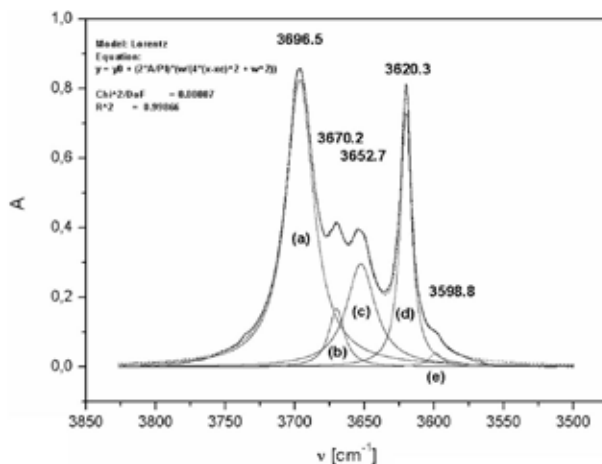
Fig. 2. **Fitted spectrum in the O–H stretching region for the f50-40 fraction of dried kaolin Sedlec Ia: v$_1$(ouOH) (a), v$_2$(ouOH) (b), v$_3$(ouOH) (c), v$_4$(inOH) (d) and v(OH) of admixtures in the**
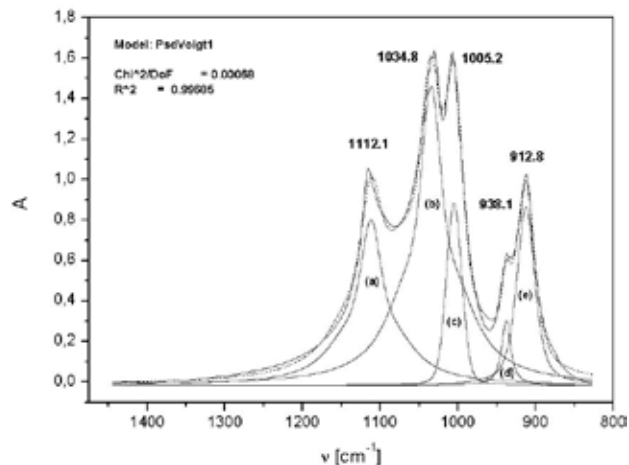
Fig. 3. **Fitted spectrum in Si–O stretching and O–H bending region of kaolin Sedlec Ia (f$_{50-40}$): v(Si-(apical)O) (a), v$_s$(Si–O–Si) (b), v$_{as}$(Si–O–Si) (c), δ$_1$(O–H) (d) and δ$_2$(O–H) (e)**
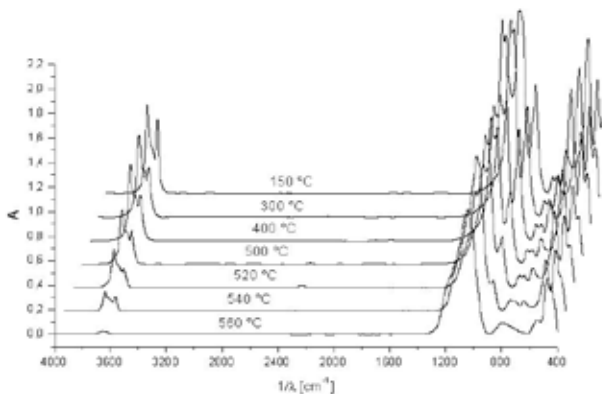
Fig. 4. **Subtracted spectra of burning kaolin Sedlec Ia (fraction f$_{50-40}$)**

Peaks   Spectroscopic   Variables
– T h e   O – H   S t r e t c h i n g   R e g i o n

The progress of the primary spectroscopic parameters, i.e. amplitude, half width and peak's center, of ν_1(ouOH) and ν_4(inOH) IR bands during kaolin thermal were compared. The dependence of peak's amplitude on the temperature and particle size is shown on Figs. 5. and 6.

While peak's amplitude as well as its area is related to amount of hydroxyl groups in sample, the peaks width pro-vides information about level of hydrogen bonds interaction. The width of bands increase together with extends of inter-molecular interaction, whereas the peak's center is degreased. Relation of peak's half-width on the temperature and particle size is shown on Figs. 7. and 8.

Peak´s amplitude and half-width show the significant positive correlation on the level $p < 0.05$. Value of correlation coefficient was calculated on 0.405.

The dependence of peak's center on the temperature and particle size is shown on Figs. 9. and 10.
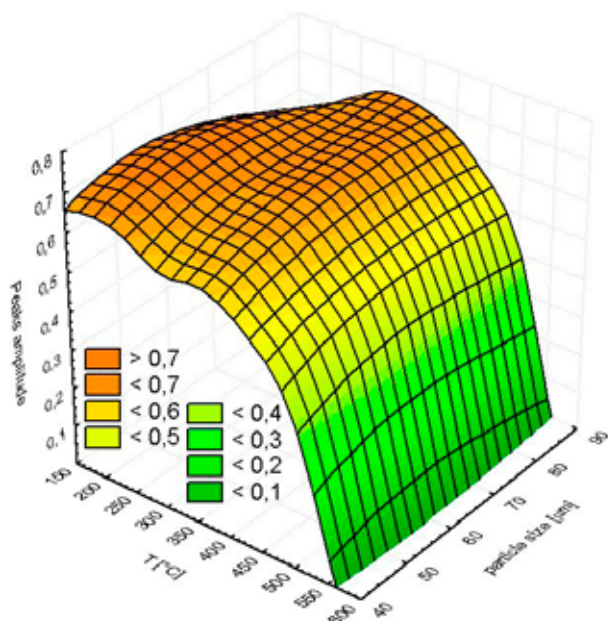
Fig. 5.   **Dependence of ν_1(ouOH) peak's amplitude on the temperature and particle size**
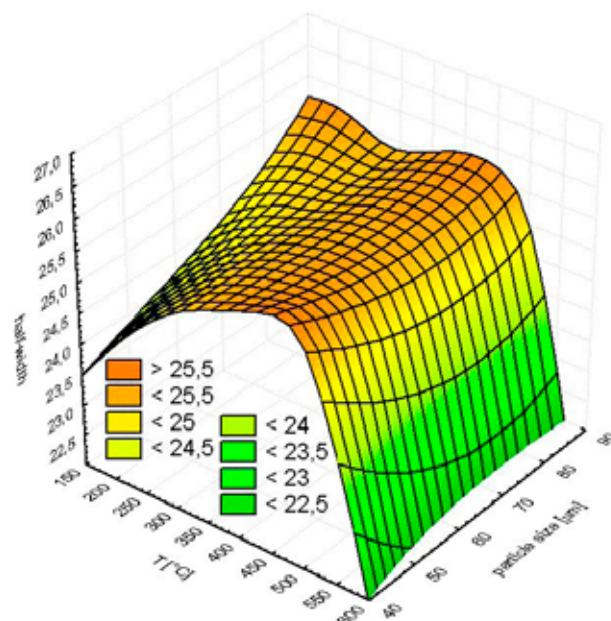
Fig. 7. **Dependence of ν_1(ouOH) peak's width on the temperature and particle size**
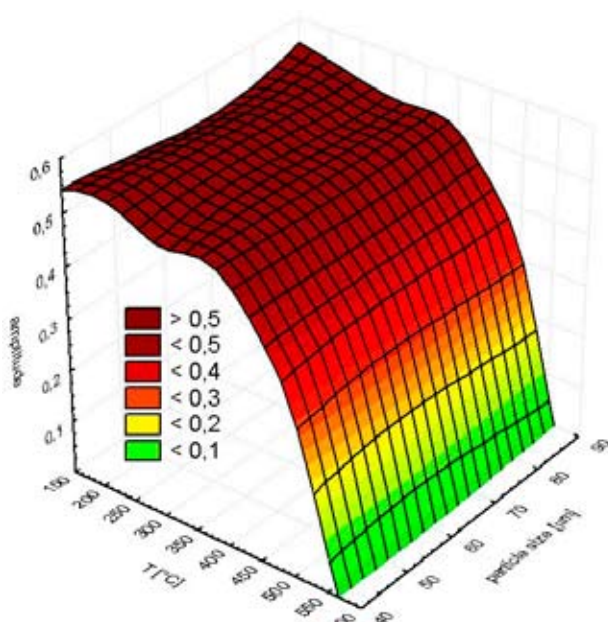
Fig. 6.   **Dependence of ν_4(inOH) peak's amplitude on the temperature and particle size**
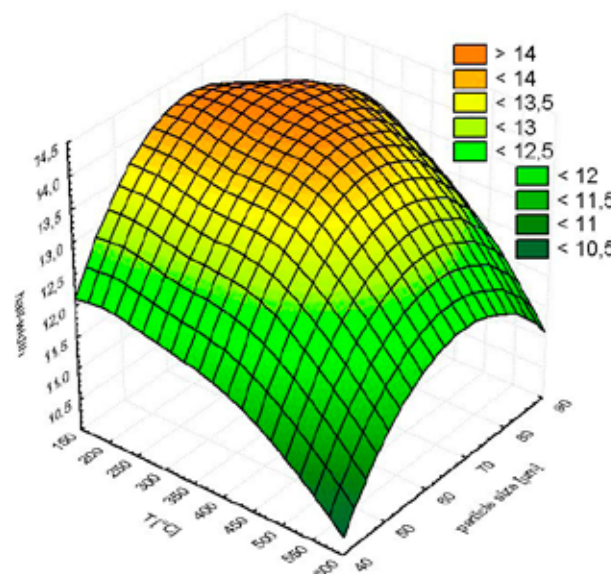
Fig. 8.   **Dependence of ν_4(inOH) peak's width on the temperature and particle size**
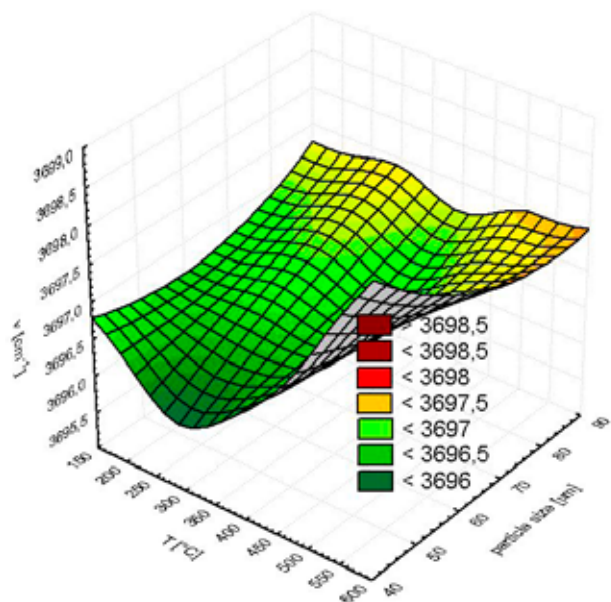
Fig. 9. **Dependence of v_1(ouOH) peak's wavelength on the temperature and particle size**
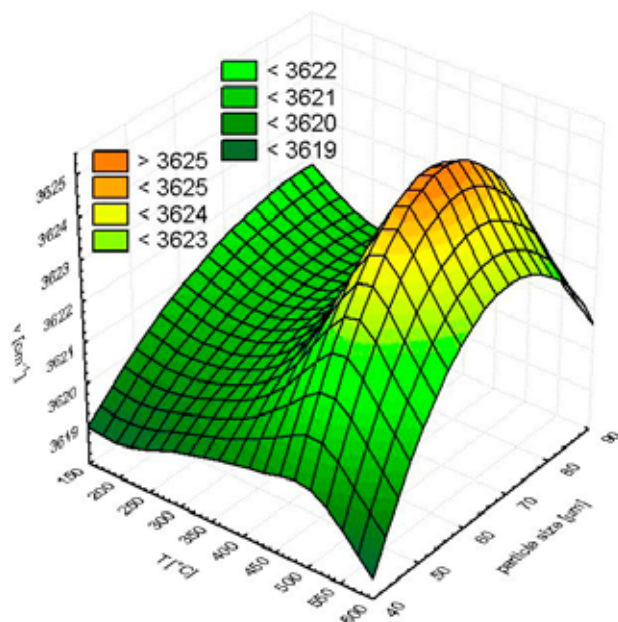
Fig. 10. **Dependence of v_4(inOH) peak's wavelength on the temperature and particle size**

P e a k s   S p e c t r o s c o p i c   V a r i a b l e s
–   T h e   S i – O   S t r e t c h i n g   R e g i o n

The band of symmetric stretching of Si–O bond in siloxane bridge (Si–O–Si) at wavelength ~ 1,033 cm^{-1} was pursued. Among other leads the thermal inducted processes during dehydroxylation of kaolinite to increasing of shape factor (m_u) of applied Voight function (1). Further sample heating leads to lose selectivity of v_s and v_{as} vibration.

Conclusions

The v_1(ouOH) and v_2(inOH) sharp spectral bands were used for dehydroxylation process study, because these stretch band can be fitted with good accuracy and selectivity they isn't lose absorbtion selectivity during dehydroxylation.

The reason for peak's amplitude decrease and its re-entry increase on temperature interval 200–350 °C is pre-dehydroxylation process, which according several authors[8], takes place on the temperature interval from 160 to 360 °C, i.e. this process precluding dehydroxylatin.

For ouOH groups has influence of predehydroxylation process on the shape of spectra decreased with growing particle size (see Fig .5.). This effect is insignificant for inner hydroxyl groups. Smaller particles show more slowly loosing of inOH groups than bigger (see Fig. 6.).

The intensive Van der Wals force for the biggest particles at low temperature is caused by capillary water, while small particles are already exsiccated. There is visible significant influence of pre-dehydroxylation process on the peks half width (see Fig. 7.).

For small particles were interactions between inOH groups decrease with temperature more quickly than bigger particles (see Fig. 8.).

Van der Wals force going to be stronger during pre-dehydroxylation process. The most intensive hydrogen bonds interaction between outer hydroxyls was found for temperature interval from 200 to 300 °C and the particles smaller than 60 µm. The process of pre-dehydroxylation takes place on this temperature interval.

Smaller particles are more sensitive to pre-dehydroxylatin, but dehydroxylation proceeds faster. Isolated OH groups are formed via this process and peak's wavelength during heating increase more rapidly than in the case of bigger particles (see Fig. 9.).

Inner hydroxyl groups show the minimum extent of hydrogen bonds interaction about 500 °C, this correspond to starts of the second dehydroxylation step, i.e. recombination of alumina octahedron and silica tetrahedron (see Fig. 10.).

The influence of dehydroxylation process on the shape of infrared spectrum was also evaluated from shape factor of peak of asymmetric stretching of Si–O bond. Increasing of m_u value with growing temperature means that peak's shape more approaching to Lorentz function profile.

REFERENCES

1. Temuujin J., Okada K., MacKenzie D. J. K., Jadambaa T. J. Eur. Ceram. Soc. *19*, 105 (1988).
2. Pérez-Rodríguez J. L., Pascual J., Franco F., Jiménez de Haro M. C., Duran A., Ramírez del Valle V., Pérez-Maqueda L. A. J. Eur. Ceram. Soc. *26*, 747 (2006).
3. Levy H. J., Hurst J. H. Fuel *72*, 873 (1993).
4. Castelein O., Soulestin B., Bonnet P. J., Blanchart P.: Ceram. Int. *27*, 517 (2001).

5. Heide K., Földvari M.: Thermochim. Acta *446*, 106 (2006).
6. Nahdi K., Llewellyn P., Rouquérol F., Rouquérol J., Ariguib N. K., Ayedi M. T.: Thermochim. Acta *390*, 123 (2002).
7. Traoré K., Gridi-Bennadji F., Blanchart P.: Thermochim. Acta *451*, 99 (2006).
8. Balek V., Murat M.: Thermochim. Acta *282/283*, 385 (1996).
9. Temuujin J., MacKenzie D. J. K., Schmücker M., Schneider H., McManus J., Wimperis S.: J. Eur. Ceram. Soc. *20*, 413 (2000).
10. Santos S. H., Campos W. T., Santos S. P., Kiyohara K. P.: Ceram. Int. *31*, 1077 (2005).
11. Hlaváč J., *Základy technologie silikátů* (trans. name: *The primer of technology of silicates*), chapter II, p. 118, SNTL, Prague 1988.
12. Franco F., Pérez-Maqueda A. L., Pérez-Rodríguez L. J., J. Colloid Interface Sci. *274*, 107 (2004).
13. Deng Y., White N. G., Dixon B. J.: J. Colloid Interface Sci. *250*, 379 (2002).
14. Zhang B., Li Y., Pan X., Jia X., Wnag X.: J. Phys. Chem. Solids *68*, 135 (2007).
15. Ptáček P., Kubátová D., Havlica J., Šoukal F., Opravil T.: Keramický zpravodaj *1*, 5 (2008).

L09 CRITICAL PARTICULATES FINENESS OF THE AIR CLASSIFICATION PROCESSES

TOMÁŠ SVĚRÁK, ONDŘEJ KOZDAS and VÍTĚZSLAV FRANK

Brno University of Technology, Faculty of Chemistry, Institute of Materials Chemistry, Purkynova 118, 612 00 Brno, Czech Republic,
sverak@fch.vutbr.cz

Introduction

Very fine powder materials are used widely in applications of material engineering, chemical industry, industry of building materials, food processing industry, production of pharmaceuticals and in various other areas. In all the here above areas of application, the use of very fine powder materials is conditioned by their granulometry: the contents of particles above the defined limit is usually strictly restricted, respectively the presence of finer particles than defined, i.e. particles below the defined limit – for example the highest acceptable content of pulverous share. In both of the here above cases, for separation of coarse particles from the finer particles, a series of sorting processes are used. Those processes are applied to the given very fine powder material in the form of a dispersion or suspension in the gaseous medium or liquid medium.

One of the basic ways of grain-size classifying of very fine powder materials used in the industry is the "dry" way of sorting of particles of materials dispersed in the flow of gas in the air classifiers. Those air classifiers (often known as "air separators") are based on the principle of competition of centrifugal forces and adrifting forces.

The very often discussed limits defined for working regimes of classification in the air classifiers[1] are the following:
- the required classifying sharpness
- adhesive forces of sorted materials
- the maximal classifying fineness attainable in operation processes
- abrasion

Hereinafter, we will deal with the attainable fineness of classified materials and classifying sharpness of air classifiers.

Experimental

D e f i n i t i o n   A r e a

Air classifiers with cylindrical rotor – see Fig. 1. and Fig. 2. – represent the type of classifying equipment that enables us to attain the maximal sorting effectiveness of very fine powder materials under the here above conditions of "dry" industrial classifying.

Functional critical balance of forces causing the movement of sorted materials is established on the level of the radius of the cylindrical turbine in case of uniform motion of particles in a straight line way with a constant speed relative
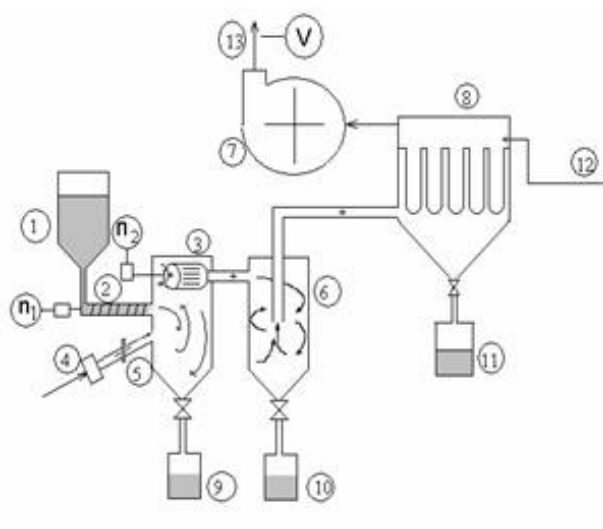
Fig. 1.　**Air classifiers function: 1 – Input material hopper, 2 – Feeder, 3 – Classifying chamber, 4 – Suction air filter, 5 – Air flap, 6 – Cyclone clarifier, 7- Centrifugal blower, 8 – Beg dust filter, 9 – Coarse share bin, 10 – Fines bin,11 – Powder fines bin, 12 – Pulsating flick air, 13 – Classification air outlet**

Fig. 2.　**Classifying cylindrical turbine of air classifiers**
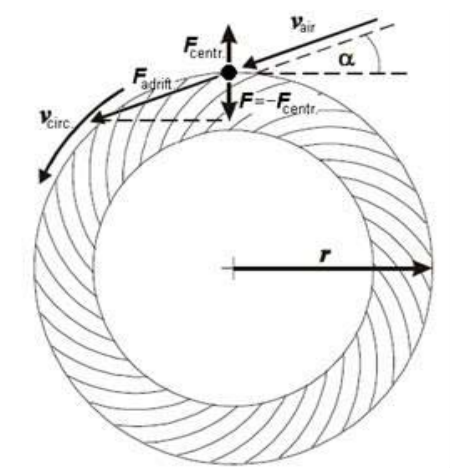
Fig. 3.　**The balance of forces in the course of particles classification for dcr**

to the sorting turbine blades. This balance depends on and is given by just and only the centrifugal and adrifting forces then. The adrifting forces are represented by the aerodynamic forces of the resistance of the particle to its relative movement in the centripetal flow of air in the classifying turbine (Fig. 3.).

The balance of forces is defined by the relations[2,3] (1)–(6):

$$F_{adrift} \cdot \sin\alpha = F_{centr} \tag{1}$$

$$F_{adrift} = \frac{1}{2} \cdot C \cdot S \cdot \rho_f \cdot v_{air}^2 \tag{2}$$

$$C = f(\text{Re}) \tag{3}$$

$$\text{Re} = v_{air} \cdot d_{cr} \cdot \rho_f / \mu \tag{4}$$

$$v_{circ} = \pi \cdot D \cdot n \tag{5}$$

$$F_{centr} = 2 \cdot m \cdot v_{circ}^2 / D \tag{6}$$

where:

$C\,[-]$ – Resistance coefficient taking into account gas flow round the particle,

$d_{cr}\,[\text{m}]$ – Critical particle size,

$d75_F\,[\text{m}]$ – Particle dimension which corresponds to the passed 75% wgt amount of the fine share

$D\,[\text{m}]$ – Effective diameter of classifier turbine,

$m\,[\text{kg}]$ – The particle mass of the critical grain dimension d_{cr},

$n\,[\text{min}^{-1}]$ – Turns of classifier turbine,

$q_d\,[\%]$ – Particle size amount

$S\,[\text{m}^2]$ – Frontal cross-section plane of the critical dimension particle,

$v_{air}\,[\text{m s}^{-1}]$ – Gas flow that drags solid particles into classifier turbine,

$v_{circ}\,[\text{m s}^{-1}]$ – Peripheral velocity of classifier turbine on its effective diameter,

$\rho, \rho_f\,[\text{kg m}^{-3}]$ – Specific mass of classified solid, gas stream density,

$\mu\,[\text{Pa s}]$ – Gas stream viskozity

$\text{Re}\,[-]$ – Reynolds number,

$T_{mod}\,[-]$ – modified Tromp number.

The classification sharpness (7) corresponds to the modified Tromp definition[3] based on the grain-size curves analysis (Fig. 4.).

$$T_{mod} = d75_F / d25_R \tag{7}$$

E x p e r i m e n t a l   F a c i l i t y   a n d
C l a s s i f i e d   M a t e r i a l

Pilot plant air classifier Hosokawa Alpine ATP-50 (Fig. 5.)

Grain sizer: granulometr LA-500 Horiba (Japonsko).

Classified material : surface treated carbonate filler on

the basis 2VA OMYA Vápenná a.s., the specific weight of which equals $\rho = 2.72$ kg m^{-3}; with additional surface treatment by higher fatty acids on the level of 0.3 % wt. (Fig. 6.).

Fig. 4.　**Definition of the classification sharpness**

Fig. 5.　**Pilot plant air classifier**
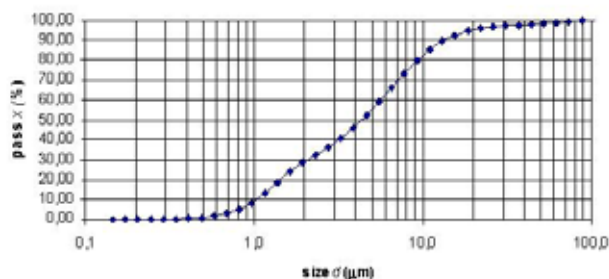
Fig. 6.　**Grain sizing curve of the filler at the inlet area of the classifier**

M e a s u r e m e n t   P r o c e d u r e

The here above carbonate filler was classified in and by the air classifier. In the course of the process, the following variables were changed[4]: Turns n of the classifying turbine, the input m_{inp} of sorted material incoming into the classifier

as well as the speed *w* of the classifying air incoming into the classifying turbine. The evaluated parameters d_{cr} and T_{mod} were obtained from the grain sizing curves of the coarse and fine shares of the classified material.

We concentrated especially on the classification of the finest particles of material, i.e. on the area with the highest turbine speed attainable in the sorting equipment used.

Results

The iterative calculation of the relations (1)–(6) in Excel® mode provided us the way to establish the classification process area (Fig. 7.). Out of the figure the following is evident: the combinations of the turns range of the classifying turbine *n* and the velocity of the classifying air *w* are needed to attain the required fineness of classifying defined by the size of the coarsest particles d_{cr}
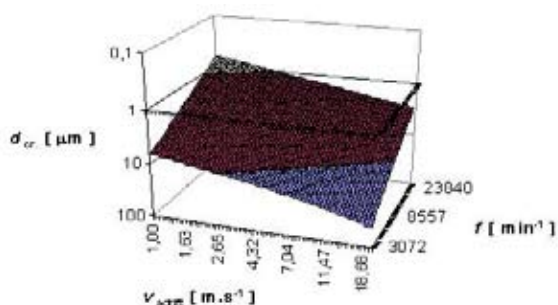
Fig. 7. **Attainable classification fineness as a function of the velocity of the classifying air w and turns of the classifying turbine n**

The analysis of the deviations of the really measured values from calculated values as well as the analysis of the airflow around the particles of material under the conditions of the transition region as well as the changes in the morphology of particles of real material will be specified in a separate publication.

This article deals especially with the limiting conditions under which it is possible to attain the highest fineness of classification. Out of the results we have achieved in the course of the measurements, we show here just the time dependence of the values of classification sharpness T_{mod} in the area of the highest fineness of the classified material and the maximal turns of the classifying turbine with the opti-
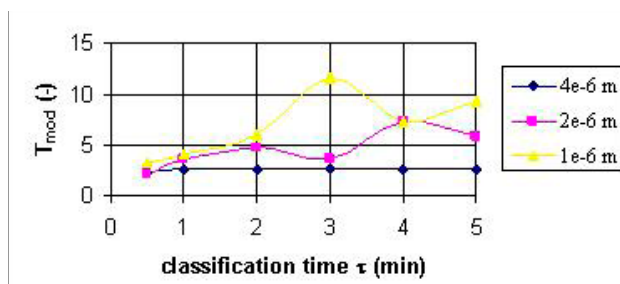
Fig. 8. **Time dependence of the classifying sharpness in the area of the highest fineness of classifying**

mal material input (Fig. 8.). The theoretical (i.e. calculated) fineness of sorting dcr set by regulating the velocity of the classifying air is shown here as a parameter.

Conclusions

The attainable level of the fineness of classification depending on the type of the classified material and the size of the classifiers amounts to several micrometers[5], the paper[6] cites 3μm and the latest catalogue of the products made by the world-renowned company Hosokawa Alpine[7] mentions 2,5 μm. What is the reason for this limitation? Why is it not possible to move the limits of the air classifying towards the higher fineness when attaining higher turns of rotors of the classifiers cannot be a principal problem these days and when the present technologies require particulate solids of higher fineness? The solution to these questions is evidently contained in the analysis relating to Fig. 8.

The chart shows that the classificatio sharpness between the fine and coarse share of the classified material decreases significantly with the set fineness of sorting. As the higher theoretical fineness is set in the classifying system at the given turns of the classifying turbine by the decreasing of the velocity of the classifying air incoming into the classification process, the problem is to keep the regular, relatively very low flow rate of the classifying air in the blades of the classifier at the extremely high turns of the classifying turbine. The measured values of the time dependence (Fig. 8.) show that the conditions for keeping regular conditions are getting worse with the increasing time of classification. Significant change for the worse is evident especially at the initial phase of classifying. On the basis of the computer simulation[4] (Fig. 9.) we assume that in the course of the classification process, at the peripheral area of the classifying turbine, a barrier layer of critical grain of material is created that partially restrains the movement of the finer fractions that have been sorted out into the exhaust of those shares that is located in the axis of the classifying turbine.
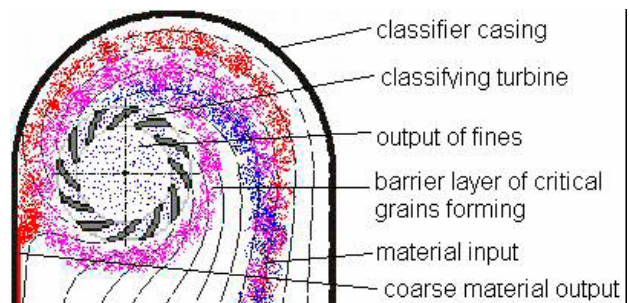
Fig. 9. **Creation of a barrier layer in the classifying process of very fine particulate solids**

As the hypothetical barrier layer of the critical grain of material has to restrain the sorting air flow into this turbine, we anticipate the occurrence of the pressure pulsation (and therefore also a flow rate pulsation) of the classifying air that carries the coarser particles into the finer fractions.

This is the mechanism that we use to explain the irregularities of the conditions under which the classifying air flows into the classifying system. Due to that mechanism, it s no more possible to achieve higher fineness in the processes of air classifying today. We arrived at the following conclusion: Any evidence that would prove occurrence of the hitherto hypothetical barrier layer of the critical sizes of grain of the classified material might result in changes in constructions and processes that could enable us to overcome the fineness classificatio limits of the present air classifiers.

REFERENCES
1. Peukert W.: Production and Handling of Nanoparticles. *Proceedings of the 5th International Conference for Conveying and Handling of Particulate Solids*, Sorento 2006.
2. Himmelblau D. M.: *Basic Principles and Calculations in Chemical Engineering*. 5th Edition, Prentice-Hall International, Inc., Englewood Cliffs, New Jersey 1989.
3. Wills B. A., Napie-Munn T.: *Mineral Processing Technology*. 7th Edition, Elsevier, London 2006.
4. Kozdas O.: Diploma thesis,FCH BUT Brno 2007.
5. Eštoková A., Števulová N.: Chem. Listy *96*, 509 (2002).
6. Sverak T.: Int. J. Miner. Process. Int J Miner Process *74*, 1 (2004).
7. *Handbook Powder and Particle Processing*. 2th Edition, Hosokawa Alpine, Augsburg 2006.

L10 DETERMINATION THE REACTION ORDER FOR FAST FORMATION OF CuS₂O₃

MIHAELA LIGIA UNGUREŞAN[a] and FRANCISC VASILE DULF[b]

[a]*Technical University of Cluj-Napoca, Chemical Department, 103–105 Muncii Bvd., 400641, Cluj-Napoca, Romania*
[b]*University of Agricultural Sciences and Veterinary Medicine, Food Quality Control Department, 3–5 Mănăştur Str., 400372, Cluj-Napoca, Romania,*
Mihaela.Unguresan@chem.utcluj.ro

Introduction

Reactions between thiosulfate and ions of metallic elements in solution have been repeatedly studied, several papers being published, for instance[1,2,3,4,5].

The theory of the method of continuous variations as given by Job is reviewed and extended to cases in which more than one compound is formed from a given pair of components.

The method was applied to the formation of CuS_2O_3. The absorption of the monochromatic light was the property measured in this case. Because only a single compound is formed, the results are independent of the wave length of the light used. Job's method was used to identify the intermediate compound formed by the reaction of the two components.

Cu^{2+} and $S_2O_3^{2-}$ react in a 1 : 1 ratio, consistent with the formation of CuS_2O_3 (ref.[6])

The reaction between Cu(II) and thiosulfate ions results from the formation of an intermediary complex, CuS_2O_3, similar with the complex $FeS_2O_3^+$.

It's considered:

$Cu^{2+} + S_2O_3^{2-} \leftrightarrow CuS_2O_3$ $\qquad$ $K = k_1/k_2$
$CuS_2O_3 + S_2O_3^{2-} \rightarrow Cu^+ + {}_4O_6^{2-}$ $\qquad$ k
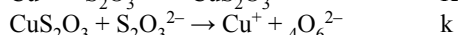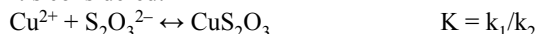
where the seconds step is determined by speed.

The formation of the reaction intermediate develops fast both ways, which implies the following relation between the speed constants: $k_1, k_2 \gg k$.

The concentration of the reactions' intermediate is the one that corresponds to the equilibrium for the first process, just as the first one does not happen.

Due to the fact that the second process takes place, the concentration of the reaction's intermediate is close the equilibrium one, no exactly it, but the approximation of pre-equilibrium is considered the one appropriate to this equilibrium[7].

The formation of this complex can be followed spectrophotometrically, but the time of this reaction is very small (10–50 ms), therefore for the study of the formation of CuS_2O_3 was used the stopped-flow technique.

Experimental

R e a g e n t s

All chemical used were analytical grade, from B&A and were used without further purification. The dilution of

Cu(ClO₄)₂, Na₂S₂O₃ and HClO₄ (60%) were made with doubly distilled water.

A p p a r a t u s

A stopped-flow apparatus[7] was used. The essential parts are: two syringes needed to rapidly inject the reactants into the mixing chamber, manually. After leaving the mixing chamber the mixture flows into a third syringe whose piston is suddenly stopped after a predetermined volume of solutions has been injected. At the moment the flow is stopped, a micro switch operated by the third piston triggers the oscilloscope of the detection system.

On the osscillogramme the variation of transmitted light intensity I_t through the solution, depending on time, for known reactant concentrations (Fig. 1.) is followed. The intensity of light at the maximum transparency, I_0, was also recorded.
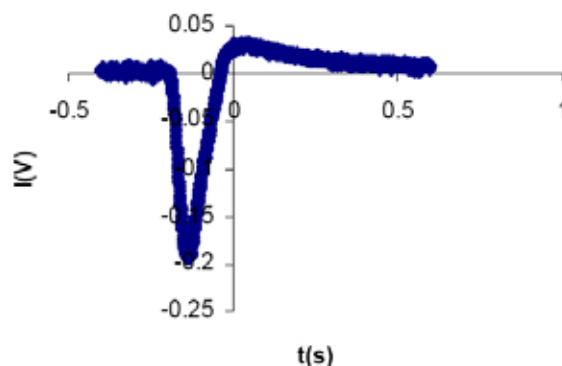
Fig. 1. **The variation of transmitted light intensity I(V) with respect to time t[s] for $[Cu^{2+}] = 5 \times 10^{-3}$ mol dm⁻³; $[S_2O_3^{2-}] = 5 \times 10^{-3}$ mol dm⁻³; λ = 430 nm; T = 21 °C**

For each set of concentrations of the two reactants there have been at least 20 experiments, the reproducibility of the experimental data obtained being very good even for really small concentrations of the reactants. ($[Cu^{2+}] = 5 \times 10^{-4}$ mol dm⁻³; $[S_2O_3^{2-}] = 5 \times 10^{-4}$ mol dm⁻³).

Results and Discussion

According to the Lambert-Beer Law, extinctions at different concentrations of the Cu(ClO₄)₂, Na₂S₂O₃ were computed. Many experimental records were done for concentrations of $[Cu(ClO_4)_2] = [5 \times 10^{-4}, 10^{-1}]$ mol dm⁻³, $[Na_2S_2O_3] = [5 \times 10^{-4}, 10^{-1}]$ mol dm⁻³, for wavelength λ = 430 nm.

The measured absorption at 430 nm, E, is made out of contributions of the colored species, which in our case is just the reaction's intermediate CuS_2O_3:

$E = \varepsilon \, l \, [CuS_2O_3]$

where the optical way is l = 1.2 cm.

The extinction of the solution has been calculated for the mixing period, $E_0 = \log (I_0/I_t)_0$. The initial concentrations of the reactants are identical in all determinations; therefore the

influence of the pre-equilibrium on the experimental reaction order could be fully manifested.

So, for example, with concentrations of $[Cu^{2+}] = 5 \times 10^{-3}$ mol dm^{-3}, $[S_2O_3^{2-}] = 5 \cdot 10^{-3}$ mol dm^{-3} and $[HClO_4] = 2 \times 10^{-2}$ mol dm^{-3}, wavelength $\lambda = 430$ nm and $T = 21$ °C, $I_0 = 1{,}493.5$ mV. The curve of formation the reaction intermediate is given in Fig. 2.
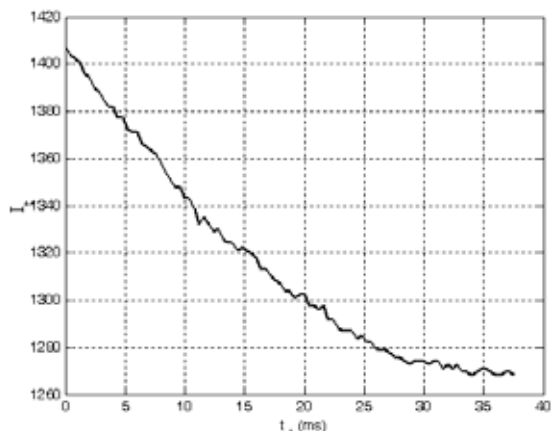
Fig. 2. **Transmitted intensity I_t (mV) as a function of time t [ms] for $[Cu^{2+}] = 5 \times 10^{-3}$ mol dm^{-3}, $[S_2O_3^{2-}] = 5 \times 10^{-3}$ mol dm^{-3} and $[HClO_4] = 2 \times 10^{-2}$ mol dm^{-3}, wavelength $\lambda = 430$ nm and $T = 21$ °C**

The calculus for the determination of the reaction order was made using Mathlab sheets. E = f(t) (Fig. 2.), lg (E) and 1/E = f(t) were represented graphically as well as dE/dt, which is a measure of the reaction rate.

Using these data, the reaction order with respect to the colored complex was calculated. The plots of logarithm of the rate vs. the logarithm of the extinction gave straight lines with slopes 1, as it is illustrated by Fig. 3., where the reaction order n = 0.98 was calculated with initial concentrations of 5 × 10–3 mol dm–3 for both reactants in aqueous acidic solution (2 × 10–3 mol dm–3 HClO4), wave length $\lambda = 430$ nm and T = 21 °C.
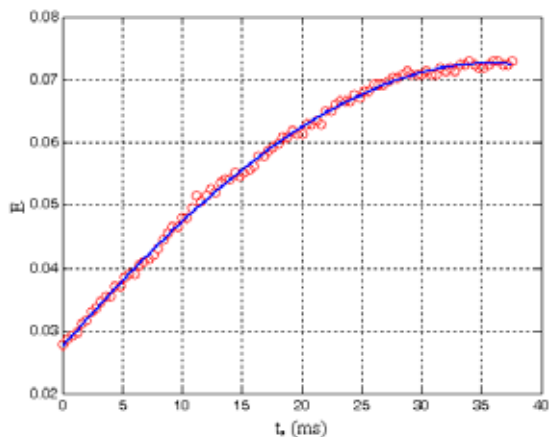
Fig. 3. **Extinction (E) as a function of time t [ms]**
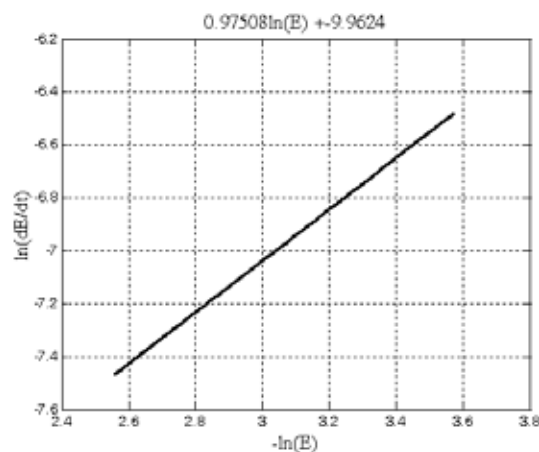
Fig. 4. **The reaction order obtained through experiments**

In conclusion, the reduction of Cu^{2+} with ions of thiosulfate is a reaction with pre-equilibrium, from kinetic point of view 8,9.

Another set of experimental data are presented in Table I.

Conclusions

Table I

The experimental data (at T = 21 °C; λ = 430 nm; $[HClO_4] = 2 \times 10^{-2}$ mol dm^{-3})

The applications of the stopped-flow technique are

Exp. no.	Initial conditions	n
1.	$[Cu(ClO_4)_2] = 10^{-1}$ mol dm^{-3}; $[Na_2S_2O_3] = 10^{-1}$ mol dm^{-3};	1.04
2.	$[Cu(ClO_4)_2] = 5 \times 10^{-2}$ mol dm^{-3}; $[Na_2S_2O_3] = 10^{-1}$ mol dm^{-3};	1.01
3.	$[Cu(ClO_4)_2] = 5 \times 10^{-2}$ mol dm^{-3}; $[Na_2S_2O_3] = 5 \times 10^{-2}$ mol dm^{-3};	0.98
4.	$[Cu(ClO_4)_2] = 10^{-2}$ mol dm^{-3}; $[Na_2S_2O_3] = 5 \times 10^{-2}$ mol dm^{-3};	1.15
5.	$[Cu(ClO_4)_2] = 10^{-2}$ mol dm^{-3}; $[Na_2S_2O_3] = 10^{-2}$ mol dm^{-3};	0.93
6.	$[Cu(ClO_4)_2] = 5 \times 10^{-3}$ mol dm^{-3}; $[Na_2S_2O_3] = 5 \times 10^{-3}$ mol dm^{-3};	0.98
7.	$[Cu(ClO_4)_2] = 5 \times 10^{-3}$ mol dm^{-3}; $[Na_2S_2O_3] = 10^{-3}$ mol dm^{-3};	1.04
8.	$[Cu(ClO_4)_2] = 5 \times 10^{-3}$ mol dm^{-3}; $[Na_2S_2O_3] = 5 \times 10^{-4}$ mol dm^{-3};	1.03
9.	$[Cu(ClO_4)_2] = 5 \times 10^{-4}$ mol dm^{-3}; $[Na_2S_2O_3] = 5 \times 10^{-3}$ mol dm^{-3};	1.01

numerous. Any reaction, which can be initiated by mixing two solutions, can be studied by the stopped-flow technique as far as the reaction is a rapid one.

This studies show that the formation of the copper thiosulfate complex (CuS_2O_3) from the rapid redox reaction between Cu(II) and thiosulfate ions proceed at 21.0 °C is a first order reaction.

REFERENCES

1. Bâldea I., Niac G.: Inorg. Chem. *7*, 1232 (1868).

2. Bâldea I., Niac G.: Inorg. Chem. *9*, 110 (1870).

3. Niac G., Cădariu I.: *Contribuţii la Studiul Reacţiei din-tre Ionul Feric şi Ionul Tiosulfuric*, Studia Universitatis Babeş-Bolyai, Series I, Fasciculus 2, p.25. Chemia, 1959.

4. Cădariu I., Niac G., Oniciu L., *Determinarea Spectrului de Absorbţie în Ultraviolet al Complexului* $FeS_2O_3^+$, *Studia Universitatis Babeş-Bolyai,* Series I, Fasciculus 1, p. 27. Chemia, 1962.

5. Niac G., Teza de Doctorat, Universitatea Babeş-Bolyai Cluj-Napoca, 1962.

6. Ungureşan Mihaela Ligia, Niac G.: Rev. Roum. Chim. *52*, 481 (2007).

7. Ungureşan Mihaela Ligia, Niac G., Surducan, E., Surducan, V.: Rev. Chim. *58*, 40 (2007).

8. Niac G., Schonberger E.: Chimie-fizică, *3* Bucureşti, Ed. Tehnică, 1970.

9. Williamson Mark A., Rimstidt Donald J., Geochim. Cosmochim. Acta 57, 3555 (1993).

L11　NEW FINDINGS ON THE CERAMIC PETROGRAPHY OF THE LOŠTICE POTTERY

MIROSLAVA GREGEROVÁ, MARTIN HLOŽEK and DALIBOR VŠIANSKÝ

Institute of Geological Sciences, Faculty of Sciences, Masaryk University, Kotlářská 2, 611 37 Brno, Czech Republic.
mirka@sci.muni.cz

Introduction

The 15th and 16th century ceramic vessels covered with "blebs" called the Loštice pottery (see Fig. 1.) represent unique products of the mediaeval and early modern Central European pottery. These tumblers were exported abroad and become famous in the whole Europe. Workshops producing this pottery were located in the village Loštice in the north Moravia (Czech Republic). Used raw material came from nearby villages' districts.

The presented research is aimed at the raw materials' identification, the examination of the Loštice pottery chemical and mineralogical composition and technological production process.

The paper summarizes the results of micropetrographic, geochemical and experimental examination of the mediaeval pottery from Loštice. The original tumblers' (based on shape and raw material petrographical composition they have been divided into five groups), assumed raw material (clay and loess) and also the experimentally fired vessels were subject to chemical analyses, optical and scanning electron microscopy (SEM) and energy dispersive (EDX) analyses. The firing temperature and the affect of garnets on the formation of "blebs" were experimentally examined.
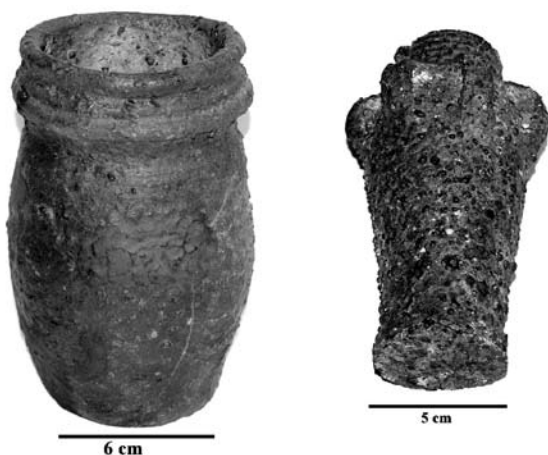
Fig. 1.　**The Loštice pottery. Collections of the Moravian Museum in Brno**

Analyses of the Loštice Pottery Artifacts and Raw Materials

Analytical Methods
- SEM and EDX analyses were done on Cameca SX 100 equipment (at 15 kV and 10 nA)
- Chemical silicate analyses were done in the ACME laboratories in Vancouver, Canada. The complete analysis of main oxides was done via ICP-emission spectrometry and trace elements via ICP-MS
- Some of the samples were analysed by so called wet analysis
- Recalculations on normative minerals were done using the MINLITH software
- Optical microscopy; analyses were carried out using covered thin sections on Olympus BX 51 petrological polarising microscope

Chemical Composition of the Assumed Raw Material and Artifacts

Silicate analyses were done to evaluate the complex chemical composition of the original raw materials. Eight original ceramic artifacts, two assumed raw material samples and four samples extracted from the furnace vault were examined. Graphical results – see Figs. 2. and 3.
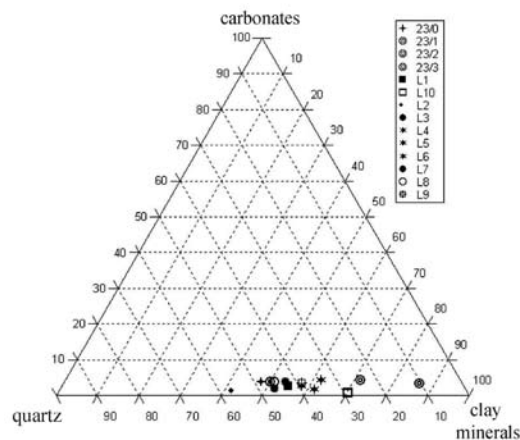
Fig. 2.　**Normative composition of examined artifacts and raw materials calculated from the chemical silicate analyses**
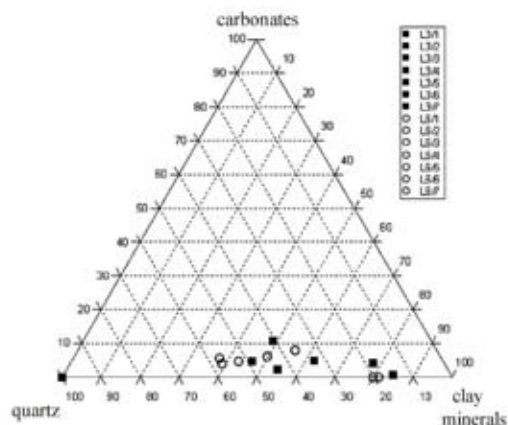
Fig. 3.　**Normative composition of examined artifacts calculated from the microchemism of glass and binder. Analyzed by P. Sulovský**

Explanations to Figs. 2. and 3.:
L1 – raw material (grey clay containing graphite)
L2 – raw material (loess soil)
L3 and L7 - ceramic artifacts of the (020) group
L4, L5 and L6 – ceramic artifacts of the (010) group
L8 – ceramic artifacts of the (030) group
L9 – ceramic artifacts of the (040) group
L10 – graphite ceramics of the (050) group
23/0 – 23/3 – samples extracted from the furnace vaults.
Chemical analyses of the 23/0, 23/1, 23/2 and 23/3 samples were done on CAMECA SX100 micro analyser. Chemical analyses of the L1–L10 samples were done by wet silicate analysis.

The recalculation results show that the (010), (020), (030) and also (040) pottery groups' chemical composition is very similar. Seven visually different samples (coming from all the five pottery groups) were chosen to verify the application of normative minerals for the identification of the Loštice pottery raw materials.

It is evident that the normative minerals recalculations from silicate and EDX analyses correspond to each other.

The presence of graphite (identified by chemical analyses and also by optical microscopy) represents the evidence of graphitic raw material application. The sorted out graphite clasts of high quality might have been used for graphitic pottery production. The material of lower quality, so called waste (clasts containing less graphite and more micas and iron oxides), might have been a suitable non-plastics supplement in the case of vessels covered with "blebs" (i.e. especially of the (010) pottery group). In the artifacts of the (010) group, graphite was present in the amount of 0.2–1.9 % wt.

Except of cordierite also sekaninaite and osumilite were be identified there – see TableI. Fig. 5. documents that these are new-formed crystals formed from the melt. Along with them, spinelides (magnetite, magnesioferrite and hercynite) occur in the pottery.

In some artifacts of the (040) group, relict garnets were determined – pyrope (94.6 % of pyrope and 4.4 % of almandine component).

The surface red colour of the (010) pottery group is caused by iron enamel with the melting addition. Except of one case, the enamel did not contain Pb. It is very probable that also the other enamels were alkalical and contained the addition of washed brick clay, which is responsible for the red up to red-purple colour of the enamel. The addition of iron clay did not have to be high. In the case of the Loštice pottery, the red colour was also caused by the interlayer under the enamel.

Experimental Firing

Miniature replicas of the Lošice pottery were made of local loess and clay soils found during the archaeological works. The raw material corresponds to tertiary deposits in the surroundings (e.g. in Litovel), which were also mined for the pottery production in later periods. Graphite was added in a form of graphitic clay. The graphitic pigment improves the clinkering properties of ceramic body. The bodies were always white, with grey streaks in the cross section. Apparent darker colour of the clay is explained by re-deposition of the raw material.

The difference between clay and loess is evident even macroscopically. Brownish colour of the fired body is caused by iron oxides.

The raw materials were mixed with water. As non-plastics, a garnet (almandine) concentrate was added to the ceramic paste.

To reach the specific surface colour, the dried replicas were coated with an engobe layer containing minerals of iron and melting addition before the firing. The firing was carried out in oxidation furnace at 1,250 °C.

The high melt content during the firing caused collapse of the vessels made of loess (see Fig. 4.).

Fig. 4. **Experimental firing of the Loštice pottery miniature replicas. The collapsed vessels were made of loess soil**
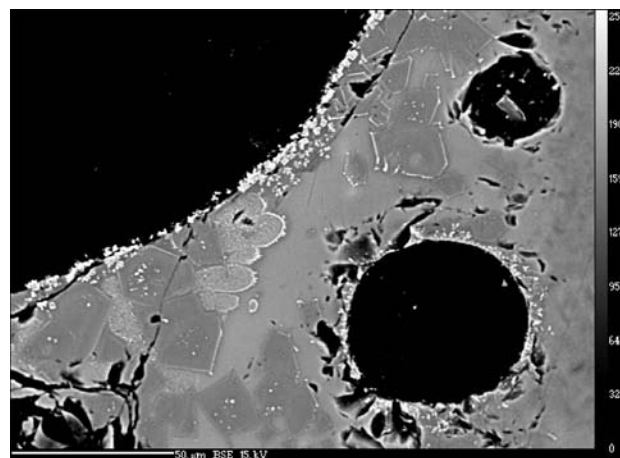
Fig. 5. **"Bleb" in the Loštice pottery of the (020) group (sample no. L 3) lined with a thin layer of spinel and glass matter containing a new-formed cordierite. Photo by R. Škoda**

The experiments bring the evidence of the use of almandine. The Loštice pottery replicas undisputedly display macroscopically the same "blebs", which are found in the original vessels. The correspondence of the mineralogical composition of the replicas and the original artifacts has been proven by optical and electron microscopy and microchemical examination of the new-formed phases (compare Table I and Table II).

Discussion

The basical plastic raw material corresponds to clay with a low content of very fine graphite (5–8 % wt.). The origi-nal raw material (pottery clay) from Loštice was used for the experiments. The products made of clay were able to resist high temperatures without a shape deformation. On the other hand, the utilization of local loess has been disproved by the experimental firing. The replicas made of loess collapsed at the temperature about 1,200 °C.

The opinion that the "blebs" on the pottery surface form by the decomposition of sulphides contained in the graphite from Svinov (Měchurová, Čejka, Zalabák 1992) has also been disproved by the experiment. The replica made of soil extracted from a pottery workshop did not contain any surface "blebs" after the experiment. The "blebs" only appeared

Table I

Chemical composition (EDX) of cordierite ($Mg_2Al_3[AlSi_5O_{18}]$), sekaninaite (($Fe^{2+}_{1.5}Mg_{0.5}$) $Al_3[AlSi_5O]_1)_8$) and osumilite ($(K_{0.75}Na_{0.25}Fe^{2+}_{1.5}Mg_{0.5})Al_{2.25}Fe^{3+}_{0.75}[Si_9Al_3O_{30}]$)

Sample Mineral/oxide	L 3	L 5	L6	L 11	L 15	L 3	L 5	L 9	L-19	L-24
	Cordierite				Sekaninaite	Osumilite				
SiO_2	47.6	49.3	47.6	47.1	47.3	58.6	59.8	60	56.5	54.5
TiO_2	0.2	0.1	0.4	0.1	0.1	0.1	0.8	1.1	1.7	1.6
Al_2O_3	36.5	32.6	33.8	32.3	32.4	11.6	18.4	23.2	13.3	14.7
FeO	7.7	7.2	8.5	14	16.7	20.3	15.8	6.6	20.2	15.7
MnO	0.1	0.1	0.1	0	0.1	0.1	0	0.1	0.2	0.4
MgO	7.8	9.1	8.7	4.9	3.2	0.6	0.9	3.1	0.4	1.4
CaO	0.1	0	0	0	0	0.9	1.2	1.2	2.7	3.5
Na_2O	0	0.2	0	0.1	0	0.8	0.2	0.7	0.2	0.7
K_2O	0.3	0.6	0.2	0.4	0.5	4.5	2.7	4.1	3.6	3.2
Cl						0		0.1	0	
F						0	0		0	
BaO						0.2	0	0.1		
P_2O_5	0.1		0	0		0.1		0		
Total	100.5	99.3	99.4	99.1	100.3	97.8	100	100.4	98.8	95.7
NaKCa										
Na	0	0	0	0		0.1	0	0.1	0.1	0.3
K	0.3	0.1	0	0	0.1	0.9	0.6	0.9	0.8	0.7
Ca									0.1	0
sum	0.3	0.1	0	0	0.1	1	0.6	1	1	1
FeMgMn										
Fe*(ii)*	0.6	0.6	0.7	1.2	1.5	1.6	1.5	1	1.4	0.9
Mn	0	0	0	0	0	0	0	0	0	0.1
Mg	1.2	1.4	1.3	0.8	0.5	0.2	0.2	0.8	0.1	0.4
Ca						0.2	0.2	0.2	0.4	0.7
Al	0.1	0	0	0		0	0		0.1	
Subtotal	1.8	2	2	2	2	2	1.9	2	2	2.1
FeAlTi										
Al						1.3	2.4	2.9	1.1	1.2
Ti						0	0.1	0.1	0.2	0.2
Fe						1.5	0.4		1.6	1.6
Subtotal						2.8	2.9	3	3	3
SiAl										
Si	4.8	5	4.8	4.9	5	10.8	10.6	10.2	10.3	10
Al	4.2	4	4.1	4.1	4	1.2	1.4	1.8	1.7	2
Sum	9	9	8.9	9	9	12	12	12	12	12
O	18.1	18	17.9	18	17.9	30.2	30	30.3	30.3	30.1

Table II
Chemical composition (EDX) of cordierite ($Mg_2Al_3[AlSi_5O_{18}]$), sekaninaite (($Fe^{2+}_{1.5}Mg_{0.5}) Al_3[AlSi_5O]_1)_8$) and osumilite ($(K_{0.75}Na_{0.25}Fe^{2+}_{1.5}Mg_{0.5})Al_{2.25}Fe^{3+}_{0.75}[Si_9Al_3O_{30}]$) in ceramic miniature replicas of tumblers experimentally fired at the temperature of 1,250 °C

Sample/oxide	1/1	1/2	1/3	1/4	1/5	2/1	2/2	4/1	4/2	4/3	4/4	4/5	4/6
SiO_2	47.6	47.3	47.9	44.6	47.1	56.0	52.5	51.1	51.7	51.7	47.7	50.7	48.9
TiO_2	0.2	0.2	0.2	0.2	0.2	0.4	0.2	0.1	0.0	0.1	0.1	0.2	0.2
Al_2O_3	34.0	34.5	33.5	36.0	34.3	24.4	27.3	32.0	32.5	32.5	29.2	32.3	36.2
FeO	7.7	7.2	7.8	8.5	7.7	14.4	14.0	3.3	2.6	3.6	1.9	4.3	3.2
MnO	0.1	0.0	0.1	0.1	0.1	0.2	0.3	0.1	0.1	0.1	0.1	0.1	0.1
MgO	8.9	9.1	8.6	9.1	8.7	2.0	3.6	11.9	12.3	11.4	4.1	11.2	10.7
CaO	0.1	0.0	0.0	0.0	0.1	0.3	0.2	0.1	0.1	0.1	15.8	0.4	0.0
Na_2O	0.1	0.2	0.1	0.2	0.1	0.0	0.0	0.0	0.0	0.0	0.4	0.0	0.0
K_2O	0.7	0.9	0.7	0.9	0.8	0.9	0.4	0.2	0.3	0.2	0.1	0.5	0.3
P_2O_5	0.0	0.0	0.0	0.0	0.0	0.3	0.1	0.0	0.0	0.1	0.0	0.1	0.0
Total	99.3	99.5	99.1	99.6	99.2	98.9	98.6	98.8	99.6	99.7	99.4	99.7	99.7
NaKCa													
Na	0.0	0.0	0.0	0.0	0.0	0.0	0.0	0.0	0.0	0.0	0.1	0.0	0.0
K	0.0	0.1	0.1	0.1	0.1	0.2	0.1	0.0	0.0	0.0	0.0	0.1	0.0
Ca	0.0	0.0	0.0	0.0	0.0	1.1	0.0	0.0	0.0	0.0	0.0	0.0	0.0
Sum	0.1	0.1	0.1	0.1	0.1	0.3	0.1	0.0	0.1	0.0	0.1	0.1	0.1
FeMgMn													
Mg	1.3	1.4	1.3	1.4	1.3	0.5	0.6	1.8	1.8	1.7	0.6	1.7	1.6
Fe	0.7	0.6	0.7	0.7	0.6	2.3	1.3	0.3	0.2	0.3	0.2	0.4	0.3
Mn	0.0	0.0	0.0	0.0	0.0	0.0	0.0	0.0	0.0	0.0	0.0	0.0	0.0
Ca	0.0	0.0	0.0					0.0	0.0		1.2	0.0	0.2
Subtotal	2.0	2.0	2.0	2.1	1.9	2.8	1.9	2.1	2.0	2.0	2.0	2.0	2.0
FeAlTi													
Al						3.0							
Fe	0.0	0.0	0.0	0.0	0.0	0.0	0.0	0.0	0.0	0.0	0.0	0.0	0.0
Ti	0.0	0.0	0.0	0.0	0.0	0.1	0.0	0.0	0.0	0.0	0.0	0.0	0.0
Subtotal	0.0	0.0	0.0	0.0	0.0	3.1	0.0	0.0	0.0	0.0	0.0	0.0	0.0
SiAl													
Si	4.8	4.8	4.9	4.5	4.8	9.9	5.6	5.1	5.1	5.1	4.9	5.0	4.8
Al	4.2	4.2	4.1	4.5	4.2	2.1	3.4	3.9	3.9	3.9	4.1	4.0	4.2
Subtotal	9.0	9.0	9.0	9.0	9.0	12.0	9.0	9.0	9.0	9.0	9.0	9.0	9.0
O	18.0	18.0	18.0	17.9	17.9	30.5	18.2	18.2	18.1	18.1	18.0	18.1	18.0

on the surface of replicas made of a raw material with the addition of almandine.

The experiments proved that the firing temperature reached 1,200–1,250 °C. The number and appearance of "blebs" depends on the content and chemical composition of almandine (garnet) in the raw material mixture. The reaction of almandine garnet (decomposed on almandine and pyrope components) with kaolinite can be summarized by the following equation:

$$Mg^{2+}_3Al_2Si_3O_{12} + 3Fe^{2+}_3Al_2Si_3O_{12} + 8Al_2Si_2O_5(OH)_4$$
$$\rightarrow \qquad (1)$$
$$2Mg^{2+}_{1.5}Fe^{2+}_{0.5}Al_4Si_5O_{18} + 8Fe^{2+}Al_2O_4 + 6H_2O + 18\ SiO_2$$
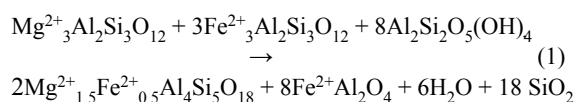
The composition of spinel, formation of cordierite, sekaninaite and possibly osumilite depends not just on the garnet composition but also on the original plastic raw material (Abbott, Clarke 1979, Green 1977).

Conclusion

The results show that the technology of the Loštice pottery production was completely different than described in older papers (e.g. Měchurová, Čejka, Zalabák, 1992).

The firing temperature of the Loštice pottery was nearly 300 °C lower than mentioned by Měchurová, Čejka and Zálabák (1992) based on XRD identification of cristobalite (1,470 °C). Cristobalite already forms at temperature above 1,000 °C.

The mineralogical analyses of the artifacts and the experiments showed that the cause of "blebs" formation was the addition of almandine.

REFERENCES

 1. Bláha R., Frolík J., Sigl J.: Archaeologia historica *28*, 525 (2003).
 2. Goš, V.: ZVOTAM *2*, 25 (1982).
 3. Goš V.: Archaeologia historica *8*, 197 (1983).
 4. Goš V.: *Loštice. Město středověkých hrnčířů*, Opava 2007.
 5. Goš V., Novák J.: Archeologické rozhledy *XXVIII*, 399 (1976).
 6. Měchurová Z., Čejka J., Zalabák P.: Časopis Moravského muzea – vědy společenské *57*, 201 (1992).
 7. Měřínský, Z.: Vlastivědný věstník moravský *21*, 1 (1969).
 8. Slivka M.: Severní Morava *46*, 65 (1983).

4.2. Posters

P01 OPTIMALIZATION OF LEAD SULPHIDE MECHANOCHEMICAL SYNTHESIS

MARCELA ACHIMOVIČOVÁ, ANNAMÁRIA MOCKOVČIAKOVÁ and ERIKA DUTKOVÁ

Institute of Geotechnics, SAS, Watsonova 45, 043 53 Košice, Slovak Republic,
achimovic@saske.sk

Introduction

Nanocrystalline lead sulphide is an important part of opto-electronic devices such as light emitting diodes and solar cells[1,2]. One of the most problematic issues of particles prepared by mechanochemical synthesis is their tendency for an aggregation, and this problem makes it very difficult to obtain particles with a high degree of dispersity. The dispersity is characterized by the particle size distribution, the particle's shape and morphology as well as their interfacial properties[3]. Stearic acid $C_{17}H_{35}COOH$ is a fatty acid that was used as a process control agent for mechanochemical synthesis of different nanocomposites where the sticking of synthesized particles and mechanical alloying was delayed[4,5]. Also the additional parameters of the mechanochemical synthesis, as the time of mechanochemical synthesis and intensity of milling (mill revolutions) strongly influence the resulting particle size distribution. The reason for this behaviour lies in the different dependencies of nucleation and growth rates on supersaturation[3]. Several authors used statistical factorial design methods for conditions optimalization of the process under study.[6–9] This factorial plan examines the given area thoroughly because it involves all possible combinations of levels of watching factors and provides the determination of an optimum value of search function from minimum number of the experiments. One of the frequently used factorial design method is the 1st order model fitting 2nd (n-number of factors). On the basis of solving of factorial plan designed matrix, it is possible to obtain objective function:

$$Y = b_0 + b_1 x_1 + b_2 x_2 + b_3 x_3 + b_{12} x_1 x_2 + b_{13} x_1 x_3 + b_{23} x_2 x_3 + b_{123} x_1 x_2 x_3 \tag{1}$$

The aim of this study was a statistical experiment design of PbS mechanochemical synthesis with determined response–mean particle size and three independent factors: time of milling, mill revolutions, the amount of stearic acid and to detect the interaction factors that can affect the output parameters.

Experimental

Mechanochemical Synthesis

Mechanochemical synthesis of PbS particles was performed in a planetary mill Pulverisette 6 (Fritsch, Germany) by high-energy milling of lead acetate and sodium sulphide with stearic acid (SA) as the process control agent in the air according to the reaction[10]:

$$(CH_3COO)_2 Pb \cdot 3H_2O + Na_2S \cdot 9H_2O \rightarrow$$
$$PbS + 2CH_3COONa + 12H_2O \tag{2}$$
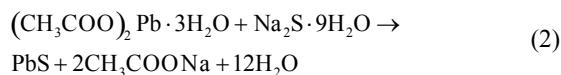
The following constant conditions were used: loading of the mill with 50 balls of 10 mm diameter; material of milling chamber and balls: tungsten carbide; weight of $(CH_3COO)_2Pb \cdot 3H_2O$: 4.75 g; weight of $Na_2S \cdot 9\,H_2O$: 3.01 g; temperature: laboratory. After the completion of reaction (2), the PbS nanoparticles have been washed and dried.

The particle size distribution of mechanochemically synthesized PbS particles was measured by a particle size analyzer HELOS (Sympatec GmbH, Germany) with wet dispergation unit SUCELL 12LA. Mean particle size of PbS particles was determined according to a mathematical model that is based on spherical systems.

Design of Experiment

One 2^3 factorial experiment with the mean particle size $D = Y$ as a response of mechanochemically synthesized PbS and 3 independent variables: time of milling-t_M, mill revolutions-n and weight of stearic acid-m_{SA} used as factors x_1, x_2, x_3 was performed. In Table I are introduced the basic level, variation interval of selected factors and two factor levels which were assigned to each of three factors $x_1 = t_M$, $x_2 = n$ and $x_3 = m_{SA}$ and these levels were varied in all kinds of combination.

Eight experiments of PbS mechanochemical synthesis were performed. Their conditions are specified in the Table II.

Table I
Levels of independent variables (factors)

Factor level	$x_1 = t_M\,[min]$	$x_2 = n\,[min^{-1}]$	$x_3 = m_{SA}\,[g]$
Basic level – x_{0i}	8	400	0.09
Variation interval – Δx_i	2	100	0.05
Low level – x_{Li}	6	300	0.04
High level – x_{Hi}	10	500	0.14

Table II
Specified conditions of PbS mechanochemical synthesis experiments

Trials series n°	$x_1 = t_M\,[min]$	$x_2 = n\,[min^{-1}]$	$x_3 = m_{SA}\,[g]$
1	6	300	0.04
2	10	300	0.04
3	6	500	0.04
4	10	500	0.04
5	6	300	0.14
6	10	300	0.14
7	6	500	0.14
8	10	500	0.14

Results

The 1st order model fitting predicting the values of mean particle size was found, where the coefficients represent the measure of the effects of variables $x_1 = t_M$, $x_2 = n$ and $x_3 = m_{SA}$. The mixed terms $x_1 x_3$ and $x_2 x_3$ indicate the measure of mutual interactions between the variables. The designed matrix, observed responses and predicted values are introduced in Table III and the regression coefficients of model function are in Table IV. Variance of reproducibility S_{Re}^2 of the mean particle size values of synthesized particles is 0.014 calculated from experiments performed in the centre of experiment (trials 9 to 14 from the factorial experiment), the mean value of Y equal to 1.33 μm respectively). On the basis of S_{Re}^2 value, the variance of regression coefficients or parameters of model function, S_{bi}^2 was calculated, that equals to 0.0098. The values of Student's test-t were calculated according to the formula:

$$t_i = \frac{|b_i|}{\sqrt{S_{bi}^2}} \quad (3)$$

The value of this t-test defines the significance of the regression coefficient: regression coefficient is significant if the calculated value of Student's test is greater than the table value, $t_{\alpha,f} = 2.57$(ref.[11]). After separation of insignificant regression coefficients the model function of PbS mechanochemical synthesis has the following form:

$$Y = 1.91 - 0.12x_1 - 0.47x_2 + 0.12x_1 x_3 - 0.43x_2 x_3 \quad (4)$$

The values of F-Fisher's test were calculated because of verifying of the factors significance according to the formula (5).

Table III
Designed matrix of PbS mechanochemical synthesis system, observed responses – Y_i^{OR} and predicted values – Y_i^{PV} of mean particle size, D

Trials series n°	x_0	x_1	x_2	x_3	$x_1 x_2$	$x_1 x_3$	$x_2 x_3$	$x_1 x_2 x_3$	Y_i^{OR} [μm]	Y_i^{PV} [μm]
1	1	−1	−1	−1	+1	+1	+1	−1	2.13	2.19
2	1	+1	−1	−1	−1	−1	+1	+1	1.66	1.71
3	1	−1	+1	−1	−1	+1	−1	+1	2.07	2.11
4	1	+1	+1	−1	+1	−1	−1	−1	1.58	1.63
5	1	−1	−1	+1	+1	−1	−1	+1	2.77	2.81
6	1	+1	−1	+1	−1	+1	−1	−1	2.95	2.38
7	1	−1	+1	+1	−1	−1	+1	−1	1.15	1.01
8	1	+1	+1	+1	+1	+1	+1	+1	0.97	1.01
9	0	0	0	0	0	0	0	0	1.25	1.25
10	0	0	0	0	0	0	0	0	1.23	1.01
11	0	0	0	0	0	0	0	0	1.23	1.01
12	0	0	0	0	0	0	0	0	1.53	1.01
13	0	0	0	0	0	0	0	0	1.36	1.01
14	0	0	0	0	0	0	0	0	1.38	1.01

Table IV
1st order model fitting results for PbS mechanochemical synthesis with mean particle size, D as optimization parameter

Variable	Regression coefficients of model function (1) b_0 b_i· b_{ij} b_{ijk}	S_i^2 variance due to factors and factor interactions	t-Student's test	F-Fisher's test
x_0 (constant)	1.91	0.5	60.83	36.34
x_1	−0.12	0.12	3.83	8.72
x_2	−0.47	1.75	14.99	127.80
x_3	0.05	0.02	1.59	1.45
$x_1 x_2$	−0.05	0.02	1.59	1.45
$x_1 x_3$	0.12	0.12	3.83	8.72
$x_2 x_3$	−0.43	1.5	13.72	109.01
$x_1 x_2 x_3$	−0.04	0.01	1.37	0.73

$$F = \frac{S_i^2}{S_{Re}^2} \quad (5)$$

According to Fisher test the factor is significant if the calculated value of F-test is greater than the table value $F = 6.61$(ref.[11]).

An adequacy of model function was verified by F-test that consist in a comparison of the variance reproducibility S_{Re}^2 and the variance S_{AD}^2 that is given by the variances of theoretical and experimental values of mean particle size Y = D, according to:

$$F_{AD} = \frac{S_{AD}^2}{S_{Re}^2} \quad (6)$$

The proposed model function sufficiently represents the course of mechanochemical synthesis process in examined region because the calculated F_{AD} value equal to 1.24 is less than the table value of $F_{AD} = 5.41$(ref.[11]).

It can be concluded from Table III, that the observed responses Y_i^{OR} are in close agreement with predicted values Y_i^{PV} of the model. It follows from the model function, that the mean particle size of PbS is mostly influenced by revolutions of mill, less by time of mechanochemical synthesis and the weight of stearic acid did not influence the mean particle size in used range 0.04–0.14 g. The twofactors interaction between the revolution of mill and the amount of stearic acid has larger effect on the PbS mean particle size. The smallest mean particle size from the particle size distribution analysis point of view (Table III) can be obtained at trials 7 and 8 of Table II, it means at high level of the factors – mill revolution and amount of stearic acid.

Conclusions

The role of the process control agent – stearic acid with the aim to decrease the ability of particles to create aggregates during the mechanochemical synthesis of PbS

in a planetary mill was studied. The 1st order model fitting with the mean particle size-Y as a measured response and three independent variables: time of mechanochemical synthesis-x_1, revolutions of mill-x_2 and weight of stearic acid-x_3 was constructed and the model function $Y = 1.91 - 0.12x_1 - 0.47x_2 + 0.12x_1x_3 - 0.43x_2x_3$ was obtained. It resulted from this function that the mean particle size of synthesized PbS nanoparticles was most influenced by revolutions of mill, less influenced by time of mechanochemical synthesis and the weight of stearic acid did not influence the mean particle size of synthesized PbS particles basically.

REFERENCES

1. Wang W., Liu Y., Zhan Y., Zheng Ch., Wang G.: Mater. Res. Bull. *36*, 1977 (2001).
2. Warner J. H., Watt A. A.R.: Mater. Lett. *60*, 2375 (2006).
3. Peukert W., Schwarzer H. Ch., Stenger F.: Chem. Eng. Process. *44*, 245 (2005).
4. Bhattacharya P., Bellon P., Averback R. S., Hales S. J.: J. Alloy. Compd. *368*, 187 (2004).
5. Byun J. S.: J. Alloy. Compd. *365*, 149 (2004).
6. Agatzini S., Burkin A. R.: Trans. Instn. Min. Metall. (Sect. C: Mineral Process. Extr. Metall.) *94*, 105 (1985).
7. Cunha M. L., Bastos M. H.: *Proceedings of 7th Int. Mineral Processing Symposium*: *Innovations in Mineral and Coal Processing* (Atak S., Őnal G., Celik M. S., eds.), p. 899. Istambul, Balkema, Rotterdam 1998.
8. Godočíková E., Baláž P., Leško M.: Uhlí-Rudy-Geologický průzkum *9*, 21 (2002).
9. Box G. E. P., Wilson K. B.: J. Royal Statist. Soc. Series B, *13*, 1 (1951).
10. Baláž P., Boldižárová E., Godočíková E., Briančin J.: Mater. Lett. *57*, 1585 (2003).
11. Eckschlager K., Horsák I., Kodejš Z.: *A Czechoslovak norm: Evaluation of the Analytical Results and Methods*. Publ. House ALFA, Prague 1980.

P02 SYNTHESIS OF DOPED LANTHANUM FERRITE PEROVSKITES

EVA BARTONÍČKOVÁ and JAROSLAV CIHLÁŘ

Brno University of Technology, Purkynova 118, 612 00 Brno, Czech Republic,
bartonickova@fme.vutbr.cz

Introduction

Multicomponent ceramic materials have a variety of industrial applications. Types of application are strongly depended on the properties such as mixed ionic and electronic conductivity, transport properties, ability working at severe reducing conditions and elevated temperatures. The main purpose for study and producing of multicomponent ceramic oxides are applications in syngas production, oxygen membranes or components of SOFCs. These properties are interdependent on the way of preparation. In general the routes of preparation can be divided into two groups. The first one is "wet" chemical routes. There are typical methods as precipitation synthesis, sol-gel processes then the novel ones as self-combustion reactions – glycine nitrate processes (GNP)[1,2], spray pyrolysis or Pechini synthesis[3]. Otherwise the conventional synthesis based on solid state reactions are still frequently applied as well[4,5]. This study is focused on the preparation of multicomponent perovskite system $La-Sr-Fe-Ti-O$ by several methods. System $La-Sr-Fe-Ti-O$ belongs to materials with high oxygen transport and sufficient mixed conductivity at high temperatures.

Doped lanthanum ferrites were studied by Tsipis and all.[6] They observed the high mixed conductivities in $La_{1-x}Sr_xFeO_{3-\delta}$ when $x = 0.5$. The high strontium content determined the high conductivity values but is associated with poorer thermodynamic and chemical stability under the large oxygen chemical potential gradient. The way to improve the stability in higher temperatures is partial substitution of iron by redox-stable cations such as transition metals e.g. titanium and chromium or cobalt what was published by several authors[7,8]. The work is focused on the preparation and study of composition of $La-Sr(Ca)-Fe-Ti-O$ perovskites.

Experimental

P o w d e r   P r e p a r a t i o n

Perovskite systems $La_{0.2}Sr_{0.8}Fe_{1-x}Ti_xO_{3-\delta}$ (LSFT) and $La_{0.2}Ca_{0.8}Fe_{1-x}Ti_xO_{3-\delta}$ (LCFT) ($x = 0.2 - 0.4$) were synthesized by two methods. Conventional solid state reaction and glycine-nitrate process (GNP) were used.

The oxides and carbonates of appropriate metals were used as starting material for SSR The suspensions of oxides in isopropanol in stechiometric ratios (Table II) were milled in planetary ball mill for 24 h then dried. These precursors were put to the furnace for SSR for 30 h at the temperature of 1,100 °C.

The nitrates and alkoxides of appropriate metals were used as starting materials in GNP process. The aqueous solutions of each cation were mixed in stechiometric ratios and

glycine was added at G/N ratio = 5/9. The concentrations are given in Table 1. Synthesized precursor was calcined (950 °C 4 h^{−1}) for decompositions of carbonates residues and SSR of oxide precursors.

Table I
The data used for preparation of suspensions for compositions ($x = 0.2, 0.4$)

Starting materials	Concentration [$mol\,dm^{-3}$] $La_{0.2}Sr_{0.8}Fe_{1-x}Ti_xO_{3-\delta}$		Concentration [$mol\,dm^{-3}$] $La_{0.2}Sr_{0.8}Fe_{1-x}Ti_xO_{3-\delta}$	
	$x = 0.2$	$x = 0.4$	$x = 0.2$	$x = 0.4$
La_2O_3	0.0838	0.0940	0.1158	0.1162
$SrCO_3$	0.7507	0.7565	–	–
CaO	–	–	0.9255	0.9345
Fe_2O_3	0.3752	0.2837	0.4627	0.3508
TiO_2	0.1876	0.3783	0.2314	0.4671

Table II
The data used for preparation of solutions

Starting materials	Concentration [$mol\,dm^{-3}$]
$La(NO_3)\cdot 9H_2O$	1.2269
$Sr(NO_3)_2$	3.0741
$Fe(NO_3)_3\cdot 9H_2O$	1.8444
$Ti(C_2H_6O)_4$	0.3074
Glycine	1.0775

P o w d e r   C h a r a c t e r i z a t i o n

The phase composition was determined by X-ray diffraction analysis. KCo wavelength (X´pert. Philips. Netherlands). The morphology of powder products was studied by scanning microscopy (SEM XL 30. Philips. Netherlands). The composition was determined by EDS detector of scanning microscopy (SEM XL 30. Philips. Netherlands). The specific surface area (SSABET) was determined by the BET method (Chembet. Quantachrome. USA). Particle size was calculated from BET values.

Table III
Properties of synthetized powders

Sample		XRD	Rietveld analysis	BET [$m^2\,g^{-1}$]	Particle size [μm]
SSR	$x = 0.2$	Cub.	*Pm3m*	1.00	1.08
LSFT	$x = 0.4$	Cub.	*Pm3m*	3.00	0.36
SSR	$x = 0.2$	Orth.	*Pbnm*	1.60	0.67
LCFT	$x = 0.4$	Orth.	*Pbnm*	1.00	1.08
GNP LFST	$x = 0.4$	Cub.	*Pm3m*	5.20	0.21

Results

All materials obtained by SSR and GNP process were composed of one phase products. The properties of synthesi-

zed powders are given in Table III. Powders prepared by conventional solid state reaction are phase pure and the particle size was in range of 300 nm to 1.2 μm. The perovskite system $La_{0.2}Sr_{0.8}Fe_{1-x}Ti_xO_{3-\delta}$ was single phase with cubic lattice symmetry (space group *Pm3m*). The perovskite system $La_{0.2}Ca_{0.8}Fe_{1-x}Ti_xO_{3-\delta}$ was single phase with orthorhombic lattice symmetry (space group *Pbnm*).

The XRD patterns of ceramic powders of several compositions are given in Fig. 1.
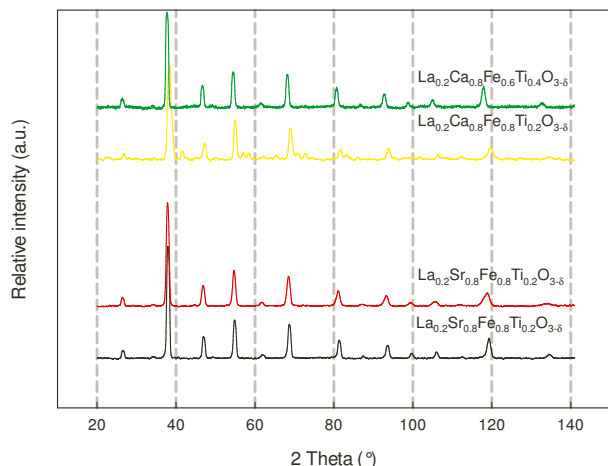
Fig. 1.　**XRD patterns of synthetized powders**

The multicomponent system was analysed by EDS SEM and the compositions are given in Table IV.

Table IV
Chemical composition analysed by EDS SEM

Expected compostition	Determined composition (EDS SEM)
$La_{0.2}Sr_{0.8}Fe_{0.8}Ti_{0.2}O_{3-\delta}$	$La_{0.21}Sr_{0.68}Fe_{0.80}Ti_{0.20}O_{3-0.91}$
$La_{0.2}Sr_{0.8}Fe_{0.6}Ti_{0.4}O_{3-\delta}$	$La_{0.21}Sr_{0.73}Fe_{0.61}Ti_{0.39}O_{3-0.41}$
$La_{0.2}Ca_{0.8}Fe_{0.8}Ti_{0.2}O_{3-\delta}$	$La_{0.23}Ca_{0.67}Fe_{0.79}Ti_{0.21}O_{3-0.16}$
$La_{0.2}Ca_{0.8}Fe_{0.6}Ti_{0.4}O_{3-\delta}$	$La_{0.15}Ca_{0.49}Fe_{0.44}Ti_{0.56}O_{3-0.75}$

Systems synthesized via both methods were single phase with cubic lattice symmetry (space group *Pm3m*). The temperature of formation of pure phase was different for each of method. The solid state reactions were performed at 1,100 °C and for 30 hours. The glycine/nitrate combustion synthesis occured several minutes after evaporation of water and was followed by SSR at 950 °C for 4 hours. The particle

(a)　　　　　　　　　　(b)
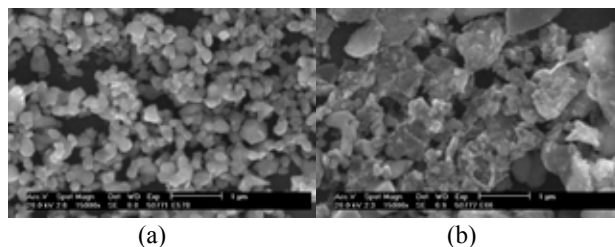
Fig. 2　**SEM micrographs of syntetized powders: (a) SSR synthesis and (b) GNP combustion reaction**

size of prepared powders is depended on method which was used. In case of SSR the particle size was around 360 nm and 210 nm for GNP process. The SEM micrographs of $La_{0.2}Sr_{0.8}Fe_{0.6}Ti_{0.4}O_{3-\delta}$ are given in Fig. 2.

Conclusions

The single phase multicomponent ceramic systems were successfully prepared via both methods – SSR and GNP. The particle size of synthesized powders was in the range of 0.21 to 1.08 um and specific surface area in the range of 1.0 to 5.2 $m^2\,g^{-1}$.

REFERENCES

1. Liu M., Wang R., Li D. F., Liang D. T.: Mater. Chem. Phys. *102*, 132 (2007).
2. Lee G. Y., Song R. H., Kim J. H., Peck D. H., Lim T. H., Shul Y. G., Shin D. R.: J. Electroceram. *17*, 723 (2006).
3. Lepe F. J., Fernández-Urbán J., Mestres L., Martínez-Sarrión M. L.: J. Power Sources *151*, 74 (2005).
4. Wang S., van der Heidea P. A. W., ChavezaC., Jacobson A. J., Adler S. B.: Solid State Ionics, *156*, 201 (2003).
5. Bayraktar D., Clemens F., et al.: J. Eur. Ceram. Soc. *27*, 2455 (2007).
6. Tsipis E. V., Patrakeev M. V., et al.: Solid State Sci., *7*, 355 (2005).
7. Fagg D. P., Kharton V. V., et al.: Solid State Ionics, *156*, 45 (2003).
8. Fagg D. P., Kharton V. V., et al.: J. Eur. Ceram. Soc. *21*, 1831 (2001).

P03 EFFECT OF HEAT TREATMENT ON THE Al + Si DIFFUSION COATINGS ON Ni-BASED ALLOYS

LADISLAV ČELKO and LENKA KLAKURKOVÁ

Brno University of Technology, Faculty of Mechanical Engineering, Institute of Materials Science and Engineering Technická 2896/2, 616 69 Brno, Czech Republic
ycelko00@stud.fme.vutbr.cz

Introduction

Diffusion barriers are a wide group of protective coatings currently used for high temperature applications. They ensure an improvement of substrate surface stability against degradation processes closely related to the working environment, oxidation and hot corrosion mainly[1]. Generally, the effect of heat treatment is possible to be divided into the protective coating formation and degradation of the coating just formed[2].

In principal, the diffusion coating production is based on thermodiffusion saturation of the substrates by aluminum or aluminum combined with other elements (e.g. Al-Cr, Al-Si). A great variety of techniques for deposition of diffusion coatings were designed. Regarding to the diffusion coating production costs, the powder mixtures with halide activators, circulating gaseous phase and slurry deposition techniques are prefered.

The first and the second technique use similar chemical process for aluminide coating formation (in a shortcut: activator decomposition, saturating gas formation, substrate surface saturation and diffusion coating growth) during annealing in relatively wide temperature range: from 500 °C to 1,200 °C[3]. Nevertheless, to co-deposit aluminum in combination with other elements, suitable pack activators and temperature range to create favourable conditions for coating formation must be found[4,5].

Instead of the techniques mentioned above, the use of slurry deposition has a series of advantages. They are as follows: preparation of arbitrary elements powder mixtures, a shorter thermal cycles necessary to the coating formation, a possibility of local and large-size substrate coating deposition. The slurry is made of saturating elements powder mixtures and of an organic binder. Diffusion annealing (commonly in the temperature range from 650 °C to 1,200 °C) ensures a complete burnout and volatilization of organic components without deteriorating the substrate and coating[2,6,7].

Experimental

Sheets of Ni (nickel of commercial purity, 99.7 % wt. Ni), Ni-Cr (commercial nichrome, Ni-20 % wt. Cr) and Inconel 713LC were used as substrates. The substrate surface was ground with abrasive paper to #600, polished with 3 μm diamond paste and washed with acetone in ultrasonic cleaning bath for 15 min. Slurry was prepared by stirring a mixture of Al, Si powders (up to 90 and 45 μm in diameter, respectively) and amyl acetate based organic binder solution
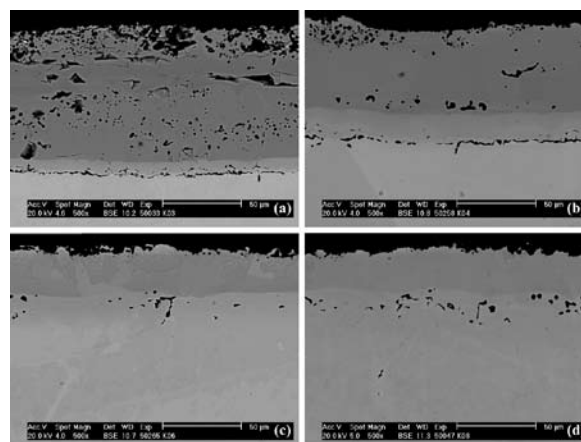
Fig. 1. **The cross-sectional SEM images of coating formed on Ni after annealing at 1,000 °C; (a) – 0 min, (b) – 60 min, (c) – 180 min and (d) – 600 min**
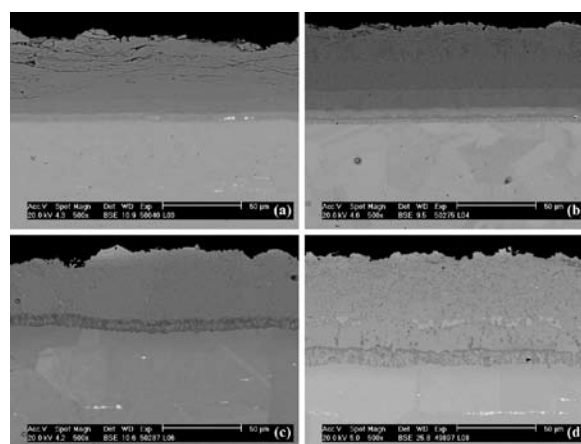
Fig. 2. **The cross-sectional SEM images of coating formed on Ni-Cr after annealing at 1,000 °C; (a) – 0 min, (b) – 60 min, (c) – 180 min and (d) – 600 min**

(100 ml to 38 g of Al and 32 g of Si powder) with propeller stirrer at 150 rpm for 15 min. Viscosity of the slurry measured by Ford Cup (Ø 6 mm, 20 °C) was 13 s. The slurry was sprayed by hand onto the sheets' surface. Specimens prepared this way were heated in a tube furnace with flowing argongas atmosphere. Heat treatment conditions were 200 °C 60 min^{-1} (Ar-gas flow 9 dm^3 min^{-1}) to decompose organic binder and 1,000 °C per 0, 60, 120, 180, 360, 600 min (Ar-gas flow 5 dm^3 min^{-1}) to investigate the intermetallic layer formation and development. After heating, the samples were cooled under Ar-gas flow to 550 °C and then in air to room temperature.

For microstructure observation, the scanning electron microscope (Philips XL30) was used. Elements interaction studies, based on energy dispersive microanalysis (EDAX), and layer thickness measurements by means of image analysis (NIS Elements AR 2.3) were performed. Microhardness tester (LM 247AT) was used for layers hardness determination.
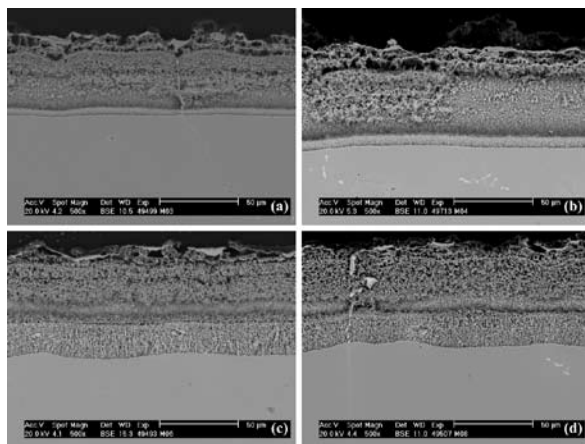
Fig. 3.　**The cross-sectional SEM images of coating formed on Inconel 713LC after annealing at 1,000 °C; (a) – 0 min, (b) – 60 min, (c) – 180 min and (d) – 600 min**

Results

Figs. 1., 2. and 3. show SEM images of the course of diffusion coating formation on Ni, Ni-Cr and Inconel 713LC substrates, respectively.

Concentration change of the elements with depth from the surface to nickel-base substrates, measured by EDS, are depicted on Fig. 4. The coating transformation diagrams, based on image analysis measurements were constructed, see Fig. 5. Hardness of the substrates decrease during annealing while the hardness of intermetallic layers is stable within 500 to 950HV.

Conclusions

The first step of annealing is necessary for organic binder decomposition. This leads to partial aluminum powder oxidation. Intermetallic phases start to form when the temperature exceeds the Al-Si eutectic point.

Relatively thin intermetallic layers of NiAl and Ni_3Al were produced at the moment when the temperature 1,000 °C was reached. The part of the coating, termed as "Al reserves", is also intermetallic in this moment but with high degree of open porosity. This layer disappears at the expense of inner layers growth during the annealing dwell.

Silicon addition in the slurry is detrimental in the case of Ni substrate (diffusion coating destroyed after 180min annealing) and beneficial for Ni-Cr and Inconel 713LC (stabilises the lower Cr-rich layer, forms Cr-Si intermetallics and/or carbides, respectively).

Fig. 4.　**Concentration change of the elements with depth from surface to substrate after annealing at 1,000 °C for (a) 0 min, (b) 600 min on Ni, Ni-Cr and Inconel 713LC substrates (from the top)**
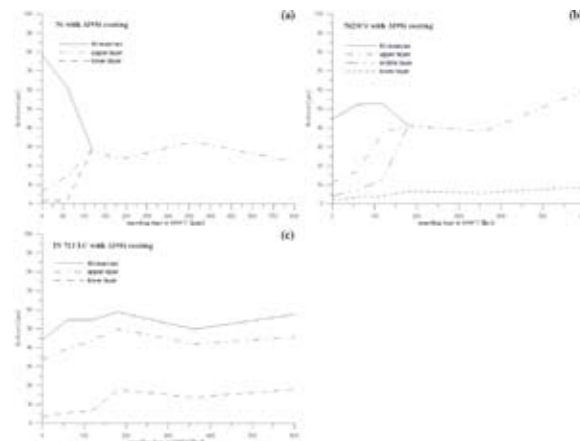
Fig. 5.　**Transformation of diffusion coating during annealing at 1,000 °C on (a) Ni, (b) Ni-Cr and (c) Inconel 713LC substrate**

REFERENCES

1. Bose T.: *High Temperature Coatings*. Elsevier, 2007.
2. Tamarin Y.: *Protective Coatings for Turbine Blades*. ASM International, Ohio 2002.
3. Houngninou C., Chevalier S., Larpin J. P.: Appl. Surf. Sci. *236*, 256 (2004).
4. Xiang Z. D., Datta P. K.: Surf Coat Technol *179*, 95 (2004).
5. Xiang Z. D., Datta P. K.: Mater Sci Eng A *356*, 136 (2003).
6. Murakami K., Nishida N., Osamura K., Tomota Y.: Acta mater. *52*, 1271 (2004).
7. Murakami K., Nishida N., Osamura K., Tomota Y., Suzuki T.: Acta Mater *52*, 2173 (2004).

P04 CHEMICAL ANALYSIS OF Al AND Si SURFACE LAYERS ON STEELS

PAVEL DOLEŽAL, LADISLAV ČELKO, ANETA NĚMCOVÁ and LENKA KLAKURKOVÁ

Brno University of Technology
Faculty of Mechanical Engineering
Technická 2896/2, 616 69 Brno, Czech Republic
pavdol@email.cz

Introduction

Great variety of surface modifications was developed in the effort to improve bearing steels' surface properties. In order to achieve an improvement in performance of the bearings working at higher temperatures, the diffusion coatings may be applied. The diffusion coatings are special group of surface modifications commonly used to improve the high temperature alloys' surface protection against degradation processes, closely related to the working environment (oxidation and hot corrosion, mainly)[1].

Several deposition techniques were designed for the diffusion coating application. The most widely used techniques are coating in powder mixtures with halide activators or the in circulating gaseous phase. These techniques use similar chemical processes for diffusion coating formation, i.e. activator decomposition, saturating gas development, substrate surface saturation and diffusion coating growth. Main disadvantages of these techniques lie in the need for favourable multicomponent co-deposition conditions design and in the substrate surface corrosion damage during the coating formation (triggered by incomplete "saturation" halide gas decomposition)[2,3].

Application of the diffusion coatings using slurry is a widely used technique, as well. The slurry is made of saturating elements powder, such as Al, Al-Cr, Al-Si, and of an organic binder. Ready-to-use slurry could be applied by various methods, such as dipping, brushing or spraying onto the substrate surface. When the coating is applied onto the surface and dried, the heat treatment designed for protective layer formation follows[4].

In this article, the influence of temperature on the silicon-alloyed aluminide diffusion coatings formation on the 100Cr6 bearing steel is investigated.

Experimental

The 100Cr6 bearing steel was used as substrate. The substrate was ground, polished and washed with acetone in ultrasonic cleaning bath. Slurry was made of 55 % Al + 45 % Si powders and of amyl-acetate based organic binder solution. The slurry was sprayed by hand onto the substrates' surface.

Samples prepared this way were heated in a tube furnace with flowing argon-gas atmosphere. The two-stage heat treatment for surface layer formation was employed; the first stage, i.e. low temperature dwell, to decompose the organic binder and the second stage, i. e. high temperature dwell, at 800, 900 and 1,000 °C 3h^{-1} for intermetallic layers formation.

For microstructure observation, the light microscope (Olympus GX71) and scanning electron microscope (Philips XL30) were used. Elemental interaction studies, based on energy dispersive microanalysis (EDS), glow discharge optical emission spectrometry (GD OES) and layer thickness
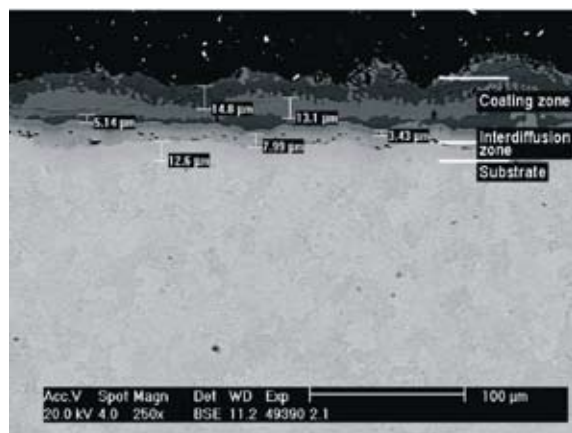
Fig. 1. **The SEM cross-sectional image of Al and Si diffusion layer after annealing at 800 °C 3h^{-1}**
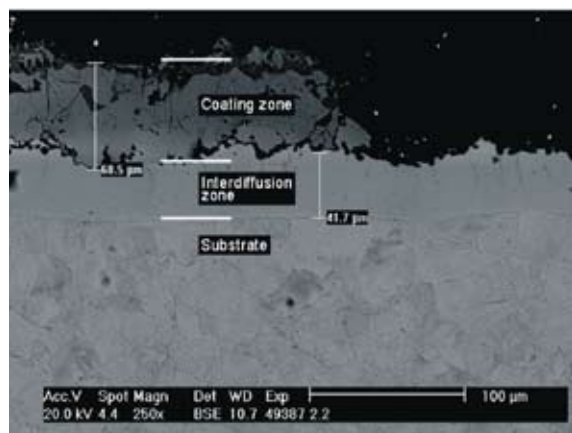
Fig. 2. **The SEM cross-sectional image of Al and Si diffusion layer after annealing at 900 °C 3h^{-1}**
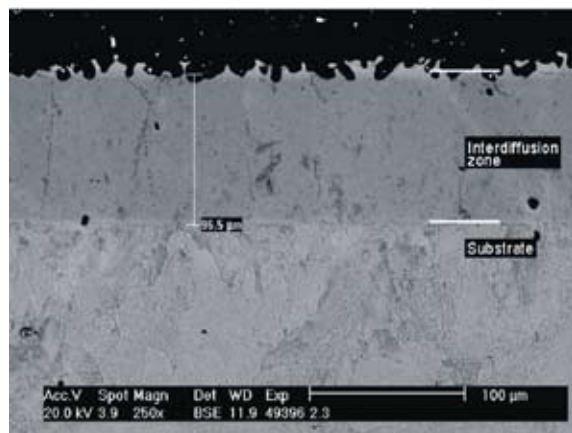
Fig. 3. **The SEM cross-sectional image of Al and Si diffusion layer after annealing at 1,000 °C 3h^{-1}**

measurements by means of image analysis (NIS Elements AR 2.3) were performed. The intermetallics' composition ranges were calculated from Al-Fe binary diagram.

Results

Figs. 1., 2. and 3. show SEM images of Al-Si diffusion coatings on 100Cr6 substrate after annealing at 800, 900 and 1,000 °C, respectively. Changes in concentration of elements with depth, measured by EDS and GD OES, are presented in Figs. 4., 5., 6. and in Figs. 7., 8., 9. for each annealing temperature, respectively. The calculated phase composition results are presented in Figs. 10,. 11. and 12. Fig. 13. shows the thickness of the interdiffusion zone, evaluated by the image analysis from SEM images.

Conclusions

The Si alloyed aluminide layers after annealing at 800, 900 and 1,000 °C were formed on the substrate of 100Cr6 bearing steel.

The coating after annealing at 800°C was divided into three continuous intermetallic layers separated by sharp Al and/or Si concentration gradient. Concentration of Al and Si decreases slowly from the top of the coating towards the substrate. Calculated intermetallics, i.e. $FeAl_3 + Fe_2Al_5$, $FeAl + FeAl_2$ and $FeAl$ were identified. The hardest "Si-rich" layer (1,050 up to 1,100 HV0.025) was identified as $FeAl + FeAl_2$.
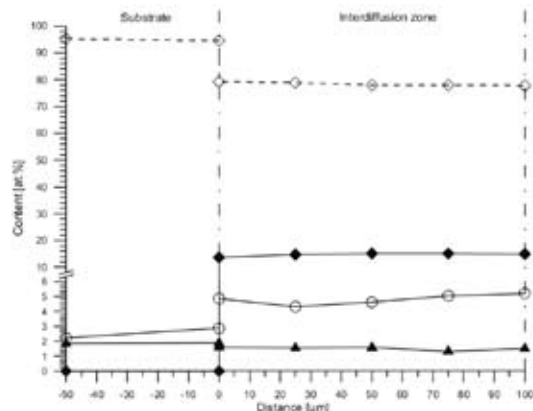
Fig. 6.   **Compositional variation with depth from substrate to surface after annealing at 1,000 °C 3h⁻¹, measured with EDS**
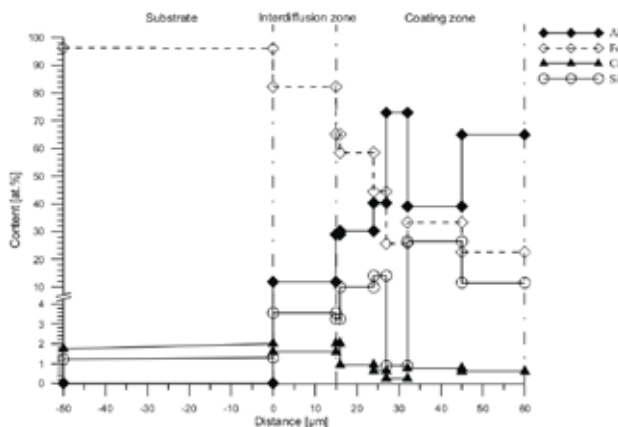
Fig. 4.   **Composition change of the elements with depth from substrate to surface after annealing at 800 °C 3h⁻¹, measured by EDS**
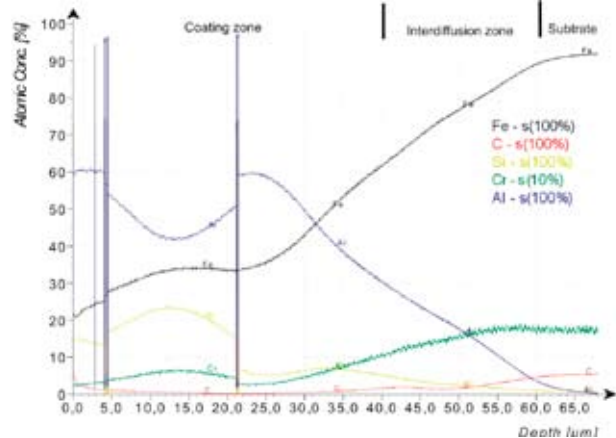
Fig. 7.   **Compositional variation with depth from surface to substrate after annealing at 800 °C 3h⁻¹, measured with GD OES**
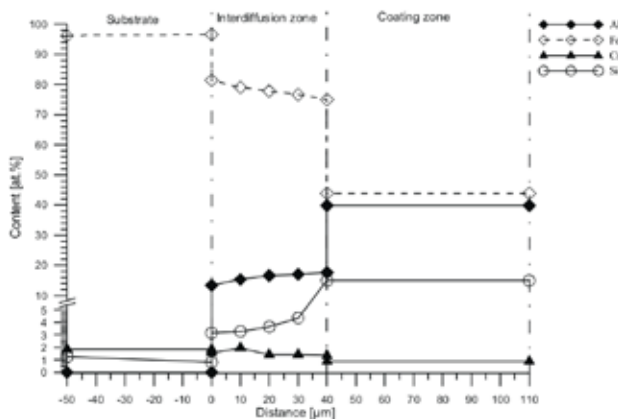
Fig. 5.   **Compositional variation with depth from substrate to surface after annealing at 900 °C 3h⁻¹, measured with EDS**
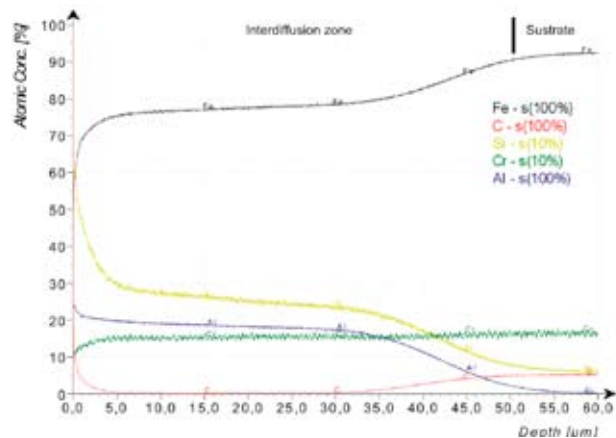
Fig. 8.   **Compositional variation with depth from surface to substrate after annealing at 900 °C 3h⁻¹, measured with GD OES**
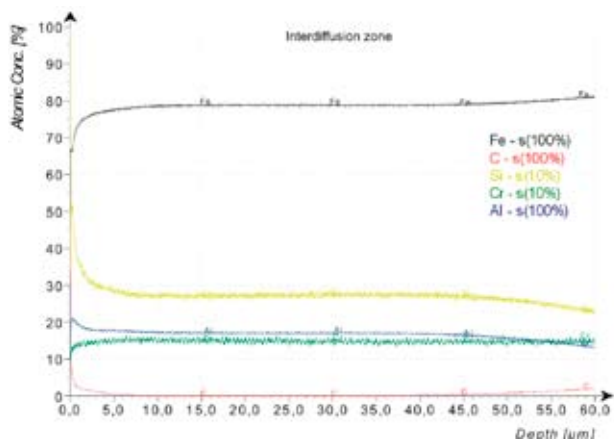
Fig. 9. **Compositional variation with depth from surface to substrate after annealing at 1,000 °C 3h⁻¹, measured with GD OES**
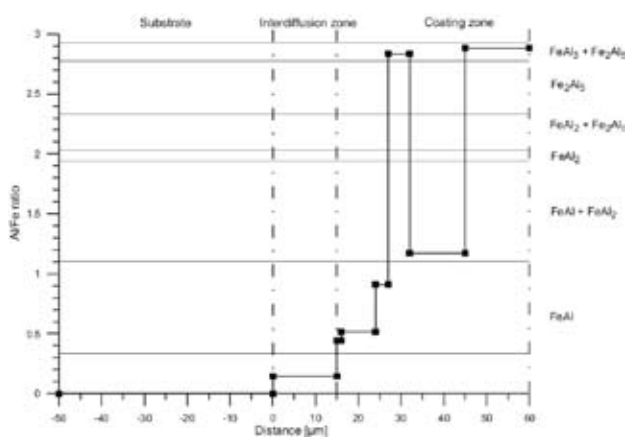
Fig. 10. **Phase composition of Al and Si surface layers calculated on the basis of Al-Fe binary system for 800 °C 3h⁻¹**
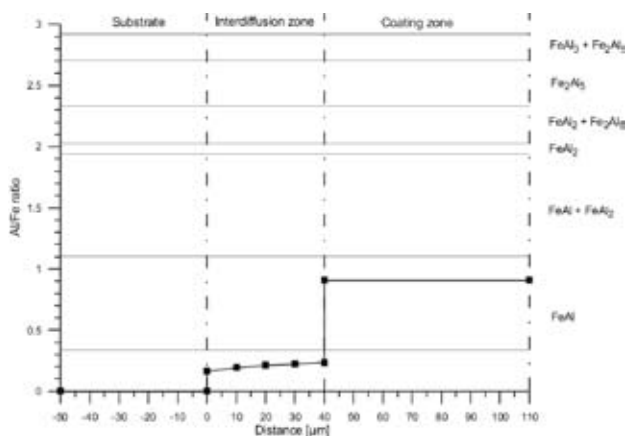
Fig. 11. **Phase composition of Al and Si surface layers calculated on the basis of Al-Fe binary system for 900 °C 3h⁻¹**

The coating after annealing at 900 °C was composed of two layers; the upper one (irregular and incompact), calculated as FeAl aluminide, and the lower one, Fe-Al solid solution, termed as interdiffusion zone.
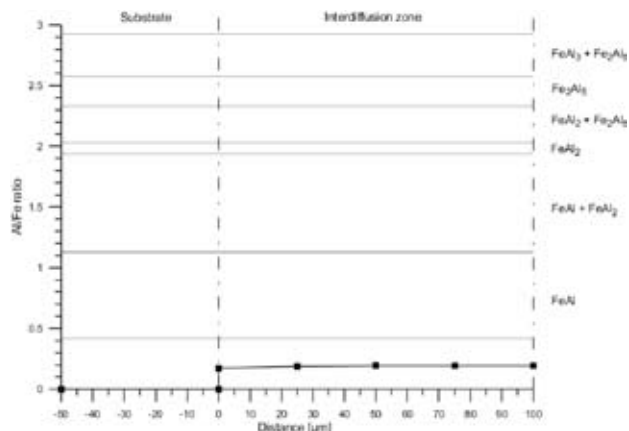
Fig. 12. **Phase composition of Al and Si surface layers calculated on the basis of Al-Fe binary system for 1,000 °C 3h⁻¹**
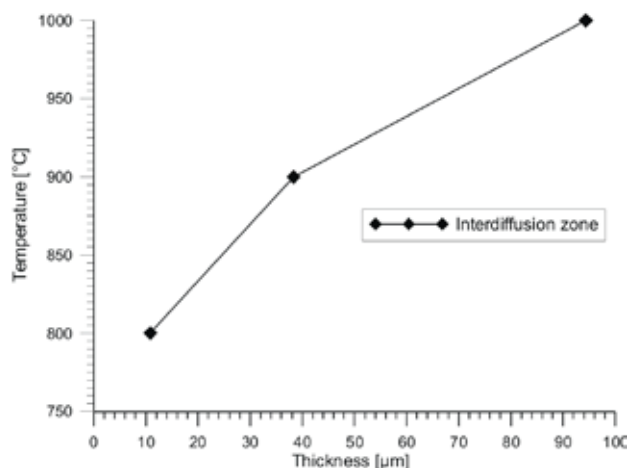
Fig. 13. **Thickness of the interdiffusion zone**

After annealing at 1,000 °C, only the interdiffusion zone was formed.

The higher temperature was used the thicker the interdiffusion zone was observed. Annealing temperature under 900 °C has to be applied to produce stable and continuous surface layer.

REFERENCES
1. Cotell C. M., Sprague J. A., Smidt F. A.: *Surface Engineering 5*, ASM, 1994.
2. Houngninou C., Chevalier S., Larpin J. P.: Appl. Surf. Sci. *236*, 256 (2004).
3. Kim M. T., Jung J. S.: Surf. Coat. Tech. *161*, 218 (2002).
4. Bose T.: *High Temperature Coatings*. Elsevier, 2007.

P05   SYNTHESIS OF BELITE CEMENT FROM COAL FLY ASH

IVANA FIĽKOVÁ and NADEŽDA ŠTEVULOVÁ

Technical University of Kosice, Civil Engineering Faculty, Institute of Building and Environmental Engineering, Vysokoskolska 4, 042 00 Kosice, Slovakia,
ivana.filkova@tuke.sk

Introduction

The growing interest is related to synthesis of reactive low-energy belite cements as an alternative to the conventional Portland cement. Cements composed by β-Ca_2SiO_4 (belite) represent great economic and environmental value, mainly because of CO_2 emission reduction and energy saving. Many investigations have been realised in order to synthesize belite cement[1,2]. Also, use of wastes and byproducts from coal combustion processes of fossil fuels in power plants and electric power stations as alternative secondary raw materials for synthesizing belite cements have become the hotspot in cement-concrete materials science at present[3,4].

In our previous works[5,6], mechanochemical synthesis of belite precursors from coal fly ash/portlandite mixture has been reported.

In this paper, hydrothermal method for structure and properties modification of fluidized coal fly ash for belite cement synthesis is presented

Experimental

Materials and Methods

Slovak coal fly ash of chemical composition (Table I) from fluidized bed brown coal combustion in power plant ENO A (Nováky) was used as raw material. In order to reach required finesses of coal fly ash the short termed milling in vibratory mill was carried out (1 min.). Starting mixture consisting of milled coal fly ash and CaO (analytical grade reagent) with CaO/SiO_2 molar ratio of 2 was prepared by homogenization.

Table I
Chemical composition of coal fly ash

LI [%]	SiO_2 [%]	Fe_2O_3 [%]	Al_2O_3 [%]	CaO [%]	MgO [%]	O_3 [%]
5.25	30.36	2.29	16.95	51.21	2.45	33.36

LI – loss of ignition

Initial mixture and demineralised water at a water-to-solid ratio of 5 was hydrotermally activated in rotating autoclave A-08 at 175 °C and 200 °C during 2 and 4 hours, respectively. The products of hydrothermal treatment were filtered and dried at 55 °C during 24 h.

The starting mixture and products of hydrothermal treatment were subsequently calcinated at temperatures of 700 °C, 800 °C and 900 °C. Crystalline phases development after hydrothermal treatment and heating of starting mixture

and all products was characterized by XRD analysis (DRON 6.0, Technabsexport, Russia).

Results and Discussion

The main crystalline phases as anhydrite, calcite, quartz, lime and portlandite (Fig. 1.) were identified in starting mixture.
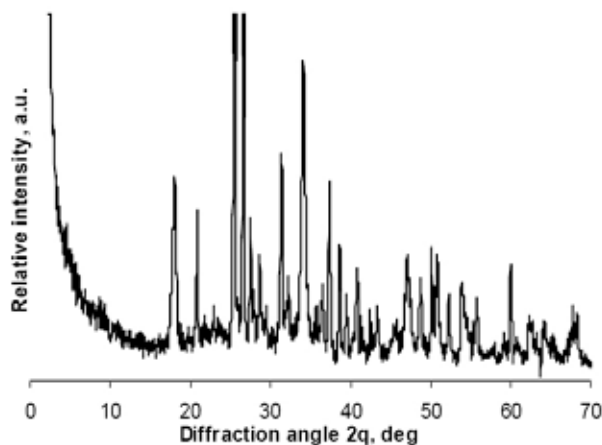
Fig. 1.   **XRD diffraction pattern of starting mixture consisting of coal fly ash and CaO (A – anhydrite, C – calcite, Q – quartz, L – lime, P – portlandite)**

Based on XRD diffraction patterns of mixtures after hydrothermal treatment at different conditions, the optimal parameters were defined for formation belite precursors: 200 °C for 4 hours. The changes in integral intensities of XRD reflections of main crystalline phases (without anhydrite) of starting mixture as a consequence of the hydrothermal treatment and subsequent calcinations can be seen in Figs. 2.–5. Formation of new profiles of low intensities corresponding to CSH
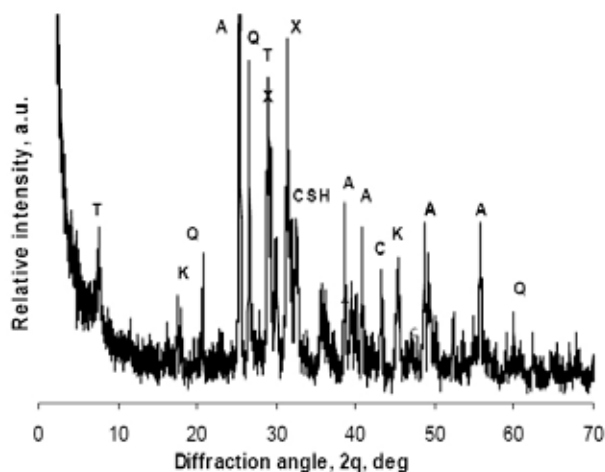
Fig. 2.   **XRD diffraction pattern of starting mixture after hydrothermal treatment at 200 °C for 4 hours (A – anhydrite, C – calcite, Q – quartz, t – tobermorite, X – xonotlite, CSH – calcium silicate hydrate, K –katoite)**
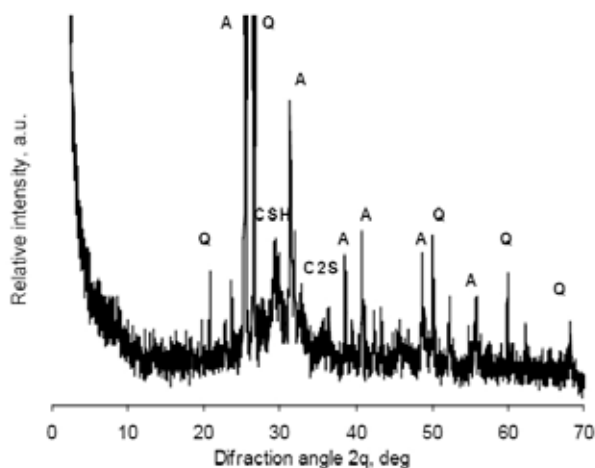
Fig. 3. **XRD diffraction pattern of starting mixture after hydrothermal treatment (200 °C; 4 h) and subsequent calcination at 700 °C (A – anhydrite, Q – quartz, CSH – calcium silicate hydrate, C2S – belite)**

Fig. 4. **XRD diffraction pattern of starting mixture after hydrothermal treatment (200 °C; 4 h) and subsequent calcination at 800 °C (A – anhydrite, Q – quartz, W – wollastonite, C2S – belite)**

phases as belite precursor as well as calcium silicates and aluminosilicates (tobermorite, xonotlite) after hydrothermal treatment of mixture was confirmed (Fig. 2). Calcination of hydrotermally treated products (Figs. 3.–5.) showed that heating at 800 °C led to transformation of CSH phases to wollastonite (CS) and belite phase (C2S). Formation of gehlenite which is known as a retarder of cement hydration was observed at 900 °C. As can be seen in Figs. 2.–5., the high CaO content fixed in anhydrite wasn't changed during the hydrothermal treatment and subsequent calcination and the same quantity of belite phase from CSH phase was reached.

Fig. 5. **XRD diffraction pattern of starting mixture after hydrothermal treatment (200 °C; 4 h) and subsequent calcination at 900 °C (A – anhydrite, Q – quartz, W – wollastonite, C2S – belite, G – gehlenite)**

The reason of low CSH phase content after hydrothermal treatment and low conversion degree of precursors to belite consists in anhydrite that is a very stable compound. Application of pre-treatment focused on decomposition of anhydrite structure in coal fly ash at high temperature for obtaining higher amount of reactive CaO could by successful but we preferred to use coal fly ash as raw material.

Conclusions

The obtained results confirm that the hydrothermal modification in combination with subsequent calcination is not suitable treatment of starting mixture based on coal fly ash with high anhydrite content for preparing belite.

REFERENCES

1. Jiang W., Roy D. M.: Am.Ceram. Soc. Bull. *71*, 642 (1992).
2. Rodriques F. A.: Cem. Concr. Res. *33*, 1525 (2003).
3. Guerrero A., Goňi S., Macias A., Luxán M. P.: J. Mater. Res. *14*, 2680 (1999).
4. Guerrero, A., Goňi, S., Campillo, I., Moraques, A.: Enviro. Sci. Technol. *38*, 3209 (2004).
5. Števulová, N., Bálintová, M., Briančin, J., Széghyová, Z.: Chem. listy *99*, 420 (2005).
6. Števulová, N., Bálintová, M., Briančin, J., Széghyová, Z.: Chimija v interesach ustojčivogo razvitija *15*, 225 (2007).

P06 MICROBIALLY INFLUENCED CORROSION OF CONCRETE

VLASTA HARBUĽÁKOVÁ, ADRIANA EŠTOKOVÁ, ALENA LUPTÁKOVÁ, NADEŽDA ŠTEVULOVÁ and LUCIA SČIGULINSKÁ

Technical University of Košice, Civil Engineering Faculty, Institute of Building and Environmental Engineering, Vysokoškolská 4, 042 00 Košice, Slovak Republic,
vlasta.harbulakova@tuke.sk

Introduction

The adverse effect of microbial activity on the long-term performance of cement materials is often not considered, despite the fact that studies on the effect of microbial activity on concrete have been ongoing for many years[1]. The corrosion process is initiated by the conversion of sulphate to sulphide by sulphate-reducing bacteria[2] (SRB) e.g. *Desulfovibrio desulfuricans* (*Dvs.d*) in anaerobic conditions. *Dvs. d.* are chemoorganotrophic, strictly anaerobic and gramnegative bacteria. Optimal growth conditions are in pH range 6.5–7.3 and temperature range 30–37 °C. Sulphur-oxidising bacteria *Acidithiobacillus thiooxidans (A.t.)* were chosen for microbially influenced corrosion (MIC) of concrete testing; because is most aggressive biological agents promoted[3]. *A.t.* as strictly autotrophic bacteria oxidizes sulphur and thiosulphate to sulphuric acid. Optimal growth temperature was 38–30 °C and pH has been in 2.0–3.5 range.

Experimental

Bacteria and Growth Condition

Sulphuretum simulated by *A.t.* and *Dsv.d.* under optimal growth conditions were chosen for experimental plan. Bacteria *Dsv.d.* were isolated from a mixed culture obtained from the potable mineral water (Gajdovka spring, the locality Kosice-north, Slovakia) and for the isolation and cultivation of these bacteria a selective nutrient medium DSM-63[4] was used. During their growth bacteria *Dsv.d.* produce a large amount of hydrogen sulphide that assures the maintenance of anaerobiosis[5].

Sulphur-oxidizing bacteria *A.t* were isolated from the mixed culture obtained from the mine water (the shaft Pech, the locality Smolník, Eastern Slovakia) and the selective nutrient medium 9K[6] was used for the isolation and cultivation of them.

Concrete Samples

Concrete cylinder samples of a 25 mm diameter and 20 mm height formed as a drilled core from real concrete cube using drilling mechanism STAM were used for experiment. The cylinder specimens were polished.

Utilized Apparatus

MIC proceeded in laboratory reactor, where sulphuretum simulation (simultaneous effect *Dvs.d.* of and A.t.) was under way. Laboratory apparatus of 1 flask with SRB and 1 flask as a trap for H_2S that were mutually joined with reactor consisted. Active bacterial SRB was in first flask and the second flask cadmium acetate contained.

Four samples in the four beakers were into reactor inserted. First beaker was filled with waste water (1), the second with acid mine drainage (2), the third with A.t. cultivating medium (3) and the fourth was with distilled water filled (4). The top of samples was by A.t. inoculated and on the bottom of reactor distilled water was poured.

The samples were every 7 days inoculated by A.t. and in the same period the change of cultivating medium for *Dvs.d.* were realized.

Methods

The weight changes were determined by gravimetric method. pH changes in leachate were evaluated as differences between initial pH and final pH after the experiment. The values of leachate pH were by pH meter PHH-3X Omega measured. The calcium concentrations in the solution were determined by atomic absorption spectrometry using Varian SpectrAA-30 spectrometer. Structural concrete surface changes were observed by stereomicroscope STM 723 ZOOM.

Results

After 50 days the concrete samples were took out of their solutions, dried and the change of the weight was determined. The results are presented in Table I.

Table I
The change of concrete samples weight

Sample	Weight of sample [g]		Change of weight	
	Before experiment	After experiment	[g]	[%]
(1)	46.1876	46.3041	0.1165	0.25
(2)	43.6003	43.4153	–0.185	–0.42
(3)	21.1463	21.1925	0.0462	0.21
(4)	25.0345	24.1245	–0.0914	–0.09

pH value has been increased into alkali after experiment for all samples. The most increment was in sample (2) and (3) registered as is evident from Table II.

Because of activity of A.t. and bacterial production of H_2SO_4 by SRB, releasing of calcium from concrete matrix was expected. The calcium concentrations in the solution determined are presented in Table III.

Table II
Change in pH value in liquid leachate

Leachate	pH leachate	
	Initial pH	Final pH
(1)	9	10.24
(2)	4	9.95
(3)	4	10.24
(4)	7.80	8.45

Table III
Calcium content in leachate

leachate	Ca [mg dm^{-3}]	
	before experiment	after experiment
(1)	87.14	8.4
(2)	128.38	24.6
(3)	45.7	37.6
(4)	0	45.1

Ca was released from concrete matrix under influence of H_2SO_4 bacterially produced. Consequently precipitations of $CaSO_4$ white crystals were attached on the concrete surface as it was in instances of samples (1)–(3) as Fig. 1 shows.

Fig. 1.   **$CaSO_4$ white crystals on the concrete samples surface (20 × 4.5 magnifications)**

The most considerable changes of concrete structure samples were visible on samples (1) and (2). For illustration, surface structure changes of sample (1) after 50 days are pictured in Figs. 2. and 3.
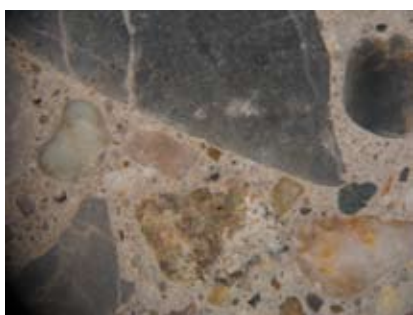
Fig. 2.   **Surface of concrete sample (1) before experiment (magnification 20 × 4.5)**

Fig. 3.   **Surface of concrete sample (1) after 50 days experiment duration (magnifications 20 × 4.5)**

For every sample except (4) was typical that some gravel components were completely removed and were significantly eroded. It is visible in white crystals probably of gypsum, which are on the surface precipitated. Accept the change of color of sample (4) into grey, there were no changes observed at this sample.

Conclusions

Concrete samples were under sulfuric acid influence corroded. The most considerable activity of microbially influenced corrosion degradation was on sample immerged into wastewater and into acid mine drainage. Experiment simultaneous effect of bacteria A.t. and SRB, which were the source of H_2S has proven.

REFERENCES
1. Sand W., Bock E.: *Seventh International Biodeterioration Symposium*, p.113. England, 1998.
2. Davis J. L., Nica D., et al: Int. Biodeterior. Biodegrad. *42*, 75 (1998).
3. Rogers R. D., Knight J. J., et al: Cem. Concr. Res. *33*, 2069 (2003).
4. Postgate J. R.: *The Sulphate Reducing Bacteria*, 2nd, Cambridge University Press, New York. (1984).
5. Beech I. B.: Microbiol. today *30*, 115 (2003).
6. Karavajko G. I., Rossi G., Agate A. D., Groudev S. N. Avakyan Z. A.: *Biogeotechnology of metals*, Centre of projects GKNT, Moscow, (1988).

P08   PREPARATION OF THAUMASITE

MARKÉTA HERMANOVÁ

Brno University of Technology, Faculty of Chemistry, Purkyňova 118, 612 00 Brno, Czech Republic,
hermanova@fch.vutbr.cz

Introduction

Thaumasite $Ca_6Si_2(SO_4)_2(CO_3)_2(OH)_{12}\cdot 24(H_2O)$ is an unusual mineral in that it contains silicon in 6-coordination with hydroxyl. It is sometimes classified as a silicate because it content silicon or as carbonate for presence of carbonate ions. But Thaumasite belongs to sulfate class and to Ettringite Group for his similarity of crystal structure and properies with ettringite.

Thaumasite Formation

Sulphate attack on concrete is considered as a source of damage. Ingressing sulphate ions can react with minerals from the cement paste to form gypsum, ettringite or thaumasite. These phases bind additional water and this effect leads to an increase in volume. If there is no space for such an expansion, micro-cracks are formed, the tension becomes higher than the tensile strength of the hardened cement paste, cracks are formed, which support access of sulphate ions and accelerate the process of destruction.

Conditions of Thaumasite Formation[1]

- a source of C–S–H,
- an external supply of sulfate ions,
- a source of carbonate ions,
- mobile water (condition pro transport iontů),
- cool temperatures(< 15 °C),
- molar ratio C/S (CaO, SiO_2), quantity of CaO, pH, temperature, humidity

Experimental part

Influence of moisture and enviroment temperature on interface of phases and creation rate of thaumasite was observed in these samples T6. Portland cement SiO_2 was used as a source. Proportion of base mixture was designed to agree with materials that are used for production of concrete

Samples were composed from Portland cement, special-milled quartz, $CaSO_4\cdot 2\,H_2O$, calcite $CaCO_3$ and H_2O.

Samples was storaged in four different conditions:

T6vt – moisture, 25 °C; T6vz – moisture, 2 °C; T6st – dry, 25 °C; T6sz – dry, 2 °C

Formula dese[6]:

$$CaSO_4\cdot 2H_2O + H_2O + CaCO_3 + SiO_2 + Ca(OH)_2 \rightarrow CaSiO_3\cdot CaSO_4\cdot CaCO_3.15H_2O \tag{1}$$
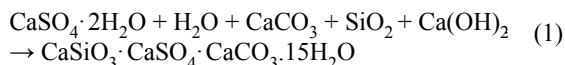
Results

It appears from RTG analyses (Table I) that thaumasit began to create in samples T6vz after 4 months. Ideal conditions for thaumasite creation are intense moisture and low temperatures. Thaumasite was created in other 2 samples (T6sz, T6vt) after 10 months. In comparison of these samples we can observe, that low temperature is more essential for creation of thaumasite. It creates faster at these temperatures than at room temperature. C–S–H gel was created in sample T6vt, which can be considered as antecedent of thaumasite. This presumtion was confirmed after 10 months.

$$CSH + H_2O + CO_3^{2-} + SO_4^{2-} + Ca^{2+} \rightarrow Thaumasite + calcite(ref.^3) \tag{2}$$
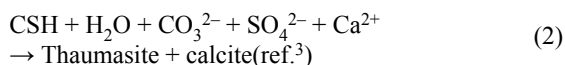
Morfologies of samples T6sz and T6vz after 10 months are presented on these images. This follows that thaumasit has crystals in columns form of lenght 3 µm.

Volume changes were occured at samples T6vz and T6sz, what is presented in the Fig. 3.. Volume change resulted in a loss of coherence, samples were plastic, which is caused by hydration suppression of Portland cement at low temperatures.

Picture from electron microscope (Fig. 4.) demonstrates baculiform crystals in sample T6st, which was placed at laboratory temperatures and at dry enviroment. These crystals can correspond to crystals of thaumasite. According to RTG analysis existence of thaumasite wasn´t confirmed. These crystals are in insignificant amount in comparison with other phases, which were created during observation, that´s why they weren´t recorded by RTG analysis. Samples didn´t change their volume during the observation.

Table I
Results of RTG analyses

T6sz	After 4 month	gypsum	calcite	SiO_2	–
	After 10 month	gypsum	thaumasite	calcite	SiO_2
T6st	After 4 month	calcite	gypsum	SiO_2	portlandite
	After 10 month	gypsum	calcite	SiO_2	–
T6vt	After 4 month	calcite	SiO2	gypsum	C–S–H
	After 10 month	gypsum	calcite	SiO_2	thaumasite
T6vz	After 4 month	gypsum	calcite	SiO_2	thaumasite
	After 10 month	thaumasite	gypsum	–	–
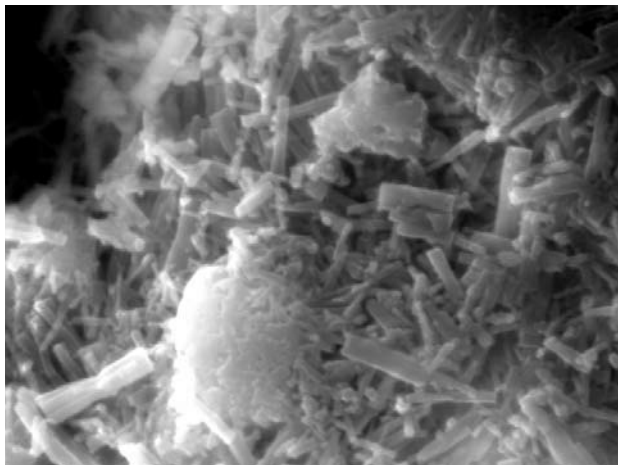
Fig. 1.   **Picture of SEM of sample T6sz after 10 months**
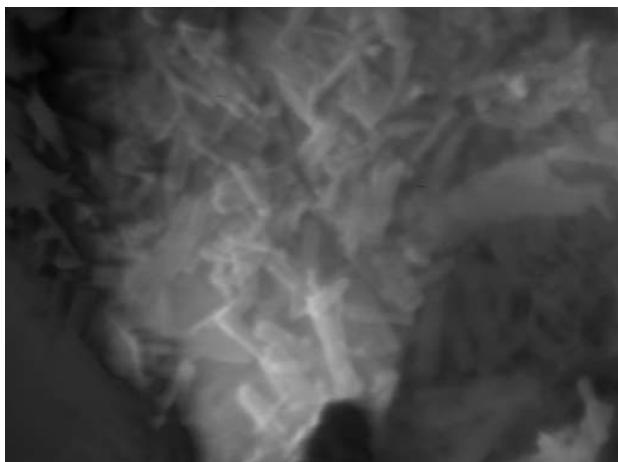
Fig. 2.   **Picture of SEM of sample T6vz after 10 months**

Fig. 3.   **Comparison of standard sample (left) without volume increase and sample T6vz with volume change**
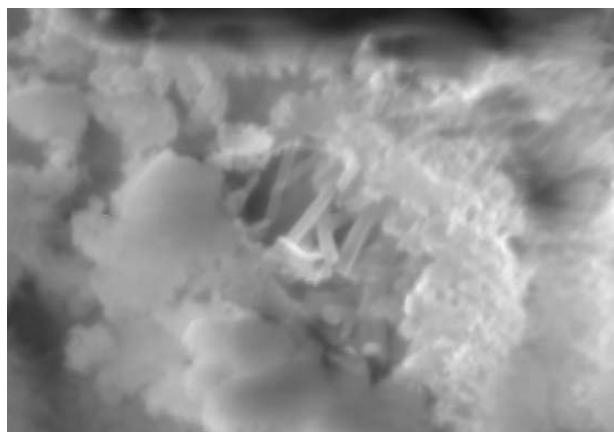
Fig. 4.   **Picture of SEM of sample T6st after 10 months**

Discussion

Preparation of thaumasite is long-term process of stabilization of the whole system, when transformation of primary material via transiant phases (portlanit or C–S–H gel) to stable phases (kalcite, gypsum, eventually SiO_2 and thaumasite) is occured.

During observation of thaumasite was discovered, that creation of thaumasite depends on physical conditions – low temperature below 10 °C and intense moisture. Dependence of moisture occured at samples T6, in the concrete at samples T6vz and T6sz, which were kept at low temperatures about 2 °C during the observation, T6vz in moist enviroment, T6sz in dry enviroment. From the RTG and SEM results of these two samples (Table I) follows that presence of water accelerates creation of thaumasite due to easy availability of water, which is necessary for crystallization of thaumasite (15 molecules of water) $CaSiO_3 \cdot CaCO_3 \cdot CaSO_4 \cdot 15H_2O$.

Dependence on temperature is visible at samples T6vz, T6vt. Phase composition of sample T6vt after 10 months was consistent with composition of sample T6vz, which was analysed after 4 months. It means, there is difference of 6 months and in comparison with the sample T1 1a (it has the same phase composition after 2 months, kept at low temperatures and in moist enviroment) there is diference of 8 months. This considerable difference is too perceptible between samples T6st and T6sz (see Table I).

REFERENCES

1. Skalny J., Marchand J., Odler, I.: *Sulfate attack on concrete*. Spon press, MCT 10, 2002.
2. Hlaváč J.: *Základy technologie silikátů*. SNTL.1988.
3. Aguilera J., Blanco Varela M. T., Vázquez T.: Cem. Concr. Res. *31*, 1163 (2001).
4. Romer M., Holzer L., Pfiffner M.: Cem. Concr. Compos. *25*, 1111 (2003).
5. Bellman F.: *Simulation of the formation of thaumasite*

P09　AN APPLICATION OF Al-Si LAYER ON NICKEL-BASED SUPERALLOYS AND THEIR ANALYSIS

SIMONA POSPÍŠILOVÁ, MARTIN JULIŠ and TOMÁŠ PODRBÁBSKÝ

Brno University of Technology, Faculty of Mechanical Engineering, Technická 2, 616 69 Brno, Czech Republic, julis@fme.vutbr.cz

Introduction

Production of new generation of aircraft gas turbine engines is based on designing new constructions and materials, which make it possible to operate under still more severe conditions. The key assembly of the engine is its turbine, whose materials and design determine the tolerable gas temperature. Increased inlet gas temperatures resulted in the shortening of the service life of the blades protected with diffusion coatings. New principles of coating deposition opened up new possibilities for purposive improvement of coating compositions and variation of their properties[1].

A diffusion barrier from Al-Si layer was developed for turbine blades of aircraft engines from nickel-base superalloy ZhS6K as oxidation and corrosion protection. The main subject of the research is application of Al-Si protect layers to alternative materials as are IN713LC and IN738LC.

Experimental

This paper is focused on microstructure and chemical analysis of protective layers created by co-deposition of Al and Si (Al + Si spray application and diffusion annealing at 950 °C for 4 h) on nickel-based superalloys IN713LC and IN738LC (chemical composition is shown in Table I) after thermal and thermal-stress exposition. It also was observed an influence of Al-Si layer on mechanical properties of basic materials with and without Al-Si layer.

An operational degrading process were simulated by high-temperature heat treatment (700 to 1,100 °C – 50 to 1,000 h), by creep tests (750 to 1,000 °C under constant load) and low fatigue tests (at 800 °C).

Table I
Alloy chemical composition [% wt.]

Element	IN713LC	IN738LC
C	0.05	0.11
Cr	12.08	15.86
Ti	0.75	3.27
Al	5.91	3.31
Zr	0.10	0.03
Nb	2.02	0.88
Ta	<0.05	1.65
Mo	4.58	1.74
W	–	2.54
Co	<0.05	8.26
Ni	Bal.	Bal.

Results

C r e e p   T e s t s   R e s u l t s

For the mutual comparison of the influence of Al-Si layer on creep-resistant properties for IN 713LC and 738LC, we applied the L-M model[2]. A graphical comparison of stress versus Larson-Miller parameter for the coated material by Al-Si layer and the uncoated material are shown in Fig. 1.
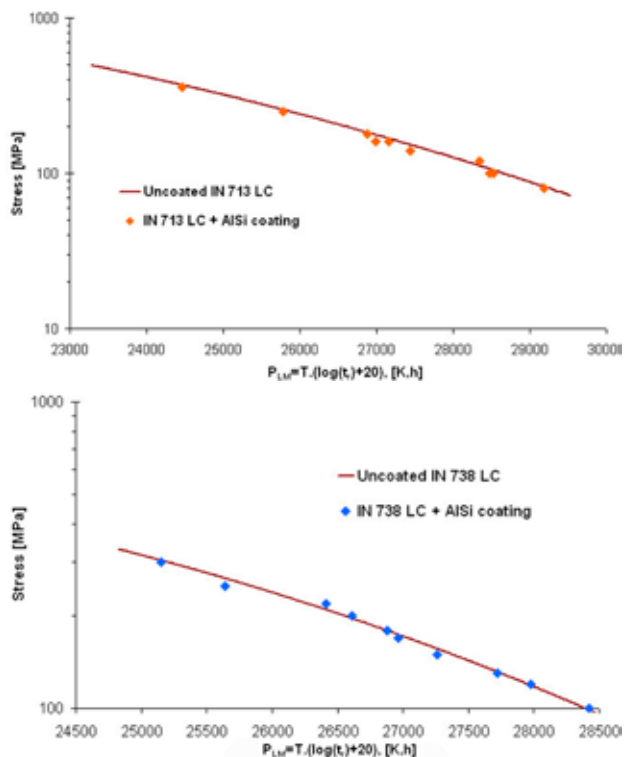
Fig. 1.　**The influence of Al-Si layer on creep- resistance**
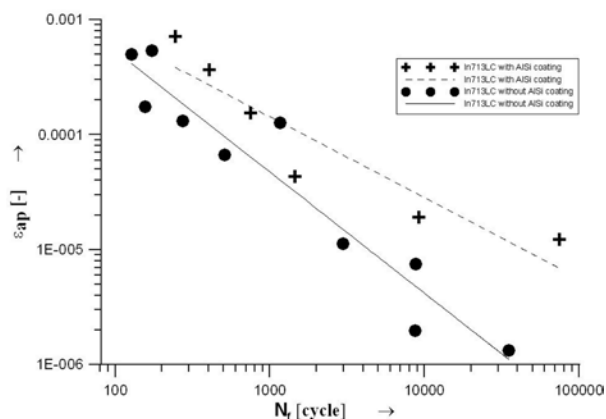
Fig. 2.　**Manson-Coffin curves of coated and uncoated IN713LC**

L o w - F a t i g u e   T e s t s   R e s u l t s

Total strain controlled tests have been performed on cylindrical specimens of polycrystalline IN713LC. Results of low cycle fatigue tests made at 800 °C on uncoated samples

are compared with similar tests carried out on specimens with Al-Si coating. Fatigue life curves are documented on Fig. 2. There is dependence plastic strain amplitude ε_{ap} at half life on number of cycles to fracture N_f in the bilogarithmic representation. Experimental data were fitted by the Manson-Coffin law[3]. It can be seen that Al-Si layer increases low cycle fatigue life of the coated specimens.

Metallographic Analysis

According to the pictures and analyses from light and scanning electron microscopy, a split into several areas is evident. The surface of the samples from both materials at the initial state is divided into four sub-layers, see Fig. 3., left. The upper layer, called "oxide layer", is very thin and discontinuous. By the spot and space analysis we detected Al_2O_3 oxides which originated by diffusion from the layer, and under these oxides we can find Cr_2O_3 which are created by diffusion from the base material. Sometimes SiO_2 oxides grow up. The second layer is a "coating zone" with Ni and Al phases. The next layer is called the "inter-diffusion zone" and contains more Si and heavy elements, such as Mo, Nb, Cr, W. Simultaneously the content of Ni and Al decreases. The last sub-layer, a "substrate diffusion zone", is actually a band without γ' phase. Sometimes, this layer can be reached in complex phases and carbides based on Co, Cr, Al with acicular morphology, Fig. 3. right.

Fig. 4. **Microstructure of Al-Si layer on IN738LC, after thermal-stress exposition 900 °C – 50 h;**
Note: 1 (Cr_2O_3), 2 (Al_2O_3), 3, 4 (solid solution mixture reached in Si, Cr), 5 (solid solution mixture reached in Si, Ti), 6, 7 (Ti, Nb complex carbide), 8 (Cr-Si-Co-Ni complex phase), 9, 10 (Co, Cr, Al complex phase)

Fig. 3. **Microstructure of AlSi layer on IN738LC, as received (left), after thermal-stress exposition 800 °C – 500 h (right)**

After thermal exposition and thermal-stress exploitation, the thickness of particular layers is changed. Several sub-layers are created while several disappear. The distribution of single elements is also changed (Fig. 4.). After exposition at temperature 1,000 °C (and higher) for longer time one layer remains and gets wider. From EDS microanalysis that followed, the oxygen stays on the surface and its content decreases with the distance from the surface. After temperature and creep exposition, the oxides Al_2O_3 and Cr_2O_3 are more created. After exposition at 1,000 °C and 200 h, this layer is somewhere cracky and sporadically is a surface without layer. However, this temperature highly exceeds the working conditions.

The surface of the samples without layer is non-uniform. There is a band without coherent γ', depleted by Cr and Al and with titanium nitrides which have an acicular morphology. This band is extended with time and temperature.

Conclusions

From performed analyses followed that the Al-Si layer improves heat-resistance of materials IN 713LC and 738LC.

It were also estimated that this layer does not nearly have an influence on creep-resistance of observed materials.

The low cycle fatigue life of IN713LC at 800 °C increases with application Al-Si coating.

REFERENCES

1. Tamarin, Y.: Protective *Coatings for Turbine* Blades. ASM Ohio, USA, 2002.
2. Seifert, B., Melzer, B.: Rechnerische *Auswertung von Zeitstandversuchen am Beispiel des Stahles 13CrMo4-4.15.*: Langzeitverhalten warmfester Stähle und Hochtemperaturwerkstoffe, Düsseldorf (1992).
3. Obrtlík, K., Man, J., Polák, J.: *Room and high temperature low cycle fatigue of Inconel 713LC, No.: 894*, In Euromat 2001, Rimini Italy, 2001.

P10   ALKALINE MODIFIED COAL FLY ASH AS AN ADDITION TO CONCRETE

JOZEF JUNÁK and NADEŽDA ŠTEVULOVÁ

Technical University of Košice, Civil Engineering Faculty Vysokoškolská 4, 042 00 Košice, Slovakia,
Jozef.Junak@tuke.sk

Introduction

Coal fly ash is well-know material utilized in civil engineering, mainly in building materials preparing such as blended cements and concretes. Traditionally, coal fly ashes are used as a pozzolanic material to enhance physical, chemical and mechanical properties of concretes. However, only amounts of 20–30 % of this waste kind are used in these terms and the excess is stored in large extension[1]. The reasons of small quantities coal fly ash exploitation consists in insufficient quality of fly ash required by the standard.

A number of hydrothermal activation methods have been proposed to activation coal fly ash using alkaline solutions (mainly NaOH a KOH solution). The traditional conversion methods differ in the molarity of the alkaline reagents, activation-solution/fly ash ratio, temperature (80–200 °C), reaction time (3–48 h) and pressure, depending on the type of coal fly ash used[2].

In our previous paper has been shown that the zeolite phase formation influences favourably process of physico-chemical consolidation at hardening of coal fly ash/cement pastes and leads to higher compressive strength in comparison to composite prepared without alkaline treatment[3].

The objective of this study was to investigate the hydrothermal alkaline treatment influence of coal fly ash/cement mixture on mechanical properties of hardened composites in dependence on temperature.

Experimental

Portland cement (CEM I 42.5) and coal fly ash originating from Slovakian power plant ENO A in Nováky were used as raw materials. Granulometric composition of original coal fly ash and cement is given in Table I.

Table II summarizes chemical composition of coal fly ash. Total amount of SiO_2 and Al_2O_3 was 82.127 %. Based on the chemical analysis, the used coal fly ash is high silica ash with molar ratio of $SiO_2/Al_2O_3 = 3.2$. The presence of crystalline phases was detected by X-ray diffraction (XRD) analysis on diffractometer DRON 2.0 with goniometer GUR-5 (Technabsexport, Russia). The following minerals as major components present in coal fly ash are quartz, mullite and hematite. Cristobalite, magnetite, illite, anhydrite, some silicates, aluminosilicates and their hydrates (albite, andalusite, kaolinite) were identified too.

Table I
Granulometric composition of coal fly ash and Portland cement

Fraction	[% wt.]	
[μm]	Coal fly ash	Portland cement
180	24.64	–
180–125	10.79	–
125–71	23.67	0.10
71–45	13.09	3.85
<45	27.81	96.05

Table II
Chemical composition of coal fly ash

Component	Content [%]
SiO_2	62.526
MgO	1.900
K_2O	2.879
Na_2O	1.683
Fe_2O_3	8.068
CaO	2.893
Al_2O_3	19.601
LOI^*	2.38

LOI^* – loss of ignition

Laboratory investigation of alkaline treatment of coal fly ash/cement mixtures with 25 % wt. cement replacement was carried out in 5M NaOH solution at solid/liquid ratio of 0.5. Comparative cement paste was prepared by mixing only cement with water (sample 1). Mixed pastes were given in forms and subsequent 24 hours heated at temperatures of 120, 160 and 200 °C (sample 2, 3, 4) in drying-oven. Hardening samples during 28 and 90 days under laboratory conditions was realized.

The compressive strengths were measured at concrete prisms (40 mm × 40 mm × 160 mm) after hardening and evaluated according to the STN EN 206.

Results

The compressive strength values of composite samples after 28 and 90 days hardening are presented in the Table III. As it can be seen, compressive strengths of hardened experimental coal fly ash/cement composites reach the values ranging from 7 to 14 MPa. Compressive strengths of concretes increase with hardening duration. However, compressive strength values of experimental composites are lower than that of comparative composite (sample 1).

The compressive strength development is closely related

Table III
Compressive strength RC of composites after 28- and 90-days hardening

Sample	RC [MPa]	
	28 days	90 days
1	32.1	33.6
2	12.4	13.6
3	7.8	9.2
4	7.1	9.8

to the temperature. As it is shown in Table III, compressive strength of composites is in indirect proporcionality with temperature increase. From all investigated composites, the highest value of 28 and 90 days compressive strength accounts the sample 2 that was 24 hours heated at temperature of 120 °C.

Based on the XRD results of hardened products, zeolitic phases such as analcime and hydroxy-sodalite during alkaline treatment of coal fly ash/cement mixtures under selected conditions were formed. It is known that hydroxysodalite can be formed by conversion of the A zeolite in alkaline solution (> 10 % wt. NaOH). According to paper[4], crystalline phase of A zeolite is created in reaction mixture with SiO_2/Al_2O_3 ratio = 2 within temperature range from 25 to 150 °C.

Structures of identified phases are different from those of NaP1 zeolite and phyllipsite designated in the case of hydrothermal alternation of alone coal fly ash in autoclave. These phases favourably influence the concrete structure matrix as well as mechanical properties of hardened composite[3] in difference from composites based on alkaline and subsequent thermally treated coal fly ash/cement mixtures.

Conclusions

According to the standard requirements of STN EN 206, the measured values of 28 and 90 days compressive strengths of composites prepared by alkaline treatment of coal fly ash/cement mixture correspond to concrete class of C 8/10.

Therefore, concretes with hydrothermal alkaline treated coal fly ash at 25 % wt. cement replacement can be used for non-load-bearing constructions.

REFERENCES

1. Puertas, F. et al.: Cem. Concr. Res. *30*, 1625 (2000).
2. Morena, N. et al.: J. Environ. Eng. *11*, 994 (2001).
3. Junák, J., Števulová, N., Kušnierová, M.: Selected Scientific Papers – J. Civ. Eng. *2*, 106 (2007).
4. Vučinič, D. et al. : *Proc. of the conference on Waste Recycling*, pp. 140, Poland, Kraków, Wydawnictwo IGSMiE PAN, 2005.

P11   ELEMENTS INTERACTION ANALYSES DURING PREPARATION OF Al-Al₃Ni EUTECTIC COMPOSITES

LENKA KLAKURKOVÁ, LADISLAV ČELKO, PAVEL DOLEŽAL, ONDŘEJ MAN and KAREL NĚMEC

Brno University of Technology, Faculty of Mechanical Engineering, Institute of Materials Science and Engineering Technická 2, 616 69 Brno, Czech Republic,
klakurkova@fme.vutbr.cz

Introduction

The Al-Ni binary phase diagram contains five intermetallic compounds (Al_3Ni, Al_3Ni_2, Al_3Ni_5, AlNi and $AlNi_3$). For high temperature coatings and structural materials the AlNi and $AlNi_3$ phases are widely used[1]. The third, considerably lower area of interest, are the aluminum-based matrix composites (AMC) strengthened by Al_3Ni and Al_3Ni_2 phases[2].

The Al-Al₃Ni eutectic composites production consists of the semi-product manufacturing (sharp interface between Al and Ni) and the following mechanical and/or heat treatment (enables the creation of Al₃Ni particles as strenghtening phase).[3–5]

In this paper, the high velocity oxyfuel deposition technique was used for semi-product manufacture. The influence of annealing, at temperatures below the Al-Al₃Ni eutectic point, and dwell time on strenghtening phase formation was studied.

Experimental

Aluminum sheet of commercial purity (99.5 % wt.Al) was used as a substrate. The substrate surface was ground with abrasive paper to #600, blasted by SiO2 particles and washed in acetone bath before plasma coating deposition. For nickel powder (45 ± 5 μm in diameter) deposition, the high velocity oxyfuel technique was employed. The thickness of the layer was approximately 200 ± 10 μm. After the deposition, the specimens were heated in a furnace. Heat treatment conditions were designed closely to the Al-Al3Ni eutectic melting point (639.9 °C). The first set of samples was heated to 600 °C for 50 and 500 h, the second set to 630 °C for 10 and 50 h. The samples were fan-cooled in air after the heat treatment.

For the microstructure observation, the scanning electron microscopes (JEOL 840 and PHILIPS XL30) were used. Eneregy dispersive x-ray microanalysis of selected points

Fig. 1.   **The cross-sectional SEM image of Al substrate coated by Ni in as-received state**

and layer thickness measurements by image analysis (NIS Elements AR 2.3) were performed.

Results

As-received state

The microstructure of Al substrate coated by Ni without heat treatment is shown on Fig. 1. The chemical concentrations measured by EDS are presented in Table I.

Table I
Chemical composition of selected points, see Fig. 1.

Point	O [% at.]	Al [% at.]	Fe [% at.]	Ni [% at.]
1	8.34	0	0	91.66
2	4.52	95.48	0	0
3	6.60	86.29	7.11	0

Annealing at 600 °C
Binary images used for image analysis based on SEM images were prepared, see Fig. 2. Chemical concentrations measured in selected points are presented in Table II. The values of Al₃Ni particles formed (count, diameter and circularity), are summarized in Table III.
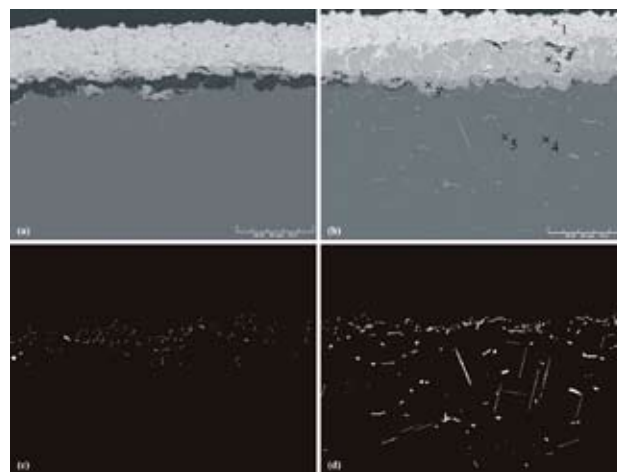
Fig. 2.   **The cross-sectional SEM images of HVOF deposited Ni coating on Al substrate and the binary images prepared for image analysis measurements after annealing at 600 °C per (a, c) 50 h, (b, d) 500 h, respectively**

Table II
Chemical composition of selected points, see Fig. 2.b

Point	O [% at.]	Al [% at.]	Fe [% at.]	Ni [% at.]
1	9.03	0	0	90.97
2	5.56	58.17	0	36.27
3	4.27	73.38	0	22.35
4	2.96	86.87	4.06	6.12
5	3.29	79.61	6.99	10.12

Table III
Image analysis data of Al$_3$Ni particles

Heat Treatment	Count [–]	Diameter [μm]	Circularity [–]
600 °C 50 h^{-1}	202	3.82	0.84
600 °C 500 h^{-1}	253	7.59	0.68

A n n e a l i n g   a t   6 3 0 ° C

Binary images used for image analysis based on SEM images were prepared, see Fig. 3. Chemical concentrations measured in selected points are presented in Table IV. The values of Al$_3$Ni particles formed (count, diameter and circularity), are summarized in Table V.
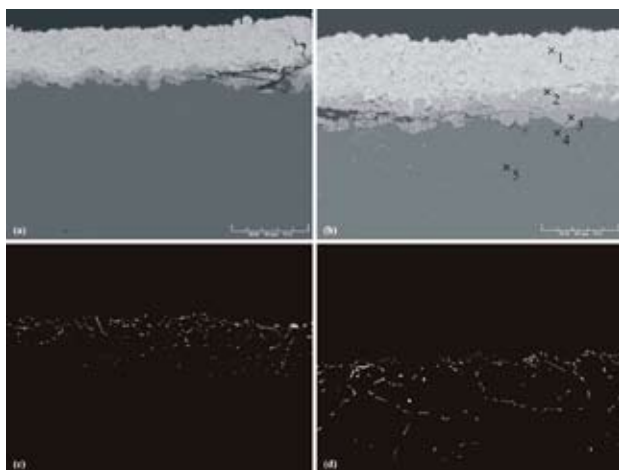
Fig. 3. **The cross-sectional SEM images of HVOF deposited Ni coating on Al substrate and the binary images prepared for image analysis measurements after annealing at 630 °C per (a, c) 10 h, (b, d) 50 h, respectively**

Table IV
Chemical composition of selected points, see Fig. 3.b

Point	O [% at.]	Al [% at.]	Fe [% at.]	Ni [% at.]
1	9.96	0	0	90.04
2	6.41	59.00	0	34.60
3	4.88	72.42	0	22.70
4	3.00	87.90	2.65	6.45
5	4.85	77.89	10.41	20.97

Dependence of annealing time and temperature height on the Al + Al$_3$Ni band thickness growth and on the Al$_3$Ni volume fraction is shown on Fig. 4.

Table V
Image analysis data of Al$_3$Ni particles

Heat Treatment	Count [–]	Diameter [μm]	Circularity [–]
630 °C 10 h^{-1}	341	3.92	0.81
630 °C 50 h^{-1}	239	5.85	0.67
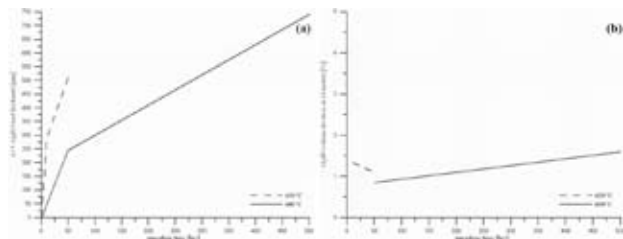
Fig. 4. **The influence of annealing time and temperature on the Al$_3$Ni + Al band (a) thickness growth, (b) volume fraction**

Conclusions

In this work, the elements interaction on Al and Ni sharp interafce during annealing below the melting point of Al+Al$_3$Ni eutectic was investigated primarily. The Al$_3$Ni$_2$ (light gray) and Al$_3$Ni phases (dark gray) between the Ni coating and Al substrate were observed and analysed. Platelet-like and needle-like particles of Al$_3$Ni phase were observed in the Al substrate; the first one formed at the grain boundaries and the second one on the favourable places inside the grains, most probably due to the grain boundary and pipe diffusion mechanisms. These mechanisms are apparently faster then volume diffusion at these "lower" temperatures. Rising temperature accelerates the diffusion of Ni into the Al and increases the thickness of Al+Al$_3$Ni band. The longer dwell time leads to the formation of coarse and less regular particles, as well.

REFERENCES

1. Morsi K.: Mat. Sci. Eng. A *299*, 1 (2001).
2. Rajan T. P. D., Pillai R. M., Pai B. C.: J. Alloys Compd. *453*, L4 (2008).
3. Zhu P., Li J. C. M., Liu C. T.: Mater. Sci. Eng A *532*, 239-240 (1997).
4. Zhu P., Li J. C. M., Liu C. T.: Mater Sci Eng A *57*, 329-331 (2002).
5. Min G., Lee J. M., Kang S., Kim H.: Mater Lett *60*, 3255 (2006).

P12   MAGNETIC PROPERTIES OF WASTE VITRIFIED IN MICROWAVE FURNACE

MILOTA KOVÁČOVÁ[a], MICHAL LOVÁS[a], MAREK MATIK[a,b] and VLADIMÍR ŠEPELÁK[a,c]

[a]*Institute of Geotechnics, Slovak Academy of Sciences Watsonova 45, 043 53 Košice, Slovakia,*
[b]*Department of Physical Chemistry, Faculty of Sciences, Palacký University, tř.Svobody 26, 771 46 Olomouc, Czech Republic,*
[c]*Institute of Physical and Theoretical Chemistry, Technical University of Braunschweig, Hans-Sommer Straße 10, D-38106 Braunschweig, Germany,*
kovacova@saske.sk

Introduction

Vitrification is a well established technology that involves the conversion of the waste in a stable and homogenous glass through a thermal treatment of melting, with the additional modification of the starting composition with glass-forming additives[1].

The paper deals with the magnetic properties of an iron-containig waste from the former nickel hydrometallurgy plant in Sereď (Slovakia). The waste, nickel leaching residue (NLR), was used as a model carrier of heavy metals (Co, Cu, Cd, Pb, Ni) from wastewater treatment, which was necessary to stabilize. Recently, microwave enegy has been applied for the waste treatment as an energy efficient alternative to current heating technologies[2]. In the presented work, microwave vitrification was used for the stabilization of heavy metals carriers.

The magnetic properties were studied by magnetic susceptibility measurement and Mössbauer spectroscopy method.

Experimental

Microwave Vitrification

The chemical composition of waste (NLR) and the raw materials used for the glasses is following: NLR 15 % SiO_2, 4.8 % Al_2O_3, 3.54 % CaO, 2.21 % MgO, 38.57 % Fe_2O_3, 22.64 % FeO, 1.06 % Cr_2O_3, 0.17 NiO, glass cullet 72.4 % SiO_2, 1.7 % Al_2O_3, 9.6 % CaO, 1.7 % MgO, 0.05 % Fe_2O_3, 13.8 % Na_2O, 0.6 % K_2O, dolomite 0.59 % SiO_2, 0.34 % Al_2O_3, 29.61 % CaO, 22.47 % MgO, 0.29 % Fe_2O_{3total}, 0.04 % Na_2O, 0.11 % K_2O, 46.35 % loss of ignition, glass sand 99 % SiO_2, soda 58 % Na_2O.

The glasses from S1 series contain 30–60 % of NLR, glass cullet and dolomite. In S2 series, the glasses include 30–50 % of NLR, glass sand and soda, besides glass cullet and dolomite. The theoretical chemical compositions of glasses measured by AAS (Varian, Australia) are described in Table I (S1) and Table II (S2).

Microwave vitrification was carried out in a microwave furnace Panasonic NN-5251B (series S1) and Panasonic NN-Q453 (series S2) with frequency 2.45 GHz and output 900 W (S1) and 1,000 W (S2). The samples were placed in thermal isolated ceramic crucibles and heated during 30 (S1) and 45 (S2) minutes. When the samples achieved the melting temperature, they slowly cooled down in the furnace.

Table I
Chemical analysis of samples from S1 series [% wt.]

Sample	SiO_2	Fe_2O_3	FeO	Al_2O_3	CaO	MgO	Na_2O	K_2O
1-S1	19.28	11.73	6.79	1.95	17.79	12.24	2.78	0.18
2-S1	13.55	15.58	9.06	2.26	17.18	12.29	1.40	0.12
3-S1	42.27	15.48	9.06	2.80	9.18	3.98	6.90	0.31
4-S1	14.99	19.41	11.32	2.71	14.57	10.26	1.40	0.10
5-S1	16.44	23.23	13.58	3.15	11.97	8.24	1.39	0.09
6-S1	30.80	23.19	13.58	3.42	7.97	4.08	4.14	0.19

Table II
Chemical analysis of samples from S2 series [% wt.]

Sample	SiO_2	Fe_2O_3	FeO	Al_2O_3	CaO	MgO	Na_2O	K_2O
1-S2	52.37	11.61	6.79	1.90	6.42	3.34	6.37	0.16
2-S2	46.15	11.64	6.79	2.02	9.86	5.67	4.15	0.20
3-S2	56.92	11.61	6.79	2.22	6.86	2.55	6.21	0.28
4-S2	48.01	11.63	6.79	2.49	9.78	3.93	8.28	0.37
5-S2	53.87	15.46	9.06	2.11	3.86	2.18	10.14	0.07
6-S2	48.92	15.47	9.06	2.38	6.78	3.56	3.45	0.16
7-S2	42.27	15.48	9.06	2.80	9.18	3.98	6.90	0.31
8-S2	46.75	19.30	11.32	2.74	3.69	1.45	5.68	0.12
9-S2	46.38	19.31	11.32	3.08	5.61	1.79	5.62	0.24

Magnetic Susceptibility and Mössbauer Spectroscopy Measurements

Magnetic susceptibility of the melted samples was measured by Kappabridge KLY-2, Geofyzika Brno in magnetic field intensity of 300 Am^{-1} with homogeneity of 0.2 % at frequency 920 Hz.

The room-temperature Mössbauer spectroscopy measurements were realized in transmission geometry using a conventional spectrometer in a constant acceleration mode. A ^{57}Co/Rh γ-ray source was used. The velocity scale was calibrated relatively to ^{57}Fe in Rh. A proportional counter was used to detect the transmitted γ-rays. Mössbauer spectral analysis software Recoil[3] was applied to provide a quantitative evaluation of the spectra.

Results

Magnetic Susceptibility Measurements

The magnetic susceptibility of the raw materials and glasses are presented in Table III, IV and V. The measured values are not depending on the iron content. Samples 2-S1 with the highest value of magnetic susceptibility in the series and 4-S2 with the lowest value of magnetic susceptibility have been chosen for Mössbauer spectroscopy measurements.

Table III
Magnetic susceptibility of raw materials

Sample	Magnetic susceptibility $\times 10^{-6}$ SI unit
NLR	135,222
Glass cullet	247
Dolomite	36
Glass sand	34

Table IV
Magnetic susceptibility of vitrified samples from S1 series

Sample	Magnetic susceptibility $\times 10^{-6}$ SI unit
1-S1	126,943
2-S1	245,918
3-S1	56,441
4-S1	189,272
5-S1	211,601
6-S1	96,101

Table V
Magnetic susceptibility of vitrified samples from S2 series

Sample	Magnetic susceptibility $\times 10^{-6}$ SI unit
1-S2	45,792
2-S2	54,739
3-S2	35,318
4-S2	15,066
5-S2	115,310
6-S2	130,587
7-S2	81,010
8-S2	99,680
9-S2	169,626

Mössbauer Spectroscopy Measurements

Fig. 1. shows the Mössbauer spectrum of NLR. The spectrum is characterized by three doublets and two sextets. The doublets correspond to iron in Fe^{2+} state and superparamagnetic Fe^{3+}. The sextets are ordered in tetrahedral and octahedral position. The parameters of NLR Mössbauer spectrum are in Table VI.

The percentage content of iron forms is possible to determine from the intensities. Spectrum 1 and 3 represents Fe^{2+} with iron content of 9.6 % and 10.9 %. The isomer shift of subspectrum 2 presents Fe^{3+} (12.7 %) in polycrystalline state. Subspectrum 4 was found to be Fe in the tetrahedral form of Fe_3O_4 (28.7 %) and subspectrum 5 in the octahedral form of Fe_3O_4 (38.1 %).

Fig. 2 shows the Mössbauer spectrum of glass 2-S1. The spectrum contains a central doublet and a magnetic sextet.
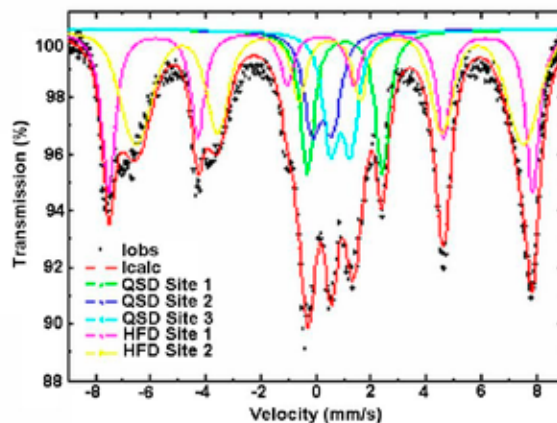
Fig. 1. **Mössbauer spectrum of NLR (Iobs–experimental spektrum, Icalc-theoretical spectrum)**

Table VI
Mössbauerspectrum parameters of NLR

Subspectrum	IS [mm s^{-1}]	QS [mm s^{-1}]	I[%]	H	σ_B
1 QSD Site 1	0.36	0.73	9.6	–	0.28
2 QSD Site 2	1.16	2.72	12.7	–	0.04
3 QSD Site 3	1.01	0.72	10.9	–	0.2
4 HFD Site 1	0.30	–	28.7	47.7	0
5 HFD Site 2	0.61	–	38.1	43.6	2.69

The structure of central doublet in the sample confirms the presence of Fe^{2+} and also Fe^{3+} ions. The central doublet corresponds to Fe cations in nanoparticles in superparamagnetic state. Magnetic sextet belongs to magnetite in a polycrystalline (ferrimagnetic) state. The wide spectral lines indicate the presence of iron containing particles with a large distribution of dimensions[4].

Mössbauer spectrum of glass 4-S2 (Fig. 3.) is fitted by three subspectrums – doublets. The presence of doublets confirmed the paramagnetic respectively superparamagnetic
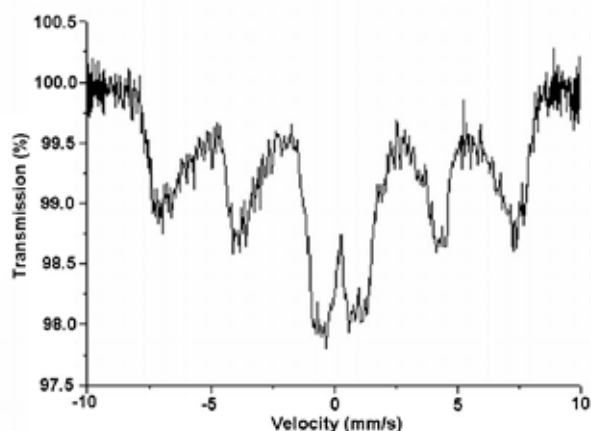
Fig. 2. **Mössbauer spectrum of vitrified sample 2-S1**
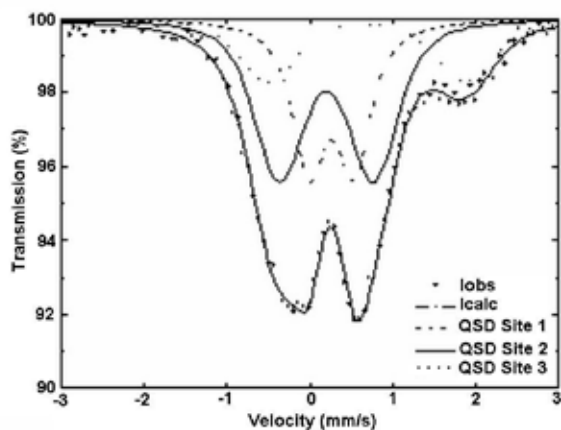
Fig. 3. **Mössbauer spectrum of vitrified sample 4-S2 (Iobs-experimental spektrum, Icalc-theoretical spectrum)**

Table VII
Mössbauer spectrum parameters of vitrified sample 4-S2

Subspektrum	IS [mm s^{-1}]	QS [mm s^{-1}]	I [%]
1 QSD Site 1	0.27	0.47	31.3
2 QSD Site 2	0.25	1.03	47.1
3 QSD Site 3	0.68	2.62	21.6

state of iron in the sample. Low magnetic susceptibility is expected for this magnetic state.

The values of isomer shift of subspectrum 1 IS(1) and subspectrum 2 correspond to polycrystalline Fe^{3+}.

The content of Fe^{3+} is 31.3 % (subspectrum 1) and 47.1 % (subspectrum 2) respecively. Subspectrum 3 represents Fe^{2+} with the content of 21.6 % (see Table VII).

Conclusions

By the Mössbauer spectroscopy measurements, the magnetic properties of vitrified samples depend on magnetic state that is influenced by grain size[5]. Magnetic susceptibility of glasses is affected by the ratio of iron content in magnetic ordered phase represented by sextet to the iron content in superparamagnetic phase represented by doublet. The grain size of glasses is mainly influeced by a cooling of molten mixture.

REFERENCES

1. Appleton T. J., Colder R. I., Kingman S. W., Lowndes I. S., Read A. G.: Appl. Energ. *81*, 85 (2005).
2. Colombo P., Brusatin G., Bernardo E., Scarinci G.: Curr. Opin. Solid State Mater. Sci. *7*, 225 (2003).
3. Lagarec K., Rancourt D.G.: RECOIL. *Mössbauer Spectral Analysis Software for Windows, version 1.02.* University of Ottawa 1998.
4. Goya G. F., Berquó T. S., Fonesca F. C., Morales M. P.: J. Appl. Phys. *94*, 3520 (2003).
5. Šepelák V., Feldhoff A., Heitjans P., Krumeich F., Menzel D., Litterst F. J., Bergmann I., Becker K. D.: Chem. Mater. *18*, 3057 (2006).

P13 THE USE OF ELECTROKINETIC POTENTIAL MEASUREMENT FOR EXAMINATION OF KAOLINITE DECOMPOSITION

DANA KUBÁTOVÁ, PETR PTÁČEK and JAROMÍR HAVLICA

Výzkumný ústav stavebních hmot, a.s., Hněvkovského 65, 617 00 Brno, Czech Republic,
kubatovad@centrum.cz

Introduction

Metakoalin represents one the important puzzolana materials that are widely used in mortar and concrete technology. It is white amorphous aluminosilicate $Al_2O_3 \cdot 2SiO_2$. It is prepared by calcination of kaolin in temperature range 500–800 °C. This process is possible to describe by the following equation:

$$Al_2O_3 \cdot 2SiO_2 \cdot 2H_2O \xrightarrow{500-800\,°C} Al_2O_3 \cdot 2SiO_2 + 2H_2O \quad (1)$$
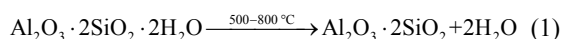
Adsorbed water is released at 100 °C and the dehydroxylation begins over 400 °C. At the temperature over 900 °C, other reactions occur. Their resultant products are silica and mullite. The dehydroxylation process affects the degree of structure orderliness, disturbances of crystal lattice, particle shape and size, type and amount of mineral admixtures, and also experimental conditions. The electrokinetic potential measurement, FT-IR spectroscopy and differential thermal analysis were used for determination of the kinetics of metakaolin thermal conversion.

Experimental
Sample preparation
Zeta potential
Industrial kaolin was calcinated at the temperatures of 105, 300, 400, 450, 500, 550, 600, 700, and 800 °C in a porcelain cup.

Infrared spectroscopy
Kaolin symples were calcinated by temperatures 440 and 500 °C and were mixed with dried KBr in weight ratio 1 : 100.
Thermal Analyse
Kaolin samples were calcinated at the temperature range 400 to 520 °C for the period of 2 hour. The heating rate was 30 °C min^{-1}.

Results
Zeta Potential
Measured values of zeta potential are displayed in the Fig. 1.

At the temperature range 105–300 °C is capillary and adsorbed water released. Volume change attending capillary water evaporation generate tension that is released by cracks' formation or disintegration of aggregate. The observed growth of zeta potential is possible to explain by the pre-dehydroxy-

lation on the surface of particles. At the temperature range 400–500 °C, dehydroxylation proceeds. Water that is fixed in ions solvation sheets is released in first step. The charge reduction that results in zeta potential decrease is possible to describe by the following reaction:

$$[= Al - O]^- [Na(H_2O)_x]^+ \xrightarrow{T} = Al - O - Na + x\,H_2O(g) \quad (2)$$
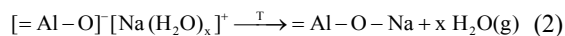
Along with the partial water vapour pressure (pH_2O), the water released from the hydration sheath, Si-O bonds of the siloxane bridges ($\equiv Si - O - Si \equiv$) tetrahedic layers and silanol groups $\equiv Si–OH$ form. The surface silanoles dissociation is connected with the surface potential increase, which leads to the zeta potential increase of the samples calcinated at 500 °C.
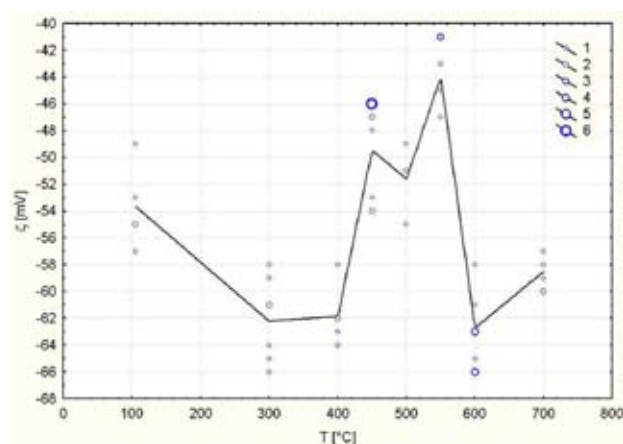
Fig. 1.　**Relation of zeta potential on the burning temperature**

Along with the temperature of the thermal treatment, the amount of water released during the condensation between $\equiv Si - OH$ a $HOAl \equiv$ bonds increases. The process may be described by the following reactions:

$$\equiv Si - O - Si \equiv + H_2O \xrightarrow{T, p_{H_2O}} 2 \equiv Si - OH \quad (3)$$

$$\equiv Si - OH + = Al - OH \xrightarrow{T, p_{H_2O}} \equiv Si - O - Al + H_2O(g) \quad (4)$$

$$2 = Al - OH \xleftarrow{T, p_{H_2O}} = Al - O - Al = + H_2O(g) \quad (5)$$
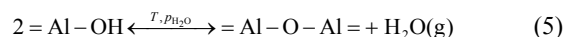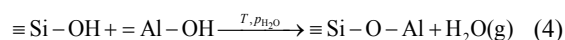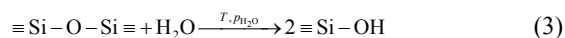
The dehydroxylation (decrease of the OH bonds abundance) connected with polykondenzation (500–550 °C) results to the kaolin zeta potential decrease. Above the temperature of 550 °C, a significant zeta potential value increase was observed. The increase can be explained by the formation of a metastable phase – metakaolin. The reconstructive phase transition is connected with the destruction of sheet structure of kaolinite. At lower temperature, the amount of crystal defects forming in the metakaolin structure is significant. The zeta potential increase can be explained by the adsorption of hydroxyl anions on these defects from dispersive environment, which increases the surface potential of a particle.

Thermal Analyse

The dehydroxylation of kaolin proceed at temperature range 400 to 670 °C and there occurs weiht decrease about 13,1%.

Overall activation energy and pre-exponential coefficient were defined from the Arrhenius equation in logarithmic form. The overall activation energy reaches 148.78 kJ mol^{-1} and pre-exponential coefficient reaches $2.71 \times 10^7 s^{-1}$, under isothermal conditions.
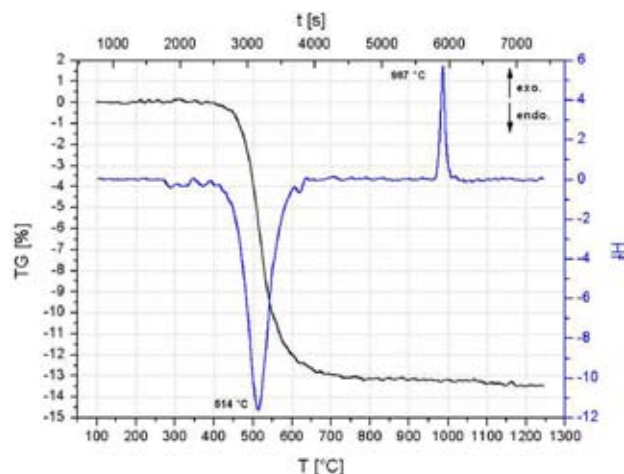
Fig. 2.   **TG-DTA curves**
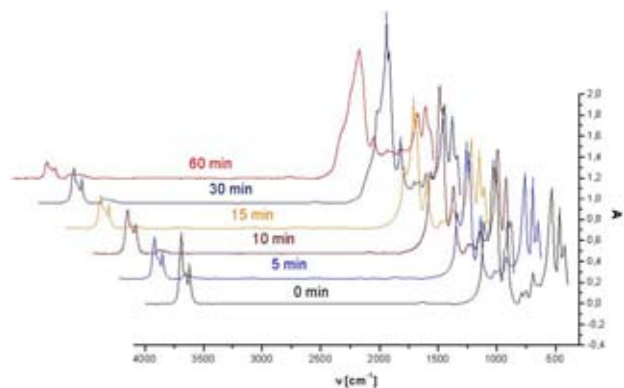
Fig. 3.   **Spectra of kaolin calcination (at 440 °C)**

Infrared Spectroscopy

The spectum shape changes show that the dehydroxylation process consists of two steps – see Fig. 3.

The major part of water molecules from layer kaolin structure leaves the structure first.

During this process, reduction of hydroxyl stretching a bendind absorption bands occurs, while SiO and AlO modes do not change. The second step is connected with the loss of selectivity of SiO and AlO modes (30 min.) because of changes in primary coordinate shell during kaolin to metakaolin conversion. The second step, at the temperature 440 °C) begins after 15 minutes. The v1 modes of ouOH groups were used for interpretation of kinetics of kaolin decomposition only. The –ln(1–y) linear dependace on time confirmed F1 model of kaoline dehydoxylation.

Conclusions

The paper demonstrates that zeta potential measurement may be used for characterization of dehydroxylation processes. Zeta potential increases during pre-dehydroxylation process. During dehydroxylation zeta potential reaches its minimum value at 550 °C. Destruction of kaolinite sheet structure during nucleation of metakaolinite leads to the repeated increase of zeta potential values. The good agreement between zeta potential measurement, thermogravimetry and infrared spectroscopy results was achieved. All the methods applied on the examination of isothermal kaolinite dehydroxylation indicate that the dehydroxylation proceeds during a single nucleation process (F1) at the temperature range from 420 to 520 °C. The overall activation energy determined by thermogravimetry reaches 148.78 kJ mol^{-1} (TG). Good agreement with literature sources was achieved. This value lies within the most frequently reported interval: 140–250 kJ mol^{-1}

REFERENCES

1. Heide K., Földvari M.: Thermochim. Acta *446*, 106 (2006).
2. Nahdi K. et al.: Thermochim. Acta *390*, 123(2002).
3. Ptaček P. et. al. Keramický zpravodaj *1*, 5 (2008).
4. Temuujin J. et. al. J. Eur. Ceram. Soc. *19*, 105 (1998).
5. Traore K., Gridi-Bennadji F., Blanchart P.: Thermochim. Acta *451*, 99 (2006).

P14 ALKALI AND VANADIUM OXIDES CORROSION OF HIGHLY ALUMINA RERRACTORIES

TOMÁŠ OPRAVIL, PETR PTÁČEK, JAROMÍR HAVLICA, FRANTIŠEK ŠOUKAL and MICHAL VRŠECKÝ

Institute of Materials Chemistry, Brno University of Technology, Purkyňova 118, 612 00, Czech Republic,
opravil@fch.vutbr.cz

Introduction

Refractory materials with height and very height alumina content are commonly used at higher temperatures under reduction conditions. These materials are based on mullite and corundum. Mullite ($3Al_2O_3 \cdot 2SiO_2$) is under ordinary pressures only stable compound in the $SiO_2 - Al_2O_3$ system and the other alumosilicates, such as silimamite, andalucite and cyanite, become to mullite at temperatures 1,545, 1,390 and 1,370 °C, respectively. Mullite confers interesting properties to the refractory materials, such as thermal and chemical stability, mechanical resistance, low thermal expansion and thermal impact strength.[1–3]

The aim of this work is study of alumina and vanadium oxides corrosion of shaped high alumina refractory material. The corrosion products were investigated by DTA, FT-IR and XRD.

Experimental

Corrosion process of corundum based refractory materials used in combustion reactor was compared. Phosphate bonded corundum heat-resistant brick Korrath K99 ($Al_2O_3 > 99$ %) can be employed to the 1900 °C under reducing condition. Material properties were enhanced by addition of Cr_2O_3 and ZrO_2. LS – Kleber 34 (94 % Al_2O_3, 4 % P_2O_5) was used as binding agent.

S i m u l t a n e o u s   T G - D T A

The TG-DTA analysis of the Korrath K99 lining fragment in an air oven at ambient atmospheric condition was carried out by TG-DTA Analyzer Setaram 92-18 up to temperature 1,400 °C. Applied heating and cooling rate was 10 °C min^{-1}.

I n f r a r e d   S p e c t r o s c o p y

Infrared spectra of samples were recorded in KBr pellets using FT-IR spectrometer Nicolet Impact 400 in the wavelengths range from 4,000 to 400 cm^{-1}. Measurements were done under resolution 8 cm^{-1}.

Grinded samples were mixed with KBr with mass ratio 1:100. Mixtures were homogenized by grinding in dish and its weighted amount was pressed under 40 kPa for 20 s and next 80 kPa for 30 s.

X - r a y   D i f f r a c t i o n

Sample phase composition was investigated by X-ray powder diffraction analysis by difractometer X´Pert (Philips).

Results

D i f f e r e n t i a l   T h e r m a l   A n a l y s i s

The DTA results of unused and corroded heat resistant brick Korrath K99 is shown on Figs. 1. and 2. There is one sharp endothermic peak at temperature 795 °C on Fig. 1. With regard to sample composition is this effect probably caused by unmixing of $Al_2O_3 - ZrO_2$ solid solution. Sample mass changes are insignificant.

Material used in refractory line show endothermic doublet at 553 and 583 °C.

This double peak was fitted by first type Voight function (1), due to specify peak's temperature of second endothermic effect – 586 °C.

$$y = y_0 + A\left[m_u \frac{2}{\pi} \frac{w}{4(x-x_c)^2 + w^2} + (1-m_u) \frac{\sqrt{4\ln 2}}{\sqrt{\pi}w} e^{-\frac{4\ln 2}{w^2}(x-x_c)^2} \right] \quad (1)$$

Where y_0 is offset, x_c peak center, A amplitude, w width and m_u shape factor of peak.

Fig. 1. **DTA of refractory material Korrath K99 unaffected by corrosion**
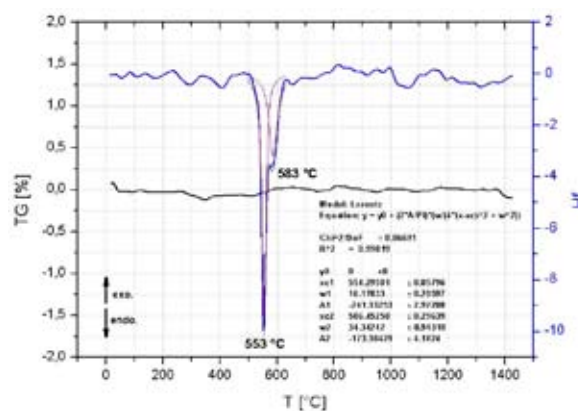
Fig. 2. **DTA of corroded refractory material Korrath K99**

The first peak on Fig. 2. belongs to thermal decomposition of the CaO·V$_2$O$_5$ (2). Reaction was connected with V$_2$O$_5$ reduction to VO$_2$.

$$2\,CaO \cdot V_2O_5 + C \rightarrow 2\,CaO + 4\,VO_2 + CO_2 \qquad (2)$$
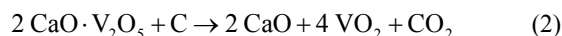
Low temperatures eutectic melts were form between product of reaction (2) and Fe or Ti compounds. Source of Fe, Ti compounds is burning aw material. The second endothermic peak is connected with eutectics melt appearance.

Infrared Spectroscopy

FT-IR spectrum of unused and corroded heat resistant brick Korrath K99 is shown on Figs. 3. and 4. While the first of them is virtually similar like the spectrum of corundum, corroded brick show more complicated XRD pattern.

There was found absorbtion band of silica and mullite. Mullite is part of basic brick material, but SiO$_2$ spectral bands belong to glassy phase of corrosion product. Silica source is heat resistant binding agent.
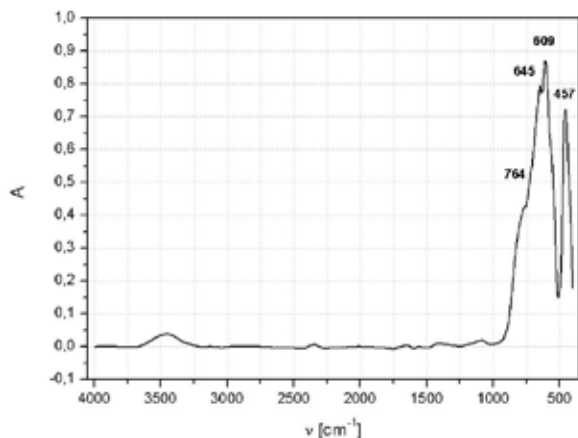
Fig. 3.   **FT-IR of unused Korrath K99 material**
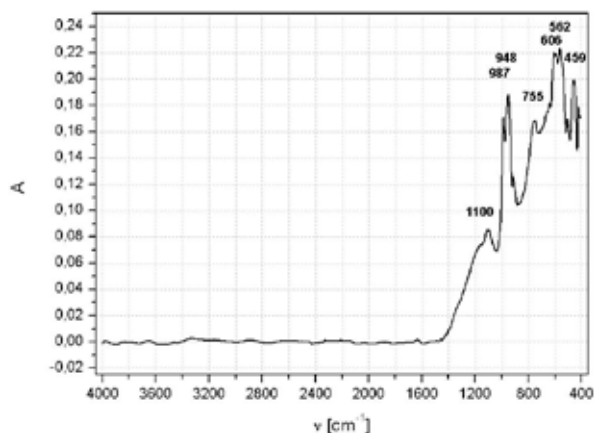
Fig. 4.   **FT-IR of corroded Korrath K99 material**

X-ray Diffraction

The XRD patterns of unused and corroded heat resistant brick Korrath K99 is shown on Figs. 5. and 6.

The Ca$_{0.17}$V$_2$O$_5$ dual oxide was identified as main crystalline product of Korrath K99 corrosion (Fig.6).
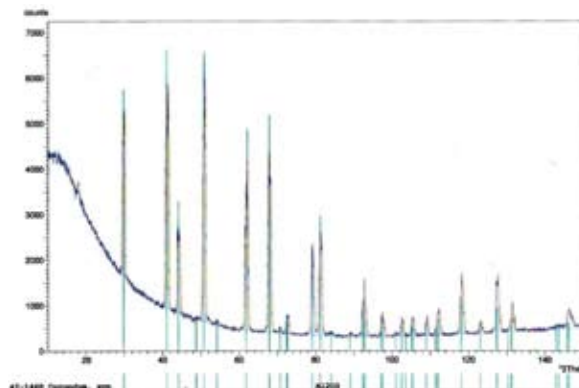
Fig. 5.   **XRD of unused Korrath K99 material**
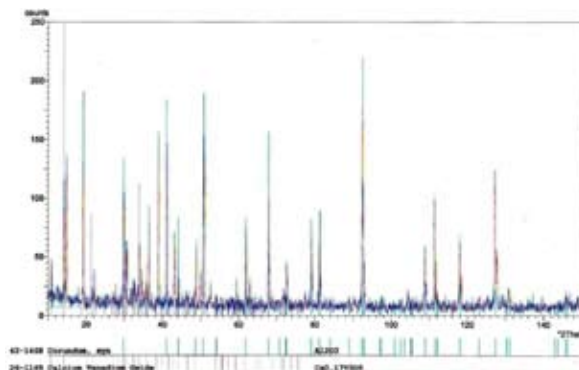
Fig. 6.   **XRD of corroded Korrath K99 material**

Conclusions

In XRD pattern of corroded material of Korrath K99 heat resistant brick wasn't found diffractions of mullite. Accord to FT-IR results is this compound more sensitive to corrosion process than corundum. There has been risk of prior corrosion of binding mullite phase.

In addition vanadium oxides corrosion of high alumina refractory line, there was formed glassy phase. Alkali oxides from raw material play significant role on its origin.

REFERENCES

1. Hlaváč J., *Základy technologie silikátů* (trans. name: *The primer of technology of silicates*), chapter II, p. 118, SNTL, Prague 1988.
2. Hanykýř V., Kutzendörfer J., *Technologie keraramiky*, Silis, Vega s.r.o., Hradec Králové, 2000.
3. Ribero D., Restrepo R., Paucar C., García C.: J. Mat. Process. Technol. (2008), aricle in press, aviable on-line *26 March 2008*.

P15 MEASUREMENT OF HEAT OF HYDRATATION OF ROMAN CEMENT

TOMÁŠ OPRAVIL, PETR PTÁČEK, FRANTIŠEK ŠOUKAL and JAROMÍR HAVLICA

Institute of Materials Chemistry, Brno University of Technology, Purkyňova 118, 612 00, Czech Republic,
opravil@fch.vutbr.cz

Introduction

The old buildings (sights) are very complicated in their composition and function. Some of these buildings survive for hundreds of years, but many of them are not in good condition, so here is a space for restorers, who want a material or materials, which will help them to conserve or repair these sights or presents from our ancestors. Restorers have to respect rules of care of historical monuments (try to use materials similar or the same as the original material of the sight is) which requires searching for materials, that will protect, restore and conserve the object with minimal harm.

This paper describes testing of lime stone from Kurovice, especially chemical, phase composition and hydraulic modulus determination.

Natural cement (Roman cement), which was used as a building material in the last century in the area of Bohemia, isn´t produced nowadays in the Czech Republic and surrounding states. The Roman cement is a historical variation of lime binder, it's important for its hydraulic properies and it is necessary to be interested in this material because of conservators.

Chemical analysis was focused on assesment of loss during annealling and oxides specification (oxides which are useful in characteristic modules calculation – CaO, SiO_2, Al_2O_3, Fe_2O_3, MgO).

For classification prepared roman cements and base materials is good analyses methods TG-DTA method, XRD method and heating microscope showed us the temperature of sintering, melting point and phase composition of tested material from stonepit in Kurovice.

Very important for classification prepared roman cements is hydratation haed. These work is suggests easy method for determination hydratation head. H_2O.

Experimental

The enthalpiometric method for the hydration heat assessment in prepared roman cements was tested. The apparatus consisting of multimeter with thermistor and styrofoam calorimetric cell with magnetic stirrer was made and whole system was connected to PC (Fig. 1.). The measurement itself was performed in styrofoam cup placed in calorimetric cell. Determined amount of distilled water was poured into the cup and after temperature stabilization the exact amount of sample of roman cement was added while slowly stirred. After the temperature stabilization (minimum 15 min of stable temperature) the measurement was finished. From the recorded data the temperature difference was determined and

together with roman cement amount, volume of used distilled water, and calorimetric constants it served for the hydration heat calculations according to (1). The number of moles of water was calculated from (2). The calculations resulted in the determination of hydration heat released from the hydration of roman cement.
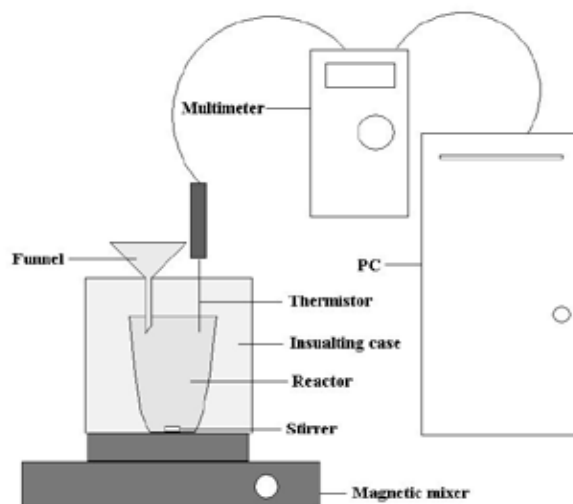
Fig. 1.　**The experiments for measuring of hydratation heat**

For calculation hydratation heat was used this formula:

$$Q_{HYD} = n_{H_2O} \cdot c_{H_2O} \cdot \Delta T \qquad (1)$$

Q_{HYD} – hydratation head [$J\,mol^{-1}$]
n_{H2O} – number of moles (water) [mol]
c_{H2O} – heat capacity (water) [$J\,K^{-1}\,mol^{-1}$]
ΔT – difference of temperatutre [°C]

For calculation number of moles was used this formula:

$$n_{H_2O} = \frac{m_{H_2O}}{M_{H_2O}} \qquad (2)$$

Table I
Composition of synthetic roman cement 1

Component	Weight [%]	Grams to 100 g
$CaCO_3$	58.98	80
$CaSO_4 \cdot 2H_2O$	3.09	4.0
$Mg(OH)_2$	1.19	1.6
Kaolinit	8.01	9.0
Fe_3O_4	4.87	6.6
SiO_2	20.65	28.0
K_2CO_3	1.91	2.6
Na_2CO_3	1.03	1.4
$Al(OH)_3$	1.62	2.2

Table II
Composition of synthetic roman cement 2

Component	Weight [%]	Grams to 100 g
$CaCO_3$	60.24	80
$CaSO_4 \cdot 2H_2O$	3.16	4.0
$Mg(OH)_2$	1.81	2.4
Kaolinit	6.78	9.0
Fe_3O_4	2.25	3.0
SiO_2	21.08	28.0
K_2CO_3	1.96	2.6
Na_2CO_3	1.05	1.4
$Al(OH)_3$	1.66	2.2

Table III
Composition of synthetic roman cement 3

Component	Weight [%]	Grams to 100 g
$CaCO_3$	60.24	80
$CaSO_4 \cdot 2H_2O$	3.16	4.0
$Mg(OH)_2$	1.81	2.4
Kaolinit	6.78	9.0
Fe_3O_4	2.25	3.0
SiO_2	21.08	28.0
K_2CO_3	1.96	2.6
Na_2CO_3	1.05	1.4
$Al(OH)_3$	1.66	2.2

Results

In this work the samples of synthetic roman cements were tested. The amount of 50 ml distilled water was poured into the cup. The exact amount of binder sample was added at once while stirring. The temperature inside the vessel was recorded each 5 sec. by thermistor.

Table IV
Results of measurement of hydratation composition of synthetic roman cement 1

Sample	ΔT	$Q [J\,mol^{-1}]$	$Q [J\,g^{-1}]$
Nature	1.2682	264.522	244.242
RC 1	3.3386	696.368	642.979
RC 2	3.5725	745.155	688.026
RC 3	2.5360	528.96	488.406

Samples of roman cements were prepared by burning out the raw meal at the temperature of 870 °C for the period of 4 hours. Synthetic roman cements were prepared by mixing the pure chemicals at a dry state. (Tables I–III). The refference sample was prepared in the same way from natural raw material from Kurovice quarry.

The results of masurment of hydratation heat are stated in Table IV.

Conclusions

It can be assumed, that the enthalpiometric determination is appropriate method for hydration heat measurement for roman cements as well as for other hydraulic binders. Mainly the easy intrumentation and short measurement times can be pointed out.

Also it was found, that roman cements prepared from natural raw material have the hydration heat values significantly lower than those prepared from pure chemicals. The reason for this is that the silicon oxide in pure state does not likely react with calcite to form dicalcium silicite and the soft lime is formed, which releases large amount of heat when hydrating.

P16 DETERMINATION OF PORTLAND CEMENT COMPOSITION BY FT-IR SPECTROSCOPY

TOMÁŠ OPRAVIL, PETR PTÁČEK, JAROMÍR HAVLICA and FRANTIŠEK ŠOUKAL

Institute of Materials Chemistry, Brno University of Technology, Purkyňova 118, 612 00, Czech Republic,
opravil@fch.vutbr.cz

Introduction

Cements show variable and sometimes unpredictable hydration behavior which may sometimes leads to operation failures. The rapid and accurate characterization method for identification of clinker and accessory minerals is needed. These requirements are for the Fourier transform infrared (FT-IR) spectroscopy fulfilled. The infrared spectrum provides informative signature of cement, in which is encoded information about its elemental and mineralogical composition. FT-IR methods can be in cement chemistry used for monitoring of hydration reactions and prediction of the performance properties[1,2].

The Portland cement composition was studied by mid-IR spectroscopy. This work is a part of wider FT-IR study about course hydrolysis of clinker minerals and kinetic of hydration processes of in aged Portland cement paste.

Experimental

The Portland cement was used in this study. The sample was characterized in wavelengths range from 4,000 to 400 cm^{-1} by FT-IR analyzer Nicolet Imact 400 with using of KBr pellets technique. Applied resolution for measurements is 8 cm^{-1}.

Dried samples were mixed with KBr with mass ratio 1:100. Mixtures were homogenized by grinding in mortar dish. Weighted amount of these mixtures were pressed under 40 kPa for 20 s and next 80 kPa for 30 s.

Results

Infrared spectrum of Portland cement is shown on Fig. 1. There were identified absorbtion bands of several clinker minerals relevant to its technical phase: allite – tricalcium-silicate (C_2S), belite – larnite (C_2S) and C_3A – tricalcium-aluminate. Further are present spectral bands of anhydrite ($CaSO_4$), gypsum ($CaSO_4 \cdot 2H_2O$) and hydration product: portlandite, calcite and hexagonal hydrates. Presence of the clinker minerals hydration products indicate that sample was slightly hydrated by air humidity.

From data published in literature[1,3–7] we put together correlation table (Fig. 1.). Portland cement IR bands assignment is summarized in Table I.

Table I
FT-IR spectrum of Portland cement

ν [cm^{-1}]	peak's assignment	compound
3,644	$\nu(OH)$	portlandite
3,550	$\nu(OH)$	water (silanol groups)
3,404	$\nu_1(OH)$	water (adsorbed on the surface)
1,685	$\nu_2(OH)$	water (hydrates)
1,621	$\nu_2(OH)$	water (adsorbed on the surface)
1,495, 1,420	$\nu_3(CO_3^{2-})$	calcite
1,138	$\nu_3(SO_4^{2-})$	anhydrite
1,118	$\nu_3(SO_4^{2-})$	gypsum
925	$\nu_3(SiO_4^{4-})$	tricalciumsilicate (C_3S)
732	$\nu_4(CO_3^{2-})$	calcite
670, 599	$\nu_4(SO_4^{2-})$	gypsum
524	$\nu_4(SiO_4^{4-})$	larnite (C_2S)
451	$\nu_2(SO_4^{2-})$	gypsum
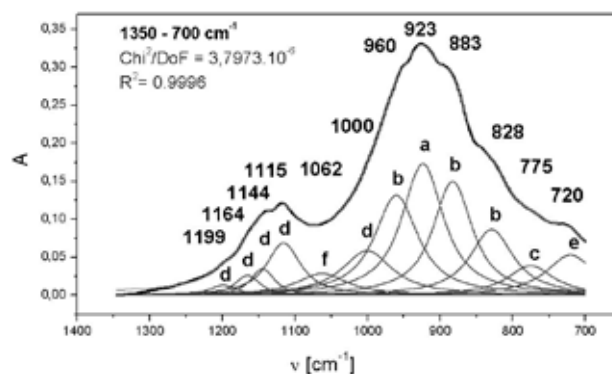
Fig. 2. **IR spectra region from 1,350 to 700 cm^{-1} fitted by Lorentz function. Peaks assignment is noted in Table II**

The peak belongs to stretching of Si–O bond in structure of C_3S, which is centered at wavelength 925 cm^{-1}, implies band complexity. This multiplet was fitted by Lorentz function (1) due to obtain other information about composition of the sample.

Fig. 1. **Subtracted infrared spectrum of Portland cement and correlation table. The Si–O stretch region was fitted by Lorentz function**

$$y = y_0 + \frac{2A}{\pi} \frac{w}{4(x - x_c)^2 + w^2} , \qquad (1)$$

where y_0 is offset, x_c is wavelength of peak's center, w is peak's half-width and A is amplitude of peak.

Fitted spectrum of the Portland cement is shown on Fig. 2. There were found absorbtion bands of anhydite, gypsum, larnite, C_2S, C_3S and calcite. Cement IR bands assignment is summarized in Table II.

Table II
Fitted FT-IR spectrum of Portland cement

$\nu\,[\text{cm}^{-1}]$	peak's assignment	compound
1,199	$\nu_3, b_1(SO_4^{2-})$	
1,164	$\nu_3, a_1(SO_4^{2-})$	anhydrite
1,144	$\nu_3, a_2(SO_4^{2-})$	
1,115	$\nu_3(SO_4^{2-})$	gypsum
1,062	$\nu(Al\text{–}O)$	hexagonal hydrates
1,000	$\nu_1(SO_4^{2-})$	anhydrite
960, 883	$\nu_3(SiO_4^{4-})$	larnite (C_2S)
923	$\nu_3(SiO_4^{4-})$	tricalciumsilicate (C_3S)
828	$\nu_1(SiO_4^{4-})$	larnite (C_2S)
775	$\nu(Al\text{–}O)$	tricalciumaluminate
720	$\nu_4(CO_3^{2-})$	calcite

Conclusions

The Fourier transform infrared spectroscopy is a suitable tool for determination of cement phase composition, because enable monitored course of hydration processes by changes of spectroscopic variables (ν, w and A) in the time. These parameters may provide secondary information about changes in the sample.

Main absorbtion area of clinker minerals is spread over spectral region from 1,000 to 400 cm^{-1}. Peaks coincidence make interpretation of spectrum more difficult, but is possible distinguished of individual peaks.

Amount of spectral bands in hydrated or partially hydrated cement has increasing due to intermolecular interaction of cations with SO_4^{2-} and CO_3^{2-} anions leading to reduction of their symmetry.

REFERENCES

1. Hughes L. T., Methven M. C., Jones J. G. T., Pelham E. S., Fletcher P., Hall Ch.: Adv. Cem. Based Mater. *2*, 91 (1995).
2. Mueller J. H., Freeman D.: Mater. Charact. *35*, 113 (1995).
3. Papoušek D., Horák M., *Infračervená spektra a struktura molekul*, Academica, Praha 1976.
5. Mollah A. Y. M., Kesmez M., Cocke D.: Sci. Total Environ. *325*, 255 (2004).
6. Smith H. D., Seshadri S. K.: Spectrochim. Acta Part A 55, 795 (1999).
7. Trezza A. M., Lavat E. A.: Cem. Concr. Res. *31*, 869 (2001).

P17 THERMAL BEHAVIOR OF POWDER PRECURSOR FOR LAS CERAMIC DOPED BY HYDROXYAPATITE

PETR PTÁČEK, HELENA KREJČOVÁ, JAROMÍR HAVLICA, FRANTIŠEK ŠOUKAL and TOMÁŠ OPRAVIL

Institute of Materials Chemistry, Brno University of Technology, Purkyňova 118, 612 00, Czech Republic,
ptacek@fch.vutbr.cz

Introduction

The performance of precision devices and instruments has been limited by the problem of thermal stress induced by the thermal expansion between different materials. To avoid this problem, one of the choices is to develop negative thermal expansion materials[1]. It has been known that thermal shock resistance of ceramics is influenced by the thermal expansion coefficient[2]. LAS ($Li_2O \cdot Al_2O_3 \cdot SiO_2$) system has been investigated extensively, because its show low, zero or even negative thermal expansion coefficient as well as high thermal shock resistance[3].

The most important crystaline phases present in the LAS system are β-eucryptite ($Li_2O \cdot Al_2O_3 \cdot SiO_2$), β-spodumene ($Li_2O \cdot Al_2O_3 \cdot 4SiO_2$), virgilite ($Li_2O \cdot Al_2O_3 \cdot 6SiO_2$), petalite ($Li_2O \cdot Al_2O_3 \cdot 8SiO_2$) as well as metastable solid solutions that are derived from the hexagonal high quartz structures by the substitution of Al^{3+} and Li^+ for Si^{4+}. These solid solutions are denoted as β-quartz (ss) and have general composition $Li_2O \cdot Al_2O_3 \cdot nSiO_2$, where n varies from 2 to 10(ref.[2]).

There are many methods to prepare ultra-fine powders for synthesis of LAS ceramic or glass-ceramic. The conventional method is melt processing, which has many problems, such as too high melting temperature and high viscosity of melt. Lately, sol-gel processing has been widely used in the manufacture of LAS. This method reduces the sintering temperature and can obtain high purity and homogenous products.[4–6]

The present study on the LAS ceramic based on spodumene is mainly concentrated to investigation of influence of $Ca_2(PO_4)_3OH$ on thermal behavior of sol-gel derived precursor. Processes whose take place during thermal treatment were analyzed by DTA and heating microscopy.

Experimental

The β-spodumene powder precursor was prepared from Li_2OH, $Al(NO_3)_3 \cdot 9H_2O$, both in analytical purity grade. Silica sol containing 30 % wt. of SiO_2 (Tosil) was applied as source of SiO_2. A weighed quantities of lithium carbonate and $Al(NO_3)_3 \cdot 9H_2O$ were first dissolved in hydrochloric acid and Tosil, respectively.

Both prepared solutions were next slowly mixed together. Resulting sol contain $LiCl$, $Al(NO_3)_3 \cdot 9H_2O$ and SiO_2 in weight ratio 1 : 1.77 : 1.89 that is equal to spodumene composition. The gelation of mixed sol at 80 °C took place after 20 min. The resulted gel was dried at 105 °C for 24 h.

Powder LAS ceramic precursor was prepared by calcination and subsequent milling of grinded xerogel at 750 °C for 2 h.

The powder precursor was next doped with 0.25, 0.50, 0.75 and 1.00 % wt. hydroxyapatite ($Ca_5(PO_4)_3OH$) working as sintering additive (agent of mineralization).

Differential Thermal Analysis

The DTA analysis of the $Ca_5(PO_4)_3OH$ doped powder precursor in an air oven at ambient atmospheric condition was carried out by TG-DTA Analyzer Setaram 92-18 up to temperature 1,400 °C. Applied heating and cooling rate was 10 °C min⁻¹.

Heating Microscopy

Test piece (cube, a = 3 mm) was prepared by pressing of precursor and hydroxyapatite mixture under pressure 1 MPa. Sample was heated in an air oven at ambient atmospheric condition up to sample melting temperature at heating rate 10 °C min⁻¹.

Results

Diferential Thermal Analysis

Fig. 1. shows the DTA curves of powder precursor with hydroxyapatite content from zero to 1 % wt.. The endothermic peak at temperature about 1,360–70 °C belong to melting of sample. Peak shape and temperature (T_m) depend on concentration of $Ca_5(PO_4)_3OH$.
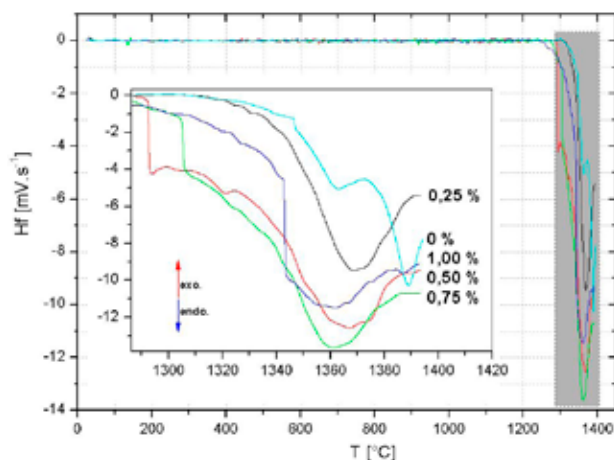
Fig. 1. **Heating step of DTA of the LAS powder precursor with 0, 0.25, 0.50, 0.75 and 1.00 % wt. $Ca_5(PO_4)_3OH$**

The values of melting temperature, that are found for individual samples is shown in Table I. This table further contains the peaks temperature shift against system without additive (ΔT).

Table I

The DTA curves of cooled powder precursor with hydroxyapatite are shown on Fig. 2. Only one exotherm was observed in each curve. This peak is associated to crystallization of glass (T_k).

Table I
Temperature of melting of LAS ceramic (T_m) and peak shift (ΔT) for different $Ca_5(PO_4)_3OH$ content. Significat correlation coeficien (R) level is typed bold

$Ca_5(PO_4)_3OH$ [%]	T_m [°C]	ΔT [°C]
0	1,388.9	–
0.25	1,368.6	–20.3
0.50	1,367.0	–21.9
0.75	1,361.1	–27.8
1.00	1,359.8	–29.1
R	**–0.888**	
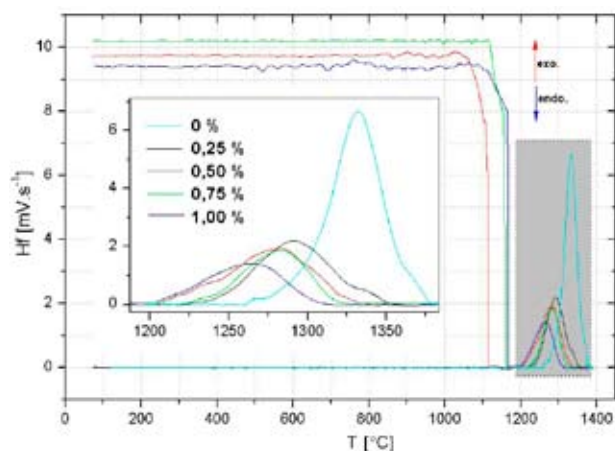
Fig. 2. **Cooling step of DTA of the LAS powder precursor with 0, 0.25, 0.50, 0.75 and 1.00 % wt. $Ca_5(PO_4)_3OH$**

The values of crystallization temperature, that are found for individual samples is shown in Table II. This table further contains shift of peaks temperature against crystallization in pure LAS system (ΔT).

Table II
Crystallization peaks temperature and peak shift (ΔT) for different $Ca_5(PO_4)_3OH$ content. Significant correlation coefficient (R) level is typed bold

$Ca_5(PO_4)_3OH$ [%]	T_k [°C]	ΔT [°C]
0	1,333.1	–
0.25	1,290.8	–42.3
0.50	1,279.8	–53.3
0.75	1,281.2	–51.9
1.00	1,267.0	–66.1
R	**–0.885**	

The shift of baseline, which takes place in samples with hydroxyapatite content equal and higher than 0.25 % wt. was recognized as high quartz solid solution phase separation. The found values are listed in Table III.

Table III
The phase separation temperature for different $Ca_5(PO_4)_3OH$ content in heating ($T_{g,1}$) and cooling ($T_{g,2}$) step

$Ca_5(PO_4)_3OH$ [%]	$T_{g,1}$ [°C]	$T_{g,2}$ [°C]
0	–	–
0.25	–	–
0.50	1,292.9	1,113.7
0.75	1,305.4	1,158.0
1.00	1,343.3	1,166.6

Heating Microscopy

The dependences of test piece on temperature were shown on Fig. 3. Height of sample without agent of mineralization has been decreased about 9.5 % on temperature interval 600–810 °C due to formation of β-spodumene. This process begin at higher temperature if samples containing the $Ca_5(PO_4)_3OH$.
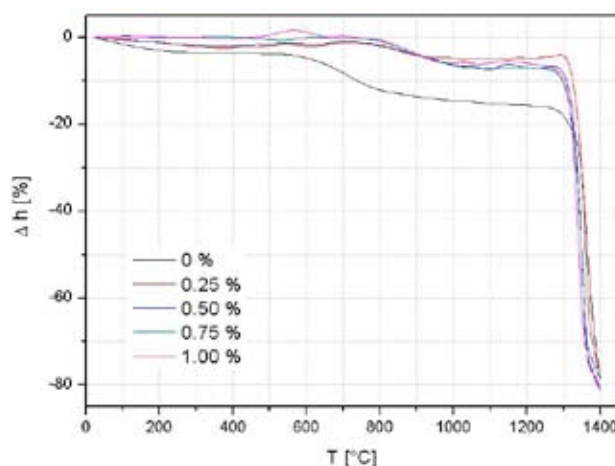
Fig. 3. **Heat microscopy of the LAS powder precursor with 0, 0.25, 0.50, 0.75 and 1.00 % wt. $Ca_5(PO_4)_3OH$**

The influence of hydroxyapatite concentration in sample on spodumene formation interval and sample melting temperature is shown in Table IV.

Photos for significant temperatures, whose were taken during thermal treatment of sample placed in heat microscope furnace are shown on Fig. 4.

Influence of $Ca_5(PO_4)_3OH$ content on temperature

Table IV
Temperature synthesis of spodumene (T_s) and melting of sample (T_m). Significant correlation coefficient (R) level is typed bold

$Ca_5(PO_4)_3OH$ [%]	T_s [°C]	T_m [°C]
0	600–805	1,335.5
0.25	792–918	1,337.0
0.50	767–1,016	1,325.2
0.75	789–997	1,325.2
1.00	789–957	1,316.1
R		**–0.933**
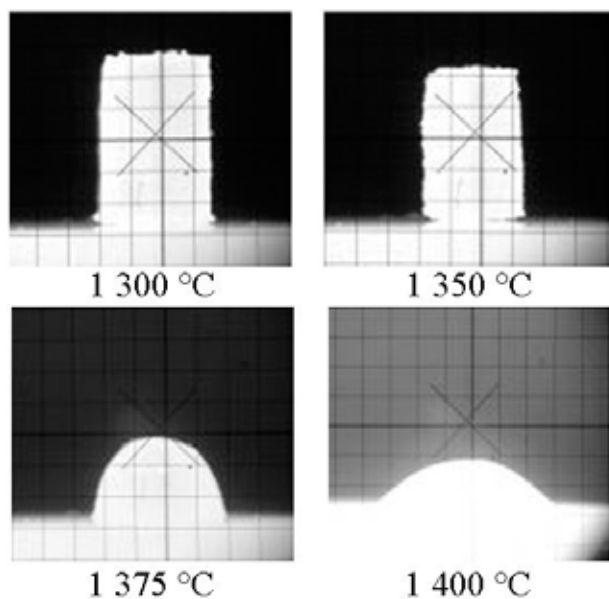
Fig. 4. **Picture of powder precursor test peace at temperature of sintering, deformation, hemisphere and pouring**

of sintering, deformation, hemisphere a pouring of melt is shown in Table V.

Conclusions

Table V
The significant thermal points of fired LAS powder precursor with different $Ca_5(PO_4)_3OH$ content

$Ca_5(PO_4)_3OH$ [%]	Sintering [°C]	Deformation [°C]
0	1,300	1,350
0.25	1,325	1,350
0.50	1,300	1,325
0.75	1,300	1,325
1.00	1,250	1,300
$Ca_5(PO_4)_3OH$ [%]	Hemisphere [°C]	Pouring [°C]
0	1,375	1,400
0.25	1,360	1,380
0.50	1,350	1,370
0.75	1,350	1,370
1.00	1,350	1,360

In presence of hydroxyapatite is spodumene stabilized in solid solution with β-SiO_2 (ss) and melting was changed from incongruent to congruent. In range from 0 to 1.0 % wt. of $Ca_5(PO_4)_3OH$ content has been melting temperature fall about 29.1 °C.

Solid solution immiscibility process was proceed in samples with $Ca_5(PO_4)_3OH$ concentration 0.50 % wt. and higher. Temperature of process has been increased with content of hydroxyapatite.

Temperature of sample melting and β-SiO_2 (ss) precipitation has been decreased with increasing content of hydroxyapatite.

In presence of hydroxyapatite in the sample, the temperature of the β-spodumene formation was shifted to higher temperature. Temperature of β-spodumene was average increased about 184 ± 6 °C.

Significant negative correlation of melting temperature on hydroxyapatite content in the sample was found by heating microscopy. In range from 0 to 1.0 % wt. can by this relationship expressed as:

$$T_m = 1337.9 - 20.24\, w_{(Ca_5(PO_4)_3OH)} . \qquad (1)$$

Significant thermal points, i.e. temperature of sintering, deformation, hemisphere and melting, has generally decreased in presence of $Ca_5(PO_4)_3OH$.

REFERENCES

1. Sheu G. J., Chen J. C., Shiu J. Y., Hu C.: Scr. Mater. *53*, 577 (2005).
2. Mandal S., Chakrabarti S., Das S. K., Ghatak S.: Ceram. Int. *33*, 123 (2007).
3. Guo X., Yang H., Han Ch., Song F.: Thermochim. Acta *444*, 201 (2004).
4. Wu S., Liu Y., He L., Wang F.: Mat. Lett. *58*, 2772 (2004).
5. Chatterjee M., Naskar N. K., Ceram. Int. *32*, 623 (2006).
6. Amini M. M., Mehraban Z., Sabounchei S. J. S., Mater. Chem. Phys. *78*, 81 (2002).

P18 SYNTHESIS AND CATALYTIC ACTIVITY OF TITANIA – KAOLINE SYSTEM

PETR PTÁČEK, MICHAL FIALA, JAROMÍR HAVLICA, FRANTIŠEK ŠOUKAL and TOMÁŠ OPRAVIL

Institute of Materials Chemistry, Brno University of Technology, Purkyňova 118, 612 00, Czech Republic,
ptacek@fch.vutbr.cz

Introduction

Heterogeneous catalysis is the most promising technology for the reduction of environmental pollution in soil, air and water. The pillared clays (PILCs) are an interesting group of microporous materials, because they combined catalytic activity, porous structure and surface acidity. The PILCs have great potential either as support or directly as catalyst. Pillared clays were prepared by calcination of intercalate of clay minerals (smectite and mica group) with polynuclear metal cation. Specific surface are higher than 300 $m^2 g^{-1}$.[1–5]

Generally is the synthesis of TILCs with well defined bidimensional zeolite structure and good thermal stability difficult, because obtaining of adequate polymeric cationic species depends on several related parameters. The bes results were reached by acidic (HCl, H_2SO_4...) hydrolysis of $TiCl_4$ or $Ti(OC_3H_7)_4$ (TTIP).[2]

Interlayer surface of TiO_2 pillared montmorillonite is hydrophobic and that hydrophobic interaction between adsorbate and interlayer surface of the pillared clay is one of the most predominant factors in adsorption of various organic compounds. Surface hydrophobicity of TiO_2 pillared clay has been increasing in the order saponite < fluorine hectorite < montmorillonite < fluorine mica.[3]

The aim of this work is preparation, characterization and study of the efficiency of the Na-kaolin/TiO_2 and metakaolin/TiO_2 catalysts. The catalytic performance was compared with pure Na-kaolin. Simultaneous TG-DTA (TG-DTA Analyzer Setaram 92-18), infrared spectroscopy (FT-IR Analyzer Nicolet Impact 400), X-ray diffraction (Difractometer X´Pert Philips) were used for investigation of prepared samples.

Experimental

Washed kaolin Sedlec Ia produced by Sedlecký kaolin a.s. was used for sample preparation. Content of kaolin is higher than 90 % wt. with equivalent diameter grain median in range 1.2–1.4 µm. The main impurities are mica group minerals and quartz. The content of colorant oxides – hematite (α-Fe_2O_3) and tetragonal TiO_2 (rutile), is lower than 0.85 and 0.2 % wt., respectively.

Two kinds of catalyst were prepared by hydrolysis of $TiCl_4$ in 30 % wt. aqueous suspension of washed Na-kaolin:

- kaolin/TiO_2,
- metakaolin/TiO_2

Titanium tetrachloride was introduced in to stirred suspension in the flow of carrier gas (argon) at laboratory tempe-

rature for 30 min. The suspension was deposit on the surface of substrate – glass balls with diameter about 5 mm. Film on the glass support was solidified by drying at laboratory temperature for 24 h. Metakaolin/TiO_2 type sample was still calcined at 600 °C for 2 h. Purely kaolin deposited on the glass support surface was used as standard.

Catalytic performance of prepared catalysts was examined on flow reactor in temperature range from 100 to 400 °C. The ordering of experiment is shown on Fig. 1. Ethanol vapor was flow (1.48 mol min^{-1}) through heated catalyst in the flow of carrier gas (12.85 cm^3 min^{-1}). In periodic interval was into reactor introduced oxygen from 356.4 cm^3 stack pressurized to 700 mbar. Concentration of oxygen in reactor leaving gas was measured by oxymeter.

1. Rotameter
2. Ethanol source
3. Escape valve
4. Thermometer well
5. Reactor
6. Oxymeter
7. O_2 stack
8. barometer
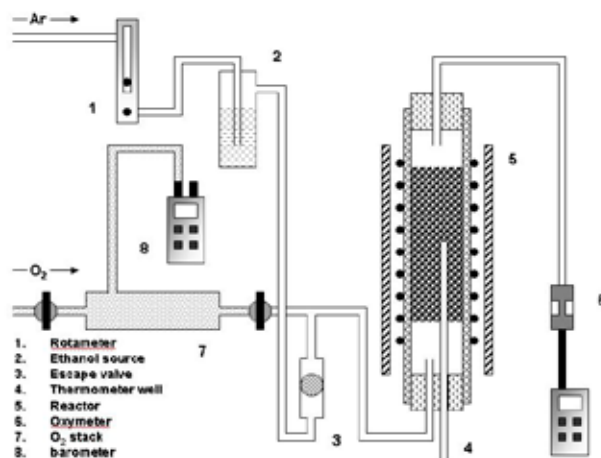
Fig. 1. **Schematic representation of the apparatus for investigation of catalytic performance**

Relative degree of conversion (α_r) and extend of reaction (ξ_r) were evaluated as follow:

$$\alpha_r = \frac{A_K - A_{KT}}{A_K}, \tag{1}$$

$$\xi_r = -\frac{A_{KT} - A_K}{3}, \tag{2}$$

There A_K and A_{KT} are peaks area obtained for pure kaolin and kaolin (metakaolin)/TiO_2 catalyst, respectively. The denominator value in (2) is equal to stoicheiometric coefficient of ethanol ($\nu_{O2} = -3$) in reaction:

$$C_2H_5OH + 3 O_2 \rightarrow 2 CO_2 + 3 H_2O \tag{3}$$
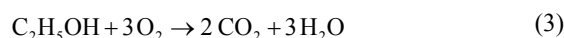
Values of α_r and ξ_r can be converting according to (4).

$$A_K \, \alpha_r = 3 \, \xi_r \tag{4}$$

Results

Thermal Analysis

TG-DTA experiments results is shown on Fig. 2. There are endothermic peak at 525 °C accompanied with sample mass decrease about 8 % wt. and exothermic peak at 984 °C. Any changes takes place at this temperature.
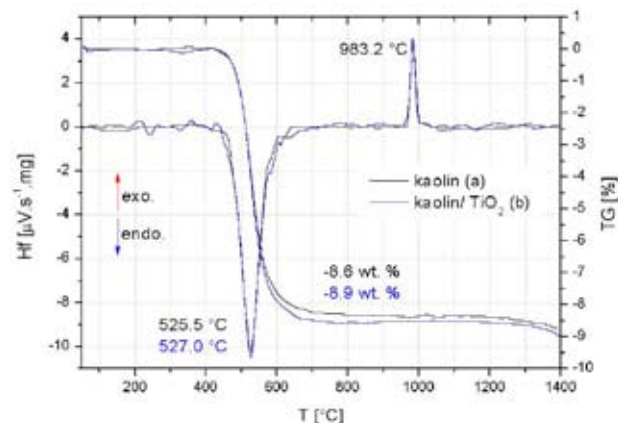
Fig. 2.　**TG-DTA of kaolin (a) and kaolin/TiO₂ catalyst (b)**

Endoterm belong to course of dehydroxylation process of kaolin to metakaolin. Cubic phase formation – spinel phase $(2Al_2O_3 \cdot 3SiO_2)$ or γ-Al_2O_3, is on the contrary exothermic process.

Infrared Spectroscopy

Fig. 3. show FT-IR spectrum of kaolin/TiO₂ and metakaolin/TiO₂ catalyst. The bands located at wavelengths 3,696, 3,673, 3,652 and 3,619 cm⁻¹ are ν_1, ν_2, ν_3 and ν_4 stretching of O–H bonds in outer (ν_{1-3}) and inner hydroxyl groups (ν_4) of kaolinite. Bending and translation modes of these groups are appeared at 939, 912 and 791, 754 cm⁻¹, respectively.

The broad band centered at 3,440 cm⁻¹ and band located at 1,634 cm⁻¹ belongs to O–H bond stretching and bending of surface adsorbed water molecules, respectively. Bands at 1,115, 1,032 and 1,007 cm⁻¹ are stretching, symmetric and asymmetric stretching of Si–(apical)O and Si–O–Si, respectively. Bending vibration is appearing at 421 cm⁻¹. The Si–O–Al and Al–O out of plane deformation shows the band at wavelengths 536 and 496 cm⁻¹, respectively.

The calcination leads to dehydroxylation of kaolinite and product of $TiCl_4$ hydrolysis – $TiO(OH)_2$. Sample may also contain a small amount of $TiOCl_2$. The O-H bands were almost disappeared during this process, but small amount of "residual hydroxyl groups" is still present. The Si–O bond stretching and bending modes show lose of his selectivity.

X-ray Diffraction

The XRD patterns on Fig. 3.(a) show intensities of kaolinite and other component of applied kaolin Sedlec Ia – montmorillonite, hematite and quartz. Anatase was formed via titanium tetrachloride hydrolysis. Metakaolin is amorphous and diffractions related to kaolinite were disappeared after sample calcination (b).
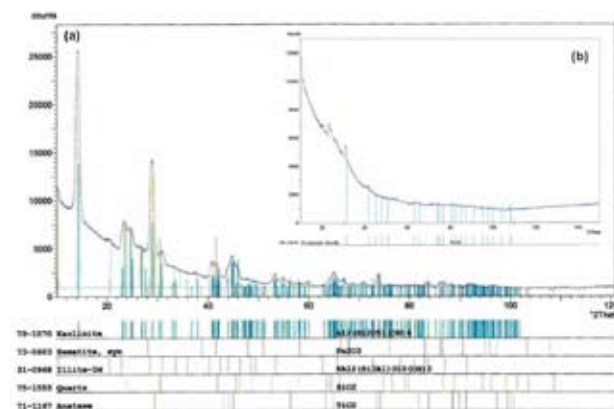
Fig. 4.　**Powder XRD patterns of the kaolin/TiO₂ catalyst before (a) and after calcination (b)**

Fig. 3.　**Baseline corrected infrared spectrum of kaolin/TiO₂ (a) and metakaolin/TiO₂ catalyst (b): ■ kaolinite bands, ● product of hydrolysis of TiCl₄, ▲ molecules of surface adsorbed water**
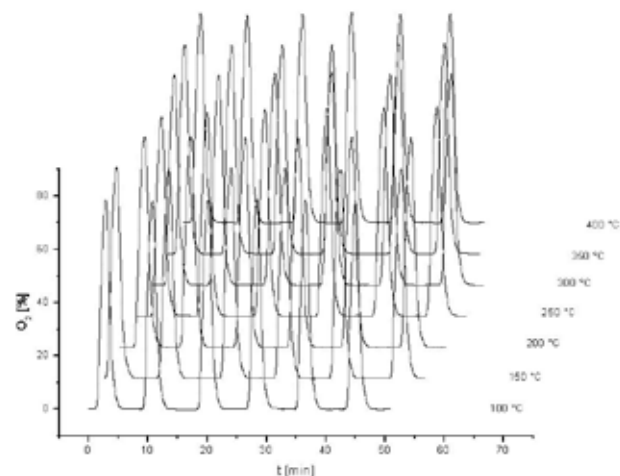
Fig. 5:　**Results obtained for kaolin Sedlec Ia**

Catalytic Performance

Recorded data about answer of catalyst on oxygen "pulse" is for kaolin shown on Fig. 5. Individual peaks were next integrated due to determination of their area, height and width. Results obtained for kaolin is of Fig. 6. Analogical procedures were applied on kaolin or metakaolin/TiO_2 catalyst.
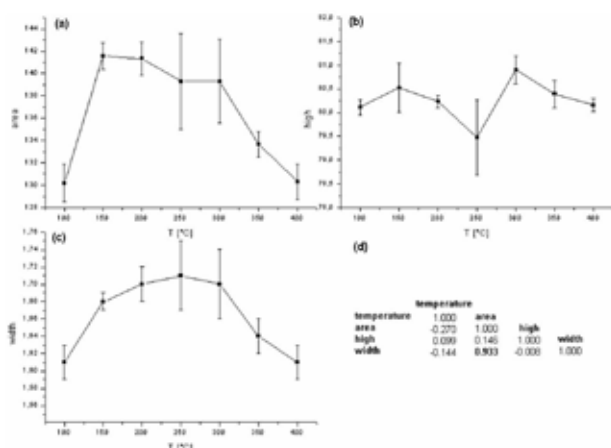
Fig. 6.　**Changes of oxygen peaks parameters with temperature for kaolin Sedlec Ia: area (a), height (b) and width (c). Correlation matrix is shown on (d). Significant correlation level is typed by bold**

Catalytic performance results obtained for kaolin/TiO_2 system is shown on Fig. 7. The process is strongly influenced by thermal behavior of product of $TiCl_4$ hydrolysis. Water evolving during dehydroxylation process was influenced of specific surface of catalyst and partial water vapor pressure (p_{H2O}) over sample. Exchange adsorption of ethanol on the internal catalyst surface is influenced by p_{H2O} value.

Temperature dependence of relative degree of conversion (α_r) and extend of reaction (ξ_r) are plotted on Fig. 9.(a) and (b). The best results were found for 300 °C.
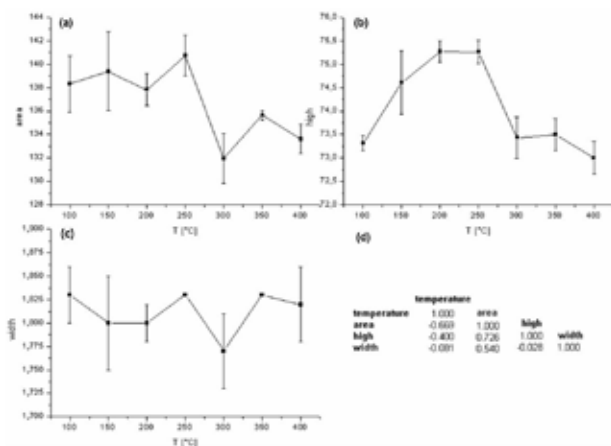
Fig. 7.　**Changes of oxygen peaks parameters with temperature for kaolin/TiO_2 system: area (a), height (b) and width (c). Correlation matrix is shown on (d)**
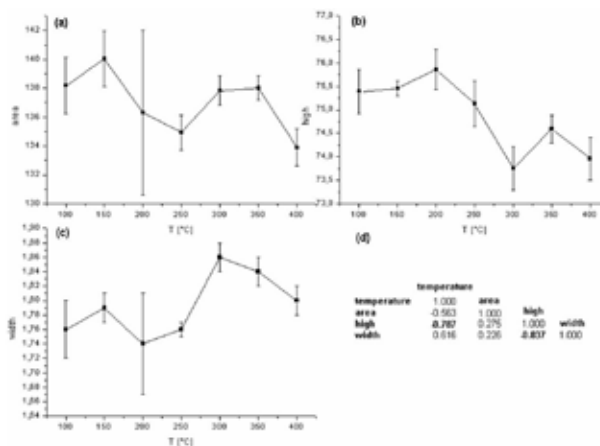
Fig. 8.　**Changes of oxygen peaks parameters with temperature for metakaolin/TiO_2 system: area (a), height (b) and width (c). Correlation matrix is shown on (d). Significant correlation level is typed by bold.**

Result obtained for metakaolin/TiO_2 system is shown on Fig.8 and temperature dependence of α_r and ξ_r are plotted on Fig. 9(c) and (d).
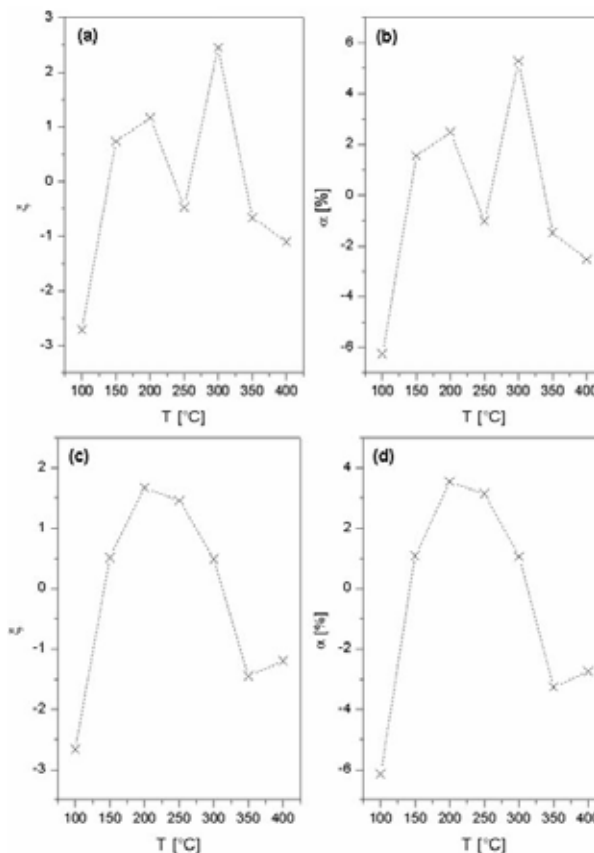
Fig. 9.　**Temperature dependences of relative degree of conversion (α_r) and extend of reaction (ξ_r)**

Conclusions

The $TiCl_4$ hydrolysis product shows any significant influence on the results of TG-DTA experiment. Dehydroxylation peak was slightly increased about 2.5 °C. Temperature formation of cubic phase isn't influenced.

Peaks height and width must depend of specific surface of catalytic system. While value of the first parameter has decreased with growth of specific surface, the second has increased.

Area of peak is directly proportional to amount of moles of oxygen. The minimum values of α_r was found for kaolin/TiO_2 catalyst at 250 °C, due to course of $TiO(OH)_2$ dehydroxylation.

High p_{H2O} value makes adsorption of ethanol on the catalyst surface more difficult. Temperature 300 °C show the best catalytic performance, because dehydroxylation of $TiO(OH)_2$ be on the wane and kaolinite dehydroxylation doesn't proceed till this time.

The metakaolin/TiO_2 catalyst show higher catalytic performance than kaolin on temperature interval from 350 to 350 °C. Dehydroxylation has in general negative influence on catalytic performance, because this process leads to specific surface reduction.

REFERENCES

1. Ding Z., Zhu Y., Greenfield P. F., Lu Q. G.: J. Colloid Interface Sci. *238*, 267 (2001).
2. Boudali K. L., Ghorbel A., Tichit D., Chiche B., Dutartre R., Figueas F.: Microporous Mater. *2*, 525 (1994).
3. Ooka Ch., Yoshida H., Suzuki K., Hattori T.: Microporous Mesoporous Mater. *67*, 143 (2004).
4. Pernyeszi T., Dékány I.: Colloids Surf., A *230*, 191 (2004).
5. Belessi V., Lambropoulou D., Konstantinou I., Katsoulidis A., Pomonis P., Petridis D., Albanis T.: Appl. Catal., B *73*, 292 (2007).

P19　DEPOSITION OF THE TiO$_2$ ON A GLASS AND CERAMICS SURFACE

ALENA RUTTEOVÁ, PETR PTÁČEK and JAROMÍR HAVLICA

Institute of Material Chemistry, Brno University of Technology, Purkynova 118, 62100 Brno, Czech Republic,
xcrutteova@fch.vutbr.cz

Introduction

Photocatalysis has recently become a common word and various products using photocatalytic functions have been commercialized. Photocatalytical self cleaning surfaces offer many advantages in household, construction, industrial and medical sectors. Among many candidates for photocatalysts, TiO$_2$ is almost the only material suitable for industrial use at present and also probably in the future. This is because TiO$_2$ has the most efficient photoactivity, the highest stability and the lowest cost[1,2].

Experimental

Deposition of the TiO$_2$ on a glass and ceramics surface was provided by precipitation of gas phase at temperature of 22, 100, 200, 300, 400 and 500 °C for 3 hours (1). TiCl$_4$ (Lachema, p.a., in gaseous state) and water vapour in current of argon were leaded into tempered tube reactor within three supports (glass or ceramics). Flow rate of argon was regulated at 30 cm^3 min^{-1}. The ordering of experiment is schematically drawing in Fig. 1.

$$TiCl_{4\,(g)} + 2H_2O_{(g)} \rightarrow TiO_{2\,(s)} + 4HCl_{(g)} \qquad (1)$$
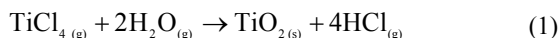
Surface of support was studied by the optical microscopy. The photos of TiO$_2$ layer were taken by Olympus BX 50F4.

Unprecipitated TiCl$_4$ went out from reactor at the temperature of 500 °C and hydrolyzed in water bath or Tosil (Koma, s.r.o., colloidal solution of SiO$_2$, 30 % wt. of SiO$_2$). Temperature of Tosil was 20, 40, 50 and 60 °C.

TiO$_2$ dispersion in water and SiO$_2$–TiO$_2$ hydrosol were analyzed by infrared spectroscopy (FT-IR spectroscope Nicolet Imapct 400), particulates size distribution (Zetasizer 3000HS), differential thermic analysis (TG-DTA Analyzer SETARAM 92–18) and X-rays diffraction.
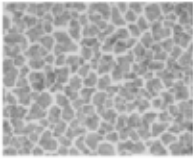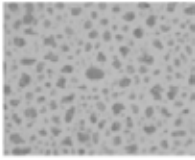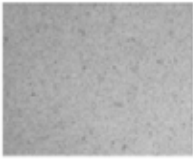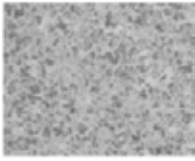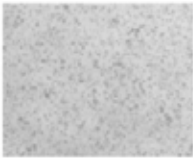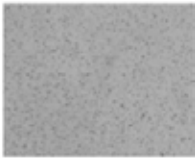
Results

The morphological properties depend on temperature. Polycrystalline agglomerates arise from decreased temperatures whereas continuous layer come up from increased temperature. Further quality of substrate's surface proves on appearance deposit layer. Sintered corundum ceramics have much more active adsorptive centres (e.g. edges and tops of crystal).

Table I
Layers of TiO$_2$ on glass and ceramics support (place in the middle of tube reactor)

T [°C]	Glass support	Ceramics support
22		
200		
500		

System which is created by hydrolysis TiCl$_4$ approaches monodispersive. It results from shape distribution curve (Fig. 2.). The fraction has major representation about 233.3 nm particles size and minor about 293.7 nm.

Distribution curves SiO$_2$–TiO$_2$ hydrosol indicate three peaks (Fig 3.). The first part shows SiO$_2$ particles size

1 - supply of Ar with TiCl$_4$
2 - supply of Ar with H$_2$O
3 - thermocouple
4 - heat insulation
5, 6 - supply of Ar
7, 8 - Erlenmeyer flask
9, 10, 12 - support
11 - winding
13 - tube reactor
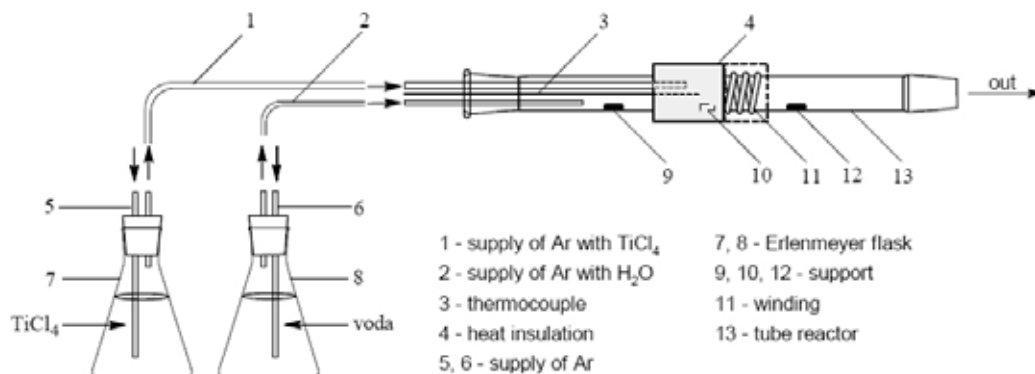
Fig. 1.　**Ordering of the experiment**
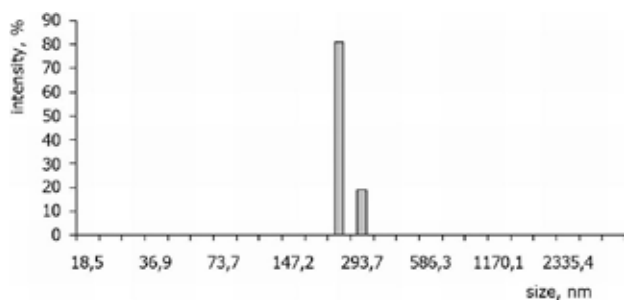
Fig. 2.　**TiO$_2$ dispersion in water**

(Fig. 3. (a) peak 7.6 nm, (b) peak 7.1 nm), the most of TiO$_2$ particles are included in the second part (Fig. 3. (a) peak 121.1 nm, (b) peak 90 nm) and the third peak proves the particles coagulation.
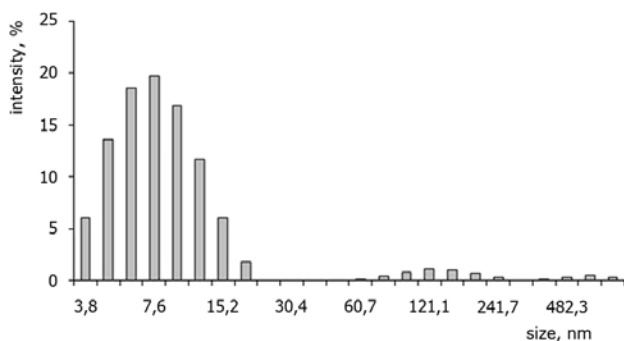
Fig. 3.　**SiO$_2$–TiO$_2$ hydrosol prepared at 20 °C under ultra-sound treatment**
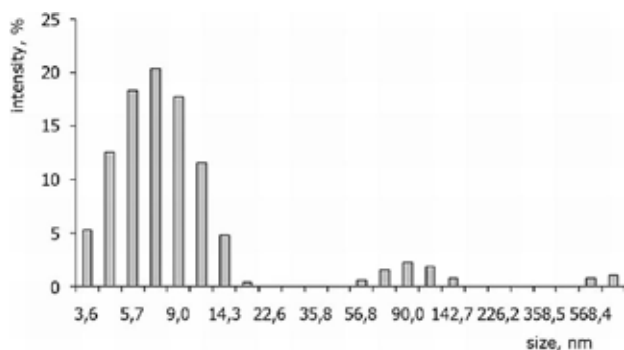
Fig. 4.　**SiO$_2$–TiO$_2$ hydrosol prepared at 50 °C under ultra-sound treatment**
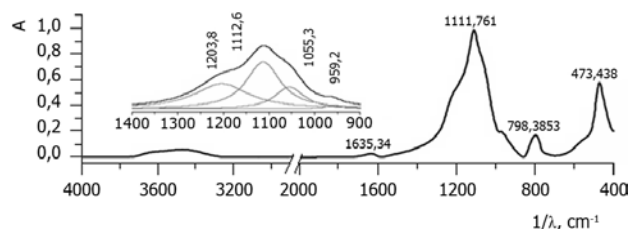
Fig. 5:　**FT-IR SiO$_2$–TiO$_2$ hydrosol prepared at 20 °C**

Table II
Peaks assignment

T [°C]	20	Assignment
	1,203.8	$\delta(Ti-OH)$
	1,112.6	$\nu(Si-O)$
$1/\lambda$	1,055.3	$\nu(Si-OH)$
[cm^{-1}]	959.2	$\nu_s(Si-O-Si)$
	798.4	$\gamma(Si-O-Si)$
	473.4	$\delta(Si-O-Si)$

The FT-IR spectrogram contains only absorption bands of silica (Fig 4.). Assign of recognized peaks are summarized in Table II.

Conclusions

The presented work compares TiO$_2$ layers on glass surface with layers on ceramics surface. Morphological characteristic TiO$_2$ layer is significantly influenced by temperature of deposition and substrates type. Smaller TiO$_2$ particles arise by hydrolysis TiCl$_4$ in Tosil than hydrolysis in water.

REFERENCES
1. Hashimoto K., Irie H., Fujishima A.: JSAP International *14*, 4 (2006). http://www.jsapi.jsap.or.jp/Pdf/Number 14/04_JJAP-IRP.pdf, download: 11.03.2007.
2. http://www.dyo.com.tr/uploads/yayinlar_ 082206163146_　yayinlar_08150683358_NEW.pdf, download: 11.03.2007.

P20 THE INFLUENCE OF P_2O_5 ON THE FORMATION OF PORTLAND CEMENT CLINKER

THEODOR STANĚK[a] and PETR SULOVSKÝ[b]

[a]*Research Institute of Building Materials, Hněvkovského 65, 617 00 Brno, Czech Republic,*
[b]*Department of Geological Sciences, Faculty of Science, Masaryk University, Kotlářská 2, 611 37 Brno, Czech Republic,*
stanek@vustah.cz

Introduction

The nature of the cement production process allows utilizing various secondary raw materials and wastes. One of such wastes is the meat and bone meal (MBM). This material, especially if coming from herds in which BSE-positive cows were identified, has to be liquidated by a high-temperature process. This can be done in incineration plants, but also in rotary cement kilns. The advantage of the latter is that MBM is utilized as a low-grade[1] fuel and at the same time it is degraded and the hazardous substances are liquidated, while its incombustible components are built in the clinker. The main problem is the relatively high P_2O_5 content, contained in the ash as calcium phosphate. P_2O_5 influences the properties of the clinker melt[2], enters the structure of clinker minerals, and influences the phase composition of clinker[3–5] and thus also the quality of cement[4,5]. So far, the common cement production practice is that only such amounts of MBM are combusted that do not adversely affect the clinker properties. Maximum safe amount is around 0.5 % wt. P_2O_5 in the clinker (only exceptionally more[6]). We assume that the study of reaction kinetics and of the phase changes in clinkers containing P_2O_5 will enable to produce clinker with much higher levels of this oxide without negative impact on clinker properties, along with discovering new findings on its influence on clinker minerals.

Methods and Results

The raw meal for laboratory experiments, prepared from common raw materials, was mixed to have the following basic chemical parameters: SLP = 98, Ms = 2.3 a Ma = 1.8. P_2O_5 was added to this basic raw meal in graded amounts of finely ground $Ca_3(PO_4)_2$ or ashed MBM.

The burning of these P_2O_5-enriched raw meals was performed in a superkantal oven in equilibrium- as well as non-equilibrium burning regime at 1,450 °C. Quantitative phase composition was determined by microscopic point counting[7] and the chemical composition of clinker minerals by spot microanalyses performed with electron microprobe CAMECA SX100 (accelerating voltage 15 kV, beam current 20 nA).

The results obtained with MBM ash were in equilibrium-burned clinkers very similar to those acquired with raw meals enriched with pure $Ca_3(PO_4)_2$. Incompletion of reactions in non-equilibrium burnings of raw meals blended with

MBM ash leads to the increased volumes of the clinker melt, to incomplete consumption of free lime at low P_2O_5 contents in clinker, and to the increase of alite proportion in clinkers high in P_2O_5. The trend of the influence of P_2O_5 on the phase composition of clinker is nevertheless the same, with critical limit around 0.7 % wt. P_2O_5 in clinker, when the C_2S and free lime proportions start to enhance on the expense of C_3S (Fig. 1.).
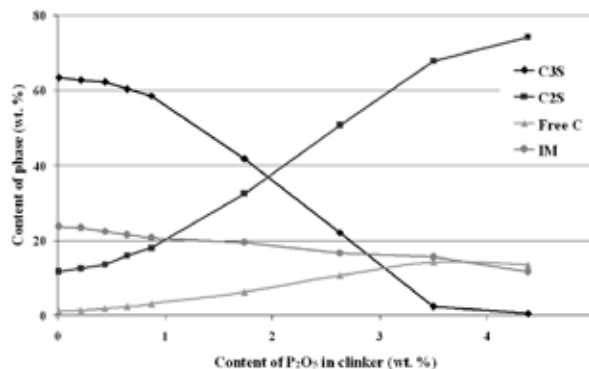
Fig. 1. **The influence of P_2O_5 content (added in the form of MBM ash) on the phase composition of non-equilibrium burned clinkers (IM – interstitial mass)**

The results of electron microanalysis indicate that both in alite and in belite the increase in P_2O_5 in clinker leads to the decrease of SiO_2, TiO_2 and MnO, and to an increase of P_2O_5, Al_2O_3, MgO, Na_2O, and K_2O. All minor oxides (besides MgO) are in belite present in higher levels than in alite.

An interesting finding ensued from the comparison of concentrations of P_2O_5 and Al_2O_3 (Fig. 2.). It occurs that P enters the structure of both clinker minerals at least partially through the so called berlinite substitution: $Al^{3+} + P^{5+} \leftrightarrow 2Si^{4+}$, where $AlPO_4$ (the berlinite component), isostructural with quartz, substitutes SiO_4 tetrahedrons. The berlinite substitution is the more important, the higher is the P_2O_5 content in clinker.

Based on the obtained results, experiments aimed on more detailed elucidation of the entry of P_2O_5 into clinker phases in the presence of Al_2O_3 were run. For the burning of clinkers without either Al_2O_3 or Fe_2O_3, raw meals were blended from pure components; the theoretical content of P_2O_5 in clinker was chosen to be 0, 1, 3 and 5 % wt. (added as $Ca_3(PO_4)_2$).

The phase composition of such equilibrium-burned clinkers without Al_2O_3 develops in relation to the P_2O_5 levels in a way similar to the common clinker with all four main oxides. The degree of alite conversion is anyway higher with increasing P_2O_5 content and as the Al_2O_3 is missing, the interstitial mass is formed above all by C_2F. In clinkers without Fe_2O_3 the evolution of phase composition is distinctly different. The alite proportion in these clinkers is at the same lime saturation lower, but the negative impact of P_2O_5 on alite formation manifests itself only at the theoretical content of 3 % wt. P_2O_5 in clinker; and at the content of 5 % wt., certain

small amount of alite still forms. Mutual comparison of alite contents in individual clinkers from all three series of experiments is shown on Fig. 3.
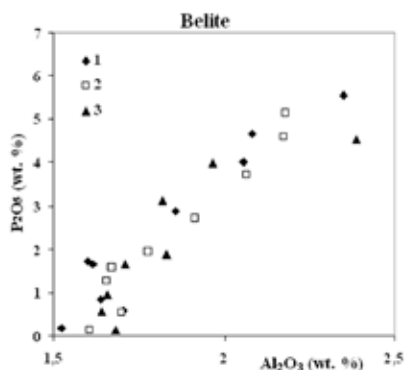
Fig. 2.   **Relationship between average P_2O_5 and Al_2O_3 contents in belite. Each point represents an average of 15–20 spot analyses. (1 – non-equilibrium burning, MBM addition, 2 – equilibrium burning, MBM addition, 3 – equilibrium burning, MBM addition, C3P addition)**
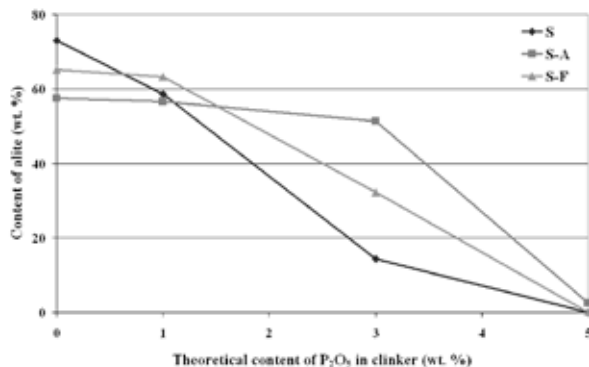
Fig. 3.   **The dependence of alite content on the theoretical concentration of P_2O_5 in clinker (S – clinkers with 4 main oxides, S-A – clinkers without Fe_2O_3, S-F – clinkers without Al_2O_3)**

Discussion and Conclusions

The experiments have confirmed that P_2O_5 has distinctly negative impact on the nucleation of alite and that it stabilizes belite by entering the structure of C_2S, forming a solid solution with C_3P.

Starting from 0.7 % wt. P_2O_5 in the clinker, negative impact of P_2O_5 on the phase composition of clinker was observed, involving the increase of belite and free lime contents on the expense of alite. Even after four hours burning at 1,450 °C, which can be considered due to their length as equilibrium, with increasing P_2O_5 full reacting of free lime with belite to alite does not happen. 4.5 % wt. of P_2O_5 in clinker completely block the formation of alite. The result of P_2O_5 addition is similar to that of SO_3(ref.[8]), but the mechanism of their operation is most probably different.

Electron microanalysis documented distinctly increasing content of P_2O_5 in the structure of clinker silicates, above all of belite, with increasing bulk P_2O_5 content in clinker. It was found that P enters the structure of both clinker silicates partially by means of the berlinite substitution: $Al^{3+} + P^{5+} \leftrightarrow 2Si^{4+}$.

These findings led to experiments with clinker composed of only three main oxides, i.e. without either Al_2O_3 or without Fe_2O_3. It was found that the raw meal mix without Fe_2O_3, characteristic for clinkers used for production of white cement, to a certain extent eliminates the negative effect of P_2O_5 on the alite formation.

REFERENCES

1. Scheuer A.: Cem. Inter. *1*, 48 (2003).
2. Timashev V. V., Osokin A. P.: Cement *9*, 4 (1982).
3. Goetz-Neunhoeffer F., Neubauer J.: *Proceedings of 20th International Conference on Cement Microscopy*, (ICMA, ed.), p. 130. Guadalajara 1998.
4. Puntke S.: *Dissertation*. Technical University at Clausthal, Clausthal, Germany, 2004.
5. Gutt W., Smith M. A.: *Proceedings of 6th International Congress on the Chemistry of Cement*, (Boldyrev A.C., ed.), p. 115. Stroyizdat, Moscow 1974.
6. Martauz P., Strigáč J., Orság Z., Tiso I., Gach F., Ježo L., Ivanka V. (PCLA Corp): CZ 291729 B6.
7. Chromý S.: Silikáty *22*, 215 (1978).
8. Staněk T.: *Proceedings of conference CEMENT 2002*, (Kostka J., ed.), p. M1. Cemdesign, High Tatras 2002.

**P22 THE STUDY OF COMPRESSIVE FLEXURAL
STRENGTH OF HIGH PERFORMANCE
CONCRETE (HPC) AS THE FUNCTION OF ITS
COMPOSITION**

PAVEL ŠILER, JOSEF KRÁTKÝ and PAVEL JEDLIČKA

*Institute of Materials Science, Faculty of Chemismy,
Brno University of Technology, Purkyňova 118, 612 00,
Czech Republic,*
siler@fch.vutbr.cz

Introduction

Lots of important material parameters of high performance concrete (HPC) can be improved by application of chemical modifying admixtures called superplasticizers (SP). Also the desired properties can be achieved by proper mixture design. This work is aimed at the study of the compressive and flexural strength of high performance concrete (HPC) as the function of its composition. The influence of the HPC composition on hydration process was observed by means of isoperbolic calorimetry.

Experimental

The mixtures composition was selected as the constitution of ordinary used HPC (Table I). Constituents used for HPC preparation were: white cement (A), silica fume (S), finely ground granulated blast furnace slag (VPS), finely ground silica (SUK), calcinated bauxite (B), polycarboxylate superplasticizer (SP) and water. The compressive and flexural strength of HPC prepared was measured after 28 day moist curing.

Table I
The constitution of mixtures

Number of mixture	A [g]	S [g]	B [g]	SUK [g]	VPS [g]	SP [g]	H₂O [g]
1	750	300	1,050	0	0	25	148
2	750	225	500	0	0	25	130
3	750	300	1,050	150	0	25	171.5
4	750	300	1,050	0	150	25	176
5	750	300	1,050	150	150	25	189
6	750	300	500	0	0	25	148
7	750	300	0	300	300	25	205
8	750	300	500	300	300	25	215
9	750	300	500	150	150	25	180
10	750	300	500	300	300	25	220
11	750	150	0	150	150	25	169.5
12	750	150	500	0	0	25	110
13	750	0	500	0	0	25	176.5
14	750	300	0	0	0	25	130
15	750	0	0	300	0	25	173
16	750	0	0	0	300	25	207
17	750	0	500	150	0	25	172
18	750	0	500	0	150	25	175

The influence of HPC composition on hydration process was observed by means of isoperbolic calorimetry. From obtained calorimetric curves, the maximal achieved temperature and time from mixing to reaching this temperature was evaluated.

Results

The controlling samples of cement and one constituent studied was prepared. Flexural strength of these mixtures decreased in the following sequence: silica fume > SUK > VPS > bauxite and compressive strength in this sequence: silica fume > VPS > SUK > bauxite.

From mixtures prepared by combination of selected components, the highest strength was measured in mixtures
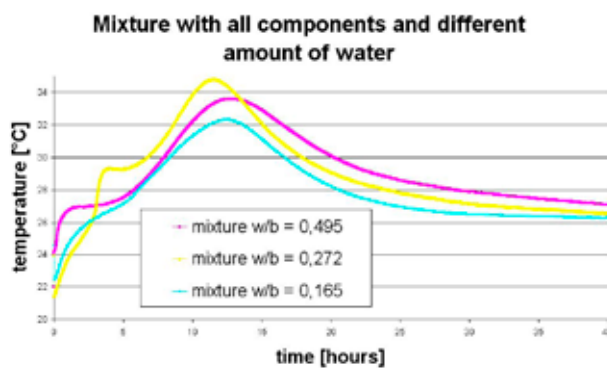
Fig. 1. **Influence of water to binder ratio on temperature
changes**

Table II
The constitution of mixtures

Number of mixture	Max. temperature [°C]	Time of max temperature [hours]	Flexural strength [MPa]	Compressive strength [MPa]
1	32.35	12.54	18.87	154.40
2	36.11	10.65	19.66	146.80
3	33.64	11.58	22.76	160.30
4	31.81	10.59	20.55	161.20
5	31.15	11.24	21.26	145.10
6	36.05	11.44	16.03	123.05
7	34.85	8.95	19.5	147.90
8	32.44	9.03	20.6	139.80
9	34.31	8.19	17.77	133.70
10	34.09	6.21	20.23	138.48
11	41.33	6.80	17.92	147.48
12	36.00	7.36	20.27	164.10
13	39.88	7.21	10.31	98.50
14	42.41	10.51	14.48	140.55
15	43.49	8.75	13.34	102.40
16	44.80	9.22	9.53	123.40
17	37.45	8.91	13.28	125.20
18	37.82	10.44	14.34	123.20

(a)

(b)
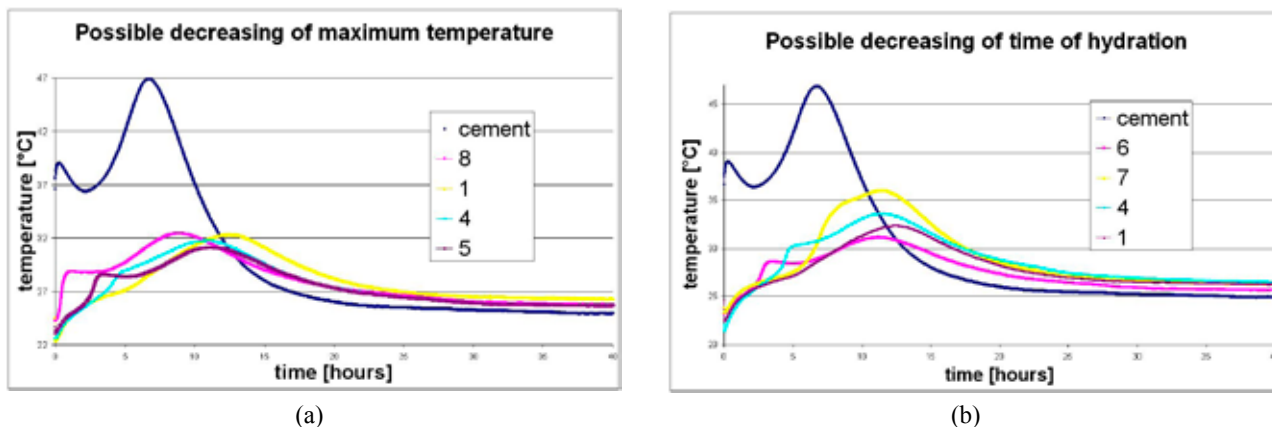
Fig. 2. **Decreasing of the maximum temperature and delaying of the second peak on the hydration curve**
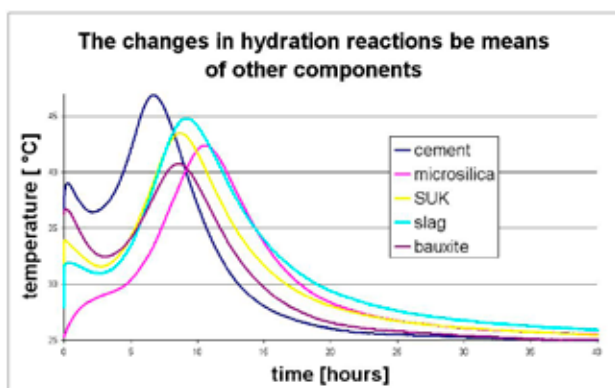
Fig. 3. **The changes in hydration process by using of other components**

with cement, silica fume, bauxite and only minimal amount of other components.

The influence of water to binder ratio on temperature changes was observed by measuring of mixture with all components and different amounts of added water.

When the w/b ratio is increased, total amount of heat is increased too. The temperature is increasing only to fixed amount of added water. Increasing the quantity of added water results in better contact of elements with water and hence supports the heat releasing hydration reaction. When the amount of added water is higher than quantum necessary for the hydration processes, this water becomes the "inert water", which does not contribute to the hydration, hence the maximum temperature reached during the hydration process is lowered.

From evaluated data (Table II) we can see, that as expected the highest temperature was reached by the mixtures with the highest amount of cement.

When some cement is replaced by other component, the maximum temperature and heat release is decreased. This decreasing is probably possible thanks to reaction of components with free lime, which going to decreasing of pH value. When the pH is changed, total heat of reactions is changed too. The bauxite is probably use as "inert element", which is effecting similarly as "inert water". For decreasing of maximum temperature are components more effectively in this sequence: bauxite > silica fume > SUK > VPS.

Some constituents studied also caused the retardation of the hydration process, which can be observed on the calorimetric curves as the shift of the second peak maximum. The constituents used are increasing time of hydration process in following sequence: silica fume > VPS > SUK > bauxite.

When we change some dosage of cement by other components, may be maximum temperature decreased by 20 °C and time of hydration increased two times. In compare with measuring of strength we can look that the highest strength is in mixtures with lower maximum temperature.

Conclusions

The compressive and flexural strength of HPC prepared was measured after 28 day moist curing. The influence of HPC composition on hydration process was observed by means of isoperbolic calorimetry. From obtained calorimetric curves, the maximal achieved temperature and time from mixing to reaching this temperature was evaluated. Flexural strength of prepared mixtures decreased in the following sequence: silica fume > SUK > VPS > bauxite and compressive strength in this sequence: silica fume > VPS > SUK > bauxite. For decreasing of maximum temperature are components more effectively in this sequence: bauxite > silica fume > SUK > VPS, for increasing time of hydration process in following sequence: silica fume > VPS > SUK > bauxite.

P23 TEMPERATURE AND MOISTURE EFFECTS ON MACRODEFCT-FREE COMPOSITE STRUCTURE AND PROPERTIES

FRANTIŠEK ŠOUKAL, JIŘÍ MÁSILKO, JAROMÍR HAVLICA, PETR PTÁČEK and TOMÁŠ OPRAVIL

Brno University of Technology, Faculty of Chemistry, Institute of Materials Science, Purkyňova 118, 612 00 Brno, Czech Republic,
soukal@fch.vutbr.cz

Introduction

Nowadays a part of hydrated cementitious materials research branch is focused on the polymer-cement composites with unusual manufacture qualities. The high-strength polymer-cement composites based on a water-soluble polymer are also known as macrodefect-free (MDF) composites. The name originates from its typical structure free of macrodefects such as large pores and flaws. MDFs have a privileged position due to its superior mechanical properties in the field of cementitious materials. Its flexural strength is reaching up to 300 MPa compared with values of about 5 MPa typical ones for ordinary Portland cement paste. The strength improvement is reached only by addition of up to 10 % of polymer and subsequent high-shear processing[1].

Macrodefect-free composites exhibit high sensitivity to moisture[2] due to its water-soluble polymer that interpenetrates throughout the whole bulk of composite forming an organo-inorganic matrix. The used polyvinylalcohol-acetate polymer forms the matrix with hydration product of aluminate cement during the high-shear processing and especially during the subsequent curing. The curing condition such as temperature and moisture plays important role in the matrix formation and further chemical composition and physical properties.

Experimental

The tested MDF composites were prepared using aluminate cement Secar 51 (Lafarge Aluminates) whose major phase is $CaO \cdot Al_2O_3$ supplemented with $12CaO \cdot 7Al_2O_3$, $2CaO \cdot Al_2O_3$ and $CaO \cdot TiO_2$ with total Al_2O_3 content above 50 % and with polyvinylalcoholacetate Sloviol P-8810 (NCHZ) of hydrolysis degree 88 % and viscosity of 4% water solution 11.6 mPa s.

Cement with polymer was mixed in amount from 2 up to 7.5 % wt. The water was added certainly to obtain an optimal consistency for subsequent high-shear processing. The water – solidus ratio varied around the value of 0.16. 1 % wt. of superplasticizer Glenium C151 (Degussa) was also added. The mixture of cement, polymer, water and superplasticizer was compacted and high-shear processed with twin-roll mixer. $100 \times 20 \times 2$ mm sized thin specimens were pressed at 5 MPa to constant pressure. These specimens were heated at 20, 40, 60, 80 and 100 °C in open atmosphere and afterwards for 1 and 7 days put into three types of surroundings – dry (polyethylene bags), moist (at almost 100% RH.) and immersed in water.

After 1 or 7 days of curing the specimen's flexural strength was tested in three-point bend instrumentation with 40 mm distance of supports.

Results

The flexural strength results of tested composites with different polymer content, cured at various temperatures and moisture conditions are shown at Figs. 1.–5. The results are divided according to moisture conditions to five histograms. The first graph at Fig. 1. represents samples cured in dry condition in closed PE bags. The effect of moisture was studied in two intensities – at almost 100% relative humidity and immersed in water, and after two periods – 1 day and 7 days, that is shown at following four histograms at Figs. 2.–5. Flexural strength is served in dependence on polymer content together with curing temperature.

	20°C	40°C	60°C	80°C	100°C
2,50%	29,07	28,78	30,3	39,94	32,23
4%	31,81	43,44	34,83	33,94	30,02
6%	44,38	42,84	55,86	33,89	41,69
7,50%	31,13	39,69	61,3	30,67	42,26
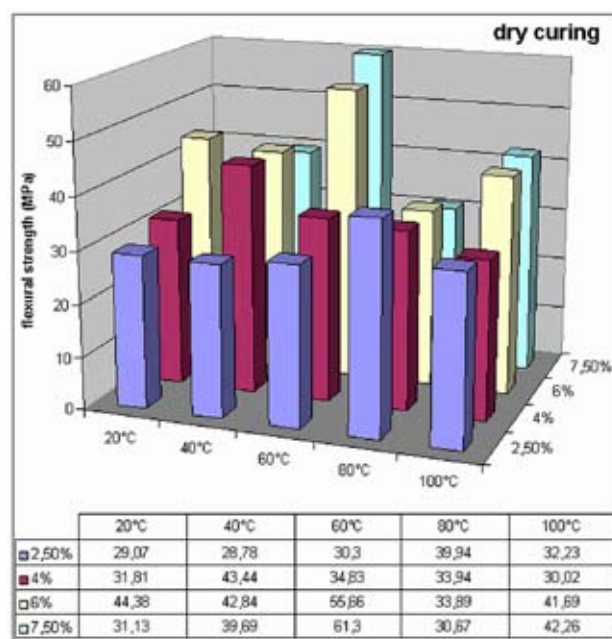
Fig. 1. **Flexural strength of MDF composites with different polymer content and curing temperature, cured in dry atmosphere**

Fig. 1. shows that composites with given polymer content have different flexural strength dependence on curing temperature stored in dry conditions. The highest flexural strengths at given polymer dosage are following: 2.5 % – 40 MPa at 80 °C, 4 % – 43 MPa at 40 °C, 6 % – 56 MPa at 60 °C and 7.5% – 61 MPa at 60 °C.

Samples cured at almost 100% relative humidity (Fig. 2. and Fig. 3.) generally exhibits lower flexural strength compared with that ones cured in dry atmosphere. The strength decrease at higher polymer content is over 50 % and at lower polymer content (2.5 %) about 30 %. It can be explained by lower initial strengths due to insufficient polymer content. At curing temperature of 60 and 80 °C the decrease is more outstanding (up to 75 %).On the other hand the most expressive
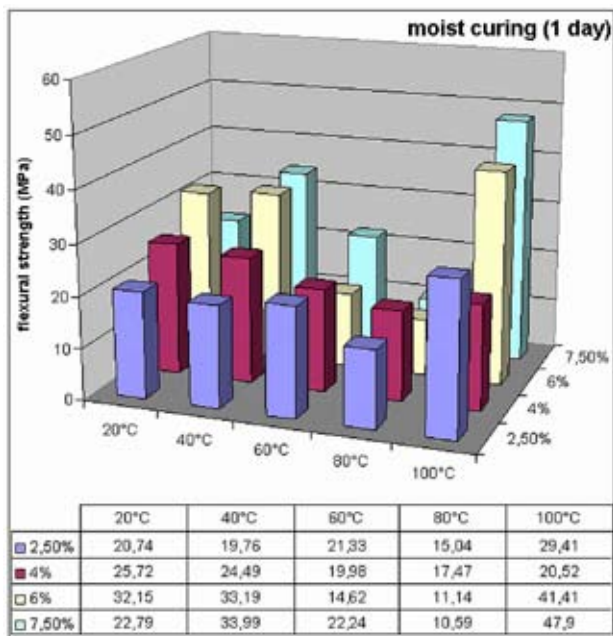
	20°C	40°C	60°C	80°C	100°C
▣ 2,50%	20,74	19,76	21,33	15,04	29,41
▪ 4%	25,72	24,49	19,98	17,47	20,52
▢ 6%	32,15	33,19	14,62	11,14	41,41
▢ 7,50%	22,79	33,99	22,24	10,59	47,9

Fig. 2. **Flexural strength of MDF composites with different polymer content, curing temperature, cured in moist atmosphere for 1 day**

	20°C	40°C	60°C	80°C	100°C
▣ 2,50%	17,08	17,83	25,79	18,51	13,27
▪ 4%	17,68	17,63	31,86	8,57	12,02
▢ 6%	19,26	13,61	39,28	8,9	9,65
▢ 7,50%	16,03	8,81	42,99	8,4	6,3

Fig. 4. **Flexural strength of MDF composites with different polymer content, curing temperature, immersed in water for 1 day**

	20°C	40°C	60°C	80°C	100°C
▣ 2,50%	21,14	20,19	20,28	16,4	19,09
▪ 4%	32,94	20,53	21,33	10,35	12,64
▢ 6%	30,22	29,76	17,91	10,74	16,8
▢ 7,50%	19,99	24,14	25,86	8,43	6,23

Fig. 3. **Flexural strength of MDF composites with different polymer content, curing temperature, cured in moist atmosphere for 7 days**

	20°C	40°C	60°C	80°C	100°C
▣ 2,50%	34,14	27,14	25,13	25,7	25,9
▪ 4%	29,17	22,9	20,86	16,86	17,52
▢ 6%	22,11	16,07	22,94	14,29	16,02
▢ 7,50%	20,65	14,89	21,28	12,72	11,36
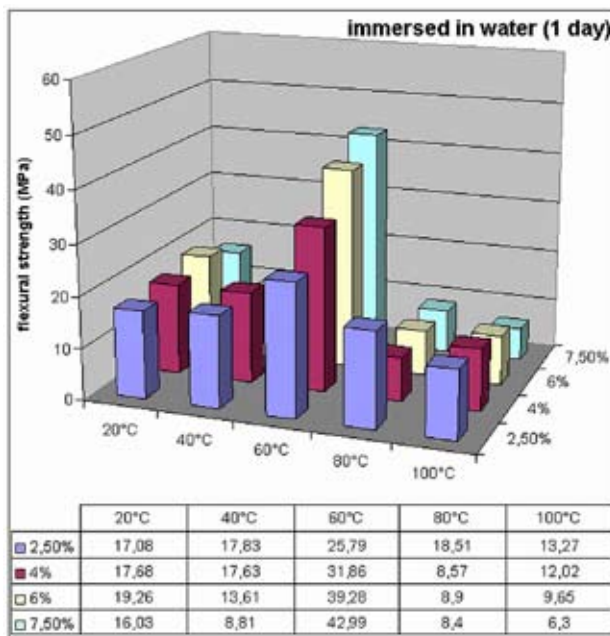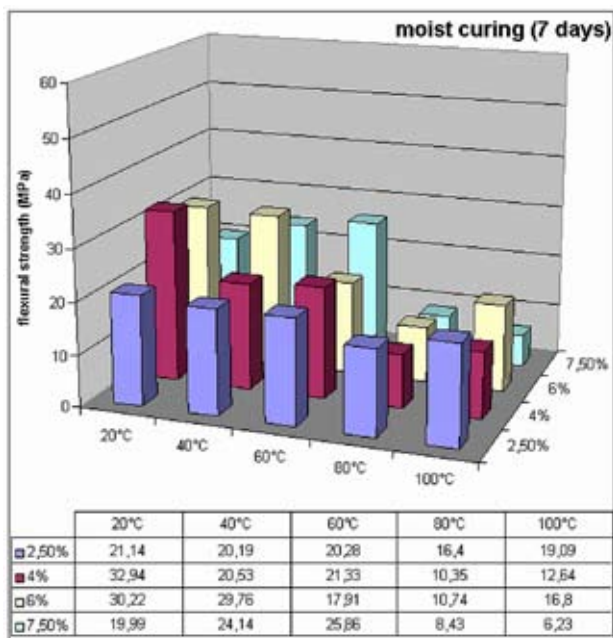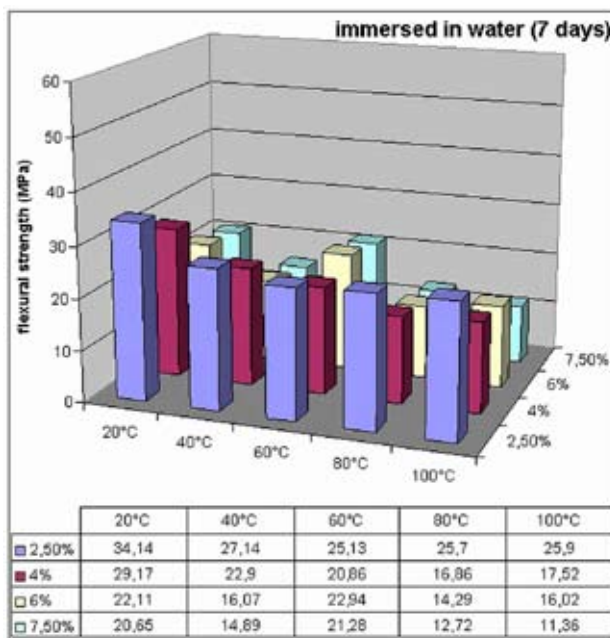
Fig. 5. **Flexural strength of MDF composites with different polymer content, curing temperature, immersed in water for 7 days**

difference is at 100 °C. After 1 day of moist curing the flexural strengths keep almost the same values compared with dry curing, whereas flexural strengths after 7 days of moist curing are very low especially at polymer content of 7.5 %, where the flexural strength exhibits only almost 10 % of the initial

value. Composites cured at other temperatures generally are not influenced by time of moist curing.

MDF composites immersed in water for 1 day (see Fig. 4.) exhibit overall more lower flexural strengths than composites cured in moist atmosphere. One significant irre-

gularity is in the case of composites cured at 60 °C. These samples have almost the same flexural strength like that ones cured in dry atmosphere. On the other hand composites immersed for 7 days exhibits markedly lower decrease of flexural strength. The lower polymer content and temperature is, the lower decrease is monitored. Polymer in MDF composites immersed in water is washed out during the first day that leads to very porous structure and lower strength. In the following period up to 7 days of immersion water come into the open pores and the non-hydrated cement grains undergoes further hydration. Large pores after polymer agglomerates are filled with $Al(OH)_3$ precipitated from solution and CAH gel forms the binder matrix. Therefore the flexural strength of MDF composites after longer immersion increases again.

Fig. 6.   **Image in polarized light of thin section of MDF composite containing 6 % of polymer after 7 days in moist atmosphere**

Conclusions

Prepared MDF composites exhibits extreme mechanical properties in terms of cementitious materials. The best reached flexural strength was 61.3 MPa in the case of 7.5 % of PVAl cured at 60 °C. Overall the best performing composite consist of 6 % of PVAl at all curing temperatures. Its best flexural strength was reached after curing at 60 °C in the value of 55.7 MPa.
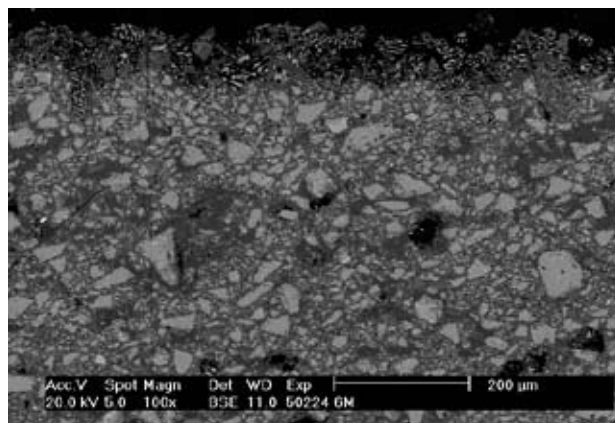
Fig. 7.   **SEM image of thin section of MDF composite containing 6 % of polymer after 7 days of immersion in water**

Generally, the mechanical properties of tested composites were significantly influenced by contact with water. Samples stored in moist atmosphere for 7 days exhibited higher strength decrease then that ones stored for only 1 day. Immersion in waterfor 1 day leads to even higher strength fault compared with moist atmosphere. On the other hand the longer storage under water evoked follow-up increase of flexural strength. In the first stage polymer was washed up from pores of composite and subsequently water hydrated exposed clinker grains throughout the open pores.

REFERENCES
1. Šoukal F.: Disertační práce, Brno: Vysoké učení technické v Brně, 2007.
2. Drabik, M., et al.: J. Therm. Anal. Calorim. *76*, 91 (2004).

P24 LATEX MODIFIED CEMENT COMPOSITES: EFFECT OF POLYMER TYPE

FRANTIŠEK ŠOUKAL, VÁCLAV VINTER, JAROMÍR HAVLICA, PETR PTÁČEK and TOMÁŠ OPRAVIL

Brno University of Technology, Faculty of Chemistry, Institute of Materials Science, Purkyňova 118, 612 00 Brno, Czech Republic,
soukal@fch.vutbr.cz

Introduction

Nowadays an extensive research is aimed to polymer-cement materials. Generally, two ways can be mentioned how to combine organic polymer with the inorganic cement. The first one is concrete impregnation with polymer, where polymer in form of solution, emulsion or dispersion is transported into the open pore structure of concrete. The second type of these materials is the polymer modified concrete (PMC), where the polymer is mixed within fresh cement paste building up two component composite binder. The nature of mineral phases – polymer chemical interactions decides on the consequent properties of composite[2].

Polymer latex modified cement composites forms within its structure two different binder – cement paste and polymer films. Properties of these binders can supplement each other due to intramolecular forces interactions. Water from latex is consumed during the hydration of cement that leads to formation of polymer films. Interactions of polymer with the surrounding mineral phases are primarily of van der Walls type. Almost no chemical bonds are supposed in this system. Latex modified mortars exhibit increased flexural strength. Elastic polymer films fulfill pores and flaws which avoids premature failure of the material. On the other hand pressure strength is not so influenced by polymer films formation. Its value is preferably determined with concretion of gel and crystalline phases of hydrated cement[1,2].

The paper deals with effect of polymer in latex on mechanical properties of latex modified cement materials.

Experimental

Preparation and Curing of PMC

There were selected 5 types of latexes according to polymer nature. Some of their basic properties are presented at Table I. Lipaton XA 491 represents styrene-vinylacrylic esters (SAE), Lipaton SB 5813 is representative of styrene-butadiene rubbers (SBR), Plextol × 4002 of polyacrylic esters (PAE), Plextol D 509 is latex of copolymer of methylmethacrylate and n-butylacrylate (MBR) and Duvilax BD-20 is latex of polyvinylacetate (PVAc). Latexes of series Lipaton and Plextol are produced by PolymerLatex company in Germany and Duvilax is produced by Duslo Šala in Slovakia. Polymer latexes were combined with Portland cement CEM I 42.5 R (Turňa nad Bodvou, Slovakia).

Polymer latexes were mixed with cement from 1 to 15 % of weight to cement. Various amount of water was added to obtain always the same consistency. Fresh pastes were formed to testing beams of dimensions of $20 \times 20 \times 100$ mm. Thereafter smples were cured in atmosphere of almost 100% relative humidity.

Table I
Basic properties of tested polymer latexes

| Properties | Polymer latex | | | | |
	Lipaton XA 491	Lipaton SB5813	Plextol X 4002	Plextol D 509	Duvilax BD–20
	SAE	SBR	PAE	MBR	PVAc
Polymer Solids content [%]	57	48.5	60	50	53.5
pH [20°C]	8.0	8.0	2.0–2.5	7.5	3.0–5.0
Density [g cm^{-3}]	1.04	1.01	1	1.05	–
Viscosity [mPa s]	500–4,000	30	100–2,000	100–2,000	4,000–19,000

Results

Mechanical Properties

The whole range of tested latexes was primarily tested in PMC pastes of polymer content of 5, 10 and 15 % of weight to cement. Compressive and flexural strength after 28 days of curing was tested as the basic mechanical parameters. For comparation a pure cement paste without latex was prepared and its compressive strength was 64.06 MPa and flexural strength was 9.14 MPa and this values are marked in graphs with red line. The experimental results are shown at Fig. 1. and Fig. 2. Polymer latexes Plextol × 4002 (PAE) and Duvilax BD-20 (PVAc) in dosage 10 and 15 % markedly fall behind the other types in strength parameters. We can see that PMC pastes with PAE and PVAc latex in dosage of 5 % exhibit almost the same flexural strength compared with pure cement paste. Higher polymer dosage leads to decrease of flexural strength up to 50 % of initial value. Polymer addition decreased the compresive strength in all cases beyond SBR latex. SBR latex decreased compressive strength under the value of pure cement paste after dosage of 15 %. PAE and PVAc
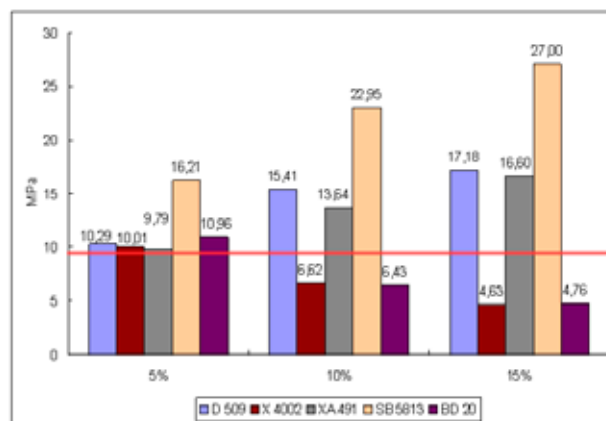
Fig. 1. **Compressive strength of PMC after 28 days of curing**

Fig. 2.   **Flexural strength of PMC after 28 days of curing**
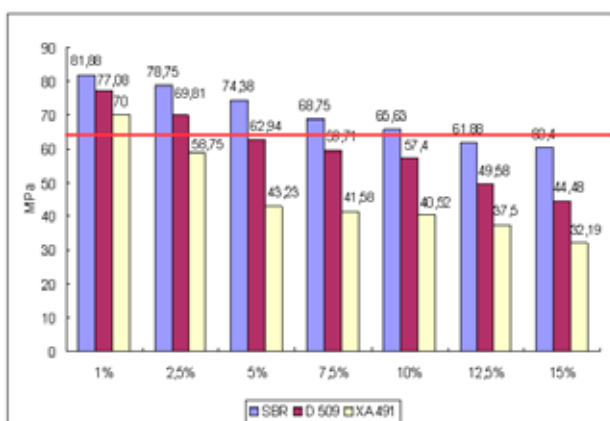
Fig. 3.   **Compressive strength of selected PMC after 28 days of curing**
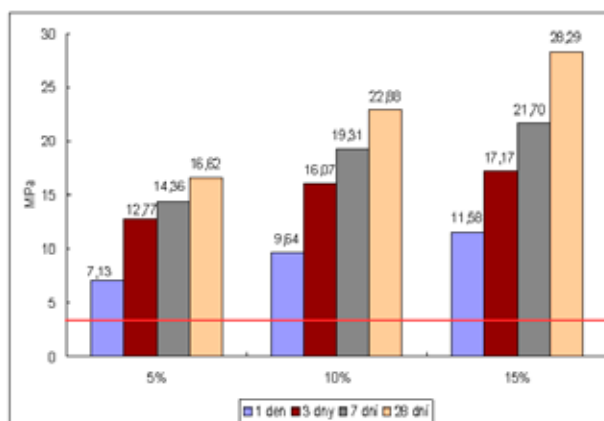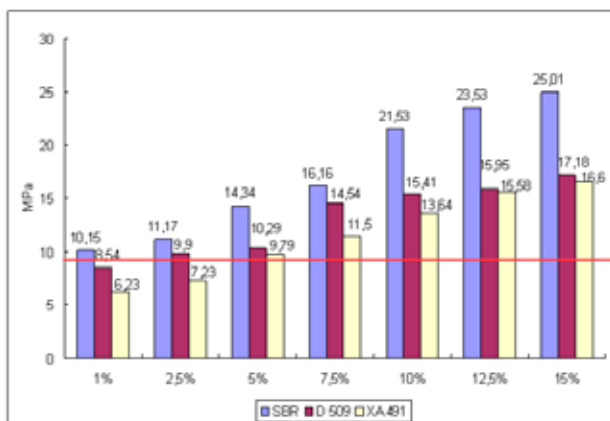
Fig. 4.   **Flexural strength of selected PMC after 28 days of curing**

latexes leads to compressive strength decrease up to 20 % of pure cement paste. Therefore the following experiments targeted the only three perspective latexes – Lipaton SB 5813 (SBR), Lipaton XA 491 (SAE) and Plextol D 509 (MBR).

Subsequently the selected polymer latexes were used to prepare PMC pastes of polymer dosage 1, 2.5, 5, 7.5, 10, 12.5

Fig. 5.   **Compressive strength development of PMC with latex SB 5813**

Fig. 6.   **Flexural strength development of PMC with latex SB 5813**

and 15 % of weight to cement. Again flexural and compressive strength was tested and its results are shown at Fig. 3 and Fig. 4. At Figs. 3. and 4. we can see that increasing content of polymer in all cases increases flexural strength and on the other hand it decreases compressive strength. The highest increase is notable in the case of SBR latex from 10.15 MPa up to 25.01 MPa. PMC pastes with 15 % of polymer reach almost double flexural strength in case of SAE and MBR latexes and paste with SBR latex reached even triple flexural strength compared to pure cement paste. SAE latex leads to flexural strength increase after 5% addition to paste and under this value flexural strength is decreased. Compressive strength decrease was lowest in pastes with SBR latex again. The pastes with polymer dosage up to 10 % exhibited higher compressive strength even than pure cement paste. PMC paste with MBR latex holds its compressive strength over the pure cement one up to 2.5% of polymer content and paste with SAE latex only at 1% dosage.

PMC paste with the most perspective SBR latex was tested also for strength development in time. The experiment were hold with 5, 10 and 15 % polymer dosage and compressive and flexural strength was test after 1, 3, 7 and 28 days of

hydration. Experimental results are introduced at Figs. 5. and 6. We can see that increasing polymer content increases also flexural strength development and decreases development of compressive strength. Producent declared 2–day flexural strength of pure cement paste is 3.3 MPa and compressive strength 31.1 MPa (red lines in Figs. 5. and 6.). Flexural strength development of tested PMC paste with SBR latex is several times faster. Strength development of PMC paste with low polymer dosage significantly slows down after 3 days of hydration in contrast to high polymer dosage PMC paste whose strength development rate is quite extensive up to 28 days of hydration. Development of compressive strength is markedly fast up to 3 days in all polymer dosage.

Conclusions

The measured strength characteristics show that the most promising type of polymer latex for preparation of polymer modified concrete is styrene-butadiene ruber latex (SBR). Its 15% addition to cement paste leads to triple flexural strength after 28 days of hydration, while compressive strength is not reduced up to 10% dosage. Its flexural strength development in time is very fast. It reaches more than 30 % of final strength after 1 day of hydration. Very good results were achieved also with styrene-vinylacrylic ester latex and methylmethacrylate n-butylacrylate copolymer latex. They higher addition leads to higher compressive strength decrease, therefore they should be preferably used in low dosage. Polyacrylic ester latex and polyvinylacetate latex exhibited decrease of the compressive even the flexural strength so that they are not suitable for PMC preparation.

REFERENCES

1. Eve S., Gomina M.,: J. Eur. Ceram. Soc. *27*, 1395 (2007).
2. V. S. Ramachandran: *Concrete admixtures handbook – properties*, science and technology, 2nd edition. ISBN O-8155–1373-93.

P25 INFLUENCE OF CONDITIONS ON HYDRAULIC CALCIUM ALUMINATE PHASES HYDRATION MECHANISMS

FRANTIŠEK ŠOUKAL, JAN KOPLÍK, JAROMÍR HAVLICA, TOMÁŠ OPRAVIL and VITĚZSLAV FRANK

Brno University of Technology, Faculty of Chemistry, Institute of Materials Science, Purkyňova 118, 612 00 Brno, Czech Republic,
soukal@fch.vutbr.cz

Introduction

Aluminate cement is known since beginning of 20th century. After a few collapses of constructions made from aluminate cement its utilization such as construction material was prohibited in many countries. Nowadays aluminate cement finds utilization especially in refractories and some non-traditional material e.g. macrodefect-free composites.

CA (CaO·Al$_2$O$_3$), the major component of common aluminate cements, is responsible for the characteristic properties of aluminate cements, namely strength and hydration rate. CA$_2$ (CaO·2Al$_2$O$_3$) mineral grossite and C$_{12}$A$_7$ (12CaO·7Al$_2$O$_3$) mineral mayenite are usually minor hydraulic phases of aluminate cements, but CA$_2$ can major component of high-aluminate cement. Their presence influences the properties of cement, chiefly hydration rate and early and late strength. C$_3$A (3CaO·Al$_2$O$_3$) is an important component of Portland cement. Although it is not major component, it plays significant role in hydration process of Portland cement especially in reactions with gypsum.

Despite of cement hydration has been studied for a long period and there were established a number of reaction mechanisms (Le Chatelier, Michaelis) and there were identified some of hydration products, the process of hydration of the individual phases has not been clearly explained. In contrast to calcium silicates primarily not all the hydration products of calcium aluminates have been identified to date as well as their hydration kinetics at various pH environments.

Experimental

Preparation of Hydraulic Calcium Aluminate Phases

Calcium aluminate phases can be prepared in several ways. The most common preparation method is based on solid phase clinkering that was used. CaCO$_3$ and Al$_2$O$_3$ in p.a. clearness were well mixed in stoicheiometric rate appropriate for the individual phases.

According to results the sintering has to be done at least twice to establish thermodynamic equilibrium and to obtain the pure phase. Throughout the first sintering the mixture was heated to 900 °C at rate of 10 °C min^{-1} for 1 hour. Then the heating continued at the same rate to the final temperature and there kept out for 5 hours. The final temperature depends on the prepared phase: CA and C$_3$A – 1,450 °C, CA$_2$ – 1,600 °C, C$_{12}$A$_7$ – 1,360 °C. The second heating was accomplished without the holding at 900 °C right to final temperature for

5 hours as well. The products were grounded after each sintering in vibration mill. The clearness of prepared calcium aluminate phases was verified with XRD analysis. Only the powder fraction with particles passed sieve mesh of 90 μm was used for the following hydration.

Hydration and Semiadiabatic Calorimetry

For the evaluation of hydration kinetics the semiadiabatic calorimeter has been utilized. The calorimeter consists of thermo-isolation cell from polystyrene foam, 250 ml reaction vessel, magnetic stirrer, thermistor, digital multimeter and data logging software in PC.

Hydration of the individual phases was monitored at four different pH values varying from neutral to high alkali: 6, 9, 11, 12.65. 30 g of the phase was poured into 50 ml of water with appropriate puffer. The pH 6 was measured in the pure distilled water. The temperature logging was started immediately after the pouring of oxide into water with logging interval of 2 seconds for following 48 hours. Afterwards the hydrated mixture was filtrated and several times rinsed with distilled water. The solid hydration products were dried at 40 °C at decreased pressure for 4 hours.

Results

Semiadibatic Calorimetry

Hydration of C$_3$A is the most intensive between 20 and 50 minutes after mixing with water depending on pH value (see Fig. 1.). This hydration process is very fast and linked with high evolution of heat and its kinetics is enough fast until 5 hours after mixing. At pH of 6, 9 and 11 can observed very weak exothermic process at 32–36 hours after mixing. Compared with other oxides the hydration of C$_3$A is the fastest. Hydration at pH value of 6 is connected with the highest temperature increase of all oxides.
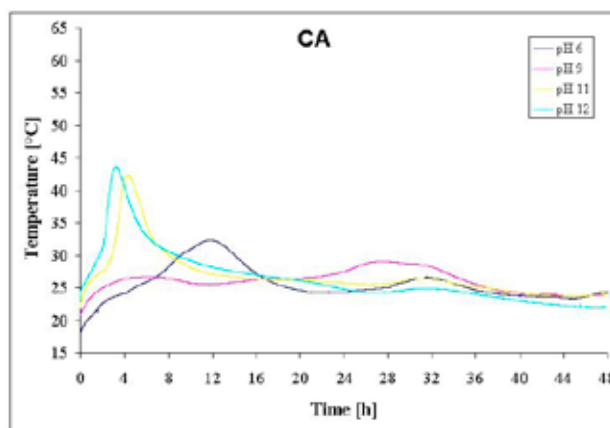
Fig. 1. **Semiadiabatic calorimetric curves of CA hydrated at pH 6–12**

Hydration of CA at all environments is characteristic by two separated processes evolving heat. The first one has maximum of rate at 3–12 hours after mixing and its rate strongly

depends on pH value (see Fig. 1.). The hydration rate is increasing with increasing pH, only hydration at pH 9 is totally inhibited in this first step. On the other hand the intensity of the second weak process occurring after 27–32 hours is higher then intensity at the other pH values. Overall hydration rate of CA is the second slowest of the examined oxides.
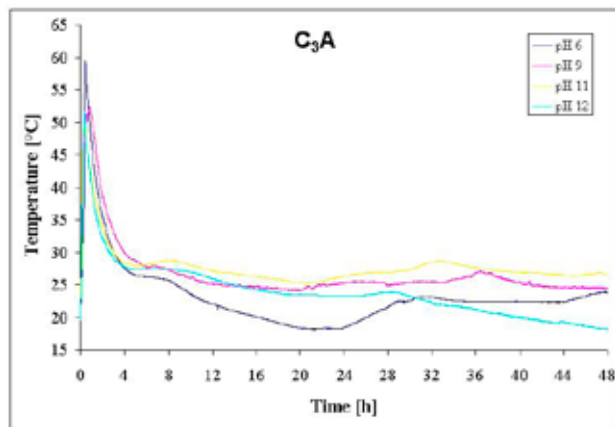
Fig. 2. **Semiadiabatic calorimetric curves of C_3A hydrated at pH 6–12**
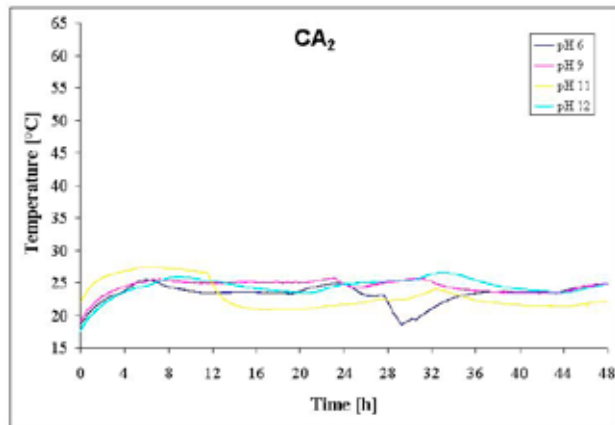
Fig. 3. **Semiadiabatic calorimetric curves of CA_2 hydrated at pH 6–12**

CA_2 exhibits the lowest hydration activity (see Fig. 1.). The hydration process starts during the first 5 hours and the evolution of heat is poorly identifiable. The hydration continues whole monitored 48 hours at very low intensity. Two weak separated processes could be found at 6–9 hours, that is most clear at pH 6, and about 23 hours of hydration detectable at pH 11 and 12.

The kinetics of hydration process of mayenite is very similar to that of C_3A (see Fig. 1.). The highest evolution of heat comes on after 40–60 minutes of hydration. This process is also very fast. A weak process can be observed at 30–36 minutes after mixing as well. $C_{12}A_7$ is the second most reactive oxide.
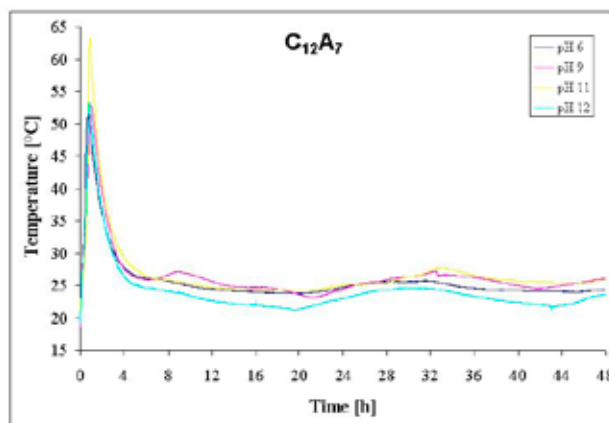
Fig. 4. **Semiadiabatic calorimetric curves of $C_{12}A_7$ hydrated at pH 6–12**

DTA and X-ray Diffraction Analysis

Samples cured at almost 100% relative humidity (Figs. 2. and 3.). The DTA curves of hydrated C_3A exhibit three endothermal effects at all pH (see Fig. 2.). XRD analysis identified only one crystalline hydration product – hydrogrossular C_3AH_6 (see Fig. 3.). The first endotherm without weight loss at 150 °C can be connected with decomposition of C_3AH_6 to C_2AH_5 and portlandite CH. The second strong endothermal effect at 310 °C is invoked by dehydration of C_2AH_5 followed by dehydration of portlandite at 460 °C. This process is confirmed by the proportion of weight loss during these dehydrations that is always strictly 5 : 1. TGA curves shows that the most amount of hydrogrossular was created at pH 9 and the least at pH 11.

The hydrated CA exhibits more hydration product than C_3A and their amount only slightly depends on pH (see Fig. 2.). As well as in the case of C_3A there can be found hydrogrossular, but only as the minor hydration product, especially at pH 12 (well observable is only endotherm at 310 °C). Endotherms at 150 and 275 °C at all pH are joined with dehydration of C_2AH_8. This hydrate was not identified by XRD (see Fig. 3.), so that it has to be of amorphous or microcrystalline nature. The amount of C_2AH_8 is comparable at all pH values. A distinct endothermal effect is connected with a crystalline hydrate that was identified also by XRD. The nature of this hydrate was not clarified. Its diffractions are not published in available XRD databases. The highest amount of this hydrate is at pH 6 and 12, the least at pH 11. Another weak endothermal maximum can be observed at 225 °C mainly at pH 11 (see Fig. 2.) and one at 320 °C noticeable at pH 6. These effects have not been assigned.

DTA curves of hydrated CA_2 are shown also at Fig. 2. DTA and TGA curves correspond with measured calorimetry results (see Fig. 1.). The extent of hydration is very low. No hydration products at pH 9 were identified. Hydration at pH 6 and partially at pH 11 and 12 leads to lower amount of hydration products. As well as in the case of CA there can
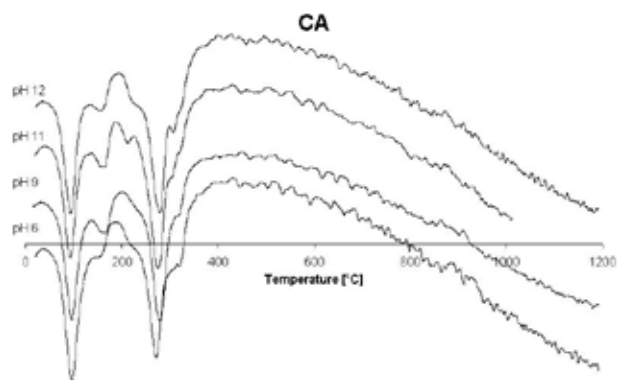
Fig. 5.   **DTA curves of hydrated CA at pH 6–12**
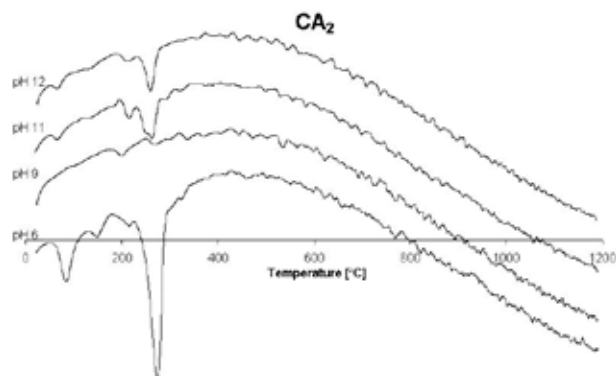
Fig. 7.   **DTA curves of hydrated CA$_2$ at pH 6–12**
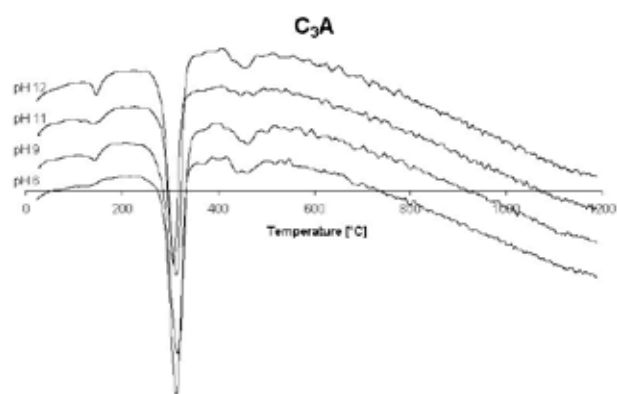
Fig. 6.   **DTA curves of hydrated C$_3$A at pH 6–12**
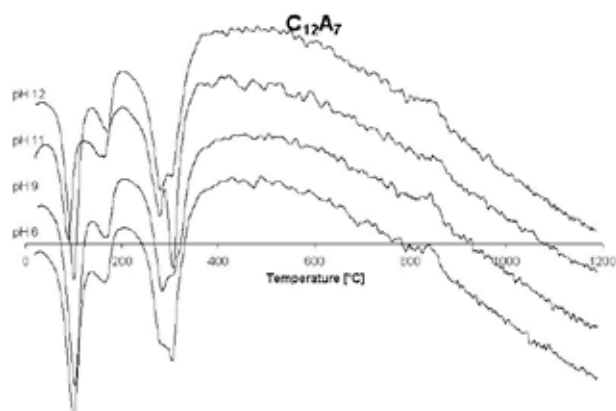
Fig. 8.   **DTA curves of hydrated C$_{12}$A$_7$ at pH 6–12**

be identified hydrate C$_2$AH$_8$ and not clarified hydration products (at 70 and 215 °C).

Hydration of mayenite leads to similar hydration products as in the case of CA. There can be identified hydrogrossular C$_3$AH$_6$ at pH 11 and 6 such as main hydration, whereas at pH 9 and 12 its amount is lower. C$_2$AH$_8$ was found mainly at pH 6, 9 and 12 as well as the not clarified crystalline hydration product at 100 °C that is the main hydration at pH 6, 9 and 12. Analogous to C$_3$A the lowest conversion of oxide to hydration products is at pH 11.

Conclusions

According to obtained results oxides C$_3$A and C$_{12}$A$_7$ exhibit highest hydration activity. Hydration products and their formation kinetics are very similar at all tested pH

values. The least reactive calcium aluminate phase is CA$_2$. Hydration of C$_3$A at all pH values evokes only one product – cubic hydrogrossular C$_3$AH$_6$. Hydration of CA at all pH and C$_{12}$A$_7$ at pH 9 and 12 leads also to formation of hydrate C$_2$AH$_8$. Less amount of C$_2$AH$_8$ was also found in hydration products of mayenite at pH 6 and 11 and CA$_2$ at pH 6, 11 and 12. During the hydration of CA and C$_{12}$A$_7$ an unidentified crystalic hydration product is generated. Its X-ray diffractions were not found in the newest databases. Generally, hydration of CA and C$_{12}$A$_7$ leads to formation of the same products, only changes are in the amount of hydrates.

P26 THE STUDY OF BUILDING BIOCORROSION

EVA TERPÁKOVÁ

Technical University of Košice, Civil Engineering Faculty, Institute of Building and Environmental Engineering, Vyso-koškolská 4, 042 00 Košice, Slovak Republic,
eva.terpakova@tuke.sk

Introduction

Biodeterioration or biocorrosion of building materials – stone, concrete, mortar, etc., can be caused by such microorganisms as bacteria, fungi, lichens, algae, and plants (Wasserbauer, 2000). Multidiscipline methods are available for the study of biodeterioration each other materials. Almost of them is bearing to biological part of problem e.g. identification of biodeteriorates, evaluating of birth biofilm or studies of metabolites. Biofilms are complex communities of microorganisms attached to surfaces of materials generally, or associated with interfaces. Bacterial biofilm formation on inert surfaces is a significant technical and economic problem in a wide range of environmental, industrial, and medical areas. Bacterial adhesion is generally a prerequisite for this colonization process and, thus, represents an attractive target.

Experimental

To the purpose of concrete corrosion study (chemical, physical and structural changes) is important to obtain the representative sample from damaged part. Drilling corps are the most suitable for these purposes. On the other hand, there is some risk to damage of biodeteriogen or biofilm in consequence of high temperature beside drilling procedure. The cores of 75 mm diameter and about 100 mm length were obtained by coring equipment Hilti. The experimental samples are from concrete material of sewerage system of 30 years old building with very aggressive environment, because mineral water sources with H_2S are in this locality. Consequently potential risk of biodeterioration follows to SRB (sulphate reducing bacteria) which living in this type of water.

Chemical impact on to concrete samples was tested by classical methods; results are in Tables II and III. From surface were taken small amounts of sample under sterile conditions for microbiological tests and examination of MID of concrete.

Analytical Evaluation

The dependence of pH values changes and aggressive ions on depth e.g. their profile was determined. The samples were separated mechanically by gradual depth up to 3.0 mm. Concrete powder after grinding procedure was collected; the each other portion of samples was dried up to constant weight at 105–110 °C. For potenciometric determination of alkality we used 1 ± 0.0005 g of samples after their separation, and dissolute in 100 ml distilate water. Solutions were shaken for 2 hours. Filtrate was used to determine Cl^- ions by potentiometric method. The result expressed as % wt. in cement stone

are in Tables II and III. The pH values were determined by potentiomeric method, too. Concentration of inorganic sulphates was determined by gravimetric method follow to Slovak standard rules (Priganc, Terpáková, 2003).

Biocorrosion Evaluation

The media used for isolation and continued cultivation of samples obtained from concrete surface were neutrophilic media (N) and acidophilic media (A) prepared follow to (Sand, 1987). Experiment continues in this time and details of biodegradation inner parts of concrete will be tested by AFM (atomic force microscope) in a future.

Results

Table I
Colonial types of bacteria cultivated from concrete

	(N)	(A)
Sample 1	Opaque, white spreader with irregular edges Small, round, creamy collared	Large, white with very good growth
Sample 2	Small, round, creamy collared Opaque, white spreader with irregular edges	Small, round, white translucent colonies Small, round, shiny yellow colonies

(N) – neutrophilic medium
(A) – acidophilic medium

Table II
Chemical results of concrete core 1

Depth of sample [mm]	Concentration [%]			
	pH ± 0.01	Cl^-	SO_4^{2-}	l.o.i 1,000 °C
0–3	9.25	0.025	0.13	12.23 ± 0.01
3–6	9.36	0.021	0.12	10.95 ± 0.02
6–9	9.40	0.020	0.11	9.86 ± 0.02
9–12	9.55	0.020	0.09	9.78 ± 0.01
12–15	9.73	0.017	0.09	9.53 ± 0.01
Comprehensive strength values [MPa]				20.3

Table III
Chemical results of concrete core 2

Depth of sample [mm]	Concentration [%]			
	pH ± 0.01	Cl^-	SO_4^{2-}	l.o.i 1,000 °C
0–3	9.12	0.028	0.16	13.40 ± 0.01
3–6	9.20	0.022	0.13	11.24 ± 0.01
6–9	9.23	0.019	0.11	10.18 ± 0.01
9–12	9.35	0.018	0.08	10.25 ± 0.01
12–15	9.62	0.015	0.07	10.13 ± 0.01
Comprehensive strength values [MPa]				19.5

Fig. 1.   **Detail view of surface sample number 1**

Fig. 2.   **Detail view of surface sample number 2**

Major colonial types of bacteria obtained from corroded concrete product are described in Table I.

Determination the typical corrosive agents confirmed their presence in the structure of concrete and consequently manifestation of sulphate corrosion and carbonisation above all.

Conclusions

Aggressive MID microorganisms can form a biofilm on the surface of samples so that when nutrients are provided the microbes remain active. The changes of physical – chemical characteristics expressed as the differences in alkaline reaction confirme the neutralisation process of cement stone due to MID up to 3–6 mm depth. Follow to alkali reaction values is possible to confirm that 2–3 degree of carbonisation concrete is present in both samples, (Matoušek, Drochytka, 1998). The statistically significant changes were obtained in case determination of loss weight by ignition too. Results of long time experiment after incubation by neutrophilic and acidophilic medium were present in future.

REFERENCES
1. Wasserbauer R.: *Biologické znehodnocení staveb*. ABF,a.s. Nakladatelství ARCH, Praha, 2000.
2. Priganc S., Terpáková E.: *Diagnostic of concrete construction parts*. TU-SvF, TULIP, Košice, 2003.
3. Matošek M. Drochytka R.: *Atmosferická koroze betónu*. IIKAS, Praha, 1998.

P27   MILLING OF OLIVINE (Mg, Fe)₂SiO₄ IN HIGH-ENERGY MILLS BY WET AND DRY WAY

ERIKA TURIANICOVÁ and PETER BALÁŽ

Institute of Geotechnics, Slovak Academy of Science, Watsonova 45, 043 53 Košice, Slovak Republic,
turianicova@saske.sk

Introduction

High-energy milling is now one of the materials processing methods that is widely used in powder technology. The advantage of high-energy milling is its simplicity and effectiveness. The disintegration of mineral particles by mechanical activation is accompanied by an increase in the number of particles and by generation of fresh, previously unexposed, surface[1,2].

Particle size reduction in olivine is produced by milling (either wet or dry), the nature of which plays an important role in the physicochemical properties of the resulting powders and in the further processing steps.[3–5] The effects of milling have been studied extensively, mainly for silicates minerals such as olivine because it is a mineral possible to use as a suitable feedstock for carbon dioxide sequestration[3,4].

The basic concept behind CO_2 disposal by means of silicates well known as mineral sequestration was originally proposed by Seifritz in 1990 and first studied in more details by Lackner. This idea mimics very slow (of thousands to millions of years) natural weathering process of silicate minerals conversion.

Mechanical activation by high-energy milling can results in major improvement of the reaction rate[1].

Experimental

Material

The olivine sample used in this study was kindly supplied by the Norwegian mining company North Cape Minerals (NCM) and originates from the production plant at Åheim (Norway).

The sample contains approximately 93 % forsterite (Mg_2SiO_4) and 7 % fayalite (Fe_2SiO_4). This olivine composition is referred to as Fo_{93}. Small amounts of accessory minerals like chlorite, chromite, enstatite, serpentinite and talc can also be found in the sample. The olivine product used in this study is a foundry sand (AFS50) and contains approximately 95 % pure olivine.

The bulk chemical composition (as analysed by NCM using X-ray fluorescence (XRF) analysis) of the sample is following: 50.2 % MgO, 41.5 % SiO_2, 7.41 % Fe_2O_3, 0.36 % Al_2O_3, 0.33 % NiO, 0.30 % Cr_2O_3, 0.08 % MnO, 0.08 % CaO, 0.01 % Na_2O, 0.01 % K_2O, LOI 0.27 %.

Mechanical Activation

Two milling models including dry and wet modes are applied in the milling processes such as mechanical activation of material and/or minerals. The comparison of the wet and dry milling effects on the structural changes usually was made at the same grinding mill.

The olivine sample was mechanically activated in two high-energy mills by various conditions:

Laboratory planetary ball mill (Pulverisette 6, Fritsch, Germany) (PM) (Fig. 1.a):
- Weight/diameter of balls: 360 g 10 min⁻¹
- Volume of milling chamber: 250 ml
- Material of milling chamber and balls: WC
- Rotation speed: 450 min⁻¹
- Weight of sample: 18 g
- Volume of added water: 0–100 %
- Milling times: 2–30 min
- Conditions of milling: ambient temperature, free access of air

Industrial nutating mill (Hicom 15, Hicom International Pty, Ltd., Australia)(NM)(Fig. 1.b):
- Weight/diameter of balls: 10 kg 5 mm⁻¹
- Volume of milling chamber: 5,000 ml
- Material of milling chamber and balls: stainless steel
- Rotation speed: 900 min⁻¹
- Weight of sample: 1,000 g
- Volume of added water: 0–50 %
- Milling times: 1–10 min
- Conditions of milling: ambient temperature, free access of air

Specific Surface Area

The specific surface area was determined by the low temperature nitrogen adsorption method in a Gemini 2360 sorption apparatus (Micromeritics, USA).

Results and Discussion

The olivine sample was mechanically activated in one laboratory and one industriall mill. Conditions of milling are described in previous part. The aim of the present investigation was to study the effects of dry and wet milling on the
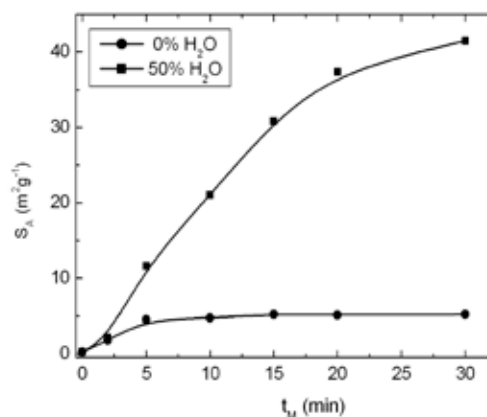
Fig. 1.   **Specific surface area S_A as a function of milling time in a planetary mill**

Table I
Milling parameters and specific surface area

Type of mill	Milling time [min]	H_2O addition [%]	Specific surface area [$m^2 g^{-1}$]	
			Dry milling	Wet milling
–	–	–		0.25
PM	2	50	1.82	2.19
PM	5	50	4.51	11.61
PM	10	50	4.76	21.06
PM	15	50	5.25	30.86
PM	20	50	5.11	37.34
PM	30	5		13.19
PM	30	20	5.21	38.29
PM	30	50		41.49
PM	30	100		40.49
NM	1	–	0.88	–
NM	3	–	1.76	–
NM	5	–	2.46	–
NM	10	5		21.64
NM	10	10	3.03	17.57
NM	10	20		12.31
NM	10	50		9.43

Fig. 3. **Specific surface area S_A as a function of milling time in a nutating mill**

Fig. 4. **Specific surface area S_A as a function of H_2O addition by nutating milling**

changes in surface area of olivine sample. Summary of the milling results is given in Table I.

As can be seen from results in Table I, milling of olivine in laboratory planetary mill produces an increase of starting surface area from 0.25 $m^2 g^{-1}$ to 5.21 $m^2 g^{-1}$ at 30 min without water addition and to 41.49 $m^2 g^{-1}$ at the same time with addition of 50 % of water (Fig. 1.). It was observed increase of specific surface area (S_A) by milling with various addition of water (0, 5, 20, 50, 100 %) at the same time (30 min). Progressive increasing up was observed in the presence of 50 % of water, in the presence of 100 % of water the S_A decrease (Fig. 2.).

The increase of specific surface area was observed by milling in industriall nutating mill from value 0.25 $m^2 g^{-1}$ to 3.03 $m^2 g^{-1}$ at 10 min without water (Fig. 3.). Special effect

has been observed by milling of olivine for 10 min in nutating mill in the presence of small amounts of water (Fig. 4.).

The less water is applied, the higher values for specific surface area have been obtained: for 5 % wt. H_2O the value of S_A was 21.6 $m^2 g^{-1}$. The effect of the addition of small amounts of a liquid to accelerate the solid-state reactions carried out by milling is called kneading in the chemical engineering. Kneading has been described as a sort of catalysis, where the small amount of solvent provides a lubricant for solid-state diffusion[6,7].

The corresponding micrographs for as-received olivine as well as for the same samples activated by dry milling for 30 min in a laboratory planetary mill and in an industriall nutating mill for 10 min are given in Fig. 5. The as-received sample shows particles irregular in shape with characteristic sharp edges. During milling the particles are rounded, fractured and diminished. Some large particles still exist but an overall reduction in size appears to have occurred as a result of high-energy milling. The evidence of well-bonded aggregates can be seen.

Fig. 2. **Specific surface area S_A as a function of H_2O addition by milling in a planetary mill**
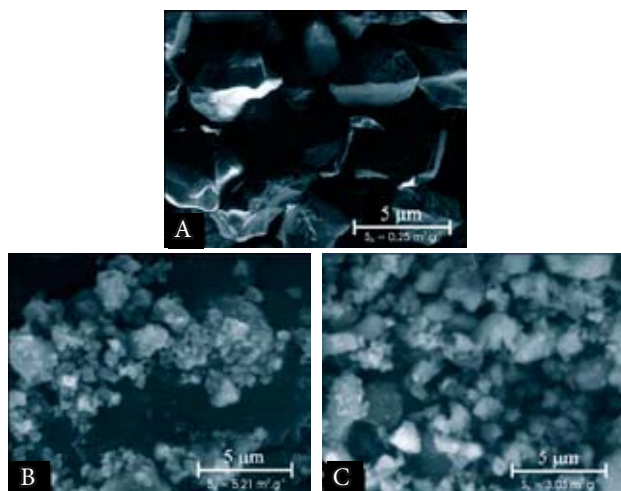
Fig. 5.　SEM photos of olivine: A – as received sample, samples after dry milling in (B) planetary mill, (C) nutating mill

Conclusions

　　Changes in specific surface area of mechanically activated olivine in high-energy mills were detected. Milling in wet mode results in the highest values of specific surface area.

REFERENCES

1. Baláž P.: *Extractive Metallurgy of Activated Minerals*. Elsevier, Amsterdam, 2000.
2. Baláž P.: *Mechanochemistry in Nanoscience and Extractive Metalurgy*. Springer, Heidelberg, 2008.
3. Tkáčová K.: *Mechanical Activation of Minerals*. Elsevier, Amsterdam, 1989.
4. Kleiv R. A., Thornhill M.: Miner. Eng. *19*, 340 (2006).
5. Huijgen W. J. J., Witkamp G .J., Comans R. N. J.: Chem. Eng. Sci. *61*, 4242 (2006).
6. Braga D., Grepioni F.: Angew. Chem. Int. Ed. *43*, 4002 (2004).
7. Braga D., Grepioni F.: Chem. Commun. 3635 (2005).

P28 NUMERICAL MODELLING AND SIMULATION FOR INTERACTION BETWEEN Cu²⁺ AND S₂O₃²⁻

MIHAELA-LIGIA UNGUREŞAN[a], MIHAIL ABRUDEAN[b], PAULA RAICA[b], EVA H. DULF[b] and TIBERIU COLOŞI[b]

[a]*Technical University of Cluj-Napoca, Chemistry Department, Romania,*
[b]*Technical University of Cluj-Napoca, Automation Department, Romania,*
Mihaela.Unguresan@chem.utcluj.ro

Introduction

Reactions between thiosulfate and ions of metallic elements in solution have been studied[1,2].

Cu^{2+} – thiosulfate reaction kinetics explanation is of interest since Cu^{2+} is used as catalyst within the reaction between Fe^{3+} and thiosulfate, allowing determining the presence of copper traces, but also because copper ions play important roles in biological processes, as enzymes components and as antioxidants[3].

The kinetics of Cu^{2+} reduction with $S_2O_3^{2-}$ in aqueous acidic solutions is not yet known, there is just one paper dealing with the reaction of $Cu[NH_3]_4^{2+}$ with $S_2O_3^{2}$, the observed half time of this reaction being about 0.15 s(ref.[4]).

Reaction between Cu(II) and thiosulfate ions results in the formation of a colored intermediate, supposed to be CuS_2O_3, similar to the intermediate $FeS_2O_3^+$, but unloaded.

The evolution of this complex can be followed spectrophotometrically, but the reaction's half time is three or four orders of magnitude smaller than the one of the $FeS_2O_3^+$-complex, therefore the disappearance of CuS_2O_3 study requires a stopped-flow apparatus.

The Analytical Modelling of the Process

For the input signal u(t) with the amplitude (u_0) and period (τ), the output light intensity y(t, p) experimentally measured can be approximated by:

$$y(t, p_1) = J(p_1) \cdot t \cdot \varepsilon^{-\frac{t}{T}}, \tag{1}$$

as shown in Fig. 1, for $p = p_1 > 0$.
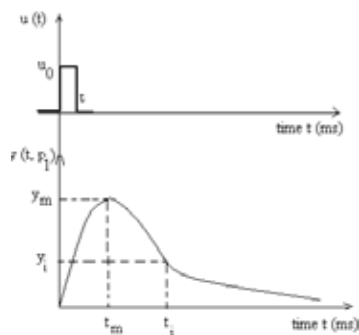
Fig. 1. **Light intensity y [mV] = f(time t [ms])**

The J(p) function it is approximated to be polynomial decreasing of the form[5,6]:

$$J(p) = J_0 + J_1 p + J_2 p_2 + J_3 p_3. \tag{2}$$

The maximum value for (1) results from:

$$\left(\frac{\partial y}{\partial t}\right)_{p_1} = J(p_1) \cdot (1 - \frac{t}{T}) = 0, \tag{3}$$

so that

$$t_m = T, \tag{4}$$

$$y_{m1} = y(t_m, p_1) = \frac{t}{\varepsilon} \cdot J(p_1), \tag{5}$$

$$\left(\frac{\partial^2 y}{\partial t^2}\right)_{p_1} = \frac{J(p_1)}{T} \varepsilon^{-\frac{t}{T}} \cdot (-2 + \frac{t}{T}) = 0, \tag{6}$$

for which

$$t_i = 2T, \tag{7}$$

$$y_{i1} = \frac{2T}{\varepsilon^2} \cdot J(p_1). \tag{8}$$

As a result, the analytical modelling for y(t, p) can be qualitatively illustrated in Fig. 2, where the maximum values ym(t, p) become proportional to curve 2, as it results from (5).
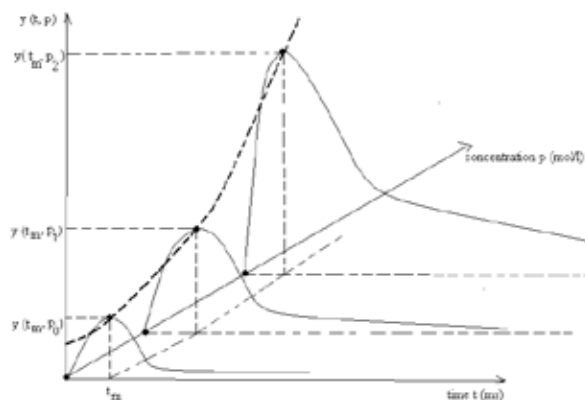
Fig. 2. **Light intensity *vs.* concentration and time**

The decreasing polynomial curve (2) results from experimental measurements and it has been approximated in the following two variants, associated to Fig. 3.

We define: $J(p_0)$, $\left(\frac{\partial J}{\partial p}\right)_{p_0}$, $J(p_f)$ and $\left(\frac{\partial J}{\partial p}\right)_{p_f}$ from which we can obtain the coefficients in (2): $J_0 = J(p_0)$;

$$J_1 = \left(\frac{\partial J}{\partial p}\right)_{p_0}; \quad J_2 = \frac{3}{p_f^2} \cdot \left[J(p_f) - J_0 - \frac{p_f}{3} \cdot \left(\frac{\partial J}{\partial p}\right)_{p_f} - \frac{2}{3} p_f \cdot J_1 \right];$$

$$J_3 = \frac{1}{p_f} \left[J(p_f) - J_0 - J_1 \cdot p_f - J_2 \cdot p_f^2 \right].$$

The variant has the advantage of following a rigorous polynomial trajectory and the disadvantage of a more difficult choice of the slopes from the ends of this curve.

We define the four points where that the polynomial curve (2) needs to pass, respectively $J(p_0)$, $J(p_1)$, $J(p_2)$ and

$J(p_f)$, finally having: $J_0 = J(p_0)$; $J_1 = \dfrac{DET1}{DET\Phi}$; $J_2 = \dfrac{DET2}{DET\Phi}$

and $J_3 = \dfrac{DET3}{DET\Phi}$. The four determinants correspond to a system of four linear algebraic equations, written in the points $(p_0, p_1, p_2 \text{ and } p_f)$ from the polynomial curve (2).

This variant has the advantage of this curve passing through those four predetermined points (usually experimental) and the disadvantage of eventually deformations of the curve between the four predetermined points.
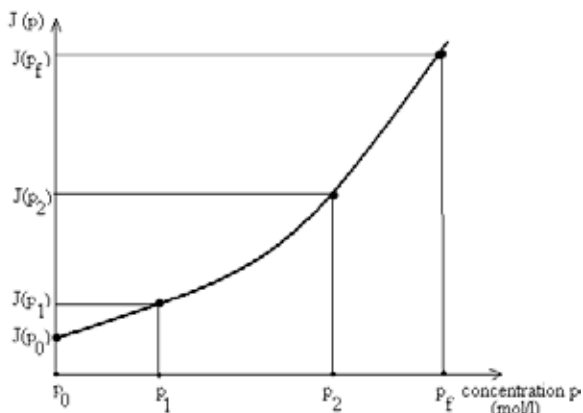
Fig. 3.　$J[mV\,ms^{-1}] = f$ (concentration p [mol dm^{-3}])

Results

The experimental measurements have been done for stoechiometric mixtures of reactants with concentrations between 5×10^{-4}–1×10^{-1} mol dm^{-3}.

The polynomial approximation (2) has been achieved by using the experimental data obtained for the domain of the above concentrations.

The results obtained by simulation for the second variant of calculus are:

(i)　$[Cu^{2+}] = 5 \times 10^{-3}$ mol dm^{-3}; $[S_2O_3^{2-}] = 5 \times 10^{-3}$ mol dm^{-3}, J = 9.54 mV ms^{-1}; $t_m = T = 59.6$ ms; $y_m = 209.3$ mV

The curve obtained by simulation overlapped on the curve obtained experimentally, for $[Cu^{2+}] = 5 \times 10^{-3}$ mol dm^{-3}; $[S_2O_3^{2-}] = 5 \times 10^{-3}$ mol dm^{-3}, is presented in Fig. 5.
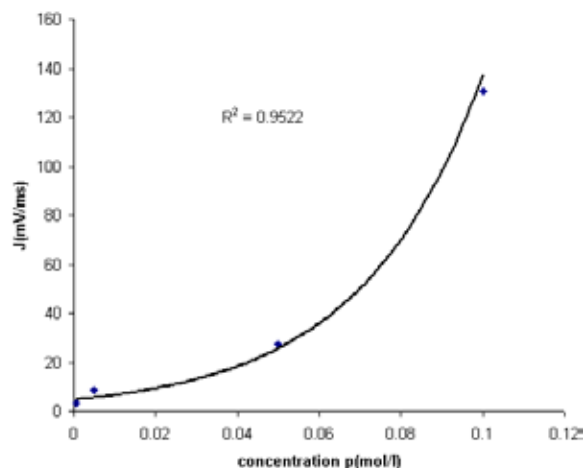
Fig. 4.　$J[mV\,ms^{-1}] = f$ (concentration p [mol dm^{-3}])
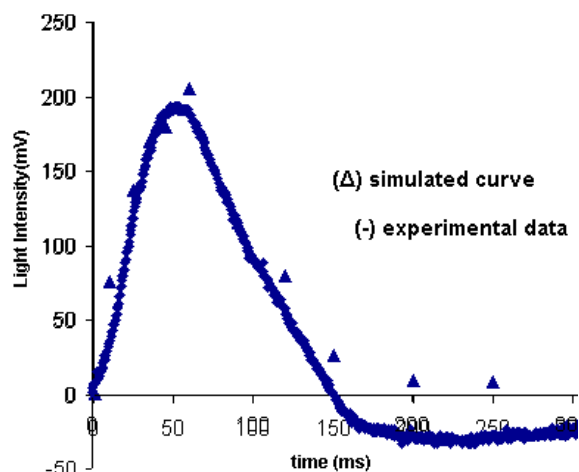
Fig. 5. **Superposition experimental curve; (-) to the simulated curve, (▲) for $[Cu^{2+}] = 5 \times 10^{-3}$ mol dm^{-3}; $[S_2O_3^{2-}] = 5 \times 10^{-3}$ mol dm^{-3}**

(ii) $[Cu^{2+}] = 10^{-1}$ mol dm^{-3}; $[S_2O_3^{2-}] = 10^{-1}$ mol dm^{-3}, J = 130.6 mV ms^{-1}; $t_m = T = 15.6$ ms; $y_m = 650$ mV.

The curve obtained by numerical simulation overlapped on the curve obtained experimentally, for $[Cu^{2+}] = 10^{-1}$ mol dm^{-3}; $[S_2O_3^{2-}] = 10^{-1}$ mol dm^{-3}, is presented in Fig. 6.

The parameters k_1, k_{-1} and k_2 and molar absorption coefficient for the initial conditions ($[Cu^{2+}] = [S_2O_3^{2-}] = 5 \times 10^{-3}$ mol dm^{-3}, $l = 0.4$ cm, $I_0 = 2,950$ mV, $E = \lg I_0/I$) is obtained by optimization, realized by multiple iterations, so as the square middle error tend to small values for a better superposition of the simulated response and the experimental response. It has to be mentioned that the flat section of the maxim was moved. This section seems to appear due to hydrodynamic conditions and due to diffusion phenomena existing in thoroidal mixing chamber, although at much reduced scale, and also due to fact that in flow time the reaction may start beyond the measuring cell.
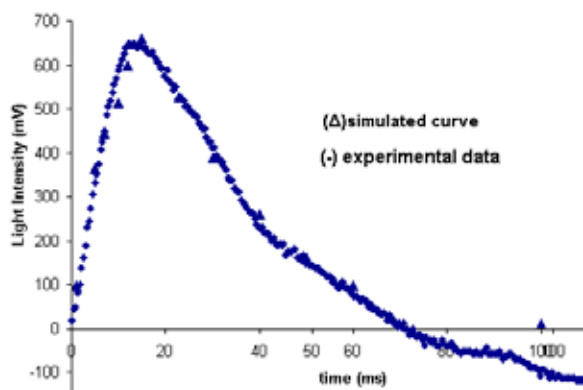
Fig. 6. Superposition experimental curve (-) to the simulated curve (▲)

Due to imperfect mix, it was necessary the translation of the experimental values – corresponding to decomposition of the intermediary compound – toward the values corresponding to forming operation of the intermediary compound.

The obtained results from the optimization of the simulated curve (Fig. 7.): $k_1 = 9.7$; $k_{-1} = 0.7$; $k_2 = 8,222.5$; $\varepsilon = 1489.7 \, M^{-1} cm^{-1}$, the reaction order for decomposition of the intermediate compound is $n = 2$.

The value of the formation constant of CuS_2O_3 at 19.5 °C is $K = k_1/k_{-1} = 13.86$.

Conclusions

It was simulated and modeled the kinetic of rapid redox reaction between Cu^{2+} and $S_2O_3^{2-}$ (Figs. 5., 6.). The proposed mathematical model, which is based on the reaction mechanism determined in conformity with the obtained experimental values, allow – by numerical simulation – the approximate calculus of the kinetic parameters: $k_1 = 9.7$; $k_{-1} = 0.7$ and $k_2 = 8,222.5$; $\varepsilon = 1,489.7 \, M^{-1} cm^{-1}$ and $n = 2$. The results obtained by analogical modeling and numerical simulation are in accordance with the experimental values.
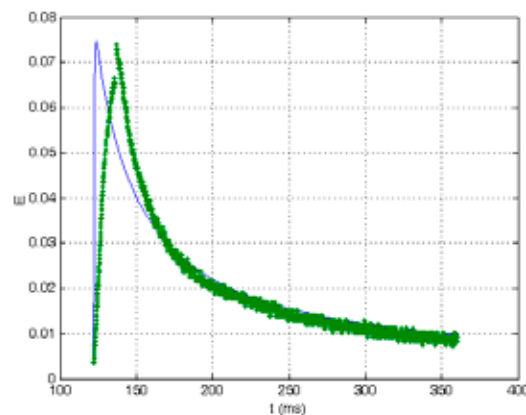
Fig. 7. **The absorbance E = f(t); experimental curve (bold); simulated curve (line)**

REFERENCES

1. Baldea I., Niac G.: Inorg. Chem. *9*, 110 (1970).
2. Cadariu I., Niac G., Oniciu L., Studia Universitatis Babeş Bolyai, Chemia *1*, 27 (1962).
3. Biesalski H. K., Grimm P.: *Taschenatlas der Ernährung*, Thieme Verlag, Stuttgart 1999,.
4. Byerley J. J., Safaa A., Rempel F., Garry L.: J.C.S.Dalton *1973,* 889.
5. Ungureşan M. L.; Abrudean M., Coloşi T.: *Nonlinear-Exponential Numerical Modelling and Simulation of the Kinetic Rapid Redox Reaction Cu^{2+} with $S_2O_3^{2-}$*, SIN-TES 12,p. 215, Craiova, 2005.
6. Dulf E., Coloşi T., Abrudean M.; Ungureşan M. L.: *Modeling and Numerical Simulation of First and Second Order Distributed Parameters Processes, using M_{dpx} Operating Matrix*, SINTES 12, p. 66, Craiova, 2005.

P29 BIOACTIVITY AND CYTOTOXICITY OF FLUORHYDROXYAPATITE CERAMIC

MARTIN VITKOVIČ, MAHA SALIH MAHAMMED NOAMAN and MARTIN PALOU

Slovak University of Technology, Faculty of Chemical and Food Technology, Radlinského 9, 812 37 Bratislava, Slovak Republic,

martin.vitkovic@stuba.sk

Introduction

There is an increasing need for medical implants, due to an increasing aged population. Bone defects resulting from trauma, disease or developmental anomalies can substantially be improved by reconstructive surgery.

Bone is essentially constituted of nanoscale inorganic materials and proteins. The inorganic materials are minerals which are structurally apatite-like, such as hydroxyapatite [HA, $Ca_5(PO_4)_3OH$], fluorapatite [FA, $Ca_5(PO_4)_3F$] and carbonate-apatite.

Therefore, composite fluorhydroxyapatite (FHA) materials have been developed by different synthesis routes and techniques in order to improve both bioactivity and mechanical properties of various orthopaedic prosthesis and dental implants. Besides bioactivity and mechanical properties, the non-cytotoxicity is one of the most important requirements for applications of these materials.

The present work deals with the bioactivity and the cytotoxicity investigation of ceramic materials on the base of apatites with general formula $Ca_5(PO_4)_3(OH)_{1-x}F_x$ (x = 0, 0.5 and 1).

Experimental

Samples Preparation

The samples of hydroxyapatite (HA), fluorapatite (FA) and fluorhydroxyapatite (FHA) were prepared by homogeneous precipitation method using $Ca(NO_3)_2 \cdot 4H_2O$ and $(NH_4)_2HPO_4$ as starting materials and ammonia solution as agents for pH adjustment. Equations (1)–(3) illustrate chemical reactions leading to the precipitation of HA, FA and FHA, respectively. A suspension of $Ca(NO_3)_2 \cdot 4H_2O$ powder was diluted in deionised water. Then, a solution of $(NH_4)_2HPO_4$ was slowly added by drop-wise to the $Ca(NO_3)_2 \cdot 4H_2O$ solution. In all experiments the pH of $Ca(NO_3)_2 \cdot 4H_2O$ solution was kept by ammonia solution at 10. The final solution was stirred at room temperature for 3 h. Then, the precipitate formed was filtered off, washed with deionised distilled water several times to the neutral pH, and finally dried in owen at 70 °C for 24 h. After drying, the samples were powdered and treated at 1,000 °C for 1 h. After heat treatment at 1,000 °C, the pellets were compressed from powdered samples and heated at the same temperature.

The chemical process leading to HA can be explained by the following reaction (1):

$$5Ca(NO_3)_2 \cdot 4H_2O + 3(NH_4)_2HPO_4 + 4NH_4OH \rightarrow Ca_5(PO_4)_3OH + 10NH_4NO_3 + 23H_2O \tag{1}$$
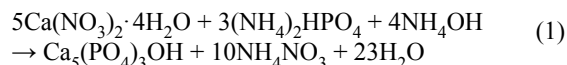
Likewise the FA was obtained according to the reaction (2):

$$5Ca(NO_3)_2 \cdot 4H_2O + 3(NH_4)_2HPO_4 + 4NH_4F \rightarrow Ca_5(PO_4)_3F + 10NH_4NO_3 + 3HF + 20H_2O \tag{2}$$
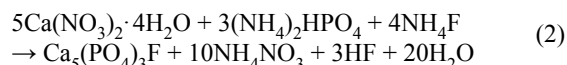
The solid solution of FHA (FA : HA = 1 : 1) was prepared according to the reaction (3):

$$5Ca(NO_3)_2 \cdot 4H_2O + 3(NH_4)_2HPO_4 + 3.5NH_4F + 0.5NH_4OH \rightarrow \\ Ca_5(PO_4)_3OH_{0.5}F_{0.5} + 10NH_4NO_3 + 3HF + 20H_2O \tag{3}$$
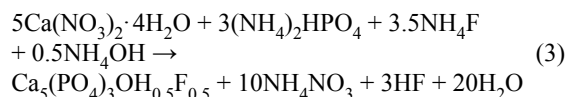
Used Methods

Obtained HA, FA and FHA powders were controlled by powder X-ray diffraction.

The bioactivity of the samples was evaluated by in vitro testing in simulated body fluid (SBF). SBF, which ion concentrations are almost identical with inorganic ion concentrations of human blood plasma, was prepared according to literature[1]. The calculated volumes of SBF (4) were poured in the plastic containers and heated up to the temperature of 36.5 °C.

$$VS = \frac{S_a}{10}, \tag{4}$$

V_S – volume of SBF [ml],
S_a – apparent surface area of specimen [mm^2].

The pellets of FA, HA and FHA were immersed in SBF for 4 weeks at 36.5 °C. Changes of the surface microstructure of the samples were observed by scanning electron microscopy (SEM).

HA, FA and FHA have also been used to investigate the cytotoxic effect on murine fibroblast. The cytotoxicity was determined using the method of direct cell counting[2]. NIH–3T3 cells were cultured with biomaterial discs for 24 h, 48 h and 72 h. The cell proliferation and the morphology were examined.

Results

The results of SEM analysis after SBF acting are showed in Figs. 1., 2. and 3., respectively. The high *in vitro* bioactivity of all samples is demonstrated by the growth of new apatite-like phase on the surface of them.

Fig. 4. shows the direct effect of HA, FA and FHA on cell proliferation evaluated at 24, 48 and 72 h of culture. HA, FA and FHA induced slight inhibition of NIH–3T3 cell proliferation. In the first time interval cells affected by biomaterials proliferated was 92.68 % for HA, 97.56 % for FA and 96.34 % for FHA. After 72 h incubation the inhibition of cell division was the same for all the biomaterials (25 %). According to this, the cytotoxicity was in the range of 5 49–27.19 %.

(a)   (b)
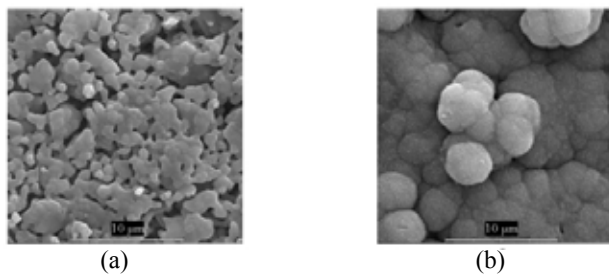
Fig. 1. **Surface microstructure of HA: (a) before immersion in SBF, (b) after 4 weeks in SBF**

(a)   (b)
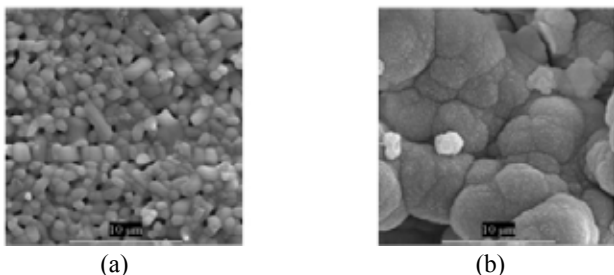
Fig. 2. **Surface microstructure of FA: (a) before immersion in SBF, (b) after 4 weeks in SBF**

(a)   (b)
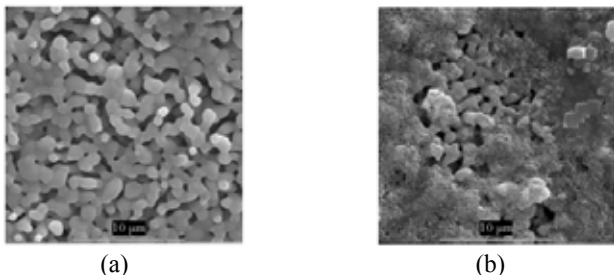
Fig. 3. **Surface microstructure of FHA: (a) before immersion in SBF, (b) after 4 weeks in SBF**

The morphology of NIH–3T3 cells grown in direct contact with apatites was completely similar to that of control cells and did not show any morphological damages.

Conclusions

The new layer of apatite-like phase covered the surface of all samples. The creation of the new biologic active layer confirmed the bioactivity of apatites.
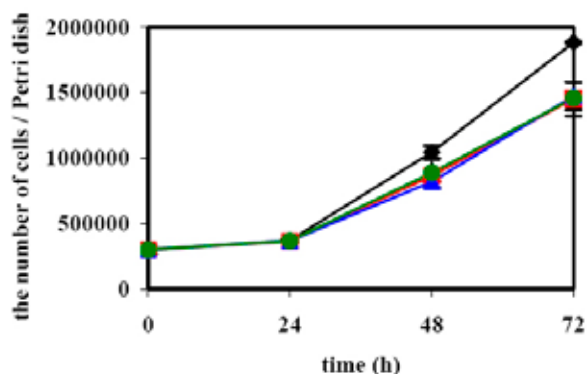
Fig. 4. Growth curve of NIH–3T3 cells cultured with biomaterials : ♦ – C; ● – FHA; ▲ - FA; ■ – HA

Control   FHA   FA   HA
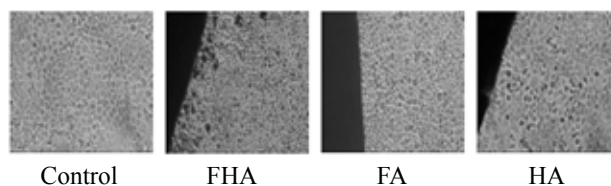
Fig. 5. **Morphological analysis of NIH–3T3 cells cultured for 72 h in presence of FHA, FA and HA. Magnification: 80×**

HA, FA and FHA induced slight inhibition of cell proliferation, which was the same for all apatites after 72 h incubation. The cell number monitoring showed their slight cytotoxicity.

The morphology of cells grown in direct contact with apatites did not show any morphological damages.

REFERENCES

1. Kokubo T., Takadama H.: Biomaterials *27*, 2907 (2006).
2. Lang H., Mertens T .H.: J. Oral. Maxillofac. Surg. *48*, 606 (1990).

P30   MICROWAVE-HYDROTHERMAL SYNTHESISOF HYDROXYAPATITE FROM CaSO₄·1/2H₂O FOR DENTAL REPARATION

P. ZAMAZALOVÁ[a,b], C. DAMIA[a], E. CHAMPION[a] and O. GEDEON[b]

[a]*SPCTS UMR 6638 CNRS, Faculté des Sciences et Techniques, 123 avenue Albert Thomas, 87060 Limoges Cedex, France,*
[b]*Department of Glass and Ceramics, ICT Prague, Technická 5, 166 28 Prague 6, Czech Republic,*
Petra.Zamazalova@vscht.cz

Introduction

The aim of present work is to obtain particles of hydroxyapatite (HA $-$ $Ca_{10}(PO_4)_6(OH)_2$) suitable for the reparation of defects occurring on the surface of dental enamel as a result of demineralization process. HA was chosen as the filling material due to its composition similar to enamel which can be chemically defined as non-stoichiometric apatite ($Ca_{10-x}(HPO_4)_x(PO_4)_{6-x}(OH)_{2-x}\cdot xH_2O$, $0<x<2$)[1]. However, particle size of HA is limited to be sub-micron by the micrometric size of surface defects.

Numerous techniques of HA synthesis have been developed during past years, particularly wet chemical methods based on the low temperature precipitation from aqueous solutions. Usually $Ca(NO_3)_2\cdot 4H_2O$ is used as a source of calcium[2], however, several authors have already reported the use of gypsum ($CaSO_4\cdot 2H_2O$)[3,4] as a starting material. Recently, microwave irradiation has been used in order to obtain nanoparticles of a variety of inorganic materials in a short time including HA.[5–7] Despite our effort we did not find any mention of the utilization of plaster ($CaSO_4\cdot 1/2H_2O$) even though its higher reactivity in aqueous solutions is well known.

Therefore, in this report the preparation of HA by microwave-hydrothermal synthesis from plaster and the application of obtained powder on tooth enamel are presented.

Experimental

$CaSO_4\cdot 1/2H_2O$ (Aldrich) and $(NH_4)_2HPO_4$ (Aldrich) were used as starting materials for the synthesis of HA according to the following equation which is the modification of the formulation reported by Katsuki *et al.*[7]:

$$10CaSO_4\cdot 1/2H_2O + 6(NH_4)_2HPO_4 \rightarrow \\ Ca_{10}(PO_4)_6(OH)_2 + 6(NH_4)_2SO_4 + 4H_2SO_4 + 3H_2O \quad (1)$$
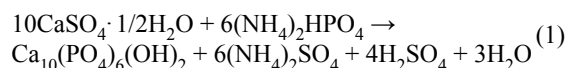
Plaster was mixed with a 1M solution of $(NH_4)_2HPO_4$ in a Teflon beaker with molar ratio of Ca/P equal to 10/6 corresponding to stoichiometric HA. The pH of the mixture was adjusted to a value between 9–10 using NH_4OH solution. Reaction mixture was then irradiated for 40 min. with a microwave power of 750 W in home microwave oven (Whirlpool JT357, 2.45 GHz). After the reaction, sample was filtered, washed by distilled water and dried at 100 °C in air.

Calcination of sample at 1,000 °C for 15 h permitted to determine the stoichiometry of powder[8]. Powder was characterized by XRD (Siemens D5000 diffractometer), FT-IR (Bomen MB2), BET (analyzer Micromeritics ASAP 2010) and SEM (Hitachi S2500 and Hitachi S4700).

For the study of defect reparation a gel of methyl cellulose containing 5 % wt. of HA powder was prepared and applied on the tooth surface using classical toothbrush. Artificial defect was created on the tooth enamel in order to facilitate microscopic observations.

Results and Disscussion

Phase composition of HA powder was studied by XRD (Fig. 1.). In non-calcined powder, large peaks of low crystalline HA occurred without any other phase (Fig. 1.a). The XRD of calcined powder confirmed full conversion of starting materials and revealed the presence of sharp peaks of HA and β-TCP (β-Tricalcium phosphate; β-$Ca_3(PO_4)_2$) (Fig. 1.b). It was reported that peaks of HA accompanied by β-TCP occur in samples with Ca/P ratios between 3/2 (stoichiometric β-TCP) and 10/6 due to the decomposition of a Ca-deficient hydroxyapatite (CDHA, $Ca_{10-x}(HPO_4)_x(PO_4)_{6-x}(OH)_{2-x}$, $0<x<1$)(ref.[2]). Therefore, it can be supposed that non-calcined powder contain CDHA.
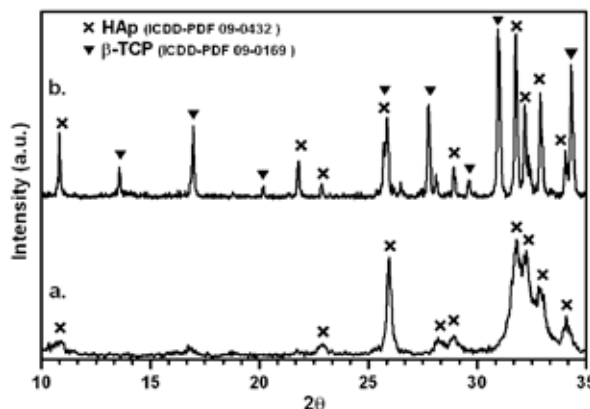
Fig. 1.   **XRD patterns of HA sample (a) non-calcined and (b) calcined**

This supposition was confirmed by FT-IR analysis (Fig. 2.) showing the presence of an absorption band of HPO_4^{2-} (874 cm⁻¹) characteristic for CDHA. Apatitic structure was supported by the observation of the splitting of PO_4^{3-} bands (602–562 cm⁻¹, 1,095–1,029 cm⁻¹) and the presence of OH⁻ bands (630 cm⁻¹, 3,570 cm⁻¹). As expected, since the sample was not calcined, bands of adsorbed water (3,433 cm⁻¹, 1,638 cm⁻¹) and carbonate (CO_3^{2-}) groups (1,420–1,500 cm⁻¹) were also visible.

The specific surface area (SSA) of HA powder obtained by BET measurement is 73.1 ± 0.7 m² g⁻¹. The microstructure of the sample can be observed in Fig.3. SEM micrographs reveal fine needle-like particles 200 nm long and 30 nm wide which corroborates BET measurement.
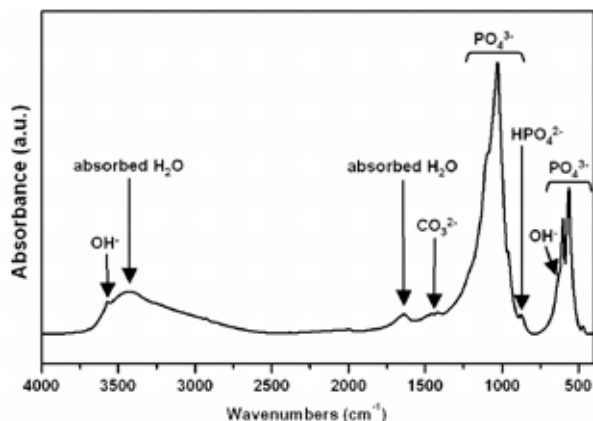
Fig. 2.   **FT-IR spectrum of non-calcinated HA powder**
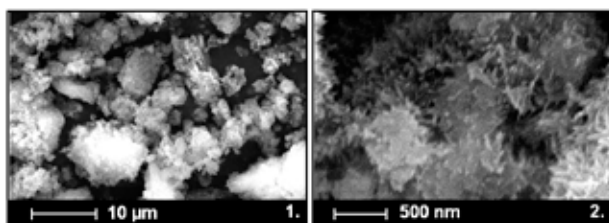
Fig. 3.   **SEM micrographs of sample HA at (1.) low magnification and (2.) high magnification**
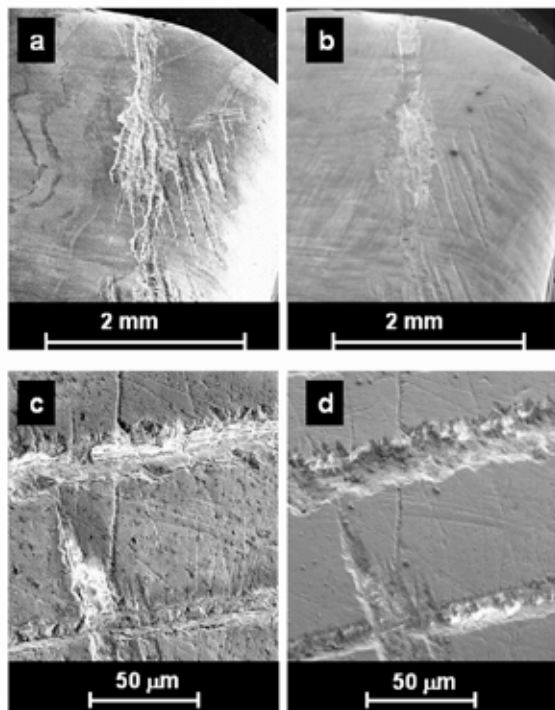
Fig. 4.   **SEM micrographs of tooth surface (a), (c) before and (b), (d) 3 days after the application of gel with HA**
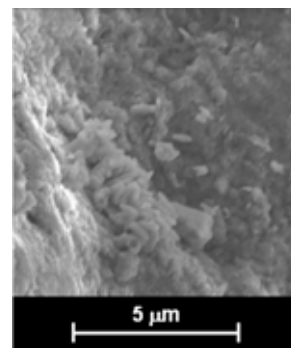
Fig. 5.   **New crystals formed in defect**

Artificial scratches are easily recognized and are much deeper than defects normally occurring on the tooth surface (Fig. 4.). Three days after the application of gel with HA particles the defect was filled in by the material and tooth surface looked smoother with homogeneous color (Fig. 4.). Apart deposited particles, newly formed crystals appear in defects (Fig. 5.) supposed to be HA which signify that application of HA gel may enhance further formation of HA from natural environment.

Conclusions

Sample HA was prepared from plaster by microwave-hydrothermal synthesis after 40 minutes of irradiation at 750 W. Characterization techniques showed that non-calcinated sample is composed from fine needle-like particles of Ca-deficient apatite. HA powder was dispersed in methyl cellulose gel and applicated on tooth surface with an artificial defect. Three days after the application defects were filled in by HA gel and newly formed crystals were observed too.

REFERENCES

1. Jenkins G. N.: *The physiology and biochemistry of the mouth*. Blackwell Scientific Publications, Oxford 1978
2. Raynaud S., Champion E., Bernache-Assollant D., Thomas P.: Biomaterials *23*, 1065 (2002).
3. Furuta S., Katsuki H., Komarneni S.: J. Mater. Chem. *8*, 2803 (1998).
4. Suzuki Y., Matsuya S., Udoh K., Nakagawa M., Tsukiyma Y., Koyano K., Ishikawa K.: Dent. Mater. J. *24*, 515 (2005).
5. Yang H., Huang Ch., Tang A., Zhang X., Yang W.: Mater. Res. Bul. *40*, 1690 (2005).
6. Teoreaunu I., Preda M., Melinescu A.: J. Mater. Sci. Mater. Med. *19*, 517 (2008).
7. Katsuki H., Furuta S., Komarneni S.: J. Am. Ceram. Soc. *82*, 2257 (1999).
8. Raynaud S., Champion E., Bernache-Assollant D., Laval J. P.: J. Am. Ceram. Soc. *84*, 359 (2001).

P31 CONVERSION COATINGS ON AMGNESIUM ALLOYS

MARTIN ZMRZLÝ

Faculty of chemistry, Brno University of Technology, Purkynova 118, 612 00 Brno, Czech Republic,
zmrzly@fch.vutbr.cz

Introduction

Magnesium alloys belong to the most perspective metallic construction materials. Besides their good mechanical properties (tensile and yield strength, uniform elongation, hardness) they also dispose by very low density. This fact makes them very popular e.g. in automotive industry, since the lighter is the construction, the lower are service costs (petrol consumption) and consequently environmental damage is diminished.

Unfortunatelly, due to very low electrochemical potential of magnesium, corrosion resistance of these alloys is very poor. In the case of alloys containing lithium is this fact even emphasised.

Typical surface treatment for magnesium alloys are conversion coating. Most effective type of coating, the chromate coating, were excluded from use by EU legislation[1] since they contained a cancerogenic hexavalent chromium. However, in laboratory scale is this type of coating still widely used as a standard of corrosion protection[2].

Goal of this work is to find a chromating solution that will make a continuous coating on the surface of alloy AZ 91. This alloy is most commom magnesium alloy in technical use. The phase structure of this alloy is quite complex, containing α-solid solution of ellements in magnesium, intermetallic compound $Al_{12}Mg_{17}$ and their eutectic mixture, see Fig. 1.

These phases differ a lot in reactivity[3]. Then it is a common result, that α-phase is covered by coating and intermetallic phases remain uncoated.

Experimental

Cast specimens of AZ 91 alloy were used. They were cut to size app. $5 \times 20 \times 20$ mm and grinded by metallographic SiC paper (Struers, No. 320). Composition of alloy is 9 %Al, 1 %Zn and ballance is magnesium.

The starting solution was established according to ref.[4] as 0.35M $K_2Cr_2O_7$ (Lachema, p.a.). Further exeperiments were carried out with solutions 0.12M, 0.035M and 0.0035M. The bath should work at room temperature. Set of solutions that diferred in pH value was also prepared. pH were 3.7; 2.9; 2.1; 1.5; 1.3; 1.2; 1.1; 1.0; 0.9; 0.8; 0.7 and 0.6. Values were set by addition of 1M solution of hydrochloric acid (Lach-Ner, p.a.) and measured by pH-meter Gryf 208

Time of immersion was varied in scale 5; 15; 30 and 60 seconds for each solution.

After the process, the specimen were rinsed by distilled water and ethanol and dried by hot air. The surface was observed on micrsocope Neophot 21 (Zeiss). This way the contiunuity of prepared coating was assessed.

Coating Weight

Coating weight was measured by stripping method[5]. The specimen was weighed (accurancy 0.1 mg) immersed for 60 second in boiling suspension of 2 g Ag_2CrO_4 in 200 ml of solution CrO_3 (15%). After this immersion the specimen was dried as stated above and weighed again.

Corrosion Resistance

Corrosion resistance was measured according to ref.[5]. Weighed specimen was placed into 3.5% solution of NaCl in distilled watter for 1 hour. Than it was rinsed by water and placed in stripping suspension of Ag_2CrO_4 (process described above). Then it was dried and weighed. In the case of coated specimens, the coating weight had to be taken into account.

All the quantitative measurement were done is sets of 3–6 measurement. Q-test for removing of statistical outliers were performed and the average of the results and the stan-

Fig. 1. **Micrograph of alloy AZ 91. Light microscope, mgf.1000×. A – solid solution α, B – eutectic of solid solution and intermetalic compound, C – intermetallic compound $Al_{12}Mg_{17}$**
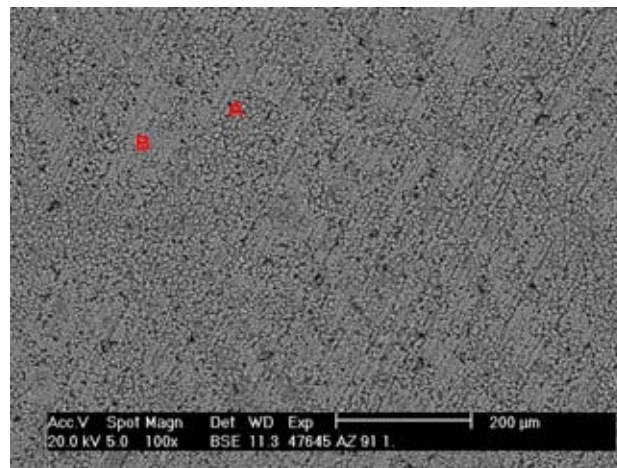
Fig. 2. **SEM Micrograph of chromate coating on alloy AZ 91. A – area, where the substrate is solid solution α, B – area, where the substrate is eutectic or intermetalic compound.**

dard deviation σ were calculated. Absolute error was taken as 2σ.

Results

According to visual assessment (microscopy), the optimal conditions were estimated as: $c_{K2Cr2O7}$ = 0.12M, pH = 0.6 and time of immersion 15 s. At these conditions the specimens were continuously coated, although there were observable differences between grain size at sites of α-phase and grain size at sites of intermetallic phases (see Fig. 2.).

The coating weight was estimated by stripping method as 660 $\mu m\,cm^{-2}$. Corrosion resistance, estimated by above described method, was obtained at both the coated and uncoated specimen. The corrosion rate of bare AZ 91 alloy was found to be 9 ± 1 mm year^{-1} and rate of alloy with chromate coating was 5 ± 1 mm year^{-1}.

Conclusions

The composition of chromating soultion convenient for prepration of standard AZ91 corrosion specimens was found, besided the optimal immersion time. Possibility of use of the NaCl solution for test of these coatings was proved. Corrosion rate of the coated specimen was approximately half the value of the uncoated AZ 91 alloy.

REFERENCES
1. EU Directive 2002/95/ES, January 27, 2003.
2. Sharma A. K.: Metal Finishing *87,*33 (1989).
3. Gray J. E. Luan H.: J. Alloys Compd. *336*, 88 (2002).
4. Magnesium Electron, Surface treatments for magnesium alloys in aerospace and defence, 2006, http://www.magnesium-elektron.com/products-services.asp?ID=9.
5. Ambat R., Aung N. N., Zhou W., Corros. Sci *42,*1433 (2000).

5. CHEMISTRY OF ORGANIC MATERIALS

5.1. Lectures

L01　EFFECT OF WETTING/DRYING ON THE CONFORMATIONAL ARRANGEMENT OF A HETEROGENEOUS ORGANIC MIXTURE AS ASSESSED BY SOLID STATE ^{13}C NMR SPECTROSCOPY

PELLEGRINO CONTE[a], ANNE E. BERNS[b], HERBERT PHILIPP[b], PETER BURAUEL[b], HANS-DIETER NARRES[b] and HARRY VEREECKEN[b]

[a]*Dipartimento di Ingegneria e Tecnologie Agro-Forestali (DITAF), Università degli Studi di Palermo, v.le delle Scienze 13, 90128 Palermo, Italy,*
[b]*Forschungszentrum Jülich GmbH, Institute of Chemistry and Dynamics of the Geosphere, Institute 4: Agrosphere, 52425 Jülich, Germany,*
pellegrino.conte@unipa.it

Introduction

Cross-polarization magic angle spinning ^{13}C-NMR (CP-MAS ^{13}C-NMR) spectroscopy is used to investigate nature of carbon skeletons in organic substances which are insoluble or poorly soluble in common NMR deuterated solvents. The technique is applied to achieve information either on the quality of complex mixtures or on the solid state structure and conformation of pure materials. One of the advantages of the technique is the possibility to analyze the structures of amorphous compounds which are not analysable by common

Fig. 1. **CPMAS ^{13}C-NMR spectra and signal attribution (black circles in the structures) of the three molecules used in our study. A – mixture before dissolution and freeze drying, B – mixture after the treatment. The non-assigned peaks are spinning side bands**

cristallographic methods (i.e. X ray diffraction)[1]. Moreover, direct quantification of molecular composition of complex organic matrices (which are not easily chromatografable such as humic substances[2]) is also possible.

The limiting factor in CPMAS ^{13}C-NMR analyses is the low spectral sensitivity that is achieved when strength of the C-H dipolar interactions is weakened by rapid molecular motions and absence of protons in the neighbourhoud of carbon atoms[1]. Moreover, presence of paramagnetic species decreases proton relaxation times, thereby allowing protons to be relaxed before full H → C cross polarization is achieved[3]. When cross polarization rates are equal to or larger than proton relaxation velocities, CPMAS ^{13}C-NMR spectra are not representative of the chemical composition of complex organic mixtures[3]. Sensitivity enhancement can be obtained by applying properly all the procedures for sample preparation as reported in Smernik[4], Blann et al.[5] and Schilling and Cooper[6].

The aim of the present paper was to understand the effect of wetting/drying treatments on the physical parameters achievable by CPMAS ^{13}C NMR spectroscopy on organic mixtures. In order to reach our goal a mixture of three different standards was prepared and analyzed by CPMAS ^{13}C NMR spectroscopy before and after water treatment and freeze-drying.

Experimental

C h e m i c a l s

Carboxymethylcellulose sodium salt (CMC), ferulic acid (FERAC) and sodium dodecylsulfate (SDS) were purchased from Sigma-Aldrich® (Steinheim, Germany) and used without further purification. They were mixed in an agate mortar with a weight ratio of 1:1:1 (corresponding to a molar ratio of 1:52:77 for CMC, SDS and FERAC, respectively). The solid mixture was divided into two portions. The first one (Mix 1) was left unchanged, whereas the second portion (Mix 2) was suspended in distilled water, stirred for one hour and then freeze-dried. Both portions were finally analyzed by CPMAS ^{13}C-NMR spectroscopy by using the conditions reported below.

S o l i d   S t a t e   N M R   S p e c t r o s c o p y

A 7.05 T NMR spectrometer Unity INOVA™ (Varian Inc., Palo Alto, CA, USA), equipped with a wide bore probe operating at a ^{13}C frequency of 75.4 MHz, was used to acquire the CPMAS ^{13}C-NMR spectra of Mix 1 and Mix 2. The samples were packed in 6 mm zirconium rotors with Teflon® bottom and top spacers and Vespel® drive tips. Temperature was kept constant at 25.0 ± 0.1 °C. Magic angle spinning was carried out at 5,000 ± 1 Hz. Acquisition time of 30 ms, [1]H 90 ° pulse of 4 μs with a power level of 49 dB at the maximum decoupler power modulation, 1k data points and a recycle delay of 10 s were applied. A ramped cross-polarisation sequence with an ascending H-ramp of 15-kHz ramp width was applied. 256 transients were used to acquire all the spectra.
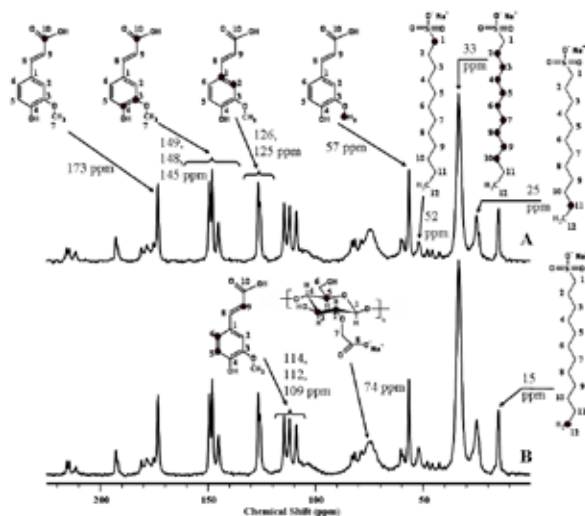
Arrayed (or pseudo-2D) experiments were performed to precisely measure cross polarization time (T_{CH}), and ^{1}H spin-lattice relaxation times in the rotating frame ($T_{1\rho}$(H)). T_{CH} was measured by variable contact time experiments (VCT) carried out by arraying 30 different contact times from 0.1 to 7.0 ms. Variable spin lock experiments were conducted according to Tekely et al.[7] to measure $T_{1\rho}$(H) values. An array of 35 spin lock times ranging from 0 to 50 ms was used. $T_{1\rho}$(H) values obtained from VCT experiments were not considered due to the overestimation of this parameter by VCT experiments as compared to delayed spin lock measurements.

Spectra Elaboration

VNMRJ software (Version 1.1 RevisionD, Varian Inc., Palo Alto, CA, USA) was used to acquire all the free induction decays (FID). Spectra elaboration was conducted by Mestre-C software (Version 4.9.9.9, Mestrelab Research, Santiago de Compostela, Spain). All the FIDs were transformed by applying, first, a 4k zero filling, and, then, an exponential filter function with a line broadening of 18 Hz. Fully automatic baseline correction using Bernstein algorithm was applied for baseline corrections. The intensities of all the peaks were measured and imported in OriginPro 7.5 SR6 (Version 7.5885, OriginLab Corporation, Northampton, MA, USA) to fit equation (1) for T_{CH} measurement, and equation (2) to obtain $T_{1\rho}$(H) values.

$$I(t) = I_0 \alpha^{-1} \left[1 - \exp\left(-\alpha \frac{t_{CP}}{T_{CH}} \right) \right] \times \exp\left(-\frac{t_{CP}}{T_{1\rho}(H)} \right) \quad (1)$$

$$I(t) = I_0 \exp\left(-\frac{t_m}{T_{1\rho}(H)} \right) \quad (2)$$

In equations (1) and (2), $I(t)$ is the signal area at the assigned t_{CP}, and t_m value, I_0 is the total nuclear magnetization of ^{13}C in thermal equilibrium, $\alpha = 1 - T_{CH}/T_{1\rho}$(H), t_{CP} is the contact time, and t_m is the spin-locking time.

Results and Discussion

Fig. 1. shows the spectra of Mix 1 (Fig. 1.A) and Mix 2 (Fig. 1.B). Structures of each standard and signal attribution are also reported. Namely, peaks at 173, 149, 148, 145, 126, 125, 114, 112, 109 and 57 ppm are assigned to FERAC and those at 52, 33, 22 and 15 ppm are due to the resonance of the SDS chain. The only visible signal of CMC is the signal at 74 ppm, as it appears in a spectral range free of other signals The signal of carbon 4 at about 82 ppm is hidden beneath the spinning side bands of FERAC appearing in this region. The resonance of carbon 1 at 104 ppm only appears as a shoulder of the FERAC signal at 109 ppm. The signals of carbons 6 and 7 (60 and 62 ppm) as well as the signal of carbon 8 (177 ppm) are also hidden under prominent spinning side bands in these regions. The reason why CMC signals are almost negligible in the spectra of Fig. 1. can be related to the
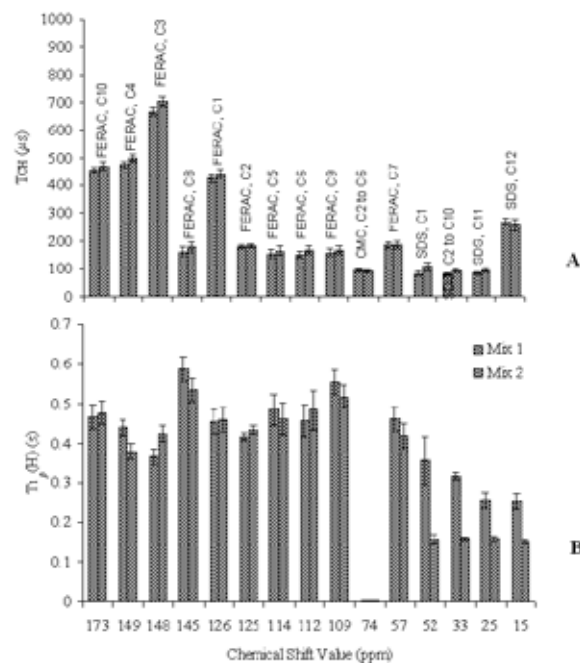
Fig. 2. T_{CH} **(A) and** $T_{1\rho}$**(H) (B) values as obtained from VCT and VSL experiments. See text for the meaning of acronyms**

amount of CMC which is 52 and 77 times lower than that of SDS and FERAC, respectively (see Experimental section).

CPMAS ^{13}C NMR experiments on Mix 1 and Mix 2 were done in VCT and VSL mode (see Experimental for details) in order to obtain information on T_{CH} and $T_{1\rho}$(H) values.

T_{CH} measures the cross polarization (CP) efficiency which depends on the strength of the C-H dipolar interactions[1]. The shorter the proton-to-carbon distances and the slower the local molecular motions, the stronger is the strength of the C-H dipolar interactions, thereby leading to faster CP rates[1] (shorter T_{CH} values).

$T_{1\rho}$(H) is associated to local molecular motions in the kilohertz (kHz) scale[1]. In particular, the faster the molecular motions in the lattice, the shorter is the $T_{1\rho}$(H) value (fast proton relaxation processes). Conversely, when the molecular motions slow down, relaxation processes are slower and longitudinal relaxation times increase[1]. However, attention must be paid when dealing with the interpretation of the molecular motions in lattices by using $T_{1\rho}$(H) values. In fact, proton relaxation times in the rotating frame are also affected by nuclear dipolar interactions. In the case of organic materials, where protons are very abundant, the H-H dipolar interactions are very strong and they predominantly control the rate of the magnetization transfer among protons in the lattice[1]. For this reason, if relaxation mechanisms related to dipolar interactions cannot be ruled out, short $T_{1\rho}$(H) values cannot be associated solely to fast molecular motions in proton-rich organic compounds[1].

The analysis of the T_{CH} values of the different carbon nuclei in FERAC (Fig. 2.A) revealed that they varied in the

order C3>C1, C4, C10>C2, C5, C6, C7, C8, C9. The cross polarization rate of the proton rich methyl group indicated as C7 (Fig. 1.) was similar to the CP rates of the monoprotonated FERAC carbons 2, 6, 7, 8 and 9. This was expected. In fact, CH_3 systems are terminal groups subjected to fast rotational motions. Fast motions weaken H-C dipolar interactions, thereby lowering CP efficiency of the highly protonated methyl groups compared to that of the less protonated methylene systems. A confirmation of a less efficient CP of non protonated C1, C4 and C10 carbons in FERAC as compared to the protonated C nuclei is also reported in Fig. 2.A. However, it must be noted that, among the cross polarization time values of the quaternary carbons (i.e. C1, C3, C4, C10), position 3 (Fig. 1.) showed the largest T_{CH} value. This was attributed to the combined effect of the non-protonation and the large rotational movements of the methoxy group directly bound to C3, which caused poor CP efficiency. Finally, the comparison of the T_{CH} values of the FERAC carbons in Mix 1 and Mix 2 (Fig. 2.A) shows that the CP mechanisms in the ferulic acid are not affected by the physical treatments to which the mixture was subjected in our study.

Fig. 2.B reports the $T_{1\rho}(H)$ values measured for the signals of FERAC, either before or after water dissolution and freeze drying. All the $T_{1\rho}(H)$ values are similar to each other and they did not change passing from Mix 1 to Mix 2. Since FERAC carbons are subjected to different molecular motions, as reported above, we may conclude that the proton longitudinal relaxation mechanisms in FERAC are affected more by H-H dipolar interactions than by fast local movements and chemical-physical treatments.

The T_{CH} values of CMC either in Mix 1 or Mix 2 are similar (Fig. 2A). Such similitude reveals that, as for FERAC, the water dissolution and the freeze drying processes did not affect the CP mechanisms in carboxymethylcellulose. Moreover, the polymeric nature of CMC should be responsible for slow molecular motions that, in turn, should provide longer $T_{1\rho}(H)$ values as compared to FERAC and SDS. Conversely, Fig. 2.B shows the shortest $T_{1\rho}(H)$ values for CMC in both Mix 1 and Mix 2. Also in CMC, as for FERAC, then, predominant relaxation mechanisms are mediated by homonuclear H-H dipolar interactions, rather than molecular motions.

Fig. 2.A shows also similarities in the T_{CH} values of the methylene carbons 1 to 11 of SDS, while the methyl C in the same material (C12) was cross polarized less efficiently due to fast rotational motions as already previously outlined.

After the treatments, the $T_{1\rho}(H)$ values of SDS were halved. Since the H-H dipolar interactions are the main responsible for the longitudinal proton relaxation mechanisms in organic materials, we may argue that the more efficient proton relaxation of SDS in Mix 2 can only be achieved by a strengthening of the homonuclear H-H dipolar interactions. This can be due to a closer proximity of the SDS alkyl chains that before freeze drying are arranged to form micelles.

Conclusions

This work revealed that water treatment and freeze drying processes do not affect the cross polarization dynamics in a mixture of three molecules having known structure and conformation in the solid state. Conversely, proton relaxation, which is affected mainly by the strong H-H dipolar interactions, was fastened only in SDS which was able to form micelles in water solution before freeze drying. Although after the drying procedure micelles cannot be present anymore, the closer proximity of the protons in the alkyl chains as consequence of SDS behaviour in water, strengthened the homonuclear proton dipolar interactions, thereby favouring shorter $T_{1\rho}(H)$ values.

REFERENCES

1. Duer M. J.: *Solid-state NMR spectroscopy: principles and applications*. Blackwell Science, Oxford 2002.
2. Conte P., Piccolo A.: Chemosphere *38*, 517 (1999).
3. Wilson M. A.: *NMR techniques and applications in geochemistry and soil chemistry*. Pergamon Press, London 1987.
4. Smernik R. J.: Eur. J. Soil Sci. *57*, 665 (2006).
5. Blann W. G., Fyfe C. A., Lyerla J. R., Yannoni C. S.: J. Am. Chem. Soc. *103*, 4030 (1981).
6. Schilling M., Cooper, W. T.: Anal. Chim. Acta *508*, 177 (2004).
7. Tekely P., Gérardy V., Palmas P., Canet D., Retournard A.: Solid State Nucl. Magn. Res. *4*, 361 (1995).

L02 AMINOACID PROFILES MONITORING FOR DIAGNOSIS

MONICA CULEA, ANDREEA IORDACHE and CORNELIA MESAROS

Babes-Bolyai University, Str. Kogalniceanu, nr.1, 3400 Cluj-Napoca, Romania,
mculea@phys.ubbcluj.ro

Introduction

Gas chromatography coupled with mass spectrometry (GC-MS) is largely used for the quantitative analyses of the organic compounds from biological fluids[1,4]. Metabolic fingerprinting, metabolite profiling or metabolite target analysis are strategies used in the metabolomics analysis for rapid diagnosis. Biological fluids are ideal candidates for diseases diagnosis because they can easily and inexpensively be isolated from the body.

The study deals with possible diagnosis of neonatal diseases caused by inborn error of metabolism using gas chromatography – mass spectrometry (GC-MS). Phenylketonuria (PKU) is a metabolic disease usually caused by phenylalanine hydroxylase deficiency, which leads to an increase of phenylalanine and a decrease of tyrosine content in plasma. Enzyme deficiency results in high levels of blood phenylalanine and an accumulation of phenylketones in the urine. Partial deficiency of the enzyme results in hyperphenylalaninemia. Maple syrup urine disease (MSUD) is a metabolism disorder caused by a gene defect, in which the body cannot break down some branched-chain amino acids[3]. In MSUD, the enzymes necessary to break down leucine, isoleucine, and valine are either absent, inactive, or only partially active. As a result of the enzyme deficiency, the branched-chain amino acids and ketoacids become elevated in the blood, resulting in an altered mental state and progressive neurodegeneration. PKU is general screened by a bacterial inhibition assay (BIA) of elevate blood phenylalanine levels on newborn filter paper samples of blood specimens. There are many chromatographic methods for screening PKU and also mass spectrometry as electrospray mass spectrometry, ESI-MS-MS[5].

The main goal of the present work was to perform a rapid and precise analysis of volatile derivatives of aminoacids from dry plasma and blood spots for diagnosis of two inborn errors diseases: PKU and MSUD. This minimum invasive method is based on profiling and quantitative determination of some amino acids in blood samples of 20 μl by using filter paper blood specimens and the GC-MS technique. The method is useful for the diagnosis of the PKU disease, by determination of phenylalanine (Phe) and tyrosine (Tyr) content in blood or for the diagnosis of the MSUD disease, by estimation of valine (Val), leucine (Leu) and proline (Pro) content.

Experimental

Chemicals and Samples

Acetyl chloride and ion exchange resin Dowex 50W-X8 50–100 mesh were purchased from Fluka, while acetone and trifluoroacetic anhydride were obtained from Merck (Darmstadt, Germany). Amino acids standards were purchased from Sigma. [^{15}N]-isoleucine (99%) was produced by chemical synthesis. All the other chemicals were from Comchim (Bucharest). The blood and urine samples were obtained from patients and volunteers from the Pediatric Clinic III Cluj-Napoca. Written informed consents were obtained from each subject's parent prior to this study.

Extraction Procedure and Derivatization of Amino Acids

The blood was placed in a screw cap vial with 200 μl methanol/HCl 0.1% and extraction was performed either 1 h at 4 °C or by sonication for 1 min. 100 μl of the extract were placed in a vial and after the addition of the internal standard and removing of the reagent using a nitrogen stream, the amino acid extract was derivatized. Amino acids of the blood samples or standard samples were derivatized as trifluoroacetyl butyl ester derivatives. Derivatization was performed in screw-cap tubes, in two steps. Dry samples were esterified with 100 μl butanol: acetyl chloride, 4:1 (v/v) for 30 min at 100 °C. The excess reagent was removed with a stream of nitrogen. The amino group was acetylated with 100 μl trifluoroacetic anhydride (TFAA) at 100 °C for 30 min. After cooling, the excess reagent was removed under nitrogen at ice temperature and ethyl acetate was added[1].

Instrumentation

A Trace DSQ ThermoFinnigan quadrupole mass spectrometer in the EI mode coupled with a Trace GC was used. The capillary column Rtx-5MS had 30 m in length, 0.25 mm as diameter and a film thickness of 0.25 μm. The experiments were performed by using a temperature program from 50 °C (1 min), then 20 °C min^{-1} to 260 °C, 100 °C min^{-1} to 300 °C, in the selected ion monitoring mode (SIM). Helium (5.5) carrier gas had a flow rate of 1 ml min^{-1}. The qualitative analysis was carried out in the 50–500 a.m.u. mass range. The following conditions were ensured: transfer line temperature 250 °C, injector temperature 200 °C, ion source temperature 250 °C, splitter 10:1, electron energy 70 eV and emission current 100 μA.

In the SIM mode, the following ions were used (Fig. 1.): m/z 168 for valine, m/z 182 for leucine, m/z 166 for proline, m/z 91 and 148 for phenylalanine (Figs. 2., 3.), m/z 203, 260, 316 (Fig. 3.) for tyrosine. 25 μg ml^{-1} of the ^{15}N-isoleucine (^{15}N-Ile, m/z 183) internal standard was added at each sample. For Val, Leu and Pro amino acids, the important ions selected in the SIM experiment from the trifluoroacetyl butyl esters derivatives mass spectra correspond to the loss of butyl ester from the molecular ion [M – COOC$_4$H$_9$]$^+$.
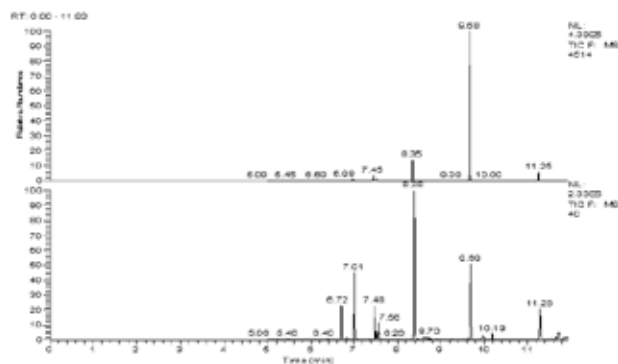
Fig. 1. **SIM-GC-MS comparison of screening of the five amino acids in a PKU blood sample (top) and a standard mixture (bottom) of the amino acids (7.01 min: Val, 7.48 min: Leu, 7.56 min: ^{15}N-Ile (IS); 8.38 min: Pro; 9.69 min: Phe and 11.28 min: Tyr**
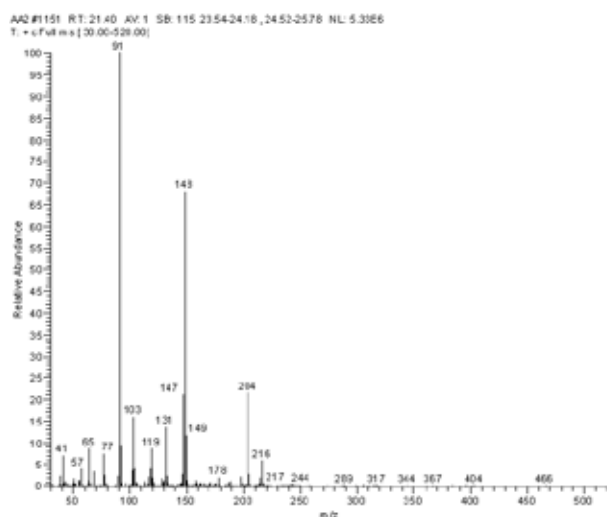
Fig. 2. **The mass spectra of trifluoroacetyl butyl ester derivatives of Phe**

Linearity of the method was calculated by representing the ratio of the selected ion peak area for each amino acid and the internal standard versus the amino acid standard concentrations (in µg ml^{-1}). The regression curves were obtained by injecting standard solutions containing amino acids in concentration of 1, 5, 10, 20, 30 and 40 µg ml^{-1} with 25 µg ml^{-1} of ^{15}N-Ile added to each standard solution per ml of blood sample. The regression curves obtained were: Val: $y = 0.0912x + 0.0555$, regression coefficient $r = 0.999$; Leu: $y = 0.0515x - 0.0097$, $r = 0.998$; Pro: $y = 0.1835x - 0.1382$, $r = 0.998$; Phe: $y = 0.1119x - 0.0665$, $r = 988$; Tyr: $y = 0.08x - 0.1938$, $r = 0.984$. The precision and the accuracy were studied by extracting four times the standard solutions of 1, 30 and 40 µg ml^{-1}. The R.S.D. values obtained ranged between 9-12.9 % for 30 µg ml^{-1} and 6.7–18.6 % for 40 µg ml^{-1} (Table I). For 1 µg ml^{-1}, the precision was between 45-50 %. Accuracy values were between 4–30% for 30 µg ml^{-1} and lower than 5.5 for 40 µg ml^{-1} (n = 4). The limit of detection (L.O.D.) was lower than 0.1 µg ml^{-1}.
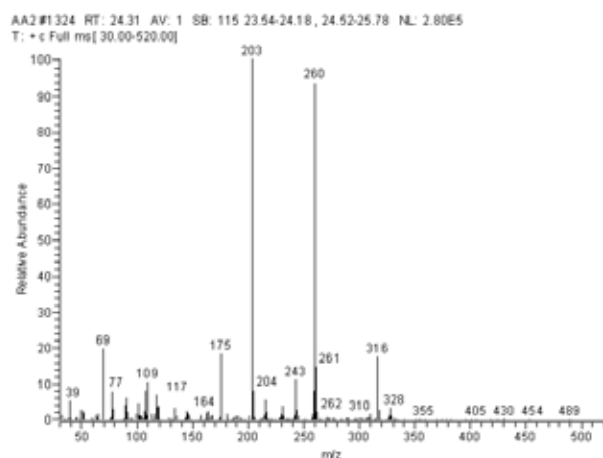
Fig. 3. **The mass spectrum of Tyr trifluoroacetyl butyl ester derivative**

Table I
Precision study for the same patient (6 spots, n = 6)

Amino acid	[µg ml^{-1}]	SD	RSD [%]
Val	4.05	0.28	6.97
Leu	3.39	0.17	5.00
Pro	3.40	0.27	6.57
Phe	1.32	0.14	10.41
Tyr	2.19	0.11	5.06

Table II
The amino acids quantitation in control blood samples, spot samples (mean values, n = 53)

Amino acid	[µg ml^{-1}]	[µM]
Val	11.66	99.62
Leu	13.19	100.71
Pro	17.82	155.00
Phe	17.15	103.95
Tyr	26.67	147.33
Phe/Tyr	0.64	0.71

Table III
Amino acids values [µg ml^{-1}] in PKU blood samples, spot samples

Val	22.27	21.73	21.47	23.22	22.16	21.51
Leu	22.96	24.56	16.97	25.84	33.16	19.92
Pro	37.76	23.67	19.85	25.64	65.66	31.42
Phe	93.18	134.13	89.75	142.7	131.3	119.3
Tyr	50.02	38.99	19.4	35.91	57.2	33.53
Phe/Tyr	1.86	3.44	4.63	3.97	2.30	3.56

In our study, 13 cases of PKU children were found, Phe/Tyr value being significantly higher than control.

Table IV
Amino acids values [$\mu g\,ml^{-1}$] in a PKU child blood samples; spots were taken at different intervals of the day; hour: 7, 9, 14 and 19

Val	8.9	10.86	10	8.95
Leu	23.16	41.3	35.59	36. 57
Pro	16.34	40.09	43.52	43. 68
Phe	262.33	608.71	548.85	491.65
Tyr	15.84	42.63	50.07	67.59
Phe/Tyr	16.56	14.28	10.96	7.27

Results

Quantitative analysis of five amino acids, valine, leucine, proline, phenylalanine and tyrosine, in blood samples, by using blood spots[1] or 0.5 ml blood[3,9] gave similar results, the coefficient of regression obtained by comparing the amino acid values in the two extraction methods gave $r = 0.91$ ($n = 4$). Fig. 1. shows the chromatogram of separation of the five amino acids by using the minim invasive method, from 20 µl blood.

The intraindividual amino acid values variation is shown in Table I. Table II shows the comparison of the results obtained for the amino acids average value in control blood samples ($n = 53$). Good amino acid precision in the same child was obtained, R.S.D. lower than 10.4 %. The results obtained by using only 20 µl of blood spots showed that the PKU diagnosis could be tested by calculating the Phe/Tyr ratio. Diagnosis of the MSUD disease should be obtained by calculating the ratio between aliphatic and aromatic amino acids in the blood samples[1]. The results for some PKU patients are presented in Tables III and IV. The high benefits of the early diagnosis and treatment are strong arguments for the neonatal screening of metabolic disorder. The classical bacterial inhibition assay (BIA) used for the diagnosis of PKU is a semi-quantitative method giving false positive results. More precise methods, such is the MS/MS technique, were developed, but they have the disadvantage of high price and less affordable equipment. By comparison, the proposed

GC/MS method is simple, inexpensive, easily operated and high-speed technique.[5–8] The internal standard used increased the precision of the method. The use of mass spectrometer as a detector for GC is important not only for its high sensitivity but also for selectivity and the identity of the analytes[9].

Conclusions

Measurements performed on amino acids from dried blood spots showed that GC-MS is a suitable method for PKU diagnosis in neonatal blood samples, from Phe/Tyr ratio and MSUD from the amino acid values[1]. The labelled internal standard used increased the precision of the method and simplified the samples injection. The method is a minim invasive, by using very small quantities of blood. Monitoring these diseases is important because once the diagnosis is made and treatment is started in the first few weeks of life, normal brain development is not disturbed or affected.

REFERENCES

1. Deng C., Li N., Wang X., Zhang X., Zeng J.: Rapid Commun. Mass Spectrom. *19*, 647 (2005).
2. Phillips M., Cataneo R. N., Cheema T., Greenberg J.: Clin. Chim Acta., *344*, 189 (2004).
3. Culea M., Bucur A., Cozar O.: Analele Univ. Vest Timisoara *45*, 89 (2004).
4. Culea M., Cozar O., Ristoiu D.: JMS *41*, 1594 (2006).
5. Nagy N., Takats Z., Pollreisz F., Szabo T., Vekey K.: Rapid Commun. Mass. Spectrom. *17*, 983 (2003).
6. Deng C., Yin X., Zhang L., Zhang X.: Rapid. Commun. Mass. Spectrom. *19*, 2227 (2005).
7 Jouvet P., Hubert P., Saudubray J. M., Rabier D., Man N. K.: Pediatric Res. *58* (2005) 278.
8 Shen X., Deng C., Wang B., Dong L.: Anal. Bioanal. Chem. *384*, 931 (2006).
9 Culea M., Hachey D. L.: Rapid Commun. Mass. Spectrom. *9*, 655 (1995).

L03 MICROWAVE-ASSISTED EXTRACTION OF ORGANIC COMPOUNDS FROM THE BROWN COAL

SILVIA ČUVANOVÁ[a] and MICHAL LOVÁS[a]

[a]*Institute of Geotechnics, Slovak Academy of Sciences, Watsonova 45, 043 53 Košice, Slovakia,*
cuvanova@saske.sk

Introduction

Microwave heating arises from the ability of some liquids and solids to transform the absorbed electromagnetic energy into heat. The heating effect originates from the microwave electric field which forces dipoles to rotate and ions to migrate; from a slower response of dipoles and ions to follow the rapid reversal of the electric field. The ability of material to increase its temperature under microwave at a given frequency and temperature is referred to the dissipation factor, defined as $\tan \delta = \varepsilon''/\varepsilon'$, where ε'' is the dielectric loss factor related to the efficiency of a medium to convert microwave energy into heat, while ε' is the dielectric constant measuring the ability of a molecule to be polarised by an electric field. The penetration depth (D_p) is the distance from the material surface where the absorbed electric field falls to $1/e$ of the electric field at the surface. The penetration depth is inversely proportional to the frequency, whereas the greatest heating is achieved at the high frequencies. However, the penetration depth at such frequencies is so low that only the exterior of the material will heat. D_p is given by (1):

$$ D_p = \frac{c}{2.\pi.f\sqrt{2.\varepsilon'}} \cdot \frac{1}{\left[\sqrt{1+\tan^2\delta}-1\right]^{1/2}} , \qquad (1)$$

where: f – frequency [Hz]; c – speed of light [ms^{-1}].

Together with the ability to dissolve reagents and products, the solvent under microwaves can play a more active role. The acceleration of a chemical reaction under microwaves depends on the dielectric properties of the solvent. Solvents that are able to directly absorb microwaves increase the reaction rate of the dissolved reagents. The solvent overheating is a phenomenon frequently observed when microwaves are applied in chemical processes. In the presence of microwaves, common solvents are found to boil at higher temperatures: for dichloromethane the difference is about 15 °C. In closed vessels this increases the pressure of the system.

The microwave applications in mining and process metallurgy have been the subject of many research studies over the past two decades. The microwaves have potential application in mineral processing and extraction of metals such as copper, gold, nickel, cobalt, lead, zinc and manganese[2], and also for the direct determination of sulphide, pyrite and organic sulphur concentrations in coals of bituminous or sub-bituminous rank[3].

Microwave-assisted extraction in the closed system has been developed as a means of avoiding the use of large amounts of solvent and to save time. The samples and solvents in the closed system reach temperatures above the boiling points of the solvents at the atmospheric pressure. As results, the extraction of samples can be completed in minutes as opposed to hours necessary when traditional methods are used[4,5]. There are many reports where PAHs are extracted with comparable efficiency to those by using Soxhlet extraction, even for extraction times of less than 30 min[4].

The microwave heating has been applied to the extraction of organic contaminants such as polycyclic aromatic hydrocarbons, pesticides, polychlorobiphenyls, herbicides, phenols, neutral and basic priority pollutants in various matrices such as sediments, soils, coal or atmospheric particles. The main purposes of the microwave heating are the reduction of extraction time and solvent quantity. The decrease of solvent waste, solvent release into the environment and human exposure is also important.[6–10]

The most common solvents used for the MAE of PAHs from the solid samples are acetone-hexane, dichloromethane, methanol, and methanol-toluene. However, the selection of solvent to extract analyses has to take into consideration the technique which will be used in the final determination. Most solvents or solvent mixtures used for PAHs extraction appear to be perfectly suited for the gas chromatography. But if liquid chromatography will be used, the solvent exchange would be necessary.[7–9,11–15]

Our article presents the influence of conditions of extraction on the occurrence of PAHs in dichloromethane extract.

Experimental

S a m p l e   C h a r a c t e r i z a t i o n

The research was carried out with the samples of the Slovak brown coal from Handlová (West Slovakia) after the hydrocyclone washing[16]. The chemical analysis of studied sample was following: A^d (Ash) = 9.01 %, M (Moisture) = 7.55 %, C^{daf} = 74.86 %, H^{daf} = 4.93 %, N^{daf} = 0.6 %, $(O + S)^{daf}$ = 19.61 %.

I n s t r u m e n t a t i o n

CHN analysis was realized using elementary analyser Carlo Erba Model 1106 equipped with the microprocessor and recorder. Helium (purity 99.998 %) was used as the carrier gas; oxygen (99.999%) was used as the oxidative agent and argon created an inert atmosphere during measurement. The chromatographic column was filled with the Porapak QS with granularity 80–100 mesh. The cyclohexanone – dinitrophenylhydrazone (content of N = 20.14 %, C = 51.79 % and H = 5.07 %) was used as the standard material.

The studied sample was pretreated in the mill and then the sample of under 0.5 mm granularity was activated by the grinding using the planetary mill Pulverisette 6 (Fritsch, Germany) in the air atmosphere at the following conditions: granularity of input – 0.5 mm, mass of sample – 20 g, grinding speed – 400 rev min^{-1}, time of grinding – 20 minutes.

SEM/EDX analysis was carried out at the Institute of Theoretical and Physical Chemistry – Braunschweig, Germany. It was used JSM – 6400 Scanning microscope (JEOL

LTD., Tokyo Japan) combined with the Microanalysis System Software, EDAX Genesis V2.50.

Microwave-Assisted Extraction and Analysis

Soxhlet extraction of the coal sample was realized in dichloromethane for 3 days. The microwave-assisted extraction was realized in the microwave Whirpool at the power 500 W and frequency 2.45 GHz. The extraction was realized in the non-polar solvent of dichloromethane at the boiling point 40 °C (it increases in microwave oven to 55 °C) for the period of 30 minutes. The boiling point of solvent in the microwave was measured using the contactless thermometer Raytek MX4. MAE was also realized in the closed pressure vessels by automatic pressure regulation within range 1.8–2 bar for the period of 20 minutes.

GC-MS analyses were realised in National Water Reference Laboratory for Slovakia in Bratislava. The chromatographic analyses were performed using Agilent 6890 gas chromatograph coupled to Agilent 5973 mass spectrometric detector (USA). Capillary GC analysis was performed on a 30 m×250 μm I.D.; 0.25 μm d_f HP-5MS column (Agilent Technilogies). Helium was used as a carrier gas. The MSD was used in the scan mode (m/z 40–550) for all samples. Mobile phase was methanol and water Milli-Q. The identification of compounds was performed using mass spectrum libraries Wiley 7n and NIST02, respectively.

The distribution of temperature in the extraction solvent was operated by modeling program Comsol, version 3.3.

Results

Microwave Heating of Dichloromethane

Coal pretreatment with dichloromethane has been reported for improvement of selective grindability of organic substances and mineral matters in coal. Table I summarizes the properties of dichloromethane.
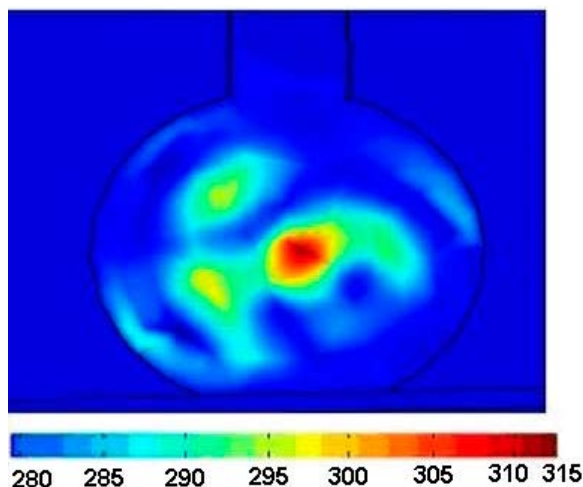
Fig. 1. **Distribution of temperature for the microwave heating of dichloromethane after 3 seconds; radius of spherical container is 10 cm**

Table I
The physical properties of dichloromethane

Density [kg m⁻³]	Diel. const.	Loss factor[17]	Heat capacity [J K⁻¹ kg⁻¹]	Thermal conduct. [W m⁻¹ K⁻¹]
1,317.0	8.93	0.042	1,190.0	0.122

The penetration depth calculated according to equation (1) for dichloromethane is 0.16 m.

Commercial final element method based on software COMSOL Multiphysics was used to modeling the dichloromethane microwave heating (Fig. 1.). Various steps involved in the modeling with COMSOL software are outlined in Fig. 2.
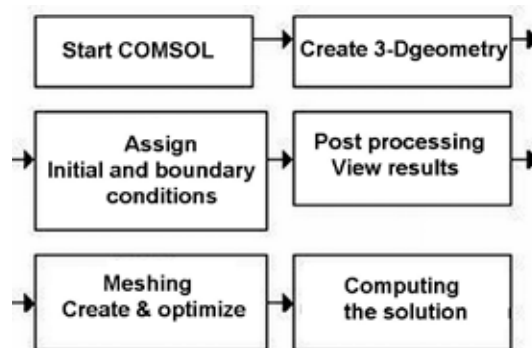
Fig. 2. **The COMSOL modeling steps**

Microwave Extraction of Samples in Dichloromethane

Fig. 3. shows the quantity of physically treated brown coal sample after the microwave-assisted extraction in dichloromethane.

The presence of elements typical for the Slovak brown coal (Table II) was confirmed.
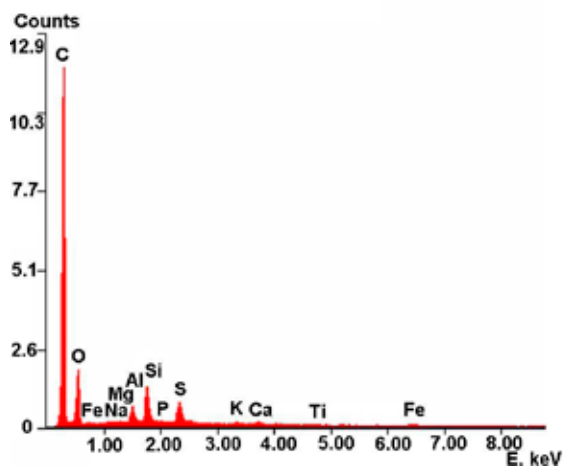
Fig. 3. **EDX spectrum of physically treated brown coal sample after the microwave-assisted extraction in dichloromethane**

Table II
Content of elements in the coal sample after the microwave-assisted extraction in dichloromethane

Element	W_t [%]	A_t [%]
C	78.52	84.61
O	16.40	13.27
Na	0.14	0.08
Mg	0.08	0.04
Al	0.83	0.40
Si	01.83	0.84
P	0.04	0.02
S	01.15	0.46
K	0.14	0.05
Ca	0.24	0.08
Ti	0.06	0.02
Fe	0.57	0.13

Table III
The composition of the Slovak brown coal extract after the Soxhlet extraction in dichloromethane

Peak number	Ion intensity [m/z]	Formula	Characterization of the compounds
1	198	$C_{15}H_{18}$	1,6-dimethyl-4-(1-methylethyl) naphthalene
2	274	$C_{20}H_{34}$	4b,8,8-trimethyl-2,10a-(2'-methylethano)-perhydrophenanthrane
3	270	$C_{20}H_{30}$	7-izopropyl–1,1,4a-trimethyl–1,2,3,4,4a,9,10,10a-oktahydrophenanthrene
4	252	$C_{19}H_{24}$	simonelit

Our attention was intent on the study of influence of Soxhlet and microwave-assisted extraction in the open-vessel and closed-vessel system, respectively.

It was also realized the blank experiment (Fig. 4.). It was prepared with 100 ml Milli Q vody and 10 ml methanol. Then it was mixed 2 hours with the blender Twister.

Fig. 5. shows the chromatogram of coal extract after the Soxhlet extraction in dichloromethane for 72 hours The presence of organic compounds with carbon numbers C15, C20 a C19 was confirmed in the extract after the Soxhlet extraction. All analyzed compounds belong to group of polycyclic aromatic hydrocarbons (Table III).

During microwave-assisted extraction in the open-vessel system the extraction time was shorten to 30 minutes at power 500 W and frequency 2.45 GHz. The following organic compounds were identified by GC-MS method: naphthalene and its derivates with the carbon numbers 14 and 15 (m/z = 184, 198), phenanthrene derivates with the carbon number 20 (m/z = 274, 276). The presence of benzene derivate $C_{15}H_{22}$, indene derivate $C_{14}H_{20}$ and other naphthalene derivate $C_{14}H_{16}$ was confirmed as well (Fig. 6., Table IV).

The microwave-assisted extraction in closed-vessel system was realized by pressure 1.8–2 bar for 20 minutes. The temperature was not possible to measure correctly. Fig. 7. shows the representative GC-MS chromatograph of the orga-

Fig. 4.　**Typical GC chromatogram of the blank experiment**
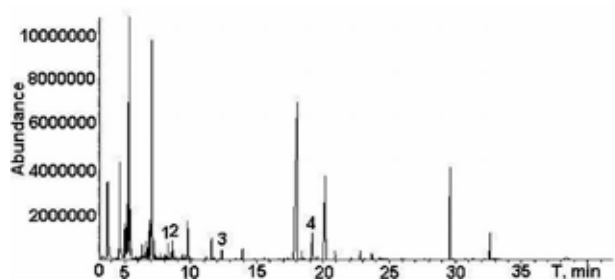
Fig. 6.　**Typical GC chromatogram of dichloromethane extract of the physically treated brown coal prepared by the microwave-assisted extraction in the open-vessel system; extraction time of 30 minutes**

Fig. 5.　**Typical GC chromatogram of dichloromethane extract of the physically treated brown coal prepared by the Soxhlet extraction; extraction time of 72 hours**

nic compounds occurrence in the microwave extract of coal sample in dichloromethane. The growing of other organic compounds was confirmed. The solvent temperature has the essential influence on number of extracted substances. The temperature is higher by microwave heating in comparison with Soxhlet extraction. Other organic compounds occurred in extract after the microwave-assisted extractions in the closed-vessel system are listed in Table V.

Table IV
The occurrence of other organic compounds in the Slovak brown coal extract after the extraction in dichloromethane; the open-vessel system

Peak number	Ion intensity [m/z]	Formula	Characterization of the compounds
1	202	$C_{15}H_{22}$	1-methyl-4-(1,2,2-tri methylcyclopenthyl) benzene
2	188	$C_{14}H_{20}$	1,1,4,6,7-pentamethyl-2,3-dihydroindene
3	184	$C_{14}H_{16}$	1,2,3,4-tetramethyl-naphthalene
4	276	$C_{20}H_{36}$	2-ethyl-2,4,8,8-tetramethyl-perhydrophenanthrene
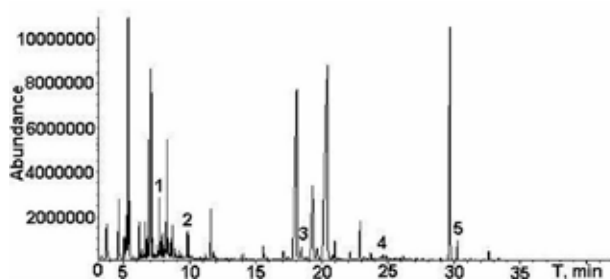
Fig. 7. **Typical GC chromatogram of dichloromethane extract of the physically treated brown coal prepared by the microwave-assisted extraction in the closed-vessel system; extraction time of 20 minutes**

Table V
The occurrence of other organic compounds in the Slovak brown coal extract after the extraction in dichloromethane; the closed-vessel system

Peak number	Ion intensity [m/z]	Formula	Characterization of the compounds
1	206	$C_{15}H_{26}$	alfa-cedrane
2	226	$C_{16}H_{34}$	hexadekane
3	272	$C_{20}H_{32}$	(5alfa, 9 alfa, 10 beta)-kaur–15-ene
4	234	$C_{18}H_{18}$	1-methyl-7-izopropyl-phenanthrene
5	366	$C_{26}H_{54}$	hexakozane

Conclusions

The focused microwave-assisted extraction in the atmospheric open-vessel systems seems to be a viable alternative method to Soxhlet extraction for the analysis of organic compounds, mainly polycyclic aromatic hydrocarbons in the coal sample from Handlová. The advantage of using MAE for the coal sample is the reduction of extraction time. The optimized conditions can be applied for extraction with good recoveries and reproducibility. This method can be used in conjunction with GC-MS for the determination of PAHs in the large number of coal samples.

REFERENCES

1. Mingos D. M. P., Baghurst D. R.: Chem. Soc. Rev. *20*, 1 (1991).
2. Al-Harahsheh M., Kingman S. W.: Hydrometallurgy *73*, 189 (2004).
3. Laban K.L., Atkin B. P.: Fuel *79*, 173 (2000).
4. Itoh N., Numata M., Yarita T.: Anal. Chim. Acta (2008, in press).
5. Karthikeyan S., Balasubramanian R., See S. W.: Talanta *69*, 79 (2006).
6. Letellier, M., Budzinski, H.: Analusis *27*, 259 (1999).
7. Čuvanová S., Lovás M., Turčániová Ľ., Hredzák S.: *The 11th International Conference on Environment and Mineral Processing*, p. 123. Ostrava, 2007.
8. Zubrik A., Turčániová Ľ., Ježová V., Čuvanová S., Skybová M.: J. Alloys Compd. *434*, 837 (2007).
9. Zubrik A.: *Dissertation*. Institute of Geotechnics, Slovak Academy of Science in Košice, Košice, Slovakia, 2008.
10. Murová I.: *Dissertation*. Institute of Geotechnics, Slovak Academy of Science in Košice, Košice, Slovakia, 2001.
11. Pensado L., Casais C., Mejuto C., Cela R.: J. Chromatogr. A *869*, 505 (2000).
12. Fabbri D., Vassura I.: J. Anal. Appl. Pyrolysis *75*, 150 (2006).
13. Liguori L., Heggstad K., T. Hove H., Julshamm K.: Anal. Chim. Acta *573-574*, 181 (2006).
14. Cai O.-Y., Mo C.-H., Wu Q.-T., Zeng Q.-Y.: Bioresour. Technol. *99*, 1830 (2008).
15. Mikošková J., Čáp L., Lemr K.: Chem. Listy *98*, 85 (2004).
16. Hredzák S.: Gospodarka Surowcami Mineralnymi *15*, 221 (1999).
17. Kappe C. O.: Angew. Chem. Int. Ed. *43*, 6250 (2004).

L04 REACTIVITY OF N−NO₂ BONDS IN NITRAMIDES

ZDENĚK FRIEDL[a] and SVATOPLUK ZEMAN[b]

[a]*Brno University of Technology, Faculty of Chemistry, Purkyňova 118, 602 00 Brno, Czech Republic*
[b]*Institute of Energetic Materials, University of Pardubice, 532 10 Pardubice, Czech Republic,*
friedl@fch.vutbr.cz

Introduction

The highly energetic character of the N−NO₂ group means that *N*-nitro-based energetic materials are of the most powerful explosives available. Different chemical properties of primary and secondary nitramines predetermine the others (e.g. RDX, HMX and HNIW) as the explosives of choice for military use[1].

Structurally related type of compounds represent nitramides where conjugated C=O group is directly bonded to N−NO₂ grouping. At present the idea of fundamental role of nitro groups is generally accepted[2,3]. The homolytic dissociation of C−NO₂, N−NO₂ or O−NO₂ represents the primary fission process of energetic materials under thermal, impact, shock and electric spark initiation stimuli. Thus, the relationships exist between characteristics of low-temperature thermal decomposition and detonation characteristics of polynitro compounds[2].

In the case of polynitro compounds as nitro aromatics, nitramines and nitramides the C−NO₂ or N−NO₂ bond fission is mostly characterized by homolytic *bond dissociation energy BDE*(N−NO₂)[4-12]. The theoretical calculations of homolytic *BDE* energies are substantially influenced from inadequate treatment of electron correlation. At present the mostly used density functional models with 6-311+G(d,p) basis set provide a much improved description of homolytic *BDE* in comparison with Hartree-Fock models. Overall, B3LYP models provide the best results and are quite close to those from the corresponding MP2 models[13,14].

Recently the elegant method was suggested to overcome this substantial drawback – the isodesmic reaction approach[4,15]. This type of virtual symmetrical chemical equilibria inherently cancels electron correlation effects accompanying homolytic bond dissociation. The application of isodesmic reaction scheme to describe N−NO₂ bond fission leads to the formulation of relative *bond disproportionation energy DISP*(N−NO₂) described by (1):

$$R-CO(N-NO_2)-R' + \begin{array}{c}\text{(piperidinone, NH)}\end{array}$$

$$\longrightarrow R-CO(NH)-R' + \begin{array}{c}\text{(N-NO}_2\text{ piperidinone)}\end{array} \quad (1)$$
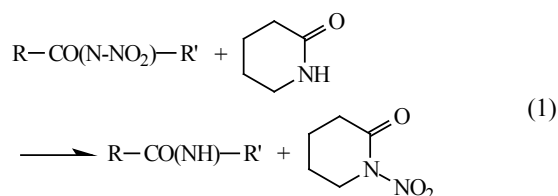
The use of closed shells reactants in (1) guarantee that the electron correlation term in bond disproportionation

energy *DISP*(N−NO₂) is irrelevant. In view of the difference in cost between theoretical calculations of open shell or neutral molecules, the latter seems the obvious choice for this purpose.

Relating to our results on initiation reactivity[2,3,12] we have recently calculated the theoretical *in silico* bond dissociation energies *BDE*(N−NO₂) and bond disproportionation energies *DISP*(N−NO₂) for 20 nitramines[16]. The energies obtained were compared with their detonation velocity *D* and heat of explosion *Q*real.

In this paper we have calculated bond dissociation energies *BDE*(N−NO₂) and bond disproportionation energies *DISP*(N−NO₂) by B3LYP/6-311+G(d,p) method for 12 nitramides of general formula RN−NO₂ (1-nitropiperidin-2-one as a standard nitramide SN−NO₂) and the energies obtained were compared with their detonation velocities *D*.
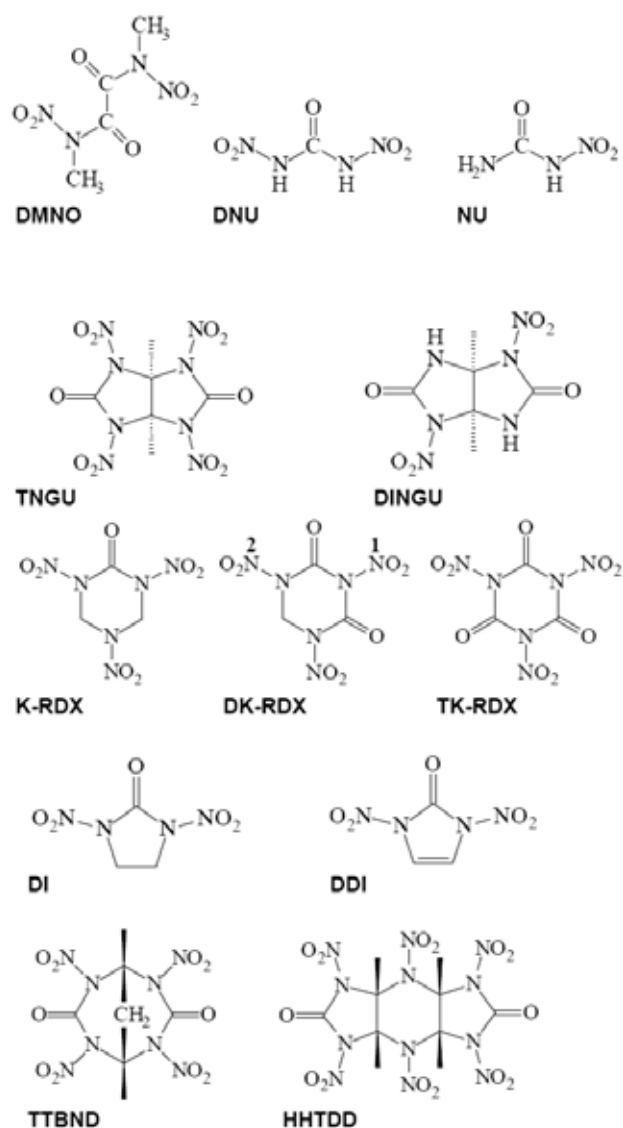
Fig. 1. **The chemical structures and names of nitramides studied with numbering of respective NO₂ groups**

Experimental

C a l c u l a t i o n s

The calculations of bond dissociation energies $BDE(N-NO_2)$ and bond disproportionation energies $DISP(N-NO_2)$ were performed by B3LYP/6-311 + G(d,p) method[17]. The calculations by total optimization gave the equilibrium geometries in the gas phase at 0 K. The optimized structures of 13 nitramides and related amides were verified by normal mode frequency analysis to exclude imaginary frequencies for the remaining $3N$-6 vibrational degrees of freedom. The relevant data are summarized in Table I.

Table I

Calculated bond dissociation energies BDE(N–NO$_2$), bond disproportionation energies DISP(N–NO$_2$) and detonation velocities D of nitramides studied

Name	BDE DISP [kJ mol^{-1}]	D [km s^{-1}]
DMNO	177.67–18.98	7.20
DNU	171.20–38.55	8.32
NU	207.18–35.44	8.35
TNGU	151.96–40.96	8.86
DINGU	173.20–3.80	8.04
K-RDX	152.39–25.24	9.01
DK-RDX N1	161.89–59.79	8.62
N2	155.12–27.06	8.62
TK-RDX	135.04–98.16	7.85
DI	164.50–2.90	7.99
DDI	252.28–20.30	8.30
TTBND	158.16–38.70	8.72
HHTDD	150.16–31.47	9.26
NPO	173.99–0.00	(3.65)

The chemical structures and names of nitramides studied with numbering of respective NO$_2$ groups are given in Fig. 1.

DMNO *N,N'*-dimethyl-*N,N'*-dinitroethanediamide, DNU *N,N'*-dinitrourea, NU *N*-nitrourea, TNGU 1,3,4,6-tetranitro-tetrahydroimidazo[4,5-d]imidazole-2,5-(1*H*,3*H*)-dione, DINGU 1,4-dinitrotetrahydroimidazo[4,5-*d*]imidazole-2,5-(1*H*,3*H*)-dione, K-RDX 1,3,5-trinitro-1,3,5-triazinan-2-one, DK-RDX 1,3,5-trinitro-1,3,5-triazinane-2,4-dione, TK-RDX 1,3,5-trinitro -1,3,5-triazinane-2,4,6-trione, DI 1,3-dinitroimidazolidin 2-one, DDI 1,3-dinitro-1,3-dihydro-2*H*-imidazol-2-one, TTBND 2,4,6,8-tetranitro-2,4,6,8-tetraazabicyclo[3.3.1]nonane-3,7-dione, HHTDD 1,3,4,5,7,8-hexanitrooctahydrodiimidazo[4,5-*b*:4,5-*e*]pyrazine-2,6-(1*H*,3*H*)-dione, NPO 1-nitropiperidin-2-one

D e t o n a t i o n　P a r a m e t e r s

The values of detonation velocities *D* were calculated using the known relationships of Rothstein & Petersen[18,19]. Summary of calculated values is given in Table I.

Results

From the published papers[2,3,20,23,24] it follows that logical relationships exist between the characteristics of low-temperature thermal decomposition and those of initiation and detonation, respectively. The homolytic character of primary fission in both the detonation and low-temperature thermal decompositions of energetic materials (for relevant quotations, see ref.[21]) was a motive factor for using the Evans–Polanyi–Semenov equation[25] (E–P–S) to study the chemical micro-mechanism governing initiation of energetic materials in the following form:

$$E_a = \alpha Q + \beta \qquad (2)$$

Application of the definition relationship[26] between detonation velocities and heats of explosion *Q* leads to the Eq. (3):

$$Q = \frac{D^2}{2(\gamma^2 - 1)} , \qquad (3)$$

where γ is the polytropy coefficient which transforms Eq. (2) into Eq. (4) named in the previous paper[23]

$$E_a = aD^2 + b \qquad (4)$$

as a modified E–P–S equation. The original E–P–S describes a relationship between activation energies E_a of the most substitution reactions of free radicals and corresponding heats of reaction ΔH of narrow sets of substance structures[25]. The equation documents that the strength of bond being split is a decisive factor in the given reaction.
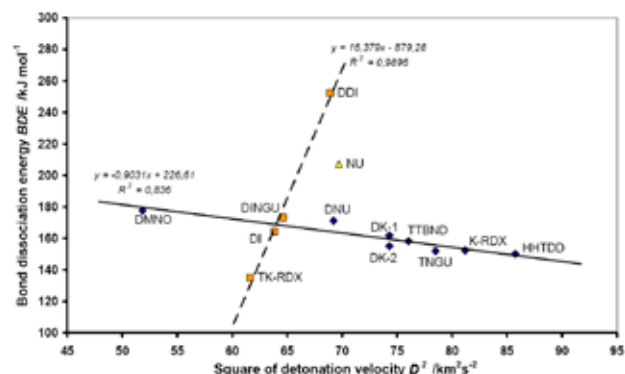
Fig. 2. **Relationship between bond dissociation energy BDE(N–NO$_2$) and square of detonation velocity D^2 of nitramides studied**

In both equations (2) and (4) the energy, E, can be the activation energy of thermal decomposition (E$_a$)[3,23,27], the slope E$_a$R^{-1} of the Kissinger relationship[3,20,24], the energy of electric spark E$_{ES}$, drop energy E$_p$, it may be substituted by the charge q^N at nitrogen atom of the most reactive nitro group in the molecule[3,20,24], by the net charge of this nitro group[23], or by the half-wave polarographic potential[20]. Sub-

stitution of the energy E in Eq. (4) by the BDE energy leads to Fig. 2.

Fig. 2. presents the relationships between dissociation energies $BDE(N-NO_2)$ and square of detonation velocities D^2. The dominant relationship with the slope of –0.90 describes the generally expected indirect rule of proportion between ease of bond fission and detonation velocity. This relationship is valid from polycyclic nitramide HHTDD till the open structure of DMNO. Nevertheless, nitramides DDI and TK-RDX, which are strictly planar and highly conjugated fail the general relationship but create a new line with the positive slope of 16.38 Similarly NU miss the plot due to its different structure.
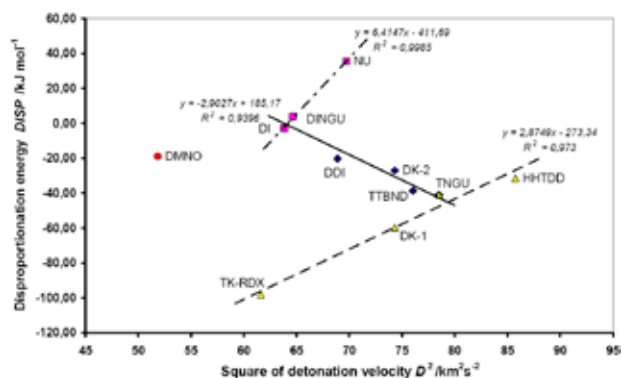
Fig. 3. Relationships between bond disproportionation energies DISP(N−NO$_2$) and square of detonation velocity D^2 of nitramides studied

Similarly, a substitution of the energy, E, in Eq. (4) by the bond disproportionation DISP energy leads to Fig. 3. Differentiation of the studied nitramides in the sense of Eq. (4) is more pronounced and corresponding relationships are closer as in the case of Fig. 2. TK-RDX and DK1-RDX are nitramides with specific group $(C=O)-(N-NO_2)-(C=O)$ and make relationship with similar positive slope as nitramides containing $NH-(C=O)-(N-NO_2)$ group, i.e., DINGU and NU. According to the Fig. 3. the remaining cyclic nitramides are differentiated into line with negative slope -2.90. Alternative expansion of this plot should probably be relationship comprising nitramides from DMNO via DK2-RDX, TNGU to HHTDD resembling the correlation of BDE in Fig. 2. Considering the detonation of nitramides studied as a "zero order" reaction, then the relationships in Figs. 2. and 3. partly reminder the LFER approach, i.e., correlation of rate constants with Hammett substituent parameters[28].

Conclusions

The homolytic dissociation of $N-NO_2$ bond represents the primary fission process of both secondary nitramines and nitramides under thermal, impact, shock and electric spark initiation stimuli. This bond fission is characterized by homolytic bond dissociation energies $BDE(N-NO_2)$. The theoretical calculations of BDE energies are substantially influenced from inadequate treatment of electron correlation. Recently the

alternative method was suggested to overcome this substantial drawback – the bond separation approach described by an isodesmic reaction $RN-NO_2 + SN-H \rightarrow RN-H + SN-NO_2$ where $SN-NO_2$ is a standard nitramide (NPO). This type of virtual symmetrical chemical equilibrium, characterized as bond disproportionation reactions, inherently cancel the electron correlation effects accompanying homolytic bond dissociation. The BDE energies correlate generally tightly with detonation velocities D of nitramides studied. The analysis of the relationship for $DISP(N-NO_2)$ leads to finding that the resulting correlations of D^2 values with these energies somewhat remind analogous relationships between the rate and Hammett constants (detonation is taken as a "zero order" reaction in this case). It seems that the mutual correlation of D^2 with $BDE(N-NO_2)$ values is more limited by molecular structure than a similar correlation with $DISP(N-NO_2)$ energies.

REFERENCES

1. Agrawal J. P., Hodgson R. D.: *Organic Chemistry of Explosives.* Wiley, Chichester 2007.
2. Zeman S., in: *Energetic Materials* (Politzer P., Murray J.S., eds.), part 2, p. 25. Elsevier, Amsterdam 2003.
3. Zeman S.: J. Hazard. Mater. *132*, 155 (2006).
4. Hehre W. J., Radom L., Schleyer P. v.R., Pople J. A.: *Ab Initio Molecular Orbital Theory.* Wiley, New York 1986.
5. Wiener J. J. M., Murray J. S., Grice M. E., Politzer P.: Mol. Phys. *90*, 425 (1997).
6. Harris N. J., Lammertsma K.: J. Am. Chem. Soc. *119*, 6583 (1997).
7. Rice B. M., Sahu S., Owens F. J.: J. Mol. Struct. *583*, 69 (2002).
8. Zhao Q., Shaowen Z., Li Q. S.: Chem. Phys. Lett. *407*, 105 (2005).
9. Shao J., Cheng X., Yang X.: Struct. Chem. *16*, 457 (2005).
10. Su X., Cheng X., Liu Y., Li Q.: Int. J. Quant. Chem. *107*, 515 (2006).
11. Shao J., Cheng X., Yang X.: Struct. Chem. *17*, 547 (2006).
12. Zeman S., Pelikán V., Majzlík J., Friedl Z.: Centr. Eur. J. Energ. Mater. *3*, 27 (2006).
13. Wiener J. J. M., Politzer P.: THEOCHEM *427*, 171 (1998).
14. Hehre W. J.: *A Guide to Molecular Mechanics and Quantum Chemical Calculations*. Wavefunction, Irvine 2003.
15. Hehre W. J., Ditchfield D., [1]Radom L., Pople J.: *J. Am. Chem. Soc. 92*, 4796 (1970).

16. Friedl Z., Zeman S., in: *Theory & Practice of Energetic Materials* (Wang Y., Huang P., Li S., eds.), vol. VII, p. 410. Science Press, Beijing/New York 2007.
17. TITAN v.1.0.8. Wavefunction, Schrödinger, Irvine 2000.
18. Rothstein L. R., Petersen R.: Propellants Explos. *4*, 56 (1979).
19. Rothstein L. R.: Propellants Explos. *6*, 91 (1981).
20. Zeman S., in: *Structure and Bonding*, vol. 125, *High Energy Density Materials* (Klapötke T., ed.), p. 195, Springer, New York 2007.
21. Zhang C., Shu Y., Huang Y., Zhao X., Dong H.: J. Phys. Chem. B *109*, 8978 (2005).
22. Zhang C., Shu Y., Wang X.: J. Energ. Mater. *23*, 107 (2005).
23. Zeman S.: *Thermochim. Acta 384*, 137 (2002).
24. Zeman S.: in: *Theory & Practice of Energetic Materials* (Wang Y., Huang P., Li S., eds.), vol. VI, p. 452. Science Press, Beijing/New York 2005.
25. Semenov N. N.: *Some problems of chemical kinetics and of reaction capability*. USSR Acad. Sci., Moscow 1958.
26. Andreev S. G., Babkin A. V., Baum F. A., Imkhovik N. A., Kobylkin I. F., Kolpakov S. V., , Ladov V. I., Odintsov V. A., Orlenko L. P., Okhitin V. N., Selivanov V. V., Solovev V. S.,. Stanyukovich K. P., Chelyshev V. P., Shekhter B. I.: *Fizika vzryva*. Fizmatlit, Moscow 2002.
27. Pepekin V. I., Makhov N. M., Lebedev Yu. A.: Dokl. Akad. Nauk SSSR *230*, 852 (1977).
28. Exner O.: *Correlation Analysis of Chemical Data*. Plenum Press, New York 1988.

L05 XRD, FT-IR AND DTA STUDY OF SOOT OBTAINED FROM PYROLYSIS OF USED TIRES

SLAVOMÍR HREDZÁK, SILVIA ČUVANOVÁ and
JAROSLAV BRIANČIN

*Institute of Geotechnics of the Slovak Academy of Sciences,
Watsonova 45, 043 53 Košice, Slovak Republic,
hredzak@saske.sk*

Introduction

Processing of used tyres by application of pyrolysis can be considered as an advanced and environmentally friendly method. It is concerned thermal degradation of substances by heating in atmosphere without oxygen or atmosphere with decreased content of oxygen. The pyrolysis of used tyres usually results in the following products: pyrolytic oil (35 %) pyrolytic gas (20–25 %), solid residuum containing pyrolytic soot (33 %) and steel wires (10–12 %). The mass yields of pyrolytic products depend on composition of feed to pyrolysis and mainly on the temperature of pyrolytic process[1, 2, 3].

Thus, the composition of soot coming from a pilot pyrolytic plant for processing of crushed used tires in Slovak leaching works – Chemistry, Inc. Hnúšťa has been studied. The specimens were prepared using a dry low intensity magnetic separation to remove the residues of thin steel wires and other Fe-bearing phases. The products of magnetic separation were subjected to XRD study. Non-magnetic product was analysed using FT-IR and DTA.

The research on grain size composition and treatment of pyrolytic soot is referred in report[4]. The paper[5] deals with the XRD study, analysis of magnetic fractions as well as of material balance of iron and combustible matter at magnetic separation of pyrolytic soot. A detailed study on phase composition of soot magnetic product is introduced in paper [6].

FT-IR spectra of various types of commercial soot are different in intensity of absorption band, but their position is identical: 3,435 cm^{-1}, 2,943 cm^{-1}, 2,860 cm^{-1}, 1,600 cm^{-1}, 1,335–1,000 cm^{-1} and 755–684 cm^{-1}. This fact is caused by difference in grain size and specific surface[7,8].

The study of clean carbon blacks and modified soot is reported in papers[9,10,11,12]. The following values of vibrations are introduced: 3,434.7 cm^{-1}, 1,728.2 cm^{-1}, 1,711.7 cm^{-1}, 1,591 cm^{-1}, 1,278.9 cm^{-1}, 1,228.9 cm^{-1}, 1,119.1 cm^{-1} and 614.3 cm^{-1}.

The paper[13] describes the synthesis of carbon materials from organic precursors. Prepared carbon materials had absorption lines: 3,423 cm^{-1}, 1,579 cm^{-1}, 1,578 cm^{-1}, 1,509 cm^{-1}, 1,383 cm^{-1}, 1,382 cm^{-1}, 1,343 cm^{-1}, 1,191 cm^{-1}, 1,183 cm^{-1}, 1,159 cm^{-1}, 841 cm^{-1}, 798 cm^{-1}, 693 cm^{-1}, 692 cm^{-1}, 624 cm^{-1} and 620 cm^{-1}.

Frequencies of vibrations for graphite, amorphous carbon and refined single-wall carbon nanotubes are reported in paper[14]. As to graphite, two weak vibration at 1590 cm^{-1} and 868 cm^{-1} are reported[14,15].

Techniques and Equipments

Magnetic Separation

The specimen of deferrized soot was prepared by dry low-intensity high gradient magnetic separation using an universal laboratory magnetic separator JONES (Fig. 1), in a cassette located between of its poles. The cassette was equipped by two finely grooved plates, made of carbon-free iron owing to ensuring of required magnetic field parameters. The separation was performed at the induction of 0.15 T. The induction has been examined at the top of grooves by teslameter with Hall´s sensing head.

Magnetic product was screened by dry way on the sieve with a mesh size of 0.3 mm. Thus, steel wires (M-W) and grainy product (M-G) have been obtained. The both products were analyzed separately.
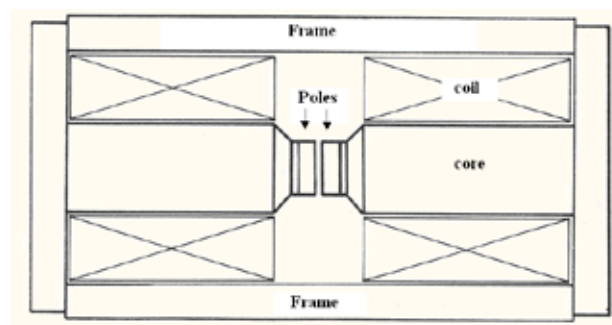
Fig. 1. **Design of the JONES separator**
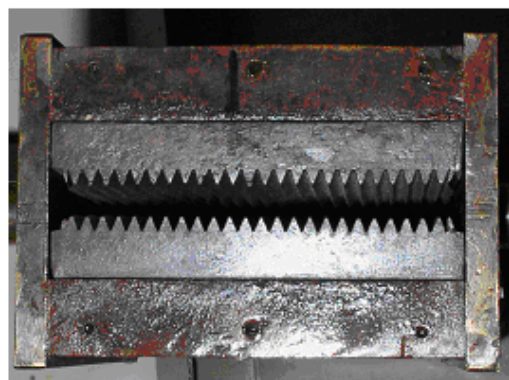
Fig. 2. **The cassette equipped by grooved plates**

Material and Products Analyses

After determination of mass yields the products of separation were subjected to chemical analyses and measurements of volume magnetic susceptibility. On the basis of mass yields and chemical analyses the recoveries of observed components into products separation were calculated according to the method of classical material balance.

Loss on ignition (LOI) at 900 °C and SiO$_2$ content were assayed gravimetrically. Other elements have been determined by atomic absorption spectroscopy using the device VARIAN with accessories: Fast Sequential AAS AA240FS, Zeeman AAS AA240Z with Programmable Sample

Dispenser PSD120, Graphite Tube Atomizer GTA120 and Vapor Generation Accessory VGA-77.

　　C, H and N were determined in the Geoanalytical laboratories of the State geological institute of Dionýz Štúr, Spišská Nová Ves using an elementary analysis with thermal conducting detector.

　　The volume magnetic susceptibility measured using the Kappabridge KLY-2, Geofyzika Brno. The following conditions were applied: a magnetic field intensity of 300 Am^{-1}, a field homogeneity of 0.2 %, an operating frequency of 920 Hz at measurement range of device $-1,999 \times 10^{-6}/$ $+650,000 \times 10^{-6}$ SI unit.

　　The XRD study of magnetic separation products was performed using the device DRON-UM1 with goniometer GUR-8 at following conditions: radiation CuKα, Cu-filter, voltage 30 kV, current 20 mA, step of goniometer 2° min^{-1}. The device id equipped by evaluating program developed by PETRA-ARTEP, Ltd. Košice, which operates on the application interface Control WEB2000.

　　FT-IR spectra were measured by means of spectrometer AVATAR 330 FT-IR ThermoNicolet. KBr tablet technique was applied. Prepared tablets has a diameter of 13 mm.

　　The tablet consisted of 0.2 g KBr and 0.002–0.003 g of studied specimen (pyrolytic soot and flaky graphite). One tablet was also prepared with half charge of soot. The conditions of measuring were as follows: a range of 4,000–400 cm^{-1}, 64 scans, a resolution of 4 cm^{-1}.

　　Differential thermal analysis was carried out using Derivatograph–C (MOM) equipped by evaluating software WINDER. The measurement has been performed in natural atmosphere up to 1,000 °C at a temperature gradient of 10 °C min^{-1}.
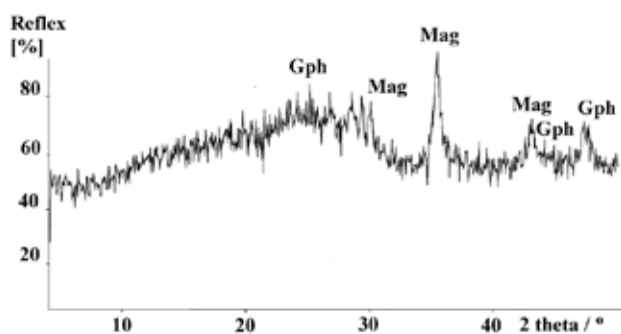
Fig. 3.　**XRD pattern of M–G product**

Table I
Quality and material balance of separation products

Product	Yield [%]	κ	Content [%]				Recovery [%]			
			LOI	Fe	Zn	S	LOI	Fe	Zn	S
M-W	1.21	852,267	0.00	98.40	0.22	0.00	0.00	45.93	0.07	0.00
M-G	1.81	107,074	59.60	23.50	2.54	2.83	1.27	16.34	1.19	2.13
N	96.98	1,412	86.72	1.01	3.92	2.43	98.73	37.78	98.74	97.87
feed	100.00	13,620	85.18	2.60	3.85	2.40	100.00	100.00	100.00	100.00

κ – volume magnetic susceptibility (10^{-6} SI unit), LOI – loss on ignition

Results

Magnetic Separation

　　The results of magnetic separation are introduced in Table I. Thus, in such way, a 62.22 % of Fe was removed from soot, whereas obtained Fe-bearing products, namely M-W (steel wires) and M-G (grainy product), attain the Fe content of 98.40 % and 23.50 %, respectively. Naturally, the content of iron clearly corresponds with the value of volume magnetic susceptibility of obtained products. Undesirable elements such as zinc and sulphur, coming from additives at tires production, are bonded with combustible matter of soot. Similarly, a 37.78 % of Fe at a content of 1.01 % remains in deferrized soot.

　　More detailed chemical composition of defferized soot is given in Table II and III. Thus, under application of dry low-intensity high-gradient magnetic separation the product with carbon content of 80.5 % can be won.

Table II
Composition of deferrized soot

LOI	Fe	Zn	S	SiO$_2$	Ca	Sum
86.72	1.01	3.92	2.43	4.12	1.13	99.33

Table III
CHN elementary analysis of deferrized soot

C	H	N	R[a]	C/H[b]
80.50	1.80	0.30	17.40	3.75

[a]Difference R = 100% – C(%) – H(%) – N(%)
[b]Ratio C/H is related to atomic weight ratio

XRD Study of Magnetic Separation Products

　　The diffractograms of grainy magnetic product (M-G) and defferized soot are introduced in Fig. 3 and Fig. 4, respectively.

　　Magnetite and graphite were identified in grainy magnetic product. The defferized soot contains the following mineral phases:
- Gph1 – Graphite – hexagonal, $a_0 = 2.463$, $c_0 = 6.714$,
- Gph2 – Graphite – hexagonal, $a_0 = 2.456$, $c_0 = 6.696$,
- Lon – Lonsdaleite – hexagonal, $a_0 = 2.52$, $c_0 = 4.12$,
- (high pressure modification of carbon),
- Cal – Calcite – CaCO$_3$,
- Ran – Rankinite – Ca$_3$Si$_2$O$_7$.

The presence of two forms of graphite is approved by its forked peaks. An enhanced background in the both samples indicates an occurrence of amorphous or cryptocrystalline, primarily carbon phase.
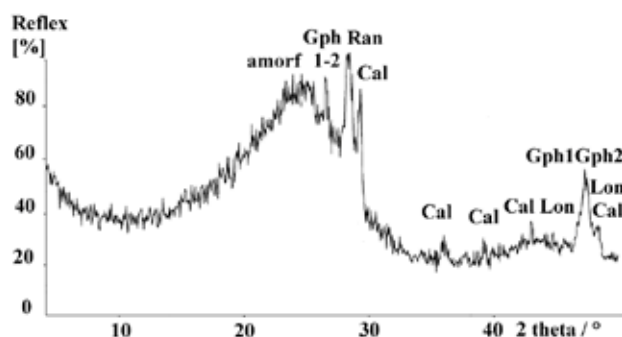
Fig. 4.　**XRD pattern of deferrized soot**

FT-IR　Study　of　Deferrized　Soot

The FT-IR spectra of deferrized soot are illustrated in Fig. 5 and Fig. 6, respectively. For comparison a FT-IR spectrum of flaky graphite is introduced in Fig. 7. The interpretation of obtained spectra of soot can be as follows:

- 3,431–3,424 cm^{-1} – ν (OH), valence vibrations of –OH bonds, intramolecular H–bond[7]. Vibrations of water, coming from tablet preparation. This band is very conspicuous.
- 2,976–2,852 cm^{-1} – ν_{as}(CH$_3$), group –(C)–CH$_3$, valence vibrations of C–H bonds of alkanes, for which is typical forked band in the range of 2,980–2,850 cm^{-1}.
- 2,064 cm^{-1} – ν (C≡C), group –C≡C–H, very small peak, at larger charge of specimen more visible, it is on the border of belt of the valence vibrations of C≡C bonds. Regarding chemical composition of studied soot it is probably concerned the bond of carbonyl group >C=O with metal. Typical band is in the range of 2,100–2,000 cm^{-1}.
- 1,635 cm^{-1}, or more precisely 1,650–1,600 cm^{-1} at larger charge – ν (C=C), group –C=C–C=C–, valence vibrations of conjugated C=C bonds, often two bands, weaker at 1,650 cm^{-1}, stronger at 1,605 cm^{-1}. About of 1,600 cm^{-1} there are also vibration of aromatic C=C bonds and water.
- 1,448–1,350 cm^{-1} – valence vibration of C–O bonds in the groups COOH.
- 1,107–1,049 cm^{-1} – valence vibration of C–C bonds.
- 800–700 cm^{-1} – vibrations of aromatic C=C bonds.

The strong vibration at 1,420 cm^{-1} as well as weak vibrations at 890–880 cm^{-1} and 700 cm^{-1} were also investigated in soot specimen, i.e. all in the fingerprint region (1,500–400 cm^{-1}). They can be considered as the peaks of calcite[17], which was also detected by XRD study.

Authors[14,15] describe weak vibrations for graphite at 1,590 cm^{-1} and 868 cm^{-1}. These vibrations were also recorded in studied specimens and in the case of flaky graphite

spectrum, several additional peaks were also detected, probably rests of flotational agents.
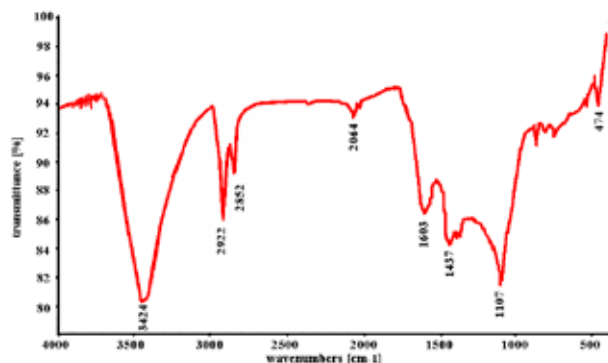
Fig. 5.　**FT-IR spectrum of deferrized soot**
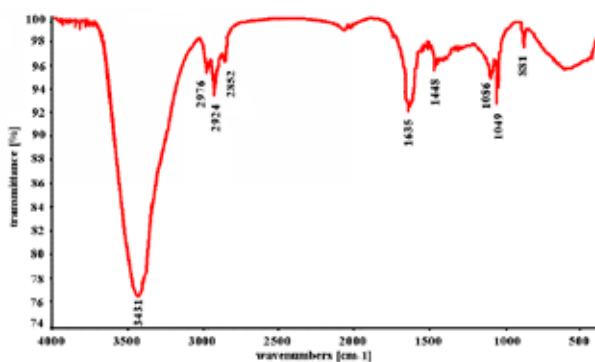
Fig. 6.　**FT-IR spectrum of deferrized soot – half charge**
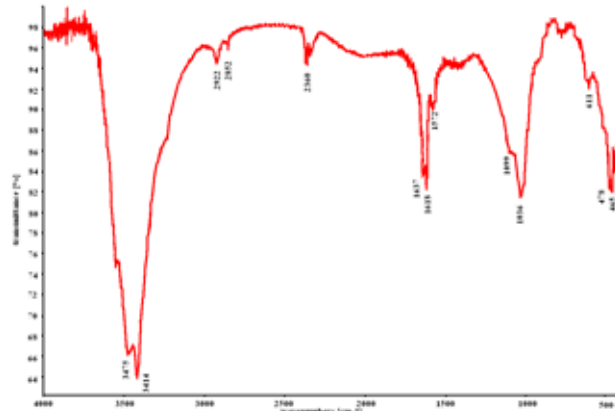
Fig. 7.　**FT-IR spectrum of flaky graphite**

Authors[14] give the following values of vibrations for amorphous carbon: 1,587 cm^{-1} (middle intensity), 1,250 cm^{-1} (strong intensity), further without description of intensity: 1,188 cm^{-1}, 1,168 cm^{-1}, 1,127 cm^{-1}, 1,090 cm^{-1} and 1,045 cm^{-1}. These vibrations were also observed in spectra of deferrized soot (Fig. 5 and 6). Thus, with regard to results of chemical and XRD analyses, it can be pointed to fact that amorphous carbon occurs in soot.

Subsequently, interpretation of given FT-IR spectra in correlation with chemical analyses can be amended as follows: bands in the region of 1,150–1,000 cm^{-1} probably appertain to valence vibrations of $C-SO_2-C$ (also in the region of 1,376–1,300 cm^{-1}) and $Si-O-Si$ bonds[18]. A small, but visible peak in the area of 740–690 cm^{-1} testifies to a presence of valence bond $C-S$[18]. In the region of 500–400 cm^{-1}, namely 474 cm^{-1} in Fig. 5, there are reported valence vibration of $Si-O-Si$ bonds by authors in papers[18,19]. Similarly as to the region of 500–400 cm^{-1} other authors[20] introduce for $Zn-O$ bonds vibrations at 532 cm^{-1} and 473 cm^{-1}, what corresponds with the spectra of studied soot.

DTA Study of Defferized Soot

DTA and TG curves are illustrated in Fig. 8. The total mass loss is running about 85 %, which is in accordance with LOI introduced in Table I and II, respectively.
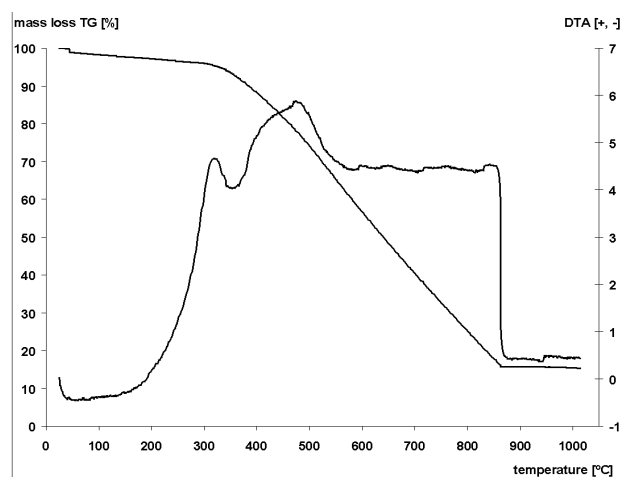
Fig. 8.   **DTA and TG curves of deferrized soot**

As to the course of DTA curve a giant exothermic effect can be observed in a temperature interval of 300–860 °C. This effect has three tops, namely at 323, 481 and 848 °C. The tops are probably connected with an occurrence of several phases of carbon and/or differences in grain sizes of burning soot.

Conclusion

The study of soot coming from pyrolysis of used tires was performed with the aim to verify the possibilities of its treatment and an application in various branches of industry as a secondary raw-material. Special attention was paid to deferrized soot.

XRD analysis showed an occurrence of two forms of graphite, lonsdaleite, calcite and rankinite in such soot.

Using FT-IR spectroscopy, graphite and amorphous carbon were identified. Vibrations of functional group of alkanes, alkenes, alkines and aromatic hydrocarbons have been also observed. Owing to presence of aromatic hydrocarbons bonds it is needed to mention paper[21], where authors studied bonds of carbon in commercial and pyrolytic soot.

Thus, these carbon blacks are different in the occurrence of aromatic hydrocarbons. Commercial soot, applied in tires production as filler, does not contain any aromatic hydrocarbons and carbon content is higher by 10 %, then in pyrolytic soot. It usually attains 90–97 %.

Other chemical components such as S, Zn, Ca, and SiO_2 determined in pyrolytic soot coming from original fillers and modifiers added to tire mixtures to obtain required properties.

Finally, studied pyrolytic soot containing of 80.5 % C is not suitable for application in tires production, because carbon content over 95 % is desired. This deferrized pyrolytic soot can be used as a filler to asphalt mixture on surface of roads, also in shoe manufacturing industry and generally in production of rubber with lower quality.

REFERENCES
 1. Sharma V. K., Fortuna F., Mincarini M., Berillo M., Cornacchia G.: Appl. Energy *65*, 381 (2000).
 2. Sharma V. K, Mincarini M., Fortuna F., Cognini F., Cornacchia G.: Energy Convers. Manage. *39*, 511 (1998).
 3. Chang, Y. M.: Resour. Conserv. Recycl. *17*, 125 (1996).
 4. Hredzák S. a kol.: Research report No. 2004SP26, Institute of Geotechnics of the Slovak Academy of Sciences, Košice, 2005.
 5. Hredzák S., Maceková J., Jakabský Š., Lovás M., Čuvanová S.: *Proc. of the Wastes Recycling X: Deferrization of pyrolytic soot.* (Fečko P. ed.), p. 115. Ostrava 2006.
 6. Hredzák S., Matik M., Štefušová K., Maceková J.: *Proc. of the 16th symposium on Ecology in selected agglomerations of Jelšava-Lubenik and Central Spiš: To occurrence of magnetite in pyrolytic soot.* (Hredzák S., Bindas Ľ. eds.), p. 209. Hrádok 2007.
 7. Rositani F., Antonucci P. L., Minutoli M., Giordano N.: Carbon *25*, 325 (1987).
 8. O'Reilly J. M., Mosher R. A.: Carbon *21*, 47 (1983).
 9. Pena J. M., Allen N. S., Edge M., Liauw C. M., Hoon S. R., Valange B., Cherry R. I.: Polym. Degrad. Stab. *71*, 153 (2001).
10. Pena J. M., Allen N. S., Edge M., Liauw C. M., Valange B.: Polym. Degrad. Stab. *72*, 31 (2001).
11. Pena J. M., Allen N. S., Edge M., Liauw C. M., Valange B., Santamaria F.: Polym. Degrad. Stab. *74*, 1 (2001).
12. Pena J. M., Allen N. S., Edge M., Liauw C. M., Valange B.: Dyes Pigm. *49*, 29 (2001).
13. Cudziło S., Huczko A., Pakuła M., Biniak S., Swiatkowski A., Szala M.: Carbon *45*, 103 (2007).
14. Bantignies J. L., Sauvajol J. L.: Phys. Rev. *B74*, *195*, 425 (2006).
15. Kuhlmann U., Jantoljak H., Pfänder N., Bernier P., Journet C., Thomsen C.: Chem. Phys. Lett. *294*, 237 (1998).

16. Patrik Kania: Infrared spectroscoppy. http://www.vscht. cz/anl/lach1/7_IC.pdf
17. http://lms.vscht.cz/Zverze/Knihovna.htm
18. Oréfice R. L, Henchb L. L., Brennan A. B.: J. Braz. Chem. Soc. *11*, 78 (2000).
19. Russell J. D.: Clay Miner. *14*, 127 (1979).
20. Kwon Y. J., Kima K. H., Limb C. S., Shim K. B.: J. Ceram. Process. Res. *3*, 146 (2002).
21. Roy C., Chaala A., Darmstadt H.: J. Anal. Appl. Pyrolysis *51*, 201 (1999).

L06 DETERMINATION OF THE YIELD OF SODA-ANTHRAQUINONE SEMICHEMICAL PULP FROM HARDWOOD MIXTURE

MICHAL LETKO, ERIKA NOVÁKOVÁ and MILAN VRŠKA

Department of Chemical Technology of Wood,Pulp and Paper, Faculty of Chemical and Food Technology, Slovak University of Technology, Radlinského 9, 812 37, Bratislava, Slovakia, michalletko@stuba.sk

Introduction

In cooperation with the NovaCell project, a central European NSSC mill, Kappa Štúrovo in Slovakia, has converted to sulphur-free production during 2004. It is a new and sulphur free process concept for manufacturing of chemical and semi chemical fibres. The starting point for the development of NovaCell process has been a 2-stage cooking process, consisting of a mild pre-hydrolysis stage with AQ in aqueous environment followed by a cooking stage with alkali. New technology consumes a cooking liquor compound from sodium hydroxide and sodium carbonate for delignification. SAQ pulp is made from mixture of three hardwood species – hornbeam, birch and poplar.

The first results for different wood resources indicated a great potential to reduce the wood consumption at a given production rate or conversely, at a given wood consumption level, the pulp production can be increased considerably compared to the Kraft process. Therefore one of the Novacell aims is high yield, higher than a modern kraft. A higher pulp yield will also contribute to a better use of the capital employed in the pulp mills[1].

Wood is the dominant cost factor for a pulp mill. Pulp yield has a major impact on the competitiveness of a mill[2]. In order to optimize pulp yield, for example by changing the operating conditions, a mill must be able to monitor the yield accurately. Traditionally, pulp yield is estimated based on wood usage and pulp sales data covering a period of 3–6 months to eliminate the mill operation dynamics. However, this approach can not be used to monitor yield changes occurring for brief periods, e.g., during evaluation of process modifications[3]. There are two general approaches available to measure mill pulp yield: the direct and indirect methods. In the direct pulp measurement method the yield is determined from the wood and pulp mass or mass flow rates. The indirect pulp yield measurement methods rely on measurement of pulp or spent pulping liquor properties to determine the yield using pre-established "calibration curves". The semichemical SAQ pulp yield is estimated by methodology developed by Duranti[4] and improved by Kovács and Pavlik[5]. It is based on dependence of semichemical pulp yield in % from specific mass according wood species charge. Woitkovich pointed out the importance of knowing the relationship between pulp properties and yield and using of indirect methods for unmensurability of yield and mensurability of physical properties [6]. Since there is not an explicit relationship between yield

and inputs, our aim was to find a mathematical relationship between yield and charge of different species of hardwoods and charge of alkali. We had a concept of a usable equation for industry, in particular for the Smurfit Kappa Štúrovo mill. There are still problems for technologists at the place.

We would like to consider which of the parameters is ruling and statistically significant. By means of mixed cooking we managed to study not only total yield but also yields of individual species of wood. This allows to compare the rate of cooking and reciprocal influences[7].

Experimental

Materials

For the experiment we used chips from Smurfit Kappa Štúrovo a.s. woodyard. Chips from three species of hardwoods (hornbeam, birch, poplar) were used for cooking SAQ semichemical pulp. Dry matter of the chips before cooking (hornbeam = 93.5 %, birch 94 %, poplar = 94.5 %) and their fractionation have been defined. Screenings from sieve with 0.705 cm mesh were used for cooking.

The cooking liquor was mixed from black and green liquor from Smurfit Kappa Štúrovo a.s. Acid-base titration was used for determination of sodium hydroxide and sodium carbonate.

Green liquor:
concentration:
$$NaOH = 27.94 \ g \, dm^{-3} \ as \ Na_2O$$
$$Na_2CO_3 = 71.14 \ g \, dm^{-3} \ as \ Na_2O$$
$$Total \ alkali = 99.08 \ g \, dm^{-3} \ as \ Na_2O$$

Black liquor:
concentration:
$$Na_2CO_3 = 48.67 \ g \, dm^{-3} \ as \ Na_2O$$
$$NaOH = 0 \ g \, dm^{-3} \ (consumed)$$
$$Total \ alkali = 48.67 \ g \, dm^{-3} \ as \ Na_2O$$

Cooking

Cooking was carried out in a 1 dm³ autoclaves electrically heated in silicone oil. 100 g of oven-dry chips with hydromodule (liquor/wood rate) 3 were added. The charge of anthraquinone was 0.5 % for oven-dry wood. Cooking temperature was 170 °C for 60 minutes (cooking time).

Cooking curve was recorded by help of a digital thermometer. Alkali charge was calculated from determined sodium hydroxide in green liquor.
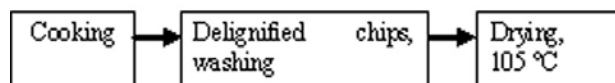
Fig. 1. **Experimental procedures**

When mixed cooking is carried out, reduction of liquor concentration is followed by the influence of more accelerated cooking of some species. However, this effect changes the conditions for other ones. This is why we wanted both total and partial yield of each wood specie. The same conditions have been provided for each wood in autoclave (separated by permeable barrier). It was entered with stainless steel bars. Calculated and weighed volumes of chips were put into

stainless container gradually. Each specie was covered with stainless steel bar. Full cooking container was inserted into autoclave and flooded with the volume of green liquor as shown in Table II. The volume was topped up to 300 ml with black liquor. When oil in boiler reached 170 °C, the prepared autoclaves were inserted. It is possible to cook three autoclaves in our boiler.

After 60 minutes the autoclaves were removed from the boiler and cooled down. Then, the autoclaves were opened and each wood specie had been washed for 48 hours in permeable polyamide bags. After cooking the liquor was taken for analysis. Washed chips were dried at 105 °C. Oven-dry chips were weighed and the yield was determined gravimetrically.

Experimental Design

Central composite rotatable design (CCRD) was used in this study[8]. The design consists of a three-factored (n = 3) factorial design with two levels. The levels, codes and interval of variation of the independent variables are given in the Table I, while the treatment combinations with responses are presented in Table III. The process variables considered were charge of hornbeam (16.4–70 g), birch/poplar ratio (0.16–1.84) and charge of alkali expressed as Na_2O (6.7–7.7 %). Center composite design was used to show the effect of charge of different hardwood and alkali charges on the pulp yield in 20 runs of which 6 were for the center point, and 14 were for noncenter point with axial distance of 1.6818 ($\alpha = 2^{n/4}$). The following second order polynomial response surface model (1) was fitted to each of the response variable where b_0, b_i, b_{ii}, and b_{ij} are the constant, linear, quadratic and cross-product regression coefficients, respectively, X_i's are the coded independent variables of X_1 (hornbeam, g), X_2 (ratio birch/poplar) and X_3 (alkali charge, %).

$$Y = b_0 + \sum_{i=1}^{3} b_i X_i + \sum_{i=1}^{3} b_i X_i^2 + \sum_{i \neq j=1}^{3} b_j X_i X_j \qquad (1)$$

Table I
Coded and uncoded levels of three variables used in cooking of hardwood mixture

Variables		Levels				Semi-range
		−1.682	−1	0	1	1.682	
Hornbeam [g]	X1	16.4	30	50	70	70	20
Birch/Poplar	X2	0.16	0.5	1	1.5	1.84	0.5
Na_2O [%]	X3	6.7	6.9	7.2	7.5	7.7	0.3

A three-dimensional response surface and contour plots of independent variables and their interactions were generated using the Statgraphics plus. Optimization of SAQ cooking was aimed at establishing appropriate levels within the independent variables such as charge of hornbeam, birch/poplar ratio and alkali charge.

Table II
Real quantities for responsible levels used in cooking of hardwood mixture

Variables	Levels				
	−1.682	−1	0	1	1.682
Hornbeam [g]	16.4	30	50	70	88.6
Birch [g]	6.9	16.7	25	30	32.4
Poplar [g]	43.1	33.3	25	20	17.6
Charge of green green liquor [ml]	240	247	258	268	276

Results

The effect of hornbeam, birch/poplar ratio and alkali charges on the yield was investigated using the CCRD statistical model. The observations for total yield, hornbeam yield, birch yield and poplar yield with different combinations of the process parameters are presented in Table III. Response surface analysis was applied to the experimental data using Statgraphic plus. The second-order polynomial response surface model (1) was fitted to each of the response variable (Y). Estimated regression coefficients of the quadratic polynomial models for the response variables, along with the corresponding R^2 and P-values, are given in Table IV. The coefficient of determination (R^2) values of all responses are quite high (>0,8) The highest (nearly 0.9) in case of total yield and the lowest in case of yield of birch.
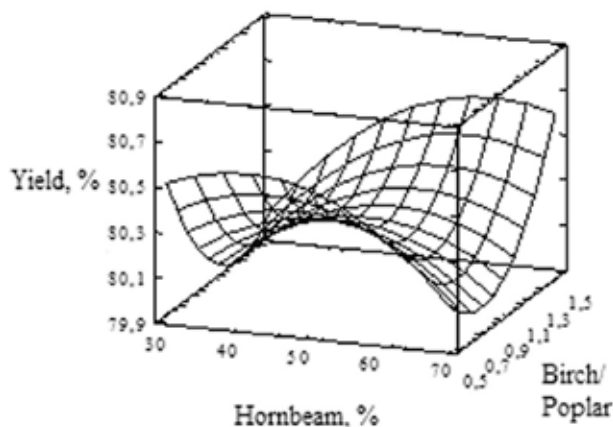
Fig. 2. **Saddle 3D response surface of the effect of hornobeam charge and birch/poplar ratio on total yield of SAQ semichemical pulp from hardwood mixture when the alkali charge was constant 7.2 % as Na_2O**

By analysis of solid residue after delignification according to treatment combinations of experiments of CCRD the values of yields were obtained. Predictive equation (2) for total yield of SAQ pulp was acquired from non-linear regression analysis.

Assessment of the effect of individual regression coefficients claimed that alkali charge has the most significant influence on pulp yield; negative sign indicates that this influence is negative. Its influence is statistically significant

in all cases (P-value is less than 0.05). Negative effect of this trend is demonstated in combinations with other parameters (in particular hornbeam charge). However, this impact is not always statistically significant.
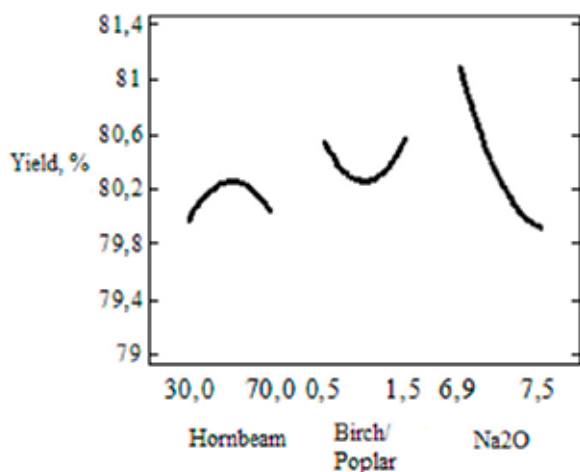
Fig. 3.   **Influence of variables on total yield of SAQ semichemical pulp from hardwood mixture**

The second important factor which can influence the yield of semichemical pulp is the birch/poplar ratio in the processed mixture. Moreover, the yield will be influenced mainly by poplar charge in the mixture which was cooked at the slowest rate in our conditions (Table III). Its effect is

negative for total yield and for poplar yield. Approximate poplar yield is not more than 2 % compared to semichemical pulp from birch and hornbeam.

Optimal values of yields and the conditions in which it is possible to get them can be read from local maximums and minimums shown in Fig. 3. Dominant position of the effect of alkali charge is confirmed by the drop of yield in dependence upon of 1 %alkali charge. The effect of other parameters is within several few tenths of percent. Generally, the results give numerous possibilities and combinations how to evaluate the effect of individual variables on the monito-red result, in this case the yield. The canonical analysis indi-cated that the predicted response surface is a saddle shaped as depicted in Fig. 2.

Since the method applied is taken after preliminary ana-lysis for determine optimal process parameters to acquire the desired (min, max) result, in Table V a combination of optimal parameters for acquirement of maximum yield is pre-sented. In our case it is not clear whether maximum yield is the suitable result. It is necessary to compare and evaluate the other qualitative parameters, for example chemical com-position.

$$Y = 225.84 + 0.34X_1 - 3.04X_2 - 40.46X_3 - 0.00061X_1^2 + 1.19X_2 + 2.83X_3^2 + 0.02X_1X_2 - 0.08X_2X_3 - 0.04X_1X_3 \qquad (2)$$

Table III
Treatment combinations for SAQ cooking with 3 variable 2nd-order response surface model designs

| Runs | Coded variables | | | Un-coded variables | | | Response | | | |
	X_1	X_2	X_3	Hornbeam	Birch/ Poplar	Na$_2$O	Yield of hornbeam	Yield of birch	Yield of poplar	Total yield
1	0	0	0	50	1	7.2	78.5	80.9	80.0	79.8
2	0	0	0	50	1	7.2	80.4	80.8	80.4	80.5
3	1.682	0	0	88.6	1	7.2	79.8	77.2	84.2	80.4
4	−1.682	0	0	16.4	1	7.2	80.5	80.1	82.1	80.9
5	0	1.682	0	50	1.84	7.2	78.9	80.1	81.6	80.2
6	0	−1.682	0	50	0.16	7.2	79.1	78.6	80.7	79.5
7	0	0	0	50	1	7.2	78.8	80.8	79.6	79.7
8	1	1	−1	70	1.5	6.9	79.1	78.9	80.0	79.3
9	0	0	0	50	1	7.2	79.6	79.6	82.0	80.4
10	0	0	−1.682	50	1	6.7	79.8	80.0	81.2	80.3
11	−1	−1	−1	30	0.5	6.9	79.0	75.7	83.2	79.3
12	0	0	0	50	1	7.2	79.0	80.4	80.8	80.1
13	−1	1	1	30	1.5	7.5	79.7	78.8	82.5	80.3
14	0	0	0	50	1	7.2	79.2	78.0	80.0	79.1
15	1	−1	−1	70	0.5	6.9	80.6	80.0	81.5	80.7
16	0	0	1.682	50	1	7.7	79.0	78.4	82.0	79.8
17	1	1	1	70	1.5	7.5	77.7	77.8	82.5	79.3
18	−1	1	−1	30	1.5	6.9	78.7	78.1	79.6	78.8
19	−1	−1	1	30	0.5	7.5	77.0	77.4	80.9	78.4
20	1	−1	1	70	0.5	7.5	77.6	77.0	77.5	78.0

Table IV
Estimated coefficients for determination of semichemical pulp yield and P-values of statistical significance

Estimated coefficients	Influenced parameter	Total yield		Yield of hornbeam		Yield of birch		Yield of poplar	
		Estimate	P-value	Estimate	P-value	Estimate	P-value	Estimate	P-value
bo		225.84		198.77		254.98		224.064	
b1	X_1	0.34	0.7415	0.53	0.4328	0.314	0.544	0.184	0.4989
b2	X_2	−3.04	0.8957	2.39	0.7966	5.142	0.650	−16.44	0.6543
b3	X_3	−40.46	0.0001*	−35.43	0.0004*	−49.32	0.001*	−36.7497	0.0017
b11	X_{12}	−0.00061	0.0202*	−0.0003	0.2433	−0.001	0.048*	−0.00069	0.0459
b22	X_{22}	1.19	0.0076*	0.58	0.1728	1.82	0.013*	1.1559	0.0387
b33	X_{32}	2.83	0.0172*	2.58	0.0392*	3.484	0.065	2.425	0.1025
b12	X_1X_2	0.02	0.0666	−0.034	0.0280*	0.031	0.155	0.0763	0.0009
b23	X_2X_3	−0.08	0.9269	−0.25	0.7812	−1.417	0.320	1.417	0.2216
b13	X_1X_3	−0.04	0.0599	−0.065	0.0146*	−0.035	0.320	−0.027	0.3423
r_2		88.70		84.26		81.88		85.42	

* value is statistically significant if P<0.05

Table V
Optimal values for maximal yield

	Optimal values			
	Total	Hornbeam	Birch	Poplar
Yield [%]	83.62	82.77	84.12	84.55
Hornbeam [%]	83.64	83.64	72.41	51.61
Ratio birch/poplar	1.84	0.39	1.79	0.16
Na_2O [%]	6.70	6.70	6.70	6.70

Conclusions

Because yields of different wood species were monitored in cooking of mixed hardwoods in additon to total yield, we are able to assess the changes of individual species when delignification is influenced by changes in alkali concentration. It varies according to the rate of delignification of individual wood species. It is possible that quickly delignified wood reduces the alkali concentration. Consequently, alkali concentration is not sufficient for wood with slower delignification. Again, this rate is more reduced with decreasing alkali concentration.

By the yields comparison of investigated wood species we found out that in mixed cooking dawns the slowest drop of yield in the case of poplar. Throughout the range upper yield up to 2 % was established.in the all range. Birch and hornbeam wood mass drops were almost equal.

The information about yields of individual wood species from mixed cooking were processed to the followingdependence (equation): yield = f(wood charge, alkali charge). It can be said on the basis of the coefficients in the equation that alkali and poplar charges show the highest effect on pulp yield. The effect of hornbeam charge in hardwood mixture was insignificant.

REFERENCES

1. Stigsson L., Berglin N.,Olm L.,Tormund D.,Tomani P., Hakansdotter-Palm L., Delin L.: *SPCI Conference: Sulphur-free pulping – The Novacell Process*. Stockholm, 2005.
2. Van Heiningen A.R.P., Gao Y., Da Silva Perez D.: *7th EWLP Conference*, p. 63. Turku, Finland, 2002.
3. Easty D. B., Malcolm E. W.: Tappi J. *65*, 78 (1982).
4. Duranti D., Colapietro M.: Cellulosa Carta *18*, 3 (1967).
5. Kovacs V., Pavlik S.: Papir Celuloza *37*, 39 (1982).
6. Woitkovich P.C.: *Mechanical pulping. Annual research review*. Project 3716, pp. 49-80. Inst. Paper Sci. Technol. Atlanta, Georgia 1991.
7. Letko M.: Diploma thesis, FCHPT-STU, Bratislava, Slovakia, 2007.
8. http://www.itl.nist.gov/div898/handbook/. NIST/ SEMATECH e-Handbook of Statistical Methods. 14. February 22, 2005.

5.2. Posters

P01 LITHIUM BROMIDE MEDIATED SYNTHESIS AND X-RAY ANALYSIS OF BISARYLMETHYLIDENES OF PIPERIDINONE SYSTEM

M. SAEED ABAEE[a], MOHAMMAD M. MOJTAHEDI[a], ROHOLAH SHARIFI[a], A. WAHID MESBAH[a] and WERNER MASSA[b]

[a]Department of Organic Chemistry, Chemistry & Chemical Engineering Research Center of Iran, P. O. Box 14335–186, Tehran, Iran,
[b]Fachbereich Chemie der Philipps-Universitaet Marburg, Hans-Meerwein-Strasse, D-35032 Marburg, Germany,
abaee@ccerci.ac.ir

Introduction

Bis(arylmethylidene)cycloalkanones as very important biologically active intermediates[1], are generally synthesized via aldol condensation of homocyclic ketones with aromatic aldehydes[2]. So far, several procedures have appeared in the literature for the synthesis of these compounds using Lewis acid catalysis[3], solid-supported reactions[4], ionic liquids[5] microwave irradiation[4a], and ultrasound mediation[4b].

In contrast, on the heterocyclic counter part much less development is achieved. In this regard, we recently disclosed Lewis acid catalyzed synthesis of several novel bisarylmethylidene derivatives of pyranone[6], thiopyranone[7], piperidinone[8], dioxanone,[9] and cyclohexenone[10] structures using very straight forward synthetic methods. The structure of these products was assigned logically based on their spectroscopic characterization. However, to distinguish between the possible isomers (Scheme 1) and to verify the proposed geometry we decided to determine the crystal structure of representative compounds.

1   **2**   **3**
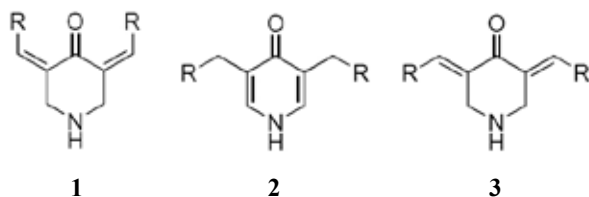
Scheme 1

In the present article, a convenient and rapid procedure is offered for the synthesis of bis(arylmethylidene) piperidin-4-ones under catalysis of LiBr which has found many applications as a mild Lewis-acid in recent years to ease up various synthetic organic transformations.[11] The X-ray structure analysis of the *p*-methoxyphenyl derivative confirms the presence of exocyclic double bonds in the products in *Z-Z* configuration **3** (Scheme 1).

Experimental

G e n e r a l

Reactions were monitored by TLC. NMR spectra were obtained on a FT-NMR Bruker Ultra Shield™ (500 MHz) as CDCl$_3$ or DMSO-d$_6$ solutions and the chemical shifts were expressed as δ units with Me$_4$Si as the internal standard. All chemicals and reagents were purchased from commercial sources.

T y p i c a l   P r o c e d u r e

A mixture of **4** (Table II) (5.0 mmol), an aldehyde (5.0 mmol), LiBr (0.5 mmol), and Et$_2$NH (10.0 mmol) in CH$_2$Cl$_2$ (15 ml) was stirred in a flask. Complete disappearance of the starting materials was observed within 2-3 hours by TLC. The mixture was diluted by dichloromethane and washed twice by water. The organic phase was dried over Na$_2$SO$_4$, the solvent was removed at reduced pressure and the product was precipitated after removal of the volatile portion. The structures of the products were assigned by spectroscopic methods.

S p e c t r a l   D a t a

3a: IR [cm^{-1}]: (KBr) v 3,235 (NH), 1,665 (C=C), 1,593 (C=O); ^{1}H NMR [ppm]: (CDCl$_3$) δ 1.68 (s, 1H, NH), 4.21 (s, 4H, H$_2$C−N−CH$_2$), 7.40–7.48 (m, 10H, Ar), 7.86 (s, 2H, CH=C); ^{13}C NMR [ppm]: (CDCl$_3$) δ 48.6 (NCH$_2$), 128.9, 129.5, 130.9, 135.4, 135.6, 136.4, 188.4 (C=O).

3b: IR [cm^{-1}]: (KBr) v 3,289 (NH), 1,657 (C=C), 1,579 (C=O); ^{1}H NMR [ppm]: (CDCl$_3$): δ 1.74 (s, 1H, NH), 2.43 (s, 6H, CH$_3$), 4.18 (s, 4H, H$_2$C−N−CH$_2$), 7.26 (d, *J* = 8 Hz, 4H, Ar), 7.32 (d, *J* = 8 Hz, 4H, Ar), 7.82 (s, 2H); ^{13}C NMR [ppm]: (CDCl$_3$) δ 21.9 (CH$_3$), 48.6 (NCH$_2$), 129.7, 131.1, 132.9, 134.8, 136.3, 139.8, 188.4 (C=O).

3c: IR [cm^{-1}]: (KBr) v 3,242 (NH), 1,667(C=C), 1,509 (C=O); ^{1}H NMR [ppm]: (CDCl$_3$): δ 1.72 (s, 1H, NH), 3.90 (s, 6H, OCH$_3$), 4.19 (s, 4H, H$_2$C−N−CH$_2$), 6.98 (d, *J* = 9 Hz, 4H, Ar), 7.40 (d, *J* = 9 Hz, 4H, Ar), 7.81 (s, 2H, CH=C); ^{13}C NMR [ppm]: (CDCl$_3$): δ 48.6 (NCH$_2$), 55.8 (OCH$_3$), 114.5, 128.4, 132.9, 133.6, 136.1, 160.7, 188.3 (C=O).

3d: IR [cm^{-1}]: (KBr) v 3,301 (NH), 1,657 (C=C), 1,584 (C=O); ^{1}H NMR [ppm]: (CDCl$_3$) δ 1.77 (s, 1H, NH), 4.15 (s, 4H, H$_2$C−N−CH$_2$), 7.35 (d, *J* = 8.5 Hz, 4H, Ar), 7.43 (d, *J* = 8.5 Hz, 4H, Ar), 7.78 (s, 2H, CH=C); ^{13}C NMR [ppm]: (CDCl$_3$) δ 48.5 (NCH$_2$), 129.3, 132.1, 134.0, 135.1, 135.6, 135.7, 187.9 (C=O).

3e: IR [cm^{-1}]: (KBr) v 3,240 (NH), 1,668 (C=C), 1,585 (C=O); ^{1}H NMR [ppm]: (DMSO–d$_6$) δ 3.40 (s, 1H, NH), 4.14 (s, 4H, H$_2$C−N−CH$_2$), 7.37 (d, *J* = 8 Hz, 4H, Ar), 7.60 (d, *J* = 8 Hz, 4H, Ar), 7.64 (s, 2H, CH=C).

3f: IR [cm^{-1}]: (KBr) v 3,350 (NH), 1,650 (C=C), 1,605 (C=O); ^{1}H NMR [ppm]: (CDCl$_3$) δ 1.70 (s, 1H, NH), 3.43 (s, 4H, H$_2$C−N−CH$_2$), 3.74 (s, 12H, OCH$_3$), 3.88 (s, 6H, OCH$_3$), 6.13 (s, 4H, Ar), 7.70 (s, 2H, CH=C); ^{13}C NMR [ppm]: (CDCl$_3$) δ 54.2 (NCH$_2$), 55.7 (OCH$_3$), 55.9 (OCH$_3$), 90.8, 107.2, 129.8, 134.9, 159.6, 162.4, 188.0 (C=O).

3g: IR [cm⁻¹]: (KBr) ν 3,291 (NH), 1,647 (C=C), 1,581 (C=O); ¹H NMR [ppm]: (CDCl₃) δ 1.85 (s, 1H, NH), 4.22 (s, 4H, H₂C−N−CH₂), 7.19 (dd, *J* = 4, 4.5 Hz, 2H), 7.38 (d, *J* = 4 Hz, 2H), 7.60 (d, *J* = 4.5 Hz, 2H), 7.98 (s, 2H, CH=C); ¹³C NMR [ppm]: (CDCl₃) δ 48.2 (NCH₂), 127.5, 128.6, 131.3, 133.0, 133.6, 139.1, 187.0 (C=O).

Table I
Crystal and experimental data for **3b**

Empirical formula	C₂₁H₂₁NO₃
Formula weight	335.39
Temperature	153(2) K
Wavelength	0.71073 Å
Habitus, color	needle, ligth-yellow
Crystal size	0.39 × 0.12 × 0.06 mm³
Crystal system	orthorhombic
Space group	Cmc2₁, Z = 4
Unit cell dimensions	a = 37.748(5) Å
	b = 7.3077(10) Å
	c = 6.0658(9) Å
Volume	1,673.3(4) Å³
Density (calculated)	1.331 mg m⁻³
Absorption coefficient	0.089 mm⁻¹
F(000)	712
Diffractometer type	IPDS–II
Theta range for data collection	2.16 to 27.09 °
Index ranges	–48 ≤ h ≤ 48, –9 ≤ k ≤ 9, –7 ≤ l ≤ 7
Reflections collected	6,300
Independent reflections	1,023 [R(int) = 0.1296]
Completeness to theta = 26.30 °	99.6 %
Observed reflections	619 [I > 2σ(I)]
Refinement method	Full–matrix least–squares on F²
Data/restraints/parameteres	1,023/1/121
Goodness–of–fit on F²	0.826
R indices (all data)	R1 = 0.0756, wR2 = 0.0854
Final R indices [I > 2σ(I)]	R1 = 0.0396, wR2 = 0.0762
Largest diff. peak and hole	0.130 and –0.187 e.Å⁻³

X - r a y   C r y s t a l   S t r u c t u r e   A n a l y s i s

A crystal of **3b** was investigated on an IPDS II area detector system (Stoe) at –120 °C using MoKα-radiation. Crystal and experimental data are given in Table I.

The structure was solved by direct methods in space group *Cmc*2₁ and refined using the SHELX97 programs[12] with anisotropic displacement parameters for all C and O atoms. All hydrogen atoms were located from a difference Fourier map but H4 at N4 only was refined. The others were kept riding on idealized positions with isotropic displacement parameters taken as 1.2U_{eq} (1.5 U_{eq} for CH₃) of their bonding

partners. No absorption or extinction correction was applied. The absolute structure was not determined, the Friedel pairs were merged. Crystallographic data (excluding structure factors) for the structure reported in this paper have been deposited with the Cambridge Crystallographic Data Center as supplementary publication no. CCDC-689654. Copies of the data can be obtained free of charge on application to CCDC, 12 Union Road, Cambridge CB2 1EZ, UK [Fax: int. Code + 44(1223)336-033; E-mail: deposit@ccdc.cam.ac.uk or via www.ccdc.cam.ac.uk/conts/retrieving.html]

Results

An equimolar mixture of piperidin-4-ones **4** and an aldehyde (as listed in Table II) was treated with LiBr (10 % mol) and Et₂NH in dichloromethane. Complete conversion of the starting materials to the desired product was observed within 2–3 hours as reactions were monitored by TLC. Control experiments confirmed the combined promoting and catalytic effects of LiBr; an alternative reaction in the absence of the catalyst led to formation of less than 10 % of the product after 24 hours.

The structure of the products was assigned with spectroscopic methods and compared with the literature data. In order to verify this structure, a single crystal of **3b** was prepared and investigated by X-ray diffraction. The result, as depicted in Fig. 1, clearly supports the proposed structure with exocyclic double bonds C2–C5 and C2'–C5'.

Table II
LiBr catalyzed aldol condensation reactions of **4**

ArCHO	Product	M.P. [°C]	Yield [%]
benzaldehyde	**3a**	175–177	92
(*p*-MeO)benzaldehyde	**3b**	196–197	93
(*p*-Me)benzaldehyde	**3c**	180–181	90
(*p*-Cl)benzaldehyde	**3d**	192–194	88
(*p*-Br)benzaldehyde	**3e**	207–208	87
2,4,6-(MeO3)C6H2CHO	**3f**	198–199	88
2-thiophenecarbaldehyde	**3g**	205–206	91
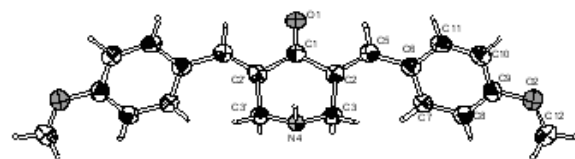
Fig. 1. **Structure of 3b at 153 K in the crystal. Displacement ellipsoids at 50% probability level. Bond lengths C1–C2 1.486(4), C2–C3 1.521(4), C2–C5 1.340(4) Å**

Conclusions

In summary, a LiBr promoted aldol condensation of piperidin-4-ones **4** with various aldehydes was carried out within few hours. Reactions proceeded with catalytic amounts of the Lewis acid, and use of harsh conditions and tedious work up procedures were avoided. High yields of the products and rapid completion of the reactions are among other advantages of this methodology. The proposed structure was confirmed by single crystal X-ray diffraction analysis.

REFERENCES

1. (a) Deli J., Lorand T., Szabo D., Foldesi A.: Pharmazie *39*, 539 (1984).;
   (b) Guilford W. J., Shaw K. J., Dallas J. L., Koovakkat S., Lee W., Liang A., Light D. R., McCarrick M. A., Whitlow M., Ye B., Morrissey M. M.: J. Med. Chem. *42*, 5415 (1999).
2. (a) Hathaway B. A.: J. Chem. Educ. *64*, 367 (1987);
   (b) Zheng M., Wang L., Shao J., Zhong Q.: Synth. Commun. *27*, 351 (1997);
   (c) Iranpoor N., Kazemi E.: Tetrahedron *54*, 9475 (1998);
   (d) Nakano T., Migita T.: Chem. Lett. 2157 (1993).
3. (a) Wang L., Sheng J., Tian H., Han J., Fan Z., Qian C.: Synthesis 3060 (2004);
   (b) Sabitha G., Reddy K. K., Reddy K. B., Yadav J. S.: Synthesis 263 (2004);
   (c) Iranpoor N., Zeynizadeh B., Aghapour A. J.: Chem. Res. 554 (1999);
   (d) Zhu Y., Pan Y.: Chem. Lett. 668 (2004);
   (e) Abaee M. S., Mojtahedi M. M., Sharifi R., Zahedi M. M., Abbasi H., Tabar-Heidar K.: J. Iran Chem. Soc. *3*, 293 (2006).
4. (a) Wang J., Kang L., Hu Y., Wei B.: Synth. Commun. *32*, 1691 (2002);
   (b) Li J., Yang W., Chen G., Li T.: Synth. Commun. *33*, 2619 (2003).
5. (a) Zheng X., Zhang Y.: Synth. Commun. *33*, 161 (2003);
   (b) Hu X., Fan X., Zhang X., Wang J.: J. Chem. Res. 684 (2004);
   (c) Zhang X., Fan X., Niu H., Wang J.: Green Chemistry *5*, 267 (2003).
6. (a) Abaee M. S., Mojtahedi M. M., Zahedi M. M., Bolourtchian M.: Synth. Commun. *36*, 199 (2006);
   (b) Abaee M. S., Mojtahedi M. M., Zahedi M. M., Sharifi R.: Heteroatom Chem. *18*, 44 (2007).
7. (a) Abaee M. S., Mojtahedi M. M., Zahedi M. M.: Synlett 2317 (2005);
   (b) Abaee M. S., Mojtahedi M. M., Zahedi M. M., Mesbah A. W., Ghandchi N. M., Massa W.: Synthesis 3339 (2007).
8. Abaee M. S., Mojtahedi M. M., Sharifi R., Zahedi M. M.: Heterocycl. Chem. *44*, 1497 (2007).
9. Abaee M. S., Mojtahedi M. M., Hamidi V., Mesbah A. W., Massa W.: Synthesis, in press.
10. Abaee M. S., Mojtahedi M. M., Zahedi M. M., Sharifi R., Mesbah A. W., Massa W.: Synth. Commun. *37*, 2949 (2007).
11. (a) Mojtahedi M. M., Akbarzadeh E., Sharifi R., Abaee M. S.: Org. Lett. *9*, 2791 (2007);
    (b) Bailey W. F., Luderer M. R., Jordan K. P.: J. Org. Chem. *71*, 2825 (2006);
    (c) Shao L. X., Shi M.: Synlett 1269 (2006);
    (d) Rudrawar S.: Synlett 1197 (2005) and references cited therein.
12. Sheldrick G. M.: SHELXS-97 and SHELXL-97, Programs for the solution and refinement of crystal structures, University of Göttingen, 1997.

P02　NOVEL DIKETOPYRROLOPYRROLES FOR MOLECULAR OPTICAL AND ELECTRICAL DEVICES

PAVEL BEDNÁŘ[a], OLDŘICH ZMEŠKAL[a], MARTIN WEITER[a], MARTIN VALA[a] and JAN VYŇUCHAL[b]

[a]*BrnoUniversity of Technology, Faculty of Chemistry, Purkyňova 118, Brno 612 00, Czech Republic,*
[b]*VUOS a.s., Rybitvi 296, Ribitvi 533 54, Czech Republic,*
bednar-p@fch.vutbr.cz

Introduction

Diketopyrrolopyrroles (DPPs) and variously substituted analogues represent class of low molecular materials with large π-conjugated system (Fig. 1.). Diketopyrrolopyrroles exhibits excellent photostability, heat and weather fastness. Furthermore, some of their physical properties such as absorption in visible area of light and high values of photoluminescence quantum yields together with semi-conducting properties are of considerable research interest.
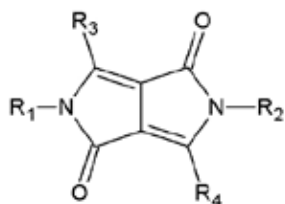
Fig. 1.　**General formula of DPPs**

The characterization of new derivatives of diketopyrrolopyrrole with different substitution and determination of their potential use in optoelectronics was the main goal of our work.

Experiments

We studied thirty derivatives of DPPs which were syntetized in VUOS a.s. However, only three materials along with the basic derivative (DPP04) are discussed in this paper (Table I).

The basic material DPP04 is insoluble in solvents with low polarity e.g. chloroform or toluene and only spectraly

Table I
DPP derivatives used in experiments

DPP	R_1, R_2	R_3, R_4
DPP04	–H	phenyl
DPP10	–C_4H_9	phenyl
DPP12	–C_7H_{15}	phenyl
DPP29	–C_4H_9	phenyl-piperidinyl

soluble in dimethylsulphoxide (DMSO). This material is therefore not usefull in spin-coating, dip or drop casting methods. The nitrogens of the basic DPP structure (R_1, R_2) were alkylated to increase the solubility in solvents like chloroform and toluene.

The substitution of piperidine groups on phenyl groups was used for modification of all properties.

The studied materials were characterized by optical and electrical methods. The absorbance and photoluminescence spectra of these materials in dimethylsulphoxide and thin layers spin-coated on the SiO_2 glass were analysed. The photoluminescence quantum yield of DPPs dissolved in dimethylsuphoxide was also determined.

The electrical masurements were obtained on sandwich structures, consisting of the transparent indium-tin oxide electrode (ITO) on glass, spin-coated PEDOT interlayer from water dispersion, spin-coated soluble DPP material, evaporated tris(8-hydroxyquinoline) (Alq_3) interlayer and finalized by evaporation of the aluminium electrode.

The PEDOT (polystyrenesulfonate/poly-(2,3-dihydrothienol-(3,4b)-1,4-dioxin) interlayer was used for the decrease of the energy barrier for the hole injection and in a similar manner the Alq_3 interlayer was used for injection of electrons.

The current-voltage and electroluminescence characterizations were performed in vacuum at room-temperature.
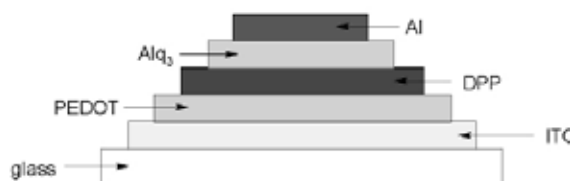
Fig. 2.　**Sandwich structure for electrical and optoelectrical measurement**

Results

The normalized absorbance and photoluminescence spectra of DPP solutions in DMSO are depicted on Fig. 3. The basic optical properties of DDP solutions are summarized in Table II.

The $\lambda_{Abx, max}$ is a wavelength of absobance maximum in a visible area of light, the ε_{max} is the molar absorption coeffitient at this wavelength and the $\lambda_{PL, max}$ is the wavelength of the photoluminescence maximum.

The absorbance spectra and the calculations (Table II) show that the alkylation of nitrogens of basic DPP structure cause hypsochromic shift and change of the shape of the spectra and decrease the molar absorption coeffitient. But these changes don't depend on length of alkyl chain. The substitution of piperidinyl groups on phenyls contributed to the large batochromic shift and increased the molar obsorption coeffitient.

The photoluminescence spectra and calculations give the results that the alkylation's of nitrogen's caused the change of

Table II
Basic optical properties of DPPs soluted in DMSO

DPP	ε_{max} [l mol^{-1}cm^{-1}]	$\lambda_{Abx,max}$ [nm]	$\lambda_{PL,max}$ [nm]	QY
DPP04	34,300	507	516	0.74
DPP10	18,500	467	530	0.69
DPP12	19,500	466	529	0.77
DPP29	42,400	536	599	0.41
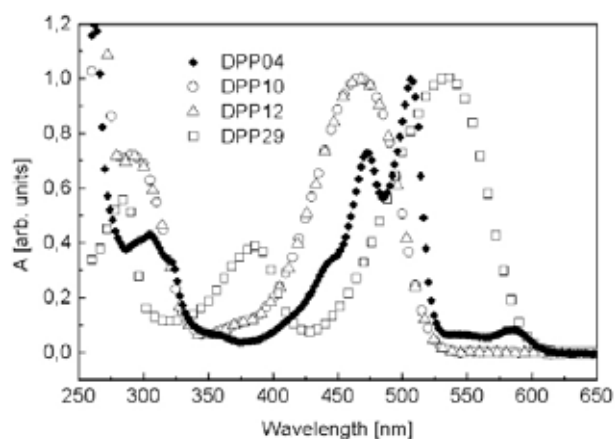
Fig. 3. **Normalized absorbance spectra of DPPs in DMSO solutions**
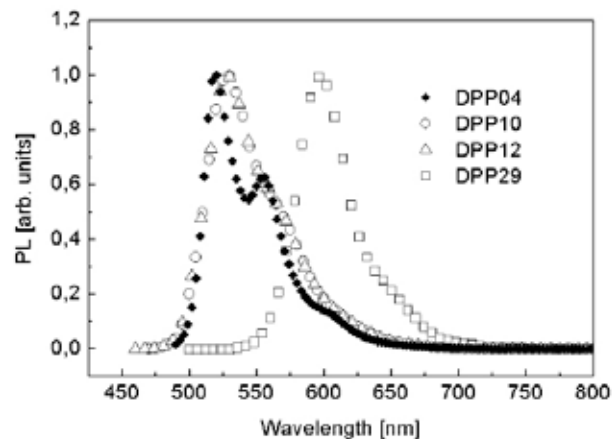
Fig. 4. **Normalized photoluminescence spectra of DPPs in DMSO solutions**

shape of the spectra but it does not depend on length of alkyl chain. The substitution of piperidinyl groups on phenyls contributed to the large batochromic shift again and the substituton decreased the photoluminescence quantum yield.

The electroluminescence spectra show that the electroluminescence does not essentially depend on legth of used
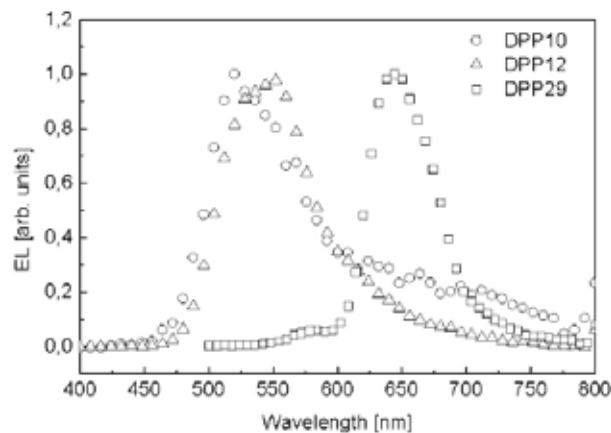
Fig. 5. **Normalized electroluminescence spectra**

alkyl chain. The substitution of piperidine groups on phenyls had the similar effect analogous to absorbance or photoluminescence spectra and contributed to the large batochromic shift.

Conclusions

This work was focused on study of number of diketopyrrolopyrroles with different substitution on nitrogens of basic skeleton of DPP and on phenyl groups.

The absorbance and photoluminescence spectra of DPPs in DMSO solutions give the result that the alkylation of nitrogens of the basic DPP structure changes the spectra, but the length of used alkyl chain doesn't have influence on the change.

The substitution of piperidinyl on phenyl groups (material U29) contributed beside the batochromic shift of all types of spectra to the increase of molar absorption coefficient and to the substantial decrease of photoluminescence quantum yield.

The all OLED prototypes showed significant electroluminescent behavior and the utilized DPP materials are of new perspective and future development. However, the electroluminescence depends on many parameters and the optimalization of multilayered structure is necessary to obtain efficient light emitting diode.

REFERENCES

1. Alp S., Ertekin K., Horn M., Icli S.: Dyes Pigm. *60*, 103 (2006).
2. Mizuguchi J.: J. Phys. Chem. *104*, 1817 (2000).

P03 DIAGNOSIS OF CIRRHOSIS BY GC/MS

CORNELIA MESAROS, MONICA CULEA and
ANDREEA IORDACHE

Babes-Bolyai University, Str. Kogalniceanu, nr.1, 3400 Cluj-Napoca, Romania,
mculea@phys.ubbcluj.ro

Introduction

Caffeine test consists in caffeine oral intake followed by measurements of blood, saliva, labelled CO_2 in the exhalation air, urine caffeine or metabolites[1,2]. The pharmacokinetic parameters of caffeine, clearance and half-life time, were usually studied by HPLC and immunoassay methods and by GC/MS[3]. Clearance of caffeine is a quantitative test of hepatic function, because caffeine is metabolized by the hepatic P-450 cytochrome oxidase system. Caffeine, 1,3,7-trimethylxanthine, has been introduced as a compound for measuring the metabolic capacity of the liver, being well tolerated when administrated orally.

The aim of the present investigation was to validate a rapid GC/MS method for plasma caffeine level determination for the characterization of some pharmacokinetic parameters in children. The application of the method on hepatitis and cirrhosis is tested.

Experimental

C h e m i c a l s   a n d   R e a g e n t s

Caffeine as a sterile caffeine sodium benzoate solution in water for injection use containing 125 mg of caffeine and 125 mg of sodium benzoate per 1 ml ampoule was obtained from pharmacy. All other reagents were from Merck (Germany). ^{15}N-theophylline, 74,2 atom % ^{15}N, labeled at the nitrogen in the position 7, synthesized in the National Institute for Research and Development for Isotopic and Molecular Technology Cluj-Napoca, was used as internal standard

E q u i p m e n t

A Hewlett Packard (Palo Alto,CA, USA) 5989B mass spectrometer coupled to a 5890 gas chromatograph were used in the conditions: EI mode, electron energy 70 eV, electron emission 300 µA and ion source temperature 200 °C, selected ion monitoring (SIM) mode. The GC/MS interface line was maintained to 280 °C, and quadrupol analyser at 100 °C. The gas chromatograph-mass spectrometer (GC/MS) assay used a HP-5MS fused silica capillary column, 30m × 0.25 mm, 0.25 µm film-thickness, programmed from 200 °C to 250 °C at a rate of 10 °C min^{-1}, the flow rate 1 ml min–1, with helium 5.5 as carrier gas. Injector temperature was 200 °C.

E x t r a c t i o n   P r o c e d u r e

0.5 ml of plasma containing caffeine was placed into a 5 ml screw-cap vial and 5 µl of internal standard ^{15}N-theophylline, 1 ml of the extraction solvent, chloroform: isopropanol 20 : 1 (v/v) and 0.2 g NaCl were added. After mechanical mixing for 1 min, the sample was centrifuged for 3 min. 3 µl of the organic layer (lower layer) were injected into the GC.

M e t h o d   v a l i d a t i o n

The method was validated in the range 0–20 µg ml^{-1} caffeine. Known amounts of caffeine 3, 5, 10, 15, 20 µg ml^{-1} and 10 µg of ^{15}N-theophylline were taken through above procedure. The regression curve, plotted as peak-area ratio of m/z 194 to m/z 181 versus caffeine concentration, gave the following linearity parameters: slope 0.5082, intercept –0.0528, r = 0.98.

Table I
Precision and accuracy of the method

Concentration added [µg ml^{-1}]	n	Concentration measured [µg ml^{-1}]	RSD [%]	Accuracy [%]
3	5	3.1	2.96	3.36
5	7	5.5	5.06	10.0

Precision gave R.S.D values lower than 5% for 5 µg ml^{-1} (n = 7) and lower than 3 % for 3 µg ml^{-1} (n = 5). Accuracy showed values lower than 10 % (Table I). Each value was obtained as an average between two measurements of the same sample. The limit of detection was 0.1 µg ml^{-1} caffeine in blood sample, signal to noise ratio 4 : 1.

P o p u l a t i o n

Caffeine concentration measurements were performed in 32 hospitalized children suffering of hepatic dysfunctions and controls. Three different groups were studied: A, formed by 19 children with hepatitis aged 3–15 years old, B, consisting from 5 children with cirrhosis, aged between 5–12 years old, and C, 8 children as control aged between 5–15 years old. The main dose was 4 mg kg^{-1}, p.o., for all groups. Blood samples were taken, at 0, 30 min, 1, 3, 6, 9 and 12 h. Blood samples were drawn into heparinized plastic tubes and immediately centrifuged. Plasma was stored at –20 °C. Written informed consents were obtained from each subject parent prior to this study.

C a l c u l a t i o n

Regression curves obtained by the GC/MS method in the SIM mode were used for pharmacokinetic parameters study. Caffeine elimination constant was calculated as follows:

$$k_{el} = (\ln C_1 - \ln C_2)/\Delta t, \qquad (1)$$

where C_1 = higher caffeine blood concentration, C_2 = lower caffeine blood concentration and Δt = the time elapsed between venous blood samples

Two points caffeine clearance was calculated as $Cl = k_{el} \cdot V_d$ and caffeine half-life as $t_{1/2} = \ln 2/k_{el}$, using a constant volume of distribution (V_d) of 0.6 liters per kg body weight.

Clearance values calculated as dose/area under curve (AUC) were compared with the two-points values.

Results

Caffeine clearance, measured in patients with cirrhosis and chronic hepatitis, was reduced and half live time was increased in children with liver disease as compared with control. The decreased metabolism observed in patients with various forms of liver disease was correlated to the disease status. Plasma concentrations of caffeine were measured in 19 patients with chronic hepatitis and 5 patients with cirrhosis and in 8 healthy subjects after caffeine (4 mg kg^{-1} p. o.) loading. The correlations of total body clearance between two-point study (sampling times 1 h and 9 h) and seven-point study (sampling times 0, 0.5, 1, 3, 6, 9, 12 h) were highly significantly, r = 0.94, p less than 0.001. These findings suggest that caffeine pharmacokinetic parameters can be estimated using two-point blood sampling procedure and GC/MS determination, following a single load. The elimination half-life ($t_{1/2}$) of caffeine was significantly longer in cirrhotic patients than in the other two groups and clearance was substantially reduced in these patients. The higher concentrations of caffeine obser-

Fig. 1.　**Caffeine plasma concentrations at time interval (1 h and 9 h) in hepatitis (n = 19)**

ved in the first hour after caffeine loading in hepatitis (Fig. 1.) compared with controls could be a possible test for hepatitis when very precise and accurate methods as isotopic dilution GC/MS are used. Significant changes (Student's paired t-test p<0.01) were observed in caffeine metabolism in children with decompensate cirrhosis.

The clearance values of 0.55 ± 0.41 ml min^{-1} kg^{-1} and half-life times of 19.11 ± 14.9 h are changed because of the reduction in "functioning hepatocyte mass". The control values for clearance and half-life time were of 1.36 ± 0.23 ml min^{-1} kg^{-1} and $t_{1/2}$ = 5.23 ± 0.85 h (n = 8). Patients with noncirrhotic liver disease showed intermediate values (Cl = 1.19 ± 0.45 ml min^{-1} kg^{-1} and $t_{1/2}$ = 6.62 ± 2.37 h) but higher values of caffeine plasma concentrations especially in the first hour after dose.

Conclusions

The method is simple, precise and rapid, useful in the analysis of xanthines. Isotopic labeled internal standard used avoids metabolites overlapping. The elimination half-life ($t_{1/2}$) of caffeine was significantly longer in cirrhotic patients and clearance was substantially reduced than in control. Caffeine pharmacokinetic parameters can be estimated using two-point blood sampling procedure by GC/MS determination, following a single load. The higher concentrations of caffeine observed in the first hour in hepatitis compared with controls could be a possible test for hepatitis.

REFERENCES
1. Park G. J., Katelaris P. H., Jones D. B., Seow F., le Couteur D. G., Ngu M. C.: Hepatology, *38*, 1227 (2003).
2. Wittayalertpanya S., Mahachai V: J. Med. Assoc. Thai. *84*, 189 (2001).
3. Culea M., Palibroda N., Panta Chereches P., Nanulescu M.: Chromatographia, *53*, 387 (2001).

P04 LEUKOTRIENE QUANTITATION BY GC-MS

MONICA CULEA, EUGEN CULEA, PARASCHIVA
CHERECHES-PANTA and ADELA PINTEA

*Babes-Bolyai University, Str. Kogalniceanu, nr. 1, 3400
Cluj-Napoca, Romania*
mculea@phys.ubbcluj.ro

Introduction

Quantitation of eicosanoid levels in biological systems is important for understanding of their role in cell function or pathological and for diagnosis. Leukotrienes quantitation is limited by sensitivity of the method. Gas chromatography – mass spectrometry (GC-MS) provides a sensitive and specific method when proper derivatization method is used.

Bronchoscopy with bronchoalveolar lavage is the gold standard to assess airway inflammation but invasiveness makes it unethical especially in children. The exhaled leukotriene B4 (LKB4) is elevated in asthmatic children compare with control. LKB4 is a non-invasive marker for airway inflammation in asthmatic children[1,2].

A preliminary work is described for GC-MS use for quantitative determination of LKB4 in exhaled breath content.

Experimental

Gas chromatography was performed on a 5% phenyl methylpolysiloxane column (30 m × 0.25 mm I.D., 0.25 µm film thickness) operated in a suitable temperature program. Helium carrier gas was of 1 ml min^{−1}. Ionization was performed by electron impact (EI) and detection in SIM mode. Arachidonic acid was used as internal standard.

Exhalaed Breath Condensate Collection

A condensing chamber (Ecoscreen II, Germany) was used to obtain exhaled breath condense (EBC). 1.5 ml of EBC was obtained after 15 minutes of breath through a mouthpiece connected to the condencer. Samples were stored at −80 °C before measurements.

Patients with asthma were recruited from Pediatric Clinic III of Cluj-Napoca. The preliminary study was for 3 patients with asthma and 3 controls.

GC-MS Method

LTB4 and arachidonic acid, the internal standard, were analyzed by GC-MS after derivatization with ethylchloroformiate and liquid-liquid extraction. A modified method was used[2]. Reagents were from Merck (Germany). Standards containing different concentration of LKB4 and the same concentration of arachidonic acid (IS) were prepared in water. Dezactivation of all glass surfaces, injector liner and vials, was made with 10% dichlorodimethylsilan in hexane for 30 minutes.

500 µl EBC, 1 µg arachidonic acid (IS), 20 µl ethylchloroformate and 40 µl pyridine were shaken few second
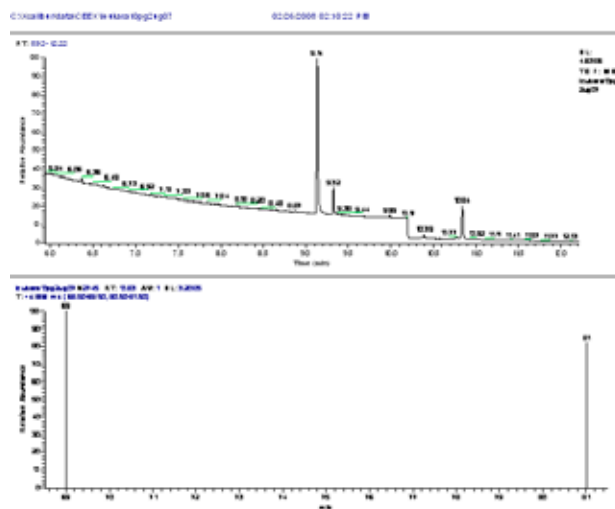
Fig. 1. **SIM chromatogram for arachidonic acid ethyl ester, the internal standard, elution time 9.33 min, and derivatized LKB₄, elution time 10.85 min: The ions m/z 69 and 81 are used in SIM mode for LKB₄. The distilled water (500 µl) was spiked with 1 µg arachidonic acid and 10 pg LKB₄**

for evaporating CO2. 0.25 ml chloroform, 0.5 ml sodium carbonate-bicarbonate solution were shaken 30 seconds. After 2 minutes of phase echilibrium, 3 µl of the lower phase was injected into the fused silica capillary column in the split-less mode. Injector temperature was 280 °C. Gas chromatography was performed on a 5% phenyl methylpolysiloxane column (30 m × 0.25 mm I.D., 0.25 µm film thickness) operated in the following temperature program: initial temperature 80 °C (1.5min), then increased with a rate of 28 °C min^{−1} at 315 °C and kept 5 minutes. The ion current chromatogram for the two compounds is presented in Fig. 1. The selected ions were m/z 79 for arachidonic acid derivative and m/z 69, 81 for LKB4 derivative. The mass spectra for the two derivatized compounds are presented in the Figs. 2. and 3.
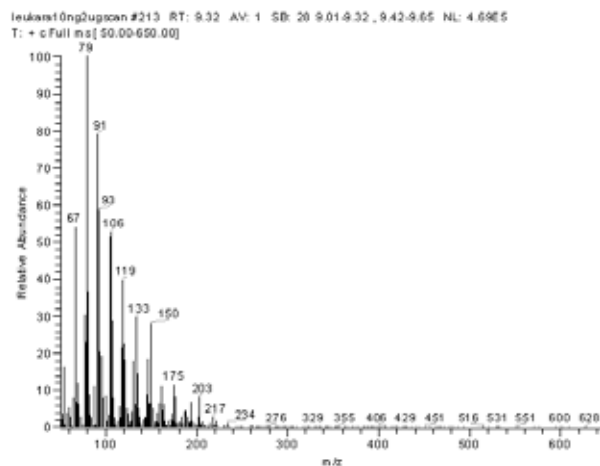
Fig. 2. **The mass spectrum of arachidonic acid ethyl ester (9.33 min), M = 332**
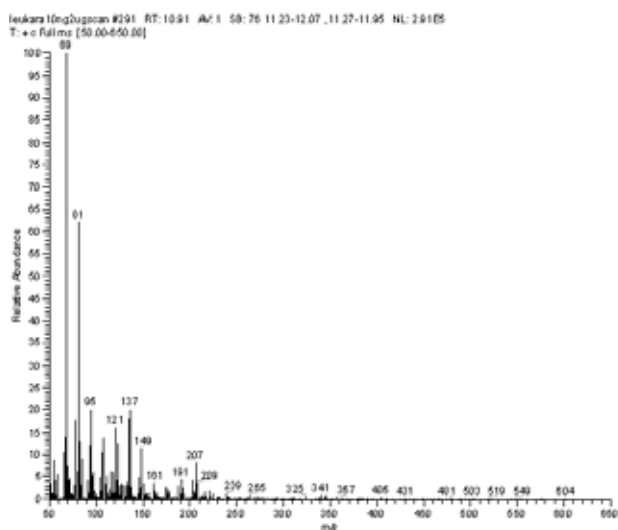
Fig. 3. **The mass spectrum of leukotriene B4 ethyl ester (10.85 min)**

Helium carrier gas flow was of $1\ ml\,min^{-1}$. Ionization was performed by electron impact (EI) and detection in SIM mode.

Results

The method provided good response linearity and precision (<30% C.V.) in the range $1–400\ pg\,ml^{-1}$, necessary to analyse leukotrene B4 in exhaled air. Arachidonic acid was used as internal standard because its structure is similar to leukotrienes, is undetectable in EBC without addition of arrachidonic acid and is stable in aqueous solution.

The linearity of the method was studied in the range $1–400\ pg\,ml^{-1}$. The regression curve obtained was:

Table I
LKB4 in EBC values in asthmatic and control children

Patient	$LKB_4\,[pg\,ml^{-1}]$	RSD [%]
1	178.2	32
2	219.5	47
3	315	35
Controls (n = 3)	78	36

$y = 0.0027x + 0.4038$, with a regression coefficient of $r = 0.99$. The detection limit was of $1\ pg\,ml^{-1}$, at a signal-to-noise of 5.

The method was applied for few cases of patients and controls. The different values of LKB4 were significant higher in asthmatic children than in healthy children.

Measurements of exhaled LKB4 are important for identifying the children with no respiratory symptoms but having inflammations which may require therapy.

Conclusions

The LKB4 was detectable in exhaled breath condense. GC-MS non-invasive method showed significant increased value for LKB4 in children with asthma than in healthy control.

REFERENCES
1. Shirley M. A., Murphy R. C.: J. Biol. Chem. *265*, 16288 (1990).
2. Cap P., Chladek J., Pejhal F., Maly M., Petru V., Barnes P. J., Montuschi P.: Thorax *59*, 265 (2004).

P05 CHARACTERIZATION OF OLIGOSACCHARIDES USING ESI-MS IN PRESENCE OF ANIONS

RICHARD ČMELÍK and JANETTE BOBÁĽOVÁ

Institute of Analytical Chemistry of the ASCR, v. v. i., Department of Proteomics and Glycomics, Veveří 97, 602 00 Brno, Czech Republic,
cmelik@iach.cz

Introduction

Knowledge of oligosaccharide sequence, inter-residual linkages, and branching are essential for understanding their biological functions and technological properties. Electrospray ionization (ESI) mass spectrometry (MS) has become one of the most important tool for structural analysis of carbohydrates[1].

For the analyses of oligosaccharides, the fragmentation of sodium or lithium adducts are commonly used to elucidate its structure, while the negative mode approach give more detailed[2] or complementary information. However, neutral oligosaccharides typically produce low signals of [M–H]$^-$ ions. An alternative way of charging a molecule to render it detectable in negative-ion mode is via either derivatization or the addition of a ammonium salt[3]. In the latter case, various anions (A$^-$) can be added in order to increase the response of saccharides to induce formation of stable and abundant anionic adducts [M + A]$^-$.

Experimental

Dextran 1000 (DEX) and ammonium salts were purchased from Fluka (Buchs, Switzerland), whereas low glucose syrup (LGS) was from Amylon (Havlíčkův Brod, Czech Republic). Maltooligosaccharides (MOS) were obtained from Sigma (St. Louis, USA). Oligosaccharides were dissolved at 30 μg ml^{-1} in methanol/water (1 : 1, v/v) containing different concentration (0, 3, 30, 100, 300 μM) of ammonium salts (bicarbonate, bisulfate, chloride, and nitrate).

ESI-MS(/MS) experiments were performed using a Esquire LC instrument (Bruker Daltonik, Germany) equipped with an ESI ion source. Samples were infused into the mass spectrometer at a flow rate of 3 μl min^{-1} via a metal capillary held at high voltage (–3,5 kV). Other potentials were modified and optimized before each experiment. Nitrogen was used as a drying (5 dm^3 min^{-1}, 250 °C) and nebulizing gas (14 psi).

Results

In this study, we reported the comparison of the malto- and isomaltooligosaccharides mixtures (MOS, LGS, and DEX) using negative-ion ESI MS. Oligosacharide samples were analyzed without additives, as well as after the addition of different amount of the ammonium salts. The effect of anion type and concentration in MS spectra have been investigated.

All oligosaccharide mixtures revealed two dominant ion series, [Glc$_x$–H]$^-$ and [Glc$_x$–H–120]$^-$. Small amount of [Glc$_x$–H+H$_2$O]$^-$ (for LGS), [Glc$_x$–H–60]$^-$ (DEX), as well [Glc$_x$–H–60–H$_2$O]$^-$ (LGS, MOS) ions were also observed. In general, higher oligomers (x≥5) formed deprotonated molecules in preference to fragments; lower oligomers were rather detected as [Glc$_x$–H–120]$^-$ ions. MS spectra of LGS dominated by [Glc$_x$–H]$^-$ (up to x = 5) or [Glc$_x$–H + H$_2$O]$^-$ ions.

The MS spectra of samples containing ammonium chloride showed [Glc$_x$+Cl]$^-$ ion series. At low nozzle-skimmer voltages under the conditions of high salt concentration (100 or 300 μM), preferential production of [Glc$_x$ + Cl]$^-$ was observed. The application of ammonium nitrate gave nitrate adducts of oligosaccharides. At the highest concentration of nitrate, the [Glc$_x$ + NO$_3$]$^-$ ions dominated. The ratio of deprotonated molecule to adducts (chloride of nitrate) and then that of [Glc$_x$–H–120]$^-$ (respectively [Glc$_x$–H + H$_2$O]$^-$ for LGS) to adducts decreased with increasing concentration of appropriate anion (Fig. 1). In both cases, the addition of anion dopant resulted in significantly simplified spectra and enhanced sensitivity and resolution.
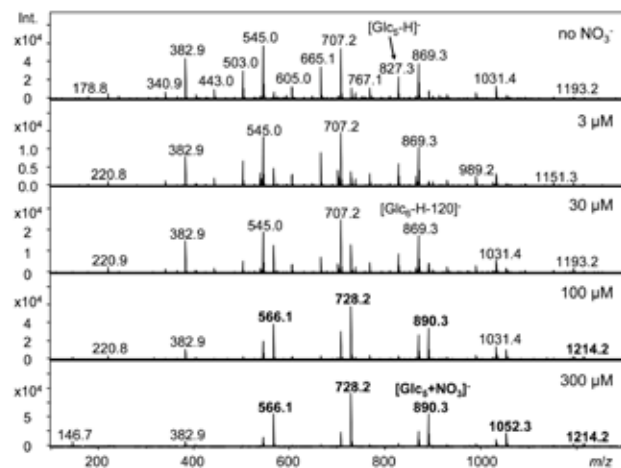
Fig. 1. **MS spectra of DEX at the different concentration of NO$_3^-$**

The behavior of bisulfate differed from the above mentioned anions. The abundance of [Glc$_x$ + HSO$_4$]$^-$ reached the maximum levels at the concentration of 30 and 100 μM of bisulfate, then HSO$_4^-$ and H$_3$S$_2$O$_8^-$ ions substantially increased. NH$_4$HCO$_3$ did not form observable adducts.

The influence of the particular studied anions on distribution of oligosaccharide derived ions is shown in Fig. 2 and Table I.

Tandem MS (MS^2) spectra generated from chloride and nitrate adduct ions of the same sample showed fragmentation pattern very similar to that for [Glc$_x$–H]$^-$, whereas a higher abundance of fragment ions was detected. On the other hand, attempts to fragment bisulfate adducts failed in all cases. Besides dominant fragments [Glc$_y$–H]$^-$ and [Glc$_y$–H–120]$^-$ (y≤x), the differences in MS^2 spectra have been observed for
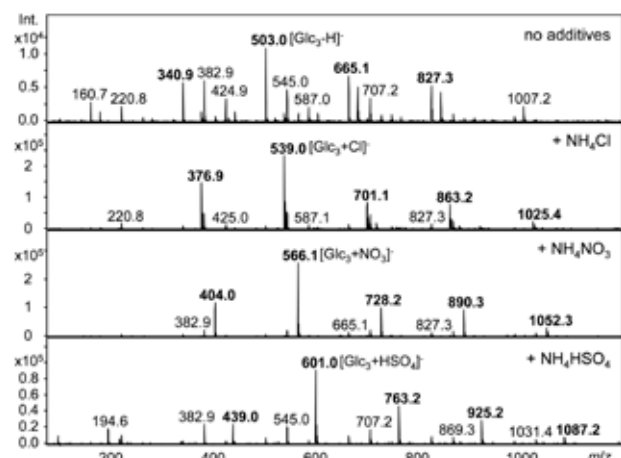
Fig. 2.   MS spectra of LGS with and without the addition of salts (300 μM)
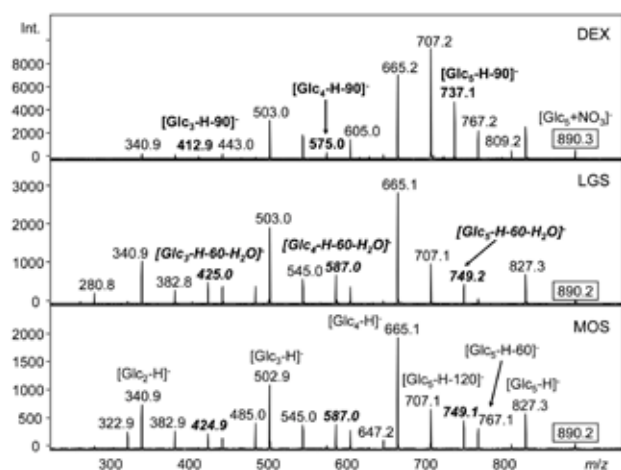
Fig. 3.   MS^2 spectra of nitrate adducts [Glc$_5$ + NO$_3$]$^-$ of DEX, LGS, and MOS

Table I
Abundant ions observed in the MS spectra of DEX, LGS and MOS with and without salts

Ion series	Range of the observed ion series – DP (x)			Salt
	DEX	LGS	MOS	
[Glc$_x$–H]$^-$	1–7	1–6	1–7	–
[Glc$_x$–H + H$_2$O]$^-$	–	4–6	–	–
[Glc$_x$–H–60]$^-$	3–6	–	–	–
[Glc$_x$–H–60–H$_2$O]$^-$	–	2–6	3–7	–
[Glc$_x$–H–120]$^-$	2–7	2–5	2–8	–
[Glc$_x$ + Cl]$^-$	2–7	2–6	2–8	Cl$^-$
[Glc$_x$ + NO$_3$]$^-$	2–7	2–6	2–8	NO$_3^-$
[Glc$_x$ + HSO$_4$]$^-$	3–7	2–6	3–7	HSO$_4^-$

Conclusions

   In the ESI negative-ion mass spectra, oligosaccharides were stabilized by adduct formation [M + A]$^-$ with several anions (A = NO$_3$, Cl). The analogous molecular mass distributions of presented glucose oligomers were obtained, whereas the adducts appeared in mass spectra in higher abundances relative to [M–H]$^-$. In addition, the in-source fragmentation was suppressed.

   MS^2 experiments enable to distinguish α-(1 → 4) and α-(1 → 6) linkages on the base of specific diagnostic product ions. A fragmentation of [Glc$_x$ + Cl]$^-$ and [Glc$_x$ + NO$_3$]$^-$ ion adducts was found to be suitable for structural determination of (iso)maltooligosaccharides because more prominent cross-ring fragmentation was observed.

REFERENCES

 1. Harvey D. J.: Proteomics *5*, 1774 (2005).
 2. Garozzo D. Giuffrida M., Impallomeni G.: Anal. Chem. *62*, 279 (1990).
 3. Jiang Y., Cole R. B.: J. Am. Soc. Mass Spectrom. *16*, 60 (2005).

particular oligosaccharide samples. The linkage included in DEX were reflected in specific cross-ring fragments [Glc$_y$–H–90]$^-$, while the presence of [Glc$_y$–H–60–H$_2$O]$^-$ appeared to be characteristic for MOS and LGS (Fig. 3).

   These observations are in agreement with the fact that DEX and MOS/LGS represent isomeric glucans differing in the prevalent α-(1 → 4), respectively α-(1 → 6) glycosidic linkage.

P06 A NEW APPROACH TO PROTEIN ENZYMATIC DIGESTION FOR FAST PROTEIN IDENTIFICATION BY MATRIX-ASSISTED LASER DESORPTION/IONIZATION TIME-OF-FLIGHT MASS SPECTROMETRY

FILIP DYČKA, MARKÉTA LAŠTOVIČKOVÁ and JANETTE BOBÁĽOVÁ

Institute of Analytical Chemistry of the ASCR, v.v.i., 602 00 Brno, Veveří 97, Czech Republic, bobalova@iach.cz

Introduction

The combination of protein separation by polyacrylamide gel electrophoresis with mass spectrometric analysis of proteins digested enzymatically in-gel is a very powerful tool for protein identification in complex biological systems. Recently several approaches have been developed for fast protein digestion. One approach is the use of modified trypsin for in-gel digestion of proteins instead of native trypsin[1]. Other promising approaches include microwave technology[2–4] or ultrasonic assisted protein enzymatic digestion[5]. The traditional sample preparation for protein identification through peptide formation is time-consuming procedure therefore we have studied and compared the variable performances of the fast enzymatic digestion of proteins using the different techniques. Most important, the new approach of protein digestion takes minutes, in contrast to several hours required by conventional methods.

The aim of this study was to demonstrate the usefulness of fast methods to apply microwave and ultrasonic device to in-gel digestion.

Experimental

Protein Separation

0.5 mg of bovine serum albumin (BSA) (Roche Diagnostics GmbH, Mannheim, Germany) was resuspended in 1 ml of sampling buffer (Laemmli Sample Buffer (Bio-Rad) with β-mercaptoethanol, 19:1). SDS-PAGE separation was performed on 12 % 1-D SDS PAGE gel. The visualization was carried out by Coomassie Brilliant Blue (CBB) G-250.

In-gel Digestion

The BSA bands separated by 1-D GE were excised manually, cut into pieces and in-gel digestion procedure was performed to the three BSA samples[6] following the protocols outlined in Table I.

Protein Identification

Obtained peptides were analyzed by MALDI-TOF/TOF MS (Applied Biosystems 4700 Proteomics Analyzer). This TOF/TOF instrument is equipped with Nd/YAG laser, 355 nm. α-Cyano-4-hydroxycinnamic acid (CHCA; 8 mg ml^{-1}, 0.1 % trifluoroacetic acid/acetonitrile (1 : 1, v/v)) was used as a MALDI matrix.

Table I
In-gel preparation, digestion, and peptide extraction using conventional, microwave (MW) and ultrasonic methods

Protocol	Solution	Convent. [min]	MW [min]	Ultrasonic [min]
Reduce	10 mM dithiotreitol.	45	45	45
Alkylate	55 mM iodoacetamide.	30	30	30
Wash	50% ACN in 0.1 M amonium bicarbonate.	30	30	30
Rehydrate	12.5 ng μl^{-1} of trypsin in 50mM ammonium bicarbonate, 5mM calcium chloride.	45	45	45
Digest	12.5 ng μl^{-1} of trypsin in 50mM ammonium bicarbonate, 5mM calcium chloride.	16 h	4	10
Extract	0.1% TFA, 50% ACN.	30	30	30
Total time		19 h	3 h, 4 min,	3 h 10 min.

Results

BSA was used as model protein to study the in-gel digestion. Three BSA samples excised from 1-D SDS PAGE gel (Fig. 1) were subjected to in-gel digestion with trypsin using conventional method, microwave irradiation and sonication in order to compare speed and convenience of new approaches.
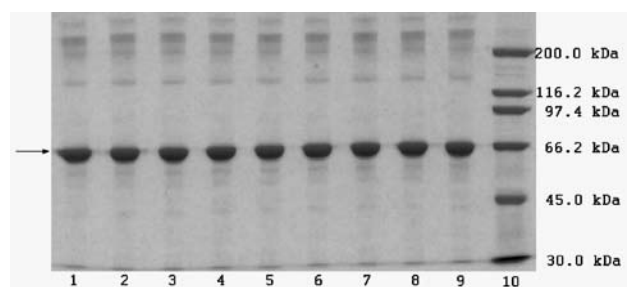
Fig. 1.　**1-D SDS PAGE separation of BSA (lane 1–9). Molecular weight markers are in lane 10. Protein bands marked by arrow were further in-gel digested by the standard, microwave or ultrasonic method and identified by mass spectrometry**

The gel particles with trypsin were incubated for 16 h at 37 °C, put into a microwave for 4 min at 350 W or put into an ultrasonic bath for 10 min at power 35 W. After in-gel digestion the peptide fragments were purified by ZipTipC$_{18}$ and directly spotted on the sample plate of the MALDI-TOF/TOF MS. Finally, CHCA was applied to each spot prior to acquiring mass spectra.

The mass spectra of tryptic peptides of BSA are shown in Fig. 2.A for conventional method, Fig. 2.B for the microwave method and Fig. 2.C for the ultrasonic method. The peptide peak patterns were almost the same for microwave and ultrasonic method, indicating that the digested peptide fragments
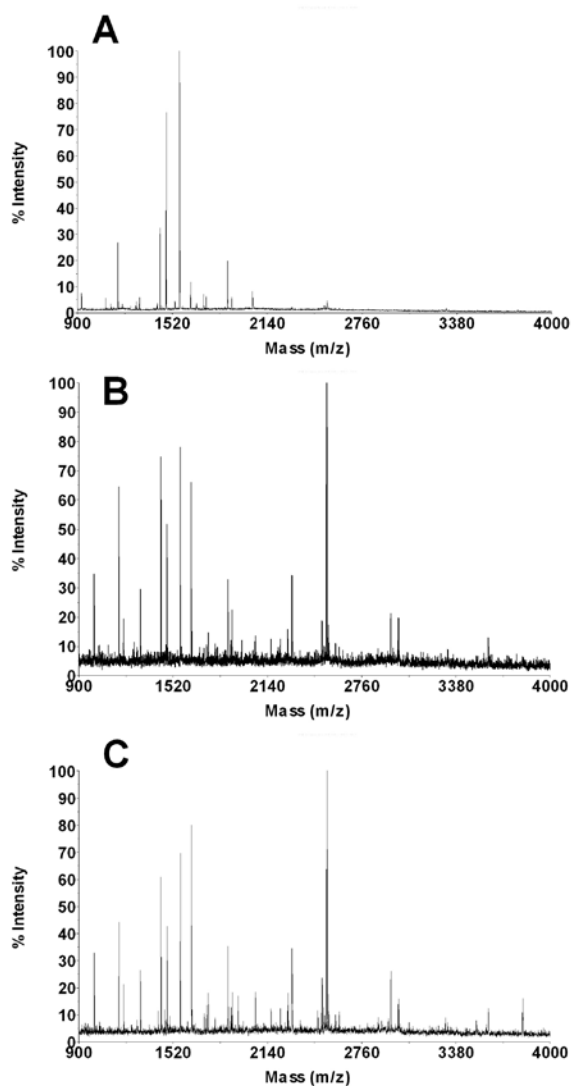
Fig. 2. **The MALDI-TOF mass spectra of BSA. The spectra were obtained after in-gel digestion: A – using conventional method; B – microwave method; C – ultrasonic method. CHCA was used as a matrix**

from two methods were similar. More relevant changes were observed between traditional method and new fast approaches. Protein identification was performed by searching the peptide masses against the NCBInr sequence database using the MASCOT search program. The methods using microwave and ultrasonic technologies gave slightly more matched tryptic fragments than the conventional method. The highest number of matched peptide and the highest score gave the method using ultrasonic device. Considering the required reaction time for the conventional method is much longer, the new methodic approaches apparently led to higher efficiency for in-gel digestion.

Conclusions

This work reports fast digestion procedures and protein identification based on the use of microwave and ultrasonic technology. These alternative metodologies can be an important advancement in proteomic research.

REFERENCES
1. Havlis J., Thomas H., Sebela M., Shevchenko A.: Anal. Chem. *75*, 1300 (2003).
2. Juan H. F., Chang S. C., Huang H. C., Chen S. T.: Proteomics *5*, 840 (2005).
3. Pramanik B. N., Mirza U. A., Ing Y. H., Liu Y.-H., Bartner P. L., Weber P. C., Bose A. K.: Protein Sci. *11*, 2676 (2002).
4. Sun W., Gao S., Wang L., Chen Y., Wu S., Wang X., Zheng D., Gao Y.: Mol. Cell. Proteomics *5*, 769 (2006).
5. Rial-Otero R., Carreira R. J., Moro A. J., Santos H. M., Vale G., Moura J. L., Capelo J. L.: J. Chrom. A *1166*, 101 (2007).
6. Shevchenko A., Wilm M., Vorm O., Mann M.: Anal. Chem. *68*, 850 (1996).

P07 THE ^{13}C AND ^{119}Sn NMR SPECTRA OF SOME TRIORGANOTIN-(IV)-N,N-DIETHYL-DITHIOCARBAMATES USED AS WOOD PRESERVATIVES

JURAJ KIZLINK[a] and LADISLAV REINPRECHT[b]

[a]*Faculty of Chemistry, Brno University of Technology, Purkyňova 118, 612 00 Brno, Czech Republic,*
[b]*Faculty of Wood Sciences and Technology, TU Zvolen, Masarykova 24., 960 53 Zvolen, Slovak Republic,*
kizlink@fch.vutbr.cz

Introduction

The organotin compounds (OTCs), mainly triorganotin compounds are very effective against fungi and were widely used for all kinds of wood preservation[1]. They are nowadays already less used to their leaking into the sweet water (brooks, lakes, rivers), but more used for sea water. OTCs are very well soluble in organic solvents and on the other hand have very low solubility in water. Many of them are irritant and harmful for human skin and some are also phytotoxic agents. For their relatively high toxicity and eco-toxicity their application is limited and are often replaced by other organic compounds now[2,3]. For this purpose the new groups of the OTCs on the base of substituted dithiocarbamic acid were synthetised and tested[4,5,6]. Till this time no cancerogenity among known OTCs was observed and reported.

Experimental

The various trialkyl-, triaryl- and triaralkyl-tin-(IV)-N,N-diethyldithiocarbamates were synthetized from corresponding trialkyl-, triaryl- and triaralkyl-tin-(IV)-chlorides (Merck s.r.o. Brno, CZ) and sodium N,N-diethyldithiocarbamate under trade name Kupral (Lachema a.s. Brno, CZ)

in ethanol or isopropanol, sometimes with methylethylketone in mixture. After removing solvent, the products as oil residue were filtrated with diatomace powder as additive throw the sinter-glass filter No. 3, under pressure of motor vacuum pump[4,5].

All these compounds were tested as wood preservatives against rot – caused by wood destroying fungi *Coniophora puteana, Coriolus versicolor, Serpula lacrymans* and against moulds.

Results and Discussion

The best antifungal results were obtained with the trialkyltin-(IV)-compounds in the order of R in the R_3Sn-group: methyl- and butyl-, comparable with commercial abroad widely used tributyltin-(IV)-naphtenate (TBTN) used as standard[4-9]. The lower efficacy was when R = cyclohexyl- or phenyl-, otherwise if R = benzyl- , the efficacy was very poor[6].

Besides these organotin-N,N-diethyldithiocarbamates we have tested also other organotin fungicides. A very good result was obtained with the compound tributyltin amidosulfonate (TBTAS), which was even comparable to the most effective, formely commercialy produced and used bis-tributyltin oxide (TBTO) as hexabutyldistannoxane and very effective against the g[+] bacteria *Streptococcus aureus*. However, this volatile compound is already out of use from technical praxis for its high toxicity and is also included in the severe poisons[10,11].

The diagrams of the biocidal efficacy for fungicides and photos of testing method (poisoned soil method) are presented on the poster at 4th Meeting on Chemistry & Life.

The ^{13}C and ^{119}Sn NMR spectra of these compounds were also measured on the JEOL spectrometer JNM-FX 100 (Japan) at 25.047 and 37.14 MHz at 300 K. The che-

Table I
^{13}C and ^{119}Sn NMR shifts for organotin compounds type $R_3SnSC(S)N(C_2H_5)_2$ at 300 K

| Compound R | Solvent | δ([119]Sn) | δ(^{13}C)/(nJ([119]Sn, ^{13}C), Hz) | | | | | | | | Ref. |
			C–1	C–2	C–3	C–4	C–5	CS	CH$_2$	CH$_3$	
C_6H_5- phenyl-	CDCl$_3$	−189.8	142.54 (604.2)	136.50 (47.6)	128.31 (62.3)	128.85 (13.4)	–	–	50.44	12.05	12
n-C_4H_9- n-butyl-	neat	12.0	17.48 (352.8)	28.71 (22.0)	26.90 (66.0)	13.58 (<5)	–	196.73	49.25	11.86	13
n-C_4H_9- n-butyl-	CDCl$_3$	23.4	17.50 (350.2)	28.74 (20.6)	26.98 (67.4)	13.58 (<5)	–	197.11	49.39	11.75	13
n-C_4H_9- n-butyl-	pdpy	14.4	18.21 (356.1)	29.38 (22.0)	27.51 (67.4)	14.00 (<5)	–	197.46	49.86	12.30	13
n-C_4H_9- n-butyl-	hmpa	−19.0	18.62 (413.2)	28.34 (24.9)	26.64 (76.2)	13.13 (<5)	–	198.58	48.17	11.55	13
CH_2=CH- vinyl-	CDCl$_3$	−202.1	140.01 (587.6)	134.86 (–)	–	–	–	195.35	49.91	11.83	15
$C_6H_5CH_2$- benzyl-	CDCl$_3$	−92.6	26.45 (303.3)	140.53 (41.5)	127.60 (30.8)	128.13 (17.6)	123.63 (22.0)	195.58	49.80	11.83	14
c-C_6H_{11}- cyklohexyl-	CDCl$_3$	−28.3	35.94 (337.0)	33.30 (17.6)	30.60 (67.4)	28.33 (<5)	–	198.81	50.85	13.47	14

mical shifts were determined relative to a suitable signal of solvent[12–15] as $CDCl_3$ (77.00 ppm), pentadeuteriopyridine (pdpy) (149.90 ppm), hexadeuteriodimethyl sulphoxide (hdso) (39.60 ppm) and hexamethylphosphor triamide (hmpa) (36.00 ppm) respectively by known method.[12–16] Achieved results are presented in the Table I.

Conclusion

Organotin compounds having three direct tin-carbon bonds have high biocidal activity[10,17], so they are useful as disinfectants and antimicrobial agents for paper, textiles, wood and even for masonry and stonework.[18–20] Their highest consumption nowadays is as antifouling paints for the wood seawater vessels against the marine organisms immersion.

REFERENCES
1. Kizlink J.: Chem. Listy *86***,** 178 (1992).
2. Paulus W.: *Microbicides for the Protection of Materials,* Chapman and Hall, London 1993.
3. Cooney J. J., Wuertz S.: J. Ind. Microbiol. *4***,** 375 (1989).
4. Kizlink J.: J. Oil Colour Chem. Assoc. *74***,** 329 (1991).
5. Kizlink J., Rattay V., Košík M.: J. Oil Colour Chem. Assoc. *76***,** 468 (1993).
6. Kizlink J., Fargašová A., Reinprecht L.: Drevársky výskum *41***,** 19 (1996).
7. Reinprecht L., Kizlink J.: Acta Fac. Xylol. Zvolen *38***,** 75 (1996).
8. Kizlink J., Fargašová A.: CHEMagazín *7*, 16 (1997).
9. Reinprecht L., Kizlink J.: Drevársky výskum *44*, 67 (1999).
10. Kizlink J.: Chem. Papers *55,* 53 (2001).
11. Kizlink J.: CHEMagazín *13*, 20 (2003).
12. Holeček J., Nádvornik M. Handliř K., Lyčka A.: J. Organometal. Chem**.** *241,* 177 (1983).
13. Nádvornik M., Holeček J., Handliř K.: J. Organometal. Chem. *275,* 43 (1984).
14. Lyčka A., Jirman J., Koloničný A.: J. Organometal. Chem. *333,* 305 (1987).
15. Handliř K., Holeček J.: Inorg. Chim. Acta *150,* 287 (1988).
16. Gielen M., Willem R., Wrackmeyer B.: *Advanced Applications of NMR to Organometallic Chemistry,* Wiley, New York 1996.
17. Fargašová A.: Bull. Environ. Contam. Toxicol**.** *60,* 9 (1998).
18. Sjoestroem E., Alén R.: *Analytical Methods in Wood Chemistry – Pulping and Papermaking,* Springer, Berlin 1999.
19. Ambrožová V.: *Nátěry dřeva,* Grada Publishing, Praha 2000.
20. Vitvar P.: *Přehled a charakteristika chemických prostředků proti biotickým škůdcům, ohni a povětrnostním vlivům*, Výzkumný a vývojový ústav dřevařský (VVUD), Praha 2000 and 2003 (handbooks).

P08　PREPARATION OF DIMETHYL CARBONATE FROM METHANOL AND CARBON DIOXIDE – THE REMOVAL OF REACTION WATER BY OLEFINS

JURAJ KIZLINK

Faculty of Chemistry, Brno University of Technology, Purkyňova 118, 612 00 Brno, Czech Republic,
kizlink@fch.vutbr.cz

Introduction

The development of suitable methods based on the carbon dioxide for the synthesis of various organic products is very attractive now. Carbon dioxide is in the last twenty years very significant waste, which is responsible for the greenhouse effect formation[1]. The preparation of dimethyl carbonate (DMC) is one of many reactions for the utilization of carbon dioxide together with methanol as significant product for various uses[2], nowadays also as additive for engine fuels[3].

The one-pot synthesis of DMC from carbon dioxide and methanol has become attractive due to the low cost of the starting materials, but the DMC yield by this way is relatively low, due to the fact that carbon dioxide is highly thermodynamically stable and kinetically inert compound and due to the deactivation of catalysts induced by water formation in the reaction process[4,5].

The main catalyst system is based on the organotin (IV) compounds, especially on the dialkyltin dialkoxides[6,7]. It has been also reported, that DMC can be synthetized in the presence of tin (IV) and titanium (IV) alkoxides[8], similar organotin compounds.[9–11] and also metal (Hg, Mg, Zn) acetates or some other (Co, Mn, Ni) acetates[12]. The values of temperatures, pressures and times range between 130–180 °C, 0.5–3.0 MPa, 2–12 hours respectively[12].

The first way is the use of the special catalyst systems, which are effective in spite of the reaction water is presented. The modified ZrO_2 catalysts promoted with phosphoric acid were used[13–15]. This catalyst was prepared by calcining of commercially available ZrO_2 It was found, that the DMC formation rate was strongly depent on the structure of zirconia catalyst and it was very depent on the calcination temperature. It was also observed and reported, that during the reaction the dimethyl ether (DME) was formed on various types of oxide catalysts (Al_2O_3, SiO_2, CeO_2, GeO_2, TiO_2, ZrO_2 a.s.o.). The other catalytic systems are based on $H_3PW_{12}O_{40}/Ce_xTi_{1-x}O_2$ compound[17], $H_3PW_{12}O_{40}/ZrO_2$ system[18], Cu-Ni/VSO system[5,19], H_3PO_4/V_2O_5 system[4] and mixtures of methyl iodide, tetrabutylammonium bromide and often potassium carbonate[20]. The formation of DME decreased by the high (supercritical) pressure of carbon dioxide[10,20,21].

The main issue is the formation of water, which can terminate this reaction in the equilibrium and also destroy the catalysts. The removal or utilization of reaction water is the important problem for this DMC preparation. Desiccants used as „water traps" were quite effective, but also very expensive.

As desiccants were applied $CaCl_2$ compound[22], Na_2SO_4, $MgSO_4$ salts[6], 2,2-dimethoxypropane (DMP) compound[23], acetals[24], dicyclohexylcarbodiimide (DCC) compound[7,8], trimethyl phosphate (TMP) compound[8], molecular sieves[25] and some epoxides as ethylene oxide (EO) named oxirane [26,27] and styrene oxide (SO) compound[28].

The second way as the novel reaction route for DMC preparation is the removal of reaction water by means of olefins. These olefins in the reaction mixture under catalysts basen on the metal oxides and zeolites in the H^+-form can react with reaction water into corresponding alcohols. The relatively high temperatures of about 180–200 °C were necessary for ethylene, when part of DMC formed was also decomposed. Better was propylene at 150–180 °C, when isopropanol was formed and the best was isobutylene at about 130–150 °C, when terc-butanol was formed. The formation of methyltercbutylether (MTBE) was also observed (highoctane additive for engine petrol). For industry, the petroleum C_4-isobutylene gas fraction from the production of the MTBE is for lower price here more suitable.

The reaction mechanism is explain often by means of NMR method mainly in the following references.[10–11,29,30]

Experimental

All reactions were carried in a stainless autoclave reactor with inner volume about 100 ml with vertical magnetic stirring[2] or horizontal shaking with electrical heating. Catalysts were prepared from commercial items (Reachim, Moscow, SU) according to references[5,6,7]. All zeolites were from the refinery Slovnaft a.s. (Bratislava, SK). Carbon dioxide and olefins were pure, min. 98% grade (Messer).

The products were analysed by GC-method with butanol, octane or toluene as internal standards, according to previous references.[6–8]

Results and Discussion

The best results by the first way with the zirconia catalysts were conversion 20 % and selectivity 80 % and so the yields up to 16 %. By the second way with olefins the conversion was about 70 %, selectivity about 8 % for ethylene, 11 % for propylene and 15 % for isobutylene, so the yields were about 5–11 %. The main problem was here the stirring of the catalysts. the contact between reaction liquids and catalysts must be effective. The addition of large amounts of desiccants e.g. DMP, TMP is not effective because of decreasing the DMC and increasing the DME formation rate.

Conclusion

The one-pot synthesis of DMC from methanol and carbon dioxide is very interesting process for the utilization of carbon dioxide. The very interesting way is here the utilization of water stable catalysts such as various metal (Ce, Ge, Mg, Sn, V, Zn, Zr) oxides. For the removal of reaction water the best way now is the utilization of ethylene oxide, when together with DMC also ethylene glycol and 2-methoxyethanol are produced. The our way for olefins must be yet more

investigated. The intention here is the utilization of carbon dioxide from large bioethanol factory in the Slovak Republic, where emissions of carbon dioxide (purity about 97 % grade) of 40,000 tons per year from the maize starch fermentation as degas waste are released into the atmosphere.

REFERENCES

1. Yamazaki N., Nakahama S.: Ind. Eng. Chem. Prod. Res. Dev. *18,* 249 (1979).
2. Sakakura T., Choi J. Ch., Yasuda H.: Chem. Rev. *107,* 2365 (2007).
3. Aresta M., Dibenedetto A.: Catal. Today *98,* 455 (2004).
4. Wu X. L., Xiao M., Meng Y. Z., Lu Y. X.: J. Mol. Catal A-Chem. *238,* 158 (2005).
5. Wu X. L., Xiao M., Meng Y. Z., Lu Y. X.: J. Mol. Catal A-Chem. *249,* 93 (2006).
6. Kizlink J.: Collect. Czech. Chem. Commun. *58,* 1399 (1993).
7. Kizlink J., Pastucha I.: Collect. Czech. Chem. Commun. *59,* 2116 (1994).
8. Kizlink J., Pastucha I.: Collect. Czech. Chem. Commun. *60,* 687 (1995).
9. Sakakura T., Saito Y., Okano M., Choi J. Ch., Sako T.: J. Org. Chem. *63,* 7095 (1998).
10. Sakakura T., Choi J. Ch., Saito Y., Matsuda T., Sako T.: J. Org. Chem. *64,* 4506 (1999).
11. Sakakura T., Choi J. Ch., Saito Y., Sako T.: Polyhedron *19,* 573 (2000).
12. Zhao T., Han Y., Sun Y.: Fuel Process. Technol. *62,* 187 (2000).
13. Tomishige K., Sakaihori T., Ikeda Y., Fujimoto K.: Catal. Letters *58,* 225 (1999).
14. Tomishige K., Ikeda Y., Sakaihori T., Fujimoto K.: J. Catalysis *192,* 355 (2000).
15. Ikeda Y., Asadullah M., Fujimoto K., Tomishige K.: J. Phys. Chem. B *105,* 10653 (2001).
16. Tomishige K., Furusawa Y., Ikeda Y.: Catal. Letters *76,* 71 (2001).
17. La K. W., Jung J. Ch., Kim H., Baeck S. H., Song I. K.: J. Mol. Catal A-Chem. *269,* 41 (2007).
18. Jiang C., Guo Y., Wang C., Hu C., Wu Y., Wang E. Appl. Catal. A-Gen. *256,* 203 (2003).
19. Wang X. J., Xiao M., Wang S. J., Lu Y. X., Meng Y. Z.: J. Mol. Catal. A-Chem. *278,* 92 (2007).
20. Fujita S., Bhanage B. M., Arai M., Ikushima Y.: Green Chem. *3,* 87 (2001).
21. Hong S. T., Park H. S., Lim J. S.: Res. Chem. Intermed. *32,* 737 (2006).
22. Jiang Q., Li T., Liu F.: Chin. J. Appl. Chem. *16,* 115 (1999).
23. Tomishige K., Kunimori K.: Appl. Catal. A-Chem. *237,* 103 (2002).
24. Choi J. C., He L. N.: Green Chem. *4,* 230 (2002).
25. Hou Z. S., Han B., Liu Z., Jiang T., Yang G.: Green Chem. *4,* 467 (2002).
26. Cui H., Wang T., Wang F., Gu Ch., Wang P. Dai Y.: Ing. Eng. Chem. Res. *42,* 3865 (2003).
27. Cui H., Wang T., Wang F., Gu Ch., Wang P. Dai Y.: Ing. Eng. Chem. Res. *43,* 7732 (2004).
28. Tian J. S., Wang J. Q., Chen J. Y., Fan J. G., Cai F., He L.N.: Appl. Catal. A-Gen. *301,* 215 (2006).
29. Holeček J., Nádvornik M:: J. Organometal. Chem. *315,* 299 (1986).
30. Suciu E. N., Kuhlman B., Knudsen G.: J.: J. Organometal. Chem. *556,* 41 (1998).

P09 AMADORI REARRANGEMENT FOR SYNTHESIS OF CHIRAL FRAGMENTS

JANA MARKOVÁ and MILAN POTÁČEK

Department of Chemistry, Masaryk University, Kotlářská 2, 611 37 Brno, Czech Republic,
21510@mail.muni.cz

Introduction

Amadori rearrangement is a reaction between sugars and amines. The rearrangement is based on the conversion of N-substituted glycosylamines to the N-substituted 1-amino-1-deoxy-2-ketoses. Amadori observed this reaction in years 1926-31. The true structure of the rearranged product exposed Weygand and Kuhn in 1937[1]. Recently, it has been found that Amadori rearrangement takes place in living cells and organisms, where sugars and amino acids coexist. There Amadori rearrangement causes the functional modification of proteins, which are characteristic for diseases *diabetes mellitus* and *arteriosclerosis*[2]. Amadori rearrangement is also known as initial phase of Maillard reaction[3] and plays an important role in the synthesis of osazone, quinoxaline, folic acid and riboflavine[4].

We have investigated conditions for Amadori rearrangement of D-glucose and 5-deoxy-D-xylose with *p*-toluidine, benzylamine and dibenzylamine. 1-Amino-3,4,5,6-tetrahydroxyhexane-2-on and 1-amino-3,4-dihydroxypentane-2-on were prepared by hydrogenolysis of benzyl group on Pd\C. These compounds are to be used for the insertion of stereogenic carbon atoms with hydroxyl groups of sugar to various organic molecules.

Experimental

Amadori rearrangement is the reaction between sugars and amines in the presence of acid catalyst. The influence of amines and acid on the course of the reaction was investigated. As acid catalysts acetic acid and diethylmalonate were used.

Reactions in the Presence of Acetic Acid

The reactions were carried out in water in the presence of 1.4 equiv. of amine and 0.04 equiv. of acetic acid. The reaction mixture was heated at 90 °C for 30 min. Then a mixture of ethanol and diethylether was added and white crystals of the product were obtained after cooling to 3–4 °C for 24 h.

1
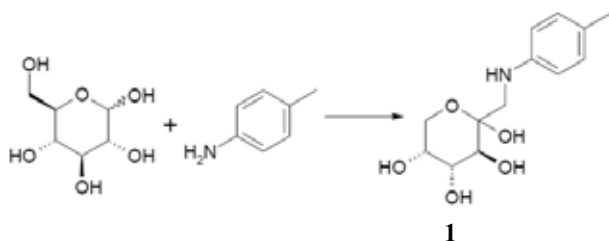
Scheme 1
Reaction of D-glucose with p-toluidine

Reactions in the Presence of Diethylmalonate

The reactions were carried out in the mixture of ethanol and diethylmalonate. 1.4 equiv of amine was used. After 2 h of reflux diethylether was added to the reaction mixture. White crystals of the product were obtained when the solution was kept at 3–4 °C for 20 h.

Hydrogenolysis of Benzyl Group on Pd/C

Product of Amadori rearrangement with dibenzylamine was hydrogenolysed on 10 % Pd/C in the presence of methanol. Reaction was carried out at room temperature and atmospheric pressure for 16 h. A yellow liquid product was obtained after the filtration and evaporation of solvent from the reaction mixture.

Results

The products of Amadori rearrangement were successfully obtained by the reaction of D-glucose with *p*-toluidine **1** (Scheme 1) and dibenzylamine **2** (Scheme 2).

On the other hand, the reaction of D-glucose with benzylamine does not follow the principles of Amadori rearran-

2
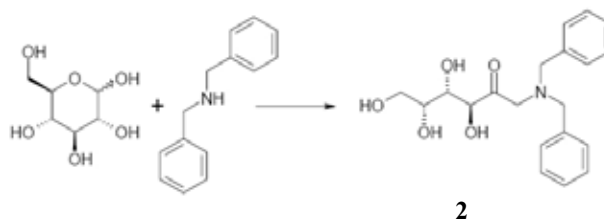
Scheme 2
Reaction of D-glucose with dibenzylamine

3
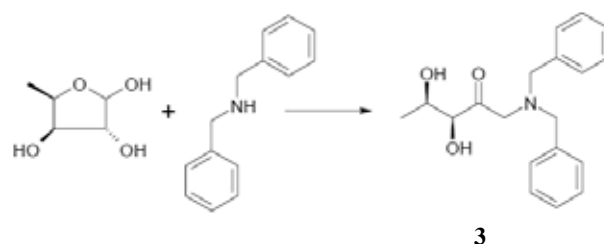
Scheme 3
Reaction of 5-deoxy-D-xylose with dibenzylamine

Table I
Reaction of D-glucose

Amine	Catalyst	Product	Yield [%]
benzylamine	CH₃COOH	glycosylamine	75
	DEM	glycosylamine	90
p-toluidine	CH₃COOH	Amadori product	61
	DEM	Amadori product	71
dibenzylamine	CH₃COOH	glycosylamine	65
	DEM	Amadori product	72

Table II
Reaction of 5-deoxy-D-xylose

	5-deoxy-D-xylose		
Amine	Catalyst	Product	Yield [%]
benzylamine	CH₃COOH	glycosylamine	68
	DEM	glycosylamine	86
p-toluidine	CH₃COOH	glycosylamine	74
	DEM	glycosylamine	78
dibenzylamine	CH₃COOH	glycosylamine	74
	DEM	Amadori product	51

gement independently on the selection of acid catalyst. The observed results and yields are summarized in Table I.

The required product of Amadori rearrangement of 5-deoxy-D-xylose was obtained only in case of the reaction with dibenzylamine, which was carried out in the presence of diethylmalonate **3** (Scheme 3).

Reactions performed under various conditions yield corresponding glycosylamines only **4** (Scheme 4).

The observed results are summarized in Table II.

4
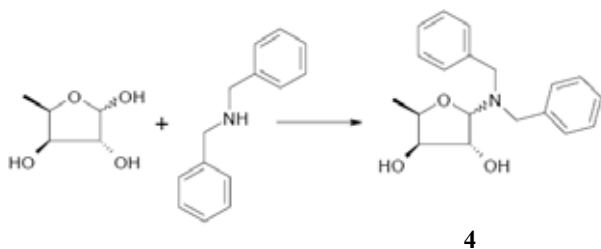
Scheme 4
Glycosylamine of 5-deoxy-D-xylose

The rearrangement of the studied sugars with *p*-toluidine yielded products containing six member ring in its structure **1** (Scheme 1). However, when dibenzylamine was used the open form **2** of the product was obtained (Scheme 2).

2   **5**
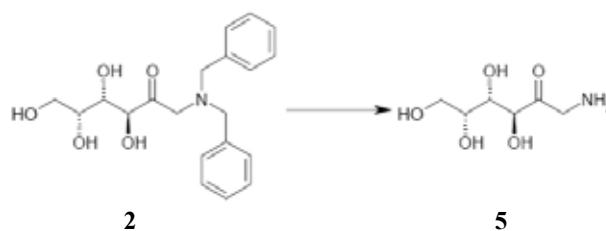
Scheme 5
Hydrogenolysis of the compound **2**

The cyclization of these products does not take place because of sterical hindrance of the large benzyl groups of amine. Both cyclic and open forms of the products were confirmed by ^{1}H and ^{13}C NMR spectroscopy.

The product with free amino group **5** was obtained after the hydrogenolysis of compound **2** on Pd/C catalyst (Scheme 5). Compound **5** with unprotected amino group can be then used in further reactions introducing stereogenic centre into an appropriate organic substrate.

Conclusions

The scope of Amadori rearrangement of D-glucose and 5-deoxy-D-xylose was searched. It was found that the structure of both sugar and amine plays an important role for course of the reaction. The rearrangement takes place more readily and with better yield in the presence of diethylmalonate when compared to acetic acid.

REFERENCES
1. Hodge J. E.: Adv. Carbohydr. Chem. *10*, 169, (1990).
2. Lederer M. O., Dreisbusch C. M., Bundschuh R. M., Carbohydr. Res. *301*, 111, (1997).
3. Stadler R. H., Blank I., Varga N., Nature *419*, 449, (2002).
4. Weygand F., Bergmann A., Chem. Ber. *80*, 255, (1947).

P10   EFFICIENT MICROWAVE-ASSISTED OXIDATIVE DEPROTECTION OF TRIMETHYLSILYL ETHERS WITH CALCIUM HYPOCHLORITE UNDER SOLVENT-FREE CONDITIONS

MOHAMMAD M. MOJTAHEDI, M. SAEED ABAEE and HASSAN ABBASI

Chemistry & Chemical Engineering Research Center of Iran, P. O. Box 14335–186 Tehran, Iran,
mojtahedi@ccerci.ac.ir

Introduction

Trimethylsilylation of alcohols is a very common practice in organic synthesis to protect hydroxyl groups[1]. Such maneuver maintains the hydroxyl functionality and prevents its oxidation during reactions. However, sometimes, it is required to convert silyl ethers into their corresponding carbonyl structures. This conversion could be either carried out in a two step desilylation-oxidation process or directly achieved in a one pot reaction. Earlier protocols for such direct oxidations include the use of chromium based procedures[2], DMSO based reagents[3], NBS[4], photochemical conversions[5], manganese based procedures[6], and some other different methods[7]. Such processes usually involve the use of harsher reaction conditions, harder work up procedures, and formation of harmful residuals. In recent years, milder reagents and reaction conditions are introduced for direct oxidation of TMS protected alcohols into their corresponding carbonyl analogues[8]. But, introduction of new and efficient methods for oxidative deprotection of trimethylsilyl ethers using inexpensive reagents and under environmentally safe conditions is still considerably attractive.

Calcium hypochlorite is a cheap and mild solid oxidant which can easily be stored[9], is relatively stable, and has recently been used efficiently for oxidation of various organic functionalities[10]. In continuation of our previous investigations to develop environmentally friendly procedures[11], we now report a one-pot oxidative deprotection of TMS ethers of benzylic alcohols on a solid support under microwave irradiation (MW) using $Ca(ClO)_2$ (Scheme 1). As a result, mild transformation of the substrates to their corresponding carbonyl compounds is observed without any undesired over oxidation.
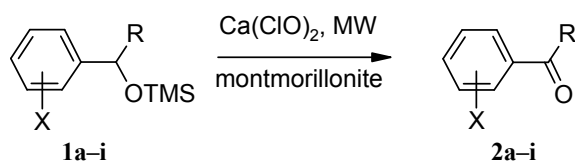
Scheme 1

Experimental

General

A commercial microwave oven (900 W) was used for irradiation of the reaction mixtures. GC analyses were recorded on a "Fison instrument Gas Chromatograph 8000" equipped with a mass detector "Trio 1000". TMS silyl ethers were prepared according to available procedures[12]. All products are known compounds and are identified by comparison of their physical and spectroscopic data with those of authentic samples[13].

Typical Procedure for Oxidative Deprotection Reactions

Montmorillonite K–10 (1.0 g) and calcium hypochlorite (286 mg, 2 mmol) were mixed thoroughly in a mortar. The resulting solid was mixed well with a TMS protected benzylic alcohol (**2a-i**) (2 mmol). The mixture was transferred to a 25 ml beaker and irradiated in microwave oven for the time periods specified in Table I. The progress of the reactions was monitored by TLC or GC. The reaction mixtures were extracted twice by 10 ml portions of diethyl ether. The combined ethereal phases were washed by water and dried over anhydrous calcium chloride. The products were obtained after evaporation of the volatile portion. ^1H NMR and IR spectra of the products were obtained and compared with those of authentic samples.

Spectral Data

2a. ^1H NMR (CDCl$_3$, δ, 80 MHz): 7.42–7.50 (m, 3H), 7.69–7.80 (m, 2H), 9.66 (s, 1H); IR (KBr disk, cm^{-1}) 1,703, 2,737, 2,819.

2b: ^1H NMR (CDCl$_3$, δ, 80 MHz): 6.52 (dd, *J* = 7.5, 15.8 Hz, 1H), 7.20–7.52 (m, 6H), 9.54 (d, *J* = 7.5 Hz, 1H); IR (KBr disk, cm^{-1}) 1,681, 2,743, 2,815.

2d: ^1H NMR (CDCl$_3$, δ, 80 MHz) 7.42 (d, *J* = 8 Hz, 2H), 7.75 (d, *J* = 8 Hz, 2H), 9.91 (s, 1H); IR (KBr disk, cm^{-1}) 1,701, 2,785, 2,859.

2e: ^1H NMR (CDCl$_3$, δ, 80 MHz): 2.36 (s, 3H), 7.20–7.31 (m, 3H), 7.69–7.80 (m, 2H); IR (KBr disk, cm^{-1}) 1,682, 3,063.
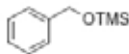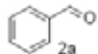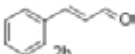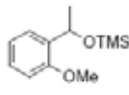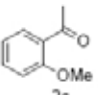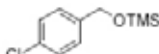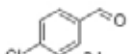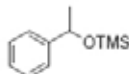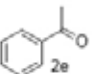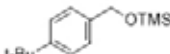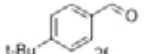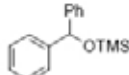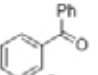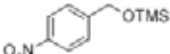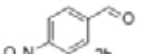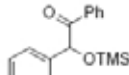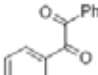
2i: ^1H NMR (CDCl$_3$, δ, 80 MHz): 7.31–7.61 (m, 6H), 7.65–7.98 (m, 4H); IR (KBr disk, cm^{-1}) 1,658, 3,063.

Results

An equimolar mixture of TMS benzylether and $Ca(ClO)_2$ on montmorillonite K-10 support was subjected to MW irradiation and complete conversion to benzaldehyde (**2a**) was performed within 60 seconds. Extraction of the product by diethyl ether followed by GC analysis showed 97% formation of **2a**. Control experiments conducted in the absence of MW irradiation at elevated or room temperature prolonged the reaction time considerably (Table I, entry 1). TMS ethers of other benzylic alcohols were subjected to the same transformation under three different sets of conditions (entries 2–9). In all cases MW irradiated samples resulted in formation of high to excellent yields of products **2b-i** in less than 2 minutes while lack of irradiation for the same mixtures took much longer time periods for reactions to complete.

The selectivity of the method was examined using an equimolar mixture of benzylsilyl ether and cyclohexylsilyl

Table I
Montmorillonite K–10 supported oxidative deprotection of TMS ethers under thermal and MW conditions

Entry	Substrate	Product	Time			Yield [%][a]			Mp or bp [°C torr^{-1}]	
			Mw [s]	40 °C [h][b]	RT [h]	Mw [s]	40 °C [h][b]	RT [h]	Found	Reported[13]
1	OTMS	O 2a	60	12	48	97	90	90	177–179	178–179
2	OTMS	O 2b	90	12	48	93	88	90	247	248
3	OTMS OMe	O OMe 2c	60	12	48	90	87	85	130/18	131/18
4	Cl OTMS	Cl O 2d	60	12	48	92	86	85	46–50	45–50
5	OTMS	O 2e	90	12	48	93	83	85	19–20	19–20
6	t-Bu OTMS	t-Bu O 2f	60	12	48	94	89	90	131/25	130/25
7	Ph OTMS	Ph O 2g	60	18	60	88	80	83	46–50	47–51
8	O₂N OTMS	O₂N O 2h	90	20	72	87	85	80	103–105	103–106
9	O Ph OTMS	O Ph O 2i	90	20	72	85	81	80	93–95	94–95

[a]Gc zields, [b]refluxing dichloromethane
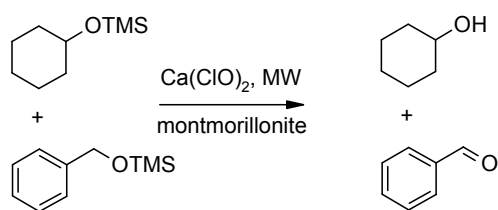
Scheme 2
Competitive oxidative deprotection of TMS ethers

ether. Under MW irradiation, formation of benzaldehyde as the sole carbonyl product was observed in 98% yield while cyclohexylsilyl ether was only deprotected giving 96 % of cyclohexanol (Scheme 2).

Conclusions

We presented an efficient, facile, and environmentally safe method for conversion of benzylic silyl ethers to their corresponding carbonyl compounds under solvent-free conditions. Rapid formation of the desired products, no over oxidation reaction, and selective oxidation of benzylic silyl ethers are the advantages of the present method.

REFERENCES

1. (a) Sartori G., Ballini R., Bigi F., Bosica G., Maggi R., Righi P.: Chem. Rev. *104*, 199 (2004);
   (b) Lalonde M., Chan T. H.: Synthesis 817 (1985);
   (c) Colvin E. W.: Chem. Soc. Rev. *7*, 15 (1978).
2. (a) Baker R., Rao V. B., Ravenscroft P. D., Swain C. J.: Synthesis 572 (1983);
   (b) Paquette L. A., Lin H. S., Junn B. P., Coghlan M. J.: J. Am. Chem. Soc. *110*, 5818 (1988).
3. Tolstikov G. A., Miftakhov M. S., Adler M. E., Komissarova N. G., Kuznetsov O. M., Vostrikov, N. S.: Synthesis 940 (1989).
4. (a) Pinnick H. W., Lajis N. H.: J. Org. Chem. *43*, 371 (1978);
   (b) Marco I. E., Mekhalfia A, Ollis W. D.: Synlett 345 (1990).
5. Piva O., Amougay A., Pete J. P.: Tetrahedron Lett. *32*, 3993 (1991).
6. Solladie G., Berl V.: Synlett 795 (1991).
7. Muzart J.: Synthesis 11 (1993).
8. (a) Karimi B., Rajabi J.: Org. Lett. *6*, 2841 (2004):
   (b) Tajbakhsh M., Heravi M. M., Habibzadeh S.: Phosphorus, Sulfur and Silicon *178*, 361 (2003).
   (c) Tajbakhsh M., Hosseinzadeh R., Niaki M. Y.: J. Chem. Res. 508 (2002);
   (d) Hajipour A. R., Mallakpour S. E., Mohammadpoor-Baltork I., Malakoutikhah M.: Tetrahedron *58*, 143 (2002).
9. (a) Hirano M., Yakabe S., Itoh S., Clark J. H., Morimotoa T.: Synthesis *1997*, 1161.
   (b) Hirano M., Yakabe S., Fukami M., Morimotoa T.: Synth. Commun. *27*, 2783 (1997).
10. (a) Lewkowski J.: ARKIVOC 17 (2001);
    (b) Cottier L., Descotes G., Lewkowski J., Skowroński R., Viollet E.: J. Heterocycl. Chem. *32*, 927 (1995);

(c) Nwaukwa S. O., Keehn P. M.: Tetrahedron Lett. *23*, 35 (1982);
(d) Nwaukwa S. O., Keehn P. M.: Tetrahedron Lett. *23*, 3131 (1982);
(e) Larionov O. V., Kozhushkov S. I., De Meijere A.: Synthesis 1916 (2003);
(f) McDonald C. E., Nice L. E., Shaw A. W., Nestor N. B.: Tetrahedron Lett. *34*, 2741 (1993);
(g) Zolfigol M. A., Mallakpour S., Khazaiae A., Vaghaie R. G., Torabi M.: Russ. J. Org. Chem. *40*, 914 (2004);
(h) Mojtahedi M. M., Saidi M. R., Bolourtchian M., Shirzi J. S.: Monatsh. Chem. *132*, 655 (2001);
(i) Inokuchi T., Matsumoto S., Nishiyama T., Torii S.: J. Org. Chem. *55*, 462 (1990).
11. (a) Heravi M. M., Oskooiee H. A., Yazdanpanah S., Mojtahedi M. M.: J. Chem. Res. 129 (2004);
    (b) Heravi M. M., Ajami D., Tabar-Heidar K., Mojtahedi M. M: J. Chem. Res. 620 (1998);
    (c) Abaee M. S., Mojtahedi M. M., Zahedi M. M., Bolourtchian M.: Synth. Commun. *36*, 199 (2006);
    (d) Mojtahedi M. M., Heravi M. M.: Indian J. Chem. B. *44*, 831 (2005);
    (e) Mojtahedi M. M., Ghasemi M. H., Abaee M. S., Bolourtchian M.: ARKIVOC 68 (2005).
12. (a) Mojtahedi M. M., Saidi M. R., Bolourtchian M., Heravi M. M.: Phosphorus, Sulfur and Silicon *177*, 289 (2002);
    (b) Mojtahedi M. M., Abbasi H., Abaee M. S.: Phosphorus, Sulfur and Silicon *181,* 1541 (2006);
    (c) Mojtahedi M. M., Abbasi H., Abaee M. S.: J. Mol. Catal. A: Chem. *250,* 6 (2006);
    (d) Mojtahedi M. M., Abaee M. S., Hamidi V., Zolfaghari A.: Ultrason. Sonochem. *14,* 596 (2007).
13. Aldrich Catalogue Handbook of Fine Chemicals, 2007.

P11   EFFICIENT IONIC LIQUID PROMOTED SYNTHESIS OF BENZOFURANS AT ROOM-TEMPERATURE

ALI SHARIFI, M. SAEED ABAEE, BAHRAM ZAMIRI and MOJTABA MIRZAEI

Chemistry & Chemical Engineering Research Center of Iran, P. O. Box 14335–186 Tehran, Iran,
sharifi@ccerci.ac.ir

Introduction

The overwhelming demand to design green and safe chemical procedures in the past three decades has dictated the use of safer and less toxic media with fewer hazards and more environmental compatibility[1]. In this context, ionic liquids have emerged as very powerful substitutes for regular molecular solvents from both economical and environmental points of view[2]. Less volatility, no chance of explosion, thermal stability, and ease of handling are among the reasons to consider ionic liquids as possible environmental benign alternates for conventional solvents. Easy separation of the products from ionic liquids is an additional advantage in many instances. Among various ionic liquids, those based on imidazolium moieties have shown great potential as eco-friendly catalytic systems for room temperature organic transformations[3].

Benzofuran derivatives constitute highly valuable heterocyclic motifs found in the structure of many natural[4] and synthetic products[5]. Derivatives of these compounds are known to possess important pharmaceutical[6], antifungal[7], antitumor[8], and other bioorganic properties[9]. In addition, benzofurans are used in cosmetic formulations[10] and have the application as synthetic precursors for optical brighteners[11]. Many multi-step synthetic approaches for the construction of the benzofuran ring exist in which the key-step includes dehydrative annulation of phenols bearing appropriate ortho vinyllic substituents[12], intramolecular cyclization of substituted allyl-aryl ethers[13], cyclization of o-formylphenoxyacetic acids or esters[14], or ring-closure of arylacetylenes[15]. Perhaps, the most straightforward method for one-pot preparation of benzofuran derivatives is the Rap-Stoermer condensation of salicylaldehyde with α-haloketones[16] providing the opportunity for the synthesis of a diverse array of benzofuran derivatives in a single step process. The reaction is traditionally carried out under basic conditions in refluxing alcoholic solvents giving low yields of products in many occasions[6–7]. In line with the context of green and sustainable chemistry, several reports are recently released to expand the synthetic applicability of Rap-Stoermer reaction by using microwave irradiation[17], solvent-free systems[18], polymer-supported reagents[19], and solid state synthesis[20]. However, these reactions are still conducted at high temperature[18–19], require the use of commercially unavailable starting materials[20], conducted in refluxing solvents[19] or need an external stimulant to proceed[17,20]. In continuation of our previous experiences on environmentally sustainable reactions[21], we would like to

herein report a novel procedure for efficient Rap-Stoermer condensation of α-haloketones with various salicylaldehyde derivatives performed at room temperature in the presence of 1-hexyl-3-methyl–1*H*-imidazolium hexafluorophosphate ([hmim]PF$_6$) (Scheme 1).

1a: R = H, X = H
1b: R = H, X = 3-OMe
1c: R = H, X = 4-NO$_2$
1d: R = H, X = 4-Br
1e: R = Me, X = H

2a: Y = H, Z = Cl
2b: Y = 4-Br, Z = Br
2c: Y = 4-OMe, Z = Br

3aa-3dc
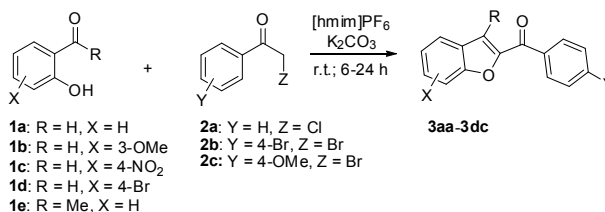
Scheme 1

Experimental

General

Reactions were monitored by TLC and GC. NMR spectra were obtained on a FT-NMR Bruker Ultra Shield™ (500 MHz) or Bruker AC 80 MHz as CDCl$_3$ solutions and the chemical shifts were expressed as δ units with Me$_4$Si as the internal standard. GC experiments were carried out using a Fisons 8000 apparatus. All chemicals and reagents were purchased from commercial sources.

Typical Procedure for [hmim]PF$_6$ Mediated Rap-Stoermer Condensations

An equimolar mixture of **1** (5 mmol), **2** (5.5 mmol), and K$_2$CO$_3$ (10 mmol) was added to 7 ml [hmim]PF$_6$ and the mixture was stirred at room temperature until TLC and GC experiments showed complete disappearance of the starting materials. The mixture was extracted with Et$_2$O (3 × 20 ml), the extracts were combined, and the volatile portion was removed under reduced pressure. The product was purified with short column chromatography over silicagel using hexane/EtOAc (7 : 1). The spectroscopic and physical properties of the products were obtained and compared with those available in the literature.

Selected Spectral Data
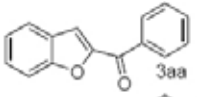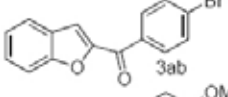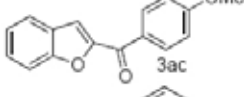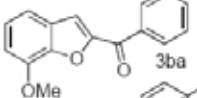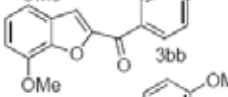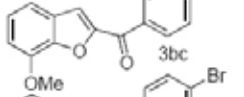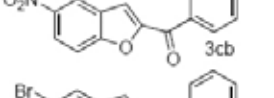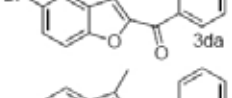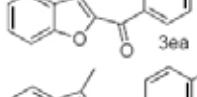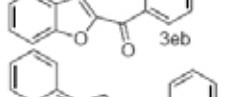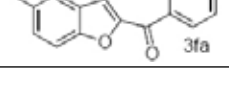
(4-Bromophenyl)(7-methoxybenzofuran-2-yl)methanone (**3bb**). Yellow crystals were obtained in 90% yield, mp 93–95 °C; IR (KBr, cm^{-1}) 1,639, 1,554, 1,280, 871; ^{1}H NMR (CDCl$_3$) δ 4.08 (s, 3H), 7.02 (d, 1H, *J* = 7.8 Hz), 7.30 (dd, 1H, *J* = 7.8, 7.8 Hz), 7.35 (d, 1H, *J* = 7.8 Hz), 7.61 (s, 1H), 7.74 (d, 2H, *J* = 8.41 Hz), 8.03 (d, 2H, *J* = 8.41 Hz); ^{13}C NMR (CDCl$_3$) δ 56.5, 110.1, 115.4, 116.7, 125.2, 128.5, 128.9, 131.6, 132.3, 136.1, 146.2, 146.5, 152.9, 183.1; MS (70 eV) m/z (%): 332, 330 (M$^+$), 251, 175, 76. Calcd. For C$_{16}$H$_{11}$BrO$_3$: C, 58.03; H, 3.35. Found: C, 58.01; H, 3.47.

(7-Methoxybenzofuran-2-yl)(4-methoxyphenyl) methanone (**3bc**). White crystals were obtained in 80% yield, mp 66–68 °C; IR (KBr, cm^{-1}) 1,664, 1,593, 1,315, 1,230, 1,160; ^{1}H NMR (CDCl$_3$) δ 3.93 (s, 3H), 4.07 (s, 3H), 6.98 (d, 1H, *J* = 7.7 Hz), 7.05 (d, 2H, *J* = 8.8 Hz), 7.26 (dd, 1H, *J* = 7.8, 7.9 Hz), 7.32 (d, 1H, *J* = 7.8), 7.56 (s, 1H), 8.19 (d, 2H,

$J = 8.8$ Hz); ^{13}C NMR (CDCl$_3$) δ 55.9, 56.5, 109.8, 114.3, 115.3, 115.8, 125.0, 129.1, 130.2, 132.5, 145.9, 146.5, 153.6, 164.0, 182.8; MS (70 eV) m/z (%): 282 (M$^+$), 252, 135. Calcd. For C$_{17}$H$_{14}$O$_4$: C, 72.33; H, 5.00. Found: C, 72.15; H, 5.12.

(4-Bromophenyl)(3-methylbenzofuran-2-yl)methanone (**3eb**). White crystals were obtained in 78% yield, mp 103–105 °C; IR (KBr, cm^{-1}) 1,643, 1,562, 1,296, 929; ^{1}H NMR (CDCl$_3$) δ 2.71 (s, 3H), 7.39 (d, 1H, $J = 6.8$, 7.8 Hz), 7.59–7.53 (m, 2H), 7.71 (d, 2H, $J = 8.5$ Hz), 7.75 (d, 1H, $J = 7.8$ Hz), 8.03 (d, 2H, $J = 8.47$ Hz),; ^{13}C NMR (CDCl$_3$) δ 10.5, 112.7, 122.0, 123.9, 128.0, 128.2, 128.9, 129.6, 131.8, 132.1, 136.9, 148.4, 154.7, 185.0; MS (70 eV) m/z (%): 315, 314 (M$^+$), 235, 207. Calcd. For C$_{16}$H$_{11}$BrO$_2$: C, 60.98; H, 3.52. Found: C, 60.59; H, 3.55.

Table I
Ionic liquid mediated Rap-Stoermer condensations

Entry	Substrate	Product	Time [h]	Yield [%]
1	**1a + 2a**	3aa	6	90
2	**1a + 2b**	3ab	24	93
3	**1a + 2c**	3ac	24	98
4	**1b + 2a**	3ba	24	98
5	**1b + 2b**	3bb	6	90
6	**1b + 2c**	3bc	24	80
7	**1c + 2b**	3cb	24	70
8	**1d + 2a**	3da	6	90
9	**1e + 2a**	3ea	24	90
10	**1e + 2b**	3eb	24	93
11	**2a + 2-hydroxy-1-napthaaldehyde**	3fa	24	90

^{a}Gc isolated yields

Results

The reaction between α-chloroacetophenone with salicylaldehyde was investigated under various sets of conditions to find the optimum conditions. A suspension of the two reactants and K$_2$CO$_3$ in the ionic liquid led to 90% formation of product **3aa** within 6 hours time period (Table I, entry 1). Conduction of the same reaction in the presence of some other ionic liquids ([bmim]PF$_6$, [hmim]BF$_4$) [bmim]PF$_6$, or bases (Et$_3$N, t-BuONa) led to formation of lower quantities of the product within the same time periods. The product was easily obtained in high purity by a simple diethyl ether. The optimized conditions were employed to investigate the Rap-Stoermer condensation of salicylaldehyde with other substrates bearing electron-withdrawing and electron-releasing groups. Therefore, reactions of **1a** with **2b** (entry 2) and with **2c** (entry 3) gave 93 and 98 % of **3ab** and **3ac**, respectively. The generality of the procedure was shown by subjecting derivatives of o-hydroxybenzaldehydes to undergo condensation with different α-haloacetophenones (entries 4–8). Furthermore, o-hydroxyacetophenone (entries 9–10) and 2-hydroxy–1-naphthaldehyde (entries 11) conveniently exhibited similar reactions. In all cases, reactions smoothly reached to completion within 6–24 hours time periods good to excellent yields of the desired products which were separable by simple ethereal extraction.

Conclusions

In summary, we have developed a novel and general procedure for room-temperature Rap-Stoermer condensation of α-haloacetophenone with various 2-hydroxyarylaldehydes mediated by [hmim]PF$_6$. Reactions complete in short time periods in the presence of no external stimulant and the procedure is applicable to both 2-hydroxyacetophenone and 2-hydroxyarylaldehydes. The versatility of the reaction, use of a recyclable media, production of pure single compounds, and easy procedure and work up are among other benefits of the present method.

REFERENCES
1. Lancaster M.: *Green Chemistry: An Introductory Text, Royal Society of Chemistry,* Cambridge, UK 2002.
2. (a) Shen Z. L., Ji S. J., Loh T. P.: Tetrahedron Lett. *46*, 3137 (2005);
   (b) Yadav J. S., Reddy B. V. S., Eshwaraiah B., Srinivas M., Vishnumurthy P.: New J. Chem. *27*, 462 (2003).
3. (a) Earle M. J., McCormac P. B., Seddon K. R.: Green Chem. *1*, 23 (1999);
   (b) Huddleston J. G., Willauer H. D., Swatloski R. P., Visser A. E., Rogers R. D.: Chem. Commun. 1765 (1998);
   (c) Wilkes J. S.: Green Chem. *4*, 73 (2002);
   (d) Bradaric C. J., Downard A., Kennedy C., Robertson A. J., Zhou Y.: Green Chem. *5*, 143 (2003);

(e) Sheldon R.: Chem. Commun. 2399 (2001);

(f) Mojtahedi M. M., Abaee M. S., Abbasi H.: J. Iran. Chem. Soc. *3*, 93 (2006).

4. (a) Simpson T. J.: *The Chemistry of Natural Products*, Blackie, London 1985;

(b) Dean F. M: *The Total Synthesis of Natural Products,* Wiley, New York 1973, vol. 1, p 513.

5. (a) Katritzky A. R., Ji Y., Fang Y., Prakash I.: J. Org. Chem. *66*, 5613 (2001);

(b) Park K. K., Seo H., Kim J.–G., Suh I.-H.: Tetrahedron Lett. *41*, 1393 (2000);

(c) Nicolaou K. C., Snyder S. A., Bigot A., Pfefferkon J. A.: Angew. Chem. Int. Ed. *39*, 1093 (2000);

(d) Park K. K., Han I. K., Park J. W.: J. Org. Chem. *66*, 6800 (2001);

(e) Shafiee A., Behnam E.: J. Heterocycl. Chem. *15*, 589 (1978).

6. Buu-Hoi N., Saint-Ruf G., Loc T. B., Xuong N. D.: J. Chem. Soc. 2593 (1957).

7. (a) Benkli K., Gundogdu-Karaburun N., Karaburun A. C., Ucucu U., Demirayak S., Kiraz N.: Arch. Pharm. Res. *26*, 202 (2003);

(b) Gundogdu-Karaburun N., Benkli K., Tunali Y., Ucucu U., Demirayak S.: Eur. J. Med. Chem. *41*, 651 (2006).

8. Baraldi P. G., Romagnoli R., Beria I., Cozzi P., Geroni C., Mongelli N., Bianchi N., Mischiati C., Gambari R.: J. Med. Chem. *43,* 2675 (2000).

9. (a) Li J., Rush T. S., Li W., De Vincentis D., Du X., Hu Y., Thomason J. R., Xiang J. S., Skotnicki J. S., Tam S., Cunningham K. M., Chockalingam P. S., Morris E. A., Levin J. I.: Bioorg. Med. Chem. Lett. *15*, 4961 (2005);

(b) Pestellini V., Giolitti A., Pasqui F., Abelli L., Cutrufo C., De Salvia G., Evangelista S., Meli A.: Eur. Med. Chem. *23*, 203 (1988).

10. Leung A. Y., Foster S.: *Encyclopedia of Common Natural Ingredients Used in Food, Drugs, and Cosmetics*, Wiley, New York 1996.

11. Elvers B., Hawkins S., Schulz G.: *Ulmann's Encyclopedia of Industrial Chemistry*, Optical Brighteners, 5th ed., Vol A18, VCH, Weinheim 1999, p153.

12. (a) Thielges S., Meddah E., Bisseret P., Eustache J.: Tetrahedron Lett. *45*, 907 (2004);

(b) Gil M. V., Roman E., Serrano J. A.: Tetrahedron Lett. *41*, 10201 (2000);

(c) Herndon J. W., Zhang Y., Wang H., Wang K.: Tetrahedron Lett. *41*, 8687 (2000);

(d) Arrault A., Touzeau F., Guillaument G., Merour J. Y.: Synthesis 1241 (1999).

13. (a) Hennings D. D., Iwasa S., Rawal V. H.: Tetrahedron Lett. *36*, 6379 (1997);

(b) Xie X., Chen B., Lu J., Han J., She X., Pan X.: Tetrahedron Lett. *45*, 6235 (2004);

(c) Youn S. W., Eom J. I.: Org. Lett. *7*, 3355 (2005).

14. (a) Bogdal D., Warzala M.: Tetrahedron *56*, 8769 (2000);

(b) Park K. K., Jeong J.: Tetrahedron *61*, 545 (2005);

(c) Bellur E., Freifeld I., Langer P.: Tetrahedron Lett. *46*, 2185 (2005);

(d) Bogdal D., Bednarz S., Lukasiewicz M.: Tetrahedron *62*, 9440 (2006);

(e) Kraus G. A., Zhang N., Verkade J. G., Nagarajan M., Kisanga P. B.: Org. Lett. *2*, 2409 (2000);

(f) Cruz M. C., Tamariz J.: Tetrahedron Lett. *45*, 2377 (2004).

15. (a) Dai W. M., Lai K. W.: Tetrahedron Lett. *43*, 9377 (2002);

(b) Bates C. G., Saejueng P., Murphy J. M., Venkataraman D.: Org. Lett. *4*, 4727 (2002).

16. (a) Rap E.: Gazz. Chim. Ital. *285*, 2511 (1895);

(b) Stoermer R.: Liebigs. Ann. Chem. *312*, 331 (1900).

17. Rao M. L. N., Awasthi D. K., Banerjee D.: Tetrahedron Lett. *48*, 431 (2007).

18. Yoshizawa K., Toyota S., Toda F., Csoregh I.: Green Chem. *5*, 353 (2003).

19. Habermann J., Ley S. V., Smits R.: J. Chem. Soc., Perkin Trans. 1 2421 (1999).

20. Varma R. S., Kumar D., Liesen P. J.: J. Chem. Soc., Perkin Trans. 1 4093 (1998).

21. (a) Sharifi A., Mirzaei M., Naimi-Jamal M.R.: J. Chem. Res. 628 (2002);

(b) Sharifi A., Mirzaei M., Saidi M. R.: Tetrahedron Lett. *40*, 1179 (1999);

(c) Sharifi A., Mirzaei M., Naimi-Jamal M. R.: Monatsh. Chem. *137*, 213 (2006);

(d) Sharifi A., Mirzaei M., Naimi-Jamal M. R., Synth. Commun. *35*, 1039 (2005);

(e) Sharifi A., Salimi R., Mirzaei M., Abaee M. S.: Synth. Commun. *37,* 1825 (2007).

P12　CRYSTAL ENGINEERING OF GLYCOLURIL DIMERS

VLADIMÍR ŠINDELÁŘ and MAREK ŠTANCL

Department of Chemistry, Masaryk University, Kotlářská 2, 611 37 Brno, Czech Republic,
sindelar@chemi.muni.cz

Introduction

Glycolurils are heterobicyclic compounds that have been used as building blocks of various supramolecular objects. Among others, glycoluril motif has been used in molecular clips[1] and macrocyclic cucurbiturils[2]. Fundamental building block of the latter compounds is methylene-bridged glycoluril dimer. In recent years Isaacs and coworkers prepared such dimers[3] to investigate mechanism of cucurbituril formation and synthesis of new cucurbituril analogues. Depending on the reaction conditions mixture of two diastereomers, S-shaped and C-shaped, was prepared. These dimers were synthesized from *N*-protected glycolurils and formaldehyde to avoid the formation of glycoluril oligomers. Substituted xylylene sidewall was used as a protecting group and was introduced to the molecule of glycoluril using alkylation. Unsubstituted glycoluril is little soluble in common solvents, therefore various groups are introduce to glycoluril in the positions 7 and 8 to increase its solubility.

We decided to expand chemistry of glycoluril by the preparation of glycoluril dimers bearing hydrogen atoms in positions 7, 8 of the glycoluril unit with different terminal units. The reason is to get more information about cucurbituril synthesis and tune the organization of the dimer molecules in the solid state by the modification of its structure.

Experimental

Synthesis of Protected Glycolurils

For the synthesis of the dimers precursors the condensation reaction between glyoxal and substituted urea was chosen at first [4]. Unfortunately, this method gives poor yields of required 1,6-substituted glycoluril and also the isolation of the product is not easy. This method was used for the synthesis of 1,6-dimethylglycoluril **1c** following published procedure[5].

1a　　　　　　**1b**　　　　　**1c**　　1a-c R = CH₃

2a, 3a　　　　　　**2b, 3b**　　2a, 2b R = *o*-C₆H₄
　　　　　　　　　　　　　　　　3a, 3b R = CH₂
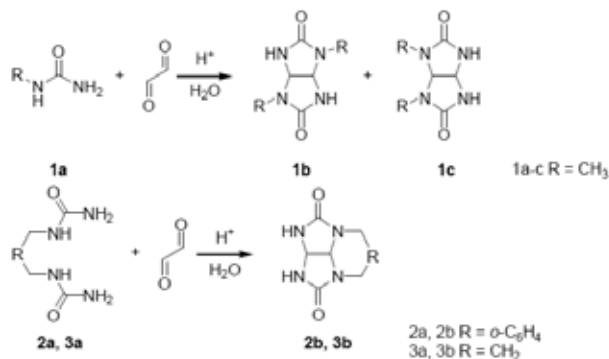
Scheme 1
Synthesis of 1,6-substituted glycolurils

Separation from 1,4-dimethylglycoluril required extensive fraction crystallization. We found, that pure product could be obtained after crystallization from 8% H_3PO_4. Despite of this improvement, the yield is 9 %.

We envisioned that the preparation of required dimer precursors could be achieved by acid catalyzed cyclocondensation reaction between bisurea and glyoxal. We selected aromatic and aliphatic bisureas **2a**, **3a** and found, that acid catalyzed reaction with glyoxal in water gives 1,6-substituted glycoluril. The product could be easily separated from the reaction mixture by filtration. Yields are modest for aliphatic derivative **3b** (47 %) and good for aromatic **2b** (75 %).

Synthesis of Glycoluril Dimers

Protected glycolurils **1c**, **2b** and **3b** were used in acid catalyzed reaction with one equivalent of formaldehyde. Reactions were carried out in concentrated HCl at 80 °C to obtain thermodynamic more stable C-shaped dimer.

2b, 3b　　　(CH₂O)n / HCl　　　**2c, 3c**　　2b, 2c R = *o*-C₆H₄
　　　　　　　　　　　　　　　　　　　　　　3b, 3c R = CH₂

1c　　　(CH₂O)n / HCl　　　**1d**　　1c, 1d R = CH₃
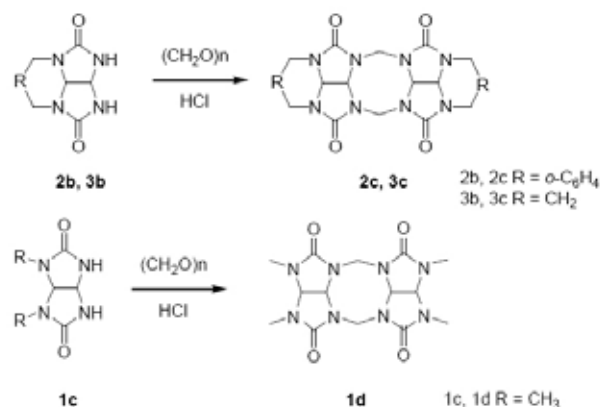
Scheme 2
Synthesis of glycoluril dimers

Glycoluril dimers **1d**, **2c**, **3c** were obtained in good yields 90, 94, 81 % respectively. We were able to obtain X-ray crystal structures of these dimers.

Results

Glycoluril dimer **2c** bearing two xylylene sidewalls is organized into dimeric aggregates; the driving force of the dimerization is the van der Waals interactions together with face-to-face π-π stacking interaction of the xylylene rings. Dimer self-assembly was also observed in the crystal structure of **3c**. In this case, the dimerization can be assigned to the van der Waals interactions only. In the crystal structure of **1d** no dimerization was observed. Instead, there is a unique three-dimensional network of molecules. Each molecule is surrounded by two molecules with the same orientation and four molecules which are rotated by 90 ° relative to the central molecule. The stacking of these motifs along the crystallographic *c*-axis results in columns in which the bowl-shaped molecules are packed on top of each other (Fig. 1).
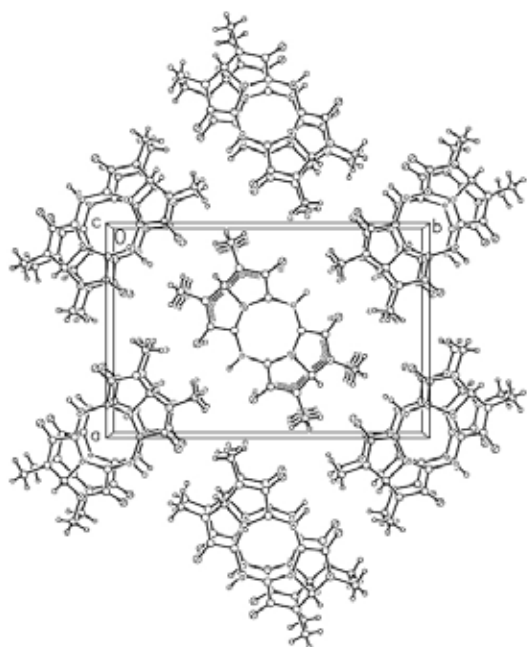
Fig. 1. **Crystal structure of methylene-bridged glycoluril dimer 1d**

Conclusion

We have prepared methylene-bridged glycoluril dimers bearing two hydrogen atoms on the convex face of the glycoluril unit. A new method for the synthesis of 1,6-substituted glycolurils was developed. In the solid state, **3c** and **2c** form dimeric aggregates whereas **1d** is organized into three-dimensional structure.

REFERENCES
1. Rowan A. E., Elemans J. A. A. W., Nolte R. J. M.: Acc. Chem. Res. *1999*, 995.
2. Lagona J., Mukhopadhyay P., Chakrabarti S., Isaacs L.,: Angew. Chem. Int. Ed. *44*, 4844 (2005).
3. Wu A., Chakraborty A., Witt D., Lagona J., Damkaci F., Ofori M., Chiles K., Fettinger J. C., Isaacs L.: J. Org Chem. *67*, 5817 (2002).
4. Krafchenko A. N., Sigachev A. S., Maksareva E. Yu., Gazieva G. A., Trunova N. S., Lozhkin B. V., Pivina T. S., Il´in M. M., Lyssenko K. A., Nelyubina Yu. V., Davankov V. A., Lebedev O. V., Makhova N. N., Tartakovsky V. A.: Russ. Chem. Bull., Int. Ed. *54*, 691 (2005).
5. Nematollahi J., Ketcham R.: J. Org. Chem. *28*, 2378 (1963).

6. PHOTOCHEMISTRY

6.1. Lectures

L01 EPR AND UV/VIS STUDY ON PHOTOCATALYTIC ACTIVITY OF TITANIUM DIOXIDE POWDERS

VLASTA BREZOVÁ, ZUZANA VRECKOVÁ and DANA DVORANOVÁ

Institute of Physical Chemistry and Chemical Physics, Faculty of Chemical and Food Technology, Slovak University of Technology in Bratislava, Radlinského 9, 812 37 Bratislava, Slovak Republic,
vlasta.brezova@stuba.sk

Introduction

The detoxification of polluted water by semiconductor photocatalysis based on the photoexcitation of titanium dioxide is nowadays accepted as promising technique also for industrial applications.[1–3] The degradation of a variety of toxic organic contaminants is initiated by non-selective attack of hydroxyl radicals generated upon ultra-band gap irradiation of TiO_2.

Our investigations are oriented on monitoring the photogenerated paramagnetic intermediates in titanium dioxide suspensions by Electron Paramagnetic Resonance (EPR) spectroscopy. The quantum efficiency of UVA-induced photocatalytic processes was evaluated.

Experimental

Titanium dioxide Aeroxide® P25 kindly provided by Degussa Company (Evonik Degussa, Germany) was used in all experiments. The formation of free radical species upon irradiation of TiO_2 suspensions in aerated aqueous media was monitored using spin trapping agents 5,5-dimethyl-1-pyrroline N-oxide (DMPO; Aldrich) and 5-(diisopropoxy-phosphoryl)-5-methyl-1-pyrroline N-oxide (DIPPMPO; Alexis® Biochemicals). Semi-stable free radicals 4-hydroxy-2,2,6,6-tetramethylpiperidine N-oxyl (Tempol), cation radical of 2,2'-azino-bis(3-ethylbenzothiazoline-6-sulfonate) (ABTS•+) and 1,1-diphenyl-2-picrylhydrazyl (DPPH) were also used to monitor TiO_2 photocatalytic activity by a continuous decrease of radical concentrations upon irradiation.

U V / V I S S p e c t r a o f T i t a n i u m
D i o x i d e S u s p e n s i o n s

UV/VIS spectra of TiO_2 aqueous suspensions in the wavelength interval 240–600 nm were recorded using a UV/VIS spectrometer UV-3600 (Shimadzu, Japan) with a large integrating sphere assembly using transmittance measurement accessory. TiO_2 suspensions with low concentrations (0.01–0.1 mg TiO_2 ml^{-1}, i.e., 1×10^{-5}–1×10^{-4} g cm^{-3}) were used in UV/VIS experiments. Titania suspensions prepared instantly before recording UV/VIS spectra were sonicated

1 minute (Ultrasonic Compact Cleaner TESON 1, Tesla, Slovak Republic), and then UV/VIS spectra were measured in duplicate. The suspensions were not stirred during spectrophotometrical measurements. The values of absorption and scattering coefficients at the individual wavelengths ($\Delta l = 5$ nm) were evaluated from the experimental data by a least-squares minimization procedure (Scientist®, MicroMath) using Kubelka-Munk model of diffuse reflectance and transmission in accordance with refs.[4,5].

E P R P h o t o c h e m i c a l E x p e r i m e n t s

The suspensions of TiO_2 containing spin trapping agents (DMPO and DIPPMPO) or semi-stable radicals (Tempol, ABTS•+ and DPPH) were prepared instantly before EPR measurements. The stock TiO_2 suspension (1 mg ml^{-1}) was homogenized in ultrasonic bath for 1 minute before dilution to final concentration of 0.5 mg TiO_2 ml^{-1}. Then the suspensions were carefully mixed by slight air stream and immediately transferred to a small quartz flat cell (WG 808-Q, Wilmad-LabGlass, USA; optical cell length 0.045 cm) optimized for the TE_{102} (ER 4102 ST) rectangular EPR cavity (Bruker, Germany). The samples were irradiated at 295 K directly in the EPR resonator, and EPR spectra were recorded *in situ* using EMX X-band EPR spectrometer (Bruker). As an irradiation source HPA 400/30S lamp (400 W, Philips; UVA irradiance of 5 mW cm^{-2}) was used. A Pyrex glass filter (thickness of 1 mm) was applied to eliminate radiation wavelengths below 300 nm. The first spectrum in the time-course of EPR spectra was measured without radiation, and subsequently we started the exposure, monitoring ten spectra upon continuous irradiation.

Results

U V / V I S S p e c t r a o f T i t a n i u m
D i o x i d e S u s p e n s i o n s

The spectrophotometrically monitored extinction in heterogeneous titanium dioxide aqueous suspensions represents combination of absorption and scattering phenomena caused by particles. Fig. 1 shows the experimental extinc-
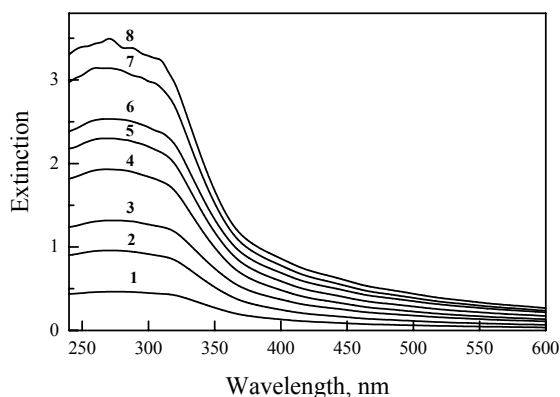
Fig. 1. **The set of UV/VIS spectra measured in aqueous suspensions of Aeroxide® P25 with increasing concentration. The numbers specify TiO2 concentration in 10⁻⁵ g cm⁻³**

tion spectra of Aeroxide® P25 in aqueous suspensions with increased concentrations measured in wavelength interval 240–600 nm.
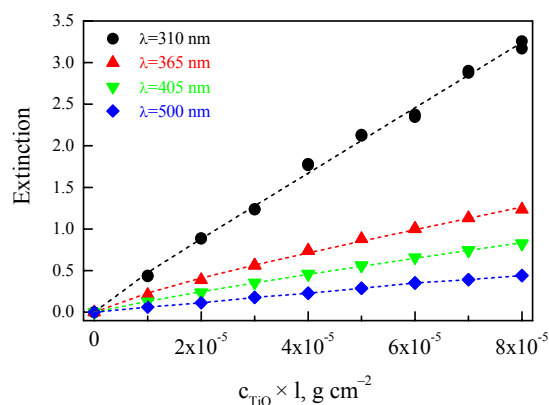
Fig. 2. **The dependence of extinction at selected wavelengths upon product of TiO$_2$ concentration and cell length obtained for Aeroxide® P25 aqueous suspensions. The symbols represent experimental data and dotted lines were evaluated by least-squares minimization procedure using Kubelka-Munk absorption and scattering model**
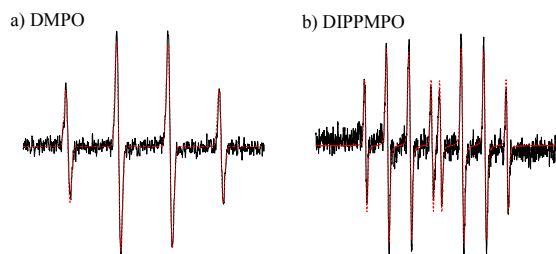
Fig. 3. **Experimental (–) and simulated (--) EPR spectra obtained in aerated irradiated Aeroxide® P25 suspensions in the presence of spin trapping agents DMPO and DIPPMPO. Magnetic field sweep: a) 7 mT; b) 15 mT**

The structure of Aeroxide® P25 sample comprises a mixture of crystalline polymorphs with 80 % anatase and 20 % rutile[3]. The energy band gap value of anatase (E$_{bg}$ = 3.2 eV), and rutile (E$_{bg}$ = 3.02 eV) correspond to absorption threshold at 384 and 410 nm, respectively. Consequently, extinction observed in the visible region, originates exclusively from the scattering on titania nanoparticles. It should be noted here that the extinction data observed for wavelengths l>410 nm are in good accordance with Rayleigh scattering (extinction = $k \times l^{-4}$). The extinction spectra of Aeroxide® P25 measured at various loadings were used for numerical evaluation of absorption and scattering coefficients at individual wavelength in accordance with Kubelka-Munk model of diffuse reflectance and transmission[4,5]. Our experiments confirmed a significant contribution of scattering phenomena in the region 240–400 nm, in accordance with previously published results.[6] The values of absorption and scattering

coefficients calculated from the extinction data were used for the construction of UV/VIS absorption and scattering spectra of Aeroxide® P25 in the wavelength interval 240–600 nm.

The sets of experimental results obtained at 310, 365, 405 and 500 nm, along with corresponding fittings to Kubelka-Munk model illustrates Fig. 2. The calculated absorption spectra of Aeroxide® P25 was used to find amount of absorbed UV radiation (300–400 nm) under the given experimental conditions (incident radiation flux in EPR cavity 6.6 × 10^{-8} Einstein s^{-1}; absorbed radiation flux 6.5 × 10^{-9} Einstein s^{-1}). Finally the quantum efficiency of photoinduced radical processes monitored by *in situ* EPR spectroscopy was evaluated[7].

Photochemical *In Situ* EPR Experiments

The photoinduced formation of reactive oxygen-centered free radicals in the aerated aqueous suspensions of Aeroxide® P25 was investigated using EPR spin trapping technique, a method for indirect detection of short-living radicals. Upon UV irradiation of aerated TiO$_2$ suspensions in the presence of DMPO, typical four-line EPR spectra were monitored, which are characterized with spin Hamiltonian parameters $a_N = a_H^\beta = 1.49$ mT and $g = 2.0058$, and are representative of the hydroxyl radical added to DMPO ($^\bullet$DMPO−OH; Fig. 3.a). The formation of hydroxyl radical adducts was evidenced also using DIPPMPO, as during photoexcitation of P25 in aqueous media dominates EPR spectrum with $a_N = 1.407$ mT, $a_H^\beta = 1.320$ mT, $a_P = 4.665$; $g = 2.0058$, characteristic of hydroxyl radical adduct ($^\bullet$DIPPMPO−OH; Fig. 3.b).

The paramagnetic signals of $^\bullet$DMPO−OH may be produced directly by the addition of photoproduced hydroxyl radicals. However, we cannot exclude an alternative mechanism assuming spin trap oxidation by photogenerated holes to cation-radical DMPO$^{\bullet+}$, which hydrolyses in the aqueous media to $^\bullet$DMPO−OH without direct hydroxyl radical formation[8]. The formal initial rate of photoinitiated $^\bullet$DMPO−OH formation was evaluated from double integrated EPR spectra monitored upon continuous UV exposure. The data obtained were used for the calculation of quantum efficiency of $^\bullet$DMPO−OH formation ($\eta_{^\bullet DMPO−OH} = (7.6 \pm 0.8) \times 10^{-4}$).

The photoinduced elimination of semi-stable free radicals (Tempol, DPPH, ABTS$^{\bullet+}$) in titanium dioxide suspensions represents an alternative technique of photoactivity testing[8].

The principle of the detection of reactive free radical formation using Tempol is based on monitoring the decrease in EPR intensity resulting from the interaction of its >N−O$^\bullet$ group with the photogenerated reactive radical species, as well as singlet oxygen[9]. The EPR spectrum of Tempol under the given experimental conditions presents a three-line signal characterized by hyperfine splitting $a_N = 1.70$ mT and $g = 2.0060$. The decrease of Tempol concentration monitored upon irradiation in aerated aqueous suspension of Aeroxide® P25 was described by the formal first-order kinetic model (Fig. 4.), and the evaluated initial rate was used in the calcu-
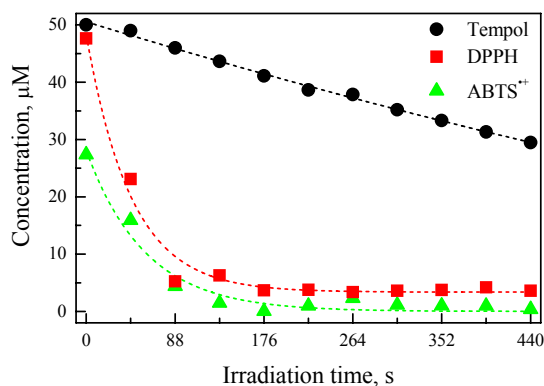
Fig. 4. **Changes in concentration of semi-stable radicals monitored upon irradiation of Tempol, DPPH and ABTS$^{•+}$ in Aeroxide® P25 suspensions. The symbols represent experi¬mental data and dotted lines were evaluated by least-squares minimization procedure using first-order kinetic model**

lation of photocatalytic process quantum efficiency (η_{Tempol} = 0.0013 ± 0.0001).

The photocatalytic experiments with DPPH were due to its lower water solubility performed in mixed water/ethanol (1 : 1; v/v.) solvent. We observed limited photochemical stability of DPPH upon irradiation also in TiO$_2$-free solutions, but the addition of Aeroxide® P25 considerably increased the rate of DPPH termination (Fig. 4.). It should be noted here that the mechanism of DPPH photocatalytic decomposition may be very complex, as DPPH molecules are capable of reacting with photogenerated electrons and hydroxyl radicals simultaneously. Probably, also from ethanol photogenerated hydroxyethyl radicals may react with DPPH producing diamagnetic products, and, consequently, the evaluated value of quantum efficiency reached the highest value (η_{DPPH} = 0.022 ± 0.002).

The EPR spectrum of ABTS$^{•+}$ is characterized by a complex hyperfine structure, but the higher value of the modulation amplitude used in the EPR spectrometer settings facilitates monitoring it as a single-line signal (g = 2.0036). The irradiation of ABTS$^{•+}$ in aqueous suspensions of Aeroxide® P25 caused efficient elimination of paramagnetic signal (Fig. 4). Our previous UV/VIS investigations of photoinduced ABTS$^{•+}$ reaction in TiO$_2$ suspensions confirmed the decrease of ABTS$^{•+}$ selective absorption bands at 735 and 415 nm, coupled with the simultaneous growth of ABTS

absorption at 340 nm. These data are in good correlation with photocatalytic reduction of cation-radical ABTS$^{•+}$ to ABTS.[8] The initial rate of ABTS$^{•+}$ reduction evaluated from EPR spectra monitored upon irradiation in P25 aqueous suspensions served as a basis for computation of quantum efficiency ($\eta_{ABTS^{•+}}$ = 0.011 ± 0.001).

Conclusions

Kubelka-Munk analysis of UV/VIS spectra measured in aqueous TiO$_2$ suspensions confirmed significant contribution of Aeroxide® P25 scattering in ultra-band gap wavelength interval 240–400 nm; the extinction data observed for wavelengths l > 410 nm are in good accordance with Rayleigh scattering on nanoparticles. EPR spin trapping technique and semi-stable radical eliminations were used to monitor photoinduced generation of reactive radical intermediates in Aeroxide® P25 suspensions, and the differences in evaluated quantum efficiencies reflected the variation of photocatalytic reaction mechanisms.

REFERENCES

1. Lee S., K., Mills A.: J. Industrial Eng. Chem. *10*, 173 (2004).
2. Herrmann J.-M.: Topics Catal. *34*, 49 (2005).
3. Carp O., Huisman C. L., Reller A.: Prog. Solid State Chem. *32*, 33 (2004).
4. Vione D., Minero C., Maurino V., Carlotti M. E., Picatonotto T., Pelizzeti E.: Appl. Catal. B: Environ. *58*, 79 (2005).
5. McNeil L. E., French R. H.: Acta Mater. *48*, 4571 (2000).
6. Cabrera M. I., Alfano O. M., Cassano A. E.: J. Phys. Chem. *100*, 200 (1996).
7. Parmon V., Emeline A. V., Serpone N.: Int. J. Photoenergy *4*, 91 (2002).
8. Brezová V., Dvoranová D., Staško A.: Res. Chem. Intermed. *33*, 251 (2007).
9. Brezová V., Gabčová S., Dvoranová D., Staško A.: J. Photochem. Photobiol. B: Biol. *79*, 121 (2005).

L02　PHOTOCATALYTIC DEGRADATION OF FORMIC ACID ON TiO₂ THIN LAYERS

JANA CHOMOUCKÁ[a], PETR DZIK[a], MICHAL VESELÝ[a], JANA DRBOHLAVOVÁ[a], ERIC PUZENAT[b] and CHANTAL GUILLARD[b]

[a]*Brno University of Technology, Faculty of chemistry, Institute of Physical and Applied Chemistry, Purkyňova 118, 612 00 Brno, Czech Republic,*
[b]*IRCELYON UMR CNRS 5634, Université de Lyon, 2 av. Albert Einstein, Villeurbanne cedex, 69626, France,* chomoucka@fch.vutbr.cz

Introduction

Environmental pollution is becoming more and more serious. Catalysis under UV irradiation, called photocatalysis, is attracting a great deal of attention from environmental purification point of view[1]. Titanium dioxide (TiO_2) photocatalysis has been focused on the elimination of toxic and hazardous organic substances and metals in wastewater, drinking water and air, which is important for the protection of the environment[2]. Heterogenous photocatalysis is a process based on the excitation of a semiconductor by light of energy equal to or higher than the bynd gap one. This excitation generates electron-hole pairs which can give rise to redox reactions with species adsorbed on the catalyst surface[3]. Among the warious semiconductors, TiO_2 is the most suitable photocatalyst because of its high activity, photostability and availability. Anyway, serious practical problems arise from the use of TiO_2 powders in the photocatalytic process – the need for post treatment separation in a slurry system. A key technology for the practical application of photocatalysis to environmental problems is the immobilization of TiO_2 as thin film on a solid substrate (even if normally the film-type photocatalysts have low surface areas and their intrinsic photocatalytic activity is usually smaller than of the powders).

TiO_2 films have been often prepared by expensive methods as pulsed laser deposition, reactive evaporation and chemical vapour deposition. Low cost preparation methods are the sol-gel process including dip-coating, spin-coating and micropiezo jet as the final step of preparation. Sol-gel method usually requires a thermal post-treatment in order to eliminate organics present in the films or to induce crystallization of the deposited material. An important requirement for improving the TiO_2 photocatalytic activity is to increase its specific surface area, which is certainly dependent on the crystal size. It is known that the smaller the catalyst is, the larger will be its specific surface area. Nevertheless, if the particles are very small, the charge carrier recombination is more probable. Thus the particle size must be optimized.

Formic acid (FA) was choosen because of simple mechanism of degradation: it undergoes a direct mineralisation to CO_2 and H_2O without the formation of any stable intermediate species[4]. Moreover, it also represents a possible final step in the photodegradation of more complex organic compounds.

Experimental

Preparation of TiO₂ Thin Films

Borosilicate glass plates ($30 \times 30 \times 2$ mm, Verre Equipements, France) were chosen as a substrate for immobilization of TiO_2 thin films. TiO_2 layers were prepared using following organometallic precursor in sol-gel process: a mixture of absolute ethanol (85 ml) and acetylacetone (3.8 ml) was added to titanium(IV) propoxide (10.3 ml) under continuous stirring, a small amount of water (0.69 ml) in ethanol was dropped at last to the previously mixed solution.

Depositions of thin films were realized by dip-coating method (withdrawal speed 120 mm min⁻¹) and by micropiezo jet. In the case of micropiezo jet one cartridge of desktop printer (EPSON R220) was filled with sol. The substrate was fixed into the holder for CD and it was printed by sol. It was possible to choose the area covered of substrate by sol or the quality of printing. The amount of printed precursor (i.e layer thickness) was determined by the gray level (dot area) of printed images. We used 2 printing speeds: slow at 720 DPI and rapid one at 360 DPI. These values are given by the printer driver setup. In the next stage, the coated substrates were dried for 30 min. at 110 °C and then calcinated for 4 hours at 450 °C with temperature ramp of 3 °C min⁻¹ which allowed us to obtain TiO_2 predominantly in anatase form.
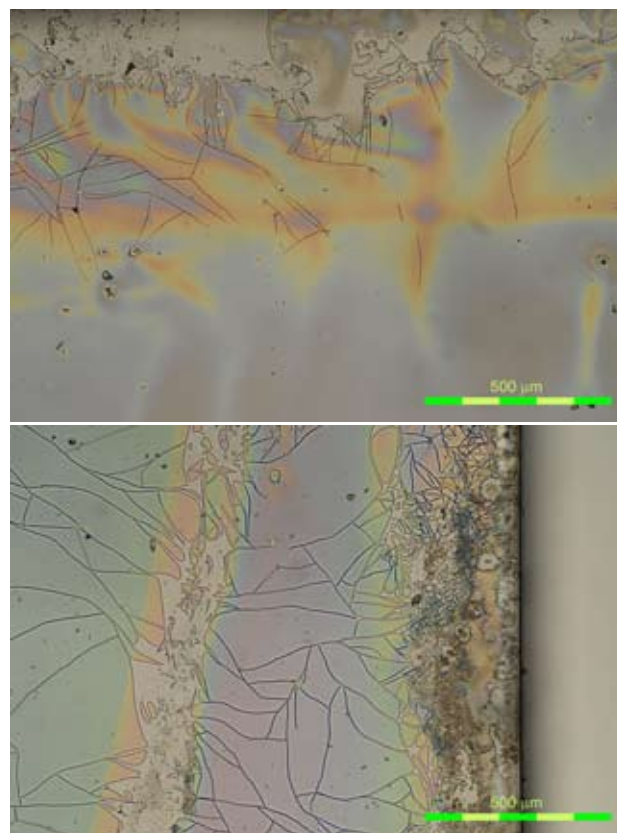
Fig. 1.　Picture from optical microscope, TiO₂ thin films prepared by dip coating method. 2 layers at the edge (upper) and 4 layers at the edge (down)

Formic Acid Photocatalytic Degradation

The formic acid reaction solution was prepared with initial concentration of 20, 50, 100, 200 and 400 mg dm^{-3}. The degradation process took place at ambient temperature in a Pyrex reactor (100 ml) with 30 ml of reaction solution under constant stirring. Before the reaction, the FA solution in the reactor was stirred during 30 min in obscurity to reach the solution adsorption equilibrium in contact with TiO$_2$ surface. During the FA photocatalytic oxidation with concentration ranging from 20 to 400 mg dm^{-3}, 0.5 ml of reaction solution was sampled every one hour for HPLC analysis. The total reaction time was 7 h. The UV irradiation was provided by high pressure mercury lamp (Philips HPK–125 W).

In order to determine the kinetic behavior of formic acid degradation on TiO$_2$ films, the initial reaction rate was estimated up to 120 min of irradiation time. The obtained values of reaction rate for various FA initial concentrations were treated using Langmuir-Hinshelwood (L-H) model.

$$v = k \cdot \theta = \frac{k \cdot K \cdot c}{1 + K \cdot c}, \text{ (per gram of photocatalyst)} \quad (1)$$

where k is the rate constant, θ is coverage degrese of surface active sites, K is adsorption constant and *c* is the initial concentration of reagents in the solution[5].
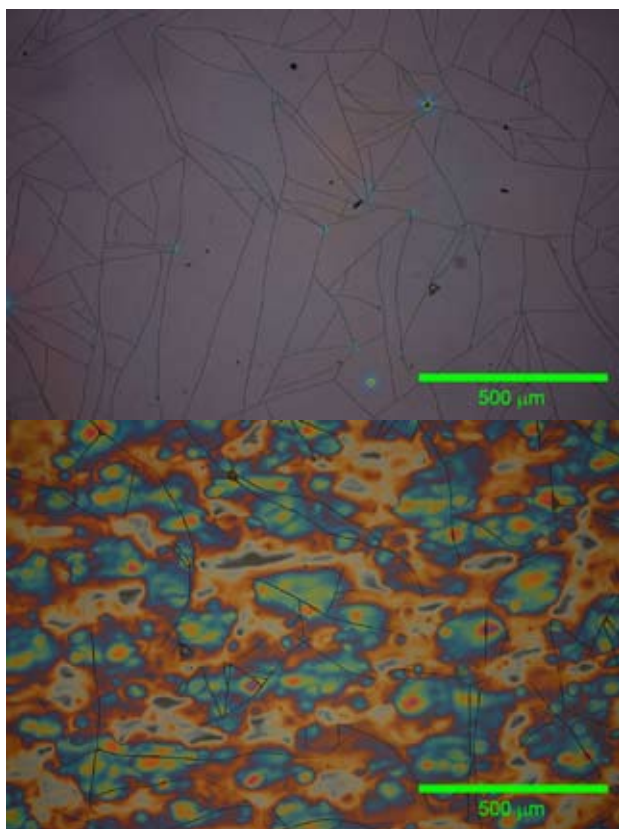
Fig. 2.   **Picture from optical microscope, TiO$_2$ thin films prepared micropiezo jet by rapid (upper) and slow (down) mode**

Results

Characterization of TiO$_2$ Thin Films Prepared by Optical Microscope

The TiO$_2$ thin films deposited on the borosilicate glass plates were optically transparent and they adhered well to the glass substrate after the calcination process. In the case of TiO$_2$ layers prepared by dip-coating method, the layers are homogenous and without cracks in the middle of a coated surface, whereas the homogeneity gets worse towards the edge of glass. The TiO$_2$ film quality slightly decreased with increasing layer number, in the case of 4 layers some cracks is appeared in the film structure (Fig. 1.).

The second method for preparation TiO$_2$ thin films was the newly adopted picropiezo jet. Surface morfology of prepared thin film greatly depends on the print setting. The TiO$_2$ prepared by micropiezo jet by rapid mode have smooth and flat surface, cracks are observed when sol loading exceeded 90% dot area. On the other hand, the layers prepared by slow mode are uneven and discontinuous (Fig. 2.).

Degradation of Formic Acid in Aqueous Phase

At first we will discused TiO$_2$ thin films prepared by dip-coating method. The reaction rate constants k depend strongly on TiO$_2$ layer number (i.e. layer thickness) whereas the adsorption constants decrease. The same behaviour we observed for two values of irradiance (7.7 and 4.6 mW cm^{-2}). The thicker TiO$_2$ film effectively absorbs the radiation, the holes can better oxidize FA (Fig. 3.).
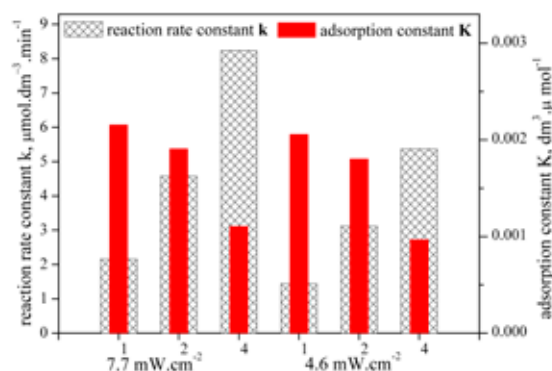
Fig. 3.   **Comparison of Langmuir-Hinshelwood parameters for different intensity of irradiance**

We observed the same characteristics in the case of thin films prepared by micropiezo jet (Fig. 4.). The photocatalytic activity grows with the value of dot area. It is caused by the growing amount of deposited TiO$_2$ and the thickness of TiO$_2$ thin film. Roughness of surface has a positive influence on the adsorption of FA on the surface of TiO$_2$. We observed decrease of adsorption constant for 60 % slow mode. It could be induced by too low coverage of substrate by TiO$_2$.
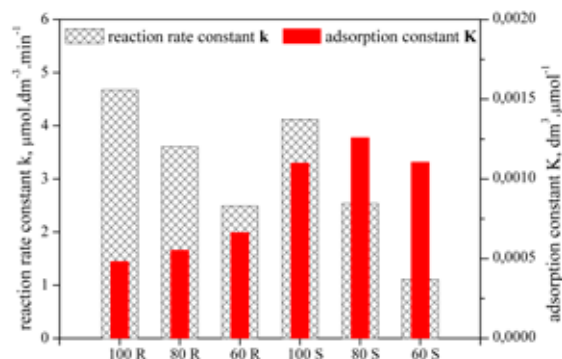
Fig. 4. **Comparison of Langmuir-Hinshelwood parameters for TiO$_2$ thin films prepared by picropiezo jet**

From the L-H model (1) we calculated the coverage of surface active sites θ by FA for different FA initial concentration (Table I and Table II). We can see that the pollutant adsorption on TiO$_2$ surface increased with increasing FA concentration. We observed a decrease in FA adsorption with increasing number of TiO$_2$ layers or sol loading. It almost achieved the value of 1 for FA initial concentration of 8.7 mmol dm^{-3}. That is nearly all active sites on TiO$_2$ surface were covered by FA molecules, which correlates well with obtained L-H kinetic behavior.

Table I
The coverage degree for different FA initial concentration, different iirradiance and for (1–4) TiO$_2$ layers

c FA [mmol dm^{-3}]	7.7 mW cm^{-2}			4.6 mW cm^{-2}		
	1	2	4	1	2	4
8.7	0.95	0.94	0.91	0.95	0.93	0.88
4.3	0.90	0.89	0.83	0.90	0.86	0.79
2.1	0.82	0.81	0.71	0.82	0.76	0.65
1.1	0.70	0.67	0.55	0.69	0.61	0.48
0.4	0.48	0.45	0.32	0.47	0.39	0.27

Table II
The coverage degree for different FA initial concentration and for TiO$_2$ thin films prepared by micropiezo jet

c FA [mmol dm^{-3}]	Rapid			Slow		
	100%	80%	60%	100%	80%	60%
8.7	0.81	0.83	0.85	0.91	0.92	0.92
4.3	0.68	0.71	0.74	0.83	0.85	0.85
2.1	0.51	0.55	0.59	0.71	0.73	0.74
1.1	0.34	0.38	0.42	0.55	0.58	0.59
0.4	0.17	0.19	0.22	0.32	0.35	0.37

Conclusions

We prepared TiO$_2$ thin layers on borosilicate glass plates by dip coating method a newly by micropiezo jet. TiO$_2$ thin films prepared by dip-coating method are homogenous and transparent as well as films prepared by micropiezo jet by rapid mode. In the case of TiO$_2$ thin films prepared by slow mode, the layers are uneven and discontinuous, partial coverage of substrate with and without TiO$_2$ is observed.

The photocatalytic efficiency of prepared coatings was evaluated by the photooxidation of FA. The kinetic parameters of FA disappearance, reaction rate constant and adsorption constant, corresponded to Langmuir-Hinshelwood behavior. It was found that the photocatalytic activity grows with the value of dot area or number of layers (i.e. thickness of film).

REFERENCES

1. Kaneko M.. Okura. I.: *Photocatalysis. Science and Technology*. Kodansha-Springer. Tokyo – New York 2002.
2. Yu J. C.. Yu J.. Zhao J.: Applied Catalysis B: Environ. *36*. 31 (2002).
3. Addamo M.. et al.: Thin Solid Films *516*. 3802 (2008).
4. Mrowetz M.. Selli E.: J. Photochem. Photobiol. A: Chem. *180*, 15 (2006).
5. Carp O.. Huisman C.L.. Reller A.: Prog. Solid State Chem. *32*, 33 (2004).

L03 KINETIC OF DEGRADATION OF HISTORICAL DOCUMENTS CONTAINING IRON-GALL INKS

MICHAL ČEPPAN, VIERA JANČOVIČOVÁ, MILENA REHÁKOVÁ and ANDREJ BUZINKAY

Faculty of Chemical and Food Technology, Slovak University of Technology, Radlinského 9, 812 37 Bratislava,
michal.ceppan@stuba.sk

Introduction

Deterioration of paper documents containing iron-gall inks is supposed to be a combination of two degradation pathways – acid hydrolysis of cellulose and oxidative degradation of cellulose. Iron gall inks contain transition metals, such as iron and copper, catalyzing the radical oxidation of the substrate, as well as acids, catalyzing its hydrolysis[1,2]. Transition metals are capable to enter Fenton and Fenton-like type of reactions[3,4] and catalyze homolytic decomposition of peroxides with production of hydroxyl radicals. Hydroxyl radicals can oxidize cellulose and induce degradation of cellulose[5].

Content and ratio of transition metals in historical iron-gall inks recipes vary. In addition to iron the most notable transition metal is cooper and the molar ration of the iron cooper to iron in these recipes get the value up to 0.7(ref.[6]). It was found that even trace amounts of cooper induce significant destruction of paper substrate[7]. The catalytic action of cooper in Fenton and Fenton-like reactions predominate over the catalytic action of iron[6,8] and the catalytic action of iron and cooper is additive[6].

The influence of transitional metals in iron-gall inks on the rate of degradation and change of optical properties of aged model documents were studied in this paper.

Experimental

Model ink systems were prepared according to the suggestion of Neevel[2]. The molar ratio of transition metal:tannine (5.5:1) and the amount of gum arabic (4.71 g 150 ml^{-1}) were kept constant. Seven model inks with the ratio of copper:iron 0 (without cooper), 0.025, 0.05, 0.10, 0.25, 0.40 (A1–A6) and model ink containing only Cu without iron (A7) were used in this study. Used chemicals: tannic acid (Sigma Aldrich), ferric sulphate heptahydrate (Lachema, Czech Rep.), cupric sulphate pentahydrate (Lachema, Czech Rep.), gum arabic (Sigma-Aldrich), cupriethylene-diamine (Sigma-Aldrich), deionised water. Water solutions of inks were applied on substrate after 15 days free staying in dark.

Whatman filter paper No. 1 (purified cotton linter cellulose) was used as a model substrate. Using a computer-guided plotter with a refillable plotter pen each ink was applied in rectangles (12 × 5 cm) and then left to dry at room temperature. The average ink amount per sample was 0.008 g cm^{-2}. Samples with pH values lying in four different regions (~ 3, ~ 4, ~ 5, ~ 6) were obtained by short immersion (2–3 s) of inked paper samples into the diluted solutions of sodium hydroxide (from 0.25M to 0.40M, as appropriate for particu-

lar sample to obtain required pH)). The samples were submitted to accelerated ageing in closed vessels at 90 °C according to the method described by Lojewski and Baranski[9].

The degree of polymerization (DP) of samples was determined viscometrically using cupriethylene-diamine as a solvent[10]. Degree of polymerization was calculated from viscometric data using Mark-Houwink-Sakurada equation and the constants according to Evans and Wallis[11,12]. Rate constants "k" of degradation of paper samples was calculated by least squares fitting of the plot DP vs. time using Ekenstam equation for degradation of linear polymers[13]:

$$(1/DP_t) = (1/DP_o) + k\ t \qquad (1)$$

where DP_t and DP_o are degrees of polymerization at the beginning of ageing and after time "t" of ageing, respectively.

Colorimetric measurements were performed using spectrocolorimeter GretagMacbeth Spectrolino keeping the standard condition for graphic arts measurements (geometry 45/0, D50 illumination, 2° standard observer, measurement without polarizing filter, black background) according to the standard[14]. Standard error of the colorimetric measurements was less than 1.0 (in ΔE^*_{ab}).

Results and Discussion

The rates constants of degradation of samples containing model inks at various pH are shown on the Fig. 1.
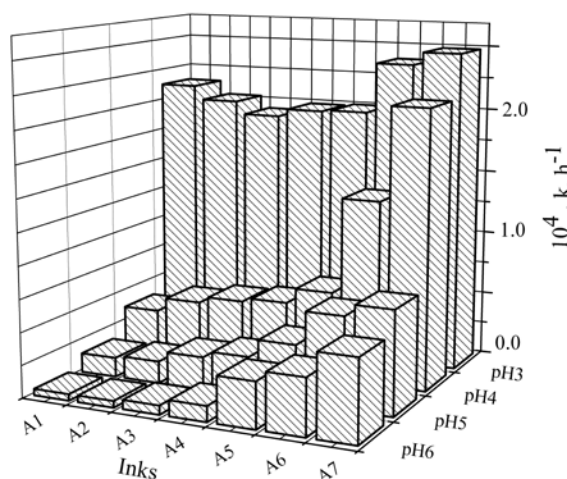
Fig. 1. **Rate constants of degradation *vs.* ratio Cu:Fe (A1–A7) and pH**

The rate constants of degradation are significantly higher at the pH value around 3, the ratio Cu:Fe in inks does not significantly affect the rate of degradation. With increasing pH the rate of degradation descends and depends on the ratio Cu:Fe in inks. Samples with higher content of copper in the inks exhibit higher constant of degradation at the same pH value.

The color changes of selected samples during ageing are on the Fig. 2.
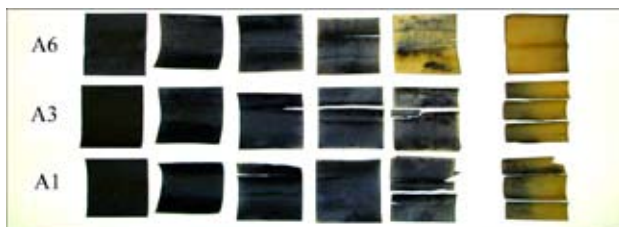
Fig. 2. Samples of inks (A1, A3, A6) at the ageing time of 0, 1, 2, 3, 4 and 24 hours, pH 3

The colorimetric changes of the samples during ageing can be summarize as follow. CIE Lab lightness of samples aged at the pH range 3 increases with prolonged ageing and this bleaching is steepest for the samples with higher content of copper (Figs. 3.–5.). At the same time CIE Lab chroma increases from small initial values (1.8) to the values up to 20 and CIE Lab hue angle is shifted from 280 ° to 76 ° (corresponds to the shift from grey to brown-yellowish color). More significant changes of chroma and hue angle during ageing were observed for the samples with higher content of cooper. The nature of these changes suggests that oxidative reactions of the iron-gall ink take place in addition to the degradation of cellulose fibers.
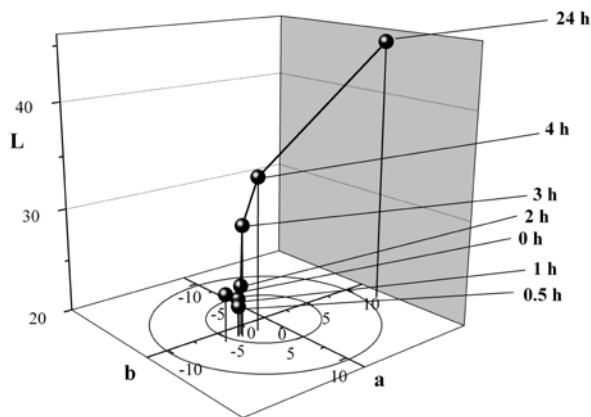
Fig. 3. Changes of colorimetric parameters (CIELab) during ageing; sample A1, pH 3

Colorimetric changes of samples aged in higher pH ranges follow the above trend, but were less significant (color difference DE^*_{ab}<3.5). Lower extend of changes of color corresponds to the lower rate of degradation in these pH ranges

In order to asses the role of hydrolytic degradation and the catalytic influence of transitional metals, the rate constants of degradation of pure substrate (Whatman paper) without ink deposition at various pH were determined (Fig. 6.).

As follows from the Figs. 6 and 7., the degradation of the samples containing iron gall inks is significantly higher than the degradation of samples of the pure substrate
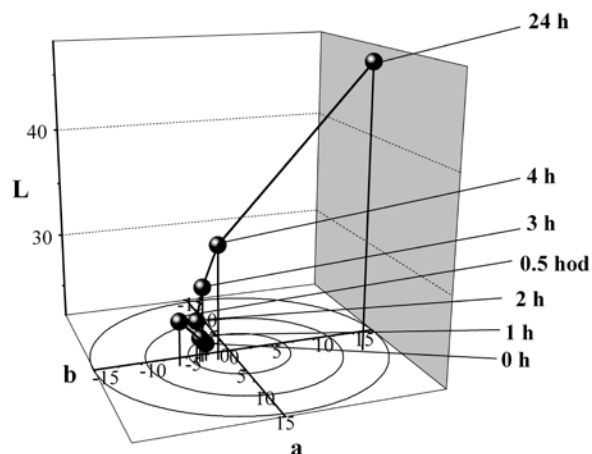
Fig. 4. Changes of colorimetric parameters (CIELab) during ageing; sample A3, pH 3
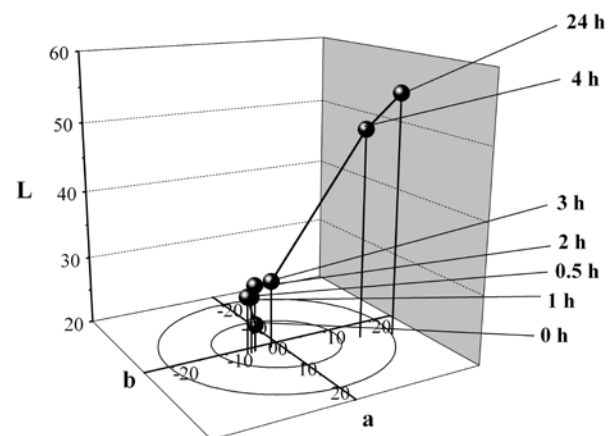
Fig. 5. Changes of colorimetric parameters (CIELab) during ageing; sample A6, pH 3

of the same pH. While the increasing of pH value of pure substrate to 3 increased the rate constant of degradation about 4-times, the change of pH value from 6 to 3 for the sample with ink A1 increased the rate constant of degradation about 20-times. This can be considered as evidence, that the accelerated degradation of samples containing transitional metals is not caused simple by increased acidity but that specific degradation reactions of cellulose fibers catalyzed by transitional metals play significant role.

Conclusions

The rate of degradation of samples of paper with iron-gall inks containing copper and iron in various ratios is the highest at the lowest pH values (around 3) and the value of rate constant of degradation does not depend significantly on the content of cooper in the ink in this pH range. Rate of degradation of the samples in less acidic regions is lower and depends on the content of cooper. The degradation of samples
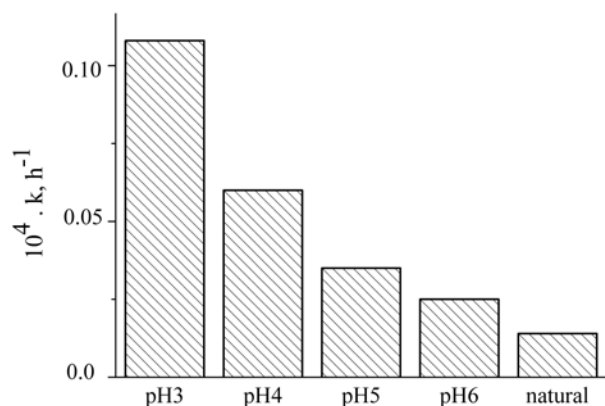
Fig. 6. **Rates constants of degradation of substrate (Whatman paper) without ink deposition at various pH and without pH adjustment (natural substrate)**

Fig. 7. **Rate constants of samples from Fig. 6 compared with rate constants of degradation of sample A1**

with inks with higher ratio copper:iron is faster, what may be caused by more significant oxidative degradation.

Accelerated degradation of samples containing transitional metals is not caused simple by increased acidity but that specific degradation reactions of cellulose fibers catalyzed by transitional metals play significant role.

Changes of colorimetric parameters during degradation of studied samples provide further indication of the running oxidation reactions.

REFERENCES

 1. Zou X., Gurnagul N., Uesaka T., Bouchard: Polym. Deg. Stab. *43*, 393 (1994).
 2. Neevel J. G.: Restaurator *16*, 143 (1975).
 3. Walling C.: ACC. Chem. Res. *8*, 125 (1975).
 4. Wardman P., Candels L. P.: Radiat. Res. *145*, 523 (1996).
 5. Bicchieri M., Pepa S.: Restaurator *17*, 165 (1966).
 6. Kolar J., Strlic M.: Acta Chim. Slov. *50*, 763 (2003).
 7. Wagner B., Bulska E., Hulanicki A., Heck M., Ortner H. M.: Fresenius J. Anal. Chem. *369*, 674 (2001).
 8. Barb W. G., Baxendale J. H., George P., Hargrave K. R.: Trans. Faraday Soc. *47*, 591 (1951).
 9. Lojwewski T., Baranski A*.: Proceedings of the International Conference Durability of Paper and Writing,* (Kolar J., Strlic M., Havermans J. B. G. A. eds.) pp. 39, Ljubljana 2004.
10. ISO 5351-1:1981, *Cellulose in dilute solutions - Determination of limiting viscosity number – Part 1: Method in cupri-ethylene-diamine (CED) solution.*
11. Evans R., Wallis A. F. A.: *Proceedeings 4th Int. Symp. Wood Chem.* p. 201 (1987)
12. Kolar J., Strlc M.: Restaurator *23*, 94 (2004).
13. Emsley A. M., Heywood R. J., Ali M., Eley C. M.: Cellulose *4*, 1 (1997).
14. ISO 13655:1996, *Graphic technology – Spectral measurements and colorimetric computation for graphic arts images.*

L04 PHOTOCHEMICAL TRANSFORMATION OF ANTICANCER DRUG IRINOTECAN

DANA DVORANOVÁ, VLASTA BREZOVÁ, ZUZANA VRECKOVÁ and MARIÁN VALKO

Institute of Physical Chemistry and Chemical Physics, Faculty of Chemical and Food Technology, Slovak University of Technology in Bratislava, Radlinského 9, 812 37 Bratislava, Slovak Republic,
dana.dvoranova@stuba.sk

Introduction

The camptothecin family of anticancer medicines has a unique mechanism of action directed to the inhibition of topoisomerase I (Topo I). It was previously shown that camptothecin (CPT) inhibits Topo I *via* the formation of ternary complex, in which the biologically active lactone ring of CPT stabilizes an irreversible Topo I/DNA covalent complex. Camptothecin molecule contains conjugated system of π-electrons representing a potential basis for UVA photoexcitation resulting in the reactive free radical species generation (e.g., ROS – Reactive Oxygen Species), which are responsible for light-mediated DNA cleavage. Consequently, alternative mechanisms of DNA damage upon the simultaneous application of CPT, Topo I and UV radiation (λ = 365 nm) were considered. A number of photoactive compounds require the contribution of a metal ion for the DNA cleavage event, therefore the biological activity of irradiated CPT has been tested also in the presence of Cu(II) ions[1,2]. Our previous investigations were oriented on study of interaction of CPT with Cu(II) and Fe(III) ions upon irradiation. The results obtained confirm the participation of these ions in the photoinitiated activation of camptothecin accompanied with the formation of reactive radical species[3,4].

Irinotecan (CPT-11 or Camptosar®) is a watersoluble semisynthetic analogue of the natural alkaloid camptothecin. The structure of CPT-11 is shown in Fig. 1.
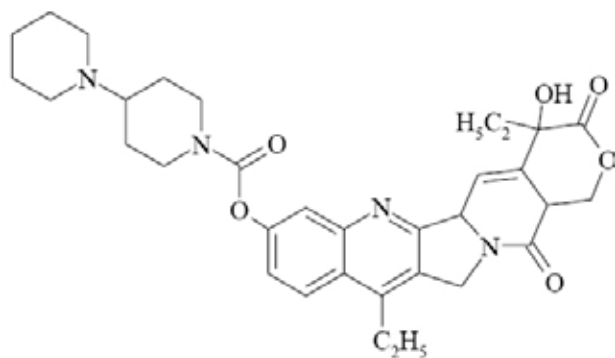
Fig. 1. **Structure of irinotecan (CPT–11)**

Irinotecan is a pro-drug, converted *in vivo* to its active metabolite. CPT-11 interfere with Topoisomerase I and cancer cells death appears to result from DNA strand breaks caused by the formation of cleavable complexes.

Our investigation was focused on photochemical transformations of CPT-11 in aqueous and dimethylsulfoxide (DMSO) solutions, and on its photoactivation in the presence of equimolar amounts of Cu(II) ions monitored by EPR spectroscopy.

Experimental

Irinotecan hydrochloride (CPT-11, Fig. 1) and cupric chloride were applied in photochemical experiments. 5,5-Dimethyl–1-pyrroline N-oxide (DMPO) and α-(4-pyridyl-1-Oxide)-N-*tert*-butylnitrone (POBN) were used as spin trapping agents, 2,2,6,6-tetramethyl-4-piperidinol (TEMPOL) was applied as spin label. The selective oxidation of 4-hydroxy-2,2,6,6-tetramethylpiperidine (TMP) *via* singlet oxygen to the paramagnetic nitroxyl radical oxyl (TEMPOL) was utilized for $^1O_2$ detection by EPR spectroscopy.

The stock solutions of CPT-11 and $CuCl_2$ (both 2×10^{-3} mol dm^{-3}) were prepared in redistilled water or dimethylsulfoxide. The CPT-11 (150 μl) were mixed with identical volume of solvent (water or DMSO) or 150 μl Cu(II) ions (to obtain equimolar solution CPT-11 : Cu(II)) and 50 μl of aqueous or DMSO solutions of spin traps/spin label were added prior to irradiation. The prepared solutions were saturated by argon or air, filled in the quartz flat cell optimized for the Bruker TE$_{102}$ EPR cavity.

The X-band EPR spectra were recorded at EPR Bruker EMX spectrometer equipped with a TE$_{102}$ (ER 4102ST) resonator. Samples were irradiated at 295 K *in situ* using HPA 400/30S lamp (400 W, λ_{max} = 365 nm, Philips, UVA irradiance 10 mW cm^{-2}). A Pyrex glass filter was applied to eliminate the radiation wavelengths below 300 nm. The simulations of the individual components in the complex EPR spectra were calculated using WinEPR and SimFonia programs (Bruker). The experimental EPR spectra were fitted as the linear combinations of these individual simulations using a least-squares minimization procedure with the Scientist Program (MicroMath).

Results

The EPR spin trapping technique enables to evidence reactive short-lived free radicals adding them to spin trapping agent under the formation of more stable paramagnetic products (spin adducts). The EPR spectrum of adducts brings information on type of reactive radical trapped.

DMPO. The dimethylsulfoxide solvent is well known for its ability to stabilize super-oxide anion radical. The EPR spectra measured after 10 min of irradiation of CPT-11 in DMSO solutions under air in the presence of DMPO confirmed the formation of two radical adducts (Fig. 2.). The spin Hamiltonian parameters of EPR signals obtained by simulation analysis revealed the generation of •DMPO–O_2^-, characterized by hyperfine splittings a_N = 1.274 mT, a_H^β = 1.035 mT, a_H^γ = 0.137 mT and g-value = 2.0058(ref.[5]). This EPR signal dominates in the experimental spectrum (relative concentration 80 %), and is produced immediately after beginning of irradiation. Additionally, a minor EPR signal was

observed, attributed to ˙DMPO–OCH$_3$ adduct (a_N = 1.330 mT, a_H^β = 0.794 mT, a_H^γ = 0.155 mT and g-value = 2.0058)[5].
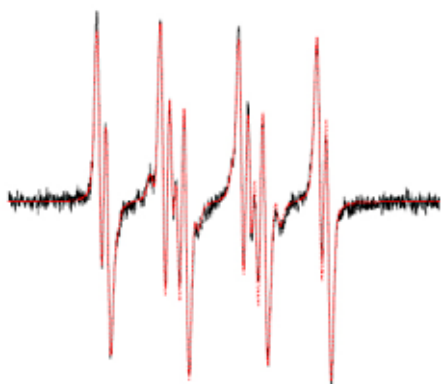
Fig. 2. **Experimental (solid line) and simulated (dotted line) EPR spectra (magnetic field sweep 7.5 mT) obtained after 10 minutes of a continuous irradiation of system CPT-11/DMPO/ DMSO/air. Initial concentration: c_0(CPT-11) = 0.86 mmol dm^{-3} and c_0(DMPO) = 30 mmol dm^{-3}**

The formation of superoxide anion radicals upon photoexcitation of CPT-11 in DMSO solvent was unambiguously confirmed by the addition of enzyme superoxide dismutase (SOD) into the solution, which caused a significant decrease of ˙DMPO–O$_2^-$ EPR intensity by the competitive reaction of SOD with O$_2^{˙-}$.

The production of ˙DMPO–OCH$_3$ adduct was established previously in aerated DMSO systems producing oxygen-centered free radicals (O$_2^{˙-}$, ˙OH). Probably, the generation of this minor adduct reflected the reaction of ROS with solvent producing ˙CH$_3$ radicals, which are in the presence of molecular oxygen transformed to CH$_3$OO˙ and trapped as ˙DMPO–OCH$_3$.

It should be noted here that the application of DMPO was not possible in systems containing Cu(II) ions and DMSO solvent, due to the formation of paramagnetic species even after mixing of individual solutions before irradiation, so the identification of photo-induced radical adducts was limited.

TEMPOL. The principle of the detection of reactive free radical formation using TEMPOL and its derivatives is based on monitoring the decrease in its EPR intensity resulting from the interaction of its >N−O˙ group with the generated reactive radical species, as well as singlet oxygen (Eqs. 1–4)[6]:

$$>N−O˙ + ˙OH → >N^+=O + OH^- \qquad (1)$$

$$>N−O˙ + ˙OH → >NOOH → >NH + O_2 \qquad (2)$$

$$>N−O˙ + ˙R → >NO\text{-}R \qquad (3)$$

$$>N−O˙ + {}^1O_2 → \text{products and/or quenching} \qquad (4)$$
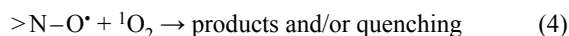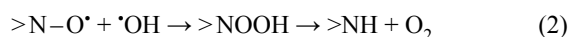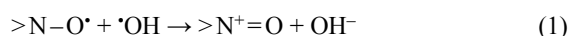
The EPR spectrum of TEMPOL in DMSO solvent in the presence of oxygen represents three-line signal characterized with hyperfine splitting a_N = 1.573 mT and g = 2.0060, as il-

lustrates inset in Fig. 3.a. Irradiation of TEMPOL in DMSO solution under air or argon confirmed its photochemical stability under given experimental conditions, as only negligible decrease of EPR signal was observed. The situation was similar if TEMPOL was irradiated in the presence Cu(II) ions. However, the addition of CPT-11 to the reaction system under air or argon led to the decrease of TEMPOL signal.
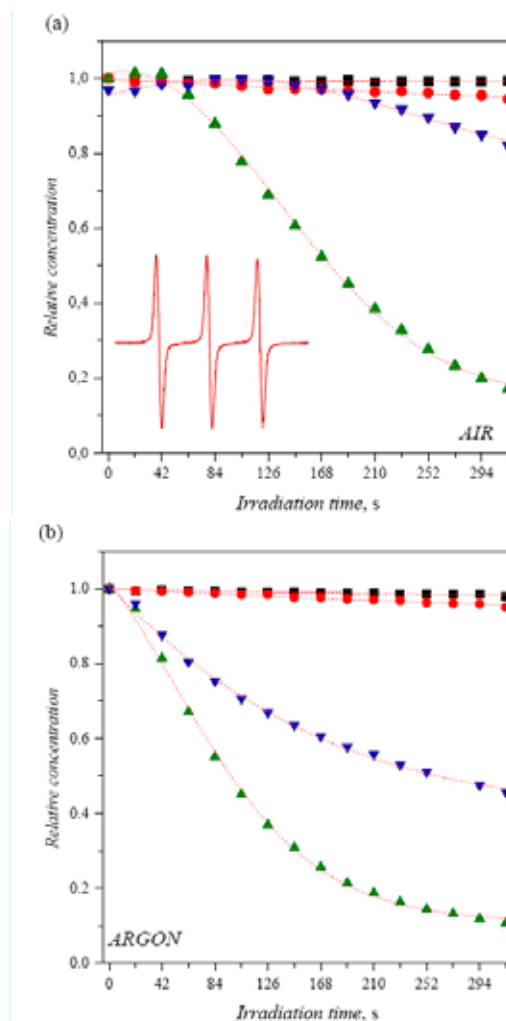
Fig. 3. **TEMPOL relative concentration monitored upon continuous irradiation (λ >300 nm) of DMSO solutions in the presence CPT-11 and/or Cu(II) ions (c_0(TEMPOL) = 43 µmol dm^{-3}) under air (a) and argon (b). Inset represents experimental and simulated EPR spectrum of TEMPOL in DMSO (magnetic field sweep 6 mT). Initial concentrations of CPT-11 and Cu(II) ions (in mmol dm^{-3}): ■ c_0(CPT-11) = 0, c_0(Cu(II)) = 0; ● c_0(CPT-11) = 0, c_0(Cu(II)) =0.86; ▲ c_0(CPT-11) = 0.86; c_0(Cu(II)) = 0; ▼ c_0(CPT-11) = 0.86, c_0(Cu(II$^+$) = 0.86**

The addition of equimolar amount of Cu(II) ions into CPT-11 solution and subsequent irradiation led to the decrease of TEMPOL signal which was less pronounced than in system with only CPT-11.

The termination of TEMPOL signal in the presence of CPT-11 indicated the formation of reactive radical species which can react with TEMPOL, forming diamagnetic products. The presence of Cu(II) ions in reaction systems with CPT-11 could cause the competitive reactions, e.g., reoxidation of Cu(II) (Eqs 5, 6):

$$Cu(II) + O_2^{\bullet-} \rightarrow Cu(I) + O_2 \qquad (5)$$

$$Cu(I) + O_2 \rightarrow Cu(II) + O_2^{\bullet-} \qquad (6)$$
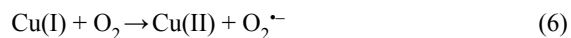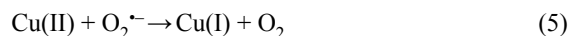
Additionally, the formation of singlet oxygen $^1O_2$ was confirmed, as irradiation of CPT-11 in the presence of TMP resulted to the formation of TEMPOL radical.

Conclusions

The work was focused on spectroscopic characterization of photoinitiated processes of irinotecan. Radical formation in the photoactivated system with CPT-11 and CPT-11/Cu(II) was monitored by spin traps DMPO and POBN under inert atmosphere and also in the presence of oxygen. DMPO was used for confirmation of photoinduced reactive radical species formation in DMSO solutions and POBN in aqueous solutions, respectively. Semi-stable free radical TEMPOL was used to verify the production of radicals upon irradiation.

REFERENCES

1. R. P. Hertzberg, M. J. Caranfa, S. M. Hecht, Biochem. *28*, 4629 (1989).
2. S. M. Hecht, Curr. Med. Chem. Anti-Cancer Agents *5*, 353 (2005).
3. V. Brezová, M. Valko, M. Breza, H. Morris, J. Telser, D. Dvoranová, K. Kaiserová, Ľ. Varečka, M. Mazúr, D. Leibfritz, J. Phys. Chem. B *107*, 2415 (2003).
4. D. Dvoranová, V. Brezová, M. Valko, A. Staško J. Photochem. Photobiol. A: Chem. *185*, 172 (2007).
5. A. S. W. Li, K. B. Cummings, H. P. Roethling, G. R. Buettner, C. F. Chignell, J. Magn. Reson. *79*, 140 (1988). (The database is available at http://epr.niehs.nih.gov).
6. V. Brezová, S. Gabčová, D. Dvoranová, A. Staško J. Photochem. Photobiol. B: Biol. *79* 121 (2005).

L05 THIN LAYERS OF TiO$_2$ PREPARED BY INKJET PRINTING

PETR DZIK, JANA CHOMOUCKÁ and MICHAL VESELÝ

Faculty of Chemistry, Brno Universityof Technology, Purkyňova 118, 612 00 Brno, Czech Republic
petr@dzik.cz

Introduction

Photocatalysis on TiO$_2$ has received much attention during last two decades. If TiO$_2$ absorbs a quantum of UV radiation of sufficient energy ($\lambda < 400$ nm), an electron is excited into the valence band and an electron-hole pair is created. The potentials of electron and hole are strong enough to oxidize water to hydroxyl radicals and reduce molecular O$_2$. Resulting reactive oxygen species (ROS) are very powerful oxidizing agents and readily attack any organic matter in their proximity until it is totally cleaved to CO$_2$ and water. Numerous applications utilizing this process for water purification, toxic waste treatment, air purification and deodorizing have been proposed and some successfully marketed. The same process can be applied for the design of self-cleaning and self-disinfecting surfaces. Moreover, the oxygen vacancy creation and subsequent photo-corrosion on irradiated surfaces of TiO$_2$ convert the surface to superhydrophilic nature, which further enhances its self-cleaning ability.

Photocatalytic systems based on slurryied powder of TiO$_2$ offer excellent performance due to their very high catalyst surface area. Upon immobilization, the free surface of catalyst inevitably decreases, resulting into a loss of catalytic performance. Nevertheless, immobilized TiO$_2$ is the preferred form of photocatalyst. for industrial application. The need of removing powder photocatalyst can prohibitively complicate any process.

So far, several forms of immobilized powder TiO$_2$ were reported, featuring glass, silica gel, quartz, stainless steel, titanium, paper and many other materials as support. There are many methods of TiO$_2$ powder immobilization, such as suspension dip-coating, electrophoretic coating, spray coating, etc. However, inferior optical and mechanical properties or resulting films restrict the use of these materials only to some type of applications, such as photocatalytic reactors.

Sol-gel technique represents a totally different approach to the preparation of TiO$_2$ thin layers. Sol-gel is one of the most successful techniques for preparing nanosized metallic oxide materials with high photocatalytic activities. By tailoring the chemical structure of primary precursor and carefully controlling the processing parameters, nanocrystalline products with very high level of chemical purity can be achieved. In sol-gel processes, TiO$_2$ is usually prepared by the reactions of hydrolysis and polycondensation of titanium alkoxides, Ti(OR)n to form oxopolymers, which are then transformed into an tridimensional network.

In this way, thin, compact and transparent layers of TiO$_2$ can be conveniently produced. Such layers find their use in the design of "smart" surfaces, such as self-cleaning glass sheets and tiles, mirrors with antifogging effect, self-disinfecting material etc. However, a suitable method for liquid sol application is needed in order to obtain a thin layer with excellent properties.

There are two traditional method of thin layer preparation from liquid precursors: spin-coating and dip-coating. Spin-coating method uses centrifugal force to form a film of liquid precursor: a sufficient volume of precursor is placed onto the support which is then rotated at a high speed. The liquid is spread by centrifugal force and a wet film of precursor is formed. The thickness of the resulting wet film depends mainly on the angular velocity of substrate rotation, precursor viscosity, precursor concentration and solvent evaporation rate[1]. In contrary, dip coating is based on dipping the substrate into liquid precursor and pulling it out at constant speed. Again, viscosity, concentration, solvent volatility and speed of pulling influence the resulting film thickness. The faster we pull, the thicker the film is.

Both these methods are widely used, yet they are burdened by several significant disadvantages, as summarized in Table I. Firstly, the coated area is rather limited. In the case of spin coating, this limitation is due to the centrifugal force. Substrates larger than a few centimeters simply can not be rotated at several thousands rpm. The area of dip coated substrates is usually also limited to centimeter scale, although devices handling large substrates up to meter size are known. Secondly, the efficiency of precursor use is extremely poor. In both spin- and dip-coating, most of the precursor is wasted, and only few percents are actually used to build up the film. Moreover, dip-coating gives us substrates coated from both sides, which is not always desired. Thirdly, both these methods are very sensitive to surface defects. A surface defect can produce traces and streaks and degrade large areas of cauted substrate. At last, these classic methods on their own are not capable of selective deposition ("patterning"), i.e. the whole area of substrate is coated.

Table I
Method comparison (adopted from[2], modified by authors)

	Spin	Dip	Inkjet
Precursor use efficiency	~ 95 % wasted	~ 95 % wasted	~ 5 % wasted
Coated area	~ cm	~ dm	~ m
Sensitivity to surface defects	☹	☹	☺
Possibility of "patterning"	☹	☹	☺

Because of these problems and limitations, a more robust method of liquid precursor application has been searched for. Inkjet printing is apparently a very good candidate for this task. In a conventional inkjet printer, small droplets of low viscosity ink are ejected from a print head and fall onto

printed substrated[3]. The movement of the print head and the substrate is precisely controlled by computer and so is the volume of ejected droplets and their loading per unit area. If we are able to replace the ink with a liquid precursor and printing paper with suitable substrate, we obtain a very robust device for the precursor deposition.

Naturally, both the printer and precursor must fulfill certain requirements in order to be employed as a thin layer deposition tool. The printer has to be able to handle rigid media so that solid materials can be used as layer support. The precursor must be of a very low viscosity (less than 20 mPa s) and must not damage the printer. If solid particles are present in the precursor, their diameter must be well below the print head nozzle diameter (50–20 μm typically) and their aggregation must be prevented. Despite these limitations, inkjet printing has been sucessfully used for the deposition of a wide variety of liquid precursors, such as conducting polymers[4], metallic nanoparticles dispersions[5], metallic precursor solutions[6], enzymes, various catalyst nanoparticles dispersions etc.

Experimental

Sol and Substrate Preparation

Sol-gel technique was applied to titanium dioxide thin films preparation using titanium(IV) propoxide as titanium precursors.

40 ml of ethanol was mixed with 3.8 ml acetylacetone. This mixture was then dropwise added to 10.3 ml titanium(IV)tetraisopropoxide (TTIP). Finally, 45 ml of ethanol was mixed with 0.69 ml water and this mixture was again dropwise added to the sol composition. Prepared sol was stored in an airtight bottle in darkness at 5 °C.

Borosilicate glass plates with sizes of $30 \times 30 \times 2$ mm (Verre Equipements, France) were chosen as a substrate for immobilization of TiO_2 thin films. This type of glass contains only 4.2 % wt. Na_2O and 0.1 % wt. of CaO. Before the preparation of the thin films, each glass was pre–treated in order to eliminate any dust, grease and other residues using an aqueous solution of industrial surfactant and dried under air flow.

Sol Application

Sol application was performed in a novel inovative way utilizing a modified office inkjet printer (Epson R220). Original ink cartridges were removed from the printer and the ink tubing and printhead were flushed and purged with anhydrous propanol. Flushing with anhydrous propanol is extremely important in order to remove any remaining aqueous ink. If this step is omitted or performed incompletely, the titanium sol will hydrolyse upon contact with residual water and precipitated TiO_2 will clog the print head nozzles.

"Virgin empty" spongeless carts were supplied by MIS Associates, USA. Titanium sol was filtered frough 0.2 μm mesh size syringe filter and loaded into one "virgin empty" cart. This cart was installed into the printer in the black position while the remaining positions were occupied by the same carts filled with dummy ink (a mixture consisting of water,

propanol, surfactant and colorant). After a series of head cleaning cycles a perfect nozzle check pattern was obtained. Cleaned glass plates were then mounted into a modified CD holder, fed into the printer and printed with "black only" driver setting. The colour of the printed pattern was varied in different levels of grey (100%, 90%, 80%, 70%, 60%) and thus glasses with correspoding *relative sol loading value* were printed.

Two print setting were adopted – *rapid* and *slow* (see Table II). The resolution, print speed and media settings were varied and their influence on the resulting TiO_2 layer properties was evaluated.

Table II
Print setting

	Rapid	Slow
Media Settings	Plain paper	CD Premium Surface
Resolution	360	720
Highspeed printing	yes (= bidirectional printing)	no (= unidirectional printing)
Absolute printing speed	appr. 1 cm^2 s^{-1}	appr. 0.05 cm^2 s^{-1}

Layer Treatment

After the previous procedure, the coated glass plates were dried in the oven at 110 °C for 30 min. Finally, the deposited layers were thermally treated in a calcination furnace at 450 °C for 4 hours with ramp of 3 °C min^{-1} to obtain the transparent photocatalytically active titanium dioxide films in anatase presupposed phase.

Study of Printed Layers Properties

Optical and SEM imaging was performed in an ordinary manner on a Nikon Eclipse E200 optical microscope equippend with Nikon D200 digital camera and Hitachi S4700 FESEM scanning electronic microscope. Recorded electronic images were also used to evaluate the layer thickness.

Surface Analysis was performed on Sanning Probe Microscopy NTegra Prima/Aura (NT-MDT).

Photocatalytic performance was evaluted by recording the dechloration rate of 2,6-dichloroindophenol (DCIP). The reaction took place in a simple single-plate reactor where the solution was circulated through a siphon by a centrifugal pump. The siphon ensured a constant level of solution over the catalyst plate during the whole reaction despite decreasing volume due to sampling. UV radiation was delivered by Philips HPA – 400 W metal halogen lamp and the intensity was 2.4 mW cm^{-2}.

The DICP concentration was determined by UV-VIS spectrophotometry at 600 nm. Samples were taken at 20 minutes intervals. Formal first order kinetic model was adopted and the reaction rate constants were calculated.

Results

L a y e r   S t r u c t u r e   a n d   M o r p h o l o g y

As far as the layer morphology is concerned, we can clearly see that there are principal differences between rapid and slow printed layers, no matter what the sol loading is. The rapid printed layers are very smooth and compact up to 80 % of sol loading (see Fig. 1.). When the sol loading value exceeds this threshold, cracking occurs (See Fig. 2.).
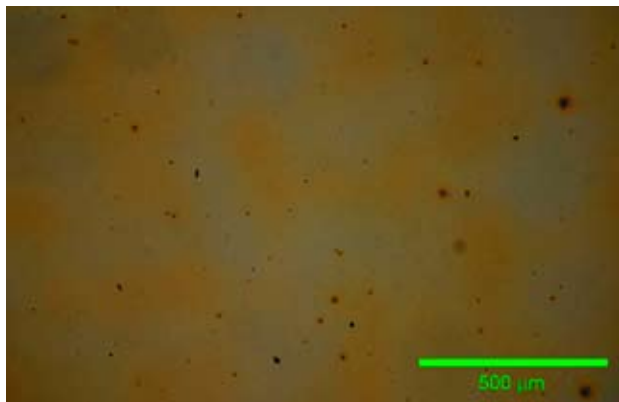
Fig. 1.   **80 % sol loading, rapid printing**
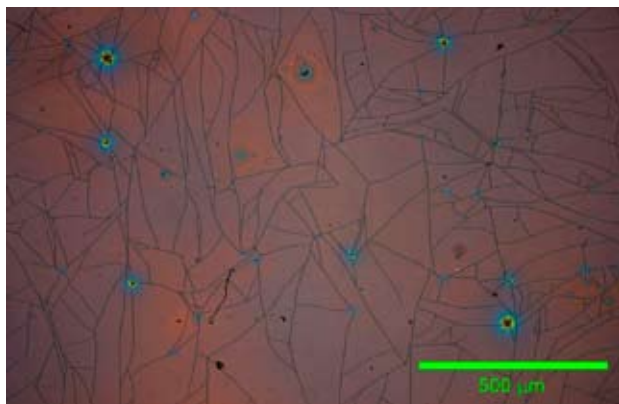
Fig. 2.   **100 % sol loading, rapid printing**

On the other hand, the slow-printed layers show completely different structure – their surface is very grooved and rough. It clearly keeps the structure of individual drops. When the sol loading value is low, we can clearly see the patterns of individual drops (see Fig. 3.). When the sol loading value increases, this pattern is still present and some cracing occurs in very thick regions (Fig. 4.).

A more detailed view is provides by the SEM imaging. Here we get a closer look at the cracks and it is also possible to estimate the thickness of the layers (Fig. 6.).

The differences in the layer structure are caused by the different speed of sol ejection: During rapid printing, the sol ejection rate is faster then solvent evaporation, and therefor a liquid film is formed on the substrate. Only then the solvent evaporates, leaving a "dry" layer of gel. However, during slow printing, the sol ejection rate is very small and the rate of evaporation exceeds it. Therefore a solig gel is formed
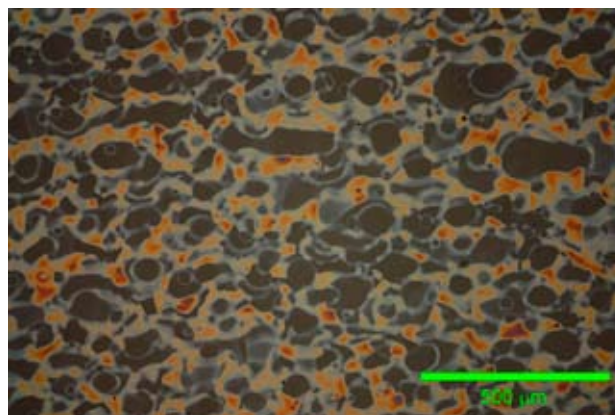
Fig. 3.   **60 % sol loading, slow printing**
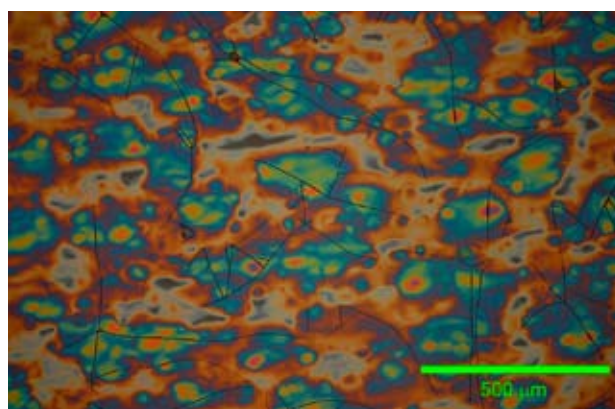
Fig. 4.   **100 % sol loading, slow printing**
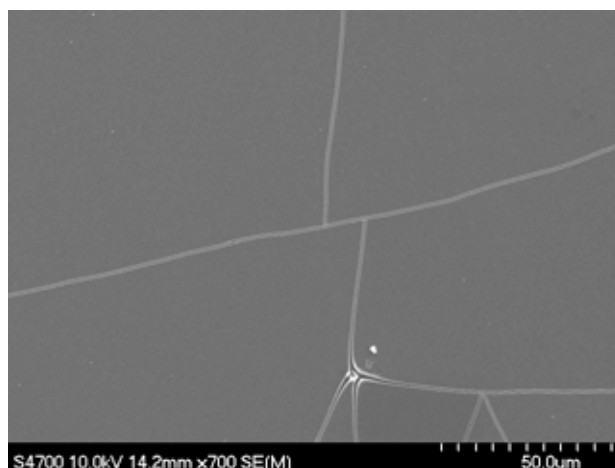
Fig. 5.   **100 % sol loading, rapid printing**

on the substrate already during printing and the last drops of sol are deposited onto dried gel. Therefore a distinctive structure develops and the resulting layer is very rough.

The roughness prepared layers was in much greater detail observed by AFM. Unfortunately, the roughness of slow printed layers was too high to be observable by our device, therefore a direct comparison is not possible at the moment. The AFM record for the rapid layer reveal a very
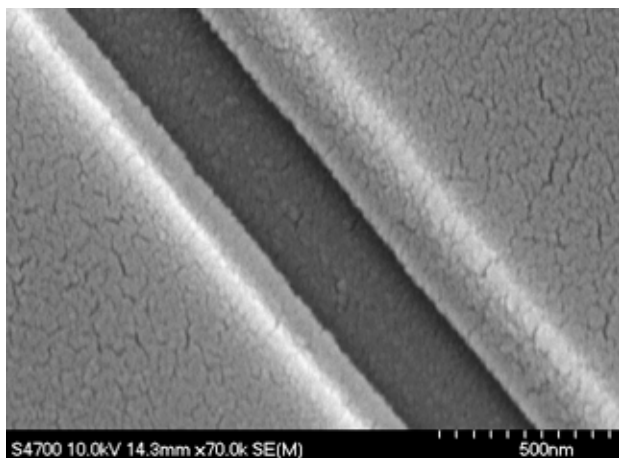
Fig. 6.   **A crack detail, 100 % sol loading, rapid printing**

smooth surface whose roughness is comparable to the roughness of support glass.
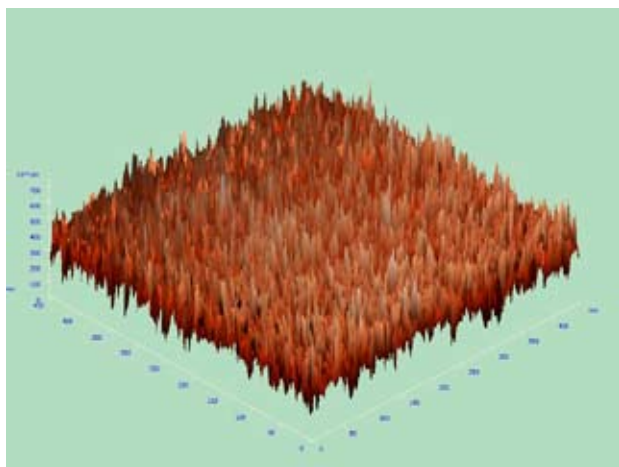
Fig. 7.   **AFM record of 100% sol loading, rapid printed layer**

P h o t o c a t a l y t i c   P e r f o r m a n c e

Fig. 7 shows the overall results for the DCIP dechloration experiment. We can clearly see that the dechloration rate increases with increasing sol loading. However, the there is a difference in the slope of this dependency. We believe that this difference can be explained by the differences in layer homogeneity. While the rapidly printed layers are very smooth and compact, the slow printed layers are grooved and rough. Therefore the catalyst surface is basically constant in the case of rapid printing and only the thickness of the layer changes. On the other hand, in the case of slow printing, both the average layer thickness and interface surface increases as sol loading increases.

Conclusion

In this letter, we demonstrate the benefits of using inkjet printing technology for the preparation of TiO$_2$ thin layers.
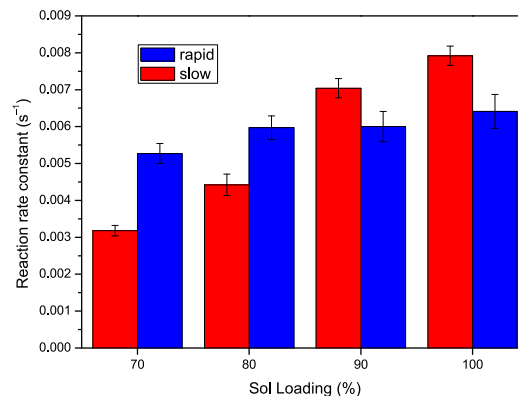
Fig. 8.   **Reaction rate constant comparison**

By utilizing the well know sol-gel chemistry used so far for spin- and dip coated layers of TiO$_2$ together with the wide deposition possibilities offered by inkjet printing, we are able pro prepare thin layers of TiO$_2$ in a very effective and clean way with minimum waste. The structure of prepared layers greatly depends on the printing conditions: If the sol ejection rate is faster then solvent evaporation, a smooth compact layer is produced. On the other hand, when the solvent evaporation rate is grater than sol ejection, we obtain highly structured and porous layer.

Slowly printed layers have structured and grooved surface giving them opaque matt apperance, but their photocatalytic performance is superior compared to rapidly printed layers. We believe this is mainly due to greater catalyst interface area. On the other hand, rapidly printed layers have better optical properties – they are glossy and transparent. However, the smooth surface results into lower mass exchange rate and therefore their photocatalytic performace is lower.

REFERENCES

1. Schubert D. W., Dunkel T.: Mat Res Innovat *7*, 314 (2003).
2. Bharathan J., Yang Y.: Appl. Phys. Lett. *72*, 2660(1998).
3. Hue P. Le, J. Imaging Sci. Technol. *42*, 49 (1998).
4. Liu Y. et al.: Solid-State Electron. *47*, 1543 (2003).
5. Park J.-W., Baek S.-G.: Scr. Mater. *55*, 1139 (2006).
6. Busato S.et al.: Sens. Actuators B *123*, 840 (2007).

L06 PROMISING PERSPECTIVES IN PHOTOCATALYSIS

C. GUILLARD, E. PUZENAT AND J.-M. HERRMANN

IRCELYON UMR CNRS 5634, Université de Lyon1, 2 av. Albert Einstein, Villeurbanne cedex, 69626, France, Chantal.guillard@ircelyon.univ-lyon1.fr

Introduction

Heterogeneous Photocatalysis based on titania originated some 40 years ago but the interest of industry for environmental applications emerged only 10 years ago. These applications mainly concerned self-cleaning materials and water and air purification and standardisation is now required. In France, French AFNOR created the B44-A photocatalytic commission in September 2007, which is composed of scientists from National and from industry.

Researches in the field of the Photocatalysis are now one of the major for remediable energy. This is a technology which took a considerable rise during these last 10 years. It is particularly well adapted to answer the new environmental stakes, insofar as she proposes solutions of for clean treatments to fight effectively against environmental pollution. The photocatalysis is a technique based on oxydo-reduction (Redox) processes, particularly well appropriate to the treatment of environmental pollution. It is quoted in the last report/ratio of the Ministry for Industry relating to "key technologies 2010" like as one of the technologies carrying for the economic development in France. These applications mainly concerned self-cleaning materials and water and air purification and standardisation is now required. In this particularly favorable context, AFNOR, the French Agency for Standardization, which has, in particular, for the mission of promoting emergent technologies and to supporting their development, has just created the Commission of Standardization named Photocatalysis B44A. At the time of during the launch the meeting of launching on May 11, 2007 which brought together some 30 people persons met, among which whom people from industry, representatives of the public authorities and scientific experts of from academic research. The scope of applications selected is relatively broad, taking into account the multiple applications considered, such as the air cleaning, the elimination of the odors, the coating materials to create self-cleaning surfaces (glass, metals, concretes, cements…), the purification, potabilisation and detoxification of water, etc. It was initially decided, to focus the work of standardization of the Commission on the applications of the photocatalysis in the field of the on air treatment.

After the presentation of the commission of standardization AFNOR "B44A" the principle of photocatalysis and the active species generated at the surface of a photocatalyst will be presented under different reaction conditions (liquid phase (water, solvents) and gas phase), corresponding to dedicated applications such as air and water treatments, self-cleaning materials, fine chemistry. Hydrogen production will be also introduced.

The comparison of reaction mechanisms occurring in aqueous and gaseous phases is made possible by identifying the intermediate products formed during the degradation of pollutants in both phases. The prediction of reaction pathways in aqueous phase is based on the attack by $OH^{\bullet}$ radicals on different families of organic pollutants and subsequently verified by the experiments. Some applications of photocatalysis (decoloration of dyes, detoxification of water, use of solar energy, air treatment (VOC and odor removal), self-cleaning materials), developed at IRCELYON will be presented and put in realistic perspectives.

Principle of Photocatalysis and Active Species

Photocatalysis is based on the double aptitude of the photocatalyst (essentially titania) to simultaneously adsorb reactants and to absorb efficient photons.

When a divided semiconductor is illuminated with photons of energy higher than or equal to its band gap energy, photo-electrons e^- and photo-holes h^+ are created. The electron is then extracted from the valence band (VB) to the conduction band (CB). This process results in a positive region in the VB (Hole h^+) and a free electron (e^-) in the CB (1). Mechanisms for the primary events occurring at the catalyst surface have been described.[1–3]

$$TiO_2 + h\upsilon \rightarrow TiO_2 + e^- (CB) + h^+ (VB) \qquad (1)$$

Reactants can adsorb and react either with electrons (acceptor molecules such as O_2) or with holes (donor molecules).

The hole, at the catalyst surface, reacts with donor molecules such as hydroxyl ions (OH^-) and adsorbs water (case of presence of water) to form free radicals ($OH^{\bullet}$). (Eqs. (2) and (3)):

$$TiO_2\,(h^+) + OH^- \rightarrow TiO_2 + OH^{\bullet}, \qquad (2)$$

$$TiO_2\,(h^+) + H_2O_{ads} \rightarrow TiO_2 + OH^{\bullet} + H^+, \qquad (3)$$
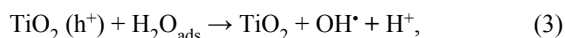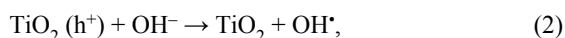
or directly with reactants (mainly in absence of water) to form $R^{+\bullet}$

$$TiO_2\,(h^+) + R \rightarrow TiO_2 + R^{+\bullet}. \qquad (4)$$
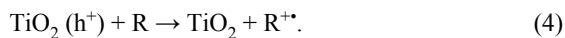
The CB electron reduces oxygen to the superoxide ion: $O_2^{\bullet-}$ (Eq. (5)). This reaction prevents the e^-/h^+ recombination, in the absence of other electron acceptors.

$$O_2 + e- \rightarrow O_2^{\bullet-} \qquad (5)$$

Water Treatment *vs.* Air Treatment

In aqueous phase, the further reduction of $O_2^{\bullet-}$ produces H_2O_2, as described in (6):

$$O_2^{\bullet-} + e- + 2H^+ \rightarrow H_2O_2 \qquad (6)$$

The superoxide ion and its protonated form subsequently dismute to yield hydrogen peroxide or a peroxide anion (Eqs. (7)–(9)):

$$O_2^{\bullet-} + H^+ \rightarrow HO_2^{\bullet} \qquad (7)$$

$$O_2^{\bullet-} + 4HO_2^{\bullet} \rightarrow 2OH^{\bullet} + 3O_2 + H_2O_2 \qquad (8)$$

$$2HO_2^{\bullet} \rightarrow O_2 + H_2O_2 \qquad (9)$$
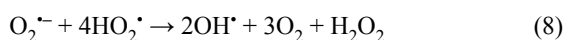
Hydrogen peroxide can also react with superoxyde *via* the Harber-Weiss reaction (10) or through the reduction of H_2O_2 by the CB e^- (11) (Ref.[4])

$$O_2^{\bullet-} + H_2O_2 \rightarrow OH^{\bullet} + OH^- + O_2 \qquad (10)$$

$$H_2O_2 + e^- \rightarrow OH^{\bullet} + OH^- \qquad (11)$$
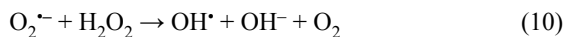
On the other hand, recombination of $OH^{\bullet}$ radicals can lead to the production of hydrogen peroxide (12):

$$OH^{\bullet} + OH^{\bullet} \rightarrow H_2O_2 \qquad (12)$$

In gas phase, organic radicals formed $R^{+\bullet}$ can react with superoxyde $O_2^{\bullet-}$ or directly with O_2 to formed oxidised compounds and in situ water, which allow to obtained a total mineralization by indirect formation of hydroxyl radical (13), (14).

$$R^{+\bullet} + O_2^{\bullet-} \rightarrow Ox \qquad (13)$$

$$R^{+\bullet} + O_2 \rightarrow Ox \qquad (14)$$

These types of reactions can also be observed in aqueous phase[5].

Principle of Self Cleaning Materials

Self cleaning materials are based on the photocatalytic and superhydrophilic properties (case of glass)[6,7] of a sub-micronic layer of photocatalyst TiO_2, deposited on their surface. Active species photogenerated, described previously (3) and (5) ($OH^{\bullet}$, $O_2^{\bullet-}$...) are able to eliminate the organic stains adsorbed on the glass surface by slow combustion at ambient temperature. Moreover, the photogeneration of these radicals induces simultaneously a phenomenon of "superhydrophili-city" on the surface of the TiO_2 layer, which takes part in the self-cleaning property of glasses, in the presence of water (rain). The proposed mechanisme occurring is presented on Fig. 1.
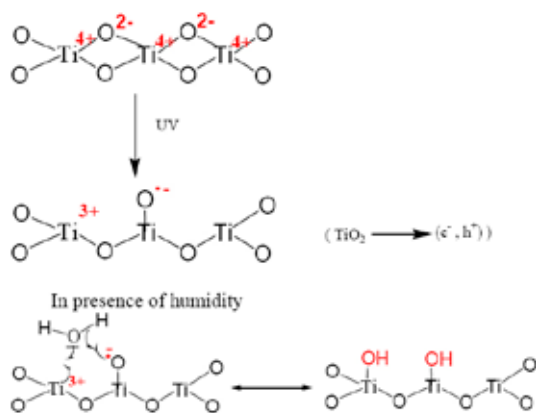
Fig. 1.   Superhydrophilicity of TiO₂

Superhydrophilicity is due to the formation of hydroxyl group on the surface of catalyst. This superhydrophilicity can occur only in the case of humide atmosphere.

Fines Chemicals *vs*. Environmental Catalysis

Indeed photocatalysis is alternatively able to induce mild and selective oxidation reactions and total oxidation reactions leading most elements to their higher oxidation state, in particular leading organic carbon to the +4 oxidation state in CO_2.

This is mainly due to the *absence* (mild oxidations) and to the *presence* (total oxidation) of water. In the first case, the active species is a neutral atomic O^* species[8] whereas in the presence of water (or humid air), $OH^{\bullet}$ radicals (2nd best universal oxidant) lead to total oxidation. Their formation is summarized in Table I.

Hydrogen Production

Scientists all over the world are very interested in hydrogen gas as the most promising energy resources to overcome the future energy crisis.

The photocatalytic decomposition of water into hydrogen and oxygen has been regarded as one of the most potential approaches ever since Fujishima and Honda reported the photoelectrochemical water splitting using a TiO_2 electrode[9].

When the surface of the TiO_2 electrode was illuminated, electrons flowed from it to the platinum counter electrode. The oxidation reaction (oxygen gas evolution) occurs at the TiO_2 electrode and a reduction reaction (hydrogen gas evolution) occurs at the Pt electrode.

The principles of photoelectrochemical water splitting have been used to guide the design of particulate systems for photocatalytic water splitting. For example, a TiO_2 particle with a small amount of Pt deposited on it is essentially a miniature photoelectrochemical cell, on which water is oxidized at the bare oxide and is reduced at the Pt-covered area to achieve the desired overall reaction.

However, particulate photocatalytic systems have the disadvantages to imply a separation of charge carriers not as efficient as with an electrode system. In addition, the back reaction between the evolved hydrogen and oxygen gases can take place. This was a problem in early work with TiO_2/Pt photocatalysts. Since, photocatalytic water splitting has been studied intensively over the past several decades. A variety of metal oxides have been examined as powder photocatalysts. These materials include transition metal oxides containing metal ions of Ti^{4+}, Zr^{4+}, Nb^{5+}, or Ta^{5+} with d^0 electronic configuration and typical metal oxides having metal ions of Ga^{3+}, In^{3+}, Ge^{4+}, Sn^{4+} or Sb^{5+} with d^{10} electronic configura-tion The record efficiency of 18.3 %, achieved on a AlGaAs/Si–RuO^2/Pt system, is very encouraging. However, these systems are so expensive that the cost of the hydrogen fuel produced would not be.competitive with other regenerative types of energy. Heterogeneous photocatalysis could provide

Table I

Features	Fine Chemicals	Environmental Catalysis
Main reaction	Mild oxidation	Total oxidation
Initial selectivity	100%	No selectivity
Final products for organics	$>C=O$	CO_2
Medium	Dry medium	Water, Humid air
Active species	O^*	$OH^\bullet$
Reaction of Formation	$O^-_{(ads)} + h^+ \rightarrow O^*_{(ads)}$	$(TiO_2) + h\nu \rightarrow e^- + h^+$ $(H_2O \leftrightarrow H^+ + OH^-) + h^+ \rightarrow H^+ + OH^\bullet$

a low-cost route for production of H_2 fuel, if the photocatalyst were able to utilize solar energy efficiently[10].

Generally, the other studies showing the photocatalytic H_2 production was initially evolved from a CH_3OH-H_2O and the mechanism implied is resume below[11].

- Dissociative chemisorption of alcohols on amphoteric OH surface groups of titania
  $R–CH_2OH_{(liq)} + (2 \text{ sites on } TiO_2) \rightarrow R–CH_2O^-_{(ads)} + H^+_{(ads)}$
- Electron transfer to metal particles as for CDIE
  $e^- + (Pt) \leftrightarrow e^-_{Pt}$
- Reaction of holes h^+ with chemisorbed alcoholate anions
  $h^+ + R–CH_2O^- \rightarrow R–CH_2O^\bullet$
- Release of a hydrogen atom and formation of a carbonyl-containing molecule (presently an aldehyde)
  $R–CH_2O^\bullet \rightarrow R–CHO + H^\bullet$
- Reverse spillover of $H^\bullet$ atoms back to the metal particle probably as protons
  $H^\bullet \rightarrow H^+ + e^-$
- Neutralization of protons at metal particles containing an excess of electrons "nano-cathodic – (like process)"
  $H^+ + e^-_{Pt} \rightarrow H^\bullet_{(Pt)}$
- Recombination of $H^\bullet$ atoms and evolution in the gas phase
  $2H^\bullet_{(Pt)} \rightarrow H_2(g)$

Research Field in Photocatalysis Developed at IRCE-LYON
Water Treatment
Removal of organic compounds – Comparison and/or coupling with other advanced oxidation processes

Removal of a large number of organic compounds such as phenolic compounds[12,13], pesticides[14–16], dyes[17,18] has been successfully degraded and chemical pathways identified in our laboratory. Their kinetics or chemical pathways compared to other advanced oxidation technologies[19–21] such as H_2O_2–UV, H_2O_2–Fe^{2+}, O_3 and ultrasound[22,23]. We have also shown that the combination between photocatalysis with these different advanced oxidation processes can improve their efficiency. For exemple the electronic affinity of ozone favor the (e^-, h^+) separation and the formation of actIve species.

The efficiency of supported TiO_2 has been evaluated and demonstrated strongly decreased the photocatalytic degradation of non-neutral compounds. This decrease has been

attributed to the presence of silica binder which decreases the adsorption of anionic compound on the photocatalyst by electrostatic repulsion.

Fate of nitrogen group

Nitrogen has always been a complex element in chemistry because of its apparent inertness as N_2, and of its multiple oxidation states, ranging from -3 to $+5$. Nitro-compounds were found to decompose into nitrite, easily oxidized into nitrate. Amino groups have been found to decompose into ammonium ions, slowly oxidizable into nitrate. Eventually, nitrogen atoms incorporated into triazinic aromatic rings were found to resist oxidation, remaining in their -3 oxidation state. This was showed by a partial oxo-degradation of *s*-triazine into cyanuric acid $C_3H_3O_3N_3$. Fortunately, cyanuric acid is innocuous because of its very high stability. It constitutes one of the very few examples of organics resisting photocatalytic degradation at room temperature. This is due *(i)* to the three bonds of N atoms involved in the aromatic ring skeleton (i.e. without aliphatic substituents) and *(ii)* to the maximum formal oxidation state of carbon $(+4)$, already reached in $C_3H_3O_3N_3$. Concerning the degradation of $(–N=N–)$ azo-groups, the mass balance in *n*-containing final products could not be obtained in aqueous phase analyses considering only the formation of NO_3^- and NH_4^+. However, this mass balance can be obtained quantifying N_2 evolution, and show that azo-groups is mainly transformed into nitrogen gas. For example, N2 evolution from Congo Red (the "terror" of printers and of paper-makers) is given in Fig. 2. During its photocatalytic
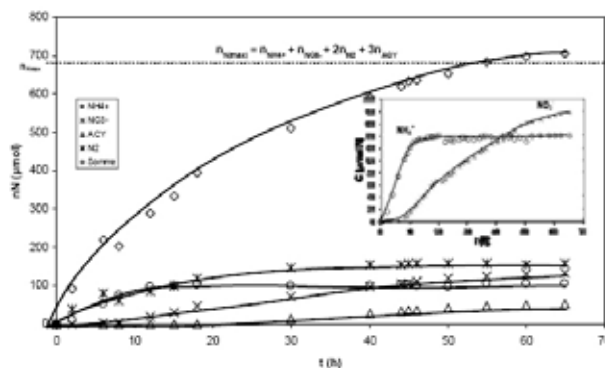
Fig. 2. **Kinetics of n-containing compound evolution, either in the aqueous or the gas phase during the photocatalytic degradation of Congo Red dye**

degradation the total nitrogen balance could be permanently established.

In the case of Amaranth a prohibited cancerigen alimentary dye or Reactive Black 5, the 100 % gaseous N2 expected could not be reached. The only 85 % and 70 % of N2 obtained were due to the presence of a hydrazone isomeric form shown below.
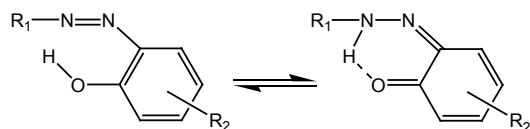
Prediction of chemical pathways – Impact of electronic density

Several studies mentioned the importance of electronic density on initial attack of hydroxyl radical, considering their electrophilic characters but also the importance of adsorption.[24–27] Taking into account these works, we used the CAChe software and the semi-empirical MOPAC package to calculate Frontier electron densities and point charges of all individual atoms in different structures (triazolidine[28], Imazapyr[29] and diuron.

Then we correlated these values with experimental results and showed that we can predict the main initial intermediates products taking into account the attack of OH• radical on the highest electronic density.

For example, electronic density can explain that amine group is mainly transformed into nitrate in the case of ammelide whereas amine group are transformed into ammonium in the case of amino-phenol (Fig. 3.)

However, this approach is a global approach and it does not explain for exemple if the monochlorohydroxylated compounds which are mainly formed in the case of diuron are obtained abstraction of hydrogen and hydroxylation or addition of OH• on the cycle and then dechlorination.

For these reasons DFT calculations have been established to determine the enthalpy of formation of each compounds considering attack by OH• radical on each atom.

Removal of micro–Organisms

Obtaining a clean air or a drinking water does not pass only by the elimination of the polluting species of chemical origin (dyes, pesticides, hydrocarbons,…), it requires also the elimination of the pollutants of biological origin (virus, bacteria, mushroom, yeast…). This operation is called disinfection or sterilization.

At IRCELYON, we work on the study of a photocatalytic disinfection process which has the advantages of proceeding at room temperature and atmospheric pressure without addition of chemical reagents and to allow a total CO_2 mineralization and H_2O. Our studies aim to better understand the mechanisms of action of the reactive species HO•, $O_2^{•-}$, $HO_2^•$, produced on the surface of the irradiated photocatalyst.

The studies began with Escherichia coli, a model micro–Organism representative of the bacteria. Correlations between chemical analyzes and biochemical are studied by determi-
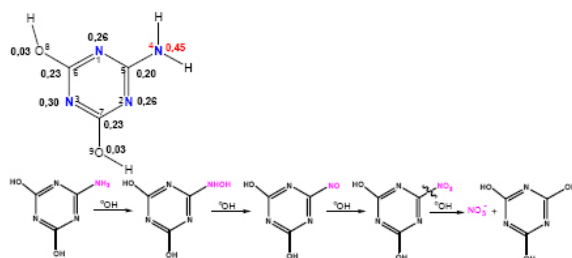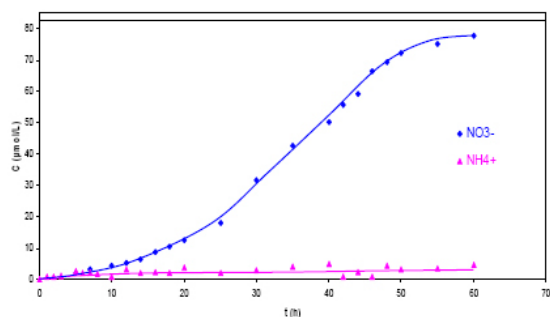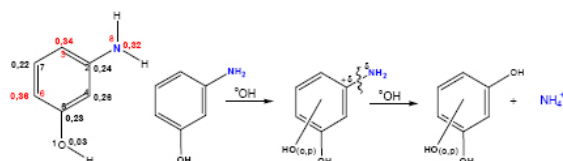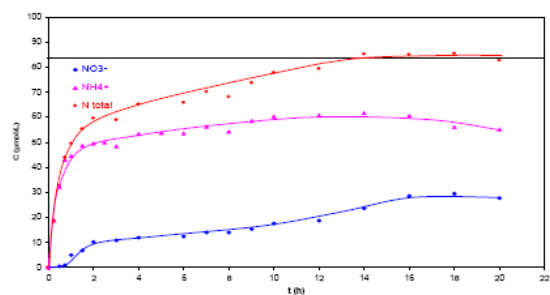
Fig. 3. **fate of nitrogen in the photocatalytic degradation of 3-amino-phenol and ammelide**
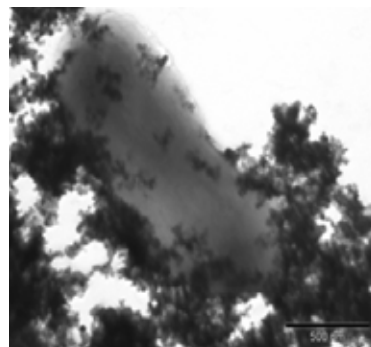
Fig. 4.   **Electronic microscopy of a suspension of *E. coli* bacteria in contact with the catalyst TiO$_2$ Degussa P–25**

nation of the photocatalytic oxidation in vitro of the nucleic acids (DNA, ARN). The first results, under UV-A irradiation
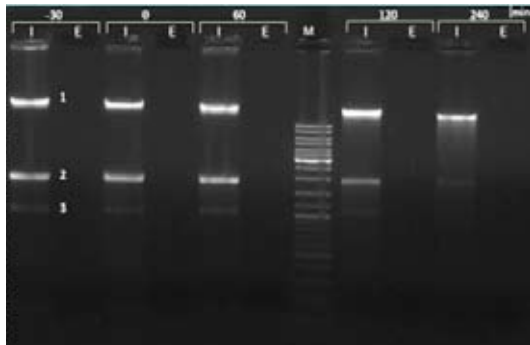
Fig. 5.   **Picture of gel electrophoresis from I: Intracellular sample, E: Extracellular sample of suspension of *E. coli* treated by UVA photocatalysis at different exposure times (0–240 min). The bands correspond to (1) chromosomic DNA, (2) 23S rRNA and (3) 16S rRNA. M: DNA molecular weight marker**

in the presence of a photocatalysor TiO_2, show the importance of the contact between micro-organisms and nanoparticules of the catalyst (Fig. 4.) which leads to the perforation of the membrane and the loss of cultivability. In parallel one observes the formation of ions ammonium and organic acids, the progressive degradation of the ARN and DNA (Fig. 5.) and the absence of nucleic acids in solution.

Used of solar energy

Various contaminants (phenol, 4-chlorophenol, 2,4-D, benzofurane, malic acid, formatante, Congo Red,…) previously studied in our laboratory, were later photodegraded in the solar pilot plant at the "Plataforma Solar de Almeria" (PSA, Spain) and it was demonstrated that the kinetic results obtained with micro-photoreactors at laboratory scale could be extrapolated to pilot photoreactors having capacities of several hundred litres by using a circulating suspension of titania. The variation in photo-efficiency under high solar flux, as well as possible thermal effects of solar light, has also been studied.[30] Some years later, European program AQUA-CAT allows us to developed and test a totally autonomous solar photoreactor, presented in Fig. 6., able to potabilize water by decontamination (chemicals) but also disinfection (bacteria).

Fig. 6.   **AQUACAT autonomous solar photoreactor prototype for water potabilization**

Air Treatment

Removal of Organic Molecules – Comparison of Reaction Mechanisms Occurring in Aqueous and Gaseous Phases

Conventional technologies for removing VOCs from the polluted air stream involved adsorption by activated carbon, biofiltration and bioscrubbling, thermal oxidation and incineration which encounter the drawbacks to be non destructive and/or expensive because of high-energy requirements and/or consumption of chemicals. A highly promising method for the destruction of VOC is photocatalytic oxidation. It offers several advantages, in comparison to the other processes, such as the destruction of organic contaminants rather than their transfer from a phase to another one, a complete mine-

(a)
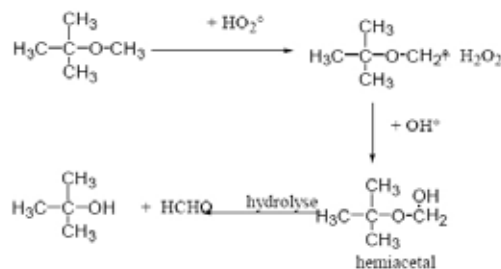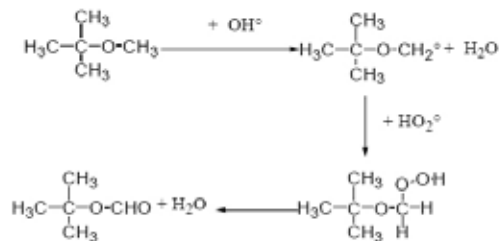
(b)
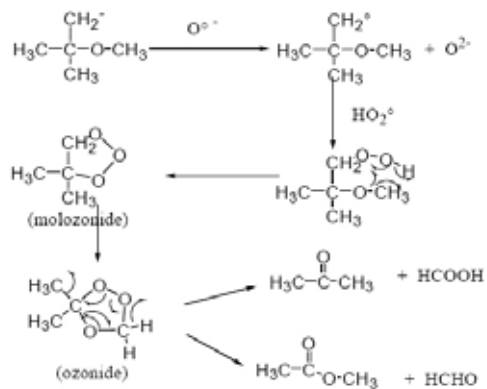
Scheme 1
Main mechanism of MTBE photocatalytic degradation in aqueous (a) or gaseous phase (b)

ralisation into carbon dioxyde and water and a wide range of VOC can be treated. Its efficiency has been demonstrated for removing a large number of VOC. In our laboratory we have shown the efficiency of the degradation of different odorous compounds[31,32] and even for the total mineralization of triple carbon-carbon bonding[33].

Moreover, utilization of this process is energetically interesting because it operates at ambient temperature and the use of solar energy to initiate photocatalytic oxidation reactions is possible.

The photocatalytic reaction mechanism is few studied in gas phase and the role of water on the mechanism not really well established. The study of humidity on mechanism of acetylene photocatalytic degradation reveals that in dry air, acetylene is slowly degraded and mainly reacts with photo-generated holes.

The comparison of the reaction mechanisms occurring in gas and aqueous phases in the photocatalytic degradation of methyl-tertio-butyl ether (MTBE), a volatile organic compound (VOC) used as a substitute for tetraethyl-lead in gasoline agree with

In aqueous phase, the main pathway is the attack on the methoxy group of MTBE by $OH^{\bullet}$ and in a less extend by $HO_2^{\bullet}$ to form tertio butyl formiate and tertio butanol while in gaz phase the attack mainly occur by hole on methyl of tertio bytyl.

In Scheme1 are represented the main mechanism of attack of MTBE in aqueous phase (a) and gaz phase (b)

Improvement of Photocatalysis by Coupling With Adsorbant or Cold Plasma

In our laboratory, we also work on the improvement of the photocatalytic efficiency. In air treatment, we have first tested the effect of the presence of adsorbant such as zeo-lithe and secondly coupled photocatalysis with non-thermal plasma.

Contrary that it will be mentioned in the literature, our results reveals that no improvement of VOC degradation occurs in presence of TiO_2 + activated carbon whereas zeolite improves the efficiency of TiO_2 supported on non woven fibre; These improvement is attributed a better dispersion on TiO_2 on fibre (Fig. 7.).

The initial reasons for coupling plasma and photocatalysis were that the photocatalysis was expected favour the total mineralization of VOC into CO_2 by decreasing intermediate compound formed in plasma reaction but also used UV generated by plasma, due to excited nitrogen relaxation, as well as activated species such as ozone, which are able to, are activate photocatalytic material.

Our results reveals that an improved of efficiency is observed when materials are present in plasma discharge. However, this improvement is mainly due to the presence of a porous material. It means that UV generated by plasma is not sufficient to activate photocatalyst.
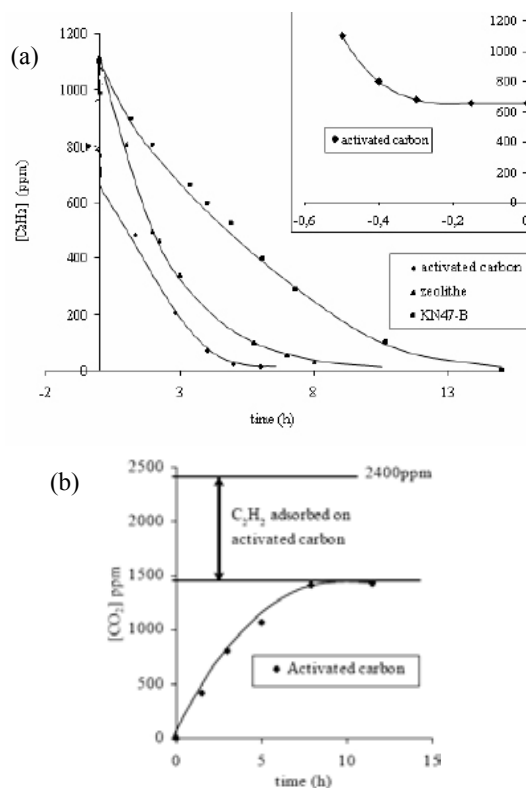
Fig. 7.   **(a) Adsorption and photodegradation of acetylene on TiO_2 coupled with adsorbing material or not and (b) Photoproduction of CO_2 by TiO_2 coupled with activated carbon**

Studies performed using additional UV indicates that a synergy is observed between plasma and photocatalysis, less CO is detected and the formation of carbon dioxide is improved. Moreover, the photocatalytic material is less easily poisoned by intermediate compounds formed due to its regeneration by plasma.

Removal of Virus

The efficiency of a photocatalytic reactor against the avian influenza virus using an aerosol flow of about 40 $m^3\,h^{-1}$ and about 10^3 $CFU\,ml^{-1}$ (CFU: Colony Forming Unit) have beeen tested. Since the A/H5N1 virus is strongly pathogenic,

Fig. 8.   **Photos of experimental device used to test the efficiency of BUXAIR reactor against the avian influenza virus**

the tests were performed on the A/H5N2 strain of the virus, chosen as the conventional research model for the A/H5N1 strain. A reference was made using no irradiation flux. The experimental set was represented in Fig. 8.

Titration results are presented in the Fig. 9.a,b. Without UV-light, we observe a 0.7 log (or 80%) reduction of the number of viruses. The addition of UV-light led to a complete elimination of viruses titrated at entry up to a 3.1 log.

(a)

(b)
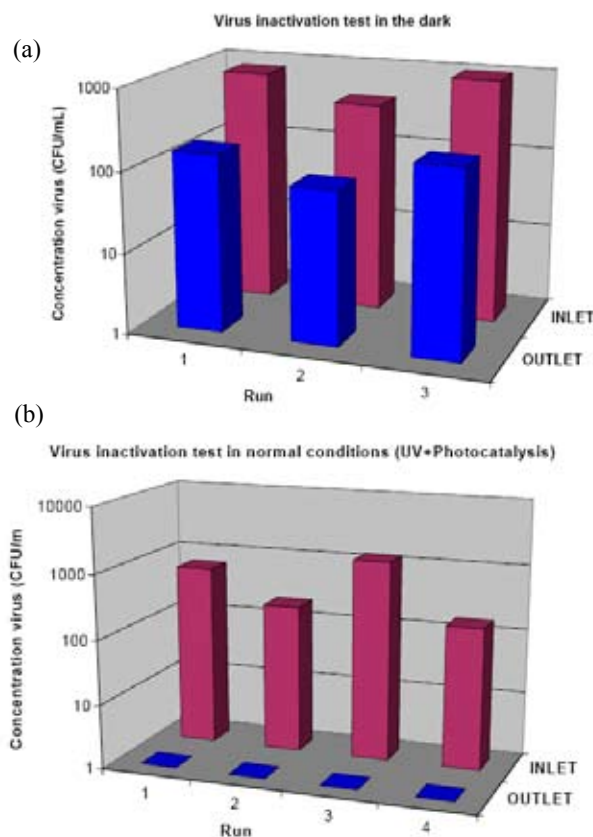
Fig. 9. **(a) Virus inactivation tested in the Imutube photoreactor in dark conditions. Air flow: 40 m3/h; (b) Virus inactivation tested in the Imutube photoreactor in UV + photocatalyst**

Self Cleaning Materials
Present Challenges in Photocatalysis

The number of publications on photocatalysis presently increases exponentially, especially from emerging countries and from the community of materials. Experts are now confronted by new challenges. Some of them concern the following points:
- Are we "condemned" to exclusively work with titania?
- Can TiO_2 be photosensitized in the visible by doping? (It is already known that cationic doping is not efficient and rather detrimental whereas anionic doping is under investigation).
- Can we find a new photocatalyst different from TiO_2 and directly active in the visible?

- Is photocatalysis suitable for preparative Fine Chemistry?
- Is photocatalysis enough bactericide in water and in air?
- Can Photocatalysis be employed as a new medical tool ("cancericide effect,….")?
- Are we able to define a few standardized and globally accepted tests for each photocatalytic application?

REFERENCES
1. Ollis D.F.: Environ. Sci. Technol. *19*, 480 (1985).
2. Serpone N.: Solar Energy Mater. Solar Cells *38*, 369 (1995).
3. Pichat P., Fox M. A. in *Photoinduced Electron Transfer* (Eds: M. A. Fox, M. Chanon), Elsevier, Amsterdam, Part D, 241,1988.
4. Pichat P., Guillard C., Laurence A., Renard A-C., Plaidy O.: Sol. Energy Mater. Sol. Cells *38*, 391 (1995).
5. Cermenati L., Pichat P., Guillard C., Albini A.: J.Phys. Chem.B *101*, 2650 (1997).
6. Mills A., Hill G., Bhopal S., Parkin I. P., O'Neill S. A.: J. Photochem. Photobiol. A: Chem. *160*, 185 (2003).
7. Watanabe T., Nakajima A., Wang R., Minabe M., Koizumi S., Fujishima A., Hashimoto K.: Thin Solid Films *351*, 260 (1999).
8. Herrmann J. M. et al.: J.Catal. *60*, 369 (1979).
9. Fujishima A., Honda K.: Nature *238*, 37 (1972).
10. Fujishima A., Zhang X., Tryk D. A.: Int. J. Hydrogen Energy *32*, 2664 (2007).
11. Pichat P, Herrmann J. M., Disdier J., et al.: Nouveau J. Chim.– New J. Chem. *5*, 627 (1981).
12. Guillard C., Disdier J., Herrmann J.-M., Lehaut C., Chopin T., Malato S., Blanco J.: Catal. Today *54*, 217 (1999).
13. Lapertot M.; Pichat P., Parra S., Guillard C.; Pulgarin C.: J. Environ. Sci. Health. Part A Environ. Sci. Health Part A Environ. Sci. Eng *41*, 1009 (2006).
14. Marinas A., Guillard C., Marinas J. M., Fernandez-Alba A. Amadeo, Aguëra A., Herrmann J.-M.: Appl. Catal. B: Environmental *34*, 241 (2001).
15. Goutailler G., Valette J.-C., Guillard C., Pad'ssé O., Faure R.: J. Photochem.Photobiol. A:Chem. *141*, 79 (2001).
16. Carrier M., Perol N, Herrmann J.-M., Bordes C., Horikoshi S., Paisse J.–O., Baudot B., Guillard C.: Appl. Catal., B *65*, 11 (2006).
17. Vautier M., Guillard C., Herrmann J. M.: J.Catal. *201*, 46 (2001).
18. Guillard C., Lachheb H., Houas A., Ksibi M., Elaloui E., Herrmann J.-M.: J. Photochem. Photobiol. A: Chem. *158*, 27 (2003).
19. Maillard C., Guillard C. Pichat P.: Chemosphere *24*, 1085 (1992).

20. Guillard C.: J. Photochem. Photobiol. A: Chem. *135*, 65 (2000).
21. Pichat P., Cerminati L., Albini A., Mas D., Delprat H., Guillard C.: Res. Chem. Intermed. *26*, 161 (2000).
22. Theron P., Pichat P., Petrier C., Guillard C.:Water Sci. Technol. *44*, 263 (2001).
23. Guillard C., Theron P., Pichat P. Petrier C.: Water Res. *36*, 4263 (2002).
24. Amalric L., Guillard C., BlanC–Brude E., Pichat P.: Water Res. *30*, 1137 (1996).
25. Palmisano G., Addamo M., Augugliaro V., Caronna T., Di Paola A., Garcia Lopez E., Loddo V., Marci G., Palmisano L., Schiavello M.: Catal. Today *122*, 118 (2007).
26. Tuazon E. C., Leod H. M., Atkinson R., Carter W. P. L.: Environ. Sci. Technol. *20*, 383 (1986); Horikoshi S., Serpone N., Zhao J., Hidaka H.: J. Photochem. Photobiol. A: Chem. *118*, 123 (1998).
27. Horikoshi S., Watanabe N., Mukae M., Hidaka H., Serpone N.: New J. Chem. *25*, 999 (2001).

28. Guillard C., Horikoshi S., Watanabe N., Hidaka H., Pichat P.: J. Photochem. Photobiol. A: Chem. *149*, 155 (2002).
29. Carrier M., Pérol N., Herrmann J.-M., Bordes C., Horikoshi S., Paďssé J. O., Baudot R., Guillard C.: Appl. Catal., B *65*, 11 (2006).
30. Guillard C., Disdier J., Herrmann J. M., Lehaut C., Chopin T., Matato S., Blanco J.: Catal. Today *54*, 217 (1999).
31. Van-Hoang C., Pichat P., Courbon H., Disdier J., Guillard C.: *Proc.4th Int.Cong.on Characterization and Control of Odors and VOCs*, p.468. Montreal, Canada, (1997).
32. Guillard C., Baldassare D., Duchamp C., Ghazzal M. N., Daniele S.: Catal. Today *122*, 160 (2007).
33. Thevenet F., Guaďtella O., Herrmann J.-M., Rousseau A., Guillard C.: Appl. Catal. B: Env. *61*, 62 (2005).

L07 PHOTOCATALYTIC PROPERTIES OF TIO₂ AND PHOTOSENSITIZING MATERIALS FOR BACTERICIDAL APPLICATIONS

C. GUILLARD[a], K. BENABBOU[a,b], T.-H. BUI[a], S. PIGEOT-REMY[a], T. PIGOT[c], S. LACOMBE[c] and P. LEJEUNE[d]

[a]Institut de recherche sur la catalyse et l'environnement de Lyon (IRCELYON), Université Lyon 1–UMR 5256 CNRS, 2 Avenue Albert Einstein 69626 Villeurbanne cedex France,
[b]Laboratoire physico-chimie des matériaux, Catalyse et environnement. Fac. Des sciences, Département de chimie, Université des Sciences et de la technologie d'Oran – B.P 1505 EL M'naouar 31000. Oran – Algérie,
[c]Institut Pluridisciplinaire de Recherche sur l'Environnement et les Matériaux (IPREM-ECP), UMR CNRS 5254, Université de Pau et des Pays de l'Adour, Hélioparc, 2 rue du Président Angot, 64053 Pau cedex 9,
[d]Microbiologie, Adaptation et Pathogénie. UMR 5240 CNRS-UCB-INSA-BCS. Domaine scientifique de la Doua. 10, rue Raphaël Dubois. Bât. Lwoff. 69622 Villeurbanne. Cedex,
Chantal.guillard@ircelyon.univ-lyon1.fr

Introduction

Several water disinfection technologies are available, such as chlorination and ozonation. However, in addition to their high costs, they can lead to the formation of harmful disinfection by-products (DBPs), among which the most dangerous are the trihalomethanes (THMs), well-known for their high carcinogenic potential[1].

Among the new oxidation methods or "Advanced Oxidation Processes" (AOP), heterogeneous photocatalysis appears as an emerging destructive technology leading to the total mineralization of pollutants at ambient temperature and atmospheric pressure using a cheap photocatalyst, TiO₂, having the possibility of using a part of solar energy as the UV source. Its principle is based on the formation of highly reactive oxygen species (ROS), such as $OH^\bullet$, $O_2^{\bullet-}$ $HO_2^\bullet$, capable of destroying chemical and biological water contaminants, under irradiation of semiconductor particles (photocatalyst) with photons of energy higher than or equal to its band gap energy. TiO₂ mediated photocatalysis has been widely investigated for a large number of organic contaminants. Their degradation pathway and their mineralization has been reported[2,3]. Nowadays, interest is directed to the use of this technique in water disinfection. Photocatalytic oxidation as a technique for microbial disinfection was first demonstrated by Matsunaga et al.[4] using TiO₂–Pt photocatalyst. Since the effects of various parameters (nature of support, nature of photocatalyst, light power, initial concentration) on the photocatalytic efficiency have been studied[5,6]

Other types of catalysts begin to appear for desinfection, such as photosensitizing materials which generate singlet oxygen under UV but also visible light. Singlet molecular oxygen (abbreviated ¹O₂) is the lowest electronic excited state of molecular oxygen. It can be readily generated by energy transfer from electronically excited dyes to ground state dioxygen, following a photochemical process called sensitization in which the excited state of the sensitizer, mostly in its triplet state, is quenched by molecular oxygen yielding singlet oxygen. Singlet oxygen is a short-lived highly reactive species that is known to inactivate air- or water-carried bacteria efficiently[7,8].

In this work, we compared the photoinduced deactivation of the model bacteria *Escherichia coli* K–12 (*E. coli*) using industrial TiO₂ photocatalysts, Degussa P25 and Millennium PC500, either suspended or supported and photosensitizers supported on silica (organic molecules derived from quinone, benzophenone, or 9,10-dicyanoanthracene). The influence of parameters, such as the nature and amount of the sensitizer or TiO₂ and of the irradiation intensity was investigated.

Experimental

Materials

Two industrial and commercial TiO₂, Degussa P25 and Millennium PC–500 and four sensitizers (9,10-Dicyanoanthracene (DCA), anthraquinone (ANT), 4-benzoyl benzoic acid (4-BB) and a new photosensitizers named X) prepared on silica[9] were used in suspension. PC–500 coated on Ahlstrom paper and commercialized by Ahlstrom firm under the reference 1048 was used as supported TiO₂.

Bacterial Strain and Growth Media

The bacteria strain used was *E. coli* K12 PHL 1273 containing a green Fluorescent protein (gfp) in ADN which enhanced the synthesis of fimbriae.

Aliquots of the overnight cultures were inoculated into fresh medium and incubated aerobically at 37 °C until the stationary growth phase was reached (15 h). Growth was monitored by optical density (OD) at 600 nm. Bacterial cells were harvested by centrifugation at 500 rpm for 10 min at 4 °C. The bacterial pellet was subsequently washed three times with the Mili-Q water. Cell suspensions were inoculated in the solution in a Pyrex cylindrical reactor to the required cell density corresponding to 10^7–10^8 colony forming units per millilitre (CFU ml⁻¹). Serial dilutions were prepared if necessary in the solution and 100 μl samples were plated on Plate-Count-Agar (PCA, Merck, Germany). Plates were incubated at 37 °C for 24 h before the bacterial counting was carried out.

Photoreactor and Light Sources

The reactor consisted on a batch Pyrex cylindrical (100 cm³) inside which 20 ml of *E. coli* aqueous solution was put into contact with the photocatalyst. The directly irradiated side of the reactor was the bottom window suprasil disk, 3 cm diameter. The light source was a HPK 125 W Philips mercury lamp, cooled with a water circulation. The irradiation spectrum was cutt–Off below 340 nm using a Corning 0.52 filter. All reactions were carried out at ambient temperature.

Results and Discussions

E f f i c i e n c y   o f   T i O$_2$

Fig.1 represents the inactivation of *E. coli* strain in presence of the two titania photocatalysts in slurry and of supported PC–500.

In suspension, TiO$_2$ PC–500 is much more efficient than TiO$_2$ P25 to inactivate *E. coli*. However, its efficiency decreases when it is supported due to the lower contact between catalyst and bacteria[10].

The more important efficiency of the PC–500 as a function of time can be explained by considering the evolution of the pH (from 6.5 to 5 after 3 hours) during the photocatalytic inactivation of *E. coli*. In this case more TiO$_2$ surface is positively charged. TiO$_2$ PC–500 should be more efficient than P25 due to the presence of more negative charges on its surface, at the working pH, taking into account the isoelectric point (IEP) of both catalysts (IEP = 7 for P–25 and 6.2 for PC 500).

Another hypothesis could also be suggested considering the smaller PC–500 particles, which could more easily penetrate between fimbriae and help more quickly to perforate the membrane. However, PC–500 particles were more agglomerated those of P25 as found by D.Gumy[5]. This hypothesis seems less probable than that based on surface charges.
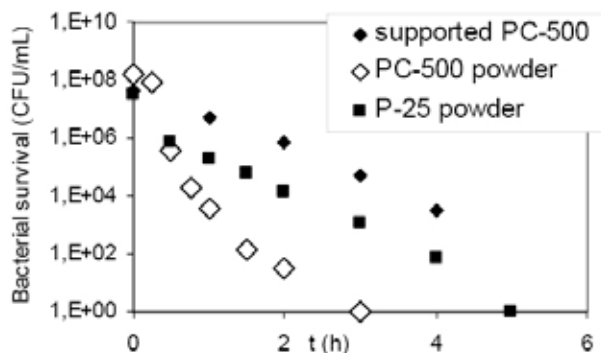
Fig. 1.   **Inactivation of *E. coli* 1273 strain in presence of 1 g dm^{-3} of TiO$_2$ Degussa P25 or TiO$_2$ Millennium PC–500 using a 3.85 mW cm^{-2}**

The effect of the amount of TiO$_2$ (P–25) and of light intensity show:

(i) that the optimal concentration of TiO$_2$ found to inactivate *E–coli* was 0.25 g dm^{-3}. Above this value a scattering effect of titania occurs,

(ii) by increasing the intensity from 0.48 to 3.85 mW cm^{-2}, the time necessary to totally inactivate *E–coli* decreased from 180 to 90 minutes and seems reach a plateau above 4 mW cm^{-2}.

E f f i c i e n c y   o f   P h o t o s e n s i t i z e r s
–   C o m p a r i s o n   w i t h   T i O$_2$

The efficiencies of the photosensitizers supported on silica elaborated by the sol-gel method, to inactivate *E.coli* are presented on Fig. 2.

Contrary to the results observed with TiO$_2$, with all the sensitizing materials a lag period is observed which can be attributed to the self-defense of the micro–Organism against active species such as $^1O_2$ (no OH$^•$ radical can be formed with these sensitizers).
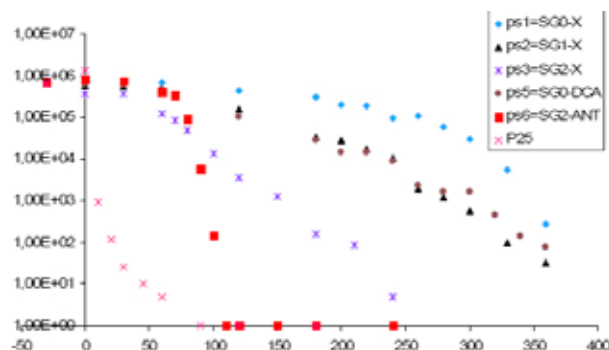
Fig. 2.   **Efficiencies of used photosensitizers**

Several parameters can influence the results obtained with these sensitizing materials, such as the nature and the concentration of the photosensitizer in the material, its method of preparation (inclusion for SG0, grafting in the xerogel for SG1 or post-grafting for SG2), or its specifice surface area. For exemple, with an original sensitizer × prepared in the lab (patent pending), it is found that a material obtained by post-grafting of the photosensitizer on silica xerogel (SG2–X) presents a higher efficiency than the same material prepared by grafting during the sol-gel process (SG1-X), itself more efficient than the material obtained by inclusion of the photosensitizer in the xerogel (SG0-X). However the se nsitizer × concentration decreases for these three materials in the order SG2>SG1>SG0 (27, 10 and 0,6 µmol g^{-1} respectively). Moreover, the increase of photosensitizer amount in the experiment leads to an increased efficiency. Comparing now different sensitizers, it is observed that SG0-DCA and SG0-X, prepared by inclusion of the sensitizer with roughly the same concentration (0,2 and 0,6 µmol g^{-1} respectively, gives the lowest efficiency. The most efficient material is an anthraquinone grafted material, SG2–ANT, with a much higher sensitizer concentration (250 µmol g^{-1}). However, additional work is needed to further correlate the known quantum yield for $^1O_2$ production and the inactivation order[11].

Compared to DEGUSSA P25 TiO$_2$, the efficiency of the photosensitizing materials is less important and a noticeable lag time before inactivation is observed. However the study of this type of catalysts to inactivate bacteria should be developed considering their potentiality to be activated by solar light.

REFERENCES

1. Lawrance C. E., Taylor P. R., Trock B. J., Reilly A. A.: Natl. Cancer Inst. *72*, 563 (1984).
2. Hoffmann M. R., Martin S. T., Choi W. Y., Bahnemann D. W.: Chem. Rev. *95*, 69 (1995).

3. Guillard C.: J. Photochem. Photobiol. A: Chem. *135*, 65 (2000).
4. Matsunaga T, Tamoda R, Nakajima T, Wake H: FEMS Microbiol. Lett *29*, 211 (1985).
5. Gumy D., Morais C., Bowen P., Pulgarin C., Giraldo S., Hajdu R., Kiwi J.: Appl. Catal. B: Environ. *63*, 76 (2006).
6. Benabbou A. K., Derriche Z., Felix C., Lejeune P., Guillard C.: Appl. Catal. B: Environ.l, *76*, 257 (2007).
7. Biological inactivation by singlet oxygen: distinguishing O_2 ($1\Delta g$) and $O_2(1\Sigma g+)$, Biochim. Biophys. Acta (G) *1117(2)*, 216 (1992).
8. Jemli M., Alouini Z., Sabbahia S., Gueddarib M.: J. Environ. Monit. *4*, 511 (2002).
9. Latour V., Pigot T., Mocho P., Blanc S., Lacombe S.: Catal. Today *101*, 359 (2005).
10. Bui T.-H., Felix C., Pigeot-Remy S., Herrmann J.-M., Lejeune P., Guillard C.: J.Adv. Oxyd. Techn., in press.
11. Cantau C., Pigot T., Manoj N., Oliveros E., Lacombe S.: ChemPhysChem. *8*, 2344 (2007).

L08 INTERACTIONS IN IRON GALL INKS IN AIR AND NITROGEN ATMOSPHERE

VIERA JANČOVIČOVÁ, MICHAELA CIGLANSKÁ, BOHUSLAVA HAVLÍNOVÁ and MICHAL ČEPPAN

Department of Printing Arts Technology and Photochemistry IPM, Faculty of Chemical and Food Technology SUT, Radlinského 9, 812 37 Bratislava, Slovak Republic,
viera.jancovicova@stuba.sk

Introduction

One of the most commonly used writing and drawing materials applied from the ancient times through Middle Ages until the modern times were the iron gall inks. In Europe they were highly used from the beginning of 11th century until the end of 20th century. The libraries and archives all over the world contain enormous amount of books (notes of Leonardo da Vinci), manuscripts, documents (US constitution proposal) and musical compositions (scores of J. S. Bach), which were written with iron gall inks.

For the preparation of iron gall inks, galls (from the chemical point of view these are polyphenols), vitriol (iron(II) sulphate), gum arabic, and as a solvent, water, sometimes wine, beer or vinegar were used. Sometimes pigments or copper (II) sulphate were added into these inks. The mixture of polyphenols with iron(II) sulphate contained complexes, which were in many cases dark coloured, while the black colour was the result of the exposure to air[1]. The manufactured inks exhibited very low pH values and represented real danger of the damage for the carrier onto which they were applied. The chemical character of inks remained very important due to the conservation problems and is very important for solving problems with the corrosion of the paper carrier. The damages included the browning of handwriting, the paper breaking, holes in carriers and the total loss of documents caused by the corrosion.

The important component that can influence the reaction between iron ions and phenolic acid is gum arabic, a binder used in the production of the ink. V. Rouchon Quilet observed in her work, that this binder might inhibit the degradation of the paper by iron gall inks[2].

Several authors have studied the structure of iron gall pigments. Wunderlich assumed that formed complex contained iron octahedrally coordinated with six oxygen atoms in four molecules of gallic acid[1]. The iron chelation properties of phenolic acids are very important also for living organism. According to authors Mabrour J. et al., plants tannins, which were used also in the ink preparation were the mixtures of several compounds (tannic acid, gallic acid and ellagic acid) and with iron cations or other metal ions were able to create chelates that composed of 3 phenolic acid units attached to one iron ion.

The evaluation of the metal chelation properties of phenolic acid has been usually done by means of UV VIS absorption spectroscopy, analysing the shifts of UV bands of polyphenolic compounds and the formation of new bands in the visible region[3].

Building on the knowledge about historical inks obtained from literature we prepared the model systems compound of gallic acid, ferrous sulphate and gum Arabic. We investigated the reaction of gallic acid with Fe(II) ions. The complex formation in the solution on air and in nitrogen atmosphere was monitored by UV VIS spectroscopy. At the same time we monitored pH value of the solutions.

Experimental

Gallic acid (3,4,5-trihydroxybenzoic acid) monohydrate, p.a. and gum arabic, p.a. were obtained from Sigma-Aldrich, ferrous sulphate ($FeSO_4 \cdot 7H_2O$) was purchased from Lachema Brno (Czech Republic).

We followed the historical recipe to prepare the model inks.[4] Prepared solution of gallic acid (3.6×10^{-4} mol dm^{-3}) and ferrous sulphate (1.8–7.2×10^{-4} mol dm^{-3}) in gum arabic solution (1 g of gum arabic 100 ml^{-1} water) were mixed immediately before the measurement. The samples were closed in the quartz cell and stored in the dark.

The solutions for study of complex formation in nitrogen atmosphere were continuously bubbled with nitrogen gas for 15 minutes before mixing. After the addition of ferrous sulphate to gallic acid, the samples were saturated with nitrogen again and then closed in quartz cell.

The UV VIS spectra of gallic acid and the changes in the spectra after addition of ferrous sulphate were recorded on UV VIS spectrophotometer PU 8800 (Philips, United Kingdom). The UV VIS spectra were measured in the wavelength range of 200–800 nm *vs.* a reagent blank containing gum arabic at specified concentrations in the cell (length = 1 cm). The pH measurements were carried out on the digital pH meter (Jenway 3510, United Kingdom).

Results

The UV VIS spectra of the colour complex occurrence on air were investigated in the solution of gum arabic (1 % wt.),
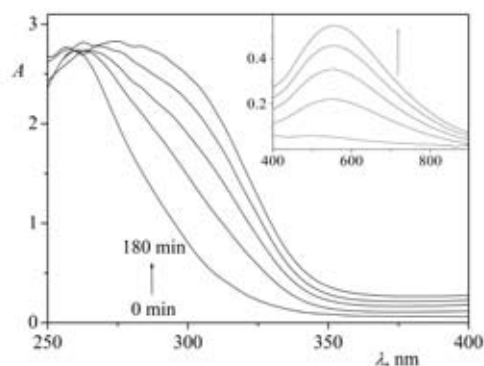
Fig. 1. **UV VIS spectra of complex formation after the addition of $FeSO_4$ to gallic acid ($[FeSO_4]_0 = 7.2 \times 10^{-4}$ mol dm^{-3}; $[gallic\ acid]_0 = 3.6 \times 10^{-4}$ mol dm^{-3}) at various time after mixing of components (0, 30, 60, 120, 180 min)**

gallic acid (3.6×10^{-4} mol dm^{-3}) and three concentrations of ferrous sulphate (1.8, 3.6 and 7.2×10^{-4} mol dm^{-3}). The new absorbance band with maxima between 560 and 590 nm was formed after the addition of ferrous sulphate to gallic acid (3.6×10^{-4} mol dm^{-3}) in gum arabic solution (Fig. 1.). This increase in absorbance indicated that gallic acid chelated iron and produced the complex that gives a colour absorbed in the visible range. The complex formation was slow and continued several hours up to several days, because the delimited reaction was the formation of unstable complex Fe(II) – gallic acid, that was the first step in the formation of the coloured Fe(III) complex. Simultaneously we observed the batochrome shift of absorbance maxima from 260 nm to 280 nm, immediately after the addition of Fe(II) ions and after 4 hours of the interaction of ink components (Fig. 1.). This shift could be caused by the structural changes in the gallic acid molecule as a consequence of the complex formation with Fe or the partial oxidation of gallic acid by the hydroxyl radicals produced *via* Fenton mechanism in the presence of Fe.
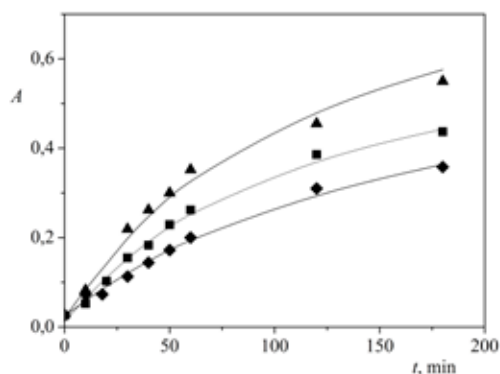
Fig. 2. **Increase of absorbance at 560–590 nm after addition of FeSO$_4$ to gallic acid ([gallic acid]$_0$ = 1.8×10^{-4} mol dm^{-3}) in solutions with various content of Fe(II) ions ([FeSO$_4$]$_0$ = 7.2×10^{-4} mol dm^{-3} ▲, 3.6×10^{-4} mol dm^{-3} ■, 1.8×10^{-4} mol dm^{-3} ◆) on air.**

The experimental time dependencies (absorbance at 560 nm) shown in Fig. 2. were fitted by a non-linear least-squares method to the general exponential function (Scientist, MicroMath), and the formal initial rate of the complex formation

$$R_{in} = \left(\frac{dA_{\lambda_{max}}}{dt} \right)_{t \to 0} \tag{1}$$

was calculated using the evaluated exponential function parameters.[5] The Fig. 2. showed that the highest rate was reached for the highest concentration of FeSO$_4$.

From Table I is evident that the initial rate of the complex formation and absorbance maxima at 560–590 nm of solutions measured in the presence of air oxygen reached after 3 hours of complex formation decreased with decline of Fe(II) contents in the solution.

Table I
The influence of initial Fe(II) concentration and atmosphere on complex formation ([gallic acid]$_0$ = 3.6×10^{-4} mol dm^{-3}, [gum arabic] = 1 % wt.); R$_{in}$ – initial rate of complex formation; A$_{3h}$ – absorbance at 560 nm after 3 hours

Fe : GA	R$_{in}$ [min^{-1}]	R$_{correlation}$	A$_{3h}$
2 : 1/air	0.00658	0.993	0.555
1 : 1/air	0.00557	0.997	0.443
1 : 2/air	0.00362	0.997	0.312
2 : 1/N$_2$	0.00075	0.997	0.343
1 : 1/N$_2$	0.00078	0.999	0.330
1 : 2/N$_2$			0.007

Parallely with the changes in the UV VIS spectra the differences in pH values of the solutions were observed. The regression in pH value occurred in the range of 4.6 to 4.1–4.3, but it was not strongly dependent on the amount of added FeSO$_4$. The decline in pH value was caused by the production of sulphuric acid that was released during the complex formation or by the oxidation of excess iron(II) sulphate by oxygen in air.
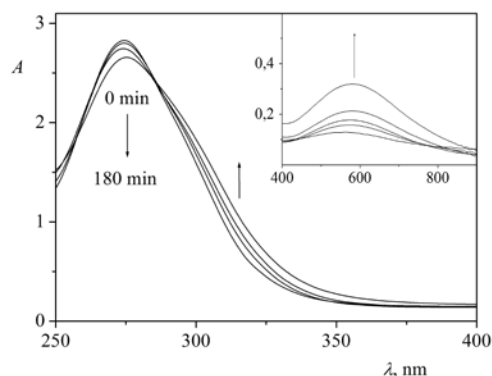
Fig. 3. **UV VIS spectra of complex formation after the addition of FeSO$_4$ to gallic acid ([FeSO$_4$]$_0$ = 7.2×10^{-4} mol dm^{-3}; [gallic acid]$_0$ = 3.6×10^{-4} mol dm^{-3}) at various time after mixing of components (0, 30, 60, 120, 180 min), bubbling with N$_2$ only immediately after prepaeration.**

The differences in UV VIS spectra were investigated in the same solutions in nitrogen atmosphere (Figs. 3., 4., Table I)), while the samples were bubbled with nitrogen gas only right after preparation, then closed in cell and repeatedly measured. In this case the flow of coloured complex formation was very similar to the ones with ratio FeSO$_4$: gallic acid 2 : 1 and 1 : 1, while in both cases the significant slow down of reaction in the beginning was observed. After 60 min the significant rise of absorbance took place, the absorbance in visible region after 4 hours was in case of 1 : 1 ratio close to the value measured without nitrogen. As the solutions were not bubbled continually, we can assume that because of untightness diffusion of air oxygen into measuring cell could took place which caused creation of coloured complex.
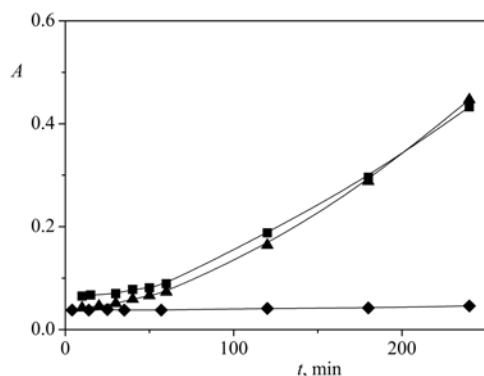
Fig. 4. **Increase of absorbance at 560–590 nm with time after addition of FeSO$_4$ to gallic acid ([gallic acid]$_0$ = 1.8 × 10^{-4} mol dm^{-3}) in solutions with various content of Fe(II) ions ([FeSO$_4$]$_0$ = 7.2 × 10^{-4} mol dm^{-3} ▲, 3.6 × 10^{-4} mol dm^{-3} ■, 1.8 × 10^{-4} mol dm^{-3} ♦), bubbling with N$_2$ only after preparation**

Fig. 5. **UV VIS spectra of complex formation after the addition of FeSO$_4$ to gallic acid ([FeSO$_4$]$_0$ = 7.2 × 10^{-4} mol dm^{-3}; [gallic acid]$_0$ = 3.6 × 10^{-4} mol dm^{-3}) at various time after mixing of components (0, 60, 120, 240 min), bubbling with N$_2$ continual**

In sample with access of gallic acid the creation of coloured complex was not observed. In this sample also change in pH during reaction did not occurred, while we observed decrease of pH approximately about 0.2 unit in the first two samples.

So that inert atmosphere was not damaged, all three observed samples were bubbled with nitrogen not only before start of measurement, but also between individual measurements. (Fig. 5) In this case only minimal changes of absorbance in visible region during measurement were determined. The absorbance in sample with the highest content of Fe(II)ions increased about 0.011 during 4 hours, in sample with equimolar content of components about 0.004 and in last sample it did not changed. Coloured complex is not created without presence of oxygen.

Conclusions

The use of UV VIS spectroscopy positively indicates the complex formation due to the absorbance increase at 650 nm and is suitable for the complex stability testing. The complex formation is most effective in solution with excess of Fe(II)

ions. The reduction in the concentration of Fe(II) ions in the solution causes the retardation of the complex formation.

The complex formation in inert atmosphere is strongly decelerated considering its formation on air, the role of oxygen is determining for colour complex formation.

REFERENCES

1. Wunderlich, C. H.: Restauro 6, 414 (1994).
2. V. Rouchon Quillet, C. Remazeilles, T. P.Nguyen, J. Bleton, A. Tchapla, in J. Kolar, M. Strlič, J. Havermans (Eds.): *Durability of Paper and Writing*, Ljubljana 2004, p. 56, Ljubljana (Slovenia), 2004.
3. Andjelković M., Van Camp, B., De Meulenaer, B., Depaemelaere, G., Socaciu, C., Verloo, M., Verhe, R.: Food Chem. 98, 23 (2006).
4. Neevel, J. G.: Restaurator 16, 143 (1995).
5. Jančovičová, V., Čeppan, M., Havlínová, B., Reháková, M., Jakubíková, Z.: Chem. Pap. 61, 391 (2007).

L13 STUDY OF INFLUENCE OF IRON-GALL INKS COMPOSITION ON PROPERTIES OF HISTORICAL DOCUMENTS

MILENA REHÁKOVÁ, MICHAL ČEPPAN and VLADIMÍR DVONKA

Slovak University of Technology in Bratislava, Faculty of Chemical and Food Technology, Radlinského 9, 812 37 Bratislava, Slovak Republic,
milena.rehakova@stuba.sk

Introduction

Iron gall inks applied on documents represent serious problem regarding conservation and preservation of documents. Problem is frequently caused by different kinds of materials and recipes used for ink preparation. Quantitative ratio of ink main components – gallic acid and ferrous sulphate – was considerably different for particular recipes. Chosen 104 historical recipes from 15th–19th century contained more iron as was necessary for creating of colour complex[1], some of them even contained hydrochloric acid or sulfuric acid to reach instant colouration and to improve solubility of pigments[2]. In 18th century it was discovered that inks with the best qualitative properties were with the ratio of gall (source of gallic acid) and green vitriol (Iron (II) sulfate heptahydrate) 3 : 1. If the ratio for $FeSO_4$ increases, ink is instable[3]. In 19th century the unification of manufacture methods of iron gall inks was noticed. Recipes contained only pure compounds – ferrous salts and gallic or tannic acids mixed in stechiometric ratios.

The aim of this work was to investigate changes of paper with applied iron gall ink under accelerated ageing for different molar compositions of main components.

Experimental

Six inks (listed in Table I) with different ratios of gallic acid (Sigma – Aldrich Lambda Life) and ferrous sulphate (Lachema Brno) and constant amount of additives – gum Arabic (Sigma – Aldrich Lambda Life) and sodium benzoate (Lachema Brno) were prepared. Inks were applied on paper Whatman (Whatman Laboratory Division, Maidstone, England, Cat No 1001917, mass per area 90 g m^{-2}, pH 7) by immersing in solution, removing extra liquid using filter paper and roller with constant pressure; the mass per area addition was 7.35 g m^{-2}. After drying on air samples were conditioned at 23 °C and RH 50 % during 24 hours. Consequently accelerated ageing was applied in covered bottles at 90 °C at different times 1, 4, 8, 14, 24 hours[4]. Following chemicals and devices were used for experiments and measurements: cupri-ethylene-diamine (Sigma – Aldrich), capillary viscosimeter according to norm ISO 5351/1 for determination of limit viscosity number, device for thermal analysis Mettler Toledo, optic fiber spectrophotometer HR 4000 CG (Ocean Optics Inc.), spectrophotometer SpectroDens A504009 Premium (Techkon).

Table I
Composition of iron gall inks

Ink	Gallic acid, GAL [mol dm^{-3}]	FeSO4 [mol dm^{-3}]	Ratio Fe : GAL
AT1	0.10	0.00	0
AT2	0.08	0.02	0.25
AT3	0.06	0.04	0.67
AT4	0.04	0.06	1.5
AT5	0.02	0.08	4
AT6	0.00	0.10	–

Results

Changes of physical and chemical properties of prepared samples caused by accelerated ageing were investigated. Attention was focused on estimation of degree of polymerization of a carrier material (method of limit viscosity number determination), determination of rate constant of depolymerization and thermal analysis – estimation of thermal stability. Using spectrophotometry in VIS/NIR area we tried to determine the course of degradation of inks. Colour changes of inks were also monitored.

The degree of polymerization (DP) of samples was determined viscometrically using cupri-ethylene-diamine as a solvent[5]. Degree of polymerization was calculated from viscometric data using Mark-Houwink-Sakurada equation with the constants (a, K) according to[6,7]. Rate constants "k" of degradation of paper samples was calculated by least squares fitting of the plot DP *vs.* time using Ekenstam equation for degradation of linear polymers[8].

$$(1/DP_t) - (1/DP_o) = k \cdot t, \tag{1}$$

where DP_t and DP_o are degrees of polymerization at the beginning of ageing and after time "t" of ageing, respectively.

The degree of polymerization during ageing in all cases decreased and differences were in between 1,500–900 (Fig. 1.). Decrease of DP of AT1–AT6 was much more considerable as of only paper Whatman. As Fig. 2. showed,
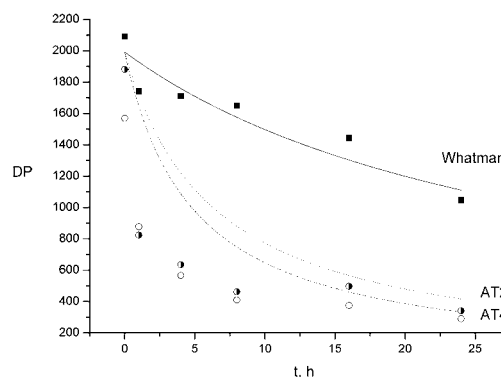
Fig. 1. **Decrease of polymerization degree during ageing; Whatman in comparison with samples AT2 and AT4 (by Ekenstam equation)**
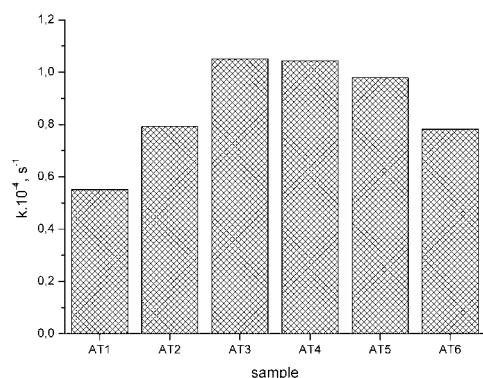
Fig. 2. **Rate constants of degradation *vs*. ratio Fe : GAL (AT1 –AT6)**

Fig. 4. **Changes of colorimetric parameter ΔE^*_{ab} (CIELab) during ageing; all samples**
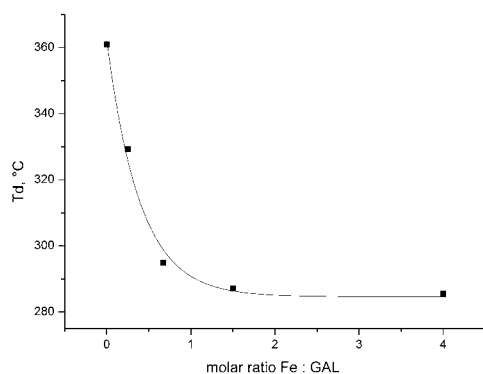
Fig. 3. **Dependence of temperature of decomposition on molar ratio of Fe : gallic acid. Samples after 24 hours ageing**

Fig. 5. **Changes of colorimetric parameter ΔL^* during ageing; sample AT3**

depolymerzation rate was considerably higher for samples AT3, AT4 and AT5. Inks with molar ratio greater or equal to 0.67 were destructing substrates faster than others. Inks which didn't contain any of complex components (AT1, AT6) weren't so aggressive to paper.

Basis of thermogravimetric analysis (TGA) consisted of warming of samples with constant rate according to controlled temperature programme in inert N_2 atmosphere and monitoring of the weight changes as a function of temperature (TG curve). Differences in material weight as a function of temperature and proportion of this change represented thermal stability of material. Samples with no ageing and maximum time of ageing were measured. Fig. 3. represented dependency of decay temperature T_d on ink composition and it showed that increasing content of iron decreased thermal stability of samples (lower value of T_d means that degradation takes course earlier).

Series of dependencies of Kubelka-Munk function (reflectance, KM) on wave number (λ) were obtained by measuring spectra in area 380–1,050 nm (VIS/NIR) of paper samples with applied iron gall inks with different ratio of gallic acid and iron for all chosen times of ageing. For evaluation of KM spectra method of factor analysis was used[8]. As a first step analysis of main components was done and

number of linear independent components in spectra was determined. These components correspond to chemical individuals that manifested in measured spectra. Analysis of main components was performed using CVD-TFA method (method of cross verification using factor analysis)[9]. Series of all spectra (non-aged and aged for all times) composed 4 independent components, series of spectra for non-aged samples represented 3 independent components, series of spectra for maximum ageing time (24 hours) represented 3 independent components and combined series of spectra composed of maximum aged and non-aged samples represented 4 independent components. The most probable explanation for these results was that in spectra of non-aged samples existed 3 chemical components, during ageing occurred formation of one new component and another was vanishing. In series of spectra of maximally aged samples occurred 3 chemical components. This method however didn't allow identify their composition.

Regarding colour axis of colour space L^*, a^*, b^* were measured and recalculated to C^* characterizing chroma of colour and h^* representing hue angle (quality of saturation). Total colour difference was calculated from values L^*, a^*, b^* and represented differences between aged and original paper samples. Total colour difference increased accor-

ding to ageing and in maximum time values total colour difference was in range 3–15 (Fig. 4.). Samples with inks AT4 and AT5 were the most inferior to ageing, the values of colour difference of inks AT1–AT3 and AT6 were acceptable (max. value 4). On the basis of these results regarding influence of ink composition on optical properties of samples it could be assumed that higher ratio of iron to gallic acid caused more considerable changes in colour of samples.

According to analysis of axis changes in colour space interesting behavior of lightness (L^*) was observed. From the beginning value L^* was slightly decreasing for all samples then break occurred and lightness started to increase (Fig. 5.). It could be caused by initial ink colouration (complex formation) on substrate which turned into bleaching (degradation of pigment structure). Chroma (C^*) gradually slightly decreased (saturation was decreasing), value of hue angle of colour tone (h^*) wasn't changing noticeably during ageing.

Conclusions

According to results it could be assumed that inks with ratio of iron:gallic acid greater than 0.67 behaved considerably destructive on paper substrate which proved negative effect of extra iron in writing inks.

REFERENCES

1. Neevel J. G.: Restaurator *16*, 143 (1995).
2. Wunderlich C. H.: Restaurator *15*, 414 (1994).
3. Sedlák F., Hanus J.: Slovenská archivistika *8*, 65 (1978).
4. ASTM D6819-02D6819-02e2, *Standard Test Method for Accelerated Temperature Aging of Printing and Writing Paper by Dry Oven Exposure Apparatus.*
5. ISO 5351-1: *Cellulose in dilute solutions: Determination of limiting viscosity number – Part 1: Method in cupri-ethylene-diamine (CED) solution* (1981).
6. Kolar J., Strlic M.: Restaurator *23*, 94 (2004).
7. Emsley A. M., Heywood R. J., Ali M., Eley C. M.: Cellulose *4*, 1 (1997).
8. Malinowski E. R.: *Factor Analysis in Chemistry*, third edition. Wiley Interscience, New York 2002.
9. Pelikán P., Čeppan M., Liška M.: *Applications of Numerical Methods in Molecular Spectroscopy.* CRC Press, Boca Raton 1994.

L14 AN OVERVIEW OF INKJET PRINTOUTS ACCELERATED AGEING METHODS

JIŘÍ STANČÍK, MICHAL VESELÝ and PETR DZIK

Brno University of Technology, Faculty of Chemistry, Purkyňova 118, Brno 612 00, Czech Republic,
xcstancik@fch.vutbr.cz

Introduction

Nowadays, digital photography is the mainstream photographic technology. It is not a new concept, it was invented by Sony in 1981, but it has taken approximately 20 years for the technology to develop into the mainstream business that it is today.

Inkjet printing has become one of the major imaging technologies used in digital printing applications. The versatility of inkjet has led to an ever increasing number of applications for this technology. Inkjet has now diversified into the business/network, wide format, photo realistic and textile printing applications. These require better image durability in order to provide a print performance as good as existing photographic, lithographic, screen or offset printing technologies. For many of these applications the print must be stable for many years for archiving or the preservation of an image exposed to the environment. The light stability of prints is of particular importance and the improvement of the photo stability of inkjet prints is an important goal[1,2].

This paper describes the various factors that affect the permanence of inkjet printouts. Accelerated test methods are described with respect to past and current standards that are widely used in imaging industry.

Image Permanence Light Fastness Tests

Standardized image permanence tests serve a number of important purposes:
- to provide guidance to consumers in selecting the longest-lasting materials which otherwise meet their needs in terms of cost, image quality, print size and convenience,
- to provide printer, ink, and paper manufacturers' research & development departments image permanence test methods to help evaluate and improve the longevity of future products,
- to enable manufacturers to understand their position in the marketplace relative to their competitors,
- to provide manufacturers image permanence data for use in promoting their products to customers,
- to provide museums and archives with data concerning the true stability properties of the imaging materials in their collections so that right conditions of the duration of display and storage can be implemented to achieve long-term preservation of the materials in their original, unchanged form.

There are several approaches for determining the light fastness of printouts. The simplest and most realistic would be to expose the print sample to actual daylight. This would indicate true lifetime of the printouts under real time conditions. However, there are many problems associated with such methods as the time taken to achieve results. The alternative, accelerated exposure testing methods have become well established allowing reproducible results to be produced in short time scales. Various standard procedures are available for accelerated ageing which detail sample type and preparation, equipment, exposure conditions, measurement and evaluation of the results[2,3].

Attitude to Evaluation of Inkjet Light Fastness Tests

There were two main types of progress in evaluation of inkjet printouts light fastness tests. The first used the existing standards for photographic materials and continued tracking changes of light fastness with densitometric measurements. Status A (for transparencies and reflection prints) and Status M (for negatives) densitometric filter sets were optimized for specific colorant systems of photographic materials. The second way tried to use evaluation of light fastness tests of textiles and dyes with simultaneously tested blue wool references. Light fastness was evaluated by noting on the scale of blue wool standards and rating the standard which has undergone a similar change to that of the print specimen[4,5].

History of Accelerated Ageing Methods

First ANSI standard for testing the permanence of color photographs was ANSI PH1.42–1969 – American National Standard Method for Comparing the Color Stabilities of Photographs. This standard did not contain "predictive" tests that could be reported in terms of years of display or the years of storage under specified conditions. It specified a series of comparative tests, including a 5.4 klx glass-filtered xenon arc test to simulate indoor display. It also included tests to simulate use in slide projectors, fluorescent viewers and direct sunlight through window glass. This early standard specified starting densities of both 1.0 and 0.5. It never achieved significant use and during the 1980's was more or less abandoned by manufacturers as well as independent labs[3].

ISO 2835: Prints and Printing Inks – Assessment of Light Fastness was published in 1974. It also did not contain "predictive" tests but it described an outdoor glass-filtered daylight test of printouts together with a standard range of eight blue dyes on wool cloth. For accelerated tests it recommended high pressure xenon lamps, light sources with spectral energy distribution very different from daylight were not permissible. Light fastness was evaluated using grey scale for assessing changes in color and blue wool references[5].

ANSI IT9.9–1990 – American National Standard for Imaging Materials – Method for Measuring was published in 1990. This document specified five comparative tests for light fading stability. The light fading tests included both 6.0 klx glass-filtered cool white fluorescent and xenon arc tests to simulate indoor display conditions. Cautions were gi-

ven with regard to possible reciprocity failures in accelerated light stability tests, and it was recommended that tests also be conducted at 1.0 klx to asses this problem. A single starting density of 1.0 was specified, but like the previous ANSI standard (PH1.42–1969), it did not specify limits of acceptability for dye fading, color balance shift, or stain formation. These important factors were left to the user to determine.

Described ANSI standard (IT9.9–1990) was adopted with little change by ISO in 1993 as ISO 10977:1993 – Photography – Processed Photographic Colour Films and Paper Prints – Methods for Measuring Image Stability. Light stability test methods were almost the same. Five light stability tests were described: 6 klx simulated indoor indirect daylight test through window glass (xenon arc lamp), 6 klx glass-filtered fluorescent room illumination test, 3 klx incandescent tungsten room illumination test, 100 klx simulated outdoor sunlight test (xenon arc lamp) and intermittent tungsten-halogen lamp slide projection test. 1 klx test for determining reciprocity failure exhibition of materials was recommended too[3,6]. Standard window glass was specified by relative spectral transmittance of float glass, together with relative spectral distributions of light sources used in light stability test methods (Fig. 1.).
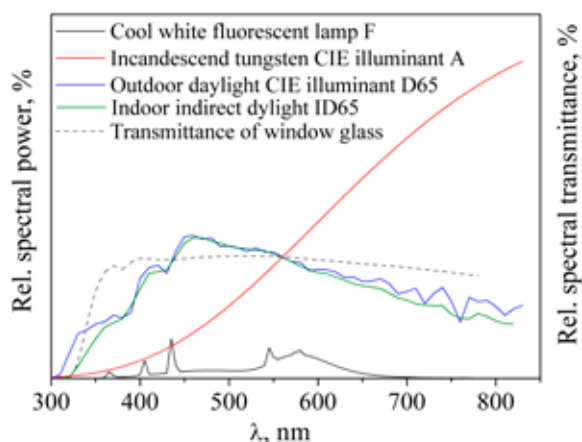
Fig. 1. Illuminants and glass window specification: cool white fluorescent lamp F-6, incandescent tungsten CIE illuminant A, outdoor daylight CIE illuminant D65, indoor indirect daylight ID65 and relative transmittance of standard window glass

In xenon arc simulated outdoor sunlight test light/dark cycles were recommended to provide good correlation with results obtained in some outdoor tests. The sample temperature during both cycles was mentioned too.

ANSI IT9.9–1996 replaced the further ANSI standard from 1990. It continued to specify a 6.0 klx illumination level for indoor light stability tests, and also specified a single starting density of 1.0(ref.[3]). In the same year an important document was published: ISO 13655:1996 – Graphic Technology – Spectral Measurement and Colorimetric Computation for Graphic Arts Images. This standard defined a methodology for reflection and transmission spectral measurement and

colorimetric parameter computation for graphic images[7]. It did not interest in light fastness tests factually, but the methodology defined here was used for evaluation of color changes in these tests later.

In 1997 first edition of ISO 12040:1997 – Graphic Technology – Prints and Printing Inks – Assessment of Light Fastness Using Filtered Xenon Arc Light was published. The method for evaluating light fastness using blue wool references corresponded with the method given by ISO 2835. It described an accelerated test method by specifying the light source and filters for daylight simulation as well as exposure of the test samples to artificial daylight[8].

Other documents dealing with theme of printouts accelerated tests were ASTM standards. ASTM D 3424 – Standard Test Methods for Evaluating the Relative Lightfastness and Weatherability of Printed Matter was published in 1998 and revised in 2001. It described a series of lightfastness tests using natural or artificial light sources. Accelerated tests were constructed to simulate outdoor weathering, daylight through window glass (both xenon arc apparatus and enclosed carbon-arc apparatus) and indoor lighting in combination with window filtered daylight (fluorescent lamp). Illumination conditions were described in $Wm^{-2}nm^{-1}$ at specified wavelength value (340 nm) for xenon arc lamp or in Whm^{-2} for fluorescent lamp apparatus[9].

In 2005 ASTM F 2366 – Standard Practise for Determining the Relative Lightfastness of Inkjet Prints Exposed to Window Filtered Daylight Using a Xenon Arc Light Apparatus was brought out. It recommended conditions of the test: an irradiance level of xenon arc lamp, the temperature (black panel or chamber air) and relative humidity. It also described the evaluation of changes in color and optical density in the printed samples. Color changes were determined either visually by comparison with the unexposed specimens or instrumentally by comparison with the color of the same specimen prior to exposure and reported as color difference, ΔE^*_{ab} (1).

$$\Delta E^*_{ab} = \sqrt{(\Delta L^*)^2 + (\Delta a^*)^2 + (\Delta b^*)^2} \qquad (1)$$

Using of spectrophotometer or colorimeter with the CIE 1964 (10°) Supplementary Standard Observer and Standard Illuminant D65 or the CIE 1931 (2°) Standard Observer and Standard Illuminant C was suggested[9,10].

The last mentioned document is ISO 18909: 2006 – Photography – Processed Photographic Colour Films and Paper Prints – Methods for Measuring Image Stability which was published in 2006. It replaced the further ISO standard (ISO 10977) and continued in inconvenient densitometric evaluations of inkjet printouts.

E v a l u a t i o n   M e t h o d s   P r o g r e s s

Modern digital printing systems employ a wide variety of pigment or dyebased colorants with markedly different spectral properties, and some use more than cyan, magenta, yellow, and black colorants to achieve enhanced color gamut and improved continuous tone properties.

In the current digital era of highly diverse colorant sets, even within a single technology class such as inkjet materials, we can no longer rely on reasonable consistency of neutral gray patch fabrication based on specified densitometric aim points. Additionally, the historical ANSI and ISO test methods only tracked losses of density from a single initial aim point of 1.0, although more starting aim points were allowed. The traditional dyebased chromogenic systems lost density uniformly across their full tonal scale, resulting in a more or less parallel shift (light fade) or linear slope change (thermal ageing) over the majority of the densitometric curve.

Today, this type of performance cannot be assumed. Catalytic fading, non-uniform printed dot dispersions and using three, four, six, seven, eight (or more) ink colorant sets with different blending levels means that the full tonal scale performance cannot be reliably inferred from measurements of just one or two initial density points, the full tonal scale behavior should be evaluated. Densitometry is no longer wholly appropriate method for measuring image quality of modern imaging systems[4].

While densitometry has long been the process control data of choice for the photo finishing and printing industries, the digital imaging market is now rapidly embracing a color-managed workflow. It is based on colorimetric characterization of monitors, printers and scanners. With regard to these facts it is better to produce samples for pictorial image quality studies using colorimetric methods rather than densitometric methods.

Some concerns have been raised that ΔE^{*}_{ab} says something about magnitude but not direction of color change. However, to generate color change one must collect the LAB data, and thus direction of change results are available if one desires to examine these trends.

Conclusions

Lightfastness tests are important guides in the area of material durability. They help both manufacturers and consumers to find out, make or buy a high-quality product. High requirements for information about inkjet print durability resulted in efforts to make the predictive test methods. Accelerated ageing tests are trying to answer these requirements. Nowadays, xenon arc lamps are predominantly used to simulate outdoor illumination or daylight filtered through window glass and white fluorescent lamps to simulate indoor illumination conditions. One have to be careful about possibility of the accelerated light stability tests reciprocity failures.

The testing and measurement of image stability is a very complex science. Standards provide recommendations and guidance on interpreting and using test data generated by the testing methods. However, these are only general recommendations and guidance because images in general have a wide range of stability requirements based on intended application, and are stored or displayed under a vast range of conditions.

As we work more and more with non-traditional photographic media (inkjet), using densitometry may lead to results that do not correlate well with actual pictorial image changes. Nowadays, attention is given to using the colorimetric characterization of image quality studies. There are some problems about CIELAB data evaluating, but new models of the colour difference are still being developed.

REFERENCES

1. Gregory P.: Opt. Laser Technol. *38*, 306 (2005).
2. Lavery A., et al.: *Proceedings of IS&T's NIP 14: International conference on digital printing technologies*, p. 123. Toronto 1998.
3. Wilhelm H.: *Proceedings of IS&T's NIP20: International conference on digital printing technologies*, p. 664. Salt Lake City 2004.
4. McCormick-Goodhart M., Wilhelm H.: *Proceedings of IS&T's Thirteenth International Symposium on Photofinishing Technologies*, p. 25. Las Vegas 2004.
5. ISO 2835: 1974 – *Prints and printing Inks – Assessment of Light Fastness*.
6. ISO 10977: 1993. – *Photography – Processed Photographic Colour Films and Paper Prints – Methods for Measuring Image Stability*.
7. ISO 13655: 1996 – *Graphic Technology – Spectral Measurement and Colorimetric Computation for Graphic Arts Images*.
8. ISO 12040: 1997 – *Graphic Technology – Prints and Printing Inks – Assessment of Light Fastness Using Filtered Xenon Arc Light*.
9. ASTM D3424-01 – *Standard Test Methods for Evaluation the Relative Lightfastness and Weatherability of Printed Matter*.
10. ASTM F 2366-05 – *Standard Practise for Determining the Relative Lightfastness of Inkjet Prints Exposed to Window Filtered Daylight Using a Xenon Arc Light Apparatus*.

L15 SUBJECTIVE AND OBJECTIVE EVALUATION OF RECOGNISABILITY OF BLACK CHARACTERS ON PAPER

ATTILA SZITÁS, MICHAL JABLONSKÝ and SVETOZÁR KATUŠČÁK

Department of Chemical Technology of Wood Pulp and Paper, Institute of Polymer Materials, Faculty of Chemical and Food Technology, Slovak University of Technology in Bratislava, Radlinského 9, 812 37 Bratislava, Slovak Republic,
attila.szitas@stuba.sk

Introduction

Visibility and recognisability of text is the key factor, influencing the information intake from printed media, billboards and other sources. As follows from several recently published papers, its importance is still increasing with the development of new technologies of spreading out the information (e. g., internet or cellular phone technology). On the other hand, a lack of attention is paid to the text visibility and recognisability, as only few published papers deal with an objective method for its determination/evaluation, respectively until present.[1–9]

The background/foreground colour contrasts, as well as the luminance of carrier are considered to be the key factors with significant impact on text visibility and recognisability. Further on, the visibility and recognisability of achromatic documents influences besides the previously mentioned also the following visual factors: letter size and style, text effects used, screen resolution, and, additionally, adaptability of reader/observer on the text displayed on screen.

The development of objective method for visibility and recognisability evaluation and prediction is of great importance. It can be later on applied for further paper quality controlling/improvement process, to affect the preferences of printing offices (to use paper of certain grades and luminance); for paper recyclation processes optimization; deacidification, modification, coating, encapsulation, scission or different conservation technologies; effect of processes of deacidification of old books and archive documents; and last but not least, to improve the communication between papermaking and printing industry and their clients/customers.

In order to obtain the objective valuable method for visibility and recognisability evaluation, it is important to find unambiguous answers on the question of the dependence or mutual correlation between subjective assessment of visibility and recognisability and the objective foreground/background contrast measurement, keeping the letter size and style constant. Additionally, the impact of carrier ageing, e.g., paper acidic hydrolysis induced destruction, as well as the influence of modern developed deacidification and stabilization procedures applied for the historical/archival document conservation and protection[10], on their visibility and recognisability is still not satisfactory proven and verified.

The aim of this work is to determine the influence of contrast between text character and background (foreground/background optical contrast) and other factors on monochromatic text visibility and recognisability and to present new valuable method of its evaluation from simultaneous comparative subjective (human observers) and objective (spectrophotometric) measurements of optical contrast. Moreover, we propose here the objective method for the determination of visibility and recognisability of documents and its prediction in aged documents in respect to all previously mentioned significant objective factors.

Experimental

Samples Characterisation

Commercial white office paper Maestro was used in all experiments. Sets of randomly generated standard black colour letters of Latin alphabet (size, 12 pt; style, Times New Roman regular (Microsoft Office® 2003)) creating the strings of constant length, printed using commercially available colour printer, (nominal resolution, 600 DPI) were printed out on paper sheet. Standardized black letters are defined in CIE $L^*a^*b^*$ system as follows:

$$L^*_c = 30.668, a^*_c = 0.714, b^*_c = -0.18 \qquad (1)$$

Subjective Visibility and Recognisability Evaluation

Observers

Ten undergraduates of an average age of 20 years with standard visual acuity and correct colour recognisability without any previous experiences with such type of testing were used as observers. Five sets of randomly generated text strings of identical length were used during the measurement with one observer. The character of strings excluded the factor of potential learning process.

Fig. 1. An example of the text string used in visibility and recognisability tests. (Contrast: background 0 % $B_{b,MS\ Word}$, text 100 % $B_{b\ MS\ Word}$).

Typical set of generated text string is shown on Fig. 1. Two trained observers moreover estimated the distinction in borders using the method of magnitude estimation as previously suggested in ref.[1]. Observers were tested to the ability to correctly recognize (read) 10 randomly selected letters from the generated strings for each contrast scale (Table I).

Evaluation of the influence of document contrast on its visibility and recognisability

Psychophysical method was used to measure the number and percentage of correctly recognized characters (R_s) at the same background/foreground contrast of documents:

Observers were asked to recognize 10 randomly selected characters from different text strings for each contrast between text characters and background. The distance l_i (cm) between the observer and text was changed continuously either to the distance $l_{100,i}$ at which still 100 % of the text was recognized correctly, or to $l_{0,i}$, with 0 % of correctly recognized letters. Using this approach, the dependence of correctly recognized letters on the distance for each colour contrast was obtained. The so obtained "absolute" individual visibility and recognisability functions $R_{S,i} = f(l')$ was normalized, in order to minimize the influence of external factors (e.g., light direction, source or intensity). Each l_i value was related to the value of l_{100}, obtained for the text string written on 100% white background (0 % $B_{b, MS\ Word}$, Table I). The so-obtained values of l'_i were used for the contrast dependent visibility and recognisability evaluation.

Objective Visibility and Recognisability Evaluation

The same text samples as utilised in subjective visibility and recognisability tests were analysed by commercially available spectrophotometer Minolta CR 200. CIE colour parameters L^*, a, and b for both, text characters (L^*_C, a_C, b_C) and for background (L^*_B, a^*_B, b^*_B, using the cylindrically shaped gape collector (gape size, 3 mm) without any filters and software correction applications. From these values the colour difference ΔE_{C-B} between the text and its background as a basic evaluation parameter was calculated using the following equation:

$$\Delta E_{C-B} = \sqrt{(L^*_C - L^*_B)^2 + (a^*_C - a^*_B)^2 + (b^*_C - b^*_B)^2} \quad (2)$$

Statistical Analysis and Data Correlation

The dependencies of l'_i and ΔE_{C-B} on text visibility and recognisability as well as the mutual correlation between these parameters were fitted to the proper mathematical function using the non-linear regression analysis. The statistical parameters of the calculation procedure (R squared, coefficient of determination and correlation, P) serve for the quality of correlation consideration.

Results

Typical dependence of averaged visibility and recognisability on relative distance from an object, obtained for different background/foreground contrasts (ΔE_{C-B}) from typical observers, is depicted on Fig. 2. For the better visualization of the text recognisability dependence on foreground/background contrasts, the obtained dependencies for each contrast were averaged and the maximum achieved distance at which just the 100% successful recognisability was achieved ($l_{100\%}$) at each contrast value was evaluated. As we have found, the continuous background "darkening" causes the gradual luminance decrease. We moreover found, that text visibility and recognisability increases significantly in the

Table I

A set of different background/foreground contrast, ΔE values obtained from (2), and subjective evaluation of the same colour system. The different contrasts between background and printed text (foreground) were achieved using Microsoft Office Word® 2003 software grey scale, setting the ratio of black colour (Bb, MS Word) to 0 % (100 % white); 5 %; 10 %; 20 %; 30 %; 40 %; 50 %; 60 %; 70 %; 80 %; 90 %; 95 %; and 100 % (totally black), respectively, as it is listed bellow

Background shading set by MS Word® Software	Blackness $B_{b\ MSWord®}$ [%]	ΔE_{C-B}	ΔE_{C-B}, visual evaluation
	100	0.0	negligible
F G H I J	95	6.1	significant
F G H I J	90	8.2	great
F G H I J	80	15.7	considerable
F G H I J	70	20.4	considerable
F G H I J	60	28.3	considerable
F G H I J	50	36.5	considerable
F G H I J	40	40.6	considerable
F G H I J	30	48.0	considerable
F G H I J	20	53.1	considerable
F G H I J	10	60.2	considerable
F G H I J	5	64.5	considerable
F G H I J	0	64.7	considerable
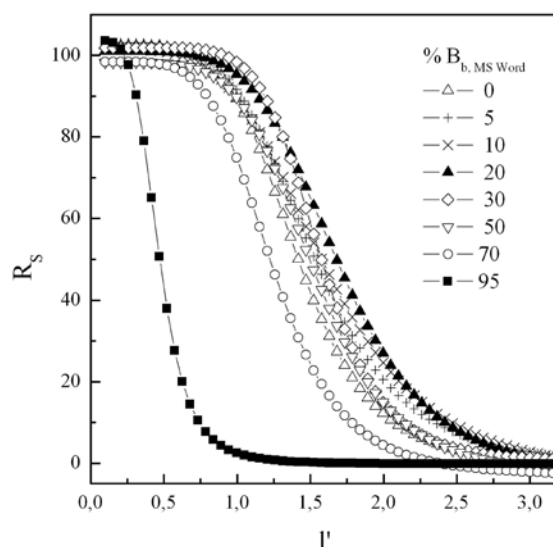
Fig. 2. **The dependence of text recognisability(R_s; %) on the relative distance from observer (l'; m), evaluated from visual test for different colour contrasts $B_{b,\ MS\ Word}$**

range of $B_{b,\ MS\ Word}$ % <10–30>, in comparison to pure white background.

The further addition of black colour (% $B_{b,\ MS\ Word}$) into background does not influence the text visibility and reco-

gnisability in any way, as the maximum distance for 100% correctness of reading is in fact, the same as if the text is printed on white background (0 % $B_{b, MS\ Word}$). As a result of additional darkening, the visibility and recognisability and correctness of text recognition dramatically decreases and at 95 % $B_{b, MS\ Word}$, which is in fact, almost pure black background of similar hue and saturation as the text in foreground, the correctness fallen down close to zero.

The dependence of visibility and recognisability on text background is better visible, when the relative distance, R_s, is plotted versus the foreground/background colour difference ΔE_{C-B}, evaluated from spectrophotometric measurements, as it is clearly depicted on Fig. 3. for the same observer. The opinion that text recognisability is in linear dependence to the optical contrast, is widely spread out. In contrary to this assumption, we found that the dependence between the visual subjective recognisability/visibility and recognisability and optical contrast ΔE_{C-B} is not linear in the whole range of ΔE_{C-B}, as is finally clearly demonstrated on Fig. 3. (theoretical course 1). At lower ΔE_{C-B} (up to 30%) the linearly growing dependence of visibility and recognisability on colour contrast is observed, while on the contrary at higher ΔE_{C-B} the saturation of text visibility and recognisability is observed, or the visibility and recognisability slightly decreases.

From the data presented on Fig. 3., the region of improved recognisability might be delimited. At optical contrast e.g., $\Delta E_{C-B} = 64.7$, $L^*_B = 93.2$ and $B_{b\ MSWord} = 0$ % the value of relative visual recognisability/visibility and recognisability reaches the value $R_S = 0.983$. If the optical contrast decrease of e.g., to $\Delta E_{C-B} = 53.1$, the R_s value increased to the value of 1.02. It means that in spite of lowered optical contrast between the foreground text and background, reader/observer is able to recognize the printed character from the longer distance than at higher optical contrast.

Data obtained in subjective visibility and recognisability tests served for the re–calculation and transformation of optical
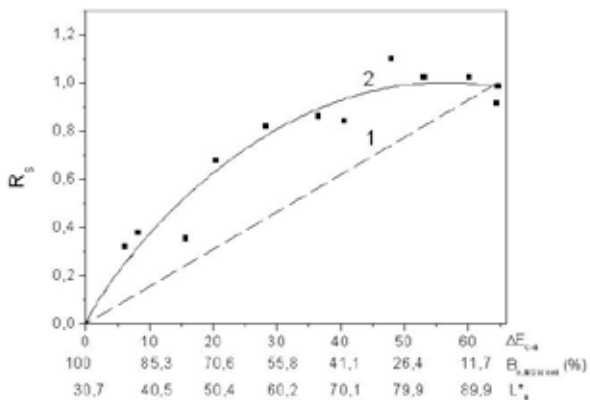
colour difference (ΔE_{C-B}) on the objective optical-device predictable visual recognisability/visibility and recognisability, expressed by the following mathematical equation:

$$R_S = \left[1 - \left(\frac{\Delta E_{C-B} - 56.4}{56.4} \right)^2 \right]^{0.87}, \tag{3}$$

which correlates well with experimental data. As follows from the data presented, change in relative recognisability is significantly dependent on the initial optical contrast, i.e. on the optical contrast of non-modified document.

Conclusions

Based on the results presented, we can conclude that the visibility and recognisability of text printed on white background (i.e., freshly produced paper just after the industrial whitening), is even worse than those, printed on grey or shaded papers. This fact can find effective application in paper recycling industry, which is nowadays of growing importance, with one of the key problems of recycled paper whitening without the influence on its mechanical or physical properties.

The evaluation of text visibility and recognisability of printed documents based on both subjective and objective assessment is presented in this paper for the first time. Objective easy-to-use methods of paper visibility and recognisability evaluation based on tristimulus values measurements are presented, based either on the relative visibility and recognisability and optical contrasts or on their relative indexes dependencies, respectively. As follows from results presented, the dependence of recognisability and visibility of printed text on respective background optical contrast has not the linear character, i.e., the higher optical contrast ("white background") can even make the visibility and recognisability of text worse than that printed on lower contrast background.

Fig. 3. **The representative dependence of text visibility and recognisability (expressed as Rs) on the colour difference (ΔE_{C-B}), evaluated from spectrophotometric measurements, whitness of background (L^*_B) and blackness ($B_{b\ MSWord}$; %). 1 – theoretical course, 2 – measuring course**

REFERENCES
1. Legge G., Rubin G., Leubker A.: *27*, 1165 (1987).
2. Knoblauch K., Arditi A., Szlyk J.: J. Opt. Soc. Am. A *7*, 1976 (1990).
3. Scharff L. F. V., Hill A. L.: Optic Express *6*, 81 (2000).
4. Paterson D.G., Tinker M.A.: J. Appl. Psychol. *30*, 454 (1946).
5. Silver N. C., Braun C. C.: Safety Sci. *16*, 615 (1993).
6. Leung C. C., Chan K. S., Chan H. M., Tsui W. K.: Pattern Recogn. Lett. *26*, 769 (2005).

7. Öquist G., Goldstein M.: Interact. Comp. *15*, 539 (2003).
8. Pescio S., Mattiello M. L. F., Álvarez R.: AIC 2004 Colour and Paints, Interim Meeting of the International Colour Association, Proceedings, 47 (2004).

9 Blackwell H. R., Blackwell O.: *Effects of lighting upon visual performance*. Columbus, Ohio State University, Illuminating Engineers Research Institute (1980).
10 Polovka M., Polovková J., Vizárová K., Kirschnerová S., Bieliková L., Vrška M.: Vib. Spec. *41*, 112 (2006).

L16 PIGMENTS FOR PHOTOCATALYTIC PAINTS

JAN ŠUBRT, JAROSLAV BOHÁČEK, LORANT
SZATMARY and PETR BEZDIČKA

*Institute of Inorganic Chemistry AS CR, v.v.i., 250 68 Řež,
Czech Republic,*
subrt@iic.cas.cz

Introduction

During recent years environmental problems play an important role in the applications of titania pigments. These include the use of their photocatalytic behavior in the development of self-cleaning surfaces for buildings, i.e. anti-soiling and antifungal growth and NO_x emissions reduction. In terms of self-cleaning paints, the idea is to limit the oxidation and chalking of the paint film to the very near surface layers such that over time with weathering rain water will wash the top layer leaving an underlying clean fresh surface. In this regard, mixtures of pigmentary rutile and nanoparticle anatase pigments appear to provide the best option, with the former inducing some level of base stability, whereas the presence of the latter gives rise to surface activity[1].

It is well known[1] that photocatalytic paints should contain two types of titania at minumum, pigmentary grade rutile serving as effcetive UV filter and nanocrystalline anatase serving as the photocatalytic component responsible for the photocatalytic function of the paint. Whereas the function of the pigment grade rutile in paints is well known and long time experience exists with this kind of material, the effect of nanocrystalline anatase is much less investigated till now. We expect that this kind of material should possess high photacatlytic activity and should be easily dispergable in the paint medium. We suppose that these demands should be fulfilled by anatase with particle size below ~ 80 nm or anatase/rutile mixtures with the same particle size. The synthetic procedure should be acceptable from environmental point of view and should be technologically viable at acceptable price.

Experimental

Synthesis of Hydrated Titania Gel Samples

Aqueous solution of titanyl sulphate containing 33 g dm^{-3} of $TiOSO_4$ was slowly neutralized with 26% aqueous NH_3 melting ice bath under stirring with magnetic stirrer; the desired pH was achieved within 20 min. After the pH was reached, the suspension was stirred for additional 30 min. The obtained precipitate was filtered off and repeatedly dispersed in water until no anions were detected. Finally, the product was washed out with distilled water and isopropyl alcohol and dried at 40 °C in air. The samples denoted as AP and RP were prepared by adding of equimolar amount of 26% aqueous NH_3 to the $TiOSO_4$ solution at 80 °C; moreover, the RP sample contains also 5 % of rutile nuclei.

Characterization Methods

In order to assess photocatalytic properties of the catalysts, kinetics of 4-chlorophenol (4-CP) decay in an aerated aqueous suspension of photocatalyst was measured. The irradiation experiments were performed in a home–made laboratory photoreactor. Probes of irradiated suspension (1 ml) are taken at desired irradiation times and analyzed by HPLC. The HPLC experiments were run on a Merck device with L-6200 Intelligent Pump, L–3000 Photo Diode Array Detector and D–2500 Chromato-Integrator. Mobile phase methanol/water (2 : 3, v/v) and a Merck column LiChro-CART 125–4 filled with LiChrosphere 100 RP–18 (5 mm) were used. Injection loop was 20 ml, and a flow rate of 1 ml min^{-1} and detection wavelength of 280 nm was applied[2,3].

Structural morphology of the samples was revealed by SEM (scanning electron microscopy). A Philips XL 30 CP microscope equipped with EDX (energy dispersive X-ray), Robinson, SE (secondary electron) and BSE (back-scattered electron) detectors was used. TEM observation was carried out on a JEOL JEM 3010 microscope operated at 300 kV (LaB6 cathode, 1.7 Å point resolution) with an EDX (energy dispersive X-ray) detector attached. Samples were reground in agate mortar, the powder was dispersed in ethanol and the suspension was treated in ultrasound for 10 min. A drop of very dilute suspension was placed on a carbon-coated Cu grid and allowed to dry by evaporation at ambient temperature.

Powder X-ray diffraction (XRD) was used for monitoring the phase composition of the samples. Unit-cell parameters, crystallite size, and weight fractions of phases were calculated by the Rietveld method. X-ray powder diffraction of annealed samples was performed on a Siemens D5005 diffractometer (Bruker AXS, Germany) using Cu Ka radiation (40 kV, 30 mA) and a diffracted beam monochromator. Qualitative phase analysis was performed with High Score software package (PANalytical, the Netherlands, version 1.0d), Diffrac-Plus software package (Bruker AXS, Germany, version 8.0), and JCPDS PDF–2 database. For quantitative phase analysis, Diffrac-Plus Topas software package (Bruker AXS, Germany, version 2.1) with structural models based on ICSD database was used.

Surface area of the samples was determined from nitrogen adsorption–desorption isotherms at liquid nitrogen temperature using a Coulter SA 3100 instrument with 15 min

Table I
Properties of the initial titania gels

Sample	Preparation pH	Surface area [m^2 g^{-1}]	Content of S [% wt.]	Wt. loss by annealing to 1200 °C [% wt.]
TIG 7	3	140	4.9	32
TIG 8	6	180	1.6	24.8
TIG 9	8	260	0.2	20.3
AP	(7)	76	2.7	21.7
RP	(7)	78	2.8	20.8

lasting outgas at 120 °C. The surface area was calculated by BET method while the pore size distribution was determined by BJH method.

Results

The characteristics of the studied titania gels are given in Table I. The results given in this Table show that all prepared hydrated titania gel samples contain remarkable content of sulphate anions (given as S content). The content of SO_4^{2-} decreases with increasing precipitation pH; at higher pH values can be prepared saples practically free of bound sulphate anions. All synthesised samples show rather high surface area, increasing with increase of the precipitation pH.

Fig. 1. shows X-ray diffraction pattern of the starting hydrated titania. The samples precipitated at higher temperature (AP and RP) contain mostly nanocrystalline anatase whereas the samples prepared at melting ice temperature TIG 7–9 are practically amorphous with signs of crystallinity at the sample TIG 7 prepared at the lowest pH 7.
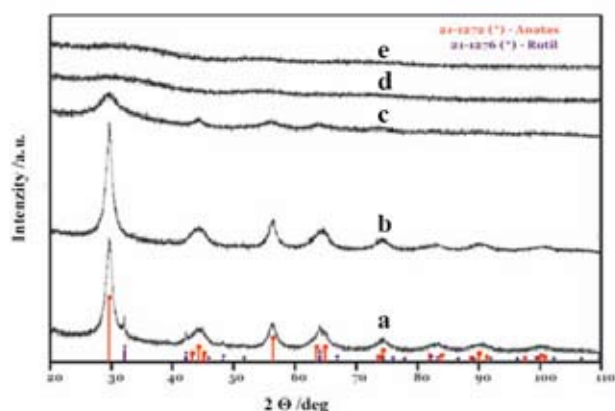
Fig. 1.   **XRD patterns of the precipitated titania gels. a – sample RP; b – sample AP; c – sample TIG 7; d – sample TIG 8; e – sample TIG 9**

Typical microstructure of the initial gels is shown on the Fig. 2. The micrograph A shows the initial sample; we can observe small (4–5 nm) crystalline zonnes randomly oriented which are surrounded by amorphous material. After annealing at 800 °C (Fig 2.B), the material is crystalline with typical crystal size in range 50–80 nm. Detail examination show that particular crystals consist of ~ 5 nm domains indicating that the crystals were formed in a self-assembly process of seeds.

It is well known that annealing of hydrated amorphous or nanocrystalline titania gels results in growth of crystalline anatase particles, at tempearture higher than 800 °C transformattion of anatase to rutile occurs. This proces has been described earlier for nanocrystalline hydrated anatse prepared by homogeneous precipitation with urea[2]. The behaviour of our samples is similar to the earlier described system but we observed that the phase composition of the
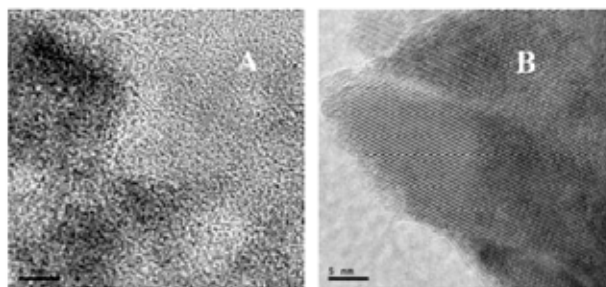
Fig. 2.   **TEM micrograph of the starting gel TIG 7 (A) and of its annealing product at 800 °C (B)**

annealed product depends significantly on the conditions of preparation of the starting gel. Fig. 2. shows the dependence of the anatase content in the annealed hydrated titania gels on preparation temperature (the rest to 100 % is rutile). We can see on this Fig. that the transition temperature from anatase to rutile is situated between 800–1,100 °C, depending on the preparation conditions of the initial gel. The lowest transition temperature was found for the RP sample (containing rutile seeds), the highest for the sample AP (prepared at 80 °C). The anatase to rutile transition of the TIG samples lies between these samples, the lower is for the TIG 7 sample prepared in weakly acidic medium whereas the higher is for the TIG 9 sample prepared in weakly alkaline medium.

The growth of the crystals during annealing is shown on the Fig. 4. We can observe continuous growth of particles during annealing in range 5–200 nm. The results presented on Figs. 3. and 4. showed that, depending on the conditions of synthesis of the starting gels (pH and temperature) and the annealing mode, both particle size and phase composition can be adjusted in rather wide range.
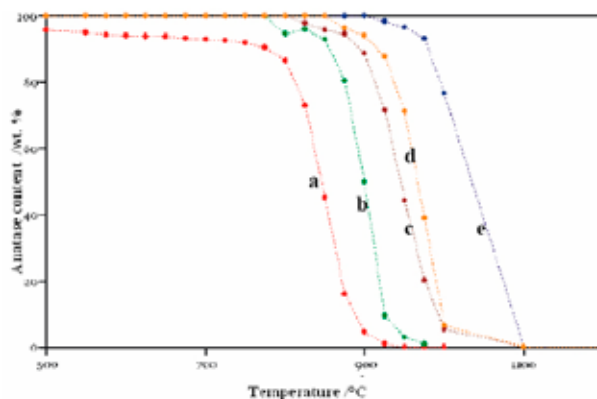
Fig. 3.   **Anatase to rutile transition of the precipitated titania gels. a – sample RP; b – sample TIG 7; c – sample TIG 8; d – sample TIG 9; e – sample AP**

The photocatalytic activity of the annealing products of the sample AP determined by decomposition of 4-chlorophenol as model reactant are given on Fig. 5. We can observe on this Fig. that the activity of some tested materials is rather high, even exceeding the Degussa P–25 material (often used
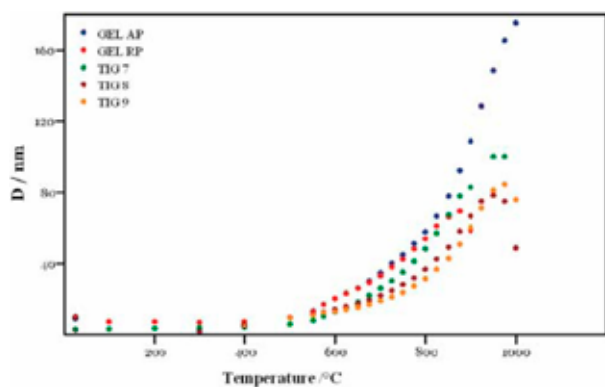
Fig. 4.   **Dependence of the particle size of TiO₂ on the annealing temperature for different starting titania gels**

Fig. 6.   **Dependence of photoactivity of the annealed AP sample on the annealing temperature**

can observe sharp peak at this graph in temperature range 800–900 °C (transition temperature anatase – rutile for this sample).

Conclusions

The described synthetic procedure for preparation of photocatalytic titanium oxide is suitable for preparation of highly active nanocrystalline material; the process enables to set both particle size and anatase/rutile ratio by controlling the parameters of synthesis. The materials were successfully tested as photoactive component in photocatalytic paints.

Fig. 5.   **Photodecomposition of 4 chlorophenol on various photocatalysts. 1 – starting AP sample; 2 – sample AP annealed at 700 °C for 30 min; 3 – sample AP annealed at 700 °C for 8 h; 4 – sample AP annealed at 800 °C for 30 min; 5 – sample AP annealed at 800 °C for 8 h; 6 – sample AP annealed at 900 °C for 30 min; 7 – sample DEGUSSA P–25**

as standard photocatalyst for comparative assessment of photocatalytic activity).

The dependence of the 1st order rate constant of photocatalyzed decomposition of 4-chlorophenol on the annealing temperature for the sample AP is given on Fig. 6. We

REFERENCES

1. Allen N. S., Edge M., Sandoval G., Verran J., Stratton J., Maltby J.: Photochem. Photobiol., *81*, 279 (2005).
2. Bakardjieva S., Subrt J., Stengl V., Dianez M. J., Sayagues M. J.: Appl. Catal., B *58*, 193 (2005).
3. Lukac J., Klementova M., Bezdicka P., Bakardjieva S., Subrt J., Szatmary L., Bastl Z., Jirkovsky J.: Appl. Catal., B *74*, 83 (2007).

L17 PHOTOLYSIS OF ARENE–IRON PHOTOINITIATORS

JAN VALIŠ[a], BOHUMIL JAŠÚREK[a], KATARÍNA REMENÁROVÁ[a] and TOMÁŠ WEIDLICH[b]

[a]*Department of Graphic Arts and Photophysics,*
[b]*Institute of Environment Protection, Faculty of Chemical Technology, University of Pardubice, Studentská 95, Pardubice, 532 10, Czech Republic,*
jan.valis@upce.cz

Introduction

Already 100 years ago G. Ciamcian predicted exploitation of photochemistry reactions in industry: "I do not believe that the industry should wait any longer before taking advantage of the chemical effects produced by light"[1]. But Roloff complain, that "large photochemical production processes are still extremely rare" in eighties[2]. Nowadays the systems cured by UV radiation, or energy-rich radiation in general, are used in many branches of industry.

Arene–iron photoinitiators are investigated relatively long time[2,3], their synthesis published Nesmeyanov in 1963[4], but only one is commercially available: (η^5–2,4-cyclopentadien–1-yl)[(1,2,3,4,5,6-η)-(1-methylethyl)-benzene]-ferrous hexa-fluorophosphate (under the commercial name Irgacure 261 by Ciba Speciality Chemicals). New types of arene–iron complexes are synthesized and tested as initiators for radical[5], hybrid[6] or mainly cationic polymerizations.[5–10 and others]

Photolysis of twelve arene-iron compounds was studied in this paper. The capability of initiation of UV polymerization was investigated previously for some of these compounds by fotocalorimetry[7] or FTIR[9,10].

Experimental

M a t e r i a l s

Eleven arene-iron salts were synthesized by exchanging the ferrocene ligand or by nucleophilic substitution reaction[7].

A mixture of ferrocene, aluminium chloride, aluminium powder in the excess of relevant arene (benzene for B, 1,3,5-trimethylbenzene – TMB, hexamethylbenzene – HMB, 1,4-diisopropylbenzene – DIPB, 1,3,5-triisopropyl-benzene – TIPB, chlorobenzene – CB, 4 methylphenol – PMP, phenyl ether – DPO and biphenyl –BP) was refluxed under nitrogen for 15 hours. After cooling, the mixture was treated with ice gradually added with constant stirring. After the end of exothermic reaction, the mixture was filtered and the phases of filtrate separated. The organic portion was extracted with water; the combined aqueous phases were extracted with diethyl ether and added to a concentrated solution of potassium hexafluorophosphate in water. The mixture was stirred, and then kept in a refrigerator for several hours. The precipitated solid was collected by filtration and dried. The raw product was purified by recrystallization from an acetone–ether mixture.

In the case of nucleophilic substitution reaction a mixture of sodium hydride, isopropyl alcohol (for IPOB, resp. *n*-propyl alcohol for NPOB) and tetrahydrofuran was stirred under inert atmosphere for about 10 min, whereupon mixture of CB (η^5-cyclopentadien–1-yl) [(η^6)-chlorobenzene]-Fe(II) hexafluoro-phosphate) and tetrahydrofuran was added. The mixture was stirred at room temperature under argon in darkness for 24 hours, whereupon it was concentrated by evaporating the solvent and treated with potassium hexafluorophosphate in water. After shaking, dichloromethane was added followed by solution of hydrochloric acid for adjustment of pH. After separation, the aqueous layer was extracted with little amount of dichloromethane; the combined organic phases were dried with salt brine, and evaporated until almost dry. The brown-red tar formed was dissolved in dichloromethane, and the product was precipitated by addition of diethyl ether.

Initiator IPB was not synthesized but commercially available initiator (Irgacure 261) by Ciba Speciality Chemicals was used. Structure formulas of tested initiators are shown in Fig. 1.
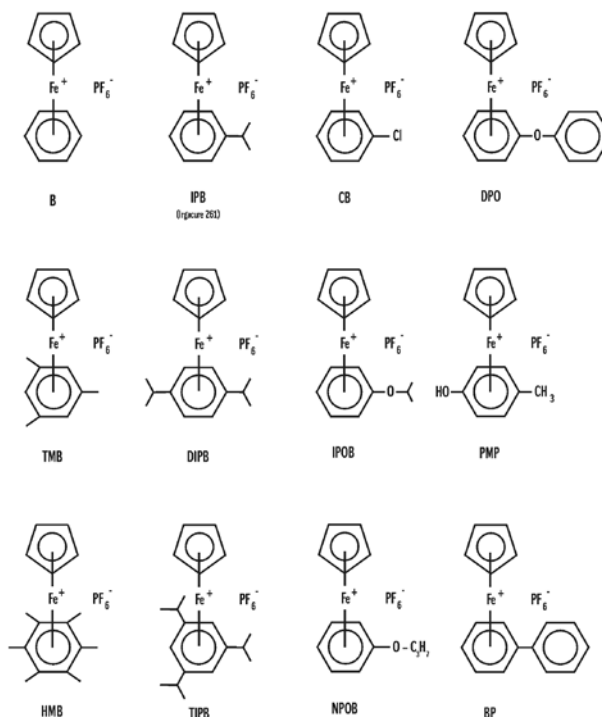
Fig. 1. **Structure formulas of tested initiators**

E x p e r i m e n t a l   A p p a r a t u s   a n d
M e a s u r e m e n t   M e t h o d

UV-VIS absorption spectra and photolysis of photoinitiators were monitored by UV-VIS spectrometer Specord 210 (Analytik Jena AG, Germany) in solutions of photoinitiators in acetonitrile at room temperature. The molar absorption coefficients were calculated using the Lambert-Beer's law. Photolysis of photoinitiators (concentration of 2×10^{-4} mol dm^{-3})

was followed by decreasing the absorption bands after irradiation by high-pressure mercury lamp (CE Green Spot from UV Source Inc., USA). The intensity of irradiation was 500 mW cm^{-2} (in the spectral region 258–380 nm). The normalized absorbance A_n was calculated by (1):

$$A_n = (A_0 - A_t)/(A_0 - A_\infty),\qquad(1)$$

where A_0 is absorbance of measured band before the irradiation, A_∞ is absorbance after the final photolysis and A_t is absorbance after the irradiation time t.

The dependence of normalized absorbance on the irradiation dose was described by (2) for first-order reaction:

$$A_n = P_1(1 - e^{-P_2 E}),\qquad(2)$$

where P_1 is maximal normalized absorbance, P_2 is rate of decomposition after irradiation and E is the irradiation dose [mJ cm^{-2}]. From (3), $E_{1/2}$ can be calculated as the energy needed to achieve the half photodecomposition.

$$E_{1/2} = \ln 2/P_2\qquad(3)$$

The degree of photodecomposition X_P of initiators for irradiation dose E was calculated from (4):

$$X_P = A_n/P_1\qquad(4)$$

Results

Photolysis spectra of [Cyclopentadien-Fe–arene] PF$_6$ photoinitiators are on Fig. 2. The concentration of photoinitiators in acetonitrile was 2×10^{-4} mol dm^{-3} and irradiation dose was 0–1,600 mJ cm^{-2}. Arrows mark the change of absorption bands during the UV exposure. Isoabsorptive points indicate that photoinitiators photodecomposition proceeded selectively without side reactions.

The degree of initiators decomposition caused by UV irradiation was evaluated from absorption changes at such wavelengths, where only respective initiators absorb (not products of its photodecomposition): 243 nm for B, CB, DIPB, DPO, IPB, IPOB, PMP, and NPOB, 245 nm for HMB, TIPB and TMB. The photolysis absorption spectra of BP are different from other tested initiators. Biphenyl produced during decomposition of BP has strong absorption band at 250 nm (Fig. 3.). From this reason, the absorption band at 290 nm was chosen.

Type of ligand has influence on absorption spectra and rate of decomposition of photoinitiators. The lowest absorption was found out for initiator B, the highest absorption for initiators with electronegative atoms in ligands. Rate of decomposition is also higher in present of ether, halogen or alcohol group. Course of decomposition was slower if methyl or propyl substituent were used on arene ligand. After UV irradiation arene ligand is released and band 243 nm decreases (except BP).
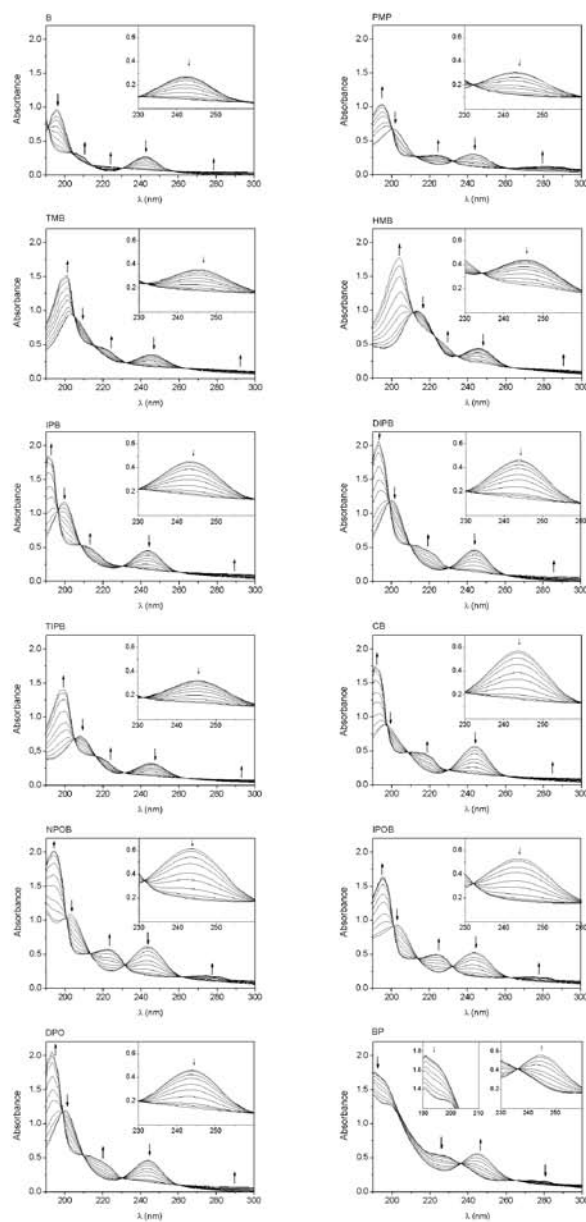
Fig. 2. **Absorption spectra of photoinitiators in acetonitrile (concentration of 2×10^{-4} mol dm^{-3}) measured after UV exposure**

The dependences of photoinitiator normalized absorbance A_n (1) on UV dose were fitted by non-linear regression according to (2). The non-linear regressions were treated by software OriginPro. The adequacy of proposed regression model with experimental data and the reliability of parameter estimates P_1 and P_2 found (Table I) were examined by the goodness-of-fit test. The determination coefficients R^2 are equal to 99.5 % or better. Applying (3) to the data according to the regression criterion, the energy needed to achieve of photodecomposition of 0.5 ($E_{1/2}$) has been estimated (Table I). Comparing the values of $E_{1/2}$ or P_2 it is apparent that speed of decomposition is higher in present of alcohol,

ether or halogen group on arene ligand. Course of decomposition was slower if methyl and propyl groups were used.
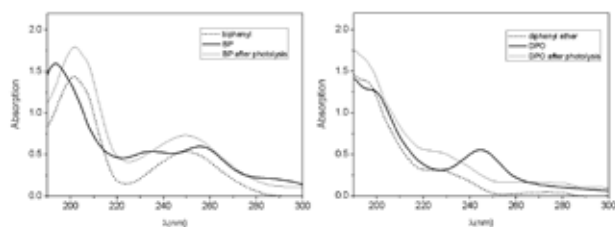
Fig. 3.   **Absorption spectra of initiators (BP and DPO) and abs. spectra of correspond ligands produced by photolysis**

Table I
Decomposition of initiators (solution in acetonitrile)

initiator	λ [nm]	ε [$dm^{-3}\,mol^{-1}\,cm^{-1}$]	P_1	P_2 [$cm^2\,mJ^{-1}$]	$E_{1/2}$ [$mJ\,cm^{-2}$]
IPB	243	11,858	1.046	0.0020	333
DIPB	243	12,024	1.055	0.0020	347
CB	243	14,830	1.020	0.0025	275
NPOB	243	16,040	1.008	0.0028	270
DPO	243	14,399	0.996	0.0035	194
PMP	243	8,043	1.008	0.0038	185
HMB	245	11,494	1.241	0.0011	645
TIPB	245	8,438	1.079	0.0017	402
TMP	245	9,254	1.036	0.0021	321
IPOB	243	13,796	1.088	0.0030	227
B	243	7,048	1.107	0.0016	406
BP	290	5,432	0.982	0.0089	71

Normalized absorbances were recalculated by (4) and the degree of photodecomposition X_p of initiators for irradiation dose E was obtained (Fig. 4.). There is apparent influence of type of ligand on the course of photolysis of photoinitiators. The sequence of initiators names in legend correspond with speed of photolysis (for initiator BP different absorption band was evaluated, so comparing with others initiators is questionable).

Conclusions

The molar absorption coefficients and degree of photodecomposition of prepared initiators was determined. Types of used ligands influence the absorption spectrum of photoinitioator, rate of decomposition and UV dose needed for achieving of $E_{1/2}$. Initiators with alcohol, ether or halogen
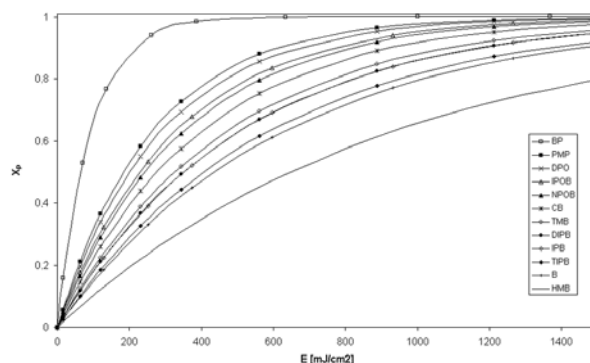
Fig. 4.   **Dependence of degree of initiators decomposition on UV dose**

substituents on ligands have higher molar absorption coefficients and decomposition of them are accelerated. The found results of decomposition efficiency correspond with results of polymerization initiation efficiency in epoxide and vinylether binders[9,10].

REFERENCES

1. Ciamician G.: Science *88*, 365 (1912).
2. Roloff A., Meier K., Riediker M.: Pure Appl. Chem *58*, 1267 (1986).
3. Crivello J. V., Lam J. H. W.: Macromolecules *10*, 1307 (1977).
4. Nesmeyanov A. N., Vol´kenau N. A., Bolesova I. N.: Dokl. Akad. Nauk. SSSR *149*, 615 (1963).
5. Bowser R., Davidson R. S.: J. Photochem. Photobiol. A: Chem. *77*, 269 (1994).
6. Jašúrek B., Vališ J., Weidlich T.: *Proceedings of RadTech Europe 07 (CD), Vienna, 13–15 November 2007*, 17 Poster sesion/01 Advences/07 Jasurek, p. 1. Vienna, 2007.
7. Vališ J., Weidlich T.: Adv. Colour Sci. Technol. *6*, 73 (2003).
8. Wang T., et al.: J. Photochem. Photobiol. A: Chem. *163*, 77 (2004).
9. Valis J., Jasurek B., Weidlich T.: Chem. listy *99*, 483 (2005).
10. Valis J., Jasurek B., Weidlich T.: *Conference Proceedings Book from The International Conference Printing Technology* SPb ´06, p.62., St. Petersburg, Russia, June 2006.

L18 KINETICS OF OXIDATIVE PROCESSES ON INKJET-PRINTED THIN LAYERS OF TITANIUM DIOXIDE

MICHAL VESELÝ, PETR DZIK, MÁRIA VESELÁ, JANA DRBOHLAVOVÁ AND JANA CHOMOUCKÁ

Brno University of Technology, Faculty of Chemistry, Purkyňova 118, 612 00 Brno, Czech Republic,
vesely-m@fch.vutbr.cz

Introduction

As the photogenerated active oxygen species are formed at the irradiated TiO_2 surface, this system can be utilized for microbes deactivation instead of the conventional methods such as UV irradiation, heat treatment or chemical disinfectant application.

The mechanism for bactericidal activity of photocatalytic oxidation was firstly[1] proposed by Matsunaga et al. in 1985. In this pioneer study, they showed that coenzyme A taking part in many biochemical processes is photoelectrochemically oxidized, which leads to the inhibition of cellular transpiration and eventually cell death. Most studies of photocatalytic microbe inactivation are focused on bacteria[2–16], less on viruses[17], yiest[18,19] and fungus[20,21]. As most of the bacteria-focused studies deals with *Escherichia coli*, this species was proposed as a standard microorganism for normalised testing of the photocatalytic activity of various substrates. One reason for this choice is definitely the fact that the presence of this bacteria indicates the contamination of water by feaces.

The mechanism for bactericidal effect of photocatalytic process on TiO_2 was in detail described on *E. coli*: Maness[22] et al. proposed, that *E. coli* was killed by the process known as lipid peroxidation. They propose that the first step is the interaction of oxidation products generated by irradiated titanium dioxide with microorganism cell wall. Here the initial oxidative damage takes place. Despite having the cell wall damaged, the cell is still viable. After the erosion of cell wall, an attack onto the cell membrane takes place. Here the peroxidation of membrane lipids takes place as the polyunsaturated phospholipids are the main components of bacterial cell membrane.

The formation of malondialdehyde was also observed, indicating the oxidative decomposition of lipids in protoplasm. This is a highly reactive compound capable of damaging proteins, nuleic acids and bases. Due to the severe erosion of membrane structures the vital biochemical processes such as respiration, semipermaeability and oxidative phosphorilation are slowed down and evetually terminated, resulting in ultimate cell death.

Sunada et al.[24] studied the destruction of *Escherichia coli* entotoxine which is an integral component of cell membrane by titanium dioxide. They proved that the cell death was accompanied by the endotoxine degradation and concluded, that the photocatalytic ptocess onto a TiO_2 thin film includes the destruction of outer bacterial mebrane.

Some differences in the susceptibility of various microorganisms to the photocatalityc stress can be observed. The difeerences are especially apparent between gram-positive and gram-negative bacteria. The gram-positive ones, although being less structurally complex then the gram-negative ones, are encapsulated by a thick peptidoglycanous layer. Similarly fungi and yiest are less sensitive to the photocalitic attack because of their strong eucariotic cellular wall representing relatively strong resisting barirrier agaist the reactive oxygen radicals generate on the surface of irradiated titanium dioxide.

Electrons reduce adsorsobed oxygen to superoxide radicals ($O_2^{\bullet-}$). Electron holes exidies OH groups into hydroxyl radical $HO^{\bullet}$, which then act as the main oxidizing agents. The heterogeneous photocatalytic process then consists of a series of reactions which may be expressed by the following set of equations:

$$TiO_2 \xrightarrow{h\nu} TiO_2(e_{cb}^-, h_{vb}^+) \longrightarrow recombination \quad (1)$$

$$TiO_2(h_{vb}^+) + H_2O_{ads} \longrightarrow TiO_2 + HO_{ads}^{\bullet} + H^+ \quad (2)$$

$$TiO_2(h_{vb}^+) + HO_{ads}^- \longrightarrow TiO_2 + HO_{ads}^{\bullet} \quad (3)$$

$$TiO_2(h_{vb}^+) + D_{ads} \longrightarrow TiO_2 + D_{ads}^+ \quad (4)$$

$$HO^{\bullet} + D_{ads} \longrightarrow D_{oxid} \quad (5)$$

$$TiO_2(e_{cb}^-) + A_{ads} \longrightarrow TiO_2 + A_{ads}^- \quad (6)$$
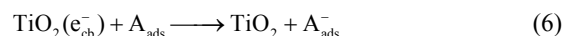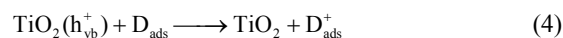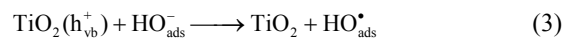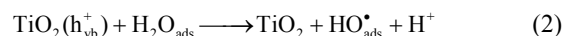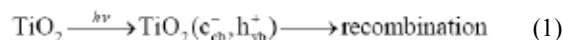
Here, **A** stands for the electron acceptor and **D** electron donor. In most cases, a complete mineralization of organic substrate takes place and CO_2 a H_2O are the final products. Dissolved oxygen is the usual acceptor in aqueous media, being transformed into superoxide anion-radicals ($O_2^{\bullet-}$), which can further initiate the formation of hydroxyl radical $HO^{\bullet}$:

$$TiO_2(e_{cb}^-) + O_{2_{ads}} + H^+ \longrightarrow TiO_2 + HO_2^{\bullet} \rightleftharpoons O_2^{\bullet-} + H^+ \quad (7)$$

Although the photocatalytic inactivation of microorganism is not suitable for the decompostion of a large quantity of matter in a short time, it became a highly effective measure to eliminate lower concentration of microorganisms and especially to prevent their further growth.

Generally, several different disinfection kinetic models are used in order to describe the microorganism killing[26]. The first empiric model for experimental data fitting was proposed by Chick and Watson in 1908:

$$\ln \frac{N}{N_0} = -k\, c^n t \,, \quad (8)$$

where N_0 and N corresponds to initial and remaining microorganism population, respectively, k is inactivation rate constant, t is reaction time, c is disinfection agent concentration and n is reaction order. In most cases n equals 1, causing the deactivation of microorganism to become a first-order

reaction. The Chick-Watson model was modified considering two different kinetic constants, k_1 describing the rate of microbial disinfection and k_2 taking into account the biocide concentration decrease:

$$\ln \frac{N}{N_0} = -\frac{k_1 c^n}{nk_2}\left[1 - \exp\left(-nk_2 t\right)\right] \qquad (9)$$

In 1972, the kinetic model of Hom was developed, which assumes a general equation for disinfection:

$$\ln \frac{N}{N_0} = -k\, c^m t^h \,, \qquad (10)$$

where k is the disinfection rate constant, *c* is the concentration of biocide, *m* is the Hom dilution coefficient, *t* is elapsed time and *h* is the Hom time exponent[29]. It should be noted that if *h* equals 1, then the equation reduces to that of the Chick-Watson model.

Some authors, who studied UV disinfection of wastewater, tried to replace the concentration of disinfectant in the previous equation (10) with the intensity φ of UV radiation[31]. Then the expression of the rate N/N_0 becomes:

$$\ln \frac{N}{N_0} = -k\, \varphi^n t = -k\, H \,, \qquad (11)$$

where *t* is time of exposure and then the product $\varphi \times t$ gives the total exposure dose H [$\mathrm{J\,m^{-2}}$].

Horie and co-authors assumed that cell deactivation obeys a second-order reaction between cells and oxidative radicals, and the death of a cell is caused by *n* times reactions on the basis of a series-event model. They derived complex equation for rate constant k' of photocatalytic disinfection in slury of titanium dioxide taking into acount titanium dioxide concentration and incident light intensity[25].

Unfortunatelly, these equagtions doesn't obeys fully to experimental data of photocatalytic disnfection of yeasts on immobilized titanium dioxide layer.

The most popular way of titanium dioxide thin layer preparation is sol-gel method. Usually the substrates are coated by dip-coating or spin-coating method. But each of them has some drawbacks. It would be very convenient to prepare these layers by way similar to spray coating. Inkjet printing is apparently a very good candidate for this task. In a conventional inkjet printer, small droplets of low viscosity ink are ejected from a print head and fall onto printed substrate. If we are able to replace the ink with a liquid precursor and printing paper with a suitable substrate, we obtain a very robust device for the precursor deposition.

By utilizing the well know sol-gel chemistry used so far spin- and dip coated layers of TiO_2 with the wide deposition possibilities offered by inkjet printing, we are able to prepare photocatalytically active thin layers of TiO_2 in a very effective and clean way with minimum waste.

Experimental

Sol-gel technique was applied to titanium dioxide thin films preparation using titanium(IV) propoxide as titanium precursors. Soda lime glass plates with sizes of $50 \times 50 \times 1.5$ mm were used as a substrate for TiO_2 thin films after treatment for surface sodium ions leaching.

Sol application was performed in a novel innovative way utilizing a modified office inkjet printer with empty carts. Cleaned glass plates were then mounted into a modified CD holder, fed into the printer and printed with "black only" driver setting. The colour of the printed pattern was varied in different shades of grey (100%, 95%, 90%, 80%, 70%, 60%) and thus glasses with varying sol loading were printed. The resolution, print speed and media settings were also varied and their influence on the resulting TiO_2 layer properties was evaluated. Two way of printer setting were chosen for thin layer of TiO_2 preparation – slow (S) and rapid (R). The sample marked as 100 R corresponds to 100 % of sol loadings printed by rapid way.

After coating, the glass plates were dried in the oven at 110 °C for 30 min and finally at 450 °C for 4 hours.

Photocatalytic killing of yeast *Candida vini* and *Candida tropicalis* were performed to study the antimicrobial properties of prepared TiO_2 layers. The yeast cells have spherical or oval, sometimes cylindrical or elongated shape of $3.0–5.5 \times 4.0–9.0$ µm in size. Generally, *Candida* is the most common cause of opportunistic mycoses (Candidiasis) worldwide. This type of endogenous infection mostly arises from overgrowth of the fungus inhabiting in the normal flora.

The yeast culture for the photocatalytic test was prepared as follows: 1 ml of yeast culture cultivated for 24 h in GPY liquid nutrient media was diluted with 9 ml of deionized water and centrifuged for 5 min at 4,000 rpm. The supernatant was separated from yeast sediment and centrifugation was repeated once again with 10 ml of deionized water. After last changing of liquid, the pure yeast suspension in water was well homogenized using minishaker. 30 µl of this suspension was dropped onto 15 min pre-irradiated TiO_2 film on glass plate and spread by micropipette for better contact of yeasts with photocatalyst surface. The sample was then put on reflective surface in Petri dish and covered by quartz plate in order to maintain a constant humidity during reaction. The sample was irradiated by four fluorescent lamps Sylvania Lynx-S 11 W with a maximum of energy at 365 nm. Irradiance of 1 mW cm^{-2} was maintained by lamp distance adjustment.

The irradiated samples were analyzed by epi-fluorescent microscopy using Acridine orange dye: 40 µl of 1.8×10^{-4} M Acridine orange (in phosphate buffer with pH 6) was added to 30 µl drop of irradiated sample placed in Petri dish. The Acridine orange dye is capable to bind to DNA in dead cell and so in epi-fluorescence microscope this complex emits red light. Then the dead cells appear as red and live cells as green in colour. A random selection of 20 places on a sample was recorded by Pixelink PL–A662 CCD camera (Pixelink Canada) and images were processed by Lucia software. On each image, the number of live and dead cells was calculated and expressed as the survival ratio (SR), i.e. number of live cells divided by total number of cells in each image using following formula:

$$SR = \frac{N_{\text{live}}}{N_{\text{live+dead}}} \qquad (12)$$

The obtained survival ratio was averaged and processed by statistical methods.

Results

By the described method of thin layer of titanium dioxide we prepared layers predominantly with crystaline structure proved by Raman spectroscopy (Fig. 1.). The Raman spectroscopic measurements of TiO_2 calcinated films revealed the anatase phase to be dominant with the small portion of rutile.
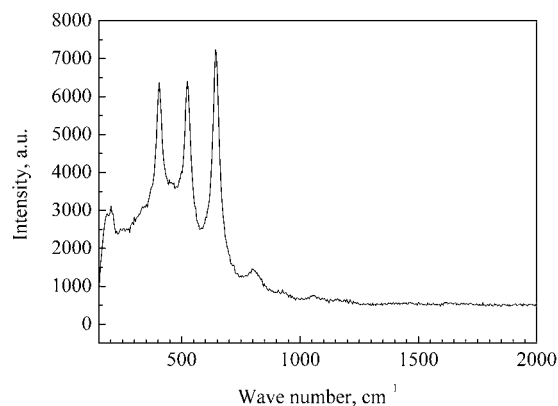
Fig. 1.   **Raman spectra of printed layer of titanium dioxide 95R**
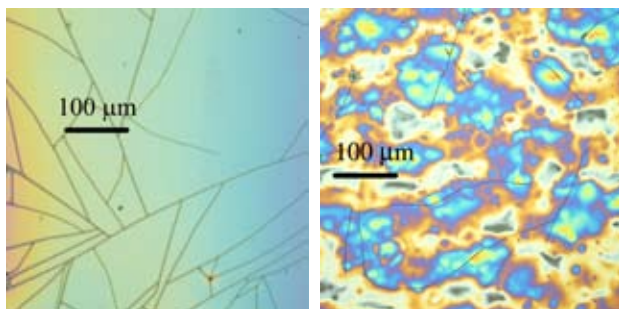
Fig. 2.   **Titanium dioxide layers: Smooth surface of rapidly printed sample 95 R (left) and structured surface of slow printed sample 95 S**

The different amount of sol printed on glass surface and two different way of sol printing resulted in various surface structure, layer homogeneity and porosity. The surface structure varied from smooth surface of fast printed layers to wrinkly surface of slow printed layers (Fig. 2.). Maximum thickness was 212 nm. The smooth layer was formed by 30 nm particles of titanium dioxide. However, this smooth layer contained cracks smaller than 700 nm (Fig. 3.).

We found that process of yeast photokilling does not significantly depend on way of printing if the surface is fully covered by TiO_2. Generally, a damage of membrane needs
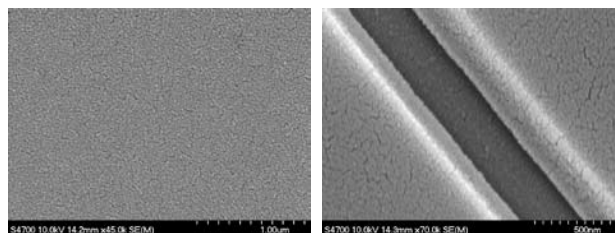
Fig. 3.   **SEM microphotography of sample 95 R**

a certain time and we observed the induction period. When a membrane was perforated, the second period occurred during which the microorganism inactivation was accelerated.

The presence of plateau in the later period of reaction was found during yeast inactivation. Inner cell components present outside the cells cause the competition between these molecules and bacteria as regards the rective oxygen species. We found similar results for both used cells of *Candida tropicalis* and *Candida vini*.
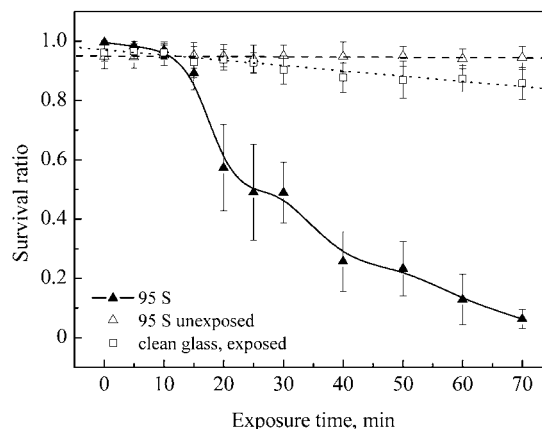
Fig. 4.   **Photocatalytic inactiovation of yeast *Candida vini* on slow printed titanium dioxide layer**

Conclusions

It was found that printed layers show photocatalytic activity. The prepared lyaers were thiner than 200 nm and transparent. Their properties were proved by phtocatalytic inactivation of yeasts. This process does not depend on the way of sol delivery by inkjet printer if the glass surface is fully covered.

REFERENCES
1. Matsunaga T., Tomoda R., Nakijima T., Wake H.: FEMS Microbiol. Lett. *29*, 211 (1985).
2. Daneshvar N., Niaei A., Akbari S., Aber S., Kazemian N.: Global NEST Journal *9*, 132 (2007).
3. Byunghoon K., Dohwan K., Donglyun C., Sungyong C.: Chemosphere *52*, 277 (2003).

4. Guimaraes J. R., Barretto A. S.: Braz. J. Chem. Eng. *20*, 403 (2003).

5. Rincón A-G., Pulgarin C.: Appl. Catal. B *49*, 99 (2004).

6. Yu J. C., Tang H. Y., Yu J., Chan H. C., Zhang L., Xie Y., Wang H., Wong S. P.: J. Photochem. Photobiol. Chem. *153*, 211 (2002).

7. Kim B., Kim D., Cho D., Cho S.: Chemosphere *52*, 277 (2003).

8. Dadjour M. F., Ogino Ch., Matsumura S., Shimizu N.: Biochem. Eng. J. *25*, 243 (2005).

9. Fernández P., Blanco J, Sichel C., Malato S.: Catal. Today *101*, 345 (2005).

10. Watts R. J., Washington D., Howsawkeng J., Loge F. J., Teel A. L.: Adv. Environ. Res. *7*, 961 (2003).

11. Kühn K. P., Chaberny I. F., Massholder K., Stickler M., Benz V. W., Sonntag H-G., Erdinger L.: Chemosphere *53*, 71 (2003).

12. Nadtochenko V. A., Rincon A. G., Stanca S. E., Kiwi J.: J. Photochem. Photobiol. Chem. *169*, 131 (2005).

13. Rincón A-G., Pulgarin C.: Appl. Catal. B *51*, 283 (2004).

14. Čík G., Priesolová S., Bujdáková H., Šeršeň F., Potheová T., Krištín J.: Chemosphere *63*, 1419 (2006).

15. Kiwi J., Nadtochenko V.: Langmuir *21*, 4631 (2005).

16. McLoughlin O. A., Fernández Ibáńez P., Gernjak W., Malato Rodríguez S., Gill L., W.: Sol. Energ. *77*, 625 (2004).

17. Lee S., Nishida K., Otaki M., Ohgaki S.: Water Sci. Tech. *35*, 101 (1997).

18. Kühn K. P., Chaberny I. F., Massholder K., Stickers M., Benz V.W., Sonntag H-G., Erdinger L.: Chemosphere *53*, 71 (2003).

19. Serpone N., Salinario A., Horikoshi S., Hidaka H.: J. Photochem. Photobiol. *179*, 200 (2006).

20. Lonnen J., Kilvington S., Kehoe S. C., Al-Touati F., McGuigan K. G.: Water Res. *39*, 877 (2005).

21. Sichel C., De Cara M., Tello J., Blanco J., Fernández-Ibánez P.: Appl. Catal. Environ. *74*, 152 (2007).

22. Maness P. C., Smolinski S., Blake D. M., Huang Z., Wolfrum E. J., Jacoby W. A.: Appl. Environ. Microbiol. *65*, 4094 (1999).

23. Pal A., Pehkonen O. S., Yu L. E, Ray M. B.: J. Photochem. Photobiol. Chem. *186*, 335 (2007).

24. Sunada K., Watanabe T., Hashimito K.: J. Photochem. Photobiol. Chem. *156*, 227 (2003).

25. Horie Y., David D. A., Taya M., Setsuji T.: Ind. Eng. Chem. Res. *35*, 3920 (1996).

26. Cho M., Chung H., Choi W., Yoon J.: Water Res. *38*, 1069 (2004).

27. Salih F. M.: Water Res. *37*, 3921 (2003).

28. Cho M., Chung H., Yoon J.: Appl. Environ. Microbiol. *69*, 2284 (2003).

29. Lambert R. J. W., Johnston M. D.: J. Appl. Microbiol. *88*, 907 (2000).

30. Sellami M. H., Hassen A., Sifaoui M. S.: JQSRT *78*, 269 (2003).

L20   A STUDY ON THE THICKNESS HOMOGENEITY AND REFRACTIVE INDEX OF THIN ORGANIC LAYERS

OLDŘICH ZMEŠKAL, OTA SALYK, MICHAL VESELÝ
and PETR DZIK

Brno University of Technology, Faculty of Chemistry, Purkynova 118, 612 00 Brno, Czech Republic,
zmeskal@fch.vutbr.cz

Introduction

This paper deals with the utilization of optical and interference microscopy for the study of thin film layers. We present a new and very simple method for the determination of refractive indexes of transparent layers based on interference phenomena. Both thin layer thickness and refractive index can be determined by this method.

We used this method for a complex analysis of sandwich and gap structures of organic semiconductor components (e.g. ITO/PEDOT/DPP/Alq3/Al) prepared by a combination of following procedures: vacuum vapour deposition and/or spin coating and/or inkjet printing. A series of photographs of one sample was recorded and analysed which gave us the thicknesses of individual layers, their homogeneity and their refractive indexes.

Recorded images were processed by means of image analysis (correlative and fractal analysis). Image analysis was performed using application HarFA (Harmonic and Fractal Image Analyser), which has a wide potential of use not only for image analysis but for analysis of video clips, signals and numerical data as well.

Results obtained by image analysis methods were confirmed and eventually further extended by ellipsometric measurements, which is unfortunately more time consuming and challenging.

Experimental

S a m p l e   P r e p a r i n g

Within the context of development of new cheap organic materials suitable for optoelectronic applications (e.g. photovoltaic cells, light emitting diodes, etc.) new techniques of their cheap production are looked for. The preparation of thin films structures by means of various methods, e.g. spin coating, vacuum evaporation or inkjet printing seems to be very perspective techniques. Structures prepared for electronic applications are mostly multilayered with a complicated structure, see Fig. 1.

It is possible to prepare complex structure of electronic component by means of suitable combination of all three procedures.

For example, structure at Fig. 1. consists of conductive thin film ITO (indium tin oxide) deposited on a glass substrate.

The other two films are composed of PEDOT (poly(3,4-ethylenedioxythiophene)) and semi conductive derivative DPP (diketo pyrrolo pyrrole). These work as an active pho-

toconductive element. It is possible to prepare these from solutions and/or dispersions by means of inkjet printer and/or spin coating, respectively.

Fig. 1.   **Example of multilayered structure for electronic applications**

Last two films consist of Alq3 (tris (8-hydroxyquinoline) and aluminium. Alq3 works as an interlayer between active semiconductor DPP and contact electrode (Al) and both layers are prepared by vacuum vapor deposition.

It is apparent that functionality of electronic component prepared in this way is dependent on the quality of prepared films, this means on homogeneity of their thickness, on their mutual contact (adhesion) and on their time and mechanical stability.

In this respect the films prepared from solution are crucial. In the case of these films it is necessary to ensure good adhesion to underlying film (for PEDOT it is ITO), to prevent agglomeration of dispersing particles and crystallization[1].

I m a g e   D a t a   R e c o r d i n g

Image analysis methods can be with advantageously utilized for the quality assessment of films prepared in this way. It is possible to use them for surface quality assessment in combination with optical microscope and digital camera. Film thickness determination is possible in combination with an interference microscope. It is also possible to determine refractive index of organic materials[2–3] using suitable interpretation of recorded results.

For example, it is possible to use the software HarFA developed by authors of this contribution for image analysis. It is necessary to eliminate image errors caused by e.g. non-homogeneity of the light, by non-linear transfer of brightness (gamma correction), and by thermal noise[4–6].
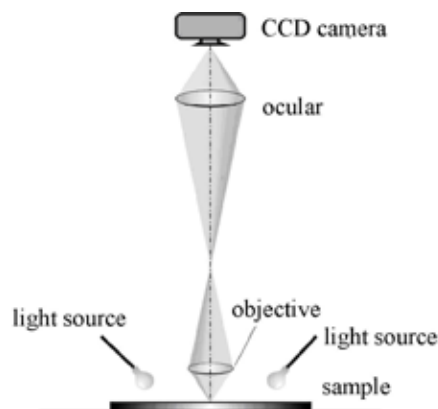
Fig. 2.   **Principle of image data recording**

Interference microscope Interphako (Carl Zeiss Jena) is used for the film thickness measurement. The principle of the measurement is based on the phase shift between beams reflected from the surface of the thin organic film and evaporated Al refractive layers. Film structure is demonstrated at Fig. 3. This phase shift is in a good agreement with double thickness of the film, as demonstrated at Fig. 3. (on the top).
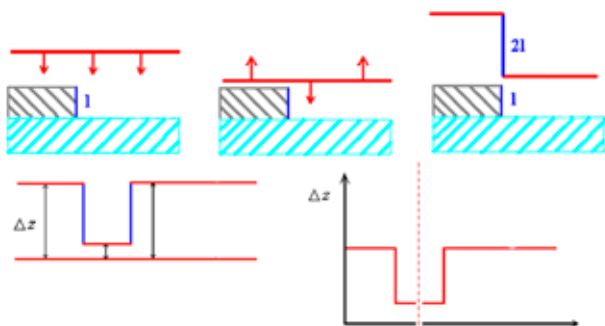
Fig. 3.   **Principle of thickness layer measurements with using of interference microscope**

Using splitting and three-dimensional shift of two parts of the Fig. and their subsequent composition it is possible to get interferential images such as those at Fig. 4.
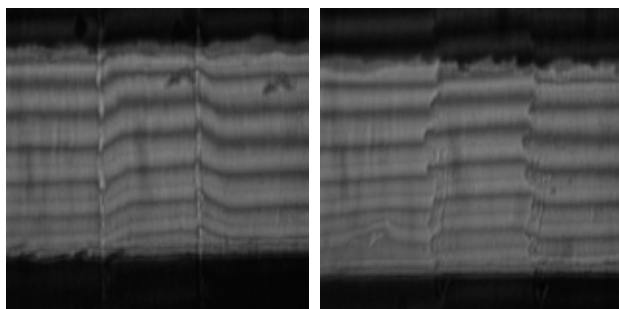
Fig. 4.   **Interference microscope images (from the "air" side) for edge of ITO (on the left) and DPP (on the right)**
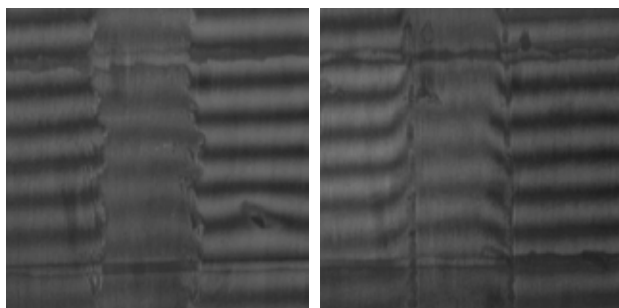
Fig. 5.   **Interference microscope images (from the "glass" side) for edge of ITO (on the left) and DPP (on the right)**

The details for two edges at aluminium contact are for ITO layer (on the left) and for DPP (on the right side). The shift of the interference line at the edge is in agreement with the Fig. 3. A similar image can be observed from the bottom

side of the sample – from the "glass" side. The results are presented at Fig. 5. We can see that shift on the edge is greater than when it is observed from the "air" side of the sample (Fig. 4.).

D a t a   A n a l y s i s

The analysis performed by HarFA consists of the following steps:

- Recording of image sequences (videos) of electrical contact from the side "air" and "glass (*Open video, File types: Images*). This step was set for more effective analysis.
- Selection of interesting part of interference images, at the place of main interference maxima (the square 512 × 512 pixels was selected).
- Selection of proper colour space for analysis (the *Brightness*, not threshold – *not BW* settings was select).
- Making of two videos (from "air" and from "glass" side) which was consist from interference image sequences (*Save square video as...*)
- Processing of correlation analysis for selected frames of videos. Selected part was vertical rectangle 256 × 512 pixels at the frame middle (*Correlation*). The results were saved as images (see Fig. 6.) and as data files (see Fig. 7.).
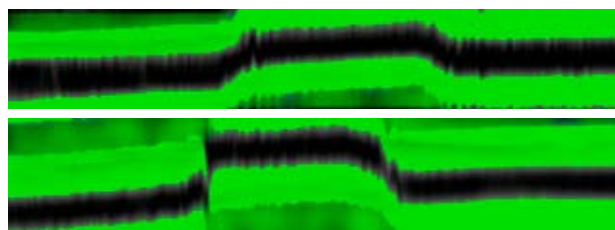
Fig. 6.   **The results of correlation analysis – sharpen lines of the same phase on the image: the split of ITO edge from the "air" (on top) and from the "glass" (bottom) measuring**

The saved data were further statistical processed by a very simple procedure. The average values of all lines were calculated and a rotation leading to horizontal zero reference line was performed. The average shift of the split and average wavelength (in pixels) from the shift of lines was calculated. The results of these very simple calculations are at Fig. 8. for ITO from "air" and "glass" side.

The thickness and refractive index of DPP and ITO can be immediately from these dependences determined. The results of calculations are summarized in Table I. The values were calculated as the average values of all pixels at the edge (Fig. 7.). The uncertainty of these values is very small; the errors are caused by the homogeneity of the measured surface.

The thickness was calculated from the known wave length $\lambda = 512$ nm, refractive index from the simple equation $n = \Delta s/\Delta l$, where Δs is so called optical line and Δl real line of the light. The profile of average phase line shift for the whole contact is presented on Fig. 8.
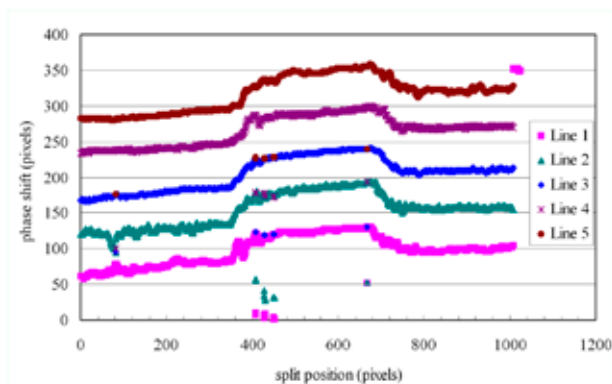
Fig. 7.   **The phase lines of the ITO edge split from the "air" side measuring**
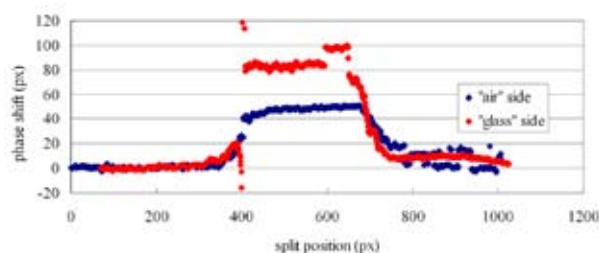
Fig. 8.   **The corrected phase lines of the ITO edge split from the both "air" and "glass" side measuring**
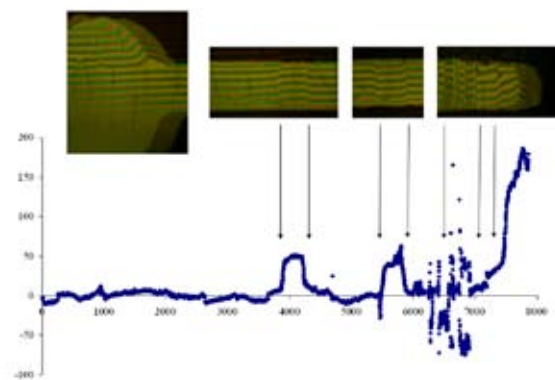
Fig. 9.   **The profile of average phase line**

The imperfect groves created by cutting to DPP layer give in maxima the same shifts of phase as the second ege (DPP). The right changes of the phase are caused by inhomogeneties on the end of glass.

Results

We can see from the results at the Table I that the ITO layer is thinner and its homogeneity is lower than DPP layer. Also refractive index value is more accurately for ITO layer.

These results confirm the dependences of refractive indexes and thicknesses on the split position of layer edge on Fig. 10. and Fig. 11. We can see that the homogeneity of the ITO thickness is greater than the momogeneity of DPP and

Table I:
The refractive index and thickness parameters of ITO and DPP layers ($\lambda = 512$ nm)

Parameter	ITO layer	DPP layer
Sample thickness [nm]	38 ± 1	80 ± 5
Optical thickness [nm]	66 ± 3	107 ± 18
Refractive index [-]	1.73 ± 0.05	1.34 ± 0.15
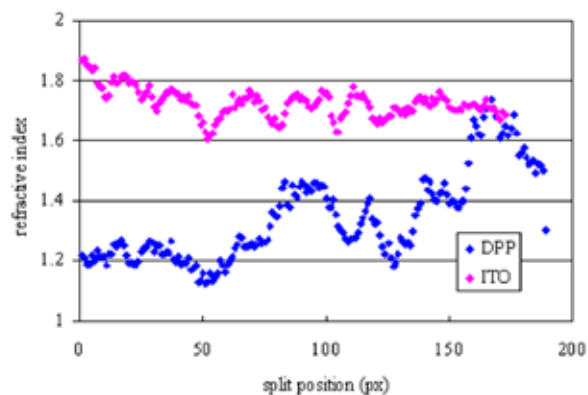
Fig. 10.   **The refractive index both ITO and DPP layer calculated from edge split reason**
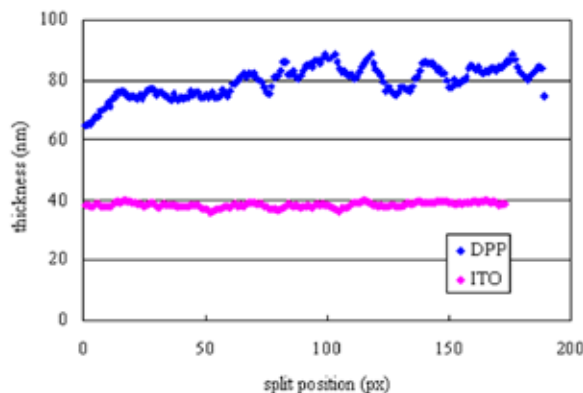
Fig. 11.   **The thickness both ITO and DPP layer calculated from edge split reason**

also the refractive index is more constant. The results are in agreement with data from ref.[7].

Conclusions

The new very simple and quick method for the determining of layer thickness and their refractive index was presented. The other advantages are that the calculation of refractive index is not dependent on the surrounding layers but only on the layer with edge. This fact is advantage in contrast to ellipsometry.

REFERENCES

1. Zmeškal O., Veselý M., Vala M., Bednář P., Bžatek T.: *In VIII Seminar in Graphic Arts. Conference Proceedings*. p. 131 Pardubice, 2007.
2. Zmeškal O., Sedlák O., Nežádal M.: *Metody obrazové analýzy dat, Digital Imaging in Biology and Medicine*, 1st ed., p. 34–43. České Budějovice: Czech Academy of Science, 2002.
3. Zmeškal O., Nežádal M., Sedlák O.: *Využití fraktální analýzy při hodnocení kvality tisku*, *IV. Polygraphic Conference*, p. 92. Pardubice, 2001.
4. Tomankova K., Jerabkova P., Zmeskal O., Vesela M., Haderka J.: J. Imaging Sci. Technol. *50*, 583 (2006).
5. Jerabkova P., Zmeskal O., Haderka J.: *Complexus Mundi*, WS. London, World Scientific. p. 305 – 312, (2006).
6. Jerabkova P., Zmeskal O., Vesela M.: *Chemisrty & Life*, 1st ed., p.292. Brno, (2005).
7. Kim J. K., Schubert M. F., Xi J.-Q., Mont F., Schubert E. F.: *Lasers and Electro–Optics* CLEO, 2007.

6.2. Posters

P01 THE STUDY OF TiO₂ THIN FILMS PHOTOCATALYTIC ACTIVITY ON DEGRADATION OF YEAST AND DYE POLLUTANTS

JANA CHOMOUCKÁ, JANA DRBOHLAVOVÁ, PETR DZIK, MÁRIA VESELÁ and MICHAL VESELÝ

Brno University of Technology, Faculty of chemistry, Institute of Physical and Applied Chemistry, Purkyňova 118, 612 00 Brno, Czech Republic,
chomoucka@fch.vutbr.cz

Introduction

Among various oxide semiconductor photocatalysts, titanium dioxide (TiO_2) appears to be a promising and important prospect for use in enviromental purification, because of its strong oxidizing power, photoinduced hydrophilicity, nontoxicity and long-term photostability. TiO_2 shows excellent photocatalytic activity for oxidative degradation of environmental pollutants[1].

The first description of antimicrobial effect of TiO_2 film was published by Japanese professor Matunago and collegues in 1985. At the beginning of the photocatalytic reaction, highly reactive groups containing oxygen atoms (ROS – reactive oxygen species) are formed. These ROS produced by photocatalysis cause different type of damage in live organisms. After a hydroxyl radical attack, the outer membrane is partially destroyed. There is no important change of cell viability during this process, but membrane permeability towards ROS is changed. At this stage, ROS can attack the cytoplasmic membrane more easily, which results in the lipid membrane peroxidation and subsequent cell death[2].

Experimental

Preparation of TiO₂ Thin Film

The substrates used as film supports were soda-lime glass plates. Boiling the glass plates in sulfuric acid removes the surface sodium ions and therefore the photoactivity of the film can be improved.

Transparent TiO_2 layers were immobilised on glass plates using sol-gel method with titanium tetraisopropoxide in ethanol as precursor. Depositions of thin films were realized by dip-coating method with withdrawal speed 120 mm min⁻¹. In the next stage, the coated substrates were dried for 30 min. at 110 °C and then calcinated for 4 hours at 450 °C with temperature ramp of 3 °C min⁻¹.

Photooxidation of 2,6-dichloroindophenol

The photocatalytic activity of the TiO_2 films was evaluated by examining the oxidation rate of water solution 2,6-DCIP (2×10^{-5} mol dm⁻³) upon UV irradiation (2.4 mW cm⁻², solar lamp Philips HPA-400 W) in a desk reactor. The concentration decrease of 2,6-DCIP was determinated spectro-

photometrically. A photochemical dechloration of 2,6-DCIP is a reaction of first order kinetics.

Antimicrobial Efect of TiO₂ Thin Film

Photocatalytic killing of yeasts *Candida tropicalis* and *Candida albicans* were performed to study the antimicrobial properties of TiO_2 films. These yeasts belong to the class of Ascomycetes, the family of Saccharomycetaceae and the kingdom of Fungi. Generally, *Candida* is the most common cause of opportunistic mycoses (Candidiasis) worldwide. This type of endogenous infection mostly arises from overgrowth of the fungus inhabiting normal flora. *C. albicans* is the most frequently encountered medical pathogen, the second one is *C. tropicalis*.

The yeast culture for the photocatalytic test was prepared as follows: 1 ml of yeast culture cultivated for 24 h in GPY liquid nutrient media was diluted with 9 ml of deionized water and centrifuged for 5 min at 4,000 rpm. The supernatant was separated from yeast sediment and centrifugation was repeated once again with 10 ml of deionized water. After the last change of liquid, the pure yeast suspension in water was well homogenized using minishaker. 30 μl of this suspension was dropped onto 15 min pre-irradiated TiO_2 film on glass plate and spread for better contact of yeasts with photocatalyst surface. The sample was put in Petri dish and covered by quartz plate. The UV irradiation was provided by fluorescent lamp Sylvania Lynx-S 11 W with intensity 1.5 mW cm⁻². After exposure suspension of yeasts, 40 ml of 1.8×10^{-4} mol dm⁻³ Acridine Orange was added to the drop of irradiated sample. Nicon Eclipse 200 with epifluorescent adapter equipped with Camera Pixelink Canada was used for dead and live cell resolution and calculation. It was calculated survival ratio of yeasts.

$$ SR = \frac{N_{live}}{N_{live+dead}} \qquad (1) $$

Results

Photooxidation of 2,6-DCIP

Fig. 1. shows that the number of layers (i.e. thickness) influences the photocatalytic activity. The higher number of TiO_2 thin layers is, the higher the photocatalytic activity is. But in the case of 4 layers, the photocatalytic activity is smaller due to its large thickness. The layer is too thick, so the generation of electrons and holes proceed deep in the semiconductor layers, and therefore they can't get to the surface and participace the reaction. It causes the decrease of photocatalytic activity.

Antimicrobial efect of TiO₂ thin film

The reaction was performed only in deionized water without the nutrient compounds to avoid their influence on yeast degradation process.

The dependence of *Candida tropicalis* and *Candida albicans* survival ratio on irradiation time and TiO_2 layer
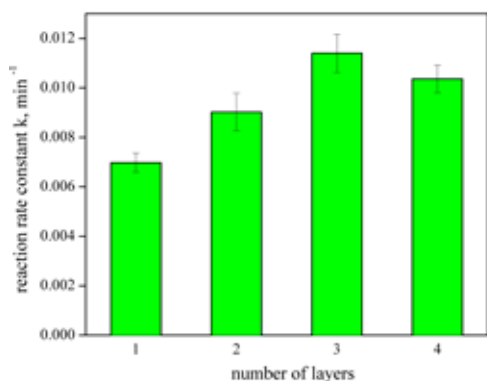
Fig. 1.   **The influence of number of TiO$_2$ thin films on the photo-catalytic efficiency 2,6-DCIP**

Fig. 2.   **The survival ratio of *Candida tropicalis* during irradiation**

Fig. 3.   **The survival ratio of *Candida albicans* during irradiation**

Conclusions

We prepared TiO$_2$ thin films on soda-lime glass plates by dip coating method. Films are homogenous and transparent.

The photocatalytic efficiency of prepared coatings was evaluated on photocatalytic oxidation 2,6-DCIP in aqueous phase, as well as on killing of microorganisms, *Candida tropicalis* and *Candida albicans* yeasts.

We found that the number of layers (i.e thickness) positively influences the photocatalytic oxidation of 2,6-DCIP.

Concerning the microorganisms killing, *Candida tropicalis* and *Candida albicans* were selected for determination of TiO$_2$ thin film antimicrobial properties, because they represent the most frequently encountered medical pathogen, causes the opportunistic mycoses. We observed that the photocatalytic degradation rate increases with increasing TiO$_2$ film thickness.

number is demonstrated at the following figures (Fig. 2. and Fig. 3.). It can be seen, there is no antimicrobial activity during UV irradiation of yeast suspension when the photocatalyst is absent.

Concerning the induction period, it is decreasing with increasing number of TiO$_2$ layer.

In the case of *Candida albicans*, we observed worse antimicrobial efficiency (Fig. 3.) therefore longer time of irradiation is necessary to kill them.

REFERENCES

1. Carp O., Huisman C. L., Reller A.: Prog. Solid State Chem. *32*. 33 (2004).
2. Sunary K., Watanabe T., Hashimoto K.: J. Photochem. Photobiol. A: Chem. *156*, 227 (2003).

P02   USING OF VIS-NIR FIBRE OPTICS REFLECTANCE SPECTRA FOR IDENTIFICATION OF IRON-GALL INKS IN HISTORICAL DOCUMENTS

MICHAL ČEPPAN[a], DANIELA PAVLISOVÁ[a], MILENA REHÁKOVÁ[a], LUKÁŠ GÁL[a], JARMILA DÓRIOVÁ[b] and JOZEF HANUS[c]

[a]*Faculty of Chemical and Food Technology, Slovak University of Technology, Radlinského 9, 812 37 Bratislava, Slovakia,*
[b]*Academy of Fine Arts and Design, Bratislava, Slovakia,*
[c]*Slovak National Archives, Bratislava, Slovakia,*
michal.ceppan@stuba.sk

Introduction

The identification of brown-grey inks is of importance to understand the history and aesthetics of an object, to evaluate the risks involved with its use, and to judge the effects of conservation treatments. Drawings may contain different brown-grey shades side-by-side, which could be due to the use of different drawing inks. Traditionally, to obtain brown-grey shades, bistre, sepia, carbon black and iron gall inks were used[1]. Iron gall inks contain transition metals, such as iron and copper, catalyzing the radical oxidation of the substrate, as well as acids, catalysing its hydrolysis[2]. These degradation processes, generally known as "ink corrosion", lead to the formation of fluorescent and brown degradation products, followed by mechanical weakening of the paper and formation of cracks. If none of these phenomena are observed, it is not easy to visually distinguish iron gall inks from other, potentially less aggressive, brown-grey inks.

Different instrumental analytical methods, e.g. SEM/EDX, XRF or FTIR have been applied to identify inks[3]. As most collection keeping institutes do not have access to these techniques, there is a need for "hands-on" methods that do not require sampling or transport of the object outside the institute. Nowadays, Fibre-Optics Reflectance Spectrometers (FORS) have reached dimensions which allow them to be transported easily to the objects to be measured.

It was shown, that brown-grey inks can be distinguished by the reflectance spectra obtained from visually comparable shades of sepia, bistre and iron gall inks, processed by chemometric factor analysis method[4]. In this paper previously developed method of factor analysis was used to process VIS-NIR fibre optics reflectance spectra measured on historical drawings and documents with grey-brown inks and identification of iron gall inks.

Computational and Experimental

Previously developed chemometric detector for identification of iron gall inks in the VIS-NIR spectral region[4] was used. Reference data set consists of 132 spectra of samples of iron gall inks. Chemometric detector is based on the testing of correspondence of studied individual spectrum with the database. This testing was performed by the method of the

Factor Analysis – namely Target Factor Analysis[5] was used. This method evaluates the deviation, call AET parameter, of tested spectrum from the projection of tested spectrum into the factor space of database spectra set. Great value of AET parameter indicates that the tested spectrum does not correspond to the database. On the other hand, low value of AET parameter indicates, that the tested spectrum corresponds to the spectra of databases. In this case we select the value of AET = 0.006 as a threshold (corresponds to the statistically evaluated reproducibility of the measurement of the database spectra).

Spectra of studied historical documents and drawings were measured with the fibre optics spectrophotometer system Ocean Optics consisting of Hi-Res spectrometer HR 4000CG-UV-NIR, UV-VIS-NIR light source DH-2000-BAL and standard reflectance accessory with 45 °/45 ° geometry. Spectra were measured at the region 500–1,050 nm. For each measurement, the detector was calibrated on the blank paper near to the inked area. In this way, changes in spectral reflectance due to ageing of the substrate were largely excluded. Original reflectance spectra were transformed into Kubelka-Munk[7] spectra. Kubelka-Munk spectra are generally preferred in the methods using linear algebra[8]. Also, each spectrum was normalized to have maximum value equal one, to enhance shape analysis.

Results and Discussion

The presence of iron gall inks was tested in the set of drawings from collection of Slovak National Gallery. Example of the analysis of VIS-NIR spectra of the drawing from 16th century is on Fig. 1.

The spectra were measured at the four locations and AET parameters indicate that the iron gall ink was used. This result is supported by the results of XRF analysis confirming the presence of iron.

The analysis of document from 19th century is on Fig. 2. VIS-NIR spectra were measured at two positions.

The AET value at of the spectrum at location A indicates that the iron gall ink was used for signature (this finding was supported by the colorimetric spot test[9]), the spectrum at location B absorbs practically all VIS-NIR light, what
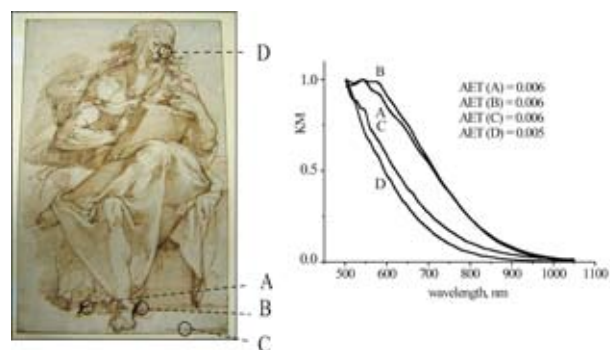
Fig. 1.   **Sitting Evangelist, Bartolomeo Passarotti, 1550–1590, Slovak National Gallery, Bratislava, Slovak Republic, Inventory No. K 96**
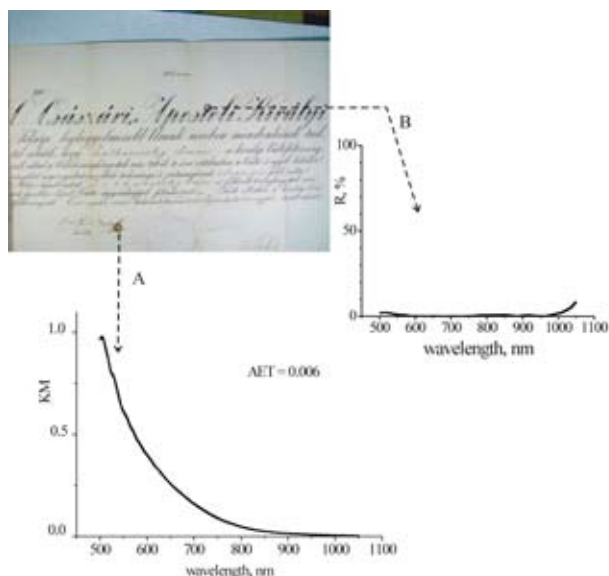
Fig. 2. **Document from 19th century, Slovak National Archives, Bratislava, Slovak Republic**

Fig. 3. **Book Historia Boiemica, 1575, older parchment sheet used as a bookbinding material, Moravian Gallery Brno, Czech Republic, inventory No. D9751**

indicates the probable presence of some kind of carbon black (Chinese) ink.

The attempt to use the detector to analyse the ink on the parchment is on the Fig. 3. The average spectrum of the typefaces corresponds to the iron gall inks spectra according to the low value of the AET parameter.

REFERENCES

1. Corrigan C.: in *Old Master Prints and Drawings – A Guide to Preservation and Conservation* (Cohn M., ed.), Amsterdam University Press, p. 76 (1997)
2. Neevel J. G.: in *Preprints of the 8th International Congress of IADA,* (Koch M. S., Palm K. J., ed.), Copenhagen, p. 93 (1995)
3. Neevel J. G., Mensch C. T. J.: in *Preprints of the 12th Triennal Meeting of the ICOM Committee for Conservation - Lyon, International Council of Museums,* (Bridgland j., Brown J., ed.), Paris, p. 528 (1999)
4. Ceppan M., Neevel J. G.: Chem. Listy, *99*, s535 (2005)
5. Malinowski E. R.: *Factor Analysis in Chemistry (Third Edition)*, Wiley, Inc., New York (2002)
6. Pelikán P., Čeppan M., Liška M.: *Application of Numerical methods in Molecular Spectroscopy*, CRC Press, Boca Raton (1994)
7. Kubelka P., Munk F.: Zeits. f. Physik *12*, 593 (1931)
8. Čeppan M., Fedák J., Dvonka V., Veselý M., Zmeskal O.: J. Imag. Sci. Technol. *47*, 171 (2003)
9. Neevel J. G.: in *Iron gall inks: on manufacture, characterization, degradation and stabilization* (Kolar J., Strlic M., ed.), Chapter 9, p. 147, Narodna i univerzitetna knjižnica, Ljubljana, Slovenia 2006

P03　THE INFLUENCE OF PHOTOINITIATORS AND ADITIVES ON THE PHOTOCHEMICAL SPEED OF METHACRYLATED PVAL

MARCELA ČERNÁ, PETR DZIK and MICHAL VESELÝ

Institute of Applied and Physical Chemistry, Faculty of Chemistry, Brno University of Technology, Purkyňova 118, 612 00 Brno, Czech Republic,
xccernam@fch.vutbr.cz

Introduction

Cross-linking is a vital tool for modification of existing polymers to achieve new and improved materials. Cross-linked gels often have different properties based on the type of cross-linking method used (chemical, physical or ionical cross-linking), as well as the fact that each method brings with it is own limitations and benefits depending on the desired use and application of the gels[1].

PVAl is largely used for the production of fiber (vinylon), film, in the paper industry, in the textile sizing, as a modifier of thermosetting resins, as pressure-sensitive adhesives, emulsifier, ect. The final properties of PVAl mainly depend on the properties of its parent polymer, poly(vinylacetate), its polymerization conditions and degree of hydrolysis. Cross-linking as well as modification of PVAl through its hydroxyl groups open new domain of application for this material[2].

Experimental

This study deals with the cross-linking reaction of methacrylated PVAl by the UV initiated non-linear polymerisation in the solid phase. For this purpose the modified PVAl had to be prepared.

Preparation of Modified PVAl

PVAl was dissolved in a mixture of DMSO and DMFA at 95 °C. Then the temperature was lowered to 70 °C. GMA and KOH ethanolic solution were added dropwise. Upon the addition of KOH, the solution changed color to yellow. After 1 hour the mixture was cooled down to room temperature and the deionized water was added. PVAl modified in this way was precipitated in ethanol and finelly washed in acetone. During this reaction a tricomponent copolymer poly(vinylalcohol-co-vinylacetate-co-vinylhydroxyprophylmethacrylate) was created.

Cross-Linking of MPVAl

A thin layer of methacrylated PVAl solution was spin-coated onto anodized aluminium plates. The coating mixture consisted of mPVAl (20 % wt.), water, surfactant and a variable amount of photoinitiators. We used three types of photoinitiators (Igacure 2959, Irgacure 2100, Irgacure 819) and their concentration was changed from 0.5 % wt. to 4 % wt. (this concentration was recommended by producer).

The spin-coated plates were exposed by UV radiation, developed in the deionized water and dyed in a Saturn Blue L4G solution. Each step of the aluminium plate was measu-

red by a densitometer. We observed the influence of photoinitiators type and concentration on the photochemical speed *S*. The photochemical speed was calculated according to the mathematical formula:

$$S = \frac{1}{H_n^{0.5}}, \tag{1}$$

where $H_n^{0.5}$ is a exposure at the normalised optical density 0.5. The value of the exposure was determined from the densitometrical measurement.

Crosslinking Above the Glass Transition Temperature

Besides the study of cross-linking below the glass transition temperature (T_g), we also investigated the kinetics of cross-linking reaction above T_g. In order to performe the cross-linking reaction above T_g, we added different types and concentration of plasticizers and we studied the dependence of this substances on the photochemical speed.

Glycerol and poly(ethylenglycol) (PEG) were used as plasticizers. We compared their plasticizing effect. The photochemical speed was determined in the same way as in case when the reaction runs below T_g.

Results

Modification of PVAl

The modified PVAl was prepared using GMA. The theoretical stechiometric degree of modification should have been 4 % mol. The real degree of the conversion was determined by UV-VIS spectroscopy[3].

Firstly, the calibration curve was constructed. The molar absorption coeficient was found out from its direction. If we knew the value of the molar absorption coeficient, the degree of conversion could be worked out. Prepared mPVAl had the degree of conversion 3.83 % mol.

The Influence of Initiators on the Photochemical Speed

The optical densities for each field of the aluminium plates were found out from the densitometrical measurement. The dependence $D_n = \log H$ was constructed. D_n is a normalized value of optical density, which was calculated as the quotient of the constituent fields of aluminium plates optical density and the full cross-linking field optical density. The value of $H_n^{0.5}$ was determined from this dependence and now we were able to calculated the photochemical speed by the formula (1).

The goal of our work was to obtain a higher *S* using two different photoinitiators (I 2100 and I 819) instead of I 2959. The spectral sensitivity of I 2959 is in the far region of UV radiation and we wanted to shift the spectral sensitivity of the studied system up to longer wavelengths because of better utilization of a radiation energy.

We didn´t reach this goal probably because the coating compositions with I 2100 and I 819 had the character of

microheterogenous mixtures. A stable emulsion was prepared in case I 2100 and a suspension was formed yet using I 819.

The results *S,* for each added initiators amount, are presented in Table I and we observe the comparison of *S* all using photoinitiators in Fig. 1. We can see that the *S* is the biggest for I 2959 and the smallest for I 819.

Table I
The photochemical speed of using commercial photoinitiators

Concentration of initiators [% wt.]	*S* of I 2959 [cm^2 J^{-1}]	*S* of I 2100 [cm^2 J^{-1}]	S of I 815 [cm^2 J^{-1}]
0.5	4,281.44	769.84	45.96
1.0	1,379.69	566.07	26.62
2.0	1,033.33	237.53	11.95
4.0	652.74	102.91	8.38
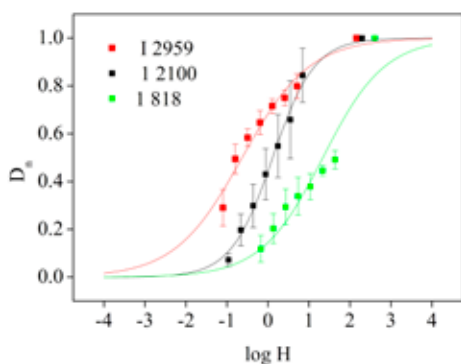
Fig. 1.   **The dependence D$_n$ = log H for all using photoinitiators, for initiators concentration 4 % wt.**

C r o s s - L i n k i n g   A b o v e   t h e   *T$_g$*

For the system with the plasticizers (glycerol and PEG), the photochemical speed *S* was determined in the same way as in the previous case. This photochemical speed was compared with *S* for the system without the plasticizer. A huge increase of *S* was observed in system with glycerol (about 50 ×).

The highest increase was achieved for glycerol concentration 5 % wt. When the concentration of plasticizer rises up above 5 % wt., the *S* decreases. This happens

Table II
The photochemical speed of systems with plasticizers

Concentration of plasticizers [% wt.]	*S*$_{glycerol}$ [cm^2 J^{-1}]	*S*$_{PEG}$ [cm^2 J^{-1}]
0	1,379.69	1,379.69
2	9,399.18	3,013.21
4	44,869.37	3,693.69
6	11,097.60	2,286.60
8	3,280.65	946.37

due to a huge increase of polymer free volume, which causes the moving away of macromolecular chains. The outgrowth is a disappearance of nearly all interaction.

The same results were reached also in case with PEG but *S* was grown up only three times. The overview of established speed can be observed in Table II. The comparison of PEG and glycero effect is noticed in Fig. 2.
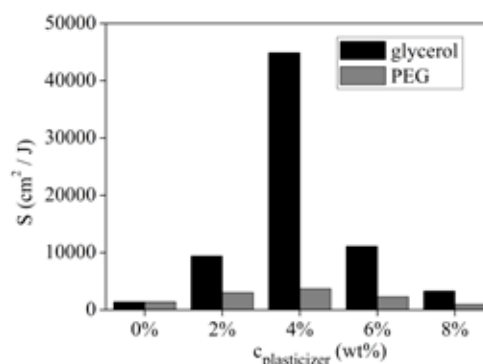
Fig. 2.   **The comparison of photochemical speed for two different plasticizers**

Conclusions

We synthesised mPVAl with the degree of conversion about 4 % mol. which secures a compromise between the system solubility in water and the content of double bonds in this system.

Our effort was to shift the spectral sensitivity up from UVC area the region of longer wavelength. This goal was accomplished but it doesn't lead to the rise of photochemical speed. It is probably caused by very slow radical transfer which comes as consequence of non-homogenous coated mixture. The coated system had heterogenous character due to limited miscibility of using compounds.

We also investigate the change of photochemical speed after plasticizer addition. We discovered that glycerol is better plasticizer than PEG because *S* grows up till 50 × in system with this plasticizer.

REFERENCES

1. Martens P., Holland T., Anseth K. S.: Polymer *43*, 6093 (2002).
2. Gohil J. M., Bhattacharya A., Ray P.: Polym. Res. *13*, 161 (2006).
3. Dzik P., Veselý M.: Chem. listy *100*, 70 (2006).

P04 TiO₂ BASED SENSOR WITH NANOSTRUCTURED SURFACE FOR GAS DETECTION

JANA DRBOHLAVOVÁ, JAROMÍR HUBÁLEK,
MARINA VOROZHTSOVA and RADIM HRDÝ

Brno University of Technology, Faculty of Electrical Engineering and Communication, Departement of Microelectronics, Údolní 53, 602 00 Brno, Czech Republic,
drbohla@feec.vutbr.cz

Introduction

On the field of environmental protection, many efforts have been done in few past years to produce a highly sensitive system for atmospheric pollutant monitoring using semiconductor metal oxide (SMO) materials[1]. More recently, the research was aimed to develope a nanostructured surface of sensing electrode in order to sufficiently increase its effective surface area and hence its sensitivity[2]. This nanostructure formation can be easily realized through a thin nanoporous Al_2O_3 template created e.g. on gold electrode. Such prepared metal nanostructures (nanowires, nanotubes, etc.) can be further modified by immobilization of previously mentioned semiconducting material. TiO_2 was found to be one of the efficient agents for this purpose, in particular for detection of different gases: O_2, H_2, CO, NH_3 as well as hydrocarbons[3,4]. Analogous to photocatalysis, the anatase phase is expected to play more important role in this case than the rutile[5,6]. Some investigators also observed a positive effect of doping the titania sensors with metals like Au, Pt, Nb, Cu or Cr[7,8].

Concerning the preparation of solid gas sensor from semiconducting material, sol-gel procedure belongs among widely used techniques despite of high precursor price and poor shelf-life of prepared sols[9,10]. However, this process allows a good control of surface properties such as composition, thickness and topology. A deposition of TiO_2 onto electrode with nanostructured surface can be then effected using dip-coating or drop-coating method. It is supposed the smaller size of semiconductor particles results in better sensitivity. Moreover, TiO_2 component should have a sufficiently porous structure.

Experimental

P r e p a r a t i o n o f A u N a n o r o d s

Nanorod-structured surface of Au electrode was fabricated using an anodisk purchased from Whatman, which consists of Al_2O_3 template sputtered on thin Au substrate. Au deposition conditions were set as follows:
- electrolyte composition of 6 g dm⁻³ of K[Au(CN)₂] and 2.32 g dm⁻³ of H_3BO_3,
- electrolyte temperature of 50 °C,
- current density of 0.25 mA cm⁻².

The deposition time *t* (s) of Au was calculated from following relationship:

$$m_{Au} = 1.2 \times 10^{-6} \cdot t \cdot \frac{I}{S}, \tag{1}$$

where m_{Au} [g] corresponds to amount of deposited Au and I/S is a current density [mA cm⁻²]. From preliminary experiments, the electrodeposition times of about 500 and 2,000 s are needed to produce Au nanorods with approximate length of 1 μm using 20 and 100 nm Al_2O_3 pore size, respectively. Finally, Al_2O_3 template was eliminated by dissolving in NaOH.

The obtained Au nanorods were characterized by SEM.

F i x a t i o n o f A u N a n o s e n s o r

Such prepared Au nanosensor was fixed on corundum plate with thick-film platinum meander heater using glass paste.

D e p o s i t i o n o f T i O₂ N a n o s t r u c t u r e s

Next step was aimed to immobilization of TiO_2 coatings by sol-gel technology starting from titanium tetrapropoxide precursor, ethanol as solvent and acetyl-acetone as stabilizing agent. The concentration of Ti was 0.35 mol dm⁻³. The sol was simply dropped onto Au surface of sensor with comb-like structure (Fig. 1), then dried at 110 °C in oven and finally annealed at 450 °C in a furnace. Also these samples were analyzed using SEM. Raman and FTIR-ATR spectroscopies were employed to characterize TiO_2 phase constitution.

Fig. 1. **Schematic illustration of gold-nanorod electrochemical gas sensor with comb-like structure**

Results

As can be seen from SEM characterization (Fig. 2), Au nanorods reached the presupposed length of about 1 μm and thickness of 0.1 μm.

Raman spectroscopic measurement showed the TiO_2 structures are predominantly in anatase phase with a small portion of rutile and organic contaminants originated from precursor (Fig. 3)[11]. The study of annealing temperature influence revealed that a composition of amorphous and rutile phase dominates in TiO_2 film dried only at 110 °C.

In addition, the presence of carbonate was also detected in samples prepared at 450 °C taking the FTIR-ATR spectra (Fig. 4). The scientists suppose the elimination of this residue detected at 1,380 cm⁻¹ requires the temperature as high as 600 °C(ref.[12]).
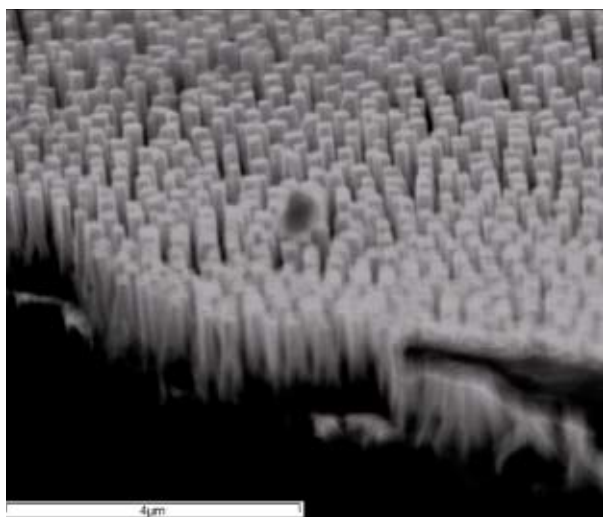
Fig. 2.   **SEM image of gold nanorods electrodeposited through Al$_2$O$_3$ template**
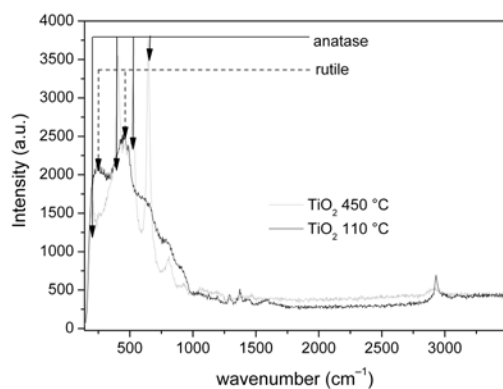
Fig. 3.   **Raman spectra of TiO$_2$ annealed at 110 °C and 450 °C**

Conclusions

At higher annealing temperature, anatase was found to be the majority phase in TiO$_2$ structure, while at lower one, TiO$_2$ was rather in the rutile form mixed with amorphous phase. Some organic and inorganic residues were also detected even after calcination at 450 °C.

Due to impedance spectroscopic measurement, we can assume our TiO$_2$ structures are homogenous and suitable for detection of various gases.
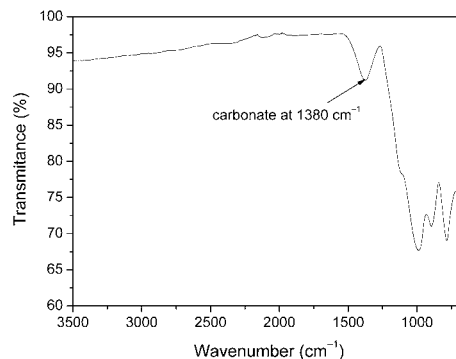
Fig. 4.   **FTIR-ATR spectrum of TiO$_2$ annealed at 450 °C**

REFERENCES

1. Khatko V., Llobet E., Vilanova X., Brezmes J., Hubalek J., Malysz K., Correig X.: Sens. Actuators B *45*, 111, (2005).
2. Klosová K., Hubálek J.: Phys. Stat. Sol. A *205*, 1435 (2008).
3. Manera M. G., Spadavecchia J., Buso D., de Julián Fernández C., Mattei G., Martucci A., Mulvaney P., Pérez-Juste J., Rella R., Vasanelli L., Mazzoldi P.: Sens. Actuators B *132*, 107 (2008).
4. Karunagaran B., Uthirakumar P., Chung S. J., Velumani S., Suh E.-K.: Mater. Charact. *58*, 680 (2007).
5. Epifani M., A. Helwig, J. Arbiol, R. Díaz, Francioso L., Siciliano P., Mueller G., Morante J. R.: Sens. Actuators B *130*, 599 (2008).
6. Francioso L., Taurino A. M., Forleo A., Siciliano P.: Sens.Actuators B *130*, 70 (2008)
7. Teleki A., Bjelobrk N., Pratsinis S. E.: Sens. Actuators B *130*, 449 (2008).
8. Alessandri I., Comini E., Bontempi E., Faglia G., Depero L. E., Sberveglieri G.: Sens.Actuators B *128*, 312 (2007).
9. Mohammadi M. R., Fray D. J.: Acta Mater. *55*, 4455 (2007).
10. Jiang H.-Q., Wei Q., Cao Q.-X., Yao X.: Ceram. Int. *34*, 1039 (2008).
11. Drbohlavova J.: *Dissertation*. Université Claude Bernard Lyon 1, Lyon, France, 2008.
12. Melián-Cabrera I., López Granados M., Fierro J. L. G.: Phys. Chem. Chem. Phys. *4*, 3122 (2002).

P05 IMAGE ANALYSIS OF OFFSET LITHOGRAPHY PRINTS

VLADIMÍR DVONKA, JÁN PANÁK MICHAL ČEPPAN
and BOHUSLAVA HAVLÍNOVÁ

Department of Graphic Arts Technology, Faculty of Chemical and Food Technology STU, Radlinského 9, 812 37 Bratislava, Slovakia,
vladimir.dvonka@stuba.sk

Introduction

Three methods of image analysis and densitometry were employed in this study to characterize influence of paper quality to quality of prints. Image analysis methods investigate the quality of printed details. The size and ink influence of printed 2% screen dots were measured by analysis of particles. Modulation transfer function (MTF) and fractal analysis were used for inspection of print edge. The 5 coated and 5 uncoated offset printing papers were tested for inspecting quality of similar samples.

Experimental Part

Screen dot size, fragmentation, fluctuation of colour (Fig. 2.) and missing dots were measured.

MTF was obtained from print edge for full printed patches[1] (Fig. 3.).

Fractal analysis method was based on Box Counting method[2] (Fig. 4., eq. (1)).

$$\ln N_{BBW}(1/\varepsilon) = \ln(K_{BBW}) + D_{BBW}\ln(1/\varepsilon) \qquad (1)$$

where ε is cell size of square net, N_{BBW} is number of black and partially black cells (Fig. 4.), D_{BBW} is fractal dimension.

Results and Discussion

Image Analysis of 2% Screen Dots

Area of screen dots

Average area of screen dot of coated samples is above of ideal screen dot size (436 μm^2) – from 509 to 608 μm^2
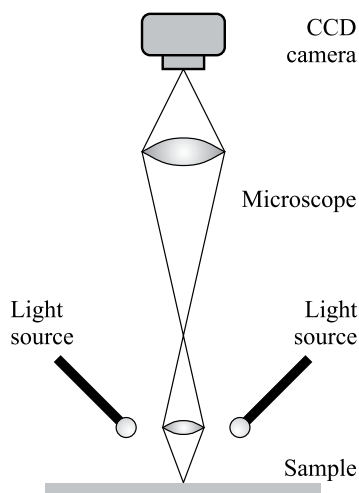
Fig. 1. **Construction of measuring equipment**

(a)   (b)
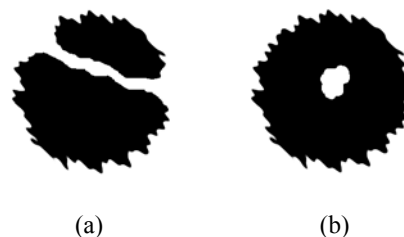
Fig. 2. **Fragmented screen dot (a), fluctuation of ink inside screen dot (b)**
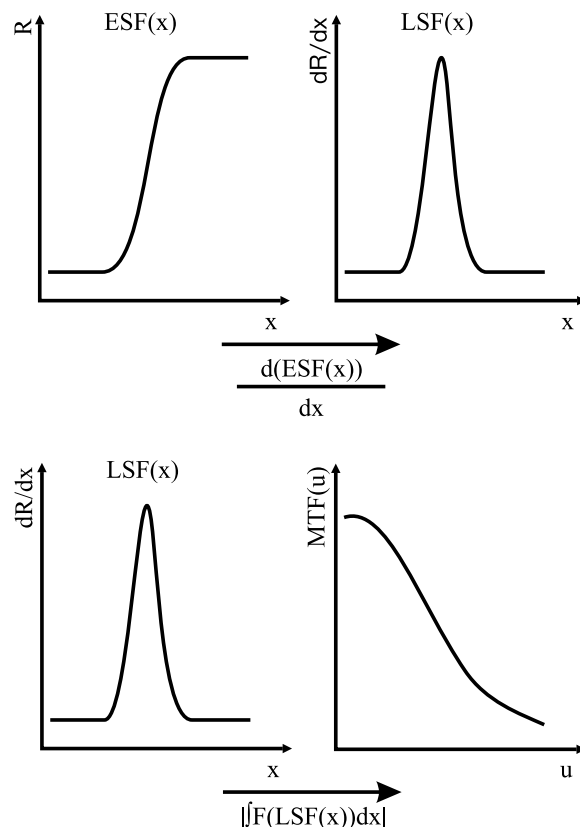
Fig. 3. **Procedure to obtain MTF, ESF/LSF – edge/line spread function, R – reflectance, u – space frequency, × – measured distance**
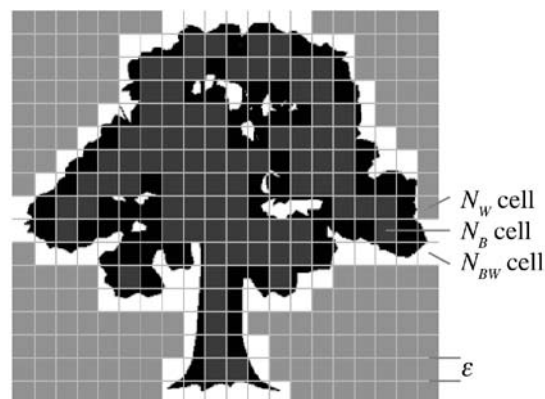
Fig. 4. **Box Counting method**

(Fig. 5.) that refers to dot gain. The biggest dot gain is by the sample 2, can be classified as the best, because of less possibility of missing dots.

Mostly opposite situation is for the uncoated paper. The lowest dot gain is by sample 6.
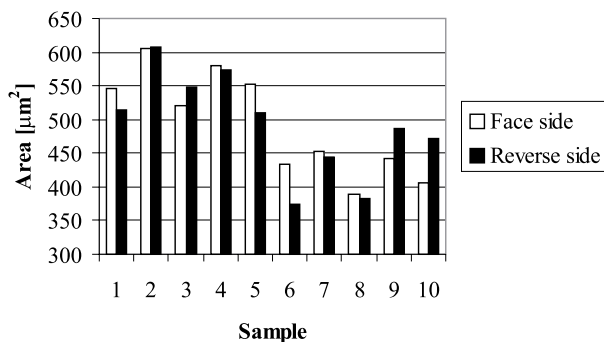
Fig. 5.   **Average area of screen dots**

Fragmented and missing screen dots

From the Fig. 6. we can conclude that uncoated samples are more predisposed to fragmentation of screen dots and to occurrence of missing screen dots. Average frequency of screen dot fragmentation is for coated samples markedly lower as for uncoated samples.
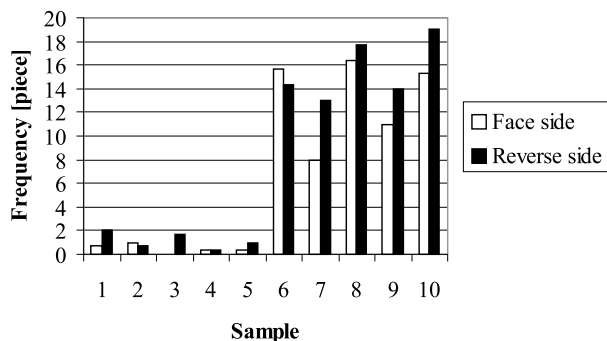
Fig. 6.   **Average frequency of fragmented screen dots**

From Figs. 7. and 8. can we draw the same conclusion as for the frequency of fragmented screen dots – higher amount of missing screen dots in uncoated samples. Black prints were the best, more resistant to missing dots as all other colour prints. We can observe more missing screen dots for cyan, magenta and then for yellow colour.

For all colours we can conclude that sample 4 is the best among the coated samples and sample 7 and 8 are the best among the uncoated samples.

M o d u l a t i o n   T r a n s f e r   F u n c t i o n

Space frequency value suggests that the samples 2 and 3 for face side and the sample 4 for reverse side are of higher quality (Fig. 9.). The lower quality sample was the sample 6.
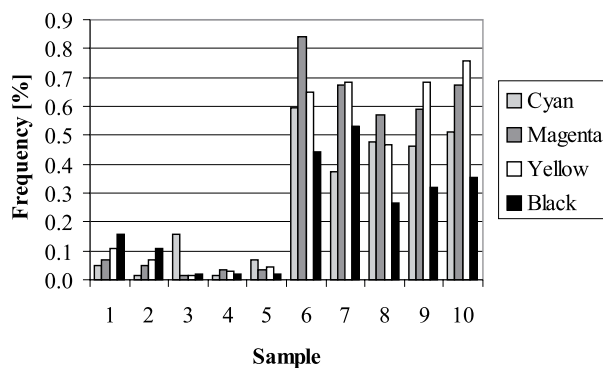
Fig. 7.   **Frequency of missing screen dots, face side**
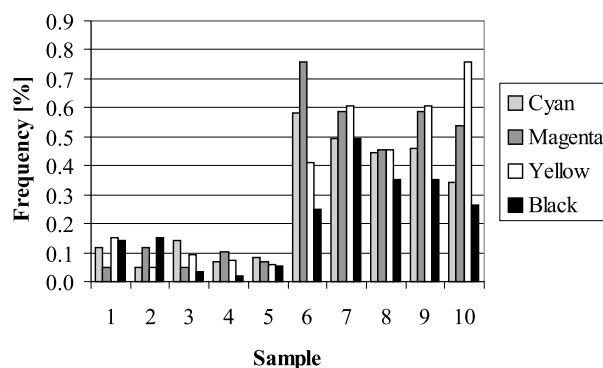
Fig. 8.   **Frequency of missing screen dots, reverse side**

F r a c t a l   A n a l y s i s   o f   P r i n t s

The results of fractal analysis clearly divided the studied samples into two groups (Fig. 10.) – coated and uncoated printing papers. The order of quality of the samples was the same for face and reverse side of printing papers – the best sample 4, the lowest quality sample 10.

D e n s i t o m e t r y

The parameters of Walker-Fetsko eq. (2)[3], except of print smoothness parameter k, gain expected values for coated and uncoated papers, with exception of samples 2 and 5 (face and reverse side).
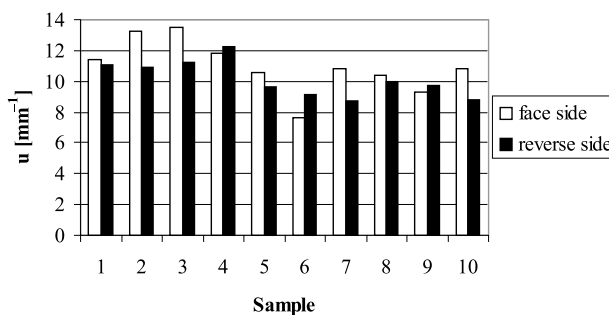
Fig. 9.   **The average space frequency u**
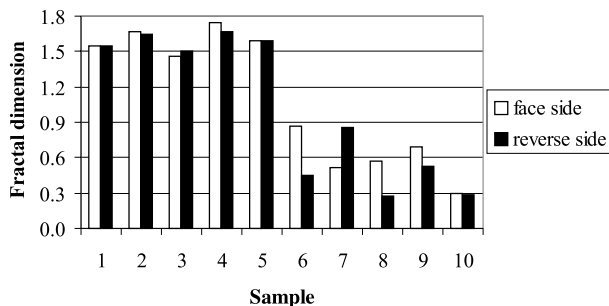
Fig. 10.   **The average value of fractal dimension**

$$y = (1 - e^{-kx})\{b(1 - e^{-x/b}) + f[x - b(1 - e^{-x/b})]\} \qquad (2)$$

where y – the amount of ink transferred to paper [$g\,m^{-2}$], x – the origin amount of ink on printing plate, k, f and b – constants obtained from graphical dependence.

The parameters of Tolenaar-Oittinen eq. (3) are more consistent. The parameters of steepness m and the parameters of sharpness radius n determined from the curve of ink consumption have markedly higher values for the coated papers.

$$D = D_\infty (1 - e^{-my^n}) \qquad (3)$$

where D_∞ – optical density for $y \rightarrow \infty$.

The trend of increasing trapping with increasing total porosity and decreasing with increasing average radius of pores for uncoated papers was observed. The opposite trend was observed for the coated papers. Interesting correlation of linear regression between trapping and solid density of inks of primary colours for the coated papers was found – 86.4 %.

The dot gain value $\Delta A_T(50\,\%)$ decreases with increasing total porosity and decreases with increasing gloss and average radius of pores. No such correlation was found for uncoated papers.

We tried also to relate image analysis parameters and densitometry values. The 96% correlation of linear regres-sion of black solid density for face and reverse side of coated papers and fractal dimension D_{BBW} confirms that image analysis is a useful method for evaluation of quality printing.

Summary

Expected correlation of densitometry values and properties of offset printing paper samples was not tight and for uncoated papers was almost none. The differences in the groups of papers were very small and taking into account errors of measurements were statistically insignificant. Dissipation of values is mostly lower for the coated papers, which refer to more homogenous surface of these samples.

Image analysis methods allowed to classify quality of samples: the sample 4 and 2 belongs to the best quality and the sample 10 and 6 belongs to the least quality printing paper.

The correlation of classical parameters of printing quality for black printing ink and parameters obtained by the methods of image analysis was investigated. Good correlations found for fractal dimension and parameters of surface roughness suggest the possible application and potential of further development.

REFERENCES

1. Koopipat C., Tsumura N., Fujino M., Miyata K., Miyake Y.: J. Imag. Sci. Technol. *45*, 591 (2001).
2. Zmeškal O., Nežádal M., Buchníček M., Čeppan M.: J. Imag. Sci. Technol. *46*, 453 (2002).
3. ISO 13656:2000: *Graphic technology–Application of reflection densitometry and colorimetry to process control or evaluation of prints and proofs* (2000).

P06 COLOR FIDELITY OF REPRODUCTION OF HISTORICAL DOCUMENTS

V. DVONKA, M. ČEPPAN, M. REHÁKOVÁ, J. PANÁK, P. AMBRÓZ and B. HAVLÍNOVÁ

Department of Graphic Arts Technology, Faculty of Chemical and Food Technology STU, Radlinského 9, 812 37 Bratislava 1, Slovak Republic,
vladimir.dvonka@stuba.sk

Introduction

The aim of this study was ability of colour reproduction of historical documents by commercial semi-professional reproduction system. Colour management systems (CMS) and colour profiles (ICC profiles) of input/output devices were used. The quality of capture and printing operations was evaluated by colour difference value[1,2].

Experimental Part

Capturing devices – CCD cameras Olympus C 7070 WZ, Fujifilm FinePix S7000, Nikon D50; scanner HP ScanJet 8300.

Output device – Epson Stylus PHOTO R2400, solvent based ink K4.

Measurement devices – spectrophotometers TECHKON SpectroDens, Spectroscan.

Lightning – two light SoLux, 4,700 K, 28,000 lx in position of sample, 45 °/0 °.

Ink-jet papers – Epson Archival Matter, Epson Premium Semigloss Photo, Epson Premium Glossy Photo, Ilford Smooth Pearl.

Test targets – analogue target IT8.7/2, Kodak Ektacolor Paper, 5"×7", 264 patches; digital target TC9.18 RGB, 918 patches.

Conversion of SRGB Colour Space to CIE L*a*b* Colour Space

Exact definition of colour space sRGB permit transformation of sRGB values to CIE L*a*b* colour space for evaluating of colour difference[2].

Calculation of XYZ colour values based on matrix equation 1 with previous modification of sRGB values[2].

$$\begin{bmatrix} X \\ Y \\ Z \end{bmatrix}_{D50} = \begin{bmatrix} 0{,}4361 & 0{,}3851 & 0{,}1431 \\ 0{,}2225 & 0{,}7169 & 0{,}0606 \\ 0{,}0139 & 0{,}0971 & 0{,}7141 \end{bmatrix}_{D50} \begin{bmatrix} R_{sRGB} \\ G_{sRGB} \\ B_{sRGB} \end{bmatrix} \quad (1)$$

XYZ colour coordinates was transformed to CIE L*a*b* colour coordinates and average colour difference values of test patches was calculated with respect to the original values.

Results and Discussion

The first step of digitizing process was test of different exposure conditions of digital cameras/scanner on reproduction of colour from original (264 colour patches) to captured
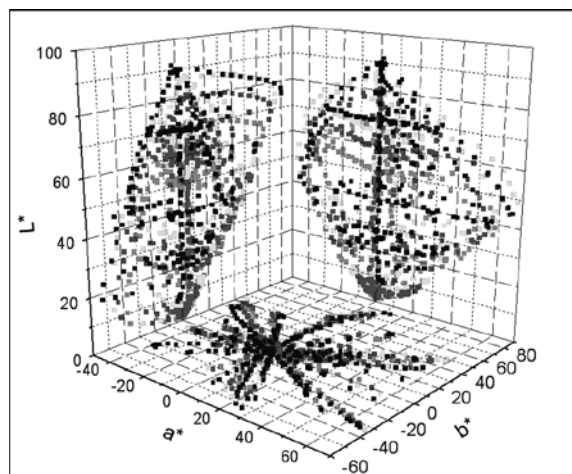
Fig. 1. **Exposure time shift, CIE L*a*b* colour space, digital camera Fujifilm, D50WS, dark grey – underexposure, light grey – overexposure, gray – right exposure, black – test target**

picture. The selection of exact white balance value was based on grey balance of captured pictures. Table I shows the influence of saturation on the colour difference value. Artificial saturation of colour increased colour difference value. Influence of exposure time on colour shift can be observed from Fig. 1. The best colour correlation to original was obtained for overexposed captured pictures. Colour profiles were prepared for all captured pictures and average colour differences of patches were calculated (Table I) before (ΔE^*_{ab1}) and after (ΔE^*_{ab2}) applying of ICC profiles.

The lowest average colour difference before applying ICC profile was obtained for Fujifilm digital camera, followed by Olympus and Nikon cameras respectively. After

Table I
Average colour differences ΔE^*_{ab} for all digital cameras, the picture name define white balance (colour temperature), saturation (S – satured, WS – without saturation), overexposed pictures (O)

Picture name	ΔE^*_{ab1}	ΔE^*_{ab2}
Fujifilm		
D50SO	14.2	9.5
D50WSO	11.1	8.2
D42SO	17.1	9.6
D42WSO	14.1	9.4
Nikon		
Picture name	ΔE^*_{ab1}	ΔE^*_{ab2}
D50SO	15.3	11.4
D50WSO	13.8	11.2
D65SO	16.1	9.3
D65WSO	14.4	9.3
Olympus		
Picture name	ΔE^*_{ab1}	ΔE^*_{ab2}
D50WSO	8.6	9.5
D42WSO	12.8	10.6

applying of ICC profile camera Fujifilm was the best followed by Nikon and Olympus cameras.

We try to set the white balance to custom mode. The results were better only in the case without using of ICC profile.

The average colour difference values for scanner (Table II) refer to better colour reproduction using embedded scanner profiling program.

The lowest average colour difference before applying ICC profile was obtained for Fujifilm digital camera, followed by Olympus and Nikon cameras respectively. After applying of ICC profile camera Fujifilm was the best followed by Nikon and Olympus cameras.

We try to set the white balance to custom mode. The results were better only in the case without using of ICC profile.

The average colour difference values for scanner (Table II) refer to better colour reproduction using embedded scanner profiling program.

Table II
Average colour differences ΔE^*_{ab}, scanner HP

ΔE^*_{ab} without CMS	ΔE^*_{ab} with ICC profile of ProfileMaker	ΔE^*_{ab} ICC profile of embedded program
12.64	6.38	4.13

The next step was printing captured images using different print conditions to minimize colour difference values. Before printing we prepare ICC profiles for different paper substrates.

Table III shows decreasing average colour difference of prints using ICC profile of printer.

Average colour difference depends on gamut size of test charts (Table III, TC9.18, IT8.7/2.

Fig. 3 shows the relations of gamuts of historical poster and capturing devices (represented by test chart). Colour gamut of 264 colour patches test chart is bigger as colour gamut of historical poster.

Table III
Average colour differences ΔE^*_{ab}, Epson printer, digital test charts TC9.18 and IT8.7/2

Paper type	ΔE^*_{ab} without ICC profile	ΔE^*_{ab} with ICC profile TC9.18	ΔE^*_{ab} with ICC profile IT8.7/2
Epson Archival Matte	34.50	18.50	9.81
Epson Premium Glossy Photo	29.87	16.56	8.72
Epson Premium Semigloss Photo	29.89	16.55	8.34
Ilford Smooth Pearl	30.39	16.68	9.22
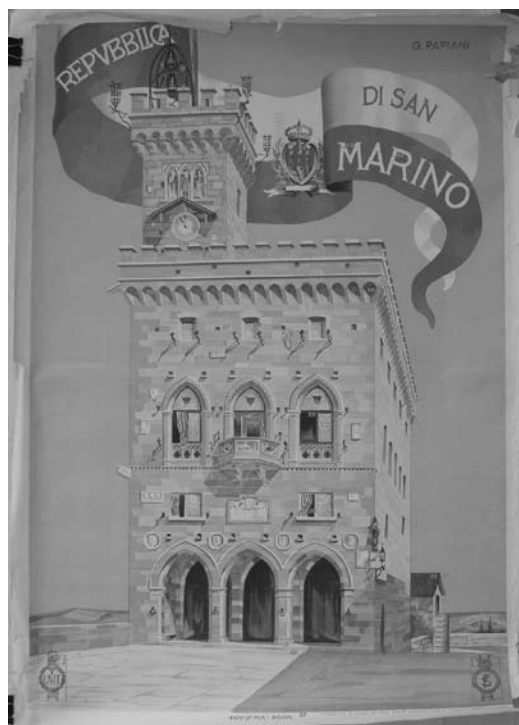
Fig. 2.   **The sample of historical poster, 43 measured points, 50 × 70 cm, 1925–1930, Fujifilm**
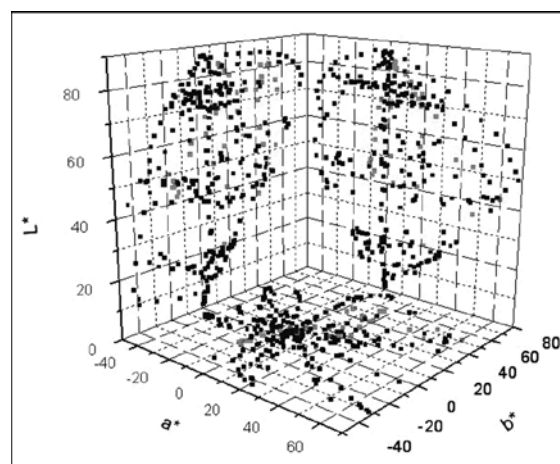
Fig. 3.   **Historical poster (gray) and test chart (black), CIE L*a*b* colour space**

Conclusion

Quality of digitized image represented by average colour difference of colour patches of digital cameras/scanner was the best for scanner – $\Delta E^*_{ab} = 4.1$. Ink-jet printer reproduced cameras images with $\Delta E^*_{ab} = 16$ for 918 patches and $\Delta E^*_{ab} = 9$ for 264 patches, result for the scanner was the best – $\Delta E^*_{ab} = 4.1$–6.5. In our case the colours of historical poster were inside the gamut space of tested input devices and mostly inside of gamut space of output device, therefore we can predict reproduction almost without any loss of colour

information caused by adaptation of out-of-gamut colours within of obtained colour difference range.

REFERENCES

1. MacDonald L.: Digital heritage: *Applying digital imaging to cultural heritage*, Elsevier, 2006.
2. Project Team 61966: *Colour management in multimedia systems – part 2: Colour management, Part 2.1: Default RGB colour space – sRGB, IEC*, 1998, http://www.w3.org/Graphics/Color/sRGB.

P07 IMPROVEMENT OF BARRIER PROPERTIES OF PAPER USING PHOTOCHEMICALLY MODIFIED POLYMER LAYERS

VIERA JANČOVIČOVÁ[a], SABINE AMBERG-SCHWAB[b], PETR DZIK[c] and MILAN MIKULA[a]

[a]Department of Printing Arts Technology and Photochemistry IPM, Faculty of Chemical and Food Technology SUT, Radlinského 9, 812 37 Bratislava, Slovak Republic,
[b]Fraunhofer-Institut für Silicatforschung ISC, 97082 Würzburg, Neunerplatz 2,Germany,
[c]Institute of Physical and Applied Chemistry, Faculty of Chemistry, Brno University of Technology, Purkyňova 118, 612 00 Brno, Czech Republic,
viera.jancovicova@stuba.sk

Introduction

The materials based on cellulose fibers (paper, card board) are sensitive to humidity and oxygen. Properties of packagings made of these materials may be improved by functionalization of paper surfaces. In combination with the characteristics of the basic materials, additional property profiles for different applications may be envisaged. Inorganic-organic hybrid polymers (ORMOCER®s: Trademark of the Fraunhofer Gesellschaft zur Förderung der angewandten Forschung e. V., Munich) are well-suited for the specific functionalization of different polymer and paper surfaces. These materials are water-based or dispersed in nontoxic solvents. Curing is performed photochemically or thermally at relatively low temperatures. Resulting layers are transparent, sturdy and chemically stable. The gas permeability of coated papers is significantly reduced and barrier properties to water vapour and odours are enhanced[1].

Papers and boards have to comply with certain demands for a successfull application of inorganic-organic hybrid polymers. The coated substrate should have a smooth, compact and non-porous surface preventing the low-viscosity coating solution penetrating deep into the paper profile and enabling even and homogeneous coating. The surface tension value should be above 40 mN m^{-1} in order to ensure a good wettability. The application of a coating primer might be necessary to fulfil these demands. With respect to the prospect application of these materials in the packaging industry, it is necessary to ensure these materials poses barrier properties and at the same time they are biodegradable and environmentally friendly.

These special material properties can be ensured by using hydrophilic water-based coating materials and a photochemical curing. Such systems feature multiple advantages, such as low VOC emission, low irrability, high speed curing, high gloss of cured coatings and simple processing. However, drying prior to curing is necessary[2].

Poly (vinyl alcohol) (PVAl), is a water soluble, film-forming, biodegradable polymer, unfortunately with insufficient resistance to water and water vapour. It is believed that modification of PVA by various organic moieties can significantly improve the barrier properties of coatings prepared from these modified grades of PVAl thus widening the application possibilities in the packaging industry.

The goal of this work was to study the ways of improving barrier properties of paper by coating it with hybrid inorganic-organic polymer ORMOCER®s. A primer consisting of UV-curable PVAl containing methacrylate moieties (poly(vinyl alcohol-co-vinyl hydroxypropyl methacrylate)) was used for planarization of the substrate. The composition of both active layers was optimized and water the vapour permeability was determined gravimetrically.

Experimental

M a t e r i a l s

Poly(vinyl alcohol) Sloviol 8-98 (NCHZ, Slovakia), glycidylmethacrylate (GMA, Merck, Germany), N,N-dimethylformamid (DMF, Lachema, Czech Republic), dimethyl sulfoxide (DMSO, Merck, Germany), ORMOCER (Fraunhofer Gesellschaft zur Forderung der angewandten Forschung, Munich, Germany), Irgacure 2959 (Ciba, Switzerland), Irgacure 184 (Ciba, Switzerland), Ethanol (Merck, Germany) and Acetone (Merck, Germany) were used.

P r e p a r a t i o n   o f   P o l y (v i n y l   A l c o h o l)
D e r i v a t i v e

10 g PVAl was dissolved at 90 °C in a mixed solvent (50 ml DMF and 50 ml DMSO). After complete dissolution, the mixture was cooled to 70 °C and 1 ml of GMA and 2.5 ml of 5 % wt. ethanolic solution of KOH was added dropwise. Mixture was kept at 70 °C for an hour and constantly agitated. Then it was cooled to ambient temperature, diluted with 25 ml of water and the product was precipitated into an excess of ethanol. The precipitate (PVAl-GMA) was collected, washed in acetone and dried to constant weight at room temperature[3].

P o l y m e r i z a t i o n   K i n e t i c s
M e a s u r e m e n t

Samples were prepared by mixing the photoinitiator initiator Irgacure 184 with ORMOCER®s and Irgacure 2959 an with aqueous solution of modified PVAl (PVAl-GMA) in varying ratios. These coating compositions were coated onto aluminum plates and cured at the light intensity 12 mW cm^{-2} (medium pressure mercury vapour lamp, 250 W).

Polymerization kinetics was evaluated on the basis of FTIR spectroscopy measurements (spectrophotometer Excalibur Digilab FTS 3000MX, USA). The absorption band at the frequency of 1,635 cm^{-1} corresponding to the C=C bonds, was monitored. The monomer conversion × was determined on the basis of decrease of the absorption band intensity according to

$$X = 1 - \frac{[A_\lambda]_0}{[A_\lambda]_t} \ , \tag{1}$$

where $[A_\lambda]_0$ and $[A_\lambda]_t$ is the absorbance measured at the chosen wavelength before and after the exposure to UV light for

the time *t*, respectively. The values of maximum conversion X_{max} were obtained from the plots of × and R_p *vs.* time.

The water Vapour Permeability Measurement

The watervapour permeability (WVP) was quantified according to a German standard DIN 53 122 and determined as an amount of the water vapour in grams passed through paper sample of a certain thickness within 24 hours at the temperature of 20–23 °C and relative humidity of 85 % provided by saturated KCl solution. Water vapour was quantitative absorbed on silicagel.

Results

In order to optimize the coating compositions we prepared samples of ORMOCER®s containing 1, 3 and 5 % wt. of Irgacure 184. During the curing process, a decrease of absorbance can be observed in the bands characteristc for carbon-carbon double bond (810 a 1635 cm^{-1}). As shown in Figure 1, the initial rate of curing is the fastest for 5 % wt. content of photoinitiator, where 70 % conversion is achieved within 40 s. Sample containing 3 % wt. of initiator takes 2 minutes to reach the same conversion while sample containing 1 % wt. of initiator takes 5 minutes. However, in the case of all three samples the curing process was completed and the conversion reached 88–90 %.
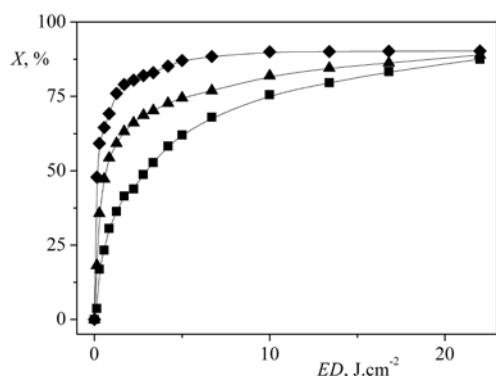
Fig. 1. **Influence of exposition dosage (ED) on the UV curing of ORMOCER®s at various Irgacure 184 concentrations (1 % ■, 3% ▲ and 5 % ♦; layer thickness 10 μm) at the light intensity 28 mW cm^{-2}**

The modification reaction performed on PVAl lead to the epoxide ring opening and the attachment of hydroxypropyl methacrylate moieties onto the PVAl macromolecular backbone. Therefore the UV curing process will be performed through radical polymerization of methacrylate groups in the lateral moieties.

As the modified product was soluble in water, also water soluble initiator was chosen (Irgacure 2959). Samples were not cured immediately after coating, but solvent water had to be evaporated first. Similarly to ORMOCER®s, samples of containing 1, 3 and 5 % wt. of Irgacure 2959 were prepared.
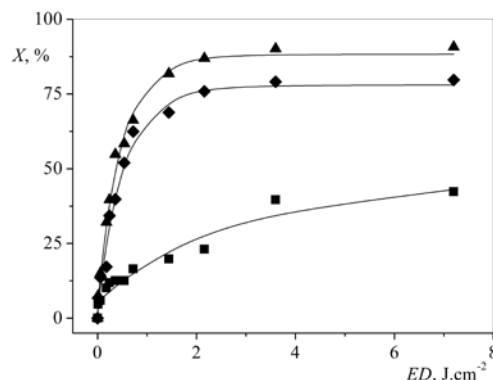
Fig. 2. **Influence of exposition dosage (ED) on the UV curing of PVAGMA at various Irgacure 2959 concentrations (1 % ■, 3% ▲ and 5 % ♦; layer thickness 10 μm) at the light intensity 12 mW cm^{-2}**

The highest conversion was achieved with 3 % wt. of initiator, sufficient curing was observed also in the case of 5 % wt. composition. However, in the case of 1 % wt. composition sufficient conversion can not be reached even after substantial extension of curing time.

Water vapour permeability (WVP) is a very important property of packaging materials. We determined the WVP of a paper and also observed the changes in WVP after coating with ORMOCER®-lacquer. Some samples featured an intercoating of PVAl-GMA, applied as s planarizing primer. With respect to the results of primary double bond conversion study, we used 3 % wt. of photoinitiators for both systems and coatings were cured for 5 minutes, this corresponds to the exposure dose 8.4 J m^{-2}. WVP was determined gravimetrically and the results are summarised in Table I.

As presented in Table I, the WVP was basically not altered by coating with PVAl-GMA. After curing this coating, the WVP decreased by 34 %. A similar value was achieved by coating the paper with the ORMOCER®-coating and curing. Significant decrease in WVP was achieved when the primer coating of PVAl-GMA was used. Since WVP is not a material constant, its value depends on the least permeable component of a system. Therefore it is possible to conclude that the 68 % decrease of WVP in the case of triple system with both coatings cured is caused by

Table I

Water vapour permeability for paper coated with photochemicall active polymers (uncured u, cured c)

Sample	WVP [g m^{-2} day^{-1}]
Paper	1,200
Paper/PVAGMA(u)	1,150
Paper/PVAGMA(c)	800
Paper/ORMOCER®s(c)	750
Paper/PVAGMA(u)/ORMOCER®s(c)	600
Paper/PVAGMA(c)/ORMOCER®s(c)	390

higher smoothness and pore closing resulting from the effect of the primer. As a direct consequence, the second layer of ORMOCER®s is more even and homogeneous and therefore its barrier effect is more pronounced.

Conclusions

The UV curable polymer films were prepared by addition of radical-type photoinitiators to ORMOCER and PVAl-GMA. According to spectroscopic monitoring of the curing process, optimal curing conditions were determined (3 % wt. of photoinitiator for both polymers, exposure dose 8.4 $J\,m^{-2}$. Paper coated with PVAl-GMA primer and ORMOCER active

layer features significantly lower WVP – a decrease by 68 % comparing with uncoated paper was observed.

REFERENCES
1. Amberg-Schwab S.: *PTS Symposium Innovative Packaging*, p. C02, Munich, 2005.
2. Decker C., Masson F., Schwalm R.: JCT Research *1*, 127 (2004).
3. Dzik P., Veselý, M.: Chemické listy *100*, 70 (2006).

P08 INFLUENCE OF AGEING ON OPTICAL PROPERTIES OF ARYLMETHANE DYES

BOHUSLAVA HAVLÍNOVÁ, VIERA JANČOVIČOVÁ and MIROSLAVA PETROVIČOVÁ

Department of Printing Arts Technology and Photochemistry IPM, Faculty of Chemical and Food Technology SUT, Radlinského 9, 812 37 Bratislava,
viera.jancovicova@stuba.sk

Introduction

Arylmethane dyes represent one of the oldest man-made dyestuffs. Primarily, Fuchsin and Methyl Violet were manufactured at the end of the 19th century. A milestone in the synthesis of arylmethane dyestuffs was the discovery (by Michler in 1867) of the reaction of phosgene with dimethylaniline. Based on this reaction, Caro and Kern prepared Crystal Violet in 1883. Fisher described, in 1887, the process of preparing Malachite Green, which is still employed on an industrial scale[1,2]. Later, other types of arylmethane dyes were prepared on the basis of hydroxyl triphenylmethane and xanthene compounds, and additionally acidic triphenylmethane dyes obtained by sulphonation of basic dyestuffs.

Damage to archive documents (bleaching, colour changes, total loss) written with tools based on arylmethane dyes, initiated the study of processes responsible for these devastating changes. The knowledge of the mechanisms of these processes opens new possibilities for the stabilization and preservation of such documents.

As arylmethane dyes in inks are water-soluble, it is essential that they are protected if aqueous conservation treatment is undertaken. Fixatives used for such a purpose must meet certain criteria (besides being able to fix the dye). In particular they must not change (or only by a minimal amount) the optical appearance of the object, i.e. neither cause colouring nor damage of the support material nor decrease the aging resistance of the dye-paper complex. The reversibility of the whole process, i.e. the possibility of removing the agent from the support, should also be taken into an account[3].

Experimental

In our experiments we used acidic, partly groundwood containing paper produced by Slavošovské Papierne (Slavošovce, Slovak Rep.)

The colorants used in the tests were arylmethane dyes (Basic Red 9, Acid Green 16). Basic Blue 9 (Methylene Blue) is a phenotiazine dye with poor lightfastness. The dyes were provided from TRIADE, Netherlands.

The fixatives used were following:

Fixing agent from Neschen company, Germany, suspension consisting of 1,2 % Mesitol NBS (Bayer AG) and 6 % Rewin EL (Chemische Fabrik Tübingen), pH = 6.2 (further marked as Neschen).

Sandofix WE – (Sandoz AG), 10% water solution, pH = 4.1.
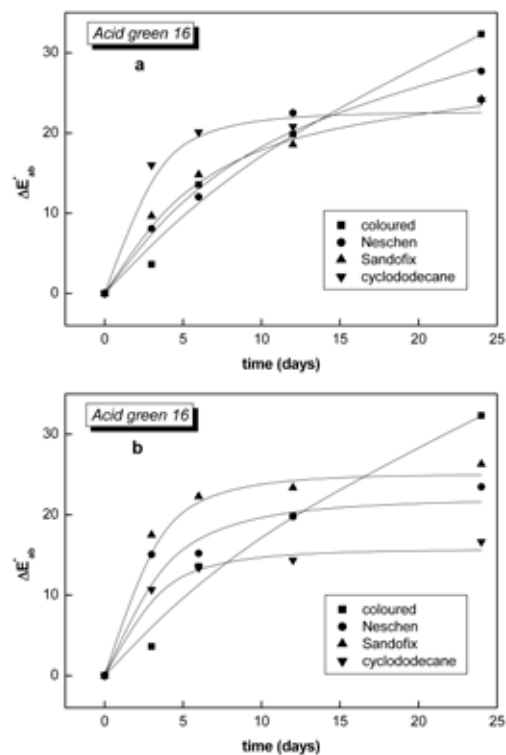
Fig. 1. **Colour Fastness of Acid Green 16 after ageing; (a) – fixation, (b) – fixation and deacidification**

Cyclododecane $C_{12}H_{24}$, solution prepared from 5 g cyclododecane and 40 g toluene.

Deacidification solution (aqueous solution of a mixture of magnesium and calcium bicarbonates, pH = 7.4) was prepared from 17 g $MgCO_3$ and 2 g $CaCO_3$ per 1 dm³ of water saturated with gaseous carbon dioxide. The samples were prepared as follows: paper rectangles measuring 7×12 cm were coloured wit solutions of different dyes (1 ml) and air dried at room temperature. Colorants Basic Red 9 (Basic Fuchsin), Acid Green 16 and Basic Blue 9 (Methylene Blue) were used as 0.2% solution in a mixture of distilled water and ethanol (1 : 1). Paper samples were immersed for 2 minutes into solutions of Neschen and Sandofix fixing agent, while cyclododecane was applied by brush on both sides on the samples.

The samples were submitted to accelerated aging by moist heat at 80 °C and 65 % RH in a climatic chamber (Feutron GmbH, Greiz, Germany (0, 3, 6, 12, 24 days). The properties of the paper samples were measured according to the Slovak Technical Standards (STN) and STN ISO Standards. A spectrophotometer Spectrolino (Gretag Macbeth AG, Regensdorf, Schwitzerland) was used for measurements of the colour components ΔL^*, Δa^*, Δb^* before and after accelerated aging on coloured paper, after fixing and after fixing and deacidification treatments.
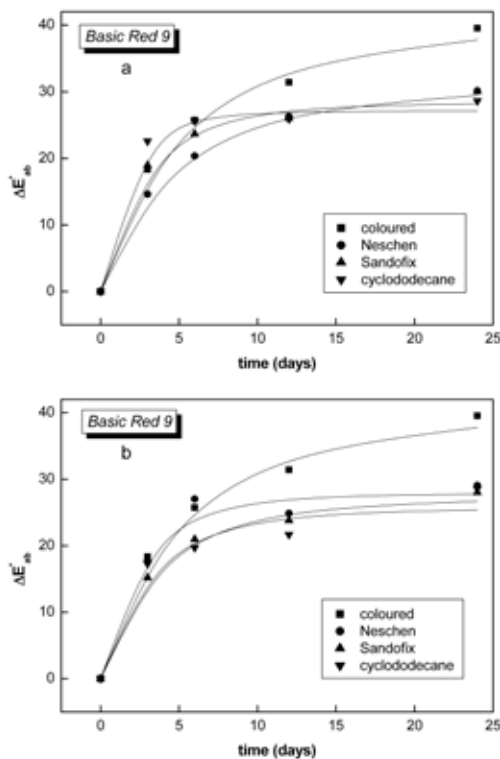
Fig. 2.   **Colour Fastness of Basic Red 9 after ageing; (a) – fixation, (b) – fixation and deacidification**

Fig. 3.   **Colour Fastness of Basic Blue 9 after ageing; (a) – fixation, (b) – fixation and deacidification**

Results

Accelerated aging of coloured paper provided complex problems because during the aging procedure the chemical and mechanical properties of the paper, as well as of the arylmethane components are changing simultaneously.

Fig. 1. presents dependency of total colour difference changes for paper coloured with 0.1% Acid Green 16, after moist heat aging. Despite an initial increase of ΔE^* caused by the fixatives, especially by cyclododecane, it can be seen that all three fixing agents caused a significant decrease after 24 days of this aging, for Sandofix and cyclododecane there was a colourfastness improvement of about 35 %. After the deacidification of samples fixed by cyclododecane another decrease (49%) was observed down to $\Delta E^*_{ab} = 11.0$ after 24 days of accelerated aging (Fig. 1.).

Fig. 2. shows the the behaviour of Basic Red 9 dye applied to paper as 0.1% ethanolic solution after moist heat aging. Moist heat fastness of the dye was improved after fixing and deacidification. This was particularly apparent from the decrease of total colour difference after 12 and 24 days of accelerated aging compared to aged, unfixed paper.

Moist heat accelerated aging of paper coloured with 0.2% Basic Blue 9 solution caused a decrease of ΔE^*_{ab} for all three fixing agents compared to non-fixed samples. The best fixing effects was shown by Sandofix (38% decrease). All three fixing agents caused about a 40% decrease of ΔE^*_{ab} after deacidification of the fixed paper samples (Fig. 3.).

Conclusions

It is possible to suppose that one universal fixing agent will have same beneficial effect on all types of dye of all archival documents.

The best lightfastness of arylmethane dyes, after being fixed with cyclododecane was shown to be Acid Green 16 and Basic Red 9 (decrease about 25 %) and followed by deacidification, Acid Green 16 and Basic Blue 9 (decrease about 46 %).

After fixing with Neschen fixing agent or Sandofix respectively and subsequent deacidification, the best light-

Table I

Total colour difference (ΔE^*_{ab}) of the coloured samples after accelerated aging (24 days) by moist heat at 80 °C and 65% RH

	Acid Green 16	Basic Red 9	Basic Blue 9
Coloured paper	32.3	39.5	23.8
Fixed by Neschen	27.7	30.1	22.6
Neschen + deacidification	23.5	29.0	13.4
Fixed by Sandofix	24.2	24.2	14.8
Sandofix + deacidification	26.3	28.0	14.7
Fixed by cyclododecane	24.1	28.6	20.8
Cyclododecane + deacidification	16.6	28.6	13.3

fastness was seen on the sample of Basic Blue 9 (decrease 44 %).

The highest resistance towards moist accelerated aging after being fixed using cyclododecane and was recorded for Acid Green 16. Good lightfastness of arylmethane dyes, after being fixed with cyclododecane and then deacidified we have seen in samples of Acid Green 16 and Basic Blue 9.

After fixing with Neschen and Sandofix fixing agents, the highest resistance towards moist accelerated aging was seen in samples of Basic Blue 9.

REFERENCES

1. Zollinger H.: *Synthese, properties and applications of organic dyes and pigments. Color Chemistry.* VCH Weinheim: 1991.
2. Bredereck K.: Restaurator *9*, 113 (1988).
3. Havlínová B., Jančovičová V., Brezová, V., Čeppan, M., Turanová M.: Restaurator *27*, 24 (2006).

P09 INVESTIGATION OF DECOMPOSITION OF PHOTOINITIATORS

BOHUMIL JAŠÚREK[a], TOMÁŠ SYROVÝ[a], JAN VALIŠ[a]
and TOMÁŠ WEIDLICH[b]

[a]*University of Pardubice, Faculty of Chemical Technology, Department of Graphic Arts and Photophysics,*
[b]*University of Pardubice, Faculty of Chemical Technology, Institute of Environment Protection, Studentská 95, 532 10 Pardubice, Czech Republic,*
bohumil.jasurek@upce.cz

Introduction

One of the most important part of UV cured systems are photoinitiators. The initiator plays a key role in that it governs both the rate of initiation and the penetration of incident light into the sample, and therefore controls the depth of cure. The rate of polymerization depends initially on the reactivity of the functional group, its concentration and the viscosity of the resin[1]. The present range of commercial photoinitiators has absorptions that covers the whole spectrum of UV and near visible light and allows the efficient formulation for majority of UV curing applications. More recent developments in photoinitiator technology are addressing particular problems that have risen in UV curing, such as that of migration from coatings into foodstuffs, etc. and the introduction of polymeric photoinitiators to counter this effect.

In this work were investigated properties (absorption spectra and molar absorption coefficients, rate of photodecomposition, number of photodecomposition products) of four photoinitiators. Two of them are commercially available initiators (Irgacure 2959, Irgacure 261) and the other two are new prepared photoinitiators (HP1 and CB). CB is cationic organometallic photoinitiator and HP1 is hybrid photoinitiator which can efficiently initiate polymerization reaction of both free radical and cationic polymerization[2]. The detailed synthesis of HP1 was described in previously publicated works[3,4] and synthesis of CB in works[5,6]. The investigated photoinitiators are shown in Fig. 1.

Experimental
U V - V I S   S p e c t r o s c o p y

UV-VIS absorption spectra and photolysis of photoinitiators were monitored by UV-VIS spectrometer Specord 210 (Analytik Jena AG, Germany) in solutions of photoinitiators in acetonitrile at room temperature. The molar absorption coefficients were calculated using the Lambert-Beer's law. Photolysis of photoinitiators (concentration of 1×10^{-4} mol dm^{-3}) was followed by decreasing the absorption bands after irradiation by high-pressure mercury lamp (CE Green Spot from UV Source Inc., USA). The intensity of irradiation was 500 mW cm^{-2} (in the spectral region 258–380 nm). The normalized absorbance A_n was calculated by equation:

$$A_n = (A_0 - A_t)/(A_0 - A_\infty), \tag{1}$$
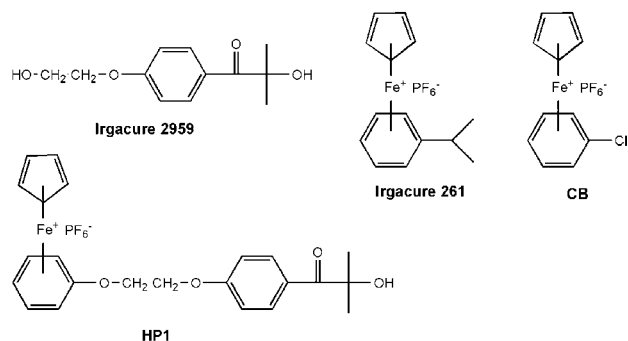
Fig. 1. **Prepared photoinitiators HP1 and CB and commercial photoinitiators Irgacure 261 and Irgacure 2959**

where A_0 is absorbance of measured band before the irradiation, A_∞ is absorbance after the final photolysis and A_t is absorbance after the irradiation time t.

The dependence of normalized absorbance on the irradiation dose was described by (2) for first-order reaction:

$$A_n = P_1(1 - e^{-P_2 E}), \tag{2}$$

where P_1 is maximal normalized absorbance, P_2 is rate of decomposition after irradiation and E is the irradiation dose (mJ cm^{-2}). From equation (3), $E_{1/2}$ can be calculated as the energy needed to achieve the half photodecomposition.

$$E_{1/2} = \ln2/P_2 \tag{3}$$

The degree of photodecomposition X_P of initiators for irradiation dose E was calculated from (4):

$$X_P = A_n/P_1 \tag{4}$$

D e t e r m i n a t i o n   o f   t h e   N u m b e r   o f D e c o m p o s i t i o n   P r o d u c t s   a f t e r   U V P h o t o l y s i s   b y   F a c t o r   A n a l y s i s

The photolysis absorption spectra of solutions of studied photoinitiators in acetonitrile were used for the determination of the number of components k in the solution by factor analysis in the INDICES algorithm. The INDICES[7,8] determines the number of dominant components present in the equilibrium mixture. In this algorithm the various indicator function Principal Components PC(k) techniques were developed to deduce the exact size of the true component space and can be classified into two general categories: *(i)* precise methods based upon the knowledge of the experimental error of the absorbance data, $s_{inst}(A)$, and *(ii)* approximate methods requiring no knowledge of the experimental error, $s_{inst}(A)$. In general, more precise and most inclining methods are based on the first criterion concerning the procedure of finding the point where the slope of the indicator function PC(k) = $f(k)$ changes. Each "real" factor corresponding to an actual absorbing component in solution will cause a dramatic decrease in PC(k) value, whereas superfluous factors cause only very small decreases. Elbergali et al.[9]

proposed a modification of index methods using derivatives to improve identification of the number of components. The second derivative SD(k) – the number of components in solution is equal to k where SD(k) has its first maximum (except $k = 2$). The third derivative TD(k) – the number of components in solution is equal to k where TD(k) has its first minimum (except $k = 2$). The derivatives ratio ROD(k) – the number of components in solution is equal to k where SD(k) has its first maximum (except $k = 2$).

Results

U V - V I S   S p e c t r o s c o p y

UV spectra of all investigated photoinitiators are shown on Fig. 2. Molar absorption coefficients at the most important emission wavelengths of the medium-pressure mercury lamp are summarized in Table I. The absorption spectrum of prepared cationic photoinitiator CB is similar to the spectrum of commercial cationic photoinitiator Irgacure 261. The exchange of isopropyl ligand by chlorine caused hypsochromic shifts from 391 nm to 377 nm and from 456 nm to 446 nm. Photoinitiator HP1 has higher molar absorption coefficients for all main emission bands of medium-pressure mercury lamp than the other tested photoinitiators (with exception of initiator Irgacure 2959 and emission band 303 nm; Table I). This is useful for commercial applications, because medium-pressure mercury lamp is often used as UV source for curing of inks, varnishes, etc.

Table I
Molar absorption coefficients ε [dm^3 mol^{-1} cm^{-1}] of photoinitiators in acetonitrile at the most important emission wavelengths of the medium-pressure mercury lamp

Photoinitiator	253 nm	303 nm	313 nm	365 nm
HP1	15,443	1,652	898	194
CB	7,129	366	242	48
Irg. 261	7,051	452	316	91
Irg. 2959	5,270	1,725	421	14

P h o t o l y s i s   o f   I n i t i a t o r s

The photolytic decomposition of initiators after UV irradiation was investigated by UV-VIS spectroscopy. Photolysis spectra of initiators are on Fig. 3. The concentration of photoinitiators was 1×10^{-4} mol dm^{-3} in acetonitrile and irradiation dose was 0–3,600 mJ cm^{-2}. Arrows mark the change of absorption bands during the UV exposure. Isoabsorptive points indicate that photoinitiators photodecomposition proceeded selectively without side reactions.

The degree of photoinitiators decomposition caused by UV irradiation was evaluated from absorption changes at such wavelengths, where only respective photoinitiator absorb (not products of its photodecomposition): 243 nm for CB, 243 nm for Irgacure 261 and 290 nm for Irgacure 2959. In case of HP1, it was difficult to analyse the decomposition spectra due to overlapping of spectra of adduct and products of photolytic reaction. Therefore it was not possible to find
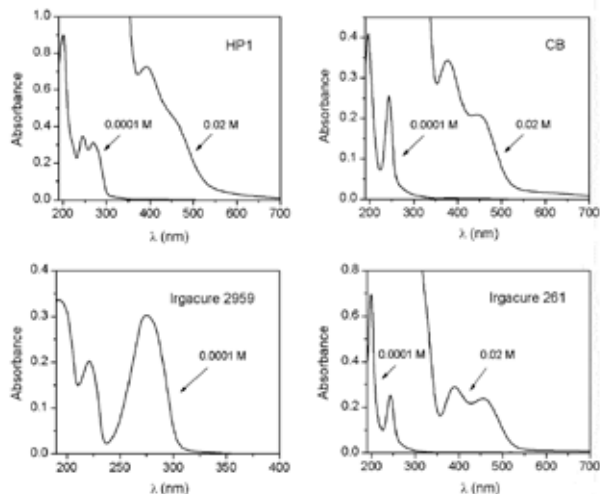
Fig. 2. **Absorption spectra of photoinitiators in acetonitrile (concentrations 1×10^{-4} and 2×10^{-2} mol dm^{-3})**
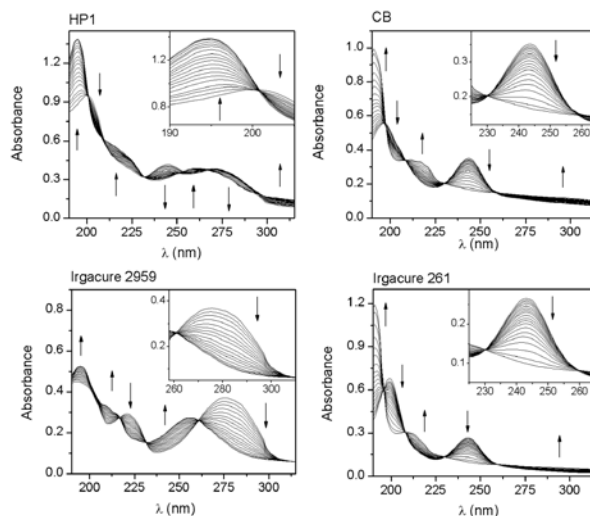
Fig. 3. **Absorption spectra of photoinitiators in acetonitrile (concentration of 1×10^{-4} mol dm^{-3}) measured after UV exposure**

the wavelength corresponding only to the decomposition of radical or cationic part of molecule. For the basic information about photolysis of HP1, the wavelength 196 nm was chosen.

The dependences of photoinitiator normalized absorbance A_n (1) on UV dose were fitted by non-linear regression according to (2) (Fig. 4.). The non-linear regressions were treated by software STATISTICA. The adequacy of proposed regression model with experimental data and the reliability of parameter estimates P_1 and P_2 found (Table II) were examined by the goodness-of-fit test. The determination coefficients R^2 are equal to 99.6 % or better. Applying (3) to the data according to the regression criterion, the energy needed to achieve of photodecomposition of 0.5 ($E_{1/2}$) has been estimated (Table II). Comparing the values of $E_{1/2}$ it is apparent
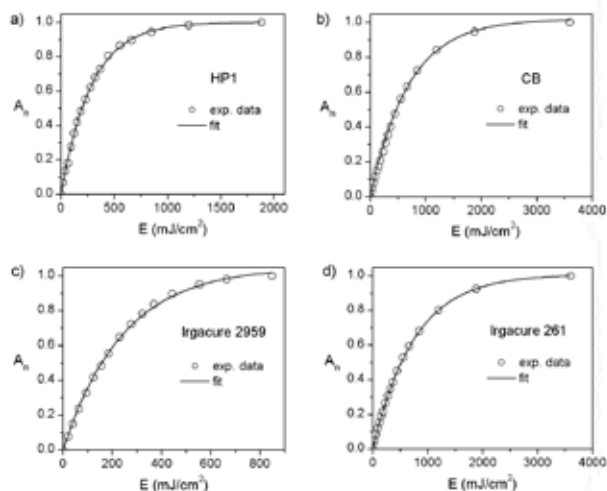
Fig. 4.   **Dependence of normalized absorbance of initiators on UV dose**

Table II
Estimated parameters P_1 and P_2, $E_{1/2}$ [mJ cm^{-2}] and determination coefficient R^2

	HP1 (196 nm)	CB (243 nm)	Irg. 261 (243 nm)	Irg. 2959 (290 nm)
P_1	0.986	1.024	1.008	1.0526
P_2	3.3×10^{-3}	1.37×10^{-3}	1.32×10^{-3}	4.1×10^{-3}
R^2	0.9960	0.9981	0,9990	0.9991
$E_{1/2}$	210	506	525	169

that prepared hybrid photoinitiator HP1 and free radical photoinitiator Irgacure 2959 needs approximately 3 times less energy for the decomposition (with high-pressure mercury lamp as UV source) and the rate of photolysis is faster as compared to cationic photoinitiators (Irgacure 261 or CB).

Normalized absorbances were recalculated by Equation 4 and the degree of photodecomposition X_P of initiators for irradiation dose E was obtained (Fig. 5.). From Fig. 5. is apparent that the course of photolysis of prepared hybrid photoinitiator HP1 is very similar to that of radical initiator Irgacure 2959 and the photolysis of these initiators is much faster than photolysis of cationic initiators CB and Irgacure 261.

Determination of the Number of Decomposition Products after UV Photolysis by Factor Analysis

The photolytic absorption spectra of photoinitiators (Fig. 3.) were used as absorption matrix for determination of number of components k in solution (after photolysis). For INDICES methods on Fig. 6 (the residual standard deviation – RSD, the root mean square error – RMS, the third derivative – TD and derivatives ratio – ROD), the dashed line denotes the value of the instrumental error, $s_{inst}(A)$. The best
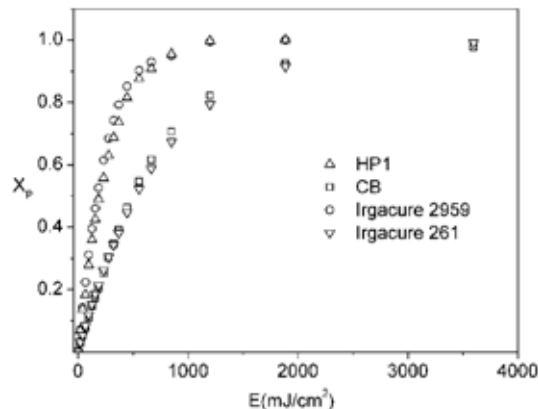
Fig. 5.   **Dependence of degree of initiators decomposition on UV dose**

approximation of $s_{inst}(A)$ for hybrid initiator HP1 was found for $k = 5$. The indices methods and their derivatives lead to estimation of five light absorbing components in the photolysis reaction system (Fig. 6.). One of them is original HP1 and the others are decomposition products. The estimated number of components (adduct and products) corresponds to the results of mass spectrometry (analysed was sample of HP1 in acetonitrile after UV photolysis). With this analytical method were detected four decomposition products with molecular weights of 218, 232, 477 and 654 g mol^{-1}.

Analysis of INDICES methods for cationic photoinitiator Irgacure 261 leads to an estimation of three light absorbing components in the photolysis reaction system.
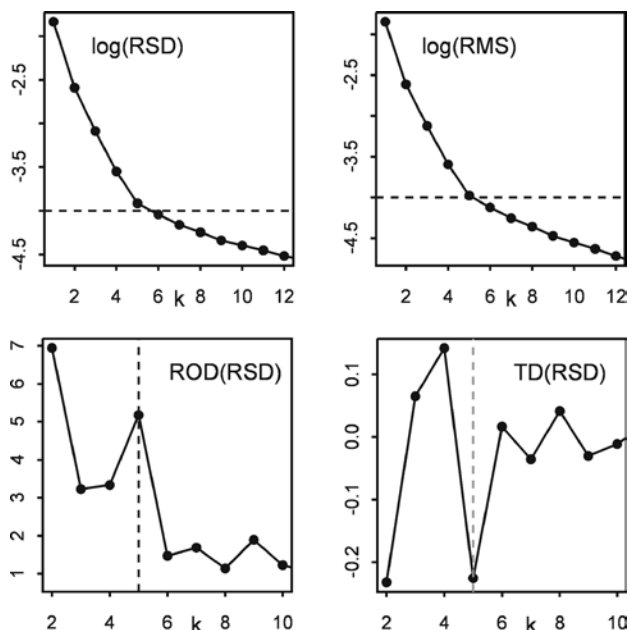
Fig. 6.   **The logarithmic dependence of representative functions of INDICES algorithm as a function of the number of principal components (k) for the absorbance matrix of photolysis equilibria of hybrid initiator HP1**

One of them is Irgacure 261 and the others are products of photoinitiator decomposition (isopropyl benzene and ferrocene), which corresponds to conclusions that have been published elsewhere[10]. During the decomposition of Irgacure 261, inorganic compound $Fe(PF_6)_2$ is also formed (non-absorbing in measured UV region).
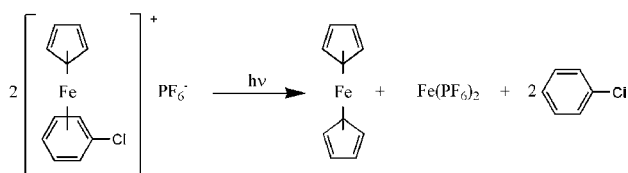
Fig. 7. **Suggested photodecomposition schema of prepared initiator CB**

All index methods proved three light absorbing components of CB photolytic equilibria (CB, ferrocene and chlorobenzene). Prepared cationic initiator CB has similar structure as cationic photoinitiator Irgacure 261 and results of factor analysis (number of decomposition products) are for both initiators the same. From UV-VIS spectra and information from literature[10,11] about photodecomposition of iron-arene complexes it can be assumed that the reaction mechanism of the decomposition of CB under UV light is similar as for Irgacure 261. The suggested decomposition schema of initiator CB is on Fig. 7. For free radical photoinitiator Irgacure 2959, the INDICES methods prove that there are four light absorbing components in the photolysis equilibria mixture. The molecular weights of individual photolysis products of Irgacure 2959 detected by mass spectrometry are 166, 314, 330 and 478 $g\,mol^{-1}$, respectively. Photolysis products of initiators Irgacure 261 and CB were not detected, which is probably caused by low molecular weights of expected decomposition products resulting in the low sensitivity of measurement with the ion trap analyzer.

Conclusions

The photodecomposition rate of prepared hybrid photoinitiator is similar to radical initiator Irgacure 2959. These two initiators need approximately 3 times less energy (high-pressure mercury lamp as UV source) than cationic organometallic photoinitiators Irgacure 261 and CB to achieve half photodecomposition. The estimated number of photodecomposition products of initiators after UV photolysis by factor analysis show good correlation with results published elsewhere[10,11] about photodecomposition of organometallic initiators or obtain from mass spectrometry.

REFERENCES

1. Decker C.: Macromol. Rapid. Commun. *23*, 1067 (2002).
2. Jašúrek B., Vališ J., Weidlich T.: *Proceedings of RadTech Europe 07 (CD),* Vienna, 2007.
3. Jašúrek B., Vališ J., Weidlich T., Knobloch J.: *RadTech Europe 2005,* Barcelona, 2005. http://www.coatings.de/survey_rte/poster.cfm,
4. Jašúrek B., Vališ J., Weidlich T., Otáhalová L.: *Proceedings of 2nd International Symposium on Novelties in Graphic (CD),* p. 140. Ljubljana, 2006.
5. Vališ J., Weidlich T.: Adv. Colour Sci. Technol. *6*, 73 (2003).
6. Jašúrek B., Vališ J., Weidlich T.: *Proceedings of RadTech Europe 2003,* p. 919. Berlin, 2003.
7. Meloun M., et al.: Anal. Chim. Acta. *423*, 51 (2000).
8. Syrový T.: *Dissertation.* University of Pardubice, Pardubice 2005.
9. Elbergali A. K., et al.: Anal. Chim. Acta *379*, 143 (1999).
10. Crivello J. V., Dietliker K.: *Chemistry and Technology of UV & EB Formulation for Coatings, Inks & Paints, Volume III: Photoinitiators for Free Radical, Cationic & Anionic Photopolymerisation,* 2nd ed., Wiley, London 1998.
11. Gill T. P., Man K. R.: Inorg. Chem. *22*, 1986 (1983).

P11   STUDY OF STABILIZATION OF DOCUMENTS CONTAINING IRON GALL INKS BY TREATMENT OF ATMOSPHERIC DBD N₂ PLASMA

MILENA REHÁKOVÁ, MICHAL ČEPPAN and MILAN MIKULA

Slovak University of Technology in Bratislava, Faculty of Chemical and Food Technology, Radlinského 9, 812 37 Bratislava, Slovak Republic,
milena.rehakova@stuba.sk

Introduction

Problems of iron gall inks corrosive effect on paper support is solved in conservation practice by basic treatment of endangered documents in deacidification solutions of Mg or Ca salts[1]. However, this treatment is not sufficient and for preservation of acceptable practical properties some other processing – like application of reinforcing agents, antioxidants or some substances which can remove excessive mobile forms of present transitional metals (iron)[2]. In recent times also favourable influence of plasma treatment on paper support leading to improvement of its mechanical properties were proven[3].

The aim of this work was study of application techniques of chitosan as reinforcing substance of alkaline nature with anti-microbiological effect for processing of paper containing iron gall ink followed by its treatment in dielectric barrier discharge (low-temperature plasma). The influence of potassium iodide – as antioxidant agent – on changes of some properties of treated papers was followed as well.

Experimental

Iron gall ink prepared according to the recipe[4] was applied to wood-free filter Whatman paper No. 1 (Cat No. 1001917), producer Whatman Laboratory Division, Maidstone, England, basis weight 90 g m⁻², pH 7, with the help of plotter (HI-1117E Image Maker, Houston Instrument) in quantity of 2.65 ± 0.05 g m⁻². In order to get a model of older writig, samples were artificially aged in a closed space[5] during 4 hours and they were named as "C" (control).

Tested samples were treated by different techniques:

- Technique A: impregnation by 0.5 % wt. of chitosan solution (Sigma-Aldrich, USA) in 0.1 mol dm⁻³ acetic acid for 10 minutes, pressing out of excessive modification agent on an inert support and drying. The samples designation: CHA.
- Technique B: continual modification in chitosan solution (for about 5 s) and drying at ambient conditions. The samples designation: CHB.
- Technique C: technique A continuing with activation of samples surface by plasma – *(atmospheric plasma surface treatment technique)* (DBD in N₂ atmosphere at atmospheric pressure: 15 kV, 5 kHz, 0.1 W m⁻¹[2], duration of action 5 s, N₂ flow rate 5 dm³ min⁻¹)[6]. The samples designation: CHP.

- Technique D: activation of paper surface by plasma under the same conditions as above mentioned technique C and subsequent application of technique B. The samples designation: PCH.

Before application of chitosan and plasma, one part of samples was immersed in 0.01 mol dm⁻³ solution of KI (Lachema Brno, Czech Republic) for 1 minute and dried between two filter paper sheets at the given pressure. The samples are marked as KI CHP (made by technique C) and KI PCH (made by technique D).

After modification the samples were pre-conditioned in bottles and artificially aged at 90 °C according to Bégin-Kaminska method[5] during 0, 2, 4, 8 and 24 hours. After ageing they were again air-conditioned (24 hours, 23 °C, 50 % RH) and tested for changes mechanical properties caused by modification treatment. They were folding endurance (MIT method according to ASTM D 2176, Tinius Olsen, 3 N, cross direction, average of 10 measurements with standard deviation 35 ± 5 %) and zero-span breaking length (equipment FDP 40).

Results

Influence of Technique of Chitosan Application

It was found out by gravimetry that the amount of chitosan deposited by two different procedures A and B described above in experimental part was the same (1.80 ± 0.02 g m⁻²). From Fig. 1. it can be seen that longer impregnation time with pressing out of modification solution (CHA) significantly increases folding endurance. For samples with shorter impregnation time but without pressing (CHB) increase of double folds was recorded comparing to the original sample, however after 2 hours of accelerated ageing the differences were negligible. It can be explained by penetrating of chitosan throughout the whole volume of sample during longer impregnating time while at the shorter time it rests mostly on the sample surface.
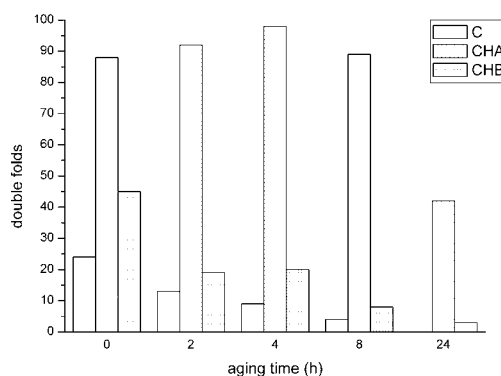
Fig. 1.   **Folding endurance of samples modified with chitosan by two different methods in aging time**

Influence of Technique of Chitosan Application and Plasma Treatment

Longer time of impregnation by chitosan followed by their treatment in plasma (technique C) seems to be more suitable (Fig. 2.a), however in the presence of KI the situation is reversed – the more suitable is plasma treatment before application of chitosan (technique D), Fig. 2.b. In that case also shorter time of impregnation by chitosan improves mechanical properties of samples. The presence of potassium iodide is unambiguously appropriate in the system. It can be suppose that plasma activates the carrier material and forms reactive spots in paper in paper already before process of chemical modification and thus stronger bonds between cellulose and chitosan can be created (by crosslinking).
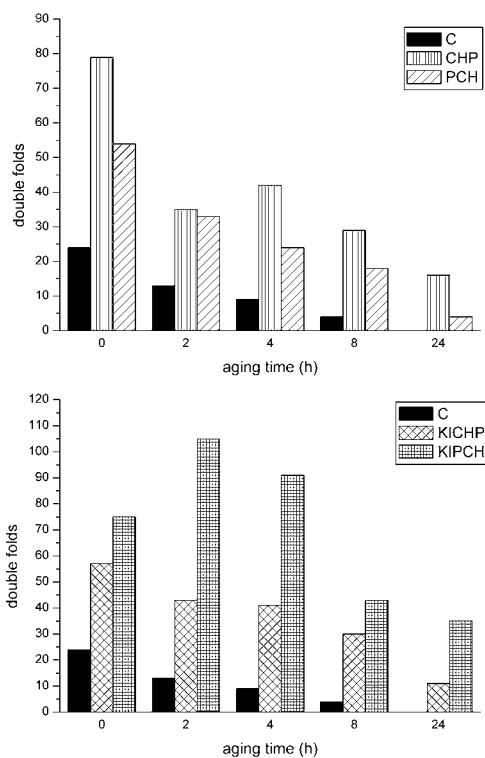
Fig. 2. **Dependence of folding endurance on aging time;
(a) – Influence of technique of chitosan and plasma application,
(b) – Influence of technique of chitosan and plasma application
at presence of KI**

Modification Treatment Efficiency

Changes of mechanical properties after modification treatment expressed by ratio of followed value of modified sample to the value of non-modified sample in certain time of ageing, called often as coefficient of permanence S confirms efficiency of selected treatment comparing to non-modified sample.

Fig. s 3, 4 express changes and results of folding endurance and zero-span breaking length for all tested modification systems applied to the samples according to the modifi-
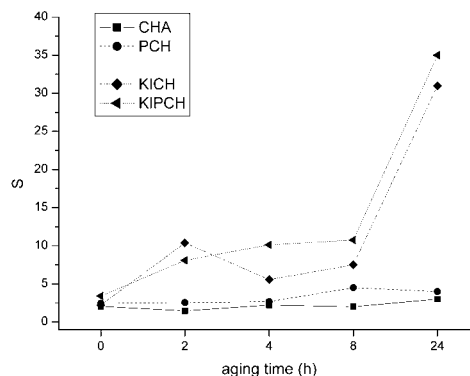
Fig. 3. **Coefficient of stability of folding endurance as dependence of aging time**
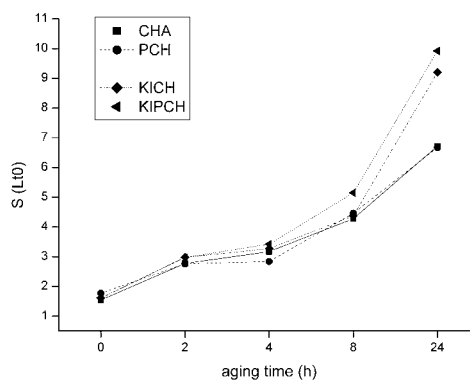
Fig. 4. **Coefficient of stability of zero-span breaking length as dependence of aging time**

cation technique B. They confirm improvement of zero-span breaking length for all modified systems during ageing time in approximately the same extent (2–8x) and also improvement of folding endurance for the most suitable systems KICH and KICHP where coefficient of permanence reached in its maximum values around 30.

Conclusions

The work was concentrated on enhancement of strength and stability of historical paper documents treated in dielectric barrier discharge (DBD) at atmospheric pressure in combination with natural polymer chitosan and/or anti-oxidizing agent. Choise of suitable modification matter and combinations of application techniques was realised.

Implementation of appropriate system for chemical modification containing antioxidant and strengthening component relatively resistant to ageing is more important than application of plasma treatment; modification systems containing potassium iodide and chitosan appeared to be suitable.

REFERENCES

1. Široký M., in: *Restaurování a konzervování archiválií a knih* (Ďurovič M.), chapter 7, p. 317, Paseka Praha 2002.
2. Malešič J., Kolar J., Strlič M., Polanc S.: e-Preservation Science 2, 13 (2005) (http://www.morana-rtd.com/e-preservationscience).
3. Nada A. M. A., El-Sakhawy M., Kamel S., Eid M. A. M., Adel A. M.: Egypt. J. Solids *28*, 359 (2005).
4. Neevel J. G.: Restaurator *16*, 143 (1995).
5. Bégin P. L., Kaminska E.: Restaurator 23, 89 (2002).
6. Mikula, M., Jakubíková, Z., Zahoranová, A.: J. Adh. Sci. Technol. *17*, 2097 (2003).

P12 THE INFLUENCE OF RECEIVING LAYER COMPOSITION ON INKJET PRINT LIGHTFASTNESS

JIŘÍ STANČÍK, MICHAL VESELÝ and PETR DZIK

Brno University of Technology, Faculty of Chemistry, Purkyňova 118, Brno 612 00, Czech Republic,
xcstancik@fch.vutbr.cz

Introduction

Papers for inkjet printing can be divided into several categories according to their printing quality or segment of application. On one hand, multipurpose office papers treated with a surface sizing agent and starch are designed for low- and middle-end applications. On the other hand, inkjet papers with high quality demands must be coated using specialty pigments and additives[1,2]. For printing high-quality photographic images, special media are used as the substrate. Currently, there are two types of special media, namely swellable polymers (based on PVAl or gelatin) and microporous media (both silica and alumina types)[3].

In many cases fillers can have a marked influence on the thermal and photochemical stability of the polymer material. They can exhibit a protective effect or alternatively they may be photoactive and sensitise the photochemical breakdown of the polymer. Research activities about the photochemical properties of titanium dioxide (TiO_2) deal with studying photochemical activity of TiO_2 in order to convert harmful organic wasteproducts into harmless environmentally acceptable materials. Another deals with minimising the photocatalytic activity of TiO_2 in order to enhance the durability of organic substrates such as polymers and coatings[4].

To enhance the durability, stabilizer additives such as ultraviolet light absorbers (UVAs) and hindered amine light stabilizers (HALS) are added to the coatings formulation[5]. One of the typical photostabilizing actions proposed for a polymer system containing HALS[6] is showed on Fig. 1.
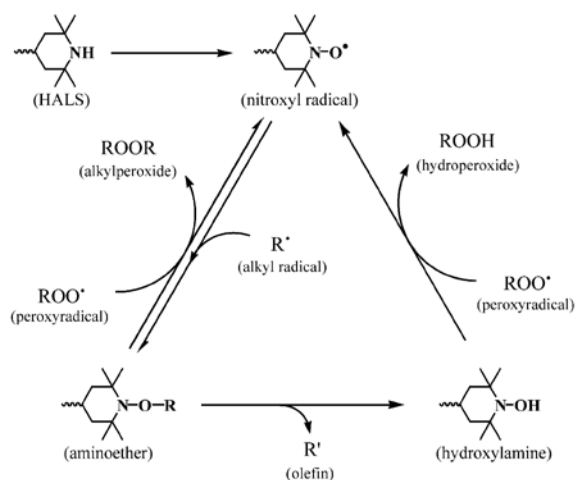
Fig. 1. **Typical photostabilizing action of HALS in the polymer system**

For printing, the three subtractive primary colours of yellow (Y), magenta (M) and cyan (C) are used. These colours are chosen because they produce the maximum number of colours by mixing (i.e. the maximum colour gamut). They can produce ca. 85 % of the 16.7 million colours theoretically possible. Inkjet dyes have to fulfil several requirements, most importantly hue (colour), vividnes, operability (reliability) and safety. Anionic water-soluble dyes (Dye-SO_3^-) are the dyes of choice for inkjet printers[3].
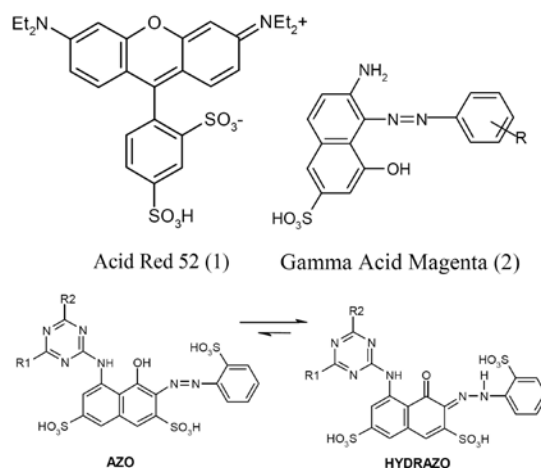
Fig. 2. **Acid Red 52, Gamma Acid Magenta and H-acid dyes**

Magenta dyes usually have the lowest lightfastness in inkjet and, indeed, in most other colour applications. The most commonly used magenta dyes for desktop inkjet printers are C. I. Acid Red 52, the H-acid dyes and dyes based on Gamma acid (they exist only in the azo form and due to higher lightfastness, compared to the other magenta dyes, they have found use in photographic applications)[7].

Experimental

Anatase pigments are generally more photoactive than the rutile types[4], what is the reason why TiO_2 of rutile type was used. It was dispersed into 5% wt. solution of poly (vinylalcohol) (PVAl) in 4 : 1 ratio. 0, 2 and 8 % wt. of water soluble stabiliser Eversorb AQ1 (blend of HALS and UVAs) was added into final dispersions. Filter paper was used as a substrate for prepared receiving layers. Layers were prepared by spreading the dispersion through a screen printing form by a blade.

Test charts were printed by Epson Stylus Photo R220 printer by dye-based inks with resolution 720 DPI. Ink set MIS Dyebase for Epson printers containing C, M, Y, K, LC and LM cartridges was used (supplied by MIS Associates Inc., USA). Test chart consisted of cyan, magenta, yellow and black colour printed with 100% and 50% dot area.

CIE $L^*a^*b^*$ coordinates of print samples were measured by spectrophotometer Gretag Macbeth Spectrolino with illuminant D65 and filter D65. The specimens were irradiated by metal-halide lamp to reach the same exposure dose. Values

of temperature, relative humidity and irradiance were taken through the exposures. Relationship (1) describes calculation of total colour difference ΔE_{ab}^*. Colour changes were evaluated from measuring after each exposure.

$$\Delta E_{ab}^* = \sqrt{(\Delta L^*)^2 + (\Delta a^*)^2 + (\Delta b^*)^2} \tag{1}$$

Results

The efect of TiO_2 added into print layers was studied using microscop Nicon Eclipse E200 and camera Nicon D200. In many plastics applications, the primary use of TiO_2 is as an opacifier[4]. In addition, it improved print quality of specimens (Fig. 3.).
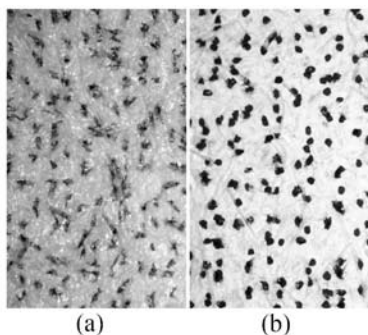
Fig. 3.   Specimens coated with PVAl (a) and with dispersion of TiO_2 in PVAl (b)

Only magenta ink results were evaluated (100% and 50% dot area). Total exposure dose acquired by irradiation was 50.6 $J\,cm^{-2}$, average temperature and relative humidity values were 27.7 °C and 24.8 %.
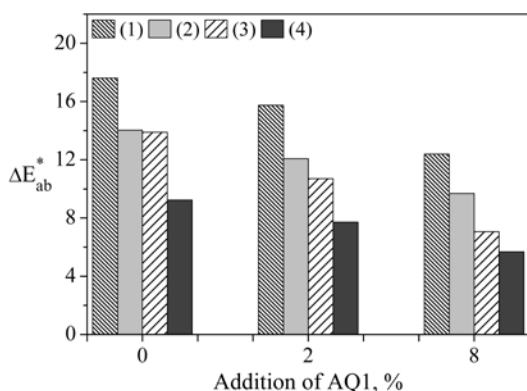
Fig. 4.   Values of total colour difference: (1) – layer with TiO_2 printed with 50% dot area, (2) – layer with TiO_2 printed with 100% dot area, (3) – layer without TiO_2 printed with 50% dot area, (4) – layer without TiO_2 printed with 100% dot area

Fig. 4. shows values of total colour differences calculated for magenta ink specimens at the end of the experiment. Fig. 5. and Fig. 6. represent receiving layers with TiO_2 filler use. The total colour difference values exceed 5 after first

exposure already. The growth of ΔE_{ab}^* values is smallest in the case of 8% addition of AQ1 stabilizer.
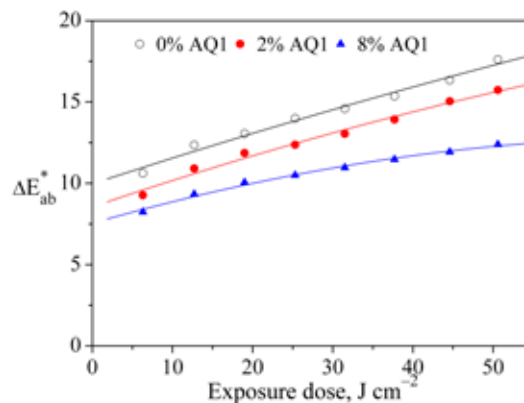
Fig. 5.   Receiving layer with TiO_2 and 50% dot area print
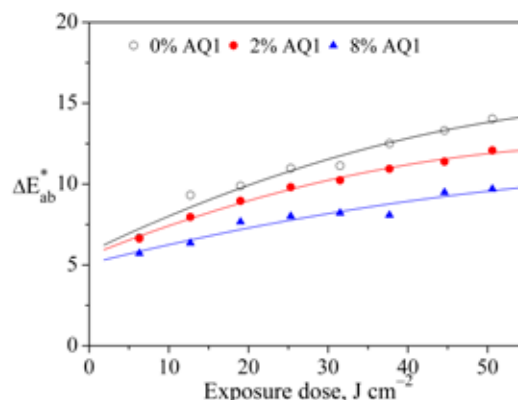
Fig. 6.   Receiving layer with TiO_2 and 100% dot area print

Fig. 7. and Fig. 8. represent receiving layers without TiO_2 filler use. The total colour difference values begun to
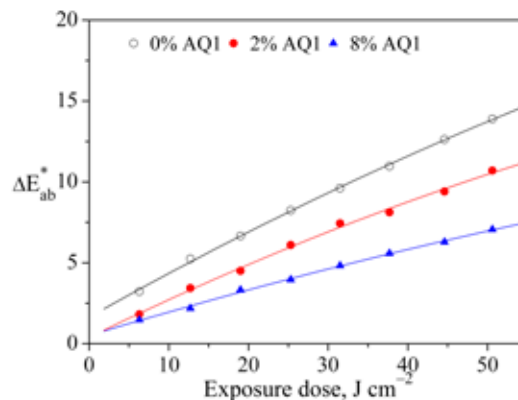
rise from the lower levels (less than 3). The growth of ΔE_{ab}^* values is smallest in the case of 8% addition of AQ1 stabilizer again.
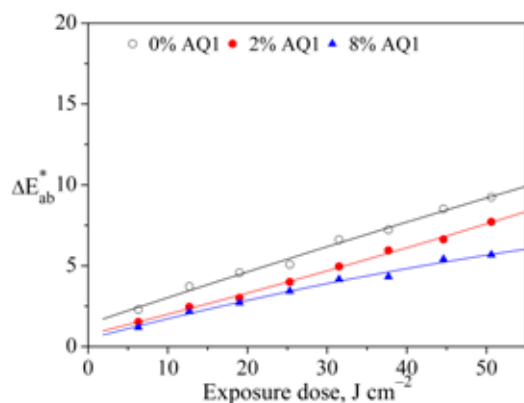
Fig. 8. **Receiving layer without TiO$_2$, with 100% dot area print**

Conclusions

Addition of TiO$_2$ into receiveng layers improved print quality and opacity of printouts, however, it decreased their lightfastnees. 50% dot area printouts faded more quickly than 100% once. An increased proportion of colour overprint and a catalytic fading can be the reason of this behaviour.

Stabilizer AQ1 had a positive influence on the lightfastness of printouts. 2% AQ1 addition decreased the progress of fading and 8% addition had even better impact on this process.

REFERENCES

1. Hladnik A.: J. Dispersion Sci. Technol. *25*, 481 (2004).
2. Londo M.: Pulp Pap. *74*, 37 (2000).
3. Gregory P.: Opt. Laser Technol. *38*, 306 (2005).
4. Allen N. S., et al.: Polym. Degrad. STable *85*, 927 (2004).
5. Ávár L., Bechtold K.: Prog. Org. Coat. *35*, 11 (1999).
6   Taguchi Y., et al.: Polym. Degrad. STable *83*, 221 (2004).
7   Lavery A., et al.: *Proceedings of IS&T's NIP 14: International conference on digital printing technologies*, p. 123. Toronto 1998.

P13 PHOTOPOLYMERIZATION OF MONOMERS WITH TWO DIFFERENT REACTIVE GROUPS

JOSEF KNOBLOCH and JOSEF SVOBODA

Department of Graphics Arts and Photophysics
Faculty of Chemical Technology, University of Pardubice,
Studentská 95, Pardubice, 532 10, Czech Republic,
josef.svoboda@upce.cz

Introduction

Glycidyl methacrylate (GMA) and 3,4-epoxy-1-butene (vinyl oxirane, butadiene monoxide, BMO) rank among monomers having two different functional groups able to polymerize by two distinct mechanisms – free radical (methacrylate and vinyl groups) and cationic (epoxy group), resp. Using suitable photoinitiators so-called hybrid photopolymerization occurs, interesting from theoretical point of view.[1–3]

Photopolymerization of GMA or mixtures of GMA with another monomers is of practical meaning as well because it gives technical useful products[4]. The oligomers prepared mainly by cationic polymerization of epoxy groups of monomers like glycidyl vinyl ether (GVE) and BMO can advantageously be used in vehicle systems[5,11].

The aim of this work was the study of the photopolymerization kinetics of bifunctional monomers in the presence of the free radical and cationic photoinitiators as well as their mixtures using Fourier transform infrared (FTIR) spectroscopy, mostly with transmission technique.

Experimental

M a t e r i a l s

Glycidyl methacrylate – Sigma-Aldrich (USA), purity >97 % wt., stabilized by 0.005 % wt. p-methoxyphenol, bp 192–197 °C

Glycidyl vinyl ether – Sigma-Aldrich, purity 97 % wt., bp 139 °C

Butadiene monoxide – 3,4-epoxy–1-butene, Sigma-Aldrich, purity 98 % wt., bp 65–66 °C

Irgacure 250 – (4-methylphenyl)[4-(2-methylpropyl) phenyl] iodonium hexafluorophosphate, Ciba-Geigy (Switzerland), a 75 % wt. solution of the active substance in propylene carbonate

Quantacure ITX – 2-isopropylthioxanthone, Great Lakes Fine Chemicals (USA), mp 62–77 °C

All the chemicals were used as purchased without any further purification.

M e a s u r e m e n t s

CE GREEN SPOT (UV Source Inc., USA) – UV radiation 300–480 nm (max. at 365 nm) source was high-pressure mercury arc lamp (100 W). UV light was guided through optical-fibre cable (diameter 5 mm), output delivery was 5 W. The distance of the optical-fibre waveguide outlet from the sample was 20 mm.

Radiometr Compact (UV Process Supply, USA) was used to calibration of UV source in the spectral range 258–380 nm (max. at 365 nm). With this device the radiation energy relative to surface up to maximum 20,000 mJ cm^{-2} can be measured.

AVATAR 320 (Nicolet Instrument Corp., USA) – FTIR spektrofotometer (beamsplitter KBr, detector DTGS KBr). Our measurements were carried out at the resolution 4 (in this case the distance of the two points in the spectrum is 1.929 cm^{-1}) using transmission, reflection and ATR (Attenuated total reflection) techniques. In all cases 32 scans were recorded and averaged.

M e a s u r e m e n t s

The photopolymerization experiments were carried out at the laboratory temperature, the average room temperature was 21 °C. For transmission technique use the defined amount of reaction mixture was placed on the grade silicon window and immediately overlayed by covering teflon foil 60 μm thick. The UV exposition was interrupted by samples analysis, time intervals between expositions were about 0.5 min. GMA reaction mixtures with photoinitiators were polymerized using specular reflexion technique and ATR technique as well. Within the photopolymerization in closed reaction space the thickness of the layer varied in the range of 5 to 7 μm.

The reactive groups concentration was determined on the basis of the respective absorption peaks areas for epoxy group and the methacrylic or vinyl double bond. As internal standard the carbonyl group absorption peak (1,719 cm^{-1}) only with GMA could be used. This peak does not change in the photopolymerization conditions. The results usually are the averaged three to five repeated analysis. The reactive groups conversion extent was expressed according to following equation[7,8]

$$x = (P_0 - P_t)/P_0, \tag{1}$$

where P_0, P_t are the sample absorbances before the UV exposition and after the irradiation total time t.

Results

FTIR spectra of the monomers used are shown in Fig. 1. During the polymerization in the presence of the free radical initiator (Quantacure ITX) the absorbances (areas) of the three peaks in the wavenumbers regions 800–950 cm^{-1} and 1,600–1,750 cm^{-1} are subsequently relatively falling. The peak at 944 cm^{-1} corresponds with methacrylate double bond of GMA[9], the second one at 1620 cm^{-1} indicates the presence of the vinylether double bond in GVE[10] and the third one at 1,641 cm^{-1} is charakteristic for the vinyl double bonds in BMO[11]. In contrast to this, initiating the monomers polymerization using the cationic photoinitiator Irgacure 250 the peaks areas at 909 cm^{-1}, 903 cm^{-1} a 818 cm^{-1} [12,9,11] are relatively falling. These peaks correspond with epoxy groups of GMA, GVE a BMO. In the presence of the cationic photoinitiator further the absorption peaks at 1,620 a 1,641 cm^{-1} are falling.
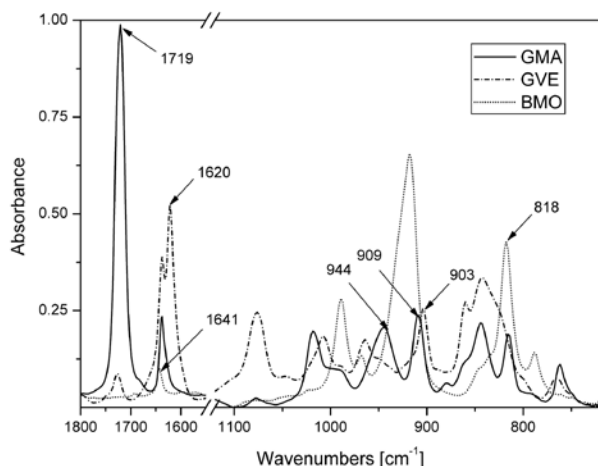
Fig. 1. **FTIR spectra of the studied monomers mixtures with photoinitiátors before UV exposition**

Fig. 2.   **Conversion curves of the double bonds (C=C) in the presence of ~ 1.1 % mol. QUANTACURE ITX and the epoxy groups (ES) in the presence of ~ 0.13 % mol. IRGACURE 250**

The experimental time-conversion curves (some typical examples are in Fig. 2.) as a rule satisfy the *n*-order kinetic equations[6]

$$\frac{dx}{dt} = k x^m (1-x)^n \qquad (2)$$

$$\frac{dx}{dt} = (k_1 + k_2 x^m)(1-x)^n \qquad (3)$$

very well. In these relations *k*, k_1 and k_2 are the reaction rate constants, *n* represents the reaction order and *m* denotes the autocatalytic exponent.

The free radical initiator concentration in the reaction mixture does not affect the attained conversion of the methacrylate double bonds in GMA which exceeded 90 % in every case. However, the necessary total irradiation time reduces as the photoinitiator concentration increases until 1.67 % mol. The vinyl double bonds conversion in BMO with the free radical initiator (~ 1.1 % mol) reached 45 % after the total irradiation time of 172 s. In the presence of the free radical photoinitiator GVE polymerizes very slowly, the vinyl ether double bonds conversion does not exceed 5 % even after irradiation time of 200 s (Fig. 2.).

During the cationic photopolymerization of the epoxy groups in GVE and BMO the reduction of the vinyl ether and vinyl absorption bands, resp. takes place at the same time. In both these cases the double bonds conversions attained are lower than those of epoxy groups. It was shown[11] that the BMO cationic photopolymerization proceed mainly by the oxirane ring opening. In our experiments GVE reacted in a similar manner, however the vinyl ether bond conversion in the initial polymerization stage was higher than the epoxy group conversion. Generally it holds however that the more reactive oxirane monomers are characterized by lower polymerization rate compared with the vinyl ether monomers[13]. During the GVE polymerization in the presence of the catio-

nic photoinitiator the mutual interference of the both reaction groups apparently occurs.

Markedly different results were obtained in monitoring the cationic photopolymerization of GMA. In oxirane ring-opening polymerization the conversions up max. 20 % were observed (Fig. 2.). On the contrary, with the increasing cationic photoinitiator concentration the polymerization rate of the methacrylate double bonds expressively rises. For example in the presence of 0.45 % mol IRGACURE 250 reach the conversion of the methacrylate double bonds 90 % after irradiation time 252 s. In comparison with GVE and BMO monomers the cationic photopolymerization of GMA in the closed thin layers is retarded hard. This matter of fact can be explained by very low reactivity of the glycidyl methacrylate epoxy groups in the experimental conditions applied. During irradiation then enforced the radical intermediates produced in diaryl iodonium salt decomposition as well.

In investigation of the hybrid monomers photopolymerization was found that the conversion curves are of the same type as those obtained in the presence of the cationic initiator alone. In every hybrid photopolymerization experiment, the initiation system was the ratio 1 : 1 % mol mixture of the free radical and cationic photoinitiators. In the case of the GMA photopolymerization the dominate reaction is the double bond polymerization again. The free radical photoinitiator addition to the cationic one enables the appreciable irradiation time shortening. Fig. 3. shows the dependence of the sum total conversions of the both functional groups vs. the hybrid initiation system concentration and irradiation time for all the monomers investigated.

Through the transmission and specular reflection techniques applied on the GMA photopolymerization in the closed thin layers with the free radical or cationic iniciators very similar results were obtained. The GMA photopolymerization monitored by the ATR technique proceeded in the air presence. This accelerated the cationic polymerization which

became the dominant reaction and the epoxy group conversion reached considerably higher values.
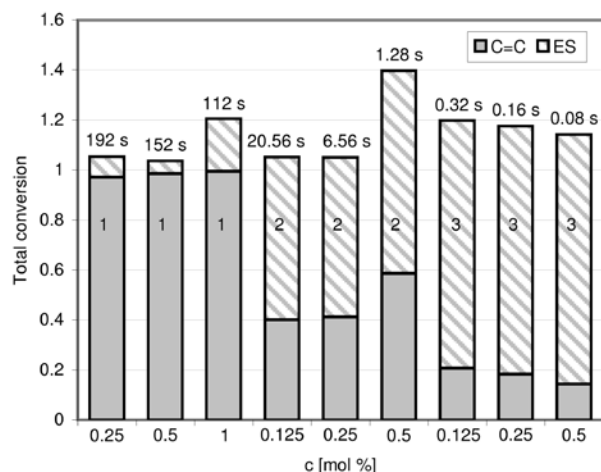
Fig. 3. **The sum total conversions of the epoxy groups and double bonds of the monomers investigated in the presence of the hybrid photoinitiator system (mol. ratio 1:1). 1 – GMA, 2 – GVE, 3 – BMO**

Conclusions

Experimental results shows the glycidyl methacrylate and butadiene monoxide monomers are able to polymerize in the presence of both the free radical and cationic photoinitiators. Within the glycidyl methacrylate photopolymerization in the closed thin layers the dominant reaction center is the methacrylate double bond even with diaryl iodonium salt photoinitiator. Glycidyl vinyl ether provides homopolymers only with the cationic photoinitiator and after irradiation finishing the conversions of the both functional groups reach the similar values. The substantial acceleration of the investigated monomers curing can be reached in the hybrid systems using suitable combination of the cationic and free radical initiators. The used mathematical models described the experimental data very well and could be applied on all the kinetic data obtained.

REFERENCES

1. Roffey C. G.: *Photogeneration of reactive species for UV curing. Wiley*, Chichester 1997.
2. Mehnert R., Pincus A., Janorsky I., Stowe R., Berejka A.: *UV and EB Curing Technology and Equipment. WILEY/SITA Series in Surface Coatings Technology, Vol. I. Wiley,* Chichester 1998.
3. Crivello J. V., Dietliker K.: *Photoinitiators for Free Radical Cationic and Anionic Photopolymerisation,* 2nd Ed. WILEY/SITA Series in Surface Coatings Technology, Vol. 3. Wiley, Chichester 1998.
4. Walter T., Höllriegl H., Schweiger H.: DE 43 07 766 C 1 (1994).
5. Minegishi S., Otsuka T., Kameyama A., Nishikubo T.: J. Appl. Polym. Sci., *43*, 3105 (2005).
6. Andrzejewska E.: Prog. Polym. Sci., *26*, 605 (2001).
7. Knobloch J.:. *MS Thesis*, University of Pardubice 2003.
8. Koenig J. L.*: Spectroscopy of Polymers*, 2nd Ed.. Elsevier, Amsterdam 1999.
9. Socrates G.: *Infrared and Raman Characteristic Group Frequencies* (3rd edn), John Wiley & Sons, Chichester, 2001.
10. Lin Y., Stansbury W. J.: Polymer, *44*, 4781 (2003).
11. Sangermano M., Falling S. N., Crivello J. V.: J. Macromol. Sci. A *38*, 919 (2001).
12. Kumar R. N., Woo C. K., Abusamah A.: J. Appl. Polym. Sci. *73*, 1569 (1999).
13. Crivello J. V., Liu S. S.: J. Polym. Sci. A *36*, 1179 (1998).

P14 A NEW APPROACH TO INKJET PRINTS LIGHTFASTNESS EVALUATION

MICHAL VESELÝ, PETR DZIK and JIŘÍ STANČÍK

Brno University of Technology, Faculty of Chemistry, Purkyňova 118, 612 00 Brno, Czech Republic,
vesely-m@fch.vutbr.cz

Introduction

The majority of printers used for colour printing in offices and homes today are inkjet printers. Inkjet is a digital printing process where the ink is ejected directly onto a substrate from a jet device driven by electronic signals. Due to its ability to print on a wide variety of substrates, inkjet technology is also increasingly being used in industrial printing and in the package printing industry.

According to the ink application it is possible to classify the inks frequently used and a method of their drying in a receiving layer: aqueous ink – absorption and evaporation, oil-based ink – absorption, UV-curable ink – absorption and the time available before cure and hot-melt/phase change – freezing.

The ink designed for ordinary portable inkjet printers can contain more than 20 various compounds, playing an important role for final printout quality. Main components of an aqueous/solvent based inkjet ink are: colorant, which gives the ink its primary function – absorbing light of a particular wavelength band (2–8 %), carrier fluid which dissolves or suspends the colorant (35–80 %), surfactant lowering the surface tension of the ink to promote wetting (0.1–2.0 %), humectant which inhibits evaporation (10–30 %), penetrant which promotes penetration of the ink into the paper structure for the purpose of accelerating ambient drying (1–5 %), dye solubilizer promoting dye solubility in the primary carrier fluid (2–5 %), anti cockle additive which reduces the interaction with paper fibres which otherwise leads to paper cockle and curl (20–50 %).

An ideal paper for inkjet printing should possess the following properties: sufficient hold out of ink dye on the surface to provide high optical print density, quick absorption of ink carrier liquid for fast drying, to prevent feathering and bleeding, low colour-to-colour bleed (well-defined diffusion of the ink), low strike-through and water- and light-fastness.

The printout fading is caused by many factors as for example chemical compounds in air (mainly aggressive ozone)[1], higher temperature, air humidity and light. The ultraviolet light is surely the most dangerous enemy of inkjet printouts. Very similar impact can be observed in the case incandescent light illumination. Any printouts should be never exposed to higher temperatures or left on moisty places.

The light fading[2,3] should be determined by exposure dose. But it was found that this process doesn´t fulfil the reciprocity law. Colour photos exposed to low intensity irradiation for a long time are often more damaged than those exposed to high irradiation for a short time with the same exposure dose.

The absorption of direct sunlight can be very dangerous for dye molecule. Its excitation can lead to forming of colourless products. Moreover, reactive oxygen radical present in illuminated layer can decompose the image dye.

The reaction pathway of the ink-forming azo dye depends on the chemical environment in which the dye molecules are bound. This environment is determined mainly by the print medium, ink-forming components and surrounding atmosphere. Depending on these conditions the dye molecule can be either reduced or oxidised. The azo dye molecule can be reduced to corresponding colourless amines in the presence of hydrogen donor. This reaction speeds up when the hydrogen donor or the azo dye itself is in the excited state. Excited dye molecules are unstable and therefore are easily degraded. The reducing hydrogen can originate from alcoholes, amines, ketones, carboxylic acids, ethers and esters. The azo dye molecules existing in hydrazone tautomeric forms attacked by singlet oxygen undergo the oxidative degradation pathway. An unstable peroxide molecule originates from this reaction. The peroxide decomposes spontaneously while nitrogen is released from the azo group. Reaction products can be coloured.

Experimental

The following inkjet paper were used: Ilford Galery Smooth Gloss – high glossy paper with microporous receiving layer, enabling fast drying of surface layer, Epson Archival Matt – matte coated paper designed for archival purposes, Ilford Galery Classic Gloss – high glossy paper with swellable polymer layer, Foma 1224 – matte coated paper for everyday printing. The test targets TC9.18 (X-Rite) were printed by printer EPSON R220 on samples of inkjet papers using dye-based inkset ESC-R200–4 (MIS Dyebase). These samples were irradiated in Q-SUN-Xe1-B (Q-PANEL) xenon chamber. Spectral irradiance was set to 0.68 W m^{-2} at 340 nm. The test targets were measured using spectrophotometer Spectrolino (X-rite) and evaluated by ProfileMaker 5.0 software.

Results

Main drawback of inkjet printing technology compared to classic silver halide photography is the overlap and mixing of individual inks in the receiving layer.

The illumination of inkjet printed photographs causes fading of individual inks with different rates – this process is called catalytic fading. During this process one ink or its decomposition products can serve as a catalyst for the second ink degradation. The results are unexpective colour shifts of printed pictures.

Test target TC9.18 with 918 patches enables to judge the results of accelerated ageing of ink overlaps. The main advantage of a great test target is the possibility to calculate ICC profile and subsequently to express the gamut in CIE L*a*b* colour space. Similarly, we evaluate the cross-sections through the gamut body at various lightness levels in CIE L*a*b* colour space. In most cases, it is sufficient to represent

the gamut as the cross-section of CIE L*a*b* colour space in 50% level of lightness (L50), eventually in 25 % and 75 % level (Fig. 1.). The other way of accelerated ageing results presentation consists of gamut volume calculation.
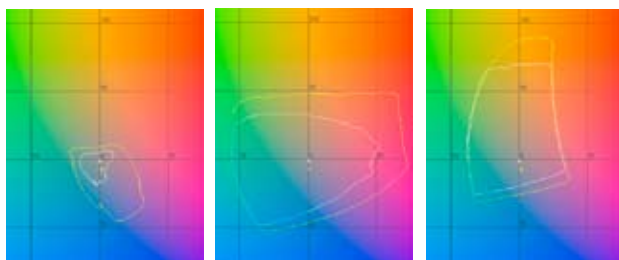
Fig. 1. **An accelerated ageing test of FOMA 1224 before (yellow lines) and after 33 hours (white lines): cross-sections of CIE L*a*b* colour space at L25 (left), L50 (middle) and L75 (right)**

After exposure dose of 80.3 kJ m^{-2} at 340 nm, we observed a considerable fading of all papers used in this test. This process is illustrated in Fig. 2 by means of counts of colour differences ΔE^*_{ab}. The distribution of colour differences ΔE^*_{ab} is narrow for papers with high resitance to fading, whereas the broader distributions indicate low lightfastness of tested inkjet papers.
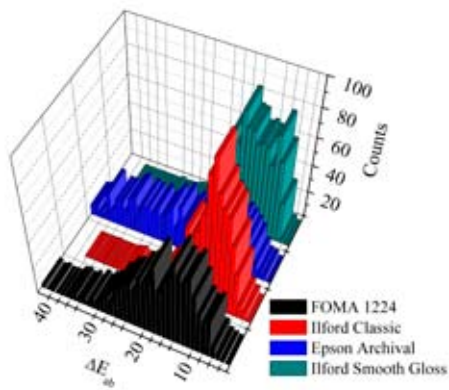
Fig. 2. **The counts of colour differences values ΔE^*_{ab} after 33 hours of accelerated ageing test measured on 918 patches of TC9.18**

All tested papers possesed a similar gamut, after accelerated ageing we found their gamut to be much smaller. Irradiation during accelerated ageing caused the loss of vivid colours printed by overlapping inks containing yellow ink. This is well visible on gamuts comparison (Fig. 4.).

Conclusions

From the presented results we can conclude that the highest image stability was observed on both Ilford papers. These papers showed the least colour fading of all tested papers. Colour gamut comparisons and the evaluation of colour differences distribution can significantly support the complex assesment of inkjet prints lightfastness.
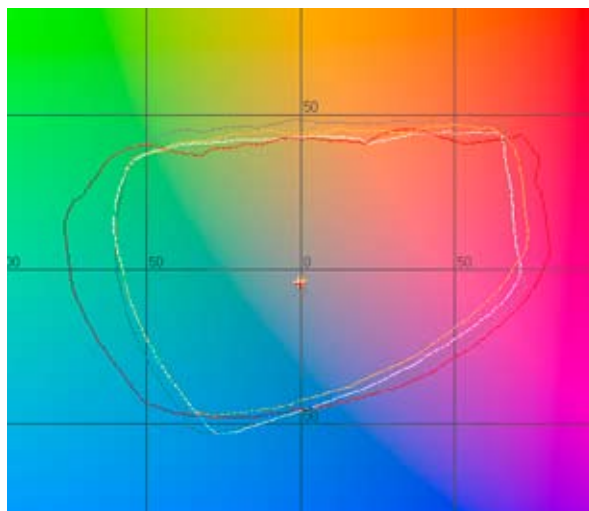
Fig. 3. **A cross-section of CIE L*a*b* colour space at L50 before test: Ilford Galery Smooth Gloss – red line, Epson Archival Matt – yellow line, Ilford Galery Classic Gloss – white line and Foma 1224 – gray line**
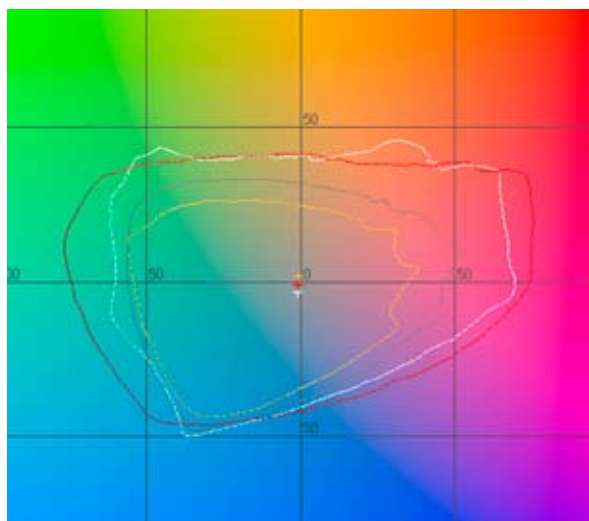
Fig. 4. **A cross-section of CIE L*a*b* colour space at L50L after 33 hours of accelerated ageing test: Ilford Galery Smooth Gloss – red line, Epson Archival Matt – yellow line, Ilford Galery Classic Gloss – white line and Foma 1224 – gray line**

REFERENCES

1. Barcock R. A., Lavery A. J.: *J Imag Sci Tech 48*, 153 (2004).
2. Feller L. R.: *Accelerated aging: Photochemical and thermal aspects*. The J. Paul Getty Trust, Michigan 1994.
3. Schwahlberg B., Wilhelm H., Brower C.: Popular Photogr *6*, 37 (1990).

7.   PHYSICAL & APPLIED CHEMISTRY

7.1. Lectures

L01 SELF-AGGREGATION OF HUMIC
AND FULVIC ACIDS STUDIED ON
IHSS STANDARDS

MARTIN DRASTÍK, ANNA ČTVRTNÍČKOVÁ and JIŘÍ KUČERÍK

Institute of Physical and Applied Chemistry, Faculty of Chemistry, Brno University of Technology, Purkyňova 118, 612 00 Brno, Czech Republic,
xcdrastik@fch.vutbr.cz

Introduction

Humic substances (HS) are ubiquitous and also the most occurring organic matter on the Earth. Due to their high heterogeneity and chemical character they tend to self-aggregate forming various molecular organisations. Despite an intensive research, the mechanisms and ways of aggregation are still not precisely known.

According to the solubility under acidic or alkaline conditions, HS are traditionally divided into three groups: humin, the insoluble fraction; humic acids (HA), the fraction soluble under alkaline but not acidic conditions (generally pH<2); and fulvic acids (FA), the fraction soluble under all pH conditions. FA may be regarded as associations of small hydrophilic molecules in which there are enough acidic functional groups to keep the fulvic clusters dispersed in solution at any pH. On the other hand, humic acids consist of associations of predominantly hydrophobic compounds which are stabilised at neutral pH by hydrophobic dispersive forces (van der Waals, $\pi-\pi$ and $CH-\pi$ bondings). Their conformations grow progressively in size when intermolecular hydrogen bondings are increasingly formed at lower values of pH, until they flocculate[1].

In 1961 Kononova introduced the concept that HS are comprised of system of polymers[2]. Piccolo, unlike foregoing theory, claims that humic constituents are supramolecular associations of relatively small heterogeneous molecules held together by weak interactions (van der Waals, $\pi-\pi$, $CH-\pi$ interactions and H-bonds)[3].

In this work the thermodynamic stability of HS standards obtained from the International Humic Substance Society (IHSS) at various concentrations was studied. In our case, the high resolution ultrasonic spectroscopy (HRUS) was the method of choice. Since in HRUS the mechanical type of waves is involved, it can succeed where classical optical methods are limited by the nature of the sample (e.g. sample concentration, pH, purity of sample, etc.). This non-destructive method has already been applied to monitor phase and thermal transitions, hydrations, coagulations and other conformational changes of various biomolecules including humic substances and proved itself as a powerful tool in colloidal chemistry due to its sensitivity (resolution down to 10–5 %) and broad possibilities of application[4,5].

Applied waves probe the elastic characteristics of materials. Compression caused by the ultrasonic wave decreases the distances between the sample molecules which then respond *via* intermolecular repulsions and, *vice versa*, the decompression probes the attractive forces. As the result, the ultrasonic velocity parameter is extremely sensitive to molecular organization and intermolecular interactions in samples.

Experimental

IHSS standards of humic acids (Suwanee River 1S101H, Leonardite 1S104H) and fulvic acids (Suwanee River 2S101F, Pahokee Peat 2S103F) were measured. Sodium salts of HA samples were prepared using following procedure. HA standard was dissolved in distilled water and the pH value was adjusted with 0.1M NaOH to 7. The sodium humate solution was freeze-dried and homogenised. FA standards were simply dissolved in distilled water.

To monitor the ultrasonic velocity, HRUS 102 device (Ultrasonic-Scientific, Dublin, Ireland) was employed. HRUS consists of two independent quartz cells which secures that complications caused by changing of water compressibility and density during non-isothermal regime are no longer significant. Cell 1 serves as a sample cell and cell 2 as a reference. Both cells are tempered by a water bath. All measurements were set up at 25.00 ± 0.02 °C, under constant stirring (600 rpm) and at ultrasound frequency of approximately 5,480 kHz. Samples were dissolved in distilled water to desired concentrations (0.01; 0.1; 1; 4 $g\,dm^{-3}$). Cell 1 was loaded up by 1 ml of a sample whereas cell 2 by 1 ml of distilled water. Temperature regime was as follows: step 1 – from 25 °C to 90 °C for 3 hours, back to 5 °C for 4 hours, step 2 – from 5 °C to 90 °C for 4 hours and back to 5 °C for 4 hours, step 3 – from 5 °C to 90 °C for 4 hours and back to 25 °C for 3 hours. The first heating cycle was used to ensure that humic samples have the same "thermal history" and that are completely dissolved. The second heating cycle was used to monitor the changes in humic solutions induced by heat, while the third one served as the reproducibility control of the experiment. During the temperature programs the ultrasonic velocity (U) was measured in both cells. The results were expressed as a difference of measured values between cell 1 and cell 2, i.e. U12.

Results

As the records from second and third step gave very similar results, we can assume that only physical and no chemical changes occurred.

HA sample of concentration 4 $g\,dm^{-3}$ (Fig. 1.) showed practically monotonous decrease of U12. At this concentration, aggregates with hydrophilic surface are present. This surface is surrounded by water shall that is due to the smaller compressibility more supportive for ultrasonic wave propagation than bulk water. With increasing temperature the relative static permittivity of water decreases which leads to the fact
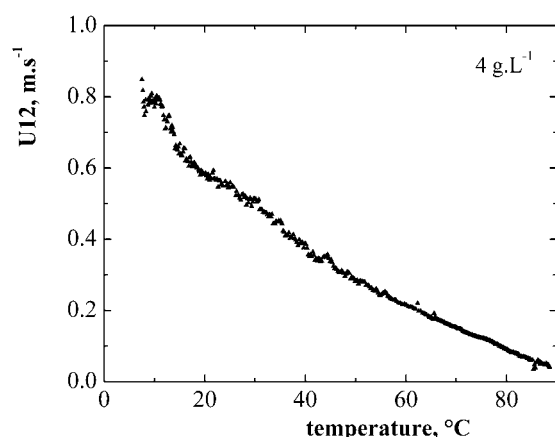
Fig. 1.   **Difference of ultrasonic velocity (U12) as a function of temperature, Suwanee River 1S101H, 4 g dm^{-3}**

that the hydration shell is weakened and U12 decreases. Furthermore, at higher temperatures the hydrophobicity of some amphiphilic headgroups increases which results in additional weakening of aggregate protecting hydration shell.

Diluting the sample solution (Fig. 2.), HA assemblies tend to form aggregates with a bit more hydrophobic exterior. The water shell is not so rigid and with increasing temperature is collapsing which results in disruption of humic aggregates. This destabilisations and consequent reaggregation can be observed as a wave-like shape of the curve.
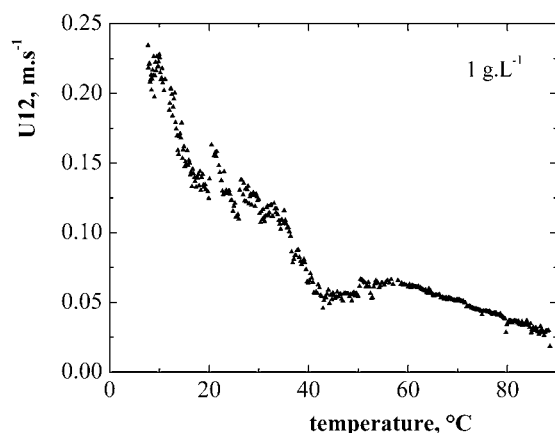
Fig. 2.   **Difference of ultrasonic velocity (U12) as a function of temperature, Suwanee River 1S101H, 1 g dm^{-3}**

It is in line with recent statement given in ref.[6] where has been demonstrated that diluting of humates is associated with decreasing in the number of relatively stable H-bonds and humic molecules are loosely bound by hydrophobic interactions such as CH$-\pi$, $\pi-\pi$ interactions or van der Waals forces[6].

Further diluting of the sample solution (i.e. under concentration of 1 g dm^{-3}) leads to formation of aggregates with

predominantly hydrophobic exterior. At some concentration, the nature of prevailing interactions holding together humic assemblies is dramatically changed. The disintegration of big aggregates into small ones or even single molecules is associated with the increase of number of water molecules in the hydration shells. With increasing temperature, the relative static permittivity of water decreases which is supportive to hydrophobic hydration. In total this leads to U12 increase (Fig. 3.).
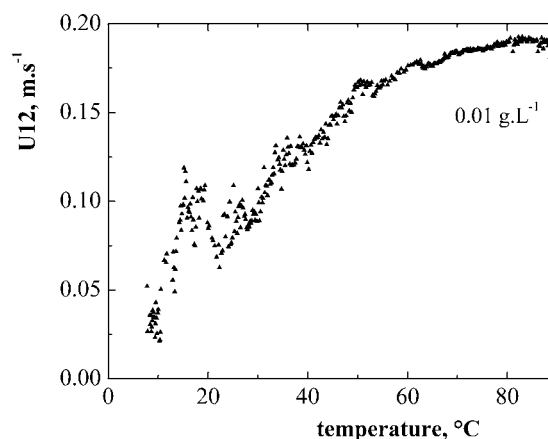
Fig. 3.   **Difference of ultrasonic velocity (U12) as a function of temperature, Suwanee River 1S101H, 0.01 g dm^{-3}**

Furthermore, the basic chemical composition (elemental analysis and carbon distribution in functional groups as revealed by liquid state ^{13}C NMR) was compared with the slope of ultrasonic velocity decrease of standards at concentration of 4 g dm^{-3} as measured by HRUS. The slope was observed steeper in line: Leonardite HA, Suwannee River HA, Pahokee Peat FA and Suwannee River FA.

As can be seen in Table I, basic chemical composition does not show clear correlation with the slope of ultrasonic velocity decrease. On the other hand, carbon distribution
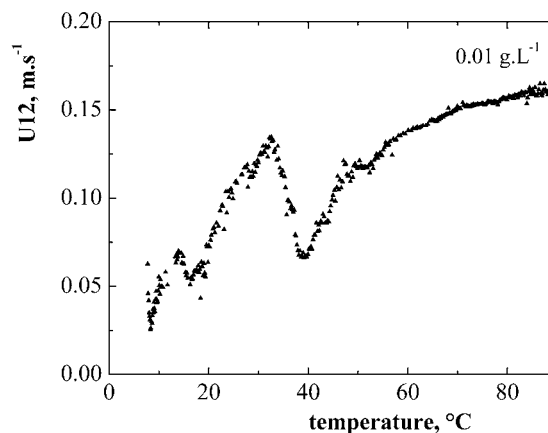
Fig. 4.   **Difference of ultrasonic velocity (U12) as a function of temperature, Leonardite 1S104H, 0.01 g dm^{-3}**

Table I
Elemental analysis of HA and FA standards (C. C – Carboxyl Carbon, Ar. C – Aromatic Carbon, Al. C – Aliphatic Carbon)

[%]	Leonardite HA	Suwannee River HA	Pahokee Peat HA	Suwannee River FA
C	63.8	52.6	51.3	52.5
H	3.7	4.4	3.5	4.3
O	31.3	42.5	43.3	42.2
N	1.2	1.2	2.3	0.7
C. C	15	19	28	20
Ar. C	58	37	34	24
Al. C	14	21	20	33

in functional groups, namely aromatic and aliphatic carbon content, can be regarded as potential indicator of the slope of ultrasonic velocity decrease. Anyway, these inferences are based on only four samples measurements thus another records are in need.

Conclusions

Results obtained by high resolution ultrasonic spectroscopy revealed differences in ultrasonic records for all samples. At the same concentration, all samples showed similar trends, nevertheless, easily distinguishable differences were observed (compare Fig. 3. with Fig. 4.). Observed differences may be explained by differences in the samples origin.

Furthermore, diluted samples brought completely different records in compare with the concentrated ones. That was attributed to the fact that at high concentrations the humic aggregates are stabilised mainly by H-bonds but at low concentrations the aggregates and/or single molecules are loosely bound predominantly via hydrophobic interactions. Elemental composition did not show clear correlation with HRUS measurements. On the other hand, slope of ultrasonic velocity decrease seemed to purvey information about carbon distribution in functional groups.

REFERENCES

1. Piccolo A.: Adv. Agron *75*, 57 (2002).
2. Kononova M. M.: *Soil organic matter. Its nature, its role in soil formation and in soil fertility.* Pergamon press, New York 1961.
3. Piccolo A.: Soil Sci *166*, 810 (2001).
4. Buckin V., Kudryashov E., Morrissey S.: Int. Labmate *27*, 23 (2002).
5. Kučerík J., Šmejkalová D., Čechlovská H., Pekař M.: Org. Geochem. *38*, 2098 (2007).
6. Conte P., Piccolo A.: Dev Soil Sci *28*, 409 (2002).

L02　ROBUST NONLINEAR CONTROL OF A SEPARATION COLUMN FOR ^{13}C ENRICHMENT BY CRYOGENIC DISTILLATION OF CARBON MONOXIDE

EVA-HENRIETTA DULF[a], CLEMENT FESTILA[a] and FRANCISC V. DULF[b]

[a]Technical University of Cluj-Napoca, Faculty of Automation and Computer Science, 400020 Cluj-Napoca, C. Daicoviciu Str., 15 Romania,
[b]University of Agricultural Sciences and Veterinary Medicine, Food Quality Control Department, 3–5 Mănăştur Str., Cluj-Napoca, Romania,
Eva.Dulf@aut.utcluj.ro

Introduction

Isotope separation columns are characterized by complex nonlinearities. Furthermore, such processes are subject to external disturbances, which are difficult to model. The controller synthesis problem for such processes is extremely challenging and has been an active area of research for the past two decades.

One approach that has proved popular is the input/output (I/O) linearization approach. In this multi-loop design methodology, Fig. 1., a coordinate transformation is utilized that results in a linear relation between the inputs and outputs (inner loop controller design). Then, an external linear controller is designed for this linear system to enforce desired performance and stability characteristics (outer loop controller design). The performance of this controller largely depends on the availability of an accurate model that leads to exact cancellation of nonlinear terms via the coordinate transformation. However, due to uncertainty and disturbance this is seldom the case and often leads to poor performance.
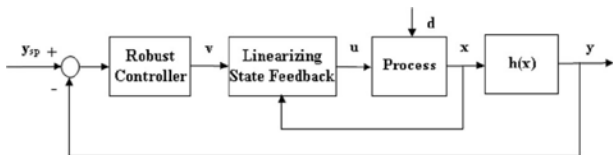
Fig. 1.　**Multi-loop robust controller design for nonlinear processes**

In principle, once the nonlinearities are canceled (or inverted), the outer-loop can be designed to impose any desired stable dynamics on the closed loop. The nonlinear model will very likely represent only an approximation of the actual plant. In addition to the modeling uncertainty, there is uncertainty in the model parameters especially in process systems. The controller in the outer loop must be designed not only for nominal stability and performance but for robustness in face of uncertainty in the model and the environment. This robustness issue can be addressed in two alternative approaches. The first approach is to consider the effect of the uncertainty in the nonlinear model and use nonlinear techniques to account for the uncertainty[1]. The second approach[2] is to consider the effect of uncertainty as a perturbation to the I/O linear model and use linear robust control techniques to account for this uncertainty.

Robust Nonlinear Control: the Linearization Approach

The first problem is to systematically design a state feedback for performance and robustness for I/O linearizable systems with parametric uncertainty. In particular, we use a multi-model approach to design a robust controller for the uncertain nonlinear system. In this multi-model approach, the state matrices are written as affine functions of the uncertain parameters and a controller is designed so that stability and performance specifications are met for all members in this polytopic family of models.

Consider the following state space model of a single input single-output (SISO) nonlinear system with parametric uncertainty

$$\dot{x} = f(x, \theta) + g(x)u$$
$$y = h(x) \qquad , \qquad (1)$$

where $x \in \Re^n$ is the state, $u \in \Re$ the control input, $u \in \Re$ the measured output, and θ is a vector of uncertain parameters that takes values in a compact set $\Theta \subset \Re^p$ $\theta \in \Theta$ we assume that f and g are smooth vector fields on , and $\Re^n$ a smooth real vector valued function. The objective is to design a controller such that the closed loop system is stable and certain performance objectives, e.g. tracking, disturbance rejection, etc., are satisfied for all $\theta \in \Theta$. To solve this problem we propose a multi-loop design approach. The inner-loop uses state-feedback to linearize the nominal process dynamics in the input-output sense. In the presence of uncertainties, these methods do not give perfectly linear models. Perturbations appear in the canonical form, as nonlinear functions, due to the presence of uncertainties. For the use of linear robust control techniques these nonlinearities have to be linearized. Standard Jacobi linearization of these nonlinear perturbations around the steady states can be used for this purpose. We note that this is different from the Jacobi linearization of the original nonlinear system. Only the perturbations arising due to uncertainties are linearized but not the whole model. The outer-loop controller is a robust controller that guarantees performance despite uncertainty in the model. The H_∞ objective in the robust controller design is to cancel the e!ect of worst-case disturbances (the nonlinear perturbations) and the H_2 objective is to obtain the optimal LQG control. This linear robust control problem can be solved via multi-objective optimization techniques such as mixed H_2/H_∞ synthesis with pole placement constraints. This technique can be used for robust design when the linear fractional representation of the plant is affne in θ. The multi-model H_2/H_∞ state-feedback synthesis places the poles such that the system has good performance for all values of θ. This problem is represented in Fig. 2., where w contains all external disturbances, e.g. d, and Z_2 and Z_∞ contains the relevant errors signals that we want to maintain small with respect to the 2-norm (average) and ∞-

norm (worst case), respectively. The generalized plant $G(\theta)$ represents the plant model together with performance and normalization weights and is affine in θ.
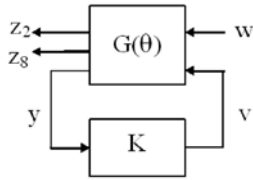
Fig. 2. Multi-model H_2/H_∞ synthesis problem

The objective is to finnd a stabilizing controller K such that

$$a\left\|T_{Z_\infty w}\right\|_\infty + b\left\|T_{Z_2 w}\right\|_2 \tag{2}$$

is minimized, for all $\theta \in \Theta$, where $T_{Z_\infty w}$ and $T_{Z_2 w}$ are linear operators mapping w to Z_∞ and w to Z_2, respectively, and *a*, *b* are positive numbers representing the trade-off between the H_2/H_∞ objectives.

The multi-objective synthesis problem for an uncertain state-space realization can be solved using linear matrix inequalities (LMI). First, the uncertain state-space model is represented as a polytopic family of systems where the state-space matrices are affne functions of the uncertain parameters, i.e. of the form

$$A(\theta) = A_0 + \theta_1 A_1 + \ldots + \theta_k A_k + \ldots \theta_p A_p, \tag{3}$$

where, *p* is number of uncertain parameters. Then, multi-objective problem (2) is solved by LMI using the following theorem.

Theorem 1. (Khargonekar & Rotea, 1991). Given a polytopic family of LTI systems, of the form

$$\dot{z} = A(\theta)z + B_1(\theta)d + B_2(\theta)v \tag{4}$$

$$Z_\infty = C_1 z + D_{11}d + D_{12}v \tag{5}$$

$$Z_2 = C_2 z + D_{22}v \tag{6}$$

The state feedback $v = Kz$ that robustly stabilizes the above system and minimizes the performance objective is given by $K = YX^{-1}$, where $\times$ and Y are obtained by solving the following LMI formulation of the multi-objective state feedback synthesis problem:

Minimize $a\gamma^2 + b$ Trace(Q) over Y, X, Q and γ^2 satisfying

$$\begin{pmatrix} A_k X + X A_k^T + B_{2k}Y + Y^T B_{2k}^T & B_{1k} & XC_1^T + Y^T D_{12}^T \\ B_{1k}^T & -I & D_{11}^T \\ C_1 X + D_{12}Y & D_{11} & -\gamma^2 I \end{pmatrix} \tag{7}$$

$$\begin{pmatrix} Q & C_2 X + D_{22}Y \\ XC_2^T + Y^T D_{22}^T & X \end{pmatrix} > 0 \tag{8}$$

$$\text{Trace}(Q) < v_0^2 \tag{9}$$

$$\gamma < \gamma_0^2 \tag{10}$$

$$f_D < 0 \tag{11}$$

where A_k, B_{1k}, B_{2k} are coefficients in the polytopic representation (as shown in (3)) of the parameter dependent state matrices A, B_1, B_2, respectively, γ and v are upper bounds on the H_∞ and H_2 norms, respectively, and f_D specifies the pole placement constraints.

Robust Nonlinear Control: Nonlinear Technique

This second approach of robust nonlinear control considers the process dynamics of the form

$$\dot{x} = f(x,\bar{u}) + \sigma(x)\dot{d} \tag{12}$$

(1) and a cost criterion L(x, u). We choose a disturbance attenuation constant, γ, and look for a nonlinear feedback control $u^*(x)$ such that[2]

$$\int_0^T L(x(t), u^*(x(t)))dt \le \gamma^2 \int_0^T |d(t)|^2 dt + D(x) \tag{13}$$

for some function of initial condition D(x) for all $d \in L_2(0,T)$, $T < \infty$. Ideally one would like γ to be nearly as small as possible. Considering the control problem as a differential game with dynamics (12), the payoff and value are given by:

$$P(x,u,d,T) = \int_0^T L(x(t), \varphi[w](t)) - \gamma^2 |d(t)|^2 dt \tag{14}$$

$$\overline{W}(x) = \inf_{\phi \in \Phi} \sup_{d \in D} \sup_{T < \infty} P(x, \phi[d], d) \tag{15}$$

If one obtains an optimal feedback control $u^*(x)$ for the game, then

$$\overline{W}(x) = \sup_{d \in D} \sup_{T < \infty} \int_0^T L(x(t), u^*(x(t))) - \gamma^2 |d(t)|^2 \tag{16}$$

which implied that (13) is satisfied.

The Isaac equation corresponding to (14) is:

$$0 = \inf_{u \in U} \sup_{d \in \Re^a} \left\{ [f(x,u) + \sigma(x)d]^T \nabla D + L(x,u) - \gamma^2 |d|^2 \right\} =$$
$$= \inf_{u \in U} \left\{ f^T(x,u)\nabla D + L(x,u) \right\} + \frac{1}{4\gamma^2} \nabla D^T \sigma(x)\sigma^T(x)\nabla D = \tag{17}$$
$$= H(x, \nabla D)$$

which is a first-order partial differential equation.

The Isotope Separation

The stable isotopes, species of any element with different number of neutrons in nucleus, exhibit today a large field of applications: research laboratories, medicine, chemical industry, etc. For each element, the natural distribution

of the isotope concentration is very well established, but in applications are necessary chemical compounds based on isotopes with higher concentration. Small differences in physical – chemical properties developed a broad range of isotope enrichment ("isotope separation") methods, technologies and equipments. For instance, by carbon, the ^{12}C and ^{13}C components have a concentration ratio of 98.9 at.%/1.1 at.%.
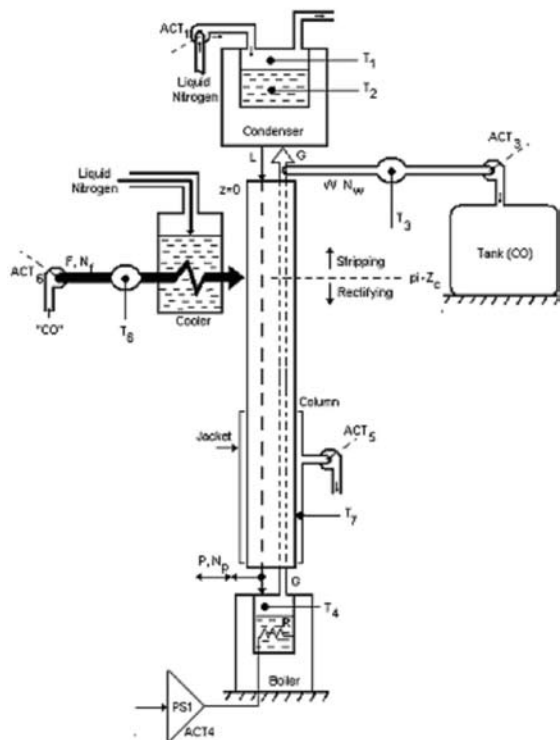
Fig. 3. **Simplified scheme of the isotope separation column**

The cryogenic isotope separation technology for ^{13}C is based on the vapor difference of ^{13}CO compared to ^{12}CO at very low temperature (about –192 °C). The isotope separation column is represented in Fig. 3. If the liquid and gaseous phases of the carbon monoxide coexist in the separation column, concentration of ^{13}CO rises in the liquid phase and ^{12}CO accumulates in the gaseous phase. In the isotope separation column a permanent ascendend gas flow and a descendent liquid flow arrises. The liquid phase is vaporized in te column base by an electric "boiler" and the vapor phase is condensed on the wall of the vessel cooled by liquid nitrogen.

The Mathematical Model of the Isotope Separation Column

Considering the above presented isotope separation column, the objective is to keep the ^{13}C isotope transfer rate ($\dot{c}$) constant by manipulating the level of N_2 in condenser (h_c) and the voltage on boiler resistor (U_B). The disturbance is the vacuum pressure in the jacket of the column (p_{vac}). Using the

physical equations for the hydrodynamic internal process, the system can be modeles as[3,4,5]

$$\dot{c} = k_{11}(\theta_B - \theta_C) - k_{12}(\theta_B + \theta_C)^2 - k_{13}p_{vac}^2 \qquad (17)$$

$$\dot{\theta}_B = -\frac{\theta_B}{T_B} + k_{21}U_B^2 + k_{22}p_{vac}^4 \qquad (18)$$

$$\dot{\theta}_C = -\frac{\theta_C}{T_C} + k_{31}h_c^{1/2} \qquad (19)$$

where θ_B is the temperature in the boiler zone, θ_C is the temperature in the condenser zone, T_B and T_C are the boiler and condenser time constants and k_{11}, k_{12}, k_{13}, k_{21}, k_{22}, k_{31} are specific constants. Choosing

$$\begin{aligned}x_1 &= c \\ x_2 &= \theta_B \\ x_3 &= \theta_C\end{aligned} \qquad (20)$$

as state variables

$$\begin{aligned}m_1 &= U_B \\ m_2 &= h_C\end{aligned} \qquad (21)$$

as manipulated variables and

$$d_1 = p_{vac} \qquad (22)$$

as disturbance, the obtained LTI model is:

$$\begin{cases}\dot{x}_1 = k_{11}x_2 - k_{12}x_3 - k_{12}x_2^2 - k_{12}x_3^2 - \\ \qquad - 2k_1k_2x_2x_3 - k_{13}d_1^2 \\ \dot{x}_2 = -\dfrac{1}{T_B}x_2 + k_{21}m_1^2 + k_{22}d_1^4 \\ \dot{x}_3 = -\dfrac{1}{T_C}x_3 + k_{31}m_2^{1/2} \\ y = x_1\end{cases} \qquad (23)$$

It is an uncertainty in the parameter k_{11} which $k_{11} = \hat{k}_{11} + c_{11}\theta$, $|\theta| < 1$ $\hat{k}_{11}$ the nominal value of k_{11} and c_{11} is a scaling constant representing the magnitude of the uncertainty.

Using this multi-model, it can be design the robust controller as described in previous sections.

Conclusions

Two design procedures were developed for the ^{13}C isotope separation column control: one design is based on I/O linearization and multi-objective H_2/H_∞ synthesis and the second one uses nonlinear techniques. The first approach combines the advantages of I/O linearization and linear robust control techniques to guarantee performance for the nonlinear system with uncertainty. The main advantage of the method is that does not require restrictive matching conditions to be satisfied. With the second approach was obtained a true, global, nonlinear H_∞ controller.

REFERENCES

1. Kolavennu S., Palanki S., Cockburn J. C.: Chem. Eng. Sci. *55*, 1583 (2000).
2. Elisante E., Rangaiah G. P., Palanki S.,: Chemical Engineering Science, *59*, 977 (2004).
3. Gligan M., Dulf E., Unguresan M. L., Festila C.,: *Proceedings of International IEEE-TTTC International Conference on Automation, Quality and Testing, Robotics AQTR 2006 (THETA 15)*, p. 155. Cluj-Napoca, 2006.
4. Dulf E. H., Unguresan L. M., Gligan M., Festila C.: *Proceedings of International IEEE-TTTC International Conference on Automation, Quality and Testing, Robotics AQTR 2006 (THETA 15)*, p. 159. Cluj-Napoca, 2006.
5. Dulf E. H., Dulf F., Festila C., Baldea A., Gligan M.: *The fifth Conference Isotopic and Molecular Processes*. Cluj-Napoca, Romania, 2007.

L04　PREDICTION OF THE ACETIC AND FORMIC ACID FORMATION IN THE PAPER DURING THE ACCELERATED AGEING BY THE CHANGE OF OPTICAL PROPERTIES

MICHAL JABLONSKÝ[a], KATARINA HROBOŇOVÁ[b] and RADOVAN TIŇO[a]

[a]Department of Chemical Technology of Wood, Pulp and Paper,
[b]Department of Analytical Chemistry, Faculty of Chemical and Food Technology, Slovak University of Technology in Bratislava, Radlinskeho 9, 812 37 Bratislava, Slovak Republic,
michal.jablonsky@stuba.sk

Introduction

The deterioration of paper as it ages is a serious problem for archival and library communities throughout the world[1]. The most important chemical reactions that occurs during the ageing of paper is the acid-catalyzed hydrolysis of cellulose in paper fibers[2–4] and oxidation of cellulose by oxygen.[2,5–7] The natural ageing processes in the paper lead to the formation of several low molecular weight compounds. Organic acids are spontaneously generated in the natural ageing of all cellulose–based papers, including alkaline papers. Easily detectable concentrations of formic (methanoic), acetic (ethanoic), lactic, glycolic, oxalic and a few others also unidentified acids accumulate within a few months of manufacture in paper stored under ambient conditions[8]. In another work Shahani[9] analyzed papers aged naturally and accelerated by ageing for carbohydrate species using ion chromatography and aliphatic acids such as formic and acetic, which we have discovered to form in surprisingly abundant concentrations, by capillary electrophoresis. In earlier works, which showed us that acidic degradation products tend to accumulate inside polyester encapsulations and other enclosures, and thereby hasten the ageing of the paper[10,11]. To stop the degradation and save millions of the books that are stored in archives different technologies of deacidification and fibre strengthening were invented[12] and considerable efforts have been devoted to find a new additives such as scavengers of free radicals, natural and synthetic compounds, inorganic compounds, solvent and improved original technologies of deacidification.[13–15]

The advantage of the optical methods in the visible part of the spectra consists in their non destructive character. Visually evaluated colour information are widely used in common praxis and in everyday life for grading, production control, sate, decisions of consumers, aesthetic and economical value evaluation, in utilisation, renovation and recycling of lignocellulosic materials and products. The objectively measured quantitative colour information are antropomorphous in nature (human-like, understandable and sometimes or to some extent proportional to the human perception).[16–19]

Experimental

Raw material

Commercial groundwood newsprint paper (grammage 45 g m^{-2}, liquor pH: 4.5–5.0) containing mechanically bleached, groundwood (55 %), bleached sulphite pulp (20 %), catch trash fibres (15 %) and clay (10 %) was used in all experiments.

Accelerated Ageing at 98 °C

Paper were conditioned for 24 hours at T = 23 ± 1 °C, RH = 50 ± 2 % by the norm TAPPI T 402 om-93. Twenty papers (sheets of paper in size A4 format) were put into PET/Al/PE bag which was subsequently completely sealed off. This bag was put into another PET/Al/PE bag which was also completely sealed off and was again put into third (final) sealed PET/Al/PE bag. Finally sample sheets were in the package consisting of three sealed bags put one in another. The bags with samples were put into the thermostat for 0, 1, 2, 3, 5, 7, 10, 15, 20, 30 and 60 days at temperature 98 ± 2 °C.

High Performance Ion-Exchange Chromatography

Approximately 2 g of the paper were accurately weighed and 15 ml of water (Millipore) was added. The mixture was mixed during 2 hour and filtered through 0.45 μm filter. Amount of 20 μl filtrate was injected into the analytical column. The used HPLC system consists of a DeltaChrom SDS 030 isocratic pump, a 7125 Rheodyne injector with a 20 μl injection loop, a thermostat Model LCT 5100, a Knauer variable wavelength detector (set at 210 nm), and CSW32 software for peak identification and integration.

Chromatographic separations of acids were performed with column Polymer IEX H-form (250 × 8 mm I.D., 8 μm). The mobile phase consisted of 9 mmol dm^{-3} sulphuric acid. The column temperature was 20 °C and the flow rate of the mobile phase was 0.8 ml min^{-1}. Formic and acetic acid were detected with spectrophotometric detection at 210 nm. The retention times were 9.7 ± 0.2 min. for formic acid and 10.7 ± 0.1 min. for acetic acid. The identification of the acids in water extract of paper was based on comparison of their retention factors (formic acid k = 1.21 ± 0.03, acetic acid k = 1.44 ± 0.03).

Calibration curves were constructed by performing a regression linear analysis of the peak area versus the concentration of acids. Based on a four-point calibration, a linear response (r = 0.99) was observed from the limit of determination to 20 mg ml^{-1} of studied acids. The limits of detection, defined as the lowest sample concentration, which can be detected (signal-to-noise ratio of 3 : 1) were 10.7 μg ml^{-1} for formic acid and 18.4 μg ml^{-1} for acetic acid. The limits of determination, defined as the lowest sample concentration, which can be quantitatively determined with suitable precision and accuracy (signal-to-noise ratio of 10 : 1) were 42.8 μg ml^{-1} for formic acid and 92.2 μg ml^{-1} for acetic acid.

Optical Properties

Changes in colour of paper surfaces due to ageing were measured using a colour measuring system ELREPHO DATACOLOR 2000. Brightness (B), yellowness (Ys), CIE-Lab L*, a*, b* and ΔE parameters were measured at five spots on each specimen and average value was calculated. The precision in the optical properties determinations brightness are estimated to be less than ± 0.05 units. The Kubelka–Munk coefficient (k/s) describing the number of chromophores present in the paper was determined on the basis of experimental values for brightness[20].

Results

On the Fig. 1. are shown correlations between each pair of variables. Fig. 1 shows Pearson product moment correlations between each pair of variables. These correlation coefficients range between –1 and + 1 and measure the strength of the linear relationship between the variables. The second number in each location of the Fig. 1. is a p-value which tests the statistical significance of the estimated correlations. P-values below 0.05 indicate statistically significant non-zero correlations at the 95% confidence level.

The most evident signs of paper are yellowing and loss of mechanical strength[21]. During the ageing of paper, decreases the lightness, brightness, but on the other side increases redness and b* coordinate, yellowness (Ys), total colour difference, Kubelka-Munk coefficient and also increases content of acetic and formic acid in paper. In modern papers the decrease of brightness is about 13–15 %, in historic papers is 3–16 %[22]. In our paper the initial value of brightness was 66.20 % ISO and after 60 days of ageing was decrease of brightness about 78 %.
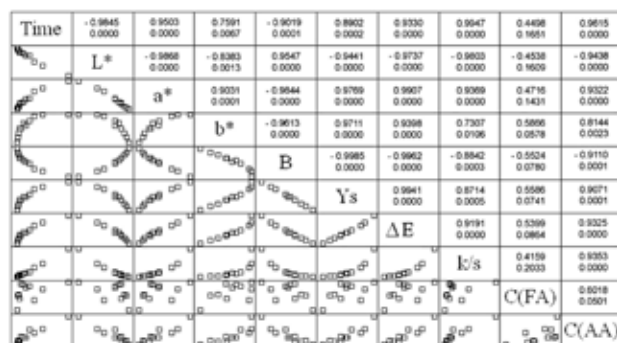
Fig. 1.   **Scatter plot for Pearson product moment correlations between each pair of variables**

The acidic products formed during the accelerated ageing accumulate inside the paper and inter-sheet spaces of the books or archival files and it results in enhanced degradation[23]. On the basis of evaluation of carboxylic acids content (formic and acetic acid) was noted unambiguous increase of acetic acid concentration during the accelerated ageing and moderate increase of formic acid concentration. During the accelerated ageing was increased concentration of acetic acid from 0.361 on the value 4.798 mg g^{-1} of paper (after 60 days).

The content of formic acid during the accelerated ageing increases from 0.185 to 0.868 mg g^{-1} of paper (after 60 days). All chemical reactions causing paper degradation are also responsible for the creation of chromophores, especially thermal oxidations and photo–Oxidations. Other reactions such as condensation, cross linking and dehydration due to heat and strongly acid environment, also produce coloured chemical compounds[23,24]. In principle, simple acid hydrolysis does not affect colour, but low-molecular-weight products are more prone to oxidation and colour formation than cellulose chains[23]. The yellowing of paper during the ageing procedure is attributed to the presence of chromophores formed by the degradation of paper components (cellulose, hemicellulose, lignin)[25,26]. The formation of macromolecular hydroperoxides in the cellulose backbone was evidenced previously in the research on paper ageing and the significant role of the produced radical species was postulated[25,26].

Correlations between optical properties and all other characteristics were mostly strong. Fig. 1. demonstrates that a few outliers did not drive the lack of correlation. It was seen earlier that a good correlation exists between C(AA) and time of accelerated ageing (r = 0.9615) and to a lesser extent between C(AA) and L* (–0.9438), k/s (0.9353), ΔE (0.9325), a* (0.9322), B (–0.9110) and Ys (0.9071).

Whereas the values for C(FA) are poorly correlated with the optical properties and time of accelerated ageing and C(AA). The correlation between content of formic acid and all other characteristics was evaluated (r < 0.61). The weak correlation were between time of accelerated ageing at 98 °C and b* coordinate (0.7591) and between b* coordinate and k/s (0.7307).

We tried to achieve a quantitative linear correlation between optical properties of ageing paper and a property related to extent of degradation formation of acetic and formic acid in paper, respectively. For our multiple regression models, we have used the model set containing samples aged in the time interval from 0–60 days at 98 °C. The output shows the results of fitting a multiple linear regression model to describe the relationship between content of acetic acid (C(AA)) or formic acid (C(FA)) and 8 independent variables. The equation of the fitted model is

$$C(AA) = -23.5965 + 0.239192T + 0.354993L^* - 0.925779a^* - 1.82714b^* - 0.311187B + 2.17738Ys - 2.7564\Delta E + 0.850291k/s$$

Since the p-value is less than 0.01, there is a statistically significant relationship between the variables at the 99 % confidence level. The R^2 parameter indicates that the model as fitted explains 99.88 % of the variability in C(AA). By the method forward selection was evaluated new multiple linear regression model are presented Table I. The R^2 parameter indicates that the model as fitted explains 96.70 % of the variability in C(AA).

The equation of the fitted model for concentration of formic acid and optical properties and time of accelerated ageing is:

$$C(FA) = -70.4895 + 0.0640916T + 0.667981L^* - 0.836883a^* - 2.84595b^* + 0.234988B + 1.19121Ys + 1.29359\Delta E - 10.578k/s$$

Table I

Parameters and estimates of fitting of linear multiple regression model for concentration of acetic acid

Dependent variable: C(AA)			
Parameter	Estimate	Standard error	p-value
Constant	1.0985	0.1303	0.0000
Time	0.2119	0.0448	0.0015
k/s	–3.6854	1.1477	0.0124
$R^2 = 0.967$			

Since the p-value is greater or equal to 0.10, there is not a statistically significant relationship between the variables at the 90% or higher confidence level. The R^2 indicates that the model as fitted explains 92.95 % of the variability in C(FA). By the method forward selection was evaluated new multiple linear regression model which is presented in Table II. The R^2 parameter indicates that the model as fitted explains 34.4 % of the variability in C(FA).

Table II

Parameters and estimates of fitting of linear multiple regression model for concentration of formic acid

Dependent variable: C(AA)			
Parameter	Estimate	Standard error	p-value
Constant	0.2990	0.1648	0.1031
b*	0.0209	0.0096	0.0578
$R^2 = 0.344$			

As was mentioned before, optical properties are physical properties which are often monitored by the conservators for the indication of chemical changes[27]. From this paper is obvious that brightness decreases during the ageing, probably because of formation of chromophore in cellulose, hemicellulose and lignin, and then it increases. In this work was confirmed that formation of acetic acid in paper depends on the time of accelerated ageing and on number of chromophores present in the paper which can be described by the Kubelka-Munk coefficient. The correlation between time of accelerated ageing, Kubelka-Munk coefficient and formation of acetic acid is strongly significant. Correlation between optical properties and time of accelerated ageing according to formation of formic acid is weak significant.

In this work was also confirmed that low-molecular product such as acetic acid have coherence with the colour information which is consequence of the accelerated ageing. Paper properties are interdependent[27] hence the change of optical properties relates with the change of chemical properties and fragility of pulp fibers during the accelerated ageing.

Conclusions

The aim of the work was to quantify the failure of acetic and formic acid estimation by optical parameters in models of ageing papers at 98 °C from 0 to 60 days. The results presented in the paper has shown that multiple linear regression model describes the relationship between acetic acid content and independent variables as time of accelerated ageing (T) and coefficient of Kubelka-Munk (k/s). The equation of the fitted model is C(AA) = 1.0985 + 0.2119T – 3.6854k/s.

The R^2 parameter indicates that the model as fitted explains 96.70 % of the variability in acetic acid content. For formic acid content the equation of the fitted model is C(FA) = 0.299 + 0.0209b*. The R^2 parameter indicates that the model as fitted explains 34.40 % of the variability in formic acid content.

Low-molecular product such as acetic acid, have coherence with the colour information which is consequence of the accelerated ageing. Formation of acetic acid in the paper depends on the time of accelerated ageing and on number of chromophores in the paper.

REFERENCES

1. Carter A. C.: Journal Chem. Edu. *73*, 1160 (1996).
2. Unsworth J., Mitchell F.: IEEE Trans. Electr. Insul. *25*, 737 (1990).
3. Bayer M., Lind A., Koch H., Fischer J.: J. Pulp Paper Sci. *25*, 47 (1999).
4. Margutti S., Conio G., Calvini P., Pedemonte E.: Restaurator *22*, 67 (2001).
5. Malesic J., Kolar J., Strlic M.: *Proceedings of the Int. Conference Chemical Technology of Wood, Pulp and Paper*, p. 382 Bratislava 2003.
6. Strlic M., Selih V. S., Kolar J.: *Proceedings of the Int. Conference Chemical Technology of Wood, Pulp and Paper*, p.385, Bratislava 2003.
7. Trnkova M., Bukovsky V.: *Proceedings of the Int. Conference Chemical Technology of Wood, Pulp and Paper*, p.444, Bratislava 2003.
8. Shahani C. J., Harrison G.: *Works of Art on Paper, Books, Documents and Photographs: Techniques and Conservation.* London 2002.
9. Shahani C. J.: *Preservation Research and Testing Division, Library of Congress.* Washington. DC.
10. Shahani C. J., Hengemihle F. H., Weberg N., in: *Amer. Chem. Soc. Symposium Series 410, S. Historic Textiles and Paper Materials II: Conservation and Characterization, American Chemical Society* (Zeronian H., Needles L.eds.), p.63, Washington DC 1989.

11. Shahani C. J.: *ASTM Workshop on the Effects of Aging on Printing and Writing Papers*, ASTM. Philadelphia PA (1994).
12. Proniewicz L. M., Paluszkiewicz C., Wesenucha-Birczynska A., Majcherczyk H., Baranski A., Konieczna A.: J. Molec. Struc. *596*, 163 (2001).
13. Cedzova M., Vrska M., Szeiffova G.: Chem. Listy *99*, 442 (2005).
14. Cedzova M., Gallova I., Katuscak S.: Restaurator *27*, 35 (2006).
15. Cedzova M., Katuscak S.: Papir Celuloza *61*, 10 (2006).
16. Katuscak S.: Drev. Vysk. *24*, 33 (1984).
17. Katuscak S., Katuscakova G.: Holzforschung *41*, 315 (1987).
18. Kucera L. J., Katuscak S.: Holz-Farbe–Gestaítung, Lignum, Zurich, 43 (1992).
19. Katuscak S., Kucera L. J.: Wood Research *45*, 9 (2000).
20. Dence, C.W., Reeve D.W.: *Pulp bleaching. Principles and practice.* Tappi Press, Atlanta 1996.
21. Vives J. M. G., Escoda J. R. M., Guerra R. A., Hernandez L. A.: Restaurator *22*, 187 (2001).
22. Bukovský M.: Restaurator *20*, 77 (1999).
23. Baranski A., Lagan J. M., Lojewski T.: *Ageing and stabilisation of paper*, p.93 Ljubljana 2005.
24. Sjostrom E.: *Wood Chemistry.* Academic Press 2, New York 1993.
25. Havlinova B., Babiakova D., Brezova V., Durovic M., Novotna M., Belanyi F.: Dyes Pigm. *54*, 173 (2002).
26. Carter H.A.: J. Chem. Educ. *73*, 1068 (1996).
27. Van Der Reyden D.: JAIC *31*, 117 (1992).

L05 EFFECT OF STABILISATION OF PAPER WITH PIPERIDINE-BASED ANTIOXIDANT ON RECOGNISABILITY OF PRINTED BLACK CHARACTERS

JANA KAZÍKOVÁ, ATTILA SZITÁS, KATARÍNA VIZÁROVÁ, MICHAL JABLONSKÝ, FRANTIŠEK POVAŽANEC, SOŇA KIRSCHNEROVÁ and SVETOZÁR KATUŠČÁK

Institute of Polymer Materials, Department of Chemical Technology of Wood, Pulp and Paper, Slovak University of Technology in Bratislava, Radlinského 9, 812 37, Bratislava, Slovak Republic,
jana.kazikova@stuba.sk

Introduction

It is well-known that the visibility, recognisability and readability of any document depend on the contrast between text characters and background[1,2,3]. The question is – how to quantify, measure objectivelly and predict the visibility of characters of text and more generally of any information in a document. Objective method enabling to predict human-like, or antropomorphous visibility and recognisability of letters of characters on paper would be of great importance. If available, such method could be widely used in paper quality control, process development and optimizing, recycling and promoting of recycled papers, in optimizing stabilisation, deacidification, modification of properties, coating, encapsulation, paper splitting and other conservation technologies, measurement of effects of ageing and conservation processes of old books and archive documents; and last but not least, to improve the communication between papermaking and printing industry and their customers. In spite of this key importance, no generally accepted method is available at the time being.

Optical properties of both paper and the printed, written, drawn or painted characters change at processes of production, ageing, recycling, conservation[4–7] and utilization. These processes influence both the visibility and recognisability of characters on the paper. The question is how. How to measure the changes of the recognisability of character objectivelly and simultaneously via human-like manner to be able to predict the changes of antropomorphous visibility, recognisability, and readability? How to objectivise and predict human-like readable and perceived information content changes caused by processes of treating the paper documents?

Visibility or legibility of a letter, or a character or an information in a document is the property expressing the ability to be seen by human eye more or less quickly, correctly, distinctly from a certain distance. It is determined and influenced by several factors, generally comprising objective properties of documents (colour contrast, light intensity, character`s font face, size...) as well as subjective quality of human eye, illumination, geometry and other objective factors.

Recognisability of a character of information in a document is closely related to visibility, and could be defined as a measure of extractability of its exact meaning.

Readability – the quality of a document expressing the ability to be understood by a human observer or intelligent optical device (CCD camera, OCR scanner.) correctly.

The semantic hierarchy of the above mentioned terms from the viewpoint of their complexity is: visibility > recognisability > readability; It means, readability includes both the visibility of characters and their recognisability. Present conservation platforms and substances for mass conservation deacidification can change mechanical, chemical and optical properties and their stability and therefore also the visibility and recognisability of black letter or characters studied in this work.

The work was aimed at determining the effect of thermally induced accelerated ageing on antropomorphous recognisability and documenting application options of developed algorithm for quantifying an effect of a selected piperidine-based antioxidant on a change in the recognisability and its stability.

Experimental

Wood-containing paper with the grammage 45 g m^{-2}, surface pH: 5.6, consisting of 55 % of the mechanically bleached groundwood, 20 % of the bleached sulphate pulp, 15 % of the recovered fibres and 10 % of clay was used in experiments. The test paper was modified by 0.5% wt. solution of a piperidine-based antioxidant DAO3 in hexamethyl-disiloxane.

The used untreated paper had the following optical parameters: $L^*_B = 84.817$; $a^*_B = -0.666$; $b^*_B = 3.763$.

The white paper used for calibration (2) between subjective psychometrically measured recognisability and objective parameters, and as white reference point in Figs. 1. and 2., with the $R/R_0 = 1$, was white office paper Maestro Standard (Mondi Business Paper SCP, a.s.) with the following CIE colour parameters: $L^* = 95.52$; $a^* = 1.98$; $b^* = -3.64$.

The paper samples were exposed to the thermally-induced accelerated ageing following the ASTM D 6819-02 standard, in a thermostat up to 15 days at temperature 98 ± 1 °C, then air-conditioned according to the ISO 187 standard at temperature 23 ± 1 °C and the relative humidity RH = 50 ± 1 %.

The CIE total colour difference ΔE_{C-B} between the text character characters (L^*_C, a^*_C, b^*_C) and its background (L^*_B, a^*_B, b^*_B,) was calculated using the following equation:

$$\Delta E_{C-B} = \sqrt{(L^*_C - L^*_B)^2 + (a^*_C - a^*_B)^2 + (b^*_C - b^*_B)^2} \quad (1)$$

where

ΔE_{C-B} – the optical contrast as expressed through total colour difference in the CIE L^*, a^*, b^* system between a printed character/letter and its background.

$L^*_C = 28.915$; $a^*_C = 0.555$; $b^*_C = -0.56$ – the optical parameters of the printed characters or letters in the model test documents used for the experiments.

The subjectively perceived recognisability (R) was calculated[8] using the optical contrast expressed by total colour difference (ΔE_{C-B}) between black character (C) and white paper (B) by the following mathematical equation:

$$R = \left(1 - \left(\frac{\Delta E_{C-B} - 62.56}{62.56}\right)^2\right)^{0.42} \tag{2}$$

Relationships between the relative recognisability R/R_0 and ΔE_{C-B} were plotted, where:

R – recognisability of a black character (C) printed on modified or unmodified, aged or unaged paper background (B).

R_0 – recognisability of the black character printed on white calibration paper with the $L^* = 95.5$; $a^* = 1.98$; $b^* = -3.64$.

Results

Currently it is generally accepted that the visibility, recognisability and readability of any document depends on the contrast between text characters and the background[1]. This hypothesis was tested and the obtained results are shown in Figs. 1. and 2. as dashed lines (2). The paper samples were subjected to accelerated ageing, which changed the paper lightness (L^*), and the optical contrast ΔE_{C-B} between a printed character and the paper, as well as the relative recognisability (R/R_0). The relationship between the relative recognisability (R/R_0), the optical contrast (ΔE_{C-B}) and the paper lightness (L^*_B) is shown in Fig. 1. The relative recognisability of characters $R/R0$ has been related to the recognisability of the same black letters /characters on white calibration paper with the following optical parameters: $L^*_B = 95.52$; $a^*_B = 1.98$; $b^*_B = -3.64$.

In Fig. 1., also the visualisation of the effect of the constant decrease of a certain optical contrast $\Delta(\Delta E^*_{C-B}) = 5$ – can be seen, caused through a 15 days ageing of paper on the human-like recognisability of black letters on a typical white paper ($L^*_B = 85$), middle light ($L^*_B = 45$) and dark paper ($L^*_B = 34$); Fig. 1. represents also a difference between the relative recognisability based on so far accepted conceptions on a dependence of recognisability on optical contrast (line 1) and actually perceived recognisability[8] based on our psychometric measurements (line 2). According to the mentioned so far accepted conceptions, visibility, recognisability and readability of any document depends on the contrast between text characters and background[1]. Following the accelerated ageing (for 15 days at $98 \pm 1\ °C$), the optical contrast ΔE_{C-B} between character and background decreased by $\Delta(\Delta E^*_{C-B}) = -8.3\%$. Stemming from a simplified linear conception on dependence on the optical contrast, the character recognisability should decrease in the same extent, i.e. by $\Delta R/R_0 = -8.0\%$. Based on our measurements of calibration between subjective and objective evaluation using eq. (2) we calculated that the actually perceived/ antropomorphous change of recognisability kept almost identical in a lighter part of document.
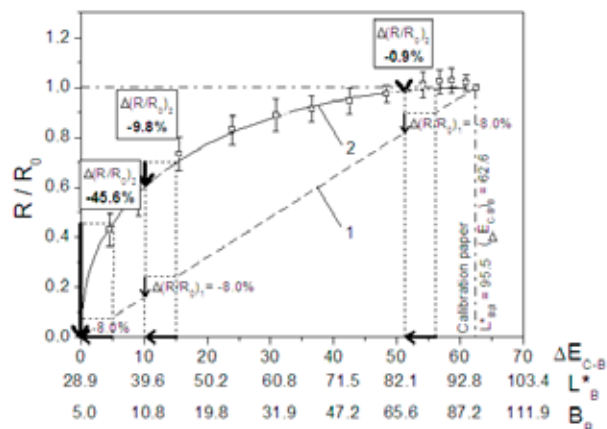
Fig. 1. **Visualisation of the effect of the constant decrease of the optical contrast $\Delta(\Delta E^*_{C-B}) = -5$ through the ageing of unmodified paper on the human-like recognisability of black letters on a typical white paper ($L^* = 85$), middle light ($L^* = 45$) and dark paper ($L^* = 34$); The relationship between the visually estimated relative recognisability index (R/R_0), and both the printed black character-paper optical contrast (ΔE_{C-B}) and the paper lightness (L^*_B); 1 – function based on the assumption of equivalency of the subjective relative recognisability and the optical contrast 2 – function according to equation (1); $\Delta R/R_0 [\%] = a$ relative decrease in recognisability related to the recognisability of the characters possessing the same black intensity colour in calibration paper with $L^*_B = 95.52$; $a^*_B = 1.98$; $b^*_B = -3.64$; Non-modified sample had the optical parameters: $L^*_B = 84.817$; $a^*_B = -0.666$; $b^*_B = 3.763$**

It follows from Fig. 1 that the hypothesis on dependence of visibility and recognisability on the optical contrast is not valid for white papers ranging from $L^* = 80$ to 95, i.e. for papers being the most important for the productiom, recycling and use of white, recycled paper for graphic and newprints usage, or other papers for printed documents production.

It can be seen in Fig. 1. that while in a light part of unmodified document or in light paper (from $L^*_B = 85$ to $L^*_B = 76$ and an optical contrast decrease by $\Delta(\Delta E^*_{C-B}) = -5$ units) the decrease in lightness does not cause any significant decrease in document characters visibility, the identical decrease of paper lightness and optical contrast (from $L^*_B = 45$ to $L^*_B = 40$ and $\Delta(\Delta E^*_{C-B}) = -5$ units, respectively) in a middle part leads to multiply decrease in recognisability (by $\Delta R/R_0 = -9.8\%$) and in document dark part with the lightness of $L^*_B = 34$ the same darkening means 45.6% loss of information ($R/R_0 = 0$).

What is the effect of antioxidant on human predicted change of visibility and recognisability?

We anticipated that the antioxidant could decelerate the paper ageing and yellowing during the ageing which, in turn, should lead to a change in the human predicted recognisability of characters in document. In Fig. 2., dependences of optical contrast and recognisability are shown for modified document with $L^*_B = 84.582$; $a^*_B = -0.586$; $b^*_B = 4.139$.
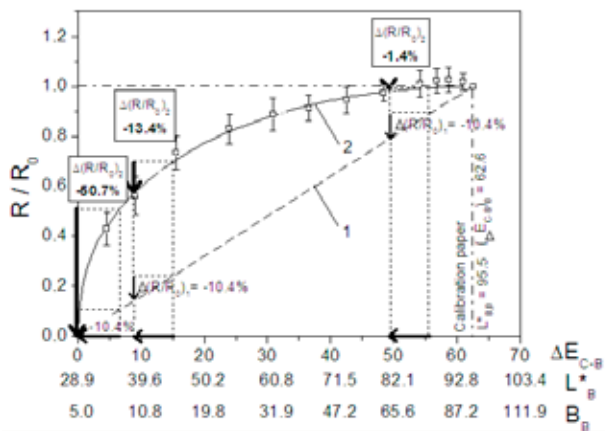
Fig. 2. **Visualisation of the effect of the constant decrease of the optical contrast $\Delta(\Delta E^*_{C-B}) = -6.5$ through the ageing of paper modified with the antioxidant DAO3 on the human-like recognisability of black letters on typical white paper ($L^* = 85$), middle light ($L^* = 45$) and dark paper ($L^* = 36$); The relationship between the recognisability index (R/R_0), the optical contrast (ΔE_{C-B}) and the paper lightness (L^*_B)**

Fig. 2. demonstrates the effect of ageing to a change in optical properties and recognisability of the paper modified by the used antioxidant. Comparing to Fig. 1. it is obvious that the effect of the antioxidant for recognisability is not significant. Using eq. (2) we came to a conclusion that antropomorphous change of recognisability in light document is −1.4 %. It is 7.4 times less than at recognisability according to so far accepted knowledge. The effect of the antioxidant thus lies in a mild decrease of antropomorphous recognisability after 15-days ageing.

What is the situation concerning a dark part of the document or dark documents from dark papers? If the ageing and antioxidant caused the same change of optical contrast, i.e. change in ΔE_{C-B} by 6.5 units, the actual human-perceived recognisability decreases due to the ageing by 13.4 %. As given by Fig. 2., a change in ΔE_{C-B} by 6.5 units from 15 to 8.5.

Conclusions

Generally it is believed that the visibility and recognisability of a document depend on optical contrast between the characters and the paper backround. The aim of this work was to test this hypothesis and to quantify the effect of accelerated ageing and paper modification with piperidine-based antioxidant on the visibility and recognisability of the black characters on paper.

It has been estimated that the hypothesis of a dependence of recognisability on the optical contrast failed – in very wide range of white papers. The dependence of recognisability is negligible in white paper documents. The less the recognisability of characters depends on the white papers the more meaningfull is the dependence in middle light paper documents and critically in dark paper documents.

The used antioxidant of piperidine type did not have meaningfull effect on paper stabilisation, neither against the changes of the paper optical properties nor the changes antropomorphous visibility and recognisability of printed information in a document caused by ageing.

REFERENCES

1. Pescio S., de Mattiello M., Álvarez R.: *Proceedings of the Interim Meeting of the International Colour Association,* p. 47, Porto Alegre 2004.
2. Eperjesi F., Fowler C. W., Kempster A. J.: Ophthalmic and Physiological Optics *15*, 561 (1995).
3. Rubin G. S., Legge G. E.: Vis Res, *29*, 79 (1988).
4. Barrow, W. J., Sproull, R. C.: Science *129*, 3356 (1959).
5. Malesic J., Kolar J., Strlic M.: *Proceedings of the Int. Conference Chemical Technology of Wood, Pulp and Paper*, p. 382-384, Bratislava 2003.
6. Strlic M., Selih V. S., Kolar J.: *Proceedings of the Int. Conference Chemical Technology of Wood, Pulp and Paper*, p. 385, Bratislava 2003..
7. Trnková M., Bukovský V.: *Proceedings of the Int. Conference Chemical Technology of Wood, Pulp and Paper*, p. 444, Bratislava 2003.
8. Szitas A., Jablonský M., Katuščák S.: Chem. listy *99*, 2008.

L06　ROLE OF AROMATICITY IN HUMIC SUBSTANCES DEGRADATION KINETICS USING NON-ARRHENIUS TEMPERATURE FUNCTIONS

JIŘÍ KISLINGER[a], FRANTIŠEK NOVÁK[b] and JIŘÍ KUČERÍK[a]

[a]*Institute of Physical and Applied Chemistry, Faculty of Chemistry, Brno University of Technology, Purkyňova 118, 612 00 Brno, Czech Republic,*
[b]*Institute of Soil Biology, Biology Centre of the Academy of Sciences of the Czech Republic, Na Sádkách 7, 370 05 České Budějovice, Czech Republic,*
xckislinger@fch.vutbr.cz

Introduction

The problem of global warming has been uncovered a long time ago. The attention of scientists and researchers in many fields is focused on possible reduction of greenhouse gases increase to the atmosphere. Such process requires principal understanding of carbon (C) stabilization in soils because the amount of organic matter stored in soils represents one of the largest reservoirs of organic carbon on the global scale. Unfortunately, the mechanisms for carbon stabilization in soils are still not perfectly clear and thus the maximal potential for C stabilization in soils remains unascertained[1].

Some important soil qualities, such as fertility or stability are directly related to its organic matter presence. Many functions of soil organic matter (SOM) are due to its stable fraction, the humified materials, and to its balance with the labile fractions. Altogether it affects, directly or indirectly, many physical, chemical and biological properties that control soil productivity and resistance to degradation. Changes in the quantity and quality of SOM and its equilibrium level depend on the interaction of several factors. As SOM enters and resides in soil, it is subjected to fundamental processes that alter its composition and quantity. These are e.g. humification, aggregation, translocation, erosion, leaching and mineralization[2]. Other changes in SOM content are related to changes in microbial biomass turnover because they reflect the balance between rates of microbial organic matter accumulation and degradation. However, SOM as a whole responds less quickly to changing soil conditions than microbial biomass. Therefore, the nature of the organic matter itself, rather than its concentration, may be more sensitive indicator of the changes in soil quality[3].

The main fraction of organic matter contained in soils, peats, sediments, low-rank coals and natural waters consists of humic substances (HS), which comprise a complex mixture of both aromatic and aliphatic moieties, having a large number of functional groups. Chemical and structural characteristics of HS are known to be better predictors of the rate of SOM turnover than SOM content itself[4].

Processes in condensed phase are extensively studied by thermoanalytical methods. Mechanisms of these processes are very often unknown or too complicated to be characterized by simple kinetic model. To describe their kinetics, of which we speak, the methods based on the single-step approximation are often used, either the model-free or model-fitting ones. It is generally recognized that the rate of the processes in condensed phase is a function of temperature (T) and conversion (α). The rate of the complex multi-step condensed-state process can be formally described as

$$\frac{d\alpha}{dt} = k(T)f(\alpha), \qquad (1)$$

where $k(T)$ is temperature function and $f(\alpha)$ conversion function. The temperature function in (1) is mostly considered to be the rate constant and the conversion function is considered to reflect the mechanism of the process[5,6]. With only for few exceptions, the temperature function is expressed by the well-known Arrhenius equation:

$$k(T) = A\exp[-\frac{E}{RT}], \qquad (2)$$

where A and E are considered the pre-exponential factor and the activation energy, respectively, T is the absolute temperature and R stands for the gas constant. It has been justified that, since $k(T)$ is not the rate constant and E cannot be mechanistically interpreted in the term of free energy barrier, there is no reason to be confined to the Arrhenius relationship and use of two non-Arrhenius temperature functions was suggested:

$$k(T) = AT^m \qquad (3)$$

$$k(T) = Ae^{DT}, \qquad (4)$$

where m and D are adjustable parameters[7]. The evaluation is carried out at fixed conversion. The isoconversional predictive procedure is huge and has already been successfully employed also in studying HS[8].

Experimental

Humic samples were extracted according to International Humic Substances Society (IHSS) procedures. They included:
- fulvic acid FA1, (B horizon of Spodo-Dystric Cambisol, mountain spruce forest, Boubín, Bohemian Forest, CZ), aromaticty: 29.0 %
- humic acid HA1, (Of horizon of Spodo-Dystric Cambisol, mountain spruce forest, Boubín, Bohemian Forest, CZ), aromaticty: 30.2 %
- humic acid HA2 (Of horizon of Podzol, mountain spruce forest, Trojmezí, Bohemian Forest, CZ), aromaticty: 46.5 %
- humic acid HA3 (Oxyhumolite lignite, Bílina mine, North Bohemia, CZ), aromaticity: 61.0 %

The aromaticity of samples was determined by ^{13}C LS NMR analysis. Thermogravimetric analyses of all samples in the dynamic air atmosphere (25 ml min^{-1}) were performed

using TA Instruments TGA Q 5000 IR. Approximately 2–3 mg of each sample were measured in open crucible at 7 different heating rates (0.5–15 K min^{-1}) from room temperature up to 600 °C.

The aim of this study lies in assessment of the stability of humic substances with different aromaticity degrees using two distinct equations, (3) and (4), as temperature functions. Such computed conversion times (having a meaning of stability – the higher the conversion time the higher the stability) serve for elucidation of role of aromaticity during the humic substances degradation.

Results

The thermogravimetric records (Fig. 1., TG) showed two or more steps of weight losses, the first one clearly attributable to loss of water (Fig. 1., part I), whereas others to degradation of organic molecules present in the humic matter (Fig. 1., part II). The latter steps were used to assess the stability of examined samples. Both the beginning as well as the end of such steps was verified by the first derivative of the TG curve (Fig. 1., DTG).
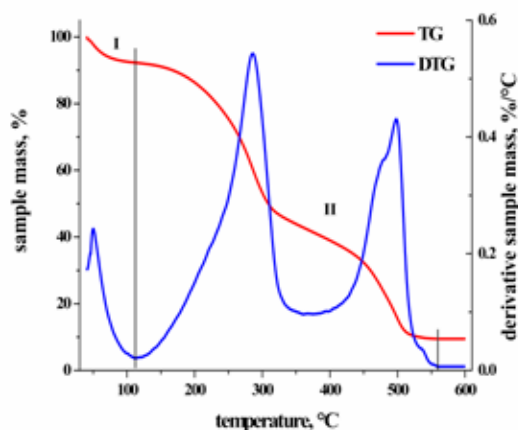
Fig. 1. **TG and DTG record of FA1, heating rate: 10 K min^{-1}**

The mass losses obtained at different heating rates were recalculated to conversion intervals (0–100 %). From this interval, several conversions were selected and for those the stabilities for 25 °C were calculated using the mathematical apparatus of integral isoconversional method at linear heating with two non-Arrhenius temperature functions. Values of conversion times served for comparison between samples with different aromatic degrees. Relative stabilities (RS) were determined as a ratio of conversion times for each conversion over the whole interval. The conversion time of sample FA1 being always the denominator (and thus the reference) because of its lowest aromatic degree. Such approach is usually used in evaluation of de-/stabilizing effect of various additives in many materials. In these cases the RS is called the protection factor with the value 1 having crucial meaning.[9] For our purposes the absolute values of RS are not of key relevance.

The induction periods (i.e. conversion times at 0% con-

version) of all samples regarding both temperature functions are summarized in Table I. Comparing the humic acids, it is obvious that the higher the aromaticity the higher the stability of the sample. The fulvic acid shows higher stability than its humic analogue having almost the same aromatic C content. This can be caused by the presence of structurally different aliphatic parts, more energy demanding for degradation than in HA1. Comparison of FA1 with HAs having the aromatic C content much higher shows that the previously described dependence is abided.

The comparison of stability curves in Figs. 2. and 3. implies the fact that both temperature functions are suitable for evaluation of thermo-oxidative stability of humic matter

Table I
Induction periods for 25 °C using both functions

Sample	IP using Eq. 3 [yrs]	IP using Eq. 4 [yrs]
FA1	0.166	0.067
HA1	0.064	0.030
HA2	0.275	0.107
HA3	1.651	0.429

because the patterns are much likely similar. A major difference can be seen in the values of RS, which is axiomatic considering the diverse temperature functions. But as stated above, if these values serve only for comparison between samples there is no reason to take the absolute values into account.
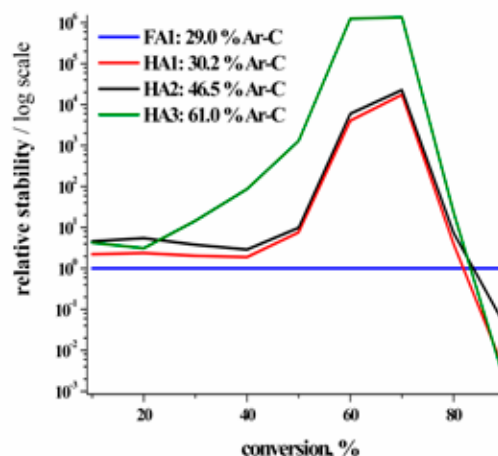
Fig. 2. **Relative stability curves of humic samples, Eq. (3)**

It is generally accepted that degradation proceeds from labile parts of humified matter to stable constituents represented by aromatic and heterocyclic cores. As suggested elsewhere[10], humic molecules tend to recombine and therefore the introduction of new, more stable molecules is probable.

Sample with the lowest aromaticity degree (FA1) has been selected as a reference and all other samples are compared to that one. It shows very low initial and also progressing
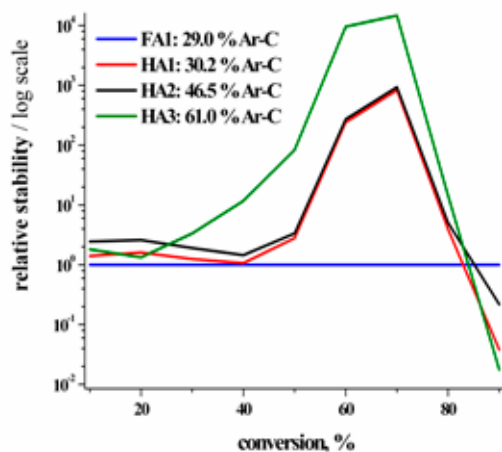
Fig. 3. **Relative stability curves of humic samples, Eq. (4)**

stability during the degradation process, meaning that first the high amount of aliphatic parts degrade. The RS of all other samples show from 70 % of conversion steep decrease indicating the presence of original or newly ocurring aromatic moieties in FA1. Stability of this sample is at the end of the degradation process the greatest of all. HA1 is of same origin as FA1 differing only in the soil horizon and in higher aromaticty, of course. Their stability progress is up to 40 % more or less the same. The stability differs from higher conversion, which can be explained by higher content of aromatic C in sample HA1 and also by distinct types of present aromatic molecules when comparing fulvic to humic acid. Although the aromaticty of sample HA2 is much larger when compared to HA1, their conversion patterns as well as stability values are very similar. Both of the samples are of soil origin, suggesting presence of analogous molecules. Slighter difference can be observed from 80 % of conversion. The explanation can lie in the fact that in HA2 very stable aromatic constituents are present and their degradation occurs in the last stage. Sample HA3 displays different shape of stability curve from the very beginning. Its stability increases until the conversion of 70 % is reached but then it decreases and at the end of the degradation process the stability is the lowest of all examined samples. A presence of absolutely different aromatic and ali-

phatic molecules in comparison with other samples is highly probable because of its origin. Aromatic molecules in lignitic humic acids are supposed to possess more extensive condensation. Thus the stability from 30 to 70 % exhibits extremely high values. The end of the degradation process shows utterly opposite progress than that of sample FA1 with the lowest aromatic C content.

Conclusions

Summarizing all the results, it can be seen that the aromaticity itself is not the absolute indicator of stability of humic materials and their origin has to be taken into account. But it can be helpful in assessment of soil organic matter depletion and help in development of remediation and soil restoration techniques. Moreover, the discovery of the right temperature function and approximation could contribute to modelling of C flux in natural systems.

REFERENCES

1. v. Lützow M., Kögel-Knaber I., Ekschmitt K., Matzner E., Guggenberger G., Marschner B., Flessa H.: Eur. J. Soil Sci. *57*, 426 (2006).
2. Dick W. A., Gregorich E. G., in: *Managing Soil Quality: Challenges in Modern ,* CABI Publishing, Oxon 2004.
3. Dell'Abate M. T., Benedetti A., Brookes P. C.: J. Sep. Sci. *26*, 433 (2003).
4. Hayes M. H. B., MacCarthy P., Malcolm R. C., Swift, R. S.: *Humic Substances II. In Search of Structure.* Wiley, New York 1989.
5. Šimon P.: J. Therm. Anal. Cal. *88*, 709 (2007).
6. Šimon P.: J. Therm. Anal. Cal. *82*, 651 (2005).
7. Šimon P.: J. Therm. Anal. Cal. *79*, 703 (2005).
8. Válková D., Kislinger J., Pekař M., Kučerík J.: J. Therm. Anal. Cal. *89*, 957 (2007).
9. Cibulková Z., Šimon P., Lehocký P., Balko J.: Polym. Degrad. Stabil. *87*, 479 (2005).
10. Kučerík J., Kamenářová D., Válková D., Pekař M., Kislinger J.: J. Therm. Anal. Cal. *84*, 715 (2006).

L07 NMR SPECTROSCOPY OF MINOR COMPOUNDS IN WINE A COMPARISON OF DIFFERENT PRE-CONCENTRATION METHODS

MILAN MAZUR, KATARÍNA FURDÍKOVÁ, MICHAL KALIŇÁK, MARIÁN VALKO, VLADIMÍR ŽÚBOR and NAĎA PRÓNAYOVÁ

Faculty of Chemical and Food Technology, Slovak Technical University, Radlinského 9, 812 37 Bratislava, Slovak Republic,

milan.mazur@stuba.sk

Introduction

The certification of the origin and geographical indications of food products has aroused increasing interest due to the introduction of European regulations for protection of agricultural products in the common market.[1–6]

Wine is a complex mixture of several hundred compounds present at different concentrations. The dominant ones are water, ethanol, glycerol, sugars, organic acids and various ions. Besides water, ethanol and glycerol, the other compounds like aliphatic and aromatic alcohols, amino acids and phenolic compounds are present at much lower concentrations[5]. Chemical analysis of complex mixtures like wine is becoming more important due to general endeavour to achieve adequate production quality. For wines particularly, differentiation according to wine variety, geographical origin and the year of production is of importance also in authenticity determination.[1–3]

High-resolution NMR spectroscopy has an outstanding position in the field of chemical analysis of food products because it is non-destructive, selective, and capable of simultaneous detection of many low molecular mass components in complex wine mixture[5]. The sample preparation for NMR spectroscopy is relatively simple and less time consuming. Another advantage of NMR spectroscopy is the possibility of detecting the magnetic resonance of different nuclei present in a molecule in different electronic and spatial environments. ^1H and ^{13}C NMR spectroscopy can successfully be used for detection of sugars, organic acids, anthocyans and amino acids present in wine as well as differences in their composition originating from different geographical area and can be used as a fingerprint for the monitoring of European wines.[5–10] Unfortunately, the weak signals of the minor compounds in NMR spectra are overlapped by the signals of other compounds present and especially by the dominant signals of water, ethanol and glycerol. For example, the amino acids are normally present in wine only at very low concentrations (in the range of 1–150 $mg\,dm^{-3}$) and therefore various techniques for the pre-concentration of the wine samples are needed.[8–10]

This contribution describes the comparison of three methods of sample preparation namely vacuum concentration, freeze-drying and argon-flow concentration with the results obtained from untreated wine for characterization of minor compounds in Slovak Chardonnay white wine by ^1H NMR spectroscopy.

Experimental

Apparatus

All ^1H NMR spectra were recorded on a Varian INOVA 600 MHz NMR spectrometer, which is located at Faculty of Chemical and Food Technology (Department of NMR and mass spectrometry, Bratislava, Slovakia), with a 5.00 mm indirect detection pulsed field gradient probe operating at 600 MHz for ^1H nuclei. The temperature during all experiments was 25 °C.

Chemicals

Deuterium oxide (99.9 %) was purchased from Aldrich and it contained 0.05% sodium 3-(trimethylsilyl)propionate –2,2,3,3,-d$_4$ (TSP) that served as an internal standard for chemical shift 0.0 ppm).

Sample preparation

Chardonnay white wine (Small Carpathian wine-growing region, Slovakia, vintage 2005) was selected for all NMR experiments. Four different groups of wine samples were prepared as follows:

- Wine samples were not pre-concentrated. In this direct analysis of wine samples 0.5 ml of wine was mixed with 0.1 ml D_2O for NMR field/frequency lock.
- Wine samples were pre-concentrated by vacuum-distillation. 5 ml of wine was pre-concentrated by vacuum distillation using rotary evaporation unit for 6 hours. The concentrate was dissolved in 1 ml of D_2O and 0.6 ml was used for measurement.
- Wine samples were pre-concentrated by freeze-drying. Again 5 ml of wine was frozen in liquid nitrogen and freeze-dried for 20 hours. The lyophylisate was dissolved in 1 ml of D_2O and 0.6 ml was used for measurement.
- Wine samples were pre-concentrated under argon-flow. Again, 5 ml of wine was dried under argon-flow for 2 hours until there was no further liquid in the sample. The dried sample film was dissolved in 1 ml of D_2O and 0.6 ml was used for measurement.

After the freeze and argon-flow- drying, close attention should be given to minimise the contamination of the dried sample with atmospheric humidity.[4,6–9] The pH values of all prepared samples were found in the interval of 3–4.

Measurement

^1H NMR spectra were acquired in 5 ml NMR tubes with and without the suppression of strong signals by presaturation. For suppression of large water signal the presaturation pulses (Varian pulse sequence PRESAT) were applied to irradiate the water signal at 4.80 ppm.

Results

It is known that ^{1}H NMR resonances of amino acids together with signals of succinic acid, glycol and buthylene glycol can be used to differentiate wines according to the wine variety, geographical origin and year of production.[3,5–10] In the present paper a different technique of the pre-concentration of the Chardonnay white wine has been investigated.

Fig. 1. shows the ^{1}H NMR spectra of the wine sample that was directly analyzed without any pre-concentration. The signal assignment in ^{1}H NMR spectra of wine samples was done according to literature[5–10] as follows: valine at 1.05 ppm, butylene glycol at 1.13 ppm, ethanol (CH₃) at 1.17 ppm, lactic acid 1.35 ppm, alanine at 1.49 ppm, isoleucine at 2.01 ppm, acetic acid/acetates at 2.04 ppm, proline at 2.34 ppm, malic acid at 2.63 and 2.82 ppm, succinic acid/succinates at 2.66 ppm, lysine at 3.04 ppm, citruline at 3.13 ppm, arginine at 3.26 ppm, ethanol (CH₂) at 3.64 ppm, glycerol (CH₂) at 3.62 ppm, glycerol (CH) at 3.76 ppm, tartaric acid at 4.79 ppm and water at 4.80 ppm.
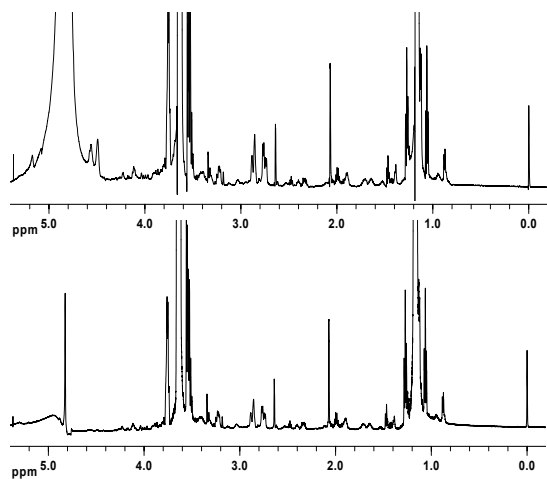
Fig. 1.   **Part of 1H NMR spectra of white wine (Chardonnay, Small Carpathian wine-growing region, Slovakia, 2005). Spectra were acquired: (a) without suppression of strong signals, (b) with suppression of water signal by presaturation. Wine samples were not pre-concentrated (direct analysis of wine samples). For assignment of selected signals of amino acids see text**

It is obvious that ^{1}H NMR spectra of wine are very crowded and many signals are overlapping (see Fig. 1.). Because of the different concentration levels of the particular compounds the signal intensities can vary by the factor of 20 or more. Therefore the small signals of minor compounds are overlapped by the signals of dominant compounds (water, ethanol and glycerol) and the correct assignment is very problematic. In accord with literature data[5–10], the region of the spectrum between 0.5–2.5 ppm contains the signals from many species including ethanol, acetic acid and acetates. Strong signal of ethanol at 1.17 ppm shows overlapping and it causes difficulties in the assignment of this region. Between 2.5–5.5 ppm the spectrum shows signals related to the principal organic acids present in wine (malic,

sucinic, lactic and tartaric). However the tails of the dominant frequencies of ethanol at 3.64 ppm and glycerol at 3.62 and 3.76 ppm obscure the weak signals in the vicinity of the strong ones. This causes problems with the assignment of ^{1}H signals in the region between 3.6–4.8 ppm, in which the signals of (CH₂) protons of amino acids and the signals of sugars are expected[7,9].

Successful suppression of intense signals improves the clarity of the spectrum and the signal to noise ratio. With the increasing amplification of the vertical scale the baseline near the strong signals is strongly affected by their tails in the spectrum without suppression, whereas in the case of suppression their influence on the surrounding is significantly reduced. Nevertheless, when using the signal suppression techniques we have to be aware that some information from the spectra close to the suppressed signals may be lost[9], because suppression causes "holes in the spectrum". The penalty is not significant considering the extra amount of information obtained.

It is common to use some kind of pre-concentration technique in the preparation procedure[4,6-9]. Most prevalent techniques are vacuum-distillation using rotary evaporation unit, lyophilization and drying under nitrogen-flow. Concentrated samples are obtained that contain not only the compounds of interest but also some portion of major constituents that may cause the signal shifting and/or line broadening[9].
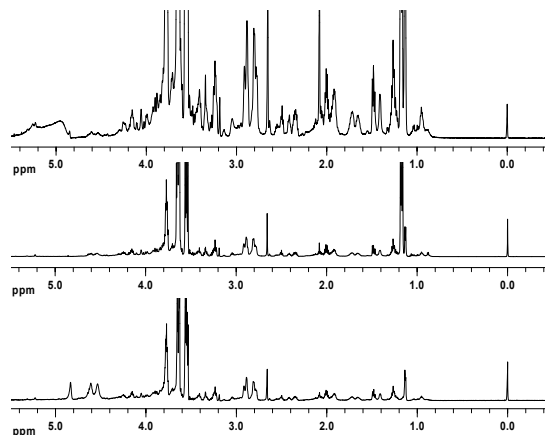
Fig. 2.   **Part of 1H NMR spectra of white wine (Chardonnay, Small Carpathian wine-growing region, Slovakia, 2005). Spectra were acquired with suppression of water signal by presaturation. Wine samples were pre-concentrated: (a) by vacuum-distillation, (b) by freeze-drying, (c) under argon-flow. For assignment of selected signals of amino acids see text**

Fig. 2. shows ^{1}H NMR spectra of Chardonnay wine samples, which were pre-concentrated by (a) vacuum-distillation, (b) freeze-drying and (c) argon-flow. The water signal (at 4.80 ppm) was suppressed by presaturation. The ^{1}H spectra of wine samples pre-concentrated by vacuum-distillation and freeze-drying (Fig. 2.a and b) still show signals at 1.17 and 3.64 ppm that demonstrate a low quantity of ethanol remained in these samples. This is in accordance with litera-

ture data.[6–10] Differences in signal intensity were also observed especially for compounds such as acetic acids and acetates at 2.04 ppm when compared to the ^{1}H spectrum of wine without pre-concentration (see Fig. 1.). The drying of Chardonnay wine by argon-flow revealed compounds between 1.0–1.5 ppm in the ^{1}H NMR spectrum (Fig. 2.c). It is clear that the ethanol signals were diminished in the spectrum of such pre-concentrated sample. As shown in literature[7], this allows the determination of butylene glycol and alanine at 1.13 and 1.49 ppm. The presence of significant resonance of lactic acid at 1.35 ppm (due to malolatic fermentation) makes difficulties to assign alanine signals. Between 2.0–3.4 ppm peaks from organic acids, arginine and proline are also observed in the ^{1}H NMR spectrum of the Chardonnay wine samples pre-concentrated by argon-flow. The 3.5–4.0 ppm region of the spectrum still shows a strong contribution of the glycerol. Then the spectral distinction of carbohydrate is extremely difficult due to peak overlap[7].

As cited in the literature[6–10], even after more than two days of freeze-drying some water and ethanol remained in the lyophylisate. Because prolonged drying is not acceptable for a procedure that should required as little time as possible, the limit ca 20 hours is a good compromise between acceptable time of sample preparation and losing sensitivity in NMR measurement. The conditions of vacuum-distillation and mainly during freeze-drying are not easily controlled and the temperature and pressure must be well monitored in order to reach a good state of reproducibility[7,9]. In vacuum-distillation, freeze-drying and argon-flow-drying it is not possible to make quantitative analysis of the volatile compounds due to their evaporation[7,9]. In complex mixture such as wine, care should be taken to pH, which may influence considerably the chemical shifts[9]. Attention should also be paid to the concentration of paramagnetic species in the wine samples.

Conclusions

High field NMR spectroscopy has been shown to be a promising method for the non-destructive analysis of minor components in wine. However, the direct analysis of minor compounds such as amino acids in wine samples by ^{1}H NMR is limited by overlapping of their weak signals by strong signals of dominant compounds (water, ethanol and glycerol).

In the wine samples pre-concentrated by vacuum-distillation (for 6 hours) a low quantity of water and ethanol, but relative high glycerol concentration still remained in the sample. The same is true for the freeze-dried samples and additionally this process is relatively long (about 20 hours) and its reproducibility is affected by many factors. Diminution of the ethanol signal was observed in ^{1}H NMR spectra of the wine samples, which were dried under argon-flow. Unfortunately, a relative high quantity of glycerol is still present in the sample even using this technique. The argon-flow drying shows advantages in the identification of compounds present as minor constituents and it is less time consuming (ca 2 hours).

REFERENCES

1. Košir I. J., Kocjančič M., Ogrinc N., Kidrič J.: Anal. Chim. Acta *429*, 195 (2001).
2. Ogrinc N., Košir I. J., Kociancič M., Kidrič J.: J. Agric. Food Chem. *49*, 1432 (2001).
3. Ogrinc N., Košir I. J., Spangenberg J.E., M., Kidrič J.: Anal. Bioanal. Chem. *376*, 424 (2003).
4. Košir I. J., Lapornik B., Andrašek S., Wondra A. G., Vrhovšek U., Kidrič J.: Anal. Chim. Acta *512*, 277 (2004).
5. Košir I. J., Kidrič J.: Anal. Chim. Acta *458*, 77 (2002).
6. Brescia M. A., Caldaroda V., De Giglio A., Banedetti D., Fanizzi F. P., Sacco A.: Anal. Chim. Acta *458*, 177 (2002).
7. Amaral F. M., Caro M. S. B.: Food Chem. *93*, 507, (2005).
8. Košir I. J., Kidrič J.: Analusis *26*, 7797 (1998).
9. Košir I. J., Kidrič J.: J. Agric. Food Chem. *49*, 50 (2001).
10. Brescia M. A., Košir I. J., Caldaroda V., Kidrič J., Sacco A.: J. Agric. Food Chem. *51*, 21 (2003).

L08　HYDROPHOBIZATION OF PAPER BY VAPOURS IN N₂ PLASMA AT ATMOSPHERIC PRESSURE

MILAN MIKULA, ZUZANA JAKUBÍKOVÁ and VIERA JANČOVIČOVÁ

Faculty of Chemical and Food Technology STU, Radlinského 9, 812 37 Bratislava, Slovak Republic,
milan.mikula@stuba.sk

Introduction

Increasing demands for new materials and solutions in printing and packaging industry cause continuous innovation in a growing market. Paper and cellulosic materials are still promising candidates for flexible materials provided suitable properties including barrier ones such as water repellence and grease resistance[1]. Other demands are focused in restoring of naturally aged papers, documents and books in archives heritage to save and stabilize them[2].

Surface modification like hydrophobization, strengthening or stabilization of paper/cellulose can be achieved by standard coatings or also by several chemical vapours deposition (CVD) techniques[1–4] mostly enhanced by plasma (PECVD) or using plasma polymerization. Plasma deposited films have several advantages: compact layers are pinhole-free, chemically inert, insoluble, mechanically tough, thermally stable and coherent and highly adherent to variety of substrates[1]. However, often thin inhomogeneous and discontinuous (island type) coatings are produced by plasma assisted deposition or grafting. Despite of just the top surface modification the surface energy is changed considerably[3,4].

Low-pressure plasma treatment is not convenient to treat common paper, because of the vacuum problems and long and expensive process. So, the atmospheric pressure discharges are preferentially used, particularly the corona discharge and several types of dielectric barrier discharges (DBD).[4–6] Next advantages of atmospheric discharges are a high effectivity of free radical, metastables and excimers creation and the ability of high rate and large scale of technological treatment. The energy of the plasma breaks the molecular bonds on the surface of the substrate. The broken bonds then recombine with the free radicals from the plasma bulk to form additional functional groups on the film surface, where grafting, polymerization or crosslinking can occur. In the presence of oxygen, the high speed oxidation occurs, that results in high surface energy, polarity, wettability, but also in degradation[6]. Under special conditions plasma etching can be applied to cleaning or even to thinning the paper. Thinning the cellulose it can convert to a low energy hydrophobic surface[7]. However, hydrophobization is mostly made by fluorinating thin layer, e.g. with fluorotrimethylsilane[3], CF_4, SF_6 or C_4F_8.[1–4]

Also organosilicon compounds (particularly hexamethyldisiloxane HMDSO) are used to achieve hydrophobization of paper/cellulose[3,5,8], where the presence of a crosslinked macromolecular structure, based on $Si-O-Si$ and $Si-O-C$ linkages was detected. Implanted functional groups (as $-Si(CH_3)_x$) at the surface layers of the paper substrates are chemically linked mainly to the lignin component on the paper[3]. Water absorption of papers was significantly reduced (from hundreds to tens $g\,m^{-2}$ of water) and the contact angle increased from $<15\,°$ to $>120\,°$ while the strength properties and brightness of the papers remained practically unaffected.

Plasma has been already used in the restoration of naturally aged paper, focusing on sterilization, cleaning and deacidifying books as well, by using alkaline plasma (nitrogen, ammonia) and strengthening them by a grafting and coating by a plasma polymerization[2,9].

In this work, we investigate the hydrophobization of different papers by vapours of HMDSO and 3 carbohydrates activated in N₂ plasma at atmospheric pressure in 2 manners.
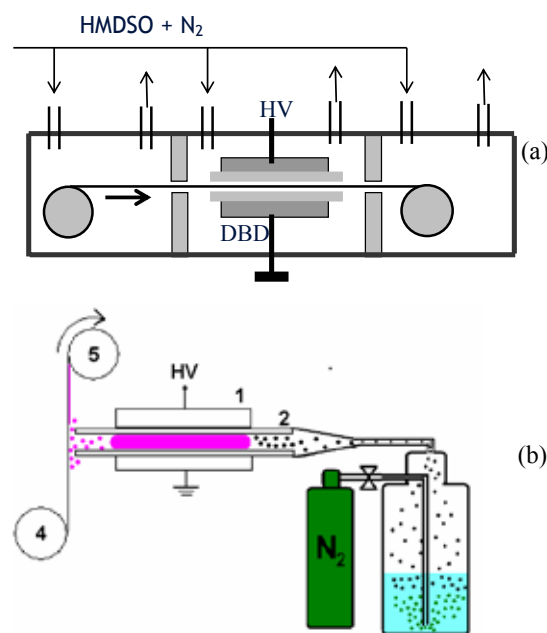
Fig. 1.　**Paper treatment inside DBD (a) and in down-stream after-DBD (b) plasma**

Experimental

- Two techniques of plasma treatment of papers were used. *(i)* The volume dielectric barrier discharge (DBD, 15 kV, 5 kHz) in standard configuration (Fig. 1.a), where the treated paper is going directly through the plasma of the mixture of N₂ and vapours, everything inside the air protective chamber ("inside-DBD" regime). *(ii)* The plasma mixture of N₂ and vapours is created in DBD and is blown onto the untreated paper passing 2 mm near the jet in common air atmosphere (Fig. 1.b, "after- DBD" regime).
- Three different paper sheets were used as substrates: cellulosic Whatman (standard filter paper, No. 1001-917, England, 90 g m⁻², thickness 280 mm), newsprint paper (NP, simulating acidic papers from 19–20ᵗʰ century,

45 g m^{-2},Vetrni, Czech. Rep.) and common office copy paper (CP, woodfree, white, 80 g m^{-2}, Europapier)

- 4 different monomers: hexamethyldisiloxane (HMDSO), n-heptane, cyclohexane and toluene were used as vapours in a mixture with nitrogen created by percolating of nitrogen through the bottle of liquid monomer.
- Paper properties were characterized by 5 ml water drop imbibition using CCD camera (SEE software 6.1, MU Brno, Czech.Rep.,) by FTIR spectroscopy (Excalibur, FTS 3000 MX, Digilab, USA, resolution 4 cm^{-1}) with total reflection (ATR) technique (25 reflections KRS-5 crystal, 45 °), and by water adsorption measurement using classical McBain balances with quartz spiral (1,230 mm g^{-1}).
- Aging stability of the modified paper was tested by artificial accelerated thermal aging according new method of Begin-Kaminska (5 days in closed bottle at 100 °C, RH 50%)[10]

Results

The papers treated in mixture plasma of nitrogen and vapours exhibited hydrophobic character as was evident from icreasing water contact angles up to 120 ° already in short exposition times Table I. However, when the water drop imbibition occurs the contact angle is not relevant parameter because of non stable drop. The changes to hydrophobic character can be better evaluated by imbibition (soaking) kinetics (Fig. 2.).

Table I
Contact angles [°] of water drop at initial and plasma treated paper surfaces, after-DBD, 60 J cm^{-2}

Papers	Initiale surface	Pure N$_2$	HMDSO	n-heptane	Cyclo-hexane	Toluene
Whatm.	n*	n*	122	90	110	105
NP	65	85	119	100	106	105
CP	85	75	120	102	105	110

n* – nonmeasurable

The flow rate of N$_2$ through the liquid monomer (HMDSO) was optimized to a value of 3.8 dm^3 min^{-1} for standard inside-DBD regime and 6.8 dm^3 min^{-1} for after-DBD regime.

Drops volumes for soaking experiments were round 5 ml and the volume of spherical cap, *V,* was calculated from the sessile drop radius *r* and height *h* and contact angle q:

$$V = \pi h^2(3r-h)/3 \qquad h = r(1-\cos\theta) \qquad (1)$$

The rate of imbibition (in ml s^{-1}) was calculated from the slope of imbibition kinetics (Fig. 3.), where some minimum was achieved for inside-DBD. It is caused by creation/degradation balance inside the plasma. Stronger hydrophobization was achieved by after-DBD, however it is less effective energetically (10 times higher exposition) than inside-DBD,

a)

b)
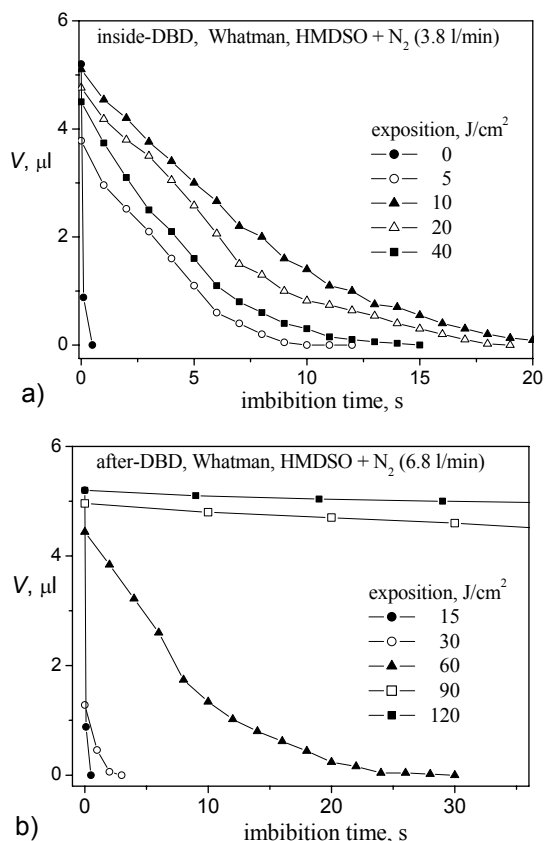
Fig. 2. **Time evolution of sessile water drop volume for Whatman and HMDSO and different expositions, for inside-DBD (a) and after-DBD (b) regimes**
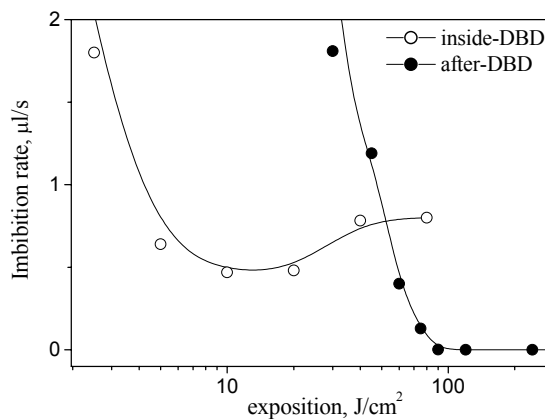
Fig. 3. **Exposition dependence of imbibition rates for Whatman treated inside-DBD and in after-DBD (N$_2$/HMDSO)**

and some problems could be in physical bonding of coating to the paper. So, the exposition was optimized to 10 J cm^{-2} for inside-DBD and to 80 J cm^{-2} for after-DBD.

Other three monomers (n-heptane, cyclohexane and toluene) were applied to treat papers just in optimized exposition doses. The level of hydrophobization correlates with reverse rate of imbibition, that is the imbibition time of 1 ml,
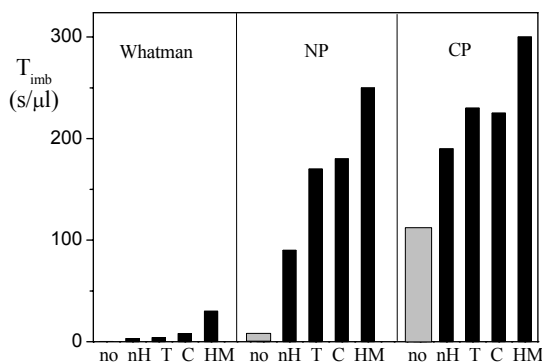
Fig. 4. **Water drop imbibition time for different vapours and treated papers in after-DBD (no – initial paper, nH – n-heptane, T – toluene, C – cyclohexane, HM – HMDSO)**
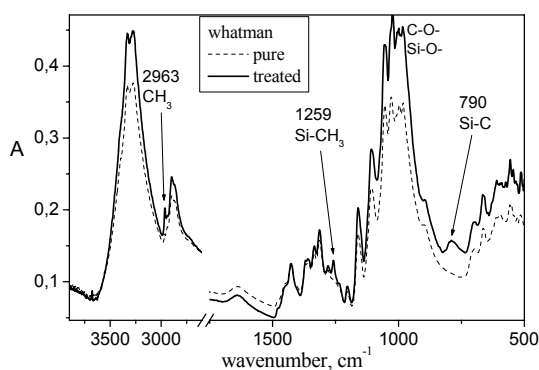
Fig. 5. **25-reflection ATR-KRS-5 IR spectra of pure and modified Whatman (after-DBD, HMDSO, 6.8 dm^3 min^{-1})**

T_{imb} [s ml^{-1}]. Calculated T_{imb} from experimental data of imbibition kinetics are shown in Fig. 4. for all vapours and substrate materials used.

The level of hydrophobization is very different for different papers, because of big differences of initial materials including wetting and roughness. The hydrophobization is most effective in case of newsprint paper (NP) and generally using HMDSO. However, the data dispersion is very high (up to 30 %), because of materials inhomogenity, DBD instabilities and inhomogenities and droplet soaking errors.

The changes of absorption IR spectra (surface ATR technique) of treated paper surfaces were generally very small. It means that very thin surface layer of paper is affected or very thin deposited layer is created, considering paper porosity. In the most successful case of HMDSO, some new functional groups are readable in FTIR spectra, Fig. 5.

The hydrophobized papers exhibited interesting performance after artificial aging. Namely in the case of inside-DBD and at long time expositions the aging causes considerable increase of hydrophobic character, probably because of recombination (and crosslinking) of long live free radicals created in plasma during long exposition.

Despite of noticeable hydrophobization in soaking process, adsorption properties of papers hydrophobized in both

manners were changed just a little, Fig. 6. The adsorption was performed at 25 °C, however, it is not typical isotherm, because of relatively quick increase of RH (1 % min^{-1}).

If slower increase were applied (0.1 % min^{-1} – equilibrium regime), the curves were nearly identical with the non-treated Whatman paper. It means that the long-term water sorption maintained unchanged, while the penetration rate was lowered due to hydrophobic surface.

It indicates that the paper porosity did not changed practically with the hydrophobization processes. Probably, the hydrophobic coating is very fine, discontinual, with an island-like character, and the thickness of coating as well as the islands dimensions are in nanometer scale.
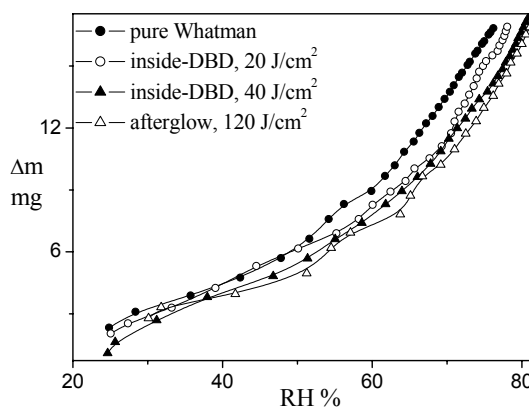
Fig. 6. **Adsorption kinetics of modified papers at 25 °C (RH increase rate: 1 % min^{-1}, samples weight: 180 mg)**

Conclusions

Different papers were continuously modified/hydrophobized by dielectric barrier discharge (DBD), inside DBD and down stream (after-DBD), using nitrogen as working gas with four organic vapors (including hexamethyldisiloxane, HMDSO). Modified papers were characterized by water imbibition (soaking), sorption and penetration kinetics and by absorption FTIR spectroscopy (surface sensitive ATR techniques).

The levels of hydrophobization of papers are very different for different papers and vapours, because of big differences of initial materials including wetting and roughness. The hydrophobization was the most effective using HMDSO and good noticeable for newsprint paper (NP) and Whatman. However, the data errors were very high (30 %) due to paper surface inhomogenities and instabilities of DBD that ought to be more controlled.

REFERENCES

1. Vaswani S.: Dissertation, Georgia Inst.of Technol., USA 2005.

2. Vohrer U., Trick I., Bernhard J., Oehr C., Brunner H.: Surface and Coatings Technol. *142*, 1069 (2001).

3. Navarro F., Davalos F., Denes F., Cruz L. E., Young R. A., Ramos J.: Cellulose *10*, 411 (2003).

4. Kloc P., Sťahel P., Buršíková V., Brablec A., Navrátil Z., Šíra M., Janča J.: Czech. J. Phys. *56*, 1345 (2006).

5. Trunec D., Navrátil Z., Sťahel P., Zajíčková L., Buršíková V., Cech J.: J. Phys. D: Appl. Phys. *37*, 2112 (2004).

6. Mikula M., Jakubíková Z., Zahoranová A.: J. Adhesion Sci. Technol. *17,* 2097 (2003).

7. Sapieha S., Wertheimer M. R.: *Application of plasma microtoming in paper science. Proc. of Int. Paper Physics Conf.*, Kailua Kona, USA (1991)

8 Šíra M., Trunec D., Sťahel P., Buršíková V., Franta D.: Czech. J. Phys. *56*, 1377 (2006).

9 Havermans J.: Abbey Newsletter *19*, 1 (1996).

10 Bégin P. L., Kaminska E.: Restaurator *23*, 89 (2002).

L09 FLUORESCENCE STUDY OF POLYSACCHARIDE IN DILUTE AQUEOUS SOLUTION

FILIP MRAVEC[a,b], TEREZA HALASOVÁ[b], MILOSLAV PEKAŘ[b] and VLADIMÍR VELEBNÝ[a]

[a]*CPN Ltd, Dolní Dobrouč 401, 561 02 Dolní Dobrouč, Czech Republic,*
[b]*IPAC FCH BUT, Purkyňova 118, 612 00 Brno, Czech Republic,*
mravec@fch.vutbr.cz

Introduction

During the last ten years, hyaluronan molecule rises in his importance. Due to its high biocompatibility and its common presence in the extracellular matrix of tissues, hyaluronan is gaining popularity as a biomaterial scaffold in tissue engineering research. Its modification can fortify hyaluronan's unique properties and opens a new fields for application this polysaccharide.

One of the most sensitive, progressive, and modern methods successfully used in investigation of polymer surfactant, is fluorescence spectroscopy. Widely used fluorescence probe method looks useful in our research; because of it contains additional information about investigated system – micellar properties, polarity, fluidity, dimensions.

We hope we are able to contribute with our results to clarification-complicated relations in this interesting system.

Experimental

Sodium hyaluronate and its derivatives (Fig. 1.) were obtained from CPN Ltd. (Dolní Dobrouč, Czech Republic). Details on the synthesis of derivatives have been published elsewhere[1]. Hyaluronate was of the molecular weight around 500 kg mol^{-1}.

All derivatives have the molecular weight around 500 kg mol^{-1}, and their substitution degrees were in the range from 10 to 70 %. Substitution degree is defined as the ratio of the mol of substituents per mol of the disaccharide unit, e.g. SD 100 % means one alkyl chain per each disaccharide unit in the hyaluronate chain. All the molecular parameters were determined and provided by the producer. The molecular weights were determined by SEC-MALLS and the substitution degree is defined from the ^{1}H NMR spectra[1]. The hyaluronate samples were dissolved in doubly distilled water
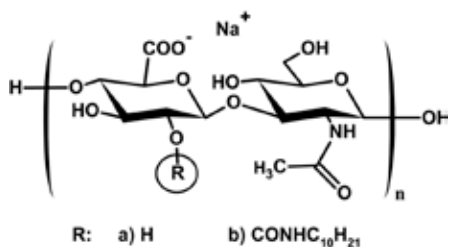
to the concentration 5 g dm^{-3}. This stock solution was stabilized by addition of sodium azide (p.a., Lachema) in final concentration 10^{-3} mol dm^{-3}.

The stock solution of pyrene (purchased from Fluka, GmbH; *for fluorescence grade*) was prepared in acetone. Probe stock solution was introduced into a vial and acetone was evaporated. The concentration of the probe in final samples was set to 5×10^{-6} mol dm^{-3}. The stock solution of HA or hHA was introduced into the vial with the probe, diluted to the desired concentration, and the resulting solution was sonicated for 4 hours and stored during next 20 hours. The fluorescence emission spectra were monitored with a luminiscence spectrophotometer (AMINCO-Bowman, Series 2) at 293.15 ± 0.1 K. The excitation and emission slit widths were set to 4 nm, and the excitation wavelength was 335 nm.

The experimental data, i.e. the pyrene I_1/I_3 ratio (y) dependency on concentration (x), were evaluated using non-linear fitting with Boltzman's curve containing four parameters – the maximum (a), the minimum (b), the inflex point (x_0), and the width of the step change (Δx) (Equation 1).

$$y = \frac{a-b}{1+e^{x_0 - x/\Delta x}} + b \qquad (1)$$

The stock solution of acridine orange (AO, purchased from Sigma-Aldrich, Co.; hydrochloride hydrate) was prepared in distilled water. Probe stock solution was introduced into after addition of HA or hHA stock solutions. The concentration of the probe in final samples was set to 5×10^{-6} mol dm^{-3}. The resulting solution was simiraly treated as pyrene's samples. The fluorescence emission spectra were monitored with a luminiscence spectrophotometer (AMINCO-Bowman, Series 2) at 293.15 ± 0.1 K. The excitation and emission slit widths were set to 4 nm, and the excitation wavelength was 492 nm.

Acridine orange is a much-studied member of a class of cationic dyes whose planar molecules aggregate in aqueous solution to cause concentration-dependent spectral changes (metachromasy).[Y] Direct evidence for the aggregation of AO has been obtained from proton chemical shifts. The concentration dependence of changes in the visible absorption spectrum of dilute AO solutions is consistent with dimerization equilibrium. The emission spectrum of AO in aqueous

Fig. 1. **Schematic structure of the sodium hyaluronate (a) and its C$_{10}$ alkyl-derivative (b)**
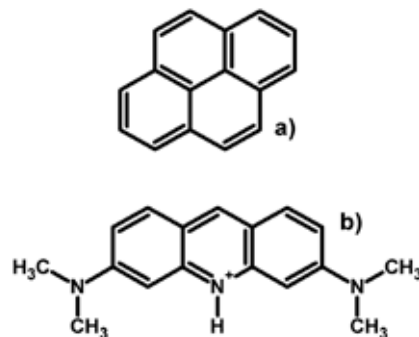
Fig. 2. **Schematic structure of the pyrene (a) and protonated form of the acridine orange (b)**

solution has a maximum at 532 nm. In the highest concentration range a new weak emission band at 630 nm is occurs. This band is related to the forbidden H-type aggregate transition. Formation of aggregates (dimers) leads to the decreasing o the fluorescence intensity.[Z]

Results
Pyrene and AO in Native Hyaluronan

Existence of hydrophobic patch, resulted from secondary structure of the hyaluronan molecule in aqueous solution, allow hyaluronan's chains aggregate to form helical structures.[X] Dissociated carboxylic groups from the *D*-Glucuronic sub-unit in aqueous solutions make hyaluronan's chain possible to interact via electrostatic interaction with a cationic species.

First measurements have been focused on possible aggregation behavior of native hyaluronan in aqueous solution. Molecular weight 500 kg mol^{-1} was selected to investigate its concentration dependencies in the presence of pyrene and acridine orange. Fig. 3. shows obtained results. It is obvious that the polarity index, ranges only from 1.40 to 1.42 through a wide concentration range. Value of the polarity index in this concentration range can be taken as constant and invariant on the hyaluronan concentration. So, from the hydrophobic polarity probe point of view no aggregation behavior was observed in these solutions and in this concentration range. Hyaluronan molecule is also known as extremely hydrophilic specie, thus it organizes water molecules around the chain resulted in water barrier. This barrier looks to be insuperable for the pyrene.
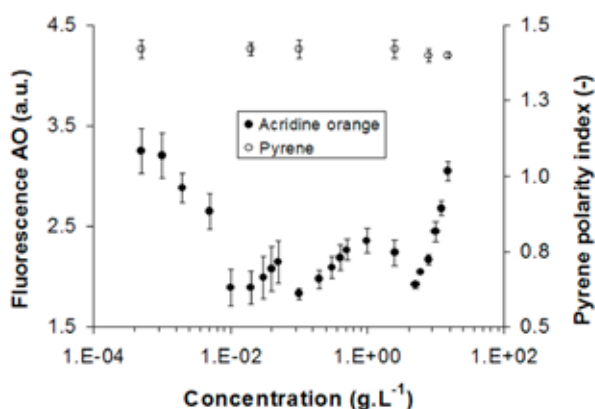
Fig. 3. **Dependencies of the pyrene polarity index and the fluorescence intensity of the acridine orange on the concentration of the native hyaluronan in aqueous solution. Hyaluronan molecular weight was 500 kg mol^{-1}**

On the other hand, electrostatic interaction between AO and hyaluronan gives interesting results. First decreasing of the AO fluorescence can be ascribed to the AO dimer formation on the HA chain. This dependency has two minimums. First, correspond to the equal point 1 mol of the AO dimer

per 1 mol of the COO$^-$ group. Second minimum corresponds to the range of the physiological concentration of the hyaluronan. In concentration around 1 g dm^{-3} a polymer domain overlay is occurs. This phenomenon will take a part in next investigation.

Pyrene in Alkyl Modified Hyaluronan

Results with hydrophobized hyaluronans, obtained for D30/30 a 1,470/30, are presented in Fig. 4. For good lucidity, concentration values are plotted in dimension g dm^{-3}. The CAC value for lower molecular weight looks to be lower than for higher molecular weight. After the conversion of the concentration dimension from "g dm^{-3}" to "10^{-6} mol dm^{-3}" the CAC value for 1.470 kg mol^{-1} (1.667 × 10^{-6} mol dm^{-3}) is 25-times smaller than for 30 kg mol^{-1} (0.068 10^{-6} mol dm^{-3}).
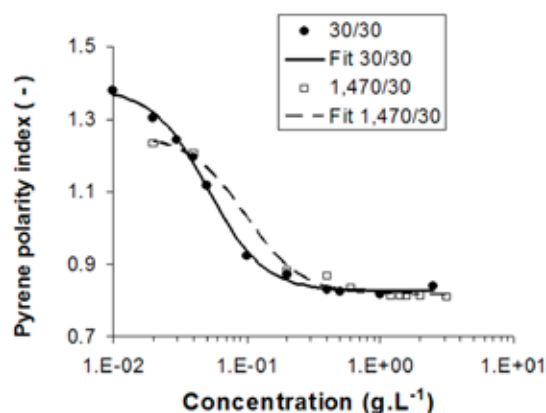
Fig. 4. **Pyrene polarity index in hydrophobized hyaluronan aqueous solution. Derivatives were in the same degree of substitution 30 % and in different molecular weights, 1.470 (□) and 30 kg mol^{-1} (●)**

Aguiar and co-workers[5] suggested a condition to select the CAC value from the pyrene polarity index. If the $x_0/\Delta x$ (cf. Eq. (1)) is less than 10, the CAC point is determined by the x-coordinate of the inflex point x_0. All of hyaluronan derivatives used in this study passed this the "less than 10-condition".

Aggregate process of the modified hyaluronan was also studied through the electrostatic interaction with AO. Aim of this study was find out if alkyl chains association has an image in processes, which can influence Stern bilayer around polyectrolyte's surface.

Fig. 5. shows comparison of the pyrene polarity index and fluorescence intensity of the AO dependencies on the concentration of the modified hyaluronan. AO dependency shows after first decreasing an area with stable values of the fluorescence intensity. This plateau is followed with next decreasing of the fluorescence intensity. According to a prediction the decreasing of the AO fluorescence is caused only by the dimer formation, in concentration range, starts near CAC point, the hyaluronan's aggregate formation cause
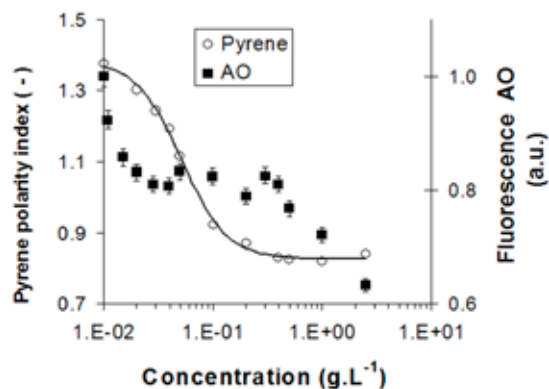
Fig. 5.   **Comparison of the pyrene polarity index (○) and fluorescence intensity of the AO dependencies (■) on the concentration of the modified hyaluronan (1.470/30)**

that newly added carboxylics group are inaccessible for AO molecules. We predicted intermolecular formation process of these aggregate types.

Conclusions

The hyaluronan alkyl derivatives, with different molecular weights and same degree of substitution, show surfactant-like aggregation behavior in aqueous solutions. Their critical aggregation concentration was comparable in dimensions g dm^{-3}. Acridine orange can be used to determine aggregation process via electrostatic interaction with the modified hyaluronan.

Aggregation properties of sodium hyaluronate (HA) in molecular weight 500 kg mol^{-1} were studied by fluorescence methods. Interactions with hydrophobic fluorescence probe pyrene showed hydrophobically-modified analogues of sodium hyaluronate, as suitable systems for drug delivery applications. Properties of hydrophobic core were studied with polarity and viscosity fluorescence probes.

Interaction with hydrophilic probe acridine orange can help to understand native hyaluronate's self-aggregation behavior in aqueous environment. Depolymerization of dye-aggregates, evidenced by fluorescence intensity, showed an abrupt change in physiological concentration region (~ 1 g dm^{-3}). Acridine orange can be also used to determine aggregation process via electrostatic interaction with the modified hyaluronan.

REFERENCES
1. Mlčochová P., Bystrický S., Steiner B., Machová E., Velebný V., Krčmář M.: Biopolymers *82*, 74 (2006).
2. De S., Girigoswami A.: J. Coll. Int. Sci. *271*, 485 (2004).
3. Wang F., Yang J., Wu X., Wang X., Feng L., Jia Z., Guo C.: J. Coll. Int. Sci. *298*, 757 (2006).
4. Scott J. E., Heatley F.: Biomacromolecules *3*, 547 (2002).
5. Aguiar J., Carpena P., Molina-Bolívar J. A., Ruiz C. C.: J. Colloid Interface Sci. *258*, 116 (2003).

L10 SPIN-TRAPPING INVESTIGATION OF RADICAL INTERMEDIATES GENERATED FROM PHENOLS SPECIFIC BEHAVIOR OF *PARA*-METHYL PHENOLS

LADISLAV OMELKA, PETR MAJZLÍK, RENATA SUPERATOVÁ and PETRA HOLUBCOVÁ

Brno University of Technology, Faculty of Chemistry, Institute of Physical and Applied Chemistry, Purkyňova 118, 612 00 Brno, Czech Republic
omelka@fch.vutbr.cz

Introduction

The formation of phenoxyl radicals is the predominating process occurring by the oxidation of monohydric phenols using different agents (PbO$_2$, MnO$_2$, RO$_2^{\bullet}$). Their stability substantially depends on the substitution in the *ortho* position. Very high stability is the typical feature of the phenoxyl radicals derived from 2,6-di-alkyl substituted phenols, especially those with bulky *tert*-butyl substituent (sterically hindered phenols). Monohydric phenols with 2,6-dialkyl substituents containing α–CH bond, as well as phenols with unsubstituted or partially substituted *ortho* position (sterically unhindered phenols) provide by the oxidation the unstable phenoxyl radicals, which can be detected only using special EPR technique, *e.g.* flow[1] or spin trapping method[2]. It was found that the addition of sterically unhindered phenoxyl radicals to aromatic nitroso spin-traps (nitrosobenzene, nitrosodurene) proceeds in the *ortho* position and leads to two different types of nitroxyl radicals (1).

(1)
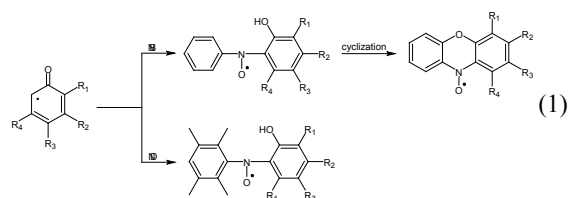
Although the generation of phenoxyl radicals, resulting from the abstraction of phenolic hydrogen atom plays an important role during the oxidation, the tendency towards the abstraction of hydrogen atom from methyl group in *para* methyl substituted phenols was also observed. The benzyl radicals formed were detected by spin-trapping technique using nitroso spin-traps[2,3]. The recombination products of benzyl radicals proved by the analysis of reaction mixture of oxidized 2,6-di-*tert*-butyl-4-methylphenol also support this mechanism, although there are also another theories interpreting their formation. To understand the specific behavior of *para* methyl group in substituted phenols in more detail, the oxidation of the series of phenols having this structure was investigated using spin-trapping method.

Experimental

All chemicals (phenols, nitroso compounds, *tert*.-butyl-hydroperoxide, PbO$_2$) were commercially available and were used without further purification. Toluene of analytical grade purity (Sigma) was used as the solvent in all experiments.

The oxidation of phenols in the presence of nitroso compounds was performed according to the following procedure: In 5×10^{-2}M toluene solution of the phenol the corresponding amount of nitroso compounds was dissolved, to adjust the molar ratio phenol : nitroso compound = 1 : 1. To 2 ml of this solution 150 mg PbO$_2$ were added under stirring. The stirring was regularly stopped in 30 min. interval and after the sedimentation of solid phase 0.3 ml of the reaction mixture were placed into the EPR tube. To obtain the high quality EPR spectra, the solution in the tube was bubbled with nitrogen for 30 sec.

Results

Hydrogen abstraction from *para*-methyl group was investigated within the series of different substituted phenols **1 – 2** in the presence of substituted nitroso compounds **3a – 3c**.

1a–1b	**2a–2e**	**3a–3b**
a: R$_1$ = R$_2$ = *t*-C$_4$H$_9$	**a**: R$_1$ = R$_2$ = R$_3$ = H	**a**: R$_1$ = R$_2$ = R$_3$ = R$_4$ = R5 = H
b: R$_1$ = R$_2$ = CH$_3$	**b**: R$_2$ = R$_3$ = H; R$_1$ = CH$_3$	**b**: R$_2$ = R$_3$ = R4 = R$_5$ = H; R$_1$ = CH$_3$
	c: R$_1$ = R$_3$ = H; R$_2$ = CH$_3$	
	d: R$_2$ = R$_3$ = H; R$_2$ = *t*-C$_4$H$_9$	
	e: R$_1$ = H; R$_2$ = R$_3$ = CH$_3$	**3c**
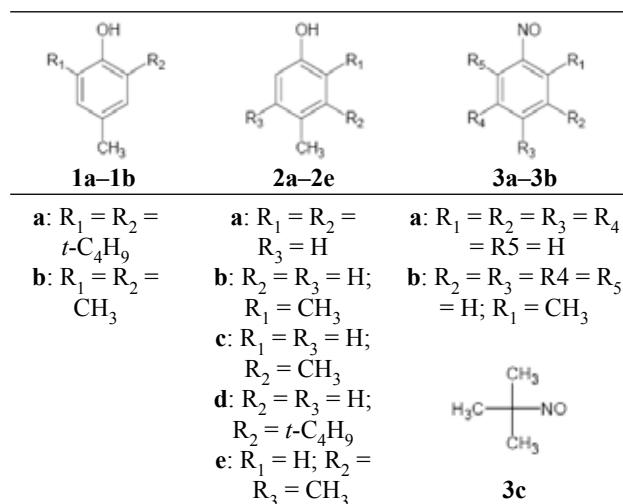
The oxidation of **1a** (R$_1$ = R$_2$ = *tert*.butyl) in the presence of nitrosobenzene (NB, **3a**) affords the mixture of radical products, where the corresponding phenoxyl radicals **4** (a$_H$(CH$_3$) = 1.094 mT, a$_H$(*m*) = 0.155 mT) together with benzyl radicals **5,** indirectly detected through the adducts **6** (X = C$_6$H$_5$; a$_N$(NO) = 1.049 mT, a$_H$(CH$_2$) = 0.565 mT, a$_H$(*o,p*) = 0.273 mT, a$_H$(*m*) = 0.092 mT)) prevail (2).

(2)
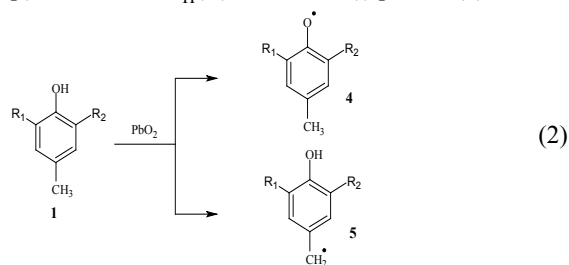
EPR parameters of **6** are similar to those observed by spin trapping of **5** with 3,5-di-*tert*.butyl-nitrosobenzene[3].

The concentration ratio between these two radicals depends on the experimental conditions and by the surplus of phenol over spin trap the pure EPR spectrum of the benzyl adduct
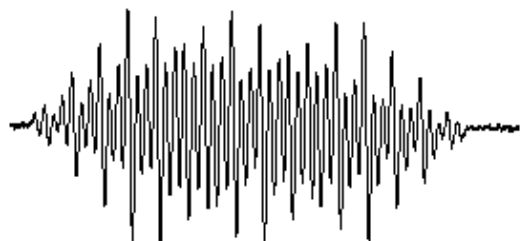
Fig. 1.   **Experimental EPR spectra of nitroxyl radical 6 prepared from 2,6-di-tert-butyl-4-methylphenol 1a**
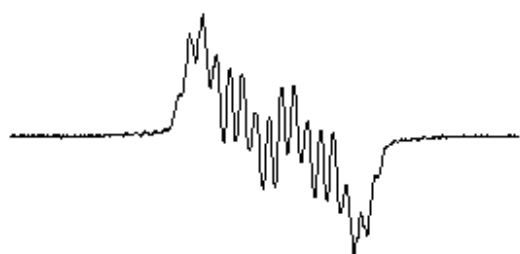
Fig. 2.   **Experimental EPR spectra of phenoxyl radical 8 prepared from 2,6-di-tert-butyl-4-methylphenol 1a**

can be observed (Fig. 1.).

Nevertheless, it was found that further changes in EPR spectra occur with time. One hour after the preparation of the sample the spectrum outlined in Fig. 1.b was detected. The g-value (g ≈ 2.0045) points out that the secondary phenoxyl radicals are formed in the consecutive steps of the oxidation. This statement is also supported by the splitting constant of two protons ($a_H = 0.15$ mT), which is the typical value of *meta* protons in phenoxyls. Other dominating splitting constants proved by the simulation of the experimental EPR spectra were attributed to one hydrogen and one nitrogen atom (Table I). Based on these experimental facts it is evident that the secondary phenoxyl radicals result from the
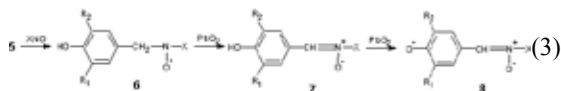
transformation of the benzyl adduct (3).

Moreover, the number of interacting nuclei suggests that the *para* position in secondary phenoxyls has the structure of the nitrone fragment $-CH = N^+O^- - C_6H_5$, which originates from the conversion of the nitroxyl moiety $-CH_2 - NO^\bullet - C_6H_5$. This implies that the nitrone **7** (X = C_6H_5) is the intermediate product, which is consequently oxidized to phenoxyl radical **8** (Fig. 2.). In the framework of further experiments the number of nitroso compounds was expanded. Besides nitro-

sobenzene other substituted derivatives X−NO (**3b**, **3c**) were studied. The analysis of EPR spectra proves that the above mentioned reaction route is valid, except for **3c**, in all cases under study.

On the other side, neither the adduct **6** nor the phenoxyl radical **8** was observed using 2-methyl-2-nitrosopropane **3c** (X = *tert*.-C_4H_9). Instead of them, only the nitroxyl radical X−NO−X (a_N(NO) = 1.555 mT) was detected, as a product of the decomposition of *tert*.-C_4H_9−NO on the surface of PbO$_2$. This fact is surprising, because the EPR parameters of the phenoxyl radical **8** (X = *tert*.-C_4H_9, Table I) produced by the oxidation of the nitrone **7** (prepared by reaction of 3,5-di-*tert*-butyl-4-hydroxybenzaldehyde with *N-tert*-butyl-hydroxylamine) using benzoyloxy radicals, are reported in the

Table I
EPR parameters of phenoxyl radicals 8 prepared by the oxidation of 2,6-di-tert-butyl-4-methylphenol 1a with PbO$_2$ in toluene solution in the presence of nitroso compounds (**3a–3c**)

X	aH(3.5) [mT]	aH(CH) [mT]	a(N) [mT]	a(X) [mT]
	0.150	0.290	0.510	0.090 (3H)
	0.150	0.280	0.490	–
	0.170 (1H) 0.150 (1H)	0.260	0.505	–

literature[4].

The experimental results obtained by PbO$_2$ oxidation of the sterically hindered 2,6-di-*tert*-butyl-4-methylphenol (**1a**) in toluene solution in the presence of different nitroso compounds X−NO initiated further investigation in this field. The tendency towards the liberation of one hydrogen atom from *para* methyl group was studied also with the methylated phenol (**1b**) and mono-, di- and tri- alkyl substituted phenols **2a–2e**. When 2,4,6-trimethylphenol (**1b**) was subjected to the oxidation, immediately after the addition of PbO$_2$ to the toluene solution of **1b** and nitrosobenzene the high concentration of benzyl adduct **6** ($R_1 = R_2 = CH_3$) was observed. Its EPR signal is stable for more then 24 hours without being overlapped by the signal of another radical. This fact seemingly points out that the suggested reaction route for **1a** (1), based on the conversion of benzyl adduct to nitrone **7** and consecutively to phenoxyl radical **8**, is not valid in this case. However, this effect can also be satisfactorily interpreted as a result of a substantially lower stability of 2,6-dimethyl-4R phenoxyl radicals in comparison with those derived from 2,6-di-*tert*.butyl-4R- phenols. The presence of nitrone **7** ($R_1 = R_2 = CH_3$) in reaction mixture was directly proved by the experiment, where *tert*.butylhydroperoxide was added to the reaction mixture 24 hours after the preparation of the adduct **6**. The high concentration of nitroxyl radical **9** with the

splitting constants (a_N(NO) = 1.049 mT, a_H(CH) = 0.175 mT, a_H(*o,p*) = 0.273 mT, a_H(*m*) = 0.092 mT) was observed in this
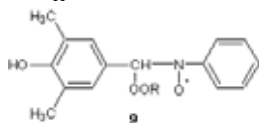
case.

The EPR parameters well agree with the published data for $RO_2{}^{\bullet}$ adducts with phenyl-*N*-phenyl nitrone[5]. The EPR signal undergoes further changes with time, which presumes the succesive degradation of hydrogen atom in nitrone fragment by peroxyl radicals.

Similarly as with **1a**, the simultaneous generation of corresponding phenoxyl and benzyl radicals is also expected in the course of the oxidation of sterically unhindered phenols **2a**–**2e** using PbO_2. In contrast to **1a**, the primary phenoxyl radical cannot be directly detected by EPR method due to their unstability. Nevertheless, by the application of spin trapping technique, they can be observed in the form of spin adducts. Due to the tendency towards the abstraction of hydrogen atom from *para* methyl substituent, the benzyl radicals

also react with nitroso spin traps and the generated adducts mostly dominate in the EPR spectrum. These EPR parameters do not substantialy differ from those observed in the case of **1a**, **1b**.

REFERENCES
1. Stone T. J., Waters W. A.: J. Chem. Soc. 213 (1964).
2. Omelka L.,Kováčová J.: Magn. Reson. Chem. *32*, 525 (1994).
3. Zhuzhgov E. I., Bazhin N. M.,Terpugova M. P.,Tsvetkov Y. D. Bull.: Acad. Sci. USSR (English translation) *23*, 2438 (1974).
4. Pacifici J. G., Browning H. L.: J. Am. Chem. Soc. *92*, 5231 (1970).
5. Cholvad V., Staško A., Tkáč A., Buchachenko A. L., Malík L.: Coll. Czech. Chem. Commun. 46, 823 (1981).

L11　VORTEX-FRACTAL-RING STRUCTURE OF MOLECULE

PAVEL OŠMERA

Brno University of Technology, Faculty of Mechanical Engineering, Technicka 2, 616 69 Brno, Czech Republic,
osmera@fme.vutbr.cz

Introduction

Most of our knowledge of the electronic structure of atoms has been obtained by the study of the light given out by atoms when they are exited. The light that is emitted by atoms of given substance can be refracted or diffracted into a distinctive pattern of lines of certain frequencies and create the line spectrum of the atom. The careful study of line spectra began about 1880. The regularity is evident in the spectrum of the hydrogen atom. The interpretation of the spectrum of hydrogen was not achieved until 1913. In that year the Danish physicist Niels Bohr successfully applied the quantum theory to this problem and created a model of hydrogen. Bohr also discovered a method of calculation of the energy of the stationary states of the hydrogen atom, with use of Planck's constant h. Later in 1923 it was recognized that Bohr's formulation of the theory of the electronic structure of atoms to be improved and extended. The Bohr theory did not give correct values for the energy levels of helium atom or the hydrogen molecule-ion, H_2^+, or of any other atom with more than one electron or any molecule. During the two-year period 1924 to 1926 the Bohr description of electron orbits in atoms was replaced by the greatly improved description of wave mechanics, which is still in use and seems to be satisfactory[1].

The discovery[1] by de Broglie in 1924 that an electron moving with velocity v has a wavelength $\lambda = h/mev$. The theory of quantum mechanics was developed in 1925 by the

Fig. 1.　**The vortex-fractal structure of the electron ray with two electrons**[19]

German physicist Werner Heisenberg. An equivalent theory, called wave mechanics, was independently developed early in 1926 by Austrian physicist Ervin Schroedinger. Important contribution to the theory were also made by the English physicist Paul Adrien Maurice Dirac. The most probable distance of the electron from the nucleus is thus just the Bohr radius r_o; the electron is, however, not restricted to this distance. The electron is not to be thought of as going around the nucleus, but rather as going in and out, in varying directions, so as to make the electron distribution spherically symmetrical[1].

This paper is an attempt to attain a new and profound model of the nature's structure using vortex, fractal and ring structures. Scientists try to explain some phenomena in Nature that have not been explained so far. The aim of this paper is the vortex-fractal modeling of vortex-ring fractal structure of atoms, molecules, and a creation of elements in the Mendeleev's periodic table with vortex-ring particles which is not in contradiction to the known laws of nature.

Electron with Vortex-Fractal-Ring Structure

The discovery of the electron was a landmark in physics and led to great technological advances. The electron emission is the process when negative charges in the form of electron, escape for example from the hot filament. Streams of electrons moving at high speed are called cathode rays or electron rays. The rays are deflected by a magnetic field too. If the N pole of a magnet is brought up to the neck of the tube, the rays move upwards, using Fleming's left-hand rule. The ratio of the charge q of an electron e to its mass m_e is called its specific charge and can be found from experiments in which cathode rays are deflected by electric and magnetic fields. It was first done by J. J. Thomson in 1897 using a deflection-type tube. His work is regarded as proving the existence of the electron as a negatively charged particle of very small mass and not, as some scientists thought a form of electro-magnetic radiation like light.

Electron is defined as a fundamental particle of matter, with negative electric charge, which populates the outer region of atoms.

The electrical force decreases inversely with the square of distance between charges. This relationship is called Coulomb's law. There are two kinds of "matter", which we can call positive and negative. Like kinds repel each other, while unlike kinds attract – unlike gravity, where only attraction occurs[2]. When charges are moving the electrical forces depend also on the motion of charges in a complicated way[2,3,4].

Fractals seem to be very powerful in describing natural objects on all scales. Fractal dimensions and fractal measures are crucial parameters for such description. Many natural objects have self-similarity or partial-self-similarity of the whole object and its part[5].

The structure of the electron in Fig. 1 presents the electron as "pure" ring fractal structure. Electrons ^0e (or e) in the electron ray ^0r hold together by photon's vortex structure ^0f (a pair of vortices).[6–20] Generally, in the fractal structure of
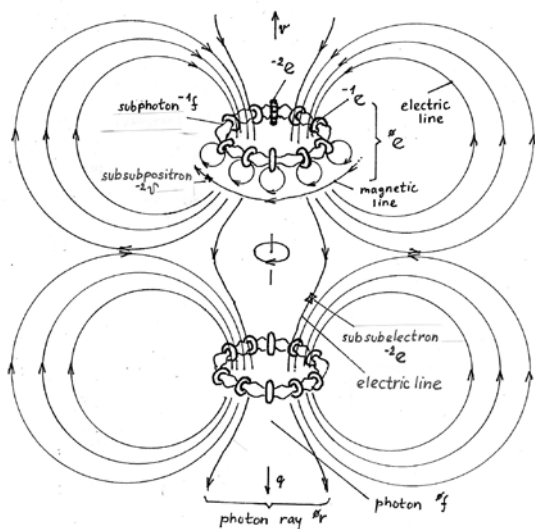
the electron, the number *n* defines the level of substructure ^{n}e. The name osmeron we derived from the name "Osmera" of Egyptian deity with 4 pairs of gods as primary creative forces (from a chaos beginning). Osmerons are too small that is why have unmeasurable size and mass. Osmerons on osmeron's trajectory creates an osmeron ray.

We know that the apparent mass of a particle changes by $1/\sqrt{(1 - v^2/c^2)}$. Does its charge do something similar? No charges are always the same, moving or not[4]. If the charge of a particle depended on the speed of the particle carrying it, in the heated block the charge of the electrons and protons would no longer balance. A block would become charged when heated. If the charge on an electron charged with speed, the net charge in piece of material would be charged in a chemical reaction. Even a very small dependence of charge on speed would give enormous fields from the simplest chemical reactions. No such effect has been observed[3,4], and we conclude that the electric charge of a single particle is independent of its state of motion.

For a calculation[9,23] of the fractal-ring electron structure we will use the structure that is shown in Fig. 1. and Fig. 2. In the ring electron structure (see Fig. 2.) the subelectrons e_o rotate with a velocity v_e and subsubelectrons e_1 with a velocity v_o. The radius of the electron is R_e and a radius of axes of subelectrons e_o is r_e. A rough estimation of number of subrings is N and number of subsubring is N^2. They are determined in the electron structure by the mass m_p of the proton structure[17].

Let us calculate properties of the electron with a vortex-fractal theory[6–20]. This requires that subelectrons are accelerated towards the center of the electron ring. The amount of the acceleration force F_a has to be in balance with two coulomb forces F_o. A whole force of attraction F_A can be calculated by Ampere's law:
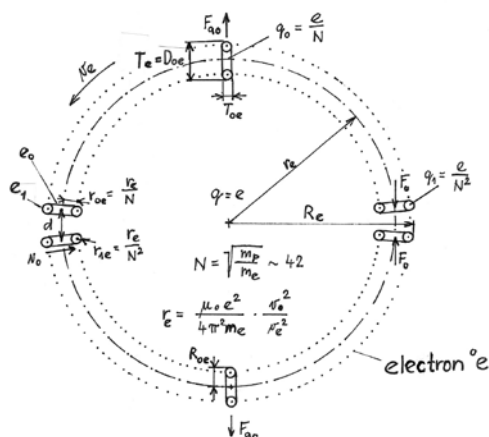
Fig. 2.   **The fractal-ring structure of the electron**[17]

$$F_a = F_A \tag{2.1}$$

The fundamental physical law for an acceleration force F_a for mass *m* with velocity *v* and distance *r* is :

$$F_a \approx m\frac{v^2}{r} \tag{2.2}$$

The mass m_{oe} of the subelectron e_o for the fractal structure of the electron is:

$$m_{oe} = \frac{m_e}{N} \tag{2.3}$$

where N is number of subelectrons. To cover creation of the proton structure and the electron structure from the same very small rings (N^2 subsubelectrons e_1)[17,22]:

$$N = \sqrt{\frac{m_p}{m_e}} \approx 42 = 2 \cdot 3 \cdot 7 \tag{2.4}$$

where m_p is the mass of the proton and me is the mass of the electron. From the fractal structure of the electron on Fig.2:

$$F_e = F_{oe} \cdot \frac{2}{\pi} \cdot \frac{N}{2} = \frac{m_e \, v_e^2}{N \, r_e} \cdot \frac{2}{\pi} \cdot \frac{N}{2} \tag{2.5}$$

The average value of forces F_{ao} for *N/2* subelectrons is on Fig.3. Their average value $2/\pi$ was calculated following way:

$$\int_0^\pi \sin x \, dx = 2 \tag{2.6}$$

$$\frac{\int_0^\pi \sin x \, dx}{\pi} = \frac{2}{\pi} \tag{2.7}$$
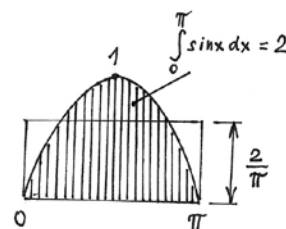
Fig. 3.   **Average value of the acceleration force F_{ao}**

The fundamental physical law for attraction force F_A (Amper's law) between two wires with a current *I*, a length *l*, a distance *d*, and a permeability μ_o of vacuum:

$$F_A \approx \frac{\mu_o}{2\pi} I^2 \frac{l}{d} \tag{2.8}$$

Electric charges *q1* in the subring *e1* create the current *I*:

$$I = \frac{dQ}{dt} = \frac{q_1 N}{T} \tag{2.9}$$

$$2\pi r_{oe} = v_o T \tag{2.10}$$

$$q_1 = \frac{e}{N^2} \tag{2.11}$$

$$I = \frac{\frac{e}{N^2} N}{T} = \frac{e}{NT} = \frac{ev_e}{N2\pi r_{oe}} = \frac{ev_e}{N2\pi \frac{r_e}{N}} = \frac{ev_e}{2\pi r_e} \tag{2.12}$$

$$d = \frac{2\pi r_e}{N} \tag{2.13}$$

Equation (2.12) and (2.13) we use in (2.8):

$$F_e = F_A = 2F_o = 2\frac{\mu_o}{2\pi} \frac{e^2 v_e^2}{4\pi^2 r_e^2} \frac{2\pi \frac{r_e}{N}}{\frac{2\pi r_e}{N}} \tag{2.14}$$

From (2.5) and (2.14):

$$\frac{m_e v_e^2}{N r_e} \frac{2}{\pi} \frac{N}{2} = 2\frac{\mu_o}{2\pi} \frac{e^2 v_e^2}{4\pi^2 r_e^2} \frac{2\pi \frac{r_e}{N}}{\frac{2\pi r_e}{N}} \tag{2.15}$$

and the radius *re* of the electron (in Fig. 2) is :

$$r_e = \frac{\mu_o e^2}{4\pi^2 m_e} \cdot \frac{v_o^2}{v_e^2} \tag{2.16}$$

If velocities of rings and subrings are:

$$v_o = v_e \approx c \tag{2.17}$$

then

$$r_e = \frac{\mu_o e^2}{4\pi^2 m_e} \approx 0.89 \times 10^{-15} \text{m} \tag{2.18}$$

We can now calculate the size of the electron with the fractal geometry on Fig. 4. Full calculation is in reference[17,19]. But it is only for the free and quite electron. The size of the electron in the hydrogen atom is not constant[19] (see Fig. 8.).

Energy E_o of the quite electron ^0e, which has velocity $v=0$ and quite mass m_{eo}, can be calculated[17] from kinetic energy of their subelectrons ^{-1}e with velocity v_{-1} (v_e), subsubelectrons ^{-2}e with velocity v_{-2} (v_o), subsubsubelectrons ^{-3}e with velocity v_{-3}, subsubsubsubelectrons ^{-4}e with velocity v_{-4}:

If velocities of substructures are:

$$v = v_e = 0 \ ,$$

$$v_o = v_{-3} \approx \frac{c}{\sqrt{2}} \ , \tag{2.19}$$

$$v_{-4} \approx c \ ,$$

their inner kinetic energy is:

$$E_o = \frac{1}{2} \frac{m_{e0}}{N^2} v_o^2 N^2 + \frac{1}{2} \frac{m_{e0}}{N^3} v_{-3}^2 N^3 + \frac{1}{2} \frac{m_{e0}}{N^4} v_{-4}^2 N^4 \approx m_{e0} c^2 \tag{2.20}$$

$$E_o \approx m_{e0} c^2 \tag{2.21}$$

This result is in coincidence with the well-known Einstein equation (2.21).
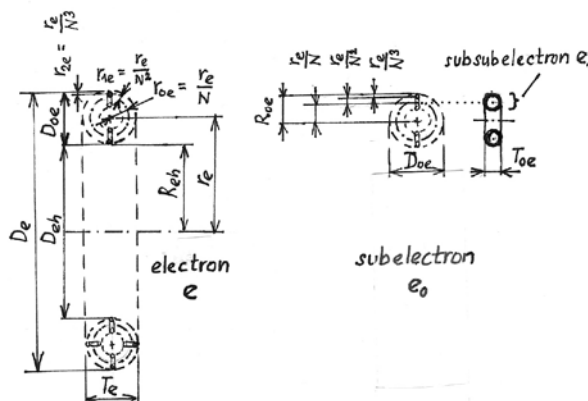
Fig. 4.   **Geometry of the electron and the subelectron[16]**

The Model of Hydrogen with Levitating Electron

The hydrogen atom can have the electron on left side or on right side (see Fig. 9.a, 9.b), thus the difference in exponents must be 2 then exp = 4. The attractive force F_+ is Coulomb's force. A distance between the electron an the proton is r :

$$F = F_+ - F_- = \frac{e^2}{4\pi\varepsilon_o}\left(\frac{1}{r^2} - \frac{A}{r^{exp}}\right) = \frac{e^2}{4\pi\varepsilon_o}\frac{1}{r^2} - \frac{e^2}{4\pi\varepsilon_o}\frac{r_o^2}{r^4} \tag{3.1}$$

For Bohr distance $r_B = r_o \approx 5.29 \times 10^{-11}$ m [18] is the resulting force $F = 0$.

$$A = r_0^2 \tag{3.2}$$

$$F = F_+ - F_- = \frac{e^2}{4\pi\varepsilon_o}\left(\frac{1}{r^2} - \frac{r_o^2}{r^4}\right) \tag{3.3}$$
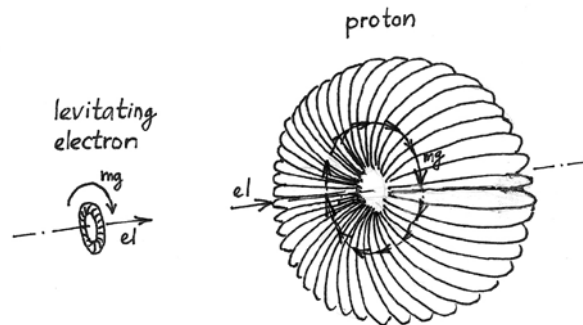
Fig. 5.   **The levitating electron in the field of the proton[18]**

Let us use equation (3.3) as a postulate for next calculations. To find the distance where F has maximum (see Fig. 3.):

$$\frac{dF}{dr} = \frac{e^2}{4\pi\varepsilon_o}\left[-\frac{2}{r^3} - \left(-\frac{4r_o^2}{r^5}\right)\right] = \frac{e^2}{2\pi\varepsilon_o r^3}\left(-1 + \frac{2r_o^2}{r^2}\right) \quad (3.4)$$

for r_o:

$$\frac{dF}{dr} = \frac{e^2}{4\pi\varepsilon_o r_o^3} = K_o \quad (3.5)$$

It is line k_o in Fig. 6

$$\frac{dF}{dr} = \frac{e^2}{2\pi\varepsilon_o r^3}\left(-1 + \frac{2r_o^2}{r^2}\right) = 0 \quad (3.6)$$

and solution is $r_{1,2} = \pm\sqrt{2}\,r_o$ for F_{max}. Energy E of the electron in the distance r:

$$E = \int \frac{e^2}{4\pi\varepsilon_o}\left(\frac{1}{r^2} - \frac{r_o^2}{r^4}\right) dr = \frac{e^2}{4\pi\varepsilon_o}\int\left(\frac{1}{r^2} - \frac{r_o^2}{r^4}\right) dr = \frac{e^2}{2\pi\varepsilon_o r}\left(-1 + \frac{2r_o^2}{r^2}\right) \quad (3.7)$$

The graph of E is on Fig. 7. Energy E_o which must be added to the electron to be free:

$$E_o = \frac{e^2}{4\pi\varepsilon_o}\int_{r_o}^{\infty}\left(\frac{1}{r^2} - \frac{r_o^2}{r^4}\right) dr = \frac{e^2}{4\pi\varepsilon_o}\left[-\frac{1}{r} + \frac{r_o^2}{3r^3}\right]_{r_o}^{\infty} = \frac{e^2}{4\pi\varepsilon_o}\left(\frac{1}{r} - \frac{r_o^2}{3r^3}\right) \quad (3.8)$$

For $E_o = 0$

$$r_{Eo} = \pm\frac{r_o}{\sqrt{3}} \approx \pm 3.05\times10^{-11}\,\text{m} \quad (3.9)$$

For r_o is E_o:

$$E_o = \frac{e^2}{4\pi\varepsilon_o}\left(\frac{1}{r_o} - \frac{r_o^2}{3r_o^3}\right) = \frac{e^2}{4\pi\varepsilon_o}\frac{1}{r_o}\frac{2}{3} = \frac{e^2}{6\pi\varepsilon_o}\frac{1}{r_o} \approx 18.13\,\text{eV} \quad (3.10)$$

$$E_o = \frac{e^2}{4\pi\varepsilon_o}\frac{1}{r_o}\frac{2}{3} \approx 27.2\frac{2}{3}\,eV \approx 18.13\,eV \quad (3.11)$$

We can calculate frequency f_o and period T_o of oscillation of the electron in the hydrogen atom around r_o if we insert K_o defined in equation (3.5) into (3.12):

$$f_o = \frac{1}{2\pi}\sqrt{\frac{K_o}{m_e}} \approx 9.3\times10^{14}\,\text{Hz} \quad (3.12)$$

$$T_o = \frac{1}{f_o} \approx 1.075\times10^{-15}\,\text{s} \quad (3.13)$$

To calculate quantum model of hydrogen we use radius r_e (2.16):

$$r_e = \frac{\mu_o e^2}{4\pi^2 m_e}\frac{v_o^2}{v_e^2} \quad (3.14)$$

$$2\pi r_e = 2\pi\frac{\mu_o e^2}{4\pi^2 m_e}\frac{v_o^2}{v_e^2} \quad (3.15)$$

We assume that[19]:

$$v_o^2 = \frac{c^2}{2} = \frac{1}{2\varepsilon_o\mu_o} \quad (3.16)$$

Subelectrons are on the orbit with the radius r_e. On this circle have to be n half-waves $\lambda/2 = h/2m_e v$ (n is quantum number):

$$2\pi r_e = 2\pi\frac{\mu_o e^2}{4\pi^2 m_e}\frac{v_o^2}{\bar{v}_e^2} = \frac{\mu_o e^2}{4\pi m_e}\frac{c^2}{\bar{v}_e^2} = \quad (3.17)$$

$$\frac{e^2}{4\pi\varepsilon_o m_e}\frac{1}{\bar{v}_e^2} = n\frac{\lambda}{2} = n\frac{1}{2}\frac{h}{m_e\bar{v}_e}$$

$$\frac{e^2}{2\pi\varepsilon_o}\frac{1}{\bar{v}_e} = nh \quad (3.18)$$

where $\bar{v}_e$ ($\bar{v}_{-1}$) is mean velocity of the subelectron ^{-1}e.

Kinetic energy[19] of the electron with mean velocity $\bar{v}$ is transformed into kinetic energy of subelectrons in 4 substruktures ($v_e, v_{-2}, v_{-3}, v_{-4}$):

$$\frac{1}{2}m_e\bar{v}_e^2 = \frac{1}{4}\frac{1}{2}m_e\bar{v}^2 \quad (3.19)$$

$$\bar{v}_e = \frac{1}{2}\bar{v} = \frac{1}{2}\frac{2}{\pi}v_m = \frac{v_m}{\pi} \quad (3.20)$$

where v_m is a maximum velocity of the electron, when the electron has the distance r_o and has minimum energy E_{min}:

$$\frac{e^2}{2\pi\varepsilon_o}\frac{\pi}{v_m} = nh \quad (3.21)$$

$$v_m = \frac{1}{n}\frac{e^2}{2\varepsilon_o h} \quad (3.22)$$

$$E_e = \frac{1}{2}m_e v_m^2 = \frac{1}{n^2}\frac{m_e e^4}{8\varepsilon_o^2 h^2} \quad (3.23)$$

For quantum number $n = 1$

$$E_{eo} = \frac{m_e e^4}{8\varepsilon_o^2 h^2} \approx 13.6\,eV \quad (3.24)$$

$$E_{eo} = E_o\frac{3}{4} = \frac{e^2}{6\pi\varepsilon_o}\frac{1}{r_o}\frac{3}{4} = \frac{e^2}{8\pi\varepsilon_o}\frac{1}{r_o} \approx 13.6\,eV \quad (3.25)$$

$$E_{eo} = \frac{m_e e^4}{8\varepsilon_o^2 h^2} = \frac{e^2}{8\pi\varepsilon_o}\frac{1}{r_o} \quad (3.26)$$

$$r_o = \frac{\varepsilon_o h^2}{m_e e^2} \approx 5.29\times10^{-11}\,\text{m} \quad (3.27)$$

$$r = n^2\frac{\varepsilon_o h^2}{m_e e^2} \quad (3.28)$$

It is the same result as Bohr obtained but with quite different hydrogen model[1].

To find the size of r where $E_o = 13.6\text{eV} = E_{qo}$ in (3.24) and (2.25) we must solve cubic equation:

$$3r^3 - 6r^2 r_0 + 2r_0{}^3 = 0 \tag{3.29}$$

The roots of equation (3.29) are:
$r_1 = 0.7223517245 r_o \sim 0.382\text{Å}$,
$r_2 = 1.792517214 r_o \sim 0.948\text{Å}$, $r_3 = -0.5148689384 \, r_o$

The values of r_1 and r_2 are the distances where the electron has velocity $v = 0$ (see Fig. 7.).

$$E_q = \frac{1}{n^2} E_{qo} \tag{3.30}$$

For quantum number $n = 1$ we calculate the maximum velocity v_m from (3.22) and the couple constant α:

$$v_m = \frac{e^2}{2\varepsilon_o h} \tag{3.31}$$

$$\frac{c}{v_m} = \frac{2\varepsilon_o hc}{e^2} = \frac{1}{\alpha} \approx 137.036 \tag{3.32}$$
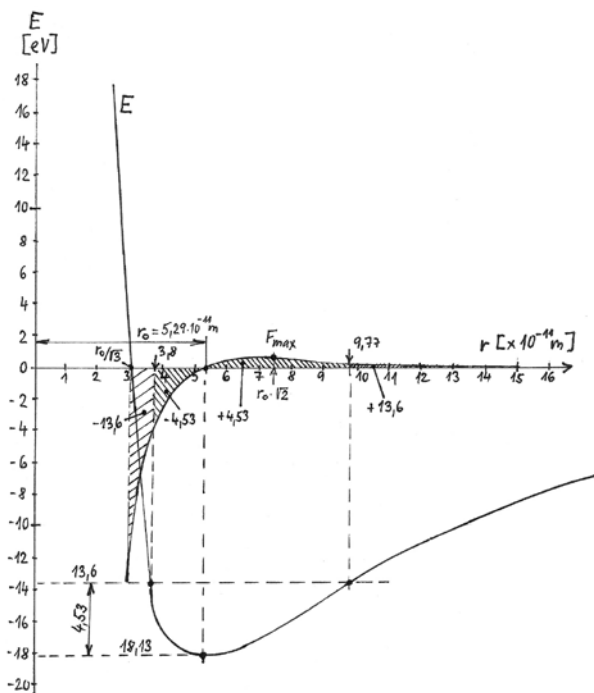
Fig. 6.   **Forces in the hydrogen atom**

In the hydrogen molecule H_2 the covalent bond has $n_e = 2$, $n_p = 1$ (see Fig. 9):

$$F = F_+ - F_- = \frac{e^2}{4\pi\varepsilon_o}\left(\frac{n_e n_p}{r^2} - \frac{r_o{}^2}{r^4}\right) \tag{3.33}$$

$$F = \frac{e^2}{4\pi\varepsilon_o}\left(\frac{2}{r^2} - \frac{r_o{}^2}{r^4}\right) = 0 \tag{3.34}$$

$$r_c = \pm \frac{r_o}{\sqrt{2}} \approx \pm 3.75 \times 10^{-11}\text{m} \tag{3.35}$$

$$d_{cp} = 2r_c \approx 7.5 \times 10^{-11}\text{m} \tag{3.36}$$

It is in coincidence with the distance between two protons for their covalent bond[1].

For the hydrogen molecule-ion $H_2{}^+$ is $n_e = 1$, $n_p = 1$ then d_{p+} (see Fig. 9.):

$$d_{p+} = 2r_o \approx 10.6 \times 10^{-11}\text{m} \tag{3.37}$$

To calculate the size of the proton structure we use fractal-coil geometry[17] (see Fig. 7.). Results are on Fig. 9.
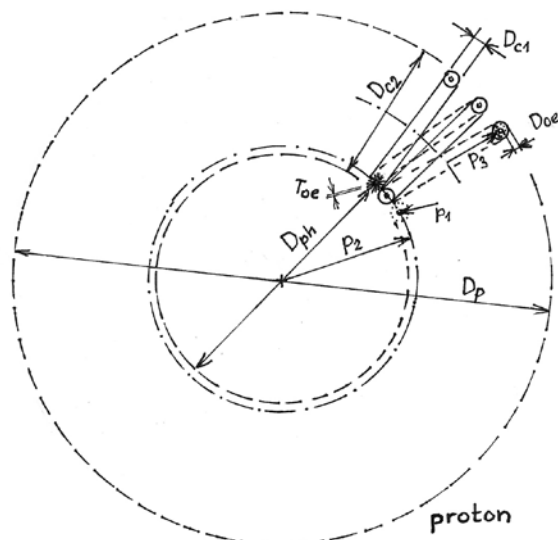
Fig. 7.   **Vortex-fractal-coil structure of the proton[18]**

The Spin of the Electron

The spin of the electron is defined as angular momentum:

$$\vec{S} = m_e (\vec{r}_e \times \vec{v}_e) \tag{4.1}$$

For the spin[19] on axis z:

$$S_z = N \frac{m_e}{N} r_e \bar{v}_e \tag{4.2}$$

$$r_e = \frac{e^2}{8\pi^2\varepsilon_0 m_e} \cdot \frac{1}{\bar{v}_e^2} \tag{4.3}$$

$$\bar{v}_e = \pm \frac{v_m}{\pi} \tag{4.4}$$

$$v_m = \frac{e^2}{2\varepsilon_o h} \tag{4.5}$$

$$r_e = \frac{e^2}{8\pi^2\varepsilon_0 m_e} \cdot \frac{\pi^2}{v_m^2} = \frac{e^2}{8\varepsilon_0 m_e} \cdot \frac{1}{v_m^2} = \frac{e^2}{8\varepsilon_0 m_e} \cdot \frac{4\varepsilon_0^2 h^2}{e^4} = \frac{\varepsilon_0 h^2}{2m_e e^2} \tag{4.6}$$
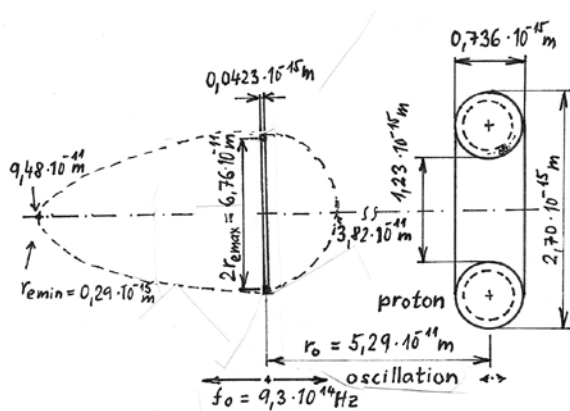
Fig. 8. **Calculated size of the electron and the proton in the hydrogen atom (in different scales)**

$$S_z = \pm m_e \bar{v} r_e = \pm m_e \frac{v_m}{\pi} r_e =$$

$$= \pm m_e \frac{e^2}{2\varepsilon_0 h} \cdot \frac{1}{\pi} \cdot \frac{\varepsilon_0 h^2}{2m_e e^2} = \pm \frac{1}{2} \cdot \frac{h}{2\pi} = \pm \frac{1}{2} \hbar = m_s \hbar \quad (4.7)$$

$$m_s = \pm \frac{1}{2} \quad (4.8)$$

The result in (4.7) is in coincidence with the generally equation for the spin, where m_s is spin quantum number.

Magnetic momentum M_z:

$$M_z = IS \quad (4.9)$$

where I is an current around a surface S:

$$T = \frac{2\pi r_e}{\bar{v}_e} \quad (4.10)$$

where T is period for calculation of I:

$$I = \pm \frac{Q}{T} = \pm \frac{\frac{e}{N} N}{\frac{2\pi r_e}{\bar{v}_e} \cdot \frac{1}{2}} = \pm \frac{e\bar{v}_e}{\pi r_e} \quad (4.11)$$

$$S = \pi r_e^2 \quad (4.12)$$

$$M_z = IS = \pm \frac{e\bar{v}_e}{\pi r_e} \cdot \pi r_e^2 \cdot \frac{m_s}{m_s} = \pm \frac{e}{m_e} S_z = \pm \frac{e}{m_e} \cdot \frac{1}{2}\hbar = \pm \mu_B \quad (4.13)$$

where μ_B is Bohr magneton.

The Size of the Electron in Hydrogen Atoms

For maximum velocity of the electron v_{em} we use analogy with (3.19):

$$v_{em} = \pm \frac{v_m}{2} \quad (5.1)$$

If we insert v_m from (3.31) into (4.3) and (5.1) we receive the maximum radius of the electron:
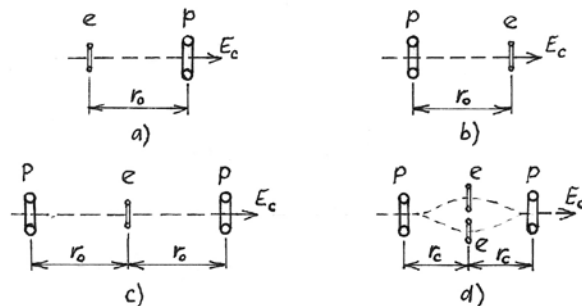
Fig. 9. **Calculated distances between the proton and the electron. a) left side orientation of hydrogen, b) right side orientation of hydrogen, c) the hydrogen molecule-ion H$_2^+$, d) the hydrogen molecule H$_2$ with covalent bond**

$$r_{emax} = \frac{e^2}{8\pi^2\varepsilon_0 m_e} \cdot \frac{4}{v_m^2} = \frac{2\varepsilon_0 h^2}{\pi^2 m_e e^2} = 3.38 \times 10^{-11}\,\text{m} \quad (5.2)$$

For minimum radius of the electron where $v=0$:

$$2\pi r_{emin} = ND_{ee} \quad (5.3)$$

$$r_{emin} = \frac{ND_{ee}}{2\pi} = 0.29 \times 10^{-15}\,\text{m} \quad (5.4)$$

The levitating electron changes the size from very small to relatively large size[19] (see Fig. 8.).

The Structure of Molecules

Atoms combine to form a molecule. Their shared air of electrons is called a covalent bond. They occupy the same orbital with opposite spins. The H$_2$ molecule atoms H share electrons. Each hydrogen atom shares its electron with another hydrogen atom to gain a full outer s shell of 2 electrons. Covalent bonding is important in carbon compounds.

There are two simple rules how to create atom nuclei:

(i) Only two protons can be on one rotational axis

(ii) Two protons cannot be connected directly with vortex nuclear bond (only the proton with the neutron can be nuclear bond)
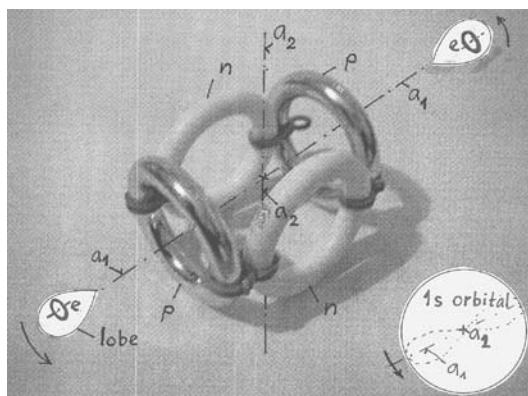
Fig. 10. **The vortex-ring structure of the nucleus of the helium $_2^4$He (alpha particle) and its orbital 1s**

Fig. 11.　**The vortex-ring structure of the atom $_6^{12}C$ to create the benzene molecule[15] (see Fig. 12.)**

Conclusions

Our science creates terrific demands on the imagination[2]. To understand the electromagnetic field requires a high degree of imagination. The degree of imagination that is required is much more extreme than that required for some of the ancient ideas. The modern ideas are much harder to imagine. We usually use mathematical equations and rules, but we used a lot of pictures to describe very complex vortex-fractal models. There is not easy to formulate mathematical models[21,23]. We can't allow ourselves to seriously imagine things, which are obviously in contradiction to the known laws of nature. We created vortex-fractal-ring model of the electron, of the proton and hydrogen and then calculated sizes, forces, energies and covalent bonds.
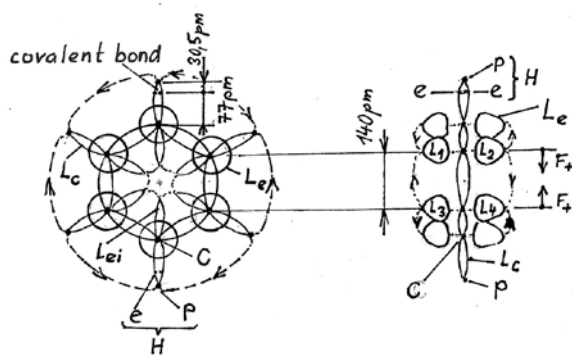
Fig. 12.　**The structure of the benzene molecule[15]**

REFERENCES

1.　Pauling L.: *General Chemistry*, Dover Publication, Inc, New York, 1988
2.　Feynman R.P. Leighton R.B., Sands M.: *The Feynman Lectures on Physics, volume I, II, III* Addison-Wesley publishing company, 1977
3.　Feynman R.P.: *QED – The Strange Theory of Light and Matter*, Princeton University Press, 1988
4.　Feynman R.P.: *The Character of Physical Law,* Penguin Books, 1992
5.　Zmeskal, O., Nezadal, M., Buchnicek, M.: Chaos, Solitons and Fractals 17 (2003) 113–119
6.　Ošmera, P.: *Proceedings of MENDEL 2005*, Brno, Czech Republic (2005) 1–6.
7.　Ošmera, P.: *Proceedings of MENDEL 2005*, Brno, Czech Republic (2005) 7–14.
8.　Ošmera, P.: *Proceedings of the 4th International Conference on Soft Computing ICSC2006,* January 27, 2006, Kunovice, Czech Republic, 111–122
9.　Ošmera, P.: *Proceedings of the 4th International Conference on Soft Computing ICSC2006,* January 27, 2006, Kunovice, Czech Republic, 123–129
10.　Ošmera, P.: *CD Proceedings of MENDEL 2006*, Brno, Czech Republic (2006) 12 pages
11.　Ošmera, P.: *CD Proceedings of MENDEL 2006*, Brno, Czech Republic (2006) 14 pages
12.　Ošmera, P.: *CD Proceedings of MENDEL 2006*, Brno, Czech Republic (2006) 10 pages
13.　Ošmera, P.: *Proceedings of MENDEL 2007*, Praha, Czech Republic (2007), 105 - 110
14.　Ošmera, P.: *Proceedings of MENDEL 2007*, Praha, Czech Republic (2007), 72 - 75
15.　Ošmera P.: *Proceedings of World Congress on Engineering and Computer Science,* San Francisco, 2007, 152–157
16.　Ošmera P.*: New Trends in Physics*, NTF 2007, Brno Czech Republic, 2007, 179–182
17.　Ošmera, P.: *Proceedings of the 6th International Conference on Soft Computing ICSC2008*, January 25, Kunovice, Czech Republic, (2008) 151 - 158
18.　Ošmera, P.: *Proceedings of the 6th International Conference on Soft Computing ICSC2008*, January 25, Kunovice, Czech Republic, (2008) 159 - 168
19.　Ošmera P.: Evolution of nonliving Nature, Kognice VIII, Prague, Czech Republic, (2008), 179
20.　Li Z., Halang W. A., Chen G.*: Integration of Fuzzy Logic and Chaos Theory;* paragraph: Osmera P: Evolution of Complexity, Springer, (2006) (ISBN: 3–540–26899–5) 527 – 578
21.　Thorne, K.S.: Black Holes & Time Warps, W.W.Norton & Company, Inc., 1994
22.　Gottvald, A.: *Proceedings of the 6th International Conference on Soft Computing ICSC2008*, January 25, Kunovice, Czech Republic, (2008) v tisku
23.　Bouchal Z.: *New Trends in Physics*, NTF 2007, Brno Czech Republic, (2007), 3–6

L12 HYDRATION OF HYALURONAN

ALENA PRŮŠOVÁ, PETRA BURSÁKOVÁ and JIŘÍ KUČERÍK

Brno University of Technology, Faculty of Chemistry, Department of Applied and Physical Chemistry, Purkyňova 118, Brno 612 00, Czech Republic,
xcprusova@fch.vutbr.cz

Introduction

During the last decades, significant advances have been made in the development of biocompatible and biodegradable materials for biomedical applications. One of an appropriate material seems to be hyaluronic acid also known as hyaluronan (HYA). It is a naturally occurring biopolymer, which serves important biological functions in bacteria and higher animals including humans. Hyaluronan is water soluble giving viscoelastic fluids[1] and it has a considerably greater ability to trap water than other polyelectrolyte polysaccharides.

Hyaluronan is a linear unbranched, high molecular weight, polar polysaccharide of the glycosaminoglycans class. Hyaluronan is composed of repeating polyanionic disaccharide units which consists of N-acetyl-D-glucoseamine and D-glucuronic acid linked by a β 1-4 glycosidic bond. The disaccharides are linked by β 1–3 bonds to form hyaluronan chains (Fig. 1.)[2].
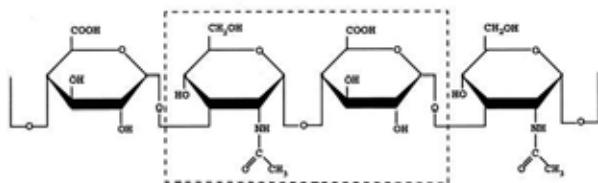
Fig. 1.　The formula of disaccharide unit of hyaluronan

The structure of water surrounding hyaluronan in the solution is affected by the the interactions between polymer and water, and thus, it exhibits different physical properties depending on their mutual distance. The aim of this work is to recognize and enumerate such hydration shells by differential scanning calorimetry (DSC), i.e. to use their different enthalpies of melting.

Experimental

S a m p l e s

Hyaluronan, isolated from Streptococcus zooepidemicus, was obtained from CPN Company (Dolní Dobrouč, Czech Republic). Five molecular weight of hyaluronan were used as follows: 100.1 kDa, 253.9 kDa, 522.1 kDa, 740 kDa and 1,390 kDa. By means of thermogravimetry (TA Instruments, Q5000IR) it was determined an equilibrium moisture content to obtain more precise results.

Low water content

Hyaluronan was placed in an aluminum pan. Excess of water was added to hyaluronan samples. Surplus water was allowed to evaporate slowly until the desired water content was obtained at room temperature. The pans were subsequently hermetically sealed and left to equilibrate at room temperature overnight. Water content (W_c) was defined as follows:

$$W_c = \frac{\text{grams of water}}{\text{grams of dry sample}} \ \text{(g/g)} \qquad (1)$$

For each molecular fraction, 7 different W_c were measured.

High water content

Hyaluronan samples were dissolved in milli-Q water. The hyaluronan concentrations was 0.1 %, 0.5 %, 1 %, 1.5 %, 2 %, 2.5 %, 3 % wt. The solutions were slowly mixed by a magnetic laboratory stirrer over a period of 24 hours to obtain perfectly dissolved and homogeneous hyaluronan sample.

DSC measurement

Differential scanning calorimetry was performed using the TA Instruments DSC Q200, equipped with a cooling accessory, and TA Universal Analysis 2000 software. Samples of approximately 10 mg were placed in hermetically sealed aluminum sample pans. High water content samples were measured immediately, to avoid condensation of water on the pan lid, which can occur if the sealed samples are stored in the cold before use. Low water content samples were measured the next day after the preparation. The thermal protocols used were as follows: equilibrate at 40.0 °C; isothermal at 40.0 °C for 2 min; cooling from 40.0 °C to –90.0 °C at 3.0 °C min⁻¹; isothermal at –90.0 °C for 2.0 min; heating from –90.0 °C to 30 °C at 3.0 °C min⁻¹.

Results

LWC – Low Water Content

Representative DSC cooling and heating curves of hyaluronan are given in Fig. 2. the sample shown is 253 kDa hyaluronan with W_c 0.75. Hyaluronan hydrogels with the lowest W_c showed almost infinitesimal fusion endothermic peak on heating curves. Nearly all water molecules are present in the form of non-freezing water in this system, and a slight amount of water molecules are present in the form of freezing-bound water which caused the observed endothermic fusion peaks. For the increasing W_c can be seen a small crystallization exothermic peak, which growth wtih the increasing W_c, on cooling curve, and consequently, on the heating curve presence of overlapped endothermic fusion peaks. Enlarged peak area is caused by larger amount of freezing and freezing-bound water. The DSC data records for higher Wc look like previous DSC records plus an increasing tendency as mentioned above.

From the obtained data it can be considered that there are tree types of water which are 'free (bulk) water' which freezes as normal water it means that this water melts, crystallized around 0 °C and enthalpy of fusion is 333.56 J g⁻¹. Only the free water contributes to the observed enthalpy change. Further 'freezing-bound water' (f-b) which freezes at
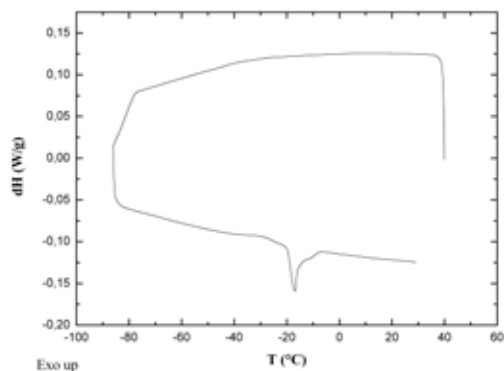
Fig. 2. **High water content – DSC record**

lower temperature than normal water but it freezes and it also exhibits a reduced enthalpy of fusion. Finally 'non-freezing water' (n-f) which does not freeze even at low temperature which was used in this work, i.e. –90 °C.

Assuming that the weight of free water is equal to the total water weight less the non-freezing water and freezing bound water, the following expression holds:

$$\frac{\Delta H_{obs}}{g_{HYA}} = \frac{\Delta H_{free\,water}}{g_{free\,water}}\left(\frac{g_{free\,water}}{g_{HYA}}\right) + \frac{\Delta H_{f\,b\,water}}{g_{f\,b\,water}}\left(\frac{g_{f\,b\,water}}{g_{HYA}}\right) \quad (2)$$

Expressing the weight of free water in terms of totalwater, freezing-bound water, and non-freezing water, one can obtain:

$$\frac{\Delta H_{obs}}{g_{HYA}} = \frac{\Delta H_{free\,water}}{g_{free\,water}}\left(\frac{g_{total\,water}}{g_{HYA}}\right) +$$

$$+\left(\frac{\Delta H_{f\,b\,water}}{g_{f\,b\,water}} - \frac{\Delta H_{free\,water}}{g_{free\,water}}\right)\left(\frac{g_{f\,b\,water}}{g_{HYA}}\right) - \frac{\Delta H_{free\,water}}{g_{free\,water}}\left(\frac{g_{n\,f\,water}}{g_{HYA}}\right) \quad (3)$$

The total amount of non-freezing water in hyaluronan hydrogels was determined directly from the X intercept. Table I reports the dependency of non-freezing water content to the molecular weight of hyaluronan reveals, although small, but evident trend of increasing number of non-freezing water with increasing molecular weight of hyaluronan. We hypothesize that large content of water in case of 1,390 kDa sample is caused by the tertiary structure of hyaluronan and by the mutual approaching of its chains to the closer proximity.

Table I
Weight of n-f water for different MW

MW [kDa]	n-f water [g 1g^{-1} HYA]
100.1	0.59
253.9	0.58
522.1	0.65
740.0	0.57
1,390	0.81

High Water Content

Fig. 3 shows record of a representative DSC cooling and heating curve for hyaluronan dissolved in water. In fact, there can be seen two phase transitions, first one in the above record which corresponds to the cooling phase and bellow one, which reflect processes of melting. Due to supercooling effect, the latter was used for enthalpy determination.
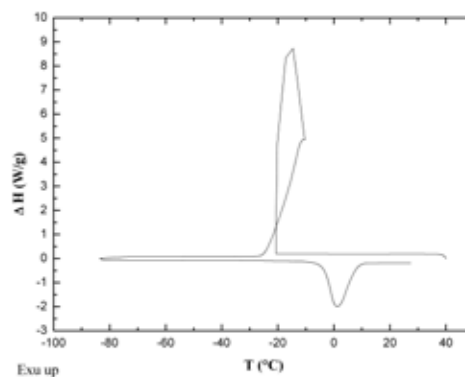
Fig. 3. **High water content – DSC record**

After the plotting the observed enthalpy change, normalized to the polymer weight, as a function of the total water content of the sample (Fig. 4.), the melting enthalpy for the free water can be obtained from the slope. The x-intercept in (3) includes terms for both the freezing-bound water and the non-freezing water. Now one can estimate the minimum amount of freezing-bound water per gram of hyaluronan in diluted and semi-diluted solutions by combination of data obtained in this part, high water content, with the data analysis from the part concerning the determination of low water content (see Table I).
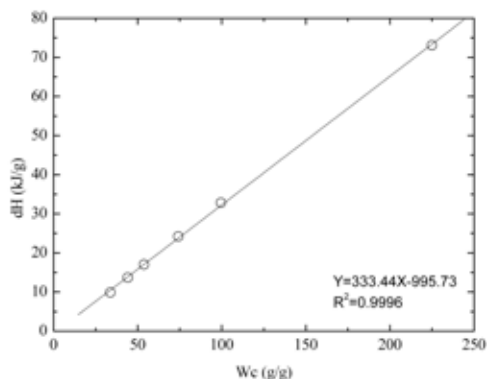
Fig. 4. **Normalized melting enthalpy versus Wc**

The content of non-freezing water was adopted from the table reporting the low water content for specific hyaluronan molecular weight (Table I). The minimum value for the enthalpy change associated with melting of the freezing-bound water was used 312 J g^{-1} ref.[3]. The determination of freezing-bound water can be carried out as follows[4]: x-inter-

cept of dependency of normalized enthalpy change on water content (Fig. 4.). This dependecy gives a value which is equal to the following formula.

$$\frac{g_{n\,f\,water}}{g_{HYA}} + \left(1 - \frac{\Delta H_{f\,b\,water}}{g_{f\,b\,water}}\frac{g_{free\,water}}{\Delta H_{free\,water}}\right)\left(\frac{g_{f\,b\,water}}{g_{HYA}}\right) \qquad (4)$$

Table II
Weight of f-b water for different M_W

M_W [kDa]	f-b water [g 1g^{-1} HYA]
100.1	38.7
253.9	38.2
522.1	29.2
740.0	70.7
1,390	76.9

Obtained values of freezing-bound water, summarized in Table II exhibit no obvious dependency. For the first three value (100.1 kDa; 253.9 kDa; 522.1 kDa), there is decrease but for the next two values (740.0 kDa; 1,390 kDa) there is increase of the values.

Conclusions

Semi-diluted hyaluronan solutions have significantly altered freezing and melting transitions of water. The results are affected by the presence of freezing-bound and of a small amount of non-freezing water strongly bound to the polymer. Those have slightly altered thermodynamic properties which were used for the enumeration of such types of water.

REFERENCES

1. Jouon N., Rinaudo M., Milas M., Desbrieres J.: Carbohydr. Polym. *26*, 69, (1995).
2. Lapčík L.Jr., Lapčík L., De Smedt S., Demeester J., Chabreček P.: Chem. Rev. *8*, 2664, (1998).
3. Yoshida H., Hatakeyama T., Hatakeyama H.: J. Therm. Anal. *40*, 483, (1992).
4. Lui J., Cowman M.K.: J. Therm. Anal. Calor., *59*, 547, (2000).

L13 ELECTROCHEMICAL ANALYSIS OF NEW INDOLE BASED ANTIOXIDANTS

MICHAL ZALIBERA[a], PETER RAPTA[a], VLADIMÍR ŠNIRC[b] and SVORAD ŠTOLC[b]

[a]Institute of Physical Chemistry and Chemical Physics, Faculty of Chemical and Food Technology, Slovak University of Technology in Bratislava, Radlinského 9, 812 37,
[b]Institute of Experimental Pharmacology, Slovak Academy of Sciences, Dúbravská cesta 9, 841 04 Bratislava, Slovak Republic,
peter.rapta@stuba.sk

Introduction

The concept of pharmacological interventions in prevention and therapy of oxidative stress-related diseases has still not found adequate application in clinical practice. One of the potential drugs intensively investigated in this area is the synthetic pyridoindole stobadine. Numerous studies in the literature were focused on its protective properties[1]. Its beneficial effects have been observed in metabolic, cardiovascular, renal, neural and hepatic systems[2]. However, only few reports deal with the electrochemical oxidation of stobadine and its derivatives[3]. Recently new indole-derived neuroprotective drugs with improved pharmacodynamic and toxicity profiles were synthesized based on the stobadine structure[4].

In this contribution a comprehensive study of the electrochemical, antioxidant and radical scavenging properties of selected indole-derived drugs (Fig. 1.) is presented. The data from three independent methods are compared including *(i)* cyclic voltammetry in DMSO and aqueous solutions, *(ii)* EPR/spin-trapping study covering the estimation of reactive radical scavenging capacity and *(iii)* estimation of Trolox equivalent antioxidant capacity (TEAC) by monitoring of ABTS[•+] cation radical and DPPH radical with UV-VIS spectroscopy, delivering information about the hydrogen/electron donating antioxidant action.

Experimental

Stobadine dihydrochloride and new stobadine derivatives SMe1EC2.HCl, SM1M3EC2.HCl, and SMe1nBuoC2.

HCl were prepared in the Institute of Experimental Pharmacology, Slovak Academy of Sciences. The analytical purity grade NaCl was from Slavus Ltd. and 5,5-dimethyl-1-pyrroline-*N*-oxide (DMPO) was the product of Sigma-Aldrich. Tetrabutylammonium perchlorate (TBAP), lithium perchlorate (LiClO$_4$) puriss., both purchased from Fluka and ferrocene (p.a.,$\geq$98.0 %), dimethyl sulfoxide (DMSO) purchased from Merck were used as received. The deionized water was used for aqueous solutions.

All cyclovoltammetric experiments were performed at room temperature under argon atmosphere. A standard three-electrode arrangement of a platinum wire (in DMSO) or glassy carbon rod (in water) as working electrodes, a platinum coil as counter electrode, and a saturated calomel electrode (SCE) as a reference electrode was used. The concentration of investigated samples was 0.5 mM in water and 1.0 mM in DMSO. The electrochemical measurements were carried out with a HEKA PG 284 (Germany) potentiostat/galvanostat using the software package PotPulse 8.53.

Standard ABTS assay was used for determination of antioxidant capacity of samples. Here, 100 µl of 0.1 mM sample solution in 10% ethanol was added to 2 ml of ABTS$^{•+}$ (70 µM) solution in 1 cm UV-cell and rigorously mixed. The decrease of absorbance at 730 nm was followed for 10 minutes. UV/VIS/NIR Shimadzu 3600 spectrometer (Japan) was used both in antioxidant tests and for the measurement of the UV-VIS spectra of samples (Fig. 2.). The difference in the absorbance in 10th minute relative to the reference, ΔA, and the calibration curve of Trolox (Sigma-Aldrich, Germany) was used to calculate the values of TEAC.
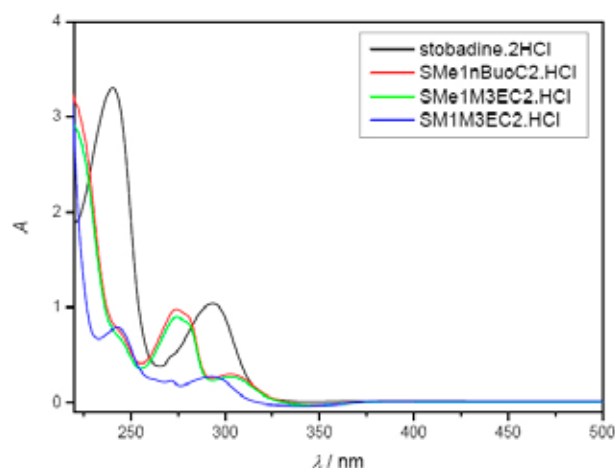
Fig. 2. **UV-VIS spectra of freshly prepared 0.15 M NaCl aqueous solutions of investigated pyridoindoles (0.5 mM)**

Antioxidant activity determination using the free DPPH radical (95%, Aldrich, Germany) was similar to the ABTS assay. 200 µl of 0.1mM sample solution in 10% ethanol was mixed with 2 ml of 0.1mM DPPH in ethanol and decrease of absorbance at 516 nm was followed for 10 minutes.

In EPR experiments the thermal decomposition of K$_2$S$_2$O$_8$ at 333 K was used as a source of reactive radicals.

Fig. 1. **Investigated indole-derived drugs**

The amount of generated radicals was monitored in air employing DMPO spin trap. 200 µl 0.5mM sample aqueous solutions, 25 µl 200mM DMPO in DMSO and 25 µl 10mM $K_2S_2O_8$ in H_2O were used in the reaction mixture.

Results

Remarkable differences in redox behavior of stobadine derivatives were observed by replacing the DMSO representing a low proton donating solvent, with highly proton donating aqueous media (see Figs. 3. and 4.). Generally, in DMSO solutions complex irreversible redox behavior in the anodic part was observed (Fig. 3.). Rich cyclovoltammetric responses with several oxidation peaks were found indicating the complexity of the stobadine oxidation in non-aqueous media.

In all cases the first irreversible oxidation peak indicates a consecutive reaction of the unstable oxidation products. Simultaneously new cathodic peaks are detected on the reverse scan in the cathodic part of voltammogram. The number of new redox couples and the corresponding oxidation potentials strongly depend on the indole substitution.

Even more complex redox behavior in the potential region from 0 V to 1 V *vs*. SCE was observed in aqueous solutions compared to DMSO, indicating the participation of water and supporting electrolyte in the formation of various forms of indoles already in the initial solutions. Fig. 4. shows the cyclic voltammograms of three selected pyridoindoles in 0.15M aqueous NaCl. The first sample is stobadine as reference. The second sample represents stobadine derivatives with metoxy group (SMe-type samples) on benzene ring instead of the methyl group in the stobadine. The third SM1M3EC2.HCl sample contains additional methyl group on the benzene ring.

In all cyclic voltammograms found in water solutions one or two consecutive products were observed in the reverse
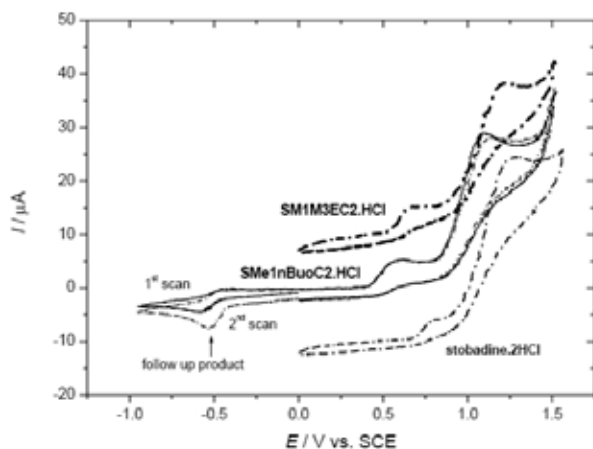
Fig. 3. **Cyclic voltammograms obtained in the oxidation of investigated stobadine and its derivatives (freshly prepared 0.1 mM solutions) in DMSO containing 0.1 M TBAP as supporting electrolyte (two CV scans including cathodic part are shown for sample SMe1nBuoC2.HCl)**

scans for SMe type structures (Fig. 4.). One of them can be again oxidized in a reversible step. These redox peaks originate from the newly formed oxidation products as illustrated in Fig. 5.
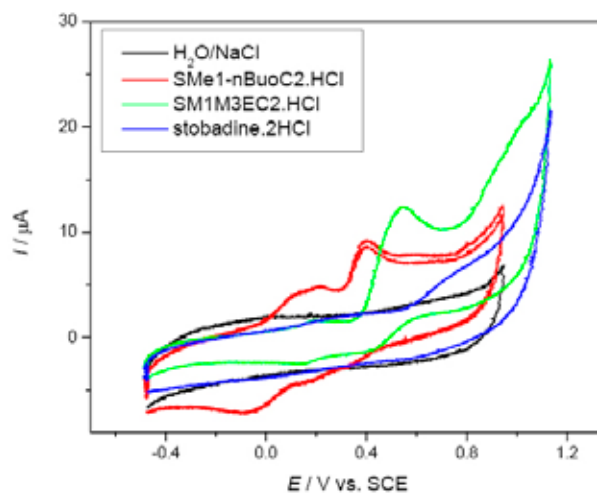
Fig. 4. **Cyclic voltammograms obtained in the oxidation of investigated stobadine and its derivatives (freshly prepared 0.5mM solutions) in H_2O containing 0.14M NaCl using glassy carbon rod working electrode**
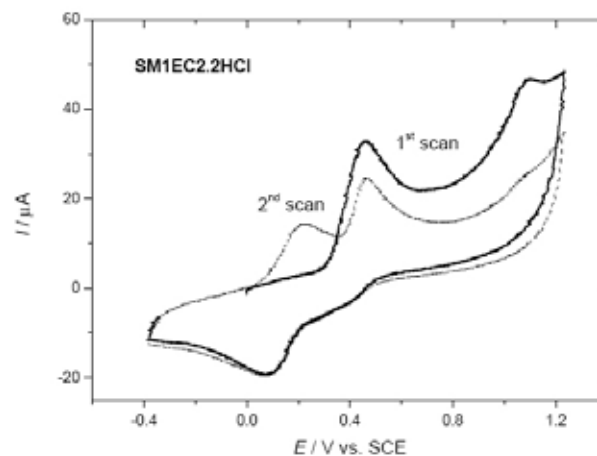
Fig. 5. **Cyclic voltammogram (1st and 2nd scan) obtained in the oxidation of SMe1EC2.HCl in H_2O containing 0.1M LiClO$_4$ using glassy carbon rod working electrode**

The low redox potentials of these products indicate the easiness of their oxidation and reduction. Therefore deviations in the relationship between electrochemical redox potentials and antioxidant and radical scavenging capacity of the investigated pyridoindoles are to be expected due to the differences in the reaction mechanisms in different media. Whereas the electrochemical redox potentials of secondary xidation products can clearly be separated from those of the parent compounds, when measuring antioxidant properties by various tests an overall activity of the parent compound and of its secondary oxidation and reduction products is measured.

Antioxidant capacity was determined by ABTS and DPPH tests, as well as EPR/spin trapping assay. The investigated samples can be divided into two groups based on the redox and radical scavenging behavior in aqueous solutions. Stobadine and SM1M3EC2.HCl exhibit higher oxidation potentials of follow up reaction products compared to the second group (SMe type derivatives). Standard ABTS and DPPH assays were used for determination of antioxidant capacity of samples expressed in TEAC (Fig. 6.).

As seen from Fig. 6. the best hydrogen/electron donating antioxidant action exhibits the sample SM1M3EC2.HCl. The lowest antioxidant activity was observed for stobadine. The total antioxidant capacity of samples was also compared with the radical scavenging capacity evaluated using the EPR/spin-trapping method (Fig. 7.).

Fig. 7. **The time course of integral EPR intensities of OH-DMPO spin adducts measured indole derivatives and Trolox in EPR/spin-trapping test**

Fig. 6. **Trolox Equivalent of Antioxidant Capacity (TEAC) of the investigated pyridoindoles determined by ABTS and DPPH tests in aqueous solutions**

The thermal decomposition of $K_2S_2O_8$ in water solutions at 333 K was used as a source of reactive hydroxyl radicals. Completely different behavior in EPR test was observed for SMe type structures in water solutions as illustrated for SMe1EC2.HCl in Fig. 7. Unusual kinetic curve was observed with a strong elimination of OH radicals formed in the reaction mixture. This confirms a special role of the methoxy group on benzene ring in stobadine-derived indoles, already indicated in the cyclovoltammetric experiments, concerning antioxidant properties of these compounds.

Conclusions

Electrochemical, UV-VIS and EPR/spin trapping investigations of new prepared indole-derived drugs were performed in order to explain in more detail the redox processes of the studied compounds in relation to their antioxidant and radical scavenging activity. Cyclic voltammetric and EPR studies indicate the formation of different oxidation products strongly depending on the pyridoindole substitution and on the solvent used. It can be concluded that similar to the most studied natural indole-type antioxidant melatonin (see recent review[5]), the indole metabolites that are formed due to oxidation, strongly contribute to the antioxidant and radical scavenging capacity of indole-based compounds both in aqueous and non aqueous media.

REFERENCES

1. Life Sciences 65 (1999*), A special issue from the International Symposium on Drug Action on Reactive Oxygen Species with Special Attention to Stobadine*
2. Yulek F., Or M., Ozogul C., Isik A. C., Ari N., Stefek M., Bauer V., Karasue C.: Arch. Med. Res. *38*, 503 (2007) and refs. cited therein.
3. Rapta P., Lichnerová E., Staško A., Šnirc V., Štolc S.: Chem. listy *99*, 221 (2005) and refs. cited therein.
4. Štolc S., Šnirc V., Májeková M., Gašparová Z., Gajdošíková A., Štvrtina S.: Cell. Mol. Neurobiol. 1495 (2006).
5. Reiter R. J., Tan D., Terron M. P., Flores L. J., Czarnocki Z.: Acta Biochim. Pol. *54*, 1 (2007).

L14 NEW COLLOIDAL SYSTEMS MADE OF HUMIC ACIDS

PETR SEDLÁČEK, MARTINA KLUČÁKOVÁ and PAVEL ONDRUCH

Brno University of Technology, Faculty of Chemistry, Purkyňova 464/118, 612 00 Brno
sedlacek-p@fch.vutbr.cz

Introduction

Humic acids (HA), as the most beneficial fraction of soil organic matter, responsible for natural detoxification of soils, provide outstanding sorption ability towards common groups of pollutants. This makes HA very promising in a production of soil remediation agents. Because of slightly acidic pH of underground waters, HA are naturally found in an insoluble state and form swelled material with high water content. Preparation of a gel form of humic substances therefore looks promising in the modeling of natural humic environments and also for a direct application of HA in agriculture or in industry.

Gelation of HA by the use of biopolymers represents rapidly evolving branch of humic research. Chitosan, polyelectrolyte biopolymer formed by a deacetylation of chitin, provides high potential on this field of study. It is known as a biocompatible material with such valuable properties as haemostatic and bacteriostatic function and sorption ability for both anionic and cationic pollutants.

Experimental

Controlled coagulation of alkalic (sodium) humate was applied in order to prepare a gel without any additional network forming agent. Solid humic acids, obtained by the method of alkalic extraction[1] from South-Moravian lignite were dissolved in 0.5 M sodium humate in solid-to-liquid ratio of 8 g dm^{-3}. This solution was precipitated by HCl addition up to pH below 1. Resulting hydrogel was separated by means of centrifugation (4,000 rpm) and washed in deionized water several times until removal of Cl$^-$ ions.

Mixed chitosan/HA hydrogels were obtained by a reaction between sodium humate and chitosan solution in volume ratio of 1 : 1. Chitosan solution was prepared by dissolution of 6.5 g of a chitosan powder (medium molecular weight, Sigma Aldrich) in 300 ml of 0.1M hydrochloric acid. pH of both solutions were adjusted to appropriate values using HCl and NaOH. After 10 minutes of continuous agitation, hydrogel was separated by either centrifugation (15 minutes, 4,000 rpm) or filtration. Hydrogel was repeatedly washed by deionized water in order to remove remaining reagents. Dry solid content of a gel was determined after drying in a laboratory oven for 5 days (at 50 °C).

For the preparation of chitosan/HA hydrogel beads, 3.3 g of chitosan flakes were dissolved in 100 ml of 5% acetic acid. This solution was slowly dropped into either 0.5M NaOH or corresponding sodium humate under continuous agitation.

In the former case, resulting chitosan beads were let to adsorb HA in the sodium humate with pH value of 8.5.

Following instruments were used for the determination of physical and chemical properties of resulting gels: Mettler Toledo 7 Easy pH-Meter, Sentron Hotline needle electrode for measurement of pH inside a gel, Hitachi U3300 UV-VIS spectrometer, Nicolet Impact 400 FT-IR spectrometer and ARG2 Rheometer from TA Instruments. Hydrogel samples were dried either via free evaporation at 25 °C or using Free-Zone 4.5 (LABCONCO) freeze dry system.

Results

Humic gel, prepared by the coagulation of sodium humate solution, represents a suitable model in order to study a pollutant transport in natural humic systems[1]. Water formed 81 % of its weight. The gel was irreversible, either freeze drying or air drying in laboratory oven provided hydrophobic humic acid powder with limited swelling ability. Main disadvantage of this gel is its high acidity (inner pH value measured by needle electrode was 1.4). Similar irreversible gel can be prepared by a precipitation of sodium humate using a solution of salt with higher valence of a cation. This method of gelation can be applied in order to mask the structural groups, responsible for the reaction between HA and metal cations (useful in diffusion experiments).

Properties of hydrogels, prepared via rection between HA and chitosan, can be dramaticaly influenced by the parameters of initial solutions (temperature, pH, ionic strength etc.). Results of an experiment, focused on the effect of initial pH showed that the highest water content of the fresh hydrogel (around 97 %) was obtained using the HA solution with the value of pH = 8.5 and chitosan solution with pH = 5.5. Also the yield of gelation (amount of a produced gel) was the highest for this way of preparation, no matter whether calculated as an amount of total gel or as an amount of dry solid content. Freeze drying of this hydrogel lead to highly porous xerogel with very fast swelling in the presence of water. Nevertheless, the structure of this xerogel was brittle; grounded or broken xerogel did not swell back into the volume of initial gel.

Another experiment determined an influence of a low-molecular electrolyte (NaCl) addition. It has been confirmed that NaCl addition causes even visually evident changes in a consistency of the gel. Small addition (~ 0.3% of the weight of mixture) increases water content of the gel, while higher addition (~ 3 %) has an opposite effect. Rheometrical measurement proved that all hydrogels show typical response of a fully cross-linked highly elastic gel; storage moduli (G') are about one order higher than the loss moduli (G'') and almost constant in a whole region of available frequencies. Addition of NaCl also affects sorption properties of gels. It was proved that isotherms for a sorption of Cu^{2+} showed typical Freundlich shape. Addition of NaCl lead to stronger binding of sorbate in a gel (during desorption experiments).

Hydrogel beads, as prepared either by reaction between chitosan solution and sodium humate or by a sorption of

humic acids on the chitosan beads, represent promissing form for industrial and agricultural application (mainly after freeze drying). Dry content of the bead is higher (~ 15% of weight). Sorption and swelling properties of this material will be taken as a focus of following experimental work.

Conclusions

This contribution introduces several preparation methods providing novel hydrogel systems made of HA. Profitable properties of resulting gels and xerogels (high swelling, sorp-tion ability, compact consistency and others) make chitosan become a material of choice for mixed biopolymer gelation of HA.

REFERENCES

1. Sedláček P., Klučáková M.: *ECCE-6, Copenhagen, Book of Abstracts* Vol. 1, p. 995. 2007.
2. Santosa S. J. et al.: Surf. Sci. *601*, 5148 (2007).
3. Ruvalcaba-Martínez A. et al.: Carbohydr. Polymer. *67*, 586 (2007).

L15　PHOTOCHEMICAL AND FREE RADICALS STUDY OF CYANOBACTERIA USING EPR SPECTROSCOPY

PAVEL STOPKA[a], BLAHOSLAV MARŠÁLEK[b] and JANA KŘÍŽOVÁ[a]

[a]Institute of Inorganic chemistry v.v.i., Czech Academy of Science v.v.i., 25068 Husinec-Řež,
[b]Institute of Botany, Czech Academy of Science v.v.i., 60365 Brno, Czech Republic,
stopka@iic.cas.cz

Introduction

We studied free radicals and their reactions in Cyanobacteria from Brno Dam on Svratka River by EPR spectroscopy. We have found free oxygen radicals on the surface of Cynobacteria. Their concentrations increase by the UV and visible light irradiation, and, in the process of their grow. By the breakdown of Cyanobacteria their concentrations falling down. These free radicals cause the health damage on the human skin and inner membranes. We have found, that some natural products cause breakdown of Cyanobacteria on the basis of their interaction with free radicals on their surface. Wheat and barley straw generate free radicals, mainly hydroxyl radicals in aqueous suspensions also. These radicals could have interaction with free radicals on Cyanobacteria to destroy it. Cynobacteria contains Fe(III) and high spin Mn(II) complexes.

Our previous experiments measured by electron paramagnetic resonance spectroscopy (EPR, ESR) proved, that actively growing cyanobacteria produce characteristic spectrum of free radicals, which may play an important role in aquatic ecosystems. Our preliminary experiments analysed by EPR also proved, that barley and wheat straw produce quite different spectrum of free radicals. Application of barley straw was published many times, but the principle remains unknown. At least on of he principle could be based on the trapping and quenching the cyanobacterial stable radicals by specific radicals produced by especially prepared natural materials. This "neutralisation" of radicals could be safe for aquatic ecosystems. We study select different natural plant materials with potential algistatic activity. Eutrophication of aquatic ecosystems and the consequent mass occurrence of harmful cyanobacterial blooms are growing problems in the entire world. Cyanobacterial blooms deteriorate water quality by toxins and odours production. Cyanobacterial toxins (microcystins, anatoxins, lipopolysacharide etc.) are known to have hepatotoxic, neurotoxic, imunotoxic, genotoxic and other adverse effects. Cyanotoxins in drinking water, fish consumption and recreational use of reservoirs represents a growing risk for human health. Besides this, cyanobacterial bloom means considerable stress for ecological stability of aquatic ecosystems, natural fish and amphibian reproduction, biodiversity of phytoplankton and zooplankton community etc. Not only toxin production is harmful, but also decrease of light intensity, pH change and excessive oxygen deple-

tion. Therefore measures to control of cyanobacterial growth are of high priority for water management. This is an actual problem in the Czech republic and many European countries For effect in shorter time algal blooms have been formerly injured by non-selective chemicals such as copper salts, but this application is no longer acceptable. Consequently there is a scope for finding of new types of algicides more selective for cyanobacteria. Except selectivity the biodegradability is the second requirement for new types of algicides. Therefore, the use of some natural agents could be acceptable and more environmental friendly way than the undesirable application of toxic algicidal chemicals. There are several references about algicidal compounds based on natural materials or extracts in the scientific literature.

Materials and Methods

Methodology for the EPR spectroscopy studies, especially *in vivo* studies was developed. The presence of free radicals on Cyanobacteria samples was measured and evaluated. The measurements of free radicals, will continue and somehypothesis regarding the content of phenolic compounds and their antioxidative capacity.

Materials

5,5-Dimethyl-1-pyrroline-N-oxide (DMPO) (Sigma-Aldrich) was used as a radical trapping agent for oxygen and nitrogen radicals. 2,2,6,6-Tetramethylpiperidine-1-oxyl (Tempol) (Sigma-Aldrich) was used as a reactant with antioxidative substances for determination of antioxidant activities. Calibration standards were Mn^{2+}/ZnS and Cr^{3+}/MgO (Magnettech, Berlin, Germany).

Electron Paramagnetic Resonance (EPR) Measurements

EPR spectra were recorded with E-540 Spectrometer X-Band (Bruker-Biospin,Germany). The following conditions were used while recording the spectra: microwave power 20 mW, magnetic modulation amplitude 0.2 mT, attenuation 20 dB, time konstant 0.5 s, scan speed $0.3\,mT\,min^{-1}$, calibration standards Mn^{2+}/ZnS and Cr^{3+}/MgO, measurement at 25 °C. WinEPR and Bruker (Bruker-Biospin, Germany) programs were used for spectra recording, handling and evaluation. The evaluation of EPR spectra was achieved according literature Weil, Bolton and Wertz[1], program Bruker-Xepr, Origin and Data Base of free radicals[2] (NIEHS, Bethesda, Maryland, USA).

Irradiation: UV and visible light irradiation of liquid sample in EPR resonator were used in the study of effect of irradiation on free radicals generation. Samples were irradiated in the EPR resonator using mercury discharge lamp for UV light irradiation (Bruker-Biospin), and halogen lamp for visible light irradiation.

Results

Typical EPR spectrum of Cyanobacteria has been shown on Fig. 1. The spectrum contains: *(i)* broad signal of low spin

Fe(III), *(ii)* organic stable radical, singlet, g = 1.99435, near to signal of free electron g = 2.0032, *(iii)* 2nd singlet of other free radical g = 2.0801, *(iv)* sextet 1 : 1 : 1 : 1 : 1 : 1 of high spin complex of Mn(II). No other signals in broad range are presented. There are new signals by the UV and visible irradiation of Cyanobacteria, see Fig. 2.
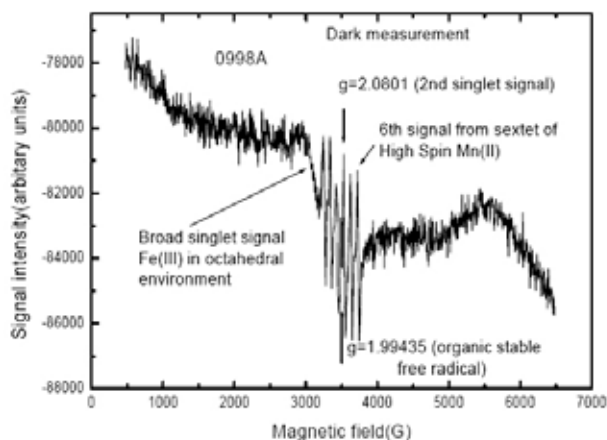
Fig. 1.　**Typical EPR spectrum of aqueous suspension of Cyanobacteria (EPR X-Band, 25 °C, microwave pover 20 mW, Magnetic modulation 0.1 mT)**

Fig. 2.　**EPR spectrum of UV irradiated aqueous suspension of Cyanobacteria (EPR X-Band, 25 °C, microwave pover 20 mW, Magnetic modulation 0.1 mT)**

The generation of unstable free radicals was studied by the spin trapping method, using DMPO as a spin trap. It has been found hydroxyl and nitroxide radicals in Cyanobacteria. Their concentrations increase by the UV and visible irradiation. It has been found hydroxyl radicals and nitroxide radicals. They generate in nature and are dangered for human skin and tissue membranes: danger of irritation, inflammation, fever.

We studied effect of copper sulfate $CuSO_4$ and cyanobacteria interaction in aqueous suspensions. The new free radicals have been found: multi line spectra: their identifica-
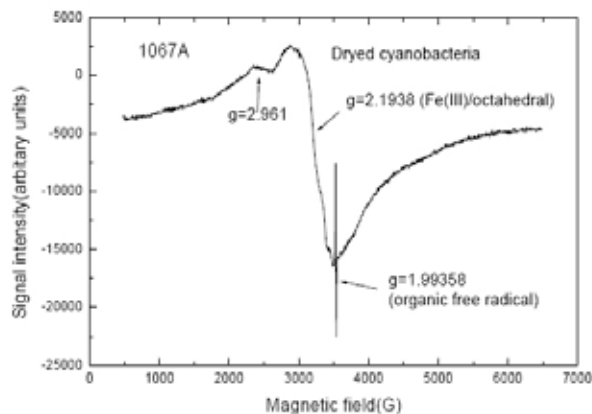
Fig. 3.　**Dryed Cyanobacteria (EPR X-Band, 25 °C, microwave pover 20 mW, Magnetic modulation 0.1 mT)**

tion was not possible. We studied effect of added hydrogen peroxide H_2O_2 to aqueous suspensions of Cynobacteria. The increasing concentration of stable organic radical (g near 2) is generated, hydroxyl and nitroxide radicals. We tried to measure dry cynobacteria. We have measured this EPR spectrum.

We studied effect of straw on free radicals on cyanobacteria surfaces and their interactions.

Wheat straw show the simply EPR spectrum: singlet signal (g = 2.0031, ΔH_{pp} = 0.6619 mT = 6.619 Gauss). There is the possibility of interaction between this radical and radical from Cyanobacteria leading to the breakdown of Cyanobacteria radical.

Barley straw show the simply EPR spectrum: singlet signal (g = 2.00325, ΔH_{pp} = 0.6317 mT = 6.317 Gauss). There is the possibility of interaction between this radical and radical from Cyanobacteria leading to the breakdown of Cyanobacteria radical.

Barley straw (aqueous suspension, bubbled by air at room temperature) show the simple EPR spectrum: singlet signal (g = 2.00, ΔH_{pp} = 0.63 mT = 6.30 Gauss). This signal increases by the UV irradiation of this sample. There is the possibility of interaction between this radical and radical from Cyanobacteria leading to the breakdown of Cyanobacteria radical.

Wheat straw (aqueous suspension, bubbled by air at room temperature): no signal, noise only.

We studied these samples in aqueous suspensions at anaerobic conditions:

Wheat straw show the anisotropic EPR spectrum: ($g_\parallel$ = 2.39, $g_\perp$ = 2.01045, ΔH_{pp} = 24 mT = 240Gauss). Probably radical with axial symmetry. There is small singlet signal in the little part of spectra: g = 1.9924, probably stable organic radical on the surface of straw. These radicals are presented in the environment of wheat straw particles.

Barley straw show the EPR spectrum: (g = 2.2331 ΔH_{pp} = 75 mT = 750 Gauss) probably low spin complex of Fe(III) and spectrum of high spin complex of Mn(II). These

radicals are presented in the environment of Barley straw particles. There is the principle of action of straw against Cyanobacteria free radicals.

Discussion

The generation of hydroxyl and nitroxide radicals on the surface of Cyanobacteria in natural waters has been found using EPR spectroscopy. These radicals could cause damage on the human skin and membranes. Their generation increase by UV and visible light irradiation. The generation of hydroxyl radicals by the breakdown of hydrogen peroxide is accelerated in the presence of Cyanobacteria. Wheat and barley straw generate free radicals, mainly hydroxyl radicals in aqueous suspensions also. These radicals could have interaction with free radicals on Cyanobacteria to destroy it. Cynobacteria contains Fe(III) and high spin Mn(II) complexes. The UV and visible light accelerate their generation and the ultimate concentration is higher. Cyanobacteria accelerate the breakdown of hydrogen peroxide and UV and visible light accelerate this effect. Wheat straw and barley straw generate free radicals which are on their surfaces and in surrounding aqueous solution. These radicals can react with free radicals located on the surface of Cyanobacteria to destroy their. Cyanobacteria (wet and dry) contain complexes of low-spin Fe (III) and high-spin Mn (II). It can play an important role for stabilization of presented unstable free radicals.

Conclusions

We have found the role of free radicals (mostly hydroxyl radicals) in ill-effects of Cyanobacteria. This result pointed to that the effect of these radicals could be eliminated by the action of straw. We have found the effect of UV and visible irradiation on the generation of hydroxyl and nitroxide radicals. Wheat straw and barley straw generate free radicals which are located on their surfaces and in surrounding aqueous solution. We have an idea to fight against Cyanobacteria using free radicals and paramagnetic metal complexes with UV and visible light irradiation.

REFERENCES

1. Weil J. A., Bolton J. R, Wertz J. E.: *Electron Paramagnetic Resonance, Elementary Theory and Practical Applications*, J.Wiley and Sons, N.York 1994.
2. Wyard S. J.: *Elektronenspinresonanz und andere spektroskopische Methoden in Biologie und Medizin*. Akademie-Verlag-Berlin 1973.
3. Stopka P., Křížová J.: Chem. listy *100*, 716 (2006).

L16 MOLECULAR ELECTRONICS: ADVANCES AND LIMITATIONS, STRATEGIES, MATERIALS, METHODS AND APPLICATIONS

MARTIN VALA and MARTIN WEITER

Brno University of Technology, Faculty of Chemistry, Purkyňova 118, Brno 612 00, Czech Republic,
vala@fch.vutbr.cz

Introduction

A molecular electronics (ME) might be defined as set of electronic behaviours in molecule-containing structures that depend upon the characteristic molecular (rather than atomic) organization of space. This behaviour is fixed at the scale of individual molecule, which is the naoscale. While the structures and devices may be macroscopic, the fundamental behavious arise at the molecular level.

Over the past several decades there have been dramatic advances toward the realization of electronic components from organic materials instead of the inorganic semiconductors. The true advencement can be achieved by utilization of the original properties of the organic materials to construct devices based on those individual features, which do not have analogies in the inorganic semiconducting physics. This is usually accomplished with the help of quantum chemical calculations, which can predict the desired properties of new materials prior to the synthesis.

The aim of this article is to introduce some of the strategies developed to take full advantage that the organic-based electronics offer. The attention is paid to solar cells, displays, and transistors representing the most developed applications. Some of them are already entering the commercial world. The last part is devoted to single molecule current switching device as the essential components of molecular memories and as good example of quantum chemistry-synthesis-device pathway used in ME research nowadays.

Materials

There is wide range of materials used in the area of ME. In the present time not only the actively performing materials (electroluminescencent, electric charge fotogenerating, etc.) but also other supporting materials are used to increase the performance of the produced devices. The materials have to cover broad range of requirements and therefore range from the low molecular weight over polymeric ones to supramolecular structures. It is therefore common strategy to tailor the properties by introducing side groups whose position, number and properties adjust the required qualities (preventing of agreagation, solubility, etc.).

However, a wide pool of posibilities exists also for the active area of the device. Many scientific groups and companies use small molecules mainly because of their intrinsic high thermal and optical stability, fatique resistance etc. On the other hand the processing usually requires thermal evaporation under vacuum which migh increase the cost of the device prepared. To increase the performance, the devices usually consists of many layeres (> 20) whose preaparation requires many precise processing steps (e.g. co-evaporation) and can increse the possibillitiy of introduction of defecst and thus might also raise the cost of such devices. Doping of these materials turned out to be a necessary strategy in order to obtain efficient devices. Examples of the materials are in Fig. 1.

The other main class of materials used consists of high molecular weight materials: polymers. The field of semiconducting polymers has it root in the 1977 discovery of the semiconducting properties of polyacetyene[1]. This breakthrough earned Alan Heeger, Alan MacDiarmid, and Hideki Shirakawa the 2000 Nobel Prize in Chemisty for "the discovery and development of conductive polymers".[2–4]

There are four specific types of semiconducting polymers:

- Filled polymers are loaded with conductive fillers, such as carbon black, graphite fiber, or metal oxide particles, and have the broadest application in electronic devices. However, they are inhomogeneous materials, which makes them hevily process-dependent and harder to reproduce.
- Ionically conducting polymers are used in such consumer electronic applications as rechargeable batteries, fuel cells, and polymer light emitting devices although their conductivity is highly sensitive to humidity.
- Conjugated polymers where delocalisation of pi-electrons allows for charge carrier conduction and is responsible for their semi-conducting properties; see Fig. 2.
- Charge-transport polymers have become the most established semiconducting organic system because of their commercial use in xerographic photoreceptors.

A special class of materials consists of molecules specially designed and synthesized to ensure a specific feature on molecular level. As an example we may mention a carotenoid-porphyrin-fullerene ($C\text{-}P\text{-}C_{60}$) triad. When porphyrin absorbs light, it donates electron to the fullerene and take electon form the carotenoid. This leads to charge separation (creation of $C^+\text{-}P\text{-}C_{60}^-$) and is analogous to the processe involved in photosysnthesis[5]. Another example will be discussed later.

Applications

Organic Solar Cells

In principle, there are four types of solar cells in terms of organic based electronics:

- Conjugated polymers based solar cells usually utilize "bulk heterojunction" between semiconducting polymer as an electron donor and low molecular weight acceptor to ensure efficient photo-induced charge generation.
- Small molecular solar cells are based on the same donor-acceptor concept but composed of low molecular weight materials and therefore require different device design and processing.

- Dye-sensitised solar cells are based on electron transfer from organic sensitizer to wide bandgap semiconductor (e.g. TiO_x) and redox reactions of mediator[6,7].
- Organic-inorganic hybrid solar cells compose of nano sized inorganic semiconductors (usually in the form of core-shell nanoparticle whose bandgap and doping levels can be easily tailored) dispersed in polymeric matrix. The charge separation occurs on the prticle-polymer interface[8]. Since our group deals with the first two types we will pay closer attention to their operational principles, material reguirements and device design and advancement.

The solar cells based on conjugated polymers in its simplest form can be acomplised as a metal-insulator-metal (MIM) diode with the metal electrodes of asymmetrical workfunction (Fig. 3.). The potential difference between electrodes have to be high enough to overcome exciton binding energy (energy needed to dissociate Coulomb attraction of the foto-generated electon-hole pair: exciton) othervise the excitons will decay geminately (either radiatively or non-radiatively). The usually used electrodes (indium tin oxide, ITO, as the transparent high workfunction metal and Aluminium as the low workunction metal) do not fulfill this requirement sufficiently. The energy conversion efficiencies are typically 10^{-3}–10^{-1} %, too low for practical applications.[9–11] To overcome this limitation various strategies have been employed to increase the photo-induced charge carrier generation.

One of the possible pathways is to introduce p-n junction by doping. The initial experiments of Chiang et al. in 1978 with p-type and n-type polyacetylene films did not succeeded[12]. The alternative way is to use a Shotky junction between conducting polymer and metal. However, neither this approach solved the problem of inefficient charge carrier generation.[13–15]

To overcome the limitation of the photo-induced charge carrier generation, a donor/acceptor (D/A) approach has been suggested.[16–19] The most widely used concept uses semiconducting polymers as an electron donor and fulerene (C_{60}) as an electron acceptor. Analogically to the p-n junction a bi-layer device can be constructed with the D/A interface between the two layers representing the heterojunction (although the actual physical processes are different). Such device has rectifying current-voltage characteristics even for the same metal electrodes on both sides. The positions of the HOMO and LUMO energy levels have to be choosen carefully to realize charge transfer rather than energy transfer, which does not lead to the charge separation. It was shown that the charge transfer from semiconducting polymers to C_{60} occurs within 50 fs after photo-excitation.[20–22] The charge transfer is therefore more than 10^3 times faster than any other competing process.

It follows that further step for efficient photo-induced charge generation is to increase the interfacial area between the donor and acceptor. Creation of so called "bulk hetero-
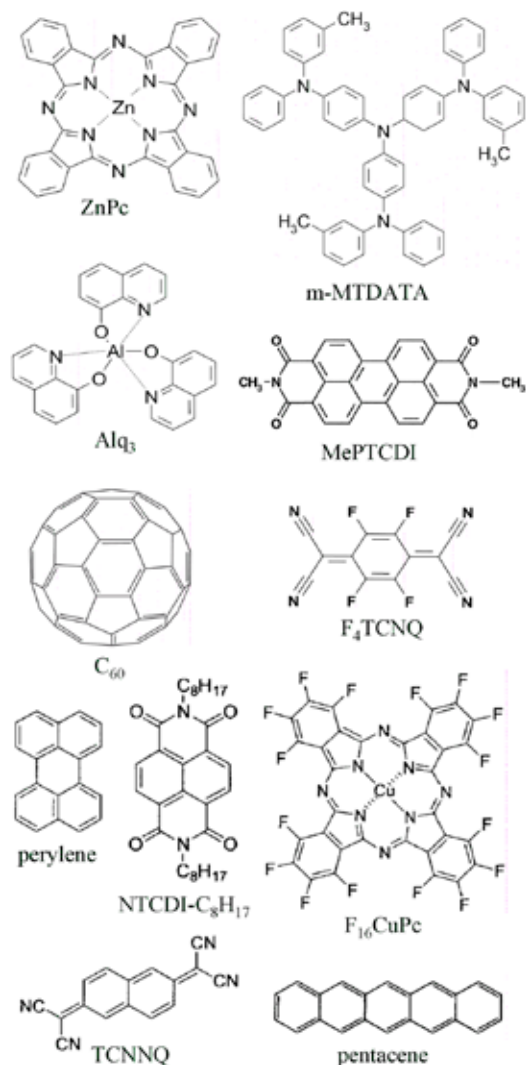
Fig. 1. **Examples of small molecular weight materials nowadays used in molecular electronics as hole transport material (zink pthalocyanine (ZnPc), tris-(phenyl–3-methyl-phenyl-amine)-triphenylamine (m-MTDATA), pentacene), electron acceptors (buckminster-fullerene (C_{60}), 2,3,5,6-tetrafluoro-7,7,8,8-tetra-cyano-quinodimethane (F_4TCNQ)) and electron transport materials (aluminium-tris-8-hydroxy-quinoline (Alq_3), m-MEPTCDI, perylene, NTCDI-C_8H_{17}, F_{16}CuPc, TCNNQ)**

junction" *via* control of the morphology of the phase separation thus have the crutial role for device efficiency[23,24]. Due to the necessity of bipolar charge transport in the bulk an interpenetrating network of D/A phase is further necessary also for equally efficient collection of charges. This approach led to increase of the solar power conversion efficiencies of around 3 %.

Although the polymer based solar cells provide promisssing concept of organic photovoltaics, the match of the absorption spectrum of the polymer with the solar spectrum is rather small and it turned out to be difficult to achieve smaller bandgap in polymers. Alternatively, small organic

dye molecules have been studied as promising materials for photovoltaic devices.[25–30] One of their advantages is their high absorption coefficient (~ 10^5 cm^{-1}) with good overlap with the solar spectrum.
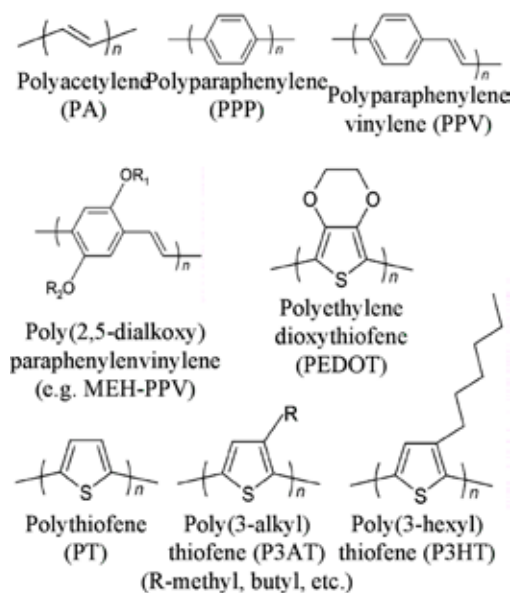
Fig. 2. **Molecular structures of a few conjugated polymers, note the bond-alternated structure responsible for the semi-conducting properties (p-type)**

The general structure of this type of solar cells is in the form of PIN (p-doped/intrinsic/n-dopoed) composed of the active layer and doped wide bandgap materials for hole and electron transport, see Fig. 4. The intrinsic layer is usualy composed of mixture of donor/acceptor molecules which create bulk heterojunction in the same way as in the case of polymer based solar cells. This approach has several advantages.

(i) The transport layers are doped in order to increase the conductivity and thus reduce the ohmic losses. *(ii)* Quenching processes at the electrode can be avoided because excitons created in the active layer cannot penetrate into the wide-gap transport layers. *(iii)* The thickness of the highly conductive spacer layers can be tuned to optimize the optical field distribution in the solar cell. *(iv)* The increased overall thickness of the devices allows higher stability and a lower probability for short cuts.

O r g a n i c   L i g h t   E m i t t i n g   D i o d e s

Since the first demonstration of efficient light emission from organic light emitting diodes (OLEDs) by the Kodak[31], the attention of following research were paid to lower operating voltages, higher efficiencies and longer lifetimes of the devices. As for the photovoltaics there are also two main clases of materials used: The polymer based LEDs mainly benefiting from the solution processing and the small molecules based LEDs with better stability and efficiency[32].
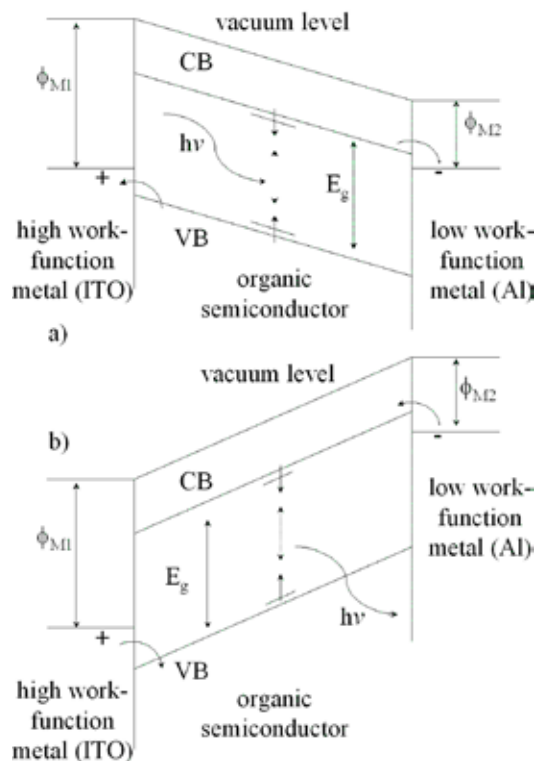
Fig. 3. **a) Charge generation in a single layer organic semiconductor device under short cut conditions (MIM structure), b) the same device under forward bias with suffitient charge injection shows light emission (electroluminiscece). VB is the valence band, CB conduction band, E$_g$ bandgap and φ workfunction**

Electroluminiscence form conjugated polymers were first reported in 1990, using poly(*p*-phenylene vinylene), PPV, as the single semiconductor layer sandwitched between metallic electrodes with different workfunctions. The MIM diode-like structure is the same as depicted for the case of single layer solar cell in Fig. 3. Under sufficient forward bias, holes from the high workfunction metal and electrons form the low workfunction metal are injected in to the thin film of organic semiconductor. Capture of oppositely charged carriers within the semiconductor can then result in photon emission.

The efficiency of the first simple LEDs based on polymers were reatively low, of the order of 10^{-4} photons generated within the device per electron injected (an internal quantum efficiency of 0.01 %)[33]. The internal quantum efficiency is defined as product of the ratio of the number of exciton formation events within the device to the number of electron flowing in the external circuit, the fraction of excitons which are formed as a singlets and the efficiency of radiative decay of these singlet excitons. In order to achieve efficient luminescence, it is therefore necessary to have good balancing of electon and hole currents, efficient capture of electons and holes within the emissive layer, strong radiative transitions

for singlet excitons, and efficient coupling of these excitons to photon states allowed in the device structure.

The electon-hole capture leads to formation of excitons. The spin wavefunction of the exciton can be either singlet or triplet. Because of the exchange energy (the difference between the singlet and triplet state) is usually large, the allowed radiative emission is from the singlet only (fluorescence). Assuming that the electon-hole capture is spin independent (Langevin model) the created excitons are in the triplet and singlet configuration in the ratio 3 : 1, therefore it is expected to loose 75 % of the electron-hole pairs. It would be therefore very attractive to use the triplet excitons. One possible approach is to introduce high-atomic-number elements with strong spin-orbit coupling to utilize the triplet luminescence (phosphorescence).[34–36] However, the triplet emission is usually red-shifted and it turned out to be rather difficult to utilize this approach for emission of green and blue colours.[34,35,37]

a)

b)

low work-
function
metal (Al)

| electron transport |
| emissive layer |
| hole transport |
| substrate |

hole blocking

electron
blocking

high work-
function
metal (ITO)
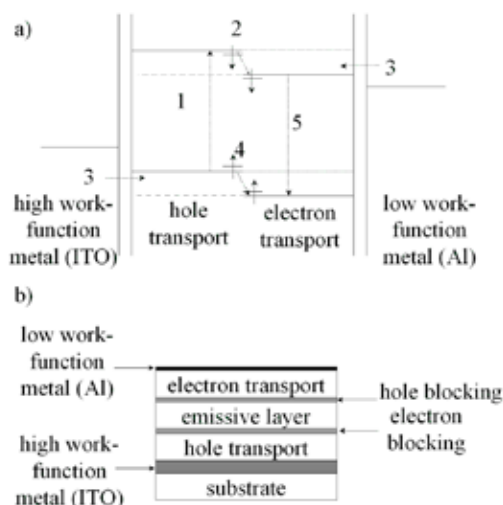
Fig. 4.   **a) Schematic diagram of a bilayer device and formation of bulk heterojunction (dotted lines) before contact of the materials is made. The charge generation process (1 – absorption, 2 – charge transfer and subsequent exciton dissociation) and light emission process (3 – charge injection, 4 – tunneling across a barrier and capture of charges and 5 – light emission), b) diagram of multilayer device configuration. Each of the layers can consist of more materials (doped) and each of the interfaces can be tailored**

Efficient electron-hole capture can be acomplished only with high density of charges in the emissive layer. Therefore great attention is paid to charge injection and transport. There exist several mechanisms that are involved for the injection of charges from metal electrodes. For diodes with large barriers either the thermionic emission or tunneling can limit the current flow. Therefore proper selection of metals used as the contact and series of pre-contact layers are employed to lower the potential barriers. Using this approach the charge injection is no more considered to limit the current flow.

Instead, the current flow is bulk-limited through the bild-up of space charge[38].

The need for balanced electron and hole current let to implementation of hole-conducting and electon-conducting layers and thus to the creation of heterojunction in the same fashion as for the solar cells, see Fig. 4. Injected charges move to the heterojunction at which they are confined by the potential barrier. Depending on the relative position of the energy position electrons or holes tunnel through this barrier and electon-hole capture lead to the electroluminescence from the respective layer. Using this approach external quantum efficiecies up to 2,5 % were obtained[39,40].

All of the principles mentioned for the polymer based LEDs are valid also for LEDs based on small molecules. In fact many of the strategies described were simultaneously or firstly discovered using this type of materials (e.g. the bilayer structures). Simirally to the solar cells the preparation technique (sublimation) offers easy way for doping and co-deposition of several materials and therefore provides additional degrees of freedom and potentially better tunability of the device performance[41]. The structures that are nowadays under study are usually composed of many layers and inter-penetrating regions with controlled thickness, level of n- or p-type doping and provides energetic barier reduction, electron or hole transport or serves as blocking layers and finaly as emissive layers with specific colour or white light emission (>20 layers). For the commercial utilization dynamic in-line deposition techniques producing efficient enough OLEDs with low operational voltages are currently under study[42].

Organic Thin-Film Transistors

Organic thin-film transistors (OTFTs) based on conjugated polymers, oligomers, or fused aromatics have been forecasted as a viable alternative to the traditional thin film transistors based on inorganic semiconductors. But because of the relatively low charge carrier mobilities (μ) in organic semiconductors OTFTs cannot rival the performance of field effect transistors based on inorganic single crystals such as Si, Ge and GaAs, which have charge carrier mobilities of three or more orders of magnitude higher[43]. Therefore, OTFTs are not suitable for high switching frequency applications. However, like in the case of photovoltaic and LED applications, OTFTs can be competitive candidates for applications requiring large area coverage, structural flexibility, low temperature processing, and especially low cost manufacturing (e.g. flat panel displays, sensors, radio-frequency identification tags (RFIDs), etc.).

Due to the weak intermolecular interaction forces, typically van der Waals with energies smaller than 10 kcal·mol^{-1}, which is close to the vibrational energy at or above RT, the upper limit of microscopic mobilities in organic molecular crystals for T = 300 K falls between 1 and 10 cm^{2}V^{-1}s^{-1} (ref.[44]). In contrast, in inorganic semiconductors such as Si, Ge and GaAs, the atoms are held together with very strong covalent bonds, which in the case of Si have energies as high as 76 kcal mol^{-1}. The charge carriers move as highly

delocalised plane waves and have a very high mobility at RT ($\mu \sim 10^3$ cm^{2}V^{-1}s^{-1}).

The boundary between band transport and hopping is defined by materials having RT mobilities of the order of 1 cm^{2}V^{-1}s^{-1}(ref.[44]). Thin films of highly oriented organic semiconductors, such as several members of the acene series including pentacene, have RT mobilities in this intermediate region. Furthermore, very high mobility values have been measured using time of flight (TOF) experiments (up to 400 cm^{2}V^{-1}s^{-1} for holes in single crystals of naphthalene at 4.2 K[45, 46]) and field effect experiments (up to $\sim 10^5$ cm^{2}V^{-1}s^{-1} for holes in single crystals of tetracene and pentacene at 1.7 K[47,48]) following a power law ($\mu \approx T^{-n}$). This gives the evidence for band-like transport in these high qualities, ultra pure single crystals. On the other hand, this behaviour is rather impossible to observe in amorphous or polycrystaline films because traps attributed to grain boundaries and other structural defects dominate transport[49]. The carrier transport takes place by hopping between localised states and carriers are scattered at every step.

Several strategies leading to increased mobilities in organic materials follow from these fundamental limits[43]. One of them is to strengthen the intermolecular interactions. Stronger interactions would lead to more rigid crystalline structures and thus it would take temperatures higher than RT to generate subtatntial scattering of charge carriers. A second way is to dramatically reduce the conduction path. If the carrier transport occurs via an array of single molecules, such as polymer chains or nanotubes the mobility is no more influenced by the grain boundary or other structural defects. Reduction of the TFT channel from micrometer to nanometer size led to mobilities of the order of 100 cm^{2}V^{-1}s^{-1} in the case of carbon nanotubes[50].

Molecular Switch

This chapter deals with construction of molecular current switch based on light driven switching of on-chain charge carrier mobility investigated at our department. To describe the proposed molecular switch, we have to briefly describe origin of traps in molecular solids first, for details see[49].

According to electrostatic approach, the ionisation energy of a crystal (I_c) is related to the molecular value (I_g) by $I_c = I_g - P$. The parameter P, referred to as the polarisation energy, represents the energy of interactions between a charge carrier localised on a given lattice site and the surrounding polarizable lattice. Local decrease of I_c in an otherwise perfect crystal lattice represents a trap for moving hole. The trap can be thus created *(i)* on a host molecule with suitably low I_g, or *(ii)* by increasing of the value of the polarization energy P contrary to that in a physically perfect material. In a molecular solid build of non-polar polarizable units, e.g. polymer segments, containing a small amount of polar guest species, its dipole moment contributes to the field acting on surrounding molecules and modifies the local values of the polarization energy. Thus, the presence of polar species may result in production of local states in their vicinity; even thus they

are not necessarily trapping sites themselves. The calculations of trap parameters (depth, extension) indicate that local perturbations of the polarization energy due to the presence of a highly polar guest molecule may result in extension over several lattice constants, and hence should influence the on-chain charge carrier mobility[51].

Changing of the dipole moment of suitably chosen side groups both, chemically attached to the polymer chain via a neutral spacer or dispersed in the matrix, thus results in changing of the on-chain charge carrier mobility. Use of photochromic side groups make it possible to modulate the charge mobility by light-activated photochromic reaction.
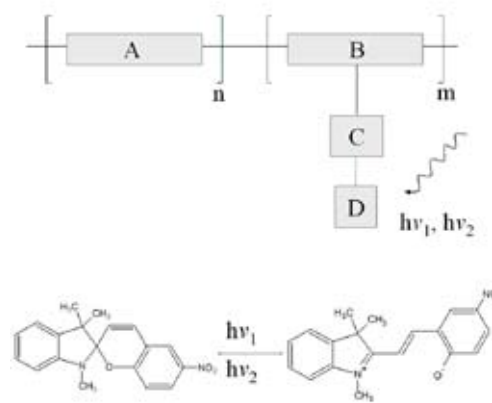
Fig. 5. **Schematic representation of light driven molecular current switch and photochromic reaction of spiropyran. The two states can be obtained using light of different wavelength (UV for the forward and VIS for the back reaction)**

The molecular current modulator is schematically demonstrated in Fig. 5. The switch consists of a molecular wire with suitable bistable side group(s). Various materials can be used to build the switch. Blocks A and B (molecular wire) can be realised by π- or σ- conjugated polymer chains as depicted in Fig. 2. The spacer C can be realised by several chemical structures, its length being easily tailored to needs resulting from e.g. model calculations. The active switching system (block D) should be selected in order to produce large dipole moment change in its two states as described above. The active moiety can be successfully realised by e.g. spiropyrans (Fig. 5.). Depending on substituents attached to their backbones, these molecules can change their dipole moment from 2–5 D to 5–13 D (theoretical calculations reveal up to 30 D)[52].

The change of the electrostatic potential due to the charge-dipole interactions shifts the transport levels. Since the position and orientations of the additive are essentially random the effect results in broadening of the distribution of transport states[53,54] and to the decrease of the charge carrier mobility[55,56,57].

In a similar way to the charge-dipole interactions resulting in mobility switching the formation of chemical traps was also demonstrated[58]. Quantum mechanical calculations

showed the possibility of the participation of the main chain electrons in the photochromic process of the side group and points to the importance of the chemical structure of the spacer. The spacer can be realised as a 'quasi-neutral' from the point of view of the charge transfer, or can freely transfer the charge. In the former case, the electrostatic contribution of the polar side groups, based on the charge-dipole interactions, is the most important factor influencing the behavior of the charges on the molecular wire. In the latter case however, the situation is more complex: the change of the chemical structure and charge redistribution on the substituent, and a charge redistribution between the molecular wire and the photochromic group may influence the ionization energy of the entire polymer segment. Such modification may results in the creation of a chemical trap on the segment.

Conclusions

Since the early times in 1970s molecular electronics went through long way from visionary (sometimes speculative) ideas over pioneering measurement of molecular-level properties to devices efficient enough enabling to start their mass production. Despite such immense development there are still many fundamental aspects that need to be answered in order to fully exploit the potential this area offers as can be seen from the examples we outlined in this article. The progress can be possible only with synergic development in many scientific areas e.g. physics, chemistry, quantum chemistry, metrology and in close cooperation of basic and applied research (science and technology).

REFERENCES

1. Chiang C. K., Fincher C. R., Park Y. W., Heeger A. J., Shirakawa H., Louis E. J., Gau S. C., MacDiarmid A. G.: Phys. Rev. Lett. *39*, 1098 (1977).
2. Heeger A. J.: Synth. Met. *125*, 23 (2002).
3. MacDiarmid A. G.: Synth. Met. *125*, 11 (2002).
4. Shirakawa H.: Synth. Met. *125*, 3 (2002).
5. Liddell P. A., Kuciauskas D., Sumida J. P., Nash B., Nguyen D., Moore A. L., Moore T. A., Gust D.: J. Am. Chem. Soc. *119*, 1400 (1997).
6. Grätzel M.: J. Photoch. Photobio. C *4*, 145 (2003).
7. Durrant J. R., Haque S. A., Palomares E.: Coordin. Chem. Rev. *248*, 1247 (2004).
8. Huynh W. U., Dittmer J. J., Teclemariam N., Milliron D. J., Alivisatos A. P., Barnham K. W.: Phys. Rev. B *67*, 115326 (2003).
9. Yu G., Zhang C., Heeger A. J.: Appl. Phys. Lett. *64*, 1540 (1994).
10. Antoniadis H., Hsieh B. R., Abkowitz M. A., Stolka M., Jenekhe S. A.: Polym. Prepr. *34*, 490. (1993).
11. Karg S., Riess W., Dyakonov V., Schwoerer M.: Synth. Met. *54*, 427 (1993).
12. Chiang C. K., Gau S. C., Fincher C. R., Park Y. W., MacDiarmid A. G., Heeger A. J.: Phys. Rev. Lett. *33*, 18 (1978).
13. Antoniadis H., Hsieh B. R., Abkowitz M. A., Stolka M., Jenekhe S. A.: Polym. Prepr. *34*, 490 (1993).
14. Antoniadis H., Hsieh B. R., Abkowitz M. A., Jenehke S. A., Stolka M.: Synth. Met. *62*, 265 (1994).
15. Rieß W., Karg S., Dyakonov V., Meier M., Schwoerer M.: J. Lumin. *60–61*, 906 (1994).
16. Sariciftci N. S., Smilowitz L., Heeger A. J., Wudl F.: Science *258*, 1474 (1992).
17. Sariciftci N. S., Braun D., Zhang C., Srdanov V., Heeger A. J., Stucky G., Wudl F.: Appl. Phys. Lett. *62*, 585 (1993).
18. Yu G., Gao J., Hummelen J. C., Wudl F., Heeger A. J.: Science *270*, 1789 (1995).
19. Halls J. J. M., Walsh C. A., Greenham N. C., Marseglia E. A., Friend R. H., Moratti S. C., Holmes A. B.: Nature *376*, 498 (1995).
20. Kraabel B., McBranch D., Sariciftci N. S., Moses D., Heeger A. J.: Mol. Cryst. Liq. Cryst. *256*, 733 (1994).
21. Kraabel B., Hummelen J. C., Vacar D., Moses D., Sariciftci N. S., Heeger A. J.: J. Chem. Phys. *104*, 4246 (1996).
22. Lanzani G., Zenz C., Cerullo G., Graupner W., Leising G., Scherf U.: Synth. Met. *111–112*, 493 (2000).
23. Brabec C. J., Shaheen S. E., Fromherz T., Padinger F., Hummelen J. C., Dhanabalan A., J. Janssen R. A., Sariciftci N. S.: Synth. Met. *121*, 1517 (2001).
24. Hoppe H., Glatzel T., Niggemann M., Schwinger W., Schaeffler F., Hinsch A., Lux-Steiner M., Sariciftci N. S.: Synth. Met. *511–512*, 287 (2006).
25. Simon J., Andre J. J.: *Molecular semiconductors*, Spring, Berlin, Heidelberg, 1985.
26. Tang C. W.: Appl. Phys. Lett., 48, 183 (1986)
27. Wöhrle D., Meissner D.: Adv. Mater. *3*, 129 (1991).
28. Petrish K., Dittmer J. J., Marseglia E. A., Friend R. H., Lux A., Rozenberg G. G., Moratiti S. C., Holmes A. B.: Sol. Energy Matter. Sol. Cells *61*, 63 (2000).
29. Debeyhu D., Männig B., Drechsel J., Leo K., Pfeiffer M.: Sol. Energy Matter. Sol. Cells *79*, 81 (2003).
30. Drechsel J., Männig B., Debeyhu D., Pfeiffer M., Leo K., Hoppe H.: Org. Electron. *5*, 175 (2004).
31. Tang C. W., VanSlyke S. A.: Appl. Phys. Lett. *51*, 913 (1987).
32. Shi J., Tang C. W.: Appl. Phys. Lett. *70*, 1665 (1997).
33. Burroughes J. H., Bradley D. D. C., Brown A. R., Marks R. N., Mackay K., Friend R. H., Burns P. L., Holmes A. B.: Nature *347*, 539 (1990).
34. Baldo M. A., O'Brien D. F., You Y., Shoustikov A., Sibley S., Thompson M. E., Forrest S. R.: Nature *395*, 151 (1998).
35. Cleave V., Yahioglu G., Le Barny P., Hwang D. H., Holmes A. B., Friend R. H., Tessler N.: Adv. Mater. *13*, 44 (2001).

36. Pfeiffer M., Forrest S. R., Zhou X., Leo K.: Org. Electron. *4*, 21 (2003).
37. Cleave V., Yahioglu G., Le Barny P., Friend R. H., Tessler N.: Adv. Matter. *11*, 285 (1999).
38. Blom P. W. M., De Jong M. J. M., Vleggar J. J. M.: App. Phys. Lett. *68*, 3308 (1996).
39. Baigent D. R., Greenham N. C., Gruner J., Marks R. N., Friend R. H., Morrati S. C., Holmes A. B.: Synth. Met. *67*, 3 (1994).
40. Becker H., Burns S. E., Friend R. H.: Phys. Rev. B *56*, 1893 (1997).
41. Pfeiffer M., Leo K., Zhou X., Huang J. S., Hofmann M., Werner A., Blochwitz-Nimoth J.: Org. Electron. *4*, 89 (2003).
42. May C., Tomita Y., Toerker M., Eritt M., Loeffler F., Amelung J., Leo K.:Current Appl. Phys. *3*, 293 (2003).
43. Dimitrakopoulos C. D., Malenfant P. R. L.:Adv. Mater. *14*, 99 (2002).
44. Pope M., Swenberg C. E.: *Electronic Processes in Organic Crystals and Ppolymers, 2nd ed.,* Oxford University Press, Oxford 1999.
45. Warta W., Stehle R., Karl N.: Appl. Phys. A *36*, 163 (1985).
46. Karl N., Marktanner J., Stehle R., Warta W.: Synth. Met. *41–43*, 2473 (1991).
47. Shön J. H., Kloc C., Batlogg B.: Org. Electron. *1*, 57 (2000).
48. Shön J. H., Kloc C., Batlogg B.: Science *288*, 2338 (2000).
49. Sworakowski J., Janus K., Nešpůrek S., Vala, M.: IEEE T. Dielect. El. In. *13*, 1001 (2006).
50. Collins P. G., Arnold M. R., Avouris P.: Science *292*, 706 (2001).
51. Nešpůrek S., Sworakowski J., Thin Solid Films *393*, 168 (2001).
52. Dürr H., Laurent H. B.: *Photochromism: Molecules and Systems, 2nd ed.,* Elsevier Science B.V., Amsterdam, 2003.
53. Toman P., Nešpůrek S., Weiter M., Vala M., Sworakowski J., Bartkowiak W., Menšík M.: Nonlinear Opt. , Quantum Opt. *36*, 289 (2007).
54. Toman P., Nešpůrek S., Weiter M., Vala M., Sworakowski J., Bartkowiak W., Menšík M.: Polym. Adv. Technol. *17*, 673 (2006).
55. Weiter M., Vala M., Zmeškal O., Nešpůrek S., Toman P.: Macromol. Symp. *247*, 318 (2007).
56. Bletz M., Pfeifer-Fukumura U., Kolb U., Baumann W.: J. Phys. Chem A *106*, 2232 (2002).
57. Vala M., Weiter M., Zmeškal O., Nešpůrek S., Toman P.: Macromol. Symp., accepted.
58. Nešpůrek S., Toman P., Sworakowski J., Thin Solid Films *438–439*, 268 (2003).

L17 MUTUAL RELATION BETWEEN FRACTAL AND STATISTICAL (RANDOM, THERMODYNAMIC) PHENOMENA IN NATURE

OLDŘICH ZMEŠKAL, MARTIN WEITER, MARTIN VALA and TOMÁŠ BŽATEK

Brno University of Technology, Faculty of Chemistry, Purkynova 118, 612 00 Brno, Czech Republic,
zmeskal@fch.vutbr.cz

Introduction

This paper deals with the unification of views on different physical and chemical fields of knowledge on natural phenomena. We put into context physical quantities defined in fractal physics, thermodynamics and statistical physics with general mathematical description by momentum of random quantities.

The mathematical tools of fractal physics enable a universal description of such phenomena as e.g. thermal radiation, conduction and convection of heat, properties of ideal and real liquids and/or gases, thermodynamic entropy of closed and open system and classic and quantum distribution functions.

This unification is not only of a theoretic importance, but enable the implementation of further modules into the HarFA application (developed by authors of this paper). The program HarFA was intended for fractal analysis of digital images, video clips, signals and numerical data sets. The new modules enable calculation of five fractal dimensions (topological, information – thermodynamic, correlative, skewness and kurtosis) which relate to corresponding moments and entropies. Thus a unification of phenomena description by different sciences is achieved.

Theoretical Backgrounds

General and Central Moments

To describe studied phenomenon, various mathematical apparatus is used in different science areas. As an example we can mention mechanics, statistical physics and physical chemistry which use general and central moments do define mean values of the respective physical qualities (e.g. position, velocity, acceleration) or their deviations form the mean values (absolute error, standard deviation, skewness, kurtosis).

Generally these moments for one variable functions can be expressed using equations (1) and (2), ref.[1].

General moments of qth order of discrete and continuous functions in real number field can be defined using the equations

$$M_q = \int_{-\infty}^{\infty} x^q f(x)\,dx \quad , \quad M_q = \sum_{i=0}^{\infty} x_i^q f(x_i) \quad . \tag{1}$$

Similarly the central moment q^{th} order of the discrete or continuous functions related to general moment of the first order (mean value μ) can be defined as

$$m_q = \int_{-\infty}^{\infty} (x-\mu)^q f(x)\,dx \;,\; m_q = \sum_{i=0}^{\infty} (x_i-\mu)^q f(x_i)\;. \tag{2}$$

Absolute Errors

To calculate absolute values of random real quantities values of qth order defined in the final interval or in final interval of random real quantities with functional values uniformly distributed ($f(x)$ = const.) can the equation (2) written as

$$r_q = \frac{1}{l}\int_0^l |x-\mu|^q\,dx \;,\; r_q = \frac{1}{n}\sum_{i=0}^{\infty} |x_i-\mu|^q\;. \tag{3}$$

The comparison of the equation (2) and (3) gives an evidence that the central moments of the even orders are in the case of uniform distribution of random quantities equal to the absolute errors of the random quantities but the odd orders differ (e.g. central moment 1st order $m_1 = 0$, r_1 is an absolute error of random value).

To compare the random samples, standardization to central moment of 2nd order (to standard deviation σ) is often employed

$$R_q = \frac{1}{l}\int_0^l \left|\frac{x-\mu}{\sigma}\right|^q dx \;,\; R_q = \frac{1}{n}\sum_{i=0}^{\infty} \left|\frac{x_i-\mu}{\sigma}\right|^q \;, \tag{4}$$

where $\sigma = r_2^{1/2}$. A simple consideration we can derive that $R_2 = 1$, R_3 is *skewness* (standardized moment of 3rd order) and R4 is *kurtosis* (standardized moment of 4th order). These equations are used as a standard DIN EN ISO 4287/ASME *Perthometer. Surface Texture Parameters* used for surface roughness evaluation although the equations have more general character.

Entropy and Fractal Dimension

The entropy is very often used for describing of statistical processes. The Kolmogorov K-entropy is important characteristic which describes a degree of chaoticity of the system. It is well-known that: in an ordered system ($K = 0$), in a random system ($K \to \infty$) and in a chaotic (semi deterministic) system ($0 < K < \infty$).

The generalized entropy K_q can be defined like the generalized dimension. From the term of generalized entropy[3] the Renyi entropy S_q of q order implicit

$$S_q = \frac{1}{1-q}\ln\int_0^l p^q\,dx \;,\; S_q = \frac{1}{1-q}\ln\sum_{i=1}^{\infty} p_i^q \;, \tag{5}$$

where p (p_i respectively) is probability of continuous (discrete) random process.

It follows form the comparison of the equations (3) and (4) that the Renyi entropy of q order is related with absolute errors of q order defined for the statistical evaluation of random samples $S_q = \ln R_q/(1-q)$ for probability (relative frequency) defined by term $p_i = (x_i - \mu)/(n\sigma)$. It is evident that for $q < 1$ will be entropy positive ($S_0 = \ln m$, so called *topological* or *Hausdorff entropy*) and for $q > 1$ will be entropy

negative already. The special case is for $q \rightarrow 1$ when the value of numerator is implicate to zero and entropy will be

numerator is implicate to zero and entropy will be

$$S_1 = \sum_{i=1}^{m} p_i \ln p_i \;\; \text{or} \;\; S_1 = k_B \sum_{i=1}^{m} p_i \ln p_i \,, \qquad (6)$$

The left term is called *information* or *Shanon entropy*, the right one (information entropy multiplied by Boltzmann constant) as a *thermodynamic entropy*. The entropies for $q = 2, 3$ or 4 are called as *correlation*, *skewness* or *kurtosis entropy*. Fractal dimensions can be assigned to individual entropies

$$S_q = -D_q \ln r \qquad (7)$$

The dimensions for $q = 0, 1, 2, 3$ or 4 are called *topological (Hausdorff)* information *(Shanon)*, *correlation*, *skewness* or *kurtosis dimension*.

Experimental

F r a c t a l   D i m e n s i o n

Statistical (e.g. thermodynamic) processes can be also understood as fractal systems. In this case the fractal algebra is used for its description. Suppose that cell with size $r = 1$ will have K states (K is so called fractal measure). The cell with dimension $r < 1$ will than have $N(r) \leq K$ states given quality according to the way the states are distributed in the cell (microstates in macrostate). The type of the distribution can be described using quantity called fractal dimension D. Relating of this number to the elementary cell unit in E-dimensional space (r^E), the density of fractal quantity $F(e)$ can be determined. Dependence of number of states $N(r)$ and density of fractal quantity $F(r)$ is defined by equations

$$N(r) = K \cdot r^D \,,\;\; F(r) = K \cdot r^{D-E} \,. \qquad (8)$$

To determine the fractal structure parameters for special cases of deterministic fractals analytical or numerical methods (e.g. radius or box counting method) can be used. The fractal parameters can be in these cases determined by the linear regression of dependence

$$\ln N(r) = \ln K + D \ln r = \ln K - S(r) \,, \qquad (9)$$

where $S(r)$ is so far unspecified entropy (5). This entropy can be determined from the statistical parameters (4). For $q = 0$ it yields

$$S(r) = \ln R(r) = \ln m(r) - \ln n \,. \qquad (10)$$

Comparing the equations (9) and (10) we can see that the fractal measure K is total number of states n and $m(r) = N(r)$ and is number of states having the defined qualities. Using the radius method it is related to number of black and white pixels threshold pictures in a selected area with the size of r. Using box counting methods it is related to a number of squares with the size $\varepsilon = 1/r$ with all pixels neither black

(N_{WBW}) or white (N_{WBW}), respectively. In this case it is also possible to determine numbers of squares with pixels neither black nor white (N_{BW}). Subsequently, from the (9) and (10) dependencies is possible to derive fractal measure K, fractal dimension D, entropy S and absolute error r (R respectively). All of these parameters can be derived with the help of HarFA 5.3. software developed by the authors of the contribution.

The new version of the HarFA 5.4. allows for determination of all of the statistical and fractal parameters mentioned above following from the moments of q order ($q = 0$, 1, 2, 3 or 4).

The area of surface and volumes under and above this area in % can be calculated from fractal measures

$$S_{BW} = \frac{K_{BW}}{K_{BBW} + K_{WBW} - K_{BW}} 100 \quad (\%) \,, \qquad (11)$$

$$V_B = \frac{K_{BBW} - K_{BW}}{K_{BBW} + K_{WBW} - K_{BW}} 100 \quad (\%) \,, \qquad (12)$$

$$V_W = \frac{K_{WBW} - K_{BW}}{K_{BBW} + K_{WBW} - K_{BW}} 100 \quad (\%) \,. \qquad (13)$$

Fig. 1.   **Fractal structure of the real sample surfaces (U10, U30)**
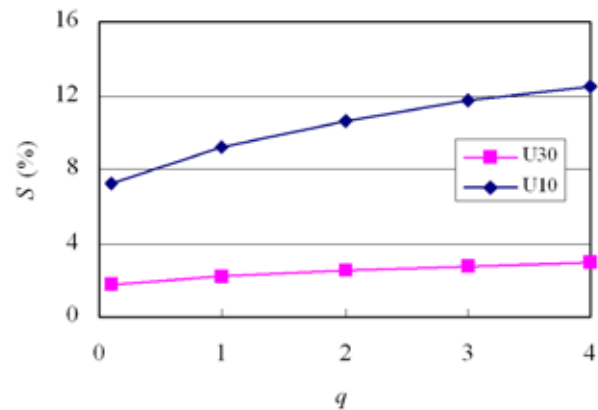
Fig. 2.   **Fractal analysis of inhomogenities of thin film layer surface for different moments of qth order**

The results of these calculations for all moments and different parts of the sample (U10, U30, see Fig. 1.) are shown

at Fig. 2. This figure shows dependence of surface size of selected part for different moments q = 0.1, 1, 2, 3 and 4.

The dependence of surface structure fractal dimensions for all these moments is at Fig. 3. We can see the decreasing fractal dimension for higher order values.
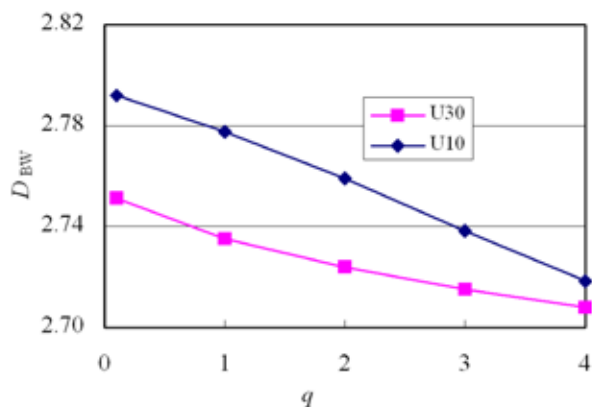
Fig. 3. **Surface structure fractal dimension of U10 and U30 samples for different moment of qth order**

Conclusions

Direct relation of the description of various physical and physical-chemical phenomenons in various science areas (statistical physics, thermodynamics, and fractal physics) is described in the contribution. It follows that the fractal analysis methods originally used to analyse threshold pictures can be easily utilized for continuous phenomenon in informatics, thermodynamics, kinetics theory of gases, etc.

REFERENCES

1. *Moment (mathematics)*, definitions in Wikipedia: http://en.wikipedia.org/wiki/Moment
2. *Perthometer. Surface Texture Parameters*. standard DIN EN ISO 4287/ASME. Göttingen: Mahr GmbH, 1999.
3. Grassberger P., Procaccia I.: Phys. Rev. Lett. *50*, 346 (1983).
4. Grassberger P.: Phys. Lett. *97*, 227 (1986).
5. Zmeskal O., Nezadal M., Buchnicek M.*:* Chaos, Solitons Fractals *17*, 113 (2003).
6. Zmeskal O., Nezadal M., Buchnicek M.: Chaos, Solitons Fractals *19*, 1013 (2004).

7.2. Posters

P01 INFLUENCE OF REGENERATED HUMIC ACIDS ON POLYVINYL ALCOHOL THERMO-OXIDATIVE STABILITY

BARBORA BAKAJOVÁ, ZOJA VLČKOVÁ and JIŘÍ KUČERÍK

Brno Univerzity of Technology ,Purkyňova 118, 612 00 Brno, Czech Republic,
xcbakajova@fch.vutbr.cz

Introduction

Transformation of coal into humic acids (HA) can be achieved by means of the oxidation process. Oxidation could be ideally considered as an inverse diagenetic process able to regenerate the molecules, which originally led to the insoluble structure of the coal. The HA produced is generally called "regenerated" humic acid (RHA) or oxyhumic acid[1]. Oxidation can be performed using many of the oxidants usually utilized in organic chemistry (HNO_3, $KMnO_4$, H_2O_2, etc.)[2].

The practical final result of the acidic treatment of the alkaline solution of humates, extracted from oxycoal, is a black, amorphous, water-insoluble regenerated HA (RHA) powder. RHA have similar characteristics and chemical behavior like the original HA, whose conversion led to coal. In fact RHA generally contain more carbon and less oxygen than HA obtained from natural environments. The major functional groups in RHA are carboxylic and phenolic groups[1].

The goal of this work is to evaluate the antioxidant or pro-oxidant efficiency of RHA as additives in polyvinylalcohol (PVA) blends.

Experimental

Line of four humic acids was obtained from South Moravian lignite and extracted by the IHSS standard alkaline method[3]. Before extraction, part of lignite sample, milled and sieved (0.2 mm) was pretreated with different oxidizing agents for 30 minutes, filtrated and washed with deionized water until agent-free.

As a reference, a HA sample was extracted from non-treated lignite. All these samples were mixed with solution of polyvinyl alcohol (PVA) (2 $g\,dm^{-3}$) to obtain, after water evaporation, final concentrations in the polymer 0.5, 2 and 5 % wt.

Thermogravimetry analysis

Thermogravimetry (TA instruments) with the dynamic air atmosphere was used for testing of PVA/RHA blends. The airflow rate was set at 25 ml per minute and the heating rates were 0.5, 1, 3, 5, 7, 10 and 15 K per minute. The measurement was carried out from room temperature to 600 °C.

As a measure of stability the induction period (IP) was determined. The thermogravimetric records showed two steps of weight loss, the first one attributable to loss of water, whereas the second one to the degradation of the polymer.

Table I
Samples of regenerated humic acids

Sample	Pretreatment agent
HA 1	–
RHA 2	5% HNO_3
RHA 3	10% HNO_3
RHA 4	20% HNO_3

The onset of the latter step corresponded to the end of IP and it was detected by the extrapolation of inclination of 1st derivative weight curve of the TG curve (DTG) for several temperature rates (Fig. 1.). The IP was determined using equations with Arrhenius temperature function (1).

$$t_i = A \exp(B/T) \tag{1}$$

t_i is a length of the induction period, A and B are adjustable kinetic parameters and T is temperature.
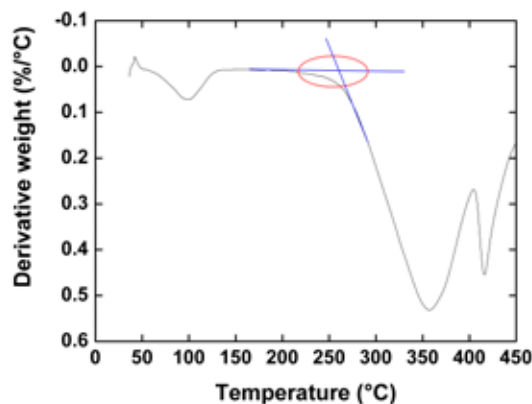
Fig. 1. **Onset temperature detected by the extrapolation of inclination of 1st derivative weight curve of the TG curve (DTG)**

Results

Antioxidant Efficiency of Regenerated Humic Acids

In our previous work[3] the antioxidant effect of South Moravian lignite humic acids and its ammonium salts in mixture with PVA was experimentally proved; while addition of sodium salts exhibited a slight pro-oxidant effect at specific concentrations. In this part we tried to find out if the oxidative modification of the parental lignite could cause any significant changes in antioxidant efficiency of extracted humic acids.

Stability of PVA/RHA blends was assessed and compared using so-called induction period (IP) measurement. The principle of this approach is given in the Experimental part. Application of Arrhenius equation as the temperature function has been demonstrated to be rather complicated due to *(i)* problems with calculation of temperature integral, *(ii)* problems associated with obtaining of unrealistic

values of induction periods and moreover *(iii)* adjustable parameters cannot be considered to have a physical meaning. On the other hand, such approach can still be used to model the kinetics of the process although without a deeper insight into its mechanism[4]. A better estimation of stabilizing effect can be obtained using the ratio of the lengths of induction periods of treated (stabilized) and nontreated material[5] so-called protection factor (PF).
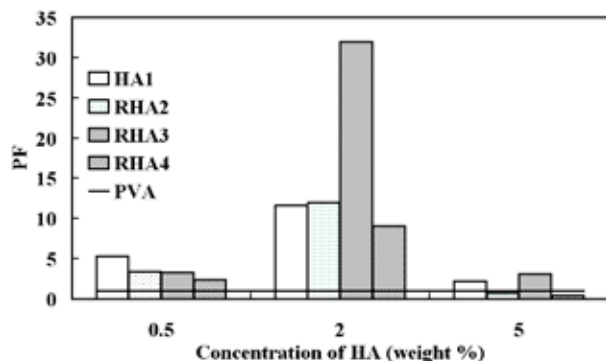
Fig. 2.   **Protection factor determined by Arrhenius kinetic**

From results reported in Fig. 2., it seems that the most efficient concentration was 2 %. In this concentration RHA 3 showed the highest efficiency to increase the stability of PVA. Further, results obtained using Eq. 1 showed, that RHA 2 and RHA 3 in concentration 2 % have higher stabilizing effect than nontreated humic acid. Stabilizing effect increases in sequence HA 4, RHA 1, RHA 2 and RHA 3. Concentration 0.5 % of humic acids also stabilizes PVA. In contrast, 5%

addition of regenerated humic acids did not bring a significant change in thermo-oxidative stability.

Conclusions

Thermal stability expressed as the length of IP of PVA with addition of humic acids was assessed by means of thermogravimetry and using a mathematical apparatus of isoconversional method. For the calculation of the induction period, Arrhenius temperature function was used.

Stabilities of PVA enriched with 3 regenerated humic acids were compared with PVA blend mixed with humic acid extracted from non-pretreated lignite. Obtained results showed, that almost all regenerated humic acids had greater stabilizing effect than humic acid extracted form paternal lignite.

REFERENCES

1. Berkowitz N.: *In The chemistry of coal,* Elsevier, Amsterdam, 1985.
2. Rausa R., Girardi E., Calemma V.: *Humic acids from coal. Production, characterization and utilization. In Humic Substances in the Global Environment and Implications on Human Health,* Elsevier Amsterdam, , pp. 1225–1244, (1994).
3. Kučerík J., Bakajová B., Pekař M.: Environ. Chem. Lett. DOI: 10.1007/s10311–007–0129, (2008).
4. Šimon P.: J. Therm. Anal. Calorim., *76,* 123 (2004).
5. Šimon P.: J. Therm. Anal. Calorim., *84,* 263 (2006).

P02 DETERMINATION OF PARTICLE SHAPE AND SIZE DISTRIBUTION

EDITA BRETŠNAJDROVÁ[a], LADISLAV SVOBODA[a]
and JIŘÍ ZELENKA[b]

[a]*University of Pardubice, Faculty of Chemical Technology, nam. Cs. Legii 565, 532 10 Pardubice,*
[b]*Synpo, a.s., S.K.Neumanna 1316, 532 07 Pardubice, Czech Republic,*
edita.bretsnajdrova@student.upce.cz

Introduction

At present great attention is given to study of preparation and properties of various nanomaterials usable in many applications. They are utilized in varied fields of human activity – e.g. in electronics, medicine, paint industry etc. Except detailed chemical structure, such nanoparticle properties as shape and size distribution are fundamental to the given application. To measure these parameters various methods are used, e.g. transmission electron microscopy (TEM), atomic force microscopy (AFM), acoustic spectrometry and methods based on the light scattering.

All above-mentioned methods were used in this work to characterize particles of two selected model types of nanomaterials – colloidal silica and sodium montmorillonite. Silica represents a material with spherical particles; tabular shapes are typical for montmorillonite materials.

Experiments proved that methods used to measure particle size distribution and based on the light scattering require very diluted dispersions to meet the needs of them. But, on the other hand, these conditions can affect the particle size distribution due to agglomeration or deagglomeration of them. For these reasons methods working with concentrated suspensions, without dilution, are more suitable to get correct results for such colloidal systems, for example acoustic spectrometry. To obtain information on the shape of particles studied TEM and AFM methods were used.

Merits and limitations of the individual methods used to evaluation of nanoparticles of various types are discussed in the work.

Experimental

Dynamic Light Scattering

Particle size distribution measurement was carried out by dynamic light scattering using Mastersizer 2000 MU.

Ultrasound Spectroscopy

The ultrasound-based technique is suitable for characterizing heterogeneous solid-in-liquid or liquid in liquid colloidal systems. This method is suitable for concentrated solutions; it is reliable in range from 5 % to 50 %. We have used equipment DT–1 200 (Dispersion technology, USA) and as standard we have used Silica Ludox with nominal particle size approx. 22 nm.

A F M

A Solver Pro M Atomic Force Microscope (NT-MDT; Russia) was used in tapping mode (semi-contact) to produce three-dimensional images of the surface. High-resolution "Golden" silicon cantilevers NSG–1 0 (Au coating, curvature radius 10 nm and cone angle less than 22°°) were used for all measurements. Set point was adjusted on 50 % of a free oscillation. Scan sizes required to evaluate the distribution of particles was 500×500 nm to several microns depending on variation of particles' sizes.

T E M

A drop of the water-diluted suspension was put on a microscopic grid covered by ultra thin carbon film and observed directly with TEM Tecnai G2 Spirit Twin (FEI).

Materials

Silicas

    Bindzil CC30
    Eka Chemicals AB, Sweden
    Dispersion of silica nanoparticles
    30% solution in water
    Particle size 7 nm

    Bindzil 30/360
    Eka Chemicals AB, Sweden
    Dispersion of silica nanoparticles
    30% solution in water
    Particle size 7 nm

Montmorillonite

    Cloisite Na$^+$
    Southern Clay
    Powder
    CEC 90 meq 100 g^{-1}

Results

Silicas

Two types of commercial silicas wear tested (Bindzil cc30 and Bindzil 30/360). These silicas are stabilized different way. While Bindzil cc30 is sterically stabilized, Bindzil 30/360 is stabilized electrostaticaly. The effect of silica concentration on zeta potential and particle size was studied for both type of stabilization. The variety of silica concentrations were prepared by dilution of original samples. Type of stabilization has crucial effect on silica concentration dependence of zeta potential (Fig. 1.).

The concentration of silica has effect on particle size and particle size distribution. Example for Bindzil cc30 is in Fig. 2.

Original sample of Bindzil cc30 has relatively broad particle size distribution. Mean value of particle size is about 40 nm. Measured value is higher than value cited by producer. Presence of bigger formations was confirmed by transmition electron microscopy (Fig. 3.).
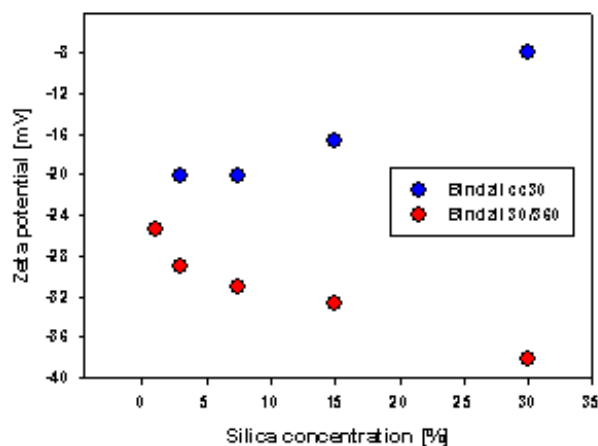
Fig. 1. **Dependence of zeta potential on silica concentration**

Bigger formations are aggregated smaller particles (Fig. 3.). These aggregates are broken up by dilution of original samples (Fig. 2.). The same conclusions can be done from AFM analysis.
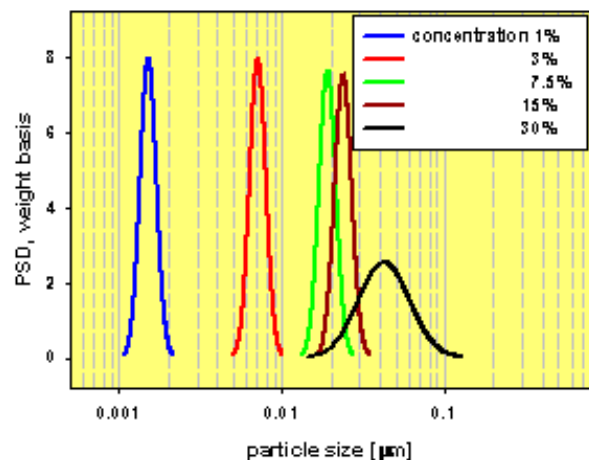
Fig. 2. **Particle size distribution on silica concentration**
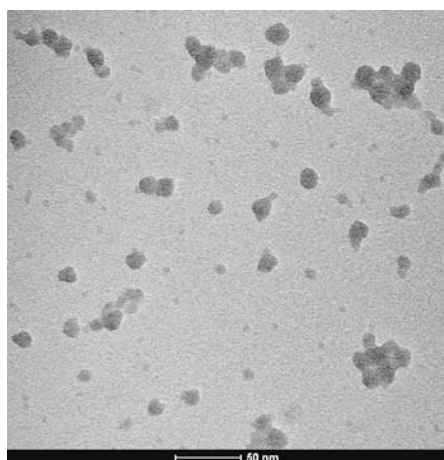
Fig. 3. **TEM photo of original sample Bindzil cc 30**
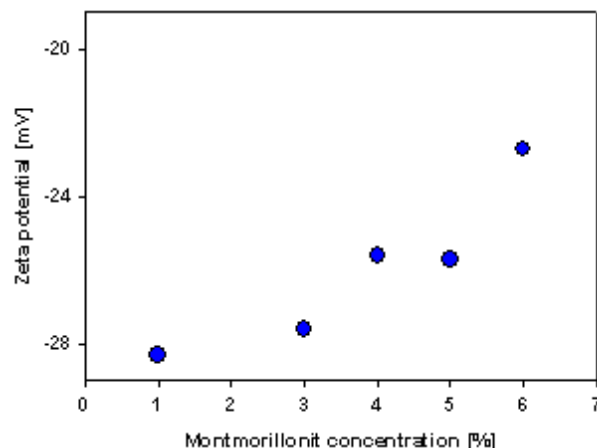
Fig. 4. **Dependence of zeta potential on montmorillonite concentration**

M o n t m o r i l l o n i t e

Zeta potential of water-based dispersion of sodium montmorillonite was influenced by filler concentration (Fig. 4.).

The particles with different shape and dimension were observed by means of different techniques (TEM, AFM). Results from AFM are in Fig 5.
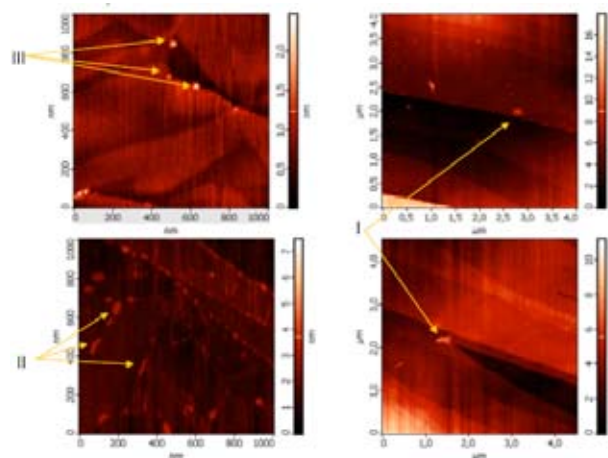
Fig. 5. **AFM photo of sodium montmorillonite sample**

Pentagon particles with particle size about 200 nm can be observed in section I of Fig. 5. Lengthwise formation with highest dimension 100 nm can be seen in part II of Fig. 5. Round particles with diameter 30 nm are in part III. Thickness of all studied particles is practically the same – about 1 nm.

Conclusions

Type of silica particle stabilization influenced behavior of colloidal solutions during dilution (particle size and zeta potential changes). All used methods (AFM, TEM and ultrasound spectroscopy) give similar results. Bigger particles (aggregates primary particles) were observed by means of AFM and TEM. These aggregates were broken up by dilution of original samples.

Commercial sodium montmorillonite is compound from elements different shapes and sizes. There are lengthwise formations, circular and pentagonal particles.

REFERENCES

1. Kosmulski M., Dahlsten P.: Colloids Surf., A *291*, 212 (2006).
2. Pierre A. C., Ma K.: J. Mater. Sci. *32*, 2937 (1997).
3. Yukselen Y., Kaya A.: Water Air Soil Pollut. *145*, 155 (2003).

P03 HYDRATION OF REGENERATED HUMIC SUBSTANCES

PETRA BURSÁKOVÁ, ZOJA VLČKOVÁ, ZDENĚK CIHLÁŘ and JIŘÍ KUČERÍK

Brno University of Technology, Faculty of Chemistry, Institute of Applied and Physical Chemistry, Purkyňova 118, 612 00 Brno, Czech Republic,
xcbursakova@fch.vutbr.cz

Introduction

Humic substances (HS) have a profound effect in many processes including cell biology of living organisms. As they are both hydrophobic and hydrophilic in nature, their function is closely related to the properties of water shell intimately bound on humic molecules and consequently on humic aggregates. A strong affinity of water molecules to stick to each other via H-bonds and formation of specific clusters is a driving force assembling humic molecules into complicated organizations.

The differences in properties of water surrounding HS can be recognized and enumerated using differential scanning calorimetry (DSC). Phase transition behaviour of sorbed water in HS-water systems was investigated as a function of water content. Three types of water can be distinguished: free water whose melting temperature and enthalpy are not significantly different from those of normal (bulk) water, those water species exhibiting large differences in transition enthalpies and temperatures (freezing-bound water), or those for which no phase transition can be observed calorimetrically, known as non-freezing water[1].

The aim of this work was to shed light on properties of hydration water in systems water/regenerated humic acids (RHA). DSC represents a technique which can help to recognize the differences in properties of water surrounding humic matter. The enumeration of water molecules is crucial in order to understand how biomolecular processes work.

Experimental

Material

The line of 8 HA was used. All of them were extracted from pretreated South Moravian lignite by standard alkaline method, purified, and freeze-dried. During the pretreatment procedure the lignite samples were soaked in solutions of either 5%, 10%, 20% nitric acid, 2%, 5% hydrogen peroxide, 20% acetic acid or 20% citric acid.

DSC Measurements

A sample was placed in an aluminum pan (~ 5 mg) and excess water was added. Surplus water was allowed to evaporate slowly at room temperature until the desired water content was obtained. Subsequently, the pans were hermetically sealed and left to equilibrate at room temperature overnight. DSC was performed by using the TA Instruments Q200 to measure phase transition of sorbed water. The measurements were conducted ranging from 40 to –90 °C and then from –90 to 30 °C at 3 °C min^{-1} under the flow of nitrogen (50 ml min^{-1}).

Water Content Determination

The thermogravimetry analysis (TGA TA Instruments Q 5000) was used to measure water content of original samples to obtain the real concentration of water (W_c). The W_c was defined as follows:

$$W_c = \frac{\text{grams of water}}{\text{grams of dry sample}} \ \text{(g/g)} . \qquad (1)$$

The obtained W_c were in range from 0.1 to 1.5 g g^{-1}. Assuming both melting enthalpies for freezing-bound water (W_{fb}) and free water (W_f) to be 334 J g^{-1} water, weights of W_{fb} and W_f (g water g^{-1} RHA) could be calculated from the endothermic heating transitions. The weight of non-freezing water (W_{nf}) was obtained using the expression:

$$W_{nf} = W_c - \left(W_{fb} + W_f \right). \qquad (2)$$

Results

RHA samples with W_c 0.1–1.5 g g^{-1} were measured. At higher water content there could be observed a large heating endotherm in the region of 0 °C whose enthalpy of transition was close to that of bulk water (334 J g^{-1}). This endotherm was ascribed to the melting of the freezing water in the hydrated RHA-water system. Some samples also showed another endothermic transition below 0 °C when the system was heated. This endothermic peak indicated the presence of freezing-bound water in a humic sample, i.e. water which is already affected by the interaction with humic molecules. Its clusters structure differs from those of bulk water and is physically recognizable by shifted temperature of melting. In fact, the enthalpy of melting differs from that ice which was attributed to the freezing water. Due to the different structure of ice such enthalpy can drop down to 312 J g^{-1}(ref.[2]). At very low water content nearly all water molecules are present in the form of non-freezing water in this system, and a slight amount of water molecules are present in the form of freezing-bound water which caused the observed endothermic fusion peak below 0 °C. Some samples showed more distinct endothermic fusion peak on heating curves. Shoulders which can be identified in this peak are possibly caused by the overlapping of different peaks which reflects the presence of several different types of freezing-bound water. Since cubic structure of freezing-bound water is thermodynamically metastable[3] such assumption is highly probable.

Representative DSC heating curve of RHA6 with water content W_c 0.7 is given in Fig. 1. where various endothermic transitions at different temperatures, attributed to the melting of different types of ice, can be observed.

The total amount of freezing water in RHA samples was calculated from the area of endothermic melting peak as follows: obtained heat of ice melting (ΔH) calculated from DSC heating curves was normalized dividing by the weight

of the dry RHA. A plot of the enthalpy change, normalized to the RHA weight, as a function of the total water content of the sample will yield the enthalpy change for the free water as a slope (Fig. 2.). The x-intercept is the point at which the total water content is equal to the amount of non-freezing water, and zero enthalpy change is observed[1].
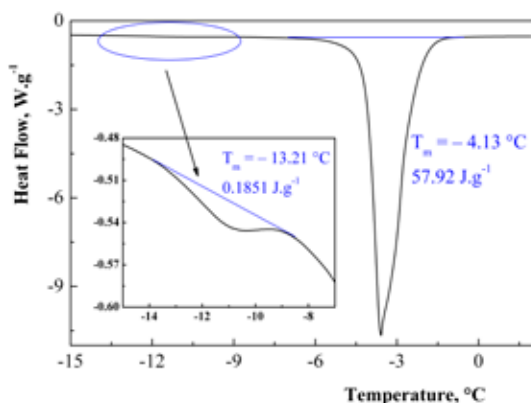
Fig. 1. **DSC heating curve for RHA6 with W$_c$ 0.7**
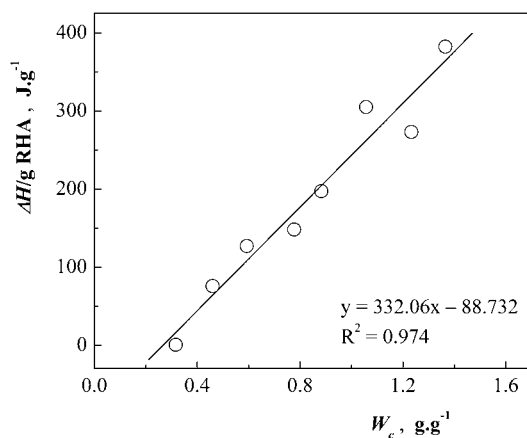
Fig. 2. **Normalized melting enthalpy versus W$_c$ for HA1**

Table I
The content of non-freezing and freezing-bound water

Sample	Pretreatment agent	W$_{nf}$ [g g^{-1}]	W$_{fb}$ [g g^{-1}]	W$_{nf+fb}$ [g g^{-1}]
HA1	–	0.267	n.d.	n.d.
RHA2	5% HNO$_3$	0.223	0.190	0.413
RHA3	10% HNO$_3$	0.081	0.219	0.300
RHA4	20% HNO$_3$	0.245	0.055	0.300
RHA5	2% H$_2$O$_2$	0.187	0.291	0.478
RHA6	5% H$_2$O$_2$	0.035	0.374	0.409
RHA7	20% acetic acid	0.238	0.142	0.380
RHA8	20% citric acid	0.078	0.218	0.296

Table I reports the content of non-freezing and freezing-bound water calculated from DSC experiments. The highest modification efficiency regarding hydration properties of HS was reached using H$_2$O$_2$ (RHA5, RHA6), 5% HNO$_3$ (RHA2) and 20% acetic acid (RHA7) as the pretreatment agents while other samples showed lower water retention capacity.

Conclusions

DSC measurements of RHA showed dependency on both concentration and used modifier. The enthalpy change of melting increased with decreasing concentration of RHA. Using of different pretreatment agents plays a significant role since some modifications can enhance hydration properties of HS. Therefore, this method can bring new information considering the function of HS in biological processes.

REFERENCES

1. Liu J., Cowman M. K.: J. Therm. Anal. Cal. *59*, 547 (2000).
2. Hatakeyama H., Hatakeyama T.: Thermochim. Acta *308*, 3 (1998).
3. Yoshida H., Hatakeyama T., Hatakeyama H.: J. Therm. Anal. Cal. *40*, 483 (1993).

P04 EVALUATION OF SORPTION ABILITIES OF NATURAL LIGNITE FOR ORGANIC SUBSTANCES

PETRA BUŠINOVÁ and MILOSLAV PEKAŘ

Brno University of Technology, Faculty of Chemistry, Institute of Physical and Applied Chemistry, Purkyňova 118, 612 00 Brno, Czech Republic,
businova@fch.vutbr.cz

Introduction

In recent years, possibilities of lignite utilization in various non-fuel applications have been investigated. Lignite as the youngest brown coal has a low degree of coalification which gives it unique chemical composition and specific properties. Therefore, lignite can be used as an interesting and versatile material in several application fields.

Studies on sorption properties have been continuously published for lignite or coals in general. Lignite, even in its natural state, is reported to have significant sorption affinity for metal ions[1,2] as well as for organic molecules, e.g. dyes[3,4].

In our laboratory, sorption properties of lignite mined in the region of South Moravia (Czech Republic) are studied. Affinity of this material for fluoride ion has previously been published[5]. This paper introduces preliminary results on a sorption of basic textile dyes and petroleum products (gasoline, diesel fuel, oils) on the natural South Moravian lignite.

Experimental

Sorption tests were performed using lignite mined in the South Moravia, Mikulčice locality. Its detailed characterization is published elsewhere[6,7]. Fraction of lignite particles smaller than 0.2 mm was used and the sample was dried at 105 °C in an oven for 24 hours. Dried product was consequently left to moisture re-equilibration at ambient atmospheric conditions in laboratory and final moisture content was about 7 %.

Six basic dyes (see Table I) have been studied. Deionized water was used to prepare the dyes solutions. UV-VIS spectroscopy (Hitachi U3300 spectrometer) was used for the determination of a dye concentration in a solution. The wave lengths of the absorption maxima of all dyes are given in Table I. In adsorption experiments, a change in the intensity of these maxima has been used in order to characterize the removal of a dye from solutions.

Sorption of dyes were carried out for four different amounts of lignite: 0.1 g, 0.2 g, 0.5 g and 1 g. Lignite was mixed with 10 ml of a dye solution with dye concentration of 1,000 $mg\,dm^{-3}$ in 50 ml screw capped plastic centrifuge tubes with conical bottom and mixtures were stirred on a rotary shaker for 24 hours. After this time period, samples were centrifuged at 4,000 rpm and 15 °C for necessary time. The supernatant solutions were pipetted out and intensity of absorption maxima were determined instantaneously using UV-VIS spectrometer.

Table I
The wave lengths of the absorption maxima of used dyes

Dye	λ_{max} [nm]
Astrazon blue 3GL (AB)	593
Maxilon yellow M-3RL (MY)	422
Maxilon red M-4GL (MR)	505
Bezacryl blue FBS (BB)	598
Bezacryl golden yellow GL 200 % (BY)	437
Bezacryl red GRL 180 % (BR)	529

Similarly, sorption tests were performed for gasoline and diesel fuel. 0.5 g of lignite was mixed with 10 ml of adsorbate in screw capped glass test tubes and rotated for 24 hours. Then a liquid portion was poured off and lignite was weighted. Consequently, it was dried at 105 °C in an oven for 24 hours and weighted again. Variation in weight was observed.

Adsorption of oils (motor and gear) was studied according to the reference[8] with slight correction. 2.5 g of lignite were weighted and evenly spread on a filter paper placed into a round stainless steel dish with a wire mesh (2 mm^2) bottom (7 cm in diameter). The dish with lignite was then placed into a square glass dish (12 × 12 × 6 cm) with 60 ml of an oil.

Table II
Residual dye concentration and percentage of dye removed from dye solution after 24 hours

Dye	Lignite amount [g]	C_R [mg dm^{-3}]	Removing [%]
AB	0.1	151.403	84.87
	0.2	–	100
	0.5	–	100
	1	–	100
MY	0.1	3.067	99.69
	0.2	–	100
	0.5	–	100
	1	–	100
MR	0.1	3.067	99.69
	0.2	1.087	99.89
	0.5	–	100
	1	–	100
BB	0.1	9.505	99.05
	0.2	0.869	99.91
	0.5	0.283	99.97
	1	–	100
BY	0.1	3.969	99.60
	0.2	1.844	99.82
	0.5	–	100
	1	–	100
BR	0.1	6.537	99.35
	0.2	0.623	99.94
	0.5	0.163	99.98
	1	–	100

– below detection limit

Table III
Amount of petroleum products sorbed on 1 g of lignite after 24 hours of drying

Petroleum product	Sorbed amount [mg]
gasoline	1425
diesel fuel	579
motor oil	350
gear oil	726

Lignite was left in contact with oil for 30 min. The stainless steel dish with sample was then removed and left to drain until the oil layer disappeared (2 hours). Then lignite was weighted. The weighting was repeated after 22 hours and obtained weights were compared.

All experimental sorption studies were performed at laboratory temperature (25 ± 2 °C).

Results

Sorption abilities of the South Moravian lignite for organic substaces were investigated. Decolorization of a single dye solution was observed, residual dye concentration in solution and corresponding percentage removal of a dye were determined. Effect of lignite to solution ratio was studied. Results are given in Table II and clearly confirm sorption ability of lignite for selected dyes. These results are also guiding for further experiments. Proper ratio between amount of lignite and volume and concentration of a solution has to be found prior for determination of sorption isotherms and kinetics.

The results of sorption tests using petroleum products, summarized in Table III, show the sorption ability of lignite towards them. Further experiments are necessary for the investigation of lignite as a suitable sorbent for removing oil spills.

Conclusions

Sorption abilities of the natural South Moravian lignite for organic substances were investigated. Obtained results show that lignite can be used as an effective sorbent for various textile dyes and that it has a positive sorption ability for petroleum products too.

REFERENCES

1. Pehlivan E., Arslan G.: Fuel Process. Tech. *88*, 99 (2007).
2. Mizera J., Mizerová G., Machovič V., Borecká L.: Water Res. *41*, 620 (2007).
3. Mohan S. V., Rao N. C., Karthikeyan J.: J. Hazard. Mater. *90*, 189 (2002).
4. Allen S. J., McKay G., Khader K. Y. H.: J. Chem. Tech. Biotechnol. *45*, 291 (1998).
5. Pekař M.: Petrol. Coal *3*, 1 (2007).
6. Kučerík J., Pekař M., Klučáková M.: Petrol. Coal *45*, 58 (2003).
7. Pekař M.; Sýkorová I.; Koutník I.: *Proc. Int. Conf. Twenty-Fourth Annual International Pittsburgh Coal Conference*, p.1. 2007.
8. Carmody O., Frost R., Xi Y., Kokot S.: J. Colloid Interface Sci. *305*, 17 (2007).

P05 MAXIMUM BUBBLE PRESSURE AND THE DU NOÜY PLATINUM RING METHOD OF SURFACE TENSION MEASUREMENTS OF SODIUM DODECYL SULFATE AND SODIUM HYALURONATE

MARTIN CHYTIL, JITKA KROUSKÁ, PAVLÍNA KULILOVÁ and MILOSLAV PEKAŘ

Institute of Physical and Applied Chemistry, Faculty of Chemistry, Brno University of Technology, Purkyňova 118, 612 00 Brno, Czech Republic,
chytil@fch.vutbr.cz

Introduction

The measurement of surface tension is a fundamental method in physical or colloidal and interfacial chemistry, assessing important parameter of liquids, surface tension (γ), surface activity of molecules in a medium, detecting *critical micelles concentration* (CMC) etc, which is very important for processing and industrial applications of given substances.

The Maximum Bubble Pressure (MBP) method is a dynamic method of measuring surface tension of liquids. Using this method, a maximum pressure inside the gas bubble, forming at the end of the capillary with a defined radius, is measured at an accurately defined rate of the bubble formation. When the pressure reaches its maximum, the bubble radius is exactly equal to that of the capillary, and the time of this point is designated as the bubble life-time[1]. For the formation of the bubble in the liquid, the surface energy must be overcome. From the surface energy, the surface tension of the liquid is calculated using the Laplace-Young equation, $\gamma = f \cdot P_{max}/2$, where f is the correction factor[2].

The Du Noüy Ring method (DNR) is a static method of surface tension measurement. The surface tension, by this method, is determined from the maximum force of lifting the, usually Pt, ring off the liquid surface just before the rupture of the liquid film having been formed on the ring surface[3].

Sodium hyaluronate (NaHA), widely known as hyaluronic acid or hyaluronan, is a naturally occurred linear polysaccharide composed of repeating disaccharide units of *D-glucuronic* acid and N-acetyl-D-glucosamine alternatively linked by β-(1 → 3) and β-(1 → 4) glycosidic bonds. Due to the presence of carboxyl groups HA is a polyelectrolyte found namely in connective tissues of vertebrate and also as a fermentation product of some *Streptococci* bacteria strains[4,5]. For its numerous unique properties, HA is used in medicine, pharmacy, cosmetics[4–6] etc. Surface tension is an important parameter for processes and applications such as formation of nanofibres from biopolymers, scaffolds in tissue engineering, drug delivery, etc. There have been only few papers reporting about HA surface activity[7], using namely static methods, e.g. pendant drop method. The purpose of this contribution was to compare the MBP and the DNR method of surface tension measurement on measurement series of aqueous solutions of a classical surfactant sodium dodecylsulfate (SDS), to man-age the data proceedings, mainly from the MBP method, and apply particularly the MBP method for the series of HA aqueous solutions. Discussion of the effect of the HA molar mass and the presence of NaCl has been also involved.

Experimental

Materials
- The bacterially produced HA of cosmetic quality with the molar masses of 4.6×10^5 and 1.69×10^6 g mol^{-1} provided by the Contipro, spol. s.r.o.
- SDS, p.a. and NaCl, p.a. by Sigma Aldrich
- Water for injection by Verkon s.r.o.

Preparation of Samples

A desired amount of dry HA was firstly stepwise sprinkled into a desired volume of water upon gently stirring and then let stirred for ca 24 h at room temperature in order to achieve a well homogenized stock solution. Afterwards, the stock solution was diluted into the series of solutions with the water or NaCl solution up to a desired concentration and ionic strength and then the series were vigorously agitated for at least 2 h. The series of SDS solutions were prepared in the same way except the long stirring of the stock solution, which lasted only 2 h in this case.

Methods

The maximum bubble pressure tensiometer BPA-800P from KSV Instruments (Finland) and KSV Sigma 701 tensiometer with the Pt ring were employed. The series of the solutions were measured at room temperature (MBP) or 25 °C (DNR). Between the measurements of each sample by the DNR method, the Pt ring was cleaned in the flame of a burner with occasional immersing into 6% (v/v) HCl. From the MBP method, the dependence of γ on the bubble life-time (t_{life}) is obtained. The measurements were performed in two different modes (Standard and Increasing Flow Rate); the results compared and final calculations were done as the average of those two measurements. By the DNR method, each sample was measured in time until it was stabilized, or for at least 40min. As a result, the plot of γ vs. time of measurement (t_{meas}) was gotten. The measurements were tripled and the other calculations were made from the mean value of all replicates.

Results and Discussions

Comparison of the MBP and the DNR Method

From the MBP method we obtained the plot of dynamic surf. tension, γ_{dyn}, against the bubble life-time, t_{life}. To determine the equilibrium surface tension, γ_{eq}, of a sample, we arranged the plot as $\gamma_{dyn} = f(1/\sqrt{t_{life}})$ (Fig. 1.) and γ_{eq} was assessed from the following equation for $t_{life} \to \infty$

$$\gamma_{dyn} = \gamma_{eq} + s_\gamma/(a_\gamma + t_{life}^{1/2}), \qquad (1)$$

where the parameters s_γ and a_γ result from the adsorption of the surfactant molecules at the solution/air bubble interface, as described elsewhere[8]. This model fitted relatively well the

data for both SDS and HA. Fig. 1 shows relatively high values of γ_{dyn} of the HA solutions even at higher concentrations (> 1 g dm^{-3}), where they began to be quite viscous, comparing to the gradually decreasing γ_{dyn} of SDS solutions with SDS concentration.

Using the DNR method the dependence of γ on the time of measurement, t_{life}, was gained and the γ_{eq} from the DNR measurements was determined as the mean of the values from the last 10 min of the measurement. Another method of γ_{eq} assessment can be the extrapolation of the γ data as a function of $1/\sqrt{t_{meas}}$, to $t_{meas} \rightarrow \infty$; nevertheless the data are theoretical and were comparable with the previous ones only except the first very diluted solutions that need more time to be stabilized.
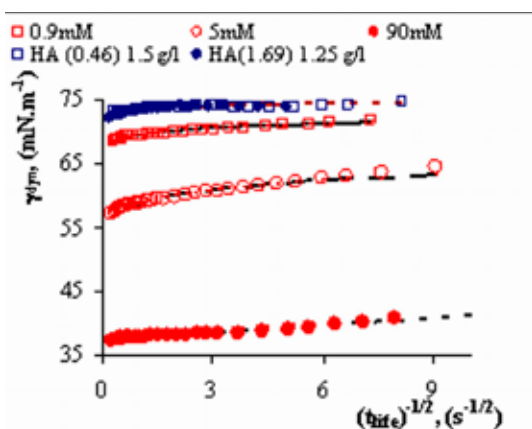
Fig. 1. **The dynamic surface tension as a function of the square-root of bubble life-time for solutions of SDS (red symbols) and HA (navy symbols) in water; the figures in the brackets refer to the molar mass of the HA in 10^6 g mol^{-1}. The lines represent the model fitted to the experimental data (see in the text)**

From the comparison of the two methods, performed on measurements of mainly SDS solutions (Fig. 2.), a clear difference can be seen. The values of γ from the MBP were higher at lower concentrations of SDS than those of the DNR method; however, they later overlapped with each other behind the CMC of SDS. The onset of γ decrease before the CMC began also at higher concentration for the MBP measurement as well as the slope of the decline was steeper for this method. From the slope, the maximum concentration of a surfactant at the air/solution interface, Γ_{max}, and other parameters can be calculated using the simplified Gibbs adsorption equation[9]:

$$d\gamma = -2.303 \cdot RT \cdot \Gamma \cdot d\log C, \qquad (2)$$

where R is the gas constant, T absolute temperature, and C molar concentration of a surfactant. The values of Γ_{max} calculated from the MBP method were thus larger than those from the DNR method and the CMC of SDS was also determined at higher surfactant concentration using the MBP method than from the DNR in water and 0.15 M NaCl as well. All the parameters are listed in Table I.

Table I
The CMC and Γ_{max} of SDS in water and 0.15M NaCl calculated from the MBP and the DNR method

	CMC [10^3 mol dm^{-3}]	Γ_{max} [10^6 mol m^{-2}]
MBP		
Water	9.8	5.5
0.15 M NaCl	1.4	5.0
DNR		
Water	5.8	3.9
0.15 M NaCl	0.9	3.3

These results clearly demonstrate a different dynamics of these two kinds of adsorption which, in fact, compete with each other and one must note more complicating dynamic balance between these two kinds of adsorption and also micellization taking place in the system during the MBP measurement. It might be suggested a higher affinity of the surfactant molecules to the flat air/solution interface than to the bubble/solution interface considering earlier onset of the decrease of γ with SDS concentration and lower CMC, which induces more negative change of free energy of micellization, ΔG°_{mic}. Nevertheless, as the surface tension drops, this decrease is more rapid for the MBP method and Γ_{max} is attained at a narrower range of SDS concentration resulting in its larger values, and thus more surfactant molecules adsorb at the bubble/solution interface.
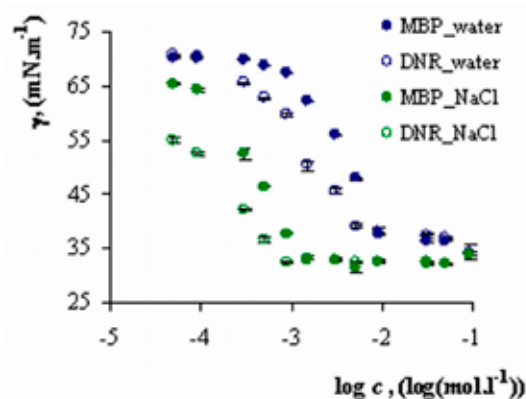
Fig. 2. **Comparison of surface tension of SDS from the MBP (full circles) and the DNR (empty circles) method in water (navy) and 0.15M NaCl (green) as a function of SDS concentration**

Surface Tension of HA Aqueous Solutions

Figs. 3. and 4. show the surface tension of HA solutions from the DNR and MBP method, respectively. A general result is that the solutions of HA exhibited the values of γ only very moderately different from those of the appropriate solvent, being mostly lower. The values γ of the HA solutions had an oscillation trend with increasing HA concentration. No particular difference between the high-molecular weight and low-molecular weight HA was observed from the
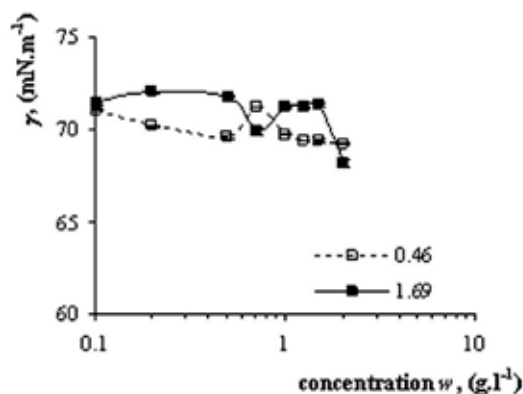
Fig. 3. **Surface tension of HA solutions in water as a function of HA concentration and molar mass from DNR method; the figures in the legend represent the molar mass of the HA in 10^6 g mol^{-1}**
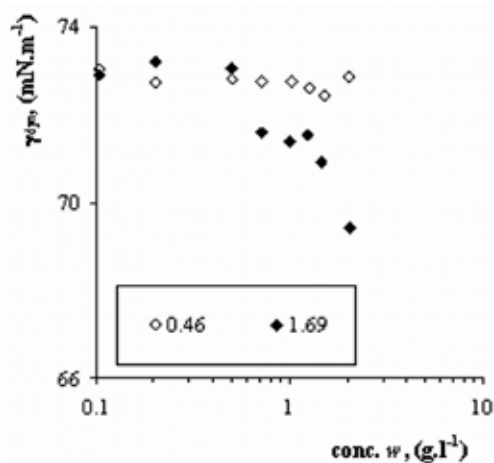
Fig. 4. **The dynamic surface tension (MBP) of HA solutions in water as a function of HA concentration and molar mass**

DNR measurements, only at low concentrations in 0.15 M NaCl, the high-molecular sample displayed slightly lower values of γ.

The similar result was obtained from the MBP measurements; however, the γ values were rather unstable. On the other hand, the opposite result to that from the DNR was observed in water, i.e. the higher-molecular weight HA displayed moderate decline of γ values with its concentration (Fig. 4.). All the samples, nevertheless, displayed a bit higher values of γ in 0.15 M NaCl than in water for both the methods. However, the differences are very small. These data are not in accordance with those found in the literature[7], in which the authors observed a decrease of γ with HA concentration

relating it to viscoelasticity of HA solutions; however, they used different method for surface tension measurement than us, i.e. the pendant drop method.

Conclusions

The comparison of two different methods of surface tension measurement, the MBP and the DNR, has been discussed on the measurements of series of SDS solutions and solutions of HA, varying in molar masses, in water and 0.15 M NaCl. Clear difference between the two methods has been seen, suggesting different dynamics and thermodynamics of adsorption of molecules at the curved air bubble surface. Although the adsorption of SDS at the bubble/solution interface occurred later than at the flat interface, the maximum concentration of the surfactant at the bubble/solution interface was larger than at the flat interface.

The HA solutions studied exhibited weak surface activity and oscillation trend in the change of γ with HA concentration. Only small difference in the behavior of the samples, due to different molar masses of the HA, has been observed, and also the presence of NaCl did not significantly alter the behavior of the HA, but the values of γ were generally a bit higher in the presence of salt. Some difference between MPB and the DNR methods has been observed during the measurement of HA in water, when higher-molar mass HA displayed slightly larger surface activity.

REFERENCES

1. *KSV BPA 800P Manual*. KSV Instruments, 48p, Finland, 2004.
2. Fainerman V. B., Mys V. D., Makievski A. V., Miller R.: J. of Coll. And Inter. Sci. *304*, 222 (2006).
3. Krouská J.: *Diploma Thesis*. Brno University of Technology, Faculty of Chemistry, Brno, Czech Republic, 2008.
4. Lapčík L. jr., Lapčík L., De Smedt S., Demeester, J., Chabreček P.: Chem. Rev. *98*, 2663 (1998).
5. Cowman M. K., Matsuoka S.: Carbohydr. Res. *340*, 791 (2005).
6. Prehm P. in: Bipolymers, *Polysaccharides I: Polysaccharides from prokaryotes* (Vandomme E. J., De Baets S., Steinbückel A. ed.), chapter 15 *Hyaluronan*, p. 379. Weinheim: Wiley-VCH 2002.
7. Ribeiro W., Mata J. L., Saramago B.: Langmuir *23*, 7014 (2007).
8. Christov N. C., Danov K. D., Kralchevsky P. A., Ananthapadmanabhan K. P., Lips A.: Langmuir *22*, 7528 (2006).
9. Zhang T., Marchant R. E.: J. of Col. And Inter. Sci., *177*, 419 (1996).

P06　SURFACE TENSION OF REGENERATED HUMIC ACIDS SALTS

ANNA ČTVRTNÍČKOVÁ, MARTIN DRASTÍK, ZOJA VLČKOVÁ AND JIŘÍ KUČERÍK

Faculty of Chemistry, Brno University of Technology, Purkyňova 118, 612 00 Brno, Czech Republic,
kucerik@fch.vutbr.cz

Introduction

The soil remediation technologies emphasize the transformation and detoxification of pollutants. For example bioremediation enables permanent elimination of pollutants by in situ remediation at low cost, however, is limited by many factors.[1] In contrast remediation using natural surfactants is gaining growing interest. Humic acids (HA) – naturally occurring surfactants are recognized to be a possible aid in soil bioremediation techniques. For example, the bioavailability of polychlorinated biphenyls (PCB) and polycyclic aromatic hydrocarbons (PAH) appeared to be increased by addition of oxygenous HA to contaminated soils[1].

Lignite represents the youngest type of coal with the age belonging between peat and brown coal. One of the most attractive ways of lignite exploitation is their use as a source of HA[2].

The aim of the work was to increase the surface activity of HA by modification of parental lignite and to find technologically appropriate composition of humic acids useful for washing technology of highly polluted soils (i.e. remediation).

Experimental

Regenerated Humic Acid

The South Moravian lignite (Mír mine, Mikulčice, Czech Republic) was used as a source of HA. The samples of "regenerated" HA were obtained from the fraction of lignite by its oxidation reaction with two oxidizers (HNO$_3$, H$_2$O$_2$) and two other agents (acetic and citric acids, respectively) according to following procedure: 20 g of raw lignite was mixed with 200 ml of appropriate modifier and stirrred 30 min, washed until agent-free. Procedure was followed by standard alkali extraction according to ref.[2]. The list of studied samples is shown in Table I.

A part of RHA samples was titrated by 0.1 M NaOH to get water-soluble sodium humate (NaRHA) and the second half remained in the protonated form. The protonated form of RHA was used for Elemental Analysis (EA). Details of the EA are given in Table II.

Surface Tension Measurement

For surface tension (ST) measurements Sigma 700 tensiometer (KSV Instruments Ltd.) using a 19mm-diameter platinum-iridium (Pt-Ir) ring was employed.

13 samples with concentrations from 0.001 to 10 g dm^{-3} of individual NaRHA were prepared by diluting humic solutions one day before measurement. Before experiment each

Table I
The list of the studied samples

Sample	Modifier	Sample	Modifier
HA	–	RHA4	2% H$_2$O$_2$
RHA1	5% HNO$_3$	RHA5	5% H$_2$O$_2$
RHA2	10% HNO$_3$	RHA6	20% acetic acid
RHA3	20% HNO$_3$	RHA7	20% citric acid

Table II
Elemental analysis of HA and RHAs [% wt.]

Sample	C [%]	H [%]	N [%]	O [%]	C/O	C/H
HA	58.1	4.44	1.53	35.9	1.62	13.1
RHA1	58.5	3.46	2.01	36.1	1.62	16.9
RHA2	58.2	3.55	2.32	35.9	1.62	16.4
RHA3	56.5	4.16	3.38	35.9	1.57	13.6
RHA4	58.0	3.62	2.15	36.2	1.60	16.0
RHA5	58.5	4.25	1.47	35.8	1.63	13.8
RHA6	58.0	3.75	2.06	36.2	1.60	15.5
RHA7	58.2	3.75	2.30	35.8	1.63	15.5

solution was stirred for 5 min in a shallow glass measuring dish. The experiment was carried out after 10 min sample repose drawing the Pt-Ir ring on the solution surface. The time of measurement was 12 hours. Obtained data were fitted by Szyszkowski equation:

$$\gamma_0 - \gamma = a \log(1 + bc), \tag{1}$$

a and b are empirical parameters of Szyszkowski equations dependence on the structure of dissolved matter, parameter a reflects the nature of surface active substances and has a constant value for the surface active moieties of one type of molecule, parameter b is different for different molecules and characterizes the efficiency of the absorbed molecules to decrease ST, and also describes the surface activity. γ_0 is the ST of the solvent (water at 25 °C: $\gamma_0 = 72.1$ mN m^{-1}), γ is the ST of the solution and c is the concentration of the solute. For the maximal surface saturation by adsorbed molecules following equation was derived[3]:

$$\Gamma_{max} = a/2.303\,RT, \tag{2}$$

where Γ_{max} is the maximal Gibbs surface excess quantity. For predicted surface excess quantity by monomolecular layer, the area of one molecule at the surface is:

$$s = 1/\Gamma_{max} \cdot N_A, \tag{3}$$

where N_A is Avogadro's number ($N_A = 6.023 \times 10^{23}$)ref.[3].

Results and Discussion

The surface tension of NaHA and NaRHAs was measured as a function of their concentration and time. In fact,

with increasing concentration of the humic samples the ST progressively decreased and equilibrium, i.e. the constant value of ST, was reached after 10 hours. Since the sorption of amphiphilic humic molecules in the surface layer is a dynamic process governed both thermodynamically and kinetically, it is likely that simultaneously desorption processes occurred. Obtained data of ST in this time were subtracted from the surface tension of the solvent (water), the results were plotted versus respective concentrations and fitted Szyszkowski equation (2) (Fig. 1.).
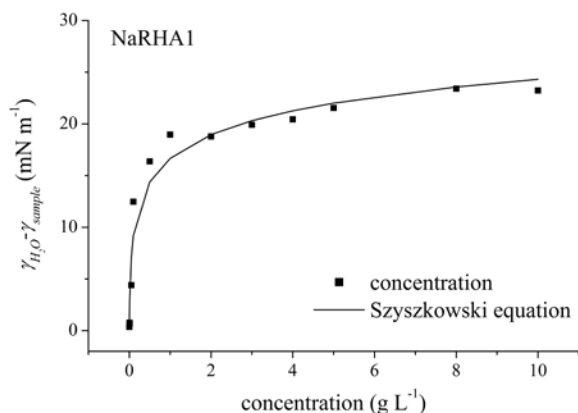
Fig. 1. **Dependence of surface tension obtained after 10 hours of the measurement of different concentrated humic samples, fitted by Szyszkowski equation**

Basically, the Szyszkowski equation was derived for water solutions of fatty acids and aliphatic alcohols[3]. We assumed that it could be used also for fitting of humic acids solutions ST measurement because the molecules adsorbed in the surface were predominantly aliphatic. The justification of this opinion is based on chemical character of HS since aliphatic molecules in humic acids are mainly lipids and alcohols. From the chemical point of view, those are amphiphiles; hence they are very likely to be excluded from bulk of water to the surface. Parameters obtained from Szyszkowski equation fitting are listed in Table III. There it can be seen almost the same value of parameter *a* for NaRHA1, NaRHA2, NaRHA3 and NaRHA4 which means that these samples include more or less the same type of molecules adsorbed at the surface. To the other group belong NaHA and NaRHA6. In the last group is NaRHA5. For example for fatty acids the value of *a* parametr is reported 12.97 $mN\,m^{-1}$.ref.[3]. Therefore, data reported in Table III are in a good agreement with this value and confirms our hypothesis.

Table III
Parameters obtained from Szyszkowski equation

Sample	*a* [$mN\,m^{-1}$]	*b* [$dm^3\,mol^{-1}$]	Γ_{max} [$10^{-3}\,mol\,m^{-2}$]	*s* [$10^{-21}\,m^2$]
NaHA	9.70	41.9	1.70	0.98
NaRHA1	7.67	147.9	1.34	1.24
NaRHA2	7.32	243.2	1.28	1.29
NaRHA3	7.97	169.7	1.40	1.19
NaRHA4	7.77	99.7	1.36	1.22
NaRHA5	8.71	382.2	1.53	1.09
NaRHA6	9.10	88.6	1.59	1.04
NaRHA7	8.25	342.2	1.45	1.15

The parameter *b* shows significantly high value 382.2 ± 274 for NaRHA5 in comparison with lower NaHA 41.9 ± 19.6. Therefore, it can be seen that the modification of parental lignite lead to production of humic acids with high surface activity. Comparison with literature data[3] shows that efficiency of NaHA sample falls between C4 (butyric) and C5 (valeric) acids (19.6 and 68.5, respectively) whereas sample NaRHA5 falls between C6 (caproic) and C7 (enanthic) acids (233 and 555, respectively).

The parameters obtained from Szyszkowski equation for all studied samples were correlated with C/O and C/H ratios from EA by Pearson correlation coefficient. The significantly high negative correlation was between the *a*-parameter and C/H ratio, the value was –0.68. It means that there was a close relationship between the type of molecule and aromaticity/aliphaticity of the sample. In fact, the larger value of *a*-parameter indicates higher aliphaticity of the sample. Positive weak relationship was between *b*-parameter and C/O ratio, the correlation value was 0.47. That reflects that with higher surface activity the oxidation degree of the samples decreases.

REFERENCES

1. Conte P., Agretto A., Spaccini R., Piccolo A.: Environ. Pollut. *135*, 515 (2005).
2. Kučerík J., Pekař M., Klučáková M.: Petrol. Coal *45*, 58 (2003).
3. Bartovská L., Šišková M. in: *Fyzikální chemie povrchů a koloidních soustav.* VŠCHT v Praze, Praha 2002.

P07 IMMOBILIZATION OF LIGNITE INTO PVAL SPONGES

PETR DZIK, VÁCLAV MACH and MICHAL VESELÝ

Faculty of Chemistry, Brno Universityof Technology, Purkyňova 118, 612 00 Brno, Czech Republic
petr@dzik.cz

Introduction

Lignite is from geological point of view the youngest form of fossil fuels. Therefore its energy content is rather low. However, much attention has been paid to non-energetic applications of lignite recently[1]. Apart from other interesting way of utilization, lignite proved to be an efficient sorbent for a number of pollutants.

Although loose finely groung lignite can be used on its own, it might be beneficial for a number of industrial application to use some immobilised form of lignite, for example for water purification. Therefore some process for lignite immobilization has to be found.

Poly(vinyl alcohol), PVAl, is a common vinyl polymer with some very special properties. It is highly hydrophilic and well soluble in polar solvents including water. Moreover, it is absolutely non toxic, biocompatible and biodegradable[2]. The reactive secondary hydroxyl groups can be used for further modification[3]. Crossliking is easily performed by a vast array of crosslinking agents[4]. Resulting hydrophilic gels are have very interesting properties and various applications, many of which include the immobilization of other active component (enzymes[5], living cells[6], heterogeneous catalyst particles[7] etc.)

Experimental

Our experiments were decicated to the preparation and study of open-pore hydrophilic sponges with immobilised lignite as sorbent. Such articles might be useful e. g. for water treatment where some immobilised form of sorbent is always preferred.

In a typical example, 10 g of 20 % wt. aqueous solution of PVAl (Mowiol 18-88, Fluka) was mixed with *A* grams of aluminum (fine powder, Fluka). After thorough mixing, 10 ml of hardener solution was added. The hardener solution consisted of two components in variable ratios: Component *B* was a solution of paraformaldehyde in sulphuric acid (10 g of paraformaldehyde was dissolved in 100 ml of 60 % wt. sulphuric acid). Component *C* was 60 % wt. sulphuric acid. After complete mixing, D grams of groung lignite was dispersed into the composition. Individual samples were then given a code (A–B/C–D) fully identifying their composition. For example, sample 0,05–7/3–2 was produced using 9 g PVAl solution + 0,05 g Al + hardener mixture made of 7 ml paraformaldehyde solution and 3 ml 60% H_2SO_4 + 2 g lignite.

After thorough mixing, the composition was transferred into PE form with perforated lid, where it was left to react for 24 hours at room temperature. During this time, formaldehyde reacted with PVAl and formalised, partially crosslinked copolymer was produced – poly(vinyl alcohol-co-vinyl acetate-co-vinyl formal).

At the same time, aluminum powder slowly reacted with sulphuric acid and hydrogen gas evolved. As the volume of hydrogen grew, the mixture was slowly foamed up and its volume increased 3–15 times, depending on the amount of aluminum added. During this process, a solid hydrophilic open-cell sponge was created.
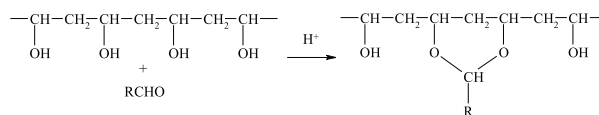
Fig. 1. **Intramolecular acetalization**
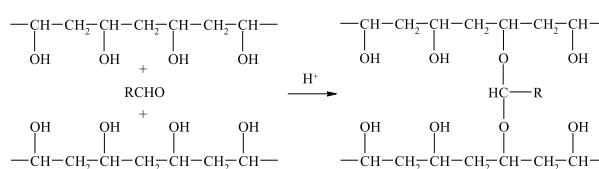
Fig. 2. **Intermolecular acetalization**

After the reaction, the form was open and the cured sponge was repeatedly washed with running tap water to remove reaction byproducts. After complete washing, the spopnges were stored soaked in 0,001 % wt. aqueous SEPTONEX solution to protect then against microbial contamination.

Table I
Composition and sample naming of PVAl sponges

Al [g]	Hardener composition [B + C, ml]	Lignite [g]	Sample code
0.05	5.5 + 4.5	2	0.05–5.5/4.5–2
		4	0.05–5.5/4.5–4
		6	0.05–5.5/4.5–6
		8	0.05–5.5/4.5–8

Adorption efficiency was studied by measuring the adsorption of Cu^{2+} ions onto pure sponge and lignite-containing sponge samples. Copper concentration was determined vy UV-VIS spectrometry by measuring the absorbance at 808 nm and the amount of of adsorbed copper was expressed as mg of copper per gram of sorbent (i.e. per total weight of sponge). The sorption capacity of lignite depends on the pH and the optimum region is 3.9–5.5. Therefore the samples were immersed in acetate buffer solution of pH = 4.5.

Results

Optical images of sponge crossection were recorded using Nickon Eclipse E200 microscope and Nikon D200 digital camera. FTIR spectra were recorded on NICOLET® Impact 400 spectrophotometer. Samples of sponges

Fig. 4.   **FT-IR spectra of raw and acetalised PVAl**

Table II
Sorprion performance

Sample	m_{Cu} [mg g^{-1}]	
	pH ~ 2,4	pH ~ 4
0.05–5.5/4.5–2	0.13	6.15
0.05–5.5/4.5–4	0.69	11.36
0.05–5.5/4.5–6	1.24	12.03
0.05–5.5/4.5–8	2.36	13.10
Lignite	*	14.43
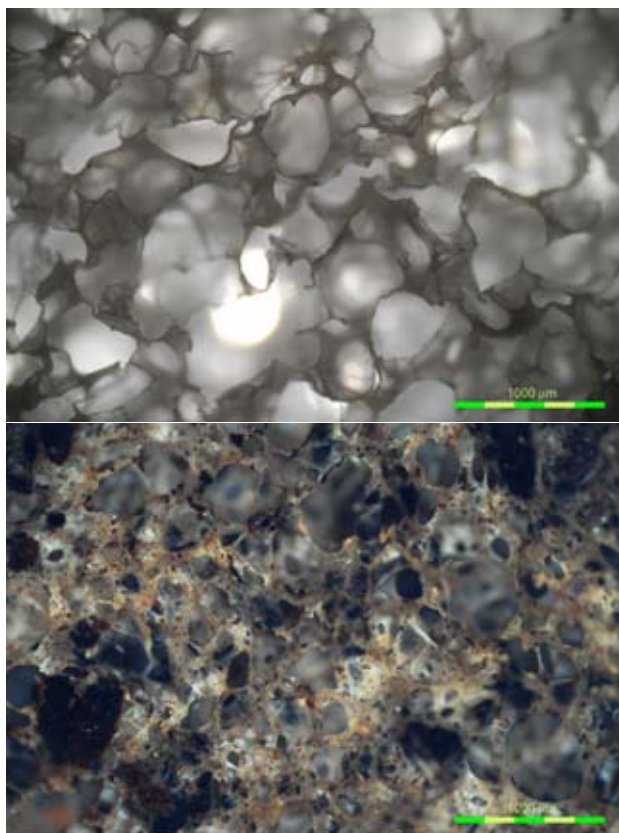
Fig. 3.   **Samples 0.05–5.5/4.5 and 0.05–5.5/4.5–6**

were finely ground to very small flakes and pressed to standard KBr tablets.

The recorded IR spectra clearly account for the reactions taking place during curing process:
- The strongly acidic environment resulting from the hardener composition yields complete hydrolysis of residual acetate groups on PVAl macromolecule. This is accompanied by total disappearance of the 1,735 cm^{-1} peak corresponding to ester vibration.
- The decreasing peak at 3,340 cm^{-1} proves the consumption of secondary hydroxyl groups for acetalization.
- C–H vibrations characteristic for formal group appeared at 2,870 and 2,790 cm^{-1} and showed increaseing intesity with increasing amount of hardener.
- Peaks at 1,189, 1,143, 1,076 a 1,033 cm^{-1} are associated with valence vibrations of $=C-O-C-$ groups and account for the formation of formal.
- Peaks at 2,360 cm^{-1} prove the presence of carbon dioxide in the tablets.

The adsorption of copper prooved to be dependent on the pH of the environment. Singe the sponges originated at highly acidic conditions, they tend to release acidity over a long period of time. Therefor the pH value had to be adjusted by the acetate buffer. Results are summarized in the following tables and figures.

Fig. 5.   **Sorption performance**

Conclusions

Our work was dedicated to the immobilization of lignite into highly porous hydrophilic sponges made of acetalized PVAl. These sponges were prepared by acidic formalization of aqueous solution of PVAl. Pores were formed by gaseous H$_2$, which originated from the reaction of powder aluminum with acid. Resulting sponges were of open-cell structure, were highly hydrophilic and had variable porosities depending on the amount of blowing agent (aluminum).

A set of sponge samples with varying lignite content was prepared and the properties of resulting sponges were studied. We also studied the sorption capacity of lignite-containing sponges on model pollutants (Cu(II) ions).

REFERENCES

1. Pekař M., Klučáková M.: CHEMagazín *13*, 8, (2003).
2. *Mowiol Polyvinyl Alcohol.* Sulzbach/Hessen: Clariant GmbH, 105 p. (1999).
3. Mleziva J., Šňupárek J.: *Polymery: výroba, struktura, vlastnosti a použití.* Praha: Sobotáles, (2000).
4. Mark H. F. *Encyklopedia of Polymer Science and Technology: Semicrystalline Polymers to Ziegler-Natta Catalysts.* 3rd ed., New Jersey: John Wiley & Sons, Inc., 2003.
5. Pourciel M. L., et al. Sens. Actuators, B 94, 330 (2003).
6. Schmedlenetal R. H.: Biomater. 23, 4325, (2002).
7. He C.-H., Gong J.: Polym. Degrad. Stab. 81, 117 (2003).

P08 FTIR AND SFS SPECTRA OF HUMIC ACIDS ISOLATED FROM LIGNITE AND CHERNOZEM

NADĚŽDA FASUROVÁ[a], ĽUBICA POSPÍŠILOVÁ[b] and EDUARD POKORNÝ[b]

[a]*University of Technology Brno,Faculty of Chemistry, Institute of Physical and Applied Chemistry, Purkyňova 118, 612 00 Brno, Czech Republic,*
[b]*Mendel University of Agriculture and Forestry, Institute of Agrochemistry, Soil Science, Microbiology and Plant Nutrition,Zemědělská 1, 613 00 Brno, Czech Republic*
fasurova@fch.vutbr.cz

Introduction

In this paper comparison of chemical structure and optical properties of humic acids (HA) isolated from various sources are presented.

Excellent sorption properties of HA are well known to depend on their chemical structure and composition.

Therefore HA isolated from different matrices (soil, lignite) were studied using FTIR and synchronous fluorescence spectroscopy (SFS) in emmision mode. FTIR spectra contributed to authentic knowing of functional groups in HA molecule. The inherent fluorescence of humic acids is an extremely sensitive measure, which allows for non-destructive analyses of samples[1,2,3]. Object of our study were HA isolated from lignite (locality Mikulčice, Czech Rep.) and Modal Chernozem (locality Bratčice, Czech Rep.).

Experimental

- HA from soil were isolated according to the international standard method IHSS[4]. HA from coal were isolated according to the Czech standard on determination of HS content in coal.
- FTIR spectra were measured using KBr technique with Nicolet Impact 400 spectrometer.
- Humic acids were dissolved in 0.5M NaOH and SFS spectra were measured by Spectrofluorimeter Aminco Bowman Series 2 within the range 320–620 nm (at $\Delta\lambda = 20$ nm and temperature 20 °C).
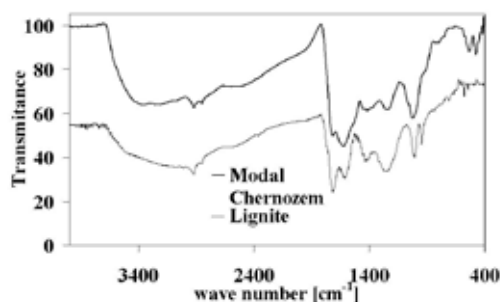
Fig. 1. **FTIR spectra of HA isolated from Lignite and Modal Chernozem**

Results

FTIR Spectra

Results showed that the main peaks observed in infrared spectra were similar for both samples (Fig. 1.). There are evident following peaks: small peaks at 3,300–3,400 cm^{-1} (OH groups, H-bonds), two small but distinct peaks at 2,930–2,850 cm^{-1} (asymmetric C of CH$_2$), sharp peak at 1,700–1,720 cm^{-1} (C= of COOH), peak at 1,650–1,655 cm^{-1} (carboxylate and amido groups), peak about 1,620 cm^{-1} (C=C in aromatic structures, C−O stretch), composed band in 1,000–1,220 cm^{-1} (aliphatic C−O stretch, OH groups and polysaccharides).

SFS Spectra

In SFS spectral range (Fig. 2.) four main fluorophore peaks were identified: at 488, 502, 470, 512 nm (at $\Delta\lambda = 20$ nm). SFS spectra of Modal Chernozem sample showed further peak at about 359 nm. The peak determined at emission 488 nm corresponded with excitation at 468 nm. This value of wavelength was more intensive then others. Maximum fluorescence intensity was shifted from shorter to longer wavelength caused by an increasing number of aromatic compounds in HA molecule. Relative fluorescence indexes (RFI) were calculated as ratio I_{488}/I_{502}. The fluorescence indexes it is supossed to be closely connected with humification degree. Higher RFI index was found in Modal Chernozem humic acid (1.13). RFI index of Lignite humic acid was lower (1.02). So we suggested higher humification degree in Modal Chernozem humic acid. These values could be also related with samples origin (mean residual time and geological age).
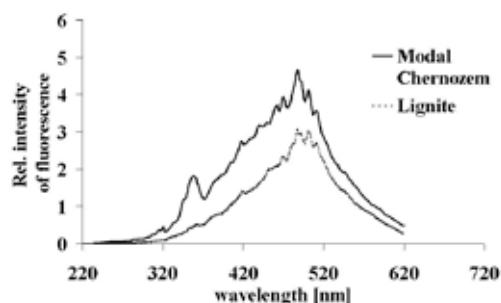
Fig. 2. **Synchronous fluorescence spectra of Lignite and Modal Chernozem humic acids at $\Delta\lambda = 20$ nm**

Fluorescence of studied samples was compared with fluorescence behaviour of Leonardite humic acid standard (IHSS). According to the literature, studied samples were included into the second group of humic substances[2]. HA in this group had two closely – spaced main excitation peaks at 450, 465 nm and emission maximum about 500–520 nm.

Conclusions

We can conclude that HA isolated from different matrices had both FTIR and SFS spectra very similar except lower wave numbers and wavelengths. Lignite and Modal

Chernozem humic acids contained the same type of fluorophore groups. More intensive fluorescence behaviour gave sample of Modal Chernozem HA. Differences in position of fluorophore peaks were not established.

REFERENCES

1. Chen J., LeBoeuf E. J., Dai S., Gu B.: Chemosphere *50,* 639 (2003).
2. Senesi N., Miano T. M., Provenzano M. R, Brunetti G.: Soil Sci. *152,* 259 (1991).
3. Senesi N., Miano T. M.: Sci. of the Total Environ. *117/118*, 41 (1992).
4. Hayes M. H. B., Wilson W. S.: R. Soc. Chem. *1997*, 83.

P09 ENHANCEMENT OF NORTHERN SOFTWOOD BLEACHED KRAFT PULP ACCESSIBILITY AND ACID HYDROLYSIS BY MEANS OF ULTRASONIC IRRADIATION

MICHAL JABLONSKÝ[a], ŠTEFAN ŠUTÝ[a] and BRANISLAV ŠVEHLA[b]

[a]*Department of Chemical Technology of Wood, Pulp and Paper, Faculty of Chemical and Food Technology, Slovak University of Technology in Bratislava, Radlinského 9, 812 37 Bratislava, Slovak Republic,*
[b]*ECOSON s.r.o., Trencianska 17, 915 01 Nove Mesto n. Vahom, Slovak Republic,*
michal.jablonsky@stuba.sk

Introduction

In the past decades, the increase in the world population and economy has resulted in a raising demand for various raw materials for industries such as raw materials for pulp and papermaking[1–4]. Many researchers have investigated the effects of the application of ultrasonic energy to pulp[1,3], recycled fiber[4], enhancement isolation of different compounds and component of wood or straw materials such as lignin[2,5,6], carbohydrate such as cellulose and hemicellulose[7,8]. The of review Willems (1962)[9] describes the use of ultrasound in pulp and paper technology for various processes like debarking, defibration, beating, impregnation and penetration, pulping, bleaching, stock preparation and grafting. The use of the ultrasound proceduce has evidenced their major potencial in the process of decreases or partial replacement of hazardous chlorine compounds during pulp bleaching alternative chemicals. Hemicellulases have been used to increase lignin extractability by partial degradation of the lignin-hemicellulose complex in the fiber, thus to improve the bleachability of pulp.[1,3,10–12]

Experimental

Raw Material

NIST standard reference material 8495 Northern Softwood Bleached Kraft Pulp was used in this study.

Ultrasonic Treatment

Sonications were carried out at 25, 40 and 80 kHz. For the ultrasonic treatment, 1 g portions of pulp (o.d.) were sonicated in 1L water using an ultrasonic generator (Model ECOSON).

Water Retention Value (WRV)

0.5 g of wet sample was swollen in 22 cm^3 deionized water for 6 hours, After this results treatment, the samples was centrifuged at 2,200 rpm. for 12 min. The dewarted sample was dried to a constant weight at 105 °C.

DRIFT FTIR Spectra

DRIFT FTIR spectra were obtained by means of a Digilab Excalibur FTS 3000MX FTIR spectrometer. Finely divided 13 mg samples of the material surface were grounded and dispersed in a KBr (260 mg). The DRIFT FTIR spectra were recorded with the nominal resolution of 4 cm^{-1} using DRIFT FTIR technique. Spectra were recorded over the range 400–4,000 cm^{-1} . Each spectrum is the average of 30 individual scans. The experimental DRIFT spectra were mathematically evaluated using OMNIC (Thermo Nicolet Corp.) and MicroCal Origin software.

Acid Hydrolysis

The resulting suspensions were then hydrolysed into microcrystals by refluxing for 5 h in 3.5M HCl.

Then the mixture was filtrated and 5 ml filtrate was added to solution of 1M NaOH buffer with pH = 7. Felingh solution I (10 ml) and Felingh solution II (10 ml) was added. This solution was warmed up to boiling point in 3 min. and following the reflux for 2 min. After heating to this sample was cooled and filtrated. Precipitated compound CuO_2 was dissolved in 20 ml 1M HCl and solution was neautralized to pH 8. Finally, this solution was titrated with the chelatone II (c = 0,01 M) using indicator murexid.

Results

The water retention value (WRV) has been extensively used to study several properties of cellulose materials. The accessibility of the cellulose material for swelling depends on several factors. The essential factors limiting the access of swelling of the fibres are: macro and microstructure of the fibres and and, in this manner, on the internal structure of cellulose and other factors such as capillary system and lumen expansion[3]. The mechanical effects of ultrasound provide a greater penetration of solvent into cellular materials and improves mass transfer[11]. The development of irradiation during ultrasonic treatment of softwood kraft pulp and different frequency 25, 40 and 80 kHz on the change of the WRV is shown on Fig. 1. On the basis of obtained results it might be said that increasing frekvence from 25 to 80 kHz in time up to 10 min. affect WRV insignificantly.With the longer
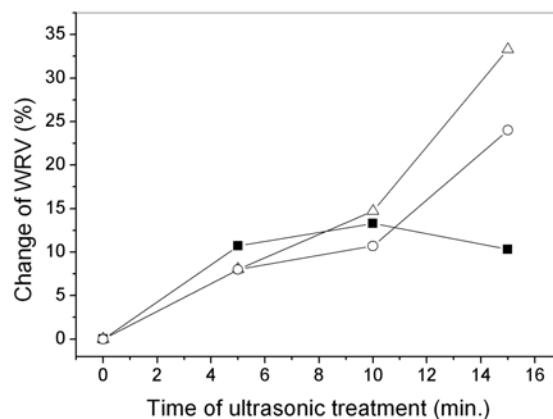
Fig. 1. **The influence of the ultrasonic treatment with the different frequency 25, 40 a 80 kHz on the change of the water retention value (WRV). -■- 25 kHz; -○- 40 kHz; -△- 80 kHz**

time of ultrasonic treatment (15 min) was found increase of WRV at 40 and 80 kHz. At 25 kHz was value of WRV didn't change. This effect of ultrasonic treatment is also confirmed by another work Wojcak and Pekarovicova, 2001[3].

The effect of the ultrasonic treatment on the pulp relates to the changes in the porosity of irradiated pulp[3]. These results were investigated in the work Laine and Goring (1977)[1] by the solute exclusion technique. They suggested that the effect of ultrasonic seems to be caused by transformation of the fibres small pores into larger ones. According to Wojcak and Pekarovicova (2001)[3] was observed that ultrasonic treatment increases the porosity of pulp. Several attempts have been made to characterize and quantify the degree of crystallinity of pure celluloses using intensities of certain bands in the infrared spectra.[13–15]
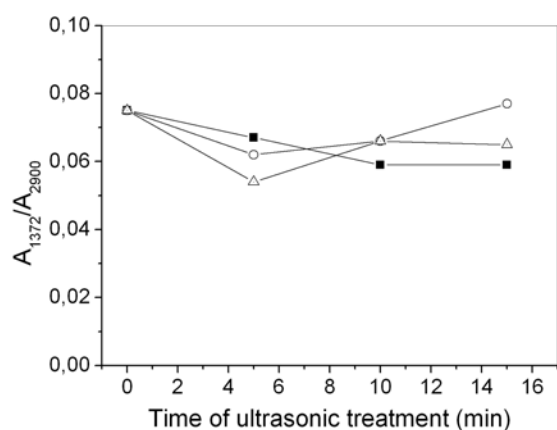
Fig. 2. **The change of the area ratio 1,372 cm^{-1} to 2,900 cm^{-1} (A1372/A2900) during the ultrasonic treatment with different frequency 80, 40 and 25 kHz. -■- 25 kHz; -○- 40 kHz; -△- 80 kHz**

The ratios of bands-heights at 1,429 and 894 cm^{-1}, at 1,372 and 2,900 cm^{-1} have been used as relative measures of cellulose crystallinites. The change in overall crystallinity has been studied by the determination of the absorbance area ratio 1,372/2,900 cm^{-1} (Fig. 2.). For the area of the band at 2,900 cm^{-1}, the baseline was drawn between the shoulders at 3,005 cm^{-1} and 2,590 cm^{-1} while for the area of the band at 1,372 cm^{-1}, the intensity of shoulder at 1,392 cm^{-1} and maximum at 1,350 cm^{-1} were used giving a common baseline for the group of bands, which occur close together in this region. The differences in the absorbane ratio of up to 0.022 units are insignificant for different frequencies which were used for ultrasonic treatment at 25, 40 and 80 kHz.

On the Fig. 3., there is shown the course of acid hydrolysis during the ultrasonic treatment with different frequency 80, 40 and 25 kHz. Samples of ultrasonification in water have exhibited higher acid hydrolysability than untreated ones. During the ultrasonic treatment increase of total content of saccharides at all frequencies was observed. The prolonged ultrasonification up to 15 minutes caused significant increase in hydrolysability. At the frequency 40 kHz was achieved significant increase of total content of saccharides at time
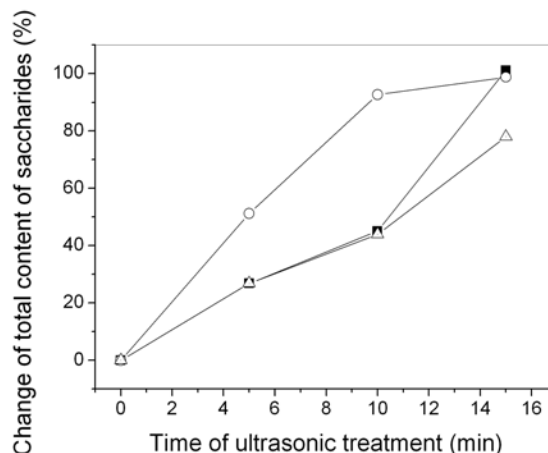
Fig. 3. **Effect of ultrasonic treatment with different frequency 80, 40 and 25 kHz on the total content of saccharides; -■- 25 kHz; -○- 40 kHz; -△- 80 kHz**

of 5 and 10 minutes of ultrasonic treatment comparing sonication at frequencies 25 and 80 kHz. At the time of 5 minutes the increase of total content of saccharides was about 90 % higher comparing to ultrasonic treatment at 25 and 80 kHz and about 106 % higher at 10 minutes of ultrasonic treatment.

Conclusions

Suspensions of northern softwood bleached kraft pulp were subjected to ultrasonic treatment at different ultrasonic frequencies 25, 40 and 80 kHz. Results revealed an increase in cellulose's accessibility in terms of water retention value (WRV) with increasing ultrasonic treatment time with the different frequency 25, 40 and 80 kHz of ultrasonic treatment. Furthermore, the acid hydrolysis of cellulose has been also successfully improved by the ultrasonic treatment. However, no significant changes in crystallinity of cellulose were noted after ultrasonic treatment which was characterized by means of FTIR.

REFERENCES

1. Laine J. E., Goring D. A. I.: Cell. Chem. Tech. *11*, 561 (1977).
2. Sun R.C, Tomkinson J. C.: Ultrason. Sonochem. *9*, 85 (2002).
3. Wojcak A., Pekarovicova A.: Cell. Chem. Tech. *3–4*, 361 (2001).
4. Tatsumi D., Higashihara T., Kawamura S., Matsumoto T.: J. Wood Sci. *46*, 405 (2000).
5. Sun R., Sun X. F. Xu X. P.: J. Appl. Polym. Sci. *84*, 2512 (2002).
6. Gadhe J. B., Gupta R. M., Elder T.: Cellulose *13*, 9 (2006).

7. Hromadkova Z, Ebringerova A., Malovikova A.: Macromolecular Symposia *232*, 19 (2006).
8. Ebringerova A., Hromadkova Z.: Ultrason. Sonochem. *9*, 225 (2002).
9. Willems P.: Pulp & Paper Magaz. Canada *63*, T455 (1962).
10. Manson T. J., Lorimer J. P.: Sonochemistry: *Theory, Applications and users of ultrasound in chemistry*, Ellis Horwood, Chichester, UK, 1988.
11. Mason T. J., Paniwnyk L., Lorimer J. P.: Ultrason. Sonochem. *3*, 253 (1996).
12. Wiikari L., Tenkanen M., Buchert J., Ratto M., Bailey M., Siikaaho M., Linko M.: *Bioconserversion of forest and agricultural residues*. (Saddler J., eds.) p.131, CAB international, Wallingford, UK 1993.
13. Fengel, D.: Holzforshung *46*, 283 (1992).
14. Evans R., Newman R. H., Roick U. C., Suckling I. D., Wallis A. F. A.: Holzforshung *49*, 498 (1995).
15. Schwanninger M., Rodrigues J. C., Pereira H., Hinterstoisser B.: Vib. Spectro. *36*, 23 (2004).

P10 MODELLING OF COMPLEXATION OF HEAVY METALS AND HUMIC ACIDS WITH UTILIZATION OF HIGH RESOLUTION ULTRASOUND SPECTROSCOPY

MARTINA KLUČÁKOVÁ, JIŘÍ KUČERÍK and MILOSLAV PEKAŘ

Institute of Physical and Applied Chemistry, Faculty of Chemistry, Brno University of Technology, Purkyňova 118, 612 00 Brno, Czech Republic,
klucakova@fch.vutbr.cz

Introduction

The high affinity of humic acids (HA) to transition metals is caused by large amount of binding sites in their structure. There is a large number of various coordination sites that are able to bind transition metals by various strengths. The most important functional groups are the carboxylic and phenolic ones. Copper was used as a model metal for experiments due to high affinity to HA and stability of formed complexes.

In previous works, quantum chemical calculations of interaction enthalpies[1] and also measurement of complexation kinetic[2,3] were carried out. On the basis of obtained results the following models have been chosen for this study: citric acid, hydroquinone, pyrocatechol, salicylic acid and EDTA. New band in UV/VIS spectra was detected as a result of complex formation for hydroquinone and pyrocatechol. Others were chosen mainly for their high affinity to metal ions, e.g. salicylic acid is frequently considered as the most suitable coordination site in structure of humic acids, which has been confirmed also by quantum chemical calculations in our works[1,3].

Experimental

Ultrasonic spectrometer with high resolution HR-US 102 (Ultrasonic Scientific, Ireland), was utilized for measurement of basic ultrasonic parameters. The device consists of two independent cells tempered at 25 °C. Both cells were filled by the same model compound (e. g. hydroquinone) and then 1.25M $CuCl_2$ (20 µl) was added into one cell. Velocity (U) and attenuation (N) in both cells was measured, the resulting differences between both cells ($U12$ and $N12$) were computed.

UV/VIS spectra were measured by means of U–3300 Hitachi spectrophotometer.

Results

Time dependencies of $U12$ for all used model are shown at Figs. 1 and 2. We can see that hydroquinone and pyrocatechol (Fig. 1.) need relatively long time for stabilization ofter addition of $CuCl_2$ than others.

Pyrocatechol, which has very strong new band in its UV/VIS spectrum after $CuCl_2$ addition, has minimum on its time-curve much higher not only than models without new band in spectra (citric and salicylic acid, EDTA – Fig. 2.) but also than hydroquinone. It seems, that relatively strong complex
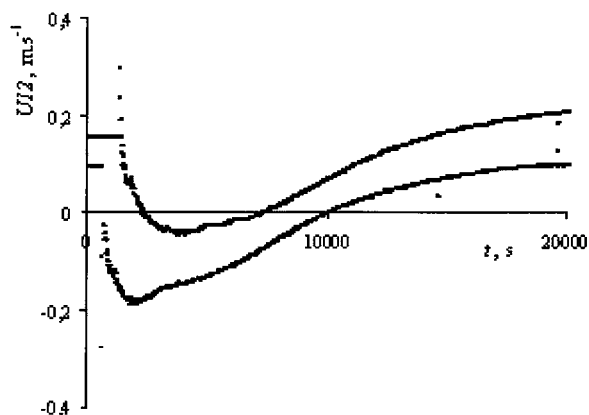
Fig. 1. **The time dependence of U12 for pyrocatechol (upper) hydroquinone after addition of CuCl₂**
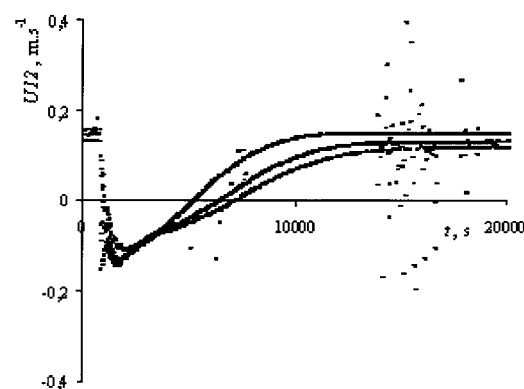
Fig. 2. **The time dependence of U12 for citric acid (upper), salicylic acid (middle) and EDTA after addition of CuCl₂**

is formed in this case, but the affinity of Cu^{2+} ions to this model is not too high, which corresponds with lower rate of the process.

On the other hand, high velocity and short time measured for salicylic acid (Fig. 2.) confirmed high ability of this structure to bind cupric ions in stable complexes. Quantum chemical calculations of interaction enthalpies[1] resulted in model of salicylic acid as a most attractive for complexation of metal ions. It is not surprising that complexation of cupric ions gives similar or better results, before its functional groups give possible similar chelating effect. In the case of EDTA is complexation rate probably influenced by molecule sizes and steric effects. But comparison with pzrocatechol and hzdroquinone shows that also this structure is more preferable. High affinity of cupric ions to these three structures probably causes that their interactions are faster than others.

Conclusions

Preliminary results of high resolution ultrasound spectroscopy are presented in this contribution. Obtained data correspond with conclusions in our previous works.[1–3] Salicylic acid, as well as citric acid and EDTA, seem to be attractive coordination sites for complexation of cupric ions.

On the hand very interesting results were obtained for hydroquinone and pyrocatechol Even though, their interaction enthalpies computed in ref.[1] are much lower than values determined for others, these structures contribute also to complexation capacity of humic acids. It corresponds with experimentally measured interaction enthalpy oh humic acids[3], which is approximately three times lower that that of salycilic acid, and EPR and FT-IR spectra of formed complexes discussed in our work[4].

REFERENCES
1. Klučáková M., Pelikán P., Lapčík L., Lapčíková B., Kučerík J., Kaláb M.: J. Polym. Mater. *17*, 337 (2000).
2. Klučáková M., Válková D., Pekař M.: *Proc. 9th International Conference on Environment and Mineral Processing* (Fečko P., Čablík V., eds.), p. 31. Ostrava, 2005.
3. Klučáková M., Pekař M., Válková D *Proceedings of the 13th Meeting of the International Humic Substances Society,* Vol. 45-I I (Frimmel F.H., Abbt-Braun G., eds.) , p. 893. Karlsruhe, 2006.
4. Čechová E., Klučáková M., Krčma F., Majzlík P., Vrajová J.: *ISPC XVIII – book of abstracts*, p. 745. Kjoto 2007.

P11   KINETICS OF SORPTION OF METAL IONS ON LIGNITIC HUMIC ACIDS

MARTINA KLUČÁKOVÁ

Institute of Physical and Applied Chemistry, Faculty of Chemistry, Brno University of Technology, Purkyňova 118, 612 00 Brno, Czech Republic,
klucakova@fch.vutbr.cz

Introduction

High sorption ability of humic acids (HA) is well known. Many authors[1–4] use Langmuir model for mathematical description of adsorption and computing HA sorption capacity. Even thought this model is in relatively good agreement with experimental data, its utilization is connected with some inaccuracies in this case, because it does not take into account the production of hydrogen ions during reactions of metal ions with acidic functional groups on the surface of humic particles. Therefore the new type of adsorption isotherm, respecting the nature of surface chemical interactions, was proposed for adsorption of metal ions on solid humic acids and proved experimentally in previous work[5].

Experimental

HA were obtained from South-Moravia lignite by means of the alkaline extraction[5–6] and characterized in[7].

The ratio 1 g of HA and 50 cm^3 of the Co^{2+} (or Ni^{2+}) salt solution was employed for the sorption experiments. The quantity of adsorbed metal ions was calculated on the basis of the decrease of absorbance (Hitachi U–3300 spectrometer) and calibration curves. The amount of liberated H$^+$ ions was measured using pH-meter Sentron Titan K185-016.

Results

The model was derived for bivalent cations and proved experimentally for sorption of cupric ions. This work deals with kinetics of sorption of cobalt and nickel ions on HA to prove above mentioned new model for metal ions with lower affinity to HA. Following equation was derived for description of adsorption kinetics for binding sites unable splitting of H$^+$ ions:

$$\rho = \ln \frac{c + c_{eq} + \dfrac{f_0 - c_0 + 1}{b_L}}{c - c_{eq}} = st + const \ , \tag{1}$$

where

$$s = k_{ads} \sqrt{\left(\frac{f_0 - c_0 + 1}{b_L}\right)^2 + 4\frac{c_0}{b_L}} \ , \tag{2}$$

c is concentration of metal ions in given time, c_0 is their initial concentration and c_{eq} is their concentration in equilibrium; f_0 is the initial concentration of free binding sites (adsorption capacity), b_L is adsorption coefficient determined on the basis

of adsorption isotherm and t is time. Because equations (1) and (2) are valid for constant pH-value, only data for $t \geq 60$ min (after pH stabilization) were used for computing values of k_{ads}. Obtained results in comparison with those published in ref.[7] for Cu^{2+} ions are listed in Table I.

Table I
Adsorption rate constants

T [°C]	k_{ads} (Co^{2+}) [dm^3 mol^{-1} s^{-1}]	k_{ads} (Cu^{2+}) [dm^3 mol^{-1} s^{-1}]	k_{ads} (Ni^{2+}) [dm^3 mol^{-1} s^{-1}]
30	1.44×10^{-6}	3.55×10^{-5}	6.57×10^{-6}
50	3.62×10^{-6}	6.28×10^{-5}	8.02×10^{-6}
70	1.17×10^{-5}	1.05×10^{-4}	9.67×10^{-6}

We can see that values obtained for Co^{2+} and Ni^{2+} ions are lower comparing with those of Cu^{2+} ions. It is caused by lower HA affinity to these metals and therefore slower adsorption. However, experimental data are in very good agreement with (1) and (2) (see Fig. 1.) and the dependence of kads on temperature can be described by Arrhenius equation similarly as in the case of Cu^{2+} ions. It confirms that developed model can be used also for adsorption of metal ions with lower affinity to HA and chemical bonds are formed in this process.
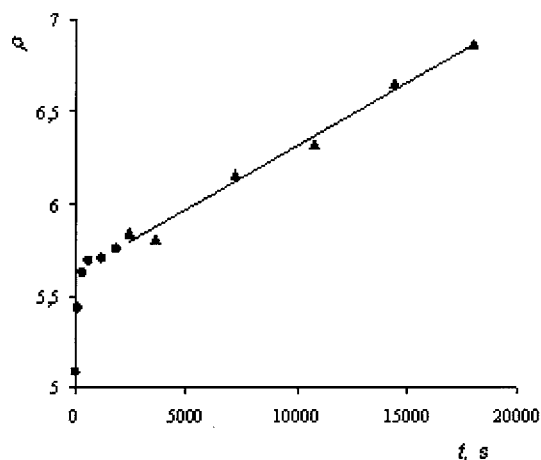
Fig. 1.   **Example of experimental data obtained for adsorption of Ni^{2+} ions at 50 °C fitted by eq. 1 (circles – H$^+$ ions are splittin off, triangles – no changes of pH)**

Conclusions

The new model published in[7] devises binding sites in humic acids into two parts: acidic functional groups, which split of hydrogen ions during surface reaction in adsorption and other binding sites as e.g. aromatic structures, which are not able to change pH value in system. One of the most important advantages of the model is that computed adsorption coefficients are not dependent on pH value as well as adsorption and desorption rate constants obtained from kinetic equation. We are able to determine directly only rate constants for adsorption and desorption, which does not cause splitting of H$^+$ ions.

REFERENCES

1. Ghabbour E. A., Davies G., Ghali N. K., Mulligan M. D.: Can. J. Soil Sci. *81*, 331 (2001).
2. Ho Y. S., McKay G.: Water Air Soil Poll. *158*, 77 (2004).
3. Mesquita M. E., Silva J.: Geoderma *106*, 219 (2002).
4. Prado A. G. S., Airoldi C.: Thermochim. Acta *405*, 287 (2003).
5. Klučáková M., Kaláb M., Pekař M., Lapčík L.: J. Polym. Mater. *19*, 287 (2002).
6. Klučáková M., Pekař M.: Colloid Surface A *252*, 157 (2005).
7. Klučáková M., Pekař M.: Colloid Surface A *286*, 126 (2006).

P12 ACID-BASE PROPERTIES OF FRACTIONATED HUMIC ACIDS

MARTINA KLUČÁKOVÁ and ONDŘEJ PILNÝ

Institute of Physical and Applied Chemistry, Faculty of Chemistry, Brno University of Technology, Purkyňova 118, 612 00 Brno, Czech Republic,
klucakova@fch.vutbr.cz

Introduction

Solid humic acids (HA) are traditionally defined according to their solubility. They are usually considered to be only partially soluble in water. The dependence of their solubility on pH-value is motivation for further fractionation. Preliminary results of the fractionation by HA dissolving in buffers with various pH values were published in ref.[1].

The same method is utilized also in this work. Acid-base properties of obtained HA fractions as well as their solubility in water are studied and compared with behaviour of original HA.

Experimental

HA were obtained from South-Moravia lignite by means of the alkaline extraction[2–3] and characterized in[4].

Batch method of fractionation using universal buffer solution (NaOH-H_3PO_4-CH_3COOH-H_3BO_3) of different pH values (4–12). Finely grounded HA (1 g) were mixed with buffer solution (50 cm^3) and stirred for 24 h. Insoluble residue was separated by vacuum filtration and concentrated HCl solution was added to the filtrate (up to pH = 1) in order to precipitate soluble HA fraction. The precipitate was washed by deionized water to remove chloride ions and dried at 50 °C.

Obtained fractions were characterized by UV/VIS (Hitachi U–3300) and FT-IR spectroscopy (Nicolet Impact 400). Content of COOH was determined by standard acetate method[5]. Acid-base properties of individual fractions as well as undissolved residues were studied by dissolving in deionized water (4–40 $g\,dm^{-3}$)[3,6].

Results

HA fractionation and study of behaviour of obtained samples showed many interesting results. While pH-values of buffers, which were before fractionation acidic decreased (up to 3.5), others were after fractionation approximately neutral, even thought dissolved HA amount was much higher. It was found that contain of acidic groups in majority of individual fractions is higher than the content of original HA samples (see Table I). Our hypothesis is that HA structure is changed during fractionation. HA can interact with individual components of buffer and re-arranged their structure, which results in apparently higher acidity of obtained fractions. The re-arrangement of HA structure probably causes, that some acidic groups inside HA aggregates, which are not able dissociate in original HA sample, can contribute to measured acidity in individual fractions.

Table I
Content of COOH groups in individual samples

Sample (fraction)	Initial pH-value	COOH [$mmol\,g^{-1}$]
original HA	–	3.3
undissolved	4	4.2
undissolved	6	3.6
undissolved	8	3.5
undissolved	10	4.2
undissolved	12	2.0
dissolved	8	6.3
dissolved	10	7.5
dissolved	12	5.3

An exception is undissolved HA residue (initial pH = 12), which has lower acidity that original HA. Surprising is that this fraction (after "exhaustion" of the largest amount of HA fraction) has several times higher solubility in water as others. Extracts had to be 30-times dissolved in order to measure UV/VIS spectra. Contradictory results were obtained in measurement of pH and conductivity. Extracts of fraction undissolved at pH = 12 had lower conductivity and very high pH values in comparison of other fractions as well as original HA sample. On the other hand, this fact corresponds with our hypothesis of re-arrangement and possible interactions with buffer, because the most "aggressive" buffer caused the most marked changes in HA properties.
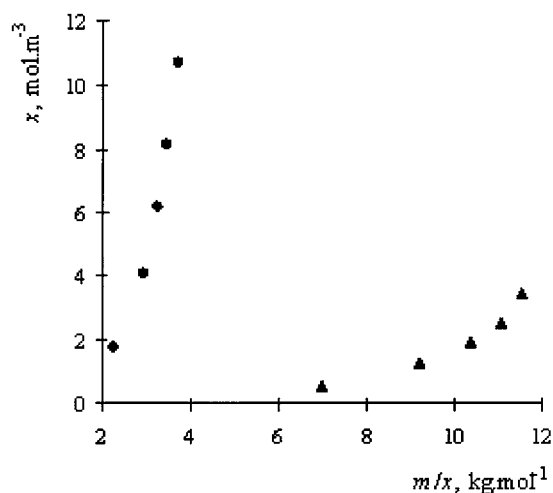
Fig. 1. **Experimental data obtained for initial pH = 6 (triangles) and 10 (circles)**

In previous works[3,6], has been deduced model of HA behaviour in water and aqueous solutions, which included dissociation both dissolved HA and undissolved solid particles. We applied this model of obtained undissolved residues, but their dissolving is different probably as a result of structural changes caused by fractionation (see above). It was derived that equilibrium constant K between dissolved and dissociated HA is

$$K = \frac{x^2}{k.m - x}, \qquad (1)$$

which can be linearized as

$$x = K.k\frac{m}{x} - K, \qquad (2)$$

where x is concentration of H^+ ions, m is content of HA in initial suspension and k is constant. While data measured for original HA agree with (2) very well and they give strong line[3], dependencies obtained for our fraction are curved and curvature increases with decreasing initial pH-value. It is other confirmation of structural changes in HA and also different behaviour of individual samples.

Conclusions

Acid-base properties of HA fractions obtained by means of extraction in buffers with various initial pH-values are studied in this work. It was found that re-arrangement and changes of HA structure are caused by this way of fractio-

nation. It results in higher acidity both dissolved and undissolved fractions in comparison with original HA sample and very high solubility of the last residue (initial pH = 12) with lowest conductivity and acidity of its extract in water.

REFERENCES

1. Klučáková M.: *Proceeding of the International Conference Humic Substances in Ecosystems 5* (Gonet S.S, Zaujec A., eds.), p. 39. Bydgoszcz, 2003.
2. Klučáková M., Kaláb M., Pekař M., Lapčík L.: J. Polym. Mater. *19*, 287 (2002).
3. Klučáková M., Pekař M.: Colloid Surface A *252*, 157 (2005).
4. Klučáková M., Pekař M.: Colloid Surface A *286*, 126 (2006).
5. Stevenson F. J.: Humus Chemistry: *Genesis, Composition, Reactions*. Wiley, New York, 1994.
6. Klučáková M., Pekař M.: Colloid Surface A *318*, 106 (2008).

P14　COMPARISON OF VARIOUS PLASMACHEMICAL PROCESSES WITH RESPECT TO THE GAS TEMPERATURE

LUKÁŠ LAZAR[a], PETR SYNEK[a], MONIKA KARÁSKOVÁ[a], MAREK ELIÁŠ[a], ONDŘEJ JAŠEK[a], LUKÁŠ KELAR[a], VILMA BURŠÍKOVÁ[a], PAVEL KONUPČÍK[b] and LENKA ZAJÍČKOVÁ[a]

[a]Department of Physical Electronics, Faculty of Science, Masaryk University,Kotlářská 2, 611 37 Brno, Czech Republic,
[b]Department of Didactic Technology, Faculty of Education, Masaryk University, Poříčí 7, 603 00 Brno, Czech Republic, *lucasl@physics.muni.cz*

Introduction

Plasma technologies have been already established a key role in many industrial products such as microelectronic devices, solar cells, protective or anticorrosion coatings on machining tools or automobile parts. However, they are still extensively studied as a tool for deposition of new materials and for better understanding of the existing processes.

Using high temperature methods, carbon nanotubes (CNTs) can be produced from carbon vapours generated by an arc discharge or by laser ablation of graphite. Alternative methods are covered by the term chemical vapour deposition (CVD). CVD offers some advantages over other mechanisms particularly in allowing synthesis on specialized surfaces and substrates. By this method, nanotubes can be produced with high purity and in well-ordered arrays of relatively uniform geometry. The CVD group can be further divided into thermal CVD processes and processes utilizing plasma discharges, the so called plasma enhanced CVD (PECVD). The PECVD technique employes combination of physical and chemical processes and is based on the molecule dissociation in the gas phase by impact of energetic electrons and atoms in metastable states followed by chemical reactions of gas radicals. PECVD technique is also one of suitable methods for the deposition of diamond-like carbon (DLC) and crystalline diamond thin films. The PECVD method enables to adjust the film properties and composition by choosing the right deposition parameters and hence make them convenient for a wide variety of applications.

Optical emission spectroscopy (OES) analysis is relatively simple tool for the investigation of plasma used for the deposition or synthesis. Among others, it can be used for the determination of neutral gastranslational temperature that is one of the important factors of the CVD processes. Hence, the OES together with numerical treatment of measured spectra was applied in this work to determine the gas temperature of different plasma processes.

Description of Plasma Processes Studied

Optical emission spectra were measured in the three types of experiments:

- atmospheric pressure microwave (mw) torch used for the synthesis of carbon nanotubes
- low pressure mw ASTeX-type discharge used for the deposition of ultrananocrystalline diamond (UNCD) films
- low pressure r.f. capacitive discharge used for the deposition of nanocomposite diamond-like carbon films

MW Torch for Synthesis of CNTs

The microwave (mw) plasma torch at atmospheric pressure has been sucessfully used for carbon nanotube (CNT) synthesis[1,2]. The whole experimental set-up (see Fig. 1.) used for the synthesis of CNTs and plasma diagnostics is described below. Microwave power is supplied by a 2.45 GHz, 2 kW generator via a standard rectangular waveguide. At the end of the waveguide there is a broadband transition to a coaxial line realized by means of a ridge waveguide. The inner conductor of the coaxial line is hollow double-walled tube accommodating a dual gas flow. A conical hollow nozzle electrode is fixed to its top. The nozzle is made of iron with a central gas flow channel. A set of holes in the outer tube wall allows for separate gas feeding by an outer channel. The central conductor is held in place by boron nitride ceramics. The outer conductor of the coaxial line is terminated by a flange.

The plasma expands from the central nozzle forming a torch discharge. A quartz tube separates the discharge from surrounding atmosphere. At the bottom it is sealed by a teflon piece to the flange of the outer coaxial conductor. At the top it is closed by an upper flange with an exhaust tube and a sealed feedthrough for a substrate holder. The substrate holder is another quartz tube fixed at the upper flange. This tube is closed at its top by a quartz window. At the opposite side, i.e. close to the discharge nozzle, two slits are cut through the tube. Substrates for the deposition (15×10 mm^2) are inserted into these 1 mm wide slits and pressed down slightly by the weight of a 20 mm piece of a narrower quartz tube.

For the CNT deposition 1,500 sccm of argon was flowing through the centre of the nozzle and an H_2/CH_4 mixture was added from the outer channel. The mw power was fixed at 400 W. The deposition of CNTs was carried out at atmospheric pressure on the silicon substrates (10–15 mm) with silicon oxide layer covered by iron (Fe) catalytic thin film.

The silicon oxide was prepared by PECVD in r.f. capacitively coupled low pressure glow discharge from the hexamethyldisiloxane/oxygen mixture and subsequently annealed at 970 K for 30 min. An iron film, 2.5–1 5 nm in thickness, was vacuum evaporated on the top of the silicon oxide

Optical emission spectra were recorded by means of the Jobin-Yvon TRIAX 320 spectrometer with a fibre optics and CCD detector. The fibre was fixed at different distances from the nozzle along the discharge axis in order to study spatial changes in the plasma emission. The measurement spot integrated by the optics was 10 mm. Appropriately, the spatial profiles were carried out with the same step.

Fig. 1.   **Microwave torch used for synthesis of carbon nanotubes**

Fig. 2.   **Microwave ASTeX-type reactor used for UNCD deposition**

M W   A S T e X - t y p e   D i s c h a r g e   f o r
U N C D   D e p o s i t i o n

The bell-jar microwave plasma CVD reactor for UNCD deposition[3] is shown in Fig. 2. The basic features of this reactor included a 10 cm in diameter silica bell-jar, that confines the plasma discharge, and 5 cm diameter substrate holder. The microwave generator (Muegge) used a magnetron to generate 2.45 GHz microwave radiation that was directed by a rectangular air filled metallic waveguide. A circulator allowed the microwave radiation to travel towards the CVD reaction chamber, but redirected any reflected microwaves into a water-cooled dummy load. In this way, any excess energy was dissipated, thus preventing damage to the magnetron. An antenna coupled the energy from the waveguide into the reactor, which was cylindrical in shape. The position of the plasma ball could be changed by bottom matching piston. The substrate was heated by the discharge.The gas mixture and the pressure range utilized were CH_4/H_2 and 4–25 kPa, respectively. The power range was typically 0.5–2 kW.

Continuous nucleation of diamond nanocrystals was achieved by capacitive coupling of r.f. power (35 W, 13.56 MHz) to the central graphite plate of the substrate holder. The outer graphite ring served as a grounded electrode. Due to different mobility of electrons and ions this resulted in a generation of dc self-bias accelerating the ions across the sheath adjacent to the graphite plate, i. e. to the substrate.

R F   C a p a c i t i v e   D i s c h a r g e   f o r
D e p o s i t i o n   o f   N a n o c o m p o s i t e   D L C
F i l m s

The DLC films with various SiO_x content were prepared in r.f. capacitive discharges at low pressures (8–11 Pa) from a mixture of methane (CH_4) and hexamethyldisiloxane (HMDSO)[4]. This basic mixture was used either without any additional gas or with an admixture of argon, hydrogen or nitrogen. The reactor was a glass cylinder with two inner parallel plate electrodes made of graphite. The bottom electrode, with the diameter of 150 mm, was coupled to the r.f. generator (13.56 MHz) via a blocking capacitor. The substrates (silicon single-crystal, glass, steel and polycarbonate) were placed on the r.f. electrode, the r.f. voltage of which was superimposed with a negative d.c. self-bias. The r.f. power was in the range 50 to 350 W. The corresponding self-bias voltage varied from –250 V to –600 V depending on the gas mixture, applied power and deposition pressure. The CH_4 flow rate was varied in the range from 1.4 sccm to 2.85 sccm. The HMDSO flow rate varied from 0 to 0.87 sccm. The flow rate of admixed gas (Ar, H_2 or N_2) ranged from 0.35 sccm to 7 sccm.

Optical emission spectra were recorded by means of the Jobin-Yvon TRIAX 550 spectrometer. Spectrum of N_2^+ (first negative system) was studied for the determination of rotational temperature.

Calculation of Rotational Temperature from Optical Emission Spectra

We have developed the program DMESS[5] for the determination of rotational temperature of diatomic molecules that is based on the least square method in which the difference between the measured and simulated data is minimized.

Nowadays, the program can be used for following vibrational transitions: N_2^+ (first negative system), CN (violet), N_2 (second positive system) and C_2 (Swan system). The line positions of the molecular spectra are calculated either using equilibrium constants that determine the vibrational and rotational constants for the particular electronic transition or, in case of N_2^+, CN and C_2 molecules, from tabulated spectroscopic constants for each vibrational level. The latter approach allows more accurate determination of the energies, i.e. the line positions, of the specific vibration levels. The intensities are convoluted with Lorentzian, Gaussian or triangular lineshapes. The program uses following fitting parameters: rotational temperature, line broadening, spectral shift of measured data and background intensity. In general, the broadening corresponds to the sum of the broadening determined by the resolution of the spectrometer, i.e. apparatus function, and the broadenings caused by physical processes. Two methods can be used for the fitting of spectra within the program, the Nelder-Mead method (known as downhill simplex method) and the Levenberg-Marquardt algorithm. The fast Nelder-Mead method starts the fitting with the user estimated values of the parameters in order to find approximately the position of the global minimum. Then, the more sophisticated Levenberg-Marquardt algorithm can be used for finding more precise parameter values.

Results and Discussion

For the mw torch discharges the gas temperature in the case of deposition mixtures was estimated as the rotational temperature from the (0,0) rotational emission band of the C_2 Swan system.

Dependence of the rotational temperature on the position of the optical fibre with respect to the nozzle electrode was measured. The calculated rotational temperatures by program DMESS show the increase of temperature approximately to position 10 mm above the nozzle electrode, where is the temperature $4,200 \pm 70$ K, and the subsequent decrease, 30 mm above the nozzle temperature is $3,100 \pm 70$ K. The comparison of measured and simulated rotational structures of C_2 (0,0) is shown in Fig. 3.
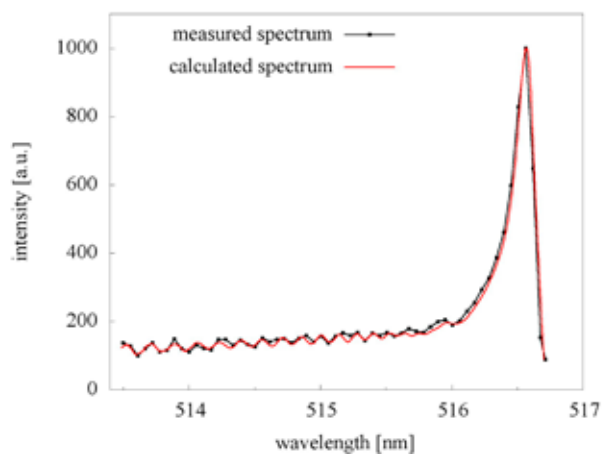
Fig. 4. **A comparison of measured and calculated spectra of C_2 (0,0) Swan system in ASTeX-type discharge used for UNCD deposition. Total line broadening was 0.12 nm**

Similary, for the ASTeX-type discharge the temperature was determined from C_2 (0,0), $T = 2,700 \pm 150$ K, but in this case only at one position of optical fibre. The total broadening of spectral lines affected the determination of rotational temperature. The estimated error was higher in less resolved spectrum of ASTeX-type discharge (Fig. 4.) then in micro-

Fig. 3. **Measured spectrum of C_2 (0,0) rotational band of the Swan system is compared with simulation in case of mw torch used for the synthesis of CNTs. The total line broadening was 0.07 nm**
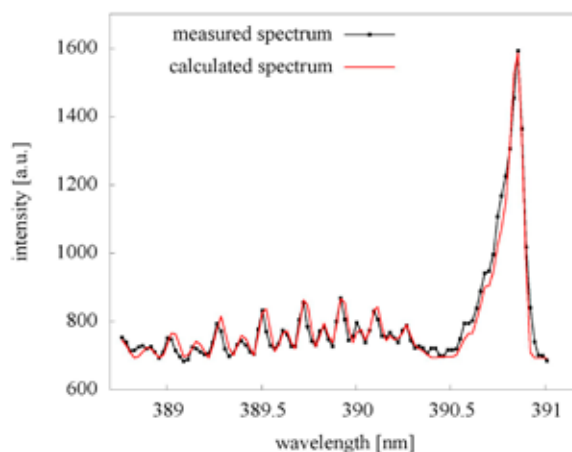
Fig. 5. **A comparison of measured and calculated spectra of N_2^+ (0,0) first negative system in the r.f. capacitive discharge used for deposition of nanocomposite nitrogen-containing DLC films. Ttotal line broadening was 0.06 nm**

wave torch discharge (Fig. 3.). Total broadening in mw torch was about 0.07 nm and in ASTeX-type discharge 0.12 nm.

The rotational temperature in case of r.f. capacitive discharge used for the deposition of nanocomposite DLC films was estimated using the N_2^+ (0,0), first negative system (Fig. 5.) if a small amount of nitrogen was added to $HMDSO/CH_4$. The calculated temperature was T = 320 ± 20 K, total broadening 0.06 nm.

Conclusions

Rotational temperatures for several types of discharges were determined from optical emission spectra by program DMESS. In the case of mw torch used for synthesis of CNTs and ASTeX-type discharge used for UNCD deposition the temperatures were estimated from the rotational emission band of the C_2 (0,0) Swan system. In the case of r.f. capacitive discharge used for the deposition of nanocomposite nitrogen-containing DLC films the N_2^+ (0,0) first negative system was employed.

REFERENCES
1. Zajíčková L., Eliáš M., Jašek O., Kudrle V., Frgala Z., Matějková J., Buršík J., Kadlečíková M.: Plasma Phys. Control. Fusion *47*, 655 (2005).
2. Jašek O., Eliáš M., Zajíčková L., Kudrle V., Bublan M., Matějková J., Rek A., Buršík J., Kadlečíková M.: Mater. Sci. Eng. C *26*, 1189 (2006).
3. Frgala Z., Jašek O., Karásková M., Zajíčková L., Buršíková V., Franta D., Matějková J., Rek A., Klapetek P., Buršík J.: Czech J. Phys. *56*, 1218 (2006).
4. Buršíková V., Dvořák P., Zajíčková L., Franta D., Janča J., Buršík J., Sobota J., Klapetek P., Bláhová O., Peřina V.: Optoel. Adv. Mater. Comm. *1*, 491 (2007).
5. Lazar L.: *Diploma thesis*. Masaryk University, Brno, Czech Republic, 2005.

P15　EPR STUDY OF NITROXIDE RADICALS GENERATED FROM SOME SECONDARY ALKYL-ARYL AND ARYL-ARYL AMINES

PETR MAJZLÍK[a], LADISLAV OMELKA[a], JAN SVĚTLÍK[b] and PETER RAPTA[c]

[a]*Brno University of Technology, Faculty of Chemistry, Institute of Physical and Applied Chemistry, Purkyňova 464/118, 612 00 Brno, Czech Republic,*
[b]*Faculty of Pharmacy, Department of Pharmaceutical Analysis and Nuclear Pharmacy, Odborárov 10, 835 32 Bratislava, Slovak Republic,*
[c]*Slovak University of Technology, Faculty of Chemical and Food Technology, Department of Physical Chemistry, Radlínského 9, 812 37 Bratislava, Slovak Republic,*
majzlik@fch.vutbr.cz

Introduction

Generally, secondary alkyl-aryl and aryl-aryl amines represent the group of very effective antioxidants. Their action is based on the reaction either with $RO_2^•$ radicals or peroxy compounds, leading to the corresponding nitroxyl radicals[1,2]. By the reaction with peroxides the intermediary formed cation radicals are involved into reaction mechanism[3]. Nitroxyl radicals, generated by both methods can be directly detected by the EPR spectroscopy. In the framework of this paper the radical products of the oxidation of some secondary amines containing one or two -NH- group in the molecule are reported.

Experimental

Within the paper the following secondary amines were studied:

1
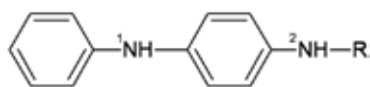
1a	$R = CH(CH_3)_2$
1b	$R = CH(CH_3)-CH_2-CH(CH_3)_2$
1c	$R = CH(CH_3)-C_6H_5$
1d	$R = C_6H_5$
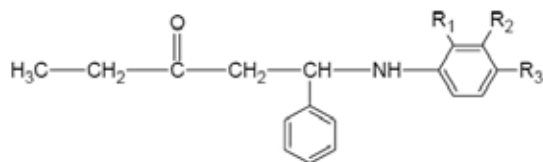
2

2a	$R_1 = R_2 = R_3 = H$
2b	$R_1 = R_2 = H, R_3 = CH_3$
2c	$R_1 = CH_3, R_2 = R_3 = H$
2d	$R_1 = R_2 = H, R_3 = Cl$
2e	$R_1 = R_3 = H, R_2 = Cl$

Oxidation of Amines with 3-Chloroperbenzoic Acid

In 10^{-2}M benzene or chloroform solution of 3-chloroperbenzoic acid (3-ClPBA), secondary amines **1**, **2** were dissolved (molar ratio 3-ClPBA: amine = 1 : 1) under stirring for 2 min. 0.5 ml of the solution was placed into the EPR cell and bubbled with nitrogen to remove the dissolved oxygen.

EPR spectra were recorded at the laboratory temperature using an EPR spectrometer SpectraNova. The simulation of the experimental EPR spectra was carried out using the simulation program Simphonia.

Results and Discussion

Within the investigation of antioxidative properties the reaction of amines **1a–1c** with 3-chloroperbenzoic acid was examined. In this way the high concentration of corresponding nitroxile radicals was obtained.

The fundamental problem, accompanying the interpretation of experimental EPR spectra, obtained by the oxidation of **1a–1c** is the attribution of generated nitroxide radicals to the structure **3** or **4** (1).
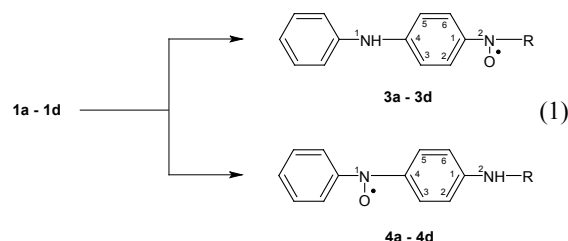
The analysis using spectral simulation has unambiguously shown that the structure **3** is responsible for the nitroxide radicals observed by the oxidation of amines **1a–1b** (structures **3** and **4** are identical in the case of **1d**). This conclusion is supported by the fact that besides the basic nitrogen splitting only the splitting constants from two hydrogen atoms in ortho position of the phenyl ring and one hydrogen atom in $-CH(CH_3)-$ group dominate in EPR spectra of **3a–3b** in benzene solution (Table I). In the case of amine **1c**, containing α-methylbenzyl substituent R, the dependence of the structure of generated nitroxide radical (**3c** *vs*. **4c**) on the solvent is documented. While in benzene the EPR spectrum of **4c** was observed, in chloroform the oxidation evidently proceeds on $-^1NH-$ group, as follows from the splitting constants of **4c**: $a_N(NO) = 1.020$ mT, $5 \times a_H(o,p) = 0.180$ mT, $4 \times a_H(m) = 0.090$ mT, $a_N(NH) = 0.045$ mT.

Characteristic feature of secondary amines **2a–2e** is the presence of only one $-NH-$ group in the molecule. By their oxidation using 3-ClPBA the EPR spectra of generated nitroxyl radicals **5** were registered (2).
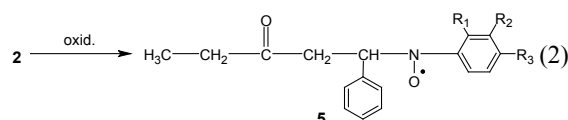
Table I

The EPR parameters of nitroxide radicals **3a–3d** prepared by the oxidation of amines **1a–1d** with 3 chloroperbenzoic acid in benzene (**3a–3d**) and chloroform (**3a–3b**) solution

Radical	a_N(NO) [mT]	a_N(NH) [mT]	Splitting constants $2a_H$(2.6) [mT]	$2a_H$(3.5) [mT]	a_H(R) [mT]	Solvent
3a	1.137	0.045	0.260	0.090	0.316	chloroform
	1.078	–	0.240	–	0.380	benzene
3b	1.127	0.045	0.216	0.085	0.336	chloroform
	1.078	–	0.225	–	0.306	benzene
3c	1.080	–	0.269	–	0.500	benzene
3d[a]	0.960	–	0.182	0.074	0.182 (3H) 0.074 (2H)	benzene

[a]splitting constants taken from ref.[4]

Table II

EPR parameters of nitroxyl radicals **5a–5e** generated by the oxidation of secondary amines **2a–2e** in toluene solution

Radical	a_N (NO) [mT]	a_H (o,p) [mT]	Splitting constants a_H (m) [mT]	a_H (CH) [mT]	a_H (CH2) [mT]
5a	1.1050	0.2730	0.0900	0.5460	0.0600 (1H) 0.0350 (1H)
5b	1.1225	0.2770 (2H) 0.2970 (3H)	0.0900 0.0350 (1H)	0.5760	0.0600 (1H)
5c	1.2000	0.1500 (2H) 0.1500 (3H)	0.0800	0.4800	–
5d	1.1000	0.2850 (2H) 0.0250 (3H)	0.0950	0.5700	0.0400 (1H) 0.0650 (1H)
5e	1.0500	0.2800	0.0820 (1H)	0.5600	0.0570 (1H) 0.0220 (1H)

In EPR sectrum of **5a**, besides the basic nitrogen splitting, the splittings from protons of phenyl ring and one hydrogen atom of –CH(Ph) were proved. Moreover, the small splitting constants from protons of $-CH_2-$ group were extracted. By the introduction of other substituents into *para* and *meta* position of phenyl ring (**2b**, **2d**, **2e**) does not bring any principal changes in spin density distribution. The only exception is represented by the nitroxyl radical **5c**. In this case, very strong *ortho* effect of methyl group, leading to the distortion of the phenyl ring from the plane of $-NO^•-$ fragment is observed. Consequently, the delocalization of spin density into this ring is reduced. The decrease of splitting constants attributed to the protons of phenyl ring is compensated by the increase of basic nitrogen splitting (Table II).

Conclusions

New types of secondary amines were subjected to the oxidation with 3-chloroperbenzoic acid in non-polar solvents. EPR spectroscopy confirmed the formation of nitroxyl radicals, the only radical products observed. Their EPR data were determined using the spectral simulation.

REFERENCES

1. Pospíšil J., Advan. Polym.Sci. *124*, 89 (1995).
2. Thomas J., J. Am. Chem. Soc. *82*, 5955 (1960).
3. Toda T., Mori E., Murayama K., Bull. Chem. Soc. Jpn, *45*, 1904 (1972).
4. Burian M., Omelka L., Ondrášová S., Brezová V., Monatsh. Chem. *134*, 501 (2003).

P16 ROUGHNESS OF PLASMA TREATED PAPERS AND FOILS AND CONDUCTIVITY OF PRINTED STRUCTURE

MILAN MIKULA, ZUZANA POBUDOVÁ and ADAM GILAN

*Faculty of Chemical and Food Technology STU, Radlinského 9, 812 37 Bratislava, Slovak Republic,
milan.mikula@stuba.sk*

Introduction

Printed electronics based on solution-processable organic inks have attracted considerable attention. It has big potential to decrease the cost of electric circuits fabrication, especially when using roll-to-roll printing[1,2]. Principal advantages are mass or large area production, low cost, flexibility of substrates and production variability. Supposed low-cost mass application includes RFID chips, flat OLEDs lightings, flexible displays and solar sells, intelligent packaging and papers etc.

Inkjet printing is applicable to print all required materials (conductors, semiconductors and dielectrics) including OLEDs and TFTs[3,4]. Inkjet was used to print conducting links based on nanosilver colloid[5] and conductive/semiconductive structures based especially on conjugated polymer chain poly(3,4 ethylenedioxythiophene) in complex with poly(styrene sulfonate), PEDOT:PSS, to create conductive links or OLED[6,7]. Conductivity of this system was increased adding organic solvents like dimethyl sulfoxide (DMSO), tetrahydrofuran[8]. The dielectric properties, wetability and roughness of printed substrates are also key parameters of resulted quality.

In this work, N_2 plasma treated coated papers and plastic foils were inkjet printed by water-based PEDOT:PSS and different solvent additives to get high conductivity structures. The influence of substrate roughness, plasma treatment and ink formulation are discussed.

Experimental

Two plastic foils: polyethylenetherephtalate (PET, $120 \, \text{g m}^{-2}$) for laser printers and ethylene-tetrafluorethylene copolymer coated by thin 70 nm silicon oxide (ETFE/SiO$_x$, $150 \, \text{g m}^{-2}$), and three coated paper sheets: $120 \, \text{g m}^{-2}$ (glossy varnish, Huber 10L9500, "L1"), $150 \, \text{g m}^{-2}$ (matt varnish,

Table I
PEDOT ink formulations, η – viscosity, γ – surface energy

PEDOT/PPS	Water	IPA	DMSO	Designation	η [mPa s^{-1}]	γ [mJ m^{-2}]
1	0	0	0	PEDOT	58.5	68.1
1	0	1/2	+5 %	IPA	–	–
1	1/2	0	+5 %	4 : 2 (5D)	21.1	67.6
1	1/4	1/4	+5 %	4 : 1 : 1 (5D)	17.5	62.4
1	1	1	+5 %	1 : 1 : 1 (5D)	16.5	45.9
1	1/2	0	+10 %	4 : 2 (10D)	20.1	68.4
1	0.3	0	0.2	4 : 1 (15D)	22.4	65.3

Huber 10L9320, "L2") and $120 \, \text{g m}^{-2}$ copy paper (Xerox Colotech, smooth, white, "CP") were used as substrates for printing.

Standard dielectric barrier discharge (DBD, 15 kV, 5 kHz) was used for plasma treatment of substrates ($30 \, \text{W cm}^{-2}$) in N_2 at atmospheric pressure (at flow rate of $10 \, \text{dm}^3 \text{min}^{-1}$).

The commercial conductive polymer PEDOT:PSS, 1.3 % wt. in water from Aldrich (hereafter PEDOT) was diluted by water, isopropanol (IPA) or DMSO in several combinations (Table I) and used as ink in inkjet printer EPSON Stylus Photo R360.

Different lines, points and full areas were printed onto all substrates, original and plasma treated, by inkjet printer in slow mode (Fig. 1.).
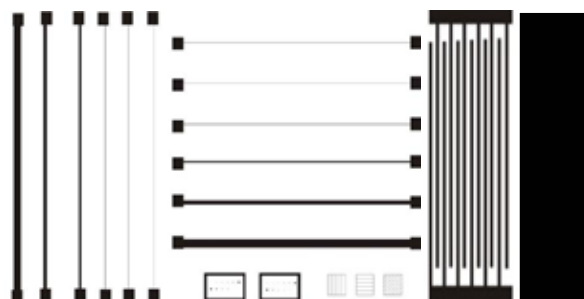
Fig. 1. **Inkjet printed figures**

Ink formulations were characterized by viscosity and surface energy, the substrates by ink wetability and AFM topography including RMS roughness and printed structures by electric conductivity and topography, using the equipments: capillary viscometer UNITEX, contact angle goniometer (SEE, MU Brno), optical and atomic force microscopy CP II, Veeco and LCR Digibridge Quadtech 1715.

Results

Addition of DMSO increased considerably the conductivity of layers (Fig. 2.). Reverse temperature dependences indicate semiconductor character of layers without DMSO and quasi-metal character of layers with DMSO.

Original high viscosity PEDOT could not be inkjet printed. It had to be diluted. Because of high dilution the coatings were very thin, so to get stable results, lines had to be printed several times on each other (more than 4) that caused misregistration problems.

Surface conductivity of printed lines depends on roughness, ink wetability and imbibition. RMS roughness of the substrates are indicated inside the legends of the Fig. 3.a and b. Conductivities on smooth foils are much higher than on papers. Specific conductivity ought to be independent on line thickness, however lines thinner than 0.5 mm are discontinuous.
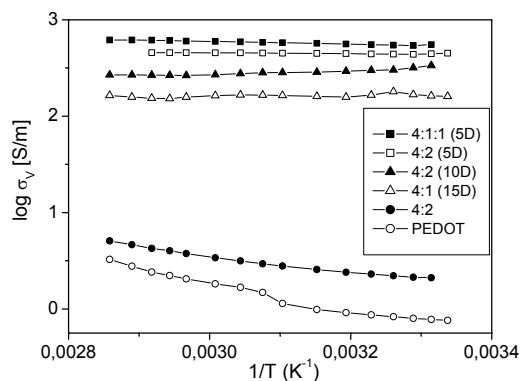
Fig. 2. **Specific volume electric conductivity of dry ink layers on clean glass substrates**
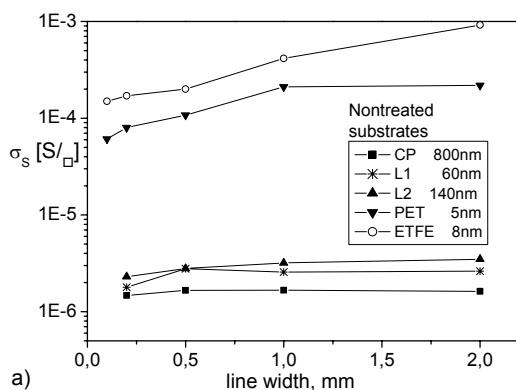
a)
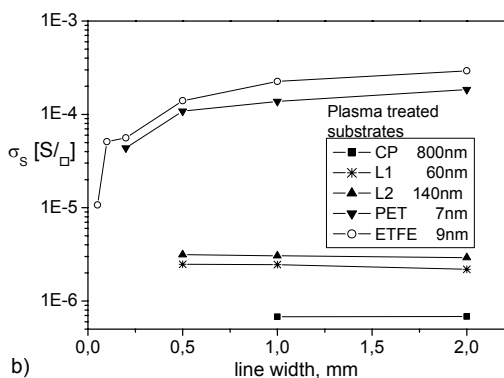
b)

Fig. 3. **Specific surface conductivities of lines 10 times printed by 4:2(5D) ink onto original (a) and plasma treated (b) surfaces**

Plasma treatment enhanced the printability of foils (conductivity results were more stable), however it increased the imbibition of copy paper resulting in conductivity decrease (Fig. 3.b).

The ink formulation 4:2 (5D) was found as the most effective considering overall topography and conductivities, but the interval allowed for dilution of PEDOT is narrow so more experiments must be done to find optimal formulation.

Conclusions

Coated and plasma treated papers and plastic foils were inkjet printed by water-based conductive inks (commercial PEDOT:PSS with additives, water, IPA and DMSO.

Addition of DMSO and water improved printability and increased conductivity of lines and full areas. Surface roughness, wetting and imbibition were key factors of features quality.

Sufficient and continuous coating and desired conductivities of lines and areas were achieved just by repeated printing (up to 10 times), so the misregistration was the limiting factor of print quality of lines and dots.

REFERENCES

1. Kallberg E.: *Inteligent Papers*, PhD. thesis, Univ. of Jyvaskyla, Finland, 2006.
2. Mäkelä, T., Jussila, S., Kosonen, H., Bäcklund, T. G., Sandberg, H. G. O., Stubb, H. Synth. Met. *153,* 285 (2005).
3. Yoshioka Y., Jabbour G. E.: *Inkjet Printing and Patterning of PEDOT-PSS*, in Conjugated Polymers, Processing and Application, eds. T. A. Skotheim, J. Reynolds, CRC Press 2006.
4. Svanholm E.: *Printability and Ink-Coating Interactions in Inkjet Printing,* PhD. thesis, Fac. of Technology and Science, Karlstad Univ. 2007, Sweden.
5. Lee H. H., Chou K. S. and Huang K.C. Nanatechnol. *16,* 2436 (2005).
6. Soltman D., Subramanian V.: Langmuir *24,* 2224 (2008).
7. Zmeškal O., Veselý M., Martin V., Bednář P., Bžatek T.: Proc. 8th Seminar in Graphic Arts, Sept.07, Pardubice, Czech Rep., . 131-7, Univ. Pardubice 2007.
8. Kim J.Y., Jung J.H., Lee D.E. Joo J. Synth. Met. *126,* 311 (2002).

P17 INFLUENCE OF DYE STRUCTURE ON ITS DECOMPOSITION BY ELECTRIC DISCHARGE IN WATER SOLUTIONS

JANA PAJURKOVÁ, ZDENKA STARÁ and FRANTIŠEK KRČMA

Brno University of Technology, Faculty of Chemistry, Purkyňova 118, 612 00 Brno, Czech Republic,
xcpajurkova@fch.vutbr.cz

Introduction

During last ten years, electrical discharges generated in water have been widely studied with a great focus on the application in water treatment. Besides classical biological, physical and chemical methods, so-called Advanced Oxidation Processes (AOP's) have been applied in removal of various pollutants. Especially degradation of phenol and some organic dyes by pulsed discharges in point-to-plane geometry have been studied by many authors, for example refs.[1–3].

Applying high energy field into water solution, various physical and chemical processes are initiated. Generation of UV light and shock waves belong to the physical processes while formation of various reactive species is the most important chemical phenomenon. Especially radicals ($^{\bullet}OH$, $^{\bullet}H$, $^{\bullet}O$), ions (O_2^-) and molecules (H_2O_2) are responsible for chemical reactions and degradation processes in water treatment. As these species have high oxidation potential they can very easily attack other molecules contained in water and caused their decomposition.

Diaphragm discharge presented in this paper belongs to the discharge configurations suitable for the purpose of water treatment, too. Its generation starts in the small orifice in the dielectric barrier separating two electrode spaces. If DC high voltage is applied, different kinds of plasma channels propagate from the orifice towards electrodes. Diversity of streamers is not only in their shape but mainly in their energy dissipation substantially influencing subsequent processes in water solution[4].

This paper presents results obtained from the treatment of solutions containing selected organic dyes. Decomposition of these model compounds was investigated from the viewpoint of diaphragm discharge conditions (electrode polarity, input power) as well as of the dye molecular structure.

Experimental

Diaphragm discharge studied in this work was generated in a batch reactor[4] using constant high voltage from the DC source that gave the input power up to 250 W (see Fig. 1.). Two planar electrodes made of stainless steel were separated by the dielectric barrier. Both electrode spaces were connected by only a small pin-hole (initial diameter of 0.25 mm) in this diaphragm. Discharge breakdown appeared just in this orifice and plasma channels propagated from this spot towards electrodes.

Each part of the reactor contained 2 litres of treated solution. Water solutions contained selected dye (initial concent-

Fig. 1. **Photograph of diaphragm discharge reactor used for decomposition of organic dyes dissolved in water**

Table I
List of used organic dyes and their characteristics

Dye	Molecular weight [$g\,mol^{-1}$]	Characteristic absorption wavelength [nm]
Direct Red 79	1,048.872	508
Direct Blue 106	741.487	608
Acid Yellow 23	534.366	428
Acid Blue 74	466.350	596

ration of ca 20 mg dm^{-3}) and a definite amount of supported electrolyte providing particular solution conductivity (initial value of 400 µS cm^{-1}). In this study, NaCl electrolyte was used for all experiments (concentration of 4 mmol dm^{-3}). Solution pH was primary adjusted by the electrolyte kind (approximately neutral in NaCl) and it was not specially modified during the experiment. Selected dyes belonged mostly to the group of azo-dyes and they could have been classified into Direct and Acid dyes. From the first group, Direct Red 79 (DR79) and Direct Blue 106 (DB106) were decomposed while Acid Yellow 23 (AY23) and Acid Blue 74 (AB74) were chosen from the second group. Their structural formulas are given below. Samples of treated solution were taken away from both electrode spaces every 5 minute and total treatment time was 40 minutes. Estimation of dye concentration was carried out by absorption spectroscopy (spectrometer Helios alfa) in the visible region (300–700 nm). Dye concentration was determined from the absorption intensity obtained at wavelength characteristic for each dye (see Table I). Decomposition rate α was calculated from the relative concentration decrease for each dye:

$$\alpha = \frac{c_0 - c}{c_0} \qquad (1)$$

where c_0 means initial dye concentration and c is dye concentration determined during the treatment.

Structural formulas of selected organic dyes are as follows:

Direct Red 79
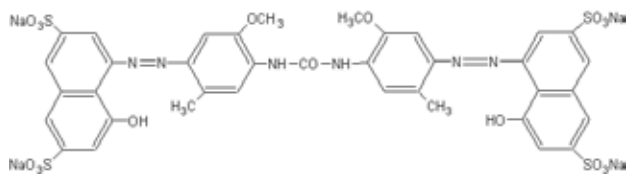
Direct Blue 106
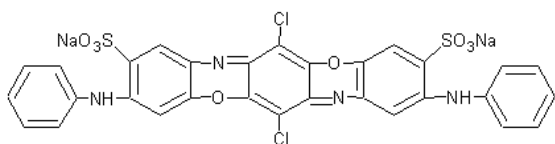
Acid Yellow 23

Acid Blue 74

Fig. 2. **Direct Blue 106 decomposition represented by relative concentration during the diaphragm discharge in the anode and cathode space (input power of 170 W, 4mM NaCl solution)**

Fig. 3. **Absorption spectra of two dyes (DR79 and DB106) before and after 20 minutes in diaphragm discharge (anode space, input power of 170 W, 4mM NaCl solution)**

Results

General Aspects of Dye Decomposition

Decomposition of all tested dyes was observed in both electrode spaces of the discharge reactor. However, removal efficiency was significantly higher in the anode space. Fig. 2. demonstrates results obtained in DB106 solution. Relative dye concentration exponentially decreased in the anode space and reached the value of less than 40 % of the initial DB106 concentration. In the cathode space, decoloration went slowly and almost linearly and final concentration dropped just below 90 %, only. Possible reasons of diverse process evaluation were assumed to be the different shape of plasma streamers (influencing different volume of treated liquid) and substantial effect of electrochemical reactions on the anode due to the application of constant DC high voltage on the electrodes[4]. Moreover, significant change of solution pH was observed during the discharge in both electrode spaces. While in the cathode space pH increased from initially neutral values of NaCl electrolyte to basic medium, situation in the anode space evaluated on the contrary, e.g. to the lower pH values and therefore remarkably acidic conditions. We expect that stronger acidic medium stimulated the degradation process of treated dyes[4]. However, clarifying of this phenomenon will be an object of our further study.

Analyses of treated dye solutions were carried out by absorption spectroscopy over visible region and recorded spectra were compared with original non-treated samples. Fig. 3. compares spectra obtained for two azo-dyes (DR79 and DB106) before and after 20 minutes of discharge treatment in the anode space. Besides remarkable decrease of absorption intensity at characteristic wavelength, certain shift of maximal absorption position could be seen. In the case of the red dye (DR79), this shift directed to shorter wavelengths while in the blue dye (DB106) the position of maximal absorption indicated its movement to longer wavelengths. We have assumed that origin of the shift in absorption came from the formation of various by-products when dye molecule was decomposed and these compounds absorbed radiation of slightly different wavelength than the original dye molecule. Determination of final products and by-products is an object of our intensive research.

Influence of Dye Structure

Effect of different molecule structure on the dye decolorization was studied for two compounds belonging to the group of Direct dyes (DR79 and DB106) and for two Acid dyes (AY23 and AB74). Evaluations of decomposition rates
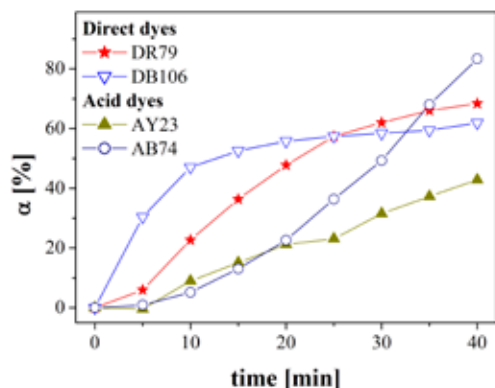
Fig. 4. **Comparison of decomposition rates obtained during diaphragm discharge in the anode space for selected dyes: Direct Red 79, Direct Blue 106, Acid Yellow 23 and Acid Blue 74 (input power of 170 W, 4mM NaCl solution)**
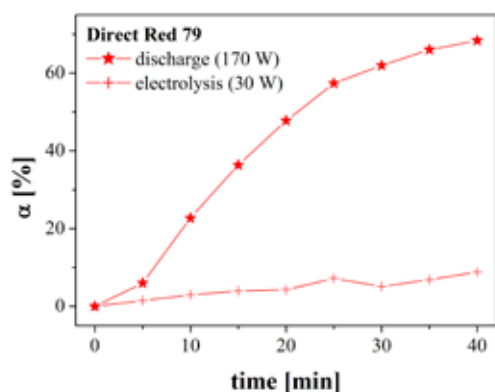
Fig. 5. **Comparison of DR79 decomposition rates obtained during diaphragm discharge (input power of 170 W) and pure electrolysis (30 W) in the anode space (4mM NaCl solution)**

determined during diaphragm discharge in the anode space are shown in Fig. 4. It was observed that removal process in direct dyes had exponential evaluation while it was linear in acid dyes. Moreover, exponential decolorization of direct dyes revealed particular residual concentration of decomposed dye. The best removal efficiency after 40 minutes of the treatment was achieved in AB74 dye (more than 80 %) which structure was on an indigoid base. The other dyes containing azo groups reached 60 % (DR79, DB106) or hardly 40 % (AY23), respectively.

Obtained results were probably caused by different mechanism of ·OH attack (or ·Cl radical coming from supported electrolyte NaCl) on the particular dye molecule, according to its size, number and kind of substitutes (see molecular structures in Experimental). The first impact of radical probably led on the azo-bond –N=N– when azo-dye is decomposed. Subsequently, this bond breaks and nitrogen is released. This reaction should be fast and its effect could explain the rapid decrease of DB106 or DR79 concenration at the beginning of the experiment.

Concerning different dye structure, molecules of acid dyes are smaller (with molecular weigth until ca 600 g·mol^{-1}) and contain lower amount of substitutes than direct dyes. Higher number of substitutes is one of the factors influencing final dye colour. Direct dyes containing more of such functional groups can be attack by active radicals from the discharge in these spots and their detachment can lead to faster decoloration of direct dyes.

On the other hand, indigo molecule (AB74) is relatively small with no substantial substitutes. And moreover, it does not contain an azo-group in its chain. Thus the degradation mechanism probably runs by different reactions and it depends on moment when the aromatic ring is finally opened.

Influence of Input Power and Electrochemical Aspects

Firstly, influence of input power applied from the DC source into the reactor on dye removal was studied for four different power magnitudes (65, 100, 130 and 170 W). From the comparison of DB106 decomposition rates obtained in both electrode spaces it was determined that increasing input power enhanced dye decomposition. Effect of power was more or less linear and with the same intensity in both electrode spaces.

More interesting results were achieved when dye decomposition by diaphragm discharge was compared with dye removal by pure electrolysis. We included this experiment into our study because we had expected a substantial effect of electrochemical reactions due to the application of constant voltage. In such case, especially electrochemical oxidation on the anode takes place and thus this reaction can be one of the factors leading to the dye decomposition.

Effect of electrolytical degradation was studied in the similar device consiting of dielectric diaphragm with one pinhole (initial diameter of 0.25 mm), stainless steel electrodes on each side and containing electrolyte solution (NaCl) of total volume of 3 litres. Constant voltage from the same DC source was applied on the electrodes. Its magnitude was adjusted on the level at which only electrolysis was kept in the reactor and the discharge was not created in the pin-hole. In that case, total power supplied into the reactor was 30 W (compared to 170 W applied during the discharge). Next procedure was carried out in the same way as the dye degradation by the diaphragm discharge.

Two dyes were selected for the comparison of degradation effect of the discharge and pure electrolysis – Direct Red 79 and Direct Blue 106. Obtained results represented as the evaluation of decomposition rates are demonstrated in Figs. 5. (for DR79) and 6. (for DB106), respectively. Results were achieved in the anode space of the reactor.

Comparison of electrolytic effect during treatment of two dyes surprisingly revealed contrary results. In DR79 solution, electrolysis had only a weak effect on the dye removal. On the other hand, DB106 dye was decomposed by both discharge and electrolysis with almost the same effect (more than 50 % of the initial dye was removed). Based on these
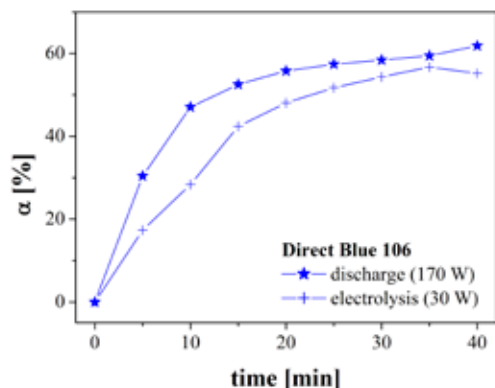
Fig. 6. **Comparison of DB106 decomposition rates obtained during diaphragm discharge (input power of 170 W) and pure electrolysis (30 W) in the anode space (4mM NaCl solution)**

results we have assumed different degradation mechanism of both dye molecules.

To compare energetic efficiency of the discharge and electrolytic treatment in the relevant criterion, efficiency η was calculated according to the following formula:

$$\eta = \frac{RDR \cdot V}{60 \cdot P} \cdot 3,600,000 , \qquad (2)$$

where RDR means the rate of dye removal in $mg\,dm^{-3}\,min^{-1}$, V is volume of the treated solution in dm^3 and P is input power in Watts (170 W for the discharge, 30 W for the electrolysis). Subsequently, efficiency was obtained in $mg\,kWh^{-1}$ and it represented amount of decomposed dye (in mg) per an energetic unit. Calculated efficiency values are given in Table II for both treated dyes.

Concerning DR79, calculated results confirmed remarkably higher efficiency when the dye was decomposed by the discharge. On the other hand, destruction of DB106 showed much higher efficiency of electrolysis (almost $1.7\,g\,kWh^{-1}$) because substantially lower power was needed for the same decomposition rate as in the discharge. We can assume that for removal of relatively larger molecules like DR79 substantially higher power is necessary to be applied while for destruction of simple molecule (DB106), electrolytic reactions initiated by lower power are sufficient.

Conclusions

Water solutions of selected organic dyes from two specific groups (Direct and Acid) were treated by diaphragm discharge generated using constant DC high voltage. Discharge reactor was divided by the dielectric barrier into two electrode spaces and the discharge itself was created in the small orifice in this barrier. Decrease of dye concentration was observed in both electrode spaces by the absorption

Table II
Energetic efficiency of dye decomposition by diaphragm discharge and electrolysis

Dye	Efficiency of diaphragm discharge – anode space $[mg\,kWh^{-1}]$	Efficiency of electrolysis – anode space $[mg\,kWh^{-1}]$
Direct Red 79	644	236
Direct Blue 106	477	1,686

spectroscopy. Study of dye removal as a function of discharge conditions gave following conclusions:

- All tested dyes were decomposed with significantly higher efficiency in the anode space than in the cathode one. The explanation could be in the different kinetic energy of electrons in plasma channels on both sides of the diaphragm as well as in the acidic conditions forming in the anode space during the discharge.
- Absorption spectra of treated solutions were recorded over the visible region. Besides decreasing absorption intensity, a remarkable shift of the position of maximal absorption was observed. Moreover, this shift was different for tested dyes. This phenomenon was probably caused by the formation of various by-products during the dye decomposition.
- Comparing molecular structure of selected dyes, significant influence of molecule size and degree of substitution was assumed as the main reason of different evaluation of dye decomposition by the diaphragm discharge.
- Increasing input power more or less linearly enhanced degradation process in both electrode spaces.

Substantial effect of electrolysis was observed during decomposition of DB106 while this effect was only negligible in DR79. Higher energetic efficiency was achieved by electrolysis in DB106 removal ($1.7\,g\,kWh^{-1}$).

REFERENCES

1. Sun B., Sato M., Clements J.S.: Environ. Sci. Technol. *34*, 509 (2000).
2. Lukeš P., Člupek M., Šunka P., Peterka F., Sano T., Negishi N., Matsuzawa S., Takeuchi K.: Res. Chem. Intermed. *31*, 285 (2005).
3. Njatawidjaja E., Sugiarto A.T., Ohsima T., Sato M.: J. Electrostatics *63*, 353 (2005).
4. Stará Z., Krčma F., Nejezchleb M., Skalný J.D.: J. Adv. Oxid. Technol. *11*, 155 (2008).

P18 NEUTRALIZATION OF MODELS OF HISTORICAL DOCUMENTS WITH MMMK

MIROSLAVA PETROVIČOVÁ[a], HANA PAULUSOVÁ[b], MICHAL ĎUROVIČ[b] and BOHUSLAVA HAVLÍNOVÁ[a]

[a]*Department of Printing Arts Technology and Photochemistry IPM of Chemical and Food Technology SUT,Radlinského 9, 812 37 Bratislava, Slovak Republic,*
[b]*National Archive in Prague, Archivní 4, 149 01 Prague 4, Czech Republic,*
miroslava.petrovicova@stuba.sk

Introduction

The corrosion of iron-gall inks is a result of their composition and is represented by two main degradation processes. On one hand, it is the hydrolytic decomposition of the paper support catalysed by acids which were added to inks during their preparation or released by a chemical reaction in the course of formation of ink colour component. The other mechanism of paper support degradation is cellulose oxidation catalysed by transitional metals, presented in iron-gall inks (Fe, Cu). Because of the presence of reductive substances, the ink lines contain ferrous ions even after centuries[2].

In the world several deacidification methods are used. These methods can be classified into water-based and non-aqueous processes. These processes make use of different combination of solvents, and they are suitable for different types of paper[1].

This work deals with the application of neutralization reagent MMMK (Methoxy magnesium methyl carbonate) and also antioxidant BHT 2,6-ditercbutyl-4-methylphenol on documents containing iron-gall inks and its influence on document properties after stabilization.

MMMK belongs to compounds suitable for deacidification of heavily damaged manuscripts. MMMK doesn't wash out iron-gall inks from substrate hence ink fixation isn't needed prior to its application.

MMMK is an organo-metallic compound which is used as a deacidification agent at Wei T'O non-aqueous process of book deacidification. It is possible to place magnesium in this form into paper structure using non-aqueous system from fluid gas[3].

BHT belongs to the group of synthetic antioxidants produced commercially, and it is also present as a natural substance in plants, e.g. in rosemary. BHT is a white powder that is used in the food industry, pharmacology, medicine for its anti-cancer effect and it is also known in the rubber industry. BHT belongs to the group of sterically hindered phenols and it had been recently introduced as a paper stabilization agent. Its effect as "chain-breaking" antioxidant is presented by deactivation of alkylperoxyle radicals[2,4].

Experimental

The experiments were performed on paper substrate using whatman No. 1 (Cat. No. 10001917) filter paper. This paper represented pure cellulose paper without any additi-ves. The set of the paper squares (8×12 cm) was immersed in a 1% gelatine solution and 5% solution of aluminium sulphate for 5 minutes.

The iron-gall ink was composed of $FeSO_4 \cdot 7H_2O$, tannin acid and gum Arabic, resulting in a molar ratio of iron and tannin acid was $5.5 : 1$.

These samples were placed into a climatic chamber for 3 hours at 50 °C, and then samples were immersed in 6% solution of methoxy magnesium methyl carbonate.

Antioxidant BHT was prepared in two concentrations (0.1% and 0.01% solution in ethanol), and samples were immersed in these solutions for 10 seconds.

One part of the samples was artificially aged in an OMT OVEN for 1 day to 24 days at 80 °C and 50 % RH. Second part of the samples was aged in the chamber APT Line Series FED for 1day to 24 days at 105 °C.

The folding endurance of paper was determined using normalized folding endurance tester Schopper according to standard ISO 5626 for the folding endurance of paper.

The changes in chemical structure of iron gall ink and iron gall ink with neutralization reagent MMMK during artificially aged was estimated by FTIR spectroscopy. FTIR spectra were recorded on a spectrophotometer Excalibur Series using transmission method by KBr pellet.

Results and Discussion

M e c h a n i c a l   T e s t

Inked samples showed low mechanical paper properties affected by artificial ageing in both cases – dry and wet ageing. Deacidification of inked samples caused retardation in decrease of mechanical properties (Figs. 1., 2.) hence it was possible to assume that also degradation of cellulose was decelerated.

In Fig. 1. obvious increase in folding endurance from 0 to 65 after neutralization of inked samples with MMMK solution was observed. However after 3 days this value decreased rapidly. Antioxidant BHT improved mechanical properties
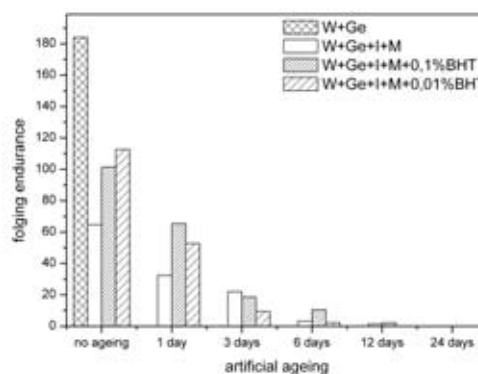
Fig. 1. **Changes of folding endurance during artificially ageing at 80 °C and 50 % RH. (W + Ge-Whatman paper modified with gelatine and sulphate, I-application of iron gall ink, M-treatment with neutralization reagent MMMK, BHT-treatment with BHT antioxidant)**
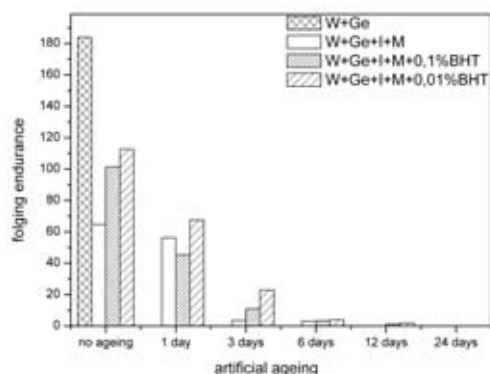
Fig. 2. Changes of folding endurance during artificially ageing at 105 °C. (W + Ge-Whatman paper modified with gelatine and sulphate, I-application of iron gall ink, M-treatment with neutralization reagent MMMK, BHT-treatment with BHT antioxidant)

only for unaged samples and samples 1 day aged. If we compared the sample without neutralization and antioxidant (that means only inked paper substrate) with 0 folding endurance even at the beginning, after neutralization with MMMK solution and subsequent stabilization with BHT antioxidant sample remained minimal mechanical properties even after 12 days of artificial ageing.

F T I R   M e a s u r e m e n t s

Fig. 3. represented comparison of FTIR spectra unaged ink and unaged neutralized ink measured in pellet. Ink neutralization with 6% solution of MMMK caused peak decrease at 1,093 cm^{-1} which is characteristic for C-O bond. Next change caused by ink neutralization was formation of new peak at 1,429 cm^{-1} which belongs to vibration of magnesium carbonate.
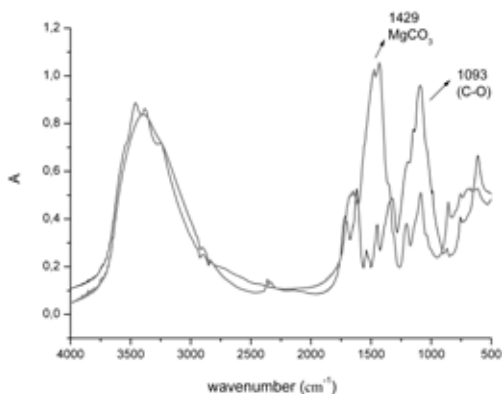
Fig. 3. FTIR spectra of iron gall ink (black line) and iron gall ink with MMMK (gray line) in pellet

Magnesium carbonate forms alkaline reserve in deacidified paper just because alkaline reserve is important from the

viewpoint of paper substrate stabilization, the peak characteristic for magnesium carbonate during ageing was observed. Fig. 4. demonstrated decrease of peak relating to vibration of magnesium carbonate (1,429 cm^{-1}) after 3 days of ageing.

FTIR spectra in Fig. 4. showed that after 12 days of ageing peak at 1,429 cm^{-1} vanished and we assumed depletion of alkaline reserve.
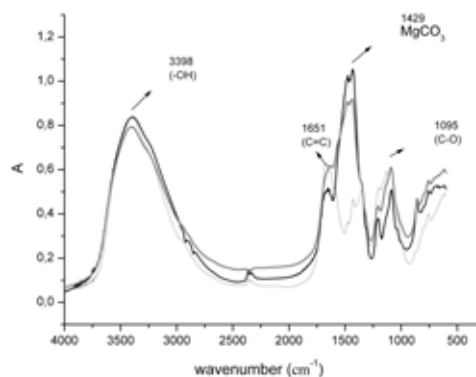
Fig. 4. FTIR spectra of iron gall ink with MMMK in pellet. Black line: no ageing, gray line: aged 3 days, light gray line: aged 12 days

Conclusion

The obtained experimental results showed that neutralization of inked samples with 6% solution of methoxy magnesium methyl carbonatu (MMMK) caused considerable improvement of optical and mechemical properties for unaged and aged inked samples. FTIR measurements confirmed the formation of alkaline reserve in neutralized ink. According to these results we could support stabilizing effect of paper neutralization with MMMK solution. However this alkaline reserve after 12 days of artificial ageing exhausted. Subsequent usage of antioxidant 2,6-ditercbutyl-4-4methylphenolu (BHT) for neutralized samples improved studied properties of unaged paper samples, nevertheless after artificial ageing stabilization effect of antioxidant wasn't approved.

REFERENCES

1. Ďurovič M.: *Research reports*. National Archive, Prague, 2000.
2. Havlínová B., Mináriková J., Hanus J., Janočovičová V., Szabóová Z. Restaurator *28*, 112 (2007).
3. Paulusová H., Novotná M.: X. Seminář restaurátorů a historiků, Litomyšl *1997*, 222.
4. Strlič M., Kolar J., Malešič J.: National and University Library, Ljubljana *2005*, 181.

P19 INFLUENCE OF BOOKSAVER DEACIDIFICATION PROCESS ON STABILITY OF ARYLMETHANE DYES ON PAPER.

BOHUSLAVA HAVLÍNOVÁ[a], MICHAL ĎUROVIČ[b], VIERA JANČOVIČOVÁ[a] and MIROSLAVA PETROVIČOVÁ[a]

[a]*Department of Printing Arts Technology and Photochemistry IPM, Faculty of Chemical and Food Technology SUT, Radlinského 9, 812 37,Bratislava, Slovak Republic,*
[b]*National Archive in Prague, Archivní 4, 149 01 Prague 4, Czech Republic,*
miroslava.petrovicova@stuba.sk

Introduction

Even after long period of time historical documents should have the ability to list in, read or possibly interpose other type of cultural experience. For population it is important for its irreplaceableness, uniqueness and attractiveness of literary works, manuscripts or paintings. Thanks to these works our history, customs and thinking could be kept. In presence problems with preservation and conservation methods of cultureal heritage have occurred[1].

Big amount of materials written in last 130 years on acid wooden papers have suffered with continuous damage process which can lead to total lost of printed or written text. The reason for this is the instability of paper substrate and meantime low chemical and light stability of dyes which represent the main component of modern inks. The most proper method against destruction of paper substrate appears to be neutralization hence formation of sufficient alkaline reserve preserving paper during ageing against acid products formed by oxidation and followed by fibre decomposition. Various deacidification methods based on waterborne and non-aqueous treatments have been developed that utilize different solvents and their combinations convenient for different types of papers.

Increase in pH value of paper substrate extends the lifetime but can damage written records mainly at unsuitable climatic conditions at deposit. The aim of this study was to investigate the influence of relative humidity and pH of paper substrate on dyes. For deacidifacation process non-aqueous deacidification was used hence no fixation was necessary[2,3].

Experimental

In this work acid, partially wooden paper with no fillers, sizes nor optical brightening agent made in Slavošovské papierne was used. Part of samples was prepared on original (acid) paper and other part on neutralized paper deacidified by Booksaver PAL method in Preservation Academy in Leipzig. Its initial properties and properties after deacidification process are listed in Table I. Samples 5×5 cm were prepared from unmodified acid paper and also from deacidified paper substrate and were treated with several dye solutions.

- Several dyes for treatment were prepared: Acid Green and Basic Red – 0.1% solutions in ethanol and Methy-

Table I
Initial properties and properties after deacidification process of paper

Property	Acid paper	Paper after deacidification
Brightness [%]	76.40	74.37
Opacity [%]	96.70	97.12
CIE L^*	91.14	94.80
CIE a^*	−1.07	−0.70
CIE b^*	3.41	2.04
pH	4.40	6.94
Alkaline reserve [%]	–	0.67

lene Blue – 0.2% solution in ethanol and water (1:1). Papers were treated with 1 ml of prepared dyes solutions and dried out on air.
- Prepared samples were treated by wet accelerated ageing in climatic chamber SANYO Gallenkamp PLC (Great Britain) at 80 °C and 3 different values of RH: 65%, 50% and 40% for 0, 1, 3, 7, 10, 18 a 30 days.

Non-aqueous deacidification (CSC) Book Saver is a method which uses carbonated magnesium propylate dissolved in n-propanol as a neutralize agent and as a carrier
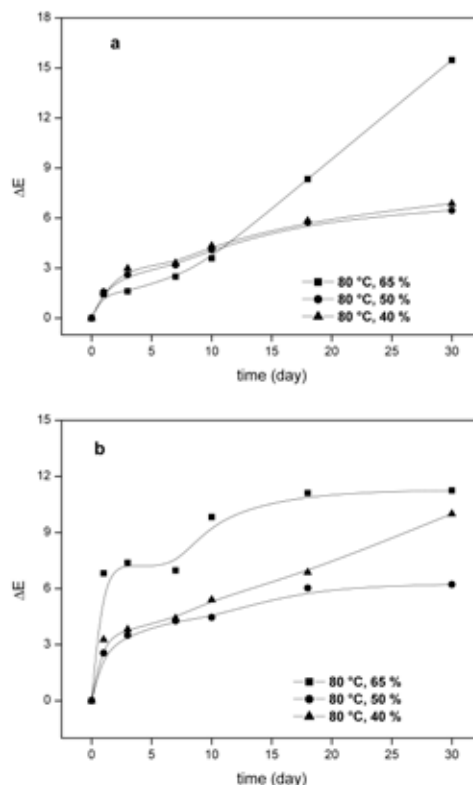
Fig. 1. **Comparison of 3 dependeces of ΔE^* of Acid Green dye on 3 different types of ageing; (a) – layered on acid paper substrat, (b) – layered on deacidified paper substrate**
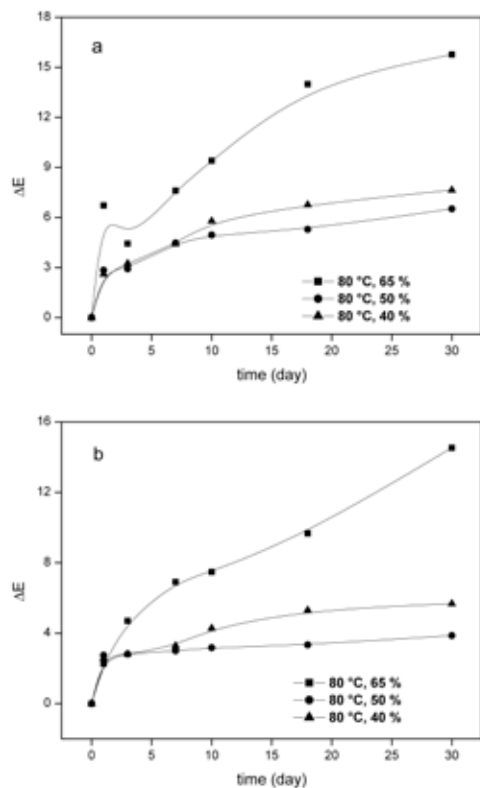
Fig. 2. **Comparison of 3 dependeces of ΔE^* of Methylene Blue dye on 3 different types of ageing; (a) – layered on acid paper substrate, (b) – layered on deacidified paper substrate**

Fig. 3. **Comparison of 3 dependeces of ΔE^* of Basic Red 9 dye on 3 different types of ageing; (a) – layered on acid paper substrate, (b) – layered on deacidified paper substrate**

is 1,1,1,2,3,3,3- heptafluoropropane (HFC 227) chosen for both mass and individual deacidification and is supplied as a spray.

Carbonated magnesium propylate is soluble in non-aqueous n-propanol and solution contains approximately 32 % of carbonate and 68 % of propanol. The composition of deacidification solutiou is: 1.06 kg of carbonated magnesium propylate, 2.25 kg of n-propanol and 190 kg of HFC 227. Neutralization agent further reacts with moisture in paper and produce alkaline reserve in the form of alkaline magnesium carbonate.

Documents were frozen to –20 °C prior to treatment. This method is convenient also for sensitive materials (parchment, leather and moreover immobilize soluble dyes and inks.

The properties of the paper samples were measured according to the Slovak Technical Standards (STN) and STN ISO Standards.

Results

Fig. 1.a showed that the lowest value of colour difference for sample Acid Green 16 on acid paper substrate was in the case of wet ageing at conditions of RH 50 % (6.46), 40 % (6.87) however for RH 65 % it was 15.48. This could be explained by axis a^* which moved by $\Delta a^* = 12.97$ from negative to zero area that means from green to grey. Fig. 1b represented Acid Green 16 on neutralized paper and the least

noticeable influence on ΔE^* colour difference had ageing at 50% RH (6.22) and for other 2 ageing types final colour difference value was measured 2 times higher.

Fig. 2.a represented Methylene Blue on acid paper substrate and the highest value of colour difference ΔE^* was monitored for wet ageing with RH 65 % (15.77). The most considerable influence on total value of ΔE^* showed axis L^* and b^* that represented significant bleaching of samples and shift of blue colour shade to grey. For ageing at RH 50 % and 40 % much lower values of ΔE^* were measured exactly $\Delta E^* = 6.52$ and $\Delta E^* = 7.64$. Similar behavior was noticed also for Methylene Blue on neutralized paper sample but after ageing the values of ΔE^* were lower (Fig. 2.b). For RH 65 % maximum value of ΔE^* was 14.53, for RH 50 % was ΔE^* 3.87 and for 40 % ΔE^* = 5.68.

Fig. 3.a monitored the influence of particular ageing condition on Basic Red 9 dye layered on acid paper. The highest value of colour difference ΔE^* was measured for ageing at RH 40 % ($\Delta E^* = 10.13$) and for RH 65 % ΔE^* = 8.51. The lowest value of $\Delta E^* = 5.88$ was obtained at RH 50 %. The sample Basic Red 9 layered on neutralized paper (Fig. 3.b) showed less stability compared to sample layered on acid paper. The most obvious instability was noticed for ageing at RH 65% where ΔE^* was 27.71 which represented the highest value for colour difference. The biggest contribution on total

value of colour difference had the colour axis a^* ($\Delta a^* = 26.88$) that moved from positive value to zero which means shift from red to grey colour. For ageing condition RH 40 % and 50 % the lowest values of colour difference ($\Delta E^* = 12.66$ and 11.29) were measured.

Conclusions

This study investigated the influence of relative humidity (40 %, 50 % a 65 % at 80 °C) and pH (acid and deacidified paper substrate) on optical properties of several arylmethane dyes (acid Acid Green 16 and alkaline Methylene Blue and Basic Red 9. ΔE^* caused by ageing was measured. The stability of arylmethane dyes on acid and deacidified paper with Booksaver method was compared.

Comparison of optical properties of acid and alkaline dye pigments showed higher stability of acid dye Acid Green 16 layered on acid as well as deacidified substrates. Lower values of RH (40–50 %) caused higher light stability and

ageing at 65 % RH influenced optical properties the most negatively. Deacidification of paper improved optical properties for all 3 types of ageing and dyes particularly Methylene Blue. However even after deacidification ageing at lower RH (40–50%) showed more sufficient.

REFERENCES

1. Zollinger H.: *Color chemistry*, Weinheim. 1991.
2. Havlínová B., Mináriková J., Švorcová L., Hanus J., Brezová V.: Restaurator *16*, 1 (2005).
3. Lewis M. L., Indig G. L.: Dyes Pigm. *46,* 145 (2000).

P20   EFFECT OF ACCELERATED AGEING PROPERTIES OF PARCHMENT

BOHUSLAVA HAVLÍNOVÁ[a], MARTINA OHLÍDALOVÁ[b], MIROSLAVA PETROVIČOVÁ[a] and BOŽENA MARUŠICOVÁ[a]

[a]*Department of Printing Arts Technology and Photochemistry IPM of Chemical and Food Technology SUT, Radlinského 9, 812 37 Bratislava, Slovak Republic,*
[b]*Institute of Chemical Technology Prague, Technická 3, 166 28 Prague 6, Czech Republic,*
miroslava.petrovicova@stuba.sk

Introduction

Parchment is a specially treated form of leather that is soft and durable, making it an excellent writing material. High quality parchment is sometimes referred to as vellum. It is known that parchment was as a writing material as early as the Ptolemaic era, and it was in fact preferred over papyrus in northern regions, where the climate can be unfavorable for papyrus, and also in Near Estern regions. Parchment as a writing material antedates aper by possibly 1500 years, although the name is derived from Pergamum, an ancient city in Asia Minor where its discovery is usally credited to King Eumenes II, in the second century 225–160[1,2].

The use of parchment for book printing in Europe continued even after the advent of prinzing from wood-blocks and moveable type, but did not survive to any extent beyond the year 1500, although for purpose of calligraphy and for printing documents a diplomas, this durable material is in demand to the present day. It was paper, however, that gave printing its real impetus, for had the expensive parchment been the only material available craft of printing could never have developed. At the process of restoration and conservation of parchment it is usually necessary to investigate the degree of parchment damage because it determines the conservation method and conservation agents. We suggest the detection method of parchment shrinking temperature[3,4].

Experimental

The aim of this study was to investigate the influence of 2 types of accelerated ageing on parchment properties.

The effects of accelerated ageing on properties of 2 different samples of parchment – goat leather (bothside grounded) and calf leather (bleached) – were investigated. The samples of parchment were cutinto squares 4×4 cm. According to norm ISO 5630/1 dry ageing at 105 °C was used during 0, 24, 72, 168 and 240 hours. The artificial ageing was performed in a multifunctional oven APT Line Series FED with the regulation R 3.1 by Fisher Scientific (Czech Republic). Second type of accelerated ageing used was wet ageing at 30 °C and 75% RH during 0, 24, 72, 168 and 240 hours according to norm ISO 5630/3. This type of wet ageing was performed in a climatic chamber Heraeus VOTSCH (Germany) situated in Slovak National Archives in Bratislava.

Measurement of Shrinking Temperature

Decay of naturally damaged skin is caused by acid hydrolytic and oxidative scission. Both processes are competitive, simultaneous and interactive. The shrinking temperature effectively reflects changes in separation of aminoacids caused by oxidation, chemical scission of tannic acids, the presence of soluble sulfates and hydrogen ions that are attached to hydrolytic scission. According to norm CSN 79 38 414 the standard measurement of shrinking temperature indicated that the initial shrinking temperature is very important for durability and speed of parchment damage. Higher initial shrinking temperature signifies higher chemical and physical stability and hence higher preservation against material damage. The disadvantage of this method is high disposal of sample material. For this reason we used microscopis method for determination of shrinking temperature.

The thermosystem FP90 Mettler Toledo with measurement chamber FP82HT was used for experiment. This device consisted of microscope with electronically heated table, concave and cover glass, scalpel, preparative needle and as a solution water was used. Few fibres (0.3 g) of parchment sample were removed using scalpel, placed on concave glass with couple drops of water and covered with glass. This way prepared sample was placed on the heated table under the microscope. The table was heated at the rate of 2 °C min^{-1} in the range of 25–80 °C. Shrinking was observed at magnification $40 \times$. Studying samples with microscope temperature T_s or temperature interval were determined when fibres started to shrink. Individual measurements were repeated at least two times.

Shrinking Process

During heating of collagen fibres in water in certain temperature interval deformation occurs. The deformation consists of fibres shrinking and depends on strength, quality and degradation degree of collagen material. This method is a measurement of combined chemical and physical material stability. The shrinking process of parchment fibres can be described in 3 temperature intervals[4].

- Interval A_1/A_2 – temperature range when fibre shrinking occurs,
- Interval – B_1/B_2 shrinking of a fibre is immediately followed by shrinking of next fibre,
- Interval C – temperature range where fibres shrink simultaneously and continuously. Initial temperature of this main interval relates to shrinking temperature T_s. The process describes following equation:

$$\Delta T = T_e - T_s, \tag{1}$$

where T_e is ending/final temperature of interval C. Shrinking process stabilizes during the intervals B_2 and A_2, however for historical parchment non of mentioned intervals can be observed. Fibres of new parchment in relation to temperature proceed following changes:
no fibre acitivity – A_1–B_1–C–B_2–A_2 – total fibre shrinking.

In practice some intervals could absent at temperature lower 40 °C and intervals B and C could not be observed when fibres lost cohesion. Final value of microscopic determination of shrinking temperature depends on the type of skin, sample preparation and subjective evaluation.

Results

Measurements of shrinking temperature for samples of goat and calf parchment indicated that dry ageing at 105 °C caused considerable damage of parchment. Ending/final shrinking temperature of both parchment samples was lower than 40 °C which indicated high degree of damage.

Fig. 1. represents dependency of shrinking temperature on time of artificial ageing of goat and calf parchment exposed to dry ageing at 105 °C during 0, 24, 72, 168 and 240 hours. Shrinking temperature decreased after 240 hours of dry ageing by 19 °C for calf skin parchment indeed only by 12 °C for goat skin parchment. However for both samples decrease of temperature below 40 °C was recorded, total degration occurred for both samples.
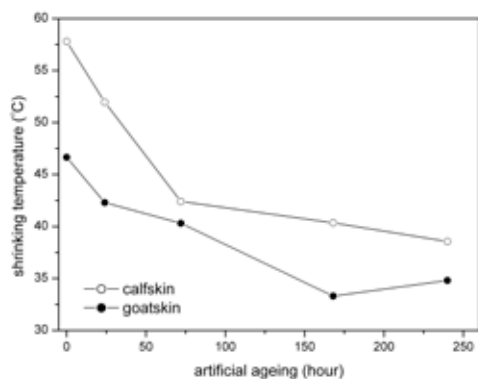
Fig. 1. **Dependency of shrinking temperature on artificial ageing of goat and calf parchment exposed to dry ageing at 105 °C durings 0, 24, 72, 166, 240 hours**
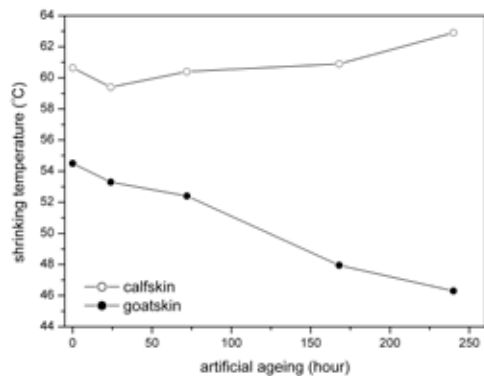
Fig. 2. **Dependency of shrinking temperature on artificial ageing of goat and calf parchment exposed to wet ageing at 30 °C and relative humidity 75 % during 0, 24, 72, 168, 240 hours**

Table I
Shrinking temperatures of goat and calf parchment for dry ageing at 105 °C

Artificial ageing [h]	Calf skin T_s [°C]	Goat skin T_s [°C]	Interval of shrinking [°C] Calf skin	Goat skin
0	57.8	46.8	57.8–66.1	46.8–52.7
24	51.9	42.3	51.9–59.7	42.3–48.6
72	42.4	40.3	42.4–52.2	40.3–46.9
168	40.4	33.3	40.4–49.2	33.3–37.9
240	38.6	34.8	38.6–43.4	34.8–40.4

Table II
Shrinking temperatures of goat and calf parchment for wet ageing at 30 °C a 75 % RH

Artificial ageing [h]	Calf skin T_s [°C]	Goat skin T_s [°C]	Interval of shrinking [°C] Calf skin	Goat skin
0	60.7	54.5	60.7–64.8	54.5–58.9
24	59.4	53.3	59.4–65.3	53.3–58.6
72	60.4	52.4	60.4–66.1	52.4–58.3
168	60.9	47.9	60.9–69.0	47.9–55.2
240	62.9	46.3	62.9–68.4	46.3–53.9

Fig. 2. indicates dependency for wet ageing at 30 °C and 75 % RH where calf skin parchment didn't show any damage not even after final ageing. The value T_s after final ageing was 63 °C and even higher compare to initial value which could correspond to measurement error or the sample was prepared from different part of skin. For goat skin parchment the value decreased after final wet ageing approximately by 8 °C hence certain damage of parchment occurred. Experimental values and their comparison indicated that wet ageing for both parchments was less drastic and total degradation didn't occur, just damage.

Conclusions

Changes of shrinking temperature reflected changes in collagen structure, agents, pH and overall storage conditions.

Initial shrinking temperature appeared to be suitable indicator of parchment durability. We could assume that higher shrinking temperature higher relative durability.

Since shrinking temperature reflects parchment's bulk condition we can recommend microscopic determination of shrinking temperature as a method for testing the damage of historical documents made of parchment and also for parchment designated for restauration.

REFERENCES

1. Ďurovič M.: *Restaurování a konzervování archiválií a knih,* Paseka 2002.
2. Larsen R., Vest M., Nielsen K. J. Leather Technol. Assoc. *77*, 154 (2006).
3. Abdel-Maksoud G., Marcinkowska E.: Restaurator *21*, 3 (2000).
4. Larsen R., Dorte V., Poulusen and Marie Vest.: Microanal. of Parchment *2002*, 55.

P21 QUALITY OF SOIL HUMIC SUBSTANCES BY SFS AND UV-VIS SPECTROSCOPY

ĽUBICA POSPÍŠILOVÁ[a] and NADĚŽDA FASUROVÁ[b]

[a]Mendel University of Agriculture and Forestry, Institute of Agrochemistry, Soil Science, Microbiology and Plant Nutrition, Zemědělská 1, 613 00 Brno, Czech Republic,
[b]University of Technology Brno, Faculty of Chemistry, Institute of Physical and Applied Chemistry, Purkyňova 118, 612 00 Brno, Czech Republic,
pospisi1@mendelu.cz

Introduction

In this paper we followed UV-VIS, SFS spectra and chemical properties of different origin soil humic subctances (HS). We selected HS from following soil types – Modal Cambisol, Litic Cambisol, Modal Chernozem, Modal Rendzina and Modal Pararendzina (Czech soil samples).

Soil quality is closely connected with HS character and chemical properties. Humic substances fractionation is contributed to specific amount of humic acids (HA) and fulvic acids (FA). Ratio HA/FA is one of the important criteria for soil quality and health. Optical curves and indexes in UV-VIS and SFS ranges indicate chemical properties and structure of HS.

Experimental

- Fractional composition of HS was made by short fractionation method according to Podlešáková et al. (1992).
- UV-VIS spectra were measured using Varian Cary 50 Probe with optical fiber within the range 300–700 nm.
- HS were dissolved in mixture of 0.1M sodium pyrophosphate and 0.1M NaOH. SFS spectra were measured after dilution (10 times) using Spectrofluorimeter Aminco Bowman Series 2 within the range 220–620 nm (at $\Delta\lambda = 20$ nm and temperature 20 °C, scan rate: 60 nm min^{-1}).
- Notes to Fig. s: Modal Cambisol (1), Litic Cambisol (2), Modal Chernozem (3), Modal Rendzina (4), Modal Pararendzina (5).
-

Fractional Composition of HS

HS fractional composition showed high FA amount in all samples.except Modal Pararendzina. HA/FA ratio was < 1 in all samples except Modal Chernozem (HA/FA = 3). Humification degree varied from middle to low as follows: Modal Chernozem (Hrušovany) > Modal Rendzina (Sloup) > Modal Pararendzina (Pouzdřany) > Modal Cambisol (Náměšť nad Oslavou) > Litic Cambisol (Ocmanice).

UV-VIS Spectra

Absorbance in UV-VIS range was the highest in Modal Chernozem (Fig. 1.). Optical indexes increased in following order: Modal Chernozem < Modal Cambisol < Modal Rendzina < Modal Pararendzina < Litic Cambisol. Practically the same sequence was found for HA/FA ratio. Increrasing of $Q_{4/6}$

indicated decreasing of HS quality. Very similar were optical indexes ($Q_{4/6}$) for Modal Rendzina, Modal Pararendzina and Modal Cambisol (about 6). Only modal Chernozem had $Q_{4/6} < 4$ which indicated high HS quality. Very high index $Q_{4/6}$ was found for Litic Cambisol (> 10) and indicated high amount of FK.
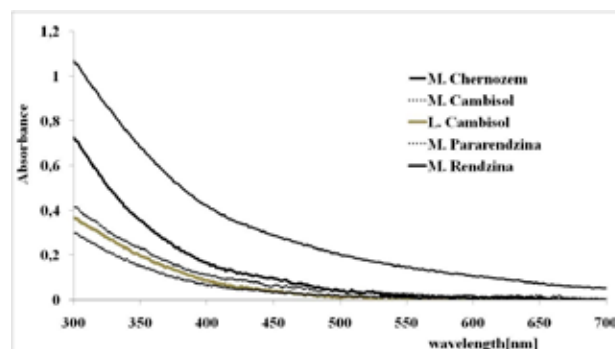
Fig. 1. **UV-VIS spectra of HA isolated from different soil types**
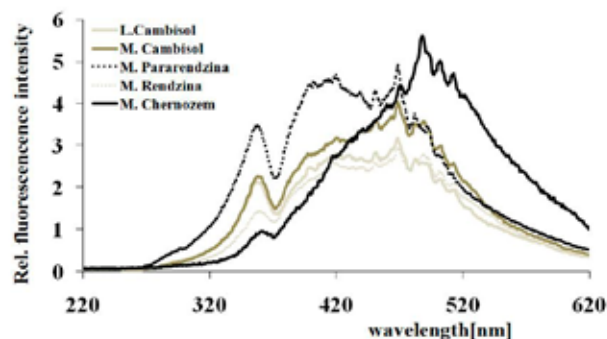
Fig. 2. **Synchronous fluorescence spectra of HA isolated from different soil types**

SFS Spectra

In SFS spectral range (Fig. 2) five main fluorophore peaks were identified: at 359, 450, 469, 489, 501 nm. Some of them gave another two peaks at 420, 513 nm (at $\Delta\lambda = 20$ nm). All samples had maximum fluorescence intensity shifted from shorter to longer wavelength and maximum at 469 or 489 nm. According to Senesi et al. (1991) there are some samples with more intensive emission (at $\Delta\lambda = 20$ nm $= (\lambda_{em.} - \lambda_{ex.})$ at 470 and others with more intensive emission at 488 nm. The last is caused by contain of aromatic compounds in HA molecule. Modal Chernozem SFS spectra showed the main peak at 489 nm and the highest relaive fluorescence to compare to others. Modal Pararendzina and Litic Cambisol contained much more aliphatic compounds and fulvic acids indicated by peaks at lower wavelegth 359 a 420 nm. Modal Cambisol had no peak at 420 nm.

Relative fluorescence indexes (F) were calculated as ratio I_{469}/I_{452}. The lowest index (F) was found for Modal Chernozem and the highest for Modal Pararendzina. The fluorescence indexes it is supossed to be closely connected with HS humification degree.

Results

In Modal Chernozem highest HA amount was found. Fulvic acids highest amount was found in both Cambisols. HA/FA ratio indicated decreasing HS quality in order: Modal Chernozem < Modal Rendzina < Modal Pararendzina < Modal Cambisol < Litic Cambisol. Linear correlation between $Q_{4/6}$ and HA sum was found.

UV-VIS spectra showed the highest absorbance in Modal Chernozem. Optical indexes $Q_{4/6}$ indicated high HS quality in Modal Chernozem and low in Litic Cambisol.

Fluorescence of studied samples was compared with literature data and/or with standard. Samples contained substitued naphtalene and coumarine derivates. Samples had similar fluorescence behaviour as Elliot soil humic acid standard (IHSS) and all samples indicated two main excitation peaks at 450, 468 nm.

Low relative fluorescence index (F) was found in Modal Cambisol (0.73). Highest index F was in Modal Pararendzina (1.16). From SFS spectra we can also suggested highest intensity of fluorescence in Modal Chernozem. These results were confirmed by HS fractionation but maximum F index in Modal Chernozem was not determined.

Conclusions

We can conclude that HS of different origin had very similar SFS and UV-VIS spectra except lower wavelengths and wave numbers. But some differences were observed in Modal Chernozem. The last had main fluorophore peak at 489 nm. Other samples contained main peak at 469 nm. UV-VIS spectra were mostly influenced by fractional composition (HA, FA content). Samples origin was therefore an important factor influencing HS quality.

REFERENCES

1. Podlešáková E. et al.: *Rozbory půd, vod a rostlin, VUMOP* , Praha, pp. 259 (1992).
2. Sierra M. M. D., Giovanela M.,Parlanti E., Soriano-Sierra E.J.: Chemosphere *58*, 715 (2005).
3. Senesi N., Miano T. M., Provenzano M. R., Brunetti G.: Soil Science *152*, 259 (1991).
4. Senesi N.: R. Soc. Chem. *1993*, 73.

P22　SENSORIC PROPERTIES OF AROMATIC AND HETEROCYCLIC COMPOUNDS WITH CONJUGATED BONDS

OTA SALYK[a], PAVEL BEDNÁŘ[a], MARTIN VALA[a] and JAN VYŇUCHAL[b]

[a]*Brno University of Technology, Faculty of Chemistry Purkyňova 118, 612 00 Brno,*
[b]*Research Institute of Organic Syntheses, Rybitvi 296, Rybitvi, 533 54, Czech Republic,*
salyk@fch.vutbr.cz

Introduction

For expected future hydrogen economy is expected vast need of hydrogen operating devices including new sensors, while nowadays sensors need extra power for hydrogen dissociation[1]. There exist a range of organic molecules with three valent nitrogen atom with high proton affinity. I case of diketopyrrolopyrrole derivatives with pyridyl, piperidyl or morpholinyl ring we obtain a pigment with potential color change while protonated. These materials are also semiconductive, so protonation can influence their conductivity. It was already observed in case of pyridyl derivative[2]. The protonation itself is tested in acids vapour so because in acid water solvent the shielding effect of water molecules prevent in proton penetration to the active centres in rhe DPP film. Protonation in real hydrogen gas is possible only after the hydrogen molecule dissociation. It proceeds on catalyzer surface of noble metal as platinum or palladium[3]. The presence of electric field supports the hydrogen dissociation, so the cluster non-conductive catalyzer layer between gap electrodes has to be obtained. It can be sputtered, evaporated or galvanically electrodeposited using anodic alumina templates[4]
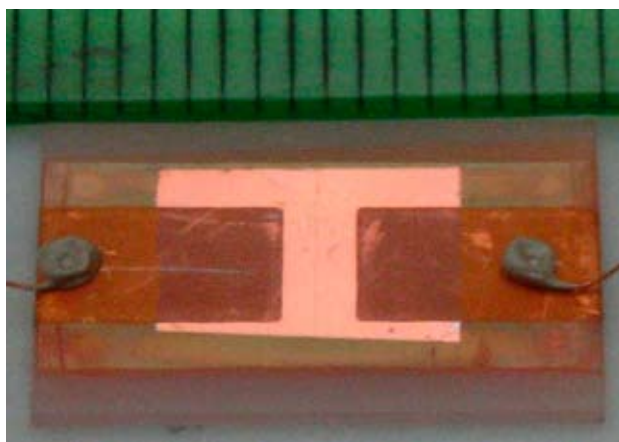
Fig. 1.　**Samples of DPP gap structure (10 μm) on glazed alumina plate with aluminium deposited contacts**

Experimental

Thin films of DPP derivative materials were prepared by vacuum evaporation method. Substances composed from heterocyclic rings appeared only poor solubility in organic solvents in case of no alkyl chain bonded to the molecule.

Table I
Series of discussed compounds with melting points T_m [°C]

U14	U15	U16
$T_m > 300$ °C	$T_m > 300$ °C	$T_m > 300$ °C

U34	U35
$T_m > 300$ °C	$T_m > 300$ °C
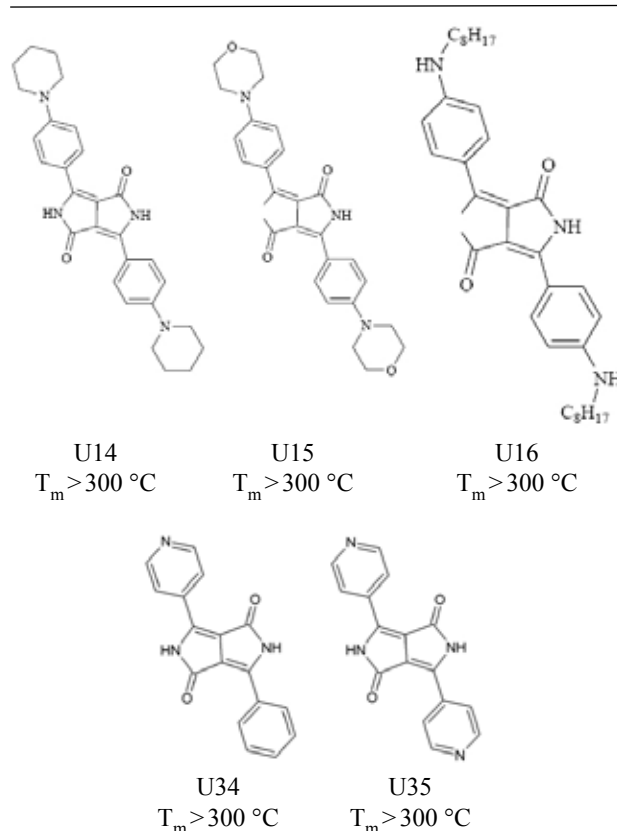
Substrates were used according to following investigation; low resistivity silicon wafers both for scanning electron microscopy (SEM) and atomic force microscopy (AFM) were used besides indium tin oxide (ITO) coated low alkali Corning glass for electro-optical testing, quartz glass for optical measurement and gap arrangement on glassed alumina plates.

The deposition of the active DPP layer was carried out in the vacuum coating facility B.55.3 HV Dresden with ultimate pressure 1×10^{-4} Pa pumped by diffusion oil pump. The crystal thin film thickness monitor was used for deposition monitoring. Thin films of thickness 200 nm were deposited on standard substrates. The material was pressed into pellets 6 mm in diameter and about 1 mm high, usually about 30 mg of mass, which was the proper dose for 200–300 nm thick layer without wasting. The sophisticated shape of the boat prevented direct radiation of the deposited layer and also focused the irradiation onto the pellet, so it decreased required heating power. This procedure allowed steady sublimation and deposition rate without sputtering of bigger clusters or drops and material melting. It also improved easy manipulation and cleanness preservation – no powder was sputtered into vacuum chamber.

The thickness measured by elipsometry typically 40–100 nm resulted. The deposition rate was typically

0.2 to 0.5 nm s^{-1}. The 10 μm gap was created by aluminium evaporation through a 10 μm tungsten wire mask.

The samples were than investigated on scanning electron microscope (SEM) FEI QUANTA 200. No grain structure in scale of 50 nm resolution was observed, so the surface appeared uniform.

The samples were than situated into quartz cell and measured on absorption on Varian UV-VIS-NIR spectrometer in hydrochloric acid solution and nitric acid vapours.

Results

Samples from Table I were investigated by acid vapour and acid solution effect on colour variation. Thin film samples U14, 15 and 16 react on HNO$_3$ vapour presence in etching dish by changing their colour from vivid violet to orange; samples U34 and U35 exhibit a colour shift from vivid red to violet at the same conditions. Similar reaction was observed in other acid vapours. Organic simple acids as formic or acetic vapours brought dissolving and destruction of the thin film.
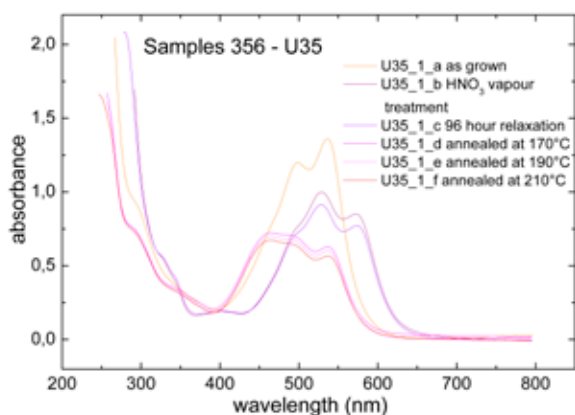
Fig. 2.   **Sample U35 – Absorption changes affected by nitric acid vapour treatment and subsequent annealing**

The attempt with water acid solution of various pH did not bring any change for samples U14, U15 and 16 and only a weak spectral shift in case of samples U34 and U35. It is explained by water molecules shielding of protons that cannot penetrate into active centres of the thin film.

Absorbance spectra in UV VIS region were scanned systematically for thin film samples U34 and U35 on quartz glass substrates. The results are presented in Fig. 2., Fig. 3. and Fig. 4. The nitric acid vapour treatment causes spectrum change, which is steady according to relaxation on air for four days. Annealing to temperature above 160 °C returned the spectrum back, but not exactly to initial shape. The change in relative intensity of the vibronic structure indicates reorganisation of the molecules geometry. The absorbance decrease is also considered as it returned to c-curve after repeated HNO$_3$. Both quantitative and qualitative reversible changes are well apparent and give an evidence of structure change. The reversibility of the spectral change was observed also
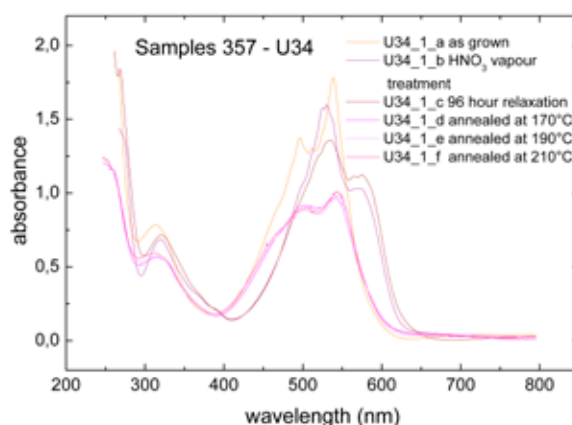
Fig. 3.   **Sample U34 – Absorption changes affected b nitric acid vapour treatment and subsewquent annealing**

Fig. 4.   **Sample U14 – Absorption changes affected by nitric acid vapour treatment**

at U14 sample after annealing at 200 °C but already at room temperature within 5 days appeared remarkable initial state regeneration.

The spectral variation has following explanation[3]: Hydrogen ion from the acid is captured on nitrogen atom in the pyridyl ring and the complex salt $(R-N-H)^+(NO_3)^-$ resulted into colour and structure change. The evolution of NO$_2$ and O$_2$ is possible as well while the free electron remains in the material. In case of dissociated hydrogen is presumed reaction, where instead of $(NO_3)^-$ ion free electron is created, which contributes to material conductivity.

However, the behaviour of the U14–U16 derivatives differs from the U34 and U35. Since the absorption spectrum of the latter derivatives undergo bathochromic shift the former derivatives shows large hypsochromic shift. The central part of the DPP unit acts as electron acceptor. Substitution of the electron donating groups (U14–U16) leads to an increase of the absorption coefficient and cause a bathochromic shift. The treatment of the derivatives under acid vapour cancelled the electron donating character of the substituents and therefore caused shift back to the absorption of non-substituted diketo-pyrrolo-pyrrole.
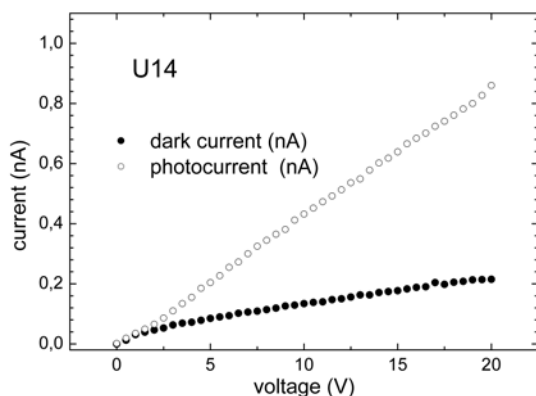
Fig. 5. **V-A characteristics of U14 as grown sample in gap structure**

The conductivity and photoconductivity of the thin film was tested as well and its changes with acid vapour treatment is also expected (Fig. 5)

Conclusions

Set of thin film samples of DPP derivatives thin films prepared by evaporating and spin coating methods were investigated by absorption spectra measurements at HNO_3 vapour treatment. The nature of electron donating groups was changed by nitric ion and absorption spectra shift was observed. Similar behaviour exhibited also other acids. This affected also conductivity. The effect was reversible. It is believed that it can be exploited for new sensing material development, especially hydrogen sensing.

REFERENCES

1. Seisler M. J.: *World Forum for Harmonization of Vehikle Regulationa (WP. 29)*, United Nations, Ženeva, March 10, 2004.
2. Mizuguchi J., Tomohiko I., Takahashi H., Yamamaki H.: Dyes Pigm. *68*, 47 (2006).
3. Takahashi H., Mizuguchi J.: J. Appl. Phys. *100*, 034908 (2006).
4. Klosová K., Hubálek J.: Phys. Stat. Sol. (a)*1–4* (2008)/ DOI 10.1002/pssa.20078169.

P23 STRUCTURE AND MORPHOLOGY OF SOME DIPHENYL-DIKETO-PYRROLO-PYRROLE DERIVATIVES PIGMENTS

OTA SALYK[a], MARTIN WEITER[a] and JAN VYŇUCHAL[b]

[a]*Brno University of Technology, Faculty of Chemistry Purkyňova 118, 612 00 Brno, Czech republic* [b]*Research Institute of Organic Syntheses, Rybitvi 296, Rybitvi, 533 54, Czech Republic,* salyk@fch.vutbr.cz

Introduction

After more than 15 years of academic and industrial research worldwide, the class of organic materials, conjugated polymers and organic molecular systems, has reached very high level of outstanding material properties and the potential for different industrial applications is now emerging. Resistors, capacitors, diodes, photodiodes, organic light-emitting diodes (OLED), field-effect transistors and optically pumped solid-state lasers can be fabricated by different methods and integrated into electronic and optoelectronic circuits[1].

In this study, a group of several derivatives of 3,6-diphenyl-2,5-dihydro-pyrrolo[3,4-c]pyrrole-1,4 dione, also known as DPP (see Table I) were investigated. DPP derivatives are mainly used as high performance pigments and are valued for their fatigue resistance; nevertheless some of their physical properties make them as potential candidates for OLED applications[2].
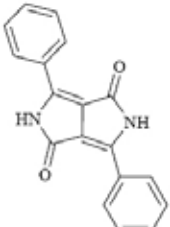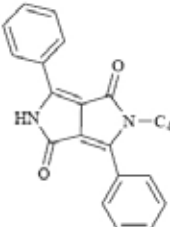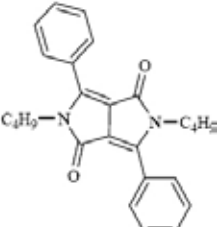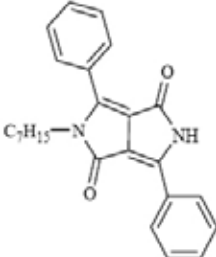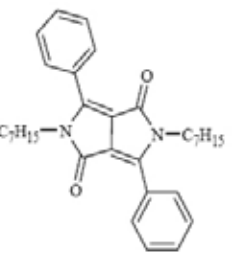
Molecular OLED devices are generally fabricated by sublimation under vacuum of successive layers of electron- and hole transporting materials. In contrast, low-cost solution-based processing techniques are usually requested for industrial production. Therefore four different derivatives of diphenyl-diketo-pyrrolopyrrole (DPP) with alkyl side groups were synthesized to increase their solubility (see Table I) and the question of relation between the chemical structure and morphology of prepared thin films were addressed.

Experimental

Thin films of DPP materials were prepared by spin coating method and by vacuum evaporation method. Low resistivity silicon substrates were used for scanning electron microscopy (SEM) and atomic force microscopy (AFM), whereas indium tin oxide (ITO) coated low alkali Corning glass were used for electro-optical and quartz glass for optical characterization, respectively. Thin layers spin-casted from chloroform-toluene solution (7:3) were typically 100–200 nm thick as measured by elipsometry.

The vacuum deposition of the active DPP layer was carried out in the vacuum coating facility B.55.3 HV Dresden with ultimate pressure 1×10^{-4} Pa pumped by diffusion oil pump. The crystal thin film thickness monitor was used for deposition monitoring. Thin films of thickness 200 nm were deposited on standard substrates. The material was pressed into pellets 6 mm in diameter and about 1 mm high, usually

Table II
Series of discussed compounds with melting points T_m [°C]

U4
$T_m > 300$

U9
$T_m = 248–252$

U10
$T_m = 118–120$

U11
$T_m = 211–213$

U12
$T_m = 109–213$

about 30 mg, which was the proper dose for 200–300 nm thick layer without wasting. The sophisticated shape of the boat prevented direct radiation of the deposited layer and also focused the irradiation onto the pellet, so it decreased required heating power. This procedure allowed steady sublimation and deposition rate without sputtering of bigger clusters or drops and material melting. It also improved easy manipulation and cleanness preservation – no powder was sputtered into vacuum chamber.

The deposition rate was typically 0.2 to 0.5 nm s^{-1}. Some samples were deposited at higher temperature, so the heated sample holder with six positions was used in order to enable preparing a series of samples at different substrate temperature. For lower than room temperature the water cooled holder combined with Peltier cell was designed. The substrate temperature –20 °C was achieved with water cooling measured by Pt100 thermometer.

The morphology of the samples was investigated by scanning electron microscope FEI QUANTA 200.
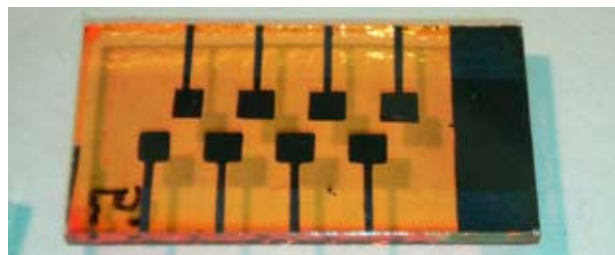
Fig. 1. **Samples of DPP sandwich structure with aluminium deposited contacts**
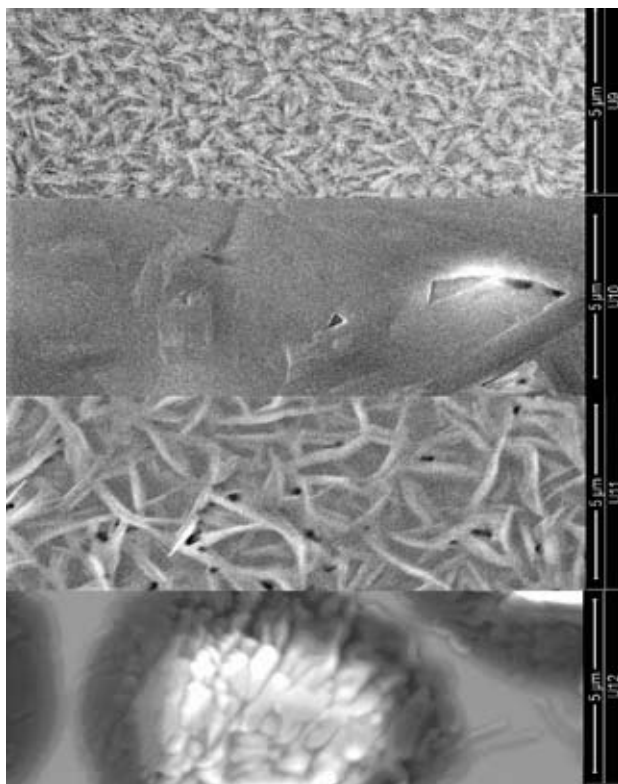
Fig. 2.　**Structure of evaporated thin films of materials U9, U10, U11 and U12**
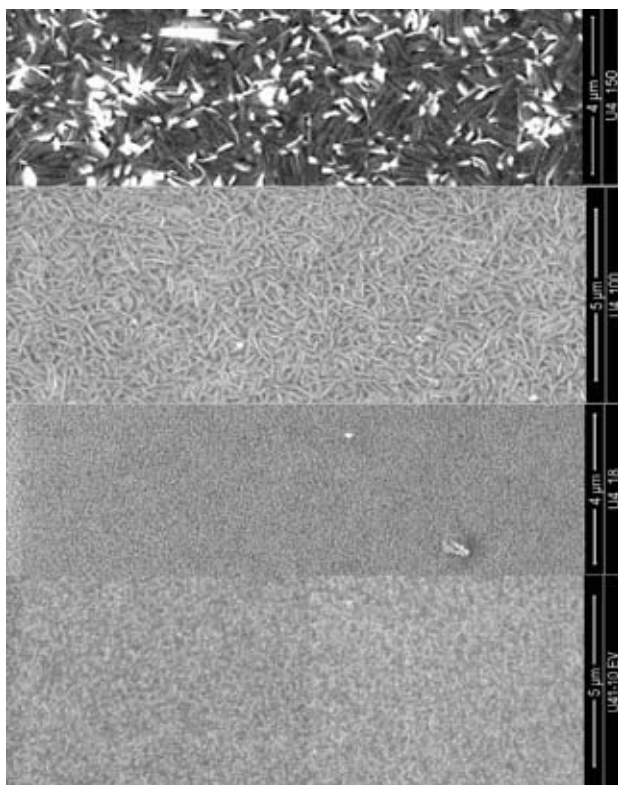
Fig. 3.　**Sample U4 prepared at various substrate temperature – 10 °C, 18 °C, 100 °C and 150 °C**
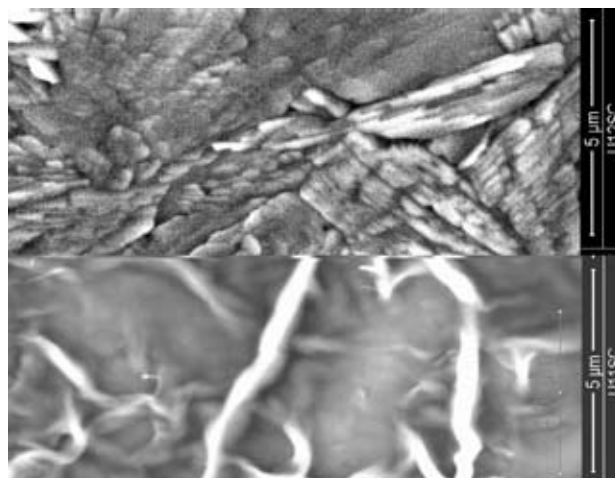
Fig. 4.　**SEM snap of U11SC and U12SC spin coated**

Results

Theory of thin film growth predict that a particle impinged onto the substrate surface can move laterally unless it losses its kinetic energy and finds the energy potential well. It is usually after joining with other particles and this particle – molecules – cluster is the nucleus of future columnar or island structure. Further more crystallization can be in process. Usually the uniform thickness and homogeneous structure is demanded in order to enable electrical thin film device to fabricate. Fig. 2. represents the series of DPP derivatives with alkyl chains symmetrically (U10, 12) and asymmetrically (U9, 11) bonded. The SEM snaps show, that they create crystalline structure with bigger and flat crystals in case of symmetric molecules and smaller and fibre crystals in case of asymmetric molecules. The melting point is lower in case of longer alkyl chain material, so it results in coarse grain structure with no amorphous phase. The island structure occurs with holes causing electrical breakthroughs in sandwich devices. The U12 material is deposited as amorphous islands, but in short time – hours – it crystallises. This effect was observed also at other materials with melting point round 100 °C and lower.

Condensation of evaporated molecules brought also problems with adhesion. The high deposition temperature causes shrinkage while cooling, more for organics than substrates and it resulted into peeling observable especially at U4–150 sample. The free crystal ends in space give high reflection in SEM due to charging and they appeared bright.

How the surface mobility of condensed molecules corresponds to surface temperature explains Fig. 3. The high melting point material was deposited by evaporation and the grain size corresponded the condensing surface temperature. The aim of the attempt should be the uniform structure, although it was achieved in scale of SEM resolution (50 nm), the electrical breakthroughs still appeared.

Samples prepared by spin coating method behave similarly, but the structure is usually continuous – no islands and visible holes m- see Fig. 4. The solvent affects blurred

transition when crystals grow just at solvent evaporation, but in case latter crystallization the grain boundaries appear sharp.

Conclusions

Set of samples of DPP derivatives thin films prepared both by evaporation and spin coating methods were investigated by SEM. Their convenience for sandwich electronic devices was criticized by the morphology appearance. The uniform thin film in scale below 100 nm grain size was not achieved due to crystallization processes. The grain size corresponded to melting point of the materials and did not vary rigorously between evaporating and spin coating method, which one gave better results due to absence of holes and continuous layer creation. Crystallization and non uniform surface appeared as well. Therefore the optimization of the chemical structure and the detail morphology studies should be done to achieve homogeneous stable layers suitable for OLED application.

REFERENCES
1. Harrop P., Das R.: *Organic Electronics: Forecasts, Players & Opportunities 2005–2025*, IDtechEx, New York, 2005.
2. Collona G., Pilati T., Rusconi F., Zecchi G.: Dyes Pigm. *75*, 125 (2007).

P24　THE INFLUENCE OF MECHANICAL ACTIVATION ON THE PRODUCTION OF THE HUMIC ACIDS IN THE BROWN COAL

M. SKYBOVA and L. TURCANIOVA

Institute of Geotechnics, Slovak Academy of Sciences
Watsonova 45, 043 53 Kosice, Slovakia
skybova@saske.sk

Introduction

One of the perspective trends of non-fuel usage of coals is the production of humic preparations on its base, which are to be used in different branches of industry and agriculture[1]. The most suitable raw material for obtaining these products is brown coals[2].

Humic acid is one of the major components of humic substances, which are dark brown and major constituents of soil organic matter humus that contributes to soil chemical and physical quality and are also precursors of some fossil fuels. They can also be found in peat, coal, many upland streams, dystrophic lakes and ocean water[3].

In the studies of Baláž[4,5] was tested the use of mechanical activation, called GACL (Grinding Aqueous Caustic Leaching) procedure which is based on the simultaneous grinding and leaching of coal. In this process of grinding was occurred significant demineralisation and detoxication. The content of humic acids increased by more than 2 times.

Recent studies using pyrolysis-FIMS and -GC/MS, multidimensional NMR and synchrotron-based spectroscopy have shown that humic substances posses both aromatic and aliphatic characteristics. The dominant functional groups, which contribute to surface charge and reactivity of humic substances, are phenolic and carboxylic groups[6].
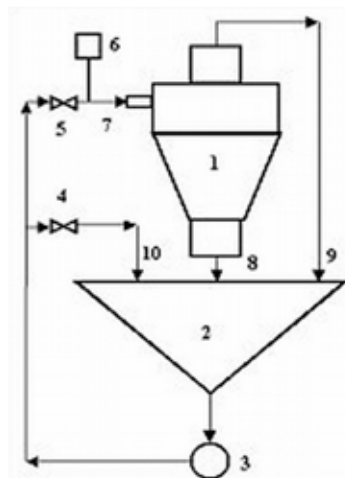
Fig. 1.　**Scheme of hydrocyclone station[7]**
1 – hydrocyclone, 2 – agitating tank, 3 – pump, 4 – valve of reverse circuit, 5 – valve for regulation of input press, 6 – pressure gauge, 7 – hydrocyclone input, 8 – heavy product – underflow, 9 – light product – overflow, 10 – circulating charge

Experimental

Hydrocyclone Separation

The steam brown coal from Handlová Colliery (central part of Slovakia) was washed in the WOC (Water-Only Cyclone). During experiments the WOC was installed in hydrocyclone station[7] (Fig. 1.). The WOC can be characterized by the following parameters: the inner diameter of cylindrical part: 150 mm; the height of this part: 200 mm; the diameter of inlet pipe 45 mm. The vortex finder and apex diameters were of 68 mm and 14.6 mm, respectively. The cone consisting of three angles (135 °, 75 ° and 20 °) was applied. The experiments have been carried out at the input pressure of 10 kPa. The concentration of solids was of 100 g dm^{-3}. The basic products of washing were collected using sieves with a mesh size of 0.5 mm. Finally, circulating slurry was collected and included into total material balance. The basic coal sample – feed (F), the obtained treatment products, i.e. washed coal – overflow (O), were dried, ground below 0.1 mm and characterized by standard analytical methods.

Extraction of Humic Acids

The coal samples (F, O) were subject to mechanical activation by the GACL (Grinding Aqueous Caustic Leaching) method in following conditions: made-up: 20 g, volume of leaching agent: 200 ml, concentration of leaching agent: 0.1%; 0.5%; 1% and 2% NaOH, leaching temperature: 60 °C, grinding period: 60 minutes, revolutions: 400 min^{-1}.

Mechanical wet grinding was performed in the attritor Molinex, type 075 Netzch, Germany with a grinding capacity of chamber – 500 ml and the grinder filling, i.e. glass balls with a weight of 685 g and 2 mm in diameter.

After the performance of the grinding test the solid phase was separated from liquid product in the centrifuge (JANETZKI T23). After through washing of the leached coal extraction in distilled water and after its drying there were determine humic acids by standard STN 441347.

^{13}C Nuclear Magnetic Resonance

The solid-state ^{13}C-NMR spectra were obtained on a Bruker Avance 500 WB/US (Karlsruhe, Germany, 2003) spectrometer.

The following experimental conditions were employed: a 4 mm ZrO$_2$ rotor with standard CPMAS pulse program, during the measuring of ^{13}C-NMR signal was applied a bipolar decupling – TPPM (two-pulse phase-modulated), a pulse length of 4.8 μs, angle of phase modulation was 15 °.

Chemical shifts were assigned according to Maciel[8].

SEM Microscopy

Scanning electron microscopy (SEM) of sample of brown coal was performed using microscope type TESLA BS 340.

Micro-shots of samples of the brown coal taken from a screening electronic microscope were enlargement of 2,000 times.

Results

The results of chemical analysis of steam brown coal and of washed WOC products are presented in Table I. It was found that WOC process reduce the amount of ash (the washed coal (O) contains lower amount of ash $A^d = 9.01$ % in comparison to the basic sample $A^d = 36.80$ %).

Table I

Characteristics of brown coal samples from Handlová Colliery. Superscripts: d – dry basis, a – analytical specimen, O^d – by difference – according to $100 - (A^d + C^d + H^d + N^d + S^d_{Total})$

Characteristics\Product	Feed	Overflow
Ad [%]	36.80	9.01
Wa [%]	9.02	7.55
Cd [%]	46.11	68.12
Hd [%]	3.04	4.49
Nd [%]	0.32	0.62
Od [%]	11.78	16.03
SiO$_2$ [%]	20.42	4.14
Al [%]	4.14	1.01
Ca [%]	0.48	0.31
Mg [%]	0.47	0.12
Fe – total [%]	1.49	0.59
S – total [%]	1.76	1.73
As [ppm]	62.00	66.00

Several procedures of preparation of humic acids make use of the traditional method of caustic treatment of brown coal with a relatively higher content of humic acids.

In Table II there is presented the influence of the concentration of leaching agent NaOH during the mechanical processing of coal before and after the WOC by the GACL method.

Table II show that a greater effect of mechanical activation by GACL process is determined by using the samples, which were not washed and which have a higher content of ash. There is the increase 1.5 in average (feed as against overflow).

In the case of mechanical activation of basic sample (after GACL method), the increase of humic acids is 2 times in comparison to the basic sample (HA – 1.62 g) before GACL method and the amount of humic acids is increased with the increase of NaOH concentration.

This same process is observed by using samples after WOC, the amount of humic acids before CACL method is 1.83 g.

The distribution of humic acids into the liquid and solid product is significant in the basic samples (liquid product $HA^{0.5} = 4.35$ g as against $HA^{0.5} = 1.04$ g in solid product).

In the samples after WOC, the distribution of the humic acids is relatively equal.

The ^{13}C-NMR spectra of the isolated coal HA are shown in Fig. 2.a), b). The spectra of HA sample were very similar and practically the minimal changes were detected.

TableII

Mechanical activation of coal using GACL process

Characteristic	HA$^{0.1}$ [g]		HA$^{0.5}$ [g]		HA^{1} [g]		HA^{2} [g]	
F: solid	1.41	3.57	1.04	5.39	1.42	4.72	1.34	6.04
liquid	2.16		4.35		3.30		4.70	
O: solid	1.02	1.94	1.43	2.83	1.92	3.92	1.45	4.85
liquid	0.92		1.40		2.00		3.40	

Concerning that, coal is very complicated nature product; its resolution of nmR spectra is very small for the most part. Inasmuch as, there is possible to estimated only basic, typical fraction of functional groups: area of 190–170 ppm – carboxylic groups or amidic carbonyls, 170–150 ppm – aromatic carbons of phenols and phenolic ester, 150–135 ppm – alcylated aromatic carbons, 135–100 ppm protonised and unprotonised bridgehead aromatic carbons, 108–100 ppm – anomeric CH of cellulose and hemiacetal carbons, 90–70 ppm – resonance area CH secondary alcohols and other carbon atoms binded to oxygen atom., 65–55 ppm – area of resonance of CH$_3$ group aliphatic and aromatic ethyleters and α-carbons of amino acids, 55–50 ppm – area of resonance of CH$_3$ group of metylesters of carboxylic groups, 50–35 ppm
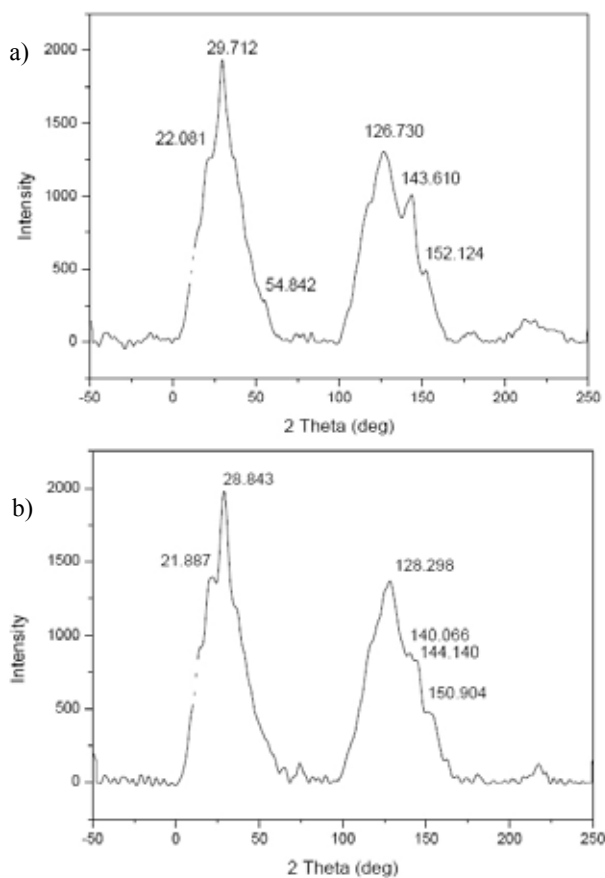
Fig. 2.   **^{13}C – nuclear magnetic resonance spectra of the humic acids – a) Overflow before the GACL process, b) Overflow after the GACL process**
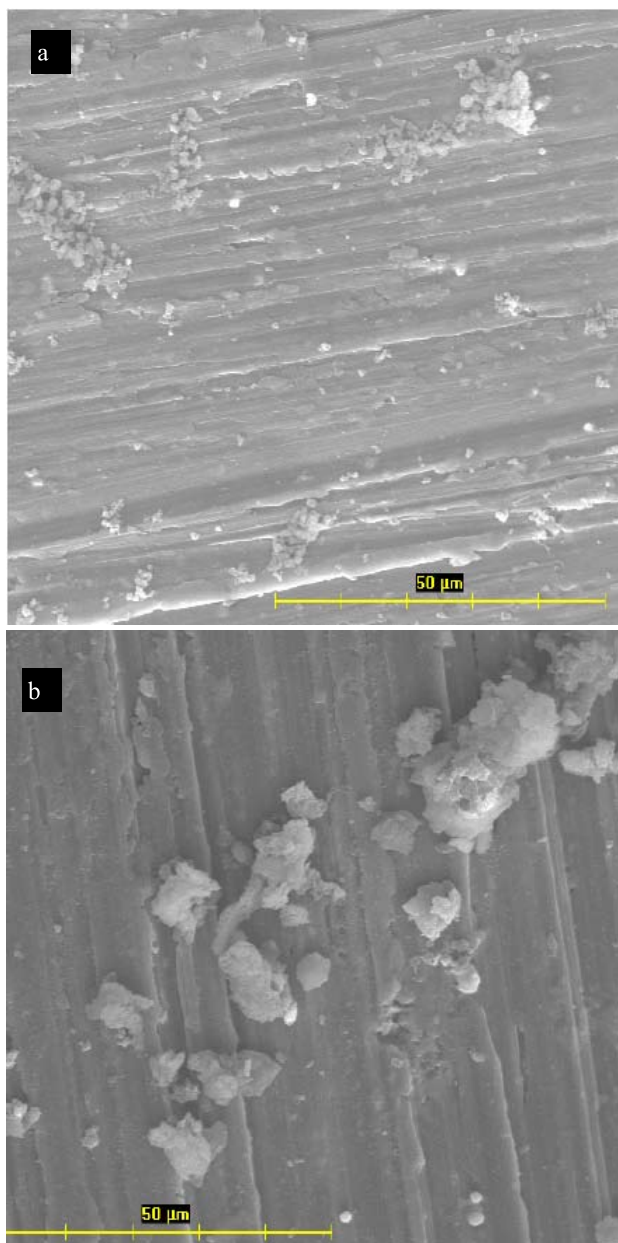
Fig. 3. **Shots of samples of the Slovak brown coal (Handlova) taken from a screening electronic microscope at a enlargement of 2,000 times: a) Overflow before the GACL process, b) Overflow after the GACL process**

– area of resonance of quarternary carbons and CH carbons, 35–25 ppm – area of resonance of CH_2 alcylic group and CH_3

acetylic group, 25–1 0 ppm – area of resonance of alcylic methyls.

Fig. 3.a) and b) show the micro-shots of the grains in mechanically active coal samples after WOC (before and after the GACL method) in the conditions of active grinding time 60 minutes

Comparing the micro-shots it may be clears that in Fig. 3.b), there is obvious aggregation of the grains in the ground stock as against 3.a). The mechanism of aggregation of ultra-fine grains cannot be definitely specified.

Conclusions

From the results presented it follow that a greater effect of mechanical activation by GACL process is determined by using the samples, which were not washed and which have a higher content of ash. In the case of leaching of the basic sample there occurs a significant selective penetration of humic acids into the liquid product. In the samples after WOC, the distribution of the humic acids into liquid and solid product is relatively equal.

REFERENCES

1. Gorlov E. G., Rodae V. V., Ryzhkov O. G., Koledin D. M.: *XXI International Mineral Processing Congress,* Rome, Italy (2000).
2. Butuzova L., Krzton A.: *European Carbon Conference. The British Carbon Group* (1996).
3. International Humic Substance Society http://www.ihss. gatech.edu/
4. Baláž P., Turčániová Ľ.: Acta Montanistica Slovaca *3*, 348 (1998).
5. Baláž P., La Count R. B., Kern D. G., Turčániová Ľ.: Fuel 80 (2001).
6. Stevenson F. J.: *Humus Chemistry: Genesis, Composition and Reaction.* Wiley, New York, (1994).
7. Jakabský Š, Lovás M., Hredzák S., Turčániová Ľ.: *Proceedings of the Fifteenth Annual International Pittsburgh Coal Conference* (1998).
8. Maciel G. E.: J. Mol. Struct. *550*, 297 (2000).

P25 NUMERIC MODELLING OF V-T PROCESS IN NITROGEN GROUND STATE UNDER POST-DISCHARGE CONDITIONS

I. SOURAL[a], F. KRČMA[a] and V. GUERRA[b]

[a]*Faculty of Chemistry, Brno University of Technology, Purkyňova 118, 612 00 Brno, Czech Republic,*
[b]*Departamento de Física, Instituto Superior Técnico, 1049-001 Lisboa, Portugal,*
xcsoural@fch.vutbr.cz

Introduction

Many scientists have tried to create the kinetic model describing the processes occurred during the nitrogen post-discharge[1,2]. These endeavours are not fully successful up to now because there are many metastable electronic and vibrational states in nitrogen and the bimolecular and trimolecular reactions among these excited states have mainly unknown reaction rate constants[3,4]. If the active discharge turns to the post-discharge period there is about 90 % of total energy in plasma dissipated into vibration at levels states of the ground state[5] and during the consequent reactions (including also the other excited species) this energy changes to the electron excitation, ionization, dissociation and other processes[6]. It means, nearly all the post-discharge kinetics starts by reactions of metastable vibrationally excited nitrogen ground state molecules. This is reason why it is necessary to study vibration distribution function of the ground state in the time evolution. Vibration distribution function is depended on different processes as V-T (Vibration-Translation transition), V-V (Vibration-Vibration transition), electron excitation, ionization and another. V-T and V-V processes are the most important for the evolution of vibration distribution function (VDF). Much work is needed for all calculations. However we have already finished V-T calculations so this work is focused on this only.

Theoretic Base of Numeric Model

There are two main well known energy transfer processes in the ground state: V-T process[7], i.e. the transfer of vibrational energy into the energy of translational motion of molecule (see R1) and V-V process[7] where the molecules exchange their vibrational excitation energy (see R2).

- V-T:
  $N_2(X\ ^1\Sigma_g^+, v) + N_2(X\ ^1\Sigma_g^+) \rightarrow$
  $N_2(X\ ^1\Sigma_g^+, v \pm 1) + N_2(X\ ^1\Sigma_g^+)$ 　　　　R1

- V-V:
  $N_2(X\ ^1\Sigma_g^+, v) + N_2(X\ ^1\Sigma_g^+, w) \rightarrow$
  $N_2(X\ ^1\Sigma_g^+, v-1) + N_2(X\ ^1\Sigma_g^+, w + 1)$ 　　R2
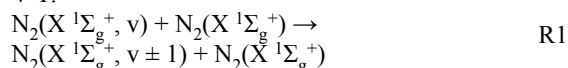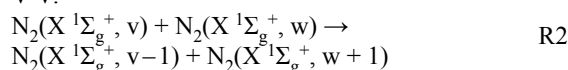
Nitrogen molecule in ground state has 60 vibrational levels (from 0th to 59th)[8]. The SSH (Schwartz-Slawsk-Herzfeld) theory was used in the presented model[9], because it is easier than quantum mechanic theory, where calculations are more complicated and need longer computation time than

SSH theory. On the other hand, SSH theory allows calculation of the rate coefficients for the first 46 vibration levels only.

The rate coefficients of all two body collisions must be known for the numeric model of V-T process. 46 different particles with 46 kind of two body reactions are used in SSH theory because the state of the second interacting particle is not resolved. Each particle can transfer its state to any from 45 others but transition with $\Delta v > \pm 1$ have very low probability at temperatures below 1,000 K and thus can be neglected.

This is reason why model calculates and uses only $P_{v,v-1}$ (probability of transition from v to $v-1$) and $P_{v-1,v}$ (probability of transition from $v-1$ to v).

Calculation of Transition

Transitions probabilities for both V-T and V-V processes were calculated using SSH theory for the lowest 46 vibrational levels using the following set of equations.

$$E_v = \hbar\omega\left[\left(v+\frac{1}{2}\right) - \chi_e\left(v+\frac{1}{2}\right)^2\right] \tag{1}$$

$$P_{v,v-1} = Z\frac{v}{1-\chi_e v}\frac{2\mu}{\mu^{A_2}}\frac{kT_g}{\hbar\omega}F(Y_{v,v-1}) \tag{2}$$

$$Z = \pi d^2 \left(8kT_g / \pi\mu\right)^{1/2} \tag{3}$$

$$F(y) \equiv \begin{cases} \frac{1}{2}\left[3 - \exp\left(-\frac{2y}{3}\right)\right]\exp\left(-\frac{2y}{3}\right) & \text{for } 0 \le y \le 20 \\ 8\left(\frac{\pi}{3}\right)^{1/2} y^{7/3}\exp\left(-3y^{2/3}\right) & \text{for } y \rangle 20 \end{cases} \tag{4}$$

$$Y_{v,v-1} = g(1 - 2\chi_e v) \tag{5}$$

$$g = \left(\frac{1}{2}\right)^{3/2}\left(\frac{4\pi^2\varpi^2 L^2\mu}{kT_g}\right)^{1/2} \tag{6}$$

$$P_{v,v-1}^{w-1,w} = Z\frac{v}{1-\chi_e^{A_2}v}\frac{w}{1-\chi_e^{B_2}\varpi}\frac{\mu kT_g}{8L^2\mu^{A_2}\varpi^{A_2}\mu^{B_2}\varpi^{B_2}}F(Y_{v,v-1}^{w-1,w}) \tag{7}$$

$$Y_{v,v-1}^{w-1,w} = \frac{\pi L}{\hbar}\left(\frac{\mu}{2kT_g}\right)^{1/2}\left|\Delta E_{v,v-1}^{w-1,w}\right| \tag{8}$$

$$\Delta E_{v,v-1}^{w-1,w} = \hbar\omega^{A_2}\left(1 - 2\chi_e^{A_2}v\right) - \hbar\omega^{B_2}\left(1 - 2\chi_e^{A_2}\varpi\right) \tag{9}$$

$$P_{v-1,v} = P_{v,v-1}\exp\left(-\frac{\hbar\omega}{kT_g}(1 - 2\chi_e v)\right) \tag{10}$$

$$P_{v-1,v}^{w,w-1} = P_{v,v-1}^{w-1,w}\exp\left(\frac{\Delta E_{v,v-1}^{w-1,w}}{kT_g}\right) \tag{11}$$

$$P_{v,v-1} = v\left(\frac{1-\chi_e}{1-\chi_e v}\right)P_{1,0}\frac{F(Y_{v,v-1})}{F(Y_{1,0})} \tag{12}$$

$$P_{v,v-1}^{w-1,w} = v\varpi\left(\frac{1-\chi_e^{A_2}}{1-\chi_e^{A_2}v}\right)\left(\frac{1-\chi_e^{B_2}}{1-\chi_e^{B_2}\varpi}\right)P_{1,0}^{0,1}\frac{F(Y_{v,v-1}^{w-1,w})}{F(Y_{1,0}^{0,1})} \tag{13}$$

$$P_{1,0} = 1{,}07 \cdot 10^{-12} T_g^{3/2} F(Y_{1,0}) \tag{14}$$

$$P_{v,v-1}[OK] = \frac{P_{v,v-1}}{\left[a + 35{,}5\left(\dfrac{v-1}{39}\right)^{0{,}8}\right]} \tag{15}$$

$$a(T_g) = 0{,}2772 \cdot T_g - 80{,}32 \tag{16}$$

$$P_{0,1}^{0,1} = 6{,}35 \cdot 10^{-17} \cdot T_g^{3/2} \tag{17}$$

$$P_v^{N_2-N} = \sum_{w\langle v} P_{v,w}^{N_2-N} \tag{18}$$

Variables	Names of variables
$a(T_g)$	Correction coefficient
d	Particle diameter
$\Delta E_{v,v-1}^{w-1,w}$	Energy difference of simultaneous transfer from level "v" to "$v-1$" and from "$w-1$" to "w"
E_v	Vibration energy
$F(y)$	Adiabatic factor
$F(Y_{1,0})$	Adiabatic factor, for transfer from 1 to 0 level
$F(Y_{0,1})$	Adiabatic factor, for transfer from 0 to 1 level
$F\left(Y_{1,0}^{0,1}\right)$	Adiabatic factor, for transfer from 1 to 0 level by first molecule and from 0 to 1 by second molecule
$F(Y_{v,v-1})$	Adiabatic factor for "v" to "$v-1$" transfer
$F\left(Y_{v,v-1}^{w-1,w}\right)$	Adiabatic factor, for transfer from "v" to "$v-1$" level by first molecule and from "$w-1$" to "w" by second molecule
g	Factor
$\hbar$	Modified Planck constant
k	Boltzmann constant
L	Parameter characterizing magnitude of repulsion potential
μ	Total reduced mass of both molecules by collision
μ^{A_2}, μ^{B_2}	Reduced mass of molecule A_2 and B_2
$P_{1,0}$	Probabilities of excitation transfer from vibration level 1 to level 0
$P_{0,1}^{0,1}$	Probability of simultaneous transfer from vibration level 1 to level 0 and from level 0 to 1 by second molecule
$P_{v-1,v}$	Probability of transfer from vibration level "$v-1$" to level "v"
$P_{v,v-1}$	Probability of transfer from vibration level "v" to level "$v-1$"
$P_{v,v-1}[OK]$	Probability of transfer from vibration level with correction (from SSH theory to quantum mechanic theory)
$P_{v,v-1}^{w-1,w}$	Probability of simultaneous transfer from vibration level "v" to level "$v-1$" and "$w-1$" to "w" by second molecule
$P_{v-1,v}^{w,w-1}$	Probability of simultaneous transfer from vibration level "$v-1$" to level "v" and "w" to "$w-1$" by second molecule
T_g	Neutral gas temperature
v	Vibration level

ω	Fundamental vibration frequency (for N_2 ground state $\omega = 4.443 \cdot 1{,}014$ Hz)
$\omega^{A_2}, \omega^{B_2}$	Vibration frequency of A_2 and B_2 molecule
χ_e	Constant of anharmonicity (second virial coefficient)
$\chi_e^{A_2}, \chi_e^{B_2}$	Anharmonicity constant for A_2 and B_2 molecule
y	Distance between molecules A2 and B2
$Y_{v,v-1}$	Factor
$Y_{v,v-1}^{w-1,w}$	Factor
Z	Collisions frequency

Our model includes two basis of calculation. The first one is based fully on theory, the second way uses experimental value of $P_{1,0}$ probability and the other probabilities are computed by SSH theory.

In presented schemes 1 and 2 you can see sequence of equations used in numeric model.
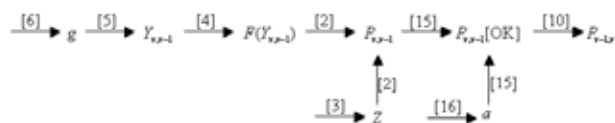
Scheme 1

Equations for calculation of probabilities for vibration-translation transfer $P_{v,v-1}$ and $P_{v-1,v}$ by SSH theory with correction to quantum mechanic theory. This scheme shows calculation of all probabilities from SSH theory.
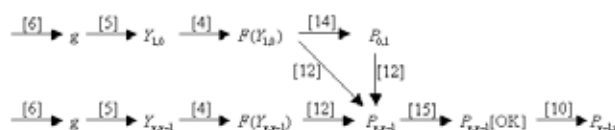
Scheme 2

Equations of calculation probabilities for vibration-translation transfer $P_{v,v-1}$ and $P_{v-1,v}$ by SSH theory with correction to quantum mechanic theory. This scheme shows calculation of probabilities from SSH with used experimentally obtained probability $P_{1,0}$ value.

Results

The gas temperature, pressure and vibrational quantum number are the main parameters of calculation. The calculated rate coefficients are shown in Figs. 1 and 2. The probabilities for the exothermic V-T transfer $P_{v,v-1}$ are higher than probabilities for endothermic V-T transfer $P_{v-1,v}$. Both these probabilities increase with the increase of vibration quantum number because energy difference between neighbour levels decreases with the increase of v according to the anharmonic potential curve of electronic state.

Also it can be seen that probabilities obtained by theory ("TH") are smaller than probabilities from theory with experimental value of $P_{1,0}$ coefficient ("EX"). These figures show the strong dependence of all probabilities on temperature. Temperature increase of about three times evokes the probability increase of about three orders in magnitude.
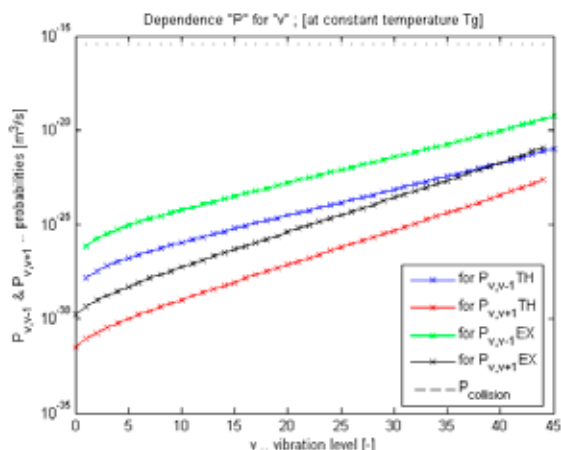
Fig. 1.   **Dependence of probabilities for vibration-translation energy transfer $P_{v,v-1}$ and $P_{v-1,v}$ on vibration level at temperature 400 K. Curves "TH" are just from theory SSH with correction, and curves "EX" are from theory with experimental value of $P_{1,0}$ coefficient**
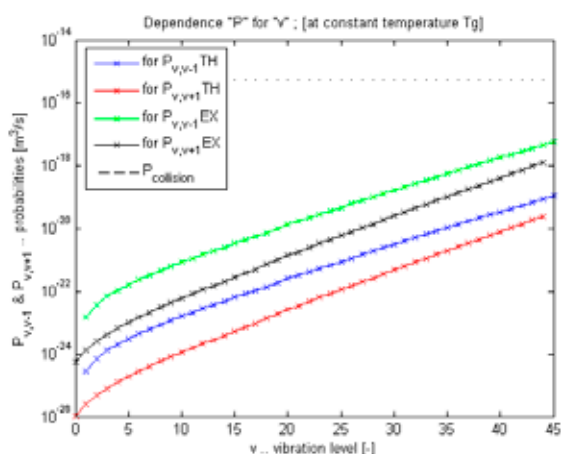
Fig. 2.   **Dependence of probabilities for vibration-translation transfer $P_{v,v-1}$ and $P_{v-1,v}$ on vibration level at temperature of 1,000 K. Curves "TH" are just from SSH theory with correction, and curves "EX" are from theory with experimental value of $P_{1,0}$ coefficient**

Vibration Distribution Function

Vibration distribution function (VDF) is time dependent during the post-discharge. The initial VDF is the same as in an active discharge and it can be calculated using active discharge conditions. Fig 4. shows VDF time evaluation at 300 K and pressure of 1,000 Pa.

Evolution of VDF shows decrease of population at the highest vibration levels. The populations at lower levels do not show any significant changes during initial part of post-discharge. As particles at higher vibrational levels have higher V-T probabilities, they are more or less in Boltzmann distribution (see blue line in Fig. 4., particles with v > 20), while particles at the lower vibration levels conserve more or less
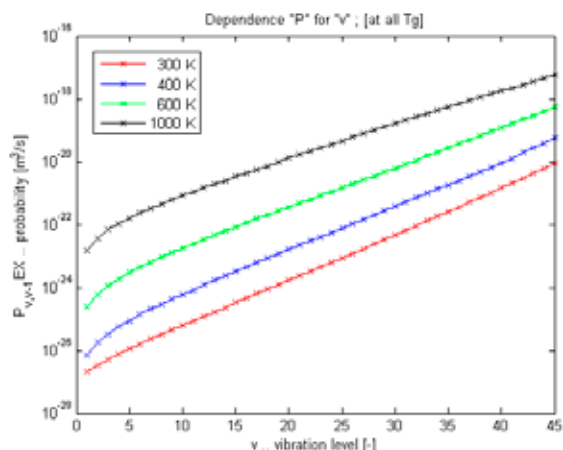
Fig. 3.   **Dependence of probabilities $P_{v,v-1}$ (from theory and experimental $P_{1,0}$) under temperature 300 K (red line), 400 K, 600 K and 1,000 K (blue lines) for vibration level**
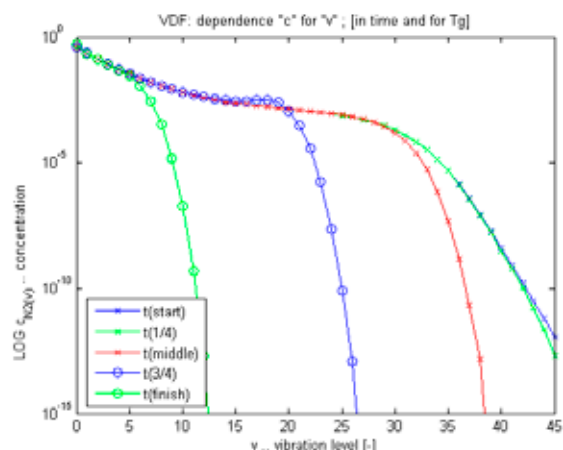
Fig. 4.   **Time evaluation of vibration distribution function at 300 K (t(start) is t = 10^{-5} s, t(1/4) is t = 10^{-3} s, t(middle) is t = 10^{-1} s, t(3/4) is t = 10^{1} s, t(finish) is t = 10^{3} s)**
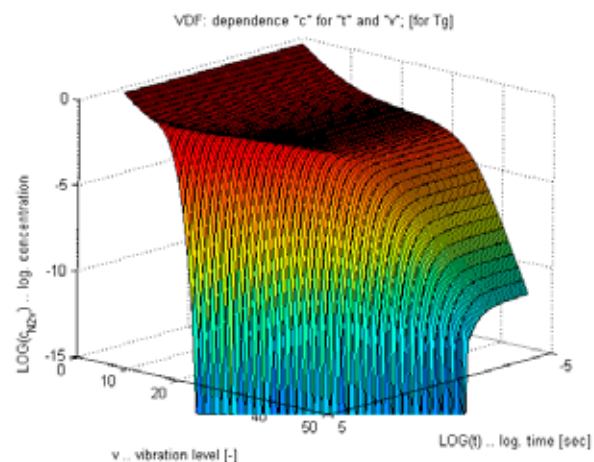
Fig. 5.   **3D diagram of vibration distribution function at 600 K**
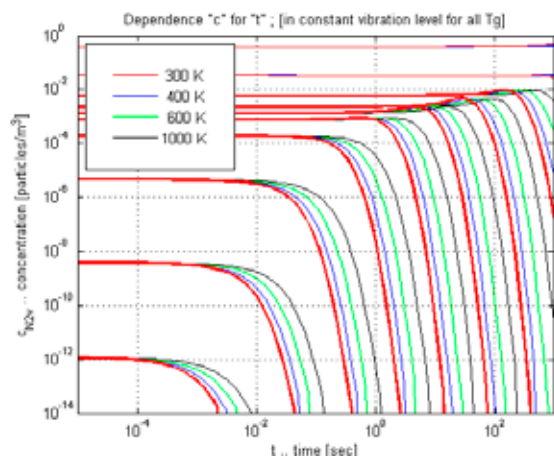
Fig. 6. **Relative populations at selected vibration levels during the post-discharge. Red lines are concentrations at temperature of 300 K and blue lines are concentrations at 400 K, 600 K and 1,000 K**

Fig. 8. **Vibration energy distribution function (EvDF) at 300 K (red lines), 400 K, 600 K and 1,000 K, t(start) is t = 10⁻⁵ s, t(1/4) is t = 10⁻³ s, t(middle) is t = 10⁻¹ s, t(3/4) is t = 10¹ s, t(finish) is t = 10³ s**

post-discharge. As particles at higher vibrational energy have higher V-T probabilities, they are more or less in Boltzmann distribution (see in Fig. 7, particles with $E_v = 0.9 \times 10^{-18}$ J), while particles at the lower vibration energy conserve more or less the initial distribution function. The same situation is described also in Fig. 8 for more temperatures.

The small increase of the population is well visible at the decay time of 10 s originates in the faster decrease of populations at higher levels.

Conclusions

This work was focused on the numeric modelling of V-T energy transfer in nitrogen molecule ground state. This process is one of the main mechanisms during the post-discharge when the systems changes its conditions from an active discharge to the common Boltzmann distribution at given (usually ambient laboratory) temperature.

Fig. 7. **Vibration energy distribution function at 1,000 K, where t(start) is t = 10⁻⁵ s, t(1/4) is t = 10⁻³ s, t(middle) is t = 10⁻¹ s, t(3/4) is t = 10¹ s, t(finish) is t = 10³ s, smooth red line is Boltzmann distribution for infinity time. EvDF is nearly the same as VDF but vibration levels are recalculated to vibration energy**

the initial distribution function. The same situation is described also in Fig. 7 for higher temperature.

Fig. 6. demonstrates the time evolution of relative vibrational populations. It can be seen that all populations are significantly higher at higher temperatures. It is also evident the populations at higher levels decrease earlier than at lower levels.

Energy vibration distribution function (EvDF) is time dependent during the post-discharge. The initial EvDF is the same as in an active discharge and it can be calculated using active discharge conditions. Fig. 7. shows EvDF time evolution at 1,000 K and pressure of 1,000 Pa.

Evolution of EvDF shows decrease of population at the highest vibration energy. The populations at lower vibrational energy do not show any significant changes during initial part of

The calculations were made using two approaches. The SSH theory with correction to the quantum mechanics was used in the first one, the second one was the same with included experimental value of $P_{1,0}$ probability. The V-T probabilities calculated by the first procedure were significantly smaller than that calculated by the other procedure. In both cases, probabilities for the exothermic V-T transfer (change of vibrational level $P_{v,v-1}$) are significantly higher than that for the endothermic (change of vibrational level $P_{v-1,v}$). The V-T transfer probability increased with the increase of vibrational quantum number due to the anharmonic potential curve of the ground electronic state. Due to this fact, the Boltzmann equilibrium distribution was reached at earlier post-discharge times at higher vibrational levels; the highest levels (over 40) were nearly the equilibrium even at begin of calculation.

The temperature had very high effect on the transition probabilities. The temperature increase of about three times evoked the V-T probability increase of three orders independently on vibrational level. On the other hand, the decrease of

vibrational populations during time is slower at higher temperatures.

The presented model showed evolution of VDF by V-T process. For the description of any real system more other processes (V-V, pooling, step-vise ionization and others) are needed to include and calculation of real system realization needs a lot of hard work and time. Its necessary to know more constants of system, new rate coefficients (that are strongly temperature dependent) and thus it is a really complex task. V-T process simulation was the first step on the way to complex numeric model of the post-discharge phenomenon.

REFERENCES

1. Guerra V., Sa P. A., Loureiro J.: J. Phys. D, Appl. Phys. *34*, 1745 (2001).
2. Guerra V., Sa P. A., Loureiro J.: Europ. Phys. J. Appl. Phys. *28*, 125 (2004).
3. Pintassilgo C. D., Loureiro J., Guerra V.: J. Phys. D, Appl. Phys. *38*, 417 (2005).
4. Krčma F., Mazánková V., Soural I.: Publications of the Astronomical Observatory of Belgrade *82*, 133 (2007).
5. Loureiro J., Ferreira C. M.: J. Phys. D, Appl. Phys. *19*, 17 (1986).
6. Paniccia F., Gorse C., Cacciatore M., Capitelli M.,: J. Appl. Phys. *61*, 3123 (1987).
7. Zelechov A., Rapp D., Sharp T. E.: J. Chem. Phys. *49*, 286 (1968).
8. Guerra V.: PhD thesis, Instituto Superior Technico, Lisbon (1998).
9. Guerra V.: *Private communications*, Lisbon, (January-May 2007).
10. Soural I., Diploma thesis, Brno University of Technology, Faculty of Chemistry, (2007).

P26   EVALUATION OF INTAKE CAPPABILITY OF LCM SURFACE BY ADSORPTION DYEDING METHOD AND ITS UTILIZATION FOR EVALUATION OF CHANGES IN SURFACE POLARITY CAUSED BY DCSBD LOW-ENERGY PLASMA

RADOVAN TIŇO, LIVIA BEŇOVÁ and SVETOZÁR KATUŠČÁK

Institute of Polymer Materials, Department of Chem. Technology of Wood,Pulp and Paper, Slovak University of Technology in BratislavaRadlinského 9, 812 37, Bratislava, Slovak Republic,
radovan.tino@stuba.sk

Introduction

Use of the color information for non destructive evaluation of wood has some advantages and drawbacks. Advantages of color information on lignocellulosics: *Visually* evaluated color information are widely used in common praxis and in everyday life for grading, production control, sale, decisions of consumers, aesthetic and economical value evaluation, in utilisation, renovation and recycling of wood materials and products. The quantified color data have shown to be valuable tool in forestry and forest products area, especially in the areas and processes of production of decorative wood[1], storage[2], drying and steaming[3]; veneers production[4], coating[5], testing of ageing[6], aesthetic evaluation[7], pulp and paper production[8], wood pyrolysis[9] tec.

The most widely used in the material engineering area inclusive wood science and technology is the CIE system.

The advantage of usage the color information for evaluation of diferences between controled and plasma modified surfaces colored with standard dyestuff solution in water is the potentialy practical readability of the method and the color information. The method would express more or less directly the water-repellent properties: the less water soluble dyestuff has been adsorbed the higher the water-repellency and the hydrophobicity. It could further correlate with the end-use properties of plasma treated wood surfaces e.g. mantainability and dirtability.

Disadvantages of color information on lignocellulosics: In spite of their value-estimating and industrial meaning analysed in the works cited above, are the color information and another optical properties of wood not so systematically known as the other physical, mechanical and chemical properties.

We have selected CIE $L^*a^*b^*$ – space as the most suitable space for the communication on the color of wood and for systematic presentation of the wood color as well as for monitoring color differences and kinetic changes of lignocellulosic materials[10,11].

For measurement of changes of surface polarity there are used methods and parameters such as: contact angle, surface energie of solid surfaces, spectroscopic methods for measurement of polar and non-polar functional groups and compounds, for an instance after their extraction from the surface of lignocellulosic materials (LCM)[12]. For characterization of LCM surfaces nowadays exists also many spectroscopic methods, which investigate functional groups of the surface, while many of them work at ultra high vacuum.[13] If it comes to the change of LCM surface ad effectum of plasma, change of ability to absorb color substances can occur. For example, when hydrophobization strikes, LCM surface takes less of polar dyeing solution or dyestuff.

Measurement of the change of surface polarity should be in such a case performable also on the basis of change colorability or change of dyestuff adsorption on the unmodified surface as well as on the surface modified with Diffuse surface coplanar barrier discharge (DCSBD).

Experimental

In experimental part was proposed new method for measurement of polarity changes on the LCM surface by means of colorimetry.

Change of colourity can be measured colorimetricaly in whole range by microspectrophotometer, which gives the exact value ΔE^*.

$$\Delta E^* = \sqrt{(\Delta L^*)^2 + (\Delta a^*)^2 + (\Delta b^*)^2} \qquad (1)$$

Value of ΔE^* refered to a plasma untreated dyed LCM surface (control sample). Measurement of color coordinates of surfaces was performed by colorimeter Minolta, CR–200.

Surface analysis offers information about chcemical composition, level of impurity, physical structure or morphology of surface.

By measuring the contact angle it is possible to study effects of wetting. For reproducibility of results of measurement contact angle is necessary to keep constant conditions: quality of testing solution, constant volume and size of drop, quality of surface (homogenity). Direct measurement of contact angle shoul be performed on lighted drop sitting on solid surface.

Contact angle θ by Surface energy evaluation system (SEE System)[14], which captures profile of solid/liquid meniscus of a liquid drop set on a solid surface with build-in camera. Images taken with camera are subsequently transfered into SEE System software, where they are processed for evaluation of surface free energy, it's portions, contact angles etc.

Preparation of Samples

Samples of European spruce (*Picea excelsa*) with dimensions of $8 \times 2.5 \times 0.5$ cm were used during the experiment. The spruce was chosen as a commercially used wood. All samples were air-conditioned prior the treatment in air-conditioned chamber with relative humidity RH = $50 \pm 2\%$ and temperature T = 23 ± 1 °C during at least 4 hours. The surface of samples was sanded by 150-grit paper. After sanding the spruce surface was blasted by air stream to remove attached dust. The spruce surface was air blasted also after the plasma treatment, in order to remove possible low molecular

fragments from the surface. Water droplet contact angle was measured with Surface energy evaluation system (SEE System)[14]. Plasma treatment of wooden samples was done by the Diffuse Coplanar Surface Barrier Discharge (DCSBD) – a planar source of the low-temperature plasma[15]. The DCSBD electrodes, consisting of 15 pairs of silver strip electrode embedded 0.5 mm below the surface of 96% Al_2O_3 ceramics, was supplied by HV generator LIFETECH VF300. The mutual distance of the 200 mm long and 2 mm wide silver strip electrodes was 1 mm. Discharge was supplied by harmonic 1,86 kHz sine high voltage of (100 ± 5) Watt, which gives 0.92 W cm^{-2} of power per treated area of sample.

The electrode was mounted inside the closed reactor chamber equipped with forced air ventilation with air flow 4 dm^3 min^{-1} .

The mutual distance d_{p-w} was adjusted by the stack of 0.13 mm thick microscope cover slips in amount (0–10 pieces) inserted between the surface of plasma electrode and surface of treated wood sample. After the treatment, samples were put again into the air-cond. chamber, where stayed another 24 hours. After this periode they were colored with 10% water solution of stain commercially known as Spoloxyl blue 6. Filter paper previously submerged 10 s in stain solution was put on the sample surface, then was loaded with 3 kg weight during 5 s and on the end, excess of stain was sucked out by clean filter paper loaded with 3 kg weight during 5 s. After this procedure, samples stayed for 4 hours in air-conditioned chamber and after that they were measured by colorimeter Minolta CR–200. Color coordinates of LCM surfaces were measured and color difference ΔE^* was calculated from them.

Measurement of Contact Angle

The thermodynamic properties of spruce wood samples were investigated by means of the sessile drop technique using the Surface Energy Evaluation System (SEE System, http://www.advex-instruments.cz,10.5.2008). The contact angles were measured directly from the images of the solid/liquid meniscus of a liquid drop set on a solid, taken with build in camera. Because the sessile drop gradually spreads over the wood surface, thus reducing its contact angle value, the initial contact angle was taken only.

Measurement of Water Uptake Time

For measurement of water uptake time was used 5-μl droplets of deionized water, which were applied onto spruce surface with Krüss single auto-dosing system D03004. Water uptake time was measured at the same time as the measurement of contact angles.The determination of water uptake time has been done in accordance with[16] in order to mutually compare obtained results. The water uptake time was the time interval from the impact of the droplet to the complete penetration of the droplet into the wood surface (no optical reflection can be seen).
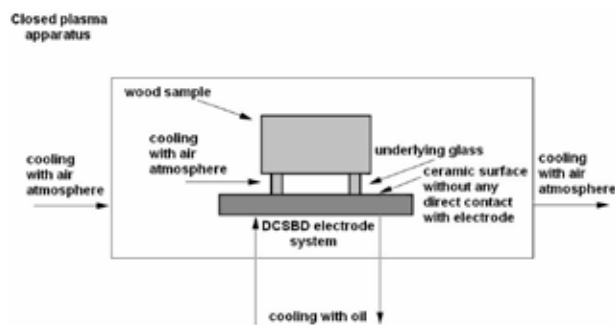
Fig. 1.   **DCSBD plasma system scheme**
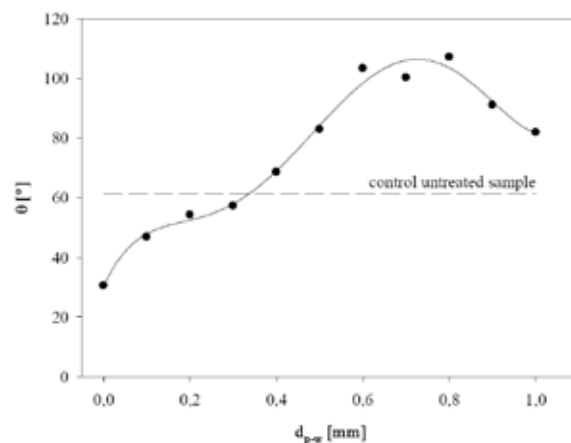
Fig. 2.   **Change of contact angle as a function of different mutual distance dp-w between surface of treated sample and surface of DCSBD plasma electrode. Dashed line represents untreated control sample**

Results

Table I sumarizes results from the measurements of color coordinates, total color difference, surface contact angle and water droplet uptake time as a function of mutual distance of the sample surface and surface of plasma electrode. By having look at color coordinates of plasma treated samples and their comparison with untreated sample is obvious, that plasma causes changes in colorability of plasma treated lignocellulosic surfaces. At the same time it is possible to say, that contact angle of plasma untreatet sample is almost the same as that treated from the distance 0.3–0.4 mm above plasma electrode. The same behaviour was observed in the case of water uptake time.

Fig. 2. shows dependance of contact angle θ on mutual distance d_{p-w} between surface of treated sample and surface of DCSBD plasma electrode. There is also present line representing value of 62 ° which matches with plasma untreated sample (control). At distance between 0.3 and 0.4 mm is contact angle of the plasma treated surface equall 62 °. Plasma makes treated surface hydrophilic (i.e. contact angle is less than 62 °). The generation of plasma at zero distance (i.e. the wood sample lying directly on the DCSBD electrode) was

Table I
Evaluation of color coordinates of stained LCM surfaces treated with DCSBD plasma by CIELab system. DCSBD plasma treated surfaces were colored with 10% water solution of stain commercially known as Spoloxyl blue 6 and are compared with plasma untreated controll sample, where: d_{p-w} – mutual distance of the surface of sample and surface of plasma electrode, θ – contact angle, τ_w-water uptake time, L^* – lightness, a^* – red-green axis, b^* – yellow-blue axis and ΔE^* – total collor difference

d_{p-w}[mm]	L^*	a^*	b^*	ΔL^{*2}	Δa^{*2}	Δb^{*2}	ΔE^*	$\theta[°]$	$\tau_w[s]$
Cont.	35.57	−8.22	−27.7	0	0	0	0	62	30
0	37.4	−11.2	−26.3	3.5	9	1.9	3.8	31	4
0.1	41.3	−13.9	−23.3	32.3	32.6	19	9.2	47	10
0.2	41.8	−14.7	−22.1	38.6	41.9	31	10.6	54	14
0.3	40.3	−14.0	−20.5	22.4	33.8	52	10.4	57	16
0.4	41.7	−13.5	−21.4	37.2	27.7	40	10.2	69	45
0.5	42.3	−15.7	−18.6	45.4	55.8	84	13.6	83	450
0.6	48.4	−15.1	−8.2	164.6	47.3	381	24.4	103	630
0.7	44.8	−13.3	−14.5	84.8	26.0	173	16.9	100	550
0.8	52.7	−12.3	−4.5	294.5	16.8	540	29.2	107	870
0.9	49.0	−15.3	−12.3	180.4	50.7	238	21.7	91	510
1	43.2	−14.3	−19.2	57.5	37.2	73	12.9	82	370

allowed due to the natural porosity and roughness of wood sample.

Samples in direct contact with the plasma electrode became more hydrophilic after the treatment which corresponds with significantly higher rate of water uptake as can be seen on Fig. 3. Samples which were more than 0,4 mm over the surface of plasma electrode became after the plasma treatment more hydrophobic which corresponds with longer period of water uptake (Fig. 3.) on their surface as well as with the higher contact angle in comparison to that of control sample.

Fig. 4 shows dependance of the total color difference on ΔE on mutual distance d_{p-w} between surface of treated spruce sample and surface of DCSBD plasma electrode. There are two peaks. First lays in the range of 0mm up to 0.4 mm. Total

color difference rises from 0 to 10.6 at d_{p-w} = 0.2mm and then slowly decreases to 10.2 at d_{p-w} = 0.4 mm which corelates with the thickness of plasma layer generated in air with the used experimental setup. By further increasing the mutual distance, ΔE^* starts to rise again and reaches maximum value of 29.2 at d_{p-w} = 0,8–0,9 mm and then starts to decrease. It seems to be, that plasma has two effects. One, when samples are in close distance up to 0.3–0.4 mm, where are treated directly with the generated plasma layer. At distances above 0.4 mm there is no visible generated plasma layer, but there is still area above the layer, which is also active at plasma

Fig. 3.   **Change of water uptake time** τ_w **as a function of different mutual distance dp-w between surface of treated spruce sample and surface of DCSBD plasma electrode. Dashed line represents untreated control sample**
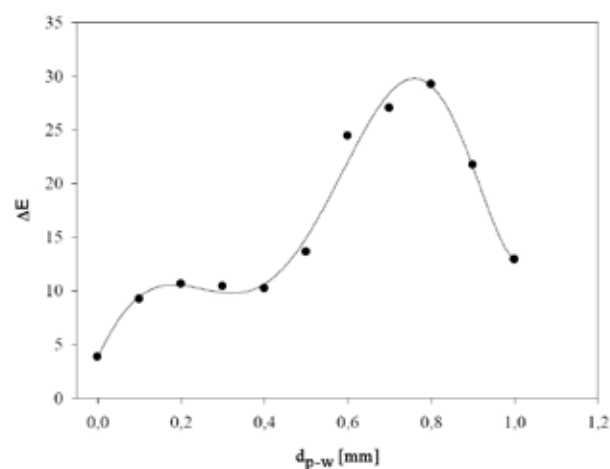
Fig. 4.   **Change of total color difference** ΔE^* **as a function of different mutual distance** d_{p-w} **between surface of treated spruce sample and surface of DCSBD plasma electrode. The biggest color difference was obtained when the sample was during the plasma tretment approximately 0.8 mm over the surface of plasma electrode. At this point also the strongest hydrophobization took the effect**

treatment. This area is responsible for hydrophobization of lignocellulosic surfaces, while are bellow 0.3 mm makes surface hydrophilic. However, whole range of distances from 0 mm up to observed 1.17 mm causes changes in colorability

Table II
Order of coefficients of correlation between results from colorimetric measurements (parameters CIELab (ΔE^*, L^*, a^*, b^*, $(\Delta L^*)^2$, $(\Delta a^*)^2$, $(\Delta b^*)^2$) and commonly used parameters describing the polarity of lignocellulosic materials (θ contact angle, τ_w – water uptake time)

Order	Parameter	Coefficient of corelation R^2 for	
		Contact angle (θ)	Water uptake time (τ_w)
1	b^*	0.91	0.93
2	ΔE^*	0.90	0.92
3	L^*	0.87	0.89
4	$(\Delta b^*)^2$	0.81	0.89
5	$(\Delta L^*)^2$	0.78	0.87
6	a^*	−0.33	−0.14
7	$(\Delta a^*)^2$	0.31	0.15

Table II shows color parameters measured at samples of spruce treated by DCSBD plasma and their correlations with the contact angle and water uptake time. Individual paramaters are ordered from that with the highest correlation with both above mentioned characteristics of surface polarity, which is parameter b^*. This parameters correlates with contact angle as well as with the water uptake time very well (91 and 93 %). Also ΔE^*, L^*, $(\Delta b^*)^2$, $(\Delta L^*)^2$ correlate quite well, so they can be used for evaluation of changes on the lignocellulosic surface caused by DCSBD plasma treatment. Parameters a^* and $(\Delta a^*)^2$ don't correlate with above mentioned characteristics of surface polarity and they are not suitable for evaluation of intake capability of lignocellulosic surfaces by adsorption dydeding method.

Conclusions

The particular aim of this paper is to propose and test characteristic color parameters and to correlate them with polarity changes on the wood surface made by DCSBD plasma treatment.

The new method for evaluation of changes in polarity of solid lignocellulosic surfaces by measurement of differencies of trichromatic components between untreated and plasma treated surface colored by given standard dye was developed. Measurement was performed in CIE Lab system. It was verified, that by measurement of color difference it is possible to evaluate polarity of lignocellulosic surfaces, what was confirmed by comparison of this method and other utilized methods for measurement of polarity changes such as measurement of water uptake time and contact angle.

REFERENCES

1. Phelps J. E., Rink G., Workman, E. C. Jr.*: Proceedings from All-Division 5 Conference „Forest Products" Vol2*, p.203, 23.–28. August 1992, Nancy.
2. Kucera L. J., Katuscak S.: *in Weinfelden: Holz-Farbe-Gestaltung, 4.-5. 11. 1992, Lignum Zürich* 1992, pp.43-52.
3. Avramidis S., Ellis S., Liu, J.: *Proceedings from All-Division 5 Conference „Forest Products" Vol.2*, 23–28 August 1992, Nancy.
4. Katuščák S. et al.: Res. Rep. 48/90, State For.Prod.Res. Institute Bratislava 1990.
5. Németh K.: Möbel und Wohnraum, Leipzig *38*, 121 (1985).
6. Plackett D. V., Dunningham E. A., Singh, A. P.: Holz als Roh- und Werkstoff *50*, 135 (1992).
7. Goncales J., Janin G., Keller R.: *Proceedings from „All-Division 5 Conference „Forest Products"*, Vol.1, 245, 23.–28. August 1992, Nancy.
8. Katuscakova G., Katuscak S.: Papir Celuloza *41*,41 (1986)
9. Bourgois J., Janin G., Guyonnet R.: Holzforschung *45*, 377 (1991).
10. Katuščák S., Katuščákova G.: Holzforschung *41*, 315 (1987)
11. Kucera L. J.: Institut für Wald- und Holzforschung ETHZ, Fachbereich Holzkunde und Holztechnologie, Zürich 1986.
12. Nováková E: *Diploma thesis*, STU, Bratislava 2007
13. Sparrow G. R., Mishmash H. E.: *ASTM STP 643, N. S. McIntyre,* Ed., American Society for Testing and Materials, 1978, pp. 164–1 81.
14. Bursikova V., St'ahel P., Navratil Z., Bursik J., Janca J.: *Surface Energy Evaluation of Plasma Treated Materials by Contact Angle Measurement.* Masaryk University, Brno, 2004.
15. Šimor M., Rahel J., Vojtek P., Brablec A., Černák M.: Appl. Phys. Lett. *81*, 2716 (2002)
16. Rehn P., Wolkenhauer A. et al Surf Coat Technol *174–175*, 515 (2003).

P27   EVALUATION OF EFFIENCY, RELEASE AND OXIDATION STABILITY OF SEABUCKTHORN MICROENCAPSULATED OIL USING FOURIER TRANSFORMED INFRARED SPECTROSCOPY

MONICA TRIF and CARMEN SOCACIU

Department of Chemistry and Biochemistry, University of Agricultural Sciences and Veterinary Medicine, Cluj-Napoca, 400372, Romania
monica_trif@hotmail.com

Introduction

Alginate and *k*-carrageenan are seaweed carbohydrate biopolymers commonly used in bioencapsulation.

The high content of polyunsaturated fatty acids, carotenoids and other oxygen sensitive lipid molecules make seabuckthorn oil susceptible to oxidation, limiting its application. This paper examines the microencapsulation efficency, the release and oxidation process of seabuckthorn oil encapsulated in ionotropically crosslinked alginate-carrageenan complex beads, using the Fourier transformed infrared (FTIR) spectroscopy.

Experimental

Sodium alginate (SA) was purchased from Promova, k-carrageenan (k-Car) from Danisco, calcium chloride (CaCl$_2$) from Sigma Aldrich, sea buckthorn oil (SBO) was extracted from the fruits of sea buckthorn, which were collected from Transilvania region, Romania.

Beads Preparation

SA (0.75 %, w/v) and *k*-Car (0.75 %, w/v) were dissolved in de-ionized water and were used to encapsulate the SBO by ionotropically cross-linked gelation. The SBO-SA-*k*-Car emulsion obtained was dropped using a syringe with a needle (0.4 × 20 mm) into a hardening bath 2% (w/v) solution of CaCl$_2$ in water.

Microscopy

Images of emulsions at magnification 10 × were obtained using an inverted microscope Olympus, with a digital camera.

FTIR-ATR measurements

The FTIR spectra were obtained with a Fourier transform spectrometer (PerkinElmer), equipped with ATR. The oxidation process induced by UV light (254 nm) after 1, 4 and 6 hours was monitored calculating the ratios between absorbance of some relevants spectral bands of free and encapsulated oil.

Encapsulation Efficiency (EE %) of the SBO

EE % was calculated taking into consideration the amount of β-carotene contained by SBO, before and after encapsulation. The amount of β-carotene was assayed spectrophotometrically at 454 nm using tetrahydrofuran (THF) as solvent, and also as a solvent to extract β-carotene from beads. The formulae (1) was used:

$$EE \% = C_1/C_2 \times 100, \qquad (1)$$

where: C_1 = β-carotene concentration content in the SA-*k*-Car beads [mg dm^{-3}] and C_2 = β-carotene concentration in SBO before encapsulation [mg dm^{-3}].

Carotenoids Release Rates Measurement from Beads

Control release of carotenoids contents fom beads in different solvents: methanol, hexane and THF were measured spectrophotometrically. The absorption spectra were obtained with a Jasco UV-VIS spectrometer the range 300–500 nm.

Results

Emulsion stability evaluations. The microscopic imaging of the SBO-SA-*k*-Car emulsion used for encapsulation reveals the presence of polydisperse oil droplets with sizes between 20–50 μm (Fig. 1.a.).

Beads characterization. Orange beads obtained from the emulsion had a diameter between 2–3 mm and spherical shapes were obtained (Fig. 1.b.).

Encapsulation efficiency of the oil. β-carotene content of SBO oil was 1.212 mg dm^{-3}. The β-carotene content in the SA-*k*-Car beads was 1.1964 mg dm^{-3}, showing that the EE% of β-carotene in beads was 98.71 %.

Carotenoid release rates measurement from beads. The carotenoid release rate was substantially slower in hexane than in the case of the methanol and the best release was obtained into THF (Fig. 1. c.). THF was demonstrated to be one of the best solvents to extract carotenoids, as mentioned elsewhere.

FTIR-ATR measurements. FTIR spectra of SBO, SA, *k*-Car and SA-*k*-Car blank beads are shown in Fig. 1.d..

The SA spectrum showed the characteristic peaks at 3242 cm^{-1} (OH$^-$ stretching), 1,596 and 1,407 cm^{-1} (COO$^-$ asymmetric and symmetric stretching), 1,081–1,024 cm^{-1} (C−O−C antisymmetric stretching), and carboxyl and carboxylate at about 1,000 to 1,400 cm^{-1}. The sign of O−H deformation of water is evident near band 1,640 cm^{-1} in all spectra.

FTIR spectrum of *k*-Car powder showed various distinct peaks: 3,514 cm^{-1} due to polyhydroxy (OH)n group; 2,953, 2,911 and 2,894 cm^{-1} due to the C−H stretch; 1,474 and 1,400 cm^{-1} due to C−H deformation; 1,223 cm^{-1} due to the S=O stretch of sulfate ester salt; 1,063 cm^{-1} C−O stretch of cyclic ethers; 924 cm^{-1} due to the C−O stretch of polyhydroxy groups attached to carbons.

In FTIR spectra of SBO some of the most significant bands are the following[1,2] the band at 3,485 cm^{-1} is assigned to the overtone of the glyceride ester carbonyl; band appearing at 3,005 cm^{-1} in the spectrum to the CH stretching of =C−H bonding; the two intensive bands at 2,922 and 2,853 cm^{-1} are assign to the aliphatic CH$_2$ asymmetric and symmetric

a

b

c

d
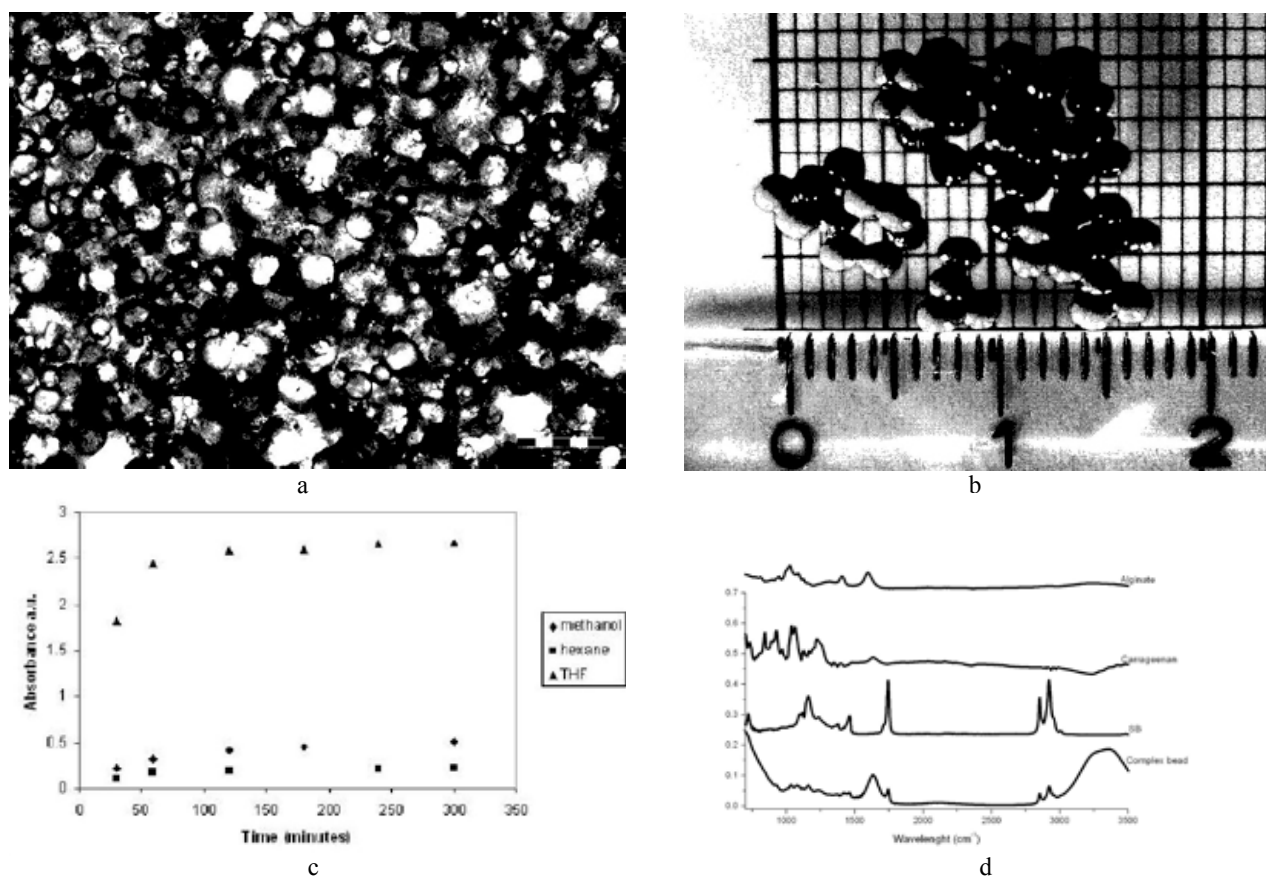
Fig. 1.   **a – the microscopic imaging of the SBO-SA-k-Car emulsion, b – SA-k-Car beads with SBO, c – carotenoid release rates measurement from beads, d – FTIR spectra of SBO, SA, k-Car and SA-k-Car blank beads**

stretching vibration, respectively; the band at 1,744 cm^{-1} is assigned to the C=O stretching vibration of the ester carbonyl functional group of the triglycerides; at 1,464 cm^{-1} is observed a band which is assigned to C=H scissors deformation vibration; the band near 1,377 cm^{-1} is assign to the bending vibration of CH$_2$ groups; the bands at 1,160 and 1,236 cm^{-1} are assign to the vibration of the C−O ester groups and CH$_2$ group.

We considered as markers of oxidation processes in SBO, the following ratios between absorbances of these important bands: $A_{2,853}/A_{3,005}$, $A_{2,853}/A_{1,744}$, $A_{2,853}/A_{1,160}$, $A_{1,744}/A_{3,005}$, $A_{1,377}/A_{3,005}$, $A_{1,160}/A_{3,005}$.

According to observations made by Guillen et al.[2], the values of ratios between absorbances of some important bands which are parameters of the oxidation level indicate a second or third stage oxidation of the pure oil comparing with the first stage of oxidation of encapsulated oil.

Conclusions

A good encapsulation efficency of 98.71 % was obtained for SBO in SA-*k*-Car complex, and the best release in THF. Encapsulation in SA-*k*-Car improved SBO stability. The encapsulated oil showed better stability against oxidation, as indicated by FTIR markers.

REFERENCES

1. Guillen M. D.and Cabo N., J. Agric. Food Chem. *47*, 709, (1999).
2. Guillen M. D.and Cabo N., J. Agric. Food Chem. *80*, 2028 (2000).

P28 ¹³C NMR SPECTROSCOPY OF HUMIC ACIDS ECTRACTED FROM INCUBATED PLANT RESIDUES IN HAPLIC LUVISOL

ANTON ZAUJEC[a], JOZEF ŠIMA[b], JURAJ CHLPÍK[a], NORA SZOMBATHOVÁ[a] and ERIKA TOBIAŠOVÁ[a]

[a]*Department of Pedology and Geology, Agricultural University of Nitra, Tr. A. Hlinku 2, 949 76 Nitra, Slovakia,* [b]*Department of. Inorganic Chemistry, Slovak Technical University of Bratislava, Radlinskeho 9, 812 37 Bratislava, Slovakia*
Anton.Zaujec@uniag.sk

Introduction

The humic acid (HA) plays an important role in determining soil characteristics by influencing its chemical, physical, and biological properties. Content of soil organic matter in soil is a reflection on the decomposition of existing humus and the formation of new humic substances from plant and animal remains. The chemical composition of post-harvest residues which is very important factor of formation of humic substances, as well as their physico-chemical properties should be taken into account Gonet and Debska[3]. The application of ¹³C-NMR spectroscopy to the study of humic substances in soils and sediments has been reviewed by Chukov[2]. In this study, the reliability of the analyses was assessed the relative abundance of different HA carbon types, derived from NMR spectra.

Experimental

Post-harvest residues with different chemical composition were used as sources of organic matter in model incubation experiment, at temperature 23–25 °C, in a constant humidity of 60 % for period one years. A laboratory incubation experiment was carried out in pots with and without the soil according to following scheme:

Variant	(symbol) materials
LO	Haplic Luvisol (soil)
WR	Wheat residues (straw and roots, 4 : 1 ratio)
LO+WR	Soil + wheat residues (LO to WR = 10 : 1)
AA	Alfalfa (hay and roots, 1 : 1.5 ratio)
LO+AA	Soil + alfalfa residues (LO to AA = 10 : 1)
MR	Maize (straw and roots, 2 : 1)
LO+MR	Soil + maize residues (LO to MR = 10 : 1)
GM	Green manures residues (oat and vetch, 3 : 1)
LO + GM	Soil + green manures (LO to GM = 10 : 1 ratio)

Humic acids (HA) were extracted, purified and measured ¹³C-NMR spectra method´s published by Zaujec et al.[6]. The relative carbon distribution was determined by integration of the signal intensity in the different chemical shift regions using an adapted integration routine supplied with the instrument software. For quantification, the spectra were used chemical shift regions described by Knicker and Ludemann[4] and Wilson[5].

Table I
Relative intensities [% of total area] for the ¹³C NMR signals of humic acids

Spectral region/ samples of HA	Alkyl-C [%]	O-alkyl-C [%]	Aryl-C [%]	Carboxyl-C [%]
LO	17.9	20.3	37.6	24.1
WR	11.3	38.1	40.3	10.3
LO + WR	17.9	27.8	36.3	18.0
AA	17.2	33.5	33.9	15.4
LO + AA	21.6	22.2	33.1	23.1
CM	17.4	33.9	36.5	12.2
LO + MR	20.7	24.7	34.1	20.4
GM	14.2	30.8	38.9	16.1
LO + GM	20.9	26.9	32.9	19.3

Results

The HA chemical composition is evaluated from the intensity distribution among the chemical region of the different functional groups in the NMR spectra. The spectra are dominated by the signal in the chemical shift region (110–160 ppm) of aromatic/olefinic C (32.9–40.3 %) and O/N-alkyl C (20.3–38.1 %) followed by that of carboxyl/amid C (10.3–24.1%) and alkyl C (11.3–21.6 %).

Extracted HA's, called "young", from incubated plant residues are characterised by significantly higher proportions of O-alkyl C (mean content 34.08 ± 3.02 %), mainly derived from hemicellulose and cellulose than HA of variants with soil (25.41 ± 2.48) and Haplic Luvisols (Table I). These data refer to an enrichment of aromaticity of HA from Haplic Luvisol relative to the HA from incubated crop residues with Haplic Luvisol or crop residues, O-Alkyl C has been degraded preferentially. The first finding is in agreement with the lignin results, indicating that crop residues are mainly composed of remaining more resistant plant tissues that have already lost part of their polysaccharide-C structures.

Based on indexes of aromaticity (α) we found Zaujec

Table II
Evaluations parameters of humic acids

Samples of HA	ID (+)	Change of ID	α (++)	alkyl-C+aryl-C/ O-alkyl-C+ carboxyl-C
LO	0.880	100%	49.6	1.249
WR	0.297	33.7	44.9	1.066
LO + WR	0.653	73.1	44.3	1.184
AA	0.513	58.3	40.1	1.045
LO + AA	0.973	110.5	43.1	1.208
CM	0.513	58.3	41.6	1.169
LO + MR	0.938	95.2	42.9	1.216
GM	0.461	52.4	46.4	1.132
LO + GM	0.779	88.5	40.7	1.164

(+) ID = Index of decomposition = (alkyl-C/O-alkyl-C)
(++) α = (aryl-C/alkyl-C + O-alkyl-C + aryl-C).100 (%)

et al.[6] that aromaticity of the HA from incubated crop residues increased as humification progressed. Ratios of alkyl C to O-alkyl C were calculated by Baldock et al.[1] as indicator for decomposition process of organic matter in soils.

The major changes that occur in an NMR spectrum after decomposition of plant residues are a decrease in carbohydrates, an increase in the relative proportion of alkyl (aliphatic chains) and carboxyl C, and partial breakdown of lignins. The relative degree of aromaticity among the HA's appears to vary as a function of the humification process. The carboxyl content and the aromaticity increase with humification. This tendency is also consistent with the nmR results discussed above and with the analytical data.

Conclusions

Comparison of the ¹³C-NMR spectra of the samples HA extracted from incubated plant residues and organic matter applied to Haplic Luvisols after incubation indicates that those from plant residues show a higher intensity in the aromatic C and O/N-alkyl C regions and a lower proportion of alkyl C and carboxyl C. The nmR spectra show that the aromaticity of humic acids extracted from incubated plant residues slowly increases during the humification process (Table II). New formed HA from humified plant residues, mainly wheat residues, decrease decomposition index and values of ratios alkyl-C + aromatic-C/O-alkyl-C + aromatic-C.

REFERENCES

1. Baldock J. A., Oades J. M., Nelson P. N., Skene T. M., Golchin A., Clarke P.: Australian J. Soil Res. *35*, 1061 (1997).
2. Chukov S. N.: Eur. Soil Sci. *31*, 979 (1998).
3. Gonet S. S., Debska B.: Rostl. Vyr. *45*, 455 (1999).
4. Knicker H., Ludemann H. D.: Org. Geochem. *23*, 329 (1995).
5. Wilson M. A.: *nmR Techniques and Application in Geochemistry and Soil Chemistry.* Pergamon Press, Oxford 1987.
6. Zaujec A., Šíma J., Liptaj T.: Procceedings of 8th Meeting of the Intern. Humic Subst. Soc.: The role of Humic Substances in the Ecosystems and Environmental Protection (Drozd J. et al., eds.), p.207. PTSH Wroclaw 1997.

L18   HS-SPME AND GC-MS AS VALID TOOLS TO ASSESS VOLATILE ORGANIC COMPOUNDS FROM SOIL NATURAL ORGANIC MATTER

C. DE PASQUALE, R. FODALE, M. GIULIVI, P. CONTE and G. ALONZO

ITAF Department – Università di Palermo Ed. 4 viale delle Scienze, 90128, Palermo, Italy
c.depasquale@unipa.it

Introduction

Humic acids (HAs) which are involved in almost all physical, chemical, and biological processes occurring in soil system[1,2] represent the most abundant fraction of soil organic matter. In particular, HAs are well known to be very active in interacting to various extents and modalities with a variety of organic and inorganic chemical contaminants[3]. Knowledge of the composition, structure, and functionalities of HAs is therefore, essential for the understanding of their chemical behavior and reactivity in environmental matrices.

Chemical analyses on HAs are traditionally done by chromatographic and spectroscopic techniques. Recent advances in the chemistry of humic substances, revealed that a detailed characterization can be better achieved when a separation of the different components is obtained[4]. Here we suggest head space solid-phase micro-extraction (HS-SPME) coupled with gas-chromatography/mass spectrometry (GC-MS) as a new analytical tool for the characterization of the volatile components released from humic substances at 80 °C.

Materials and Methods

S o i l

Two surface horizons were sampled from the ancient caldera of Vico (nearby Rome) and Monte Faito (Naples) in Italy. Detailed characterization of the two soils are reported elsewhere[5].

HA Extraction

Humic acids (HAs) were extracted by using common procedures[6]. Namely, 100 g of each soil were suspended in 500 ml of 1M NaOH and 0.1M $Na_4P_2O_7$ and centrifuged at 7,000 rpm for 20 min. The supernatant was then treated with 37% HCl until pH 1 was reached to precipitate HAs. Humic acids were purified by a series of dissolutions in 1M NaOH followed by flocculations in 6M HCl. Each HA was then shaken twice in a 0.25M HCl/HF solution for 24 h, dialyzed agaist distilled water till Cl-free and freeze-dried.

CPMAS ^{13}C-NMR Spectroscopy

CPMAS ^{13}C-NMR experiments were performed on a Bruker Avance 400 spectrometer operating at 100.6 MHz on carbon-13 and equipped with a 4 mm standard bore solid state probe. The rotor spin rate was set at 13,000 Hz. Samples were packed in 4 mm Zirconia rotors with Kel-F caps. A contact time of 1 ms, a recycle delay of 2 s, an acquisition time of 35 ms and a RAMP sequence to account for inhomogeneities of the Hartmann-Hahn condition at high rotor spin rates were used. Spectra acquisition was done with Topspin 2.0, whereas data elaboration was done with Mestre-C 4.9.9.9 by using a line broadening (LB) of 50 Hz and an automatic baseline correction with a 3rd order polynomial and Bernstein algorithm. Semi-quantitative results were obtained by integrating the spectral regions in the intervals 184–159 ppm (COOH), 159–110 ppm (aromatic C), 110−88 ppm (anomeric C), 88–62 ppm (C−O), 62–48 ppm (C−N) and 48–0 ppm (alkyl C). All the areas were normalized to the total spectral areas and content percent was obtained.
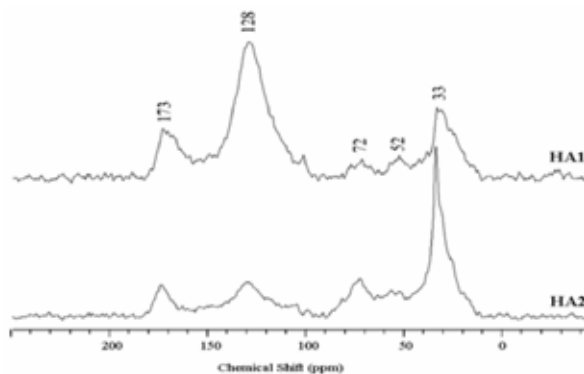
Fig. 1.   **CPMAS ^{13}C-NMR spectra of the two humic acids used in the present study**

H S - S P M E   E x t r a c t i o n

A polydimethylsiloxane fiber (PDMS 100 µm, Supelco, Bellefonte, PA – USA) was used to sample the head space in equilibrium with 20 mg of the two HAs placed in 15 ml glass vials. These were sealed with a poly(tetrafluoroethylene) silicon septum-lined cap (Supelco, Bellefonte, PA, USA) and heaten 30 min at temperatures of 80 °C. The sampling time for was 5 min maintaining the 80 °C temperature.

G C - M S   A n a l y s i s

The gas-chromatographic analyses were run on a Hewlett-Packard 5890 GC system interfaced with a HP 5973 quadrupole mass spectrometer. A HP5–MS column was used (5% diphenyl − 95% dimethylpolysiloxane 30 m × 0.2 mm, 0.25 µm film, J & W Scientific, Folsom CA, USA). The fibre was manually inserted in a GC inlet port equipped with a specific glass liner for SPME injection (0.75 mm i.d.). Analyses were carried out in splitless mode with helium as carrier gas at 1 ml min^{-1}. Chromatographic conditions were: injector temperature 250 °C, oven temperature program: 1 min at 60 °C followed by a linear temperature increase of 5 °C min^{-1} up to 280 °C held for 15 min. The MS full-scan conditions were: source temperature 230 °C, interface temperature 280 °C. The electron impact ionization spectra were obtained at 70 eV, recording mass spectra from m/z 40 to 550.

Results and Discussion

The HS-SPME extraction method allowed the identification of 31 chemical components in each HA. Analyses at different temperatures have been done (data not repoted).

The optimal temperature conditions for the qualitative discrimination of HAs 80 °C giving a relative standard deviation [RSD, %] of ≤10 % for each identified component. Moreover, the amount of volatile components sampled in the head space was significantly representative of the whole HA systems as assessed by analyses with icreasing HA material. Table I reports the class of substances identified over the two solid state humic acids. Eight classes of organic compounds were discriminated. Among those, the largest contribution was from aromatic materials. In fact, HA1 revealed 66.77 % of aromatic moieties in the volatile mixture, whereas HA2 was 81.55 % (Table I). The amount of volatile aromatic molecules in HA1, smaller than in HA2, appears at variance with the content of aromatic systems obtained from CPMAS ^{13}C-NMR spectroscopy (Fig. 1, Table II). The aromatic C content by NMR (159–110 ppm) was the largest in HA1, thereby leading to the hypothesis that such material should produce a larger amount of volatile aromatic components than HA2. The contradictory HS-SPME GC-MS and CPMAS ^{13}C NMR results could be explained by considering the different natures of the soils from which the HAs were extracted. In fact, HA1 was extracted from a buried soil whereas HA2 was obtained from a surface horizon of a different volcanic soil. Organic material in buried conditions undergoes to anaerobic and abiotic degradation. Conversely, aerobic and biotic transformations occur in organic materials placed on surface soil horizons. The abiotic degradation in anaerobic conditions may produce highly condensed aromatic systems. Due to the larger molecular size of the condensed aromatic substances in HA1, these are less available for head space sampling

Table I

Composition of the volatile components released by the two HAs at 80 °C. The compounds were grouped according to their functional groups. The reported correspondent percent amounts [%] of identified compounds are the medium value of three different chromatographic analyses

	Content [%]	
Compounds	HA1	HA2
Acids	18.64	7.30
Aldehydes	3.56	1.19
Ketones	1.36	0.00
Alcohols	0.53	0.40
Amines	0.57	0.40
Olephins	1.21	1.11
Aromatics	66.77	81.55
Alkanes	7.19	8.27

than the corresponding aromatic systems formed in aerobic and biotic transformations. Except for the aromatic moieties which were in disagreement when comparing the gas-chromatographic data with the NMR results, the remaining components be have similarly. In fact, Tables I and II report the same trends for all the relative amounts revealed by the two analytical techniques used in the present study.

Conclusions

In the present study we used a new analytical tool for the characterization of the volatile components in humic substances. Results showed that the amount of volatile aromatic moieties was depending on the nature and genesis of the soils from which the HAs were extracted. Moreover, a number of fatty acids, as well as alkane-systems were also found in the head space in equilibrium with the solid humic substances. The relevant novelty was that we expected fatty acids and hydrophobic alkanes to be confined mainly inside the hydrophobic and chemically protected core of the supramolecular humic acids. For this reason the volatilization to the head space was thought to be difficult. Conversely, our findings appeared to confirm CPMAS ^{13}C NMR results from Conte and Berns (2008)[7] which described the conformation of humic substances as made mainly by a hydrophobic aromatic core surrounded by long carbon chains. The HS-SPME-GC-MS technique appears to be a very promising tool in obtaining relevant information on the lighter fraction of organic components weakly bound to humic materials.

REFERENCES

1. Schulten H.-R.: Fresenius' J. Anal. Chem. *351*, 72 (1995).
2. Shevchenko S. M., Bailey G. W., Akim L. G.: J. Mol. Struct. *460*, 179 (1999).
3. Pignatello J. J.: Adv. Colloid Interface Sci. *76–77*, 445 (1998).
4. Conte P., Spaccini R., Piccolo A.: Anal. Bioanal. Chem. *386*, 382 (2006).
5. Conte, P., Piccolo, A., van Lagen, B., Buurman P., De Jager, A.: Geoderma *80*, 327 (1997).
6. Stevenson, F. J.: *Humus Chemistry: Genesis, Composition, Reactions*, 2nd ed. Wiley, New York, 1994.
7. Conte P., Berns A. E.: Anal. Sci. 2008 accepted.

Table II
Content [%] by CPMAS ^{13}C NMR of the different groups in HAs

Soil humic acid	COOH	Aromatic C	Anomeric C	C−O	C−N	Alkyl C
	184–159 ppm	159–110 ppm	110–88 ppm	88–62 ppm	62–48 ppm	48–0 ppm
HA1	12	55	5	4	4	21
HA2	9	21	3	14	8	45

8.　POLYMERS & POLYMER COMPOSITES

8.1. Lectures

L01　THE WAY OF STEREOREGULARITY DETERMINATION OF POLYPROPYLENE

ADAM HOZA[a], JAN KRATOCHVÍL[a,b] and SOŇA HERMANOVÁ[a]

[a]*Institute of Materials Science, Faculty of Chemistry, Brno University of Technology, Purkyňova 118, 612 00 Brno, Czech Republic,*
[b]*Polymer Institute Brno, Ltd., Tkalcovská 36/2, 656 49 Brno, Czech Republic,*
xchoza@fch.vutbr.cz

Introduction

Polypropylene (PP) is an important member of the family of the most worldwide produced thermoplastics namely because of its specific properties involving easy processability, low specific gravity and low production cost. One of the key molecular parameters defining physico-chemical properties of PP is the stereoregularity of the polymer chains, i.e. tacticity. It is well known that heterogeneous Ziegler-Natta catalytic systems due to a multiple-site character of active species produce PPs with varying degree of stereoregularity[1]. Since the stereoregularity of polymer chain has an important influence on mechanical properties of PP product, the accurate assessment of PP stereoregularity (isotacticity) is an important task. Stereoregularity can be characterized by isotactic index.

Several methods of PP isotactic index determination differing in principle, complexity of a measurement procedure and an information capability are known from the literature. The most common method used for determination of the isotactic index is an extraction by hydrocarbon solvents (e.g. pentane, hexane, heptane, and octane) at their boiling point[2].

Another method is based on a solubility of the atactic PP in hydrocarbons. Neat PP is divided into fractions (i.e. soluble and insoluble one) by complete dissolving it in high temperature boiling solvents (xylene, decahydronaphthalene (decalin), and 1,2,3,4-tetrahydronaphthalene (tetralin)) and cooling polymer solutions down to 23 °C[3].

Moreover, stereochemical structure of PP can be determined directly by ^{13}C-NMR or after separation of atactic part by extraction or solubility method. Some authors evaluate the PP stereoregularity via crystallinity determined by DSC[4].

The aim of this work was to evaluate and compare several extraction and solubility methods of the isotactic index determination, applied on the PP homopolymer. A series of nine PP homopolymer samples in a powder form having molecular weights in the range from 156×10^3 to 910×10^3 g mol^{-1} was fractionated using both these methods and the results were compared.

Experimental

Studied polymer samples were kindly supplied by PIB Company; a sample denoted as H4b, 17.5.06, was supplied by Chemopetrol. Characteristics of the samples are summarized in the Table I. Polymerizations were carried out in the 50 dm^3 reactor at propylene pressure of 2.2 MPa for 1 h. Typical polymerization conditions were: high-yield Ziegler-Natta MgCl$_2$-supported catalyst, co-catalyst triethylaluminium (TEA), electron donor dicyclopentyldimethoxysilane (DCPDMS), Al/Si/Ti = 60/6/1 mol/mol/mol, polymerization temperature 75 °C.

Table I
Characteristics of PP samples

Sample	M_w [kg mol^{-1}]	M_w/M_n	MFI$_{21 N}$, 230 °C [g 10 min^{-1}]	Flexural modulus [MPa]
H556	910	5.9	0.16	1,545
H526	509	5.3	0.92	1,560
H464	309	4.4	15.8	1,608
H460	289	5.6	21.7	1,624
H433	236	5.2	42.9	1,670
H449	207	5.3	104.4	1,716
H435	156	5.3	291.3	1,756
H4b, 17.5.06[*]	344	4.7	3.5	1,420
H420[**]	233	5.3	22.5	1,220

F r a c t i o n a t i o n　M e t h o d s

A modified Kumagawa extractor was used for the fractionation according to the ISO 9113 : 1993 Standard. The extractions were carried out on 5 g of polymer sample in a powder form. The extraction time was 6 h. The soluble fractions were recovered by evaporating the solvent.

The solubility assessment was carried out according to ISO 6427 : 1982 (E), Annex B Standard. Polymer sample (1.25 g) was completely dissolved during 1 h in o-xylene (125 ml) at its boiling point of 144.4 °C, and in tetralin (125 ml) at 160 °C yielding 1 % wt. solutions. 2 g of PP sample was completely dissolved in decalin (100 ml) at 160 °C during 1 h and 2 % solution was obtained. The solutions were cooled down to 23 °C, and kept at that constant temperature for 18 h. After centrifugation, the insoluble fraction was collected by filtration. The soluble fraction was recovered by evaporating the filtrate. First, fractionations of a standard PP sample were performed by both methods; ten runs were carried out to evaluate the reproducibility of results. The reproducibility of the amount of fractions obtained from original PP using the extraction method was ± 0.09 %. The reproducibility of results of ± 0.13 % obtained by the solubility method was very good as well.

C h a r a c t e r i z a t i o n　M e t h o d s

^{13}C-NMR spectra were recorded on a 500 MHz Bruker DRX spectrometer operating at 125 MHz. The

pulse angle was 83 °, pulse interval 20 s, decoupling Waltz 16.

PP melting points were measured with a Perkin-Elmer DSC-7 apparatus. The polymer sample was in the form of thin square-shape films of the weight of about 5 mg. Measurements were carried out using the aluminum pans in the temperature range from 40 °C to 200 °C under N_2 atmosphere (70 ml min⁻¹). The used procedure conditions were as follows: *(i)* heating from a room temperature to 200 °C at a rate 40 °C min–1, *(ii)* 10 min isothermal period at 200 °C, *(iii)* air cooling to 35 °C, and *(iv)* heating to 200 °C at a rate 10 °C min⁻¹. The second heating data were used for the analysis.

The molecular weight averages (M_n, M_w, and M_z) and the index of polydispersity (M_w/M_n) of PP and its fractions were determined using a PL-GPC 220 high temperature chromatograph (Polymer Laboratories) equipped with three PL gel 10 μm MIXED-B columns set and two detectors (PL–220DRI and VISCOTEC 220R). Calibration was done with polystyrene standards (Waters and Polymer Laboratories) using 1,2,4-trichlorobenzene solvent (LiChrosolv, Merck) containing 0.025 % Santonox R at a flow rate of 1 cm³ min⁻¹ and 160 °C. The polymer samples were measured as a 0.1 % wt. solution in a mobile phase.

Table II
Isotactic index determination by extraction

Sample	Isotactic index [%]		
	pentane	hexane	heptane
H4b, 17.5.06	99.28	98.86	96.21
H449	99.08	98.56	95.03
H460	99.15	99.05	96.54
H640	99.21	99.09	96.82
H435	98.63	98.40	94.46
H433	99.23	99.15	96.92
H526	99.35	99.32	98.07
H556	99.17	98.84	97.61
H420	98.70	98.26	94.15

Results
I s o t a c t i c   I n d e x   D e t e r m i n a t i o n   b y
E x t r a c t i o n

A series of nine PP samples was extracted by three refluxing n-alkane solvents (pentane, hexane, and heptane). Each extraction yielded two fractions; the soluble, and the insoluble one. Extraction by octane was not completed because of partial swelling of PP material on the glass frit. Isotactic indexes of PPs were calculated from the amount of insoluble fractions (see Table II) It was found out that the isotactic index of all the examined PP materials decreased with increasing boiling point of the solvent used for the extraction procedure. Thus, the use of alkane with increasing boiling point caused an increase of the weight percent of material removed from the original polymer sample.

Fractions of the representative PP sample H420 obtained by both kinds of separation methods were precisely analyzed using the ¹³C-NMR, DSC, and SEC methods. The insoluble fraction of PP sample consisted of isotactic PP, whereas the soluble one comprised mostly atactic PP. The contents of mmmm pentads present in insoluble fractions were in the range of 93.6–95.5 %, which means that insoluble fraction contains mainly high molecular weight isotactic PP. It was found out that with increasing boiling point of the solvent, the soluble fraction was enriched by low molecular weight isotactic PP, and so-called stereoblocks. An increased content of higher molecular weight atactic PP chains was observed as well.
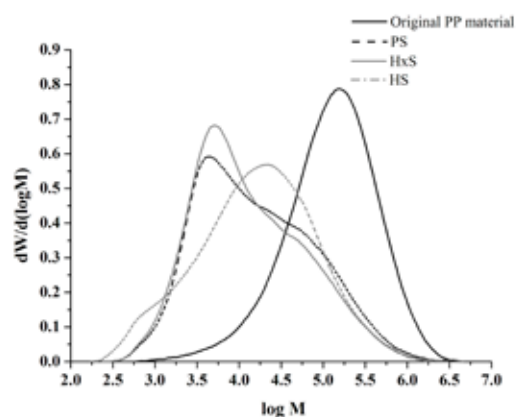
Fig. 1.   **Molecular weight distribution of the representative PP sample H420 and of the soluble fractions obtained by extraction with pentane (PS), hexane (HxS) and heptane (HS)**

From the shape of the MWD curve of soluble fractions (see the Fig. 1) it is evident, that pentane and hexane dissolved mainly low molecular weight polymer chains from the original sample. These low molecular weight chains appeared to be short chains of a-PP and short chains of i-PP. Hexane is characterized by slightly higher extraction efficiency in comparison with pentane by 0.4 % wt.

On the other hand, heptane extractable fraction was significantly higher (5.8 % wt.) and contained a much higher portion of high molecular weight chains, mostly of an atactic and stereoblock structure. An asymmetric shape of the distribution curve in the area of the lowest molecular weights is evidently an artefact, caused either by a contamination of the sample during preparation or a measuring error of the SEC method. In the right manner, the distribution curves in the area of the lowest molecular weights for all the three solvents should coalesce.

Then, the fractions of representative sample H420 were characterized by the DSC method; melting points of insoluble fractions and crystallinity of soluble fractions were compared. Calculation of crystallinity α from values of ΔH obtained from the second heating cycle was done according to the equation:

$$\alpha = \frac{\Delta H_m}{\Delta H_m^*} \cdot 100 \quad , \qquad (1)$$

$\alpha = [\%]$

ΔH_m – melting enthalpy of measured sample

ΔH_m^* – melting enthalpy of 100% crystalline polypropylene, $\Delta H_m^* = 207 \, J g^{-1}$ ref.[5].

Fig. 2. shows melting points of insoluble fractions of the representative sample obtained by pentane, hexane and heptane extractions. A decrease of melting points due to increasing boiling point of the solvent is evident. It is probably caused by higher separation efficiency of solvents having higher boiling point. Consequently, a decrease of amount of shorter isotactic PP chains occurred.

From the values showed in the Fig. 3., a dependence of increasing crystallinity on increasing boiling point of the solvent was found out. PP fractions soluble in solvents with higher boiling point contain larger amounts of crystallizable short chains of isotactic PP.
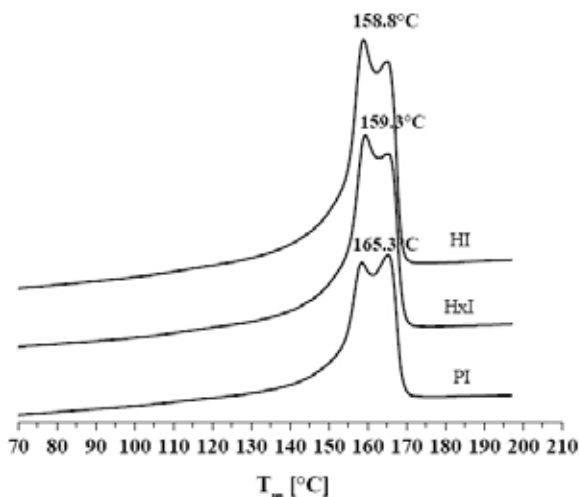
Fig. 2. **DSC melting curves of insoluble fractions of the representative sample H420 after extraction (PI pentane insoluble, HxI hexane insoluble, HI heptane insoluble)**
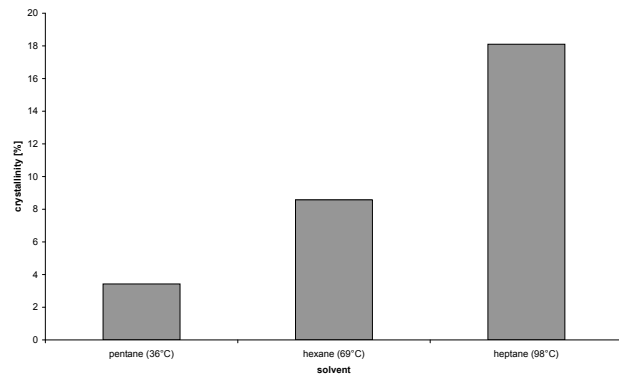
Fig. 3. **Dependence of crystallinity α (DSC) of extracted fractions of the sample H420 on the boiling point of the solvent used at extraction**

Table III
Determination of the soluble fraction content by the solubility method

Sample	Part of soluble fraction [%]		
	o-xylene	decalin	tetralin
H4b, 17.5.06	3.03	4.07	6.01
H449	2.43	3.42	4.54
H460	2.27	3.66	4.58
H640	2.23	3.10	4.83
H435	2.63	4.37	4.25
H433	2.07	4.06	3.19
H526	2.41	4.67	3.36
H556	3.30	5.01	4.30
H420	4.18	6.91	7.73

Determination of Soluble Fractions by Solubility Methods

PP samples were completely dissolved in three solvents (xylene, decalin, and tetralin) at increased temperature and after cooling at 23 °C, amounts of the fractions, which remained dissolved in solution, were determined. From these values, the contents of fractions, that remained dissolved after cooling the perfect solution of PP down to 23 °C, were calculated. The results are summarized in Table III. For all the PP samples, xylene soluble fraction was the lowest. Generally, it was not possible to specify the difference between the separative efficiency of decalin, and tetralin.
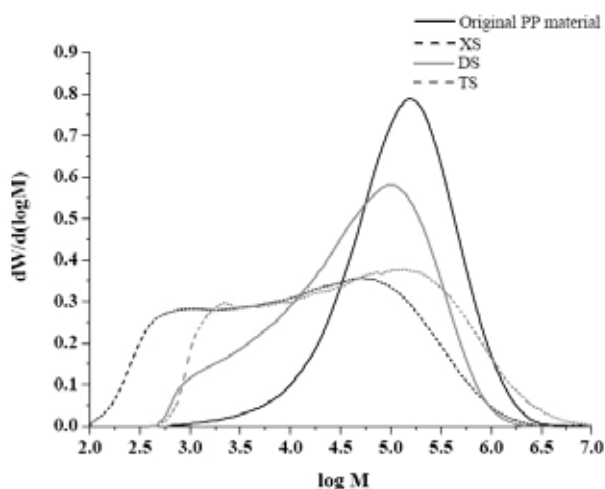
Fig. 4. **Comparison of molecular weight distribution of soluble fractions of the sample H420 obtained by solubility methods (XS = xylene soluble, DS = decalin soluble, TS = tetralin soluble)**

Characterizations of polymer fractions were carried out for the representative sample H420 by ^{13}C-NMR, SEC, and DSC methods again. A qualitative composition of soluble fractions determined by ^{13}C-NMR shows that fractions soluble in decalin and tetralin contain a higher part of longer

atactic chains as well as shorter isotactic chains and stereoblocks in comparison to o-xylene soluble fraction. Insoluble fraction was again marked as isotactic PP.

From the SEC results it is evident, that xylene soluble fraction had the lowest molecular weight part, followed by decalin soluble, whereas the tetralin soluble fraction had the highest content of a high molecular weight portion. The difference consists mainly in the area of higher molecular weights. On the other hand, the decalin soluble fraction contained a much higher portion of high molecular chains of predominantly stereoblock, partially crystalline character. The tetralin soluble fraction was characterized by a similar MWD curve as compared with the xylene soluble fraction, but it contained a portion of much higher molecular weight chains. Average molecular weight M_w of fractions, that remained dissolved, was the lowest for o-xylene, followed by decalin, and tetralin till almost the value of original sample (M_w = 233,000 g mol^{-1}, M_w/M_n = 5.3).

A narrowing of the molecular weight distribution was noted: the xylene soluble fraction had the broad molecular weight distribution (M_w/M_n = 43.5), followed by the tetralin soluble one (M_w/M_n = 34.6). The decalin soluble fraction had the narrowest molecular weight distribution (M_w/M_n = 12.2).

The presence of low molecular chains in the xylene soluble fraction is probably an artefact again.

Fig. 5. shows melting points of insoluble fractions of the representative sample obtained by solubility methods. Melting point values of insoluble fractions increased from decalin, followed by o-xylene to tetralin.

It corresponds with the crystallinity values (Fig. 6.), being the highest in the decalin insoluble fraction, followed by the xylene insoluble one, and the tetralin insoluble one. The tetralin insoluble fraction contained probably lower por-
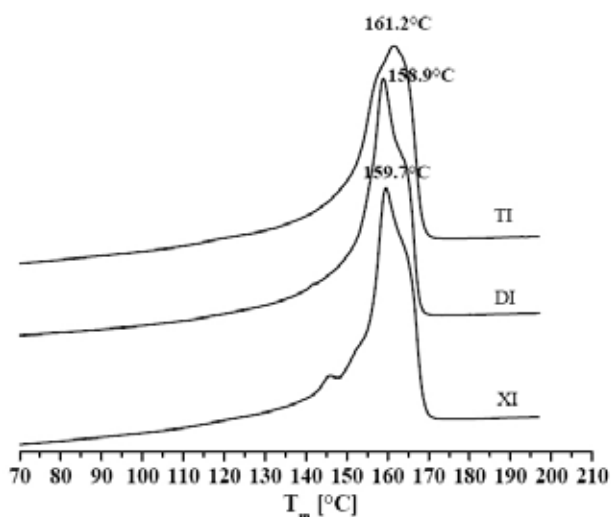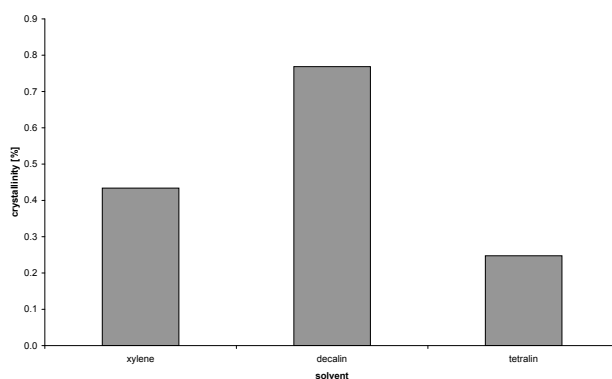
Fig. 6. **Dependence of crystallinity α (DSC) of soluble fractions of the representative sample H420 on the quality of the solvent**

tion of isotactic chains. It follows from the melting point of the tetralin insoluble fraction.

Fig. 6. shows the highest crystallinity in the case of the decalin soluble fraction, followed by the o-xylene soluble one, and the tetralin soluble one. It is probably because of the decalin insoluble fraction contained higher portion of low molecular weight isotactic chains being able to crystallize. It is also confirmed by the results of ^{13}C-NMR of the representative sample. The tetralin insoluble fraction contained the lowest part of chains able to crystallize.

The highest crystallinity of the decalin soluble fraction can be ascribed to a chemical similarity of decalin, and polypropylene molecules. In both cases, they are aliphatic hydrocarbons with a dominant presence of CH_2 and CH groups. Whereas, the molecule of tetralin is half aromatic and the molecule of xylene is fully aromatic.

Conclusions

Both kinds of fractionation methods provided very good reproducibility and good fractionation efficiency and can be recommended for determination of the isotactic index of PP.

By the extraction methods, a strong dependence of the isotactic index on the boiling point of the solvent was proved. The highest separative efficiency was found for heptane, which had the highest boiling point of all the solvents used for extractions. With using the high boiling point hydrocarbon (octane), a swelling of polymer sample happened and resulted in impassability of the frit and it was impossible to carry out the extraction. Results of analyses performed on the representative sample showed that increasing the boiling point of the solvent increases the portion of extractable longer atactic chains, shorter chains of i-PP and stereoblocks. Now separative efficiency of pentane, hexane, and heptane by extraction at the same temperature is being examined to prove a dominant influence of increasing temperature of boiling point of solvent on isotactic index.

Results of the solubility methods evaluation showed that the lowest content of the soluble fraction for all the samples under examination was obtained with use of o-xylene. At the same time, this part contained the lowest portion of isotac-

Fig. 5. **DSC melting curves of insoluble fractions of the representative sample H420 (XI xylene insoluble, DI decalin insoluble, and TI tetralin insoluble fraction)**

tic PP (measured by the presence of mm triads and mmmm pentads by ^{13}C-NMR). Decalin and tetralin showed higher separative efficiency than xylene and also dissolved a higher portion of partially isotactic or stereoblock chains. From the results of analyses, it is evident that in contrast to decalin, which dissolves significantly higher volume of high molecular weight isotactic or stereoblock chains, the efficiency of tetralin and xylene to separate the shorter and also the longer chains is almost the same. It results in a broad molecular weight distribution of soluble fractions.

Upon the performed separations and determination of their structure, the solubility methods using o-xylene, and tetralin at 23 °C can be suggested as the most correct for the determination of the isotactic index. All the other examined methods include an indispensable amount of isotactic or stereoblock chains in separated part of PP.

REFERENCES

1. Virkkunen V., Laari P., Pitkänen P., Sundholm F.: Polymer *45* (2004).
2. Kawamura H., Hayashi T., Inoue Y., Chûjô R.: Macromolecules *22* (1989).
3. Lehtinen A., Paukkeri R.: Macromol. Chem. Phys. *195*, 1539 (1994).
4. Philips R. A., Wolkowicz M. D.: *Structure and Morphology. Polypropylene Handbook (Moore, E.P.)*, Carl Hanser Verlag, Munich, Vienna, New York (1996).
5. Bicerano J.: J. Macromol. Sci. – Rev. In Macromol. Chem. and Phys. *C38*, 391 (1998).

L02 THE CRYSTALLIZATION KINETICS IN SEMICRYSTALLINE NANOCOMPOSITES

KATEŘINA HYNŠTOVÁ, JAN KALFUS and JOSEF JANČÁŘ

Institute of Materials Chemistry (IMC), Faculty of Chemistry, Brno University of Technology, Purkynova 118, 612 00, Brno, Czech Republic
xchynstova@fch.vutbr.cz

Introduction

Polyolefins represent the most important commodity plastics used in broad range of applications. In majority of cases, their processing is based on the melting step followed by cooling down in various forms and shapes. Properties of semicrystalline polymers are greatly affected by their morphology and, hence, the process of crystallization is of primary importance. High density polyethylene (HDPE) is a semicrystalline polymer with high portion of crystalline phase. The amorphous and crystalline lamellar regions are organized into the spherulites of approximately spherical shape[1,2].

Below the melting point, nuclei start to appear in the polymer melt due to the density fluctuations. These local volumes of higher molecular order growth with a rate well described by the Lauritzen – Hoffman surface nucleation theory[3,4]. According to the Lauritzen-Hoffman theoretical model, the spherulite growth rate, G, can be expressed for the case of medium undercooling as follows:

$$G_{II} = b_0 (2ig)^{1/2} \qquad (1)$$

where b_0 is the thickness of the crystalline layer added to the surface, i is the surface nucleation rate and g is the substrate completion rate. Equation (1) holds for the crystallization regime II in which multiple nucleation that is necessary for a chain segment to be attached to the single substrate takes place.

The expression for the surface nucleation rate, *i*, has been derived by Hoffman and Miller in the form[5]:

$$i = C_0 \frac{\kappa}{[(2/3)\pi]} \left(\frac{kT}{h}\right) \left[\frac{kT(\Delta h_f)(\Delta T)}{4b_0 l_u \sigma^2 T_m}\right] \exp\left(\frac{-Q_D^*}{RT}\right) \times \exp\left(\frac{-4b_0 \sigma \sigma_e T_m}{\Delta h_f (\Delta T) kT}\right) \qquad (2)$$

The substrate completion rate, *g*, involving chain reptation as main diffusion mechanism of chains can be expressed in the form:

$$g = a_0 \left(\frac{\kappa}{\frac{2}{3}n}\right) \left(\frac{kT}{h}\right) \left(\frac{a_0(\Delta h_f)(\Delta T)}{\sigma T_m}\right) \exp\left(\frac{-Q_D^*}{RT}\right) \times \exp\left(\frac{-q}{kT}\right) \qquad (3)$$

For the case of linear PE, the following parameters were utilized[5,6]: the activation energy for reptation in the neat matrix $Q_D^* = 24$ kJ mol^{-1}, $T_m = 418.7$ K, $\Delta T = 15.8$–23.8 °C (Regime II), heat of fusion $\Delta h_f = 2.8108$ J m^{-3} (2.8×10^9 erg cm^{-3}), crystalline surface free energy e = 0.093 J m^{-2} (93 erg cm^{-2}), work of chain folding q = 20.48 kJ mol^{-1} (4,900 cal^{-1} mol^{-1}), stem dimensions $a_0 = 4.55 \times 10^{-10}$ m and $b_0 = 4.15 \times 10^{-10}$ m.

Parameter κ used in equation (3) is a result of incorporation of the chain reptation motion into the secondary surface nucleation theory and can be estimated as:

$$\kappa = h \exp\left(\frac{Q_D^*}{RT_0}\right) \exp\left(\frac{q}{N_A kT}\right) / \xi_0 l_g^{*2} \qquad (4)$$

The parameter Q_D^* corresponds to activation energy for reptation motion and the monomer friction coefficient, ξ_0, equals to 2.2×10^{-12} kg s^{-1}. Particular details of the surface nucleation theory can be found elsewhere.[3–6]

It has been shown by Jancar and Kalfus[7], that the chain diffusion can be considerably reduced in nano-filled polymer well above its glass transition temperature. Hence, it is supposed that the presence of weakly interacting silica nanoparticles would be able to increase the activation energy of chain diffusion in the polyethylene melt resulting in the indispensable change of its crystallization kinetics.

Nucleation Activity of Silica Filler in HDPE

To examine the nucleation ability of the silica nano-filer in HDPE, a method suggested by Dobreva et al.[8–10] to estimate the nucleation activity of solid substrates in polymer melt was employed. Nucleation activity, Φ, is a factor by which the work of nucleation decreases with the addition of a solid substrate. Its value is in the range from 0 to 1 from extremely active to inert particles. For homogeneous nucleation in a melt under low undercooling, the cooling rate can be expressed as follows:

$$\log r = A - \frac{B}{2.3\Delta T_p^2}, \qquad (5)$$

while for heterogeneous case

$$\log r = A - \frac{B^*}{2.3\Delta T_p^2}, \qquad (6)$$

and

$$\phi = \frac{B^*}{B}, \qquad (7)$$

where r is the cooling rate, A is the constant and ΔT_p is the undercooling, $\Delta T_p = T_m - T_c$; T_c corresponds to the crystallization temperature determined from the DSC curves. Parameter B can be expressed as:

$$B = \frac{\omega \sigma^3 V_m^2}{3nkT_m \Delta S_m^2 n}, \qquad (8)$$

where ω is the geometrical factor; σ is the specific energy, V_m is the molar mass volume of crystallizing substance, *n* is the Avrami exponent, ΔS_m is the entropy of melting and *k* is the Boltzman constant.

Experimental

Fumed silica (Sigma Aldrich, USA) with specific surface area of 390 $m^2 g^{-1}$ and mean particle diameter d = 8 nm was used as a nano-filler. High density polyethylene Liten MB 71 (Chemopetrol, CZ) was used as a polymer matrix. Nanocomposite samples were prepared by adding of silica into the polymer solution at 130 °C under ultrasonic filed and intensive mixing. Dried nanocomposite samples were press molded at 170 °C (Fontijne TP400, NL) into the form of 1 mm thick plates. Thin slices cut out from press molded plates were melted between two glass slides at 170 °C. These pressed films of thickness between 5 and 10 μm were used for microscopy observations under polarized light (BX50, Olympus, Japan + hot-stage Linkam LTS 350, UK). Before each measurement of the spherulite radius, the specimen was melted at 170 °C. After 5 min isothermal step, the specimen was cooled below the melting temperature (T_m = 147 °C) at a rate of 10 °C min^{-1}. The spherulite growth rate was measured isothermally at temperatures 125 °C, 126 °C, 127 °C and 128 °C, respectively. The nucleation activity of the silica nano-filler in HDPE was estimated according to Dobreva et. al.[9–12] The samples were heated in a differential scanning calorimeter (Pyris 1, Perkin Elmer) up to 170 °C at a rate of heating 10 °C min^{-1}. After 2 min isothermal step at 170 °C, cooling down to the room temperature was carried out at rates of cooling 2, 5, 10, 20 and 40 °C min^{-1}, respectively. Crystallization temperatures were obtained from the peak maxima.

Results

The isothermal crystallization of HDPE was investigated using the polarized light microscopy. Samples with 0–8 % vol of silica nano-filler were analyzed. In Fig. 1., there is shown the early stage of HDPE spherulites growth.

The spherulite radii were analyzed as a function of time. The experimentally obtained data were correlated with the Lauritzen-Hofmann surface nucleation theory, where the chain diffusion motion via the reptation mechanism was included. The limit value of diffusion motion activation energy was

calculated from L-H equation as 24 kJ mol^{-1} for neat HDPE and with increasing filler volume content considerably higher activation energy of diffusion motion is required (Fig. 2.). In other words, larger portion of chains is immobilized at the filler surface and its motion is restricted, proportionally to the surface area and mutual interactions. Thus, the retardation of chains diffusion motion is believed to be the principal mechanisms causing changes in crystallization kinetics and morphology of filled polymers.
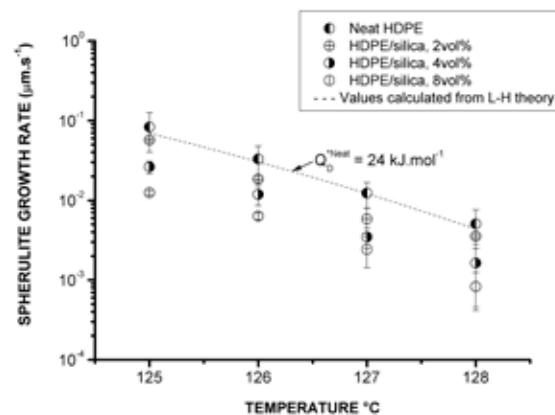
Fig. 2. **Spherulite growth rate of neat and nano-filled HDPE in dependence on temperature**

The nucleation activity Φ can be calculated using the equations 6 and 7 as the ratio of slopes of log r versus $1/\Delta T_{p2}$ for neat HDPE and filled HDPE system. The dependences are shown in Fig. 3. The nucleation factor is unity for all cases within experimental error suggesting that the silica nano-filler does not act as a nucleation agent in HDPE matrix.
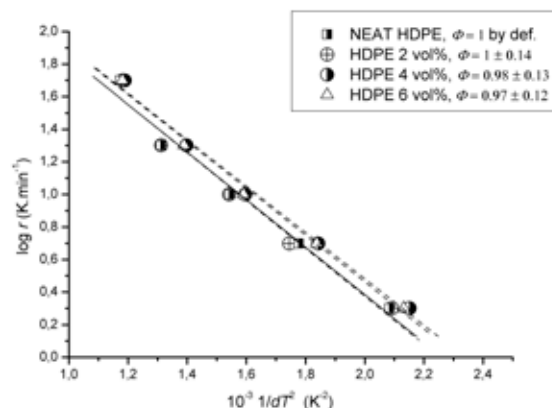
Fig. 3. **The silica nucleation activity estimation. The nucleation coefficient, Φ, is the ratio of the slopes neat/filled HDPE**

Conclusions

Crystallization kinetics of HDPE-silica nanocomposite was shown to be changed significantly by the addition of silica nanoparticles. Based on the correlation between experimental data and the Lauritzen-Hoffman model, the immobi-

Fig. 1. **The POM micrograph of the HDPE crystallization early stage**

lization of HDPE chains in presence of silica of large surface area was identified as the primary mechanism leading to the observed behavior.

REFERENCES

1. Sperling L. H.: *In Introduction to Physical Polymer Science;* Wiley: New York, (2006).
2. Woodward A. E.: *In Understanding Polymer Morphology;* Hanser: New York, (1995).
3. Lauritzen J. I. Jr., Hoffman J. D.: J. Res. Natl. Bur. Stand. – A *64*, 73 (1961).
4. Hoffman J. D., Lauritzen, J. I. Jr.: J. Res. Natl. Bur. Stand. – A *65*, 297 (1961).
5. Hoffman J. D., Miller R. L.: Polymer *38*, 3151 (1997).
6. Armistead J. P., Hoffman J. D.: Macromolecules *35*, 3895 (2002).
7. Kalfus J., Jancar, J.: J Polym Sci: Part B: Polym. Phys. *45*, 1380 (2007).
8. Dobreva A., Gutzov I.: J Non-Cryst Solids 162 (1993).
9. Dobreva A., Gutzov I.:J Non-Cryst Solids 162 (1993).
10. Alonso M., Melasco J. I., Saja J. A.: Eur Polym J *33*, 255 (1997).
11. Kim S. H., Ahn S. H.: Polymer; 44, 562 (2003).

L03 EFFECT OF HEXAMETHYLDISILOXANE SOLUTION OF ZIRCONIUM PROPOXIDE ON PERMANENCE OF PAPER

SOŇA KIRSCHNEROVÁ, KATARÍNA VIZÁROVÁ and SVETOZÁR KATUŠČÁK

Institute of Polymer Materials, Department of Chemical Technology of Wood, Pulp and Paper, Faculty of Chemical and Food Technology, Slovak University of Technology, Radlinského 9, 831 07 Bratislava, Slovakia
sona.kirschnerova@stuba.sk

Introduction

Ageing of lignocellulosic carries of information is natural process influenced by different factors. Of the outdoor impacts, relative humidity, oxides of sulphur and nitrogene and others, while of the indoor factors, type of fibres, sizing agent, filling agent, etc. may be introduced[1,2,3].

Influence of ageing leads to formation of other compounds, which accelerate degradation of paper, e.g. organic compounds[4,5,6].

To stop ocurring these processes, conservation techniques, such as deacidification of paper are used[7]. Efficient deacidification systems have been applied in both polar and nonpolar medium in conservation practice. If this modification system is in the polar medium, it is supposed that diffusion of low molecular compounds to the cell wall, fibrils, microfibrils, elementary fibrils and to the molecular level of other units are to be performed.

Double alkoxides, combination of chemical elements Al-K, Sn-Mg, Zr-Ca are used as a neutralizing agent in suitable solvents, such as alcohols, fluoro-chlorohydrocarbons, hydrocarbons and siloxanes. Disadvantage of the above mantioned alkoxides lies in the formation of visible deposit[8,9].

For papermaking industry, water solutions of zirconium compounds are of particular importance, for example adhesions supporting cohesion to the different surface, etc[10].

This work was aimed at verifying the effect of hexamethyldisiloxane (HMDO) solution of zirconium propoxide on the permanence of newsprint paper.

Experimental

R a w   M a t e r i a l s

Newsprint paper with extract pH 5.5–6.0; grammage $m_s = 45\,g\,m^{-2}$, containing 55 % of mechanical bleached groundwood, 20 % of bleached kraft pulp, 15 % scrap fibres and 10 % clay was used as received.

M o d i f i c a t i o n   S y s t e m

Two different solution of zirconium propoxide (70 % wt. in 1-propanol, Aldrich) in hexamethyldisiloxane (≥98 %, Aldrich): 0.02M solution and 0.04M solution were used.

Sheets were modified for 10 minutes at regulat stirring in a laboratory shaker. Subsequently, sheets were dryed free in sieves.

A c c e l a r a t e d   A g e i n g

Samples of paper were conditioned for 24 hours at T = (23 ± 1) °C, RH = (50 ± 2) % before the accelerated ageing. Subsequently were aged in hermetically sealed bags at 98 ± 2 °C during 0, 1, 2, 3 and 5 days according to standard ASTM D 6819-02[11].

P r o p e r t y   M e a s u r e m e n t

Changes of folding endurance[12] (ω), breaking length[13] (lt), Kubelke-Munke intensity of $1{,}735\,cm^{-1}$ peak by FTIR[14] (KM intensity), $pH_{extract}$[15] and total color difference[16] (ΔE) were studied at modified and aged samples.

Folding endurance was expressed as a coefficient of permanence[17,18] in the time of ageing (t):

$$S_{\omega,t} = \frac{\omega_{modified,t}}{\omega_{control,t}} \qquad (1)$$

- if $S_{\omega,t} > 1$ – permanence increased
- if $S_{\omega,t} < 1$ – permanence decreased
- if $S_{\omega,t} = 1$ – is it not change.

Results

The permanence of paper samples modified with HMDO solution of zirconium propoxide was studied. Permanence of paper was evaluated by the change of folding endurance (ω), breaking length (lt), KM intensity of $1{,}735\,cm^{-1}$ peak (KM intensity), $pH_{extract}$, and total color difference (ΔE).
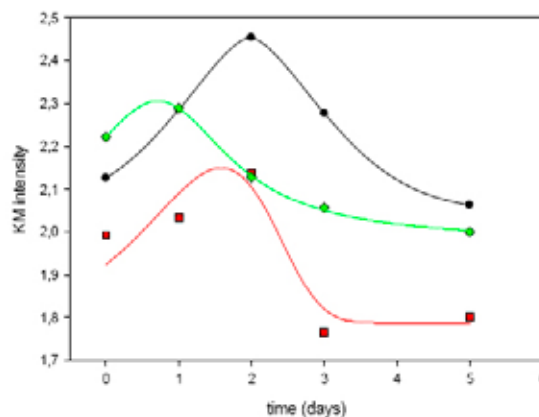
Fig. 1. **Depedence of KM intensity peak 1,735 cm⁻¹ on the time of accelerated ageing obtained by evaluation of FTIR DRIFT spectra of control (•) and samples modified by 0.02M zirconium propoxide in HMDO (■) and 0.04M zirconium propoxide in HMDO (♦)**

Increased formation of carbonyls and carboxyls depends on time of ageing. In Fig. 1., values of KM intensity absorption peak at $1{,}735\,cm^{-1}$, which relate to binding vibration C=O groups are shown. Modification system restricts creation of carbonyls and carboxyls. Marked decrease of absorption peak at $1{,}735\,cm^{-1}$ was observed at lower concentration of effective component compared with the control sample during the modification. This trend is held during all

accelerated ageings. Higher concentration of zirconium propoxide in HMDO causes increased formation of carbonyls and carboxyls with unaged control sample immediately after the modidfication. However during the accelerated ageing a decrease compared with control sample is observed.
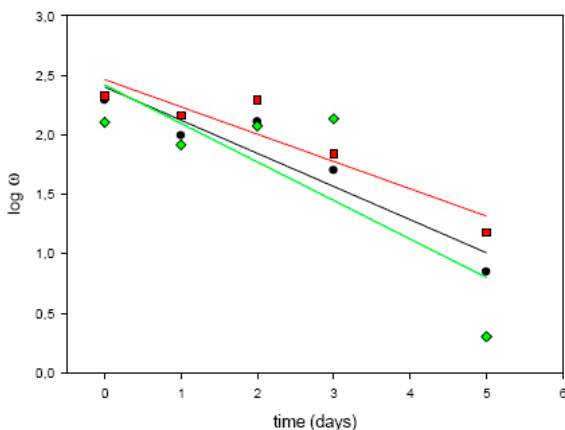
Fig. 2. Dependence of common logarithm values of folding endurance during the accelerated ageing for samples modified by 0.02M zirconium propoxide in HMDO (■), 0.04M zirconium propoxide in HMDO (♦) and control sample (•)

Folding endurance moderately increased at lower concentration of effective component ($S_{\omega,0} = 1.1$) just after the modification. During the accelerated ageing, stability values of folding endurance compared with unmodified control sample were followed. Stability effect of folding endurance after 5 days of accelerated ageing reached value 2.1 ($S_{\omega,5} = 2.1$). Higher concentration of zirconium propoxide in HMDO influences only slightly the folding endurance. It leads to an expressive decrease of this property after 0 and 5 days ($S_{\omega,0} = 0.7$ a $S_{\omega,5} = 0.3$).
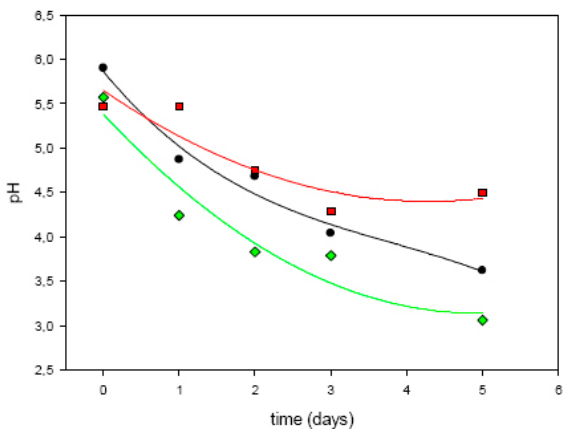
Fig. 3: Dependence of pH of cold extract samples modified by 0.02M zirconium propoxide in HMDO (■), 0.04M zirconium propoxide in HMDO (♦) and control – unmodified sample (•) during the accelerated ageing.

Cold extract of pH modified samples are comparable with unmodified sample (pH ≈ 5.5). However pH of sample with lower concentration of zirconium propoxide in HMDO (pH = 4.5) is more mild decreased after 5 days of accelerated ageing in comparison with unmodified control sample (pH = 3.6).

Table I
Breaking length values of samples modified with 0.02M zirconium propoxide in HMDO (0.02M), 0.04M zirconium propoxide in HMDO (0.04M) and unmodified samples (control) during accelerated ageing

Days	Control	0.02 M	0.04M
0	3,720 ± 570	3,860 ± 280	3,830 ± 410
1	3,760 ± 490	3,790 ± 390	4,000 ± 230
2	3,280 ± 670	3,770 ± 310	3,530 ± 550
3	3,600 ± 380	3,460 ± 490	3,560 ± 270
5	2,910 ± 430	3,340 ± 320	3,200 ± 380

Values of breaking length obtained from modified samples were higher than those of unmodified ones.

Samples modified with zirconium propoxide in hexamethyldisiloxane show decrease of measured properties in comparison with unmodified control sample. System of modification suppresses the formation of carbonyls and carboxyls. It indicates retardation of ageing process. Effect of modification causes that brittlenes of paper decreases and that folding endurance rises. Disadvantage of this modification system is low values of pH, which are comparable with unmodified paper. Combination of studied system with compound able to increase pH and thus alkaline reserve (for an instance MgO or other from lines of magnesium or calcium compounds) can help to solve this problem.

Advantage of this modification system is in the presence of polar element, 1-propanol, which is solvent of zirconium propoxide and at the same time, offers the use of non-polar carrier of effective compound. Non-polar solvent causes smooth surface of modified paper without warps and formation of visible deposits on the surface. Polar ingredient compiles presumption of facilitate intersection of effective zirconium compound to the structure of paper.

Lower concentration is more favourable in term of observed properties. This fact is shown on the look of modified paper. At a higher concentration of the effective component, e.g., at 0.04M solution, the total colour difference measured *vs*. the original unmodified paper is much more expressive ($\Delta E = 23.6$) than that at at lower concentration of zirconium compound ($\Delta E = 17.5$).

Conclusions

Solution of zirconium propoxide in HMDO exhibits a positive influence on the permanence of paper, and/or on measured properties. Utilization of studied modification system resulted in smooth surface of modified paper without warps and formation of visible deposits on the surface.

It leads to a decreased formation of carbonyl and carboxyl groups. There was also observed decrease intensity of the peak at 1,735 cm^{-1} (carbonyl groups) in comparison with control sample measured by FTIR.

It enhances the effect of stability of folding endurance – decreases brittleness of the measured sample in comparison with unmodified one.

Artificial ageing causes decrease of l_t by about 15 % in comparison with the control paper.

A more favourable effect offered solution of zirconium propoxide with lower concentration. Disadvantage of this system is its pH in comparison with pH of unmodified paper.

Combination of studied system with compound able to increase pH and thus alkaline reserve (for an instance MgO or other from lines of magnesium or calcium compounds) can help to solve this problem.

REFERENCES

1. Ďurovič M. et al: *Starnutie archiválií a kníh.* Paseka, Praha 2002.
2. Porck H. J.: *Rate of paper degradation: the predictive value of artificial aging tests.* European Commission on preservation and access, Amsterdam 2000.
3. Barrow W. J.: *Deterioration of book stock: causes and remedies: two studies on the permanence of book paper.* Virginia State Library, Richmond 1959.
4. Shahani C. J., Harrison G.: *Works of art on paper, books, documents and photographs: techniques and conservation, Baltimore, United States, 2-6 September 2002*, p. 189.
5. Hroboňová K., Lehotay J., Jablonský M., Katuščák S.: *13th International Symposium on separation sciences and 13th AACI. Štrbské Pleso, High Tatras, Slovak Republic, June 27.-29., 2007.*
6. Figedyová S., Hroboňová K., Jablonský M., Katuščák S.: *5th International Student's Seminar. Chemistry and Technology of Wood, Pulp and Paper, Brno, Trade Fair EmbaxPrint, 21.5 2007.* poster presentation.
7. Porck H. J. *Mass Deacidification: an Update of Possibilities and Limitations on Preseravtion and Access.* Washington D. C., 1996.
8. Rauleder et al. (E. I. du Pont de Nemours and Copany): US Patent 6 294 682 (C08F 10/00).
9. Wittekind et al. (Battelle Ingenieurtechnik GmbH): US Patent 5 322 558 (B41M 7/00).
10. Lebtinen E.: *Pigment Coating and surface sizing of paper. Papermaking Science and Techmology, Book 11.* Fapet OY, Helsinki 2000.
11. ASTM D 6819-02: *Standard test method for accelerated temperature aging of printing and writing paper by dry oven exposure apparatus.*
12. ASTM D 2176 - 97a: *Standard Test Method for Folding Endurance of Paper by the M.I.T. Tester*
13. STN ISO 1924-2 50 0340: *Paper and board. Determination of tensile properties. Part 2: Constant rate of elongation method*
14. Polovka M., Polovková J., Vizárová K., Kirschnerová S., Bieliková L., Vrška M: Vib. Spectrosc *41*, 112 (2006).
15. STN ISO 6588 50 0381: *Paper, board and pulps – Determination of pH of aqueous extracts.*
16. Panák J. et al.: *Polygrafické minimum.* TypoSet, Bratislava 2000.
17. Katuščák S. et al.: *Preservation, Stabilization and Conservation of Traditional Information Carriers of the Slovak Republic.* State project of research and development, *Report* 2004.
18. Cedzová M.: *Disseretation.* Slovak University of Technology, Bratislava, Slovakia 2006.

L04　MODIFICATION OF POLYPROPYLENE THROUGH RADICAL GRAFTING IN MELT

FRANTISEK KUČERA

Brno University of Technology, Faculty of Chemistry, Institute of Materials Science, Purkynova 118, 612 00 Brno,
kucera-f@fch.vutbr.cz

Introduction

Pure polypropylene (PP) is sufficient material for many applications; however utilization of PP in some applications, such as composites, needs improvement of matrix properties for better adhesion, miscibility, dyeability etc. Chemical modification of PP is a way to formation of new material without searching new monomers for polymerization. Industrial and scientific interest gained in recent years grafting of polar monomers onto PP chain[1–5], most of modification reactions target the change of PP hydrophobia. Reaction of PP with maleic anhydride (MA) is recently the best known modification process[6,7], which is generally used for improvement of polypropylene adhesion to metals, glass fibres or to other polymers such as nylon or polyethyleneterephthalate. Grafting reaction by reactive extrusion can be used for grafting of MA or other polar compounds onto PP chain in a melt state of polymer and in presence of free radical initiator. Possibility of grafting other polar substances, such as other carboxylic derivates, vinyl or acrylic molecules, were studied.[8–11] Itaconic anhydride (IA), styrene (S) are monomers used for grafting to PP backbone in this work, another monomers such as acrylic acid, methylmethacrylate, vinylacetate etc. can be also tested.

Experimental

Two initiators were used for grafting reaction on PP:
- 2,5-dimethyl–2,5-bis(tert-butylperoxy)hexane (Luperox 101) for oth styrene and itaconic anhydride monomers
- dicumylperoxide for styrene grafting onto PP backbone.

Method for PP-g-IA Preparation and Conversion of Itaconic Anhydride Determination

Experiments of PP-g-IA and preparation were carried out in laboratory mixer Brabender 50 ml at 30 rpm, at temperature 210 °C. Polymer was at first melted about 5 minutes and then was monomer dispergated in polymer for time 1 minute. After that grafting reaction was started by addition of initiator and carried out for time 6 minutes. Unreacted monomer was removed by precipitation amount of 2.5 g sample dissolved in 100 ml of boiled xylene to 700 ml of acetone. Purified PP-g-IA was filtered and washed using 50 ml o acetone and dried in vacuum oven at 40 °C.

Conversion of grafted itaconic anhydride were determined using FT-IR spectroscopy measurement of integral intensity of C=O stretching vibrations at 1,770–1,780 cm^{-1}

and intensity of peak at 1,170 cm^{-1} belonged to vibration of –CH_3 of PP.

Second method of bounded IA concentration determination was alkalimetric titration. Weight 0.5 g of precipitated PP-g-IA was dissolwed in boiling xylene and then titrated usin 0.005M KOH and bromthymolic blue as end-poin indicator.

Method for PP-g-S Preparation and Analysis

Preparation of PP-g-S was caried out the same way as was described in the last section. Styren was poured into mixer using glass pipette.

Analysis was accomplished using FT-IR spectroscopy of PP-g-S. Polymer was at first purified by the precipitation into acetone or ethanole as was described former. FT-IR spectras were taken out using polymeric film. Comparison of integral intensity of peaks of aromatic ring vibration around 700 cm^{-1} and vibration of –CH_3 at 1,170 cm^{-1} was used to attached styrene concentration determination.

Results

Two molar ratio of initiator to monomer (1 : 0.6 and 1 : 0.8) were used in experimental part to comparison efficiency of grating IA and MA. Experimental data of maleic anhydride grafting were get from the same methods as for PP-g-IA. Results of ascertained monomers conversions are shown in Table I.

Table I
Results of IA and MA monomer conversion in grafting reaction for two molar ratio of initiator:mo monomer

Monomer	w_0(monomer) [% wt.]	α(1 : 0.6) [%]	α(1 : 0.8) [%]
IA	0.25	23.9	26.7
IA	0.5	32.4	37.1
IA	1.0	62.8	55.4
MA	0.25	47.6	42.4
MA	0.5	41.9	42.3
MA	1.0	61.1	64.1

The efficiency of IA grafting in comparison to MA grafting process is apparently less due to probable homopolymerization of IA, which is removed from grafted polymer by purification. Graft length is higher in case of PP-g-IA compare to PP-g-MA and less stability o IA homopolymeric graft less could be the second reason of decreased conversion of IA.

PP-g-PS sample precipitated into ethanol contain both PP-g-PS and PS homopolymer, which could be formed by homopolymerization of styrene. Sample precipitated into acetone contain only PP-g-PS, because PS is in acetone soluble. The grafting efficiency is decreased with increased concentration o initiator. Amount of about 30 to 45 % of bounded styrene was present as a homopolymeric PS, other

Table II
Content of styrene $\omega(S)$ in PP-g-PS for concentration 1 % wt. of dicumylperoxide or 2,5-dimethyl–2,5-bis(tert-butylperoxy)hexane for initial concentration of styrene $\omega_0(S)$ from 1 to 20 % wt

Sample	$\omega_0(S)$ [wt%]	$\omega(S)$ [wt%]	
		DCP	Luperox 101
PP-g-PS+	1	0.66	1.07
PS + S	5	3.76	3.62
(non-purified)	10	5.28	6.92
	20	9.22	12.00
PP-g-PS + PS	1	0.89	0.88
(precipitated	5	2.56	2.25
into ethanol)	10	3.77	7.06
	20	6.98	8.58
PP-g-PS	1	0.74	1.07
(precipitated	5	0.99	2.24
into acetone)	10	2.57	4.13
	20	3.89	6.00

as PP-g-PS. Luperox 101 is more efficient initiator for grafting of styrene onto PP.

Conclusions

First part of work was focused to grafting of itaconic anhydride and maleic anhydride onto PP backbone. Comparison of both monomers conversion results shown, that grafting of IA bring about worse conversion due to more complex reaction mechanism and possibility of formation of less stable IA homopolymeric grat.

Second experimental part was concentred to found better initiator for styrene grafting onto PP. Luperox 101 can

be good choice for prepared grafting of mixture IA+S for grafting onto PP backbone. However analysis of amount of homopolymeric PS during radical grafting of styrene onto PP shown that complex mechanism of IA+S mixture grafting could be expected.

REFERENCES
1. Al-Malaya S.: *Reactive modifiers for polymers*. Chapman & Hall, London, UK 1996.
2. Yazdani-Pedram M., Vega H., Retuert J., Quijada R.: Polym. Eng. Sci. *43*, 960 (2003).
3. Yazdani-Pedram M., Quijada R., Lopez-Manchado M. A.: Macromol. Mater. Eng. *288*, 875 (2003).
4. Sain M. M., Kokta B. V.: J. Reinf. Plast. Compos. *13*, 38 (1994).
5. Sain M. M., Kokta B. V.: Polym. Plast. Technol. Eng. *33*, 89 (1994).
6. Shi D., Yang J., Yao Z., Wang Y., Huang H., Jing W., Yin J., Costa G.: Polymer *42*, 5549 (2001).
7. Ghahari S. M., Nazokdast H., Assempour H.: Int. Polym. Process. *18*, 285 (2003).
8. Yazdani-Pedram M., Vega H., Quijada R: Polymer *42*, 4751 (2001).
9. Yazdani-Pedram M., Vega H., Quijada R.: Macromol. Chem. Phys. *199*, 2495 (1998).
10. Moncada E., Quijada R., Lieberwirth I., Yazdani-Pedram M.: Macromolecular Chemistry and Physics *207*, 1376 (2006).
11. Pesetskii S. S., Jurkowski B., Makarenko O. A.: J. Appl. Polym. Sci. *86*, 64. (2002).

L05　PROPERTIES OF HOT COMPACTED POLYPROPYLENE PLATES INCLUDING ORIENTED POLYPROPYLENE TAPES

J. KUČERA, J. SADÍLEK and B. RÝZNAROVÁ

Polymer Institute Brno, spol. s r.o., Tkalcovská 36/2, 656 49 Brno, Czech Republic,
kucera@polymer.cz

Introduction

The polypropylene homopolymer (PPH) sheets are used in many common applications. The strength of such material is about 33 MPa, however, the toughness is not very high, especially at low temperatures at which PPH is brittle. The strength can be increased for example by reinforsing PPH with short fibres but the low temperature impact resistance still remains low. The toughness can be improved by incorporating EPR rubber into PPH matrix (impact polypropylene copolymer PPIC), but the strength of such material is substantially lower. Another way of improving both properties is to combine oriented and unoriented PPH and to construct sandwich-like composite plates.[1–4]

The polypropylene composite plates can be produced by hot pressing several layers of oriented PPH tapes and potentially by adding unoriented PPH thin layers (films). The production conditions must be held in a specific "temperature window" to avoid complete relaxation of the oriented polypropylene chains and to facilitate a lateral welding of PPH.

Some results concerning behaviour of PPH tapes at high temperatures (near to the PPH melting point), lateral welding of tapes or PPH woven fabric and properties of PPH self reinforced composites are presented in this paper.

Experimental

Material and Samples Preparation

Commercial grade of polypropylene Mosten TB 002 (MFR = 2.73 g 10min⁻¹) was used in this work. A film of 200 or 400 μm thickness (PF) was prepared by chill roll technique. This film was drawn up to ratio 5 : 1 in the first step, then it was cut into tapes (10 mm width) and those were drawn on a hot plate to the final draw ratio 8 : 1 in the second step (TB).

A part of the tapes was annealed (TB-T) at different temperatures from 120 to 170 °C. Both ends of each annealed tape were fixed to avoid the longitudinal shrinkage of the tape.

To characterise the lateral adhesion a couple of tapes was passed through a tempered channel where a short perpendicularly acting force took place to cause a lateral weld of these tapes. The length of the tempered part of tapes was fixed to avoid the relaxation of tapes.

The composite plates were hot pressed at different temperatures (160 °C to 170 °C) in an open mould. The number of PPH woven fabric layers (WF) was different (four to twelve) and the unoriented PF layers were potentially stuck in between fabric layers to improve the "weld adhesion".

Measurement

The basic information about the supermolecular structure of the PPH tapes was received by recording the fusion curve of a tape using a DSC instrument (TA Instruments Q100) under following conditions: specimen weight about 1.5 mg, heating rate 10°C min⁻¹, initial 50 °C and end temperature 200 °C.

The tensile properties of the tapes were measured at laboratory temperature using an INSTRON 4302 machine. The active length of the specimens were 100 mm, the testing speed was 100 mm min⁻¹ref.[5]. The tensile properties of pressed plates were measured according to the same method; the strips of 170 mm length and of 15 mm width were cut from the plate.

The lateral weld adhesion of a couple of tapes was characterised by the T-peel test[6] or the coherence of the composite compact by method for floating roller peel resistance[7] (INSTRON 4302, 100 mm min⁻¹).

The intensity of the relaxation process in the tape at elevated temperatures was evaluated by a DMA (R.M.I. DX04T) measurement. The constant fluctuating stress [$\sigma_m \pm \sigma_a$ (σ_m = 2, 5, 10, 15, 20 MPa, σ_a = 1 MPa), sin oscillations, 1 Hz] was applied during the temperature scan from 30 °C to 180 °C, 2°C min⁻¹. The initial distance between grips (= gauge distance) was 30 mm and the change of this quantity was recorded during the test. The complex modulus was measured, too.

The ductility of final material was measured by the instrumented puncture test (CEAST 6790/000: inside diameter of clamped support ring = 40 mm, diameter of striker = 10 mm, impact velocity = 3.6 m s⁻¹, T = 23 °C or –20 °C)[8].

Results

DSC Measurements

The information about the changes in supermolecular structure of annealed PPH tapes was evaluated only qualitatively by comparing the shapes of DCS melting records (see Fig. 1.). We interpreted these DSC records based on relaxation of oriented chains and subsequent recrystallization of PPH that took place during annealing of the tape. These processes begin at annealing temperature (approximately at 150 °C). A second melting DSC peak occurs at 155 °C. The recrystallization processes became more intensive at higher annealing temperatures (an example is given for 160 °C); the second melting peak gets larger and it is shifted to higher melting temperature. Process of recrystallization at annealing temperature 170 °C starts to change substantially the crystallite character of the tape. The thicker lamellae are built-up (higher T_m) and the orientation of chains decreases rapidly.

Tensile Tests

The results of tensile tests (tensile strength and elongation at break) are presented in Fig. 2. Tensile strength decreases with annealing temperature in the whole annealing temperature range, because the above mentioned recrystallization process decreases orientation of polymer chains.
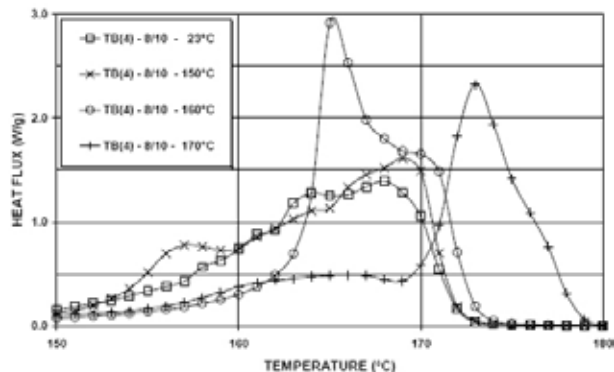
Fig. 1.　**Heat fluxes of PPH tapes (heating rate of 10 °C min⁻¹). Original tape (23 °C -□-) and annealed tapes: 150 °C (-×-), 160 °C (-◇-) and 170 °C (-+-)**

Elongation at break increases only up to annealing temperature 160 °C and then it drops. This fact could be also attributed to the polypropylene recrystallization (see above) and subsequent destruction of the tape orientation.

Adhesion of Tapes

The strength of lateral weld adhesion of a couple of tapes is depicted in Fig. 3. The adhesion increased with the welding temperature, however, the experimental results exhibited higher scatter. At temperature below 164 °C no measurable adhesion was detected and above 169 °C considerable melting of tapes was observed and this technique of measurement was not applicable.

Relaxation of Oriented Tapes

The relaxation of internal stresses was assessed only qualitative till now. The static deformation of a tape specimen with respect to the mean level of a fluctuating stress at constant heating rate were taken as a measure of intensity of the relaxation process at given temperature (see Fig. 4.). It is evident that at low mean stress levels (2, 5, 10 MPa) the shrinkage of the tape is much more intensive than the creep deformation and contrariwise at high stress level (20 MPa). A balance is held for a stress of about 15 MPa.

Properties of Pressed Composite Plates

The hot pressed composite plates have a specific structure composed of well distinguishable layers because the pressing requires specific conditions (temperature) for receiving relatively good cohesion and preserving a substantial part of molecular chain orientation in the tapes. An example of a microtomic section is presented in Fig. 5.

Fig. 4: Dependence of stationary deformation of the tape under constant fluctuating stress on temperature during the DMA measurements. The mean stress levels are: 2, 5, 10, 15 and 20 MPa.

Finally, the basic tensile properties were measured (Fig. 6). The tensile strength and also the elongation at break remain stable in the chosen temperature interval of pressing
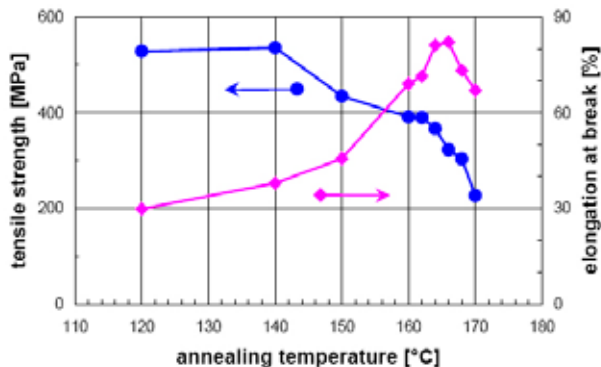
Fig. 2.　**Dependencies of tensile strength (-○-) and elongation at break (-◇-) of PPH tapes TB on annealing temperature**
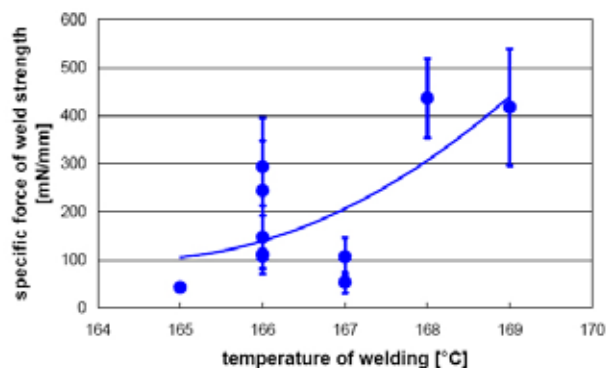
Fig. 3.　**Dependence of weld adhesion (-○-) of PPH tapes TB on temperature of short time welding**
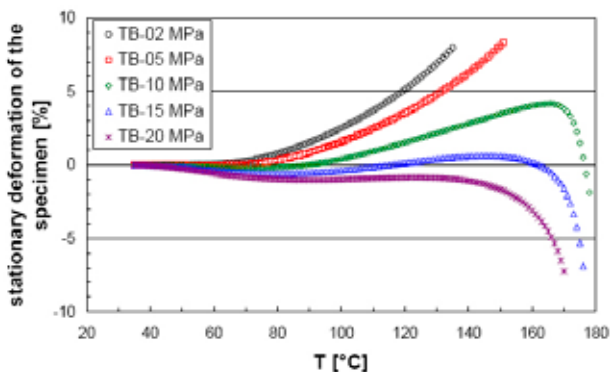
Fig. 4.　**Dependence of stationary deformation of the tape under constant fluctuating stress on temperature during the DMA measurements. The mean stress levels are: 2, 5, 10, 15 and 20 MPa**

and it is remarkable that the strength of the composite is about two times higher than the strength of unoriented PPH. The elongation at break is lower compared with PPH but it is high enough to conclude that the composite materials are not brittle at the laboratory temperature.

The composite samples were further tested by dart drop (Fig. 7). The maximum force (or maximum force at first break) and the puncture energy were recorded. The evalua-
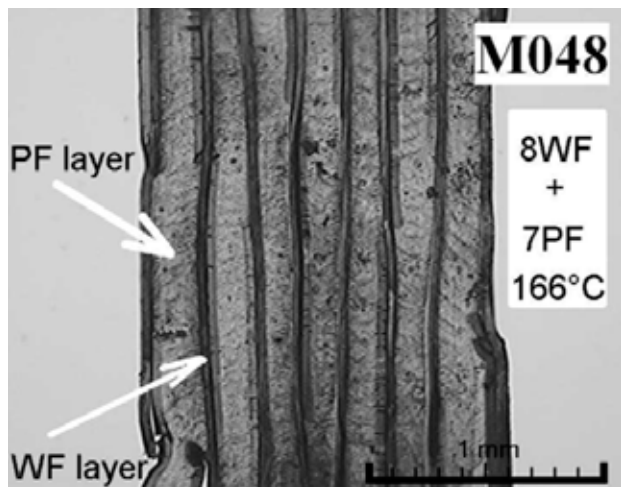
Fig. 5. **Micrograph of the layer structure of the composite plate consisting of 8 layers of PPH woven fabric (WF) and 7 layers of PPH film (PF). (Pressing temperature 166 °C)**

Fig. 6. **Dependencies of tensile strength and elongation at break on pressing temperature for hot pressed composite plates: 8 layers of PPH woven fabric (8WF) or 8 layers of PPH woven fabric and 7 layers of PPH film (8WF + 7PF)**

tion was complicated by the fact that the thickness of the composite plates varied from sample to sample and that the simple relation between the value of measured quantity and the thickness of the plate is not known. Therefore the set of unoriented PPH plates (the same type of PPH resin) of different thickness were pressed and the corresponding properties were measured at the same conditions. For evaluation the ratio between the value of composite property and the interpolated value (into the same thickness) of the same property for PPH plate was used. We found that the properties of the composite plates are noticeable better than the properties of PPH unoriented plates in the "pressing window" 160 °C /164 °C especially at testing temperature –20 °C. The common PPH homolymer is brittle and it splitters during the impact test. To the contrary, the composite plate exhibits no splitter at this temperature (Fig. 9.).

Important factor is the internal cohesion of the composite plates. It was assessed by a modified peeling test. A strip of the surface fabric layer of 15 mm in width was peeled up from the pressed composite plate to evaluate the cohesion of the plate with respect to the different pressing temperatures. The results of measured specific forces are depicted in Fig. 8. It is evident that the welding of oriented tapes starts approximately at 160°C and is significantly better for the material consisting of oriented tapes and unoriented PPH film layers.

Conclusions

It has been demonstrated that a "pressing window" exists for PPH tapes in the temperature range around 164°C where some reasonable adhesion between PPH tapes is formed and the high strength of tapes is kept.

Only a part of the PPH material melted and recrystallized during processing at this temperature.

The complete recrystallization of an oriented tape is connected with the loss of molecular chain orientation and then also with the loss of the tensile strength.
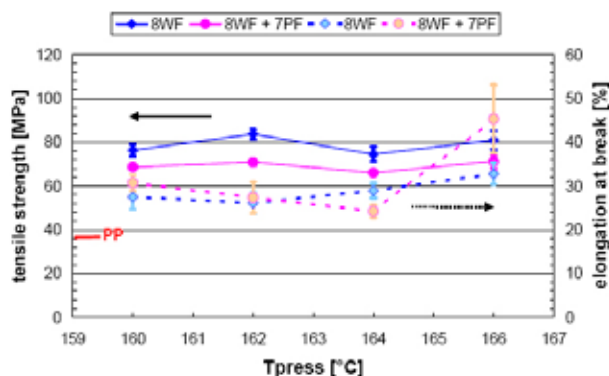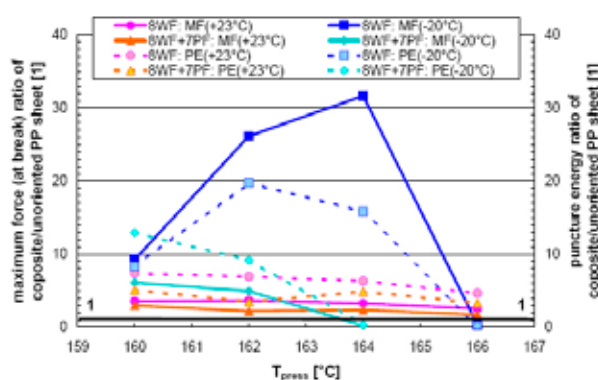
Fig. 7. **Dependencies of maximum force and puncture energy on pressing temperature at + 23 °C and –20 °C for hot pressed composite plates: 8 layers of PPH woven fabric (8WF) or 8 layers of PPH woven fabric and 7 layers of PPH film (8WF + 7PF)**
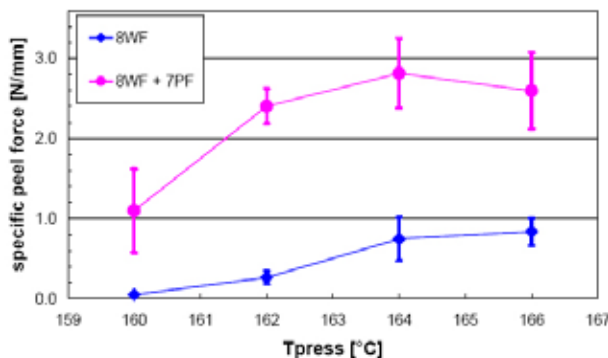
Fig. 8. **Dependencies of specific peel force on the pressing temperature. Peeling of surface fabric layer from different composite plates: tensile strength (-○-) and elongation at break (-◇-) of PPH tapes TB on annealing temperature**

The cohesion of pressed plate can be improved by adding an unoriented PPH film.
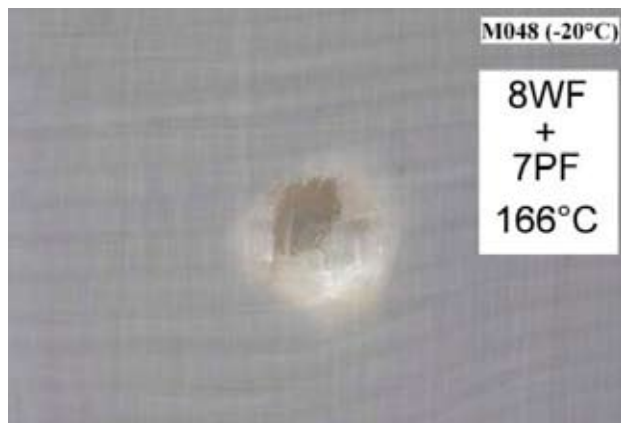
Fig. 9.   **Photograph of puncture at –20 °C of the composite plate consisting of 8 layers of PPH woven fabric (WF) and 7 layers of PPH film (PF). (Pressing temperature 166 °C)**

Some distinct layer structure is observed in the composite plates pressed according to described procedure.

A shrinkage stress around 15 MPa was found in the PPH tapes at drawing ratio of 8 : 1 and it has to be compensated during processing.

The decrease of dart drop strength is the main competitive process with respect to the improvement of the homogeneity and the cohesion of the composite plate. This process closes the "processing window" for higher temperatures.

The self reinforced PPH composite plates exhibit very good low temperature toughness comparing to the same grade of polypropylene homopolymer and they do not splitter by the low temperature impact.

REFERENCES
1.   Ward I. M., Hine P. J.: Polymer Eng. Sci., *37*, 1809 (1997).
2.   Hine P. J., Boner M., Brew B., Ward I. M.: Plast. Rubber Compos. Process. Appl., *27*, 167 (1998).
3.   Hine P. J., Ward I. M., Jordan N. D., Olley R., Bassett D. C.: Polymer, *44*, 1117 (2003).
4.   Hine P. J., Ward I. M., Jordan N. D., Olley R., Bassett D. C.: Polymer, *44*, 1133 (2003).
5.   ISO Standard 527–3 *Plastics. Determination of tensile properties – Part 3: Test conditions for films and sheets.*
6.   ASTM Standard D 1876 *Standard Test Method for Peel Resistance of Adhesives (T-Peel Test).*
7.   ASTM Standard D 3167 *Standard Test Method for Floating Roller Peel Resistance of Adhesives.*
8.   ISO Standard 6603–2 *Plastics. Determination of puncture impact behaviour of rigid plastics – Part 2: Instrumented puncture test.*

L06 BIODEGRADATION OF MODIFIED POLYURETHANE FOAMS

STANISLAV OBRUČA, IVANA MÁROVÁ, VLADIMÍR ONDRUŠKA, LUCY VOJTOVÁ and JAN DAVID

Brno University of Technology, Faculty of Chemistry, Department of Food Chemistry and Biotechnology, Purkyňova 118, 612 00 Brno, Czech Republic,
xcobruca@fch.vutbr.cz

Introduction

Polyurethanes (PUR) are unique family of polymeric materials that is able to pose wide range of properties to suit many requirements. Some of the applications of this versatile polymer include foams, elastomers, paints, fiber, adhesives and sealants[1].

Biodegradation is natural process of material decomposition which is based on the fact that synthetic polymeric materials could serve as carbon and energy sources for many microorganisms including bacteria, moulds and yeasts. Despite its xenobiotic origin PUR was found to be susceptible to biodegradation by naturally occurring microorganisms[2,3].

Biodegradability of material can be influenced by many factors. Very important are structure properties such as molecular orientation, crystallinity, cross-linking and chemical groups presented in the molecular chain. For example, increase of molecular weight or crystallinity usually leads to increasing material durability. Thus, variations in the degradation patterns of different PUR are attributed to many properties of PUR such as topology and chemical composition[3,4].

Other important factors which influence process of biodegradation in nature are presence of susceptible microbial population and environmental conditions. PUR biodegradation activity was observed for many microorganisms including bacteria (e.g. *Corynebacterium sp.*, *Pseudomonas aureginosa*, *Comamonas acidovorans*, *Pseudomonas chlororaphis*, *Pseudomonas flourscens*, *Acinetobacter calcoaceticus* and *Arthrobacter globiformis*) and fungi (*Culvularia senegalensis*, *Fusarium solani*, *Aerobasidium pollulans*, *Cladosporium sp.*, *Cheatomium globosum* and *Aspergillus terreus*)[3].

In this work, biodegradability of modified PUR foams was tested using single bacterial strain (*Arthrobacter globiformis*), mixed bacterial culture (*Thermophillus* sp.) and selected moulds strains (*Fusarium solani*, *Alternaria alternata*). In a complex comparative study standard biodegradability tests in laboratory conditions, in model composting conditions and also in different natural environments were used.

Experimental

PUR foams were modified by following biopolymer components: 10 % of acetyl- (AC), hydroxyethyl- (HEC) cellulose, 10; 20; 30 % of carboxymethyl cellulose (CMC), 10% acetylated starch (AS), 10 % glutein (PB). Modifying agents partially replaced polyether polyol. Reference sample without modification agent was tested too.

Flask biodegradation tests were carried out in 50 ml of defined media under permanent shaking (120 rpm). One sample of PUR was represented by 0.25 g of PUR. Growth characteristics and chemical oxygen demand were determined in regular intervals. At the end of cultivation (about 300 hours) PUR mass decreases were measured gravimetrically and PUR surface changes were analysed microscopically. PUR foams were tested in complete medium as well as the only carbon and/or nitrogen source. Single strain *Arthrobacter globiformis* CCM 193 was cultivated at 25 °C in Nutrient broth NB1 and in Minimal inorganic medium containing glucose as carbon source and $(NH_4)_2SO_4$ as nitrogen source. Mixed aerobic thermophillic culture *Thermophillus sp.* was originally obtained from sludge of wastewater treatment in Bystřice pod Hostýnem. Cultivation was carried out at 60 °C on Minimal inorganic medium with minerals and vitamins. The mould strain *Fusarium solani* F-552 was cultivated on Minimal inorganic medium according *A. globiformis*. *Alternaria alternata* was identified during the study with *A. globiformis* as a common air contaminant. *A. alternata* was cultivated on Minimal inorganic medium too.

Model composting experiments were carried out under controlled conditions in presence of culture *Arthorbacter globiformis*. Model experiment under composting conditions was performed according to ref.[1]. PUR mass changes and surface patterns were analysed at the end of the experiment.

Test of biodegradability in natural condition. PUR foams were exposed to three different natural envitoment for 50 days. After the end of exposition, mass decreases of foams were analysed and a total bacterial microflora (quantified as colony forming units) in each environment was determined.

Results

All flask biodegradation tests proved that crucial for the course of PUR degradation are type and concentration of modification agent (see Fig. 1. and Fig. 2.).

Generally, PUR mass decreases during flask biodegradation tests were practically identical in presence and/or in
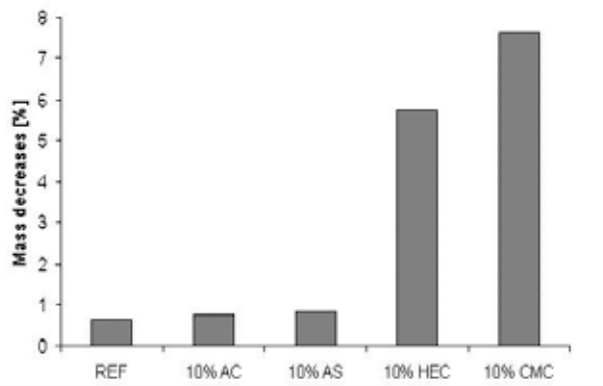
Fig. 1.　**Mass decreases of PUR samples modified by different agents (flask biodegradation test)**
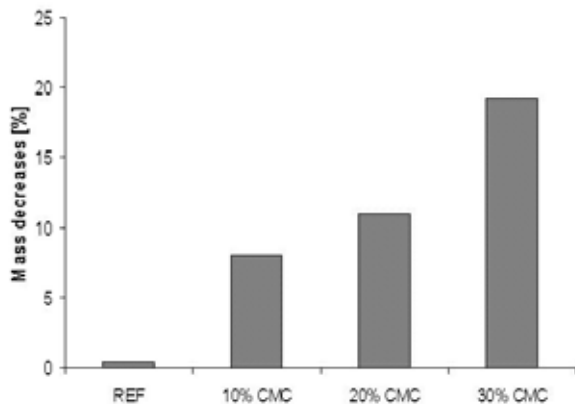
Fig. 2. **Mass decreases of PUR samples modified by different concentration of the same modification agent (flask biodegradation test)**

absence of bacterial culture. On the other side, the presence of PUR foam influenced the growth of culture. These two effects could be explained as two-step biodegradation process. First, abiotic destruction of foams occurred, which was followed by the second step – utilization of degradation products by the bacterial culture.

The growth of culture in presence of individual PUR samples was dependent on type of modifying agent. The highest growth of both cultures was observed in PUR modified by CMC.

Experiments with PUR foams used as the only carbon or nitrogen source for thermophillic culture showed that all modified PUR foams could serve as the only nitrogen source. Surprisingly, PUR modified by CMC and AS were better nitrogen sources than inorganic salt. On the other side, only PUR foam modified by AS supported the growth of culture when no other carbon source was present.

In all experiments with fungi, a typical distribution of biomass between PUR surface and medium was observed. *Alternaria alternata* utilized all PUR as the only carbon source. Foams modified by CMC and by AS strongly supported absorption of biomass on PUR surface. Under nitrogen limitation practically the whole biomass was adsorbed on foam surface.

Fusarium solani was able to use modified PUR as the only carbon as well as nitrogen source. This strain also stron-

gly preferred growth on surface of PUR foams, mainly under both carbon and nitrogen limitation.

In model composting conditions, the highest loss of biomass was observed in PUR modified by 10 % of CMC.

All tested natural environments disposed PUR biodegradation activity. In environments different total bacterial activity was found. Individual environments exhibited also different degree of exposition of foams to natural conditions (weather, water, etc.) which could be considered to be important abiotic factors.

It seems that in early stages of long-term natural degradation microbial and abiotic factors act simultaneously, but abiotic processes are more efficient. The highest degradability degree was shown repeatly in PUR modified by CMC and AS.

Conclusions

Tested PUR foams could be biodegraded by microorganisms used in this study. Degree of degradation is strongly dependent on type and concetration of used modifying agents. The highest tendency to biodegradability by most of tested microorganisms was observed in PUR modified by CMC and AS. Mainly in early stages of degradation abiotic and microbial factors act simultaneously. It seems that microorganisms are able to utilize degradation fragments formed during abiotic decomposition.

The effect of mould sorption on PUR surface could be important for biotechnological application. Surface sorption degree depended on type of used modifying agent, mould strain and also on cultivation conditions.

REFERENCES

1. Young D. K., Sung Ch. K.: Polym. Degrad. Stab. *62*, 343 (1998)
2. Wypych G.: *Handbook of Material Weathering, 3rd ed.;* ChemTec Publishing, 2003.
3. Howard G. T.: Int. Biodeter. Biodegrad. *49*, 245 (2002).
4. Chiellini E. et al.: *Biorelated Polymers – Sustainable Polymer Science and Technology;* Springer–Verlag, 2001.

L07 REINFORCING MECHANISMS IN LAYERED SILICATE POLYMER NANOCOMPOSITES

LUKÁŠ RECMAN, JOSEF JANČÁŘ AND JAN KALFUS

Brno University of Chemistry, Institute of Material Science, Purkyňova 118, Brno 612 00, Czech Republic,
jancar@fch.vubr.cz

Introduction

In last decade vast literature has been published on polymer nanocomposites reinforced with layered silicate. As it might be thought that the past decade possess a time long enough to fully understand principles of mechanical reinforcement of layered silicate nanocomposites. It is mostly truth in the opposite way. According to the amount of published literature and increasing interest from industrial sphere, we have decided to highlight the reinforcing mechanism in layered silicate nanocomposites. Polymer nanocomposites based on layered silicate were first prepared by Toyota researchers twenty years ago. Compared to the traditional composites, they possess optimal mechanical properties at low filler content, improved barrier properties. Interesting in this material is that a very small amounts of silicate resulted in pronounced improvements of mechanical and barrier properties[3].

The commonly used layered particles belong to the family of silicates. Among them montmorillonite, hectorice and saponite are the commonly used. Their crystal structure consists of layers stacked together. These layers are connected by van der Walls forces and form an interlayer or a gallery. They show two interesting abilities. The first ability is the possibility to disperse into individual layers. And the second is the ability to fine-tune their surface through ion exchange reactions. Layered silicates are mixed with plenty of polymer matrices. Glassy, Semicrystalline, Crystalline, liquid crystalline or biodegradable matrices are the most popular ones. But the physical mixture of polymer and layered silicate may not form a nanocomposite. This situation is analogous to polymer blends and leads to discrete phases and to separation. The immiscible systems correspond to the more conventionally filled polymers with poor physical interactions between organic and inorganic component. If a satisfactory result is expected a thoroughly particle distribution and dispersion must occur. Never then less a three limiting cases existed. *(i)* Floculated, where clay particles remain in their pristine form without dispergation, this system is equal to a common microcomposite, *(ii)* Intercalated, where a polymer matrix penetrates the gallery of layered particles, but they are still arranged in the "hair-like" fashion. *(iii)* Exfoliation where separate clay particles are homogenously distributed in the matrix posses the highest possible aspect ratio given by the platelet dimensions. All systems can be characterized with increasing an aspect ratio of a particle and increasing the gallery spacing[1].

Below their T_g polymers remains in so called glassy state. It means that only energy driven elasticity may occur. It is due the low thermal energy level of polymer chains which alows only anchored movement of small parts of segment conformation or only the vibration. Well above the T_g the energy is much more higher that the energy barrier of the chain movement. This allows chain to posses a large variety of segmental movement and conformations. Therefor the elastic response of the material above T_g is primarily an entropy driven. The polymer remains in rubbery or rubbery liquid state. In semicrystalline polymers the discription is more complicated because of the presence of the crystal phase. Polymer of this kind can be termed as a composite with crystal reinforcement in amorphous matrix. The elastic behavior of glassy portions is more complex. The chain movement is hindered with presented crystalline domains or they undergo a multiphase morphology like the chains anchored in crystalline domains.

There is no doubth that the adition of the filler to matrix leads to the enhancement of its mechanical properties. Like strength, stiffness and modulus[4]. Three basic mechanisms stiffening may be considered. *(i)* Replace of softer matrix with stiffer filler, *(ii)* A stress transfer from matrix to filler (For non-spherical inclusions). *(iii)* a polymer immobilisation on the surface of the filler as a consequence of matrix filler interactions. In amorphous matrices above their T_g this is the most pronounced reinforcement effect. Below the T_g where all the chains are already immobilized the remaining two mechanisms prevails. In semicrystalline polymer between the temperature range T_g and T_m an amorphous phase can contribute to the reinforcement via the chain immobilization. The other remaining mechanisms are active as well. Additionaly a neglecting effect must be taken into a consideration like the particle agregation, low intercalation or exfoliation, voids and bulk non-homogenities. This complicates the modulus predictions based on material parameters and aspect ratio as a function of filler concentration[1].

In this article we attempt to make an analysis of published data on the elastic modulus of layered silicate nanocomposites for amorphous and semicrystalline polymers. Simple Halpin-Tsain model was used to determine the upper and lower limiting values of the elastic modulus of weakly and strongly interacting systems.

Methodology Used

An experimental data published on clay minerals in polymer matrices were colected. Amorphous and semicrystalline polymers were taken into a consideration. The values for amorphous matrices were taken below T_g and for semicrystalline matrices below T_m. The boundary lines for upper and lower limiting values were calculated using simple Halpin-Tsai model[2]

$$\frac{E_C}{E_m} = \frac{1 + \zeta \eta f}{1 - \eta f},\tag{1}$$

where $\dfrac{E_c}{E_m}$ ratio represents the relative modulus, E_c refers to complex modulus and E_m to matrix modulus. ζ is termed

as shape parameter and is related to the aspect ration with equation

$$\zeta = 2A_R. \tag{2}$$

$$A_R = \frac{length}{thickness} \tag{3}$$

η is a material parameter related to the elastic modulus of constituents with equation

$$\eta = \left(\frac{E_f}{E_m} - 1\right)\left(\frac{E_f}{E_m} + \zeta\right)^{-1} \tag{4}$$

Based on simple micromechanical model represented by Halpin-Tsai model we may consider the aspect ratio equal 1 for no intercalated systems and equel 250 for fully intercalated systems. The values of limiting aspect ratios were roughly estimated from microscopic observations of commercional layered silicate nanocomposites.

Results and Discussion

In amorphous polymers below T_g the chains remain in a frozen state. No low temperature conformations are considered. Hence no further immobilisation can take place while embedded the filler. As a result there are only two reinforcing mechanisms that were left to consider, reinforcement based on elastic modulus and aspect ratio. Experimental data taken from the literature for glassy polymers reinforced mostly with MMT particles completely fell between the boundaries predicted by micromechanical model calculated by equation (1).[5–18]
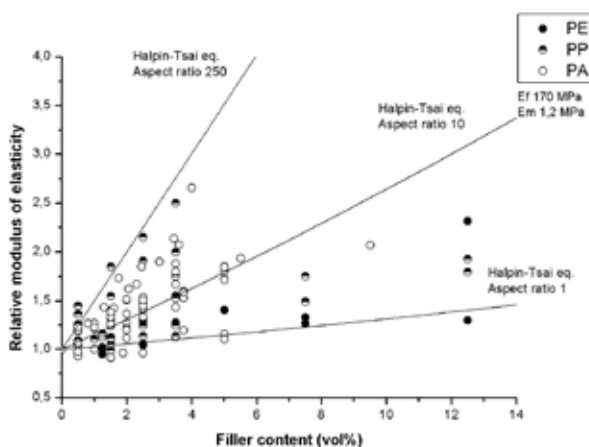
Fig. 1. **Relative modulus of elasticity for PE, PP and PA matrices**

In semicrystalline polymers one may take into a consideration an existance of two distinct temperature regions.[19–32]. $T<T_g$ for the amorphous phase and $T_g<T<T_m$. Below the T_g the reinforcing mechanism is the same as for the amorphous polymers below their T_g. The presence of platelets did not

alter the crystalline regions during solidification. On the other hand the semicrystalline polymer in the temperature range $T_g<T<T_m$ represent more complex behaviour. The amorphous phase above the T_g shows a nano-scale reinforcement mechanism base on segmental immobilization becomes more important. The overall contribution is proportional to the amount of amorphous portion in semicrystalline polymer able to be immobilized. From H-NMR and Raman spectroscopy measurement only 5–20 % of chains is mobile in the case of common polyolefines at room temperature. It is not surpising that the reinforcement for semicrystalline polymers is not as pronounced as for amorphous polymers. It seems that the main reinforcing mechanism for semicrystalline polymers is the same as for the glassy polymer matrices – stress transfer into a platelet shape filler. This hypothesis is supported by the observation of systems reinforced with fillers with high intercations like (polyamides) compared with the systems with weakly filler matrix interactions (polyolefines) at the same filler content.

Conclusions

An experimental data published in literature on the relative elastic modulus of amorphous and semicrystalline layered silicate nanocomposites were analyzed using a simple micromechanical model. It was demonstrated that the mechanism of reinforcement for amorphous polymers beneath their T_g and for semicrystalline polymers beneath their T_m originates primarily from the substitution of matrix with stiffer filler and from the stress transfer. Most of the published data fell within an upper boundary with aspect ratio 250 and the lower boundary with aspect ration 1. The upper bound has not been achieved because of the low degree of intercalation of platelets, non-homogeneus dispersion and random orientation of the particles. The upper bound is truly related to the idealised dispersion and intercalation.

REFERENCES

1. Ray S. S., Okamoto M.: Prog. Polym. Sci. *28* 1539 (2003).
2. Halpin J. C., Kardos J. L.: Pol. Eng. Sci. *16* (1976).
3. Vaia R. A., Wagner H. D.: *Materials Today* (2004).
4. Nielsen L. E., Landel R. F., Dekker M.: New York, second edition (1994).
5. Pinnavaia T. J., Beall G. W.: *Polymer-clay nano-composites,* Chichester, Wiley, (2000).
6. Koerner H., Mistra D., Drummy L., Mirau P., Vaia R.: Polymer, *47*, 3426 (2006).
7. Zhou Y., Pervin F., Biswas M.A., Rangari V. K.: S. Mat. Lett, *60* 869 (2006).
8. Xue S., Pinnavaia T. J.: Microporous Mesoporous Mater. 2007 in press.

9. Ha S. R., Ryu S. H., Park S. J., Rhee K. Y.: Mat. Sci. Eng. A, *448*, 264 (2007).
10. Bozkurt E., Kaya E., Tanoglu M.: Comp. Sic, Tech., *67* 3394 (2007).
11. Chozhan C. K.: J. Polym. Res. *14*, 319 (2007).
12. Ingram S. E., Liggat J. J., Pethrick R. A.: Polym Int. *56*, 1029 (2007).
13. Chang J. H., Kim S. J., Joo Y. L.: S. Im, Polymer *45*, 919 (2004)
14. Fu X., Qutubuddin S.: Polymer *42*, 807 (2001)
15. Gurmendi U., Eguiazabal J. I., Nazabal J.: Comp. Sci. Tech. *66*, 1221 (2006)
16. Su S., Jiang D. D., Wilkie C. A.: Pol. Deg. Stab. *83*, 321 (2004)
17. Uhl F. M., Davuluri S. P., Wong S. C. Webster D. C.: Polymer, *45*, 6175 (2004)
18. Gong F., Feng M., Zhao C., Zhang S., Yang M.: Pol. Test. *23*, 847 (2004)
19. Wan C., Qiao X., Zhang Y.: Pol. Test. *22*, 453 (2003)
20. Lepoittevin B., Devalckenaere M., Panoustier N.: Polymer *43*, 4017 (2002)
21. Yu S. Z., Zhao J. H., Chen G., Juay Y. K.: J. Mat. Proc. Tech. *192–193*, 410 (2007)
22. Wilkinson A. N., Man Z., Stanford J. L.: Comp. Sci. Tech. 2007 in press
23. Alexandre M., Dubois P.: P. Mat. Sci. Eng. *28* 1 (2000)
24. Fornes T. D., Yoon P. J., Keskkula H., Paul D. R.: Polymer *42*, 9929 (2001)
25. Paul D. R., Fornes T. D.: Polymer *44*, 4993 (2003)
26. Liu T. X., Liu Z. H., Ma K. X., Shen L.: Comp. Sci. Tech. *63*, 331 (2003)
27. Fornes T. D., Hunter D. L., Paul D. R.: Polymer *45*, 2321 (2004)
28. Luduena L. N., Alvarez V. A., Vazquez A.: Mat. Sci. Eng. A, *460–461*, 121 (2007)
29. Liu X., Wu Q.: Polymer *42*, 10013 (2001)
30. Pozsgay A. G.: PhD Thesis, Budapest Univeristy of Technology and Economics, 2003.
31. Mittal V.: J. Appl. Pol. Sci. 2007 in press.
32. Ding C., Jia D., He H., Guo B., Hong H.: Pol. Test. *24*, 94 (2005)

L08 THE EFFECT OF MODIFICATION OF PAPER BY MAGNESIUM COMPOUNDS ON HORNIFICATION AND STRENGTH OF PAPER DURING ACCELERATED AGEING

ŠTEFAN ŠUTÝ, KATARÍNA PETRILÁKOVÁ, SVETOZÁR KATUŠČÁK, SOŇA KIRSCHNEROVÁ, MICHAL JABLONSKÝ AND KATARÍNA VIZÁROVÁ

Institute of Polymer Materials, Department of Chemical Technology of Wood, Pulp and Paper, Faculty of Chemical and Food Technology, Slovak University of Technology, Radlinského 9, 831 07 Bratislava, Slovakia,
stefan.suty@stuba.sk

Introduction

Hornification is one of the main reasons leading to brittlenes of fibres on paper recycling[1]. Brittlenes of recycled fibres is explained by hornification which is measured as a loss of the ability of fibres to retain water. This phenomenon was observed with lignin-cellulose fibres when they were repeatedly wetted and dried.

Hornification is one of the presumed processes occurring also during accelerated ageing of paper. However, the effect of hornification on changes in strength properties of paper has not been expressly proved so far. Hornification manifests itself in lignin-cellulose fibres as their lower ability to retain water and it is determined by WRV.

To determine the degree of hornification and to determine the changes on absorption of water, several methods can be used, for example the method determining the ability to retain water (WRV) or the method determining the point of saturation of fibres (FSP). WRV is calculated as a ratio of the mass of water in saturated fibres dipped into water, with subsequent removal of superfluous amounts of water in a centrifuge to the mass of absolutely dry fibres. The FSP is calculated as the total volume of pores, in other words the total content of water in the pores of the cell wall, and can be determined by free discharge or absorption of nitrogen. If the content of water is lower, WRV decreases linearly with increasing dry matter. This situation shows that hornification can occur when the content of water falls under critical level. If the content does not fall under FSP, hornification shall not occur. Both WRV and FSP fall in value when the fibres get repeatedly wetted, from dry state.

The chemical treatment, that is usually used to prevent hornification, gets effective under the condition that it disrupts the creation of hydrogen bonds between cellulose-cellulose and that it becomes strong enough to inhibit serious changes in the inner structure of the paper.

To prevent the process of hornification one can use chemicals that can cause the fibres to swell. Some studies have shown that alkalic NaOH causes the fibres to swell on the basis of ion-exchange reaction.[2–6] The swelling occurs in reaction to osmotic pressure, generated by cations present in the solution (Donnan Effect). The level of swelling increases with the following order of cations: $Al^{3+} < H^+ < Mg^{2+} < Ca^{2+} < Li^+ < Na^+$.

The known modification processes that are to protect the lignin-cellulose carriers of information, as for example the Bookkeeper process[7–11] or the Wei T'o Canada[9,12], run on the basis of compounds that contain magnesium.

The neutralising agents for the Bookkeeper process are the particles of magnesium oxide (MgO) that are smaller than 1μm and are dispersed in perfluorheptane. Some part of the content of magnesium oxide neutralises the present acids, while the non-regenerated part creates alkalic reserve. The magnesium oxide reacts with the acids and with the moisture in the paper in reactions described in the work[13].

The deacidification agent of Wei T'o Canada is methoxy-magnesium-methyl-carbonate (MMMK). This alkoxide is soluble in organic solvents. It is an organic-metallic compound, having the formula: $CH_3O-Mg-O-CO-O-CH_3 \times xCO_2$, where x depends on solvents and on temperature[14].

The MMMK reacts with the moisture of the paper, but most of all with the air humidity, as expressed by the reaction[13]:

$$H_3O-Mg-O-CO-O-CH_3 + 2H_2O \rightarrow Mg(OH)_2 + CH_3OH + CO_2$$
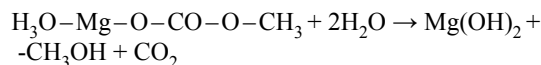
There occur some other reactions liberating magnesium di-hydroxid $Mg(OH)_2$, magnesium carbonate $MgCO_3$ and magnesium oxide MgO, that react with the acids present in paper, thus creating neutral salts. The magnesium compounds, namely, $Mg(OH)_2$, $MgCO_3$ and MgO, gradually absorb the moisture and carbon dioxide CO_2 from the air to form basic magnesium carbonate $MgO \cdot MgCO_3 \cdot Mg(OH)_2$ that gets deposited into the fibres of the substrate, thus creating alkalic reserve that is able to protect the paper against acids.

The end-products from the previously mentioned reactions have a deacidification effect on the products of acid hydrolysis in the paper. Simultaneous swelling reactions of the fibres can occur and they lead to increased flexibility and antihornification effect.

This study reports on the effect of some magnesium compounds on improved ability of fibres to retain water in the process of accelerated ageing. The ability to retain water is a measure of hornification that is one of the mechanisms of fibre brittlenes.

Experimental

Thermally Accelerated Ageing

Paper samples held 24 hours in climatic conditions at 23 °C, and RH = 50% were put in sacks made of layered polyethylene foils with aluminium layer and hermetically closed. The sacks were conditioned at temperature t = 98 ± 2 °C, in time periods 0, 1, 2, 3, 5, 10, 15, 20 and 30 days according to standard ASTM D 6819-02 ref.[15].

Paper

The experiment was performed on newspaper produced by Jihočeské papírny Větřní a.s. The newspaper was wood-

based, callendered, nonsized, with basis weight 45 g m^{-2}, containing 55 % bleached ground wood pulp, 20 % white sulphate pulp, 15 % trapped waste fibres, 10 % clay, pH (surface): 4.5–5.0.

Modification Suspensions

In the fight against the ageing processes, the procedures commonly used to modify paper are the processes Bookkeeper and Wei T'o. These processes are based on the concept of binding particles of magnesium compounds onto the paper fibre surface. Used modification surpensions were:

- Suspension of MgO in perfluorheptane (Bookkeeper), Preservation Technologies, L.P. (PTLP), Cranberry. Township, PA (USA). The PTLP declares that their dispersion of Bookkeeper contains three basic groups of components[16].
- Methoxy-magnesiummetyl-carbonate in methanol, 2% solution, (MMMK), produced by SNK, Martin.

Measuring of Mechanical Properties

The tensile test to determine breaking length was performed on a universal tensile strength tester INSTRON 1122, Instron Ltd., High Wycombe, Buckinghamshire, England, pursuant to the specification *STN ISO 1924–1 (500340): Paper and cardboard. Determination of tensile properties.* Changes of folding endurance[17] (w) were studied on modified and aged samples.

Water Retention Value

The test is carried out by placing a pad of moist fibers in a centrifuge tube that has a fritted glass filter at its base. The centrifuge is accelerated at 900 g to remove water from the outside surfaces and lumens of the fiber (a higher force is used according to some European standards). The remaining water is believed to be associated with submicroscopic pores within the cell wall. The centrifuged fiber pad is weighed, dried at 105 °C, and then reweighed. The WRV equals the ratio of the water mass to the dry mass according to standard ISO 23718:2007.

Results

The previous works report that a modification by Bookkeeper is more or less just a surface modification and a modification of the paper by MMMK can be considered as running inside the volume because it is present in the whole volume of the paper. A similar difference can be found as to the content of magnesium in the paper on modification[18].

Fig. 1. shows changes in the WRV parameter of modified papers as related to the period of ageing. The lowest slump of WRV is in connection with the non-modified paper. With the papers modified by compounds of magnesium, the decrease of WRV with time of ageing is less dramatic. The process of modification in surface, that works with a lower content of magnesium than the process of modification in volume, led to an increase of WRV by 17 %, while the modi-
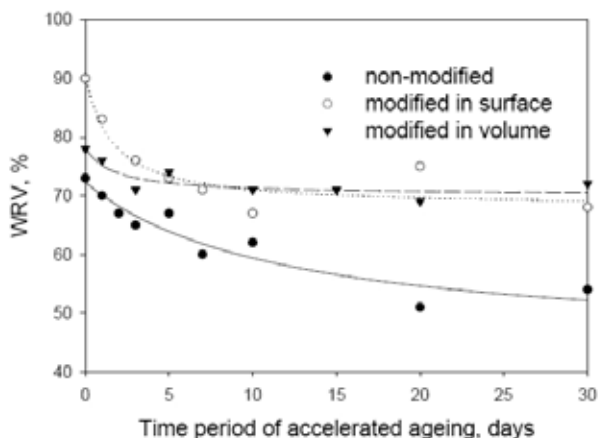
Fig. 1. **WRV as a function of accelerated ageing time period for different modified papers**

fication in volume saw the increase just by 5 %.When one compares the curve of this characteristic and how it develops during ageing, one can see that for the volume modification the trend of WRV to decrease is not significant, the value of WRV decrease is rather stable in the range between 78 % and 72 %. However, in the process of surface modification the WRV value falls from 90 % to 70 %.

When one compares changes of the relative WRV to the changes of WRV for non-aged paper, as dependent on time for given modification processes (Fig. 2.), the trends in decrease for this value are similar. With non-modified paper this relation has a decreasing characteristic, while with modified samples the decreasing trend looks as if it has stopped and is not continuing any more. Out of this relation the best seems to be the modification at which magnesium has been distributed into the whole volume of paper, as the decrease of relative WRV is the slightest. It could be caused by the moisture in the paper itself. Probably, during ageing of the paper, mag-
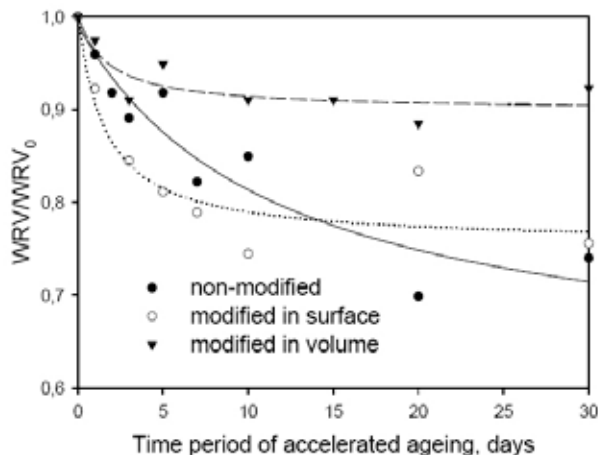
Fig. 2. **Relative value of WRV that is a ratio of WRV and WRV time = 0 as a function of accelerated ageing time period for different modified papers**
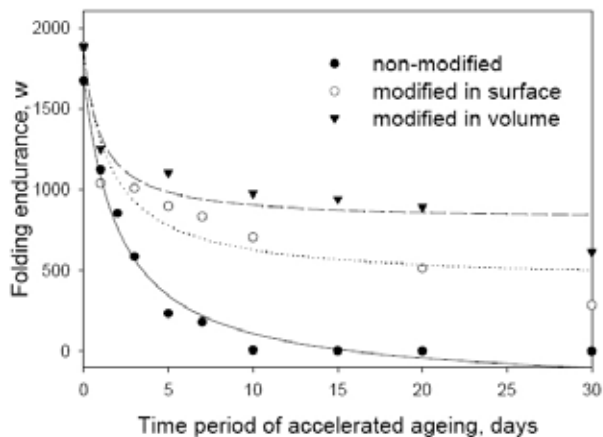
Fig. 3. **Folding endurance as a function of accelerated ageing time period for different modified papers**
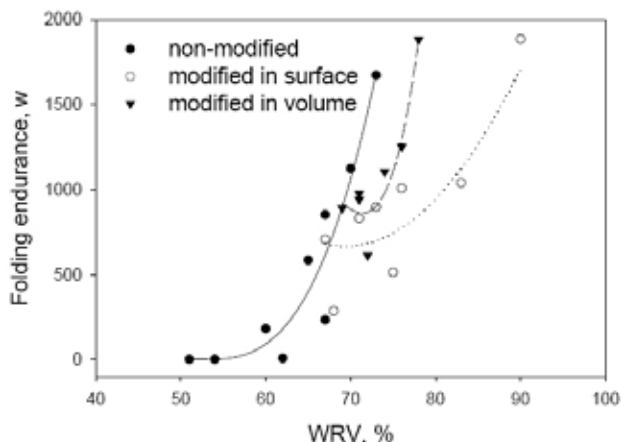
Fig. 5. **Relationship between folding endurance and WRV**
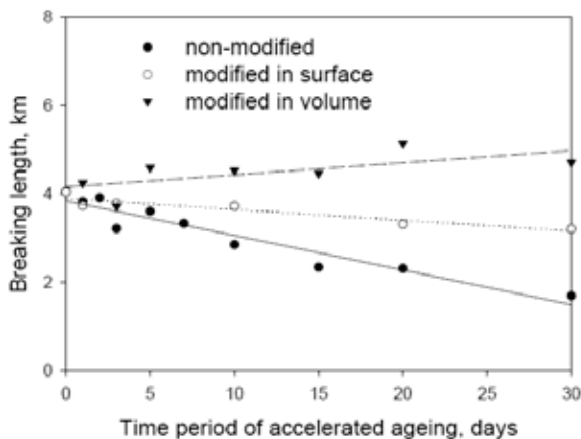
Fig. 4. **Changes in breaking length during accelerated ageing for different modified papers**
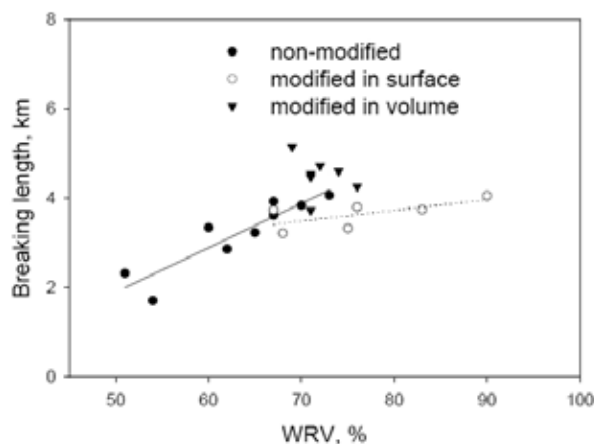
Fig. 6. **Breaking length as a function of WRV for different modified papers**

nesium reacted with the moisture present in the paper which caused swelling of the fibres, thus leading to better results of the process of hornification.

Fig. 3. shows the dependence of number of double-folds during accelerated ageing on time. The effect of magnesium compounds on the number of double-folds is clearly positive. Improvements in the number of double-folds can be seen also in non-aged samples, in which case the papers modified in volume or surface prove higher number of double-folds than non-modified paper. The curves reflecting the changes of double-folds are similar for all samples. The greatest decrease can be seen with the non-modified paper. All the samples show the greatest decrease in the number of double-folds in the first ten days of accelerated ageing, later there is a tendency to certain stabilisation of the decrease of the measured quantity. A similar development of relation can be seen for the WRV.

Fig. 4. shows dependences of breaking length on time of accelerated ageing. Even in this relation one can see the posi-

tive effect of paper modification via magnesium compounds. Even more, modification in volume increases the breaking length of paper during accelerated ageing. Similarly, paper modification in surface considerably contributes to its breaking length. In the case of non-aged papers, no differences can be seen for the parameter of breaking length.

Fig. 5. documents dependence of the number of double-folds on WRV of papers modified in different way. All the measured dependences reflect the fact that with growing values of WRV the number of double-folds grows as well. For non-modified paper the number of double-folds falls to zero. For modified papers the minimum values are considerably higher and they do not fall to zero.

For non-modified paper, the breaking length depending on WRV changes linearly, but with growing value of WRV the breaking length increases. For paper modified in surface, a similar dependence has been obtained, but with smaller angle of inclination. The paper modified in volume does not show this dependence.

Conclusions

Modification of lignin-cellulose fibres by magnesium compounds leads to their better retention of water. Modification by magnesium compounds inhibits hornification of fibres along the process of ageing. The probable mechanism of the modification is based on reaction of magnesium compounds that are transported into the paper in organic phase by water present in the paper. Magnesium compounds react with residual moisture giving alkalic substances that improve the ability of fibres to retain water. The fibres thus adjusted are more flexible; they undergo only a limited process of hornification and are more stable on bending than non-modified fibres.

REFERENCES

1. Gullichsen J., Paulapuro H.: *Papermaking Science and Technology, Book:* 7:*Recycled fiber and deinking* (Göttsching L., Pakarinen H),,Fapet Oy, Helsinki, p. 359 (2000).
2. Alanko K.: *M.Sc. thesis,* Helsinki University of Technology, Department of Forest Products Technology, Espoo, Finland, (1993).
3. Scallan A., Tigerstrom A. C.: *CPPA 1st Research Forum on Recycling,* Montreal , p.149, 1991.
4. Gurnagul N.: Tappi J. *78,* 119 (1995).
5. Katz S., Liebergott N., Scallan, A.M.: Tappi J. *64,* 97 (1981).
6. Laine J., Stenius P.: Paperi Puu *79,* 257 (1997).
7. Buchanan S. et al.: *An Evaluation of the BOOKKEEPER Mass Deacidification Process: Technical Evaluation Team Report for the Preservation Directorate,* Library of Congress. Preservation Directorate, Library of Congress. Washington 1994.
8. http://www.loc.gov/preserv/deacid/bkkeep2.html
9. *Technical Evaluation Team Report: An Evaluation of the Bookkeeper Mass Deacidification Process.* Pittsburgh, PA, 1994.
10. *Supplement E.: An Evalution of the Bookkeeper Mass Deacidifikation Process* (S. M..Melnick, Ed.), Preservation Directorate, Library of Congress, Washington (1994).
11. http://aic.stanford.edu/sg/bpg/annual/v15/bp15–17.html
12. Kaminska E. M., Burgess H. D.: *Evaluation of Commercial Mass Deacidification Processes: akzo-dez, Wei T'o. New and Artificially Aged Modern Papers.* Canadian Conservation Institute, Ottawa 1994.
13. Kirschnerová S.: *M.Sc. Thesis,* Slovak University of Technology, Bratislava, Slovakia 2005.
14. Brandt A. CH.: *Mass Deacidication of Paper. A Comparative study of existing processes.* Bibliothéque Nationale, Paris 1992.
15. ASTM D 6819-02: *Standard test method for accelerated temperature aging of printing and writing paper by dry oven exposure apparatus.*
16. Bieliková L: *M.Sc. Thesis,.* Slovak University of Technology, Bratislava, Slovakia 2005.
17. *ASTM D 2176 – 97a: Standard Test Method for Folding Endurance of Paper by the M.I.T. Tester*
18. Majerčáková K.: *M.Sc. Thesis,* Slovak University of Technology, Bratislava, Slovakia 2006.

L09 IMPACT OF PROCESSING ON DEGRADATION OF POLYPROPYLENE IMPACT-COPOLYMER

JIŘÍ TOCHÁČEK[a], SOŇA HERMANOVÁ[b], JOSEF JANČÁŘ[b] and JAN KALFUS[b]

[a]*Polymer Institute Brno, Ltd., Tkalcovská 36/2, 656 49 Brno, Czech Republic,*

[b]*Institute of Materials Chemistry, Faculty of Chemistry, Brno University of Technology, Purkyňova 118, 612 00 Brno, Czech Republic,*

tochacek@polymer.cz

Introduction

During processing by extrusion polymers undergo harsh thermo-mechanical exposure, which usually induces chemical reactions leading to the changes in polymer backbone. Conditions in extruder cylinder are very specific as to the access to oxygen, which basically impacts the chemistry of degradation. A certain limited amount of oxygen originally dissolved in polymer matrix is consumed at the initial zone of cylinder. The following path through cylinder is characterized by no oxygen access. Different kinds of reactions thus take place during extrusion[1,2].

In the case of polypropylene homopolymer (PPH), the traces of oxygen are consumed by the reactions with R• radicals, originating from the thermo-mechanical cleavage of C−C and C−H bonds. These reactions give rise to the formation of oxygen containing intermediates such as RO• and ROO• radicals, the cleavage of which leads to the decrease in molecular weight. These reactions, however, are of limited extent just because of the limited amount of oxygen entering the reaction. When oxygen is consumed, the thermomechanical cleavage of C−C backbone plays the dominating role. This mechanism is typical for the processing in an extruder. Carbon centered R• radicals formed in this way are not able to propagate in the absence of oxygen and in the case of polypropylene they terminate by disproportionation giving rise to $CH_2=C(CH_3)$- end groups. Due to the methyl substitution, the end double bond cannot add R• radicals. Thus in the case of PP no crosslinking occurs and processing degradation leads exclusively to the decrease in molecular weight, reflected by the increasing melt-flow rate[1,2].

PP homopolymer degradation mechanism has been well described in literature.[1-4] On the other hand degradation of PP impact-copolymer is much less documented[5,8]. PP impact-copolymer is typical with the heterogeneous structure, consisting of PP homopolymer, ethylene-propylene rubber and a relatively small portion of PE homopolymer phases[6,7]. The degradation processes induced here by extrusion are thus more complicated and influenced by the presence of ethylene units, the quantity and distribution of which substantially influences the overall behaviour of the material. The target of this work is to elucidate phenomena taking place in PP impact-copolymer during extrusion.

Experimental

Materials

Polypropylene, a medium-impact copolymer of Innovene technology (gas-phase process) – *(i)* non-stabilized fluff (total ethylene content 6.4 % wt.) and *(ii)* commercial grade (total ethylene content 5.4 % wt.) both of melt-flow index (MFI) 6 dg min^{−1}. (230 °C 2.16 kg^{−1}) were used for the experiments. Polypropylene homopolymer of the same technology, commercial grade of MFI 6 dg/min. (230 °C 2.16 kg^{−1}) was used as a reference. Both commercial grades were pelletized and stabilized with the same stabilizer system.

Methods and Measurement

Processing stability was carried out on a Brabender single-screw extruder 19mm, l/d=30, at 260 °C 100 rpm;

Melt-flow index (MFI) was measured at 230 °C, 2.16 kg (ISO EN 1133).

Yellowness index (YI) – according to ASTM D 1925 (DataColor SF650) measured on pellets

GPC analysis – carried out at PL-GPC 220 with detectors PL–220DRI and VISKOTEK model 220R, 3 × column PL gel 10 μm MIXED-B, 300 × 7.5 mm, mobile phase TCB, flux 1.0 ml min^{−1}.

Mechanical properties were measured on Instron 4466 and Zwick 5102; specimens injection moulded at 200–230 °C were used.

Solvents successive extractions were carried out using a Soxhlet extractor. Extractions varied from 12 to 20 hours; 5 g of polymer were extracted, solvent volume was 800 ml.

Results

Processing of Commercial Grades

Processing stability

A commercial PP impact-copolymer (ICPP) and its homopolymer reference (PPH) were subjected to multiple extrusion on a laboratory Brabender extruder at 260 °C. Because both the starting materials were received in the form of pellets, the pelletization step at the producer´s facility at 240 °C was denoted as zero extrusion, while the other ones carried out on a Brabender at 260 °C were numbered 1st to 5th extrusion. After selected extrusions, material properties were determined (Tables I and II).

In spite of the different chemical compositions of both of the polymers, processing characteristics induced by multiple extrusion were found very similar. The presence

Table I

Properties of commercial ICPP after multiple extrusion at 260 °C

	MFI [dg min^{−1}]	Yellowness index (YI)	OIT 180 °C [min]
0. extrusion	6.1	−3.4	22.1
1st extrusion	6.9	-0.9	15.3
3rd extrusion	8.7	1	12.6
5th extrusion	11.5	2.3	13.8

Table II
Properties of commercial PPH after multiple extrusion at 260 °C

	MFI [dg min^{-1}]	Yellowness index (YI)	OIT 180 °C [min]
0. extrusion	6.2	–4.4	9.5
1st extrusion	7.1	–1.4	Not measured
3rd extrusion	8.6	-0.6	Not measured
5th extrusion	11.1	0.3	8.5

of ethylene units in ICPP did not exhibit any special impact on melt behaviour, so that as to the melt rheology, one could conclude that both the materials behaved similarly. Higher levels of colour development in ICPP may be accounted for to the phenol conversion, favoured by a higher level of oxygen dissolved in its amorphous phase. The presence of oxygen and phenol consumption are also likely responsible for faster OIT drop in ICPP. Regardless to their absolute values, OIT changes also indicate that the stabilizer system is faster consumed in ICPP.

　　More intensive changes in ICPP macromolecules are indicated by GPC data. It shows that average number molecular weight Mn drops due to multiple extrusion by 21 % rel. in ICPP and only about 8 % rel. in PPH (Tables III and IV).

Table III
Molecular weight distribution of ICPP after multiple extrusion at 260 °C

PP- impact copolymer	M$_n$ [× 10^3]	M$_w$ [× 10^3]	M$_z$ [× 10^3]	M$_w$/M$_n$	Intrinsic viscosity [ml g^{-1}](GPC)
0. extrusion	62	342	1,059	5.6	166.6
1st extrusion	49	262	708	5.4	135.6

Table IV
Molecular weight distribution of PPH after multiple extrusion at 260 °C

PP- impact copolymer	M$_n$ [× 10^3]	M$_w$ [× 10^3]	M$_z$ [× 10^3]	M$_w$/M$_n$	Intrinsic viscosity [ml g^{-1}](GPC)
0. extrusion	51	314	986	6.2	158.4
1st extrusion	47	260	705	5.6	138.3

Mechanical properties
　　The changes in mechanical properties, as a consequence of processing, were monitored. It was found that in spite of relatively strong thermo-mechanical impact of multiple extrusion at 260 °C, tensile and flexural properties did not change substantially. Attained values, such as shown in Tables V and VI, more or less lie within the range of experimental error in the cases of both polymers.
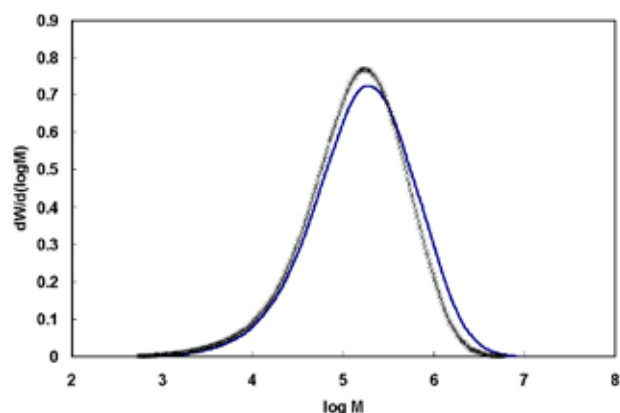
Fig. 1. **Molecular weight distribution of ICPP after multiple extrusion at 260 °C, (full line = 0.extrusion; shredded line = 5th extrusion)**

　　The only parameter reflecting the changes is Charpy impact strength at +23 °C, visibly decreasing with the number of extrusions. Beside lower absolute values, the higher relative drop in Charpy values was observed in PPH.

　　While a more intensive drop in molecular weight was found in an ICPP during melting, the complexity of ICPP solid phase caused that its consequences were far not so dramatic. Relatively stronger decrease in Charpy values in PPH is likely the result of scission of the longest macromolecules, serving as tie molecules among the crystalline areas. Very similar phenomena must logically take place also in ICPP, where PPH phase occupies about 95 % of the mass of the polymer.

Table V
Mechanical properties of ICPP after 0. and 5th extrusions at 260 °C

	0.extrusion	5th extrusion
Stress at yield [MPa]	29.9 ± 0.1	29.2 ± 0.1
Elongation at yield [%]	3.8 ± 0.1	3.9 ± 0.1
Elongation at break [%]	67.3 ± 23	56.3 ± 18
Flexural modulus [MPa]	1,671 ± 15	1,647 ± 19
Impact strength Charpy +23 °C [kJ m^{-2}]	8.6 ± 0.3	7.0 ± 0.3

Table VI
Mechanical properties of PPH after 0. and 5th extrusions at 260 °C

	0.extrusion	5th extrusion
Stress at yield [MPa]	33.9 ± 0.4	34.2 ± 0.2
Elongation at yield [%]	7.5 ± 0.1	7.5 ± 0.1
Elongation at break [%]	>335	101– >335
Flexural modulus [MPa]	1,597 ± 24	1,566 ± 30
Impact strength Charpy +23 °C [kJ m^{-2}]	3.6 ± 0.1	2.6 ± 0.3
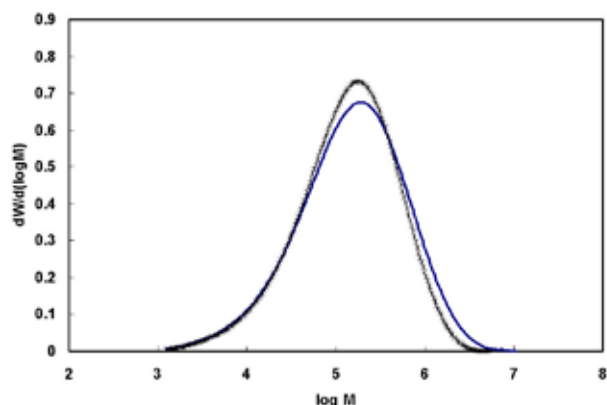
Fig. 2. **Molecular weight distribution of PPH after multiple extrusion at 260 °C, (full line = 0.extrusion; shredded line = 5th extrusion)**

Fig. 3. **Molecular weight distribution of non-stabilized ICPP fluff after triple extrusion (full line = 0. extrusion; shredded line = 5th extrusion)**

However, the presence of rubbery (EPR) domains in ICPP causes that crack propagation rate is still fairly moderated and the loss of some portion of tie molecules is thus compensated. Then the relative drop in Charpy + 23 °C values is rather moderate in ICPP.

Despite certain degradation changes, such as partial crosslinking, may also take place in EPR phase, their role as energy dissipaters is still not lost[8]. Hence, coming out of the above results it can be confirmed that as to mechanical properties, the negative consequences of processing degradation are less pronounced in ICPP than in PPH.

Processing of Non-Stabilized ICPP

In the previous part, commercial ICPP and its PPH reference were investigated. Both were stabilized. Since the stabilizer system moderates degradation and diminishes its consequences, another measurements were carried out with a non-additivated ICPP fluff. With respect to the absence of

Table VII
Melt-properties of non-stabilized ICPP after multiple extrusion at 260 °C

ICPP fluff	MFI [dg min^{-1}]
0. extrusion	6.0
1st extrusion	20.1
3rd extrusion	42.3

Table VIII
Molecular weight distribution of non-stabilized ICPP fluff after triple extrusion at 260 °C

PP- impact copolymer	M_n [$\times 10^3$]	M_w [$\times 10^3$]	M_z [$\times 10^3$]	M_w/M_n	Intrinsic viscosity [ml g^{-1}](GPC)
0. extrusion	46	305	907	6.7	148.7
3rd extrusion	30	185	472	6.2	99.5

stabilization only three processing extrusions were adopted. Samples after 0. and 3rd extrusion were tested.

Degradation of non-stabilized ICPP was found very intensive even after three extrusions at 260 °C, strong increase in melt-flow index was observed. The samples after 0. and 3rd extrusion were subjected to successive extraction by organic solvents in order to separate individual polymer fractions and determine changes in their quantities as a consequence of processing.

As solvents, non-polar hydrocarbons with increasing boiling temperatures – n-hexane, n-heptane and n-octane were used according to scheme in Fig. 4. Polymers were dissolved in boiling solvent and precipitated from the solution at room temperature. Each solvent extracted different fraction of polymer. In this way, four fractions – hexane solubles (HEX-sol), heptane solubles (HEP-sol), octane solubles (OCT-sol) and octane insolubles (OCT-ins) were attained. Their composition, previously determined by NMR, FTIR and DSC techniques[9,10] is shown in Table IX.
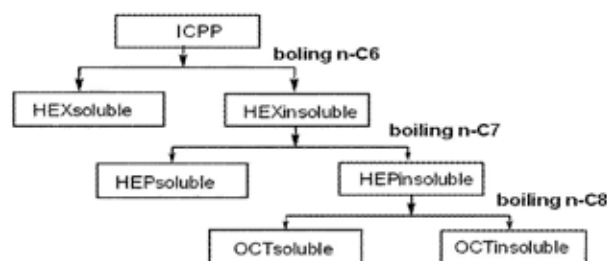
Fig. 4. **Scheme of successive extractions of a non-stabilized ICPP**

Considering the effect of processing on quantities of individual fractions it was found that hexane and heptane solubles mostly vary only within an experimental error and their quantities do not exhibit any impact processing.

Biggest changes due to processing took place in both octane fractions. Drop in octane insolubles indicates that the longest isotactic homopolymeric chains were reduced

Table IX
Overview of fractions available by successive solvents extractions from ICPP matrix[9,10]

	PE-homo	PE-homo	PP-atactic	PP-isotactic
HEX-sol	•	XX	X	
HEP-sol	x	x	XX	
OCT-sol		•		XX
OCT-ins				XX

XX – prevailing, X – much, x – little, • – nearly nothing

in molecular weight. Increase in octane solubles portion on the other hand provides information on the degree of solubility of the scission products. No increase in heptane solubles then confirms, that the scission products are only highly crystalline PP homopolymeric chains.

The solvent successive extraction thus provided evidence that in ICPP the biggest extent of degradation changes induced by processing took place in a PP homopolymeric phase.
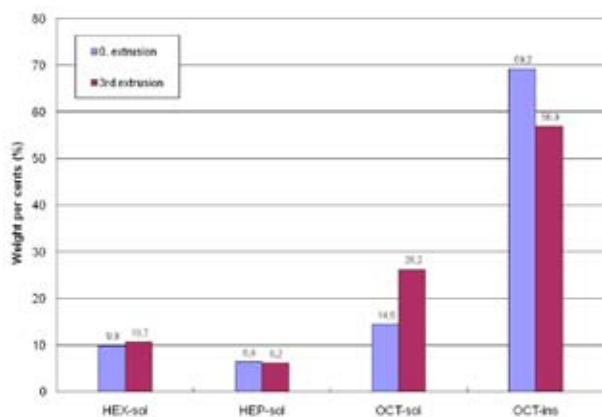
Fig. 5. **ICPP solvent successive extractions overview – mass balance**

Conclusions

The above processing experiments have revealed, that despite higher extent of backbone scission taking place in ICPP, in terms of melt viscosity both polymers behaved in a similar way. It can be concluded that both ICPP and PPH, tested under the same processing conditions and using the same stabilizer systems, exhibit the same processing stabilities.

In the solid state some differences were observed. While the tensile and flexural characteristics were not affected by

processing at all, impact properties dropped down and indicated certain changes in polymer morphology. Although the biggest portion of degradation changes took place in the homopolymeric phases of both polymers, the presence of rubbery domains diminished their effect in ICPP. Due to the ability of moderating the crack propagation rate, EPR phase compensated the loss of some tie molecules and partly retained the impact resistance. Then it is evident that multiple extrusion caused relatively less harm in ICPP also in its solid state.

The results obtained in this work, together with the data of our previous experiments, step by step reveal the mechanism of ICPP processing degradation and allow us to learn where and in what extent degradation takes place.

REFERENCES

1. Zweifel H.: *Stabilization of Polymeric Materials,* Springer-Verlag Berlin, Heidelberg, New York 1998.
2. Gächter R., Müller H.: *Plastics Additives,* 3rd Edition, Hanser Publishers, Munich, Vienna, New York, 1990.
3. Hawkins W. L.: *Polymer Stabilization*, Wiley, New York 1972.
4. Scott G.: *Mechanisms of Polymer Degradation and Stabilisation,* Elsevier Applied Science, London and New York, 1990.
5. Tocháček J., Jančář J., Kalfus J.: *A poster presented at 8th Austrian Polymer Meeting 2006,* Johannes Kepler University, Linz, Austria, 2006.
6. Hongjun C., Xiaolie L., Dezhu M., Jianmin W., Hongsheng T.: J.Appl.Polym.Sci. *71*, 93 (1999).
7. Hongjun C., Xiaolie L., Xiangxu C., Dezhu M., Jianmin W., Hongsheng T.: J.Appl.Polym.Sci. *71*, 103 (1999).
8. Tocháček J., Jančář J., Kalfus J., Šimková P., Buráň Z.: Polym. Degrad. Stab. *93*, 770 (2008).
9. Hermanová S., Jančář J., Tocháček J., Kalfus J.: *Plastko 2008 Conference,* Zlín, Czech Republic, 2008.
10. Hermanová S., Jančář J., Tocháček J., Kalfus J.: accepted for publication at Macro 2008, Polymers at Frontiers of Science and Technology, Taipei, Taiwan, June 29-July 4 2008.

L10 POLYMER SEMICONDUCTORS FOR FUTURE MOLECULAR ELECTRONIC DEVICES

MARTIN WEITER and MARTIN VALA

Brno University of Technology, Faculty of Chemistry, Purkyňova 118, 612 00 Brno, Czech Republic,
weiter@fch.vutbr.cz

Introduction

Polymer semiconductors are poised as never before to transform the world of circuit and display technology. After more than 20 years of academic and industrial research worldwide the conjugated polymers has reached a very high level of outstanding material properties that are particularly attractive for the electronic industry. There are many potential applications including light-emitting devices, photovoltaic solar cells, plastic field-effect transistors, non-linear optical devices. Major electronics firms such as Sony, Philips, Samsung, Siemens and Pioneer are now developing the low cost and sometimes surprisingly high performance organic electronic and optoelectronic devices. Large-scale multicolor displays together with flexible active matrix of organic thin film transistors (OTFT) are now commercially available. Functional polymers are applied even in the logical circuits, which give rise to a new branch – "Plastic Logic".

For this to become a reality, an intensive research has to be done. The first highly conducting organic polymer, chemically doped polyacetylene, was reported in 1977[1]. Although initially these doped conducting polymers were unstable in air, brittle, and difficult to process, new generations of these materials are stable and easily processable from a wide variety of solvents. The electrical conductivities now range from those typical for insulators ($<10^{-10}$ S cm^{-1}), to those typical of semiconductors such as silicon ($\sim 10^{-5}$ S cm^{-1}), to those greater than 10^4 S cm^{-1} (nearly that of copper, 5×10^5 S cm^{-1}). At the end of the 1980s poly(phenylenevinylene) (PPV) has been one of the most studied polymers. This intense research led to the discovery of the polymer-based light emitting diode (LED)[2] in 1990 by the Cambridge group in England. At the same period the high-performance electroluminescent devices made of multilayer of vacuum-sublimed dye films at Eastman Kodak[3], field-effect transistors made from polythiophene[4,5] and from small conjugated oligomers[6,7] were demonstrated. This was a breakthrough improvement since it made it possible to combine the good mechanical and processing properties of polymers with semiconducting behavior (providing processibility under well established techniques, such as spin or dip coating). From that time, wide range of semiconducting polymers is now commercially available from different suppliers, for different quantities and qualities.

In spite of great progress that has been made, there is still much to be understood about the underlying science that controls the properties of the organic electronic devices. Organic materials have often proved to be unstable and when exposed to air, water, or ultraviolet light, their electronic properties can degrade rapidly. Making reliable electrical contacts to organic thin films is difficult and the metal-polymer interface is a matter of intensive study[8]. The low carrier mobilities characteristic of organic materials[9] obviates their use in high-frequency (greater than 10 MHz) applications. These shortcomings are compounded by the difficulty of both purifying and doping the materials. Finally, in many types of organic semiconductors, the processes connected with the photogeneration and transport of charge carriers under the influence to electric field are still not well understood and are open to conjecture. The better understanding of these basic phenomena can enhance speed and efficiency of organic electronic devices, which is the fundamental motivation of our work.

Organic photovoltaics currently lag behind the inorganic one because of low solar energy conversion efficiency about 1–6 %. It is well known that photodissociation can be highly efficient in two component donor-acceptor systems, as evidenced by the photovoltaic response of several systems. To improve the efficiency, the combination of photoconducting polymer substrates and quest materials such as fullerenes were employed, nevertheless the experimental results published by different authors are diverse. In order to enter an electrode the photogenerated charges have to move over the bulk of the solar cell and overcome the potential barrier in electrode region. On molecular level the charge transport can be affected by introducing the guest molecules, whose energy levels are in general different from the energy levels of the host. The transport of charges is affected by recombination during the journey to the electrodes – particularly if the same material serves as transport medium for both electron and holes. Also, interaction with atoms or other charges may slow down the travel speed and thereby limit the current. It is often observed that the distribution in the length of the conjugated segments caused by kinks or chemical defects increases disorder in conjugated polymers as compared to their oligomeric counterparts or other small molecules. Thus, in organic photovoltaic devices based on the combination of additives and polymer substrates the interaction between the moving charges and the additives seems to be a crucial process affecting the efficiency of photovoltaic conversion. Therefore, the aim of our study was to describe the influence of charge traps induced by additives on the efficiency of charge carrier transport.

Experimental

Polymer devices were manufactured as a sandwich cell with a dielectric multilayer. Samples consisted of transparent indium tin oxide (ITO) electrode on a glass substrate on to which the 15 nm thin layer of poly(2,3-dihydrothieno-1,4-dioxin) (PEDOT) was spin cast from water solution to decrease the injection barrier for holes. Then, the active polymer layer, typically 150 nm thick, was spin coated from chloroform solutions of MDMO-PPV (Poly[2-methoxy-5-(3',7'-dimethyloctyloxy)-1,4-phenylenevinylene]) with 0/30 % wt. of spiropyran 6-nitro-1',3',3',-trimethylspiro[2H-1-benzopyran-2,2'-indoline] (SP). To decrease the contact injection

barrier for electrons a thin 10 nm layer of Alq$_3$ (8-hydroxyquinoline, aluminium salt) was vacuum evaporated and the structure was completed by evaporation of aluminium top electrode 100 nm thick. Average device area was 3 mm^2.

The photochromic reaction of SP was activated using a Xenon lamp with band filter (360 ± 20) nm. In our previous work it has been shown that after photochromic conversion the charge traps are created in the vicinity of a polymer chain and charge carrier mobility decreases which lead to to the current decrease[10]. The electric response of the samples on the spiropyrane photoswitching was studied by measuring the current-voltage (*I-V*) characteristics of the samples by Keithley 6517A electrometer.

Results

The photoswitching of polymer conductivity and photoconductivity was studied by standard current-voltage *j(V)* measurement. The results for typical devices are shown as log-log plot in Fig. 1. The variation of the dark current before and after photochromic conversion is depicted by dark symbols, whereas the variation of the photocurrent during irradiation of the sample with halogen lamp with cut off UV filter (<420 nm) is shown by white symbols. In organic thin film devices the current is typically contact limited in low field region, whereas at higher field region space-charge or charge-trap limited conductivity are commonly accepted. The results show this behavior. At low forward-bias voltages below 10 V the increase of *j* with *V* is relatively small, whereas in the higher field region the slope of the dependence is more pronounced, which is in accordance with Space-charge limited current (SCLC) theory. This theory proposes that the space charge which limits conduction is stored in the traps. In the case of energetically discrete trapping level, the SCL current can be expressed as

$$j_{SCL} = \frac{9}{8}\varepsilon\varepsilon_0\mu\vartheta\frac{V^2}{L^3},$$ (1)

where ε and ε_0 is the relative permittivity and permittivity of vacuum, μ is the charge carrier mobility, V is the applied voltage, L is the electrode distance and ϑ is the ratio of free to total charge carriers.

However, in cases of practical interest traps are usually distributed in energy. In that case traps will be filled from the bottom to the top of the distribution as applied electric field increases. This is equivalent to an upward-shift in the quasi-Fermi level with electric field. As a consequence, ϑ increases with electric field and the *j(V)* characteristics becomes steeper. In terms of present work, the distribution of charge traps describes those induced by spiropyrane to merocyanine photochromic conversion. The presence of distribution of traps opens additional pathways to the relaxation of charge carriers towards steeper states. A zero order analytic description of the effect can be based on the Hoesterey and Letson formalism. The latter is premised on the argument that the carrier mobility in a system with relative trap concentration *c*

is the product of the mobility in the trap-free system μ_0 multiplied by trapping factor:

$$\mu(c) = \mu_0\left[1 + c\exp\left(\frac{E_t}{kT}\right)\right]^{-1},$$ (2)

where E_t is the energy of trapping level, k is the Boltzmann constant and T is the temperature. Consequently, the current flowing in a sample with enhanced number of trap states will be less than in sample without traps.

The surprisingly large increase of the photocurent after the photochromic conversion can be explained by the charge transfer mechanism and by the presence of polar merocyanine molecules. This phenomenon indicates that there is a high tendency for charge separation as well as good ability to retain charges once induced by electric field. However the elucidated the detailed mechanism of the photogeneration, a detailed studies of exciton generation, charge separation and following transport should be done.
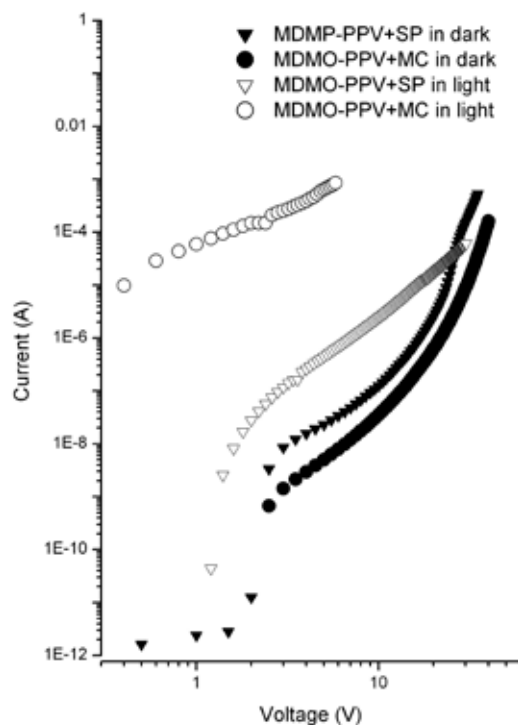
Fig. 1. **The current-voltage characteristics of the ITO/PEDOT/ MDMO-PPV:SP/Al (20 % wt.) sample before (triangles) and after (circles) the photochromic conversion of spiropyran molecules by irradiation of UV ligh as measured in the dark (filled symbols) and by irradiation (open symbols)**

Conclusions

The utilization of organic semiconductors in electronic and optical devices was described. The new molecular device based on photoswitching of polymer conductivity and photoconductivity was demonstrated. The experimental behavior of the system explored by means of SCLC method showed

a change of the density of states in the bandgap of the polymer. Reversible creation of new trapping level during the photochromic conversion was observed. According to the trap controlled hopping model for the description of charge transport, the presence of new trapping level results in the decrease of the charge carrier mobility as predicted by the theoretical calculations.

REFERENCES
1. Chiang C. K., Fincher C. R. Jr., Park Y. W., Heeger A. J., Shirakawa H., Louis E. J., Gau S. C., MacDiarmid A. G.: Phys. Rev. Lett. *39*, 1098 (1977).
2. Burroughes J., H., Bradley D. D. C., Brown A. R., Marks R. N., Mackay K., Friend R. H., Burn P. L., Holmes A. B.: Nature *347*, 539 (1990).
3. Tang C. W., VanSlyke S. A.: Appl. Phys. Lett. *51*, 913 (1987).
4. Koezuka H., Tsumura A., Ando Y.: Synth. Met. *18*, 699 (1987).
5. Tsumura A., Koezuka H., Ando, Y.: Synth. Met. *25*, 11 (1988).
6. Horowitz G., Fichou D., Peng X. Z., Xu Z., Garnier F.: Solid State Commun. *72*, 381 (1989).
7. Garnier F., Horowitz G., Peng X. Z., Fichou D.: Adv. Mater. *2*, 592 (1990).
8. Murdey R. J., Salaneck W. R.: Jap. J. Appl. Phys. *44*, 3751 (2005).
9. Baessler H.: *Semiconducting Polymers – chemistry, Physics and Engineering* p. 365 – 410, Eds. By Hadziioannou, G., and van Hutten, P., F., Wiley, New York, 2000.
10. Weiter M, Vala M, Zmeškal O., Nešpůrek S., Toman P.: Macromol. Symp. *247*, 318 (2007).

L11   MOLECULAR MODELING OF MATERIALS WITH NETWORK STRUCTURE

JAN ŽÍDEK and JOSEF JANČÁŘ

Institute of Materials Science, Brno University of Technology, Purkynova 118, 612 00 Brno, Czech Republic,
zidek@fch.vutbr.cz

Introduction

Numerous different polymeric materials are from structural point of view macromolecular networks. Network-like polymers can have various forms, such as gels, rubbers and glasses. Their properties depend on microscopic properties such as crosslink density, chemical composition. Variability of behaviors is caused by different theoretical principles influencing their properties. Deformation properties can be as a consequence either of intermolecular interactions or of the change of combinational entropy.

Macromolecular networks are known for a long time. First theories were proposed by Flory, Kuhn and Grun[1], and James and Guth[2]. In the 70s as a consequence of the single chain elasticity model proposed by Treloar[3]

$$\sigma = \frac{1}{3} E \sqrt{N} L^{-1} \left(\frac{\lambda}{\sqrt{N}} \right), \tag{1}$$

where E was Young modulus; N – number of segments of the chain; λ – draw ratio (elongation) of the chain and L^{-1} was the inverse Langevin function.

Since the development of this theory, have been many refinements and extensions, such as the model of 8 chains cell proposed by Arruda and Boyce[4] which approaches to the real behavior of rubbery networks. The main results about rubbery networks were summarized on a large review work by Puso[5]. In the first work of Termonia[6], was the single chain elasticity theory was successfully applied to the prediction of spider silk elasticity. However, the simple network is not realistic. Therefore the models should reflect real structure of the networks.

Second principle of polymer loading is acting of intermolecular interactions[7]. The interactions can be either bonding or nonbonding. During the deformation, the bonds and the nonbonding pairs are shifted from their equilibrium positions. The exact molecular theories were introduced by Lennard Jones potential. This is a model of potential where the atoms approaching each to other are subjected to strong repulsive interaction whereas the in the long distance are not interacting. The distance of such potential is a function of interatomic distance:

$$U = 4\varepsilon \left[\left(\frac{r_{12}^0}{r_{12}} \right)^6 + \left(\frac{r_{12}^0}{r_{12}} \right)^{12} \right], \tag{2}$$

where ε is energy of nonbonding interaction and r_{12}^0 is distance where the energy is zero.

Intermolecular interaction is mostly used in the Molecular Dynamics and Molecular Mechanics. These two techniques are used to investigation of molecular theories. The molecular mechanics is to find the optimum atomic positions in the molecule. Molecular dynamics is based on solution of Newton equations. It enables to describe effects hanging together with molecular motion such as effect of temperature and pressure. Task of molecular dynamics simulation can be defined in the box with periodic boundary conditions.

Position restrains are the functions that can fix the nod at one certain position.

Experimental

The simulation consisted of three phases: *(i)* system building, *(ii)* simulations, and *(iii)* calculation of material properties.

Building of Rigid Networks

The material was considered a network composed of macromolecular chain. The chains were composed of atoms and atomic groups. The atomic groups were coupled together according to their connectivity. Building of network was made by in-house builder. Input properties of the builders were crosslink density and the density of material. The results of the builder were coordinates of atoms and topology of groups. The material is represented by representative sample volume (RSV). The RSV was a cubic box.

Deformation of Network

The cubic box was deformed and the position restrains were set to the model. The position restrains were introduced to topology and applied to boundary atoms. Two types of deformation were applied. Tensile deformation was applied to one boundary in perpendicular direction to plane of box side. The shape in other axes was compressed. The second was shear deformation applied to the boundary atoms. It was applied in parallel direction to the boundary plane of cubic box.

Optimization of structure and calculation of potential energy was applied by GROMACS software. Input properties were coordinates of atomic groups and topologies of atoms. The result was a potential energy calculated for each deformed state. The potential energy density was considered a function of deformation tensor.

$$u = f(\varepsilon) \tag{3}$$

Calculation of Material Properties

Important material properties are Young Modulus and Poisson ratio. The tensile curve was calculated as a gradient of equation (1).

$$\sigma(\varepsilon) = grad(u) = \left(\frac{\partial u}{\partial \varepsilon_{xx}}, \frac{\partial u}{\partial \varepsilon_{yy}}, \frac{\partial u}{\partial \varepsilon_{zz}}, \frac{\partial u}{\partial \tau_{xy}}, \frac{\partial u}{\partial \tau_{xy}}, \frac{\partial u}{\partial \tau_{yz}} \right) \tag{4}$$

Material described here was isotropic; therefore, the deformation was performed only in one axis. The Young modulus was considered a derivative of the tensile curve.

$$E = \left(\frac{d\sigma_{zz}}{d\varepsilon_{zz}}\right)_{\lim \varepsilon \to 0} \quad (5)$$

Poisson ratio was calculated from shear modulus (μ) and tensile modulus.

$$\nu = \frac{E}{2\mu} - 1 \quad (6)$$

Rubbery Networks

The polymer material was considered affine rubbery network. It was composed by tetra-functional affine nods and freely joined chains with both fixed ends. The deformation of single chain was calculated from Treloar equation.

The input properties of the model were crosslink density and number of segments between two nods. The network was built and deformed. The result of the software was a tensile curve. Young modulus of rubbery network was calculated from tensile curve. Poisson ratio for rubbery network is from theory 0.5 as the networks are incompressible.

Results

Three types of macromolecular network of crosslink density were built. All the networks were composed of carbon or hydrocarbon groups and they differed in crosslink density. The set of materials was composed of one example of sparse network (vulcanized rubber), one example of dense network (ebonite) and one example of the crystalline structure (diamond).

First was a rubbery network where the distances between crosslinks were too long. There was presumed rubbery behavior of network. Example of predictive power can be shown on example of vulcanized natural rubber. Network model was applied to the measured data from literature. The recipe of natural rubber contained 1.96 % sulfur[8]. Theoretical crosslink density considering only the disulfide bridges was 337 $mol\,m^{-3}$. Tensile curve is shown in Fig. 1. The modulus was higher than measured modulus. The measured experimentally crosslink density was 91 $mol\,m^{-3}$. It can be caused by two reasons. First, not all the sulfur will participate on reaction. The disulfide bridge is only a model crosslink. In reality, the crosslinks are poly-sulfide bridges.

In the ebonite, crosslink density was calculated from composition. The average fraction of sulfur in ebonite is 30 weight percent. Considering that two atoms of sulfur form a tetrafuctional nods are connected by connected 6 freely joined segments. Taking density 1.3 $g\,cm^{-3}$ we get 0.006 crosslinks cm^{-3}. That means 0.012 elastically active chains. The volume of nods was negligible. The chain with 6 segments cannot be considered a statistical chain. Therefore the rubber elasticity of such network was not calculated. The potential as a function of deformation is shown in Fig. 2.
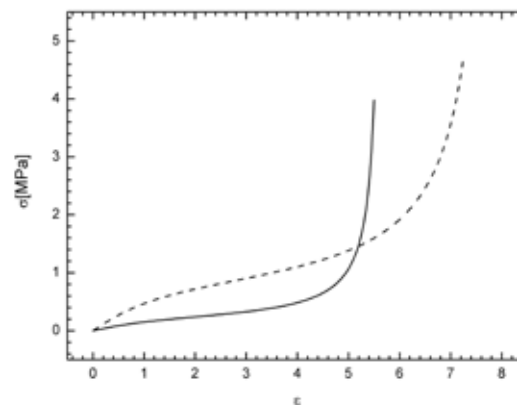
Fig. 1. **Stress-strain function of model vulcanized rubber calculated from rubber elasticity theory solid line: calculated from experimental density; dashed calculated from theoretical crosslink density**
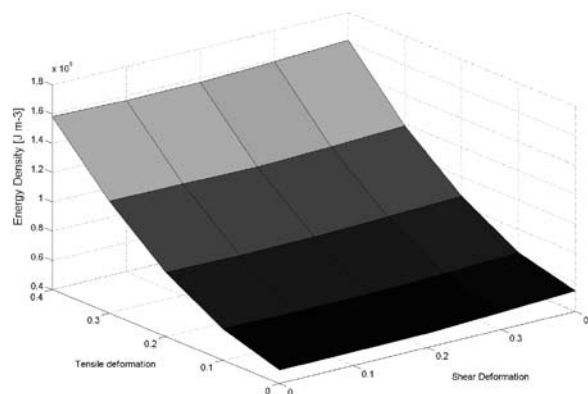
Fig. 2. **Potential energy density calculated from molecular interactions. A function of tensile and shear deformation**

The tensile curve was calculated from the potential energy density of ebonite network. The stress strain characteristics was calculated as a gradient of function of energy density. Function of stress on relative elongation is shown in Fig. 3.

All the stress-strain functions were applied to calculation of material properties. As the method was not sensitive to shear deformation, the poisson ratio could not be calculated. The Young modulus was calculated and compared to experimental data in Table I.

The vulcanized rubber properties are driven by entropic interaction whereas the ebonite and diamond were influenced by intermolecular interactions.

In the rubbery material, the modulus calculated from theoretical crosslink density is higher than experimental modulus. The modulus calculated from experimental crosslink density is lower than the experimental modulus. The model network even with experimental crosslink density is not yet realistic description of structure. It was negligible the volume
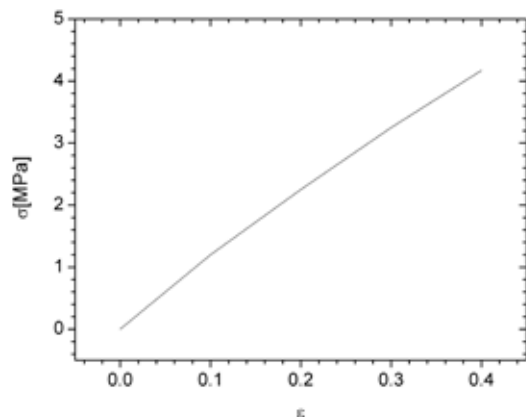
Fig. 3. **Stress-strain function of model material ebonite calculated from intermolecular interaction**

of crosslinks, that will act as increase of Young modulus. Moreover, the model and material showed different elongation at break. It shows that there could be some unstable crosslinks such as two macromolecular chains coupled with weak interaction. These nods can disappear and re-appear during the tabnsile test.

The calculated modulus of ebonite and diamond was lower than experimental. It can be caused by not exact structure of both models and non exact force fields. The ebonite had model density 0.5 g mol^{-1} whereas the real density was 1.4 g mol^{-1}. Also the diamond had density 11 g mol^{-1} whereas experimental density of diamond was 3.45 g mol^{-1}.

Conclusions

Macromolecular networks show different deformation behavior even if they have composition. It is caused by different principles of their deformation. Loading of materials can be caused by rubber elasticity or by intermolecular interactions.

The vulcanized rubber, ebonite and diamond are material based on carbon structures. The vulcanized rubber is a sparse network, ebonite is a dense network and diamond is a regular lattice. Their deformation properties were calculated: vulcanized rubber from rubber elasticity theory, ebonite and diamond by molecular mechanics. The calculated values were lower than the experimental data. The densities were different form experimental densities of material. It is necessary to approach the structural properties to real structure of materials.

REFERENCES
1. Kuhn W., Grün F.: Kolloid Z. *101*, 248 (1942).
2. James H. M., Guth E.: J. Chem. Phys. *11*, 455 (1943).
3. Treloar L. R. G.: *The physics of rubber elasticity*; Oxford: Clarendon Press, 1975.
4. Boyce A.: J Mech. Phys. Solids *9*, 389 (1993).
5. Puso M.*: Mechanistic Constitutive Models for Rubber Elasticity and Viscoelasticity;* University of Californina, Davis, 1994, Davis, USA.
6. Termonia Y.: Macromolecules *27*, 7378 (1994).
7. Rapaport D. C.: *The art of molecular dynamic simulation;* Cambridge University Press; 2004.
8. Ostad-Movahed S., Yasin K. A., Ansarifar A., Song M., Hameed S.: Journal of Applied Polymer Science *109*, 976 (2008).
9. Agrawal S.L.: Rub Tech Track *2*, 14 (2004).
10. Djemia P., Tallaire A., Achard J., Silva F., Gicquel A.: Diamond & Related Materials, *16*, 962 (2007).

8.2. Posters

P01　PHYSICO-CHEMICAL PROPERTIES OF FUNCTIONALIZED TEMPERATURE-SENSITIVE BIOCOMPATIBLE BLOCK COPOLYMERS

JAN DAVID, LUCY VOJTOVÁ, LENKA MICHLOVSKÁ, JIŘÍ KUČERÍK, LUDMILA MRAVCOVÁ, MARTIN CHYTIL, MILOSLAV PEKAŘ, MILADA VÁVROVÁ and JOSEF JANČÁŘ

Faculty of Chemistry, Brno University of Technology, Purkyňova 118, 612 00, Brno, Czech Republic
xcdavid@fch.vutbr.cz

Introduction

Copolymers of poly(lactic acid), poly(glycolic acid) and poly(ethylene glycol) (PLGA-PEG) are presenting interesting features, such as biodegradability, no toxicity and thermal induced sol-gel transition, for their potential use in tissue engineering and controlled drug delivery[1,2]. The aqueous solution of the copolymer is free flowing sol at room temperature and becomes a non flowing gel at body temperature[3].

Various architectures of PLGA copolymers with PEG were studied in the past few years and they have been also modified with different kinds of crosslinkers[4].

The goal of this work is to discover the possibilities of synthesis of PLGA-PEG copolymer and its modification with itaconic anhydride (ITA) in order to prepare crosslinkable macromonomer for the use in tissue engineering and bone repair. ITA is obtainable from natural resources and was recently used for functionalization of poly(ε-caprolactone)[5].

Experimental

R a w　M a t e r i a l s

Poly(ethylene glycol), (PEG, M_n = 1,500, Aldrich, Germany), D,L-lactide and glycolide (DLLA, GA, 99.9 %, Polysciences, U.S.A.), stannous 2-ethylhexanoate, (95 % Aldrich, Germany), itaconic anhydride (ITA, 97 %, Aldrich, Germany). All chemicals were used as received.

S y n t h e s i s

The PLGA-PEG triblock copolymer (see Fig. 1.) was prepared via ring opening cationic polymerization of DLLA and GA in a bulk using the PEG as initiator and stannous 2-ethylhexanoate as catalyst under inert athmosphere. PLGA-PEG product was modified by ITA in the bulk under inert athmosphere.
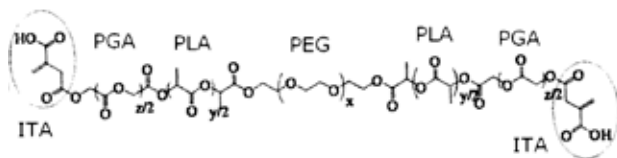
Fig. 1.　**PLGA-PEG-PLGA/ITA macromonomer structure**

C h a r a c t e r i z a t i o n

The molecular weight and the molecular weight distribution (PDI) was determined by gel permeation chromatography (GPC) using Agilent technologies 1100 Series GPC with RI detector at the temperature of 30 °C in tetrahydrofurane mobile phase.

The product structure was studied by means of Fourier transformed infra-red spectroscopy on Nicolet Impact 400D FTIR spectrometer using KBr pellets.

Proton nuclear magnetic resonance spectra (^{1}HNMR) analysis was performed on the Bruker 500 MHz nmR spectrometer, when 20 mg of copolymer sample were dissolved in 1 ml of CDCl$_3$.

Thermal analyses (TA) of copolymer sample were made using TA Instruments TGA Q500 machine for thermogravimetric analysis (TGA), temp. ramp of 10 °C min^{-1} from 40 °C to 600 °C under 25 ml min^{-1} nitrogen purge and also by means of TA Instruments DSC Q200 machine for differential scanning calorimetry (DSC), temp. ramp of 3 °C min^{-1} from –90 °C to 200 °C under 50 ml min^{-1} nitrogen purge.

S o l - G e l　T r a n s i t i o n　A s s e s s m e n t

The sol-gel transition was determined by the test tube inverting method (TTIM) in the temp. ramp from 24 °C to 50 °C by the 1 °C 10 min^{-1} rate in a water bath. Samples of copolymers were dissolved in the vials in the concentration step of 2 % wt. from 2 % wt. to 24 % wt. The transition temperatures were determined according to a flow (sol)/no flow (gel) criterion.

Moreover, rheology was used for the sol-gel transition determination. Samples of copolymers were dissolved in the vials at the concentrations of 15, 20 and 25 % wt. and measured by the TA Instruments AR-G2 rheometer equipped with plate-plate geometry using 25 mm standard steel parallel plate and 1,000 μm gap. Measurements were proceeded at the temp. ramp step tests of 0.5 °C min^{-1} rate from 15 to 60 °C under oscillation stress of 0.40 Pa and angular frequency of 1 rad s^{-1}.

Results

P o l y m e r　C h a r a c t e r i z a t i o n

The GPC analyses of PLGA-PEG (M_n = 4 861; M_w = 6 392; PDI = 1.32) and PLGA-PEG/ITA (M_n = 4 989; M_w = 6 663; PDI = 1.34) showed very similar values of M_n and PDI before and after the functionalization by ITA indicating no side reactions within functionalization process.

The ^{1}H nmR spectroscopy proved the incorporation of itaconic acid to the end of polymer through the characteristic peaks of lactic acid (O−(CH$_3$)CHO) protons (δ = 1.5–1.75 ppm) and (O−(CH$_3$)CHO) protons (δ = 5.1–5.35 ppm), glycolic acid (OCH$_2$O) protons (δ = 4.6–4.95 ppm), backbone PEG (OCH$_2$CH$_2$O) protons (δ = 3.55–3.8 ppm) and itaconic acid double bond (OC(CH$_2$)CCH$_2$COOH) protons (δ = 5.7–5.8 ppm and δ = 6.35–6.5 ppm).
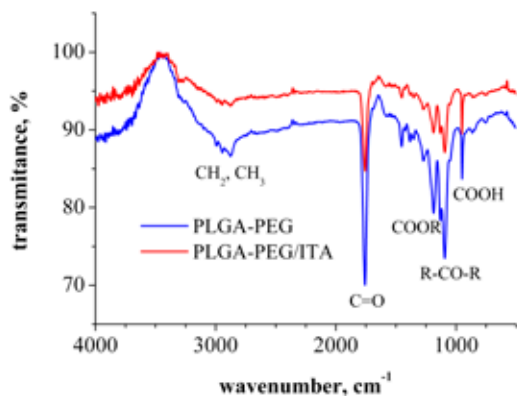
Fig. 2.   **FTIR spectra of copolymers**

S t r u c t u r e   A n a l y s i s

FTIR spectroscopy analysis showed characteristic ester, C=O, acidic and alkyl bands. The spectra are presented on Fig. 2.

T h e r m a l   A n a l y s i s

Thermal degradation of copolymers proceeds in two steps, the first is ascribed to PLGA blocks, the second to PEG
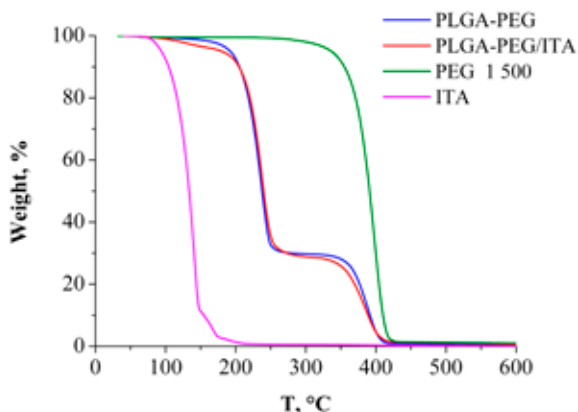
Fig. 3.   **TGA curves of copolymers, PEG and ITA**

chain, as it is described in the literature[6]. Indistinctive degradation step around 110 °C by the PLGA-PEG/ITA copolymer can be assigned to the ITA groups. ITA itself tends to degrade from 90–110 °C which has a conclusion for further modification conditions. The thermograms are shown in Fig. 3.

DSC analysis showed a broad glass transition peak in temperatures from −65 °C to 0 °C with inflexes at −14.9 °C and −23.9 °C for PLGA-PEG and PLGA-PEG/ITA copolymers, respectively.

S o l - G e l   T r a n s i t i o n

Rheology showed two storage modulus (G') peaks and tan δ valleys for PLGA-PEG copolymer sol, which are assigned to amber and white gel respectively, but one G' peak and tan δ valley for PLGA-PEG/ITA copolymer. Both TTIM and rheological analysis proved the uprise of amber gel state of both the copolymer sols in concentrations higher than 15 % wt. and temperatures from 35 °C to 45 °C. In higher temperatures, the gels turn white and then separate to suspension. The TTIM phase diagram and rheology charts are shown on Fig. 4 and Fig. 5.

Conclusions

PLGA-PEG copolymer and PLGA-PEG/ITA macromonomer were synthesized successfully and characterized via FTIR, GPC and ^{1}HNMR. The molecular weight of both products is similar. The presence of ITA in the polymer chain caused decrese in temperature stability, glass transition temperature and critical gel temperature. Storage moduli of gels increase with concentration. TTIM results correspond with those obtained by rheology. Both gels exhibit suitable mechanical properties at the concentrations of 15 % wt. and higher for biomedical applications (bone adhesives).

Fig. 4.   **Sol-gel phase diagram obtained by TTIM**
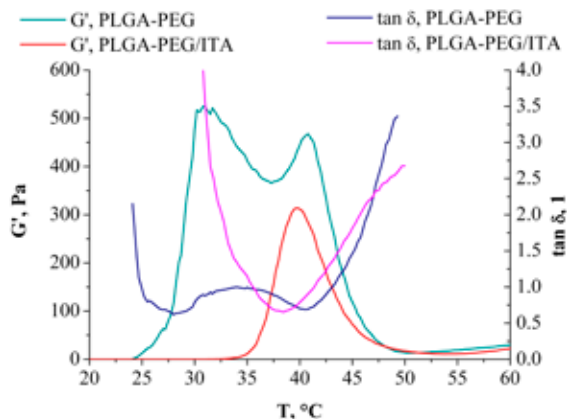
Fig. 5.   **Rheology analysis of 20 % wt. copolymer sols**

REFERENCES

1. Hoffman A. S.: Adv. Drug Deliv. Rev. *43*, 3 (2002).
2. Jeong B., Kim S. W., Bae Y. H.: Adv. Drug Deliv. Rev. *54*, 37 (2002).
3. Jeong B., Choi Y. K., Bae Y. H., Zentner G., Kim S.W.: J. Control. Release *62*, 109 (1999).
4. Hiemstra C., Zhong Z. Y., Li L. B., Dijkstra P. J., Feijen, J.: Biomacromolecules *7*, 2790 (2006).
5. Turunen M. P. K., Korhonen H., Tuominen J., Seppälä J. V.: Polym. Int. *51*, 92 (2001).
6. D'Antone S., Bignotti F., Sartore L., D'Amore A., Spagnoli G., Penco, M.: Polym. Degrad. Stab. *74*, 119 (2001).

P02 PROPERTIES OF RECYCLED CARBON FIBERS

JAN GRÉGR, VLADIMÍR KOVAČIČ, MIROSLAV VALEŠ, BEDŘICH ŠTEKNER and KAREL CIHELNÍK

Department of Chemistry, Faculty of Education, Technical University of Liberec, Studentská 2, 461 17 Liberec, Czech Republic,
jan.gregr@tul.cz

Introduction

Fibers in high performance composite materials are very expensive. For this reason is suitable to interesting about recycling waste products from fabrication of composites and composite parts after its lifetime. We made some experiments to obtain reinforcing carbon fibers from waste products and we evaluated properties of this recycled fibers. These fibers can be suitable for next exploitation. In contribution we demonstrate products of recycling and its properties. In Aeronautical Research and Test Institute, Prague are developed experimental test system for fibrous thermosetting composite breakdown. This system was designed and realized during 2006 in cooperation with the company Elektrické pece Svoboda, Světice near of Říčany. The base of the system consists of a thermal reactor, where under conditions of high temperatures and normal or inert atmosphere, decomposition of composite takes place. The results of process are remaining fibrous or other reinforcement and gasified components of matrix, which are conducted into cooling and filtration parts. These parts enable to obtain additional components from material breakdown, depending on the type of material and processing technology. The whole system is fully programmable and variably adjustable as to temperature or inert media flow. Several restrictors, suck-in valves and flaps can also control the movement of gaseous products. The system also allows for monitoring of many parameters of the process, in particular the temperature inside of furnace inside of charge, temperature at cooler and filter unit outlets. Furthermore the mass decrement of the material processed and, gaseous products of breakdown are monitored, especially O_2, CO, CO_2, H_2, NO, NO_2, SO_2 or C_XH_Y contents. Of course, it is possible to transmit measured values to PC for further analyses[1].

Experimental

On the Department of Textile materials, Faculty of textile engineering and Department of chemistry, Faculty of education, Technical university of Liberec are develop testing methods for evaluating of recycled high performance fibers. We made analysis by the optical, gravimetric and SEM method; we realized tests of strength and wetting characteristics of these fibers.

Results

Fibers at standard temperature of recycling are much damaged. The standard temperature is temperature optimized

Table I
Results of optical analysis recycled carbon fibers

Fiber/Process	Environ	Diameter [µm]	Yield [%]
standard	air	5.06	36
standard −50 °C	air	5.55	43.7
standard −100 °C	air	7.07	70.3
standard −100 °C	N_2	8.26	96
virgin		8.43	–

Table II
Results of gravimetric analysis recycled carbon fibers

Fiber/Process	Environ	Diameter [µm]	Yield [%]
standard	air	4.94	42.7
standard −50 °C	air	6.39	71.4
standard −100 °C	air	7.38	94.5
standard −100 °C	N_2	7.43	95.6
virgin		7.71	–

Table III
Results of mechanical tests of recycled carbon fibers

Fiber/process	Elongation [%]	Tensile strength [MPa]	Modulus [GPa]
st. – air	1.41	820	83
st. −50 °C – air	1.52	1,122	104
st. −100 °C – air	1.89	1,496	102
st. −100 °C – N_2	2.04	1,731	105
virgin	1.53	990	91

for perfect decomposition of epoxy resin in composite. Ends of fibers are etched after oxidative treatment of air oxygen. In probe are much released microfibrils. Damaging after treatment on temperature below 50 °C on air is also obvious. Some ends of fibers appear as hollow fibers. On the surface are etch pits and released microfibrils. Surface of fibers after recycling at standard temperature minus 100 °C on air have only very small damaging. The bright speckles are rests from weft glass fibers. Carbon fiber after recycling at standard temperature minus 100 °C in nitrogen is smooth without remarkable
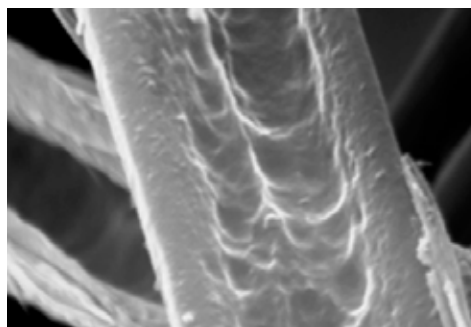
Fig. 1. **SEM image of the most damaged fiber end**

damaging. On the surface of virgin fibers are fine striation advanced with structure of polyacrylonitrile precursor.
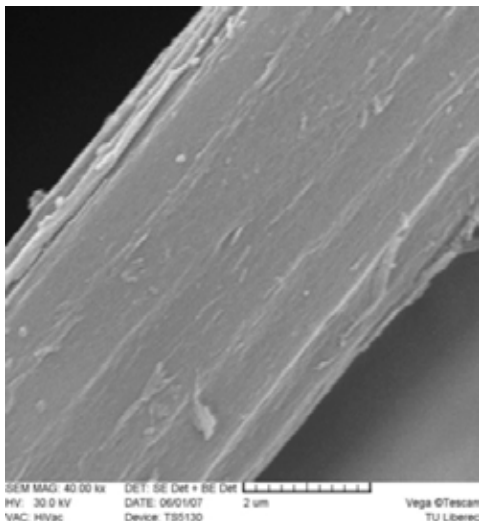
Fig. 2.   **SEM image of typical carbon fiber recycled at standard temerature**
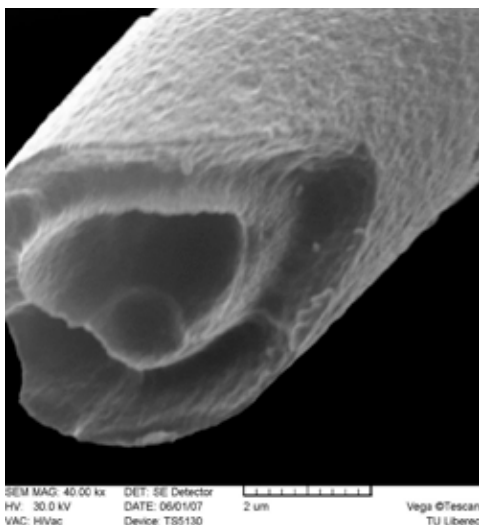
Fig. 3.   **SEM image of hollow carbon fibers after recycling**

Conclusions

In this time we are trying to another way of recycling of carbon composites. We study surface properties of recycled fibers and hazard factors of carbon fiber dust. We searching possibilities of utilization of recycled carbon fibers no only for termoplastioc composites, but also for special purpose for example electric conductive paper and so on. We assume that recycling of composites will be in next time very significant.[2–6]
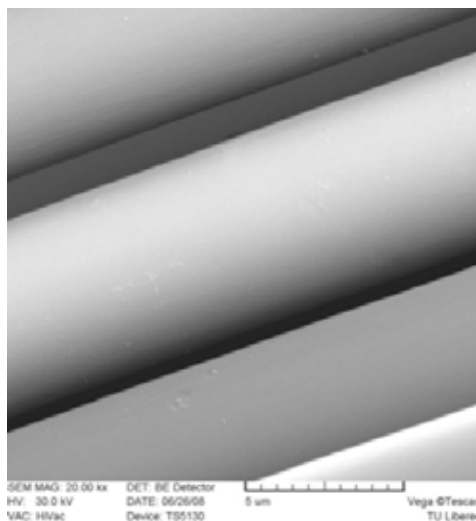
Fig. 4.   **SEM image recycled carbon fibers at standard temperature minus 100 °C**
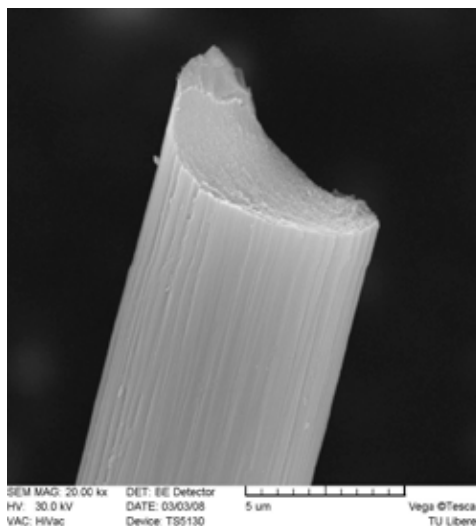
Fig. 5.   **SEM image of vigin carbon fiber end**

REFERENCES

1. Valeš M., Štekner B., Cihelník K., Grégr J., Kovačič V.: *Czech Aerospace Proceedings No. 3/2007,* p. 27.
2. Pickering S. J..: Composites: Part A *37*, 1206 (2006).
3. Cunliffe A. M., et all.: J. Anal. Appl. Pyrolysis *70*, 315 (2003).
4. Perrin D., et al.: Waste Management *28*, 541 (2008).
5. Dang W., et al.: Polymer *43*, 2953 (2002).
6. Hyde J. R., et al.: Composites: Part A *37*, 2171 (2006).

P03　HALOSILYL-SUBSTITUTED CYCLOPENTADIENYL TITANIUM COMPLEXES AS CATALYSTS FOR STYRENE SYNDIOSPECIFIC POLYMERISATION

SOŇA HERMANOVÁ[a], JAN MERNA[b], MILAN ERBEN[c], MICHAL DUŠEK[c] and ZDENĚK SVAČINA[a]

[a]Institute of Materials Science, Faculty of Chemistry, Brno University of Technology, Purkynova 118, 612 00 Brno, Czech Republic,
[b]Department of Polymers, Institute of Chemical Technology, Prague (ICTP), Technicka 1903, 166 28 Praha 6, Czech Republic,
[c]Department of General and Inorganic Chemistry, Faculty of Chemical Technology, University of Pardubice, Čs. Legií 565 square, 532 10 Pardubice, Czech Republic,
hermanova-s@fch.vutbr.cz

Introduction

Syndiotactic polystyrene (s-PS) is an interesting material with a high melting point of 275 °C and a fast crystallization rate as compared with isotactic polymer. Its interesting properties which are similar to those of some more expensive engineering plastics are the reason for further scientific interest[1,2]. In our previous work we reported the catalytic behaviour of novel half-sandwich titanium complexes in syndiotactic styrene polymerisation (see in Fig. 1). The variation of halosilyl substitutent on cyclopentadienyl ligand affected both the catalytic activity and the properties of s-PS[3].

In this contribution a series of polymerisation runs was carried out in a time scale of 20–120 min in order to compare the activity dependence of examined complexes on reaction time and thus to better evaluate their polymerisation behaviour.
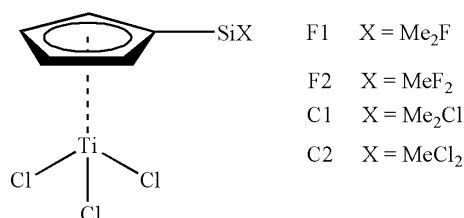
Fig. 1.　**Half-sadwich titanium precursors for styrene polymerisations**

Experimental

All manipulations of air- and moisture-sensitive materials were carried out under nitrogen atmosphere, using either a dual vacuum/nitrogen line and standard Schlenk techniques or a high vacuum line. Methylaluminoxane (MAO) was purchased from Crompton GmbH (10 % wt. in toluene). Toluene (Lachema) was freshly distilled from sodium benzophenone ketyl prior to use. Styrene (Aldrich) was dried over calcium hydride and freshly distilled under vacuum prior to use. Investigated complexes and reference compounds $CpTiCl_3$, Cp^*TiCl_3, $[Si(CH_3)_2FCp]TiCl_3$ (F1), $[Si(CH_3)F_2Cp]TiCl_3$ (F2), $[Si(CH_3)_2ClCp]TiCl_3$ (C1), $[Si(CH_3)Cl_2Cp]TiCl_3$ (C2) were prepared according to the known procedure.

Polymerisation and Polymer Characterisation

Styrene polymerisations were carried out in a magnetically stirred (600 rpm min^{-1}) glass double-jacket reactor (100 ml) under nitrogen atmosphere. The reactor was successively charged by toluene (30 ml), styrene (0.0156 mol, 1.8 ml) and MAO. The MAO/Ti ratio of 800 was used for all polymerisation runs. Afterwards the rector was thermostated at 50 °C and titanium complex in toluene (9×10^{-6} mol) was injected to initiate the polymerisation. After selected period of time (20–120 min) the reaction was quenched by adding 10 ml of *sec*-butyl alcohol. The resulting mixture was poured into acidic methanol (500 ml). The polymer was collected by filtration and dried under vacuo to constant weight. The reproducibility of obtained polymer yields was estimated to be ± 10 %. Representative PS samples were extracted with boiling methyl ethyl ketone for 6 h to remove any atactic material. The syndiotactic polymer was determined as the amount of material insoluble in methyl ethyl ketone.

^{13}C nmR spectra were recorded on a 500 MHz Bruker Avance spectrometer operating at 125 MHz. The pulse angle was 83 °, pulse interval 20 s, decoupling Waltz 16. Melting points were measured with a Perkin-Elmer DSC–7.

Results

The catalytic behaviour of four titanium complexes with varying halosilyl substituent on Cp ligand and MAO for syndiospecific styrene polymerisation was investigated. Polymerisations were performed in toluene at 50 °C in the range of polymerisation time of 20–120 min.

The catalytic efficiency of complexes was evaluated according to the polymerisation activity, which is defined as a yield of PS per mol of titanium and per 1 h of polymerisation (see in Fig. 2). The activity of all studied complexes was dependent on the polymerisation time. A maximum activity was reached after a short induction period of about 20 min whereafter the activity decreased. The decrease could be attributed to the deactivation of the active species or to the occlusion of part of the catalyst in the precipitating polystyrene.

The average catalytic acitivity decreased in the order F1 > F2 > C1 > C2. Such decrease of activities may result from an increase of steric bulk of halosilyl substituent hindering the monomer coordination to active species. The highest activity was 207 kgPS mol$_{Ti}^{-1}$ h^{-1} using $[Si(CH_3)_2FCp]TiCl_3$ (F1)/MAO catalytic system.

Further the polymerisations catalyzed by well known complexes $CpTiCl_3$ and Cp^*TiCl_3 ($Cp^* = C_5Me_5$) and MAO were carried out under identical experimental conditions. Complex $CpTiCl_3$ in combination with MAO reached maximum polymerisation activity of 91 kgPS mol$_{Ti}^{-1}$ h^{-1}. However, the complex with Cp^* ligand, which is a stronger electron

donor and exerts a greater sterical hindrance, possessed a slightly lower maximum activity of 86 kgPS $mol_{Ti}^{-1} h^{-1}$ at the same polymerisation conditions. In all cases halosilyl-substituted titanium complexes were more active than the reference $CpTiCl_3$ and Cp^*TiCl_3 compounds.
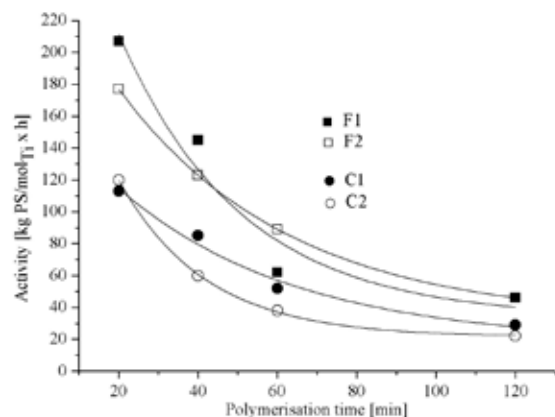
Fig. 2. **Dependence of polymerisation activity on polymerisation time**

Polystyrenes prepared by examined substituted half-sandwich titanium complexes and MAO exhibited melting points in the range of 264–266 °C. Melting point of PS obtained by $CpTiCl_3$/MAO system was lower approximately by 10 °C. The percentages of fractions insoluble in boiling methyl ethyl ketone were in the range of 92–99.9 %. The syndiotacticity of PSs was not possible to be evaluated by means of ^{13}C nmR namely because of the insolubility of highly syndiotactic fractions obtained after extraction procedure.

Conclusions

The introduction of halosilyl substituent onto Cp ligand of half-sandwich titanium complex affected both the catalytic activity and syndiotacticity of product. The catalytic acitivity on average decreased in the order F1 > F2 > C1 > C2.

REFERENCES
1. Kaminsky W., Lenk S., Schulz V., Roesky H. W., Herzog A.: Macromolecules *30*, 7647 (1997).
2. Sun, X., Xie J., Yhang H., Juany, J.: Eur. Polym. J. *40*, 1903 (2004).
3. Erben M., Merna J., Hermanová S., Císařová I., Padelkova Z., Dušek M.: Organometallics *26*, 2735 (2007).

P04   SYNTHESIS OF MODIFIED CUCURBIT[N]URILS

MUHAMMAD SHAMSUL AZIM KHAN and VLADIMÍR ŠINDELÁŘ

Department of Chemistry, Masaryk University, Kotlářská 2, 611 37 Brno, Czech Republic
sindelar@chemi.muni.cz

Introduction

Cucurbit[n]urils (CB[n], n = 5–10), a remarkably robust macrocyclic host molecule, have gained much attention in the new millennium for their exceptional molecular recognition ability. The pumpkin-shaped molecule has a hydrophobic cavity and two identical carbonyl-laced portals. While the hydrophobic interior provides a potential inclusion site for nonpolar molecules, the polar ureido carbonyl groups at the portals allow CB[6] to bind ions and molecules through charge-dipole and hydrogen bonding interactions. The unique structure and recognition properties make CB[n] attractive not only as a synthetic receptor but also as a building block for the construction of supramolecular architectures. Compared to the chemistry of cyclodextrins and calixarenes, however, that of CB[n] has developed slowly until recently, which may be attributed mainly to their poor solubility in common solvents and inability to functionalize these molecules. Our research is aimed to the synthesis, characterization, purification and separation of new functionalized CB[n].

Experimental

Generally modified CB[n] was synthesised from an acid-catalyzed condensation reaction of glycoluril or substituted glycoluril and formaldehyde (paraformaldehyde) or mixture of aldehydes.

The indirect method of functionalization of CB[n] involves acid-catalyzed self-assembly of an equimolar mixture of unsubstituted glycoluril (A) with two different aldehydes (B and C), the results of which would give CB[n] functionalized at the methylene bridges of CB[n] (Scheme 1).
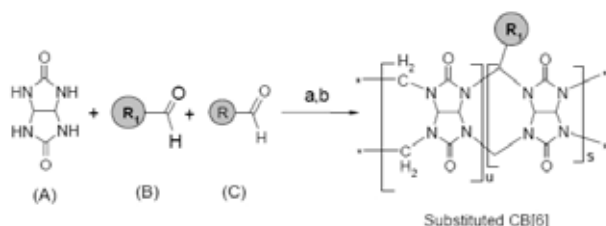
Scheme 1

P u r i f i c a t i o n

Isolation of mono-functionalized CB[6] from the crude mixture was a very tedious and time consuming job which took most of our research time. The primary purification was based on the preferential solubility or stepwise precipitation of variously substituted and unsubstituted CB[n] as well as other glycoluril oligomers. Water, methanol, acetone and 2-propanol were used to precipitate solids from the crude mixture. MALDI-TOF MS was used to determine molecular weight distributions of all collected fractions and the results were compared to select the most relatively pure fraction for further purification treatment. It was found that for some specifically substituted CB[n] 0.1M NaOH can selectively extract monosubstituted and unsubstituted CB[6] from di- and tri-substituted CB[6] and other minor components. Dilute aqueous HCl (for example 7 % or 21 %) solution was also used in the combination with the basic medium. Component enriched with the monosubstituted CB[6], was subjected further purification on the strong acid cation exchange resin. As a solvent system mixture of HCl and HCOOH was used and numerous fractions were collected and analyzed by ^{1}H-NMR. Please note that in no case completely pure monosubstituted CB[6] was obtained although MALDI spectrum in some case showed a single molecular ion peak for the corresponding component. This might be rationalized due to lack of optimization of chromatographic conditions such appropriate composition of mobile phase and right length of stationary bed. As stationary phase, we used DOWEX50WX8(mesh no. 100–200) in one case and DOWEX50WX2(mesh no 200–400, p.a) in other case.

C h a r a c t e r i z a t i o n

The purified sample was analyzed by ^{1}H and ^{13}C-NMR spectra using Bruker AVANCE 300 MHz and 75 MHz spectrometer respectively and molecular weight distribution was obtained on a MALDI-TOF mass spectrometer Reflex IV, Bruker Daltonics.
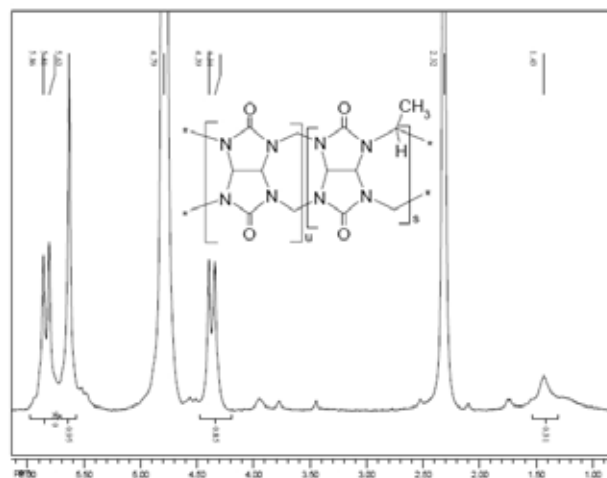
Fig. 1.   **[1]H nmR spectrum (300 MHz, D$_2$O)**

^{1}H-NMR spectrum shows three typical CB[6] peaks: two doublets at δ 5.34–5.39 ppm, 5.81–5.86 ppm and a singlet at 5.63 ppm. Besides these signals, there is one more singlet of methyl group at δ 1.43 ppm. It should be mentioned here that from ^{1}H-NMR spectra we can hardly confirm about the composition of the substance after final purification step.
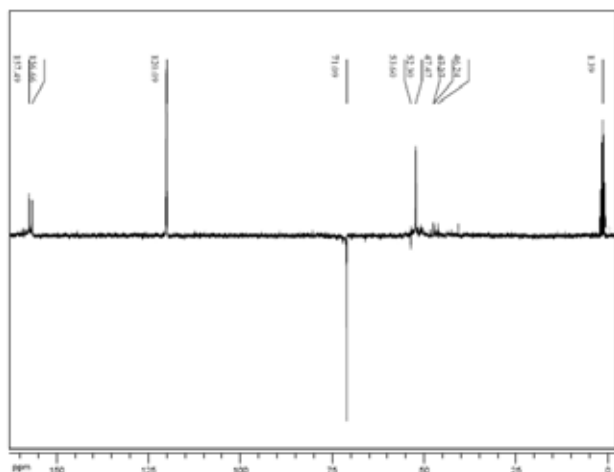
Fig. 2.   **¹³C APT nmR spectrum (75 MHz, CD₃CN-D₂O)**
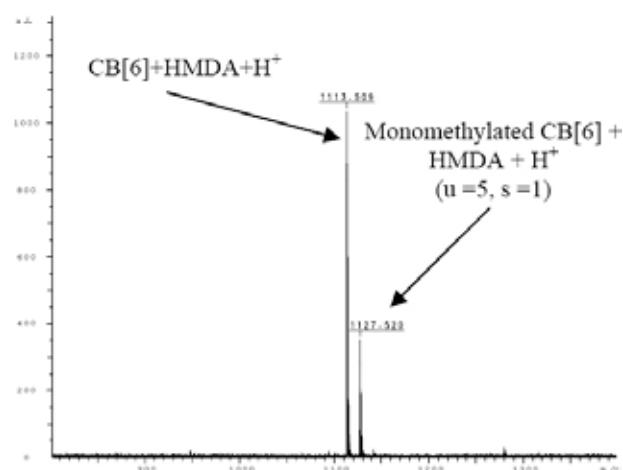
Fig. 3.   **MALDI-TOF Mass spectrum of monomethylated-cucurbit[6]uril [hexamethylenediamine (HMDA) was used as guest molecule to prove it's formation]**

¹³C nmR APT spectrum shows two C=O peaks at δ 156.66, and 157.49 ppm, one of which nicely indicates the formation

of a second type of CB[6], that is, monomethylated CB[6]. The peak at δ 53.60 ppm indicates -CH₃ substitution at the methylene bridge position.

MALDI-TOF MS spectrum shows that the purified sample contains mixture of monosubstituted CB[6] (m/z 1,127.5 as complexed with hexamethylenediamine (HMDA) as well as unsubstituted CB[6] (m/z 1,113.5 as complexed with HMDA) as major product. HMDA was used to improve the sample solubility.

Conclusion and Perspectives

Though the parent molecule CB[6] is a century old, the chemistry of the CB family seems beginning to blossom. The recent developments, including the synthesis of CB homologues and derivatives, have brought dynamism to CB chemistry, as witnessed from the increasing interest in various interdisciplinary application fields such as artificial ion channels, vesicles, stationary phases in chromatography, ISEs, polymers, nanomaterials, and many others for the last several years. In this poster we have demonstrated a new one pot synthetic method for the preparation of new functionalized CB[n] derivatives. As the yield and purity of compound is not yet satisfactory more time is still required to optimize the purification method.

REFERENCES

  1. Freeman W. A., Mock W. L.: J. Am. Chem. Soc *103*, 7367 (1981).
  2. Day A. I., Arnold A.P., Blanch R. J.: Molecules *8*, 74 (2003).
  3. Day A. I.; Arnold A. P., Blanch R. J.: J. Org. Chem *66*, 8094 (2001).
  4. Lagona J., Mukhopadhyay P., Isaacs L.: Angew. Chem. Int. Ed. *44*, 4844 (2005).

P05 DETERMINATION OF COLOR TRANSITION TEMPERATURE FOR PROCESSING OF THERMOCHROMIC POLYMERIC MATERIALS

FRANTIŠEK KUČERA and PETRA SLÁNSKÁ

Brno University of Technology, Faculty of Chemistry, Institute of Materials Science, Purkynova 118, 612 00 Brno, Czech Republic,
kucera-f@fch.vutbr.cz

Introduction

Thermochromic behaviour means a reversible colour change with temperature change and it has been observed for a variety of compounds with temperature variation[1]. A more precise definition has been given by Day: "Thermochromism is defined operationally as an easily noticeable reversible colour change in the temperature range limited by the boiling point of each liquid, the boiling point of the solvent in the case of solution or the melting point for solids"[2]. While Day's definition is applicable for majority of inorganic and organic substances, we can use the term thermochromic also in important technical fields, which demands another external impulse together with temperature of the observed colour change (e.g. thermochromic pigments).

Thermochromic dispersions are manufactured for use in aqueous ink and coating systems, but can be applied in dried encapsulated form also into polymeric materials such as polyolefines. As the temperature rises, they change from coloured form to colourless one. They get back their coloured state when the temperature is decreased again. Colour change induced by thermochromism occurs when certain temperature of thermochromic transition is reached. This transition temperature varies for different thermochromic compounds. Colour change is usually slow process; hence it can appear to occur in some temperature range. There can be observed a kind of thermal hysteresis, which means that the temperature needed to regain its former colour is significantly less than the temperature needed to obtain required colour change[3].
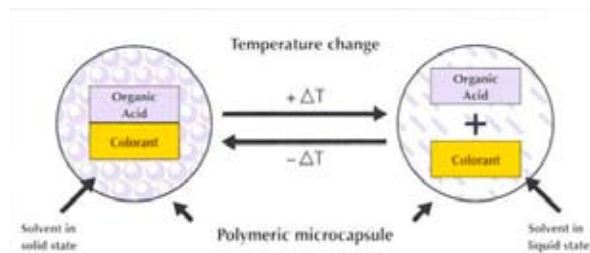
Fig. 1. **Principle of colour change in thermochromic dispersions**

There are two components in thermochromic dispersion systems: a solvent and a colorant. If the temperature is below the melting point of the solvent, these two parts stick together and the system is coloured because of the electron interactions. But if we increase the temperature of the system and this temperature reaches the melting point of the solvent, these two parts separate resulting in decolorization of the system (see Fig. 1.).

Experimental

Experimental part is based on the usage of the thermochromic granules of ThermChrom BG, VB, OY containing about 20 % of thermochromic compounnd in polypropylene matrix. Temperatures used in the polymer processing could be relatively high (from 200 to 260 °C) so it was essential to find out how the thermochromic compounds respond to exposure to temperatures.

Determination of Thermochromic Transition Temperature

Determination of thermochromic transition temperature (TTT) needed to be stated for further processing with the thermochromic compounds. Sample of thermochromic material was fixed to the tip of the thermocouple. Thermocouple with the granule of pigment was placed into the beaker with distilled water. Magnetic stirrer was set to warm up distilled water to 37 °C. Colour of the thermochromic granule was observed using Gretag Macbeth SpectroScan. Process was repeated five times for each type of thermochromic pigment and average TTT value was calculated.

Determination of the Thermal Color Stability of Thermochromic Compound

First tests of thermal stability of color transition were done in drying oven Venticell, BMT, a.s. (200 °C, 230 °C and 260 °C) as Method 1. Tests served as preliminary ones because the ovens did not have the exact control of temperature. Deviation was ± 10 °C. One pellet of each sample of thermochromic material was heated at apropriate temperature for 5 minutes and pellet was left in the opened and turned-off drying oven to cool down slowly to the room temperature. There was a necessity of tempering the oven before placing samples in it, the tempering period was 20 minutes.

Other tests (by Method 2) were done using hot-air pistol Steinel HL2305LCD and a thermocouple for determination of the exact temperature of test. Hot-air pistol was placed on a stand by holders and under the pistol there was a basin made of tinfoil. Hot-air pistol was turned on and the temperature nearby tinfoil basin was measured by thermocouple. When the temperature reached desired value (either 260 °C, 280 °C), a granule of thermochromic material was placed into the basin. Pellets were placed into the basin separately (unlike heating in an oven) and were heated for 5 minutes.

Results

Determination of Thermochromic Transition Temperature

Samples were heated to pre-set temperature (37 °C) and they were observed during the whole process of heating. Tem-

perature was written down when the colour of the samples began to change.The colours of the samples returned to the initial ones after cooling samples down to room temperature. We can state that the thermochromic transition is reversible for these types of thermochromic compounds after testing at given temperatures.

Table I. shows the temperatures of thermochromic transition of samples used. The lowest TTT was measured for the sample VB and it was 29.6 °C, almost the same TTT was measured for sample GB –29.8 °C. The highest measured TTT was 30.6 °C of the sample OY.

Table I
Temperatures of thermochromic transition of thermochromic compounds

ThermChrom Measurement number	BG	VB	OY
1	29.5	29.6	30.4
2	29.8	29.7	30.6
3	29.9	29.8	30.6
4	29.9	29.4	30.8
5	29.9	29.6	30.7
Average TTT	29.8	29.6	30.6

Determination of the Thermal Color Stability of Thermochromic Compound

Samples were heated to 37 °C and sample colour was observed during the whole process of heating. Temperature was noted when the colour of the thermochromic material changed.

Table II shows the measured temperatures of thermochromic transitions for all three samples tested after the thermal conditioning. There is only slight difference between

those temperatures for each sample at given temperature. For example TTT of sample BG varies only by 0.3 °C and this difference can be caused by measurement deviation. Generaly were TTTs slowly decreased after melting of samples. After materials cooling down they all got into their beginning colours. Thermochromism was not lost by exposing thermochromic granules to the temperatures up to 260 °C.

Temperature of thermochromic transition has decreased by approximately 1.5 °C for the sample BG and 2 °C for the sample OY when heating up. The changes in TTT were almost the same no matter if we heated it to 200, 230, 260 or 280 °C.

Measured temperature of thermochromic transition for VB has not almost changed. The difference between all done measurements is 0.8 °C which can be neglected having in mind that the observation was only visual and on that account subjective. The fault of the measuring TTT of VB is also because the change in colour from violet to blue was not as obvious as when measurements were done with BG and OY.
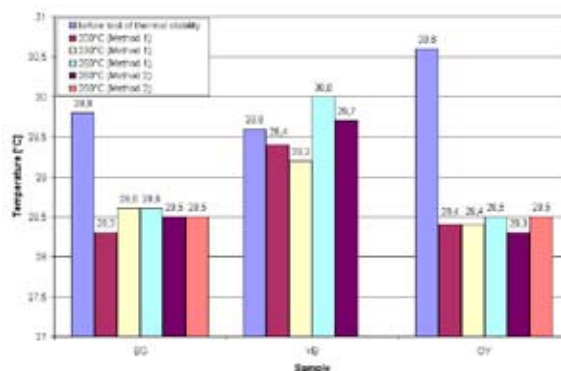
Fig. 2.   **Comparison of TTT before and after the thermochromic material tests of thermal stability**

Table II
Temperatures of thermochromic transition of thermochromic compounds after the test of thermal stability at 200 °C, 230 °C and 260 °C (by Method 1) and 260 °C, 280 °C (by Method 2)

Therm Chrom	Measurement number	Method 1			Method 2	
		tested at 200 °C TTT [°C]	tested at 230 °C TTT [°C]	tested at 260 °C TTT [°C]	tested at 260 °C TTT [°C]	tested at 280 °C TTT [°C]
BG	1	28.3	28.5	28.5	28.4	28.5
	2	28.4	28.5	28.6	28.4	28.7
	3	28.3	28.7	28.6	28.6	28.4
	Ø	28.3	28.6	28.6	28.5	28.5
VB	1	29.5	29.0	29.9	29.5	–
	2	29.4	29.4	30.0	29.7	–
	3	29.4	29.1	30.1	29.8	–
	Ø	29.4	29.2	30.0	29.7	–
OY	1	28.5	28.3	28.5	28.3	28.6
	2	28.3	28.4	28.6	28.3	28.7
	3	28.4	28.5	28.5	28.4	28.2
	Ø	28.4	28.4	28.5	28.3	28.5

Conclusions

Preliminary tests were done with samples to see how they behave at increased temperature. All of them exhibited thermochromic colour transition at approximately 30 °C. Another set of tests was done to find out the ceiling temperature they can be exposed to. These tests of thermal stability were important because thermochromic compounds were intended to manufacture by processes where temperatures reach 260 °C. It was found out that ThermChrom BG and OY stand the temperatures up to 280 °C whereas ThermChrom VB is suitable for using at 260 °C at most. Tests of thermal stability proved the thermochromic compounds are suitable for processing without substantiall TTT change by all common technology for plastics materials.

REFERENCES

1. Crano J.C., Guglielmetti R.J.: *Organic Photochromic and Thermochromic Compounds, Volume 2, Physicochemical Studies, Biological Applications, and Thermochromism,* Kluwer Academic/Plenum Publishers, New York (1999).
2. Day J. H.: Chem. Rev. *63*, 65 (1963),
3. Principle of thermochromism, last update: 1st November 2005 Available from: http://www.chromazone.co.uk/Thermochromism.htm

P06 POLYMER PHOTOELECTRONIC DEVICES BASED ON INTERACTION BETWEEN π-CONJUGATED POLYMER MATRICES AND PHOTOCHROMIC MOLECULES

JIŘÍ NAVRÁTIL, MARTIN WEITER and MARTIN VALA

Faculty of Chemistry, Brno University of Technology
Purkynova 118, 612 00 Brno, Czech republic,
xcnavratil@fch.vutbr.cz

Introduction

Nowadays, after more than 15 years of academic and industrial research worldwide, the class of organic materials, conjugated polymers has reached a very high level of outstanding material properties and the potential for different industrial applications is now emerging. Various polymers are used in organic light-emitting diodes (OLED) and flat organic displays equipped with organic field-effect transistors, some other expect applications including optical sensors are very close to industrial applications. Printing technology is currently enabling the production of these high-efficiency organic devices. Given the need for very low-cost circuits for everything from smart cards carrying personal information, to building entry cards, to inventory control, it is reasonable to assume that within 10 years, the square footage of organic circuitry might exceed that of silicon electronics, though one expects that silicon transistors would still vastly outnumber and outperform those fabricated from organic materials[1].

Experimental

Polymer devices were manufactured as a sandwich cell with a dielectric layer of MDMO-PPV (Poly[2-methoxy-5-(3',7'-dimethyloctyloxy)-1,4-phenylenevinylene]) containing 0–30 % wt. of admixed spiropyrane (6-nitro-1',3',3',-trimethylspiro[2H-1-benzopyran-2,2'-indoline]). The device and material structure is depicted in Fig. 1. The active polymer layer was spin coated from chloroform solutions on transparent indium tin oxide (ITO) electrode covering part of the glass substrate. The thickness of the active layer was about 150 nm. The structure was completed by evaporation of aluminium top electrode. Average electrode area that delimitate the active area of the device was 3 mm^2. The same
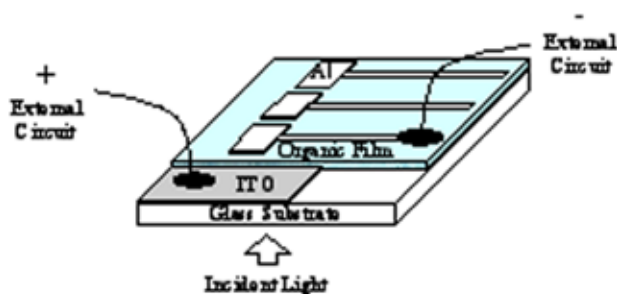
Fig. 1. **Schematic structure the devices used for characterization**

solutions of active materials were spin cast on quartz substrates for optical measurements. The photochromic reaction of spiropyrane was activated using a Xenon lamp with blue filter transmitting UV light 340 nm. Optical switching was studied using standard absorption and photoluminescence spectroscopy (PL) with excitation at 450 nm. The electric response was studied by measuring the current-voltage $j(V)$ characteristics of the samples in the dark with Keithley 6517A electrometer. The measurements were performed in vacuum cryostat at room temperature.

Results

Optical Switchning

Under irradiation of an appropriate light energy, the spiropyran exhibits photochromism as shown in Fig. 2 and Fig.3. The photochromic reaction is accompanied by a charge redistribution resulting in a significant increase of the dipole moment of the molecule. The studied spiropyran (SP) is stable in its colourless closed ring isomeric form, while UV irradiation produces a metastable open ring isomer merocyanine (MC) absorbing at 550–600 nm. The maximum of absorption band of MDMO-PPV is situated at 450 nm, the addition of SP increases the absorption of the sample in the UV region as shown in Fig.3. After irradiation with UV light the spectra exhibit a significant absorption band at 590 nm caused by the colored merocyanine form. Annealing in dark or irradiation with a red light gradually restores the original spectrum, the change is fully reversible.
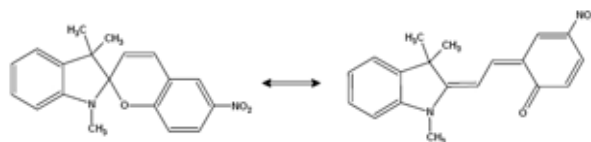
Fig. 2. **Photochromic reaction of the spiropyran (SP) into (photo)merocyanine (MC) manifests itself as color change of the system**

A strong photoluminescence (PL) quenching after the photochromic conversion caused by radiative energy transfer was observed as figured in Fig. 4. The stable form of spiropyran does not show any luminescence contrary to its MC form. MDMO-PPV show their own luminescence and creation of MC form via the photochromic reaction therefore could result in the photoluminiscence bands decrease of the MDMO-PPV. However, MC possesses a high dipole moment which generally causes a quenching of luminescence. The quenching was found to be strong even in the case when the SP → MC conversion was very weak, even not observable in absorption spectra. Furthermore the PL of MC could be triggered through the polymer excitation. This means that the energy absorbed by polymer (donor) is transferred to MC molecules (acceptor). According to the Forster-Dexter theory the dipole-dipole energy transfer probability is, among other, related to the overlap of donor emission and acceptor absorption. After the reverse (MC → SP) reaction was com-

pleted, the polymer PL was recovered, the reversibility of the process was, however, influenced by photodegradation of the polymer matrix.
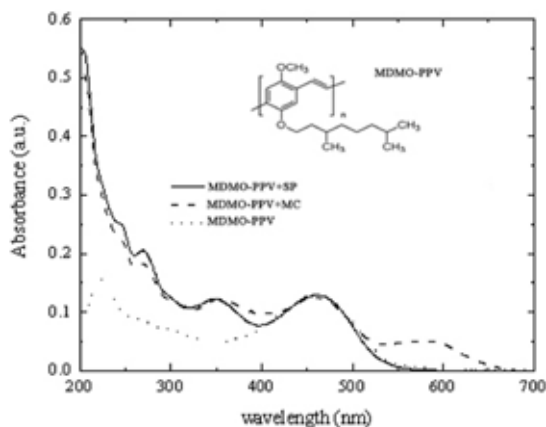
Fig. 3. **The dotted line shows the UV-VIS absorbance spectrum of MDMO-PPV polymeric matrix. Full line represents the absorbance spectrum of MDMO-PPV:SP mixture. The spectrum after the photochromic conversion (dashed line) shows distinct appearance of a band peaking at 590 nm. The inset show the chemical formula of MDMO-PPV unit**
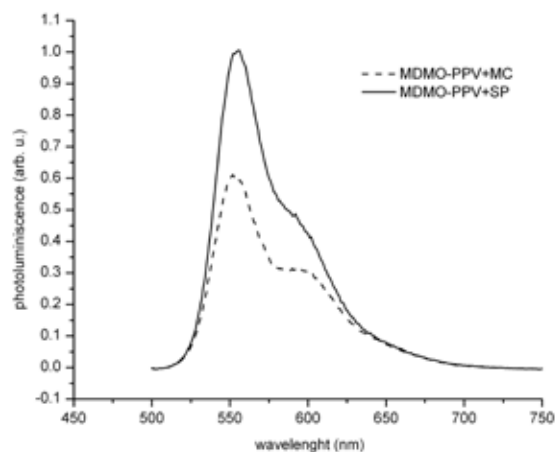
Fig. 4. **Photoluminiscence quenching after the photochromic conversion is liquid state. After photochromic covnersion (dashed line) is the photoluminiscence decrease apparent**

Current-Voltage Measurements

The photoswitching of charge carrier mobility was studied by standard current-voltage $j(V)$ measurement. The results for typical devices are shown as log-log plot in Fig. 5. The curent-voltage characteristics show a typical decrease of the current after the excitation of photochromic spiroparane. These prove that the presence of created polar MC molecules
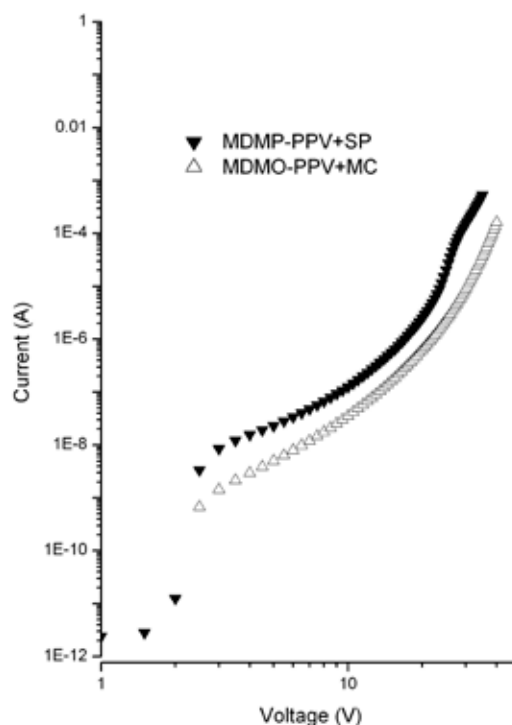
Fig. 5. **Current-voltage characteristics of the 20% mixture of the MDMO-PPV:SP measured in dark**

in the vicinity of a polymer chain modifies the distribution of on chain site energies. Thus the ditribution of hopping transport states is broadened and charge carrier mobility decreases which lead to to the current decrease. These findings are in good agrement with our previous theoretical studies by means of quantum-chemistry calculations[2].

Conclusions

The experimental behaviour of the system explored by means of current-voltage characterization showed a significant decrease of the current thorough the sample after irradiation.

REFERENCES

1. Harrop P., Das R.: *Organic Electronics: Forecasts, Players & Opportunities*. IDtechEx, New York 2005.
2. Toman P, Nešpůrek S., Weiter M., Vala M., Sworakowski J., Bartkowiak J., Menšík M.: Nonlin.Opt., Quant. Opt. *37*, 87 (2007).

P07   ANALYSIS OF THE WOOD SURFACE TREATED BY DIFUSE COPLANAR SURFACE BARIER DISCHARGE TYPE ATMOSPHERIC PLASMA

ERIKA NOVÁKOVÁ, MICHAL LETKO, RADOVAN TIŇO, JÁN MARTÁK and LÍVIA BEŇOVÁ

Department of Chemical Technology of Wood, Pulp and Paper, Faculty of Chemical and Food Technology, Slovak University of Technology, Radlinského 9, 812 37, Bratislava, Slovakia,
erika.novakova@stuba.sk

Introduction

DCSBD plasma sources proved their potential for surface treatment of wide spectrum of polymer materials[1,2]. The treatment of wood with atmospheric-pressure plasma offers at least three advantages: expensive vacuum equipment is not required, continuous in-line processing can be realised and processing times are short[3].

Surface treatment of wooden materials by atmospheric coplanar barier plasma discharge can improve homogenity of wood surface, which has mostly unequal structure. Unequality comes from the fact, that wood surface contains spots with different affinity to water (hydrophobicity and hydrophylicity).

Changes of wood surface pH and composition of water extract influence the adhesion of urea-formaldehyde resins[4]. Therefore the study of plasma treatment effect for surface pH can contribute to the improvement of coating technology.

Experimental

Wood surface was treated by atmospheric plasma generated by diffuse coplanar surface barrier discharge (DCSBD) in air atmosphere. The plasma exposure time of wood surface was 5 s.

pH Measurement

Determination of surface pH of three wood species was performed according to standards (STN ISO 50 0374 and Tappi T 529 om-88). Measurement was carried out with electrode with flat head Sentek P17/BNC conected with Jenway 3510 pH-meter. Clean (dustless) wooden surface was air-conditioned for 24 hours at 23.5 °C and at 48.65 % of humidity prior the measurement. Wooden surface was during the plasma treatment in direct contact with plasma electrode surface (0 mm).

Acid-Base Titration

Cold water extracts (5 ml) of three wood species (*Picea excelsa L., Fagus silvatica L., Quercus robur L.*) were prepared. Cold extract was acquired from area of 3.037 cm^2 with the assistance of extraction cell attached on the wood sample. Extraction was done at constant conditions. Thickness of extracted surface layer can be different. Extraction time was 3 minutes (the same as the measurement of surface pH).

Cold water extract was titrated with 0.01M solution of sodium hydroxide on phenolphthalein indicator. Amount of acid components was determined from sample surface treated in distance 0 mm, 0.39 mm, 0.65 mm up to 1.04 mm from plasma electrode.

Isotachophoretic Determination

Extraction time of cold water extract was 60 minutes. Wooden surface was in direct contact on plasma electrode surface (0 mm).

Electrophoretic analyser type EA 100 (Villa, SK) was applied for electrophoretic determination of carboxylic acids, which is given for capillary isotachophoresis (ITP). Standards of formic acid, acetic acid, propionic acid and butyric acid were used for determination.

Composition of electrolytes: 5 mol m^{-3} MES (Morpholineethanesulphonate) + HIS (Histidine buffer), 10 mol m^{-3} HISCl (Histidine chloride buffer) + 10 mol m^{-3} HIS + 0.1% MHEC (Methylhydroxyethylcellulose), pH = 6.

Results

From Table I is evident that by plasma treatment the increase of acidity was detected at all wood species. It was evinced from decrease of pH value about 2 units in case of spruce and beech and 1 unit in the case of oak.

Values of surface pH were stabilized faster in case of plasma treated samples than untreated samples. Value of pH was stabilized slowlier in case of untreated samples because gradual release of acid components from wooden surface. Wood surface treatment caused greater acidity and acid components were releasing faster.

Table I
Surface pH of three wood species before and after the plasma treatment

Sample	pH value before plasma treatment	pH value after palsma treatment
Spruce	6.23 ± 0.03	4.18 ± 0.03
Beech	5.77 ± 0.02	3.72 ± 0.03
Oak	4.74 ± 0.02	3.68 ± 0.03

Total change of acid components concentration was determined by the acid-base titration. In this case was also measured dependence of concentration of acid content on distance between wood surface and surface of plasma electrode. The highest concentration of acid content was observed when surface of wood was in direct contact with plasma electrode. By increasing the distance between surface plasma electrode and surface of wood, concentration of acid content was falling down gradually (Table II).

Total acidity in comparison to untreated sample demonstrated the least increase (43 %) of acid components after the plasma treatment at spruce sample. The highest increase of acid components up to 95 % was achieved at oak wood, which surface was in direct contact with plasma electrode.

Value of increase of acid components in beech sample was similar to oak sample (94 %). Value of acid components in the distance of 1.04 mm from surface of electrode was near to value of untreated sample (Table II, III).

Table II

Acid components concentration (c) of three wood species in air atmosphere in different distances of wood surface from surface of electrode (d)

d [mm]	c Spruce $[10^4\,\mathrm{mol\,dm^{-3}}]$	c Beech $[10^4\,\mathrm{mol\,dm^{-3}}]$	c Oak $[10^4\,\mathrm{mol\,dm^{-3}}]$
0	3.3972	4.9259	6.9643
0.39	2.8876	3.7369	5.2657
0.65	2.5479	3.0575	4.5862
1.04	2.3780	2.7178	3.7369

Table III

Acid components concentration at wood samples before the plasma treatment (c)

Sample	$c\,[10^4\,\mathrm{mol\,dm^{-3}}]$
Spruce	2.3780
Beech	2.5479
Oak	3.5671

By means of carboxylic acids standards (formic acid, acetic acid, propionic acid, butyric acid) we confirmed presence of these carboxylic acids in the samples of spruce, beech and oak. We found that plasma treatment caused increase of formic acid content. It was located at all measured wood samples against to untreated samples. The highest increase of formic acid concentration up to 56.2 % was achieved at oak sample (Table VI). Otherwise the least increase of this acid was measured at spruce sample where percentage of increase moved at level 11 % against to untreated sample (Table IV). Concentration of formic acid increased up to 39.2 % in the beech sample (Table V). On the other hand, concentration of acetic acid decreased after the plasma treatment at all wood species. The highest decrease was observed at spruce sample up to 49.7 % and the least decrease was measured at oak sample where concentration dropped to level 6.4 %. Concentration at oak sample dropped to 11.2 %.

The highest concentration among investigated acids had propionic acid but change of concentration influenced by the

Table IV

Acid concentrations at spruce sample determined by isotachophoretic method before the plasma treatment (c_1) and after the plasma treatment (c_2)

Carboxylic acids	$c_1\,[10^3\,\mathrm{mol\,dm^{-3}}]$	$c_2\,[10^3\,\mathrm{mol\,dm^{-3}}]$
formic acid	0.0082	0.0091
acetic acid	0.0153	0.0077
propionic acid	0.0242	0.0234
butyric acid	0.0171	0.0145

Table V

Acid concentrations at beech sample determined by isotachophoretic method before the plasma treatment (c_1) and after the plasma treatment (c_2)

Carboxylic acids	$c_1\,[10^3\,\mathrm{mol\,dm^{-3}}]$	$c_2\,[10^3\,\mathrm{mol\,dm^{-3}}]$
formic acid	0.0079	0.0110
acetic acid	0.0089	0.0079
propionic acid	0.0218	0.0235
butyric acid	0.0181	0.0138

Table VI

Acid concentrations at oak sample determined by isotachophoretic method before the plasma treatment (c_1) and after the plasma treatment (c_2)

Carboxylic acids	$c_1\,[10^3\,\mathrm{mol\,dm^{-3}}]$	$c_2\,[10^3\,\mathrm{mol\,dm^{-3}}]$
formic acid	0.0089	0.0139
acetic acid	0.0078	0.0073
propionic acid	0.0236	0.0219
butyric acid	0.0180	0.0131

plasma treatment was in this case the least. It is only one acid which demonstrated both increase and decrease in depence of wood species. Propionic acid concentration decreased by plasma treatment against to untreated sample (3,3 % and 7,2 %) at the spruce and oak sample. Concentration of propionic acid increased at oak sample up to 7,8 % against to untreated sample.

After the plasma treatment, decrease of concentration in case of butyric acid in all wood species as in case of acetic acid occured. Concentration decreased up to 15,2 % at spruce sample, 23,8 % at beech sample and 27,2 % at oak sample.

Conclusions

Formic, acetic, propionic and butyric acid were in water extract before and after plasma treatment, but their concentration differed. As formic acid is out of the all above mentioned acids strongest one and it can be stated, that this acid contributes to the total acidity of wooden surface the most. The highest increase of formic acid concentration was found at oak wood (56 %). The lowest fall of concentration was found at propionic acid, which dropped down just about 3 % after the plasma treatment in comparison to untreated sample.

Extraction method allows semiquantitative determination of acids and relative comparison of plasma treated and plasma untreated samples. Therefore the data of acids concentrations relate only to the volume of water extract and to area of exposed surface of sample.

REFERENCES

1. Šimor M., Rahel J., Vojtek P., Brablec A., Černák M.: Appl. Phys. Lett. *81*, 2716 (2002).
2. Černák M., Ráhel J., Šimor M: Slovak Patent Appl. PP 0136–2003.
3. Tóth A., Černáková L., Černák M., Kunovská K.: Holzforschung *61*, 528 (2007).
4. Medved S., Resnik J.: Acta Chim. Slov. *51*, 353 (2004).

P08　STRATEGIES FOR ENHANCING POLY(3-HYDROXYBUTYRATE) PRODUCTION IN SELECTED BACTERIAL STRAINS

STANISLAV OBRUČA, SOŇA MELUŠOVÁ, IVANA MÁROVÁ and ZDENĚK SVOBODA

Brno University of Technology, Faculty of Chemistry, Department of Food Chemistry and Biotechnology, Purkyňova 118, 612 00 Brno, Czech Republic,
xcobruca@fch.vutbr.cz

Introduction

Polyhydroxyalkanoates (PHAs) are a group of hydroxyacid polyesters that are produced and accumulated in the form of intracellular granules by a wide variety of bacterial strains. These strains use PHA as carbon, energy and reducing power storage material[1]. Of the big family of PHAs, a homopolymer of 3-hydroxybutyrate, poly(3-hydroxybutyrate) (PHB), is the most widespread in nature and the best characterised. PHB aroused much interest in industry and research thanks its biocompatible, biodegradable, thermoplastic and piezoeletric properties. PHB appears to find many pottential applications in medical, industrial and agricultural fields[2].

Generally, the main problem of PHB is high cost in comparison with traditional plastics from petrochemical routes. That is why strategies for enhancing of PHB production are developed. Typical strategy, which is widely used for enhancing PHB production, is limitation with nitrogen, phosphorus or another element when excess amount of carbon source is present[3].

Among the factors restricting the economy of PHB production very important is the cost of carbon source. In PHB production, about 40 % of the total cost is for raw materials. Cheap waste substrates, for instance cheese whey or waste potato starch, are very attractive from this point of view. Effective utilization of waste subtrates should lead to reduction of PHB cost[4].

The positive influence of stress factors (such a peroxide stress, osmotic stress, ethanol stress or heavy metal stress) on accumulation of differents secondary metabolites were reported[5]. However, to this time only little is known about accumulation of PHA under exogenous stress condition.

The aim of this work was to compare different strategies that could enhance PHB production and reduce costs of PHB. Limitations with nitrogen and/or phosphorus source were tested. The influence of several exogenous stresses on PHB production was compared. Finally, production of PHB was studied in synthetic and organic medium as well as using cheese whey as a cheap waste substrate.

Experimental

Bacterial Strain

Cultivations were performed with culture *Bacillus megaterium* CCM 2037.

Cultivation Condition

Cultivations were carried out at 30°C under permanent shaking (150 rpm) in 100 ml of media. Several media were tested, as the first synthetic medium (SM) containing glucose as the only carbon source, KH_2PO_4 and Na_2HPO_4 (1 : 1) as the phosphorus source and $(NH_4)_2SO_4$ as the nitrogen source was used. SM was used for limitation experiments. Culture was transferred (centrifugation 20 min., 6,000 rpm) into limited medium (medium without nitrogen or/and phosphorus source) after 20 hours of growth on complete medium. After following 15 hours, biomass and PHB concentration were determined. SM was also used for stress experiments. The second tested medium was *Bacillus* medium (BM) containing peptone and beef extract. The last medium was cheese whey obtained from cheese manufactury Pribina Přibyslav. Thermal denaturation and sulphuric acid were used for precipitation and removing of whey proteins before cultivation. Whey was tested with and/or without addition of salts according to SM.

Analytical methods

Biomass concentration was analyzed spectrophotometrically at 630 nm after suitable dilution with distilled water. Relationship between absorbance A 630 nm and dry cell mass was evaluated. Before PHB determination biomass was lyophillized. Dryied cell material was hydrolyzed and derivatized in a mixture of 0.8 ml acidified methanol (15 % v/v H_2SO_4) and 1 ml chloroform at 100 °C for 140 min. Resulting methyl esters of 3-hydroxybutyric acids were determined using gas chromatography with MS or FID detection. Commercial PHB (Fluka) was used as the external standard[6].

Results

First, the effect of nitrogen and/or phosphorus source limitation was tested. All tested limitations led to enhancing PHB content in bacterial cell biomass in comparison with cultivation without limitation. However, it seems that for *Bacillus megaterium* limitation with nitrogen source is probably the best stimulating factor for PHB production (see Table I).

Table I
PHB production under limitation (35 hours)

Limitation	PHB content [% dry wieght]	PHB yield [g dm^{-3}]
Without limitation	14.164 ± 1.248	0.234 ± 0.025
N limitation	24.035 ± 1.406	0.360 ± 0.029
P limitation	14.857 ± 0.826	0.177 ± 0.009
N + P limitation	17.648 ± 0.691	0.237 ± 0.018

Also some other tested exogenous stress factors influenced positively the productivity of culture in comparison with control. Ethanolic stress as well as Na_2SO_4 supported PHB accumulation.

Mainly ethanolic stress resulted in improving PHB production. This effect could be caused by the fact, that ethanol

is metabolised *via* acetyl-coenzym A, which is starting meta-bolite for PHB production. It is not clear if enhanced PHB production was casued by ethanolic stress or by utilization of ethanol alone. Both factors could be involved. The culture could utilize ethanol with the aim to remove toxic substance from medium. Increase of acetyl-coenzym A concentration led then to enhanced PHB accumulation.

Table II
PHB production under exogenous stress (35 hours)

	Biomass [$g\,dm^{-3}$]	PHB content [%]	PHB yield [$g\,dm^{-3}$]
H_2O_2	0.047 ± 0.001	*	*
NaCl	0.134 ± 0.039	6.864 ± 0.082	0.016 ± 0.001
EtOH	1.812 ± 0.029	20.793 ± 0.358	0.377 ± 0.007
$NiCl_2$	0.053 ± 0.000	*	*
Citrate	1.739 ± 0.025	14.620 ± 0.054	0.254 ± 0.001
Na_2SO_3	1.744 ± 0.050	19.881 ± 0.612	0.345 ± 0.011
Control	1.762 ± 0.009	17.030 ± 0.179	0.300 ± 0.003

* no PHB production was observed

Table III
PHB production on different media (45 hours)

	Biomass [$g\,dm^{-3}$]	PHB content [%]	PHB yield [$g\,dm^{-3}$]
BM	1.288 ± 0.015	0.050 ± 0.011	0.001 ± 0.000
BM + glucose	2.602 ± 0.050	44.720 ± 3.290	1.164 ± 0.086
BM + starch	2.150 ± 0.110	21.054 ± 0.711	0.453 ± 0.012
Whey	0.389 ± 0.033	*	*
Whey + salts	1.612 ± 0.033	15.464 ± 0.181	0.249 ± 0.003

* no PHB production was observed

Addition of Na_2SO_3 led to higher PHB production too. This effect could be caused by reducing properties of Na_2SO_3, but the effect on PHB production was relatively low.

Other stress factors inhibited the growth of culture and/or PHB accumulation. Because of relationship between stress factor concentration and its biological effect further experiments will be needed. Detailed analysis of concentration effects was not included into this pilot study.

Because of relatively low PHB amount (14–20 % of total biomass) other media then SM were tested. Culture growing

on BM medium itself did not contain almost any PHB after 45 hours of growth. However, when glucose was added, production of relatively high PHB amount was observed. This is probably caused by the fact, that culture depleted nitrogen and phosphorus sources of BM medium, but carbon source (sugar) was still present. Culture was able to utilize sugar for the growth as well as for PHB accumulation.

Finally, cheese whey was tested as a component of medium for PHB production. Low growth and no PHB production were observed when cultivations were performed on whey itself. Addition of salts (according to SM) led to the strong increase of growth and production properties of culture.

Conclusions

All strategies tested in this work could be used for enhancing PHB production in *Bacillus megaterium* CCM 2037. Limitation with nitrogen seems to be a strong stimulating factor for PHB production.

Positive effect of two exogenous stress factors on PHB production was observed. Ethanolic stress and Na_2SO_3 enhanced PHB production. However, the mechanism and optimal concentration of stress factors have to be clarified.

Culture was able to utilize organic substrates (BM, cheese whey) and product high amount of PHB. The highest yield of PHB (1.16 $g\,dm^{-3}$) was obtained during growth in BM medium with glucose. *Bacillus megaterium* is also able to use cheap cheese whey or starch as a carbon source. That should lead to reducing of PHB cost. However, further otimization studies are needed.

REFERENCES

1. Lee S. Y.: Biotechnch. Bioeng. *49*, 1 (1996)
2. Reddy C. S. K. et al.: Bioresour. Technol. *87*, 137 (2003).
3. Choi J., Lee S. Y.: Appl. Microbiol. Biotechnol. *51*, 13 (1999).
4. Solaiman D. K. Y. et al.: Appl. Microbiol. Biotechnol. *71*, 783 (2006).
5. Marova I. et. al: Ann. Microbiol. *54*, 78 (2004).
6. Brandl H. et. al: Appl. Enviroment. Microbiol. *54*, 1977 (1988).

P09　COMPARISON OF BIODEGRADABILITY OF MODIFIED POLYURETHANE FOAMS AND POLYURETHANE ELASTOMERIC FILMS

STANISLAV OBRUČA, IVANA MÁROVÁ, JANA PIECHOVÁ, LUCY VOJTOVÁ, MAREK NOVOTNÝ and JAN DAVID

Brno University of Technology, Faculty of Chemistry, Department of Food Chemistry and Biotechnology, Purkyňova 118, 612 00 Brno, Czech Republic,
xcobruca@fch.vutbr.cz

Introduction

Polyurethanes (PUR) are a widespread group of polymeric materials involved in many aspects of modern life. They are widely used in medical, automotive or industrial fields. PUR are very variable group of materials because they could be prepared in many forms ranging from flexible or rigid foams, solid elastomers, coating, adhesives and sealants[1].

Polymeric materials could serve as carbon (but also nitrogen and other atoms) and energy source for heterotrophic microorganism including bacteria, moulds and yeasts. This natural process of material decomposition is called biodegradation[2].

After the years of PUR production manufactures found PUR susceptible to biodegradation. Microbial degradation of PUR as well as other polymeric materials is dependent on many properties of the polymer such as molecular orientation, crystallinity, cross-linking and chemical groups present in the molecular chain. Very small variations in the chemical structure may result in large differences in the term of biodegradability[3].

This work was focused on the comparison of biodegradability of two different forms of the same PUR material - modified PUR foams and modified PUR elastomeric films. Several types of biopolymers were used as modyfying agents that should enhance biodegradability of both PUR forms. For laboratory biodegradtion tests mixed thermophillic culture *Thermophillus sp.* was used.

Experimental

PUR foams and elastomeric films were modified by 10 % of acetyl-cellulose (CA), 10 % carboxymethyl cellulose (CMC) and 10 % acetylated starch (AS). Modifying agents partially replaced polyether polyol. Both PUR foams and PUR elastomeric films were prepared from the identical raw materials. The only difference was that in film preparation blowing agent (water) was not used.

Biodegradation Tests

Biodegradation tests were performed with mixed thermophillic culture *Thermophillus sp.* Cultivations were carried out at 60 °C under permanent shaking in 100 ml of defined media. One sample of PUR was represented by 0.25 g of PUR. Growth characteristics, chemical oxygen demand and glucose concentration were determined in regular intervals. At the end of cultivation (about 100 hours) PUR mass decreases were measured gravimetrically and PUR surface changes were analysed microscopically.

Results

The presence of PUR material influenced growth of bacterial culture in comparison with culture without PUR. Generally, PUR foams supported the growth of bacterial culture, on the contrary PUR elastomeric films weakly inhibited biomass production. The inhibition effect was exhibited mainly during early stages of growth when long lasting lag-phase was observed. This effect was probably caused by formation and/or by release of some toxic component(s) which inhibited the start of the growth. Because toxic effect was not observed in PUR foams, it is possible that toxic component(s) was by some way removed during the foaming process.

Modifying agent type was other important factor which influenced the growth of culture. From this point of view, CMC seems to be the best modifying agent because it strongly supported the growth of culture grown both in presence of PUR foams as well as PUR films.

Mass decreases of foams and films were very similar, however, in some experiments higher degradation degree was observed in PUR films. It is surprising because PUR films are expected to be more rigid than PUR foams.

It seems that modification agent type is probably more important factor than the form of PUR material. The highest losses of material were observed in PUR foams and films modified by CMC (see Fig. 1.). High mass decreases of CMC PUR materials could be partially caused by water solubility of carboxymethyl cellulose itself.
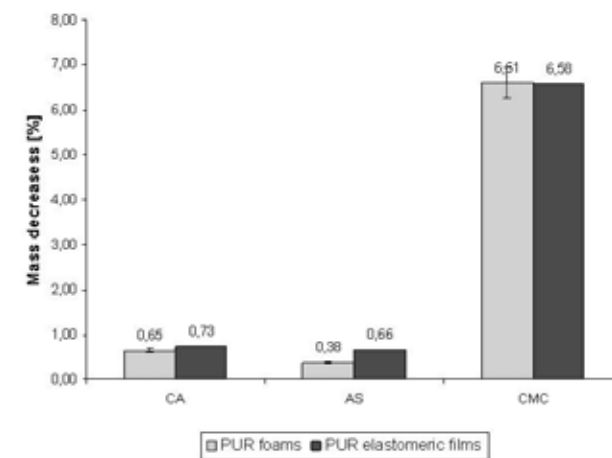
Fig. 1.　**Mass decreases of PUR foams and films**

Conclusions

In conclusion, modified PUR foams as well as elastomeric films could be degraded by thermophillic bacteria. Differences between foams and films are surprisingly small. It seems that for biodegradation degree more important factor is the modification agent type than PUR material form. Carboxymethyl cellulose appears to be the best modifying agent

from biodegradation point of view. In relatively short-time lasting tests (about 100 hour) PUR materials modified by carboxymethyl cellulose exhibited almost 7 % of weight loss. CMC PUR materials also strongly supported the growth of bacterial culture.

REFERENCES

1. Oertel G.: *Polyuretane handbook*, 2nd ed., Hanser Publisher, 1993.
2. Wypych G.: *Handbook of Material Weathering*, 3rd ed.; ChemTec Publishing, 2003.
3. Howard G. T.: Int. Biodeter. Biodegrad. *49*, 245 (2002).

**P10 SYNTHESIS OF SUBSTITUTED
　　　POLYSILYLENES USED AS
　　　SEMICONDUCTIVE POLYMERS**

IMAD OUZZANE[a], SOŇA HERMANOVÁ[a], MARTIN
VALA[a], MARTIN WEITER[a] and STANISLAV
NEŠPŮREK[b]

[a]*Brno University of Technology, Faculty of Chemistry, Pur-
kyňova 118, 612 00 Brno, Czech Republic,*
[b]*Institute of Macromolecular Chemistry Academy of Sciences
of the Czech Republic Heyrovsky Sq. 2, 162 06 Prague 6,
Czech Republic,*
ouzzane@fch.vutbr.cz

Introduction

　　Polysilylenes are of considerable research interest
because of their electronic, photoelectrical and nonlinear
optical properties.

　　Polysilylenes are most often obtained by Wurtz reduc-
tive coupling of organosilanes with sodium metal in reflu-
xing toluene (Scheme 1). Therefore the metal is easily dis-
tributed throughout the solution. Unfortunately, the yields of
polymers and the reproducibility of the reaction are usually
quite poor. Up to now there is no satisfactory mechanistic
theory to determine the best procedure, and the reaction con-
ditions must be optimized for each polymerization. Reaction
conditions close to optimum could be achieved by evaluating
the trends. This contribution reports on the methods and pro-
cedure based on new operatory conditions that allowed us to
gain in yield and quality of product obtained.
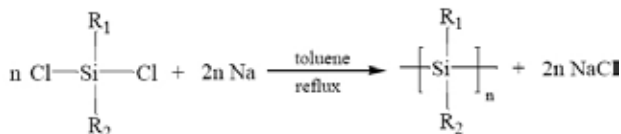
Scheme 1

Experimental

General Synthesis (Procedure A)
of Poly[methyl(phenyl)silylene]
PMPSi.

　　The polymers were prepared by the Wurtz synthesis
from dichloro(methyl)phenylsilane with sodium dispersion
in refluxing toluene under inert and dark atmosphere during
the whole process. To a three-necked Schlenk flask equipped
with stirring bar, condenser and dropping funnel was added
freshly cut sodium (7.5 g, 0.33 mol). Dry toluene (100 ml)
was transferred with a canulla to the reaction flask and heated
to reflux. The solution of freshly distilled dichloro(methyl)p
henylsilane (25 ml, 0.13 mol) in 25 ml of toluene was added
dropwise into the dispersion until the color of the reaction
mixture changed to blue, indicating the start of the reaction.
The rest of the monomer solution was then dropped in the
course of 1 h. After 1 h 30 min under reflux, the reaction
was quenched at room temperature by addition of 1 ml of

BuLi solution. The residual sodium was reacted, under ice
bath cooling with 25 ml of ethanol and then with 25 ml of
water. The organic layer was separated and taken directly to
centrifuge. Cross-linked and insoluble portions were sepa-
rated by centrifugation at 12,000 rpm for 15 min.). Desired
polymer fraction was recovered by precipitation of the tolu-
ene solution into methanol. For purification, it was repreci-
tated from THF solution with methanol. The white solid was
collected by filtration, washed with methanol and dried in a
vacuum oven.

Modified Procedure (B) for the
synthesis of Poly[methyl(phenyl)s
ilylene] PMPSi

　　The solution of freshly distilled dichloro(methyl)phe
nylsilane (25 ml, 0.13 mol) in 25 ml of toluene was added
rapidly (5 min) into the dispersion Extreme care had to be
exercised due to great rate of polymerization. After that the
reaction mixture was stirred under mild reflux for 1 h. The
mixture was then allowed to cool to room temperature for
quenching with 1 ml of distilled water. While cooling in an
ice bath water (2×25 ml) was added carefully to neutralize
the excess of sodium.

Polymer Characterization

　　^{1}H, ^{13}C NMR spectra were recorded with a Bruker
Avance 300 Varian aparatus at a working frequency of
300 MHz for ^{1}H and 75 MHz for ^{13}C in CDCl$_3$ using TMS as
the internal standard. Chemical shifts are given in ppm. The
molecular weight and the molecular weight distribution of
the polymers were determined by GPC method using Agilent
Technologies 1100 Series instrument equipped with a refrac-
tive index detector and UV detector, two PLgel Mixed C
columns of 300×7.5 mm with particle size of 5 mm, degas-
ser, pump and auto sampler. Tetrahydrofurane was used as the
mobile phase at a flow rate equal to 1 ml min^{-1}. The average
molecular weight was calculated using a series of polystyrene
standards ($M_p = 316,500 - 162$).
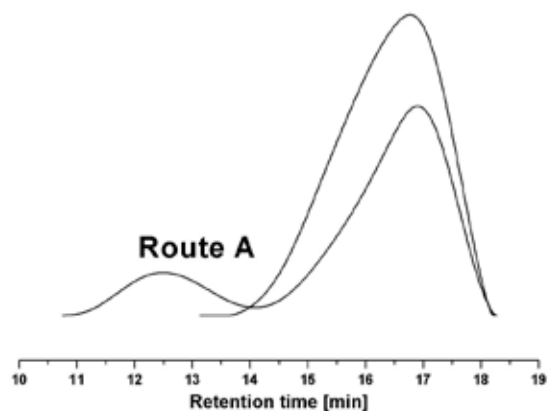
Fig. 1.　**Molecular weight distribution of polymer produ-
cts obtained by route A, M_w = 6.2 kg mol^{-1}, M_w/M_n(PD) = 2,
M_w = 47 kg mol^{-1}, M_w/M_n(PD) = 14**

Results

The present study is focused on properties of polymers obtained using proposed experimental conditions.

The data collected on NMR indicates the presence and purity of the product obtained: The peaks of methyl group resonating around 1.2 ppm and the aromatic protons of the phenyl group resonating around 7 ppm. Peaks are slightly shifted due to the Silicon bonding compared to the Carbone one.

Typical analytical data after precipitation: ^{1}H NMR (CDCl$_3$): δ/ppm = −1.0–1.3 (br, m, 3H, CH$_3$), 6.0–8.4 (br, m, 5H, aromatic H). ^{13}C NMR (CDCl3): δ/ppm = −6.3 (br), 127.1 (br), 129.1 (br), 133.3 (br), 134.8 (br), 136.2 (br).

GPC analyses (Fig. 1.) confirmed that the new procedure (Fig. 2.) allowed us to access to new longer chain polymers with higher polydispersity(PD). The yields of such kind of synthesis varies from 40–60 % and is well described in literature.

The Wurtz coupling reaction was conducted in low quantities and many times extracted so that we could obtain more or less pure long chain polymers separated from olygomers. Some low yields obtained are due to a lower scale reaction and drastic separation methods. Better yields can be obtained working on higher scale and determining better single chain molecular weight as we observed total conversion of starting products.

Conclusions

Methods used for the synthesis of PMPSi are well known in chemical industries and are usually drastic and therefore expensive and polluting. The way we explored allowed us to access higher yield polymers of very reasonable cost. The biggest advantage of it is that it uses also less hazardous products or polluting solvent. We could get through this new fashion synthesis high value polymers at lower cost and using only water and ethanol for reaction's ending and extraction which makes it part of the "green chemistry" or at least towards it.

The other aim of our work would be to synthesize new model of polysilylenes attached directly to functional chromophores throughout a Suzuki coupling and investigate their electrical and optical properties. The proposed structure should be capable of light driven switching between high conductive and low conductive regime, and therefore to be used as current switch or actuator.

Fig. 2. **Molecular weight distribution of polymer products obtained by route A, M$_w$ = 58 kg mol^{-1}, M$_w$/M$_n$(PD) = 18.4, M$_w$ = 89 kg mol^{-1}, M$_w$/M$_n$(PD) = 12.9**

REFERENCES

1. Jones R. G.: Polym. Int. *55*, 711 (2006).
2. Jones R. G., Wong W. K. C., Holder S. J.: Organometallics *17*, 59 (1998).
3. Jones R. G., Budnik U., Holder S. J., Wong W. K. C.: Macromolecules *29*, 8036, (1996).
4. Matyjaszewski K., Greszta D., Hrkach J. S., Kim H. K.: Macromolecules *28*, 59 (1995).
5. Weiter M., Vala M., Salyk O., Zmeškal O., Nešpůrek S., Sworakowski J.: Mol. Cryst. Liq. Cryst. *430*, 227 (2005).
6. Nešpůrek S., Zakrevskyy Y., Stumpe J., Sapich B., Kasashchuk A. : Macromolecules *39*, 690 (2006).
7. Nešpůrek S.: Mat. Sci. Eng. C *8*, 319 (1999).
8. Nešpůrek S., Sworakowski J., Kadashchuk A., Toman P.: J. Organomet. Chem. *685*, 269 (2003).
9. Kminek I., Brynda E., Schnabel W.: Eur. Polym. J. *27*, 1073 (1991).
10. Suzuki M.: J. Am. Chem. Soc. *123*, 10099 (2001).

P11   AUTOMATION OF PE-CVD PROCESS FOR PREPARING OF NANOSTRUCTURED FILMS

RADEK PŘIKRYL

*Brno University of Technology, Faculty of Chemistry, Purky-
ňova 464/118, 612 00, Brno, Czech Republic,*
prikryl@fch.vutbr.cz

Introduction

Plasma Enhanced Chemical Vapor Deposition (PE-CVD) is a power tool for designing of nanostructured films. The PE-CVD technology is relatively complicated and condition-intensive in term of resulting material's reproducibility. The deposition system has many input parameters have to be set or continuously regulated. A controlling of the process parameters using an automation technique can increase a reproducibility of experiments. The automated measured data recording enables additional check of deposition process. The aim of presented work is a design and development of programmable automation system for deposition process with a view of parameters controlling.

Plasma polymerization is a powerful tool for a deposition of thin films whose physicochemical properties can be controlled in wide ranges and thus the technology enables adjusting of the material properties with respect to an appli-cation. Recently the interest in nanolayers and nanoscrutures preparation increases. Preparation of the layers and/or complicated structures offers controlling of many process parameters in real time. A success of the coating technique depends on a suitable technological system, as the vacuum quality and film reproducibility are the crucial parameters[1]. With respect to the necessary accuracy of synchronization of all controlling component during the plasma processes the high level of deposition process automation is requisite.

The Developed System

We have developed a capacitive coupling system for creative design and application of complex film systems in smart materials. The internal setup of our deposition chamber using plan-parallel electrodes was derived from a typical capacitive coupling system, but our apparatus was equipped with many non-standard components described in other papers[1]. The electronic components of the deposition system were choosing according to the possibility of remote controlling in term of needed deposition system automation during the system designing. The wiring of the components, its communication ports or bus channels and/or analog channels was realized.

The system for PE-CVD process controlling used for a research in the lab conditions is complicated in term of a needed great versatility of the system, its peripheries, and
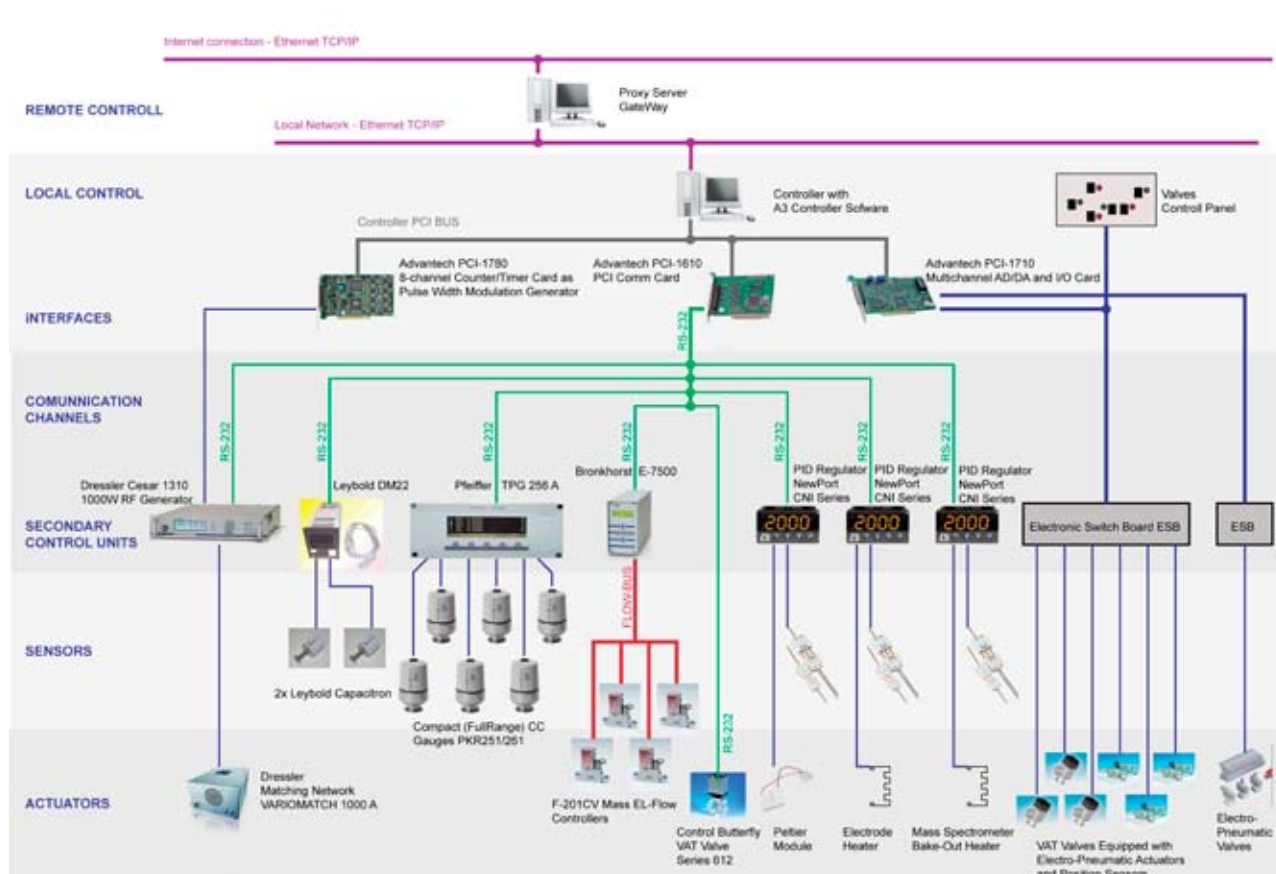
Fig. 1.   **Block scheme of communication between the third control unit and the connected peripheries**

a variability of deposition process conditions. The setup of the technological system to an exactly defined state requires a data reading from many sensors and offers controlling of many components of the system. The needed parameters of the deposition process are a function of time in the case of a multilayer or a gradient structures preparation. In fact the process is synchronized controlling and/or tracing regulation of process parameters defined in the real time. The full controlling of the system is realized using three computers -control units:

- The first of them controls spectroscopic in situ ellipsometer Yobin – Ivon. The communication is realized by TCP/IP protocol via commercially used software.
- The second control unit communicates with mass spectrometer Hiden and oscilloscope Hameg using serial channel RS – 232 via commercially made software.
- The third of control units supplies a pressure measuring, a process gases flow, a temperature measurement and a regulation, a vacuum valves position controlling, a communication with rf plasma generator and so on.

A block scheme in the Fig. 1. describes the realized solution of communication between the third control unit and the connected peripheries. The system was designed according to a possibility of basic operation of the deposition process independently of the control units operation in case of their failure. Therefore all sensors and actuators are connected via their autonomic primary control units equipped basic user interface which enables to obtain the needed values and/or elementary control the sensor/actuator function. The interfaces are relatively complicated and not user friendly, therefore they are not usable for common work of operator. The primary control units are connected *via* RS-232 serial channel to a multi-serial interface installed in the main control unit. The system of vacuum control is realized using a digital input/output interface of the multi-channel measuring card Advantech. The digital signal is adjusted by system of electronic switches controlling electro pneumatic actuators of the vacuum valves.

The plasma polymerization technology often uses a pulsed mode of the plasma discharge. The plasma generator Cesar 1310 (Advanced Energy company) is equipped with an internal timer for the pulse mode. The change of pulse mode parameters is belated by a time needed for a communication between the control unit and the generator. Therefore the solution is not suitable for stepless control of the pulse mode parameters. Fort the reason the main control unit is equipped with a multi-channel timer/counter module Advantech working in the pulse width modulation (PWM) regime. The signal controls the pulse mode parameters during complicated high-speed process operations.

The developing of control software for the main control unit was necessary as well. The elemental control units are not distributed with suitable communication software mostly. Therefore the software components for the communication between the elemental control units and the main control unit were developed using Borland Delphi tool. The components were implemented to a developed main software user interface named as A3-Controller. The software enables to an operator comfortably and easily to control all peripheries mentioned in the block scheme in Fig. 1. as well as to obtain and record the process values. In addition the main software was equipped with a timing functions, an automated control of a pumping speed, and a module fore a vacuum tightness checking etc. The three main control units are connected via Ethernet to the Internet network therefore the PE – CVD system is controllable from any PC connected to Internet.

REFERENCES
1. Prikryl R., Čech V., Studýnka J.: Czech. J. Phys. *56*, 468 (2006).

P12 CRYSTAL STRUCTURE OF A LANTHANIDE SANDWICH COMPLEX $(C_5Me_5)_2NdCl_2Li(OEt_2)_2$

LUKÁŠ RICHTERA, SOŇA HERMANOVÁ, VOJTĚCH JANČÍK and JAROSLAV CIHLÁŘ

Brno University of Technology, Faculty of Chemistry, Institute of Materials Science, Purkyňova 118, 612 00 Brno, Czech Republic,
richtera@fch.vutbr.cz

Introduction

The potential of lanthanide sandwich complexes of general formula $(C_5Me_5)_2LnCl_2Li(OEt_2)_2$ (where Ln = Nd, Sm) in polymerisation catalysis is nowadays well established[1]. *In situ* alkylation of the dichloro lanthanidocene precursor by dialkylmagnesium results in a production of efficient active species for ethylene oligomerisation. The propagation takes place *via* a controlled ethylene growth chain transfer reactions between active centres and dialkylmagnesium yielding tailor-made oligomers possessing narrow molecular weight distributions. These transfer reactions are reversible, very effective even at higher temperature and could thus be considered as living.

The reaction mechanism of ethylene oligomerisation was published few years ago but there was no reliable proof of the structure of $(C_5Me_5)_2LnCl_2Li(OEt_2)_2$ even though its synthesis was described already in 1981 by Tiley et al. and well grown blue crystals of this compound could be easily isolated[2]. The structure of $(C_5Me_5)_2LnCl_2Li(OEt_2)_2$ was first proposed based on the similarity with the spectral data of compounds $(C_5Me_5)_2LnCl_2Li(OEt_2)_2$ (Ln = Ce, Sm) whose structures were known[3,4] as well as for some other lanthanide sandwich complexes (Pr, Nd, Gd, Dy, Yb and Lu) with different organic donors (e.g. THF or TMEDA) and various substituents on the cyclopentadienyl rings.

Although many structures of lanthanidocenes with the general formula $Cp_2LnCl_2MD_2$ (Cp = cyclopentadiene or its derivative, Ln = lanthanide, M = alkali metal, D = organic donor) are known, others have been reported to have a quite unconventional structures and/or coordinations numbers[5]. Therefore we have focused on the determination of the crystal structure of the title species *(i)* to confirm or negate the structure predicted in already published studies; *(ii)* to get the missing experimental data for quantum mechanical study of this compound[6].

Experimental

The density data were collected on a KUMA KM–4 CCD kappa-axis diffractometer using a graphite monochromatized Mo-Kα radiation (λ = 0.71069 Å).

Results

The selected compound $(C_5Me_5)_2LnCl_2Li(OEt_2)_2$ was prepared according to the known procedure[2]. Blue crystals were obtained from the reaction mixture and after various kinds of recrystallization in diethylether suitable crystals for X-ray analysis were obtained. The data collection details are tabulated in Table I and selected bond lengths and angles are reported in Table II.

Table I
Crystal data and structure refinement for $(C_5Me_5)_2NdCl_2Li(OEt_2)_2$

$(C_5Me_5)_2NdCl_2Li(OEt_2)_2$	
formula	$C_{28}H_{50}Cl_2LiNdO_2$
formula weight	640.76
crystal system	Tetragonal
space group	$\overline{4}_1m$
temp [K]	120(2)
λ [Å]	0.71073
a = b [Å]	11.181(2)
c [Å]	12.647(3)
V, [Å³]	1581(1)
Z	2
$\rho_{calcld.}$ [g cm⁻³]	1.346
μ [mm⁻¹]	1.831
F(000)	662
crystal size [mm³]	0.10 × 0.10 × 0.04
θ range for data collection, deg	3.22 to 25.02
no. of reflns collected	18864
no. of indep. reflns (R_{int})	1,497 (0.0117)
no. of data/restraints/parameters	1497/372/205
GoF on F²	1.145
R_1,[a] wR_2[b] (I > 2σ(I))	0.0168, 0.0419
R_1,[a] wR_2[b] (all data)	0.0177, 0.0428
abs. struct. par.	–0.01(2)
largest diff. peak / hole [e Å⁻³]	0.601/–0.352

[a] $R_1 = \Sigma ||F_o| - |F_c||/\Sigma |F_o|$.
[b] $wR_2 = [\Sigma w (F_o^2 - F_c^2)^2/\Sigma (F_o^2)^2]^{1/2}$

Table II
Bond lengths [Å] and angles [°] for $(C_5Me_5)_2NdCl_2Li(OEt_2)_2$

Bonds and angles	Å or °
Cl(1)−Li(1)	2.354(7)
Li(1)−O(1)	1.98(2)
Nd(1)−Cl(1)	2.750(1)
Li(1)−Cl(1)−Nd(1)	88.9(2)
O(1)−Li(1)−O(1A)	105.4(7)
Cl(1)−Li(1)−Cl(1A)	100.1(4)
Cl(1)−Nd(1)−Cl(1A)	82.0(1)

Conclusions

The title compound crystallizes in the tetragonal space group $P\overline{4}_1m$ with one quarter of a molecule in the asymmetric unit and it is isomorphous with the cerium analogue. The molecule is localized on the mm symmetry site, which together with a heavy disorder of all organic residues made the structure determination rather difficult. However, it was possible to obtain data of satisfactory quality and finally confirm the molecular structure of this species (see in Fig. 1.).
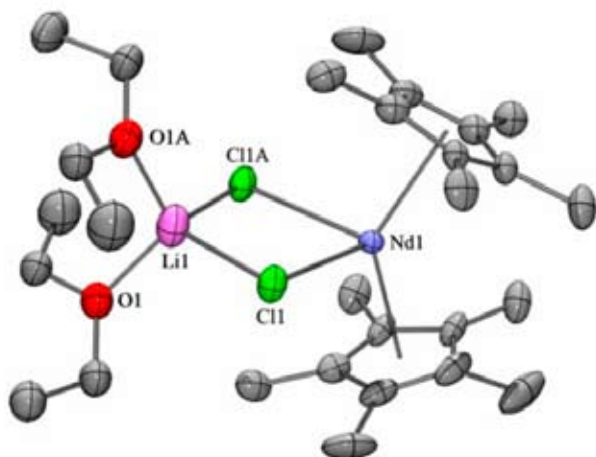
Fig. 1. **Crystal structure of (C₅Me₅)₂NdCl₂Li(OEt₂)₂. All hydrogen atoms as well as second positions of the disordered moieties have been omitted for clarity**

REFERENCES

1. Bogaert S., Chenal T., Mortreux A., Carpentier J.-F.,: J. Mol. Catal. A *90*, 207 (2002).
2. Tilley T. D., Andersen R. A.: Inorg. Chem., *20*, 3267 (1981).
3. Rausch, M. D., Moriarty K. J., Atwood J. L., Weeks J. A., Hunter W. E., Brittain H. G.: Organometallics *5*, 1281 (1986).
4. Junk P. C., Smith M. K.: Appl. Organomet. Chem. *18*, 252 (2004).
5. Zhongsheng J., Yongsheng L., Wenqi C.: Sci. Sin., Ser. B (Engl. Ed.) *30*, 1136 (1987).
6. Kroutil O., Hermanová S., Richtera L., Žídek J., Jančář J.: *1st Workshop on Multi-Scale Modelling of Nanostructured and Functional Polymeric Materials.* Brno, Czech Republic, 2007.

P13 COMUTING EFFECTIVE PROPERTIES OF COMPOSITES *VIA* FEM SIMULATIONS

MIROSLAV ROLNÍK, JAN ŽÍDEK and JOSEF JANČÁŘ

Brno University of Technology, Faculty of Chemmistry, Pur-kyňova 464/118, 612 00 Brno, Czech Republic,
xcrolnik@fch.vutbr.cz

Introduction

Composite materials take more and more important role in modern material science. It is influenced by several reasons, however mainly for their good mechanical properties and very cheap preparation. For estimation of properties of such materials were introduced many models with different assumptions and with different quality of approximation. The method which was used by us was mathematical homogenization method which follows from asymptotical properties of differential equations describing given physical phenomenon – linear elasticity in our case, however method can be used for wider spectrum of equations. The input of this method is representative volume element (RVE) – unitary cube (denoted by *Y*) which represents whole material. It has to be determined theoretically or from experimental results. The space conformation of phases can be arbitrarily complex also we can compute with more than only two phases (matrix, reinforcements). We supposed spherical shape of reinforcements, the inclusions are uniformly distributed in matrix and have random diameters. For generating such conformation was used discrete version of random sequential algorithm (RSA). All computings were done in Matlab 7.1 and in Comsol Multiphysics 3.2.

Aromatic thermotropic liquid crystalline polymer (TLCP) dispersed in polypropylene (PP) could serve as high modulus and high strength deformable inclusions. Modeling of relation between its morphology and mechanical behavior is useful way in development of new materials with tailored properties. It can eliminate certain polymer structures prior to the costly process of its preparation, processing and testing.

Experimental

Hard Sphere Problem, RSA Algorithm

Problem of placing spheres in unit cube is in literature refered as hard sphere problem – we have to randomly place *n* spheres with radius r_i to which corresponds volume V_i in such way that following holds:

(i) $\sum_{i=1}^{n} V_i = \varphi, \quad 0 \leq \varphi < 1$

(ii) the spheres do not intersect each other

(iii) the spheres are uniformly distributed in space

(iv) the space is composed from periodical copy of this unit cube so it has to be periodic wrt. spheres

For creating of such structure were designed several algorithms, we introduce two of them:

- Algorithm 1.: we randomly generate new position of sphere and then we test if it satisfies conditions *(ii)* and *(iii)*, if it does then we save this position and generate position for next sphere, if it doesn't we generate again new position and do test, we repeat this procedure untill we place all spheres, this algorithm is denoted as random sequential algoritm(RSA)

- Algorithm 2.: we begin with all spheres placed in some lattice(often it is FCC lattice) and then we randomly move each sphere so that condition *(ii)* holds, after enough movements the condition *(iii)* is also satisfied.
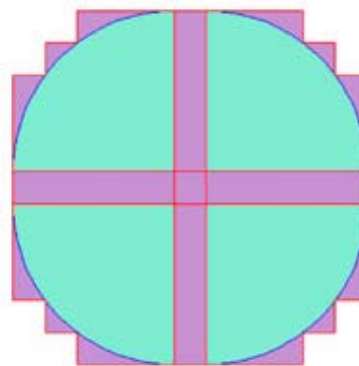
Fig. 1. **Discrete approximation of disc, original disc divided to four parts is coloured by shadow green (area S_{orig}), extra space due to discrete approximation is coloured by shadow violet. Whole object has area S_{disc}**

The advantage of Algorithm 2. is that it quarantee, that all spheres are placed and also much higher cover efficiency (up to 74 % against 38 %, what is theoretical jamming limit for Algorithm 1.). Disadvantage is that it is applicable only for spheres with same or very close diameters, if this doesn't hold than there arises problem with starting conformation.

Table I
Illustration of quality of an approximation of disc with different fineness of space division

# of units per radius	S_{disc}/S_{orig}	# of units per radius	S_{disc}/S_{orig}
1	1.9099	50	1.0590
2	1.8209	75	1.0395
5	1.4565	100	1.0298
10	1.2796	200	1.0149
20	1.1450	300	1.0099
30	1.0986	400	1.0075
40	1.0737	500	1.0059

On the other hand disadvantage of algorithm 1 is possible infinite time or sometimes impossibility to succesfully finish algorithm. This disadvantage was partially removed by our improvement of this algorithm. The space was dividend to small cubes(discretization), which then form unity in discrete space(the approximation of sphere in this space is shown on Fig. 1., Table I gives us information about quality of such

approximation). Possibility of placing the center of the next sphere to some cube was indicated by 1 and negative of this by 0. By this algorithm we can also trace the decreasing amount of free space available for place center and from this value we can estimate how much effort we need in algorithm 1, this is shown on Fig. 2. One of generated structures used for computing is shown on Fig. 3.
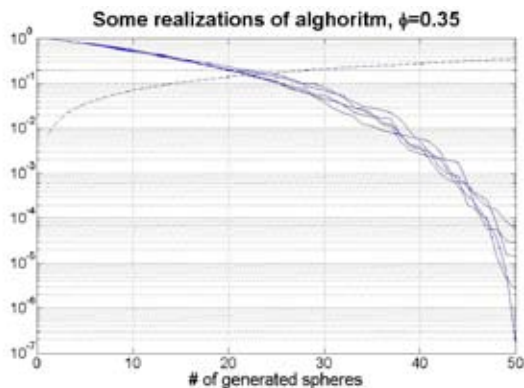
Fig. 2. **Progress of algorithm, solid lines depict decrease of space available to place another sphere, dashed line shows volume of placed spheres, n was set to 50 and φ to 0.35**

Mathematical Homogenization Method

Mathematical theory of homogenization was developed in early 60s of 20th century by many mathematicians. We used results ot this theory for system of elliptic PDE's (linear elasticity equation)[1] to computing mechanical properties of composites. Formulas for tensor describing material characterics of resulting composite material are (we are using Einstein summation convence, A is tensor of original material, A^0 is tensor of homogenized material)

$$A^0_{ijkl} = \frac{1}{\int_Y dx} \int_Y A_{ijkl} - A_{ijlm} e_{lm}(\chi^{kh}) dx, \qquad (1)$$

where χ_l^{kh} are solutions of following problems

$$-\frac{\partial}{\partial x_j}(A_{ijlm}\frac{\partial \chi_l^{kh}}{\partial x_m}) = -\frac{\partial A_{ijkh}}{\partial x_j} \text{ in } Y, i = 1, ..., n,$$

$\chi_l^{kh} \; Y-$ periodic

$$\int_Y \chi_l^{kh} dx = 0$$

and

$$e_{lm}(\chi^{kh}) = \frac{\partial}{\partial x_l}\chi^{kh} + \frac{\partial}{\partial x_m}\chi^{kh}$$

is linearized strain tensor.
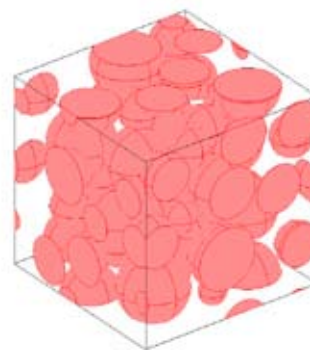
Fig. 3. **Example of generated structure for n = 40 and φ = 0.3**
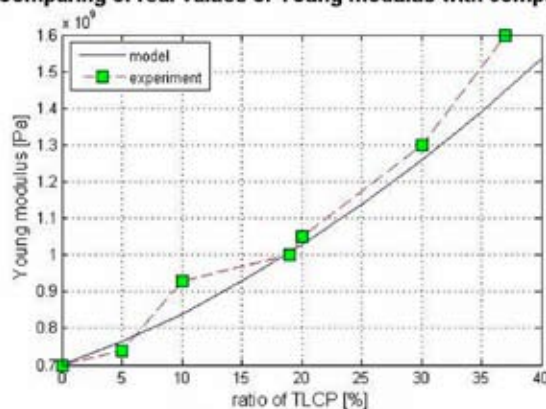
Fig. 4. **Results of model compared with experimental data**

Results

Computed results compared with experimental ones (PP matrix reinforced with TLCP, where portion of TLCP goes from 0 % to 40 %) are shown on Fig. 4. We can conclude that for small amounts of TLCP prediction is quite good and our curve fits well to experimental data, for bigger amounts of TLCP this doesn't hold, this can be influenced by the fact that particles of TLCP can interact between them or by the fact that that our sphere model is inadequate to reality.

Conclusions

Discrete version of RSA seems to be good way how to analyze evolution of algorithm. It shows us that possibility of place another sphere goes rapidly down. So ordinaly RSA can be insufficiently slow or it won't lead to solution at all.

Prediction possibilities of homogenization algorithm are sufficiently good, for better description of behaviour is needed to know much precisely microstructure of composite material.

REFERENCES

1. Cioranescu D., Donato P.: *An Introduction to Homogenization,* Oxford University Press, 2000.

P14 EFFECT OF THERMAL HISTORY ON STRUCTURE-PROPERTY RELATIONSHIP IN ORIENTED POLYPROPYLENE FILMS AND TAPES

JIŘÍ SADÍLEK and JAROSLAV KUČERA

Brno University of Technology, Faculty of Chemistry, Purky-ňova 118, 612 00 Brno, Czech Republic,
xcsadilek@fch.vutbr.cz

Introduction

The orientation is technological process for foils, tapes and fibrils preparation. Oriented monofilaments have better mechanical properties (e.g. tensile strength, modulus, resistivity to cyclic deformation[1]) than unoriented.

Annealing of an oriented sample causes relaxation, polymeric chains integrate into the existing lamellae and the lamellae thicknesses increase. An increase of crystallographic symmetry, decrease of orientation of crystalline phase, an disorientation of amorphous phase and a decrease of some mechanical properties is caused by annealing[1,2].

Experimental

Material and Samples Preparation

Commercial grade of polypropylene Mosten TB 002 was used in this work (MFR = 2,73 10 min^{-1}). This material was extruded and film of 400 μm thickness was prepared by chill roll technique. Primary film was drawn up to ratio 5:1 in the first step, then the film was cut to tapes (10 mm) and those were drawn on the hot plate to the final draw ratio 8:1 in the second step.

A part of tapes TB(4)-8/10 were continual annealed in the next step. This lable of tapes means: TB is polypropylene Mosten TB 002, (4) is thickness of primary foil (400 μm), 8 is drawn ration and 10 is cutting width of tape before drawing (10 mm). Testpieces passed throught temperated channel; both ends of samples were fixed to minimize shrinkage and annealed at 150, 160 and 170 °C.

Unannealed and annealed testpieces were tested. Strength and elongation at break (tensile properties), degree of crystallinity and structure characteristics (DSC) and chain orientation (RTG) were measured.

DSC, Tensile Tests and RTG

A circle specimens of 1 to 4 mg of weight were cut from the tapes. Each specimen was put into the aluminum pan and heated up in apparatus TA Instruments Q100. The test conditions were: heating rate of 10 °C min^{-1}, inert nitrogen atmosphere, the test was started at 50 °C and stopped at 200 °C. The endotherm peaks were recorded out and the fusion enthalpy, maximal temperature and the half-width of the peak were evaluated.

The tensile properties of unannealed and annealed polypropylene tapes were tested using INSTRON 4302. Tensile tests were performed at laboratory temperature and at test speed of 100 mm min^{-1}. The cylindrical iron clamps of the axises distance (100 mm) were used. The maximal tensile strength and elongation at break were recorded.

The RTG measurements were done in a laboratory of UTB FT Zlín using difractometer HZG-6 in transition and reflection modes. The tapes were measured longitudinal and transversely to the draw direction.

Results

DSC

The melting curves of polypropylene tapes are shown in Fig. 1, the main characteristics are given in Table I. The first curve represents melting of unannealed oriented material TB(4)-8/10 - 23 °C and the others with changed shape represent melting of annealed tapes.

We interpreted change of shape in this way. Structure has changed during recrystallization. The part of the oriented chains relaxed and a lamellar structure was created. The beginning of the process is represented by the curve of TB(4)-8/10-150 °C.

Annealing at 160 °C. The peak is higher and is shifted to higher temperature. Lamellae of regular structure increased in the thicknesses.

Process of recrystallization at annealing temperature 170 °C starts to change substantially the crystallite character in the tape. The thicker lamellae are built-up (higher T_m) and the orientation of chains becomes to decrease (see RTG).
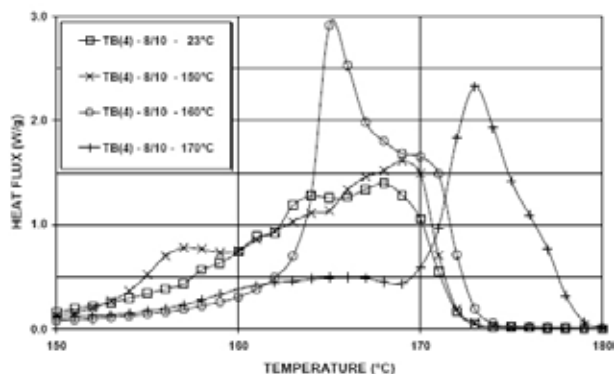
Fig. 1. **Heat fluxes of PP tapes – TB(4)–8/10. Test were done with heating rate of 10 °C min^{-1}. Materials were without ageing (23 °C -□-) and aged at 150 °C (-×-), 160 °C (-○-) and 170ºC (-+-)**

Table I
DSC characteristics of PP tapes

Sample	ΔH_m [J g^{-1}]	Half-width [°C]
TB(4)-8/10-23 °C	114.7	10.80
TB(4)-8/10-150 °C	118.5	10.1
TB(4)-8/10-160 °C	119.9	6.83
TB(4)-8/10-170 °C	116.4	4.42

Tensile Test

The results of tensile tests are presented in Table II (tensile strength and elongation at break). Tensile strength

decreases with annealing temperature in the whole annealing temperature range, because the above mentioned recrystallization decreases orientation of polymer chains.

Elongation at break increases only up to annealing temperature 160 °C and then it drops. This fact could be attributed to polypropylene recrystallization process (see above) and subsequently destruction of the tape orientation.

Table II
Results of tensile tests

Sample	Tensile strength [MPa]	Elongation at break [%]
TB(4)-8/10-23 °C	513 ± 20	41 ± 3
TB(4)-8/10-150 °C	419 ± 40	96 ± 14
TB(4)-8/10-160 °C	328 ± 16	158 ± 8
TB(4)-8/10-170 °C	201 ± 14	97 ± 7

R T G
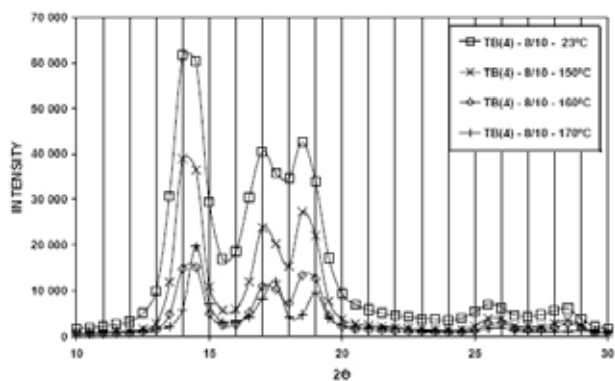
Fig. 2. **WAXS patterns measured longitudinal to draw direction (tapes TB(4)–8/10, unannealed (23 °C -□-) and annealed at temperatures (150 °C -×-, 160 °C -◇-, 170 °C -+-))**

The maximums of diffraction intesity are located at the same 2Θ angles for tape annealing temperatures 23 °C, 150 °C and 160 °C (Fig. 2.). TB(4)-8/10-170 °C sample has those maxima shifted to higher angles. The intensities of peaks are changed in accordance with annealing temperature, because the number of crystallites in the drawing direction has decreased.

Measured intensities in transversal direction are very low, i.e. the tapes have practically no reflection planes per-
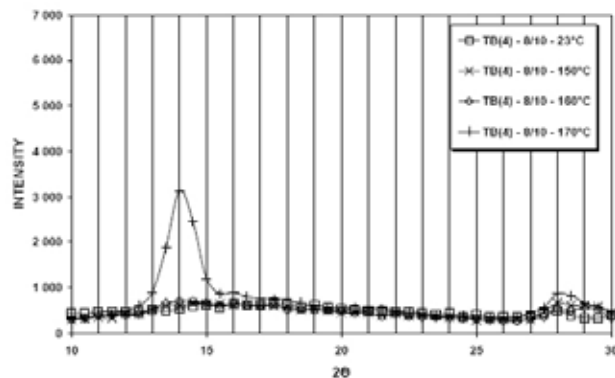
Fig. 3. **WAXS patterns measured transversely to draw direction. PP tapes, unannealed (23 °C -□-) and annealed at temperatures (150 °C -×-, 160 °C -◇-, 170 °C -+-)**

pendicular to the draw direction. Material TB(4)-8/10-170 °C has some few crystallites in the transversal direction. Probably, some of crystallites were created during recrystallization in this direction.

Conclusions

Results of DSC, tensile tests and RTG are presented in this paper.

DSC results show that annealing of PP tapes increase dimensions of crystals and above 170 °C a complete recrystallization started.

The tensile strength decreases in the whole range of the annealing temperature. Deformation increases up to 160 °C, then it decreases. This phenomenon should be interpreted by above mentioned recrytallization processes.

The crystallite orientation decreases in the drawing direction with increasing annealing temperature. The samples have no or very low amount of crystallites orientated in transversely direction, because of absence of WAXS peaks.

REFERENCES

1. Meissner, B., Zilvar, V.: *Fyzika polymerů, Struktura a vlastnosti polymerních materiálů.* SNTL, Praha 1987.
2. Karger-Kocsis, J.: *Polypropylene: structure, blends and composites, Vol. 1. Structure and morphology.* Chapman a Hall, London 1995.

P15 BIORESORABLE COLLAGEN-HYALURONIC ACID SCAFFOLDS CROSS-LINKED USING A WATER-SOLUBE CARBODIIMIDE

ALEXANDRA SLOVIKOVÁ, LUCY VOJTOVÁ and JOSEF JANČÁŘ

Institute of Materials Chemistry, Brno University of Technology, Purkyňova 464/118, 612 00 Brno, Czech Repulic,
xcslovikova@fch.vutbr.cz

Introduction

Porous collagen scaffold matrices containing hyaluronic acid (HA) are promising materials for tissue regeneration. Collagen, a well-known material has been widely used in medical applications[1]. It is extensively used for wide-area parenchyma bleeding and for laparoscopic procedures as a haemostatic agent[2]. HA is important component of extracellular matrix, having high water retention capacity. HA is involved in cell migration and cell differentiation which support wound healing process[3]. By combination of collagen and HA, the material with haemostatic and healing properties can be created.

In this study, collagen was blended with hyaluronic acid and cross-linked by carbodiimide at different period of time in order to evaluate the swelling and degradation properties used for certain biological applications.

Experimental

Bovine collagen type I (VUP a. s., CZ) and hyaluronic acid (CPN spol. s.r.o., CZ, $Mn = 150$ kDa) were used. Cross-linking solution mixture of 25 $mmol.l^{-1}$ of N-(3-dimethyla-mino-propyl)-N'-ethylcarbodiimide hydrochloride (EDC, Sigma Aldrich, D) and 12,5 $mmol.l^{-1}$ of N-hydroxysuccinimide (NHS, Sigma Aldrich, D) in 98 % of ethanol was prepared.

Sample Preparation

Collagen and hyaluronic acid were mixed in two different ways. The Coll-HA-1 matrix was made by combination of freeze drying and air drying method while the Coll-HA-2 one was only freeze dried which is commonly used method.

Prepared matrices were subsequently cross-linked using EDC/NHS system for three periods of time: 0.25, 1 and 2 h.

Characterization

The morphology of a surface structure and cut profiles of collagen-HA matrices was compared using scanning electron microscopy (SEM).

For water uptake determination each scaffold was cut up and weighted. The pieces were consequently immersed to physiological solution (PS) and in 1 hour the pieces were removed and re-weighted. The water content was calculated according to formula (1), where w_s is weight of swollen scaffold and w_d is weight of the dry scaffold.

$$\text{Water uptake} = \frac{w_s - w_d}{w_s} \times 100 \qquad (1)$$

The hydrolytic degradation of collagen-HA samples was studied in PS at 37 °C which simulated human body fluids. The degradation resistances were measured within a period of 30 days and determined using gravimetric method.

The bioinduction differences were evaluated just between matrices of pure collagen and collagen includes hyaluronic acid. The samples were tested at the laboratory of cells regeneration and plasticity (Liběchov, Czech Republic). The collagen scaffolds were colonized with mesenchymal cells and cultivated for 10 days in order to monitor both the stability in the cells solution and cells activity.

Results

SEM images of collagen-HA surfaces at Fig. 1.a and Fig. 1.b demonstrate differences between scaffold structures. Samples of Coll-HA-1 embodies smooth surface in comparison with porous surface of Coll-HA-2. Cut profiles scan (Fig. 1.c and Fig. 1.d) show that Coll-HA-1 is porous only in the middle part but the smooth just on the surface. The Coll-HA-2 shows porous structure in all volume.

The fastest hydrolytic degradation (of about 1 hour) yield the non cross-linked Coll-HA-2 porous sample while the other non cross-linked Coll-HA-1 sample exhibit higher stability by degrading up to 90 % in physiological solution at 37 °C within 30 days. The degradation stability of all samples increased markedly after the cross-linking by EDC/NHS, however, the different cross-linking period of time did not shown considerable dependences. Based on the results, the samples truckled to the degradation between 20–30 % (Coll-HA-1) or 30–40 % and (Coll-HA-2) in 30 days as can be seen in Fig. 2 and Fig. 3 respectively.
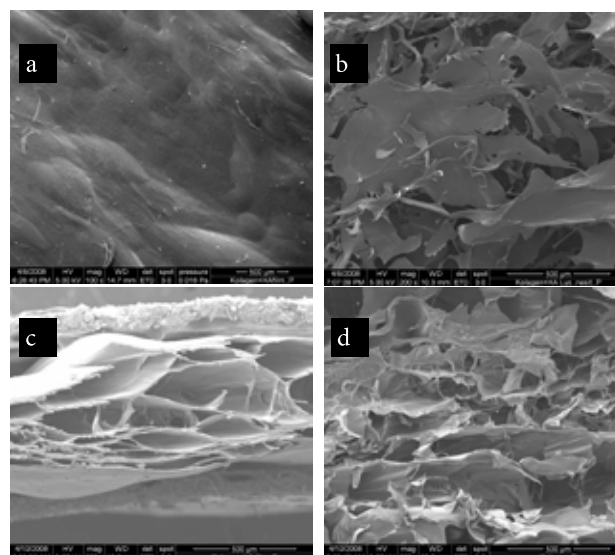
Fig. 1. **Scanning electron images of collagen-hyaluronic scaffolds a) Coll-HA-1 surface, b) Coll-HA-2 surface, c) Coll-HA-1 cut profile, d) Coll-HA-2 cut profile**
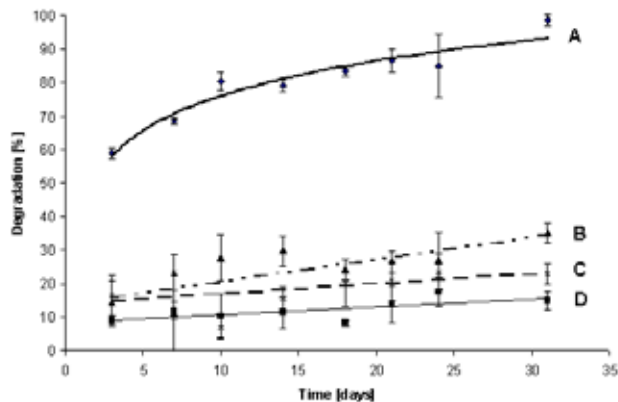
Fig. 2. **Degradation of Coll-HA-1 sample cross-linking at A) 0 hour, B)1 hour, C)2 hours, D) 0.25 hours**
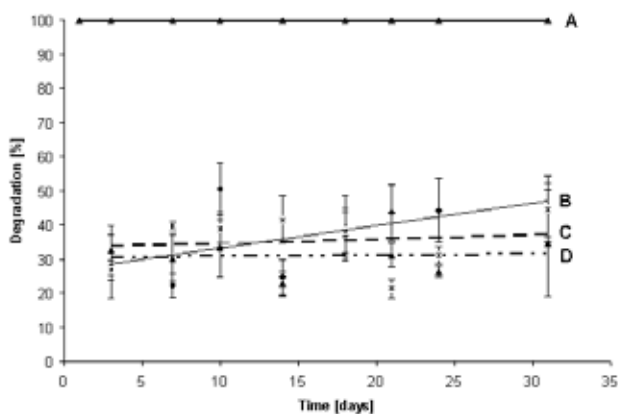
Fig. 3. **Degradation of Coll-HA-2 sample cross-linking at A) 0 hours, B) 0.25 hours, C) 2 hours, D) 1 hour**

Moreover, different water uptake behavior of collagen-HA matrices were observed. As presupposed, more stable Coll-HA-1 samples absorbed smaller amount of water in comparison with Coll-HA-2 samples. The time of cross-linking did not have considerable influence on the water uptake behavior as shows Fig. 4.

Compared with pure collagen the collagen-HA scaffolds indicated higher shape resistant and better density of cultivated mesenchymal cells after 10 days of cultivation.

Conclusions

Collagen and hyaluronic acid are poorly miscible when the amount of hyaluronic acid increases. Two different samples of collagen-HA were prepared (Coll-HA-1 and Coll-HA-2), cross-linked by EDC/NHS system and analyzed.

Scanning electron images showed differences in porosity of both samples. The Coll-HA-1 sample was porous just in the middle part between two smooth surface layers which probably protect the material against external effects resulting to slowest degradation rate and lower uptake in comparison with fully porous Coll-HA-2 sample. While non cross-linked Coll-HA-1 sample degraded at 90 % after 30 days,
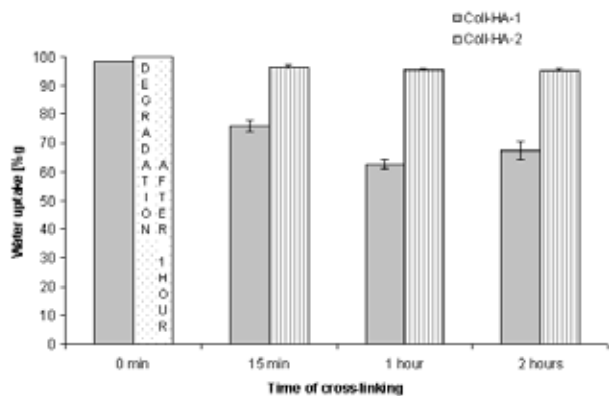
Fig. 4. **Water uptake of collagen-HA matrices for different time of cross-linking**

the non cross-linked Coll-HA-2 sample fully disintegrate in one hour. The cross-linking of both samples stabilized the matrices against the hydrolytic degradation. In 30 days the cross-linked Coll-HA-1 sample degraded to 30 % compared to 40 % of Coll-HA-2. As for water uptake behavior, the Coll-HA-2 sample absorbed 90 % wt. of water in one hour in contrast to 60 % wt. of Coll-HA-1 samples where the bilayer decreases the water absorption. However, the cross-linking time did not have considerable influence in both swelling and degradation behaviors.

It is assumed that after the formation of collagen-hyaluronic acid mixture, carboxyl groups of hyaluronic acid react promptly with amino groups of collagen. This result in small amount of free amino groups applicable to cross-linking thereupon the time, needed for the sufficient cross-linking degree, is surprisingly short – 15 minutes.

The collagen-HA matrices showed better bioinduciton effect in both shape resistance and cells density in comparison with pure unmodified collagen samples.

The results showed that collagen-HA materials prepared in various ways exhibited different properties useful for wide range of applications. Particularly, Coll-HA-1 might be used as material needed higher stability, whilst Coll-HA-2 is suitable for systems required higher absorption ability.

REFERENCES

1. Lee Ch. H., Singla A. Yugyung L.: Int. J. Pharm. *221*, 1 (2001).
2. Wagner W. R., Pachence J. M., Ristich J., Johnson P. C.: J. Sugical Res. *66*, 100 (1996).
3. Park S., Lee H. J., Lee K. H., Suh H.: Biomat. *24*, 1631 (2003).
4. BubnisW. A., Ofner C. M.: Anal. Biochem. *207*, 129 (1992).

P17 SPIN PROBE DYNAMICS IN RELATION TO FREE VOLUME AND RELAXATION DYNAMICS OF POLY(ISOBUTYLENE)

HELENA ŠVAJDLENKOVÁ and JOSEF BARTOŠ

Polymer Institute of the Slovak Academy of Sciences, Dúbravská cesta 9, 842 36 Bratislava, Slovak Republic,
Helena.Svajdlenkova@savba.sk

Introduction

The local structure and dynamics of glass-forming systems can be studied by means of reporter stable free radicals, the so-called spin probes.[1–4] The ESR spectra reflect rotational mobility of paramagnetic molecules which is closely related to both internal and external factors. We attempt to understand the rotational dynamics of the spin probes which is dependent on the microstructure of a matrix and its static and dynamic fluctuations as well as the spin probe parameters, i.e. the size (volume, mass) and shape as a function of temperature.

The physical microstructure of disordered former can be characterized using the free volume concept[5,6]. In the past, this idea was utilized to interpret spin probe dynamics by formulating the various versions of free volume models of spin probe rotation in polymers.[7–9] Recent progress in positron annihilation lifetime spectroscopy (PALS)[10,11] allowed to relate the directly measurable free volume to individual matrix dynamics[12] as well as to the spin probe mobility[13,14]. Recent PALS and ESR studies on a series of polymers revealed the connection between crossover of regimes for the small spin probe TEMPO at characteristic ESR temperature T_{50G}[15] and the appearance of a certain mean free volume hole which confirmed the independence of the chemical structure of matrices[13,14]. For further clarification ot the role of free volume in spin probe mobility are nedded more detailed free volume PALS data.

Investigations of glass-formers within ESR *vs.* PALS analysis supported the idea that primary α-process in the matrix plays the role in mobility of larger spin probes[4,16] and that the secondary processes are important for the smaller ones[16]. We present cross analyses of the spin probe dynamics results in the context of the microstructure and microdynamic data of pure matrix from PALS and BDS studies.

Experimental

Poly(isobutylene) $-[CH_2-C(CH_3)_2]_n-$ from a recent PALS study[18] was used. Molecular weight $\overline{M}_n = 1.3 \times 10^6$ g mol^{-1} and glass transition temperature from differential scanning calorimetry (DSC) $T_g^{DSC} = 207 \pm 1$ K. The spin probes 2,2,6,6-tetramethyl-1-piperidinyloxy, known as TEMPO, 4-Maleinimido-2,2,6,6-tetramethyl-1-piperidinyloxy (MI-TEMPO) from Aldrich Chemical Comp., Inc and 1,5-dioxa-3,3-bis(brommethyl)-8,8,10,10-tetramethyl-9-azospiro [5,5] undecaneoxy (Br-TEMPO) were used. They were introduced into the polymer matrix by diffusion from the vapour phase at a temperature near their corresponding

melting points. The structure and basic molecular parameters of spin probes are presented in Fig. 1 obtained by means of the simulation software Cerius[2], Accelrys Inc.

	TEMPO	MI-TEMPO	Br-TEMPO
M_W	156.1	251.1	412.0
V_P^W	170.1	230.6	305.9
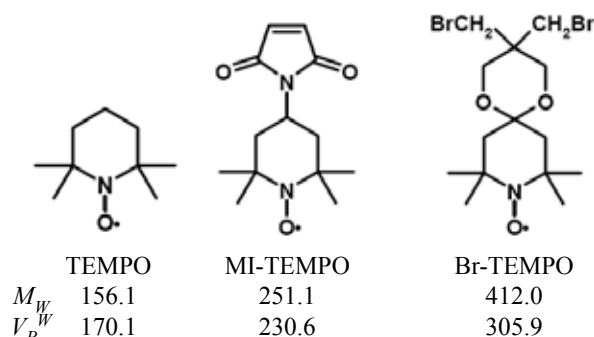
Fig. 1. **Structure, molar mass in g mol^{-1}, and van der Waals volumes in Å^3 of a series of spin probes used**

ESR investigations were performed on the X-band Brucker-ER 200 SRL with a Brucker BVT100 temperature variation controller unit. The ESR spectra were registered over a wide temperature range from 100 K up to 400 K. The ESR spectra were analyzed via two parameters of the rotational dynamics. The spectral parameter of mobility, $2A_{ZZ'}$, and the correlation time, τ_c being determined by the standard formulae[1,2,16].

Results

ESR Data

The ESR signal of all the three nitroxyl radical change from a broad triplet at lower temperatures to a narrow triplet in a higher temperature region, which corresponds to a slow rotational regime with a high spectral parameter of the $2A_{ZZ'} \sim 68$ G changing to a rapid rotational regime with lower values of $2A_{ZZ'} \sim 35$ G. Fig. 2. shows the spectral parameter of mobility, $2A_{ZZ'}$, i.e. the distance between the outer peaks of the triplet signal of the spin probes, as a function of the temperature from 100 K up to 400 K. A typical sigmoidal curve reflects the crossover from the slow regime to the rapid one. This crossover is characterized by the operationally defined ESR parameter, T_{50G}, at which the extrema of separation reaches just 50 Gauss[15]. In general, the T_{50G} value is expected to be dependent on the size (volume and mass) and the shape of the spin probe used. For the smallest quasi-spherical spin probe TEMPO $T_{50G} = 263$ K. In addition, crossovers in the $2A_{ZZ'}-T$ plot within the slow and rapid regimes define the two characteristic ESR temperatures at $T_{X1}^{2A} = 205$ K or $T_{X2}^{2A} = 347$ K, respectively. On the other hand, the temperature dependences of the spectral parameter $2A_{ZZ'}$ for the two larger non-spherical spin probes MI-TEMPO and Br-TEMPO, which differ in their volume by a factor of 1.35 and in their masses by a factor of 1.64, are rather similar with the corresponding T_{50G} values of 330 K or 333 K, respectively.

For the quasi-spherical spin probe TEMPO, the second parameter of mobility can be used to characterize its motional state, i.e., the rotational correlation time, τ_c, which was
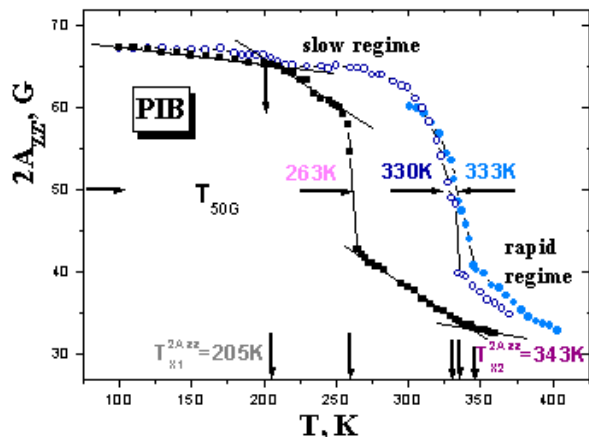
Fig. 2. **Spectral parameter of mobility, $2A_{zz}$, as a function of temperature ,over a wide temperature range for a series of spin probes in PIB. The characteristic ESR temperatures of TEMPO (■) and larger spin probes: MI-TEMPO (○), Br-TEMPO (●) are T_{50G} at 263 K or 330 and 333 K, respectively. Moreover, the additional characteristic temperatures at $T_{X1}{}^{2A} = 205$ K and $T_{X2}{}^{2A} = 347$ K were determined for the TEMPO**

Fig. 3. **Arrhenius plot log τ_c vs. $1/T$ for PIB/TEMPO system showing the presence of four regions of different motional behaviour with following Arrhenius parameters: slow-A: $\tau_\infty = 3.2 \times 10^{-9}$ s, $E_c = 3.2$ kJ mol^{-1}, slow-B: $\tau_\infty = 2.5 \times 10^{-10}$ s, $E_c = 7.7$ kJ mol^{-1}, rapid-A: $\tau_\infty = 4.0 \times 10^{-13}$ s, $E_c = 21$ kJ mol^{-1}, rapid-B: $\tau_\infty = 3.3 \times 10^{-18}$ s, $E_c = 52$ kJ mol^{-1}**

estimated by using the standard formulae[1,2,16]. In the case of a slow motional regime, the Goldman – Bruno – Polnaczek – Freed equation (1) has been applied:

$$\tau_c = a[1-S(T)]^b \tag{1}$$

where, $S(T) = A_{ZZ}(T)/A_{ZZ}(T_{ref})$ and represents the extrema line separation $2A_{ZZ}$, of the triplet spectra at temperature T and some reference value of $2A_{ZZ}$, usually at $T_{ref} = 77$ K. The a and b coefficients depend on the motional model of spin probe reorientation used. In the case of organic matrices/ small spin probe systems such as our PIB/TEMPO pair, the jump diffusion mechanism was found to be hold, for which $a = 2.55 \times 10^{-9}$ s and b = −0.615 (ref.[1,2,16]). In the rapid rotation regime the Freed – Fraenkel equation (2) was used:

$$\tau_c(T) = A\Delta H_{+1}[I_{+1}/I_{-1}]-1]^{1/2} \tag{2}$$

where $A = 6.7 \times 10^{-10}$ s, ΔH_{+1} – the line width of the low-field line of the triplet spectrum and I_{+1}, I_{-1} are the intensities of the lines of the low- and high-field component of the triplet spectrum. The results are displayed in the Arrhenius representation in Fig. 3. Four regions of different motional regime having the Arrhenius character:

$$\tau_c = \tau_\infty \exp[E_c/RT] \tag{3}$$

where, τ_∞ is pre-exponent and E_c is activation energy, can be distinguished. Intersection points of the linear regimes define the characteristic ESR temperatures $T^\tau_{X1} = 208$ K, and $T^\tau_{X2} = 320$ K. The first two bend effects in Fig. 3. are consistent with the characteristic ESR temperatures $T_{X1}{}^{2A}$, T_{50G} from Fig. 2. Dynamic change between the rapid sub-regimes at T^τ_{X2} is approximately consistent with $T_{X2}{}^{2A}$ from $2A_{ZZ}$, vs. T plot.

The observed reorientation behaviour of a series of spin probes can be related to the o-Ps annihilation and free volume information from PALS[18], as well as to the relevant literary dynamic results from broadband dielectric spectroscopy (BDS)[19] and nuclear magnetic resonance (NMR)[20].

PALS Data in Relation to ESR Findings

The PALS technique provides a unique information about the free volume microstructure of a matter[10,11]. This method is based on the annihilation behaviour of microscopic ortho-positronium probe (o-Ps) which is very sensitive indicator of local regions of low electron density, the so-called free volume. According to quantum-mechanical model[21–23], the o-Ps lifetime, τ_3, is a measure of the radius, R_h, of a spherical free volume hole by equation (4):

$$\tau_3 = \tau_{3,0}\{1-R_h/(R_h + \Delta R) + (1/2\pi)\cdot \sin[2\pi R_h/(R_h + \Delta R]^{-1}\} \tag{4}$$

where $\tau_{3,0}$ is the statistically averaged para-Ps and ortho-Ps lifetime (0.5 ns) and $\Delta R = 1.66$ Å is the thickness of electron layer around the hole whose value is determined by fitting the observed lifetimes in molecular crystals and zeolites of known vacancy or cages sizes.[21–23] The corresponding mean hole volume is simply $V_h = (4/3)\pi R_h{}^3$. In reality, however, the shape of free volume holes is not strictly spherical, so that equation (4) is used as the equivalent sphere radius or volume. In addition, free volume holes in condensed media, generally, have no uniform size, so that the free volume size distribution function is relevant[22]. If a one-to-one correspondence between the o-Ps lifetime and the free volume hole radius is assumed to be valid, the o-Ps lifetime distribution can be transformed into the free volume hole radius distribution, $f(R_h)$:

$$f(R_h) = -2\Delta R\{\cos[2\pi(R_h/R_0)]-1\}\alpha(\lambda_3)/R_0^2 \qquad (5)$$

where $\lambda_3 = 1/\tau_3$. Finally, by transformation of $f(R_h)$ we arrive at the free volume distribution function $g(V_h)$ (6):

$$g(V_h) = f(R_h)/4\pi R_h^2 \qquad (6)$$

The influence of local free volume on the rotational dynamics of the spin probes from ESR measurements can be evaluated at both the phenomenological and geometrical levels.

Phenomenological comparison of ESR and PALS data search for the mutual relationships between characteristic ESR temperatures T_{50G} and T_X and the characteristic PALS temperatures[12]. These temperatures are determined by analysis of the o-Ps annihilation quantities as obtained from the continuous term analysis of the PALS spectra by means of the LT 9.0 program[23]. Fig. 4. shows the mean o-Ps lifetime, τ_3, and the width of the o-Ps lifetime distribution, σ_3, in the same PIB sample as a function of the temperature over the temperature range from 130 K up to 350 K[18].

Three different regions of the o-Ps annihilation can be described by a best linear fit[12]:

- region I: 133 K < T < 203 K
  $\tau_3(T) = (3.85 \pm 0.94) \times 10^{-4}T + (1.21 \pm 0.02);$ (7a)
  $r = 0.889$

- region II: 213 K < T < 263 K
  $\tau_3(T) = (7.73 \pm 0.24) \times 10^{-3}T - (0.31 \pm 0.06)$ (7b)
  $r = 0.997$

- region III: 273 K < T < 353 K
  $\tau_3(T) = (1.59 \pm 0.01) \times 10^{-2}T - (2.56 \pm 0.38)$ (7c)
  $r = 0.997$

Intersection points define two characteristic PALS temperatures T_g^{PALS} and T_{b1}. Similarly, four different regions in the σ_3-T plot can be distinguished. The first two characteristic PALS tmeperatures T_g^{PALS} and T_{b1}^{σ} agree with the previous ones, while the third one lying at $T_{\sigma3} = 320$ K has not direct analogy in the o-Ps lifetime.

By comparing ESR and PALS responses, following coincidences were found. The bend effect within the slow rotational regime of TEMPO at $T_{X1}^{2Azz} = 205$ K (Fig. 2.) lies in the vicinity of the glass transition. Further, a crossover between slow and rapid regimes at $T_{50G} = 262$ K is in an approximate coincidence with $T_{b1} = 270$ K in τ_3, σ_3 *vs.* T plot. The acceleration of TEMPO in a rapid rotational regime at $T_c^{\tau} = 320$ K is comparable to the plateau at T_{b2}^{σ} from Fig. 4. Moreover, a crossover of MI-TEMPO and Br-TEMPO at $T_{50G} = 330$ or 333 K in Fig. 2. lies slightly above T_{b2}^{σ}.

All these phenomenological coincidences suggest the common origin in the underlying processes. This aspect will be discussed later by considering the dynamic data of PIB.

Geometrical aspect consists in a direct comparison of the spin probe sizes V_p^W with free volume hole sizes as well as free volume hole distributions as obtained from analysis of PALS spectra by using the LT 9.0 programme[18]. Fig. 5. shows the mean hole volume, $<V_h>_n$ and the mean hole volume dispersion σ_{Vh} as a function of temperatures in relation to V_{Tempo}^W 170 Å^3. It follows that TEMPO reaches the mean free volume size at $T \sim 348$ K in the vicinity of $T_{X2}^{2Azz} = 343$ K from Fig. 2. which indicates the presence of a sufficient mean local free volume. On the other hand, two remaining probes are larger than the mean free volume hole size.

Subsequently, another ESR *vs.* PALS analysis applies a direct comparison of VdW volumes of the spin probes V_p^W with the free volume hole distributin $g_n(V_h)$ at several temperatures in Fig. 6. At low temperatures, the spin probe sizes are larger than the hole volume and they lie well outside of the free volume hole distribution $g_n(V_h)$. This means that the spin probes form a certain type of perturbation in the matrix.

Fig. 4. **The mean o-Ps lifetime τ_3 (■) and the width σ_3 (□) of o-Ps lifetime distribution in PIB as a function of the temperature. The characteristic PALS temperatures $T_g^{PALS} = 207$ K, $T_{b1} = 270$ K, $T_{b2}^{\sigma} = 320$ K are related to the ESR findings as follows: $T_{X1}^{2Azz} \cong T_g^{PALS}$, T_{50G}(TEMPO) $\approx T_{b1}$, and T_{50G} (larger probes) $\cong T_{b2}^{\sigma}$.**
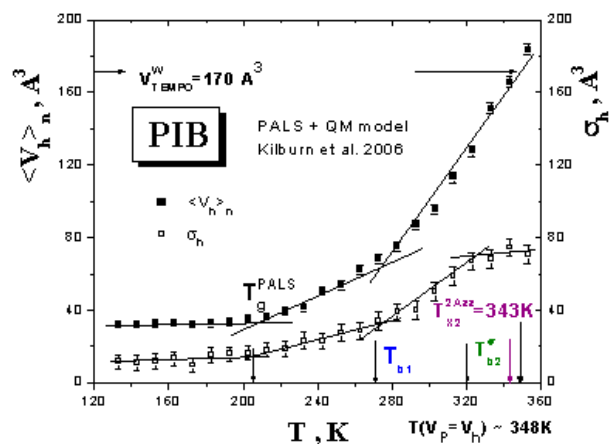
Fig. 5. **The mean hole volume, $<V_h>_n$ (■) and the mean hole volume dispersion, σ_h (□), as a function of the temperature for pure PIB.**

On increase the temperature, $g_n(V_h)$ approaches the vdW volume of TEMPO and at T_{50G}, it crosses the high-value tail of the corresponding distribution. Similar finding is valid for the MI-TEMPO and Br-TEMPO probes at $T_{50G} \cong 330$ K. However, the same values of T_{50G} suggest that the presence of local free volume is a necessary condition, but not a sufficient condition for a crossover phenomenon. Finally, at higher temperatures, the bend effect in the rapid regime of the TEMPO at $T_{X2}^{2Azz'} = 343$ K in Fig. 2. is related to the maximum of $g_n(V_h)$, when is the maximal probability of the occurrence of free volume holes being almost equal to the vdW volume of the TEMPO probe. This is fully consistent with Fig. 5.
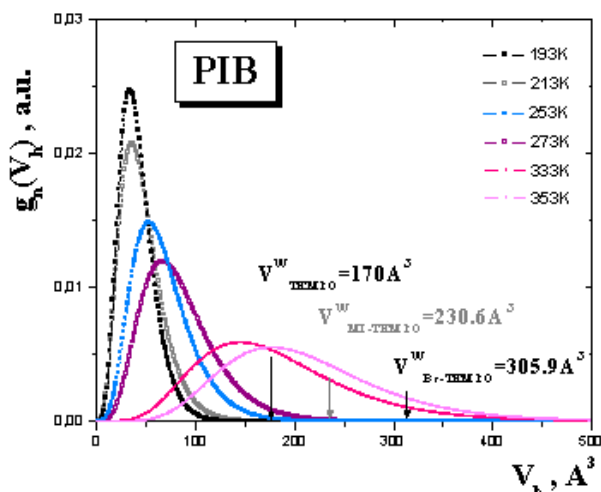
Fig. 6. **Relationships between the free volume distributions $g_n(V_h)$ at selected ESR temperatures in PIB: (■) – 193 K, (○) – 213 K, (●) – 253 K, (Δ) – 273 K, (◆) – 333 K, (◇) – 353 K. The arrows depict the van der Waals volumes of a series of the spin probes used**

P A L S   a n d   E S R   D a t a   *v s .*   D y n a m i c s   R e l a t i o n s h i p s

This section discusses the ESR crossover phenomena in relation to internal dynamics of PIB. Fig. 7 displays the relaxation map for the all relaxation processes in PIB as obtained from BDS and NMR studies[19,20]. Amorphous PIB exhibits a slow primary α process and two secondary β – and δ – processes. In this plot, the o-Ps lifetimes at the characteristic ESR temperatures T_{50G} are compared with the mean characteristic times of the secondary relaxation processes. In the case of the smallest probe TEMPO, the o-Ps lifetime at T_{50G}, $\tau_3(T_{50G}) = 1.75$ ns crosses the δ – process at 282 K, which is quite close to the first characteristic PALS temperature at $T_{b1} = 270$ K and not too distant from the $T_{50G} = 263$ K. On the other hand, the o-Ps lifetime at T_{50G} for larger spin probes $\tau_3(T_{50G}) = 2.7$ ns reaches the time scale of the extrapolated β- process at 322 K in good agreement with the plateau temperature $T_{b2}^{\sigma} = 320$ K as well as $T_{50G} = 330$ or 333 K, respectively.
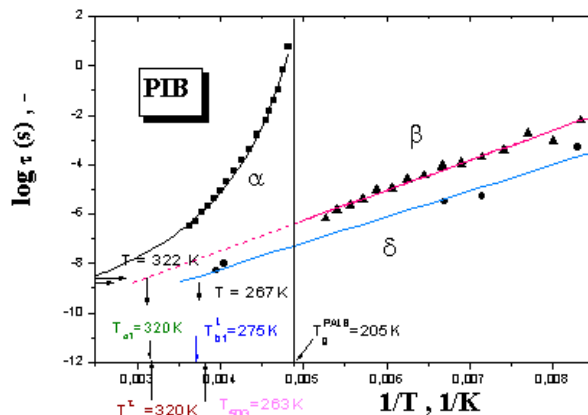
Fig. 7. **Arrhenius plot for the primary α- (□) and the two secondary β – (■) and δ – (▲) processes[19,20]. The shorter arrow depicts the o-Ps lifetime at T_{50G} for TEMPO which crosses the δ-process at around 282 K. The longer arrow marks the o-Ps lifetime $\tau_3(T_{50G})$ for larger spin probes which crosses the extrapolated β-process at 322 K**

Conclusions

In summary, from the mutual cross-comparisons of three responses it follows that the changes in the spin probe TEMPO dynamics are closely related to the fluctuaction of the local free volume due to secondary δ-process. On the other hand, the local dynamics of the β-process is responsible for the occurrence of plateau at T_{b2}^{σ} as well as for the ESR crossovers at T_{50G} for the larger spin probesMI-TEMPO and BR-TEMPO in PIB.

REFERENCES

1. Berliner L. J (Ed.): *Spin labelling theory and applications, vol.1,* Academic Press, New York 1976.
2. Cameron G. G*.: Comprehensive Polymer Science Vol.1.*, Pergamon Press, Oxford 1989;
3. Veksli Z., Andreis M.: Rakvin B, Prog. Polym. Sci. *25*, 949 (2000).
4. Andreozzi L., Faetti M., Giordano M.: Recent Res. Dev. Phys.Chem. *5*, 2895 (2001).
5. Ferry J.D.: *Viscoelastic properties of polymers*. 3[rd]ed Wiley, New York 1980.
6. Crank J., Park G.: *Diffusion in Polymers*, Academic Press, New York 1968.
7. Kusumoto N., Sano S., Zaitsu N., Motozato Y.: Polymer *17,* 448 (1976).
8. Bullock A. T., Cameron G. G., Miles I. S.: Polymer *23*, 1536 (1982).
9. Bartoš J. Hloušková Z.: Colloid and Polym. Sci., *266* 624 (1988).

10. Jean Y. C., Malton P. E., Schrader D. S. (Eds.): *Principles and Application of Positron and Positronium Chemistry,* World Scientific, Singapore 2003.

11. Bartoš J in: Meyers.R. A. (Eds.), Encyclopedia of Analytical Chemistry, Wiley, Chichester 2000.

12. Bartoš J., Šauša O., Bandžuch P., Zrubcová J., Krištiak J.: J. Non-Cryst. Solids; *307*, 417 (2002).

13. Bartoš J., Hloušková Z.: Polymer *34*, 4570 (1993).

14. Bartoš J., Andreozzi L., Faetti M., Šauša O., Račko D., Krištiak J.: J. Non-Cryst.Solids *352*, 4785 (2006).

15. Rabold G. P.: J. Polym. Sci., A1 *7*, 1217 (1969).

16. Törmälä P.: J. Macromol. Sci. Rev. Macromol. Chem., *C17*, 297 (1979).

17. Andreozzi L., Faetti M., Giordano M., Leporini D.: J. Phys.-Cond. Mat.,*11*, 131 (1999).

18. Kilburn D., Wawryzczuk J., Dlubek G., Ponteck J., Hässler R., Alam A.: Macromol. Chem. Phys. *207*, 721 (2006).

19. Richter D., Arbe A., Colmenero J., Monkenbusch M., Farago B., Faust R.: Macromolecules, *31*, 1133 (1998).

20. Slichter W. P.: J. Polym. Sci. *14*, 33 (1966).

21. Tao S. J.: J. Chem. Phys. *56*, 5499 (1972)

22. Eldrup M., Lightbody D., Sherwood J. N.: Chem. Phys., *63*, 51 (1981).

23. Nakanishi H., Wang S. J., Jean Y. C.: *Positron Annihilation Studies of Fluids,* World Scientific, Singapore, pp.292 (1988).

24. Gregory R. B.: J.Appl.Phys. *70*, 4665 (1991).

25. Kansy J.: Nucl. Instr. Methods Phys. Res.; A *374*, 235 (1996).

P18 TOUGHNESS VERSUS STRENGTH AND STIFFNESS OF POLYPROPYLENE FILLED WITH SUBMICRON CaCO₃ PARTICLES

PETR VESELÝ, EVA NEZBEDOVÁ and BOHUMIL VLACH

Brno University of Technology, Institute of Material Science and Engineering, Technická 2, 616 69 Brno, Czech Republic,
wesa@email.cz

Introduction

Polypropylene (PP) as one of the most important commodity polymer is widely used in technical applications. The advantage of this material is good processability, relatively high mechanical properties, great recyclability and low cost. However, due to its impact resistance especially, the usefulness of PP as an engineering thermoplastic is still limited[1]. The challenge of improving the impact toughness of this semi-crystalline polymer continues to receive considerable interest in recent years. It is well known that the addition of the mineral fillers to PP can profoundly change the mechanical properties of a polymer system. The properties themselves (size, shape, material properties, surface treatment) and distribution of this particles can have a significant effect on the global behavior of the composites. Generally, the addition of rigid particles to a polymer matrix will have an embrittling effect on the composite[2]. A new concept is the usage of filler particles as toughening agent. The general idea is to mimic the rubber toughening mechanism using rigid filler particles. The rigid particles must debond and create free volume in the blend on a sub-micron size level. This is much like the cavitation mechanism in rubber toughened systems[3]. The micro-mechanistic model for this toughening effect is consisting of three stages (stress concentration, debonding and shear yielding)[4].

In this paper, the toughening of polypropylene with calcium carbonate particles on submicron size level is studied. First, the influence of matrix molecular weight and the nucleation agent on the toughening behavior was evaluated. Following results o this experiment was preparing optimized polymeric matrix. The next step was compounding of a composites system from optimized matrix and submicron size CaCO₃ particles. The influence of the size and mass content of the particles on the mechanical properties of composites were investigated. Particularly, the stiffness, strength and toughness were chosen as relevant parameters. The stiffness and strength were estimate by the means of tensile test while for toughness the J-R curve procedure was utilized. The results were correlated with microscopic observation. Further we were interested on deformation behavior of the composite system.

Experimental

The izotactic polypropylene (iPP) matrix with MFR 37 g 10min⁻¹ (230 °C, 2.16 kg) and molecular weight M_w = 194,000 was prepared. Further, this iPP matrix was modified by beta nucleation agent NJ Star NU-100 from Rika International (GB).

As filler we used to commercial available CaCO₃ particles from Solvay production concretely SOCAL 312 with these parameters: Average diameter d_{50} = 0.07 μm and specific surface (BET) 19 m² g⁻¹, that was with surface treatment already from production. The composite was prepared with two weight percents of filler (5 % wt., 10 % wt.), see (Table I).

Table I
Types of prepared composites

Sign as	Material
N5	Native iPP and 5 % wt. CaCO₃
N10	Native iPP and 10 % wt. CaCO₃
B5	Beta nucleated iPP (0.03 % wt. β) and 5 % wt. CaCO₃
B10	Beta nucleated iPP (0.03 % wt. β) and 10 % wt. CaCO₃

Compounding of the materials was done using APV 25 twin screw extruder. After compounding, the blends were injection moulded into "dog-bones" using Battenfeld 750 CD injection moulding machine in accordance with ČSN EN ISO 527-1.

T e n s i l e   T e s t
The tensile tests were carried out on the testing machine ZWICK Z020 in accordance with ČSN EN ISO 527-1. The
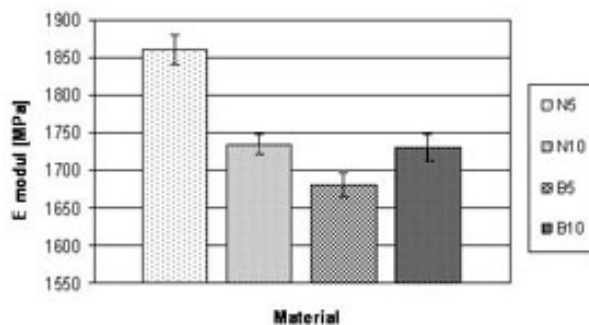
Fig. 1. **Dependence of mechanical properties (tensile modulus) on the type of composite materials**

deformation rate was 10 mm min⁻¹ and the temperature of measurement was 23 °C. The following values were estimated: Tensile Modulus (E), Tensile Stress at Yield (σ_y), and Tensile Strain at Yield (ε_y). Extensometer with accuracy class 0.5 was used to measure the strain during the tensile test.

The tensile test results (Figs. 1., 2.) exhibit lower tensile modulus and slightly lower yield strength with the increasing of fillers content. This trend was shown distinctive in the case of composite with beta nucleated matrix.

Comparing of tensile plots (Fig. 3.) and energy to break Wb (Fig. 4.) from these composite materials interpret the
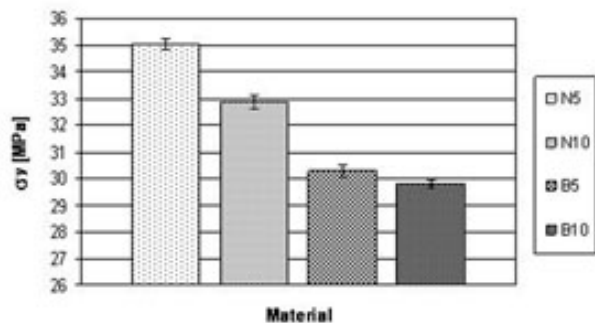
Fig. 2. **Dependence of mechanical properties (Yield strength) on the type of composite materials**
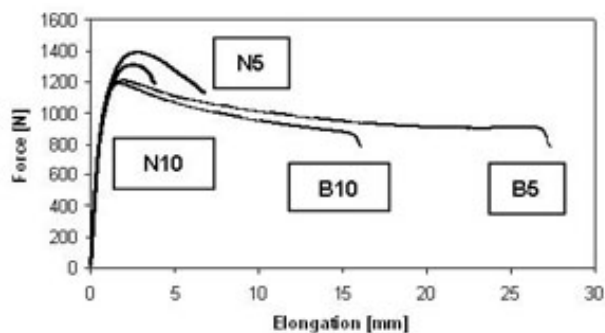
Fig. 3. **Tensile plots of individual composite materials**
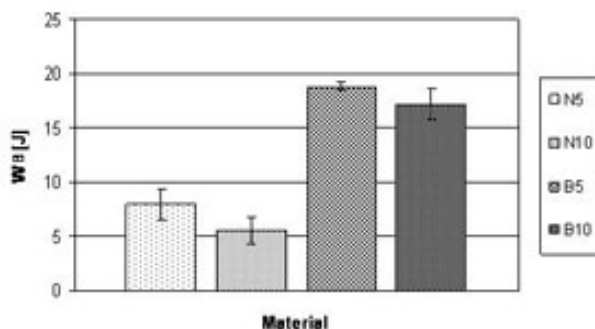
Fig. 4. **Dependence of mechanical properties (Energy to break) on the type of composite materials**

difference in deformation behavior. Composite materials with beta nucleated PP matrix exhibit higher elongation to break and higher energy to break. This enhancement grown to double in composite with 5 % wt. of particle content (material B5).

J - R   C u r v e s

Resistance curve tests were made by multiple specimen technique in accordance with ASTM 6068-96 on the testing machine ZWICK Z1120 (deformation rate was 10 mm min^{-1}, support distance 40 mm).

Tree point bend test (SENB) specimens were used ($4 \times 10 \times 80$) with total notch depth 5 mm (4 mm using mechanical saw and 1 mm by sliding fresh razor blade.)

The fracture toughness of composites with native PP matrix and beta nucleated PP matrix were determined in terms of the J-R curves. As the fracture characteristics the J integral value at crack extension of 0.05 mm ($\Delta a = 0.05$ mm) was chosen ($J_{0.05}$).

The results of fracture tests are summed up in (Fig. 5.) and (Fig. 6.), respectively. Particularly, J-R curves of individual composite systems are given in (Fig. 5.) and the $J_{0.05}$ values for native or beta nucleated PP matrix with 5 % wt. and 10 % wt. composite systems are shown in (Fig. 6.).
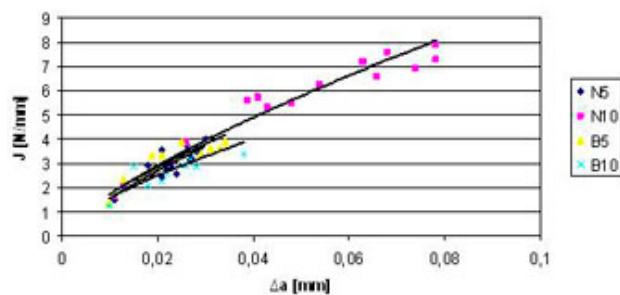
Fig. 5. **J-R curves of individual composite materials**
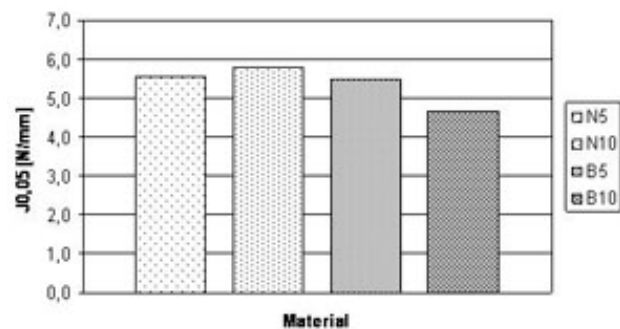
Fig. 6. **Dependence of fracture toughness characteristic ($J_{0.05}$) on the type of composite materials**

As shown in Fig. 6. the composite material with beta nucleated PP matrix and 10% wt. content of $CaCO_3$ particles (material B10) exhibit decrease trend of $J_{0.05}$ characteristic. This effect means possible lower crack resistance of mentioned system. Generally, the crack resistance of all this systems is considerably higher in comparison with PP matrix materials without $CaCO_3$ fillers.

M i c r o s t r u c t u r e

The structure of composite materials was evaluated by optical microscopy in polarized light on microscope Zetopan-Pol. It was preparing by the method of ultrathin cuts (5 µm) on Mikrotom Leica. Ultrathin cuts were extracted from the middle part of injected molded specimens perpendicularly to this direction (Fig. 7.).
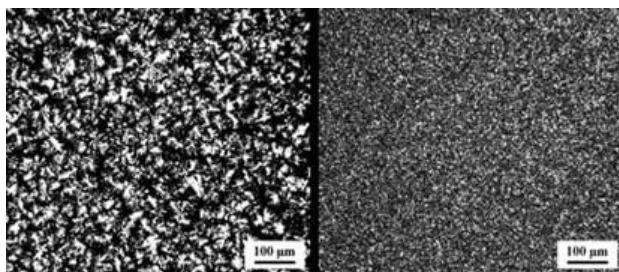
Fig. 7.   Microstructure of individual types of composite materials. (Polarized light, 5 µm ultrathin cuts)
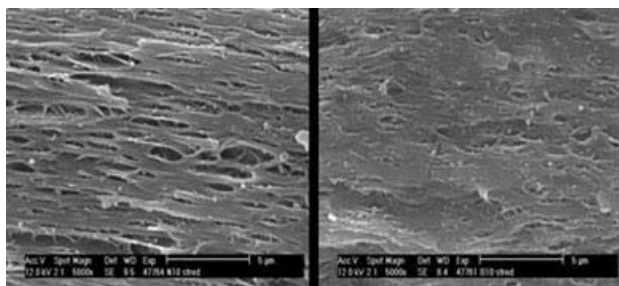
Fig. 8.   Microstructure of individual types of composite materials. (SEM, total magnification 5,000 ×, 10 % wt. From left: PP – native matrix composite, PP – beta nucleated matrix composite)

We can see markedly difference between composites with native PP matrix and beta nucleated PP matrix. The native matrix compopsites shows spherulite structure with small size of spherulites. In the case of beta nucleated PP matrix composites is any spherulite structure visible. Further it was the crystallization process examined under temperature 135 °C. The addition of $CaCO_3$ particles affect this behavior and reduce the crystallization time from 1 hour to 10 min. The filler particles increase number of crystallization centers and accelerate the crystallization process. In the case of beta nucleated matrix is mentioned effect involved by higher ability of this nucleation agent.

Morphology of PP specimens was study by scanning electron microscopy (SEM).

These samples were prepared from part of composite material specimens after tensile test in axial direction. Separating of samples was in liquid nitrogen and than they was evaporate coated. The fracture areas were observed in $5,000 \times$ total magnification (Fig. 8.). Not least we evaluated distribution of $CaCO_3$ filler particles.

 The characteristic morphology changes of samples in a study are shown in (Fig. 8.). The particles are dispersed reasonably well, although there are only small agglomerates visible. On both pictures we can see formation of tree stage micro-deformation mechanism. This result is in good agreement with literature[3,4].

Conclusions

The mechanical properties and morphologies of PP composites filled with $CaCO_3$ particles are in good accordance with literature. It was clear that type of PP matrix had key effect on composite properties and behavior. The addition of fillers particles lead to increase stiffness and crack initiation resistance and improve too the deformation behavior especially in the case of beta nucleated PP matrix. Further the filler particles increase number of crystallization centers and accelerate the crystallization process. It was confirmed forming of 3-stage deformation mechanism in investigated systems.

REFERENCES

1. Yang K., Yang Q., et al.: Polym. Compos. 443 (2006).
2. Rothon R. N.: *Particulate-Filled Polymer Composites (Second Edition)*. Rapra Technology Ltd., Shawbury UK, p. 542 (2003).
3. Zuiderduin W. C .J., Westzaan C., Huétink J., Gaymans R. J.: Polymer *44*, 261 (2003).
4. Kim G.M., Michler G.H.: Polymer *39*, 5699 (1998).

P19 POLYSACCHARIDES MODIFIED ELASTOMERIC POLYURETHANE

LUCY VOJTOVÁ[a], MAREK NOVOTNÝ[a], STANISLAV OBRUČA[b], JANA PIECHOVÁ[b], IVANA MÁROVÁ[b] and JOSEF JANČÁŘ[a]

[a]Institute of Materials Science,
[b]Institute of Institute of Food Science and Biotechnology,
Faculty of Chemistry, Brno University of Technology, Purky-
ňova 118, 612 00, Brno, Czech Republic,
vojtova@fch.vutbr.cz

Introduction

Polyurethanes (PUs) are widely commercially produced material because of possibility to obtain various properties by changing raw materials resulting in flexible or rigid foams, solid elastomers, coatings, adhesives and sealants. PUs are usually produced by the polyaddition reaction of a polyfunctional isocyanate with polyol or other reactants containing two or more groups reactive with isocyanates[1]. Nowadays, with increasing PUs consumption, the chemistry of preparation is focused on the possibilities of recycling and/or degradation of the plastic materials in order to avoid environmental pollution by non-degradable polymer waste dump. The elimination of expenses connected with recycling of these materials becomes a vital target of all producers[2]. One of the ways how to reduce the price along with increasing the degradability of these materials is addition of cheap biodegradable filler to the structure of PURs, which can partly or fully substituted one of the raw material, mostly polyol. Several research works using bio-polyols containing more than one hydroxyl group (-OH) in the main chain suitable for coupling reaction has been carried out.[3–7]

In this paper, new elastomeric PUs with specific mechanical as well as biological properties were prepared by one-shot process. Commercial non-degradable polyether polyol derived from petrochemical feed stocks was partly substituted by the bio-polyols based on cellulose or starch derivatives. Prepared samples were tested for mechanical properties by tensile measurements. Moreover, the biodegradability was evaluated by thermophilic bacteria.

Experimental

Briefly, water-free tolylene diisocyanate (TDI), water-free polyether polyol (PEP), tin catalysts and degassed bio-polyol (cellulose or starch derivatives) were mixed together in one shot process, stirred under the vacuum and poured into the 1 mm thick metal frame placed between two polypropylene sheets. The reacting mixture was left to cure for 2 days at laboratory temperature. Cellulose or starch derivatives with different degree of substitution (DS) of -OH groups like acetylated starch (DS = 0.1), acetylcellulose (DS = 2.4), 2-hydroxyethylcellulose (DS = 0.6) and carboxymethylcellulose sodium salt (DS = 0.7), AS, AC, CMC, HEC, respectively, were used for substitution of common PEP in amount from 1 to 10 % wt.

Scanning Electron Microscopy (SEM)

The samples morphology was observed on SEM FEI Quanta 200 Mk2 microscope at 20 kV. Specimens were frozen in liquid nitrogen and broken. 2 nm thin layer of gold and platinum (60 : 40 wt. ratio) was deposited onto the breaked surfaces. The magnification of 1500 times was applied with a view to see incorporation of bio-polyol particles into the PU matrix.

Tensile Measurements

Prepared samples were tested on Zwick Z010/Roell machine according to ISO 527–2/5A/50. The measurements proceeded on 500 N head at the velocity of 50 mm min^{-1} and 0.2 N pre-load at the laboratory temperature. The dimensions of cut dumb-bells testing specimens were 75 mm long and 4 mm wide in the middle part with 1 mm thickness. Each sample was measured 5 times and data were averaged to get the standard deviation.

Biodegradability Evaluation

Resulting BIO-PU elastomers filled with AC, AS, CMC and HEC were undergone microbial degradation using a bacteria of mixed thermophillic culture namely *Thermophillus sp.* that produce a large amount of hydrolytic enzymes capable of degrading polymeric materials. 0.25 g of each PU sample was degraded at 60 °C for 100 h under permanent shaking in 100 ml of media. In regular intervals the concentration of biomass (g of cells dm^{-3} of medium), chemical oxygen demand and glucose concentration were determined as well as the total weight loss of modified PU samples after the biodegradation.

Results

Morphology

Based on the SEM pictures (Fig. 1.) of PU specimens it is evident that all added fillers were not dissolved in polyol and prepared samples have character of composite materials. Fig. 1.a shows one big particle of CMC (approx. 250 μm) with bad adhesion to the PU matrix. The surface of HEC particles looks flat with several sharp borders showing little bit better adhesion to the matrix than CMC (Fig. 1.b). On the other hand, some molecules from the bio-filler surface could be dissolved in the polyether polyol and thus integrated to the polymer structure. This probably happened in the case of AC and AS bio-polyol because their surface is smooth and particles are fully incorporated in PU matrix (Fig. 1.c and d). The AC particles are strongly porous and their adhesion to the matrix is very good. There is no evident separation between the AC and PU surface. However, specimens filled by AS shows excellent adhesion to the PU matrix which either stays on the surface of particles or the particle breaks apart with the matrix during the breaking of the specimen.

All mentioned SEM pictures show evident influence on both size and chemical composition of filled bio-polyols on the modified PUR morphology. The best adhesions show both AC and AS even if their particle sizes and shapes are

different. However, the morphology does not say anything about the mechanical properties of resulted polymer composite materials, which have to be evaluated by tensile measurement.
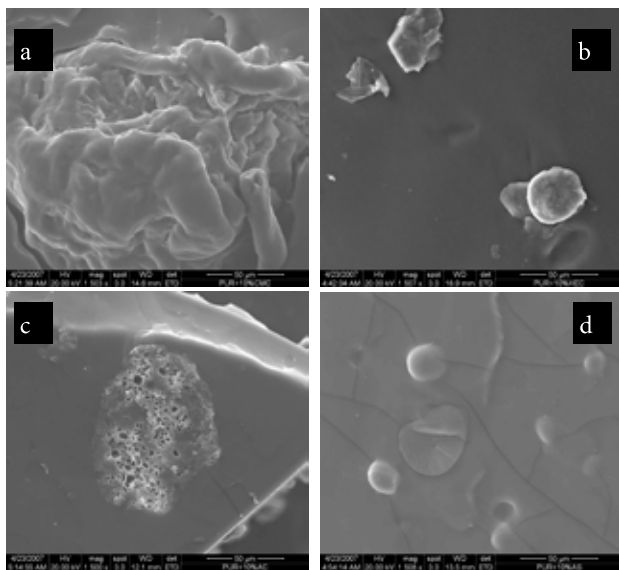
Fig. 1.　**1,500 × magnification of PU matrix filled with CMC (a), HEC (b), AC (c) and AS (d)**

Tensile Characteristics

Based on the stress-strain curves all prepared specimens behaved like tough materials without yield point. The reaching the elasticity limit was followed up by a long extension ended with the break. Better elongation at break then reference PU sample embodied only specimens having 1 and 5 % wt. of CMC and all PU elastomers filed with hyperbranched AS polysaccharide. Fig. 2. shows that the addition of the bio-filler increased the Young's modulus in all cases except the specimens filled with 1 % wt. of HEC, AC and AS, which should not be taken into deep account due to the relatively high standard deviation of Ey.

Based on the results it is evident that there are two groups of fillers which influence the properties of final material. CMC, HEC and AC forms the first group of the linear cellulose molecules incorporated in PU matrix. 1 % wt. of these bio-polyols in PU matrix increase the tensile strain at break ε_B [%]of prepared specimen and in the case of 1 % wt. of CMC also tensile stress at break σ_B [MPa]. σ_B of 1 % wt. of HEC and AC is lower than σ_B of REF. All cellulose based derivatives filled specimens with content of 5 % wt. of fillers in polyol part have increased σ_B but only in case of 5 % wt. of CMC increased also ε_B. In case of substitution of 10 % wt. of polyol by CMC, HEC or AC have all specimens slightly increased σ_B but decreased ε_B, whereupon, it is possible to say that only addition of 5 and 10 % wt. of CMC can improve the mechanical properties of PU matrix, which corresponded with stress-strain curves, even if SEM microscopy had not proved good adhesion of CMC to PU matrix. The CMC
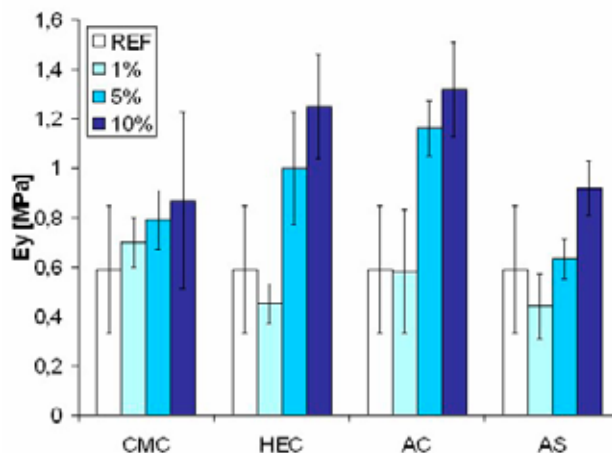
Fig. 2.　**Young's moduli of prepared specimens**

particles are probably very tough composed of long agglomerated fiber, which might improve the elongation during the mechanical straining. On the other side, porous particles of AS showing good adhesion resulting in increase the Young's modulus but also reduce the elongation at break.

The second group include the specimens made of polyol partly substituted by AS which consists of branched amylopectin and linear amylose whose -OH groups of their polymer chains are partly substituted by acetate group $-C(O)CH_3$ with degree of substitution DS = 0.1. Addition of 1 % wt. of AS has increased ε_B and its values of σ_B are very close to REF sample whereas addition of 5 and 10 % wt. have both values higher resulting in improved mechanical properties of above mentioned samples in comparison with reference PU elastomer also proved by SEM pictures. Starch particles are probably more flexible then cellulose ones implicating the increase in elongation at break.

Biodegradation

The growth of thermophillic bacteria in the presence of control and modified PU elastomeric films is illustrated in Fig. 3. It is evident that PU films weakly inhibited the initial
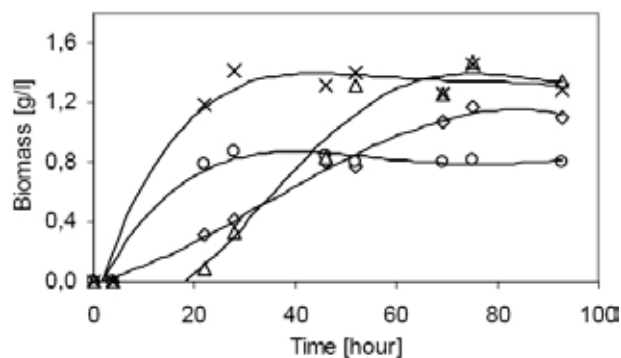
Fig. 3.　**Growth of thermophillic bacteria in the presence of PU biofilms filled with AC (◇), CMC (△) AS (○) and control (×)**

growth phase of bacterial culture where the lag-phase is dependent on the type of modification agent.

Conclusions

Proposed work proved that synthesis of the new cost-effective biodegradable PU elastomers can improve mechanical properties of commercially available polyurethane materials. Applied methods showed that prepared samples have character of particle reinforced composite materials.

In a pilot study, biodegradation of modified polyurethane elastomers by mixed culture of thermophillic bacteria exhibited unusual growth characteristics strongly dependent on the type of biopolymer filler.

REFERENCES

1. Oertel G.: *Polyuretane handbook*, 2nd ed., Hanser Publisher. 3 (1993).
2. Ehrig R. J.: *Plastics Recycling: Products and Processes,* Carl Hanser Verlag, Munich (1992).
3. Boggs F.W.: US Patent 2,908,657, September 15 (1954).
4. Dosmann L.P., Steel R.N.: US Patent 3,004,934, October 31 (1957).
5. Hostettler F.: US Patent 4,197,372, January 16 (1978).
6. Ge J., Zhong W., Guo Z., Li W., Sakai K.: J. Appl. Pol. Sci. *77*, 2575 (2000).
7. Saraf V.P., Glasser W.G.: J. Appl. Polym. Sci. *29*, 1831 (1984).

P20 MODELS OF ORGANIZED SUPERMOLECULAR STRUCTURES: APPLICATION TO COLLAGEN FIBRILS AND DENDRIMERS

JAN ŽÍDEK, JOLANA ŠČUDLOVÁ and JOSEF JANČÁŘ

Institute of Materials Science, Brno University of Technology, Purkynova 118, 612 00 Brno, Czech Republic,
zidek@fch.vutbr.cz

Introduction

Contribution describes simulation of selected supermolecular structures: dendrimers and collagen fibril. Research was focused to relation between its supermolecular structure and macroscopic physical properties derived from the structure.

Dendrimers are synthetic macromolecules with regular and highly branched architecture. They are synthesized with series of controlled reactions, where each step (generation) results in an exponential increase in the number of monomers[1]. Structure of such materials has also impact on their applications such as catalysis or biomedical applications[2,3].

They are interesting from viewpoint of theoretical research because they have simply defined supermolecular structure. It enables building a model of such structures with high fidelity. Second, they have no more stuctural levels between supermolecular and macroscopic structure. This enables instant validation of modeling results with measured properties. Mainly the dendrimer solutions are described in literature. Therefore, modeling of its solvation can be useful.

Collagen is fibrous protein that is found in connective tissue – bone, tendons, and skin. This function requires special properties. The crucial property is high elasticity. The tendons are deformed and relaxed many times during life. Dissipation of a lot of energy could lead to its damage. Moreover, the plastic deformation would lead to permanent deformation of tendons. Neither dissipation of energy nor the permanent deformation is observed in nature.

One of collagen components is composed from complex helical structure. Three factors were taken into account: triple helical supermolecular structure, presence of strong intermolecular interaction, and the layout side chains outside the triple helical structure[5]. Model can be hepful in analysis of the factors. Unlike real experiment, in the model one factor can be switched off and isolated effect other factors can be analyzed separately.

Experimental

Buliding of supermolecular structures as well as deformation and salvation of supermolecular structures were performed by in house software.

Molecular simulations and visualization were realized by general public license software GROMACS [6] and ArgusLab[7].

Building Structure of Dendrimer and its Solvation

Input properties of dendrimers are shown in Fig. 1. The result of the model is a molecule. The molecules were built either in vacuum or in water.
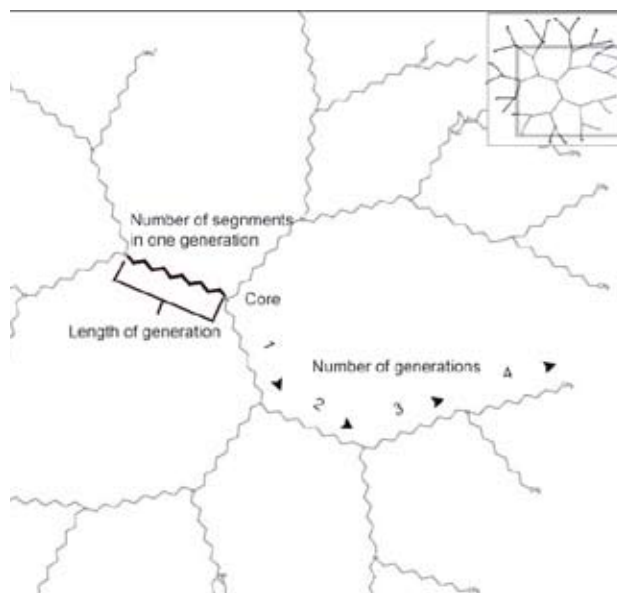
Fig. 1.　**Parametrization of dendrimer molecule**

Building structure and Deformation of Collagen Fibrils

Parameters of collagen triple helix are shown in Fig. 2. Builder outputs are analogous to previous chapter.

The structure was optimized by energy minimalizaion method. A deformation was applied to the collagen fibril by position restrains.
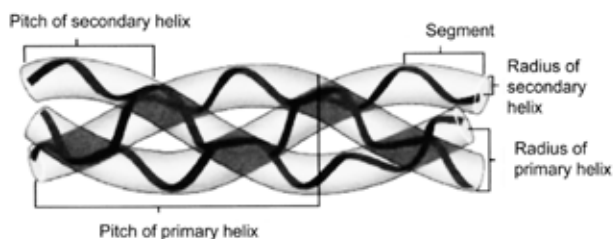
Fig. 2.　**Parametrization of collagen fibril**

Results

Solvation of Dendrimers

Dendrimer of CH_2 group was build of 1st, 2nd and 5th generation. The structures were optimized in vacuum. Introduction of solvent led to steep increase of potential energy. 3.7×10^6 kJ mol^{-1}.

However, the increase of energy may be caused by repulsive intermolecular energy. Two atoms were in close vicinity. The interactions must be analyzed and dendrimer builder with higher fidelity should be programmed.

Deformation of Collagen Fibrils

First, structure of collagen without hydrogen bonds was built. Structure was optimized. The combination of triple helix and weak London interactions were sufficient to conserve main helices; however, they were not sufficient to conserve secondary helix. In this structure, increase of energy during deformation was lower than statistical deviation of energy in undeformed strate. Thus, the deformation was not calculated.
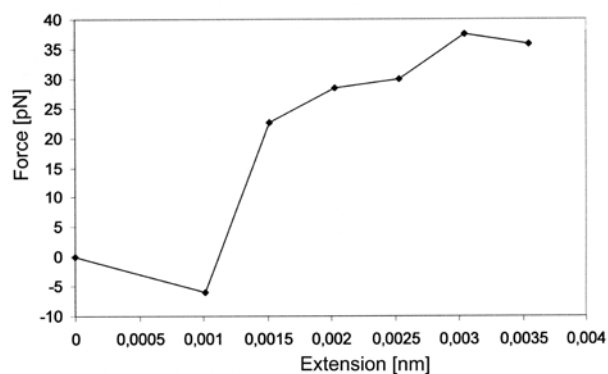
Fig. 3. **Function of force on extension of single collagen fibril**

In case of structure with hydrogen bonds, increase of energy was significant. Deformation was performed until the elongation limit 0.0035 nm. The resulting force is shown in Fig. 3.

Until elongation 0.001 nm no force was registered. Then, the interaction increased. The atoms were probably slightly out of equilibrium in the first phase of simulation.

Conclusions

Properties of selected supermolecular structures: dendrimers and collagen fibrils were investigated. They were calculated by molecular mechanics method. First process was salvation of dendrimer by water. Energy of molecular box increased significantly during solvation. It is not in correlation with real solution. The factor responsible for increase of energy should be analyzed. Deformation of collagen model molecule corresponded to real behavior of collagen fibrils.

REFERENCES
1. Suek N. W., Lamm M. H.: Macromolecules *39*, 4247 (2006).
2. Holister P.,Vas C. R., Harper J. W.: Dendrimers, (2003) http://cientifica.eu/files/Whitepapers/dendrimers_WP.pdf.
3. Opitz W. A, Wagner J. N.: N. Wiley; *44*, 3062.
4. Meyer P.Y., Chen A., Lin Y.M., Seki Y.: Progress in Materials Science *53*, 1 (2008).
5. Okuyama H., Narita T., Kawaguchi K., Noguchi Y., Tanaka N., Nishino N.: Biopolymers *86*, 212 (2007).
6. Gromacs; *Molecular dynamics simualtion: User Manual;* http://www.gromacs.org.
7. ArgusLab: A molecular modeling, graphics, and drug design program http://www.arguslab.com.

9. AUTHOR INDEX

Matulová, D. s777

Matúš, P. s355

Maxová, M. s795

Mazanec, K. s728

Mazur, M. s1089

Melušová, S. s1255

Merna, J. s1243

Mesaros, C. s936, s961

Mesbah, A. W. s956

Michlovská, L. s1238

Mihăiescu, R. s441

Mihăiescu, T. s441

Mika, O. J. s425

Mikula, M. s1051, s1061, s1092

Mikula. M. s1164

Mikulášik, R. s552, s730

Mikulíková, R. s592, s595, s597, s716, s724

Milata, V. s521

Minea, R. s663

Mirzaei, M. s978

Mládková, Z. s428

Mocák, J. s556, s706, s736

Mockovčiaková, A. s834, s864

Mojtahedi, M. M. s956, s975

Momeu, C. s622

Moos, M. s430, s432, s497

Morales, F. J. s610

Moreno, F. s435, s733

Mravcová, L. s290, s437, s459, s461, s511, s1238

Mravec, F. s1096

Mrázová, V. s556, s736

Muchová, Z. s718

Müller, L. s682

Müller, P. s371

Muntean, E. s439, s441

Muntean, N. s439, s441

Munteanu, M. F. s739

Musilová, J. s489

N

Nápravníková, M. s375, s445, s771

Navrátil, J. s1250

Negrea, O. s589, s726

Nehyba, S. s371

Nemcová, K. s599

Němec, K. s884

Németh, L. s544

Nešpůrek, S. s1259

Nesterenko, P. s319

Nezbedová, E. s1276

Němcová, A. s871

Niculescu, V. s479

Niksic, M. s406

Noaman, M. S. M. s927

Noskovič, J. s395

Novák, F. s1086

Novák, J. s420

Nováková, E. s952, s1252

Novotný, M. s1257

Nôžková, J. s626, s628, s680

O

Obruča, S. s1219, s1255, s1257

Ohlídalová, M. s1175

Omelka, L. s1099, s1162

Omelková, J. s630, s660, s742, s745

Ondruch, P. s1115

Ondruška, V. s747, s1219

Opravil, T. s822, s847, s891, s893, s895, s897, s900, s910, s913, s916

Orolínová, Z. s834, s839

Ošmera, P. s1102

Ouzzane, I. s1259

P

Pajurková, J. s1166

Pállová, Z. s839

Palou, M. s927

Panák, J. s1045, s1048

Pařilová, K. s624, s647, s724

Pasquale de, C. s1284

Pauliková, A. s399, s402

Paulusová, H. s1170

Păun, N. s479

Pavlisová, D. s1039

Pečinková, D. s689

Pekař, M. s1096, s1137, s1139, s1152, s1238

Pešková, K. s428

Petriláková, K. s1224

Petrovičová, M. s1054, s1170, s1172, s1175

Piechová, J. s1257

Pigeot-Remy, S. s1007

Pigot, T. s1007

Pilný, O. s1156

Pintea, A. s579, s589, s619, s749, s803, s963

Pleskačová, H. s461

Pobudová, Z. s1164

Podborská, M. s751

Podrbábský, T. s880

Podunavac-Kuzmanović, S. O. s753, s757, s762

Pokorný, E. s1147

Polívka, Ľ. s810

Polovka, M. s552, s560, s765, s797

Pospíšilová, Ľ. s1147, s1178

Pospíšilová, S. s880

Potáček, M. s973

Poustka, J. s375, s445, s571, s694, s771

Považanec, F. s1083

Praščáková, M. s415

Přikryl, R. s1261

Princz, E. s482

Prokeš, O. s487, s844

Z

Zachariášová, M. s571, s694, s700

Zachová, L. s657

Zajíčková, L. s1158

Zalibera, M. s1112

Zamazalová, P. s929

Zamiri, B. s978

Zaujec, A. s463, s525, s1200

Zbořil, F. s386

Zdeňková, M. s819

Zdráhal, Z. s647, s724

Zechmeistrová, L. s742

Zelenka, J. s1132

Zeman, S. s943

Zemanová, J. s795, s817

Zemanová, L. s527

Zlámalová Gargošová, H. s359, s529

Zmeškal, O. s959, s1033, s1127

Zmrzlý, M. s931

Znamenáčková, I. s531

Zrostlíková, J. s282

Zubrik, A. s534

Ž

Ždánská, P. s720

Žídek, J. s1235, s1265, s1282

Žúbor, V. s1089

10. LIST OF PAPERS

51. mezinárodní strojírenský veletrh

MSV 2009

5. mezinárodní veletrh dopravy a logistiky

Transport a Logistika

14.–18. 9. 2009

Brno – Výstaviště

www.bvv.cz/msv
www.bvv.cz/imt

Central European Exhibition Centre

Veletrhy Brno, a.s.
Výstaviště 1
647 00 Brno
tel.: +420 541 152 926
fax: +420 541 153 044
e-mail: msv@bvv.cz
www.bvv.cz/msv

BVV
Veletrhy Brno